

EANM'16



Annual Congress
of the
European Association of Nuclear Medicine
October 15 – 19, 2016
Barcelona, Spain

Abstracts

European Journal of Nuclear Medicine and Molecular Imaging
Volume 43, Supplement 1
10.1007/s00259-016-3484-4

This supplement was not sponsored by outside commercial interests. It was funded entirely by the association's own resources.

Table of Contents

Content	Page
Welcome Message.....	S3
Programme at a Glance.....	S4
Oral Sessions.....	S7
e-Poster Walks.....	S209
Poster Walks.....	S243
e-Posters.....	S254
Posters.....	S545
Technologist Posters.....	S641
Authors Index.....	S674
ESMIT.....	S732
EANM'17.....	S734

Welcome to the EANM Congress 2016 in Barcelona

With great pleasure the European Association of Nuclear Medicine welcomes you to its 29th Annual Congress in Barcelona, Spain.

The Annual EANM Congress 2016 offers attendees from all over the world the broad perspective on basic, translational and clinical science that makes nuclear medicine such an exciting and vibrant profession. The EANM Committees have made a tremendous effort to put together a high-quality program for you to attend. You will not only recognize the traditional elements that make our meeting stand out, but also some novelties to further enhance your experience during the meeting. Next to the clinicians, scientists and technologist in nuclear medicine, we are especially proud to extend a special welcome to the numerous guests from outside our community, who will deliver lectures and discuss multimodality molecular imaging, therapy, physics, basic science, technology from their perspective.

The 2016 plenary sessions will traditionally open on Sunday, October 16 with Clinical Molecular Imaging (including the Marie Curie Lecture by Prof. Sally Barrington from London, UK on the role of nuclear medicine in malignant lymphoma), followed by “Radiation – facts and figures” on Monday, October 17. As part of the M2M - Molecule to Man track, which has rapidly expanded to a track running over the full duration of the meeting, the plenary session on Tuesday, October 18 will focus on New Developments in Cancer Imaging and Therapy. We are honored that Prof. Maria Blasco, one of leading scientists in cancer research, will give a lecture based on her world-class research. The traditional conclusion of the meeting on Wednesday, October 19 will be the Highlights Lecture, presented by Prof. Françoise Kraeber-Bodéré and Prof. Eric Aboagye.

The joint efforts of the EANM Committees will be visible throughout the congress. Multi-committee collaborations are reflected in the Molecule to Man (M2M) track which addresses basic and translational research and in the Dosimetry and Molecular Radiotherapy (Do.MoRe) tracks. Both tracks will run throughout the Congress. To highlight the best proffered papers in M2M and Do.MoRe tracks, both tracks will feature a Rapid Fire session chaired by distinguished experts in the field, in which the authors of the very best papers in these tracks are invited to give a short plenary pitch of their work, followed by discussions with you while gathering around posters detailing the work. The third Rapid Fire session will again summarize the best presentations in field of clinical oncology.

You will experience the best that clinical, translational and fundamental nuclear medicine has to offer in an open, truly multidisciplinary setting that is characterized our profession. The Scientific Program Committee, representing all EANM Committees, received a total of 2201 abstracts, of which 1881 were accepted for oral sessions (509 presentations) or poster sessions (1372 presentations). For the first time the EANM Congress will feature the Presidential session, a one-of-a-kind session during the meeting presenting you works of excellence and late-breaking science.

In the pre-congress and the joint symposia, a large number of experts from disciplines outside nuclear medicine together with experts from the EANM Committees will provide new data and will share with you how nuclear medicine contributes to better science and enhanced patient care throughout the areas in which nuclear medicine is active. A special symposium on radionuclide therapy has been organized by Dr. Savvas Frangos, commemorating the pioneering work of Prof. Saul Hertz, who performed the first radioiodine treatment of thyroid disease 75 years ago. In collaboration with the European School of Nuclear Medicine, the EANM Committees organized a full track of CME sessions, again featuring many interactive sessions. As hybrid imaging is one of the core contributions of nuclear medicine to today’s patient care, educational lectures on cross-sectional imaging to support interpretation of molecular imaging are an important part of the educational program. The EANM Technologist Committee contributes to a successful meeting with a full parallel program of oral and poster sessions as well as Continuing Technologist Education (CTE) sessions and courses.

It has been a true privilege for me to be allowed to act as your Congress Chair for the EANM’16 Congress. The content of the meeting reflects the team work of many professionals in our field who have devoted time and effort to deliver the program in all its diversity. I am very grateful to all members of the EANM Committees, the staff of the EANM Executive Office, all speakers and session chairs and everyone involved in putting this meeting together.

On behalf of the EANM community, I welcome you to the 29th EANM Congress Barcelona’16. I sincerely hope that you will enjoy, discuss, learn and get inspired for the bright future of our profession and that you will appreciate the many wonderful features that Barcelona has to offer.

Prof. Dr. Wim J. G. Oyen
EANM Congress Chair 2014-2016

Saturday, October 15, 2016												
Time/Room	Auditorium	111	112	113	114	115	116	117	118	119	120	
Capacity	3000	800	800	800	800	800	800	800	800	800	800	
08:00 - 19:00				EANM Advisory Council Meeting (11:00 - 13:00)	EANM Delegates Assembly (13:45 - 15:45)	Pre-Symposium 1: Imaging for Therapy with Statistical SPECT/PET Reconstruction (09:00 - 16:00)	Pre-Symposium 2: Radionuclide Therapies of Brain Tumours (09:00 - 12:00)	Pre-Symposium 4: EANM/ASNC Myocardial Perfusion Imaging in Clinical Routine: From SPECT/PET to Hybrid Imaging (09:00 - 12:00)	EANM Members Assembly (16:00 - 18:30)	Pre-Symposium 6: Advances in Hybrid Imaging in Musculoskeletal Infections (09:00 - 12:00)	Pre-Symposium 8: Challenging the Brain: Imaging Neurotransmitter Release (09:00 - 16:00)	Poster Setup (08:00 - 20:00)
19:30 - 20:30	OPENING CEREMONY (19:30 - 20:30) & WELCOME RECEPTION (20:30 - 23:00)											

Sunday, October 16, 2016												
Time/Room	Auditorium	111	112	113	114	115	116	117	118	119	120	
Capacity	3000	800	780	800	800	800	800	800	800	800	800	
08:00 - 09:30	CME 1 Paediatrics/Oncology/ELI PET in Lymphoma: What are the New Fields in Adult and Paediatric Practice?	Joint Symposium 1 EANM/EULAR Spondyloarthropathies	Technologists Opening (08:00 - 08:12) CTE 1 Radiation Protection and Dose Optimisation (Tech Guide Book Launch) (08:15 - 09:45)	Do.Molle Clinical Dosimetry for 20Y Radioembolisation	M2M - Featured PSMA Targeting	Pitfalls & Artifacts - Interactive Endocrine and Exocrine Imaging - Interpretation and Misinterpretation	Clinical Oncology Gastrointestinal			Conventional & Specialised Nuclear Medicine Urology		(08:30 - 09:30) Poster Walk PW-1, PW-3 in Poster Area e-Poster Walks E-PW1, E-PW2, E-PW3
10:00 - 11:15	Primary 1 incl. Marie Curie Lecture Clinical Molecular Imaging		209 In Auditorium Primary 1 incl. Marie Curie Lecture Clinical Molecular Imaging									
11:30 - 13:00	CME 2 Dosimetry/Radionuclide Therapy Dosimetry for Clinical Trials	Joint Symposium 2 EANM/ICRP Dosimetry-Guided Personalized Therapy - Are We Prepared for February 6, 2018?	Technologists CTE 2 - Interactive Technologist Competencies Round Table		M2M New Radionuclides - Brain	Physics & Instrumentation & Data Analysis Advanced Quantification & Kinetic Modeling		Special Symposium 1 Key Issues in Cardiovascular Nuclear Medicine	Clinical Oncology Rapid Fire Session	310 Conventional & Specialised Nuclear Medicine Paediatrics		
13:00 - 14:30				Sanofi Genzyme Symposium			Styer Symposium	BTC Symposium				Young EANM Daily Forum
14:30 - 16:00	CME 3 Oncology/EORTC Metabolic Response Assessment in Solid Tumours	Joint Symposium 3 EANM/E-DIB Consortium Dementia with Lewy Bodies (DLB): What Have We Learned in the Last Years?	Technologists (14:30 - 15:00) Mini Course 1 Updates in Radiopharmaceuticals for SPECT (15:15 - 16:45) Mini Course 2 Updates in Radiopharmaceuticals for PET	Do.Molle - Featured PSMA Imaging & Therapy	M2M PET/CT & Metabolism - Preclinical	Teaching Session - Interactive TBA	Clinical Oncology Image Guided Surgery	Physics & Instrumentation & Data Analysis SPECT Image Processing & Reconstruction	Conventional & Specialised Nuclear Medicine Infection & Inflammation 1	Late Breaking Abstracts "The Presidential Session"		(16:00 - 16:30) Poster Sessions (P-01 - P-08)
16:30 - 18:00	CME 4 Radiopharmacy/Drug Development Antibody-Based Radiopharmaceuticals	Joint Symposium 4 EANM/ESTRO SBT - Tried or the Next Change in a Treatment Paradigm?	403c (17:00 - 18:00) Mini Course 3 Updates in Radiopharmaceuticals for Radionuclide Therapy	Do.Molle - Featured Thyroid Dosimetry	M2M - Featured SPECT/CT - Preclinical	Teaching Session - Interactive TBA	Clinical Oncology Head & Neck	Committee Symposium EANM/EASL Why Your Centre should be EARL Accredited - The Nuclear Medicine Physician Point of View/ The Physicist Point of View	Cardiovascular System Cardiac Sarcofollis, Amyloidosis & (Large) Vessel Vasculitis	Neurosciences Miscellaneous		

Monday, October 17, 2016

Time/Room	Auditorium	111 800	112 780	113 800	115 360	111 360	116 360	112 360	113 360	114 360	Area 4 + 5 - Poster Exhibition
08:00 09:30	CME 5 Radiobiology/Radiation Biology Markers of Radiation Damage	601 Joint Symposium 5 EANN/EACVI Imaging Atherosclerosis: From Inflammation to Calcification	603 Technologists Oral Presentations 1	604 Do.MoRe Thyroid & Parathyroid	605 M2M PET/CT - Preclinical	606 Pitfalls & Artefacts - Interactive Pitfalls in Paediatrics Bone Imaging	Clinical Oncology Breast & Gynaecology	608 Physics & Instrumentation & Data Analysis Multimodality Systems & Quantification	609 Special Session Sustainability of Supply of Medical Radioisotopes in the EU	610 Neurosciences Data Analysis & Quantification	08:30 - 09:30 In-Poster Area e-Poster Walks E-PW3, E-PW4, E-PW5, E-PW10
10:00 11:15	701 Plenary 2 Radiation Facts and Figures		703 In Auditorium Plenary 2 Radiation Facts and Figures								
11:30 13:00	CME 6 Neuroimaging Alzheimer's Disease and Amyloid PET: News and Views 2016	802 Joint Symposium 6 EANN/EAU Imaging for Staging Prostate Cancer	803 Technologists Oral Presentations 2			806 Cardiovascular System Myocardial Sympathetic Innervation	807 Clinical Oncology - Featured NET	808 Physics & Instrumentation & Data Analysis PET/CT Performance & Instrumentation	809 M2M Rapid Fire Session	810 Neurosciences Basic Science	
13:00 14:30				GE Healthcare Symposium		Sirtex Symposium	EB Lilly Symposium			Young EANN Daily Forum	
14:30 16:00	CME 7 Cardiovascular/Inflammation & Infectious/EACVI Imaging Sarcoidosis, Endocarditis and Amyloidosis by PET	902 Joint Symposium 7 EANN/SEMIN Latest Advances in Multidisciplinary Management of Tumours of the Digestive System	903 Technologists CTE 3 Joint Session with SNMMI Dose Optimisation	904 Do.MoRe Bone Palliation	905 M2M Radiolabelled Peptides	906 Teaching Session - Interactive TBA	907 Clinical Oncology Prostate	908 Physics & Instrumentation & Data Analysis Practical & Clinical SPECT Systems & Performance	909 Conventional & Specialised Nuclear Medicine Endocrinology & Gastroenterology	910 Neurosciences Dementia	16:00 - 16:30 Poster Sessions (P-09 - P-17)
16:30 18:00	CME 8 Physics/Translational Molecular Imaging & Therapy DA/OC Preclinical Systems and Practical Imaging Procedures	1002 Joint Symposium 8 EANN/EASD The Infected Diabetic Foot – Consensus Meeting	1003 Technologists CTE 4 Nuclear Medicine Oncology beyond FDG	1004 Do.MoRe Neuroendocrine Tumours	1005 M2M New Chemistry & Instrumentation	1006 Teaching Session - Interactive TBA	1007 Clinical Oncology Haematology (LMM + MM)	1008 Special Symposium 2 The Soul Hertz Symposium – 75 Years of Radioisotope Therapy	1009 Cardiovascular System Imaging of Cardiovascular (Vulnerable) Plaques	1010 Neurosciences Movement Disorders & Neurodegeneration	

Tuesday, October 18, 2016

Time/Room	Auditorium	111 800	112 780	113 800	115 360	111 360	116 360	112 360	113 360	114 360	Area 4 + 5 - Poster Exhibition
08:00 09:30	CME 9 Drug Development/ Radiopharmaceutical/Translational Molecular Imaging & Therapy Strengths and Limitations of Techniques and Instrumentation	1102 Joint Symposium 9 EANN/ENIT/S/OPEN Strategies in Endocrine Tumors: Neuroblastoma & Paraganglioma	In Area 4 + 5 - Poster Exhibition Technologists Poster Sessions TP-01, TP-02, TP-03, TP-04	1104 Committee Symposium EANN Do.MoRe: Feasibility of Treatment Planning for Radioisotope Therapy	1105 M2M - Featured Radioisotope Production	1106 Pitfalls & Artefacts - Interactive Joint Session EANN/ESR Basic Artefacts in Hybrid Imaging (SPECT/CT, PET/CT and PET/MR): Pitfalls and Solutions	1107 Clinical Oncology - Featured PSMA Theranostics	1108 Cardiovascular System Myocardial Perfusion - Conventional SPECT			08:30 - 09:30 Poster Walks PW-4 In-Poster Area e-Poster Walks E-PW6, E-PW7, E-PW8
10:00 11:15	1201 Plenary 3 New Developments in Cancer Imaging and Therapy		1203 In Auditorium Plenary 3 New Developments in Cancer Imaging and Therapy								
11:30 13:00	CME 10 Translational Molecular Imaging & Therapy/Radiopharmacy Developments on Radioisotope and Radiopharmaceutical Manufacturing and Automation	1302 Joint Symposium 10 EANN/EORTC Apoptosis and Proliferation – Two Important Hallmarks of Cancer: From Bench to Bedside	1303 Technologists Oral Presentations 3		1305 M2M Oncology - Preclinical	1306 Physics & Instrumentation & Data Analysis PET/CT Image Analysis & Quantification	1307 Clinical Oncology - Featured PET/MR in Clinical Oncology	1308 Cardiovascular System Myocardial Perfusion - Gated SPECT	1309 Do.MoRe Rapid Fire Session	1311 In Hall 130 Joint Session EANN/SNMMI Paediatric Dose Optimisation	
13:00 14:30				Hall 133/134 AAA Symposium		Noirige Symposium	Spectrum Dynamics Medical Symposium			Young EANN Daily Forum	
14:30 16:00	CME 11 Paediatric/Inflammation & Infectious/ESPGHAN/ESR Inflammatory Bowel Disease (Adults and Children)	1402 Joint Symposium 11 EANN/ETA-CRN New Approaches in Thyroid Cancer Management	1403 Technologists CTE 5 Joint Session with ESTRO Radiotherapy Planning	1404 Do.MoRe Thyroid	1405 M2M/Do.MoRe - Featured Radioisotope Therapy - Preclinical	1406 Teaching Session - Interactive TBA	1407 Clinical Oncology Prostate PSMA	1408 Cardiovascular System Myocardial Perfusion - CZT	1409 Conventional & Specialised Nuclear Medicine Musculoskeletal - Benign		16:00 - 16:30 Poster Sessions (P-18 - P-26)
16:30 18:00	CME 12 Oncology/Radioisotope Therapy/ESO Therapeutic Options for Hepatic, Primary and Secondary Tumours	1502 Joint Symposium 12 EANN Developments with Cardiovascular Tracers		1504 Do.MoRe Cellular Dosimetry Response	1505 M2M Protein-Based Radiotracers	1506 Teaching Session - Interactive TBA	1507 Clinical Oncology Lung	1508 Cardiovascular System Myocardial Perfusion - PET		1510 Neurosciences Psychiatry & Neurotransmission	

Wednesday, October 19, 2016											
Time/Room Capacity	112 800	113 780	114 800	115 800	116 800	117 800	118 800	119 800	120 800	121 800	Area X Y 5: Poster Exhibition
08:00 - 09:30	1601 CME 13 - Interactive Bone & Joint/ESSR The Post-Operative Spine	1602 Joint Symposium 13 EANM/ISNM GMP Meets Drug Development	1603 Technologists CTE 6 Positron Emission Mammography	1604 Du.Molle Clinical Dosimetry - 177Lu Peptides	1605 M2M - Featured Nuclear & Optical Imaging	1606 Pitfalls & Artifacts - Interactive Breast Cancer and PET with Various Tracers FDG, Fluoride, Fluoroestradiol and Others	1607 Clinical Oncology CNS Tumours	1608 Special Symposium 3 (Part I) EANM/ESSO Advances in Radionuclide Intervention for Biopsy of Occult Lesions and Sentinel Nodes	1609 Joint Symposium 15 EANM/ISNM Standardisation of Imaging and Harmonisation Criteria of the Scanning Protocols for FDG, Ammonia and Amyloid PET of the Brain		
10:00 - 11:30	1701 CME 14 Thyroid/ETA Non-isotopic Diagnostic Thyroidology - An Update for Nuclear Medicine Physicians	1702 Joint Symposium 14 EANM/ESMI Best of EMM 2016			1705 M2M Nanoparticles & Macromolecules	1706 Physics & Instrumentation & Data Analysis Dosimetry, Radiation Safety & Miscellaneous	1707 Clinical Oncology Lymphoma	1708 Special Symposium 3 (Part II) EANM/ESSO Advances in Radionuclide Intervention for Biopsy of Occult Lesions and Sentinel Nodes	1709 Conventional & Specialised Nuclear Medicine Infection & Inflammation 2		
11:45 - 13:20	1801 (11:45 - 12:15) Awards Ceremony (12:15 - 13:15) Highlights Lecture (13:15 - 13:20) Closing Ceremony		1803 in Auditorium Awards Ceremony (12:15 - 13:15) Highlights Lecture (13:15 - 13:20) Closing Ceremony								

- Pre-Program Meetings/Sessions & Industry Sponsored Symposia / Young EANM Daily Forum
- Primary Sessions
- Continuing Medical Education Sessions
- Scientific Symposia
- Technologist Track
- Poster Sessions
- Parallel Sessions
- Du.Molle Track
- M2M Track
- M2M & Artifacts / Teaching Session

Oral Sessions

PS1 – Saturday, October 15, 2016, 09:00 - 16:00, Hall 115

Pre-Congress Symposium 1: Imaging for Therapy with Statistical SPECT/PET Reconstruction

PS01

General Introduction on Pre-Therapy Imaging for Predicting Biodistribution under Therapy

G. Glatting; Medizinische Fakultät Mannheim der Universität Heidelberg, Medizinische Strahlenphysik/Strahlenschutz, Mannheim, GERMANY.

PS02

Introduction to Problems Related to Quantitative Imaging of SPECT and PET

M. Ljungberg; Lund University, Dept Medical Radiation Physics, Lund, SWEDEN.

PS03

Statistical Reconstruction Methods

M. Defrise; UZ Brussel, Department Nuclear Medicine, Brussels, BELGIUM.

PS04

Compensation Methods in Statistical Reconstruction Methods

H. de Jong; UMC Utrecht, Utrecht, NETHERLANDS.

PS05

Quantitative Y-90 PET Imaging

H. de Jong; UMC Utrecht, Utrecht, NETHERLANDS.

PS06

Quantitative Y-90 SPECT Bremsstrahlung Imaging

M. Ljungberg; Lund University, Dept Medical Radiation Physics, Lund, SWEDEN.

PS07

Quantitative Lu-177 SPECT Imaging

K. Sjögren Gleisner; Lund University Hospital, Clinical Sciences, Lund, Medical Radiation Physics, Lund, SWEDEN.

PS08

Quantitative I-124 SPECT Imaging

W. Jentzen; Klinik für Nuklearmedizin, Essen, GERMANY.

PS09

Quantitative I-131 SPECT Imaging

Y. K. Dewaraja; University of Michigan, Department of Radiology, Ann Arbor, UNITED STATES OF AMERICA.

PS10

Developments in New Hardware

S. Walrand; Saint-Luc, Université Catholique de Louvain, Nuclear Medicine Center, Brussels, BELGIUM.

PS2 – Saturday, October 15, 2016, 09:00 - 12:00, Hall 111

Pre-Congress Symposium 2: Radionuclide Therapies of Brain Tumours

PS12

WHO 2016 Classification of CNS Tumours; Incorporation of Diagnostic and Prognostic Molecular Markers

P. Wesseling; Radboud UMC, Nijmegen, NETHERLANDS.

PS13

Challenges in Imaging for Diagnosis and Management of Brain Tumours

A. Waldman; Charing Cross Hospital, Department of Imaging, London, UNITED KINGDOM.

PS14

The Potential of PET for Guiding Therapy in Brain Tumours

K. Herholz; University Of Manchester, Wolfson Molecular Imaging Centre, Manchester, UNITED KINGDOM.

PS16

Surgical Management with Standard Techniques and New Approaches

J. Barcia; Hospital Clínico San Carlos, Department of Neurosurgery, Madrid, SPAIN.

PS17

Treatment Management in Adults and Children with Brain Tumours - Insight on Clinical Trials

A. Salmaggi; Ospedale di Lecco, Lecco, ITALY.

PS18

Radiotherapy and Brain Tumours - How and When?

A. L. Grosu; University Medical Center Freiburg, Department of Radiation Oncology, Freiburg, GERMANY.

PS19

Radionuclide Therapy in Brain Tumours

F. Forrer; Kantonsspital St. Gallen, Department of Radiology and Nuclear Medicine, St. Gallen, SWITZERLAND.

PS4 – Saturday, October 15, 2016, 09:00 - 12:00, Hall 116

Pre-Congress Symposium 4: Myocardial Perfusion Imaging in Clinical Routine - From SPECT/PET to Hybrid Imaging

PS20

How to Speak Cardiology - Risk Factors, Medications, the ECG, Stress Testing

H. Verberne; Academic Medical Center, Department of Nuclear Medicine, Amsterdam, NETHERLANDS.

PS21

Clinical Indications for SPECT and PET MPI - Patient Selection delete etc.

D. Wolinsky; Cleveland Clinic Florida, Weston, UNITED STATES OF AMERICA.

PS22**SPECT/CT and PET/CT Hybrid Imaging - How and When?**

S. Dorbala; Brigham and Women's Hospital, Department of Radiology, Boston, UNITED STATES OF AMERICA.

PS23**Patient-Centered Imaging and Radiation Dose Reduction Strategies**

E. Depuey; Mount Sinai Hospital, New York, UNITED STATES OF AMERICA.

PS24**Case Review - A Systematic Approach to Interpreting and Reporting MPI SPECT(/CT)**

A. Todica; Klinikum Großhadern, University of Munich, Department of Nuclear Medicine, Munich, GERMANY.

PS25**Case Review - A Systematic Approach to Interpreting and Reporting MPI PET(/CT)**

R. Sciagra; University of Florence, Department of Nuclear Medicine, Florence, ITALY.

PS26**Effective Reporting for Patient Risk Stratification and Management**

B. Abbott; Rhode Island Hospital, East Greenwich, UNITED STATES OF AMERICA.

PS6 – Saturday, October 15, 2016, 09:00 - 12:00, Hall 113

Pre-Congress Symposium 6: Advances in Hybrid Imaging in Musculoskeletal Infections**PS28****What do Clinicians Want to Know from the Imaging Specialists?**

P. Jutte; Orthopaedic Surgery, University Medical Center Groningen, Groningen, NETHERLANDS.

PS29**New Available Tests to Diagnose Musculoskeletal Infections**

A. Cataldo; National Institute for Infectious Diseases, Clinical Department, Rome, ITALY.

PS30**Radiologic Imaging of Musculoskeletal Infections**

V. Cassar-Pullicino; The Robert Jones and Agnes Hunt Orthopaedic Hospital, Department of Diagnostic Imaging, Oswestry, UNITED KINGDOM.

PS31**Hybrid Imaging of the Painful Joint**

W. van der Bruggen; Slingeland Ziekenhuis, Dept. Radiology and Nuclear Medicine, Doetinchem, NETHERLANDS.

PS32**Imaging the Painful Spine (Including the New Joint Society Endorsed Guidelines for Imaging Spondylodiscitis)**

E. Lazzeri; Centro Regionale Medicina Nucleare, Azienda Ospedaliero Universitaria Pisana, Pisa, ITALY.

PS33**Imaging Peripheral Bone Infection (Including the New Joint Society Endorsed Guidelines)**

A. Glaudemans; University Medical Center Groningen, Nuclear Medicine and Molecular Imaging, Groningen, NETHERLANDS.

PS34**Imaging Prosthetic Joint Infection (Including the New Joint Society Endorsed Guidelines)**

O. Gheysens; KU Leuven, Leuven, BELGIUM.

PS8 – Saturday, October 15, 2016, 09:00 - 16:00, Hall 114

Pre-Congress Symposium 8: Challenging the Brain: Imaging Neurotransmitter Release**PS36****Radiotracers for Measuring Endogenous Neurotransmitter Release**

C. Halldin; Psychiatry Section, Department of Clinical Neuroscience, Stockholm, SWEDEN.

PS37**Methodological Considerations for Measuring in Vivo Neurotransmitter Release**

A. Lammertsma; VU University medical center, Department of Nuclear Medicine & PET Research, Amsterdam, NETHERLANDS.

PS39**Striatal Dopamine Release - From Pharmacologic to Non-Pharmacologic Challenges**

J. Booij; Academic Medical Center, Nuclear Medicine, Amsterdam, NETHERLANDS.

PS40**Extrastriatal Dopamine Release**

E. van de Giessen; Academic Medical Center, University of Amsterdam, Nuclear Medicine, Amsterdam, NETHERLANDS.

PS42**Serotonin Release - Promises and Pitfalls**

G. Knudsen; Copenhagen University Hospital Rigshospitalet, Neurobiology Research Unit 9201, Copenhagen, DENMARK.

PS43**New Ways to Image Noradrenaline**

S. Finnema; Yale University, PET Center, New Haven, UNITED STATES OF AMERICA.

PS45**Measuring Endogenous GABA Release**

J. Myers; Imperial College London, Division of Brain Sciences, Centre for Neuropsychopharmacology, London, UNITED KINGDOM.

PS46**Effects of Psychotropic Medications on the Developing Brain (ePOD) - A Case for Pharmacological MRI**

L. Reneman; Academic Medical Center, Department of Radiology, Amsterdam, NETHERLANDS.

PS3 – Saturday, October 15, 2016, 13:00 - 16:00, Hall 111
Pre-Congress Symposium 3: Strategies in Endocrine Tumours

PS49

Novel Developments in Adrenocortical Carcinoma
C. Bluemel; University of Wuerzburg, Wuerzburg, GERMANY.

PS50

F-18-Choline-PET/CT vs MIBI-Scintigraphy in Parathyroid Adenomas
W. Langsteiger; St Vincent's Hospital, PET - CT Center LINZ, Nuclear Medicine & Endocrinology, Linz, AUSTRIA.

PS51

Renaissance of Redifferentiation in Thyroid Cancer
J. Nagarajah; University Hospital Essen, Nuclear Medicine, Essen, GERMANY.

PS52

New MTC Guidelines and Role of Nuclear Medicine
G. Treglia; Oncology Institute of Southern Switzerland, Bellinzona, SWITZERLAND.

PS53

Low versus High Activities in Ablation - Open Discussion
U. Mallick; FREEMAN HOSPITAL, NCCC, ONCOLOGY, Newcastle Upon Tyne, UNITED KINGDOM.

PS54

Low versus High Activities in Ablation - Open Discussion
F. A. Verburg; University Hospital Aachen, Dept. of Nuclear Medicine, Aachen, GERMANY.

PS5 – Saturday, October 15, 2016, 13:00 - 16:00, Hall 116
Pre-Congress Symposium 5: Multimodality Imaging – Opportunities and Challenges

PS56

Multimodality Imaging – Opportunities and Challenges – General Aspects
G. van Dam; University of Groningen, Groningen, NETHERLANDS.

PS57

Opportunities and Challenges of Compounds for Multimodality Imaging

PS58

In Vivo Imaging of Tumor Metabolism and Acidosis by Combining PET and MRI-CEST pH Imaging
S. Aime; Molecular Imaging Center, Torino, ITALY.

PS59

Combined Optical and Nuclear Medicine Imaging
W. Cai; University of Wisconsin-Madison, Department of Radiology and Medical Physics, Madison, UNITED STATES OF AMERICA.

PS7 – Saturday, October 15, 2016, 13:00 - 16:00, Hall 113
Pre-Congress Symposium 7: Radionuclide Support Crisis – An Update: what will happen?

PS61

Global Update on Mo-99
S. Schwarz; Washington University School of Medicine, Washington, UNITED STATES OF AMERICA.

PS62

Overview from the European Industrial Perspective
J. VANDERHOFSTADT; I.R.E., Fleurus, BELGIUM.

PS63

Cyclotron-Produced Tc-99m
R. Harper; Centre for Probe Development and Commercialization Hamilton Health Sciences, Hamilton, CANADA.

PS64

Alternative Cyclotron-Produced Radionuclides
L. Perk; Radboud university medical center, Radboud Translational Medicine, Nijmegen, NETHERLANDS.

101 – Sunday, October 16, 2016, 08:00 - 09:30, Auditorium
CME 1 - Paediatrics/Oncology/ELI: PET in Lymphoma: What are the New Fields in Adult and Paediatric Practice?

OP001

Early Response PET in Paediatric Lymphoma - Qualitative Criteria or qPET?
R. Kluge; Universität Leipzig, Klinik und Poliklinik für Nuklearmedizin, Leipzig, GERMANY.

OP002

PET in Peripheral T Cell Lymphoma
A. Cottreau; Henri Mondor, Nuclear Medicine, Paris, FRANCE.

OP003

PET Combined with Biological Data in Lymphoma
A. Gallamini; A. Lacassagne Cancer Center, Research, Innovation and statistics department, Nice, FRANCE.

102 – Sunday, October 16, 2016, 08:00 - 09:30, Hall 211
Joint Symposium 1 - EANM/EULAR: Spondyloarthropathies

OP004b

Clinical Challenges in the Management of Spondyloarthropathies: What the Clinician Wants to Know From SPECT/CT and PET/CT Imaging?
G. Hayem; Hospital Bichat - Claude-Bernard, Department of Rheumatology, Paris, FRANCE.

OP005

Radiopharmaceuticals for Imaging Rheumatic Diseases (RA, SS, Vasculitis)
A. Versari; S. Maria Nuova Hospital, Nuclear Medicine, Reggio Emilia, ITALY.

OP006**Advances in the Radiologic Assessment of (Suspected) Spondyloarthropathy: Role and Limitations of Whole-Body MRI**

V. Zubler; Universitätsklinik Balgrist, Radiologie, Zurich, SWITZERLAND.

OP007a**Radionuclide Imaging in Spondyloarthropathy: A Revival Through Hybrid Imaging?**

A. Versari; S. Maria Nuova Hospital, Nuclear Medicine, Reggio Emilia, ITALY.

103 – Sunday, October 16, 2016, 08:15 - 09:45, Hall 117

CTE 1: Radiation Protection and Dose Optimisation (Tech Guide Book Launch)**OP008****Interaction of Radiation with Matter**

Á. K. Krizsán; Medical and Health Science Center, University of Debrecen, Nuclear Medicine, Debrecen, HUNGARY.

OP009**Radiobiology Principles**

L. Lundholm; Stockholm University, Centre for Radiation Protection Research, MBW Department, Stockholm, SWEDEN.

OP010**Nuclear Medicine and PET Department Design Considerations**

E. A. Bailey; Royal North Shore Hospital, Department of Nuclear Medicine, Sydney, AUSTRALIA.

104 – Sunday, October 16, 2016, 08:00 - 09:30, Hall 112

Do.MoRe: Clinical Dosimetry for 90Y Radioembolisation**OP011****Personalized treatment planning in radioembolization of Hepatocarcinoma with 90 Y glass microspheres: update of clinical outcomes in the Milan experience**

M. Maccauro¹, C. Spreafico², C. Chiesa¹, M. Mira¹, M. De Nila¹, R. Romito³, C. Morosi², C. Sposito³, S. Bhoori³, G. Aliberti¹, E. Seregni¹, G. Tagliabue⁴, F. Crippa¹, A. Marchianò², V. Mazzaferro³; ¹Department of Nuclear Medicine, Fondazione IRCCS Istituto Nazionale Tumori, Milan, Milan, ITALY, ²Department of Radiology, Fondazione IRCCS Istituto Nazionale Tumori, Milan, Milan, ITALY, ³Department of Surgery, Fondazione IRCCS Istituto Nazionale Tumori, Milan, Milan, ITALY, ⁴Department of Epidemiology, Fondazione IRCCS Istituto Nazionale Tumori, Milan, Milan, ITALY.

Aim: to compare the clinical outcome of radioembolization (TARE) with ⁹⁰Y glass microspheres in Hepatocarcinoma (HCC), after ^{99m}Tc-MAA SPECT personalized treatment planning with respect to the standard “120 Gy to lobe” glass microspheres indication. **Methods:** two sequential cohorts of intermediate/advanced HCC patients were treated. 52 patients (cohort 1) were enrolled in a phase II prospective study (Mazzaferro Hepatology 2013) with tight exclusion criteria: tumor burden >50%, anti-tumor therapy including drug treatment within 30 days before TARE, previous TACE, complete PVT. Therapeutic activity was chosen according to the standard indications (120 Gy to lobe). 166 sequential

“real life” patients were enrolled in cohort 2. Child A of this cohort were treated according to a ^{99m}Tc-MAA SPECT personalized treatment planning. This aimed to the maximal tumor dose with a dose limit to whole parenchyma of 75 Gy, in order to keep the liver decompensation rate below 15%, as obtained in cohort 1. Further dose reduction for Child B cases was applied. For a meaningful comparison, we tried to identify a subcohort 2 of 110 patients, homogeneous to cohort 1, applying retrospectively most of the exclusion criteria of cohort 1: complete PVT, tumor burden >50%, concomitant sorafenib. Patients with previous TACE were included. Liver decompensation within 6 months was considered excluding cases clearly attributable to progression. **Results:** Treatment related liver decompensation rate in Child A patients of subcohort 2 (15/106=14%) was maintained as in cohort 1 (6/43=14%), as programmed. The median overall survival of subcohort 2 was identical to cohort 1: 15 months, 13 months for PVT and 17 months for non PVT patients. **Discussion:** The absence of the expected gain in survival is attributed to tumor volumes of subcohort 2 of double size than in cohort 1. Lesion volume in subcohort 2 versus cohort 1 were average 186 cc vs 93 cc, median 70 cc versus 22 cc (p<0.001); for non PVT median 49 cc versus 9 cc (p=0.001) and for PVT, median 83 cc vs 31 cc (p=0.02). **Conclusion:** Personalized treatment planning was able to maintain the same overall survival and toxicity rate previously obtained with standard method, despite patient of subcohort 2 were less selected, representing the real life, and with twice larger lesion volumes. In order to validate the impact of personalized treatment planning on patient outcome, we recommend a new setting of a randomized study, with deep attention to many clinical details.

OP012**Subjective vs Objective Y90 dosimetry based on MAA**

M. Tann¹, P. Haste¹, V. Aaron¹, T. Laroche¹, T. Mauxion², M. R. Dreher², S. Persohn¹, M. S. Johnson¹; ¹Indiana University Health, Indianapolis, IN, UNITED STATES, ²BTG, London, UNITED KINGDOM. Distribution of ^{99m}Tc-MAA and ⁹⁰Y Glass Microspheres in Hepatocellular Carcinoma: A Subjective Versus Objective Analysis

Aim: The ideal radioembolization treatment provides optimal therapeutic dose to the tumor without exceeding the tolerable dose to normal liver tissue. Pre-treatment personalized dosimetry, based on the absorbed dose distribution calculated from ^{99m}Tc-MAA, shows potential for improving radioembolization treatment. Currently, most pre-treatment absorbed dose (AD) calculations assume that ^{99m}Tc-MAA and ⁹⁰Y have the same distribution. These assumptions are mainly based off subjective similarities in appearance. Our goal was to compare subjective analysis of the distribution of ^{99m}Tc-MAA and ⁹⁰Y, in both tumor and whole liver normal tissue (WLNT), with objective absorbed doses calculated from ^{99m}Tc-MAA/SPECT and ⁹⁰Y PET/CT. **Material/Methods:** From 2013-2014, 84 patients with HCC underwent ⁹⁰Y glass microsphere radioembolization with pre-treatment ^{99m}Tc-MAA SPECT and post-treatment ⁹⁰Y PET/CT. SPECT, PET, and CT images were fused (3 blinded reviewers) and the WLNT and the largest lesions (5 lesions maximum) were segmented (MIM software Inc.). The AD was calculated using the MIRD methodology. Two Nuclear Medicine radiologists then subjectively evaluated the SPECT and PET images and graded tumor to background uptake (4 point scale) for all tumors on both SPECT and PET. Direct subjective comparison between ^{99m}Tc-MAA and ⁹⁰Y, in both tumors and WLNT, was performed using a 3 point scale (complete/near complete, moderate, poor/no agreement). Objective and subjective agreements between reviewers and between ^{99m}Tc-MAA and ⁹⁰Y (Bland Altman - 95% limit of agreement [LoA], Non parametric Kruskal-Wallis, Mann-Whitney and Wilcoxon tests) were analyzed. **Results:** Objective analysis demonstrated a clinically acceptable LoA between ^{99m}Tc-MAA and ⁹⁰Y for WLNT AD (LoA= [-15;15] Gy; Bias=0 Gy). However, the LoA for tumor AD was deemed clinically unacceptable

(LoA= [-355;327] Gy; Bias=-14Gy). Subjectively, 87%±3% of patients show either moderate to complete agreement between ^{99m}Tc -MAA and ^{90}Y distribution for WLNT and 90%±5% of patients show moderate to complete agreement in distribution within tumors. Agreement between reviewers was found clinically acceptable but non-statistically significant ($p>0.05$). We also found a significant correlation between AD and subjective tumor to background uptake for both agents ($p<0.05$), particularly for one reviewer ($p<0.001$). Conclusion: ^{99m}Tc -MAA and ^{90}Y demonstrate a subjectively similar distribution, in both tumors and WLNT, for the majority of the cases. However, this subjective similarity does not match the poor objective agreement between ^{99m}Tc -MAA and ^{90}Y in tumors. Importantly, the objective correlation between ^{99m}Tc -MAA and ^{90}Y in WLNT is clinically acceptable, agreeing with the subjective impressions.

OP013

Downstaging intermediate and advanced HCC using radioembolization therapy, a difficult but achievable strategy

M. Manfredi^{1,2}, P. Carbonatto¹, A. Codegone¹, E. Richetta¹, M. Tabone¹, R. E. Pellerito¹; ¹Azienda Ospedaliera Ordine Mauriziano, Torino, ITALY, ²Azienda Ospedaliero-Universitaria Città della Salute e della Scienza, Torino, ITALY.

In patients with unresectable hepatocarcinoma (HCC) due to portal venous thrombosis, large or multifocal tumour, or vascular proximity, Y-90 radioembolization (TARE) results in a good benefit in overall survival (OS). This approach also raises the possibility of patient downstaging, showing promising results in allowing salvage surgery for large HCCs, as evaluated in this prospective pilot study. Between 2011 and 2014, 22 patients with HCC unsuitable for chemoembolization, showing conserved liver function and good performance status, were enlisted to receive TARE with downstaging purpose. According to hepatic angiography and Tc-99m scintigraphy, due to technical reasons, TARE was not feasible for 5 patients, that received the best possible care. The remaining 17 patients underwent one or more TARE treatments and were re-evaluated for restaging. The downstaging was possible in 5 out of 17 cases: 4 patients underwent resection surgery and 1 underwent transplantation. On the opposite, surgery was not possible for the other 12 patients, in 11 cases for insufficient tumor regression, unsuitable tumor localization or pathology progression, while in the remaining patient the transplantation was feasible, but no liver was available leading the patient to suffering from pathology progression. All the patients were followed until death or until March 2016. This prospective pilot study defines three subgroups of patients with significant differences in OS (Log-rank test $P=0.03$): (1) the ones that are not suitable for TARE, with no other possible therapy than Sorafenib or palliative treatments, probably due to a more aggressive pathology, as suggested by significantly higher Alpha-fetoprotein and tumor dimension compared with the other groups (median survival: 11 months); (2) the ones that, despite TARE treatment, did not achieve surgical requirements, showing better survival rates, comparable to chemoembolization treatment (median survival: 17 months); and (3) a group that following TARE had access to surgery, that showed the better OS with more than 50% patients alive at the end of the study. In conclusion, downstaging was possible in a small subgroup of patients, moreover TARE treatment alone was sufficient to increase survival. This study suggests a new possible approach for the treatment of intermediate and advanced HCC that, although not validated by extensive studies, can be safely applied in centers where TARE is available, following accurate selection of patients. However, further investigation is needed, to better define the HCC population in which TARE could lead to surgery.

OP014

Dose-Response Relationship Evaluation in Selective Intraarterial Radionuclide Therapy

N. Alan Selcuk¹, T. Toklu¹, S. Karaaslan², A. Ozgen³, O. Eren⁴, L. Kabasakal⁵; ¹Yeditepe University Hospital, Dept. of Nuclear Medicine, Istanbul, TURKEY, ²Yeditepe University, Dept. of Physics, Istanbul, TURKEY, ³Yeditepe University Hospital, Dept. of Radiology, Istanbul, TURKEY, ⁴Yeditepe University Hospital, Dept. of Oncology, Istanbul, TURKEY, ⁵Istanbul University, Cerrahpasa Medical School, Dept. of Nuclear Medicine, Istanbul, TURKEY.

Aim: To evaluate dose-response relationship in transarterial radioembolization (TARE) using microspheres loaded with Yttrium-90 in the treatment of primary and metastatic tumors of the liver. **Methods:** A retrospective analysis were performed on 25 adult patients with primary (4 patients) and secondary (21 patients) tumors of the liver who underwent 39 course of treatment. Twenty-nine of them were standard TARE and 10 were superselective TARE. Four patients had primer liver cancer, 8 patients had metastasis of colorectal carcinoma, 4 patients had metastatic breast carcinoma, 3 patients had gastric cancer and 6 patients had other cancer with liver metastases. Tumor, healthy injected liver dose (HILD) and total healthy whole liver doses (HWLD) were evaluated. Doses were calculated using Medical Internal Radiation Dosimetry (MIRD) with partition model. Treatment results were grouped as complete or partial response, and progression of disease in the targeted area. Dose values were compared in these two groups. Follow-up of the patients were made by using PET-CT and contrast enhanced magnetic resonance imaging and/or computed tomography. **Results:** Mean follow-up time was 7.8 months. Progression was observed in 7 patients, while complete or partial response were detected in the rest of the patients. Four patients were died because of extrahepatic disease while one was died due to liver failure during follow-up. Mean tumor dose, HILD and HWLD were 204.7±77.2 Gy, 72.2±20.3 Gy and 25.4±13.0 Gy, respectively. Radiation induced liver disease (RILD) was not observed in any patient. Mean tumor dose was 183.3±65.5 Gy in progressive group while 207.1±79.2 Gy in responsive group. **Conclusion:** According to our results, minimum of 200 Gy tumor dose seems to be necessary for a successful treatment, although statistically significant difference in tumor doses was not observed. HILD of up to 110 Gy is generally tolerated by liver.

OP015

Correlation Between Pre-Treatment ^{99m}Tc -MAA SPECT and Post-Radioembolization ^{90}Y PET

N. M. Maughan, K. J. Fowler, R. Laforest, A. Sharma, J. Olsen, C. K. Speirs, T. DeWees, S. Markovina, P. J. Parikh, N. E. Saad; Washington University in St. Louis, Saint Louis, MO, UNITED STATES.

Aim: In this study, we investigated the role of pre-treatment ^{99m}Tc -MAA SPECT to predict individual lesion response, as well as its correlation with post-treatment PET. **Materials and Methods:** 22 patients who received standard-of-care pre-treatment ^{99m}Tc -MAA SPECT/CT, ^{90}Y radioembolization, and follow-up imaging at our institution were included in this retrospective analysis. Patients received a PET/MRI after radioembolization according to an IRB-approved protocol. Regions of interest were drawn and approved by a board-certified radiologist on the contrast-enhanced MRI from PET/MRI and on 3-6 month follow-up imaging. We classified response based on vRECIST criteria. Both ^{90}Y PET and ^{99m}Tc -MAA SPECT images were rigidly registered and fused to the contrast-enhanced MRI. Dose from ^{90}Y PET was calculated by convolving the activity with a dose point kernel (DPK), with dose from the lower resolution ^{99m}Tc -MAA SPECT calculated using the local deposition method. Dose was normalized and scaled according the amount of

delivered ^{99m}Tc -MAA and ^{90}Y activities, respectively. Dose metrics previously shown to be predictive of response—D70 and D_{average} —were compared between ^{99m}Tc -MAA SPECT and ^{90}Y PET using Spearman's Correlation test. D70 and D_{average} from ^{99m}Tc -MAA SPECT and ^{90}Y PET were also assessed for their ability to predict response using Logistic Regression. Results: A total of 83 lesions were identified in both PET/MRI and follow-up imaging: 41 metastatic colorectal cancer (mCRC), 39 hypervascular lesions (hepatocellular carcinoma, neuroendocrine tumor, and thymic carcinoid), and 3 metastatic esophageal cancer. D70 and D_{average} were correlated between SPECT and PET for hypervascular lesions ($r=0.53$ and 0.57 , $p<0.05$) and for mCRC ($r=0.31$ and 0.36 , $p<0.05$). While D70 and D_{average} from ^{90}Y PET were predictive of response in mCRC ($p<0.05$), neither of these dose parameters from ^{99m}Tc -MAA SPECT were predictive of response in any group ($p>0.05$). There was a strong and significant correlation for D_{average} in the treated lobe of the liver between ^{99m}Tc -MAA and ^{90}Y ($r=0.89$, $p<0.0001$). Conclusion: The strong correlation for D_{average} in the treated lobe of the liver between ^{99m}Tc -MAA and ^{90}Y may be useful for estimating possible toxicity levels. The weaker correlation between tumor dose measured on the two modalities suggests that the pre-treatment ^{99m}Tc -MAA SPECT may be useful for qualitative predictions of microsphere distribution but not for quantitative predictions of lesion response. This may be due to changes in liver blood flow or catheter position. This study further emphasizes the unique role of post-treatment dosimetry in ^{90}Y radioembolization.

OP016

Usefulness of ^{99m}Tc -MAA scan for ^{90}Y -Radioembolization planning in 532 patients

L. Sancho, M. Rodríguez-Fraile, E. Prieto, V. Morán, D. Martínez-Urbistondo, D. Martínez-Urbistondo, M. Iñarrairaegui, J. Marti-Climent, J. Arbizu, J. Bilbao, B. Sangro; Clínica Universidad de Navarra, Pamplona, SPAIN.

AIM: To determine whether ^{99m}Tc -MAA scan results that will contraindicate ^{90}Y -Radioembolization as it was initially designed can be predicted from baseline patient and tumor characteristics. **MATERIALS AND METHODS:** A single-centre retrospective study of patients that underwent ^{99m}Tc -MAA scan planning for radioembolization using ^{90}Y resin microspheres was conducted between 2006 and 2015. Baseline tumor and patient characteristics were compared between the group of patients in which the results of ^{99m}Tc -MAA scan led to contraindication of ^{90}Y -Radioembolization and the group that was treated as initially planned. Patients were dismissed as the result of the ^{99m}Tc -MAA for three main causes, two objective ones [high lung shunt fraction (HLSF) and extrahepatic uptake (EU)] and a single subjective one [mismatch between ^{99m}Tc -MAA and intrahepatic tumor distribution (MM)]. Variables that carried an independent risk of resulting in contraindication were identified by logistic regression analysis. The ability of these variables to predict contraindication was obtained. **RESULTS:** A total of 532 patients (365 males) with hepatocellular carcinoma ($n=217$), cholangiocarcinoma ($n=31$) and liver metastases from colorectal cancer ($n=142$), neuroendocrine tumors ($n=49$), or other tumors ($n=93$) were identified. ^{90}Y -Radioembolization was contraindicated in 48 patients as the result of the ^{99m}Tc -MAA scan findings due to objective causes [HLSF ($n=29$) or EU ($n=19$)] and in 73 patients as a result of subjective causes (MM). For objective dismissal, an association was found between HLSF and vascular invasion (VI) (OR 5.58[95%CI:2.56-12.2] $p<0.01$) and for EU the association was found with the presence of secondary tumors (ST) (OR 3.6 [95%CI:1.75-7.39] $p<0.01$) and prior intraarterial chemotherapy (OR 2.3 [95%CI:1.06-4.9] $p<0.01$). The negative predictive value (NPV) for VI and high LSF was 97%, for ST and EU was 99% and for both of them versus contraindication was 92%. Variables significantly related with the subjective cause of dismissal (MM) were the presence of unimodular tumors (OR 0,839 [95%CI: 1,227-4,367] $p<0,01$) and prior

antiangiogenic drugs (OR 1,036 [95%CI:1,583-5,018] $p<0,01$), both of them with a NPV of 89%. **CONCLUSION:** The presence of vascular invasion, secondary tumors, unimodular tumors and antiangiogenic drugs independently predicted ^{90}Y -Radioembolization contraindication based on the results of the ^{99m}Tc -MAA scan. Nevertheless, the lack of strong discrimination power emphasizes the value of ^{99m}Tc -MAA scan in the workup of ^{90}Y -Radioembolization. The absence of either of them identifies a group of patients with very low risk of contraindication. However, the severity of complications encourage the use of ^{99m}Tc -MAA scan.

OP017

Advancing Post-Radioembolization Yttrium-90 Imaging: The Clinical Impact of Time-of-Flight in Next-Generation Digital PET/CT versus Conventional PET/CT Systems

C. L. Wright¹, K. Binzel¹, J. Zhang¹, E. Wuthrick¹, P. Maniawski², M. V. Knopp¹; ¹The Ohio State University, Columbus, OH, UNITED STATES, ²Philips Healthcare, Cleveland, OH, UNITED STATES.

Aim: Yttrium-90 (^{90}Y) microspheres are used to selectively embolize tumor-associated neovasculature as well as deliver therapeutic doses of radioactivity to unresectable malignant/metastatic liver lesions (radioembolization). Bremsstrahlung is currently used for post-therapy detection of ^{90}Y microsphere radioactivity, but is limited by poor ^{90}Y -to-background contrast and quantitative dosimetry. ^{90}Y produces a small fraction of annihilation photons which can be imaged using conventional photomultiplier tube-based PET (cPET). New, solid-state, digital photon counting PET (dPET) detectors produce best-in-class time of flight (ToF) timing resolution, ~325 ps. This study evaluates the clinical impact of ToF on image quality and post-therapy volumetric assessment of ^{90}Y radioactivity following radioembolization using both cPET/CT and dPET/CT. **Materials and Methods:** Standard bremsstrahlung (bSPECT, Symbia T16, Siemens) was performed for 15 patients within a few hours following interventional radioembolization with ^{90}Y microspheres, with an acquisition time of 22m. Pre-commercial release dPET/CT (Vereos, Philips) and cPET (Gemini TF 64, Philips) imaging was performed. Both were performed 4 - 50 h following radioembolization with an acquisition time of 21m each. PET data were reconstructed with and without ToF. ^{90}Y image characteristics and isocontoured activity volumes were evaluated by matched comparison using the Intellispace Portal workstation including comparison with bSPECT/CT. **Results:** When compared with bSPECT/CT, dPET detection of ^{90}Y radioactivity provided markedly improved image quality, exceptional ^{90}Y -to-background contrast and more precise volumetric assessment of intrahepatic ^{90}Y activity when ToF enabled reconstructions were utilized. On the other hand, non-ToF dPET reconstructions demonstrated ^{90}Y -to-background contrast and image quality which was poorer than ToF dPET but better than bSPECT. For dPET, no significant differences in the intrahepatic ^{90}Y activity volumes were noted for ToF and non-ToF reconstructed data sets when using 1% isocontours. ^{90}Y activity volumes were consistently larger on cPET. Non-ToF cPET volumes were even more greatly skewed. **Conclusion:** Currently ^{90}Y imaging is arduous due to long image acquisition times necessary for cPET imaging or the low image quality/limited quantitative capability of bremsstrahlung imaging. These results demonstrate that ToF dPET image quality is superior to non-ToF dPET as well as cPET and bSPECT. The faster timing resolution of ToF dPET likely contributes to more precise localization of ^{90}Y internal pair production events and less partial volume effect. It is expected that dPET technology will enable new strategies for ^{90}Y image acquisition and reconstruction, contributing to faster imaging with better image quality, dose quantification and predictive response assessment in patients treated with existing and new ^{90}Y -based theranostics.

OP018**Differences Between Free-Breathing and Breath-Hold CT for Application in SIRT Dosimetry**

A. Thyroff¹, J. C. Sanders^{1,2}, T. Kuwert¹, M. Beck¹, P. Ritt¹; ¹Clinic of Nuclear Medicine - University Hospital Erlangen, Erlangen, GERMANY, ²Pattern Recognition Lab - University of Erlangen-Nuremberg, Erlangen, GERMANY.

Aim In Selective Intra-arterial Radio Therapy (SIRT) of liver tumors with Y-90 loaded microspheres, prevailing compartment models for dosimetry assume that the deposited energy dose due to treatment is proportional to the injected Y-90 dose and inversely proportional to the liver volume. For the pre-therapeutic SPECT/CT-based dosimetry, a wide range of SPECT/CT systems is used, including numerous devices which are not suited for achieving the necessary scanning speed for breath-hold CT imaging of the abdomen. Respiratory artifacts in these slow CT acquisitions could result in an erroneous CT-based volume determination, which would lead to incorrect dosimetry. The aim of this study was to assess the differences in liver volume determination between slow, free-breathing and fast, breath-hold CT acquisitions. **Material and Methods** In 14 patients, breath-hold (Siemens Biograph mCT, 40 CT detector slices) as well as free-breathing (Siemens Symbia T2, 2 detector slices) CTs were acquired. The time difference between the two acquisitions was 8.7±3.8 (1-15) days. The liver volume was determined by manual segmentation of the transaxial CT slices by one experienced reader. The breath-hold CT was considered as ground-truth. Additionally, the intra-reader variability was measured by segmenting 10 acquisitions for a second time after sufficient temporal distance. **Results** The average volume difference between breath-hold and free-breathing CT was 5.8±4.6% (p<0.001), ranging 0.1-14.1%. This corresponds to a volume difference of 101±82 (1-271) ml. The intra-reader variability was 0.4±0.3% (0.1-1.3%). 5 and 8 datasets had lower and higher volumes, respectively, in the free-breathing versus the breath-hold acquisitions, with one dataset having an equal volume. **Conclusion** Determination of liver volume based on free-breathing CT examinations results in significant volume inaccuracies. These errors directly affect SIRT dosimetry, and, depending on the respiratory movement relative to the patient table motion during the CT acquisition, the volume may be either over- or under-estimated.

105 – Sunday, October 16, 2016, 08:00 - 09:30, Hall 115

M2M - Featured: PSMA Targeting

OP019**PSMA Targeting**

K. Kopka; DKFZ, Radiopharmazeutische Chemie, Heidelberg, GERMANY.

OP020**Synthesis and comparative evaluation of three ¹⁸F-AmBF₃ derivatives of Glu-ureido-Lys for imaging PSMA expression in prostate cancer with positron emission tomography**

H. Kuo¹, J. Pan¹, H. Merckens¹, J. Lau¹, C. Zhang¹, Z. Liu², D. M. Perrin², F. Benard¹, K. Lin¹; ¹BC Cancer Agency, Vancouver, BC, CANADA, ²University of British Columbia, Vancouver, BC, CANADA.

OBJECTIVES: Expressed in most prostate cancers (PCa), the membrane-bound glycoprotein prostate specific membrane antigen (PSMA) is an attractive diagnostic and therapeutic target. In recent years, several PSMA-targeting radiotracers have successfully entered the clinic for imaging PCa. Among them, ¹⁸F-DCFPyL is one of the most sensitive tracers for the identification of PSMA-positive PCa. However, the

reported radiosynthesis of ¹⁸F-DCFPyL involves multiple steps, and is challenging for automation using GMP-compliant synthesis modules. In this study, three ¹⁸F-labeled PSMA-targeting Glu-ureido-Lys derivatives (HTK01069, HTK01070 and HTK01130) that could be radiolabeled via a one-step ¹⁸F-¹⁹F isotope exchange reaction on the ammoniomethyl-trifluoroborate (AmBF₃) motif were synthesized and evaluated for PSMA imaging. **METHODS:** HTK01069 was synthesized by coupling succinimido 4-(*N*-trifluoroborylmethyl-*N,N*-dimethylammonio) methylbenzoate to Glu-ureido-Lys. HTK01070 and HTK01130 were prepared by coupling 2,3,5,6-tetrafluorophenyl 4-(azidomethyl)benzoate and 2,3,5,6-tetrafluorophenyl 6-(azidomethyl)nicotinate, respectively, to *t*-butyl protected Glu-ureido-Lys, followed by deprotection and click reaction with *N*-propargyl-*N,N*-dimethyl-ammoniomethyltrifluoroborate. Radiolabeling was conducted via ¹⁸F-¹⁹F isotope exchange reactions and tracers were purified by HPLC. The stability of the tracers was assessed in mouse plasma. PET imaging and biodistribution studies were performed in mice bearing PSMA-expressing LNCap PCa xenografts. For blocking studies, mice were co-injected with 0.5 mg of DCFPyL. **RESULTS:** ¹⁸F-HTK01069, ¹⁸F-HTK01070 and ¹⁸F-HTK01130 were obtained in 3 - 9% average decay-corrected radiochemical yields with > 99% radiochemical purity and ≥ 29.6 GBq/μmol average specific activity. All tracers were stable (>99% intact) after 2 h incubation in plasma. From PET images, all three tracers successfully delineated PSMA-expressing LNCap xenografts at 1 h post-injection (p.i.) with excellent tumour-to-background contrast. The clearance of these tracers was predominantly renal with minor involvement of the hepatobiliary pathway. At 1 h p.i., ¹⁸F-HTK01070 exhibited higher tumour uptake (8.28 ± 1.25 %ID/g) than ¹⁸F-HTK01069 (5.82 ± 1.09 %ID/g) and ¹⁸F-HTK01130 (4.22 ± 0.44 %ID/g). ¹⁸F-HTK01070 was also superior to ¹⁸F-HTK01069 and HTK01130 in terms of tumour-to-muscle ratio (37.7 ± 9.53 vs. 18.9 ± 6.05 and 21.6 ± 5.46) and tumour-to-blood ratio (16.0 ± 1.37 vs. 11.9 ± 4.60 and 7.89 ± 3.13). With PSMA blockade, uptake in tumours reduced by > 90% for all tracers. **CONCLUSION:** Three AmBF₃-conjugated Glu-ureido-Lys derivatives were successfully radiolabeled with ¹⁸F-fluoride and evaluated for imaging PSMA expression with PET. With high tumour uptake, excellent tumour-to-background contrast, and ease of synthesis, ¹⁸F-HTK01070 warrants further investigation as a PSMA imaging agent.

OP021**High Affinity F-18 Labeled PSMA Inhibitors: Preclinical Evaluation and Comparison to ⁶⁸GaDKFZ-PSMA-11**

J. M. Kelly, A. Amor-Coarasa, A. Nikolopoulou, D. Kim, C. Williams, Jr., S. Ponnala, J. W. Babich; Division of Radiopharmaceutical Sciences, Department of Radiology, Weill Cornell Medicine, New York, USA, New York, NY, UNITED STATES.

Aim: Current clinical imaging of PSMA-positive prostate cancer (PCa) by positron emission tomography (PET) mainly feature ⁶⁸Ga-labeled tracers, notably DKFZ-PSMA-11. The longer half-life of ¹⁸F offers significant advantages over ⁶⁸Ga in both clinical and production environments. Therefore we aimed to develop high affinity PSMA inhibitors labeled with ¹⁸F as alternatives to ⁶⁸GaDKFZ-PSMA-11 for imaging PCa. **Methods:** Six Glutamate-urea-Lysine (EuK) based triazoles and their alkyne precursors were synthesized starting from H-Glu(OtBu)-OtBu. 2-Azidoethyltosylate was synthesized from 2-bromoethanol. PSMA binding affinities were determined in a competitive binding assay on LNCaP cells. Radiofluorination was achieved using Cu(I)-catalyzed click chemistry after preparation and distillation of [¹⁸F]fluoroethylazide. [¹⁸F]fluorinated triazoles were isolated using prep-HPLC. [¹⁸F] labeled compounds were evaluated in nude mice bearing LNCaP tumors (n=2-5), with imaging at 1, 2, 4 and 6hrs p.i. The same mice were imaged with ⁶⁸GaDKFZ-PSMA-11 within 24 hours. Biodistribution studies were performed on the two tracers with the highest imaged-derived tumor uptake

(5 mice/time point) at 1, 2 and 4hrs post-injection. PSMA specific uptake was confirmed by co-administration of PMPA. **Results:** [^{18}F]Fluoroethyl-triazoles were prepared with an overall decay corrected RCY of 21–43% and >98% radiochemical and chemical purity. PSMA binding was in the range 8–25 nM (IC_{50}). Preference for substitution on the phenyl ring was in the order 3 > 4 > 2, and direct conjugation of the triazole with the phenyl alkyne moiety was preferred to insertion of a spacer group. Image-derived tumor uptake was calculated for each of the injected mice and ranged from 6 to 14% ID/g (at 2 hrs). By the same calculation, uptake of ^{68}Ga DKFZ-PSMA-11 in the tumor was 5% ID/g. Biodistribution studies of the compounds displaying the highest imaged-derived tumor uptake (also highest PSMA affinity) gave tumor uptakes of $8.3 \pm 2.5\%$, $10.9 \pm 1.0\%$, and $10.3 \pm 1.9\%$, and $12.7 \pm 1.6\%$, $14.3 \pm 2.5\%$, and $13.9 \pm 2.1\%$ at 1, 2 and 4hrs p.i., respectively. The biodistribution of ^{68}Ga DKFZ-PSMA-11 was determined at 1hr post-injection and tumor uptake was found to be $5.32 \pm 1.56\%$. **Conclusions:** Six urea-based triazoles were [^{18}F]fluorinated by click chemistry in good radiochemical yield. The compounds showed PSMA-specific uptake in LNCaP tumors as high as 14% ID/g, nearly a 3-fold increase over ^{68}Ga DKFZ-PSMA-11. The facile and high yielding radiosynthesis of these F-18 labeled urea-based triazoles as well as their promising *in vitro* and *in vivo* characteristics make them worthy of clinical development for PET imaging of PCa.

OP022

^{18}F -PSMA-1007: The Optimal Variant of Radiofluorinated PSMA Ligands Derived from PSMA-617

J. Cardinale¹, M. Schäfer¹, M. Geerlings¹, M. Benešová¹, M. Eder¹, U. Bauder-Wüst¹, A. Baranski¹, O. Neels¹, K. Leotta¹, U. Haberkorn², F. Giesel², K. Kopka¹; ¹German Cancer Research Center, Heidelberg, GERMANY, ²University Hospital, Heidelberg, GERMANY.

Aim: Urea-based inhibitors of the prostate-specific membrane antigen (PSMA) show promising results for the diagnosis (1,2) and endoradiotherapy (3) of prostate cancer. The aim of the project was the development of F-18 labeled PSMA ligands derived from PSMA-617. So far, the compound PSMA-1007 offered the most promising characteristics in preclinical experiments. To further investigate the structure activity relationships, a variety of PSMA inhibitors with altered linker modifications have been developed. Therefore, we especially aimed at high internalization ratios. **Materials and Methods:** The PSMA binding-motif Glu-NH-CO-NH-Lys was synthesized on a solid phase (chlorotrityl-resin) (4), and subsequently amino acid linkers were built up by fmoc-based solid phase synthesis (SPPS). After separation from the resin and deprotection, the peptidomimetics were conjugated using the prosthetic group 6-fluoronicotinic acid TFP-ester. The non-radioactive reference compounds were also prepared by SPPS. The K_i -values of all compounds were determined by competitive binding assay on LNCaP cells against ^{68}Ga -PSMA-10 using the respective cold reference compounds. Additionally, the internalization of the radiofluorinated ligands was analyzed. **Results:** The no-carrier-added radiofluorination of the new PSMA inhibitors with 6-fluoronicotinic acid TFP-ester was accomplished with good radiochemical yields. With one exception the K_i -values of all compounds were in between 1.0–15.0 nM while internalization ratios up to 65 % of the total bound activity were observed. Within the novel series PSMA-1007 still shows the best characteristics for clinical translation (6.7 ± 1.7 nM, 65% int. ratio). Thus, PSMA-1007 was selected as the leading candidate for the translation into the clinic. **Conclusions:** Based on PSMA-617, a series of promising radiofluorinated PSMA ligands was developed and evaluated *in vitro* and (partly) *in vivo*. Amongst those, PSMA-1007, showed the most promising characteristics *in vitro*. Since a further improvement of the binding characteristics could not be achieved, PSMA-1007 was selected as candidate for clinical translation. **Literature:** (1) A. Afshar-Oromieh et al., EJNMMI 2015, 42, 197–209. (2) Z. Szabo et al., Mol. Imaging Biol. 2015, 17, 565–574. (3) C.

Kratochwil et al., JNM 2016, Ahead of print, PMID: 26985056. (4) M. Eder et al., Bioconjugate Chem. 2012, 23, 688–697.

OP023

^{44}Sc -labeling of PSMA-617 for dosimetry of prostate cancer

E. Eppard¹, A. de la Fuente², M. Benesova³, S. Kürpig¹, K. Kopka³, F. Rösch², M. Essler¹; ¹University Hospital Bonn, Bonn, GERMANY, ²Johannes Gutenberg University, Mainz, GERMANY, ³German Cancer Research Center, Heidelberg, GERMANY.

OBJECTIVES By conjugation the prostate-specific membrane antigen (PSMA) inhibitor Glu-NH-CO-NH-Lys(Ahx) with the complexing agent DOTA a broad pool of radionuclides becomes available for its radiolabeling. This allows the visualization of the biological behavior over different periods of time depending on the half-life of the respective radionuclide (^{68}Ga $t_{1/2} = 68$ min; ^{44}Sc $t_{1/2} = 3.9$ h). Additionally, different imaging modalities and peptidomimetic mediated radionuclide therapy (i.e. targeted endoradiotherapy) can be applied depending on the employed radionuclide (e.g. ^{44}Sc (PET); ^{111}In (SPECT); Gd (MRT); $^{90}\text{Y}/^{177}\text{Lu}$ (Therapy)). **METHODS** PSMA-617 was obtained from ABX (Radeberg, Germany). ^{44}Sc was obtained from a $^{44}\text{Ti}/^{44}\text{Sc}$ generator in Mainz, where ^{44}Ti decays with a half-life of 60 years to no-carrier-added (n.c.a) ^{44}Sc . Radiolabeling with ^{44}Sc was performed in 3 mL 0.25 M ammonium acetate buffer at 95°C. Stability studies and cell studies (internalization and binding assay) were performed. Quality control was performed using radioHPLC and radioTLC. A PTW torso phantom with ^{44}Sc and ^{68}Ga was measured 5 min every 30 min over 2.5 h. **RESULTS** ^{44}Sc -PSMA-617 was effectively labeled at 95 °C. Subsequent cartridge-based solid-phase-extraction (C-18) resulting in a radiochemical purity of the final tracer of $\geq 98\%$. Stability studies with ^{44}Sc -PSMA-617 showed the high stability against transchelation and transmetallation of the compound. In cell studies ^{44}Sc -PSMA-617 showed similar behavior like ^{68}Ga -PSMA-617 and ^{177}Lu -PSMA-617. Radiochemical purity could be analyzed effectively using radioHPLC and radioTLC. Measurement of a torso phantom applying ^{44}Sc into the spheres and ^{68}Ga into the surrounding was done. **CONCLUSIONS** The radiolabeling of PSMA-617 with the new generator-derived PET radionuclide ^{44}Sc was investigated in detail. ^{44}Sc -PSMA-617 was investigated *in vitro*. Also a radiolabeling and quality control protocol along the lines of the monograph of the European Pharmacopoeia for ^{68}Ga -DOTATOC was developed and validated to produce ^{44}Sc -PSMA-617 suitable for clinical investigations.

OP024

Guiding the Arrow: A Dual Targeted Approach to Prostate Cancer Therapy

J. M. Kelly¹, A. Amor-Coarasa¹, T. Wuestemann¹, A. Nikolopoulou¹, P. Barelli², C. Williams, Jr.¹, D. Kim¹, B. Hu³, S. DiMagno³, D. Hage⁴, D. Warren², X. Zheng⁵, J. W. Babich¹; ¹Division of Radiopharmaceutical Sciences, Department of Radiology, Weill Cornell Medicine, New York, USA, New York, NY, UNITED STATES, ²Milstein Chemistry Core Facility, Department of Biochemistry, Weill Cornell Medicine, New York, NY, USA, New York, NY, UNITED STATES, ³Department of Medicinal Chemistry and Pharmacognosy, University of Illinois at Chicago, Chicago, IL USA, Chicago, IL, UNITED STATES, ⁴Department of Chemistry, University of Nebraska-Lincoln, Lincoln, NE, USA., Lincoln, NE, UNITED STATES, ⁵Department of Medicinal Chemistry and Pharmacognosy, University of Illinois at Chicago, Chicago, IL USA, Chicago, IL, UNITED STATES.

Aim: Several prostate specific membrane antigen (PSMA) targeted radiotherapeutics based on the Glu-urea-Lys (EuK) pharmacophore are currently under clinical investigation and showing anti-tumor activity in

mCRPC. However, these compounds localize to the salivary and parotid glands, as well as kidney, which may present dose-limiting organs or lead to related long term adverse events effecting quality of life. We therefore sought to modulate pharmacokinetics through interaction with serum albumin (HSA) which might limit normal tissue uptake without affecting tumor targeting. **Methods:** A series of small molecules (< 600 Da) possessing the *EuK* moiety and an albumin-binding moiety were synthesized and evaluated in vitro and in vivo. HSA binding affinity was determined by high-performance affinity chromatography. PSMA affinity was determined using a competitive binding assay in LNCaP cells, and uptake and internalization of the radiolabeled compounds were measured both in the presence and absence of HSA. Radiolabeling with I-131 or I-124 proceeded via iodo-destannylation. Four compounds were labeled with I-131 and biodistributions determined in nude mice bearing LNCaP tumors at 1, 6, 12, 24 and 48h post-injection (n=4). The compound with the most promising pharmacokinetics was labeled with I-124 for PET imaging at 1, 3, 6, 24 and 48h post-injection. **Results:** Calculated IC₅₀s for PSMA were 8–15 nM and K_d for HSA 1–53 μM. For all compounds in vitro cell uptake was lower in the presence of HSA with uptake inversely related to HSA affinity. Compounds with K_d < 2 μM had extended blood residence over 48h and decreased tumor uptake while those compounds with K_d > 20 μM were rapidly cleared from the blood and elevated kidney uptake. One compound was identified to show dramatically improved pharmacokinetics, with prolonged tumor retention (9% ID/g at 1h vs. 5.5% ID/g at 48h) leading to high tumor:kidney and tumor:blood ratios after 24h. Imaging with a ¹²⁴I-labeled analogue confirmed the excellent targeting and contrast. **Conclusions:** The improved pharmacokinetics of a dual targeting ligand by tailoring HSA binding represents a potentially valuable development in the design of targeted radiotherapeutics for prostate cancer. Preliminary pre-clinical data suggest that the compound has lower uptake in non-target tissue and consequently presents a greater therapeutic index. The ligand may be suitable for treatment of prostate cancer in man when labeled with therapeutic doses of I-131 or the alpha emitter At-211.

OP025

Protecting salivary glands: Displacement of off-target bound prostate-specific membrane antigen ligands

T. Wüstemann¹, A. Nikolopoulou¹, A. Amor-Coarasa¹, D. Kim¹, J. M. Kelly¹, C. Williams, Jr.¹, U. Haberkorn², J. W. Babich¹; ¹Division of Radiopharmaceutical Sciences, Department of Radiology, Weill Cornell Medicine, New York, USA, New York, NY, UNITED STATES, ²Department of Nuclear Medicine, University Hospital Heidelberg, Germany, Heidelberg, GERMANY.

Aim: Prostate-specific membrane antigen (PSMA)-targeted endoradiotherapy has recently shown significant promise in metastatic castrate resistant prostate cancer. Radiolabeled small molecule inhibitors of PSMA developed to date show high specificity to its molecular target in vivo and promising results in the clinic. However, as PSMA is also expressed in several normal tissues, radiation doses especially to kidneys and salivary and parotid glands may limit therapeutic dosing. Developing ligands with less binding to normal tissues remains challenging and until such compounds are found alternative approaches to protect normal tissues are needed. A promising pharmacological approach has been explored by us to displace off-target PSMA-associated renal radioactivity (J Nucl Med. 2015 Feb;56(2):293–8). We now apply this approach to protection of the salivary glands with the intent of minimizing xerostomia. **Methods:** 2-(Phosphonomethyl)pentane-1,5-dioic acid (PMPA) was used to selectively displace the PSMA PET tracer, ⁶⁸Ga-labeled HBED-CC-(Ahx)Lys-NH-CO-NH-Glu (68Ga-HBED-CC), localized to the salivary glands of healthy male Sprague-Dawley rats. The salivary glands were first localized by ^{99m}Tc-pertechnetate imaging using μSPECT/CT (Inveon^R, Siemens). Rats were then injected with ⁶⁸Ga-

HBED-CC followed by μPET/CT imaging of the head, at 2 h pi, to define baseline uptake in the salivary glands. After acquisition of baseline images rats were administered PMPA (1–10 mg/Kg), or saline, either by tail vein injection or as a mouth rinse imitating a gargle. μPET/CT imaging was then repeated 30 min post PMPA or saline administration to assess displacement. **Results:** Localization of the salivary glands was achieved by μSPECT/CT imaging. ⁶⁸Ga-HBED-CC μPET/CT showed colocalization to the glands. Intravenous injection of PMPA led to a near complete displacement of ⁶⁸Ga-HBED-CC at 10mg/Kg and 80% reduction at 1mg/Kg. PMPA gargle also achieved significant, but lower reduction, with 80% displacement at 10mg/Kg and 50% at 1mg/Kg. Saline infusion or gargle showed no reduction in ⁶⁸Ga-HBED-CC retention in salivary glands. **Conclusions:** This study indicates that gargling a PMPA solution 2h after injection of PSMA radiopharmaceuticals can reduce PSMA-specific localized activity in the salivary glands. The low toxicity of PMPA and the simplicity of administration suggest this finding could easily be implemented in the clinic and should be investigated to improve PSMA-based therapy and preserve the quality of life of the prostate cancer patient.

106 – Sunday, October 16, 2016, 08:00 – 09:30, Hall 111

Pitfalls & Artefacts - Thyroid/Radionuclide Therapy: Endocrine and Exocrine Imaging – Interpretation and Misinterpretation

OP026

Pitfalls in Differentiated Thyroid Cancer Imaging with I-124 and I-131
B. de Keizer; UMC Utrecht, Radiology & Nuclear Medicine, Utrecht, NETHERLANDS.

OP027

Incidentalomas in FDG PET/CT

M. Hoffmann; Medical University Vienna, Nuclear Medicine, Vienna, AUSTRIA.

OP028

Pitfalls in Ga-PET/CT (DOTA-SSA and PSMA)

A. Pfestroff; Universitätsklinikum Marburg-Gießen Standort Marburg, Klinikum für Nuklearmedizin, Marburg/Lahn, GERMANY.

107 – Sunday, October 16, 2016, 08:00 – 09:30, Hall 116

Clinical Oncology: Gastrointestinal

OP029

Metabolic tumor volume in FDG PET/CT is a useful predictor for survival in patients with unresectable esophageal squamous cell carcinoma treated by definitive chemoradiotherapy

S. Watanabe¹, M. Myoujin², K. Itoh², K. Hirata¹, O. Manabe¹, K. Kobayashi¹, Y. Onodera², K. Kanegae³, H. Takahashi³, M. Hosokawa², N. Tamaki¹; ¹Hokkaido University Graduate School of Medicine, Sapporo, JAPAN, ²Keiyukai Sapporo Hospital, Sapporo, JAPAN, ³Keiyukai 2nd Hospital, Sapporo, JAPAN.

Objective FDG PET/CT has predictive values in the prognosis of esophageal carcinoma. Identification of additional prognostic factors could improve risk-adapted treatment strategies to select patients who would benefit from intensified treatment. Since usefulness of volumetric analysis of FDG PET/CT in relation to patient prognosis has not been fully known, we aimed to investigate the prognostic value of pretreatment metabolic tumor volume (MTV) in a population of patients with unresectable

esophageal squamous cell carcinoma (ESCC). **Methods** We retrospectively reviewed 98 (aged 65 ± 9 years; 87 men) patients with pathologically proven ESCC who underwent pretreatment FDG PET/CT in Keiyukai Sapporo Hospital. All of them were clinically diagnosed as T4 stage without distant metastasis based on endoscopy, endoscopic ultrasound, CT, MRI, esophagography, endobronchial ultrasound and FDG PET/CT. MTV and maximum standardized uptake value (SUVmax) for the primary tumor were measured on FDG PET/CT. A fixed-threshold-based analysis, using an SUV of 2.5, was chosen for the measurement of MTV. The prognostic significance of MTV, SUVmax, clinical parameters and overall survival (OS) was assessed by univariate and multivariate Cox proportional hazards regression analysis. To further evaluate and compare the predictive performance of MTV and SUVmax, time-dependent receiver operating characteristic curve (ROC) analysis was used. **Results** At the time of analysis, 61 (62.2%) patients had died and 37 (37.8%) were alive. Median follow-up period for surviving patients was 24 months (range, 15–37 months). Median overall survival time was 15 months [95%CI, 13–17 months], with 2-year cumulative survival of 39%. MTV ranged between 7.9 cm^3 and 196.0 cm^3 , with median of 65.7 cm^3 and mean of 72.2 cm^3 . SUVmax ranged between 6.2 and 35.5, with median of 16.8 and mean of 17.0. In the univariate analysis, MTV (HR 1.008, $P = 0.013$) of the primary tumor was a significant predictor of survival. Age, sex, SUVmax and the location of the primary tumor, presence of clinical lymph metastasis, and radiation dose did not correlate with the OS. On multivariate analysis, MTV (HR 1.011, $P = 0.005$) was the only independent predictive factor associated with short OS. SUVmax was not a significant factor (HR 0.974, $P = 0.357$). On time-dependent ROC analysis, MTV (AUC = 0.647) achieved better predictive performance for OS than SUVmax (AUC = 0.549). **Conclusion** MTV of the primary lesion before definitive chemoradiotherapy is an important independent prognostic factor for survival in patients with unresectable ESCC.

OP030

Dual-tracer 18F-Fluorocholine and 18F-FDG PET/CT can impact BCLC classification and treatment allocation in patients with hepatocellular carcinoma

J. Chalaye¹, C. Costentin², A. Luciani³, G. Amaddeo², N. Ganne-Carrie⁴, E. Evangelista¹, D. Azoulay⁵, O. Seror⁶, A. Mallat², C. Duvoux², J. Nault⁴, V. Eder⁷, E. Itti¹; ¹Department of Nuclear Medicine, H. Mondor Hospital, Assistance Publique-Hôpitaux de Paris/Paris-Est University, Creteil, FRANCE, ²Department of Hepatology, H. Mondor Hospital, Assistance Publique-Hôpitaux de Paris/Paris-Est University, Creteil, FRANCE, ³Department of Medical Imaging, H. Mondor Hospital, Assistance Publique-Hôpitaux de Paris/Paris-Est University, Creteil, FRANCE, ⁴Liver Unit, Hôpital Jean Verdier, Hôpitaux Universitaires Paris-Seine-Saint-Denis, Assistance-Publique Hopitaux de Paris, Bondy, FRANCE, ⁵Department of Digestive, Hepatobiliary and Pancreatic Surgery and Liver Transplantation, Henri-Mondor Hospital, Assistance publique-Hôpitaux de Paris, Creteil, FRANCE, ⁶Radiology Department, Hôpital Jean Verdier, Hopitaux Universitaires Paris-Seine-Saint-Denis, Assistance-Publique Hopitaux de Paris, Bondy, FRANCE, ⁷Department of Nuclear Medicine, AP-HP, Avicenne Hospital, Bobigny, FRANCE.

Introduction: Conventional imaging allows staging of hepatocellular carcinoma (HCC) according to the BCLC classification, which links staging to therapeutic modalities. The aim of our study was to assess the impact of dual tracer 18F-Fluorocholine and 18F-FDG PET/CT on tumor staging and treatment allocation. **Methods:** 154 dual-tracer PET/CT were performed in 138 patients with HCC between 2012 and 2015 in two institutions. Diagnosis of HCC was based on histological (n=108) and/or radiological findings. For these patients, we retrospectively reviewed HCC staging according to the BCLC classification based on the conventional

imaging and treatment proposition. Then, we collected any new lesion detected, as well as any change in BCLC classification and treatment allocation based on the dual-tracer PET/CT. Modification of BCLC classification and treatment allocation according to the dual tracer PET/CT were defined in a multidisciplinary meeting. **Results:** Patients were mostly men (n=122; 88%) with cirrhosis in 106 patients (77%). BCLC staging was 0 or A in 52 patients (34%), B in 32 patients (23%), C in 25 patients (16%). No typical active tumor was identified with conventional imaging in the remaining 45 patients (29%). 18F-FDG PET/CT detected new lesions in 21 patients (14%), upgraded BCLC staging in 15 patients (10%) and modified the treatment in 17 patients (11%). Dual-tracer 18F-Fluorocholine and 18F-FDG PET/CT detected new lesions in 30 patients (19.4%). BCLC staging was upgraded in 22 patients (14%), and dual tracer PET/CT had an impact on treatment decision in 23 patients (15%). New intrahepatic lesions were detected in 7 patients, extrahepatic lesions in 16 patients and both intra and extrahepatic lesions in 7 patients. Ten patients had new bone lesions, 6 vascular invasion, 8 tumoral nodes, 3 lung metastasis and 1 adrenal metastasis. In patients waiting liver transplantation, staging was modified in 9% of the patients with active lesion (n=34) and in 4% of patients without tumor remaining after curative treatment (n=26). BCLC staging was modified in 19% of the patients assessed before percutaneous treatment or resection (n=36), in 10% of the patients assessed before palliative treatment (n=30). Staging was modified in 23% of the patients with doubtful extra-hepatic lesions (n=17) and in 36% of the patients with increased AFP without typical lesions at conventional imaging (n=11). **Conclusion:** In our population, dual-tracer 18F-Fluorocholine and 18F-FDG PET/CT allowed the upstaging in the BCLC classification in 13.6 % of the patients with HCC and treatment modification in 14.9% of the cases.

OP031

FDG-PET/CT in Primary Staging of Cholangiocarcinoma

A. Sabaté-Llobera¹, L. Gràcia-Sánchez¹, J. Mestres-Martí¹, I. Puig-Povedano¹, J. L. Vercher-Conejero¹, E. Llinares-Tello¹, L. Rodríguez-Bel¹, J. J. Robles-Barba¹, M. Cortés-Romera¹, L. Lladó-Garriga², T. Serrano-Piñol³, E. Ramos-Rubio², C. Gámez-Cenzano¹; ¹PET Unit, Department of Nuclear Medicine - IDI. Hospital U. de Bellvitge-IDIBELL, L'Hospitalet de Llobregat (Barcelona), SPAIN, ²Department of Surgery, Hospital U. de Bellvitge-IDIBELL, L'Hospitalet de Llobregat (Barcelona), SPAIN, ³Department of Pathology, Hospital U. de Bellvitge-IDIBELL, L'Hospitalet de Llobregat (Barcelona), SPAIN.

AIM: To assess the role of FDG-PET/CT in cholangiocarcinomas, identifying the primary tumor and staging, both in intrahepatic (IHC) and extrahepatic (EHC) lesions. **MATERIAL AND METHODS:** Between 2012 and 2015, 50 patients (27 men, mean age 68 years) with confirmed or suspected cholangiocarcinoma were studied with FDG-PET/CT at initial staging, as well as diagnostic CT and MRI. Thirty-one patients (62%) had an IHC and 19 (38%) an EHC. Metabolic parameters of primary lesions (SUVmax and lesion-to-normal-hepatic-activity ratio (L/NHA)) as well as performance of FDG-PET/CT for detection of regional lymph node metastasis and distant disease were compared between EHC and IHC. **RESULTS:** All IHC (31/31 patients-100%) showed an increased FDG uptake with a median SUVmax of 8.7 (3.6–19.5) and a median L/NHA ratio of 2.86 (1.06–7.22). By contrast, only 13/19 EHC (68%) showed an increased FDG uptake with a of median SUVmax of 4.5 (2.6–9.6) and a median L/NHA ratio of 1.45 (1–1.96). SUVmax and ratio L/NHA were significantly higher in primary lesions of IHC compared to EHC ($p < 0.01$). In 14/31 (44%) patients with IHC FDG-PET/CT detected regional/distant disease: isolated regional lymph node metastases in 7 (22%) (not biopsy-proven), and both regional and distant metastases in 7 (22%), located in peritoneum (3), bone (2), liver and mediastinum, with biopsy-proven disease in peritoneal and mediastinal sites. Additionally, a synchronous colorectal cancer was diagnosed. In patients

with EHC, 6/19 (32%) primary tumors did not show increased FDG uptake. Histologically there were one mucosecretor adenocarcinoma, one poorly-differentiated adenocarcinoma, three moderately-differentiated, and one well-differentiated adenocarcinoma. In these 6 patients with non-FDG avid tumors surgery discovered non-FDG avid metastases: regional lymph nodes in 3 and peritoneal metastases in 1. In 1/13 FDG-avid primary EHC, FDG-avid regional and distant metastases (supraclavicular nodes) were confirmed. **CONCLUSION:** FDG-PET/CT appears to be a useful technique in primary staging of cholangiocarcinoma, with better results in intrahepatic compared to extrahepatic lesions. IHC and its metastases seem more FDG-avid, whereas EHC are more heterogeneous, limiting the assessment of disease extension. These results must be confirmed by larger number of patients and biopsy-proven lesions.

OP032

Prognostic value of combined [^{99m}Tc-MAA-SPECT/CT and [¹⁸F]Fluoroethylcholine-PET/CT in patients suffering from advanced hepatocellular carcinoma prior to radioembolization

M. Hartenbach¹, S. Weber², S. Hartenbach³, M. Zacherl⁴, P. M. Papprottka⁵, R. Tiling⁶, P. Bartenstein⁴, M. Hacker¹, N. L. Albert⁴, A. Haug¹; ¹Medical University of Vienna, Dep. of biomed. imaging and image guided therapy, Vienna, AUSTRIA, ²Medical University of Vienna, Vienna, AUSTRIA, ³German Armed Forces Hospital, Institute of Pathology, Vienna, AUSTRIA, ⁴Univ. of Munich, Department of Nuclear Medicine, Munich, GERMANY, ⁵University of Munich, Clinical Institute of Radiology, Munich, GERMANY, ⁶University of Munich, Dept. of Nuclear Medicine, Vienna, GERMANY.

Hepatocellular carcinomas (HCC) are increasingly treated with radioembolization (RE). However, prognostic factors with regard to survival are needed for better patient selection. **Methods** 24 patients with advanced HCC underwent MAA-SPECT/CT und FEC-PET/CT prior to RE. We evaluated various uptake parameters, tumor-to-spleen-ratio and volumetric overlap of uptake on MAA-SPECT/CT and FEC-PET/CT using Hermes Hybrid 3D viewer. This data was analyzed with regard to survival. We used ROC analysis, Youden-index, multiple logistic regression analysis and Kaplan-Meier analysis for statistical analysis. **Results** All patients died with a median survival of 437±71 days. A high overlap of MAA SPECT/CT and FEC PET/CT was significantly associated with a shorter survival (AUC=0,75; P<0,05). A combination of SUV values, tumor-to-spleen-ratio and volumetric data using multiple logistic regression had an AUC of 0.87 (P=0.004) with a sensitivity of 100%, specificity of 75%, accuracy of 92%, a NPV of 89% and a PPV of 100% (P<0.001). Regression analysis was able to separate patients with regard to prognosis (median survival 531±68 days versus 840±96 days; log rank: 5.7; P=0.017) **Conclusion** Patients suffering from advanced HCC and a combination of high overlap of MAA-uptake (as a parameter for high tumor vascularization) and FEC-uptake have a significantly shorter survival as the remaining patients. This finding may aid to enhanced patient selection for RE.

OP033

Evaluation of the predictive role of ¹⁸F-FDG PET/CT in patients with locally advanced rectal cancer submitted to neoadjuvant therapy: correlation with tumour characteristics and treatment response

E. Puta¹, F. Orsini¹, L. M. Leva¹, L. Deantonio², L. Turri², R. Grasso², S. Torrente², A. Caroli², F. Apicella², D. Ferrante³, M. Krenghi², G. M. Sacchetti¹; ¹Nuclear Medicine Department, University Hospital “Maggiore della Carità”, Novara, ITALY, ²Radiotherapy Dept., University Hospital “Maggiore della Carità”, Novara, ITALY, ³Biostatistics & Clinical Epidemiology, University Hospital “Maggiore della Carità”, Novara, Italy, Novara, ITALY.

Aim [¹⁸F]FDG PET/CT has an important role in staging and treatment planning of rectal cancers. Neo-adjuvant chemo-radiotherapy (CT-RT) in locally advanced rectal cancer (LARC) helps to obtain tumour downsizing/downstaging. According to the literature data about 20% of these patients reach pathological complete response (pCR) after neo-adjuvant CT-RT leading to the concept of non-surgical approach aiming at organ preservation. The aim of our study was to evaluate whether baseline [¹⁸F]FDG PET/CT could help to predict histopathological response in LARC in patients treated with neoadjuvant CT-RT. **Materials and Methods** Fifty-six patients (37 males, 19 females; median age 69yrs) with LARC underwent a baseline [¹⁸F]FDG PET/CT study within 5 days from CT simulation scan. All patients had neoadjuvant CT-RT followed by radical surgery. For each patient we calculated the pre-treatment PET/CT values of SUVmax, SUVmean, Metabolic Tumour Volume (MTV) and Total Lesion Glycolysis (TLG) and we analysed their correlation with clinical parameters (cT3 and cT4) and histopathological data (Tumour Regression Grade TRG1 vs TRG2-5). **Results** According to TRG classification, 10/56 patients (17.9%), were classified as TRG1 (ypT0N0) corresponding to pCR and 46/56 patients (82.1%) as TRG2-5 (ypT1-4N0-2). SUVmax and TLG were significantly different between T-stage classes (p=0.05; p=0.002) and histopathological response (p=0.05; p=0.03). MTV was significantly different only between T-stage groups (p=0.008). SUVmean was not significantly different between T-stage (p=0.07) or histopathological response groups (p=0.18). We fit all the SUV variables in a logistic regression model and considered as a cut-off the median value of each SUV parameter. Values of SUVmax and SUVmean higher than the median resulted in a significant prediction of T4 primary tumour (p= 0.01 and p= 0.05). Higher SUVmax was associated with TRG2-5 (OR 5.2; CI95% 1.0-27.2), and SUVmax, SUVmean, MTV and TLG with T-stage (OR 5.3; CI95% 1.0-27.7). **Conclusions** Our data suggest that pre-treatment [¹⁸F]FDG PET/CT SUVmax and TLG are significantly lower in patients with pCR and SUVmax, MTV and TLG are significantly lower in patients with less extended primary disease (cT3). This study suggests that the baseline [¹⁸F]FDG PET/CT could predict treatment response; however the present results require validation in larger cohort.

OP034

Value of PET/CT in the characterization of extra-hepatic lesions in patients with hepatocellular carcinoma before liver transplantation

M. Houseni¹, L. zidan²; ¹National Liver Institute, Menoufia University, Menoufia, EGYPT, ²Faculty of Medicine, Cairo University, cairo, EGYPT.

Aim: Evaluate the role of FDG-PET/CT in the differentiation between neoplastic and benign extra-hepatic lesions in patients with hepatocellular carcinoma before liver transplantation. **Methods:** A total of 106 patients (89 male, 17 female with mean age 57 y) diagnosed with hepatocellular carcinoma and have extra-hepatic lesions detected during their assessment before liver transplantation enrolled in this study. FDG-PET/CT with multiphase CT was performed at same time. All finding were confirmed with histopathology or clinical and imaging follow-up for at least 24 months. **Results:** Thirty-seven patients have extra-hepatic metastases. The extra-hepatic findings were benign in 69 patients. The prevalence of extra-hepatic metastases was 34.9%. The sensitivity, specificity, accuracy, positive predictive value and negative predictive value for FDG-PET/CT were 83.8%, 85.5%, 84.9%, 75.6% and 90.8%, respectively. **Conclusion:** FDG-PET/CT can be of value in the assessment of patients with hepatocellular carcinoma before liver transplantation. PET/CT imaging play an important role in the characterization of extra-hepatic disease and expedite the transplantation process especially when the test is negative due to high negative predictive value.

OP035**18F-FDG PET/CT for restaging gastric cancer after surgical resection: is there a role in the assessment of local relapse?**

G. Polverari¹, F. Ceci¹, V. Ambrosini¹, P. Castellucci¹, P. Guidalotti¹, D. Campana², A. Matti¹, G. M. Lima¹, S. Fanti¹; ¹Service of Nuclear Medicine, S.Orsola-Malpighi University Hospital, University of Bologna, Bologna, ITALY, ²Department of Internal Medicine and Surgery, S.Orsola-Malpighi University Hospital, University of Bologna, Bologna, ITALY.

Aim: to investigate the performance of 18F-FDG-PET/CT in the evaluation of local recurrence in resected gastric cancer (GCa) patients, presenting 18F-FDG uptake in remnant stomach or anastomotic site. Secondary aim was to assess if clinical and diagnostic features might have an influence on the images reading process. **Materials and methods:** inclusion criteria were: 1) proven GCa treated with surgery with curative intent; 2) 18F-FDG-PET/CT performed during follow-up to restage the disease; 3) 18F-FDG uptake observed in remnant stomach or anastomotic site; 4) validation of PET/CT results obtained by histology and/or clinical/radiological follow-up. Exclusion criteria were: 1) no 18F-FDG uptake in remnant stomach or anastomotic site; 2) no validation of PET/CT results. 58 patients were retrospectively enrolled (35 male and 23 female). The 22.4% (13/58) performed total gastrectomy, while the 77.6% (45/58) performed subtotal gastrectomy. The mean time between surgery and 18F-FDG-PET/CT was 22 months (median 11 months). The overall performance of 18F-FDG-PET/CT (sensitivity, specificity, positive predicting value (PPV), negative predictive value (NPV) and accuracy) was calculated in accordance with an informed reading performed by two experienced readers aware of all the clinical and diagnostic data. A blind reading was performed in order to assess if clinical and diagnostic features might have an influence on the images reading process. A lesion suspected for malignancy was considered with focal and intense uptake with/without pathologic lesions in CT. A non-malignant lesion was suspected with faint and diffused uptake without pathologic lesions in CT. **Results:** at the informed reading, aware of the type of surgery (radical vs. partial) and the time from surgery to 18F-FDG-PET/CT, the 46.5% of scans (27/58) were considered suspected for local GCa relapse, while the 53.5% (31/58) were considered as not suspected for local relapse. Histological confirmation was obtained in the 48.3% of patients (28/58), while in the 51.7% (30/58) were validated with follow-up. Local GCa recurrence was proved in the 41.4% (24/58) of patients. 18F-FDG-PET/CT sensitivity, specificity, PPV, NPV and accuracy were 96%, 88%, 85%, 97% and 91%, respectively. Considering a blind reading of the images 18F-FDG-PET/CT sensitivity, specificity, PPV, NPV and accuracy were 58%, 76%, 64%, 72% and 69%, respectively. **Conclusion:** in our patient-series, 18F-FDG-PET/CT showed good performance for the assessment of local recurrence in resected GCa patients. An informed reading of the images could help physicians, with type of surgery and time from surgery to 18F-FDG-PET/CT as the main criteria for differentiating malignant vs. non-malignant lesions.

OP036**Visual scoring system for the assessment of treatment response in patients with oesophageal and gastro-oesophageal junction carcinoma**

E. Cong¹, M. Lee^{1,2,3}, A. Chicco⁴, M. Lin^{1,4,3}, J. Yap⁴, P. Lin^{1,4,3}, T. Tran², I. Ho-Shon^{1,4,3}; ¹University of New South Wales, Sydney, AUSTRALIA, ²Cancer Therapy centre, Liverpool Hospital, Sydney, AUSTRALIA, ³Western Sydney University, Sydney, AUSTRALIA, ⁴Department of Nuclear Medicine and PET, Liverpool Hospital, Sydney, AUSTRALIA.

Aim: To evaluate the prognostic value of a 5 point FDG-PET/CT visual scoring system in patients with newly diagnosed oesophageal or gastro-

oesophageal junction (GOJ) cancer that have received neoadjuvant or definitive radiotherapy and/or chemotherapy. **Methods:** Ninety seven patients with endoscopically confirmed oesophageal or gastro-oesophageal junction carcinoma treated with definitive or neoadjuvant therapy received pre-treatment PET-CT scans, and of these, sixty seven received post-treatment PET/CT scans. Primary tumours were assessed using a 5 point visual scoring system (visual score of the primary tumour: PVS) for both the pre and post-treatment scans. The score is derived from comparisons between tumour uptake and background references adapted from the Deauville score used to assessment treatment response in lymphoma. Cox regression was used to analyse the relationship between pre-treatment PVS (prePVS), post-treatment PVS (postPVS), change in PVS (deltaPVS) and survival (overall survival: OS, progression free survival: PFS). Log-rank tests were used to separate PVS into two prognostic categories with the greatest survival separation. Tumours were independently scored by 4 experienced observers blinded to all other information. Agreement was assessed using Cohen's kappa for individual scores and for two categories of scores (postPVS 1-3 vs 4-5 and deltaPVS (-4)-(-2) vs (-1)-1). **Results:** On multivariate analysis postPVS and deltaPVS were significant predictors of survival. Patients with postPVS of 1 to 3 had significantly greater median OS (ranging from 53.3-56 months between all observers) compared to patients with postPVS 4-5 (15.2-23.6 months; all observers). Patients with primary tumours experiencing a reduction of 2 or more points had much greater median OS (56 months - not reached in study; all observers) compared to patients whose tumours only experienced a point reduction of 1, had no change, or increased in points by 1 (15.1-21.8 months; all observers). Agreement for high uptake at site of primary tumour in the post-treatment scan (postPVS = 4-5) versus low uptake at site of primary tumour (postPVS = 1-3) was good with kappa ranging from 0.70 to 0.88 for paired combinations of all four readers. **Conclusion:** A visual assessment based on tumour uptake relative to reference background structures has the potential to provide valid and reproducible prognostic information following neoadjuvant or definitive radiotherapy +/- chemotherapy for oesophageal or GOJ carcinoma. These scores also have the potential to stratify treatment responders and non-responders, thus influencing management.

109 – Sunday, October 16, 2016, 08:00 - 09:30, Hall 113

Conventional & Specialised Nuclear Medicine: Uro-nephrology**OP037****The reliability of estimated glomerular filtration rate in South African oncology patients**

J. Holness, H. Simonds, P. Barnardt, J. Warwick; Stellenbosch University, Cape Town, SOUTH AFRICA.

Aim: Due to the nephrotoxicity of platinum-based chemotherapy, it is essential that patients' kidney function is measured accurately prior to commencing treatment, and monitored closely during therapy. Although glomerular filtration rate (GFR) is widely accepted as the best measure of kidney function, it is not feasible to measure in all patients. Consequently, GFR is usually estimated from the serum creatinine concentration using one of a variety of equations. However, these equations have been shown to perform poorly in many non-Caucasian populations around the world, including South Africans, and it is hypothesized that they will be even less accurate in cancer patients. The aim of this study is to determine whether estimated GFR can be used routinely for the measurement of kidney function in South African cancer patients. **Materials and methods:** This was a retrospective review of 233 cancer patients who had a GFR study to determine renal function prior to or during treatment with platinum-based chemotherapy, between January 2011 and May 2015. For GFR determination (mGFR), 40 MBq of ^{99m}Tc-diethylenetriamine pentaacetic acid (^{99m}Tc-DTPA) was administered

intravenously. Venous blood samples were taken at 2, 3 and 4 hours after injection. GFR was calculated using the slope-intercept method. The mean Brochner-Mortensen correction was applied after correction for body surface area. Serum creatinine was measured within seven days of the GFR study with patients receiving no treatment between the two measurements. Estimated GFR (eGFR) was calculated using the Cockcroft-Gault, Modification of Diet in Renal Disease (MDRD), and Chronic Kidney Disease Epidemiology Collaboration (CKD-EPI) equations. The correlation, bias, accuracy, and impact on patient management of the estimated GFR was determined for each equation. **Results:** The correlation between eGFR and mGFR was poor with $R^2 = 0.25-0.5$. All three equations generally over-estimated GFR with a mean bias of 12–20 ml/min/1.73m². The precision of the three equations, expressed as the percentage of estimated GFR values within 30% of mGFR (P_{30}), was 53–69%. Use of eGFR would have led to inappropriate management in 11–13% of cervix cancer patients, with 5–8% receiving too high a dose or the incorrect drug, and 4–7% having the drug withheld or the dose reduced unnecessarily. **Conclusion:** Estimated GFR using Cockcroft-Gault, MDRD or CKD-EPI equations cannot be used as replacement for measured GFR in South African cancer patients requiring nephrotoxic chemotherapy.

OP038

Assessing four kidney function parameters with dynamic FDG-PET/MR: a feasibility study

B. K. Geist, S. Rasul, A. Staudenherz, M. Hacker; Medical University of Vienna, Vienna, AUSTRIA.

Aim: The routinely used sugar-like PET tracer FDG participates in several crucial kidney processes: it is filtered, reabsorbed and extracted. The renal time activity curves (TACs) of FDG therefore might contain information about certain kidney functions. The aim was, to extract four kidney parameters (clearance, split function, transit time, renal blood flow) from one dynamic FDG-PET/MR scan and to compare the results to standard methods. **Method:** In a current study in the General Hospital in Vienna, kidneys of 20 healthy volunteers are examined with a PET/MR scan (Siemens Biograph mMR), including two MR pictures of the abdomen, in which the regions of interest in both kidneys were drawn; and one 30 minutes dynamic PET scan directly after injection (2 Mbq/kg) with FDG, from which TACs were extracted after image fusion. From renal cortex TAC, the slope of the Patlak-Rutland-Plot and the integral over the first 3 minutes were calculated. Maximum transit time and renal blood flow were calculated with the - from the image derived aorta input function - deconvoluted renal cortex TAC. Kidney volume was determined solely from the according MR pictures. As reference method, volunteers undergo a renography with Tc-MAG3 for determination of split function and transit times. Additionally, blood samples were drawn for determination of glomerular filtration rate and renal blood flow (methods by Cockcroft-Gault and Bubeck, respectively). **Results:** So far, 11 healthy volunteers have been evaluated (estimated study end: June 2016), between 25 and 59 years. The slope of the Patlak-Rutland-Plot, reflecting the initial filtration process, multiplied with the kidney volume correlates with the glomerular filtration rate significantly ($r = 0.86$, $p < 0.001$). Split function from renography varies between 45 % and 57 % (left kidney) and correlates well with cortex FDG-TAC split function ($r = 0.8$, $p < 0.001$). Maximum transit times and renal blood flow also correlate well with reference methods ($p < 0.0001$ and $p < 0.0005$, respectively). **Conclusion:** The kidney parameters extracted from a dynamic FDG-PET/MR scan show promising preliminary results compared to routinely used methods in nuclear medicine. Four crucial parameters can be estimated from FDG-TACs if the cortex region and the kidney volume can be determined accurately from MR scans. As a consequence, kidney function might be assessed simultaneously to a routine PET/MR scan. The results of the finished study will be presented in detail.

OP039

The effect of measurement errors on glomerular filtration rate: a comparison of the slope-intercept, single-sample and slope-only methods

J. Holness¹, J. Fleming², J. Warwick¹; ¹Stellenbosch University, Cape Town, SOUTH AFRICA, ²University Hospital Southampton NHS Foundation Trust, Southampton, UNITED KINGDOM.

Aim: Glomerular filtration rate (GFR) is conventionally measured using the slope-intercept method (SI-GFR), which has acceptable accuracy provided strict attention is paid to avoid technical errors at a number of stages. Single-sample GFR estimates (SS-GFR) have recently been shown to be as accurate as SI-GFR, while having the advantage of taking less time to perform. A third method, slope-only GFR (SO-GFR), based exclusively on the slope of the terminal exponential of the plasma clearance curve, obviates the need for a standard or measurement of the doses, height or weight. The aim of this paper is to use patient data to model GFR measurement error resulting from the SI-GFR, SS-GFR and SO-GFR methods. **Materials and methods:** Departmental records were reviewed to identify all GFR studies that were performed using Tc-99m DTPA between Jan 2008 and March 2016, in which at least 3 blood samples were taken (2h, 3h and 4h after injection). Using the original data, GFR was calculated using 8 methods: SI-GFR:3-sample (2h 3h 4h); SI-GFR:2-sample (2h 3h); SI-GFR:2-sample (2h 4h); SI-GFR:2-sample (3h 4h); SS-GFR:2h (Fleming's method); SS-GFR:3h; SS-GFR:4h; SO-GFR. These values were regarded as the reference GFR values. Realistic, normally distributed, random errors were subsequently introduced to all measurements: height (2.5cm), weight (2kg), syringe masses (0.005g), standard flask volume (1%), pipetting volumes (2%), sampling times (2 min) and count rates ($\sqrt{\text{counts}}$), to generate 30 GFR realisations per study. The mean errors in GFR were then compared, and correlated with GFR. **Results:** A total of 780 GFR studies were included. GFR ranged from 15 to 158 ml/min/1.73m² (median 85 ml/min/1.73m²). Mean measurement error in GFR was highest using SI-GFR:2 sample (3h 4h) (95% CI 3.27–3.45 ml/min/1.73m²) and lowest using SS-GFR:4h (95% CI 1.84–1.87 ml/min/1.73m²). However, none of the methods differed significantly. Mean error increased with GFR for all methods ($p < 0.001$). **Conclusion:** Using all GFR calculation methods, the measurement errors that can be expected in a busy clinical Nuclear Medicine department are small compared to intra-patient variation of repeat measurements. These findings support emerging evidence in favour of using the shorter SS-GFR over SI-GFR or SO-GFR in busy clinics with high patient throughput.

OP040

Clinical usefulness of advanced quantitative analysis of diuresis renogram in patients with equivocally obstructed upper urinary tract

S. BEATOVIĆ¹, M. Janković², D. Sobić Saranović¹, E. Jaksic¹, V. Antić³, M. Blagić³, V. Artiko¹; ¹University of Belgrade Faculty of Medicine, Center for Nuclear Medicine, Clinical Center of Serbia, BELGRADE, SERBIA, ²University of Belgrade Faculty of Electrical Engineering, BELGRADE, SERBIA, ³Center for Nuclear Medicine, Clinical Center of Serbia, BELGRADE, SERBIA.

Introduction: Advanced parameters of diuretic renography - output efficiency (OE) and normalized residual activity (NORA) help to distinguish between obstructed and non-obstructed kidneys. Unfortunately, algorithm for their calculation is not widely available. Non-commercial software developed by International Atomic Energy Agency (IAEA) enables this comprehensive analysis, but till now, it has not been widely implemented in the nuclear medicine institutions in developing countries. The aims of this study were: a) to calculate, by means of the International Atomic Energy Agency (IAEA) software, the values of ^{99m}TcDTPA renogram parameters in obstructed kidneys and hypotonic unobstructed

kidneys and to determine significance of OE and NORA in the assessment of equivocally obstructed urinary tract. Subjects and methods: 153 patients with suspected obstruction (age range: 18–83 years; mean: 51.8 years) underwent ^{99m}Tc DTPA dynamic scintigraphy with furosemide stimulation at 20 minute. 164 kidneys were investigated. 40-minutes acquisition with 240 10-sec images was applied. Post-void static image was acquired at 50 minute. Studies were analyzed by two observers and, according to assessment of images and renograms, kidneys were classified as obstructed (56), hypotonic unobstructed (63) and equivocal (45). IAEA software was applied to each study. Parameters analyzed were: OE at 20 minute (OE_{20}) and 20 minutes after injection of furosemide (OE_{F+20}), NORA at 20 minute (NORA_{20}), NORA on the post-micturition acquisition (NORA_{PM}) and residual kidney counts on post-micturition acquisition normalized to maximum kidney counts (PM/max). Results for obstructed kidneys were: OE_{20} : $56.8 \pm 10.1\%$; OE_{F+20} : $69.5 \pm 7.1\%$; NORA_{20} : 2.28 ± 0.52 ; NORA_{PM} : 0.40 ± 0.12 ; PM/max: 0.21 ± 0.05 . Results for hypotonic unobstructed kidneys were: OE_{20} : $52.8 \pm 10.1\%$; OE_{F+20} : $87.9 \pm 3.7\%$; NORA_{20} : 2.38 ± 0.52 ; NORA_{PM} : 0.12 ± 0.04 ; PM/max: 0.061 ± 0.02 . Difference between obstruction/dilatation was significant for OE_{F+20} , NORA_{PM} and PM/max ($p < 0.001$). Linear regression analysis between OE_{20} and NORA_{20} was significant ($r = -0.975$; $p < 0.001$). Among 45 kidneys with equivocal findings according to standard parameters, calculation of OE_{F+20} revealed 26 kidneys to be non-obstructed. In 2 kidneys obstructive pattern was converted into non-obstructive according to NORA_{PM} and PM/max value. In remaining 17 kidneys both parameters were in obstructive range. Conclusion: Results of OE_{20} , OE_{F+20} , NORA_{20} and NORA_{PM} for obstructed and unobstructed kidneys, calculated by the use of IAEA software showed excellent agreement with previously reported values of these parameters for ^{99m}Tc DTPA. High correspondence between OE and NORA gives the opportunity of replacing OE with NORA, when algorithm for OE could not be applied. OE_{F+20} , NORA_{PM} and PM/max contribute to clarify equivocal findings of diuresis renography.

OP041

Blood-Pool Compensation Method Revisited: Similarity and Difference in Comparison with Patlak-Rutland Plot

M. Samal¹, A. Brink², V. Ptacnik¹, H. Jiskrova¹, D. Skibova¹, J. Kubinyi¹; ¹Charles University Prague @ General University Hospital in Prague, Prague, CZECH REPUBLIC, ²Red Cross War Memorial Children's Hospital, Cape Town, SOUTH AFRICA.

A slope of Patlak-Rutland plot (PRP) has been used to calculate differential kidney function not affected by vascular background in the kidney ROI. Blood-pool compensation method (BPC) claims that it further corrects for extravascular (interstitial) background [EJNMMI 2016;43:550]. The aim of this study was to examine the assertion in more detail. Method: Performance of PRP and BPC has been compared with simulated and patient data (107 MAG_3 dynamic renal studies in adults and 173 in children). Renal curves were simulated as "zero-output curves" (without outflow) - scaled integrals of a monoexponential plasma clearance curve. Vascular backgrounds were simulated as scaled plasma curves, extravascular backgrounds as weak kidneys. In the patient data, PRP and BPC were applied to a fixed interval between 1 - 2 minutes. Both the heart and the liver ROIs have been used to generate input functions and a circumferential kidney ROI was chosen to represent kidney background. Differential kidney functions calculated by PRP and BPC under various conditions were compared using Passing-Bablok regression. Results: Using the same time-activity curves, PRP and BPC provided almost identical results. PRP has been found more robust with better linear relationship between the plotted variables. In all simulated experiments, the ratio of PRP slopes was identical to the ratio of BPC intercepts. Differential function was not affected by vascular background in the kidney ROI and by extravascular background in the heart or the liver

ROI. However, it was affected by extravascular background in the kidney ROI. Despite this fact, an independent analysis has confirmed the main result of the EJNMMI paper above: BPC with the liver ROI input curve (without additional background subtraction) provides the same result as PRP with the heart ROI input curve and circumferential background subtraction from the kidney ROI. Whether this is the result of renal extravascular background compensation by BPC or another effect (related to the liver ROI curve rather than kidney curve) still remains to be established. Conclusion: BPC method definitely extends a tool kit for calculation of differential kidney function. It has also been shown that in case of absence of the heart in the field of view, the liver can be used as an excellent substitution in either BPC or PRP. It is interesting that such a possibility has already been proposed 30 yrs ago by C.S.Patlak [JCBFM 1985;5:584] but remained overlooked in renal nuclear medicine by now.

OP042

Clinical validation of comprehensive non-commercial software for renogram analysis: values of washout parameters in healthy individuals

S. BEATOVIĆ¹, M. Janković², D. Sobić Saranović¹, E. Jaksic¹, V. Artiko¹; ¹University of Belgrade Faculty of Medicine, Center for Nuclear Medicine, Clinical Center of Serbia, BELGRADE, SERBIA, ²University of Belgrade Faculty of Electrical Engineering, BELGRADE, SERBIA.

A decade ago IAEA initiated the work on comprehensive non-commercial software for processing of renogram on a simple p-computer, but the software hasn't been completed and only the draft version was available. Furthermore, the accuracy of numerical outputs of the software has not been assessed in comparison with commercial software. Purpose: The aims of this study in healthy individuals were: to implement IAEA software into analysis of Tc-99m DTPA and Tc-99m MAG_3 dynamic scintigraphy and to validate results of obtained renogram parameters against their reference values. Patients and Methods: Study population consisted of 104 healthy subjects who were evaluated by dynamic scintigraphy for kidney donation. 54 of them underwent Tc-99m DTPA scintigraphy and 50 ^{99m}Tc MAG_3 scintigraphy. 208 kidneys were analyzed in total. IAEA software was applied to process the studies. Parameters analyzed were: time to maximum activity (T_{max}), time to half maximum ($T_{1/2}$), output efficiency at 20 minutes (OE_{20}), residual kidney counts at 20min normalized to the 1-2min counts (NORA_{20}), residual kidney counts on post-micturition acquisition normalized to the 1-2min counts (NORA_{PM}), residual kidney counts on post-micturition acquisition normalized to maximum kidney counts (PM/max), whole kidney mean transit time (MTT) and mean parenchymal transit time (MPTT). Correspondence between OE_{20} and NORA_{20} , was evaluated by Pearson correlation coefficient and linear regression analysis. The results for Tc-99m DTPA were: T_{max} : 3.6 ± 0.9 min; $T_{1/2}$: 9.1 ± 3.5 min; OE_{20} : $88.1 \pm 2.3\%$; NORA_{20} : 0.66 ± 0.1 ; NORA_{PM} : 0.07 ± 0.02 ; PM/max: 0.06 ± 0.01 ; MTT: 2.08 ± 0.54 min and MPTT: 1.77 ± 0.37 min. Results for ^{99m}Tc MAG_3 : T_{max} : 3.8 ± 0.7 min; $T_{1/2}$: 6.9 ± 1.9 min; OE_{20} : $92.0 \pm 2.4\%$; NORA_{20} : 0.38 ± 0.1 ; NORA_{PM} : 0.03 ± 0.01 ; PM/max: 0.02 ± 0.01 ; MTT: 2.44 ± 0.61 min and MPTT: 1.80 ± 0.33 min. The excellent agreement was observed between obtained values of renogram parameters and their reference values in the literature. Significant linear correlation between NORA_{20} and OE_{20} was observed ($r = -0.936$, $p < 0.01$). Conclusion: IAEA software gives reliable numerical indices of kidney excretion. The values for normal kidneys were almost identical with previously reported reference values for DTPA and MAG_3 parameters. NORA_{20} highly corresponds with OE_{20} and could replace the former parameter in the evaluation of kidney drainage. The obtained results should be an incentive for IAEA to continue its work on completion of software in order to standardize technique of dynamic renal scintigraphy.

OP043**Evaluation of interobserver agreement in interpretation of indirect radionuclide cystography**

B. Caliskan, A. N. Korkmaz; Abant Izzet Baysal University, Department of Nuclear Medicine, Bolu, TURKEY.

Aim: Indirect radionuclide cystography (IRC) offers chance to investigate vesico-ureteric reflux (VUR) without bladder catheterization and it has an advantage of lower radiation burden compared with radiological micturating cystogram. We aimed to investigate the interobserver agreement in interpretation of IRC. **Material and methods:** Indirect radionuclide cystograms of 47 patients were retrospectively evaluated independently by 2 experienced nuclear medicine physicians. The mean age of the patients was 8.25 ± 3.75 and 37 of the patients were females (79%). All patients had routine dynamic renal scintigraphy. Subsequently IRC's were performed by collecting 3-second frames during voiding. Curves were generated by drawing region of interests over bladder and two kidneys. IRC's were interpreted in a stepwise fashion involving visual images, compressed images and curves, respectively. The diagnosis of VUR was recorded as a result of the final decision of physician. The interobserver agreement between the two physicians in determining the VUR was investigated using the Kappa statistics. A Kappa-value >0.80 was considered as "excellent", $0.61-0.80$ as "good", $0.41-0.60$ as "moderate" and 0.40 or less as "poor". **Results:** The interobserver agreement was found to be poor when the physicians made their decision with only visual images ($k=0.242$, $p=0.102$). There was a moderate interobserver agreement in assessment of VUR with the evaluation of compressed images of IRC ($k=0.564$, $p<0.001$) and there was no difference between the observers in determining the VUR by curves. When a final diagnosis of VUR was made with taking of all three kind of processes into consideration, there was a moderate agreement between the two observers to assess the VUR in IRC ($k=0.589$, $p<0.001$). **Conclusions:** The diagnosis of VUR in IRC is more reliable when all of the visual images, compressed images and curves are taken into consideration. Interpretation of only the visual images decreases the interobserver agreement in IRC.

OP044**Non-infectious complications of peritoneal dialysis detected by Peritoneal scintigraphy - our experience**

A. Fernandes, T. Faria, A. Oliveira, V. Alves, M. Perez, A. Pinto, J. Pereira; Hospital São João, Porto, PORTUGAL.

Introduction/Aim: The use of Continuous Ambulatory Peritoneal Dialysis (CAPD) is increasing. Despite its confirmed advantages (compared with haemodialysis), several complications have been recognized - including infectious and pressure-related ones. The infusion into the peritoneal cavity leads to increased intra-abdominal pressure with potential leakage. Dialysate leakage occurs in more than 5% of patients in the first year of CAPD. Leaks may present as pericatheter drainage, but more often present as subcutaneous swelling and oedema, weight gain, peripheral or genital oedema, and apparent ultrafiltration failure. When dialysate leakage occurs into subcutaneous tissues, it is sometimes difficult to evaluate. Available diagnostic methods include radiography, CT with contrast material, and peritoneal scintigraphy. Our aim was to analyse our results and ascertain the diagnostic value of peritoneal scintigraphy. **Materials/Methods:** We reviewed data from all patients who underwent peritoneal scintigraphy at our department from 2008 to March 2016 ($n=81$), and used indirect follow-up criteria to verify leakage: surgical intervention to the catheter/CAPD suspension - "confirmation"; maintenance of CAPD with no further surgical interventions - "non-confirmation". Peritoneal scintigraphy protocol: the abdominal cavity was drained of all dialysate, and 185 MBq of Te-99m-MAA (in 1 L of dialysate solution) were instilled via the peritoneal catheter. Images were acquired 5 hours

after instillation: planar images of the peritoneal cavity (anterior/lateral projections), obtained both with the patient in a supine position and standing-up, before and after drainage of the dialysate. When necessary, SPECT/CT was performed. **Results:** Scintigraphies were performed because of abdominal wall swelling, inguinal/genital swelling, poor drainage/ultrafiltration, or pleural effusion. We detected leaks in 57 patients (70%), some with multiple sites, resulting in 62 leaks (48.4% in the umbilical region, 17.7% in the hypogastric region, 16.1% in the iliac region, 6.5% in the lumbar region, 4.8% in the pleural cavity, 3.2% in the genital region, and 3.2% in other locations). Of these 57, we confirmed leakage in 41; 6 patients maintained CAPD with no further surgical interventions; we couldn't assess the follow-up of 10 patients. Of the 24 negative studies, 21 maintained CAPD with no further surgical interventions; two patients had otherwise diagnosed leakage; we couldn't assess the follow-up of 1 patient. The positive predictive value (PPV) was 87.2% and the negative predictive value (NPV) was 91.0%. **Conclusion:** Peritoneal scintigraphy is a simple, safe, low-radiation-exposing, non-invasive method of determining the site of dialysate leak, allowing diagnosis, post-surgery evaluation and follow-up. In our series we found high PPV and NPV.

201/203 – Sunday, October 16, 2016, 10:00 - 11:15, Auditorium

Plenary 1: Clinical Molecular Imaging (incl. Marie Curie Lecture)**OP045****Guiding Therapy in Heart Disease: Role of Hybrid Imaging**

P. Kaufmann; University Hospital Zurich, Department of Nuclear Medicine, Cardiac Imaging, Zurich, SWITZERLAND.

OP046**Cancer, Inflammation and the Immune System**

A. Mantovani; Humanitas University, Rozzano, ITALY.

OP047**PET/CT in Malignant Lymphoma**

S. Barrington; St. Thomas' Hospital, PET Imaging Centre, London, UNITED KINGDOM.

301 – Sunday, October 16, 2016, 11:30 - 13:00, Auditorium

CME 2 - Dosimetry/Radionuclide Therapy: Dosimetry for Clinical Trials**OP048****Requirements for Acquiring Dosimetry in Clinical Trials with Diagnostic Radiopharmaceuticals**

U. Eberlein; Universitaetsklinikum Wuerzburg, Klinik fuer Nuklearmedizin, Wuerzburg, GERMANY.

OP049**Requirements for Acquiring Dosimetry in Clinical Trials with Therapeutic Radiopharmaceuticals**

M. Cremonesi; I.E.O. European Institute of Oncology, Health Physics, Milan, ITALY.

OP050**Dosimetry in Daily Practice – The Physician's Point of View**

R. P. Baum; Zentralklinik Bad Berka GmbH, Klinik für Molekulare Radiotherapie Zentrum für Molekulare Bildgebung (PET/CT), ENETS Center of Excellence, Bad Berka, GERMANY.

302 – Sunday, October 16, 2016, 11:30 - 13:30, Hall 211

Joint Symposium 2 - EANM/ICRP: Dosimetry-Guided Personalised Therapy – Are We Prepared for February 6, 2018?

OP051

Introductory Presentation on the EU Council Directive 2013/59/ EURATOM

G. Flux; Royal Marsden NHS Trust & Institute of Cancer Research, Joint Department of Physics, Sutton Surrey, UNITED KINGDOM.

OP052

Current Status and Preparedness to Comply to the Directive (Report on European Survey)

K. Sjögreen Gleisner; Lund University Hospital, Clinical Sciences, Lund, Medical Radiation Physics, Lund, SWEDEN.

OP053a

ICRP View on Dosimetry Guided Personalised Therapy

S. Mattsson; Lund University, Lund, SWEDEN.

OP053b

ICRP View on Dosimetry Guided Personalised Therapy

Y. Yonekura; National Institute of Radiological Sciences, Tokyo, JAPAN.

OP054a

Patient's View on Dosimetry Guided Personalised Therapy

J. Mailman; Oakland, UNITED STATES OF AMERICA.

303 – Sunday, October 16, 2016, 11:30 - 13:00, Hall 117

CTE 2: Technologist Competencies Round Table

OP055

Nuclear Medicine Technologists within EFRS

W. van den Broek; Radboud University Medical Center, Department of Nuclear Medicine, Nijmegen, NETHERLANDS.

OP056

Controversies in Competencies, Accreditation and Education

G. Testanera; Istituto Clinico Humanitas, Department of Nuclear Medicine, Milan, ITALY.

OP057

Nuclear Medicine Technologists: European Qualification Framework Level 6 and Level 7

P. A. Frago Costa; University Carl von Ossietzky, Oldenburg, GERMANY.

305 – Sunday, October 16, 2016, 11:30 - 13:00, Hall 115

M2M: New Radiotracers - Brain

OP058

Evaluation of two new radiotracers for alpha synuclein PET imaging

E. Levigoureux^{1,2}, W. ZEINYEH³, T. BILLARD³, F. CHAUVEAU¹, M. VERDURAND¹, L. ZIMMER^{1,2,4}, S. LANCELOT^{1,2}, ¹Université Claude Bernard Lyon 1, Lyon Neuroscience Research Center,

INSERM, CNRS, Lyon, FRANCE, ²Hospices Civils de Lyon, Lyon, FRANCE, ³Université Claude Bernard Lyon 1, Institute of Chemistry and Biochemistry, CNRS, Villeurbanne, FRANCE, ⁴CERMEP-Imaging Platform, Bron, FRANCE.

Aim Alpha-synuclein (α -syn) aggregation is a neuropathological hallmark of neurodegenerative diseases called synucleinopathies, including Parkinson's disease, dementia with Lewy bodies and multiple system atrophy. The purpose of this study was to evaluate two new radiotracers, the N-{4-[(E)-2-(1,3-benzoxazol-2-yl)ethenyl]phenyl}-4-fluoro-N-methylbenzene-1-sulfonamide or [¹⁸F]ZW27 and N-{4 [(E)-2-(1,3-benzoxazol-2-yl)ethenyl]phenyl}-2-fluoro-N methylbenzene-1-sulfonamide or [¹⁸F]ZW31, as possible probes for PET imaging of cerebral α -syn plaques. **Material and methods** To investigate the selectivity of the two radiotracers, we tested the ability of [¹⁸F]ZW27 and [¹⁸F]ZW31 to bind to synthetic α -syn and A β 1-42 fibrils. Synthetic fibrils were obtained by incubating human recombinant proteins at 200 μ M, 37 °C. The quality of the fibril formation was determined by ThT fluorescence and transmission electron microscopy, before the binding assays. Fibrils (400 nM) were incubated with increasing concentrations of [¹⁸F]ZW27 and [¹⁸F]ZW31 (0.5-200 nM). These reactions were duplicated in the presence of unlabeled molecules at a concentration of 50 μ M to evaluate the non-specific binding. Binding data were analyzed with a curve fitting software that calculates the Kd and Bmax using nonlinear regression. **Results** Analyses indicated that [¹⁸F]ZW27 bound on α -syn fibrils with a low affinity (Kd = 155.4 nM and Bmax = 2.073 pmol/nmol of fibrils) and with a better affinity on A β 1 42 fibrils (Kd = 7.74 nM and Bmax = 0.802 pmol/nmol of fibrils). In contrast, [¹⁸F]ZW31 bound on α -syn fibrils with a high affinity (Kd = 3.291 nM and Bmax = 0.128 pmol/nmol of fibrils) and with a lower affinity on A β 1-42 fibrils (Kd = 145.3 nM and Bmax = 0.592 pmol/nmol of fibrils). **Conclusion** These preliminary results suggest that [¹⁸F]ZW31 is potentially a radiotracer for α -syn imaging while [¹⁸F]ZW27 is more interesting for amyloid imaging studies. These molecules have now to be evaluated in postmortem studies in synucleinopathies and Alzheimer' disease patients in order to confirm this trend and to envisage a possible first-in-man study.

OP059

Novel compounds for specific visualization of α -synucleinopathies by PET

B. Hooshyar Yousefi¹, M. Mohring¹, T. Arzberger², G. Höglinger³, H. Wester⁴, M. Schwaiger¹; ¹Klinikum rechts der Isar, Technical University Munich, Nuclear med. Dept., Munich, GERMANY, ²Neurobiobank München, Center for Neuropathology and Prion Research, Department of Psychiatry and Psychotherapy, Ludwig-Maximilians-Universität München, Munich, GERMANY, ³Klinikum rechts der Isar, Technical University Munich, Department of Neurology and German centre of neurodegenerative diseases (DZNE), Munich, GERMANY, ⁴Technical university Munich, LS Pharm. Radiochemistry, Garching, GERMANY.

PET is increasingly applied for diagnosis of neurodegenerative diseases such as Alzheimer's disease by targeting neuroproteopathies like cerebral amyloid (A β), PHF-tau and NFTs. Tracer delineating α -synuclein protein expression would be invaluable for early diagnosis of α -synucleinopathies (α -syn) and clinical trials testing of therapeutic strategies aimed at lowering α -synuclein protein levels in the brain. Hence, the objective of this study was to find chemical entities that can be transformed into radiolabeled tracers for selective imaging of α -synuclein depositions. **Methods:** Among the compounds screened in our lab, a promising series of candidates based on 4,4'-diaryl-2,2'-bithiazole (DABTA) was identified as specific markers for α -syn as opposed to other proteopathies (eg. A β and tau). Pharmacokinetics of these radioligands were investigated using biodistribution and in-vivo stability studies. Furthermore, blood-brain-barrier penetration and specific binding

have been studied with longitudinal PET, ex vivo/ in vitro autoradiography and IHC using transgenic E46K rats. **Results:** The search for α -syn tracers revealed several compounds with nanomolar affinity for α -syn suitable for ^{11}C - or ^{18}F -labeling. The first biological evaluation of [^{18}F]DABTA-11, 4-(benzo[d][1,3]dioxol-5-yl)-4'-(4-(2-[(^{18}F] fluoroethoxy)phenyl)-2,2'-bithiazole), indicated a high initial brain uptake ($> 5\%$ ID/g at 5 min, $\log D=2.9$) and fast brain clearance (5/30 min brain uptake ratio > 5.7 , $n=5$) with high binding ($K_i < 10\text{nM}$), and high selectivity (> 120 -fold) over A β and tau. Moreover, [^{18}F]DABTA-11 PET in 2 month old E46K rats showed accumulation in medulla oblongata which became more prominent after 6 months of age and a detectable uptake in substantia nigra. **Conclusion:** A library of DABTAs was screened and preclinically evaluated as α -syn imaging agents. [^{18}F]DABTA-11 PET showed excellent accumulation in medulla oblongata followed by substantia nigra (known α -syn rich regions) in E46K rats at 6 month. These findings suggest that DABTA-11 is the first promising and selective α -synuclein tracer that may allow early diagnosis of α -synucleinopathies such as Parkinson's disease and dementia with Lewy bodies or multiple system atrophy.

OP060

Evaluation of the Ligand [^{18}F]IMA201 as a Novel Radiotracer for Aggregated Alpha-Synuclein in Parkinson's Disease

E. J. Smyth¹, S. Tang¹, I. Ahmed², L. A. Wells¹, C. Plisson¹, J. Passchier¹; ¹Imanova Ltd, London, UNITED KINGDOM, ²Parkinson's UK Brain Bank, Imperial College London, London, UNITED KINGDOM.

Alpha-synuclein is found in an aggregated state in many neurodegenerative diseases such as Parkinson's disease (PD). The availability of a PET ligand selective for α -synuclein would greatly help in drug development for PD in addition to the diagnosis and prognosis of α -synuclein associated diseases. The aim of this study was to evaluate [^{18}F]IMA201 as a potential PET ligand for delineation of α -synuclein in patients with PD. Animal experiments were conducted in accordance with the UK Animals (Scientific Procedures) Act 1986. [^{18}F]IMA201 was prepared following the recently developed copper II-mediated ^{18}F -fluorination methodology.¹ Human tissue was ethically sourced from the Parkinson's UK Brain Bank. Anatomically adjacent fresh frozen tissue sections (10 μm) from the grey matter area of the midbrain or cortical region of three individual PD patients were cut and fixed in 4% paraformaldehyde. Sections were incubated with increasing concentrations of [^{18}F]IMA201 (0.3, 1, 10nM) for 45 minutes, washed twice and opposed to phosphor-imager plates. Specific binding (SB) was identified by homologous block (10 μM) and ligand binding was quantified using a standard curve. The presence of α -synuclein was confirmed with immunohistochemistry in anatomically adjacent slides. Dynamic PET scans were conducted under baseline conditions and following pre-treatment with unlabelled IMA201 (2 mg/kg *i.v.*) to determine *in vivo* regional brain uptake of [^{18}F]IMA201 in a healthy male rat. IMA201 was successfully labelled with ^{18}F with a radiochemical yield of 150–400MBq and mean specific activity of 10 ± 11 GBq/ μmol ($n=3$). [^{18}F]IMA201 demonstrated a heterogeneous SB signal in brain tissue of three patients at three different concentrations (**0.3nM:** 6.2, 22 and 6.5 DLU/mm²/Bq; **1nM:** 0, 120 and 40 DLU/mm²/Bq; **10nM:** 390, 370 and 100 DLU/mm²/Bq). Percentage SB ranged from 0 - 87%, which was consistent with the heterogeneous expression of α -synuclein between patients as determined by immunohistochemistry. [^{18}F]IMA201 demonstrated good brain penetration in a healthy rodent with reversible kinetics during the time of the scanning period. The successful labelling, SB characteristics and good *in vivo* kinetic profile of [^{18}F]IMA201 suggest that this is a potential candidate for monitoring α -synuclein in the CNS. Radiosynthesis optimisation to allow clinical translation and further studies investigating the selectivity of [^{18}F]IMA201 for α -synuclein over other misfolded proteins in patient brains, including the

evaluation of a SB signal in a rodent model of PD, are required to confirm the potential of [^{18}F]IMA201 in clinical applications and neurodegenerative drug development. **Reference:** 1. C. Plisson et AL *J Label Compd Radiopharm* 2015, 58 (S1), S268

OP061

Identification of PF-06684511 as a novel β -secretase (BACE) selective radioligand lead for PET imaging

L. Zhang¹, M. A. Brodney¹, E. M. Beck¹, J. K. Dutra², B. T. O'Neill², L. M. Buzon², T. J. McCarthy¹, C. E. Nolan¹, A. Villalobos¹, L. Chen²; ¹Pfizer Inc., Cambridge, MA, UNITED STATES, ²Pfizer Inc., Groton, CT, UNITED STATES.

Aim Amyloid β (A β) plaque accumulation in brain is a hallmark of Alzheimer's disease (AD) pathology. A β production occurs by consecutive cleavage of amyloid precursor protein by β - and γ -secretase. Limiting A β production via inhibition of β -secretase (BACE) is an attractive strategy to develop a disease-modifying AD therapy. We are interested in developing a BACE-specific PET ligand to facilitate clinical characterization and assessment of BACE inhibitors. Herein, we report PF-06684511 as a potent and selective PET radioligand lead that demonstrated high specific binding *in vivo*. **Materials and methods** The existing chemical matter was prioritized based on potency/selectivity, physicochemical, and *in vitro* pharmacokinetic properties. Specifically, we targeted central nervous system PET multi-parameter optimization (CNS PET MPO > 3); passive permeability (RRCK $> 10 \times 10^{-6}$ cm/s) and multi-drug resistance efflux (MDR BA/AB ≤ 2.5); and brain fraction unbound (F_u > 0.05). The *in vivo* specific binding was assessed in a LC-MS/MS based "cold-tracer" method in mice. PF-06684511 was dosed in tracer amount (10 $\mu\text{g}/\text{kg}$, *iv*). Concentrations were quantified in cerebellum, frontal cortex, hippocampus and striatum at 45 minutes post administration. The specific binding was defined by comparison between a wild-type (WT) group and a BACE-knockout (KO) group ($n=5$ per group). Vehicle and three doses of a selective BACE inhibitor (1, 10 and 80 mg/kg, *sc*) were tested in male 129/sve mice to determine target occupancy (TO). **Results** Prioritization of existing chemical matter (~ 800 compounds) led to rapid identification of PF-06684511 as a promising radioligand lead. Structurally PF-06684511 is amenable to either [^{11}C] or [^{18}F] labeling. It showed high BACE potency ($\text{IC}_{50} = 0.7$ nM), high RRCK (17.5×10^{-6} cm/s), low MDR BA/AB (1.6) and favorable F_u (0.06). In the LC-MS/MS "cold-tracer" study, PF-06684511 showed high brain uptake and bio-distribution consistent with BACE expression. A significant reduction of PF-06684511 binding was observed in KO mice (e.g. 0.7% ID/g vs. 2.3% ID/g WT in hippocampus), indicating high specific binding. Furthermore, binding of PF-06684511 in these brain regions was reduced by a selective BACE inhibitor in a dose-dependent manner, confirming its potential for TO determination. **Conclusions** Using a set of PET ligand design parameters, PF-06684511 was rapidly identified with favorable *in vitro* attributes and structural handles for PET radiolabeling. Further evaluation in a LC-MS/MS "cold-tracer" study revealed high specific binding to BACE *in vivo*. Taken together, these data suggested PF-06684511 is a promising radioligand lead for BACE PET imaging.

OP062

Fluorinated Derivatives of Puromycin for PET Imaging of Protein Synthesis

H. M. Betts¹, S. Milicevic Sephton², C. Tong³, R. O. Awais³, P. J. Hill³, A. C. Perkins³, F. I. Aigbirhio²; ¹Nottingham University Hospitals NHS Trust, Nottingham, UNITED KINGDOM, ²University of Cambridge, Cambridge, UNITED KINGDOM, ³University of Nottingham, Nottingham, UNITED KINGDOM.

Introduction and Aims: Disruption of cellular protein synthesis (PS) is a hallmark of numerous diseases including cancer and neurodegeneration. The ability to visualise and quantify PS is an important goal in diagnosis, treatment and monitoring of these conditions. Radiolabelled amino acids have been investigated widely for this purpose, but their application suffers from several key limitations, including the inability to distinguish between active transport and PS.¹ At present, there is no ideal radiotracer for imaging PS by PET. The aim of this project was to develop a radiotracer which is not an amino acid but enables measurement of PS *in vivo*, and can be radiolabelled with fluorine-18, via [¹⁸F]fluoride. Puromycin (PURO) is an antibiotic that inhibits PS in both bacteria and eukaryotes by mimicking aminoacyl-tRNA at the ribosome.² We hypothesised that a fluorine-18 labelled PURO analogue could be used for PS imaging, and previously reported a single derivative as a potential candidate.³ We now describe the synthesis and PS inhibitory potency of a series of PURO analogues containing a fluorine substituent. **Materials and Methods:** A previously reported common intermediate was employed for further derivatisation.⁴ The novel PURO analogues were analysed in a PS assay using Gaussia Luciferase as a bioluminescent reporter, and their potency compared with that of commercially available PURO. The radiosynthesis of the most potent candidate was achieved by direct nucleophilic [¹⁸F]fluorination of a tosylate precursor followed by deprotection. **Results:** Fifteen novel PURO analogues were prepared from the common intermediate in 20–90% yields. Fluoroethylpuromycin (FEPURO) proved the most potent PS inhibitor of the class, exceeding the inhibitory activity of PURO itself in the assay. Three-step radiosynthesis of [¹⁸F]FEPURO was achieved in 140 min in 2±1% radiochemical yield (not corrected for decay) and with radiochemical purity >99%. **Conclusions:** From the series of novel PURO analogues, FEPURO was identified as a potential candidate for PET imaging of PS. Radiosynthesis of [¹⁸F]FEPURO was successfully accomplished in modest yield and excellent radiochemical purity. Characterisation of [¹⁸F]FEPURO *in vivo* is underway in our laboratories. ¹P. Laverman, O.C. Boerman, F.H.M. Corstens, W.J.M. Oyen, Eur. J. Nucl. Med. 2002, 29(5), 681. ²D. Nathans, Proc. Natl. Acad. Sci. 1964, 51(4), 585. ³H.M. Betts, R.O. Awais, J.C. Luckett, A.C. Perkins, Eur. J. Nucl. Med. Mol. Imaging 2014, 41 (Suppl 2), S416. ⁴S. M. Sephton, F. I. Aigbirhio, ACS Med. Chem. Lett. 2016, doi: 10.1021/acsmchemlett.6b00093.

OP063

[¹⁸F]F13640 preclinical evaluation as a 5-HT1A receptor agonist for PET neuroimaging, from rodent to non-human primate

B. Vidal¹, S. Fieux¹, T. Billard², O. Barret³, G. Tamagnan³, A. Newman-Tancredi⁴, L. Zimmer^{1,5,6}; ¹Université Claude Bernard Lyon 1, Lyon Neuroscience Research Center, INSERM, CNRS, Lyon, FRANCE, ²Université Claude Bernard Lyon 1, Institute of Chemistry and Biochemistry, CNRS, Villeurbanne, FRANCE, ³Molecular NeuroImaging, New Haven, CT, UNITED STATES, ⁴Neurolix Inc., Dana Point, CA, UNITED STATES, ⁵Hospices Civils de Lyon, Lyon, FRANCE, ⁶CERMEP - Imaging Platform, Bron, FRANCE.

Aim: Serotonin 1A receptors are known to play an important role in many psychiatric and neurodegenerative disorders. Currently, all available 5-HT1A fluorinated PET radiopharmaceuticals are antagonists. As agonists bind preferentially to the high-affinity (G-protein-coupled) state of receptors, it would be of great interest to develop agonist radioligands which could provide a measure of the functional 5-HT1A receptors in pathophysiological processes. The agonist 5-HT1A radiotracer candidates we proposed recently had interesting *in vitro* properties but were not optimal in terms of *in vivo* imaging (Eur J Nucl Med 2010, 37(3): 594–605; J Nucl Med 2012, 53(6): 934–41). We propose now a new selective agonist with a suitable affinity for 5-HT1A receptors. **Materials and methods:** F13640 is a ligand with a high affinity (1nM) and a high selectivity for 5-HT1A receptors. Its nitro-precursor was synthesized and radiolabeled via a

fluoro-nucleophilic substitution. Its radiopharmacological characterization included autoradiographic studies, biodistribution and metabolic studies, PET scans in rats, cats and non-human primates. Several of these results were compared with studies using the antagonist [¹⁸F]MPPF, a validated 5-HT1A radiopharmaceutical. **Results:** The radiochemical purity of [¹⁸F]F13640 was > 98%. [¹⁸F]F13640 *in vitro* binding was consistent with the 5-HT1A receptors distribution. Biodistribution studies revealed that 1% of the radiotracer rapidly entered the brain and led to few brain radiometabolites. [¹⁸F]F13640 binding was decreased by co-injection of WAY-100635, a 5-HT1A antagonist, or blocked by pre-injection of 8-OH-DPAT, a 5-HT1A agonist (-40% and -85% in the rat, respectively). [¹⁸F]F13640 *in vivo* distribution differed from the classical distribution observed with [¹⁸F]MPPF. As an example, in the three studied species, [¹⁸F]F13640 binding was high in the dorsal raphe nucleus and the cingulate cortex, but moderate in the hippocampus. Finally, *ex vivo* and microPET studies in rat revealed a high sensitivity of [¹⁸F]F13640 to endogenous serotonin, with a binding decrease after low doses of fenfluramine (a serotonin releaser). **Conclusions:** [¹⁸F]F13640 has suitable characteristics for probing *in vitro* and *in vivo* the high-affinity states of the 5-HT1A receptors. Interestingly, this study reveals that the binding pattern of a selective agonist radiotracer can differ significantly from the binding of a selective antagonist radiotracer. Quantification analyses with kinetic modelling are in progress to prepare the first-in-man study of [¹⁸F]F13640.

OP064

In vivo characterization of a novel [¹⁸F]-labelled radiotracer for PET imaging of multidrug resistance or drug toxicity

P. Kannan¹, J. Collins², T. Falls², W. Ladno², S. Dizdarevic³, M. van Dam², J. Lee², D. Maheshwari¹; ¹Avaant Pharmaceuticals Inc, Woburn, MA, UNITED STATES, ²Crump Institute for Molecular Imaging, Department of Molecular and Medical Pharmacology, David Geffen School of Medicine at UCLA, Los Angeles, CA, UNITED STATES, ³Avaant Pharmaceuticals Inc, Brighton and Sussex University Hospitals NHS Trust and Brighton and Sussex Medical School, Brighton, UNITED KINGDOM.

Background: Multidrug resistance (MDR) is a major impediment in the treatment of cancer and various neurological disorders. Two efflux transporters from the ATP-binding cassette (ABC) family, ABCB1 (P-gp) and ABCG2 (BCRP), commonly contribute to MDR by restricting the entry of therapeutic drugs into target organs, including into brain across the blood brain barrier and tumours. Contrary, constitutionally low expression of ABC transporter proteins is linked with drug toxicity and susceptibility to ABC-mediated disease. **Aim:** The goal of this work was to characterize the specificity, brain uptake, and metabolism of the new tracer, AVT-011, with an ultimate aim for detecting and investigating the function of ABC-transporter proteins, MDR or drug toxicity *in vivo*. **Methods:** To enhance clinical utility, AVT-011 was radiolabelled with [¹⁸F]. The specificity of the radiotracer [¹⁸F]-AVT-011 for ABCB1 and/or ABCG2 was measured using three groups of mice (FVB background strain, females): wild-type (n = 5), those genetically lacking *abcb1a/1b* (n = 5), and those genetically lacking *abcg2* (n = 5). Brain uptake was assessed quantitatively and reported as standardized uptake value (SUV) from dynamic PET scans performed over 120 mins following intravenous injection of approximately 3–4 MBq [¹⁸F]-AVT-011. The plasma protein binding of the radiotracer was determined using human plasma proteins, while the metabolism of the radiotracer was determined using human microsomes. **Results:** AVT-011 was successfully radiolabelled with [¹⁸F], resulting in a decay-corrected yield of 3.7 ± 1.0% (n=4) and specific activity of 143 ± 31 (n=4) GBq/μmol. At 120 min, brain uptake of [¹⁸F]-AVT-011 was 2 times higher in mice lacking ABCB1 (0.15 ± 0.04 SUV) and 1.4 times higher in mice lacking ABCG2 (0.10 ± 0.02 SUV) than in wild-type mice (0.075 ± 0.013 SUV). Brain

uptake remained stable out to 120 mins, with peak uptake occurring within the first minute. Plasma protein binding of the radiotracer was $43.6 \pm 4.0\%$, and 91% of the radiotracer remained in its unchanged form at 30 min. **Conclusions:** AVT-011 can be readily labelled with [^{18}F] at sufficiently high specific activity and yield for in-vivo imaging. The radiotracer [^{18}F]-AVT-011 is a substrate for ABCB1 and ABCG2 at the mouse blood brain barrier, is stable metabolically, and has good bioavailability. Since many drugs are dual substrates for ABCB1 and ABCG2, and these transporters are often co-expressed in causing MDR in multiple disease, [^{18}F]-AVT-011 seems to be a promising new radiotracer for dual ABC/MDR imaging.

306 – Sunday, October 16, 2016, 11:30 - 13:00, Hall 111

Physics & Instrumentation & Data Analysis: Advanced Quantification & Kinetic Modeling

OP065

Supervised Cluster Analysis for Automatic Extraction of Reference Region in Dynamic [^{18}F]THK5317 PET

M. Jonasson^{1,2}, A. Wall², K. Chiotis³, K. Heurling¹, L. Saint-Aubert³, G. Antoni^{1,2}, A. Nordberg³, M. Lubberink^{1,2}, ¹Uppsala University, Uppsala, SWEDEN, ²Uppsala University Hospital, Uppsala, SWEDEN, ³Karolinska Institutet, Stockholm, SWEDEN.

Objectives: [^{18}F]THK5317 is a PET tracer for in-vivo imaging of tau pathology which is associated with neurodegeneration and cognitive impairment. Research investigation on tau pathology imaging with PET is facilitated by the availability of simplified analysis methods such as standardized uptake value ratios (SUVr). However, previous work has shown modest correlation between SUVr and binding potential (BP), with the latter assumed to be better representation of tau accumulation. Parametric images based on dynamic [^{18}F]THK5317, showing BP at voxel level, are preferred for investigation of tau distribution in the brain. Reference tissue models, used to compute these images, require a reference region time-activity curve (TAC). The aim of this study was to evaluate a supervised clustering analysis method (SVCA) for automatic extraction of a reference region and compare with parametric images computed using MRI-based cerebellum volume of interest (VOI) as reference input. **Methods:** Sixteen subjects (5 healthy controls, 8 AD and 3 MCI) received a 60 min dynamic [^{18}F]THK5317 PET scan and a T1-weighted MRI scan. A set of four predefined kinetic classes was defined based either on the five healthy subjects (cerebellum reference class) or five randomly selected AD subjects (white matter, grey matter and blood pool class). The SVCA algorithm segments voxels in the dynamic PET volume based on the shape of their TACs with no spatial constraint. Voxels with TACs most resembling the kinetic behavior of the proposed reference region are selected and a reference TAC can be obtained. Reference Logan DVR-1 and SUVr-1 (40-60 min p.i.) images were computed for the remaining AD and MCI subjects using both MRI-based and SVCA-based reference. Nine representative regions were used for the evaluation. Correlation and agreement of DVR-1 and SUVr-1 values of the two methods were assessed by linear regression. **Results:** Correlation and agreement between DVR-1 values of all nine regions, based on MRI and SVCA reference regions, were high: $R^2=0.92$ and 0.87 , slope= 1.09 and 1.05 for DVR-1 and SUVr-1 values respectively. When evaluating single regions, correlation was somewhat lower; e.g. $R^2=0.76$ and 0.74 , slope= 0.94 and 1.21 , for DVR-1 and SUVr-1 values in hippocampus, respectively. **Conclusion:** The results indicate that supervised clustering may be used to obtain a reference TAC from a dynamic [^{18}F]THK5317 PET scan. This would allow for automated computation of parametric images without the need for an MRI scan. The presented method needs to be evaluated in a larger number of subjects.

OP066

[^{11}C]flumazenil kinetics in the rat brain: model preference and the impact of non-specific and non-selective binding in reference region modeling

I. Lopes Alves¹, D. Vález García¹, A. Parente¹, J. Doorduyn¹, A. Marques da Silva², M. Koole³, A. T. M. Willemsen¹, R. Dierckx¹, R. Boellaard¹; ¹University Medical Center Groningen, Groningen, NETHERLANDS, ²Pontificia Universidade Católica do Rio Grande do Sul, Porto Alegre, BRAZIL, ³KU Leuven, Leuven, BELGIUM.

Aim: The analysis of [^{11}C]flumazenil pre-clinical studies currently follows the quantitative models validated in the clinical setting. Since tracer kinetics can differ between species, [^{11}C]flumazenil kinetic modeling was evaluated for the rat brain. **Material and Methods:** 60min [^{11}C]flumazenil brain PET scans with arterial sampling were performed in two groups of male Wistar rats (n=10, tracer dose only; n=2, pre-saturated with 330nM of flumazenil). Time-activity curves (TACs) were generated for frontal cortex, hippocampus, cerebellum, medulla and pons (reference). Next, noiseless TACs (n=10) were simulated using an average input function and representative rate constants from animal data. A three-tissue compartment model including a compartment for non-selective binding was simulated with different levels of specific-binding (k_3 ranging from 0.2 to 2.6min^{-1}). For animal and simulated data, distribution volume (V_T) and distribution volume ratios (DVR) were calculated using one and two-tissue compartment models (1TCM and 2TCM) and spectral analysis (SA). Binding potential (BP_{ND}) was determined from full and simplified reference tissue models with one or two-tissue compartments for the reference (FRTM, SRTM and SRTM-2Ref). Parameter agreement was assessed by Spearman's correlation and Bland-Altman plots. Akaike information criterion (AIC) was used to determine model preference. **Results:** 1TCM and 2TCM V_T of regions with high specific-binding (frontal cortex, hippocampus and cerebellum) showed similar AIC (143 ± 7 and 148 ± 10 respectively), strong correlation ($r_s=0.99$) and good agreement (0.1% difference). In contrast, low specific-binding regions (pons and medulla) showed worse correlation ($r_s=0.77$) and agreement (17.6% difference), while AIC were lower for 2TCM (134 ± 10) than for 1TCM (161 ± 8). The pre-saturated group displayed similar results to those of low specific-binding regions. High levels of non-specific and/or non-selective binding (2TCM $V_T=2.5 \pm 0.4$) was observed in pons and affected BP_{ND} estimation by all tested reference tissue models. Simulations showed a similar pattern: 2TCM V_T demonstrated better agreement ($<8.0\%$ bias) than 1TCM for all levels of specific-binding, while 1TCM V_T demonstrated smaller bias with increasing specific-binding (from -55.1% to 3.1%). SA generated accurate V_T ($<0.9\%$ bias) for all specific-binding levels. 1TCM DVRs resulted in the largest BP_{ND} overestimation (up to 58% bias), while SRTM-2Ref showed an overall smaller bias ($<1.5\%$). **Conclusion:** [^{11}C]flumazenil kinetics in rats was substantially different from that in humans, especially in low specific-binding regions. In those, the 2TCM is preferred and the standard 1TCM and SRTM can lead to major errors in parameter estimation. Instead, models which can better account for non-specific and/or non-selective binding should be used, such as 2TCM or SA.

OP067

Quantitative Assessment of Osteoblastic Tumor Burden with Threshold-based Volumetric Na ^{18}F PET/CT Methodologies - Challenges and Opportunities

C. I. Odom, C. L. Wright, P. Subramanian, J. Zhang, M. V. Knopp; The Ohio State University, Columbus, OH, UNITED STATES.

Aim: Although routinely used for ^{18}F -FDG PET, maximum lesion SUVs for Na ^{18}F -avid lesions demonstrate very high values even in benign areas of increased bone turnover. Total lesion fluoride (TLF) and fluoride tumor volume (FTV) are recently described metrics that may enable better prognostic information for ^{18}F -avid malignant/metastatic osteoblastic lesions.

These metrics can be rapidly established using whole-body threshold-based isocontouring but are confounded by the inadvertent inclusion of benign regions of increased bone turnover. This study assessed methodologies for evaluating and quantifying osteoblastic tumor burden in oncologic patients. **Materials and Methods:** 20 patients who underwent routine Na¹⁸F PET/CT studies for prostate, breast, thyroid, and head/neck cancers were retrospectively evaluated. Visual assessment of ¹⁸F-avid osteoblastic lesions was performed by a reader panel. Quantitative isocontour assessment of ¹⁸F-avid osteoblastic tumor burden was performed using either automated threshold-based whole body contouring or manual contouring of individual lesions. Using a MIM workstation, the following parameters were assessed: highest SUV_{max} for all osteoblastic lesion (hSUV_{max}), average of SUV_{max} values over all ¹⁸F-avid osteoblastic lesions, fluoride tumor volume (FTV) for all isocontoured lesions, and the whole-body total lesion fluoride (TLF) uptake. **Results:** Qualitative assessment demonstrated a spectrum of ¹⁸F-avid osteoblastic tumor burden ranging from no lesions to extensive multifocal osteoblastic disease. In addition, there was a wide spectrum of osteoblastic degenerative disease burden. Quantitative whole-body isocontour assessment of ¹⁸F-avid osteoblastic activity using a minimum threshold SUV of 10 were sufficient to capture osteoblastic metastatic lesions but it also captured benign degenerative disease which confounded the automated whole-body results (Automated analysis: hSUV_{max} = 56 ± 43, average SUV_{max} = 15 ± 6, FTV = 153 ± 111 mL, and TLF = 2371 ± 1956 SUV*³mL). Although labor-intensive, manual lesion-by-lesion isocontouring of ¹⁸F-avid osteoblastic metastatic lesions (Manual analysis: hSUV_{max} = 48 ± 48, average SUV_{max} = 16 ± 10, FTV = 33 ± 58 mL, and TLF = 884 ± 1777 SUV*³mL) minimizes false-positive tumor activity from underlying benign osteoblastic disease and provides more accurate quantification of tumor-specific osteoblastic disease burden. **Conclusion:** Confounding factors like degenerative disease limits the clinical utility of automated or semi-automated whole body threshold-based methodologies for quantifying tumor-specific osteoblastic disease burden. The alternative approach of using manual lesion-by-lesion quantitative assessment produces more robust and more accurate metrics for quantifying osteoblastic disease burden.

OP068

Investigation into the optimal model for whole tumour and voxel FMISO kinetics analysis

D. R. McGowan^{1,2}, R. E. Macpherson², S. L. Hackett¹, F. V. Gleeson², G. S. Higgins¹, J. D. Fenwick^{1,3}; ¹University of Oxford, Oxford, UNITED KINGDOM, ²Oxford University Hospitals NHS Foundation Trust, Oxford, UNITED KINGDOM, ³University of Liverpool, Liverpool, UNITED KINGDOM.

Purpose A study is presented of the relative abilities of different kinetics compartmental models to describe whole tumour and voxel FMISO uptake time-activity-curves (TACs). **Methods** Two-, three- and four-compartment models were fitted to 28 TACs obtained for 14 tumour structures in 8 patients with advanced stage lung cancer, each imaged twice as part of an ongoing clinical trial. Descriptions of the TACs provided by fits of the models were compared using the Wald-Wolfowitz runs test, Akaike and Bayesian information criteria (AIC/BIC), and leave-one-out cross-validation. The accuracy and precision with which fitted model parameters estimated the uptake kinetics were calculated using statistical simulation procedures carried out for several different ground-truths. These analyses were performed both for whole tumour volumes as well as for individual voxels. **Results** An irreversible three-compartment model, 3C5K, provided the best overall description of the FMISO uptake time-courses of whole tumours according to AIC, BIC and cross-validation scores totalled across TACs. Fits of the 3C5K model and a more complex four-compartment model, 4C7K, passed the runs test for 23/28 and 28/28 TACs respectively. However, the simulation studies indicate that 3C5K fits provided the most accurate and precise estimates

of FMISO uptake kinetics (10% precision for tumour fractional blood volumes and FMISO binding rate-constants), even for TACs described better by the 4C7K model. The 3C5K model also provided the best overall description of time-courses of FMISO uptake in individual voxels according to AIC and BIC measures. However, simulation studies indicated that 2C3K model fits provide the most accurate and precise estimates of voxel FMISO uptake kinetics (39% precision for tumour fractional blood volumes and 37% for FMISO binding rate-constants): the higher noise-levels within single voxel uptake time-courses means that the greater stability of this simpler model outweighs its less accurate descriptions of their time-courses. **Conclusion** Fits of an irreversible three-compartment model provide the best descriptions of uptake time-courses of whole tumours, and the most precise and accurate estimates of their uptake kinetics. For single voxels the three-compartment model also provides the best descriptions of uptake time-courses, however fits of a simpler irreversible two-compartment model provide more precise and accurate estimated of uptake kinetics in single voxels.

OP069

A comparative analysis between SVM and PCA plus Logistic Regression for the construction of a discriminative glucose metabolic brain pattern in ALS

M. Devrome, J. Ceccarini, D. Van Weehaeghe, P. Van Damme, K. Van Laere, M. Koole; KU Leuven, Leuven, BELGIUM.

Introduction The differential diagnosis of neurodegenerative disorders may be difficult on clinical grounds only, especially at an early stage. [¹⁸F]FDG brain PET imaging allows the identification of several disease-specific metabolic patterns such that a differential diagnosis is facilitated. Two different machine learning methods, Support Vector Machine (SVM) and regularized Logistic Regression (LR) combined with Principal Component Analysis for feature extraction (PCA-LR), were used for the construction of a discriminative brain pattern in Amyotrophic Lateral Sclerosis (ALS) and were evaluated in terms of classification performance. **Methods** PCA-LR is based on the method of Spetsieris et al. [1]. First, PCA is performed by selecting a limited number of eigenvectors of the data covariance matrix. Regularized LR is then applied to find the weights discriminating the most between the ALS and healthy controls PCA features, where the weighted sum of the selected eigenvectors corresponds to a discriminative brain pattern for ALS. SVM is a sparse kernel technique obviating the feature selection prior to training of the classifier. A linear kernel is considered, because this leads to a straightforward construction of the ALS specific discriminative pattern. Static [¹⁸F]FDG-PET scans were selected from a prospective cohort of 175 patients with a clinical diagnosis of ALS [2]. 20 ALS scans were randomly selected and combined with the 20 scans of age matched healthy controls to generate a realistic training set. Performance was tested using a leave-one-out cross-validation. **Results** The PCA-LR approach resulted in a sensitivity of 91%, a specificity of 96%, an accuracy of 93.5% and an Area Under Curve (AUC) of 96.1% for the Receiver Operating Characteristic (ROC) curve. For SVM, a sensitivity of 90.5%, a specificity of 97.5%, an accuracy of 94% and an AUC of 96.6% for the ROC curve was found. Both methods generated a discriminative metabolic brain pattern for ALS where known regions of relative hypo- and hyper-metabolism could be clearly identified. **Conclusion** A discriminative voxel-wise metabolic brain pattern for ALS was constructed, based on both a SVM and PCA-LR approach. In terms of discriminative performance, similar results were obtained for both methods for a relatively small but realistic sample size, with a comparable discriminative brain pattern. [1] Spetsieris et al. Identification of Disease-related Spatial Covariance Patterns using Neuroimaging Data. *J Vis Exp*. 2013. [2] Van Weehaeghe et al. Prospective Validation of ¹⁸F-FDG Brain PET Discriminant Analysis Methods in the Diagnosis of Amyotrophic Lateral Sclerosis. *J Nucl Med*. 2016.

OP070**Partial Volume Effect correction (PVC) improves the sensitivity of SPM for the detection of focal cortical dysplasia on refractory epilepsy**

J. Silva-Rodríguez¹, J. Cortés², X. Rodríguez-Osorio³, Á. Ruibal², P. Aguiar¹; ¹Fundación Ramón Domínguez, Santiago de Compostela, SPAIN, ²Nuclear Medicine Department, University Hospital, Santiago de Compostela, SPAIN, ³Neurology Department, University Hospital, Santiago de Compostela, SPAIN.

Introduction: In latter years, PET has gained a leading role in the presurgical evaluation of refractory epilepsy. The availability of co-registered PET/MRI images has improved the interpretation of images of both modalities, while the use of quantification techniques, such as Statistical Parametric Mapping (SPM), has improved the interpretation of PET images. SPM is a well-known quantification technique in PET neuroimaging, but its sensitivity in epilepsy is still relatively low when compared with other applications such as dementia. This might be related with the Partial Volume Effect (PVE) and the low resolution of PET images when dealing with small focal hypometabolisms, such as those observed in epilepsies associated with focal cortical dysplasias (FCDs). Due to this, techniques that can provide an improvements on PET resolution are promising in order to improve the localization of these focal hypometabolisms. On a previous work, our group has shown how PVE correction improves the sensitivity of both quantification and visual inspection on temporal lobe epilepsy, which was associated to an improved visualization of the hippocampal region. **Aim:** In this work, we investigate the impact of PVE correction on the sensitivity of SPM for the localization of small focal hypometabolisms associated with FCD on refractory epilepsy. **Methods:** This study was performed on 14 patients diagnosed with refractory epilepsy caused by a FCD reported on the MRI examination (11 FCD-I, 2 FCD-II and 1 FCD-III). All of them underwent surgery with positive outcome. PET images were visually evaluated using PET/MR co-registered images. The analysis was complemented by with a SPM statistical analysis comparing the patient to 87 controls. PET images were corrected using a novel PVE correction method. The quantification results with and without PVE correction were compared. Co-registered images and quantitative analysis were provided by IQ-Brain (QubioTech Health Intelligence S.L). **Results:** On the original evaluation, the visual inspection of PET/MR co-registered images reported hypometabolism associated with the FCD on 85.7% (12/14) of the patients, while SPM performed very poorly, being positive only for 57.1% (8/14) of the patients. After the correction, the SPM statistical analysis showed a sensitivity of 85.7% (12/14), which implies an improvement of a 28.6% and is comparable to the sensitivity of the visual inspection. These results are in good agreement with the ones previously obtained on TLE patients. **Conclusions:** PVE correction showed potential to improve the sensitivity of SPM on the detection of the hypometabolisms associated with FCD in refractory epilepsy.

308 – Sunday, October 16, 2016, 11:30 - 13:00, Hall 212

Special Symposium 1: Key Issues in Cardiovascular Nuclear Medicine**OP071****Current Role of PET for CAD Evaluation**

N. Tamaki; Hokkaido University Graduate School of Medicine, Department of Nuclear Medicine, Sapporo, JAPAN.

OP072**Emerging Applications of Vessel Imaging with PET and SPECT**

H. Strauss; Memorial Sloan-Kettering Cancer Center, New York, UNITED STATES OF AMERICA.

OP073**PET/MR versus PET/CT in Cardiovascular Medicine**

M. Schwaiger; Klinikum R. D. Isar der Technischen Universität München, Nuklearmedizinische Klinik und Poliklinik, Munich, GERMANY.

309 – Sunday, October 16, 2016, 11:30 - 13:00, Hall 113

Clinical Oncology: Rapid Fire Session**OP074****Value of ¹¹¹In-PSMA-radioguided surgery for salvage lymphadenectomy in recurrent prostate cancer: correlation with histopathology and clinical follow-up**

I. Rauscher, T. Maurer, M. Wirth, M. Schottelius, H. Wester, J. E. Gschwend, M. Schwaiger, M. Eiber; Klinikum rechts der Isar, Munich, GERMANY.

Aim: With the advent of ⁶⁸Ga-HBED-PSMA PET hybrid imaging techniques even small and atypical localized metastatic lesions of prostate cancer (PCa) can be visualized. Previously, the novel technique of PSMA-radioguided surgery (PSMA-RGS) to localize those metastatic lesions using a γ -probe after injection of a radiolabelled PSMA-ligand has been described. However, follow-up of these salvage surgery cases is necessary to determine its possible role in clinical routine. Thus, the aim of this study was to evaluate the feasibility of preoperative injection of ¹¹¹In-labeled PSMA-I&T SPECT/CT for facilitated intraoperative identification of PSMA-positive lesions using a γ -probe in recurrent PC and to correlate these results with postoperative histopathological results of the resected lymph nodes. Further, the impact of PSMA-RGS was tested using postoperative prostate-specific antigen (PSA) values and clinical recurrence-free survival. **Material and Methods:** 22 consecutive patients with localized recurrent prostate cancer (PCa) underwent PSMA-RGS with ¹¹¹In-labeled PSMA ligand during April 2014 to March 2015. Preoperative median PSA was 1.38ng/ml (range: 0.19 - 13.90ng/ml). Results of ex vivo radioactive rating (positive vs. negative) of resected tissue were compared to findings of postoperative histological analysis. Best PSA response without additional treatment was determined 8-16 weeks following PSMA-RGS and PCa-specific additional treatments were recorded. **Results:** In 21/22 patients PSMA-RGS could identify the lesions intraoperatively. One patient without identification of the metastatic lesion in the deep internal region exhibited a PSA of 0.45ng/ml. On follow-up PSMA-PET imaging lesion was still present. In total, 85 surgical specimens were removed and 34 showed metastatic involvement at histological analysis. 32 were correctly classified as metastatic and 47 as cancer-free, 2 specimens were false negative and 4 false positive compared to standard histological evaluation. Follow-up information was available for 21/22 patients. PSA reduction >50% were observed in 16/21 patients and >90% in 10/21 patients. In 11/21 patients a PSA drop below 0.2ng/ml could be observed. 9/21 patients received further PCa-specific treatment after median 4 months after PSMA-RGS (range: 3 - 13 months), the remaining 12 patients remained treatment free at a median follow-up of 10 months (range: 7 - 17 months). **Conclusion:** PSMA-radioguided surgery proved to be of high value for intraoperative detection of even small metastatic lesions in PCa patients scheduled for salvage lymphadenectomy and might have a beneficial influence on further disease progression. However, identification of suitable patients on the basis of PSMA-PET imaging is critical to obtain satisfactory results.

OP075**Predictive and prognostic potential of volume-based metabolic variables with 18F-FDG PET/CT in locally advanced breast cancer**

A. Garcia Vicente¹, J. Pérez-Beteta², M. Tello Galán¹, D. Molina-García², G. Jiménez Londoño¹, V. Pérez-García², A. Martínez-González², F. Pena Pardo¹, A. Soriano Castrejón¹; ¹Nuclear Medicine Department. Hospital General Universitario de Ciudad Real, CIUDAD

REAL, SPAIN, ²Instituto de Matemática Aplicada a la Ciencia y a la Ingeniería. UCLM., CIUDAD REAL, SPAIN.

Aim: To investigate the usefulness of metabolic variables of breast lesions obtained in 18F-FDG PET/CT in the prediction of neoadjuvant chemotherapy (NC) response and prognosis in locally advanced breast cancer (LABC). **Material and methods:** Prospective study including 67 patients with LABC and NC indication and a baseline 18F-FDG PET/CT. After breast tumor segmentation, SUV variables (SUV_{max}, SUV_{mean} and SUV_{peak}) and volume-based variables as metabolic tumor volume (MTV) and total lesion glycolysis (TLG) were obtained. Breast specimens were grouped into molecular phenotypes and classified as responders or no responders after completion of NC. Univariate analysis was performed with the use of Kaplan-Meier and Cox proportional hazards models to study the potential of metabolic variables, molecular phenotypes and histologic response to predict: disease-free status (DFs), disease-free survival (DFS) and overall survival (OS). **Results:** Sixty patients underwent NC. 14 were classified as responders. 56 patients had a DFs during the follow-up. Median±SD of DFS and OS was 43 ±15 and 46±13 months respectively. SUV and volume-based variables showed significant relations ($p<0.005$) with the histological response with higher values in responders compared to no responders (median, mean and SD of SUV_{max}, SUV_{mean}, SUV_{peak}, MTV and TLG of 13.77, 13.34 and 5.79; 8.85, 8.35 and 3.73; 11.33, 10.7 and 4.88; 13.44, 26.60 and 34.58 and 96.39, 258.12 and 384.63 for responders vs 6.04, 7.84 and 5.26; 3.42, 4.77 and 3.20; 4.79, 6.06 and 4.08; 9.88, 13.63 and 12.48 and 33.78, 70.17 and 97.94 for non responders respectively). MTV and TLG showed significant association with DFs ($p=0.015$ and $p=0.038$ respectively). Median, mean and SD of MTV and TLG for patients with DFs were: 8.90, 13.72 and 15.12 and 33.78, 90.54 and 144.64 respectively. Median, mean and SD of MTV and TLG for patients with a non-DFs were: 16.72, 29.70 and 31.09 and 90.89, 210.98 and 382.80 respectively. No significant relations were observed with SUV variables and DFs. No significant relations were obtained for none metabolic variable with DFS and OS. **Conclusion:** Volume-based metabolic variables obtained with 18F-FDG PET/CT, differently to SUV based variables, were good predictors of neoadjuvant chemotherapy response and disease free status in patients with locally advanced breast cancer.

OP076

Ga68 RM2 PET/MRI Evaluation of Gastrin-Releasing Peptide Receptor Status in Patients with Biochemically Recurrent Prostate Cancer and Negative Conventional Imaging

A. Iagaru, I. Sonni, R. Minamimoto, A. Loening, S. Vasanawala; Stanford University, STANFORD, CA, UNITED STATES.

Background: ⁶⁸Ga-labeled DOTA-4-amino-1-carboxymethyl-piperidine-D-Phe-Gln-Trp-Ala-Val-Gly-His-Sta-Leu-NH₂ (⁶⁸Ga-RM2, formerly known as ⁶⁸Ga-Bombesin or BAY86-7548) is a novel synthetic bombesin receptor antagonist that targets gastrin-releasing peptide receptors (GRPr). GRPr are highly overexpressed in several human tumors, including prostate cancer (PC). Because of their low expression in BPH and inflammatory prostatic tissues, imaging GRPr has potential advantages over current choline- and acetate-based radiotracers. We now present data on the use of ⁶⁸Ga-RM2 PET/MRI in patients with biochemically recurrent prostate cancer (BCR PC) and non-contributory conventional imaging (CI). **Methods:** We enrolled 28 men with BCR PC, 59-83 year-old (mean±SD: 68.4±6.7) in an IRB-approved prospective study. Imaging started at 40-69 minutes (mean±SD: 50.1±7.2) after injection of 3.6-4.1 mCi (mean±SD: 3.8±0.2) of ⁶⁸Ga-RM2 using a time-of-flight enabled simultaneous PET/MRI scanner. MRI sequences consisted of T1-weighted, T2-weighted and DWI. SUV_{max} and SUV_{mean} measurements were recorded in normal tissues and areas of uptake outside the expected physiological biodistribution. **Results:** All patients had rising PSA (range: 0.3-

36.4 ng/mL; mean±SD: 6.9±7.9) and non-contributory CI (CT, MRI, ^{99m}Tc MDP bone scan). ⁶⁸Ga-RM2 uptake had the highest value in the pancreas and bladder, while moderate uptake was noted in the esophagus, kidneys, blood pool, stomach, small bowel and colon. High ⁶⁸Ga-RM2 uptake (SUV_{max}: 12.7 ± 7.8 [range: 2.6 - 33.5], SUV_{mean}: 5.7 ± 2.5 [range: 1.7 - 10.8]) corresponded to pelvic lymph nodes (7 patients), retroperitoneal lymph nodes (5 patients), prostate bed (3 patients), seminal vesicle (2 patients), supraclavicular lymph node (2 patients), mesenteric lymph nodes (1 patient), mediastinal lymph node (1 patient), liver (1 patient), lung (1 patient) and bone marrow (1 patient). ⁶⁸Ga-RM2 PET findings were compatible with recurrent prostate cancer in 19 of the 28 participants. MRI identified findings compatible with recurrent prostate cancer in 8 of the 28 patients (lymph nodes in 6 patients, prostate bed in 1 patient, lung in 1 patient and bone marrow in 1 patient). **Conclusions:** ⁶⁸Ga-RM2 produces high quality PET images for assessment of GRPr expression in patients with BCR PC. High uptake in multiple areas compatible with cancer lesions suggests that ⁶⁸Ga-RM2 is a promising PET radiopharmaceutical for localization of disease in participants with BCR PC and non-contributory conventional imaging.

OP077

⁶⁸Ga-PSMA PET/CT for early restaging prostate cancer. Preliminary results of a prospective trial in patients with biochemical failure after radical therapy and PSA levels < 2 ng/mL

F. Ceci, P. Castellucci, T. Graziani, C. Fonti, F. Lodi, S. Boschi, S. Fanti; Service of Nuclear Medicine, S.Orsola-Malpighi Hospital, University of Bologna, Bologna, ITALY.

Aim: the goal of this mono-centric prospective trial was to assess the performance of ⁶⁸Ga-PSMA-PET/TC in detecting the site of relapse in prostate cancer (PCa) patients who experienced biochemical recurrence (BCR) after primary treatments. **Materials and methods:** this prospective trial was approved by the local ethical committee (protocol "PSMA-PROSTATA"). Inclusion criteria were: 1) histological proven diagnosis of PCa; 2) radical therapy with radical prostatectomy (RP) or primary external-beam radiotherapy (EBRT) (with/without adjuvant therapies); 3) proven BCR with rising PSA values comprised between 0.2-2 ng/mL; 4) Gleason Score (GS) ≥7; 5) Age ≥35 years. The study was designed to enrol a homogenous cohort of 100 consecutive patients, with stringent selection criteria for preventing heterogeneity in our cohort. From March 2016 to April 2016, 50 patients have been so far enrolled and included in the present analysis. 47/50 (94%) patients were treated with RP + pelvic lymph-node (LN) dissection, while 3/50 (6%) received EBRT as primary therapy. 12/50 (24%) patients received salvage radiotherapy during follow-up for BCR. Only 2/50 (4%) patients were receiving androgen deprivation therapy at the time of ⁶⁸Ga-PSMA-PET/TC. The mean PSA values at the time of scan were 0.89 ng/mL (median=0.77 ng/mL); mean age=69,7 years-old (median=70); median GS=7. Correlative imaging with choline-PET/CT and/or pelvic magnetic resonance (MR) was available in 27/50 (54%) patients. **Results:** ⁶⁸Ga-PSMA-PET/TC resulted positive in 31/50 patients (positivity rate=62%). Local uptake (prostate bed or prostate gland and/or pelvic LNs) was observed in 15/50 patients (30%); distant uptake (retroperitoneal LNs and/or bone) in 10/50 patients (20%); local and distant uptake in 5/50 patients (10%); lung uptake in 1/50 (2%). The mean PSA values in PET-positive patients was 1.04 ng/mL (median=0.91 ng/mL), while in PET-negative patients was 0.65 ng/mL (median=0.31 ng/mL). In 26/31 PET-positive patients (83.9%) were observed not more than 1 or 2 lesions (oligometastatic disease). In PSA range values comprised between 0.2-0.5 ng/mL ⁶⁸Ga-PSMA-PET/TC resulted positive in 6/18 patients (positivity rate=30%). Correlative imaging was available in 18 of 31 PET-positive patients and resulted negative/inconclusive in 14/18 (77.8%) of cases. 1/50 (2%) patient had negative ⁶⁸Ga-PSMA-PET/TC and positive choline-PET/CT. The lung lesion was later confirmed as PCa relapse by histology.

Conclusion: the preliminary results of this prospective trial confirmed the promising performance of ^{68}Ga -PSMA-PET/CT for early restaging PCa patients with BCR. The validation of ^{68}Ga -PSMA-PET/CT in the clinical setting and its comparison with histology and/or other techniques would facilitate the routine implementation of this modality.

OP078

F-18-FDG PET/CT in the evaluation of tumour response after neoadjuvant chemoradiation (nCRT) in locally advanced oesophageal cancer

M. J. Valkema¹, B. J. Noordman¹, B. P. L. Wijnhoven¹, J. P. Ruurda², G. A. P. Nieuwenhuijzen³, M. I. Van Berge Henegouwen⁴, M. N. Sosef⁵, J. J. B. Van Lanschot¹, R. Valkema¹; ¹Erasmus MC University Hospital, Rotterdam, NETHERLANDS, ²University Medical Centre, Utrecht, NETHERLANDS, ³Catharina Hospital, Eindhoven, NETHERLANDS, ⁴Academic Medical Centre, Amsterdam, NETHERLANDS, ⁵Atrium Medical Centre, Heerlen, NETHERLANDS.

Aim: Neoadjuvant chemoradiotherapy (nCRT) with "CROSS" (NEJM 2012) is effective in reducing tumour load preoperatively. Many patients (92%) had radical resections after nCRT, with pathologically complete response (tumour regression grade = TRG1) in 29%. In future, we aim at postponing surgery using adequate clinical response evaluations (CRE) until residual locoregional disease without distant metastases has been identified. A multicentre feasibility study is underway (preSANO trial, NL41732.078.13) including endoscopy, biopsies, ultrasound and FDG-PET/CT with surgery 12 weeks after nCRT. The current preliminary analysis focuses on FDG-PET/CT to predict residual vital tumour (minimal: $\leq 10\%$ vital cells = TRG1+2, substantial: $>10\%$ = TRG3+4) after nCRT. **Methods:** FDG-PET/CT at baseline and CRE was performed according to EANM guidelines 1.0 (2.3MBq/kg F-18-FDG; scanning 60±5min.). Visual assessment: presence of residual tumour and/or metastases. SUV and SUV/lean body mass (SUL) measurements at tumour, lymph nodes, oesophagus, liver and bloodpool were recorded and compared with pathology (resection specimen). **Results:** Of 75 patients analysed, 7 withdrew before CRE. Ten patients had no surgery (1 died, 1 metastases before CRE, 5 FDG-positive metastases, 3 surgery postponed). Eight patients had surgery without FDG-PET/CT at CRE. In the remaining 50 operated patients FDG-PET/CT at CRE was positive in 36 (72%). In 3/36 patients tumours appeared irresectable, 33/36 patients had radical resections. In 18/33 TRG3 or TRG4 residual tumour was found. SUL-max in these tumours was 3.67 ± 0.97 and SUL-max-ratio tumour/oesophagus (SULR) 1.83 ± 0.41 . In 8/33 patients TRG2 residual tumour was present; SUL-max 4.35 ± 2.52 and SULR 2.24 ± 1.41 . In 1/33 patients TRG score was missing. In total, FDG-PET/CT was true positive in 29/36 patients (81%). 6/36 patients had no vital tumour (TRG1; 17% false positive); SUL-max 2.84 ± 0.97 , SULR 1.60 ± 0.69 . In 14/50 operated patients FDG-PET/CT at CRE was negative. No vital tumour (TRG1) was found in 6/14 patients (43% true negative); SUL-max 1.94 ± 0.29 , SULR 1.14 ± 0.16 . Conversely, 1 patient had minimal (TRG2) and 7/14 patients had substantial residual tumour (TRG3 or TRG4); SUL-max 2.49 ± 0.71 , SULR 1.43 ± 0.09 . Two patients (1 irradical resection) had non-FDG avid baseline scans, 6 (1 irradical resection) had good FDG-response compared to baseline. **Conclusion:** Positive FDG-PET/CT after nCRT predicts substantial residual tumour in 81% of patients. However, visual and quantitative FDG-PET/CT alone is not sufficiently accurate for detection or exclusion of substantial vital tumour; results of FDG-PET/CT performance combined with endoscopy, biopsies, ultrasound have to be awaited.

OP079

Using dynamic ^{18}F -FDG PET for lung tumour segmentation and quantitative assessment of glucose metabolism for different histological types

T. W. H. van Zon-Meijer¹, L. F. de Geus-Oei^{2,3,4}, E. P. Visser³, W. J. G. Oyen⁵, M. G. Looijen-Salamon⁶, D. Visvikis⁷, A. F. T. M. Verhagen⁸, J. Bussink¹, D. Vriens²; ¹Department of Radiation Oncology, Radboud University Nijmegen Medical Centre (Radboudumc), Nijmegen, NETHERLANDS, ²Department of Radiology, Leiden University Medical Center (LUMC), Leiden, NETHERLANDS, ³Department of Radiology and Nuclear Medicine, Radboud University Nijmegen Medical Centre (Radboudumc), Nijmegen, NETHERLANDS, ⁴Biomedical Photonic Imaging Group, MIRA Institute for Biomedical Technology and Technical Medicine, University of Twente, Enschede, NETHERLANDS, ⁵The Institute of Cancer Research and The Royal Marsden NHS Foundation Trust, London, UNITED KINGDOM, ⁶Department of Pathology, Radboud University Nijmegen Medical Centre (Radboudumc), Nijmegen, NETHERLANDS, ⁷INSERM, UMR 1101, LaTIM, Université de Bretagne Occidentale, Brest, FRANCE, ⁸Department of Cardiothoracic Surgery, Radboud University Nijmegen Medical Centre (Radboudumc), Nijmegen, NETHERLANDS.

OBJECTIVES: Combined radiochemotherapy is the standard treatment for irresectable stage III non-small cell lung cancer (NSCLC). The aim of this prospective cohort study was dual. Firstly, to answer whether 4D dynamic is superior to static ^{18}F -FDG PET for tumor delineation using pathology volumes as Gold standard. Secondly, to describe tumor regional variation in pharmacokinetic rate constants of ^{18}F -FDG metabolism (K_1 - k_3) and fractional blood volume (V_B) in regions with different levels of glucose metabolic rate (MR_{glc}) and compare these between histologies. **METHODS:** One-hour dynamic ^{18}F -FDG PET/CT scans were acquired in 38 patients with resectable NSCLC of at least 30mm in diameter. Two datasets were obtained: a static image 50-60min post injection and a parametric image of Patlak MR_{glc} values. Lesions were delineated on both using three strategies: (i) a threshold of 50% of the maximum voxel value, (ii) an adaptive threshold method of 40% of the background subtracted maximum voxel value and (iii) using the fuzzy locally adapted Bayesian (FLAB) algorithm. The pathological volume was calculated from three orthogonal tumor diameters. For the second aim, the tumor was divided in three equal volumes of increasing MR_{glc} , in which, K_1 - k_3 and V_B were computed. **RESULTS:** 35 patients having 36 primary malignancies were available for analysis. These included 20 squamous cell carcinomas (SCC), 12 adenocarcinomas (AC) and 4 lesions with another malignant histology. Pathological volumes were significantly larger than image volumes, except for FLAB volumes in a subset of 23 patients without macroscopic necrosis. Static PET volumes were significantly larger than volumes determined on MR_{glc} images. The volume determined by FLAB on the static PET corresponded best with the pathological volume. In SCC compared to AC, lesion MR_{glc} and k_3 were significantly higher and V_B was significantly lower. AC showed less heterogeneity relative to SCC in terms of mean MR_{glc} , k_3 and V_B . In SCC, a significant higher value for k_3 and lower value for V_B was found in regions with higher values of MR_{glc} . **CONCLUSIONS:** FLAB delineation on static ^{18}F -FDG PET scans resulted in volumes in best agreement with pathology. There was significant difference in glucose metabolic rate, phosphorylation rate (k_3) and fractional blood volume between the major pathological subtypes of NSCLC. In SCC, tumor regions with higher MR_{glc} showed higher phosphorylation rate and lower fractional blood volumes compared to regions with less intense metabolism. These differences in metabolism between NSCLC histologies might be relevant for targeting therapies and radiotherapy dose escalation.

OP080**Quantification of FDG uptake to detect residual nodal disease in locally advanced head and neck squamous cell carcinoma (LAHNSCC) after chemoradiotherapy (CRT): which threshold is optimal?**

N. Helsen^{1,2}, T. Van den Wyngaert^{1,2}, L. Carp^{1,2}, O. Hoekstra³, F. De Geeter⁴, A. Maes⁵, K. Spaepen⁶, J. Cambier⁷, F. Homans⁶, D. Van den Weyngaert⁸, S. Stroobants^{1,2}; ¹University of Antwerp, Antwerp, BELGIUM, ²Antwerp University Hospital, Wilrijk, BELGIUM, ³VU university medical center Amsterdam, Amsterdam, NETHERLANDS, ⁴Sint-Jan, Brugge, BELGIUM, ⁵AZ Groeninge, Kortrijk, BELGIUM, ⁶Sint-Augustinus, Wilrijk, BELGIUM, ⁷Jessa Hospital, Hasselt, BELGIUM, ⁸Middelheim Hospital, Antwerp, BELGIUM.

Background Surveillance of the neck with FDG-PET/CT after CRT in LAHNSCC patients is a valid alternative to routine neck dissection (Mehanna H, et al. N Engl J Med 2016). However, image interpretation remains largely unstandardized and quantification may further improve diagnostic accuracy. **Methods** Different $SUV_{body\ weight}$ thresholds and lesion-to-background ratios were explored in a prospective multicenter study of FDG-PET/CT 12 weeks after CRT in newly diagnosed LAHNSCC patients (ECLYPS). Whole-body (WB) and dedicated head-and-neck (H&N) series were acquired in 5 PET centers with scanner cross-calibration and image reconstruction according to EANM EARL criteria. Reference standard was histology or >1y negative clinical follow-up after imaging. Time-dependent receiver-operator characteristics (ROC) curves were used to determine the optimal cut-off thresholds and ratios at 1 year after CRT. Prognostic value was assessed with Cox regression. Thresholds were validated in an independent retrospective cohort of HNSCC patients referred for suspicion of disease recurrence using non-standardized FDG-PET/CT scans as performed in routine clinical care ($n=127$; median interval of imaging after CRT: 13 weeks, mean FU time 29.2 months). **Results** A total of 152 patients were enrolled, with 125 (male 93; median age 59) having primary tumor control and entering clinical follow-up. With a median follow-up of 20.4 months, 23 nodal neck recurrences were observed (prevalence 18.4%; 95% CI: 12.0–26.3%). A threshold of $SUV_{50}=2.1$ yielded an optimal AUC on both WB series (AUC=0.88, sensitivity=79.7% and specificity=80.8%) and H&N series (AUC=0.84, sensitivity=73.1% and specificity=79.8%), but only the WB series outperformed visual assessment (AUC=0.79; sensitivity=73.1%, specificity=85.0%; $p=0.040$). lesion-to-background ratios were not superior to visual assessment for WB (SUV_{50}/SUV_{liver} ; threshold=0.96; AUC=0.89; $p=0.056$) and H&N ($SUV_{90}/SUV_{parasp\ muscle}$; threshold=2.7; AUC=0.84; $p=0.507$) images. Validation of thresholds in an independent cohort yielded similar AUC values: WB $SUV_{50}=0.84$, WB $SUV_{50}/SUV_{liver}=0.90$, HN $SUV_{90}/SUV_{parasp\ muscle}=0.88$. WB SUV_{50}/SUV_{liver} had best sensitivity (74.6%) and specificity (94.8%), and outperformed visual read ($p=0.011$). The SUV_{50}/SUV_{liver} ratio was the most prognostic metric in the prospective and retrospective study for prediction of nodal recurrence (HR 6.98 and 13.2; 95% CI: 3.03–16.09 and 6.94–25.4; $p<0.0001$) and survival (HR 6.78 and 4.31; 95% CI: 2.46–18.71 and 2.29–8.12; $p<0.0001$). **Conclusion** FDG uptake quantification improves the diagnostic performance of FDG-PET/CT in LAHNSCC patients 1 year after CRT and contributes clinically meaningful prognostic information. When using EARL standardized PET acquisitions and reconstruction, absolute SUV metrics prove robust, yet ratios may be more useful in routine clinical care with less standardized imaging protocols.

OP081**Feasibility and results of a comprehensive whole-body PET/MR protocol for staging non-small cell lung cancer**

M. Soussan, C. Comtat, S. Djelbani, V. Brulon, I. Buvat, B. Helal; IMIV, CEA-Inserm, Univ Paris Sud, CNRS, Université Paris Saclay, Orsay, France, Orsay, FRANCE.

OBJECTIVES: For non-small cell lung cancer (NSCLC) staging, FDG-PET/MR might be superior to PET/CT in the detection of mediastinal invasion and metastatic disease. We evaluated the feasibility of a comprehensive PET/MR protocol for NSCLC staging. **METHODS:** 23 patients underwent a dual-imaging protocol consisting of a PET/CT scan (Biograph, Siemens) followed by PET/MR scan (Signa, GE healthcare) for lung cancer staging. PET/CT scans were performed 63 ± 11 min after injection of 4MBq/kg of 18F-FDG (head to mid-tight, 3 min/bed position ($n=7$ beds), FORE+OSEM reconstruction, 6 iterations/8 subsets). Subsequently (108 ± 14 min after injection), PET/MR was performed (2–3min/bed position, 5–6 beds) and PET data were reconstructed using TOF- OSEM, 2 iterations/28 subsets. MR sequences included a Dixon sequence for attenuation correction and a 5mm section axial T2- T2W FRFSE, with respiratory triggering (duration ~2–3 min). Axial T1-weighted 3D dual-GE sequence (LAVA-Flex) in the thorax was then performed (duration ~1 minute, $n=10/23$). Then, MR brain imaging was performed ($n=15/23$), including a FLAIR and a post contrast 3D-T1-weighted sequences (duration ~8 min). Thoracic lesions were identified visually in PET/CT and PET/MR. The number, location, SUVmax, and largest diameter were compared between both modalities. **RESULTS:** 50 hypermetabolic lesions were identified: 26 lung lesions, 22 lymph nodes (LN), one adrenal and one bone lesions. All lung lesions (mean CT size: 28 ± 23 mm [3–81 mm] seen on CT were also identified on T2W images, with an excellent correlation in lesion size ($r=0.99$) and with no significant difference between MR and CT-estimated size ($p=0.4$). Mediastinal hypermetabolic LN were measurable in 17/22 and 16/22 of cases in PET/CT and PET/MR, respectively. Correlations in LN size and SUVmax were excellent: $r=0.95$ and $r=0.92$, respectively. Pooling all lesions, SUVmax were 79 ± 63 % higher in PET/MR than PET/CT, due to both the ~45 min delay between PET/MR and PET/CT, and the different generation of PET scanners (TOF vs non-TOF). Thoracic T1W sequence, for T staging purpose, was feasible and provided good contrast between tumor with mediastinum or thoracic wall. Brain imaging was feasible and showed brain metastasis in 5/15 patients. **CONCLUSION:** PET/MR including thoracic and brain imaging is feasible for the TNM staging of NSCLC, with scan duration less than 45 min. Lesion-size measurements in PET/MR for lung and mediastinal lesions are comparable to those in PET/CT. PET/MR imaging might thus be considered as a “one-stop shop” modality for the staging of NSCLC.

OP082**Comparison between LUGANO, EORTC, PERCIST And IHP Criteria At Interim PET In Patients With Follicular Non-Hodgkin's Lymphoma**

L. Baratto¹, O. Jegede², F. Hong², B. Kahl³, A. M. Evens⁴, A. Quon¹; ¹Division of Nuclear Medicine and Molecular Imaging, Department of Radiology, Stanford University, Stanford, CA, UNITED STATES, ²Department of Biostatistics and Computational Biology, Dana-Farber Cancer Institute, Harvard Chan School of Public Health, Boston, MA, UNITED STATES, ³Department of Medicine, Washington University School of Medicine, St. Louis, MO, UNITED STATES, ⁴Division of Hematology/Oncology, Tufts University School of Medicine, Tufts Cancer Center, Tufts Medical Center, Boston, MA, UNITED STATES.

OBJECTIVES: FDG PET/CT is a standard clinical tool for response assessment in aggressive lymphoma. The aim of this preliminary study is to compare different PET interpretation criteria at interim therapy (i-PET) to find out which is the best predictor of clinical response. **METHODS:** This study is part of an Eastern Cooperative Oncology Group (ECOG) randomized phase II multicenter trial, (ECOG protocol E2408), that enrolled 250 patients with a histologically confirmed diagnosis of follicular non-Hodgkin lymphoma. Among these 250, 90 patients were included in our analysis. All patients performed at least two 18F-FDG PET/CT scans: at diagnosis (baseline PET) and after 3 cycles of

chemotherapy (i-PET). Response evaluation at i-PET was retrospectively performed according to LUGANO criteria, EORTC (European Organization for Research and Treatment of Cancer), PERCIST (PET Response Criteria in Solid Tumors) and IHP (International Harmonization Project), classifying the patients into 4 categories: complete metabolic response (CMR), partial metabolic response (PMR), stable metabolic disease (SMD), and progressive metabolic disease (PMD). All criteria were correlated to the best-observed response after 6 cycles of chemotherapy (referred to as “step 1” or end of initial round of treatment). RESULTS: LUGANO, EORTC and IHP were registered in 90 patients; PERCIST was recorded in 81 patients. For the first group (90 patients), the best observed response was CMR in 67/90 patients (74.5%), PMR in 19/90 (21.1%), SMD in 2/90 (2.2%) and PMD in 2/90 (2.2%). In the second group (81 patients), the best observed response was CMR in 62/81 (76.5%), PMR in 17/81 (21%), SMD in 0% and PMD in 2/81 (2.5%). According to LUGANO criteria, the rate of CMR at i-PET was 92.5% (62/67), for EORTC and IHP was 89.5% (60/67). For all these three criteria the rate of PMR was 21% (4/19), the rate of SMD and PMD was 50% (1/2). For PERCIST CMR rate at i-PET was 90.3% (56/62), PMR 17.7% (3/17), SMD 0% and PMD 50% (1/2). The overall response rate (defined by i-PET indicating at least stable disease or better) for LUGANO and IHP was 96.5%, for EORTC was 95.3% and for PERCIST was 93.7%; all criteria gave the same percentage for progressive disease. The rate of SMD was higher with LUGANO, EORTC and IHP criteria; no significant differences between them and PERCIST. The strongest correlation (~90% or higher) for all criteria was between CMR and the best-observed response at step 1. CONCLUSION: Our study demonstrated a strong correlation between interim-PET CMR assessed with all the criteria and treatment response after 6 cycles of chemotherapy. We are still evaluating patients to confirm these data.

OP083

Localisation of insulinoma using Glucagon-like Peptide-1 Receptor (GLP-1R) SPECT/CT, GLP-1R PET/CT and MRI: Preliminary results of a prospective clinical study

K. Antwi¹, M. Fani¹, T. Heye¹, G. Nicolas¹, E. Merkle¹, J. Reubi², B. Gloor³, E. Chris³, D. Wild¹; ¹University Hospital Basel, Basel, SWITZERLAND, ²University of Bern, Bern, SWITZERLAND, ³University Hospital Bern, Bern, SWITZERLAND.

Purpose: We aimed at prospectively comparing the detection rate of GLP-1R PET/CT vs GLP-1R SPECT/CT vs standardized contrast enhanced 3T MRI in patients with endogenous hyperinsulinemic hypoglycemia. Preliminary results of an ongoing study are reported. Methods: Thirty-three consecutive patients with neuroglycopenic symptoms due to endogenous hyperinsulinemic hypoglycemia were enrolled. A standardized contrast enhanced 3T MRI was performed. Afterwards the patients received a SPECT/CT at 4 and 72 hours after injection of ¹¹¹In-DOTA-exendin-4 and a PET/CT 2.5 hours after injection of ⁶⁸Ga-DOTA-exendin-4 in a randomized order. Six independent blinded Nuclear Medicine Physicians and Radiologists reviewed the scans. Standard of comparison was the histological diagnosis after surgery. Results: Previously performed cross-sectional imaging (CT/MRI) was negative or not conclusive in 25/33 (76%) of patients. So far 22 patients have been operated. In this collective, the histological diagnosis of a benign insulinoma was confirmed in 19 patients, 1 patient had adult islet cell hyperplasia. In 1 patient both intraoperative palpation as well as the histological diagnosis did not confirm an insulinoma. In 1 patient symptoms of endogenous hypoglycemia ceased postoperative but histological diagnosis did not confirm the diagnosis of a benign insulinoma or nesidioblastosis. Only this patient was excluded from evaluation, as the final diagnosis remained unclear. Two patients refused surgery. Five patients are awaiting surgery. In 4 patients PET/CT, SPECT/CT as well as the previous performed conventional imaging did not find any suspicious

lesion and were thus not operated up to date. In this interim analysis overall pooled sensitivity was 95% for PET/CT, 73% for SPECT/CT, and 81% for MRI. PET/CT was the only modality which correctly identified the area of islet cell hyperplasia (adult nesidioblastosis) within the pancreas. Conclusion: Our interim analysis suggests that GLP-1R PET/CT performs better than MRI and GLP-1R SPECT/CT at a lower radiation dose and shorter examination time. GLP-1R PET/CT might be a useful diagnostic tool in patients where cross sectional imaging (CT/MRI) fails to localize the insulinoma.

310 – Sunday, October 16, 2016, 11:30 - 13:00, Hall 114

Conventional & Specialised Nuclear Medicine: Paediatrics

OP084

I-131-meta-iodobenzylguanidine therapy improves survival in high-risk neuroblastoma patients with I-123-mIBG positive residual metastatic disease

M. C. Schmidt¹, B. Hero¹, B. Decarolis¹, A. Eggert², F. Berthold¹, A. Drzezga¹, T. Simon¹; ¹University Hospital of Cologne, Cologne, GERMANY, ²Charité Berlin, Berlin, GERMANY.

Background: Randomized trials on the first-line treatment of high-risk neuroblastoma are limited. Therefore, we analyzed the national data base on the impact of I-131-meta-iodobenzylguanidine (I-131-mIBG) therapy, local radiotherapy, and single agent ch14.18 immunotherapy in the first-line therapy of high-risk neuroblastoma. Methods: Patients of two consecutive national neuroblastoma trials in Germany were included if they met all key criteria: (1) stage 4 neuroblastoma, (2) age at diagnosis 18 months or older, (3) N5/N6 induction chemotherapy, (4) non-progressing residual I-123-mIBG positive metastatic disease after induction chemotherapy prior to myeloablative chemotherapy and autologous stem cell transplantation, (5) diagnosis between 1997 and 2012. I-131-mIBG therapy was scheduled for non-progressing I-123-mIBG positive lesions. Local radiotherapy 36-40 Gy was scheduled for I-123-mIBG positive residual disease at the primary site. Single agent ch14.18 was stratified according to open trials. Results: A total of 232 patients were analyzed. The median observation time was 8.8 years. I-123-mIBG positive residual metastases were present prior to myeloablative chemotherapy in 92 patients. The median interval between I-131-mIBG therapy and stem cell transplantation was 21 days. The median I-131-mIBG activity applied was 7.4 GBq. Event-free survival was very similar between patients who underwent I-131-mIBG therapy (5yEFS 32.2+/-7.1%) compared to no I-131-mIBG therapy (5yEFS 27.9+/-6.9%, p=0.553). In contrast, a trend for better overall survival was found after I-131-mIBG therapy compared to no I-131-mIBG therapy (5yOS 58.1+/-7.6% vs. 38.9+/-7.5%, p=0.086). Multivariable analysis including MYCN, I-131-mIBG therapy, local radiotherapy, and immunotherapy with ch14.18 revealed an independent impact of MYCN amplification (p=0.028, hr 1.987) and ch14.18 treatment (p=0.004, hr 0.441) on EFS, and MYCN amplification (p<0.001, hr 3.476), ch14.18 treatment (p=0.008, hr 0.560), and I-131-mIBG therapy (p=0.047, hr 0.426) on OS. Conclusions: I-131-mIBG therapy can improve survival in patients with incomplete metastatic response to induction chemotherapy. These results warrant a prospective multicenter trial on I-131-mIBG therapy. Moreover, this analysis confirmed the efficacy of immunotherapy with ch14.18.

OP085

Towards an International mIBG Skeletal Score for High Risk Neuroblastoma: A SIOPEN-COG cooperation

U. Pötschger¹, A. Naranjo², G. Yanik³, M. Castellani⁴, A. Boubaker⁵, B. Lambert⁶, V. Lewington⁷, A. Kaminska⁸, K. Taborska⁹, M. Parisi¹⁰, B. Shulkin¹¹, J. Park¹², S. Kreissman¹³, K. Matthay¹⁴, R. Ladenstein¹; ¹Children's Cancer Research Institute, Vienna, AUSTRIA,

²Children's Oncology Group Statistics and Data Center, Gainesville, FL, UNITED STATES, ³University of Michigan Medical Center, Ann Arbor, MI, UNITED STATES, ⁴Instituto Nazionale Tumori di Milano Nuclear Medicine Division, Milan, ITALY, ⁵Centre Hospitalier Universitaire Voudois, Lausanne, SWITZERLAND, ⁶Ghent University, Department of Nuclear Medicine, Ghent, BELGIUM, ⁷Guy's and St. Thomas NHS Foundation Trust, London, UNITED KINGDOM, ⁸Children's Memorial Health Institute, Warsaw, POLAND, ⁹Motol University Hospital, Prague, CZECH REPUBLIC, ¹⁰Seattle Children's Hospital, University of Washington, Seattle, WA, UNITED STATES, ¹¹St. Jude Children's Research Hospital, Memphis, TN, UNITED STATES, ¹²Seattle Children's Hospital, University of Washington, Seattle, WA, UNITED STATES, ¹³Duke University Medical Center, Durham, NC, UNITED STATES, ¹⁴University of California, San Francisco, CA, UNITED STATES.

PURPOSE: A collaborative effort was undertaken to derive an internationally agreed semi-quantitative meta-iodobenzylguanidine (mIBG) scoring method in neuroblastoma by harmonising previously established scoring systems, which were each found to have prognostic value at the end of induction (Yanik JNM 2013). The aim of this analysis was to investigate the individual effect on event-free-survival (EFS) of the two components of the scoring system: 1) the number of involved anatomic regions and 2) the scoring value within each segment and to evaluate the prognostic value of the new proposed scoring system. **PATIENTS AND METHODS:** COG and SIOPEN merged data of children with stage 4, mIBG avid, neuroblastoma entered on the COG-A3973 (216pts) and the SIOPEN/HR-NBL1 trial (341 pts) for first line therapy. Two independent nuclear medicine review teams scored mIBG scans pre and post induction according to Curie- and SIOPEN-methodologies. Here, the SIOPEN score evaluating the skeletal (mIBG) uptake on a 0-6 scale in 12 anatomical regions was chosen for the statistical analysis due to the greater range of values. The two study cohorts were investigated separately and a bootstrap-based internal validation was performed. **RESULTS** In 557 pts the cumulative SIOPEN-score post induction had a significant prognostic impact with 5-years EFS of 41%, 33% and 15% for total scores of 0, 1-3 and greater than 3, respectively. However, no increasing hazards with increasing scores per segment were observed. In contrast, the number of positive segments alone had a highly significant impact with 5-year EFS of 41%, 32% and 14% for patients with 0, 1-2 and greater than 2 positive segments post induction. **CONCLUSION** The number of positive segments was the most important prognostic factor. Weighting the involvement within segments did not improve the prognostic value of the scoring system. These results suggest a possible simplification of mIBG scoring, facilitating future international collaborations.

OP086

¹⁸F-FDG PET-CT scan versus bone marrow biopsy in Pediatric Hodgkin's Lymphoma: A quantitative analysis

M. Siddique, A. Hassan, H. Bashir, S. Riaz, M. Nawaz; Shaukat Khanum Memorial Cancer Hospital & Research Centre, Lahore, PAKISTAN.

Background: The present study investigates whether combined positron emission tomography/computed tomography using Fluorine-18 fluorodeoxyglucose (¹⁸F-FDG PET-CT scan) predicts clinically important bone marrow involvement (BMI) by Hodgkin's Lymphoma (HL) in pediatric population with sufficient accuracy to replace routine staging iliac bone marrow biopsy (iBMB). We also characterized distribution patterns of BMI in HL as determined by ¹⁸F-FDG PET-CT scan in accordance with bone marrow biopsy findings. **Methods:** Retrospectively analysis of scans, histology reports and treatment records of all pediatric patients diagnosed as HL between July 2010 and June 2015 who underwent ¹⁸F-FDG PET-CT scan and iBMB as part of staging work up were analyzed. Different patterns of FDG uptake in patients with BMI were

reviewed visually as well as quantitatively. BMI was defined as positive iBMB and/or foci of marrow uptake on ¹⁸F-FDG PET-CT scan that behaved concomitantly with other sites of lymphomatous involvement on post treatment evaluation scans. Clinical/radiological stage according to the Ann Arbor staging system was recorded. Significant marrow uptake (SUV_{max}) on ¹⁸F-FDG PET-CT scan was evaluated by using Student's *t*-test. **Results:** 788 patients were enrolled. 656(83.2%) male, 132(16.8%) females; male to female ratio [5:1]. Age range: 2-18 years (mean 10.3 years). Overall 108 of 788(13.7%) had BMI. The results of iBMB and ¹⁸F-FDG PET-CT scan in the detection of BMI were concordant in 734(93%); positive concordance was observed in 60, and negative concordance was observed in 674. Out of discordant cases (n=54,6.8%), four were upstaged by iBMB with normal uptake on ¹⁸F-FDG PET-CT scan, while 44 with negative iBMB findings were upstaged due to increased focal medullary uptake that normalized after treatment. Based on PET findings, out of 108 cases with BMI, four had no uptake, six had diffuse, 21 had uni/bifocal and 77 multifocal. Overall, visual assessment of BMI on ¹⁸F-FDG PET-CT scan had a sensitivity, specificity, positive predictive value (PPV), negative predictive value (NPV) and accuracy of 96%, 99%, 95%, 99%, 98% respectively versus 59%, 100%, 100%, 93%, 94% for iBMB. On a quantitative assessment, BM-SUV_{max} was significantly higher in patients with BM involvement (p<0.05). **Conclusion:** ¹⁸F-FDG PET-CT scan demonstrated BMI in 13.7% of newly diagnosed pediatric HL. Diagnosis of BMI in HL by ¹⁸F-FDG PET-CT scan was more sensitive than iBMB with potential upstaging in 6% of patients. Multifocal FDG uptake (at least three foci) is more indicative of BMI; however, in case of diffuse FDG uptake, iBMB is still an indispensable procedure for staging.

OP087

Prognostic Value Of Different F-18 FDG PET/CT Quantitative Analytical Methodologies In Pediatric Hodgkin's Lymphoma

O. Serry¹, A. A. Kandeel², M. A. El-Sayed², A. E. M. Hussein³, W. S. Omar⁴; ¹Children's Cancer Hospital Foundation, Cairo, EGYPT, ²Nuclear Medicine Department, Faculty of Medicine, Cairo University, Cairo, EGYPT, ³Nuclear Medicine Department, Faculty of Medicine, Sohag University, Cairo, EGYPT, ⁴Nuclear Medicine Department, National Cancer Institute, Cairo University, Cairo, EGYPT.

Introduction and aim of work: Assessment of the individualized SUVs, PET-derived total metabolic tumor volume (TMTV) and the product of both parameters, termed total lesion glycolysis (TLG) in both initial and interim PET if it carries a better PPV in early assessment of response to therapy in pediatric Hodgkin's lymphoma (PHL) patients. **Patients and Methods:** Retrospective analysis of PET/CT results was performed on 60 patients (42 males and 18 females; mean age 8.7±4.2 years). To assess the prognostic value of initial and interim ¹⁸F-FDG PET/CT, different semi-quantitative parameters such as SUV_{max}, SUV_{mean}, Total lesion glycolysis (TLG) and TMTV of all lesions using SUV_{max} & mean including SUV_{2.5} and 40% of SUV_{max} as cut-off values were calculated. Follow up for 24 months from initial treatment with calculation of Disease Specific Survival (DSS). According to the recommendations of Deauville criteria interim PET (PET2) results were identified into three groups; PET2-negative (PET2-ve), PET2-positive (PET2+ve), and PET2-minimal residual uptake (PET2-MRU), the cut-off between PET2+ve and PET2-MRU was 3-4 in the 5-point scale. **Results:** Out of the 60 interim-PET scans, 50 scans were considered as PET2-ve (83.3%), 5 scans as PET2+ve (8.3%) and 5 scans as PET2-MRU (8.3%). The risk of the disease and the visual scoring assessment were significantly correlated with patient's outcome (whether Negative or Residual/Relapse) (p < 0.0001). Different results were obtained; the most important were TLG_{max2.5} (cut-off 2.5), TLG_{mean2.5} (cut-off 2) and TMTV_{2.5} (cut-off 0.75 ccm) in interim PET showed the highest sensitivity, specificity, PPV and NPV (58.5%, 97.9%, 87.5% and 90.3% respectively for the 3 parameters). **Conclusion:** LG_{max2.5},

TLGmean2.5 and TMTV2.5 are the most relevant parameters for predicting the outcome in patients with PHL, and can add a significant prognostic insight to interim PET response assessment. This may guide clinicians in their choice of therapeutic strategy.

OP088

Differentiated Thyroid Carcinoma in Children, Adolescents and Young Adults- a bicentric Analysis with long-term Follow Up in 354 Patients

A. Thoma¹, A. Todica², P. A. Bartenstein², K. Scheidhauer¹, M. Schwaiger¹, **M. Mustafa¹**; ¹Klinikum rechts der Isar, Dept. of Nuclear Medicine, Munich, GERMANY, ²Klinikum der LMU, Dept. of Nuclear Medicine, Munich, GERMANY.

Aim: Differentiated Thyroid Carcinoma (DTC) has a worldwide peak incidence between 40 and 50 years of age. In children and adolescents it remains a rare disease, presenting with a different and usually more widespread clinical stage, nonetheless prognosis is supposed to be excellent. This bicentric study aimed at investigating a cohort of pediatric and young patients with DTC, who received radioiodine ablation with regards to differences in primary presentation at diagnosis and long-term follow up. **Methods:** All patients, who underwent radioiodine ablation between 01/2000 and 12/2015 at both university hospitals in Munich, Germany, were retrospectively analyzed for pediatric and young patients under 30yrs: Group A=83 pts ≤20 yrs. and Group B = 271 pts ≤30 yrs were included. The two cohorts were investigated with regards to histological data (maximum size of tumors, multifocality, aggressive subtypes), extent of lymphadenectomy (number of lymphnodes resected, number of lymphnode metastases), initial presentation at post-ablation radioiodine WBS, follow-up WBS (diagnostic or post-therapeutic), clinical and ultrasound follow-up examinations and additional imaging (including MRI and PET/CT where available) to determine progression free survival (PFS). **Results:** The median follow-up was 4,8 years. The initial presentation of patients in both groups did not differ with regards to gender (78% female A and B), tumor size according to TNM-classification and maximum diameter (1,5cm in A and 1,4cm in B), average dissected lymph nodes (15,0 Gr. A vs. 15,5 Gr. B), lymph node metastases (N1 54% Gr. A vs. 50% Gr.B; fraction of excessive lymph node metastases defined as >5 LNM). There were significant differences in initial M1 stage (12,0% Gr. A vs. 2,6% Gr. B), 90% of M1 metastases being pulmonary. Of all M1 metastases 80% were radioiodine avid in Gr. A and 86% in Gr. B, complete remission was achieved in 40% (A) and 83% (B). In Gr.A 13,3% of pts and Gr. B 6,3% had persistent or progressive disease, PFS was significantly longer in Gr. A (26 vs. 18months). **Conclusion:** In this large cohort of pediatric patients and young adults presenting with DTC initial presentation and response to radioiodine ablation and therapy were comparable. Significant differences were to be found in rates of distant metastases at initial presentation, whereas radioiodine avidity was similar and lead to complete remission in a majority of patients.

OP089

Can FDG PET/CT predict the outcome of pediatric rhabdomyosarcoma?

E. El-kholy¹, I. El-Antably¹, E. El-Nadi², M. S. Zaghoul³, S. Ahmed³, H. Hafez⁴, O. Shawky⁴, T. Rafaat⁵, N. El-Kilini⁶, A. Younis⁷, G. Taha⁷; ¹Nuclear Medicine National cancer Institute (NCI) and Children Cancer Hospital Egypt (CCHE), Cairo, EGYPT, ²Pediatric Oncology, Faculty of Medicine Benisuef University and Children Cancer Hospital Egypt (CCHE), Cairo, EGYPT, ³Radiotherapy Department, Children Cancer Hospital Egypt (CCHE), Cairo, EGYPT, ⁴Medical Oncology, Children Cancer Hospital Egypt (CCHE), Cairo, EGYPT, ⁵Radiology Department, National cancer Institute (NCI), Children Cancer Hospital Egypt (CCHE), Cairo, EGYPT, ⁶Pathology Department, Children Cancer

Hospital Egypt (CCHE), Cairo, EGYPT, ⁷Surgical Oncology, Children Cancer Hospital Egypt (CCHE), Cairo, EGYPT.

Aim: to establish whether initial 18F-FDG SUV can add prognostic information to clinical staging in pediatric rhabdomyosarcoma patients. **Materials and methods:** 98 patients (48 female, 50 male, Age ranged 4 mo-17.5 years, mean age: 5.8±4.5) with pathologically proven RMS underwent PET/CT for initial cancer staging were included in the study. We retrospectively assessed whether or not FDG PET/CT using primary SUVmax and primary/liver ratio, could predict event-free survival (EFS) or overall survival (OS) in patients with pediatric RMS who received specific therapy according to the standard Children Cancer Hospital-Egypt (CCHE) protocol. Correlation with other prognostic factors was also obtained. **Results:** High SUVmax was significantly related to the presence of nodal or distant metastasis. With marked cutoff values of (3.6) and (2.1) by ROC curve for SUV primary and SUV primary/liver ratio respectively, OS (for 36 months) and EFS proved to be higher in patients with SUVmax below these values. Patients with SUVmax primary/liver less than the cutoff of 2.1 had OS 60.8% and EFS 48.1% compared to 44.5% and 14.8% to those above the cutoff, yet, this semi-quantitative evaluation failed to attain statistical significance. (P value 0.92 & 0.16 respectively). Similar results were obtained in assessment of primary SUVmax with (P value 0.76 and 0.62 respectively). There was prevalence of high SUV primary and SUV primary/liver ratio among those patients with less favorable clinico-pathological features (unfavorable primary site, high and intermediate risk & alveolar pathological type), yet was not statistically significant. **Conclusion:** In this preliminary study, FDG PET/CT may be an additional predictor of outcome in pediatric rhabdomyosarcoma, further studies are needed to correlate between assessment of therapy response by PET/CT and final outcome and survival. **Key words:** FDG PET/CT, rhabdomyosarcoma, prognosis.

OP090

Sulesomab in Pediatric Musculoskeletal Infection

A. Javid¹, S. Usmani², M. U. Khan³, I. AlShammari¹; ¹Farwania Hospital, Farwania, KUWAIT, ²Faisal Bin Essa Hospital, Saba Area, KUWAIT, ³Al Jhara Hospital, Jahara, KUWAIT.

Introduction: Bone and joint infections are one of the major causes of morbidity in infants and children. Early diagnosis with prompt treatment, are key to prevent the complications and morbidity. **Objective:** The objective of this study is to evaluate the diagnostic accuracy of Tc-99m labeled anti-granulocyte monoclonal antibody fragment Fab' (Sulesomab, Leukoscan®) for the detection of musculoskeletal infection in pediatric population. **Material and Method:** This is a prospective study of 55 pediatric patients (30 males and 25 females) with a mean age of 6 years and 9 months (range 1 month to 15 years and 8 months). These patients were referred from out-door clinic or admitted cases in Pediatrics and Medical wards to the Nuclear Medicine Department. The monoclonal antibody scan and the three phase bone scan were carried out with a maximum interval of 7 days. The patients was injected with age adjusted dose according to Webstre's rule taking 20 mCi (750 MBq) as adult dose. The minimum injected dose was 3.5 mCi (130 MBq). Imaging was performed after one and 4-hour after injection and in eight cases at 24-hours. Bone scan was acquired according to standard protocols. The sulesomab scan results was compared with final diagnosis, provided by the primary physician on 2-months clinical follow-up along with biochemical tests. **Results:** The accuracy of the Sulesomab scan was 92.7% for the diagnosis of acute musculoskeletal infection. The calculated sensitivity, specificity, negative & positive predicted values were 95.8%, 90.3%, 96.5% and 88.4% respectively. No patient had adverse events. **Conclusion:** Sulesomab was well tolerated with no apparent side effects. It was found highly accurate and had high sensitivity and negative predicted values. So, this agent can be used with confidence to rule out acute musculoskeletal infection in pediatric age group.

OP091**Can we predict definitive or transient hypothyroidism in new born under one month with iodine scintigraphy?**

A. LEGENDRE, Jr., G. PETYT, D. BELLEVRE, G. COLLET, C. HOSSEIN FOUCHER, H. LAHOUSSE; CHRU de Lille, LILLE, FRANCE.

AIM: Iodine scintigraphy in diagnostic of congenital hypothyroidism is very specific to determine location of thyroid and dysgenesis. Usually we wait 2 years to know if hypothyroidism is definitive or transient. In our study we tried to determine factors predictive of definitive or transient hypothyroidism in new born with congenital hypothyroidism. **MATERIEL** and **METHOD:** We included 114 children under one month, retrospectively between 2004 and 2014 in CHRU of LILLE who had iodine scintigraphy in diagnostic of congenital hypothyroidism with TSH Superior to 12 mUI/ml. 100 of them had definitive hypothyroidism and only 14 transient with a decline of two years when TSH without levothyrox was measured in order to confirm or not definitive hypothyroidism. We evaluated location of thyroid in scintigraphy, thyroid area on scintigraphy, TSH on Guthrie test, sex and percent of decrease fixation rate after perchlorate discharge test when we saw a thyroid. **RESULTS:** TSH on Guthrie test is predictive of definitive hypothyroidism (p inferior to 0.0001 Wilcoxon Two Sample Test), higher is TSH more hypothyroidism has chance to be definitive. With TSH superior to 58mUI/L sensitivity is of 84% and specificity of 92% either in 44 children with thyroid in orthotopic position (p=0,001), with TSH superior to 60mUI/ml sensitivity of 60% and specificity of 93%. Concerning location of thyroid all 70 dysgenesis became definitive hypothyroidism. Other 44 children with thyroid in orthotopic location had for 30 definitive hypothyroidisms and 14 transient hypothyroidisms. There is more definitive hypothyroidism in dysgenesis group (p inferior to 0.0001). There is no significant difference of area thyroid test between definitive and transient hypothyroidism (respectively p=0.29 student test. Percent of decrease fixation rate after perchlorate discharge test is significantly higher in definitive hypothyroidism p= 0.02(Wilcoxon two sample test). For increase of 10 percent sensitivity of perchlorate discharge test is of 67% and specificity of 87.5%. **CONCLUSION:** TSH on Guthrie test, location of thyroid on iodine scintigraphy and percent of increase of iodine rate after perchlorate discharge test are significantly predictive of definitive or transient hypothyroidism. They can be useful for improving the therapeutic education depending on the depth of hypothyroidism.

YE1 – Sunday, October 16, 2016, 13:00 - 14:30, Hall 114
Young EANM Daily Forum 1: TBA

OP092

TBA

401 – Sunday, October 16, 2016, 14:30 - 16:00, Auditorium
CME 3 - Oncology/EORTC: Metabolic Response Assessment in Solid Tumours

OP093**Methodological Considerations**

R. Boellaard; VU University Medical Center, Nuclear Medicine & PET Research, Amsterdam, NETHERLANDS.

OP094**Breast and Gynecological Tumors**

L. Kenny; Imperial College London, Faculty of Medicine, Department of Surgery & Cancer, London, UNITED KINGDOM.

OP095**Gastrointestinal Tumors**

A. Hendlisz; Institute Jules Bordet, Digestive Oncology / Gastro-Enterology, Brussels, BELGIUM.

OP096**Bone and Soft Tissue Sarcomas**

W. Fendler; University of California at Los Angeles, Ahmanson Translational Imaging Division, Munich, UNITED STATES OF AMERICA.

402 – Sunday, October 16, 2016, 14:30 - 16:00, Hall 211

Joint Symposium 3 - EANM/E-DLB Consortium: Dementia with Lewy Bodies (DLB): What Have We Learned in the Last Years?**OP097****New Data and New Visions in Clinical Assessment**

D. Aarsland; Center for Age-Related Medicine, Stavanger University Hospital, Stavanger, NORWAY.

OP098**The Concept of Prodromal Dementia of Lewy Body is Ongoing**

L. Bonanni; G. d'Annunzio University, Aging Research Centre, Department of Neuroscience and Imaging, Chieti, ITALY.

OP099**DAT Imaging : Always Impaired?**

Z. Walker; University College London, Mental Health Sciences, London, UNITED KINGDOM.

OP100**Metabolic Network Underlying Dementia of Lewy Body**

S. D. Morbelli; San Martino Hospital, Nuclear Medicine, Genova, ITALY.

403a – Sunday, October 16, 2016, 14:30 - 15:30, Hall 117

Mini Course 1: Updates in Radiopharmaceuticals for SPECT**OP101****SPECT Radiopharmaceuticals: In-111-Exendin, an Example from Preclinical to Clinical studies**

P. Laverman; Radboud University Nijmegen Medical Centre, Department of Nuclear Medicine, Nijmegen, NETHERLANDS.

OP102**SPECT Radiopharmaceuticals: An Update**

J. Sosabowski; Barts Cancer Institute, Queen Mary University of London, Centre for Molecular Oncology, London, UNITED KINGDOM.

403b – Sunday, October 16, 2016, 15:45 - 16:45, Hall 117

Mini Course 2: Updates in Radiopharmaceuticals for PET**OP103****New PET Tracers and Oncology**

P. Kolenc Peitl; University Medical Centre Ljubljana, Department For Nuclear Medicine, Ljubljana, SLOVENIA.

OP104**New PET Tracers and Neurology**

E. Demirci; Cerrahpasa Medical Faculty, SISLI ETFAL TRAINING&RESEARCH HOSPITAL, Istanbul, TURKEY.

403c – Sunday, October 16, 2016, 17:00 - 18:00, Hall 117

Mini Course 3: Updates in Radiopharmaceuticals for Radionuclide Therapy**OP105****Radiolabelling of PRRT****Radiopharmaceuticals in Small-scale Radiopharmacies and the Evolution of PRRT Radiopharmaceuticals**

J. O. Brillhante; Unipessoal Lda, Viseu, PORTUGAL.

OP106**Radiotherapeutics and Radiodiagnostics: Yin and Yang?**

B. Vanbilloen; U.Z. Gasthuisberg, Department of Nuclear Medicine (Radiopharmacy), Leuven, BELGIUM.

404 – Sunday, October 16, 2016, 14:30 - 16:00, Hall 112

Do.MoRe: PSMA Imaging & Therapy**OP107****Gallium-68-PSMA-HBED-CC PET/CT in patients with biochemical recurrence after treatment with curative intent: potential impact on patient management**

R. Valkema, M. B. Busstra, I. L. Bakker, T. De Vringer, C. H. Bangma, J. F. Verzijlbergen; Erasmus MC University Hospital, Rotterdam, NETHERLANDS.

Aim: Radical prostatectomy (RP) or radiation therapy (RT) are curative options for patients with localized prostate carcinoma (PCa). Local salvage therapy is considered when prostate specific antigen (PSA) becomes detectable after RP at 0.2 - 0.5 ng/mL, or rises >2ng/mL above nadir after RT. However, only half of the patients will benefit of local salvage therapy, which has important side effects. Current imaging methods are not accurate enough to identify patients with only local recurrence. **Methods:** Fifty-three patients (42 post-RP and 11 post-RT) were referred for ⁶⁸Ga-PSMA-HBED-CC PET/CT to find the substrate for elevated PSA: prostate fossa (PF), locoregional lymph nodes (LN), or more distal metastases (M). PET/CT was performed 60 min after injection of 104 ± 30 MBq ⁶⁸Ga-PSMA-HBED-CC. Nominal activity was 1.5 MBq/kg for 3 min/bed; time/bed was extended with less administered activity. Most patients had a delayed partial scan at 120 min p.i., after furosemide. Scans were systematically read (positive, equivocal, negative) for the PF, LN and M regions. **Results:** In 26/42 post-RP patients PET/CT was positive, in 3/42 equivocal and in 12/42 negative. Negative scans were found in 10/25 (40%) of patients with PSA 0.2 - 0.5 ng/mL, in 2/8 (25%) with PSA 0.6 - 2.0 ng/mL and in 0/10 with PSA >2.0 ng/mL. In all 11 post-RT patients (PSA 1.3 - 37 ng/mL) PET/CT was positive. In 21/53 patients, positive LN or M lesions, although unconfirmed, suggested that not local salvage, but alternative options should be considered, thus to avoid side effects associated with (futile) salvage therapy. **Conclusion:** ⁶⁸Ga-PSMA-HBED-CC PET/CT is promising for sensitive detection of PCa lesions in patients with PSA recurrence after initial RP or RT, even at low PSA levels. Prospective studies are warranted to confirm the accuracy of ⁶⁸Ga-PSMA-HBED-CC PET/CT and its role in patient management and outcome.

OP108**Detection Rates of ⁶⁸Ga-PSMA PET/CT in Patients with Biochemical Relapse from Prostate Cancer after Radical Prostatectomy and PSA Values < 1 ng/ml: Preliminary Results from a Prospective, Multicenter Trial**

J. B. Nielsen, Jr.^{1,2}, H. D. Zacho^{1,2}, K. Dettmann³, N. C. Landkilde⁴, J. B. Jensen³, U. Haberkorn⁵, L. J. Petersen^{1,2}; ¹Dept. of Nuclear Medicine, Aalborg University Hospital, Aalborg, DENMARK, ²Dept. of Clinical Medicine, Aalborg University, Aalborg, DENMARK, ³Dept. of Urology, Holstebro Regional Hospital, Holstebro, DENMARK, ⁴Dept. of Urology, Aalborg University Hospital, Aalborg, DENMARK, ⁵Dept. of Nuclear Medicine, University Hospital of Heidelberg, Heidelberg, DENMARK.

Aim: To evaluate the clinical value of ⁶⁸Ga-labelled prostate-specific membrane antigen (⁶⁸Ga-PSMA) used in PET/CT at low PSA levels (PSA < 1 ng/ml) in patients with recurrent prostate cancer. **Materials and Methods:** This study was a prospective, GCP-monitored clinical trial (EudraCT number 2014-005073-37) of ⁶⁸Ga-PSMA-HBED-CC ⁶⁸Ga-PSMA PET/CT in recurrent prostate cancer. This report included twenty-six patients with biochemical relapse of prostate cancer after radical prostatectomy (RP) with PSA < 1 ng/ml. The administered dose was 2 MBq/kg; scan time was 60 ± 15 min. **Results:** The mean age was 67 years. Mean PSA level at the time of ⁶⁸Ga-PSMA PET/CT was 0.4 (range 0.2-0.9 ng/ml). A total of 20 of 26 patients had a PSA level < 0.5 ng/ml. Biochemical relapse occurred after mean of 40 months (6-128) after RP; 7 did not reach postoperative PSA < 0.1 ng/ml. Mean activity was 175 MBq ⁶⁸Ga-PSMA (128-223). Definitive pathological uptake of ⁶⁸Ga-PSMA was observed in 4 patients and equivocal uptake in 2 patients (23.1%, 95% confidence interval 6.9-39.3%). In all patients with pathological ⁶⁸Ga-PSMA uptake (n=6), mean PSA was 0.6 ng/ml (0.2-0.9) versus 0.3 ng/ml (0.2-0.7) in PSMA-negative patients. Mean PSA doubling time were 7 months (0-24) and 18 (0-89) months in the patients with and without pathological ⁶⁸Ga-PSMA uptake, respectively. Mean injected dose and time to scan did not differ among these groups. The location of relapse was at lymph node level in three patients and bone in two patients (one patient had both lymph node and bone involvement). Equivocal lesions were located in the prostatic bed and bone. Control scans in 18 patients participating in a staging protocol, confirmed pathological uptake in all patients with a mean target-to-background ratio of 27, indicating satisfactory scan sensitivity. **Conclusion:** Pathological uptake of the ⁶⁸Ga-PSMA tracer was detected in 6 of 26 patients (23.1%) with biochemical relapse and low PSA values (PSA < 1 ng/ml) after radical prostatectomy. Pathologic ⁶⁸Ga-PSMA uptake was shown in lymph nodes and bones but no uptake was shown in the prostatic bed. The detection rate of recurrent prostate cancer in this study was far below previous detection rates reported from a number of large retrospective series.

OP109**Pre - (¹⁷⁷Lu-PSMA) Therapy Response Prediction by Textural Heterogeneity Parameters in ⁶⁸Ga-PSMA PET Scans among Patients with Metastatic Prostate Cancer**

Z. Khurshid¹, H. Ahmadzadehfar¹, F. Gaertner¹, L. Papp², N. Zsótér², M. Essler¹, R. Bundschuh¹; ¹Uniklinikum Bonn, Bonn, GERMANY, ²Mediso Medical Imaging Systems, Budapest, HUNGARY.

Objective: Prostate cancer is the most common tumor in men and is the cause of significant patient mortality and morbidity globally. In newer diagnostic agents PSMA linked ones are specifically important due to its significant up regulation in tumor cells. In this era of personalized therapy emphasis is being placed on earlier response prediction and risk stratification of patients even before the start of therapy. Analysis of textural heterogeneity parameters has been associated with determination of innately aggressive and therapy resistant cell lines thus emphasizing their importance in therapy planning. In our study, we aimed to determine pre (¹⁷⁷Lu-PSMA) therapy response prediction by textural heterogeneity parameters as assessed by pre therapy ⁶⁸Ga-PSMA PET scan in metastatic prostate cancer patients.

Materials and Methods: Retrospective analysis of 36 patients was performed. All patients had metastatic prostate cancer and were planned to undergo ^{177}Lu -PSMA therapy. Pre therapy ^{68}Ga -PSMA PET scans were used for analysis. Interview Fusion (MEDISO Medical Imaging) was used for entire analysis. 3D volumes (VOIs) for 3 lesions each in bones and lymph nodes were manually delineated in static PET images (also in prostate and liver when applicable). In addition to conventional parameters, 10 PET based textural heterogeneity parameters were determined. Results obtained were then compared with clinical parameters including pre and post therapy PSA, alkaline phosphate, bone alkaline phosphate levels and ECOG criteria. Spearman correlation was used to determine statistical dependence among variables. **Results:** Two heterogeneity parameters entropy ($p=0.046$) and homogeneity ($p=0.034$) in pre therapy scans showed statistically significant correlation with the change in pre and post therapy PSA levels. Entropy showed positive correlation with therapy outcome while homogeneity showed negative. Any of the conventional PET parameter did not show any statistical significance. **Conclusions:** Analysis of pre therapy heterogeneity parameters showed the potential for response prediction with the help of baseline scan only instead of waiting for change in clinical parameters determined before and after the therapy. This can help in risk stratification and advanced strategy making for personalized therapy. The predictive values of heterogeneity parameters were also seen to be superior to conventional PET parameters with high value of entropy showing better treatment response and high homogeneity showing decreased response. These results will be verified with time to progress and overall survival in further studies.

OP110

Protection of Normal Tissue in Molecular Radiotherapy with ^{177}Lu -labeled PSMA-Targeting Peptides using Preloading

P. Kletting¹, D. Hardiansyah², A. J. Beer¹, G. Glatting³; ¹Department of Nuclear Medicine, Ulm University, Ulm, GERMANY, ²Medical Radiation Physics/Radiation Protection, Universitätsmedizin Mannheim, Medical Faculty Mannheim, Heidelberg University, Mannheim, GERMANY, ³Medical Radiation Physics/Radiation Protection, Universitätsmedizin Mannheim, Medical Faculty Mannheim, Heidelberg University, Ulm, GERMANY.

Purpose: In molecular radiotherapy with ^{177}Lu -labeled prostate specific membrane antigen (PSMA) peptides, the kidneys, salivary and lacrimal glands are considered to be potentially dose limiting. The aim of this simulations study was to determine the effect of cold PSMA specific peptide applied prior to therapy on the time-integrated activity coefficients (TIACs) of critical organs and tumor and thus on the therapeutic index. **Methods:** A recently developed physiologically based pharmacokinetic (PBPK) model for PSMA-specific peptides was modified and implemented. Model parameter values were taken from the literature. Salivary and lacrimal glands, kidneys and tumor TIACs were determined for different dissociation constants K_D , peptide amounts and injection times used for preloading. The optimal TIACs tumor-to-kidneys, tumor-to-lacrimal and tumor-to-salivary glands ratio were identified for each scenario. **Results:** The simulations suggest that the application of high affinity ($K_D \leq 0.1$ nM) PSMA specific peptides 5-30 min before therapy has substantial effect on the therapeutic indices. The optimal preload depends on the affinity of the used ligand. For $K_D = 0.1$ nM the model predicts an optimal preload of 128 nmol improving the tumor-to-kidneys, tumor-to-lacrimal and tumor-to-salivary-glands TIAC ratios 1.6 fold. **Conclusion:** Based on model predictions, preloading using the optimized amount of a high affinity peptide seems to be an interesting option to improve the therapeutic indices in molecular radiotherapy with ^{177}Lu -labeled PSMA-specific peptides.

OP111

Automatic image segmentation for efficient 3D dosimetry with reduced influence of registration-errors and noise in Lu-177 DKFZ-PSMA-617 therapy using a robust cluster algorithm on sequential SPECT data and subsequent voxel-wise re-scaling

L. Vomacka, A. Delker, A. Gosewisch, W. Fendler, F. Gildehaus, A. Brunegrab, P. Bartenstein, G. Böning; University of Munich, Munich, GERMANY.

Objectives: In Lu-177 DKFZ-PSMA-617 therapy the estimation of 3D-dose distributions in tumours and radiation-sensitive organs such as the kidneys supports individualized therapies. However, common methods which provide 1D-organ- or lesion-doses based on a manual delineation of volumes-of-interest are time-consuming and observer dependent. Therefore we have studied a method for automatic and efficient determination of 3D-dose distributions with reduced influence of image-registration artefacts in sequential SPECT data. **Methods:** Ten patients with mCRPC received multiple therapy-cycles with the administration of either 3.6GBq or 6GBq Lu-177 DKFZ-PSMA-617 per cycle. In each cycle quantitative 3D-SPECT images were measured 24, 48 and 72h p.i., of which one was performed in SPECT/CT mode. Robust k-means based dynamic-cluster-segmentation (DCS) was established to automatically segment eight clusters containing voxels with similar dynamics and activity values in quantitative 4D-SPECT studies, followed by a labeller to segment each individual connected VOI. For comparison 78 tumour and 36 kidney-cortex VOIs were defined by manual-threshold-segmentation (MTS, $\text{th}=40\%$ of maximum). For each volume the accumulated activity was derived from a mono-exponential fit on the mean time-activity-curve and re-scaled voxel-wise based on the activity values measured 24h p.i. Finally the 3D-map filled with accumulated activities was convolved with an S-value kernel obtained from Monte Carlo simulation in soft tissue in combination with a CT-based mass-scaling. **Results:** DCS successfully found all considered tumours and 32 kidneys. DCS of the kidneys failed in two studies due to overlap with high-uptake lesions or marginal uptake in the kidneys. The mean tumour dose estimate was $1.9\pm 1.6\text{Gy/GBq}$ with DCS and $1.8\pm 1.7\text{Gy/GBq}$ with MTS. The estimated dose to the kidney cortex was $0.6\pm 0.2\text{Gy/GBq}$ for DCS and $0.7\pm 0.2\text{Gy/GBq}$ for MTS. We found a strong correlation of dose estimates from both methods for tumours and kidneys (Pearson, $p < 0.001$). However, dose estimates of both methods were significantly different in tumours and kidneys (paired T-Test, $p < 0.01$). This observation may be linked to slightly larger tumour volumes delineated by MTS compared to DCS and to fitting inaccuracies due to a lack of late measurement points. **Conclusion:** This preliminary study showed that automatic dynamic-cluster-segmentation is a promising approach for the efficient estimation of 3D-tissue dose in radionuclide therapy. Further enhancements such as an organ- or lesion-based co-registration, advanced fit-models, or the inclusion of anatomical information into a multi-dimensional and multi-modal automated dose estimation approach are conceivable.

OP112

PSMA Radioligand Therapy of Metastasized Prostate Cancer Using Lu-177 PSMA I&T and Lu-177 PSMA-617: First comparative Dosimetric Results

C. Schuchardt, H. R. Kulkarni, S. Wiessalla, M. Shahinfar, A. Singh, R. P. Baum; THERANOSTICS Center for Molecular Radiotherapy and Molecular Imaging, BAD BERKA, GERMANY.

Aim: The prostate-specific membrane antigen (PSMA) is significantly over expressed in prostate cancer cells compared to normal prostate tissue. The aim of our study was to determine and compare the kinetics and dosimetry in patients undergoing PSMA radioligand therapy (PRLT) of castrate resistant metastasized prostate cancer (mCRPC) using Lu-177 labeled PSMA I&T and PSMA-617. **Methods:** Fiftysix patients with progressive mCRPC (aged 71 ± 8 years) were included in the analysis.

High PSMA expression was verified before treatment by Ga-68 PSMA PET/CT. 37 patients received 3.4 - 7.6 GBq Lu-177 PSMA I&T and 19 patients were treated with 4.9 - 8 GBq Lu-177 PSMA-617. The time-dependent whole-body, organ and tumor activities were determined based on conjugated planar whole-body scintigraphies and SPECT/CT acquisitions. Dosimetric calculations (MIRD scheme) were performed using OLINDA/EXM software. To analyze the kinetics, we used the following parameters (median values): effective half-life (hours) and uptake (%IA, fraction of injected activity), which were calculated using the fit of the time-dependent activity curve to a mono- or bi-exponential function. **Results:** Relatively intense uptake in the metastases as well as significant uptake in the kidneys, the parotid and lacrimal glands was observed in all patients. A higher uptake of Lu-177 PSMA-617 was found for whole-body as well as parotid and lacrimal glands. The renal uptake was higher for PSMA I&T. Despite the longer half-life of PSMA-617 in kidneys and parotid glands, the renal dose was higher for PSMA I&T (PSMA I&T 0.95 Gy/GBq, PSMA-617 0.78 Gy/GBq); and the dose to parotid glands was comparable for both PSMA ligands (1.1 Gy/GBq). Concerning malignant lesions we distinguished between bone and lymph node metastases. All tumor lesions demonstrated a higher initial uptake for therapy using PSMA I&T followed by a faster wash out at later time points, which was confirmed by a longer half-life of PSMA-617. The longest half-life was determined for bone lesions when using PSMA-617 (PSMA-617 71h, PSMA I&T 44h) but the highest tumor dose was estimated for lymph node metastases in case of PSMA I&T (PSMA I&T 8Gy/GBq, PSMA-617 6 Gy/GBq). No clinically relevant renal or salivary gland toxicity was observed in any of the patients. **Conclusions:** These results demonstrate the different kinetics of both PSMA ligands in mCRPC patients. Additionally, the results revealed a large inter-patient variability of the dosimetric parameters, which leads to the conclusion that individual patient dosimetry is important for the concept of personalized radioligand therapy.

OP113

Differential Response of Bone versus Lymph Node Metastases After Lu-177 Labelled PSMA Radioligand Therapy in Patients with Metastatic Castration-Resistant Prostate Cancer

H. R. Kulkarni, A. Singh, R. P. Baum; THERANOSTICS Center for Molecular Radiotherapy and Molecular Imaging, Bad Berka, GERMANY.

Aim: The aim of this study was to assess the response of bone and lymph node lesions on Ga-68 PSMA PET/CT after prostate specific membrane antigen (PSMA) targeted radioligand therapy (PRLT). **MATERIALS AND METHODS:** One hundred and twenty patients with progressive metastatic castration-resistant prostate cancer (mCRPC) underwent PRLT using Lu-177 labeled PSMA inhibitor. A total of 61 skeletal and 73 lymph node metastases, also measurable on CT, were included in the analysis. Response after at least 2 cycles of PRLT was determined applying molecular (EORTC) and morphological (RECIST) imaging criteria, using Ga-68 PSMA PET/CT. **RESULTS:** Molecular response (reduction in the SUV of the target lesion on PET/CT by > 25%) after 2 or more PRLT cycles was observed in 32/61 (52.4%) bone lesions and 48/73 (65.7%) lymph node lesions, whereas progression (increase of SUV by > 25%) was noted in 5/61 (8.2%) bone and 10/73 (13.7%) lymph node lesions. On the other hand, CT detected decrease in size in only 4/61 (6.6%) skeletal metastases and 29/73 (39.7%) lymph node metastases. All lesions responding on CT revealed a significant decrease in SUV. There was a progression on CT in 10/73 (13.7%) lymph nodes, all of which showed concordant progression on PET/CT. Interestingly, there was an increase in size on CT of 2 osteoblastic lesions in a patient who had a molecular and biochemical complete remission (Ga-68 PSMA PET negative and PSA undetectable, respectively) after 2 PRLT cycles. **CONCLUSIONS:** Lymph node

metastases of mCRPC respond better to PRLT than bone metastases. This may be explained by a higher and more uniform absorbed radiation dose by lymph node metastases as compared to bone lesions, probably due to attenuation of radiation in bone lesions due to the normal surrounding bone tissue. In addition, the biological differences in radiation sensitivity must be considered. Ga-68 PSMA PET/CT is superior in response assessment of skeletal metastases compared to CT alone, in which the actual size of the osteoblastic metastases is difficult to measure and change in size difficult to appreciate. The paradoxical increase in size of the osteoblastic lesions in a patient with complete remission was most probably due to osteosclerosis after therapy (flare phenomenon). Even in lymph node metastases, Ga-68 PSMA PET/CT detects response at an earlier stage than CT (i.e. molecular response precedes morphological changes).

405 – Sunday, October 16, 2016, 14:30 - 16:00, Hall 115

M2M: PET/CT & Metabolism - Preclinical

OP114

Development and Evaluation of Radiocobalt-labelled Affibody Molecule for Next Day PET Imaging of HER3 Expression

M. Rosestedt¹, B. Mitran¹, K. G. Andersson², J. Löfblom², S. Ståhl², V. Tolmachev³, A. Orlova¹; ¹Dept. of Medicinal Chemistry, Div. of Molecular Imaging, Uppsala University, Uppsala, SWEDEN, ²Div. of Protein Technology, KTH, Royal Institute of Technology, Stockholm, SWEDEN, ³Dept. of Immunology, Genetics and Pathology, Rudbeck Laboratory, Uppsala University, Uppsala, SWEDEN.

Aim: The human epidermal growth factor receptor type 3 (HER3) recently received attention as a candidate for anti-cancer targeted therapy. HER3 is involved in the development of a variety of cancer types, as well as in the resistance towards tyrosine kinase-targeted therapies. Affibody molecules have in preclinical and clinical studies demonstrated that high contrast imaging is possible a few hours after injection, which is due to the fast blood clearance of the unbound tracer and rapid tumour penetration. Recent preclinical studies have shown that imaging contrast can be improved over time. ⁵⁵Co is a positron-emitting nuclide with a suitable half-life (17.5h) allowing for imaging at the day of injection as well as the next day. In this study, we evaluated targeting properties of radiocobalt-labelled anti-HER3 affibody in mice bearing HER3-expressing xenografts. **Materials and methods:** ⁵⁷Co was used as a surrogate for ⁵⁵Co. An anti-HER3 affibody molecule Z₀₈₆₉₈ with a picomolar affinity, having a HEHEHE-tag on the N-terminus and NOTA chelator on C-terminus was evaluated. The HEHEHE-Z₀₈₆₉₈-NOTA affibody molecule was labelled with ⁵⁷Co using ammonium acetate buffer, pH 5.5. Binding specificity and cellular processing were evaluated in vitro. To evaluate the targeting of HER3-expressing tumours in vivo, BALB/C nu/nu mice bearing LS174T colorectal cancer xenografts were used. Mice were injected with 2 µg of ⁵⁷Co-HEHEHE-Z₀₈₆₉₈-NOTA and the biodistribution was studied at 3 and 24h post injection (pi). **Results:** HEHEHE-Z₀₈₆₉₈-NOTA was labelled with ⁵⁷Co with high stability and >99% purity. The binding of ⁵⁷Co-HEHEHE-Z₀₈₆₉₈-NOTA to HER3-expressing cell lines (LS174T, BT474) was specific. Pattern of cellular uptake for LS174T and BT474 cell lines was similar; the internalized fraction did not change over time (3.7% for LS174T; 6.8% for BT474, from cell associated radioactivity). Injected dose of 2 µg resulted in a tumour uptake of 2.6±0.2%ID/g at 3h and 1.9±0.1%ID/g at 24h pi, which significantly (p<0.05) exceeded the liver uptake, 1.1±0.7%ID/g. Injection of 70 µg of protein demonstrated a saturation of HER3 in xenografts, indicating on a specific tumour uptake. At 3h pi, the tumour-to-blood, tumour-to-liver, tumour-to-muscle and tumour-to-bone ratios were 5.0±0.5, 0.9±0.06, 18.4±3 and 11.6±0.7, respectively. Because of good tumour retention and significant decrease of radioactivity concentration in blood over time, the tumour-to-blood ratio reached the level of 8.2±0.3

and tumour-to-liver was 1.3 ± 0.05 at 24h pi. LS174T xenografts were visualized using microSPECT. **Conclusion:** Radiocobalt-labelled anti-HER3 antibody molecule Z₀₈₆₉₈ is a promising tracer for imaging of HER3 expression in tumours.

OP115

First Real-Time Kinetic *in vitro* Method for Rapid Prediction of P-glycoprotein Interactions of Newly Developed Radioligands

C. VRAKA^{1,2}, T. Rac³, C. Philippe¹, C. Rami-Mark³, K. Wagner², M. Hacker¹, W. Wadsak¹, M. Mitterhauser^{1,4}; ¹Division of Nuclear Medicine, Medical University of Vienna (MUW), Vienna, AUSTRIA, ²Department for Nutritional Science, University of Vienna, Vienna, AUSTRIA, ³Medical University of Vienna (MUW), Vienna, AUSTRIA, ⁴LBI for Applied Diagnostics, Vienna, AUSTRIA.

Aim: The demand of radioligands for cerebral application and tumor diagnostic and therapy (theranostic) is expanding rapidly. One main cause of candidate exclusion and failed tumor theranostics is the efflux mechanism via permeability-glycoprotein (P-gp/MDR1/ABCB1). P-gp is expressed at blood brain barrier, in different peripheral tissue and it is highly expressed on diverse tumors. In detail, pharmaceuticals contact to P-gp can cause drug resistance, poor brain uptake or clinical relevant drug-drug interaction. Aim is to develop an *in vitro* screening method to distinguish between P-gp substrates, inhibitors or radioligands without P-gp interaction in early stage of drug development. **Materials and Methods:** Madin-Darby Canine Kidney cell line, overexpressing human MDR1, (MDCKII-hMDR1) and the MDCKII-wild type (MDCKII-WT) purchased from NKI Amsterdam (Netherlands) were cultivated in DMEM GlutMAXTM (10% FCS & 0.5% Pen/Strep) in the oblique plane of a petri dish. Experiments were carried out with serum free medium to avoid unspecific binding of the tracer to FCS. For P-gp mediated binding or transport *in vivo* kinetics with various PET tracers ((R)-[¹¹C]Verapamil, [¹⁸F]FE@SNAP, [¹⁸F]FEMeNER-D2 etc.) were performed using LigandTracer@Yellow technology (Ridgeview Instruments AB develop). The half life of each tracer was corrected automatically by LigandTracer@ software and the uptake behavior (kinetic) was used for qualitatively interpretation and the slope (k) was calculated for quantitative assessment. **Results:** [¹¹C]Verapamil shows a steep kinetic ($k=0.27 \pm 0.01$, $n=3$) in the MDCKII-hMDR1 cells, which is replaceable with non labelled verapamil. Whereas on MDCKII wildtype cells uptake is moderate ($k=0.12 \pm 0.01$) and not replaceable. The uptake behavior of [¹⁸F]FEMeNER-D2 ($k=0.35 \pm 0.03$, $n=3$) does not differ in the two cell lines. Additionally, no changes in the kinetics and slopes were observed by replacement with known P-gp inhibitors. No uptake of [¹⁸F]FE@SNAP was observed in hMDCKII-MDR1. In contrast, on MDCKII-WT cells and when the P-gp transporter was blocked in hMDCKII-MDR1 cells an uptake of [¹⁸F]FE@SNAP was observed ($k=0.06 \pm 0.03$, $n=5$). **Conclusion:** A simple and rapid *in vitro* real time kinetic model was developed for prediction of P-gp interaction of radiopharmaceuticals. [¹¹C]Verapamil could be verified as P-gp inhibitor. The missing kinetic of [¹⁸F]FE@SNAP on MDCKII-hMDR1 cells in contrast to the uptake in wild type cells proof that [¹⁸F]FE@SNAP is a substrate of P-gp and discharged via the transporter. These data correlate with *in vivo* PET quantifications. As a result, newly developed tracer can be distinguished easily into three groups: I. P-gp inhibitors [¹¹C]Verapamil II. P-gp substrates ([¹⁸F]FE@SNAP) III. No P-gp interaction ([¹⁸F]FEMeNER-D2)

OP116

Monitoring the effects of combined treatment with EGFR and MET inhibitors in non-small cell lung cancer and synergy quantification by 18F-FLT PET/CT

F. Iommelli¹, V. De Rosa¹, M. Monti², M. Panico¹, S. Del Vecchio²; ¹Institute of Biostructures and Bioimages, National Research Council, Naples, ITALY, ²Department of Advanced Biomedical Sciences, University “Federico II”, Naples, ITALY.

Aim: In non-small cell lung cancer (NSCLC) patients refractory to treatment with EGFR tyrosine kinase inhibitors (TKIs), mutational and genetic profile of resistant tumors showed that MET amplification may coexist with EGFR bearing T790M mutation or wild type EGFR. Therefore combination therapies simultaneously targeting both receptors may be required to overcome resistance. However, no imaging technique is currently available to detect *in vivo* drug synergy using a noninvasive approach. Here we tested whether ¹⁸F-FLT PET/CT can detect drug synergy between MET and EGFR inhibitors in refractory NSCLC by comparing imaging findings with the rate of proliferation in excised tumors. **Materials and Methods:** NSCLC cells bearing MET amplification and wild type EGFR (H1993) or EGFR T790M (H820) were selected and tested for the effects of EGFR and MET inhibitors, used alone or in combination, on cell viability and levels of pAKT/AKT, pERK/ERK and cyclin D1. Then, H1993 tumor-bearing mice underwent ¹⁸F-FLT PET/CT scan before and after treatment with escalating doses of EGFR and MET inhibitors, alone or in combination, and post-treatment changes of ¹⁸F-FLT uptake in tumors were determined. At the end of imaging studies, tumors were removed and tested for cyclin D1 levels by morphodensitometric analysis of western blot signal as well as for Ki67 immunostaining. Synergistic effect was evaluated for *in vivo* and *in vitro* data set by determining the combination index (CI) using the CompuSyn software. **Results:** In the selected cell lines, the highest dose-dependent reduction of cyclin D1 and other signaling mediators levels was obtained by combined treatment with EGFR and MET inhibitors as compared with single agent alone. Imaging studies showed a significant reduction of ¹⁸F-FLT uptake in response to combined treatment with escalating doses of EGFR and MET inhibitors ranging between -38.9% and -69.2%. Treatment with EGFR inhibitor alone did not cause any significant change of ¹⁸F-FLT uptake whereas a reduction of tracer uptake ranging between -24.5% and -42.5% was obtained in response to MET inhibitor alone. Analysis of imaging data set showed a combination index <1 indicating drug synergism. Furthermore a significant positive correlation was found between reduction of ¹⁸F-FLT uptake and percentage decrease in cyclin D1 levels ($r=0.94$, $p=0.016$) and Ki67 positive stained cells ($r=0.92$, $p=0.022$). **Conclusion:** Our findings indicate that ¹⁸F-FLT PET/CT may be used as a surrogate biomarker for synergy quantification in NSCLC patients receiving combined treatment with EGFR and MET inhibitors thus contributing to personalized therapy.

OP117

Experimental study on Multiple Tracers PET/CT in the differentiation of C6 glioma and different inflammation

L. CAI, S. GAO, Y. WANG, Y. LI, H. YANG; PET/CT Center, General Hospital of Tianjin Medical University, Tianjin, CHINA.

Aim To study the value of ¹⁸F-FDG, ¹¹C-MET and ¹¹C-CHO PET/CT in the differentiation of C6 glioma and different inflammation in experimental rat models. **Materials and Methods** (1)48 male SD rats were randomly divided into 8 groups: group 1 and 2 consisted of 8 rats bearing both C6 glioma and turpentine oil-induce acute inflammation; group 3 and 4 consisted of 8 rats bearing both C6 glioma and turpentine oil-induce chronic inflammation; group 5 and 6 consisted of 8 rats bearing both C6 glioma and BCG-induced granuloma. (2) ¹⁸F-FDG and ¹¹C-MET PET/CT were performed on group 1, 3 and 5; ¹⁸F-FDG and ¹¹C-CHO PET/CT were performed on group 2, 4 and 6. The lesion-to-muscle(L/M) ratios and a tumor selectivity index, $SI=(\text{tumor } SUV_{\max} - \text{muscle } SUV_{\max})/(\text{different inflammation } SUV_{\max} - \text{muscle } SUV_{\max})$, were calculated. (3)After that, the lesions were excised. Immunohistochemical stain were used to demonstrate the situation of glucose transporter-1(GLUT-1),hypoxia inducible factor-1 α (HIF-1 α), and CD98. (4)A unpaired *t* test and nonparametric Kruskal-Wallis *H* test were used to make statistical analyses. **Results** (1) ¹⁸F-FDG and ¹¹C-MET uptake in C6 glioma were higher than that in different inflammatory tissues, and the differences of

two tracers uptake between C6 glioma and acute inflammation, and chronic inflammation, and C6 glioma and granuloma were significant (all $P < 0.05$). The ^{11}C -CHO uptake between different lesions were no significant (all $P > 0.05$). In group 1 models, mean SI_{MET} 4.22 ± 2.96 was significantly higher than SI_{FDG} 1.77 ± 0.86 ($P = 0.030$); in group 5 models, mean SI_{MET} 4.89 ± 2.08 was significantly higher than SI_{FDG} 1.72 ± 0.769 ($P = 0.042$), but in group 3 models, mean SI_{MET} 3.84 ± 2.71 was higher than SI_{FDG} 2.28 ± 1.14 ($P = 0.076$). (2) Immunohistochemical study showed that there were significant differences of the expression of HIF-1 α , CD98 between different lesions (all $P < 0.05$), and no significances of expression of GLUT-1 between different lesions ($P = 0.061$). Nemenyi test showed that there was significant difference between C6 glioma and acute inflammation, C6 glioma and granuloma in CD98 (all $P < 0.05$), and between C6 glioma and chronic inflammation in HIF-1 α , CD98 (all $P < 0.05$). **Conclusions** ^{11}C -MET is more tumor selective than ^{18}F -FDG and ^{11}C -CHO, therefore, ^{11}C -MET PET/CT is able to differentiate glioma from different inflammation. ^{11}C -CHO PET/CT is not able to differentiate tumor from different inflammation.

OP118

^{68}Ga]Pentixafor for CXCR4 Imaging in a PC-3 Prostate Cancer Xenograft Model - comparison with ^{18}F]FDG PET/CT, MRI and ex-vivo receptor expression

S. M. Schwarzenböck¹, J. Stenzel¹, T. Otto¹, J. Kurth¹, S. Polei¹, T. Lindner¹, A. Hohn¹, H. Wester², B. Vollmar¹, B. J. Krause¹; ¹Rostock University Medical Center, Rostock, GERMANY, ²Pharmaceutical Radiochemistry, Technische Universität München, Garching, GERMANY.

Introduction: Chemokine receptors, i.e. the subtype CXCR4, play a significant role in tumor progression, metastasis, recurrence and angiogenesis. CXCR4 has been demonstrated to be highly overexpressed in prostate cancer. Thus, ^{68}Ga]Pentixafor, targeting CXCR4, might serve as a promising tracer for imaging of aggressive and metastasizing prostate cancer. **Aim:** The aim of this study was to characterize the properties of ^{68}Ga]Pentixafor as tracer for prostate cancer imaging in an aggressive PC-3 prostate cancer xenograft mouse model by small animal PET/CT and to investigate its correlation with ^{18}F]FDG uptake, functional/morphological MRI and CXCR4 immunohistochemistry (IHC). **Methods:** A dual tracer small animal PET/CT study was conducted comparing ^{68}Ga]Pentixafor and ^{18}F]FDG. The androgen-independent human prostate cancer cell line PC-3 was implanted subcutaneously in both flanks of NMRI (nu/nu) mice ($n = 19$). Mice - 4 weeks post xenograft implantation - were injected with 15 MBq ^{68}Ga]Pentixafor and ^{18}F]FDG, respectively, on two separate days. Static PET imaging was performed 60 min p.i. with an Inveon animal PET/CT scanner (Siemens Preclinical Solutions, Knoxville), respectively. VOIs using a threshold of 60% were placed in transaxial slices in tumor, muscle, liver, kidney and blood pool. Diffusion weighted MRI (ADC-Trace, 4 b-values), morphological MRI and ^1H MR spectroscopy was performed (7T small animal MRI, Bruker BioSpec 70/30). Uptake of ^{68}Ga]Pentixafor and ^{18}F]FDG was compared to MRI (DWI derived ADC values, T2 weighted MRI derived tumor volume and spectroscopy data). Imaging data were correlated with ex-vivo tumor expression of CXCR4 (assessed via IHC and mRNA). Statistics were performed using SPSS. Ex-vivo biodistribution of ^{68}Ga]Pentixafor in tumor, muscle, liver, kidney and blood was assessed. **Results:** Tumor uptake of ^{68}Ga]Pentixafor was significantly lower compared to ^{18}F]FDG (mean % ID/g 1.8 / standard deviation (SD) 0.6 and 5.8 / SD 1.2 , respectively). No significant correlation was found between the uptake of the two tracers. There was no significant correlation of ^{68}Ga]Pentixafor or ^{18}F]FDG uptake and mean ADC values (mean 1.0 / SD 0.05), respectively. Expression of chemokine receptors on tumor cells was demonstrated qualitatively by IHC as well as quantitatively via mRNA analysis. **Conclusion:** In a PC-3 prostate cancer xenograft model tumor visualization was feasible using ^{68}Ga]Pentixafor

PET/CT; ^{68}Ga]Pentixafor tumor uptake was lower compared to ^{18}F]FDG uptake. No significant correlation was found between tracer uptake and mean ADC values. Expression of chemokine receptors in a model of aggressive and undifferentiated prostate cancer was shown qualitatively and quantitatively as a correlate of ^{68}Ga]Pentixafor uptake.

OP119

Zirconium-89-girentuximab PET/CT imaging in renal cell carcinoma: first in man results

M. Hekman, M. Rijpkema, P. Mulders, E. Oosterwijk, O. Boerman, W. Oyen; Radboudumc, Nijmegen, NETHERLANDS.

Background: More advanced imaging methods are needed to reliably distinguish benign small renal masses (SRM) from renal cell carcinoma (RCC) to prevent invasive biopsies or unnecessary surgeries. Similarly, imaging methods need to be improved for unambiguous detection of lesions suspect for metastatic and relapse RCC during follow-up. Girentuximab is an antibody against Carbonic Anhydrase IX (CAIX), an antigen that is expressed on the cell surface of 95% of clear cell RCC (ccRCC). Zirconium-89-girentuximab PET/CT may be a valuable imaging technique in the diagnosis of patients with RCC. The aim of the present study is to show the impact of the Zirconium-89-girentuximab PET/CT in the clinical management of ccRCC patients. Here we present our first results with Zirconium-89-girentuximab PET/CT for diagnosing patients presenting with either a small renal mass or with a history of ccRCC. **Methods:** Thirty patients suspect of or with a history of ccRCC in whom conventional imaging methods are inconclusive will be included. In these patients a PET/CT will be acquired 4-5 days after injection of 5 mg Zirconium-89-girentuximab (37 MBq). **Results:** So far, 5 patients have been included in this clinical study. One patient presented with a Bosniak 3 lesion in a solitary kidney. Another patient presented with a SRM (31 mm) and a synchronous lung carcinoma. In both patients the SRM showed clear uptake of Zirconium-89-girentuximab and a partial nephrectomy was performed. Histology confirmed ccRCC in the first patient, surgery of the second patient is scheduled. A third patient presented with multiple bilateral growing renal masses. None of the masses showed uptake of Zirconium-89-girentuximab on the PET/CT and repeated biopsies showed the presence of oncocytomas. Two patients with a history of ccRCC and a suspicion of metastases were included. A growing lymph node in the first patient showed no uptake of Zirconium-89-girentuximab on PET/CT. Histology showed that the lymph node contained a CAIX-expressing metastasis of a papillary growing ccRCC. In the second patient clear uptake of Zirconium-89-girentuximab in a large liver lesion and in multiple pulmonary lesions was seen, and therefore a biopsy could be avoided and systemic therapy with pazopanib was initiated. **Conclusion:** These preliminary results suggest that Zirconium-89-girentuximab PET/CT can be a valuable aid in the diagnosis of patients suspected of ccRCC.

OP120

Differential regulation of glucose metabolism by ERK1/2 and AKT pathways in EGFR-driven NSCLC

V. De Rosa¹, F. Iommelli¹, M. Monti², S. Del Vecchio²; ¹Institute of Biostructures and Bioimaging, National Research Council, Naples, ITALY, ²Department of Advanced Biomedical Sciences, University of Naples "Federico II", Naples, ITALY.

Aim: In a previous study we showed that inhibition of EGFR signaling causes a metabolic switch from aerobic glycolysis to oxidative phosphorylation by reducing hexokinase II (HKII) and phosphorylated form of pyruvate kinase M2 (p-PKM2 Tyr105) and upregulation of mitochondrial complexes (OXPHOS) in NSCLC cells and in vivo in animal models. To test the existence of a cause-effect relationship between the reduced levels of relevant glycolytic enzymes and OXPHOS upregulation, silencing of HKII and

PKM2 mRNAs was performed using targeted or scrambled siRNAs followed by inhibition of EGFR cascade. Furthermore, we tested whether the selective inhibition of AKT and ERK1/2 pathways could differentially modulate glycolysis and oxidative phosphorylation. **Materials and Methods:** Erlotinib-resistant H1975 and H1993 NSCLC cells were transfected with 100 nM specific and scrambled siRNAs using Dharmafect reagent and after 24 h they were treated with 1 μ M erlotinib, WZ4002, PHA-665,752 or vehicle for additional 48 h. AKT and ERK1/2 pathways were differentially inhibited by treatment with wortmannin (1 μ M, 10 μ M, 20 μ M) or U0126 (1 μ M, 10 μ M, 20 μ M), respectively. Levels of HKI, HKII, PKM1, PKM2 and LDH-A as well as phosphorylation status of PKM2 in the glycolytic cascade along with OXPHOS and PGC-1 α were tested in response to each treatment. **Results:** The downregulation of HKII and PKM2 do not cause an increase of OXPHOS levels but enhances the effect of EGFR signaling inhibition on the upregulation of OXPHOS. Furthermore, when cells were exposed to increasing concentration of AKT inhibitor, a dose-dependent increase of OXPHOS levels was obtained whereas no changes of HKII and p-PKM2 Tyr105 levels were observed. Conversely, treatment with ERK1/2 inhibitor caused a dose-dependent decrease of HKII and p-PKM2 Tyr105 levels whereas no changes of OXPHOS levels were observed in treated cells. **Conclusion:** Our findings indicate that aerobic glycolysis and oxidative phosphorylation are differentially regulated by ERK1/2 and AKT pathways, respectively, providing a mechanistic clue for rational combinations of anti-cancer agents targeting EGFR pathways and glucose metabolism.

OP121

MicroRNA-342-3p Suppresses Warburg Effect and Tumor Proliferation by Targeting Insulin-like Growth Factor 1 Receptor in Hepatocellular Carcinoma

L. Kang¹, Y. Huo¹, R. Wang¹, X. Xu²; ¹Peking University First Hospital, Beijing, CHINA, ²Academy of Military Medical Sciences, Beijing, CHINA.

Objective: ¹⁸F-FDG PET has been widely used in the detection of malignant tumors based on Warburg effect. Better understanding the regulated factors in Warburg effect can improve the utility of ¹⁸F-FDG. miR-342-3p has been proved to play an inhibitory role in some malignant tumors. However, the function of miR-342-3p in Warburg effect remains poor understood. The objective is to investigate the role of miR-342-3p in the regulation of glucose metabolism and potential mechanism in hepatocellular carcinoma (HCC). **Methods:** The HepG2 cells stably overexpressing miRNA and empty vector were constructed by lentiviral vector transfection. Quantitative real-time PCR (qRT-PCR) was used to evaluate the expression level of miRNA-342-3p in HCC cell lines. Then, the role of miR-342-3p was determined on cell proliferation, migration, invasion, and FDG uptake in HCC cell lines. FDG PET imaging and biodistribution study was performed to evaluate the role of miR-342-3p *in vivo*. Finally, a luciferase reporter assay was performed to confirm the target gene of miR-342-3p and the relative proteins are evaluated by Western blotting. **Results:** miR-342-3p is down-regulated in HCC cell lines, and its overexpression induced significant inhibition of HCC cell proliferation and invasion in HCC cell lines, as well as tumor growth and metastasis in xenograft and metastasis mice. In addition, micro PET showed that miR-342-3p repressed FDG uptake in xenograft and metastasis mice. Furthermore, we identified 3'-UTR of insulin-like growth factor 1 receptor (IGF1R) as a target of miR-342-3p and miR-139-5p suppressed FDG uptake via IGF1R/PI3K/AKT/GLUT1 pathway. **Conclusion:** miR-342-3p exhibits a negative role in the regulation of glucose metabolism and FDG uptake via inhibition of IGF1R/PI3K/AKT/GLUT1 pathway.

406 – Sunday, October 16, 2016, 14:30 - 16:30, Hall 111

Teaching Session: TBA

OP122

TBA

407 – Sunday, October 16, 2016, 14:30 - 16:00, Hall 116

Clinical Oncology: Image Guided Surgery

OP123

Sentinel lymph node biopsy using ^{99m}Tc-tilmanocept (Lymphoseek®) in patients with oral cavity squamous cell carcinoma: Safety results from Phase III clinical trial

S. Y. Lai¹, F. Civantos², A. Agrawal³; ¹Department of Head and Neck Surgery, The University of Texas MD Anderson Cancer Center, Houston, TX, UNITED STATES, ²Department of Otolaryngology, University of Miami Hospital and Clinics/Sylvester Comprehensive Cancer Center, Miami, FL, UNITED STATES, ³Department of Otolaryngology—Head and Neck Surgery, Arthur G. James Cancer Hospital and Richard J. Solove Research Institute, The Ohio State University Wexner Medical Center, Columbus, OH, UNITED STATES.

AIM: In clinically N0 early-stage (T1-2) oral cavity squamous cell carcinoma (OSCC), surgeons presently favour resection of regional lymphatics although up to ~80% of early stage patients are pN0 and may be over-treated, with significant potential morbidity. Sentinel lymph node biopsy (SLNB) has been shown to be a safe and effective alternative to complete elective neck dissection (END) for early-stage OSCC. A recently published multi-centre trial of ^{99m}Tc-tilmanocept (Lymphoseek®), the first and only receptor-targeted (CD206) molecular SLNB agent, was evaluated in head and neck cancer (HNC) patients undergoing SLNB. The study's primary objective was to determine the false negative rate (FNR) of ^{99m}Tc-tilmanocept localized SLNs versus END [published Agrawal *et al*, *Ann Surg Oncol*, 2015; 22(11):3708-3715]. Here we report safety findings from the study. **MATERIAL AND METHODS:** A Phase III, multicenter, open-label, within-patient trial of ^{99m}Tc-tilmanocept was conducted for detection of SLNs in OSCC and cutaneous SCC patients (T1-4aN0M0). Patients received a single dose (50mcg) of ^{99m}Tc-tilmanocept, radiolabeled with 18MBq (for same-day surgery) or 74MBq (for next-day surgery). Patients underwent preoperative lymphoscintigraphy and SLNB with a handheld gamma detector followed by requisite END. Adverse events, vital signs, electrocardiograms, physical exams, and clinical laboratory parameters were collected. **RESULTS:** 85 patients (79 OSCC, 6 cutaneous SCC) received ^{99m}Tc-tilmanocept and were included in the safety analysis. No deaths occurred in the study, and no serious adverse events (SAEs) were related to the agent. Of the 13 non-drug related SAEs, 11 were considered by the investigators to be related to surgical procedures. Overall, 36 patients (31 OSCC, 5 cutaneous) reported at least 1 AE; most AEs were mild (62%) and unrelated to ^{99m}Tc-tilmanocept (85%), and no event led to discontinuation from the study. There were no reports of injection site pain, and only 1 report of mild injection site irritation. No clinically meaningful changes were noted for laboratory parameters, vital signs, physical examinations, and ECG values. Patient level FNR for SLNB with ^{99m}Tc-tilmanocept was 0.0256 (95% CI=0.0006,0.1349). The mean number of SLNs per evaluable patient was 3.9 (median 4), whereas the mean number of END nodes was 34 (maximum 82). **CONCLUSIONS:** Use of Lymphoseek was well tolerated by the studied population. The strong safety profile in HNC patients and low FNR observed in this trial suggest that ^{99m}Tc-tilmanocept may allow for safe and effective use for SLNB as an alternative to END, with the potential for substantially reduced morbidity.

OP124**Bilateral and contralateral sentinel node identification with ^{99m}Tc-tilmanocept (Lymphoseek®) in oral cavity squamous cell carcinoma patients**

S. Y. Lai¹, F. Civantos², A. Agrawal³; ¹The University of Texas MD Anderson Cancer Center, Houston, TX, UNITED STATES, ²University of Miami Hospital and Clinics/Sylvester Comprehensive Cancer Center, Miami, FL, UNITED STATES, ³Arthur G. James Cancer Hospital and Richard J. Solove Research Institute, The Ohio State University Wexner Medical Center, Columbus, OH, UNITED STATES.

AIM: In clinically N0 early-stage (T1-2) oral cavity squamous cell carcinoma (OSCC), surgeons presently favour resection of regional lymphatics although ~70-80% of early-stage patients are pN0 and may be over-treated, with significant potential morbidity. Sentinel lymph node biopsy (SLNB) has been shown to be a safe and effective alternative to elective neck dissection (END) for early-stage OSCC. ^{99m}Tc-tilmanocept (Lymphoseek®), the first and only receptor-targeted (CD206) molecular SLNB agent, was evaluated in a trial of head and neck cancer patients undergoing SLNB [Agrawal *et al*, *Ann Surg Oncol*, 2015; 22(11):3708-3715]. The primary objective was to determine the false negative rate (FNR) of ^{99m}Tc-tilmanocept-localized SLNs versus END [2.6%]. Here we report bilateral and contralateral SLN identification from the study. **MATERIAL AND METHODS:** A Phase III, multicenter, open-label, within-patient trial of ^{99m}Tc-tilmanocept was conducted for detection of SLNs in OSCC and cutaneous SCC patients (T1-4aN0M0). Patients received a single dose (50mcg) of ^{99m}Tc-tilmanocept, radiolabeled with 18MBq (for same-day surgery) or 74MBq (for next-day surgery). Patients underwent preoperative lymphoscintigraphy and SLNB with a handheld gamma detector followed by requisite END. **RESULTS:** 85 patients (79 OSCC, 6 cutaneous SCC) received ^{99m}Tc-tilmanocept; 2 did not undergo protocol-defined surgery and are censored from efficacy analyses. Of 83 evaluable patients, 8 had midline tumors (within 1cm; 6 floor-of-mouth [FOM], 1 oral tongue, and 1 mucosal lip); 5 had bilateral SLNs identified in the neck, of which 4 patients had pathology-positive SLNs (1 bilateral positive SLNs, 3 unilateral positive SLNs). The other 3 patients with midline tumors had SLNs identified on one side of the neck, and 2 of the 3 had positive pathology in the SLNs. 24% of patients with single-sided tumors (18 of 75) had contralateral SLNs. Of these, 11 had pathology-positive SLNs: 5 (4 tongue, 1 lower alveolar ridge) had pathology only in the ipsilateral SLN(s); 4 (3 FOM, 1 tongue) had pathology in both ipsilateral and contralateral SLNs; and 2 (both FOM) had pathology only in the contralateral SLN(s). **CONCLUSIONS:** ^{99m}Tc-tilmanocept for SLNB is highly predictive in staging the cN0 neck. In this study, ^{99m}Tc-tilmanocept identified bilateral and contralateral draining nodes that may have not been removed using standard-of-practice END, in some cases identifying the only pathology-positive lymph nodes. In fact, without SLNB, ≥7.2% of the patients treated with standard END would have left behind a positive node. These and other data suggest SLNB with ^{99m}Tc-tilmanocept may be an alternative to END in OSCC.

OP125**Real time robotic arm assisted FDG PET/CT-guided percutaneous metabolic biopsy: Initial Experience**

R. Kumar, B. R. Mittal, R. K. Radhakrishnan, A. Bhattacharya, A. Sood, A. Sood; PGIMER, Chandigarh, INDIA.

Objective: The aim of this prospective study was to evaluate the feasibility and diagnostic utility of automated robotic arm (ARA) assisted ¹⁸F-FDG PET/CT guided real-time metabolic biopsy from various organs during the diagnostic PET scan or with inconclusive prior biopsy results. **Materials and Methods:** In this prospective study we evaluated 31 patients (12 females and 19 males) with median age 54.64 years (20-69 years) who were either directly subjected to a diagnostic ¹⁸F-FDG PET/CT scan and per-cutaneous biopsy or had inconclusive prior biopsy

results. All the patients underwent whole body FDG PET/CT and site of the biopsy was planned from the most accessible FDG avid lesions. Biopsy was performed after 2 hrs of initial diagnostic study by obtaining one table position PET/CT. The biopsy needle was placed into the lesion with the help of automated robotic arm (ARA) needle navigation technique. The real time tissue sampling was done from the highest metabolically active tissue by confirming the position of the needle tip with a check CT scan. For reviewing the accuracy of the procedures and confirmation of negative results histopathological examination, clinical or imaging follow up results were reviewed. **Results:** Out of the total 31 patients, PET guided biopsy was done from lung (n=17), bone (n= 6), liver (n=2) lymph nodes (n=3), chest wall (n=1), breast (n=1) and abdominal mass (n = 1). Adequate representative tissue sample were retrieved in all the patients and diagnostic results were yielded in all the biopsy procedures; 23 were positive for malignancy (lung -13, liver-1, lymph node-1, breast-1, chest wall -1, bone-5 and abdominal mass-1) and eight had no evidence of malignancy (organising pneumonia-3, tuberculosis-1, reactive lymphoid hyperplasia-2, granulomatous hepatitis-1 and no excess plasma cells-1). All the 15 patients with negative prior CT guided FNAC/biopsy from the lung lesions were found to be positive for malignancy on PET guided biopsy. We noticed complications in four patients only (two had mild pneumothorax while two had hemoptysis) with no life threatening event. The diagnostic yield of real time PET guided metabolic biopsy procedure was 100%. **Conclusion:** We conclude that ARA directed FDG PET/CT guided real time metabolic percutaneous biopsies are technically feasible and are of great help in patients with prior negative lung biopsies. Additionally ARA guided biopsy is a promising tool in targeting the metabolically active site with high accuracy in bone biopsies and help in avoiding unsuccessful and painful blind biopsy procedures.

OP126**Lymphoscintigraphic detection of the sentinel lymph node in breast cancer patients: peritumoral injection versus single subareolar injection**

P. B. Gouveia, R. Teixeira, R. Brito, R. Castro, I. Amorim; Centro Hospitalar do Porto, Porto, PORTUGAL.

Aim: Preoperative lymphoscintigraphy is without doubt a valid method for the detection of the sentinel lymph node (SLN). However, uncertainty remains regarding the best method of radiotracer injection. The purpose of our study was to evaluate the lymphoscintigraphic identification rate of peritumoral (PT) injection versus a single subdermal subareolar (SA) injection in the detection of SLNs in breast cancer. **Material and Methods:** A retrospective study was conducted on a cohort of 433 patients with biopsy proven breast cancer that underwent 442 SLN biopsy procedures between January 2008 and February 2016. Nine patients had bilateral breast cancer. Patients with ductal carcinoma in situ diagnosed at needle core biopsy and patients with multifocal breast cancers were included in the study. Patients with cytological positive lymph nodes, with previous ipsilateral axillary surgery, and patients who received neoadjuvant chemotherapy before surgery were excluded from the study. A total of 96 procedures (Group A) were performed using a PT deep injection of radiotracer while 337 procedures (Group B) adopted a single SA injection of radiotracer. Chi-square test was performed to compare the rate between the different groups. P<0.05 was considered to be statistically significant. **Results:** SLNs were identified in the lymphoscintigram in 93/96 cases (96.86%) of Group A (PT injection) and in 322/ 337 cases (95.55%) of Group B (PA injection). Furthermore, in 2/96 patients (2.08%) of Group A, internal mammary lymph nodes were found at lymphoscintigraphy, whereas 4/337 (1.19%) were found in the Group B patients. The intraoperative identification rate of axillary SLNs was 98.95% (95 of 96) in the Group A patients and 99.65% (334 of 337) in the Group B patients. There was no significant difference in the two groups between the incidence of the number of SLNs detected and the incidence of identification of positive SLNs. **Conclusion:** PT versus single SA injection of radiotracer showed comparable success rates for SLN identification. We

believe that a single SA injection is to be considered the method of choice in the identification of SNLs, since it is less painful for the patient and it is easier to perform. Furthermore, as SA injection requires a single subareolar injection site, the tumor does not have to be located by other techniques, and the “shine-through phenomenon” is avoided, when the tumor is located near the axilla.

OP127

Role of Pleural Pathway in Determining Drug Shunt During Hyperthermic Isolated Lung Perfusion: a Radioisotope Leakage Study

F. Fiz¹, G. Villa¹, E. Ferrari², M. Manitto², E. Pomposelli¹, S. Morbelli¹, M. Sicignano¹, A. Alloisio², D. Pende³, R. Meazza³, C. Gereloni⁴, G. Ratto², C. Marini², G. Sambuceti¹; ¹Nuclear Medicine Unit, Department of Health Sciences, University of Genoa, Genoa, ITALY, ²Department of Thoracic Surgery, IRCCS San Martino-IST, Genoa, ITALY, ³Immunology Laboratory, IRCCS SAn Martino-IST, Genoa, ITALY, ⁴TFPCC Foundation, IRCCS Policlinico San Matteo, Pavia, ITALY, ⁵National Council of Research, IBFM, Genoa, ITALY.

Rationale: Hyperthermic isolated lung perfusion (HILP) is a growing surgical treatment modality, used to deliver supra-maximal chemo- or immunotherapeutic drug dosage to the lung, while sparing the remaining organism from toxicity. Avoiding shunts from the isolated to the systemic circulation is key. Radioisotopic leakage monitoring has been validated for a long time in the setting of isolated limb perfusion; in the lung, double circulation and pleural re-uptake could complicate the task. In this project, we used a radioisotope technique to test the contribution of pleural shunt in determining drug leakage. **Patients and Methods:** Eleven patients, with multiple lung metastases, were submitted to a total of 15 HILP, using TNF- α as active agent. Leakage from isolated circuit was monitored by serial blood sampling (from both the isolated and systemic circulation) and by a radio-isotopic method. Briefly, patients' erythrocytes were in-vivo labeled with ^{99m}Tc and stannous agent, using a ten-fold dose for the isolated circuit. A probe was placed on the temporal artery and real-time counts with respect to baseline were used to compute the percent leakage factor (RLF). TNF- α concentration in the pleural aspirate reservoir (PRC) was measured at the end of the procedure. **Results:** Average PRC was 429 \pm 271 ng/ml, not significantly different from mean circuit concentration 700 \pm 374 ng/ml (p=ns), but markedly higher than peripheral blood concentration 0,6 \pm 1,2 ng/ml (p<0.01). The integral of TNF- α concentration in the perfusion circuit positively correlated with PRC (R=0,64, p<0,05). By contrast, PRC showed a definite negative correlation with RLF (R=0,8, p<0,01), indicating that inefficient removal of pleural fluid could aggravate drug leakage. Accordingly, difference in TNF- α concentration between the isolated circuit and the pleural reservoir showed a positive correlation with RLF (R=0,74, p<0,01). **Conclusions:** Radioisotopic leakage monitoring is able to correctly TNF- α leakage during HILP. Pleural shunt plays a major role in drug leakage determination: efficient removal of pleural fluids is pivotal in ensuring the patients' safety during the procedure.

OP128

Diagnostic value of additional SPECT/CT in sentinel lymph node mapping in breast cancer patients

S. Stanzel¹, B. Pernthaler¹, G. Pregartner², T. Schwarz³, V. Bjelic-Radicic⁴, R. M. Aigner¹; ¹Medical University of Graz, Department of Radiology, Division of Nuclear Medicine, Graz, AUSTRIA, ²Medical University of Graz, Institute for Medical Informatics, Statistics and Documentation, Graz, AUSTRIA, ³Department of Radiology, Division of Nuclear Medicine, Graz, AUSTRIA, ⁴Medical University of Graz, Department of Gynecology and Obstetrics, Graz, AUSTRIA.

Aim: In scientific literature for sentinel lymph node mapping (SLNM) different examination protocols are reported. The objective of the study was to demonstrate the diagnostic value of SPECT/CT in SLNM in patients with invasive breast cancer. **Materials and methods:** One hundred and fourteen patients with invasive breast cancer with clinically negative lymph nodes were included in this study as they were referred for SLNM with ^{99m}Tc-nanocolloid. Planar image acquisition was accomplished in a one-day or two-day protocol depending on the schedule of the surgical procedure. Low-dose SPECT/CT was performed after the delayed planar images. The sentinel lymph node biopsy (SLNB) was considered false negative if a primary recurrence developed within 12 months after SLNB in the axilla from which a tumor-free SLN had been removed. The false-negative rate was determined as the ratio of false-negative results to the total number of positive nodes (false-negative nodes plus true-positive nodes). **Results:** Between December 2009 and December 2011, 114 patients underwent SLNM with SPECT/CT. 139 SLNs were detected with planar scintigraphy alone and 290 SLNs with additional SPECT/CT. In 5 patients, no SLN could be detected with planar scintigraphy. In 4 of the last patients, SLNs were identified with the aid of SPECT/CT. Thus, with SPECT/CT significantly more SLNs were detected than with planar scintigraphy alone (p>0,001). Consequently, 32 patients (28%) had therapy change (axillary lymph node dissection). No patient had lymph node metastasis within 12 months after SLNB in the axilla from which a tumor-free SLN had been removed resulting in a false-negative rate of 0% (0/18). **Conclusion:** Among patients with breast cancer, the use of SPECT/CT-aided SLNM correlated due to a better anatomical localization and identification of planar not visible SLNs with a higher detection rate of SLNs. This led to therapeutic consequences and an excellent false-negative rate.

OP129

Late acquisition with SPECT/CT lymphoscintigraphy improves Sentinel Lymph Nodes detection in vulvar cancer patients

A. Olivier, E. Leblanc, A. Oudoux, E. Tresch, L. Delcroix, C. Leprince, F. Narducci, H. Kolesnikov-Gauthier; Oscar lambret center, lille, FRANCE.

AIM: We assessed the interest of late planar acquisition and single photon emission computed tomography (SPECT/CT) lymphoscintigraphy (LSG) for sentinel lymph node (SLN) detection and dissection in patients with vulvar cancer. **MATERIALS AND METHODS:** 73 consecutive patients underwent a preoperative SLN tracking with 4 intradermal injections of Technetium 99m - nanocolloid (mean total injected dose: 60MBq) and subsequent early planar (mean time after injection: 38.4 minutes), late planar (mean time after injection: 4.2 hours) and SPECT/CT LSG. Directly before radioguided intraoperative detection, 52 of the 73 patients were injected with patent blue dye. We retrospectively analyzed detection rates of early planar (n= 73), late planar (n=59) and SPECT/CT (n=46) LSG, and intraoperative detection. Histologic results for all dissected LN were collected. **RESULTS:** Detection rates of SLN with early planar, late planar, SPECT/CT LSG and patent blue dye were respectively 82.2%, 91.5%, 95.7% and 80.8%. Late planar LSG identified more inguinal and iliac SLN than early planar [respectively per patient: mean value 2.4 (SD 1.7) and 1 (SD 1.1) versus 1.8 (SD 1.5) and 0.6 (SD 0.9)] (p<0.001). SPECT/CT LSG identified more inguinal SLN than late planar [mean value 3 (SD 2) versus 2.4 (SD 1.7)] (p=0.004), and also more iliac SLN than late LSG [mean value 2 (SD 1.8) versus 1 (SD 1.1)] (p<0.001). We analyzed all removed LN who were not radioactive. This could be observed in 3 situations. 1/ Sixteen patients had unilateral isotopic SLN detection (14 patient with midline tumor and 2 with unilateral tumor but positive SLN on the first side). Thirteen patients subsequently had an inguinofemoral lymphadenectomy of the other side. Five of them had metastatic LN in the groin dissection. 2/ Blue dye procedure finds 2 LN who were not detected by isotopic method. None were metastatic in

final histology. 3/ At surgery, 5 not radioactive LN were visually suspect and therefore dissected. Two of them were metastatic. **CONCLUSION:** In vulvar cancer patients, SPECT/CT lymphoscintigraphy leads to a higher identification compared to early or late LSG. Its higher resolution provides better anatomical localization of SLN and improves the detection rate. Systematic SPECT/CT could decrease the number of inguinofemoral lymphadenectomies and so reduce associated comorbidity.

OP130

A pilot study of absolute quantitative SPECT/CT for sentinel lymph node mapping in endometrial cancer

S. Sahbai¹, F. Fiz¹, F. Taran², S. Brucker², D. Wallwiener², C. la Fougère¹, H. Dittmann¹; ¹Nuclear Medicine, University Hospital Tuebingen, GERMANY, ²Gynecology and Obstetrics, University Hospital Tuebingen, GERMANY.

Introduction: Our previous study indicated that high venous drainage, as visualized by significant bone marrow uptake, was the most important factor associated with sentinel lymph node (SLN) detection failure in endometrial cancer. Aim of this study was to use absolute quantification in order to further explore actors disturbing successful SLN detection with SPECT/CT after pericervical 99m Tc-Nanocolloide injection. **Methods:** Fifty-three patients underwent four pericervical injections of 99m Tc-Nanocolloide (200-300 MBq) and preoperative SPECT/CT of abdomen and pelvis (2:30-6:00h p.i.). We compared imaging findings of patients with SLN detection failure (n=14) to a randomized matched cohort of patients (n=14) who showed at least 2 detected SLNs at SPECT/CT. Activity concentration (MBq/ml), percentage of injected dose (%ID) as well as absolute activity (MBq) were assessed by means of a commercial software (GE Healthcare Q.metrics) in volumes of interest: SLN, liver, spleen, injection site and body remainder within the field-of-view. Mann-Whitney U-test was used for statistics. **Results:** Fifty-four SLN were visualized in the 14 patients with successful detection in SPECT/CT. Mean SLN activity concentration was 0.05 MBq/ml (range 0.003-0.22). In case of successful detection, percentage of injected dose and absolute activity at the injection site were significantly higher than in patients with detection failure (53±25 %ID vs. 29±18 %ID, p<0.01 and 73 ±31 MBq vs. 43±37 MBq, p<0.05). Failure to detect SLN tended to be associated with higher liver mean uptake through not reaching significance (26±20 vs. 12±7 KBq/ml, p=0.17). Moreover, we observed a trend for higher activity fraction in the body remainder in negative SLN scans (15±7% vs. 11±4%; p=0.13) and a lower overall %ID (58±27% vs. 75±10%; p=0.16) the latter finding indicating a loss of activity after application. Successful SLN detection was not correlated with the amount of injected activity and the time gap between injection and imaging. **Conclusion:** This pilot study indicates that SLN with a nanocolloide activity concentration as low as 0.003 MBq/ml could be detected on SPECT/CT. Furthermore, SLN detection is associated with a higher persisting activity at the injection site and low venous drainage highlighting the relevance of meticulous injection technique. Further studies, with larger cohorts of patients are needed to confirm these preliminary results.

408 – Sunday, October 16, 2016, 14:30 - 16:00, Hall 212

Physics & Instrumentation & Data Analysis: SPECT Image Processing & Reconstruction

OP131

Penalised Deconvolution of SPECT Images for Tumour Dosimetry

I. Murray¹, M. Gray¹, G. Flux²; ¹Royal Marsden NHS Foundation Trust, Sutton, UNITED KINGDOM, ²Royal Marsden NHS Foundation Trust / Institute of Cancer Research, Sutton, UNITED KINGDOM.

Introduction: The partial volume effect remains a challenge for the quantification of SPECT data for dosimetry. The aim of this work was to develop methods for partial volume correction in the image domain. The Lucy-Richardson (LR) iterative algorithm is used to deconvolve images given the point spread function (psf). It is a particular example of the MLEM algorithm where the system matrix is described by the psf. Penalised MLEM reconstruction techniques use penalty functions that favour a solution reflecting some assumed prior knowledge of the image. However, available anatomical imaging may not always reflect functional boundaries. **Methods:** An adaption of the LR algorithm was developed to include a Bowsher prior function [1]. The purpose of this function is to favour local smoothness between neighbouring voxels classified as having the same tissue type, whilst maintaining high spatial resolution at the tumour edge. Tissue type was defined by using a fuzzy locally adaptive Bayesian algorithm (FLAB), a segmentation method developed for PET images in the context of radiotherapy planning [2]. The algorithm was applied to OSEM reconstructed SPECT images of a NEMA Image Quality phantom. The phantom was filled with known concentrations of ^{99m}Tc in both the background and spherical insert (10mm - 37mm diameter) compartments. Recovery of the mean counts in each sphere was measured as a function of sphere-size, LR iterations and the β parameter used to describe the weighting given to the Bowsher prior. **Results:** Without application of the penalised LR algorithm full recovery of the counts within in each sphere was not obtained for any size sphere. Application of the penalised LR algorithm resulted in 100% recovery for the three largest spheres. Recovery was improved from to 47% to 82%; 33% to 60%; and 27% to 48% for the 17mm, 13mm and 10mm spheres respectively. The algorithm was shown to converge as a function of both iterations and β . Further iterations did not increase image noise. **Conclusions:** An algorithm has been developed for SPECT / PET images demonstrating the potential for substantial partial volume correction in the calculation of absorbed dose to small tumours. 1. Bowsher, J.E., et al. Utilizing MRI information to estimate F18-FDG distributions in rat flank tumors. in Nuclear Science Symposium Conference Record, 2004 IEEE. 2004. 2. Hatt, M., et al., A fuzzy locally adaptive Bayesian segmentation approach for volume determination in PET. IEEE Trans Med Imaging, 2009. 28(6): p. 881-93.

OP132

A fast GPU code for full Monte Carlo based SPECT reconstruction

T. Magnander¹, J. Heydom Lagerlöf¹, J. Hemmingsson¹, M. Båth¹, J. Svensson², P. Gertsson³, P. Bernhardt¹; ¹Department of Radiation physics, Sahlgrenska Academy, Gothenburg, SWEDEN, ²Department of Oncology, Sahlgrenska Academy, Gothenburg, SWEDEN, ³Department of Clinical Physiology, Sahlgrenska Academy, Gothenburg, SWEDEN.

To improve image quality in SPECT/CT reconstructions, various approximate recovery resolution techniques have been developed and implemented in clinical practice. However, optimal image reconstruction requires accounting for all physical interactions of the emitted photons in the individual patient. The objectives for this study were to develop a novel Monte Carlo (MC) code for fast simulation of individual image projections, and to implement these projections in ordered subset expectation maximum (OSEM) reconstructions of SPECT/CT images. **Method:** The MC code was written in Compute Unified Device Architecture language for a computer with four graphic processing units (GeForce GTX Titan X, Nvidia, USA). This enables simulations of parallel photon emission from the voxels matrix (128³ or 256³). Each CT number was converted to attenuation coefficients for photo absorption, coherent scattering and incoherent scattering. The type of interaction was determined by the ratio of attenuation coefficients in the CT voxels. For photon scattering the deflection angle was determined by the differential scattering cross sections. The accepted angle for photon interaction with the crystal was determined from the diameter and height of the collimator hole. Predefined energy and spatial resolution kernels for the crystal were used.

The MC code was implemented into OSEM reconstruction of ^{177}Lu , ^{111}In and $^{99\text{m}}\text{Tc}$ SPECT/CT images. The National Electrical Manufacturers Association (NEMA) image quality phantom was used to evaluate the performance of the MC reconstruction in comparison with clinical standard OSEM reconstructions and clinical state-of-the-art OSEM reconstructions with recovery resolution corrections. Results and conclusion: The performance of the MC code was 500 millions photons/s. The required number of photons emitted per voxel for obtaining low noise in the simulated image was 400 for a 128^3 voxel matrix. With this number of emitted photons/voxel the MC-based OSEM reconstruction with 10 subsets was performed within 60 s/iteration. The images converged after 2–4 iterations, depending on the sphere sizes in the NEMA phantom. Thereby, the reconstruction time was <4 minutes. The contrast-to-noise level was slightly improved with increased number of emitted photons/voxel, and the reconstruction time was linearly depending on the number of emitted photons/voxel. The signal-to-background for the spheres in the NEMA phantom was clearly improved with MC-based OSEM reconstruction: e.g. for ^{177}Lu the improvement was 37% compared to standard OSEM and 20 % compared to state-of-the-art OSEM. Furthermore, visual inspection of clinical investigations revealed clearly improved resolution and contrast with MC-based reconstruction.

OP133

Optimized Respiratory Gating Strategy for Myocardial Perfusion SPECT

D. Zhang, G. S. P. Mok; University of Macau, Macau, MACAO.

Aim: Different respiratory gating methods are feasible for motion reduction in cardiac SPECT. However, the efficiency of different methods has not been evaluated. This study aims to evaluate three gating methods for respiratory gated SPECT. **Materials and methods:** We used the digital 4D XCAT phantom to model a normal male patient with Tc-99m-MIBI activity distribution. We simulated (i) regular respiratory cycles with 25 mm axial amplitude and 5 s duration; (ii) irregular respiratory cycles with 25, 27.5, 30 mm axial amplitudes and 4, 5 and 6 s respective duration. Each respiratory cycle was divided into 96 frames which were grouped to 6 gates with 3 different methods: (1) equal time gating (TG); (2) equal amplitude gating (AG) and (3) amplitude gating with equal counts (CG). Average of all frames was used to represent static SPECT, while average activity and attenuation maps in each gate represented gated SPECT and CT respectively. Realistic noisy projections were generated using an analytical LEHR projector and reconstructed by OS-EM algorithm using gated CT for AC for up to 30 updates. Reconstructed images of each gate were registered to end-expiration phase using affine+b-spline method and then averaged and reoriented to generate polar plots. Polar plots from static SPECT and end-expiration phase were also obtained. Relative difference (RD) of the average intensity was computed for each segment using end-expiration phase as the reference in 17-segment analysis. Two regions-of-interest (ROIs) were chosen in the basal-anterolateral and mid-septal regions of the polar plots to calculate the intensity ratio (IR). Normalized standard deviation (NSD) of the ROI in mid-septal region was calculated to assess the noise. **Results:** Amplitude-based gating methods (AG and CG) showed less motion artifacts from visual assessment. The TG and CG methods had more uniform NSD distribution among all gates as compared to AG, i.e., their SDs were 0.022, 0.007 and 0.040 respectively. The RDmean for TG, AG and CG were 6.15%, 6.48% and 5.60% for regular breathing cycle and 6.68%, 6.70% and 5.47% for irregular cycle respectively. The IR of static, TG, AG and CG were 51.24%, 88.68%, 91.52% and 86.07% for regular cycle and 48.74%, 75.57%, 82.23% and 85.00% for irregular cycle respectively. **Conclusion:** Out of three respiratory gating approaches, the CG method shows better motion reduction and more uniform noise distribution. Patients with regular respiratory cycles show better gating results. Amplitude-based gating method is preferable for respiratory gated SPECT implementation.

OP134

Navigation of a robot-integrated fluorescence laparoscope in preoperative SPECT/CT and/or intraoperative freehand SPECT data

M. N. van Oosterom¹, N. S. van den Berg¹, M. Engelen¹, G. H. KleinJan¹, H. G. van der Poel², T. Wendler³, C. J. van de Velde¹, N. Navab³, F. W. B. van Leeuwen¹; ¹LUMC, Leiden, NETHERLANDS, ²NKI-AVL, Amsterdam, NETHERLANDS, ³TUM, Munich, GERMANY.

Introduction Robot-assisted laparoscopic surgery is becoming the standard-of-care for prostatectomy and is also increasingly being explored for other types of cancer (e.g. rectal cancer). Preoperative (molecular) imaging can provide the surgeon with three-dimensional insight into the location of lesions and their surrounding anatomy, but it remains a challenge to translate this information to the setting of robotic surgery. Navigation technologies can be a solution, especially when they are directly linked to technologies that provide intraoperative confirmation of the navigation accuracy e.g. fluorescence imaging. In this phantom study, we studied the navigation of a robot-integrated fluorescence laparoscope. **Methods** Both preoperative SPECT/CT and intraoperative freehand SPECT data sets were used to navigate the robot-integrated Firefly laparoscope via an augmented reality overlay provided in the laparoscopic video feed. Errors of the navigation were initially measured in soft-tissue phantoms, followed by studies in a torso phantom. **Results** In both phantom setups, the feasibility of the robotic navigation concept could be successfully demonstrated. Mean navigation accuracy found for SPECT/CT-based navigation was 2.25 mm (coronal) and 2.08 mm (sagittal). For the freehand SPECT-based navigation the respective average accuracy was 1.92 mm (coronal) and 2.83 mm (sagittal). These navigation errors remain well below the < 1 cm detection limit for fluorescence imaging, allowing refinement of the navigation process using fluorescence findings. **Conclusions** The phantom experiments performed suggest that SPECT-based navigation of the robot-integrated laparoscope may aid fluorescence guided surgery procedures.

OP135

Computational-Based Bone Recognition and Tracer Quantification in Patients with Disseminated Prostate Cancer: a SPECT/CT study

F. Fiz¹, S. Sahbai¹, M. Weissinger¹, C. Campi², M. Piana², G. Sambuceti³, C. la Fougère¹; ¹Nuclear Medicine Unit, Department of Radiology, University of Tübingen, Tübingen, GERMANY, ²Department of Mathematics, University of Genoa, Genoa, ITALY, ³Nuclear Medicine Unit, Department of Health Sciences, University of Genoa, Genoa, ITALY.

Rationale: Evaluating multiple skeletal metastases on hybrid SPECT/CT systems implies significant information flow, which could be simplified by computer-assisted algorithms. The validation of an automated tool is however complex, as it implies the capability to detect and isolate osteoblastic areas within the skeleton and to quantify the morpho-functional data. In this project, a dedicated software application was developed and tested against clinical data. **Material and Methods:** Seventy-six $^{99\text{m}}\text{Tc}$ -DPD SPECT/CT scans, from patients with disseminated bone metastases were analyzed with a dedicated software application. Outputs included volumes, average HU density (HU) as well as blood-pool normalized counts (target-to-background ratio, TBR) in three different bone volumes: total (TBV), compact (CBV) and trabecular (IBV). Volumes and HU values were compared with controls from a published normalcy database. TBV and mean TBR were compared with the corresponding outputs, obtained from a validated commercial quantitative analysis tool. As a measure of osteoblastic reaction, percentage of CBV in TBV (CBV%) and HU in CBV were compared with the number of visible tracer foci at SPETC MIP, with the current PSA values and with the presence of a “superscan” status on NM images. **Results:** Whole-body

HU was increased in both IBV and CBV with respect to controls (240 ±77 vs. 161±39 and 612±113 vs. 547±45, respectively, $p<0,001$). Volumetric estimates of TBV and mean TBR provided by our application tightly correlated with the outputs of the commercial application ($R=0,93$ and $0,96$, $p<0,001$, respectively). The number of visible foci correlated with CBV% ($R=0,6$, $p<0,01$) as well as with whole-body HU/TBR in CBV ($R=0,55$ and $0,69$, respectively, $p<0,01$). PSA values correlated with TBR in both IBV and CBV ($R=0,61$, $p<0,01$ and $R=0,49$, $p<0,05$, respectively), as well as with %CBV ($R=0,62$, $p<0,01$). Patients with “superscan” status presented increased CBV% ($66\pm5\%$ vs. $61\pm5\%$, $p<0,001$) with respect to the other patients; this difference was even more marked in the axial skeleton ($59\pm6\%$ vs. $51\pm9\%$, $p<0,001$). “Superscan” patients had also increased HU and TBR in both IBV and CBV ($p<0,001$). Conclusions: These results show that computational-based compact bone identification is able to detect significant changes in patients with osteoblastic metastases, as well as in the patients’ subset with scintigraphic signs of advanced disease. Moreover, CT-based segmented volumes and SPECT-based counting rate correlated with an accepted standard for SPECT/CT quantification.

OP136

Standardisation and Optimisation of Quantitative Radioiodine SPECT/CT Imaging for Dosimetry in the Multicentre SEL-I-METRY Trial

R. Gregory^{1,2}, I. Murray^{1,2}, J. Gear^{1,2}, S. Chittenden^{1,2}, J. Merrett^{3,4,5}, J. Scuffham^{3,5}, A. Fenwick⁴, M. Stuffs⁶, S. Micholopoulou⁶, S. Jeans⁷, B. Murby⁷, J. Tipping⁷, G. Flux^{1,2}; ¹Royal Marsden NHS Foundation Trust, Sutton, UNITED KINGDOM, ²Institute of Cancer Research, Sutton, UNITED KINGDOM, ³Royal Surrey County Hospital, Guildford, UNITED KINGDOM, ⁴National Physical Laboratory, Teddington, UNITED KINGDOM, ⁵The University of Surrey, Guildford, UNITED KINGDOM, ⁶University Hospital Southampton, Southampton, UNITED KINGDOM, ⁷The Christie NHS Foundation Trust, Manchester, UNITED KINGDOM.

Aims: The aim of this study was to set up the first network of centres to perform standardised quantitative radioiodine imaging for comparable dosimetry measurements in the United-Kingdom for a phase II clinical trial (SEL-I-METRY). The trial will evaluate the ability of the MEK inhibitor Selumetinib to stimulate radioiodine uptake in iodine refractory thyroid cancer and the subsequent potential benefit from radioiodine therapy. Absorbed doses will be measured on pre-radioiodine therapy ¹²³I and post-therapy ¹³¹I NaI SPECT/CT images. **Materials and Methods:** The SPECT acquisition protocol for the trial was developed to comprise 20% wide energy windows and 72 views, providing high-count projections. Six-percent wide energy windows are included for triple-energy-window scatter correction. High-energy general-purpose collimators are used for ¹³¹I imaging and medium-energy general-purpose collimators for ¹²³I to avoid septal penetration. A standardised calibration protocol was developed for partial-volume effect (PVE) and dead-time correction and used at all centres. A body-shaped phantom with six 0.7 to 196 ml cylindrical inserts filled with 0.25 MBq/ml radioiodine was imaged using the trial protocol, for both ¹²³I and ¹³¹I. Volumes of interest (VOI) were defined on the reconstructed images about the internal wall of the cylinders. A sigmoidal fit was applied to the VOI’s cps/MBq/ml versus volume. The plateau was set to the average cps/MBq/ml for oversized VOIs defined about the 3 largest cylinders to give a calibration factor in the absence of PVE. Dead-time was also characterised for 20 to 2800 MBq ¹³¹I in a 6 L cylindrical phantom. Measured count-rates for activities below 100 MBq were linearly extrapolated to higher activities to determine these rates in the absence of dead time. Paralyzable and non-paralyzable models were fitted. **Results:** The PVE correction factors varied between systems for both ¹²³I and ¹³¹I. The curves had a plateau ranging from 0.7 to 1.4 cps/MBq/ml for ¹³¹I and 1.8 to 3 cps/MBq/ml

for ¹²³I. The GE systems need to operate in ‘fast’ mode for high ¹³¹I activities to avoid reaching the peak count rate below 2.8 GBq. Dead-time losses were below 20%. A non-paralyzable model fitted these count rates to provide a simple correction. **Conclusions:** Accurate dosimetry results that are comparable between centres are vital to identify absorbed dose relationships and are reliant on the quantitative accuracy of the SPECT/CT images. The variations in correction factors between these centres demonstrate that this program of standardised calibration measurements is essential for a multicentre dosimetry trial.

OP137

3D Lung quantification using SPECT/CT

D. Gillett, N. Bird, H. Cheow; Addenbrooke’s Hospital, Cambridge, UNITED KINGDOM.

Introduction: Functional assessment of lung perfusion using Technetium-99m (Tc-99m) macro aggregated albumin (MAA) has been available for many years. It is commonly used for lung assessment prior to lung volume reduction surgery (LVRS). It is based on dividing a planar perfusion study into three equal portions and calculating the percentage of each portion with respect to the lung. We describe a technique of using SPECT with low dose CT (SPECT/CT). **Method:** Patients were intravenously administered with 90 MBq (+/- 10%) of Tc-99m-MAA then immediately underwent a SPECT/CT. The CT is used to do attenuation correction of the SPECT and to manually draw regions of interest (ROIs) around each anatomical lung lobe. These ROIs were transferred onto the SPECT images using the size and location information from the DICOM header. The number of counts and area of each 2D ROI are added together to create 3D ROI for each lobe. This data is then used to generate the relative function (RF), approximate volumes and mean counts per voxel (MCV) for each lobe. Validation of the technique was done using a torso phantom with known ratios of activities and concentrations between the lung regions. The imaging protocol used on patients was used with the phantom. **Results:** Analysis of the phantom experiments ($n=3$) demonstrated that the RF and MCV calculations were within 1% of the known activities and concentrations that were added to the phantom. Retrospective analysis of patient data ($n=19$) yielded significantly different RF results for the three lobes of the right lung when the SPECT/CT technique was compared to the planar technique ($p<0.05$). The left lung was excluded from the comparisons because the planar technique divides it into three lobes and the SPECT/CT method divides into two in accordance with the anatomical regions. **Conclusion:** Using SPECT/CT in combination with manual region drawing of lung lobes generates RF and MCV estimates that closely match known ratios of activity added to a phantom. This result along with comparisons between planar and SPECT/CT lobar analysis in patients suggests that SPECT/CT can be a useful tool in patients undergoing LVRS. The SPECT/CT technique is currently time consuming because of the manual region drawing and would benefit from an automated lung segmentation algorithm.

OP138

Quantitative Optimisation of Triple Energy Windowing and Deconvolution for Artefact Reduction in I-131 Imaging

A. Grimwood¹, F. Barrack¹, L. Livieratos², J. Scuffham¹; ¹Royal Surrey County Hospital, Guildford, UNITED KINGDOM, ²King’s College London, London, UNITED KINGDOM.

Patients undergoing radioiodine treatment for thyroid cancer are given a post-ablation whole body scan to assess therapeutic effectiveness and check for potential metastatic spread or nodal involvement. This is typically indicated by localised regions of activity away from the main tumour/resection site. However, Compton scatter and septal penetration

from high energy gamma emissions introduce noise and imaging artefacts, especially where foci of high activity are present against a low background. Such effects can obscure the presence of involved nodes or distant metastases. Triple energy windowing (TEW) and deconvolution techniques can be used as a means of artefact reduction. In both cases, optimisation is crucial to maximise image correction whilst minimising the effects of over-correction (such as a loss of contrast or the presence of negative counts). Using a Monte Carlo model of the GE Optima 640, the collimator-detector response function was characterised for a range of I-131 scans. By separating list-mode data into contributions from Compton scatter, septal penetration and geometric components, it was possible to quantitatively optimise both TEW and deconvolution methods. A GATE Monte Carlo model of the GE Optima 640 was developed and validated against a real system to ensure clinical relevance. List mode data was recorded from both experimental and simulated systems and used to reconstruct images. Optimisation was performed on simulated data and the resulting image quality was quantified. TEW window widths were selected according to the ratio of scatter fraction to geometric fraction in list-mode. An analytic expression for the point spread function was derived from simulations. This was used for Lucy-Richardson deconvolution with input parameters optimised accordingly. The Optima 640 model accurately represented the clinical system at energies close to the 365 keV primary photopeak, exhibiting a sensitivity and energy resolution of $\pm 15\%$ and $\pm 10\%$ respectively compared to the actual system. Simulated images produced a contrast to noise ratio (CNR) within 1% difference from experimental acquisitions and a similarly close spatial resolution. For a specific acquisition geometry, the optimised TEW images provided a CNR equal to the original image with a negative count ratio of $<10\%$. For deconvolution, CNR was degraded by 28%, however, overall scatter background was reduced by 75% whilst resolution improved 32%. Combining both TEW and deconvolution produced a synergistic effect, effectively removing imaging artefacts.

409 – Sunday, October 16, 2016, 14:30 - 16:00, Hall 113

Conventional & Specialised Nuclear Medicine: Infection & Inflammation 1

OP139

Normal variability of FDG uptake after prosthetic heart valve implantation

W. E. Vlemmings¹, J. Faggiday¹, E. Daeter², R. Kauling³, R. Keijsers¹, M. van Buul¹; ¹St Antonius hospital, Nieuwegein, NETHERLANDS, ²St Antonius hospital, cardiothoracic surgery, Nieuwegein, NETHERLANDS, ³St Antonius hospital, cardiology, Nieuwegein, NETHERLANDS.

Introduction: Limited data exist on physiologic FDG uptake in and around artificial heart valves after replacement. In this retrospective study, the metabolic activity in various prosthetic valve types in different valve positions was measured in patients without any suspicion of endocarditis. Data were compared with those of native heart valves. **Methods:** Thirty-eight FDG PET/CT studies in 29 patients in which PET/CT was obtained for noncardiac indications, 2 weeks-260 months (mean 21,5 m) after prosthetic valve implantation, were included. Definite and suspected endocarditis were excluded on basis of the modified Duke's criteria. Maximal standardized uptake values (SUVmax) were measured as well as the ratio between SUVmax around the valves and SUVmean in the descending aorta (SUVmax/SUVmean DA). Statistical analysis was performed to determine differences by Mann-Whitney U testing. **Results:** 22 M and 7 F, mean age 69,4 y (39-90 y). The aortic valve group contained 5 native aortic valves, 13 trans catheter valve replacements (TAVI), 12 Bentall procedures and 8 aorta valve replacements (AVR). The mitral group contained 9 mitral valve replacements (MVR) and 29 native mitral valves. The tricuspid group contained 34 native valves and 4 replaced tricuspid valves (TVR). All pulmonary valves were native.

Compared to native aortic valve, average SUVmax was significantly higher in TAVI, Bentall procedures and AVR (2.1 vs 2.5, 3.8 and 4.1, respectively). Av. SUVmax of TAVI was significantly higher than after AVR, while there was no difference between TAVI and Bentall or between Bentall and AVR. Av. SUVmax/SUVmean DA was only significantly higher in AVR (1.4 vs 2.4). In MVR, both parameters, av. SUVmax and av. SUVmax/SUVmean DA, were significantly higher compared to native mitral valve, av. SUVmax 3.5 vs 2.5 and av. SUVmax/SUVmean DA 1.4 vs 2.0. In the tricuspid group, only the av. SUVmax/SUVmean DA of TVR was significantly higher, 1.3 vs 1.8. Average SUVmax of the pulmonary valve was 2.6 and av. SUVmax/SUVmean DA was 1.5. **Conclusion:** physiologic FDG uptake in native and artificial heart valves after replacement is given. Compared to native heart valves, average SUVmax increases significantly in all aortic and mitral valve prosthesis. In aortic valve prosthesis, the highest uptake was found after full surgical replacement. In Tricuspid valve prosthesis, only the average SUVmax/SUVmean AD ratio value was significantly higher.

OP140

18F-FDG PET/CT in the Evaluation of Large-Vessel Vasculitis: Comparison Between Visual and Semi-Quantitative Analysis and Their Correlation with Clinical and Biochemical Data

L. M. P. Pires¹, R. Silva^{1,2}, P. Lapa¹, G. Costa¹, J. P. Lima^{1,2}; ¹Centro Hospitalar e Universitário de Coimbra, Coimbra, PORTUGAL, ²Instituto de Ciências Nucleares Aplicadas à Saúde, Coimbra, PORTUGAL.

AIM: Recent scientific evidence has demonstrated the potential use of 18F-FDG PET/CT for the evaluation of large-vessel vasculitis (LVV). It has been postulated that 18F-FDG PET/CT may have superior sensitivity in an early stage, because of its ability to identify metabolism changes that precede structural alterations. However, studies have shown notable variability regarding the diagnostic criteria used for the differentiation between affected and unaffected vessels. In this study we aim to compare two different visual and semi-quantitative quantification methods and their correlation with clinical data in patients with suspected LVV. **MATERIAL AND METHODS:** The clinical charts of 52 patients (19 males and 33 females, 64.2 \pm 15.5 years) who performed F18-FDG PET/CT due to a clinical suspicion of LVV were retrospectively reviewed. In each patient, presence or absence of LVV was confirmed or excluded by case base work-up, including clinical work-up, inflammatory markers, other imaging modalities, response to corticosteroid treatment (CST) and biopsies. The clinician's decision was used to classify a patient as a LLV or not. Patients were thus divided into 3 groups: (1) 18 patients with active LLV without CST, (2) 23 patients with LVV under CST, (3) 11 patients in whom LLV was excluded. F18-FDG uptake was evaluated in the aorta and its major branches using a visual scoring system (0-no uptake, 1-less than liver uptake, 2-similar to liver uptake, 3-superior than liver uptake, positive if >1) and a semi-quantitative method (average SUVmax in 4 ROI manually generated in each arterial compartment). Also, all available biochemical data, including inflammatory markers, was recorded. Statistical analysis was performed using IBM[®] SPSS[®] Statistics, version 22. **RESULTS:** 18F-FDG PET/CT was positive in at least one arterial compartment in 94.4% of group 1 patients, in 30.4% of group 2 patients and in 0% of group 3 patients ($p < 0.05$). A statistical significant difference was found between SUVmax values in the 3 groups ($p < 0.05$). Also a statistical significant correlation was found between the visual scoring system and the semi-quantitative method (Spearman rho: 0.942, $p < 0.05$). The only clinical variables correlated with SUVmax were haemoglobin and reactive protein C, and with the sedimentation rate in the visual scoring system. **CONCLUSION:** In this study F18-FDG PET/CT was able to differentiate between patients with active LVV without CST, patients with active LVV with CST and patients without active LVV, using both visual scoring system and the semi-quantitative method. Both scoring methods were strongly correlated.

Also, some clinical variables were correlated with SUVmax and the visual scoring system.

OP141

Evaluation of predictor variables of diagnostic [18F] FDG-PET/CT in fever of unknown origin

K. Okuyucu¹, E. Alagoz¹, S. Demirbas², S. Ince¹, A. Karakas³, B. Gunalp¹, A. O. Karacalioglu¹, N. Arslan¹; ¹Gulhane Military Medical Academy, Department of Nuclear Medicine, Ankara, TURKEY, ²Gulhane Military Medical Academy, Department of Internal Medicine, Ankara, TURKEY, ³Gulhane Military Medical Academy, Department of Infectious Diseases, Ankara, TURKEY.

Aim Fever of unknown origin (FUO) is defined as an illness having fever which lasts at least 3 weeks of duration and is higher than 38.3 °C on several measurements. The causes are infections, malignancies, noninfectious inflammatory diseases and miscellaneous. If [18F]FDG-PET/CT helps the final diagnosis, it is called contributory. The aim of the study is to evaluate the predictor variables effecting a contributory PET/CT for the diagnosis. Methods This is a retrospective cohort study conducted between June 2004 and May 2015 including 76 patients. The evaluated predictor variables are age, sex, ESR, CRP, fibrinogen, ferritin, albumin, haemoglobin level, platelet count, total leukocyte count, neutrophil percentage, lymphocyte percentage, ALP, LDH, ALAT, ASAT, GGT, total bilirubin, CK, RF, ANA, urinalysis, chest radiography, abdominal US, lymphadenopathy, duration of fever, comorbid diseases and previous therapies. Results ESR (p=0.001), CRP (p=0.001), fibrinogen (p=0.009), lymphopenia (p<0.001), neutrophilia (p<0.001), ferritin (p<0.001), leukocytosis (p=0.003), duration of fever before PET/CT (<3 months) were found to be statistically significant for positive contribution of PET/CT results to the diagnosis. Conclusions [18F]FDG-PET/CT is helpful and contributory for the diagnosis of FUO in patients having higher levels of CRP, ESR, ferritin, fibrinogen, leukocytosis, neutrophilia and shorter durations of fever (<3 months).

OP142

Anti-granulocyte SPECT-CT for detection of sub-clinically infected neurostimulator lead prior to implantation of internal pulse generator

S. Vermeulen, M. Huylebrouck, L. Goethals, P. Gykiere, J. Heemskerck, M. Moens, H. Everaert; Universitair Ziekenhuis Brussel, BRUSSELS, BELGIUM.

Background: Neurostimulation (NS) by means of an implantable device is a well-validated technique in the treatment of medically intractable neuropathic pain. Because not all patients will benefit sufficiently from NS the effectiveness is measured during week(s) with NS-leads (subcutaneously implanted insulated wires delivering pulses to spinal cord) temporarily connected to an external pulse generator (EPG). In patients benefitting from NS the EPG will be replaced by a much more expensive internally placed pulse generator (IPG). During the period of EPG patient are at risk for (subclinical) infection that becomes apparent months after insertion of the IPG and will ultimately necessitate explantation of entire device. The aim of this work was to evaluate whether anti-granulocyte SPECT/CT can be used to demonstrate subclinical infection of the NS-lead prior to the insertion of the IPG. Methods: In 77 patients (32 M, 45 F) with EPG the NS-leads were evaluated for infection using ^{99m}Tc anti-granulocyte SPECT/CT (^{99m}Tc-Besilesomab, 25 mCi, acquisition 4 hrs pi) immediately prior to the insertion of the IPG. Scans were interpreted visually and the results were confronted with clinical follow up. Results: In 5 patients focal tracer accumulation adjacent to the NS-lead was observed suggesting infection. All these patients developed clinical signs of

NS-lead infection 2 weeks - 5 months after insertion of the IPG requiring antibiotics and explantation of the device. None of the patients with negative ^{99m}Tc anti-granulocyte SPECT/CT developed clinical signs of infection during ≥ 5 m follow-up period. Conclusion: ^{99m}Tc anti-granulocyte SPECT/CT can be used to accurately demonstrate presence / absence of subclinical infection of NS-leads prior to the insertion of IPG. A prospective trial using ^{99m}Tc anti-granulocyte SPECT/CT as a gate-keeper to decide about explantation of the NS-lead in case of suspected clinical infection prior to insertion of IPG is warranted. The cost effectiveness of systematic screening for subclinical infection using ^{99m}Tc anti-granulocyte SPECT/CT in this indication should be investigated.

OP143

Comparative effectiveness of ¹⁸F-FDG PET-CT and contrast-enhanced CT in the diagnosis of suspected large-vessel vasculitis

S. Vaidyanathan, A. Chattopadhyay, S. Mackie, A. F. Scarsbrook; Leeds Teaching Hospitals NHS Trust, Leeds, UNITED KINGDOM.

Aims: To compare the accuracy of 2-[18F]-fluoro-2-deoxy-D-glucose positron emission tomography - computed tomography (FDG PET-CT) and contrast-enhanced CT (CECT) in the evaluation of a cohort of patients with suspected large vessel vasculitis (LVV). The aim was to validate the use of CECT assessment of vessel mural thickening as a surrogate to metabolic activity in a European population. Materials and Methods: A retrospective institutional database search for patients with suspected LVV undergoing both CECT and PET-CT between December 2011 to March 2016 yielded demographics, time interval between scans and type of vasculitis. Qualitative and quantitative PET-CT data analyses were performed including aorta:liver FDG uptake, bespoke FDG uptake distribution scores and vascular maximum standardized uptake values (SUVmax). Quantitative CECT data assessment for wall thickness and mural/lumen ratio were also performed. ROC curves were constructed to evaluate comparative diagnostic accuracy and a correlational analysis was conducted between SUVmax and wall-thickness. Results: 36 adults (17 proven LVV, 19 controls without LVV) with a mean age (range) 63 (38 - 89) years, of which 17 (47%) were males were included. Time interval between CT and PET was mean (standard deviation (SD)) 1.9 (1.2) months. Estimated mean (SD) SUVmax was 3.0 (1.0) and wall thickness was 2.37 (1.05) mm. Both parameters demonstrated a significant difference between patients with and without LVV, with a mean difference (95% confidence interval (CI)) for SUVmax 1.6 (1.1, 2.0) and wall thickness 1.25 (0.68, 1.83) mm, respectively. The area under the curve (AUC) (95% CI) for SUVmax was 0.95 (0.88-1.01), for mural thickening was 0.83 (0.66-0.99), and with a highly significant correlation (P < .0001, R = 0.62) between the two parameters. Conclusion: FDG PET-CT demonstrated excellent accuracy whilst CECT mural thickening showed good accuracy in the diagnosis of LVV, and both parameters showed a highly significant correlation. In hospitals without access to FDG PET-CT or in patients unsuitable for PET-CT (e.g. uncontrolled diabetes) CECT offers a viable alternative for assessment of suspected LVV. **Table . Baseline and group characteristics.**

OP144

Effect of CRP value on ¹⁸F-FDG PET vascular positivity in Takayasu arteritis: a systematic review and per-patient based meta-analysis

L. Gomez¹, P. Chaumet-Riffaud^{1,2}, N. Noël³, E. Durand^{1,2}, F. L. Besson^{1,2}; ¹Department of Nuclear Medicine, Bicêtre university hospital APHP, 78 rue du Général Leclerc, 94270 Le Kremlin-Bicêtre, FRANCE, ²IR4M, UMR 8081, Université Paris Sud/CNRS, Université Paris Saclay, 91405 Orsay, FRANCE, ³Department of Internal Medicine, Bicêtre university hospital APHP, 78 rue du Général Leclerc, 94270 Le Kremlin-Bicêtre, FRANCE.

Purpose. The aim of this study was to conduct a systematic review and perform a meta-analysis on the potential effect of CRP value on vascular

activity assessed with ^{18}F -FDG PET in Takayasu arteritis (TA). **Methods.** The PUBmed/MEDLINE, database was searched from January 2000 to December 2015. Original articles focusing on TA and ^{18}F -FDG PET were reviewed and qualitatively analysed. To assess the relation between CRP and FDG PET vascular activity, studies that fulfilled the following criteria were included in a quantitative analysis: 1) Takayasu vasculitis according to the ACR criteria 2) No case mixed vasculitis 3) More than 5 cases per article 4) CRP values available 5) Per patient data 6) Predefined PET positivity criteria. Pooled Standard Mean Difference (SMD) of CRP values between positive and negative PET were computed using a fixed effect model. **Results.** Nine complete articles (210 patients) were qualitatively reviewed. A relationship between CRP and ^{18}F -FDG PET was observed in four studies, whereas five did not find any association. The meta-analysis of six selected studies (121 patients) provided the following results: Standard mean difference 0.54 [0.15; 0.92]; Heterogeneity $\text{Chi}^2 = 3.35$; $I^2 = 0\%$; Test for overall effect: $Z = 2.70$ ($P = 0.007$). **Conclusion.** In TA vasculitis, CRP value has a medium effect on ^{18}F -FDG PET vascular positivity.

OP145

Integrate FDG PET/CT Imaging for the assesment of plaque vulnerability in carotid stenosis compared to inflammation biomarkers, plaque echogenity and microembolic signals (MES)

S. Nicolosi, E. Giovannini, E. Borsò, P. Lazzeri, A. Chiti, E. Giorli, A. Mannironi, G. Celoria, M. Del Sette, A. Ciarmiello; Ospedale S.Andrea La Spezia, La Spezia, ITALY.

Background and Goal of study: ^{18}F -FDG-PET/CT is a noninvasive imaging modality able to quantify carotid plaque inflammation, which seems to be a crucial event in plaque vulnerability and increased risk of ischemic stroke. ^{18}F -FDG-PET/CT has been used to evaluate atherosclerotic plaque metabolic activity, and through its uptake by macrophages is believed to have the potential to identify vulnerable plaques, to predict plaque progression and subsequent cerebrovascular events. The main aim of this study is to assess the correlation between ^{18}F -FDG uptake on PET scan of carotid plaques in symptomatic and asymptomatic patients, with other vulnerability markers, such as echogenicity of plaque on ultrasound, microembolic signals (MES), histological assessments of plaque inflammation and peripheral blood markers of inflammation. **Materials and Methods:** A total of 44 consecutive patients with carotid stenosis, 17 symptomatic and 27 asymptomatic, underwent Colour Duplex ultrasound, transcranial Doppler for MES monitoring, ^{18}F -FDG-PET and blood tests. ^{18}F -FDG-PET scans were acquired after fasting for 8 h, 190 min after intravenous administration of ^{18}F -FDG (350-370 MBq) performed by a PET/CT Discovery T710 scanner, (GE Healthcare), 20 min/each bed position in the region of head-neck. Patients were stratified into two groups on the basis of presence or absence of previous stroke. Plaques were defined symptomatic when associated with ipsilateral cerebral ischemic symptoms within 15 days prior to inclusion. In symptomatic patients PET evaluation was made considering ipsilateral and contralateral sides. Plaques were assessed histologically following endarterectomy. The level of agreement between ^{18}F -FDG uptake (TLG: Total Lesion Glicolysis), and target-to-background ratio, symptoms, blood and histological evidence of inflammation has been assessed. **Results and Discussion:** Analysis of variance with the one-way anova was performed on preliminary data from 45 patients. Symptomatic patients have a higher ipsilateral plaque metabolic rate than asymptomatic patients ($P < 0.05$). Furthermore, a strong correlation was found between symptomatic patients with higher ipsilateral plaque uptake and lipid core ratio, erosion, MMP9, Plasmacells, presence of Calcium, Lipids, ac. Uric and PCR ($P < 0.05$). **Conclusion:** Our data shows that ^{18}F -FDG uptake on PET is higher in patients with symptomatic as opposed to asymptomatic carotid artery plaques. This data is confirmed by the strong correlation with inflammation biomarker.

These results support the use of ^{18}F -FDG-PET for carotid plaque risk stratification.

OP146

Standardized Uptake Values in FDG PET/CT for Prosthetic Heart Valve Endocarditis: Need for Standardization of Acquisition and Reconstruction

A. M. Scholtens¹, H. J. te Kolste², L. E. Swart³, R. P. J. Budde³, M. G. E. H. Lam⁴, H. J. Verberne⁵; ¹Meander Medical Center, Amersfoort, NETHERLANDS, ²VU Medical Center, Amsterdam, NETHERLANDS, ³Erasmus Medical Center, Rotterdam, NETHERLANDS, ⁴University Medical Center, Utrecht, NETHERLANDS, ⁵Amsterdam Medical Center, Amsterdam, NETHERLANDS.

Purpose: ^{18}F -fluorodeoxyglucose positron emission tomography combined with computed tomography (FDG PET/CT) is of increasing interest and clinical impact in prosthetic heart valve endocarditis (PVE). The significance of and threshold values for the standardized uptake value (SUV) to diagnose PVE are unclear at present. We therefore evaluated the range of SUVs in a small cohort of patients with a prosthetic heart valve but without signs of PVE to ascertain a normal range and compared these values to the available literature on SUVs in PVE. **Methods:** Twelve patients, referred for FDG PET/CT for suspicion of PVE, with no signs of PVE on FDG PET/CT and without evidence of PVE during follow up (minimum two months) were retrieved from our database. Time since prosthetic heart valve implantation ranged from 1 day to 117 days. FDG PET/CT scans were performed according to the European Association of Nuclear Medicine Research Ltd. (EARL) scanning and reconstruction specifications. The SUV in the area of the prosthetic valve was measured. A review of the literature was subsequently performed to assess the currently available data on SUV in PVE which was compared to the values in our cohort. **Results:** Median SUVmax in our cohort was 2.70 (range 1.73-3.46). In the literature, SUVs for definite, possible and rejected PVE according to the modified Duke criteria varied across studies, most likely due to differences in acquisition, reconstruction and measurement protocols, with median SUVmax values for rejected PVE ranging from 0.5 to 4.9. **Conclusion:** SUV varies according to acquisition and reconstruction protocols, meaning potential cutoff values are not interchangeable between sites. Standardization of quantification on reconstructions based on EARL specifications is desirable, with normal SUVmax values likely in the range of 1.5-4.0.

410 – Sunday, October 16, 2016, 14:30 - 16:00, Hall 114

Late-Breaking Abstracts: "The Presidential Session"

OP147

Striatal Phosphodiesterase 10A and Thinning of the medial Prefrontal Cortex in Schizophrenia - a PET and MRI study

R. Boden, J. Persson, A. Wall, M. Lubberink, L. Ekselius, E. Larsson, G. Antoni; Uppsala University, Uppsala, SWEDEN.

Objectives: The enzyme phosphodiesterase 10A (PDE10A) is abundant in medium spiny neurons of the striatum and is crucial for cell energy metabolism and thus neural function. PDE10A has been implicated in the pathophysiology of schizophrenia in animal models and is investigated as a possible new pharmacological treatment target. A reduction of medial prefrontal cortical thickness has repeatedly been observed in patients with schizophrenia, but how this relates to PDE10A expression is unknown. The primary objective of this study was to compare the striatal non-displaceable binding potential (BPND) of the PDE10A ligand [^{11}C]LuAE92686 between patients with chronic schizophrenia and healthy controls. A second objective was to assess the correlation of PDE10A BPND to cortical thickness. **Methods:** Ten male patients with

chronic schizophrenia treated with clozapine, olanzapine or quetiapine and 16 healthy controls underwent 90 min dynamic scans after injection of circa 370 MBq [^{11}C]LuAE92686 on an ECAT Exact HR+ PET scanner. MRI was performed for structural information. Clinical assessments of symptoms and cognitive function were performed and the antipsychotic dosage recorded. Volumes of interest were placed in the PET images over the striatal subregions putamen, caudate and nucleus accumbens, as well as thalamus, substantia nigra, globus pallidus and cerebellum, and PET data were analysed using the simplified reference tissue model using grey-matter cerebellum as reference tissue, giving BPND. Cortical thickness maps were calculated using Freesurfer. Results Patients with schizophrenia had a significantly lower BPND of [^{11}C]LuAE92686 in whole striatum than healthy controls (Mean \pm SD BPND 3.3 ± 0.7 versus 4.3 ± 1.0 , $p = 0.003$). Differences were significant in all striatal subregions and thalamus, but not in substantia nigra and globus pallidus. Striatal BPND significantly correlated to cortical thickness in the medial prefrontal cortex and superior frontal gyrus in both patients with schizophrenia and healthy controls. No significant correlation was observed between striatal BPND of [^{11}C]LuAE92686 and age in patient and control groups, and between BPND and schizophrenia symptoms, antipsychotic dosage, coffee consumption, smoking, duration of illness, or cognitive function in the patient group. Conclusions Striatal PDE10A expression is lower in patients with schizophrenia than in healthy controls. The degree of PDE10A expression is also correlated to cortical thickness of distant frontal cortical areas. PDE10A may thus be important for functioning in the striato-cortical interaction and in the pathophysiology of schizophrenia.

OP148

Integrity of neurocognitive networks in dementing disorders as measured with simultaneous PET/fMRI

T. Stadhouders, C. Sorg, J. Diehl-Schmid, T. Grimmer, I. Yakushev, Klinikum Rechts der Isar, Technische Universität München, Munich, GERMANY.

Background: Disrupted integrity of resting state networks (RSNs) in patients with Alzheimer's disease (AD) and frontotemporal dementia (FTD) have been reported by a number of functional magnetic resonance imaging (fMRI) studies. Of particular interest have been so-called neurocognitive networks, such as default mode (DMN), salience (SN), and central executive networks (CEN). As neuronal activity is closely linked to glucose consumption, positron emission tomography with [^{18}F]fluorodeoxyglucose (FDG-PET) represents an attractive tool for mapping RSNs. The aim of this combined FDG-PET/fMRI study was to characterize alterations in network integrity in patients with AD and FTD. **Methods:** Twenty seven patients with mild AD, 16 matched patients with FTD, and 26 healthy subjects underwent a simultaneous resting state fMRI and FDG-PET on a hybrid PET/MR system. After a standard pre-processing, images were subjected to spatial independent component analysis. Thus, a number of networks were extracted in a user-independent manner separately from fMRI and PET data. For PET, we quantified so-called loading coefficients, a degree of network expression in each subject. For fMRI, a goodness-of-fit of each network to a standard network template was calculated. Thus, fMRI- and PET-based indices of network integrity were derived for each network and subject. **Results:** Relative to healthy subjects, integrity of SN was reduced in FTD, while DMN and CENs were affected in both AD and FTD in fMRI data. In PET data, SN integrity was reduced in FTD, DMN in AD, while CEN was affected in both disease groups. In fMRI data, no significant differences between the AD and FTD groups were found. In PET data, SN integrity was reduced in FTD relative to AD ($p < 0.001$), while DMN integrity was reduced in AD relative to FTD ($p < 0.05$). In a step-wise binary logistic regression, PET indices of SN integrity alone differentiated between

the AD and FTD groups with an accuracy of 81.4 % ($p < 0.005$). Correlations between the PET- and fMRI-based indices of network integrity were low. **Conclusions:** These preliminary results in mildly affected patients with AD and FTD indicate limited disease specificity of neurocognitive networks in general and DMN in particular. Only SN as measured with FDG-PET appeared to discriminate between two patients groups. FDG-PET and fMRI seem to track partly different aspects of network integrity.

OP149

Theranostic perspectives of [$^{67}\text{Ga}^{111}\text{In}^{177}\text{Lu}$]NeoBOMB1 in prostate cancer - First evidence for clinical translation with [^{68}Ga]NeoBOMB1 and PET/CT

B. A. Nock¹, T. Maina-Nock¹, A. Kaloudi¹, A. Giarika¹, E. Lymperis¹, A. Singh², H. R. Kulkarni², I. Klette², E. P. Krenning³, M. de Jong³, R. P. Baum²; ¹Molecular Radiopharmacy, INRASTES, NCSR Demokritos, Athens, GREECE, ²Theranostics Center for Molecular Radiotherapy & Molecular Imaging, Zentralklinik, Bad Berka, GERMANY, ³Department of Radiology and Nuclear Medicine, Erasmus MC, Rotterdam, NETHERLANDS.

Aim: The gastrin releasing peptide receptor (GRPR) is highly expressed in prostate cancer and hence represents an attractive target for diagnosis and therapy with BBN-like radiopeptides. Especially, those based on GRPR-antagonists have recently shown excellent pharmacokinetics and higher biosafety for human use compared to agonists. We hereby introduce NeoBOMB1, (DOTA-*p*-aminomethylaniline-diglycolic acid-DPhe-Gln-Trp-Ala-Val-Gly-His-NH-CH[CH₂-CH(CH₃)₂]₂), based on a potent GRPR-antagonist and derivatized with DOTA to allow for labeling with diagnostic and therapeutic radiometals. The respective [$^{67}\text{Ga}^{111}\text{In}^{177}\text{Lu}$]NeoBOMB1 radioligands have been evaluated in GRPR-expressing prostate cancer PC-3 cells and mice models for potential application in prostate cancer diagnosis and therapy. In addition, first evidence for clinical translation with [^{68}Ga]NeoBOMB1 and PET/CT has been acquired in prostate cancer patients.

Materials and Methods: The affinity of NeoBOMB1 and [$^{nat}\text{Ga}^{nat}\text{In}^{nat}\text{Lu}$]NeoBOMB1 for the GRPR was determined by competition binding assays against [^{125}I -Tyr⁴]BBN in PC-3 cell membranes. The internalization of [$^{67}\text{Ga}^{111}\text{In}^{177}\text{Lu}$]NeoBOMB1 at 37°C in PC-3 cells was compared at 1 h. Mouse blood collected 5 min post-injection (pi) of [$^{67}\text{Ga}^{111}\text{In}^{177}\text{Lu}$]NeoBOMB1 was analyzed by HPLC to evaluate in vivo stability. Biodistribution of [$^{67}\text{Ga}^{111}\text{In}^{177}\text{Lu}$]NeoBOMB1 was studied in SCID mice bearing subcutaneous PC-3 xenografts; for in vivo GRPR-blockade 40 nmol [Tyr⁴]BBN were co-injected in mice. [^{68}Ga]NeoBOMB1 was administered in prostate cancer patients and PET/CT scans were acquired. **Results:** NeoBOMB1 and [$^{nat}\text{Ga}^{nat}\text{In}^{nat}\text{Lu}$]NeoBOMB1 showed comparable high affinity for the GRPR (IC₅₀s of 1-2 nM). At 37°C [$^{67}\text{Ga}^{111}\text{In}^{177}\text{Lu}$]NeoBOMB1 strongly and specifically bound to the cell-membrane of PC-3 cells (35-40% at 1 h), as expected for radioantagonists. [$^{67}\text{Ga}^{111}\text{In}^{177}\text{Lu}$]NeoBOMB1 were detected >95% intact in peripheral mouse blood at 5 min pi. In mice, [$^{67}\text{Ga}^{111}\text{In}^{177}\text{Lu}$]NeoBOMB1 showed comparably high and GRPR-specific uptake in the PC-3 xenografts (e.g. $30.6 \pm 3.9\%$ ID/g, $28.6 \pm 6.0\%$ ID/g and $>35\%$ ID/g at 4 h pi, respectively). In prostate cancer patients [^{68}Ga]NeoBOMB1 rapidly localized in pathological lesions achieving high contrast imaging. **Conclusions:** Regardless of the radiometal used, [$^{67}\text{Ga}^{111}\text{In}^{177}\text{Lu}$]NeoBOMB1 displayed comparable behavior in prostate cancer models, highlighting the theranostic strength of NeoBOMB1. Translational evidence in patients was acquired after visualization of prostate cancer lesions by [^{68}Ga]NeoBOMB1 PET/CT with excellent target-to-background ratios and high diagnostic accuracy.

OP150

Therapeutic Efficacy of CXCR4-targeted Endoradiotherapy with Lu-177-pentixather in Patient-Derived Xenograft (PDX) Models of Leukemia

M. Schottelius¹, S. Habringer², P. Herhaus², A. Poschenrieder¹, K. Steiger³, M. Schwaiger⁴, U. Keller², H. Wester¹; ¹Pharmaceutical Radiochemistry, TU Munich, Garching, GERMANY, ²III. Medical Department, Klinikum rechts der Isar, TU Munich, Munich, GERMANY, ³Institute of Pathology, Klinikum recht der Isar, TU Munich, Munich, GERMANY, ⁴Nuclear Medicine, Klinikum rechts der Isar, TU Munich, Munich, GERMANY.

First results in patients with multiple myeloma have demonstrated the therapeutic efficacy of [¹⁷⁷Lu] pentixather as a CXCR4-directed endoradiotherapeutic agent. To assess its potential for the therapy of human leukemic diseases, [¹⁷⁷Lu]pentixather was now evaluated in two PDX models of human-derived T-cell acute lymphoblastic leukemia (T-ALL). Murine PDX models were established by intravenous injection of patient-derived T-ALL cells with comparable CXCR4 expression, but different aggressiveness (ALL230:high, ALL0:low) into NOD/SCID/γ mice. Upon disease manifestation (monitored via ex vivo analyses and [⁶⁸Ga]pentixafor-PET), mice were treated with 25–35 MBq [¹⁷⁷Lu]pentixather. Animals were sacrificed 3d and 7d after therapy, and biodistribution studies were performed. Spleen and bone marrow (BM) of treated and control (injection of unlabeled peptide only) mice were isolated, and the effect of [¹⁷⁷Lu]pentixather therapy on human ALL infiltration and on the murine BM niche were evaluated using FACS analysis and colony forming unit (CFU) assays. Biodistribution studies revealed high [¹⁷⁷Lu]pentixather uptake in ALL-infiltrated spleens and BM (ALL230: 22.9±16.6 and 1.1±0.5%ID/g, ALL0: 2.4±1.4 and 0.6±0.03%ID/g in spleen and femur (3d p.i.), respectively), which correlates with the different extent of ALL infiltration in the two PDX models (Additional Information). Accordingly, upon [¹⁷⁷Lu] pentixather treatment, the spleen size, which reflects ALL infiltration, was reduced by a factor of 12.1 (47.6) and 2.0 (2.8) compared to control in the high-tumor-burden (ALL230) and low-tumor-burden (ALL0) model at 3d (7d) p.i., respectively. FACS analysis of spleen, BM and blood confirmed a reduction of ALL infiltration by 83%, 61% and 47% in the ALL230 model versus 15% reduction of BM infiltration in the ALL0 model (7d p.i.). Despite low affinity of [¹⁷⁷Lu]pentixather to murine CXCR4, mouse hematopoietic progenitor cells in the BM are indirectly targeted by crossfire effect and are almost completely eradicated by [¹⁷⁷Lu] pentixather therapy in both PDX models (CFU count Control vs. [¹⁷⁷Lu] pentixather: 29.5±20.9 vs 0±0 (ALL230), 130.5±20.0 vs. 33.2±9.6 (ALL0) (3d p.i.)). In contrast, mesenchymal stromal cells isolated from the murine BM niche of [¹⁷⁷Lu] pentixather-treated animals were reduced, but able to regenerate, as shown by their potential to support the self-renewal and differentiation of mouse hematopoietic stem cells in co-culture experiments. CXCR4-targeted endoradiotherapy using [¹⁷⁷Lu] pentixather is highly efficient in reducing leukemia in murine ALL PDX models. Under consideration of the necessity of stem cell support, [¹⁷⁷Lu] pentixather thus represents a highly promising therapeutic option for patients with leukemia, complementing diagnostic [⁶⁸Ga] pentixafor-PET to a first powerful CXCR4-targeted theranostic concept, which is currently being translated into the clinic.

OP151

Comparison between the antagonist ⁶⁸Ga-OPS202 and the agonist ⁶⁸Ga-DOTATOC for somatostatin receptor PET/CT in gastroenteropancreatic NET patients: results of a phase 1/2 study

G. Nicolas¹, N. Schreiter², F. Kaul¹, J. Uijters², R. Mena², A. Bauman¹, J. Kaufmann², H. Bouterfa², J. Reubi³, J. Rivier⁴, H. Maecke⁵, R. Cathomas⁶, E. Christ⁷, M. Fani¹, D. Wild¹; ¹Dept of Radiology and Nuclear Medicine, University of Basel Hospital, Basel, SWITZERLAND, ²OctreoPharm Sciences, Ipsen Group, Berlin,

GERMANY, ³Division of Cell Biology and Experimental Cancer Research, Institute of Pathology, University of Berne, Berne, SWITZERLAND, ⁴Clayton Foundation Laboratories for Peptide Biology, Salk Institute, La Jolla, CA, UNITED STATES, ⁵Department of Nuclear Medicine, University Hospital Freiburg, Freiburg, GERMANY, ⁶Dept of Oncology, Kantonsspital Graubünden, Chur, SWITZERLAND, ⁷Department of Endocrinology, University Hospital of Berne, Berne, SWITZERLAND.

Introduction/Background: ⁶⁸Ga-DOTATOC PET/CT is a reference method for imaging somatostatin receptor expressing neuroendocrine tumours (NET). Presence and extent of metastases, especially liver metastases, impact highly on patient management and prognosis. **Aims:** To investigate safety, biodistribution, dosimetry and preliminary efficacy of ⁶⁸Ga-OPS202, a radiolabelled somatostatin receptor antagonist for PET/CT imaging of gastroenteropancreatic (GEP) NET (ClinicalTrials.gov NCT02162446). **Materials and Methods:** Twelve metastatic G1/G2 GEP-NET patients were enrolled in a prospective phase 1/2 study. Safety, biodistribution, dosimetry and preliminary efficacy were assessed after administration of 2 single doses of ⁶⁸Ga-OPS202 (A: 15µg then B: 50µg within 3 to 4 weeks). Both ⁶⁸Ga-OPS202 PET/CT were compared to ⁶⁸Ga-DOTATOC PET/CT (~15 µg) in the same patient and using the same scanner. Uptake in normal organs (SUVmax) and tumour-to-background uptake ratios were compared for matched pairs using the Wilcoxon signed rank test. Two independent readers blinded from clinical information and type of scans reviewed the PET/CT. Follow-up imaging up to 9 months were used as standard of reference. **Results:** ⁶⁸Ga-OPS202 was well tolerated and no adverse reaction requested treatment. The median time between ⁶⁸Ga-OPS202 (dose A) and ⁶⁸Ga-DOTATOC PET/CT was 34 days. On the 1 hour post-injection scans, each ⁶⁸Ga-OPS202 dose showed lower SUVmax in the normal liver, the pancreas and the gastro-intestinal (GI) tract (p<0.05), but similar uptake in malignant lesions in comparison with ⁶⁸Ga-DOTATOC; thus image contrast and tumour detection rate were significantly improved over the agonist. The liver-lesions-to-normal-liver uptake ratio (mean±σ) increased from 3.0±4.1 for ⁶⁸Ga-DOTATOC to 5.7±6.9 (A)/6.0±7.4 (B) for ⁶⁸Ga-OPS202 (p<0.05). On a per-lesion basis sensitivity and diagnostic accuracy (pooled for both readers) improved from 52 and 52% for ⁶⁸Ga-DOTATOC to 81 and 83% (for ⁶⁸Ga-OPS202 dose A) and 89 and 90% for dose B respectively. **Conclusion:** ⁶⁸Ga-OPS202 is well tolerated, significantly improves imaging contrast, sensitivity and diagnostic accuracy compared to ⁶⁸Ga-DOTATOC PET/CT, especially in the liver. The lower GI and pancreatic uptake of the antagonist may increase the sensitivity of PET for detecting sites of primary tumours of GEP origin.

OP152

Radiolabeled Gastrin-Releasing-Peptide receptor antagonist (⁶⁸Ga-RM2) PET/CT in newly-diagnosed prostate cancer (PCa), compared and combined with multiparametric prostate MRI

L. Michaud, I. Sandler, B. Beatty, A. Gopalan, S. Lyaschenko, N. Taunk, J. Lewis, H. Hricak, A. Vargas, K. Touijer, W. Weber; MSKCC, New York, NY, UNITED STATES.

Purpose: We evaluated the ability of ⁶⁸Ga-RM2 PET/CT to localize newly-diagnosed PCa, comparing it to MRI and assessing the additional value of combined ⁶⁸Ga-RM2 PET/CT-MRI. **Methods:** As part of an ongoing prospective study, we have so far included sixteen men (age 46–68 y) with biopsy proven PCa (2 low, 8 intermediate and 6 high risk). PSA range was 1.4–64.4 ng/mL with Gleason scores ranging between 6 and 9. All patients underwent multiparametric prostate MRI, no more than 4 weeks prior ⁶⁸Ga-RM2 PET/CT. PET/CT scans, from mid thighs to top of skull, were performed 60 minutes after injection of 150–200 MBq ⁶⁸Ga-RM2. All patients underwent radical prostatectomy and lymph node dissection no more than 2 weeks after the PET/CT scan. For data analysis the prostate was divided in 4 areas (right anterior, right posterior, left

anterior and left posterior; total 64 prostatic areas). The presence of PCa was evaluated using a 5-point scale by a genitourinary radiologist for MRI and 2 nuclear medicine physicians for PET/CT. Lesions with a score of 4 or 5 were considered as positive. In addition, uptake of ^{68}Ga -RM2 uptake within each area was quantified by standardized uptake values (SUVmax). After the independent analysis of PET/CT and MRI a combined analysis of PET/CT fused to MRI was performed. Whole mount, step-section pathology of the prostate served as the reference standard. Presence of extracapsular extension (ECE), seminal vesicle involvement (SVI), and lymph node metastasis was also recorded. **Results:** On histology, PCa was present in 55 of the analyzed regions. Sensitivity of MRI, PET/CT and combined analysis was 67%, 81%, 84%; specificity 89%, 78%, 89%; accuracy 70%, 81%, 84%, respectively. Receiver-operating characteristic (ROC) analyses for SUVmax yielded an area under the curve of 0.79 (95% confidence interval 0.618–0.956, $p = 0.006$). Twelve patients had ECE; 11/12 were identified by MRI, only 4 detected by PET/CT. 4/16 tumors showed SVI; 2/4 reported on MRI, non on PET. 3/16 patients had lymph node (LN) metastasis; 2 detected only by MRI and 1 only by PET. One patient was false positive for LN metastasis on MRI. **Conclusion:** According to this preliminary analysis, ^{68}Ga -RM2 PET/CT is promising for detection and localization of primary PCa. Combined ^{68}Ga -RM2 PET-MRI provided complementary value for the evaluation of newly-diagnosed PCa.

OP153

Comparison between CT-based and PERCIST criteria for evaluation of response to immune checkpoint inhibitors in Non-Small Cell Lung Cancer (NSCLC): is there a role for 18F-FDG PET/CT?

M. Bauckneht¹, G. Rossi², R. Piva¹, C. Genova², E. Rijavec², G. Barletta², F. Biello², S. Menella³, M. Dal Bello², R. Di Stefano², G. Cittadini³, D. Merlo⁴, G. Sambucetti¹, F. Grossi², **S. Morbelli¹**, ¹Nuclear Medicine Unit, IRCCS San Martino - IST, University of Genoa, Genoa, ITALY, ²Lung Cancer Unit, IRCCS San Martino - IST, Genoa, ITALY, ³Radiology Department, IRCCS San Martino - IST, Genoa, ITALY, ⁴Epidemiology, Biostatistics and Clinical Trials Division, IRCCS San Martino - IST, Genoa, ITALY

Background: Immune checkpoint inhibitors exert their activity by blocking inhibitory signaling therefore enhancing T-cell activity against tumor cells. This peculiar mechanism of action may hamper dimensional CT-based response evaluation due to infiltration of inflammatory cells. The aim of this study was to compare CT-based and PERCIST criteria for evaluation of response to immune checkpoint inhibitors in NSCLC. **Methods:** From May 2015 to April 2016, 74 patients with advanced pretreated NSCLC were treated with the checkpoint inhibitor nivolumab in the frame of a single-institutional translational research trial. The patients underwent both contrast enhanced (ce)CT and 18F-FDG-PET at baseline and every four cycles. We evaluated the response to treatment by ceCT scan with either RECIST and Immuno-related Response Criteria (irRC) and metabolic response by means of PERCIST criteria. Concordance between CT-based and PERCIST criteria was computed with kappa value. **Results:** A low concordance between both CT-based criteria and PERCIST was highlighted with a relatively higher concordance between PERCIST and RECIST criteria ($k=0.500$). In particular PERCIST seems to underestimate the presence progressive disease (PD). In fact, 46% and 55% of patients defined in progression with RECIST and irRC criteria were considered in stable metabolic disease (SMD) according to PERCIST. Among these, only 50% were alive at 6 months and only one of them reached a partial metabolic response (PMR) by continuing treatment with nivolumab. Conversely, 9% and 18% of the patients considered in progression with irRC and RECIST criteria were classified as PMR with PERCIST. Of note, all these patients are still alive with a survival rate similar to those defined in partial response with RECIST and irRC criteria (>9 months). Capability of both CT-based and PERCIST criteria to predict overall survival could not be evaluated as patients' sample have not yet reached the median overall survival. **Conclusion:** Given the peculiar mechanism of

action of immune checkpoint inhibitors, 18F-FDG-PET as evaluated with PERCIST criteria is not informative when patients are classified as SMD. SMD group includes both not- and late-respondents patients. In fact, when SMD patients were classified as PD according to RECIST they maintained (despite their metabolic stability) a poor prognosis compared to patients classified as RECIST-stable. Conversely, PERCIST evaluation could provide relevant information when it defines a PMR in presence of RECIST progressive disease. These patients seem to have a longer survival and thus 18F-FDG PET might impact on clinician's decision making in patients with suspected CT-based PD in the future.

OP154

Dose escalation experience with Ac-225-PSMA-617 in PSMA targeting alpha-radiation therapy of patients with mCRPC

C. Kratochwil¹, F. Bruchertseifer², F. L. Giesel¹, C. Apostolidis², U. Haberkorn¹, A. Morgenstern²; ¹University Hospital Heidelberg, Heidelberg, GERMANY, ²European Commission - Joint Research Centre, Institute for Transuranium Elements, Karlsruhe, GERMANY

Aim: To develop a standard treatment protocol for Ac-225-PSMA-617 PSMA targeting alpha-radiation therapy. **Methods:** Treatment dose in kBq per kg body-weight (kBq/kgBW) was stepwise increased from 50 kBq/kg (n=2), 100kBq/kgBW (n=2), 150kBq/kgBW (n=2) and 200 kBq/kgBW (n=4). Additionally, a 2-monthly fractionation regime was compared with a 4-monthly administration interval (n=4). Hematological toxicity, clinical exam and patient self-reported side-effects were assessed every 4 weeks, in case of irregular findings every 2 weeks. In addition PSA was also checked every 4 weeks. **Results:** Severe xerostomia was dose-limiting before hematological toxicity became relevant. 3 patients with 200kBq/kg and 1 patient with 150kBq/kg requested dose reduction. Thus 100kBq/kgBW was defined as standard treatment dose per cycle. 2/4 patients with a 4-monthly treatment interval had PSA-progression before the succeeding cycle, which then also demonstrated also to be less effective than the 2nd cycle during the 2-monthly treatment regime. With doses above or equal to 100 kBq/kgBW per cycle tumor response in regard to a PSA-decline of >50% was demonstrated in about 70% of the treated patients. **Conclusions:** A standard treatment dose of 100kBq/kgBW administered every two month seems both associated with remarkable anti-tumor activity and tolerability. In our hospital it became the standard treatment activity for the first phase of routinely clinical application as a salvage therapy for mCRPC.

501 – Sunday, October 16, 2016, 16:30 – 18:00, Auditorium

CME 4 - Radiopharmacy/Drug Development: Antibody-Based Radiopharmaceuticals

OP155

The Site-Specific Modification of Antibodies for Molecular Imaging and Therapy

B. M. Zeglis; Center for Translational and Basic Research (CTBR), Hunter College, CUNY, Department of Chemistry, New York, UNITED STATES OF AMERICA.

OP156

Pre-Targeting Approaches with Antibodies for Cancer Imaging and Therapy

J. Barbet; Inserm, Université de Nantes, Centre de Recherche en Cancérologie de Nantes-Angers, Nantes, FRANCE.

OP157

Good Manufacturing Practice (GMP) Production of Antibodies and Antibody Conjugates

M. Mattarella; Philochem AG, Otelfingen, SWITZERLAND.

502 – Sunday, October 16, 2016, 16:30 - 18:00, Hall 211

Joint Symposium 4 - EANM/ESTRO: SBRT - Trend or the Next Change in a Treatment Paradigm?

OP158

Early Stage Lung Cancer - SBRT as an Alternative to Treatments with Curative Intent

X. Geets; Université Catholique de Louvain, St-Luc University Hospital, Radiation Oncology Dept & Center for Molecular Imaging and Experimental Radiotherapy, Louvain, BELGIUM.

OP159

Early Stage Lung Cancer - Role of PET/CT as a Guide to SBRT in Treatment Planning and Follow-Up

R. C. Delgado-Bolton; San Pedro Hospital - Centre for Biomedical Research of La Rioja (CIBIR), Servicio Riojano de Salud (SERIS), Department of Diagnostic Imaging (Radiology) and Nuclear Medicine, Logroño - La Rioja, SPAIN.

OP160

Oligometastatic Disease - SBRT as an Alternative to Treatments with Curative Intent

M. Høyer; Aarhus University Hospital, Department of Oncology, Aarhus, DENMARK.

OP161

Oligometastatic Disease and SBRT - Role of PET/CT as a Guide in Treatment Planning and Follow-Up

P. Vera; CENTRE HENRI BECQUEREL, Rouen, FRANCE.

504 – Sunday, October 16, 2016, 16:30 - 18:00, Hall 112

Do.MoRe - Featured: Thyroid Dosimetry

OP162

Personalized Treatment of Thyroid Cancer

M. Lassmann; Universitätsklinikum Wuerzburg, Klinik fuer Nuklearmedizin, Wuerzburg, GERMANY.

OP163

Cellular Distribution and Small-scale Dosimetry of [¹⁸⁸Re]-perrhenate: A Potential Therapeutic Radiotracer for Thyroid Disease

K. Chuamsaamarkkee^{1,2}, A. Divoli³, P. J. Blower², L. Livieratos^{2,4}; ¹Nuclear Medicine, Ramathibodi Hospital Mahidol University, Bangkok, THAILAND, ²Division of Imaging Sciences and Biomedical Engineering, King's College London, London, UNITED KINGDOM, ³Institute of Cancer Research and the Royal Marsden NHS foundation Trust, London, UNITED KINGDOM, ⁴Nuclear Medicine, Guy's & St Thomas' Hospitals NHS Foundation Trust, London, UNITED KINGDOM.

Background: Our recent studies with preclinical MIRD dosimetry (“macrodosimetry”) showed promising results for [¹⁸⁸Re]-perrhenate as candidate for therapy of thyroid benign disease. However, macrodosimetry assumes uniform distribution of radiotracer throughout the organ and this assumption is not always correct. Iodine (e.g. [¹³¹I]-NaI) is taken up by follicular cells then incorporated into thyroid hormone and stored in colloid until exported. We hypothesise that, in contrast, non-metabolised tracers (e.g. [^{99m}Tc]-pertechnetate, [¹⁸⁸Re]-perrhenate) not involved in hormone synthesis are solely localised within thyrocytes, being imported by NIS but not

further metabolised. No experimental data are available to confirm this. Therefore, this study aims to examine the cellular distribution of [^{99m}Tc]-pertechnetate and [¹⁸⁸Re]-perrhenate in a thyroid model and use the resulting data for small-scale dosimetry (“microdosimetry”) to assess the potential of [¹⁸⁸Re]-perrhenate for radionuclide therapy of thyroid disease. **Methods:** [¹⁸⁸Re]-perrhenate was intravenously injected into Wistar rats. After 1 h, thyroids were harvested and cryosectioned to determine radionuclide distribution by microautoradiography (MAR). After developing and fixing, the combined MAR emulsion and tissue section was fluorescently stained with DAPI and viewed under a fluorescence microscope. Post-processing technique was used to enhance the silver grains. For microdosimetry, a geometrical model was derived from MAR images propagated in 3D. The matrix size was 128 x 128 x 5 voxels with voxel size 16 μm³. Input files for the MCNPX version 2.5.0 Monte Carlo code were created using an IDL interface OEDIPE with tissue compositions taken from ICRU 44. Absorbed doses were recorded at each voxel and dose volume histograms were created using IDL. **Results & Discussion:** MAR showed that perrhenate localised only in thyrocytes and not present in colloid (the reverse of the known distribution of radioiodine). Microdosimetry demonstrated that [¹⁸⁸Re]-perrhenate has potential dosimetric advantages over [¹³¹I]-iodide. By assuming follicular cells as targets for cell killing, ¹⁸⁸Re distributed in follicular cells resulted in absorbed doses higher and more uniform (FWHM: 10.62 - 19.86 mGy/MBq.s) than ¹³¹I localised in colloid (FWHM: 6.03 - 17.78 mGy/MBq.s). **Conclusion:** Radiation dose delivered to the thyrocyte is strongly dependent on sub-cellular distribution of radiotracers. These pilot data provide microdosimetric support for the macrodosimetric prediction that [¹⁸⁸Re]-perrhenate for treatment of thyroid disease may have advantage or complementarity, encouraging radiobiological evaluation of [¹⁸⁸Re]-perrhenate treatment to assess the feasibility of clinical translation.

OP164

Automatic acquisition and analysis of whole-body time activity curves demonstrates distinct compartments during NaI treatment.

D. P. Rushforth, J. I. Gear, S. J. Chittenden, B. E. Pratt, I. A. Murray, G. D. Flux; The Joint Department of Physics, Sutton, UNITED KINGDOM.

Introduction: Following molecular radiotherapy (MRT), multiple measurements of whole-body activity (WBA) retention are required to determine the whole-body absorbed doses (WBD), excretion rates and external dose rates. This is necessary for treatment validation, as required by European council directive 2013/95/Euratom, and accurate radiation protection advice, as described by ICRP94. **Aims:** To provide a complete package for the acquisition of cumulated WBA measurements and the automatic production of WBDs and radiation protection advice. To investigate the potential of the system for improving personalised MRT treatment. **Method:** A program was created that interfaces with three Geiger counters, each positioned above beds within different therapy rooms. An intuitive interface was designed to make it easy for staff to collect multiple precise and accurate measurements throughout the day. The display constantly displays a live count rate from each detector and maximum visiting times, based on local dose constraints. A quality control mode facilitates testing of the detectors and an export function automatically saves data to the secure hospital network. Whole-body time activity curves, consisting of multiple simultaneous exponential phases, are derived using an algorithm that automatically determines the curve stripping solution with the least square residual; allowing standardised WBDs and restriction times to be calculated instantly. **Results:** To date the system has been used for 31 I-131 NaI treatments for thyroid carcinoma (ablation and therapy) and 11 Y-90 DOTATATE treatments, with an average of 6 readings per patient per day. In the case of the NaI treatments, all patients demonstrate a phase with a 13.0 ± 2.6 hour half-life. 70 % of patients also demonstrate a phase with a shorter 4.09 ± 1.83 hour half-life containing 17 ± 14 % of the total cumulated activity (max of 47 %). Slower phases with half-lives of 46 and 86 hours (81 and 87 % of total cumulated activity) were also detected in two patients with heavy disease burden, for whom later measurements were

made. Conclusion: A system was created which has enabled the acquisition of high quality WBA data and reduced the time necessary for dosimetry calculations. Analysis of the stripped phases has led to the observation of two well defined compartments that demonstrate consistency across patients. Results indicate that a third compartment may be identified from measurements made at later time points. Further work aims to determine if this compartmental approach can be used to localise the deposition of dose in individual patients.

OP165

A set of realistic thyroid phantoms for personalized radioiodine uptake measurement

T. BEAUMONT¹, P. CALDEIRA IDEIAS², O. CASELLES³, D. BROGGIO¹, D. FRANCK¹; ¹Institut de Radioprotection et de Sûreté Nucléaire (IRSN), Fontenay-aux-Roses, FRANCE, ²Institut de Radioprotection et de Sûreté Nucléaire (IRSN), Le Vésinet, FRANCE, ³Institut Universitaire du Cancer Toulouse - Oncopole, Toulouse, FRANCE.

Purpose According to the EANM recommendations for benign thyroid diseases therapy, the absorbed dose should be personalized. Consequently, the iodine thyroid uptake should be accurately measured. Calibration phantoms are quite crude representations of neck anatomy. In order to better simulate thyroid volumes and patient variability, a set of realistic thyroid phantoms with varying volumes have been developed and 3D printed. **Materials and methods** The designed thyroid shape follows the MIRDC committee recommendations and includes the isthmus and two ellipsoidal lobes. Five volumes have been selected from 3.24 to 30 cm³, following ICRP recommendations, to cover different clinical cases: children, adolescents, standard and pathologic adults. The linear attenuation coefficient of the selected material was determined by spectroscopic measurements at the photopeak energy of ¹³¹I and the isthmus-neck distance was chosen accordingly. Neck, vertebra, spinal cord and trachea were also designed and put together to create the final phantoms. Care was taken to ensure the waterproofness and robustness over time of thyroid inserts: special epoxy glue and nylon screw have been used. The design was performed with a Computer Aided Design software and then the phantoms were 3D printed. For measurements, the thyroid inserts have been filled with a liquid ¹³³Ba solution (¹³¹I substitute). **Results** An exponential fit of the experimental data gave an attenuation coefficient of 0.116 cm⁻¹ at 356 keV, bearing out that the material can be considered as tissue equivalent. As a first experiment, the sensibility of a germanium (HPGe) probe was measured for each phantom. At contact with the probe, a 25 % difference in sensitivity between the smallest volume and the 19.05 cm³ volume was observed, decreasing to 10% at 15 cm. Currently, measurements are underway for a NaI probe and gamma-camera in a nuclear medicine department. The goal is to compare the standard calibration procedure with ANSI phantom and a ¹³¹I seed with a new procedure using the developed phantoms filled with an iodine solution. **Conclusion** With ¹³¹I filled realistic thyroid phantoms of different volumes, the assessment of the time-dependent fractional uptake will be improved. Practically, volume dependent calibration factor can be measured and then used after ultrasonic evaluation of the thyroid volume. This procedure might be particularly interesting for children and to reduce the toxicity. Furthermore, the set of phantoms can be used for *in situ* thyroid monitoring of nuclear medicine workers which are presumably subject to chronic exposure.

OP166

Calculating dose to risk organs for complex differentiated thyroid cancers treated with combined I-131 and EBRT using Monte Carlo simulations

J. Nilsson¹, O. Ardenfors^{1,2}; ¹Department of Medical Physics, Karolinska University Hospital, Stockholm, SWEDEN, ²Medical Radiation Physics, Department of Physics, Stockholm University, Stockholm, SWEDEN.

Background: Patients with differentiated thyroid cancer are commonly treated with adjuvant radionuclide therapy (RNT) using I-131 after surgery. In more advanced disease with locoregional invasion and metastasis, adjuvant external beam radiotherapy (EBRT) in the head and neck region is sometimes also employed. For thyroid cancers with tracheal or esophageal invasion, RNT could cause high doses to the organs at risk (OAR). Tumour dose in EBRT is constrained by the doses to different OAR and not accommodating the RNT dose contributions can result in excessive combined OAR doses. Conventional RNT dosimetry using MIRD formalism is not feasible for complex and invasive cancers. The aim of this work was to estimate the dose contributions from RNT using Monte Carlo (MC) methods and to establish their impact on dose limits in EBRT. **Methods:** A patient with a non-radically excised intratracheal thyroid cancer underwent combined RNT and EBRT at our hospital in 2015. Three tumour/remnant sites and two OAR (trachea and esophagus) were delineated on a post-therapeutic SPECT/CT scan. The cumulated activity of iodine in the uptake sites were calculated from two SPECT/CT-acquisitions and three gamma probe measurements. The maximum and mean absorbed doses to OAR were calculated using MC simulations of gamma and beta doses with the code MCNP6. The MC simulations were performed on CT-based geometry and the absorbed doses were calculated from cumulated activity in the three uptake sites. The results were evaluated with regard to dose constraints commonly employed for the OAR in EBRT. **Results:** Mean absorbed doses to the OAR from MC simulations were 0.8 Gy to the trachea and 0.6 Gy to the esophagus (only gamma contributed to the dose). The corresponding maximum absorbed doses to the OAR were 117 Gy to the trachea and 5 Gy to the esophagus (only gamma contributed to the dose). The maximum tracheal dose was at the site of tumour invasion. Mean absorbed doses to the three tumour/remnant sites as calculated by MC simulation were 810 Gy, 560 Gy and 190 Gy. **Conclusions:** The results showed that RNT in non-radical complex tumours can cause doses that risk exceeding OAR limits in EBRT. The calculated doses were in agreement with previously published data for tumour/remnant doses. Monte Carlo dosimetry for RNT is a viable method for planning combined RNT and EBRT in differentiated thyroid cancer.

OP167

Preivisional and post therapy Red Marrow Dosimetry in differentiated thyroid cancer : a method to optimize treatment and efficacy

G. ROSSI¹, M. Camarda¹, P. D'Avenia¹, E. Di Nicola¹, L. Montani¹, C. Bartolozzi¹, F. De Angelis¹, A. Dente¹, N. Gasparini¹, E. Brianzoni², S. Fattori¹; ¹Medical Phisic Unit, Macerata Hospital, MACERATA, ITALY, ²Nuclear Medicine Unit, Macerata Hospital, MACERATA, ITALY.

Introduction In multi treated DTC patients(pts)it is fundamental knowing the maximum tolerated dose(MTD) to the red marrow(RM) in order to administer the best therapy, and subsequently verify the effective absorbed dose to evaluate the clinical utility and define the correct staging. **Materials and methods** We enrolled 66 pts(35 M 31 F)with DTC. 10 pts with 2 evaluation and 3 with 3, for a total of 85 calculations.All pts were in thyroid hormone withdrawal.On the first day,TSH,hTG,AbhTG,Ioduria and aematochemical routine were evaluated then ¹³¹I was administered(median 18 MBq, range 8-21),fasting and no urine excretion for 2 hours. According to the AIFM protocol we collected blood sample(BS)and whole body(WB)counts at 2-24-48-96-120 h.We calculated tau(SAAMII)and the MTD(OLINDA/EXM)after blood/RM approximation considering the 2 GY/RM limit and 2960 MBq of WB retention at 48^oh(if pulmonary metastases).Then considering dosimetry we administered the ¹³¹I-therapy MTD(range 1019-9334 MBq) sometimes modulated.In therapy we repeated the data collection and calculations.Pts have made every 20 days for three months aematochemical routine.Results No pts overcame 2 Gy/RM.The pre-post comparison shows differences greater than 50% for WB in 18/66 pts(27%, 12 lower 6 higher),for the RM in 14/66(20%, 1 higher and 13

lower). The absorbed RM dose range is 0.17–1.9 Gy. In the 10 multidosimetry pts we found big deviation between different dosimetric evaluation: for 2/10 more than 400% (19–21 months between treatments), for 7 dosimetries from 3% to 76% for WB and 2% to 53% for RM (6–12 months). No side effect of elevated grade for the aemathological syneresis. Conclusions The previsional dosimetry allows to avoid to overcome 2 Gy/RM. High variation pre-post often is due to a significative modification of the staging at the WB scan post treatment. It is then desirable to repeat dosimetry for further treatment and to study metastases to modulate the following one.

OP168

Accuracy, Precision and Operator-Variability of Co-registered Early CT with Delayed SPECT in Quantitative Parathyroid Scans

S. Razavi, B. Ziebarth, L. Zuckier, R. Klein, **W. Zeng**; The Ottawa Hospital, Ottawa, ON, CANADA.

Introduction Dual phase parathyroid scintigraphy utilizing early (15–20 min) and delayed (2 hour) planar or SPECT images of the neck and the upper chest following ^{99m}Tc SestaMIBI is a well-established procedure for the diagnosis of parathyroid adenoma or hyperplasia. SPECT-CT allows for anatomical localization and attenuation correction, and is added to imaging at either early or delayed SPECT-CT in many centres; both early and delayed SPECT-CT is not usually performed due to concern over duplicated CT exposure. The goal of this study was to assess feasibility and reproducibility of reconstructing delayed SPECT-CT images by fusing early CT and delayed SPECT images. **Methods** 15 patients with suspected parathyroid adenoma or hyperplasia who had both early and delayed SPECT-CT of the neck were included for retrospective analysis. Delayed SPECT images were reconstructed using attenuation, scatter, and resolution recovery correction derived from the contemporaneous delayed CT and quantified in SUV units (HERMES HybridRecon); these were considered the gold standard values. Delayed SPECT (with all corrections) was manually co-registered with early CT on 3 occasions by an experienced technologist and once by a novice physicist. Maximum SUV of the thyroid lobes, parathyroid adenomas and ectopic parathyroid adenoma were measured by a board certified nuclear medicine physician on all 5×15 image sets. Bland-Altman and correlations analyses was used to evaluate accuracy, intra-operator variability of the experienced technologist, and inter-operator variability, and the results of which were summarized using bias, absolute SUV and relative to mean reproducibility coefficient (RPC = 95th percentile of errors) and Pearson r^2 . **Results** Maximum SUV measurements were obtained for 14 right thyroids, 10 left thyroids, 6 parathyroid adenomas, and 4 ectopic adenomas. Due to the small sample size and challenging co-registration, ectopic adenomas were excluded from the analysis. For the 30 remaining regions, the accuracy on the 3 sets of reconstructed image from experienced-operator was excellent (no bias, $p=0.2$), with good reproducibility of true SUV at $\text{RPC}=0.63$ (33%), $r^2=0.82$. Suboptimal reproducibility of true SUV was recorded in images reconstructed by the novice operator, with $\text{RPC}=0.88$ (44%), $r^2=0.70$. Intra-operator reproducibility for experienced operator was excellent at $\text{RPC}=0.22$, (12%), $r^2=0.85$, but the agreement with the novice operator was less optimal at $\text{RPC}=0.49$ (48%), $r^2=0.64$. **Conclusions** Delayed quantitative SPECT imaging of the parathyroid using manually registered early CT imaging is feasible, precise and accurate by experienced technologists. Training of technologists for accurate and reproducible co-registration is essential to achieve optimal quantitative measurements.

505 – Sunday, October 16, 2016, 16:30 – 18:00, Hall 115

M2M - Featured: SPECT/CT - Preclinical

OP169

SPECT/CT - Preclinical

O. Boerman; Radboud University Nijmegen Medical Centre, Nuclear Medicine, Nijmegen, NETHERLANDS.

OP170

Truncated CD31 as a new molecular target for imaging of inflammation

J. Vigne^{1,2}, J. Senemaud², N. Anizan³, S. Delbosc², D. Diallo³, A. Truffier², L. Louedec², A. Nicoletti², F. Rouzet^{1,2,3}, G. Caligiuri^{1,2}, D. Le Guludec^{1,2,3}; ¹Bichat University Hospital, Paris, FRANCE, ²INSERM UMRS 1148 - LVTS, Paris, FRANCE, ³University Paris Diderot, Paris, FRANCE.

FDG PET offers sensitive detection of inflammation but suffers from poor specificity and physiologic uptake in heart and brain. There is room for novel imaging agents of inflammation. CD31 is a transmembrane glycoprotein receptor constitutively expressed by leukocytes, platelets, and endothelial cells. Due to its homophilic and inhibitory functions it exerts a crucial role in the homeostasis of the circulation. In pro-inflammatory conditions, the homophilic portion of receptor is lost due to a cleavage and activated cells express a truncated CD31. We have identified a small peptide, named P8RI, able to specifically bind the truncated CD31 on activated endothelial cells, platelets and leukocytes, all present in close vicinity at sites of ongoing inflammation. The main objective of this work was to develop a ^{99m}Tc labelled-P8RI and test its potential as a radiotracer for molecular imaging of inflammation. Hydrazinonicotinamide (HYNIC) was coupled to the N-terminal amino-acid of P8RI. ^{99m}Tc labelling of HYNIC-P8RI was performed using tricine and EDDA as coligands. Radiochemical purity (RCP) was determined using HPLC. The radiolabelled peptide stability (% RCP) and protein binding (size exclusion chromatography) have been assessed in human plasma at 37°C over 4h. ^{99m}Tc P8RI biodistribution and specific uptake by activated platelets and leukocytes have been evaluated in a rat model of chronic vascular inflammation: the experimental abdominal aorta aneurysm (AAA) induced by local infusion of elastase. Immediately after intravenous injection of 74 MBq of radiolabelled HYNIC-P8RI, sequential whole-body acquisitions (every 10 minutes for the first hour) were performed with a hybrid SPECT/CT camera (NanoSPECT/CT, Bioscan Inc.). The RCP of [^{99m}Tc]EDDA/HYNIC-P8RI was >93% without any purification, and the specific activity was >71 GBq/μmol. There was no significant release of degraded radiolabelled peptide (RCP > 89%) and the radiotracer binding to plasma proteins was low (< 5% after 4 h incubation). In vivo blood clearance of the tracer was almost exclusively renal with a peak activity in kidneys and bladder 1 h after injection, corresponding to the unaltered form of the peptide on HPLC. In addition, ^{99m}Tc -HYNIC-P8RI uptake by AAA was detectable from 30 min after injection in animals and associated with activated platelets and leukocytes on immunohistochemistry. By specifically targeting activated cells involved in inflammation expressing truncated CD31, and with a rapid blood clearance, radiolabelled P8RI offers a promising novel approach in inflammation imaging. Further experiments will allow to determine its diagnostic value comparatively to FDG, particularly in models of heart or brain inflammation.

OP171

Prospects of targeting the gastrin releasing peptide receptor, the chemokine c-x-c motif receptor type 4 and the somatostatin receptor subtype 2 in primary breast cancer and metastases

S. U. Dalm¹, W. A. M. E. Schrijver², A. M. Sieuwerts¹, M. P. Look¹, A. C. J. Ziel - van der Made¹, V. de Weerd¹, J. W. Martens¹, P. J. van Diest², M. de Jong¹, C. H. M. van Deurzen¹; ¹Erasmus MC, Rotterdam, NETHERLANDS, ²University Medical Center Utrecht, Utrecht, NETHERLANDS.

Background: Imaging and therapy using somatostatin receptor (SSTR) radioligands targeting SSTRs overexpressed on tumor cells are methods successfully used in patients with neuroendocrine tumors. Based on this success, gastrin releasing peptide receptor (GRPR) and chemokine c-x-c motif receptor type 4 (CXCR4) radioligands are currently being investigated for the same purposes. Previous research has demonstrated GRPR, CXCR4 and SSTR2 expression on breast cancer (BC) cells. These studies were solely performed in primary BC, probably due to scarcity of tumor material from metastatic lesions. However, targeting these receptors with radioligands could especially be advantageous for treatment of metastatic BC, since distant metastases are often not accessible for resection and most systemic agents are accompanied by severe side effects. Furthermore, imaging of primary and metastatic BC can offer possibilities such as image guided surgery/biopsy, disease monitoring and sentinel node visualization. Therefore, the aim of this study was to determine GRPR, CXCR4 and SSTR2 expression in primary BC and corresponding regional and distant metastases, in order to study the prospects of targeting these receptors in BC patients. **Materials and methods:** Fifty-two primary BCs and corresponding regional lymph node or distant metastases (lung, liver, brain and ovarian) were selected for this study. GRPR, CXCR4 and SSTR2 mRNA levels were determined on macro-dissected tumor cells using RT-qPCR. Receptor expression levels of primary BC and corresponding metastases were compared and correlated with clinico-pathological factors. Furthermore, GRPR and SSTR2 expression of 12 paired primary BC and regional lymph node metastases were analyzed by in vitro autoradiography using GRPR-targeting ^{111}In -JMV4168 and SSTR-targeting ^{111}In -DOTA-Tyr³-octreotate, and correlated with corresponding mRNA levels. **Results:** There was no significant difference in GRPR and CXCR4 mRNA levels between primary BCs and corresponding metastases from different sites. SSTR2 mRNA expression of liver and ovarian metastases was significantly lower than that of corresponding primary tumors ($p=0.02$ and $p=0.03$, respectively). GRPR and SSTR2 mRNA levels showed a significant positive correlation with estrogen receptor (ER) expression in primary BC ($p<0.001$ for both receptors) and metastases ($p<0.001$, $p=0.02$, respectively). CXCR4 mRNA expression showed no significant association with the studied clinico-pathological factors. Binding of GRPR and SSTR2 radioligands to tumor tissue was target-specific and correlated significantly with receptor mRNA expression. **Conclusion:** Targeting the GRPR, CXCR4 and SSTR2 for nuclear imaging and/or treatment might improve BC care in primary and metastatic disease. GRPR and SSTR2 (but especially GRPR) could be good candidates for imaging and treatment of ER-positive primary and metastatic BC.

OP172

Influence of the N-terminal amino acid sequence on imaging properties of ^{111}In -labeled anti-HER2 scaffold protein ADAPT6

J. Garousi¹, S. Lindbo², H. Honarvar¹, J. Vellella¹, B. Mitran³, M. Altai¹, A. Orlova³, V. Tolmachev¹, S. Hober²; ¹Department of Immunology, Genetics and Pathology, Uppsala University, Uppsala, SWEDEN, ²Department of Protein Technology, KTH - Royal Institute of Technology, Stockholm, SWEDEN, ³Preclinical PET Platform, Department of Medicinal Chemistry, Uppsala University, Uppsala, SWEDEN.

Aim. ADAPTs (ABD-based Derived Affinity ProTein) constitute a novel type of imaging probes derived from an albumin-binding domain (ABD) scaffold of the protein G. Previous study concerning influence of purification tag composition on biodistribution of radiolabeled anti-HER2 ADAPT6 indicated that N-terminal amino acid sequence (DEAVDANS) may have an impact on targeting using ADAPTs. This sequence is a part of the scaffold, but does not participate in recognition of a molecular target. The aim of this study was to evaluate if modification of composition of the N-terminal sequence

can improve imaging properties of ADAPTs. **Materials and methods.** A series of ADAPT6 variants with different N-terminal sequences GCH₆DANS, GC(HE)₃DANS, GCDEAVDANS and GCVDANS were constructed. A parental variant with GCSS(HE)₃DEAVDANS sequence was used for comparison. DOTA chelator was site-specifically conjugated to a unique N-terminal cysteine of new constructs, and ADAPTs were labeled with ^{111}In . HER2-expressing cell lines, ovarian carcinoma SKOV-3 and breast carcinoma BT474, were used for evaluation of binding and cellular processing in vitro. Pre-saturation of receptors with anti-HER2 antibody trastuzumab was used to test the binding specificity. A series of comparative biodistribution studies in normal NMRI and BALB/C nu/nu mice bearing SKOV-3 xenografts was performed. **Results.** Affinity to HER2 was in the range of 1.0–2.7 nM (SPR measurements) for all ADAPT variants. All radiolabelled variants demonstrated specific binding to HER2-expressing cells. The internalization of all conjugates by HER2-expressing cells was rather slow (less than 50% after 24 h). The internalization of all variants was slow. The major finding of this study was the strong influence of the N-terminal sequence on uptake of ADAPTs in normal tissues and tumor xenografts in mice. In vivo comparison of ^{111}In -labelled DOTA-GCSS(HE)₃DEAVDANS-ADAPT6, DOTA-GCH₆DANS-ADAPT6 and DOTA-GC(HE)₃DANS-ADAPT6 demonstrated that a presence of a hexahistidine tag is associated with elevated hepatic uptake. Uptake in blood, lung, spleen and muscle for all new variants was lower than for the parental variant. ^{111}In -DOTA-GC(HE)₃DANS-ADAPT6 and ^{111}In -DOTA-GCVDANS-ADAPT6 were the best variants, and provided tumor uptakes of 14.6 ± 2.4 and 12.5 ± 1.3 %ID/g at 4 h p.i., respectively. The tumor uptakes of these variants were significantly ($p<0.05$) higher than the uptake of the parental ^{111}In -DOTA-GCSS(HE)₃DEAVDANS-ADAPT6 (9.1 ± 2.0 %ID/g). Tumor-to-blood ratios for ^{111}In -DOTA-GC(HE)₃DANS-ADAPT6 and ^{111}In -DOTA-GCVDANS-ADAPT6, was 395 ± 75 and 419 ± 91 at 4 h p.i., respectively. **Conclusion.** The composition of N-terminus sequence of ADAPT molecules influences their biodistribution and targeting properties. The imaging contrast might be appreciably improved by selection of an optimal variant.

OP173

Comparison of In-111- and Tc-99m-labeled exendin-3 for determination of the beta cell mass with SPECT

L. Joosten, M. Brom, O. C. Boerman, M. Gotthardt; Radboud University Medical Center, Nijmegen, NETHERLANDS.

Aim The beta cell mass (BCM) plays a key role in the development and progression of diabetes. A non-invasive method to determine the BCM *in vivo* would allow measurement of the BCM during the development and progression of type 1 and 2 diabetes. Exendin-3 is a stable glucagon-like peptide-1 (GLP-1) analogue with high affinity for the GLP-1 receptor (GLP-1R). Recently, targeting of the GLP-1R on beta cells was proven to be a successful method to determine the beta cell mass *in vivo* in a rat model of chemically induced beta cell loss. In this study we compared the *in vivo* BCM quantification with SPECT with In-111- and Tc-99m-labeled exendin-3. **Materials and methods** Exendin-3 was conjugated with DTPA or HYNIC to the C-terminal Lysine residue to enable radiolabeling with In-111 or Tc-99m, respectively. The IC₅₀ for the GLP-1R of both tracers was determined in a competitive binding assay using CHL cells, stably transfected with the GLP-1R. To assess SPECT quantification to determine the BCM, diabetes was induced by alloxan injection in twenty C57BL/6 mice and ten mice only received vehicle. When elevated blood glucose levels were measured in the alloxan-treated mice, either 15 MBq In-111-DTPA-exendin-3 or 10 MBq Tc-99m-HYNIC-exendin-3 was injected intravenously. SPECT/CT was acquired 2 h p.i., animals were euthanized afterwards and pancreas and relevant

organs were dissected, weighed and the radioactivity in the organs was measured in a gamma counter. **Results and conclusion** IC₅₀ values were 7.8 nM (DTPA-exendin-3) and 13.1 nM (HYNIC-exendin-3). Biodistribution studies revealed higher uptake in pancreas for In-111-DTPA-exendin-3 (10.3 ± 0.7 %ID/g) than for Tc-99m-HYNIC-exendin-3 (6.6 ± 0.6 %ID/g). However, accumulation of Tc-99m-HYNIC-exendin in the kidneys was lower (94 ± 16 vs. 258 ± 25), resulting in a favorable kidney-to-pancreas ratio for Tc-99m-HYNIC-exendin-3 (26.0 ± 3.5 vs. 16.2 ± 2.0). With SPECT the pancreas could be visualized after In-111-DTPA-exendin-3 as well as Tc-99m-HYNIC-exendin-3 injection. The correlation between SPECT-based pancreatic tracer uptake and pancreatic uptake as determined determined *ex vivo* was higher for In-111-DTPA-exendin-3 (Pearson $r = 0.82$, $p = 0.0002$) than for Tc-99m-HYNIC-exendin-3 (Pearson $r = 0.71$, $p = 0.0066$). In conclusion, the pancreas can be visualized with both radiotracers and tracer uptake can be determined based on quantitative analysis of the SPECT images. This study shows a preference for In-111 labeled tracer when measuring the BCM, since the correlation of SPECT quantification with *ex vivo* counting is better.

OP174

131I Labeled CendR Peptide for Imaging Neuropilin-1 Positive Tumor

P. Dong, H. Cai, L. Li; West China Hospital of Sichuan University, Chengdu, CHINA.

Introduction: Neuropilin-1 (NRP-1) is a multifunctional single-pass transmembrane protein, which is overexpressed in a variety of cancers (eg. non-small cell lung cancer). CendR sequence motif (R/KXXR/K) could efficiently and specially bind with NRP-1, and transport diagnostic molecules into tumor cells based on the transmembrane capability of NRP-1. This study aimed to evaluate the use of ¹³¹I-Tyr-tLyp-1, a kind of ¹³¹I-labeled CendR peptide, as a diagnostic agent for SPECT imaging of NSCLC. **Methods:** Truncated Lyp-1 was designed to expose its C-end motif (R/K)XX(R/K), and conjugated to Tyrosine for radiolabeling. *In vitro* targeted binding of the Tyr-tLyp-1 peptide was evaluated by fluorescent cellular analysis. Radiolabeling of the conjugate with ¹³¹I produced ¹³¹I-Tyr-tLyp-1 in high radiochemical yield (≥95%). Mice bearing A549 (a kind of human NSCLC cell line) tumors (n=4 for each group) were subjected to static whole-body SPECT scans at different points after intravenous injection of ¹³¹I-Tyr-tLyp-1. Dynamic scans were also obtained for A549 tumor-bearing mice. All mice were sacrificed at 72h after injection of ¹³¹I-Tyr-tLyp-1 and biodistribution studies were performed. **Results:** Tyr-tLyp-1 displayed high and specific binding to A549 cells under micromole concentration, whereas this binding was depend on surface NRP-1 in cells and could be inhibited by NRP-1 antibodies. *In vivo* ¹³¹I-Tyr-tLyp-1 SPECT imaging demonstrated that the subcutaneous NSCLC A549 tumor could be visualized and the tumor uptake of ¹³¹I-Tyr-tLyp-1 was 4.8 times ($p < 0.05$) higher than in muscles at 6h after injection. **Conclusion:** Truncated Lyp-1 peptide specifically localized in NRP-1 positive tumors, highlighting the high potential of using ¹³¹I-Tyr-tLyp-1 as a targeted imaging probe for NRP-1 positive tumors.

OP175

Characterization of [¹¹¹In]-labeled Glucose-Dependent Insulinotropic Polypeptide as a Radiotracer for Neuroendocrine Tumors

S. M. A. Willekens, L. Joosten, O. C. Boerman, M. Brom, M. Gotthardt; Dept of Radiology and Nuclear Medicine, Radboudumc, Nijmegen, NETHERLANDS.

Aims Nowadays, somatostatin receptor scintigraphy (SRS) is considered the gold standard for non-invasive imaging of neuroendocrine

tumors (NET). However, not all NETs overexpress somatostatin receptors, or the subtypes relevant for imaging, hampering their detection using SRS. Therefore, the search for novel targets to visualize NETs, expressing low somatostatin receptor levels, is ongoing. Since many of these NETs have been shown to express the glucose-dependent insulinotropic polypeptide (GIP) receptor, this receptor might be a novel target for NET imaging. Therefore, we investigated whether imaging of NET with DTPA-conjugated GIP radiolabeled with ¹¹¹In is feasible. **Methods** The N-terminally acetylated GIP analogue [Lys³⁷(DTPA)]GIP₁₋₄₂ was synthesized, labeled with ¹¹¹In and the stability of the tracer was assessed in human serum. Receptor targeting was investigated *in vitro* using BHK-GIP receptor positive tumor cells, NES2Y cells (human beta cell line) and isolated islets of Langerhans of C3H mice. *In vivo*, GIP receptor targeting was examined in BALB/c nude mice with a subcutaneous BHK-GIP receptor positive tumors or subcutaneous NES2Y tumors, and optimal peptide dose and time point for *in vivo* imaging was assessed. **Results** [Lys³⁷(DTPA)]GIP₁₋₄₂ was radiolabeled with a specific activity of up to 1.2 TBq/μmol and [Lys³⁷(¹¹¹In-DTPA)]GIP₁₋₄₂ was stable in human serum up to 24h *in vitro*. *In vitro*, [Lys³⁷(¹¹¹In-DTPA)]GIP₁₋₄₂ showed preferential binding to BHK-GIP receptor positive cells, NES2Y cells and isolated islets that could be blocked with an excess of unlabeled ligand. Biodistribution studies revealed optimal tumor targeting 4 hours post-injection, at a peptide dose of 0.1 μg. Four hours post-injection, co-administration of an excess unlabeled peptide lowered GIP receptor positive tumor uptake from 4.2 ± 0.2 %ID/g to 0.8 ± 0.1 %ID/g ($p = 0.04$), indicating GIP receptor mediated accumulation *in vivo*. Also in mice with NES2Y tumors, a more relevant model for diseased human beta cells, preferential tumor uptake was observed (0.5 ± 0.1 %ID/g). **Conclusion** [Lys³⁷(DTPA)]GIP₁₋₄₂ shows receptor mediated binding *in vitro*. Furthermore, the tracer specifically accumulated in BHK-GIP receptor positive tumors and preferential tumor uptake was observed in NES2Y tumors. Therefore, [Lys³⁷(¹¹¹In-DTPA)]GIP₁₋₄₂ is a promising tracer for SPECT imaging of somatostatin receptor negative NET.

506 – Sunday, October 16, 2016, 16:30 - 18:00, Hall 111

Teaching Session: TBA

OP176

TBA

507 – Sunday, October 16, 2016, 16:30 - 18:00, Hall 116

Clinical Oncology: Head & Neck

OP177

Relationships between preoperative FMISO and FDG PET parameters and the prognosis in patients with oral squamous cell carcinoma

J. Sato¹, Y. Kitagawa¹, S. Watanabe², K. Hirata², S. Okamoto², N. Ohga¹, T. Asaka¹, M. Miyakoshi¹, T. Shiga², M. Shindoh³, T. Nagara²; ¹Oral Diagnosis and Medicine, Hokkaido University Graduate School of Dental Medicine, Sapporo, JAPAN, ²Nuclear Medicine, Hokkaido University, Sapporo, JAPAN, ³Oral pathology and Biology, Hokkaido University, Sapporo, JAPAN.

OBJECTIVES: Hypoxia is considered to be resistant to chemotherapy and radiotherapy in head and neck cancer. HIF-1α is a key player of the transcriptional response to hypoxia in cancers. We have already reported that ¹⁸F-Fluoromisonidazole (FMISO)-PET uptake in oral squamous cell carcinoma (OSCC) can reflect a hypoxic environment with HIF-1α expression (*JNM*; 2013). Although Some PET parameters are reported as prognostic factors in patients with OSCC,

no studies demonstrated the relationship between hypoxic volume (HV) of the tumor and the prognosis in patients with OSCC. The aim of this study is to elucidate the relationships between FMISO and FDG-PET parameters including HV of the tumor and the prognosis after surgery in patients with OSCC. **METHODS:** A total of 23 patients (Age: 42–84; M/F: 15/8) with OSCC who underwent radical surgery were enrolled in this study. Each patient underwent FMISO and FDG-PET CT before surgery. The HV was measured by FMISO-PET CT, defining as hypoxic area if FMISO tumor to muscle ratio (TMR) was more than 1.25. Metabolic tumor volume (MTV) was measured using the cut off values with 2.5 of SUV max of FDG-PET. In statistical analyses, the cutoff values of PET parameters were determined using ROC curves. The follow-up periods of the 23 patients were more than four years. Disease free survival (DFS) rates are calculated by Kaplan-Meier methods. **RESULTS:** The medians of HV and MTV were 0.45ml, ranged from 0 to 7.7ml and 5.8ml, ranged 0.3–36.1ml, respectively. The HV was significantly higher in patients with T3+T4 than T1+T2 tumors (medians; 2.8ml vs. 0 ml, $P=0.02$). However, the MTV was not significant different between T1+T2 and T3+T4 tumors (medians; 3.5ml vs. 15.5ml, $P=0.07$). During follow-up after radical surgery, there were 6 cases with locoregional recurrences, 3 cervical lymph node metastases and one distant metastasis. There was a significant difference of DFS rate between the patients with high and low HV volumes of the tumor ($P=0.01$, cutoff value: 3.6ml). However, the MTV was not a significant factor to be relating to DFS. The HV and MTV were not significant factors to be related to overall survival (OS) rates ($P=0.08$ and 0.17). **CONCLUSIONS:** This study first suggests that the HV of the tumor evaluated by pre-operative FMISO-PET CT may reflect the prognosis of the patients with OSCC treated by radical surgery.

OP178

Multiparametric imaging in predicting prognosis of patients with primary hypopharyngeal squamous cell carcinoma using 18F-FDG PET/CT heterogeneity and dynamic contrast-enhanced or diffusion-weighted MRI parameters

S. Chan¹, S. Ng², C. Hsu²; ¹Keelung Chang Gung Memorial Hospital, Keelung, TAIWAN, ²Linkou Chang Gung Memorial Hospital, Taoyuan, TAIWAN.

Background: The prognostic significance of combination of 18F-FDG PET heterogeneity with dynamic contrast-enhanced MR imaging (DCE-MRI) or diffusion-weighted MR imaging (DWI) parameters for the prediction of survival in patients with primary hypopharyngeal cancer is not clear. In this study, we investigate the utility of multiparametric imaging in the prognosis prediction of these patients. **Methods:** We examined 61 patients with primary hypopharyngeal cancer who underwent pretreatment ¹⁸F-FDG PET/CT, DCE-MRI and DWI. Conventional and heterogeneity parameters from ¹⁸F-FDG PET as well as DCE-MRI and DWI parameters were analysis in relation to recurrence-free survival (RFS) and overall survival (OS). Independent prognosticators were identified by Cox regression analysis. **Results:** The median follow-up time was 3 years for the survival patients. Twenty-two patients were expired and 32 had tumor recurrence. After multivariate analysis, higher DCE-MRI parameter K^{trans} ($p=0.031$, Hazard ratio (HR) = 0.448), total lesion glycolysis ($p=0.031$, HR = 3.398), and PET heterogeneity parameter entropy ($p=0.033$, HR = 4.042) values independently predicted RFS. DCE-MRI parameters V_p ($p=0.026$, HR = 2.831), V_e ($p=0.005$, HR = 0.203), and PET heterogeneity parameter uniformity ($p=0.005$, HR = 0.243) retained their independent prognostic significance for OS. Integrating the PET heterogeneity parameter with DCE-MRI parameters allowed distinct prognostic stratification by dividing the patients into three groups with OS ($p=0.234$, 3-year rates=83.2%/47.9%/14.3%) and four groups with RFS ($p<0.042$, 3-year rates=51.2%/31.3%/0%). **Conclusions:** The

heterogeneity parameters of ¹⁸F-FDG PET appeared to be the independent prognostic factors of overall and recurrence-free survivals for hypopharyngeal cancer patients. Multiparametric imaging combining PET heterogeneity with DCE-MRI parameters could be used to improve prognostic stratification of these patients.

OP179

Performance evaluation of 18F-FDG PET/CT tumour delineation methods for volume assessment in head and neck cancer (SCCHN)

R. Lorenz¹, A. Boehm², M. Fischer², L. Kurch¹, T. W. Georgi¹, D. Hasenclever³, G. Wichmann², A. Dietz², O. Sabri¹, R. Kluge¹; ¹University Hospital Leipzig, Department of Nuclear Medicine, Leipzig, GERMANY, ²University Hospital Leipzig, Department of Otorhinolaryngology, Leipzig, GERMANY, ³University Leipzig, Institute for Medical Informatics, Statistics and Epidemiology (IMISE), Leipzig, GERMANY.

Aim: The aim of this study was to evaluate the performance of automated tumour delineation methods for 18F-FDG PET, to investigate factors potentially affecting the segmentation result and to deduce recommendations for the use of certain delineation methods. **Method:** Eight different 18F-FDG PET delineation methods were applied to assess the primary metabolic tumour volume (MTV) of 39 patients with untreated head and neck cancer. All volume segmentations based on region growing algorithms with varying SUV-thresholds (T) calculated as follows: $T=1.5 \times \bar{x}BG$; $T=\bar{x}BG+3SD$; $T=1.5 \times \bar{x}BG+2SD$; $T=2 \times \bar{x}BG+2SD$; $T=0.4 \times SUV_{max}$; $T=0.5 \times SUV_{max}$; $T=0.4 \times (SUV_{max}-\bar{x}BG)+\bar{x}BG$; $T=0.5 \times (SUV_{max}-\bar{x}BG)+\bar{x}BG$. All regional voxels greater than these calculated intensity values were assigned to the FDG-avid vital tumour volume. For methods requiring a mean background uptake ($\bar{x}BG$) a cuboid volume of interest (VOI) of 30 millilitres was positioned in the right lobe of the liver. The volume error (VE) was determined using manual CT-morphologic delineations (GTV) as reference standard. Additionally, volumetric information, different SUV-parameters (SUV_{mean} , SD_{SUV} , SUV_{max} , SUV_{min}), the tumour-to-background ratio (TBR), plasma glucose level, administered activity, time interval to image acquisition, and body mass index were correlated with VE using Spearman's rho. **Results:** The median VE was lowest with $T=2 \times \bar{x}BG+2SD$ (0.88ml; 6.34%); $T=0.4 \times SUV_{max}$ (0.92ml; 10.20%); $T=0.5 \times SUV_{max}$ (-3.01ml; 27.54%) and $T=0.4 \times (SUV_{max}-\bar{x}BG)+\bar{x}BG$ (-2.48ml; 28.25%). VE interquartile range (IQR) varied between 6.15ml for $T=0.4 \times (SUV_{max}-\bar{x}BG)+\bar{x}BG$ to 16.50ml for $T=\bar{x}BG+3SD$. Rank analysis of VE showed that $T=0.4 \times SUV_{max}$ and $T=0.4 \times (SUV_{max}-\bar{x}BG)+\bar{x}BG$ were the two best performing algorithms. Correlation analysis revealed that the tumour volume itself (GTV or MTV) noticeably affects the segmentation result. The impact of other parameters on VE was more variable and less systematic. **Conclusion:** Although performance of central tendency was satisfactory for some algorithms, statistical dispersion is a major limitation of automated delineation methods. Considering the tumour volume for method selection may improve the accuracy of tumour segmentation.

OP180

18F-FDG PET/CT In The Diagnosis Of Suspected Recurrence In Patients With Head And Neck Cancer (HNC)

S. Rizkallah Monzon, S. Rodado Marina, M. Coronado Poggio, Y. Ramirez Escalante, G. Villoria Almeida, C. Escabias del Pozo, M. Orduña Diez, I. Santos Gómez, J. Guzmán Cruz, L. Domínguez Gadea; Hospital Universitario La Paz, Madrid, SPAIN.

OBJECTIVE: The aim of this retrospective study was to determine the benefits of hybrid 18F-FDG PET/CT in diagnosis of suspected recurrence of HNC and distant metastases after treatment, and study its accuracy regard other imaging techniques (CT, RM)/ physical examination.

METHODS: 77 FDG PET/CT examinations were performed to 72 patients (50 men, 22 woman, mean age: 63, 5 years) between January 2014 and November 2015; all of them curatively treated for HNC. 59 studies were performed in patients with high recurrence suspicion (findings in CT, RM or physical examination) and 18 in follow-up. All patients underwent a whole-body 18F-FDG examination that was classified by visual analysis as: positive, negative or indeterminate. The final diagnosis was determinate by histopathology findings or clinical/imaging follow up (gold standard) **RESULTS:** The primary tumor location was larynx (27), oral cavity (20), oropharynx (8), nasopharynx (5), hypopharynx (4), maxilar (4), salivar gland (3) and nasal cavity (1). The final diagnosis was determined by histopathological 34 studies and 25 by imaging/clinical follow-up. In the 59 studies with recurrence suspicion, 50 were detected by imaging (CT/RM) and 9 by physical examination. The whole-body 18F-FDG PET/CT examinations had positive results in 28 studies, negative in 26 and indeterminate in 5. Only one of who exhibited abnormal 18F-FDG uptake in the head and neck area did not have confirmed recurrence (false positive). The other 27 had proven recurrence. All negative PET/CT, were negative for recurrence in the final diagnosis. The sensitivity and specificity of 18F-FDG PET/CT was 100% (27/27) and 96% (26/27) respectively. The positive predictive value was 96% (27/28) and the negative predictive value was 100% (26/26). The overall accuracy was 98%. In the 27 positive PET/CT studies with positive final diagnosis, the CT/RM results were positive in 74% (20/27) and indeterminate in 26% (7/27). In the group with PET/CT performed as a follow up (18), the PET/CT was: positive in 2 (both positive in the final diagnosis), negative in 14 (all negative in final diagnosis) and indeterminate in 2 (both negative in final diagnosis). **CONCLUSIONS:** The high diagnostic performance of FDG PET/CT in detecting recurrence in curatively treated patients with HNC supports its use in clinical practice for patient follow-up, obviating further radiologic imaging. Further studies are needed to evaluate the prognostic utility of PET/CT in the follow-up of HNC in patients without suspected recurrence.

OP181

High FDG Uptake on Pre-radiotherapy PET/CT and Preferential Sites of Local Relapse after Chemoradiotherapy for Locally Advanced Head and Neck Cancer

A. CHAPUT¹, J. CALAIS^{2,3}, P. ROBIN¹, S. THUREAU³, D. BOURHIS¹, R. MODZELEWSKI³, U. SCHICK¹, P. VERA³, P. SALAÛN¹, R. ABGRAL¹; ¹Brest University Hospital, Brest, FRANCE, ²Bichat University Hospital, Paris, FRANCE, ³Henri Becquerel Center, Rouen, FRANCE.

Purpose: The potential benefits of 18F-fluorodesoxyglucose positron emission tomography (FDG-PET/CT) imaging for radiotherapy (RT) planning treatment of head and neck cancer (HNC) are increasingly being recognized. It has been suggested that intra-tumor sub-volumes with high FDG avidity are potential target for selected dose escalation. Our aims were to demonstrate that pre-RT FDG PET/CT can identify intra-tumor sites at increased risk of local relapse (LR) after RT and to determine an optimal maximum standardized uptake value (SUVmax) threshold to delineate smaller RT target volumes that would facilitate RT dose escalation without impaired tolerance. **Methods:** The study included 72 consecutive patients with locally advanced HNC treated by radiotherapy ± concurrent chemotherapy. All patients underwent FDG PET/CT at initial staging (PET_A) and during systematic follow-up (PET_R) in a single institution. FDG PET/CT acquisitions were co-registered on the initial CT scan with a rigid method. Various subvolumes (A_X; X=30, 40, 50, 60, 70, 80 and 90% SUVmax thresholds) within the initial tumor and in the subsequent LR (R_X; X=40 and 70% SUVmax thresholds) were

pasted on the initial PET/CT and compared together [Dice, Jaccard, overlap fraction (OF), common volume/baseline volume, common volume/recurrent volume] **Results:** Nineteen patients (26%) had LR. Using a 40% of SUVmax threshold, initial metabolic tumor volume (MTV) was significantly higher in all relapse patients (local and distant relapse) than in controlled patients (mean: 11.3 ± 9.8 vs. 5.1 ± 4.9 cc, p = 0.001) as well as total lesion glycolysis (TLG) (mean: 134.6 ± 116 vs. 60.6 ± 80.4, p=0.002). For both using methods, the overlap index between A₃₀, A₄₀, and A₅₀ sub-volumes on PET_A and the whole metabolic volume of recurrence R₄₀ and R₇₀, on PET_R showed a moderate agreement (between 0.40 and 0.60). **Conclusion:** We confirm that TLG and MTV are independently correlated with recurrence-free survival in patients with HNC. Due to sub-optimal co-registration, we could not reach high overlap index values between initial tumor and recurrence sub-volumes. Further larger prospective studies with FDG-PET/CT performed in the same RT position and with a validated elastic registration method are needed.

OP182

Diagnostic Performance Of ¹⁸F - FDG PETCT In Suspected Recurrence In Treated Cases Of Oral, Pharyngeal and Laryngeal Malignancy

S. Padma, P. Shanmuga Sundaram, B. R Arun; Amrita School of Medicine, Amrita Institute of Medical Sciences, COCHIN, INDIA.

Introduction: Excluding local recurrence in treated cases of oropharyngeal, laryngeal malignancies is a challenge as there is local tissue distortion and edema after chemoRT and surgery. Anatomical imaging modalities fair poorly in the identification of local recurrence. It is also imperative to accurately assess the disease extension in order to plan the most appropriate treatment, which has important implications for patient outcomes. Data is controversial on the role of PET in post chemoRT setting in patients with suspected recurrence. **Aims & Objectives:** To determine the diagnostic performance of ¹⁸F FDG PETCT in suspected cases of local recurrence and its ability to assess disease extension in treated cases of oral, pharyngeal, laryngeal cancers. **Materials & Methods:** Data of 52 treated cases of oropharyngeal, laryngeal malignancy (M: F= 40:12, mean age 58 yrs), who presented to our dept for PETCT between Jan 2013 to Nov 2014 with suspected local recurrence were retrospectively analysed. Imaging was performed after a minimum interval of three months post treatment. PETCT findings were correlated with histopathology from the PET detected site of local recurrence. Statistical analysis was also performed. **Results:** 32/52 pts revealed FDG avid lesions locally (tongue; alveolus; floor of mouth; pyriform sinus; vocal cord; pharynx = 10: 3: 3: 14: 2) with no corresponding CT lesion. Dual timepoint imaging was conducted in 23/32 pts to rule out inflammation. PETCT was negative in 20/52 pts. Biopsy correlation was performed in all. Sensitivity, Specificity, Positive Predictive Value and Negative Predictive values for detection of local recurrence were found to be 87.5%,80%,87.5% and 80% respectively. 9/32 (28%) pts (tongue : alveolus : floor of mouth : pyriform sinus = 4 : 1 : 3 : 1) had unsuspected lymphnodal involvement & same was also correlated with histopathological findings. Sensitivity, Specificity, Positive Predictive Value and Negative Predictive values for detection of local recurrence were found to be 100%, 89 %, 100 %, 89% and 80% respectively. **Conclusion:** ¹⁸F FDG PETCT is reliable in the assessment of local recurrence in oropharyngeal and laryngeal malignancy. High negative predictive value of FDG PETCT performed at least 8 weeks post chemoRT allows prevention of unnecessary diagnostic invasive procedures and neck dissection, with a significant impact on clinical outcome. Dual timepoint imaging serves as a useful tool in decision making. FDG PETCT is superior as it identifies viable tumour within the treated region, thus overcoming the known limitations of morphological imaging modalities.

OP183**Initial feedback of 18F-FDG PET/MR in head and neck oncology in clinical practice**

R. de Laroche^{1,2}, M. Sahli-Amor³, G. Bera², C. Bertolus⁴, G. Herve⁵, N. Pyatigorskaya³, M. Soret², M. Bertaux², M. Habert², A. Kas²; ¹University Hospital of Brest, Department of Nuclear Medicine, Brest, FRANCE, ²Hôpital de la Pitié-Salpêtrière, Department of Nuclear Medicine, Paris, FRANCE, ³Hôpital de la Pitié-Salpêtrière, Department of Neuroradiology, Paris, FRANCE, ⁴Hôpital de la Pitié-Salpêtrière, Department of Oral and Maxillofacial Surgery, Paris, FRANCE, ⁵Hôpital de la Pitié-Salpêtrière, Department of Cytopathology, Paris, FRANCE.

Aim Hybrid PET/MR imaging is a promising tool for initial assessment of head and neck cancers. Combination of the metabolic information from 18F-FDG PET with the high soft tissue contrast and multiparametric characterization of MRI should yield to a better understanding and management of these poor prognosis malignancies. Our objective is to evaluate the feasibility and the potential interest of 18F-FDG PET/MR in head and neck oncology in clinical practice. **Materials and Methods** Between October 2015 and April 2016, 62 patients (31 men, 31 women, mean age 61±18) underwent PET/MR for head and neck malignant tumor. Images were acquired 1 hour after injection of 3.7 MBq/kg on a hybrid TOF 3T Signa PET/MR (GE Healthcare). Imaging workflow comprised dedicated head and neck 18F-FDG PET acquisition simultaneously with axial T1w, axial T2 IDEAL, and axial diffusion weighted imaging sequences, and after gadolinium injection coronal T2 IDEAL, T1w 3-dimensional and axial T1 IDEAL sequences, followed by a whole body (4 beds) PET and MRI (Lava-Flex, GE Healthcare) acquisition. For head and neck attenuation correction, two methods were tested : the MR based method (Dixon sequence) and the pseudo CT-based atlas method. Useful MR sequences have been selected in order to reduce the time of acquisition. **Results** Thirty-two patients were scanned for initial staging, 22 for restaging, 2 for carcinoma of unknown primary, 3 for therapeutic assessment and 3 for characterization of a suspicious lesion. A total of 37 squamous cell carcinomas, 8 adenoid cystic carcinomas, 3 adenocarcinomas, and 11 other carcinomas was explored. Distant metastases were identified for 6 patients (10 %) and suspicious cervical lymph nodes for 25 patients (40 %). Total acquisition time was about 50 minutes. The atlas method for attenuation correction was not suitable. For all patients, PET/MR images accurately defined local extension of primary tumor site. Both MRI and PET, particularly when there were void artifacts on MRI images, contributed to tumor delineation. Both PET and morphologic MRI sequences were helpful to characterize cervical lymph nodes. Fusion quality, image quality and anatomic location of focal uptake were good on both head and neck and whole body images. **Conclusion** This initial feedback confirmed the feasibility of 18F-FDG PET/MR for head and neck oncology in clinical practice. The added value lies particularly on the improved specificity from the registration of PET and MR images. Attenuation correction in this region is still insufficient, further studies are needed to improve it.

OP184**Advancing Precision Nuclear Medicine for Head and Neck Cancers with Higher Definition Digital PET/CT**

C. L. Wright, A. D. Bhatt, K. Binzel, P. Bhatia, P. Subramanian, J. Zhang, M. V. Knopp; The Ohio State University, Columbus, OH, UNITED STATES.

The introduction of next-generation, solid-state, digital photon counting PET detector (dPET) technology represents an innovative leap over conventional photomultiplier tube-based PET (cPET) technologies to enable precision nuclear medicine practices for oncology patients. This dPET technology enables higher definition PET imaging with smaller voxel volumes which reduces partial volume effects. The objective of this study

is to evaluate the clinical capabilities of dPET technology as it relates to patients with head and neck cancer. In an intra-individual matched pair comparison study, 12 head and neck cancer patients underwent both ¹⁸F-FDG dPET/CT (pre-commercial release Vereos, Philips) and cPET/CT (Gemini TF 64, Philips). Standard cPET/CT was performed using a target dose of 481 MBq FDG at ~75 min p.i. and investigational dPET/CT was performed at ~55 min p.i. or ~95 min p.i. All images were reconstructed with ToF using a standard definition (SD) voxel volume of 4x4x4 mm³. In addition, the dPET images were reconstructed at high definition (HD, 2x2x2 mm³) and ultra-high definition (UHD, 1x1x1 mm³). Independent visual assessment for overall image quality, background quality, lesion detectability, and diagnostic confidence for cPET and dPET image sets were performed by a blinded reader panel. All 12 cPET and dPET data sets were evaluable. The UHD dPET reconstructions were consistently rated the best in terms of overall image quality for evaluating primary and metastatic lesions with no appreciable effect on the background FDG intensity. Higher definition dPET data sets consistently demonstrated improved lesion detectability for small lesions (< 15 mm) when compared with cPET. The clinical impact of UHD dPET was consistently rated preferable compared to cPET, indicating that it can potentially impact clinical outcome. This improved lesion detectability likely relates to the faster timing resolution of dPET (~325 ps) compared with cPET (~550 ps) and the higher definition reconstructions, both of which decrease partial volume effects. In head and neck cancer, FDG PET imaging is clinically invaluable for the routine detection of occult malignancy, staging and assessment of treatment response. This study demonstrates that HD and UHD dPET imaging of head and neck cancer improves lesion detectability (especially for smaller lesions), lesion characterization (especially in heterogeneous masses) and overall diagnostic confidence for the reader. These essential advances strengthen the utilization of PET as an imaging biomarker in head and neck cancer, where large, heterogeneous primary tumors and small metastatic lesions are common, further lending support to the vision of precision nuclear medicine.

508 – Sunday, October 16, 2016, 16:30 - 18:00, Hall 212

Committee Symposium - EANM/EARL: Why Your Centre should be EARL Accredited - The Nuclear Medicine Physician Point of View/The Physicist Point of View**OP185b****Physics Aspects of PET/CT Harmonization and Accreditation for Quantitative Multicenter Studies**

R. Boellaard; VU University Medical Center, Nuclear Medicine & PET Research, Amsterdam, NETHERLANDS.

OP186**EARL Accreditation and Standardization from the Nuclear Medicine Perspective – Including Reporting Results from Survey**

N. Aide; Service de Médecine Nucléaire, Centre Régional de lutte contre le cancer François Baclesse, Caen, FRANCE.

OP187**Experiences and Results of the PET/CT Accreditation Program: The 150 Sites Milestone**

T. Sera; University of Szeged, Department of Nuclear Medicine, Szeged, HUNGARY.

OP188**FDG PET/CT: Can We Really Use it as Quantitative Imaging Biomarker in Multicenter Studies?**

P. Bourguet; CRLCC Centre Eugène Marquis, Service de Médecine Nucléaire, Rennes, FRANCE.

509 – Sunday, October 16, 2016, 16:30 - 18:00, Hall 113

Cardiovascular System: Cardiac Sarcoidosis, Amyloidosis & (Large) Vessel Vasculitis

OP189

Comparison of Contrast-enhanced MRI versus ^{68}Ga -DOTATOC-PET/CT in Patients with Suspected Cardiac Involvement of Sarcoidosis

F. C. Gaertner¹, U. Schlesinger-Irsch², C. Pizarro³, T. Reiter⁴, D. Skowasch³, W. R. Bauer⁴, D. Thomas², R. A. Bundschuh¹, C. Lapa⁵; ¹Department of Nuclear Medicine, Universitaetsklinikum Bonn, Bonn, GERMANY, ²Department of Radiology, Universitaetsklinikum Bonn, Bonn, GERMANY, ³Department of Internal Medicine II, Universitaetsklinikum Bonn, Bonn, GERMANY, ⁴Department of Internal Medicine I, Universitaetsklinikum Wuerzburg, Wuerzburg, GERMANY, ⁵Department of Nuclear Medicine, Universitaetsklinikum Wuerzburg, Wuerzburg, GERMANY.

Purpose: Cardiac involvement is rare but important for the prognosis and therapy decisions in patients with sarcoidosis. Diagnosis is demanding and often based on cardiac function. Recently late contrast enhancement in magnetic resonance imaging (MRI) as well as somatostatin-receptor positron emission tomography has been described for diagnosis of cardiac sarcoidosis. In this analysis we directly compared both imaging modalities to each other. **Material and Methods:** 16 patients from two centers with proven sarcoidosis who underwent contrast enhanced MRI and ^{68}Ga -DOATATOC PET/CT due to clinical suspicion of cardiac involvement were retrospectively analyzed. In MRI data presence of late enhancement was analyzed using the 17-segment American Heart Association model. ^{68}Ga -DOTATOC uptake was analyzed using the same model. **Results:** In 6 patients pathological uptake was found in PET as well as late enhancement in MRI, here in average 72.4 % of the segments did overlap. In 4 patients with negative PET findings, late enhancement was found in MRI. The remaining 6 patients were negative in PET and MRI. In patients with PET positive findings, the ratios lesion-to-blood-pool and myocardium-to-blood-pool showed better ability to differentiate between lesions and normal myocardium compared to SUV. **Conclusion:** In 75 % of the patients PET and MRI showed agreement in diagnosis of cardiac involvement of sarcoidosis. Lesion localization showed an overlap of 72 %. For quantitative discrimination in PET, ratios of the uptake compared to blood pool showed better discrimination than absolute uptake values (SUV). However late enhancement in MRI showed pathological findings in 4 PET-negative patients. This may either be due to differences in sensitivity of the modalities (e.g. caused by differences in spatial resolution) or due to scar tissue without active inflammation showing late enhancement in MRI. Further clinical follow-up might help to clarify this point.

OP190

Quantification of ^{11}C -PIB uptake in cardiac amyloidosis

T. Kero¹, J. Sörensen¹, G. Antoni², H. Wilking², K. Carlson³, O. Vedin³, G. Wikström³, M. Lubberink¹; ¹Surgical sciences, Uppsala, SWEDEN, ²Medical Chemistry, Uppsala, SWEDEN, ³Medical Sciences, Uppsala, SWEDEN.

Aim: Recent studies have shown promise for ^{11}C -PIB PET as a non-invasive diagnostic and quantitative tool in cardiac amyloidosis. The aims of this study were to determine the optimal tracer kinetic model of ^{11}C -PIB and to evaluate the performance of two simplified methods, retention index (RI) and standardized uptake value (SUV), in the quantification of cardiac ^{11}C -PIB uptake in amyloidosis. **Materials and methods:** Six patients with systemic amyloidosis and cardiac involvement underwent dynamic 35-min

^{11}C -PIB PET scans with arterial blood sampling for measurement of blood radioactivity and metabolite analysis. Volumes of interest were drawn over the left myocardial wall according to the 17 segment model of the American Heart Association. Single-tissue and reversible and irreversible two-tissue models were fitted to the data using a metabolite-corrected arterial input function, both based on individual metabolite data and on a population-average metabolite correction. The optimal kinetic model was determined using the Akaike information criterion (AIC) and Akaike weights. RI and SUV (15-25 min p.i.) were compared with the rate of irreversible binding (K_i). In a retrospective analysis, data from 10 amyloidosis patients and 5 healthy controls for which no blood data was available were analysed in a similar way using a population-average metabolite correction. **Results:** The irreversible two-tissue (2Tirr) model was preferred based on AIC and Akaike weights and robustness of fits. RI and SUV correlated moderately well with the rate of irreversible binding (K_i) from the 2Tirr model ($r^2=0.73$ and $r^2=0.66$ respectively). Correlation ($r^2=0.86$) and agreement (ICC=0.91) were high between K_i using individual metabolite corrections versus K_i using population-averaged metabolite correction. In the retrospective analysis using population-averaged metabolite correction, K_i was higher in amyloidosis patients than in healthy controls ($p=0.008$). However, there was an overlap between the lowest K_i in amyloidosis patients and the highest K_i in controls, whereas both RI and SUV both showed higher values in patients than controls ($p=0.001$ for both), without an overlap in values. **Conclusion:** An irreversible two-tissue model best describes the ^{11}C -PIB uptake in cardiac amyloidosis. RI and SUV showed modest correlation with quantitative results from this kinetic model. However, RI and SUV are more feasible for use in clinical routine and also showed better discrimination between amyloidosis patients and controls than K_i . Therefore, RI and SUV are preferred in clinical diagnosis of cardiac amyloidosis.

OP191

Quantitative assessment of cardiac amyloid burden in patients with suspected transthyretin cardiac amyloidosis (ATTR): a feasibility study

S. Ben-Haim^{1,2}, M. Smechov¹, E. Goshen¹, M. Arad¹, I. Medini³, A. Bar-Shalev³, J. Bomanji², L. Menezes²; ¹Chaim Sheba Medical Center, Ramat-Gan, ISRAEL, ²University College London and UCL Hospitals, London, UNITED KINGDOM, ³GE Healthcare, Nuclear Medicine, Haifa, ISRAEL.

Objectives: 99mTc-diphosphono-propano-dicarboxylic acid (Tc-DPD) can be used for the diagnosis of ATTR by visual interpretation. Recent developments in therapy may require a more precise quantitative assessment. We have assessed the feasibility of absolute quantitation of myocardial Tc-DPD in patients with suspected ATTR using a quantitative software package (Q.Metrix, GE Healthcare). **Methods:** Tc-DPD whole body planar and SPECT/CT studies of the chest of 80 patients with suspected ATTR were evaluated. Data were corrected for patient motion, attenuation and collimator blurring, and absolute quantitation was performed given the injection information and system sensitivity. Mean cardiac uptake (MBq/ml), % injected dose within the heart (%ID) and the ratio of heart/spine concentrations were obtained and were compared to semi-quantitative visual assessment (Perugini score [PS] 0 - no cardiac uptake to PS 3 - cardiac uptake greater than bone). **Results:** At 3 hours after injection there were 68 patients with PS 0. Cardiac activity was seen in 12 patients on planar and on SPECT/CT studies ($m=10$, age: 76.6 ± 6.8 years). There was one patient with PS1, eight had PS2 and 3 had PS3. %ID in PS1 was 0.41 , compared to 2.54 ± 0.53 and 2.72 ± 0.5 in PS2 and PS3, respectively. The average concentration in the heart was 0.015 MBq/ml in PS1, 0.048 ± 0.01 in PS2 and 0.042 ± 0.0 in PS3. The ratio of heart/spine concentrations was 0.34 in PS1, 2.11 ± 0.6 in PS2 and 2.44 ± 0.8 in PS3. **Conclusion:** Absolute quantitation of cardiac Tc-DPD uptake is feasible using Q.Metrix. These initial findings suggest significantly lower

cardiac uptake in PS1, whereas no significant differences were demonstrated between PS2 and PS3, suggesting perhaps patients with PS2 and patients with PS3 can be grouped together. Further assessment in larger patient cohorts is needed to determine the clinical relevance of these findings.

OP192

Comparison of MIBG and Diphosphonate scintigraphy in patients with aTTR-FAP

R. CHEQUER¹, H. REGAIEG¹, R. BEN AZZOUNA¹, V. ALGALARRONDO², B. MAHIDA¹, E. PIEKARSKI¹, M. SLAMA², D. LE GULUDEC¹, F. ROUZET¹; ¹BICHAT HOSPITAL, PARIS, FRANCE, ²CARDIOLOGY DPT HOPITAL BECLERE, PARIS, FRANCE.

Background. In familial aTTR amyloid polyneuropathy (FAP), cardiac involvement is of major prognostic value. Two approaches using radio-nuclide imaging proved relevant in the assessment of aTTR-related cardiac amyloidosis: detection of amyloid deposits with diphosphonates (DPD) and of sympathetic denervation with MIBG. The study aimed to compare the respective value of both approaches in patients with aTTR-FAP with suspected cardiac involvement. **Methods.** 76 consecutive patients with genetically proven aTTR-FAP were prospectively included (males 62%, Val30Met: 42%, domino-liver transplantation 13%, symptomatic 57%, interventricular septum (IVS)≥12 mm: 52%; left ventricular ejection fraction: 63±10%). They underwent both MIBG and DPD scintigraphy in a delay <3 months. For DPD SPECT, acquisitions were performed 3 hours after tracer injection. Cardiac uptake was visually scored as present or absent and quantified by the ratio of 3D isocount volume of interest generated over the myocardium to a standard volume in lung (H/L). For MIBG, heart-to-mediastinum ratio (HMR) was calculated on planar acquisitions performed 4 hours after tracer injection. Cardiac MIBG was classified as normal, mildly, moderately, or severely abnormal. **Results:** The delay between MIBG and DPD 6±12 days. MIBG was abnormal in 50 patients (66%) and DPD in 30 patients (39%; p=0.002). When MIBG was normal (n=26), DPD scintigraphy was normal except for 1 patient. When MIBG was abnormal (n=50), DPD scintigraphy was normal in 21 patients (42%). The uptake of DPD increased with the denervation score (normal: 0.6±0.2; mild: 0.6±0.4, moderate: 3.4±3.3; severe: 4.5±3.7; p<0.001 between normal and moderate/severe). In patients with a previous domino liver transplantation (n=10), the overall pattern was similar. In asymptomatic patients (n=31), all those with a normal MIBG (n=17) had a normal DPD; MIBG was abnormal in 45% (n=14), 50% had a normal DPD. In addition, HMR was greater (1.8±0.3 vs. 1.6±0.4; p=0.008) and H/L was lower (1.7±2.3 vs. 3.2±3.5; p=0.04) compared to symptomatic patients. **Conclusion:** in patients with suspected cardiac involvement of aTTR-FAP, MIBG was abnormal more frequently than DPD. In particular, DPD abnormalities are delayed compared to MIBG since it was abnormal only when denervation was moderate or severe. In the group of asymptomatic patients, only half of those with cardiac denervation had a positive DPD scintigraphy. This suggests that innervation abnormalities detected by MIBG are more frequent and appears earlier than amyloid deposits detected by Diphosphonates.

OP193

Usefulness of combined FDG-PET/MR to diagnose active cardiac sarcoidosis

R. Abgral^{1,2}, M. R. Dweck^{1,3}, M. G. Trivieri¹, P. M. Robson¹, N. Karakatsanis¹, V. Mani¹, M. Padilla⁴, J. Sanz⁵, J. Narula⁵, V. Fuster⁵, J. Contreras⁵, J. C. Kovacic⁵, Z. A. Fayad¹; ¹Translational and Molecular Imaging Institute, Icahn School of Medicine at Mount Sinai, New York, NY, UNITED STATES, ²Department of Nuclear Medicine, European

University of Brittany, EA3878 GETBO, IFR 148, CHRU Brest, Brest, FRANCE, ³British Heart Foundation/University Centre for Cardiovascular Science, University of Edinburgh, Edinburgh EH16 4SB, Edinburgh, UNITED KINGDOM, ⁴Division of Pulmonary, Critical Care and Sleep Medicine, Icahn School of Medicine at Mount Sinai, New York, NY, UNITED STATES, ⁵Cardiovascular Institute, Icahn School of Medicine at Mount Sinai, New York, NY, UNITED STATES.

Aim: Sarcoidosis is a granulomatous disease of unknown etiology affecting commonly lung and mediastinal lymph nodes. Heart involvement poses an increased risk of sudden death but is probably underdiagnosed due to frequent absence of clinical symptoms and the inability to easily diagnose cardiac sarcoidosis (CS) with a non-invasive method. Several imaging techniques are already used to assess CS including 18F-fluorodesoxyglucose/positron-emission tomography (FDG-PET) to underline inflammatory disease and magnetic resonance (MR) with late Gadolinium enhancement (LGE) to determine the pattern of myocardial injury. Recent advances now allow combining these 2 techniques to benefit from the best of these modalities. Our aim was to assess the usefulness of FDG-PET/MR in the diagnosis of CS. **Methods:** Patients with previous histologically proven extra-cardiac sarcoidosis and/or clinical symptoms consistent with CS were referred to our department for PET/MR imaging. PET data were reconstructed using a Dixon-MR attenuation correction map. Different quantitative parameters were measured on images: mean and maximal myocardial standardized uptake values (SUVmax, SUVmean) around area positive for LGE, if present; mean T2 mapping value (T2mean) in the same volume; target-to-blood pool ratios (TBRmax, TBRmean); and target-to-negative LGE myocardium ratios (TNRmax, TNRmean). A final diagnosis of active cardiac sarcoidosis (CS+) or no (CS-) was defined by a consensus of clinical experts. Mean values of imaging parameters in CS+ and CS- patients were compared using a Student t-test and a ROC analyses was performed to assess their diagnostic accuracy. **Results:** Twenty-five patients (11M/14F; 55.2±9.7 yo) were prospectively enrolled in 9 months. They underwent a PET/MR 68.6±9.4 min after injection of 4.8±0.2 MBq/Kg of FDG. Eight patients were considered as CS+ and 17 as CS-. There was no statistically significant difference in terms of SUVmax (p=0.266), T2mean (p=0.320), TBRmax (p=0.239) and TBRmean (p=0.248) between CS+ and CS- patients. Mean TNRmax were respectively 1.68±0.41 and 1.09±0.08 in CS+ and in CS- patients (p<0.0001). Mean TNRmean were respectively 1.52±0.27 and 1.03±0.14 in CS+ and in CS- patients (p<0.0001). ROC analysis revealed a threshold of TNRmax=1.21 (AUC=0.978) and TNRmean=1.24 (AUC=0.993) to differentiate all patients as being CS+ or CS- (accuracy=96%). Two previously unknown cases of sarcoid involvement (bone, liver) were identified. FDG-PET/MR identified an alternative cause for cardiac symptoms in 6 (35%) of CS- patients. **Conclusion:** Our results show the usefulness of combined FDG-PET/MR in the diagnosis of CS using TNR measurements and confirm its clinical ability to evaluate extra-cardiac involvement of sarcoidosis and in assessing alternative myocardial pathologies.

OP194

Does quantification of FDG uptake with TBR improve the assessment of disease activity in Takayasu arteritis ?

B. Emsen¹, K. Benali¹, D. Larivière², B. Mahida¹, T. Papo², K. Sacré², F. Hyafil¹; ¹Department of Nuclear Medicine, Bichat Hospital, AP-HP, PARIS, FRANCE, ²Department of Internal Medicine, Bichat Hospital, AP-HP, PARIS, FRANCE.

Background. Takayasu arteritis (TA) is a rare autoimmune vasculitis, which predominantly affects the aorta and its branches. The role of FDG-PET imaging for the assessment of the disease activity remains controversial. **Objective.** The aim of this study was to assess whether the precise quantification of FDG uptake in the vessel wall using tissue

to background ratio (TBR) might be useful for the assessment of disease activity at the time of diagnosis and for monitoring the efficacy of immunosuppressive therapy (IS). **Methods.** A total of 62 FDG-PET scans with TA were analyzed retrospectively. All patients received corticosteroids or immunosuppressive treatments. The diagnosis of TA was based on the American College of Rheumatology criteria. TBR were calculated as the ratio between max. SUV in the aortic wall and mean SUV of blood. For each patient, the disease was established as clinically active or inactive at the time the FDG PET imaging based on the clinical criteria included in the NIH assessment of disease activity for TA patients. **Results.** A total of 15 patients were included in this study and imaged on average 5 times with FDG-PET scans. Eight patients were imaged before the initiation of IS therapy. An average of 5 ± 2 vascular lesions were present on the first FDG-PET scan with a maximal TBR of 2.7 ± 0.9 . On the second FDG-PET scan after introduction of IS therapy, the max. TBR was reduced by ca. 40 % with a mean TBR value of 1.45 ± 0.5 on the second PET scan. In the 24 FDG-PET scans of patients classified as inactive after initiation of therapy, TBR was always $< 2.3 \pm 0.3$. The disease was classified as clinically active in 40 % of patients with max. TBR value > 2.3 and in only 27 % of the patients with max. TBR between 1.6 and 2.3. Max. TBR measured in vascular lesions changed by $+ 51 \pm 64\%$ when the disease became active, $- 18 \pm 25\%$, when the disease became inactive and $- 5 \pm 26\%$ when the disease was considered as stable. **Conclusions.** In TA patients, high TBR value are measured at the time of diagnosis but decrease by ca. 40 % after initiation of IS therapy. During follow-up, we confirmed important discrepancies between clinical activity and vascular FDG uptake for intermediate values of TBR on FDG-PET imaging.

OP195

Semiquantitative analysis of 18F-FDG PET/CT in the follow-up of large vessel vasculitis

M. Jimenez-Alonso¹, I. Martinez-Rodriguez¹, C. Lavado-Perez¹, J. Lopez-Defillo¹, R. Quirce¹, J. Jimenez-Bonilla¹, M. De Arcocha-Torres¹, D. Meza-Escobar¹, J. Loricera², M. Gonzalez-Gay², I. Banzo¹; ¹Nuclear Medicine Service. Molecular Imaging Group (IDIVAL). Marqués de Valdecilla University Hospital. University of Cantabria, Santander, SPAIN, ²Rheumatology Service. Marqués de Valdecilla University Hospital. University of Cantabria, Santander, SPAIN.

Aim: Large vessel vasculitis (LVV) is the most common type of systemic vasculitis, especially in older female population. Treatment of LVV includes steroids and immunosuppressive drugs. 18F-FDG PET/CT has proven its value for diagnosis and evaluation of the extent of disease. However, its role in the follow-up is not well established. Our aim was to evaluate the usefulness of the semiquantitative analysis of 18F-FDG PET/CT in the follow-up of these patients. **Materials and methods:** This study included 38 patients (28 women and 10 men, mean age: 66.5 ± 9.8 y.) with LVV who had an initial (at diagnosis) and follow-up 18F-FDG PET/CT scan. Follow-up PET/CT was carried out 3-12 months after the initial scan (mean time: 7.5 ± 2.9 months). 18F-FDG PET/CT scan was obtained 180' after intravenous injection of 7 MBq/Kg 18F-FDG. A semiquantitative analysis of images based on the target (aortic wall) to background (aortic blood pool) ratio (TBR) was performed. The initial and the follow-up scans results and clinical and biochemical outcome were compared. **Results:** Overall, mean TBR decreased significantly from 1.71 ± 0.5 in the initial scan to 1.41 ± 0.28 in the follow-up ($p=0.0002$). In a patient-based analysis, TBR decreased in 30 out of 38 patients (19 of them had clinical improvement), and increased in 8 patients (6 of them presented clinical worsening). In the 21 patients with clinical improvement the mean TBR decreased significantly from 1.83 ± 0.59 to 1.47 ± 0.29 ($p=0.0002$). In the 17 patients with no changes or clinical worsening the mean TBR decreased from 1.56 ± 0.24 to 1.48 ± 0.28 , although the difference was not significant ($p=0.1848$). Twenty-four out of 38 patients showed biochemical data improvement. The mean

TBR decreased from 1.74 ± 0.57 to 1.52 ± 0.34 ($p=0.0097$). In the other 14 patients who presented worsening of biochemical data, TBR decreased from 1.65 ± 0.29 to 1.4 ± 0.14 ($p=0.0041$). Mean TBR was higher at the initial scan in patients who presented clinical and/or biochemical improvement, although the difference were not significant ($p=0.0859$ and 0.7737 , respectively). **Conclusions:** The semiquantitative analysis of 18F-FDG PET/CT is useful in the follow-up of patients with LVV. In addition, it could identify patients with a favorable clinical outcome. Although mean TBR decreased in the follow-up, some degree of vascular uptake remained. No relationship was found between mean TBR and biochemical data.

510 – Sunday, October 16, 2016, 16:30 - 18:00, Hall 114

Neurosciences: Miscellaneous

OP196

Decreased Cerebral Glucose Metabolism Associates with Risk Factors for Poor Neurodevelopmental Outcome in Very Low Birth Weight Infants

H. Kim, K. Won, B. Song, H. Lee, S. Lee, C. Kim, J. Park; Keimyung University, School of Medicine, Daegu, KOREA, REPUBLIC OF.

Purpose: Although brain MRI shows no structural abnormality in very low birth weight infants (VLBWI), these VLBWI have an increased risk of poor neurodevelopment. The aim of this study was to evaluate clinical significance of decreased cerebral glucose metabolism in VLBWI without structural abnormality on brain MRI. **Methods:** Forty VLBWI (gestational age (GA): 24 - 29 weeks) who had no structural abnormality (severe intraventricular hemorrhage, cystic periventricular leukomalacia, punctate lesion, loss of volume, and ventricular dilatation) on brain MRI were enrolled in this study. All infants performed brain MRI and fluorine-18 fluorodeoxyglucose (F-18 FDG) brain PET at term-equivalent age. F-18 FDG brain PET images were quantitatively analyzed using the infant automated anatomic labeling template after spatial normalization. The regional glucose metabolic ratio (MR) and asymmetric index (AI) for each VOI of the cerebral cortices, striatum and thalamus were calculated. Asymmetric glucose metabolism was considered as significant when AI is higher than 110% or lower than 90%. The relationships between regional MR and risk factors, including multiple gestations, gestational diabetes mellitus (GDM), pregnancy induced hypertension, premature rupture of membrane (PROM), GA, birth weight, bronchopulmonary dysplasia (BPD) and Apgar score at one and five minutes, were evaluated. **Results:** Seventeen infants (42.5%) had right > left asymmetry and three infants (7.5%) had right < left asymmetry of the cerebral glucose metabolism. The MRs of the left cerebral cortices, striatum and thalamus were significantly lower than those of right cerebral cortices, striatum and thalamus. The MRs were significantly correlated with GA, birth weight and Apgar score at one minute. The MRs in infants with multiple gestations, GDM, PROM or BPD were significantly lower than those in infants without multiple gestations, GDM, PROM or BPD. **Conclusion:** VLBWI had relatively low glucose metabolism of the left cerebral hemisphere compared with the right cerebral hemisphere. Decreased cerebral glucose metabolism associates with risk factors for poor neurodevelopmental outcome in VLBWI. Future studies will be required to assess predictive accuracy of F-18 FDG brain PET for predicting long-term neurodevelopmental outcomes.

OP197

Hybrid PET/MRI Imaging in Healthy Unsedated Newborn Infants with Quantitative rCBF Measurements using ¹⁵O-water PET

J. B. Andersen, U. Lindberg, O. V. Olesen, D. Benoit, C. N. Ladefoged, H. B. W. Larsson, L. Højgaard, G. Greisen, I. Law; Copenhagen University Hospital, Rigshospitalet, København Ø, DENMARK.

Aim: The purposes of this study was to investigate the feasibility of quantitative regional cerebral blood flow (rCBF) in healthy newborn subjects using PET with low-activity ^{15}O -water and an image derived input function (IDIF) previously developed in a piglet model on a hybrid PET/MRI scanner (Andersen JB, *J Cereb Blood Flow Metab*, 2015). Especially we wished to establish a proof-of-concept of the applied PET method for medical research use in newborn infants. **Materials and methods:** Four healthy full-term newborn subjects with a mean age of 2.5 days (range 2–3 days) and mean weight of 3.4 kg (range 3.3–3.7 kg) were scanned in a PET/MRI (Siemens mMR) during natural sleep injecting a median dose of 14 MBq ^{15}O -water. This corresponds to an upper effective dose limit of 0.33 mSv, which is the approximate background radiation dose per month for the general public in Denmark (4.0 mSv/year). The study was approved by the Regional Scientific Ethical Committee of the Capital Region of Denmark, and oral and written informed consent was obtained from the children's' parents according to the Helsinki II declaration. Regional CBF was quantified using a 1-tissue compartment model (PMOD version 3.3) employing an image derived input function (IDIF) from a dynamic sequence of images of the left ventricle. Volumes of interest (VOIs) were drawn individually including whole brain, periventricular unmyelinated white matter, thalamus, striatum, mesencephalon and cortex. **Results:** PET rCBF distribution showed relatively high rCBF in the striatum, thalami, mesencephalon, pons, cerebellar vermis, and medulla, and to a lesser degree in the perirolandic cortex, mesial occipital cortex and hippocampal area. The global CBF was mean 17.8 ml/100g/min. The mean rCBF in periventricular unmyelinated white matter and thalami were 10.3 ml/100g/min and 31.3 ml/100g/min, respectively. The average white matter/thalamic ratio CBF was 0.36. **Conclusions:** Minimally invasive PET using ^{15}O -water with a very small radiation dose yielded expected values of global and regional CBF using an image derived non-invasive obtained arterial input function. The method may be used for quantitative rCBF measurements in unsedated newborn infants for clinical research purposes.

OP198

Investigating the Utility of FDG-PET/CT for Pediatric Encephalitis

P. Martineau¹, R. Lambert², J. Decarie², S. Turpin²; ¹The University of Ottawa, Ottawa, ON, CANADA, ²CHU Sainte-Justine, Montréal, Québec, CANADA.

Introduction: Encephalitis in children is a potentially debilitating neurological condition associated with a host of different etiologies. Treatment of this condition depends on the cause; however, clinical diagnosis can be difficult, and conventional radiological findings can be non-specific. To date, there have been few studies examining the role of FDG-PET/CT in the diagnosis of encephalitis, particularly in the pediatric setting. To better understand the PET manifestations of this condition, we conducted a retrospective study comparing the findings on Fluorine-18 fluorodeoxyglucose positron emission tomography (FDG-PET/CT) to those of magnetic resonance imaging (MRI) in a cohort of children with acute encephalitis. **Methods and Materials:** A retrospective study of 55 pediatric patients with suspected encephalitis who underwent FDG-PET/CT was performed. Areas of abnormal brain metabolism were identified by both qualitative and quantitative analysis. Quantitative analysis was performed using commercially available software (NeuroQTM). These findings were then compared with the MRI results and the final clinical diagnosis. **Results:** MRI was performed in 48 patients and was abnormal in 23 (48%), while FDG-PET/CT was visually abnormal in 37 of 55 (67%) patients. Using quantitative analysis to compare to a normal pediatric database, 54 (98%) studies were found to contain abnormalities. The pathologies represented in our cohort included collagen-vascular diseases, psychiatric conditions, anti-NMDAR encephalitis, Hashimoto's encephalitis, infectious encephalitis, PANS/PANDAS, ADEM, chorea, and patients in which a definitive etiology for

encephalitis could not be determined. Anti-NMDA encephalitis was associated with a large number of abnormal MRI (4/5) and FDG-PET/CT (5/5). Both patients with ADEM had abnormal MRI but normal qualitative FDG-PET/CT. Only one of seven patients with collagen-vascular disease had MRI anomalies. In this group qualitative FDG-PET/CT was abnormal in 4 and quantitative in 6. Similarly, no patients with PANS/PANDAS had abnormal MRIs, while qualitative FDG-PET/CT was abnormal in 2 of five. 11 of 16 patients had encephalitis of aseptic, infectious or unknown etiology with abnormal MRIs while FDG-PET/CT was positive in all cases. Of 7 patients presenting with chorea, 4 of 6 had abnormal MRI results while all had abnormal PET findings. Finally, qualitative FDG-PET/CT and MRI were normal in the majority of patients with neuropsychiatric symptoms (7/10 for PET and 7/8 for MRI). **Conclusion:** Our results suggest that FDG-PET/CT was more sensitive than MRI for the detection of encephalitis and sensitivity was improved by the use of quantification. Different metabolic abnormalities seemed to be characteristic of particular types of encephalitis.

OP199

Distinct Cerebral 18F-FDG PET Metabolic Patterns in Anti-N-methyl-D-aspartate Receptor Encephalitis Patients with Different Trigger Factors

J. Ge, B. Deng, C. Zuo, X. Chen; Huashan Hospital, Shanghai, CHINA.

Aim: Anti-N-methyl-D-aspartate receptor (anti-NMDAR) encephalitis is a subgroup of treatable autoimmune encephalitis, characterized by rapid development of psychosis, cognitive impairments and seizures. Etiologically, anti-NMDAR encephalitis could be divided into three subgroups, which are paraneoplastic (especially associated with ovarian teratoma), viral encephalitis-related and cryptogenic. Each type is different in clinical course, treatment strategies and prognosis. Cerebral glucose metabolic abnormalities have been reported in patients with anti-NMDAR encephalitis using 18F-fluorodeoxyglucose (FDG) positron emission tomography (PET) imaging. While previous studies commonly demonstrated a general pattern of FDG PET abnormalities associated with the disease, this study aim to investigate distinct cerebral metabolic patterns of encephalitis patients confirmed with antibodies against NMDAR according to different trigger factors. **Materials and Methods:** Twenty patients with anti-NMDAR encephalitis from Huashan Hospital, Shanghai were consecutively recruited in this study. All patients were diagnosed based on clinical manifestations and positive anti-NMDAR antibodies both in serum and in CSF samples. Each patient was classified into an etiological subgroup (paraneoplastic, viral encephalitis-related and cryptogenic) by two senior neurologist based on clinical and laboratory information. 18F-FDG PET brain imaging was performed after confirmed diagnosis. To evaluate the cerebral metabolic activity of recruited patients, the PET images of individual patients were compared with those of the same ten normal controls using a voxel-wise statistical parametric mapping analysis, respectively. **Results:** Twelve patients with anti-NMDAR encephalitis were divided into cryptogenic group, four patients were paraneoplastic and the remaining four were considered secondary to virus infection of central nervous system. Both groups of patients with cryptogenic and paraneoplastic anti-NMDAR encephalitis showed bilateral hypermetabolism in the frontal-temporal lobes and basal ganglia, covarying with bilateral hypometabolism in the occipital regions. Notably, the changes of hypermetabolism in the cortical and subcortical regions were usually asymmetric in the patients with cryptogenic encephalitis, but relative symmetric in those associated with tumor. Moreover, the anti-NMDAR encephalitis patients secondary to viral encephalitis presented with significant hypometabolism in the bilateral occipital regions, as well as in the unilateral temporal lobes and basal ganglia (also is virus infection side), but hypermetabolism in the contralateral temporal areas and basal ganglia. **Conclusion:** This study revealed that anti-NMDAR encephalitis patients triggered by different factors presented distinct cerebral metabolic patterns. We propose that

awareness of these patterns may help to better understand the various occurrence and development of anti-NMDAR encephalitis in each subgroup, and could offer valuable information to the diagnosis, treatment and prognosis of this elusive, but treatable disorder.

OP200

PISCOM: PET-FDG Interictal Subtracted ictal SPECT Coregistered with MRI for seizure focus localization

A. Perissinotti¹, A. Niñerola-Baizán¹, S. Rubi², F. Maite¹, C. Mar¹, A. Donaire¹, N. Bargalló¹, J. Rumià¹, A. Tapia¹, J. Pavia¹, F. Lomeña¹, X. Setoain¹; ¹Hospital Clínic de Barcelona, Barcelona, SPAIN, ²Hospital Universitari Son Espases, Palma de Mallorca, SPAIN.

Aim: To develop and validate a new processing nuclear imaging procedure consisting of ictal perfusion SPECT studies subtracted with interictal FDG-PET images coregistered to MRI (PISCOM) for seizure focus (SF) localization in patients with intractable complex partial seizures. **Methods:** A retrospective selection from our clinical practice between 2008 and 2012 included 18 patients (8 male and 10 female, from 18 to 61 years - mean age: 37 years) who had been diagnosed of medically refractory epilepsy, studied with MRI, ictal SPECT, interictal SPECT, interictal FDG-PET and also that remained seizure free for at least two years after surgical resection of the SF. To perform PISCOM analysis, interictal FDG-PET images were resampled and filtered to obtain a same matrix, voxel size and a similar degradation to that of 99mTc-interictal perfusion SPECT. Finally, a brain mask was used to avoid extracerebral differences between both radiotracers. PISCOM and SISCOM images were obtained using Focus-DET software and SF localization in PISCOM and SISCOM studies was determined blinded for clinical data by two nuclear medicine experts. Results of both studies were compared with each other and with the known surgical site of resection (15 temporal and 3 extratemporal). **Results:** PISCOM and SISCOM showed localizing findings in the same cerebral lobule in 15/18 (83.33%) cases. The SF was correctly identified as compared to surgical resection brain area and post-surgical outcome in 15/18 patients by both PISCOM and SISCOM, with a good concordance among them (global agreement of 88.89% and a Kappa coefficient equal to 0.60). In two cases only one of the studies (PISCOM or SISCOM) correctly identified the SF. In two subjects both modalities failed to correctly identify SF, one of them with both PISCOM and SISCOM concordant incorrect localizing findings. In 4/18 (22%) cases MRI (not blinded from clinical data and other tests) failed to identify SF: three of them were successfully identified by both PISCOM and SISCOM, and in the remaining case SF was exclusively identified by PISCOM. **Conclusions:** Even though further research is needed, the preliminary findings of this new processing nuclear imaging technique are promising as a high rate of PISCOM/SISCOM concordance for correct seizure focus localization has been found. Possibly, with further development of the PISCOM technique, the need to obtain interictal SPECT images could be minimized or even be avoided and replaced by interictal FDG-PET images.

OP201

Grey matter metabolism in relation with white matter lesions in older hypertensive patients with subjective memory complaints: a pilot voxel-based analysis study

A. Verger¹, G. Hossu², A. Kearney-Schwartz³, S. Bracard⁴, V. Roch¹, A. Van der Gucht¹, R. Fay⁵, A. Benetos³, P. Marie¹, L. Joly³; ¹Nuclear Medicine Department CHRU Nancy, Nancy, FRANCE, ²CIC-IT, CHRU Nancy, Nancy, FRANCE, ³Geriatric Medicine Department CHRU Nancy, Nancy, FRANCE, ⁴Neuroradiology CHRU Nancy, Nancy, FRANCE, ⁵CIC-P, CHRU Nancy, Nancy, FRANCE.

Aim. This study aimed at assessing the changes in brain metabolism, related to white matter magnetic resonance (MR) hyperintensities of presumed vascular origin, with a voxel-based quantitative analysis of [¹⁸F]-fluorodesoxyglucose Positron Emission Tomography (FDG-PET) imaging. **Methods.** Sixty older hypertensive patients with subjective memory complaints (75±5 years, 34 women) were prospectively referred to FDG-PET and MRI brain imaging. The Statistical Parametric Mapping software was used to assess the correlation between brain distribution of FDG and white matter hyperintensities assessed by the Fazekas score on MRI images. **Results.** The Fazekas score was inversely related to FDG uptake, independently of age and gender, within 14 Brodmann areas located mainly in the frontal lobe but also in certain limbic, insular and temporal areas. This relationship was also found to be largely independent of the volume of grey-matter expressed in % of cranial volume, an index of atrophy. **Conclusions.** White matter MR hyperintensities of presumed vascular origin are cross-sectionally associated with a lower grey-matter metabolism, mainly but not only within frontal areas and independently of age, gender and grey-matter atrophy. **Keywords:** White matter lesions, Brain FDG-PET, Brain MRI, hypertension.

OP202

Moderate regional differences in sequential FDG brain PET images caused by bio-kinetic heterogeneity can be detected regardless of the acquisition technique (static vs. flow-motion)

G. Berding^{1,2}, F. Wilke³, M. Kessler^{1,2}, N. Owsianski-Hille¹, M. Mamach^{1,2,3}, L. Geworski³, F. Bengel¹; ¹Department of Nuclear Medicine, Hannover Medical School, Hannover, GERMANY, ²Cluster of Excellence Hearing4all, Hannover Medical School, Hannover, GERMANY, ³Department of Medical Physics and Radiation Protection, Hannover Medical School, Hannover, GERMANY.

Aims Sequential F-18-Fluorodeoxyglucose (FDG) brain-PET within 70min post injection revealed a characteristic difference pattern in regional glucose metabolism (relative frontal increase and cerebellar decrease). We evaluated, if this pattern can be related to bio-kinetic differences between brain regions and is present at later time points as well. Moreover, we investigated, whether a new acquisition technique, flow motion - aiming for increased uniformity of the sensitivity profile in axial (z) direction - is capable to detect such differences equally to static imaging. **Methods** 108 FDG brain-PET/CT (Biograph mCT, Siemens) scans were enrolled. In three groups of oncologic patients (mean-age 56, 24 female) without malignancy in the brain or neuropsychiatric disease always two sequential scans were acquired at the following times post injection: (i) n=21, flow-motion 84min, static 108min, (ii) n=23, static 78min, flow-motion 105min, (iii) n=10 static 82 and 112min. After proportional scaling of PET data, VOI and SPM analyses were applied (paired t-test). Additionally, 9 dynamic 50min FDG brain scans without appreciable findings were enrolled (mean patient-age 58, 3 female). These scans were quantified including simultaneously obtained arterialized venous blood samples using a 2-tissue compartment model with and without fitting for k4 (PMOD 2.9). **Results** Based on VOI data the most pronounced differences (p<0.0025) in all three comparisons were: uptake increase early to late in frontal cortex (Flow-motion/static: +2.8%, static/flow-motion: +1.1%, static/static: +2.2%) and relative decrease early to late in cerebellum and occipital cortex (Flow-motion/static: -2.5%, -0.8%, static/flow-motion: -2.1%, -1.6% static/static: -2.7%, -1.8%). Clearly the same pattern was detected in SPM analyses. Bio-kinetic modeling revealed significantly higher net influx of FDG in the frontal cortex compared to the cerebellum (Ki: 0.034 vs. 0.018, p=0.001). Conversely, k4 was significantly higher in the cerebellum compared to the frontal cortex (0.021 vs. 0.016, p=0.002). **Conclusions** The difference pattern between sequential FDG scans up to 70min post injection is also observable later. Therefore constant uptake duration has to be ensured in longitudinal studies even for late imaging time points. The difference

pattern seems to be caused by a bio-kinetic heterogeneity, notably higher influx and lower reflux of FDG in the frontal cortex compared to the cerebellum. Relatively higher occipital uptake in early images might be related to the eyes open condition after tracer injection in oncologic patients. Since the present differences could be detected regardless of the acquisition technique (flow-motion vs. static) both seem to be interchangeable in follow-up scans of brain glucose metabolism.

OP203

18F-FDOPA PET for the differential diagnosis between brain tumor recurrence and radiation necrosis: correlation with pathological results obtained from surgery

J. Darcourt^{1,2}, M. Dufour¹, A. Schiazza^{1,2}, F. Almairac³, C. Zwarthoed¹, V. Bourg³, M. Ouvrier¹, P. Bondiau¹, D. Benisvy¹, L. Mondot³, F. Vandenbos^{3,2}; ¹Centre Antoine Lacassagne, Nice, FRANCE, ²Université de Nice, Nice, FRANCE, ³CHU, Nice, FRANCE.

During the follow-up of patients treated for a malignant brain tumour, the differential diagnosis between recurrence (REC) and radiation necrosis (RN) is often difficult on MRI (pseudoprogression...). 18F-FDOPA PET can be used in this situation. We report on a retrospective study in which PET 18F-FDOPA findings are compared to pathological results obtained from surgery. **Materials and methods** 25 patients mean age 59 years old (11M; 14F) were included: 10 GBM, 3 grade III oligoastrocytomas, 12 metastases. They were studied after initial treatment by 18F-FDOPA PET for differential diagnosis between recurrence and radiation necrosis. A 10 min static PET-CT was performed 20 min post injection of 2 MBq/kg of 18F-FDOPA (mCT-Siemens; OSEM 5 it and 24 subsets). MRI T1 weighted images were coregistered to PET data. Images were graded visually using Lizarraaga et al. criteria (JNM 2014), comparing tumour uptake with striatal activity: 0 lesion not visible, 1 uptake inferior to striatum, 2 lesion uptake equal to striatum and 3 uptake higher than striatum. PET was considered positive for a score > 1. SUV values were measured for quantitative analysis. All patients underwent neurosurgery for suspicion of REC based on MRI and PET data (mean delay 37 days; 8-70). The final diagnosis of REC and RN was based on pathologist diagnosis. Aminoacid transporter LAT1 expression was measured by immunohistochemistry using a semiquantitative score (from 0 to 400). **Results** 20 patients showed REC and 5 RN. 18F-FDOPA PET was positive in all REC and was negative in 3 and positive in 2 of the 5 RN (sens 100%; spec 60%). Tumour to striatum SUV values were significantly higher in REC ($p < 0,005$) than in RN. The 2 false positive 18F-FDOPA patients had high astrocytic LAT1 expression (270 and 300) despite pure RN without REC explaining 18F-FDOPA uptake. **Conclusion** In the difficult situation of post initial treatment differential diagnosis between REC and RN in brain tumours, 18F-FDOPA PET has a high sensitivity. However, over expression of LAT1 in radiation necrosis tissues may decrease its specificity.

601 – Monday, October 17, 2016, 08:00 - 09:30, Auditorium

CME 5 - Dosimetry/Oncology/ESTRO: Radiobiology/Radiation Biology Markers of Radiation Damage

OP204

Radiation-Induced Abscopal Effects by Radiotherapy and Radionuclide Therapy

G. Hanna; Queen's University Belfast, The School of Medicine, Dentistry and Biomedical Sciences, Belfast, UNITED KINGDOM.

OP205

Radiotherapy Combined with Immunotherapy: Present Status and Future Perspectives

P. Lambin; MAASTRO Clinic, Radiation Oncology, Maastricht, NETHERLANDS.

OP206

Towards Imaging of Repair/Recovery Mechanisms in Response to Radiation Exposure

B. Cornelissen; RRI, Dept.of Oncology, univ. of Oxford, Oxford, UNITED KINGDOM.

602 – Monday, October 17, 2016, 08:00 - 09:30, Hall 211

Joint Symposium 5 - EANM/EACVI: Imaging Atherosclerosis: From Inflammation to Calcification

OP207

Current Concepts in Atherosclerosis

J. Knuuti; Turku University Hospital, Turku PET Centre, Turku, FINLAND.

OP208

Imaging Atherosclerosis with PET (Protocols Inflammation/Calcification etc.)

F. Hyafil; CHU Bichat, AP-HP, Nuclear Medicine, Paris, FRANCE.

OP209

Imaging Atherosclerosis with CT (Protocols, (Vulnerable) Plaques etc.)

P. Maurovich-Horvat; Semmelweis University, Budapest, HUNGARY.

OP210

Risk Stratification PET/CT

J. Bucarius; Maastricht University Medical Center, Maastricht University, Department of Nuclear Medicine, Maastricht, NETHERLANDS.

603 – Monday, October 17, 2016, 08:00 - 09:30, Hall 117

Technologist Oral Presentations 1

OP211

Pediatric low-dose CT: How low can we go?

G. Caan, **A. Almeida**, M. Segbers; ErasmusMC, Rotterdam, NETHERLANDS.

Aim: It is well known that pediatric patients are more sensitive to radiation than adults. We therefore reduced the dose for low-dose CT's in this patient group. We studied the effect on image quality and investigated the behavior of Automatic Exposure Control (Caredose4D) for pediatric patients. **Materials and Methods:** We performed a retrospective study of 40 patients scanned on Siemens Biograph mCT40 and 128 slice scanners. To reduce dose, scanner parameters were set to 80kV and 40 reference mAs (ref.mAs). In comparison adults are scanned at 120kV and 40 ref.mAs. Patients ranged from 1 to 16 years of age, with body mass varying from 6.5kg to 58kg and length from 0.68m to 1.65m. To quantify image quality in all subjects, a circular ROI with a fixed diameter of 3cm was drawn in one slice in a homogeneous part of the liver. The noise level was derived by computing the standard deviation (SD) within the ROIs. The noise level was used as a parameter for image quality. The noise was then correlated to patient parameters as body mass, body mass per length and BMI. **Results:** Eff.mAs values were in between 20 and 40 mAs. CT dose index (CTDI) was from 0.39 to 1.82. The range of SD was 27 to 89 with a mean value of 54. SD showed the best significant correlation with body mass per length ($p < 0.001$, $R^2=0.3$) and BMI ($p < 0.001$, $R^2=0.3$). Body mass gives $p < 0.001$, $R^2=0.25$. In general, image quality was best for the smallest patients. For larger patients the image quality was reduced. All parameters showed a significant correlation with CTDI. The best significant correlation was found for body mass length ($p < 0.001$, $R^2 = 0.6$). CTDI remained virtually constant (0,40-0,50) for patients up to 45 kg. Over 45 kg

there was a clear increase of dose. **Conclusion:** The scan protocol resulted in unwanted variations in image quality (noise). CareDose4D does not adapt the dose such that the image noise level is constant across all patient sizes. Image noise for large patients was too high. The dose should be increased in our pediatric low-dose CT protocol.

OP212

Feasibility study of a human tissue equivalent phantom for PET/CT

M. Szoliková¹, G. Nagy¹, A. Forgács¹, M. Zentai², I. Garai¹; ¹ScanoMed Ltd., Debrecen, HUNGARY, ²Mediso Medical Imaging Systems, Budapest, HUNGARY.

Aim: A proper CT based attenuation correction of a positron emission tomography (PET) image is essential for reliable quantification. To check the comparability of the goodness of the attenuation corrections applied by different manufacturers makes the necessity of a phantom, which can represent the whole range of the attenuation coefficient specific for human body. In the study we aimed to create an in-house human tissue equivalent phantom, which includes lung, fat, muscle and bone equivalent material containing F-18 isotope. **Methods:** The lung equivalent compartment was Styrofoam® beads surrounded by F-18 and water solution ((-650 Hounsfield Unit (HU)) - (-800 HU)), as it is frequently applied for anthropomorphic phantoms. To mimic the fat tissue, firstly the F-18 FDG synthesized in water was evaporized, then it was diluted in isopropyl alcohol, finally it was mixed with the oil. With this method a homogeneously distributed F-18 FDG isotope was created in oil in the range of (-50) - (-100) Hounsfield Unit (HU), accordingly to the fat HU range. The muscle was simulated by ballistic gel mixed with F-18 FDG, resulting (+50) - (+100) HU material. The bone was a hollow shin bone of a cattle. Finally the phantom was measured on two PET/CT scanners. **Results:** F-18 FDG diluted in ballistic gel and oil were feasible to extend the HU scale. The phantom covered the whole Hounsfield Unit spectrum of human body, measured from the lung till the bone. With the help of this phantom the two compared PET/CT systems provided the same standard uptake values within 3% error. **Conclusion:** The introduction of the ballistic gel and the oil as a possible candidate of new phantom material, facilitates the construction of a human tissue equivalent phantom to assist a new way of comparing PET/CT scanners.

OP213

Radiation dose reduction using a bismuth-coated latex shield over the eye lens in Brain SPECT/CT

N. Matsutomo¹, M. Fukunaga², T. Yamamoto¹, H. Onishi³; ¹Kyorin University, Mitaka, JAPAN, ²Kurashiki Central Hospital, Kurashiki, JAPAN, ³Prefectural University of Hiroshima, Mihara, JAPAN.

Purpose For brain SPECT/CT, although CT images provide precise anatomical information and accurate attenuation correction, their use increases the radiation dose to the patient, especially to the eye lens. The eye lens is particularly radiosensitive: ICRP has reviewed that the threshold in absorbed dose for the eye lens is considered to be 500 mGy. Therefore, because of the radiation effect, the eye lens is at high risk when brain SPECT/CT is performed. The purpose of this study was to assess the usefulness of a bismuth-coated latex shield (B-shield) as an eye protectant during brain SPECT/CT. **Methods** Three types of B-shields containing heavy metal bismuth (0.15, 0.25 and 0.35 mm lead equivalent) were employed. Each B-shield was placed over the cylindrical phantom and the eyes of a 3-dimensional brain phantom filled with Tc-99m solution. Subsequently, SPECT/CT was performed on the phantoms both with and without the B-shields. The CT scan parameters were set to 30-200 mA and 130 kV. Dose reduction due to the supposed radioprotection was measured using a pencil-shaped ionization

chamber. In addition, the image artifacts (changes in CT number), linear attenuation coefficients, coefficients of variation (CV) on SPECT images and the relative radioactivity concentrations were evaluated for the protective effect of the B-shield. **Results** The B-shields decreased the average radiation dose by 60.1%, 68.6% and 73.5%. The radiation doses with/without the B-shield were 0.62-0.93 mGy and 2.31 mGy. Although increasing the mean CT number caused by B-shield, it was just beneath the surface level on the phantom. Beam hardening was detected as streaks of higher density in close proximity to the underside of the B-shield. The linear attenuation coefficients and CVs were not significantly different between phantoms with/without the B-shield. The relative radioactivity concentrations when using Tc-99m were not affected by B-shield thickness. **Conclusions** The B-shields decreased the radiation dose without affecting attenuation correction or radioactivity concentration. Although B-shields increased artifacts in the surface level, the SPECT image quality was acceptable. The use of B-shields could prove beneficial in pediatric patients and those with preexisting eye disease.

OP214

Design and physical performance of a plastic scintillator detector to control radioactive waste in a nuclear medicine unit

F. Zito¹, A. D'Alessio², G. Galetta³, L. Rossi², R. Benti¹; ¹FONDAZIONE IRCCS CA' GRANDA Ospedale Maggiore Policlinico, Milan, ITALY, ²Specialization School of Medical Physics Università di Milano, Milan, ITALY, ³Specialization School of Medical Physics Università di Milano, FONDAZIONE IRCCS CA' GRANDA Ospedale Maggiore Policlinico, Milan, ITALY.

Purpose: Management of solid radioactive waste produced in a nuclear medicine unit (NM-unit) has to be arranged according with country regulatory requirements. For disposal of waste, containing radionuclides with half life less than 75 days, the exempt activity concentration < 1 Bq/g is fixed by the Italian regulation. Aim of the present work is to describe physical performance of a plastic scintillator detector dedicated to control boxes containing contaminated solid materials produced during nuclear medicine activities (residuals of radiopharmaceutical preparations and administrations, absorbing papers and tissues contaminated by biological fluid of administered patients and any object suspected of contamination). **Methods :** Three polyvinyl-toluene (PVT) modules, each of 35 cm x 15 cm size and 2 cm thickness coupled to a photomultiplier (PMT), were assembled to realize a 35 cm width x 45 cm height detector surface (ELSENUCLEAR Milan-Italy). This surface sufficiently covered the largest face of the waste box. After assessing background level, sensitivity was determined for the principal radionuclides used in a typical NM-unit: ^{99m}Tc, ¹²³I, ¹³¹I, ¹¹¹In and ¹⁸F. For each radionuclide a calibrated radioactive solution was prepared and a source realized with 0.5 ml volume in a tube of 1 cm diameter was positioned at the container center at a distance of 15 cm from the detector surface. Minimum detectable activity (MDA) at 4.65 standard deviation of the background (SD-bkg) and at 2 SD-bkg were determined. Sensitivity for a ¹³⁷Cs point source with certified activity was also assessed and used for periodical check of equipment stability response. A mean weight of 4 Kg was supposed for waste containers. The detector system was equipped with auditory and red light alarms activated when net counts of the container under control are higher or equal to the set threshold level. **Results:** Background level was 350 cps. For 1 minute acquisition, for all considered radionuclides, moving from the lowest to the highest energy radionuclides (^{99m}Tc, ¹²³I, ¹¹¹In, ¹³¹I, ¹⁸F) MDA values were: 4.4, 3.4, 2.5, 1.6, 0.7 KBq at 4.65 SD-bkg and 1.8, 1.4, 1.1, 0.7 and 0.3 KBq at 2 SD-bkg. By assuming the 4Kg mean weight of the containers MDA resulted sufficiently lower than exempt activity concentrations (< 1 kBq/kg). For ¹³⁷Cs the sensitivity was 750 net cpm/KBq. **Conclusion:** The designed PVT detector showed good sensitivity and a threshold set to 2SD-BKg is suitable and conservative to control radioactivity concentrations of waste containers produced by a conventional NM-unit.

OP215**Evaluation of the use of the scatter limit option to reduce wash-out artefacts on the GE Discovery 710**

C. Abreu, L. C. Pike; PET Imaging Centre, Division of Imaging Sciences and Biomedical Engineering, King's College London, King's Health Partners, St. Thomas' Hospital, London, London, UNITED KINGDOM.

Patient motion during PET/CT acquisitions causing misalignment between CT and PET images can result in wash-out artefacts due to incorrect scatter correction scaling. The GE Discovery 710 includes a scatter limit (SL) option in the reconstruction to limit scaling and reduce artefacts. The aim of the study was to investigate image quality and quantitative accuracy using the SL option for ^{18}F -FDG-PET/CT for eliminating wash-out artefacts. This study analysed wash-out artefacts in ^{18}F -FDG PET/CT images acquired from 81 patients and from a NEMA image quality phantom. Images were acquired of the NEMA image quality phantom using six hot spheres (10, 13, 17, 22, 28 and 37mm diameter) to background ratio of 4. To simulate arm motion, a cylinder of 8.5 cm radius was filled with the same ^{18}F solution as the phantom background. PET/CT data were acquired with the arm correctly aligned and then the cylinder misaligned on CT. A hot syringe was placed by the side of the cylinder and on top of the phantom, to simulate a tissue injection. PET data were reconstructed using ordered subset expectation maximisation (OSEM) with and without time-of-flight (TOF) information. Images were also reconstructed using a proprietary GE reconstruction 'QClear'. Comparisons were made of the PET images reconstructed with the correctly aligned CT versus the misaligned CT both with and without the SL option on. Clinical PET images were retrospectively reconstructed without the scatter correction and with SL on, and analysed for the presence of artefacts. With SL off, the maximum error between matched and mismatched images was 83.8, 72.1 and 54.7% for non-TOF, TOF and QClear, for the 10mm sphere. The highest percentage errors for the 10 and 37mm spheres were 83.6% and 50.5% with SL off and 40.1% and 57.8% with SL on, respectively. There was improvement in quantitative accuracy for all spheres and background with SL on. From the 81 patients analysed, 3 of those required rescanning. Whilst image quality was improved using SL, quantitative accuracy was still significant with underestimation of uptake in the region near the artefact. SL worked better eliminating artefacts caused by arm motion. The results of our study show using SL is useful and could be used clinically to reduce wash-out artefacts and improve quantitative accuracy. The SL option must be used with caution particularly if there is a lesion in the vicinity of the artefact, rescanning may still be required so a clinical opinion should be sought.

OP216**Radiation Exposure of the Nuclear Medicine Personnel during new therapy procedures, the Lutetium-177 DOTATATE Production, Administration and Imaging**

B. G. Hoving, B. J. de Wit-van der Veen; Antoni van Leeuwenhoek Hospital, Amsterdam, NETHERLANDS.

Introduction The Antoni van Leeuwenhoek hospital started with Lu-177-DOTATATE therapy. The administered dose is 7.4 GBq per cycle which is repeated every 10 weeks for 4 cycles. To assess the dose distribution, 4 post-injection scans are performed each cycle. Thus for 25 patients, 100 productions and 400 extra scans per year are needed, resulting in a potentially increase of radiation dose to our personnel. **Aim** This study will determine the impact of Lu-177-DOTATATE therapy on the radiation dose of the personnel involved in the labelling, quality control (QC), dose administration and imaging procedure. **Materials and Methods** The Lu-177-DOTATATE therapy workflow is divided into three sub-procedures; I. production (including labelling using the automated system, QC and syringe preparation), II. patient administration, and III. imaging. Lu-177 DOTATATE is prepared on a fully automated

system (Scintomics GmbH, Germany). QCs are performed with HPLC and administration was done using a shielded dispensing cart. The durations of all actions were denoted, and a dose rate monitor (Thermo Eberline ESM FH 40 G-L) was used to estimate the dose rate for each action. We measured during 5 productions, 4 administrations and 16 imaging procedures. **Results** The administered dose to the patient was 7233 ± 55 MBq. On average, the dose rate during production was $7.2 \mu\text{Sv/h}$, with removing the Lu177-DOTATATE vial after labelling ($35 \mu\text{Sv/h}$) and preparing the synthesis system ($13.9 \mu\text{Sv/h}$) being the most crucial steps. The dose rate during administration was $5.6 \mu\text{Sv/h}$, with the crucial actions being dismantling of the cart ($7.9 \mu\text{Sv/h}$) and patient transport to the scanner ($14.8 \mu\text{Sv/h}$). Imaging had an average dose rate of $21.4 \mu\text{Sv/h}$, with helping the patient throughout the first scan as critical action ($52.6 \mu\text{Sv/h}$). Still, the time-corrected total average dose during production, administration and imaging was 3.1, 5.2 and $8.3 \mu\text{Sv}$, respectively. The radiation dose to one person from a Lu-177 DOTATATE cycle is $16.6 \mu\text{Sv}$, with a total handling time of 2 hours and 25 minutes. **Conclusion** The impact of the 4 patients with 1 cycle Lu-177 therapy on the personnel radiation dose is rather small, $66.3 \mu\text{Sv}$. The Lu-177 therapy of 25 patients leads to an extra radiation dose of 1.66 mSv per year. This extrapolated dose will be divided over >10 persons of different disciplines. The current effective dose to technicians is below the legal annual limit ($< 6 \text{ mSv/yr}$) with an average dose of 1.5 mSv/yr in our hospital.

OP217a**A European phantom study to cross-calibrate myocardial ^{123}I -mIBG scintigraphy**

E. Poel¹, D. O. Verschure¹, K. Nakajima², K. Okuda³, B. L. F. van Eck-Smit¹, G. A. Somsen⁴, H. J. Verberne¹; ¹Academic Medical Center, Amsterdam, NETHERLANDS, ²Kanazawa University Hospital, Kanazawa, JAPAN, ³Kanazawa Medical University, Uchinada, JAPAN, ⁴Cardiology Centers of the Netherlands, Amsterdam, NETHERLANDS.

Aim: Planar ^{123}I -meta-iodobenzylguanidine (^{123}I -mIBG) scintigraphy is a highly reproducible technique to assess cardiac sympathetic activity and helps differentiating high and low risk heart failure patients. ^{123}I -mIBG has a small inter- and intra-observer variation. However differences in the collimators used is one of the most important factors that cause variation in the commonly used heart-to-mediastinum ratio (H/M) among institutions and studies. Therefore standardization among various gamma camera-collimator combinations is needed. Previously a phantom for ^{123}I -mIBG planar imaging has been developed to cross-calibrate different acquisition conditions in Japan. However, data from European institutions is still lacking. Therefore, to further cross-calibration of ^{123}I -mIBG in Europe, the aim of this study was to accumulate ^{123}I -mIBG data for the H/M from common vendors in Europe. **Methods:** A total of 163 phantom experiments were performed in 21 institutions in Austria, Belgium and the Netherlands to calculate cross-calibration coefficients of H/M. Based on the phantom study, a conversion coefficient for each gamma camera-collimator system was created, including low-energy (LE) ($n = 93$) and medium-energy (ME) ($n = 70$) collimators. An average conversion coefficient from the most common ME group was used to calculate a standardized H/M. **Results:** On average the LE collimator derived H/Ms were significantly lower compared to the ME-collimator derived H/Ms. The mean conversion coefficients from the individual gamma camera-collimator combination to the mathematically calculated reference H/M ranged from 0.53 to 0.67 for the LE collimator group and from 0.91 to 1.00 for the ME collimator group. A conversion coefficient of 0.88 was established that unifies H/Ms from all acquisition conditions. **Conclusion:** H/Ms can be converted into standardized H/Ms by using the reference H/M and

conversion coefficients for each acquisition condition. This standardization is also important for identifying appropriate thresholds for differentiating high and low risk heart failure patients. In addition this cross-calibration would enable a better comparison between European and Japanese data.

OP217b

Audit on staff exposure when administering Radium 223 Dichloride Therapy

A. S. F. Ribeiro, S. Summers, L. Causer, T. Shepherd, I. Murray, J. Gear, G. Flux, M. Meintjes, Y. Du; Royal Marsden Hospital, Sutton, UNITED KINGDOM.

Background: Prostate cancer is the fourth most common cancer in both sexes combined and the second most common cancer in men. In 2012 an estimated 1.1 million men worldwide were diagnosed with prostate cancer according to the World Health Organization. Radium dichloride therapy (^{223}Ra) has a half-life of 11.4 days which emits short-range alpha-particles with high-energy that selectively targets areas of increased bone turnover such as bone metastases. A range of methods to administer ^{223}Ra have been reported from using protective suits with face masks to more commonly personal protective equipment such as gloves and aprons. This audit intends to evaluate our current practice with regards to staff exposure and method of administration of ^{223}Ra . **Materials and Methods:** Since 2004 we have been involved with administering ^{223}Ra . We currently perform an average of four patients a week (clinical and research). Data from 18 administrations was collected over a period of 3 months. Specialized techniques, such as two staff members for therapy administration, use of personal protective equipment (double gloves, apron and Inco pad sheets) are current practice when administering the therapy within our general Nuclear Medicine Service. Administration is currently performed under the Ionising Radiations Regulations 1999 (IRR99) by a team of four experienced members of staff (two clinical nurse specialists; two nuclear medicine research technologists). The average patient activity was 4.35 MBq of ^{223}Ra , ranging from 3 MBq - 6.7 MBq. A dose meter was used at a 50 cm distance from the syringe (approximate distance from administrator to syringe) as well as Electronic Personal Dosimeter (EPD). **Results:** Our data showed the average dose rate from administering the therapy was 3.67 $\mu\text{Sv/hr}$ (± 1.4). No EPD readings were observed for all 18 administrations. The room monitoring (injection chair; trolley and surrounding areas) and self-monitoring were both not significant. **Conclusion:** This audit confirmed that according with the methods and practices used in our service, most Nuclear Medicine Departments can potentially deliver this treatment, providing adequate staff training is in place as well as good communication with all teams involved. ^{223}Ra can be administered with safety for both patients and staff involved.

OP218

Design and Development of a Dedicated Robotic SPECT System for Cardiac Imaging

M. R. Ay¹, B. Teimourian², S. Sajedi¹, A. Akbarzadeh¹, S. Kaviani¹, M. Farahani¹, S. Farzanefar³, Z. Shapouri¹; ¹Research Center for Molecular and Cellular Imaging, Tehran University of Medical Sciences, Tehran, IRAN, ISLAMIC REPUBLIC OF, ²Faculty of Physics and Nuclear Engineering, Amir Kabir University of, Tehran, IRAN, ISLAMIC REPUBLIC OF, ³Department of Nuclear Medicine, Valiasr Hospital, Tehran University of Medical Sciences, Tehran, Iran, Tehran, IRAN, ISLAMIC REPUBLIC OF.

Introduction: Cardiac imaging has become an integrated part in the diagnostic and prognostic work-up of patients with cardiovascular disease. In order to improve the quality of cardiac imaging dedicated cardiac scanners with small field of view introduced in last couple of years. We designed and developed a dedicated cardiac SPECT system in our lab for cardiac imaging called RoboSPECT. This name was chosen because of robotics motions of detectors and arms in this scanner. The reclining seat design of the scanner provides maximum patient comfort. It should be noted two perpendicular detector heads designed and optimized for cardiac imaging. The aim of this study is to introduce the concept design of the scanner and also evaluates and characterizes the performance of RoboSPECT based on NEMA-NU2 2007 standards for gamma cameras. **Method:** The detector of the scanner is based on NaI(Tl) crystal and 24 rectangular PMTs (76x76 mm) in 4x6 form cover the detection area. Rectangular shape of PMT allows the full coverage of active crystal area without any dead zone. The scanner equipped with LEHR lead Parallel-hole collimators with 1.5 mm hexagonal holes, 35 mm hole length, and 0.2 mm septal thickness. The gantry of the scanner is based on robotic motion of both arm and detectors that fixed in 90 degree position. All readout electronic in the detector designed based on our US patient called non linear recursive filter. **Results:** The experiments showed that the intrinsic spatial resolution was 3.6 mm on the surface of crystal. The system spatial resolution and the sensitivity of the system on the collimator surface were 7.8 mm and 179 cps/MBq, respectively. The extrinsic energy resolution was determined as about 9.3 %. In addition, the integral uniformity and the differential uniformity, after uniformity correction, in UFOV were measured 2.2% and 1.2%, respectively. Also the absolute and differential linearity were evaluated 0.8 and 0.1 mm in UFOV. In order to validate the accuracy of images acquired by this scanner 50 patients were scanned both with RoboSPECT and ADAC camera. The results showed good agreement between the images of both scanners. **Conclusion:** This study showed that the designed scanner called RoboSPECT has acceptable performance for cardiac imaging.

604 – Monday, October 17, 2016, 08:00 - 09:30, Hall 112

Do.MoRe: Thyroid & Parathyroid

OP219

Role of single-nucleotide polymorphisms (SNPs) of glucose transporter 1 (GLUT1) in differentiated thyroid cancer (DTC) patients

V. Stebner¹, N. Becher-Boveleth¹, S. Ting², A. Sabet¹, A. Bockisch¹, J. Nagarajah³; ¹Department of Nuclear Medicine, Medical Faculty, University Duisburg-Essen, Essen, GERMANY, ²Department of Pathology, Medical Faculty, University Duisburg-Essen, Essen, GERMANY, ³Department of Radiology, Memorial Sloan Kettering Cancer Center, New York, NY, UNITED STATES.

Aim: The human genome has about 35 million SNP. Some SNP are more common than other. Our aim was to identify SNP, which are presented more frequently in patients with DTC or which change for the worse of this disease. GLUT1 is up regulated in solid tumors like DTC and patients with higher standardized uptake values (SUV) on F-18-FDG (FDG)-PET show a poorer prognosis. For this we evaluated the effect of the three mostly reported SNP XbaI, HpyCH4V and HaeIII for the GLUT1 on progression free survival and overall survival in DTC patients. **Methods:** A total of 69 patients (P) with DTC and a follow-up of minimum 60 months were included in this retrospective study. All these patients had archival tumor free tissues for SNP analyses. Restriction fragment length polymorphism (RFLP) technique was used to identify SNP. Progression was defined as either increasing Tg-values and/or progress on imaging. FDG-PET was performed for all P and SUVmax was used to quantify glucose uptake. Kaplan Meier curve was made for progression-free and overall survival. **Results:** The allele frequencies were: XbaI G>T: G=0,37 , T=0,63; HpyCH4V A>T: A=0,15 , T=0,85; HaeIII T>C:

T=0,17, C=0,83. XbaI GT has a shorter PFS than GG/TT (Median: GT 23 months (m) vs. GG/TT 55,5 m; p=0,045). The PFS of HpyCH4V and HaeIII show a strong correlation with each other (p=0,0001). There is an implied correlation between XbaI and M-stage. There is a linear trend between XbaI and UICC-stage. XbaI GT shows a higher SUVmax. in FDG-PET/CT than GG/TT. Conclusion: XbaI GT SNP of GLUT1 seems to be correlated with a lower PFS and a higher SUVmax. HpyCH4V and HaeIII seems to co-occur in these patients.

OP220

Circulating Tumor Cells, a New Prognostic Factor In Minimally Invasive Follicular Thyroid Carcinoma

C. Badulescu^{1,2}, A. Piciu^{1,2}, M. Larg¹, E. Barbus¹, C. Pesteau¹, M. Saftencu², O. Barbos¹, G. Chereches¹, N. Bejinariu¹, **D. Piciu**^{1,2}; ¹Institute of Oncology, CLUJ-NAPOCA, ROMANIA, ²University Of Medicine and Pharmacy "Iuliu Hatieganu", Cluj-Napoca, ROMANIA.

Introduction: Follicular thyroid carcinoma (FTC) is a well-differentiated carcinoma, with a worldwide incidence of 5-15 %. FTC has been classified, according to histological criteria, as minimally invasive (MIFC) or widely invasive carcinoma (WIFC). Objectives: The aim of this study was to determine the presence of circulating tumor cells (CTC) in the blood of patients with MIFC, in order to define the treatment and the prognosis. **Methods:** Between January-June 2015, we conducted a study on 16 cases of MIFC who underwent total thyroidectomy. One month after the surgery, we recorded: gender, age, histological features, tumor size, serum thyroglobulin (Tg) and we analyzed the presence of CTC from venous blood on an immunomagnetic segregation method. **Results:** Females were 81.3%; the mean +/- SD age was 47.2 +/- 15.79 years. The tumoral size mean +/- SD was 2.2 +/- 1.74 cm; 5 patients had tumor size <1 cm; 5 patients presented capsular and vascular invasion, 4 only capsular invasion; 10 patients out of 16 had CTC present one month after surgery, with values ranging between 1 CTC/6ml to 13 CTC/6ml. This study shows the relation between the type of invasion and CTC value. Patients with a change in CTC status from positive to negative had a good prognosis, as well as patients without baseline CTC. **Conclusion:** This study opens the opportunity to improve the management of MIFC, making the CTC status a part of the therapy algorithm. Further studies are needed to determine the accuracy of the test and its role in the long-term follow-up.

OP221

Predictive and prognostic value of 18F-DOPA PET/CT in patients affected by recurrent medullary carcinoma of the thyroid

F. Caobelli¹, A. Chiaravalloti², L. Evangelista³, M. Vadrucchi⁴, F. Scalorbi⁵, D. Donner⁵, P. Alongi⁶, Y. Working Group¹; ¹Universitätsspital Basel, Basel, SWITZERLAND, ²Università Cattolica del Sacro Cuore, Roma, ITALY, ³Istituto Oncologico Veneto, Padova, ITALY, ⁴Università Milano Statale, Milano, ITALY, ⁵Hospital of Trento, Trento, ITALY, ⁶San Raffaele G. Giglio Institute, Cefalu' (PA), ITALY.

Background. Medullary thyroid carcinoma (MTC) is a malignancy that originates from thyroid parafollicular C cells and accounts for about 5% of thyroid cancers. The measurement of calcitonin in washout fluids of thyroid nodule aspirate is widely used to monitor disease progression. However, prognostic factors to predict outcomes and allow the planning of the most appropriate therapy are highly warranted. 18F-DOPA PET/CT has been investigated in patients with MTC, and showed promise in diagnosing, staging, detecting recurrent lesions, and monitoring treatment response. Specifically, this technique has been demonstrated to be superior to 18F-FDG PET/CT in detecting disease recurrence, also for low carcinoembryonic antigen (CEA) and calcitonin levels. It remains unclear, whether 18F-DOPA PET/CT can have a prognostic role

in the restaging process. **Methods.** 60 patients affected by MTC (mean age: 63.6±13 years, range 44-82 years) were eligible from a multicenter database. All patients underwent a restaging 18F-DOPA PET/CT, performed at least 6 months from surgery or first-line therapy. CEA/calcitonin levels, local recurrences, nodal involvement and distant metastasis at PET/CT were recorded. SUVmax-SUVmean (normalized using mediastinal uptake as reference) and metabolic tumoral volume were automatically calculated for each lesion, by placing a volume of interest (VOI) around the lesion with a 30% threshold. The patients were clinically and radiologically followed up for a period of 19±10 months. ROC curve was used to determine the best cut-off value for CEA and calcitonin to predict a positive PET/CT. Progression free survival (PFS) and overall survival (OS) were calculated by using Kaplan-Meier curves. Increased odd ratio was also assessed using Cox regression analysis by testing all parameters associated to the lesions revealed. **Results.** Optimal thresholds to predict a recurrence of disease at 18F-DOPA PET/CT were 400 ng/L for calcitonin (AUC 0.81; p<0.001) and 5 ng/ml for CEA (AUC 0.78; p=0.007). PFS was significantly longer in patients with a negative PET/CT scan (median survival: 37 vs 29 months respectively for negative and positive PET; p=0.019). Similarly, a negative PET/CT study was associated with a significantly higher 2-year OS than a positive PET/CT examination (100% vs 61%; p<0.001). The hazard ratio for OS of a positive PET/CT study was 4.3 (95% confidence interval: 1.244-8,982). Neither SUVmax nor SUVmean thresholds were found to be predictive of a worse PFS and OS in patients with recurrent MDT. **Conclusions.** A high correlation between 18F-DOPA PET/CT results and biochemical assessment was demonstrated. Moreover, PET/CT seems to have an important prognostic value in predicting disease progression and mortality rate. Therefore, an effective therapy planning might effectively rely on 18F-DOPA PET/CT findings.

OP222

⁶⁸Ga-HBED-CC-PSMA PET/CT to visualize PSMA expression in metastatic differentiated thyroid cancer

S. Lütje¹, B. Gomez¹, J. Cohnen¹, L. Umutlu¹, M. Gotthardt², T. D. Poeppel¹, A. Bockisch¹, S. Rosenbaum-Krumme¹; ¹University Hospital Essen, Essen, GERMANY, ²Radboud university medical center, Nijmegen, NETHERLANDS.

Aim: The prostate-specific membrane antigen (PSMA), which was originally thought to be specific for prostate carcinoma, was recently shown to be overexpressed on endothelial cells of the neovasculature of several malignancies. Here, we evaluate the role of ⁶⁸Ga-HBED-CC-PSMA (⁶⁸Ga-PSMA) PET/CT for the detection of PSMA expression in patients with metastasized differentiated thyroid cancer (DTC). **Material and methods:** Five patients with ¹³¹I-iodine-negative and [¹⁸F]-fluorodeoxyglucose (FDG)-positive metastasized DTC (mean TG: 1906.2 ng/ml) received 80±9 MBq of the ⁶⁸Ga-labeled PSMA ligand and underwent PET/CT at 61±7 min p.i.. 2 patients additionally underwent ⁶⁸Ga-PSMA PET/MRI. Data were analyzed regarding the tumor accumulation capacity of the tracer and the detection rate of local recurrences and metastases compared to [¹⁸F]-FDG. Tracer uptake was quantified in terms of the maximal standardized uptake value (SUV_{max}) within a spheroidal volume of interest (VOI). A characterization for malignancy was made in consensus taking into account existing prior examinations. **Results:** In all patients, sites of putative metastatic disease could be identified using ⁶⁸Ga-PSMA PET/CT. All lesions detected with ⁶⁸Ga-PSMA PET/CT (n=50) could be visualized with ⁶⁸Ga-PSMA PET/MRI. The tumor lesions detected included local recurrences (2/5 patients), lymph node lesions (5/5 patients), bone lesions (4/5 patients) as well as soft-tissue metastases (5/5 patients). Using ⁶⁸Ga-PSMA PET/CT and PET/MRI, all tumor lesions identified with [¹⁸F]-FDG-PET/CT imaging could be visualized in 3/5 patients. In 2 patients, only the most prominent lesions detected with [¹⁸F]-FDG-PET/CT imaging were visualized with the PET component of

^{68}Ga -PSMA PET/CT and PET/MRI. ^{68}Ga -PSMA uptake ranged from low in 1 patient (mean SUV_{max} 3.3) to intermediate (1 patient, mean SUV_{max} 6.1) to intense (3 patients, mean SUV_{max} 12.8, 16.2 and 18.3). The highest SUV_{max} were observed for soft-tissue lesions, reaching 39.7. **Conclusion:** These preliminary results indicate that ^{68}Ga -PSMA PET/CT and PET/MRI are suitable for staging of patients with metastasized DTC. ^{68}Ga -PSMA PET/CT and PET/MRI could be useful for the identification of patients that might qualify for PSMA-based endoradiotherapy due to high PSMA uptake.

OP223

^{68}Ga -PSMA HBED-CC PET/CT imaging may be useful in detection of differentiated thyroid cancer: a comparative study with ^{68}Ga -DOTA-TATE PET/CT and ^{18}F -FDG PET/CT imaging

B. Vatankulu¹, E. Akgün¹, M. Ocak², E. Demirci¹, L. Uslu¹, S. Sağer¹, M. Halaç¹, L. Kabasakal¹, K. Sönmezoglu¹; ¹Istanbul University Cerrahpaşa Medical Faculty Department of Nuclear Medicine, İstanbul, TURKEY, ²Istanbul University Cerrahpaşa Medical Faculty Department of Pharmacy, İstanbul, TURKEY.

Aim: The prostate-specific membrane antigen (PSMA) is overexpressed in the neovasculature of several malignancies, therefore it might serve as a target in oncology. Although ^{68}Ga PSMA HBED-CC PET/CT (PSMA PET/CT) is most commonly used in the diagnosis of prostate cancer, few cases described that PSMA PET/CT could show avid uptake in differentiated thyroid cancer (DTC). The aim of this study was to evaluate the diagnostic value of PSMA PET/CT in DTC and to compare with ^{68}Ga DOTA-TATE PET/CT (TATE PET/CT) and FDG PET/CT imaging. **Materials and methods:** Twelve DTC patients with progressive rising thyroglobulin (Tg) levels and negative iodine-131 wholebody scan were prospectively enrolled to this study. All patients underwent PSMA PET/CT and TATE PET/CT and FDG PET/CT scan were performed to 10 of 12 patients within interval of two months. PET/CT analysis was done based on a lesion wise, location wise and per patient basis. PET/CT lesion were examined in according to four categories as local, nodal, pulmonary and skeletal. Detection rates of metastatic lesions were compared between all these functional imaging studies. **Results:** The study group consisted of 8(67%) females and 4(33%) males with a mean age of 58 years. The mean levels of Tg and anti-thyroglobulin were 616.5 mg/dl (min-max:38.2-1000 mg/dl) and 166.4 pg/dl (min-max:20-207 pg/dl) with thyroid hormone suppression therapy, respectively. In patient based analysis, we observed at least one focus of abnormal uptake in 11 of 12 patients in both of PSMA and TATE PET/CT, 10 of 12 patients in FDG PET/CT scans. One of 12 patients who had lower Tg levels (38.3 mg/dl) compared to other patients had no pathological uptake in both PSMA and TATE PET/CT scan. In the lesion based analysis, 92 lesions were detected with FDG PET/CT, 159 lesions with TATE PET/CT and 154 lesions with PSMA PET/CT. There are no difference in location wise analysis between all imaging modalities. **Conclusions:** PSMA PET/CT may be an efficient imaging modality in DTC patients with increased Tg levels for localizing metastatic disease.

OP224

^{68}Ga]DOTATATE-PET/MRI and ^{18}F]FDG-PET/CT are complementary and superior to diffusion weighed MR imaging for radioactive-iodine-refractory differentiated thyroid cancer

A. Vrachimis, L. Stegger, C. Wenning, M. Schäfers, B. Riemann, M. Weckesser; University Hospital Münster, Münster, GERMANY.

Purpose: Whether ^{68}Ga]DOTATATE-PET/MRI with diffusion weighted imaging (DWI) can replace or complement ^{18}F]FDG-PET/CT in patients with radioactive-iodine-(RAI)-refractory differentiated thyroid cancer

(DTC). **Methods:** 12 thyroidectomized and remnant ablated DTC patients underwent ^{18}F]FDG-PET/CT and ^{68}Ga]DOTATATE-PET/MRI within 8 weeks of each other. Localization of recurrent cancer was evaluated on a per-patient, per-organ and per-lesion basis. Histology, prior and follow-up examinations served as standard of reference. **Results:** Tumor masses were correctly identified in all of the 11 from 12 DTC patients with RAI-refractory tumor burden by ^{68}Ga]DOTATATE-PET/(MRI), whereas one patient with local relapse was missed by ^{18}F]FDG-PET/CT. In the lesion based analysis overall lesion detection rates were 79/85 (93%), 69/85 (81%) and 27/82 (33%) for ^{18}F]FDG-PET/CT, ^{68}Ga]DOTATATE-PET/MRI and DWI respectively. ^{18}F]FDG-PET/(CT) was superior to ^{68}Ga]DOTATATE-PET/(MRI) in the overall evaluation and with regards to detection of pulmonary. For the extrapulmonary metastases, ^{68}Ga]DOTATATE-PET/(MRI) showed a superior sensitivity over ^{18}F]FDG-PET/(CT), to the disadvantage of specificity. On the contrary, DWI achieved only poor sensitivity rates and was significantly different from ^{18}F]FDG-PET in the lesion based overall evaluation, pulmonary metastases and overall evaluation excluding pulmonary metastases. **Conclusion:** ^{18}F]FDG-PET/CT overall performs better than ^{68}Ga]DOTATATE-PET/MRI in RAI-refractory DTC mostly due to the superiority in the detection of lung metastases. However, in the evaluation of extrapulmonary lesions ^{68}Ga]DOTATATE-PET/(MRI) is the more sensitive and ^{18}F]FDG-PET/(CT) the more specific imaging modality. Furthermore, DWI is not essential in clinical PET/MRI protocols and cannot replace ^{18}F]FDG-PET for monitoring postoperative DTC patients with suspected RAI-refractory tumor burden.

OP225

The relationship of mRNA ABCC1 expression and uptake of MIBI-Tc99m in patients with hyperparathyroidism

M. Listewnik¹, H. Piwowska-Bilska¹, M. Kurzawski¹, K. Safranow¹, M. Ostrowski¹, A. Borowiecki¹, M. Laszczyńska¹, M. Chosia¹, K. Jasiakiewicz², J. Iwanowski¹, T. Sulikowski¹, **B. Birkenfeld**¹; ¹Pomeranian University of Medicine in Szczecin, SZCZECIN, POLAND, ²Independent Public Clinical Hospital No 1 in Szczecin, SZCZECIN, POLAND.

Introduction: The genetic factors influencing parathyroid MIBI-Tc99m uptake in patients with hyperparathyroidism were postulated in many publications. The aim of our study was to elucidate this issue. **Material and Methods:** A total number of 332 (93 men and 239 females) prospectively investigated patients, aged 11-89 (mean 56,1) years, referred to nuclear medicine department for preoperative parathyroid scintigraphy with clinical, biochemical and/or sonographical suspicions of hyperparathyroidism were included for analysis. Primary, secondary and tertiary hyperparathyroidism was diagnosed in 241 (72,6%), 79 (23,8%), 12 (3,6%) patients, respectively. All of them were genotyped for MDR1 (ABCB1) and MRP1 (ABCC1) genes. They underwent double phase-one tracer ("washout") SPECT/CT scintigraphy with MIBI-Tc99m. All together 413 scintigraphic examinations with 618 lesions of increased tracer uptake (early and delayed planar scintigraphy) were analyzed. Among them 70 patients were operated. During surgery 116 tissue specimens suspected for parathyroid adenoma were removed and in 69 of them mRNA expression was analyzed. **Results:** Different parameters of MIBI-Tc99m uptake in parathyroid adenoma was calculated. Maximal uptake in tumor divided by uptake in 10 minutes (TBR10max) and 120 minutes (TBR120max) background after i.v. injection showed statistically significant relationship ($p=0,00034$ and $p=0,000914$ for TBR10max and TBR120max, respectively) with mRNA expression of MRP1 (ABCC1) gene. **Conclusion:** Genetic background for MIBI-Tc99m uptake was confirmed and relationship of mRNA ABCC1 expression and TBR max in early and delayed phase was found. GRANT support N N402 463339, Ministry of Science & Higher Education, Republic of Poland.

OP226**Carbon-11-Methionine PET/CT derived functional parameters in patients with primary hyperparathyroidism reflect PTH-secretory activity of parathyroid glands: a retrospective single-centre evaluation**

C. Caldarella¹, S. Annunziata¹, M. Isgro², A. Giordano¹; ¹Institute of Nuclear Medicine, Università Cattolica del Sacro Cuore, Rome, ITALY, ²Clinical Chemistry and Hematology Laboratory, Ospedale di Circolo e Fondazione Macchi, Varese, ITALY.

Aim: Positron Emission Tomography/Computed Tomography (PET/CT) using Carbon-11-Methionine (C-MET) is a reliable imaging method for detecting abnormal parathyroid glands in patients with primary hyperparathyroidism (pHPT). Uptake mechanisms of C-MET in abnormal glands are not yet fully understood, although it is presumed to be involved in the synthesis of PTH precursors. Aim of our study was to determine whether C-MET PET/CT-derived functional parameters reflect PTH-secretory activity. **Materials and Methods:** Medical records of patients with pHPT undergoing C-MET PET/CT from September 2014 to January 2016 were reviewed. Patients with renal failure and/or no evidence of C-MET uptake were excluded. Intact serum PTH (iPTH) levels were collected. Several PET/CT-derived functional parameters of C-MET-positive lesions, such as SUV_{max}, SUV-R (lesion SUV_{max}/SUV_{mean} of lungs) and functional lesion volume (FLV) at SUV_{max} thresholds 40%, 70% and 90% of SUV_{max} (FLV₄₀, FLV₇₀ and FLV₉₀, respectively) were obtained. Different regression models were explored and relative R² coefficients evaluated to assess a possible correlation between these functional parameters and abnormal glands' secretory activity expressed as iPTH levels. Mann-Whitney U-test was performed to detect a possible association between FLVs values and positive/negative findings on neck ultrasonography and/or ^{99m}Tc-MIBI scintigraphy. **Results:** According to the aforementioned criteria, 25 patients with pHPT were included. SUV_{max}, SUV-R, FLV₄₀, FLV₇₀ and FLV₉₀ median values were 3.73 [interquartile range (IQR) 2.87-5.22], 7 [IQR 5.52-11.39], 0.77 cm³ [IQR 0.4-1.46], 0.32 cm³ [IQR 0.16-0.71] and 0.12 cm³ [IQR 0.06-0.16], respectively. Regression models performed (linear, power, sigmoid and exponential) showed a positive correlation between iPTH levels and C-MET PET/CT functional measures, even though at different degrees. Among all, FLV₇₀ showed to better correlate with iPTH levels, according to an exponential model (R² = 0.959, P<0.001), thus demonstrating an excellent direct linear relation between FLV₇₀ measure and log₁₀[iPTH] or log₁₀[iPTH]. Only FLV₄₀ resulted significantly higher in 13/23 patients with positive findings on ^{99m}Tc-MIBI scintigraphy (median 1.38 cm³, IQR 0.51-2.75 vs median 0.59 cm³, IQR 0.23-0.84; P = 0.03). **Conclusions:** In a small cohort of patients with pHPT, for the first time, we propose C-MET PET/CT functional parameters as in-vivo reliable measures of PTH-secretory activity of abnormal glands, demonstrating a remarkably high positive relation between FLV₇₀ and iPTH levels. The potential clinical usefulness of these findings still has to be determined; however, the possibility to non-invasively explore the biochemical behaviour of abnormal glands may allow to take the first steps towards a deeper insight in pHPT physiopathology.

605 – Monday, October 17, 2016, 08:00 - 09:30, Hall 115

M2M: PET/CT - Preclinical

OP227**Zr-89 Labelling of Immunotherapeutic Tumour Specific T-Cells to measure L-Selectin Dependent Homing in a Murine Cancer Model**

S. J. Paisey, J. Ohme, C. Marshall, A. Ager; Cardiff University, Cardiff, UNITED KINGDOM.

Aim: L-selectin sufficient tumour specific T cells have been shown to control the growth of solid tumours more effectively than L-selectin

deficient cells. This is thought to be due to L-selectin mediated homing to sentinel lymph nodes where T cells are activated by tumour derived antigens. The aim of this study was to label murine tumour specific CD8+ T-cells with Zr-89-Oxine and use micro-PET/CT to follow L-selectin dependent homing to lymphoid organs and tumour tissue following adoptive transfer to tumour bearing mice. **Materials and methods:** Freshly harvested CD8+ T cells from L-selectin sufficient and L-selectin deficient CD90.2 mice were labelled with Zr-89 Oxinate4 using published methods 1,2 and cell viability was assessed by trypan blue staining. Labelled cells were then injected intravenously via the tail vein into CD90.1 mice which were PET/CT scanned for up to 14 days after injection. Cell distribution was assessed by roi assessment of images and confirmed by flow cytometric and immunohistochemical analysis of post mortem tissues for donor CD90.2 cells. **Results:** Labelling yields of up to 2MBq in 20x10⁶ cells were obtained without significantly reducing cell viability. Labelled cells survived in vivo and cell tracking was possible for the imaging period. Significant differences between the biodistribution of L-selectin deficient and L-selectin sufficient cells CD8+ were observed. The radioactive biodistribution pattern matched the distribution of CD90.2 donor cells in lymphoid and non-lymphoid organs observed at post mortem. **Conclusions:** The Zr-89 Oxine cell labelling technology can be translated to track the migration pathways of immunotherapeutic cell grafts. This technology will be used in future studies to dissect the relationship between T lymphocyte accumulation inside tumour tissue and tumour progression. **References:** 1) Gattinoni L1, Klebanoff CA, Palmer DC, Wrzesinski C, Kerstann K, Yu Z, Finkelstein SE, Theoret MR, Rosenberg SA, Restifo NP. J Clin Invest. 2005 Jun;115(6):1616-26. 2) Ferris, Trevor J., Putthiporn Charoenphun, Levente K. Meszaros, Gregory E. D. Mullen, Philip J. Blower, and Michael J. Went.. Dalton Transactions 43, no. 39 (16 September 2014): 14851-57. 3) Charoenphun, Putthiporn, Levente K. Meszaros, Krisanat Chuamsaamarkkee, Ehsan Sharif-Paghaleh, James R. Ballinger, Trevor J. Ferris, Michael J. Went, Gregory E. D. Mullen, and Philip J. Blower. European Journal of Nuclear Medicine and Molecular Imaging 42, no. 2 (February 2015): 278-87.

OP228**Feasibility of gene-transferred glucagon-like peptide 1 receptor gene as a novel imaging reporter gene**

Y. Zhang¹, Y. Pan¹, J. Lv¹, M. Yang², D. Pan²; ¹Rui Jin Hospital, Shanghai Jiao Tong University School of Medicine, Shanghai, CHINA, ²Ministry of Health, Jiangsu Key Laboratory of Molecular Nuclear Medicine, Jiangsu Institute of Nuclear Medicine, Wuxi, CHINA.

Nuclear medicine molecular imaging techniques, especially the radionuclide reporter gene imaging systems, could provide much information on underlying processes at the molecular level or noninvasively monitor the fate of transplanted therapeutic cells, which have attracted considerable attention. Glucagon-like peptide 1 receptor (GLP-1R) is a G protein-coupled receptor, the natural or analogue ligands of which have been radiolabelled in different methods and mainly been used to image the GLP-1R highly-expressing normal (e.g. islets β cells) or abnormal (e.g. insulinoma) tissues in recent studies. In this study, we firstly put forward the idea of utilizing this GLP-1R gene and its radionuclide-labelled ligands as a novel receptor-based reporter gene imaging system. We constructed the human GLP-1R gene within a baculoviral vectors, which combined the adeno-associated virus-derived inverted terminal repeats for higher transgene expression (BV-AAV). Real-time PCR revealed that BV-AAV vectors-mediated GLP-1R mRNA expression level in human umbilical cord blood-derived mesenchymal stem cells (hUCB-MSCs) was about 6-fold higher than INS-1 insulinoma cells type and much higher than another insulinoma cells type RIN-m5f. Micro-PET imaging with synthetic radiotracer [¹⁸F]AIF-NOTA-MAL-Cys³⁹-exendin-4

showed that the BV-AAV-infected hUCB-MSCs were clearly imaged at 30, 60 and 120 time points after radiotracer administration with an excellent target-to-background ratio, while the mock-infected cells were not detected. And the radiotracer accumulation could be blocked by high-dose exendin-4 administration. In addition, the rodent endogenous GLP-1R expressing tissues like pituitary gland, lung and pancreas were imaged as well. These results indicated that the gene-transferred GLP-1R gene has the tremendous potential of being ideal and broadly accepted radionuclide reporter gene, considering its distinctive advantages like excellent target-to-background ratio, less endogenous GLP-1R interference, and numerous types of deeply developed radionuclide-labelled ligands, some of which (like the radiotracer in this study) even has the blood-brain-barrier passing effects, also implying its great potential in brain reporter gene imaging.

OP229

Feasibility of Gallium-68 Chelates as Diffusible PET Tracers for Cardiac Imaging

S. España¹, T. Arias¹, C. Velasco^{1,2}, J. Pellico^{1,2}, F. Herranz^{1,2}, J. Ruiz-Cabello^{1,2}, J. Mateo^{1,2}, ¹CNIC, Madrid, SPAIN, ²Ciber de Enfermedades Respiratorias (CIBERES), Madrid, SPAIN.

Introduction PET radiotracers for assessment of myocardial perfusion include ¹³NH₃, ⁸²Rb and H₂¹⁵O. However, their short half-life limits widespread clinical use due to the need of a nearby cyclotron (¹³N and ¹⁵O) or of expensive generators (⁸²Rb). Furthermore, current techniques for assessment of extracellular volume fraction (ECV) as late gadolinium-enhancement MRI are limited for detection of diffuse or interstitial myocardial fibrosis and have limited spatial coverage. In contrast, ⁶⁸Ge/⁶⁸Ga generators have a low cost and provide easy access to positron emitting radionuclides compared with those produced by a cyclotron. We propose the use of ⁶⁸Ga-DOTA PET imaging for quantification of myocardial perfusion and ECV. The results obtained in pig studies are presented here. **Methods** Pigs with induced cardiac infarcts by 40 min ischemia of the left anterior descending coronary artery followed by chronic reperfusion were used in the PET/CT studies 7- (n=5) and 45-days (n=5) after infarction. In addition, a series of PET scans at intervals of 30 min were obtained in healthy pigs (n=4) during intravenous infusion of adenosine (0, 100, 200, 400, 600, and 800 mg/kg/min). Each PET scan was performed as a 10-min dynamic scan started 50 s before tracer injection (~100 MBq). ⁶⁸Ga-DOTA was intravenously injected as a 10-s bolus with an automated pump. The amount of free tracer in plasma was determined from blood samples withdrawn at different time-points under rest and stress conditions. Segmentation of the myocardium, ventricles and aorta was performed. Time-activity curves were introduced in a single-tissue compartment model implemented obtaining the perfusion and ECV values at the ROI and voxel levels. **Results** Myocardial perfusion values obtained in the infarcted areas were significantly reduced in comparison to remote regions in both groups, 7- and 45-days post-infarction. ECV was considerably increased in the infarcted areas in pigs 7-days after infarction while the other group showed only minor increase. Polar plots showing full myocardial information were also obtained (see figure 1). Dose-response studies with adenosine showed an increase in perfusion that was in agreement with previous studies using different radiotracers². **Conclusions** ⁶⁸Ga-DOTA PET allowed us to successfully quantify myocardial perfusion and ECV in pigs with induced myocardial infarction and in healthy pigs. This technique provides wide access to quantitative measurement of both perfusion and ECV with PET imaging.

OP230

Imaging atherosclerosis of aortic arch and pulmonary arteries with ¹⁸F-FDG and ¹⁸F-NaF in high-fat western diet ApoE knockout rats

X. Zhuang¹, F. Yue², Q. You², Y. Chen², J. Li¹; ¹General Hospital of Ningxia Medical University, Yinchuan, CHINA, ²Southwest Medical University, Luzhou, CHINA.

Aims: Inflammation and calcification are risk factors of atherosclerosis, but their relationship is still unknown. This study was designated to investigate the correlation of inflammation and calcification, and the difference of atherosclerotic plaque between aorta and pulmonary arteries using ¹⁸F-FDG and ¹⁸F-NaF PET/CT imaging in high-fat western diet apoE knockout rats. **Materials and Methods:** Male ApoE knockout rats (n=19) (Biocytogen, Beijing, China) were maintained on high-fat western diet (42% fat) from 12 wk. Combined PET and CT imaging was performed with a hybrid scanner (Siemens Inveon PET/CT) at 12 wk (before high-fat western diet), 27 wk and 46 wk. Rats were imaged at 1 h after ¹⁸F-FDG or ¹⁸F-NaF injection after 12 h fasting. Maximal and mean standardized uptake values (SUV_{max} and SUV_{mean}) were measured over aortic arch and pulmonary arteries. Gross examination and dissection microscopy also were performed. **Results:** Plaque regions have not shown to take ¹⁸F-FDG and ¹⁸F-NaF always simultaneously. Uptake of ¹⁸F-FDG is mainly on aortic arch, meanwhile ¹⁸F-NaF on pulmonary arteries. From 12 wk to 46 wk, uptake of ¹⁸F-FDG on aortic arch and ¹⁸F-NaF on pulmonary arteries is increased, related to the size of lesions. In aorta, ¹⁸F-FDG SUV_{mean} is increased from 1.17±0.38 to 1.44±0.48 to 1.87±0.62, respectively, SUV_{max} from 1.96±0.73 to 2.66±1.17 to 3.45±1.36, respectively, both p<0.05. In left pulmonary artery, ¹⁸F-NaF SUV_{mean} is increased from 0.69±0.09 to 0.79±0.24 to 0.95±0.38, respectively, SUV_{max} from 1.01±0.16 to 1.33±0.26 to 1.50±0.48, respectively, both p<0.05. In right pulmonary, ¹⁸F-NaF SUV_{mean} is increased from 0.82±0.12, to 0.85±0.21, to 0.91±0.31, respectively, SUV_{max} from 1.12±0.15 to 1.33±0.28 to 1.43±0.4, respectively, both p<0.05. Morphological observations show that atherosclerotic lesions in pulmonary arteries were severer than in aortic arch. **Conclusion:** Based on apoE knockout rat studies, we found that atherosclerotic uptake of FDG and NaF is different between pulmonary and aortic arch, implying that calcification is independent of inflammation in atherosclerosis, and inflammation is not the precondition of calcification. **Research Support:** This work was supported by the NNSF of China (No.81360226).

OP231

Dynamic PET/CT Receptor Imaging Using ⁶⁸Ga-Labelled asialoglycoprotein

q. xia; Ren Ji Hospital, School of Medicine, Shanghai Jiao Tong University, Shanghai, CHINA.

Background: Liver asialoglycoprotein receptor (ASGPR), a specific endocytic receptor on the surface of hepatocytes, is an accurate index reflecting liver reserve function, and the quantity of ASGPR expression directly reflects the level of functional reserve of the liver. This study was the development of labeling the ASGP using ⁶⁸Ga to construct a new type of positron molecular probe ⁶⁸Ga-NOTA-LSA to target ASGPR in the liver for the potential use with dynamic PET/CT imaging. **Methods:** LSA was synthesized by conjugating α-lactose to human serum albumin (HSA) by reductive amination. LSA was conjugated with 2- (p-isothiocyanatobenzyl) -1,4,7-triazacyclononane-1,4,7-triacetic acid (SCN-NOTA) and the resultant NOTA-LSA was labeled with ⁶⁸Ga at 37 °C. For quality control thin-layer chromatography (TLC) technique were evaluated. Stability of ⁶⁸Ga-NOTA-LSA was studied in phosphate-buffered saline (PBS). Biodistribution and dynamic PET/CT studies of ⁶⁸Ga-NOTA-LSA were performed in SD rat following tail vein injection of radiotracer. Time-activity curves (TAC) for liver and other organs were generated and corresponding parameters calculated. **Results:** ⁶⁸Ga-NOTA-LSA can be produced with high radiochemical purity. The best TLC methods for determining potential free ⁶⁸Ga include 0.1 M sodium citrate as eluent. Stability after 120 min incubation at 37 °C was high in PBS (>95 % intact tracer). Biodistribution and animal PET/CT studies showed specific retention of ⁶⁸Ga-NOTA-LSA in liver following intravenous administration. ⁶⁸Ga-NOTA-LSA rapidly accumulated and persisted mainly in the liver at 40mins after injection. Other organs including heart, bone,

marrow, kidney and bladder with the uptake were much lower than liver. **Conclusion:** This study provides a promising new ^{68}Ga -labelled compound for evaluation of hepatic function by PET/CT is important for optimizing treatment and improving the prognosis of functional diseases of the liver.

OP232

^{68}Ga /PET imaging and quantification of fibrosis using peptide-based tracers

I. Velikyan^{1,2}, U. Rosenström³, O. Eriksson², G. Antoni²; ¹Uppsala PET Centre, Uppsala, SWEDEN, ²Division of Molecular Imaging, Uppsala University, Uppsala, SWEDEN, ³Division of Organic Pharmaceutical Chemistry, Uppsala University, Uppsala, SWEDEN.

Aim: Positron emission tomography (PET) being a powerful non-invasive and quantitative molecular imaging technique may enable accurate diagnosis and progression monitoring of fibrosis involved in many chronic diseases. Imaging agents specifically targeting collagen present in fibrotic tissue are under development for the realization of such diagnostic technology. **Materials and Methods:** Eighteen amino acid residue cyclic peptide conjugated either to 2-(4,7-bis(2-(tert-butoxy)-2-oxoethyl)-1,4,7-triazonan-1-yl)acetic acid (NOTA(tBu)₂) or 4-(4,7-bis(2-(tert-butoxy)-2-oxoethyl)-1,4,7-triazacyclononan-1-yl)-5-(tert-butoxy)-5-oxopentanoic acid (NODAGA(tBu)₃) via ethylene glycol linker (EG₂) was synthesized and labelled with ^{68}Ga . Organ distribution in rat was investigated ex vivo at 5, 10, 20, 40, 60, and 120 min time points as well as in vivo by dynamic scanning for both imaging agents. The pharmacokinetics was analyzed. The extrapolation of the biodistribution data was conducted for the estimation of human organ and total body absorbed and total effective doses using Organ Level Internal Dose Assessment Code software (OLINDA/EXM 1.1) assuming similar organ distribution pattern between the species. **Results:** The peptide bioconjugates were synthesized with chemical yield ranging from 40 to 55%. The subsequent ^{68}Ga -labelling demonstrated high radioactivity incorporation of over 90%. Ex vivo and in vivo organ distribution results demonstrated fast blood clearance and renal excretion. The analogues differed in total charge of the [^{68}Ga]Ga-chelator moiety which resulted in the lower uptake in liver, spleen, and kidney for the positively charged one. The dosimetry estimations revealed the highest organ absorbed dose was for kidneys (0.1 mGy/MBq), still it would allow for the administration of over 1460 MBq per year. It was the total effective dose that was the limiting parameter for both analogues, allowing for at least six examinations with total administration of 621 to 643 MBq yearly before reaching the annual limit of 10 mSv. **Conclusions:** Peptide based agents for the imaging of fibrosis by PET were developed and preclinically investigated. The rat organ distribution of the analogues differed in liver, spleen, and kidney uptake dependent on the total charge of [^{68}Ga]Ga-chelator moiety. The fast radioactivity clearance from normal lung, heart, and liver was observed indicating strong potential for the visualization of fibrosis in these organs. Dosimetry estimations revealed possibility of at least six examinations per year that might be sufficient for the adequate disease monitoring in longitudinal studies and routine clinical setup.

OP233

Metabolic pattern of transgenic mice overexpressing lipocalin-2: a microPET study

A. Buschiazzo¹, F. Ticconi¹, E. Principi², L. Garaboldi¹, A. Bozzano¹, A. Orengo¹, I. Calamia¹, S. Morbelli¹, C. Ghersi¹, A. Democrito¹, C. Marini³, S. Tavella², G. Sambuceti¹; ¹Nuclear Medicine Unit, Department of Health Sciences, University of Genoa and IRCCS AOU San Martino-IST, Genoa, ITALY, ²Laboratorio di medicina rigenerativa e ingegneria dei tessuti, Department of Experimental Medicine, University of Genoa and IRCCS AOU San Martino-IST, Genoa, ITALY, ³CNR Institute of Bioimages and Molecular Physiology, Section of Genoa, Genoa, ITALY.

Aims. Recent literature suggests that the overexpression of Lipocalin-2 (Lcn2) contributes to the development of metabolic syndrome through largely ignored mechanisms. To explore Lcn2 target tissues, we tested glucose consumption in the whole body and in specific tissues (skeletal muscle-SM, brown adipose tissue-BAT and liver) of wild type (WT, n=6) and transgenic mice overexpressing Lcn2 (Lcn2-Tg, n=6). **Materials and Methods.** The Licensing and Ethical Committee approved animal experiments. All mice were submitted to FDG-PET imaging after 6 hours fasting with a dedicated microPET system (Albira, Bruker, US) injecting 3-4 MBq of FDG through a tail vein, soon after start of a list-mode acquisition lasting 50 minutes. Animals were studied, twice in random sequence, 15 minutes after intraperitoneal glucose load (1.5 g/Kg) or saline with a time gap of two weeks. A volume of interest (VOI) was manually drawn in the left ventricular chamber to define tracer input function that was used to estimate glucose metabolic rate (MRGlu) in BAT and SM of hindlimb using the Patlak routine of a dedicated software (PMOD, Zurich, CH). To avoid the interference of variable hormone concentrations, liver tracer handling was estimated only under fasting conditions by a previously validated approach that combines arterial input function with tracer-concentration curves in gut and liver VOIs. **Results.** Fasting serum glucose level was lower in Lcn2-Tg than in WT mice (76 ±38 vs 144±38 mg/100mL, respectively, p<0.05) but not after glucose load. However, this effect was not related to increased monosaccharide utilization. In fact, whole body glucose disposal, calculated with the conventional stochastic analysis, was lower in Lcn2-Tg than in WT mice under fasting conditions (0.19±0.15 vs 0.42±0.13 μmol/min/g body weight, p<0.05), but not after glucose load. Similarly, MRGlu was significantly lower in Lcn2-Tg than in WT mice both in SM (0.23±0.31 vs 1.57±1.42 μmol/min/100 g, p<0.05) and BAT (12.5±6.5 vs 5.8±4.9 μmol/min/100 g, p<0.05). Again, this difference disappeared after glucose load. Moreover, under fasting conditions, tracer entrapment in hepatocytes (k_{tr}) was significantly higher in Lcn2-Tg than in WT mice (0.11±0.05 vs 0.001±0.001 min⁻¹ p<0.01) while FDG dephosphorylation rate (k_{fm}) was superimposable in both groups. **Conclusion.** In mice overexpressing Lcn-2, serum glucose level is reduced under fasting condition. This behaviour reflects an increased liver entrapment of FDG by phosphorylation and not an increased glucose utilization by peripheral tissues.

OP234

Pretargeting trastuzumab and cetuximab with ^{18}F -tetrazine tracer

O. Keinänen^{1,2}, J. Pourat², J. S. Lewis^{2,3}, A. J. Airaksinen¹, M. Sarparanta^{1,2}; ¹Laboratory of Radiochemistry, Department of Chemistry, University of Helsinki, Helsinki, FINLAND, ²Department of Radiology, Memorial Sloan Kettering Cancer Center, New York, NY, UNITED STATES, ³Program in Molecular Pharmacology, Memorial Sloan Kettering Cancer Center, New York, NY, UNITED STATES.

Aim: We have used ^{18}F -labeled tetrazine (5-[^{18}F]fluoro-5-deoxy-ribose-tetrazine, [^{18}F]TAF)¹ for *in vitro* pretargeting of two clinically used antibodies, trastuzumab and cetuximab. Pretargeted PET-imaging experiments are currently underway. Trastuzumab is known to internalize making it possibly out of reach for a tracer that doesn't internalize. We wanted to explore the sensitivity of [^{18}F]TAF to locate trastuzumab inside living cancer cells and compare this to pretargeting cetuximab, that is mainly bound to the cell membrane. **Materials and methods:** Trastuzumab and cetuximab were functionalized with TCO groups (2 TCO-groups/antibody). Pretargeting of HER2 expressing cancer cells with trastuzumab was tested using BT-474 and SKOV3 cell lines. A549 cell line was used for pretargeting EGFR expressing cancer cells with cetuximab. The cells (1x10⁶ per well on a 6-well plate) were preincubated with TCO-antibody in DMEM media for 60 min at 37 °C (n=6), followed by incubation with [^{18}F]TAF in cell media for 60 min at 37 °C. The free and cell-associated fractions of radioactivity were determined by automated gamma counting. Three control sample sets were used. First control had 50 eq. excess of antibody incubated (60 min at 37 °C) with the cells

before incubating with TCO-antibody. In second control 100 eq. excess of cold TAF was added to compete with the [^{18}F]TAF. In third control [^{18}F]TAF was incubated with cells without preincubation with TCO-antibody. **Results:** *In vitro* binding of [^{18}F]TAF to TCO-antibody pretreated cells exceeded nonspecific uptake by untreated cells over 10-fold, 20-fold, and 8-fold in BT474, SKOV3, and A549 cells, respectively. A significant reduction of radioactivity bound to cells was observed when presaturated with antibody or under competition with large excess of cold TAF. **Conclusions:** We have demonstrated that [^{18}F]TAF binding depends on the interaction of TCO-antibody with receptors and on the reaction between [^{18}F]TAF and TCO, thus confirming *in vitro* pretargeting. Surprisingly, *in vitro* pretargeting was more efficient with trastuzumab than with cetuximab. Optimization of the *in vitro* assay is being done to ensure that the system hasn't been saturated with the amount of [^{18}F]TAF. *In vivo* pretargeted PET-imaging studies in xenograft models are currently underway. **Acknowledgements:** Supported by the Academy of Finland, CHEMS Doctoral Program, Memorial Sloan Kettering Cancer Center core grant P30 CA008748, Mr. William H. Goodwin and Mrs. Alice Goodwin and the Commonwealth Foundation for Cancer Research and The Center for Experimental Therapeutics at Memorial Sloan Kettering Cancer Center **References:** 1. Keinänen O et al *ACS Med Chem Lett.* 2016;7:62–66

606 – Monday, October 17, 2016, 08:00 - 09:30, Hall 111

Pitfalls & Artefacts - Paediatrics/Bone & Joint: Pitfalls in Paediatrics Bone Imaging

OP235

Imaging of the Developing Skeleton

M. Roca Bielsa; Hospital Universitari Vall d'Hebron, Servei Medicina Nuclear, Barcelona, SPAIN.

OP236

Diagnostic Pitfalls of an Apparently Solitary Lesion

D. De Palma; Ospedale di Circolo, Serv. di Medicina Nucleare, Varese, ITALY.

OP237

Work-Up of Diffuse/Multifocal Skeletal Lesions

F. Paycha; Hôpital Lariboisière, Paris, FRANCE.

OP238

The Painful Joint

T. Van den Wyngaert; Antwerp University Hospital, Nuclear Medicine, Antwerp, BELGIUM.

607 – Monday, October 17, 2016, 08:00 - 09:30, Hall 116

Clinical Oncology: Breast & Gynaecology

OP239

^{68}Ga -Pentixafor PET for Imaging of Chemokine Receptor CXCR4 in Patients with Breast Carcinoma and Correlation with Histopathology

T. Vag¹, A. Rossmann¹, S. Paepke², K. Steiger³, M. Niemeier², H. Wester⁴, M. Schwaiger¹; ¹Clinic of Nuclear Medicine, Klinikum Rechts der Isar, Munich, GERMANY, ²Clinic of Gynecology, Klinikum Rechts der Isar, Munich, GERMANY, ³Institute of Pathology, Klinikum Rechts der Isar, Munich, GERMANY, ⁴Faculty of Pharmaceutical Radiochemistry, Technical University Munich, Munich, GERMANY.

Purpose: CXCR4 is a chemokine receptor that is overexpressed in several types of human cancers including breast cancer and is

reported to have a key role in signaling pathways of metastases. The aim of this study was to assess the feasibility of CXCR4 directed imaging in patients with breast cancer using the novel CXCR4 targeted Positron Emission Tomography (PET) probe ^{68}Ga -Pentixafor. **Material and Methods:** 10 patients suffering from breast cancer (9 patients with primary breast cancer, one patient with local recurrent breast cancer) underwent PET imaging (either PET/MR or PET/CT) using ^{68}Ga -Pentixafor. The lesions included 9 invasive ductal carcinomas (IDC) and one invasive lobular cancer (ILC). Four of the patients were known to have lymph node or distant metastases detected by previously performed imaging modalities. Maximum standardized uptake values (SUVmax) and tumor-to-background ratios (T/B ratio) were determined in the breast cancer lesions and metastases and correlated with immunohistochemistry, when available. **Results:** 8 of 10 breast cancers were visually detectable with a mean SUVmax of 3.1 (range 1.7 to 4.5) and a mean T/B ratio of 2.8. The visually undetectable lesions included the case of ILC and one IDC (T2 Grade 2). Immunohistochemistry revealed highest CXCR4 staining intensity in the patient with local recurrent breast cancer which also showed highest T/B ratio of all examined lesions. Lowest CXCR4 staining intensity was observed in the visually undetectable case of ILC. T/B ratio of metastases were similar to T/B ratios of corresponding breast carcinomas. **Conclusion:** CXCR4 directed PET imaging of breast cancer is feasible. Based on our first observations in this small patient cohort, CXCR4 expression profile on the tumor cell surface seems to correlate with signal intensity in PET imaging. Moreover, CXCR4 expression of breast cancer metastases seems to be similar to primary lesions.

OP240

Metabolic tumor burden assessed by dual time point 18F-FDG PET/CT in breast cancer: Relation with tumor biology

A. Garcia Vicente¹, J. Pérez-Beteta², M. Tello Galán¹, D. Molina-García², G. Jiménez Londoño¹, V. Pérez-García², A. Martínez-González², F. Pena Pardo¹, Á. Soriano Castrejón¹; ¹Nuclear Medicine Department, Hospital General Universitario de Ciudad Real, CIUDAD REAL, SPAIN, ²Instituto de Matemática Aplicada a la Ciencia y a la Ingeniería. UCLM., CIUDAD REAL, SPAIN.

Aim: To investigate the influence of dual time point 18F-FDG PET/CT in the SUV and volume-based metabolic variables of breast lesions and their relation with biological characteristics and molecular phenotypes. **Material and methods:** Prospective study including 67 patients with locally advanced breast cancer (LABC). All patients underwent a standard 18F-FDG PET/CT (PET-1) followed by a delayed acquisition (PET-2). After breast tumor segmentation following a tridimensional methodology, semiquantitative metabolic variables (SUVmax, SUVmean and SUVpeak) and volume-based variables as metabolic tumor volume (MTV) and total lesion glycolysis (TLG) were obtained. Biologic prognostic parameters, such as the receptor status, p53 and HER2 expression, proliferation rate (Ki-67) and grading were obtained and molecular phenotypes and risk-classification [low: luminal A, intermediate: luminal B HER2 (-) or luminal B HER2(+) and high: HER2pure or triple negative] were established. Spearman test was used to study the relation between clinical and biologic variables with all the metabolic parameters. **Results:** Metabolic variables obtained in the PET-1 showed high and significant relations between them and the same happened for the obtained in the PET-2, except for the MTV and SUV variables (SUV max, SUV mean and SUV peak). PET-1 metabolic variables showed significant and high association with the obtained in PET-2 except for the MTV and SUV variables, with low but significant association. SUV variables showed associations with receptor status (p<0.001) and risk-classification attending phenotype (p<0.005). With respect to volume-based variables, only

TLG showed association with receptor status, risk-classification and grade ($p=0.001$, $p<0.01$ and $p<0.05$ respectively). Receptor negative tumors, high grade tumors and high-risk phenotypes showed higher values compared to the others. No association was found with the Ki-67, HER2 and p53 expression. **Conclusion:** Most of PET-1 SUV and volume-based variables were predictors of the obtained in PET-2. PET-derived parameters, such as the SUV variables and TLG, could act as predictors of tumor biology based on their association with histopathological factors of breast cancer.

OP241

Breast cancer grading of ^{18}F -FDG-PET/CT and patient-derived statistical features based on supervised machine-learning approaches

L. Papp¹, T. S. Nakuz¹, H. F. Magometchnigg², K. Pinker², A. Haug¹, T. H. Helbich², T. Beyer³, M. Hacker¹, G. Karanikas¹; ¹Medical University of Vienna, Division of Nuclear Medicine, Vienna, AUSTRIA, ²Medical University of Vienna, Division of Radiology, Vienna, AUSTRIA, ³Medical University of Vienna, Center for Medical Physics and Biomedical Engineering, Vienna, AUSTRIA.

Introduction To date, breast cancer grading is possible only through histopathological biopsy analysis. We propose a novel, non-invasive method of tumour grading in breast cancer. Specifically, we had the following objectives: (1) to identify [^{18}F]FDG-PET/CT features and patient characteristics that correlate with tumour grades as derived from histopathological analysis, and (2) to define a novel computer-aided decision support system to automatically predict grading of breast cancer built on pre-selected features. **Materials and Methods** To date, 51 data sets ([^{18}F]FDG-PET/CT and histology-based grades ranging from G1 to G3 of which 44 were IDC and 7 ILC) of breast cancer patients were included. Tumour and reference regions (mediastinum) were delineated manually on PET/CT using the Hybrid-3D software (Hermes Nuclear Diagnostics, Stockholm, Sweden). The voxel values of each [^{18}F]FDG-PET tumor regions were normalized to the mean of the respective reference region to calculate tumour-to-background ratio (TBR). The following features were calculated for each tumour region from both [^{18}F]FDG-PET TBR and CT: mean, variance, min, max, volume (general); entropy, homogeneity, contrast, correlation, uniformity, dissimilarity (Textural grey-level co-occurrence matrix (GLCM)); coarseness, contrast, busyness (Textural neighbourhood grey-tone difference matrix (NGTDM)); and patient age (Non-image). To identify relevant key features for classifying tumours, a novel machine-learning algorithm was implemented that builds on evolutionary algorithm (EA) principles. In each iteration of the EA, a second machine-learning algorithm was executed over the residual features to optimize the variables of our classifier model by a Levenberg-Marquardt (LM) approach. The classifier model utilized weighted fuzzy clustering of features to grade breast cancer regions. The EA and LM methods were programmed to minimize the summed Receiver Operator Characteristic distance of the grade-groups. Our optimized classifier was validated (sensitivity and specificity) with histopathological grading serving as standard-of-reference. **Results** The EA algorithm selected the following features as relevant for classification: [^{18}F]FDG-PET TBR (min, max, variance, volume, entropy-GLCM, dissimilarity-GLCM, uniformity-GLCM, correlation-GLCM, busyness-NGTDM), CT (min, max, homogeneity-GLCM, contrast-NGTDM, correlation-GLCM) and patient age. Based on these features the LM algorithm provided the following sensitivity and specificity values for the grade groups: 98% and 94% (G1), 89% and 96% (G2), as well as 91% and 96% (G3), respectively. **Conclusions** We have successfully tested a novel machine-learning approach that automatically selects relevant features and optimizes classifier variables to generate a computer-aided decision making model for grading breast cancer patients.

OP242

Prognostic evaluation of ^{18}F -FDG-PET/CT in endometrial cancer

A. A. Lund^{1,2}, M. H. Vilstrup¹, K. Jochumsen^{1,2}, P. Hoiland-Carlsen^{1,2}, S. Hess^{1,3,2}; ¹Odense University Hospital, Odense, DENMARK, ²University of Southern Denmark, Odense, DENMARK, ³Hospital of Southwest Jutland, Esbjerg, DENMARK.

Aim: To ascertain if semi-quantitative measurements derived from ^{18}F -FDG-PET/CT can be used as prognostic markers in patients with newly diagnosed endometrial cancer. This may help stratify patients, who may benefit from a more aggressive treatment plan or closer surveillance.

Materials and methods: Included were patients with high-risk endometrial cancer (grade 3 endometrial adenocarcinoma or non-endometrioid histology) or clinically suspected spread of disease at the time of initial diagnosis. All underwent ^{18}F -FDG-PET/CT before curatively intended treatment. The scans were evaluated using standard uptake values (SUVmax and partial volume corrected SUVmean) and whole-body partial volume corrected total lesion glycolysis (TLG), which were analyzed as prognostic factors in relation to overall survival. ROC curves were performed on all three PET measurements to find the optimal cut-off for predicting high risk of mortality. Multivariate COX proportional regression models were used for exploring the relationship between survival and the following explanatory variables: SUVmax, SUVmean, TLG and other known prognostic factors. **Results:** 83 patients (mean age 69.7 years, range 26.8-91.1) with high-risk endometrial cancer or suspected high FIGO stage were included. Mean follow-up time was 3.48 years (range 0.31-6.87), 24 patients died during follow-up. Regional lymph node involvement, lymphovascular space invasion, SUVmax and TLG were associated with overall survival in univariate analyses, whereas FIGO stage, histological type and grade, peritoneal cytology, and age were not. In multivariate analyses with adjustment for other known prognostic factors, a SUVmax of ≥ 14.3 and SUVmean of ≥ 12.7 of the primary tumor yielded a HR for higher risk of mortality of 3.18 (1.19-8.49) and 1.93 (0.80-4.68), respectively. Whole-body TLG of ≥ 176.1 yielded an HR of 5.70 (1.94-16.78) for higher risk of mortality in a multivariate analysis. **Conclusion:** Preoperative SUVmax and TLG showed potential as independent prognostic markers of overall survival in patients with high-risk endometrial cancer. SUVmean was not a strong prognostic marker in this patient group. SUVmax and TLG might help identify patients who could benefit from a more aggressive treatment strategy or closer surveillance.

OP243

Advanced ^{18}F -FDG PET/CT Imaging Analysis In Selected Series Of Breast Cancer Patients

L. Antunovic¹, F. Gallivanone², A. Sagona¹, G. Manfrinato¹, M. Sollini³, M. Kirienko¹, I. Castiglioni², A. Chiti³; ¹Humanitas Clinical and Research Center, MILAN, ITALY, ²Institute of Molecular Bioimaging and Physiology, National Research Council, MILAN, ITALY, ³Humanitas University, MILAN, ITALY.

Aims Texture analysis of medical images has been proposed as a non invasive tool for tumour heterogeneity assessment, containing information about tumour histology, disease stage, tumour metabolism and even patient outcome. The main purpose of our study was to evaluate imaging biomarkers obtained from ^{18}F -FDG PET/CT enabling to 'in vivo' characterize breast cancer. **Methods** 44 patients with breast cancer (age 51.9 ± 13.9 , range 35-88 years), who underwent staging ^{18}F -FDG PET/CT over a time period of 4 years (2012- 2015), were reviewed. Thirty-nine patients had ductal invasive breast cancer, while 3 had lobular cancer; the remaining 2 were unclassified. According to molecular tumor subtype, 13 patients were classified as luminal A, 16 as luminal B, 6 as luminal B Her-2 positive, 5 patients had HER2-enriched tumor subtype and 4 were classified as basal-like tumors. Metabolic Tumor Volume (MTV) of breast lesions was obtained using a fully automatic

image segmentation method, combining an automatic threshold-based algorithm for the definition of MTV and a k-means clustering algorithm for the estimation of the background. Average and maximum SUV of the primary lesion were calculated within the segmented MTV. Mean SUV was corrected for partial volume effect and Total Lesion Glycolysis (TLG) was calculated as the product between mean SUV and MTV. Texture-based features were evaluated using the segmented MTV. Fourteen features were extracted as first order statistics features enabling to describe the characteristics of the histogram of the PET voxel intensities within the segmented MTV. Four shape and size features were extracted, enabling to describe the shape and size of the segmented MTV. Univariate correlation between imaging quantitative features and histological parameters was performed and values of $p \leq 0.05$ were considered significant. **Results** On image analysis, considering standard quantitative measures, statistically significant correlation was found between partial volume corrected (PVC)-SUV and tumor grade ($p < 0.05$), Ki67 level ($p = 0.01$), overexpression of HER2 receptor ($p < 0.05$) and presence of local vascular invasion ($p < 0.05$); PVC-TLG also correlated with Ki67 level ($p < 0.05$). Histogram Energy was found correlated with tumor grade ($p < 0.002$), Ki67 level ($p < 0.01$) and molecular subtype ($p < 0.05$), while other intensity-based features (maximum, mean, median, root mean square) correlated with molecular tumor subtype ($p < 0.05$). **Conclusions** This initial experience generate interesting data from PET images, beyond standard quantitative parameters. Further analysis are needed in order to define clinical impact of these features, especially regarding correlation with patient outcome.

OP244

Reproducibility of Response Assessment in Metastatic Breast Cancer Patients with Contrast-enhanced CT and FDG PET/CT

L. Lebron¹, C. Riedl¹, N. Long¹, K. Pinker-Domenig^{1,2}, W. Weber¹;
¹Memorial Sloan-Kettering Cancer Center, New York, NY, UNITED STATES, ²Medical University Vienna, Vienna, AUSTRIA.

Objectives: To evaluate the reproducibility of PERCIST 1.0 and RECIST 1.1 criteria in metastatic breast cancer patients receiving systemic therapy. **Materials and Methods:** Retrospective study of patients with metastatic breast cancer who received first or second line systemic therapy on protocol, from 2007 to 2012, and underwent contrast-enhanced (CE)-CT of the chest, abdomen, and pelvis and FDG PET/CT within 4 weeks prior and 3 months after treatment initiation. Two radiologists with specialty training in Oncologic Body Imaging and Molecular Imaging assessed response by PET/CT using PERCIST 1.0. Two different radiologists with specialty training in Oncologic Imaging assessed response by CE-CT based on RECIST 1.1. The degree of agreement between observers was quantified by kappa statistics, using the four categories defined by RECIST and PERCIST: complete response, partial response, stable disease and progression of disease. Results were also dichotomized into responders (complete response and partial response) and non-responders categories (stable disease and progression of disease), and kappa was again calculated. After the analysis, reasons for discrepancies were identified in consensus. **Results:** Sixty-five patients met the inclusion criteria. Kappa was 0.81 (95% confidence interval (CI) 0.70, 0.93) between PET/CT readers (PERCIST) and 0.67 (95% CI 0.51, 0.82) between CT readers (RECIST) when 4 response categories were used. Agreement increased amongst PET/CT readers ($k = 0.94$; 95% CI 0.85, 1.0) for the classification of cases as either responders or non-responders. Agreement was moderate between CT readers when cases were classified as responders or non-responders ($k = 0.54$; 95% CI 0.32, 0.76). Discordant results between CT readers were due to measurement differences in 10 cases and differences in interpretation of findings in 3 cases. Among PET/CT readers, all differences were due to differences in interpretation ($n = 9$). **Conclusion:** In patients with metastatic breast cancer, response assessment with FDG PET/CT and PERCIST is highly reproducible and the variability of response assessment compares favorably with response assessment by RECIST.

OP245

Predictive Value of Intratumoral Metabolic Heterogeneity in terms of Disease Free Survival in Hormone Receptor Positive Invasive Ductal Carcinoma Breast

A. S. Bedmutha, N. Singh, M. Pereira, A. Nair, P.D.Hinduja National Hospital and Medical Research Center, Mumbai, INDIA.

Aim: Malignant component within solid neoplasms has distinct heterogeneity regarding cell proliferation, metabolism, angiogenesis and necrosis and this heterogeneity is represented as phenotypic and behavioural alterations of the neoplasm, including proliferative and metastatic potential which has reliably been demonstrated by F-18 FDG on autoradiography. It has been shown to correlate significantly with disease outcome in sarcomas and cervical cancer. This study was performed to evaluate the significance of intratumoral heterogeneity in predicting disease free survival of patients with hormone receptor (HR) positive invasive ductal carcinoma (IDC) breast. **Materials and methods:** Thirty female patients (age group 38-65 years) with HR positive (ER/PR positive or triple positive) local or locally advanced invasive ductal carcinoma breast, excluding multicentric/ multifocal tumours and patients with other co-existing or past malignancy, who underwent pre-treatment fluorodeoxyglucose positron emission tomography/ computed tomography (F-18 FDG PET/CT) scan were retrospectively evaluated. Maximum transaxial dimensions of primary tumours ranged from 1.3cm - 7cm. Metabolic parameters such as standardized uptake value maximum (SUVmax) and metabolic tumour volume (MTV) were noted. Intratumoral heterogeneity factor (HF) was defined as the derivative (dV/dT) of a volume threshold function from 40-80%, quantified for each primary tumour. Patients were clinically and radiologically followed up for minimum period of 3 years post completion of treatment. Events of recurrence/ metastasis were compared to PET/CT parameters by receiver operating characteristic (ROC) curve analysis. **Results:** HF ranged from 0.025 to 1.37, with mean values for recurrence and disease free group being 0.83 and 0.15 respectively. It correlated well with MTV (correlation coefficient 'r' = 0.984, $p < 0.01$). ROC curve analysis demonstrated significant association of both HF and MTV with disease free survival (area under curve = 0.967 for HF and 0.955 for MTV; $p < 0.001$ for both). HF was found to be higher in higher T stage tumours. Optimal cut-off values of HF > 0.34 and MTV $> 12.03 \text{ cm}^3$ were found to have high sensitivity and specificity in predicting recurrence, and hence affecting prognosis. SUVmax was not found to be a reliable predictor of DFS. **Conclusion:** Intratumoral heterogeneity correlates well with MTV, and is a potentially reliable predictor of DFS in patients with hormone receptor positive local or locally advanced IDC breast. It can be evaluated as a tool to decide management strategy in selected group of patients.

OP246

Prognostic significance of FDG-PET/CT derived parameters in a first metastatic breast cancer relapse

E. Depardon¹, S. Kanoun¹, O. Humbert¹, J. Riedinger¹, I. Tal², J. Vrigneaud¹, M. Lasserre¹, M. Toubeau¹, A. Berriolo-Riedinger¹, I. Dygai-Cochet¹, P. Fumoleau³, F. Brunotte¹, A. Cochet¹;
¹Department of Nuclear Medicine, Centre Georges-François Leclerc, Dijon, FRANCE, ²Beth Israel Deaconess Medical Center, Boston, MA, UNITED STATES, ³Department of Medical Oncology, Centre Georges-François Leclerc, Dijon, FRANCE.

Aim: To investigate the prognostic value of fluorodeoxyglucose (FDG) positron emission tomography/computed tomography (PET/CT) derived parameters (metabolic tumour volume [MTV]) in a first metastatic breast cancer recurrence (MBCR). **Methods:** From December 2006 to August 2013, 49 women with a first MBRC were retrospectively included. FDG-PET/CT was performed within one month before systemic treatment.

Three sets of MTV were calculated with Beth Israel (BI) software: based on an absolute threshold selecting voxel with standardized uptake value (SUV) >2.5 ($MTV_{2.5}$), applying a per-lesion threshold of 41% of the maximum SUV (SUV_{max}) (MTV_{41}) and using a per-patient adapted threshold based on PERCIST definition of measurable target lesion defined by $SUV > 1.5$ -fold greater than liver $SUL_{mean} + 2$ standard deviations (SD) (MTV_p). Patients were also classified as mono-organ (only one organ involved) or multiorgan relapse according to PET/CT uptake. MTV analysis was dichotomised by median value and overall survival (OS) with each MTV methodology was determined by Kaplan-Meier survival curves and log rank test. Spearman rank order correlation was performed to establish the correlation between MTV_p and CA15-3 value. **Results:** Median follow-up period was 34 months (range: 8-72 months) during which 21 patients died. Median MTV value for $MTV_{2.5}$, MTV_{41} and MTV_p were respectively 24 ml (range: 0-1302), 34.5 ml (range: 1.4-876.8), 26.9ml (range: 0.38-1796.1). By log-rank analysis, a high MTV value after dichotomisation by the respective median value was able to predict OS using all methodologies ($p=0.031$, 0.027 and 0.002 respectively). Time delay longer than 5-y between initial diagnosis and recurrence (26 patients) was also predictor of OS ($p < 0.001$). When the patients were classified into four groups according to the combined factors of MTV_p and delay, MTV_p was predictive of OS in patients with a relapse time <5 years (mean survival time: 60 months versus 27 months; $p = 0.026$), but not in patients with time delay longer than 5-y. Mono-organ invasion (27 patients) predicted longer overall survival than multiorgan invasion (56 months versus 34 months; $p = 0.003$) whatever the number of metastases involved. SUV_{max} , initial diagnosis stage, SBR status and CA15-3 value were not predictors of OS. No statistically significant relationship was observed between MTV_p and CA15-3 value. By cox multivariate analysis, recurrence delay and mono-organ invasion remained independent predictors of survival. **Conclusion:** In a first MBCR, MTV, recurrence delay and multiorgan invasion are significant prognostic biomarkers. Recurrence delay <5 years and multiorgan recurrence being unfavourable independent prognostic biomarkers.

608 – Monday, October 17, 2016, 08:00 - 09:30, Hall 212

Physics & Instrumentation & Data Analysis: Multimodality Systems & Quantification

OP247

Reproducibility of MR-based attenuation correction maps for PET/MRI: Variations with free breathing and breath-hold protocols

S. K. Øen¹, M. L. Lassen², I. Rausch², M. O. Myrthue³, L. Eikens¹, T. Beyer², ¹Norwegian University of Science and Technology, Trondheim, NORWAY, ²Medical University of Vienna, Vienna, AUSTRIA, ³St. Olavs Hospital, Trondheim, NORWAY.

Objectives Combined PET/MRI systems are well-suited for long-term follow-up studies given the lowered ionizing radiation burden. Here, we investigate the variability of DIXON-based attenuation correction (AC) maps acquired in free breathing and breath-hold for longitudinal PET/MRI studies in a scan-rescan set-up. **Materials/Methods** Nine healthy volunteers (3m/6f) were included in this study. All subjects were positioned with arms-down in a whole-body PET/MRI scanner (Siemens Biograph mMR) and underwent the MRI-part for the generation of MR-based AC. AC maps of thorax were acquired during free breathing (FB) and breath-hold (BH) in a scan-rescan set-up. All scans were acquired again on a second day. Attenuation correction coefficients (ATN) in mediastinum, lungs and liver were calculated for all AC maps. Further, total lung volume and artifacts were calculated for all subjects and scans.

Image artifacts were categorized into: (ASF) air misclassified as soft tissue/fat, (SFA) soft tissue/fat misclassified as air, (LSF) lung tissue misclassified as soft tissue/fat, (LA) lung tissue misclassified as air and (TI) tissue inversion of soft tissue and fat. **Results** Mean lung volumes across subjects were $2.1 \pm 0.5L$ (FB) and $2.3 \pm 0.6L$ (BH). Population based day-to-day variation in lung volume was $2.5 \pm 2.6\%$ (FB) and $0.4 \pm 1.1\%$ (BH). Lung ATN values were $0.0232 \pm 0.0034 \text{cm}^{-1}$ (FB) and $0.0233 \pm 0.0044 \text{cm}^{-1}$ (BH), with average day-to-day variations of 0.3% and 3.5%, respectively. Mediastinum- and liver-ATN values were 0.1cm^{-1} with no day-to-day variations. ASF, SFA and LSF misclassifications in the AC maps were observed in 36/36 scans acquired in FB. Further, LA misclassifications were reported in 12/36 and TI in 3/36 scans. For BH-protocols, ASF and SFA were reported in 36/36 scans and LSF in 16/36. LA and TI were reported in 8/36 and 3/36, respectively. **Conclusion** Day-to-day variation of- ATN values and lung volumes are very small (non-significant) on population-basis. Breath-hold acquisitions improved the quality and accuracy of the AC maps and, thus, should be used for thorax-studies.

OP248

The use of RESOLUTE brain attenuation correction in [¹⁸F]-fluoro-ethyl-tyrosine (¹⁸F-FET) PET/MRI of gliomas

C. N. Ladefoged, I. Law, C. Hassing, L. Højgaard, F. L. Andersen; Rigshospitalet, Copenhagen, DENMARK.

AIM: Evaluating glioma patients using [¹⁸F]-fluoro-ethyl-tyrosine (¹⁸F-FET) PET scanning is critically dependent on accurate and reliable tissue activity quantification. However, the vendor-provided attenuation correction (AC) maps in present PET/MRI scanners are incorrect particularly close to the skull. The glioma patients are often scanned post-operative with MRI artifacts from titanium craniotomy fixation plugs, which may also challenge atlas or template-based AC methods. The aim of this study was to determine the use of the subject-specific MR-derived AC method RESOLUTE in post-operative glioma patients. **METHODS:** We analyzed 61 postsurgical glioma patients with static PET images acquired 20-40 minutes after injection of 200 MBq [¹⁸F]-FET on a PET/MRI scanner (Siemens mMR) followed by separate same day acquisition of low dose CT as “gold standard” AC. Furthermore, MRAC maps were acquired using the Dixon water fat separation sequence and ultra short echo time (UTE) sequences, and calculated using a patient specific segmentation-based method with continuous bone density values assigned - RESOLUTE (Ladefoged, PMB 2015). For each subject and AC method the tumor was segmented using an isocontour including tracer uptake above a tumor-to-brain background activity (B), ratio of 1.6. We measured B, tumor mean and maximal activity (T_{mean} , T_{max}), and tumor volume (T_{vol}) calculating T_{mean}/B and T_{max}/B , and the Jaccard index of tumor delineation. **RESULTS:** A single patient was excluded from analyses due to disruptive signal voids from the metal plugs. The average %-difference within the tumor was for T_{mean} : -15%, -8%, and -3% for Dixon, UTE, and RESOLUTE, respectively. The absolute difference of T_{max}/B relative to CT was 0.13 ± 0.13 for Dixon (max: 0.6), 0.07 ± 0.09 for UTE (max: 0.4), 0.03 ± 0.05 for RESOLUTE (max: 0.2). The absolute difference in T_{vol} was 5.2 ± 6.2 ml for Dixon (Jaccard: 73%), 2.3 ± 3.0 ml for UTE (Jaccard: 84%), and 1.6 ± 2.0 ml for RESOLUTE (Jaccard: 87%). **CONCLUSIONS:** The AC method RESOLUTE robustly produced AC maps in postsurgical glioma patients with metal plugs. Only a single case had signal voids near the metal extending into the brain. Using RESOLUTE resulted in a large decrease in the average error in the tumor uptake. As a T_{max}/B level >2.4 is used as a cut-off to identify active tumor tissue this decrease in error (mean, SD and maximum) is instrumental for correct assessment. The accuracy of the tumor volume and delineation also increased, which indicates a potential use of the method in therapy planning.

OP249**Accuracy of a new atlas-based attenuation correction method in comparison to standard MR-based attenuation correction of the skull region in PET/MR imaging**

I. Rausch¹, L. Rischka¹, C. N. Ladefoged², M. Fenchel³, A. Hahn¹, R. Lanzenberger¹, T. Traub-Weidinger¹, T. Beyer¹; ¹Medical University of Vienna, Vienna, AUSTRIA, ²Rigshospitalet University Hospital, Copenhagen, DENMARK, ³Siemens Healthcare GmbH, Magnetic Resonance, Erlangen, GERMANY.

Aim: To evaluate the influence of different attenuation correction approaches in positron emission tomography (PET)/magnetic resonance imaging (MR) on clinical evaluation of dynamic [18F]FET imaging. **Methods:** Up to date, 12 patients who underwent a 40 min (0–40 min post injection) dynamic PET/MR (Siemens Biograph mMR) examination following the injection of 250 MBq [18F]FET were included in this ongoing study. Dynamic PET data was reconstructed using an OP-OSEM algorithm (3 iterations, 21 subsets, 3mm FWHM Gaussian post filtering) into 8 frames of 2x2 min, 4x4 min and 2x10 min using four different attenuation correction methods: (A) Standard implemented Dixon-based AC, (B) Standard implemented UTE-based AC, (C) a model-based post-processing approach incorporating spatially variant bone attenuation values into the attenuation map from (A) (non-commercial prototype software by Siemens Healthcare) and (D) CT-based AC. For each reconstruction, a threshold-based volume of interest (VOI) was segmented using a threshold of 90% of the maximum pixel in the respective lesion on summed images (20–40 min). An additional spherical background VOI was placed on the contralateral side to calculate a lesion-to-background ratio (LBR). The VOIs were copied to the different timeframes to calculate the time activity curves (TAC). From the last time frame, volumes of the VOIs and LBR were extracted. An experienced reader with 5 y of experience in dynamic [18F]FET imaging assigned each TAC to two curve patterns: 1) constantly ascending or peaking followed by a plateau and 2) peaking followed by a descent. The volumes and LBRs were compared, and differences to (D) were calculated. For the TAC patterns, changes in assignments relative to the pattern found in (D) were investigated. **Results:** Extracted VOI volumes changed on average by (A): -14±29%, (B) -7±38% and (C) 0±23% relative to (D). LBR were in general similar for all AC methods with an average difference to (D) of (A): -2±2%, (B) -2±5%, and (C) 0±3%. The assignment of the TACs to the different uptake patterns changed for 2/12 cases for (A) and for (B). For (C), no change in uptake pattern assignment could be observed. **Conclusion:** The use of different AC methods in PET/MR can influence the clinical diagnosis in dynamic [18F]-FET glioma imaging. This is mainly attributed to changes in the segmentation of VOIs when using threshold-based segmentation approaches. Nevertheless, LBR seems to be comparable for all evaluated AC approaches.

OP250**Implementation of routine sequential PET/MR of the rat heart in an in-line preclinical scanner**

J. M. Vrigneaud¹, P. Walker^{2,3}, A. Camacho⁴, A. Courteau², A. Oudot¹, M. Guillemin¹, F. Brunotte^{1,2,3}; ¹CGFL Preclinical Platform, Dijon, FRANCE, ²Le2i-UMR CNRS 6306, Dijon, FRANCE, ³CHU, Dijon, FRANCE, ⁴MR Solutions, Guildford, UNITED KINGDOM.

Introduction: Cardiac imaging is one of the important potential applications of PET/MR studies as MRI and PET are the most accurate methods to respectively collect functional and molecular data during the same examination. Several clinical PET/MR Scanners are now marketed and permit cardiac clinical investigation but surprisingly no pre-clinical cardiac PET/MR scanner is available. The present system is made of an 8

head SiPM PET module with Dual-layer LYSO matrix and an effective axial field of view of 50.4 mm. The PET detector is clipped-on at the extremity of a 3T 17 cm bore cryogen-free superconducting magnet with 400 mT/m gradients. The bed movements and PET operation are fully integrated in the software controlling MRI. The aim of the present study is to detail the implementation of heart imaging and the first results obtained with this scanner. **Methods:** The present study comprised two steps. The first step was to adapt the PET/MR scanner to cardiac imaging of the rat. The second step was to obtain cardiac acquisitions after injection of 10–40 MBq of 18F-FDG. PET was acquired in list mode and images were reconstructed using 3D OSEM. MR images of the left ventricle were acquired in cine-MRI using 2 mm thick short- and long-axis FLASH sequences. Cardiac gating was obtained all over the PET and MR examinations using cutaneous electrodes. All the MR acquisitions were respiratory gated in expiratory position using a pneumatic cushion placed on the abdomen. **Results:** The adaptation of the PET/MR scanner comprised the development of a bed Technical Support Unit adapted to anaesthesia, ECG acquisition, passage of the perfusion line with adequate shielding in order to reduce the noise in MR induced by the ECG wires. A quadrature coil was also developed with a sufficient diameter to permit the movement of the animal bed. Ten consecutive rats were imaged with 16 images per cardiac cycle acquired sequentially with each modality in less than 90 minutes. **Conclusion:** Rat heart PET/MR imaging can be easily obtained in less than 90 minutes with a temporal resolution of 16 images per heart cycle and a spatial resolution better than 1 mm. This study opens the way to routine use of PET/MR in cardiac preclinical imaging.

OP251**Impact of respiratory motion compensation in patients with solid tumors undergoing PET/MR**

M. Soussan, S. Djelbani, C. Comtat, V. Brulon, B. Helal, I. Buvat; IMIV, CEA-Inserm, Univ Paris Sud, CNRS, Université Paris Saclay, Orsay, France, Orsay, FRANCE.

Objective: For chest and abdominal imaging, respiratory motion can create blurring and suboptimal quantification in PET imaging. We evaluated the impact of bellow-based respiratory compensation to mitigate motion both in MR and PET images during oncologic routine PET/MRI. **Methods:** Twenty patients underwent a FDG-PET/MR (Signa, GE Healthcare) (107±15 min after FDG injection, 4MBq/kg, 4–6 beds, 3–4 min/bed position, time-of-flight OSEM reconstruction, 2 iterations/28 subsets, no post reconstruction filter) for solid tumor staging. Respiratory signal was recorded using a respiratory bellow. MR sequences consisted in a Dixon sequence for attenuation correction, and a thin section (5mm) axial T2W-FRFSE, with respiratory triggering (duration ~2 min). PET data were reconstructed using 3 approaches: the entire data set (Static), the end-expiration quiescent period only (PET frame with around 50% of the counts; GE, Q-Static), and gated data set registered to a single time frame using a non-rigid technique (GE, Q-Freeze). All that were clearly distinct from adjacent lesions or surrounding background were included for analysis. Lesions were evaluated using SUVmax and SUVpeak. Noise in PET images was estimated in the liver parenchyma by drawing a region of interest (ROI) over the right hepatic lobe, using the standard deviation (SD) of SUV divided by the mean SUV in that ROI. **Results:** Forty-eight lesions were included in the analysis: 23 mediastinal lymph nodes (LN), 19 lung nodules and 6 abdominal lesions. The noise measurements showed that noise level was significantly higher in motion corrected PET images than in static images : 0.21±/0.04, 0.31±/0.09 and 0.25±/0.04, in Static, Q-Static, and Q-Freeze images respectively (p<0.001). 46% (22/48) of lesions had a consistent increase in SUVpeak after motion correction with both methods: these changes were mostly related

to motion correction given that SUV_{peak} is little affected by noise. Among these 22 lesions, 11/22 were lung nodules (SUV_{peak} increase: 7+/-6.5% with Q-Static and 8+/-5% with Q-Freeze) and 9/22 were LN (SUV_{peak} increase: 4.1+/-3% with Q-Static and 17+/-24% with Q-Freeze). Interestingly, only 27% (13/48) of lesions showed an increase in SUV_{max} with both Q-Static and Q-Freeze, suggesting that the impact of motion correction is not properly characterized using SUV_{max}. Conclusions: Respiratory triggering and motion correction methods are feasible during routine PET/MR protocols, and affect lesion quantification in about half of lesions in our cohort. Changes in SUV_{max}, being sensitive to the noise level that is affected by motion compensation, do not properly reflect the number of lesions benefiting from motion correction.

OP252

Validation of Zero-Echo Time PET-MR against stand-alone PET using dynamic dopamine transporter imaging

J. M. Sousa¹, L. Appel¹, S. Papadimitriou², D. Nyholm², J. Sörensen¹, T. Danfors¹, E. Larsson¹, G. Delso³, F. Wiesinger³, H. Ahlström¹, M. Lubberink¹; ¹Department of Surgical Sciences, Uppsala, SWEDEN, ²Department of Neurosciences, Uppsala, SWEDEN, ³GE Healthcare, Zürich, SWITZERLAND.

Objectives: Zero echo time (ZTE) MR has been proposed as a skull segmentation method for MR-based attenuation correction (MRAC) which may reduce the quantitative bias of PET data. The aim of this study was to evaluate quantitative measures of dopamine transporter availability and relative cerebral blood flow based on a dynamic ¹¹C-PE2I-PET scan acquired on a PET-MR scanner using ZTE-MRAC. Data from the same subjects acquired on a stand-alone PET system with rotating ⁶⁸Ge rod sources for attenuation correction, considered the gold standard for quantitative brain-PET, was used as reference. **Methods:** Six patients evaluated for Parkinsonism underwent two 80-min dynamic ¹¹C-PE2I PET scans within 6 months on a stand-alone PET (ECAT HR+) and a time-of-flight integrated PET-MR (Signa PET-MR). ECAT and PET-MR scans were reconstructed using resolution-matched OSEM, with MRAC based on 2-point Dixon with ZTE as well as the standard head atlas method. Volumes of interest were defined using a probabilistic template on co-registered T1 images and transferred to the PET datasets. Binding potential (BP_{ND}), reflecting dopamine transporter availability, and relative cerebral blood flow (R₁) were estimated with a simplified reference tissue model using cerebellar cortex as reference tissue. Correlation and agreement between BP_{ND} in putamen and R₁ in anterior cortical, posterior cortical, limbic and striatal regions for both modalities were assessed using regression and Bland-Altman analysis. **Results:** High correlation (R² 0.97) was found between BP_{ND} values for putamen based on PET-MR with ZTE-MRAC and stand-alone PET, with no significant bias. For R₁, highest correlations were observed in limbic and striatal regions (R² 0.94 and 0.91, respectively), with somewhat lower correlations in anterior and posterior cortex (R² 0.82 and 0.78). PET-MR R₁ values were higher in posterior cortex (bias 0.07) and lower in striatum and limbic regions (bias -0.18 and -0.05), but biases were not significant. Correlation and agreement between PET-MR and ECAT was considerably better for ZTE than for head atlas MRAC, especially in anterior and posterior cortex where head atlas showed a significant positive bias. **Conclusion:** A good correlation and agreement was found between PET-MR with ZTE-MRAC and stand-alone PET for quantitative measures of dopamine transporter availability and relative cerebral blood flow based on dynamic PET scans. Besides extension of the number of patients, further studies will have to show whether the remaining observed differences are due to MRAC only or to other factors influencing quantitative accuracy.

OP253

PET/MR in radiation oncology - how to correct for attenuation caused by flat table top?

S. Witoszynskyj¹, P. Andrzejewski², I. Rausch³, M. Hacker⁴, D. Georg², B. Knäusl³; ¹Div. of Nuclear Medicine, Dept. of Biomedical Imaging and Image-guided Therapy, Vienna General Hospital, Vienna, AUSTRIA, ²Dept. of Radiation Oncology, Comprehensive Cancer Center, Medical University Vienna, Vienna, AUSTRIA, ³Center for Medical Physics and Biomedical Engineering, Medical University Vienna, Vienna, AUSTRIA, ⁴Div. of Nuclear Medicine, Dept. of Biomedical Imaging and Image-guided Therapy, Medical University Vienna, Vienna, AUSTRIA.

Introduction: PET and MR provides complementary information useful in many aspects of radio-therapy (RT). The implementation of PET/MR scanners overcame issues of PET-MR image registration. However, to assure patient positioning during imaging and RT, dedicated MR-compatible flat table tops (FTT) are required. However, these FTT cause attenuation and scatter and can lead to a significant degradation of PET image quality (IQ). This study's goal was to evaluate the impact of a FTT on PET IQ and to introduce a correction method. Materials and methods: PET images of a 12l cuboid canister, a cylinder phantom and a modified NEMA body phantom (all spheres of 11.3ml volume; activity-to-background ratio of 8:1) were acquired on a Biograph TrueV PET/CT and a Biograph mMR PET/MR (Siemens). All phantoms were filled with 18F-FDG in aqueous solution containing 0.9% NaCl and 0.2mmol/l Gd-DO3A-butrol. Measurements were performed with and without FTT (X-tend ApS). A transmission scan (PET-TS) of the FTT was acquired using a GE Advance PET. MR markers visible in PET were used for co-registration. An attenuation map (μMap) was derived from PET-TS and used for PET/(MR) image reconstruction. Activities measured in the spheres of the body phantom and activity profiles in the cylinder were compared between PET/CT and PET/MR images. Canister images were evaluated by computing a uniformity index (UI) using a sliding window approach with a 5x5 voxel ROI on slice-by-slice basis. Advantages of using PET-TS were compared to standard correction methods. Results: The (MAX-MIN)/AVG ratios of the mean activities in the body phantom's spheres were as follows (without and with the FTT, respectively): PET/CT 1.7% and 6.2%; PET/MR 2.6% and 6.8%. The best IQ was found in PET/CT without FTT. Compared to these images, PET/MR images were degraded. PET/CT with FTT exhibited attenuation artifacts. In PET/MR scans, scatter and attenuation artifacts were observed. IQ was significantly improved using FTT's PET-TS μMap. Discussion: Using PET-TS derived μMap reduces artifacts in PET/MR. The deteriorated AC observed in PET/CT images is caused by the transformation from CT attenuation to PET attenuation not being valid for materials used in the FTT. This proves that CT based AC may not be sufficient to perform AC in PET/MR scanner. Although the UI measure provides an indication of IQ, it is of limited use for evaluating systematic artifacts caused by incorrect AC. Further improvements are currently explored to improve quality of the PET-TS μMap and to integrate it into image reconstruction.

OP254

PET Detection Capabilities of Siemens Biograph PET/CT and PET/MR Systems

L. B. Aasheim¹, L. Eikenes², **A. M. Karlberg**¹; ¹Department of Radiology and Nuclear Medicine, St. Olavs Hospital, Trondheim, NORWAY, ²Department of Circulation and Medical Imaging, Norwegian University of Science and Technology, Trondheim, NORWAY.

Aim: With improvements in PET technology such as time-of-flight (TOF) capability, point-spread-function (PSF) modelling, reconstruction algorithms, detector design and materials, PET image quality and resolution have increased significantly, and with it the capability of detecting smaller lesions. The existing international standard for assessing PET image quality (NEMA NU 2-2012) does however not assess uptake volumes below 10 mm, even though current PET systems are more than capable of detecting lesions smaller than this. The purpose of this study was therefore to quantitatively assess, and compare the detectability of small uptake volumes in two state-of-the-art PET systems; Siemens Biograph mCT (PET/CT) and mMR (PET/MR). Furthermore, the dependence of detection capability of different reconstruction settings was evaluated. **Materials and Methods:** The PET Esser phantom with small hot spheres (inner diameters 4, 5, 6, 8, 12 and 20 mm) was used for evaluation of mCT and mMR image data. The background-to-hot-sphere activity concentration was 1:8 and 1:4. The phantom was prepared once for each concentration and scanned on both systems consecutively with clinical routine protocols. Attenuation correction was CT based in both mCT and mMR PET data. Iterative reconstruction (3D Ordered Subset Expectation Maximization (OSEM) algorithm) was employed (2-8 iterations), with/without PSF modelling and for the mCT additionally with/without TOF. Contrast-to-noise ratio (CNR) was evaluated for different reconstruction settings, and the Rose criterion ($CNR \geq 5$) was applied as a measure of detectability/visibility in phantom data. In order to validate the phantom results, a patient with lung tumours (5-9 mm) was included in the study. **Results:** For the mCT, highest CNR for small uptake volumes was found with PSF&TOF and 2-3 iterations, while for the mMR corresponding settings were PSF and 3-4 iterations. Using optimal reconstruction settings, uptake volumes down to 5 mm (1:8 activity concentration) and 8 mm (1:4 activity concentration) were visible ($CNR \geq 5$) in both mCT and mMR phantom images. For the clinical data a 5 mm lung lesion was observed in the PET images from both systems. **Conclusion:** The same uptake volumes were detected on both systems in phantom and clinical data, when using optimal reconstruction settings. Reconstruction improvements, such as TOF and PSF should be used, when available, to maximize the possibility of detecting small lesions.

610 – Monday, October 17, 2016, 08:00 - 09:30, Hall 114

Neurosciences: Data Analysis & Quantification

OP255

Quantitative imaging of cell viability after graft in stroke rodent model with [^{18}F]-FHBG

A. SALABERT^{1,2}, L. Vaysse¹, M. Beaurain¹, M. Alonso², J. Besombes¹, I. Loubinoux¹, M. Tafam^{1,2}, P. Payoux^{1,3}, ¹INSERM U1214, Toulouse, FRANCE, ²University hospital, Radiopharmacy unit, Toulouse, FRANCE, ³University hospital, Nuclear medicine unit, Toulouse, FRANCE.

Aim: Cell transplantation is an innovative therapeutic approach particularly after brain injury to compensate tissue damage and neuronal loss. However, before translation to the clinic, we need to better understand the underlying mechanisms of graft and to ensure the safety of this kind of approach. To have a real-time longitudinal monitoring of cell graft, we propose a molecular imaging approach using a gene encoding thymidine kinase (HSV1-tk) and [^{18}F]-FHBG) as a reporter probe to image the expression of this enzyme. HSV1-tk phosphorylates the radiotracer leading to its intracellular accumulation only in cells expressing HSV1-tk. The first step of this study was to standardize the method. **Material and methods:** Five million of HSV1-tk stably transfected Neuro2a cells were incubated with 5,55 MBq of [^{18}F]-FHBG during 3 hours. Calibration

ranges from 10 000 to 3 000 000 cells were realised and were counted in a gamma-counter or analysed by PET-camera. In parallel, we tested graft procedure in a model of rat stroke. Brain lesion was induced by stereotaxic injection of malonate toxin 3M (5 μL). 15 days after the surgery; we performed a stereotaxic graft, into the lesion, with different quantity of cells. Image acquisition of rats was then performed during 15 min in PET-CT. Data analysis and quantification was performed on homemade software (Sisyphé) on co-registered image. Results: [^{18}F]-FHBG cell uptake rate was stable, around 2.61% \pm 0.8 (n = 9). Calibration range analysis show no significant difference (p=0, 75, n= 6) between signal on gamma counter and PET (Bq) as a perfect correlation and reproducibility between the number of cells and the signal intensity. In vivo, we also observed a linear correlation between PET signal in brain rats and number of grafted cells (r = 0.996, p <0.00001, n =18), matching with the calibration range. Scalp attenuation was insignificant. These acquisitions also allowed the validation of stereotaxic injection quality. We noticed three types of injection variability: reflux in cisterna of CSF, cell reflux on the scalp and brain diffusion if the lesion was too small. **Conclusion:** We proved that molecular imaging with [^{18}F]-FHBG allows to quantify the number of grafted cells and to monitor the quality of cell injection. We plan to use this tracer to achieve a graft longitudinal follow up to quantify cell viability and biodistribution several weeks after injection. The repeated, non-invasive tracking of grafted cells will accelerate the development of effective stem cell therapy in stroke.

OP256

Reconstruction of Input Function for Rapid PET measurement of CBF, OEF, and CMRO₂

N. Kudomi¹, Y. Maeda², H. Yamamoto¹, Y. Yamamoto¹, T. Hatakeyama¹, Y. Nishiyama¹; ¹Faculty Of Medicine, Kagawa University, KAGAWA, JAPAN, ²Clinical Radiology, Kagawa University Hospital, KAGAWA, JAPAN.

Objectives: CBF, OEF and CMRO₂ images can be quantitatively measured using ¹⁵O-PET. Recently, we have developed a novel protocol allowing a short PET scan time. In that protocol, two tracers of ¹⁵O₂ and H₂¹⁵O were sequentially administrated with 10-minute interval during a single PET scan for CBF, OEF, and CMRO₂ (DBFM) [1]. One of problems, so far, is need for invasive arterial blood withdrawal for input function. The aim of the present study was to develop a new method for image-derived input function (IDIF) for quantitative CBF, OEF and CMRO₂ from the dynamic PET single scan image. **Methods:** Our technique consisted of formula based on the single tissue compartment model for expressing inputs for water and oxygen from a tissue curve with parameters of rate constants: K_1^w and K_1^o for water and oxygen, respectively. For multiple tissue curves extracted from brain regions in a PET dynamic image, the rate constants were estimated so as to minimize a sum of square differences for expressed inputs expressed from the tissue curves. Using the estimated rates, IDIFs were reconstructed for all applied tissue curves, and mean of reconstructed inputs was estimated as IDIF. To test validity, 20 subjects with suspected cerebrovascular disorder were studied with DBFM protocol. Arterial blood was sampled during scan time and activity concentration was determined to serve as reference measurements. The CBF, OEF and CMRO₂ values were computed by the IDIF and measured input functions. **Results:** The estimated IDIFs were well reproduced compare to the measured ones. The mean of calculated CBF, OEF, and CMRO₂ values were 0.46 \pm 0.16 and 0.46 \pm 0.16 ml/min/g by the measured and IDIF, 0.46 \pm 0.08 and 0.44 \pm 0.08, and 0.037 \pm 0.014 and 0.035 \pm 0.013 ml/min/g, respectively and differences were \pm 7.1%, \pm 6.7% and \pm 8.3% for those functions, respectively. Regression analysis showed tight correlation between IDIF and measured input methods as: r=0.97, 0.93, and 0.97, for CBF, OEF and CMRO₂, respectively. **Conclusion:** The presented results demonstrate that IDIF can be

estimated directly from tissue TACs extracted from dynamic PET image for DBFM method. This suggests the possibility to enable the noninvasive assessment of CBF, OEF and CMRO₂. [1] Kudomi et al JCBFM (2013) 33; 440-448

OP257

Healthy ageing assessed by simultaneous high-resolution TOF PET/MR brain imaging: partial-volume corrected cerebral glucose metabolism versus white matter microstructure

S. M. A. Willekens^{*1}, J. Ceccarini^{*1}, M. Koole¹, K. Goffin¹, S. Sunaert², K. Van Laere¹; ¹Division of Nuclear Medicine, University Hospitals Leuven and KU Leuven, Leuven, BELGIUM, ²Translational MRI, Division of Radiology, University Hospitals Leuven and KU Leuven, Leuven, BELGIUM.

Aims Cognitive decline in neurodegenerative disorders such as Alzheimer's disease and frontotemporal dementia, is marked by underlying grey matter (GM) atrophy, impairment in brain metabolism and white matter (WM) integrity. To comprehensively understand the effect of healthy ageing on cerebral glucose metabolism combined with GM and WM integrity, we studied age-related changes in simultaneously acquired ¹⁸F-FDG PET and diffusion tensor imaging (DTI) using high resolution time-of-flight (TOF) PET/MR. **Methods** ¹⁸F-FDG PET and DTI data were acquired simultaneously in 24 cognitively healthy individuals as part of an ongoing normal dataset project, with an age range of 20 to 78 years (n=4/decade; mean age 49.8±18.2 years, 10M, 14F). Dynamic ¹⁸F-FDG brain PET data and MR sequences (volumetric T1, T2 FLAIR and DTI) were acquired for 60 minutes on a GE SIGNA PET/MR scanner. Partial volume corrected (PVC) PET images were analyzed VOI-based (Hammers atlas, PNEURO v3.6) and voxel-based (SPM12). Regional 40-60 min ¹⁸F-FDG uptake values were normalized to average whole-brain activity. DTI data were analyzed using ExploreDTI. Fractional anisotropy (FA) was evaluated as diffusion tensor parameter in pre-defined WM ROIs (Johns Hopkins University WM atlas). Associations between regional ¹⁸F-FDG uptake, FA and age were assessed using linear regression and voxel-wise analyses (SPM12; p_{height}<0.005; K_{ext}>50). **Results** PVC VOI-based analysis showed negative correlations between age and ¹⁸F-FDG uptake in the frontal and prefrontal lobes, mainly in the middle (r=-0.50-0.54) and superior frontal gyrus p=0.007-0.01), and in the anterior cingulate gyrus (r=-0.46, p=0.03). These observations were confirmed in the voxel-based SPM analysis (P_{FWE-corrected}<0.005, T=5.2). Pearson correlation analysis showed a negative correlation between FA and age in the superior corona radiata and posterior thalamic radiation (r=-0.44, p=0.03). Age-related decrease in prefrontal metabolism correlated positively with WM FA decline with the age in the anterior (r=-0.43, p=0.04) and superior corona radiata (r=-0.44, p=0.03). **Conclusion** Partial volume-corrected cerebral glucose metabolism and WM FA decline with age, especially in frontal brain regions, indicating aging effects that surpass grey matter atrophy. Furthermore, prefrontal glucose metabolism decline is related to decreases in WM integrity in the anterior and superior corona radiata, demonstrating connected deterioration of frontal projection networks upon healthy ageing. The joint study of metabolism and GM/WM integrity with PET/MR can enable a more refined composite picture of the ageing healthy and diseased brain.

OP258

Evaluation of a novel quantitative metric, Volumetric Statistical Amyloid Burden (VSAB), for 18-F florbetaben PET using a probabilistic gray matter brain mask

A. Swallen, A. Nelson, J. Piper; MIM Software, Inc, Cleveland, OH, UNITED STATES.

PURPOSE/OBJECTIVES: Our goal is to evaluate the use of VSAB, the volume of gray matter that exceeds a z-score threshold when compared to a database of healthy controls, for distinguishing amyloid+ from amyloid- patients using a probabilistic gray matter mask (GMM) for florbetaben PET scans. **MATERIALS/METHODS:** MRI scans from 10 subjects were segmented using FreeSurfer into gray matter and white matter. The segmentations were transferred to corresponding florbetaben PET images for the same patients and transformed into template space using the florbetaben template registration. A mask was constructed for computing VSAB which includes only voxels which are at least 50% more likely to contain gray matter than white matter. One-hundred fourteen florbetaben PET scans acquired 90-110 minutes after injection were selected for analysis. All scans were classified as amyloid positive or negative by three expert readers and the majority read result was taken after assessment. For the quantitative analysis, MIMneuro 6.6 was used to deformably register each scan to a common template space comprised of 3 florbetaben PET templates. Z-scores were computed for every voxel, using the whole cerebellum as reference, as compared to 49 healthy controls within a probabilistic GMM. Z-score thresholds from 1.65 to 7 were considered for the computation of VSAB, defined as the percentage of voxels within the GMM that exceeded the z-score threshold. The z-score volume threshold was defined by finding the best separation of the two groups. **RESULTS:** Agreement with consensus reads for VSAB at z-score thresholds 1.65, 3, 4, 5, 6, 7 were kappa = 0.95, 0.95, 0.95, 0.95, 0.93, 0.86, respectively. The VSAB used were 22.65, 2.1, 0.45, 0.066, 0.007, 0.0007 %, respectively. Using z-score 3, 4, and 5 threshold the percent of patients classified correctly were 97.4%. For the visually positive cases, 60/62 (96.8%) were correctly classified and for the visually negative cases, 51/52 (98.1%) were correctly classified. **CONCLUSION:** VSAB using a probabilistic GMM was found to have high accuracy and excellent agreement with expert visual assessment. The level of agreement with expert visual assessment suggests that VSAB has the potential to serve as a valuable quantitative metric in the evaluation of florbetaben PET images.

OP259

Regional Visual Read Inspection of [¹⁸F]Flutemetamol Brain Images from a Large Autopsy Cohort

G. Farrar¹, M. Zanette²; ¹GE Healthcare, Amersham, UNITED KINGDOM, ²GE Healthcare, Boston, MA, UNITED STATES.

Introduction Visual interpretation of PET amyloid images obtained with [¹⁸F]flutemetamol as normal (negative) or abnormal (positive) relies upon a systematic review of 5 brain regions (frontal, parietal, posterior cingulate & precuneus, striatum and lateral temporal lobes). For a brain to be deemed amyloid-positive there must be an elevated cortical signal in at least one of these grey-matter regions. Analysis of a 106-patient autopsy cohort was performed to examine which regions were assessed as visually positive to contribute to the overall assignment of 'amyloid positive'. **Methods** 180 end-of-life subjects were scanned following 185-370 MBq of intravenous [¹⁸F]flutemetamol and 106 of these came to autopsy. PET images were read by 5 blinded readers trained using an electronic program, who independently classified as positive or negative each of the 5 regions in each of the 106 images. The majority interpretation (made by at least 3 of the 5 readers) was used as the imaging endpoint. **Results** Of the 106 images, 71 (67%) were positive and 35 (33%) were negative. Of the positive images, 54 (76%) were positive in all 5 regions and 14 (20%) were positive in 4 regions. There were 3 brains that read positive with 3, 2 or one region each. Posterior cingulate & precuneus always read positive in each of the 71 abnormal brains. **Conclusion** When interpreting PET [¹⁸F]flutemetamol images the reader should systematically review each of the 5 review regions. This is particularly important when assigning a scan as negative as there can be cases with a positive PET signal restricted to one or more regions. The majority of positive [¹⁸F]flutemetamol images showed positivity in 4 or 5 of the

review regions in this cohort of end-of-life subjects. In summary the methodology for the visual read of [¹⁸F]flutemetamol offers a robust assessment of 5 individual cortical brain areas which potentially allows different regions to be discretely studied if required.

OP260

Agreement Between Automatic Quantification and Experienced Reviewers in the Reporting of Amyvid PET/CT Scans

D. Fakhry-Darian^{1,2}, S. R. Khan², N. H. Patel^{1,2}, K. S. Nijran^{1,2}, K. L. Wallitt², S. Khan², W. Svensson², T. D. Barwick², Z. Win²; ¹Radiological Sciences Unit, Imperial College Healthcare NHS Trust, London, UNITED KINGDOM, ²Nuclear Medicine, Imperial College Healthcare NHS Trust, London, UNITED KINGDOM.

Aim: Florbetapir ¹⁸F (Amyvid, Eli Lilly) is a PET radiopharmaceutical used to detect the presence of β -amyloid plaques in the brain - an early stage indicator of Alzheimer's disease. The recent release of Hermes Amyvid BRASS allows for quantification of these studies by comparing SUV_r in six regions of the brain (relative to the cerebellum) against a database of 80 healthy control patients. In order to validate this software the agreement between trained reviewers and automatic quantification in BRASS was assessed. **Materials and Method:** 100 patients, age range 41-88 years, median age 68 years, were blind reported by 3 experienced reviewers with one final clinical report decided upon by all reviewers. The images were quantitatively evaluated in BRASS and the outcome was compared against the agreed clinical report. Studies were blind reported as either positive or negative and the subtype of the scan was identified amongst reviewers. The BRASS result was classed as positive if two out of the six automatic regions showed increased uptake more than 2 SD from the mean database score (z -score ≥ 2). Each patient underwent the same preparation and imaging: 370 MBq (max) florbetapir-¹⁸F, imaged 40 minutes p.i. for 20 minutes, list mode acquisition, on a Siemens Biograph 64. The 20 minute study was assessed for motion visually and any frames with obvious motion were left out of the final reconstruction (OSEM 2D 4i 14s, 3 mm Gauss, 168 matrix, min. 10 minutes). **Results:** 70 patients have so far been reported by all reviewers and quantified in BRASS. Moderate to good agreement was observed between the clinical report and BRASS quantification, $k = 0.66$ (95% CI 0.49-0.84). The false positive rate (FRP) was 29% (11 FP results) and the false negative rate (FNR) was 3% (1 FN result). Of the 12 results that disagreed, 10 displayed significant motion or were of atypical appearance (non-subtype A). Agreement between clinical reviewers and BRASS for type A scans only (56/70) was much better, $k = 0.79$ (95% CI 0.63-0.95). FPR = 16%, FNR = 4%. **Conclusions:** Hermes BRASS can support clinical reporting of Amyvid studies. Scan subtype should be identified prior to BRASS quantification. In the case of scans with atypical appearance a re-evaluation of Z-scores is necessary so as not to increase the occurrence of FP results. Motion should be identified prior to the final reconstruction and only the most stable frames should be used.

OP261

Comparison of F-18 FDG Brain PET Data Acquired Sequentially on Hybrid PET/CT and PET/MR Systems

Ü. Ö. Akdemir, U. Aydos, M. Özçelik, N. &. Karabacak, L. Ö. Atay Kapucu; Gazi University Faculty of Medicine, Nuclear Medicine Department, Ankara, TURKEY.

Aim: We aimed to compare brain F-18 FDG PET data of the same patients acquired sequentially on PET/CT and hybrid PET/MR cameras in a mixed patient group of neurodegenerative diseases and epilepsy. **Materials and Methods:** Brain PET/CT imagings were done on a PET/CT system (Discovery ST PET/CT, GE) 45 minutes after injection

of 0.1 mCi/kg of F-18 FDG in resting state. The acquisition time for PET emission was 12 minutes. Subsequently brain PET/MR acquisitions were done on a hybrid PET/MR system (Signa PET/MR, GE) in patients who gave informed consent and had no contraindications for MR without additional F-18 FDG administration. The PET/MR protocol consisted of a PET emission acquisition (15 minutes) and simultaneous MR imaging which included a T1w-DIXON sequence for attenuation correction of PET data. The two sets of brain F-18 FDG PET data were quantitatively compared using spm2 using a paired t-test model with $p < 0.05$, *FWE*-corrected and extent-threshold of 100 voxels. Spatial normalizations of PET data were done using an institutionally created F-18 FDG PET template. **Results:** Eleven patients with neurodegenerative diseases (5 dementia and 6 parkinsonism; mean age = 65 (\pm 10)) and 12 patients with epilepsy (mean age = 19 (\pm 9)) were included. Three separate spm2 analyses were done: One for the whole group and two separately for each patient groups. In the whole group analysis PET images from the PET/MR system showed lower values in bilateral frontal-temporal and higher values in bilateral parietal and right temporal regions in comparison to PET images from the PET/CT system. In the neurodegenerative diseases group PET images from the PET/MR system showed lower values in left frontal lobe and higher values in left parietal-posterior cingulate, right frontal, right primary auditory regions and right cerebellum. In the epilepsy group PET images from the PET/MR system showed lower values in left frontal lobe, right cerebellum and higher values in left primary visual, right premotor and posterior cingulate cortical regions. **Conclusion:** We observed significant quantitative differences between paired brain F-18 FDG PET data acquired sequentially on PET/CT and PET/MR systems in a mixed clinical patient population, which might be caused by differences in spatial resolution of PET cameras and methods of attenuation correction of PET data. These results indicate that for the quantitative analysis of brain PET images a camera specific spatial normalization procedure and normal database should be used.

OP262

A PET/CT approach to spinal cord metabolism in amyotrophic lateral sclerosis

E. Pomposelli¹, A. Cistaro², C. Campi³, M. Pennone¹, A. Buschiazzo¹, F. Bongioanni¹, F. Nobili⁴, E. Monteverde¹, P. Gancitano¹, A. Massone⁵, G. Sambuceti¹, A. Chio⁶, M. Piana³, C. Caponnetto⁷, C. Marini⁸; ¹Nuclear Medicine Unit, Department of Health Sciences, University of Genoa and IRCCS AOU San Martino-IST, Genoa, ITALY, ²Positron Emission Tomography Centre IRMET S.p.A., Euromedic inc., Turin, ITALY, ³Department of Mathematics, University of Genoa, Genoa, ITALY, ⁴Clinical Neurology, IRCCS AOU San Martino-IST, Genoa, ITALY, ⁵CNR-SPIN Institute for Superconductors, Innovative Materials and Devices, Genoa, ITALY, ⁶Department of Neuroscience "Rita Levi Montalcini", University of Turin, Turin, ITALY, ⁷Department of Neuroscience, IRCCS AOU San Martino-IST, Genoa, ITALY, ⁸CNR Institute of Bioimages and Molecular Physiology, Section of Genoa, Genoa, ITALY.

Aim. Amyotrophic lateral sclerosis (ALS) is fatal late-onset neurodegenerative disorder of adult life, characterized by a progressive impairment of motor function. We recently developed new software able to recognize the spinal canal and spinal cord (SC) tracer uptake on PET/CT images. Our study aims to investigate whether this method permits to identify abnormalities in SC metabolism in ALS patients. **Materials and Methods.** We studied 30 patients with spinal-onset ALS at different clinical stage, submitted to FDG-PET/CT following 1-36 months (median 14) after diagnosis. Obtained data were compared with corresponding findings in age and sex-matched healthy controls selected from a published normalcy database. Image analysis was performed according to a previously validated algorithm able to identify all vertebrae from the image data set and to extract the spinal canal as the non-osseous space within the spine volume. The output

of the software was therefore the extraction and the 3D-representation of spinal canal volume that served as a mask to recognize SC using a segmentation algorithm based on Hough transformation. Thereafter, mean standardize uptake value (SUV) of cervical and dorsal SC, normalized to the liver (NSUV), was evaluated in comparison with normal subjects. Results. No differences were found in SC volume between patients and controls. FDG uptake was slightly, yet significantly, higher in ALS patients in the whole SC (NSUV 0.82 ± 0.28 vs 0.70 ± 0.14 $p < 0.05$) and in cervical segment (NSUV 0.99 ± 0.37 vs 0.85 ± 0.20 , $p < 0.05$). During follow-up 13 patients died. A potential prognostic role of SC metabolism was suggested by the observation of a higher SC_NSUV in non-survivors compared with the survivor patients (0.71 ± 0.26 vs 0.55 ± 0.16 , $p < 0.05$). Kaplan-Meyer approach confirmed the predictive value of SC-NSUV while multivariate analysis confirmed the additive nature of metabolic information (HR = 24.3, 95% CI 2.2-262.8). By contrast no association with prognosis was observed for age, ALSFRS-R score, time elapsed from diagnosis to PET scanning or presence/absence of riluzole treatment. Conclusion. Our computational approach might represent a new window to explore SC metabolism from PET/CT images. Whether confirmed in larger prospective studies, the prognostic significance of SC metabolic pattern in ALS patients might suggest a relevant role for SC inflammatory response in ALS progression.

701/703 – Monday, October 17, 2016, 10:00 - 11:15, Auditorium
Plenary 2: Radiation Facts and Figures

OP263

Radiation Exposure and Dose Limits: Understanding the Effects of Radionuclides for Diagnosis and Therapy

M. Lassmann; Universitaetsklinikum Wuerzburg, Klinik fuer Nuklearmedizin, Wuerzburg, GERMANY.

OP264

Radiation Dose from Nuclear Medicine Procedures: A Dose of Reality

M. Stabin; Vanderbilt University, Nashville, UNITED STATES OF AMERICA.

OP265

Potential of Combined EBRT and Systemic Radionuclide Therapy

U. Nestle; Universitaetsklinikum Freiburg, Klinik für Strahlenheilkunde, Freiburg, GERMANY.

801 – Monday, October 17, 2016, 11:30 - 13:00, Auditorium

CME 6 – Neuroimaging: Alzheimer’s Disease and Amyloid PET: News and Views 2016

OP266

Amyloid PET Reading and Reporting: A Tale of Four Tracers

A. Drzezga; Uniklinik Köln, Cologne, GERMANY.

OP267

Quantification and Semi-Quantification in Amyloid Imaging - Controversies and Unsolved Issues

A. Lammertsma; VU University medical center, Department of Nuclear Medicine & PET Research, Amsterdam, NETHERLANDS.

OP268

Suspected Non-Amyloid Pathology - What is it?

F. Nobili; Clinical Neurophysiology, Dept. of Neuroscience, Ophthalmology and Genetics (DINO), Genova, ITALY.

802 – Monday, October 17, 2016, 11:30 - 13:00, Hall 211

Joint Symposium 6 - EANM/EAU: Imaging for Staging Prostate Cancer

OP269

The Clinician’s Point of View

J. Walz; Institute Paoli-Calmettes, Dept. of Urology, Marseille, FRANCE.

OP270

Bone Imaging with Nuclear Medicine Methods

M. Beheshti; PET-CT Center Linz - St. Vincent's Hospital, Nuclear Medicine & Endocrinology, Linz, AUSTRIA.

OP271

Radiological Imaging at Staging

F. Lecouvet; Clinique Universitaires Saint-Luc UCL Brussels, Department of Radiology, Brussels, BELGIUM.

OP272

PET Imaging at Staging with New Tracers

K. Herrmann; Universitaetsklinikum Wuerzburg, Nuclear Medicine, Wuerzburg, GERMANY.

803 – Monday, October 17, 2016, 11:30 - 13:00, Hall 117

Technologist Oral Presentations 2

OP273

Quantification of FDG PET/CT dual-time-point imaging in recurrent breast cancer

C. Baun¹, **K. Falch**¹, **O. Gerke**¹, **J. Hansen**¹, **A. Alavi**², **P. F. Høilund-Carlson**¹, **M. G. Hildebrandt**¹; ¹Dept. of Nuclear Medicine, Odense University Hospital, Odense, DENMARK, ²Department of Radiology, Perelman School of Medicine, University of Pennsylvania, Philadelphia, PA, UNITED STATES.

Aim: To investigate quantification measurements of whole-body dual-time-point FDG-PET/CT in patients with suspected recurrent breast cancer using semi-quantitative analysis with partial volume correction. **Material and methods:** Patients with suspected recurrent breast cancer underwent whole-body PET/CT scans 1 hour (1 h) and 3 hours (3 h) after intravenous injection of FDG. Scans were evaluated semi-quantitatively by estimating standard uptake values (SUV_{max}, SUV_{mean}) in suspected malignant lesions along with lesion volume and partial volume corrected SUV_{mean} (cSUV_{mean}). The change in SUV from 1h to 3h was calculated, and SUV_{mean} was compared to cSUV_{mean} for all subgroups. Reference measurements were obtained in healthy liver tissue for all patients. Metastases were verified by biopsy, but for ethical reasons most patients had only one biopsy, and follow-up data were used to verify other metastatic sites. **Results:** Of 102 patients included in the study, 99 had data for analysis and 41 of these had recurrent disease with a total of 337 malignant lesions. Overall, SUV_{max} of malignant lesions increased by 28% ($p < 0.0001$) from 1h to 3h imaging, i.e., SUV_{max} was 6.36 ± 3.4 [0.9-19.7] (mean \pm SD, min and max) at 1h versus 8.14 ± 4.4 [0.7-29.7] at the 3h time point. For healthy liver reference tissue, SUV_{max} decreased by 11% ($p < 0.0001$), i.e., from 3.32 ± 0.67 [2.2-6.1] to 2.97 ± 0.51 [2.1-4.2] at 1h and 3h imaging, respectively. Metastases in breast, lung, lymph nodes and bone showed significant ($p < 0.0001$) increase in SUV_{max} between 1h and 3h by 25%, 40%, 33% and 27% respectively. Metastases in the lungs showed the highest increase%

in SUV_{max}, i.e., from 5.05±3.5 [1.2–15.2] at 1h to 7.05±4.8 [1.7–18.8] at 3h. Overall, partial volume correction increased SUV_{mean} significantly at 1h by 63% with a mean factor of 2.51 [2.14 - 2.88] and at 3h by 71% with a mean factor of 3.64 [3.22 - 4.06]. The highest impact was in breast lesions at 3h, where cSUV_{mean} increased by 87% compared to SUV_{mean}, whereas the smallest change was noted in liver lesions at 1h, where cSUV_{mean} was 39% higher than SUV_{mean}. No difference was seen between cSUV_{mean} and SUV_{mean} in healthy liver reference tissue. **Conclusion:** Standard uptake values increased significantly between 1h and 3h in malignant lesions of recurrent breast cancer, and particularly in lung lesions. The use of partial volume correction increased these values significantly, especially in breast lesions.

OP274

Use of PET / MRI hybrid systems in cancer recurrent prostate: pioneering study in Latin America

T. M. Ionescu, T. Vitor, K. M. Martins, S. A. Nogueira, J. Wagner, R. H. Baroni, M. F. Barboza, M. L. Cunha, G. C. Campos Neto; Hospital Israelita Albert Einstein, São Paulo, BRAZIL.

In recent year hybrid imaging scanners have emerged, achieving superior results by combining several techniques imaging advantages. PET/CT is the most widely used hybrid imaging system in oncologic diseases, including prostate cancer. PET/CT imaging of prostate cancer has been significantly improved with the introduction of the highly specific tracer ⁶⁸Ga-PSMA-11. Prostate cancer is the most frequent cancer in men worldwide and relatively high rates of recurrences, however, it is often more difficult to evaluate in its early stages using PET/CT. The main drawback of CT is its poor soft-tissue resolution. Recently the emerging PET/MRI systems improve this aspect using the excellent soft-tissue contrast and resolution of MRI and less radiation exposure. The aim of this study was present the clinical relevance of PET/MRI in prostate cancer compared to PET/CT. Since the acquired and the implementation of the Biograph mMR PET/MRI scanner (Siemens Medical Solutions, Erlangen, Germany) by Hospital Albert Einstein in Brazil, images were analyzed retrospectively and compared to the PET/CT scans performed with a Biograph mCT scanner (Siemens Medical Solutions, Erlangen, Germany). The PET/CT examinations were performed 60 minutes after intravenous injection of 148–222Mq ⁶⁸Ga-PSMA-11. A typical prostate whole body parameters were used for PET/CT images including: 120kV, modulated mAs, 1.5mm collimation, abdomen window, 4–5min per bed position, 200mm field-of-view (FOV), zoom 1.0, 2 interactions, 21 subsets and UltraHD PET at reconstruction method using a 3.0mm Gaussian filter. Following PET/CT the patients directly underwent PET/MRI examinations without any further intravenous injection or contrast agent. PET/MRI was acquired with attenuation correction using a dual echo VIBE Dixon sequence separating water and fat. The anatomical MRI sequences used were axial T2, axial T1 In_Out, diffusion and sagittal T2. The simultaneously acquired PET scan used following parameters: 500mm FOV, 400mm anterior-posterior FOV, 1.0 zoom, 3 interactions, 21 subsets, HD PET as reconstruction method and 2.0mm Gaussian filter. Both images were analyzed and compared retrospectively. New molecular imaging permit accurately assess the status of the disease and the progress of therapy and facilitate the selection of optimal treatment and improve patient outcomes. Our results show important advantages of PET/MRI regarding the evaluation and spatial characterization of lesions, including their expansive and invasiveness. We thereby believe that PET/MRI can achieve significant improvement in the diagnosis and therapy of recurrent prostate cancer in cases of poor resolution of soft-tissue contrast of PET/CT. In the future PET/MRI imaging should be employed in such cases.

OP275

Respiratory gated FLT and FAZA PET-CT imaging in patients with tumour motion

D. C. Vines¹, B. D. Driscoll¹, H. Keller¹, A. Lin¹, D. Glick¹, H. Raziee¹, M. Giuliani¹, A. Sun¹, D. A. Jaffray²; ¹Princess Margaret Cancer Centre, TORONTO, ON, CANADA, ²Princess Margaret Cancer Centre and TECHNIA Institute, TORONTO, ON, CANADA.

Objectives: Respiratory gated PET (gPET) with FDG has been shown to quantitate radioactivity more accurately in the presence of motion. Other PET radiotracers such as ¹⁸F-Fluorothymidine (FLT) or ¹⁸F-Fluoroazomycin arabinoside (FAZA) do not typically have the same high target-to-background ratios as FDG. The purpose of this study was to evaluate feasibility and potential benefit of using gPET for imaging lung tumors with motion using either FLT or FAZA. **Methods:** A retrospective study combining 10 patients (non-small cell lung cancer) with motion from 2 different PET trials was performed. Patients were imaged at 1 and 2h post-injection with either FLT or FAZA (n=6,4, respectively). Attenuation correction (AC) was performed using a helical CT (hCT) for both non-gated (NG) and gPET using 6 bins (hCT-gPET). A respiratory gated cine CT (4DCT) was then also used to reconstruct the matching phase of the gPET to create phase-matched AC gPET (PM-gPET). Scans were analyzed in patients having tumor motion greater than 5mm as assessed by 4DCT. Uptake of FLT and FAZA in the primary tumor was measured as SUV_{max} and SUV_{peak}. For both gPET methods (hCT and PM) only the exhale bin was used. To allow comparison of both gPET methods to NG data, the original 1200s NG scan was re-binned to 200s to match the gPET bin time. Evaluation of the effects of gated PET was performed by comparing SUV's for both hCT- and PM-gating methods to NG. **Results:** Tumour motion ranged from 5.7–26.1mm. SUV_{max} values for NG, hCT- and PM-gating were 3.04±1.6, 2.99±1.8, and 2.97±1.7, respectively, while SUV_{peak} values were 2.37±1.3, 2.39±1.5, and 2.36±1.4. It appears there is little difference in uptake between both gPET methods and NG, as well as for SUV_{max} and SUV_{peak}. Within FLT and FAZA there were also little differences. However, gPET showed some differences in spatial distribution of uptake in some cases. **Conclusions:** Both gated FLT and FAZA PET were feasible, however, the potential benefit of gating was not as evident as previous FDG data suggest. Additional data with tumor motion is required to determine if there are differences in the potential benefit of gPET using uptake metrics of SUV_{max} and SUV_{peak}. Although there seems to be little difference between quantitative results in patients with tumor motion, there may nevertheless, be differences in spatial distribution of the uptake regions within tumors among the 3 imaging methods. The impact of method on spatial distribution requires further investigation.

OP276

The diagnostic quality of 18-F-FDG PET images from the PET/MR in comparison with the PET/CT

E. Voets, M. G. W. Visser, F. M. Mottaghy, S. Vöö; Maastricht UMC, Maastricht, NETHERLANDS.

Aim: The purpose of this study was to compare and correlate the diagnostic quality level of PET images based on Magnetic Resonance Attenuation Correction (MRAC) from the hybrid PET/MR (Siemens Biograph mMR) with those derived from Computed Tomography Attenuation Correction (CTAC) of the PET/CT (Philips Gemini TF TOF 64) at our department. **Material and methods:** Nine consecutive oncology patients (54 years ±18.6) which were included in this research underwent a whole body 18-F-FDG PET/CT and a whole body PET/MR. The PET/MR was subsequently performed after the routine PET/CT, approximately 15 minutes later, for validation of our new PET/MR system and in order to avoid unnecessary administration of additional 18-F-FDG radioactive tracer. Visual assessment

was performed by four experienced nuclear medicine physicians and included the overall image parameters contrast-to-noise ratio (CNR), signal-to-noise ratio (SNR), and the delimitation of lesions based on a Likert scale 0–5. Quantitative assessment was determined in ROI measurements on MR/CT PET images. Volume of interest (VOI) were drawn over four normal structures (liver, spleen, mediastinal blood pool, and muscle gluteus maximus). SUV_{max} and SUV_{mean} values were determined in VOI on the MRAC and CTAC images. Between correspondent SUV_{mean} and SUV_{max} on MRAC and CTAC the difference was determined on Bland Altman plots. The study was approved by the internal ethical review board and all subjects gave written informed consent prior to inclusion in the study. **Results:** The Likert scale based analyses show a good inter observer agreement with regard to SNR and delimitation of lesions (median 0) and a good agreement for CNR (median 0.25). The Bland Altman test showed < 0.4 mean difference between SUV_{max} (MRAC-CTAC) indicating a very good agreement (SUV_{max} liver 0.04, mediastinal blood pool, 0.02 and muscle gluteus maximus 0.16) and a relatively good agreement for the spleen (SUV_{max} spleen 0.38). The same was available for the SUV_{mean} (liver 0.16, spleen -0.27, mediastinal blood pool 0.11, and muscle gluteus maximus -0.14). **Conclusions:** Our results show an overall agreement for the visual and quantitative image quality between MRAC and CTAC from the PET/MR and PET/CT. Differences observed between MRAC and CTAC derived SUV values are negotiable and may be attributed to the time-delay between the PET/CT and PET/MRI scans and biologic clearance of radiotracer. Further studies are required to assess SUV measurements when performing different MR attenuation correction techniques.

OP277

Optimisation of Time per Bed Position in ^{18}F -FDG PET/CT Lung Cancer Studies

A. List, E. Souza, N. H. Patel, J. W. Hubber, H. Tam, S. Khan, N. D. Soneji, Z. Win, K. S. Nijran; Imperial College Healthcare NHS Trust, London, UNITED KINGDOM.

Aim: To find the minimum time required per bed position for a ^{18}F -FDG PET/CT scan while maintaining diagnostic image quality, lesions detectability, and clinical diagnosis. **Methods:** Forty patients with lung cancer referred to the PET/CT imaging centre took part in the study. A standard half body protocol (eyes to mid-thigh) with three minutes per bed position, was performed on the Siemens Biograph-64 PET/CT scanner at our institute followed by an extra 10 minutes bed position over the lungs collected in list mode. The data was subsequently histogrammed to replicate bed position times of 2 min to 4 min in 30sec increments. A minimum bed position time of 2 minutes was determined from previous phantom studies which demonstrated a high confidence level for image quality when acquiring for ≥ 2 minutes. Transverse slices were reconstructed using attenuation and scatter-corrected iterative reconstruction 3D OSEM (4 iterations, 8 subsets, 5mm FWHM Gaussian post reconstruction filter, 168 x 168 matrix size). Reconstructed images from datasets at different time per bed position (i.e. 2 min, 2.5 min, 3 min, 3.5 min and 4 min) were independently reviewed by three Nuclear Medicine radiologists while blinded to the dataset used for image reconstruction. The number of lesions, the maximum standard uptake value (SUV_{max}), and a confidence score of diagnosis and image quality using a scale of 1 to 5 (1 indicating low confidence of diagnosis, 5 indicating high confidence in diagnosis) were collected. **Results:** For each patient, the mean SUV_{max} of all lesions and nodes between the different time per bed position was evaluated with z-statistics. The confidence scores for the different time per bed positions were evaluated with a score ≥ 4 indicating high confidence of diagnosis and image quality. Kappa analysis was performed to determine inter-observer and final report agreement. Initial results show good agreement between the observers for a 2.5 minutes bed position time. The SUV_{max} of each lesion and node, the mean SUV_{max} for all lesions and nodes, and the diagnostic confidence for each time per bed-

position will be presented at the meeting. **Discussion and Conclusion:** The optimal time required per bed position for lung cancer patients from our initial findings is 2.5 minutes. We will work towards implementing an optimised protocol for lung cancer patients. Future work will look at optimising the time per bed position for different clinical applications.

OP278

First clinical experience with SUVmax quantification by a dedicated breast PET compared to PET-CT.

R. SANCHEZ JURADO, J. FERRER REBOLLEDA, M. COZAR SANTIAGO, J. AGUILAR BARRIOS, R. BRISA VAZQUEZ, A. VICEDO GONZALEZ; ERESA MEDICAL GROUP, Valencia, SPAIN.

Methods: Twenty-five patients with invasive breast cancer (20 ductal, 3 lobular, 2 other) prior to chemotherapy and surgery, underwent both ^{18}F -FDG breast PET/CT and MAMMI-PET in prone position with hanging breasts. PET/CT and MAMMI-PET were performed 60 min and 90 min after injection of 223 (+/- 15) MBq of FDG, respectively. Primary tumor detection was assessed and FDG uptake, expressed as maximum standardized uptake value (SUV_{max}) was calculated in both and compared the results. **RESULTS:** Twenty-five patients evaluated, and focused only in the breast imaging: 34 lesions detected by PET/CT and 42 lesions by MAMMI-PET. All lesions were confirmed by histology. Also, MAMMI-PET revealed a heterogeneity uptake of the tumor. Agreement in FDG uptake between PET/CT and MAMMI-PET was high ($r=96$, 97% CI 0.92-0.98). SUV_{max} quantification differences were observed between PET/CT and MAMMI-PET. 0.3 points of SUV higher in MAMMI-PET than PET/CT. **CONCLUSION:** The dedicated high-resolution breast PET (MAMMI-PET) was able to visualize all breast tumors including in its field of view (about 2 cms upper limit of pectoral muscle). Actually SUV_{max} values by MAMMI-PET are directly comparable to standard PET-CT. The high-resolution of MAMMI-PET provides a better visualization of tumoral heterogeneity with possible impact in the management of the patients. However, further studies will be necessary to support the use of MAMMI-PET for tumor quantification.

OP279

Amyloid brain PET: Does SUVr semi-quantitation help reader confidence including cases of suspected mixed proteinopathies?

N. Gulliver, G. Havariyoun, D. Ruiz, A. Eccles, N. Mulholland, G. Vivian; King's College Hospital, London, UNITED KINGDOM.

Introduction: Amyloid brain PET-CT is a relatively new tool for in-vivo investigation of suspected Alzheimer's disease and the availability of new amyloid-binding ligands has generated intense interest in this area. Three fluorine-18 tracers (^{18}F -florbetaben, ^{18}F -florbetapir, ^{18}F -flutemetamol) have now entered clinical use in a limited number of centres in the UK. However, since the routine clinical use of amyloid PET is not publicly funded, it is rare for reporting physicians to see significant numbers of scans. **Aim:** We aim to describe our single scanner centre experience thus far with amyloid ligands in investigating aetiology of memory loss. In addition, we aim to assess the impact of semi-quantitation on reader confidence of amyloid brain PET scans. **Clinical criteria** for use of amyloid PET includes patients who satisfy a core criteria but with mixed aetiology presentation. In these cases, the clinical question is to assess degree of amyloid burden with co-existing synucleinopathies. **Methods:** We retrospectively reviewed patients seen within our department from February to December 2015 who were imaged with amyloid-binding PET ligands as part of their routine clinical investigation. All scans were reported visually. Images were binary read (abnormal/positive or normal/negative) using Hermes Hybrid Viewer by two reporting clinicians having received multiple ligand-specific reader training, stating a confidence level from 1 to 5 (1 = not confident at all, 5 = extremely confident). Images were then assessed by semi-quantitative

analysis using Hermes BRASSTM software with SUV_r calculated for frontal, anterior cingulate, lateral temporal, precuneus, posterior cingulate and parietal brain regions with a cut-off of $Z < -2.5SD$ from database template. Confidence scoring was with then repeated. Statistical analysis was performed using SPSS. Results: The mean age of patients was 67 (range 50–80), with 6 male and 4 female. 50% of patients had previous examinations with findings consistent with Parkinson's disease (PD) or PD“plus” syndromes. Results indicated a statistically significant increase in confidence post quantitation for both reporting physicians ($p=0.005$). Global amyloid findings based on ligand-specific criteria for interpretation were changed from positive to negative in four (reader 1) and two (reader 2) cases. There was a statistically significant increase in inter-observer agreement (from $k=0.2$ pre quantitation to $k=1$ post quantitation) for overall scan result. Conclusions: although a larger sample size is needed to confirm this, early indications suggest semi-quantitation with Hermes BRASS software has some benefits in improving reader confidence and inter-observer agreement including for amyloid plaque burden assessment in patients with PD.

OP280

Correlation between TNM staging and tumor metabolic parameters assessed in vivo by FDG-PET/CT in patients with lung cancer

P. Cegla¹, K. Tyczynska², R. Czepczynski³, W. Cholewinski⁴; ¹Greater Poland Cancer Center, Poznan, POLAND, ²Affidea Medical Center, Poznan, POLAND, ³Department of Endocrinology, Metabolism and Internal Medicine, Poznan University of Medical Sciences, Poznan, POLAND, ⁴Chair and Department of Electroradiology, Medical University in Poznan, Poznan, POLAND.

OBJECTIVES: Lung cancer is the most common cancer in men and globally the leading cause of death in both sexes. Although CT is the primary diagnostic method that provides relevant information about the morphology and location of the tumor, the introduction of PET/CT allowed greater accuracy for determining the stage of the process and acquiring in vivo information on the biology of cancer cells. Commonly used TNM staging, despite the proven benefits has the limitations of pure morphological assessment. Several parameters of the biological activity of tumor in PET images have been introduced based on SUV and its derivatives as metabolic tumor volume (MTV) and TLG (total lesion glycolysis), calculated for primary tumor [TLG] and all foci of the cancer [TLGtotal]. The aim of the study was to compare the TNM stage of the cancer with biological parameter as MTV and TLG in patients with lung cancer. **MATERIAL AND METHODS:** The analysis was performed in 65 patients (40M,25F) aged 70 ± 10 y with a histologically confirmed lung cancer before treatment. PET scans were acquired on Gemini TF PET/CT scanner 60min after IV injection of ¹⁸F-FDG with the mean activity of 364 ± 75 MBq, with the area being examined from calvaria to half way down the thigh. The reconstructed PET images were evaluated using MIM 6 Software for MTV and TLG values. For MTV calculation a phantom study was performed for simulation of the variety of activity and volume. **RESULTS:** The analysis of the cancer stage showed stage IV-17patients, stage IA and IIIA-12 patients, stage IIA-11patients, 8 patients with stage IB, stage IIB at 5 patients. The lowest TLG values were observed in stage IA (19.05 ± 17.5) and the highest in stage IIB (415 ± 384). Other groups showed TLG values: stage IB (155 ± 108), stage IIA (210 ± 254), stage IIIA (278 ± 348), stage IV (275 ± 381). TLGtotal values were as follows: stage IA (19.5 ± 17.2), stage IB (156 ± 107), stage IIA (216 ± 251), stage IIB (433 ± 403), stage IIIA (299 ± 344) and stage IV (433 ± 464). An expected strong and significant correlation was found between the MTV and feature T but there was no correlation between the stage and both parameters of TLG and TLGtotal. **CONCLUSION:** Metabolic parameters of the tumor and proliferative process expressed with TLG values represent different from TNM staging system biological description of lung cancer, which may be important for the treatment and prognosis.

OP281

Image quality of PET ¹⁸F-FDG for patients with a high body weight

J. Hagerman¹, B. Olsson¹, A. Stenvall², F. Hedeer¹, H. Almquist¹, J. Oddstig², C. Hindorf²; ¹Clinical Physiology and Nuclear Medicine, Lund, SWEDEN, ²Radiation Physics, Lund, SWEDEN.

Aim The image quality for patients that undergoes ¹⁸F-FDG PET examination and has a body weight over 100 kg is lower than for patients with body weight less than 100 kg. In the clinical protocol patients are administered an activity of 4 MBq/kg body weight, maximum 400 MBq, and images are acquired for 2 min/bed position. The aim of this study was to investigate whether the image quality could be improved after increasing the maximum activity to 500 MBq and prolonging the acquisition time. **Material and Methods** 23 patients were included in the study. Nine patients had a weight <100 kg (63–95 kg) and 14 patients had a weight >100 kg (108–147 kg). The patients were injected with 4 MBq/kg, maximum 500 MBq, and imaged after 60 minutes on a GE Discovery PET/CT 690. The acquisition time for patients <100 kg was 2.0 min/bed. For patients with a weight >100 kg the acquisition time per bed was prolonged: 105–125 kg, 2.5 min/bed; 126–150 kg, 3.0 min/bed. Listmode allowed studies for patients >100 kg to be truncated to correspond to acquisition of maximum 400 MBq and 2.0 min/bed. Three regions-of-interest were drawn in the liver. The SNR (signal-to-noise ratio) was calculated as the ratio of the mean value of the activity concentration (kBq/ml) and the standard deviation. Two expert readers scored the studies for image quality independently. Scores were given by a five grade image quality scale (1=unacceptable image quality and 5=very high image quality). **Results** SNR for patients <100 kg was 10.5. For patients >100 kg the SNR increased from 7.8 to 9.3 ($p < 0.05$) when the maximum activity was increased to 500 MBq and the time per bed was prolonged. The SNR for patients >100 kg with the new protocol was not statistically different from patients <100 kg. The mean value of the scored image quality for patients <100 kg was 3.1. For patients >100kg the mean image quality score increased from 2.2 to 2.9 ($p < 0.05$) when increasing the injected activity and prolonging the time per bed position. The image quality score increased in 9 and 10 of 14 patients, respectively, for the two readers. **Conclusions** Increasing the maximum injected activity to 500 MBq and prolonging the acquisition time for patients with a body weight over 100 kg improved the image quality to become similar to the image quality in patients with a body weight less than 100 kg.

806 – Monday, October 17, 2016, 11:30 - 13:00, Hall 111

Cardiovascular System: Myocardial Sympathetic Innervation

OP282

Does cardiac ¹²³I-mIBG scintigraphy predict appropriate ICD-therapy in stable chronic heart failure patients?

D. O. Verschure^{1,2}, J. R. de Groot¹, S. Mirzaei³, O. Gheysens^{4,5}, B. L. F. van Eck - Smit¹, G. A. Somsen⁶, H. J. Verberne¹; ¹Amsterdam Medical Center, Amsterdam, NETHERLANDS, ²Zaans Medical Center, Zaandam, NETHERLANDS, ³Wilhelminenspital, Vienna, AUSTRIA, ⁴University Hospitals Leuven, Leuven, BELGIUM, ⁵KU Leuven, Leuven, NETHERLANDS, ⁶Cardiology Centers of the Netherlands, Amsterdam, NETHERLANDS.

Aim: Chronic heart failure (CHF) is a life-threatening disease, in part due to sudden cardiac death (SCD). Implantable cardioverter defibrillators (ICD) for primary prevention of SCD have improved overall survival of CHF patients. However, a high percentage of patients never receives appropriate ICD therapy. Moreover, ICD's are associated with malfunction, (operative) complications (e.g. infection, inappropriate ICD shocks) and high cost. Therefore, optimization of current selection criteria for

primary ICD is needed. This prospective multicenter study evaluated whether cardiac sympathetic activity assessed by planar ^{123}I -mIBG scintigraphy could identify high-risk CHF subjects most likely to experience appropriate ICD therapy. **Materials and Methods:** A total of 135 stable CHF subjects (age 64.5 ± 9.3 years, 79% male, LVEF $25 \pm 6\%$) referred for primary prevention ICD implantation in 12 centres in Austria, Belgium and the Netherlands were enrolled. All subjects underwent planar cardiac ^{123}I -mIBG imaging before ICD implantation. Planar images were acquired at 15 minutes (early) and 4 hours (late) after i.v. administration of 185 MBq ^{123}I -mIBG. Early Heart/Mediastinum ratio (H/M), late H/M and ^{123}I -mIBG washout (WO) were calculated. Cross-calibrated phantom study-data were used to correct these values for differences in collimator-gamma-camera combinations. Cox proportional hazards regression was used to determine the association between ^{123}I -mIBG derived parameters (i.e. H/M and WO) and appropriate ICD therapy. Furthermore, the association between H/M and WO and the combined endpoint of appropriate ICD therapy, NYHA functional class progression and SCD was investigated, expressed as hazard ratio (HR) with 95%-confidence interval (95%CI). **Results:** The mean early H/M was 2.05 ± 0.39 , late H/M 1.79 ± 0.38 and ^{123}I -mIBG WO 12.4 ± 9.2 . During a median follow-up of 29 ± 16 months (2–64 months), 21 subjects (15.6%) experienced a cardiac event (appropriate ICD therapy [10], NYHA functional class progression [6] and SCD [5]). In multivariate analysis, WO was associated with occurrence of the combined endpoint (HR 1.063 [95%CI: 1.016–1.112], $p=0.008$). WO had an almost statistical significant association with appropriate ICD therapy (HR 1.065 [95%CI: 1.000–1.135], $p=0.051$). No association was observed between H/M and appropriate ICD therapy or combined endpoint. **Conclusion:** There is a significant association between cardiac sympathetic activity as assessed by planar ^{123}I -mIBG WO and the combined endpoint of appropriate ICD therapy, worsening of heart failure and SCD in stable CHF subjects with an ICD for primary prevention. Planar myocardial ^{123}I -mIBG scintigraphy derived WO trended toward an association with appropriate ICD therapy. Therefore, ^{123}I -mIBG scintigraphy seems to identify CHF subjects most likely to experience appropriate ICD therapy.

OP283

Polymorphism of SLC6A2 gene does not influence outcome of myocardial ^{123}I -mIBG scintigraphy in patients with chronic heart failure

D. O. Verschure^{1,2}, F. Baas¹, B. L. F. van Eck-Smit¹, G. A. Somsen³, H. J. Verberne¹; ¹Amsterdam Medical Center, Amsterdam, NETHERLANDS, ²Zaans Medical Center, Zaandam, NETHERLANDS, ³Cardiology Centra Netherlands, Amsterdam, NETHERLANDS.

Aim: Chronic heart failure (CHF) results in both increased cardiac sympathetic activity and myocardial inflammation. The aim of this study was to identify the relationship between severity of heart failure (i.e. NTproBNP and LVEF), cardiac sympathetic activity (^{123}I -mIBG scintigraphy) and markers of inflammation in subjects with stable, optimally treated CHF. In addition, the predictive value for cardiac events (ventricular arrhythmia, progression of CHF, cardiac death) of ^{123}I -mIBG parameters and these inflammatory markers was evaluated. **Materials and Methods:** Fifty-five CHF patients (age 66.3 ± 8.0 years, 78% male, LVEF 22.4 ± 6.3) referred for cardiac ^{123}I -mIBG imaging were included. At 15 minutes (early) and 4 hours (late) after i.v. administration of ^{123}I -mIBG (185 MBq), planar images were acquired. Early Heart/Mediastinum (H/M), late H/M and ^{123}I -mIBG washout (WO) were calculated. NT-proBNP and inflammatory markers (i.e. C-reactive protein (CRP), IL-1 β , IL-6, IL-8, IL-10, IL-12p40, tumour necrosis factor- α (TNF- α), soluble (s)E-selectin, myeloperoxidase (MPO), plasminogen activator inhibitor-1 (PAI-1), tPA, tumor necrosis factor receptor 1 (TNFR1) and TNFR2) were measured in blood plasma samples, taken just before ^{123}I -mIBG administration. **Results:** Mean early H/M was 2.12

± 0.39 , late H/M 1.84 ± 0.40 and ^{123}I -mIBG WO 13.0 ± 10.9 . LVEF was the only independent predictor of late H/M (adjusted $R^2 = 0.100$, $p = 0.011$). NT-proBNP was an independent predictor of ^{123}I -mIBG WO (adjusted $R^2 = 0.090$, $p = 0.015$). None of the inflammatory markers was related to late H/M or ^{123}I -mIBG WO. During a median follow-up of 31 months (2 - 58 months), 13 patients experienced a cardiac event (ventricular arrhythmia (4), progression of CHF (4) and cardiac death (5)). Univariate Cox regression analysis showed that the risk of a cardiac event was associated with CRP (HR 1.047 [95% CI: 1.013–1.081]), NT-proBNP (HR 1.141 [95% CI: 1.011–1.288]), MPO (HR 0.998 [95% CI: 0.996–1.000]) and late H/M (HR 0.182 [95% CI: 0.035–0.946]). Multivariate Cox regression analysis showed that only CRP, NT-proBNP, MPO and IL-12p40 were predictors of a cardiac event. **Conclusion:** In this specific CHF population inflammatory markers and ^{123}I -mIBG assessed cardiac sympathetic activity are both prognostic indicators.

OP284

Validation of the 2-year cardiac mortality risk model using I-123 meta-iodobenzylguanidine in chronic heart failure

K. Nakajima¹, T. Nakata², T. Doi³, T. Kadokami⁴, S. Matsuo¹, T. Konno¹, T. Yamada⁵, A. Jacobson⁶; ¹Kanazawa University Hospital, Kanazawa, JAPAN, ²Hakodate-Goryokaku Hospital, Hakodate, JAPAN, ³Obihiro-Kosei Hospital, Obihiro, JAPAN, ⁴Saiseikai-Futsukaichi Hospital, Tsukushino, JAPAN, ⁵Osaka Prefectural General Medical Center, Osaka, JAPAN, ⁶Diagram Consulting, Kihei, HI, UNITED STATES.

Purpose: A 4-parameter risk model for predicting cardiac mortality was developed based on a Japanese pooled database consisted of 1280 patients with chronic heart failure (CHF), who underwent I-123 meta-iodobenzylguanidine (MIBG) imaging (EHJ Cardiovasc Imaging 2015/12/24). This study aimed to validate this 2-year risk model in a new cohort of CHF patients. **Methods:** A total of 546 patients (392 males, 72%; age, 66 ± 17 ; 14 years) with either suspected or definitive CHF who underwent I-123 MIBG imaging were selected retrospectively from 4 hospitals. Baseline conditions were 126 patients (23%) with NYHA class III-IV, left ventricular ejection fraction (LVEF) 39 ± 17 ; 14%, and ischemic etiology in 198 (36%) patients. Late anterior imaging of the chest was performed 3–4 hours after injection of 111 MBq I-123 MIBG, and heart-to-mediastinum ratio (HMR) was calculated on-site. Since low-energy (LE) and low-medium-energy collimators were used at the participating hospitals, HMRs were adjusted to LE-collimator comparable values using institutional collimator-specific conversion coefficients as previously established. The 2-year cardiac mortality risk prediction model used was developed using 4 variables: age, New York Heart Association (NYHA) functional class, I-123-MIBG HMR and LVEF. Patients were classified into 3 risk categories using commonly acceptable threshold of 2%/y and average of the 2-year cardiac mortality risk (12%); namely 2-year cardiac mortality of low (<4%), intermediate (4–12%) and high (>12%) risk. **Results:** Adjusted late HMR was 1.51 ± 17 ; 0.30. The average 2-year cardiac mortality risk calculated by the model was 12 ± 17 ; 11%, ranging from 0.4% to 52%. Mortality risk for 2 years was estimated to be 2.4 ± 0.9% (n=85), 7.5 ± 2.2% (n=291), and 24.9 ± 11.1% (n=170) for low, intermediate and high-risk groups, with predicted numbers of cardiac deaths of 1, 22, and 42, respectively. During the 2-year follow-up, cardiac mortality occurred in 1 (2%), 24 (8%), and 82 (48%) patients in the 3 risk groups. The predicted and actual numbers of cardiac deaths were comparable for low and intermediate risk groups, but the model underestimated cardiac mortality in the high-risk group. This probably reflected more severe CHF in the validation population in a hospital versus the derivation population (2-year cardiac mortality in class III-IV: validation population 51%; derivation population 20%). **Conclusion:** The present results demonstrated validity of the 2-year risk model, particularly for

differentiating low and intermediate risk patients from high-risk patients. In these CHF patients, the model may have practical applications to assist in clinical management decisions.

OP285

Characteristics of gamma cameras with medium-energy-type collimators in cardiac ^{123}I -MIBG imaging: A multicenter MIBG phantom study in Japan

K. Okuda¹, K. Nakajima², C. Kitamura³, M. Hori³, Y. Kirihara³, S. Matsuo², J. Taki², M. Hashimoto¹, S. Kinuya²; ¹Kanazawa Medical University, Uchinada, JAPAN, ²Kanazawa University Hospital, Kanazawa, JAPAN, ³FUJIFILM RI Pharma Co., Ltd., Tokyo, JAPAN.

Objectives: We have proposed a standardization method using a dedicated phantom for the determination of the ^{123}I -metaiodobenzylguanidine (MIBG) heart-to-mediastinum ratio (HMR) for the calibration of the characteristics of gamma cameras with collimators. We have been accumulating the calibration factors obtained from different combinations of gamma cameras and collimators in Japan. The purpose of this study was to characterize the calibration factors for various gamma camera with medium-energy (ME)-type collimators in a multicenter phantom study. **Methods:** A total of 667 planar phantom images were acquired by using gamma cameras manufactured by ADAC Laboratories (n = 28), GE Healthcare (n = 107), Philips Healthcare (n = 48), Shimadzu Medical Systems (n = 28), Siemens Healthcare (n = 262) and Toshiba Medical Systems (n = 210). The low-medium-energy general-purpose (LMEGP, n = 328), ME/MEGP/ME general-all-purpose (GAP) (n = 249) and ME low-penetration (MELP, n = 90) collimators were used in the multicenter phantom study. The mean acquisition time was 309 ± 126 s (95% range, 70–600 s). Planar images were obtained with 64×64 (n = 2), 128×128 (n = 30), 256×256 (n = 495) and 512×512 (n = 140) matrices. The calibration factor was calculated by using a dedicated software program, and defined as the conversion coefficient K. The K value shows an approximate range of 0.5 to 1.0, corresponding to low-energy to ME collimators. **Results:** The mean K value for all of the ME-type collimators was 0.863 ± 0.054 (95% range, 0.765–0.976). When the conversion coefficients were evaluated for each of the collimators, the mean K values for the LMEGP, ME/MEGP/MEGAP and MELP were 0.834 ± 0.043 (95% range, 0.829–0.839), 0.880 ± 0.044 (0.874–0.885) and 0.922 ± 0.046 (0.913–0.932), respectively ($P \leq 0.0001$). The mean K values for the LMEGP showed significantly higher in SIEMENS (0.845 ± 0.042 , 95% range, 0.839–0.851) than Toshiba (0.822 ± 0.033 , 0.816–0.829) ($P < 0.0001$). The mean K values were equivalent among the manufacturers in the ME/MEGP/MEGAP and MELP collimators. **Conclusions:** The characteristics of the gamma cameras and collimators could be determined by using the conversion coefficient K, derived from the multicenter phantom study. Since the K values for the LMEGP collimators differed significantly, depending on the manufacturers, we might apply cross-calibration to ^{123}I -MIBG imaging to obtain standardized HMR.

OP286

Characterization of cardiac sympathetic denervation and innervation after ischemia-reperfusion injury as assessed by a novel PET tracer [^{11}C]Me@HAPTHI for the norepinephrine transporter

X. Li¹, M. Dumanic¹, A. Kiss², C. Philippe³, N. Berroterán-Infante⁴, M. Mitterhauser⁴, W. Wadsak², B. Podesser², M. Hacker²; ¹Vienna General Hospital, Vienna, AUSTRIA, ²Medical University of Vienna, Vienna, AUSTRIA, ³Medical university of vienna, Vienna, AUSTRIA, ⁴Medical University of Vienna, Vienna, AUSTRIA.

Background and Aim: Disorders of sympathetic nervous system was recognized as key underlying pathophysiology after myocardial ischemia

reperfusion (IR). Norepinephrine transporter (NET) is located in the noradrenergic neurons and is responsible for the synaptic reuptake of extracellular norepinephrine. In this study, a novel PET tracer [^{11}C]Me@HAPTHI with high affinity and selectivity to the NET was used to characterize sympathetic denervation and innervation after myocardial ischemia. **Method:** Myocardial uptake of [^{11}C]Me@HAPTHI was compared [^{11}C]mHED which is an analogue PET tracer of the NE using PET/CT. In vivo dynamic [^{11}C]Me@HAPTHI gated PET imaging and ex-vivo autoradiography was performed to determine rat myocardial sympathetic nerve denervation (1day, 3days, 1week, 4 weeks) following transient ischemia of 20 minutes. Tracer's biodistribution and kinetics was analysed. Specificity of tracers was evaluated by PET imaging with NET blocking agent Nisoxetine (2mg/kg). Immunohistochemical stains of H&E and Tetrazolium chloride (TTC) assay were used to determine myocardial defect area and remote region. TH staining was quantified to assess sympathetic innervation density. Region-of-interest analysis was used to determine uptake ratios for the ischemic region related to the remote area. **Results:** Significant myocardial uptake of [^{11}C]Me@HAPTHI compared with [^{11}C]mHED PET was observed (Fig.A). After transient ischemia, reduced [^{11}C]Me@HAPTHI uptake was detected from day 1 to 4 weeks, which was confirmed by increased uptake ratio of ischemic area to the non-ischemic area (Fig. A), and increased uptake ratio of non-ischemic area to the blood pool. Representative time-course PET/CT images are shown in figure A. Correspondingly, in autoradiography, decreased uptake in the ischemia region with myocardial injury was observed, which was determined by histology (Fig.C); moreover, innervation in the heart was confirmed during the time course (Fig.B). In the kinetics analysis, the ratio of myocardium to blood radioactivity was reduced by the pre-injection of blockers (Fig. B) confirming the high specificity of cardiac uptake. **Conclusion:** [^{11}C]Me@HAPTHI PET can be used for specific imaging and quantitative method for cardiac adrenergic nerve function with high specific myocardial uptake through NET. It enable in vivo monitoring dynamic repair process after transient ischemia. Further therapeutic studies with remote ischemic conditioning will be conducted at left limb of rats to achieve protection against IR injury and evaluated by [^{11}C]Me@HAPTHI PET scan.

OP287

Abnormal cardiac adrenergic neuron activity assessed by ^{123}I -MIBG is an early marker of cardiac dysfunction in doxorubicin-induced cardiomyopathy in rats

B. Collin^{1,2}, A. Oudot¹, J. M. Vrigneaud¹, S. Delemasure³, M. Guillemin¹, P. M. Walker^{4,5}, A. Lalande^{4,5}, A. Cochet^{1,5}, F. Brunotte^{1,5}; ¹Centre Georges-François Leclerc, Dijon, FRANCE, ²ICMUB - UMR CNRS 6302, UBFC, Dijon, FRANCE, ³Cohiro Biotech, Dijon, FRANCE, ⁴CHU François Mitterrand, Dijon, FRANCE, ⁵Le2i - UMR 6306, UBFC, Dijon, FRANCE.

Aim: Several antitumor agents are well known to induce cardiac dysfunction such as anthracyclines (e.g. doxorubicin) and trastuzumab (Herceptin®). Thus, it is very important to identify, as early as possible, patients at risk of cardiac toxicity induced by cancer therapies, especially when combination therapies are necessary. Echocardiography and nuclear functional imaging such as Single Photon Emission Computed Tomography (SPECT) are common techniques to determine Left Ventricle (LV) functional parameters during anticancer treatment. Interestingly, SPECT could also be a valuable tool to go further, regarding its ability to assess the cardiac neurons activity within the heart with the noradrenaline analog ^{123}I -Metaiodobenzylguanidine (^{123}I -MIBG). Thus, the purpose of the present study was to follow and compare over time the evolution of cardiac function (echocardiography) and sympathetic innervation (SPECT) in a rat model of doxorubicin-induced cardiac failure. **Materials and methods:** Wistar Rats were respectively treated with doxorubicin (DOX, cumulative dose of 15 mg/kg) or with a saline solution (control, CTRL) and followed-up over a 6 weeks period. Transthoracic

micro-echocardiography (functional cardiac parameters such as Fractional shortening - FS) and ^{123}I -MIBG SPECT (cardiac sympathetic innervation) of rats was performed at baseline, two, four and six weeks. Cardiac injury biomarkers (troponin I - Tn-I and N-Terminal Pro-Brain Natriuretic Peptide - NT-proBNP) concentrations were determined in plasma by ELISA at 6 weeks. **Results:** Body weight evolution of DOX group was significantly lowered compared to CTRL group from week 2 (W2) to week 6 (W6). Echocardiography showed that DOX significantly impaired the FS at W6 ($31.4\pm 1.7\%$ vs $46.1\pm 2.1\%$, $p < 0.001$) whereas SPECT demonstrated a significant sympathetic denervation through the decrease of ^{123}I -MIBG uptake in DOX group as early as W2 and this effect was maintained until W6 (Heart to mediastinum ratio at W6: 3.05 ± 0.20 vs 1.21 ± 0.10 , $p < 0.001$). At W6, plasma levels for both Tn-I and NT-proBNP were dramatically increased in the DOX group when compared to CTRL (respectively: 628.0 ± 245.0 pg/mL vs 2.4 ± 2.4 pg/mL, $p < 0.01$ and 463.0 ± 236.0 pg/mL vs 0.0 ± 0.0 pg/mL, $p < 0.05$). **Conclusion:** Our results suggest that ^{123}I -MIBG SPECT imaging could constitute a reliable biomarker of doxorubicin-induced-cardiomyopathy much earlier than echocardiography did with functional parameters. Thus, molecular imaging of cardiac sympathetic innervation in this cardiotoxicity model could be particularly relevant to evaluate either new cardioprotective drugs in a preclinical setting or to set up cardioprotective regimens for clinical purpose.

OP288

Standardization of dietary regimen to highlight the metabolic effect of doxorubicin administration on myocardium in mice: a microPET study

G. Ferrarazzo¹, M. Bauckneht¹, F. Pastorino², F. Fiz^{1,3}, M. Ponzoni², G. Bottoni¹, A. Buschiazzo¹, F. Ticconi¹, L. Emionite⁴, A. Bozzano¹, A. Nieri¹, M. Pennone¹, C. Marini⁵, S. Morbelli¹, G. Sambucetti¹; ¹Nuclear Medicine Unit, IRCCS-IST San Martino, University of Genoa, Genoa, ITALY, ²Laboratory of Oncology, Istituto Giannina Gaslini, Genoa, ITALY, ³Nuclear Medicine Unit, Department of Radiology, Uniklinikum Tübingen, Tübingen, GERMANY, ⁴Animal facility, IRCCS AOU San Martino-IST, Genoa, ITALY, ⁵Institute of Bioimaging and Molecular Physiology, CNR, Milan, Genoa Section, Genoa, ITALY.

Aim. Several in vitro studies documented that antracycline-related cardiomyopathy is at least partially related to the capability of these drugs to impair mitochondrial function. The reduced oxidative phosphorylation rate and the consequent decrease in ATP availability accelerate glycolytic flux far before the development of contractile dysfunction. Accordingly, an increased ^{18}F -FDG uptake in the left ventricular myocardium might represent an early predictor of toxic doxorubicine (DXR) effect. However, this hypothesis has not been fully tested, since myocardial FDG uptake is profoundly influenced by dietary regimen in the days preceding the scan, despite a correct fasting period before tracer injection. The aim of the present study was to verify whether and to what degree DXR increases cardiac FDG uptake in a series of mice, exposed to the same dietary condition before microPET scanning. **Materials and Methods.** Animal experiments were reviewed and approved by the Italian Ministry of Health. Five-week-old female, athymic mice were treated once a week for 3 weeks, with DXR (5 mg/kg, n=7) or saline (n=7). Time points of PET scans were at baseline and 3 weeks after treatment beginning. FDG imaging was preceded by 6-hours fasting, with a dedicated micro-PET system (Albira, Bruker, US). After intraperitoneal administration of ketamine/xylazine (100 and 10 mg/kg, respectively), mice were weighted and serum glucose level was tested. A dose of 3-4 MBq of FDG was injected through a tail vein, while 10 minutes image acquisition was performed 40 minutes later. An operator unaware of mice treatment manually identified a volume of interest on the left ventricular myocardium and hind limb skeletal muscle (internal control). Average standardized uptake values (SUV) within both regions were thus calculated and termed LV-SUV and SM-SUV, respectively. **Results.** DXR markedly increased the ratio between LV- and SM-SUV from 2.3

± 0.5 at baseline to 4.6 ± 1.4 at the end of the experiment ($p < 0.05$). Conversely, the same ratio remained stable in control animals, starting from 2.2 ± 0.2 and resulting 2.3 ± 0.2 in the second PET scan ($p = \text{ns}$ vs. baseline; $p < 0.05$ vs. DXR group). **Conclusions.** Administration of high DXR doses result in increased cardiac FDG uptake in mice fed with a standardized dietary regimen. Further studies, including lipid-rich diet, are needed to clarify the potential additive value of diet regimen standardization in the early detection of myocardial metabolic injury related to DXR, especially in patients with Hodgkin Lymphoma submitted to serial ^{18}F -FDG imaging and treatment protocols encompassing DXR.

807 – Monday, October 17, 2016, 11:30 - 13:00, Hall 116

Clinical Oncology - Featured: NET

OP289a

NET

D. Wild; University Basel Hospital, Nuclearmedicine, Basel, SWITZERLAND.

OP289b

First Clinical Study of Gastroenteropancreatic Neuroendocrine Tumor (GEP-NET): Patient Dosimetry Assessment with the Somatostatin Receptor Antagonist ^{68}Ga -OPS202

S. Beykan¹, G. P. Nicolas², M. Fani², R. Mena³, J. Kaufmann³, H. Bouterfa³, R. Bejot³, D. Wild², M. Lassmann¹; ¹University of Würzburg, Department of Nuclear Medicine, Würzburg, GERMANY, ²Division of Nuclear Medicine, University of Basel Hospital, Basel, SWITZERLAND, ³OctreoPharm Sciences GmbH, Ipsen Group, Berlin, Germany, Berlin, GERMANY.

Aim: Radiolabeled somatostatin receptor antagonists are a promising class of radiotracers for imaging and treatment of neuroendocrine tumor patients. We report here on the biodistribution and dosimetry of ^{68}Ga -OPS202 PET/CT in gastroenteropancreatic neuroendocrine tumors (GEP-NET) in a phase I trial (ClinicalTrials.gov NCT02162446). **Materials and Methods:** In-vivo patient studies in metastatic G1/G2 GEP-NET patients (5 female, 7 male, weight: 55 ± 19 kg) were performed with approximately 158 ± 34 MBq ^{68}Ga -OPS202 (amount of peptide: $15\mu\text{g}$). Biodistribution and dosimetry of ^{68}Ga -OPS202 were investigated. A series of whole-body PET/CT scans were conducted, multiple blood and urine samples were taken up to 4 hours after intravenous injection. Time-activity curves (TACs) were generated for blood and selected organs delineated on fused PET/CT images. Organ-specific time-integrated activity coefficients (TIACs) were calculated by using the NUKFIT software tool (Kletting et al., MedPhys 2013;40:102504) for the corresponding TACs. Blood- and image-based (LV2-LV4) time-activity curves were integrated to calculate the bone marrow TIACs. Based on these data, the absorbed organ dose coefficients for a 74kg patient were calculated using the OLINDA/EXM software and applying the ICPR60 weighting factors. **Results:** The highest calculated absorbed doses were registered in urinary bladder wall ($1.01\text{E-}01$ mGy/MBq), the kidneys ($8.43\text{E-}02$ mGy/MBq) and the spleen ($6.02\text{E-}02$ mGy/MBq). The calculated mean absorbed dose, based on imaging, for the bone marrow was $1.13\text{E-}02$ mGy/MBq. None of the absorbed doses exceed organ toxicity levels. An analysis of the activity in the urine samples shows that, $8.1\pm 2.8\%$ of the injected activity (min: 3.3%, max: 12.4%) and $1.6\pm 0.6\%$ of the injected activity (min: 0.6%, max: 2.6%) are excreted 2 h and 4 h respectively after administration of the activity. The effective dose coefficient for ^{68}Ga -OPS202 is $2.4\text{E-}02$ mSv/MBq which is comparable to previous studies with ^{68}Ga -DOTATATE ($2.6\text{E-}02$ mSv/MBq), ^{68}Ga -DOTATOC ($2.2\text{E-}02$ mSv/MBq), and lower than the values for ^{111}In -DTPA-octreotide ($8.0\text{E-}02$ mSv/MBq). The effective dose for an injection of 150 MBq ^{68}Ga -OPS202 is 3.6 mSv. **Conclusion:** ^{68}Ga -OPS202 is well tolerated and

exhibits a favorable dosimetry delivering absorbed doses to organs that are comparable to other ^{68}Ga -labeled somatostatin receptor ligands. As expected, the main pathway of excretion is the urinary tract.

OP290

^{68}Ga -Pentixafor-PET/CT in Neuroendocrine Tumors - a triple tracer approach

R. A. Werner¹, A. Weich², H. Wester³, M. Scheurlen², J. Brumberg¹, T. Higuchi⁴, S. Samnick¹, M. Lassmann¹, C. Blümel¹, M. Rudelius⁵, A. K. Buck¹, C. Lapa¹, K. Herrmann¹; ¹Department of Nuclear Medicine, University Hospital Würzburg, Würzburg, GERMANY, ²Department of Internal Medicine II, Gastroenterology, University Hospital Würzburg, Würzburg, GERMANY, ³Pharmaceutical Radiochemistry, Technische Universität München, Munich, München, GERMANY, ⁴Comprehensive Heart Failure Center, University Hospital Würzburg, Würzburg, GERMANY, ⁵Institute for Pathology, University of Würzburg, Würzburg, GERMANY.

Introduction: Diagnostic imaging of neuroendocrine tumors (NETs) is the domain of somatostatin receptor (SSTR) agonists as well as FDG PET/CT in dedifferentiated tumors. SSTR also serves as target for receptor directed peptide therapy. More recently, specific ligands targeting the chemokine receptor 4 (CXCR4) were introduced potentially offering an additional theranostic option in NETs. Here we evaluated the CXCR4 expression using ^{68}Ga -Pentixafor PET/CT in NET patients in comparison to ^{68}Ga -DOTATOC and ^{18}F -FDG PET/CT. **Material and Methods:** 11 consecutive patients with histologically proven advanced NETs were retrospectively analyzed (3 female; mean age, 69±10 years; Ki67 36±36%). 5/11 (45%) suffered from pancreatic NETs, 3/11 (27%) from ileum NETs, 2/11 (18%) from cancer of unknown primary and 1/11 (9%) was classified as a gastric NET. DOTATOC, FDG and Pentixafor PET/CT were performed in all patients within 4 weeks to confirm target expression of SSTR, CXCR4 and to detect dedifferentiated tumor lesions. Image analysis was performed visually. Immunohistochemical CXCR4 expression was evaluated in biopsy samples using monoclonal anti-human anti-CXCR4 antibodies. **Results:** 7/11 (63%) initially presented with lymph node metastases, 3/11 (27%) with bone metastases, 9/11 (82%) with liver metastases, 2/11 (18%) with lung metastases and 1/11 (9%) with a brain metastasis. On visual analysis, Pentixafor was positive in 4/11 (36%), FDG in 9/11 (82%) and DOTATOC in 9/11 (82%) patients, respectively. Of the nine SSTR positive patients seven and three were also FDG- and CXCR4-positive. Two DOTATOC negative patients were FDG positive and one of them also Pentixafor positive. Three patients were positive on all three PET/CT scans. In 2/4 Pentixafor-positive patients, biopsy samples revealed intense CXCR4 expression. **Conclusions:** In this pilot study, only one third of NET patients were CXCR4 positive. However, one NET patient without SSTR expression was Pentixafor positive. Hence, CXCR4-directed radionuclide therapy can be envisioned for selected patients with SSTR-negative tumors.

OP291

^{11}C -hydroxy-tryptophan-PET/CT of Small Intestinal Neuroendocrine Tumours

N. Casta¹, K. Fröss-Baron², U. Garske-Roman¹, A. Sundin¹; ¹Surgical Sciences, Dept. Radiology & Molecular Imaging, Uppsala, SWEDEN, ²Inst. Immunology, Genetics and Pathology, Dept Oncology, Uppsala, SWEDEN.

Aim: In a retrospective study, PET/CT with the serotonin precursor ^{11}C -hydroxy-tryptophan (5-HTP) was assessed for staging and restaging in small intestinal neuroendocrine tumour (SI-NET) patients. **Materials and methods:** 83 patients (48 men/35 women, median age 60 years) with a

histopathological diagnosis of SI-NET underwent Whole-Body 5-HTP-PET/CT without i.v. contrast-enhancement for staging or restaging purposes. The imaging results were compared to those at diagnostic contrast-enhanced CT of the thorax and abdomen (n=76), MRI (n=3) and US (n=4) of the abdomen performed within 3 months of PET/CT. The imaging results were correlated to those at surgery, and clinical and imaging follow-up. **Results:** 5-HTP-PET/CT showed 47 true positive, 30 true negative, 4 false negative and 2 false positive observations and a resulting patient-based 92% sensitivity, 94% specificity, 96% positive predictive value (PPV) and 88% negative predictive value (NPV). 5-HTP-PET/CT detected 384 tumours out of a total of 398 lesions resulting in 96% lesion-based detection rate. The detection rate was 93% for liver metastases, 100% for lymph nodes metastases and peritoneal tumours, 100% for bone lesions and 91% for breast metastases. In the 12 patients who underwent surgery of the primary tumour 5-HTP-PET/CT detected 4 (33%). 5-HTP-PET/CT missed 14 small (less than 6mm) hypervascular liver metastases and 1 breast metastasis that were diagnosed by CT. Three false positive observations were a lesion in the stomach and in the duodenum, that could not be verified at follow-up, and an adrenal tumour that was found to represent a pheochromocytoma. In 5 patients 5-HTP-PET/CT correctly diagnosed 19 SI-NET metastases (12 in liver, 6 in abdominal lymph nodes, 1 ovarian metastasis) that were missed by CT. **Conclusion:** This first report on PET/CT with 5-HTP shows high patient based sensitivity and specificity and high lesion detection rates, consistent with previous reports on stand alone 5-HTP-PET. Especially detection of metastases in bone, lymph nodes and liver were advantageous by 5-HTP-PET/CT although small hypervascular liver metastases were missed. Consequently, contrast-enhanced CT is needed in conjunction with 5-HTP-PET/CT.

OP292

Use of ^{68}Ga -DOTATOC PET/CT in initial or recurrent ectopic Cushing's syndrome: a single centre experience

O. Bélassant Benesty, V. Nataf, J. Ohnona, M. Gauthé, L. Michaud, T. Cassou-Mounat, J. Talbot, F. Montravers; Hôpital Tenon, Paris, FRANCE.

Aim: Ectopic Cushing's syndrome (ECS) is rare, but localisation of the causative tumour is of paramount importance: treatment consists of resection of the tumour to avoid morbidity and mortality linked to chronic glucocorticoid excess. Neuroendocrine tumours (NETs) of low grade are frequently involved but can be of small size, hardly seen on conventional imaging, leading to up to 20% of tumours still occult after years. ^{68}Ga -somatostatin receptor-PET/CT (SR-PET) with different peptides (DOTATOC, DOTANOC or DOTATATE) has been shown to be promising, mainly for the detection of the primary NET, but its role in the detection of the cause of recurrence of ECS has been less often reported. In this review we share our experience with DOTATOC PET/CT in localising of the cause of ECS, for both the detection of the primary NET and for the restaging in case of recurrence. **Materials and Methods:** We performed a retrospective review of all patients who underwent DOTATOC PET/CT for ECS in our centre between January 2011 and March 2016. Thirteen patients (11 females, 2 males, aged from 31 to 66 years) underwent 18 examinations. Eight examinations were performed for detection of a primary NET, five for persistence or recurrence of ECS in patients who had previously surgical resection of a primary NET, without SR-PET before surgery (three lung carcinoids and one thymic NET), and five for surveillance after resection of primary or secondary NETs detected on a DOTATOC PET/CT performed in our centre, all with complete resolution of clinical symptoms and biologic anomalies after surgical removal of the tumour. **Results:** Among the eight examinations performed to search for primary NET, four were positive: three carcinoid lung tumours were confirmed after surgical resection and one lung focus is not confirmed yet. Four examinations were negative. Among the five examinations performed for persistence or recurrence of ECS after surgery, four were positive showing mediastinal lymph nodes, three confirmed after

surgical resection and one not confirmed yet, and one was negative. All examinations performed for surveillance after resection of NETs previously detected on a DOTATOC PET/CT were negative. Maximum Standard Uptake Values in the true positive lesions ranged from 2.9 to 8.5, with high tumour to background ratios. **Conclusion:** DOTATOC PET/CT seems to be a valuable tool not only for detection of the causal tumour in ECS, but also in the detection of the cause of persistence or recurrence of ECS after surgery.

OP293

Interim Results in 19 Patients on the Influence of Lanreotide on Uptake of [68Ga]-DOTATATE in Patients with Metastatic or Unresectable NET: No Evidence for Discontinuation of Lanreotide before [68Ga]-DOTATATE PET/CT

E. A. Aalbersberg, L. J. Saveur, M. E. T. Tesselaar, M. P. M. Stokkel; Netherlands Cancer Institute, Amsterdam, NETHERLANDS.

Introduction: Somatostatin receptor imaging with [68Ga]-DOTATATE PET/CT has become common practice in patients with neuroendocrine tumors (NET). Current guidelines (from both the EANM and SNMMI) recommend discontinuing treatment with somatostatin analogues before obtaining a [68Ga]-DOTATATE PET/CT scan. The assumption is that unlabeled somatostatin may lower the detectability of lesions. However, both guidelines also state that this issue is still being debated. **Aim:** The aim of this study is to investigate the influence of lanreotide on the uptake of [68Ga]-DOTATATE in tumor- and normal tissue. **Materials and methods:** Patients with metastatic or unresectable NET being treated with lanreotide and scheduled for [68Ga]-DOTATATE PET/CT are included prospectively in this study. A [68Ga]-DOTATATE PET/CT scan is made on the day before and the day after lanreotide injection in each patient. PET images were acquired 45 minutes post injection of 100 MBq [68Ga]-DOTATATE. [68Ga]-DOTATATE uptake in the primary tumor, metastasis, and normal tissue are quantified as SUV_{max} , SUV_{peak} , and $SUV_{mean50\%}$. A maximum of three target lesions per metastatic site (liver, bone, lung, peritoneal, lymph nodes, and other) were quantified in each patient. Normal tissue measurements were performed in the liver, spleen, adrenal gland, pituitary gland, thyroid gland, and parotid gland. **Results:** 19/34 patients have been included up to March 2016. No significant difference was seen in uptake of [68Ga]-DOTATATE in tumor lesions, neither in primary tumors or metastatic lesions, before or after injection of lanreotide. This held true for all metastatic sites investigated. Mean SUV_{max} was 21.01 before and 21.47 after lanreotide ($p=0.26$), mean SUV_{peak} was 16.62 before and 16.82 after lanreotide ($p=0.34$), and mean $SUV_{mean50\%}$ was 14.54 before and 14.64 after lanreotide ($p=0.59$). In normal tissue, the SUV_{max} of [68Ga]-DOTATATE in spleen, liver, and the thyroid gland were significantly lower after injection of lanreotide. **Conclusion:** The administration of lanreotide does not change the uptake of [68Ga]-DOTATATE in tumor lesions, but lowers the background uptake in the liver, spleen, and thyroid gland. This contradicts the current guidelines for [68Ga]-DOTATATE PET/CT imaging.

OP294

Comparison of ⁶⁸Ga-DOTA-TOC and ¹⁸F-FDG-PET/CT in the follow-up of neuroendocrine tumor patients after first full PRRT cycle

B. Nilica, D. Waitz, V. Stevanovic, C. Uprimny, D. Kendler, S. Buxbaum, L. Gerardo, B. Warwitz, B. Henninger, I. Virgolini, **M. Rodrigues**; Medical University, Innsbruck, AUSTRIA.

Purpose: to determine the value of ⁶⁸Ga-DOTA-TOC and ¹⁸F-FDG-PET/CT for initial and follow-up evaluation of NET patients treated with PRRT. **Methods:** We evaluated 66 patients who had histologically proven NET and underwent both PRRT and 3 combined ⁶⁸Ga-DOTA-TOC and ¹⁸F-FDG-PET/CT studies. ⁶⁸Ga-DOTA-TOC-PET/CT was performed before PRRT,

3 months after completion of PRRT and 6-9 months thereafter. ¹⁸F-FDG-PET/CT was done within 2 months of ⁶⁸Ga-DOTA-TOC-PET/CT. Follow-up ranged 11.8-80.0 (mean:34.5) months. **Results:** All patients were ⁶⁸Ga-DOTA-TOC-PET-positive initially and at follow-up after first full PRRT. Overall, 62/198 (31%) ¹⁸F-FDG-PET were true-positive in 38/66 (58%) patients. 28 patients (G1,5; G2,23 patients) were ¹⁸F-FDG-negative initially and during follow-up (group 1), 24 patients (G1,5; G2,13; G3,6 patients) were ¹⁸F-FDG-positive initially and during follow-up (group 2), 9 patients (G1,2; G2,6; G3,1 patient) were initially ¹⁸F-FDG-negative, but converted to ¹⁸F-FDG-positive during follow-up (group 3), and 5 patients (all G2) were initially ¹⁸F-FDG-positive, but converted to ¹⁸F-FDG-negative during follow-up (group 4). ¹⁸F-FDG-PET showed more and/or larger metastases than ⁶⁸Ga-DOTA-TOC-PET in 5 patients of group 2 and 4 patients of group 3, all with progressive disease. In 3 patients (progressive disease, died during follow-up) SUV_{max} of tumors increased 41-82% from first to last follow-up investigation. **Conclusions:** In NET patients, the presence of ¹⁸F-FDG-positive tumors correlates strongly with a higher risk of progression. Initially ¹⁸F-FDG-negative NET patients may show ¹⁸F-FDG-positive tumors during follow-up. Also G1 and G2 NET patients may have ¹⁸F-FDG-positive tumors. Therefore, ¹⁸F-FDG-PET/CT is a complementary tool to ⁶⁸Ga-DOTA-TOC-PET/CT with clinical relevance for the molecular investigation.

808 – Monday, October 17, 2016, 11:30 - 13:00, Hall 212

Physics & Instrumentation & Data Analysis: PET/CT Performance & Instrumentation

OP295

Evaluation of System Characteristics of Next Generation Digital Photon Counting Compared to Current Photomultiplier Tube PET/CT

J. Zhang¹, K. Binzel¹, M. Miller², M. V. Knopp¹; ¹The Ohio State University, Columbus, OH, UNITED STATES, ²Philips Healthcare, Cleveland, OH, UNITED STATES.

Purpose: To measure, evaluate and compare system physics characteristics of next generation digital photon counting (DPC) PET/CT with current photomultiplier tube (PMT) PET/CT. **Materials and Methods:** Physical characteristics of timing resolution and energy resolution as well as NEMA 2012 based spatial resolution, sensitivity, count loss and image quality were measured on both a pre-commercial release DPC PET/CT system (Vereos) (dPET) and a conventional PMT PET/CT system (Gemini TF 64) (cPET). A 1110 MBq (30 mCi) ¹⁸F acquisition was performed for count loss and noise equivalent counting rate determination over ~16hours. CQIE PET uniformity was measured in a quarterly manner on both systems. Sensitivity, timing, energy and spatial resolution were characterized across the clinically relevant count rate range. Overall system characteristics were evaluated and compared on both systems regarding its potential impact in clinical applications. **Results:** The dPET system demonstrated robust system physics characteristics with <2% variability in timing resolution, ±0.4% change in energy resolution, <2% change in spatial resolution, <10% variations in detector temperature and humidity as well as <5% change of the SUV or uniformity profile over a 12 month monitoring period. NEMA 2012 testing found for dPET a spatial resolution (in mm FWHM) of 4.10 transverse / 3.96 axial at 1 cm and 5.79 / 6.20 at 20 cm compared to cPET with 4.70 / 4.71 at 1cm and 6.5 / 7.1 at 20cm. For dPET, a 325 ps timing and 11.1 % energy resolution were consistently obtained, versus 550 ps timing and 11.7% energy on cPET. While NEMA sensitivity showed a 5.7: 7.0 (in kcps/MBq) for dPET/cPET, the clinical effective sensitivity was 24.1:17.0 correspondingly. The peak

of NECR failed to exceed 250kcps at ~25kBq/mL for cPET, whereas dPET achieved > 680 kcps peak true rate (>160% improvement) even at 50 kBq/mL revealing a substantially broader dynamic range. NEMA IQ demonstrated improved hot sphere contrast (from ~62%±2% (10 mm) to ~88%±2% (22 mm)) as well as significantly better image uniformity and quality on dPET than on cPET. CQIE performance testing showed significantly improved uniformity with ~3% variances on dPET vs. ~10% variances on cPET. **Conclusion:** The digital photon counting PET/CT system demonstrated excellent system characteristics, most notably in dynamic range, clinical sensitivity and timing resolution which promise to improve clinical PET imaging compared to conventional photomultiplier tube based systems.

OP296

Comparison of SUVs based on different ROIs and VOIs definitions: a multicenter respiratory phantom study

M. L. Lambrecht¹, M. La Fontaine², J. Sonke², R. Boellaard³, M. Verheij², C. W. Hurkmans¹; ¹Catharina ziekenhuis, Eindhoven, NETHERLANDS, ²Netherlands cancer institute, Amsterdam, NETHERLANDS, ³University Medical Center Groningen, Groningen, NETHERLANDS.

Background:In the context of the EORTC LungTech trial, a QA procedure including a PET/CT credentialing has been developed. This procedure will ultimately allow us to pool data from 23 institutions with the overall goal of investigating the impact of tumour motion on quantification. As no standardized procedure exists under respiratory conditions, we investigated the variability of 14 SUV metrics to assess their robustness over respiratory noise. **Methods:**The customized CIRS-008A phantom was scanned at 13 institutions. This phantom consists of a 18 cm long body, a rod attached to a motion actuator, and a sphere of either 1.5 or 2.5cm diameters. Body, rods and spheres were filled with homogeneous ¹⁸F¹⁸FDG solutions representative of activity concentrations in mediastinum, lung and tumour for a 70kg patient. Three respiratory patterns with peak-to-peak amplitudes and periods of 15mm/3sec, 15mm/6sec and 25mm/4sec were tested. Prior to scanning in respiratory condition, a 3D static PET/CT was acquired as reference. During motion, images were acquired using 3D or 4D gated PET (average image) according to institutional settings. 14 SUV (mean) metrics were obtained per acquisition varying ROI/ROI shape and location. Three ROIs and three VOIs with respective radii of 0.5, 0.6 and 0.8cm were investigated. These ROIs/VOIs were first centred on the maximum activity voxel; a second analysis was made changing the location from the voxel to the region (ROI5voxels) or the volume (VOI7voxels) with the maximum value. Two additional VOIs were defined as 3D isocontours respectively at 70% and 50% of the maximum voxel value. The SUV metrics were normalized by the corresponding 3D static SUV. Converting to recovery coefficients (RC) allowed us to pool data from all institutions, while maintaining focus solely on motion. For each RC from each motion setting we calculated the mean over institutions, we then looked at the standard deviation (Sd) and spread of each averaged RC over each motion setting (formula [1], [2], Figure1). **Results:**For the institutions visited we found that RC_{VOI70%} and RC_{VOI50%}, yielded over the 14 metrics the lowest variability to motion with Sd of 0.04 and 0.03 respectively. The RCs based on ROIs/VOIs centered on a single voxel were less impacted by motion (Sd: 0.08) compared to region RCs (Sd: 0.14). The averaged Sd over the RCs based on VOIs and ROIs was 0.12 and 0.11 respectively. **Conclusion:**Quantification over breathing types depends on ROI/VOI definition. Variables based on SUV max thresholds were found the most robust against respiratory noise.

OP297

Amplitude-based respiration-gated PET and patient-specific breathing-instructed CT to improve the spatial alignment in PET/CT

C. S. van der Vos^{1,2}, A. P. W. Meeuwis¹, W. Grootjans^{1,3}, E. P. Visser¹, L. de Geus - Oei^{1,2,3}; ¹Radboud university medical center, Nijmegen, NETHERLANDS, ²University of Twente, Enschede, NETHERLANDS, ³Leiden University Medical Center, Leiden, NETHERLANDS.

Respiratory motion can introduce a spatial mismatch between PET and CT images during combined PET/CT imaging, possibly reducing quantitative accuracy of PET images. It is therefore important to have a good spatial alignment to obtain a correct PET interpretation. In this study, the effect of patient-specific breathing-instructed CT on the spatial alignment between CT and amplitude-based optimal respiration-gated (ORG) PET images was investigated. **Materials and Methods:** FDG PET/CT imaging was performed in 20 patients. Images were acquired using a Siemens Biograph 40 mCT PET/CT scanner. Respiratory gating was performed using ORG (HD.Chest). The respiratory signal was obtained using a pressure sensor integrated in an elastic belt placed around the patient's upper abdomen. In addition to the standard free-breathing low-dose (LD) CT (CT_{st}) an additional LD CT was made with patient-specific breathing instructions (CT_{bh}). These breathing instructions were provided using the amplitude limits of the ORG PET reconstructions. Patients were instructed to hold their breath at the same amplitude level. Lesions were segmented manually on CT images and on PET images using a fixed threshold at 40% of the maximum standardized uptake value (SUV_{max}). For both CT_{st} and CT_{bh}, the mismatch was quantified using the position differences between the lung-liver transition in PET and CT images (Δ_{LL}), the distance between PET and CT lesions' centroids (Δ_C) and the amount of overlap indicated by the Jaccard similarity coefficient (JSC). Furthermore, the effect of attenuation correction was quantified using the SUV_{max} of PET images reconstructed with both types of CT scans. Statistical analysis was performed using the Wilcoxon Signed Ranks test, statistical significance was defined for $p < 0.05$. **Results:** Three out of 20 patients did not follow the breathing instructions and were excluded. The remaining 17 patients had 29 lung lesions. Regarding quantification of spatial overlap, the following values were found when comparing CT_{st} and CT_{bh}, respectively: Δ_{LL} was 5.0±7.0 and 1.4±6.7 mm ($p=0.036$), Δ_C was 5.7±6.7 and 3.7±2.1 mm ($p=0.050$), JSC was 0.32±0.16 and 0.37±0.17 ($p=0.151$), and SUV_{max} was 10.6±6.4 and 10.9±1.3 g/cm³ ($p=0.139$). **Conclusion:** There was a significant improvement in the spatial alignment of the lung-liver transition for these 17 patients. The same trend was visible for the alignment of the lesions. The effect on SUV_{max}, however, was small. The results indicate that the breathing instructions can improve spatial alignment and possibly quantification of ORG PET and CT.

OP298

Performances comparison of five commercial 4D-PET/CT devices

J. N. BADEL¹, V. ISNARDI¹, E. SPASIC², D. DONNARIEIX³, A. CHEMIN⁴, J. M. VRIGNEAUD⁵, T. MOGNETTI¹; ¹LEONBERARD, LYON, FRANCE, ²Institut Curie, PARIS, FRANCE, ³JEAN-PERRIN, CLERMONT-FERRAND, FRANCE, ⁴Institut BERGONIE, BORDEAUX, FRANCE, ⁵GEORGES-FRANCOIS LECLERC, DIJON, FRANCE.

Introduction: Use of the 4D-PET/CT technology is growing in radiotherapy planning of mobile lesions. This technique allows a reduction of breathing-related PET image degradation (underestimation of tracer uptake, overestimation of the lesion volume, etc.) and thus improves the delineation of metabolic tumor volume (MTV). Several respiratory gated 4D-PET/CT acquisition techniques have been developed by constructors. In this study, we propose a comparative study of five commercial 4D-

PET/CT gating devices for use in the context of radiotherapy applications. **Material and method:** Five commercial built-in 4D-PET/CT technologies were evaluated: Ingenuity TF (A), Gemini TF Big Bore (B), IQ (C), Discovery 710 (D) and Biograph mCT-Flow (E). The A, B and E devices use a respiratory monitoring system based on pressure sensor whereas C and D use an opto-electronic system. The 4D-PET/CT's impact on the quantification and the definition of MTV was compared among five devices. A CIRS-008A dynamic thorax phantom was used to simulate a spherical lesion's motion in the lung parenchyma. Three volumes of fillable spheres were tested: 0.5, 2 and 8 ml. To simulate the breathing motion, a cosine equation was used with 20 mm longitudinal peak-to-peak amplitude and 4 seconds breathing cycle. Three acquisitions were done with each size of spheres: a standard 3D without respiratory motion (3D reference acquisition), a standard 3D and retrospective 4D (4 and 10 phases reconstructions) with respiratory motion. The emission times per bed position were 2 and 8 minutes for 3D and 4D acquisitions respectively. The gain on the quantification provided by the five 4D technologies was estimated by calculating the SUV ratios (max and peak) between 3D and 4D acquisitions. The impact of 4D-PET/CT on the definition of MTV was measured by comparing the measured volume to the actual volume of spheres from volume recovery coefficients (VRC). The alignment between 4D-PET and 4D-CT images was tested by calculating the Dice coefficient on the spheres volume. **Results:** Differences in the quantification among systems were relatively small (max 20%). The ratio between 3D and 4D SUV ranged between 1.7 and 3.2 depending on the sphere's size and the number of phases reconstructed. The VRC ranged between 1.1 and 2.9 according to the same parameters. **Conclusion:** The 4D-PET/CT gating technology significantly improves the quantification and the MTV's definition. The five commercial systems tested offer relatively similar performances, and no technology really stands out.

OP299

Characterisation of Scatter and Attenuation in GE Discovery 530c using Monte Carlo simulations

M. Peterson, M. Ljungberg; Department of Medical Radiation Physics, Lund University, Lund, SWEDEN.

Introduction: New SPECT systems, based on CZT (Cadmium-Zinc-Telluride) solid-state detectors, have been commercially introduced during the last 5-10 years. The characteristic of CZT differs significantly from common NaI(Tl)-based scintillation crystal cameras in that an electrical signal is produced directly at the photon interaction site. Effects such as recombination and charge charring results, however, in a detector response that differ from NaI(Tl) scintillators and therefore is it important to characterize the energy spectrum to investigate, for example, the usefulness of scatter compensation methods, based on acquisition in additional energy windows. **Material and Methods:** The Monte Carlo code SIMIND has previously been modified to model CZT detectors. By simulations using a digital version of an elliptical torso phantom with a cardiac insert (Data Spectrum Inc) we create projections for the GE Discovery 530c system (a pinhole collimation using 19 CZT detectors in different positions with 180 degrees angular coverage). Simulated SPECT projections are then imported to the Xeleris workstation by patching a Dicom file and the clinical routine reconstruction program is used to create horizontal-axis, vertical-axis and short-axis images. Comparisons with measurements have been made to validate the simulation procedure. In addition, we have studied a) the scatter fraction in the main energy peak and in additional lower energy windows, b) the distribution of primary good events resulting from incomplete charge collections c) the effect of attenuation and d) defect contrast. **Results:** Comparisons between measured and simulated energy spectrum shows a good agreement even down in the lower parts of the spectrum. Visually, reconstructed images on the GE Xeleris workstation compared well with measurements, as do profiles through short-axis images. The myocardial-

to-defect contrast, $[C_{\max}-C_{\text{def}}]/C_{\text{def}}$ is 1.25 in measured data and 1.04 in simulated data with an overall good agreement between the two polar plots. Despite the lower energy resolution (in the order of 5% FWHM at 140 keV) the scatter-to-total fraction is about 30.5% for a 20% energy window, 25.1% for a 15% energy window and 19.2% for a 10% energy window. **Conclusion:** The Monte Carlo simulations of the 19 detectors pinhole GE 530c SPECT system, based on CZT detectors, have shown good agreement with measurement projections. The ability to separate the events into components of primary events, scatter, penetration event etc. makes it suitable for optimization of acquisition parameters and to understand if commonly used scatter correction method are applicable.

OP300

Initial performance evaluation of a preclinical PET scanner available as a clippable assembly in a sequential PET/MRI system

J. M. Vrigneaud¹, J. Mc Grath², R. Pegg², A. Camacho², G. Martin², N. Schramm³, F. Brunotte^{1,4}; ¹CGFL, preclinical imaging platform, Dijon, FRANCE, ²MR Solutions, Guildford, UNITED KINGDOM, ³Central Institute of Engineering (ZEA-2), Research Center, Juelich, GERMANY, ⁴Le2i - CNRS 6306, UBFC, Dijon, FRANCE.

AIM: we evaluated the performance characteristics of a new preclinical PET scanner available as an easy clippable assembly that docks to the MRI system to perform sequential PET/MR imaging using a unified interface. **MATERIALS AND METHODS:** The single ring version of the PET system consists of 8 detectors, each of which comprises 12×12 SiPMs ($50.2 \times 50.2 \text{ mm}^2$) coupled with a dual layer of offset scintillation crystals to measure depth of interaction. The crystal arrays have 30×30 (29×29 for the outer layer) 6 mm long LYSO crystals (4 mm for the outer layer). The ring diameter is 119.2 mm and the axial field of view is 50.4 mm. The NEMA NU-4-2008 protocol was followed for studying the PET performance. The following tests were performed: counting-rate performance, scatter fraction, sensitivity and image quality. Image quality was assessed using the 3D-OSEM algorithm implemented in the system with one iteration and 64 subsets. FWHM and FWTM spatial resolutions in all three directions were estimated on FBP reconstructed images by fitting line profiles in each direction with a Gaussian function. To evaluate the resolution experienced in practice, a Jaszczak phantom was also acquired (0.7-1.2 mm) and reconstructed with 3D-OSEM. **RESULTS:** The peak system absolute sensitivity was 4.56% at the center of the field of view (FOV). The uniformity with the image-quality phantom was 13.6% and the spillover ratios in the images of the water and air filled chamber were 0.16 and 0.31, respectively. Recovery coefficients ranged from 0.20 to 0.76. The radial spatial resolution was nearly constant as a function of the radial offset, varying from 1.27 mm FWHM at a distance of 5 mm from the center to 1.58 mm FWHM at a distance of 25 mm from the center. The tangential spatial resolution ranged from 1.67 mm FWHM to 1.98 mm FWHM in the same conditions. The axial spatial resolution remained nearly constant (less than 2.0 mm) within a radial offset less than 15 mm from the center. Using the Jaszczak phantom, the 0.9 mm diameter rods were resolved after one iteration of the 3D-OSEM, 2-3 iterations resolved the 0.8 mm diameter. **CONCLUSION:** These first results indicate excellent spatial resolution performance of this preclinical PET system for use with animal studies. Moreover, the clippable assembly can be upgraded to accept a second ring of SiPMs modules, leading to improved sensitivity and axial coverage.

OP301

Breast-dedicated PET scanner based on partial geometry

A. Emami^{1,2,3}, H. Ghadiri^{1,2}, P. Ghafarian^{4,5}, P. Geramifar⁶, M. Ay^{1,2}; ¹Department of Medical Physics and Biomedical Engineering, Tehran University of Medical Sciences, Tehran, IRAN, ISLAMIC REPUBLIC

OF, ²Research Center for Molecular and Cellular Imaging, Tehran University of Medical Sciences, Tehran, IRAN, ISLAMIC REPUBLIC OF, ³International Campus, Tehran University of Medical Sciences, Tehran, IRAN, ISLAMIC REPUBLIC OF, ⁴Chronic Respiratory Diseases Research Center, National Research Institute of Tuberculosis and Lung Diseases (NRITLD), Shahid Beheshti University of Medical Sciences, Tehran, IRAN, ISLAMIC REPUBLIC OF, ⁵PET/CT and cyclotron Center, Masih Daneshvari Hospital, Shahid Beheshti University of Medical Sciences, Tehran, IRAN, ISLAMIC REPUBLIC OF, ⁶Research Center for Nuclear Medicine, Shariati Hospital, Tehran University of Medical Sciences, Tehran, IRAN, ISLAMIC REPUBLIC OF.

Breast cancer is the most frequent type of cancer in women all over the world. Mammography, ultrasound (US), and magnetic resonance imaging (MRI) are employed as diagnostic tools for diagnosis of breast cancer and help raise sensitivity for several years. Molecular imaging techniques such as Positron Emission Tomography (PET), has the potential to significantly enhance the diagnostic and reflects metabolic changes that often occur before morphological. However, because of the limited resolution and partial volume effect of most whole-body PET scanners, sensitivity for detection of small tumors is generally low. To improve the visualization and quantification of primary breast tumors, several dedicated breast PET devices have been developed. Most of them consist of tightly packed discrete detector module to improve efficiency. Our aim is to assess the possibility of reducing the number of detector elements per ring, while maintaining image quality by employing compressed sensing (CS) techniques, accuracy, and lower cost compared with current screening tools. The simulation of dedicated breast PET scanners was performed using GATE (GEANT4 application for tomographic emission) for assisting, optimizing and finding the best detector configuration system. Using GATE, different detector geometries were generated assuming different numbers and width for a system polygon. The system has two detector rings that each ring consist of 10 modules. Each detector block is composed of 50 mm × 50 mm array of LYSO crystals coupled to photodiodes, with transaxial field of view (FOV) of 170 mm in diameter and 80 mm axial FOV. In order to investigate the possibility of reducing number of detectors and provide geometric flexibility in lower price, the partial geometry of dedicated breast PET scanners lead to gaps between the detector modules and result in loss of PET data during measurement. So, we applied the compressed sensing minimization method to PET image reconstructions in order to reduce the artifacts caused by gaps. Simulation results predicted a 60–100% relative increase of photon sensitivity for the proposed dedicated breast PET system geometry. Also, simulation results indicated that spatial resolution values below 4 mm were measured in most of the FOV, and the partial ring incorporating CS method could control gap artifacts, recovered the PET image with minimal error in image quantification and generated image from its partially sampled data. Decreasing the number of detector module including some advantages specially reducing the cost of scanner to make it more accessible to users, and scan time.

OP302

Design and Performance evaluation of a Novel Brain PET Geometry Based on Partial Cylindrical Detector using Monte Carlo simulation

P. Sheikhzadeh^{1,2}, H. Sabet³, H. Ghadiri^{1,2}, P. Ghafarian^{4,5}, **M. Ay**^{1,2},
¹Department of Medical Physics and Biomedical Engineering, Tehran University of Medical Sciences, Tehran, IRAN, ISLAMIC REPUBLIC OF, ²Research Center for Molecular and Cellular Imaging, Tehran University of Medical Sciences, Tehran, IRAN, ISLAMIC REPUBLIC OF, ³Massachusetts General Hospital, Harvard Medical School, Charlestown, MA, UNITED STATES, ⁴Chronic Respiratory Diseases Research Center, National Research Institute of Tuberculosis and Lung Diseases (NRITLD), Shahid Beheshti University of Medical Sciences,

Tehran, IRAN, ISLAMIC REPUBLIC OF, ⁵PET/CT and Cyclotron Center, Masih Daneshvari Hospital, Shahid Beheshti University of Medical Sciences, Tehran, IRAN, ISLAMIC REPUBLIC OF.

Aim: The aim of this study is to introduce a novel PET system dedicated to brain imaging which we refer to as HoodPET, and evaluate its performance characteristics compared with other brain dedicated PET systems. In the conceptual design of HoodPET, we are seeking a compact, low cost, and portable design which can provide brain image(s) at different patient positions. **Materials and methods:** Our design is based on cylindrical geometry with partially populated detector modules such that the front and back of the patient head is open, and the detector modules cover the top and the sides of the patient head. We simulated different variations of this open geometry in GATE simulation code. In one design, the ring diameter is 240mm and axial FOV is 317mm. A total of 72 block detectors arranged in 6 rings of 12 blocks per ring that cover ~3/4 circumference of the cylinder. Each block comprises of an array of 2.3×2.3 mm² LYSO crystals. For comparing the performance of our design with conventional cylindrical brain PET, a cylindrical scanner with 300 mm ring diameter and 227mm axial FOV and 72 block detector contains of 2.3×2.3 mm² LYSO crystal array was simulated. For sensitivity evaluation in both scanners the NEMA 70cm sensitivity phantom with 1 MBq 18F activity and a 10cm radius Polymethyl methacrylate sphere was modeled as a head phantom. A spherical source with radius of 2cm that emits back to back gamma photons with activity of 1 MBq positioned in the 7cm offset in phantom to model the brain lesion. **Results:** The sensitivity of 23.61 and 36.42 kcps/MBq was calculated for NEMA and head phantoms, respectively. The mentioned sensitivities for conventional design were 17.00 and 21.58 kcps/MBq. This results show that our design has higher sensitivity than conventional cylindrical PET with the same number of block detectors. This is because of compatibility of our design with head and brain anatomy. **Conclusion:** Preliminary simulation results shows that our design for a brain-dedicated PET scanner can provide higher sensitivity than conventional cylindrical PET scanner for brain imaging. The results are very encouraging in that a non-cylindrical PET geometry can potentially provide better performance than a cylindrical PET geometry for brain imaging. We will further optimize the geometry of the HoodPET to increase the sensitivity while taking advantage of detectors with depth of interaction information which is a necessity in non-symmetric geometries with small FOV.

809 – Monday, October 17, 2016, 11:30 - 13:00, Hall 113

M2M: Rapid Fire Session

OP303

Radio-labeling and initial evaluation of a novel beta-secretase (BACE)-selective PET radioligand, [¹⁸F]PF-06684511, in nonhuman primates

A. Takano¹, L. Chen², S. Nag¹, M. A. Brodney³, N. Amini¹, C. Chang², R. Arakawa¹, S. Doran², J. Dutra², T. McCarthy³, C. Nolan³, B. O'Neil², A. Villalobos³, L. Zhang³, C. Halldin¹; ¹Karolinska Institutet, Department of Clinical Neuroscience, STOCKHOLM, SWEDEN, ²Pfizer Inc., Worldwide Research and Development, Groton, CT, UNITED STATES, ³Pfizer Inc., Worldwide Research and Development, Cambridge, MA, UNITED STATES.

Aim Beta-secretase (BACE) is a key enzyme in the generation of beta-amyloid. BACE inhibitors are being developed to decrease beta-amyloid accumulation in the brain and to reduce the risk of Alzheimer disease. BACE-selective PET radioligands would enable target occupancy measurement and inform optimal dose selection in clinical trials. PF-06684511 was identified by Pfizer and has shown high specific binding in rodents. In this study, we aimed to radio-label PF-06684511 with F-18 and evaluate the

brain distribution and quantitative methods of [^{18}F]PF-06684511 as PET radioligand for BACE in nonhuman primates (NHPs). **Materials and methods** [^{18}F]PF-06684511 radiolabelling was accomplished from Boc protected precursor, PF-06816649 by a two-step synthesis, comprising a nucleophilic substitution followed by hydrolysis of the protected group. Brain PET measurements were performed for 180 min at baseline and after oral administration of 5 mg/kg of PF-06738879, a selective BACE inhibitor, in two cynomolgus monkeys. Arterial blood was collected to evaluate kinetic compartment models. Total distribution volume (V_T) (mL/cm 3) was estimated from one tissue compartment model (1TC) and two tissue compartment model (2TC). The target occupancy was calculated using the Lassen plot. **Results** Radiolabeling was accomplished successfully with an incorporation radiochemical yield of 4–12% from fluorine-18 ion. The radiochemical purity was higher than 99% and the specific radioactivity was 73 ± 38 GBq/ μmol at the time of administration. Whole brain uptake of [^{18}F]PF-06684511 reached peak (approximately 220% SUV) at approximately 20 minutes and thereafter decreased (approximately 100% SUV at 180 min). Pretreatment with PF-06738879 significantly blocked the brain binding of [^{18}F]PF-06684511, confirming its *in vivo* specificity. There were no radioactive metabolites showing higher lipophilicity than [^{18}F]PF-06684511. In most brain regions, 1TC and 2TC fit well to the time activity curves while 2TC fit better in some regions such as the hippocampus. V_T of two monkeys were 7.6 and 6.1 in the cerebellum and 19.5 and 13.6 in the amygdala at the baseline PET measurements. Non-displaceable distribution volumes (V_{ND}) estimated by Lassen plot were 2.7 and 3.1. The estimated BACE occupancy was greater than 90% after a single 5 mg/kg oral dose of PF-06738879. **Conclusions** [^{18}F]PF-06684511 demonstrated favorable *in vivo* binding and brain kinetics in NHPs. The target occupancy was able to be estimated using the Lassen plot. [^{18}F]PF-06684511 could be a valuable PET imaging translational tool to facilitate the clinical development of BACE inhibitors as potential treatment for Alzheimer disease. Further evaluation is expected in human subjects.

OP304

ImmunoPET of uPA/uPAR signaling: broad applicability in cancer imaging

H. Hong¹, D. Yang¹, C. A. Dougherty¹, G. W. Severin², D. Chen¹, A. P. Mazar³; ¹University of Michigan, Ann Arbor, MI, UNITED STATES, ²Technical University of Denmark, Kongens Lyngby, DENMARK, ³Northwestern University, Evanston, IL, UNITED STATES.

Aims: Mounting evidences have suggested that urokinase plasminogen activator (uPA) and its receptor (uPAR) play a central role in tumor cell survival, growth, migration, angiogenesis, and metastasis. The fact that uPA/uPAR can be identified in nearly all solid tumors and their confined expression pattern (almost undetectable in healthy, quiescent tissues) make them attractive targets for tumor detection. The goal of this study was to develop an ^{89}Zr -labeled, antibody-based positron emission tomography (PET) tracer for quantitative imaging of uPA/uPAR system. **Materials and Methods:** An anti-uPA monoclonal antibody named ATN-291 was conjugated to desferrioxamine via the reaction of p-SCN-Bn-Df and subsequently labeled with ^{89}Zr . Flow cytometry, microscopy studies, and competitive binding assay were conducted to validate the binding affinity and specificity of Df-ATN-291 against uPA. PET imaging with ^{89}Zr -Df-ATN-291 was carried out in six different tumors with distinct expression levels of uPA. Biodistribution and *ex vivo* histology examination were performed to validate the results from PET, while Western blot of tumor lysate was conducted to correlate the uptake of ^{89}Zr -Df-ATN-291 with uPA/uPAR expression level. **Results:** ATN-291 retained the binding affinity and specificity against uPA after Df conjugation, confirmed by flow cytometry, fluorescence microscopy, and competitive binding assay. ^{89}Zr -labeling of ATN-291 was achieved in good yield and high specific

activity. Serial PET imaging demonstrated that, in most tumors (except uPA⁺ LNCaP), the uptake of ^{89}Zr -Df-ATN-291 was higher than all other organs at 120 h post-injection, which provided excellent tumor contrast. The tumor-to-muscle ratio of ^{89}Zr -Df-ATN-291 in U87MG was as high as 45.2 ± 9.0 at 120 h p.i. ($n = 4$). *In vivo* uPA specificity of ^{89}Zr -Df-ATN-291 was confirmed by successful blocking of tumor uptake with ATN-291 in U87MG tumors. Interestingly, the tumor uptakes obtained from PET correlated with both uPA and uPAR expression in tumor measured by Western blotting. **Conclusion:** The tumor uptake of ^{89}Zr -Df-ATN-291 from PET quantification reflects tumor uPA/uPAR expression level as a whole system *in vivo*. Quantitative immunoPET imaging of uPA/uPAR in tumors can facilitate oncologists to adopt more relevant treatment planning in future clinical investigations.

OP305

The use of somatostatin receptor antagonists may provide a role for receptor-mediated nuclear imaging and therapy of breast cancer

S. U. Dalm, J. Haeck, G. N. Doeswijk, E. de Blois, C. H. M. van Deurzen, M. de Jong; Erasmus MC, Rotterdam, NETHERLANDS.

Background: Somatostatin receptor (SSTR) mediated imaging and therapy using radiolabeled SSTR agonists are successfully used for imaging and treatment of patients with neuroendocrine tumors. Recently, radiolabeled SSTR antagonists have been described that show superior tumor targeting (≥ 11 times higher tumor dose) compared to radiolabeled SSTR agonists. SSTRs are also expressed on breast cancer (BC) cells. Sufficient SSTR expression is a pre-requisite for successful SSTR-mediated tumor targeting, but SSTR expression on BC seems to be lower and more heterogeneous compared to neuroendocrine tumors. Since radiolabeled SSTR-antagonists proved to be more efficient for SSTR-mediated targeting of neuroendocrine tumors, the use of these antagonists might provide a role for SSTR-mediated imaging and/or treatment of BC. We therefore compared the tumor-targeting property of the radiolabeled SSTR agonist DOTA-Tyr³-octreotate versus that of the SSTR antagonist DOTA-JR11, in BC tumor tissue and a BC xenograft mouse model. **Materials and methods:** Binding of DOTA-Tyr³-octreotate and DOTA-JR11 to 40 primary BCs was analyzed by *in vitro* autoradiography. Tumors were incubated with 10^{-9} M ^{111}In -DOTA-Tyr³-octreotate or ^{111}In -DOTA-JR11, with or without 10^{-6} M unlabeled peptide to determine specificity of binding. Radioligand binding of the radiotracers to tumor tissue was quantified and compared. Furthermore, SPECT/MR imaging was performed in an orthotopic SSTR2-expressing patient-derived xenograft mouse model, T126. When tumor size reached ± 1300 mm 3 , animals were injected with 20 MBq/200 pmol ^{177}Lu -DOTA-Tyr³-octreotate or ^{177}Lu -DOTA-JR11. Four hours post injection T1 and T2 weighted MR images and focused SPECT images were acquired. After imaging, animals were euthanized and tumors were excised to determine radioactivity uptake. **Results:** Specific binding of the receptor antagonist ^{111}In -DOTA-JR11 to tumor cells was significantly higher (up to 21 times higher, $p < 0.0001$) than binding of the agonist ^{111}In -DOTA-Tyr³-octreotate. Regarding *in vivo* imaging of the xenograft mouse model, the T1 and T2 weighted MR images showed homogenous tissue signal intensity throughout the tumor, indicating viable tumor tissue. SPECT images showed superior tumor targeting of the receptor antagonist vs. the agonist, in agreement with the measured tumor uptake (2.3 vs. 0.9% ID/g tissue, respectively). **Conclusion:** Our findings indicate that the radiolabeled SSTR2 antagonist DOTA-JR11 is superior to the SSTR agonist DOTA-Tyr³-Octreotate for targeting of low SSTR-expressing tumors such as BC. Therefore, the use of a radiolabeled SSTR antagonist might lead to better results than previously obtained with the agonist, shedding new light on the potential role for SSTR-mediated imaging and/or treatment of BC.

OP306**Sensitive ¹¹¹In-labeled SPECT/CT imaging to monitor anti-IL-22 treatment in experimental arthritis**

T. van der Geest¹, D. M. Roeleveld², T. K. Nayak³, C. Klein⁴, B. Walgreen², M. M. Helsen², J. M. Metselaar^{5,6}, P. Laverman¹, M. I. Koenders², **O. C. Boerman¹**; ¹Department of Radiology and Nuclear Medicine, Radboud university medical center, Nijmegen, NETHERLANDS, ²Department of Experimental Rheumatology, Radboud university medical center, Nijmegen, NETHERLANDS, ³Roche Pharmaceutical Research & early Development, Innovation Center, Basel, Basel, SWITZERLAND, ⁴Roche pharmaceutical Research & Early Development, Innovation Center Zurich, Schlieren, SWITZERLAND, ⁵Department of Experimental Molecular Imaging, University and Helmholtz Institute for Biomedical Engineering, RWTH-Aachen University, Aachen, GERMANY, ⁶Department of Targeted Therapeutics, MIRA Institute, University of Twente, Enschede, NETHERLANDS.

Rheumatoid arthritis (RA) is a chronic autoimmune disease leading to progressive destruction of cartilage and bone. RA patients show elevated levels of IL-22 and IL-22-producing T helper cells that correlate to erosive disease, suggesting a role for this cytokine in the pathogenesis of RA. The purpose of this study was to determine the feasibility of ¹¹¹In-28H1 SPECT/CT imaging to monitor the therapeutic potential of neutralizing IL-22 during experimental arthritis. Collagen-induced arthritis (CIA) was induced in male DBA/1J mice. Mice (N=6) were treated 3 times per week with anti-IL-22 antibodies (8 mg/kg), while the control group (N=6) received rat IgG1 isotype control antibodies. To monitor the therapeutic effect after 2 weeks of treatment, SPECT/CT images were acquired 24 h after injection of ¹¹¹In-labeled DTPA-conjugated anti-FAP antibody, 28H1. After image acquisition, mice were euthanized and dissected. Imaging results were compared with the macroscopic arthritis score. Blocking IL-22 during CIA was a potent approach to prevent arthritis development, reaching a disease incidence of only 50%, versus 100% in the control group. Imaging showed that joint uptake was significantly ($p = 0.02$) lower in treated mice (4.3 ± 5.4 %ID/g) compared to the control group (12.8 ± 9.0 %ID/g). This was confirmed by macroscopic scores, histological scores and bone damage scores that all were lower in treated mice compared to the control group. These findings suggest that IL-22 plays an important role in the development of experimental arthritis, and targeting this cytokine seems an attractive new strategy in RA treatment. Most importantly, SPECT/CT imaging with ¹¹¹In-DTPA-28H1 can be used to specifically monitor response to therapy and is potentially more sensitive in disease monitoring compared to the gold standard method of macroscopic arthritis scoring.

OP307**Differentiating Cancer From Inflammation: Positron Emission Tomography With A Boron-Derived Leucine Mimic**

Z. Liu, D. Kieseewetter, G. Niu, X. Chen; National Institute of Health, Chevy Chase, MD, UNITED STATES.

AIM Non-invasively differentiating tumor from inflammation is a long-standing challenge for cancer diagnosis. Therefore, a biopsy or surgery is still required in many occasions to justify the malignancy of a neoplasm. Previously, positron emission tomography (PET) with ¹⁸F-FDG is the standard non-invasive technique for cancer imaging. However, FDG highlights any tissue with high energy consumption and is not tumor-specific. In addition to accumulating in fast growing tumors, FDG accumulation may be observed in a variety of healthy tissues and ones affected by various non-neoplastic pathologic conditions, such as acute and chronic inflammations and infections. Herein we report a boron-derived leucine derivative (B-Leu) to distinguish cancer from inflammation by using PET imaging. **METHOD** A boron-derived leucine derivative was synthesized

to mimic Leu, of which the transportation depends on L-type amino acid transporter type one (LAT-1). ¹⁸F-¹⁹F isotope exchange reaction was conducted for radiolabelling and quality control was performed by both HPLC and radioTLC. The metabolic stability of ¹⁸F-B-Leu was assessed both *in vitro* and *in vivo*. PET imaging and bio-distribution studies were performed in mice bearing UM22B xenografts on the right shoulder and inflammation in the left hind limb (Inflammation was introduced by intramuscular injection of turpentine 72 h prior to PET scan). **RESULT** The cellular uptake of B-Leu was found to be highly LAT-1 dependent, and a nearly linear correlation was observed between B-Leu intake and LAT-1 expression. Remarkably, ¹⁸F-B-Leu exhibited superior metabolic stability over ¹¹C-labelled natural Leu, resulting in better tumor-specificity as an imaging probe. As expected, PET images showed that ¹⁸F-B-Leu has intense accumulation in UM22B tumor (12.5 ± 3.1 %ID/g) and low uptake in the rest of the body (liver, 2.23 ± 0.46 %ID/g; muscle, 2.01 ± 0.53 %ID/g; and blood, 1.49 ± 0.82 %ID/g). The tracer had predominant renal clearance but with low kidney retention. Comparing with ¹¹C-Leu and ¹⁸F-FDG, ¹⁸F-B-Leu showed higher tumor uptake in UM22B xenografts (¹⁸F-B-Leu: ¹¹C-Leu: ¹⁸F-FDG = 12.5 ± 3.1 : 6.5 ± 2.2 : 10.7 ± 2.3 %ID/g), and notably lower uptake in healthy tissues. In addition, PET images and biodistribution demonstrated that ¹⁸F-B-Leu does not accumulate, but ¹⁸F-FDG does accumulate, in the inflammatory lesion. **CONCLUSION** A boron-derived Leu derivative has been developed for imaging LAT-1 expression with PET. Administration of ¹⁸F-B-Leu allowed for clear visualization of tumor xenografts, with almost negligible uptake in the inflammatory foci, suggesting a unique advantage over ¹⁸F-FDG on distinguishing cancer from inflammation.

OP308**Non-invasive imaging of CD146 in hepatocellular carcinoma with a dual-labeled monoclonal antibody**

W. Cai, R. Hernandez, H. Sun, C. G. England, H. F. Valdovinos, T. E. Barnhart, Y. Yang; University of Wisconsin-Madison, MADISON, WI, UNITED STATES.

Objective: Overexpression of CD146 has been correlated with aggressiveness, recurrence rate, and poor overall survival in hepatocellular carcinoma (HCC) patients. The goal of this study was to develop a CD146-targeted probe for high-contrast non-invasive *in vivo* positron emission tomography (PET) and near-infrared fluorescence (NIRF) imaging of HCCs. **Methods:** *In vitro* expression levels of CD146 were characterized in two HCC cell lines, HEPG2 (CD146+) and Huh7 (CD146-) via western blot, flow cytometry, and immunofluorescent staining. YY146, an anti-CD146 monoclonal antibody, was conjugated to the zwitterionic NIRF dye ZW800-1 and to deferoxamine (Df) for radiolabeling with ⁸⁹Zr. Sequential PET and NIRF imaging was performed after intravenous injection of 5.6-7.4 MBq (400 pmol) of ⁸⁹Zr-Df-YY146-ZW800 in athymic nude mice bearing HepG2 or Huh7 subcutaneous (s.c.) xenografts. Orthotopic tumors were generated by stereotactic injection of stably luciferase-transfected HepG2 cells into the left lobe of the liver and their progression was monitored by regular bioluminescence imaging. Multimodality imaging was carried out in mice with confirmed orthotopic liver tumors using the condition described for s.c. tumors. A terminal imaging time-point was acquired at 168 h post-injection (p.i.) of the tracer, after which tissues were collected for *ex vivo* NIRF imaging, biodistribution, and histological studies. **Results:** *In vitro* assays revealed high and low CD146 expression levels in HepG2 and Huh7 cells, respectively. Flow cytometry showed similar CD146-binding affinity between the native and conjugated YY146 mAb. PET and NIRF imaging unveiled a prominent and persistent uptake of ⁸⁹Zr-Df-YY146-ZW800 in HepG2 tumors that peaked at 31.7 ± 7.2 %ID/g (n=4) at 72 h p.i. Owing to such marked accumulation, the detection of orthotopic HepG2 tumors was successful, despite the relatively high liver background. CD146-negative Huh7 and CD146-blocked HepG2 tumors exhibited

significantly lower $^{89}\text{Zr-Df-YY146-ZW800}$ accretion (6.1 ± 0.5 and 8.1 ± 1.0 %ID/g at 72 h p.i., respectively; $n=4$), demonstrating CD146-specificity of the tracer *in vivo*. *Ex vivo* biodistribution and immunofluorescent staining corroborated the accuracy of the imaging data and correlated $^{89}\text{Zr-Df-YY146-ZW800}$ uptake with *in situ* CD146 expression. **Conclusion:** $^{89}\text{Zr-Df-YY146-ZW800}$ showed excellent properties as a PET/NIRF imaging agent, including high *in vivo* affinity and specificity for CD146-expressing HCC. CD146-targeted molecular imaging using dual-labeled YY146 has great potential for early detection, prognosis, and image-guided surgical resection of liver malignancies. Currently, we are devoting efforts to improve imaging by using antibody fragments that can allow for faster imaging and enhanced liver contrast, and to assess the potential of YY146 as a targeted therapeutic agent.

OP309

Dual Isotope Labeled Multimeric PSMA Ligands

A. Wurzer¹, C. Seidl², A. Morgenstern³, F. Bruchertseifer³, H. Wester¹, J. Notni¹; ¹Pharmaceutical Radiochemistry, TU Munich, Garching, GERMANY, ²Department of Nuclear Medicine, TU Munich, Garching, GERMANY, ³Institute for Transuranium Elements, Karlsruhe, GERMANY.

Exact quantification of biodistribution and tumor uptake of endoradiotherapeutics is highly desirable for therapy optimization. Currently, therapy planning for radiometallated compounds (e.g., sst2- or PSMA-ligands labeled with Y-90, Lu-177, or Bi-213) often relies on the respective Ga-68 PET tracers, thus lacking precision because pharmacokinetics of the structurally different diagnostics and therapeutics are not identical. Dual-isotope labeled tracers could circumvent this problem by allowing for direct PET-based dosimetry. **Methods:** Phosphinate chelators with selectivity for Ga-68 (TRAP) and lanthanides (DOTPI) were tethered together and further equipped with 3 copies of DBCO-Ahx-KuE or PA-Ahx-KuE (DBCO = 5-aza-1,3-dibenzocyclooctyne, Ahx = 6-aminoheptanoic acid, KuE = Glu-urea-Lys, PA = 4-pentynoic acid), employing Cu(I)-catalyzed (CuAAC) as well as strain-promoted click chemistry (SPAAC). The TRAP chelating site of the resulting constructs DOTPI(PA-Ahx-KuE)₃(TRAP) (1) and DOTPI(DBCO-Ahx-KuE)₃(TRAP) (2) was selectively saturated with cold Ga(III) by reaction with excess Ga(III) and subsequent by removal of DOTPI-bound Ga(III) with Na₂EDTA, followed by manual labeling with Lu-177 and Bi-213. Likewise, the compounds containing cold Lu(III) or Bi(III) in the DOTPI cage, obtained by M(III) complexation and subsequent treatment with Na₃DTPA, were labeled with Ga-68 in a standard automated procedure. Lu-177 and Ga-68-labeled compounds were used for biodistribution studies and PET imaging, respectively, in LNCaP-xenografted SCID mice. **Results:** For DOTPI-TRAP conjugates 1 and 2, the complementary chelation selectivity of DOTPI (lanthanides and large trivalent metal ions) and TRAP (trivalent gallium) enabled site-specific complexation of the respective (radio)metal ions and thus, chemoselective radiolabeling with two independent radionuclides. The nonradioactive compounds, [^{nat}Bi][^{nat}Ga]-1, 2, and [^{nat}Lu][^{nat}Ga]-2 exhibited comparably high PSMA affinities ($IC_{50} = 2.5 \pm 0.2$, 1.8 ± 0.4 and 2.8 ± 0.3 nM, respectively). Presence of the DBCO moieties effected a less pronounced hydrophilicity of [^{nat}Lu][⁶⁸Ga]-2 ($\log D = -3.8 \pm 0.1$) compared to [^{nat}Bi][⁶⁸Ga]-1 (-4.4 ± 0.1). Bi-213 labeling of [^{nat}Ga]-1 required lower concentration than DOTA, pointing at a higher Bi-213 labeling efficiency of DOTPI than DOTA. Comparable PET imaging results were obtained for [^{nat}Bi][⁶⁸Ga]-1 and [^{nat}Lu][⁶⁸Ga]-2 for which a ROI-based tumor uptake of 3.35 ± 0.17 %ID/g (60 min p.i., $n=4$) was found. **Conclusions:** DOTPI-TRAP conjugates allow for preparation of theranostic pairs consisting of a Ga-68-PET tracer and a radiometallated therapeutic with identical chemical structure. Their co-injection enables exact PET-based dosimetry, which is particularly attractive for combinations of Ga-68- and Bi-213-labeled compounds due to comparable nuclide half lives (68 and 43 min, respectively) and the lack of other imaging possibilities for Bi-213.

OP310

In Vivo Evaluation of [¹⁸F]PF-06445974, a Novel Phosphodiesterase 4D Sparing PET Radioligand for the Phosphodiesterase 4 Enzyme, In Nonhuman Primates

L. Chen¹, K. Zasadny¹, E. M. Beck¹, C. Chang¹, T. Chappie², R. V. Coelho¹, S. Doran¹, K. Fan¹, K. Kuszpit¹, M. B. Skaddan¹, A. Villalobos², J. M. Young¹, L. Zhang²; ¹Worldwide Research & Development, Pfizer Inc., Groton, CT, UNITED STATES, ²Worldwide Research & Development, Pfizer Inc., Cambridge, MA, UNITED STATES.

Aim: Phosphodiesterase 4 (PDE4) is a major regulator of cyclic adenosine monophosphate and consists of multiple subtypes such as PDE4A, PDE4B, PDE4C and PDE4D. PDE4D-sparing PDE4 inhibitors, with low affinity to PDE4D and high affinity to other subtypes, were hypothesized to be as effective as non-selective PDE4 inhibitors for treating diseases such as psychosis but without emesis side effects. [¹⁸F]PF-06445974 is a novel PDE4D-sparing PDE4 PET radioligand. In this study, we aimed to evaluate the brain distribution and the baseline test-retest variability (TRV) of the total volume of distribution (V_T) by [¹⁸F]PF-06445974 in nonhuman primates (NHPs). In addition, [¹⁸F]PF-06445974 was applied to measure the target occupancy (TO) of a PDE4D-sparing PDE4 inhibitor ABI-4 in NHPs. **Materials and methods:** Three cynomolgus monkeys were scanned with [¹⁸F]PF-06445974 (IV, 37 MBq/kg) PET for 180 minutes at baseline twice to measure the TRV. Four doses (0.005, 0.025, 0.01, and 0.1 mg/kg, IV, 30 minute pretreatment time) of ABI-4 were tested to measure the TO. Arterial and venous blood samples were collected to measure the percent parent and ABI-4 concentration in plasma respectively. Time-activity curves (TACs) were generated for various brain regions. V_T was calculated with the one tissue (1T), two-tissues (2T) and MA1 kinetic models. TO was estimated using Lassen plots. An Emax model was fitted between the TO and the mean plasma ABI-4 exposure. **Results:** The percent parent of [¹⁸F]PF-06445974 in plasma decreased gradually and reached about 67% at 180 minutes. [¹⁸F]PF-06445974 showed the highest uptake in thalamus, followed by putamen and caudate, various cortical regions and lower uptake in cerebellum and hippocampus. The baseline TACs reached peak concentration (SUV ~1.5-3.5) in less than 30 minutes post tracer injection at all brain regions. The 2T model fit the data the best, though the MA1 and 1T models produced a more robust estimate of V_T . The mean TRV of baseline V_T were 9.5%, 6.6% and 7.7% for 2T, 1T and MA1 models respectively. Significant blockade of the brain uptake of [¹⁸F]PF-06445974 was achieved with the pretreatment of ABI-4. The measured TO (36.2% to 93.7%, MA1) and the plasma ABI-4 exposure were fitted nicely with an Emax model, with an estimated free plasma EC₅₀ of 2.24 nM. **Conclusions:** [¹⁸F]PF-06445974 demonstrated favorable *in vivo* binding and brain kinetics and good baseline TRV in NHPs. It could be a valuable PET radioligand for measuring the TO of PDE4D-sparing PDE4 inhibitors upon further evaluation in human subjects.

OP311

Feasibility of in vivo imaging of VEGFR2 expression using high affinity antagonistic biparatopic affibody construct Z_{VEGFR2}-Bp₂

B. Mitran¹, R. Güler², E. Lindström¹, F. Fleetwood², V. Tolmachev¹, S. Ståhl², A. Orlova¹, J. Löfblom²; ¹Uppsala University, Uppsala, SWEDEN, ²KTH Royal Institute of Technology, Stockholm, SWEDEN.

Aim: Vascular endothelial growth factor receptor 2 (VEGFR2) is a key mediator of angiogenesis. Therefore it has emerged as a promising target in a wide variety of malignancies and several ophthalmological disorders. Molecular imaging of VEGFR2 expression may enable patient stratification for therapies targeting VEGF-VEGFR signaling axis. Z_{VEGFR2}-Bp₂ is an antagonistic biparatopic affibody construct (14.4 kDa) with equally high affinity to human and murine VEGFR2. The aim of this study was to

develop an imaging probe for in vivo visualization of VEGFR2 expression in tumors using the $Z_{\text{VEGFR2-Bp}_2}$ derivative. **Materials and methods:** Maleimido derivative of NODAGA was site-specifically conjugated to a unique cysteine at C-terminus of HEHEHE- $Z_{\text{VEGFR2-Bp}_2}$. HEHEHE- $Z_{\text{VEGFR2-Bp}_2}$ -NODAGA was radiolabeled with ^{111}In . In vitro specificity, binding affinity and cellular processing were investigated using VEGFR2-expressing MS1 murine endothelial cell line. The biodistribution of ^{111}In -HEHEHE- $Z_{\text{VEGFR2-Bp}_2}$ -NODAGA was studied in BALB/c nu/nu mice bearing MS1 xenografts. Experimental imaging was performed using SPECT/CT for small rodents. **Results:** HEHEHE- $Z_{\text{VEGFR2-Bp}_2}$ -NODAGA was radiolabeled with ^{111}In with >98% radiochemical yield and the specific activity of 15 GBq/ μmol . ^{111}In -HEHEHE- $Z_{\text{VEGFR2-Bp}_2}$ -NODAGA demonstrated specific binding to VEGFR2-expressing MS1 cells. The internalized fraction was 58% of cell-associated radioactivity after 24h. The dissociation constant (K_D) of ^{111}In -HEHEHE- $Z_{\text{VEGFR2-Bp}_2}$ -NODAGA binding to MS1 cells was 33 ± 18 pM. Tumor targeting and biodistribution studies showed specific dose-dependent uptake in tumors (3.1 ± 0.7 %ID/g for 1 μg , 2.4 ± 1.3 %ID/g for 4 μg , 0.8 ± 0.1 %ID/g for 20 μg at 2 h p.i.). Uptake in liver, spleen and lungs was also saturable, indicating VEGFR2-mediated accumulation. Variation in tumor uptake over time was negligible up to 24 h (1.9 ± 0.2 %ID/g at 6h p.i., 1.9 ± 0.4 %ID/g at 24h p.i.). At 6 h p.i., lung uptake decreased by approximately 60% compared to 2 h p.i. There was no statistically significant decrease of ^{111}In -HEHEHE- $Z_{\text{VEGFR2-Bp}_2}$ -NODAGA in other organs. The tumor-to-organ ratios at 6 h p.i. were 9.1 ± 0.6 , 4.7 ± 0.4 , 27 ± 2 , for blood, muscle and brain, respectively. MS1 xenografts were visualized using ^{111}In -HEHEHE- $Z_{\text{VEGFR2-Bp}_2}$ -NODAGA. **Conclusion:** ^{111}In -HEHEHE- $Z_{\text{VEGFR2-Bp}_2}$ -NODAGA was able to specifically target VEGFR2 in vivo. Tumor-to-blood ratio for anti-VEGFR2 antibody construct was higher than for other anti-VEGFR2 imaging probes. While the high uptake in major metastatic sites such as liver, lungs and bones limit the diagnostic potential in most cancers, ^{111}In -HEHEHE- $Z_{\text{VEGFR2-Bp}_2}$ -NODAGA could be a promising probe for imaging of VEGFR2 expression in glioblastoma.

810 – Monday, October 17, 2016, 11:30 - 13:00, Hall 114

Neurosciences: Basic Science

OP312

Imaging synaptic density in the living human brain using positron emission tomography

S. J. Finnema¹, N. B. Nabulsi¹, T. Eid², K. Detyniecki³, S. Lin¹, M. Chen¹, R. Dhaher², E. Baum¹, D. Holden¹, D. D. Spencer⁴, J. Mercier⁵, J. Hannestad², Y. Huang¹, R. E. Carson¹; ¹Yale PET Center, New Haven, CT, UNITED STATES, ²Yale University, Department of Laboratory Medicine, New Haven, CT, UNITED STATES, ³Yale University, Department of Neurology, New Haven, CT, UNITED STATES, ⁴Yale University, Department of Neurosurgery, New Haven, CT, UNITED STATES, ⁵UCB Biopharma, Braine-l'Alleud, BELGIUM.

Aim: Synaptic changes are associated with numerous brain disorders, including epilepsy and Alzheimer's disease. However, quantification of synaptic density in living patients has been limited to studies of surgically resected or post-mortem tissues. Here, we validated positron emission tomography (PET) imaging with the synaptic vesicle glycoprotein 2A (SV2A) radioligand ^{11}C -UCB-J as a novel approach for the quantification of synaptic density in the living primate brain. **Materials and methods:** In a validation study, one baboon was studied with ^{11}C -UCB-J. After completion of the PET scan, the baboon was euthanized and the brain harvested. Tissue samples from 12 brain regions were analyzed with western blot analyses (for SV2A and synaptophysin (SYN)) and SV2A homogenate binding assays. Regional V_T values were estimated with arterial input functions using the one-tissue compartment model. Furthermore, three patients (3 men, 52 ± 6 years of age) with temporal lobe epilepsy (TLE) and mesial temporal sclerosis (MTS) were examined in the HRRT PET system after

injection of ^{11}C -UCB-J. Parametric binding potential (BP_{ND}) maps were generated with the simplified reference tissue model 2 using the centrum semiovale as a reference region for non-displaceable binding. **Results:** Western blot analyses demonstrated strong and specific SV2A and SYN signals in all gray matter regions, and weak/absent signals in the white matter (centrum semiovale). The correlation between SV2A and SYN was linear across all gray matter regions examined. In the homogenate binding assays, the regional SV2A density ranged between 2.1-20.6 pmol/mg protein. There was a good correlation between regional *in vitro* B_{max} values and the corresponding SV2A optical density as well as with the *in vivo* V_T values measured with PET. In all three epilepsy patients, there was a large unilateral decrease in hippocampus binding ipsilateral to the MTS seen on MRI. The unilateral uptake of ^{11}C -UCB-J was region specific, with no asymmetry observed in the fusiform. Regional asymmetry indices were much higher in the hippocampus ($52 \pm 13\%$ vs. $-9.6 \pm 5.4\%$, 3 patients) and amygdala ($47 \pm 13\%$ vs. $-8.4 \pm 15\%$, 2 patients) of epilepsy patients than in 5 previously examined healthy subjects. **Conclusion:** Validation studies confirmed that SV2A is a valid alternative synaptic density marker to SYN. PET studies in TLE patients confirmed that ^{11}C -UCB-J binding is sensitive to synaptic loss. Thus, ^{11}C -UCB-J PET imaging is a promising biomarker approach for *in vivo* quantification of synaptic density with several potential applications in diagnosis and therapeutic monitoring of neurological and psychiatric disorders.

OP313

Complete hearing loss changes activity pattern and inhibitory neurotransmission in the auditory system of rodents detected with PET

M. Mamach^{1,2,3}, M. Kessler^{1,2}, J. P. Bankstahl¹, T. L. Ross¹, L. Geworski³, F. M. Bengel¹, G. Berding^{1,2}, S. Kurt^{2,4}; ¹Department of Nuclear Medicine, Hannover Medical School, Hannover, GERMANY, ²Cluster of Excellence Hearing4all, Hannover, GERMANY, ³Department of Medical Physics and Radiation Protection, Hannover Medical School, Hannover, GERMANY, ⁴Department of Otolaryngology, Hannover Medical School, Hannover, GERMANY.

Aim: In inferior colliculus (IC), medial geniculate body (MGB) and auditory cortex (AC), F-18-Fluorodeoxyglucose (FDG) enables detection of activation in the auditory system and F-18-Flumazenil (FMZ) quantification of inhibitory GABA_A receptors. Ex-vivo studies provided evidence that the GABAergic system is involved in adaptive/plastic changes after hearing loss. The present longitudinal study aims to detect such changes before/after induction of complete hearing loss *in vivo*. **Methods:** Six Sprague Dawley rats were studied before (PRE) and after (POST1: 1-7days, POST2: 29-36days) inducing complete hearing loss by either cochlear ablation or noise trauma. After trauma all animals showed a complete loss of the hearing thresholds. 12-20MBq FMZ or 18-22MBq FDG were injected intravenously during isoflurane anesthesia. Imaging was performed dynamically for 45min after injection of FMZ and after injection of FDG plus 40min of acoustic stimulation by laboratory background noise of 55dB (BG) for 30min using an Inveon PET system (Siemens). Data were analyzed using PMOD3.6 software and Schwarz's VOI atlas to match changes to anatomical locations. Non-displaceable binding potentials (BP_{nd}) of GABA_A receptors were determined based on Logan's reference tissue method (using the pons as a reference). Changes of activity in auditory regions during BG from PRE to POST conditions were assessed after proportional scaling. All parameters were determined at all time points in the somatosensory cortex (SC) as well as control for unspecific changes in the brain. **Results:** Compared to PRE the activity during BG decreased significantly ($p < 0.05$) in the IC (POST1 -19%, POST2 -18%) and the AC (POST1 -9%, POST2 -7%). No significant change was observed in the MGB. Significant changes ($p < 0.05$) in GABA_A receptor BP_{nd} compared to PRE were detected in AC (BP_{nd} PRE = 1.24 ± 0.15) at POST2 (decrease: -0.14 ± 0.05) and MGB (BP_{nd} PRE = 0.69 ± 0.09) at POST1 (increase: $+0.09 \pm 0.03$) as well as POST2 (increase: $+0.09 \pm 0.03$). No significant change in

BPnd could be observed in the IC. The control region (SC) did neither show differences in activity during BG condition nor changes in GABA_A receptor BPnd between the given time points. **Conclusions:** We demonstrated reduced activity in IC and AC but not in MGB in rats with complete hearing loss. GABA_A receptor binding in AC decreased significantly for the later time point. Conversely, the region without change in activity (MGB) showed an increase in BPnd. The present data provide first-time an evidence for the involvement of the inhibitory GABAergic system in adaptive/plastic changes *in vivo* after complete hearing loss.

OP314

Differential cerebral plasticity after bilateral audio-vestibular damage in a rat model: A comparative [¹⁸F]FDG-μPET behavioral analysis

E. Eilles¹, L. Günther¹, G. Xiong¹, R. Oos², A. Zwergal³, P. Bartenstein², R. Beck¹; ¹German Center for Vertigo and Balance Disorders, University Hospital of Munich, Department for Nuclear Medicine, Munich, GERMANY, ²University Hospital of Munich, Department for Nuclear Medicine, Munich, GERMANY, ³German Center for Vertigo and Balance Disorders, University Hospital of Munich, Munich, GERMANY.

Aim: The aim of the study was to analyse the regeneration of balance control after a bilateral audio-vestibular inner ear damage by behavioral testing and to correlate the results with changes of the regional glucose metabolism (rCMRglu) in the cerebral audio-vestibular system. **Methodology:** 7 SD rats underwent a bilateral chemical labyrinthectomy (BL) by transtympanale injection of bupivacain/arsenilat in the inner ear. For control (Sham) 0.9% NaCl solution was applied to 8 other rats. On day 1,2,3,7,15,30 and 60 post Op behavioral testing was carried out with all animals (apparative gait analysis (catwalk), apparative movement analysis (open-field)). In addition, behavioral testing was followed by serial cerebral [¹⁸F]FDG-μPET-scans on the respective days. **Results:** All BL-animals showed a pronounced stance and gait ataxia as well as a hearing decrease, which persisted up to day 60 after surgery. Corresponding serial [¹⁸F]FDG-μPET-scans showed a permanent bilateral reduction of the rCMRglu in the *colliculi inferiores* compared to the Sham-animals. The gait analysis of the directed walk in the catwalk system revealed an assimilation of gait parameters after day 15 post surgery. Accordingly a bilateral reduction of the rCMRglu in the *nuclei vestibulares* was visible in the [¹⁸F]FDG-μPET just up to day 15 post BL. The movement analysis in the open-field showed a permanently hyperlocomotion up to day 60 post BL compared to the Sham-animals. Referring to this, indicated the rCMRglu of the BL-animals an activation of limbic regions. **Conclusions:** Using the [¹⁸F]FDG-μPET differential cerebral plasticity after bilateral audio-vestibular damage could be visualised. The findings of the [¹⁸F]FDG-μPET correspond with the results of behavioral testing. While no relevant change appeared in the central audiological system a vestibular compensation could be proved in the central vestibular system. The hippocampal system showed a persistent activation.

OP315

Inhibition of P-gp and BCRP-mediated efflux transport of [¹¹C]erlotinib at the non-human primate blood-brain barrier

N. Tournier¹, S. Goutal¹, S. Auvity¹, A. Traxl², S. Mairinger², T. Wanek², I. Buvat¹, M. Soussan¹, F. Caillé¹, O. Langer²; ¹CEA, Orsay, FRANCE, ²Austrian Institute of Technology, Seibersdorf, AUSTRIA.

Aims: The epidermal growth factor receptor (EGFR) targeting tyrosine kinase inhibitor erlotinib poorly penetrates the blood-brain barrier (BBB) due to efflux transport by P-glycoprotein (P-gp) and breast cancer resistance protein (BCRP) thereby limiting its utility in the treatment of non-small cell lung cancer brain metastases. Pharmacological strategies to inhibit P-gp/BCRP-mediated efflux transport at the BBB have been successfully developed in rodents, but it remains unclear if these can be translated to humans given

pronounced species differences in BCRP/P-gp expression ratios at the BBB. We assessed the efficacy of two different P-gp/BCRP inhibitors (elacridar and high-dose erlotinib) to enhance brain distribution of [¹¹C]erlotinib in non-human primates as a model of the human BBB. **Methods:** Three adult male *Papio anubis* baboons underwent arterial blood sampling and PET scans of the brain following i.v. injection of [¹¹C]erlotinib under baseline conditions ($n = 4$), during i.v. infusion of high-dose erlotinib (10 mg/kg/h, $n = 4$) and during i.v. infusion of elacridar (12 mg/kg/h, $n = 3$). Brain distribution of [¹¹C]erlotinib was expressed as total volume of distribution (V_T) estimated with Logan plot analysis using an arterial plasma input function. Data were statistically compared using an ANOVA with Tukey's *post-hoc* test. **Results:** Under baseline conditions, [¹¹C]erlotinib distribution to the brain ($V_T = 0.23 \pm 0.015$ mL/cm³) was markedly lower ($P < 0.001$) than its distribution to muscle tissue surrounding the skull ($V_T = 0.86 \pm 0.10$ mL/cm³). Elacridar infusion resulted in a 3.7-fold increase in [¹¹C]erlotinib distribution to the brain ($V_T = 0.81 \pm 0.21$ mL/cm³, $P < 0.01$), reaching comparable levels as in muscle tissue, without changing [¹¹C]erlotinib plasma pharmacokinetics. During high-dose erlotinib infusion [¹¹C]erlotinib brain distribution was also significantly (1.7-fold) increased ($V_T = 0.38 \pm 0.033$ mL/cm³, $P < 0.05$) with a concomitant increase in [¹¹C]erlotinib plasma exposure. The 3-7-fold increase in [¹¹C]erlotinib brain distribution in non-human primates following P-gp/BCRP inhibition with elacridar was remarkably similar to a previously performed mouse study (5.3-fold increase). **Conclusion:** We successfully translated P-gp/BCRP inhibition protocols from rodents to non-human primates resulting in pronounced increases in distribution of [¹¹C]erlotinib to the non-human primate brain. Such inhibition protocols may ultimately find application for a more effective treatment of patients with brain tumors using drugs that undergo efflux transport at the BBB.

OP316

Target occupancy of PF-06663195 measured with a beta-secretase (BACE) PET radioligand [¹⁸F]PF-06684511 in non-human primates

R. Arakawa¹, L. Chen², A. Takano¹, M. A. Brodney³, S. Nag¹, C. Chang², N. Amini¹, S. Doran², T. McCarthy³, C. Nolan³, L. Zhang², C. Halldin¹; ¹Center for Psychiatric Research, Department of Clinical Neuroscience, Karolinska Institutet, Stockholm, SWEDEN, ²Worldwide Research & Development, Pfizer Inc., Groton, CT, UNITED STATES, ³Worldwide Research & Development, Pfizer Inc., Cambridge, MA, UNITED STATES.

Aim PF-06684511 is a promising PET ligand lead identified by Pfizer that has shown high specific binding in rodents to beta-secretase (BACE). To further evaluate its potential as a BACE selective PET ligand, PF-06684511 was successfully radio-labeled with F-18 and evaluated with a baseline/blocking study in non-human primates (NHPs) with PET imaging. [¹⁸F]PF-06684511 showed high brain uptake in NHPs and the brain uptake was significantly reduced by a high dose of a BACE inhibitor PF-06738879, demonstrating high target binding specificity. To further develop [¹⁸F]PF-06684511 into a clinically usable PET radioligand, we assessed the relationship between BACE target occupancy in the brain and the plasma exposure for a BACE inhibitor, PF-06663195, in NHPs. **Materials and methods** Four cynomolgus monkeys were used in this study. Brain PET measurements for 120 min were performed three times in each NHP, one at baseline and two after intravenous administration of one of four different doses of PF-06663195. Total distribution volume (V_T) by two tissue compartment (2TC) model with metabolite corrected plasma radioactivity as the input function was calculated. The target occupancy was estimated by Lassen plot as there was no good reference region for BACE binding observed in NHPs. The relationship between average plasma concentration of PF-06663195 determined by area under the curve during 120min PET scan and the brain occupancy was estimated by an E_{max} model with the following equation: Occupancy (%) = $C / (EC_{50} + C) \times E_{max}$, as C is the plasma concentration of PF-06663195, EC_{50} is the plasma concentration required to achieve 50% of the maximum occupancy, and E_{max} is the maximum occupancy. **Results** The uptake of [¹⁸F]PF-06684511 decreased in all brain regions with

administration of PF-06663195. 2TC model was fitted well to estimate the V_T s. The target occupancy estimated using Lassen plot was 39.5% - 98.1%, as showing at a dose dependent manner. Exposure-occupancy curve was well fitted with an E_{max} model. EC_{50} was estimated to be 3.75 ng/mL. **Conclusions** These data suggest that PF-06663195 might fully block the target enzyme, BACE. [^{18}F]PF-06684511 can estimate the BACE activity specifically in NHP brain *in vivo* and may be a promising PET radioligand for estimating BACE activity in human brain upon further evaluation.

OP317

Microglia, Amyloidosis and TREM2 Progress in Parallel during the Life Course of PS2APP Mice

M. Brendel¹, A. Jaworska², S. Lindner¹, F. Gildehaus¹, N. Albert¹, R. Beck¹, P. Bartenstein¹, J. Herms², G. Kleinberger², C. Haass², A. Rominger¹; ¹University of Munich, Munich, GERMANY, ²DZNE, Munich, GERMANY.

Aims: TREM2 as an innate immune receptor on myeloid cells has a potential impact on the linkage between neuroinflammation and amyloidosis. Therefore we aimed to investigate amyloid and TSPO μ PET estimates together with TREM2 levels at different stages of age in PS2APP mice, an Alzheimer's disease model with severe amyloid pathology. The main focus was on regional mapping of microglia activation and amyloidosis during the life course of the animals tracked by dual small animal PET in a cross-sectional design. **Materials and Methods:** Groups (N=8) of PS2APP and C57Bl/6 wild-type mice of four ages (5-16 months of age) were examined *in vivo* by F-18-GE180 (microglial activity) and F-18-florbetaben (amyloidosis) μ PET, followed by biochemical quantification of TREM2 *post mortem*. μ PET data was analysed voxel-wise by statistical parametric mapping including (all FDR-corrected; $p < 0.05$). Pathology affected brain regions were compared between tracers (dice similarity coefficients) and pseudo-longitudinally. μ PET results of both tracers were correlated with terminal TREM2 levels. **Results:** Microglial activation was already elevated at early ages of PS2APP mice in large parts of the brain (5mo: 11% brain volume; 8mo: 32% brain volume; versus WT) where fibrillary amyloidosis only occurred punctually ($\leq 3\%$ brain volume, dice similarity $\leq 12\%$). Both neuropathological hallmarks consecutively reinforced each other during the advancing life course. Finally at 16 months of age neuroinflammation and amyloidosis indicated an overlap in 37% of the total brain volume (dice similarity 67%). Dual *in vivo* μ PET data and *post mortem* TREM2 levels were closely associated with each other ($R=0.86$; $p < 0.001$) and progressed in parallel during the life course of PS2APP mice. **Conclusion:** The study reveals a strongly correlated and age-dependent progression of microglial activation and amyloidosis together with TREM2, allowing interventional designs to detect interdependence of each other. Especially early anti-inflammatory treatment and its effect on amyloidogenesis is of highest interest.

OP318

PET *in vivo* imaging of 18kDa TSPO expression in a mouse model of temporal lobe epilepsy using [^{18}F]DPA-714

D. NGUYEN, C. WIMBERLEY, I. BUVAT, R. BOISGARD, V. BOUILLERET; CEA/I2BM/Service Hospitalier Frédéric Joliot, Gif sur Yvette, FRANCE.

Introduction: Mesial temporal lobe epilepsy (MTLE) is the most common type of epilepsy. Several studies in animal models showed a high neuroinflammatory signal using PET with 18kDa TSPO tracer during the constitution of the seizures. In rat models of epilepsy previously established, the disease-related signal decreases and even disappears at later time points, whereas it persists in the human. The intrahippocampal kainate injection mouse model reproduces the pattern of hippocampal sclerosis and the

persistent life-time of spontaneous recurrent seizures of MTLE better than the rat model. We studied whether [^{18}F]DPA-714 PET of 18kDa TSPO was a good marker of neuroinflammation to investigate the disease process in the mouse model. **Methods:** The model was induced by unilateral injection of kainic acid (KA) into the right dorsal hippocampus of male C57/Bl6 mice. Sham mice were also prepared by injecting saline at the same location. To investigate the epileptic process, 60 minutes dynamic [^{18}F]DPA-714 PET/CT scanning were performed at 2 different groups (i) during the constitution of the epileptic process at 7 days and (ii) during the recurrence of the seizures 1 and 6 months after injection. Brain PET/CT images were reconstructed using OSEM 2D algorithm including attenuation correction. These images were then coregistered to a MRI atlas in PMOD 3.6 to identify regions of interest. The uptake within the right and left hippocampus reported here were normalized to the cerebellum uptake. **Results:** For the first group (5 KA and 5 sham mice), 7 days after the injection, an increased uptake was observed in both hippocampi, predominant in the injected hippocampus compared to the sham mice (right: 1.06 ± 0.04 vs 0.88 ± 0.03 , $p < 0.0001$; left: 0.96 ± 0.03 vs 0.83 ± 0.02 , $p < 0.0001$). For the second group (5 KA and 5 sham mice), one month after the KA injection the TSPO uptake decreased but remained always higher than in sham (right: 0.94 ± 0.03 vs 0.79 ± 0.03 , $p < 0.0001$; left: 0.82 ± 0.03 vs 0.74 ± 0.05 , $p = 0.0154$), and persisted even 6 months after injection (right: 0.93 ± 0.04 vs 0.82 ± 0.01 , $p = 0.0003$ and left: 0.85 ± 0.03 vs 0.77 ± 0.02 , $p = 0.0011$). **Conclusion:** For the first time, we showed that [^{18}F]DPA-714 PET could detect the inflammatory process in a mouse model of MTLE *in vivo* up to 6 months after the induction of a lesion. More sophisticated processing and quantification should help precisely characterize TSPO expression in longitudinal studies in the hippocampus and in other brain regions. **Acknowledgement:** This work was supported by the EU FP7 INMiND (Grant agreement no. 278850)

OP319

Evaluation of Logan's graphical method with reference tissue input as a simplified approach for quantification of GABA_A receptor binding in rats

M. Kessler^{1,2}, M. Mamach^{1,2,3}, J. P. Bankstahl¹, T. L. Ross¹, F. Wilke³, L. Geworski³, F. M. Bengel¹, S. Kurt^{2,4}, G. Berding^{1,2}; ¹Department of Nuclear Medicine, Hannover Medical School, Hannover, GERMANY, ²Cluster of Excellence Hearing4all, Hannover, GERMANY, ³Department of Medical Physics and Radiation Protection, Hannover Medical School, Hannover, GERMANY, ⁴Department of Otolaryngology, Hannover Medical School, Hannover, GERMANY.

Aim: In rodent models for hearing loss GABA_A receptors have been demonstrated to play a key role in adaptive/plastic changes in the auditory system. Therefore we aimed to implement a simplified approach for measurements of GABA_A receptor non-displaceable binding potentials (BPnd) in rats using F-18-flumazenil (FMZ) PET. **Methods:** 12-20MBq FMZ were injected via the tail veins of 6 normal-hearing female Sprague Dawley rats under isoflurane anaesthesia. Simultaneously a 45min list-mode acquisition was started employing an Inveon PET (Siemens) system. Data were reconstructed iteratively into 31 time consecutive frames (5x2s, 4x5s, 3x10s, 8x30s, 5x60s, 5x5min, 1x10min) including Co-57-transmission-source-based attenuation-correction. Analyses were performed using PMOD3.6 software. Three bio-kinetic models were applied: (i) a 2-tissue-compartment-model with an image derived input function not corrected for metabolites (2T), (ii) a 2-tissue-compartment-model with an image derived input function including metabolite correction based on data from literature (2T-corr) and (iii) a Logan-plot with a reference tissue input function obtained from the pons (Logan). The values of BPnd for auditory cortex (AC), inferior colliculus (IC), mediate geniculate body (MGB) and somatosensory cortex (SC) were calculated with the pons as a reference region based on a standard VOI atlas. **Results:** Using the 2T-corr procedure, BPnd was 1.53 ± 0.26 for AC,

1.47±0.21 for IC, 0.81±0.15 for MGB and 1.38±0.30 for SC. Pairwise t-test between bio-kinetic models revealed significant difference in BPnd with a hierarchy of values 2T-corr > Logan > 2T for all regions. In the AC 2T-corr showed the highest difference of +35% to 2T (p<0.001) and +12% to Logan (p<0.05), while Logan was 23% higher than 2T (p<0.001). Linear regression analyses revealed highly significant (p<0.001) correlation between BP values determined using 2T-corr and Logan for all regions, i.e. R²=0.9970 for AC, R²=0.9873 for IC, R²=0.9444 for MGB and for SC R²=0.9956. Conclusion: Considering 2T-corr as a gold standard, omitting metabolite correction (2T) produced distinctly lower values. Employing Logan's reference tissue model partly compensated for this effect and resulted in only moderately lower absolute BPnd values which strongly correlate to BPnd values determined by 2T-corr. Therefore our data indicate that using the simpler Logan approach seems to be adequate for analysis of data from one research center. However, if absolute values of BPnd should be compared to other centers' values or to other methodological approaches 2T-corr would be preferable. Furthermore, the relatively low BPnd values determined for MGB might be explained by partial volume effects related to this anatomically small structure.

YE2 – Monday, October 17, 2016, 13:00 - 14:30, Hall 114

Young EANM Daily Forum 2: TBA

OP320

TBA

901 – Monday, October 17, 2016, 14:30 - 16:00, Auditorium

CME 7 - Cardiovascular/Inflammation & Infection/EACVI: Imaging Sarcoidosis, Endocarditis and Amyloidosis by PET

OP321

Patient Preparation and Possible Pitfalls in 18F-FDG PET/CT Imaging of Cardiac Infection and Inflammation

A. Scholtens; Meander Medical Center, Nuclear Medicine, Amersfoort, NETHERLANDS.

OP322

Endocarditis: 18F-FDG and Other (PET) Tracers

P. Erba; University of Pisa Medical School, Nuclear Medicine, Pisa, ITALY.

OP323

Cardiac Sarcoidosis: 18F-FDG PET and Other Tracers

O. Gheysens; KU Leuven, Leuven, BELGIUM.

OP324

Cardiac Amyloidosis with (Non-)PET Tracers, Echo, CT and MRI

K. Wechalekar; University College London (Royal Free Campus), National Amyloidosis Centre, London, UNITED KINGDOM.

902 – Monday, October 17, 2016, 14:30 - 16:00, Hall 211

Joint Symposium 7 - EANM/SEMNM: Latest Advances in Multidisciplinary Management of Tumours of the Digestive System

OP325

The Surgeon's Point of View: An Insight into Minimally Invasive Surgery, Image Guided, 3D and Robot-Assisted Surgical Advances

J. Mayol; Hospital Clínico San Carlos, Department of Surgery, Madrid, SPAIN.

OP326

The Nuclear Medicine Physician's Point of View: Impact of FDG PET on Patient Management

R. C. Delgado-Bolton; San Pedro Hospital - Centre for Biomedical Research of La Rioja (CIBIR), Servicio Riojano de Salud (SERIS), Department of Diagnostic Imaging (Radiology) and Nuclear Medicine, Logroño - La Rioja, SPAIN.

OP327

The Medical Oncologist's Point of View: An Insight into New Biomarkers and Targeted Therapies

P. Gascón; Hospital Clínic, Medical Oncologist, Barcelona, SPAIN.

OP328

The Nuclear Medicine Physician's Point of View: Textural Parameters of Tumour Heterogeneity in ¹⁸F-FDG PET/CT for Therapy Response Assessment and Prognosis

M. Schwaiger; Klinikum R. D. Isar der Technischen Universität München, Nuklearmedizinische Klinik und Poliklinik, Munich, GERMANY.

903 – Monday, October 17, 2016, 14:30 - 16:00, Hall 117

CTE 3 - Joint Session with SNMMI: Dose Optimisation

OP329

PET Protocol Optimization for Dose Reduction

G. Testanera; Istituto Clinico Humanitas, Department of Nuclear Medicine, Milan, ITALY.

OP330

Dose Optimization for Diagnostic Procedures – The SNMMI Point of View

F. Fahey; Children's Hospital Boston, Nuclear Medicine and Molecular Imaging, Boston, UNITED STATES OF AMERICA.

OP331

Dose Optimization in Paediatric Radionuclide Imaging

D. De Palma; Ospedale di Circolo, Serv. di Medicina Nucleare, Varese, ITALY.

904 – Monday, October 17, 2016, 14:30 - 16:00, Hall 112

Do.MoRe: Bone Palliation

OP332

223Ra-dichloride treatment: the European Institute of Oncology experience

M. Colandrea, Jr., S. M. Baio, S. L. V. Fracassi, L. Gilardi, L. L. Travaini, P. A. Rocca, M. Cossu Rocca, A. Gaetano, D. Cullurà, E. Verri, S. Papi, A. Carollo, F. Nolè, C. M. Grana; IEO, Milan, ITALY.

Introduction: 223Ra-dichloride is a novel radiopharmaceutical approved for the treatment of bone metastases of castration resistant prostate cancer (mCRPC). Its chemical affinity with calcium and the high dose delivered, make Ra-223 dichloride a relevant radiopharmaceutical for targeting areas of increased bone turnover. **Aim:** To present the IEO single-centre experience with 223Ra-dichloride in the treatment of patients with mCRPC, in terms of evaluation of feasibility, efficacy and management of a multidisciplinary patient. **Methods:** Nine progressive and symptomatic patients with multiple bone metastases without involvement of any other organ (age 62±9.3 yrs,

medium PSA 150.8 ng/mL) are under treatment; they are receiving 223Ra-dichloride 50 kBq/kg i.v. on day 1 every 28 days for a maximum of 6 cycles. So far 3 patients have completed the treatment, and we are planning to present the complete report during the congress. Pretreatment evaluation was performed with CT scan and bone scan. Patients have been evaluated at every cycle with complete blood chemistry and pain scale and QoL evaluations. A multidisciplinary team followed patients during both screening and treatment period. **Results:** No problems in vial manipulation, dose preparation, administration and radiation protection issues occurred. Therapy was well tolerated in all patients and none presented acute side effects. No cycles were delayed due to blood toxicity, and no patient discontinued the treatment. Most of patients had bone pain relief and reduced pain drugs intake, also during the treatment. No patient presented anorexia; only one case of diarrhoea was observed during the first 4 cycles. At the current timepoint our patients received 33 cycles of 223Ra-dichloride. Three patients have already completed the treatment: we found G3 anemia in 1 patient; G2 neutropenia and G2 thrombocytopenia in 1 patient. Biomarkers response showed different results: 1 patient with increase in ALP and 1 with decline, 1 patient with a stable value. We have no significant data on PSA. At the first CT and bone scan evaluations, the three patients presented bone stable disease and one patient presented visceral metastases. **Conclusion:** our single-centre experience shows the feasibility of radiometabolic therapy with 223Radium-dichloride in patients with mCRPC in a multidisciplinary team. Palliative effect allows decreasing pain drugs consume with a mild toxicity profile (at this first evaluation), allowing the use of 223Ra-dichloride in combination with other treatments. We are planning to compare the ALP, PSA and bone scintigraphy results before and after treatment.

OP333

Two Years Of Experience Of 223Ra-Dichloride In Clinical Practice: Have We Started Treating At Earlier Stage Of Bone Disease?

S. Dizdarevic^{1,2}, M. Jessop¹, P. Begley¹, M. Aplin¹, A. Hosur¹, A. Nikapota¹, A. Robinson¹; ¹Brighton and Sussex University Hospital NHS Trust, BRIGHTON, UNITED KINGDOM, ²Brighton and Sussex Medical School, Brighton, UNITED KINGDOM.

Background: Extent of bone disease as assessed by pre-treatment bone scintigraphy is a predictive imaging biomarker of the overall survival of patients with castrate resistant prostate cancer (CRPC) treated with 223Ra-dichloride. However very often those patients were referred to Nuclear Medicine (NM) department at very late stage with severe metastatic bone burden. Aim: Aim of this study was to demonstrate a change in the pattern of referrals for 223Ra-dichloride treatments in our clinical practice in the second year in comparison with the first year of service and further to implementation of strong collaborative Uro-Oncology/NM multidisciplinary referrals pathways. Methods: All patients treated in period March 2014 to March 2016 were included. Extent of bone disease (EOBD) was categorised from a pre-treatment bone scan in accordance with Alsympeca trial (EOBD1 = less than 6 metastases, EOBD2 = 6-20, EOBD3 >20, EOBD4 = superscan). Data from the first year of service were compared with the second year. Overall survival was defined as the time from first clinic visit to the date of death, regardless of cause. A log-rank test was applied to Kaplan-Meier survival analysis. Results: Fifty two patients underwent 223Radium-dichloride treatments from March 2014 to March 2016; in the first year 26 patients were treated and in the second year 24 patients completed their treatment and two are on their sixth cycle. The percentage of patients referred in each EOBD group in the first year versus the second year was: EOBD1 (4% vs. 23%), EOBD2 (35% vs. 27%), EOBD3 (23% vs. 35%), EOBD4 (38% vs. 15%). All patients with EOBD 1 completed their treatment with 6 cycles and no patient from group EOBD1 died. Patients in EOBD2 underwent an average of 4.6 cycles [SD: ±1.5]; EOBD3, 4.3 cycles [±1.9]; EOBD4, 3.1 cycles [±2.1]. In addition, we have previously demonstrated a statistically significant difference in survival between EOBD2/3 and EOBD4 (p < 0.03 and p < 0.05,

respectively), but no significant difference between EOBD2 and EOBD3. Conclusion: In the 2nd year of 223Ra service we have noticed reverse pattern in EOBD1 and EOBD4 referrals with 19 % increase in EOBD1 and 23% decrease in EOBD4 treatments. We continue treating EOBD2/3 with similar rate. Treating more patients with lower bone burden subsequently has resulted in significantly better overall outcomes. Coherent uro-oncology/NM interface with increased confidence of referring clinicians for earlier intervention is a key for successful treatment with 223 Ra-dichloride.

OP334

Pain Response and Acute Hematologic Toxicity in Castration-Resistant Prostate Cancer (CRPC) patients (pts) treated with ²²³Ra-dichloride: a Single-Center Clinical Series

G. A. Follacchio, V. Frantellizzi, M. Liberatore, F. Monteleone, G. De Vincentis; Sapienza University, Dept of Radiology, Oncology and Human Pathology, Rome, ITALY.

Aim. Alpha-emitter ²²³Ra-dichloride has been recently approved for treatment in mCRPC pts with symptomatic bone metastases due to its significant impact on OS associated to a low hematologic toxicity profile. Since its approval, 59 pts have been referred to our center to undergo ²²³Ra treatment, currently consisting in 50 kBq/kg IV q4wks for 6 cycles. This interim retrospective analysis was conducted to evaluate pain response and occurrence of acute hematologic toxicity in our series. **Methods.** Complete blood counts were recorded at baseline and before each ²²³Ra administration. Pain score was assessed through Brief Pain Inventory-Short Form at baseline and after each ²²³Ra infusion. To further evaluate pain response, EORTC questionnaires QLQ-C30 and QLQ-BM22 were submitted to pts at baseline and after each treatment and analyzed according to published guidelines. Data were retrospectively collected and summarized using descriptive statistics. **Results.** 206 ²²³Ra cycles were delivered to 59 pts (mean age 74y, mean Gleason Score 8, mean ECOG Performance Status 1.3, no known visceral metastases). Skeletal tumor burden evaluated at baseline bone scan was classified as low (0-6 mets) in 8% of pts, intermediate (6-20 mets) in 80% pts and high (>20 mets) in 12% pts. 49% of pts received prior docetaxel. Baseline pain was mild in 27% of pts, moderate in 46%, severe in 27%. During ²²³Ra treatment, 3 out of 59 pts developed G3/4 thrombocytopenia, while 6/59 pts received blood transfusions during the course of treatment due to G3 anemia. Discontinuation rate of ²²³Ra treatment was 22% (13/59) due to disease progression (46%), bone marrow failure (23%) and death (31%). Prior docetaxel use was associated to a higher discontinuation rate (66% vs 34%). 54% of pts experienced an improvement of bone pain, 39% had no changes in pain scale and 7% reported worsening bone pain. **Conclusions.** This interim analysis confirmed ²²³Ra favorable hematologic toxicity profile. Bone pain response was not correlated to baseline hematologic status in our series. ²²³Ra was effective in pain relief in the majority of pts. Notably, all pts with high tumor burden at baseline experienced an improvement in bone pain. Prior docetaxel use was associated to a higher discontinuation rate; this should support the opinion that ²²³Ra treatment should be delivered in an upfront therapeutic setting in mCRPC patients.

OP335

Response Evaluation to Radium-223-Dichloride in Castration-Resistant Metastatic Prostate Cancer using 11C-choline PET/CT and Bone Scintigraphy

P. Ghedini¹, T. Graziani¹, E. Lodi Rizzini¹, G. M. Lima¹, A. Matti¹, I. Bossert¹, F. Ceci¹, G. C. Montini¹, F. Monari², A. Morganti³, P. Castellucci¹, S. Fanti¹; ¹Nuclear Medicine Department, University Hospital S.Orsola-Malpighi, Bologna, ITALY, ²OU Radiotherapy, University Hospital S.Orsola-Malpighi, Bologna, ITALY, ³OU Radiotherapy, University Hospital S.Orsola-Malpighi, Bologna, ITALY.

Aim: our purpose was to investigate the response to Radium-223-Dichloride therapy using 11C-choline PET/CT in comparison with Bone Scintigraphy in patients with bone metastasis in castration-resistant prostate cancer (mCRPC). **Material and Methods:** 11 patients were retrospectively enrolled (age mean 75.4 yr, range 58–86). Our inclusion criteria were 1) symptomatic bone metastasis in mCRPC; 2) 6 months treatment with Radium-223-Dichloride; 3) Bone scintigraphy and 11C-choline-PET/CT performed before (SCI1; PET1) and two months after withdrawal of therapy (SCI2; PET2). PSA and Alkaline phosphatase (ALP) values were measured before (PSA1; ALP1) and after the end of treatment (PSA2; ALP2). PET2 and SCI2 were reported as complete response (CR), partial response (PR), or stable disease (SD). The appearance of a new lesion at PET2 or SCI2 was considered progression disease (PD). Clinical, radiological and laboratory follow-up were performed within 3 months. We measured the SUVmax of the detectable lesions, Δ SUV values between PET1 and PET2 and SUVmax of bone marrow in both scans. Limitations of our study are the small number of patients and the short duration of follow up. **Results:** the 72.7% (8/11) of patients showed PR at PET2; 27.3% (3/11) showed a CR of bone metastasis. Considering the 8 patients with PR, the 75% (6/8) showed increasing PSA-trend while considering the 3 patients with CR at PET2, the 66.6% (2/3) showed increasing PSA-trend. 100% of patients of both groups showed a significant decrease of ALP (mean reduction of 44.1%). 81.8% (9/11) of patients showed PR at SCI2; 18.2% (2/11) of patients showed PD at SCI2. PET2 and SCI2 were accordant in 7 patients, while 4 patients obtained a discordant result (2 PET2 classified as CR showed a PR at SCI2; 1 CR PET2 demonstrated a PD at SCI2; 1 PET2 reported as PR was classified as PD at SCI2). All patients with PD at PET2/SCI2 were confirmed by clinical or radiological follow-up. The mean SUVmax reduction (Δ SUV) in PR patients at PET2 was 56.7%; in CR patients SUVmax of the lesions at PET2 was <1.5. All patients showed an increased SUVmax of bone marrow at PET2. **Conclusion:** to better evaluate the real state of the disease in discordant patients a prolonged follow up is needed. PSA trend don't seem able to foresee PET or SCI outcome. Furthermore, ALP trend demonstrate the efficacy of the treatment on bone lesions, without any implications in the final outcome.

OP336

Lesion dosimetry for ^{223}Ra therapy of bone metastases from castration-resistant prostate cancer: patients eligibility criterion and update of dosimetric assessments

M. Pacilio¹, B. Cassano², G. De Vincentis³, G. Ventroni⁴, V. Frantellizzi³, G. A. Follacchio³, R. Pellegrini⁵, E. Di Castro³, P. Ialongo⁶, L. Mango⁴, R. Pani⁷; ¹Department of Medical Physics, Azienda Ospedaliera San Camillo Forlanini, Rome, ITALY, ²"Sapienza" University of Rome, Rome, ITALY, ³Department of Radiological, Oncological and Anatomopathological Sciences, Rome, ITALY, ⁴Department of Nuclear Medicine, Azienda Ospedaliera San Camillo Forlanini, Rome, ITALY, ⁵Department of Molecular Medicine, "Sapienza" University of Rome, Rome, ITALY, ⁶Department of Radiology, Azienda Ospedaliera San Camillo Forlanini, Rome, ITALY, ⁷Department of Medico-surgical Sciences and Biotechnologies, "Sapienza" University of Rome, Rome, ITALY.

AIM: Dosimetry of bone metastases from castration-resistant prostate cancer in ^{223}Ra -dichloride therapy, by in-vivo quantitative planar imaging, was recently demonstrated to be feasible, obtaining preliminary values of absorbed dose (AD) to lesions using exclusively the MIRD S factor of ^{223}Ra . The aim of this study were: to assess an eligibility criterion for patient dosimetry; to evaluate more reliable ADs, considering the S factors of all ^{223}Ra decay daughters. **Materials and methods:** The study included 36 patients, treated with 6 injections of 50 kBq per kg. For a subgroup of 25 patients (69 lesions), the visibility of lesions (with area > 900 mm²) on ^{223}Ra images at t=24 h from the administration was described by ROC curve, using the lesion/soft tissue $^{99\text{m}}\text{Tc}$ -MDP whole-

body contrast ratio as score value. The lesions visibility was examined independently in anterior and posterior views, so obtaining a group of 138 data. Gamma-camera calibrations for ^{223}Ra included measurements of sensitivity and transmission curves. After the first injection, patients were statically imaged for 30 min, using a MEGP collimator, double-peak acquisition, and Wiener filtering to improve the image quality. For most patients, three serial acquisitions were performed: between 18–24 h, 48–60 h and 7–10 days. Lesions were delineated on $^{99\text{m}}\text{Tc}$ -MDP whole-body images, and the ROIs superimposed on the ^{223}Ra images (if lesions were visible) after image coregistration. The overall number of patients resulting eligible for dosimetry was 20 (38 lesions). The activity was quantified with background, attenuation, and scatter corrections. ADs were assessed from the OLINDA/EXM S factors for soft-tissue spheres of ^{223}Ra and decay daughters, evaluating the lesion mass by CT images delineation and 1.4 g/cm³ density. D_{RBE} values were calculated multiplying ADs by the cycles number (6) and alpha particles RBE (5). **Results:** The ROC analysis yielded: AUC=0.972; optimal threshold=10 (accuracy of about 92%). The mean effective half-life of ^{223}Ra (mean [range]) was 7.7 [4.2–11.4] days. The AD was 3.6 [0.8–9.7] Gy, $D_{\text{RBE}}/A_{\text{adm}}$ was 4.5 [1.1–12.1] Gy/MBq, and D_{RBE} was 108 [24–291] Gy. **Conclusion:** In-vivo quantitative imaging and lesions dosimetry in ^{223}Ra therapy resulted feasible if the lesion/soft tissue $^{99\text{m}}\text{Tc}$ contrast ratio is higher than 10. The D_{RBE} to lesions was much higher than that of other bone-seeking radiopharmaceuticals. Further studies are ongoing to evaluate the dose-response correlation in a clinical context.

OP337

Early bone SPECT/CT for prediction of prognosis in patients with castration resistant prostate cancer treated with ^{223}Ra

G. Paone, L. Ceriani, T. Ruberto, G. Treglia, L. Giovanella; Oncology Institute of Southern Switzerland, Lugano, SWITZERLAND.

Aim: The purpose of this study was to assess the prognostic value of early Bone-SPECT/CT (BS), using treatment-related changes in skeletal tumor burden (active tumor volume) compared with visual assessment, in patients with metastatic castration resistant prostate cancer (mCRPC) treated with ^{223}Ra dichloride (^{223}Ra). **Materials and Methods:** Eleven patients with a mCRPC underwent bone SPECT/CT before and after 3 cycles of ^{223}Ra therapy for evaluation of skeletal metastatic disease. In order to determine skeletal tumor Burden semi-automatic isocontour ROIs, normalized to highest normal bone uptake, were performed on pre-treatment and post 3-cycle BS. A 1-cm spherical VOI was placed on right femur to compute the maximum normal bone uptake (NBup) and threshold defined was > 4NBup. Active tumor volume (ATV) and maximum metastatic bone uptake (MBup) on base line BS and their changes post 3-cycle BS were recorded and compared with visual analysis for predicting event-free survival (EFS), in terms of no treatment discontinuation and absence of skeletal related events (SRE), using receiver-operating-characteristic (ROC) analysis. Survival curves were estimated with Kaplan-Meier analysis. A correlation with treatment-related changes in prostate-specific antigen (PSA) and alkaline phosphatase (ALP) was assessed. **Results:** With visual analysis, the accuracy of early BS to predict EFS was 64%. An optimal cutoff value of 47% ATV reduction from baseline to mid-therapy obtained from ROC analysis ($p < 0.0001$; 95% CI 0,715 to 1,000) yielded an accuracy of 91%. EFS was 17% in patients with ATV reduction $\leq 47\%$ (Mean 7,1 months; 95% CI 4,496 to 9,837) compared with 80% (Mean 11,8 months; 95%CI 9,696 to 13,904) in those with reduction > 47% ($p 0,0485$). Corresponding ALP levels reduction was more evident (66,7%) in the group α ATV > 47%. No good correlation was found with the heterogeneous variation of PSA. **Conclusion:** These data suggest that quantitative assessment on 3-cycles bone scan during ^{223}Ra therapy could be considered as predictive biomarker improving the prognostic value, in terms of no treatment discontinuation and absence of skeletal related events (SRE), compared with visual analysis in mCRPC. Further studies are needed to support these conclusions.

OP338**Re-treatment of Radium-223 From an International, Multicenter, Prospective, Single-Arm Trial in Patients With Castration-Resistant Prostate Cancer and Bone Metastases**

A. Schwartz¹, O. Sartor², N. Mariados³, J. A. Vallejo Casas⁴, C. Thellenberg Karlsson⁵, A. Peer⁶, G. Procopio⁷, S. J. Frank⁸, K. Pulkkanen⁹, S. Severi¹⁰, J. M. Trigo Perez¹¹, R. Li¹², J. Garcia-Vargas¹², D. Keizman¹; ¹Meir Medical Center, Kfar-Saba, ISRAEL, ²Tulane Cancer Center, New Orleans, LA, UNITED STATES, ³Associated Medical Professionals of New York, PLLC, Syracuse, NY, UNITED STATES, ⁴Hospital Universitario Reina Sofia, Cordoba, SPAIN, ⁵Cancer Center Norrlands University, Umeå, SWEDEN, ⁶Rambam Medical Center, Haifa, ISRAEL, ⁷Foundation IRCCS National Cancer Institute, Milan, ITALY, ⁸Hadassah Hebrew University Medical Center, Jerusalem, ISRAEL, ⁹Kuopio University Hospital, Kuopio, FINLAND, ¹⁰Romagnolo Scientific Institute for the Study and Care of Cancer—IRST IRCCS, Meldola, ITALY, ¹¹Hospital Universitario Virgen de la Victoria, Málaga, SPAIN, ¹²Pharmaceuticals Division of Bayer, Whippany, NJ, UNITED STATES.

Aim: Given the acceptable safety profile in phase 3 ALSYMPCA, re-treatment with radium-223 may be well tolerated after initial exposure and provide added benefit to patients who had disease progression following an initial course of 6 radium-223 injections. In addition, recent revision of US National Institute of Standards and Technology (NIST) standardization and its impact on radium-223 dosing is clinically important for nuclear medicine physicians. Reported here are safety and efficacy findings of radium-223 re-treatment from an international prospective open-label trial (NCT01934790) and updated radium-223 labeling based on a new NIST standardization requirement. **Materials and Methods:** Eligible patients had bone-metastatic castration-resistant prostate cancer and 6 radium-223 injections with no bone progression during initial treatment. Eligible patients had clinical or radiologic bone progression after prior exposure to radium-223 treatment, and adequate hematologic values. Concomitant agents were allowed at investigator discretion, excluding initiation of new abiraterone or enzalutamide, and cytotoxic treatment. Primary end point was safety; exploratory end points included time to radiographic bone progression and radiographic progression-free survival (rPFS) based on MRI/CT and bone scans every 3 months. Dose labeling was updated based on NIST revision of radium-223 primary standardization (Zimmerman et al. *J Res NIST*. 2015). **Results:** Radium-223 re-treatment was based on a 50-kBq/kg dose (55 kBq/kg following NIST update). The NIST update does not change the amount of radioactivity administered, but translates to a labeled increase from 1000 to 1100 kBq/mL in the 6-mL vial, as of April 18, 2016. Of 44 radium-223 re-treatment patients, 29 (66%) received all 6 injections. At baseline, 18 (41%) patients had <6 bone metastases, 15 (34%) had 6-20, 6 (14%) had >20, and 5 (11%) had superscan. Median time from last dose of initial radium-223 treatment was 6 months. There were no marked alterations in treatment-emergent adverse event (TEAE) incidence compared with ALSYMPCA. No grade 4 or 5 hematologic TEAEs were reported; 3 (7%) patients had grade 3 or 4 treatment-related TEAEs. Maximum follow-up time for radiographic bone progression and rPFS was 12.8 months. Only 1 patient had radiographic bone progression. Median rPFS was 9.9 months. **Conclusions:** Re-treatment with radium-223 was well tolerated with minimal hematologic toxicity and provided continued control of disease progression in this small dataset. Radium-223 labeling was recently updated following NIST standardization; 50 kBq/kg is now 55 kBq/kg. However, the amount of radioactivity administered has not changed from that in ALSYMPCA.

OP339**Effect of ¹⁵³Samarium Ethylene Diamine Tetra Methylene Phosphonate therapy on pain and analgesic requirement in patients with multiple skeletal metastases**

K. Reddy, Dr. Dhanapathi. H, Dr. Madhusudhanan. P, Dr. Gunaseelan. K, Dr. Biswajit. D.; Jawaharlal Institute of Postgraduate Medical Education & Research, Puducherry, INDIA.

Aim: This study was aimed to assess the effect of Sm-153 EDTMP therapy on pain and analgesic requirement in patients with painful multiple skeletal metastases. **Materials and Methods:** *Study design:* Prospective observational study *Sample population:* The patients who attended to Nuclear Medicine OPD of JIPMER for bone pain palliation during the period September 2013 to July 2015. *Methods:* Patients with multiple painful bone metastasis documented on bone scan within last 8 weeks were included. Pain and performance were assessed using the visual analog scale, Karnofsky performance scale, mobility score and analgesic score. The dose of Samarium-153 EDTMP administered was 37 MBq/kg (1mCi/kg) body weight, by intravenous route on an out-patient basis. Whole body scan was done after 2 hours to see the radio-pharmaceutical distribution. The patients were followed up at 4, 8 and 12 weeks after therapy with recording of complaints, blood investigations, VAS pain score, analgesic-score, mobility score and Karnofsky performance scores. **Results:** 45 patients were recruited for the study. 24 out of 45 patients completed the 12-week follow up and all of them responded to Samarium-153 EDTMP therapy. Eight (33.3%) patients showed complete response to therapy. After therapy, pain scores (VAS scale) were significantly reduced ($P < 0.001$). Maximum reduction of pain was seen around 4-8 weeks in most of the patients. Analgesic scores were not changed significantly after the therapy. There was a significant difference in the class of analgesic used after Samarium-153 EDTMP therapy ($P < 0.01$). No statistically significant change was seen in Karnofsky scores pre- and post-therapy. Statistically significant ($P < 0.002$) change was seen in mobility scores before and after therapy. Only 3/24 patients showed grade III anaemia, 8/24 patients showed grade II anemia, 4/24 patients showed grade II leucopenia and 2/24 patients showed grade III and IV thrombocytopenia. No other significant side effects were seen immediately after the administration and during the study period. **Conclusion:** Multimodality approach is needed to relieve bone pain in patients with multiple skeletal metastases. Sm-153 EDTMP is an effective adjuvant in relieving skeletal metastatic pain. Most of the patients show good response to therapy that lasts for a long duration. It helps in decreasing the use of more potent opioids that produce side effects. Temporary myelosuppression can be seen after the therapy, but recovery occurs in most of the patients.

905 – Monday, October 17, 2016, 14:30 - 16:00, Hall 115

M2M: Radiolabelled Peptides**OP340****[⁶⁸Ga]NeoBOMB1, a new candidate in the diagnosis of breast cancer: First results in GRPR-expressing cells and animal models**

T. Maina-Nock¹, A. Kaloudi¹, A. Giarika¹, E. Lymperis¹, S. U. Dalm², F. Orlandi³, D. Barbato³, M. Tedesco³, M. de Jong², B. A. Nock¹; ¹Molecular Radiopharmacy, INRASTES, NCSR Demokritos, ATHENS, GREECE, ²Department of Radiology and Nuclear Medicine, Erasmus MC, Rotterdam, NETHERLANDS, ³Advanced Accelerator Applications, Colliere Giacosa, ITALY.

Aim: The gastrin releasing peptide receptor (GRPR) is a promising molecular target for diagnosis and therapy of prostate and breast cancer. We have recently introduced NeoBOMB1, a potent GRPR-antagonist coupled to DOTA at the N-terminus (DOTA-*p*-aminomethylaniline-

diglycolic acid-DPhe-Gln-Trp-Ala-Val-Gly-His-NH-CH[CH₂-CH(CH₃)₂]₂) for facile labeling with diagnostic and therapeutic radiometals. The respective [^{67/68}Ga/¹¹¹In/¹⁷⁷Lu]NeoBOMB1 radioligands have shown excellent theranostic properties at the preclinical level for application in prostate cancer. In the present work, we have investigated the potential impact of [⁶⁸Ga]NeoBOMB1 in the diagnosis of breast cancer, using [⁶⁷Ga]NeoBOMB1 as a surrogate and GRPR-positive T-47D cells and animal models. **Materials and Methods:** The affinity of NeoBOMB1 and [^{nat}Ga]NeoBOMB1 for the GRPR was studied during competition binding assays against [¹²⁵I-Tyr⁴]BBN in T-47D cell membranes. The internalization of [⁶⁷Ga]NeoBOMB1 at 37°C in T-47D cells was studied over time (15 min - 2 h intervals). Mouse blood collected 5 and 30 min post-injection (pi) of [⁶⁷Ga]NeoBOMB1 was analyzed by HPLC to assess in vivo stability. Biodistribution was performed at 1, 4 and 24 h pi of [⁶⁷Ga]NeoBOMB1 (100 µL bolus, 37 kBq, 200 pmol total peptide) in female SCID mice bearing subcutaneous T-47D xenografts; for in vivo GRPR-blockade an additional 4-h animal group received 40 nmol NeoBOMB1 together with the radioligand. **Results:** NeoBOMB1 and [^{nat}Ga]NeoBOMB1 showed identical affinity for the GRPR (IC₅₀s of 2.2±0.2 nM and 2.5±0.2 nM, respectively). At 37°C [⁶⁷Ga]NeoBOMB1 strongly and specifically bound to the cell-membrane of T-47D cells (45.8±0.4% at 2 h) with only a small portion internalizing (up to 10% at 2 h), as consistent to a radioantagonist profile. [⁶⁷Ga]NeoBOMB1 was found more than 90% intact in peripheral mouse blood at 30 min pi. In mice bearing T-47D xenografts, [⁶⁷Ga]NeoBOMB1 rapidly and specifically localized in the tumor (8.68 ±2.9%ID/g vs. 0.6±0.1%ID/g in GRPR-blocked at 4 h pi). Interestingly, tumor values remained unchanged between 1 and 24 h pi. **Conclusions:** This study has revealed the potential of [^{67/68}Ga]NeoBOMB1 to target GRPR-positive breast cancer with excellent prospects for clinical translation.

OP341

Biodistribution, radiation dosimetry and first preliminary results of a novel ¹⁸F-fluoroethyl triazole [Tyr³] octreotate analogue for PET imaging in locally advanced and metastatic Neuroendocrine tumour patients

S. R. DUBASH¹, n. Keat², P. Mapelli¹, F. Twyman¹, L. Carroll¹, K. Kozlowski¹, A. Al-Nahhas¹, A. Saleem², m. Huiban², A. Frilling³, T. Barwick¹, A. Rockall¹, R. Sharma⁴, E. O. Aboagye¹; ¹department of surgery and cancer, Imperial College, LONDON, UNITED KINGDOM, ²Imanova centre for imaging studies, LONDON, UNITED KINGDOM, ³Department of Surgery, Imperial College Healthcare NHS Trust, LONDON, UNITED KINGDOM, ⁴Department of medicine, Imperial College, LONDON, UNITED KINGDOM.

Background Despite advances, detection and quantification of neuroendocrine tumour activity by imaging remains a challenge. We present results of the first in-man study of ¹⁸F-fluoroethyl triazole [Tyr³] octreotate (¹⁸F-FET-βAG TOCA) in NET patients to evaluate biodistribution, dosimetry, and safety and the preliminary results of comparison between ¹⁸F-FET-βAG TOCA versus ⁶⁸Ga-DOTATATE PET/CT. **Materials and methods** ¹⁸F-FET-βAG TOCA was synthesized via the click reaction (Iddon L et al, 2011). Fourteen patients with histologically confirmed NET were evaluated. Cohort 1 (biodistribution and dosimetry), nine patients (6 female, 3 male) were enrolled into study. Eight patients with sporadic NET and 1 MEN1 syndrome. Patients underwent whole body PET-CT multi-bed scanning over 4 h and venous blood samples were taken at intervals to measure ¹⁸F radioactivity concentration in blood and plasma. Regions of interest were drawn, to derive individual and mean organ residence times; effective dose (ED) was calculated with OLINDA 1.1. Comparison of ¹⁸F-FET-βAG TOCA versus ⁶⁸Ga-DOTATATE was assessed in all patients. Images were reviewed by 2 independent radiologists and patient data was blinded. SUV_{max} in all

patients was assessed by a lesion-by-lesion analysis. SUV measurements were performed side-by-side on corresponding lesions on fused image datasets and obtained by outlining whole tumour volumes. In regions of >5 lesions, 5 target lesions all ≥2cm were chosen. **Results** All patients tolerated ¹⁸F-FET-βAG TOCA with no adverse events. Over 60% parent tracer was present in plasma at 60 minutes. High tracer uptake was observed in tumours (primary and metastases). Physiological uptake was seen in pituitary, salivary, thyroid and spleen, with low background uptake in liver, an organ where metastases commonly occur. The organs receiving highest absorbed dose were gallbladder, spleen, stomach, liver, kidneys and bladder. The calculated ED over all subjects was 0.029mSv/MBq (SD ± 0.004). There was high tumour to background ratio with both ¹⁸F-FET-βAG-TOCA and ⁶⁸Ga-DOTATATE. The ¹⁸F-FET-βAG-TOCA and ⁶⁸Ga-DOTATATE PET/CT were both positive in 12 (86%) and negative in 2 (14%) patients. In those negative on ⁶⁸Ga-DOTATATE and ¹⁸F-FET-βAG-TOCA, both patients were confirmed as having high grade (G3) NET. **Conclusion** We present the first in-man study of ¹⁸F-FET-βAG-TOCA. The favourable safety, imaging and dosimetric profile makes it a valuable candidate in staging and management of NETs. Head to head comparison of ¹⁸F-FET-βAG-TOCA versus ⁶⁸Ga-DOTATATE show comparable accuracy in detection of lesions. Clinical studies in an expanded cohort are ongoing to clinically qualify ¹⁸F-FET-βAG-TOCA.

OP342

CCK-2 Receptor Targeting by Tc-99m-Demogastrin in Patients with Medullary Thyroid Carcinoma

A. C. Fröberg¹, M. de Jong¹, T. Maina², R. Valkema¹, F. van Nederveen³, M. W. Vernooij¹, B. A. Nock², J. W. A. Burger⁴, W. W. de Herder⁵; ¹Erasmus MC, Department of Radiology & Nuclear Medicine, ROTTERDAM, NETHERLANDS, ²Molecular Radiopharmacy, INRASTES, NCSR "Demokritos", Athens, GREECE, ³Laboratorium voor pathologie, Dordrecht, NETHERLANDS, ⁴Erasmus MC, Department of Surgery, ROTTERDAM, NETHERLANDS, ⁵Erasmus MC, Department of Internal Medicine, ROTTERDAM, NETHERLANDS.

Aim: In medullary thyroid carcinoma (MTC), surgery is still the only curative therapy. No well tolerable, effective systemic therapy exists. Unfortunately, conventional imaging modalities (such as ultrasound or CT/MRI) often fail to localize metastatic lesions, both preoperatively and in suspected recurrent MTC. Therefore, there is a need for more sensitive imaging, to enable local treatment of local recurrences and/or oligometastatic disease. As > 90% of MTC show overexpression of cholecystokinin-2 receptors (CCK2R), these may represent excellent targets for peptide receptor radionuclide scintigraphy. After first promising results of ^{99m}Tc-N₄-Gly-(D)Glu-(Glu)₅-Ala-Tyr-Gly-Trp-Met-Asp-Phe-NH₂ (^{99m}Tc-Demogastrin 2), patients with a diagnostic challenge have been referred for CCK2R-scintigraphy. In the present study, we give an overview of the results of all (first) ^{99m}Tc-Demogastrin 2 scans. **Patients and methods:** 42 patients (28 f. 16-76 y, calcitonin range 0.27-823 (median 83) times the upper reference value) were included; 9 patients were scanned prior to planned neck surgery, the others after surgery; 11 had ≥1 known tumour lesion and 22 patients had elevated serum calcitonin levels but earlier conventional imaging had not detected tumour. Imaging was performed at 4, 8 and 24 h post injection of 800 MBq ^{99m}Tc-Demogastrin 2. Positive and equivocal findings were correlated with CT, MRI and/or ultrasound, already available or directed by scintigraphic results. If feasible, fine needle aspiration cytology of neck lesions was performed. **Results:** Side-effects were minor and as expected similar to those of Pentagastrin® tests. Scintigraphy was positive in 28 pts, false positive in 1, negative in 7 and "false negative" (tumour discovered < 6 months) in 3 pts. In 1 patient not yet confirmed. Two scans were true negative (serum calcitonin elevation at referral, no elevation nor tumour in follow up). In the subgroup of 21 pts in whom earlier conventional imaging was

negative, 10 scans were positive; in 9 of these, lesions were confirmed. Seven patients underwent local therapy. Two patients with distant metastases could not be treated. For 1 lesion follow up is needed. Of scans made prior to surgery, 2 showed clear uptake in the primary tumour, 3 in primary tumour and neck metastases and 3 in primary tumour, neck and distant metastases. One scan was false negative. Conclusion: Our results suggest CCK2R scintigraphy to be a very promising diagnostic tool in MTC, both preoperatively and in case of recurrent tumour. Because of the clear clinical need for better treatment of MTC, further investigation to optimize CCK2R scintigraphy is imperative.

OP343

A direct comparison of four ^{68}Ga -labelled RGD peptides to image $\alpha_v\beta_3$ integrin expression in a human tumour xenograft mouse model

D. Lobeek¹, G. M. Franssen¹, J. D. M. Molkenboer-Kuening¹, A. Eek¹, M. Rijpkema¹, M. T. Ma², H. Wester³, C. Decristoforo⁴, S. Y. A. Terry², W. J. G. Oyen^{1,5}, O. C. Boerman¹; ¹Department of Radiology and Nuclear Medicine, Radboud University Medical Center Nijmegen, Nijmegen, NETHERLANDS, ²Department of Imaging Chemistry and Biology, King's College London, London, UNITED KINGDOM, ³Lehrstuhl für Pharmazeutische Radiochemie, Technische Universität München, Garching, GERMANY, ⁴Department of Nuclear Medicine, Medical University Innsbruck, Innsbruck, AUSTRIA, ⁵Institute of Cancer Research, Royal Marsden NHS Trust, London, UNITED KINGDOM.

Introduction: Angiogenesis plays an important role in tumour proliferation and tumour cell migration. During angiogenesis, $\alpha_v\beta_3$ integrin is overexpressed on newly formed blood vessels. A series of radiolabelled cyclic RGD analogues with a high affinity for $\alpha_v\beta_3$ integrin has been developed. Dimeric and trimeric RGD analogues have shown enhanced accumulation in $\alpha_v\beta_3$ integrin expressing tumours as compared to their monomeric counterparts. In the current study four multimeric cyclic RGD-based radiotracers were selected: ^{68}Ga -DOTA-E-[c(RGDfK)]₂, ^{68}Ga -TRAP-(RGD)₃, ^{68}Ga -fusarinine-C-(RGD)₃, and ^{68}Ga -THP-(RGD)₃, and the *in vitro* and *in vivo* $\alpha_v\beta_3$ integrin targeting characteristics of each tracer were determined under standardized conditions. **Methods:** DOTA-E-[c(RGDfK)]₂ and TRAP-(RGD)₃, were labelled with fractionated eluted ^{68}Ga in HEPES buffer at pH 3.8. Fusarinine-C-(RGD)₃, and THP-(RGD)₃ were labelled in NaOAc buffer at pH 5. The IC₅₀-values of the RGD analogues were determined in a solid phase $\alpha_v\beta_3$ integrin binding assay. The *in vivo* $\alpha_v\beta_3$ targeting properties of the four tracers (i.v. injection of 0.5 nmol, 10 MBq per mouse) were determined in mice with s.c. $\alpha_v\beta_3$ integrin expressing SK-RC-52 xenografts using microPET/CT and biodistribution studies at 1 hour post injection. **Results:** ^{68}Ga -DOTA-E-[c(RGDfK)]₂, ^{68}Ga -TRAP-(RGD)₃, ^{68}Ga -fusarinine-C-(RGD)₃, and ^{68}Ga -THP-(RGD)₃ were produced with specific activities ranging from 40–48 MBq/nmol and a radiochemical yield of >95%, as determined by RP-HPLC and ITLC. IC₅₀-values of DOTA-E-[c(RGDfK)]₂, TRAP-(RGD)₃, fusarinine-C-(RGD)₃, and THP-(RGD)₃, were: 3.79 ± 0.65 nM, 10.0 ± 1.81 nM, 9.02 ± 1.61 nM, and 11.38 ± 1.88 nM, respectively. Tracer accumulation in the SK-RC-52 tumours was 5.1 ± 2.7 %ID/g, 4.3 ± 0.8 %ID/g, 8.5 ± 1.4 %ID/g, and 5.3 ± 0.6 %ID/g for ^{68}Ga -DOTA-E-[c(RGDfK)]₂, ^{68}Ga -TRAP-(RGD)₃, ^{68}Ga -fusarinine-C-(RGD)₃, and ^{68}Ga -THP-(RGD)₃, respectively. Mice with ^{68}Ga -fusarinine-C-(RGD)₃ and ^{68}Ga -THP-(RGD)₃ showed a higher concentration of the tracer in non-tumour tissues. ^{68}Ga -fusarinine-C-(RGD)₃ resulted in a high blood level, possibly due to interaction with plasma proteins. Consequently, tumour-to-blood ratios of ^{68}Ga -DOTA-E-[c(RGDfK)]₂ (17.81 ± 9.39), ^{68}Ga -TRAP-(RGD)₃ (31.46 ± 15.79), and ^{68}Ga -THP-(RGD)₃ (13.47 ± 1.54) were higher than those of ^{68}Ga -fusarinine-C-(RGD)₃ (4.24 ± 1.83). **Conclusion:** In this model, all tracers allowed *in vivo* visualization of the tumour and showed IC₅₀-values in the same nM range. ^{68}Ga -DOTA-E-[c(RGDfK)]₂ and ^{68}Ga -TRAP-(RGD)₃

showed optimal *in vivo* $\alpha_v\beta_3$ integrin targeting properties, due to higher tumour-to-blood ratios and lower tracer uptake in non-tumour tissue, compared to ^{68}Ga -fusarinine-C-(RGD)₃ and ^{68}Ga -THP-(RGD)₃.

OP344

Design and validation of a ^{68}Ga -radiolabelled PET imaging agent for *in vivo* evaluation of angiomin expression

A. Moyon¹, P. Garrigue¹, P. Brige², J. Stalin¹, S. Fernandez², M. Blot-Chabaud¹, F. Dignat-George¹, B. Guillet¹; ¹UMR_S1076 VRCM, Marseille, FRANCE, ²CERIMED, Marseille, FRANCE.

This study aimed to develop a ^{68}Ga -radiolabelled PET imaging agent for assessing tissular angiomin (AMOT) expression, as a regulator of angiogenic processes in ischemic tissues. On that basis, we developed in this work an AMOT-targeting ^{68}Ga -radiolabelled radiotracer, ^{68}Ga -NODAGA-AM007, and performed the first *in vivo* evaluation on a hindlimb ischemia model in mice. Hindlimb ischemia was induced by ligation and resection of the right femoral artery in mice and limb perfusion evaluated by LASER-Doppler imaging up to 30 days after surgery. AMOT expression was evaluated by histology on gastrocnemius muscle. NODAGA-conjugates of AM007 were synthesized and radiolabeled with ^{68}Ga (25°C for 15 minutes). Gallium was obtained in $^{68}\text{Ga}^{3+}$ form using a commercial TiO₂-based $^{68}\text{Ge}/^{68}\text{Ga}$ generator (Obninsk). ^{68}Ga -NODAGA-AM007 (8–14 MBq) PET imaging was performed on SHAM and ischemic mice 1, 2, 5, 10, 15 and 21 days after surgery using $\mu\text{PET}/\text{CT}$ (nanoPET/CT®, Mediso). We demonstrated by immunohistochemistry a significant overexpression of AMOT from Day 1 up to Day 21 after hindlimb ischemia in mice (ipsi=444±102 μm^2 ; contro=18.7±4.7 μm^2 , $P < 0.0001$, on day 5) whose intensity was significantly correlated with post-ischemic reperfusion. Mean ^{68}Ga -NODAGA-AM007 radiochemical purity was 93.1%±2.0 ($n=10$) and stability in serum evaluated up to 2 hours at 90 ± 1.5%. In mice, ^{68}Ga -NODAGA-AM007 showed a rapid plasmatic clearance (6.0±2.0 min) and a pharmacokinetic profile compatible with PET imaging. In hindlimb ischemia model, ipsi- to contralateral hindlimb (i/c) ratio of ^{68}Ga -NODAGA-AM007 uptake 40 min after injection showed a specific radiotracer uptake in ischemic hindlimb from day 1 (i/c=1.85±0.6; $n=11$; $P < 0.05$) up to day 30 (i/c=1.13±0.1; $n=7$), peaking on day 5 (i/c=2.67±1.1; $n=7$; $P < 0.001$) confirming our previous observations of AMOT expression time profile. Moreover, we also observed a significant positive i/c ratio assessed by μPET on Day 15 and the ischemic hindlimb reperfusion assessed by LASER-Doppler on day 28 ($R^2=0.77$; $n=8$, $P=0.009$). Based on the increased AMOT expression after hindlimb ischemia in mice, we developed an AMOT-targeting imaging agent, ^{68}Ga -NODAGA-AM007, and showed that ^{68}Ga -NODAGA-AM007 presented a specific uptake in ischemic hindlimb up to 21 days using μPET imaging. Correlation of post-ischemic ^{68}Ga -NODAGA-AM007 uptake with delayed hindlimb perfusion recovery allows us to postulate that ^{68}Ga -NODAGA-AM007 could represent a promising and innovative radiotracer for tissue angiogenesis assessment.

OP345

A comparison of ^{68}Ga and ^{89}Zr labelled minigastrin bioconjugates in animal imaging

D. Summer¹, G. Franssen², P. Laverman², H. Haas³, E. von Guggenberg¹, C. Decristoforo¹; ¹Department of Nuclear Medicine, Medical University, Innsbruck, AUSTRIA, ²Department of Nuclear Medicine, Radboud University Medical Center, Nijmegen, NETHERLANDS, ³Division of Molecular Biology/Biocenter, Medical University, Innsbruck, AUSTRIA.

Background: Over the last 5 years ^{89}Zr has attracted tremendous interest as radionuclide for PET applications. Due to a relatively long half-life

(3.2d) compared to the well-established ^{68}Ga (67.6 min.), ^{89}Zr seems to be the right choice for tracers with slow pharmacokinetics or when late time point imaging is needed. Recently our working group showed that Fusarinine C - a hexadentate bifunctional chelator - is suitable for labelling tetravalent ^{89}Zr without being fully coordinated. Introducing an additional charge and its influence on imaging abilities as well as the direct comparison to ^{68}Ga -labelled counterparts was the matter of this study.

Methods: Mono- and multimeric compounds were synthesized by utilizing Fusarinine C (FSC) from fungal culture followed by coupling of minigastrin (MG11) peptides via maleimide chemistry. Radiotracers were labelled with ^{68}Ga as well as with ^{89}Zr following standard radiolabeling protocol and labelling efficiency was monitored by radio-HPLC for ^{68}Ga and radio-ITLC for ^{89}Zr respectively. Small animal imaging ($\mu\text{PET}/\text{CT}$) was carried out in tumour xenograft bearing balb/c nude mice. Static imaging was made after one and two hours for ^{68}Ga -labelled tracers and after one, four and 24 hours for ^{89}Zr -labelled counterparts. Furthermore dynamic imaging was performed with a few selected derivatives over a period of one hour. **Results:** First of all ^{68}Ga as well as ^{89}Zr -labelled radiotracers showed no significant release of radionuclide when imaging was performed, this indicating excellent complex stability. ^{68}Ga -labelled multimeric conjugates showed higher tumour uptake but kidney retention also increased severely compared to the monomeric tracer. This effect could be confirmed by comparing the dynamic imaging of ^{68}Ga -labelled monomer with the trimeric conjugate. Comparing ^{89}Zr -labelled compounds the monomer showed fast tumour wash out after four and 24 hours respectively whereas multimeric radiotracers showed better uptake. In comparison to their ^{68}Ga -labelled counterparts overall tumour uptake was lower at early time points i.e. one hour but increased retention in tumour tissue was observed at late time points. Furthermore kidney retention was more intense; this may be related to the additional charge of not fully coordinated ^{89}Zr . **Conclusion:** In summary we could show that ^{68}Ga -labelled mono and multimeric minigastrin bioconjugates showed a similar behaviour compared to their ^{89}Zr -labelled counterparts including slight variations in tumour uptake at early stages and overall kidney retention.

OP346

Preclinical Characterization of Ga-68-Avebehexin, a Specific Probe for the "Cancer Integrin" $\alpha\text{v}\beta6$

J. Notni¹, K. Steiger², C. Mendler³, D. Reich¹, O. V. Maltsev⁴, T. G. Kapp⁴, F. Hoffmann¹, W. Weichert², H. Kessler⁴, M. Schwaiger⁵, H. Wester¹; ¹Pharmaceutical Radiochemistry, TU Munich, Garching, GERMANY, ²Institute for Pathology, TU Munich, Munich, GERMANY, ³Department of Nuclear Medicine, TU Munich, Garching, GERMANY, ⁴Center for Integrated Protein Science, TU Munich, Garching, GERMANY, ⁵Department of Nuclear Medicine, TU Munich, Munich, GERMANY.

$\alpha\text{v}\beta6$ -integrin expression is restricted to epithelial cells and is upregulated by carcinomas (epithelial cancers), particularly in connection with tumor invasion and metastasis. For many cancers, for example pancreatic, ovarian and gastric carcinoma, it has thus been recognized as a prognostic marker, associated with poor survival. Hence, $\alpha\text{v}\beta6$ -integrin imaging could primarily be useful for prognosis and tumor staging, but also for imaging of idiopathic pulmonary fibrosis (IPF) where $\alpha\text{v}\beta6$ -integrin has been shown to play a role as well. **Methods:** Avebehexin was obtained by conjugation of TRAP (triazacyclononane-triphosphinate) to the cyclic nonapeptide c(FRGDLAFp(NMe)K(pentynoic acid)) on the pentynoic acid-functionalized lysine side chain by means of click chemistry (CuAAC). Fully automated Ga-68-labeling (HEPES-buffered eluate of an IThemba generator, pH 2, followed by SPE cartridge purification) delivered Ga-68-Avebehexin, which was used for biodistribution studies and dynamic as well as static $\alpha\text{v}\beta6$ -integrin PET imaging in H2009 (human lung adenocarcinoma) and FaDu (human squamous cell carcinoma) tumor xenografted mice. $\alpha\text{v}\beta6$ -integrin affinities were determined

by ELISA on immobilized integrins. Expression density of αv - and $\beta6$ -integrin chains were analyzed by immunohistochemistry (IHC) in paraffin slices of tumors and other tissues (αv : LS-Bio 6179; $\beta6$: clone 442.5C4, Calbiochem 407317). **Results:** Ga-68-Avebehexin possesses high $\alpha\text{v}\beta6$ -integrin affinity (260 ± 17 pM) and pronounced hydrophilicity (logD: -3.7). Biodistribution studies in H2009 mice showed moderate tumor uptake (0.65 ± 0.04 %ID/g) but also significant uptakes in lung (0.41 ± 0.01 %ID/g) and stomach (0.52 ± 0.04 %ID/g), all of which were blockable by co-injection of $100\ \mu\text{g}$ nat-Ga-Avebehexin. Virtually no uptake was observed in the pancreas (0.07 %ID/g), giving rise to a tumor/pancreas ratio of ~ 10 . $\beta6$ -integrin levels determined by IHC were found to correlate with these data, in particular, confirming only moderate $\beta6$ expression in tumor tissue. Dynamic ^{68}Ga -PET showed fast renal clearance and low background, enabling clear delineation even of tumors with moderate $\alpha\text{v}\beta6$ -integrin expression densities. **Conclusion:** Ga-68-Avebehexin enables high-contrast PET imaging of $\alpha\text{v}\beta6$ -integrin expression, suggesting applicability for imaging of various carcinomas as well as fibrosis. Particularly the good tumor/pancreas ratio rises high expectations for diagnosis and staging of pancreatic carcinoma.

906 – Monday, October 17, 2016, 14:30 - 16:30, Hall 111

Teaching Session: TBA

OP347

TBA

907 – Monday, October 17, 2016, 14:30 - 16:00, Hall 116

Clinical Oncology: Prostate

OP348

Detection of prostate cancer with the [^{68}Ga]-labeled bombesin antagonist RM2 in patients undergoing radical prostatectomy - a Phase I/II study

M. Beheshti¹, P. Taimen², J. Kemppainen³, A. Mueller⁴, G. Broinger⁵, W. Loidl⁶, E. Kaehkoenen⁷, M. Kaekelae³, M. Berndt⁴, A. W. Stephens⁴, H. Minn⁸, W. Langsteger¹; ¹PET-CT Center Linz, Department of Nuclear Medicine & Endocrinology, St. Vincent's Hospital, Linz, AUSTRIA, ²Department of Pathology, Turku University Hospital, Turku, FINLAND, ³Turku PET Centre, University of Turku and Turku University Hospital, Turku, FINLAND, ⁴Piramal Imaging GmbH, Berlin, GERMANY, ⁵Department of Pathology, Krankenhaus der barmherzigen Schwestern, Linz, AUSTRIA, ⁶Department of Urology, Krankenhaus der barmherzigen Schwestern, Linz, AUSTRIA, ⁷Department of Surgery, Division of Urology, Turku University Hospital, Turku, FINLAND, ⁸Department of Oncology and Radiotherapy, Turku University Hospital, Turku, FINLAND.

Background: Gastrin-releasing-peptide receptor (GRPr) is overexpressed in prostate carcinoma (PCa) and offer new means to detect prostate cancer foci. The bombesin derivative RM2 (DOTA-4-amino-1-carboxy-methyl-piperidine-D-Phe-Gln-Trp-Ala-Val-Gly-His-Sta-Leu-NH₂) is a GRPr antagonist with strong binding affinity (K_d 3 nM). Based on promising results from a first-in-man study on PCa detection in patients with local disease, a Phase I/II study was initiated. **Methods:** A Phase I/II study was performed with a pre-specified interim analysis after 30 biopsy-positive PCa subjects had been enrolled, stratified into high, intermediate and low pretreatment risk of prostate Ca recurrence as defined by NCCN criteria. All enrolled subjects had documented PCa by transrectal needle biopsy and were scheduled to undergo prostatectomy with pelvic lymph node (LN) dissection in intermediate and high risk patients. The patients received an intravenous dose of 140 MBq of [^{68}Ga]RM2 followed by imaging for at least 20 min at 60 min p.i. Twenty-five (25/30) subjects had concomitant [^{18}F]-fluoromethylcholine

(^{18}F]FCH) PET/CT imaging. All intra-prostatic and pelvic nodal PET/CT findings were correlated with histopathologic results. **Results:** High uptake of [^{68}Ga]RM2 is seen in pancreas and the urinary system with very low background in the rest of the abdomen or thorax. Despite of high bladder activity, focal intraprostatic uptakes were well detectable. Lesion-based analysis of [^{68}Ga]RM2 PET/CT revealed 35 true-positive tumor lesions, 6 false-positive lesions, and 8 false-negative lesions resulting in a sensitivity of 81%. Five (5/6) false-positive intraprostatic lesions were determined to be BPH or inflammation based on whole-mount prostatectomy sections. [^{68}Ga]RM2 PET/CT successfully detected the index lesions in 20 of 24 subjects (83%). Lesion-based analysis of [^{18}F]FCH PET/CT revealed 27 true-positive tumor lesions, 11 false-positive lesions, and 13 false-negative lesions resulting in a sensitivity of 68%. Eight (8/11) false-positive intraprostatic lesions were determined to be BPH or inflammation based on whole-mount prostatectomy sections. [^{18}F]FCH PET/CT successfully detected 17 index lesions in 21 subjects (81%). There was no difference in sensitivity or index lesion detection between the NCCN risk groups with either agent. [^{68}Ga]RM2 PET/CT correctly detected 2 histopathologically verified LN metastases in 2 high risk patients, while [^{18}F]FCH PET/CT only identified the LN lesion in 1 patient. **Conclusion:** [^{68}Ga]RM2 is a promising new tracer with a high detection rate for intraprostatic and extracapsular PCa. Although the index lesion detection rate is similar, [^{68}Ga]RM2 performs notably better than [^{18}F]FCH in the detection of intraprostatic lesions largely because of improved specificity for cancer vs. BPH.

OP349

^{11}C -choline (CHOL) PET/CT outcome prevented potential toxic local salvage therapy in 47% of men with radio-recurrent prostate cancer

M. S. Vallinga¹, J. Pruijm^{1,2}, M. Rybalov³, A. J. Breeuwsma⁴, I. J. de Jong¹; ¹University Medical Center Groningen, Groningen, NETHERLANDS, ²Univeristy of Stellenbosch, Stellenbosch, SOUTH AFRICA, ³Pavlov Saint-Petersburg State Medical University, Saint-Petersburg, RUSSIAN FEDERATION, ⁴Elisabeth-TweeSteden Ziekenhuis, Tilburg, NETHERLANDS.

Aim: So far studies on ^{11}C -choline (CHOL) PET/CT for restaging patients with recurrent prostate cancer, involved a heterogeneous population or patients with concomitant androgen deprivation use. There is no data on the clinical impact of restaging with CHOL PET/CT on selection for and outcome of local salvage therapy in a homogeneous post-radiotherapy population. We studied the clinical impact of screening with CHOL PET/CT to exclude patients with extra prostatic activity and thus avoid a potential toxic salvage cryoablation. Secondary we aimed to reveal the outcome of salvage therapy after screening with CHOL PET/CT, without distorted results due to simultaneous androgen deprivation use. **Materials and Methods:** A total of 116 patients with biochemical recurrence after radiotherapy (Phoenix definition: PSA nadir + 2 ng/mL) were retrospectively studied. All patients were restaged with a CHOL PET/CT and prostate biopsies. Patients received 200 MBq ^{11}C -choline and were scanned with an mCT Siemens Biograph system, 5 minutes post-injection. Patients with equivocal lesions on CHOL PET/CT underwent additional imaging, biopsy or lymph node dissection for histological confirmation. Clinical impact of CHOL PET/CT outcome on therapy was rated as major (no salvage cryoablation because of metastases or lack of local recurrence on PET/CT), minor (local salvage treatment, but different technique or after additional diagnostics) or none (salvage cryoablation). The outcome of salvage cryoablation was measured by biochemical failure (phoenix definition) and clinical progression to metastasis or start of hormonal therapy. **Results:** Of 116 patients who were restaged with CHOL PET/CT, 59 (51%) underwent cryoablation, 3 underwent other local salvage treatment and 5 patients could be actively surveillanced after a negative scan. In 42% (49/116) treatment changed from cryoablation to delayed hormonal therapy because extra-prostatic tumor activity was seen. Impact of CHOL PET/CT outcome on therapy was rated as major, minor and none in

respectively 46%, 23% and 31%. After salvage cryoablation, the biochemical recurrence free rate was 66% with a mean follow-up post-scan of 38 months (range 6-71). 12.5% did not show a PSA response after cryoablation. Clinical progression to metastasis and start of hormonal therapy, was seen in respectively 15% and 17% of patients post-cryoablation. **Conclusion:** ^{11}C -choline PET/CT showed a significant clinical impact on therapy choice for salvage cryoablation. A potential toxic salvage cryoablation could be abandoned in almost half of men. Outcomes of salvage cryoablation were encouraging with few men with clinical progression and a long biochemical recurrence free survival.

OP350

Observer Agreement of Treatment Responses on Planar Bone Scintigraphy in Prostate Cancer Patients: Importance of the Lesion Assessment Method

R. F. Fonager¹, H. D. Zacho^{1,2}, S. Albertsen³, J. Fledelius⁴, J. A. Ejlersen⁴, M. H. Christensen⁵, R. Aleksyniemi¹, J. A. Biurrum Manresa⁶, L. J. Petersen^{1,2}; ¹Dept. of Nuclear Medicine, Aalborg University Hospital, Aalborg, DENMARK, ²Dept. of Clinical Medicine, Aalborg University, Aalborg, DENMARK, ³Dept. of Urology, Aalborg University Hospital, Aalborg, DENMARK, ⁴Dept. of Nuclear Medicine, Herning Hospital, Herning, DENMARK, ⁵Dept. of Clinical Physiology, Viborg Regional Hospital, Viborg, DENMARK, ⁶Dept. of Health Science and Technology, Aalborg University, Aalborg, DENMARK.

Aim: The aim of this study was to assess observer agreement in the evaluation of treatment responses of bone metastases using three different scoring methods in prostate cancer patients. **Materials and methods:** A total of sixty-three paired bone scans (BSs) were selected from prostate cancer patients with two or more BSs within twelve month at Aalborg University Hospital from January 2009 to November 2014. BS was performed before initiation of a therapy and minimum twelve weeks within treatment. Experienced nuclear medicine physicians, blinded to clinical and laboratory data, evaluated the whole-body BS by three different methods, A) standard clinical assessment (improved, stable, or worse), B) MD Anderson criteria (complete response, partial response, stable disease, or progression), and C) Prostate Cancer Working Group 2 criteria (non-progression versus progression, defined as two or more new lesions). Individual BS were evaluated for presence (M1) or absence (M0) of bone metastases, superscan (absent/present), and number of lesions per region. Observer agreement was assessed by Cohen's kappa and reported by Landis & Koch strength of agreement terminology. **Results:** There was substantial agreement on bone response when using Prostate Cancer Working Group 2 criteria (Cohen's kappa at 0.84, 95% CI 0.69-0.99). Cohen's kappa for standard clinical assessment and MD Anderson criteria were 0.52 (95% CI 0.36-0.69) and 0.56 (95% CI 0.40-0.71), respectively, corresponding to moderate agreement. However, the latter methods have more response categories and this is known to affect agreement negatively. Excellent agreement was demonstrated with regards to M0/M1 (Cohen's kappa 0.94, 95% CI 0.82-1.00), and substantial agreement was found in assessment of superscan (Cohen's kappa 0.78, 95% CI 0.49-1.00). Bland-Altman analysis showed a large variation in the assessment of number of lesions per region, e.g. in column, which showed the largest variation, limits of agreement (Bland Altman analysis) ranged from -14 to 15, with median number of lesions of 7 (range 0 to >20). The average difference in number of lesions between readers though was low, maximum 1.0 in all regions, meaning that no reader assessed the number of lesions systematically higher or lower than another. **Conclusion:** Variations in BS response assessment strongly depended on the method of analysis. Separate counting of lesions on repeated BSs without access to prior scans cannot be recommended. Furthermore, variation in classification of progression versus non-progression might have significant impact on clinical decision-making, emphasizing the need for a uniform approach in bone response monitoring.

OP351**PET imaging of prostate cancer using the GRPr-targeting ligand Sarabesin 3 prior to radical prostatectomy**

I. L. Bakker¹, A. C. Fröberg¹, M. B. Busstra¹, J. F. Verzijlbergen¹, I. Schoots¹, G. J. L. H. van Leenders¹, E. de Blois¹, J. Veenland¹, W. M. van Weerden¹, T. Maina², B. A. Nock², M. de Jong¹; ¹Erasmus MC, Rotterdam, NETHERLANDS, ²NCSR "Demokritos", Athens, GREECE.

Aim: Even though [⁶⁸Ga]PSMA-PET shows impressive results in the detection of prostate carcinoma (PCa) metastases, still a selection of lesions are missed. Gastrin releasing peptide receptor (GRPr) targeting tracers may improve the detection of PC. We selected the gallium-68-labelled GRPr-antagonist Sarabesin 3 ([⁶⁸Ga]SB3) for further clinical investigation because of its excellent results in (pre)clinical pilot studies. The aim of the study was to assess safety and to investigate the diagnostic potential of [⁶⁸Ga]SB3 PET-CT imaging in prostate carcinoma. To enable correlation with gold standard histopathology, this pilot study was performed in therapy-naïve PCa patients prior to prostatectomy. **Materials & Methods:** Nine therapy-naïve patients with biopsy-proven PCa scheduled for curative prostatectomy were included in the study. [⁶⁸Ga]SB3 (178±91 MBq, 40±5 µg) was administered, followed by an extensive scan protocol. To enable optimal imaging of the prostatic region, the bladder was flushed continuously. Scans were separately interpreted by two experienced nuclear physicians who reached consensus. After prostatectomy, the pathologist determined tumour localisations and Gleason Scores (GS). In vitro autoradiography was performed to investigate GRPr expression. Available multiparametric MRI scans were matched to PET-CT. Results were evaluated per patient and per lesion. **Results:** [⁶⁸Ga]SB3 administration did not induce side-effects, though the urinary catheter caused some discomfort. Up to now, 7 patients have been evaluated. In all of them tumour lesion(s) were visible on [⁶⁸Ga]SB3 PET-CT-scans. All positive lesions on scintigraphy that were analysed showed GRPr overexpression. Eleven of 12 tumour lesions (5xGS6, 5xGS7, 2xGS8) were identified on scintigraphy. In one patient a lesion of <2 mm was missed (sensitivity 92%), unfortunately in-vitro autoradiography was not possible of this lesion. Two lesions judged positive on scintigraphy showed no histologic confirmation and are considered false positive (specificity 85%). Correlation with MR showed concordance of correct PCa detection in 3 patients; concordance of underestimation in 1 patient; in 1 patient MR showed an underestimation, tumour was correctly assessed by PET-CT; a false positive lesion on PET-CT was correctly not detected by MR in 1 patient; in the last patient number of lesions was overestimated on PET-CT, MR was false negative. The GRPr-expressing pancreas showed high physiological uptake. We observed fast renal excretion and very low radioactivity in liver. Diffuse, low tracer uptake was visible in the gastrointestinal tract, lower oesophageal and rectal sphincters. **Conclusion:** This data shows that [⁶⁸Ga]SB3 PET-CT is a promising diagnostic tool in the imaging of prostate carcinoma and might be helpful in PCa.

OP352**Fluciclovine (¹⁸F) for the Characterisation and Detection of Primary and Recurrent Prostate Cancer: Results of a Single-Centre Experience**

F. Willoch¹, W. Picker², J. Kieboom², A. Chau³, P. Ward³; ¹University of Oslo, Oslo, NORWAY, ²Aleris Helse AS, Oslo, NORWAY, ³Blue Earth Diagnostics Ltd., Oxford, UNITED KINGDOM.

Aims: To evaluate the ability of the amino acid analogue PET radiotracer, fluciclovine (¹⁸F) to detect recurrent prostate cancer according to PSA values in a biochemical relapse (BR) cohort, and to characterise primary prostate cancer. **Materials and Methods:** Data were obtained from a single-centre in

Norway from patients with either BR of prostate cancer or biopsy-confirmed high-risk primary prostate cancer who underwent fluciclovine (¹⁸F) PET/CT scanning. These data are part of a retrospective observational study (BED001) designed to analyse results across multiple research sites in Norway, Italy and USA. Scans were acquired on a GE 690 PET/CT in 3D mode using a 3.5 MBq/kg fluciclovine (¹⁸F) dose. A 15 minute dynamic scan was acquired centred over the prostate beginning immediately after injection, followed by a whole body acquisition using 2.5 min/bed. Detection rate (DR) in the BR cohort was analysed according to baseline PSA; the diagnostic performance in primary disease was evaluated versus histology. **Results:** 146 BR patients (mean [SD] age: 65.1 [7.2] years; Gleason score: 8.0 [1.1]; baseline PSA: 4.9 [7.9] ng/mL; 26.7% D'Amico high risk) and 51 primary patients (mean [SD] age: 66.1 [9.1] years; Gleason score: 8.0 [1.0]; baseline PSA: 16.9 [19.3] ng/mL; 62.7% D'Amico high risk) were included. In the BR cohort, the DR according to baseline PSA (ng/mL) at the subject level was: ≤0.2, 3/9 (33.3%); >0.2-0.5, 16/22 (72.7%); >0.5-1.0, 9/11 (81.8%); >1.0-2.0, 12/14 (85.7%); >2.0-5.0, 19/22 (86.4%); >5.0, 30/32 (93.8%). The DR in the prostate/bed was: ≤0.2, 0/9 (0%); >0.2-0.5, 5/23 (21.7%); >0.5-1.0, 2/8 (25.0%); >1.0-2.0, 6/16 (37.5%); >2.0-5.0, 13/22 (59.1%); >5.0, 19/29 (65.5%). The DR in the extra-prostatic region was: ≤0.2, 3/10 (30.0%); >0.2-0.5, 12/21 (57.1%); >0.5-1.0, 9/11 (81.8%); >1.0-2.0, 9/13 (69.2%); >2.0-5.0, 10/20 (50.0%); >5.0, 21/29 (72.4%). In patients with primary prostate cancer, fluciclovine (¹⁸F) was true positive in all patients (N=32) at prostate level (100% sensitivity and positive predictive value (PPV)) and had 50% sensitivity, 73% specificity, 67% PPV and 58% NPV for disease detection in the extra-prostatic region (N=31). **Conclusions:** Fluciclovine (¹⁸F) is effective for visualising locations of prostate cancer relapse across a wide range of PSA values in BR; DR was proportional to PSA. Fluciclovine (¹⁸F) may also be used to assist pre-treatment staging of patients with high-risk primary prostate cancer, in particular for extra-prostatic disease detection.

OP353**18F-Choline PET/CT and multiparametric MRI for the detection of local recurrence of prostate cancer initially treated by radiotherapy: comparison with systematic transperineal mapping biopsy**

S. Kanoun^{1,2,3}, P. Walker^{1,2}, J. Vrigneaud³, E. Depardon³, V. Barbier⁴, O. Humbert^{1,3}, M. Moulin⁴, G. Créhange³, L. Cormier⁴, R. Loffroy⁴, F. Brunotte^{1,3,2}, A. Cochet^{1,3,2}; ¹Le2i CNRS UMR 6306, Dijon, FRANCE, ²CHU Dijon, MRI unit, Dijon, FRANCE, ³Centre Georges Francois Leclerc, Dijon, FRANCE, ⁴CHU Dijon, Dijon, FRANCE.

Purpose: To compare the diagnostic performance of ¹⁸F-Fluorocholine PET/CT (FCH PET/CT), multiparametric prostate MRI (mpMRI) and combination of both techniques for the detection of local recurrence of prostate cancer initially treated by radiotherapy. **Methods:** This was a retrospective single-institution study of 32 patients with suspicion of prostate cancer recurrence, who underwent both FCH PET/CT and 3T mpMRI (T2-weighted, diffusion-weighted and dynamic contrast-enhanced sequences) for detection of recurrence within 3 months. All included patients had to be cleared for a metastatic recurrence. The reference standard was systematic transperineal prostate biopsies for the final assessment of local recurrence. Both imaging modalities were analyzed blindly of clinical data by two experienced readers. FCH PET/CT was considered positive for a local recurrence in case of a focal uptake in the prostate, and mpMRI in case of concordant abnormalities in at least two MRI sequences. The analysis was made per-patient and per-segment using a 4-segments model. **Results:** The median PSA at the time of imaging was 2.92ng/mL. The mean PSA doubling time was 14 months. Of the 32 patients, 31 had a positive transperineal mapping biopsy for a local relapse. On a patient-based analysis, detection rate was 71% (22/31) for mpMRI and 74% (23/31) for FCH PET/CT. On a segment-based analysis, the sensitivity and specificity were 32% and 87% for mpMRI, 34% and 87% for FCH PET/CT, and 43% and 83% for the combined

analysis of both techniques. Accuracy was 64, 65 and 66% respectively. Seven segments on 128 were discordant between FCH PET/CT and mpMRI procedure (Kappa=0.84). The inter-observer agreement was kappa=0.92 for FCH PET/CT and kappa=0.74 for mpMRI. **Conclusion:** Both mpMRI and FCH PET/CT shows limited sensitivity but good specificity for the detection of local cancer recurrence after radiotherapy, when compared with transperineal mapping biopsy. Prostate biopsy still appears mandatory to diagnose a local relapse and select patients who could benefit for a local salvage therapy.

OP354

Diagnostic performance of ^{18}F -FACBC PET/CT, PET/MRI and MRI in primary prostate cancer

J. Kempainen¹, I. Jambor^{2,3}, A. Kuisma⁴, M. Kim¹, S. Ramadan⁴, O. Eskola⁵, H. J. Aronen², E. Kähkönen⁶, P. Taimen⁷, H. Minn^{4,3}; ¹Turku University Hospital, Turku PET Centre, TURKU, FINLAND, ²Department of Radiology, Turku University Hospital, TURKU, FINLAND, ³Turku University Hospital, Turku PET Centre, Turku, FINLAND, ⁴Department of Oncology and Radiotherapy, Turku University Hospital, TURKU, FINLAND, ⁵Turku PET Centre, Radiopharmaceutical Chemistry Laboratory, University of Turku, TURKU, FINLAND, ⁶Department of Surgery, Division of Urology, Turku University Hospital, TURKU, FINLAND, ⁷Department of Pathology, Turku University Hospital, TURKU, FINLAND.

Purpose: Uptake of ^{18}F -amino-3-fluorocyclohexane-1-carboxylic acid (^{18}F -FACBC) tracer depicts amino acid transportation, which has shown to be elevated in PCa cells. The diagnostic accuracy of ^{18}F -FACBC PET/CT, PET/MRI and MRI for the detection of primary prostate cancer (PCa) was prospectively evaluated in this study. **Materials and Methods:** Twenty-six patients with histologically confirmed PCa who were scheduled for radical prostatectomy underwent dynamic and static ^{18}F -FACBC PET/CT examination followed by PET/MRI. Multiparametric MRI scan consisted of T2-weighted, diffusion weighted (DWI), second order rotating frame (RAFF) imaging, T2 mapping and contrast enhanced imaging. Presence of PCa was assessed in 12 prostatic regions with histopathological reference. Sensitivity, specificity, accuracy and area under the curve (AUC) values were determined for each imaging modality. **Results:** Altogether 41 tumor foci larger than 0.5 cm³ were identified. In the region-based analysis, 164 (53%, 164/312) regions contained PCa. The sensitivity, specificity and accuracy were 88%, 56% and 72% respectively for PET/CT, 79%, 93% and 86% for PET/MRI and 78%, 99%, and 88% for multiparametric MRI. AUCs of both PET/MRI and MRI were significantly ($p < 0.01$) higher (0.85 and 0.88, respectively) than that of PET/CT (0.72) while no significant differences were present between PET/MRI and MRI. **Conclusion:** ^{18}F -FACBC PET/CT had the highest sensitivity but lacked specificity in PCa detection. Combined PET/MRI has significantly higher specificity than PET/CT. This highlights the importance of adding MRI rather than CT with PET for PCa imaging. However, ^{18}F -FACBC together with PET/CT or PET/MRI provided limited added value to multiparametric MRI imaging of prostate cancer.

OP355

Impact of ^{11}C -CHOLINE PET-CT in the management of prostate cancer patients candidate to Radiation Therapy

E. Lopci¹, G. D'Agostino¹, C. Iftode¹, C. Franzese¹, M. Rodari¹, E. Villa², M. Scorsetti¹, A. Chiti³; ¹Humanitas Clinical and Research Hospital, Milano, ITALY, ²Humanitas Gavazzeni, Bergamo, ITALY, ³Humanitas University, Milano, ITALY.

Purpose: The aim of the present study was to verify the impact of Choline PET imaging in treatment planning of prostate cancer (PCa) patients eligible for radiotherapy (RT). **Materials and Methods:** From

September 2011 to April 2016, 135 consecutive patients (median age 69 years, range 53-89) referred to our Institution and investigated with ^{11}C -choline PET prior to radiotherapy, were enrolled. The planned therapy was with radical intent (n=29), adjuvant to surgery (n=13), salvage therapy (n=50), re-irradiation (n=18) or palliative treatment of distant metastases (n=25). Clinical-tumor volumes (CTV), planning-tumor volumes (PTV) and organs at risk (OAR) were outlined on CT slices with Eclipse Varian Medical System software, whereas gross tumor volume (GTV) was defined on ^{11}C -choline PET using a PETVCAR software on Advantage GE workstation. Patients were monitored for a median period of 41.1 months. **Results:** The indication to RT was modified in a total of 65 cases (48.2%) on the basis of PET results. The median PSA before and after treatment in this subgroup of patients was 35.2ng/ml (range 0.19-387) and 3.46ng/ml (range 0.01-337), respectively. Among the 29 patients evaluated before radical RT, 11 received an additional boost on positive nodes, while 1 patient presented with metastatic disease and was treated according to the new stage. Adjuvant or salvage therapy was planned in 63 patients: 23 patients (36.5%) received a boost on positive nodes, 3 oligometastatic patients received RT on visible lesions, while the remaining patients presented multiple metastases. Out of 18 patients candidate to re-irradiation: 3 were upstaged for distant metastases and excluded, 5 were excluded because of a negative scan. Out of 25 patients scheduled for target RT on metastatic lesions, 12 had a change in their treatment plan (48%). Overall, ^{11}C -choline PET influenced RT planning in 41.4% of patients candidate to radical RT, 52.4% of patients undergoing adjuvant or salvage RT, 46.5% of patients with relapsed or metastatic disease. **Conclusion:** Choline PET confirmed to have a significant impact on RT planning of patients affected from prostate cancer, determining a change in the treatment management in 48.2% of cases.

908 – Monday, October 17, 2016, 14:30 - 16:00, Hall 212

Physics & Instrumentation & Data Analysis: Preclinical & Clinical SPECT Systems & Perfusion

OP356

Towards fast ^{123}I / $^{99\text{m}}\text{Tc}$ -sestaMIBI parathyroid imaging with CZT camera : a preliminary study

Y. R. PETEGNIEF, M. VERSTRAETE, R. SABBAH, C. DROUET, H. BOULAHDOUR; CHRU Jean Minjot, BESANCON, FRANCE.

Introduction : Cadmium-Zinc-Telluride (CZT) detectors have recently emerged as an alternative to conventional NaI(Tl)-based Anger cameras for cardiac and breast imaging. It is likely to improve sensitivity and resolution and limits crosstalk between isotopes for dual isotope $^{99\text{m}}\text{Tc}$ MIBI/ ^{123}I parathyroid SPECT. This study focuses on the evaluation of a new method for simultaneous reconstruction of subtracted $^{99\text{m}}\text{Tc}$ and ^{123}I clinical data using a dedicated cardiac CZT system in comparison with conventional Anger cameras imaging. **Material :** Stationary projections (600 s) obtained with pin-hole collimators and the ^{123}I energy window (159 keV, 18 keV width) were adaptively weighted and then subtracted from the $^{99\text{m}}\text{Tc}$ projections (141 keV, 15 keV width) in order to simulate a 'scatter-like' additional window for MIBI correction during MAP OSEM OSL reconstructions. Image reconstructions were repeated with the $^{99\text{m}}\text{Tc}$ and ^{123}I raw projections and the subtracted ones. We adaptively varied the coefficient of correction of $^{99\text{m}}\text{Tc}$ projections C till achieving optimal visualization of parathyroid adenoma. Resulting images were reoriented and simultaneously reviewed with ^{123}I thyroid images to localise the lesions and were compared to SPECT Anger iterative reconstructions (A-SPECT) for localisation of primary parathyroid adenomas. **Results :** The ^{123}I / $^{99\text{m}}\text{Tc}$ ratio of counts in anterior projection at the thyroid location varied from 0,4 to 1 in CZT studies. Ratios in the reconstructed slices (range 0.15-1.9) were not correlated with A-SPECT ratios. With weighted ^{123}I projections (C varying from 0.25 to

1 - step 0.25), higher C demonstrated artifactual patterns of activity around the thyroid location whereas lower coefficients gave an homogeneous activity level within the parenchyma of the thyroid affecting detection of lower activity foci. For $C=0.5$, the parathyroid to thyroid ratio (PTTR) of counts showed huge variations from one patient to the other (range 0.4–36) in comparison to the raw Tc99m slices (PTTR 0.13–1.3) and A-SPECT (0.37–1.45). **Conclusion**: CZT imaging demonstrated very promising preliminary results for high contrast fast parathyroid imaging. OSEM MAP OS� improved contrast of adenomas with pre-processed 99mTc projections. Further work is required for automatic dual-isotope processing and comprehensive evaluation of the technique with regards to the established Anger camera protocols.

OP357

SPECT image quality parameters for lesion detection task

K. Kacperski, D. Świtlik; Centre of Oncology - Institute, Warsaw, POLAND.

Clinical task-based image quality assessment is regarded the most relevant in the context of medical imaging. However, such approach, involving evaluation of series of simulated or experimentally generated images by human observers is usually time consuming and often impractical, when many combinations of scanning, reconstruction and post-processing parameters are to be tested for optimal performance. In this paper we search for an easily computable parameter of the type of contrast-to-noise ratio, which could predict the results of a human observer experiment of hot lesion detection on reconstructed SPECT images. **Materials & Methods**: We used cylindrical numerical phantoms of the diameter 42 cm filled uniformly with water solution of 200 MBq 99mTc. Spherical hot lesions of diameters from 4.2 mm to 50 mm, and contrasts from 1:2 up to 1:15 have been placed randomly within the phantom. SPECT scans have been simulated for a range of parallel hole collimators from ultra high resolution to high sensitivity and different scanning times. The images were reconstructed using ML-EM/OSEM iterative algorithms with different number of iterations, subsets and inter-iteration filters. Depending on the lesion type and scanning/reconstruction parameters, images with lesions clearly visible to hardly detectable have been obtained. Sets of 60 images (30 with lesions and 30 lesion free) were evaluated by several human observers in free-choice ROC (FROC) studies with the task to mark all the lesions and rate the level of confidence on a 5-point scale. Average Jafroc figures of merit (JFOM) have been used as a gold standard quantifying the performance of human observers. On the other hand, several types of contrast-to-noise ratio (CNR) parameters have been computed on the evaluated sets as well as on ensembles of images with fixed lesion position. Correlations between the JFOM and the corresponding CNRs have been computed. **Results**: The CNRs correlate relatively well with the JFOMs for a wide range of image qualities, however, several significant outliers can also be noticed for the fixed lesion based CNRs. Those values display lower variance for a given number of sample images, but their predictive value is lower. CNRs computed on images with random lesions, although of higher variance, are better correlated with lesion detectability. CNR type parameters are well correlated with the FROC figures of merit and are good predictors of human observer studies on SPECT images, provided they are computed on a population of reconstructed images with randomly placed lesions of the same type.

OP358

The use of fast acquisition SPECT/CT for the assessment of suspected bone metastases

H. D. Zacho^{1,2}, J. B. Manresa³, J. A. Ejlersen⁴, J. Fledelius⁴, R. Aleksyniene¹, H. Bertelsen¹, L. J. Petersen^{1,2}; ¹Dept of Nuclear Medicine, Aalborg University Hospital, Aalborg, DENMARK, ²Department of Clinical Medicine, Aalborg

University, Aalborg, DENMARK, ³Department of Health Science and Technology, Aalborg University, Aalborg, DENMARK, ⁴Department of Nuclear Medicine, Heming Hospital, Heming, DENMARK.

Aim: To assess whether standard SPECT/CT used as an ‘add-on’ to whole body bone scintigraphy (WB-BS) can be replaced by a fast acquisition SPECT/CT for the investigation of bone metastases. **Materials & Methods**: Consecutive cancer patients referred for WB-BS were included in the study if SPECT/CT was conducted as ‘add-on’ due to suspicious or equivocal findings of bone metastasis on WB-BS or if the patients had localized cancer-suspicious pain despite the findings on WB-BS. A standard SPECT, a fast acquisition SPECT and a low-dose CT was performed. Standard SPECT-parameters: Matrix 128x128, zoom factor 1, 20 seconds per view (32 views), 180 degrees detector rotation (non-circular orbit, step and shoot), flash 3D iterative reconstruction (four iterations, eight subsets) with scatter correction applied. Fast acquisition SPECT had identical parameters except for 10 s per view using 16 views. A low-dose CT (25 mA, 130 keV, scan time 13.55 s, 30 mAs, slice thickness 0.6 mm) was acquired and used for both standard and fast acquisition SPECT. Four nuclear medicine physicians participated in the evaluation. A three category scale was used in the evaluation: M0 for no bone metastases, M1 for bone metastases, and Me for equivocal findings. A diagnosis was reached in consensus by two observers for each set of images (WB-BS + standard SPECT/CT and WB-BS + fast acquisition SPECT/CT). Images were evaluated in random order with at least four weeks between evaluations. Agreement between acquisition methods was assessed by Cohen’s Kappa. **Results**: A total of 104 patients were included in the study, the majority were diagnosed with prostate cancer (n=71). According to WB-BS + standard SPECT/CT, 71 (68%) patients had M0, 19 (18%) had M1, whereas 14 (14%) patients had Me. Agreement between WB-BS + standard SPECT/CT and WB-BS + fast acquisition SPECT/CT using the three category-scale was: unweighted Cohen’s Kappa=0.86 (95% CI 0.76–0.96), linear weighted Cohen’s Kappa=0.91 (95% CI 0.84–0.97), and quadratic weighted Cohen’s Kappa=0.94 (95% CI 0.90–0.99). This corresponds to excellent agreement between the two SPECT/CT acquisition-methods. The use of fast acquisition SPECT versus standard SPECT reduced SPECT-acquisition time from 16 to 4 minutes. The use of SPECT/CT provided a definitive classification in 90 of 104 cases in which the WB-BS was not entirely diagnostic. **Conclusion**: Investigation for bone metastases can be conducted using a fast acquisition SPECT/CT as ‘add-on’ to WB-BS without compromising the diagnostic confidence and with notable reduction in acquisition time.

OP359

Keel- versus Knife-Edge Slit-Hole Collimation in Small-Animal SPECT: a GATE Monte Carlo Study

H. Mahani^{1,2}, G. Raisali², A. Kamali-Asl³, **M. Ay**^{4,1}; ¹Research Center for Molecular and Cellular Imaging (RCMCI), Tehran, IRAN, ISLAMIC REPUBLIC OF, ²Radiation Application Research School, Nuclear Science and Technology Research Institute (NSTRI), Tehran, IRAN, ISLAMIC REPUBLIC OF, ³Radiation Medicine Engineering Department, Shahid Beheshti University, Tehran, IRAN, ISLAMIC REPUBLIC OF, ⁴Department of Medical Physics and Biomedical Engineering, Tehran University of Medical Sciences, Tehran, IRAN, ISLAMIC REPUBLIC OF.

Aim: Performance of knife-edge SPECT collimators is usually limited by a considerable edge penetration, leading to inferior spatial resolution. The problem is severe in slit-hole collimation where there is a long narrow aperture. In this research, we were aiming at making a comparison between imaging performance of a keel- and a knife-edge slit-hole collimator, a novel collimation offering a high detection efficiency. **Materials and Methods**: The slit-hole is a single slit aperture extended across long-axis of scanner’s head, allowing to collect much more photons. To meet

the data-sufficiency condition, the collimator has to spin around its central-axis at each regular SPECT angle. To doing so, HiReSPECT camera, a dedicated small-animal SPECT scanner developed in our department, benefiting from the slit-hole collimator was modeled within the GATE. Slit's edges differed in channel height ranging from 0 (knife-edge) to 1.2 mm (full-keel), and slit width was 0.6 mm. Percentage edge-penetration (normalized to that of the knife-edge), full-width-at-tenth-maximum (FWTM) of the reconstructed point-source images, and system sensitivity were evaluated. The channel height was then optimized for two common collimator materials: lead and tungsten. The slit-hole collimation data were iteratively reconstructed using a dedicated in-house 3D MLEM algorithm. **Results:** Edge-penetration exponentially falls off as channel height raises, for both lead and tungsten. A 6 mm channel height results in a decreased percentage edge-penetration by a factor of 1.49 and 2.25 for lead and tungsten, respectively. A 1.2 mm height outcomes a decreased reconstructed FWTM of 1.35 and 1.57 times which observed with a knife-edge geometry, for lead and tungsten, respectively. Increasing channel height also simultaneously improves spatial resolution and mitigates image background. In contrast, sensitivity drops when channel height increases. A 6 mm channel height tungsten collimation gives rise to a decreased background-subtracted system sensitivity of 7.46 cps/ μ Ci compared to 8.18 cps/ μ Ci obtained by a knife-edge one, all at a 30 mm distance. The gains in percentage edge-penetration and FWTM obtained by increasing channel height also compromises field-of-view of the camera. Therefore, a tungsten keel-edge slit-hole collimation benefited from a 0.6 mm channel height provides the best compromise for technetium-99m molecular imaging using the HiReSPECT system. **Conclusion:** The results highlight that there is a trade-off among spatial resolution, edge-penetration, sensitivity, and FOV for slit aperture design. As a conclusion, a keel-edge collimator offers SPECT image quality superior to a knife-edge one.

OP360

Design Optimisation of 3D Printed Parallel-Hole Tungsten Collimators for High Activity I-131 Imaging

J. Gear, G. Flux; Royal Marsden NHSFT, Sutton, UNITED KINGDOM.

Introduction: With the advent of power bed laser melting (3D printing) the clinical introduction of tungsten based collimators could soon be realised. This could have a significant impact on quantitative imaging for I-131 dosimetry. I-131 imaging is affected by several factors including scatter, septal-penetration, system resolution and camera dead-time. Commercial high-energy lead collimators are designed for diagnostic imaging and optimised for detection efficiency. High activity administrations of therapeutic I-131 do not suffer from a lack of counts and tungsten collimators could therefore be designed to reduce system deadtime and to improve image quality. **Method:** Designs for lead and tungsten parallel-hole collimators were optimised by iteratively solving analytical formulae for penetration, efficiency and resolution. A cost-function to determine the optimal septal length, thickness and hole-size was reduced using benchmarking inputs for the desired collimator characteristic. Optimised collimator geometries were then used as input into the Monte Carlo program SIMIND to demonstrate the improvement in I-131 image quality that could be achieved. Simulated images for each collimator were used to generate NEMA system characteristics. Comparisons with physical measurements for commercial collimators were also made. **Results:** A good agreement between physical and simulated measurements was observed for commercial lead collimators. For the optimised collimators NEMA system-sensitivity was reduced by a factor of 5 compared to commercial alternatives. However, sensitivity also includes scattered and penetrating photons which were reduced from 30% to 10%. Spatial resolution improved from 14 mm to 6 mm FWHM. A simulation of a thyroid remnant demonstrated clearer foci with the optimised collimator with peak counts only 50% less than commercial

lead HEGP, indicating that such collimators may also be suitable for general use. Estimations of costs and collimator mass indicate that tungsten collimators would weigh approximately 170 kg and have material cost 35 times that of current lead alternatives. However, 3D printing options of tungsten offset the expensive machining costs required for lead and therefore such collimators are becoming financially viable.

OP361

A Qualitative and Quantitative Comparison of Step-and-shoot, Acquire-during-step and Continuous SPECT Acquisition Modes

N. A. Bebbington¹, H. B. Joergensen², V. Ovtchinnikova², J. B. Medhus², P. C. Holdgaard²; ¹Siemens Healthcare A/S, Aarhus, DENMARK, ²Nuclear Medicine Department, Vejle Sygehus, Vejle, DENMARK.

AIMS: Time savings of >3 minutes/acquisition or dose reduction for equivalent time can be made with continuous or acquire-during-step (ADS) acquisitions, compared with step-and-shoot (SS). Comparisons made ≥ 20 years ago favoured continuous acquisition mode due to greater angular sampling, despite a small increase in image blurring, yet clinically, SS is most common. However, given the improved image quality with modern SPECT reconstruction techniques, an up-to-date comparison is necessary. This study provides thorough qualitative and quantitative comparisons of images acquired with continuous, ADS and SS modes under clinically realistic conditions. **MATERIALS AND METHODS:** SPECT-CT studies of a Tc-99m-filled NEMA-IEC image quality phantom were acquired on a Siemens Symbia Intevo 6, with different settings used clinically (LEAP/LEHR collimator; 128/256 matrix, 60/120 projections; 5, 10, 20 minutes scan time) under four tracer conditions (high contrast (8:1) hot spheres with high and low activities; low contrast (7:2) hot spheres with low activity; medium contrast (1:6) cold spheres with high activity). Flash3D (resolution recovery) reconstructions were made with optimal iterations and Gaussian filter for the given conditions (consistent between acquisition mode) and CT attenuation correction. Five experienced observers blind-scored confidence in uptake from 0 (no uptake) to 5 (certain significant uptake) for each sphere (10-37mm) in 90 datasets (30 per mode). Contrast-to-noise ratios (CNR) were also measured under the four conditions. Results for were plotted on a curve (sphere size (mm) vs confidence; sphere size (mm) vs CNR) and AUC compared by acquisition mode. **RESULTS:** High contrast hot spheres: ADS gave highest CNR at high activities (AUC: ADS 366; cont 320, SS 270) but confidence scores were comparable (AUC: ADS 109.9; SS 109.2; cont 107.2). Yet, at low activities ADS gave lowest CNR whilst SS and continuous were comparable (AUC: SS 260; cont 259; ADS 179), and continuous gave greatest confidence in lesion detectability (AUC: cont 94.5; ADS 88.0; SS 85.7). Low contrast hot spheres: CNR and confidence scores were greatest for SS (CNR AUC: SS 91; ADS 83; cont 63; confidence AUC: SS 62.0; cont 52.7; ADS 51.4). Cold spheres: CNR and confidence scores were most favourable for continuous mode (CNR AUC: cont -121; ADS -92; SS-82; confidence AUC: cont 70.8; SS 68.6; ADS 67.5). **CONCLUSIONS:** For equivalent counts and reduced time to SS, continuous mode acquisitions showed favourable qualitative and quantitative results in assessing high contrast hot lesions and cold defects, although it was considered inferior to SS for low contrast hot lesions.

OP362

A Comparative Phantom Study: Digital-CZT vs Analog SPECT

E. Goshen¹, L. Beilin², R. Goldkom¹, S. Ben-Haim¹; ¹Chaim Sheba Medical Center, Ramat Gan, ISRAEL, ²Molecular Dynamics, Caesarea, ISRAEL.

Purpose We have assessed the performance of a novel digital SPECT camera with multiple pixelated cadmium zinc telluride (CZT) detectors and high sensitivity collimators (Digital SPECT; Valiance X12 prototype,

Molecular Dynamics). The system's architecture enables gantry rotation, as well as radial and swivel detector motion, providing multiple degrees of freedom for the scanning pattern. These features are used to minimize the patient-detector distance, providing patient-tailored imaging. **Materials and Methods** Images of both Tc-99m filled Hoffman 3-D Brain phantom, and Tc-99m filled Jaszczak phantom with cold rod and solid sphere inserts (rod diameter 4.8–12.7 mm, spheres 9.5–31.8 mm), were compared to images acquired on a standard NaI based analog (Anger) SPECT system. The images acquired on the digital SPECT camera with high sensitivity collimators (Valiance X12) were compared to the images obtained on the analog SPECT system fitted with high resolution collimators (Discovery NM/CT 670, GE). All images (digital and analog SPECT) were iteratively reconstructed and evaluated visually for resolution. Contrast was calculated using standard methodology. **Results** The digital SPECT images of Hoffman Brain phantom displayed improved resolution compared to the analog SPECT images. The contrast calculated in the region corresponding to the anatomic site of basal ganglia was higher in digital SPECT compared to the analog system (72% vs. 26% respectively). Digital SPECT of Jaszczak phantom demonstrated cold rods in reconstructed transaxial slices of 5 segments with rod diameters of 12.7, 11.1, 9.5, 7.9, 6.4 mm, and in five external rows in the sixth segment (diameter 4.8 mm). Analog SPECT demonstrated rods in 4 segments and in part of the 5th (down to 6.4mm). Spheres were resolved on digital SPECT with contrast of 92.9%, 87.8%, 82.7%, 68.2%, 66.3% and 51.7% (for sphere diameters measuring 31.8, 25.4, 19.1, 15.9, 12.7 and 9.5 mm, respectively). Analog SPECT yielded contrast of 63.5%, 52.8%, 44.4%, 39.3%, 26.4%, and 18.6% for the same spheres, respectively. See fig. 1: **Top** - Jaszczak phantom cold rods section: Left - Valiance X12 prototype; Right - NaI based analog SPECT system. **Center and Bottom** - Transaxial slices of Hoffman 3-D Brain phantom with horizontal profile plots through section corresponding to anatomical site of basal ganglia: Left - Valiance X12 prototype; Right - NaI based analog SPECT system. **Figure Conclusion** Contrast and resolution of digital SPECT consistently surpassed standard analog SPECT performance in the phantom studies reported. The superior image quality will likely prove useful in clinical settings.

OP363

Optimization of Preclinical I^{125} SPECT in Conventional and CZT Cameras using Universal Image Quality Indices

J. A. Kennedy^{1,2}, M. Weiler-Sagie¹, R. Lugassi¹, Z. Gil¹, M. Amit¹; ¹Rambam - Health Care Campus, HAIFA, ISRAEL, ²Technion - Israel Institute of Technology, Haifa, ISRAEL.

Purpose: To optimize preclinical imaging of iodine-125 (I^{125}) in conventional and solid-state CZT cameras according to indices relevant to the human visual system (HVS). **Method:** SPECT images were obtained of a small 33 mL phantom with an activity of 36.7 MBq of I^{125} solution on conventional (Discovery 670 SPECT/CT) and CZT cardiac (Discovery 570c SPECT/CT) cameras for durations of 30 and 15 min respectively. For image quality (IQ) comparison, Poisson resampling and list mode provided virtual acquisitions at 1/8, 1/4, and 1/2 of the full acquisition time. SPECT with energy windows of $\pm 13.5\%$, $\pm 27\%$ and $\pm 54\%$ centered at 27.5 keV were compared to SPECT at the monochromatic γ -peak (35.5 keV $\pm 15\%$). Metrics for IQ comparison were contrast, contrast-to-noise ratio, mean-squared error (MSE), and the structural similarity index (SSIM) reflecting known HVS characteristics, with higher SSIM or lower MSE values indicating superior IQ. Optimized acquisition parameters were used to obtain SPECT images of 3 mice at 36 hours post-injection of 11 MBq I^{125} solution. These were an euthyroidic C57BL/6, one athyroidic C57BL/6 and an athyroidic athymic nude mouse with a human papillary thyroid cancer (PTC) flank xenograft, the latter two being thyroidectomized one day prior to the study and treated with thyrotropin-alpha. The PTC case was sacrificed at 8 hours post- I^{125} injection to see total body distribution. **Results:** Of the evaluated IQ metrics, SSIM improved monotonically with

increased acquisition time, a known IQ determinant. For the CZT camera, the $\pm 54\%$ energy window gave the best SSIM (0.398) compared to the $\pm 27\%$ and $\pm 13.5\%$ cases (0.388 and 0.363 respectively) or to the monochromatic γ -peak case (0.274), with MSE giving comparable results (6.85 vs. 7.00, 7.39 and 10.44 respectively). The conventional camera IQ indices were also superior for the $\pm 54\%$ energy window (0.409 vs. 0.406, 0.395 and 0.349 respectively for SSIM, and 7.54 vs. 7.72, 7.58 and 8.34 respectively for MSE). With both cameras, the thyroid was clearly visible in the euthyroidic case as was stomach uptake in the athyroidic case. The total body distribution was well delineated in both studies for the PTC case. **Conclusion:** I^{125} SPECT performed on conventional and CZT cameras provides a good imaging tool for preclinical research and should be performed with a wide energy window. The CZT camera provided similar IQ as the conventional camera in half the acquisition time. Using SSIM to model HVS provides an effective index for IQ optimization.

909 – Monday, October 17, 2016, 14:30 - 16:00, Hall 113

Conventional & Specialised Nuclear Medicine: Endocrinology & Gastroenterology

OP364

Effect of glycemc control on exendin-based beta-cell mass quantification

M. Buitinga, W. A. Eter, C. Frielink, L. Claessens-Joosten, D. Bos, M. Brom, M. Gotthardt; RadboudUMC, Nijmegen, NETHERLANDS.

Background and aim: Targeting of the glucagon-like peptide-1 receptor (GLP-1R) with radiolabeled exendin, a GLP-1R agonist, is an attractive approach to determine the beta-cell mass (BCM) (1-3), which is of high interest in diabetes research. Hence, the effect of metabolic status/chronic hyperglycemia on GLP-1R expression and exendin uptake remains to be elucidated. Here, we investigated the effect of chronic hyperglycemia on ^{111}In -exendin uptake in diabetic mice with intramuscular islet transplants.

Materials and methods: Syngeneic transplantations of 200 islets were performed in the calf muscle of alloxan-induced diabetic C3H mice (n=6). Glycemic state was regulated using insulin pellets. Three groups of glycemic state were analyzed; 4 weeks of hyperglycemia (HG, blood glucose levels >25mM, n=6), 4 weeks of normoglycemia (NG, blood glucose levels <10mM, n=6), and 2 weeks of normoglycemia followed by four weeks of hyperglycemia (NGHG, n=6). Mice were injected intravenously with 15 MBq of ^{111}In -exendin and SPECT was acquired 1h post-injection. Exendin uptake was determined by autoradiography and was normalized for insulin area (determined by immunohistochemistry).

Results: Islet grafts were clearly visualized by SPECT in all recipient groups. Tracer uptake was significantly influenced by glycemic state with an accumulation of 19.0 ± 1.6 counts/insulin area for the NG mice and 7.5 ± 2.0 and 9.1 ± 1.3 for the HG and NGHG mice, respectively ($p < 0.01$, ANOVA with a bonferroni correction for multiple group comparisons). Despite this two-fold reduction in tracer accumulation, tracer uptake linearly correlated with insulin area (Pearson's Correlation Coefficient r for NG= 0.86, HG= 0.95 and NGHG=0.63). **Conclusion:** Our results indicate that exendin uptake is influenced by glycemic control. The observation that tracer uptake linearly correlates with insulin area, even under chronic hyperglycemia, indicates that BCM quantification using exendin is a valid technique provided that tracer uptake will be corrected for the glycemic state of the subject. These results have significant clinical implications for the interpretation of exendin scans in subjects with diabetes. 1. M. Brom et al., Non-invasive quantification of the beta cell mass by SPECT with (^{111}In)-labelled exendin. *Diabetologia* (2014), doi:10.1007/s00125-014-3166-3. 2. M. Brom, L. Joosten, C. Frielink, O. Boerman, M. Gotthardt, ^{111}In -exendin Uptake in the Pancreas Correlates With the β -Cell Mass and Not With the α -Cell Mass. *Diabetes*. **64**, 1324-1328 (2015). 3. I. van der Kroon et al., Noninvasive imaging of islet transplants with ^{111}In -exendin-3. *J. Nucl. Med.*, 1-24 (2016).

OP365

Imaging beta cell mass with ⁶⁸Ga-exendin PET in patients with remission of type 2 diabetes mellitus (T2DM) after Roux-en-Y gastric bypass (RYGB) surgery

L. N. Deden¹, M. Boss², E. O. Aarts¹, H. de Boer¹, M. Buitinga², I. M. C. Janssen¹, M. Brom², F. J. Berends¹, M. Gotthardt²; ¹Rijnstate, Arnhem, NETHERLANDS, ²Radboud University Medical Center, Nijmegen, NETHERLANDS.

Background In more than 60% of T2DM patients, diabetes remission is seen after Roux-en-Y Gastric Bypass (RYGB) surgery, the underlying mechanisms is not completely understood. Possibly, preoperative beta cell activity (BCA) or mass (BCM) play a role and have a predictive value for T2DM remission. BCM could be measured *in vivo* using the radiolabeled glucagon-like peptide-1, exendin, which specifically accumulates in the islets of Langerhans. In this study the difference in pancreatic ⁶⁸Ga-exendin uptake, as measure for BMC, in patients with and without complete T2DM remission after RYGB is evaluated in PET. **Methods** In 24 T2DM patients ⁶⁸Ga-exendin PET will be performed at least one year after RYGB, 12 patients with complete T2DM remission (responders) and 12 patients without complete T2DM remission (non-responders). Pancreatic uptake corrected for injected dose (kBq/MBq) was quantified by delineation of the pancreas in PET images and compared between responders and non-responders (student's T-test). BCA was measured by arginine stimulation and oral glucose tolerance test (OGTT). Additionally, optimal acquisition moment and time were determined based on the first six patients. PET was acquired one and two hours after injection of 100 MBq ⁶⁸Ga-exendin in list mode with 10 minutes per bed position (reconstructions for 2, 5, 7 and 10 minutes per bed position). Optimal acquisition was based on image quality, pancreatic and kidney uptake and activity distribution within the scans. **Results** So far, three responders and three non-responders have completed the study. Preoperative and weight loss parameters were comparable, only fasting c-peptide was lower in non-responders compared to responders (0.4 versus 0.8 nmol/l, P=0.049). Pancreatic uptake was 36% lower in non-responders (2.2±0.42 kBq/MBq) compared to responders (3.5±1.9 kBq), although this is not a significant difference (P=0.3). Pancreas volume was smaller in non-responders (42±1 ml) compared to responders (74±7 ml; P=0.089). BCA was impaired in non-responders compared to responders; stimulated c-peptide was 0.8 versus 1.8 nmol/l and during OGTT maximum c-peptide was 1.3 versus 4.2 nmol/l, with largest glucose levels in non-responders. Pancreatic and kidney uptake, corrected for decay, and activity distribution were similar one and two hours after injection. Image quality was best one hour after injection. Pancreatic uptake was similar for increasing acquisition time, but image quality increased for acquisition time of 7 and 10 minutes. **Conclusion** Preliminary results suggest that pancreatic uptake of ⁶⁸Ga-exendin is lower in non-responders compared to responders after RYGB. Optimal acquisition is performed is one hour after injection with seven minutes per bed position.

OP366

Obesity-associated alterations of glucose metabolism are ameliorated after chronic stimulation of abdominal vagus nerve

C. Malbert¹, M. Genissel¹, J. Georges¹, F. Legouevic¹, J. Divoux², C. Picq², L. Guillemetz², C. Henry³; ¹INRA, Saint-Gilles, FRANCE, ²Axonix, Vallauris, FRANCE, ³LivaNova, Clamar, FRANCE.

Obesity alters glucose metabolism with specific reference to insulin resistance. We have previously demonstrated that chronic stimulation of abdominal vagus nerve (VNS) was able to restore insulin sensitivity in obese animals (Malbert et al, Obesity facts, 2015). The aim of this study is to evaluate the capability of vagal stimulation to recover the altered glucose metabolism induced by obesity. 15 adults age-matched minipigs

were divided into three groups: lean (33±1.6 kg), obese (49±1.1 kg) and obese with VNS (47±1.3 kg). Obesity was induced by 3 months of obesogenic diet. Once obese, the obese and obese-stimulated groups were fitted with cuff electrodes around the abdominal vagi using laparoscopy. VNS was applied in obese-stimulated group only. Obese and obese-stimulated groups were tested after 5 months of obesogenic diet whereas lean group remained on normal diet. Oxidative and non oxidative glucose metabolism were evaluated using indirect calorimetry coupled with euglycemic clamp. Brain, hepatic and skeletal muscle metabolism were quantified as insulin-mediated glucose uptake using FDG dynamic PET imaging coupled with continuous arterial input function measurement also during clamp. Brain glucose uptake was obtained by kinetic modeling of PET and arterial data whereas hepatic and skeletal muscle glucose uptake were calculated using Patlak method. Glucose oxidative metabolism was unchanged in lean, obese and obese-stimulated animals (p>0.05). On the contrary, non oxidative glucose metabolism was significantly reduced by obesity and partially restored by VNS (4.5±0.65, 2.9±0.26 and 4.1±0.19 mg/kg/min for lean, obese and obese stimulated, p<0.01). Whole brain glucose metabolism was also reduced by obesity, a feature restored by VNS to lean condition. ROI based analysis showed that this pattern was similar in all brain areas. Liver and skeletal muscle glucose metabolism followed the same trend. Chronic vagal stimulation was able to restore whole body glucose metabolism altered by obesity. This restoration was equally effective on the main organs involved in glucose metabolism e.g. brain, liver and skeletal muscle demonstrating that restoration of insulin sensitivity by VNS was organ independent.

OP367

Gelofusine inhibits the renal uptake of ¹¹¹Indium-labeled exendin in humans

M. Buitinga¹, M. Boss¹, M. Behe², M. Brom¹, M. Gotthardt¹; ¹RadboudUMC, Nijmegen, NETHERLANDS, ²Paul Scherrer Institut, Villigen, SWITZERLAND.

Background and aim: Targeting of the glucagon-like peptide-1 receptor (GLP-1R) with radiolabeled exendin, a GLP-1R agonist, is an attractive approach to determine the beta-cell mass (BCM) (1-3). However, the high kidney uptake is hampering SPECT-based quantification of pancreatic uptake. It has been demonstrated in rats that the renal reabsorption of ¹¹¹In-exendin can be reduced by co-infusion of succinylated gelatin (Gelofusine, Braun) (4). Here, we studied the effects of a low-dose Gelofusine infusion on the renal uptake of ¹¹¹In-exendin in humans. **Materials and methods:** Ten healthy volunteers, 5 men and 5 women, were given 50 MBq ¹¹¹In-exendin, in combination with normal saline or Gelofusine (bolus of 1 mL/kg body mass during 10 minutes followed by 0.02 mL/kg/min for 3 hours). SPECT images were obtained after 24 hours. After a period of three weeks, the procedure was repeated; participants who received normal saline during the first session, were given Gelofusine, and vice versa. Blood and urine samples were taken to monitor radioactivity concentrations. Uptake of ¹¹¹In-exendin was determined by drawing regions of interest around the kidneys and in the pancreas. **Results:** Normal saline or Gelofusine injections did not induce any changes in blood pressure or heart rate and did not cause any other clinical side effects. Analysis of the scans of the first 5 patients showed that a low dose of Gelofusine is able to effectively reduce the kidney retention. The observed reduction in kidney uptake varied between 14% and 53% with a mean reduction of 27%. Assessment with t-test for paired data showed that this reduction was significant (p=0.013). Gelofusine injections did not alter the uptake of ¹¹¹In-exendin in the pancreas (paired t-test, p=0.41). ¹¹¹In-exendin was rapidly cleared from the blood. When gelofusine was administered, the excretion of ¹¹¹In-exendin in the urine was increased from 2.0%ID to 3.2%ID in 24 hours. **Conclusion:** The present study shows that a low-dose Gelofusine infusion effectively reduces the renal uptake of ¹¹¹In-exendin, without any side effects. This decrease in kidney uptake does not only reduce the radiation exposure, but

also the kidney:pancreas ratio. 1. M. Brom *et al.*, *Diabetologia*. 57, 950-959 (2014) 2. M. Brom *et al.* *Diabetes*. 64, 1324-1328 (2015). 3. I. van der Kroon *et al.* *J. Nucl. Med.*, 1-24 (2016). 4. E. Vegt *et al.* *Eur. J. Nucl. Med. Mol. Imaging*. 37, 226-34 (2010).

OP368

Increased Proliferative Activity in Parathyroid Scan in Hyperplastic Parathyroid Glands, measured by PCNA and Ki-67 Expression: Impact on specific surgical treatment

S. Dugonjic, Sr., S. Cerovic, M. Siscic, B. Ajdinovic; Military Medical Academy, Belgrade, SERBIA.

Background. Improvement of sensitivity of parathyroid scintigraphy (PS) for hyperplastic parathyroid glands (HPG) visualization requires determination of many factors which influence intensity of Tc99m-MIBI uptake. **Aim.** The aim of this study was to correlate the degree of PS Tc99m-MIBI uptake with proliferative activity of hyperplastic PG, measured by PCNA and Ki-67 expression. **Methods.** Twenty-seven patients with primary/secondary parathyroid hyperplasia underwent PS before surgery. Static scintigrams of neck/chest were performed, 15 minutes and 2 h after *iv.* inj. of 740 MBq of Tc99m-MIBI. Four hours later, after *iv.* inj. of 185 MBq Tc99m, thyroid scintigraphy was performed. After normalization and motion correction, subtraction was done. Scintigraphic results were graded from 1-5, depending on the intensity of Tc99m-MIBI uptake. PS graded 3, 4 and 5 were considered positive. Commercial mice monoclonal anti-human antibody DAKO: PCNA and Ki-67 were used. Visualization system, EnVision™ DAKO kit and chromogen DAKO DAB liquid, was used. As a positive immunohistochemical (IMH) response, exclusively nuclear immunoreactivity, using standard formula for the number of cells (1000 cells) and proliferative parameters at high microscopic magnification were established. Positive control for the IMH method represented by samples from 10 PG, removed incidentally at normocalcaemic patients (during thyroidectomy), and negative control, IMH procedure using buffer instead of antibodies. Proliferative activity was determined as positive and negative, by the expression of PCNA and Ki-67 antibody, at standard preparations. **Results.** PS localized 51 from 73 HPG, 60 nodular hyperplastic (NHPG), 13 diffuse hyperplastic PG (DHPG), with sensitivity of 70%. From HPG, 92% were PCNA positive, while 15% were Ki-67 positive. Control PG (50 PG) were 98% PCNA and 100% Ki-67 negative. Significant statistical difference was found between HPG and control PG comparing PCNA and Ki-67 expression, $p < 0.0001$. PCNA expression was positive in 100% DHPG and in 90% NHPG with statistically not significant difference. Ki-67 expression was negative in all DHPG, and positive in 18.3% NHPG, with statistically important difference, $p < 0.0001$, between two groups. Between PS and PCNA expression significant positive correlation was found, $p < 0.0001$. Significant negative correlation was found between scintigraphic and Ki-67 positivity, $p < 0.0001$. **Conclusion.** Increased proliferative activity of HPG was demonstrated, with high sensitivity of PCNA, and high specificity of Ki-67. Increased proliferative activity is one of the factors responsible for higher Tc99m-MIBI uptake in hyperplastic parathyroid glands. Finding that scintigraphic negative HPG have less pronounced proliferative activity, imply that these HPG are PG of choice whose remnant should be left during subtotal parathyroidectomy.

OP369

⁷⁵SeHCAT in the diagnosis of bile acid malabsorption in patients with crohn's disease. correlation with pathologic study and treatment

P. TALAVERA RUBIO, M. BELLÓN GUARDIA, P. OLIVENCIA PALOMAR, N. DISOTUAR RUIZ, E. DE LA SANTA BELDA, V. POBLETE GARCÍA, G. JIMENEZ LONDOÑO, M. TELLO GALÁN, A. GARCÍA VICENTE, J. CORDERO GARCÍA, A. SORIANO CASTREJÓN; HGUCR-SESCAM, CIUDAD REAL, SPAIN.

Aim: To study the diagnosis with ⁷⁵SeHCAT scintigraphy in bile acid malabsorption (BAM) in patients with Crohn's disease (CD) and its possible correlation with the severity of the disease, indicated by histological study, and treatment received. **Material and Methods:** We analyzed the studies that we have performed on patients diagnosed with Crohn's disease, to assess the existence of BAM etiology associated with the persistence of diarrhea despite the treatment received (surgical/immunotherapy). The images of abdominal region were acquired at 3 hours and 7 days after administration of a capsule containing 0.01 mCi of ⁷⁵SeHCAT (previous fasting). Background images were also obtained immediately before and after the acquisition of patient's images, at 3 h and 7 days. The study was considered pathological when the retention rate was $\leq 10\%$. The results of the technique were correlated with pathological alteration detected by endoscopic biopsy (normal-mild/moderate-severe) and previous treatment administered to the patient (medical/surgical resection) **Results:** We performed a total of 32 studies (15 women and 17 men, age range: 21-77 years). 23 of them had a pathological retention rate in ⁷⁵SeHCAT scintigraphy (72%). 11/32 patients had been treated with ileal surgery and 21/32 not (⁷⁵SeHCAT scintigraphy was pathological in 8 and 15 of them, respectively). 19/32 patients had received medical treatment and 13 not (⁷⁵SeHCAT scintigraphy was pathological in 13 and 10 of them, respectively). 5 patients of the 9 with ⁷⁵SeHCAT scintigraphy normal and 10 of 23 with pathological scintigraphy showed moderate-severe damage in the endoscopic study. No statistically significant correlation between the result of the technique and the variables analyzed (disease severity and prior treatment) was found. **Conclusion:** We found a high association between BAM and Crohn's disease (nearly 3/4 of patients), but no correlations with the severity of the disease, nor the type of prior treatment received.

OP370

Diagnostic Accuracy Of ^{99m}Tc MAA Whole Body Shunt Scintigraphy In Patients With Suspected Hepatopulmonary Syndrome

P. Shanmuga Sundaram, S. Padma; Amrita School of Medicine, Amrita Institute of Medical Sciences, COCHIN, INDIA.

Aim: Hepatopulmonary syndrome (HPS), a severe complication of cirrhosis is associated with poor survival. It is characterized by hypoxaemia due to pulmonary vasodilatation and shunting (i.e. Pulmonary arteriovenous fistula PAVF formation). Pts are managed conservatively or by liver transplant. 2D transthoracic contrast echocardiogram (CE) is accurate and an established imaging modality in HPS. ^{99m}Tc MAA Whole body shunt scintigraphy (MAA scan) is less commonly used. This study was designed i) to assess the diagnostic accuracy of MAA scan in suspected HPS patients in comparison to CE (ii) to evaluate the clinical significance of semiquantitative analysis of shunts as assessed by both techniques. **Materials & Methods:** Prospective study was conducted in 22 consecutive cirrhotic patients with portal hypertension (all males, age 17 to 59 yrs, Jan 2013 to 16) planned for liver transplant. All underwent clinical evaluation, pulse oximetry, MAA scan and CE. Presence of PAVF (interatrial shunt) is depicted by extrapulmonary MAA distribution followed by shunt percentage calculation. Semiquantitative analysis of shunt severity was also performed by CE in all (Grade 0 no bubbles; 1 occasional filling with less than 20 bubbles; 2 moderate filling; 3 complete opacification). **Results:** Dyspnoea, digital clubbing, cyanosis and spider angiomas were present in all. Hypoxemia was documented in all. 20/22 pts (91%) had positive CE and MAA scan. In 2 pts CE was erroneous. MAA shunt of more than 6% was observed in all patients, except 2 who were negative for shunt. Grade of shunt severity by CE was found to be equivalent to that of MAA shunt calculation. MAA shunt was grade 3 (more than 25%) in 6 pts, grade 2 (more than 15%) in 5 pts & grade 1 (6 to 15%) in 9 pts. A significant correlation was found between CE and MAA shunt grading (P less than 0.0001). A χ^2 test for linear trend showed significant association

between CE & MAA shunt grading, P less than 0.0001. Conclusion: Wholebody MAA shunt scintigraphy is an effective modality to assess and grade HPS in cirrhotic liver patients. Presence of HPS indicates a worse prognosis thus early initiation of therapy is imperative. The grade of shunt severity as assessed by CE is equivalent to MAA shunt percentage calculation. Thus MAA shunt scintigraphy is a reliable, reproducible investigation with excellent diagnostic accuracy and can be used at par with CE in identifying and prognosticating HPS pts scheduled for liver transplant.

OP371

Ectopic gastric mucosa scintigraphy: retrospective review of a series

M. R. Victor, A. Prata, S. Carmona, J. G. Santos, J. A. Sequeira, A. I. Santos; Hospital Garcia de Orta, Almada, PORTUGAL.

Introduction: Ectopic gastric mucosa scintigraphy (EGMS) is a simple nuclear medicine procedure indicated in Meckel's Diverticulum (MD) suspicion. The radiopharmaceutical used, ^{99m}Tc -pertechnetate, is taken up and excreted by the mucus-secreting gastric cells, present superficially in all different types of gastric glands. Aim: To review our series of EGMS regarding presenting symptoms, referral data, scan results and clinical follow-up. Material and methods: Retrospective analysis of referrals for EGMS between July 1998 and December 2015, characterizing age, clinical referral, symptoms, scintigraphic results, surgery and corresponding histological findings. Results: A total of 105 EGMS were performed to a population of 99 patients, 78 children with median age and interquartile range of 6 [2.5;12] years; and 21 adults with median age and interquartile interval of 39 [28;47.5] years. In the pediatric patients, the majority of the referrals came from pediatric surgery (30%) and pediatric emergency ward (25%). The adult patients were mainly referred from gastroenterology appointments (52%). The most prevalent presenting symptoms were lower gastro-intestinal bleeding (49% children and 67% adults) and abdominal pain (29% children and 14% adults). A total of 16% of patients were asymptomatic (20% pediatric and 5% adult), electively studied after incidental MD finding during abdominal or pelvic surgery, and all of them had a negative EGMS. In 6 (5.7%) EGMS there was scintigraphic evidence of ectopic gastric mucosa (positive result), being 5 children and 1 adult; they underwent surgery and all had histologic confirmation of gastric mucosa. Within the population with negative EGMS, 5 patients were operated, one of which had a MD resection with histological confirmation of presence of gastric mucosa. The remaining four had a different final diagnosis (gastric duplication, appendicitis, enteric herniation and peptic ulcer, respectively). Conclusions: The most frequent symptom for referral was gastrointestinal bleeding, in accordance with the literature. There were no false positive results, in agreement with the known high specificity of this diagnostic procedure. The only false negative case raises the need of further data on mass/volume and type of gastric cells present on the ectopic mucosa, in order to understand the limitations of the exam. The low prevalence of positive results indicates that there is a possible need for better referral criteria definition. All the asymptomatic patients who were referred after incidental intraoperative finding of MD had a negative EGMS, questioning the appropriateness of this indication.

910 – Monday, October 17, 2016, 14:30 - 16:00, Hall 114

Neurosciences: Dementia

OP372

GLP-1 Analog Raises Glucose Transport Capacity of Blood-Brain Barrier in Alzheimer's disease

A. Gjedde¹, M. Gejl², J. Rungby¹, B. Brock²; ¹University of Copenhagen, Copenhagen N, DENMARK, ²Aarhus University, Aarhus, DENMARK.

Introduction: Glucose enters the brain tissue from plasma by facilitated diffusion across the two membranes of the endothelium of the blood-brain barrier (BBB), mediated by the glucose transporter 1 (GLUT1). There is evidence in Alzheimer's disease (AD) of reduction of glucose transport across the blood-brain barrier, due to diminished GLUT1 translocation and expression at the BBB. Reduced BBB GLUT1 expression is known to aggravate AD pathology and further impair cognitive function, implying that GLUT1 may be a potential target of therapy directed towards AD neurovascular dysfunction and degeneration. The incretin hormone GLP-1 prevents the decline of the cerebral metabolic rate of glucose that signifies cognitive impairment, synaptic dysfunction, and disease evolution in AD, and GLP-1 may directly activate GLUT1 transport in brain capillary endothelium. For this reason, we here claim that the GLP-1 analog liraglutide may prevent the decline of blood-brain glucose transfer in AD. Methods: In this 26-week test of the hypothesis, we randomized 38 patients with AD to treatment with the GLP-1 analog liraglutide (n=18) or placebo (n=20). We determined blood-brain glucose transport capacity (Tmax) with [^{18}F]FDG (FDG) (ClinicalTrials.gov NCT01469351). Results: Unlike the placebo treatment, the GLP-1 analog treatment significantly ($P < 0.0001$) raised Tmax in cerebral cortex as a whole from 0.72 to 1.1 mmol/hg/min, a 50% increase (2-way ANOVA of qui-squared). Conclusion: The results are consistent with the claim that GLP-1 analog treatment raises GLUT1 activity in the BBB and hence may represent a therapeutic target for neurovascular dysfunction and degeneration in AD.

OP373

Interaction between education and clinical expression of Alzheimer's disease across European countries: an 18F-FDG PET study of the European Alzheimer's Disease Consortium (EADC)

A. Buschiazzo¹, G. Frisoni^{2,3}, S. Galluzzi², R. Perneczky^{4,5}, A. Drzezga^{6,7}, B. van Berckel⁸, R. Ossenkoppele⁸, E. Guedj⁹, M. Didic¹⁰, P. Mecocci¹¹, M. Dottorini¹², M. Bauckneht¹, G. Sambucetti¹, F. Nobili¹³, S. Morbelli¹; ¹Nuclear Medicine Unit, Department of Health Sciences, University of Genoa and IRCCS AOU San Martino-IST, Genoa, ITALY, ²LENITEM Laboratory of Epidemiology and Neuroimaging, IRCCS S. Giovanni di Dio-FBF, Brescia, ITALY, ³University Hospitals and University of Geneva, Geneva, SWITZERLAND, ⁴Neuroepidemiology and Ageing Research Unit, School of Public Health, Faculty of Medicine, The Imperial College London of Science, Technology and Medicine, London, UNITED KINGDOM, ⁵Department of Psychiatry and Psychotherapy, Technische Universität, Munich, GERMANY, ⁶Department of Nuclear Medicine, Technische Universität, Munich, GERMANY, ⁷Klinik und Poliklinik für Nuklearmedizin, Universität zu Köln, Köln, GERMANY, ⁸Department of Nuclear Medicine & PET Research, VU University Medical Center, Amsterdam, NETHERLANDS, ⁹APHM, CHU Timone, Service de Médecine Nucléaire, CERIMED, INT CNRS UMR7289, Aix-Marseille University, Marseille, FRANCE, ¹⁰APHM, CHU Timone, Service de Neurologie et Neuropsychologie, Aix-Marseille University, INSERM U, Marseille, FRANCE, ¹¹Institute of Gerontology and Geriatrics, Department of Medicine, University of Perugia, Perugia, ITALY, ¹²Nuclear Medicine Unit, Azienda Ospedaliera di Perugia, Perugia, ITALY, ¹³Clinical Neurology, Department of Neuroscience, Rehabilitation, Ophthalmology, Genetics, and Mother-Child health (DINO GMI), University of Genoa and IRCCS AOU, San Martino-IST, Genoa, ITALY.

Aims. Owing to its easy measurability, education is one of the most straightforward used proxies for Cognitive Reserve (CR). We hypothesized that the link between education and cognitive meta-skills needed to maintain daily functioning against the AD-related damage may be influenced by the educational gradient of the elderly at different latitudes across Europe. **Methods.** 62 patients with

prodromal (p)AD (34 female, age 72.3±8.2 years, baseline 27.0±1.5 mmse) and 109 controls (57 females, age 66.8±6.5, MMSE 29.3±1.0) were recruited from EADC centers in Italy, the Netherlands, France, and Germany. All subjects underwent 18F-FDG PET at baseline. Patients were divided into two groups according to the educational gradient of their country of belonging: 1 higher educational gradient (Germany and The Netherlands; HEG) and 2 lower educational gradient (Italy and France; LEG). To confirm the effect of education as RC proxy, the whole CTR group was first compared with pAD subgroups divided into highly (high-educ) and poorly educated (low-educ pAD) according to their individual educational level (lower or higher than median years of education; 11 years). Then CTR were independently compared with high-educ and low-educ pAD belonging to HEG and LEG countries, respectively. Finally high-educ and low-educ HEG pAD were compared with education matched LEG pAD (significance: $p < 0.001$ uncorrected at peak and FDR-corrected at cluster level). pAD subgroups were not different with respect to age and baseline MMSE score; however age, sex, MMSE score and center of belonging were included as nuisance. **Results.** The effect of CR was present in the whole group of pAD. In low-educ pAD hypometabolism was evident only in bilateral posterior cingulate and parietal cortex while in high-educ pAD a larger cluster of hypometabolism involved also temporal cortex bilaterally and left dorso-lateral frontal cortex. When subgroups of pAD were independently compared with CTR, HEG-poorly-educated pAD showed hypometabolism in posterior cingulate while LEG-poorly-educated pAD showed a larger area of hypometabolism involving also left posterior parietal cortex. Finally, LEG poorly educated pAD showed more marked hypometabolism with respect to HEG poorly educated pAD in bilateral temporo-lateral cortex. **Conclusions.** Poorly educated pAD from European countries with lower educational gradient have higher CR with respect to pAD patients belonging to countries with higher educational gradient with the same years of formal education. This finding suggests that relevance of education and hence its influence on clinical expression of dementia varies with latitude across Europe.

OP374

Role of 18F-FDG-PET and amyloid-PET imaging on patient management in mild cognitive impairment or dementia

C. Gámez-Cenzano¹, L. Rodríguez-Bel¹, J. Gascón-Bayarri², R. Reñé-Ramírez³, J. Campdelacreu-Fumado⁴, J. Turón-Sans³, C. Soriano-Mas⁵, J. Vercher-Conejero¹, L. Gràcia-Sánchez¹, E. Llinares-Tello¹, A. Pons-Escoda⁶, C. Majós-Torro⁶, C. Aguilera-Grijalvo⁶; ¹PET Unit. Nuclear Medicine Department. IDI. H. de Bellvitge-IDIBELL., L'HOSPITALET DE LLOBREGAT. BARCELONA, SPAIN, ²Neurology Department. Hospital de Bellvitge-IDIBELL., L'HOSPITALET DE LLOBREGAT. BARCELONA, SPAIN, ³Neurology Department. H. de Bellvitge-IDIBELL., L'HOSPITALET DE LLOBREGAT. BARCELONA, SPAIN, ⁴Neurology Medicine Department. H. de Bellvitge-IDIBELL., L'HOSPITALET DE LLOBREGAT. BARCELONA, SPAIN, ⁵Psychiatry Department. H. de Bellvitge-IDIBELL., L'HOSPITALET DE LLOBREGAT. BARCELONA, SPAIN, ⁶RM Unit. IDI. H. de Bellvitge-IDIBELL., L'HOSPITALET DE LLOBREGAT. BARCELONA, SPAIN.

Aim: To evaluate the role of FDG-PET and amyloid-PET on patient management and outcomes in mild cognitive impairment or dementia. **Material and Methods:** Prospective study including 142 patients (77 women) with mean age of 68 years old (range: 50–82), with cognitive impairment where Alzheimer Disease (AD) was considered as a possible cause. Patients underwent brain FDG-PET and 18F-Florbetapir-PET scans, CT or MRI and a battery of laboratory and neuropsychological tests. History of depression, hypothyroidism and diabetes and the standardized Mini-Mental State Examination (SMMSE) were recorded. The APOE genotype and

cerebrospinal fluid biomarkers for AD were available in 43 and 10 patients, respectively. The FDG-PET brain analysis was visual and quantitative (CortexID-GE Healthcare) and scans were classified in 2 patterns: AD (temporoparietal hypometabolism) and non-AD (others). The amyloid-PET images were classified as positive or negative by visual interpretation, using additional fusion with MRI in cases with cerebral atrophy. The FDG-PET and amyloid-PET results were compared between them and correlated with final probable clinical diagnosis. **Results:** Most patients (132/142) presented a recent history of significant memory problems and the remaining patients showed other predominant symptoms as depression, incontinence, aphasia, aggressive behaviour or agoraphobia. FDG-PET studies were abnormal in 77/142 patients (54%): 52 AD (52/52 positive amyloid-PET) and 25 non-AD (4/25 positive and 21/25 negative amyloid-PET, on of them with primary progressive aphasia). FDG-PET scans were normal in 65/142 patients (66%), but 33 of them had a positive amyloid-PET (15 APOE of risk). Amyloid-PET studies were positive in 82/142 patients (58%). The SMMSE were significantly lower in patients with abnormal FDG-PET compared with the normal scans (mean: 19 vs 26) but no statistical differences were founded between patients with positive amyloid-PET and those with negative scans (mean: 22 vs 23). **Conclusions:** Brain PET is a useful diagnostic tool in patients with cognitive impairment, where FDG and amyloid provide different and complementary information. FDG-PET helps to identify typical patterns of AD and frontotemporal dementia. Amyloid-PET may have a major impact in patients with negative or abnormal FDG-PET with non-AD pattern, when negative to exclude AD (psychiatric scenarios) or when positive to confirm AD in younger patients (< 70 years old).

OP375

PET-amyloid (18F-Florbetaben) and CSF: biomarkers agreement for Alzheimer disease diagnosis

N. Testart Dardel^{1,2}, E. Triviño-Ibáñez^{1,2}, R. Sánchez Vañó³, A. González Jiménez^{1,2}, C. Carnero-Pardo¹, A. Rodríguez-Fernández^{1,2}, M. Gómez-Río^{1,2}, J. Llamas-Elvira^{1,2}; ¹Complejo Hospitalario Universitario de Granada, Granada, SPAIN, ²IBS, Granada, SPAIN, ³Hospital 9 de Octubre, Valencia, SPAIN.

OBJECTIVES: The development of reliable biomarkers in Alzheimer's disease (AD) has become one of the main areas of interest, because of the enormous impact that would have its diagnosis and treatment. The **aim** of this work is to study the relationship of CSF biomarkers (CSFb) and molecular imaging by amyloid-PET 18F-Florbetaben (FBB-PET). **METHODS:** A preliminary series of patients with mild cognitive impairment fulfilling clinical criteria for FBB-PET (early and/or atypical onset cognitive impairment) were included. In all patients data of demographic, clinical and biochemical determination of CSFb (beta-amyloid, total and phosphorylated tau protein) were collected. FBB-PET protocol: Siemens Biograph 16. CT: Low-Dose: 50mAs; 120kV. Slow injection, dose: 300 mBq; acquisition: 90 min p.i.; 3D; 30 min (1.5x10⁶ trues accumulated). Reconstruction: OSEM-OM: 168x168; 4 it/24 sub; zoom=2; FWHM=3. CSFb were considered quantitatively and as positive/negative. FBB-PET was evaluated according visual and semiquantitative analysis. ROIs were established at cerebellar white matter, anterior pole of the temporal lobe, frontal cortex and posterior cingulate, in both hemispheres, estimating the ratio between the SUVmax at each ROI and the cerebellum (reference region). **Results:** Ten patients were included (3 women / 7 men, mean age of 58.7 ± 9.1 years). Amyloid PET was considered positive in 7/10 patients and negative in 3/10 patients. CSFb were positive in 6/10 and negative in 4/10 patients. Only one patient had discordant findings between CSFb and PET, with positive FBB-PET, positive beta-amyloid and negatives CSF, total tau (t-tau) and phosphorylated tau (p-tau). The rest of cases (positive and negative) were concordant. The mean values of beta amyloid, t-tau and p-tau levels at CSF were significantly higher in the positive PET amyloid patients than in negative subgroup (779,3 ± 37,5 vs 364,7 ± 113.5

ng/L; 126.3 ± 2.3 vs 338.4 ± 165.9 ng/mL; 24.0 ± 1.7 vs 50.0 ± 21.3 ng/L, $p < 0.05$ respectively). The uptake ratio from all ROIs showed a positive correlation with the CSF levels of beta amyloid, t-tau and p-tau. **CONCLUSIONS:** Our preliminary results showed a high agreement between the diagnostic classification on basis CSFb and FBB-PET and suggesting a positive correlation between absolute value of CSFb and the uptake index at target ROIs.

OP376

Conversion of aMCI subjects to AD in relation to [¹⁸F]flutemetamol Amyloid status, white matter hyper-intensities and hippocampal volume in a phase III longitudinal study

C. J. Buckley¹, M. Zanette², A. Cherubini³; ¹GE Healthcare, Amersham, UNITED KINGDOM, ²GE Healthcare, Marlborough, MA, UNITED STATES, ³Institute of Molecular Bioimaging and Physiology (IBFM-CNR), National Research Council, Catanzaro, ITALY.

Introduction Previously, GE Healthcare conducted a three-year outcome study in which 232 patients with amnesic mild cognitive impairment (aMCI) underwent baseline amyloid PET imaging with [¹⁸F]flutemetamol to determine time to conversion to dementia in relation to baseline amyloid status. Conversion was determined by an independent clinical adjudication committee, which reviewed the results of 6-monthly neuropsychiatric testing for up to 36 months. While amyloid positivity was a significant and independent predictor of conversion, a fraction (23%) of the amyloid-negative subjects also converted while 77% did not convert in the three year study window. In this post-hoc analysis, we determined the association of hippocampal atrophy and white-matter lesion load with conversion to dementia with the ultimate aim of improving conversion prediction. **Methods** Baseline MRI scans from the study cohort were analysed quantitatively for hippocampal volume and white-matter lesion load in a post-hoc analysis. ANOVA was used to compare hippocampal volume by conversion to dementia status and amyloid status by dichotomous [¹⁸F]flutemetamol PET image visual read. A similar model included white matter lesion load as the dependent variable. **Results** Among amyloid-negative patients, converters had both a significantly higher white matter lesion load ($p=0.0033$) and a significantly lower hippocampal volume ($p<0.0001$) than non-converters. For amyloid-positive patients, converters had a significantly lower hippocampal volume than non-converters ($p=0.0140$) but the difference between converters and non-converters in white-matter load was not statistically significant. **Discussion** Subjects who are amyloid-negative by [¹⁸F]flutemetamol at baseline are less likely to progress in the short term to dementia than those with a positive scan. The results above provide evidence that amyloid-negative aMCI subjects who converted to dementia had significant levels of either a white-matter lesion load or hippocampal atrophy as compared to the amyloid-negative non-converters. This presentation elucidates the relationship between the assessment of amyloid PET and MRI biomarkers which can be combined to predict conversion from aMCI to symptomatic dementia.

OP377

Effects of scanner and acquisition-time on brain amyloid PET evaluation: possible impact on the follow-up

J. Arbizu¹, A. Danilenko², E. F. Guillen¹, E. Prieto¹, L. Imaz¹, B. Garcia-Garcia¹, M. Riverol¹, J. M. Martí-Climent¹; ¹University of Navarra Clinic, PAMPLONA, SPAIN, ²Centre Léon Bérard. CHU, QUÉBEC, QC, CANADA.

Objectives : To investigate the impact on visual and quantitative evaluation of 18F-Florbetapir PET/CT performed on new generation or standard scanners and at different acquisition times. **Methods :** Two consecutive studies

were conducted using Biograph PET/CT scanners (Siemens): DUO using OSEM reconstruction, and mCT using OSEM reconstruction with PSF and TOF (sequence was selected randomly). A Hoffman 2-D Multi-Compartment Brain Phantom™ was filled with 18F simulating different ratios between grey and white-matter (1:1, 2:1, 4:1). We included 20 patients (57 to 89 y.o.; MMSE: 23 to 29): 4 probable AD, 2 possible AD, 7 amnesic MCI, and 7 MCI plus. Additionally, 9 patients (58 to 74 y.o.; MMSE: 17 to 29; 8 MCI, 1 possible AD) were studied in the mCT scanner using list mode acquisition between 40 to 70 minutes after injection. Images were evaluated visually (positive or negative), and quantitatively using the SUVR. Agreement between visual readings, and concordance (exchangeability and agreement) between SUVR values were analysed. Results : An overestimation of phantom ratios was measured using DUO or overfiltered mCT images. Visual reading agreement between scanners exhibited a kappa of 0.83. Three out of 20 patients were classified as doubtful in the DUO and negative in the mCT. SUVR values exhibited significant differences between visual categories using both scanners ($p<0.001$). A systematic bias of higher DUO SUVR values was found. Bland-Altman LOA showed mild agreement between scanners, although SUVR average differences were almost significant ($p=0.054$), but there was not clear exchangeability between SUVR values (some Lin's Concordance Coefficient were lower than 0.9). White-Matter/Cerebellum values were higher when images were acquired firstly than when acquired secondly in the sequence ($p<0.01$). When SUVR mean of 9 patients (5 positive, 4 negative) were plotted against acquisition times (40, 50 and 60 minutes after injection), both increases and decreases were observed (unrelated to amyloid load condition). Within subject SD ranges from 0.01 to 0.06 (mean: 0.03). All regional SUV decrease slopes were homogeneous along time. **Conclusions :** Clinical Amyloid-PET reading is not significantly affected by the type of the scanner, although new scanners reduce the number of possible doubtful cases and estimate more precisely quantitative values. Fluctuations on the SUV decrease slopes along time have possible major impact on SUVR values. Consequently, amyloid-PET studies should be acquired at a similar uptake-time and scanner during the follow-up of patients with cognitive impairment.

OP378

Scan time-windows and diagnostic performance of florbetaben amyloid PET imaging

H. Barthel¹, A. Jovalekic², S. Bullich², S. DeSanti², N. Koglin², A. Stephens², S. Dresel³, P. Bartenstein⁴, J. Seibyl⁵, O. Sabri¹; ¹Leipzig University, Leipzig, GERMANY, ²Piramal Imaging, Berlin, GERMANY, ³Helios Hospital Berlin-Buch, Berlin, GERMANY, ⁴Ludwig-Maximilian University, Munich, GERMANY, ⁵Institute for Neurodegenerative Disorders, New Haven, CT, UNITED STATES.

Introduction: [¹⁸F]florbetaben (FBB) is approved in the European Union, the USA, and South Korea for clinical use to image beta-amyloid plaques. Depending on the marketing authorization, different PET acquisition time windows are possible. In a phase 2A study, following FBB administration the accuracy of the visual read for earlier acquired PET images (45-60min p.i.) did not differ compared to later acquired PET images (90-110min p.i. and 110-130min p.i.) (Barthel et al., Lancet Neurol 2011). The analysis presented here aimed to further investigate the diagnostic properties of earlier FBB images analysed quantitatively. **Methods:** The FBB Phase 2A study was carried out in 18 centres on 3 continents. The present analysis examined the FBB PET data of 77 patients with probable Alzheimer's disease (AD, age 55 years or older, mini-mental state examination [MMSE] score=18-26, clinical dementia rating [CDR]=0.5-2.0) and of 69 age-matched healthy controls (HCs, MMSE ≥ 28 , CDR=0). Volumes of interest (modified AAL template, PMOD) were defined to calculate neocortical composite SUV ratios (cSUVRs) using the cerebellar cortex as the reference region. Clinical diagnosis served as the Standard of Truth. **Results:** cSUVRs were significantly higher for the AD patients vs. HCs in all three time-windows

($p < 0.0001$, Cohen's effect sizes = 1.54, 1.37, and 1.44). Receiver-operating characteristics curve derived cSUVR thresholds resulted in sensitivities/specificities of 78%/93%, 74%/94%, and 75%/91% for the three time-windows. For the AD patients, the binary cSUVR readouts at 45–60min p.i. showed 86% and 88% concordance with those of the 90–110min p.i. and 110–130min p.i. images, respectively. For the HCs, the concordance was 99% and 97%, respectively. **Conclusion:** Diagnostic accuracy is not compromised when quantitatively analysing FBB PET data at the 45–60min time-window. As this time-window has not yet reached steady state of the FBB cSUVR time-activity curve, further research is needed to address the question whether the use of this time-window could influence the analysis in longitudinal studies. Research support: Piramal Imaging, Berlin, Germany

OP379

Alzheimer's disease in Down Syndrome: a FDG and Amyloid PET study

V. Camacho¹, A. Fernandez-Leon¹, F. Sampedro², M. Carmona-Iragui^{3,4,5}, D. Lopez¹, E. Vilaplana^{3,5}, J. Fortea^{3,4,5}, S. Videla⁴, A. Lleó^{3,5}, R. Blesa^{3,5}, I. Carrió¹; ¹Nuclear Medicine Department. Hospital de la Santa Creu i Sant Pau, Barcelona, SPAIN, ²Faculty of Medicine. Autonomous University of Barcelona, Barcelona, SPAIN, ³Memory Unit, Neurology Department. Hospital de la Santa Creu i Sant Pau, Barcelona, SPAIN, ⁴Down Medical Centre. Fundació Catalana Síndrome de Down, Barcelona, SPAIN, ⁵Centre of Biomedical Investigation Network for Neurodegenerative Diseases (CIBERNED), Barcelona, SPAIN.

Most patients with Down's syndrome (DS) develop young onset Alzheimer disease (AD). However, the natural history of AD in DS remains unclear. The objective of this study was to evaluate the use of 18F-Florbetapir PET and 18F-FDG PET in DS patients with prodromal AD. Material and methods: we included 16 consecutive DS patients (10 without cognitive decline and 6 with prodromal AD) who underwent 18F-Florbetapir PET-CT and 18F-FDG PET-CT studies. The studies were evaluated visually and quantitatively. The quantitative analysis for FDG and Florbetapir studies was performed according to the Alzheimer's Disease Neuroimaging Initiative methodology, obtaining SUVr values in AD-related regions of interest. Results: The FDG visual analysis showed that all patients without cognitive decline presented preserved brain metabolism in FDG studies, while 2 of 6 patients with prodromal AD showed hypometabolism in parietotemporal regions. The Florbetapir visual analysis showed cortical Florbetapir uptake in 2 of 10 subjects without cognitive decline, and in all patients with prodromal AD. These results were supported by quantitative FDG and Florbetapir analysis: patients with prodromal AD showed a significant decrease in FDG SUVr values (1.36±0.08 vs 1.22±0.1; $p=0.012$), and a significant increase in Florbetapir SUVr values (1.02±0.08 vs 1.19±0.1; $p=0.003$). Conclusion: FDG and Florbetapir studies may be both useful in clinical diagnostic of dementia in DS patients and might give complementary information. Florbetapir uptake starts in the preclinical phase of the disease and is present in all presymptomatic patients, while hypometabolism observed in the FDG starts later in the symptomatic phase of the disease.

1001 – Monday, October 17, 2016, 16:30 - 18:00, Auditorium
CME 8 - Physics/Translational Molecular Imaging & Therapy: QA/QC Preclinical Systems and Preclinical Imaging Procedures

OP380

Keynote – QA/QC of Preclinical Imaging System

S. Vandenberghe; Universiteit Gent, Medisip Elis-Ibitech, Ghent, BELGIUM.

OP381

Acceptance Testing and QA of Small Animal PET/MRI System

M. Kranz; Helmholtz-Zentrum Dresden-Rossendorf, Neuroradiopharmaceuticals, Leipzig, GERMANY.

OP382

First Experiences with Small Animal PET/CT and PET/MR Systems (Acceptance Testing Application)

M. Huisman; VU University Medical Centre, Amsterdam, NETHERLANDS.

OP383

Standardisation of Molecular Preclinical Imaging Procedures

C. Kuntner-Hannes; Biomedical Systems, Seibersdorf, AUSTRIA.

1002 – Monday, October 17, 2016, 16:30 - 18:00, Hall 211

Joint Symposium 8 - EANM/EASD: The Infected Diabetic Foot – Consensus Meeting

OP384

The Infected Diabetic Foot - Clinical Point of View

B. Lipsky; University of Oxford, Division of Medical Sciences, Oxford, UNITED KINGDOM.

OP385

The Infected Diabetic Foot - Radiological Point of View

L. Sconfienza; IRCCS Policlinico San Donato, Servizio di Radiologia, Milan, ITALY.

OP386

The Infected Diabetic Foot - Nuclear Medicine Point of View

R. M. Chakravarty; Kings College Hospital NHS Foundation Trust, Kings College London, Nuclear Medicine Department, London, UNITED KINGDOM.

1003 – Monday, October 17, 2016, 16:30 - 18:00, Hall 117

CTE 4: Nuclear Medicine Oncology beyond FDG

OP387

PET/CT Imaging Beyond 18F-FDG: 18F and 68Ga-labelled tracers

L. Lezaic; Klinični center Ljubljana, Klinika za Nuklearno Medicino, Ljubljana, SLOVENIA.

OP388

Current Status of F-18 DOPA Imaging in Neuroendocrine Tumours

D. Huic; University Hospital Center Zagreb, Clinical Department of Nuclear Medicine and Radiation Protection, Zagreb, CROATIA.

OP389

PET-CT Imaging with C11 tracers

G. Testanera; Istituto Clinico Humanitas, Department of Nuclear Medicine, Milan, ITALY.

1004 – Monday, October 17, 2016, 16:30 - 18:00, Hall 112

Do.MoRe: Neuroendocrine Tumours

OP390

Absorbed kidney doses in patients treated with different activities of Lu-177-octreotate - results of the first 100 patients treated in the Helsinki University Hospital

V. Reijonen, J. Heikkonen, H. Mäenpää; Helsinki University Hospital Cancer Center, Helsinki, FINLAND.

Aim: The routine activity of 7.4 GBq in ¹⁷⁷Lu-octreotate treatment is often reduced by 25% or 50% for clinical reasons. The effect of this reduction on absorbed kidney doses is studied. **Materials and methods:** Between February 2011 and December 2015, 100 patients had received 3.3 to 8.8 GBq of ¹⁷⁷Lu-octreotate with protecting amino acid solution. The standard protocol was to administer 7.4 GBq four times at eight week interval, but the activity was reduced to either 75% or 50% due to older age, previous chemotherapy, diabetes, hypertension, fragility, or signs of bone marrow toxicity sustained during earlier treatment cycles. The kidney region of the patients was imaged using either Symbia T2 or Intevo T6 SPECT/CT (Siemens Healthcare) at 24 hours after each treatment and also at 168 hours after the first and third treatment. The first 58 patients were scanned at 1, 72 and/or 120 hours in addition to the later standard 24 and 168 hours after each treatment to establish the method for estimating the absorbed dose to the kidneys. The activities in the left and right kidney were determined from SPECT images and the kidney volumes were defined from the axial CT slices. Also a small volume (SV) of interest (4 cm³) was selected from the volume of maximal counts in the kidney region to estimate the maximum absorbed dose for the kidney. **Results:** We divided the treatments into three groups according to the administered activity: group 1 (n=38, range 3283–4266 MBq), group 2 (n=55, range 4600–6432 MBq), and group 3 (n=244, range 6600–8790 MBq). In group 1, the median whole kidney dose was 1.8 Gy (range 0.9–4.9 Gy) and median SV dose 3.1 Gy (range 1.4–8.4 Gy), while in group 2 and group 3, the median whole kidney doses were 3.5 Gy (range 1.0–7.6 Gy) and 3.2 Gy (range 1.0–9.2 Gy), and the median SV doses 5.6 Gy (range 1.8–19.7 Gy) and 5.5 Gy (range 1.4–16.3 Gy), respectively. The median whole kidney and SV doses were significantly smaller in group 1 than in groups 2 and 3 (Mann-Whitney, p<0.05), while there was no significant difference between groups 2 and 3 (p=0.976 and p=0.778). **Conclusion:** In our patient cohort, kidney doses were significantly smaller when the administered activity was reduced to about 50% of the standard protocol. However, when the administered activity was reduced to 75% of the standard protocol, the kidney doses did not scale down accordingly.

OP391

Characterisation of a planar dosimetry method estimating the absorbed dose to the bone marrow during ¹⁷⁷Lu-DOTATATE treatment

L. Hagmarker¹, J. Svensson², T. Magnander¹, J. Hemmingsson¹, P. Gjertsson³, P. Bernhardt¹; ¹Department of Radiation Physics, Sahlgrenska Academy, University of Gothenburg, Göteborg, SWEDEN, ²Department of Oncology, Sahlgrenska Academy, University of Gothenburg, Göteborg, SWEDEN, ³Department of Clinical Physiology, Sahlgrenska University Hospital, Göteborg, SWEDEN.

Aim: An image based method for bone marrow dosimetry, earlier presented by our research group, has shown a significant correlation between the absorbed dose to the bone marrow and haematological toxicity in ¹⁷⁷Lu-DOTATATE treatment. The aim of this study was to further evaluate and optimise the method. **Materials and Methods:** 46 patients with advanced neuroendocrine tumours were treated with ¹⁷⁷Lu-DOTATATE on 2–6 occasions. The patients were evaluated using the 4 planar gamma camera images collected at 2, 24, 48 and 168 hours after injection. The whole body was divided into a high- and a low uptake compartment, using a threshold based segmentation tool in the image platform PhONSAi, developed in-house. The segmentation tool starts by including the highest uptake focus and then gradually includes foci with lower and

lower uptakes until a threshold is reached where the number of foci escalates. The threshold determines the proportion of the foci that is included in the two compartments. Visual inspection was used to determine the threshold value where all high uptake tissues (i.e. kidney, spleen, liver and tumours) were included in the high uptake compartment. For thresholds around this value the activity in the two compartments was determined by the conjugate view method and the bone marrow dose was calculated as a sum of the self and cross dose in the low uptake compartment and the cross dose from the high uptake compartment. **Results:** The visual analysis implies a threshold value of 10 % of the maximum number of foci. A correlation was found between the absorbed bone marrow dose and haematological toxicity with p-values ranging from 0.001 to 0.02 for thresholds between 2 % and 25 %, the strongest correlation was found at 15 %. The mean absorbed bone marrow dose were 0.20–0.22 Gy per 7.4 GBq for threshold values between 10–25 %, and increased to 0.28 Gy for the lower values. No significant difference was observed in coefficient of variation (8.2–8.7 %) for the individual mean absorbed doses when varying the threshold value. **Conclusion:** The individual variation in absorbed dose is maintained at a low level when varying the threshold value for the determination of the compartment sizes. This implies that the method is stable for estimation of bone marrow doses and its correlation to haematological toxicity.

OP392

Simulation study to determine an optimal sampling schedule for dynamic PET measurements for treatment planning in peptide-receptor radionuclide therapy

D. Hardiansyah^{1,2}, A. A. Attarwala^{1,2}, L. D. Jimenez^{1,2}, P. Kletting³, F. M. Mottaghy^{4,5}, G. Glatting¹; ¹Medical Radiation Physics/Radiation Protection, Universitätsmedizin Mannheim, Medical Faculty Mannheim, Heidelberg University, Mannheim, GERMANY, ²Department of Radiation Oncology, Universitätsmedizin Mannheim, Medical Faculty Mannheim, Heidelberg University, Mannheim, GERMANY, ³Department of Nuclear Medicine, University Hospital Ulm, Ulm, GERMANY, ⁴Klinik für Nuklearmedizin, University Hospital, RWTH Aachen University, Aachen, GERMANY, ⁵Department of Nuclear Medicine, Maastricht University Medical Center (MUMC+), Maastricht, NETHERLANDS.

Aim: To determine the optimal sampling schedule for dynamic PET measurements to obtain an accurate prediction of time-integrated activity coefficients (TIACs) in peptide-receptor radionuclide therapy (PRRT). **Methods:** Parameters of a physiologically based pharmacokinetic (PBPK) model were individually fitted to the biokinetic data of 15 patients after injection of ¹¹¹In-DTPAOC. True mathematical patient phantoms (true MPPs) were build using the fitted parameters from the PBPK model. Dynamic PET simulations with two bed positions were performed after i.v. injection of 150 MBq of ⁶⁸Ga-DOTATATE (25 µg total peptide amount) for 3 different sampling schedules (SS), i.e. SS1 consisting of 1 dynamic PET scan at approximately 30 min, SS2 consisting of 1 dynamic PET scan at approximately 4 h, and SS3 which is a combination of SS1 and SS2. Four frames, with duration of 5 min each, were collected for each bed position. Organ activities of the kidneys, liver and spleen were taken from the first bed position (first 4 frames), while the tumor activities were taken from the second bed position. A PET noise model was used to add noise to the simulated data. The PBPK model was fitted again to the simulated noisy PET data using Bayesian information calculated as the mean and SD of the population. The fitted parameters were used to build the PET-predicted MPPs. A therapeutic injection of 5 GBq of ⁹⁰Y-DOTATATE in a 30 min infusion was simulated in both the true and the PET-predicted MPPs followed by the calculation of their TIACs. Relative variability values (v) between the therapeutic TIACs of the true and the PET-predicted MPPs for the tumor, kidneys, liver, spleen and whole body (WB) were calculated and analyzed. **Results:** Relative

variability values from the SS1 were accurate enough to predict TIACs of the organs at risk during PRRT, i.e. $v_{\text{kidneys}}=(3.5\pm 1.8)\%$, $v_{\text{liver}}=(2.9\pm 1.3)\%$, $v_{\text{spleen}}=(3.5\pm 1.6)\%$, and $v_{\text{WB}}=(3.9\pm 1.9)\%$. The variability values from SS2 and SS3 presented small differences when compared to the SS1 variabilities, i.e. for SS2 $v_{\text{kidneys}}=(2.6\pm 1.7)\%$, $v_{\text{liver}}=(2.6\pm 1.8)\%$, $v_{\text{spleen}}=(2.6\pm 1.8)\%$, and $v_{\text{WB}}=(3.8\pm 3.4)\%$; and for SS3 $v_{\text{kidneys}}=(1.6\pm 0.9)\%$, $v_{\text{liver}}=(1.1\pm 0.5)\%$, $v_{\text{spleen}}=(1.6\pm 0.9)\%$, and $v_{\text{WB}}=(0.5\pm 0.3)\%$. However, variabilities of predicted TIACs in the tumor showed inaccurate results for all protocols, e.g. SS1 $v_{\text{tumor}}=(19.1\pm 12.6)\%$, SS3 $v_{\text{tumor}}=(16.1\pm 13.4)\%$ and SS3 $v_{\text{tumor}}=(17.2\pm 7.7)\%$. **Conclusions:** Dynamic PET scans at approximately 30 min or 4 hours p. i. in combination with the use of a PBPK model with population-based Bayesian parameters may allow both simplifying the treatment planning workflow in PRRT and improving the accuracy of predicted TIACs.

OP393

Definition of a reference organ for lesion thresholding on ^{68}Ga -DOTATATE PET/CT

G. Marin^{1,2}, H. Levillain¹, B. Vanderlinden¹, T. Guiot¹, I. Karfis¹, Z. Wimana¹, S. Vandenberghe², P. Flamen¹; ¹Institut Jules Bordet, ULB, Bruxelles, BELGIUM, ²MEDISIP, Ghent University, Ghent, BELGIUM.

Aim: ^{68}Ga -DOTATATE has become the radiolabeled peptide of choice for well-differentiated neuroendocrine tumors diagnosis and follow-up. Still, there are no established guidelines for lesion segmentation. The aim of this work was to define a reference organ for lesion thresholding, assessed by their inter- and intra-patient variability. **Materials and methods:** Twelve patients from the LuMen trial underwent 3-5 ^{68}Ga -DOTATATE PET/CT every 3 months preceding each ^{177}Lu -DOTATATE administration. Long acting somatostatin analogs were discontinued 4 weeks prior to ^{68}Ga -DOTATATE PET/CT. A mean \pm SD activity of 1.91 ± 0.32 MBq/kg was administered. Whole body images were acquired 63.5 \pm 9.5 minutes after injection on a Discovery 690 PET/CT (GE-Healthcare) with 10 bed positions of 2.5-3 minutes. Images were reconstructed with 3D OSEM algorithm (18 iterations, 3 subsets, 6.8 mm Gaussian post filtering, time of flight and resolution recovery corrections). Healthy kidneys, spleen and liver mean SUVs (normalized for body weight) were determined from three spherical volumes of interest (2 cm diameter) placed in each organ. Inferior left/right and superior left kidney cortex areas were considered, thus avoiding liver activity spill-in. Two larger volumes of interest were drawn in left and right buttocks. Additionally, mean and maximum SUVs were measured in a sphere centered on the pituitary. Inter-patient coefficient of variation (CoV) of mean SUVs was computed for each organ based on the baseline ^{68}Ga -DOTATATE PET/CT of each patient. Intra-patient CoV of mean SUVs was computed for each organ of each patient from the acquisitions. Median and interquartile range (IQR) of CoVs were then calculated for each organ. The same methodology was also applied to the different considered areas in the kidneys. **Results:** Regarding inter-patient variability, the kidneys had the smallest CoV (20 % versus 25, 27, 46, 32 and 36 % respectively for mean spleen, liver, buttocks, pituitary SUV and maximum pituitary SUV). No difference was noticed between the considered kidneys areas. Intra-patient CoV results were more balanced with median[IQR] equal to 12[9], 13[16], 17[11], 11[16], 16[26] and 25[25] % respectively for mean kidneys, spleen, liver, buttocks, pituitary SUV and maximum pituitary SUV. For the kidneys, the best results were found for the right kidney (12[5] % versus 16[12] and 13[15] % for the superior and inferior left). **Conclusion:** These results indicate that kidneys are the organs with the smallest inter- and intra-patient variability on ^{68}Ga -DOTATATE PET/CT and could therefore be used as a reference for lesion thresholding.

OP394

NETTER-1 Phase III in Patients with Midgut Neuroendocrine Tumors Treated with ^{177}Lu -Dotatate: Efficacy and Safety Results

J. Strosberg¹, E. Wolin², B. Chasen³, M. Kulke⁴, D. Bushnell⁵, M. Caplin⁶, R. P. Baum⁷, P. Kunz⁸, T. Hobday⁹, A. Hendifar¹⁰, K. Oberg¹¹, M. Lopera Sierra¹², D. Kwakkeboom¹³, P. Ruszniewski¹⁴, E. Krenning¹⁵; ¹H. Lee Moffitt Cancer Center, Tampa, FL, UNITED STATES, ²Markey Cancer Center, University of Kentucky, Lexington, KY, UNITED STATES, ³University of Texas MD Anderson Cancer Center, Houston, TX, UNITED STATES, ⁴Dana-Farber Cancer Institute, Boston, MA, UNITED STATES, ⁵University of Iowa, Iowa City, IA, UNITED STATES, ⁶Royal Free Hospital, London, UNITED KINGDOM, ⁷Zentralklinik, Bad Berska, GERMANY, ⁸Stanford University Medical Center, Standford, CA, UNITED STATES, ⁹Mayo Clinic College of Medicine, Rochester, Rochester, MN, UNITED STATES, ¹⁰Cedars Sinai Medical Center, Los Angeles, CA, UNITED STATES, ¹¹University Hospital, Uppsala, Uppsala, SWEDEN, ¹²Advanced Accelerator Applications, New York, NY, UNITED STATES, ¹³Erasmus Medical Center, Rotterdam, NETHERLANDS, ¹⁴Hopital Beaujon, Clichy, Clichy, FRANCE, ¹⁵Erasmus Medical Center, Rotterdam, Rotterdam, NETHERLANDS.

Background: Currently, there are limited therapeutic options for patients with advanced midgut neuroendocrine tumors progressing on first-line somatostatin analog therapy. **Methods:** NETTER-1 is the first phase III multicentric, randomized, controlled trial evaluating ^{177}Lu -DOTA⁰-Tyr³-Octreotate (Lutathera®) in patients with inoperable, progressive, somatostatin receptor positive midgut NETs. 230 patients with grade 1-2 metastatic midgut NETs were randomized to receive Lutathera 7.4 GBq every 8 weeks (x4 administrations) versus Octreotide LAR 60 mg every 4 weeks. The primary endpoint was PFS (RECIST 1.1), with tumor assessment every 12 weeks. Secondary objectives included ORR, OS, toxicity, and quality of life (QoL) based upon EORTC QLQ-C30 and QLQ-G.I.NET21 questionnaires. **Results:** The centrally confirmed disease progressions or deaths were 23 in the Lutathera arm and 68 in the Octreotide LAR 60 mg arm. The median PFS was not reached for Lutathera and 8.4 months with control, $p<0.0001$, HR 0.21. The number of CR+PR was 18 (18%) with Lutathera and 3 (3%) with control ($p=0.0008$; $n=201$). At the time of the NDA submission, interim OS analysis (14 deaths in Lutathera group and 26 in control group; $p=0.0043$) suggests an improvement in OS. The median TTP was not reached for Lutathera and 8.7 months with control, $p<0.0001$, HR 0.17. Among patients treated with Lutathera, only 5% (6 patients) experienced dose modifying toxicity. Adverse events, grade 3 or 4 neutropenia, thrombocytopenia and lymphopenia occurred in 1%, 2% and 9% of patients in Lutathera arm vs. none in controls. Health related QoL surveys indicated a slight improvement in the global health status under Lutathera treatment, demonstrating that the treatment benefit of Lutathera is not offset by a negative impact on patient quality of life. **Conclusions:** The phase III NETTER-1 trial provides evidence for a clinically meaningful and statistically significant increase in PFS, TTP and ORR, and suggests an OS benefit in patients with advanced midgut NETs treated with Lutathera. The Lutathera safety and QoL profile was found to be favorable.

OP395

Tandem peptide radionuclide therapy with $^{90}\text{Y}/^{177}\text{Lu}$ -DOTATATE clinical results and long term side effect - 10 years' experience

J. Kunikowska¹, D. Pawlak², M. Bak³, B. Kos-Kudla⁴, R. Mikolajczak², L. Krolicki¹; ¹Nuclear Medicine Department, Medical University of Warsaw, Warszawa, POLAND, ²National Centre for Nuclear Research, Radioisotope Centre POLATOM, Otwock-Swierk, POLAND, ³Department of Gastroenterology and Internal Medicine, Medical University of Warsaw, Warszawa, POLAND, ⁴Division of

Endocrinology, Department of Pathophysiology and Endocrinology, Medical University of Silesia, Katowice, POLAND.

PRRT with ^{90}Y and ^{177}Lu is a form of molecular targeted therapy for the inoperable/or disseminated neuroendocrine tumors (NEN). De Jong was the first one, who described the use of combination treatment consisting of 50% ^{177}Lu -DOTATATE and 50% ^{90}Y -DOTATOC in rats; which demonstrated 3 times longer survival rates. It was confirmed in human in our previous trial. The aim of the study was to evaluate clinical results and long term side effects of combination treatment - tandem $^{90}\text{Y}/^{177}\text{Lu}$ -DOTATATE in patients with disseminated neuroendocrine tumors. **Materials and methods:** 59 patients with disseminated NEN were included in the study prospectively. Therapy protocol was based on combined 1:1 $^{90}\text{Y}/^{177}\text{Lu}$ -DOTATATE with activity 3.7 GBq/m² body surface area in 3-5 cycles. Blood tests for hematology, kidney and liver function, and chromogranin A (CgA) were evaluated before therapy. All patients underwent CT scans and somatostatin receptor imaging (SRI; $^{99\text{m}}\text{Tc}$ -HYNICTATE or ^{68}Ga -DOTATATE). Mixed amino-acids infusion over 8 hours was used for the kidney protection. **Results:** At the time of treatment all patients showed progressive disease confirmed by CT, SRI and/or increasing CgA level. Ki-67 of primary tumours in examined group was below 20%. Clinical response defined as increase in clinical symptoms (diarrhoea, flushes, wheezing, hypoglycemia or dyspnea) was observed in 97 % patients with hormone-related syndromes before PRRT. During a median follow up of 75.8 months (range 11-121 months) the observed PFS was 32.2 months and OS was 82 months, 25 patients died. The observed 5-years overall survival was 63% and 2-years risk of progression was 39.4%. At the time of restaging 3 patient died. Treatment response according to RECIST 1.1 criteria consisted of complete response 2%, partial response in 22%, stable disease in 65% and progressive disease in 6% patients. The disease control rate was 89%. Objective Response Rate (ORR), defined as proportion of patients achieving partial (PR) or complete response (CR), was 24%. PRRT was well tolerated by all patients. One patients (2%) revealed MDS five years, after receiving after total activity 29.6 GBq. No other hematological grade 3 and 4 was observed. Renal toxicity grade 3 was observed in one patient (2%), no grade 4 was observed. **Conclusions:** The tandem $^{90}\text{Y}/^{177}\text{Lu}$ DOTATATE therapy is effective and safety treatment option for patients with disseminated or inoperable neuroendocrine tumors. Long term follow up revealed high disease control rate and long PFS with small number of side effects.

OP396

Correlation Between Somatostatin Receptor Expression and Molecular Response to Peptide Receptor Radionuclide Therapy in Head and Neck Paragangliomas evaluated by ^{68}Ga -DOTANOC

G. Ferreira, I. L. Sampaio, L. Sobral Violante, J. P. Teixeira, H. Duarte; Instituto Português de Oncologia Francisco Gentil, Porto, PORTUGAL.

Aim: To correlate pre-treatment somatostatin receptor expression with molecular response after completion of three peptide receptor radionuclide therapy (PRRNT) cycles, using ^{68}Ga -DOTANOC PET/CT in patients with head and neck paraganglioma (HNPGL). **Materials and methods:** Twenty-one patients (3 men and 18 women; mean age \pm SD, 59.0 years \pm 13.5) with HNPGL evaluated between 2011 and 2015 were included. All patients performed two ^{68}Ga -DOTANOC PET/CT studies, one at baseline and another after completion of three PRRNT cycles with ^{177}Lu -DOTATATE. Median time between baseline ^{68}Ga -DOTANOC PET/CT and first PRRNT cycle was 2.2 months (IQR 1.2) and between PRRNT completion and post treatment ^{68}Ga -DOTANOC PET/CT was 6.1 months (IQR 2.2). The median inter-scan period was 14.4 months (IQR 3.1). Somatostatin receptor expression was assessed using 2 measures of standardized uptake value (SUV): maximum SUV (SUV_{max}) and tumor-to-spleen SUV ratio (SUV_{T/S}). SUV_{max} variation ($\Delta\text{SUV}_{\text{max}}$) percentage and SUV_{T/S} variation ($\Delta\text{SUV}_{\text{T/S}}$) percentage were used to define four categories of molecular response, based on European

Organization for Research and Treatment of Cancer Criteria: Complete Metabolic Response (CMR), Partial Metabolic Response (PMR), Stable Metabolic Response (SMR) and Progressive Disease (PD). According to metabolic response, patients were divided in responders (CMR and PMR) and non-responders (SMR and PD). Wilcoxon-Mann-Whitney for independent samples tests and Spearman rank correlation tests were used ($P < 0.05$). **Results:** SUV variation percentage after PRRT was highly asymmetrical in both evaluation methods, $\Delta\text{SUV}_{\text{max}}$ (mean \pm SD, -16.0% \pm 40.3, min -78.1%, max 83.5%) and $\Delta\text{SUV}_{\text{T/S}}$ (mean \pm SD, -7.0% \pm 42.3, min -69.8%, max 102.5%). Metabolic responses based on $\Delta\text{SUV}_{\text{max}}$ percentage were: 10 PMR, 8 SMR, 3 PD and 0 CMR. Baseline SUV_{max} did not correlate significantly to $\Delta\text{SUV}_{\text{max}}$ percentage after PRRT ($\rho = -0.34$, $P = 0.134$). Although responders (PMR) registered a higher baseline median SUV_{max} compared to non-responders, the difference was not statistically significant (13.0 vs. 9.2, $P = 0.159$). Metabolic responses based on $\Delta\text{SUV}_{\text{T/S}}$ were: 9 PMR, 9 SMR, 3 PD, 0 CMR. A statistically significant correlation between baseline SUV_{T/S} and $\Delta\text{SUV}_{\text{T/S}}$ percentage after PRRT was found ($\rho = -0.44$, $P = 0.022$). Responders (PMR) had statistically significant higher median baseline SUV_{T/S} than non-responders (14.89 vs. 8.08, $P = 0.012$). **Conclusion:** Initial ^{68}Ga -DOTANOC PET/CT uptake values may contribute usefully to select HNPGL patients for PRRT. We found a statistically significant correlation between baseline SUV_{T/S} and $\Delta\text{SUV}_{\text{T/S}}$ percentage ($\rho = -0.44$, $P = 0.022$). Also, responders had statistically significant higher median baseline SUV_{T/S} than non-responders (14.89 vs. 8.08, $P = 0.012$). Baseline SUV_{T/S} value was therefore superior to SUV_{max} for predicting molecular response to PRRT. Clinical correlations remain to be assessed.

1005 – Monday, October 17, 2016, 16:30 - 18:00, Hall 115

M2M: New Chemistry & Instrumentation

OP397

A Novel and Rapid [^{11}C]CO₂ to [^{11}C]CO Conversion Methodology via Disilane Species

C. Taddei, S. Bongarzone, A. D. Gee; King's College London, London, UNITED KINGDOM.

Introduction: Carbon-11 carbon monoxide ([^{11}C]CO) is used to produce functionalised [^{11}C]molecules, such as amides, esters and ketones.[1] [^{11}C]CO is traditionally produced by gas-phase reduction of [^{11}C]CO₂ at elevated temperatures.[2] We recently reported a novel chemical conversion of [^{11}C]CO₂ to [^{11}C]CO via [^{11}C]silicarboxylic acids.[3] This methodology avoids the use of high temperatures by implementing a simple and readily available set-up. It does, however, require the careful preparation of silane lithium derivatives and the addition of an activator to trigger the release of [^{11}C]CO. A recent synthetic chemistry publication reported the use of disilanes as CO releasing agents in the presence of fluoride sources.[4] Herein, we show the application of disilane species to carbon-11 chemistry. This approach obviates time consuming preparation of reagents and simplifies the experimental set-up needed. Furthermore, the generated [^{11}C]CO is transferred to a second vial containing carbonylation reagents to yield ^{11}C -labelled products of interest. Method and Results: A simple two-vial reaction set-up on an Eckert & Ziegler Modular-Lab system was used. In a first vial, a disilane species and catalytic amount of a fluoride source were dissolved in a dry aprotic solvent. [^{11}C]CO₂ was delivered from the cyclotron by a helium stream and instantaneously converted to [^{11}C]CO at 20 °C by a fluoride activated disilane carboxylate species. The released [^{11}C]CO was transferred to a second vial where a palladium-mediated carbonylation reaction was performed. The transfer of the produced [^{11}C]CO to a second vial was time-monitored. As model reactions, [^{11}C]N-benzylbenzamide and [^{11}C]tert-butyl acrylate were obtained in high radiochemical purity ($\geq 85\%$) and short synthesis time (≤ 10 min from EOB). Conclusion: The development of a new [^{11}C]CO₂ to [^{11}C]CO conversion methodology via

disilanes was successfully achieved. This methodology yields [^{11}C]CO in up to 35% under very mild and rapid reaction conditions, with no time-consuming reagent preparation or complex automation required. Moreover, it represents an attractive route to synthesise [^{11}C]carbonyl-containing molecules avoiding the need for traditional high temperature gas-phase infrastructure. Research Support: This work was supported by European Commission, FP7-PEOPLE-2012-ITN (316882, RADIOMI), Medical Research Council (MRC, MR/K022733/1) and Biomedical Research Centre award to Guy's&St Thomas' NHS Foundation Trust. References: [1] B. Långström *et al* (2007) *J. Labelled Compd. Radiopharm.*, 50, 794. [2] S.K. Zeisler, *et al* (1997) *Appl. Radiat. Isot.*, 48, 1091. [3] C. Taddei *et al* (2015) *Chem. Commun.*, 51, 11795. [4] C. Lescot *et al* (2014) *J. Am. Chem. Soc.*, 136, 6142.

OP398

Novel Chemoselective [^{18}F]-Radiolabeling of Thiol-Containing Biomolecules under Mild Aqueous Conditions

A. Chiotellis¹, F. Sladojevich², L. Mu², A. Mueller-Herde², I. E. Valverde³, V. Tolmachev⁴, R. Schibli², S. M. Ametamey², T. L. Mindt²; ¹University of Nottingham, Nottingham, UNITED KINGDOM, ²ETH Zurich, Zurich, SWITZERLAND, ³University Hospital of Basel, Basel, SWITZERLAND, ⁴Uppsala University, Uppsala, SWEDEN.

Aim: Although prosthetic groups based on maleimide chemistry are established tools for the selective and controlled introduction of an [^{18}F] label into thiol-containing (bio)molecules, there are certain limitations. These mainly include susceptibility of the addition product to hydrolysis or exchange reactions with biologically relevant reactive thiols and the formation of racemic mixtures. Recently it was reported that 2-(methylsulfonyl)-5-phenyl-1,3,4-oxadiazole reacts rapidly and specifically with thiols of biomolecules with excellent chemoselectivity at biological pH to provide conjugates with superior stability compared to the corresponding maleimide-based analogues.¹ Herein, we report a novel prosthetic group based on this oxadiazole scaffold, termed [^{18}F]FPOS (fluoroethoxyphenyl-oxadiazole methylsulfone), and its utility for the [^{18}F]-radiolabeling of thiol containing molecules. **Methods:** A nosylate precursor for labeling and non-radioactive reference FPOS were synthesized from methyl-4-hydroxybenzoate in a total of 6 steps and good overall yield. FPOS was conjugated with two model thiols (dodecylthiol, methyl acetyl-L-cysteinate) and two single-cysteine containing tumor targeting biomolecules; bombesin analogue AcCys(β Ala)₃[Nle¹⁴]BBN (7-14)NH₂, a high affinity peptide for the gastrin-releasing peptide receptor and affibody Z_{HER2:2395}-Cys which effectively targets the human epidermal growth factor receptor-2 (HER-2). The corresponding [^{18}F]-labeled molecules were synthesized by a two-step procedure; (i) aliphatic nucleophilic substitution of the nosylate precursor with [^{18}F] and (ii) subsequent coupling with the corresponding thiols. *In vivo* PET imaging was performed with [^{18}F]Z_{HER2:2395}-Cys using CD1 nude mice bearing HER2-positive SCOV3 xenografts. Nude mice with HER2-negative RAMOS xenografts were used as control. **Results:** Prosthetic group [^{18}F]FPOS was efficiently prepared within 60 min in good radiochemical yield (27±6%, d.c.) with an activity of 6-16 GBq after HPLC purification. [^{18}F]FPOS readily reacted with the two model thiols within 15 min at 37 °C to give quantitatively the corresponding [^{18}F]-labeled compounds. Reaction of [^{18}F]FPOS with AcCys(β Ala)₃[Nle¹⁴]BBN(7-14)NH₂ at 3.5 mM in PBS, quantitatively yielded the [^{18}F]-labeled peptide at 37 °C after 15 min with a specific activity of 54 GBq/ μ mol. [^{18}F]FPOS reacted with Z_{HER2:2395}-Cys in PBS (50 °C, 15 min) to give [^{18}F]Z_{HER2:2395}-Cys with 40% conversion and 17 GBq/ μ mol specific activity. PET imaging of the [^{18}F]-labeled affibody showed substantial accumulation of radioactivity in the SCOV3 xenografts with excellent tumor-to-background ratio whereas negligible uptake was observed in the RAMOS tumors. **Conclusion:** The novel prosthetic group based on the oxadiazole scaffold, [^{18}F]FPOS, meets all criteria for the effective and

chemoselective radiolabeling of thiol containing (bio)molecules and thus represents a true alternative to the maleimide-based approaches. [1] N. Toda *et al.*, *Angew. Chem.* 2013, 52(48), 12592-12596.

OP399

From [^{11}C]CO₂ To [^{11}C]Amides And [^{11}C]Ureas: A Rapid One-Pot Mitsunobu Reaction

S. Bongarzone, A. Runser, C. Taddei, A. Haji Dheere, A. D. Gee; Division of Imaging Sciences and Biomedical Engineering, King's College London, London, UNITED KINGDOM.

Background The existence of reliable chemical methods for labeling organic molecules such as ureas and amides with ^{11}C are key to the production of novel radiotracers intended for PET imaging studies. A rapid single-pot radiosynthetic approach for the production of [^{11}C]amides and [^{11}C]ureas starting from cyclotron-produced [^{11}C]CO₂ is presented. **Materials and Methods** A vial containing a solution of an amine and 1,8-Diazabicycloundec-7-ene (DBU) in acetonitrile (ACN) was placed on an Eckert & Ziegler Modular-Lab automatic system. [^{11}C]CO₂ was bubbled through the solution producing the corresponding [^{11}C]carbamate derivative. Mitsunobu reagents, tributylphosphine (Bu₃P) and di-tert-butyl azodicarboxylate (DBAD), were added to activate the [^{11}C]carbamate derivative and subsequently reacted with either a) an amine^{1,2} or b) a Grignard reagent to give the corresponding [^{11}C]ureas or [^{11}C]amides respectively. The reactions were quenched with H₂O and the crude product was analysed by radio-HPLC. **Key Results** A novel strategy for radiolabeling ureas and amides starting from cyclotron-produced [^{11}C]CO₂ is presented. [^{11}C]amides and [^{11}C]ureas are obtained in moderate to excellent radiochemical purity (30-90 %) in short synthesis times (2 - 5 mins from end of [^{11}C]CO₂ delivery). This strategy was applied to radiolabel [^{11}C]melatonin with good radiochemical yield (36%) within 2 mins from end of [^{11}C]CO₂ delivery. **Conclusion** A rapid method to radiolabel ureas and amides starting from [^{11}C]CO₂ has been developed. This strategy has been successfully applied to radiolabel melatonin, a biologically relevant amide derivative. **References** [1] Haji Dheere AK, Yusuf N, Gee A (2013). Rapid and efficient synthesis of [^{11}C]ureas via the incorporation of [^{11}C]CO₂ into aliphatic and aromatic amines. *Chem. Comm.*, 49, 8193-8195. [2] Haji Dheere AK, Bongarzone S, Taddei C, *et al.* (2015). Synthesis of ^{11}C -Labelled Symmetrical Ureas via the Rapid Incorporation of [^{11}C]CO₂ into Aliphatic and Aromatic Amines. *Synlett* 26(16), 2257-2260. **Acknowledgements** This work was supported by Medical Research Council (MRC, MR/K022733/1), European Commission, FP7-PEOPLE-2012-ITN (316882, RADIOMI), and Biomedical Research Centre award to Guy's & St Thomas' NHS Foundation Trust.

OP400

^{68}Ga in vivo chelation with tris(hydroxypyridinone) ligands

C. Imberti, S. Y. A. Terry, S. Nawaz, J. Baguña Torres, M. T. Ma, J. D. Young, S. Karagiannis, P. J. Blower; King's College London, London, UNITED KINGDOM.

Aim: Gallium uptake in several cancers is well documented and has been extensively exploited in Ga-67 citrate scans¹. In healthy individuals Ga³⁺ accumulates in the bones, liver and spleen while slowly clearing from the blood renally². In order to increase image contrast, chelation of non-tissue associated gallium might be advantageous. Tris(hydroxypyridinone) ligands (THP) are promising chelators for $^{68/67}\text{Ga}$ owing to their ability to rapidly chelate Ga³⁺ under unusually mild conditions (neutral pH, room temperature)³. Here we investigate the ability of THP chelators to radiolabel with ^{68}Ga in biological systems: *in vitro*, by testing their ability of binding $^{68/67}\text{Ga}$ in presence of serum and gallium-avid cancer cells and *in vivo*, by investigating the effect of THP on ^{68}Ga biodistribution in

healthy mice. **Methods:** ^{68}Ga acetate or ^{67}Ga citrate was incubated with serum, THP (10–30 μM) was then added. Speciation pre- and post-addition of THP was determined by size exclusion chromatography. A375 melanoma cells were incubated for 30 minutes with THP (1–100 μM) or PBS, followed by ^{68}Ga acetate addition and further 30 minutes incubation. Percentage cellular uptake of ^{68}Ga was measured by γ -counting. The experiment was repeated in reverse order, i.e. ^{68}Ga first followed by THP. Balb/c mice (female, 7–8 weeks) were anaesthetised, and intravenously injected with acetate buffered ^{68}Ga for dynamic nanoPET/CT scanning. THP (1–20 μg) or saline (control group) were injected at different time points after ^{68}Ga injection. Upon procedure completion, animals were sacrificed and biodistribution assessed by γ -counting. **Results:** THP is able to decrease ^{68}Ga binding to serum proteins and A375 melanoma cells when added either before or after ^{68}Ga incubation. Intravenous injection of THP (≤ 20 $\mu\text{g}/\text{mouse}$) resulted in a sudden change of ^{68}Ga biodistribution in healthy mice, clearly visible in the PET scans. Biodistribution data confirmed a significant increase in ^{68}Ga renal clearance (from 4.9 ± 1.2 ID/g to 30.3 ± 6.6 ID/g measured in kidney) and decreased bone uptake (from 6.1 ± 1.1 ID/g to 2.8 ± 0.2 ID/g measured in femur). HPLC analysis of the urine confirms formation of the radiolabelled THP complex. **Conclusions:** This study shows the potential of *tris*(hydroxypyridinone) chelators for ^{68}Ga -labelling in biological systems, at low concentrations, successfully dealing with competing ligands. $^{68/67}\text{Ga}$ *in vivo* chelation is a useful tool to control biodistribution and excretion of ligand-free gallium in molecular imaging. **References:** 1. Larson, S.M., *Seminars in Nuclear Medicine*, 1978, **8**(3), 93–203. 2. Sohn, M.H. *Journal of Nuclear Medicine*, 1993, **34**(12), 2135–2143. 3. Berry, D.J. *Chemical Communications*, 2011, **47**(25), 7068–7070.

OP401

A 3D Printed Automated Synthesizer for the Rapid production of C-11 Fatty Acids

A. Amor-Coarasa, J. M. Kelly, P. Kothari, W. Qu, D. Kim, J. W. Babich; Division of Radiopharmaceutical Sciences, Department of Radiology, Weill Cornell Medicine, New York, NY, UNITED STATES.

Aim: Swift, robust and reliable synthesis of C-11 tracers is vital in clinical and research settings. Here we present a fully 3D printed automated synthesis unit (ASU) that exploits the advantages of solid phase fatty acid (FA) synthesis and different trapping materials for $\text{CH}_3-(\text{CH}_2)_n-\text{COOH}$ of chain length, $n=0$ to 14. **Methods:** A fully automated FA ASU (approximately $25\text{h} \times 25\text{w} \times 15\text{d}$ cm) was designed using AutoCAD and all components were manufactured exclusively using a 3D printer. Moving parts for turning valves and syringe pumping were printed in nylon while the rest of the primary structure was printed in acrylonitrile butadiene styrene (ABS). High torque motors and linear actuators were used for valve turning and syringe loading/dispensing, respectively. A 24 channel USB servo controller was used for control while Maestro[®] software controlled sequenced automation. A 13X zeolite cartridge was coupled to a 5 port DMSO-resistant manifold containing a Grignard reagent, washing and elution solutions, and a compressed gas line for assisting liquid transfers. $^{11}\text{CO}_2$ was trapped on zeolite with the box in “loading mode”. Once $^{11}\text{CO}_2$ is trapped, the automated sequence is activated, lasting 5.5–8.5 min (depending on the fatty acid) and yielding a radiolabeled product with final formulation dependent on chain length and solubility. **Results:** The synthesizer was mainly used to synthesize ^{11}C -acetate, ^{11}C -propionate and ^{11}C -palmitate. A total of 22 sequential syntheses were performed without mechanical failure. Short target bombardments (5 min for investigational study and 15 min for pre-clinical dose preparation) were sufficient for FA production. Using a 5 min bombardment, up to 0.59 GBq ^{11}C -acetate (96.7% RCP), 2.12 GBq (65% RCP) ^{11}C -propionate and 2.98 GBq ^{11}C -palmitate (94% RCP) were obtained preformulation. Following the 15 min bombardments 1.16 GBq (97.5% RCP) ^{11}C -acetate, 0.45 GBq (99.7%) ^{11}C -propionate and 1.06 GBq (96.7% RCP) ^{11}C -palmitate were obtained in a final formulation suitable for injection. The chemical identity of each FA product was confirmed by comparison with

known standards. **Conclusions:** A 3D printed ASU was designed, manufactured and shown to be robust and reliable in a pre-clinical research environment. Furthermore, it was compatible with high starting activities comparable to clinical syntheses and overcomes high internal pressures without leakage of liquids or radioactivity. On this basis, the 3D printed ASU is a practical, lower cost alternative to commercially available ASUs for the pre-clinical and clinical synthesis of fatty acids labeled with carbon-11.

OP402

Intrinsically ^{89}Zr -Labeled Self-Destructing Mesoporous Silica Nanostructures for In Vivo Tumor Vasculature Targeting

W. Cai, S. Goel, F. Chen, S. Shi, H. F. Valdovinos, T. E. Barnhart; University of Wisconsin-Madison, MADISON, WI, UNITED STATES.

Objective: We present a systematic study of in vitro/in vivo behavior of biodegradable mesoporous silica nanoparticle (bMSN), designed to carry multiple cargos (both small and macromolecular drugs) and subsequently self-destruct over time after drug release. Chelator-free labeling of bMSNs with ^{89}Zr ($t_{1/2}=72.8$ h) was used to track their in vivo pharmacokinetics and CD105 targeting capability via PET imaging. **Methods:** Multi-generational bMSNs with tunable pore diameters were synthesized using a bi-phase stratification approach and thoroughly characterized. In vitro degradation and dual drug loading and release studies were carried out in simulated body fluid (SBF) for 14 days and assessed using standard techniques. bMSNs were intrinsically radiolabeled with oxophilic radionuclide ^{89}Zr , followed by conjugation with polyethylene glycol (PEG) and TRC105 (an antibody specific for CD105) to form (^{89}Zr)bMSN-PEG-TRC105 for in vivo PET imaging in 4T1 breast cancer model. Comprehensive in vitro/in vivo/ex vivo experiments were carried out to evaluate the stability, pharmacokinetics, and tumor vasculature targeting of the nanoconjugates. **Results:** Degradation of nanoconjugates into biocompatible and non-toxic byproducts presents a favorable prospect for their clinical translation. We engineered dendritic bMSNs with spoke-like radiating bimodal mesoporous channels. The hierarchically structured large pore size (5.4 nm and 12 nm) of bMSNs resulted in rapid and complete degradation in SBF within 21 days, while solid silica and mesoporous silica (with smaller pore size) controls showed marginal degradation. The mesostructure further allowed greater co-encapsulation and gradual pH-dependent release of small and large biomolecular drugs. Excellent ^{89}Zr -labeling yield ($\sim 98\%$ within 2 h) and radiostability ($>95\%$ up to 72 h) were observed. CD105 specificity of (^{89}Zr)bMSN-PEG-TRC105 was confirmed in vivo with PET imaging showing significantly enhanced tumor uptake (4.5 ± 0.6 , 11.2 ± 2.1 , 11.5 ± 1.3 and 11.2 ± 0.9 %ID/g at 0.5, 6, 24 and 48 h post-injection; $n=4$), compared to non-targeted and blocking controls. CD105 specificity was further confirmed with ex vivo biodistribution and histological examination. **Conclusion:** We report the first systematic in vivo study of intrinsically ^{89}Zr -labeled bMSNs, targeting CD105 that is overexpressed on tumor neovasculature. The simple, versatile and readily tunable approach shows great potential for bench-to-bedside transition of personalized nanomedicine. The nanoconjugates can be readily tailored to (i) label a plethora of diagnostic/therapeutic radioisotopes without the need for tiresome specific chelator chemistries, (ii) carry small molecule and large biomolecular drugs concurrently for combination therapy, (iii) target multiple tumor types since CD105 is overexpressed on most solid tumor neovasculature, and (iv) auto-destruct and excrete from the body overtime.

OP403

How to gain higher specific radioactivity? A Quality Control (QC) approach

L. Nics¹, B. Steiner¹, E. Klebermass¹, M. Hacker¹, M. Mitterhauser², W. Wadsak¹; ¹Medical University of Vienna, Vienna, AUSTRIA, ²Ludwig Boltzmann Institute for Applied Diagnostics, Vienna, AUSTRIA.

Aim: Time is the limiting factor regarding preparation of radiopharmaceuticals labeled with short-lived radionuclides (e.g. carbon-11, nitrogen-13, gallium-68), especially when both high radioactive yield and specific radioactivity are desired. It is well known, that radioactive decay starts immediately after end of bombardment - even before delivery of the radionuclide to the synthesis unit. After quality control (QC) and final release of the product there is no more influence from the lab's side. Concerning in-vivo applications, it is of utmost importance for radiotracers binding to saturable targets such as receptors and transporters that for high occupancy at the binding sites, high specific radioactivity is crucial. Optimization of the chemical synthesis process as well as the subsequent purification can lead to a significant time reduction. So far, QC procedures are not considered to its full extent in that regard. When determining specific radioactivity and radiochemical purity, high performance liquid chromatography (HPLC) is mostly the method of choice. Knowing, that HPLC is the most time consuming step in QC process, aim of present work was to implement an ultra-HPLC ((U)HPLC) method¹ for different carbon-11 based radiotracers such as (+)-[¹¹C]PHNO², [¹¹C]Harmine, [¹¹C]mHED and [¹¹C]Erlotinib to shorten this HPLC-based QK-step and enhance specific radioactivity. **Methods:** HPLC analyses were performed on an (U)HPLC Agilent 1260 system equipped with: quaternary pump/multi-wavelength UV-detector/manual injector/radio-detector/Elysia-Raytest software. HPLC column: Waters X-Bridge BEH Shield RP-18 (4.6x50mm, 2.5µm, 130Å); mobile phase: (A) 100mM ammonia-phosphate-buffer, pH 2.1 including 5mM sodium-1-octasulfonate; (B) 90% ACN/10% aquadest. (v/v); (C) Aqua purificata (HPLC grade); (D) 50mM ammonia-phosphate-buffer, pH 9.3. HPLC conditions: (+)-[¹¹C]PHNO: 33%A/20%B/14%C/33%D, flow rate 1.6mL/min (0-30"), then 1.0mL/min, wavelength 280nm; [¹¹C]Harmine: 44%B/56%D, flow rate 1.7mL/min (0-15"), then 1.0mL/min, wavelength 246nm; [¹¹C]mHED: 34,5%A/11%B/20%C/34,5%D, flow rate 1.6mL/min (0-45"), then 1.0mL/min, wavelength 275nm; [¹¹C]Erlotinib: 25%A/36%B/39%C, flow rate 1.7mL/min (0-17"), then 1.5mL/min (17"-35"), then 1.0 mL/min, wavelength 334nm. **Results:** Retention times for precursors/products/total HPLC runtimes (rt): (+)-HNO 23sec, (+)-PHNO 41sec,rt 1.0min; Harmol 20sec, Harmine 39sec, rt 55sec; Metaraminol 56sec, mHED 1min18sec, rt 1min35sec; 6-O-desmethylerlotinib 25sec, Erlotinib 46sec, rt 1min5sec. **Conclusion:** The present work demonstrates the importance of shortening the QC process especially time consuming HPLC analyses when working with short-lived radiopharmaceuticals. The resulting increase in specific radioactivity of up to 15% for all tested compounds ((+)-[¹¹C]PHNO, [¹¹C]Harmine, [¹¹C]mHED and [¹¹C]Erlotinib) suggests an implementation of these optimized chromatographic protocols into routine QC. References: ¹Nakao R et al. J PharmBiomed Anal, 2009.; ²Nics L et al. EJNMMI Research, 2016.

1006 – Monday, October 17, 2016, 16:30 - 18:00, Hall 111

Teaching Session: TBA

OP404 TBA

1007 – Monday, October 17, 2016, 16:30 - 18:00, Hall 116

Clinical Oncology: Haematology (LMM + MM)

OP405

Prospective non-invasive evaluation of CXCR4 expression for diagnosis of MALT lymphoma using ⁶⁸Ga-Pentixafor PET/MRI- initial experience

A. Leisser¹, M. Raderer², M. Mayerhöfer³, W. Wadsak¹, M. Mitterhauser¹, M. Hartenbach¹, S. Pfaff¹, S. Kropf⁴, M. Hacker¹, A. R. Haug¹; ¹Medical University of Vienna, Division of Nuclear Medicine, Vienna, AUSTRIA, ²Medical University of Vienna, Department of Internal Medicine I, Vienna,

AUSTRIA, ³Medical University of Vienna, Department of Biomedical Imaging and Image-guided Therapy, Vienna, AUSTRIA, ⁴Scintomics GmbH, Fuerstenfeldbruck, GERMANY.

Aim: MALT lymphomas are a challenge for non-invasive diagnosis. So far, biopsy is still needed for staging and re-staging. MALT lymphoma express the chemokine receptor CXCR4 on a regular basis, and ⁶⁸Ga-Pentixafor has shown to quantify CXCR4 expression non-invasively (1-4). Based on these findings, we evaluated for the first time ⁶⁸Ga-Pentixafor PET/MRI for non-invasive diagnosis of MALT lymphoma. **Materials and methods:** We prospectively included 10 patients with MALT lymphoma in this pilot study (5 male, mean age 67). Localisations were stomach (n=3), lung (n=3), kidney (n=2), palatine tonsil and orbita (n=1). Precursor for ⁶⁸Ga-Pentixafor synthesis was provided by Scintomics in GMP grade. 60 minutes after application of 172 MBq ⁶⁸Ga-Pentixafor whole-body PET images were acquired with 5 minutes per bed position. Simultaneously the following MRI sequences were acquired: axial T1 vibe Dixon, coronal T2 haste, axial diffusion weighted images (ADC, b_50, b_800). We evaluated the uptake (SUVmax, SUVmean, SUVpeak) and volume in MALT lymphoma and the SUVmax in the liver as background. All MALT lymphomas were verified by biopsy. **Results:** In all patients the MALT lymphoma showed increased uptake of ⁶⁸Ga-Pentixafor. Mean SUVmax was 12.3 (range 4.1-25.4), SUVmean 6.0 (range 2.9-10.2), and SUVpeak 7.3 (range 7.1-22.7; 2 patients with low tumor volume were not evaluable). The mean SUVmax of the liver was 1.8. The tumor-to-background ratio was excellent with mean 7.1 (range 2.4-14.9). The mean tumor volume was 90 ml (range 3.4-306). **Conclusion:** In this pilot study all MALT lymphoma had high ⁶⁸Ga-Pentixafor uptake with excellent tumor-to-background ratios and, therefore, enabling non-invasive detection. 1. Gourni E, Demmer O, Schottelius M, et al. PET of CXCR4 expression by a (⁶⁸Ga)-labeled highly specific targeted contrast agent. J Nucl Med. 2011;52:1803-1810. 2. Demmer O, Gourni E, Schumacher U, Kessler H, Wester HJ. PET imaging of CXCR4 receptors in cancer by a new optimized ligand. ChemMedChem. 2011;6:1789-1791. 3. Herrmann K, Lapa C, Wester HJ, et al. Biodistribution and radiation dosimetry for the chemokine receptor CXCR4-targeting probe ⁶⁸Ga-pentixafor. J Nucl Med. 2015;56:410-416. 4. Wester HJ, Keller U, Schottelius M, et al. Disclosing the CXCR4 expression in lymphoproliferative diseases by targeted molecular imaging. Theranostics. 2015;5:618-630.

OP406

Prognosis value of baseline total metabolic tumor volume (TMTV) in advanced Hodgkin lymphoma (HL) : Ancillary study of AHL2011 LYSA trial

S. Kanoun^{1,2,3}, A. Berriolo-Riedinger², I. Tal⁴, V. Edeline⁵, A. Cottreau⁶, P. Brice⁷, R. Bouabdallah⁸, G. Salles⁹, A. Stamatoullas¹⁰, J. Dupuis⁶, M. Andre¹¹, N. Mounier¹², C. Ferme¹³, M. Meignan⁶, R. Casasnovas¹⁴; ¹LE2I, UMR CNRS 6306, Dijon, FRANCE, ²Centre Georges Francois Leclerc, Dijon, FRANCE, ³CHU Dijon, Dijon, FRANCE, ⁴Beth Israel Deaconess Medical Center, Boston, MA, UNITED STATES, ⁵Institut Curie, Paris, FRANCE, ⁶Hopital H. Mondor, Creteil, FRANCE, ⁷AP-HP at Saint-Louis Hospital, Paris Diderot- Sorbonne University, Paris, FRANCE, ⁸Cancer Center Institut Paoli-Calmettes, Marseille, FRANCE, ⁹University De Lyon, Hospices Civils De Lyon, Lyon, FRANCE, ¹⁰Centre Henri Becquerel, Rouen, FRANCE, ¹¹Centre Hospitalier Universitaire Mont-Godinne, Dinant, BELGIUM, ¹²CHU l'Archet, Nice, FRANCE, ¹³Institut Gustave Roussy, Villejuif, FRANCE, ¹⁴Hôpital Le Bocage, Dijon, FRANCE.

Aim: The TMTV assessed on the baseline FDG-PET is a novel approach of tumor burden measurement. It has been reported to influence HL outcome in a retrospective series (Kanoun, EJNM 2014). We designed a study evaluating the TMTV prognosis value in patients (pts) prospectively

enrolled in a phase III randomized trial testing a treatment strategy driven by PET, compared to a standard treatment not monitored by PET. Methods: Eligible pts had to be enrolled in the AHL2011 trial (NCT01358747) and to have a baseline PET (PET0) available for central review and TMTV calculation. Pts were 16–60 y, with a previously untreated advanced HL (Ann Arbor stage III, IV or high risk IIB) and were randomly assigned to a treatment strategy driven by PET after 2 escalated BEACOPP (BEA) cycles (PET2), delivering 4 cycles of ABVD for PET2- pts and 4 cycles of BEA for PET2+ pts or a standard treatment not monitored by PET and delivering 6 cycles of BEA. PET2 were centrally reviewed and interpreted according to Deauville criteria. TMTV was computed on PET0 by summing the metabolic volumes of the individual lesions using the 41% SUVmax thresholding method already described in lymphoma. Results: 392 pts with a median age of 30 y were included: 64% were male, 89% had stage III/IV, and 59% an IPS \geq 3. Median TMTV was 200 ml (23–2149). Using a X-tile method a 350 ml cut off value was identified from a training set (n = 262) and confirmed in a validation set (n = 130) of pts obtained from the whole series. With a 16 months median follow up, 2y-PFS was 81% vs 93% in pts with high and low TMTV respectively in the whole population (p = 0.0015; HR = 3). PET2 positivity was also related to a lower 2y-PFS compared to PET2- pts (76% vs 92%; p<0.0001). Then 3 groups could be identified: pts with either [high TMTV and PET2+ (n = 23; 6%)], or [high TMTV and PET2-, or low TMTV and PET2+ (n = 103; 27%)], or [low TMTV and PET2- (n = 261; 67%)] had a 61%, 88%, 94% 2y-PFS respectively (p<0.0001). Conclusions: TMTV predicts the outcome of young advanced HL pts independently of the early metabolic response to treatment. The combination of TMTV and PET2 allows identifying 3 subsets of HL pts with significantly different outcome that may help clinician to better tailor therapy.

OP407

FDG-PET/CT at Relapse Predicts Survival in Multiple Myeloma

B. JAMET, 44000. C. Bailly, L. Planche, T. Carlier, T. Eugene, C. Touzeau, C. Ansquer, P. Moreau, F. Kraeber-Bodéré, C. Bodet-Milin; University Hospital, Nantes, FRANCE.

AIM: Multiple myeloma (MM) is a B-cell neoplasm characterized by aberrant expansion of plasma cells, typically within the bone marrow but with increased extramedullary sites with disease relapse/progression, which arises inevitably. At relapse, recommended imaging includes skeletal survey and MRI and interest of FDG-PET/CT should be confirmed. This retrospective study evaluated the benefit of FDG-PET/CT to predict the survival of MM patients, at suspected or biochemical proved relapse. **MATERIALS AND METHODS:** 45 patients with a history of MM have been included, all initially treated as recommended by the IMWG's guidelines (median time from diagnosis to suspected or biochemical proved relapse: 42 months (range, 5 to 169)). All patients were examined with FDG-PET/CT. Visual focal lesions (FLs), bone marrow involvement (BMI), extra-medullary disease (EMD) and quantitative PET parameters (SUVmax, metabolic tumor volume (MTV) and total lesion glycolysis (TLG) of hottest lesions, whole-body MTV (MTVT)) were evaluated. Kaplan-Meier method, Logrank tests, univariate and multivariate Cox analyses were used to analyze whether PET and usual international prognostic parameters (International staging system score (ISS), cytogenetic abnormalities (FISH analysis of del(13q), t(4;14), del(17p)) could predict free-progression survival (PFS) and overall survival (OS). **RESULTS:** The median age at diagnosis was 61 years (range, 33 to 80) and median follow-up after PET/CT was 18 months (range, 1 to 64) for living and 19 months (range, 7 to 28) for dead patients. 34/45 patients had a positive FDG-PET/CT, including 6/11 (54,5%) without abnormality of electrophoresis or free light chain level (FLC). The first multivariate analysis performed in the entire cohort showed that positive FDG-PET/CT affected PFS, (P=0.02) whereas ISS and cytogenetic abnormalities did not. Univariate analysis realised in positive FDG-PET/CT patients showed that

presence of \geq 2 EMD lesions was correlated with shorter OS (P<0.001) and presence of \geq 17FLs (P=0.003), \geq 4FLs in the appendicular skeleton (P=0.0057), SUVmax (P=0.04) and TLG \leq 24.22 (P=0.01) predicted shorter PFS. MTV, ISS, cytogenetic abnormalities were not predictive for PFS or OS. Multivariate analysis performed in this subgroup of positive FDG-PET/CT patients highlighted that only presence of \geq 17FLs (P=0.03) was an independent variable adversely affecting PFS whereas presence of \geq 2 EMD had a limit prognostic value for OS (P=0.06). **CONCLUSION:** Our study showed interest of FDG-PET/CT in MM patients with suspected relapse, especially in patients with normal electrophoresis and FLC. Positive FDG-PET/CT predicted PFS and number of FLs, SUVmax, TLG, and presence of EMD lesions showed prognostic value.

OP408

Chronic Lymphocytic Leukemia: Computational analysis of PET/CT images as new window for evaluating disease clinical course

R. Piva¹, F. Fiz^{1,2}, S. Matis³, A. Ibatci⁴, M. Miglino⁴, C. Neumaier⁵, A. Nieri¹, M. Bauckneht¹, S. Morbelli¹, A. Orengo¹, M. Piana⁶, G. Cutrona³, G. Sambucetti¹, F. Fais⁷, C. Marini⁸; ¹Chair of Nuclear Medicine, Genoa University, IRCCS San Martino-IST, Genoa, Italy, Genoa, ITALY, ²Nuclear Medicine Unit, Department of Radiology, Uni-Klinikum Tübingen, Germany, Tübingen, GERMANY, ³Molecular Pathology Unit, Genoa University, IRCCS San Martino-IST, Genoa, Italy, Genoa, ITALY, ⁴Department of Haematology and Bone Marrow Transplants, IRCCS Martino-IST, Genoa, Italy, Genoa, ITALY, ⁵Department of Radiology, Genoa University, IRCCS San Martino-IST, Genoa, Italy, Genoa, ITALY, ⁶Department of Mathematics, University of Genoa, Italy, Genoa, ITALY, ⁷Department Experimental Medicine, University of Genoa, Genoa, Italy, Genoa, ITALY, ⁸CNR Institute of Molecular Bioimaging and Physiology, Milan, Section of Genoa, Genoa, Italy, Genoa, ITALY.

Aim. Chronic Lymphocytic Leukemia (CLL) is a heterogeneous disease, characterized by low-grade proliferation of immature B-cell clone. Existing evidence indicates that interaction between neoplastic clone and bone marrow (BM) environment is key in disease progression. The present study utilized a computational application to quantify bone alterations and metabolic changes in a cohort of patients, with different disease stages, submitted to whole-body FDG-PET/CT. **Materials and Methods.** FDG-PET/CT images of 33 CLL patients (12 Binet A, 13 Binet B and 8 Binet C, mean age 70 \pm 11 years) were analyzed. The algorithm measured the ratio between trabecular and total bone volume (IBV/SV). Active "red" BM volume, defined as all intrabone voxels with SUV>1.11 according to our previously published normalcy data-base, was normalized for ideal body weight (IBW). Data in the whole skeleton and on axial/appendicular districts were compared with corresponding findings in 36 sex/age-matched controls. **Results** IBV/SV ratio was markedly increased in CLL patients with respect to controls (39 \pm 4% vs. 30 \pm 6%, p<0.001), signaling presence of cortical bone erosion in these subjects. This phenomenon was particularly pronounced in Binet C patients (42.7 \pm 5.6%, p<0.01 vs. Binet A/B) and equally involved axial and appendicular skeleton. Likewise, CLL was associated with an expansion of active BM (10.4 \pm 3.4 vs. 7.4 \pm 3.2 ml/Kg IBW, p<0.05) whose normalized value reached its maximum Binet C stage (13.8 \pm 3.7, p = 0.01 vs. Binet A/B). Similarly, CLL progression was paralleled by an acceleration in glucose metabolism of hematopoietic tissue whose mean SUV was significantly higher in stage C patients with respect to A/B ones, both in total (1.9 \pm 0.5 vs 1.66 \pm 0.12, p=0.01 vs A/B) and in axial body skeleton (2.0 \pm 0.5 vs 1.7 \pm 0.14, p<0.001 vs A/B). **Conclusions.** CLL is associated with bone erosion and increased glucose consumption of active BM. Degree of these manifestations is stage-dependent. Computational analysis of PET/CT images might represent a new window for evaluating the CLL clinical course.

OP409**Computational-Based PET/CT Evaluation Can Detect and Stage the Metabolic Changes, Linked to the RANKL/RANK Loop, in Chronic Lymphocytic Leukemia**

F. Fiz¹, R. Piva¹, S. Matis², A. Neri¹, S. Bruno², G. Ferrarazzo¹, P. Giannoni³, D. De Toter², M. Bauckneht¹, S. Morbelli¹, A. Orenco¹, G. Cutrona², F. Fais², G. Sambuceti¹, C. Marini⁴; ¹Nuclear Medicine Unit, Department of Health Sciences, University of Genoa, Genoa, ITALY, ²Molecular Pathology Unit, University of Genoa, Genoa, ITALY, ³Department of Experimental Medicine, University of Genoa, Genoa, ITALY, ⁴National Council of Research, IBFM, Genoa, ITALY.

Aim. Chronic Lymphocytic Leukemia (CLL) is a heterogeneous disease, characterized by progressive insensitivity to apoptotic signals and to cytotoxic treatments. In CLL, overexpression of surface receptor associated with nuclear-factor kB and its ligand (RANK/RANKL) share the capability to bolster clonal proliferation and to prevent apoptosis. Furthermore, they can disrupt the niche environment via osteoclast activation. Both clone activation and skeletal erosion can potentially be detected by PET/CT. Accordingly, we recently reported that bone-erosion, detected at X-ray CT, is a strong predictor of disease outcome. This study aimed to verify the correlation between cellular expression of RANKL/RANK and bone marrow metabolism (as an index of CLL cells proliferation) as well as between RANKL expression and skeletal alterations. **Materials and Methods.** We applied dedicated software to estimate total (TBV) trabecular (IBV) and compact bone volumes (CBV) as well as total active bone marrow asset, in 30 prospectively enrolled CLL patients submitted to ¹⁸F-fluoro-deoxyglucose PET/CT imaging. Before tracer injection, blood was sampled to evaluate expression of RANK/RANKL and CD38%. Whole-body FDG imaging was performed according to the standard procedure while SUV of intrabone volume was normalized for blood-pool (N-SUV). **Results.** Skeletal erosion was confirmed in this population with IBV/TBV displaying a progressive increase from Binet A to Binet C stage. Bone erosion was more pronounced in patients with >20% CD38+ cells with respect to the remaining ones (37±4% vs. 41±4%, respectively, p<0.05). Percentage of cells positive for both markers significantly and progressively increased from Binet A to Binet C stage (9.8%±0.5% vs. 19%±3.5%, respectively, p<0.05). Bone marrow N-SUV in the whole skeleton significantly correlated with double positive cells (R=0.61, p<0.01). This relationship was reproduced in the axial bone segments while it was relatively less pronounced in the appendicular ones. **Conclusion.** Our imaging study documents that RANK/RANKL loop contributes to bone marrow involvement by CLL. Integrated analysis of PET/CT images can improve accuracy of CLL staging.

OP410**¹¹C-Methionine PET/CT in Multiple Myeloma: Comparison with ¹⁸F-FDG PET/CT and Diagnostic Value through Clinical and Biological Parameters**

B. Garcia, M. Morales, E. F. Guillen, R. Figueroa, M. Marcos, V. Moran, R. Ramos, J. San-Miguel, M. J. Garcia-Velloso, J. A. Richter; Clinica Universidad de Navarra, Pamplona, SPAIN.

AIM Multiple Myeloma (MM) remains as incurable hematologic malignancy arising from clonal plasma cells. The purposes of this study were to analyse the diagnostic accuracy of PET/CT performed with ¹¹C-methionine (MET) as a radiolabelled amino acid tracer compared with ¹⁸F-FDG, to correlate the results with clinical and biological parameters, and to evaluate the clinical usefulness of the aforementioned radiotracers by studying their diagnostic yield. **MATERIALS AND METHODS** The study group comprised 26 patients (53% women, ranged 32-73 years) with plasma cells malignancy (4 solitary plasmacytomas, 3 smoldering myelomas, and 19 MM) who underwent both MET- and ¹⁸F-FDG-PET/CT for

staging or restaging the disease. Tracer uptake in focal lesions (FL) was evaluated, and the number of FL and the standard uptake values (SUV) were interrelated with clinical/biological parameters of disease activity. **RESULTS** Concerning the definite diagnosis per patient, the accuracy values of MET (Sensitivity=100%, Specificity=88%, Positive-Predictive-Value=95%, Negative-Predictive-Value=100%) seemed to be superior to those reached with ¹⁸F-FDG (Sensitivity=94%, Specificity=75%, Positive-Predictive-Value=89%, Negative-Predictive-Value=86%). MET detected FL in 16/26 subjects (61%) and ¹⁸F-FDG in 17/26 (65%). The number of FL observed with MET was higher than that with ¹⁸F-FDG in 56% of these patients (mean=4 in the subjects who presented <20FL) markedly in the cranial vault. Only in 2 patients ¹⁸F-FDG revealed FL that were negative with MET, one of which was demonstrated by biopsy as non-malignant; the other one was considered as a false-positive result of ¹⁸F-FDG in the definite diagnosis using standard clinical criteria. SUV was calculated in 46 FL and the values with MET were significantly higher than those obtained with ¹⁸F-FDG [median (IQR)= 4.96 (2.05 - 6.71) vs 1.86 (1.32 - 3.03); p<0.001]. Cohen's kappa coefficient between both radiotracers (0.81) showed a very good agreement (p<0.001). The levels of M-component and the kappa/lambda ratio were associated with a significant increase in the SUV only with MET PET/CT (p<0.05) and not with ¹⁸F-FDG PET/CT. **CONCLUSION** Uptake of MET tended to be higher than that of ¹⁸F-FDG, and an equal or greater number of FL per patient was mostly depicted by MET, particularly shown in the cranial vault. The data also suggested that MET is a more accurate tracer of tumour burden and disease activity than ¹⁸F-FDG.

OP411**¹⁸F-FDG PET/CT in diagnosis of Plasma cell disorders: From MGUS to Multiple Myeloma - correlation with histopathology**

A. S. Manglunia, A. D. Puranik, S. D. Vitalkar, T. V. Dhote, N. R. Thaker; Bombay Hospital & Medical Research Centre, Mumbai, INDIA.

Introduction: Multiple myeloma is a malignant disorder of plasma cells, which is characterized by infiltration of bone marrow and excess production of monoclonal immunoglobulins. The disease classification varies widely from monoclonal gammopathy of undetermined significance (MGUS) to symptomatic multiple myeloma (MM). Usual investigations include serum protein electrophoresis, bone marrow aspirate (BMA) and biopsy (BMB), x-ray skeletal survey, CT or MRI. The role of imaging in multiple myeloma is crucial - in the initial staging of the disease, to assess complications, and in the evaluation of treatment response. However, there is a lack of standardized imaging protocol for both recently diagnosed patients and patients on follow-up. Our study was aimed to assess the role of ¹⁸F-FDG PET-CT in the patients with suspected multiple myeloma. **Materials and Methods:** We carried out prospective study of the patients clinically suspected to have multiple myeloma and referred to PET/CT department of our hospital. 39 patients, comprising of 21 males and 18 females underwent whole body PET/CT with intravenous contrast. SUV max was documented for every lesion. CT imaging features were also considered. Mean age of the patients was 62.5 years (SD 10.2 years). Most common presenting symptom was backache and the median symptomatic period was 2 months. Out of 39 patients, 17 patients were eventually diagnosed with Multiple Myeloma based on the BMB, 5 were diagnosed with plasmacytoma and 4 were classified as MGUS. Rest 13 patients were diagnosed with other medical conditions. **Results:** For multiple myeloma, the sensitivity of whole body FDG PET/CT was 94.12% (16/17) and specificity was 84.62%. SUV max of MM patients ranged from 6.5 to 28.0 (mean 13.35). PET-CT correctly diagnosed 4 out of 5 patients with solitary plasmacytoma. In the 4 patients diagnosed with MGUS, PET-CT study showed no

metabolically active disease or lesion, thus corroborating with the biochemical diagnosis. **Conclusion:** The results showed that PET/CT is a valuable tool to confirm MM in cases of clinical suspicion. In addition, quantitative parameter of SUV max can help differentiate between active myeloma and MGUS. Multiplicity of lesions helps in differentiating between MM and plasmacytoma. Overall, PET/CT with its metabolic dimension and morphological features has been shown to have high sensitivity and specificity in patients clinically suspected of multiple myeloma.

OP412

Use of 99m-Tc labeled Zolendronic acid in Myeloma patients

V. Y. Sukhov¹, K. Zaplatnikow²; ¹ARCEM n/a A.M.Nikiforov of MES Russia, St. Petersburg, RUSSIAN FEDERATION, ²MÁZ, Department for Nuclear Medicine, NÜRNBERG, GERMANY.

OBJECTIVES: Resistant to cleavage by bisphosphonates (BPs) - synthetic analogues of natural bone matrix pyrophosphates, were shown to be effective in treatment of patients with different malignant tumors, including primary diagnosed or relapsed multiple myeloma (MM). Zolendronic acid (ZdA) most strongly inhibits osteoclasts activity, since it has unique ability to block synthesis of mevalonate, which is basic substance in formation and upkeep of osteoclasts activity. However, recently there was no possibility of direct prediction of BFs action and evaluation of their effectiveness. Introduction of new tracer labeled ZdA allowed visualization of BFs accumulation in bone. **METHODS:** Study included 37 patients with newly diagnosed MM, average age of 62 (29-79) y.o., 16 men and 21 women with radiographic evidence of osteolytic lesions. Besides of other diagnostics methods algorithm also included Whole-body Bone Scan (WbBS) with 99m-Tc-ZdA. As a treatment posology 90 mg of pamidronate or 4 mg of ZdA were additionally prescribed to 9 and 29 patients, respectively, as i.v. infusions every 3-4 weeks. All patients underwent repeated WbBS procedures after BFs each treatment. **RESULTS:** 99m-Tc-ZdA was successful in finding of known osteolytic lesions in 32 patients, while equivocal results were in 5 cases. BFs therapeutic procedures (range 1 to 6) were prescribed upon WbBS results of ZdA focal uptake. Majority of patients with high 99m-Tc ZdA uptake at WbBS showed good response to BFs therapy. Partial response (PR) was achieved in 86% of cases (32 of 37 patients) from ZdA-group, noted by reduction number of lesions and/or decrease of 99m-Tc-ZdA uptake and also lowering levels of biochemical markers of bone metabolism. In 1 patient treated with ZdA and all pamidronate-treated patients no PR was observed (registered progression of disease), which necessitated use of other therapeutic schemes. **CONCLUSION:** Study showed that WbBS with a labeled analogue of a therapeutic agent 99m-Tc-ZdA is a feasible and affective diagnostic procedure. We can suggest prediction of response to treatment with BPs and evaluation its effectiveness. Level of response depends on tracer uptake in MM pathological foci. This information is greatly valuable for correct agent choice from available spectrum of BPs to prevent further progression of disease and obtain therapeutic effect. WbBS with ZdA contributes to correct pathogenetic understanding of specific disease stages that helps identifying choice of therapeutic regimens and use of definite BF. It helps to determine various forms and stages of MM that require different therapeutic modes and schemes of BFs use.

1008 – Monday, October 17, 2016, 16:30 - 18:00, Hall 212

Special Symposium 2: The Saul Hertz Symposium – 75 Years of Radionuclide Therapy

OP413b

The Ideal Targeted Therapy - Radioiodine and the Thyroid

V. McCready; Sutton Surrey, UNITED KINGDOM.

OP414

Radionuclide Therapy of Bone and Joint Diseases - A New/Safe Procedure?

M. Fischer; IBA Molecular, Kassel, GERMANY.

OP415a

Fifty Years of Targeting Neuroendocrine Tumors

C. A. Hoefnagel; Badhoevedorp, NETHERLANDS.

1009 – Monday, October 17, 2016, 16:30 - 18:00, Hall 113

Cardiovascular System: Imaging of Cardiovascular (Vulnerable) Plaques

OP416

Combined ¹⁸F-fluorocholine PET and MR imaging of vulnerable atherosclerotic plaques: prospective study with immunohistochemical validation

S. Vöö¹, R. Kwee¹, J. Sluimer¹, F. Schreuder¹, R. Wierst¹, R. van Oostenbrugge¹, M. J. Daemen², F. M. Mottaghy¹, M. E. Kooi¹; ¹Maastricht University Medical Center, Maastricht, NETHERLANDS, ²Amsterdam Medical Center, Amsterdam, NETHERLANDS.

Purpose: ¹⁸F-fluorocholine (¹⁸F-FCH) emerges as a possible molecular tracer for positron emission tomography (PET) in assessing macrophage infiltration and detecting active inflammation. We hypothesized that ¹⁸F-FCH PET is a valuable imaging tool for the identification of vulnerable plaques and associated intraplaque inflammation. **Methods and Materials:** Ten consecutive stroke patients (90% men, median age 66.0 years, range 51.7-77.4) with ipsilateral >70% carotid artery stenosis and who underwent carotid endarterectomy (CEA) were included. Prior to CEA, all patients underwent PET+MRI to assess maximum ¹⁸F-FCH uptake in ipsilateral symptomatic carotid plaques and contralateral asymptomatic carotid arteries (given as maximum target-to-background ratio, TBRmax) and plaque components. Macrophage content was assessed in all CEA specimens as percentage of CD68⁺-staining per whole plaque area (CD68⁺) and as maximum CD68⁺ percentage (CD68max) in the most inflamed section/plaque. **Results:** Dynamic PET imaging demonstrated that an interval of 10 minutes between ¹⁸F-FCH injection and PET acquisition is appropriate for carotid plaque imaging. TBRmax in ipsilateral symptomatic carotid plaques correlated significantly with CD68⁺ ($\rho=0.648$, $p=0.043$) and CD68max ($\rho=0.721$, $p=0.019$). TBRmax was significantly higher in symptomatic carotid plaques compared to the asymptomatic carotid arteries (median of 2.0, interquartile range [IQR], 1.6-2.6 versus median of 1.2, IQR 1.1-1.5, $p=0.047$). In univariate linear regression, TBRmax was not significantly related to carotid artery stenosis grade. TBRmax correlated significantly with the percentage of plaque lipid-rich necrotic core on MR ($p<0.05$), but not with the degree of plaque calcifications. **Conclusion:** ¹⁸F-FCH uptake in human carotid atherosclerotic plaques correlated strongly with the degree of intraplaque inflammation and recent symptoms. Therefore, ¹⁸F-FCH PET is a promising tool for the evaluation of vulnerable carotid plaques.

OP417

Non-invasive assessment of atherosclerotic carotid plaques by 18F-FDG positron emission tomography/computed tomography (PET/CT) imaging and microwave radiometry (MWR): validation with histopathological and immunohistochemical findings

A. Georgakopoulos¹, I. Koutagiari², N. Pianou¹, G. Benetos², E. Athanasiadis³, G. Agrogiannis⁴, K. Filis⁵, N. Bessias⁶, C. Klonaris⁷, G. Spyrou³, E. Tsiamis², E. Siores⁸, D. Tousoulis⁹, K. Toutouzas², C. D. Anagnostopoulos¹; ¹Biomedical Research Foundation of the Academy

of Athens, Center for Clinical Research, Experimental Surgery and Translational Research, Athens, GREECE, ²Athens Medical School, Hippokraton Hospital, Athens, GREECE, ³Center of Systems Biology, Biomedical Research Foundation of the Academy of Athens, Athens, GREECE, ⁴Department of Pathology, Athens Medical School, Athens, GREECE, ⁵First Department of Cardiology, Hippokraton Hospital, Athens, GREECE, ⁶Department of Vascular Surgery, General Hospital "Korgialenio-Benakio National Red Cross", Athens, GREECE, ⁷University of Athens, Laiko Hospital, Department of Propedeutic Surgery, Athens, GREECE, ⁸University of Bolton, Centre for Materials, Research and Innovation, Bolton, UNITED KINGDOM, ⁹Athens University Medical School, Athens, GREECE.

Background and aim: ¹⁸F-Fluorodeoxyglucose (¹⁸F-FDG) PET/CT imaging is a robust technique for atherosclerosis assessment, however high cost and patient exposure to radiation limit its use in everyday practice as a screening tool for evaluation of plaque inflammation. Microwave Radiometry (MWR) is a low cost non-invasive and safe diagnostic modality allowing in vivo evaluation of carotid inflammation by measuring internal temperatures of tissues. In this study, we explore the relationship between temperature measurements and carotid ¹⁸F-FDG uptake and assess their association with histological and immunohistochemistry findings in patients with high-grade carotid artery (CA) stenosis. **Materials and Methods:** Twenty one consecutive patients scheduled to undergo carotid endarterectomy due to high grade asymptomatic carotid artery stenosis were included. ¹⁸F-FDG uptake was evaluated as target-to blood ratio (TBR) across each CA, by obtaining measurements in consecutive axial slices 2cm below to 2cm above the carotid bifurcation. Temperature difference (ΔT) was assigned as the maximum-minimum measurements over the corresponding carotid segments. Degree of calcification, extent of lipid core and expression of CD68 were evaluated semi-quantitatively. **Results:** There was a significant positive correlation between ¹⁸F-FDG uptake and ΔT values for the total carotid arteries ($R=0.40$ $p=0.01$). In contrast, no correlation was demonstrated between TBR or ΔT and the percentage of luminal stenosis ($R=-0.28$, $p=0.86$ and $R=-0.02$, $p=0.91$, respectively). TBR values were lower in patients with specimens containing increased calcification compared to those with limited calcification ($p=0.003$). Conversely, there was a trend for higher TBR values in patients with plaques containing an extended lipid core ($p=0.06$). In contrast, there was no difference in ΔT values between specimens with increased extension and specimens with low extension of lipid core ($p=0.45$). Similarly, there was no difference in ΔT values of specimens with high and low extension of calcification ($p=0.95$). Specimens with high CD68 expression had higher ΔT and TBR values compared to those with low CD68 count ($p=0.04$ and $p=0.005$, respectively). **Conclusions:** Inflammatory process within carotid atheromatic plaques is not correlated with structural changes, as reflected by luminal stenosis, illustrating the different pathobiological processes taking part in atherosclerosis. MWR values are correlated with ¹⁸F-FDG PET/CT measurements and with immunohistochemical findings suggesting that both techniques can be used for an indirect detection of plaque inflammatory activation in vivo. However, ¹⁸F-FDG PET/CT parameters are also influenced by histological plaque features too, indicating that PET/CT is a more accurate technique than MWR for plaque characterisation.

OP418

Evaluation of carotid atherosclerotic plaques using a simple semi-quantitative score based on FDG PET and CT angiography

N. Mikail¹, E. Meseguer², M. Mazighi³, C. Guidoux², L. Cabrejo², A. Touati¹, G. Lesèche⁴, D. Le Guludec¹, P. Amarenco², F. Hyafil⁵; ¹Department of Nuclear Medicine, Bichat Hospital, AP-HP, PARIS, FRANCE, ²Department of Neurology, Bichat Hospital, AP-HP, PARIS, FRANCE, ³Department of Neurology, Lariboisière Hospital, AP-HP, PARIS, FRANCE, ⁴Department of Vascular Surgery, Bichat Hospital, AP-HP, PARIS, FRANCE.

Background. There is currently a lack of imaging criteria to define high-risk plaques with FDG-PET imaging. **Objective.** Our aim in this study was to develop a simple semi-quantitative score for the classification of carotid plaques based on morphological and functional imaging criteria extracted from FDG-PET and CT angiography, respectively. **Material and methods.** A total of 54 patients with carotid plaques were imaged with PET 2 hours after injection of 4 MBq/kg of FDG followed by CTA of the supra-aortic trunks. Carotid plaques were evaluated in the region with the highest degree of luminal stenosis and graded using a semi-quantitative CT score based on plaque morphology (maximal score = 6) and a PET score based on the intensity of FDG uptake (maximal score = 4). A combined score was calculated for each carotid artery by summing the CT and PET scores (maximal score = 10). The combined score was first tested in 23 patients undergoing carotid endarterectomy. Plaque obtained after carotid endarterectomy was classified as complicated (thrombus, plaque rupture or intra-plaque haemorrhage) or non-complicated. The combined score was then evaluated in a cohort of asymptomatic patients with carotid stenosis > 50 % followed for occurrence of clinical events. **Results.** 54 patients with carotid stenosis > 50 % (31 symptomatic; 23 asymptomatic) were imaged in this study. Among the 29 atherosclerotic plaques obtained from carotid endarterectomy, 23 plaques were classified macroscopically as complicated. Combined score measured in complicated vs. non-complicated plaques was 6.1 ± 1.9 vs. 3.7 ± 2.0 ($p < 0.05$). A combined score ≥ 4 identified complicated plaques with a sensitivity of 90 % and a specificity of 67 % (accuracy 83%). This threshold value of combined score was then tested in a cohort of asymptomatic patients with carotid stenosis > 50 % ($n = 16$). During a mean follow-up of 13 ± 9 months, 5 patients (1 acute ischemic cerebral event, 4 carotid endarterectomy with complicated plaques) met the primary endpoint: 4 patients in the group with combined score ≥ 4 and 1 in the group of a combined score < 4 (odds ratio = 3,9 for a combined score ≥ 4). **Conclusions.** A simple semi-quantitative score based on combined FDG-PET-CTA imaging can help for the identification of complicated carotid plaques in symptomatic patients and helped to stratify the risk of clinical events in a small cohort of asymptomatic patients with carotid stenosis.

OP419

Detection of culprit non-stenotic plaques with FDG PET CT angiography in patients with unknown cause of ischemic stroke

N. Mikail¹, M. Mazighi², E. Meseguer³, C. Guidoux⁴, L. Cabrejo⁴, I. Klein⁵, D. Le Guludec⁶, P. Amarenco⁴, F. Hyafil⁶; ¹Department of Nuclear Medicine, Beaujon Hospital, AP-HP, PARIS, FRANCE, ²Department of Neurology, Lariboisière Hospital, AP-HP, PARIS, FRANCE, ³Department of Neurology, Bichat Hospital, AP-HP, PARIS, FRANCE, ⁴Department of Neurology, Bichat Hospital, AP-HP, PARIS, FRANCE, ⁵Department of Radiology, Bichat Hospital, AP-HP, PARIS, FRANCE, ⁶Department of Nuclear Medicine, Bichat Hospital, AP-HP, PARIS, FRANCE.

Background. Non-stenotic carotid can rupture and cause ischemic stroke but are difficult to identify owing to the high prevalence of carotid stenosis < 50 % in the population. CT angiography (CTA) and ¹⁸F-fluorodeoxyglucose positron emission tomography (¹⁸F-FDG PET) imaging allows for the detection of specific morphological and functional features associated with complicated carotid plaques. **Objective.** The aim of this study was to investigate the prevalence of features of complicated plaques using FDG-PET-CTA in non-stenotic plaques of patients with ischemic stroke of unknown origin. **Methods.** 37 patients with ischemic stroke of unknown origin < 14 days were evaluated in this study. PET imaging of carotid arteries was acquired 2 hours after injection of 4 MBq/kg of FDG and followed by CTA of the supra-aortic trunks. The presence of hypodense areas (< 30 Hounsfield units) and its extent were identified on CTA. The intensity of FDG uptake was quantified using tissue to background ratio (TBR) with PET on 3 adjacent slices centered on each plaque (TBR max.) and on 12 axial slices along each carotid artery (TBR

mean). Results. Patients (mean age: 63 ± 27 ; 38% female) were imaged 7 days (1–12 days) after ischemic stroke. A total of 34 non-stenotic plaques were identified in the carotid artery ipsilateral to stroke and 7 in the artery contralateral to the stroke. The prevalence of hypodense plaques was significantly higher in the carotid artery ipsilateral vs. contralateral to the stroke (47% vs. 16%; respectively, $p < 0.05$) but maximal hypodense area in plaques did not differ significantly ($1.5 \pm 1.5 \text{ mm}^2$ vs. $1.1 \pm 1.5 \text{ mm}^2$; $p = 0.53$). Maximal and mean TBR were significantly higher in ipsilateral vs. contralateral carotid artery (2.75 ± 1.18 vs. 2.05 ± 0.55 and 2.20 ± 0.95 vs. 1.65 ± 0.52 respectively); $p < 0.05$ for both). Non-stenotic plaques combining hypodense area and TBR max. > 1.80 were found significantly more frequently in the ipsilateral carotid artery vs contralateral to the stroke (71% vs. 34%, $p < 0.05$, respectively). Conclusions. In this study, we found an increased prevalence of non-stenotic plaques combining hypodense area on CTA and high FDG uptake on PET in carotid arteries ipsilateral to the stroke suggesting a causal role for these plaques in patients with unknown cause of stroke and a role for FDG-PET-CTA for their more specific detection.

OP420

Higher arterial wall inflammation in familial combined hyperlipidemia (FCH) compared to heterozygous familial hypercholesterolemia (hFH): insights from a pilot ^{18}F -FDG PET/CT study

N. Piana¹, K. Toutouzias², I. Koutagiari², A. Georgakopoulos¹, J. Skoumas², G. Benetos², P. Kafouris³, S. Galanakis², M. Metaxas¹, A. Rigatou², G. Spyrou³, A. Peters⁴, D. Tousoulis², C. D. Anagnostopoulos¹; ¹Biomedical Research Foundation of the Academy of Athens, Center for Clinical Research, Experimental Surgery and Translational Research, Athens, GREECE, ²Hippokraton General Hospital, First Department of Cardiology, Athens, GREECE, ³Center of Systems Biology, Biomedical Research Foundation of the Academy of Athens, Athens, GREECE, ⁴Division of Clinical and Laboratory Investigation, Brighton and Sussex Medical School, Brighton, UNITED KINGDOM.

Background and aims: Familial hyperlipidemia (FH) of either heterozygous (hFH) or combined (FCH) type is the most common atherogenic disorder of lipid metabolism leading to accelerated atherogenesis and increased cardiovascular risk. It is usually characterized by LDL receptors deficiency or increased production of very low density lipoproteins (VLDL)/apolipoprotein B in the liver driving a pro-atherothrombotic lipid profile and systemic inflammatory activation. VLDL production depends on the amount of fat accumulated in the liver resulting in non-alcoholic fatty liver disease in up to 76% of individuals with FH. The aim of this study was to investigate the effect of hFH and FCH on inflammation of the arterial wall and liver using ^{18}F -FDG PET/CT. **Methods:** Twenty patients (6 female) with hFH ($n=10$) or FCH ($n=10$) with no difference in age, blood glucose levels, smoking, hypertension or family history of cardiovascular disease and free of statin therapy for at least 6 months, and 10 non-dyslipidaemic individuals (3 female) of similar age were included. FDG uptake was evaluated in the wall of the ascending aorta (AA) in axial slices every 5mm as target-to blood ratio (TBR) by dividing SUVmax with the superior vena cava blood mean SUV to correct the arterial FDG uptake for blood pool activity. FDG uptake was also assessed in the liver by dividing SUVmean with the mean SUV of the left ventricular cavity. Lipid profile was obtained in all patients. **Results:** FH patients had higher TBR values in AA compared to controls ($p < 0.001$) and FCH patients exhibited higher TBR values than those with hFH (2.3 ± 0.2 vs. 2 ± 0.3 , $p=0.03$). However, liver FDG uptake did not reach statistically significant difference between controls and FH patients (2.08 ± 0.48 vs. 2.11 ± 0.42 vs. 2.54 ± 0.76 , for controls, hFH

and FCH patients respectively, $p=0.18$). Total cholesterol and low density lipoprotein (LDL) values were higher in hFH patients (338 ± 43 vs. $282 \pm 46 \text{ mg/dL}$, $p < 0.01$ and 249 ± 41 vs. $175 \pm 29 \text{ mg/dL}$, $p=0.001$, respectively), but triglyceride levels were higher (347 ± 172 vs. $108 \pm 33 \text{ mg/dL}$, $p=0.002$) in FCH patients. **Conclusions:** Increased vascular inflammation as assessed by ^{18}F -FDG PET/CT imaging was observed in FH patients. In particular, we have demonstrated for the first time that FCH patients are characterized by higher arterial wall inflammation compared with hFH, likely reflecting different pathophysiological substrate of the atherosclerotic process. We have observed no differences in FDG liver uptake between patients and controls in this pilot study, but this needs further assessment in a larger sample size.

OP421

Metabolic interplay between arterial plaques and trabecular bone osteoblastic activity: an insight into mineral metabolism in atherosclerosis, based on ^{18}F -NaF PET/CT Data

F. Fiz¹, M. Bauckneht¹, C. Campi², A. Nieri¹, G. Ferrarazzo¹, R. Piva¹, V. Ceriani¹, E. Pomposelli¹, N. Artom³, S. Morbelli¹, P. Ameri³, M. Canepa⁴, M. Piana², C. Marini⁵, G. Sambucetti¹; ¹Nuclear Medicine Unit, Department of Health Sciences, University of Genoa, Genoa, ITALY, ²Department of Mathematics, University of Genoa, Genoa, ITALY, ³Department of Internal Medicine, University of Genoa, Genoa, ITALY, ⁴Department of Cardiology, University of Genoa, Genoa, ITALY, ⁵National Council of Research, IBFM, Genoa, ITALY.

Rationale: Atherosclerosis progression is linked to osteoblast-like cells, contributing to calcium deposition within the arterial plaque (AP): this phenomenon can be exploited to quantify plaque metabolism using ^{18}F -Natrium Fluoride (^{18}F -NaF) PET/CT. There is accumulating evidence hinting that atherosclerosis is part of a systemic alteration of mineral metabolism. To test this hypothesis, we analyzed the correlation of average density and ^{18}F -NaF uptake between AP and trabecular bone, as this latter tissue constitutes the physiological calcium reserve. **Patients and Methods:** Seventy-nine ^{18}F -NaF PET/CT, from prostate cancer patients, were retrospectively analyzed. After visual identification, a VOI was constructed on every aortic AP, using a region-growing algorithm, with lower bound set at 130 Hounsfield Units. From each VOI, mean plaque density (pHU) and blood-pool normalized activity (target-to-background ratio, pTBR) were calculated. Likewise, mean density and activity were extracted from trabecular bone (bHU and bTBR, respectively), using a segmentation program based on edge recognition. In the skeletal analysis, a segment that was consistently free from metastases (MTS) was selected (i.e. femoral diaphysis). The lumbar vertebrae were analyzed if no MTS were detectable ($N=35$) and the entire skeleton was considered if the patient was free from disease localizations ($N=19$) **Results:** An inverse correlation between pHU and bHU was observed ($R=0.3$, $p < 0.01$); this correlation was more evident when considering lumbar vertebrae ($R=0.33$) or MTS-free patients only ($R=0.39$). There was a positive correlation between pTBR and bTBR ($R=0.31$, $p < 0.01$), even more evident in patients whose lumbar segment was MTS-free ($R=0.59$, $p < 0.001$). Finally, in patients with both pHU and pTBR above the median value, levels of bTBR were significantly higher with respect to those with pTBR below the median value ($p < 0.01$). **Conclusion:** Our data highlighted an inverse correlation between calcification density and trabecular bone thickness, suggesting the existence of systemic signaling mechanisms, misdirecting calcium deposition from bones to the growing plaques. Functional data support this hypothesis as NaF uptake, as a marker of mineral turnover, correlated in the two districts. Conversely, patients presenting plaques with high density and low activity (as seen in aged, stable calcifications) had the lowest bone TBR. These data can lay the path for understanding the causes and mechanisms underlying the development of a "pro-calcifications environment".

OP422**In vivo molecular imaging of glutamate carboxypeptidase II expression in re-endothelialisation after percutaneous balloon denudation in a rat model**

F. M. Mottaghy¹, H. Endepl², S. Simsekylmaz³, J. Bucerius⁴, F. Vogt⁵, O. Winz¹, R. Richarz², P. Krapf², B. Neumaier², B. D. Zlatopolskiy², A. Morgenroth¹; ¹Dept. Nuclear Medicine, University Hospital, RWTH Aachen, Aachen, GERMANY, ²Institute of Radiochemistry and Experimental Molecular Imaging, Koeln, GERMANY, ³Institute for Molecular Cardiovascular Research, University Hospital, RWTH Aachen, Aachen, GERMANY, ⁴Cardiovascular Research Institute Maastricht, MUMC+, Maastricht, NETHERLANDS, ⁵Dept. Cardiology, Pneumology, Angiology, and Internal Intensive Care Medicine, University Hospital, RWTH Aachen, Aachen, GERMANY.

The short- and longterm success of intravascular stents is dependent on a proper re-endothelialisation after the intervention-induced endothelial denudation. The aim of this preclinical study was to evaluate the potential of in vivo molecular imaging of glutamate carboxypeptidase II (GCPII) expression as a marker of re-endothelialisation. Angioplasty of the common carotid artery was performed under isoflurane anaesthesia in eight Sprague Dawley rats. The external carotid artery was tied off distally, and via transverse arteriotomy, a balloon dilatation catheter (2.0 x 8.0mm) guided by a flexible angioplasty wire was advanced into the common carotid artery (CCA) by 1 cm. Complete and uniform endothelial denudation was achieved by expanding the balloon for 5 seconds with a pressure of 12 bar. Molecular imaging using a fluorinated GCPII inhibitor (F-GCPII) was performed at two time intervals, 5-8d and 11-13d post intervention, additional immunostaining was performed. The contralateral CCA served as a reference. Semiquantitative analyses of CCA F-GCPII uptake revealed significantly higher values for treated CCA (0.0305 ± 0.0245 vs. 0.0165 ± 0.014 , $p = 0.018$). At late time point, uptake values in treated CCA remained higher but reached no significance (0.0142 ± 0.0067 vs. 0.0106 ± 0.0074 , $p = 0.068$). By immunohistochemistry, specific expression of GCPII in treated CCA was confirmed. In conclusion, by using a molecular imaging marker of GCPII expression, we provide the first non-invasive in vivo delineation of re-endothelialisation after angioplasty.

OP423**Targeting mannose receptor (MR) expressed on macrophages for imaging of atherosclerosis in a murine model using tilmanocept**

Z. Varasteh¹, F. Hyafil², D. Diallo³, R. Aid⁴, N. Anizan³, M. Mohring¹, J. Vigne², S. Nekolla¹, J. Fabre², D. Le Guludec², D. Vera⁵, M. Schwaiger¹; ¹Klinikum rechts der Isar der Technischen Universität München, München, GERMANY, ²Department of Nuclear Medicine, Hôpital Bichat, Paris, FRANCE, ³Fédération de Recherche en Imagerie Multimodale, Université Paris Diderot, Paris, FRANCE, ⁴Hôpital Bichat, Paris, FRANCE, ⁵Moore's UCSD Cancer Center University of California, San Diego, CA, UNITED STATES.

Atherosclerosis, which was previously considered as a cholesterol storage disease, has come to be regarded as a chronic inflammatory disorder of the vessel wall. Despite the significant advances in the diagnosis and management of atherosclerosis-related diseases, they remain common health problems worldwide. Primary plaque rupture prevention was reported to modify the course of disease. Therefore, imaging of atherosclerosis may help to identify plaques at risk of rupture and apply early the therapies aimed at plaque stabilization. Monocyte-derived macrophage infiltration is the main characteristic of vulnerable plaques. Besides classically activated M1-macrophages, the presence of alternatively activated M2-subset is reported for human atherosclerotic plaques. Therefore it is

reasonable to target mannose receptor (MR, CD206), which is an M2-macrophage marker, for plaque imaging. In this study our aim was to use diethylene triaminepentaacetic acid (DTPA)-mannosyl-dextran (tilmanocept) for in-vivo detection of atherosclerotic plaques in Apolipoprotein E-knockout (ApoE-KO) mouse model. Tilmanocept is a MR-targeting molecule, with molecular weight of 17 kDa and molecular diameter of 7 nm. ^{99m}Tc-tilmanocept with a trade name of Lymphoseek, is the first FDA approved receptor targeted lymphatic mapping radiopharmaceutical. **Methods:** Tilmanocept was labeled with ¹¹¹In at room temperature. The labeling stability and biodistribution of the tracer were checked in control mice (C57BL/6). The binding specificity of tilmanocept to receptor-positive organs was tested in controls. For in-vivo as well as ex-vivo imaging studies, ¹¹¹In-tilmanocept was injected into ApoE-KO mice and controls intravenously and scanned 90 minutes p.i. using nanoSPECT-CT. To test the specificity of ¹¹¹In-tilmanocept uptake in plaques, a group of mice was co-injected with excess amount of non-labeled tilmanocept. Upon imaging, the whole aortas were excised free from adventitial tissue for autoradiography. **Results:** The radiochemical yield was greater than 97% and the tracer was used for all the studies without further purification. In biodistribution studies, high liver, spleen and kidney uptake was observed. However, only low residual blood radioactivity was detected (0.18 ± 0.02 %ID/g, 1 h p.i.). The specific uptake was detected in MR⁺ organs, i.e. liver and spleen. The focal signal could be also detected in atherosclerotic plaques. SPECT signals from the lesions in the far end of abdominal aorta were well matched with the signals observed in ex-vivo autoradiography. **Conclusion:** The feasibility of ¹¹¹In-tilmanocept to image small dimension atherosclerotic plaques was presented in ApoE-KO mouse model. ¹¹¹In-tilmanocept may accumulate in high-risk vulnerable plaques (which are rich in CD206 expressing macrophages) and allow to identify them from low-risk stable lesions.

1010 – Monday, October 17, 2016, 16:30 - 18:00, Hall 114

Neurosciences: Movement Disorders & Neurodegeneration

OP424**Development and Validation of a PGJ2 Induced Rat Model of Parkinson's Disease**

A. Nikolopoulou^{1,2}, C. Corwin³, Y. Kang¹, P. Kothari², W. Qu², M. Nunez-Santos³, D. Kim², S. Vallabhajosula¹, M. E. Figueiredo-Pereira³, J. W. Babich^{1,2}; ¹Division of Radiopharmaceutical Sciences, Department of Radiology, Weill Cornell Medicine, New York, NY, UNITED STATES, ²Citigroup Biomedical Imaging Center, Weill Cornell Medicine, New York, NY, UNITED STATES, ³Department of Biological Sciences, Hunter College and the Graduate Center, CUNY, New York, NY, UNITED STATES.

Aim: Our earlier efforts to develop a mouse model of neuroinflammation (NI) revealed that repeated microinjections of prostaglandin J2 (PGJ2) into the substantia nigra (SN) led to Parkinsonian-like pathology with reduction of dopaminergic neurons in SNpc, activation of microglia/astrocytes and impaired gait and balance. To improve our ability to perform longitudinal quantitative imaging with μ PET, we sought to establish a similar NI model in rats with the ultimate intent of studying therapeutic interventions. We report here our initial findings in rats unilaterally lesioned with PGJ2 using μ PET imaging to characterize microglial activation and pre- and post-synaptic dopaminergic neuronal loss. **Methods:** Adult male SD rats received treatment of two unilateral injections (a week apart) of 2 μ L PGJ2 (33.4 μ g in DMSO/PBS) or vehicle (DMSO/PBS) into the right SN. The intact contralateral side served as internal control. Dynamic 60-min scans with [¹¹C](R)PK11195 (PK) (42 ± 5 MBq) were performed 4 and 8 weeks post treatment. PK- μ PET images were analyzed using the Logan plot and vena cava IDIF. Dynamic 90-min dopamine transporter (DAT) imaging

with [^{11}C]PE2i (PE2i) (32 ± 2 MBq) and 60-min dopamine D_2 receptor imaging with [^{11}C]Raclopride (RAC) (26 ± 7 MBq) were performed 14 weeks post treatment. Binding potentials (BP_{ND}) for PE2i and RAC were estimated with SRTM with cerebellum as reference. **Results:** At week 4 post treatment, the lesioned side of rat brains showed significantly higher PK uptake than the contralateral side with average V_T ratio of 1.55 ± 0.10 for PGJ2 and 1.23 ± 0.16 for vehicle ($P=0.01$). At week 8 post treatment, the PK average V_T ratio dropped to 1.37 ± 0.15 for PGJ2 ($P=0.02$) while vehicle returned to baseline. At week 14 post treatment, PE2i BP_{ND} ratios were 0.81 ± 0.05 for PGJ2 and 0.97 ± 0.04 for vehicle ($P=0.02$) while no PGJ2 related alterations in RAC binding were found (BP_{ND} ratios: 1.00 ± 0.10 for PGJ2 and 0.95 ± 0.11 for vehicle). **Conclusion:** We have developed a Parkinsonian-like rat model of neuroinflammation. Our data reveal sustained microglial activation with subsequent moderate loss of pre-synaptic dopaminergic neurons in response to PGJ2 detected with PK- μPET and PE2i- μPET , respectively. NI persisted in the PGJ2 rats beyond the sham (vehicle) injection which returned to control (contralateral) levels by 8 weeks post treatment. No loss of post-synaptic neurons was detected by RAC- μPET . Long-term dopaminergic degeneration in PGJ2 lesioned rats is still under investigation. This model will be used to test pharmacological interventions for reversal of NI.

OP425

18F-THK5351 PET in Patients with Clinically Diagnosed PSP

A. Rominger, M. Brendel, S. Schonecker, G. Höglinger, S. Lindner, A. Danek, J. Levin, P. Bartenstein, N. Okamura; University of Munich, Munich, GERMANY.

Background: The pathophysiology of progressive supranuclear palsy (PSP) is characterized by deposition of fibrillar aggregates of 4-repeat tau protein in neurons. These deposits are a key finding leading to the neuropathological diagnosis of “definite PSP”, which is usually established *post mortem*. The diagnosis of PSP *in vivo* according to current criteria does not take tau pathology into consideration. In light of future intervention trials biomarkers to establish a molecular diagnosis and also as potential markers of disease progression become increasingly important. 18F-THK5351 as a novel Tau-PET ligand may allow *in vivo* visualization and quantification of tau deposits, therefore the aim of the study is to investigate characteristics of 18F-THK5351 binding in patients with clinically diagnosed PSP and correlate tau-tracer uptake with clinical findings. **Methods:** Ten patients with probable PSP according to current criteria underwent 18F-THK5351 PET scanning. PET scans were acquired 30-70 min p. i. and were coregistered to the individual MRI. Standardized uptake value ratio (SUVR) in predefined brain regions were generated using the cerebellar cortex as reference region. Additionally disease severity measured by the PSP Rating Scale (PSPRS), functional independence measured by Schwab and England Activities of Daily Living scale (SEADL) and disease duration were assessed and correlated with PET findings. **Results:** In 9/10 patients significantly increased 18F-THK5351 binding was found predominantly in midbrain (SUVR 2.8-3.9), compared to a historical subject with AD (SUVR 2.2). 40-60 min p.i. time window revealed robust quantitation. One subject with a PSPRS of 33/100 and additional innate hydrocephalus did not show an elevated mid-brain uptake (SUVR 2.1), suggesting no underlying tauopathy responsible for the clinical presentation. Midbrain uptake correlated significantly with PSPRS ($R=0.58$; $p<0.05$). **Conclusions:** 18F-THK5351 binding patterns correlated well with the known distribution of tau-pathology at autopsy in PSP and with clinical severity. 18F-THK5351 seems to be a useful biomarker of tau deposition and may therefore facilitate earlier and more reliable diagnosis of PSP.

OP426

Human brain PET imaging of PDE10A in Parkinson's disease and progressive supranuclear palsy

R. Ahmad¹, M. Koole¹, J. Ceccarini¹, S. Bourgeois¹, H. Hudyana¹, M. Schmidt², G. Bormans¹, W. Vandenberghe¹, K. Van Laere¹; ¹KU Leuven, Leuven, BELGIUM, ²Janssen Pharmaceutica NV, Beerse, BELGIUM.

Objective: Phosphodiesterase 10A (PDE10A) hydrolyzes cAMP and cGMP and is strongly enriched in striatal medium spiny neurons (MSNs), regulating the responsiveness of MSNs which is of particular importance in movement disorders and several neuropsychiatric diseases. In this study, we have used ^{18}F -JNJ42259152 and PET to evaluate PDE10A binding in patients with Parkinson's disease (PD) and progressive supranuclear palsy (PSP), compared to healthy controls. **Methods:** Ten patients with PD (age 69.0 ± 7.5 ; 8M/2F; Unified Parkinson Disease Rating Score (UPDRS) III 10-38, mean 23; Hoehn and Yahr range 1-3, mean 1.7) and 5 PSP patients (age 73.8 ± 3.1 ; 2M/3F; PSP rating scale 26-44, mean 35) were included and compared to 6 healthy controls (CON) (age 61.1 ± 9.1 ; 2M/4F). Subjects received a bolus of 167 ± 11 MBq ^{18}F -JNJ42259152, and underwent dynamic PET scanning for 90 minutes. A volume of interest (VOI) analysis was performed using individual volumetric T1-weighted MRI. Partial volume correction was applied and the frontal cortex was used as reference region. Left and Right Putamen (LPT - RPT) and left and right caudate nucleus (LCNc - RCNc) PDE10A binding potential (BP_{ND}) was calculated using a Multilinear Reference Tissue Model (MRTM). **Results:** BP_{ND} was significantly decreased in PSP compared to CON both in CNc and PT ($p_{\text{HC vs PSP}} < 0.05$). For PD, BP_{ND} values were also lower than CON, but showed only a trend for CNc ($p=0.08$). For both PSP and PD however, the average CNc/PT ratio was decreased compared to CON ($p=0.01$ and $p=0.03$, respectively). There was no significant difference between PD and PSP. Taking clinically affected side into account for PD did not alter the findings. BP_{ND} values were not correlated to UPDRS III motor scores for PD. For the PSP group, a Pearson correlation showed a trend towards a negative correlation with PSPRS (gait and midline) ($r = -0.83$; $p = 0.08$). Discriminant analysis did not allow to separate PD and PSP. **Conclusions:** Striatal PDE10A expression is decreased in both PD and PSP patients compared to CON. However, VOI-based analysis of PDE10A PET using ^{18}F -JNJ42259152 does not allow to distinguish PD from PSP patients.

OP427

Value of ^{123}I -ioflupane DaT SPECT quantification in the assessment of patients with movement disorders or dementia

J. Booi¹, D. Pryma², J. Dubroff³, J. Yu⁴, R. Agarwal⁵, P. Lakhani⁶, P. Kuo⁷; ¹University of Amsterdam, Academic Medical Center, Amsterdam, NETHERLANDS, ²University of Pennsylvania School of Medicine, Philadelphia, PA, UNITED STATES, ³University of Pennsylvania Medical School, Philadelphia, PA, UNITED STATES, ⁴Fox Chase Cancer Centre, Philadelphia, PA, UNITED STATES, ⁵University of Pennsylvania Health System, Philadelphia, PA, UNITED STATES, ⁶Thomas Jefferson University Hospital, Philadelphia, PA, UNITED STATES, ⁷Banner University Medical Center, Tuscon, AZ, UNITED STATES.

The visual assessment of the striatal dopamine transporter with ^{123}I -ioflupane SPECT is well-established for the differentiation of degenerative parkinsonian syndromes (PS) from essential tremor (ET) and probable dementia with Lewy bodies (pDLB) from Alzheimer's disease (AD). This study investigated the impact of image quantification on accuracy and reader confidence compared to visual interpretation alone. Striatal binding ratios were determined with the DaTQUANT™ software in 304 ^{123}I -ioflupane SPECT (DaTscan™) images from 3 multi-center, Phase 3/4 trials, enrolling subjects with a clinical diagnosis of PS, non-PS, pDLB and AD

established after a minimum follow-up of 12 months. Images were assessed by five blinded Nuclear Medicine physicians who had limited prior clinical experience of ^{123}I -ioflupane interpretation (i.e. between 5 and 50 prior assessments). In two reads, with at least a 1 month interval, readers were presented with either visual only or combined (i.e. visual plus quantitative) data. Readers were asked to rate confidence of image interpretation (from 1 - very challenging to 5 - very easy) and judge scans as easy or difficult to read. Accuracy, positive percent agreement (PPA) and negative percent agreement (NPA) were also determined. Compared to the visual read, the combined analysis showed a small, non-significant increase of mean NPA (87.9% vs 89.9%) and equivalent PPA (80.1% vs 80.2%). Readers who initially read in the combined analysis had significantly greater accuracy (85.8% vs 79.2%, $p=0.0178$) and were closer to the accuracy of the expert readers in the original studies (range 83.3% to 87.2%). Mean confidence of image interpretation was high for both read methodologies but was significantly greater for the combined analysis (i.e. 4.25 visual vs 4.37 combined, $p<0.0001$). In difficult to read cases, PPA remained high for both visual and combined assessment while NPA in the combined read trended to increase relative to the visual assessment as levels of difficulty increased. Intra- and inter-reader agreement was very high ($\kappa>0.85$). The combined read improved the percentage of agreement among all readers from 82.8% (visual) to 89.9% (combined) and kappa values from 0.85 to 0.91. The addition of quantification allowed readers with limited experience of ^{123}I -ioflupane SPECT to perform as well as the more experienced readers used for the original clinical studies. We observed minor but consistent improvements in diagnostic accuracy while offering an increase in reader confidence that may result in fewer scans being considered difficult to read.

OP428

Striatal dopamine depletion in young onset versus late onset Parkinson's disease

A. Damian¹, C. Pascovich¹, D. Muñoz¹, M. Langhain¹, I. Amarin², A. Lescano², J. Higgin², R. Buzó², R. Ferrando¹; ¹Nuclear Medicine and Molecular Imaging Centre, Clinical Hospital, University of the Republic, Montevideo, URUGUAY, ²Neurology Institute, Clinical Hospital, University of the Republic, Montevideo, URUGUAY.

Even though many studies have described differences in clinical presentation and treatment response between patients with young onset Parkinson's disease (<50 years old) and late onset Parkinson's disease (LOPD), the underlying pathophysiology of these differences and the corresponding manifestation in presynaptic dopamine imaging is still a matter of discussion. Therefore, the aim of this study is to assess the differences in dopamine depletion between these two subtypes of PD at a similar time of disease duration. Material and methods: Retrospective study of 54 PD patients, 17 with young onset Parkinson's disease (YOPD, 36.2 ± 11 years old, 6 women) and 37 with LOPD (61.1 ± 6 years old, 23 women) matched for disease duration (7.1 ± 4.7 years) that underwent 99mTc-TRODAT-1 SPECT scan between 2011 and 2015. Specific putaminal, striatal and caudate nucleus binding uptake ratios (SUR, striatal mean counts - occipital mean counts/occipital mean counts) and asymmetry index ($2 \times [(ipsilateral\ SUR - contralateral\ UR)/(ipsilateral\ SUR + contralateral\ SUR)] \times 100$) were quantified, and Hoehn and Yahr scale (HYS) of disease severity was compared in both groups. The correlation between SUR, age of disease onset and time of duration in all patients was explored using multiple lineal regression. $P<0,05$ was considered significant. Results: Patients with YOPD showed higher HYS score in comparison with LOPD (2.5 ± 1.2 and 1.75 ± 0.8 respectively, $p=0.02$). Asymmetry index was 0.42 ± 0.3 in YOPD and 0.24 ± 0.2 in LOPD ($p=0.023$). Although putaminal SUR was lower in YOPD (0.27 ± 0.17) in comparison with LOPD (0.38 ± 0.23) this finding did not reach statistical significance ($p=0.1$). Putaminal SUR showed a significant negative correlation with time of disease duration ($p=0.017$, correlation coefficient -0.009) but not with the age of onset ($p=0.119$, correlation

coefficient -0.002). Conclusion: Patients with YOPD showed more severe clinical presentation than LOPD with a similar progression time and more asymmetrical dopamine deficit. Although putaminal dopamine impairment was lower in YOPD, it did not reach statistical significance. We could not find a correlation between age of onset of PD and absolute dopamine depletion measured with 99mTc-TRODAT-1.

OP429

Clinical impact of 18F - FDOPA PET for parkinsonian syndromes management

A. SCHIAZZA, C. ZWARTHOED, D. BENISVY, N. SAPIN, M. BORG, J. DARCOURT; CENTRE A. LACASSAGNE, NICE, FRANCE.

Introduction: The diagnosis of parkinsonian syndromes (PS) remains a challenge in various clinical situations. Unlike DAT SPECT the clinical utility of 18F-FDOPA PET has not been investigated yet. The aim of our study was to perform this evaluation through a prospective survey sent to the referring physicians. Materials and methods: During a six month period, for all patients referred to our department for 18F-FDOPA PET for movement disorder evaluation, a survey was sent out to the ordering neurologist ($n=192$). The survey included 3 types of questions. The first addressed the indication and purpose of the study. The second concerned the diagnosis (pre-PET clinical diagnostic hypothesis, post-PET final diagnosis and correlations between clinical examination and PET results). The third evaluated the practical impact on the diagnosis, the management and the follow-up of patients with PS. 18F-FDOPA PET consisted in a 10 min static PET-CT acquisition 90 min post injection of 2 MBq/kg of 18F-FDOPA (mCT-Siemens; OSEM 5 it and 24 subsets). Each study was analyzed visually by 2 observers. The final diagnosis of the referring neurologist served as reference for the 18F-FDOPA PET performances evaluation. Results: We obtain 91 answers for 91 patients with PS (mean age: 71.4). The response rate was 47%. Clinical examination of the neurologist and PET results were considered coherent in 78% of the cases ($n=71/91$). 18F-FDOPA PET induced a change in the final diagnostic in 33% of the cases when a Parkinson Disease (PD) was suspected and in 50% when another PS was suspected. 18F-FDOPA PET improved physician confidence in the initial diagnosis in 71.4% of the cases. It induced changes in the intended management in 57% of the patients. These changes were a therapeutic modification in 73% of the cases. Sensitivity of 18F-FDOPA PET was 78% and specificity 98%. Conclusion: These results demonstrate that 18F-FDOPA PET is feasible in routine clinical evaluation with good performances. The results change significantly the diagnosis (more in other PS than in PD). They also induce changes in the patient management in more than 50% of the cases.

OP430

Relationship between brain metabolism and cognitive/behavioral functioning in ALS-FTD

J. Evens*¹, S. M. A. Willekens*², D. Van Weehaeghe², P. Van Damme¹, K. Van Laere²; ¹Division of Neurology, University Hospitals Leuven and KU Leuven, Leuven, BELGIUM, ²Division of Nuclear Medicine, University Hospitals Leuven and KU Leuven, Leuven, BELGIUM.

Aims Amyotrophic lateral sclerosis (ALS) is a fatal neurodegenerative disease characterized by progressive death of motor neurons, leading to progressive muscle weakness and death within 3-5 years. ALS shows significant clinical, pathological and genetic overlap with frontotemporal dementia (FTD) and 10-15% of all ALS patients develop FTD (ALS-FTD), resulting in poorer prognosis. The aim of this

study was to relate the degree of regional brain glucose metabolism to cognitive and behavioral impairments in ALS patients. **Methods** 75 patients diagnosed with ALS, underwent ECAS scoring and ^{18}F -FDG PET/CT. According to their ALS-specific ECAS score, patients were divided in three groups: cognitively normal ALS patients (ALS-CN), patients with cognitive or behavioral impairment (ALS-Ci/Bi) and patients with ALS-FTD. Static ^{18}F -FDG PET images were acquired 30 min after injection of approximately 150 MBq ^{18}F -FDG. PET images were analyzed using a VOI-based (Hammers atlas, PNEURO v3.6) and a voxel-based (SPM8) approach. ^{18}F -FDG uptake was normalized to the average whole-brain grey matter uptake. Correlation between regional ^{18}F -FDG uptake were assessed using linear regression analyses with ALS-specific ECAS score and the sub-scores verbal fluency and executive functioning. For all statistical analyses, the level of significance was set at $p < 0.05$ and Bonferroni correction was performed to correct for multiple testing. **Results** A voxel-wise group comparison revealed significant relative hypometabolism in the middle frontal gyrus and subcallosal area of ALS-FTD patients when compared to ALS-CN patients ($P_{FWE-corrected} < 0.001$, $T=3.3$, $kE = 20$ voxels). No differences in cerebral metabolism were found between patients with ALS-FTD and ALS-Ci/Bi. As for the VOI-based correlation analyses, a positive correlation was found between ALS-specific ECAS score and ^{18}F -FDG uptake in the prefrontal cortex (PFC) ($r = 0.50$, $p < 0.001$) and the anterior cingulate cortex (ACC) ($r = 0.56$, $p < 0.001$) with the strongest correlation observed in the subcallosal area ($r = 0.54$, $p < 0.001$). In addition to the correlation with ALS-specific ECAS score, verbal fluency correlated with ^{18}F -FDG uptake in PFC ($r = 0.40$, $p < 0.001$) and ACC ($r=0.42$, $p<0.001$) while executive functioning was only correlated to ACC activity ($r = 0.41$, $p < 0.001$). **Conclusion** ECAS performance, indicating cognitive impairment and executive disturbances in ALS, is associated with prefrontal and anterior cingulate hypometabolism. These results corroborate previous findings that ^{18}F -FDG PET could be an early marker for cognitive and behavioral decline in ALS and development of ALS-FTD.

OP431

Amyloid brain deposition in idiopathic normal pressure hydrocephalus assessed by 11C-PIB PET/CT

J. F. Jimenez-Bonilla¹, R. Quirce¹, M. De Arcocha-Torres¹, I. Martínez-Rodríguez¹, J. M. Carril¹, M. Jiménez-Alonso¹, I. Banzo¹, A. Pozueta², R. Martín-Laez³, E. Rodríguez-Rodríguez²; ¹Servicio de Medicina Nuclear. Hospital Universitario Marques de Valdecilla. Grupo de Imagen Molecular IDIVAL. Universidad de Cantabria., SANTANDER, SPAIN, ²Servicio de Neurología. Hospital Universitario Marques de Valdecilla. Grupo de enfermedades Neurodegenerativas IDIVAL. Universidad de Cantabria., SANTANDER, SPAIN, ³Servicio de Neurocirugía. Hospital Universitario Marques de Valdecilla., SANTANDER, SPAIN.

Aim: Idiopathic normal pressure hydrocephalus (INPH) is a potentially treatable cause of cognitive impairment by surgical diversion of cerebrospinal fluid (CSF). An important comorbidity with Alzheimer's disease (AD) has been described in these patients, so an accurate selection of candidates for surgery is desirable. 11C-PIB PET/CT can detect in vivo the amyloid cerebral deposition. The aim of our work was to detect the presence and distribution of regional cerebral amyloid deposition on 11C-PIB PET/CT in patients with INPH, candidates to CSF shunting. **Materials and Methods:** Thirteen patients with clinical diagnosis of INPH (7 women and 6 men, mean age 73 ± 6 y) who had criteria for CSF shunt surgery and 7 healthy controls (4 women and 3 men; mean age 64 ± 10 y) were included in the study. Static 11C-PIB PET was acquired between 60' -90' after the intravenous administration of 555 MBq of 11C-PIB. PIB cerebral retention in INPH patients was compared

with those detected in controls. Visual and semiquantitative analysis of the studies was performed. SUV regional indices were obtained by drawing manual ROIs in cerebellar, temporal, frontal, anterior cingulate, occipital, parietal and posterior cingulate cortex. Using the cerebellar cortex as reference region, SUVratios (SUVr) and global SUVratios (gSUVr) were obtained. **Results:** Visual analysis classified the studies as positive in 3, equivocal in 2 and negative in 8 patients. Semiquantitative analysis showed no overall statistically differences between the mean of gSUVr of INPH and controls ($p=ns$). In the group of visual positive patients, significant differences were appreciated in the mean of gSUVr compared with controls (2.297 ± 0.188 vs 1.230 ± 0.238) ($p < 0.001$). SUVr for each region was 2.152 ± 0.4879 for temporal area; 2.163 ± 0.089 for occipital area; 2.309 ± 0.169 for frontal area; 2.396 ± 0.506 for anterior cingulate; 2.319 ± 0.506 for parietal area and 2.445 ± 0.188 for posterior cingulate. All regions showed significant regional differences with control values ($p < 0.001$). In the groups of equivocal and negative visual analysis, there were no statistically significant differences with controls ($p = ns$). **Conclusion:** Cerebral amyloid deposition was detected in 23% of INPH patients. PIB cerebral deposition was higher in frontoparietal and posterior cingulate regions. Further post-surgical studies would be desirable to elucidate if the presence of cerebral amyloid deposition may be a prognostic factor, and if this deposition is in agreement with cerebral amyloid distribution in AD patients.

1101 – Tuesday, October 18, 2016, 08:00 - 09:30, Auditorium

CME 9 - Drug Development/Radiopharmacy/Translational Molecular Imaging & Therapy: Strengths and Limitations of Techniques and Instrumentation

OP432

New Cyclotrons to Serve the Future of Nuclear Medicine

M. Jensen; Hevesy Lab., DT-NUTECH, Roskilde, DENMARK.

OP433

Maximising the Impact of LC-MS/MS on Tracer Discovery

V. Barth; Eli Lilly, Neuroscience, Indianapolis, UNITED STATES OF AMERICA.

OP434

Simultaneous PET-MR: Strengths and Weaknesses from Instrumentation to Applications

A. Hammers; King's College London, PET Imaging Centre, London, UNITED KINGDOM.

1102 – Tuesday, October 18, 2016, 08:00 - 09:30, Hall 211

Joint Symposium 9 - EANM/ENETS/SIOPEN: Strategies in Endocrine Tumors: Neuroblastoma & Paraganglioma

OP435

Non MIBG Radiopharmaceuticals in the Evaluation and Follow Up of Neuroblastoma and Paraganglioma

E. Lopci; Istituto di Ricerca e Cura a Carattere Scientifico (IRCCS), HUMANITAS (Rozzano), Nuclear Medicine, Milano, ITALY.

OP436

Strategies in Paraganglioma: ENETS' Point of View

A. Grossmann; University of Oxford, Churchill Hospital, Radcliffe Dept. of Medicine, Oxford, UNITED KINGDOM.

OP437

Imaging Based Prognostic Factors in the Assessment of Neuroblastoma
F. Giammarile; Centre Hospitalier Universitaire de Lyon, Lyon, FRANCE.

OP438

PRRT for Paraganglioma and Neuroblastoma

L. Bodei; European Institute of Oncology, Division of Nuclear Medicine, Milan, ITALY.

1104 – Tuesday, October 18, 2016, 08:00 - 09:30, Hall 112

Committee Symposium Do.MoRe: Feasibility of Treatment Planning for Radionuclide Therapy

OP439b

Quantitative Imaging and Treatment Planning for Radiopeptide and PSMA Therapy

J. Kurth; University Medical Centre Rostock, Department of Nuclear Medicine, Rostock, GERMANY.

OP440

Image Segmentation and Treatment Planning for Y-90 Radioembolisation
C. Chiesa; Fondazione IRCCS Istituto Nazionale Tumori, Milan, ITALY.

OP441

Time-Activity Curve Evaluation, Dosimetry Calculation and Absorbed Dose Constraints

M. Bardies; Centre de Recherche en Cancérologie de Toulouse, Toulouse, FRANCE.

OP442a

Clinical Objectives in Treatment Planning for Patient-Specific Therapy, Consequences for Patient Care

A. Sundlöv; Skåne University Hospital, Lund, SWEDEN.

1105 – Tuesday, October 18, 2016, 08:00 - 09:30, Hall 115

M2M - Featured: Radionuclide Production

OP443

Radionuclide Production

T. Eriksson; General Electric, Uppsala, SWEDEN.

OP444

Production and Automated Separation of Cyclotron Produced Cu-64 for Preclinical Purposes

V. Gupta, S. Schweitzer, S. Stricker, M. Schäfer, A. Runz, K. Kopka; German Cancer Research Center, Heidelberg, GERMANY.

Aim: Among the non-standard positron emitters, Cu-64 exhibits favorable decay characteristics ($t_{1/2} = 12.7$ h, $E_{\beta^+, \max} = 0.656$ MeV) for PET imaging of radiotracers with slow or delayed pharmacokinetics. The main focus of this study is on a self-constructed automated system for separation of Cu-64 produced from a 32 MeV negative-ion departmental cyclotron for preclinical research purposes. **Materials and Methods:** Cu-64 was produced via $^{64}\text{Ni}(p,n)^{64}\text{Cu}$ reaction bombarding 11.7 MeV protons at $45\mu\text{Ah}$ on 100 mg of enriched Ni-64 (Chemotrade, 99.3% enrichment, thickness $350\mu\text{m}$) electroplated on a gold disc. The radiochemical separation of Cu-64 from the irradiated Ni-64 target, consisting of

by-products for e.g. radioisotopes (Co-55, Co-57, Ni-57, Co-61), was achieved by a self-constructed automated system using the principle of anion and cation exchange chromatography (Dowex 1X8, 100-200 MESH) with diluted mixtures of hydrochloric acid in organic solvents¹. A first prototype to automate the Cu-64 separation has been developed and successfully tested. It is based on an EtherCAT PLC System which is able to operate with any kind of actuators and sensors irrespective of manufacturers available in the market. The assembly contains two self-designed reactors and the module construction itself. It holds 4 Tevisio RD2007 activity sensors, 14 standard Bürkert valves, 3 Thomas Denver peristaltic pumps SR10/30, 2 custom made heating coils from Hotset and 2 ion exchange columns. **Results and Conclusion:** The fully automated set-up for the separation of Cu-64 from Ni-64 and by-products has been successfully implemented and tested. The complete separation process takes ca. 120 min with marginal absorbed effective. The purified Cu-64 was obtained as $[\text{}^{64}\text{Cu}]\text{CuCl}_2$ in 400 μL of 0.1M HCl, and Ni-64 was successfully recovered for further usage. The production yield of Cu-64 was 111 MBq/ μAh , the radiochemical yield of $[\text{}^{64}\text{Cu}]\text{CuCl}_2$ after the separation process was about 82%. Radionuclide purity of the $[\text{}^{64}\text{Cu}]\text{CuCl}_2$ solution was > 99.9% after 12h. **Reference** Smith SV, Waters J, Di Bartolo N., "Separation of ^{64}Cu from ^{67}Ga waste products using anion exchange and low acid aqueous/organic mixtures"; *Radiochimica Acta* 75, 65-68 (1996)

OP445

Cyclotron production of theranostic pair ^{43}Sc - ^{47}Sc on calcium targets

A. Bilewicz¹, R. Walczak¹, A. Majkowska¹, R. Misiak², J. Choinski³, M. Sitarz³, A. Stolarz³, J. Jastrzębski³; ¹Institute of Nuclear Chemistry and Technology, Warsaw, POLAND, ²Institute of Nuclear Physics, Cracow, POLAND, ³Heavy Ion Laboratory, University of Warsaw, Warsaw, POLAND.

Aim: The ^{43}Sc ($t_{1/2} = 3.89$ h) is an ideal β^+ - emitter in PET diagnosis. It can be used as an alternative to ^{68}Ga , because ^{43}Sc has longer half-life and forms theranostic pair with β^- emitter ^{47}Sc , that is important in planning radionuclide therapy. In comparison with ^{44}Sc -other proposed isotope of scandium - ^{43}Sc has half-life and beta plus radiation similar to ^{44}Sc , moreover gamma-ray energy emission and intensity is much lower (372 keV, 23%) than in case of ^{44}Sc (1157 keV, 99%) what is not negligible for patient and medical personnel. On the other hand ^{47}Sc - low energy β^- emitter is attractive candidate for radioimmunotherapy. In our work we propose new way for cyclotron production of ^{43}Sc in $^{42}\text{Ca}(d,n)^{43}\text{Sc}$ nuclear reaction and ^{47}Sc by proton irradiation of ^{48}Ca target in p,2n reaction. **Materials and methods:** In the present work we used enriched $^{42}\text{CaCO}_3$ and $^{48}\text{CaCO}_3$ targets (Isoflex, Russia). To manufacture the targets enriched $^{42}\text{CaCO}_3$ or $^{48}\text{CaCO}_3$ powder was pressed with graphite powder (10-25%) and mounted to a water cooled target holders and irradiated with beam of proton and deuteron at different energies. The activity of the samples were measured with high resolution γ -ray spectrometry. CaCO_3 targets were dissolved in 0.2 M HCl and an ion exchange resin Chelex 100 was used to separate ^{43}Sc and ^{47}Sc from calcium target materials. **Results:** . The obtained by deuteron irradiation of ^{42}Ca radionuclide of ^{43}Sc was radionuclidally pure. In the product no other than ^{43}Sc radionuclides not detected. In the case of proton irradiation of ^{48}Ca obtained product contained a mixture of an radionuclides ^{47}Sc and ^{48}Sc . At optimal irradiation energy and the thickness of the target content of ^{48}Sc impurity was less than 16%. It is worth be noted that ^{48}Sc is also low energy β^- emitter but emits also high energy gamma quanta. **Conclusion:** The proposed methods allow to obtain high activity of ^{43}Sc and ^{47}Sc . Scandium isotopes were separated from the targets on iminodiacetic resin with efficiency of more than 90% and eluted in volume of 0.3 ml. The level of Ca^{2+} in ^{43}Sc and ^{47}Sc fraction is less than 3 $\mu\text{g/ml}$. The recovery of the calcium target is nearly quantitative making the proposed production process economically

feasible. This work was carried out as a part of the projects of the National Center for Applied Research of Poland Nr PBS3/A9/28/2015.

OP446

A Fully Automated GMP-Compatible Two-in-One Dissolution-Purification Module for Extraction of Tc-99m from Irradiated with Cyclotron Mo-100 Targets

S. V. Selivanova¹, J. A. Sader², A. Zyuzin²; ¹Centre Hospitalier Universitaire de Sherbrooke, Sherbrooke, QC, CANADA, ²Advanced Cyclotron Systems Inc, Vancouver, BC, CANADA.

Aim: Direct production of ^{99m}Tc with cyclotrons, utilizing ¹⁰⁰Mo as starting material, can be a viable alternative to conventional reactor-based technology. GMP-compatible manufacturing process is an essential requirement for obtaining manufacturing authorisation. Our objective was to develop a safe and reliable procedure where dissolution of solid target and processing of target solute would be combined and controlled within a single automated module. In addition, the procedure should be easily transferred to a GMP-compliant environment. **Methods:** A prototype dissolution system was designed in-house (Advanced Cyclotron Systems Inc.). The dissolution system consisted of a dissolution chamber assembly, which accommodated high-current target, and a neutralisation vial, where target solute was collected. Commercially available cassette-based automated module (MiniAIO, Trasis) was used to add reagents and solvents to the dissolution system and to process resulting target solute. To achieve controls via Trasis software, both systems were hard-wired via digital outputs of the MiniAIO unit. Layout of the MiniAIO hardware layer was redesigned to include control valves and switches of the dissolution system. Feedback was displayed through external digital inputs. The system was first optimised under simulated conditions with non-irradiated targets prepared from natural molybdenum and spiked with generator-eluted ^{99m}Tc target solute. Then, the procedure was tested using irradiated targets made of ¹⁰⁰Mo. **Results:** The prototype dissolution system was successfully interfaced with automated cassette-based purification module. This allowed uninterrupted automated target dissolution and processing. Controls of the dissolution system, including solvent addition, were entirely integrated with MiniAIO functionalities. Single program sequence included on-line conditioning of all cartridges, target dissolution, and ^{99m}Tc extraction and purification. **Conclusions:** We developed and tested an automated GMP-compatible combined dissolution-purification procedure for extraction of ^{99m}Tc from irradiated with cyclotron ¹⁰⁰Mo targets. It can permit a trained technician to perform routine productions following a standard operating procedure.

OP447

Titanium-45 as an innovative radionuclide for PET imaging: from cyclotron production to potential biomedical applications

P. Costa^{1,2}, L. F. Metello^{1,3}, F. Alves⁴, S. Carmo⁴, M. D. Naia²; ¹Nuclear Medicine Department, ESTSP.IPP, Vila Nova de Gaia, PORTUGAL, ²CEMUC® - Physics Department, ECT-UTAD, Vila Real, PORTUGAL, ³Nuclear Medicine Department, IsoPor SA, Porto, PORTUGAL, ⁴Institute for Nuclear Sciences Applied to Health, ICNAS-University of Coimbra, Coimbra, PORTUGAL.

Introduction: In recent times, several groups are working worldwide in the extension of the number and availability of positron emitting radionuclides for PET imaging, in the way to avoid the strict dependence on ¹⁸F, ¹¹C, ¹³N and ⁶⁸Ga, so increasing the number of available tools for a truly practice of personalized Nuclear Medicine. From few years ago, our group is busy studying ⁴⁵Ti, assuming it as a potential candidate, since it presents many interesting properties: physical half-life of 3.09h, together with relevant chemical properties, that enable radiolabelling with

bifunctional chelates, direct labelling of specific chemical ligands or even to be used in the radiolabelling of titanium (di)oxide nanoparticles. **Aim:** This work presents our experimental results on the determination of excitation function of ⁴⁵Sc(p,n)⁴⁵Ti nuclear reaction, that is being studied as the most interesting route to efficiently produce ⁴⁵Ti in low energy cyclotrons. **Material and Methods:** Cyclotron beam energy was calibrated using a copper stacked foil. The stacked foil technique was then applied using 99,5% pure Sc foils mounted on an inhouse, internally developed, aluminum target holder interspaced in some positions with 99,999% pure Cu foils. Short irradiations (~1µA during 100 seconds) in an 18 MeV cyclotron (CYCLONE 18/9, from IBA®) were implemented. Results of this activation study were evaluated using HPGe spectroscopy (always considering dead time losses ≤ 5%). **Results:** Results concerning the excitation function of the main route under study were collected, with the addition of some information regarding concurrent reactions leading to ^{44m}Sc and ⁴⁴Sc. Experimental results were also compared with the Monte Carlo simulation results obtained using TALYS code calculations. Our results confirm TALYS predictions and are completely comparable to other few (even incomplete) results already published. Specifically, cross-section values for the ⁴⁵Sc(p,n)⁴⁵Ti nuclear reaction presented maximum values for beam energies between 10-15 MeV, presenting an approximated plateau shape in this region. Energies higher than 16 MeV lead to co-production of ⁴⁴Ti, ⁴⁴Sc and ^{44m}Sc. **Conclusion:** Considering our results, the production of ⁴⁵Ti seems feasible in low energy cyclotrons, with maximum yields obtained for 10-15 MeV proton beams, allowing its production in an appropriate manner to be used in several potential biomedical applications.

OP448

Development of Pt-195m Cisplatin and Derivatives as New Imaging Agents

K. Codee-van der Schilden, O. Zwaagstra; NRG, Petten, NETHERLANDS.

Aim: Cisplatin is worldwide one of the most used anticancer agents and is applied in standard treatment procedures for several malignant tumor types. However, significant differences appear between patients and between tumors, and treatment outcome cannot be predicted. Moreover, Cisplatin can cause severe toxic side effects. We have developed Pt-195m Cisplatin as a SPECT imaging agent to enable studies of patient specific interactions with Cisplatin with the aim to improve treatment outcome and reduce toxic side effects in a personalized approach. We also developed a Pt-195m Cisplatin derivative as a new SPECT imaging probe ideally suitable for linkage to biologically active compounds to allow to study their behavior in vivo in a noninvasive manner. **Materials and Methods:** Platinum-195m was produced by thermal neutron irradiation of enriched Platinum-194 in the High Flux Reactor in Petten, the Netherlands for four to eight days. After sufficient cooling time, the irradiated Platinum was dissolved and analyzed by UVVIS and gamma spectroscopy. Radioactive Cisplatin and Platinum-195m ethylenediammine dinitrate were synthesized by slight modification of known procedures¹. An identification test was developed using UVVIS. Radiochemical purity was assessed by HPLC, radionuclide purity was determined using gamma spectroscopy and chemical purity was evaluated using nonradioactive counterparts. **Results:** Eight days of irradiation resulted in highest specific activity of approximately 1 mCi/mg Pt at End of Irradiation (EOI). Thorough washing of the diiodide Platinum intermediate resulted in sufficient separation of Gold and Iridium radioactive side products. UVVIS of the synthesized product showed a maximum at 301 nm and a minimum at 246 nm, which are characteristic for Cisplatin. Radiochemical purity was greater than 95 %, impurities of silver were below acceptable levels, radionuclide purity was greater than 99 %. **Conclusion and future prospects:** Pt-195m Cisplatin and [Pt(NH₃)₂(NO₃)₂] have been successfully synthesized with good quality. In collaboration with the Dutch Cancer Institute quantification of Pt-

195m using SPECT has been shown. Automatization of Pt-195m Cisplatin has been started to enable GMP production of the product. 1: Hoeschele, J.D., Butler, T.A., Roberts, J.A., Guyer, C.E. Analysis and refinement of the microscale synthesis of the ^{195m}Pt-labeled antitumor drug, *cis*-Dichlorodiammineplatinum(II), *cis*-DDP. *Radiochimica Acta* 31, 27-36 (1982).

1106 – Tuesday, October 18, 2016, 08:00 - 09:30, Hall 111

Pitfalls & Artefacts - Oncology: Basic Artefacts in Hybrid Imaging (SPECT/CT, PET/CT and PET/MR): Pitfalls and Solutions

OP449b

General Radiology Perspective

L. Umutlu; Universitätsklinikum Essen (AöR), Institut für Diagnostische und Interventionelle Radiologie und Neuroradiologie, Essen, GERMANY.

OP450

SPECT/CT Perspective

R. Hustinx; Centre Hospitalier Universitaire, Service de Médecine Nucléaire, Liège, BELGIUM.

OP451

PET Perspective

B. Sattler; University Hospital Leipzig, Department for Nuclear Medicine, Leipzig, GERMANY.

OP452

PET/MR Perspective

P. Veit-Haibach; University Hospital Zurich, Klinik für Nuklearmedizin, Zurich, SWITZERLAND.

1107 – Tuesday, October 18, 2016, 08:00 - 09:30, Hall 116

Clinical Oncology - Featured: PSMA Theranostics

OP453

PSMA Theranostics: State of the Art

U. Haberkorn; University Hospital Heidelberg, Department of Nuclear Medicine, Heidelberg, GERMANY.

OP454

Ac-225-PSMA-617 for PSMA targeting alpha-radiation therapy of 28 patients with mCRPC

C. Kratochwil¹, F. Bruchertseifer², F. L. Giesel¹, C. Apostolidis², U. Haberkorn¹, A. Morgenstern²; ¹University Hospital Heidelberg, Heidelberg, GERMANY, ²European Commission - Joint Research Centre, Institute for Transuranium Elements, Karlsruhe, GERMANY.

Aim: We evaluate imaging and tumor marker response as well as clinical and hematological toxicity of targeted alpha-radiation therapy with Ac-225-PSMA-617 (TAT) in inter-individual comparison to Lu-177-PSMA-617 in dependency of prognostic factors.

Methods: Retrospective analysis of case series about patients treated either with Ac-225-PSMA-617 (n=28) or Lu-177-PSMA-617 (n=30), after treatment stratification based on PSMA-imaging. Tumor spread, previously applied treatments and lab tests were used to analyse the prognostic profile of both cohorts. After treatment, lab tests and tumor markers were determined at least every 4 weeks. After 3 cycles (6 months) radiological restaging was performed. **Results:** The TAT group was in more advanced stage

and more heavily pre-treated. Hematological toxicity was tolerable in both groups, with limitation that Lu-PSMA was restricted to oligo-multifocal bone metastases while TAT also included patients with diffuse type red marrow infiltration. Moderate xerostomia occurred occasional in the beta-radiation group but frequently and more severe during TAT. However, both imaging response and tumor markers were in favor for TAT, e.g. PSA-response was seen with 95% (Ac-225) vs 75% (Lu-177) after week-8 and 75% (Ac-225) vs 50% (Lu-177) after week-24. After TAT, 20% of patients achieved complete remission (CR) in regard to imaging and tumor markers. Some radiological CR but no biochemical CR was found after beta-radiation therapy.

Conclusions: In regard to mCRPC alpha-emitters seem superior in comparison to beta-nuclides when tagged to the identical carrier molecule.

OP455

The Value of Ga-68-PSMA-PET/CT as a Gatekeeper for Ra-223-Dichloride Therapy

A. Bode, K. Rahbar, J. Konner, M. Bögemann, L. Stegger; University Hospital Münster, Münster, GERMANY.

Purpose. ²²³Ra-dichloride is a novel therapeutic option for the treatment of osseous metastases in castration-resistant prostate carcinoma. Application is currently approved for patients with symptomatic bone metastases but without visceral metastases. A successful treatment depends on an adequate uptake of ²²³Ra in metastases, predicted by bone scintigraphy. The purpose of our study was to investigate whether ⁶⁸Ga-PSMA-PET/CT performed in patients intended for ²²³Ra-dichloride therapy has incremental value over conventional staging in order to detect visceral metastases or osseous metastases without adequate uptake in bone scintigraphy. **Materials/Methods.** Additional ⁶⁸Ga-PSMA-PET/CT was performed in 27 patients intended for ²²³Ra-dichloride therapy. Conventional staging included bone scintigraphy and computer tomography of the thorax, abdomen and pelvis. Visceral metastases diagnosed by ⁶⁸Ga-PSMA-PET/CT but not by conventional staging were recorded. In addition, the tumour extent visible with ⁶⁸Ga-PSMA-PET/CT was compared to the extent and intensity of tracer uptake in bone scintigraphy. Both image data sets were evaluated for mismatch patterns with absent or low uptake in the bone scan in relation to the tumour distribution. Patients with either newly diagnosed visceral metastases or significant areas of osseous tumour without adequate uptake in bone scintigraphy were re-evaluated with the option to undergo experimental ¹⁷⁷Lu-PSMA-Radioligand-Therapy instead. **Results.** In two patients previously unknown visceral metastases were detected by ⁶⁸Ga-PSMA-PET/CT. In four patients comparison of ⁶⁸Ga-PSMA-PET with bone scintigraphy revealed large volumes of tumour within the spine without adequate uptake in bone scintigraphy, most likely owing to extended bone marrow involvement with little activation of bone. In these patients the efficacy of ²²³Ra therapy was called into question. In six other patients ⁶⁸Ga-PSMA-PET/CT revealed a minor mismatch with detection of smaller additional metastases mainly in the thorax and the extremities. In these patients the bulk of the tumour showed good uptake in bone scintigraphy and ²²³Ra-dichloride therapy was performed as planned. **Conclusion.** Additional ⁶⁸Ga-PSMA-PET/CT in patients intended for ²²³Ra-dichloride therapy can provide significant incremental information that may change subsequent therapeutic decisions. This scan can reveal previously unknown visceral metastases but it can also identify patients with extended areas of tumour with good PSMA expression but inadequate uptake in bone scintigraphy. The latter is of tremendous importance given the availability of the new ¹⁷⁷Lu-PSMA-Radioligand-Therapy, probably the more effective therapeutic option in these patients compared to ²²³Ra-dichloride.

OP456**⁶⁸Ga-PSMA PET/CT early detection of Prostate Cancer bone metastases: the end of the osteoblastic era?**

C. ARTIGAS, T. KAMOUN, C. GARCIA, Z. WIMANA, G. GHANEM, R. VAN VELTHOVEN, F. OTTE, T. GIL, P. FLAMEN; Institut Jules Bordet, Brussels, BELGIUM.

Introduction and Aim: Bone metastases (BM) are present in 90% of patients who die of Prostate Cancer (PCa). However, diagnosis of BM is usually done in advanced stages of the disease with bone scan being recommended in EAU guidelines only for PSA values >20ng/ml. Identifying those lesions in an early stage before osteoblastic activity may have a prognostic value and influence the treatment choice going from local to systemic therapies and better selecting patients candidates for oligometastatic therapeutic approach. The aim of this communication was to determine if ⁶⁸Ga-PSMA PET/CT is able to early detect BM, even before osteoblastic/osteolytic reaction becomes detectable. **Material and methods:** We retrospectively analyzed a cohort of 223 consecutive ⁶⁸Ga-PSMA PET/CT performed at our institution for PCa biochemical relapse (BCR) after local treatment with curative intent (surgery, radiotherapy or both) between November 2014 and February 2016. All patients had PSA <20ng/ml [mean 4.4ng/ml (range 0.3-15.6)]. Focal bone uptake was considered as suspected for BM if the SUVmax lesion-to-background ratio was >2. Validation criteria included the confirmation by other imaging techniques (bone scan, MRI or CT), clinical follow-up with PSA decrease after targeted therapy or increase in PSA and in number of lesions after watchful waiting period. BM were divided into (a) osteolytic, (b) osteoblastic and (c) none based on CT images. **Results:** 38/223 patients presented with at least one suspected BM at ⁶⁸Ga-PSMA PET/CT. Mean SUVmax lesion-to-background ratio was 15 (range 2-74). 33/38 (87%) of patients had at least one validation criteria confirming BM. 4/38 patients with suspected BM didn't have confirmation and are still on follow-up. Only one lesion was a false positive resulting in a vertebral hemangioma. A total of 235 bone lesions were detected. 32 (13%) were osteolytic, 64 (27%) osteoblastic and 163 (69%) showed no abnormality on CTscan and were considered as bone marrow lesions. Finally 26/38 (68%) patients presented with ≤3 suspected BM (oligometastatic disease). **Conclusion:** This retrospective study suggests that ⁶⁸Ga-PSMA PET/CT is a useful technique to early detect PCa BM in patients with BCR after local treatment with curative intent, even before those lesions become osteoblastic/osteolytic. This fact could substantially influence therapeutic strategy decision, especially for those patients with oligometastatic disease.

OP457**Validation of ⁶⁸Ga-PSMA-Ligand-PET/CT in Primary Staging of Prostate Cancer Patients**

C. Uprimny, A. Kroiss, C. Decristoforo, L. Scarpa, D. Kendler, L. Geraldo, E. von Guggenberg, B. Nilica, S. Buxbaum, I. Virgolini; Medical University Innsbruck, Innsbruck, AUSTRIA.

Purpose: Prostate cancer (PC) cells usually show a high level expression of prostate-specific membrane antigen (PSMA) as can be assessed by ⁶⁸Ga-PSMA-ligand-PET/CT. The aim of this study was to assess the intensity of PSMA-expression of the primary tumour and metastases in patients with biopsy proven PC prior to therapy, and to determine if there exists an association of PSMA-expression and Gleason score (GS) or prostate specific antigen (PSA)-level. **Methods and Materials:** 82 patients with transrectal ultrasound (TRUS) biopsy proven PC (GS 6-10; median PSA: 10.0 ng/ml) referred for ⁶⁸Ga-PSMA-ligand PET/CT were retrospectively analysed (diagnostic CT: n=20). PET scans were acquired 60 minutes after injection of ⁶⁸Ga-PSMA-ligand (Glu-NH-CO-NH-Lys-HBED-CC) using a median activity of 145 MBq. PET images were

analysed visually. In addition, maximum standardized uptake values (SUVmax) of the primary tumour and pathological lesions suspicious for lymphatic or distant metastases were calculated and compared to physiological background activity of normal prostate tissue (BGp) and the gluteal muscle (BGg). SUVmax of the primary was compared to the PSA-level and GS of the TRUS-biopsy specimen. **Results:** 76 patients (92.7%) demonstrated pathological tracer uptake within the prostate gland (median tumour SUVmax: 12.0). In comparison the median SUVmax of BGp and BGg was 3.85 and 1.3, respectively. PC with GS 6 and 7 showed a lower PSMA-expression (median SUVmax: 7.6) compared to patients with GS >7 (median SUVmax: 24.3). PC patients with PSA >10.0 ng/ml exhibited a higher PSMA-ligand uptake in the tumour compared to those with PSA-levels <10.0 ng/ml (median SUVmax: 17.0 versus 7.8). 23 patients (28%) showed lymph nodes (LN) with pathologic tracer accumulation consistent with metastases (n=75; median SUVmax: 11.15). In 10 patients (12.2%) pathologic skeletal lesions suspicious for bone metastases were found (n=27; median SUVmax: 8.4). **Conclusion:** The majority of TRUS-biopsy proven PC patients showed a pathologic ⁶⁸Ga-PSMA-ligand accumulation in the primary tumour on ⁶⁸Ga-PSMA-PET/CT. However, PC patients with GS >7 and PSA >10.0 ng/ml exhibited a higher PSMA-expression than those with low GS (6 and 7) and PSA <10.0 ng/ml. The data allow the conclusion that the higher PSMA-ligand uptake related to both PSA >10 ng/ml and GS >7 should be considered in the selection of PC patients referred to ⁶⁸Ga-PSMA-PET/CT for primary staging.

OP458**Comparison of ⁶⁸Ga-PSMA and ¹¹C-Choline using a tri-modality PET/CT-MR (3.0T) system with a dedicated shuttle**

O. Alonso^{1,2}, G. dos Santos^{1,2}, M. García Fontes¹, M. Rodríguez Taroco¹, H. Engler¹; ¹Centro Uruguayo de Imagenología Molecular (CUDIM), Montevideo, URUGUAY, ²Hospital de Clínicas, Universidad de la República, Montevideo, URUGUAY.

Multiparametric MR has shown high sensitivity and specificity for the detection of relapses in prostate cancer patients. Besides, PET/CT with ⁶⁸Ga-PSMA has been proposed as a promising tracer for imaging patients with biochemical recurrence (BR) at low PSA levels. The aim of this study was to prospectively compare the detection rate of ⁶⁸Ga-PSMA versus ¹¹C-Choline in prostate cancer patients with BR using a tri-modality PET/CT-MR system. **Material and methods.** Patients with BR after initial treatment were included between August 2015 and March 2016. Within 1-2 weeks PET/CT scans were performed with ¹¹C-Choline followed by ⁶⁸Ga-PSMA studies, with doses of approximately 400 MBq and 300 MBq, respectively. A 64-slice PET/CT scanner with TOF correction was used. Additionally, for the ⁶⁸Ga-PSMA scans, acquisitions with a PET/CT-MR (3.0 T) system with a dedicated shuttle, were included. An abbreviated MR protocol was planned with T1 and T2 sequences beginning at aortic bifurcation. High-resolution thin slices with T2 sequence at prostate bed and focal and panoramic diffusion (DWI) and ADC maps were obtained. MR images were performed during 30 minutes, starting 30 minutes after tracer injection. **Results.** A total of 36 patients were included in te study. Twenty-four (67%) underwent radical prostatectomy whereas 12 were treated with radiotherapy. The median PSA level was 3.3 ng/mL, ranging from 0.2 to 138 ng/mL. In 18 patients (50%), both scans were positive and in 8 (22%), negative. Nine patients were positive with ⁶⁸Ga-PSMA alone (25%) and one only with ¹¹C-Choline (3%). A total of 185 lesions were detected by at least one tracer. ⁶⁸Ga-PSMA had a significantly higher SUVm compared to ¹¹C-Choline: 7.0 (1.5-46) versus 4.3 (1.0-16.5), median and range for each tracer, respectively (P < 0.0001). Furthermore,

^{68}Ga -PSMA detected more lesions per patient compared to ^{11}C -Choline: 2.0 (0-93) versus 1.0 (0-57), respectively ($P=0.023$). The number of detected lesions per patient was lower for ^{11}C -Choline in patients with PSA < 3.3 ng/mL ($P=0.03$), but the difference was not statistically significant for ^{68}Ga -PSMA. Regarding pelvic evaluation, metastases were found in 25 patients (69%) with ^{68}Ga -PSMA PET/CT; 21 (58%) with MR (3.0 T) and 18 (50%) with ^{11}C -Choline PET/CT. MR was very useful in cases classified as indeterminate by means of PET/CT alone. Conclusion: ^{68}Ga -PSMA detected more lesions than ^{11}C -Choline in patients with prostate cancer with biochemical recurrence, regardless of PSA levels. PET/CT-MR (3.0 T) system is a feasible imaging modality that adds relevant information for patient management.

OP459

PSMA Radioligand Therapy (PRLT) of Metastatic Castration-Resistant Prostate Cancer: Safety, Efficacy and Dosimetry using the PSMA Inhibitor 617

H. R. Kulkarni, C. Schuchardt, A. Singh, K. Niepsch, R. P. Baum; THERANOSTICS Center for Molecular Radiotherapy and Molecular Imaging, Bad Berka, GERMANY.

AIM: We have already had experience with the PSMA inhibitor I&T in 56 patients with progressive metastatic castration-resistant prostate cancer (mCRPC). The objective of this study was to analyze the safety and efficacy of Lu-177 labeled prostate specific membrane antigen (PSMA) ligand Lu-177 PSMA-617 in progressive mCRPC. **MATERIALS AND METHODS:** Thirty-nine mCRPC patients underwent a total of 78 cycles (1: n=15, 2: n=11, 3: n=11, 4: n=2) of PSMA radioligand therapy (PRLT) using Lu-177 PSMA-617. The median administered activity per treatment was 6.04 GBq (3.2 - 8.4). Ga-68 PSMA-HBED-CC (Ga-68 PSMA) PET/CT (contrast-enhanced CT) was used for patient selection and follow-up after PRLT. Response after at least 2 cycles was available at the time of analysis in 15 patients. Hematological status, renal and hepatic function and serum prostate specific antigen (PSA) levels were documented before and after therapy. Dosimetry was performed in 15 patients. **RESULTS:** Lu-177 PSMA-617 demonstrated intense accumulation in the metastases on post-therapy whole-body scans. The uptake was moderately intense in the kidneys and salivary glands, and mild to moderate in the intestine. The mean absorbed tumor dose was 5.1 mGy/MBq (median). Parotid glands received a higher dose (1.0 mGy/MBq) than kidneys (0.7 mGy/MBq). All patients tolerated the therapy well without any acute adverse effects. The only long-term clinical adverse effect was mild xerostomia observed in 5 patients. Grade (G) 1 hematological toxicity was noticed in 9 patients, G2 toxicity in 4 and G3-4 pancytopenia in 2 patients. Mild erythrocytopenia was the commonest sequel. Higher-grade toxicity was observed in patients (n=6) having received chemotherapy or Ra-223 treatment before. The severity of pain was significantly reduced in 4/12 (33.33 %) symptomatic patients after PRLT. Decrease in PSA was noted in 30/39 (76.9 %) patients. Molecular response evaluation (Ga-68 PSMA PET/CT) revealed complete remission (CR) in 1, partial remission (PR) in 7, stable disease (SD) in 2 and progressive disease (PD) in 5 patients. CT exhibited PR in 3, SD in 7, and PD in 5 patients. Over this period of analysis, 3 patients died (2 due to progression of disease and 1 due to myocardial infarction). The median overall and progression-free survival have not been reached yet. **CONCLUSION:** Lu-177 PSMA-617 appears to be safe and effective in progressive mCRPC with kinetics and dosimetry similar to Lu-177 PSMA-I&T, the first-ever PSMA inhibitor used at our center. Ga-68 PSMA PET/CT enables appropriate selection and follow-up of patients, applying the theranostics concept.

1108 – Tuesday, October 18, 2016, 08:00 - 09:30, Hall 212

Cardiovascular System: Myocardial Perfusion - Conventional SPECT

OP460

Long-term Negative Predictive Value of Stress Myocardial Perfusion Imaging and Coronary Computed Tomography Angiography: A Meta-analysis

V. Cantoni¹, R. Green¹, W. Acampa¹, R. Assante¹, E. Zampella¹, V. Gaudieri², C. Nappi¹, M. Manganelli¹, M. Petretta¹, A. Cuocolo¹; ¹University of Naples, Naples, ITALY, ²Institute of Biostructure and Bioimaging, National Council of Research, Naples, ITALY.

Aim: We conducted a meta-analysis to compare the long-term negative predictive value (NPV) of stress single-photon emission computed tomography myocardial perfusion imaging (MPI) and coronary computed tomography angiography (CCTA) for the prediction of cardiovascular events in patients with suspected or known coronary artery disease (CAD). **Materials and Methods:** We searched PubMed, Cochrane, Web of Science and Scopus database between January 2000 and December 2015 for stress MPI and CCTA studies. We included studies that followed-up ≥ 100 subjects with a follow-up ≥ 5 years and providing data on annualized event rate (AER). Summary risk estimates for normal perfusion at MPI or <50% coronary stenosis at CCTA were derived in random effect regression analysis, and causes of heterogeneity for demographic or clinical variables were determined in meta-regression analysis. **Results:** We identified 22 eligible articles (13 MPI and 9 CCTA) including 47,596 participants (34,492 in MPI and 13,104 in CCTA studies) with suspected or known CAD. The outcome of interest was the occurrence of the primary end-point considered of each study. The pooled NPV for the primary endpoint was higher in CCTA than MPI studies ($p<0.05$), ranging from 82% to 96% for MPI and from 79% to 98% for CCTA. The pooled annualized event rate (AER, per 100 person-years) was lower in CCTA than MPI studies ($p<0.05$), ranging from 0.69 to 2.28 for MPI and from 0.21 to 4.13 for CCTA. Among the studies selected, 13 MPI and 5 CCTA reported the AER for the occurrence of hard events (death and non-fatal myocardial infarction). Considering these studies, the pooled NPV for the occurrence of hard events was higher in CCTA than MPI studies ($p<0.05$) and the NPV ranged from 82% to 96% for MPI and from 87% to 99% for CCTA. Conversely, the pooled AER was lower in CCTA than MPI studies ($p<0.05$), ranging from 0.69 to 2.28 for MPI and from 0.21 to 2.63 for CCTA. A high level of heterogeneity ($P<0.0001$) was observed between studies for NPV for both MPI ($I^2=97.77\%$) and CCTA ($I^2=93.80\%$). At meta-regression analysis, a significant association between AER and hypertension ($p<0.005$) and diabetes ($p<0.01$) was found only for MPI. **Conclusions:** Stress MPI and CCTA have a high long-term NPV for adverse cardiac events. The lower AER in CCTA studies probably emerged for the heterogeneity of patient population included in the meta-analysis.

OP461

Prognostic value of coronary artery calcium scanning, coronary CT angiography and stress myocardial perfusion imaging in patients with suspected coronary artery disease

C. Nappi¹, S. Daniele², V. Gaudieri¹, W. Acampa¹, S. Segreto¹, V. Cantoni¹, R. Green¹, A. Mirabile¹, M. Imbriaco¹, M. Petretta¹, A. Cuocolo¹; ¹University of Naples, Naples, ITALY, ²Institute of Biostructure and Bioimaging, National Council of Research, Naples, ITALY.

Aim: We compared the prognostic value of coronary artery calcium (CAC) scanning, coronary computed tomography angiography (CCTA) and stress single-photon emission computed tomography myocardial perfusion imaging (MPI) in assessing cardiovascular risk in patients with suspected coronary artery disease (CAD). **Material and methods:** We prospectively evaluated 172 consecutive patients (age 62±11 years) at low-intermediate pre-test probability of CAD undergoing CAC scanning, CCTA and stress MPI for suspected CAD. CAC score was measured according to the Agatston method and patients were categorized into 3 groups (0, 0.01–300, and >301). Coronary artery stenoses were quantified by visual estimation as significant in the presence of ≥50% luminal narrowing. Summed stress score (SSS), summed rest score (SRS) and summed difference score (SDS) were automatically calculated. Ischemia was defined in the presence of a SDS ≥2. Major cardiac events (MACE) were considered cardiac death, nonfatal myocardial infarction and unstable angina requiring coronary revascularization. **Results:** Follow-up was 91% complete during a mean period of 82±34 months. In 156 subjects, 22 events occurred (4 cardiac deaths, 2 nonfatal myocardial infarctions, and 16 revascularizations for unstable angina) with cumulative event rate of 14%. Cardiac event risk increased with worsening of CAC categories. In patients with CAC of 0 (n=42) no event was observed; whilst patients with CAC 1–300 (n=98) and >300 (n=16) had 14 and 8 events, respectively (14% and 50%, respectively; P<0.001). MACE occurred in 27% of patients with ≥50% stenosis at CCTA and in 34% of patients with ischemia at stress MPI. At univariable Cox regression analysis, male gender, ln(CAC + 1), ≥50% stenosis at CCTA, SSS and SDS resulted significant predictors of MACE (all P<0.05). At multivariable analysis, only ln(CAC + 1) and SDS (both P<0.001) resulted independent predictors of events. The addition of MPI data improved the prognostic strength of the model including in hierarchical order clinical data, CAC score and CCTA findings increasing the global chi-square from 36.17 to 41.99 (P<0.05). Conversely, CCTA data did not provide significant incremental prognostic power over the model including clinical data, CAC score and stress MPI findings (global chi-square from 38.84 to 41.99 (p=0.08). **Conclusions:** Patients at low-intermediate pre-test probability of CAD without CAC do not need further cardiac imaging investigations. Both CCS and MPI, but not CCTA, are independent predictors of MACE. Moreover, functional data by stress MPI improves risk stratification over clinical variables, CAC scanning and CCTA findings.

OP462

Future Cardiac Events in Patients with Ischemic ECG Changes during Adenosine Infusion as a Myocardial Stress Agent with Normal Cardiac Scan.

H. A. AMER, K. Niaz, H. Samiri, M. Sheikh, M. Alothman, M. Alhammad; King Abdulaziz Hospital for National Guards, Al-Ahsa 31982, SAUDI ARABIA.

Background. The development of ischemic changes during adenosine myocardial perfusion imaging (MPI) has been shown to be a predictor of CAD and consequently subsequent cardiac events and worse outcome. Some published data shown that ST-segment depression develops during adenosine administration appear to be at increased risk for future cardiac events compared with similar patients without ECG evidence of ischemia. We sought to determine the prognostic importance of adenosine-induced ischemic ECG changes in patients with normal SPECT myocardial perfusion images. **Methods:** We performed a retrospective analysis of 750 patients undergoing adenosine MPI. Patients with baseline electrocardiographic (ECG) abnormalities and/or abnormal scan were excluded. The data were collected from the nuclear medicine database identifying all the reported Gated myocardial perfusion SPECT with adenosine stress tests between January 2013 and January 2015. Images were graded using the 17-segment model. Follow-up information was obtained from hospital records. All cardiac events (cardiac death, nonfatal myocardial infarction [MI], percutaneous coronary

intervention, coronary artery bypass grafting, or angiography) were verified with hospital records. **Results:** Overall, 67 patients (9%) had ischemic ECG changes during adenosine infusion in the form of ST depression of ≥1mm. Of these, 29 (43% [3.8% of all patients]) had normal MPI (positive (+) ECG group). An age- and sex-matched group of 108 patients with normal MPI without ECG changes served as control subjects (negative (-) ECG group). During a mean follow-up of 27 +/- 12 months, patients in the +ECG group had no significantly more adverse cardiac events than those in the -ECG group (nonfatal myocardial infarction and cardiac death did not differ between the 2 groups). There were no cardiac deaths in either group. One (0.9%) patient within the negative ECG group had a nonfatal MI (0.7% annual event rate after a negative MPI). Two also in this group (1.8%) patients admitted with a diagnosis of CAD where they have been ruled out by angiography. A fifth case was admitted due to heart failure that proved to be secondary to pulmonary cause and not of CAD. **Conclusions.** Patients with normal myocardial perfusion scintigraphy in whom ST-segment depression develops during adenosine stress test appear to be with no increased risk for future cardiac events compared with similar patients without ECG evidence of ischemia and consequently myocardial perfusion scan remain a main predictor for future cardiac events and worse outcome.

OP463

Cardiac stress test modalities during myocardial perfusion scintigraphy in type-2 diabetic patients: are they relevant for prognosis? A Substudy of the BARDOT Trial

F. Caobelli, J. Chronis, G. Haenny, M. Brinkert, M. E. Pfisterer, M. J. Zellweger; Universitätsspital Basel, basel, SWITZERLAND.

Objectives: to assess clinical characteristics able to predict the stress test modality and the impact of exercise level achieved on cardiovascular risk. **Background:** the Basel Asymptomatic high-Risk Diabetics' Outcome Trial (BARDOT) demonstrated that asymptomatic diabetic patients with an abnormal myocardial perfusion scintigraphy (MPS) were at increased risk of major cardiac events (MACE). It still remains unclear whether in such patients some comorbidities can predict the stress modality and whether, in patients undergoing physical stress test, the exercise level achieved can provide further risk stratification. **Methods:** four hundred patients with type-2 diabetes and neither history nor symptoms of CAD were evaluated. They underwent clinical evaluation and MPS with either physical or pharmacologic stress test. Those able to perform an exercise stress were divided into two groups based on METs achieved (i.e <6 and ≥6, corresponding to vigorous exercise). Patients were followed up for 2 years. MACE were defined as myocardial infarction or cardiac death. **Results:** A large proportion of patients (305/400, 76.3%) could perform an adequate ergometric test, defined by reaching 85% of the predicted max heart rate. Of these, 244 (80%) could reach 6 METs. Independent predictors of a pharmacologic stress test with adenosine were smoking (OR 2.6, 95%CI 1.5–2.7, p=0.009), Body Mass Index >30 (OR 2.7, 95%CI 1.9–3.1, p=0.006), presence of peripheral neuropathy (OR 2, 95%CI 1.3–2.3, p=0.04) and peripheral arterial disease (OR 4.3, 95%CI 2.8–4.7, p<0.001). Patients undergoing pharmacological stress had a higher rate of MACE than physically stressed patients (3.2% vs 0.9%, p=0.03). Patients reaching < 6 METs during physical stress had a significantly higher MACE rate than those achieving ≥6 METs (4.9% vs 0.4%, p=0.01). Even in those patients achieving ≥6 METs, MPS showed an incremental prognostic value over pre-test information (chi-square 20.1 vs 5.4, p=0.01). **Conclusions:** In asymptomatic diabetic patients at high cardiovascular risk, specific comorbidities are highly predictive of the stress test modality used. Patients undergoing pharmacologic stress had a higher rate of MACE, similarly to those unable to reach 6 METs during physical exercise. Even in patients with preserved exercise capability, MPS provided incremental prognostic value.

OP464**Possible application of stress-only protocol in myocardial perfusion imaging**

M. M. Włodarczyk¹, J. Kuśmierk², A. Plachcińska¹; ¹Department of Quality Control and Radiological Protection, Medical University of Lodz, Poland, Lodz, POLAND, ²Department of Nuclear Medicine, Medical University of Lodz, Poland, Lodz, POLAND.

Aim: The purpose of this study was to determine in which patients it is possible to use a stress-only (SO) strategy to assess myocardial perfusion. **Material and methods:** 154 patients (65F, 89M, mean age 61 years) without prior myocardial infarction, history of coronary artery by-pass grafting or cardiomyopathy underwent two day stress/rest Gated-SPECT/CT MPI using ^{99m}Tc-MIBI (11MBq/kg) as a radiopharmaceutical. Exercise or dipyridamole (0,7mg/kg) was used as a stressor. Studies were processed on GE Xeleris2 station without (NC) and with use of attenuation correction (AC). Two experienced nuclear medicine specialists assessed visually myocardial perfusion (a consensus) using 4-point scale (4p): 1-normal (n), 2-probably normal (pn), 3-probably abnormal (pa), 4-abnormal (a). At first stress-only images were evaluated without and with AC, then stress/rest (S/R) images without and with AC. Regional and global wall motion was also evaluated. Patients with LVEF<50% (N=14) were eliminated from further analysis. Coefficients of agreement between SO and S/R assessments were calculated in 4p scale (including Cohen's kappa) and after dichotomizing results to normal (n+pn) and abnormal (a+pa) - 2-point scale (2p). Agreement was also analyzed in subgroups (male, female, BMI<30, BMI≥30). **Results:** Agreement of assessments in the whole cohort (N=140) in 4p scale was equal to 58%, k=0,41 (NC) and 74%, k=0,51 (AC); in 2p scale: 80% (NC) and 89% (AC), p=0,019. Among discordant results there were statistically significantly more abnormal results in S/R evaluation than in SO (17% vs 3%, p=0,0003 for NC and 10% vs 1%, p=0,006 for AC). Agreement in subgroups in 2p scale with AC was: for male patients with BMI<30 - 93%, with BMI≥30 - 76%, for female patients - 94% and 88%, respectively. **Conclusions:** Agreement of assessments of SO and S/R studies was higher after application of AC. Higher percentage of abnormal S/R study interpretations among discordant results indicates that some of myocardial perfusion defects were underestimated in SO protocol. Application of SO protocol is possible in patients with BMI<30 provided that AC is used.

OP465**The Prognostic Value of Mechanical Dyssynchrony by GSPECT vs Electrical Dyssynchrony by QRS in Patients with CAD and Ejection Fraction >35%**

S. Borges-Neto, M. Fudim, P. Hess; Duke University, Durham, NC, UNITED STATES.

Background: Whether mechanical dyssynchrony measured by phase analysis of gated single-photon emission computed tomography myocardial perfusion imaging (GSPECT MPI) adds prognostic information to electrical dyssynchrony or is independently associated with death among patients with an ejection fraction >35% is incompletely understood. **Methods:** We identified consecutive patients with angiographically significant coronary disease who underwent GSPECT MPI. Serial Cox proportional hazards models consisting of clinical variables only, clinical variables plus mechanical dyssynchrony according to the duration of the cardiac cycle during which 95% of the ventricle is initiating contraction (phase bandwidth), clinical variables plus electrical dyssynchrony as measured by QRS duration, and a final model inclusive of all of these variables were fitted. **Results:** A total of 1,157 patients were identified. The median age was 64 (interquartile range (IQR) 55-72 years). Patients were predominantly white (73.8%), of male sex (67.7%), and had hypertension (76.7%). A minority had congestive heart failure (21.9%),

peripheral vascular disease (10.5%), and cerebrovascular disease (12.2%). The median QRS duration was 92 (IQR 84-103) ms, while the median bandwidth was 58 (IQR 41-90)°. The median duration of follow-up was 4.3 (IQR 3.0-6.4) years. A total of 293 deaths were observed. Mechanical dyssynchrony added prognostic information independent of standard clinical variables and electrical dyssynchrony (p<001). **Conclusions:** Mechanical dyssynchrony measured by GSPECT MPI is independently associated with death and adds prognostic information above that provided by standard clinical covariates and electrical dyssynchrony.

OP466**The Impact of Appropriate Use Criteria 2013 on the diagnostic accuracy of SPECT-MPI**

D. DATTA, K. NARVESH, S. GAMBHIR; SANJAY GANDHI POST GRADUATE INSTITUTE OF MEDICAL SCIENCES, LUCKNOW, INDIA.

ABSTRACT Background - Appropriate Use Criteria have been developed by ASNC to aid in the optimal use of SPECT- myocardial perfusion imaging (MPI), a technique that is a mainstay of risk-assessment for ischemic heart disease. In this study, we have tried to evaluate the impact of appropriate use criteria on the diagnostic value of SPECT-MPI. The sensitivity, positive predictive value and overall accuracy of SPECT-MPI is calculated under the 'appropriate' category. **Methods and Results-** A retrospective study of 100 consecutive patients undergoing outpatient, community-based SPECT-MPI and Invasive coronary angiography was conducted. The maximum time-interval between the two tests was 30 days. Subjects were categorized as normal and abnormal SPECT-MPI. The abnormal MPI test includes presence of stress-induced ischemia or non-viable myocardial tissue. The normal MPI test consists of absence of stress-induced ischemia or non-viable myocardial tissue. The coronary angiography was called positive if there was presence of more than 50% stenosis or plaquing in any coronary arteries, and was called negative in case of normal coronaries or less than 50 % stenosis in any of the coronary arteries. In the appropriate category, those with only positive coronary angiography (more than 50 % stenosis) were considered in this study, among which positive and negative Myocardial perfusion scans occupied 91% and 09% respectively. In the appropriate criteria, the Sensitivity (95 % Confidence Interval), Positive Predictive Value, and Overall Accuracy of SPECT-MPI is 90.8% (82.8 - 95.4%) , 97.8% and 89% respectively. **Conclusion-** The Appropriate Use Criteria has a definite impact on the diagnostic accuracy of SPECT-MPI. When performed for appropriate indications, SPECT-MPI continues to demonstrate high diagnostic value. Overall results indicate the appropriateness of cardiac diagnostic care in SGPGI meets international standards. **Key words:** myocardial perfusion imaging, appropriate use criteria, diagnosis, SPECT.

OP467**Assessment of Left Ventricular Remodeling by Gated SPECT Myocardial Perfusion Imaging in Diabetic Patients: a Propensity Matched Cohort Analysis**

V. Gaudieri¹, C. Nappi², W. Acampa², S. Daniele¹, R. Assante², E. Zampella², M. Petretta², A. Genova², P. Buongiorno², A. Cuocolo²; ¹Institute of Biostructure and Bioimaging, National Council of Research, Naples, ITALY, ²University Federico II, Naples, ITALY.

Aim: Left ventricular (LV) geometry is an important parameter in the pathophysiology of heart failure. Diabetes is an independent risk factor for the development of heart failure. Measures of LV remodeling automatically derived from gated single-photon emission tomography (SPECT) provide incremental and independent information over standard clinical and nuclear markers for the identification of patients with heart failure. The aim of this study was to

compare LV shape parameters and indices of diastolic function in a propensity score-matched cohort of diabetic and non-diabetic patients with normal stress myocardial perfusion imaging and preserved LV systolic function. **Materials and Methods:** We evaluated 1168 consecutive patients (806 non-diabetic and 362 diabetic patients) without a documented history of coronary artery disease, with normal myocardial perfusion and normal LV ejection fraction at stress gated SPECT. To account for differences in baseline characteristics between diabetics and non-diabetics patients, we created a propensity score-matched cohort considering clinical variables. An automated software program was used to calculate indices of LV diastolic and systolic function and parameters indicating shape distortion (stress end-diastolic, SIED, stress end-systolic, SIES, shape index and eccentricity index). A cut-off of 0.54 was considered to identify patients with abnormal SIES. **Results:** Before matching, diabetic patients were younger with a greater body mass index and higher prevalence of male gender, hypertension, dyslipidemia, smoking, family history of coronary artery disease and chest pain (all $P < 0.001$). After matching, clinical characteristics were comparable in 332 diabetic and 332 non-diabetic patients. Diabetic patients showed significantly higher SIED and SIES values and lower eccentricity index compared to non-diabetic patients (all $P < 0.001$). Patients with diabetes also had higher prevalence of abnormal SIES compared to those without diabetes (33% vs. 16%, $P < 0.001$). Indices of LV diastolic function did not differ between diabetic and non-diabetics patients. **Conclusions:** After balancing clinical characteristics by propensity score analysis, diabetic patients with normal myocardial perfusion and preserved LV systolic function, showed a higher prevalence of abnormal LV shape parameters compared to non-diabetic subjects. Thus, shape indexes by gated-SPECT are useful for identifying early LV remodeling in patients with diabetes.

1201/1203 – Tuesday, October 18, 2016, 10:00 - 11:15, Auditorium
Plenary 3: New Developments in Cancer Imaging and Therapy

OP468

Beyond Somatostatin Receptors: Potential for Therapy?

M. De Jong; Erasmus MC Rotterdam, Department of Nuclear Medicine, Rotterdam, NETHERLANDS.

OP469

Imaging CXCR4 in Haematologic and Solid Tumours

H. Wester; Technische Universität München, Garching, GERMANY.

OP470

The Hallmarks of Aging: The Road to Personalised Medicine in Prevention and Cancer Care?

M. Blasco; Centro Nacional de Biotecnología, Madrid, SPAIN.

1301 – Tuesday, October 18, 2016, 11:30 - 13:00, Auditorium
CME 10 - Translational Molecular Imaging & Therapy/Radiopharmacy: Developments on Radionuclide and Radiopharmaceutical Manufacturing and Automation

OP471

An Overview on Developments on Radionuclide Production, Synthesis Modules, QC Equipment and Approaches for QC

J. Koziorowski; Universitetssjukhuset, Linköping, SWEDEN.

OP472

Let's be Precise! ...And Make it Fast!

W. Wadsak; Medical University of Vienna, Nuclear Medicine, Vienna, AUSTRIA.

OP473

Microfluidics in Radiochemistry: Pros and Cons

G. Pascali; ANSTO - Australian Nuclear Science and Technology Organisation, Camperdown, AUSTRALIA.

1302 – Tuesday, October 18, 2016, 11:30 - 13:00, Hall 211

Joint Symposium 10 - EANM/EORTC: Apoptosis and Proliferation – Two Important Hallmarks of Cancer: From Bench to Bedside

OP474

Preclinical and Clinical Experience in Proliferation Imaging

A. Buck; University of Wuerzburg, Nuklearmedizinische Klinik und Poliklinik, Wuerzburg, GERMANY.

OP475

Imaging Apoptosis – Ready for Clinical Use? PET

Tracers

E. O. Aboagye; Hammersmith Hospital, Department of Cancer Medicine, London, UNITED KINGDOM.

OP476

Imaging Apoptosis – Ready for Clinical Use? SPECT Tracers

C. Reutelingsperger; Maastricht University, Maastricht, NETHERLANDS.

1303 – Tuesday, October 18, 2016, 11:30 - 13:00, Hall 117

Technologist Oral Presentations 3

OP477

Utility of myocardial perfusion SPECT images reconstructed from early dynamic acquisition with a cadmium zinc telluride camera Comparison with conventional late acquired images

C. Kullberg¹, S. Akil², F. Hedeer¹, H. Engblom², C. Hindorf³, J. Oddstig³; ¹Clinical Physiology and Nuclear Medicine, Lund, SWEDEN, ²Lund University, Department of Clinical Sciences Lund, Clinical Physiology, Skane University Hospital, Lund, SWEDEN, ³Radiation Physics, Lund, SWEDEN.

Introduction The cadmium zinc telluride (CZT) SPECT camera enables imaging of the entire myocardial volume simultaneously. Thus, myocardial perfusion SPECT (MPS) based on this technique could potentially enable quantification of absolute myocardial blood flow using early dynamic list-mode image acquisition. If static perfusion images, reconstructed from this early dynamic image acquisition, could replace conventional late imaging (approximately 1 hour after administration of ^{99m}Tc-tetrofosmin) the examination time would be significantly shortened. The aim of this study was to investigate whether static perfusion images reconstructed from early dynamic imaging could replace conventional late static images for diagnosing decreased perfusion in patients undergoing MPS. **Materials & Methods** The study included 39 dynamic examinations from patients with suspected or established stable ischemic heart disease (25% women, mean BMI=27). 31 examinations were performed at rest and 8 with adenosine stress. A 12-minute dynamic list-mode image acquisition, started at the time of ^{99m}Tc-tetrofosmin administration (mean activity 375MBq), as well as a conventional 8-minute static image acquisition approximately 1 hour later were performed using a CZT camera (GE NM530c). Static perfusion images were reconstructed from the early list-mode dynamic acquisition using the last 8 minutes of the 12-minute acquisition. An experienced observer visually graded both early and late perfusion images regarding image quality (poor=1 to excellent=4),

presence of extracardiac uptake (none=1 to 4=unacceptable) and diagnosis based on presence or absence of decreased perfusion (pathologic with high certainty=1, probably pathologic=2, probably non-pathologic=3, non-pathologic with high certainty=4). All image analysis were performed with the observer blinded to all patient data and timing of the acquisition. **Results** In the early reconstructed images, mean score for image quality was 2.8 (range: 2-4) and 72% of the patients had extracardiac uptake disturbing perfusion assessment. For the conventional late reconstructed images, mean score for image quality was significantly higher (3.5, range: 2-4; $p < 0.001$) and 13% of the patients had disturbing extracardiac uptake. The diagnosis (pathological vs non-pathological) based on images reconstructed from early dynamic acquisition matched the diagnosis obtained using late conventional imaging in 87% (34/39 patients). The over all agreement of perfusion score showed a kappa value of 0.3. **Conclusion** The early static images reconstructed from the dynamic image acquisition can not be recommended for clinical routine, mainly because of significant extracardiac uptake in the majority of the patients.

OP478

Dual isotope Gated SPECT and PET CT imaging in evaluation of coronary artery disease

A. Ghilardi, G. Medolago, L. Pozzi, N. Brambati, E. Iampietro, R. Rota, L. Madaschi, C. Bianchi, A. Bruno; ASST Papa Giovanni XXIII, BERGAMO, ITALY.

Aim: we report our experience in the evaluation of extent of myocardial damage in CAD: scar, viability and ischemia using dual isotope Gated SPECT and PET CT imaging. **Methods:** We distinguish three different conditions: the first [A], the most common: the evaluation of extent of myocardial scar/viability comparing Rest[Stress] Gated_Spect MPI [Tc^{99m} Sestamibi] to $F^{18}DG$ PET_CT after glucose loading. The second [B]: the evaluation of direct imaging of stress-induced myocardial ischemia with $F^{18}DG$ PET_CT [no glucose loading] compared to Tc^{99m} -Sestamibi stress/rest Gated-SPECT. The third [C]: the identification of acute ischemia in patients referred to ED for acute chest pain with low/intermediate risk [not significant ECG changes, normal enzymes and no wall motion abnormalities] using Tc^{99m} -Sestamibi rest Gated SPECT and $F^{18}DG$ PET_CT [no glucose loading]. Gated_SPECT [Tc^{99m} Sestamibi Tc^{99m}] was performed using Siemens Symbia S equipped with LEHR; PET images were obtained with Siemens Biograph-6. Transaxial images were reconstructed with iterative displayed as a series of short-long[sagittal-horizontal]-axis. **Results:** In viability evaluation [A] the typical pattern is the mismatch perfusion/metabolism with focal $F^{18}DG$ uptake in hypoperfused segments: glucose loading is needed. If stress Gated_SPECT is performed also ischemia can be evaluated. In the second [B] in stress-induced ischemic myocardium $F^{18}DG$ uptake is present [hot spot] in stress hypoperfused or normal perfused segments: no glucose loading is needed. In the third [C], $F^{18}DG$ PET_CT better than rest Gated_SPECT identifies acute ischemic segments highlighting so “called metabolic stunning” as a “hot spot” even after restoration of blood flow [no glucose loading]. In all cases it is preferable not to include diabetic patients. In A the issue is to demonstrate viability in infarcted segments that may benefit from revascularization or in presence of severe coronary stenosis. In B we prefer to study patients with multivessel coronary disease to overcome so “called balanced ischemia”: focal ischemic uptake of $F^{18}DG$ in normal perfused segments is a marker of anaerobic metabolism activation. Finally in C, $F^{18}DG$ PET_CT may represent an accurate and sensitive procedure superior to Gated_SPECT in identifying acute myocardium ischemia because metabolic recovery lags behind perfusion for almost 24-30 hours. **Conclusions:** In our experience dual isotope Gated_SPECT - PET_CT imaging is an effective and accurate tool to evaluate the extent of myocardial damage in CAD in subgroups of patients in which standard usual Gated_SPECT can't fully address clinical decision making.

OP479

Radium-223 Therapy in Metastatic Castration - Is post treatment bone scan helpful to assess treatment response ?

D. Aniceto, M. Botelho Cruz, A. Nunes, V. Lewington, H. Fahim, S. Allen, C. Mills; Nuclear Medicine Service Guys and St. Thomas NHS Trust, London, UNITED KINGDOM.

Background: Prostate cancer is the 2nd commonest cause of cancer death in UK men and frequently metastasis to bone. The bone seeking radiopharmaceutical radium-223 dichloride ($^{223}RaCl_2$) has been shown to prolong survival and delay bone complications in men with castrate resistant prostate cancer (CRPC). Our aim was to assess the role of ^{99m}Tc MDP bone scintigraphy as a response marker in men undergoing $^{223}RaCl_2$ therapy and to compare this with the impact of treatment on quality of life. **Methods:** Data from patients with metastatic CRPC who had completed 6 cycles of $^{223}RaCl_2$ treatment at Guys and St Thomas' NHS Trust between 2015 and 2016 were reviewed retrospectively. Patients' Quality of Life (QoL) was assessed by EORTC QLQ-C30 questionnaires as part of the routine therapy procedure. All patients underwent a ^{99m}Tc MDP bone scan within two months of starting $^{223}RaCl_2$ therapy and within three months of completing the sixth cycle. Skeletal metastatic involvement was assessed semi-quantitatively using the Soloway score system. Pre and post treatment scans were compared and correlated with QoL responses for each patient. **Results:** 39 patients were treated, median age of 72.3 years. The interval between first evidence of metastases and first cycle of was 0.5-7.7 years. QoL scores revealed an overall sustained improvement in patients' wellbeing. Of the 77% patients who reported bone pain at the beginning of treatment, 35% recorded reduced pain score. Comparison of pre and post treatment bone scans showed skeletal metastatic progression in 44%, stable disease in 19% mixed metabolic response in 31% and improvement in 6% of patients. **Discussion:** Our results support published evidence that $^{223}RaCl_2$ treatment delivers improved QoL in men with metastatic CRPC. This improvement does not appear to correlate with metabolic treatment response as assessed by ^{99m}Tc MDP bone imaging, however. **Conclusion:** Whilst bone scintigraphy is a pre requisite for planning $^{223}RaCl_2$ molecular radiotherapy, routine post therapy imaging does not seem a useful means of assessing response and / or clinical outcome.

OP480

SPECT Myocardial Perfusion Imaging Quantification in Obese Subjects: Influence of Adipose Tissue in the Attenuation Correction with Computed Tomography Attenuation Maps

I. Melo¹, O. Stakhiv², M. Jessop², P. Begley², S. Dizdarevic², E. Sousa¹; ¹Escola Superior de Tecnologia da Saúde de Lisboa, LISBOA, PORTUGAL, ²Nuclear Medicine, Department of Imaging, Brighton and Sussex University Hospital NHS Trust, Brighton, UNITED KINGDOM.

Introduction: Myocardial Perfusion Imaging (MPI) is a well implemented technique for assessment of Coronary artery disease (CAD). Obese subjects have a larger amount of adipose tissue (AT) that attenuates gamma rays emitting from the heart potentially causing false positive results due to attenuation artefacts. **Aim:** To evaluate the influence of thoracic and abdominal AT, on the perfusion quantification for subjects with Body Mass Index (BMI) between 30 and 35, and above 35. **Materials and Methods:** A sample of 72 subjects, who underwent two day protocol stress-rest SPECT MPI, was divided into 4 groups by gender and BMI. The activity of ^{99m}Tc -tetrofosmin administered was adjusted using ranges based on the weight of the patients. All patients were referred for suspected CAD. Images were analysed with and without the incorporation of computed tomography attenuation correction (CTAC), for stress and rest studies and reconstructed by OSEM/MLEM. All image segmentation and quantification was done by myocardial wall regions for

perfusion: Anterior, Inferior, Lateral, Septal and Apical, using QGS/QPS. Each study was processed three times by one operator, and average value was used. The AT in thoracic (T7 to T8) and abdominal (T9) regions was calculated from CT acquired for attenuation correction, using ImageJ automatic threshold for segmentation, with selected Hounsfield Units from -190 to -30. Regression analyses were performed, between the thoracic and abdominal AT quantity and the difference in the perfusion values with CTAC and without CTAC. **Results:** The sample was split into 4 groups: 47 with BMI between 30 and 35 Kg/m² (27 male (M1) and 20 female (F1)) and 24 (13 male (M2) and 11 female (F2)) with BMI between 30 and 35 Kg/m² above 35 Kg/m². Although expecting influence of thoracic AT in women in lateral and anterior perfusion, these results showed no strong correlation. Abdominal AT influenced inferior perfusion as expected (F2: R²=0.46). For men the results showed no strong relationship for abdominal AT, but thoracic AT showed influence on septal rest (M2: R²=0.55), inferior rest (M2: R²=0.56), and apical stress (M2: R²=0.47). **Conclusion:** The influence of AT in the abdomen and thorax does not affect all groups in the same way, however the effect is more marked in the male group with large BMI.

OP481

Scintimammography in the assessment of early and final response of breast cancer to neoadjuvant chemotherapy: results of single center prospective study

S. N. Novikov, S. Kanaev, P. Krivorotko, P. Krzhivitskiy, T. Semiglazova, Z. Bryanzeva, E. Turkevich, L. Jukova; N.N. Petrov Institute Oncology, St Petersburg, RUSSIAN FEDERATION.

Purpose: to determine whether scintimammography (SMG) with 99mTc-MIBI performed after 2-3 cycles and/or at the end of neoadjuvant chemotherapy (NAC) can be used to predict complete pathologic response in breast cancer (BC). The secondary objective was to correlate accuracy of SMG with biologic subtypes of BC. **Material and methods:** 120 patients with advanced BC were included in prospective single center comparative study of taxane or taxane-doxorubicin (+/-trastuzumab) based NAC. Planar SMG with 740 MBq of 99mTc-MIBI was performed before the start, after 2-3 and at the end of NAC. Pathologic response was assessed according Miller-Payne V grade classification. Scintigraphic response was estimated as follows: progression (grade I); stabilization (II); partial effect (III); prominent efficacy (IV); complete response (V). We evaluate accuracy of grade IV-V SMG response mentioned after 2-3 cycles of NAC for predicting complete pathologic response (pCR) at the end of treatment. We determine accuracy of grade V SMG response at the end of NAC for predicting pCR. Additionally we evaluate predictive value of SMG in patients with different biologic subtypes of BC. **Results:** Grade IV-V scintigraphic response after 2-3 cycles of NAC demonstrated moderate (84%) accuracy (Ac) in predicting pCR: sensitivity (Sen) - 78%, specificity (Sp) - 84%, positive predictive value (PPV) - 56%, negative predictive value (NPV) - 94%. Grade V scintigraphic response at the end of NAC characterized by high (92%) Ac in predicting pCR: Sen - 95%, Sp - 91%, PPV - 76%, NPV - 98%. We mentioned significant differences in frequency of pCR in women with luminal (pCR - 3%) and non-luminal (pCR-19%) BC but we didn't find significant differences in accuracy of SMG for predicting pCR in women with various biologic subtypes of BC.

Conclusion 1. SMG is accurate method for predicting pCR in patients with BC. 2. Its Sen and PPV are higher at the end of NAC. 3. We didn't find correlation of BC biologic subtype and efficacy of SMG in predicting pCR.

OP482

Nuclear Medicine Departmental experience in providing efficient treatment and care for ²²³Ra Dichloride Therapy

A. S. F. Ribeiro, S. Summers, L. Causer, T. Shepherd, I. Murray, J. Gear, G. Flux, M. Meintjes, Y. Du; Royal Marsden Hospital, Sutton, UNITED KINGDOM.

Background: Prostate cancer is unique among solid tumours, the greatest threat to patient's survival and quality of life is posed by bone metastases rather than visceral involvement. Radium dichloride therapy (²²³Ra) is currently used to treat advanced castration-resistant prostate cancer. Our Nuclear Medicine Department has been providing ²²³Ra since 2004 and currently we perform an average of four treatments a week, both clinical and research patients. Our Nuclear Medicine Department provides a variety of diagnostic (both conventional nuclear medicine & PET/CT) and therapy services within a leading specialist cancer treatment hospital. Our department includes a Radioisotope Therapy Consultant (RTC), two Clinical Nurse Specialists for radioisotope therapy (CNSr), and two Research Technologists (RT) who all work together to safely deliver ²²³Ra. **Materials and Methods:** Our pathway starts with initial referral from clinical team; patients are seen by the RTC and the CNSr/RT who advise patient on treatment and coordinate all 6 treatments, liaise directly with the clinical team (usually Urology) and patient. Our in house Radiopharmacy dispenses the solution for injection ready to be administered; the CNSr and RT rotate in accessing the patient for suitable venous access (similar to chemotherapy access) and administering the therapy. Between cycles patients are closely monitored up either by the Urology team or the research team which normally include blood tests and scans. Our technique to administer the treatment is simple yet effective; protective personal equipment is always used: double gloves, apron, incontinence pads and always two staff members present; one member administers the treatment while the other assists and collects the radioactive waste. We also operate in a quiet environment to avoid distractions and to ensure there is no contamination. Thorough close monitoring of the room/equipment used and self-monitoring are carried out as standard of practice. **Results:** Our recent audit on staff exposure when administering ²²³Ra has demonstrated average dose rate recorded of 3.67µSv/hr (±1.4) with room contamination and self-monitoring not significant and no recorded EPD readings. Our service has been visited by other institutions to observe our practice and we have taken part in teaching sessions both across the hospital (liaising with wards and clinical teams) as well as outside training sessions. **Conclusion:** This study aims to disseminate our experience in providing ²²³Ra therapy both in clinical and research settings, including our challenges and improved outcomes.

OP483

Automated production of ⁶⁸Ga-DOTATATE: an overview of yield and quality

T. Young-Mylvaganan, E. A. Aalbersberg, M. Geluk-Jonker, B. J. de Wit-van der Veer; The Netherlands Cancer Institute, Amsterdam, NETHERLANDS.

Introduction ⁶⁸Ga-DOTATATE PET/CT is an important imaging technique used for the visualization of somatostatin receptor (SSTR)-positive neuroendocrine tumours. In 2012 the NKI-AVL initially started ⁶⁸Ga-DOTATATE synthesis with a semi-automated module. In December 2014 a fully automated commercial system was purchased, which led to an increase in production over the past two years. Aim To present our ⁶⁸Ga-DOTATATE syntheses experiences and evaluate the production-rates between December 2014 and March 2016. **Materials and Methods** ⁶⁸Ga-DOTATATE is prepared on a fully automated system (Scintomics GmbH, Germany) using the ⁶⁸Ge/⁶⁸Ga-generator produced by iThemba LABS (IDB Holland bv). Quality control (QC) procedures include tests for radiochemical purity (the percentage of ⁶⁸Ga DOTATATE), pH, filter integrity, sterility, ⁶⁸Ge breakthrough and HEPES content. Before the batch is released for clinical use, all QC tests except sterility, ⁶⁸Ge breakthrough and HEPES need to be performed. Instant thin-layer chromatography (ITLC) and solid phase chromatography were used to determine radiochemical purity in the final product. The pH of each batch was assessed with an universal indicator strip. ⁶⁸Ge breakthrough was measured using gamma-ray spectrometry after complete ⁶⁸Ga decay (>48

hour). 2-week culture of the final product in Tryptose soya broth (TSB) indicated whether the final product was sterile. Finally, HEPES content was determined by ITLC. Results A total of 116 ^{68}Ga -DOTATATE syntheses were performed using two generators, of which 110 (95%) proved suitable for injection. 3 productions failed due to technical difficulties and 3 were rejected due to failed QC for both ^{68}Ga (III) ions and ^{68}Ga colloids. In respectively 5 and 2 cases the ^{68}Ga (III) ions and ^{68}Ga colloids were too high; these were released for patient administration by the local pharmacist. The final yield of ^{68}Ga DOTATATE was 613.00 MBq (range 285.7–1034.00 MBq) with an average radiochemical purity of 97.96% (range 87.77–99.00%). The average ^{68}Ga (III) ions were 0.79% (range 0.25–5.16%) and ^{68}Ga in colloidal form was 1.50% (range 0.56–7.49%). The average breakthrough of ^{68}Ge was 0.00032%, and was too high (>0.001%) in 2 batches of which 1 was released for clinical use. All productions were sterile and HEPES concentration exceeded the maximum limit in only 1 case. The measured pH (limit 4.0–8.0) and the filter integrity never exceeded the allowed limits. Conclusion Automated production of ^{68}Ga -DOTATATE has been implemented successfully with low failure rates (5%) and yields sufficient to prepare 2–3 syringes for patient administration per batch.

OP484

Inter operative imaging of Sentinel node procedure with use of a portable gamma camera: An technologist's perspective

L. A. van Kronenburg-Rooze, T. Young-Mylvaganan, E. C. Streefkerk, B. G. Hoving, B. J. de Wit- van der Veen; Netherlands Cancer Institute-Antoni van Leeuwenhoek, Amsterdam, NETHERLANDS.

Introduction Since 2015 technologist are performing intra-operative imaging during sentinel node (SN) procedures, primary for head/neck (HN) and penile carcinoma, using a portable gamma camera (PGC) in our institute. This specific approach assists the surgeon with accurate localization of lymph nodes. Aim Working in the operation room (OR) is a new and challenging task for nuclear technologists, so the aim of this descriptive evaluation is to provide a technologist's insight on intra-operative SN imaging. Methods /materials All OR-procedures were performed on the same (1-day protocol) or the next day (2-day protocol), depending on the OR planning. The 2-day protocol is based on the 1-day protocol, with an increased radiopharmaceutical dose due to the larger time interval. Three technologists are currently selected for the rotational intra-operative imaging team, and all underwent the 'Working in the OR'-training and are internally certified for working with the PGC. The standard SN-workflow constitutes of; Pre-operative: planar and SPECT/CT imaging by a technologist at the nuclear medicine department. SNs were appointed by a Nuclear physician and marked on the skin of the patient. Pre-operative images were also assessed by the OR-technologist. Intra-operative: the OR-technologist acquired and interpreted the PGC images in the OR. The surgeon uses the pre- and intraoperative images, a gamma probe and blue dye to excise the allocated lymph nodes. Result In 2015, 80 penile (46x 1-day and 34x 2-day protocol) and 65 HN (35x 1-day and 12x 2-day protocol) SN-procedures were performed with use of the PGC imaging on OR. The average time a technologist was needed was 88 min. for penile and 124 min. for HN procedures. The 2-day protocol had a 79% larger time interval between imaging and OR compared to the 1-day protocol (90 MBq), and doses were adjusted (180 MBq) In penile cancer 46 and 109 were marked; 182 and 136 were removed on OR for 1-day and 2-day protocols, respectively. In HN-SN 160 and 34 were marked; 296 and 49 were removed on OR for 1-day and 2-day protocols, respectively. Conclusion Technologists have successfully assisted in 145 image guided SN-procedures at our institute. The positive feedback from technologist, surgeons and nuclear physicians on the use of intraoperative imaging by technologists suggests an increase of procedures for next year. Nonetheless, due to logistics and available material, there is now a limit of 3 sequential OR' s per day.

OP485

Time-to-peak ratio. What does it mean in myocardial perfusion imaging using IQ SPECT in patients with manifested coronary artery disease?

L. Hehenwarter, G. Schweighofer Zwink, C. Pirich; Uniklinik Salzburg, Salzburg, AUSTRIA.

Aim: To assess the added diagnostic value of time-to-peak ratio (TPR) for risk stratification in patients with manifested coronary artery disease undergoing accelerated myocardial perfusion imaging (MPI) using IQ SPECT. **Material and Methods:** Retrospective analysis of 183 patients with priory angiographically proven coronary artery disease (CAD) referred to our department for risk stratification with MPI performed using a two-day pharmacological stress protocol with adenosine or regadenoson and gated Tc-99m-Tetrofosmin SPECT (4 MBq/kg body weight). Data were acquired in 17 views (17 sec. each) with a Siemens Symbia T6 camera using IQ-SPECT collimators. The results were generated with Corridor 4DM software. The SSS, SRS, SDS, EF, TID, extent of ischemia in % of left ventricular area, extent of scar tissue in % of left ventricular area and TPR values of five segmented model were statistically analyzed using SPSS software. The following TPR indices were calculated: sum of defect-diagram (TPRdefect), sum of normalized diagram (TPRsumND), minimum of normalized diagram (TPRminND), maximum of normalized diagram (TPRmaxND), standard deviation of normalized diagram (TPRsdND) and range of normalized diagram (TPRranND). Results: 183 patients (130 males, 53 females) with a mean age of 67 (± 11) years were analyzed of whom 90, 47 and 30 patients had 3-, 2- or 1-vessel disease, respectively. 16 patients had different disease. The following TPR indices were significantly different in patients with 3-VD compared to the remaining participants: TPRminND (44.1 ± 7.3 vs. 46.9 ± 6.6 ; $p < 0.007$), TPRranND (13.8 ± 7.8 vs. 11.2 ± 7.8 ; $p < 0.023$), TPRsdND (20.7 ± 11.6 vs. 17.0 ± 12.0 ; $p < 0.033$). TPR indices were significantly related to the following MPS parameters: TPRminND to SSS ($r = -0.251$; $p < 0.001$), SRS ($r = -0.295$; $p < 0.001$), scar ($r = -0.283$; $p < 0.001$), EF post stress ($r = 0.476$; $p < 0.001$) and EF rest ($r = 0.390$; $p < 0.001$). TPRranND was significantly related to SSS ($r = 0.428$; $p < 0.001$), SRS ($r = 0.447$; $p < 0.001$), scar ($r = 0.375$; $p < 0.001$), EF post stress ($r = -0.629$; $p < 0.001$) and EF rest ($r = -0.525$; $p < 0.001$). TPRsdND was significantly related to SSS ($r = 0.459$; $p < 0.001$), SRS ($r = 0.464$; $p < 0.001$), scar ($r = 0.409$; $p < 0.001$), EF post stress ($r = -0.612$; $p < 0.001$) and EF rest ($r = -0.519$; $p < 0.001$). Conclusion: In 3-VD patients TPRminND, TPRranND and TPRsdND are different compared to the other patients, while the indices TPRdefect and TPRsumND are not.

1305 – Tuesday, October 18, 2016, 11:30 – 13:00, Hall 115

M2M: Oncology - Preclinical

OP486

In Vivo Study on Re-oxygenation of Tumor after Heavy Carbon-Ion Beam and Photon Beam Irradiation Using animal ^{18}F -MISO PET/CT

j. cheng¹, J. Lu², Y. Sheng³, Z. Jiang⁴, Z. Li⁴, Y. Zhang¹; ¹Department of Nuclear Medicine, Shanghai Proton and Heavy Ion Center, Fudan University Cancer Hospital, Shanghai, CHINA, ²Department of Radiation Oncology, Shanghai Proton and Heavy Ion Center, Shanghai, CHINA, ³Department of Medical Physics, Shanghai Proton and Heavy Ion Center, Shanghai, CHINA, ⁴Department of Nuclear Medicine, Shanghai Proton and Heavy Ion Center, Shanghai, CHINA.

Objective: Heavy carbon-ion irradiation can kill both hypoxic and non-hypoxic tumor cells. In this study, the human breast cancer ER(+) xenografts were exposed to low/medium/high dose of heavy carbon-ion and photon beam to observe the early and later re-oxygenation phenomenon with respect to different types and dose. **Methods:** The xenograft was performed ^{18}F -MISO animal PET/CT imaging, and the naturally

occurring chronic hypoxia was identified using $TBR > 1.4$ as the threshold. Xenografts were divided into photon group and heavy carbon-ion group. Every group included three sub-groups of different dose as high dose group (single dose of 15GyE), medium (10GyE) and low (5GyE). The volume of tumor was observed and the growth curve was drawn. The animal ^{18}F -MISO PET/CT scans were performed on the high dose sub-group of photon and the low / medium / high dose sub-groups of heavy carbon-ion. The changes of oxygenation were observed on the 1st/3rd/5th/7th day for early term and on the 5th/10th/15th day for later term.

Results: In photon group, only high dose sub-group (15GyE) inhibited tumor growth ($t=15.24$, $P < 0.001$). While in heavy carbon-ion group, medium and high dose sub-group both inhibited tumor volume evidently ($P < 0.001$ both). Early oxygenation status: in low dose heavy carbon-ion group, the TBR and HV increased slightly in the 1st and 3rd day's observations and then remained stable. In medium/high dose heavy carbon-ion groups, the phenomenon of "transient severe hypoxia" appeared in the 1st day's observation, and disappeared in the 7th, which was more remarkable in high dose heavy carbon-ion group. In high dose photon group, TBR and HV increased in the 3rd day's observation and recovered in the 7th. Later oxygenation status: in low dose heavy carbon-ion group, the TBR and HV increased obviously. In medium dose heavy carbon-ion group, the TBR and HV kept stable at first but increased at last. In high dose heavy carbon-ion group, the TBR and HV decreased continuously. In low dose photon group, the TBR and HV decreased in 5th day's observation and recovered finally. **Conclusion:** The early oxygenation status reveals that time window of "re-oxygen" of photon is the first 3-5 days after irradiation. However, no "re-oxygenation" phenomenon exists in heavy carbon-ion irradiation. The "transient severe hypoxia" will appear after heavy carbon-ion irradiation depending on the dose delivered. The inhibition / killing effect of heavy carbon-ion irradiation on tumor is not dependent on the degree of tumor oxygenation.

OP487

Novel CMKLR1-targeted peptide conjugates for molecular imaging and therapy of breast cancer

S. Erdmann, L. Niederstadt, E. L. Koziolok, N. Beindorff, J. D. C. Gomez, S. Prasad, A. Wagener, J. L. Körner, S. Hallmann, S. Exner, S. Bandholtz, V. Prasad, W. Brenner, C. Grötzinger; Charité - Universitätsmedizin Berlin, Berlin, GERMANY.

Aim Targeted imaging and therapy is a promising approach in nuclear cancer medicine. Knowledge about molecular properties as overexpression of certain receptors is thereby offering a powerful tool for tumor-selective imaging and treatment of cancer cells. We utilize novel chemerin-based peptides for receptor-ligand binding-mediated targeting of CMKLR1 overexpressing tumors in small animal models. By conjugation with radiolabeled chelator DOTA we obtain highly specific and affine tracers. The novel contrast agents enable multimodal *in vivo* imaging with positron emission tomography, single photon emission computed tomography and complementary biodistribution studies and provide the means for continuative targeted therapy. **Materials and Methods** We developed highly specific and affine peptide ligands for the G protein-coupled receptor CMKLR1 by substitution of wild type chemerin-9 and structure-activity relationship analysis. The combination of these peptides linked to radiolabeled (^{68}Ga / ^{177}Lu) chelator DOTA and an established target-positive tumor model in immunodeficient nude mice enabled tumor-specific imaging *in vivo*. Therefore, we acquired small animal PET/MR and SPECT/CT images, assessed biodistribution by *ex vivo* measurements and investigated the tracer specificity by blocking experiments. **Results** Our novel chemerin peptide conjugates demonstrated significantly improved properties compared to the wild type peptide concerning biological activity, affinity and metabolic stability. Their target is known to be overexpressed in different pathologies, including cancer. Beside other tumor entities like pancreatic cancer, we could demonstrate CMKLR1

overexpression in breast cancer patient tissue and exemplarily in the breast cancer cell line Du4475. After establishment of the cancer model with both, a target-positive and -negative tumor, PET/MR (^{68}Ga) and SPECT/CT (^{177}Lu) imaging along with complementary biodistribution studies revealed a strong CMKLR1-specific uptake ($\leq 9\%$ ID/g) of the targeted tracers in positive tumor tissue for up to twenty-four hours. More strikingly, tumor uptake of our tracers could not only be blocked by excess of unlabeled peptide, but also significantly depended on the number of receptors expressed by the tissue. Tumor uptake, organ distribution and corresponding kinetics strongly correlated with the chemical and physical properties of the different conjugates. **Conclusion** We found the receptor CMKLR1 to be overexpressed in different tumor entities such as breast cancer. With the cell line Du4475, we had a model endogenously expressing our target to evaluate our optimized chemerin peptides as stable ligands with high affinity. Eventually, we demonstrated the applicability of our novel ^{68}Ga - and ^{177}Lu -labeled tracers by visualizing CMKLR1-positive breast cancer tumors in PET/MR and SPECT/CT imaging and thus developed promising theranostics for potential clinical Translation.

OP488

CXCR4 chemokine receptor imaging: evaluation and validation of a new configurationally restricted tetraazamacrocyclic CXCR4 antagonist, ^{64}Cu -CB-bicyclam

C. S. Miranda^{1,2}, B. P. Burke^{3,2}, R. E. Lee^{3,2}, S. Nigam^{3,2}, G. Clemente^{1,2}, J. A. Thompson^{4,2}, T. Ruest², T. D'huys⁵, D. Schols⁵, J. Greenman¹, C. Cawthorne^{1,2}, S. J. Archibald^{3,2}; ¹School of Biological, Biomedical and Environmental Sciences, University of Hull, Hull, UNITED KINGDOM, ²Positron Emission Tomography Research Center, Hull, UNITED KINGDOM, ³Department of Chemistry, University of Hull, Hull, UNITED KINGDOM, ⁴Hull York Medical School, Hull, UNITED KINGDOM, ⁵Rega Institute for Medical Research, Leuven, BELGIUM.

Introduction: There is particular interest in imaging CXCR4 expression levels in cancer, as over-expression of CXCR4 has been linked to an aggressive phenotype and poor prognosis.¹ Attempts have been made to radiolabel small molecule CXCR4 antagonists such as AMD3100 and AMD3465 with copper-64, however, results have been unsatisfactory due to high non-specific liver uptake which may be linked to complex instability.^{2,3} Incorporation of an ethylene cross bridge is known to result in a higher stability copper(II) complex along with increased receptor affinity and residence time.⁴ **Aim:** The aim of this study is to validate the cross-bridged bis-cyclam derivative ^{64}Cu -CB-bicyclam as a new CXCR4 targeted imaging agent, by evaluation of tracer specificity and stability in a U87/U87-CXCR4 xenograft model. **Materials and methods:** U87 and U87-CXCR4 cells were incubated with 37 kBq of ^{64}Cu -CB-bicyclam ($IC_{50} = 24$ nM) to determine tracer uptake. Dynamic PET/CT imaging studies were carried out in CD-1 nude mice bearing U87/U87-CXCR4 xenografts on a Sedecal SuperArgus PET-CT scanner after injection of 9.6 ± 0.7 MBq ^{64}Cu -CB-bicyclam and uptake in various tissues quantified using tumour-to-muscle ratios. Biodistribution studies were carried out in non-tumour bearing CD-1 nude mice after injection of 740 kBq ^{64}Cu -CB-bicyclam to determine *in vivo* stability. Blocking studies were performed after pre-injection of 5 mg/kg of high affinity CXCR4 antagonist (Cu_2CB -bicyclam, $IC_{50} = 4$ nM). **Results:** ^{64}Cu -CB-bicyclam showed higher uptake in U87-CXCR4 than U87 cells (incubated dose $28.2 \pm 0.63\%$ and $0.2 \pm 0.02\%$ respectively). Dynamic PET/CT imaging studies showed higher tracer accumulation in U87-CXCR4 vs. U87 tumours. Tumour-to-muscle ratio at 90 min in U87-CXCR4 tumours was > 8 -fold higher than for U87 (23.6 ± 2.7 vs 3.0 ± 0.5). Blocking studies with Cu_2CB -bicyclam resulted in $> 92\%$ reduction of radioactivity in U87-CXCR4 tumours (SUVmax 7.9 vs 0.5) and 89% reduction in liver (SUVmax 5.3 vs 0.6). This agrees with the biodistribution carried out in non-tumour bearing mice which showed $> 90\%$ reduction in liver uptake. **Conclusions:** To target CXCR4, a new configurationally restricted tetraazamacrocyclic CXCR4 antagonist was

developed and radiolabelled with copper-64. *In vitro* and *in vivo* data showed high specificity for the CXCR4 receptor. The significant reduction in liver uptake suggests higher *in vivo* stability. (1) J. Burger et al, Blood, 2006, 107, 5; (2) S. Nimmagadda et al., Cancer Res., 2010, 70, 3935; (3) R. A. De Silva, et al., J. Nuc. Med., 2011, 52, 986; (4) A. Khan et al., J. Am. Chem. Soc., 2009, 131, 3416.

OP489

SPECT/CT imaging of the PD-1/PD-L1 immune checkpoint pathway in syngeneic murine tumor models

S. Heskamp, J. D. M. Molkenboer-Kuenen, R. H. A. M. van de Vondervoort, O. C. Boerman; Radboud University Nijmegen Medical Centre, NIJMEGEN, NETHERLANDS.

Introduction: Programmed-death 1 (PD-1) is expressed by T-cells and is a major co-inhibitory immune checkpoint. Its ligand PD-L1 is expressed by tumor cells. By upregulating PD-L1, tumors are capable of escaping immune recognition and attack. Clinical trials with anti-PD-1/PD-L1 immune checkpoint inhibitors have shown impressive and durable antitumor activities. However, a large number of non-responding patients is unnecessarily exposed to ineffective, expensive treatment. To use these drugs more effectively, there is an urgent need for a biomarker. The aim of this study is to develop an imaging technique to non-invasively assess PD-L1 expression and PD-1+ tumor infiltrating T-lymphocytes (TILs). **Material and methods:** Anti-murine PD-1 and PD-L1 antibodies were radiolabeled with In-111. The *in vitro* binding characteristics were assessed using EL-4 (PD-1+) and Renca (PD-L1+) cells. Subsequently, the optimal antibody dose (1 - 1,000 µg) and time point (4, 24, 48, 72, 168 h) for imaging were assessed by *ex vivo* biodistribution studies and microSPECT/CT imaging in mice with *s.c.* syngeneic Renca, 4T1, CT26, or LLC1 tumors. Tumors and relevant organs were stained immunohistochemically for the expression of PD-L1 and TILs. **Results:** In-111-labeled antibodies specifically bound to PD-1 and PD-L1 expressing cell lines *in vitro*. The optimal antibody dose to target PD-L1-expressing Renca tumors was 30 µg and highest tumor-normal tissue contrast was obtained 24 to 72 h post injection. Tumor uptake in Renca, 4T1, CT26, and LLC1 was 15 ± 5 %ID/g, 16 ± 6 %ID/g, 11 ± 6 %ID/g, and 6 ± 3 %ID/g, respectively, and correlated with PD-L1 expression as determined immunohistochemically. Enhanced uptake was also observed in spleen (17 ± 2 %ID/g), brown fat (19 ± 2 %ID/g), and duodenum (10 ± 2 %ID/g). Immunohistochemistry confirmed PD-L1 expression in these organs. The optimal antibody dose to target PD-1 was 3 µg. MicroSPECT/CT showed heterogeneous uptake of the radiolabeled anti-PD-1 antibody in 4T1 tumors. *Ex vivo* biodistribution studies showed a tumor uptake of 14 ± 4 %ID/g. Other organs which showed uptake of the anti-PD-1 antibody were thymus (10 ± 2 %ID/g), spleen (10 ± 3 %ID/g), and lymph nodes (14 ± 5 %ID/g). **Conclusion:** These studies demonstrate that PD-L1 and PD-1 can be imaged with microSPECT/CT. These techniques can potentially be used to non-invasively select tumors that are most likely to respond to immune checkpoint inhibitor therapy and to monitor PD-1/PD-L1 during conventional anti-cancer treatment and disease progression.

OP490

Characterising ¹¹¹In-anti-γH2AX-TAT in Targeting the DNA Damage Signal Associated with Wnt Activated Colorectal Cancer

M. Konstantinou¹, J. Knight², T. Hay¹, P. Shaw¹, M. Smalley¹, B. Cornelissen², A. R. Clarke¹; ¹Cardiff University, Cardiff, UNITED KINGDOM, ²University of Oxford, Oxford, UNITED KINGDOM.

Objectives: Colorectal cancer (CRC) is the second most commonly diagnosed cancer has a poor 60% 5-year survival rate. The Wnt signalling

pathway is fundamental for homeostasis of the intestinal epithelium. Its deregulation drives development of CRC and induces DNA damage. Histone-2AX (H2AX) is a component of the nucleosome whose phosphorylated form, γH2AX, is a marker of DNA damage. The VillinCreERApcl/fl mouse model is an inducible genetically engineered mouse model of CRC, where tamoxifen-induced deletion of the APC gene induces Wnt signalling and precipitates a crypt-progenitor-like phenotype. Here, we assess whether the DNA damage generated in this CRC mouse model with Wnt signalling deregulation can be targeted using ¹¹¹In-anti-γH2AX-TAT, a γH2AX-imaging agent we developed previously. **Methods:** ¹¹¹In-anti-γH2AX-TAT, based on anti-γH2AX antibodies conjugated to the cell-penetrating peptide TAT to allow cellular internalisation and nuclear localisation, was produced as previously described. The VillinCreERApcl/fl model was induced by tamoxifen three times in a day by either intraperitoneal (IP) injection (80 mg/kg) or gavage (60 mg/kg). γH2AX immunohistochemical analysis was performed three days post induction to assess γH2AX levels. Three days post induction, another group of mice was injected intravenously with ¹¹¹In-anti-γH2AX-TAT or isotype control RIC (5 µg/mouse; 1 MBq/µg). At 24h post-injection SPECT/CT imaging and biodistribution studies were performed. **Results:** Immunohistochemical analysis showed that on day three post-induction using either IP injection or gavage, overall intestinal γH2AX levels were significantly elevated compared to controls. However, the intensity of γH2AX staining was higher by IP injection compared to gavage. *In vivo* experiments highlighted that ¹¹¹In-anti-γH2AX-TAT uptake is more prominent in the induced intestine (2.46 ± 0.57 % ID/g) compared to controls (1.41 ± 0.29 % ID/g, $p < 0.05$). **Conclusion:** Irrespectively of the technique used for inducing VillinCreERApcl/fl model, DNA damage levels were elevated as a result of Wnt signalling activation. Nonetheless, the extent of the DNA damage is different when comparing gavage with IP injection, highlighting IP injection as the technique that generates higher grade of DNA damage. The *in vivo* ¹¹¹In-anti-γH2AX-TAT accumulation is significantly higher after Wnt signalling activation. Taken together, these promising results suggest that γH2AX imaging could be exploited for early detection of CRC.

OP491

Targeted *in vivo* PET/CT imaging of integrin α2β1 in a orthotopically-implanted non-small cell lung cancer model

C. Huang¹, S. Hsu¹, Y. Chung¹, W. Chang¹, Y. Lin¹, T. Yen^{1,2}, F. Huang³; ¹Center for Advanced Molecular Imaging and Translation, Chang Gung Memorial Hospital, Taoyuan, TAIWAN, ²Department of Nuclear Medicine, Chang Gung Memorial Hospital, Taoyuan, TAIWAN, ³Department of Biochemical Science and Technology, National Taiwan University, Taipei, TAIWAN.

Introduction: The mounting evidences clearly demonstrate the pro-oncogenic role of integrin α2β1 and its aberrant expression might contributes to non-small lung cancer (NSCLC) induced invasion and metastasis. Therefore, the development of integrin α2β1 targeted agent may significantly increase the detection specificity towards various lung cancer types increased with their malignancy level. **Methods:** The orthotopic A549 human NSCLC model was established by tail vein injection with 2×10^6 cells. The mice (n = 5) were imaged in the prone position in the microPET/CT scanner. The tumor-bearing mice were injected with $6.6 - 7.4$ MBq of ⁶⁸Ga-A2B1 tracer and the 15 min acquisition of static scans was obtained at 15 min after injection. The average radioactivities of regions-of-interest (ROIs) were determined by multiple regions of interest volumes manually using 50% of maximum minus minimum %ID/g value within a tumor or an organ. At the end of each scan, the animals were sacrificed. The tumor and major tissues and organs were dissected, and *ex vivo* autoradiography and immunohistochemistry images were acquire to confirm the tracer distribution results. **Results:** The PET/CT images of the orthotopic NSCLC mouse model unambiguously demonstrated the accumulation of integrin tracers in the tumor lesions. The average tumor

uptake was measured as 1.05 ± 0.12 SUVmax ($n=5$), the ratios of tumor/normal (T/N) was 2.29 making the tumor is clear visible. The autoradiography is further performed to compensate the resolution limitation of microPET results, which showed that integrin tracers penetrated the lung capillaries and located in the tumor nodules as early as 15min post-injection. The integrin targeting tracer showed the high T/N ratio in the excised lung tumor autoradiography and the value was calculated as 4.59, which was much higher than that of the PET imaging-derived data. The biodistribution data expressed as a percentage of injected dose/gram of tissue (%ID/g) were calculated. The tracers mainly located in the liver (2.53 ± 0.47) and kidney (8.25 ± 2.61), respectively. The combined PET/CT imaging data were analyzed to provide unique diagnostic parameter such as aggressive potential, which were correlated with histological changes during the tumor growth. **Conclusion:** The development of an accurate noninvasive imaging technique to detect primary, recurrent and metastatic non-small cell lung cancer is critical for the effective management of this group of patients. The integrin $\alpha 2\beta 1$ tracer ^{68}Ga -A2B1 can more subjectively adequate evaluate the integrin profiling, which potentially leading to better evaluate the disease course and therapeutic efficacy at the earliest stages of treatment.

OP492

Comparison of PSMA protein expression and radiopeptide internalization of prostate cancer models with and without castration resistance

B. Meller, F. Bremmer, C. O. Sahlmann, C. Bouter, L. Trojan, J. Meller, P. Thelen; Georg-August-University Göttingen, Göttingen, GERMANY.

Aim: Investigation if prostate specific membrane antigen (PSMA) protein expression and tracer internalization is influenced by castration resistance and androgen deprivation. **Methods:** Human prostate cancer cells were grown permanently with testosterone (T, revCRPC) or without T (CRPC) with and without abiraterone acetate (AA). RevCRPC-cultures represent therefore the androgen sensitive cell type, CRPC the castration resistant and CRCAA the androgen deprivation tolerant cell type. In these cell lines PSMA protein expression was determined by western blot analysis and visualized by immunohistochemical staining. In parallel cultures androgen deprivation was increased by testosterone withdrawal and AA supplementation. Beside determination of the PSMA mRNA by qPCR over 4 w, the cell surface bound and internalized fraction of ^{68}Ga -PSMA-HBED-CC was investigated. **Results:** In contrast to castration resistant cells androgen sensitive cells exhibited significant lower PSMA proteins (<10%). The highest expression was determined in the AA insensitive cell type. These results could be verified by immunohistochemical staining. In internalization experiments these results could be confirmed whereby the ratio between membrane bound and internalized fraction remained nearly constant (25-35%). Androgen deprivation treatment over 4 w resulted in significantly increasing PSMA mRNA expression in revCRPC (>900 %) as well as in CRPC (>500 %). Short-time (48 h) androgen deprivation of androgen sensitive revCRPC cells by testosterone withdrawal and abiraterone acetate treatment resulted in inhibition of proliferation as well as in increasing uptake of ^{68}Ga -PSMA-HBED-CC on a higher level than in abiraterone acetate insensitive CRCAA cells. **Conclusions:** The PSMA protein expression was directly correlated with castration resistance and/or tolerance against AA in the investigated systems. PSMA expression could be stimulated by increasing androgen deprivation in androgen sensitive and castration resistant cells. This should be considered in repeated PSMA-PET/CT investigations and might be useful to increase therapy efficiency of PSMA-directed therapies.

1306 – Tuesday, October 18, 2016, 11:30 - 13:00, Hall 111

Physics & Instrumentation & Data Analysis: PET/CT Image Analysis & Quantification

OP493

Does digital PET fit EARL accreditation specifications for tumour imaging?

D. Koopman¹, M. L. Groot Koerkamp², H. Arkies¹, P. L. Jager¹, S. Knollemans¹, C. H. Slump², P. G. Sanches³, J. A. van Dalen⁴; ¹Isala, Department of Nuclear Medicine, Zwolle, NETHERLANDS, ²MIRA Institute for Biomedical Technology and Technical Medicine, Enschede, NETHERLANDS, ³Philips Healthcare, Eindhoven, NETHERLANDS, ⁴Isala, Department of Medical Physics, Zwolle, NETHERLANDS.

Background: Recently, a prototype digital PET system (Philips Healthcare) with digital photon counting technology using silicon photomultipliers was introduced. In clinical practice, EARL FDG-PET/CT accreditation specifications for tumour imaging are widely used for standardization and multi-centre trials. However, EARL specifications are based on analog PET systems. The aims of this study were (1) to evaluate whether a prototype digital PET system can fit EARL accreditation specifications for tumour imaging and (2) to determine the minimal scan duration for digital PET, compared to a state-of-the-art analog PET system, that results in image noise levels fulfilling EARL requirements. **Method:** As a part of system acceptance tests, we performed a phantom study using the NEMA image quality phantom filled with FDG-activity, with sphere-to-background ratio 10:1. The background was filled with 2.0 kBq/mL. We acquired PET/CT scans with 10 minutes scan duration on both prototype digital PET and analog state-of-the-art PET (Ingenuity TF, Philips Healthcare). PET data were reconstructed using default settings with $4 \times 4 \times 4$ mm³ voxels. For digital PET data, we performed additional reconstructions using a Gaussian post-smoothing filter with varying kernel widths of 1-8 mm. We determined mean and maximum contrast recovery coefficients (CRC) for all spheres. Results were compared with EARL accreditation specifications. Additionally, we performed reconstructions using multiple shorter scan times per bed position, using list mode clipping, for both digital and analog PET. In each reconstructed image, we measured the covariance in the background, which was defined as standard deviation divided by the mean value. For both systems we determined the acquisition time at which the covariance was 15%, which is the minimum EARL requirement. **Results:** For digital PET using default reconstruction settings, the maximum CRC for the smallest phantom sphere was above the EARL upper limit. Applying a Gaussian post-smoothing filter of 3 mm resulted in CRCs that best fitted within EARL specifications. Using PET reconstructions consistent with EARL, covariance levels of 15% were found at an acquisition time of 54 seconds in analog PET and at 38 seconds in digital PET, given a fixed FDG-activity. **Conclusion:** Digital PET fits EARL specifications when using default PET reconstructions with $4 \times 4 \times 4$ mm³ voxels and a 3 mm Gaussian post-smoothing filter. To reach similar image noise levels, this study indicates that the administered FDG-activity or scan time per bed position can be reduced by typically 30% with digital PET, compared to a state-of-the-art analog PET system from the same vendor.

OP494

First clinical experience of dose and acquisition duration reductions in PET ^{18}F FDG imaging with a BGO PETCT system .The added value of Bayesian Penalized Likelihood reconstruction algorithm: Prospective study on 116 patients

c. frederic, D. Vallot, L. chaltiel, A. Fernandez, S. Zerdoud, L. Dierickx, M. Bauriaud, S. Brillouet, O. Caselles; institut universitaire du cancer de Toulouse Oncopole, toulouse, FRANCE.

Introduction Traditional PET image reconstruction algorithms, such as Ordered Subsets Expectation Maximization (OSEM), cannot be run to full convergence because image noise increases with each iteration. Therefore,

the convergence is stopped after a predetermined number of iterations, typically two or four. However, under-converged images may introduce bias that can directly impact lesion quantitation. New technology now enables PET images to be reconstructed to full convergence using a Bayesian Penalized Likelihood (PL) reconstruction algorithm that aims to improve the signal-to-noise ratio (SNR) and standard uptake value (SUV) accuracy. Full BGO PET CT is reported to have a NEMA sensitivity of 22 cps/kBq and a larger axial field of view (26 cm) that could allow to reduce both the injected activity and the acquisition time per bed position. However, no clinical evaluation of the PL reconstruction algorithm on this new PET system has not been reported so far **Methods** We performed a prospective study on 116 patients, injected with a median of 2.19 MBq/kg of ^{18}F -FDG. Images were reconstructed using two different algorithms: OSEM and PL regularization algorithm. The SNR was calculated in the liver and SUV_{peak} was also determined in lesions or focal physiological uptake. Differences between the two algorithms were analyzed using the Wilcoxon test for paired samples. P-values below 0.05 were considered statistically significant **n** algorithm that aims to improve the signal-to noise ratio (SNR) and standard uptake value (SUV) accuracy. **Results** 116 patients (48 males and 68 females) weighing between 45–125 kg were analyzed. The median injected activity of ^{18}F -FDG was 2.19 MBq/kg, with a range of 1.67–4.01 MBq/kg depending on the patient's body mass index (BMI). The total amount of injected activity per patient ranged from 75.10 to 401.45 MBq. The entire duration of the PET acquisition was 10 minutes. The use of the full convergence PL reconstruction improved the SNR (median of 12%, increasing with patient's BMI), increased the lesion's SUV_{peak} (p below 0.0001) and lowered the volume of injected activity. **Discussion-Conclusion** PL reconstruction demonstrated the capability to reduce both injected activity and acquisition duration by 50% compared to the guidelines without visually impairing the image quality, SNR and lesion's SUV_{peak} . The clinical benefit of increased SUV value due to PL reconstruction on lesion detectability remains to be established.

OP495

A new Zeolite PET phantom to test accuracy of PET image quantitative analysis

F. Zito¹, C. Soffientini², E. De Bernardi³, R. Casati¹, R. Benti¹, G. Baselli²; ¹FONDAZIONE IRCCS CA' GRANDA Ospedale Maggiore Policlinico, Milan, ITALY, ²DEIB, Department of Electronics, Information, and Bioengineering, Politecnico di Milano, Milan, ITALY, ³Department of Medicine and Surgery, Tecnomed Foundation, University of Milano Bicocca, Milan, ITALY.

Purpose: The use of ^{18}F -FDG PET images for diagnosis or treatment planning requires accurate quantification of lesion volume and uptake. Automatic segmentation algorithms (AS) can allow correct definition of lesion borders by overcoming operator dependence of manual delineations. The assessment of PET-AS algorithms requires both realistic data sets and ground truth contours. Physical phantoms satisfy the second requirement, but regular shapes, homogeneous activity, and cold object walls commonly limit the realism of the uptake pattern. This work presents the design of a phantom in which radioactive zeolites, immersed in a warm heterogeneous background, simulate realistic-wall-less lesions with irregular shape and known activity. **Methods:** Zeolites, aluminosilicate minerals, having adsorbing properties, were characterized and used to simulate lesions. Selected samples were heated to eliminate the adsorbed humidity, soaked in an ^{18}F -FDG radioactive solution, extracted and wrapped in Parafilm before being inserted in a proper phantom. Three different types of zeolites (PRODAC and ZEOVIT clinoptilolites, St Cloud cabazite) were evaluated in terms of homogeneity and radioactive uptake, and also of CT contrast useful for contouring ground truth in PET/CT scans. After zeolite family selection, ^{18}F -FDG soaking solutions for lesion simulations were planned. Heterogeneous lesions were simulated by the perfect matching of two parts of broken zeolites, loaded in two different radioactive solutions.

Heterogeneous background was obtained by immersing tissue paper balls with about 2mm diameter and polypropylene sponge pieces of about 2cm x 2cm x 2cm (560 g/m³) into a warm solution. Background mean activity and variability was a posteriori assessed by drawing ROIs on phantom PET images. The phantom was assembled using the PH-24 Myocardial Phantom (Capintec, Inc); the two lung cavities were filled with radioactive pieces of sponge; the mediastinum was filled with a ^{18}F -FDG water solution and a little plastic box containing radioactive paper balls was positioned in its centre. **Results:** Natural PRODAC clinoptilolite resulted the most suitable zeolite for PET lesion simulation. The heterogeneous background showed an uptake variability from 269% to 443% times higher than that obtained with a uniform radioactive solution. The assembled phantom included 7 lesions with volumes ranging from 1.86ml to 7.24ml and background contrasts in the range of 4.8:1 to 21.7:1. **Conclusions:** A novel phantom for the evaluation of PET-AS algorithms and for assessing PET quantitative accuracy was developed providing a data set with both reference contours and activity ground truth, in a wide range of volumes and lesion to background contrasts.

OP496

Quantification of tumor uptake with molecular breast imaging (MBI)

S. Bache, B. Lopez, G. Rauch, B. Adrada, A. Jessop, S. C. Kappadath; UT MD Anderson Cancer Center, Houston, TX, UNITED STATES.

Aim: Molecular Breast Imaging (MBI) uses small dual-headed semiconductor-based gamma camera in a mammographic configuration to obtain functional images of $^{99\text{m}}\text{Tc}$ -sestamibi uptake in breast. Currently, MBI images are purely qualitative. We have developed a novel attenuation correction algorithm to quantify uptake with MBI; the accuracy and robustness of this methodology is presented together with clinical applications. **Materials and Methods:** A 7cm thick phantom containing $^{99\text{m}}\text{Tc}$ -water simulating breast tissue and fillable spheres simulating tumors were imaged with a GE 750b MBI system. Six spheres ranging in diameter from 9mm to 27mm were imaged with sphere-to-background ratios (SBRs) of 3.5, 2.6, 1.7 and located at depths of 2cm, 4cm, 6cm within the water-bath (total of 54 unique scenarios). Sphere images were acquired in-air for ground truth. Decay-corrected projection images were scatter-corrected using a custom dual-energy-window technique (Bache et al, J Nucl Med 56(3):45, 2015). To estimate true counts, T, from each sphere, the geometric mean (GM) of the counts within square ROIs circumscribing the sphere on the two projections was calculated as $T = [C_1 C_2 \exp(-\mu x) F]^{1/2}$, where C is counts, μ is linear attenuation coefficient of water, and x is detector separation. We introduce 4 unique definitions of F to account for background activity: standard GM (GMstd), background-subtracted GM (GMbc), MIRD Primer 16 factor (GMmird16), and a novel "volumetric" factor (GMvol). Error in T was estimated with respect to in-air conditions. The quantitative accuracy of T using different GM definitions was calculated as a function of SBR, depth, and sphere size. Tumors in serial MBI scans of patients undergoing neo-adjuvant chemotherapy were delineated by radiologists. GMvol was used to compute $^{99\text{m}}\text{Tc}$ -sestamibi SUV. **Results:** Mean errors (95%CI range) for all 54 unique scenarios were 167%(-127%, 460%), -16%(-38%, 5%), 19%(-17%, 55%), 3.8%(-24%, 17%) for the GMstd, GMbc, GMmird16, and GMvol. GMmird16 varied the most under differing SBR with COV of 209%, while GMbc and GMvol were least sensitive to SBR with COVs of 25% and 19%. GMvol was the least sensitive to variations in sphere diameter with COV of 28%, compared to 37% and 110% for GMbc and GMmird16. All 3 non-standard GM formalisms were insensitive to depth with COV of ~5%. Tumor SUV changes correlated well with pathological response. **Conclusion:** Using our novel geometric mean formalism, GMvol, we obtained accurate estimates of tumor uptake in MBI images (error <5%; 95%CI ~20%) under a variety of SBRs, tumor sizes, and depths. Research support: GE Healthcare.

OP497**The impact of prompt gamma compensation on myocardial blood flow measurements in dynamic rubidium-82 PET**

I. S. Armstrong, M. J. Memmott, C. M. Tonge, P. Arumugam; Central Manchester University Hospitals, Manchester, UNITED KINGDOM.

Introduction: There is increasing evidence demonstrating a clinical role for myocardial blood flow (MBF) and myocardial flow reserve (MFR) - the ratio of MBF at stress to rest. There are however technical factors that might have an impact on these measurements. The desire for a standardised technique necessitates an understanding of these factors. Unique to rubidium-82 is the Prompt Gamma Compensation (PGC) to compensate for the 776 keV gamma-ray emissions that can cause erroneous coincidence events. PGC has been shown to improve image quality but its impact on MBF or MFR has not been evaluated. **Methods:** 50 sets of routine dynamic rubidium-82 stress and rest images from 29 male (median [inter-quartile range] BMI: 28.4 [25.2-30.5]) and 21 female (median [inter-quartile range] BMI: 33.8 [26.7-38.7]) were acquired on Siemens Biograph mCT. 1110 MBq of rubidium-82 was used for stress and rest; 18-frame dynamic images were reconstructed with and without Siemens PGC using 3D-OSEM (2i24s, 6.5mm post-filter). The area under the curve (AUC) for the blood input function (BIF) was calculated. Stress MBF, rest MBF and resulting MFR were calculated using Siemens syngoMBF. Relative differences of values with and without PGC were calculated along with Wilcoxon rank test and Mann-Whitney U test for statistical analysis. **Results:** With PGC applied, the BIF AUC was significantly greater by +14.0% stress and +14.6% at rest ($p < 0.001$) with no significant differences between the relative BIF AUC increases during stress or rest. Over all patients, no significant differences were observed for stress MBF, rest MBF or MFR. However, significant differences in stress and rest MBF were seen in obese (BMI > 30) patients ($n=23$) but not in non-obese patients. With PGC applied, the median [inter-quartile range] relative change of MBF was -7.0% [-13.3% to +1.8%] for stress ($p < 0.01$) and -5.8% [-16.1% to +3.0%] for rest ($p=0.02$) in the obese patients. No significant difference was observed in MFR for either obese patients or non-obese patients. **Conclusion:** The use of PGC in rubidium-82 dynamic image reconstruction can result in a small but significant reduction of measured absolute MBF in obese patients. Stress and rest values are reduced by similar relative amounts and, as such, MFR is preserved. The use of PGC does not appear to result in any significant differences in MBF or MFR for non-obese patients.

OP498**Radiomics texture features variability and Reproducibility in advance image reconstruction setting of oncological PET/CT**

I. Shiri¹, A. Rahmim^{2,3}, H. Abdollahi¹, P. Ghafarian^{4,5}, A. Bitarafan^{1,6}, M. AY^{7,8}, M. BakhshaishKaram^{4,5}; ¹Department of Medical Physics, Iran University of Medical Sciences, Tehran, IRAN, ISLAMIC REPUBLIC OF, ²Department of Radiology, Johns Hopkins University, Baltimore, MD, UNITED STATES, ³Department of Electrical and Computer Engineering, Johns Hopkins University, Baltimore, MD, UNITED STATES, ⁴Chronic Respiratory Diseases Research Center, National Research Institute of Tuberculosis and Lung Diseases (NRITLD), Shahid Beheshti University of Medical Sciences, Tehran, IRAN, ISLAMIC REPUBLIC OF, ⁵PET/CT and Cyclotron Center, Masih Daneshvari Hospital, Shahid Beheshti University of Medical Sciences, Tehran, IRAN, ISLAMIC REPUBLIC OF, ⁶Cardiovascular Intervention Research Center, Rajaie Cardiovascular Medical and Research Center, Iran University of Medical Sciences, Tehran, IRAN, ISLAMIC REPUBLIC OF, ⁷Department of Medical Physics and Biomedical Engineering, Tehran University of Medical Sciences, Tehran, IRAN, ISLAMIC REPUBLIC OF, ⁸Research Center for Molecular and Cellular Imaging, Tehran University of Medical Sciences, Tehran, IRAN, ISLAMIC REPUBLIC OF.

Aim Radiomics features derived from oncological PET images are now recognized as valuable tool for future prognostic and predictive models, knowledge about their variability and Reproducibility is essential. The purpose of current study was to investigate the variability and reproducibility of radiomics texture feature in oncological PET/CT due to different advance image reconstruction parameters. **Material and method** PET images of the NEMA-IQ phantom containing 6 hot spheres (diameter 10 to 37mm) were acquired on GE Discovery 690 PET/CT scanner. The 3D iterative reconstruction was done using OSEM + PSF and OSEM+ PSF + TOF with two and three iteration and eight post-reconstruction filters width 1 to 6.4 mm. The five largest spheres were analyzed. PET-based VOIs were drawn automatically by applying a threshold of 50% of SUVmax. All analysis was performed in Matlab R2013b. For each VOI, 80 radiomic features were based on intensity histograms (IH), gray level co-occurrence (GLCM), gray level run-length (GLRLM), neighborhood-difference matrices (NDM), gray level size-zone texture matrices (GLSZM) and SUV statistics. All radiomics features were categorized into 4 groups based on coefficient of variation (COV): a very small ($COV \leq 5\%$), small ($5\% < COV \leq 10\%$), intermediate ($10\% < COV \leq 20\%$) and large ($COV > 20\%$) range of variation with respect to the mean. **Result** Approximately 71% of the radiomics features (57/80) had a significantly smaller variance. TLG, SUVmean, 10 SUV statistics and 27 texture feature had the best performance with a COV less than 5%. 18 features had COV between 5 and 10%, 12 features had COV between 10 and 20%, Whereas 11 features such as LZE and HGLZE from GLSZM were the least robust. SUVskewness, Coarseness, RLV are in the large variation group for all reconstruction algorithms. **Conclusion** The sensitivity of PET Radiomics textural features to advance reconstruction parameters is feature-dependent. Therefore, texture Features with high COV are more prone to errors if employed to quantitative oncological PET image. Radiomics texture Features with low COV over different reconstruction are better candidates for reproducible tumor quantification. Robustness of (57/80) texture feature between different advance images reconstructions may be high enough to allow the extraction of texture feature values for oncological PET image.

1307 – Tuesday, October 18, 2016, 11:30 - 13:00, Hall 116

Clinical Oncology - Featured: PET/MR in Clinical Oncology

OP499**PET/MR in Clinical Oncology - State of the Art**

P. Veit-Haibach; University Hospital Zurich, Klinik für Nuklearmedizin, Zurich, SWITZERLAND.

OP500**Evaluation of primary prostate pathologies by large-scale analysis of non-invasive PET-MRI features with Machine-Learning approaches**

L. Papp¹, S. Hartenbach², A. Duhovic¹, P. Baltzer³, I. Rausch⁴, T. Beyer⁴, M. Susani⁵, L. Kenner⁵, C. Seitz⁶, S. Shariat⁶, M. Hacker¹, M. Hartenbach¹; ¹Medical University of Vienna, Division of Nuclear Medicine, Vienna, AUSTRIA, ²German Armed Forces Hospital Ulm, Institute of Pathology, Ulm, GERMANY, ³Medical University of Vienna, Division of General and Paediatric Radiology, Vienna, AUSTRIA, ⁴Medical University of Vienna, Center for Medical Physics and Biomedical Engineering, Vienna, AUSTRIA, ⁵Medical University of Vienna, Clinical Institute of Pathology, Vienna, AUSTRIA, ⁶Medical University of Vienna, Department of Urology, Vienna, AUSTRIA.

Introduction Prostatic tissue offers a wide range of pathologies from benign alterations and non-significant cancers up to aggressive tumor patterns. So far imaging has played a minor role in tissue characterization. Our goal was to provide a PET-MRI based classification model built on

large-scale analysis of multi-modal and parametric features incorporating supervised Machine-Learning (ML) approaches. **Materials and Methods** To date, 30 of 60 collected prostate patients were processed having a dual-tracer multiparametric PET/MRI (^{18}F -FMC, ^{18}F -FMC+ ^{68}Ga -PSMA^{HBED-CC} (dual-tracer) PET, and ADC-map) together with the respective histopathological analysis to serve as a reference. Manual retrospective delineation of IgPIN, hgPIN, BPH, Prostatitis, Gleason 3 and Gleason >3 regions over PET/MRI images was performed on the Hybrid-3D software (Hermes Nuclear Diagnostics, Stockholm, Sweden) when at least one PET/MRI parameter matched the pathology in a lesion >5mm axial size. Tumour-to-background ratio (TBR) of PET region voxel values were calculated (background: gluteal muscle). Overall 56 general and textural (neighbourhood grey-tone difference matrix (NGTDM), grey-level co-occurrence matrix (GLCM)) based parameters were calculated over PET TBR, T2 and ADC delineated regions of each case. An automated feature selection and feature weight estimation ML algorithm was implemented to minimize the classification error of a multivariate weighted-Gaussian classifier function over predefined grading clusters. The ML algorithm was first executed as a binary classifier to separate Benign (Prostatitis, IgPIN, hgPIN, BPH) and Tumour (all Gleason) groups, then as a unary classifier to separate BPH, Gleason 3 and Gleason 4 groups. Both classifiers were validated by comparing their results to histology-derived grading values serving as reference to calculate sensitivity and specificity over a multivariate confusion matrix. **Results** The binary classification resulted 98% sensitivity and 94% specificity where the ML-selected features were: dual-tracer TBR (homogeneity-GLCM, complexity-NGTDM), ^{18}F -FMC TBR (homogeneity-GLCM, uniformity-GLCM, busyness-NGTDM), T2 (homogeneity-GLCM, contrast-GLCM, complexity-NGTDM), ADC (volume, dissimilarity-GLCM, busyness-NGTDM). In case of the unary classification the sensitivity and specificity values were: BPH: (98%, 96%), Gleason 3: (78%, 94%) and Gleason 4: (94%, 89%) respectively with ML-selected features of: dual-tracer TBR (mean, homogeneity-GLCM, dissimilarity-GLCM, contrast-NGTDM), ^{18}F -FMC TBR (mean, variance, homogeneity-GLCM, contrast-GLCM, contrast-NGTDM), T2 (homogeneity-GLCM, coarseness-NGTDM, contrast-NGTDM, complexity-NGTDM), ADC (mean, volume, dissimilarity-GLCM, contrast-NGTDM). **Conclusions** Both the binary and the unary classification validations have shown high sensitivity and specificity indicating that there is a high potential in characterizing prostate lesions based on PET/MRI-derived textural parameters. As a next step, our method will be validated in an approved prospective clinical trial setting in our working group (Clinicaltrials.gov: NCT02659527).

OP501

Comparison of integrated ^{18}F -FDG PET/MRI and MRI alone for the evaluation of patients with lymphoma

J. Grueneisen¹, L. M. Sawicki², B. M. Schaarschmidt², V. Ruhlmann¹, M. Forsting¹, L. Umutlu¹; ¹University Hospital Essen, Essen, GERMANY, ²University Hospital Dusseldorf, Dusseldorf, GERMANY.

Aim: To compare the diagnostic performance of integrated ^{18}F -FDG PET/MRI and MRI alone for whole-body staging of patients with lymphoma. **Material and Methods:** A total of 48 consecutive patients underwent 52 whole-body ^{18}F -FDG PET/MRI (Biograph mMR, Siemens) examinations for pretreatment staging as well as for therapy monitoring and surveillance of lymphoma disease. Two physicians analyzed the MRI datasets, followed by a second reading of ^{18}F -FDG PET/MRI datasets. Both readers were instructed to identify the total number of tumor lesions. Apparent diffusion coefficients (ADC) and standardized uptake values (SUV) were determined and served as an orientation for a differentiation between malignant and benign lesions. Sensitivity, specificity, positive predictive value, negative predictive value and diagnostic accuracy for the identification of patients with lymphoma disease as well as the detection of malignant lesions

were calculated for ^{18}F -FDG PET/MRI and MRI alone. **Results:** Malignant lesions were present in 28 of the 52 examinations. ^{18}F -FDG PET/MRI enabled correct identification of disease presence with a sensitivity, specificity, positive predictive value, negative predictive value and diagnostic accuracy of 100%, 92%, 93%, 100% and 96%. The respective values for MRI alone were 89%, 83%, 86%, 87% and 87%. Differences between the two imaging modalities were not statistically significant ($p > 0.05$). Furthermore, a total 96 nodal regions were analyzed of which 62 (65%) were affected with active lymphoma disease. ^{18}F -FDG PET/MRI revealed significantly higher values for the detection of lymphoma lesions (97%, 91%, 95%, 94% and 95%) when compared to MRI alone (84%, 74%, 85%, 71% and 80%). Calculated statistical values for the identification of extranodal sites did not show a significant difference between ^{18}F -FDG PET/MRI and MRI alone ($p > 0.05$). **Conclusion:** The present study underlines the usefulness of ^{18}F -FDG PET data as a valuable additive to MR imaging for a more accurate evaluation of patients with lymphomas. Combining high-quality MR and simultaneous PET-imaging, integrated ^{18}F -FDG PET/MRI enables an accurate staging of lymphoma patients and may serve as a valuable alternative/adjunct for the clinical work-up.

OP502

Evaluation of PET and MR datasets in an integrated ^{18}F -FDG PET/MRI setting: comparison of different MR sequences for whole-body staging of patients with a suspected tumor recurrence of breast cancer

J. Grueneisen¹, J. Kirchner², A. Wetter¹, V. Ruhlmann¹, M. Forsting¹, L. Umutlu¹; ¹University Hospital Essen, Essen, GERMANY, ²University Hospital Dusseldorf, Dusseldorf, GERMANY.

Aim: To assess the diagnostic value of different MR sequences and ^{18}F -FDG PET data, acquired with an integrated PET/MR scanner, for whole-body restaging of breast cancer patients. **Material and Methods:** A total of 35 consecutive patients with a suspected tumor recurrence of breast cancer were prospectively enrolled for a whole-body ^{18}F -FDG PET/MRI (Biograph mMR, Siemens) examination. The whole-body MR protocol comprised: 1) T2w HASTE ax., 2) DWI ax. and 3) post-contrast T1w VIBE ax. Two readers evaluated the following datasets, while in each reading session a different constellation of available MR sequences was utilized: 1. MRI alone, 2. PET/MR-HASTE/DWI, 3. PET/MR-HASTE/VIBE, 4. PET/MR-HASTE/DWI/VIBE. they were instructed to identify the total number of tumor lesions in each reading session. The diagnostic confidence for each detected lesion (3 point ordinal scale) and the lesion conspicuity (4 point ordinal scale) for the three different MR sequences were additionally rated. **Results:** Tumor recurrence was present in 24/35 (69%) patients and a total of 155 lesions (malignant, $n = 112$; benign, $n = 43$) were described. On a lesion based analysis, MRI revealed a sensitivity, specificity, positive predictive value, negative predictive value and diagnostic accuracy of 81%, 86%, 94%, 64% and 83%, respectively and a confidence level (CL) of 2.23 ± 0.70 for the identification of tumor recurrence. In all three PET/MR readings higher values than for MRI alone were obtained (PET/MR-HASTE/DWI: 92%, 91%, 96%, 81% and 92%, CL: 2.44 ± 0.67 ; PET/MR-HASTE/VIBE: 94%, 91%, 96%, 85% and 93%; CL: 2.65 ± 0.53 ; PET/MR-HASTE/DWI/VIBE: 95%, 93%, 97%, 87% and 94%, CL: 2.72 ± 0.49). Furthermore, mean values for lesion conspicuity were 3.31 ± 0.80 (VIBE), 3.01 ± 0.84 (HASTE) and 2.84 ± 1.14 (DWI), respectively and differed significantly from each other. **Conclusion:** Our results demonstrate the usefulness of ^{18}F -FDG PET data as a valuable additive to MR imaging for more accurate restaging of breast cancer patients. Furthermore, the presented data underline the benefit of contrast-enhanced MR sequences and questions the use of DWI. Since well-considered MR protocols are required for an accurate and effective oncological work-up of breast cancer patients using integrated PET/MRI, the omission of DWI may enable a distinctive reduction in scan-duration accompanied by improved patient comfort.

OP503

Real-time PET/Hyperpolarized MRS/Ultrasound Molecular Imaging Fusion for Focal Prostate Cancer Detection and Guided Biopsy

K. S. Valluru, J. Park, S. V. Bachawal, C. Liu, V. Taviani, P. K. Gulaka, Y. Saenz, S. A. Felt, J. G. Vilches-Moure, B. Daniel, Z. Cheng, D. M. Spielman, **J. K. Willmann**; Stanford University, Stanford, CA, UNITED STATES.

Background: Blinded transrectal ultrasound (TRUS) biopsy can fail to identify prostate cancer (PCa) in 10–25% of patients. Also, many men without PCa undergo unnecessary biopsies, with attendant morbidity. Accurate prostate imaging could help eliminate unnecessary biopsies or improve their yield. Hyperpolarized ^{13}C Magnetic Resonance Spectroscopy (HMRS) provides metabolic MR imaging of cancer with substantially enhanced signal-to-noise ratios, with ^{13}C -pyruvate reported as safe and effective in PCa patients. Furthermore, ultrasound molecular imaging (USMI) with vascular endothelial growth factor receptor type-2 (VEGFR-2)-targeted microbubbles ($\text{MB}_{\text{VEGFR2}}$), and PET imaging with gastrin-releasing peptide receptor-targeted tracer reported promising results. In this study, we investigated the clinical translational feasibility of real-time PET/HMRS/USMI fusion and TRUS biopsy using an *in vivo* canine PCa model. **Materials and Methods:** 60×10^6 Ace-1 cells were orthotopically-transplanted in the prostate of immunosuppressed sexually mature (18–30 months, 10–12Kg) dogs ($n=3$). Two weeks later, simultaneous prostatic PET/HMRS/USMI was performed with ^{68}Ga -NODAGA-RM1 ($\sim 1\text{mCi}$) dynamic PET scan in all the dogs and an additional ^{18}F -FDG ($\sim 2\text{mCi}$) scan in dogs 2 and 3. ^1H -MRI and ^{13}C HMRS (250mM pyruvate, 0.8mL/Kg) images were acquired using ^{13}C /1H dual-tuned endorectal receive and ^{13}C clamshell transmit coils. Subsequently, USMI (BR55, 0.05mL/Kg) and real-time fusion with TRUS (dog 1: HMRS/MRI, dog 2: PET/HMRS/MRI, dog 3: PET/HMRS/MRI+Biopsy) was implemented followed by histological analysis (H&E) of the resected prostate and biopsy samples. **Results:** In all dogs, Ace-1 tumors were seen on TRUS and T_2 -weighted MRI, while USMI revealed peripheral binding in tumors, associated with rapid clearance (~ 3 minutes), possibly due to low affinity of BR55 for canine VEGFR-2. In dog 1, ^{68}Ga PET showed no specific uptake but HMRS showed increased ^{13}C -lactate production in tumor (lactate/pyruvate=0.5). H&E confirmed PCa with ~ 1 mm heterogenic nests surrounded by inflammatory cells. In dog 2, FDG-PET and HMRS showed elevated metabolic activity with lactate/pyruvate=0.64 in tumor, with no ^{68}Ga -tracer uptake. On H&E, extracapsular growth of PCa was confirmed. In dog 3, ^{18}F -FDG and ^{68}Ga showed uptake in tumor with little signal observed on HMRS. Overall, in each dog the tumors were confirmed to be viable at least by one physiological imaging modality showing the benefit of multimodality imaging in improving the diagnosis of PCa. **Conclusion:** Real-time fusion of PET/HMRS/MR images with TRUS is feasible and allows guided PCa biopsy. Our study lays the groundwork for potential clinical translation of this approach for improved guided biopsy results in patients.

OP504

Imaging patients with breast and prostate cancers using combined ^{18}F -NaF/ ^{18}F -FDG and TOF simultaneous PET/MRI

I. Sonni, R. Minamimoto, V. Taviani, A. Loening, S. S. Gambhir, S. Vasanawala, A. Iagaru; Stanford University, Stanford, CA, UNITED STATES.

Introduction: We previously reported the pilot evaluation of a simultaneous PET/MRI scanner with TOF capability, as well as the use of combined ^{18}F NaF/ ^{18}F FDG PET/CT in cancer patients. Here we prospectively compared the combined ^{18}F NaF/ ^{18}F FDG PET/ MRI against $^{99\text{m}}\text{Tc}$ -MDP in patients with breast and prostate cancers for the detection of metastatic disease. **Methods:** Thirty-seven patients referred for $^{99\text{m}}\text{Tc}$ -MDP bone

scans were prospectively enrolled from Oct 14 to April 2016. The cohort included 26 men with prostate cancer and 11 women with breast cancer, 41 - 85 year-old (average 63.4 ± 12). ^{18}F NaF (0.7–2.2 mCi, mean: 1.1 mCi) and ^{18}F FDG (3.6–5.5 mCi, mean: 4.1 mCi) were subsequently injected from separate syringes. The PET/MRI was done 6–30 days (average 9.3 ± 3.2) after bone scan. The whole body MRI protocol consisted of T_2 -weighted, DWI, and contrast-enhanced T_1 -weighted imaging. Lesions detected with each test were tabulated and the results were compared. **Results:** All patients tolerated the PET/MRI exam, and PET image quality was diagnostic despite the marked reduction in the administered dosage of radiopharmaceuticals (80% less for ^{18}F NaF and 67% less for ^{18}F FDG compared to standard protocols). Sixteen patients had no bone metastases identified on either scans. Bone scintigraphy and PET/MRI showed osseous metastases in 20 patients, but more numerous bone findings were noted on PET/MRI than on bone scintigraphy in 9 patients. One patient had negative bone scan, but bone metastases were seen on PET/MRI. Lesions outside the skeleton were identified by PET/MRI in 7 patients. **Conclusion:** The combined ^{18}F NaF/ ^{18}F FDG PET/MRI is superior to $^{99\text{m}}\text{Tc}$ -MDP scintigraphy for evaluation of skeletal disease extent. Further, it detected extra-skeletal disease that may change the management of these patients, while allowing a significant reduction in radiation exposure from lower dosages of PET radiopharmaceuticals administered. A combination of ^{18}F NaF/ ^{18}F FDG PET/ MRI may provide the most accurate staging of patients with breast and prostate cancers prior to the start of treatment.

OP505

Comparison of ^{18}F -FDG PET/MRI and MRI for whole-body staging of patients with primary cervical cancer

J. Grueneisen¹, L. M. Sawicki², B. M. Schaarschmidt², A. Wetter¹, V. Ruhlmann¹, L. Umutlu¹; ¹University Hospital Essen, Essen, GERMANY, ²University Hospital Dusseldorf, Dusseldorf, GERMANY.

Aim: The aim of this study was to compare the diagnostic potential of integrated ^{18}F -FDG PET/MRI and MRI alone for the assessment of the primary tumors as well as whole-body staging of patients with cancers of the uterine cervix. **Material and Methods:** The study was approved by the local institutional ethics committee. A total of 42 consecutive patients with histopathologically proven primary cancers of the uterine cervix were prospectively enrolled in this trial. All patients underwent an integrated whole-body ^{18}F -FDG PET/MRI examination, which comprised a contrast-enhanced whole-body MR protocol including dedicated imaging of the female pelvis. Two physicians separately evaluated the MRI data, followed by readings of the ^{18}F -FDG PET/MRI datasets. They were asked to determine the local tumor spread of primary tumors as well as the occurrence of nodal and distant metastases. **Results:** Both, MRI and ^{18}F -FDG PET/MRI allowed for the correct identification of 41 of the 42 primary cervical tumors. In one patient with FIGO stage Ia, the tumor could not be identified based on either imaging technique. Furthermore, MRI and ^{18}F -FDG PET/MRI showed an equivalent diagnostic performance and enabled correct determination of the T-stage in 37 (85.7%) out of the 42 patients. In 19 of the 42 patients lymph node metastases were present. ^{18}F -FDG PET/MRI revealed higher values for sensitivity (84% vs. 68%), specificity (92% vs. 87%) and diagnostic accuracy (88% vs. 79%) in comparison to MRI alone for the identification of nodal positive patients. A total of 3 patients had distant metastases which could be correctly detected with both imaging modalities. **Conclusion:** The present results demonstrate the usefulness of ^{18}F -FDG PET data as a valuable additive to MR imaging for more accurate nodal staging of patients with primary cervical cancer. For the determination of the local tumor spread ^{18}F -FDG PET/MRI and MRI performed equally. Combining high-quality MR and simultaneous PET-imaging, integrated ^{18}F -FDG PET/ MRI enables an accurate primary staging of tumors of the uterine cervix and may serve as a valuable alternative/adjunct for the clinical work-up in a pretreatment setting.

1308 – Tuesday, October 18, 2016, 11:30 - 13:00, Hall 212

Cardiovascular System: Myocardial Perfusion - Gated SPECT**OP506****Left and right ventricular peak emptying and filling rates measured by gated tomographic radionuclide angiography using a cadmium-zinc-telluride SPECT gamma camera in chemotherapy-naïve cancer patients**

N. L. Hansen, B. Zerahn; Herlev Hospital, Herlev, Copenhagen, DENMARK.

Aim: To establish normative data of left and right ventricular peak emptying and filling rates assessed with ^{99m}Tc -Human Serum Albumin equilibrium radionuclide angiography using a cadmium-zinc-telluride (CZT) SPECT gamma camera. **Materials and Methods:** The study included 718 newly diagnosed cancer patients (393 females) without diabetes mellitus or known cardiovascular diseases referred for routine baseline assessment of left ventricular function prior to potential cardiotoxic chemotherapy. Each acquisition was analysed twice and mean values of left ventricular emptying (LPER), left ventricular filling (LPFR), right ventricular emptying (RPER), and right ventricular filling (RPF) peak rates were obtained. **Results:** LPER and RPER did not differ between gender; LPFR and RPF were higher in women (Students t test, $p < 0.03$). Mean and SD were: LPER (women -3.41 ± 0.9 ml/s, men -3.53 ± 0.8 ml/s), RPER (women -2.26 ± 0.6 ml/s, men -2.28 ± 0.56 ml/s), LPFR (women 3.03 ± 0.86 ml/s, men 2.7 ± 0.83 ml/s), RPF (women 1.82 ± 0.62 ml/s, men 1.73 ± 0.7). An index defined as peak filling rate/peak emptying rate (PFR/PER) for left and right ventricle was introduced, as this was less dependent of heart rate. Left ventricle PFR/PER was -0.91 ± 0.23 (women), and -0.78 ± 0.23 (men). Right ventricle PFR/PER was -0.82 ± 0.24 (women), and -0.77 ± 0.27 (men). LPER increased numerically with age in women ($p < 0.0001$, $R^2 = 0.044$), RPER increased numerically with age in both genders ($p = 0.01$, $R^2 = 0.013$). LPFR decreased with age in both genders ($p < 0.004$, $R^2 = 0.017$ in women, $R^2 = 0.076$ in men), RPF decreased with age in women ($p = 0.005$, $R^2 = 0.016$). Left and right PFR/PER decreased numerically with age for both genders ($p < 0.004$, R^2 varied between 0.02 and 0.13). In patients where rates for early filling and atrial filling could be obtained separately ($n=516$, 416 women), we calculated right and left E/A ratio (early/atrial filling rate), which decreased with age in both genders ($p < 0.00001$, R^2 varied between 0.06 and 0.25). **Conclusion:** Reference values for ventricular peak filling and emptying rates in chemotherapy-naïve cancer patients without cardiopulmonary disease are presented. Filling rates tended to be higher in women and decrease with age, the latter in accordance with age-related increasing fibrosis. Emptying rates generally increased numerically with age, which could be related to age-related changes in heart rate and size.

OP507**Impact of spatial resolution on the assessment of left and right ventricular function by gated bloodpool SPECT: a simulation study using the 4D-MCAT phantom**A. Fernando¹, N. Delcroix², P. Segars³, D. Mariano-Goulart⁴, F. Ben Bouallègue⁴, A. Manrique¹; ¹EA4650 Université de Caen Normandie, Caen, FRANCE, ²CNRS UMS 3408 GIP Cyceron, Caen, FRANCE, ³Duke University, Carl E. Ravin Advanced Imaging Laboratories, Durham, NC, UNITED STATES, ⁴CHRU de Montpellier - Inserm U1046 - CNRS UMR 9214, Montpellier, FRANCE.

Introduction: The new CZT based cameras improve spatial resolution in cardiac perfusion SPECT. However, the impact of the increased resolution on gated bloodpool SPECT (GBPS) measurements is poorly documented. **Materials and methods:** 15 different dynamic three-dimensional mathematical cardiac torso (MCAT) phantoms with increasing ventricular size were generated. We simulated a 360° SPECT acquisition using a Matlab program (72 projections every 5°) with two different Poisson noise levels. The spatial resolution was successively set to 6 mm and 12 mm to mimic both CZT and conventional Anger camera resolutions. All sinograms were then reconstructed using filtered backprojection (Hamming filter). Finally, the 60 reconstructed datasets were converted into a DICOM format and processed using software based on a watershed immersion algorithm (Tompool®, Montpellier University, France) to assess the left ventricular (LV) and right ventricular (RV) ejection fractions (EF) and volumes (end-diastolic volume: EDV or end-systolic volume: ESV). **Results:** Simulated LVEDV ranged from 26 to 277 ml. GBPS post-processing using Tompool was successful in 52/60 cases, but failed in 8 cases with smallest hearts size examined at low (12 mm) resolution. Compared to true values, GBPS overestimated left and right ventricular volumes (LVEDV: 156 ± 77 ml vs. 125 ± 80 ml, LVESV: 58 ± 26 ml vs. 38 ± 25 ml, RVEDV 200 ± 108 ml vs. 170 ± 109 ml, RVESV: 106 ± 60 ml vs. 86 ± 55 ml, all p values < 0.0001 vs. true volumes) and underestimated left and right EF (LVEF: $62 \pm 7\%$ vs. $69 \pm 1\%$, $p < 0.0001$; RVEF: 47 ± 5 vs. $49 \pm 1\%$, $p < 0.01$). A linear model analysis demonstrated that spatial resolution, but not the noise level, significantly impacted the assessment of LV and RV volumes and ejection fractions, the increase in spatial resolution leading to a reduced measurement bias (all p values < 0.001). The correlation between measured and true volumes was high for RVEDV and LVEDV (r^2 values range: 0.92-0.98) whatever the resolution. For LVESV, the correlation was higher using 6-mm ($r^2 = 0.95$) compared to 12-mm resolution ($r^2 = 0.80$). Due to larger systolic volumes, this difference was not observed for RVESV (6mm: $r^2 = 0.99$; 12mm: $r^2 = 0.98$). **Conclusion:** This phantom study demonstrated that spatial resolution has a significant impact on left and right ventricular function assessment using GBPS, suggesting an increased accuracy when using a CZT-like spatial resolution.

OP508**Gamma-cameras are likely to be less vulnerable to small heart motions when equipped with CZT detectors**L. IMBERT^{1,2,3}, J. SALVADORI³, Y. PETEGNIEF⁴, R. SABBAH⁴, H. BOULAHDOUR⁴, G. KARCHER^{1,2,5}, P. MARIE^{1,2,6}; ¹CHU NANCY HOPITAL BRABOIS ADULTES, VANDOEUVRE LES NANCY, FRANCE, ²Plateforme d'Imagerie Expérimentale, Nancy, FRANCE, ³Institut de Cancérologie de Lorraine, Vandoeuvre-lès-Nancy, FRANCE, ⁴CHRU DE BESANCON, BESANCON, FRANCE, ⁵Université de Lorraine, Faculté de Médecine, Nancy, FRANCE, ⁶INSERM, U1116, Nancy, FRANCE.

Introduction. Solid-state CZT cameras provide high-quality images, with better contrast and signal-to-noise ratio than conventional Anger cameras, but it is not known whether they are vulnerable to small cardiac motions, which are frequently documented during patients' SPECT recordings. This study was aimed to assess the motion-related increase in the heterogeneity of the myocardial activity recorded on a left ventricular phantom with 2 CZT cameras, the Discovery NM-530c (GE) and the D.SPECT (Spectrum Dynamics) in comparison with an Anger camera (Symbia T2, Siemens) equipped with an astigmatic (IQ.SPECT) or parallel-hole (Conv.SPECT) collimator. **Methods.** The left ventricular insert, which walls were filled-in with a solution containing ^{99m}Tc , was placed at the center of the field of view and for the second half of the SPECT recordings, this insert was

translated with various amplitudes in 6 different directions (-X/+X, -Y/+Y et -Z/+Z). SPECT images were reconstructed with the parameters recommended for clinical routine for each of the 4 cameras. Mean activity was determined for 17 left ventricular segments with the QPS software, and the motion-related increase in heterogeneity between segments' activities was assessed with: 1) the coefficient of variation of the segments' activities (ratio of the standard deviation to the mean) and 2) the number of segments becoming definitely abnormal with a mean activity < 60% of maximal voxel activity. **Results.** The coefficient of variation of the segments' activities was markedly lower in static conditions for the two CZT cameras (D.SPECT: 5.2% Discovery: 5.4%) than for the Anger ones (IQ.SPECT: 9.5%, Conv.SPECT: 8.0%) and these coefficients exhibited further deteriorations according to motion amplitude. For motions of 10-mm, these coefficients were on average: 6.0% for D.SPECT, 7.0% for Discovery, 11.5% for IQ.SPECT and 8.3% for Conv.SPECT. Up to motions of a 10-mm amplitude, the mean number of segments becoming definitely abnormal was low for the CZT cameras (none for D.SPECT and 1 for Discovery) and higher for the Anger ones (3 for both IQ.SPECT and Conv.SPECT). **Conclusions.** When compared with Anger cameras on phantom recordings, CZT cameras exhibit a lower vulnerability to small heart motions, with a lower number of artefactual segmental defects. This may be explained by the higher homogeneity of the activity recorded with CZT detectors and by the limited deteriorations associated to small motions.

OP509

Myocardial Perfusion Imaging with CZT SPECT: Dual Cardiac and Respiratory Gating and Motion-Free SPECT Diastolic Images

D. Daou^{1,2}, R. Sabbah³, C. Coaguila⁴, H. Boulahdour³; ¹Cochin Hospital, APHP, Paris, FRANCE, ²EA 7334 REMES, Université Paris-Diderot, Sorbonne Paris-Cité, Paris, FRANCE, ³CHU Jean Minjot, Besançon, FRANCE, ⁴Centre Hospitalier de Bigorre, Tarbes, FRANCE.

Aim: We recently developed a data-driven respiratory-motion (RM) correction program (REGAT) to process myocardial perfusion (MPI) with CZT SPECT and reported its clinical feasibility and interesting impact on image characteristics. In this MPI CZT SPECT pilot study, we evaluate the feasibility of dual cardiac-respiratory gating with REGAT, its capacity to generate motion-free diastolic SPECT images and its impact on image characteristics. **Materials and Methods:** Were included 7 patients addressed for a stress/rest 99mTc-Tetrofosmin MPI. All patients had prone stress (2 MBq/Kg, 5 min) than rest MPI 3-hours later (6 MBq/Kg, 10 min) on Discovery NM 530c. Only rest list mode acquisitions were processed to generate dynamic SPECT studies using a sampling duration equal to mean ECG RR/16 msec. Each dynamic SPECT study was processed to calculate a data-driven RM curve and generate a mean RM GSPECT study (16 bins). The ECG trigger contained in the list mode was used to generate a mean ECG GSPECT study (16 bins) which was used to generate a corresponding diastolic SPECT study -does not account for RM- by summing bins 1 and 12 to 16 (D-SPECTs) (38% of RR ~4 min acquisitions). The RM curve and the list mode ECG trigger were also used to generate a mean dual cardiac-respiratory gated study (256 bins). The above RM GSPECT was reconstructed and summed either without (SPECTs) or after rigid realignment of cardiac RM. The calculated cardiac RM shifts in the patient's 3-axis were used to process and realign the mean dual cardiac-respiratory gated SPECT projections generating a mean RM-free ECG gated SPECT study. This served to generate a RM-free study by summing all bins (SPECTs-RMfree) and a diastolic RM-free study by summing bins 1 and 12 to 16 (D-SPECTs-RMfree). Were noted for each study the maximal RM in

the cranio-caudal (CC), minimum left ventricular cavity counts (LV-Min), maximum LV myocardial counts (LV-Max), FWHM of anterior (FWHM-ant) and inferior (FWHM-inf) LV myocardial wall. Contrast = (LV-Max - LV-Min)*100/(LV-Max + LV-Min). **Results:** CC was 12±5 mm and > 10 mm in 4/7 pts. D-SPECTs and D-SPECTs-RMfree were very good quality. For SPECTs, D-SPECTs, SPECTs-RMfree, and D-SPECTs-RMfree:

FWHM-ant were	5.9±0.7	5.5±0.6	5.5±0.7	and 5±0.4 mm
FWHM-inf were	6.7±0.6	6.5±0.8	6.2±0.3	and 6.1±0.7 mm
Contrast	83±6	91±5	86±7	and 93±6 %.

Conclusion: Dual cardiac and respiratory gating of MPI CZT SPECT is feasible with REGAT. It provides very good quality cardiac and RM-free diastolic SPECT images with the best image characteristics.

OP510

CZT SPECT Cardiac Radionuclide Angiography: Feasibility of Data-Driven Respiratory-Motion Gating with REGAT Software

D. Daou^{1,2}, R. Sabbah³, C. Coaguila⁴, H. Boulahdour³; ¹Cochin Hospital, APHP, Paris, FRANCE, ²EA 7334 REMES, Université Paris-Diderot, Sorbonne Paris-Cité, Paris, FRANCE, ³CHU Jean Minjot, Besançon, FRANCE, ⁴Centre Hospitalier de Bigorre, Tarbes, FRANCE.

Aim: We recently reported the clinical feasibility of a data-driven respiratory-motion (RM) correction program (REGAT) to process 99mTc-Tetrofosmin myocardial perfusion (MPI) with CZT SPECT. In this preliminary study, we evaluate the feasibility of dual cardiac-respiratory gating with REGAT to process CZT SPECT cardiac radionuclide angiography (RNA). **Materials and Methods:** Were included 18 patients having a rest cardiac 99mTc-Angiocard RNA on Discovery NM 530c (500 MBq, 5 min acquisition). List mode acquisitions were processed to generate dynamic SPECT studies using a sampling duration equal to mean ECG RR/16 msec. Each dynamic SPECT study was processed to calculate a data-driven RM curve and generate a mean RM GSPECT study (16 RM bins). The ECG trigger contained in the list mode was used to generate a mean ECG GSPECT study (16 ECG bins). The RM curve and the list mode ECG trigger were also used to generate a mean dual cardiac-respiratory GSPECT study (256 bins). RM GSPECT was reconstructed and rigidly realigned focusing on left and right ventricles. The calculated cardiac RM shifts in the patient's 3-axis were used to process and realign for RM the mean dual cardiac-respiratory GSPECT projections generating a mean RM-free ECG GSPECT study by summing all respiratory bins (ECG-GSPECTs-RMfree, 16 ECG bins, it maintains all acquired counts) or by summing only end-expiratory bins corresponding arbitrarily to 30% of respiratory time (ECG-GSPECTs-EE, 16 ECG bins). Were noted: quality of RM curves and image quality of GSPECT, and the maximal respiratory motion in the 3 axis: cranio-caudal (CC), left-right arm (LR) and ventral-dorsal (VD) axis. **Results:** REGAT generated good quality RM curves. Cardiac motion was the largest in CC (7.2±5.8 mm). CC was ≥ 10 mm (2-FWHM) in 5/18 pts and ≥ 15 mm (3-FWHM) in 2/18 pts. LR and VD cardiac motion were 1.72±1.31 mm and 0.59 ±0.47 mm. LR and VD were < 5mm in all 18 patients. ECG-GSPECTs-RMfree were good quality. But ECG-GSPECTs-EE were of insufficient quality. **Conclusion:** Dual cardiac and respiratory gating of RNA CZT SPECT appears feasible with REGAT. It provides cardiac RM magnitude in the 3-axis globally concordant with those in the literature. ECG-GSPECTs-RM-free was of good quality but may suffer limitations inherent to rigid alignment. ECG-GSPECTs-EE does not need alignment but provides inadequate image quality

due to restricted respiratory bin sampling. To overcome this, it needs to be evaluated on longer acquired studies. Their impact on quantification of cardiac function needs to be evaluated.

OP511

Differences in attenuation pattern in myocardial perfusion SPECT between CZT and conventional gamma cameras

J. Oddstig¹, E. Martinsson², F. Hedeer³, H. Engblom³, C. Hindorf¹; ¹Radiation Physics, Skane University Hospital, Lund University, Lund, SWEDEN, ²Radiation Physics, Lund University, Lund, SWEDEN, ³Department of Clinical Physiology and Nuclear Medicine, Skane University Hospital, Lund, SWEDEN.

Background A new generation of gamma cameras with cadmium zinc telluride (CZT) detectors and pinhole collimators has been introduced. The use of pinhole collimators and static gantry result in different image appearance compared to conventional gamma cameras with parallel-hole collimators and rotating gantry. To what extent the attenuation pattern differs between the two cameras is not known. Therefore, the aim of the present study was to compare the position, extent and depth of attenuation defects in myocardial perfusion SPECT (MPS) for a CZT and a conventional gamma camera. **Material and Methods** Phantom measurements were performed on both a CZT camera (GE NM 530c) and a conventional gamma camera (GE Ventri) using a cardiac phantom including lung insert (Data Spectrum Corporation). Twenty patients underwent a 2-day stress-rest protocol (4MBq/kg, stress and rest) and were examined on both cameras approximately 1 hour after administration of ^{99m}Tc-tetrofosmin. All images were corrected for attenuation by an externally acquired CT. Reconstruction parameters recommended by the manufacturer were used. The localization, extent and depth of the attenuation defect was quantified using the software Segment (version 1.9) by comparing the attenuation-corrected and non-attenuation-corrected images for both phantoms and patients. The extent of attenuation for each camera was defined by visual delineation of the ratio between the attenuation-corrected and non-attenuation-corrected phantom images. **Results** The localization of an attenuation defect was shifted counter-clockwise from the inferolateral wall to the lateral wall for the CZT camera compared to conventional camera in both the patient and the phantom measurements. Based on the manual delineation of the attenuation in the phantom ratio images the attenuation threshold was 0.90 and 0.85 for the CZT and conventional camera, respectively. When applying these thresholds in patients the attenuation defect was 23% and 14% ($p < 0.05$) of the total myocardium (mean) for the CZT and conventional camera, respectively. In the phantom experiments the percent of maximum counts within the attenuation defect was 73% and 67% for the CZT and conventional gamma camera, respectively. For the attenuation defect in the patient images was the percent of maximum counts 72% for the CZT and 68% ($p < 0.05$) for the conventional camera. **Conclusions** Attenuation defects have different location, extent and depth when comparing a CZT camera to a conventional gamma camera which needs to be taking into consideration when evaluating perfusion images.

OP512

Interstudy repeatability of left and right ventricular peak emptying and filling rates using a cadmium-zinc-telluride SPECT gamma camera for radionuclide angiography

N. L. Hansen, B. Zerahn; Herlev Hospital, Herlev, DENMARK.

Aim: To assess interstudy repeatability of left and right ventricular peak emptying and filling rates assessed with ^{99m}Tc-Human Serum Albumin equilibrium radionuclide angiography using a cadmium-zinc-telluride (CZT) SPECT gamma camera. **Materials and Methods:** The

study included 46 newly diagnosed cancer patients (35 females) without diabetes mellitus or known cardiovascular diseases referred for routine baseline assessment of left ventricular function prior to potential cardiotoxic chemotherapy. A dose of 550-600 MBq ^{99m}Tc-labeled human serum albumin (HSA) was administered intravenously to each patient. Two acquisitions were performed on a CZT cardiac SPECT gamma camera, GE Discovery 530c (GE Healthcare, Milwaukee, WI, USA), between which the patient was repositioned. Each acquisition was analysed twice by two experienced technologists using a Xeleris 3 Imaging workstation reorientation software (version no. 3.0562) and Cedars-Sinai QBS processing software (revision 2009.0), and mean values of left ventricular emptying (LPER), left ventricular filling (LPFR), right ventricular emptying (RPER), and right ventricular filling (RPFR) peak rates were obtained. Interstudy repeatability was assessed by calculating the intraclass correlation coefficient (ICC) with 95% confidence intervals for the two acquisitions. Furthermore, Bland-Altman analysis was carried out in order to assess proportional bias. **Results:** One patient had an extremely high influence on the simple linear regression analysis carried out for identification of proportional bias (Cook's distance > 1). A review of the raw data revealed a high intra-observer variation for both acquisitions. Subsequently, this patient was excluded from the analysis. ICC and 95% confidence intervals for LPER, RPER, LPFR, and RPFR were 0.99 (0.99-1.00), 0.94 (0.89-0.97), 0.99 (0.98-0.99), and 0.84 (0.72-0.91) respectively. There was no significant proportional bias for any of the variables. **Conclusion:** The CZT camera provides reproducible estimates of left and right ventricular peak emptying and filling rates. Peak filling and emptying rates might be useful for monitoring cardiac function in cancer patients receiving potential cardiotoxic chemotherapy. However, in cases where a high intra-observer variation is found, outcome should be interpreted with caution.

1309 – Tuesday, October 18, 2016, 11:30 - 13:00, Hall 113

Do.MoRe: Rapid Fire Session

OP513

Targeted radionuclide therapy of non-Hodgkin B-cell lymphoma using ¹⁷⁷Lu-lilotomab or ¹⁷⁷Lu-rituximab: a radiobiological approach

A. Pichard¹, S. Marcatili², A. Courteau², R. Ladjohounlou¹, G. Cartron³, I. Navarro-Teulon¹, A. Repetto-Llamazares⁴, H. Heyerdahl⁴, M. Bardiès², J. Dahle⁴, J. Pouget¹; ¹IRCM/INSERMU896, Montpellier, FRANCE, ²UMR 1037 INSERM/UPS, Centre de Recherche en Cancérologie de Toulouse, Toulouse, FRANCE, ³Centre Hospitalier Universitaire de Montpellier, Montpellier, FRANCE, ⁴Nordic Nanovector ASA, Oslo, NORWAY.

Aims. We investigated *in vitro* and *in vivo* in mice the therapeutic efficacy of ¹⁷⁷Lu-lilotomab, a monoclonal antibody targeting CD37 receptor expressed by B lymphoma cells. **Materials and methods.** *In vitro*, Ramos (Burkitt) and DOHH2 (follicular) lymphoma cell lines were exposed for 18 hours to increasing activities (0–6 MBq/mL) of ¹⁷⁷Lu-rituximab, ¹⁷⁷Lu-lilotomab, of the non-specific ¹⁷⁷Lu-cetuximab or to unlabelled mAbs (0-40µg/mL). A radiobiological model considering the cytotoxic effects of radiation alone, of cold antibody alone or of the ARC was established using a mathematical model. This model was next used for predicting the *in vivo* therapeutic efficacy of the three latter ARC in mice bearing Ramos or DOHH2 tumour xenografts. The approach relied on *in vitro* and *in vivo* absorbed dose assessment using MIRD formalism. **Results.** We showed in Ramos and DOHH2 cells the highest cytotoxicity of ¹⁷⁷Lu-rituximab, followed by ¹⁷⁷Lu-lilotomab and the lowest for ¹⁷⁷Lu-cetuximab. The highest sensitivity to ARC was observed in DOHH2 presumably because of their p53 wild type status. Unlabelled rituximab was more efficient in killing cells than lilotomab mainly through apoptosis induction. We determined that in the radiation sensitive DOHH2 cell line, radiation produced by ¹⁷⁷Lu could counterbalance the lower efficacy of lilotomab compared with rituximab, such that

^{177}Lu -lilotomab or ^{177}Lu -rituximab showed the same cytotoxicity. The contribution of radiation to cell killing was much lower in the radiation resistant Ramos cells and ^{177}Lu -rituximab was then more efficient than ^{177}Lu -Lilotomab in that cell line. *In vivo* we showed that ^{177}Lu -rituximab was more toxic than ^{177}Lu -lilotomab and led to a lower maximum tolerated activity. In addition, we showed that one injection of naked rituximab or lilotomab in Ramos tumour xenograft was accompanied by similar increase in median survival. This suggests that under these conditions, naked antibodies have similar (and rather weak) efficacy *in vivo*. Therefore, only final tumour absorbed dose explained the differences in therapeutic efficacies of ^{177}Lu -rituximab and ^{177}Lu -lilotomab. In this respect, we confirmed that the median survival of mice treated with ^{177}Lu -rituximab, ^{177}Lu -cetuximab or ^{177}Lu -lilotomab was proportional to the tumour absorbed dose and was greater for the latter antibody. Similar analysis is ongoing in DOHH2 tumour xenograft treated with ARC. **Conclusion.** We established *in vitro* a radiobiological model to predict *in vivo* the therapeutic efficacy of ^{177}Lu -rituximab, ^{177}Lu -lilotomab or ^{177}Lu -cetuximab. This model was validated by *in vivo* data showing that in mice with Ramos tumour xenograft, ^{177}Lu -lilotomab was more efficient than the two other ARCs.

OP514

Simultaneous PET-MR First Pass Perfusion Imaging using a Novel Cardiac Perfusion Phantom

J. O Doherty¹, E. Sammut¹, P. Schleyer², J. Stirling¹, P. Marsden¹, A. Chiribiri¹; ¹King's College London, London, UNITED KINGDOM, ²Siemens Healthcare UK, London, UNITED KINGDOM.

Background: PET-MRI scanners are increasingly being employed for quantitative myocardial perfusion imaging. We describe a feasibility study of simultaneous first-pass PET-MRI of gadolinium-based contrast agent (GBCA) and PET radiotracer in a dedicated hardware cardiac perfusion phantom, showing repeatability in the quantified perfusion measurements of the resulting simultaneous dynamically acquired traces. Methods: [18F]-NaF and GBCA were injected simultaneously into the phantom using a range of ground-truth myocardial perfusion rates (F_T) of 1 ml/g/min to 5 ml/g/min. MRI and PET data analysis was performed to compare signal time traces in the aorta and the myocardial sections of the phantom, which simulate an image-derived arterial input function (AIF) and myocardial uptake respectively. PET quantification of perfusion flow resulting in values of K_1 (ml/g/min) was performed using a single tissue compartmental model, while MR relative perfusion measurements of the tissue impulse response function ($h(t)$) were calculated using a diluted prebolus of contrast ($h(t)_{PB}$) as the input function using a signal deconvolution technique. Results: Image analysis show simultaneous dynamic PET and MR signal traces at the aorta input and through the myocardial compartments. Calculation of perfusion parameters showed both K_1 and $h(t)_{PB}$ to be linearly related with F_T and also linearly related to each other ($R^2=0.99$). The highest difference in perfusion values between K_1 and F_T was at 1 ml/g/min of 16% but the mean difference for other flow rates was <3%. Conclusion: This study shows that the novel perfusion phantom allows reliable, reproducible simulation of the myocardial kinetics for simultaneous PET-MR imaging, and will find use in protocol design, comparison of PET quantification software and development of MR-based quantification techniques.

OP515

Effect of Data-Driven Respiratory Gating on Lu-177 SPECT/CT Scans

J. C. Sanders^{1,2}, T. Kuwert², A. H. Vija³, A. K. Maier¹, P. Ritt²; ¹Pattern Recognition Lab, University of Erlangen-Nuremberg, Erlangen, GERMANY, ²Clinic of Nuclear Medicine, University Hospital Erlangen, Erlangen, GERMANY, ³Siemens Healthcare GmbH, Molecular Imaging, Hoffman Estates, IL, UNITED STATES.

Aims: Due to long projection times, traditional SPECT imaging suffers from blurring caused by patient breathing motion. This may adversely affect personalized dosimetry for targeted Lu-177 therapies that relies on precise volume of interest (VOI) delineation and quantitation. A data-driven respiratory gating method was recently proposed for Tc-99m liver acquisitions to mitigate this effect, but due to the lower resolution and different activity distributions in Lu-177 imaging, it is yet to be established whether or not this method is applicable for the latter isotope. This study aimed to apply the data-driven respiratory gating method to Lu-177 scans and investigate its effectiveness in these cases. **Methods:** 7 patients undergoing targeted radionuclide therapy were injected with 6.1 ± 1.0 GBq of either Lu-117-PSMA (2 patients) or -DOTATATE (5 patients) prior to SPECT/CT acquisitions at 4, 24, 48, and 72 h.p.i., yielding a total of 28 datasets. Data was acquired with a Symbia T2 SPECT/CT (Siemens Healthcare) for 60 15sec views, and a data-driven respiratory gating method was used to subdivide list-mode data into 5 gates, which were reconstructed separately using prototype xSPECT Quant software (20iterations/1subset, attenuation and scatter correction, 10mm post-smoothing). VOIs were defined at spinal and ilial bone lesions (BL , $n=20$), bladders (B , $n=16$), left/right kidneys (KL/KR , $n=20$), and liver lesions (LL , $n=31$) using a 50% iso-contour in the SPECT image. VOIs were excluded where spillover into neighboring tissue with high activity concentration (e.g. pancreas) precluded clear delineation. The center of mass in each VOI was calculated for each reconstructed gate. Using the beginning inspiration gate as reference, maximum translation along the head/foot axis during the respiratory cycle was then recorded. **Results:** Translations of BL and B VOIs were -0.1 ± 1.8 and -0.5 ± 2.3 mm, respectively, and insignificant ($p=0.89$ and 0.43). Motions in KL , KR , and LL VOIs were -7.2 ± 3.8 , -5.8 ± 4.1 , and -8.1 ± 3.9 mm, respectively. All motions in the latter group were significantly greater than zero with $p < 0.001$. There was no significant difference between the magnitude of left and right kidney motion ($p=0.31$). **Conclusion:** In this preliminary study, translations after respiratory gating were found to be insignificant in tissues assumed to be unaffected by respiratory motion (spinal and ilial bone lesions, bladder), whereas those in regions known to be affected by respiration (liver, kidneys) were significant. These results indicate that the respiratory gating method is indeed able to capture breathing motion for Lu-177 imaging. More patients must be analyzed to characterize its performance and assess clinical utility.

OP516

A software for characterizing intra-tumor heterogeneity in multimodality imaging and establishing reference charts

C. NIOCHE¹, F. ORLHAC¹, M. SOUSSAN², S. BOUGHDAD³, J. ALBERINI³, I. BUVAT¹; ¹IMIV, CEA, Inserm, CNRS, Univ. Paris-Sud, Université Paris Saclay, CEA-SHFJ, 91400, Orsay, FRANCE, ²HU-Paris Seine Saint Denis site Avicenne ap-hp, 93000 Bobigny, FRANCE, ³Institut Curie-Hôpital René Huguenin, 92210 Saint-Cloud, FRANCE.

Objectives: Textural analysis is gaining considerable interest in medical imaging, in particular to characterize tumor heterogeneity. Yet, values corresponding to heterogeneous tumors are unknown. We developed an easy-to-use freeware enabling calculation of a broad range of conventional, textural and shape indices from PET, MR and CT images to speed up the creation of reference charts. **Methods:** The LIFEx freeware does not rely on any commercial libraries. LIFEx is dedicated to researchers, radiologists, nuclear medicine physicians and oncologists and includes a user interface displaying conventional indices (eg SUV, metabolic volume and total lesion glycolysis in FDG PET) and a large variety of histogram, textural and shape indices. Calculation options (eg, resampling method and number of grey

levels for textural analysis) can be changed by the user. LIFEx reads DICOM images locally or over a network using a DICOM browser, is compatible with Osirix and includes a powerful 3D reconstruction-based slice viewer. Volumes of interest can be imported, drawn and manipulated using LIFEx. Results are exported in Excel format files. LIFEx runs on Windows, MacOs and Linux platforms. It is distributed with examples and includes a tutorial. Users can contribute to the gathering of index values in different tissue types and different images. A public database of reference values is being built and integrated in the software for assisting result interpretation. **Results:** LIFEx has been distributed to research labs, nuclear medicine and radiology departments for investigating different tumor types (gliomas, cervix, lung, breast, and colorectal tumors). The intuitive interface made it fast to master for staff, and allowed us to start building databases of normal textural values in brain (white and grey matter), breast, liver, lung, fat, and muscles for various imaging equipments and protocols in PET and CT, while MR data are currently being collected and processed. The collected data resulted in a large set of reference charts characterizing the values and variability of the textural indices in PET and CT as a function of the organ, scanner and imaging protocol when using identical calculation formula. **Conclusions:** The availability of a free software to calculate indices characterizing tumor heterogeneity facilitates the collection of data by independent centers. The on-going creation of reference charts for various indices, organs, imaging modalities and protocols should contribute to a better understanding of the potential and limitation of textural analysis in PET, CT and MR.

OP517

Dynamic scanning, kinetic modelling and parametric images reveal lung inflammation

I. Velikyan¹, J. Sörensen¹, J. Retamal², F. Suarez-Sipmann², S. Jalkanen³, G. Antoni⁴, G. Hedenstierna², A. Roivainen⁵, A. Larsson⁶, M. Lubberink¹; ¹Section of Nuclear Medicine and PET, Department of Surgical Sciences, Uppsala University, Uppsala, SWEDEN, ²Hedenstierna laboratory, Department of Surgical Sciences, Uppsala University, Uppsala, SWEDEN, ³MediCity Research Laboratory and Department of Medical Microbiology and Immunology, University of Turku, Turku, FINLAND, ⁴Department of Medicinal Chemistry, Uppsala University, Uppsala, SWEDEN, ⁵Turku PET Centre, University of Turku, Turku, FINLAND, ⁶Hedenstierna laboratory, Department of Surgical Sciences, Uppsala, SWEDEN.

Aim: Development of radiopharmaceuticals for fast, noninvasive, specific and quantitative imaging of acute lung inflammation is a challenging task. The apparent uptake in positron emission tomography (PET) images is a manifestation of a number of physiological processes. Dynamic scanning, kinetic modelling, and parametric net influx rate (K_i) images were employed in order to elucidate target specific binding of [⁶⁸Ga]Ga-Siglec-9/PET-CT in porcine model of acute respiratory distress syndrome (ARDS). **Material and Methods:** Pigs with induced ARDS were first intravenously administered with [¹⁵O]water (421±4 MBq) for dynamic scanning during 10 min. Then ⁶⁸Ga-labeled 1,4,7,10-tetraaza cyclododecane-1,4,7-tris-acetic acid-10-ethylene glycol-conjugated Siglec-9 motif peptide ([⁶⁸Ga]Ga-Siglec-9; 120±36 MBq) was intravenously administered for dynamic scanning during 90 min followed by whole-body examination. Arterial blood samples (1 mL) were collected at 0.5, 1, 2, 5, 7, 10, 15, 20, 30, 45, 60, 75, 80 and 90 min post injection. Lung tissue perfusion was quantified from dynamic [¹⁵O]water/PET. The dynamic [⁶⁸Ga]Ga-Siglec-9/PET data from the lung was fitted to a reversible two-tissue compartment model. Net uptake rate ($k_i=K_i*k_3/(k_2+k_3)$) was calculated as the slope of the linear portion of the

time-activity-curve TAC, starting at 15 min post injection. Parametric K_i images were generated using a basic function method. **Results:** Injured lungs demonstrated 10-fold lower tissue perfusion and 2-fold lower standardized uptake value (SUV) as compared to that of the healthy ones. The right and left ventricular TACs of [¹⁵O]water/PET fit best as input function respectively in the healthy and injured lungs. The kinetics of [⁶⁸Ga]Ga-Siglec-9 distribution was described by the reversible two-tissue compartment model well. K_i value was 2.2 times higher for the healthy lungs, however when normalized to the tissue perfusion the value was found 4 times higher for the injured lungs. The retention of the tracer was also statistically higher for the injured lungs. **Conclusions:** The correction for the tissue perfusion, that strongly influences the accessibility of [⁶⁸Ga]Ga-Siglec-9 to the target, revealed higher net influx rate for the injured lungs thus allowing the detection of pulmonary inflammation. This finding would not be possible on the bases of SUV readings only. Furthermore the parametric K_i images improved the quantification accuracy and image contrast.

OP518

BRAF V600E Mutation In Papillary Thyroid Cancer: Its Influence On Radioiodine Postsurgical Therapy - Preliminary Results

M. Domínguez-Ayala¹, P. Mínguez-Gabiña², A. Expósito Rodríguez¹, E. Rodeño Ortiz de Zarate², T. Gutiérrez Rodríguez¹, B. Barrios Treviño¹, M. Paja Fano¹, A. Gómez Palacios¹; ¹H.U. Basurto, Bilbao, SPAIN, ²H.U. Cruces, Barakaldo, SPAIN.

OBJECTIVE: The BRAF V600E mutation in papillary thyroid cancer (PTC) has been related to resistance to iodine in recurrent disease. However, this influence is not known in the early stages of disease. Our aim was to evaluate the effect of the BRAF V600E mutation in PTC after the postsurgical ablation of thyroid remnants with ¹³¹I. **MATERIALS AND METHODS:** A prospective cohort study was designed, from September 2015 to February 2016, which included patients with PTC receiving ablative ¹³¹I therapy after surgical treatment. All of them were operated by the same surgical centre and by the same surgical team. Two different groups were established: patients who had BRAF V600E mutation (BRAF +) and those without it (BRAF-). Variables were described of age, gender, tumor stage, thyroglobulin values after 6 months of the radioiodine therapy, and the therapeutic administered activity. To determine the influence of the mutation in the radioiodine uptake in the remnants, SPECT/CT based dosimetry of thyroid remnants was performed. **RESULTS:** 17 patients giving in total 32 thyroid remnants with an average of 1.8 per patient were included. 76% of patients were women and 59% of patients were BRAF +. In both BRAF + and BRAF - patients, age was similar. BRAF + patients had more advanced tumor stages (II and III) (50% vs 29%). Thyroglobulin values at 6 months were significantly higher for the BRAF + group (mean 0.91 vs 0.18; $p = 0.47$) and also was the administered activity (mean 3638 MBq vs 2590 MBq; $p = 0.053$). The BRAF + patients had a lower absorbed dose to thyroid remnants per administered activity (5.5 Gy/GBq vs 12.4 Gy/GBq; $p = 0.18$) and a lower remaining activity in remnants per the unit mass and per administered activity at 7 days (0.006 %/g vs 0.022 %/g $p = 0.28$). The effective half-life of the radioiodine in the remnants was higher for BRAF- patients (69 h vs 47 h $p = 0.26$). **CONCLUSIONS** According to the initial results, more than half of patients with PTC showed BRAF V600E mutation. After postsurgical ablation with ¹³¹I, the mutation involved a lower absorbed dose per administered activity, lower relative activity per unit mass after 7 days and faster washout of the radioiodine. We need more long-term studies with a larger population to confirm these results and know their clinical consequences.

OP519**Induction and Maintenance Regimen with Peptide Receptor Radionuclide Therapy Lu-177-DOTA-TATE (PRRT) Improves Progression Free Survival (PFS) in Patients with Advanced Neuroendocrine Tumours (NETs)**

A. J. B. McEwan¹, M. Wieler¹, M. B. Sawyer¹, D. W. Morrish¹, B. A. Schaitel², L. D. Schrader², D. Murray¹, W. Makis¹, T. McMullen¹; ¹University of Alberta, Cross Cancer Institute, Edmonton, AB, CANADA, ²Alberta Health Services, Cross Cancer Institute, Edmonton, AB, CANADA.

Introduction: A PRRT protocol of induction (4 cycles) and maintenance (up to 8 cycles) treatments is a novel and effective therapeutic option for patients with advanced gastrointestinal and pancreatic NETs (GEPNETs). **Aims:** We hypothesize long-term and ongoing therapy with Lu-177 improves outcomes, and is effective and safe for these patients. We evaluated PFS in a cohort with GEPNETs following an induction regimen of Lu-177 (4 cycles of up to 6.11 GBq/cycle every 10 - 14 weeks) and maintenance (up to 8 cycles of up to 4.07 GBq/cycle every 5.5 - 10 months). **Materials and methods:** A subset of 139 participants enrolled in this Lu-177 study have PNETs (n=44), GNETs (n= 85), or presumptive GNETs (n=10)). Of these 139 participants, 30 had 1-2 cycles, 26 had 3-4 cycles, 34 had 5-6 cycles, 28 had 7-8 cycles, 13 had 9-10 and 8 had 11-12 cycles of Lu-177 therapy. Cumulative mean administered dose was 5.76 ± 2.39 GBq (1-2 cycles); 17.90 ± 3.35 GBq (3-4 cycles); 23.67 ± 3.87 (5-6 cycles); 32.98 ± 4.34 GBq (7-8 cycles); 40.25 ± 2.88 GBq (9-10 cycles) and 48.88 ± 6.02 GBq (11-12 cycles). Doses were modified by defined algorithm for age, metastatic burden and renal function. **Results:** 111 patients remain on treatment and 28 have stopped treatment: 1 is surgically confirmed disease free (after 4 cycles); 13 discontinued due to biochemical, anatomic or symptomatic progression between cycles (after 1-2 cycles, n=2; after 3-4, n=3; after 5-6, n=1; after 7-8, n=4; after 9-10, n=2; after 11-12, n=1); 14 died (after 1-2 cycles, n=4; after 3-4, n=1; after 5-6, n=5; after 7-8, n=3; after 9-10, n=1). Mean time from first treatment was: 12.4 weeks, 1-2 cycles; 36.8 weeks 3-4 cycles; 17.7 months 5-6 cycles; 34.2 months 7-8 cycles; 46.9 months 9-10 cycles and 58.1 months 11-12 cycles. A Kaplan-Meier survival curve shows median PFS has not yet been reached at 59.3 months. Transient Grade 3 renal and haematological toxicity were seen; no Grade 4 toxicity was observed. **Conclusion:** These data support our hypothesis that a long term regimen of induction and maintenance therapy with Lu-177 improves PFS in patients with GEPNETs, and supports the hypothesis of low dose hypersensitivity as the mechanism of action for PRRT in GEPNETs. This regimen is more effective than literature reported treatment regimens; in this cohort, median PFS has not been reached at 59.3 months.

OP520**Secondary glioblastoma multiforme - local alpha emitters targeted therapy with ²¹³Bi-DOTA-substance P**

L. Królicki¹, A. Morgenstern², J. Kunikowska¹, H. Koziara³, B. Królicki³, M. Jakuciński⁴, D. Pawlak⁵, C. Apostolidis⁶, F. Bruchertseifer⁶; ¹Nuclear Medicine Department, Medical University of Warsaw, Warszawa, POLAND, ²European Commission, Joint Research Centre, Institute for Transuranium Elements, European Commission, Joint Research Centre, Institute for Transuranium Elements, Karlsruhe, GERMANY, ³Department of Neurosurgery, Institute of Psychiatry and Neurology, Warszawa, POLAND, ⁴Department of Nuclear Medicine, Brodnowski Hospital, Warszawa, POLAND, ⁵Radioisotope Centre POLATOM, National Centre for Nuclear Research, Otwock-Swierk, POLAND, ⁶European Commission, Joint Research Centre, Institute for Transuranium Elements, Karlsruhe, GERMANY.

Glioblastoma multiforme (GBM) is the most common and malignant brain tumor. GBM may be primary or secondary. Primary GBM develop rapidly in elderly patients without histologic evidence of a less malignant precursor lesions. Secondary GBM origin from low-grade diffuse astrocytoma or anaplastic astrocytoma, with manifestation in younger patients. Histologically, primary and secondary GBM are largely indistinguishable, but they differ in their genetic and epigenetic profiles. Secondary GBM accounted for about 9% of all GBM. The median overall survival time in patients with secondary GBM without treatment is 7.8 months, and in patients after surgery and radiotherapy - 27.1 months. Advancements in the past decades have not significantly increased the overall survival of patients with this disease. GBM has been demonstrated NK-1 receptor system and substance P can be used as a ligand for targeted therapy. Alpha emitter, like ²¹³Bi offers the new potential for selective irradiation of tumors, with minimizing damage to adjacent tissue. **Material and methods:** In general, 50 patients with different glia tumors were treated in the study. Secondary glia tumor IV was diagnosed in 7/50 patients. In all cases standard therapy were performed. Following intracavitary or intratumoral insertion of 1-2 catheter systems, patients were treated with 2-8 doses of 2 GBq ²¹³Bi-DOTA-Substance P (²¹³Bi-SP) in intervals of 2 months. ⁶⁸Ga-DOTA-Substance P (⁶⁸Ga-SP) was co-injected with the therapeutic doses to assess biodistribution using PET/CT. Therapeutic response was monitored with MRI. Study was approved by the ethical committee of the Medical University of Warsaw. **Results:** Clinically, treatment with activity up to 13 GBq ²¹³Bi-SP was well tolerated and PET/CT imaging showed high retention of the radiolabeled peptide at the tumor site. No any serious adverse reactions was shown. Median progression free survival was 13.6 months. Median overall survival from the diagnosis time was 46.8 months. Follow up of therapeutic responses and toxicity is continued and patient recruitment is ongoing. **Conclusions:** Treatment of secondary GBM with ²¹³Bi-SP is safe and well tolerated. Targeted alpha therapy with ²¹³Bi-SP may evolve as a promising novel option for treatment of secondary GBM.

OP521**Assessing Yttrium-90 Microsphere Delivery Systems Following Radioembolization: A Feasibility Study Using Digital Photon Counting PET/CT Technology**

C. L. Wright¹, K. Binzel¹, J. Zhang¹, M. Jedlicka¹, R. L. Anderson¹, P. Maniawski², M. V. Knopp¹; ¹The Ohio State University, Columbus, OH, UNITED STATES, ²Philips Healthcare, Cleveland, OH, UNITED STATES.

Aim: It has been demonstrated that ⁹⁰Y generates a small fraction of discrete annihilation photons which can be detected and imaged using conventional photomultiplier tube-based PET systems. A recent technological innovation has led to the replacement of these photomultiplier tubes in the PET gantry with new, solid-state, digital photon counting PET detectors (dPET). The objective of this study is to assess the technical capability of a dPET/CT system for imaging very low doses of residual ⁹⁰Y activity within microsphere delivery systems. **Materials and Methods:** Imaging was performed using a pre-commercial release dPET/CT system (Vereos, Philips). In this feasibility study, six ⁹⁰Y delivery systems were imaged following radioembolization procedures. Residual ⁹⁰Y activities in the delivery systems ranged from 9 - 288 MBq. One source vial of unused ⁹⁰Y microspheres was also imaged. Two dPET acquisitions were obtained in list-mode using total imaging times of 7 min and 60 min. These datasets were reconstructed with ToF and using a standard definition voxel size of 4x4x4 mm³. In addition, list-mode clipping of the dPET data was used to generate subsampled reconstructions in order to simulate virtual faster image acquisition times ranging from 50 min down to 7 min. Matched comparison of image quality for the actual and simulated dPET datasets was performed using the

Intellispace Portal workstation by a blinded reader panel. **Results:** Digital PET imaging of low levels of residual ^{90}Y activity within the delivery system is feasible and produces evaluable images. There was consistent ^{90}Y activity detected in the source vial and, in some cases, activity in the catheter tubing. Although the 60 min acquisitions yielded more ^{90}Y counts, there was no qualitative difference in ^{90}Y detectability or image quality when compared with 7 min acquisitions. Likewise, subsampled listmode dPET datasets produced simulated 7 min acquisitions which were visually identical to the actual acquisitions. **Conclusion:** Our study demonstrates that dPET/CT detection of residual ^{90}Y activity within microsphere delivery systems is feasible. In particular, this new digital photon counting PET detector technology allows for fast image acquisition and promises even faster acquisition with no significant impact on the qualitative assessment of this residual ^{90}Y activity. Continued refinement of ^{90}Y dPET image acquisition and image reconstruction methodologies will enable both fast and accurate evaluation of ^{90}Y microsphere delivery systems in the case of ^{90}Y misadministration events.

OP522

Radiation exposure of the kidneys affects haematological response during ^{177}Lu -DOTATATE treatment

J. Svensson¹, **R. Hermann**², **K. Holgersson**¹, **B. Wängberg**³, **A. Sundlöf**⁴, **J. Tennvall**⁴, **K. Sjögreen Gleisner**⁵, **P. Bernhardt**²; ¹Department of Oncology, The Sahlgrenska Academy, Gothenburg University, Göteborg, SWEDEN, ²Department of Radiation Physics, The Sahlgrenska Academy, Gothenburg University, Göteborg, SWEDEN, ³Department of Surgery, The Sahlgrenska Academy, Gothenburg University, Göteborg, SWEDEN, ⁴Department of Clinical Sciences, Lund University, Lund, SWEDEN, ⁵Department of Medical Radiation Physics, Lund University, Lund, SWEDEN.

Aim Radionuclide therapy with ^{177}Lu -DOTATATE is a valuable treatment option in the management of patients with neuroendocrine tumours overexpressing somatostatin receptors. The amount of treatment is usually restricted by a fixed absorbed dose limit to the kidneys, or by persistent haematological toxicity. To better understand which patients will tolerate the treatment, and who should be considered for other treatment; clinical background information is important, including renal and bone marrow function, tumour burden and previous treatment. In this study, the impact of absorbed renal dose on the haematological response was investigated. *Materials and methods* This study analyses the results from 34 of the 80 patients included in the prospective ILLUMINET study (EUDRACT 2011-000240-16), treated with 7.4 GBq of ^{177}Lu -DOTATATE on one to eight occasions. Patients included in the study had a progressive disease according to RECIST criteria, tumours judged to overexpress somatostatin receptors by SSTR imaging and a GFR of ≥ 50 ml/min. Treatment was given as a 30 min infusion together with kidney protecting amino acids, at 8 to 12 week intervals until a BED of 27 Gy (Stage 1 of the study) or 40 Gy (Stage 2) to the kidneys was reached. Some patients ended treatment earlier because of persisting haematological toxicity or disease progression. For dosimetry planar whole-body images were acquired at 1.5, 24, 48 and 168 h p.i. and a SPECT/CT at 24 h p.i. Dosimetry was based on a hybrid technique utilising both planar and SPECT activity data. Patient bone marrow function was monitored by blood sampling for haemoglobin, white blood cell and platelet counts weekly. *Results* The development of haematological toxicity was correlated to the total absorbed renal dose according to the decline in haemoglobin ($r=-0.40$, $p=0.04$) and platelet counts ($r=-0.43$, $p=0.02$), but not to the activity amount given. Baseline GFR also affected the haematological toxicity according to haemoglobin values ($r=0.49$, $p=0.01$). *Conclusion* The correlation between

radiation exposure of the kidneys and the decline in haemoglobin and platelet values during ^{177}Lu -DOTATATE treatment can not be explained by the total amount of activity given. Instead renal function at baseline seems to be a risk factor, and possibly also the magnitude of the radiation of the kidneys, which may affect the ability to produce erythropoietin in response to the decline in haemoglobin.

YE3 – Tuesday, October 18, 2016, 13:00 - 14:30, Hall 114
Young EANM Daily Forum 3: TBA

OP523

TBA

1401 – Tuesday, October 18, 2016, 14:30 - 16:00, Auditorium
CME 11 - Paediatrics/Inflammation & Infection/ESPGHAN/Inflammatory Bowel Disease (Adults and Children)

OP524

Clinical Presentation of IBD in Adults and Children

G. Pujol Muncunill; Hospital Sant Joan de Déu, Barcelona, SPAIN.

OP525

MRI in Crohn's Disease

F. Maccioni; University of Rome La Sapienza, School of Medicine, Department of Radiological Sciences, Rome, ITALY.

OP526

Microscopical Endoscopy in IBD

M. Neurath; Universitätsklinik Erlangen, Medizinische Klinik 1 - Gastroenterologie, Pneumologie und Endokrinologie, Erlangen, GERMANY.

OP527

Role of Nuclear Medicine in IBD

O. Catalano; Harvard University, PET/MR imaging, Cambridge, UNITED STATES OF AMERICA.

1402 – Tuesday, October 18, 2016, 14:30 - 16:00, Hall 211

Joint Symposium 11 - EANM/ETA-CRN: New Approaches in Thyroid Cancer Management

OP528

Tc99m-sestaMIBI and F-18-FDG-PET/CT in Evaluating Thyroid Nodules

L. Giovannella; Oncology Institute of Southern Switzerland, Department of Nuclear Medicine, Bellinzona, SWITZERLAND.

OP529

New ATA Guidelines in Differentiated Thyroid Cancer – The Endocrinologist's Perspective

B. Jarzab; MSC Memorial Cancer Center and Institute of Oncology, Gliwice Branch, Dept. of Nuclear Medicine and Endocrine Oncology, Gliwice, POLAND.

OP530

New ATA Guidelines in Differentiated and Medullary Thyroid Cancer – The EANM Perspective

F. A. Verburg; University Hospital Aachen, Dept. of Nuclear Medicine, Aachen, GERMANY.

1403 – Tuesday, October 18, 2016, 14:30 - 16:00, Hall 117

CTE 5 - Joint Session with ESTRO: Radiotherapy Planning

OP531

Introduction to Radiobiology and Novel Radiotherapy Technologies

M. Coffey; Trinity College Dublin, Radiation Therapy, Faculty of Health Sciences, Dublin, IRELAND.

OP532

The Clinical Use of PET-CT in Radiotherapy Planning Head and Neck Cancer

V. Gregoire; Université Catholique de Louvain, Cliniques Universitaires St-Luc, Clinical and Experimental Research Institute, Cancer Center and Department of Radiation Oncology, Brussels, BELGIUM.

OP533

Physics and Technical Aspects of PET-CT Scanning for Radiotherapy Planning

N. Patel; Imperial College Healthcare NHS Trust, London, UNITED KINGDOM.

1404 – Tuesday, October 18, 2016, 14:30 - 16:00, Hall 112

Do.MoRe: Thyroid

OP534

The diagnostic value of I-124 PET/ CT in the follow-up of patients with differentiated thyroid carcinoma

E. I. Klaver, H. Arkies, S. Mijnhout, A. Franken, P. L. Jager; Isala Klinieken, Zwolle, NETHERLANDS.

Purpose: The aim of this retrospective study is to evaluate the diagnostic role of I-124 PET/ CT in the evaluation 6 month or 1 year after ablation-therapy of patients with well differentiated thyroid cancer (DTC). **Methods:** The results of 29 eligible I-124 PET/ CT-scans performed in XX48 DTC patients between February 2013 and February 2016 are evaluated. PET was done using 74 MBq I-124, imaging at 24 and 96 hours with recombinant thyroid hormone (rTSH) stimulation. Thyroglobulin (Tg) and antibodies (Ab) were measured. Findings on the I-124 PET/ CT were compared with subsequent I-131 post-treatment scan in 6 cases and in the remaining with combination of laboratory, radiological, pathological or surgical outcome data over max. 2,5 year follow up. Recurrence was based on laboratory findings (Tg), positive imaging as interpreted by experts. **Results:** 23 I-124 scans showed no uptake and in all there were no signs of recurrence. In 11 scans (8 patients) the I-124 scan showed uptake: in 2 rest thyroid tissue, 1 lymph node metastases in the neck and 2 both (in these 2 metastases were unexpected and led to upstaging from N1a tot N1b). All of these 5 patients received a therapeutic dose of I-131, and the PET findings were concordant on the post-treatment scan. In the remaining 6 cases 2 scans of the same patient were considered false-positive because of a histologically proven ductus thyroglossis cyst, and one given I-131 therapy was retrospectively unjustified. In the other 4 scans the I-124 showed aspecific uptake, and I-131 therapy was not given. In 1 patient the I-124 scan did not detected miliairy lungmetastases, although positive on the I-131 post-treatment scan, but CT was normal. This leads to a sensitivity for the detection of Iodine avid remnants or metastases of 80%, specificity 96%, positive predictive value 80% and negative predictive value 96%. **Conclusion:** in this retrospective study the I-124 PET/ CT proved to be a reliable diagnostic tool for the evaluation of I-131 ablation in patients with DTC.

OP535

Differentiated Thyroid Cancer lymph-node relapse. Relevance of adjuvant RAI after lymphadenectomy. A multicentric study

G. Bottoni¹, F. Bertagna², M. Puntoni¹, A. PICCARDO¹, G. Treglia³, M. Bertoli⁴, L. Foppiani¹, U. Catrambone¹, A. Arlandini¹, B. Dib¹, M. Massollo¹, I. Bossert¹, M. Cabria¹, L. Giovannella⁵; ¹AZIENDA OSPEDALIERA GALLIERA, GENOVA, ITALY, ²Department of Nuclear Medicine, University of Brescia and Spedali Civili di Brescia, Brescia, ITALY, ³Department of Nuclear Medicine and PET/CT Centre, Oncology Institute of Southern Switzerland, Switzerland., Bellinzona, SWITZERLAND, ⁴Department of Nuclear Medicine, University of Brescia and Spedali Civili di Brescia., Brescia, ITALY, ⁵Department of Nuclear Medicine and PET/CT Centre, Oncology Institute of Southern Switzerland, Bellinzona, SWITZERLAND.

Aim: Lymphadenectomy is the therapy of choice when differentiated thyroid cancer (DTC) lymph-node relapse is detected on neck ultrasonography and cytologically confirmed. Radioiodine therapy (RAI) is the adjuvant treatment after thyroidectomy for intermediate/high risk DTC patients. However, its adjuvant role after lymph-node dissection for DTC relapse, is not established. Our aim is to evaluate the impact of adjuvant RAI on progression free survival (PFS) and on overall survival (OS) in patients affected by DTC lymph-node relapse and previously treated with lymphadenectomy. We also assessed the association between PFS and OS and the main prognostic factors able to influence DTC outcome. **Materials and methods:** we retrospectively evaluated DTC patients treated with lateral lymph-node dissection for disease relapse. All patients were previously treated with total thyroidectomy and radioactive remnant ablation for intermediate/high risk DTC. Clinical and histological data obtained during follow-up were used to assess the response and outcome. The association between adjuvant RAI, thyroglobulin levels on suppressive levothyroxine treatment after lymphadenectomy (Tg-on) and other risk-factors and either PFS and OS was evaluated through univariate and multivariate analyses, respectively. **Results** We evaluated 113 patients of which 64 were treated with adjuvant RAI (median activity 4440 MBq). During a median 5.7-year follow-up, 27 patients showed recurrence and 13 died. Kaplan-Meier PFS and OS curves showed that age on diagnosis, histology, tumor dimension, nodal status on diagnosis, percentage of positive nodes on relapse, tumor histology, DTC virulence, and Tg-on were all associated with prognosis. On the other hand, adjuvant RAI itself was not associated with PFS and OS. However, the adjuvant RAI effect was significantly different between patients with Tg-on ≥ 1 ng/ml and those with Tg-on < 1 ng/ml (interaction p value=0.002 for PFS and 0.03 for OS). Indeed, patients with Tg-on ≥ 1 ng/ml treated with adjuvant RAI showed a better PFS (p=0.0005) and OS (p=0.005) than untreated ones. When we adjusted risk using a multivariate Cox model, Tg-on (HR 16,1, p=0.0001) and adjuvant RAI (HR: 0.37, p=0.03) remained the most important factors associated with PFS but only Tg-on remained associated with OS (HR: 8.6, p=0.01). Nonetheless, a trend towards a lower risk of mortality (HR: 0.34, p=0.09) emerged for patients treated with adjuvant RAI. **Conclusions:** Adjuvant RAI after lymphadenectomy for DTC relapse is significantly associated with a better PFS. However, its use should be reserved only for DTC patients with Tg-on ≥ 1 ng/ml.

OP536

The sensitivity and positive predictive value (PPV) of ¹³¹I-post-therapy whole body scan is higher than serum Tg values in detecting metastases in early stage of differentiated thyroid cancer patients

A. Campenni¹, S. Pignata¹, M. Mure¹, F. Di Mauro¹, M. Stipo¹, M. Siracusa¹, R. Ruggieri², S. Baldari¹; ¹Unit of Nuclear Medicine of Messina, Messina, ITALY, ²Unit of Endocrinology of Messina, Messina, ITALY.

AIM: Differentiated thyroid cancer (DTC) is a rare tumor but is the most common malignancy of the endocrine system. The work-up of DTC

patients includes (near)total-thyroidectomy [(n)TT], thyroid remnant ablation (TRA) with ^{131}I -radioiodine and long life follow-up. ^{131}I -post therapy whole body scan (pT-WBS) and serum thyroglobulin (Tg) are used in identifying metastatic patients. Some authors evaluated the possibility to use post-surgical Tg values in deciding for or against TRA. The aim of our study was to verify the sensitivity and PPV of ^{131}I -pT-WBS compared to serum Tg levels in detecting metastases in early stage of DTC patients.

MATERIAL AND METHOD: We retrospectively reviewed the records of 1102 consecutive patients affected by DTC and referred to our Nuclear Medicine Unit in the last five years. For the study, we selected 570 out of 1102 (52%) patients affected by pT1-pT3 DTC (F= 450, M= 120, mean age 48.5 ± 13.2 , ranges 17-82 years; F/M ratio= 3.7:1). Exclusion criteria were: 1) presence of loco-regional or distant metastases at the time of recruitment; 2) age ≤ 16 years; 3) positive thyroglobulin-antibody (Tg-Ab); 4) pT4 stage, 5) poorly-differentiated thyroid cancer. The majority of patients (560/570, 98.2%) were affected by papillary carcinoma while the remaining (1.8%) had follicular carcinoma. Before TRA, all patients underwent neck-ultrasonography, laboratory test and, if treated in hypothyroid state, radioiodine thyroid uptake. Patients underwent TRA in hypothyroid state (321/570, 56%) or after recombinant-human-TSH stimulation (249/570, 44%). Serum Tg values evaluated both before TRA (on L-T4 therapy) and at TRA were matched with ^{131}I pT-WBS results.

RESULTS: ^{131}I pT-WBS discovered metastases in 82 out of 570 (14.4%) patients. Seventy-three out of these patients (90.2%) showed serum Tg levels ≤ 1 ng/ml in post-surgical period. At the time of TRA, forty of them (54%) maintained serum Tg levels ≤ 1 ng/ml. Comparing pT-staging, 33, 2 and 5 patients had pT1, pT2 and pT3 lesions, respectively. The majority of these patients (38/40, 95%) showed regional lymph-node metastases at ^{131}I -pT-WBS while three had lung metastases (one of them also showed lymph-node metastasis). The metastases were confirmed by targeted morphological studies.

CONCLUSION: Serum Tg levels obtained in post-surgical period cannot be used to decide for or against TRA and to predict the outcome of patients. In early stage of DTC, ^{131}I -pT-WBS is an accurate method in detecting metastases also in patients with stimulate serum Tg values ≤ 1 ng/ml, showing sensitivity and PPV significantly higher than serum Tg (100% vs 29.3% for both).

OP537

Clinical outcome of postoperative radioiodine therapy with high dose and low dose in intermediate risk differentiated thyroid cancer patients

J. Jeong¹, E. Kong², S. Jeong¹, S. Lee¹, J. Lee¹, K. Chun², B. Ahn¹; ¹Kyungpook National University Hospital, Daegu, KOREA, REPUBLIC OF, ²Yeungnam University Hospital, Daegu, KOREA, REPUBLIC OF.

Purpose: We evaluated the response to radioiodine (RAI) therapy with high dose (HD) or low dose (LD) using two criteria (with or without whole body scan (WBS)) and re-classification system in Korean differentiated thyroid cancer (DTC) patients with intermediate risk (IR). Additionally we evaluated long-term clinical outcomes. **Methods:** A total of 204 DTC patients with IR who underwent postoperative RAI therapy at two hospitals from 2003 to 2004 were enrolled retrospectively. 124 patients were treated with 3.7 to 7.4GBq (HD) in one center and 80 patients were treated with 1.1GBq (LD) in the other center. Patients were categorized as having excellent (ER), indeterminate (IDR), biochemical incomplete (BIR), or structural incomplete response (SIR) according to re-classification system at during the first 2 years of follow-up using thyroglobulin, ultrasonography, and WBS. Data were also assessed the success rate of RAI therapy with or without WBS results. Recurrence was defined as newly detected pathologically proven lesion. **Results:** There was no significant difference in the success rate between HD and LD groups regardless of whether WBS was included in the criteria or not (54.84% vs. 46.25% with WBS results, $p=0.23$; 60.48% vs. 62.5% without WBS results, $p=0.77$). On the basis of re-classification system, ER was observed in 54.84% of patients treated with HD and in 45.0% of those treated with

LD, IDR was found in 34.68% of patients treated with HD and in 30.0% of patients treated with LD, BIR was found in 4.03% of HD group and in 13.75% of LD group, SIR was found in 6.45% of HD group and in 11.25% of LD group ($p=0.04$). BIR or SIR rate was lower in patients treated with HD compared to patients treated with LD (HD, 10.48%; LD, 25.0%, $p=0.01$). At last follow-up (HD, median 11 years; LD, median 10 years), patients with ER maintained no evidence of disease state. After initial RAI therapy, additional RAI therapies were given to 8 patients of HD group and 18 patients of LD group who got the IDR or BIR. However 7 patients (5 patients with IDR, 2 patients with BIR) in HD group and 7 patients (5 patients with IDR, 2 patients with BIR) in LD group had a recurrence. **Conclusion:** This study suggested that LD therapy seems to be insufficient to DTC patients with IR. In LD group, there were more BIR or SIR to initial therapy and more additional RAI therapies were needed.

OP538

Effectiveness of pre-therapy red marrow and blood dosimetry in ^{131}I treatment of metastatic thyroid cancer

E. Richetta, G. Lo Moro, M. Pasquino, C. Cutaia, S. Valzano, L. Radici, R. Pellerito, M. Stasi; AO Ordine Mauriziano, Turin, ITALY.

AIM Despite the therapy of the metastatic thyroid cancer with ^{131}I is well consolidated some patients still are refractory because of the treatment's sequence. A single high activity treatment seems to improve the outcome compared to several lower activity ones, but it can be inhibited by excessive irradiation at organ at risk such as red marrow or blood as surrogate. A personalized dosimetry could help the physician in determining the optimal activity. To this aim pre-therapy residence time and doses were compared to in-therapy results in order to investigate repeatability and effectiveness of different dosimetric methods. **MATERIALS AND METHODS** We analyzed 88 advanced metastatic thyroid patients (32M, 56 F); after the administration of a ^{131}I tracer activity (15.7 MBq) 114 pre-therapy dosimetries to red marrow (AIFM and Traino Methods) and to blood (EANM Method) were performed and then repeated after therapy (7600 ± 750 MBq). Blood samples (2, 24, 48 and 96 h p.a.) converted into activity-curves allowed the estimation of the blood residence time (τ_{B}). Whole-body AP-PA measurements were performed at same time of blood sampling during pre-therapy and AP every 2 h during hospitalization with detectors placed on patient's bed, to evaluate residence times (τ_{WB}). Pre-therapy (PT) and in-therapy (IT) residence times and doses to red marrow and blood per activity unit were compared with Wilcoxon paired-samples test. Percentage dose differences were also evaluated. **RESULTS** Blood mean residence times τ_{B} were 0.000656 h/ml and 0.000668 h/ml for PT and IT respectively with a mean percentage difference equal to 1.6 ± 25.4 %; p -value (0.991) did not show a statistical significant difference. Whole-body mean τ_{WB} were 23.86 h and 25.056 h for PT and IT, respectively (percent difference 0.5 ± 32 %); p -value (0.043) showed a statistical difference probably due to the different measurements scheduling-time. The statistical analysis confirmed a significant differences for whole-body component of doses (AIFM 0.0146, Traino 0.0196 and EANM 0.016). The different dosimetric method showed similar percentage differences between PT and IT dosimetry (AIFM and Traino -2.02 ± 22.5 %, EANM -1.4 ± 23.1 %) and 69.5 % of patients showed a difference within 20 %. **CONCLUSION** Pre-therapy red marrow ^{131}I dosimetry predicts accurately the in-therapy results and can be safely implemented to help the physician in the determination of a personalized therapeutic activity.

OP539

Early and Late Adverse Effects of Radioiodine Therapy for Pediatric Differentiated Thyroid Cancer

D. Albano, Sr., F. Bertagna, G. Magri, M. Panarotto, R. Giubbini; Spedali Civili Brescia, Brescia, ITALY.

Aim: radioiodine therapy (I131) for differentiated thyroid cancer is generally a safe and efficient treatment, but has some potential side effects consequent to radioiodine. These potential adverse effects are well described in adults and little analyzed in pediatrics. Our aim was to analyze early and late adverse events of radioactive iodine-131 in pediatric patients. **Materials and methods:** all consecutive patients <18 years treated for pediatric differentiated thyroid cancer in our department in the period 1980-2015 were evaluated for early and late side effects of radioiodine therapy. Early side effects, which occur during or shortly after therapy, include gastrointestinal symptoms (nausea and emesis), radiation thyroiditis, sialadenitis/xerostomia, dry mouth and transient bone marrow suppression. Late complications include permanent salivary gland dysfunction, permanent bone marrow suppression, pulmonary fibrosis, secondary cancers and fertility problems. Statistical analysis was carried out with the Student's t test. P-Value of ≤ 0.05 was considered as statistically significant. **Results:** 105 patients (77 female, 28 male; median age 15 years, range 4-17 years) were treated with 131I for differentiated thyroid cancer in our department. Totally, they underwent 302 radioiodine treatments (overall 46092 mCi): 50 children underwent only one radiometabolic treatment for ablation of thyroid remnant. Median follow-up time was 150 months (range 8-348 months). Thirty-six patients (34%) had almost one early adverse event; 31 had nausea and/or emesis; 24 sialoadenitis/xerostomia, 20 thyroiditis, 15 dry mouth and 5 transient bone marrow suppression. All early side effects were correlated with the amount of radio-activities administrated in any single treatment ($p < 0.001$). Fourteen children (13%) developed ≥ 1 late complication: 2 permanent salivary gland dysfunction, 4 permanent bone marrow suppression, 5 pulmonary fibrosis, 4 secondary malignancies (2 breast cancer and 2 leukemia) and 5 fertility alterations. All late adverse events, except fertility alterations, were correlated with number of radiometabolic therapies and cumulative activities of 131I. Early and late adverse events were not correlated with sex, age and histotype. **Conclusions:** radioiodine therapy in pediatric is a safe and efficient treatment. The risk of developing some early and late side effects is not different than of adults. Early side effects are associated with the amount of administrated activities of any treatment, while the late effects are correlated with number of treatments and cumulative activities of radioiodine, except for fertility problems.

OP540

The influence of single dose recombinant human thyroid stimulating hormone on the efficacy of radioiodine therapy in patients with subclinical hyperthyroidism with low RAIU

S. Abdelrazek, M. Mojsak, P. Szumowski, J. Mysliwiec, A. Polak, M. Janica, K. Lomperta; Department of Nuclear Medicine, Medical University of Bialystok, BIALYSTOK, POLAND.

The aim of our study was to evaluate the influence of recombinant human thyroid-stimulating hormone (rhTSH) on the efficacy of radioiodine therapy in patients with subclinical hyperthyroidism (SHT) with low RAIU. **Materials and methods:** The study was performed on 40 patients with subclinical hyperthyroidism all with multinodular goitre (MNG) referred for radioiodine therapy (32 females and 8 males, aged 32-75 years). Qualification of these patients were based on: normal levels of serum fT3 and fT4, low levels of serum TSH (< 0.1 mU/L), and RAIU $< 15\%$. Thyroid volume ranged between 70-145ml. Malignant changes were excluded in all nodules by fine needle aspiration biopsy. All the patients had serum TSH levels < 0.1 mU/L and low RAIU (7-14%), 24 h after a diagnostic dose of I-131 (4 MBq). All the patients received a single intramuscular dose of 0.05 mg rhTSH (thyrogen). 24 h later diagnostic dose of ^{131}I was administered and thyroid scan with RAIU after 24 and 48 h was estimated. Therapeutic dose of I-131 was given on the third day of rhTSH administration. Serum levels of TSH, fT4 and fT3 were determined, 24 and 72 h after rhTSH administration and on the 3rd day after radioiodine therapy. The therapeutic activity of I-131 calculated by Marinelli's formula and

ranged between 280 and 600 MBq. The absorbed dose ranged between 150 and 220 Gy. Follow up control was done every 6 weeks. Thyroid ultrasound, and thyroid scan were done again after 6 and 12 months of radioiodine therapy. **Results:** A significant increase (3-11 fold) in 24 h RAIU was observed after rhTSH administration. The distribution of radioiodine was more homogeneous 48 h after rhTSH administration. After 12 months 91% of patient were in euthyroid state and 9% develop hypothyroidism. After 6 months the mean reduction in goitre volume was 30% and 45-55% after 12 months. The medium therapeutic activity of I-131 was 400 MBq. **Conclusions:** Pre-treatment with rhTSH reduce the therapeutic dose of I-131 by 50-58% without compromising the result of thyroid volume reduction. rhTSH makes radioiodine therapy more effective in the patients with subclinical hyperthyroidism with low RAIU.

OP541

Feasibility of thyroid uptake measurements with the CoTI device

E. J. Kranenborg, R. van der Boor, A. E. Gelderblom, K. A. J. van Gils, J. B. A. Habraken; St. Antonius Hospital, Nieuwegein, NETHERLANDS.

Introduction The CoTI (Collar Therapy Indicator) is a portable device for thyroid uptake measurements. It consists of two gamma detectors which are placed in a collar worn by the patient. This makes it a convenient device for thyroid measurements. However, it may be susceptible to errors due to patient movement or poor positioning. **Aim** The aim of this study is to assess the feasibility of performing thyroid uptake measurements using the CoTI, particularly regarding detector positioning. **Methods and materials** *Preliminary tests* To assess the influence of collar movement, we performed preliminary tests with 18 volunteers to determine the maximum shift in collar position due to movement or intra-operator variability in positioning the collar. We also determined the maximum shift from the anatomical position necessary to achieve the highest count rate in 23 patients scheduled for thyroid measurements. *Patient tests* Based on these maximum shifts, we measured the effect on the count rate in 25 patients scheduled for I-123 uptake measurements. We placed the collar at the anatomical position (baseline) and shifted it 2.0 cm right, 2.0 cm left, 2.0 cm caudal and 1.0 cm cranial. We compared the measured counts of the combined detectors to the baseline position. *Phantom tests* To determine the accuracy of the position of each detector in the collar we used an anthropomorphic thyroid phantom. We measured the count rate for each detector at 49 different positions and compared them to the baseline (midline of the collar at the centre of the phantom). **Results** Results are presented as a percentage of the baseline count rate. The patient tests show a decrease in average count rate in relation to the baseline at right lateral shift (90.6%), left lateral shift (91.8%) and cranial shift (77.0%). Caudal shift leads to an increase (122.1%). The phantom tests show an increase in count rate in relation to the baseline for each detector at medial shift, with a maximum score of 245%. Shifting the detector in lateral, caudal or cranial direction shows a decrease, with a minimum score of 21%. **Conclusion** The placement of the collar on the patient can easily vary and the detectors are generally not in the optimal position in the collar. Both aspects can lead to a difference in count rate, which linearly affects the calculated uptake. Therefore a more sophisticated collar or stringent procedures are necessary to accurately measure thyroid uptake using the CoTI.

1405 – Tuesday, October 18, 2016, 14:30 - 16:00, Hall 115

M2M/Do.MoRe - Featured: Radionuclide Therapy - Preclinical

OP542

Molecular Radiotherapy Leads to the Future

M. W. Konijnenberg; Erasmus MC, Nuclear Medicine, Rotterdam, NETHERLANDS.

OP543**Therapeutic Potential of ⁴⁷Sc in Comparison to ¹⁷⁷Lu and ⁹⁰Y: Preclinical Investigations**

K. Siwowska; Paul Scherrer Institute, Villigen, SWITZERLAND.

Aim: The concept of theragnostic application (PET/ β^- -therapy) with the matched pair of Sc-nuclides (⁴⁴Sc/⁴⁷Sc) was recently proposed and exemplified in our group. The aim of the present study was to evaluate ⁴⁷Sc ($T_{1/2} = 3.35$ d, $E_{\beta^-} = 162$ keV) for therapeutic purposes using a DOTA-folate conjugate and compare it to the effects obtained with the same compound labeled with ¹⁷⁷Lu and ⁹⁰Y. **Materials and methods:** Labeling of a DOTA-folate with ⁴⁷Sc, ¹⁷⁷Lu and ⁹⁰Y was performed at a specific activity of 10 MBq/nmol. ⁴⁷Sc-folate was compared with the ¹⁷⁷Lu- and ⁹⁰Y-labeled compounds *in vitro* using FR-positive IGROV-1 tumor cells. *In vivo* studies were performed with tumor-bearing mice for comparison of the anti-tumor effects obtained with each of the radiofolates applied at 10 MBq ⁴⁷Sc-folate, 10 MBq ¹⁷⁷Lu-folate and 5 MBq ⁹⁰Y-folate, respectively. The mean absorbed tumor and kidney doses were calculated based on biodistribution results, under the assumption that the tissue distribution would be equal for all radiofolates. **Results:** Radiolabeling of the folate conjugates was achieved with >96% radiochemical purity. *In vitro* cell uptake was FR-specific, proven by a reduced uptake (<1%) when cells were co-incubated with excess folic acid. The calculated tumor doses were determined as 17 Gy, 21 Gy and 21.5 Gy for mice treated with ⁴⁷Sc-folate, ¹⁷⁷Lu-folate and ⁹⁰Y-folate, respectively. *In vivo* experiments confirmed the dose-dependent effect, as the relative time which passed until the tumors reached a ten-fold increased size was determined to be 1.5 for ⁴⁷Sc-folate-treated mice, 1.8 for ¹⁷⁷Lu-folate-treated mice and 2.0 for ⁹⁰Y-folate-treated mice, compared to 1.0 for untreated controls. The average survival time of ⁴⁷Sc-folate-treated mice was significantly increased (33 days) as compared to the survival time of untreated controls (21 days). The average survival time for ¹⁷⁷Lu-folate and ⁹⁰Y-folate-treated mice was 43 and 41 days, respectively. Significant accumulation of all folates in the kidneys resulted in kidney doses of 18 Gy, 23 Gy and 22 Gy for ⁴⁷Sc-folate, ¹⁷⁷Lu-folate and ⁹⁰Y-folate, respectively, all below the critical limit of ~25 Gy. **Conclusion:** *In vitro* and *in vivo* studies confirmed a dose-dependent and FR-specific therapeutic efficacy of ⁴⁷Sc-folate. The low β^- -energy of ⁴⁷Sc is clearly preferred to the high-energy β^- -particles of ⁹⁰Y, which comprise a higher risk of undesired effects to normal tissue. The excellent decay characteristics of ⁴⁷Sc, together with the fact that a diagnostic match for PET exists, make ⁴⁷Sc highly attractive for clinical translation.

OP544**Role of ADAMTS2 and ADAMTS5 Genes in Radioiodine Induced Damage to the Salivary Glands of Rats: Genetic, Immunohistochemical and Histopathological Evaluations**M. SADIC¹, K. DEMIREL¹, S. O. HALACLI², E. KARAKOK³, G. KOCA¹, O. EKINCI³, K. DEMIRCAN⁴; ¹Ministry of Health Ankara Training and Research Hospital, ANKARA, TURKEY, ²Hacettepe University, School of Medicine, ANKARA, TURKEY, ³Gazi University, Faculty of Medicine, ANKARA, TURKEY, ⁴Turgut Ozal University, Faculty of Medicine, ANKARA, TURKEY.

Background: Aim of this study which is the first in this area was to determine the role of the ADAMTS2 and ADAMTS5 genes on parotid gland (PG) and submandibular gland (SMG) damage occurred after high dose RAI administration. **Methods:** Sixty four male Wistar albino rats (mean weight 285±55 gr, 6-8 months) were included and sacrificed as follows; Control (n=20): Group 1: 4th hour (n=6), : 24th hour (n=20), Group 3: 48th hour (n=6), Group 4: 7th day (n=6), Group 5: 30th day (n=6) after RAI administration. 3 mCi I-131 was administered to all rats except control group. According to the sacrifice, PG and SMG were removed

surgically. Biodistribution and histopathologic studies were performed on the removed SGs. Real time PCR and immunohistochemical analysis were applied to show mRNAs and protein expression levels of ADAMTS genes. Differences between groups were statistically evaluated. **Results:** In biodistribution studies, the highest values were observed in 4 hours in PG. In RAI treated groups, ADAMTS2 and ADAMTS5 gene expression was observed to increase while there is no any mRNA or protein expression in the control group. ADAMTS2 expression in Groups 2 and 3, ADAMTS5 expression in Groups 2 and 5 for SMG, ADAMTS2 expression in Groups 3 and 5, ADAMTS5 expression in Groups 2 and 4 for PG were statistically significant (Table). By means of immunohistochemistry analysis, the staining pattern in the extracellular source was also observed to in the overexpressed ADAMTS2 and ADAMTS5 groups. Nuclear coarsening and partial focal subnuclei vacuolization were determined in all RAI administered group by histopathologic examinations. **Conclusion:** An increase mRNA expression levels of ADAMTS2 and ADAMTS5 genes were detected in RAI administered groups. These results suggested that ADAMTS2 and ADAMTS5 genes might play role on radioiodine induced SGs changes. Further studies are needed to understand better the subpathways related to ADAMTS genes.

OP545**Localized irradiation of cell membrane by Auger electrons is cytotoxic through non-targeted effects involving p38 and JNK signaling pathways**S. Paillas^{1,2}, R. Ladjohounlou¹, C. Lozza¹, A. Pichard¹, V. Boudousq¹, M. Jarlier³, E. Deshayes¹, J. Sosabowski², T. Chardès¹, I. Navarro-Teulon¹, R. Mairs⁴, J. POUGET¹; ¹IRCM/INSERMU896, Montpellier, FRANCE, ²Barts Cancer Institute, Queen Mary University of London, London, UNITED KINGDOM, ³ICM, Montpellier, FRANCE, ⁴Institute of Cancer Sciences, University of Glasgow, Glasgow, UNITED KINGDOM.

Aims: We have investigated *in vitro* and *in vivo* the contribution of bystander effects to the efficacy of Auger electron emitter (¹²⁵I) labeled monoclonal antibodies (¹²⁵I-mAbs) targeting the cell membrane. **Materials and methods:** *In vitro*, colorectal HCT116 cells were exposed to increasing activities (0-4MBq/mL) of either non-internalizing anti-CEA, internalizing anti-HER1 or of the non-targeting PX ¹²⁵I-mAbs. Cells were also exposed up to 20 kBq/ml of 5-[(¹²⁵I)]jodo-2'-deoxyuridine (¹²⁵IuDR). Direct and bystander cytotoxic effects were measured using clonogenic assays and standard medium transfer protocol. DNA damage, lipid raft formation and activated signaling pathways were also measured. Activated signaling pathways were further investigated using protein arrays together with pharmacological inhibitors. The role of oxidative stress was investigated using N-Acetyl-L-Cystein (NAC) or dimethyl sulfoxide (DMSO), two radical scavengers. ¹²⁵I-radioimmunotherapy was carried out *in vivo* using mice bearing intraperitoneal tumors and the relationship between energy deposition in tumors using digital autoradiography and spatial distribution of 53BP1 foci was determined by immunofluorescence. **Results:** No cytotoxicity was observed either both donor or recipient cells after donor cells were treated with the ¹²⁵I-PX antibody. Bystander effects measured in recipient cells were associated with lipid raft formation in donor cells treated with anti-CEA or anti-HER1 ¹²⁵I-mAbs and their disruption with filipin or methyl- β -cyclodextrin (MBCD) significantly reduced the bystander response. Incubation of donor cells with either NAC or DMSO, increased the survival of donor and recipient cells indicating the involvement of oxidative stress in the observed bystander effects. We have identified that p38 and c-Jun N-terminal kinase (JNK) were the predominant proteins involved in lipid-raft activated signaling cascades and participated in subsequent cytotoxic effects of targeting ¹²⁵I-mAb in both donor and recipient cells. In addition, we have also shown that the bystander response induced by ¹²⁵I-mAbs against cell surface receptors was comparable to that obtained with ¹²⁵IuDR targeting the cell nucleus. *In vivo*, our results indicate DNA damage in mouse tumor xenograft sections beyond the expected Auger electron range suggesting the involvement of bystander effects also *in vivo*. Moreover, we found that the

statistical significance of tumor growth delay induced by ^{125}I -mAb was removed after inhibition of lipid raft formation. **Conclusion:** Our *in vitro* and *in vivo* results provide evidence that the cell membrane plays an essential role in the mediation of the bystander response induced by anti-CEA or anti-HER1 ^{125}I -mAb. p38 and JNK appear to be the main proteins responsible for cytotoxic effects measured in donor and recipient cells.

OP546

Modulation of glutathione synthesis for radio-sensitization of Breast Cancer Stem cells: a novel therapy concept

A. Morgenroth¹, T. Miran¹, N. Drude¹, A. T. Vogg¹, F. M. Mottaghy^{1,2},
¹University of Aachen, RWTH Aachen, Aachen, GERMANY, ²Maastricht University Medical Center, Department of Nuclear Medicine, Maastricht, NETHERLANDS.

The estrogen receptor, progesterone receptor and HER2neu negative breast cancer phenotype exhibits enhanced treatment unresponsiveness. These cells represent a cancer stem cell (CSC) population whose unique therapy resistance is attributed to reactive oxygen species (ROS) defense through up-regulation of glutathione (GSH) synthesis. Since efficiency of cancer therapies rely on generation of ROS and induction of oxidative stress, targeting of antioxidant system may impair ROS defense ability of CSC and thereby sensitize them to endogenous nanoirradiation. We evaluated therapeutic potential of I-125-ITdU for targeting of breast CSC after inhibition of ROS scavenging enzyme GSH synthase with Buthionine Sulfoximine (BSO). For CSCs isolation, MDA MB-231 cells were incubated with CD24 and CD44 MicroBeads. The CD Marker expression was investigated by FACS. Cells were incubated with 1.0 mM BSO for 2d under hypoxia and normoxia. The GSH and ROS were evaluated using Thiol Green dye and H₂DCFDA by FACS, respectively. Apoptotic cells were identified using PI by FACS and γ -H2AX staining by microscopy. For therapy study, BSO treated (5mmol/kg) and untreated SCID breast CSC xenografted mice received 3 injections of 5-7 MBq I-125-ITdU (6 h p.i. BSO, cycle per week). Therapy efficiency was monitored by FDG- μ PET. The purity of isolated CSC was more than 98%. BSO treatment of CSC yielded a decreased GSH and an increased ROS level. The modulation of GSH level affected the therapeutic efficiency of I-125-ITdU. In the therapy study, BSO pre-treated animals showed a significant reduction in tumor size and an improved survival as compared to the BSO-untreated control group. No radiotoxicity was detected in liver, spleen and small intestine. This is the first report to demonstrate that modulation of GSH increases radiosensitivity in highly resistant stem cells of breast cancer.

OP547

NeoBOMB1, a novel GRP analog, for theranostic use in oncology

S. U. Dalm¹, I. L. Bakker¹, E. de Blois¹, G. N. Doeswijk¹, F. Orlandi², D. Barbato², M. Tedesco², T. Maina³, B. A. Nock³, M. W. Konijnenberg¹, M. de Jong¹,
¹Erasmus MC, Rotterdam, NETHERLANDS, ²Advanced Accelerator Applications, Colleretto Giacosa, ITALY, ³INSRATES NCSR Demokritos, Athens, GREECE.

Background: Overexpression of the gastrin releasing peptide receptor (GRPR) has been reported on several major cancers, including prostate and breast cancers. Targeting this receptor with radiolabeled peptide analogs for imaging and therapy could have a significant impact on the staging and treatment of GRPR-expressing tumors. NeoBOMB1 is a novel DOTA-coupled peptide with high GRPR affinity and excellent *in vivo* stability. The aim of our preclinical study was to explore the theranostic use of ^{68}Ga -NeoBOMB1 and ^{177}Lu -NeoBOMB1 at two different specific activities, in order to find the peptide amount with the most optimal tumor to background ratios. Materials and methods: Biodistribution and imaging studies were performed in Balb c nu/nu mice

xenografted with the GRPR-expressing PC-3 cells. For the biodistribution studies animals were injected with either 13 MBq ^{68}Ga -NeoBOMB1 (in total 250 pmol peptide) or 1 MBq ^{177}Lu -NeoBOMB1 (in total either 200 pmol or 10 pmol peptide). At different time points post injection (p.i.) animals were euthanized, organs and tumors were excised and radioactivity uptake (%ID/g) was determined. Biodistribution data was used to determine pharmacokinetics, mouse dosimetry and predict patient dosimetry. In addition, PET/CT and SPECT/MRI was performed with ^{68}Ga -NeoBOMB1 and ^{177}Lu -NeoBOMB1, respectively. Results: Biodistribution studies with ^{68}Ga -NeoBOMB1 resulted in a tumor and pancreas uptake of 12.4 \pm 3.3 and 22.7 \pm 3.3 %ID/g at 2 h p.i., respectively, with clearance half-lives of 6.9 \pm 2.8 h and 12.9 \pm 4.0 h. With the ^{177}Lu -NeoBOMB1 the tumor uptake at 4 h p.i. was 17.9 \pm 3.3 and 11.6 \pm 1.3 %ID/g, leading to an absorbed tumoral dose of 570 and 435 mGy/MBq, for the 200 pmol and 10 pmol peptide dose, respectively, with clearance half-lives of 36 \pm 3 h and 29 \pm 3 h. Uptake in the GRPR-expressing pancreas was 19.8 \pm 6.9 and 105 \pm 13 %ID/g at 4 h p.i. for the 200 pmol and 10 pmol peptide dose of ^{177}Lu -NeoBOMB1, respectively, but with faster clearance half-lives than those from tumors. In mice the absorbed dose tumor/pancreas ratio increased with increasing peptide amount (from 0.2 to 2.2, with 10 pmol and 200 pmol, respectively). The uptake kinetics of ^{68}Ga -NeoBOMB1 provided good indications of doses achieved with ^{177}Lu -NeoBOMB1. Using the data to predict patient dosimetry we found a kidney, pancreas and liver exposure of 0.10, 0.65 and 0.06 mGy/MBq, respectively. Furthermore, imaging studies resulted in good tumor visualization. Conclusion: Our findings indicate that the GRPR-antagonist $^{68}\text{Ga}/^{177}\text{Lu}$ -NeoBOMB1 is a very promising theranostic pair with favorable biodistribution characteristics for nuclear imaging and therapy, especially with the higher peptide amount applied. Table:

OP548

Chimeric Version of the Anti-CD37 Antibody Radionuclide Conjugate Betalutin® (NNV009) elicits an Anti-Tumour Response in Non-Hodgkin Lymphoma and Chronic Lymphocytic Leukemia Models

H. Heyerdahl¹, A. O'Shea¹, K. B. Melhus¹, B. Eiriksdottir², A. H. V. Repetto-Llamazares¹, J. Dahle¹,
¹Nordic Nanovector ASA, Oslo, NORWAY, ²ArcticLAS ehf, Reykjavik, ICELAND.

Aim: The novel antibody-radionuclide-conjugate (ARC) ^{177}Lu -DOTA-lilotomab (^{177}Lu -DOTA-HH1; Betalutin®) is based on the murine anti-CD37 antibody lilotomab and is currently in a clinical phase 2 trial for treatment of non-Hodgkin Lymphoma (NHL). A chimeric version of the lilotomab antibody (NNV003) is currently under development and may have potential advantages over the murine antibody by reduced immunogenicity and immunotherapeutic effects of the naked antibody through ADCC induction. The objective of the current study was to investigate the immunological ADCC and CDC potency as well as the therapeutic potential and adverse effects of the naked and radiolabeled antibody in NHL and Chronic Lymphocytic Leukemia (CLL) models. **Materials and Methods:** ADCC and CDC assays were performed in four different NHL and CLL cell lines; DOHH-2 (transformed follicular lymphoma), REC-1 (mantle cell lymphoma), Ramos (Burkitt's lymphoma) and MEC-2 (CLL), using FcR γ 3a immortalized NK92 cells as effector cells. For *in vivo* studies, the NNV003 antibody was conjugated with p-SCN-Bn-DOTA prior to labelling with ^{177}Lu to make the ARC NNV009. Biodistribution was measured in mice with NHL (DOHH-2) and CLL (MEC-2) xenografts. Therapeutic and adverse effects of the naked antibody and ARC were investigated in mouse models bearing disseminated NHL and CLL human xenografts. Toxicity was additionally tested in immunocompetent Balb/c mice. **Results:** The NNV003 antibody elicited ADCC lysis in all four cell lines tested. Minimal CDC activation was observed. Biodistribution was relevant in both mouse models with specific tumour uptake. Survival was significantly extended in DOHH-2 xenograft-bearing RAG2 mice treated with NNV003 naked antibody (2-30 mg/kg) and ARC NNV009 (200-400

MBq/kg) compared to groups given NaCl and isotype control naked and ^{177}Lu -labeled antibody ($p < 0.0002$). Survival was extended in MEC-2 xenograft-bearing SCID mice treated with NNV009 (100 MBq/kg) compared to mice treated with NaCl, NNV003 (0.5 mg/kg) and isotype control (100 MBq/kg) ($p < 0.05$). Transient hematological effects were observed in the highest radioactivity groups in all studies, with reduction of white blood cell and platelet counts 1.5–3 weeks after injection, recovering after 5 weeks. Naked antibody NNV003 at doses ≤ 40 mg/kg was well tolerated with no observed adverse effects. **Conclusion:** *In vitro* and *in vivo* studies have shown that the chimeric naked antibody NNV003 elicits ADCC in NHL and CLL cell lines. Both NNV003 and ^{177}Lu -labeled antibody NNV009 showed statistically significant survival increases in mouse models with disseminated NHL and CLL xenografts. The results provide a good rationale for clinical testing in patients suffering from CD37-expressing B-cell malignancies.

1406 – Tuesday, October 18, 2016, 14:30 - 16:30, Hall 111

Teaching Session: TBA

OP549

TBA

1407 – Tuesday, October 18, 2016, 14:30 - 16:00, Hall 116

Clinical Oncology: Prostate PSMA

OP550

Australian multicentre evaluation of clinical management intent utilising Ga68-PSMA PET scans in patients with prostate cancer

P. Roach^{1,2}, R. Francis^{3,2,4}, L. Emmett⁵, E. Hsiao¹, A. Kneebone¹, G. Hruby¹, T. Eade¹, Q. Nguyen^{6,7}, B. Thompson^{7,6}, M. McCarthy⁸, C. Tang⁴, P. Brenner⁹, P. Stricker^{9,6}, A. Scott^{10,2}; ¹Royal North Shore Hospital, St Leonards, AUSTRALIA, ²Australasian Radiopharmaceutical Trials Network, Sydney, AUSTRALIA, ³University of Western Australia, Perth, AUSTRALIA, ⁴Sir Charles Gairdner Hospital, Perth, AUSTRALIA, ⁵St Vincent's Hospital, Sydney, AUSTRALIA, ⁶The Garvan Institute of Medical Research, Sydney, AUSTRALIA, ⁷Australian Prostate Cancer Research Centre – New South Wales (APCRC-NSW), Sydney, AUSTRALIA, ⁸Fiona Stanley Hospital, Perth, AUSTRALIA, ⁹St Vincent's Prostate Cancer Centre, Sydney, AUSTRALIA, ¹⁰Olivia Newton-John Cancer Research Institute, Melbourne, AUSTRALIA.

Aim: Conventional imaging has limitations in the accurate evaluation of Prostate cancer (PCa). Ga68-Prostate Specific Membrane Antigen (PSMA) PET scanning is a new imaging technique that has been shown to be more accurate than conventional imaging techniques in many patients. This Australian multicentre study sought to determine whether the findings of PSMA PET imaging impacts on planned clinical management. **Materials:** Four centres throughout Australia participated in this prospective study. Local institutional ethics approval was obtained at each site. Prior to undertaking Ga68-PSMA PET imaging, referring medical specialists were required to complete a survey detailing relevant demographic and clinical data as well as the proposed management plan. Once the referring specialist was provided with the Ga68-PSMA PET scan results, they were asked to complete a follow up survey, primarily seeking to determine whether their management plan would change based on the PSMA PET scan finding. **Results:** For the period between August 2015 and March 2016, 285 patients with PCa had pre- and post-Ga68 PSMA management plans completed by their referring specialists. Scans were performed for primary staging in 22% patients and for a rising PSA following surgery and/or radiotherapy in 78% of patients. On the pre-

PSMA management plan, the most common treatment intent was for targeted or localised treatment (66%), followed by systemic therapy (18%) and surveillance (16%). On the post PSMA survey the clinicians indicated that the PSMA scan lead to a change in planned management in 55% of patients. The PSMA scan revealed disease that was not previously suspected in the prostate bed (30% of patients), locoregional lymph nodes (36% of patients) and distant disease (16% of patients). In those in whom there was no management change, the survey indicated this was most often due to no additional information being provided from the PSMA scan. **Conclusions:** These preliminary results indicate that PSMA PET scans detect previously unsuspected disease and change planned clinical management in a high proportion of patients with prostate cancer. This demonstrates the potential clinical value of PSMA PET in treatment planning in this patient group.

OP551

Staging primary prostate cancer with ^{68}Ga -PSMA^{HBED-CC} / [^{18}F]Fluorocholine-PET/MRI

M. Hartenbach¹, P. Baltzer¹, S. Hartenbach², M. Susani³, C. Seitz⁴, L. Kenner³, G. Kramer⁴, A. R. Haug¹, W. Wadsak¹, M. Mitterhauser¹, A. Ponholzer⁵, M. Lamche⁵, S. Shariat⁴, M. Hacker¹; ¹Medical University of Vienna, Dep. of biomed. imaging and image guided therapy, Vienna, AUSTRIA, ²German Armed Forces Hospital, Institute of Pathology, Ulm, GERMANY, ³Medical University of Vienna, Institute of Pathology, Vienna, AUSTRIA, ⁴Medical University of Vienna, Dep. of Urology, Vienna, AUSTRIA, ⁵Hospital St. John of God, Urology, Vienna, AUSTRIA.

Introduction/Objectives Staging primary prostate cancer lacks of accuracy and reliability although invasive methods are used for clinical staging nomograms. The aim of this study was to determine the clinical impact and staging performance of non-invasive hybrid multiparametric ^{68}Ga -PSMA^{HBED-CC} / [^{18}F]Fluorocholine-PET/MRI (dtPET/MRI) in patients with biopsy proven prostate cancer, scheduled for radical prostatectomy. **Methods** 80 patients, scheduled for radical prostatectomy, underwent dtPET/MRI for primary staging. cTNM-staging was performed prospectively according to UICC 2009. dtPET/MRI impact on guideline-conform treatment decision was corrected, when conventional, guideline-conform imaging modalities delivered equal information (CT/bone scan). Clinical pre-therapeutic TN-prediction was performed using the MSKCC-prediction nomogram. dtPET/MRI and prediction nomogram were correlated with post-surgery results. dtPET/MRI M1b-staging was verified by histology or follow-up exams. '2x2' tables were evaluated. Two-tailed Fisher Exact was used for level of significance. **Results** In 56 of 80 patients (70%), radical prostatectomy was still chosen as primary treatment, but 5 had additional radiotherapy (RT)/anti-hormonal therapy (aHT). 5 had primary RT due to T4-status, 2 RT + aHT due to N1-status, 9 chose active surveillance (minimal tumor burden), 4 palliative TUR-P+aHT/chemotherapy (cT3b/T4, N+/M+) and 6 primary aHT/chemotherapy. Initial mean PSA was 11.88ng/ml (n=80). Treatment changed in 28/80 patients (35%) due to imaging, and in 24/80 patients (30%) due to dtPET/MRI. dtPET/MRI T2 vs. T3a/b staging had a sens./spec/acc./npv/ppv/rel.risk of: 84%/72%/77%/67%/88%/5.3 ($P < 0.001$). MSKCC nomogram: 67%/44%/54%/48%/63%/1.3 ($P = 0.54$). N-staging dtPET/MRI sens./spec/acc./npv/ppv/rel.risk: 67%/97%/91%/86%/92%/10.3 ($P < 0.001$) MSKCC nomogram: 25%/100%/83%/100%/82%/5.7 ($P = 0.044$). dtPET/MRI M1b-status sens./spec/acc./npv/ppv were 100% respectively ($P < 0.001$; $n = 32$). **Conclusions** Hybrid multiparametric dtPET/MRI prior primary treatment of prostate cancer patients led to a remarkable change in the therapeutic management in this dual center evaluation. Furthermore, non-invasive dtPET/MRI was more reliable than common used invasive staging nomograms and provided additional highly accurate information on patient's M-status.

OP552**The clinical impact of additional late PET/CT-imaging with ⁶⁸Ga-PSMA-11 (HBED-CC) in the diagnosis of recurrent prostate cancer**

A. Afshar-Oromieh¹, L. Sattler¹, C. Kratochwil¹, F. Giesel¹, K. Kopka², U. Haberkorn¹; ¹University Hospital of Heidelberg, Heidelberg, GERMANY, ²Div. of Radiopharmaceutical Chemistry, German Cancer Research Center, Heidelberg, Germany, Heidelberg, GERMANY.

Aim: PET/CT with the small molecule inhibitor of the prostate-specific membrane antigen ⁶⁸Ga-PSMA-11 is regarded as a significant step forward in the diagnosis of prostate cancer (PCa). While ⁶⁸Ga-PSMA-11 PET/CT is routinely performed at 1h p.i., it is known that later images show most tumor lesions with higher tracer uptake and contrast. The aim of this retrospective evaluation was to investigate the clinical impact of late PET-imaging with ⁶⁸Ga-PSMA-11. **Methods:** 117 patients with recurrent PCa (median PSA 2.6 ng/ml) who were referred to ⁶⁸Ga-PSMA-11 PET/CT were included in this evaluation. All of them were scanned 1h p.i. and a 3h p.i. in order to increase the probability of tumor detection or to clarify unclear findings. Both scans were analyzed with regard to tumor detection. Quantitative assessment of tracer uptake (SUVmax) of 222 tumor lesions in 83 patients was performed in both scans. **Results:** In 84 of 117 patients (71.8%), at least one tumor suspicious lesion was detected in, both, early and late scans. 7 of 117 patients (6%) showed each one suspicious finding in early scans which, however, could not be confirmed as PCa lesions in late scans[AA1]. 5 patients who showed no suspicious findings in early scans presented with one PCa lesion in late scans. Overall, 18 of 222 lesions (8.1%) in 14 of 83 (16.9%) different patients were visible in late scans only. Amongst them, local relapse lesions demonstrated the highest rate: 5 of overall 15 local relapses (33.3%) were visible in late images only. 73.9% of all tumor lesions presented with significantly higher uptake in late images whereas 15.3% of them presented with significantly lower uptake in late images. **Conclusion:** ⁶⁸Ga-PSMA-11 PET/CT at 3h p.i. is a powerful method to clarify unclear findings in early images and to find additional lesions in patients with PCa.

OP553**⁶⁸Ga-PSMA PET/CT in Staging and Restaging of prostate Cancer Patients: Comparative Study with ¹⁸F-Choline PET/CT**

W. Langsteger¹, L. Imamovic¹, H. Geinitz², C. Schiller¹, F. Moinfar³, A. Rezaee¹, L. Pallwein-Prettner⁴, W. Loidl⁵, M. Beheshti¹; ¹PET-CT Center Linz, St. Vincent's Hospital, Linz, AUSTRIA, ²Department of Radiation Oncology, St. Vincent's Hospital, Linz, AUSTRIA, ³Department of Clinical Pathology, St. Vincent's Hospital, Linz, AUSTRIA, ⁴Department of Radiology, St. Vincent's Hospital, Linz, AUSTRIA, ⁵Prostate Cancer Center Linz, Department of Urology, St. Vincent's Hospital, Linz, AUSTRIA.

Aim ¹¹C- and ¹⁸F-choline PET/CT have been established in the assessment of prostate cancer (PCa) patients. However, it suffers to differentiate malignant vs benign prostate hyperplasia and detect small lesions. Recently, ⁶⁸Ga-PSMA (PSMA) PET/CT was introduced as promising imaging in assessment of PCa. This study was designed for comparison of detection rate between PSMA and ¹⁸F-fluoromethylcholine (FCH) PET/CT scan in staging and recurrent Pca patients. **Material & Methods** In this prospective study 22 consecutive PCa patients (mean age 68±7) underwent both PSMA and FCH PET/CT with a maximum interval of 4 weeks without any treatment in between. Patients with systemic therapy and known second cancer were excluded. Pathologic findings in each imaging modalities have to be clarified histopathologically or by conventional imaging modalities and/or clinical follow-up. **Results Staging:** 10 histopathologically verified high-risk PCa patients were examined. The mean of PSA was 32.2 ±26.4 ng/ml (range: 1.29 - 61.33). Both imaging modalities were able to detect the index

lesion in the prostate gland. Overall, a total number of 25 and 20 positive lymph nodes (LN) were detected on PSMA PET/CT and FCH PET/CT, respectively. Malignant LN showed significantly higher uptake on PSMA-comparing FCH PET/CT [mean SUVmax: PSMA PET/CT: 12.8 (range: 2.8-34); FCH PET/CT: 6.6 (range: 2.3-12.3)]. Bone metastases (BM) were detected in 3 patients by FCH PET/CT but PSMA PET/CT was negative in one patient with BM in the pelvic skeleton. **Restaging:** 12 patients with biochemical recurrence were included in this study. The mean of PSA was 7.3 ng/ml (range: 0.07 - 42.02). Local recurrences (LR) with pathologically increased tracer uptake were detected in 2 patients on both imaging modalities; However, LR show markedly higher uptake on PSMA PET/CT (SUVmax: PSMA: 12.4; FCH: 4.9). In addition, PSMA PET/CT was able to detect higher number of metastatic LN compared with FCH PET/CT (7 vs 6) with significantly better tumor to background ratio (SUVmax 8.7 on PSMA vs 4.45 on FCH). Both imaging modalities were able to detect 5 BM. One false positive bone lesion was detected on PSMA PET/CT. **Conclusion** PSMA PET/CT reveals a more promising role in staging and re-staging of prostate cancer patients even with low PSA level. Markedly higher tumor to background contrast is seen on PSMA PET/CT which allows higher detection rate especially in the small lesions. However, the value of this modality in the assessment of bone metastases should be further evaluated in future studies.

OP554**Probability of positive ⁶⁸Ga-PSMA PET/CT as a function of serum PSA: an optimal PSA cut-off in patients with biochemical recurrence after radical prostatectomy?**

L. Tosco^{1,2}, O. Gheysens^{3,1}, W. Everaerts^{2,4}, M. Albersen^{2,4}, L. Cromphout², C. M. Deroose^{3,1}, K. Van Laere^{3,1}, S. Joniau^{2,4}, K. E. Goffin^{3,1}; ¹Department of Imaging and Pathology, KU Leuven, Leuven, BELGIUM, ²Urology, UZ Leuven, Leuven, BELGIUM, ³Nuclear Medicine, UZ Leuven, Leuven, BELGIUM, ⁴Department of Development and Regeneration, KU Leuven, Leuven, BELGIUM.

Introduction: After radical prostatectomy (RP), 20-30% of patients experience biochemical recurrence (serum PSA increase). ⁶⁸Ga-PSMA PET/CT is useful to detect locoregional and distant recurrences of prostate cancer, with an increasing detection rate depending on the PSA level. In this study, we investigated the relationship between ⁶⁸Ga-PSMA PET/CT positivity and PSA level in depth to determine an optimal PSA cut-off value to guide the indication for ⁶⁸Ga-PSMA PET/CT imaging after RP. **Materials and methods:** We retrospectively evaluated all consecutive ⁶⁸Ga-PSMA PET/CT scans (n=129) in patients with biochemical recurrence after RP between January 2015 and April 2016. A ⁶⁸Ga-PSMA PET/CT scan was considered positive when there was focal uptake above background not corresponding to physiologic uptake. To evaluate the effect of PSA on the positivity of the ⁶⁸Ga-PSMA PET/CT, we performed a logistic regression analysis. A ROC curve analysis was applied to determine an optimal PSA cut-off value. **Results:** The median PSA value was 1.16 ng/ml (range 0.02-56.2). The probability of a positive ⁶⁸Ga-PSMA PET/CT scan in function of PSA values followed a sigmoidal curve on a logarithmic PSA scale, and varied from 41% at a PSA value of 0.02 ng/ml, 50% at 0.58 ng/ml, 75% at 2.45 ng/ml to up to 100% at PSA values above 10 ng/ml. The odds ratio for PSMA PET/CT positivity per logarithmic unitary increase in PSA level was 1.82 (95% confidence interval (CI): 1.29-2.60). The area under the ROC curve for PSA was 0.78 (95% CI 0.70-0.85). A PSA value of 0.38 ng/ml was identified as the optimal cut-off for maximal combined sensitivity/specificity to have PSMA PET/CT positivity and therefore a clinically helpful scan (sensitivity 85%, specificity 60%). **Conclusion:** The probability of a positive ⁶⁸Ga-PSMA PET/CT scan in patients with biochemical recurrence after RP increases with PSA value in a log-sigmoidal fashion. Our study showed that a PSA value of 0.38 ng/ml can be regarded an optimal threshold for ⁶⁸Ga-PSMA PET/CT positivity. However, even at the lowest PSA values, the calculated probability of a positive scan was still above 40%.

OP555**68Ga-PSMA PET/CT in Preoperative Staging of Intermediate and High Risk Prostate Cancer Patients**

C. Schiller¹, M. Beheshti¹, H. Geinitz², B. Aschacher², F. Moinfar³, G. Broinger³, L. Pallwein-Pretner⁴, W. Loidl⁵, W. Langsteiger¹; ¹PET-CT Center Linz, St. Vincent's Hospital, Linz, AUSTRIA, ²Department of Radiation Oncology, St. Vincent's Hospital, Linz, AUSTRIA, ³Department of Clinical Pathology, St. Vincent's Hospital, Linz, AUSTRIA, ⁴Department of Radiology, St. Vincent's Hospital, Linz, AUSTRIA, ⁵Prostate Cancer Center Linz, Department of Urology, St. Vincent's Hospital, Linz, AUSTRIA.

Aim 68Ga-PSMA (PSMA) PET/CT is introduced as new promising imaging in assessment of prostate cancer (PCa). This study assesses the impact of PSMA PET/CT in preoperative staging of intermediate and high risk Pca patients. **Material & Methods** Sixty-one histopathologically proven consecutive intermediate risk (5) and high risk (56) PCa patients (mean age 69 ± 8) who underwent PSMA PET/CT for preoperative staging, were included in this study. Patients with previous hormone and/or radiotherapy and known second cancer were excluded. PET/CT imaging was performed 60 min. after intravenous injection of 140 MBq Glu-NH-CO-NH-Lys-(Ahx)-[68Ga(HBED-CC)] (68Ga-PSMA) with 3min/bed position acquisition time. Pathologic findings in each imaging modalities have to be clarified histopathologically or by other imaging modalities and/or clinical follow-up. **Results** Patients had a mean PSA level of 27.2 ± 38.4 ng/ml (range: 0.78 - 224.7 ng/ml) and median Gleason score of 8. At least one malignant lesion was detected in the prostate gland in all patients. PSMA PET/CT detected lymph node metastases in 18 patients, bone metastases in 12 patients and both bone and lymph node metastases in 6 patients. All extraglandular metastases were detected in high risk patients while none of intermediate risk patients showed lymph nodes or bone metastases. No significant difference in mean PSA value was found in patients with lymph nodes (44.9 ± 55.8) and bone metastases (52.6 ± 69.3). PSMA PET/CT changed patients' management in 20 % (12/61) of high risk PCa patients. **Conclusion** PSMA PET/CT showed a promising role in staging of high risk prostate cancer patients. It was well able to detect lymph nodes as well as bone metastases and changed the patients' management in 20 % of the cases.

OP556**Intra-individual comparison of the PSMA-ligand ^{99m}Tc-MIP-1427 with ^{99m}Tc-MDP bone scan in patients with osseous metastasized prostate cancer**

H. Rathke¹, F. L. Giesel¹, A. Afshar-Oromieh¹, S. Haufe¹, W. Mier¹, J. W. Babich², U. Haberkorn¹, C. Kratochwil¹; ¹University Hospital Heidelberg, Heidelberg, GERMANY, ²Division of Radiopharmaceutical Sciences, Department of Radiology, Weill Cornell Medicine, New York, NY, UNITED STATES.

Purpose: To evaluate the diagnostic potential of the PSMA-targeting tracer ^{99m}Tc-MIP1427 in comparison to conventional bone scan with ^{99m}Tc-MDP in patients with known osseous metastasized prostate cancer using identical imaging equipment/protocol. **Methods:** In this ongoing evaluation patients with known metastatic disease were staged with both, conventional bone scan and PSMA-scintigraphy, within a time-frame of <10days. Until know, n=20 patients were evaluated with a blind-read by two experts in nuclear medicine. Imaging included planar whole-body scans and two bed positions SPECT or SPECT/CT 3h after injection of either 500-750 MBq ^{99m}Tc-MIP1427 or 600-750 MBq ^{99m}Tc-MDP. Lesions were scored: typical tumor / equivocal / benign lesion / normal, within a standard reporting schema divided into defined anatomical regions. **Results:** One patient had a PSMA-negativ tumor phenotyp. In one patient the PSMA-ligand demonstrated only faint tumor uptake but,

nevertheless, was diagnosed identical to the high uptake bone scan. 5 patients demonstrated equal findings in both examinations. 5 patients presented with additional visceral metastases in PSMA-imaging, which were predictably not diagnosed with conventional bone scan. However, SPECT/CT was required to distinguish between soft tissue uptake and overlapping bone. 4 patients had superscan character in bone scan, in contrast extend of red marrow involvement was evaluable more detailed by PSMA-imaging. In two patients PSMA-scan found tumor-typical lesions in more regions than MDP. In the rest of the patients identical pathological findings were reported with both tracers, however with bone scan more of the lesions were scored equivocal or presumably benign while PSMA more often resulted in tumor typical appearance. **Conclusion:** In the intra-individual analysis between the ^{99m}Tc-labeled PSMA-ligand and conventional bone scan the directly tumor targeting PSMA-tracer demonstrated clearly superior in comparison to bone scan which is based on secondary reactions of the tumor stroma environment. However, SPECT or SPECT/CT is often pivotal to differentiate between bone metastases and extra-osseous tumor lesions. Rare cases of PSMA-negative tumor phenotypes remain limitations.

OP557**Safety Evaluation and Cardiovascular Responses of the ⁶⁸Ga-PSMA Ligand used for PET/CT Imaging in Patients with Prostate Cancer in a Prospective, Multicenter Trial**

J. B. Nielsen, Jr.^{1,2}, H. D. Zacho^{1,2}, U. Haberkorn³, L. J. Petersen^{1,2}; ¹Dept. of Nuclear Medicine, Aalborg University Hospital, Aalborg, DENMARK, ²Dept. of Clinical Medicine, Aalborg University, Aalborg, DENMARK, ³Dept. of Nuclear Medicine, University Hospital of Heidelberg, Heidelberg, GERMANY.

Aim: Safety reviews of non-marketed drugs are mandatory for obtaining regulatory approval for clinical or experimental use in many countries. Often safety reporting is scarcely reported in imaging trials, largely due to retrospective data collection. The aim of this study was to evaluate the safety profile and cardiovascular response of the ⁶⁸Ga-PSMA ligand used for PET/CT imaging in prospective clinical trials. **Materials and Methods:** A total of 77 patients with newly-diagnosed or recurrent prostate cancer participated in two prospective trials. Safety reporting was identical in the two trials. Patients were actively asked to report any AE during the ⁶⁸Ga-PSMA administration and until the end of the day of the PET/CT scan. Any AE was classified as mild, moderate or severe by the patients and categorized by Common Terminology Criteria for Adverse Events (CTCEA) v4.0 by the physician. Blood pressure (BP) and heart rate (HR) were measured prior to injection (baseline), immediately after the tracer injection, and at 1, 10 and 60 min post-injection (p.i.). A final assessment was made after the PET/CT scan. The definitions of hemodynamic adverse events were as defined: Bradycardia (HR < 50 beats per minute), tachycardia (HR > 100 beats per minute), hypertension (systolic BP > 180 mmHg) or hypotension (systolic BP < 100 mmHg). **Results:** There was no reported AE. Mean systolic BP was 149 mmHg at baseline, and 145, 145, 139, 147 and 150 mmHg at injection, 1, 10, 60 minutes p.i. and after the PET/CT scan, respectively. There was no significant change in BP ($p=0.74$, ANOVA). Additionally, mean HR was 67 beats per minute at baseline, and 65, 62, 64, 62 and 62 beats per minute at injection, 1, 10, 60 minutes p.i. and after the PET/CT scan, respectively. There was no significant changes in mean heart rate ($p=0.78$). No patients developed de novo hypertension, hypotension, bradycardia, or tachycardia. Five patients presented with hypertension at baseline, but did not increase their systolic BP during/after the scan. Six patients showed bradycardia at baseline, none of these patients showed further decrease in HR p.i. **Conclusion:** ⁶⁸Ga-PSMA PET/CT is very well tolerated. None of the patients experienced any AE and there were no changes in blood pressure or heart rate. We conclude that ⁶⁸Ga-PSMA is safe for human application.

1408 – Tuesday, October 18, 2016, 14:30 - 16:00, Hall 212

Cardiovascular System: Myocardial Perfusion - CZT

OP558

First Validation of Myocardial Flow Reserve (MFR) by Dynamic SPECT Acquisitions using CZT camera in Comparison with O¹⁵-water PET in patients with Stable Angina. Preliminary Results of Waterday Study

D. Agostini¹, V. Roule¹, C. Nganoa¹, J. Wain-Hobson¹, D. Peyronnet¹, M. Maguet¹, R. Baavour², N. Roth², F. Beygui¹, A. Manrique¹; ¹CHU Caen, Caen, FRANCE, ²Spectrum Dynamics Medical, Caesara, ISRAEL.

Introduction. Quantification of myocardial blood flow has previously demonstrated diagnostic incremental value in patients with CAD using PET imaging. The advent of novel CZT camera has opened new perspectives for perfusion quantification using dynamic SPECT acquisitions. We appraised the feasibility of myocardial flow reserve (MFR) estimation using CZT camera in patients with stable angina and its correlation to MFR as measured using O¹⁵-water PET data. **Materials and methods.** 16 patients (12 M, 4 F; 66± 7 yo) with stable CAD (intermediate risk factors with angina 9/16 pts) and positive ischemia test (10/16 pts) were prospectively included during the angiographic procedure (clinicaltrials.gov: NTC 02278497). 6-min dynamic SPECT acquisitions using an injector to deliver a bolus injection of ^{99m}Tc-sestamibi [(3 MBq/kg at rest and 9 MBq/kg after regadenoson (400 µg,IV))] were performed using a CZT camera (D-SPECT, Spectrum Dynamics, Israel). The whole procedure lasted for 60 min for a patient in a supine position. The same procedure was done for O¹⁵-water PET within 2 weeks. For SPECT, reconstructed frames were automatically segmented to extract the vascular input function and the myocardial uptake curve. One-compartment kinetic modeling was used to estimate global uptake values, and then MBF was derived using Leppo correction. MBF at rest and stress were assessed and then MFR as a ratio of stress MBF/rest MBF. For PET, parametric MBF images were generated and analyzed quantitatively using Corridor 4DM, INVIA (Ann Arbor,USA). An ischemia by PET and SPECT was considered present if MFR was lower than 2. **Results.** Rest vs stress injected activity was 310 ±67 vs 817 ±166 MBq, respectively; P<0.05. The total injected dose was 1127±228 MBq. Global stress and rest MBF by SPECT correlated well with those measured by PET [DSPECT(MBF) = 0.078 + 0.74 x PET(MBF); r²=0.84; P= 10⁻⁴]. Stress MBF with SPECT was significantly lower (1.99± 0.66) than that with PET (2.51± 0.87 ml/min/g; P= 0.0011). Rest MBF with SPECT was significantly lower (0.706± 0.27) than that with PET (0.926± 0.22 ml/min/g; P= 0.002). However, MFR with SPECT was slightly higher (3.10± 0.74) than that with PET (2.91± 0.88; P= 0.05). **Conclusion.** SPECT estimations of MBF and MFR using dynamic CZT camera acquisitions appear to correlate well with O¹⁵-water PET measurements in patients with stable CAD.

OP559

Assessment of Myocardial Flow Reserve (MFR) by Dynamic SPECT using CZT camera and Comparison with invasive Fractional Flow Reserve (FFR) Measurements in Patients with Stable Angina. Preliminary Results of Waterday Study

D. Agostini¹, V. Roule¹, C. Nganoa¹, J. Vigne¹, T. Salomon¹, J. Wain-Hobson¹, M. Maguet¹, R. Baavour², N. Roth², F. Beygui¹, A. Manrique¹; ¹CHU Caen, Caen, FRANCE, ²Spectrum Dynamics Medical, Caesara, ISRAEL.

Introduction. Quantification of myocardial blood flow has previously demonstrated diagnostic incremental value in patients with CAD using

PET imaging. The advent of novel CZT camera has opened new perspectives for perfusion quantification using dynamic SPECT acquisitions. We appraised the feasibility of MFR estimation using a CZT camera in patients with stable angina and its pertinence with respect to angiographic and FFR data. **Materials and methods.** 19 patients (15 M, 4 F; 66± 8 yo) with stable CAD (intermediate risk factors and angina 9/19 pts) and positive ischemia test (13/19 pts) were prospectively included during the angiographic procedure (clinicaltrials.gov: NTC 02278497). 6-min dynamic SPECT acquisition using a contrast injector to deliver a bolus injection of ^{99m}Tc-sestamibi (3 MBq/kg at rest and 9 MBq/kg after regadenoson 400 µg, IV) were performed using a CZT camera (D-SPECT, Spectrum Dynamics, Israel). The whole procedure lasted for 60 min for a patient in supine position. Reconstructed frames were automatically segmented to extract the vascular input function and the myocardial uptake curve. One-compartment kinetic modeling was used to estimate global uptake values, and then MBF was derived using the Leppo correction. Global stress and rest MBF were assessed and then MFR as the ratio of stress MBF/rest MBF was done. All patients underwent 3 FFR measurements (LAD+CX+RCA) during the angiography. A stenosis was considered obstructive if greater than 50% and an FFR abnormal if ≤ 0.8. An ischemia by SPECT was considered present if MFR was lower than 2. **Results.** Rest vs stress injected activity was 310 ±67 vs 817 ±166 MBq, respectively; P<0.05. The total injected dose was 1127±228 MBq. Global stress MBF (1.99± 0.66 ml/min/g) was significantly higher than rest MBF (0.706± 0.27, P= 0.002). Pts with FFR≤ 0.8 showed a trend of decreasing stress MBF (1.64± 0.78 ml/min/g) vs pts with FFR> 0.8 (stress MBF= 1.99± 0.76 ml/min/g; P= 0.05). In pts with FFR ≤ 0.8: MFR tended to drop to 2.22± 1.31 when compared with pts FFR> 0.8: MFR was 3.10± 0.74; P= 0.05. With the cutoff of 2, the sensitivity, specificity and accuracy of MFR were, respectively, 71%, 93% and 89.5% for the detection of abnormal FFR. The total (rest+stress) effective dose was 8.92±1.81 mSv. **Conclusion.** Dynamic SPECT estimations of global stress MBF and MFR using CZT camera appear feasible, reliable and correlate well with invasive angiographic findings as FFR measurements in patients with stable CAD.

OP560

High diagnostic performances of 82Rubidium PET as compared to 99mTechnetium MIBI with CZT gamma cameras for detection of coronary artery disease in women and overweight people

F. Hyafil¹, R. Chequer¹, E. Sorbets², C. Estellat³, F. Rouzet¹, H. Regaieg¹, S. Leygnac¹, M. Milliner¹, R. Ben Azzouna¹, L. Imbert⁴, P. Marie⁴, D. Le Guludec¹; ¹Department of Nuclear Medicine, Bichat Hospital, AP-HP, PARIS, FRANCE, ²Department of Cardiology, Avicennes Hospital, AP-HP, Bobigny, FRANCE, ³Unité de Recherche Clinique, Bichat Hospital, AP-HP, PARIS, FRANCE, ⁴Department of Nuclear Medicine, Brabois Hospital, Vandoeuvre-les-Nancy, FRANCE.

Background. In obese patients and women, most non-invasive tests offer poor diagnostic performance for the detection of coronary artery disease (CAD). CZT gamma cameras owing to their cardiac-centred design and ⁸²Rubidium(Rb)-PET thanks to accurate attenuation correction might prove particularly interesting in this population. **Purpose.** The objectives of this study were to compare the diagnostic performance and associated radiation exposure of ⁸²Rb-PET-MPS and ^{99m}Tc-MIBI-MPS with CZT gamma cameras for the detection of CAD in women and overweight people. **Methods.** Men with BMI ≥ 25 and women referred for MPS with a pre-test intermediate prevalence of CAD were considered for inclusion. All patients underwent a gated MPS with ^{99m}Tc-MIBI using CZT cameras in association to the best stress test feasible (exercise and combined tests were prioritized) and a gated MPS with ⁸²Rb-PET and pharmacological stress using dipyridamole. Patients with at least one MPS considered as positive were referred for coronary angiography (CA). Patients were classified as positive for myocardial ischemia in case of significant stenosis

on CA or, in absence of CA, occurrence of cardiovascular event during the following year. After exclusion of 17 patients with missing information, diagnostic performance of each MPS were compared in the remaining 294 patients using the Mc Nemar test. Effective doses related to the injection of each radiotracer and CT acquisitions were calculated using the recommendations of ICRP. **Results.** A total of 311 patients (143 women) with mean BMI of 31.8 ± 6.5 were included in the study. Three patients had a MPS with ^{82}Rb -PET-CT not interpretable and were excluded from the analysis. Sixty CA were performed and 35 showed significant stenosis. CA could not be performed in 12 patients with at least one positive MPS and 2 patients were lost to follow-up. In the remaining 294 patients, sensitivity for the detection of CAD was significantly higher with ^{82}Rb -PET-MPS than with $^{99\text{m}}\text{Tc}$ -MIBI-MPS (83.3 [95% CI: 71.1; 95.5] vs. 55.5 [39.3; 71.7], respectively; $p = 0.02$), whereas the specificity was equally high for both tests (93.4 [90.4; 96.4] vs. 95.7 [93.2; 98.2], respectively; $p = 0.22$). Mean total effective dose per patient for MPS was significantly lower with ^{82}Rb -PET-CT as compared to $^{99\text{m}}\text{Tc}$ -MIBI-scintigraphy with CZT cameras (4.1 ± 1.4 vs. 10.0 ± 3.3 mSv; $p < 0.05$). **Conclusions.** In women and overweight patients, ^{82}Rb -PET-MPS offers higher diagnostic performances and lower radiation exposure for the detection of CAD as compared with $^{99\text{m}}\text{Tc}$ -MIBI-MPS using CZT cameras.

OP561

Comparison of myocardial perfusion scintigraphy (MPS) between CZT detector cardiac gamma camera and conventional dual head gamma camera

S. S. SINGH; Narayana Hrudalaya, BANGALORE, INDIA.

INTRODUCTION: SPECT MPI is a widely used non-invasive method for the detection of suspected obstructive coronary artery disease (CAD). Conventional SPECT uses Thallium doped Sodium Iodide i.e. NaI(Tl) crystals for myocardial perfusion imaging in which there is indirect conversion of the gamma rays to an image after passing through number of intermediate steps. The new cardiac camera with Cadmium Zinc Telluride (CZT) semiconductor crystals, converts radiation to electronic signals directly without intermediate conversion steps, resulting in improved sensitivity and spatial resolution. **AIM OF THE STUDY:** Comparison of Myocardial perfusion scintigraphy between new CZT detector cardiac camera and conventional dual head gamma camera. **MATERIALS AND METHODS:** This prospective study involved 52 patients with significant coronary artery disease (mean age group of 60 ± 15 years, 50males and 2females). Clinical history and investigation details comprising of symptoms, ECG, coronary angiogram details were collected. Patients had undergone $^{99\text{m}}\text{Tc}$ -sestamibi 1 day stress rest protocol/ rest stress protocol and stress and rest image acquisition was performed on CZT dedicated cardiac gamma camera and conventional dual head NaI(Tl) within 10 minutes of each other as per ASNC guidelines. Image processing and reconstruction was done on Xeleris-3 workstation using ECTool box (version 3.2) to generate corresponding slices and polar plots. Interpretation of stress and rest images was done by two experienced Nuclear Medicine Physicians and summed stress score (SSS), summed rest score (SRS) and summed difference score (SDS) was derived. Correlation between above parameters and was done using Spearman correlation coefficient and cronbach alpha. **RESULTS:** Correlation coefficient between two observers for CZT detector camera was determined as 0.92 ($p < 0.001$) for SSS, 0.94 ($p < 0.001$) for SRS, 0.82 ($p < 0.001$) for SDS and for conventional gamma camera was determined as 0.95 ($p < 0.001$) for SSS, 0.96 ($p < 0.001$) for SRS, 0.91 ($p < 0.001$) for SDS. Internal consistency between two cameras for LAD territory was determined as 0.99 for SRS and 0.79 for SDS,

for LCX territory was determined as 0.94 for SRS and 0.94 for SDS and for RCA territory was 0.96 for SRS and 0.54 for SDS. **CONCLUSIONS:** In the present study, there is overall good to excellent correlation between perfusion images obtained from both the cameras. Territory wise, there is poor agreement between the data obtained from two cameras in the RCA territory, good agreement in LAD territory and excellent agreement in LCX territory. **KEYWORDS:** ASNC: American Society of Nuclear Cardiology, LAD: left anterior descending, LCX: left circumflex, RCA: right coronary artery.

OP562

Myocardial scintigraphy with D-SPECT: How much can we reduce patient radiation dose without decreasing image quality and diagnostic confidence?

E. Olsson¹, A. Davidsson¹, J. Engvall¹, B. Holmberg¹, M. Ochoa-Figueroa¹, V. Sanchez-Rodriguez¹, G. Varelogianni¹, P. Norberg²; ¹Department of Clinical Physiology, Department of Medical and Health Sciences/Cardiovascular Medicine, Linköping University, Linköping, SWEDEN, ²Department of Medical Physics and Department of Medical and Health Sciences, Linköping University, Linköping, SWEDEN.

Aim Image quality has become increasingly important in SPECT myocardial perfusion imaging (MPI) in terms of accurate reporting of ischemia with reliable quantitative measurements of myocardium at risk. Dedicated cardiac gamma camera CZT-systems with increased sensitivity produce improved image quality and may allow injected dose and radiation exposure to be lowered. The choice of count level and its impact on image quality and diagnosis is still debated. Our aim was to identify the lowest count level that still maintained diagnostic confidence. **Materials and Methods** A thorax-heart phantom was used to simulate two patient studies, one with two ischemic and another with two infarct defects. Imaging was performed with a D-SPECT camera (Spectrum Dynamics) with four count levels; 1, 0.75, 0.5 and 0.25Mcounts. 34 patients examined with clinically indicated MPI (tetrofosmin, 6MBq/kg) were retrospectively included, aiming at 10 with normal, 10 with intermediary and 14 with pathological (ischemia/infarct) MPI results. The images with the three lower count levels were digitally generated from the clinical 1Mcount image. The 136 patient and 8 phantom cases were visually assessed in random order by 6 physicians, using a four grade scale, assessing 3 questions on image quality and 5 regarding diagnosis. Statistical analysis was performed using Visual Grading Regression with $p < 0.05$ considered significant. Quantification of defects (percentage of LV myocardium) was performed for both the phantom and the patient studies for all four count levels looking for a 5% change. **Results** Image quality decreased gradually for all count levels ($p < 0.05$). For the diagnostic questions the result was non-significant between the 1 and 0.75Mcount level for identifying normality ($p = 0.07$), ischemia ($p = 0.13$) and infarct ($p = 0.42$). For false positive findings the result was non-significant for the intermediary ($p = 0.11$) and the ischemia/infarct ($p = 0.27$) groups, but in the group with normal MPI result diagnostic confidence was gradually lower for each reduction in counts ($p < 0.01$). Quantitative evaluation of the patient study is in process. The results in the phantom study showed similar diagnostic confidence in all questions ($p > 0.05$) and similar defect size ($p > 0.05$) for the four count levels. **Conclusion** Visual assessment indicated significant differences in image quality between the four count levels. Diagnostic questions suggest that the count level could be reduced to 0.75Mcounts, at a cost of increasing false positive findings in the group with normal MPI. The phantom study indicated that further dose reduction was possible, which was not corroborated when using real patient data.

OP563**Routine evaluation of left ventricular function with CZT-SPECT, low injected activities and limited recording times**

L. IMBERT¹, M. CLAUDIN¹, W. DJABALLAH¹, V. NICOLAS¹, S. POUSSIER², V. ROCH¹, M. PERRIN¹, A. VERGER¹, H. BOUTLEY², G. KARCHER¹, P. MARIE¹; ¹CHU NANCY HOPITAL BRABOIS ADULTES, VANDOEUVRE LES NANCY, FRANCE, ²GIE NANCYCLOTEP, NANCY, FRANCE.

Purpose. Gamma-cameras, equipped with Cadmium-Zinc-Telluride (CZT) detectors, allow to perform myocardial perfusion imaging (MPI) with protocols involving low injected activities and limited recorded counts and recording times. This study aimed at determining whether the routine assessment of left ventricular (LV) function with such limited counts protocols and a 16-interval gated-SPECT compares well with reference values from cardiac MRI. **Methods.** The study included patients having undergone cardiac MRI and a MPI routinely planned on a CZT camera with a low-dose protocol (120MBq of Tc-99m Sestamibi for stress and 360 MBq at rest for 75kg body weight) and while targeting the recording of only 500 myocardial kcounts in order to limit the recording times (<10 min for stress, <4 min for rest). SPECT-images were reconstructed with a specific method maintaining sufficiently high spatial (8 mm) and temporal (16 frames/cycle) resolutions. **Results.** Seventy-six patients were included among whom 44 had evidence of myocardial infarction at MRI. Mean ejection fraction was 45±13% at MRI and mean effective dose was 3.5±1.7 mSv for the total MPI protocol. Correlations between CZT-SPECT and MRI were good to excellent for ejection fraction ($r^2=0.77$), end-diastolic ($r^2=0.88$) and end-systolic ($r^2=0.93$) volumes, with global underestimations for end-diastolic (-46±25 mL) and end-systolic (-20±19 mL) volumes. The analysis of segmental contractility correlated well between the two techniques (kappa score=0.72±0.02). **Conclusion.** LV function, routinely assessed by 16-interval gated-SPECT on a CZT camera with low injected activities, limited recording times and an adapted method of image-reconstruction, correlates well with the reference assessment from cardiac MRI.

OP564**The effect of dose reduction on left ventricular volumes and ejection fraction assessed by cadmium-zinc-telluride SPECT gamma camera gated tomographic radionuclide angiography**

T. Q. Nguyen, J. Rydberg, B. Zerahn, B. Kristensen; Herlev Hospital, Herlev, DENMARK.

Aim: To examine the effect of reducing dose when measuring left ventricular ejection fraction (LVEF) and left ventricular volumes by cadmium-zinc-telluride (CZT) SPECT gamma camera gated tomographic radionuclide angiography (MUGA). **Materials and methods:** From September 2015 to March 2016, two consecutive MUGAs were performed on 46 patients who were injected first with a quarter of a full dose and subsequently adding up to a full dose of 550 MBq 99m Tc-HSA. All acquisitions were performed on a dedicated cardiac CZT SPECT gamma camera, GE Discovery 530c, using 16 bins and requesting 600 accepted beats in a 20% energy window centered on 140 keV. Each acquisition was then analyzed twice by two experienced technologists using a Xeleris 3 Imaging workstation reorientation software (version no. 3.0562) and then a Cedars-Sinai QBS processing software (revision 2009.0). Data on heart rate (HR), left ventricular end diastolic volume (LVEDV), left ventricular end systolic volume (LVESV), LVEF, and count rate were registered. Intraobserver variation was assessed in terms of interclass correlation coefficient (ICC) for each dose level and comparisons were done with paired Student's t-test. **Results:** The quarter dose series of acquisitions

had a median count rate of 1.30 kcounts/sec (range: 0.58 - 2.78) while the median count rate for full dose was 4.40 kcounts/sec (range: 2.02 - 8.39). Dose reduction gave rise to significantly lower LVEDV (mean: 91.4 mL vs. 96.0 mL; $p = 0.001$) and LVESV (mean: 34.2 mL vs. 38.4 mL; $p < 0.001$). Subsequently this gave rise to a significantly higher LVEF (mean: 63.4 % vs. 60.5 %; $p < 0.001$). There was significantly higher HR during quarter dose acquisition compared to full dose (70.9 vs. 69.6; $p = 0.004$). Reducing dose did not significantly change the intraobserver variation as the ICC between the two observers remained above 0.99 for all test variables with overlapping 95% confidence intervals. **Conclusion:** Reduction of dose in CZT detector based MUGA causes a decrease in ventricular volumes and a higher LVEF which can be explained by a partial volume effect. The significantly higher HR may also contribute to this effect and was most likely caused by nervousness from the patient at the start of the examination. However, reproducibility in terms of intraobserver variation is not compromised by dose reduction. Subsequently, it is possible to adjust CZT-detector based MUGA outcome to a reference method without compromising reproducibility within the dose range mentioned above.

OP565**Agreement between conventional and CZT cameras for the assessment of myocardial viability**

B. Vagne, R. DE PAOLA CHEQUER, N. MIKAIL, H. REGAIEG, A. HALKOVICH, F. HYAFIL, D. LE GULUDEC, F. ROUZET; Hopital Bichat, Paris, FRANCE.

Introduction: ²⁰¹Thallium (Tl-201) myocardial SPECT is well established to assess myocardial viability. New generation of *solid-state detectors gamma-camera* (CZT) offers technical advantages over conventional cameras (CC). So far, both systems have been compared exclusively in the detection of myocardial ischemia. The objective of the present study was to evaluate the agreement between quantitative analysis obtained on CC and on CZT for the assessment of myocardial viability. **Methods:** Patients referred for viability assessment during a 16-month period were prospectively included. Four hours after injection of 1 MBq/Kg Tl-201, they underwent sequentially and in a random order an acquisition on both a CC (INFINIA, GEMS) and on a CZT (D-SPECT, Spectrum Dynamics). The necrosis extent was quoted on the 17-segments model. The tracer uptake value in the necrosis area was quantified both automatically (QPS software, Cedars-Sinai) per vascular territory (% of pixel maximal value) and manually using the ratio between a manually drawn regions of interest (ROI) on the necrosis area (≥ 1 per patient) and remote healthy myocardium (using pre-set threshold values: non viable < 0.50 ≤ indeterminate < 0.65 ≤ viable). Quantitative continuous values obtained on both cameras were compared by use of Bland-Altman plots, and the agreement between cameras for viability ratings was assessed by weighted kappa coefficient. **Results:** The study population consisted of 57 patients (mean age: 67±13 years; 12% women; LVEF: 38±14 %; ≥ 2 -vessel disease: 72%). The mean difference between CC and CZT in necrosis extent was 0.05 segment [-1.60; 1.71] and the mean difference in uptake value per vascular territory was 2.0% [11.0; 15.1], with a bias proportional to the uptake value. Out of 65 necrosis areas analyzed, 49 were concordant (75%) and the agreement was considered substantial (kappa: 0.7). In most cases of discordance, the difference in uptake ratio was <5% but on either side of a threshold value. The most frequent discordance related to areas considered as indeterminate on the CC and non viable on the CZT. **Conclusion:** the present study suggests substantial agreement between CC and CZT cameras in the quantification of myocardial Tl-201 uptake, thus supporting the use of new generation systems for viability assessment and subsequent dose reduction. Follow-up studies are required to determine the need to refine threshold values.

1409 – Tuesday, October 18, 2016, 14:30 - 16:00, Hall 113

Conventional & Specialised Nuclear Medicine: Musculoskeletal - Benign**OP566****In-vivo PET Imaging of $\alpha v\beta 3 / \alpha 5\beta 1$ Integrin Expression Using Ga-68-Avebetrin and Ga-68-Aquibeptrin in Mouse Models of Rheumatoid Arthritis**

P. Sommer¹, J. Notni², K. Steiger³, G. Topping⁴, S. Ziegler⁴, W. Weichert³, M. Schwaiger⁴, H. Kessler⁵, R. Meier¹, H. Wester²; ¹Department of Diagnostic and Interventional Radiology, TU Munich, Munich, GERMANY, ²Pharmaceutical Radiochemistry, Garching, GERMANY, ³Institute for Pathology, TU Munich, Munich, GERMANY, ⁴Department of Nuclear Medicine, TU Munich, Munich, GERMANY, ⁵Center for Integrated Protein Science, TU Munich, Garching, GERMANY.

Rheumatoid Arthritis (RI) is the most common chronic inflammatory joint disease. Symptoms are painful, swollen joints and joint degradation, caused by an autoimmune reaction induced by a combination of genetic and environmental factors. Currently, diagnosis is mainly based on clinical symptoms, while detection of RI onset prior to physiological manifestation could enable early treatment and improve long-term outcome for risk patients. We investigated the suitability of $\alpha v\beta 3 / \alpha 5\beta 1$ integrin targeted PET imaging with Ga-68-Avebetrin and Ga-68-Aquibeptrin, respectively, for early detection of RI. *Methods:* Collagen-induced arthritis (CIA) mouse models were generated according to Nat. Protocols 2007;2:1269 by intradermal injection of an emulsion of type II collagen (CII) ion in complete Freund's adjuvant (CFA) (induction), followed after 14d by another injection of CII in incomplete Freund's adjuvant (IFA) (boostering), into the tail base of arthritis-susceptible DBA/1 mice. Starting 21 days after boosting, 5 cohorts of 6 mice each were investigated (one cohort per week). Animals were subjected to paw scoring, MR imaging (7T small animal scanner), and static PET imaging (Ga-68-Avebetrin and 6h later with Ga-68-Aquibeptrin, each 20 MBq, 0.5 nmol, 1.5 h p.i.), and subsequently sacrificed. Paws, ankle and knee joints were removed, decalcified and slices analyzed by histology and immunohistochemistry (MOVAT staining / $\beta 3$ - and $\alpha 5$ -IHC). *Results:* Uptake of both Ga-68-Avebetrin and Ga-68-Aquibeptrin was observed not only in arthritic paws and ankles/knees but also in some hidden joints not accessible for physical examination (shoulder/pelvis), and in some physically inconspicuous limb joints. Accumulation in arthritic joints was comparable for both tracers (2.6 ± 0.3 %IDg), while normal joints showed background uptakes < 0.5 %ID/g. Joint uptakes could be reduced to 10-20 % by means of coinjection of 100 μ g of the respective precursor, proving integrin-specificity. Negative cross-blockade studies with 100 μ g of the respective other precursor proved selectivity of both tracers for their respective integrin targets. Presence of $\beta 3$ and $\alpha 5$ integrin in PET-positive joints was confirmed by IHC. *Conclusions:* Ga-68-Avebetrin and Ga-68-Aquibeptrin PET enabled selective imaging of elevated $\alpha v\beta 3 / \alpha 5\beta 1$ integrin expression in arthritic joints of mice, suggesting that these integrins can act as biomarkers for RI. Moreover, our results indicate that $\alpha v\beta 3 / \alpha 5\beta 1$ integrin PET can detect RI already in pre-symptomatic stages, which is potentially useful for improved management of RI in risk patients.

OP567**Feasibility of Ultra High Definition Dynamic PET/MR for Evaluation of ACL Graft Viability**

K. Binzel¹, R. Moore¹, X. Liu¹, M. U. Knopp², R. Magnussen¹, C. Kaeding¹, D. Flanigan¹, M. V. Knopp¹; ¹The Ohio State University, Columbus, OH, UNITED STATES, ²Pepperdine University, Malibu, CA, UNITED STATES.

Injury to the anterior cruciate ligament (ACL) is common. Cases of a complete tear usually require surgical placement of a graft to restore stability and function to the knee. We have previously demonstrated the utility of a combined ultra-low dose PET/CT/MR approach for a molecular imaging assessment of graft healing. Here we demonstrate the feasibility of further refinement by use of ultra-high definition (UHD) reconstruction. 10 patients with recent ACL surgery underwent MRI and dynamic PET on a next-generation pre-commercial release digital PET/CT system (Veres Philips). Using an ultra-low dose (< 111 MBq) ^{18}F -FDG protocol, images were acquired continuously for 75 minutes. The PET listmode data were then reconstructed using standard definition (SD) 64 mm^3 voxel volume with frame times of 5 and 15 minutes. Ultra-high definition (UHD) images with 1 mm^3 voxel volume were reconstructed for the same frame durations. PET images were manually co-registered with MRI. Regions of interest (ROIs) were placed over the distal, middle, and proximal portions of the graft, the femoral and tibial tunnels, the posterior cruciate ligament (PCL) and quadriceps muscle for reference. Matched ROIs were placed over the contralateral knee. The kinetic characteristics of FDG uptake was assessed over the 75 minute acquisition. Dynamic PET reconstruction with UHD settings could be completed for all patients. As expected, the noise level in the fourfold increased reconstruction matrix or $1/64^{\text{th}}$ voxel volume increased which was mitigated by modified iterative reconstruction with lower number of subsets. The anatomic detail and ability to more precisely delineate the graft and anatomical structures was markedly improved by the considerable reduction in partial volume. Consistent with prior studies, the uptake kinetics of FDG in the graft and bone tunnels was elevated shortly after surgery with a lower level in the less than 6 month group. With time, the uptake intensity decreased, eventually becoming equivalent to that in the healthy knee. Ultra-High definition reconstruction is feasible even in ultra-low dose dynamic acquisition of the knee to assess graft viability using next generation digital PET. The larger reconstruction matrix reduces partial volume and thus enables the more precise assessment especially of small structures, such as those in the knee. The FDG PET/MR approach to evaluate graft viability continues to mature into a clinically feasible molecular imaging tool.

OP568**Idiopathic inflammatory myopathy: Quantification of $^{99\text{m}}\text{Tc}$ -pyrophosphate uptake by SPECT/CT**

K. F. Thøgersen^{1,2}, S. Hvidsten², L. P. Diederichsen³, S. Jacobsen⁴, P. F. Høilund-Carlsen^{2,5}, J. A. Simonsen²; ¹Aalborg University Hospital, Aalborg, DENMARK, ²Odense University Hospital, Dept. of Nuclear Medicine, Odense, DENMARK, ³Odense University Hospital, Dept. of Rheumatology, Odense, DENMARK, ⁴Rigshospitalet, Dept. of Rheumatology, Copenhagen University Hospital, Copenhagen, DENMARK, ⁵University of Southern Denmark, Dept. of Clinical Research, Odense, DENMARK.

Aim Diagnosing idiopathic inflammatory myopathy (IIM) can be challenging and is currently based on clinical examinations, blood analyses and muscle biopsies. Imaging is not routine. Due to the patchy distribution of pathological muscle changes in IIM, biopsies may be falsely negative, which calls for non-invasive, accurate tests to detect inflammation. We present a way to distinguish between IIM patients and healthy controls using technetium-99m-pyrophosphate ($^{99\text{m}}\text{Tc}$ -PYP) SPECT/CT, where increased uptake indicates inflammation. **Materials and methods** We compared $^{99\text{m}}\text{Tc}$ -PYP SPECT/CT scans of 77 patients, 56 women and 21 men, aged 23-78 years, diagnosed with polymyositis (PM), dermatomyositis (DM) or cancer associated myositis (CAM) with scans of 48 healthy controls. We performed semi-quantitative assessment by

calculating mean standard uptake values (SUV_{mean}) in volumes of interest (VOIs) in selected muscles and a qualitative assessment scoring the amount of tracer uptake by scores of 1 to 4 with 4 indicating highest uptake, by visual assessment to determine the uptake pattern (patchy versus not patchy). **Results** Patients had significantly higher SUV_{mean} in all muscles of interest compared with controls (right m. triceps brachii 46.0 g·mL⁻¹ vs. 30.1 g·mL⁻¹, $p < 0.0004$, left 45.3 g·mL⁻¹ vs. 30.1 g·mL⁻¹, right m. biceps brachii 48.6 g·mL⁻¹ vs. 37.7 g·mL⁻¹, left 50.0 g·mL⁻¹ vs. 36.1 g·mL⁻¹, right m. quadriceps proximally 39.0 g·mL⁻¹ vs. 28.7 g·mL⁻¹, left 39.9 g·mL⁻¹ vs. 28.6 g·mL⁻¹, right m. quadriceps mid-thigh 39.8 g·mL⁻¹ vs. 29.1 g·mL⁻¹, left 38.4 g·mL⁻¹ vs. 28.1 g·mL⁻¹, right m. quadriceps distally 33.2 g·mL⁻¹ vs. 24.1 g·mL⁻¹, left 31.5 g·mL⁻¹ vs. 23.0 g·mL⁻¹, p for all < 0.00001). Qualitative scores were distributed significantly different between groups with a larger fraction of patients being scored as “patchy” compared to controls (24% vs. 6% for the upper limbs, 21% vs. 6% for the lower limbs, p for both < 0.02). Compared with controls, patients had a higher median visual score (2 vs. 1, $p < 0.0001$) for their upper limbs but the same median visual score of 2 for their lower limbs. As an added bonus, qualitative assessment allowed also for localization of hot spots relevant to biopsy. **Conclusions** Quantitative assessments by ^{99m}Tc-PYP SPECT/CT consistently showed 30%–50% higher muscular uptake in IIM patients than in controls. Qualitative assessment showed higher visual uptake in the upper limbs and the patchy pattern typical of IIM was seen more often in patients than in controls. These findings put ^{99m}Tc-PYP SPECT/CT forward as having a potential role in the diagnosis and monitoring of IIM.

OP569

Innovative positioning and immobilisation techniques to refine SPECT-CT imaging of the foot and ankle

N. Soneji, D. Dalili, Y. Berkowitz, M. Vartzokas, J. Hubber, S. Yusuf, K. Wallitt, N. Davey, S. Khan, D. Amiras, H. Tam; Imperial College Healthcare NHS Trust, London, UNITED KINGDOM.

Purpose: The investigation of foot and ankle pain can be challenging due to the complexity of the osseous anatomy and numerous articulations. Each imaging modality offers different benefits and limitations. SPECT-CT with ^{99m}Tc-MDP or HDP has a high sensitivity for identifying osseous/articular pain generators (OAPG) and provides precise anatomical localisation. Failure to accurately co-register the SPECT and CT dataset through movement artefact has significant potential to lead to erroneous treatment. Various deformation-based software co-registration regimes can partially overcome this issue but may introduce other misregistration artefacts that can be more difficult to detect than the simpler image overlay method. The image overlay method, however, can only perform simple corrections for linear movements but is inadequate when there is movement at the joints. Manual correction for co-registration is also time consuming. Limb immobilisation is a simple solution that keeps the limb in an anatomical position during image acquisition and reduces movement artefact, thereby minimising the need to correct co-registration. We investigated the added value of utilising a standard Aircast® boot to immobilise the affected limb(s) and maintain anatomical alignment of the foot during SPECT-CT acquisition, comparing the diagnostic quality of these studies with those performed with the traditional use of immobilisation with tape. **Methods and Materials:** Retrospective review was performed of 10 consecutive patients referred for foot and ankle SPECT-CT immobilised with an Aircast® boot during image acquisition compared with 10 consecutive patients immobilised using the traditional tape method. The SPECT-CT images were then evaluated independently using a qualitative score by 2 nuclear medicine radiologists and a musculoskeletal radiologist with respect to the following categories: 1) the quality of the images 2) spatial localisation and 3) diagnostic certainty. Inter-rater

agreement was compared using Fleiss kappa statistics. Performance categories of Aircast-immobilised and tape-immobilised studies were compared with Fisher's exact test. **Results:** Inter-rater agreement was “substantial-perfect” (0.80–0.94) for assessment of the 3 parameters. Aircast-immobilised studies showed superior image quality ($p = 0.014$) and spatial localisation ($p < 0.0001$) over tape-immobilised studies. This led to an improvement in diagnostic certainty where 70% of tape-immobilised scans provided optimal diagnostic certainty compared to 100% in Aircast-immobilised scans which was however non-significant ($p = 0.211$). **Conclusion:** The use of an Aircast® boot during acquisition of both SPECT and CT greatly improves the quality and spatial localisation of potential OAPG.

OP570

Bone scintigraphy of feet: Considerations when moving from planar imaging to SPECT/CT alone

P. C. Holdgaard, H. C. Larsen; Department of Nuclear Medicine, Vejle, DENMARK.

AIM: Our standard imaging of feet was previously planar in 2–5 projections. We have experienced an increased use of supplementary SPECT/CT. Static images of feet require a long acquisition time and an additional SPECT/CT increases the time. We wanted to examine if the same information and conclusions could be obtained by a SPECT/CT alone, eliminating the need for planars. **METHODS AND MATERIALS:** Thirteen consecutive patients were scanned with both planar of feet in 5 projections and SPECT/CT with and without X-SPECT® reconstruction. Eleven of the thirteen also had a whole-body acquisition. All data were blinded and planar and SPECT/CT were first evaluated separately. All lesions were marked on an anatomical bone image and scored (1–5) for localisation certainty, intensity, intensity certainty and pathological degree. Also a conclusion was given and overall score (1–5) for the reporters diagnostic certainty, difficulty to interpret and time usage. Finally the exams were unblinded and the results were compared side by side for each patient. X-SPECT® reconstruction was qualitatively compared with the SPECT/CT **RESULTS:** SPECT/CT scored better for localisation ($p < 0.01$), a tendency to score lesions more intense ($p = 0.07$), a little higher pathological degree on lesion basis ($p = 0.01$), same intensity certainty ($p = 0.97$) and same number of lesions ($p = 0.23$). Overall conclusion on patient basis: the planar scored higher on diagnostic certainty ($p = 0.02$), felt easier to interpret ($p = 0.01$) and were faster to interpret ($p < 0.01$). Overall X-SPECT® reconstructions showed the same lesions as SPECT/CT but with reduced intensity, consistent with planar findings. General learning points were: Characterisation of lesions on CT (5 of 13 patients) can help the aid diagnosis. Appropriate thresholding of SPECT images is difficult in minor lesions. Absolute quantification would be helpful. CT volume rendering was useful for localisation in the small bones where cross-sectional imaging is difficult. In future acquired planar images could be substituted with reprojections from the SPECT. **CONCLUSION:** The SPECT/CT alone images in all the patients gave the same information as planars and as expected, improved localisation and reduced the total acquisition time when done without planars. Awareness of interpretation should be given to small weak lesions that look more pathologic on SPECT/CT compared with reporting practice for planars.

OP571

Hybrid SPECT/CT images in the evaluation of patient with rheumatoid arthritis of the hand: Correlation with clinical features and MRI

M. Yoo¹, S. Ha¹, J. Paeng¹, D. Lee¹, J. Chung¹, K. Kang¹, S. Hong², Y. Song³, G. Cheon¹; ¹Department of Nuclear Medicine, Seoul National University Hospital, Seoul, KOREA, REPUBLIC OF, ²Department of Radiology and Institute of Radiation Medicine, Seoul National University College of

Medicine, Seoul, KOREA, REPUBLIC OF, ³Division of Rheumatology, Seoul National University Hospital, Seoul, KOREA, REPUBLIC OF.

Purpose: The assessment of rheumatoid arthritis (RA) involvement in hand has been limited to multipinhole single photon emission computed tomography (SPECT) in nuclear medicine due to the small size of the hand joints. We investigated the diagnostic value of SPECT-CT hybrid images in small joint arthritis of hand in patients with rheumatoid arthritis. **Methods:** Hybrid SPECT-CT scan with Technetium-99m methylene diphosphonate and 3-tesla magnetic resonance imaging (MRI) were prospectively performed in 15 patients with rheumatoid arthritis, and 3 healthy control subjects. Total 338 joints consist of 170 metacarpophalangeal (MCP) joints and 168 proximal interphalangeal (PIP) joints were investigated. SPECT-CT hybrid images were analyzed using semi-quantitative assessment by region-of-interest (ROI) analysis. For MR images analysis, synovitis and bone inflammation were scored following the subscores of the Rheumatoid Arthritis MRI Score (RAMRIS). The clinical symptoms about tenderness and swelling of the finger joints were also investigated. **Result:** The SPECT-CT uptake ratio of total joints demonstrated significant correlation to the RAMRIS score ($r=0.671$, $p<0.0001$). The mean uptake ratio of hand joints in healthy control subject and patient with rheumatoid arthritis were 1.48 ± 0.27 and 2.66 ± 1.89 , respectively. The SPECT-CT uptake ratio of total joints showed significant difference according to the presence of swelling and tenderness (2.13 ± 1.40 vs 3.70 ± 2.28 , $p<0.01$ and 2.13 ± 0.9 vs 3.11 ± 2.34 $p<0.01$, respectively). In PIP joints group, SPECT uptake ratio showed significant difference between the subgroups which stratified by the score of RAMRIS ($p<0.01$). But in MCP joints group, the SPECT-CT uptake ratio only showed significant difference between normal and severe synovitis subgroups ($p<0.01$). **Conclusion:** Hybrid SPECT/CT images of the small finger joints in patients with RA can reflect the severity of bone inflammation affected by severity of the synovitis. Hybrid SPECT/CT images can be useful to localize and measure the severity of active arthritis in hand with RA.

OP572

Can the associated use of SPECT/CT in vertebral bone scintigraphy help to identify different lesions in patients with previous spinal fusion?

A. L. Santos Carreño, O. Ajuria Ilarramendi, A. Ortega Manrique, M. E. Rioja Martin, P. Paredes Rodriguez, J. M. Castro Beiras; Hospital Universitario Ramon y Cajal, Madrid, SPAIN.

Purpose: The aim of this study is to compare the findings of ^{99m}Tc HDP bone selective planar scintigraphy with SPECT/CT in patients with previous spinal fusion. **Materials and methods:** We analyzed 118 patients with spinal fusion, since July/2011 until April 15/2016, who were referred for a bone scintigraphy study. A two-phases vertebral bone scan was performed with ^{99m}Tc HDP including pool imaging followed by a delayed selective image. A SPECT/CT imaging centred over the localization of spinal fusion was subsequently performed. The median age was 60,5 years. 66 were female and 35 male. The median time from surgery for the study was 23,5 months with a range of 5 to 278 months. **Results:** We review 118 patients. 7 patients were excluded because they didn't have spinal fusion at the time of the study; we didn't found planar image in 4 and SPECT/CT in 6. Finally 101 patients have been analyzed. The planar study and SPECT/CT were normal in 3 patients. 37 patients had normal planar study, but in the SPECT/CT were found different kinds of lesions; 22/37 patients had screw loosening in the SPECT/CT, and 15/37 had degenerative changes or uptake (abnormal/normal) in the bone in-jert of posterior fusion. 61 patients had abnormal uptake in the planar study and the SPECT/CT. 33/61 patients had screw loosening in the SPECT/CT, 24 of these patients had only non-specific changes (degenerative) in the planar study, 2 were classified by compression fracture in planar, and 7 were classified as pathological by viewing the bone in-jert of posterior fusion. 12 patients had

compression fracture in the SPECT/CT, 3 also viewed in planar, and one of them with screw loosening associated. The compression fracture was only viewed in SPECT/CT in 9 patients. The remaining patients had minor injuries like degenerative changes or uptake (abnormal/normal) in the bone in-jert of posterior fusion. **Conclusion:** In patients who have previous spinal fusion, the associated use of SPECT/CT in vertebral bone scintigraphy, allows to increase the sensitivity for identifying lesions and also contributes to help detect other different types of injuries.

OP573

Stress injury detection with three phase dynamic Tc-99m MDP bone scan in adult athletes with calf pain; Contribution of SPECT/CT, preliminary findings

A. Ayan¹, **B. Gunalp**¹, **E. Balkan**¹, **S. İnce**¹, **K. Okuyucu**¹, **A. Orsçelik**², **N. Arslan**¹; ¹Gulhane Military Medical Academy, Department of Nuclear Medicine, ETLIK/ANKARA, TURKEY, ²Gulhane Military Medical Academy, Department of Sports Medicine, ETLIK/ANKARA, TURKEY.

Aim : Stress fractures in the lower extremity are common injuries among individuals who participate in endurance , high load bearing activities as running, military training. Therefore require proper diagnosis which is necessary for appropriate management . Our aim in this study was to evaluate stress injury type with three phase bone scan, contribution of SPECT/CT and relation of symptom duration in adult athletes with calf pain. **Patients and Methods :** 128 patients (10 female, 118 male) with a mean age of $23,63 \pm 5,96$ with tibial pain who had undergone a three phase dynamic Tc-99m MDP bone scan between January 2014 and March 2016 were included to the study. Their medical histories, radiologic examinations, bone scan findings and SPECT/CT findings were reviewed retrospectively . Stress injury types were determined up to their uptake features and intensity in three phase dynamic images. In case of subtle, inappropriate or other sites of uptake in whole body images then a SPECT /CT was performed. Among 128 patients 36 had also undergone a SPECT /CT scan. Duration of symptoms were statistically analyzed. **Results :** 63/128 bone scan revealed one or more foci compatible with stress injury. 36/128 patients had also a SPECT /CT scan . 17 /63 patients who have stress injury in bone scans had positive findings bilaterally. SPECT /CT images revealed stress fractures of metatarsal region in nine patients and also demonstrated five other causes of Tc-99m MDP uptake which were a fibroxantoma , a giant cell bone tumour, a polyostothotic bone disease , an osteoid osteoma and a unilateral sacroileitis. Duration of tibial pain symptoms was $21,17 \pm 19,95$ weeks Our statistical analysis demonstrated that in 5/31 patients with stress injury symptoms lasting more than 36 weeks only five had a positive bone scan or a stress injury compatible lesion in SPECT/CT findings whereas the positive bone scan and SPECT/CT findings were 39/58 patients with symptoms lasting less than 36 weeks. ($p < 0,0001$). **Conclusion:** Dynamic -three phase bone scan is a conventional method in assessing stress injuries. Perfusion and blood pool images are essential parts of bone scan in definition of stress injuries. SPECT/CT imaging has a leading role for better anatomic and morphologic characterization of injury and for also other musculoskeletal disorders that may offer a different opportunity for treatment and follow ups. Duration of symptoms may also be an important factor in defining probable stress injury patients.

1501 – Tuesday, October 18, 2016, 16:30 - 18:00, Auditorium

CME 12 - Oncology/Radionuclide Therapy/ESSO: Therapeutic Options for Hepatic Primary and Secondary Tumours

OP574

Role of Preoperative Molecular Imaging in Planning Radionuclide Therapy of NET Liver Metastases

M. Bozkurt; Hacettepe University Medical School, Department of Nuclear Medicine, Ankara, TURKEY.

OP575**Systemic Therapy of NETs with 90Y/177Lu-DOTA Peptides - A Surgeon's Perspective**

G. Poston; University of Liverpool, Surgery, Liverpool, UNITED KINGDOM.

OP576**Intraarterial Y-90 Microsphere Therapy of Primary and Metastatic Liver Tumors**

V. Vilgrai; Beaujon University Hospital, Radiology Department, Paris, FRANCE.

OP577**Traditional Resections and Liver Transplantation**

O. Abbasoğlu; Hacettepe University Medical School, Department of Nuclear Medicine, Ankara, TURKEY.

1502 – Tuesday, October 18, 2016, 16:30 - 18:00, Hall 211

Joint Symposium 12 - EANM: Developments with Cardiovascular Tracers**OP578****Atherosclerosis - The Clinical Need for Molecular Imaging**

M. Schäfers; Westfälische Wilhelms Universität, European Institute for Molecular Imaging, Münster, GERMANY.

OP579**Translational Evaluation of PET Tracers for**

Imaging of Atherosclerosis

A. Kjaer; Rigshospitalet, Nuclear Medicine & PET, Copenhagen, DENMARK.

OP580**Tracers to Investigate Atherosclerotic Processes**

P. Elsinga; University Medical Center Groningen, Nuclear Medicine and Molecular Imaging, Groningen, NETHERLANDS.

1504 – Tuesday, October 18, 2016, 16:30 - 18:00, Hall 112

Do.MoRe: Cellular Dosimetry Response**OP581****Mono-layer cell culture kinetics and dosimetry for intracellular uptake of ¹⁷⁷Lu-DOTA-octreotate in the Golgi apparatus**

M. W. Konijnenberg¹, D. C. van Gent², M. de Jong¹, J. Nonnekens²; ¹Radiology & Nuclear Medicine, Erasmus MC, ROTTERDAM, NETHERLANDS, ²Molecular Genetics, Erasmus MC, ROTTERDAM, NETHERLANDS.

Background: The dose-response relation is not well known for tumour cell survival after Peptide Receptor Radionuclide Therapy (PRRT) with ¹⁷⁷Lu-DOTA-octreotate. Dosimetry models for spherically shaped cells are available, e.g. MIRDcell dosimetry. Monolayer cultured cells and especially their cytoplasm are far from spherical, but more spread-out. Possible source compartments within the cell are cell membrane, cytoplasm, Golgi apparatus and cell nucleus. Exact dosimetry is needed for somatostatin-receptor subtype 2 (SSTR2)-positive cells after escalating amounts of ¹⁷⁷Lu-DOTA-octreotate to evaluate the radiobiology of low dose rate PRRT in comparison to external beam exposure. **Materials and**

Methods: 10⁵ Human osteosarcoma cells stably expressing SSTR2 were plated in 12-well plates (1.12 cm²). The next day the cells were incubated for 4h with 5×10⁻⁸M/2.5MBq or 5×10⁻⁹M/0.25MBq ¹⁷⁷Lu-DOTA-octreotate (specific activity 53MBq/nmol) and the medium was refreshed. Both uptake and clearance kinetics of ¹⁷⁷Lu-DOTA-octreotate in medium, cell surface and intracellular fraction were determined at 15 minutes intervals during the 4h incubation phase and then at 24h intervals over a 6 day irradiation phase. The morphology of the cells was determined using fluorescent confocal microscopy. A stylized fluid drop model of 5x5 cells was developed in the Monte Carlo code MCNP6. The cell membrane, cytoplasm and Golgi apparatus were modelled as source volumes within the central cell. The emission spectra from ¹⁷⁷Lu were used to calculate absorbed doses to all cell compartments, both in the source cell as in neighbouring cells. **Results:** Cellular uptake of ¹⁷⁷Lu-DOTA-octreotate from the medium proceeded with a half-life of 31.1±0.2 minutes and reached 13.1±0.3 %AD (Added Dose) after 4h. The internalized activity of 0.0135±0.0002 %AD/cell showed a bi-phasic clearance: 97% with 14.7±0.6h half-life and 3% with T_{1/2}>160 h. Staining showed that the intracellular uptake was >90% confined to the Golgi apparatus. The resulting absorbed dose S-values were within 15% of the MIRDcell S-values, but the S-value for activity in the Golgi was 45% lower than a homogeneous activity distribution in the cytoplasm. The absorbed dose to the cells was 1.5Gy for 0.25MBq and 2.4Gy for 2.5MBq. Homogeneous cytoplasmic uptake of the internalized activity would have led to absorbed doses of 2.4 and 3.7Gy, respectively. **Conclusion:** ¹⁷⁷Lu-DOTA-octreotate targets to the Golgi apparatus after internalisation. A mono-layer dosimetry model for the in-vitro cell plating experiments has been developed and led to significant changes in the cell dosimetry for source activity in the Golgi apparatus. More reliable dose-effect curves are now possible in cell survival after PRRT.

OP582**CD 44 Glioblastoma stem cells and resistance to alpha ionizing radiation: new insights into therapy**

E. Rosiak¹, R. Matyskiel¹, H. Koziara², B. Królicki², L. Królicki¹; ¹Department of Nuclear Medicine, Medical University of Warsaw, Warsaw, POLAND, ²Department of Neurosurgery, Maria Skłodowska-Curie Memorial Cancer Center and Institute of Oncology, Warsaw, POLAND.

AIM: Alpha-particles have a particular advantage in targeted therapy because of their high potency and specificity. Targeted alpha therapy with ²¹³Bi-labeled DOTA-Substance P (²¹³Bi-SP) is a promising novel option for local therapy in patients with recurrent glioblastoma multiforme (GBM). Glioblastoma multiforme (GBM) resistance to ionizing radiation has been hypothesized to be mediated by a tumor subpopulation, called cancer stem cells (CSCs). The aim was to investigate whether CD44 (+) CSCs contribute to the radioresistance of GBM to alpha therapy. **MATERIALS:** CD 44 (+) CSCs and CD44(-) GBMs cells *in vitro* were obtained from surgical tumor samples from 58 patients with histologically confirmed of GBM. The glioblastoma cells were treated with single dose of 1,2MBq ²¹³Bi-SP/1ml medium and cultured for 10 days under normoxia. **METHODS:** Following flow cytometry, CD44(+) CSCs and CD44(-) GBM cells were isolated using magnetic cell separation. The level of apoptosis and necrosis we performed by flow cytometry. Expression of VEGF (Vascular Endothelial Growth Factor) mRNA and stem cell marker CD44 mRNA were analyzed by semiquantitative RT-PCR. Experimental data was obtained at 1 h, 3 h, 6 h, 12 h, 24 h, 48 h, 72 hours and 10 days after application of isotopes for cell cultures. **RESULTS:** 72 hours after the treatment with ²¹³Bi-SP apoptosis level was significantly higher in CD44 (-) GBM cells than in CD44 (+) CSCs (74± 3.46 % v 49± 2.00 p=0.001). 10 days after treatment 32,00 ± 7.06 % of the CD44(+) CSCs survived and 100% ± 0.00% of CD44 (-) GBM cells died (p = 0.001). 10 days after irradiation CD44 (+) CSCs and CD44 (-) GBM cells had significantly higher the expressions of VEGF than before irradiation (3.8-fold and 3-

fold respectively). We found fourfold increased gene expression of CD44 in CD44 (-) GBM cells. **CONCLUSION:** CD44(+) stem cells play an important role in radioresistance of GBM. These cells possess a greater potential to survive alpha radiation and may contribute to the recurrence of GB. Therefore therapeutic strategies that selectively target CD44(+) CSCs, combined together with alpha ionizing radiation and anti-angiogenic agents need further evaluations.

OP583

Evaluation of S Values for Beta Particles with Monte Carlo Code Gate V6.2 for Unit Density Spheres of Various Sizes

A. BORA; Yeditepe University, ISTANBUL, TURKEY.

Objective: In this study, it was aimed to test the efficiency of Monte Carlo Code GATE V6.2 in dosimetric applications for small structures by evaluation of S-values for unit density spheres in various radii. **Method:** Spheres with various radii (0.133650 cm to 6.203505 cm) and masses (0.01 g to 1000 g) are simulated. All the spheres are filled with water. Different sources (^{131}I , ^{90}Y , ^{18}F) with 10MBq activity are used. Source related decay data are acquired from MIRD RADTABS program. GATE V 6.2 includes DoseActor tool for internal dosimetry applications was preferred to use. Calculation of absorbed dose is made as follows; (1) dose due to a particle is calculated (Gy/Particle), (2) the result is multiplied by the abundance of the related radionuclide, (3) unit conversion is made from Gy/Bq-s to mGy/MBq-s. Data that are acquired from the simulation is compared with the reference data from Radiation Dose Assessment Resource (RADAR). **Results:** For ^{131}I , spheres with masses 0.01g. to 0.5 g have relative errors between 8.16-10.41 %, while spheres with masses 1g - 1000 g have relative errors between 4.13% to 6.73%. For ^{90}Y , spheres with masses 0.01g. to 40 g have relative errors between 14.71-6.94 %, while spheres with masses 100g to 1000 g have relative errors between 6.01 % to 1.44 %. For ^{18}F , spheres with masses 0.01g. to 0.5 g have relative errors between 6.69-6.12 %, while spheres with masses 1g to 1000 g have relative errors between 2.72 % to 3.68 %. **Conclusion:** Unit Density Sphere model (UDSM) S-value results are accurate when compared to the reference values especially for bigger sphere masses. As the structure of sphere (tumor or cancer cell clusters) gets smaller, radionuclide properties becomes significant for dose calculations. The administered dose depends on tumor structure and radionuclide properties. Monte Carlo Code GATE V6.2 is an efficient code for assessment of internal dosimetry applications. Simulation results are highly correlated with reference values.

OP584

Development of an early brain metastasis geometric model for Geant4-DNA simulation

N. Falzone¹, X. Liu¹, M. Bernal², A. Corroyer-Dulmont¹, M. Sarmiento Soto¹, N. R. Sibson¹, K. A. Vallis¹; ¹University of Oxford, Oxford, UNITED KINGDOM, ²UNICAMP, Campinas, BRAZIL.

AIM: Brain metastases develops frequently in patients with lung and breast cancers, however treatment is mainly palliative and commonly comprises whole-brain irradiation. The pressing therapeutic challenge presented by brain metastases is the need to treat the whole brain in a molecularly targeted manner at an early stage when relatively few metastatic tumour cells have invaded the brain parenchyma. The aim of this preliminary study is to develop a geometric model of early brain metastasis to evaluate the theoretical efficacy of α - and β -emitting radionuclides for molecular radiotherapy (MRT). **MATERIALS AND METHODS:** Histological sections of mouse brain parenchyma were used to inform vessel diameter and cell geometry. The Geant4-DNA general purpose Monte Carlo (MC) simulation toolkit was used to

simulate the coupled transport of charged particles and photons of ^{212}Pb (an α emitter) and ^{177}Lu (a short range β^- emitter) and tallied the energy losses produced when the complete decay spectra interacted with liquid water. Energy deposition was evaluated at various positions as a radial function from the point source at the centre of the vessel. The energy deposition phase space at some discrete radius value were superimposed on a atomic resolution DNA geometrical model to estimate single- and double-strand break yields. In particular, double-strand break yield can serve as an indicator of the biological effectiveness of the radiation qualities in question. **RESULTS:** Energy deposition decreased as a function of radial distance from the linear source represented by the vessel, and the range of the particulate radiation. ^{212}Pb may be more suitable for short range targeting of early invasive cancer cells than ^{177}Lu . Double-strand break yield tends to increase with the capacity of radiation to form energy deposition clusters. **CONCLUSION:** MC simulation of an early brain metastatic model could provide invaluable insight into the potential efficacy of α - and β -emitting radionuclides for MRT. Furthermore, the model can be extended as a predictive indicator of DNA double-strand break production by specific radionuclides.

OP585

The mTOR inhibitor temsirolimus acts as a radiosensitizer in neuroendocrine tumor cells

S. Exner, S. Erdmann, V. Prasad, C. Grötzinger; Charité - Universitätsmedizin Berlin, Berlin, GERMANY.

Neuroendocrine tumors (NETs) express somatostatin receptors that are currently utilized for diagnostic and therapeutic approaches. For peptide receptor radionuclide therapy (PRRT), somatostatin analogs are coupled to radionuclides like ^{90}Y or ^{177}Lu , which after injection are bound and taken up specifically by NETs. PRRT can deliver radiation doses of up to 250 Gy to the tumors. Nevertheless, complete remission is extremely rare, compared to similar radiotherapies for thyroid cancer and non-Hodgkin lymphoma. The additional use of radiosensitizing agents could be a promising approach. In that way, mTOR inhibitors like temsirolimus may contribute to an improved therapeutic outcome of PRRT. To investigate this, NET cell lines of different origin were incubated with or without temsirolimus and exposed to different radiation doses from an external ^{137}Cs source between 0 and 10 Gy. Cells were harvested at distinct timepoints, stained with propidium iodide and the cell cycle distribution was assessed by FACS analysis. In addition, proliferation and viability were assessed by alamar blue assay, cell counting and clonogenic assay. Initially, the response of five neuroendocrine tumour cell lines (BON, H727, QGP-1, LCC18, UMC11) to temsirolimus was investigated. The treatment with different concentrations resulted in a biphasic inhibition of cell proliferation with two IC50 values in the nanomolar and micromolar range, respectively. Further on, temsirolimus induced a G1 arrest in the tumor cells after 24 hours as measured by cell cycle analysis. In radiation experiments all tested NET cell lines showed a radiation-induced decline in G1 cells as well as a G2/M arrest and a reduced clonogenic survival after radiation. In contrast, additional pretreatment with temsirolimus revealed an increase of cells in G1 and a decrease of the radiation-induced G2/M arrest. The combined therapy also showed a reduced viability and clonogenic survival of the tumor cells compared to radiation or temsirolimus treatment alone. In this particular case, the G1 arrest seems to sensitize NET cells to radiation therapy. Further experiments using ^{177}Lu -Octreotate instead of an external radiation source are planned to simulate PRRT in vitro. Additional studies, especially in vivo, are needed to better understand the influence of radiosensitizing agents like temsirolimus on neuroendocrine tumor cells to pave the way for a significant increase in the overall therapeutic efficacy of PRRT.

OP586**Synergistic Treatment of KLK10 and Iodine-131 in PC3 Cell Line**

J. Hu¹, Q. Qu¹, Y. Miao¹, Y. Wu², B. Li¹; ¹Department of Nuclear Medicine, Rui Jin Hospital, Shanghai Jiaotong University, School of Medicine, Shanghai, CHINA, ²Department of Pathophysiology, Key Laboratory of Cell Differentiation and Apoptosis of Chinese Ministry of Education, Shanghai Jiaotong University, School of Medicine, Shanghai, CHINA.

Aim: The tumour suppressor role of KLK10 gene in PC3 cell line has been proven in our previous study, by repressing proliferation, enhancing apoptosis and decreasing glucose metabolism. Radiotherapy is also an important treatment method for prostate cancer. Based on this, our study is to investigate the effect of synergistic therapy of KLK10 gene and radioactive iodine 131 in PC3 cell line. **Materials and methods:** To transfer KLK10 and sodium/iodide symporter (hNIS) gene into PC-3 with the recombinant lentiviral vector (pLVX-KLK10-IRES-hNIS-puro) to up-regulate the KLK10 and hNIS expressions. The high-purity, high KLK10 and hNIS stable expressing cell line, named as PC-3-KLK10-hNIS, was obtained by puromycin selection, and confirmed by western blot. Via the same method, PC-3-0-hNIS cell line was obtained as radiation therapy control, PC-3-KLK10-0 cell line as single gene therapy control, PC-3-CON cell line as negative control. Iodine 125 uptake, efflux, as well as uptake-inhibition by NaClO₄ assays were undergone in these four cell lines to detect the function of hNIS protein. After iodine 131 treatment, experiments of CCK-8 cell proliferation, cell clone formation and cell cycle were done with these radiation and non-radiation cell lines to evaluate the treatment effect. **Results:** The stable NES1 expression in PC-3-KLK10-0 and PC-3-KLK10-hNIS cell lines was validated by western blot. Interestingly, the hNIS expression could be detected in PC-3-KLK10-0 and PC-3-CON cell lines, although it was much lower than that in PC-3-0-hNIS and PC-3-KLK10-hNIS cell lines. However, the function of hNIS protein in PC-3-KLK10-0 and PC-3-CON cell lines was almost invalid respectively, because the uptake level of iodine 125 was extremely low. The hNIS over-expressed cell lines had the obvious iodine 125 uptake ability. The peak value and peak time in PC-3-0-hNIS was 6.2 times than that in PC-3-CON and at 60 min, as well as those in PC-3-KLK10-hNIS was 4.6 times and at 120 min. And NaClO₄ could inhibit the uptake abilities of these two cell lines. Iodine 125 efflux from cell cytoplasm to extracellular could be detected constantly lasting for 2 hours. After 16 h radiation of iodine 131 (3.7 MBq per 4*10⁵ cells), the growth rate of PC-3-KLK10-hNIS was lowest in all cell lines, consistent with the result of cell clone formation assay. Cell cycle assay showed a cell arrest in G1 phase of PC-3-KLK10-hNIS cell line. **Conclusion:** The effect of synergistic therapy of KLK10 gene and radioactive iodine 131 in PC3 cell line was better than single method treatment.

1505 – Tuesday, October 18, 2016, 16:30 – 18:00, Hall 115

M2M: Protein-Based Radiotracers**OP587****A new bifunctional chelator for ⁸⁹Zr-immuno-PET: DFO*-pPhe-NCS and the comparison with the current clinical standard DFO-pPhe-NCS**

D. J. Vugts¹, C. Klaver¹, C. Sewing¹, A. J. Poot¹, K. Adamzek¹, S. Huegli², C. Mari², I. E. Valverde³, G. Gasser², T. L. Mindt^{4,5}, G. A. M. S. van Dongen¹; ¹VU University Medical Center, Amsterdam, NETHERLANDS, ²University of Zurich, Zurich, SWITZERLAND, ³University of Basel Hospital, Basel, SWITZERLAND, ⁴ETH, Zurich, SWITZERLAND, ⁵General Hospital of Vienna, Vienna, AUSTRIA.

Objectives: Desferrioxamine (DFO) is currently the chelator used in clinical ⁸⁹Zr-immuno-PET studies. This chelator, however, does not provide full coordination of Zr⁴⁺ and leaves two coordination sites available for coordination of e.g. water molecules, which are relatively labile ligands.

The incomplete coordination of ⁸⁹Zr by DFO has been suggested to result in instability of the complex and as a consequence, in unwanted bone uptake of the radionuclide *in vivo*. Recently, DFO*, the octadentate version of DFO has been developed, which provides full coordination of ⁸⁹Zr. This new chelator showed excellent *in vitro* stability in DFO challenging experiments.¹ Following this promising result, now DFO*-pPhe-NCS has been synthesized and used to prepare ⁸⁹Zr-DFO*-mAb conjugates which are *in vitro* and *in vivo* compared with the current standard ⁸⁹Zr-DFO-mAb. **Methods:** DFO* was reacted with *p*-phenylenediisothiocyanate resulting in bifunctional DFO*-pPhe-NCS. Next, DFO*-pPhe-NCS and DFO-pPhe-NCS (i.e. DFO-Bz-NCS, Macrocyclics) were reacted with trastuzumab, cetuximab and rituximab and radiolabeled with ⁸⁹Zr according to literature procedures.² For *in vitro* and *in vivo* comparison, trastuzumab was used as model protein. *In vitro* stability experiments were performed in 0.9% NaCl, histidine/sucrose and serum. *In vivo* the two complexes were compared in a N87 tumor xenograft model. **Results:** All antibody conjugates could be radiolabeled with >80 % efficiency at 0.5 mg/mL resulting in radioimmunoconjugates with a good radiochemical purity (>97.5%) and optimal immunoreactive fraction (>90%). *In vitro* stability of ⁸⁹Zr-DFO*-trastuzumab was superior over ⁸⁹Zr-DFO-trastuzumab in 0.9% NaCl showing after 3 days at 4°C for ⁸⁹Zr-DFO-trastuzumab 57.6% intact tracer and for ⁸⁹Zr-DFO*-trastuzumab 94.5% intact tracer. In histidine/sucrose both products were stable and there was no difference in stability. In human serum ⁸⁹Zr-DFO*-trastuzumab was also more stable than ⁸⁹Zr-DFO-trastuzumab: after 72 h at 37°C 97.5% and 77.7% intact tracer was left, respectively. The *in vivo* tumor uptake of both conjugates was comparable: 32.6 ± 12.0 and 29.1 ± 8.7 % ID/g for DFO* and DFO-conjugates at 144 hr post injection, respectively. Bone uptake was gradually increasing for ⁸⁹Zr-DFO-trastuzumab, while gradually decreasing for ⁸⁹Zr-DFO*-trastuzumab resulting in a >3.6 fold higher uptake in bone containing organs for DFO. **Conclusion:** The octadentate chelator DFO* holds great promise as new chelator for ⁸⁹Zr-immuno-PET studies given its improved *in vitro* stability and *in vivo* performance. **References:** 1. M. Patra et al., Chem. Commun. 2014, 50, 11523-11525. 2. M.J.W.D. Vosjan et al, Nature Protocols 2010, 5, 739-743.

OP588**MA-NOTA: a new chelator for efficient ⁶⁴Cu antibody radiolabeling**

M. Moreau¹, S. Poty¹, J. Vrigneaud², P. Walker³, M. Guillemin², O. Raguin⁴, A. Oudot², C. Bernhard¹, C. Goze¹, F. Boschetti⁵, B. Collin^{1,2}, F. Brunotte^{2,3}, F. Denat¹; ¹ICMUB - UMR CNRS 6302, Dijon, FRANCE, ²Centre G.-F. Leclerc, Dijon, FRANCE, ³Le2i - UMR CNRS 6306, Dijon, FRANCE, ⁴Oncodesign, Dijon, FRANCE, ⁵CheMatech, Dijon, FRANCE.

Introduction: ⁶⁴Cu has an ideal half-life for studies of labeled fragments of antibodies and such radiotracers have attracted considerable interest in the field of targeted radionuclide therapy and diagnosis. Unfortunately, the chelation of copper is not as easy as that of other metals and the release of copper is a limiting issue for its use. We hypothesized that MA-NOTA might be a highly efficient chelator for ⁶⁴Cu labeling and the aim of the present study was to compare the biodistribution of the radioactivity after intravenous injection of Fab-fragments of antibodies conjugated to various bifunctional chelators (BFC), DOTA, DOTA-GA, NODA-GA and MA-NOTA in mice bearing subcutaneous tumors. **Method:** These four chelators, bearing a *p*-benzyl-isothiocyanate functionalization group, were conjugated to Fab-trastuzumab - which targets the HER2/neu receptor - and were radiolabeled with ⁶⁴Cu. Stability of the formed complexes was evaluated by competition with 2,000 fold EDTA at 37°C. *In vitro* binding assays were performed on HCC1954 cells to determine affinity and immunoreactivity of the four radioimmunoconjugates. Finally, PET/MR imaging and biodistribution studies were performed in mice-bearing breast cancer BT-474 xenografts overexpressing HER2 in order to compare the four radiolabeled Fab-trastuzumab. **Results:** The degree of

conjugation ranged from 2.4 to 4.3 macrocycles per Fab. Radiolabeling of the immunoconjugates with ^{64}Cu was performed in high yields after 45 min at 37 °C, and the purity of each ^{64}Cu -BFC-Fab-trastuzumab reached 97 % after purification. The complexes showed relatively good stability during competition with 2,000 molar excess of EDTA at 37°C (88 % to 95 % at 48 h). The affinity of each ^{64}Cu -BFC-Fab-trastuzumab ranged from 10.1 ± 2.5 nM to 49.3 ± 5.9 nM as evaluated by *in vitro* binding assays using HCC1954 breast cancer cell, and immunoreactivity was > 30 %. BT-474 tumors were clearly visualized on PET images at 4 and 24 h post-injection. The tumor uptakes of ^{64}Cu -BFC-Fab-trastuzumab reached 8.9 to 14.2 %ID/g 24 h post-injection and significant differences in liver uptake were observed depending on the attached BFC, with the lowest uptake for MA-NOTA-conjugated fragments. **Conclusion:** As the liver uptake of the ^{64}Cu has been shown to increase with the instability of the chelation, the present results suggest that *p*-NCS-MA-NOTA stands out from the other chelators, including the commonly used DOTA and NODA-GA, as the most promising BFC for radiolabeling antibodies with ^{64}Cu .

OP589

Development and application of first ^{44}Sc -labeled Affibody molecule

H. Honarvar¹, C. Müller², N. van der Meulen², S. Cohrs², K. Westerlund³, A. Eriksson Karlström³, R. Schibli², V. Tolmachev¹; ¹Rudbeck Laboratoriet, Uppsala, SWEDEN, ²Paul Scherrer, Villigen-PSI, Zurich, SWITZERLAND, ³School of Biotechnology, KTH Royal Institute of Technology, Stockholm, SWEDEN.

Aim: Treatment with the anti-HER2 antibody trastuzumab improves survival of breast cancer patients with tumours having high HER2-expression (3+ according to immunohistochemistry using HercepTest). Affibody molecules are small (7 kDa) scaffold proteins, which can be used as molecular imaging probes. A clinical study has demonstrated that PET-imaging using ^{68}Ga -labeled Affibody molecules enables discrimination between breast cancer metastases with high (3+) and low (2+ or less) HER2-expression. The best discrimination was obtained at 4 h p.i.; however the half-life of ^{68}Ga resulted in low activity in tumours. Scandium-44 (94.27% β^+ branching) is a positron-emitting radionuclide with 3.5-fold longer half-life than ^{68}Ga , which is favourable for imaging over several hours. The aim of this study was to develop and evaluate ^{44}Sc -labelled HER2-binding Affibody molecules for PET imaging. **Material and Methods:** The synthetic second generation anti-HER2 DOTA- $Z_{\text{HER2}:2891}$ Affibody molecule was labelled with ^{44}Sc and, for comparison, with ^{68}Ga . *In vitro* binding specificity and cellular processing of radioconjugates was studied using HER2-expressing SKOV3.ip cells. An *in vitro* competitive binding assay was performed using ^{111}In -DOTA- $Z_{\text{HER2}:2891}$ and conjugates loaded with non-radioactive gallium and scandium. The biodistribution of ^{44}Sc -DOTA- $Z_{\text{HER2}:2891}$ and ^{68}Ga -DOTA- $Z_{\text{HER2}:2891}$ was compared in nude mice bearing SKOV3.ip xenografts. To verify *in vitro* specificity, mice with HER2-negative Ramos xenografts were used. Imaging studies were performed with a G8 benchtop PET/CT scanner. **Results:** The difference between IC_{50} for ^{68}Ga -DOTA- $Z_{\text{HER2}:2891}$ (5 ± 2 nM) and ^{44}Sc -DOTA- $Z_{\text{HER2}:2891}$ (6 ± 2 nM) was not significant. The binding of the ^{44}Sc -DOTA- $Z_{\text{HER2}:2891}$ to SKOV3.ip was HER2-specific *in vitro* and *in vivo*. Biodistribution patterns of ^{44}Sc - and ^{68}Ga -DOTA- $Z_{\text{HER2}:2891}$ were similar. There was no significant difference between tumour uptake of ^{44}Sc -DOTA- $Z_{\text{HER2}:2891}$ (12.8 ± 1.6 %ID/g) and ^{68}Ga -DOTA- $Z_{\text{HER2}:2891}$ (14.4 ± 2.1 %ID/g), at 3h p.i., however the tumour-to-blood ratio for ^{68}Ga -DOTA- $Z_{\text{HER2}:2891}$ (46 ± 9) was higher than for ^{44}Sc -DOTA- $Z_{\text{HER2}:2891}$ (15 ± 2). The radioactivity concentration in blood and normal organs decreased significantly for ^{44}Sc -DOTA- $Z_{\text{HER2}:2891}$ at 6h p.i., resulting in

tumour-to-blood ratio of 51 ± 8 . The tumour uptake was 8.2 ± 2.1 %ID/g at this time point. PET/CT imaging confirmed the results of biodistribution experiments showing distinct uptake of the ^{68}Ga - and ^{44}Sc -labeled Affibody molecules in SKOV3.ip tumours while accumulation in Ramos tumours was almost absent. **Conclusion:** For the first time ^{44}Sc was successfully used for labelling of an Affibody molecule. In this pilot preclinical study ^{44}Sc -DOTA- $Z_{\text{HER2}:2891}$ proved to be useful for imaging of HER2-expressing tumours at several hours after injection. Our results hold promise for future application of ^{44}Sc -labeled Affibody molecules in the clinics.

OP590

Anti HER2 Nanobody Labeled with ^{225}Ac as a Potential Radiopharmaceutical for TRT

M. Pruszyński¹, E. Cędrowska¹, V. Radchenko², K. D. John², F. Bruchertseifer³, A. Morgenstern³, M. D'Huyvetter⁴, T. Lahoutte⁴; ¹Institute of Nuclear Chemistry and Technology, Warsaw, POLAND, ²Los Alamos National Laboratory, Los Alamos, NM, UNITED STATES, ³Joint Research Centre – Institute for Transuranium Elements, Karlsruhe, GERMANY, ⁴Vrije Universiteit Brussel, Brussels, BELGIUM.

Aim: Human epidermal growth factor receptor type 2 (HER2) is overexpressed in breast, ovarian, non-small cell lung, gastric and colon cancers, and portends poor prognosis. Intact mAbs are not always ideal vectors for radioimmunotherapy due to their slow pharmacokinetic and normal-tissue clearance. Nanobodies (Nbs) are single domain antibodies derived from *Camelidae*. Their small size (~15kDa), nM-range affinity, low immunogenicity, rapid clearance from blood and normal tissues and ease of tumor penetration make them a very attractive platform for targeted radionuclide therapy (TRT). The goal of this study was to develop and characterize a potential molecular-targeted drug based on the anti-HER2-Nb labeled with ^{225}Ac . **Materials and methods:** The anti-HER2 2Rs15d-Nb was conjugated with *p*-SCN-Bn-DOTA, purified and DOTA-2Rs15d-Nb analyzed by mass spectrometry. DOTA-2Rs15d-Nb was labeled with ^{225}Ac and with the more conventional radioisotope ^{177}Lu for comparison, and finally obtained radiobioconjugates were evaluated by TCA precipitation, ITLC, and gel electrophoresis. Stability was determined in PBS, human serum and cell culture medium for 10 days at RT and 37°C. Binding specificity and affinity assays were evaluated using SKOV-3 (HER2+) and MDA-MB-231 (HER2-) cells; immunoreactive fraction (IF) by the Lindmo method. Cell viability was assessed using the MTS colorimetric assay. **Results:** DOTA-2Rs15d-Nb conjugate was labeled with ^{177}Lu and ^{225}Ac with an efficiency of $81.1 \pm 15.4\%$ ($n = 3$) and $87.2 \pm 8.8\%$ ($n = 8$), respectively. TCA precipitation, ITLC, and SDS-PAGE indicated that >95% of radioactivity was protein-associated. Stability in biological solutions, according to ^{225}Ac radionuclide, was above 90% over 10d. Radiobioconjugates bound specifically to HER2 on SKOV-3 cells with 69-83% IF and a K_d of 4.06 ± 0.45 nM. Blocking of HER2 with 100>excess of cold 2Rs15d-Nb reduced binding almost 30-fold, whereas cold Trastuzumab did not compete with radiobioconjugates to binding sites. Low level of binding (0,3%) was observed for MDA-MB-231 (HER2-) cell line. Internalization assay indicated about 40% of initially bound radioactivity was trapped intracellularly for ^{177}Lu -DOTA-2Rs15d-Nb over 24h. Cytotoxicity studies demonstrated that ^{225}Ac -DOTA-2Rs15d-Nb significantly reduced SKOV-3 cell viability in a dose dependent manner. The estimated median lethal dose values (LD_{50}), after 24-h incubation, were equal to *ca.* 1.5 kBq/mL and 350 kBq/mL for ^{225}Ac -DOTA-2Rs15d-Nb and ^{225}Ac -DOTA, respectively. **Conclusions:** ^{225}Ac -DOTA-2Rs15d-Nb showed strong *in vitro* therapeutic potential. Therefore, this radiobioconjugate is a promising agent that warrants future *in vivo* evaluation and TRT in SKOV-3 xenografted mice. This work was supported by the Polish National Science Center under grant 2013/09/D/ST4/03791.

OP591

Improving of molecular design of a novel Affibody-fused HER2-recognition anticancer toxin using radionuclide-based techniques

M. Altai¹, H. Liu², A. Orlova³, V. Tolmachev¹, T. Gräslund⁴; ¹Immunology, Genetics and Pathology, Uppsala University, Uppsala, SWEDEN, ²DIVISION OF PROTEIN TECHNOLOGY, KTH, Stockholm, SWEDEN, ³Department of Medicinal Chemistry, Division of Molecular Imaging, Uppsala, SWEDEN, ⁴DIVISION OF PROTEIN TECHNOLOGY, KTH, Uppsala, SWEDEN.

Aim. Targeted delivery of drugs and toxins is a promising approach for treatment of disseminated cancers. Several antibodies-based toxin conjugates and fusion proteins are under development. However, the large size of antibodies results in poor tumor penetration. Small size toxin-fused antibody domains have short plasma half-life and low bioavailability. We have constructed a series of novel Affibody-fused toxins (affitoxins). The affitoxins include the deimmunized PE38X8-toxin fused to the HER2-binding Affibody molecule Z_{HER2:2891}. A role of fusion with albumin binding domain ABD₀₃₅ for the half-life extension and the use of (HE)₃ tags for reduction of hepatic uptake was evaluated using nuclide-based techniques. We expected that radionuclide-based techniques would permit for more sensitive tracking and more accurate quantification of cellular processing and tissue distribution compared to alternative approaches. **Methods.** The H₆-Z_{HER2}-PE38, (HE)₃-Z_{HER2}-PE38X8, and (HE)₃-Z_{HER2}-ABD-PE38X8 HER2-specific constructs and control (HE)₃-Z_{Taq}-ABD-PE38X8 were conjugated with a CHX-A³-DTPA chelator and labelled with ¹¹¹In. The binding specificity to and cellular processing by HER2-expressing cells was studied using SKOV-3 cell line. Affinity of labelled constructs to HER2-expressing cells was measured using LigandTracer Yellow. The influence of the composition of the histidine-containing tags tag on hepatic uptake of the affitoxin and the feasibility of extending its plasma half-life using ABD₀₃₅ was evaluated in NMRI mice. Mice bearing SKOV-3 xenografts were injected with ¹¹¹In-(HE)₃-Z_{HER2}-ABD-P38X8 and sacrificed at 1, 4 and 24 p.i. To confirm HER2 mediated uptake of the affitoxin, an additional group of mice was injected with the non-HER2-specific affitoxin, ¹¹¹In-(HE)₃-Z_{Taq}-ABD-PE38X8. **Results.** All affitoxins were efficiently labelled with ¹¹¹In (yield=84–95%) with preserved specificity of binding to HER2-expressing cells and a picomolar affinity. ¹¹¹In-(HE)₃-Z_{HER2}-ABD-P38X8 demonstrated more rapid internalization by SKOV-3 cells in vitro compared to the control H₆-tag containing variant. In vivo, the incorporation of more hydrophilic (HE)₃-tag reduced the liver uptake by 20% compared to H₆-tag containing variants. The residence time of the ABD₀₃₅-fused affitoxin, ¹¹¹In-(HE)₃-Z_{HER2}-ABD-PE38X8, in the blood was on average 28-fold higher than that of ¹¹¹In-(HE)₃-Z_{HER2}-PE38X8 and the kidney uptake was on average 6-fold lower. ¹¹¹In-(HE)₃-Z_{HER2}-ABD-PE38X8 targeted HER2-expressing xenografts in mice specifically. The tumour uptake of the HER2-affitoxin peaked at 24 h p.i. (5.5±1 %ID/g). **Conclusion.** Novel affitoxin construct (HE)₃-Z_{HER2}-ABD-PE38X8 demonstrated reduced hepatic uptake, longer residence in circulation and specific targeting of HER2-expressing xenografts. A particular advantage of radiolabelling is that it enabled to study quantitatively the biodistribution of several alternative constructs. Thus it represents a powerful tool in drug development.

OP592

Dual-targeting of tissue factor and CD105 for PET imaging of pancreatic cancer

W. Cai, H. Luo, C. G. England, S. Shi, S. A. Graves, R. J. Nickles; University of Wisconsin-Madison, MADISON, WI, UNITED STATES.

Objective: Pancreatic adenocarcinoma is a highly aggressive cancer, currently treated with limited success and dismal outcomes. Early detection and treatment offer the potential to reduce cancer morbidity and mortality,

yet over 80% of patients are diagnosed with advanced disease. Developing highly-specific non-invasive imaging probes for pancreatic cancer is essential to improving diagnostic accuracy and monitoring therapeutic intervention, which was the goal of this study. **Methods:** A bispecific heterodimer was synthesized by conjugating an anti-tissue factor (TF) Fab (i.e. ALT-836-Fab) with an anti-CD105 Fab (i.e. TRC105-Fab), via the bioorthogonal “click” reaction between tetrazine (Tz) and *trans*-cyclooctene (TCO). The heterodimer was labeled with ⁶⁴Cu for positron emission tomography (PET) imaging of nude mice bearing BXP-3 xenograft and orthotopic pancreatic tumors. **Results:** A competitive binding assay was performed to determine and compare the binding affinities of heterodimer, ALT-836-Fab, and TRC105-Fab to BXP-3 cells. The results of the binding isotherm showed a concentration-dependent displacement of bound ⁶⁴Cu-NOTA-heterodimer with IC₅₀ values of 11.35±1.04, 288.9±18, and 583.9±36 nM for heterodimer, ALT-836-Fab, and TRC105-Fab, respectively. Only a partial displacement of the bound radioligand at high concentrations (μM) of the competing antibody fragments demonstrated the bivalent nature of heterodimer binding. PET imaging of BXP-3 xenograft tumors (which express high levels of both TF and CD105) with ⁶⁴Cu-labeled heterodimer displayed significantly enhanced tumor uptake (28.8±3.2 %ID/g; n = 4) at 30 h p.i., as compared to each of their mono-specific Fab tracers (12.5±1.4 and 7.1±2.6 %ID/g; n = 3). In addition, the activity-concentration ratio allowed for effective tumor visualization (tumor/muscle ratio of 75.2 ±9.4 at 30 h p.i.; n = 4). Blocking experiments were performed to confirm tracer specificity in vivo. Tracer uptake in all major organs was similar between ⁶⁴Cu-NOTA-heterodimer and ⁶⁴Cu-NOTA-heterodimer with TF or CD105 blockade, except the BXP-3 tumor (significantly higher in the former), further confirming the TF and CD105 dual-specificity of ⁶⁴Cu-NOTA-heterodimer. Furthermore, ⁶⁴Cu-NOTA-heterodimer enabled sensitive detection of orthotopic pancreatic tumor lesions in mice with an uptake of 17.1±4.9 %ID/g at 30 h p.i. and tumor/muscle ratio of 72.3 ± 46.7 (n=3). **Conclusion:** This study demonstrates that dual-targeting of TF and CD105 provided synergistic improvements in both affinity and specificity of the heterodimer. Dual-targeted imaging agents of pancreatic and other cancers may allow for earlier pancreatic cancer detection, as well as reliable monitoring of therapeutic response.

OP593

The value of Zirconium-89 Positron Emission Tomography (⁸⁹Zr-PET) during the phase 1 study of a new antibody construct: ⁸⁹Zr-labeled cergutuzumab amunaleukin as an example

B. J. de Wit - van der Veen¹, M. Huisman², O. S. Hoekstra², M. P. M. Stokkel¹, E. van Brummelen¹, E. Mulder², G. A. M. S. van Dongen², D. J. Vugts², H. Verheul², T. K. Nayak³, J. Saro⁴, S. Evers⁴, J. H. M. Schellens¹, C. W. Menke-van der Houven van Oordt²; ¹The Netherlands Cancer Institute, Amsterdam, NETHERLANDS, ²VU University Medical Centre, Amsterdam, NETHERLANDS, ³Roche Pharma Research and Early Development, Basel, SWITZERLAND, ⁴Roche Pharma Research and Early Development, Zurich, SWITZERLAND.

Aim: Zirconium-89 Positron Emission Tomography (⁸⁹Zr-PET) can be used in Phase I trials as a tool to elucidate potentially uncertain distribution patterns of an antibody in tissues and tumour lesions. A step-wise ⁸⁹Zr-PET approach evaluates: I. biodistribution at low antibody dose, II. tumour accumulation at maximal dose, and III. biodistribution alterations throughout therapy cycles. This methodology was implemented in the Phase I trial with cergutuzumab amunaleukin, an engineered Interleukin-2 variant (i.e., abolished CD25 binding) antibody targeting Carcinoembryonic Antigen (CEA-IL2v). **Methods:** Patients (pts) with solid CEA-positive or -negative (CEA+/-) tumours were divided in three groups: I. CEA+/- dosed at 6 mg, II. CEA+/- dosed at 30 mg, and III. CEA+ dosed at 20-30 mg. Administrations during cycle 1 contained radiolabelled CEA-IL2v (± 50 MBq/2 mg ⁸⁹Zr-CEA-IL2v), pts in sub-group III received ⁸⁹Zr-CEA-IL2v in cycle 4 if tumour uptake was visible in cycle 1. ⁸⁹Zr-PETs were acquired

at day 2 and 5. Visible tumour uptake higher than surrounding tissue was regarded as 'positive' by a Nuclear Physician. Results: *Tumour accumulation* In group I (4 pts CEA+, 3pts CEA-), tumour accumulation was observed at 6 mg in 1/4 CEA+ pts. No uptake was seen in CEA- pts. At the maximum tolerated dose of 30 mg (group II, 4 pts CEA+, 4 pts CEA-) tumour accumulation was observed in 4/4 CEA+ pts, compared to 0/4 CEA- pts, indicating that tumour uptake is related to CEA-status. In group III (20 mg dose followed by 30 mg maintenance, 8 pts CEA+), the second ⁸⁹Zr-CEA-IL2v administration in cycle 4 showed reduced uptake in tumour lesions. These results indicate that levels of cold antibody at start and during treatment are an important factor to consider for tumour accumulation. *Biodistribution* In all groups accumulation was observed in the liver, spleen and lymph nodes independent of CEA-status, suggesting IL-2 receptor mediated accumulation in lymphoid tissues. Marked differences were observed in cycle 4 compared to cycle 1 with reduced accumulation in the spleen and increased accumulation in the liver. Also, ⁸⁹Zr-CEA-IL2v blood plasma levels showed a faster decline in cycle 4. These results indicate an altered pharmacokinetic-profile. Conclusion: ⁸⁹Zr-PET visualized biodistribution and tumour accumulation during this Phase 1 study with cergutumab amunaleukin, thereby shedding light on the complex relation between pharmacokinetics and -dynamics related to the targets CEA and IL2v. The proposed methodology is generic, and can be considered to visualize in vivo behaviour of novel ⁸⁹Zr-labeled multi-target drugs.

OP594

Anti-HER2 Single Domain Antibody 2Rs15d Labeled with ¹⁸F Using a Residualizing Label: Preliminary Evaluation

G. V. Vaidyanathan¹, Z. Zhou¹, D. McDougald¹, T. Lahoutte², M. R. Zalutsky¹; ¹Duke University Medical Center, Durham, NC, UNITED STATES, ²Free University of Brussels, Brussels, BELGIUM.

Aim: We have evaluated the utility of an anti-HER2 single domain antibody (sdA) 5F7, labeled with ¹⁸F using the residualizing label [¹⁸F]JRL-I, as a potential tracer for determining HER2 status in preclinical breast cancer (bc) models (*Org. Biomol. Chem.* 2016;14:1261-1271; *J. Nucl. Med.* 2016; PMID: 26912425). Unlike 5F7, sdA 2Rs15d does not compete with trastuzumab for HER2 binding, and should be more suitable for the determination of response to trastuzumab therapy. A phase I study of this sdA labeled with ⁶⁸Ga was recently performed and delineation of both primary and metastatic cancer was possible (*J. Nucl. Med.* 2016; 57:27-33). In the current work, 2Rs15d was labeled with the versatile PET radionuclide ¹⁸F using [¹⁸F]JRL-I and evaluated in vitro and by microPET imaging. Methods: 2Rs15d was labeled using [¹⁸F]JRL-I in borate buffer, pH 8.5. Radiochemical purity (RCP) of [¹⁸F]JRL-I-2Rs15d was determined by TCA precipitation, ITLC, SEC and SDS-PAGE. Binding affinity and immunoreactive fraction (IRF) of [¹⁸F]JRL-I-2Rs15d to HER2 was determined using HER2-expressing BT474M1 cells. Internalization in BT474 M1 cells in vitro was performed in a paired-label format along with 2Rs15d labeled using [¹²⁵I]SGMIB (*Nat. Protocols* 2007;2:282-286). MicroPET/CT imaging was done in a BT474M1 xenograft-bearing SCID mouse after administering [¹⁸F]JRL-I-2Rs15d. Results: 2Rs15d was coupled to [¹⁸F]JRL-I in 47.8 ±2.6% yield and with a RCP of >95%. [¹⁸F]JRL-I-2Rs15d had a Kd of 7.1 ±0.4 nM and an IRF of 78.8±7.6%. The percentage of initially-bound radioactivity that was internalized in BT474 M1 cells at 1, 2 h and 4 h was similar for ¹⁸F (43.7±3.6, 36.5±2.6 and 21.8±1.3) and ¹²⁵I (49.2±2.2, 39.6±1.1 and 23.6±0.1) (*P* < 0.05 at 1 h). MicroPET/CT imaging clearly delineated the tumor, which exhibited uptake and retention of radioactivity — 13.3±5.7, 13.7±5.4, and 13.2±5.3 %ID/g (SUV: 2.3±0.9, 2.4±0.9, 2.3±0.9) at 1, 2 and 3 h, respectively. The tumor uptake is 58% and 70% of that obtained by microPET imaging for [¹⁸F]JRL-I-5F7 at 1 h and 2 h, respectively. However, uptake of [¹⁸F]JRL-I-2Rs15d observed in this study is considerably higher than that reported for ⁶⁸Ga-labeled 2Rs15d, albeit in the SK-OV-3 mouse model (*J. Nucl. Med.* 2013; 54:776-784). Kidneys and bladder were the only other organs that were visible. Conclusion: Given that high contrast PET

image was obtained with [¹⁸F]JRL-I-2Rs15d as early as 1 h, it warrants further evaluation as an agent for determination of HER2 status, and especially for determining response to therapy with trastuzumab in bc patients.

1506 – Tuesday, October 18, 2016, 16:30 - 18:00, Hall 111

Teaching Session: TBA

OP595

TBA

1507 – Tuesday, October 18, 2016, 16:30 - 18:00, Hall 116

Clinical Oncology: Lung

OP596

Validation of high-risk CT & PET features for prediction of local recurrence after SBRT

K. Wagner¹, S. Adebahr^{1,2}, E. Gkika¹, T. Brunner^{1,2}, J. Ruf³, H. Rischke^{1,3}, A. Grosu^{1,2}, W. Vach⁴, U. Nestle^{1,2}; ¹Department of Radiation Oncology, Freiburg University Medical Center, Freiburg, GERMANY, ²German Cancer Consortium (DKTK), Heidelberg, Partner Site Freiburg, Freiburg, GERMANY, ³Department of Nuclear Medicine, Freiburg University Medical Center, Freiburg, GERMANY, ⁴Center of Medical Biometry and Medical Informatics, Freiburg University Medical Center, Freiburg, GERMANY.

Background and purpose: Detection of local recurrence (LR) after stereotactic body radiotherapy (SBRT) for lung lesions using RECIST-Criteria can be difficult because of radiation-induced CT lung changes. The role of PET/CT in this aspect has not yet been determined. High-risk CT-features (HR-CTF) for prediction of LR have been proposed in a case control study that included a blinded read by two teached radiation oncologists after appropriate teaching (Huang et al., *Radiother Oncol.* 2012 and 2013). In consensus formation (CF), the presence of ≥ 3 HR-CTF was highly sensitive and specific for LR (both ≥ 90%). The aim of the current study was to validate these CT-criteria in combination with PET-imaging features without teaching and CF in a prospective SBRT trial cohort. **Materials and methods:** In Interviews, CT image datasets of a prospective patient group treated with SBRT (57 patients with 65 pulmonary lesions), who had as well FU-PET/CTs were scored by 4 experienced blinded observers (two radiation oncologists + one nuclear medicine physician = observer 1-3; and one radiologist) using a structured questionnaire. RECIST results and all single HR-CTF were assessed. In a prospective time-point ordered sequence of follow up –CT datasets of each patient, observers determined their suspicion of LR. When this was the case, available PET/CT images of this time point were shown and analyzed qualitatively, then quantitatively. Review sequence was stopped as soon as the observer diagnosed LR in both CT and FDG-PET. For observer 1-3 inter-observer variability (IOV) was determined using Cohen's kappa. Regarding LR-detection, accordance of observers' results with the reference standard (defined by clinical long term courses including information on imaging and biopsy if available) was analyzed, sensitivity and specificity were calculated. **Results:** IOV between the Observers 1-3 were "slight" to "fair" for CT-Criteria (k=0.120 to k=0.357), with additional PET information it was "almost perfect", qualitative and quantitative (both k=0.862). For observers 1-4 sensitivity and specificity for RECIST were 46% and 95% and for single HR-CTF it were 17-58% and 56-96%, respectively; If ≥ 3 HR-CTF pertained, sensitivity and specificity were 50% and 81% respectively. PET/CT analysis was highly sensitive (100%) but varyingly specific (44-91%). **Conclusion:** While neither RECIST nor the previously defined HR-CTF could be validated as reliable predictors of LR, PET/CT seems to offer more accurate and diagnostic information about local recurrence after SBRT leading to a higher inter observer agreement in independent review.

OP597**Role of Dynamic FDG PET/CT Acquisition in Evaluation of Response to Chemotherapy in Advanced NSCLC**

A. Sharma, A. Mohan, A. S. Bhalla, P. K. Julka, C. S. Bal, M. C. Sharma, C. Patel, A. K. Pandey, C. Das, S. Thulkar, V. Sreenivas, G. Kumar, A. Sharma, R. Kumar; All India Institute of Medical Sciences, Delhi, INDIA.

Introduction: The role of Dynamic PET/CT acquisition in Oncological patients is currently limited and primarily used for research purposes. However, when used as a routine procedure in patients evaluated following chemotherapy, dynamic PET/CT may carry additional value in predicting response in these patients. **Aim:** The current study aims to evaluate the possible role of dynamic PET/CT in patients with advanced stage NSCLC at baseline as well as following 4 cycles of chemotherapy. **Material and Methodology:** Seventeen patients (10 males and 7 females) with mean age 59.5 years with histopathologically diagnosed NSCLC (10 Squamous Cell Carcinoma and 7 Adenocarcinoma) were enrolled into this prospective study. Each patient underwent a prechemotherapy and post 4 cycle of chemotherapy dynamic acquisition with the primary tumor in the FOV for 60 minutes immediately followed by a routine whole-body static acquisition. Kinetic parameters from dynamic study (namely Ki and MRglu) were estimated at 30 and 60 minute as per Patlak graphical analysis. Routinely employed whole body quantification parameters (SUVmax, SUVavg, MTV, TLG) were also evaluated and included for analysis. The response evaluation was performed as per RECIST 1.1 and EORTC criteria. Appropriate statistical methods were applied and results were obtained with P value of less than 0.05 considered statistically significant. **Results:** Of the 17 patients, 3 had TNM stage 3 disease while 14 were at stage 4 on baseline evaluation. When we compared prechemotherapy and postchemotherapy PET/CT scan as per predefined response criteria, 11 patients were classified as responders (all Partial Response) and 6 as non-responders (2 Stable Disease, 4 Progressive Disease). With paired samples t-test, excepting MTV and TLG, the difference in means of pre-therapy and post-therapy SUVmax, SUVavg, TBR, Ki30, Ki60, MRglu30 and MRglu60 were all statistically significant (P < 0.05). To assess the discriminatory ability for non-responders, ROC curve analysis was performed between the Delta values (representing percent change) of kinetic parameters (Ki60, Ki30, MRglu60, MRglu30) and static semiquantitative parameters (SUVavg, SUVmax, TBR). ROC curve analysis showed more robust AUC values for DeltaKi60 (0.864), DeltaKi30 (0.900), DeltaMRglu60 (0.918) and DeltaMRglu30 (0.936) as against for DeltaSUVmax (0.845), DeltaSUVavg (0.845) and DeltaTBR (0.755); the Delta values for kinetic parameters obtained at 30 minutes of dynamic study had maximum AUC values. **Conclusion:** Our study suggests that dynamic PET/CT kinetic parameters, particularly the percent changes in the MRglu values, carry a higher discriminatory ability for non-responders in patients undergoing chemotherapy for advanced NSCLC.

OP598**Role of 18F-FDG PET/CT scan in predicting a pathological non-invasive status in solid-type Stage-I pulmonary adenocarcinomas**

A. Filice¹, F. Lococo², C. Rapiceta², D. Formisano³, A. Tartaglione¹, S. Bellafiore⁴, M. Roncali¹, S. Taddei⁵, F. Fioroni⁶, M. Paci², A. Versari¹; ¹Nuclear Medicine Unit IRCCS-Arcispedale Santa Maria Nuova, Reggio Emilia, ITALY, ²Unit of Thoracic Surgery IRCCS-Arcispedale Santa Maria Nuova, Reggio Emilia, ITALY, ³Department of Infrastructure Research and Statistics IRCCS-Arcispedale Santa Maria Nuova, Reggio Emilia, ITALY, ⁴Unit of Pathology IRCCS-Arcispedale Santa Maria Nuova, Reggio Emilia, ITALY, ⁵Unit of Pulmonology IRCCS-Arcispedale Santa Maria Nuova, Reggio Emilia, ITALY, ⁶Medical Physics Unit IRCCS-Arcispedale Santa Maria Nuova, Reggio Emilia, ITALY.

Objective: ¹⁸F-FDG-PET/CT is currently utilized for the characterization of solitary pulmonary nodules but there are various factors that can lead to false-negative results in PET/CT. On the other hand, low ¹⁸F-FDG uptake can predict a non invasive status in this context. We aim to clarify possible factors causing false-negative PET results in solid-type pulmonary adenocarcinomas (PA), and to evaluate the relationship between ¹⁸F-FDG uptake and histologic subtypes of PA because low ¹⁸F-FDG uptake can identify possible candidates for sublobar resection. **Methods:** we retrospectively reviewed PET/CT-records, clinical information, preoperative thin-section CT-images, and pathological features (classified by the IASLC/ATS/ERS subtyping criteria) of 94 consecutive patients, 58 males and 36 females (mean age= 68.7 yrs, range 42-85), with solid-type Stage-I NSCLCs. Patients underwent surgical resection at Our Institution from 01/2007 to 12/2014. Univariate and multivariate logistic analysis were used to identify and weigh the independent predictors of PET-findings: body weight, blood glucose level, tumor-size, and histological classification. **Results:** seventeen lesions (18.1%) were judged as PET-negative and 77 lesions (81.9%) as PET-positive. Overall, mean SUVmax was 8.0 (range 0-35) with higher SUVmax-values (p<0.001) in PA>2cm (mean SUVmax=10.6) than PA<2cm (mean SUVmax=4.8). PET false-negative (FN) results were also differently distributed (27.9% in PA <2cm vs 9.8% in PA>2 cm, p=0.023). Most lesions with positive PET/CT findings were located in the upper zones of the lung. When we divided the PA in 2 histological groups (Group 1 [“colloid/mucinous/lepidic”] vs Group 2 [“micropapillary/solid/acinar/papillary”]), the radiometabolic patterns were significantly different [mean SUVmax 3.8 in Class-A vs 9.9 in Class-B, p<0.001]. Similarly, a different distribution of PET FN-cases was observed (38.7% FN in Class-A vs 7.9% FN in Class-B, p=0.001). Both the tumor-size (cut-off=2cm) and IASLC/ATS/ERS aggregated clusters were clinically relevant factors for determining whether PET results were negative or positive, but only histology was statistically significant (OR:6.1, 95%CI: 1.85-20.15, p=0.003). **Conclusions:** tumor-size and histopathological findings were significantly associated with ¹⁸F-FDG-uptake in solid-type PA. Although lesions ≤2cm and “colloid/mucinous/lepidic” adenocarcinomas have a tendency for a very low ¹⁸F-FDG uptake we know that this pattern can be a favorable predictive factor to identify a non invasive status of the neoplasms and patients could be candidates for sublobar resection. However, in presence of a solitary pulmonary nodules newly diagnosed, in order to avoid diagnostic errors it is very important to discuss the cases in a multidisciplinary setting.

OP599**Multiparametric evaluation of [¹⁸F]FLT uptake and perfusion in EGFR-mutated NSCLC patients undergoing treatment with a EGFR Tyrosine Kinase Inhibitor**

R. Iqbal, G. M. Kramer, V. Frings, E. F. Smit, O. S. Hoekstra, R. Boellaard; VU University Medical Center, Amsterdam, NETHERLANDS.

Background: 3'-deoxy-3'-[¹⁸F]fluorothymidine ([¹⁸F]FLT) was proposed as an imaging biomarker for the assessment of *in vivo* cellular proliferation with positron emission tomography (PET). The aim of the current study was to gain insight in the parametric relationship between [¹⁸F]FLT uptake and perfusion in non-small cell lung cancer (NSCLC) patients undergoing treatment with a tyrosine kinase inhibitor (TKI). **Methods:** Six patients with metastatic NSCLC, having an activating epidermal growth factor receptor (EGFR) mutation were included in this study. Patients underwent [¹⁵O]H₂O and [¹⁸F]FLT PET/CT scans at three different time points: 7 d before treatment, and 7 and 28 d after start of treatment with a TKI (gefitinib or erlotinib). Parametric analyses were performed to generate quantitative 3D images of both perfusion and [¹⁸F]FLT volume of distribution (V_T). Next, multiparametric

classification was performed by classifying voxels as low and high perfusion and/or low and high V_T using an absolute threshold based on the average tumor values of all lesions (for all time points). By combining these initial classifications, voxels were allocated to 4 categories (low perfusion-low V_T ; low perfusion-high V_T ; high perfusion-low V_T and high perfusion-high V_T). **Results:** A total of 17 perfusion and 20 [^{18}F]FLT PET/CT scans were evaluated. The average tumor values across all lesions were 0.53 ± 0.26 mL/mL/min and 4.25 ± 1.71 for perfusion and [^{18}F]FLT V_T , respectively. Multiparametric analysis suggested a shift in voxel distribution, particularly regarding V_T : from at least 47% voxels of each lesion classified in the “low- and high perfusion-high V_T -category” to at least 77% voxels classified in the “low- and high perfusion-low V_T -category”. The shift was most prominent 7 d after treatment and remained relatively similar afterwards. Changes in perfusion and its distribution were minimal. **Conclusion:** The present data indicate that parametric changes in [^{18}F]FLT uptake do not seem to be the result of parametric changes in perfusion, suggesting that [^{18}F]FLT uptake distribution and its change is independent of perfusion. **Keywords:** positron emission tomography (PET), non-small cell lung cancer (NSCLC), [^{18}F]FLT, perfusion, tyrosine kinase inhibitors (TKIs)

OP600

FDG PET-CT SUVmax and IASLC/ATS/ERS histologic classification: a new profile of lung adenocarcinoma with prognostic value

M. Suárez-Piñera¹, L. Pijuan², A. Rodríguez-Fuster³, A. Mestre-Fusco¹, M. Cufí⁴, A. Taus⁵, A. Sánchez-Font⁶, N. Rodríguez de Dios⁷, F. Zuccarino⁴, V. Curull⁶, F. Fernández-Alarza⁴, J. Belda-Sanchis³; ¹Nuclear Medicine Department, Hospital del Mar Parc de Salut Mar, Barcelona, SPAIN, ²Pathology Department, Hospital del Mar Parc de Salut Mar, Barcelona, SPAIN, ³Thoracic Surgery Department, Hospital del Mar Parc de Salut Mar, Barcelona, SPAIN, ⁴Radiology Department, Hospital del Mar Parc de Salut Mar, Barcelona, SPAIN, ⁵Oncology Department, Hospital del Mar Parc de Salut Mar, Barcelona, SPAIN, ⁶Pneumology Department, Hospital del Mar Parc de Salut Mar, Barcelona, SPAIN, ⁷Radiotherapy Department, Hospital de la Esperanza Parc de Salut Mar, Barcelona, SPAIN.

Aims: Tumor stage is the strongest prognostic factor in lung adenocarcinoma (LA) and the best guide for treatment decisions. Histopathological and metabolic criteria may be useful to overcome the heterogeneity problem in LA. The aims of this study were to determine whether the F18-FDG PET/CT standard uptake value (SUVmax) can provide information about IASLC/ATS/ERS histological subtypes of LA and to evaluate whether the combination of both parameters can prognostically stratify these patients. **Methods:** 103 cases of surgically resected LA with pre-surgical FDG-PET/CT were retrospectively reviewed. FDG uptake was quantified using SUVmax. All resected specimens were histologically classified according to IASLC/ATS/ERS classification of LA adenocarcinoma in situ -AIS-, minimally invasive adenocarcinoma -MIA- and invasive adenocarcinoma (divided into lepidic, papillary, acinar, solid, micropapillary and mucinous based on the predominant pattern). These lesions were grouped in 3 categories using prognostic criteria: Group 1; low grade (AIS, MIA), group 2; intermediate grade (lepidic, acinar, papillary) and group 3; high grade (micropapillary, solid and mucinous). One way analysis of variance and Bonferroni's test were performed to evaluate statistical differences between groups. Overall and disease-free survival rates were calculated by the Kaplan-Meier method. **Results:** The distribution of histological subtypes were: AIS (n=4), MIA (n=4), lepidic predominant (n=13), acinar predominant (n=51), papillary predominant (n=12), micropapillary predominant (n=2), solid predominant (n=12) and invasive mucinous adenocarcinoma (n=5). SUVmax values (mean±SD) were: 2.4 ± 2.7 in group 1, 7.7 ± 6.6 in group 2 and 8.3 ± 5.6 group 3. Mucinous adenocarcinomas (group 3) showed a low mean SUVmax (2.6 ± 1.4) despite its high histological grade, probably related to

the mucus content. Acinar adenocarcinoma (group 2) showed a high variability SUVmax 8.6 ± 6 , no statistical differences were found with solid tumors (group 3) SUVmax 10.1 ± 4.9 . A reason for these results in the acinar tumor could be the variability of the second cellular component. We obtained a significantly highest SUVmax value in acinar tumors accompanied by a second histological subtype intermediate or high grade than pure acinar or accompanied by the low grade subtype Increased SUVmax were associated with poor prognostic tumors. We found significant differences in SUVmax among 3 subgroups corresponding to recurrence risk ($p < 0.0001$) **Conclusions:** SUVmax can be an orientative parameter of histological LA subtypes according the proposed IASLC/ATS/ERS classification, specifically for high-intermediate grade. The heterogeneity observed in LA seems to be related to different histologic subtypes and metabolic behaviour (SUVmax), reflecting different malignant grade and different prognosis.

OP601

The role of FDG-PET/ccCT in peritoneal mesothelioma

A. Skanjeti¹, J. Dubreuil¹, P. Rousset², D. Rubello³, N. Bakrin⁴, G. Passot⁴, S. Isaac⁵, O. Glehen⁴, F. Giammarile¹; ¹Hospices Civils de Lyon - Nuclear Medicine, Lyon, FRANCE, ²Hospices Civils de Lyon - Radiology, Lyon, FRANCE, ³Santa Maria della Misericordia Hospital - Nuclear Medicine, Rovigo, ITALY, ⁴Hospices Civils de Lyon - General and oncologic surgery, Lyon, FRANCE, ⁵Hospices Civils de Lyon - Pathology, Lyon, FRANCE.

Purpose. To assess glucose metabolism of Multicystic Peritoneal Mesothelioma (MPM) and Epithelioid Peritoneal Mesothelioma (EPM), by FDG-PET/CT and to assess the prognostic impact of FDG uptake. **Material and Methods.** Twenty-three patients (9 males, age 54 ± 16 years) scheduled for peritoneal mesothelioma treatment by cytoreductive surgery and intraperitoneal chemotherapy, underwent FDG-PET/CT between September 2009 and March 2014. No previous treatment was performed. FDG-PET/CT was interpreted by two nuclear physicians as positives or negatives for the presence of EPM or MPM, respectively. SUVmax of each lesion was measured retrospectively based on lesions described on post-surgery data. At laparotomy, disease extension was estimated with the Peritoneal Cancer Index (PCI). Median follow-up was 27 months (95%CI 12.9-37.8), time to recurrence were recorded. **Results.** Nine patients had MPM and 14 EPM. PET showed a mild focal uptake in one case of MPM, while in 8 patients no abnormal uptake was observed at the site of the primary disease. PET was positive in 12/14 patients with EPM. Sensitivity, specificity and accuracy were respectively 86%, 89%, and 87%. Nine patients with EPM had recurrent disease, 3 died during follow-up, while no patients with MPM had recurrent disease. MPM histology was associated with a lower $\text{SUVmax}_{\text{lesion}}$, $\text{SUVmax}_{\text{lesion/liver}}$, PCI, younger age, and it was observed only in women. $\text{SUVmax}_{\text{lesion}}$ and age were associated with Progression Free Survival (PFS) in patients with EPM. **Conclusion.** FDG-PET/CT showed significant differences between MPM and EPM while $\text{SUVmax}_{\text{lesion}}$ was associated with PFS in EPM. Then, FDG-PET/CT is a promising tool in patients with EPM.

OP602

Effect of segmentation method on texture parameters' reproducibility and predictive / prognostic ability when derived from 18F-FDG PET scans in patients with non-small cell lung cancer

U. Bashir, G. Azad, M. Siddique, N. Patel, S. Dhillon, D. Landau, V. Goh, G. J. Cook; St. Thomas' Hospital, London, UNITED KINGDOM.

Background: 18F-FDG PET derived measures of tumour heterogeneity are increasingly being reported as potential biomarkers of cancer classification, prognostication, and response prediction. A number of

segmentation methods have been used but their effects on repeatability and predictive / prognostic power have not been evaluated. Purpose: The purpose of our study was to compare three segmentation techniques, i.e. freehand, threshold-based, and fuzzy locally adaptive bayesian (FLAB), on 18F-FDG PET scans from patients with NSCLC i) to measure inter-observer reproducibility and ii) to determine the effects of different segmentation methods on the predictive ability of multiple texture features in terms of overall survival and response to chemoradiotherapy. Materials & Methods: 18F-FDG PET scans acquired before chemoradiotherapy on 53 patients (mean age: 65.8 years; 31 males, 22 females) with non-small cell lung cancer were examined retrospectively. Three readers (clinical oncologist, radiologist and nuclear medicine physician) drew freehand regions of interest around the tumours and the freehand ROIs were then processed by software (implemented in MATLAB 2013b) to generate segmentation ROI maps based on intensity threshold (40% of maximum) and FLAB. For each segmentation technique, the agreement between the three observers was assessed using the intra-class correlation (ICC) coefficient. Univariate cox regression was used to examine the association between each of the PET texture parameters and patient survival time, taking 0.01 as p-value cut-off to determine statistical significance. This conservative cut-off was chosen to correct for the large number of texture parameters. The differences between mean texture-values of responders and nonresponders were assessed using Mann-Whitney U test. Results: Compared with FLAB, threshold-based segmentation showed significantly higher ICC in 24 of 85 parameters, whereas freehand ROIs showed lower ICC in 36 parameters and higher ICC in 1. On survival analysis, threshold-based segmentation yielded the greatest number of significant associations between survival and texture values (8 vs. 2 for FLAB and 1 for freehand). Responders and nonresponders showed statistically different mean texture values for 6 features when tumour were segmented using FLAB, compared with 5 and 2 features using freehand and 40% threshold respectively. Conclusion: The tumour segmentation techniques - FLAB, freehand, and threshold-based - overlap in their ability to predict survival and response to treatment and seem generally comparable. However, 40% threshold-based ROI segmentation shows significantly less inter-observer variability than the other two, a property that makes it a favourable choice for tumour segmentation from 18F-FDG PET images.

OP603

FDG-PET early identifies lesions at risk of recurrence under treatment by tyrosine kinase inhibitors in patients with metastatic (EGFR)-mutated lung adenocarcinoma

A. ADENS, G. PETYT, A. CORTOT, H. LAHOUSSE, G. COLLET, C. HOSSEIN-FOUCHER, D. BELLEVRE; CHRU Lille, Lille CEDEX, FRANCE.

Background: ^{18}F -FDG PET/CT is used to evaluate the response to treatment and to detect earlier the recurrence in patients with lung cancer. The aim of the study was to determine the predictive value of metabolic parameters measured by PET/CT to identify lesion with higher risk of progression, in patient treated by tyrosine kinase inhibitor (TKI) in first line for metastatic lung adenocarcinoma harboring activating epidermal growth factor receptor (EGFR) mutation. **Methods:** Thirteen patients were retrospectively analyzed. Eighty-nine lesions among patients with multiple lesions were analyzed. SUVmax, SUVmean, Metabolic Tumor Volume (MTV) and Total Lesion Glycolysis (TLG) were measured on ^{18}F -FDG PET/CT for each lesion at baseline and at first treatment evaluation. At baseline, lesions were separated into tertile, depending on their metabolic activity. At first evaluation, lesions were divided in two groups as follow: incomplete response (metabolic lesion was still measurable) and complete response (no visually detected lesion). In the patient-based analysis, progression free survival (PFS) was compared regarding complete or incomplete response status at first treatment evaluation PET/CT. **Results:** At baseline, a lesion with high metabolic parameters (SUVmax, MTV, TLG) was significantly associated to earlier progression

($p=0.0028$, $p=0.0028$ $p=0.0032$ respectively). At time of first evaluation, lesions considered in incomplete response were significantly associated with high risk of progression (OR= 9.6, $p=0.0004$). On patient based analysis, complete response on first PET/CT evaluation, was predictive of a significantly better PFS (354 days vs. 184 days, $p=0.03$). **Conclusion:** Lesions with incomplete early metabolic response were significantly associated with a high risk of progression, in patients with lung adenocarcinoma treated by TKI. Identification of these lesions could affect therapeutic management such as close follow-up or local therapy.

1508 – Tuesday, October 18, 2016, 16:30 - 18:00, Hall 212

Cardiovascular System: Myocardial Perfusion - PET

OP604

Does fractional flow reserve truly identify coronary artery stenosis causing myocardial ischemia?

R. Assante¹, E. Zampella¹, C. Nappi¹, V. Gaudieri², T. Mannarino¹, G. Rossi¹, W. Acampa¹, M. Petretta¹, G. Arena³, P. Golino³, A. Cuocolo¹; ¹University Federico II, Naples, ITALY, ²Institute of Biostructure and Bioimaging, National Council of Research, Naples, ITALY, ³Cardio-thoracic and respiratory sciences, Second University of Naples, Naples, ITALY.

Aim: Despite the clinical importance of coronary physiological assessment, the relationship between coronary flow reserve (CFR) and fractional flow reserve (FFR) remains poorly defined. We aimed at studying the relationship between absolute CFR and FFR in patients with stable coronary artery disease. **Material and Methods:** A total of 54 patients with stable coronary artery disease underwent Rb-82 positron emission tomography (PET)/computed tomography (CT) cardiac imaging at rest and after pharmacological stress test (dipyridamole 0.142 mg/kg/min for 4 min). Thereafter, all patients also underwent invasive coronary angiography with FFR assessment. At PET/CT cardiac imaging, resting and hyperemic myocardial blood flow (MBF) and CFR were automatically quantified. CFR was calculated as the ratio of hyperemic to baseline MBF and was considered reduced when <1.74 . At coronary angiography, FFR was measured during intracoronary administration of adenosine (200 μg) and was considered abnormal when ≤ 0.8 . A total of 60 coronary artery stenoses were studied. **Results:** A significant, albeit modest, correlation between CFR and FFR ($r=0.38$, $P=0.003$) was found. In particular, of the 34 coronary artery stenoses with an abnormal FFR value ≤ 0.8 , 18 (53%) showed a reduced CFR, while the other 16 (47%) coronary artery stenoses had a normal CFR. In contrast, of the 26 coronary artery stenoses with a FFR value above 0.8, only 5 (19%) showed a reduced CFR, while the other 21 (81%) had a normal CFR. **Conclusions:** In this preliminary series, FFR values >0.8 , indicating a non-significant coronary artery stenosis, show an excellent correlation with absolute CFR, while pathological FFR values (<0.8) poorly correlate with a reduced CFR. This discordance should be probably taken into account when facing the choice of recommending revascularization solely on the basis of FFR values.

OP605

Role of microvascular dysfunction in the weak association found between stress myocardial blood flow measured with ^{82}Rb rubidium PET and FFR values measured during coronary angiography?

R. Chequer¹, E. Sorbets², A. Touati¹, S. Leygnac¹, M. Milliner¹, N. Mikail³, H. Regaieg¹, R. Ben Azzouna¹, G. Ducrocq⁴, F. Rouzet¹, D. Le Guludec¹, F. Hyafil¹; ¹Department of Nuclear Medicine, Bichat Hospital, AP-HP, PARIS, FRANCE, ²Department of Cardiology, Avicennes Hospital, AP-HP, Bobigny, FRANCE, ³Department of Nuclear Medicine, Beaujon Hospital, AP-HP, Clichy, FRANCE, ⁴Department of Cardiology, Bichat Hospital, AP-HP, PARIS, FRANCE.

Background. Fractional flow reserve (FFR) allows for invasive hemodynamic evaluation of the impact of coronary stenosis on blood flow. 82 Rubidium(Rb)-positron emission tomography (PET) provides noninvasive quantification of absolute myocardial blood flow (MBF) during pharmacological stress. **Purpose.** The aim of this study was to test whether stress MBF quantified noninvasively with Rb-PET predicted the FFR measured invasively in corresponding coronary arteries. **Methods.** A total of 20 patients who underwent MPS with Rb-PET and coronary angiography (CA) with measurement of FFR were included in this study. PET was acquired in a dynamic mode during the injection of 10 MBq/kg of 82 Rubidium and intravenous dipyridamole-induced hyperemia. Stress MBF values were calculated for the left ventricle (global LV MBF) and for each of the 17 segments of the AHA classification using the FlowQuant software. FFR was measured in 29 different coronary arteries with stenosis > 50 % after intra-coronary injection of adenosine. The lowest value of stress MBF quantified with Rb-PET in a coronary territory was compared to the minimal FFR value measured along the corresponding coronary artery. **Results.** Among the 29 coronary arteries evaluated with FFR, 14 had a FFR \leq 0.80 and 15, a FFR > 0.80. Only a weak correlation was found between minimal stress MBF quantified with Rb-PET and minimal FFR in corresponding coronary artery ($r = 0.28$; $p = 0.13$). Using a threshold for minimal stress MBF < 1.8 ml/mn/g in each coronary arterial territory, sensitivity and specificity for the detection of FFR \leq 0.80 was 100 % and 50 %, respectively. In coronary arteries with a FFR \leq 0.80 during CA, all corresponding arterial territories had a minimal stress MBF \leq 1.8 ml/mn/g quantified with Rb-PET (mean MBF = 1.2 ± 0.3 ml/mn/g). In the remaining 15 coronary arteries with FFR > 0.80, 8 arterial territorial presented a minimal stress MBF < 1.8 ml/mn/g. In all these patients, global LV MBF was < 2 ml/mn/g in absence of 3-vessel disease suggesting diffuse microvascular dysfunction, whereas in the remaining 7 coronary arteries the global LV MBF was > 2 ml/mn/g (mean global LV MBF = 1.4 ± 0.3 vs. 3.0 ± 0.7 ml/mn/g, respectively; $p = 0.001$). **Conclusions.** In this study, only weak correlation was found between stress MBF quantified with Rb-PET and FFR measured invasively during CA, mostly because of the addition of microvascular dysfunction to the impact of epicardial coronary stenosis in stress MBF measurements.

OP606

Rubidium-82 PET myocardial blood flow compared to fractional flow reserve in patients with coronary artery disease

J. J. Boer, J. M. H. de Klerk, E. A. de Vrey, B. J. G. L. de Smet; Meander medical centre, Amersfoort, NETHERLANDS.

Purpose Measurement of the fractional flow reserve (FFR) is the current gold standard in assessing the significance of coronary stenosis. Rubidium-82 (Rb-82) allows non-invasive measurement of myocardial bloodflow (MBF) during stress and rest down to the microvascular level allowing the detection of microvessel disease. In this retrospective study we compared the Rb-82 derived MBF measurements introduced in our hospital in 2014 to FFR measurements and other coronary angiography (CAG) findings. **Method and materials** In 2014 RB-82 myocardial perfusion PET was performed in 482, 182 of these patients underwent coronary angiography. In these patients we correlated the findings of FFR and degree of visual stenosis in each major coronary vessel to the Rb-82 derived flow measurements. We documented the result in treatment with regard to revascularization or conservative drug therapy. **Results** A total of 182 CAG and 42 FFR findings in 482 patients were found. FFR measurements were rarely performed in patients with perfusion deficits corresponding with a visual significant epicardial stenosis, due to immediate intervention. In 46% of the vessels with visual stenosis > 50% both the FFR and MBF were normal. In 48% of the cases there was discrepancy between the FFR and Rb-82 derived MBF. In 20% of all patients there was a decreased FFR and normal MBF. There was no significant correlation between the MBF and visual degree of stenosis. All patients with a FFR below 0,8 received revascularization. In the subgroup of patients (n=9) with decreased coronary stressflow and FFR above

0,8 none underwent revascularization. **Conclusion** There is a significant number of patients with discrepancy between MBF and FFR measurements. Possible explanations include the difference between focal versus more diffuse epicardial coronary artery disease and the presence of microvessel disease. Further investigation is required to determine whether rubidium-82 derived MBF can be of additional value in identifying culprit lesions and to select patients for revascularisation.

OP607

Combined Assessment of Myocardial Perfusion and Coronary Flow Reserve by Hybrid Rb-82 PET/CT Imaging Improves the Identification of Obstructive Coronary Artery Disease

E. Zampella¹, R. Assante¹, W. Acampa¹, C. Nappi¹, V. Gaudieri², M. Panico², T. Mannarino¹, V. Vultaggio¹, P. Buongiorno¹, M. Petretta¹, A. Cuocolo¹; ¹University Federico II, Naples, ITALY, ²Institute of Biostructure and Bioimaging, National Council of Research, Naples, ITALY.

Aim: Positron emission tomography (PET)/computed tomography (CT) myocardial perfusion imaging (MPI) allows the incorporation of coronary flow reserve (CFR) into clinical protocol. We sought to determine whether the combined analysis of MPI and CFR improves the diagnostic accuracy of PET/CT to predict obstructive coronary artery disease (CAD). **Materials and Methods:** We evaluated 130 consecutive patients (age 60±11 years) with suspected or known CAD referred to stress Rb-82 PET/CT imaging and invasive coronary angiography. Myocardial perfusion was quantified automatically for left anterior descending (LAD), left circumflex (LCX) and right (RCA) coronary artery territories as ischemic total perfusion defect (ITPD) for 390 vessels. Resting and hyperemic myocardial blood flow (MBF) and CFR were automatically quantified. CFR was calculated as the ratio of hyperemic to baseline MBF and was considered reduced when <1.74. Obstructive CAD was defined as \geq 75% stenosis at coronary angiography. Logistic regression analyses were used to determine the variables associated with obstructive CAD. Net reclassification improvement (NRI) was calculated to assess whether CFR can reclassify patients with obstructive CAD. **Results:** MPI was normal in 65 (50%) patients. Mild-moderate (ITPD 1-9%) and severe (ITPD \geq 10%) reversible perfusion defects were observed in 44 (34%) and 21 (16%) patients, respectively. In the overall population, obstructive CAD was present in 40 (31%) patients. Patients with obstructive CAD had a higher prevalence of reduced CFR (<1.74) (47% vs. 22%, $P < 0.05$) and a higher ITPD value (8.6 ± 7 vs. 2.9 ± 3 , $P < 0.001$) compared to those without. At univariable analysis, age ($P < 0.05$), reduced CFR ($P < 0.05$) and ITPD ($P < 0.001$) were significant predictors of obstructive CAD. At multivariable analysis, only reduced CFR ($P < 0.05$) and ITPD ($P < 0.001$) were independently associated with presence of obstructive CAD. The addition of CFR to clinical data and ITPD increased the global chi-square value of the model in predicting obstructive CAD (chi-square from 46 to 52, $P < 0.05$). At per-vessels analysis, 55 (14%) vessels showed obstructive stenosis and 335 (86%) did not. The mean CFR was significantly lower in coronary vessels with obstructive stenosis as compared to other vessels (1.7 ± 0.7 vs. 2.3 ± 0.8 , $P < 0.01$). NRI obtained by adding CFR to a model including clinical data and ITPD was 0.6. **Conclusions:** CFR provides incremental information about the presence of obstructive CAD over established cardiac risk factors and MPI parameters. A combined use of MPI and CFR can help to predict more accurately the presence of obstructive CAD.

OP608

Myocardial Blood Flow Quantification in PET: Can We Agree on Values?

S. V. Nesterov^{1,2}, J. M. Knuuti¹; ¹Turku PET Centre, Turku, FINLAND, ²Institute of Evolutionary Physiology and Biochemistry RAS, St. Petersburg, RUSSIAN FEDERATION.

PET myocardial blood flow (MBF) quantification needs dedicated software (SW). The number of existing SW tools and tracer-kinetic models they implement is substantial and grows; they all are separately validated and then used in research or clinic; however, the global standard for PET MBF quantification is yet missing. To standardize, we must assess the agreement between the existing SW tools. AIM. To assess the agreement between the SW tools for PET MBF quantification using Rb-82, O-15 water and N-13 PET. MATERIALS AND METHODS. We finalized cross-comparing Rb-82 (N=48 and 10 SW) and O-15 water (N=91; 5 SW) PET data from CAD-suspected patients, and are in the process of comparing N-13 PET (11 SW). SW tools included CardiacVUer, Carimas, Corridor4DM, FlowQuant, HOQUTO, ImagenQ, MunichHeart, QPET, PMOD, Syngo.MBF, and UW-QPP. Experts have used one of the SW tools each to analyze global, regional (LAD, LCx and RCA) and segmental MBF and MFR using dynamic PET scans—rest and pharmacologically induced stress. We applied a custom linear mixed model for the repeated measures to produce the two agreement metrics—intraclass correlation coefficient (ICC) and difference between the values from the models—calculated pairwise. Differences below 20% of median values with corresponding ICCs above 0.75 witnessed to good reproducibility. RESULTS. Rb-82: differences between global and regional MBF values as measured with different SW tools could be as large as 130%; nonetheless, the tools that implemented the 1-TCM (Lortie et al. 2007) could be used interchangeably on global and regional levels. On the segmental level, however, only four tools—Carimas, PMOD, QPET, and syngo MBF—fulfilled the criteria for agreement. O-15 water: the studied SW tools demonstrated good intraobserver reproducibility, yet the agreement between the tools did not fulfill the predetermined criteria even on the global and regional levels. CONCLUSION. Values received from PET MBF quantification depend on the implemented kinetic model and, to a certain extent, depend on the software tool used. The extent, in our studies, depended on the PET tracer.

OP609

Validation of Carimas2.9 vs Carimas1 on ¹⁵O-water cardiac perfusion ischemic cutoff value

C. Han, J. Knuuti; Turku PET Centre and Turku University Hospital, TURKU, FINLAND.

Purpose: Carimas is a widely used analysis tool for ¹⁵O-labeled water cardiac perfusion study, developed in Turku PET Centre of Finland (<http://www.turkupetcentre.fi/carimas>). Cutoff value for ischemia in absolute terms has been validated in Carimas1 as 2.4 ml/g/min for stress study (Circ Cardiovasc Imaging 2011). However, it is unknown that if this value is still validated in new generation of Carimas (Carimas2). This study was designated to investigate the validation of this absolute cutoff value in Carimas2 based on clinical cardiac perfusion study data.

Materials and Methods: 96 patients with moderate (30%–70%) pretest likelihood of coronary artery disease underwent ¹⁵O-labeled radio water PET studies during adenosine stress were enrolled. Patient images were analyzed using Carimas1 and Carimas v2.9 independently. Absolute myocardial blood flow was calculated. The patients and the vessel regions (LAD, RCA and LCX) then were classified as normal or abnormal based on a cutoff value of 2.4ml/g/min. Cohen's Kappa analysis was employed for validation. **Results:** Total number of vessel regions is 288 (96*3) in 96 patients. Application of cutoff value of 2.4ml/g/min to Carimas2 results in: true positive 79, false positive 10, false negative 19, and true negative 180, respectively. Cohen's Kappa is 0.773 and agreement 0.899. In patient-based analysis: true positive 31, false positive 3, false negative 2, and true negative 60, respectively. Cohen's Kappa is 0.885 and agreement 0.947. **Conclusions:** Using the same absolute cutoff of 2.4 ml/g/min for evaluating ischemia on ¹⁵O-labeled radio water cardiac perfusion study, new generation of Carimas (Carimas v2.9) gives a substantial agreement of accuracy compared with Carimas 1. Therefore, new generation of Carimas can be used for analyzing cardiac PET perfusion studies.

OP610

Absolute Stress Myocardial Blood Flow Determines Ventricular Function and Synchrony Better than Myocardial Perfusion Reserve: a ¹³N-ammonia PET Study

L. Juárez-Orozco¹, E. Alexanderson², R. A. Dierckx¹, H. H. Boersma¹, C. J. Zeebregts¹, N. Prakken¹, R. A. Tio¹, R. H. J. A. Slart³; ¹University Medical Center Groningen, Groningen, NETHERLANDS, ²Instituto Nacional de Cardiología "Ignacio Chávez", Mexico City, MEXICO, ³University of Twente, Enschede, NETHERLANDS.

Introduction. Cardiac PET represents the reference technique for the absolute quantification of myocardial blood flow (MBF) and perfusion reserve (MPR). EKG-Gated PET datasets additionally assess ventricular function in three complementary spheres: systolic, diastolic and ventricular synchrony. Stress MBF and MPR have proved superior diagnostic performance to relative measurement of myocardial tracer retention and recent studies suggest that stress-MBF may outperform MPR in the detection of significant coronary artery disease (CAD). Our aim was to evaluate whether stress MBF or MPR better relates with integral ventricular function in patients with known or suspected CAD. **Methods.** We studied 248 patients who underwent a rest - adenosine-stress PET perfusion scan with ¹³N-ammonia for the evaluation of myocardial ischemia. Quantitative perfusion was assessed by stress MBF and MPR. Ventricular systolic function was evaluated through the left ventricular ejection fraction (LVEF), diastolic function through the mean filling rate in the first third of diastole (MFR/3) and ventricular synchrony through entropy (E). Clinically relevant variables considered were: gender, age, body mass index (BMI), hypertension (HTN), dyslipidemia, type-2 diabetes mellitus (DM2), smoking habit, prior MI, scar extent and semi-quantitative ischemic burden (SDS). We performed a multivariate analysis of variance (GLM) inputting LVEF, MFR/3 and E as the dependent variables (integral ventricular function). We included both stress-MBF and MPR into the model along with the relevant covariates. The independent significance of the included predictors was tested using Pillai's trace criterion F-statistic. **Results.** Our sample included 166 men and 82 women with a mean age of 63±11 and 67±11 years. There were 60% of patients with HTN, 55% with dyslipidemia, 21% with DM2, 45% of smokers and 34.7% with a previous MI. Quantitative perfusion documented a mean stress-MBF of 1.99±0.74 mL/g/min and a mean MPR of 2.54±0.92. Ventricular function measurements showed a mean LVEF=61.6±15%, mean MFR/3=1.12±0.38 EDV/s and mean E=45.6±11.2%. The multivariate analysis demonstrated that stress-MBF is a significant predictor (F[3,174]=7.25, p<0.001) for integral ventricular function (LVEF, MFR/3 and E) while MPR only showed a trend towards significance (F[3,174]=2.47, p=0.063). Gender, age, DM2 and extent of previous MI were also significantly related to the dependent variables. **Conclusions.** Stress MBF is better related to integral ventricular function than MPR, as evaluated by PET, when accounting for relevant covariates. Our results suggest that the reported better performance of stress MBF for diagnosing significant CAD could be, at least partially, linked to its stronger relationship to ventricular function measurements. Further research into the preferential application of stress MBF in cardiac PET imaging is warranted.

OP611

Diffuse subendocardial hypoperfusion leads to transient left ventricular cavity dilation by ¹³N-ammonia perfusion PET imaging in hypertrophic cardiomyopathy patients

H. Yalcin¹, I. Valenta², F. Yalcin¹, A. Tahani², N. Kucukler¹, N. Vasquez¹, I. Pozios¹, Y. Zhou², M. Pomper², T. Abraham¹, T. Schindler², M. R. Abraham¹; ¹JOHNS HOPKINS UNIVERSITY, Hypertrophic Cardiomyopathy Center of Excellence, Department of Medicine, BALTIMORE, MD, UNITED STATES, ²JOHNS HOPKINS UNIVERSITY, Division of Nuclear Medicine, Department of Radiology, BALTIMORE, MD, UNITED STATES.

Objectives: To investigate the mechanisms underlying vasodilator-induced transient left ventricular cavity dilation (LVCD) in HCM. **Background:** Vasodilator-induced transient LVCD has been linked to reduction in global myocardial blood flow, but direct proof for subendocardial hypo-perfusion during LVCD by positron emission tomography (PET) is lacking in HCM patients. **Methods:** Rest and stress ejection fraction (LVEF) and MBF were quantified in the subepicardial and subendocardial regions of the LV and globally, in 104 HCM patients, using $^{13}\text{NH}_3$ -PET. HCM patients were divided into two groups, based on the presence or absence of LVCD ($\text{LV volume}_{\text{stress}}/\text{LV volume}_{\text{rest}} > 1.13$). LV wall thickness, LV outflow tract gradients (LVOTG), diastolic function (E/E') were assessed by Echocardiography. Analysis of baseline and stress EKGs was performed digitally using Cardio Calipers software. **Results:** Transient LVCD was seen in 55 patients (52%). Maximum LV wall thickness (2.19 ± 0.6 vs 1.94 ± 0.4 cm; $p=0.02$), stress LVOTG (65 ± 51 vs 44 ± 34 mmHg; $p=0.016$), mitral E/E' (20 ± 9 vs 15.1 ± 5.14 , $p=0.001$) and ischemic ST-T changes following vasodilator infusion ($p=0.008$) were significantly higher in HCM patients with LVCD, when compared to patients without LVCD. Rest LVEF was preserved and similar in the 2 groups. Patients with LVCD had lower stress-LVEF (43 ± 11 vs 53 ± 10 ; $p < 0.001$), lower stress-MBF in the subendocardial region (1.69 ± 0.77 vs 2.33 ± 1.03 ml/min/g; $p < 0.001$) and greater regional myocardial perfusion abnormalities (SDS score: 7.0 ± 6.1 vs 3.9 ± 4.3 ; $p=0.004$) by PET, than patients without LVCD. The transmural perfusion gradient (subendocardial MBF /subepicardial MBF ratio), an indicator of subendocardial perfusion was similar in HCM patients with/without LVCD at baseline. Notably, HCM patients with LVCD had greater reduction in the transmural perfusion gradient ($\sim 62\%$) following vasodilator, when compared to HCM patients without LVCD ($\sim 25\%$), resulting in lower stress-transmural perfusion gradients in LVCD patients (0.85 ± 0.22 , LVCD⁺ vs 1.09 ± 0.39 , LVCD⁻; $p < 0.001$). Global myocardial flow reserve (MFR), stress-LVEF and stress-transmural perfusion gradient were associated with LVCD. **Conclusion:** Diffuse subendocardial hypoperfusion and myocardial ischemia resulting from microvascular dysfunction, contribute to development of transient PET-LVCD in HCM.

1510 – Tuesday, October 18, 2016, 16:30 - 18:00, Hall 114

Neurosciences: Psychiatry & Neurotransmission

OP612

JDTic-based radiotracers for Kappa Opioid Receptor PET Imaging: Design, Synthesis, Pharmacology, Molecular Modeling Studies, Radiolabelling, in vivo Characterization and Metabolic Investigation

C. Perrio¹, S. Schmitt¹, J. Delamare¹, O. Tirel¹, M. Dhilly¹, F. Fillesoye¹, N. Colloc'h², ¹UMR 6301 ISTCT, LDM-TEP, CNRS, CEA, Université Caen Normandie, CAEN, FRANCE, ²UMR 6301 ISTCT, CERVOxy, CNRS, Université Caen Normandie, CAEN, FRANCE.

Aim. JDTic belongs to a unique class of compounds exhibiting pure opioid antagonist activity that may prove useful in the treatment of obesity, psychosis and depression, as well as opioid and cocaine abuse and other central nervous system disorders.¹ We anticipated that ^{11}C - and ^{18}F -radiolabelled derivatives of JDTic would represent attractive radiopharmaceuticals to investigate drug addiction and associated psychiatric disorders (schizophrenia, depression) by PET imaging. **Methods.** We designed and synthesized a series of *N*, *O*-methyl and fluoroalkyl derivatives of JDTic. We compared their opioid receptor properties in both in vitro assays and modeling approach. The *N*-methyl and *N*-fluoropropyl JDTic derivatives were concluded to possess favorable properties to be considered as a valuable candidates as imaging agent. We performed their radiolabelling with carbon-11 and fluorine-18 by ^{11}C -methylation and ^{18}F -fluoropropylation respectively. We determined their biodistribution and specific binding after pre-treatment with U50,488 in mouse and rats by microTEP and microdissection. Additional radiometabolization and metabolization studies were

undertaken in vivo and in vitro in mouse or human liver microsomes by UPLC-MS. **Results.** We found that all new fluorinated compounds bound selectively KOR but in less extent than JDTic and its *N*-methylated derivative. *N*-Fluoroalkylation was preferable to *O*-alkylation to keep a selective KOR binding. Modeling studies based on the crystal structure of the JDTic/KOR complex revealed that fluorine atom in the *N*-fluoropropyl JDTic derivative was involved in the selective KOR binding. Radiochemistry was performed efficiently to lead to the two target radioligands. The *N*- ^{11}C -methyl JDTic derivative (10% total radiochemical yield, 60 min total synthesis time, RAS = 1.5–4.5 GBq/ μmol) was found to display a high specific binding in vivo whereas the *N*- ^{18}F -fluoropropyl JDTic (5% total radiochemical yield, 2.5 h total synthesis time, RAS = 41–89 GBq/ μmol) was quickly metabolized. In vitro metabolization investigation revealed identity of a piperidine as the major metabolic fragment of *N*-fluoropropyl JDTic. Under similar conditions, JDTic itself was found to be stable. **Conclusion.** Our finding demonstrates that *N*- ^{11}C -methyl JDTic derivative represents a promising KOR radioligand but *N*-fluoroalkylation is detrimental for in vivo stability. However, JDTic remains a lead KOR antagonist for the development of new metabolically stable drugs. (1) Thomas et al, J. Med. Chem. 2003, 46, 3127.

OP613

The neuroinflammatory and behavioral response to recurrent psychosocial stress: An ^{11}C PBR28 PET imaging study in stress-sensitized aged rats

P. Kopschina Feltes^{1,2}, E. F. J. de Vries¹, L. E. Juárez-Orozco¹, D. Vázquez García¹, C. M. Moriguchi-Jeckel², R. A. J. O. Dierckx¹, J. Doorduyn¹; ¹University of Groningen, Groningen, NETHERLANDS, ²Pontificia Universidade Católica do Rio Grande do Sul, Porto Alegre, BRAZIL

Introduction: Neuroinflammation plays an important role in the relationship between psychosocial stress and depressive-like behavior. However, it is still unknown if prior exposure to psychosocial stress has long-term influences in the response to a recurrence of the stressful stimulus later in life. The present study aimed to evaluate the behavioral and neuroinflammatory profile after repeated social defeat (RSD) in stress-sensitized and stress-naïve aged rats. **Methods:** Fourteen months old stress-sensitized Wistar rats ($n=10$), exposed during adolescence to 5-days of RSD, underwent the same RSD protocol after one year. Stress-naïve age-matched rats ($n=8$) were subjected to RSD without previous adolescent RSD exposure. The RSD protocol was performed by introducing the experimental rat (intruder) inside the home cage of a dominant Long Evans (resident) rat for a total of 60 min each day (experimental days 0–4). The protocol was considered successful when the intruder indicated defeat by adopting a submissive posture for at least 3 sec. Anhedonic behavior was assessed through the sucrose preference test on day -2 and 5. On day -1 and 11, neuroinflammation was measured by a 30-min static PET scan, performed 45 min after injection of ^{11}C -PBR28. **Results:** Decreased sucrose preference (-25% , $p=0.003$) was observed in stress-sensitized rats only on day 5, while no difference was found in stress-naïve rats after RSD. On day 11, within-group comparison demonstrated that stress-naïve rats showed an increased ^{11}C -PBR28 uptake in the frontal cortex association ($+16\%$, $p=0.035$), cingulate cortex ($+21\%$, $p=0.008$), orbitofrontal cortex ($+20\%$, $p < 0.001$), and medial/prefrontal cortex ($+27\%$, $p < 0.001$), while stress-sensitized rats had a decreased ^{11}C -PBR28 uptake in the cerebellum (-9% , $p=0.004$), frontal cortex association (-12% , $p < 0.001$), medial/prefrontal cortex (-12% , $p=0.002$), and orbitofrontal cortex (-13% , $p < 0.001$). Notably, the between-group comparison on day -1 showed a significant increased ^{11}C -PBR28 uptake in stress-sensitized rats for the cingulate cortex (25% , $p=0.022$), frontal cortex association (33% , $p=0.001$), orbitofrontal cortex (45% , $p < 0.001$) and medial/prefrontal cortex (47% , $p < 0.001$). No differences between groups were observed on day 11. **Conclusion:** Rats that were stress-sensitized at adolescence showed higher

neuroinflammatory levels in areas associated with depression at old age than stress-naïve rats. RSD exposure at old age provoked anhedonic-like behavior and decreased microglia activation in stress-sensitized rats. In contrast, stress-naïve rats demonstrated an increased neuroinflammatory profile in the same areas after RSD exposure at old age, but without anhedonic symptoms. This distinctive neuroinflammatory and behavioral response to psychosocial stress warrants further research into the long-term effects of early-life stress exposure.

OP614

¹⁸F FDG-PET and fMRI-based Connectivity Analysis of the Posterior Cingulate Cortex/Precuneus in Social Anxiety Disorder

A. Doruycer¹, L. Taljaard¹, D. Stein², P. Dupont³, C. Lochner¹, J. Warwick¹; ¹Stellenbosch University, Cape Town, SOUTH AFRICA, ²University of Cape Town, Cape Town, SOUTH AFRICA, ³KU Leuven, Leuven, BELGIUM.

Aim: Resting-state functional connectivity (RFC) in SAD has been investigated almost solely using temporal correlations of blood oxygen level dependent (BOLD) signal on functional magnetic resonance imaging (rs-fMRI). Nuclear methods possess several advantages to rs-fMRI in neuroimaging research and remain underutilized. In light of evidence that the default mode network (DMN) may play a role in social cognition we investigated RFC of the posterior cingulate cortex/precuneus (PCC/Precun) seed, a core node of this network, in SAD using both rs-fMRI and F-18 FDG-PET. **Materials and methods:** SAD participants and healthy controls (HCs) completed the Liebowitz Social Anxiety Scale (LSAS) and underwent resting-state FDG PET and MRI (rs-fMRI and T1-weighted structural). The State Trait Anxiety Inventory (STAI-S) was completed at both imaging visits. Preprocessing was performed in SPM-12. Seed-to-voxel, whole-brain RFC analysis was performed on a PCC/Precun seed described by Greicius using the functional connectivity toolbox and customized scripts in SPM-12. Conjunction analysis was performed to identify shared correlations in the FDG-PET analysis. In the SAD group, a correlation between connectivity and disease severity (LSAS score) was investigated. Statistical threshold was set at $p < 0.001$ uncorrected (voxel level) combined with $p < 0.05$ FDR-corrected at the cluster level. **Results:** Ten SAD participants and 10 age and gender-matched HCs were included. STAI-S scores were similar at imaging visits. On rs-fMRI the SAD group demonstrated reduced connectivity between the PCC/Precun seed and a cluster overlapping left striatum and thalamus. On FDG-PET the SAD group demonstrated reduced connectivity between the PCC/Precun seed and clusters overlapping bilateral insula and right medial orbitofrontal cortex. Conjunction analysis of the FDG-PET data did not detect any significant shared correlations with the PCC/Precun seed in the two groups. On rs-fMRI, disease severity was negatively correlated with connectivity between PCC/Precun and a cluster in left temporal pole. **Conclusion:** Our findings suggest disrupted BOLD connectivity in SAD between PCC/Precun and subcortical structures as well as disrupted metabolic connectivity between this seed and brain regions implicated in the fear circuit. The negative correlation between disease severity of SAD and BOLD connectivity between PCC/Precun and left temporal pole is interesting in light of the latter region's purported role as a store for social conceptual information. Differences in biological signal origin likely explain differences in RFC defined on fMRI and FDG-PET, highlighting the complementary value of these techniques.

OP615

Cerebral dopamine release and glutamatergic transmission relate to different subjective effects of acute alcohol: an in vivo multimodal imaging study

G. Leurquin-Sterk¹, J. Ceccarini¹, C. L. Crunelle^{2,3}, A. Weerasekera⁴, B. de Laat⁴, U. Himmelreich⁴, G. Bormans⁵, K. Van Laere^{1,4}; ¹Department of Nuclear Medicine & Molecular Imaging, University

Hospitals Leuven, KU Leuven – University of Leuven, Leuven, BELGIUM, ²Toxicological Center, University of Antwerp, Antwerp, BELGIUM, ³Department of Psychiatry, University Hospital Brussels, Brussels, BELGIUM, ⁴Biomedical MRI/MoSAIC, Department of Imaging and Pathology, KU Leuven - University of Leuven, Leuven, BELGIUM, ⁵Laboratory for Radiopharmacy, KU Leuven – University of Leuven, Leuven, BELGIUM.

AIM: Converging preclinical evidence has linked both extrastriatal dopamine release and glutamatergic transmission via the metabotropic glutamate receptor 5 (mGluR5) to the rewarding properties of alcohol intake. To date, direct human evidence is lacking on how and where in the brain these effects occur. This study aimed to assess whether the rewarding effects of alcohol intake in healthy humans are related to both extrastriatal dopamine release and baseline cerebral mGluR5 availability. **METHODS:** Eleven non-smoking male subjects (age = 40.1 ± 12.2 years), who were social drinkers verified by history and quantitative hair analysis, were included in the study. Mesocorticolimbic dopamine release upon monitored intravenous alcohol administration and mGluR5 availability were measured on two days using a single-session D₂/D₃ receptor ¹⁸F-fallypride positron emission tomography (PET) and a ¹⁸F-FPEB PET, respectively. Additionally, baseline and post-alcohol glutamate-glutamine levels in the anterior cingulate cortex were measured using magnetic resonance spectroscopy. Neuroimaging data were related to the subjective rewarding effects of alcohol. **RESULTS:** Intravenous alcohol induced significant dopamine release in various extrastriatal regions ($p < 0.05$, Bonferroni corrected), which correlated with the 'liking' and 'wanting' subjective effects for the anterior cingulate, orbitofrontal and left ventromedial prefrontal cortices (r range 0.60 - 0.86; $p < 0.05$, uncorrected). In contrast, baseline mGluR5 availability was positively associated with the 'high' effect of alcohol in dorsolateral, ventrolateral and left ventromedial prefrontal cortices, and in the medial temporal lobe, left thalamus and left caudate nucleus (r range 0.61 - 0.67; $p < 0.05$, uncorrected). Although glutamate-glutamine levels were not affected by alcohol intake, baseline anterior cingulate glutamate levels were negatively associated with the alcohol 'high' effect ($r = -0.80$; $p < 0.003$). **CONCLUSION:** These data reveal new mechanistic neurobiological accounts for alcohol effects on human behavior. We found the first *in vivo* evidence that alcohol-induced dopamine release is related to alcohol 'liking' and 'wanting' effects in specific prefrontal areas underlying value processing and motivation. In contrast, our findings suggest that mGluR5 availability in distinct subcortical-prefrontal-temporal regions is related to the 'high' effect of alcohol.

OP616

Exploration of the concept of 5-HT1A receptor biased agonists: a PET-MRI study

B. Vidal¹, M. Villien², S. Fieux¹, D. Le Bars^{2,3}, A. Newman-Tancredi⁴, N. Costes², L. Zimmer^{1,2,3}; ¹Université Claude Bernard Lyon 1, Lyon Neuroscience Research Center, INSERM, CNRS, Lyon, FRANCE, ²CERMEP - Imaging Platform, Bron, FRANCE, ³Hospices Civils de Lyon, Lyon, FRANCE, ⁴Neurolix Inc., Dana Point, CA, UNITED STATES.

Aim: In neuropharmacology, the recent concept of "biased agonism" implies the capacity of highly specific agonists to target specific intracellular pathways in specific brain areas. In the context of serotonin pharmacotherapy, 5-HT1A receptor biased agonists could be of great interest to optimize pharmacological treatments of several neuropsychiatric disorders. The aim of this study was to bring additional support to this concept thanks to simultaneous fMRI and PET molecular imaging. We compared two biased agonists, F13640 (a drug-candidate for the treatment of L-DOPA-induced dyskinesia) and F15599 (a drug-candidate for the treatment of breathing deficits in Rett syndrome), at different doses, in anaesthetized cats. The drug

occupancy was measured by PET imaging with [18F]MPPF, a 5-HT1A receptor radiotracer, after administration of both agonists and was correlated with the consequent brain activation patterns (pharmac-MRI). **Materials and methods:** PET and fMRI data were acquired simultaneously using a Siemens Biograph mMR hybrid camera (CERMEP-Imaging Platform). [18F]MPPF was injected in a 90-min perfusion (bolus followed by a constant infusion) in isoflurane-anesthetized cats. After a post-injection equilibrium period of 50 min, F13640 or F15599 was injected i.p. The 5-HT1A receptor occupancy was quantified by comparing [18F]MPPF binding potential values, before and after the pharmacological challenge. Thirty minutes after the beginning of the PET acquisition, continuous T2* EPI MRI acquisitions (TR = 2s) were performed to measure the BOLD signal. The fMRI session was divided into 20 minutes of baseline and 20 minutes after drug injection. A voxel based analysis of the fMRI data was performed at an individual level, followed by a second-level analysis, in a block design using a General Linear Model (GLM) approach. This PET-MRI protocol was replicated for each cat (n=4) with increasing concentrations of F13640 and F15599 (0.04 - 0.08 - 0.16 mg/kg ip). **Results:** PET and fMRI data, taken together, showed clear differences between the two agonists in terms of binding and subsequent activation patterns. F13640 displayed similar affinities for presynaptic and postsynaptic 5-HT1A receptors and elicited BOLD modifications in multiple brain regions. In comparison, F15599 showed a preference for postsynaptic receptors, with little capacity to elicit 5-HT1A activation in the raphe nucleus. **Conclusions:** This study is the first simultaneous exploration of a drug 5-HT1A receptor occupancy and its consequences in terms of brain activation. PET-fMRI represents a powerful tool in neuropharmacology and opens new ways to address the innovative concept of biased agonism.

OP617

The Effect of Brain-Derived Neurotrophic Factor (BDNF) Polymorphism Val66Met on Central Serotonin Transporter (5-HTT) Availability and body mass index (BMI) in Adults: A [¹¹C]DASB-PET Study

M. Drabe^{*1,2}, P. Hinderberger^{*1,2}, M. Rullmann^{1,2}, J. Luthardt¹, Y. Böttcher², G. Becker¹, M. Patt¹, M. Blüher², R. Regenthal³, T. Ploetz³, O. Sabri^{1,2}, S. Hesse^{1,2}; ¹Department of Nuclear Medicine, University of Leipzig, Leipzig, GERMANY, ²Leipzig University Medical Center, IFB AdiposityDiseases, Leipzig, GERMANY, ³Institute of Clinical Pharmacology, University of Leipzig, Leipzig, GERMANY.

Background: BDNF is currently being discussed as a potential modulator of weight control. Val66Met, a single nucleotide polymorphism (SNP) of the BDNF-encoding gene, leads to impaired intracellular trafficking and reduced activity-dependent secretion of the mature peptide. It has been suggested that a connection exists between Val66Met and body weight. However, current literature renders ambiguous about the exact effect of their relationship in which brain 5-HT is believed to have a regulatory role as well. The aim was therefore to investigate the influence of Val66Met genotype on body weight as well as 5-HTT availability (as a proxy for 5-HT tone) in selected brain regions in highly obese and normal-weight individuals. **Methods:** 29 non-depressed obese (mean BMI, 36.7±10.4 kg/m², 8 men; mean age, 37±10 years; range, 21-59 years) and 14 normal-weight (mean BMI, 22.5±2.6 kg/m²; 5 men; mean age, 36±7 years; range, 21-49 years) were scanned with dynamic PET and 484.1 ±9.9 MBq [¹¹C]DASB. TaqMan assay was performed for targeted BDNF SNP genotyping. Statistical analyses of 5-HTT binding potential BP_{ND}, Val66Met genotype and body-mass-index were first carried in both volume-of-interest (VOI) and voxel-based approach. **Results:** A significant increase of BP_{ND} in the anterior cingulate

cortex ($p = 0.02$) and medial prefrontal cortex ($p = 0.03$) were found in Met carriers compared to the homozygous Val/Val group. Additionally, a general linear model was then applied to account for covariates (e.g., age, sex, sunshine duration) which revealed an increased age-corrected BMI for Met-carriers compared to the homozygous Val genotype ($p = 0.04$). **Conclusion:** In our study sample, Val66Met genotype was associated with *in-vivo* 5-HTT availability and BMI. Whether such associations in regions important for reward processing, personality, and decision-making are linked to trait characteristics and neurobehavioral models has to be determined by further studies in human obesity.

OP618

Imaging drug-drug interaction using PET: investigating the impact of diazepam on buprenorphine-induced respiratory depression

D. Vodovar^{1,2,3}, G. Pottier¹, S. Auvity¹, B. Mégarbane^{2,3}, I. Buvat¹, F. Caillé¹, N. Tournier¹; ¹IMIV, CEA, Inserm, CNRS, Univ. Paris-Sud, Université Paris Saclay, CEA-SHFJ, Orsay, FRANCE, ²INSERM UMRS 1144, Paris-Diderot University, Paris, FRANCE, ³Assistance Publique - Hôpitaux de Paris, Paris, FRANCE.

Aims: Buprenorphine (BUP) is a partial mu-opioid receptor (MOR) agonist with “ceiling effect” that is supposed to prevent respiratory depression during pain management or opioid maintenance therapy. However, fatal respiratory depression with typical opioid toxidrom has been reported mainly when BUP has been co-ingested with benzodiazepines such as diazepam (DZP). In rats, we previously demonstrated that DZP (20 mg/kg s.c) or BUP (30 mg/kg i.p) did not lead to respiratory depression while their combination resulted in severe respiratory depression. Based on *in-vitro/ex-vivo* experiments, we hypothesized benzodiazepine-induced alterations in MOR affinity/density, which may provide a mechanistic explanation for the interaction between DZP and BUP *in vivo*. **Methods:** The *in vivo* effects of acute DZP exposure on BUP brain kinetics and affinity were investigated using [¹¹C]BUP PET imaging (~37 MBq, 90 min) in Sprague Dawley rats. Baseline brain [¹¹C]BUP kinetics (vehicle, n=4) were compared to kinetics obtained *i)* after displacement with unlabeled pharmacological BUP dose (0.3 mg/kg) administered at 20 min after [¹¹C]BUP (n=3) and *ii)* pre-treatment with DZP (20 mg/kg s.c) administered 15 min before PET (n=4). SUV-normalized [¹¹C]BUP PET images were co-registered in a template to generate time-activity curves (TACs) in several brain regions. ¹¹C-BUP binding potential (BP_{ND}) was estimated using the simplified reference-tissue model (SRTM) using the cerebellum as the reference region. **Results:** Baseline [¹¹C]BUP brain kinetics in the cerebellum (SUV_{90min} = 0.29±0.07) was influenced neither by the displacement (SUV_{90min} = 0.24±0.02) nor by DZP pretreatment (SUV_{90min} = 0.38±0.05) which makes it possible to use the cerebellum as reference tissue region. In the striatum, a MOR-rich region, baseline SUV_{90min} = 0.89±0.26 was significantly decreased by displacement (SUV_{90min} = 0.51±0.10; $p < 0.05$), showing the reversibility of [¹¹C]BUP binding, but not by DZP-pretreatment (SUV_{90min} = 0.90±0.13). Kinetics modeling indicated that [¹¹C]BUP BP_{ND} was not influenced by DZP pretreatment in all tested regions including the striatum, frontal cortex, midbrain, pons, amygdala and medulla. **Conclusion:** [¹¹C]BUP brain kinetics, reported for the first time in rodents, corresponds to the known distribution of MOR in the rat brain and can be described using SRTM. [¹¹C]BUP BP_{ND} was not influenced by DZP, indicating the absence of any measurable regulation of BUP affinity for MOR *in vivo*. Our results indicate that respiratory depression attributed to BUP/benzodiazepine combination observed in patients may result from the synergistic effects of these two drugs on respiratory function rather than from alteration of MOR availability or affinity for BUP. Dominique Vodovar received a joined grant from CEA and AP-HP.

OP619**Baseline binding potential of [11C]raclopride at true transient equilibrium predicts magnitude of amphetamine-stimulated dopamine release**

Y. Kumakura, A. Gjedde; University of Copenhagen, Copenhagen N, DENMARK.

Objectives: Quantitation of binding of [11C]raclopride in human brain is challenged by extreme changes of synaptic concentration of endogenous dopamine after intravenous administration of amphetamine. We used the exact approach of True Equilibrium Bolus Estimation (TREMBLE, Soelling et al., 1997; Wong et al., 1998) to quantify binding of tracer raclopride at true transient equilibrium by simple rearrangement of differential kinetic equations. We tested the hypothesis that baseline binding (BPND) of raclopride predicts the receptor occupancy by stimulated dopamine release in relation to baseline dopamine in young healthy volunteers. **Methods:** We selected PET data of 23 males and 14 females aged 19–29 years (mean 22.4; SD 3.1) from a cohort of 84 subjects (Kuwabara et al., 2012). Subjects underwent two consecutive 90-min PET sessions with [11C]raclopride. A high specific activity intravenous bolus injection was administered at the beginning of each scan. The first scan was preceded at 5 min by i.v. injection of saline; the second scan was preceded at 5 min by 0.3 mg/kg AMPH. Arterial blood was sampled at rapid intervals initially, with increasing intervals. Selected samples were analyzed by HPLC for radioactive plasma metabolites. The imaging protocol included as many as 30 acquisitions, frame durations increasing from 15 sec to 6 min. First, the raw time-activity-curves (TACs) of striatum and reference tissues were interpolated and resampled every 0.1 min. Then, we employed the Savitzky-Golay polynomial filter (Savitzky and Golay, 1964) to calculate first-order differential terms by numerical differentiation. We analyzed the filtered noise-attenuated TACs with TREMBLE to obtain BPND at the time of the transient true equilibrium (TEQ). Linear regression analysis was performed between baseline BPND (BPND_b) and receptor occupancy (%). Outliers that exceeded 2 SDs were excluded from final analysis. **Results:** Mean and SD estimates of baseline BPND for caudate and putamen were 3.36 ± 0.38 and 4.09 ± 0.46 , respectively. Mean estimates of amphetamine BPND were 3.25 ± 0.39 and 3.50 ± 0.31 . Mean estimates of RO (%) were 2.3 ± 14.9 and 13.2 ± 13.0 , meaning significantly smaller “displacement” in caudate. The slopes of linear regression analysis were significantly non-zero, at the significance levels of $P < 0.0002$ for caudate, and $P < 0.0001$ for putamen. We observed negative RO estimates in some subjects with the lowest baseline BPND. **Conclusions:** We conclude that the sensitivity of D2 receptors to saturation appears to be associated inversely with the degree of receptor occupancy at baseline, as predicted by the baseline binding potential obtained with this novel kinetic approach.

1601 – Wednesday, October 19, 2016, 08:00 – 09:30, Auditorium

CME 13 (Interactive) - Bone & Joint/ESSR: The Post-Operative Spine**OP620****Overview of Current Spinal Surgery Techniques**

P. Guigui; Hôpital européen Georges-Pompidou (HEGP), Chirurgie orthopédique et traumatologie, Paris, FRANCE.

OP621**Radiological Imaging of the Post-Operative Spine**

C. Pfirmann; Universitätsklinik Balgrist, Zurich, SWITZERLAND.

OP622**Radionuclide Imaging of the Post-Operative Spine**

T. Van den Wyngaert; Antwerp University Hospital, Nuclear Medicine, Antwerp, BELGIUM.

OP623**Teaching Cases**

F. Paycha; Hôpital Lariboisière, Paris, FRANCE.

1602 – Wednesday, October 19, 2016, 08:00 – 09:30, Hall 211

Joint Symposium 13 - EANM/SNMMI: GMP Meets Drug Development**OP624****Introduction and European Regulation for Clinical Trials**

C. Decristoforo; Universitätskliniken - Landeskrankenhaus Innsbruck, Medizinische Universität Innsbruck, Universitätsklinik für Nuklearmedizin, Innsbruck, AUSTRIA.

OP625**US Clinical Trials Regulation and Inspection Based on USP Chapter 823**

S. Schwarz; Washington University School of Medicine, Washington, UNITED STATES OF AMERICA.

OP626**PET in Drug Development Utilizing carbon-11 and fluor-18 tracers - GMP Aspects from Daily Practice**

A. Windhorst; VU University Medical Centre, Department of Radiology & Nuclear Medicine, Amsterdam, NETHERLANDS.

OP627a**GMP Requirements for a Clinical Trial with 68GaPSMA-11 - Experience from a Multi-Centre Trial**

O. Neels; German Cancer Research Center, Division of Radiopharmaceutical Chemistry, Heidelberg, GERMANY.

1603 – Wednesday, October 19, 2016, 08:00 – 09:30, Hall 117

CTE 6: Positron Emission Mammography**OP628****Recent Progress in Instrumentation for PEM Imaging**

J. Varela; Technical University of Lisbon, Lisbon, PORTUGAL.

OP629**The Clinical Use of Positron Emission Mammography in Diagnosis of Breast Cancer**

F. Müller; Praxis für Radiologie und Nuklearmedizin, Ludwigshafen, GERMANY.

OP630**Technologist Involvement in Positron Emission Mammography: Roles and Responsibilities**

T. A. ALAHmad; Kuwait Cancer Control Center, Nuclear Medicine Department, Kuwait City, KUWAIT.

1604 – Wednesday, October 19, 2016, 08:00 – 09:30, Hall 112

Do.MoRe: Clinical Dosimetry - ^{177}Lu Peptides**OP631****Performances of the collapsed cone superposition algorithm for the dosimetry of ^{177}Lu -PRRT**

A. Dieudonné¹, M. Sanchez-Garcia¹, I. Gardin², O. Hentic³, M. Palazzo³, P. Ruzsiewicz³, R. Lebtahi¹; ¹Department of Nuclear Medicine, Beaujon University Hospital, HUPNVS, APHP, Clichy, FRANCE, ²Department of Nuclear Medicine, Henri Becquerel Cancer Center and Rouen University, QuantIF – LITIS [EA 4108], Rouen, FRANCE, ³Department of Gastroenterology, Beaujon University Hospital, HUPNVS, APHP, Clichy, FRANCE.

The collapsed cone superposition algorithm (CCS) has been recently implemented for photon emitters (Sanchez-Garcia *et al.*, Phys Med Biol 2015). The objective is to compare CCS 3D-dosimetry of ^{177}Lu peptide receptor radionuclide therapy (PRRT) with other methods. **Methods:** We compared CCS with dose-kernel convolution with a simple density correction (DKCd) and without correction (DKC) in the case of ^{177}Lu -PRRT, taking Monte Carlo simulations (MCS) as reference. The clinical case was a patient treated by ^{177}Lu -PRRT for a neuroendocrine cancer with 1 lung lesion and 3 bone lesions: 2 in the iliac crest and 1 in the sacrum. The absorbed dose-rate (ADR) in $\text{Gy}\cdot\text{h}^{-1}$ was calculated from SPECT/CT data acquired 24h after injection of ^{177}Lu -octreotate. Regions of interest (ROIs) were drawn on normal tissues: lung, bone marrow, liver, kidneys and spleen, and on the 4 lesions. All calculations were done through the software tool VoxelDose. MCS were run with 10^7 histories on a 40 nodes cluster. The comparison was done in terms of relative difference ΔADR at the region level and Spearman correlation ρ_{sp} between ΔADR and mass density at the voxel level. Additionally, p , the probability of having no correlation was calculated. **Results:** For CCS, ΔADR were below 1% at the region level. At the voxel level, no or very low correlation existed between ΔADR and density ($\rho_{sp}<0.12$, $p<0.01$, $p=0.96$ for kidneys and 0.7 for sacrum lesion) showing the good performances of the algorithm whatever the tissue density. For DKC, ΔADR was between -1.5 and 0% for soft-tissue organs, between 2.4 and 10% for bone lesions, -8.6% for the lung lesion and -68% for lung. A correlation of ΔADR with density was found in lung and bone lesions ($\rho_{sp}>0.5$, $p<0.01$). For DKCd, ΔADR was between -1.5 and 0% for soft-tissue organs and all lesions, except for one iliac lesion ($\Delta\text{ADR}=-4\%$) and the lung ($\Delta\text{ADR}=23\%$). A correlation was found between ΔADR and density in lung ($\rho_{sp}=0.25$, $p<0.01$) and bone lesions ($-0.43<\rho_{sp}<-0.25$, $p<0.01$), showing that this method is sensitive to tissue density even in case of a density correction. **Conclusion:** CCS provided the best agreement with MCS, making it a clinically relevant alternative to DKC for ^{177}Lu -PRRT, while being less computationally demanding than MCS. The absorbed dose rate calculated with DKC was in very good agreement with MCS in soft-tissues, but underestimated the dose in lung. DKCd improved the agreement in lung, but with an overestimation.

OP632**Estimation Precision of Time-integrated Activity Coefficients: A Comparison of a Physiologically Based Pharmacokinetic and an Analytical Model in Peptide Receptor Radionuclide Therapy**

J. Sachs¹, C. Maaß², F. Mottaghy³, G. Glatting¹; ¹University Heidelberg, Medical Faculty Mannheim, GERMANY, ²Massachusetts Institute of Technology, Cambridge, MA, UNITED STATES, ³RWTH Aachen University, Aachen, GERMANY.

Aim: The aim of this study was to (1) determine time-integrated activity coefficients (TIACs) and their coefficients of variance (CVs) in peptide

receptor radionuclide therapy (PRRT) with ^{111}In -DTPAOC in 15 patients using an analytical model with (a) a mono- and (b) a biexponential function and to (2) compare them to their corresponding estimated TIACs and CVs obtained using a physiologically based pharmacokinetic (PBPK) model. **Materials and Methods:** Fifteen patients with proven neuroendocrine tumors (NETs) were investigated. Planar whole-body scans using a double-head γ -camera (ECAM, Siemens, Erlangen, Germany) were performed at 45 min, 4 h, 1, 2 and 3 or 5 d and serum measurements were taken at 5 min, 0.5, 1, 2, 4 h and 1, 2, 3 or 5 d after injection of ^{111}In -DTPAOC. An analytical model with mono- and bi-exponential functions was set up in MATLAB (Version: R2015a, The MathWorks, Natick, Massachusetts, USA) and fitted to the data, including a start value search and the calculation of the coefficients of variance (CVs). The precision (described by the CVs) of the estimated TIACs for tumour and kidneys were compared to the corresponding values resulting from a PBPK model. **Results:** CVs of TIACs for (1a) the mono-exponential fit were $19 \pm 6\%$ (median: 20 %, min: 7 %, max: 35 %) for kidneys and $28 \pm 22\%$ (median: 22 %, min: 3 %, max: 77 %) for tumour and (1b) the bi-exponential fit $37 \pm 51\%$ (median: 27 %, min: 2 %, max: 199 %) for kidneys and $14 \pm 20\%$ (median: 5 %, min: 0 %, max: 62 %) for tumour. The corresponding results (2) from the PBPK model were $8 \pm 3\%$ (median: 6 %, min: 5 %, max: 14 %) for kidneys and $12 \pm 10\%$ (median: 10 %, min: 2 %, max: 46 %) for tumour. **Conclusion:** The use of exponential functions in the calculation of TIACs is a common way to determine absorbed doses in PRRT. However, CVs (i.e. the precision) for tumour and kidneys may be significantly larger compared to the CVs obtained using a PBPK model. Thus, the results obtained from exponential functions should be interpreted cautiously.

OP633**Can the cumulative kidney dose be predicted on the basis of the first cycle in the standard ^{177}Lu -octreotate treatment?**

V. Reijonen, J. Heikkonen, H. Mäenpää; Helsinki University Hospital Cancer Center, Helsinki, FINLAND.

Aim: We studied how well the kidney dose calculated from the first cycle of ^{177}Lu -octreotate predicts the cumulative dose from the following cycles. **Materials and methods:** 40 patients (24 males, 16 females; age 29–69 y) with metastatic neuroendocrine tumours treated in the Helsinki University Hospital, Finland, received ^{177}Lu -octreotate according to the standard protocol (7.4 GBq administered four times at eight week intervals) with amino acid solution to decrease renal uptake. The kidneys of the patients were scanned using either Symbia T2 or Intevo T6 SPECT/CT (Siemens Healthcare) at 24 hours after each treatment and at 168 hours after the first and third treatment. The activities in the left and right kidney were determined from SPECT images with defining kidney volumes from the axial CT slices, and the mean absorbed dose to the whole kidney was then calculated based on a method utilising OLINDA® software. **Results:** The median administered activity was 7479 MBq (range 6839–8761 MBq) in cycle 1, 7481 MBq (6026–8790 MBq) in cycle 2, 7478 MBq (7220–8352 MBq) in cycle 3 and 7445 MBq (6600–8752 MBq) in cycle 4. The mean kidney-dose divided by the administered activity was 0.45 Gy/GBq (0.20–0.77 Gy/GBq) in cycle 1, 0.43 Gy/GBq (0.17–0.78 Gy/GBq) in cycle 2, 0.44 Gy/GBq (0.17–0.73 Gy/GBq) in cycle 3 and 0.45 Gy/GBq (0.17–0.73 Gy/GBq) in cycle 4. A paired-samples T-test indicated that there was not a significant difference in kidney dose per activity in the first cycle and the three following cycles; $t(39)=1.26$, $p=0.215$. When cumulative kidney dose was then calculated based on the kidney dose per activity in cycle 1 and the total activity administered to the patient (thus simulating that patient is imaged only in cycle 1 and the total kidney dose from the rest of the cycles is estimated based on this) and compared to the results based on dosimetric imaging in every cycle, the highest overestimation was 32% (19.4 Gy vs. 14.7 Gy) and underestimation 22% (10.2 Gy vs. 13.2 Gy). For altogether 15

patients the difference in the cumulative kidney dose was higher than 10 %, and for five patients higher than 20 %. **Conclusion:** Estimating the cumulative kidney dose on the basis of the first cycle can lead to considerable inaccuracy for a significant number of patients.

OP634

Development of a PBPK model of arginine biokinetics in humans to optimize kidney protection during peptide receptor radionuclide therapy

L. D. Jimenez, D. Hardiansyah, G. Glatting; Medizinische Fakultät Mannheim der Universität Heidelberg, Mannheim, GERMANY.

Aim: To develop a physiologically based pharmacokinetic (PBPK) model of the arginine biokinetics in humans to allow optimization of kidney protection during peptide-receptor radionuclide therapy (PRRT). **Methods:** Serum arginine data after intravenous injection of L-arginine with infusion rates similar to the one used in PRRT (<0.5 g/min) were collected from 3 different studies (4 datasets in total). The collected information were used to develop a PBPK model consisting of a central serum compartment, a compartment for all the organs excluding the kidneys (remainder) and a detailed five compartment model for the kidneys. The kidney compartments were: vascular, interstitial space, apical membrane, intracellular space and basolateral membrane. Metabolic clearance of arginine in the remainder compartment was considered in the model as well as arginine synthesis in the kidneys and arginine excretion through the urine. Affinity parameters of the arginine to its main transporters in the apical and basolateral membranes in the renal tubular cells were also considered. Bayesian values were used for parameter estimation. Data from a study where a ^{111}In -DTPAOC pre-therapy bolus was co-injected with a 120 minute intravenous infusion of 25 g of lysine and 25 g of arginine (LysArg) were used to optimize the radiopharmaceutical injection schedule. A proportional relationship between the interstitial concentration of arginine and the inhibition of ^{111}In -DTPAOC uptake by the kidneys was assumed. A similar behavior of arginine and lysine in the body was also assumed. The area under the curve (AUC) of the ^{111}In -DTPAOC after interaction with arginine in the interstitial space was used to determine the optimum injection schedule. **Results:** According to our model, the predicted optimum injection time for ^{111}In -DTPAOC is at 28.3 ± 2.0 min after the start of the co-infusion of LysArg. Additionally, the predicted optimal distribution for the 50 g of LysArg is approximately over 210 min with peptide injection at 65.8 ± 1.8 min which would yield a reduction of $6.4 \pm 0.8\%$ in the AUC when compared to a typical PRRT protocol. **Conclusions:** A PBPK model for arginine was successfully developed and used for optimization of kidney protection during PRRT. The currently-used peptide injection at minute 30 after amino acid infusion seems to be optimal according to our prediction. Additionally, a distribution of the 50 g of the kidney protective solution over 210 minutes may present a slight decrease of the AUC (also decreasing the absorbed dose in the kidneys) and may reduce possible adverse effects due to the amino acid infusion.

OP635

Design and Fabrication of Kidney Phantoms for Internal Radiation Dosimetry using 3D Printing Technology

J. Tran-Gia, S. Schlögl, M. Lassmann; University of Würzburg, Department of Nuclear Medicine, Würzburg, GERMANY.

AIM: Currently, the calibration of gamma cameras using phantoms of variable sizes and shapes is impeded by the lack of suitable, commercially available phantoms. Therefore, the aim of this study was to design and manufacture a set of kidney dosimetry phantoms using 3D printing techniques for obtaining phantom-specific SPECT/CT

calibration factors. **MATERIALS AND METHODS:** A set of kidney phantoms between 9 ml and 123 ml was designed based on the data provided by MIRDO Pamphlet 19 (Bouchet et al., JNM 2003) in Autodesk Inventor 2016 (CAD) and exported to the STL format. After conversion to machine-readable G-code, 3D printing was performed using the FDM-based Renkforce RF1000. The phantoms were coated with an epoxy casting resin for waterproofing and chemical stability. To examine the influence of the kidney geometry on image quantification, a set of spheres matching the kidney volumes was additionally produced. SPECT/CT acquisitions (Siemens Symbia T2) were performed with Tc-99m (0.90 MBq/ml), Lu-177 (0.99 MBq/ml) and I-131 (0.26 MBq/ml). The kidneys/spheres were mounted in a water-filled body phantom (IEC61675-1). A bottle of the same specific activity was placed next to the phantom as attenuation-free reference. After data acquisition, a CT-based VOI analysis was performed to determine calibration factors and examine their dependence on the VOI size. **RESULTS AND DISCUSSION:** A set of refillable, waterproof and chemically stable kidneys and spheres was successfully manufactured. Average calibration factors of $186.3 \text{ MBq}^{-1}\text{s}^{-1}$ (Tc-99m), $26.9 \text{ MBq}^{-1}\text{s}^{-1}$ (Lu-177) and $90.2 \text{ MBq}^{-1}\text{s}^{-1}$ (I-131) were obtained in the attenuation-free reference. For the largest phantom (adult), the VOIs had to be enlarged by 1.2 mm (Tc-99m), 2.5 mm (Lu-177) and 4.9 mm (I-131) in all directions to obtain calibration factors comparable to the attenuation-free reference bottle. This isotope-dependency of the VOI size can be explained by spill-out effects which are in turn dependent on the resolution of the collimator used (Tc-99m: LEHR, Lu-177: MELP, I-131: high-energy). While decreasing calibration factors were observed for decreasing phantom volumes (average percentage difference between reference and kidney phantom: 8.6% (8.6 ml), 4.6% (24.2 ml), 2.4% (44.4 ml), and 0.1% (122.9 ml), the difference between corresponding sphere/kidney pairs was small (<1.1% for all ages). The volume-dependent systematic deviation of the calibration factors results from partial volume effects. **CONCLUSION:** The presented 3D printing setup holds the potential for the design and fabrication of a wide range of anthropomorphic phantoms with an accuracy sufficient with respect to the resolution of clinically available SPECT/CT systems.

OP636

Comparative Dosimetric Evaluation on the course of PRRT using non carrier added LU-177 DOTATATE (i.a., i.v.), non carrier added LU-177 DOTATOC (i.v.) and carrier added LU-177 DOTATATE (i.v.)

M. Paphiti¹, R. V. McCready¹, E. Z. Dimitriadi¹, G. S. Limouris²; ¹Royal Sussex County Hosp, Brighton, UNITED KINGDOM, ²National and Kapodistrian University of Athens, Athens, GREECE.

Aim: Peptide receptor radionuclide therapy using radiolabelled somatostatin analogues is a well defined treatment option for patients with neuroendocrine tumours. It is aimed to compare patients treated with n.c.a. ^{177}Lu -DOTATATE (i.a., i.v.) to those treated with n.c.a. ^{177}Lu -DOTATOC and c.a. ^{177}Lu -DOTATATE, i.v. infused. **Methods:** Three groups of twelve patients with liver disseminated GEP-NETs were included in the study; n.c.a. ^{177}Lu -DOTATATE / ^{177}Lu -DOTATOC and c.a. ^{177}Lu -DOTATATE were administered in a dosage of 7.3 ± 2.3 GBq per session to each patient. Cycles did not exceed 6-fold in total. Amino-acid infusions were in parallel applied for nephroprotection. Planar scintigraphic images for the three groups were obtained at 24, 48, 96 and 120 hrs post injection. ROIs were drawn for tumour and critical organs to determine residence time and radionuclide uptake. Dosimetric calculations were performed using the patient specific scintigraphic data by the OLINDA /EXM/ 1.0 code. **Results:** Intravenous infusions of n.c.a. peptides were reached their max uptake to tumour lesions up to 20 hrs p.i. whereas the c.a. ones showed their max uptake peak at 24 hrs p.i. Intra-arterial infusions of n.c.a. DOTATATE resulted immediately, just after the end of the infusion with a tumour absorbed dose 3 folds higher than the i.v. one.

For i.v. infused n.c.a. DOTATATE / DOTATOC absorbed doses for a liver tumour of 10gr spherical mass were 33.0 mGy/MBq and 13.0 mGy/MBq, respectively and for blood and kidneys 0.030 mGy/MBq / 0.034 mGy/MBq and 0.46 mGy/MBq / 0.66 mGy/MBq. For i.v. infused c.a. DOTATATE, tumour dose was 4.4 mGy/MBq and for blood and kidneys 0.1 mGy/MBq and 0.9 mGy/MBq. **Conclusion:** Intra-arterial infusions with n.c.a. ^{177}Lu -DOTATATE reached its tumour max uptake immediately and 3 fold higher than the i.v. one. Intravenous infusions with n.c.a. ^{177}Lu -DOTATATE / ^{177}Lu -DOTATOC showed approximately the same dosimetric results whereas for c.a. ^{177}Lu -DOTATATE the absorbed dose in tumour was markedly lower but higher in critical organs.

1605 – Wednesday, October 19, 2016, 08:00 - 09:30, Hall 115

M2M - Featured: Nuclear & Optical Imaging

OP637

Nuclear & Optical Imaging

F. van Leeuwen; Leiden University Medical Center, Leiderdorp, NETHERLANDS.

OP638

Intrinsically ^{89}Zr -labeled $\text{Gd}_2\text{O}_3\text{:Eu}$ nanoprobles for in vivo PET and γ -ray-induced radioluminescence imaging

W. Cai¹, **Y. Zhan**², **F. Ai**³, **F. Chen**¹, **J. Liang**², **T. E. Barnhart**¹, **J. Tian**⁴;
¹University of Wisconsin-Madison, MADISON, WI, UNITED STATES,
²Xidian University, Xi'an, CHINA, ³Nanchang University, Nanchang, CHINA, ⁴Chinese Academy of Sciences, Beijing, CHINA.

Objective: Cerenkov luminescence imaging (CLI) is a non-invasive imaging technique showing immense promise for clinical translation. However, weak signal intensity and poor tissue penetration depth are two shortcomings that limit its clinical applications. γ -ray-induced optical luminescence imaging, combining the merits of CLI with optical imaging, has the capacity to overcome the current limitations of CLI. In this study, $\text{Gd}_2\text{O}_3\text{:Eu}$ nanoparticles, radiolabeled with ^{89}Zr , were optimized for in vivo sentinel lymph node (SLN) mapping using PET and γ -ray-induced optical luminescence imaging. **Methods:** Uniform, cubic and mono-dispersed $\text{Gd}_2\text{O}_3\text{:Eu}$ nanoparticles (diameter ~20nm) were synthesized using a thermal decomposition method. These highly biocompatible and water-soluble nanoparticles were prepared using a single polyethylene glycol (PEG) modification. The nanoparticles were comprehensively characterized, before undergoing chelator-free radiolabeling with ^{89}Zr , for in vivo SLN mapping in BALB/c mice. Extensive in vitro, in vivo, and ex vivo experiments were performed to evaluate the pharmacokinetics, stability, and toxicity of these nanoparticles. **Results:** Highly biocompatible and water-soluble ^{89}Zr - $\text{Gd}_2\text{O}_3\text{:Eu}$ nanoparticles were successfully synthesized, using chelator-free technology, for in vitro and in vivo lymph node mapping. The nanoparticles were successfully excited by γ -rays emitted from ^{89}Zr in vitro after hydrophilic modification. Upon subcutaneous injection of ^{89}Zr - $\text{Gd}_2\text{O}_3\text{:Eu}$ @PEG nanoparticles (40 μL , ~2.26 MBq) into the left foot pad of normal BALB/c mice, serial PET scans were performed. Accumulation of ^{89}Zr - $\text{Gd}_2\text{O}_3\text{:Eu}$ @PEG in the popliteal lymph node was found to be 8.6 ± 4.1 , 13.4 ± 3.3 and 4.4 ± 1.7 percentage of injected dose per gram of tissue (%ID/g) at 0.5, 2, and 6 h post-injection, respectively (n=3). Moreover, the accumulation of ^{89}Zr - $\text{Gd}_2\text{O}_3\text{:Eu}$ @PEG in lymph nodes was clearly detected by γ -ray excited optical luminescence imaging at 0.5 and 2 h post-injection regardless of open filter (detecting both Cerenkov signal of ^{89}Zr and γ -ray-induced luminescence signal) or 620 nm filter (detecting only γ -ray-induced luminescence signal, but NOT Cerenkov signal of ^{89}Zr). Quantitative analysis further illustrates that the intensity of luminescence from the ^{89}Zr - $\text{Gd}_2\text{O}_3\text{:Eu}$ @PEG in 620 nm filter was 10-fold lower than that in open filter, but the potential application in vivo is prominent compared with CLI. Ex vivo studies corroborated our

findings in vivo, providing additional evidence that ^{89}Zr - $\text{Gd}_2\text{O}_3\text{:Eu}$ @PEG nanoparticles may be successfully employed for SLN mapping with γ -ray-induced optical luminescence. **Conclusion:** This study successfully employed ^{89}Zr -labeled europium-doped Gd_2O_3 nanoparticles for SLN mapping with PET and γ -ray-induced optical luminescence imaging, improving upon the current limitations of CLI in vivo and providing a new path for the development of dual-modality PET/optical imaging technologies.

OP639

How the chemical structure of cyanine dyes influences the in vivo properties of receptor targeted tracers - exemplified using hybrid cRGDyK-analogues

T. Buckle, D. M. van Willigen, S. J. Spa, S. van der Wal, M. M. Welling, N. S. van den Berg, F. W. B. van Leeuwen; LUMC, Leiden, NETHERLANDS.

Background: The success of fluorescence-based image guided surgery is directly linked to the specific (*in vivo*) characteristics of the tracer used. Although often missing, systematic and quantitative assessment of tracer-affinity and -kinetics is critical. Using hybrid imaging labels that contain both a radiolabel and a fluorescent dye we systematically evaluated the effect of the composition of cyanine dyes with different substituents and wavelengths on the molecular imaging properties of an RGD-based targeting vector. **Methods:** Hybrid labels containing a DTPA chelate, a range of nine Cy5-dyes, a Cy3-dye or a Cy7-dye were synthesized together with reference compounds. These hybrid labels were subsequently conjugated with the $\alpha_v\beta_3$ -integrin targeting c[RGDyK] peptide. Affinities (Kd) were determined *in-vitro* using GE β_3 cells. *In vivo* biodistribution of the tracers was assessed in 4T1 tumor bearing Balb/c nude mice (n=6/group) using ^{111}In (%ID/g and SPECT). For the most optimal structure the optimal dose (range 0.1-1 nmol) for fluorescence imaging was determined as well as the optimal tracer administration-imaging window (4h or 24h). *In vivo* SPECT findings were complimented by *in-* and *ex vivo* fluorescence imaging using a clinical grade fluorescence endoscope. Detectability and in depth signal penetration of the different dyes was also assessed. **Results:** Affinities ranged between 21.9 and 142.3 nM. %ID/g findings and SPECT imaging, demonstrated that the dye structure heavily influenced the *in vivo* kinetics. Only one dye (Cy5-Methyl(SO3)) showed improved kinetics over the no-dye-containing hybrid reference compound. This dye also outperformed its Cy3-Methyl(SO3)- and Cy7-Methyl(SO3)-derivatives by providing e.g. lower liver and kidney retention and a two-fold higher signal-to-background ratio. While SPECT imaging was possible at all doses, *in vivo* fluorescence imaging was optimal at 1.0 nmol. Superior signal-to-background ratios were obtained at the 24h time-interval. The Cy5 derivative also showed the best *in vivo* visibility and tissue penetration using fluorescence imaging. **Conclusion:** *In vivo* tracer properties were significantly influenced by the chemical composition of the cyanine dyes used. This suggests that functionalization of a targeting vector with a fluorescent dye requires extensive structural optimization. The RGD-peptide merely provides a proof-of-concept and the same kind of tracer optimization should be applied during the development of other fluorescent (receptor-targeted) imaging tracers.

OP640

CEA-targeted dual-modality imaging with Indium-111-DTPA-labetuzumab-IRDye800CW can detect occult pulmonary metastases in a CEA-expressing tumor model

M. Hekman¹, M. Rijpkema¹, D. Bos¹, E. Oosterwijk¹, D. Goldenberg², P. Mulders¹, O. Boerman¹; ¹Radboudumc, Nijmegen, NETHERLANDS, ²Immunomedics, Morris Plains, NJ, UNITED STATES.

OBJECTIVES: Intraoperative dual-modality imaging can help the surgeon distinguish tumor from normal tissue. This technique may prove particularly valuable if small (occult) tumors need to be removed that are difficult to detect with the naked eye. The humanized anti-CEA monoclonal antibody, labetuzumab (hMN-14), can be used as a tumor-targeting agent in colorectal cancer (CRC), since CEA (carcinoembryonic antigen) is overexpressed in approximately 95% of CRC. Dual-labeled labetuzumab, labeled with both a near-infrared fluorescent dye (IRDye800CW) and a radioactive label (Indium-111), can be used to perform dual-modality imaging. This study aimed to assess whether intraoperative dual-modality imaging using Indium-111-DTPA-labetuzumab-IRDye800CW can detect CEA-expressing pulmonary micrometastases. **METHODS:** Pulmonary GW-39 human colonic carcinoma microcolonies were induced in athymic BALB/c mice by intravenous injection of 100 μ L of a 10% GW-39 cell suspension obtained from subcutaneous tumors. At 4, 11, 18, and 25 days after tumor cell injection, mice (n=7 per time point) were injected i.v. with Indium-111-DTPA-labetuzumab-IRDye800CW (10 μ g, 25 MBq). Three days later, mice were euthanized and the lungs were fixed by intratracheal injection of 4% formalin. Then microSPECT/CT images and optical images were acquired. Finally, the biodistribution of the dual-labeled tracer was determined. Formalin fixed sections of the lungs were analyzed using fluorescence imaging, autoradiography and immunohistochemistry. **RESULTS:** Submillimeter pulmonary tumor colonies could be visualized with both microSPECT and fluorescence imaging from the first week of tumor growth, before they became visible with the naked eye. After three weeks of tumor growth, pulmonary tumors could be resected by using fluorescence imaging. Mean uptake of the dual-labeled tracer in tumor nodules was 17.2 ± 5.4 %ID/g and 17.0 ± 8.3 %ID/g in weeks 3 and 4, respectively. Immunohistochemical analysis of the tumorous lungs showed that the distribution of the radioactive and fluorescent signal co-localized with CEA-expressing tumor nodules. **CONCLUSION:** Dual-modality imaging after injection of Indium-111-labetuzumab-IRDye800CW can be used to detect submillimeter CEA-expressing pulmonary colonies, before they become visible with the naked eye. A clinical study will be initiated to evaluate the feasibility of CEA-targeted intraoperative dual-modality imaging in CRC patients with peritoneal carcinomatosis scheduled for cytoreductive surgery and HIPEC.

OP641

Characterization of a triple-modality anti-PSMA targeting agent for immuno-SPECT/CT, near-infrared fluorescence imaging and targeted photodynamic therapy of PSMA-expressing tumors

S. Lütje¹, S. Heskamp², M. Hekman², S. Ekim², M. Gotthardt², A. Bockisch¹, O. C. Boerman²; ¹Clinic for Nuclear Medicine, University Hospital Essen, Essen, GERMANY, ²Department of Radiology and Nuclear Medicine, Radboud University Medical Center, Nijmegen, NETHERLANDS.

Aim: The prostate specific membrane antigen (PSMA) was shown to be overexpressed on prostate cancer as well as in the neovasculature of other malignancies, which renders it a target for imaging and therapy of cancer. Targeted photodynamic therapy (tPDT) is a highly selective cancer treatment approach based on targeting molecules conjugated to photosensitizers which can induce cell destruction upon exposure to near-infrared (NIR) light. Here, the development and *in vivo* characterization of the multi-modality anti-PSMA targeting agent ¹¹¹In-DTPA-D2B-IRDye700DX is described for both pre- and intra-operative tumor localization, image-guided surgery, as well as for eradication of tumor tissue by PSMA-targeted PDT. **Materials and methods:** The anti-PSMA monoclonal antibody D2B was conjugated with IRDye700DX and DTPA and subsequently radiolabeled with ¹¹¹In. To determine the optimal dose and time point of tPDT, BALB/c nude mice with PSMA-expressing s.c. LS174T-PSMA xenografts received 3, 10, or 30 μ g of

the conjugate intravenously (8 MBq/mouse, n=5 per group) followed by μ SPECT/CT and NIR fluorescence imaging at 24, 48, 72, and 168 h p.i. Tumor growth and overall survival of 3 mice treated with 30 μ g of the conjugate followed by 30 min of NIR light irradiation at 72 h p.i. was compared to mice that did not receive any treatment. The tumor lesions were resected under image-guidance using intraoperative NIR fluorescence imaging and stained for marker for double strand DNA breaks (H2AX and 53BP1). **Results:** PSMA⁺ tumors were clearly visualized both with SPECT/CT and NIR fluorescence imaging. Highest tumor accumulation was observed in mice treated with 30 μ g at 72 h p.i., which was confirmed by quantitative analysis of the SPECT data ($73 \pm 10\%$ ID/g) and biodistribution studies at 168 h p.i. ($52 \pm 16\%$ ID/g). tPDT with 30 μ g of the tracer and irradiation at 72 h p.i. caused significant inhibition of tumor growth in the treatment group compared to the control tumors: Median survival in the treatment group was significantly improved from 12.6 to 23.3 days. **Conclusion:** These studies provided proof-of-principle that ¹¹¹In-DTPA-D2B-IRDye700DX enables pre- and intra-operative visualization of PSMA⁺ tumors with radionuclide and fluorescence imaging, image-guided surgery and PSMA-targeted PDT.

OP642

Two different approaches to treat tumor-positive resection margins using targeted radioactive imaging and fluorescence-guided surgery

M. A. Stammes¹, H. J. M. Handgraaf², A. B. Chan³, C. J. H. Velde, van de², A. L. Vahrmeijer², L. de Geus-Oei²; ¹LUMC/Perucuros, Leiden, NETHERLANDS, ²LUMC, Leiden, NETHERLANDS, ³Perucuros, Leiden, NETHERLANDS.

Aim: By using a targeted multimodal probe with both a radioactive and near-infrared (NIR) fluorescent moiety, radioactive imaging can be used to obtain a total body overview and to locate tumors prior to surgery. During surgery, the fluorescence signal can exactly show the surgeon the boundaries of the tumor. Nowadays, the translation of pre-operative imaging to the intraoperative situation is often challenging. Surgeons therefore mostly need to rely on visual inspection and palpation when discriminating between healthy and tumor tissue. Consequently, tumor positive resection margins are still too high. The aim here is to show proof of concept for two probes, one with an antibody as targeting moiety and the second with a small molecule. **Materials & Methods:** For the first approach, trastuzumab-DTPA is coupled to the NIR fluorophore IRDye800CW and subsequently labeled with ¹¹¹In-Cl. For the second approach, cRGD-IRDye800CW-TCO in combination with Tz-DOTA is used, in here DOTA was also labeled with ¹¹¹In-Cl. The labeled product was intravenously injected in nude mice bearing subcutaneous HT-29 human colon cancer tumors on the back. Images were performed at different timepoints post injection using the μ SPECT, IVIS Spectrum, Pearl Impulse and Artemis. After the last imaging time point, mice were sacrificed and several tissues were excised, weighed, and counted for radioactivity to determine the percentage of the injected dose per gram (%ID/g). **Results:** Both *in vivo* fluorescence and radioactive images showed the same location of the probe. In addition, the *ex vivo* results, obtained with the gammacounter, confirmed that the majority of the probe was located in the tumor ($22.1\% \pm 10.9\%$ ID/g for ¹¹¹In-DTPA-CW800-Trastuzumab and $12.2\% \pm 1.2\%$ ID/g for ¹¹¹In-DOTA-Tz-TCO-CW800-cRGD). In general, the most optimal tumor-to-background ratio was found at 96h post injection for ¹¹¹In-DTPA-CW800-trastuzumab (combined FLI/RA TBR of $5.6\% \pm 0.8$) and already at 6h for ¹¹¹In-DOTA-Tz-TCO-CW800-cRGD (combined FLI/RA TBR of $4.8\% \pm 2.0$). **Conclusion & discussion:** These proof of concept preclinical experiments show that trastuzumab as well as cRGD coupled to IRDye800CW and ¹¹¹In-Cl can be visualized in a colorectal cancer model. Nevertheless, it still is a preclinical model and needs clinical validation. Trastuzumab is already a well-known clinical available antibody and cRGD is in the middle of the process of clinical translation. Furthermore, the Artemis is also being used in the surgical theatre. We therefore do not foresee major hurdles in further translating these promising constructs.

OP643**Hybrid detection modalities for intraoperative detection of multi-modal tracers**

G. H. KleinJan^{1,2}, D. Hellingman^{2,3}, N. S. Van den Berg^{1,2}, M. N. Van Oosterom¹, K. Hendricksen², S. Horenblas², R. A. Valdes Olmos^{1,2}, F. W. B. Van Leeuwen¹; ¹Leiden University Medical Centre, Leiden, NETHERLANDS, ²The Netherlands Cancer Institute - Antoni van Leeuwenhoek Hospital, Amsterdam, NETHERLANDS, ³Oncovision, Valencia, NETHERLANDS.

Introduction Multimodal tracers for image-guided surgery purposes gain more interest. An example of such a hybrid (multimodal) tracer is indocyanine green (ICG)-^{99m}Tc-nanocolloid (fluorescent and radioactive) which is a clinically applied during sentinel node (SN) procedures. Detection of these signals require both gamma and fluorescence detection modalities in the operating theater. A logical step would be to combine/integrate both modalities as such to create a hybrid detection modality for intraoperative guidance. This clinical feasibility study evaluates the combination of a commercially available fluorescence camera (FC) with a gamma-ray detection probe (GP) or a portable gamma camera (GC). **Methods** Two clip-on devices were designed and 3D printed. With these clip-on devices the FC could be attached to the GP (FC-GP) or GC (FC-GC) resulting in true hybrid detection modalities. The FC-GP and FC-GC were evaluated in five and six patients with penile cancer scheduled for SN biopsy, respectively. Logistics and data interpretation for both combined modalities were evaluated. During the operation, fluorescence-guided and radioguided SN detection rates were scored at distances varying from 0-30cm. **Results** The 3D designed clip-on system helped to successfully attach the FC to the GP and GC. Upon coupling of the devices, it was easy to place and replace them during surgery. Acoustic feedback produced by the GP provided directional guidance towards the 9 SNs in the FC-GP combination. Here gamma detection rates were 55.6% at 30cm and 20cm, and 88.9% at 10cm and 100% at 0cm. For the fluorescence detection these values were 77.8%, 77.8% and 100% for 30cm, 20cm and 10cm, respectively. Fluorescence detection at 0cm was not possible; here the camera was out of focus. In the evaluation of the FC-GC *in vivo*, all 10 SNs could be visualized with the GC. The fluorescence detection was 80% at 30cm and 20cm and 90% at 10cm working distance. **Conclusion** The current study provides a proof-of-concept for the generation of a hybrid imaging modality that allows combined intraoperative gamma and fluorescence imaging. Overall gamma tracing was best for the rough localization (30-10cm range) of the SNs, while fluorescence provided more detailed visualization within the 10cm range.

1606 – Wednesday, October 19, 2016, 08:00 - 09:30, Hall 111

Pitfalls & Artefacts: Breast Cancer and PET with Various Tracers - FDG, Fluoride, Fluoroestradiol and Others**OP644****Staging with FDG**

L. Mansi; Azienda Ospedaliera Universitaria, Seconda Università degli Studi di Napoli, Naples, ITALY.

OP645**FDG for Recurrence, Restaging and Treatment Monitoring**

L. Evangelista; Istituto Oncologico Veneto I.R.C.C.S., Medicina Nucleare, Padova, ITALY.

OP646**Tracers for Theranostics**

S. Balogova; St. Elisabeth Oncology Institute, Comenius University of Bratislava, Nuclear medicine, Bratislava, SLOVAKIA.

OP647**Other non-FDG Fluorinated Tracers**

J. Talbot; Hopital Tenon, Service de Médecine Nucléaire, Paris, FRANCE.

1607 – Wednesday, October 19, 2016, 08:00 - 09:30, Hall 116

Clinical Oncology: CNS Tumours**OP648****Automated grading of Glioma based on MET-PET and patient-derived features utilizing multi-layer machine learning approaches**

L. Papp¹, N. Pötsch¹, M. Mitterhauser¹, W. Wadsak¹, T. Beyer², M. Hacker¹, T. Traub-Weidinger¹; ¹Medical University of Vienna, Division of Nuclear Medicine, Vienna, AUSTRIA, ²Medical University of Vienna, Center for Medical Physics and Biomedical Engineering, Vienna, AUSTRIA.

Introduction [¹¹C]Methionine (MET) is well established in PET imaging of glioma. Several quantitative features can be used to characterize the amino acid metabolism in these brain tumours. Our goal was to establish a novel machine learning approach to automatically generate a classification algorithm that is based solely on MET-PET and patient-derived features. **Materials and Methods** This study relates to a cohort of 160 glioma patients who underwent MET-PET between 2000-2013 prior to therapy. Tumour grading was based on the WHO-2007 classification and histopathology. To date, 30/160 patients were analysed: astrocytoma grade 2 (10 patients), astrocytoma grade 3 (10) and glioblastoma multiforme (GBM, 10). Delineation of the tumour and a contra-lateral background region was performed manually in consensus by two experienced physicians using the Hybrid-3D software (Hermes Nuclear Diagnostics, Stockholm, Sweden). Tumour-to-background ratios (TBR) were calculated over each tumour voxel value for normalization. Several general features (mean, variance, minimum, maximum, volume), textural grey-level co-occurrence matrix (GLCM) derived features (homogeneity, entropy, contrast, dissimilarity, uniformity, correlation), textural neighbourhood grey-tone difference matrix (NGTDM) derived features (coarseness, contrast, busyness), and patient-derived features (age, Karnofsky score) were calculated for each normalized tumour regions. A novel multi-layer machine learning algorithm was implemented to automatically select relevant features for building a classification model for automated grading. The first layer selected the subset of features by a combined simulated annealing and genetic algorithm mimicking natural selection, crossover and mutation. The second layer determined weights for each residual feature of the first layer by a Nelder-Mead optimization method. Tumour classification was based on multiple Gaussian kernel functions - one for each feature of the three possible grades - to perform clustering across the selected features. Sensitivity and specificity were calculated for the machine learning derived classification results with histopathological grading serving as reference-standard. **Results** Sensitivity and specificity of the automated grading algorithm were 90% and 94% (grade 2 gliomas), 97% and 98% (grade 3), and 89% and 94% (grade 4), respectively. The following features were selected as relevant for tumour classification: [¹¹C]MET-PET TBR-derived: volume (general), homogeneity, entropy, contrast, correlation (GLCM) as well as patient-derived: age, Karnofsky score. **Conclusions** The present study demonstrates that joint analysis of heterogeneous image and patient-based features serve as a stable predictor of histology-derived grading.

OP649**[¹¹C]Methionine PET as Prognostic Parameter in Newly Diagnosed Glioma Patients**

N. Pötsch, A. Wöhrer, J. Furtner, D. Wilhelm, M. Weber, I. Rausch, A. Haug, G. Karanikas, M. Mitterhauser, W. Wadsak, M. Hacker, T. Traub-Weidinger; MEDICAL UNIVERSITY OF VIENNA, Vienna, AUSTRIA.

Background: [¹¹¹C]Methionine (MET) PET is well established in glioma imaging. Nevertheless, only few publications with small study population exist regarding MET PET and prognosis in glioma patients. **Methods:** A total of 160 glioma patients (89 men, 71 women, mean age: 45, range 18–84 years) were included in this study, who underwent a MET PET prior to any therapy between 2000 and 2014 at the Medical University of Vienna. The PET scans were evaluated visually (focal, focal with a branch, multifocal with branches, areal or visually negative) and semiquantitatively by SUV tumor to background (T/N) ratios. Following T/N ratios were evaluated: T/N_{standard} (i.e. $SUV_{\text{max}}/SUV_{\text{mean}}$), T/N_{peak} (i.e. $SUV_{\text{peak}}/SUV_{\text{mean}}$), T/N_{max} (i.e. $SUV_{\text{max}}/SUV_{\text{max}}$) and T/N_{pp} (i.e. $SUV_{\text{peak}}/SUV_{\text{peak}}$) and related to patients' survival. **Results:** Our patient group was evenly distributed between low (LGG) and high grade gliomas (HGG) (46%, 54%) according to the latest WHO classification (2007). Visually negative PET scans were predominantly found in LGG (82%). Focal pattern with a branch was observed in 78%, a multifocal pattern with branches in 70% of HGG. Patients with areal uptake pattern showed longest mean survival times (114 ± 15 months), followed by visually negative tumors (103 ± 9 months), whereas multifocal pattern with branches was associated with the worst prognosis (44 ± 6 months). T/N_{standard} ratio, by means of the AUC of a ROC-curve performed slightly better than other evaluated T/N ratios distinguishing LGG from HGG. T/N_{standard} ratio thresholds of 2.1 for differentiating LGG from HGG (AUC: 0,79) and 3.5 for separating grade III from GBM (AUC: 0,77) were found applicable. Significant survival differences were seen for these 3 threshold based groups ($p < 0.001$). Furthermore, the mean time to event (death [$n=63$] or lost to follow-up) was 47 months. Independent of histopathology, using the median T/N_{standard} ratio of 2.4 as cut-of, mean survival differed significantly ($p < 0.01$; mean survival: 123 months \pm 9 versus 66 ± 7 months). Additionally, multivariate testing showed WHO grading, surgical approach, tumor crossing midline, parietal tumor localisation, T/N_{standard} ratio value and histology as prognostic parameters by decreasing order of significance ($p < 0.001$ to $p = 0.041$). **Conclusion:** This analysis of a large population of newly diagnosed glioma demonstrates the impact of MET PET as prognostic marker on survival by visual as well as by semiquantitative analysis.

OP650

3D analysis of glioma heterogeneity with pseudo-kinetic and pharmacokinetic model parameters in dynamic 18F-FET PET

L. Vomacka, N. L. Albert, E. Mille, B. Suchorska, M. Unterrainer, A. Gosewisch, P. Bartenstein, G. Böning; University of Munich, Munich, GERMANY.

Objectives: Glioma grading with dynamic 18F-FET PET is typically performed by analysis of tumour 18F-FET uptake over time based on mean time-activity-curves delineated on late summation images (20–40min. p.i.). The aim of this work was to investigate tumour heterogeneity with quantitative parameters derived from pseudo-kinetic and pharmacokinetic models in dynamic 18F-FET PET (0–40 min p.i.). **Methods:** For each of the 42 patients with glioma (WHO2: 12; WHO3: 17; WHO4: 13) one blood volume-of-interest (VOI; 55% iso-contour) and one tumour VOI ($SUV_{\text{max}}/1.8 \times \text{background}$) were segmented. Furthermore, within each tumour VOI, sub-VOIs including voxels with similar time-to-peak (TTP) were defined. Kinetic parameters for the entire tumour VOI and the TTP-dependent sub-VOIs were derived from Patlak-plot, RE-plot, 2- and 3-compartment models (2CM, 3CM), and a linear fit to the late frames (15–40 min). **Results:** The differentiation between low grade (WHO grade 2) and high grade (WHO grade 3 and 4) glioma ($p < 0.01$) was successful with TTP, SUV at TTP, linear fit (slope and intercept), Patlak-plot (VT), RE-plot (VT and intercept), 2CM (K_1 and k_2), and 3CM (k_4 , K_1/k_2 and k_3/k_4). No significant differences were found for the remaining parameters.

None of the parameters allowed for the differentiation of grade 3 and 4 glioma ($p > 0.1$). The analysis of each tumour's TTP-dependent sub-VOIs showed that approximately 65% of the voxels of each high grade tumour volume had a maximum activity between 5 and 20 min p.i. (3CM: $K_1/k_2=0.7$, $k_3/k_4=1.3$), whereas only 15% of the voxels exhibited a peak activity after 30 min. p.i. (3CM: $K_1/k_2=0.7$, $k_3/k_4=3.7$). In the low grade glioma, 55% of the voxels presented their maximum activity later than 30 min. p.i. (3CM: $K_1/k_2=0.4$, $k_3/k_4=3.2$). However 22% of the voxels in low grade glioma revealed a peak between 10 and 20 min. p.i. (3CM: $K_1/k_2=0.4$, $k_3/k_4=2.5$). **Conclusion:** Areas with early peak uptake could be detected with a voxel-based analysis within histologically proven WHO grade 2 gliomas, supporting the identification of tumour heterogeneities. In combination with other parameters, e.g. a high uptake rate, this observation might raise suspicion for the presence of aggressive sub-areas. Whether this may have an impact on clinical procedures and patient's prognosis has to be further investigated in future studies.

OP651

Comparison of F18-Fluorodopa, F18-Fluorocholine and F18-Fluorodeoxyglucose PET/CT for detection of recurrence in patients with primary brain tumors

A. Sharma, M. Singh, A. Garg, M. Tripathi, S. Gupta, H. KP, C. Bal; ALL India Institute of Medical Sciences, New Delhi, INDIA.

Objectives- Recurrence in brain tumors is notoriously difficult to distinguish from radiation necrosis on routine Magnetic Resonance Imaging (MRI). Unlike necrotic tissue, the recurrent tumor is metabolically active. Positron Emission tomography (PET/CT) can provide this additional metabolic information (glucose metabolism by F18-FDG, lipid metabolism by F18-FluoroCholine, amino-acid metabolism by F18-Fluorodopa) over structural information provided by MRI and thus can aid in diagnosis. **Methods-** 11 post-op patients (mean age 34 years; M:F 6:5) suspected for recurrence (6 grade II, 3 grade III, 2 grade IV) were included. Of these 6 had equivocal findings on MRI. They underwent F18-FDG PET/CT (40 min post 8–10 mCi IV injection), F18-Fluorocholine PET/CT (70 min post 5–7 mCi IV), F18-Fluorodopa PET/CT (20 min post 3–5 mCi IV) on 3 separate days within a period of 15 days. Any uptake more than the contralateral normal brain parenchyma was considered positive and tumor to normal SUV_{max} (T/N) ratios were calculated. The scans were anonymized and nuclear medicine physician reporting the scans was also blinded to patient history as well as other PET/CT scans and MRI. **Results-** 12 lesions were documented (4 frontal, 4 parietal, 2 temporal, 2 cerebellar). One patient had multifocal tumor. 5 patients had surgery, 1 stereotactic biopsy (5 showed conversion to grade IV, one ischemic changes). Other 5 were followed up for average 9.8 months (6–11 months; one patient died after 6 months). Of these 3 had follow up MRI, 1 died due to clinical worsening and 1 was diagnosed with clinically progressive recurrent disease. All the lesions showed 100 percent concordance on F18-fluorocholine and F18-fluorodopa PET/CT. F18-FDG was able to diagnose 7 lesions correctly (4 true positive, 3 true negative) but 5 were false negative. F18-Dopa and F18-Choline diagnosed 9 lesions correctly (8 true positives, 1 true negative) but 2 were false positives and 1 was false negative. T/N ratios were higher for F18-choline (14.17) than F18-Dopa (3.18), but neither these ratios nor SUV_{max} showed any correlation with tumor grade or proliferative indices (mib-1). **Conclusion-** F18-Fluorocholine is as efficient as F18-Fluorodopa in diagnosis of recurrent brain tumors, but provides better tumour visualisation (higher T/N ratios). Both of these agents provide more information than F18-FDG, particularly in patients with low grade tumors or in patients with recurrence with extensive radiation changes.

OP652**¹⁸F-fluoromethylcholine (FMC) PET/CT and proton magnetic resonance spectroscopy; imaging and tissue biomarkers of cell membrane turnover in primary brain gliomas - a pilot study**

M. Grech-Sollars^{1,2}, K. L. Ordidge^{2,1}, B. Vaqas², L. Honeyfield^{2,1}, S. Khan², S. Camp², D. Towey³, D. Peterson², F. Roncaroli⁴, K. S. O'Neill², T. Barwick^{2,1}, A. D. Waldman^{5,1}, ¹Imperial College London, London, UNITED KINGDOM, ²Imperial College Healthcare NHS Trust, London, UNITED KINGDOM, ³Northampton General Hospital NHS Trust, Northampton, UNITED KINGDOM, ⁴The University of Manchester, Manchester, UNITED KINGDOM, ⁵The University of Edinburgh, Edinburgh, UNITED KINGDOM.

Background: Choline is a biomarker of interest in gliomas and relates to cell membrane turnover - a hallmark of aggressive tumour behaviour. Pilot C-11/F-18 choline PET studies show differential uptake between benign and malignant tumours, however the cellular and molecular basis of this uptake and MRS-visible choline containing compounds (Cho) is not well understood. Choline kinase (CHK) α phosphorylates choline, an essential step in membrane synthesis, and is known to be expressed by malignant tumours, including prostate, lung and brain. Here we investigate the relationship between choline metabolism detected in vivo using MRS and PET, and tissue markers of choline synthesis and glioma proliferation. **Method:** Prospective pilot study of 14 patients with suspected primary glioma underwent multimodal 3T MRI (including multi-voxel MRS) and dynamic 45 minute list mode ¹⁸F-FMC PET/CT with venous sampling prior to surgery. Time activity curves were generated and tumour SUVmax and tumour to background ratio (TBR: SUVmax tumour/SUVmean contralateral white matter) were assessed. Co-registered PET and MRI data were used to identify regions of high and low choline and targeted biopsies were performed using a surgical planning tool. Immunohistochemistry for expression of CK α expression in this biopsied tissue is being performed. **Results:** All tumours showed increased tracer uptake relative to contralateral white matter. Metabolite analysis showed fast metabolism of choline, with steady state being reached after 20 minutes. Significant differences in TBR were found between WHO grade IV (11.7–44.0, mean 25.5) and WHO grades I, II & III (5.2–13.8, mean 8.2) tumours in ¹⁸F-FMC uptake (t-test, p<0.05) and between WHO grades IV&III and grades I&II using Cho/Cr ratios on MRS (t-test, p<0.05). Combining PET and MRS data showed spatial concordance between regions of high PET uptake and highest Cho/Cr ratio, however there was no correlation between the actual levels of uptake (TBR) and the Cho/Cr ratio in these regions. Furthermore, regions of contrast enhancement on MRI showed high uptake on PET. CK α expression assays are pending. **Conclusion:** There was significantly higher choline uptake in grade IV gliomas compared to other grades. Combining ¹⁸F-FMC uptake and Cho/Cr ratio on MRS may help further distinguish between high and low grade glioma. Correlation between CK α expression in tissue and imaging markers will probe the molecular basis of this uptake/signal.

OP653**Overall survival and progression free survival in patients with primary brain tumors after treatment. Is ¹⁸F FDOPA PET/CT a prognostic factor in these patients?**

A. Chiaravalloti^{1,2}, A. Fiorentini¹, V. Villani³, C. Carapella⁴, A. D'Elia⁵, P. Sannino², M. Zinzi⁶, N. Urbano¹, G. Grillea⁶, E. Palombo¹, O. Schillaci^{1,7}; ¹Department of Biomedicine and Prevention, University Tor Vergata, Rome, ITALY, ²IRCCS Neuromed, Pozzilli, ITALY, ³Neuro-Oncology Unit, Regina Elena National Cancer Institute of Rome, Rome, ITALY, ⁴Division of Neurosurgery "Regina Elena" National Cancer Institute of Rome, Rome, ITALY, ⁵Department of neurosurgery, IRCCS Neuromed, Pozzilli, ITALY, ⁶IRCCS Neuromed, Rome, ITALY, ⁷IRCCS Neuromed, Pozzilli, AUSTRIA.

Aim: to investigate the progression free survival (PFS) and the overall survival (OS) in a populations affected by primary brain tumors (PBT) evaluated with [18 F]-L-dihydroxyphenylalanine (¹⁸F FDOPA) Positron Emission Tomography/Computed Tomography. **Materials and methods:** 124 subjects with PBT (65 women and 59 men, mean age 45 \pm 10 years old) underwent ¹⁸F FDOPA PET/CT after treatment. According to WHO score, 7 were grade I, 51 were grade II, 37 were grade III and 29 were grade IV. The strategy of treatment adopted for grade IV was radiotherapy (RT) plus continuous daily temozolomide, followed by six cycles of adjuvant. For grade III we used RT followed by chemotherapy (CHT) with temozolomide or lomustine and procarbazine 60 mg/m² orally on days 8 to 21. Grade II were subjected to standard adjuvant temozolomide treatment while grade I were subjected to surgery only. Intervals from surgery, CHT and RT were 42.28 (\pm 39.24), 17.05 (\pm 30.1) and 24.7 (\pm 32.4) months respectively. PET/CT was scored as positive or negative when pathological uptake was identified and, in particular, when an area of focal tracer uptake superior to the background was visually detected. Data concerning OS were collected and PFS was established according to clinical criteria. **Results:** Patients were observed for a mean of 24 months. Median OS was 13 months in positive PET/CT scans and 27 in PET/CT negative scans. OS curves were significantly different (P<0.0001 in Mantel-Cox test and Gehan-Breslow-Wilcoxon test). At 12 months, the survival proportions were 82% in subjects with a negative PET/CT scan and 28% in subjects with a positive PET/CT scan. The hazard ratio resulted equal to 4.62 (95% CI of ratio: 11.99 to 106.1). Median PFS was 4 months in positive PET/CT scans and 25 in negative PET/CT scans. PFS curves were significantly different (P<0.0001 in Mantel-Cox test and Gehan-Breslow-Wilcoxon test). At 12 months, the progression proportions were 14% in subjects with a negative PET/CT scan and 85% in subjects with a positive PET/CT scan. The hazard ratio resulted equal to 4.51 (95% CI of ratio: 13.03 to 43.74). **Conclusions:** a positive ¹⁸F FDOPA PET/CT scan is related to a poor OS and PFS in subjects with PBT. This imaging modality could be considered as a prognostic factor in these subjects.

OP654**Value of F-DOPA PET in the long term follow up of radionecrotic brain metastases after radiosurgery: comparison with MRI**

F. Cicone¹, L. Carideo¹, C. Scaringi², A. Romano³, A. Bozzao³, G. Minniti², F. Scopinaro¹; ¹Unit of Nuclear Medicine, Sant'Andrea Hospital, "Sapienza" University of Rome, ROME, ITALY, ²Unit of Radiation Oncology, Sant'Andrea Hospital, "Sapienza" University of Rome, ROME, ITALY, ³Unit of Neuroradiology, Sant'Andrea Hospital, "Sapienza" University of Rome, ROME, ITALY.

Aim. To analyse the value of sequential F-DOPA PET/CT scans in the long term follow-up of predominantly radionecrotic brain metastases after stereotactic radiosurgery. Comparison with MRI-derived parameters is given. **Materials and Methods.** Eighty-one patients with previously irradiated brain metastases who underwent F-DOPA PET at our institution for differential diagnosis between radionecrosis (RN) and progression (PD) were screened. Inclusion criteria were i) initial negative or borderline uptake values (rSUV) defined according to a previously published method, ii) availability of repeated F-DOPA scans over an observational period >12 months. Standard patient monitoring in this setting includes repeated MRI and F-DOPA scans every 3-6 and 6-12 months, respectively. F-DOPA PET/CT consisted of a 20 min acquisition starting 15 minutes after tracer injection. rSUV was calculated as the ratio between the lesion SUVmax and the SUVmax of the contralateral background. Tumor maximal transverse diameter (Dmax) was calculated on contrast-enhanced, T1-weighted sequences; tumour volumes were calculated by assuming a spherical geometry with Dmax as diameter. Cerebral blood flow (rCBV) was derived from perfusion-weighted images and quantified

relative to the normal contralateral white matter. Δ rSUV, Δ Dmax and Δ Vol were calculated between first and last time point imaging; PD vs RN group comparisons were made with two-tailed Student's t test. **Results.** Twenty patients (12 F, 8 M) with a total of 70 F-DOPA scans were included. Median follow-up was 30.5 months (range:13-51). So far, 4 (20%) patients have died because of intracranial (n=3) or extracranial (n=1) PD. Eleven (55%) metastases remained in histologically confirmed (n=5) or unconfirmed RN, while 9 (45%) showed a slow PD (n=3 histological confirmations) over time. All PD showed a steady rSUV increase over time; however, F-DOPA was false positive in one case of histologically confirmed RN. In two RN, there was an increase of rSUV followed by a subsequent slight decrease. An increase in Dmax was observed in all patients but two cases of RN. rCBV was falsely negative in 2 (22%) PD and falsely positive in 5 (45%) RN. Initial rSUV did not differ between groups (p=0.75), while final rSUV and Δ rSUV were significantly different between PD and RN (p<0.001 and p=0.006, respectively). All MRI derived parameters were not significantly different between PD and RN (all p>0.25). **Conclusion.** F-DOPA PET/CT is a reliable tool to assess the evolution over time of predominantly radionecrotic brain metastases after stereotactic radiosurgery. In this setting, performances of MRI including perfusion-weighted imaging are lower.

OP655

Prognostic significance of molecular and imaging biomarkers in primary brain tumors

E. Lopci¹, M. Riva¹, L. Olivari², F. Raneri², A. Bizzi³, B. Fernandes¹, P. Navarria¹, F. Pessina¹, M. Roncalli⁴, L. Bello¹, A. Chiti²; ¹Humanitas Clinical and Research Hospital, Milano, ITALY, ²University of Milan, Milano, ITALY, ³Fondazione IRCCS Istituto Neurologico Carlo Besta, Milano, ITALY, ⁴Humanitas University, Milano, ITALY.

Purpose: We evaluate the relationship between carbon-11-methionine PET (11C-METH PET) metrics with molecular biomarkers in patients affected by brain gliomas candidate to surgery. **Materials and Methods:** A consecutive series of 109 patients with pathologically proven gliomas (M:F=64:45; median age 43 years; 40 LGG, 69 HGG), referred to our Institution from March 2012 to January 2015 for tumor resection and submitted to pre-operative 11C-METH PET, was analyzed. The trial was registered at www.clinicaltrials.com (NCT02518061). Semi-quantitative metrics for 11C-METH PET included SUVmax, SUVratio to normal brain and metabolic tumor volume (MTV). Imaging findings were correlated to disease outcome expressed in terms of progression-free survival (PFS), and compared to other clinical-biological data, comprising IDH1 mutation, 1p/19q co-deletion and MGMT promoter methylation. The cohort was monitored for a mean period of 16.7 months (median 13 months). **Results:** In all patients, tumors were identified on 11C-METH PET: median SUVmax 3.3, median SUVratio 2.3, and median MTV 9.6 cm³. We observed a statistically significant difference for SUVmax, SUVratio and MTV values based on tumor grade (p<0.001). According to molecular analyses, IDH1 resulted mutated in 49 patients, 1p/19q co-deleted in 58 patients and MGMT promoter methylated in 74 patients. A statistically significant correlation between SUVmax and SUVratio and IDH1 mutation was observed (p<0.001). Relapse or progression was documented in 48 cases (median PFS 8.7 months). A statistically significant correlation was observed for SUVmax and SUVratio, tumor grade, IDH1 mutation, 1p/19q co-deletion and MGMT-promoter methylation to PFS. **Conclusions:** 11C-METH PET metrics significantly correlate with histological grading and IDH1 mutation status in primary brain tumors. Grading, molecular biomarkers, SUVmax and SUVratio resulted prognostic factors to PFS in this cohort of patients candidate to surgery.

1608 – Wednesday, October 19, 2016, 08:00 - 09:30, Hall 212

Special Symposium 3 (Part I) - EANM/ESSO: Advances in Radioguided Intervention for Biopsy of Occult Lesions and Sentinel Nodes

OP656

Interventional Molecular Imaging and Radioguided Lesion Excision
R. Valdes Olmos; Leiden University Medical Centre, LUMC, Nuclear Medicine, Leiden, NETHERLANDS.

OP657

Synergism of SPECT/CT and Portable Gamma Cameras for Intraoperative Sentinel Node Biopsy in the Pelvis
S. Vidal Sicart; Hospital Clinic Barcelona, University Barcelona, Nuclear Medicine, Barcelona, SPAIN.

OP658

FreehandSPECT Applications in Radioguided Surgery
C. Bluemel; University of Wuerzburg, Wuerzburg, GERMANY.

OP659

Combining Radiotracers and Fluorescence for Sentinel Node Localization in Complex Anatomical Areas
N. S. van den Berg; Leiden University Medical Center, Radiology, Leiden, NETHERLANDS.

OP660

Radioguided 125I-seed Localization in Breast Conserving Surgery
M. Vrancken Peeters; Netherlands Cancer Institute, Surgical Oncology Division, Department of Surgery, Amsterdam, NETHERLANDS.

1609 – Wednesday, October 19, 2016, 08:00 - 09:30, Hall 113

Joint Symposium 15 - EANM/JSNM: Standardisation of Imaging and Harmonisation Criteria of the Scanning Protocols for FDG, Aminoacid and Amyloid PET of the Brain

OP660a

A Neurologist's Perspective on Standardization of Brain FDG and Amyloid PET Imaging
K. Ishii; Tokyo Metropolitan Institute of Gerontology, Tokyo, JAPAN.

OP660b

A Practical Guide to Cross Platform Brain Imaging Standardisation
R. Boellaard; VU University Medical Center, Nuclear Medicine & PET Research, Amsterdam, NETHERLANDS.

OP660c

Phantom Criteria and a Site Qualification Program for Standardization of Brain PET Imaging
M. Senda; Kobe University / Graduate School of Medicine, Kobe, JAPAN.

OP660d

Perspectives for Hybrid MR-PET in Multicenter Dementia Research and Prevention Trials
H. Barthel; University of Leipzig, Department of Nuclear Medicine, Leipzig, GERMANY.

1701 – Wednesday, October 19, 2016, 10:00 - 11:30, Auditorium
CME 14 - Thyroid/ETA: Non-Isotopic Diagnostic Thyroidology - An Update for Nuclear Medicine Physicians

OP661**Laboratory**

L. Giovannella; Oncology Institute of Southern Switzerland, Department of Nuclear Medicine, Bellinzona, SWITZERLAND.

OP662**Sonographic Diagnosis of Thyroid Cancer, Thyroid Bed and Lymph Node Metastases**

M. ERDOĞAN; University of Ankara, School of Medicine, Ankara, TURKEY.

OP663**Cytopathology**

M. Bongiovanni; CHUV - Centre hospitalier universitaire vaudois, Médecin chef - Cytopathologie, Institut universitaire de pathologie - IUP, Lausanne, SWITZERLAND.

1702 – Wednesday, October 19, 2016, 10:00 - 11:30, Hall 211

Joint Symposium 14 - EANM/ESMI: M2M Symposium**OP664**

TBA

OP665

TBA

OP666

TBA

OP667

TBA

1705 – Wednesday, October 19, 2016, 10:00 - 11:30, Hall 115

M2M: Nanoparticles & Macromolecules**OP668****In Vitro Bioactivity Evaluation of Synthesized ¹⁸F-FDG-Grayanotoxin-Gadolinium Nanoparticles**

T. S. Akkaya, **P. Unak**, O. K. Guldu, I. Ince; Ege University, İzmir, TURKEY.

Introduction: Grayanotoxin III (GTX-III) compounds can be found naturally in *Rhododendron ponticum* L. (Ericaceae family) and “mad honey”. This natural toxic compound can cause depolarization on the cell membrane by inhibiting the voltage gated sodium channels (VGSCs) which are also associated with cancer cells. Recently, magnetic nanoparticles and radioisotopes are widely used and helpful for diagnostic and targeted therapy against cancer disease. **Methods:** In this study, we extracted GTX-III compounds from the leaves and flowers of the forest rose and mad honey. The extracted compound then conjugated with Gadolinium nanoparticles (GdO@Si-NP). Synthesized Gadolinium nanoparticles were conjugated

and radiolabelled with 2-deoxy-2-(F-18) floro-D-glucose (18F-FDG). Besides, after conjugation of Grayanotoxin-III with GdO@Si-NP bioactivity of the conjugation products were investigated by applying to Human Breast Adenocarcinoma (MCF7) and Human Prostate Adenocarcinoma (PC3) cell lines and evaluated together with the MR image contrasts. GTX-III compounds were extracted from dried leaves and flowers of the forest rose and then purified by High Performance Liquid Chromatography (HPLC). However, GTX-III separated from the mad honey with solid phase extraction (SPE). GTX-III compounds were identified with Liquid Chromatography - Mass Spectrometry (LC-MS) and Nuclear Magnetic Resonance (NMR) spectroscopy. Gadolinium nanoparticles were synthesized by co-precipitation and they were modified via silication of nanoparticles. Size and characterization of the nanoparticles were determined with Dynamic Light Scattering (DLS) and Scanning Electron Microscopy (SEM). By using 1, 1'-carbonyldiimidazole/N-Hydroxysuccinimide (CDI/NHS) conjugation method, synthesized GdO@Si-NP were conjugated with GTX-III compounds. Bioactivity of the conjugated nanoparticles was investigated by applying cytotoxicity and incorporation tests on PC3 and MCF7 cell lines. Incorporation values were evaluated with MR image contrast of the PC3 and MCF7 cell cultures. Conjugation of ¹⁸F-FDG with GTX-III coupled GdO@Si-NP, was carried out with CDI/NHS method. **Results and Discussion:** GTX-III compounds extracted from forest rose and mad honey, showed significant cytotoxic effect to MCF7 and PC3 cell lines. However, GdO@Si-NP decreased the cytotoxicity to MCF7 while increasing PC3 cells. It was shown that incorporation studies can be carried out by using Gadolinium NP contrasts of MCF7 and PC3 cell lines, which was determined with calibrated MR images. Besides, ¹⁸F-FDG was conjugated to GTX-III-GdO@Si-NP with a good yield by using CDI/NHS method. **Conclusion:** As a result of the study, the synthesized ¹⁸F-FDG-GTX-III-GdO@Si-NP compounds have the potential of being used as theranostics for prostate and breast cancers. **Keywords:** *Rhododendron ponticum* L., Mad Honey, Grayanotoxin, Gadolinium nanoparticles, MCF7, PC3, Breast cancer, Prostate cancer, MRI, ¹⁸F-FDG, Radiolabeling

OP669**Intrinsically radioactive metal-organic frameworks (MOF) nanomaterials as a novel PET-guided drug delivery nano-vector**

H. Hong, D. Chen, D. Yang, H. Wu, W. Lu; University of Michigan, Ann Arbor, MI, UNITED STATES.

Aim: Porous metal-organic frameworks (MOF) nanomaterials, which are built from metal ions/clusters bridged by organic linkers, have been successfully employed as drug delivery vehicles attributing to their enormous porosity, high surface area, and good biocompatibility. Different imaging “labels” have also been incorporated into MOFs and used for MRI, CT, or optical imaging. However, *in vivo* PET imaging with MOF has not been achieved. The aim of this study is to produce an intrinsically radioactive MOF nanoparticle based on the ⁸⁹Zr-hybrid UiO-66 nanostructure. Nucleolin, a selective tumor cell surface marker, was selected as the target-of-interest in this study. **Materials and Methods:** ⁸⁹Zr-incorporated MOF nanoparticle (⁸⁹Zr-MOF in abbreviation) was synthesized via a solvothermal method using ⁸⁹ZrCl₄ as a precursor. Further functionalization was conducted via a pyrenyl-PEG derivative. F3 peptide, a strong binding agent for nucleolin, was introduced as a tumor-targeting ligand. The structure of ⁸⁹Zr-MOF was characterized by TEM and DLS. The stability, targeting efficacy and specificity, and tissue distribution of these ⁸⁹Zr-MOF conjugates were systematically investigated. **Results:** ⁸⁹Zr-MOF has an isotope loading capacity of up to 20 GBq/mg. These ⁸⁹Zr-MOF nano-conjugates had diameters of ~ 100 nm based on TEM and hydrodynamic diameters of ~ 240 nm based on DLS. Superior radiochemical stability was achieved with ⁸⁹Zr-MOF conjugates: > 99.99% ⁸⁹Zr stayed within the structure of ⁸⁹Zr-MOF after a 120 h incubation with

mouse serum at 37°C. Flow cytometry and fluorescence microscopy examination confirmed the targeting specificity of F3 peptide attached ^{89}Zr -MOF conjugates against cellular nucleolin. Potent and persistent uptake of ^{89}Zr -MOF@Py-PEG-F3 in orthotopic MDA-MB-231 tumors (nucleolin⁺) was witnessed (~8 %ID/g at 4 h post-injection) when compared with non-targeted MOF (^{89}Zr -MOF@Py-PEG, ~2 %ID/g at 4 h post-injection). Histology evaluation also confirmed the accumulation of ^{89}Zr -MOF@Py-PEG-F3 in tumor correlated well with nucleolin expression pattern while they were non-specifically captured in liver and spleen. In addition, these GO conjugates can serve as good drug carriers with satisfactory drug loading capacity (e.g. for doxorubicin, 1,000mg/g). Enhanced drug delivery efficiency in MDA-MB-231 tumors was demonstrated in DOX-loaded ^{89}Zr -MOF@Py-PEG-F3 by fluorescence imaging. Toxicity evaluation (body weight, major tissue histology evaluation, and blood biochemical assays) confirmed the safety of these ^{89}Zr -MOF conjugates. **Conclusion:** This is the first PET study using a MOF nanomaterial as the imaging contrast agent. This ^{89}Zr -MOF based nanoplatform can serve as a useful tool for early tumor detection and PET-guidable delivery of therapeutics into a variety of tumors.

OP670

Evaluation of Co-57 labelled Layered Double Hydroxide as a Tumor Imaging Agent

J. Park¹, J. Lee¹, T. Kim², J. Oh²; ¹Korea Atomic Energy Research Institute, Jeongeup, KOREA, REPUBLIC OF, ²Yonsei University, Wonju, KOREA, REPUBLIC OF.

Aim: Layered double hydroxide (LDHs) have various advantages as drug delivery carrier, especially for anticancer therapy. They have layer-by-layer stacking structure between positively charged metal hydroxide nanolayers. Most imaging moieties are generally introduced at outer surface of nanomedicine, and thus they can be detached inside the biological system when administered, resulting in false-tracing of nanomedicine. Therefore, it is feasible that imaging moieties are introduced inside of LDHs and it leads to be more stable *in vivo* than those of outer surface of nanomaterials. In this study, we directly incorporated radioisotope Co-57 into LDH nanomaterial and both *in vitro* cellular uptake and *in vivo* biodistribution test were performed. **Material and Method:** We synthesized LDH particles consisting of Mg-Al hydroxide framework with homogenous particle size of ~150 nm through coprecipitation-hydrothermal treatment. LDHs were characterized with XRD, SEM and Zetasizer. Co-57 was incorporated to lattice of LDH framework by treating LDHs with 880 μCi of $^{57}\text{CoCl}_2$ solution per 5 mg of LDH in 150°C hydrothermal condition for 2 h. The resulting mixture was cooled down at room temperature, and then centrifuged to remove free Co-57 under 10,000 rpm for 5 min. Comparison of cellular uptake using LDHs in 3 different cell lines {CT-26 (Mouse colon), MCF-7 (Breast cancer), HepG2 (Liver hepatocellular carcinoma)}. CT-26 bearing balb/c mice of 5 weeks old weighing 25-30 g were used for the biostudies of [^{57}Co]LDHs. **Results and Conclusion:** we prepared uniform size and morphology MgAl-LDHs and successfully incorporated radioisotope Co-57 into LDH frameworks through hydrothermal assisted substitution reaction preserving physical properties of LDH nanoparticles. We found that Co-57/LDH exhibited significantly high cellular uptake in CT-26 and HepG2 cell lines, suggesting efficient radioactivity delivery capacity of LDH nanoparticles. *In vivo* biodistribution result of Co-57/LDH with CT-26 xenografted balb/c mice showed that LDH nanoparticles could deliver radioactivity to tumor with relatively high tumor-to-organ ratios for clearance organs like liver, kidney and spleens. Thus it concluded that LDH could be utilized to deliver radioisotope for diagnosis activity to tumors avoiding serious clearance and biological removal. Successful demonstration of *in vitro/in vivo* tumor targeting with Co-57/LDH makes them suitable nanoplatforms for tumor theragnostics.

OP671

PS-b-PEO polymeric micelles: dependence of biodistribution and tumor uptake on micellar dose and size

C. Santini¹, A. Laan², M. de Jong¹, A. Denkova², M. Bernsen¹; ¹Erasmus MC, Rotterdam, NETHERLANDS, ²TU Delft, Delft, NETHERLANDS.

Introduction. PS-b-PEO are amphiphilic block copolymers able to aggregate in stable polymeric micelles. They are easy to load with different agents and tunable in size, resulting in an extremely versatile vehicle for the delivery of encapsulated drugs. Size is considered one of the main factors influencing biodistribution of nanoparticles including tumor delivery efficiency. In contrast, little is known on the biological role of the applied dose, for instance regarding saturation limits of different tissues and, as a consequence, the potential therapeutic efficacy and toxicity. This study is the first assessing the biodistribution and tumor uptake of PS-b-PEO micelles of two different sizes, applied at two different doses, in tumor-bearing mice. With this study we aim to elucidate the potential of the newly developed carrier for therapeutic use. **Materials and Methods.** PS-b-PEO micelles, of size (radius) of 89 nm or 50 nm, were synthesized and radiolabeled with ^{111}In at doses 1.7 mg/mL (~1.9 MBq/mL) and 7 mg/mL (~1.1 MBq/mL) using a one-step co-solvent evaporation method. Four combinations were obtained: big micelles at high and low dose (BMH and BML, respectively) and small micelles at high and low dose (SMH and SML). Groups of 5 tumor-bearing mice were injected with 200 μL of a given preparation. Mice were subjected to SPECT/CT at 0.5, 24 and 48 hrs post-injection, followed by *ex vivo*-based biodistribution analysis. **Results.** Images and biodistribution studies showed highly comparable distribution patterns of the four micelle combinations in terms of % injected activity per gram of tissue (% IA/g) with tumor uptake up to 5% IA/g, and high clearance levels in spleen and liver in average 55% and 19% IA/g, respectively. However, due to size and concentration differences in the micellar formulations, considerable differences were found in terms of absolute amount of polymer reaching the various organs. The differences were consistent in every tissue including tumor, and suggest that, at the applied dose, BM might incur in a saturation mechanism, which is not reached by SM at the doses tested. **Conclusions.** PS-b-PEO micelles are extremely versatile and valuable tool for therapeutic applications, by being easy to radiolabel and tunable in size. Next to size, we have here determined nanoparticle-specific, dose-dependency on biodistribution. This indicates that the dose is also an important parameter to consider when applying nanoparticles in drug delivery.

OP672

Gold nanoparticles labelled with ^{211}At conjugated to substance P and trastuzumab - new radiopharmaceuticals for alpha particle therapy

A. Bilewicz¹, L. Dziawer¹, P. Koźminski¹, M. Pruszyński¹, A. Majkowska-Pilip¹, A. Stolarz², K. Szkliniarz³, J. Jastrzębski², G. Celichowski⁴, J. Grobelny⁴, E. Tomaszewska⁴; ¹Institute of Nuclear Chemistry and Technology, Warsaw, POLAND, ²Heavy Ions Laboratory, University of Warsaw, Warsaw, POLAND, ³Department of Physics, Silesian University, Katowice, POLAND, ⁴University of Lodz, Lodz, POLAND.

Aim: Among the others α -emitting radionuclide ^{211}At has attractive properties for use in targeted radionuclide therapy, especially for small tumours and cancer metastasis. ^{211}At is produced via $^{209}\text{Bi}(\alpha, 2n)^{211}\text{At}$ nuclear reaction and has a 7.2 h half-life - a sufficient time for its production, synthetic chemistry, transportation and medical application. However, many astatine compounds that have been synthesized are unstable *in vivo*, providing motivation for seeking other ^{211}At labeling strategies. In our work we propose to utilize formation of strong bond between metallic gold and astatine to bind

the ^{211}At to two biomolecules, peptide substance P and trastuzumab. **Materials and methods:** The gold nanoparticles with diameter of 5 and 20 nanometers were synthesized by Turkevich methods. The nanoparticles were characterized by SEM, STEM and DLS technique. The obtained gold nanoparticles were conjugated to substance P 5-11 (short peptide fragment having high affinity to NK1 receptors on the glioma cells) and trastuzumab (antibody having affinity to Her2 receptor). In first step polyethylene glycol with disulfide or thioctic acid with N-succinimidyl ester as a linkers were conjugated with biomolecules. After twenty four hours product was purified, lyophilized and spontaneously bound to gold nanoparticles. The obtained bioconjugates were labelled with ^{211}At produced in cyclotron at the Heavy Ion Laboratory, University of Warsaw. Before labeling astatine was reduced to At⁻ using 0.01 M Na_2SO_3 solution. Stability of the obtained radiobiocconjugates were tested in biological fluids: sodium chloride, cysteine, glutathione and human serum for 2, 4 and 19 hours. **Results:** The Au- PEG-Substance P (5-11) and Au- PEG-trastuzumab bioconjugates were successfully synthesized. The HPLC analysis has shown that bioconjugates are covalently attached to the gold surface, using the thiol approach. The labeling yield of ^{211}At was higher than 99%. The ^{211}At bioconjugates were very stable in human blood serum and cerebrospinal fluid. Less than 0.1% of the ^{211}At radioactivity was found in solution. Also agglomeration of the nanoparticles was not observed. In-vitro biological studies indicate that ^{211}At - Au- PEG-Substance P (5-11) radiobiocconjugate exhibits high affinity and cytotoxicity to the human glioma T98G cell line while ^{211}At -Au- PEG-trastuzumab to the SKOV3 ovarian cell line. **Conclusion:** We have shown that gold nanoparticles labelled with ^{211}At functionalized with substance P and trastuzumab presents a prospective solution for the use of the ^{211}At as a therapeutic tool for targeting glioma cells and HER2 positive breast and ovarian cancers. This work was supported by National Science Center of Poland (Grant 011/01/M/ST406756).

OP673

Synthesis, preparation and characterization of $^{99\text{m}}\text{Tc}$ -PEI-MP: a potential radiopharmaceutical for the diagnosis of bladder cancer

S. M. Ferreira¹, A. M. Abrantes², M. Laranjo², J. Casalta-Lopes³, A. C. Gonçalves⁴, A. B. Sarmiento-Ribeiro⁴, J. Zeevaert⁵, W. Louw⁵, C. Pais⁶, I. Dormehl⁷, M. F. Botelho²; ¹Biophysics Unit, Faculty of Medicine, University of Coimbra; Centre of Molecular and Environmental Biology, School of Sciences, University of Minho; Nuclear Medicine Course, School of Allied Health Technologies of Porto's Polytechnic Institute, Coimbra, Braga, Porto, PORTUGAL, ²Biophysics Unit, Centre of Investigation on Environment, Genetics and Oncobiology; Institute for Biomedical Research on Light and Image; Faculty of Medicine, University of Coimbra, Coimbra, PORTUGAL, ³Biophysics Unit, Faculty of Medicine, University of Coimbra, Coimbra, PORTUGAL, ⁴Centre of Investigation on Environment, Genetics and Oncobiology; Applied Molecular Biology and Hematology Group; Faculty of Medicine, University of Coimbra, Coimbra, PORTUGAL, ⁵Radiochemistry Department, NECSA, Pretoria, SOUTH AFRICA, ⁶Centre of Molecular and Environmental Biology, School of Sciences, University of Minho, Braga, PORTUGAL, ⁷Department of Internal Medicine, University of Pretoria, Pretoria, SOUTH AFRICA.

Introduction and Aim: Polyethyleneiminomethyl phosphonic acid (PEI-MP) was initially synthesized for palliative therapy of bone metastases after suitable radiolabelling. Biodistribution studies with radiolabelled PEI-MP, demonstrated that the bladder wall was a critical organ, demonstrating the affinity of PEI-MP to bladder cells and possibly to bladder cancer cells. The aim of this work was to reconstitute the cold kit of PEI-MP to be radiolabelled with technetium- $^{99\text{m}}$ and to characterize the $^{99\text{m}}\text{Tc}$ -PEI-MP in terms of hydrophilic

character and *in vitro* cellular uptake. **Material and Methods:** PEI-MP was synthesized by condensation of polyethyleneimine (PEI), phosphorous acid and formaldehyde in the presence of hydrochloric acid. The reconstitution of the PEI-MP labelling kits were performed by adding 500 mg of PEI-MP/25 ml of water and 0.05 ml of $\text{SnCl}_2 \cdot 2\text{H}_2\text{O}$ (pH = 5.0-6.0). The volume of this solution was adjusted with water and 1ml was dispensed into sterile vials, and then lyophilized. $\text{Na}^{99\text{m}}\text{TcO}_4$ (1739 to 1850 MBq) was added to the PEI-MP kit, and left to stabilize at room temperature for 15 minutes. The radiochemical purity of $^{99\text{m}}\text{Tc}$ -PEI-MP was evaluated hourly until 5 hours after the radiolabelling, using ascendant thin-layer chromatography (ITLC-SG/acetone and Whatman 3MM/citrate buffer). To determine the hydrophilicity of $^{99\text{m}}\text{Tc}$ -PEI-MP, it was calculated the 1-octanol/water partition coefficient ($\log P_{o/w}$), hourly until 4 hours after radiolabelling. For cellular uptake and retention studies human cell line of transitional cell carcinoma of the bladder (ATCC® CRL1472™) was used. Cellular uptake and retention studies were performed using $^{99\text{m}}\text{Tc}$ -PEI-MP and $^{99\text{m}}\text{Tc}$ -Pertechnetate. Cell samples were collected during 4 hours, centrifuged to separate supernatant and pellet. Subsequently, the radioactivity of each portion was counted to determine percentage of uptake and retention. **Results:** The radiochemical purity of $^{99\text{m}}\text{Tc}$ -PEI-MP (89-92%) demonstrated to be high. The partition coefficient of $^{99\text{m}}\text{Tc}$ -PEI-MP ranged between -3.28 and -3.82, demonstrated the water solubility of $^{99\text{m}}\text{Tc}$ -PEI-MP. The maximum uptake of $^{99\text{m}}\text{Tc}$ -PEI-MP (1.16), demonstrated to be significantly higher ($p=0.001$, 5%) than $^{99\text{m}}\text{Tc}$ -Pertechnetate (0.27). The minimum retention of $^{99\text{m}}\text{Tc}$ -PEI-MP (3.89), demonstrated to be significantly higher ($p<0.001$, 5%) than $^{99\text{m}}\text{Tc}$ -Pertechnetate (1.03). **Conclusions:** The high radiochemical purity of $^{99\text{m}}\text{Tc}$ -PEI-MP revealed the stability of the kit formulation. The $^{99\text{m}}\text{Tc}$ -PEI-MP demonstrated its hydrophilic character that could be an advantage in terms of unnecessary liver and fat tissue uptake, and a faster kidney-uptake *in vivo*. The high value of uptake and retention of $^{99\text{m}}\text{Tc}$ -PEI-MP, demonstrated the affinity of PEI-MP to bladder cancer cells, revealing that $^{99\text{m}}\text{Tc}$ -PEI-MP could be an excellent agent for imaging *in vivo*.

OP674

Lanthanum phosphate nanoparticles as carriers for ^{225}Ac , ^{223}Ra & ^{225}Ra for targeted alpha therapy

S. Mirzadeh¹, J. V. Rojas², M. F. McLaughlin³, J. D. Woodward¹, D. Robertson³, S. Kennel⁴; ¹Medical Radioisotope Program, Oak Ridge National Laboratory, Oak Ridge, TN, UNITED STATES, ²Department of Mechanical and Nuclear Engineering, Virginia Commonwealth University, Richmond, VA, UNITED STATES, ³Department of Chemistry and University of Missouri Research Reactor, University of Missouri, Columbia, MO, UNITED STATES, ⁴Graduate School of Medicine, University of TN, Knoxville, TN, UNITED STATES.

Targeted alpha therapy (TAT) has the potential for killing micro-metastases with minimum collateral damage to surrounding healthy tissue. *In-vivo* generator radionuclides, such as ^{225}Ac , ^{223}Ra , and ^{225}Ra are of special interest as they emit multiple α -particles during their decay. Utilizing appropriate carriers capable of retaining both the parent radioisotope as well as daughter products is important for the effective delivery of the radioisotope to the tumor site while mitigating global *in vivo* radiotoxicity. In this work, LaPO_4 core and core+2 shells nanoparticles (NPs) (NPs with 2 layers of cold LaPO_4 deposited on the core surfaces) were synthesized containing either ^{223}Ra or $^{225}\text{Ra}/^{225}\text{Ac}$ and the retention of the parents and daughters within the NPs *in vitro* was investigated. XRD and TEM analysis revealed that the NPs crystallized with mean diameters of 3.4 and 6.3 nm for core and core+2 shells, respectively. The core LaPO_4 NPs retained up to 88% of ^{223}Ra over 35 days. In the core+

2 shells NPs, the retention of ^{223}Ra and its daughter, ^{211}Pb , was improved to >99.9% over 27 days. The retention of $^{225}\text{Ra}/^{225}\text{Ac}$ parents was >99.98% and ~80% for the ^{221}Fr and ^{213}Bi daughters over 35 days for the core+2 shells NPs. Conjugation of LaPO_4 NP's to mAb 201B was achieved using a lipoamide polyethylene glycol (dPEG)-COOH linker with gold-coated $\text{La}_{0.5}\text{Gd}_{0.5}\{^{225}\text{Ac}\}\text{PO}_4$ NPs. The conjugates showed an antibody-mediated uptake of 30% injected dose/organ in the target lung, vasculature which was enhanced to 47% when the reticuloendothelial system was temporarily paralyzed. Further, the core-shell NPs retained a large fraction of the daughter products at the target site without compromising the tumoricidal properties of the α -radiation; retention of the ^{213}Bi daughter in endothelial tissue was over 70% at 1 h and about 90% at 24 h post-injection. In a model of lung metastases, treatment of mice with lung-targeted $\text{La}\{^{225}\text{Ac}\}\text{PO}_4$ NPs reduced EMT-6 lung tumor colonies significantly over control treatments. In conclusion, the high *in vitro* retention of both parents and daughters suggest that LaPO_4 NPs are potentially effective carriers of Ac and Ra isotopes, and the NPs-antibody construct is indeed stable *in vivo* with very high antibody-directed uptake.

1706 – Wednesday, October 19, 2016, 10:00 - 11:30, Hall 111

Physics & Instrumentation & Data Analysis: Dosimetry, Radiation Safety & Miscellaneous

OP675

Production yield and isotopic purity of medical Sc radioisotopes formed by proton, deuteron and alpha particle beams

M. Sitarz¹, K. Szkliniarz², R. Walczak³, J. Jastrzębski¹, J. Choiński¹, A. Majkowska³, A. Stolarz¹, A. Trzecińska¹, W. Zipper², A. Bilewicz³; ¹Heavy Ion Laboratory, University of Warsaw, Poland, POLAND, ²Institute of Physics, University of Silesia, Katowice, Poland, POLAND, ³Institute of Nuclear Chemistry and Technology, Warsaw, Poland, POLAND.

Aim. Recently there has been steadily growing interest in the medical applications of Sc radioisotopes. This is due to the convenient half-life of $^{43,44}\text{gSc}$, the prospect of using $^{44\text{m}}\text{Sc}$ as an *in vivo* $^{44\text{m}}\text{Sc}/^{44\text{g}}\text{Sc}$ generator and the therapeutic properties of ^{47}Sc which represents an ideal theranostic pair for the β^+ emitting ^{44}Sc or ^{43}Sc radioisotopes. The production efficiency and impurities generated in the formation of these radioisotopes by p, d and α projectiles are determined. **Materials and methods.** These Sc radioisotopes were produced using α particles from the K=160 heavy ion cyclotron and protons and deuterons from the medical PETtrace p/d cyclotron at the Heavy Ion Laboratory, University of Warsaw. Higher energy protons from the C30 cyclotron at the NCNR in Świerk were also employed. The targets were in CaCO_3 form, natural and enriched, mixed with graphite powder in various proportions. After target irradiation the properties of the produced radioisotopes were first investigated at HIL via gamma-ray spectroscopy techniques and subsequently transported to the Institute of Nuclear Chemistry and Technology in Warsaw for further chemical investigations. **Results.** A 20-30 MeV α -particle beam can produce from a cheap, easily affordable $^{nat}\text{CaCO}_3$ target the prospective PET radioisotope ^{43}Sc with an activity of about 100 MBq/ μAh and isotopic purity better than 10^{-3} . $^{44\text{g}}\text{Sc}$ is produced by the (p,n) reaction at 16 MeV on a 95% ^{44}Ca target with a yield of 700 MBq/ μAh and isotopic purity better than 10^{-4} . $^{44\text{m}}\text{Sc}$ can be produced by a 29 MeV α -particle beam on a 68% ^{42}Ca target with a yield of 4 MBq/ μAh . It can also be formed using a 16 MeV proton beam: for 50 μA proton intensity, 12 h irradiation and 48 h cooling time its activity will be about 1 GBq without the directly produced $^{44\text{g}}\text{Sc}$ activity. The (p,2n) reaction on a 96% ^{48}Ca target in the energy range 30-16 MeV and 10 μA beam intensity produces after 6 h irradiation 6.4 GBq of the therapeutic ^{47}Sc (see R.Walczak et al., abstract at NRC9, Finland and this conference). The

^{48}Sc contamination is 16% of this activity at EOB and decreases with target cooling time. **Conclusions.** All medically interesting Sc radioisotopes can be produced via the accelerator route with intensities and purities acceptable for clinical applications. However, cyclotrons accelerating α particles and protons to energies of about 30 MeV are in some cases necessary. Support by NCBiR grant PBS3/A9/28/2015 is acknowledged.

OP676

Nuclear Medicine Eye Dosimetry: Preliminary Results from a UK Nuclear Medicine and PET/CT centre

G. Havariyoun, M. N. Branco, P. Clinch, E. Kalogianni, A. Mistry, D. Ruiz, G. Vivian; King's College Hospital NHS Trust, London, UNITED KINGDOM.

Introduction In light of the recently recommended occupational exposure limit of 20mSv per year for the lens of the eye, an eye dose measurement study for Nuclear Medicine (NM) Technologists at a UK NM and PET/CT centre was initiated¹⁻². **Aim** The aim of the project was to determine whether there would be any concerns regarding the new exposure limit to the eye for the technologists due to the high dose rates experienced in PET/CT. **Methods** Seven Li-F Thermo-Luminescence $\text{H}_p(3)$ Eye Dosimeters (TLDs) with a dose range of 0.15mSv to 20mSv and an energy detection range of 16keV to 662keV were allocated to NM Technologists to be worn above the right eye. The headbands were worn for a one-month period in addition to the routinely issued body and finger dosimeters. Technologists were involved in both PET/CT and routine NM procedures. A monthly rota is implemented to rotate technologists on a weekly basis. Two of the seven bands were to be worn at all times by the two PET/CT operators. The other five bands were allocated to 5 individual technologists. The number and types of procedures carried out by the five technologists during this period was audited. **Results** A total number of 109 PET/CT procedures were carried out during the above mentioned period. Both headbands worn throughout all 109 PET/CT procedures had readings below the lower dose limit of the TLDs. All but one of the five headbands worn throughout a mixture of routine NM and PET/CT procedures had readings below the lower dose limit of the TLDs and were hence set to 0mSv. Only one headband had a reading of that equal to the lower limit (0.15mSv). **Conclusions** The new recommended annual eye dose limit of 20mSv would lead to a monthly limit of 1.6mSv. Preliminary results indicate that this is not exceeded with the current practice. We believe that the radiation protection measures in place such as use of an automatic radiopharmaceutical dispenser, staff rota and appropriate use of shielding has contributed to these low eye dose measurements. The results will be further validated with phantom measurements and longer use of eye dosimeters. **References** 1. International Commission on Radiological Protection (2011). **Statement on Tissue Reactions** (ICRP ref 4825-3093)1464. <http://www.icrp.org/docs/2011%20Seoul.pdf>. Accessed 01 January 2016. 2. Official Journal of the European Union. **Basic Standards Directive 2013/59/ Euratom** (2014) <https://ec.europa.eu/energy/sites/ener/files/documents/CELEX-32013L0059-EN-TXT.pdf> Accessed 20 April 2016

OP677

Intercomparison of radionuclide calibrators in Belgian hospitals

C. Saldarriaga Vargas¹, L. Struelens¹, S. Rodríguez Pérez¹, K. Baete², S. Pommé³, J. Paepen³, R. Van Ammel³; ¹Belgian Nuclear Research Centre (SCK-CEN), Mol, BELGIUM, ²UZ Leuven Gasthuisberg, Leuven, BELGIUM, ³Institute for Reference Materials and Measurements, Geel, BELGIUM.

Radionuclide calibrators are used in nuclear medicine to determine the amount of activity in a radiopharmaceutical. Their response not only

depends on the characteristic emissions of the particular radionuclide, but also on geometrical characteristics of the chamber and sample. Commercially available activity calibrators are typically calibrated inside the factory, thus establishing traceability for specific measurements. After commissioning, periodic quality control of the chamber is carried out by means of long-lived reference sources, like e.g. Co-57, Cs-137 or Ba-133. However, there is an increasing demand to investigate the accuracy of activity calibrator measurements for clinical isotopes using an SI-traceable standard solution. An intercomparison exercise has been performed of radionuclide calibrator measurements of F-18, In-111 and Tc-99m in 15 Belgian hospitals, involving 37 radionuclide calibrators. Four sessions were held in different geographical regions between December 2013 and February 2015. For each radionuclide a 10 ml Greer vial and a 10 ml syringe filled with 3 ml of stock solution were prepared. For both vial and syringe, an average activity at start was prepared of 100 MBq for Tc-99m, 15 MBq for In-111 and 115 MBq for F-18. The reference values for the massic activity of the solutions were provided by the Joint Research Centre of the European Commission in Geel following two traceability chains to the SI-unit Becquerel. For Tc-99m, about 90% of the calibrators are within $\pm 5\%$ of the reference value for vial and syringe. A maximum underestimation of 16% is observed. For F-18, about 70% of the measured activities are within $\pm 5\%$ of the reference for both containers. All results are correct within $\pm 10\%$ for the F-18 vial. For In-111 the results are worse, with only 40% of the results within $\pm 5\%$ of the reference value for the vial and none for the syringe. Whereas 80% comply within $\pm 10\%$ for the vial measurements, this is true only for 6% of the syringe measurements. For 30% of the calibrators, the In-111 syringe measurements overestimated the activity by more than 30%, up to a maximum deviation of 70%. This intercomparison exercise demonstrates that there is significant room for improvement in the activity measurements of clinical radionuclides. Traceability is best established by a systematic calibration of the radionuclide calibrator for each relevant nuclide, using well characterized standards in identical, reproducible geometrical conditions as applied in daily practice. Such measures are recommended to comply with the growing need for quantitative accuracy in nuclear medicine.

OP678

Measurement of Hg-197 and Hg-197m by a dose calibrator

R. Freudenberg, M. Vogel, M. Andreeff, J. Kotzerke; University Hospital Dresden, Dresden, GERMANY.

Aim: Radiomercury isotopes Hg-197m and Hg-197 are two prospecting isotopes for theranostic applications in nuclear medicine. Hg-197m (half life: 23.8 hours) decays by electron capture (8.9 %) to Au-197 (stable) or by internal transition to Hg-197 (half life: 64.1 hours). The mercury isotopes are produced by proton irradiation of a gold target using a cyclotron. At the end of bombardment the ratio of both radionuclides is approx. 1:1. By solid state spectroscopy it is possible to estimate the activities of both isotopes inside a radioactive probe separately. But it is challenging to do the same by a dose calibrator due to the transient equilibrium and the missing spectroscopic features of an ionization chamber. **Method:** At first we calibrated an HPGe solid state detector (Canberra GC2018-7500SL, Meriden, USA) by reference sources to measure absolute activities of Hg-197m and Hg-197. Additionally, a geometric model of the HPGe detector was constructed to perform Monte Carlo simulations using Geant4 to verify the calibration procedure. In the next step, we created reference source (vials, syringes) of different sizes containing Hg-197/Hg-197m solutions to cross calibrate a dose calibrator (MED Isomed 2010, Dresden, Germany). The radiomercury solutions were measured with and without shielding to determine both activities separately. Therefore we tested shielding of different materials and thickness to optimize the accuracy of measurement. **Results:** The Monte Carlo simulations revealed a good accordance to the HPGe measurements of

calibration sources. Hence we were able to estimate Hg-197(m) activities within 95 % accuracy by using the HPGe. We created vials containing total activities between 5 and 20 MBq within a volume between 2 and 10 ml as well as 1 ml, 2 ml, 5 ml and 10 ml syringes with different volumes. We present the results of dose calibrator measurements by using plastic, aluminum, copper and lead shielding to differentiate between Hg-197 and Hg-197m. **Conclusion:** Based on our results it is possible to upgrade the isotope table in the dose calibrator to measure Hg-197 and Hg-197m routinely. Hence it would be possible to measure radiomercury when it is successfully translated to clinical applications.

OP679

Radiation exposure in 177Lu-PSMA & the possibility of applying outpatient treatment rules

M. Abuqbeith, M. Demir, N. Yeyin, L. Uslu, B. Vatankulu, L. Kabasakal, K. Sönmezoglu; Istanbul University, İstanbul, TURKEY.

Aim: The aim of this study is to develop outpatient treatment protocol for new-emerging 177Lu-PSMA therapy and to evaluate the related radiation safety. **Materials and Methods:** This study analyzed the dose rate of 23 patients treated by 200 mCi 177Lu-PSMA at different distances (0.0, 0.25, 0.50, 1.0 and 2.0 m) in various time points (0, 1, 2, 4, 18, 24, 48 and 120 h) after infusion. Blood samples were withdrawn from 17 patients within the same group in 3, 10, 20, 40, 60, and 90 min and 2, 3, 24 h after infusion. Different 7 patients were asked to collect urine until 24 h and gamma well counter used for samples counting. Family members were invited to wear optically stimulated luminescence (OSL) dosimeter whenever they are in proximity of patients up to 4-5 days. Total dose of medical team including radiopharmacist, physicist, physician, nurse, and nuclear medicine technologist was estimated by electronic personnel dosimeter (EPD). Finger dose was determined using ring thermoluminescent dosimeter (TLD) for radiopharmacist and nurses. **Results:** Dose rate at 1 m after 4 and 6 h was 23 ± 6 μ Sv/h and 15 ± 4 μ Sv/h respectively. Mean total dose to 23 caregivers was 202.3 ± 42.7 μ Sv (120-265 μ Sv). Nurses and radiopharmacist had a total dose of 6 and 4 μ Sv per patient respectively, whereas physicist and physician dose was 2 μ Sv/patient. Blood distribution and early elimination half life was 0.41 ± 0.1 h and 5.1 ± 1 respectively. 7 patients excreted a mean of 45% (range: 32%-65%) of the initial activity during 6 hours following administration. **Conclusion:** Our study supports 177Lu-PSMA as a safe modality to be performed within outpatient treatment protocol, since dose rate decreases below the determined threshold after approximately 5 hours to < 30 μ Sv/h and after 6 hours degrades to 20 μ Sv/h.

OP680

First Ex-Vivo experience of Radioguided Surgery Technique with beta- radiation in a meningioma patient

C. M. Grana¹, R. Faccini², M. Schiariti³, M. Colandrea¹, M. E. Ferrari¹, S. Papi¹, E. Solfaroli Camillocci², P. Ferrolì³, S. Morganti⁴, M. Cremonesi¹, S. Fracassi¹, S. M. Baio¹, L. Gilardi¹, A. P. Rocca¹, L. L. Travaini¹; ¹European Institute of Oncology, Milano, ITALY, ²Dip Fisica Sapienza Università, Roma, ITALY, ³Istituto Neurologico Besta, Milano, ITALY, ⁴INFN, Roma, ITALY.

Introduction: Radioguided surgery (RGS) is a technique aimed at assisting the surgeon to reach a complete resection of the tumoral lesion, while minimizing the amount of healthy tissue removed. Established methods make use of a gamma-emitting tracer with a gamma detecting probe. Since gamma radiation can travel through large amounts of tissue, any uptake of the tracer in nearby healthy tissue represents a non-negligible background, strongly limiting and often preventing the use of this technique. **Aim:** To overcome these limits and extend the range of

applicability of RGS, it was suggested to use pure beta- emitting radioisotopes, as ^{90}Y , which are characterized by a penetration of only few millimeters of tissue. This novel approach allows to develop a new probe which, detecting electrons and operating with low radiation background, provides a clearer delineation of the margins of lesions. We started on evaluating tumors expressing somatostatin receptors, where we can study the uptake of ^{90}Y -DOTATOC, as in brain (meningioma and glioma) and neuroendocrine tumors. These studies started from PET images with ^{68}Ga -DOTATOC and, assuming that the biodistribution of the tracer did not change when labeled with ^{90}Y , with a simulation program (FLUKA) estimated the signal rate on the probe. **Materials and Methods:** A 68 years female patient with radiological diagnosis of meningioma, after giving written informed consent, received a ^{68}Ga -DOTATOC/PET, two weeks prior to surgery. PET revealed that the tumor had an average SUV of 2.3. Twenty-four hours before surgery, the patient was injected with 300 MBq of ^{90}Y -DOTATOC. Before surgery the probe was placed in proximity to the skin of the patient in several spots to estimate the level of background. **Results:** After surgery, that was performed as routine clinical indicated, the extracted tumor and the attached dura were sectioned in 7 samples. Then the probe was put in contact with each sample to measure its activity: all the samples identified by the probe as malignant were actually of tumor tissue, as histologically routine detected. **Conclusions:** This first ex-vivo RGS test proved that administering 4MBq/kg of ^{90}Y -DOTATOC, induced on the probe a signal that allows to discriminate very strongly between tumor and nearby healthy tissues. Now we are enrolling a second meningioma patient. Further developments of the probe could further increase its sensitivity, in order to reduce the dose for a given administered activity.

1707 – Wednesday, October 19, 2016, 10:00 - 11:30, Hall 116

Clinical Oncology: Lymphoma

OP681

Prognosis value of FDG-PET Parameters at Diagnosis and after Induction in Patients with Mantle Cell Lymphoma, Interim Results from the LyMa-PET Project, a LYSA study

C. Bailly¹, T. Carlier¹, M. Meignan², C. Gallazzini Crepin³, A. Beriolo Riedinger⁴, A. Devillers⁵, F. Kraeber Bodere¹, S. Le Gouill¹, C. Bodet Milin¹; ¹University Hospital, Nantes, FRANCE, ²University Hospital, Creteil, FRANCE, ³University Hospital, Grenoble, FRANCE, ⁴Cancer Center, Dijon, FRANCE, ⁵Cancer Center, Rennes, FRANCE.

OBJECTIVES: Positron emission tomography using ^{18}F -fluoro-2-deoxy-glucose (FDG-PET) has emerged as an important predictor of clinical outcome in lymphomas. Yet, its role and its prognostic value in mantle cell lymphoma (MCL) is less well defined as its utility for assessing disease burden and response to therapy remains unclear. The objective of the study was to analyse whether quantitative indices derived from FDG-PET at diagnosis and after induction can provide prognostic value for untreated MCL patients. Our work is an ancillary study of the prospective phase III LyMa trial (Le Gouill et al. ASH 2014 ; ASH 2015) (NCT00921414). Herein, we present the first results performed from the database of first planned interim-analysis. **METHODS:** FDG-PET of 94 MCL patients have been independently and centrally reviewed by 2 lymphoma expert nuclear physicians. Quantitative metrics including SUV_{max}, SUV_{mean}, SUV_{peak}, total lesion glycolysis (TLG) were extracted from the area with the highest uptake, at diagnosis and before ASCT (iPET). Whole-body functional volume and whole-body TLG (TLG_{wb}) were derived considering all detected lesions at diagnosis. Visual analysis with Deauville scale was also performed at iPET. The best cut-off values were determined for each metric using X-tile® analysis. Prognostic value was assessed using univariate analysis by Kaplan-Meier estimates of progression-free survival (PFS). **RESULTS:** The

studied population did not differ from the entire LyMa cohort (n=299). At diagnosis, univariate analysis showed a prognostic value on PFS of 4 metrics: SUV_{max} (p<0.001), SUV_{mean} (p<0.001), SUV_{peak} (p<0.001) and TLG (p=0.03). The prognostic value of SUV_{max} was reinforced when combined with MIPI. Indeed, patients can be separated in 3 prognostic groups including a group of patients with a very good outcome (low SUV_{max} plus MIPI inter/low). Whole-body functional volume and TLG_{wb} were not associated with PFS. Results of iTEP showed that SUV_{max}, SUV_{peak}, SUV_{mean} but also $\Delta\text{SUV}_{\text{max}}$, $\Delta\text{SUV}_{\text{peak}}$, $\Delta\text{SUV}_{\text{mean}}$ before ASCT were predictive of PFS. FGD-PET before ASCT's analysis according to Deauville scale (positivity cut-off: Deauville score ≥ 4) was not associated with PFS. **CONCLUSION:** The LyMa-PET project is the largest study addressing the question of FDG-PET in a homogeneously treated population of MCL. Results show a strong prognostic value on PFS of quantitative parameters such as SUV_{max} determined on FDG-PET at diagnosis and after induction in MCL untreated patients. Update results and patients' outcome according to randomization arms will be presented for the time of the meeting.

OP682

18F FDG-PET/CT In Gastric Malt Lymphoma: A Bicentric Experience To Establish Correlations With Histological And Morphological Features

D. Albano¹, P. Ferro², M. Bertoli¹, M. Spallino², G. Bosio¹, M. Picchio², F. Bertagna¹, F. Fallanca², L. Gianolli², R. Giubbini¹; ¹Spedali Civili Brescia, Brescia, ITALY, ²IRCCS San Raffaele Scientific Institute, Milano, ITALY.

Aim: gastric mucosa-associated lymphoid tissue (MALT) lymphoma is the most common extranodal MALT lymphoma. The role of ^{18}F -FDG PET/CT in evaluating this type of lymphoma is still controversial. In literature the detection rate of ^{18}F -FDG PET/CT in patients with gastric MALT is variable (9-77%) and the reason of this heterogeneity is not still clear. Our aim was to compare the metabolic behavior of gastric MALT with epidemiological, histopathological, Ann Arbor staging and gross morphological features. **Materials and methods:** sixty seven patients (26 female, 41 male; median age: 60 years; age range, 27-83) from two center (Department of Nuclear Medicine of Spedali Civili Brescia and of IRCCS San Raffaele Scientific Institute) with histologically-confirmed diagnosis of gastric MALT who underwent a ^{18}F -FDG PET for initial staging before any treatment were included. PET images were qualitatively and semi-quantitatively analyzed by measuring the maximum standardized uptake value (SUV_{max}), lesion-to-liver SUV_{max} ratio and lesion-to-blood pool SUV_{max} ratio and compared with epidemiological (age,sex), histological (presence of gastritis, ulcer, H. pylori infection, plasmacytic differentiation and Ki67 index) and morphological (diameter max lesion, superficial or mass-forming lesions) characteristics. Proliferative activity expressed by Ki-67 was evaluated in 60 patients. Forty nine patients were stage I, 4 stage II, 4 stage III and 10 stage IV. **Results:** thirty five patients had positive ^{18}F -FDG-PET/CT showing ^{18}F -FDG uptake (average SUV_{max} was 8.9 ± 6.7 ; lesion-to-liver SUV_{max} ratio 3.7 ± 2.6 ; lesion-to-blood pool SUV_{max} ratio 4.8 ± 3.3) at the corresponding gastric lesion; the remaining 32 were not ^{18}F -FDG-avid. 54 (81%) patients had gastritis, 32 (49%) had gastric ulcer, 28 (42%) had H. pylori infection. Thirty four MALT (51%) presented with superficial gastric lesion, while 33 (49%) with mass forming lesions; plasmacytic differentiation was present in 9 patients (13%); median diameter maximum measured with morphological imaging like CT or endoscopy was 1.7 cm (range:0.2-8.7 cm). ^{18}F -FDG avidity was significantly associated with morphological features (mass forming and high maximum diameter), Ann Arbor stage and Ki67 index (p<0.001). SUV_{max}, lesion-to-liver SUV_{max} ratio and lesion-to-blood pool SUV_{max} ratio correlated significantly with Ki67 index (p<0.001) and no other features. **Conclusions:** ^{18}F -FDG avidity was noted in 52% of gastric MALT lymphoma and this avidity is correlated with gross morphological characteristics, tumor stage and Ki-67 index. SUV_{max}, lesion-to-liver SUV_{max} ratio and lesion-to-blood pool SUV_{max} ratio are correlated only with Ki-67 index.

OP683**Interobserver Agreement of Interim ¹⁸F-FDG PET/CT in Diffuse Large B-Cell Lymphoma (DLBCL): Impact of Baseline Imaging Modality and Disease Localization**

C. N. Burggraaf¹, A. C. Cornelisse¹, J. M. Zijlstra¹, O. S. Hoekstra¹, H. C. W. De Vet¹, P. J. Lugtenburg², F. Celik³, J. E. Huijbregts⁴, A. I. J. Arens⁵, B. De Keizer⁴, On behalf of the HOVON imaging working group: ¹VU university medical center, Amsterdam, NETHERLANDS, ²Erasmus MC Cancer Institute, Rotterdam, NETHERLANDS, ³Deventer Ziekenhuis, Deventer, NETHERLANDS, ⁴university medical center Utrecht, Utrecht, NETHERLANDS, ⁵Radboud university medical center, Nijmegen, NETHERLANDS.

Aim: International guidelines recommend ¹⁸F-FDG PET/CT for staging and for end-of-treatment response assessment in DLBCL patients. The role of interim ¹⁸F-FDG PET/CT (iPET) in DLBCL is less clear. Our aim was to assess the interobserver agreement of iPET using the Deauville 5-point scale (DS) in patients with DLBCL as a function of the baseline imaging modality (¹⁸F-FDG PET/CT or CT only) and of the localization of residual ¹⁸F-FDG uptake. **Materials and methods:** iPET scans of DLBCL patients were collected from the HOVON84 study, an international multicenter randomised controlled trial. Patients received R-CHOP immuno-chemotherapy and were randomized to receive rituximab intensification in the first four cycles or not. iPET was made after 4 cycles. Scans were scored according to the DS by two central reviewers from a pool of ten experienced nuclear medicine physicians. Reviewers were blinded to clinical outcomes. DS results were dichotomized (DS 1-3: 'negative', DS 4-5: 'positive'). Besides Cohen's kappa we calculated the agreement separately for the positive and the negative scores, expressed as positive agreement (PA) and negative agreement (NA). Definition of positive agreement: given one reviewer scores positive, the probability that another reviewer scores positive as well. (de Vet et al. BMJ 2013). **Results:** 488 iPET scans were reviewed centrally; a baseline ¹⁸F-FDG PET/CT was available in 76%, and CT in the remaining cases. Kappa for iPET interobserver agreement was 0.65, NA was 92.1% and PA was 72.5%. Kappa and PA of the 369 iPET cases with a baseline ¹⁸F-FDG PET/CT available were 0.68 and 75.6% versus 0.52 and 60.9% in the 119 iPET cases with only a baseline CT scan for reference (p=0.10 and 0.16, respectively). Negative agreement for involved localizations was 97.8-100%. Lowest positive agreement was observed for mediastinal and mesenteric lymph nodes, spleen, GI and skeletal localizations (30.0-65.2%). **Conclusion:** Availability of a baseline ¹⁸F-FDG PET/CT seems to give a better interobserver agreement of iPET, although not statistically significant. Despite reasonable kappas, the relatively low PA indicates that observer agreement needs to be improved before iPET can be used in treatment escalation trials in DLBCL patients. These data can help to set the agenda for further training and research on iPET interpretation.

OP684**FDG PET-CT parameters in the therapy evaluation of patients with Hodgkin's lymphoma**

M. Tuncel¹, T. M. Kutluk², P. Ö. Kiratlı¹, B. Aydın², B. Erbas¹, C. Akyüz²; ¹Hacettepe University, Department of Nuclear Medicine, ANKARA, TURKEY, ²Hacettepe University, Department of Pediatric Oncology, ANKARA, TURKEY.

Aim: FDG PET-CT is the modality of choice for staging and therapy response evaluation of patients with Hodgkin's lymphoma (HL). However the optimal quantitative or qualitative parameter that predicts therapy response and prognosis is a matter of debate. In this study we aimed to compare the accuracy of several FDG PET-CT parameters in the evaluation of patients with HL. **Material and method:** FDG PET-CT was

performed in 70 pediatric patients with HL (mean age: 12.6±4, range: 4-20 yrs) at baseline(1) and after 2-3rd cycles of chemotherapy(interim)(2). End of therapy imaging(3) was available in 50 patients. The median follow-up was 31 months(6-60). Images were interpreted according to the Deauville 5-point score(DS), Revised DS(that accepts milimetric residual upper cervical lymph node with DS ≥4 as DS:1) and SUVmax of the lesion, total tumor volume(TTV) and total lesion glycolysis (TTVxSUVmean). Percentage change(%Δ) of these quantitative parameters were measured. The ROC curves were obtained to determine the AUC values and the optimal cut-off of parameters to predict relapse. **Results:** Interim FDG PET-CT was normal in 77%(54/70) of patients. DS4-5 was in 23%(16/70) of group. Six patients had progression or relapse during follow-up. SUV2[0.6 ±1.2 vs 7.3 ±7.4, p=0.001], SUV3[0.6 ±1.6 vs 6.9 ±9.3, p=0.001], TTV2 [1.9 ±8.6 vs 31.2 ±46.3, p=0.0001] and TLG2[3 ±13 vs 133 ±190, p=0.0001] values were different in remission and relapse sub-groups. The AUC values were 0.83(p=0.008) for SUV2, 0.936(p=0.02) for SUV3, 0.77(p=0.027) for TTV2, 0.78(p=0.021) for TLG2, 0.78(p=0.026) for %ΔSUV2, 0.73(p=0.08) for %ΔTTV and 0.73(p=0.087) for %ΔTLG respectively. The best cut-off values were 2.7, 6.5, 16, %55, %96 and %97 with a sensitivity and specificity of 93% and 71.4% for SUV2, 95% and 66.7% for TTV2, 98% and 66.7% for TLG2, %94.2 and 66.2 for %ΔSUV2, 94% and 60% for %ΔTTV, 94% and 60% for %ΔTLG respectively. Progression free survival(PFS) in patients with DS 1-3 was better than in patients with DS 4-5 (Log-rank, p=0.002) According to ROC analysis, revisedDS performed better than DS(AUC:0.83 P=0.005 vs AUC:0.78 p=0.017). Patients with values below the cut-off of SUV2, TTV2, TLG2, %ΔSUV2, %ΔTTV and %ΔTLG had longer PFS than patients with higher values (Log-rank, p=0.005, p=0.0001, p=0.0001, p=0.016, p=0.0001 and p=0.012). **Conclusion:**FDG PET-CT was useful for the evaluation of pediatric patients with HL. Interim Revised DS 4-5 and high TTV2 and TLG2 were the best predictors of shorter PFS. Our results should be confirmed in further studies with larger number of patients.

OP685**Evaluating early interim fluorine-18 fluorodeoxyglucose PET/CT with SUVmax-based criteria for predicting the outcome in DLBCL**

Y. Fan¹, Y. Zhang², Z. Yang¹, N. Zhou¹, C. Liu¹, Z. Ying¹, J. Zhu¹, X. Wang¹; ¹Peking university cancer hospital, Beijing, CHINA, ²Peking university cancer hospital & Institute, Beijing, CHINA.

Purpose: To investigate whether the SUV_{max}-based criteria could be a superior method for evaluating early interim PET compared with the Deauville five-point scale (5-PS) and reduction rate of the maximum standardized uptake value (ΔSUV_{max}) criteria.**Methods:** A total of 119 patients with DLBCL underwent ¹⁸F-FDG PET/CT at baseline (PET0) and after two chemotherapy cycles (PET-2) were enrolled in this study. PET-2 were evaluated with the SUV_{max}-based, 5-PS, and ΔSUV_{max} criteria. The optimal threshold of the SUV_{max}-based criteria was calculated via reproducibility and prognostic analyses using the liver SUV_{max} as reference. Using the three criteria, prognostic factors were compared by the survival analysis. Uni- and multivariate analyses of outcomes were performed using clinical variables and PET-2.**Results:** The optimal threshold for the SUV_{max}-based criteria is 1.6 fold of the liver SUV_{max}. The Cohen's *k* values for reproducibility of the SUV_{max}-based criteria were above 0.90 and were superior to the 5-PS or ΔSUV_{max} interpretation. Using the SUV_{max}-based criteria, the 3-year progression-free survival (PFS) and overall survival (OS) were 75.1% and 78.6%, respectively, for patients with a positive residue compared with 15.8% and 36.9%, respectively, for patients with a negative residue (P < 0.001). The SUV_{max}-based criteria demonstrated a slight superior prognostic value compared with the other two criteria. Uni- and multivariate

analyses revealed that the PET-2 viewing via SUV_{max} -based criteria was an independent predictor for PFS ($P < 0.001$) and OS ($P = 0.003$). **Conclusion:** Together, these data indicate that early interim ^{18}F -FDG PET/CT effectively predicts the outcome in patients with DLBCL using the SUV_{max} -based criteria.

OP686

Baseline Metabolic Tumour Volume to Predict Outcome in Diffuse Large B Cell Lymphoma: Which Method?

F. Rahman¹, N. G. Mikhaeel¹, L. C. Gormsen², J. T. Dunn³, T. C. El-Galaly⁴, H. Ilyas³, D. Smith¹, H. Möller⁵, L. J. Petersen⁶, M. H. Vendelbo², A. Elser⁷, S. F. Barrington³; ¹Department of Clinical Oncology, Guy's and St Thomas' Hospital, London, UNITED KINGDOM, ²Department of Nuclear Medicine & PET Centre, Aarhus University Hospital, Aarhus, DENMARK, ³PET Imaging Centre at St. Thomas' Hospital, King's College, London, UNITED KINGDOM, ⁴Department of Hematology, Aalborg University Hospital, Aalborg, DENMARK, ⁵Cancer Epidemiology, Population and Global Health, King's College, London, UNITED KINGDOM, ⁶Department of Nuclear Medicine, Aalborg University Hospital, Aalborg, DENMARK, ⁷Hermes Medical Solutions, Stockholm, SWEDEN.

Aim: Baseline total Metabolic Tumour Volume (tMTV) has been reported to be prognostic in Diffuse Large B Cell Lymphoma (DLBCL) using two methods, which have differing complexity and delineation time. The aim of this study was i) to determine whether the methods accurately predicted progression free survival (PFS) using commercial software in an unselected population of patients with DLBCL and ii) if measurement of MTV in the bulkiest lesion(s) could be used as a surrogate for tMTV. **Methods:** Consecutive patients with DLBCL staged with ^{18}F Fluorodeoxyglucose PET-CT and treated with RCHOP(-like) chemotherapy were included from two institutions from UK and Denmark. Tumour was segmented with Hermes Medical Hybrid 3D viewer© software using the standardised uptake value ($SUV \geq 2.5$ (MTV2.5) and $\geq 41\%$ of maximum SUV (MTV41%). Tumour volume(s) were edited to exclude physiological uptake and summed to calculate tMTV. The MTV of the lesion with the greatest overall bulk (MTVbulk) and the sum of the two bulkiest lesions above and below the diaphragm (MTVsum) were also measured. Correlation between methods was tested using Pearson's, and Kendall-tau rank correlation. Receiver operator characteristics (ROC) analysis was performed to determine the optimal threshold to predict PFS for each method. Kaplan-Meier analysis was used to examine the association between MTV and PFS using these thresholds. Results are available from 246 patients, median follow up 43.8 months (range 0.62-121.6 months). Mean tMTV2.5 (sd) was $969 \pm 1301 \text{ cm}^3$. Mean tMTV41% (sd) was $295 \pm 465 \text{ cm}^3$. Total MTV2.5 and tMTV41% correlated strongly ($R=0.79$) and ranked patients in similar order ($\text{Tau}=0.75$). MTVbulk and MTVsum also correlated strongly with total MTV using both methods. [MTVbulk2.5 vs. tMTV2.5 $R=0.84$; MTVsum2.5 vs. tMTV2.5 $R=0.86$. MTVbulk41% vs. tMTV41% $R=0.93$; MTVsum41% vs. tMTV41% $R=0.94$.] Optimal cut-off values were 426 cm^3 (tMTV2.5) and 99 cm^3 (tMTV41%). Using the derived cut-offs to separate patients into high and low MTV, the six methods were all predictive of PFS, with tMTV2.5 being the most significant ($\log \text{rank}=23.3$, $p < 0.00$). 5y-PFS was 79% vs. 50% for patients with low and high tMTV2.5 respectively and 75% vs. 51% for low and high bulkMTV2.5 respectively. **Conclusions:** Baseline MTV predicts PFS in DLBCL using both published methods, but the optimal threshold is dependent on the method used. The MTV of the bulkiest lesion predicted PFS almost as well as the total MTV. This would reduce the time needed to measure MTV making it feasible for routine reporting.

OP687

The Oncology Biomarker Qualification Initiative (OBQI): Multi-institutional Demonstration Using FDG-PET in Non-Hodgkin's Lymphoma

J. Zhang¹, N. C. Hall², H. Schoder³, L. P. Schwartz⁴, W. H. Wilson⁵, G. Kelloff⁶, M. V. Knopp¹; ¹The Ohio State University, Columbus, OH, UNITED STATES, ²Philadelphia VA Medical Center, Philadelphia, PA, UNITED STATES, ³Memorial Sloan Kettering Cancer Center, New York, NY, UNITED STATES, ⁴Columbia University, New York, NY, UNITED STATES, ⁵National Institutes of Health, Bethesda, MD, UNITED STATES, ⁶National Cancer Institute, Bethesda, MD, UNITED STATES.

Purpose: OBQI was initiated in January 2006 in USA via an FDA-NCI-CMS consortium to qualify new cancer biomarkers. The Imaging and Radiation Oncology Core (IROC) Ohio served as one of the six NCI-designated quality assurance centers and managed this multi-institutional project with the goal to qualify FDG-PET as an imaging biomarker in non-Hodgkin's lymphoma. This presentation is to introduce, evaluate and demonstrate the overall experiences within this clinical trial and the established quality assurance workflows and standards. **Methods:** To ensure consistent and objective imaging biomarker assessment for treatment response, a standardized workflow supporting such multi-institutional clinical trials was established to manage the continuum from trial initiation to closure. Four advanced components of imaging performance and protocol compliance from site credentialing to central review analysis were implemented and evaluated. 15 itemized criteria within 4 categories in data quality control were established and standardized. A 'heat-mapping' approach for quantitative data assessment was developed and utilized for effective trial performance and quality control management. All imaging aspects of this trial was coordinate between the Imaging Committee of the NCI network group and the responsible Imaging Core Lab. **Results:** Within 5 years patient enrollment and data accrual for this biomarker study, a total of 173 patients with 538 PET/CT studies from 57 specifically credentialed institutions within the US were included in the assessment. The overall data compliance rate was at the start of the trial ~50% and improved to greater than 90% due to the implemented quality control procedures. The QC scoring system found for the 538 studies 92% were rated compliant, 5% acceptable and 3% noncompliant. Focusing on 173 accessible patients found 92% were compliant, 7% acceptable and 1% noncompliant. The most common imaging protocol deviations were uptake time, scanner consistency and timing of follow up. The blinded reader assessment found a 92% agreement in quantitative biomarker analysis (discrepancies: PC2 positive 5%, PC2 negative 3%, PC6 0%). **Conclusion:** We report on the established best practices and experiences in quality assurance workflows, site credentialing strategies, imaging protocol standards and central imaging review for the national biomarker initiative. Our experience should lead to refined best clinical imaging trial practices and strengthen the effort to establish validated PET Biomarker capabilities not only for lymphoma but for all clinical trials.

OP688

Somatostatin Receptor Expression in Lymphomas: ^{68}Ga -DOTANOC PET/CT Imaging and Immunohistochemical Analysis

T. Ruuska^{1,2,3}, Y. Escala-Ramirez^{4,5}, S. Vaitinen^{1,6,3}, M. Gardberg^{6,3}, E. Alanne^{2,3}, A. Kiviniemi^{7,3}, I. Jambor^{7,1}, P. Marjamäki^{8,1}, J. Kempainen^{9,8,3}, S. Jyrkkio^{2,3}, H. Minn^{2,3}; ¹University of Turku, Turku, FINLAND, ²Department of Oncology and Radiotherapy, Turku, FINLAND, ³Turku University Hospital, Turku, FINLAND, ⁴Department of Radiology, Madrid, SPAIN, ⁵University of Madrid, Madrid, SPAIN, ⁶Department of Pathology, Turku, FINLAND, ⁷Department of Radiology, Turku, FINLAND, ⁸Turku PET Centre, Turku, FINLAND, ⁹Department of Nuclear Medicine, Turku, FINLAND.

INTRODUCTION: ^{68}Ga -DOTANOC PET/CT is routinely used to image neuroendocrine tumors (NETs). Incidentally we saw a patient whose pancreatic diffuse large B-cell lymphoma (DLBCL) mimicked NET in ^{68}Ga -DOTANOC-PET/CT. This prompted us to determine somatostatin receptor (SSTR) status in patients with lymphoma at ^{68}Ga -DOTANOC PET/CT and by immunohistochemical analysis of SSTR subtypes 2, 3 and 5 (SSTR_{2,3,5}). **METHODS:** 21 patients with newly diagnosed lymphoma were referred to ^{68}Ga -DOTANOC and FDG PET/CT prior any treatment. Tracer uptake was evaluated visually by two nuclear medicine specialists. Maximum standardized uptake values (SUVmax) were determined from 14 lymph node and two extranodal regions (if any) with highest uptake in each patient. Lesions were then graded with Deauville score (1-5) in FDG PET/CT and modified Krenning score (0-4) in ^{68}Ga -DOTANOC PET/CT, respectively. SSTR_{2,3,5} status was analyzed from routine biopsies of lymphomatous tissue and matched to corresponding PET/CT findings. **RESULTS:** 20/21 patients had FDG-positive lymphoma (Deuville score ≥ 3). Uptake of ^{68}Ga -DOTANOC was regarded as positive if modified Krenning score was ≥ 2 (uptake less or equal to liver) and resulted in 14 of 21 (67%) patients having ^{68}Ga -DOTANOC-positive lymphomas. Highest ^{68}Ga -DOTANOC SUVmax values were seen in Hodgkin's lymphoma of nodular sclerosis subtype and DLBCL (median 9.8 and 9.7, respectively). Both cases showed strong SSTR₂ immunopositivity in tumor cells. Some patients had SSTR₂ immunopositivity predominantly in endothelial and dendritic cells and follicular centers of lymph nodes contributing to a positive PET/CT with probably low tumor-specific uptake. SSTR₃ and SSTR₅ were mainly negative in all lymphoma subtypes. **CONCLUSION:** According to this pilot study, ^{68}Ga -DOTANOC PET/CT is positive in some lymphoma subtypes which express SSTRs. These tumors may be amenable to treatments targeting SSTR and present a potential risk to be classified as NET if representative tumor sample is not available.

1708 – Wednesday, October 19, 2016, 10:00 - 11:30, Hall 212
Special Symposium 3 (Part II) - EANM/ESSO: Advances in Radioguided Intervention for Biopsy of Occult Lesions and Sentinel Nodes

OP689

Intraoperative Breast Cancer Surgery with ^{18}F FDG Cerenkov Luminescence

M. Cariati; King's College London, Research Oncology Department, London, UNITED KINGDOM.

OP690

Sestamibi-Guided Biopsy of Radiologically Occult Breast Lesions

L. M. Pereira Arias - Bouda; Leiden University Medical Centre, Nuclear Medicine Section, Department of Radiology, Leiden, NETHERLANDS.

OP691

Dedicated PET for Breast Cancer Imaging and Biopsy

M. Herranz; University Hospital Santiago de Compostela, Molecular Oncology and Imaging, Santiago De Compostela, SPAIN.

OP692a

Round Table with EANM and ESSO Delegates: The Future of Radioguided Surgery

D. Rubello; Ospedale 'S. Maria della Misericordia' - Rovigo, Nuclear Medicine Service - PET Unit, Rovigo, ITALY.

OP692b

Round Table with EANM and ESSO Delegates: The Future of Radioguided Surgery

F. Giammarile; Centre Hospitalier Universitaire de Lyon, Lyon, FRANCE.

OP692c

Round Table with EANM and ESSO Delegates: The Future of Radioguided Surgery

M. Leidenius; HELSINKI UNIVERSITY HOSPITAL, BREAST SURGERY UNIT, Helsinki, FINLAND.

OP692d

Round Table with EANM and ESSO Delegates: The Future of Radioguided Surgery

O. Gentilini; Ospedale S. Raffaele, Milan, ITALY.

1709 – Wednesday, October 19, 2016, 10:00 - 11:30, Hall 113

Conventional & Specialised Nuclear Medicine: Infection & Inflammation 2

OP693

The role of ^{18}F -FDG PET/CT in the diagnosis and response to medical treatment of inflammatory aneurysms of abdominal aorta. A prospective pilot study

M. Lavalle¹, V. Alberti², S. Annunziata¹, L. Leccisotti¹, M. Orrico², S. Ronchey², N. Mangialardi², A. Giordano¹; ¹Institute of Nuclear Medicine, Università Cattolica Sacro Cuore, Roma, ITALY, ²Institute of Vascular Surgery, Presidio Ospedaliero San Filippo Neri, Roma, ITALY.

Aim: Normal aortic wall contains few inflammatory cells in contrast to aneurysm of abdominal aorta (AAA) tissue, which demonstrates a progressive accumulation of inflammatory cells from relatively non-inflammatory (niAAA) to inflammatory AAA (iAAA). Computed tomography (CT) sensitivity in identifying iAAA is ~83% and medical treatment with steroids can lead to regression of the inflammation without a reduction in aneurysm size. To date, limited data are available on the role of metabolic imaging in iAAAs by ^{18}F -FDG PET/CT. Therefore, the aim of this pilot study is to evaluate prospectively the role of ^{18}F -FDG-PET/CT in iAAA diagnosis and response to medical treatment. **Methods:** We prospectively evaluated 6 patients (all male, mean age 65±6 yrs) with symptomatic iAAA (mean diameter 7.17±1.93 cm). Five male patients with asymptomatic niAAA undergone ^{18}F -FDG-PET/CT for oncological purposes were included as age and size-matched controls. All patients with iAAA underwent ^{18}F -FDG-PET/CT before and after steroid treatment for three months. In all patients AAA SUVmax and target to background ratio (TBR) were calculated (a VOI was placed on the area of most intense aortic wall ^{18}F -FDG uptake and the superior cava vein was used for background). All PET parameters were compared with serum inflammation levels. After steroids, clinical examination, especially a prompt reversal of symptoms, was used as response criteria in iAAA patients. **Results:** All iAAAs showed significantly increased FDG uptake before steroid therapy compared to asymptomatic niAAAs (mean SUVmax 9.61±2.43 vs. 2.28±0.23, mean TBR 5.49±1.60 vs. 1.40±0.31; p<0.05). After medical treatment, all PET parameters significantly decreased in all iAAAs compared to baseline values (mean SUVmax 3.29±1.12 and mean TBR 1.58±0.49; p<0.05). Mean SUVmax and TBR reductions were respectively 65±12% (range 50%-79%) and 69±11% (51%-83% range). Mean C-reactive protein value slightly decreased after steroid therapy without reaching statistical significance (7.70±3.43 vs. 5.84±1.22 mg/dl after steroids; p=n.s) and maintaining levels higher than laboratory cut-off in all iAAAs. All iAAAs were considered responders to medical treatment by clinical examination. **Conclusions:** The preliminary

data of this prospective pilot study show that all symptomatic iAAAs exhibit highly increased ^{18}F -FDG uptake compared to asymptomatic niAAAs. Moreover, ^{18}F -FDG uptake changes seems to correlate with clinical response to steroid therapy more than serum inflammation parameters suggesting that PET/CT may become a useful method of monitoring response to medical treatment.

OP694

Correlation of tissue to blood standard uptake ratio (SUR) derived from static ^{18}F -FDG-PET scans with the metabolic uptake rate derived from dynamic ^{18}F -FDG-PET scans for quantification of lung inflammation in experimental ARDS

A. Braune, L. Oehme, T. Kiss, T. Bluth, J. Kotzerke, M. Gama de Abreu; University Hospital Carl Gustav Carus at the Technische Universität Dresden, Dresden, GERMANY.

AIM: PET imaging using ^{18}F -FDG followed by mathematical modelling of the pulmonary metabolic uptake rate of ^{18}F -FDG (ki) is goldstandard for the assessment of pulmonary inflammation in acute respiratory distress syndrome (ARDS). However, dynamic PET requires 60–75min and covers only a 15cm cranio-caudal field of view. It has been shown in experimental ARDS in dogs, the tissue to blood standard uptake ratio (SUR), derived from the last 300s-frame of a 58min dynamic ^{18}F -FDG-PET scan, highly correlated with ki measurements [Chen DL et al., JNuclMed2004]. In this study we investigated whether ki measurements also correlate with SUR derived from static ^{18}F -FDG-PET in experimental ARDS, which would allow a much faster acquisition of the whole lung. We also investigated, whether the 15cm cranio-caudal field of view of dynamic PET was representative for inflammation of the whole lung. **METHODS:** Lung injury was induced by saline lavage and ventilation with high tidal volumes in 8 pigs. After injury (day1) and after 24h of mechanical ventilation (day2) ^{18}F -FDG uptake was quantified as kiP using the Patlak analysis of dynamic PET frames 15–75min after ^{18}F -FDG injection. Mean kiP values were calculated for 5 isogravimetric subregions (ROIs15cm) along the ventro-dorsal gradient of the captured 15cm cranio-caudal lung field. Immediately after dynamic PET scanning and 77–80min after ^{18}F -FDG injection, static ^{18}F -FDG-PET scans of the whole lung were obtained. Mean SUR values (SUR15cm) were calculated for the same ROIs as used for kiP analysis, thus covering only a 15cm cranio-caudal lung field, using plasma activity measurements at the timepoint of static PET scanning. In addition, mean SUR values (SURwholeLung) were calculated for 5 ROIs using the ventro-dorsal expansions of ROIs15cm but the whole cranio-caudal lung dimensions. Correlation of kiP and SUR15cm and of SURwholeLung and SUR15cm were investigated by means of linear regression of all ROI on day1 and day2, respectively, and coefficients of determination (r^2) were compared. **RESULTS:** SUR15cm linearly correlated with kiP within all ROIs, both on day1 and day2 ($r^2=0.8581$ and 0.9643 , respectively). SUR15cm highly correlated with SURwholeLung, both on day1 and day2 ($r^2=0.9069$ and 0.9909 , respectively). **CONCLUSION:** Compared to dynamic PET and Patlak analysis, SUR determined with static PET is a valuable alternative for determination of pulmonary inflammation. It allows assessment of inflammation of the whole lung within a much shorter time range. In this ARDS study the inflammation within a 15cm cranio-caudal lung field was representative for inflammation of the whole lung.

OP695

The diagnostic value of F-18-FDG PET/CT in patients suspected for LVAD infection

N. Avramovic¹, A. Dell'Aquila², J. Sindermann², M. Schäfers¹, C. Wenning¹; ¹Department of Nuclear Medicine, University Hospital Münster, Münster, GERMANY, ²Department of Cardiac Surgery, University Hospital Münster, Münster, GERMANY.

Continuous-flow left ventricular assist device (CF-LVAD) is a new gold standard in supporting end-stage heart failure patients, bridging them to heart transplantation. Infection is one of the major complications associated with LVAD implants. The goal of this study is to evaluate the potential impact of F-18-FDG PET/CT in the diagnosis of infection in patients with implanted CF-LVAD. We examined 57 patients with an implanted LVAD who underwent an F-18-FDG PET/CT, who were either suspected to have a driveline infection or the infection of the LVAD itself or who received PET/CT for other reasons. Three groups were compared: Group A (n=21) consisted of patients suspected of LVAD/driveline infection due to positive blood cultures and/or leukocytosis or elevated CRP but without wound healing disorder; Group B (n=30) included patients with clinically apparent wound healing disorder; a control group (n=6) consisted of patients without signs of infection who received PET/CT for other reasons. First, PET/CT was graded visually as positive or negative in order of pathological uptake along the driveline and/or the device. Second, uptake was measured quantitatively (SUVmax) in the attenuation corrected images at the driveline skin penetration point and at the subcutaneous portion of the driveline. A semi-quantitative target-to-background ratio (TBR) using the uncorrected PET images was calculated in order to measure the activity around the LVAD aggregate. Out of 21 patients in Group A 13 (62%) had a positive finding in PET/CT. 27 of 30 patients (90%) in Group B were graded positive in PET/CT. In the Control group, 1 of 6 patients was falsely positive. At the driveline skin penetration point we observed significantly higher SUVmax in Group A (4.23 ± 0.67 vs. 2.02 ± 0.84 , $p=0.02$) and Group B (6.57 ± 0.78 vs. 2.02 ± 0.84 , $p<0.001$) compared to controls. At the subcutaneous portion of the driveline only Group B showed significantly higher SUVmax (8.66 ± 0.89 vs. 3.09 ± 0.19 , $p<0.001$). The TBR of the aggregate did not differ significantly. The area under the ROC curve was 0,744 at the driveline skin penetration point and 0,768 at the subcutaneous portion of the driveline. Sensitivity/specificity (Group B as reference) was 90%/83%. F-18-FDG PET/CT is a valuable tool in the diagnosis of infection in the patients with CF-LVAD at the driveline skin penetration point and at the subcutaneous portion of the driveline. However, the identification of the infection around the LVAD aggregate may be challenging. Finally, F-18-FDG PET/CT might be useful in guiding therapeutic decisions.

OP696

Respective role of ^{18}F -FDG PET/CT and WBC SPECT/CT in the diagnosis of cardiac implantable electronic devices infection.

J. CALAIS, A. TOUATI, N. GRALL, K. BENALI, B. MAHIDA, F. HYAFIL, B. IUNG, X. DUVAL, D. LE GULUDEC, F. ROUZET; Hopital Bichat, Paris, FRANCE.

Rationale: Although the role of nuclear imaging in the management of cardiovascular infections is acknowledged, its diagnostic value in CIEDs infection remains debated and nuclear techniques have not been included in the recently issued ESC/EANM joint guidelines. Some studies showed good diagnostic values of both FDG PET/CT and radiolabelled WBC scan in patients with high prevalence of the disease. The aim of the study was to evaluate the respective role of both techniques in a population with intermediate prevalence of CIEDs infection. **Methods:** Our institution's database has been reviewed for a 3-year period to identify patients with a suspicion of CIEDs infection who underwent both FDG PET/CT and radiolabelled WBC scan in a time span of <1 month. Whole-body PET/CT was acquired 1 h after injection of FDG. SPECT/CT acquisitions were performed 4 and 24 hours after reinjection of $^{99\text{m}}\text{Tc}$ -HMPAO labelled WBC, included planar and SPECT/CT. The final diagnosis of CIEDs infection was based on the modified Duke classification after 3-month follow-up (rated as: definite, possible or rejected) with the addition of positive culture of the extracted material and clinically patent pocket infection as major criteria for infection. The readers of FDG PET and WBC SPECT were blinded to the results of the other technique and to the patients' clinical record. Each scan was rated for diagnosis of infection as positive

or negative. Results: 48 consecutive patients were included (age 70±11 years; female: 50%; prosthetic heart valve: 60%; Staphylococcus species: 38%). Thirty-two (67%) patients were receiving antibiotic therapy at the time of imaging (mean duration >1 month). The final diagnosis of CIED infection was: definite in 29%, possible in 23% and rejected in 48%. The diagnostic sensitivity, specificity, PPV, NPV and accuracy of FDG PET were respectively: 71%, 82%, 71%, 82%, 78% and of WBC SPECT: 50%, 100%, 100%, 76%, 77%. WBC SPECT was always negative when FDG PET was negative. By combining FDG PET as a first line modality with WBC SPECT only when PET was positive, the diagnostic sensitivity, specificity, PPV, NPV and accuracy were respectively: 70%, 100%, 100%, 57%, 79%. Conclusion: In a study population with intermediate prevalence of CIEDs infection, FDG PET has a good overall diagnostic value although the sensitivity may have been decreased by prior antibiotherapy. WBC SPECT is highly specific of infection and thus strongly supports CIED extraction when positive.

OP697

Does antibiotic treatment effect the diagnostic accuracy of F18-FDG PET/CT studies?

O. Kagna, M. Kurash, Z. Keidar, O. Israel; Rambam Health Care Campus, Haifa, ISRAEL.

Introduction: F18-FDG PET/CT plays a significant role in the assessment of various infectious processes. Patients with suspected or known sites of infection are often referred for FDG imaging while already receiving antibiotic treatment. To the best of our knowledge the effect of antibiotic treatment on the uptake of FDG is not yet well established. Current study aims at assessing the impact of antibiotic therapy on the detectability rate of infectious processes by FDG PET/CT. **Methods:** FDG PET/CT studies of 105 consecutive hospitalized patients (71M, age 18-88 years) evaluated for fever of unknown origin (n=64) and suspected vascular graft infection (n=41) were analyzed. The presence and duration of antibiotic treatment prior to performing the FDG-PET/CT study was recorded. The final diagnosis of an infectious process was based on microbiological and pathological as well as on clinical and radiological data available at follow-up. **Results:** Ten of the 64 patients who presented with FUO were diagnosed as having a non-infectious process and were excluded from further analysis. Thus the final study population included 95 patients. FDG-PET/CT was true positive and diagnosed an infectious process in 49 of the 95 patients (51%). Furthermore there were 31 (33%) true negative and 15 (16%) false positive FDG-PET/CT studies. Sixty-nine of the 95 patients (73%) received antibiotic treatment prior to the PET/CT study for a period ranging from 1 to 73 days (mean 9.57± 13.23 days). Forty patients with true positive studies (82%) were under antibiotic therapy. No false negative results were found among the whole population of 95 patients included in this study group. **Conclusion:** PET/CT correctly identified increased FDG uptake compatible with infection in more than half of the study population including 82% of the patients who were on antimicrobial therapy prior to the study. No false negative results were found in this study group including 73% of patients receiving antibiotic treatment over a wide range of duration. Current results in a group of 95 patients suggest that antimicrobial therapy appears to have no clinically significant impact on the diagnostic accuracy of FDG PET/CT performed for evaluation of known or suspected infectious processes.

OP698

¹⁸F-FDG PET/CT For Prosthetic Valve Endocarditis And Cardiac Device Infection Diagnosis: An Additional Tool

A. Jiménez-Ballvé, C. Sánchez-Enrique, M. J. Pérez-Castejón, M. Martínez de Bourio, A. Ortega-Candil, I. Vilacosta, D. Vivas, M. E. Fuentes-Ferrer, J. L. Carreras-Delgado; Hospital Clinico San Carlos, Madrid, SPAIN.

Aim: The aim of this study was to assess the usefulness of FDG PET/CT in the diagnosis of prosthetic valve endocarditis (PVE) and cardiac device infection (CDI) as an additional tool to the modified Duke criteria and echocardiography, as both seems to have limitations for these challenging diagnosis. **Materials and methods:** We performed a prospective study including 41 patients with infection suspicion (PVE/CDI) from November-2012 to January-2015. PET/CT was considered positive when FDG uptake was present in the region of interest in both PET images (corrected and non-corrected); and negative if there was no uptake or did not persist in the non-corrected images. Histopathologic result was considered the gold standard in patients who underwent cardiac surgery. Those without surgery, final diagnosis was established according to clinical consensus of the endocarditis team. **Results:** In the 41 PET/CT studies, we analyzed 62 foci with infection suspicious, 42 PVE (27 mechanical and 15 biological) and 20 CDI. Duke criteria classified 28 (45%) foci as definitive endocarditis and 34 (55%) as possible endocarditis. Echocardiography was positive in 30 (48%) foci; PET/CT was positive in 40 (65%); we obtained a final diagnosis of infection in 32 (52%) foci. PET/CT had a sensitivity (Se), specificity (Sp), positive predictive value (PPV), negative predictive value (NPV) and area under de curve (AUC) of 100%, 73%, 80%, 100%, 0,86, respectively; and Duke criteria had 84% Se, 96% Sp, 96% VPP, 85% VPN and 0,90 AUC. Both tools presented statistically significant differences of Se (p<0,020) and Sp (p<0,011), with a similar AUC (p=0,49) and a moderate Kappa Index (0,56). Echocardiography had 75% Se, 80% Sp, 80% VPP, 75% VPN and AUC of 0,78. Kappa Index between PET/CT and echocardiography was moderate (0,43). When only using transesophageal echocardiography data just before PET/CT, Se, Sp, VPP, VPN and AUC were 55%, 96%, 94%, 67% and 0,76, respectively; with a low Kappa Index (0,38) with PET/CT. Additionally, PET/CT detected systemic septic emboli in 12 patients (29%) (8 spleen, 3 lung parenchyma, 3 spondylodiscitis, 1 liver and 1 kidney) and in 6 patients (15%) we detected incidental malignancies leading to changes in therapeutic management. **Conclusion:** ¹⁸F-FDG PET/CT seems to be a promising diagnostic tool for prosthetic valve endocarditis and cardiac device infection with high sensitivity in infection diagnosis as well as detecting systemic septic emboli. It has become an imaging technique complementary to echocardiography in the new modified criteria for the diagnosis of endocarditis.

OP699

Potential role of WBC-SPECT/CT to assess antibiotic treatment

J. Dubreuil¹, I. Morelec², A. Skanjeti², M. Moret³, P. Michon³, D. Matanza⁴, M. Frayssé⁴, C. Thivolet³, J. Vouillarmet³; ¹CHU Lyon Sud, Pierre-Bénite, FRANCE, ²Nuclear Medicine - Hospices Civils de Lyon, Lyon, FRANCE, ³Endocrinology - Hospices Civils de Lyon, Lyon, FRANCE, ⁴Radiopharmacy - Hospices Civils de Lyon, Lyon, FRANCE.

Background : Diabetic foot osteomyelitis (DFO) is a frequent complication of diabetes, and an important risk factor of amputation. However, the duration of antibiotic therapy is difficult to define in the absence of a marker to diagnose osteomyelitis remission at the end of the treatment. The aim of this study is to evaluate the performance of Tc99m-White Blood Cell (WBC)-SPECT/CT to diagnose DFO remission. **Material and methods:** Patients with DFO proved were included and scheduled to perform a WBC-SPECT/CT at the end of antibiotic treatment. WBC-SPECT-CT included planar acquisitions at 2h and 20h post-injection and a SPECT-CT at 20h. All exams were retrospectively read by 2 nuclear physicians, blind to clinical results, with consensus (IM and JD). Successful treatment of DFO was defined by absence of DFO relapse in the same site within 1 year. **Results:** Sixty patients were included in this study between March 2010 and April 2015. Nine were excluded of analysis due to absence of follow-up or absence of SPECT-CT. Median activity injected was 437 MBq, and median labelling yield was 82%. Of the 51 patients included in the analysis, 9 (17.6%) showed DFO relapse during follow-up. Sensitivity, specificity, negative predictive value, positive predictive value and accuracy of WBC-SPECT/CT to predict relapse of DFO in the same area were 77.8%, 83.7%, 94.7%, 50% and 82.6% respectively.

Conclusion: These preliminary results confirm the potential role to assess treatment of DFO especially due to his high negative predictive value. This exam could be used in the future to decrease the duration of DFO treatment.

OP700

SPECT-based semi-quantitative assessment of ^{123}I -SAP scintigraphy in patients with amyloidosis

R. W. J. van Rheenen, B. P. C. Hazenberg, W. Noordzij, R. A. J. O. Dierckx, R. H. J. A. Slart, A. W. J. M. Glaudemans; UMCG, Groningen, NETHERLANDS.

INTRODUCTION: ^{123}I -Serum Amyloid P (SAP)-scintigraphy is used to image the extent and distribution of amyloid deposition in patients with systemic AA, AL and ATTR amyloidosis in a non-invasive manner. In the context of follow-up and inter-observer agreement, the standard visual assessment method has proven to be suboptimal. The aim of this study was to develop a SPECT(-CT) organ/blood pool ratio-based quantitative assessment system with clear cut-off values to define organ involvement with a high specificity. **MATERIAL & METHODS:** Between January 2009 and January 2016 in 145 patients with amyloidosis a ^{123}I -SAP with SPECT(-CT) was performed to evaluate the extent and distribution of the amyloidosis. In all patient's amyloidosis had been proven by means of a fat biopsy. The patients were divided in four groups: AL type (n=86), AA type (n=20), ATTR type (n=18), AL localized type (n=21). A fived disease-control group without amyloidosis (n=24) was used to calculate the reference cut-off values for each organ ratio. The validity of these new values was tested by comparing ratio-based results to visual grading as well as to clinical parameters. **RESULTS:** Based on data of the control group the following cut-off ratios were calculated: liver 1.0, spleen 1.5, and kidney 1.1. When comparing ratio-based organ results to visual grading of the organs, normal values within the reference range were present in all amyloidosis patients visually graded 0. Values above the reference range were present in patients visually graded 2 or higher. Normal values, however, were often found in spleens and kidneys visually graded 1. When comparing organ values to the respective clinical parameters, modest correlations were found for liver values and Alkaline Phosphatase ($r = 0.33$; $p=0.028$), kidney values and eGFR ($r = -0.21$; $p=0.032$), and kidney values and proteinuria ($r = 0.45$; $p=0.04$). This correlation was not present using the standard visual grading. **DISCUSSION & CONCLUSIONS:** The ratio-based assessment of SAP-scintigraphy enables us to obtain a very specific, although less sensitive organ evaluation of liver, spleen and kidney compared with our current visual assessment of these organs. Besides, the ratio-based method hints at a physiologically increased SAP binding within the spleen of controls. The amount of SAP binding in kidney and liver somewhat reflects clinical disease and probably the amyloid load of these organs. The latter may indicate utility of this quantitative method for monitoring patients with amyloidosis during the course of their disease and especially for assessing the effect of treatment.

1801/1803 – Wednesday, October 19, 2016, 12:15 - 13:15, Auditorium
Plenary 4: Highlights Lecture

OP701

Highlights Lecture

F. Kraeber-Bodéré; Hotel Dieu, Service de Médecine Nucléaire, Nantes, FRANCE.

OP702

Highlights Lecture

E. O. Aboagy; Hammersmith Hospital, Department of Cancer Medicine, London, UNITED KINGDOM.

e-Poster Walks

E-PW1 – Sunday, October 16, 2016, 08:30 – 09:30, e-Poster Area
e-Poster Walk 1 – Clinical Oncology: Radioguided Surgery & PET Malignancies in Women

EPW01

Distinguishing breast tumor from normal breast using textural indices in FDG-PET

S. Boughdad¹, C. Nioche², F. Orhac³, L. Champion¹, J. Alberini¹, I. Buvat²; ¹Institut Curie-Hôpital René Huguenin, Saint-Cloud, FRANCE, ²IMIV CEA, Inserm, CNRS, UnNiv Paris Sud, CEA-SHFJ, Orsay, FRANCE, ³IMIV CEA, Inserm, CNRS, UnNiv Paris Sud, CEA-SHFJ, IGR, Orsay, FRANCE.

Introduction: Breast cancer (BC) is the most common cancer in women in western countries. Previous studies have shown a significant correlation between histological data and SUV or textural indices (TI) measured from PET images. However, little is known about textural characteristics of normal breast tissue. We assessed TI in normal breast tissue in comparison to BC to define “normal” values for those index. **Method:** Normal breast tissue group (NBT group) was defined from a population of 112 women who underwent a F18-FDG-PET/CT in our institution for initial staging of various cancers (discarding BC, endometrial, or ovarian cancers) for comparison to our BC sample population consisting of 58 patients. SUV (max, mean and peak), TLG (total lesion glycolysis, mL) and TI (homogeneity, entropy, LRE, SRE, LGZE and HGZE) were measured in a tumor volume of interest (T-VOI) in the BC group obtained using a threshold method (40% of SUVmax). The same VOI was mirrored in the contralateral breast (CL-VOI). A VOI with a volume identical to the average volume of T-VOI in our BC group was then drawn on both breasts of the NBT group (B-VOI) to derive “normal” SUV and TI. A ROC analysis was performed to assess SUV and TI performances for distinguishing normal breast tissue and BC. **Results:** Fifty-four T-VOI were drawn in the BC group and 54 VOI were drawn in the contralateral breast of this group. Patients with bilateral breast cancer were excluded. A total of 224 VOI were drawn in the NBT group. The SUV and TI measured in the T-VOI significantly differ from those measured in the CL-VOI in the BC group and from those measured in the B-VOI from the NBT group (table 1). There was no significant difference between SUV and TI in the CL-VOI of the BC group and in the B-VOI of the NBT group using a Mann-Whitney test ($p > 0.05$ for SUV and TI except for SRE and LRE). **Conclusion:** Our study showed significant differences in SUV and textural indices between BC and NBT. For the first time, “normal” TI values in non-pathological breast tissues are reported and might be useful for early detection of BC in seemingly normal breast tissues, especially in contralateral breast of patients with unilateral BC at initial staging.

EPW02

Preoperative prediction for invasive components in breast ductal carcinoma in situ with FDG PET/CT

H. Hwang, L. Kim; Hallym Sacred Heart Hospital, Anyang-si, KOREA, REPUBLIC OF.

Objectives: Preoperative diagnosis of ductal carcinoma in situ (DCIS) on needle biopsy specimen is limited role in treatment decision because it can provide only partial information for the entire tumor tissue. The limited specimens obtained from biopsy frequently resulted in underestimation of invasive components. This study investigated the role of FDG PET/CT to predict invasive cancer components in ductal carcinoma in situ at core needle biopsy. **Methods:** This retrospective analysis focused on 85 biopsy confirmed DCIS patients (age: mean 50.3±10.2) who

performed F-18 FDG PET/CT preoperatively, and underwent curative surgery, between 2009 July to 2015 December. We analyzed FDG PET/CT, visually and semiquantitatively, and assessed histopathologic characteristics. We evaluated the areas under the receiver operating characteristic curve (AUC) for SUVmax. After surgery, final pathology was categorized as pure DCIS (DCIS-P), DCIS with microinvasion (DCIS-MC), DCIS and invasive ductal carcinoma (IDC) (DCIS-MX), or IDC. DCIS-MX and IDC were classified as invasive components. **Results:** Final pathology confirmed 48 DCIS-P, 13 DCIS-MC, 12 DCIS-MX, and 12 IDC. AUC of SUVmax for invasive components was 0.758 (CI: 0.652-0.844) at the cutoff value of SUVmax to predict underestimation of invasive component was 2.1 (sensitivity: 83.33%, specificity: 62.30, $p < 0.0001$). SUVmax was significantly correlated with pathologic IDC size ($p = 0.0001$), PET axillary LN uptake ($p = 0.0004$), and pathologic LN metastasis ($p = 0.001$). The pathologic invasive components was significantly correlated with SUVmax ($p < 0.0001$), and mildly correlated with PET axillary LN uptake ($p = 0.031$), but not correlated with PET tumor size ($p = 0.22$) and nuclear grade at preoperative needle biopsy ($p = 0.63$). **Conclusions:** The SUVmax of primary tumor on preoperative FDG PET/CT was most important to predict the invasive components in cases of DCIS at core needle biopsy.

EPW03

Performance of a newly developed parallel detector PEM in detection of small breast cancer less than 2 cm

M. Itoh¹, S. Itoh², H. Hirakawa³, F. Yano¹, M. Soma¹, R. Sugai¹, I. Odano¹, M. Tashiro⁴, H. Sato², A. Yoshikawa⁵, S. Yamamoto⁶, A. Yanai⁷; ¹Sendai Medical Imaging Center, Sendai, JAPAN, ²Furukawa Scintitec Corporation, Iwaki, Fukushima, JAPAN, ³Tohoku Kosai Hospital, Sendai, JAPAN, ⁴Cyclotron RI Center, Tohoku University, Sendai, JAPAN, ⁵Institute for Material Science, Tohoku Univ., Sendai, JAPAN, ⁶Graduate School of Medicine, Nagoya Univ., Nagoya, JAPAN, ⁷Graduate School of Medicine, Tohoku Univ, Sendai, JAPAN.

Aim of the Study A high resolution wide field of view positron mammograph (PEMGRAPH) comprised of novel scintillation crystals, praseodymium-doped lutetium aluminium garnet, Pr:LuAG, was developed under collaboration of Tohoku University and Furukawa Ltd, Japan. Its clinical utilities were evaluated in detection of small breast cancers less than 2 cm as compared with whole-body PET/CT, Siemens Biograph. **Subjects and Methods** The PEMGRAPH is comprised of two 140×200 mm² (field of view) opposing detectors made of Pr:LuAG scintillation blocks coupled with position-sensitive PMTs (Hamamatsu H8500). The spatial resolution was 2.1 mm FWHM in the directions parallel to the detector faces. The time resolution and energy resolution were 3.1 ns FWHM and 11.6 % FWHM (at 511 keV), respectively at the center of the detector block. The peak count rate was 51.4 kCPS using a flood phantom having 35.7 kBq/ml ¹⁸F-solution. Eighty-one subjects having biopsy or cytology proven breast cancer before operation participated the study. The inclusion criteria was as follows; subjects who has breast cancer less than 2 cm in size and agreed to participate with a written informed consent. The tumor volume and its position relative to the nipple were measured by ultrasound in the same day prior the injection of FDG. ¹⁸F-FDG was injected via cubital vein at the amount of 3.7 MBq/kg. After 75 minutes of uptake time whole body isotope distribution was measured using a PET/CT, Siemens Biograph 16 for two minutes at each couch position. Then PEM images were obtained in the mediolateral direction with subjects sitting on an electric driven up-down chair. Breast images tangential to the chest wall was also obtained with 15 cm detector separation in case of the tumor was close to the pectoral muscles. Scan time was between 3 to 5 minutes at each position. **Results** Twenty-eight breast tumors were not detected by PET/CT in which 15 tumors were detected by PEM The detection sensitivity was

66.3%, 75.9% and 84.3% for PET/CT, PEM and the both combined respectively. PEM missed 7 cases which were detected by PET/CT. In cases of breast tumors less than 1.0 cm the sensitivity were 36.8%, 57.9%, and 68.4% for PET/CT, PEM and the both combined respectively. **Conclusion** The detection sensitivity by FDG molecular imaging for UICC T₁ breast cancer was 84% if PET/CT and PEM were combined in this study. The chest wall scanning with PEM was useful for tumors close to the pectoral muscles.

EPW04

5 Year-Follow-up: Value and Efficacy of Sentinel Lymph Node Diagnostics in Patients with Penile Carcinoma with Non-Palpable Inguinal Lymph Nodes

U. Lützen, M. Marx, M. Zuhayra, Y. Zhao, M. Jüptner, K. Jünemann, M. Naumann; Universitätsklinikum Schleswig-Holstein, KIEL, GERMANY.

Introduction and Aim For some years, sentinel lymph node excision (SLNE) has been described as a minimally invasive method for lymph node staging in patients with a penile carcinoma and non-palpable inguinal nodes in the guidelines of the German Society of Nuclear Medicine (DGN), the European Association of Urologists (EAU) and the European Society for Medical Oncology (ESMO). However, this method is rarely used in Germany due to the initial unreliable results and the methodical demands associated with the application of radioactive tracers as well as the radiation burden. The aim of this study was to validate the reliability and morbidity of this method. **Material and Methods** We recorded all cases of lymph node recurrence and complications in patients with initially non-palpable inguinal lymph nodes and histologically negative sentinel lymph nodes in a prospective approach. We calculated the rates of false negative findings and morbidity as qualitative criteria. Inguinal regions with palpable lymph nodes and/or evidence of metastases were not considered here in accordance with the expert society guidelines. **Results** 28 patients with histologically negative sentinel lymph nodes in 47 groins with non-palpable inguinal lymph nodes were included in this study. There were 17 T1(a/b) stages, 8 T2 and 3 T3-stages. Tumor differentiation was good in 4, moderate in 22 and poor in 2 patients. During a median follow-up of 68 (4-131) months, we observed one case of bilateral lymph node recurrence as well as one case of prolonged inguinal lymphorrhea, which could be managed conservatively. Per inguinal region, the false negative rate was 4.25% and the morbidity rate was 2.12%; seen per patient the rates were both 3.57%. **Conclusions** SLNE under use of radioactive tracers is a reliable method of lymph node staging in patients with penile carcinoma and non-palpable inguinal lymph nodes. Its higher methodical complexity is justified by high reliability and low radiation exposure for both patient and medical staff as well as low morbidity rates.

EPW05

Development and evaluation of a high sensitivity gamma imaging probe for axillary sentinel lymph node mapping

M. Georgiou¹, G. Loudos², E. Fysikopoulos³, E. Lamprou⁴, K. Mikropoulos³, A. Shegani⁵, P. Georgoulas¹; ¹Department of Nuclear Medicine, Medical School, University of Thessaly, Larissa, GREECE, ²Technological Educational Institute of Athens, Athens, GREECE, ³BioEmission Technology Solutions, R&D, Athens, Greece, Athens, GREECE, ⁴Department of Medical Physics, Medical School, University of Patras, Patra, GREECE, ⁵Institute of Radioisotopes and Radiodiagnostic Products, NCSR “Demokritos”, Athens, GREECE.

Aim: Sentinel lymph node (SLN) mapping is very important for the recognition and the dissection of the first lymph nodes (LN) that drain the breast tumor. The detection of the lymph nodes using blue-dyes and acoustical gamma probes can be improved with a gamma imaging probe

acquiring real-time images. The aim of this work is the construction and performance evaluation of “λ-eye”, a gamma imaging probe, optimized in terms of sensitivity for Sentinel Lymph Node (SLN) mapping. **Methods:** The optimization of “λ-eye” was based on theoretical calculations, presented in a previous published work of our group. The system was constructed based on these results and was evaluated using phantoms and performing animal studies. All critical parameters for the evaluation of gamma imaging probes were measured according to similar studies for the characterization of small gamma imaging devices. The systems’ spatial and energy resolution, sensitivity, count rate performance Integral (IU) and Differential Uniformity (DU) in the Useful-Field-of-View (UFOV) and in the Central-Field-of-View (CFOV) were measured using phantoms. Finally, a proof-of-concept animal experiment was carried out for the imaging of the lymph nodes of normal mice using a clinical and a novel radiotracer. **Results:** The energy resolution of individual scintillator pixels was found equal to 22%±1.6%, while the system’s total energy resolution was measured 36%±2%. The spatial resolution was 2.2mm at 2mm source-collimator distance and ~10mm at 50mm respectively. The sensitivity of the system was measured to be ~1.5cps/kBq. The values of the IU in the UFOV and in the CFOV were found to be 5.2% and 1.7%, while the DU was measured equal to 2.1% and 0.75% respectively. Finally, clear visualization of the lymph nodes of the mice was obtained using both radiotracers. **Conclusion:** The “λ-eye”, dedicated for SLN mapping, provides a combination of high sensitivity (~1.5cps/kBq) and good spatial resolution (~6mm FWHM @ 20mm and ~10mm FWHM @ 50mm distance), which makes it an appropriate tool for fast and accurate real-time intraoperative imaging of the lymph nodes.

EPW06

Lymphoscintigraphy for sentinel node identification after neo-adjuvant therapies in breast cancer: feasibility

S. M. Baio, L. Gilardi, S. L. Fracassi, M. Colandrea, L. Travaini, P. Rocca, G. Corso, B. Ballardini, P. Veronesi, V. Galimberti, C. M. Grana, F. Bassi, P. Maisonneuve, N. Rotmensz; European Institute of Oncology Milan, Milano, ITALY.

Introduction Neo-Adjuvant Treatment (NAT) is a consolidated approach for the care of locally advanced Breast Cancer (BC). The main objective of NAT is to obtain a tumour down-staging with a cytoreductive surgery that may comprise the sentinel lymph-node biopsy (SNB). To date, the role of SNB in patients receiving NAT still remains controversial, as it has been theorized that systemic chemotherapy as local radiotherapy are responsible to alter lymphatic drainage causing a false negative rate in the SN detection during lymphoscintigraphy. In fact, some institutes discourage the SNB after NAT, due to the high failure of SN identification rate. **Aim** The aim of this study was to assess the SN identification rate at lymphoscintigraphy and its technical feasibility after NAT. **Materials and Methods** Between 2000 and 2013, 444 consecutive patients (median age 44 years) affected by primary locally advanced BC were enrolled in this study. All individuals were eligible for NAT, including hormone therapy alone, chemotherapy alone, or chemotherapy plus hormone therapy. All patients gave informed consent and use of anonymized data was approved by the Institute's Review Board. Lymphoscintigraphy was performed as already described: a subdermal injection of the radiotracer, ^{99m}Tc-labeled human albumin colloid particles was performed 2-20 hours before surgery in correspondence of the skin projection of the tumour. Planar images of involved breast and axillary regions were acquired 15-30 min post-injection. The images showed a single area or, less frequently, two or multiple hot spots, corresponding to the SNs. After the acquisition of the last scan, the skin projection of these hot spots were marked with a suitable pen. During surgery the SN was identified by a gamma ray detection probe. This method allows the surgeon to remove the sentinel node and to send it for histopathological examination. **Results** Almost one sentinel node was identified during lymphoscintigraphy in

430 cases. The detection rate at lymphoscintigraphy was 96.9% (95% CI, 94.8–98.1%). Considering the correlation between specific treatments and sentinel node identification rate, we verified that the detection rate did not vary significantly ($p=0.53$) according to the type of neo-adjuvant therapies administered to the patients. **Conclusion** Our results demonstrated that lymphoscintigraphy for sentinel node identification is a safe and feasible procedure after neo-adjuvant therapies, independently of treatment types.

EPW07

Radioguided surgery in non palpable lung lesions. Our preliminary experience

M. Salcedo-Pujantell¹, I. Navales², I. Bello³, E. Pallisa⁴, J. Blanco-Cano¹, D. Varona⁴, M. Deu³, M. Simó-Perdigó¹, J. Castell-Conesa¹; ¹Hospital Universitari Vall d'Hebron. Nuclear Medicine, Barcelona, SPAIN, ²Hospital Universitari Vall d'Hebron. Nuclear Medicine. Institut de Diagnòstic per la Imatge, Barcelona, SPAIN, ³Hospital Universitari Vall d'Hebron. Thoracic Surgery, Barcelona, SPAIN, ⁴Hospital Universitari Vall d'Hebron. Radiology, Barcelona, SPAIN.

Aim: Radioguided resection of ground glass opacities and deep small solid lung nodules by video-assisted thoracic surgery (VATS) is a demanding scenario. Even though this procedure is well documented and there's enough clinic evidence about its utility, it has not become widespread yet. We report our initial experience implementing this technique in our center. **MATERIAL AND METHODS:** We prospectively added our first 14 patients (60,54± 18,79 years, 4W): 9pts were referred for suspected malignancy of a solitary lung lesion based on a radiological follow-up (7 pure ground-glass opacity, 1 subsolid and 1 solid nodule) whereas the others 5pts had solid nodule that were suspected to be pulmonary metastases of known previous extrathoracic malignancies. The mean size of the solid nodules was 6mm, and for the ground glass opacities/subsolid pulmonary lesions were 14mm. Intralesional percutaneous 99mTc-MAA CT-guided injection was performed in all patients. Subsequent gamma probe localization of the lesion was performed during VATS (Dylon Navigator GPS). **RESULTS:** Regarding the injection procedure, there were no significant complications. Only minor asymptomatic hemorrhages in the needle path and small pneumothorax were seen in some patients. There were no cases of pleural diffusion. The whole procedure, including the scintigraphy (planar and/or SPECT images), was completed in an average time of 74m, this allowed for the surgery to be performed on the same day. The detection rate at surgery was 100%. Only in the first patient an intentional thoracotomy was chosen by the thoracic committee in order to test the gamma probe localization technique. In the other 13pts a two incisions VATS was performed, and just one case required conversion to a thoracotomy because the nodule was too deep to securely resect it. After wedge resection, histological examination showed malignancy and margins free of tumour in all lesions (5 metastases and 9 lung primary adenocarcinomas). In 7pts with lung primary adenocarcinomas a completion lobectomy was performed, (the remaining 2 pts had not enough cardiopulmonary reserve to stand a lobectomy). **CONCLUSIONS:** Radioguided surgery is a reliable procedure that allows the identification and resection of nonpalpable lung lesion, such as ground glass opacities, subsolids and small deep nodules by VATS. While it requires a good interdisciplinary communication, this technique can be done in one day step. Even though we have only performed it on 14 patients, we found it easy to learn. Excellent detection rate and the lack of surgical complications, encourages us to recommend this technique.

EPW08

Phase II study of prophylactic radiotherapy in cN0 HNSCC patients based on sentinel node(s) SPECT/CT

E. Longton¹, G. Lawson², B. Bihin³, S. Deheneffe¹, I. Mathieu⁴, J.

Installé⁴, T. Vander Borgh⁵, M. Laloux⁶, J. Daisne¹; ¹Clinique et Maternité Sainte-Elisabeth, Radiation Oncology, Namur, BELGIUM, ²CHU Dinant-Godinne, Head and Neck Surgery, Yvoir, BELGIUM, ³Namur Research Institute for Life Sciences NARILIS, Unit of Biostatistics, Namur, BELGIUM, ⁴Clinique et Maternité Sainte-Elisabeth, Nuclear Medicine, Namur, BELGIUM, ⁵CHU Dinant-Godinne, Nuclear Medicine, Yvoir, BELGIUM, ⁶Clinique et Maternité Sainte-Elisabeth, Head and Neck Surgery, Namur, BELGIUM.

Purpose/Objectives: Due to a risk of 18 to 45% of occult nodal metastases in cN0 HNSCC patients, prophylactic neck irradiation is often mandatory. Anyway, it leads to a large irradiation of normal tissues because bilateral drainage is the rule in only 30 to 50 % of individuals. Moreover, 15 to 30 % of the tumors drain in unpredicted nodal basins (risk of geographical miss). SPECT/CT lymphoscintigraphy of sentinel lymph nodes (SLN) could help individualizing prophylactic irradiation levels in cN0 patients and, hence, reduce irradiated volume and improve quality of life (QoL). This ongoing prospective phase II study investigates its oncological safety. **Materials and Methods:** Twenty-seven patients with newly diagnosed cN0 SCC of the oral cavity, oropharynx, larynx or hypopharynx were included. All patients were imaged with SPECT/CT after 99mTc nanocolloid injection around the tumor. The neck levels containing up to four hottest SLN were identified and selected for prophylactic irradiation (CTVn-LS) by volumetric modulated arc therapy. A comparative virtual planning was performed with volumes selected according to international guidelines (CTVn-IG). QoL was assessed using EORTC C30 and HN25 scales. **Results:** Migration was observed in all of the 27 patients (one with gamma probe only) with an average of 3.1 sentinel nodes detected per patient. CTVn-LS was totally encompassed by CTVn-IG in all patients but two with an unpredicted drainage in homolateral retropharyngeal levels. More than half of the patients has only a unilateral drainage. CTVn-LS and related PTV were systematically smaller than IG ones, by a factor of two on average. This led to significant dose decrease in identified OAR as well as remaining volume at risk. With a median follow-up of 30 months, no regional relapse was observed while 3 patients had a local one (11%). Crude overall survival rate is 89%. **Conclusions:** SPECT/CT lymphoscintigraphy of SLN allows individualizing prophylactic node CTV in cN0 HNSCC patients eligible for definitive radiotherapy. Both CTV and PTV are significantly reduced, which results in a significant dose decrease in OAR. At a median follow-up of 30 months, no regional relapse was observed but further follow-up and recruitment are necessary to ensure the oncological safety.

EPW09

18F-FDG PET-CT and DWI-MRI in staging cervical cancer patients: role of metabolic and volumetric parameters

C. Crivellaro^{1,2}, P. A. Bonaffini³, M. Cuzzocrea¹, L. Baratto¹, E. De Ponti⁴, F. Elisei², A. Buda⁵, L. Guerra², P. Guglielmo¹, S. Sironi³, C. Landoni¹; ¹University Milan-Bicocca, Milan, ITALY, ²Nuclear Medicine, ASST-San Gerardo, Monza, ITALY, ³Radiology, University Milan-Bicocca, Milan, ITALY, ⁴Medical-Physics, ASST-San Gerardo, Monza, ITALY, ⁵Gynaecology-Oncology, ASST-San Gerardo, Monza, ITALY.

Aim. To evaluate the role of metabolic and volumetric parameters obtained in pre-operative PET and MRI studies of patients with cervical cancer. **Materials and Methods.** 29 females (range 28–76 years) with histologically proven cervical cancer were enrolled. Before surgery (hysterectomy, bilateral salpingo-oophorectomy and lymphadenectomy), all patient underwent to both a ¹⁸F-FDG PET-CT and pelvic 1.5T MRI scan, including DWI (b : 0–1000 mm²/sec). On PET images, SUVmax and SUVmean, metabolic tumor volume (MTV) and total lesion glycolysis (TLG) of cervical lesions were calculated, using an iterative threshold segmentation. On MRI scan, ADC values and DWI tumor volume were considered. All parameters were statistically analysed and correlated to

histological analysis (parametrial and lymphovascular invasion, tumor grade, nodes metastases) and relapse (by using Kruskal-Wallis test). **Results.** In G3 lesions, SUVmax (mean 13.5 g/ml), MTV (mean 21.6 ml), TLG (mean 164 g), DWI-V (mean 34.6 ml) were significantly higher than SUVmax (9.2 g/ml; $p=0.02$), MTV (6.5 ml; $p=0.001$), TLG (50.5 g; $p=0.005$) DWI-V (11.1ml; $p=0.04$) of G2 lesions, respectively. A significant association was found between the presence of LN metastases (7/29 pts, incidence 24%) and SUVmax ($p=0.09$), MTV ($p=0.02$) and DWI-V ($p=0.002$), respectively. Mean ADC value of cervical cancer was significantly lower ($0.85\pm 0.12\times 10^{-3}\text{mm}^2/\text{sec}$) than normal myometrium ($1.15\pm 0.20\times 10^{-3}\text{mm}^2/\text{sec}$). No other statistically significant differences were obtained, in particular no correlations were found between PET and MRI parameters and relapse (median follow-up 48 months). **Conclusion.** At metabolic and DWI-MRI parameters analysis, SUVmax, MTV, TLG and DWI-V were significantly higher in G3 lesions. SUVmax, MTV and TLG were correlated to the presence of nodal metastases, while none of these parameters was predictor of recurrence.

EPW10

Detection of extraregional tumor recurrence with ^{18}F -FDG-PET/CT in patients with recurrent gynecological malignancies being considered for pelvic exenteration

U. Metsler; University of Toronto, Toronto, ON, CANADA.

Background: Pelvic exenteration may be offered as a salvage procedure for patients with central recurrent or persistent gynecologic cancer, including cervical, endometrial, vaginal, or vulvar cancer. This procedure is the only potential curative therapy for these patients but is associated with significant morbidity and mortality; therefore, appropriate patient selection, and exclusion of extra-regional metastases is paramount. **Objective:** To compare the detection rate of extraregional metastases in patients with recurrent gynecological malignancies being considered for pelvic exenteration with FDG-PET/CT (=PET) compared to conventional imaging. **Methods:** A retrospective review was performed of all patients in a provincial database with recurrent gynecological malignancies being considered for pelvic exenteration that underwent restaging with PET between March 2011 and October 2014. Findings on PET and conventional imaging (CT \pm pelvic MRI) were abstracted. Disease sites were classified according to location (regional nodal metastases, extra-regional nodal metastases, peritoneum or other distant sites) and diagnostic certainty (definitive or equivocal). The proportion of patients positive for extraregional recurrence was calculated for PET and conventional imaging. In addition, the proportion of patients with indeterminate lesions only was calculated for each modality and the sites of indeterminate findings were tabulated. **Results:** There were 85 patients (median age, 50 years; range: 30-81) with carcinoma of cervix ($n=51$), endometrium ($n=18$), vagina ($n=6$), or vulva ($n=10$). Extraregional recurrence was detected in 8/85 (9.4%) and 24/85 (28.2%) patients on conventional imaging and PET, respectively ($p=0.0017$). The greatest impact of PET compared to CT was in detection of extraregional nodal metastases, including above the diaphragm (27 vs. 6 nodal basins, respectively). There were 61 equivocal lesions on CT in the entire patient cohort and 22/61 (36%) were above the diaphragm. PET was positive in only 12/61 (20%) of CT equivocal lesions and negative in 44/61 (72.1%). PET had significantly fewer examinations equivocal for extraregional recurrence versus CT (6/85 [7.1%] and 29/85 [34.1%], respectively; $p<0.001$). **Conclusion:** In patients with recurrent gynecologic malignancies being considered for pelvic exenteration, PET identifies significantly more extraregional recurrence than conventional imaging. PET also results in fewer equivocal lesions. The impact of these results on patient management and outcome should be confirmed in future prospective trials.

E-PW2 – Sunday, October 16, 2016, 08:30 - 09:30, e-Poster Area
e-Poster Walk 2 – Do.MoRe: PSMA & Bone Palliation

EPW11

Initial experience with aggressive treatment of metastatic prostate cancer using 3 cycles of 7.4 GBq [^{177}Lu]-PSMA every 4 weeks

A. R. Haug^{1,2}, S. Shariat³, H. Eidherr^{1,2}, C. Vraka^{1,2}, W. Wadsak², M. Mitterhauser², G. Kramer³, M. Krainer⁴, H. Duan^{1,2}, M. Hacker^{1,2}, M. Hartenbach^{1,2}; ¹University of Vienna, Vienna, AUSTRIA, ²Division of Nuclear Medicine, University of Vienna, Vienna, AUSTRIA, ³Department of Urology, University of Vienna, Vienna, AUSTRIA, ⁴Department of Internal Medicine I, University of Vienna, Vienna, AUSTRIA.

Aim: Treatment with [^{177}Lu]-PSMA has emerged as treatment option in metastatic prostate cancer. However, so far treatment schemes have been adopted mainly from experiences based on PRRT of NET. Given the more aggressive biological features of metastatic prostate cancer, a more aggressive treatment might be more appropriate. **Materials and methods:** We have treated 15 patients (mean age 69 years) with intended 3 cycles of [^{177}Lu]-PSMA every 4 weeks. 14/15 were castration resistant, 7/15 resistant to chemotherapy. All patients have been examined with [^{68}Ga]-PSMA PET/MRI to validate PSMA expression of all metastatic lesions. We monitored haemoglobin (Hb), platelets (Pl), leucocytes and creatinine for assessment of toxicity. The highest toxicity grade during therapy was reported and additional toxicity grade 3 months after the last cycle. Scintigraphy of the salivary glands using $^{99\text{m}}\text{TcO}_4$ before treatment, and after the third cycle has been used to assess salivary toxicity. For treatment response we evaluated PSA values before the first and after the third cycle. For RECIST based response 12/15 patients were examined with [^{68}Ga]-PSMA PET/MRI 4 weeks after the last cycle. **Results:** 12/15 patients were treated with all 3 cycles; In 2/15 treatment was stopped after the second cycle due to progressive disease, in 1/15 patient treatment was stopped due to PSA response (-52%) and minimal tumor load. 11/15 patients (73%) had a decreasing PSA (mean -53%), 6/15 (40%) with a decline of more than 50%. According to RECIST 5/12 patients showed PR (42%), 4/12 SD (33%) and 3/12 PD (25%). Treatment was excellent tolerated with no grade 2 toxicity. 1/15 patients showed an increase of Hb toxicity of grade 0 to 1; 2/15 had an increase of Pl toxicity from grade 0 to 1 and 4/15 of leucocytes toxicity, which resolved after 3 months, respectively. We experienced no toxicity regarding creatinine. We did not experience any relevant loss of function neither in scintigraphic monitoring of the salivary glands nor from patient reports. **Conclusion:** In the presented small preliminary patient cohort aggressive [^{177}Lu]-PSMA treatment was safe and effective. As our reported response rates are comparably high, treatment with high doses every 4 weeks might better reflect the more aggressive nature of castration resistant metastatic prostate cancer.

EPW12

Predictors of better response to radioligand therapy of metastatic castrate-resistant prostate cancer with ^{177}Lu -PSMA-617

J. Ferdinandus, E. Eppard, S. Kürpigg, F. Gärtner, R. Fimmers, A. Yordanova, S. Hauser, M. Essler, G. Feldmann, H. Ahmadzadehfahr; University Hospital Bonn, Bonn, GERMANY.

Aim: Radioligand therapy (RLT) with ^{177}Lu -PSMA-617 (Lu-PSMA) (prostate-specific membrane antigen) is a novel targeted therapy for metastatic prostate cancer. In this study we evaluated the effect of different pretherapeutic parameters on therapy response measured by PSA two months after RLT. **Methods:** RLT was performed in 40 hormone and/or chemo refractory patients with distant metastases and progressive disease (mean age: 71.4 y/o). ^{68}Ga -PSMA PET/CT was performed in all patients

one to two weeks prior to RLT. SUV max and mean were determined by region of interest. SUV values were recorded for up to five bone and lymph node lesions as well as for relevant normal organs such as liver and spleen as background for the calculation of lesion/background. CBC, renal and liver functions, different previous therapies, pain medication and SUVs were evaluated. **Results:** All patients were treated with a mean of 6 GBq. PSA was controlled two months after RLT. A proportion of 67.5% showed a PSA decline, with 45% and 35% showing a decline of more than 30% and 50%, respectively. In the univariate analysis, older age, a lower Gleason score, a lower number of platelets, lower CRP, no need for pain medication and lower LDH reflected a positive impact of better therapy response; however, multivariate analysis revealed that the most significant independent factors were the number of platelets and no need for pain medication. The response was independent of the amount of PSMA uptake, previous therapies with enzalutamide, abiraterone, Ra-223 and chemotherapy, and other measured factors. **Conclusion:** RLT with Lu-PSMA is an effective therapy in hormone-refractory patients. The metastases should be just PSMA-positive but the response is independent of the amount of PSMA expression. A better treatment response was observed in older patients with a lower Gleason score as well as in patients with platelets in the lower normal limit and without regular need for pain medication.

EPW13

PSA-response and acute toxicity with 4, 6 or 7.4 GBq/cycle of ¹⁷⁷Lu-PSMA-617 in patients with mCRPC

H. Rathke¹, F. L. Giesel¹, F. Paul¹, K. Kopka², W. Mier¹, U. Haberkorn¹, C. Kratochwil¹; ¹University Hospital Heidelberg, Heidelberg, GERMANY, ²Division of Radiopharmaceutical Chemistry, German Cancer Research Center (dkfz), Heidelberg, GERMANY.

Aim: PSMA targeting radionuclide therapy (PSMA-RLT) with ¹⁷⁷Lu-PSMA-617 is an upcoming treatment option for patients with mCRPC and presents promising dosimetry. However, the bone-marrow reserve might be reduced after previous chemotherapy and tolerance limits have to be interpreted with care; thus making it difficult to define the optimal treatment regime based on dosimetry only. Here we retrospectively report our empiric dose escalation experience. **Methods:** Patients (n=30) with PSMA-positive tumor phenotype were selected with PSMA-imaging. The PSMA-RLT was performed bi-monthly with single fraction treatment activities of 4 GBq, 6 GBq or 7.4 GBq (n=10, respectively). The treatment regime was applied to 10 consecutive patients, respectively before the treatment activity was escalated. After each cycle blood cell count, clinical symptoms and tumor markers were checked at least every 4 weeks. **Results:** All patients tolerated the first therapy cycle well. The only G3/4 hematological toxicity was observed with 4 GBq in a patient with diffuse type red marrow infiltration which consecutively was considered a contra-indication against ¹⁷⁷Lu-PSMA-RLT; thereafter no dose limiting hematological toxicity was observed even in the 7.4 GBq group. Initial PSA-response (> 50% decrease in comparison to baseline) was observed in the 4 GBq-group in 4 of 10 patients, 3 of 10 in the 6 GBq and 5 of 10 in the 7.4 GBq-group. However, with 4 GBq only 2/10 intention-to-treat (ITT) patients could accomplish 3-cycles per protocol before PSA re-progression. In the 6 GBq and 7.4 GBq group out 5/10 patients could stay per protocol and were still in PSA-response after 3 cycles (6 month follow-up). In our cohort 70% of patients were pre-treated with chemotherapy. **Conclusions:** If patients with diffuse red marrow infiltration are excluded a priori, the maximum tolerated dose is not reached with treatment activities of up to 7.4 GBq and bi-monthly repetition, even in a patient collective with previous chemotherapy. A positive dose-effect relationship in regard to response duration emphasizes that escalation to even higher treatment activities is warranted.

EPW14

Treatment response according to PSA changes in patients undergo more than one cycle of ¹⁷⁷Lu-PSMA-617 therapy

S. Wegen, E. Eppard, S. Kürpig, M. Essler, A. Yordanova, S. Hauser, H. Ahmadzadehfard; University Hospital Bonn, Bonn, GERMANY.

Aim: Radioligand therapy (RLT) with ¹⁷⁷Lu-PSMA-617 (Lu-PSMA) (prostate-specific membrane antigen) is a novel targeted therapy for metastatic prostate cancer. About 70% of patients show PSA decline after the first cycle. The aim of this study was to evaluate the treatment response considering PSA changes after the second cycle and to determine whether the patients without any response after the first cycle show a good response to further treatments. **Methods:** One hundred five RLT were performed in 39 hormone and/or chemorefractory patients (2-5 cycles; median: 3 cycles) with distant metastases and progressive disease (mean age: 72 y/o). Gleason-Score was 6-10 (median: 9). Mean PSA was 798 ng/ml (range: 4.7-5910). The median interval between the therapy cycles was 2 months. The PSA level was measured every 4 weeks after each cycle; however, the PSA value 8 weeks after each cycle was considered for the evaluation of therapy response. **Results:** The median administered activity was 6.0 GBq per cycle. Two months after the first cycle, 26/39 patients (66.7%) showed a PSA decline. All 39 patients received the second cycle independent of the treatment response. Two months after the second cycle, 21 patients (53.8%) showed a PSA decline compared to baseline PSA prior to the first cycle. The patients who did not show any treatment response according to PSA changes after the first cycle did not show any positive response after the further cycles, either. **Conclusion:** The patients without any PSA-decline after the first cycle did not show a PSA decline after the further cycles. However, this does not mean that these patients did not profit from RLT. This should be evaluated in a long-term follow-up with measurements of the overall survival of both groups in comparison to patients who did not receive any RLT.

EPW15

Dosimetry for Lu-177-PSMA therapy of patients with mCRPC: A comparison of 3D SPECT and 2D planar methods

A. Delker¹, A. Gosewisch¹, S. Rieger¹, H. Ilhan¹, W. Fendler², F. Gildehaus¹, P. Bartenstein¹, G. Böning¹; ¹University of Munich, München, GERMANY, ²UCLA, Los Angeles, CA, UNITED STATES.

Aim: In nuclear medicine the new radioligand Lu-177-DKFZ-PSMA-617 was developed for the treatment of patients with mCRPC. In a recent dosimetry study an elevated tracer uptake in the intestine was observed in the majority of patients which in planar images superimposes the kidneys. In this study we compared two approaches for planar 2D dosimetry with the 3D dosimetry calculations based on quantitative SPECT. **Methods:** For 8 patients an anterior and posterior planar image with a subsequent SPECT image acquisition was performed at 1h, 24h, 48h and 72h after administration of 3.7 GBq Lu-177-PSMA. Quantitative 3D SPECT was regarded as overlay-free reference. The kidney dose was determined by fitting and integrating the activity signal of the co-registered images by use of an exponential function and subsequent multiplication of the accumulated activity with the kidney specific S-value. Two methods for planar dosimetry were investigated: In the first method (planar1), according to the MIRDOSE concept, all images were corrected for scatter and attenuation and calibrated with the known activity. In the second method (planar2) the effective half-life of each kidney was determined from the posterior planar acquisitions which were only corrected for scatter, and adjusted to an overlay-free fully calibrated data point from quantitative SPECT before calculating the dose. **Results:** The mean estimated dose was 1.46 ± 0.53 Gy for SPECT, 3.89 ± 2.03 Gy for planar1 and 1.48 ± 0.56 Gy for planar2. A significant difference (t-test $p < 0.001$) and no correlation (Pearson $\rho = 0.43$) was observed between SPECT and planar1. No significant difference ($p = 0.92$) and a

very strong correlation ($\rho = 0.96$) was observed with planar2. **Conclusions:** In Lu-177-PSMA therapy we noted an overestimation of kidney dose from anterior and posterior planar images compared to the corresponding 3D dosimetry. This observation can be addressed to extra-renal activity in the intestine which apparently has an emphasized effect onto the anterior view. Solely utilizing the posterior view and consequently omitting attenuation correction improved planar dosimetry, provided that appropriate calibration of the time-activity curve is performed. Although we used quantitative SPECT for this purpose, the application of other calibration methods based on the planar data may be feasible.

EPW16

PSMA Radioligand Therapy (PRLT) using Lu-177 PSMA I&T and Lu-177 PSMA-617: Intra-individual comparison of kinetics and dosimetry

C. Schuchardt, H. R. Kulkarni, S. Wiessalla, M. Shahinfar, A. Singh, R. P. Baum; THERANOSTICS Center for Molecular Radiotherapy and Molecular Imaging, BAD BERKA, GERMANY.

Aim: PRLT using Lu-177 labeled PSMA ligands is a promising therapy option for metastasized castrate-resistant prostate cancer (mCRPC). Goal of the study was the intra-individual comparison of the kinetics and mean absorbed dose in organs and tumor lesions in PRLT using Lu-177 PSMA I&T and Lu-177 PSMA-617. **Methods:** Four patients (P1-P4) suffering from mCRPC were enrolled (intense PSMA expression verified before using Ga-68 PSMA PET/CT). Three patients (P1-P3) initially received Lu-177 PSMA I&T (P1-P3: 5, 6, 5.4 GBq respectively), in the following cycle PSMA-617 (6.4 GBq each patient). P4 was treated using 6 GBq Lu-177 PSMA 617 in the first cycle, followed by 7.4 GBq Lu-177 PSMA I&T in the next cycle. The kinetics were determined by means of planar whole body scintigraphies plus SPECT/CT acquisitions and dose estimations performed according to MIRD-scheme (OLINDA/EXM). For intra-individual comparison, the following parameters were analyzed: effective half-life, uptake and mean absorbed dose. **Results:** P1: PSMA-617 showed a higher uptake, longer half-life and higher mean absorbed dose for all normal organs. In contrast, the analyzed bone lesion demonstrated a higher uptake, longer half-life and higher tumor dose when using PSMA I&T for therapy. P2: The half-life of PSMA-617 was longer in normal organs, the uptake of both ligands in kidneys (similar doses) and parotid glands was comparable, but the dose to parotid glands was higher for PSMA I&T. In opposition to P1, a longer half-life, higher uptake and therefore a higher tumor dose was found for a bone lesion in case of PSMA-617. P3: Regarding normal organs and a bone metastasis, a longer half-life, higher uptake and higher doses were determined for PSMA I&T. P4: Therapy using PSMA-617 revealed higher uptake, and dose, as well as longer half-lives for whole body and parotid glands. The renal parameters were comparable. A higher uptake and longer half-life were also found for the lymph node metastasis for PSMA-617. **Conclusions:** These first comparative investigations demonstrate the different kinetics of Lu-177 PSMA I&T and Lu-177 PSMA-617 which represent higher uptake in normal organs for therapy using PSMA-617. Due to the different biodistribution and mean absorbed doses to normal organs and tumor lesions, individual dosimetry should be performed.

EPW17

Impact of treatment delay in Radium-223 Dichloride therapy of metastatic castration-resistant prostate cancer patients

M. Ø. Fosbøl, S. Holm, P. M. Petersen, G. Daugaard, J. Mortensen; Rigshospitalet, Copenhagen, DENMARK.

Aim: A global temporary shortage of Radium-223 Dichloride ($^{223}\text{RaCl}_2$) occurred for 7 weeks in the fall of 2014 due to production irregularities. The

objective of this study was to assess the impact of treatment delay due to non-disease related causes in $^{223}\text{RaCl}_2$ therapy of patients with metastatic castration resistant prostate cancer (mCRPC). **Materials and methods:** Retrospective cohort study of mCRPC patients who initiated $^{223}\text{RaCl}_2$ therapy in the period from March to November 2014. End points were number of completed $^{223}\text{RaCl}_2$ cycles, overall survival (OS) and hematological toxicity defined as grade 2-4 anemia, leucopenia or thrombocytopenia according to Common Terminology Criteria for Adverse Events 4.0 (CTCAE). Bone scintigraphy, hematological status, PSA and alkaline phosphatase were evaluated prior to first dose and after 3rd and 6th treatment, respectively. Follow-up period was 17 months after first $^{223}\text{RaCl}_2$ dose. **Results:** 30 consecutive patients initiated $^{223}\text{RaCl}_2$ therapy in the time period. Median age 70 years (range 51-82 years), median baseline PSA 172 $\mu\text{g/l}$ (range 18-2098) and alkaline phosphatase 181 U/l (range 29-1850). 23 patients (77%) had extensive metastatic disease with ≥ 20 bone metastases or superscan. 17 of 30 patients were affected by delivery problems. Median delay was 4 weeks (range 3-9 weeks). Five of the 17 patients did not recommence $^{223}\text{RaCl}_2$ therapy, four patients due to progressive disease and one patient for reasons not related to $^{223}\text{RaCl}_2$ therapy or prostate cancer. For the 13 patients not affected by delivery delay mean number of completed treatment cycles was 3.5 (SD 1.9) vs. 4.5 cycles (SD 1.5) in the delay group. Median OS from the first $^{223}\text{RaCl}_2$ dose was 9.0 months (95% CI 5.9-11.5) for the patients without delivery delay and 15.1 months (95% CI 8.2-21.9) for the patients impacted by treatment delay (Hazard ratio 0.62, $P=0.304$). There was no significant difference in frequency or severity of hematological toxicity. Hematological toxicity grade 2 occurred in 6 (46%) of the patients without delivery delay vs. three patients (17.6%) of the patients affected by delivery issues ($P=0.09$). For Grade 3 toxicity the numbers were 2 (15%) vs. 5 (29%) ($P=0.36$). No cases of grade 4 hematological toxicity were observed. **Conclusion:** Results from this small retrospective cohort do not suggest that a short treatment pause due to non-disease related causes has negative impact on number of completed treatment cycles or overall survival in mCRPC patients receiving $^{223}\text{RaCl}_2$ therapy.

EPW18

Radium-223 dichloride treatment for prostate cancer with bone metastases: A symptomatic outcome review of 12 months experience

H. H. Lee¹, N. C. McAddy¹, P. O'Sullivan¹, P. Crawley¹, S. Beesley², M. Naji¹; ¹Nuclear Medicine Department, Maidstone and Tunbridge Wells NHS Trust, Maidstone, UNITED KINGDOM, ²Oncology Department, Maidstone and Tunbridge Wells NHS Trust, Maidstone, UNITED KINGDOM.

Background Radium-223 dichloride (Ra-223) is an alpha emitting radiopharmaceutical that has been approved under the National Institute of Health and Care Excellence (NICE) guidelines for the treatment of patients with castration-resistant prostate cancer (CRPC) and symptomatic bone metastasis. Bone metastases disrupt the normal balance of bone formation by osteoblasts and bone resorption by osteoclasts, which in many cases, are associated with significant pain. This has a direct impact on patients' morbidity, mortality as well as quality of life. Ra-223 has shown to be an effective therapy that targets osteoblastic bone lesions to prolong survival and life expectancy in CRPC. In this study we reviewed the symptomatic outcome of the treatment and effect on pain score and quality of life. **Methods** 43 Patients, who commenced Ra-223 treatment between March 2015 and January 2016, were prospectively reviewed. They were asked to rate their severity of pain and the impact on quality of life at three time points (pre-treatment, mid treatment and at the end of treatment). Pain scores and overall quality of life scores were given on a scale of 0 to 10. Data were analysed to look for whether there is a clinical and symptomatic improvement during and following a full course of treatment. Ra-223 is given as an intravenous injection each month over a total period of 6 months. **Results** In 8 patients the treatment course was abandoned due to clinical deterioration or death. In most patients, who completed a full 6-month course of treatment, there was a measurable pain improvement. The

effect on quality of life was somewhat variable; it was improved in some patients but it remained stable or deteriorated in others. **Conclusion** The current regime of treatment with Ra-223 for symptomatic bone metastasis for CRPR has shown a favourable symptomatic outcome in the majority of patients. The pain score has reduced in most patients and quality of life has also improved in some patients, however, a small minority of patients felt that their quality of life has deteriorated despite an improvement in pain score. This may be related to the general progression of the disease and occasionally patients were being referred late for this particular treatment. Nonetheless, in our experience Ra-223 treatment has been generally well-tolerated and resulted in symptomatic improvement in most patients.

EPW19

Correlation between Bone Lesion Dosimetry and Pain Outcome in Patients (pts) with Castration-Resistant Prostate Cancer (CRPC) undergoing ^{223}Ra -dichloride Therapy

G. A. Follacchio¹, V. Frantellizzi¹, M. Pacilio², B. Cassano¹, R. Pani¹, R. Pellegrini¹, G. De Vincentis¹; ¹Sapienza University, Rome, ITALY, ²San Camillo-Forlanini Hospital, Rome, ITALY.

Aim. ^{223}Ra is an alpha-emitting radiopharmaceutical indicated in CRPC pts with symptomatic bone metastases. We recently confirmed the feasibility of bone lesion dosimetry in pts treated with ^{223}Ra . Aim of this work was to evaluate correlation between Cumulative Absorbed Dose to bone lesions and pain outcome in pts undergoing ^{223}Ra therapy. **Patients and methods.** 59 pts affected by mCRPC undergoing ^{223}Ra treatment in our institution were evaluated for bone lesion dosimetry on the basis of baseline $^{99\text{m}}\text{Tc}$ -diphosphonate bone scan acquired a month before first ^{223}Ra administration. Pts presenting relevant bone lesions characterized by a Tumor/Soft Tissue Contrast Ratio (TST-CR) ≥ 10 were enrolled. Pts with lesions with TST-CR < 10 and pts with low compliance due to an ECOG Performance Status > 2 were excluded. Pts underwent serial planar static images based on ^{223}Ra γ -emitting component (double-peak acquisitions on thoracic or pelvic district, energy window centred at 84 and 164 keV, each 20% wide, MEGP collimator, 256x256 matrix, acquisition time 30") acquired after 24h, 48h and 7 days from first ^{223}Ra administration. Absorbed Dose (D) to bone lesions with the highest uptake was calculated, accounting for all radioactive decay daughters, and Cumulative D_{RBE} was obtained by multiplying D for α -particles RBE ($=5$) and for the number of administered ^{223}Ra cycles. Pain scores during ^{223}Ra treatment were acquired through Brief-Pain Inventory 0-10 Numeric Rating Scale at baseline and after every ^{223}Ra cycle. **Results.** 10/59 pts were studied. On the basis of pain outcome, pts were classified in improved pain score (4/10), constant pain score (3/10) and pts with worsening pain (3/10). A total of 10 lesions were selected over 10 pts. Mean Cumulative D_{RBE} to lesions resulted: 73 Gy for the first group of pts, 43 Gy for the second group and 36.5 Gy for the third group. **Conclusions.** Bone lesion dosimetry in pts undergoing ^{223}Ra therapy was feasible in pts with bone scan TST-CR ≥ 10 . As general trend, the bone pain outcome seems to improve with increasing of the Mean Cumulative D_{RBE} to bone lesions with the highest uptake. Clinical trials are currently evaluating the possibility to rechallenge ^{223}Ra treatment and to modulate ^{223}Ra dosage. This preliminary results suggest that dosimetric assessment in patients undergoing ^{223}Ra treatment could lead to a personalized therapeutic approach. Statistical significance of the observed trend will be studied in a larger number of patients.

EPW20

First Italian Multicentre Experience in using Ra-223 in patients with metastatic castration resistant prostate cancer (mCRPC)

S. Mazzarri¹, G. Boni¹, C. Cianci², L. Galli², A. Farnesi², P. Ghidini³, F. Monari⁴, F. Massari⁵, E. Borsatti⁶, C. Gobitti⁷, R. Bortolus⁷, L. Fraterno⁸,

A. G. Morganti⁴, S. Fanti³, D. Volterrani¹; ¹Regional centre of Nuclear Medicine, AOU Pisa, Pisa, ITALY, ²Medical Oncology Division, AOU Pisa, Pisa, ITALY, ³Nuclear Medicine, Policlinico Sant'Orsola, Bologna, ITALY, ⁴Radiotherapy, Policlinico Sant'Orsola, Bologna, ITALY, ⁵Medical Oncology Division, Policlinico Sant'Orsola, Bologna, ITALY, ⁶Nuclear Medicine Unit, CRO-IRCCS, Aviano, ITALY, ⁷Radiation Oncology Department, CRO-IRCCS, Aviano, ITALY, ⁸Medical Oncology Division, CRO-IRCCS, Aviano, ITALY.

Aim: Radium-223 is a novel bone-targeted α -emitter associated with a survival benefit. We present first Italian multicentre experience in using Ra-223 in mCRPC patients. **Material and methods:** Data from mCRPC patients submitted to Ra-223 treatment over 3 years (August 2013 - February 2016) were retrospectively collected. Information included Gleason score, age, prior treatments, bone symptoms, analgesic requirements, imaging and blood results. Ra-223 (50 kBq/kg) was administered every 4 weeks, up to the recommended 6 therapy cycles. Endpoints assessed included Overall Survival, pain score using Visual Analog scale (VAS), side effects, skeletal related events (SREs), disease biomarkers (PSA & ALP levels) and haematological parameters. **Results:** 90 patients received Ra-223 in three Italian Radiotherapy/Nuclear Medicine Departments. Up to April 2016 only Pisa Nuclear Medicine Department data are available, while analysis of data from other centres is still ongoing. Median age was 69 yr (range 52-85 yr). Median follow-up was 8,6 months (range 1-18 months). Mean Gleason score was 7. All patients received 3 previous lines of treatment on average. All bone scans showed foci of abnormal uptake. CT scans was used to exclude visceral involvement and the presence of pathologic lymph nodes with a diameter ≥ 3 cm. 16/32 pts completed the recommended 6 cycles, of whom: 5 had bone pain reduction, 3 had worsening, 8 had absence of bone pain, remaining stable and not requiring analgesia. 16 pts stopped treatment: 3 cases of delay due to lack in radiopharmaceutical supplies, 9 developed extra skeletal disease/skeletal progression, 3 deteriorated clinically, 1 experienced SRE during treatment. About non-haematological toxicity we observed 3 cases of G3 anorexia, 3 cases of G1 diarrhoea, 2 cases of G2 asthenia. No patients developed SREs during follow-up. Concerning haematological toxicity, bone marrow failure resulted in 8 cases of G2 anaemia, 6 cases of G3 anaemia, 2 cases of G2 leucopenia, 1 case of G2 thrombocytopenia. Regarding biomarkers, median ALP decline was 50%, median LDH decline was -5%, 32% of pts showed a reduction in PSA level. OS mean is at the present date about 8 months, and median OS has not been achieved yet. **Conclusion:** Ra-223 has a major impact on serum ALP levels, with negligible effect on PSA levels. Therefore, ALP appears to be a useful biomarker of therapy response. Haematological and non-haematological side effects were acceptable. Stability in pain or palliative effects occurred in the majority of pts.

E-PW3 – Monday, October 17, 2016, 08:30 - 09:30, e-Poster Area
e-Poster Walk 3 – Clinical Oncology: FDG PET in Oncology

EPW21

Hepatic nodules characterization with FCH-PET/ccCT: preliminary results

J. Dubreuil^{1,2}, A. Skanjeti^{1,2}, P. Rousset^{3,2}, C. Houzard¹, O. Guillaud⁴, F. Giammarile¹, C. Houzard¹, O. Dumortier⁴, P. Valette³; ¹Nuclear Medicine - Hospices Civils de Lyon, Lyon, FRANCE, ²Equipe Mixte de Recherche 3738, Lyon, FRANCE, ³Radiology - Hospices Civils de Lyon, Lyon, FRANCE, ⁴Hepatology - Hospices Civils de Lyon, Lyon, FRANCE.

Background: The diagnostic of hepatocellular carcinoma (HCC) is a challenge for medical imaging. MRI is the gold standard, however its accuracy is limited, especially in small tumors. The aim of

this study was to evaluate the potential of fluorocholine (FCH)-PET to diagnose HCC. **Material and method:** Twenty-six cirrhotic patients were prospectively included in this observational study. FCH-PET/CT was performed with enhanced triple phase CT after IV contrast injection (ceCT). MRI and PET were realized within 3 months (median interval: 24 days). Gold standard was considered Liver Imaging Reporting and Data System (LI-RADS) classification based on MRI. A total of 77 liver nodules were classified as follows: 45 HCC (LI-RADS 4-5) and 32 negative lesions (LI-RADS 1 to 3). All hepatic nodules were recorded by a nuclear physician blinded to MR results and classified using the LI-RADS classification based on ceCT. FCH uptake higher than background (on visual analysis) was used as an ancillary feature to favor HCC. Each nodule was matched between both techniques for comparison. McNemar test was used to compare the performances of ceCT, FCH-PET, and FCH-PET/ceCT. Correlation coefficient was used between FCH uptake and size of HCC. **Results:** The sensitivity, specificity and accuracy were respectively 75.6%, 87.5%, 80.5% for ceCT, 73.3%, 84.4%, 77.9% for FCH-PET and 82.2%, 81.3%, 81.8% for FCH-PET/ceCT. FCH-PET/ceCT was superior to ceCT ($p=0.03$) and FCH-PET ($p=0.03$). There was no difference between ceCT and FCH uptake ($p=1$). FCH uptake was positive in 3 of 4 HCC nodules (75%) inferior to 10 mm, 16 of 22 (72.7%) HCC nodules with size between 1 and 2 cm and in 14 of 18 (77.7%) HCC nodules with size superior to 20 mm. No correlation was observed between size of HCC and FCH uptake ($r=0.10$). **Conclusion:** These preliminary results confirm the potential interest of FCH-PET/ceCT in HCC, in particular shows the significant and synergic improvement of diagnosis produced by FCH-PET and contrast enhanced CT acquired in “one stop shop”. Furthermore, the size of the nodules does not seem to impact significantly the sensitivity of FCH-PET.

EPW22

Recurrent bladder carcinoma: clinical and prognostic role of 18F-FDG PET/CT

P. Alongi¹, R. Gentile², A. Stefano³, G. Russo³, S. Baldari², M. Gilardi³, M. Midiri⁴; ¹San Raffaele G. Giglio Institute, Cefalù, ITALY, ²University of Messina, Messina, ITALY, ³IBFM-CNR, Cefalù, ITALY, ⁴DIBIMEF - University of Palermo, Palermo, ITALY.

Aim: the performance of 18F-FDG-PET/CT (FDG-PET) for the restaging of patients (pts) with bladder carcinoma (BC) were shown in the literature in a small number of studies. Furthermore, its prognostic role remains still undefined. The aims of this retrospective study were to evaluate the accuracy, the effects on treatment decision and the prognostic value of FDG-PET/CT in pts with suspicious of recurrent BC. **Materials and Methods:** data from 41 pts affected by BC, who underwent FDG-PET for suspicious of recurrent disease were collected. The diagnostic accuracy of visually interpreted FDG-PET was obtained by considering histology (n=8), other diagnostic imaging modalities (ceCT in 38/41 pts and MRI in 15/41 pts) and clinical follow-up (n=41pts). Semi-quantitative PET values were calculated by using a graph-based method. Progression-free survival (PFS) and overall survival (OS) were assessed by using Kaplan-Meier method. The risk of progression (Hazard Ratio-HR) was computed by Cox regression analysis by considering all available variables. **Results:** suspicious of recurrent BC was confirmed in 20/21 pts with a positive FDG-PET scan. Overall, the sensitivity, specificity, positive predictive value, negative predictive value and accuracy of FDG-PET were 87%, 94%, 95%, 85%, 90%. AUC was 0.9 (95%IC 0.8-1; $p<0.05$). Likelihood ratio analysis results were as follows: LH+=14.5; LH-=0.13. FDG-PET findings influenced significantly the therapeutic management in 12 patients (modified therapy in 7 PET positive pts; watch and wait in 5 PET negative pts). After 2 years of follow-up, PFS was

significantly longer in pts with a negative vs. a positive FDG-PET scan (85% vs 24%, $p<0.05$). Moreover, a negative study was associated with a significantly longer OS than a positive one (88% vs 47% after 2 years and 87% vs 25% after 3 years, respectively; both $p<0.05$). Furthermore, a positive PET scan was associated with an increased risk of disease progression (HR=12.4; $p=0.001$). At semi-quantitative PET analysis, thresholds SUVmax>6 and TLG>8.5 were recognized as the unique values predicting significantly ($p<0.05$) the PFS rate (2 year PFS rate for SUVmax<6 vs SUVmax>6= 62% vs 15%; 2 year PFS rate for TLG<8.5 vs TLG>8.5= 66% vs 18%). **Conclusion:** FDG-PET/CT has a valuable diagnostic performance in pts with suspicious of recurrent BC and provided a change in treatment decision in about 30% of cases. Moreover, FDG-PET showed an important prognostic value in assessing the risk of disease progression and survival outcomes in this setting of pts.

EPW23

¹⁸F-FDG PET/CT in the evaluation of adrenal masses in patients with oligometastatic state non-small cell lung cancer: a histopathologic comparison after laparoscopic adrenalectomy

Y. Kordan¹, F. Sen², O. Kaygisiz¹, G. Ozmerdiven¹, I. Yavascaoglu¹; ¹Uludag University Department of Urology, BURSA, TURKEY, ²Uludag University Department of Nuclear Medicine, BURSA, TURKEY.

Aim: Adrenal glands comprise one of the most common site for an oligometastatic involvement of non-small cell lung cancer (NSCLC). Patients with such limited metastatic site has the opportunity to be treated surgically and improved survival rate. First-line staging of NSCLC patients with ¹⁸F-FDG PET/CT (PET/CT) has made an increase in the frequency of adrenal mass detection. However the accurate diagnosis of the lesion, whether benign or malignant, is challenging and preoperative imaging with combined PET/CT help to avoid the patient from aggressive treatment modalities. We aimed to determine the reliability of PET/CT for characterizing the mass in the adrenal glands in patients with oligometastatic NSCLC by comparing results after adrenalectomy. **Materials and Methods:** This was a retrospective study of all laparoscopic adrenalectomy performed with curative intent between March 2004 and January 2014 in our clinic. Patients who had histologically proven NSCLC with detected adrenal masses on staging PET/CT scans were included in the study. Patients who were staged without PET/CT or patients who received chemotherapy before imaging were excluded. Patient demographics, analysis of both PET and CT components of adrenal lesions on PET/CT and histopathological results after adrenalectomy were determined. The intensity of FDG uptake expressed as a standard uptake value (SUV) with ratio of SUV in adrenal mass to normal liver uptake was recorded. These parameters were compared statistically between benign and malignant pathologies. **Results:** A total of 22 patients met the inclusion criteria. All but three were females. The mean age was 58.3± 8.35. Metastasis was found in 16 of the adrenal masses (72.7%). SUVmax and SUV ratio values were found significantly higher in the metastatic group ($p=0.001$ and $p=0.009$, respectively). The HU value in CT was greater than 10 in all the patients. No metastasis was found in patients with adrenal mass SUV max smaller than 3, all the patients with SUVmax greater than 4.1 were found to have metastases. There was only one patient with SUV ratio less than 1. The smallest SUV ratio among the adrenal metastases was 1.07. Using ROC curve analysis the best SUV ratio threshold to differentiate benign and metastatic adrenal lesions was 1.2 with a sensitivity of 87.5% and specificity of 83.3%. **Conclusion:** When evaluating the adrenal masses of patients with NSCLC, PET/CT can reliably predict adrenal metastases and oligometastatic state and aid decision making by means of follow-up or surgical resection.

EPW24**Circulation Tumor Cells in Resected Nonsmall Cell Lung Cancer: The Association With Early Relapse and 18F-FDG PET Uptake**

C. Ramos-Font¹, A. Rodríguez-Fernández¹, C. Bayarri-Lara¹, D. de Miguel-Pérez², M. J. Serrano³, E. Triviño-Ibáñez¹, R. Sánchez-Sánchez¹, M. Gómez-Río¹, J. M. Llamas-Elvira¹; ¹COMPLEJO HOSPITALARIO UNIVERSITARIO DE GRANADA, GRANADA, SPAIN, ²GENYO. Centre for Genomics and Oncological Research: Pfizer / University of Granada, GRANADA, SPAIN, ³1.-GENYO. Centre for Genomics and Oncological Research: Pfizer/University of Granada. 2.-Integral Oncology Division, San Cecilio Clinical University Hospital, GRANADA, SPAIN.

Objective: More than 20% of lung cancer patients develop recurrence, even after curative resection. It is hypothesized that relapse may arise from dissemination of circulating tumor cells (CTCs). The present study investigated the association between CTCs and primary tumor 18F-fluorodeoxyglucose (FDG) uptake on PET scan. Secondly, we evaluated the influence of CTCs detection on recurrence rate in surgically resected nonsmall cell lung cancer (NSCLC). **Methods:** In this single center prospective study, blood samples for CTCs analysis were obtained from 102 patients with previously untreated, stage IIIA NSCLC both before and one month after radical resection. CTCs were isolated using immunomagnetic techniques. CTCs presence was correlated with standardized uptake value (SUVmax) measured on preoperative FDG PET/CT. Recurrence and disease free survival (DFS) analysis was performed. **Results:** CTCs were detected in 39.2% of patients before surgery and in 27.5% one month after surgery. In the 85% (34 out of 40) of patients with CTCs at baseline showed a decrease in CTC count after surgery. CTC presence after surgery was significantly correlated with SUVmax on PET scan, pathological stage and with surgical approach. But only SUVmax on PET was an independent predictor of CTC presence after the operation in multivariate analysis (HR=3.71, 95% CI 1.3210.37, p=0.013). 36 patients (35.3%) experienced recurrence during a median follow up period of 19 months. CTCs presence after surgery was significantly associated with early recurrence (p=0.006) and with a shorter DFS, with a 1 year DFS rate of 52.1% compared to 79.1% for CTC negative group (log rank test p=0.005). In multivariate analysis CTCs presence after surgery was associated with a shorter DFS, independently of disease staging. **Conclusion:** Detection of CTCs one month after radical resection might be an useful marker to predict early recurrence in stage III NSCLC. SUVmax value of the primary tumor on preoperative PET scan was associated with CTCs presence one month after the operation.

EPW25**Correlation of metabolic information on FDG-PET with the tissue expression of immune markers in patients with non-small cell lung cancer (NSCLC) candidate to upfront surgery**

E. Lopei¹, L. Toschi¹, F. Marchesi¹, F. Grizzi¹, D. Rahal¹, L. Olivari², G. Castino¹, S. Marchetti², N. Cortese¹, M. Alloisio¹, P. Allavena³, A. Santoro³, A. Chiti³; ¹Humanitas Clinical and Research Hospital, Milano, ITALY, ²University of Milan, Milano, ITALY, ³Humanitas University, Milano, ITALY.

Purpose: Eliciting antitumor T-cell response by targeting the PD-1/PD-L1 axis with checkpoint inhibitors has emerged as a novel therapeutic strategy in non-small cell lung cancer (NSCLC). The identification of predictors of sensitivity or resistance to these agents is therefore needed. Herein, we investigate the correlation of metabolic information on FDG-PET with tissue expression of immune-checkpoints and other markers of tumor-related immunity in resected NSCLC patients. **Materials and Methods:** All patients referred to our Institution for upfront surgical resection of NSCLC, who were investigated with FDG-PET prior to

surgery, were consecutively included in the study. From January 2010 to May 2014, 55 patients (stage IA-IIIB; M:F=42:13; mean age 68.9 years) were investigated. Sampled surgical tumor specimens were analyzed by immunohistochemistry (IHC) for CD68-TAMs (tumor-associated macrophages), CD8-TILs (tumor infiltrating lymphocytes), PD-1-TILs and PD-L1 tumor expression. The immunoreactivity was evaluated and scores compared with imaging findings. FDG-PET images were analyzed to define semi-quantitative parameters: SUVmax and SUVmean. Metabolic information on FDG-PET were correlated with tissue markers expression, and both with disease-free survival (DFS) considering a median follow-up of 16.2 months. **Results:** Thirty-six adenocarcinomas (ADC), 18 squamous cell carcinomas (SCC), and 1 sarcomatoid carcinoma were analyzed. All tumors resulted positive at FDG-PET: median SUVmax 11.3 (range: 2.3-32.5) and SUVmean 6.4 (range: 1.5-13) resulted both significantly higher in SCC compared to other NSCLC histotypes (p=0.007 and 0.048, respectively). IHC demonstrated a median immunoreactive surface covered by CD68-TAMs of 5.41% (range: 0.84-14.01%), CD8-TILs of 2.9% (range: 0.11-11.92%), PD-1 of 0.65% (range: 0.02-5.87%), and PD-L1 of 0.7% (range: 0.03-10.29%). We found a statistically significant correlation between SUVmax and SUVmean with the expression of CD8 TILs (rho=0.31; p=0.027) and PD-1 (rho=0.33; p=0.017 and rho=0.36; p=0.009, respectively). The other tissue markers correlated as follows: CD8 TILs and PD-1 (rho=0.45; p=0.001), CD8 TILs and PD-L1 (rho=0.41; p=0.003), CD68-TAMs and PD-L1 (rho=0.30; p=0.027), PD-1 and PD-L1 (rho=0.26; p=0.059). With respect to patients' outcome, SUVmax, SUVmean and disease stage showed a statistically significant correlation with DFS (p=0.002, 0.004 and <0.001, respectively). **Conclusions:** The present study shows a direct association between metabolic parameters on FDG-PET and the expression of tumor-related immunity markers, suggesting a potential role for FDG-PET to characterize the tumor microenvironment and select NSCLC patients candidate to checkpoint inhibitors.

EPW26**Role of F-18 FDG PET/CT in non-conjunctival origin ocular adnexal mucosa-associated lymphoid tissue (MALT) lymphomas, in comparison with orbital MRI**

H. Park¹, J. Kim², S. Kim¹, J. O¹, S. Yang¹, S. Cho¹; ¹Seoul St. Mary's Hospital, Seoul, KOREA, REPUBLIC OF, ²Taeam Health center and County Hospital, Seoul, KOREA, REPUBLIC OF.

Purpose: Despite the widespread use of F-18 fluorodeoxyglucose positron emission tomography/computed tomography (FDG PET/CT) in the diagnosis and response assessment of patients with lymphoma, few studies have assessed its value in ocular adnexal lymphomas. The purpose of this study was to evaluate the role of FDG PET/CT in staging of non-conjunctival origin ocular adnexal MALT lymphomas (OAML), and to compare its diagnostic sensitivity to magnetic resonance imaging (MRI). **Methods:** FDG PET/CT of 124 patients with pathologically proven OAML between January 2009 and February 2016 were retrospectively reviewed. The patients with MALT lymphoma originating from conjunctiva were excluded. Total 50 patients with non-conjunctival origin OAML were assessed. Maximum standardized uptake value (SUVmax) was measured for all lesions. Sensitivity for primary tumor detection was compared to MRI. **Results:** Ten patients had bilateral OAML and total 60 OAML lesions were analyzed. MRI was missing in one patient. The tumor locations were: eyelid, 9; lacrimal gland, 18; orbit, 33. Fifty lesions (83.3%) showed perceptible FDG uptake with mean±SD SUVmax 4.8±2.4 (range 2.0~11.1). The mean SUVmax according to tumor location were: eyelid, 3.7±1.1 (2.8~5.3); lacrimal gland, 3.6±1.4 (1.4~6.4); orbit, 5.7±2.6 (2.0~11.0). Mean SUVmax among the 3 locations were statistically different (p=0.010 by Kruskal-Wallis test). The sensitivity was

calculated as 83.1% (49/59) for FDG PET/CT and 89.8% (53/59) for MRI, which were statistically comparable ($p=0.219$ by McNemar's test). Seven of 50 patients (14%) were upstaged by detect on of extraocular lesions by FDG PET/CT (1 kidney and lung, 1 tonsil, 4 cervical LNs, 1 sacral foramen). Conclusion: Non-conjunctival origin OAML showed perceptible FDG uptake in 83.3% of the lesions, with comparable sensitivity to that of MRI. FDG PET/CT detected extraocular lymphoma involvement in 14% of the patients. FDG PET/CT performed for non-conjunctival origin OAML has a role in guiding the therapeutic plan.

EPW27

The Prognostic Utility of Pre-Treatment 18F-FDG-PET for Salvage Re-Irradiation in Head and Neck Cancer Patients

K. Musaieva¹, O. Solodyannikiva², Y. Kmetiyuk¹; ¹All-Ukrainian Center of Radiosurgery, Kyiv, UKRAINE, ²National Cancer Institute, Kyiv, UKRAINE.

Background. Statistical image features from hybrid PET/CT scans were studied for their potential to predict clinical outcome of salvage re-irradiation treatment. We analyzed tumor metabolic features from pre-treatment 18F-FDG-PET scans as related to clinical outcomes in patients treated with intensity modulated radiotherapy (IMRT) for recurrent squamous cell carcinoma of head and neck (HNSCC). **Materials and Methods.** Pretreatment PET/CT scans and after treatment PET/CT scans (2.5 to 4.5 months) of 11 patients (9 males, 2 females) who underwent re-irradiation for recurrent HNSCC, were retrospectively evaluated. Semi-quantitative analysis of PET/CT were performed. Metabolic response was assessed using PET response criteria for solid tumors (PERCIST). None of the patients underwent a salvage surgery. Multiple statistical image features related to the standard uptake value (SUV) were computed: metabolic tumor volume, maximum SUV, mean SUV, total lesion glycolysis (TLG), whole-body total lesion glycolysis, whole-body metabolic tumor volume. The correlation between the image features and local control and overall survival was calculated. **Results.** Between 2012 and 2015 eleven patients with recurrent HNSCC underwent IMRT re-irradiation; interval since previous radiation is 21.5 months (3-72). Complete tumor metabolic response (CMR) was achieved in 5 patients (45.5%). Six patients failed to achieve CMR: progressive metabolic disease was in 4 patients (36.4%); stable metabolic disease in one patient (9.1%); one patient had partial metabolic response (9.1%). The median follow-up time was 18.2 months; by the time of this report three patients who failed to achieve CMR died. Out of the calculated image features, only pre-treatment tumor TLG (individual tumor volume multiplied by its mean SUV) correlated with tumor metabolic response in the early PET/CT follow-up: mean tumor TLG in the group with CMR was 71.74; while the mean tumor TLG in the group who failed to achieve CMR was 224.75. Also dividing the patient population based on the median tumor TLG showed a split of the Kaplan-Meier survival curves. **Conclusions.** The tumor TLG of pre-treatment PET/CT scans has important information on the failure risk to achieve CMR in recurrent HNSCC patients. It is necessary to obtain additional patients data to validate these results and to find correlations of the calculated image features with metabolic outcome, local control, progression-free survival and overall survival.

EPW28

The Role Of 18F-FDG PET/CT In Diagnosis And Staging Of Gastric Cancer

E. ARSLAN¹, F. D. CAN TRABULUS², S. BAYRAK², H. E. PASAOGLU³, N. DURSUN³, T. F. CERMIK⁴; ¹ISTANBUL RESEARCH AND EDUCATIONAL HOSPITAL CLINIC OF NUCLEAR MEDICINE, ISTANBUL, TURKEY, ²ISTANBUL RESEARCH AND EDUCATIONAL HOSPITAL CLINIC OF GENERAL SURGERY, ISTANBUL, TURKEY,

³ISTANBUL RESEARCH AND EDUCATIONAL HOSPITAL DEPARTMENT OF PATHOLOGY, ISTANBUL, TURKEY, ⁴SAKARYA SCHOOL OF MEDICINE,NUCLEAR MEDICINE DEPARTMENT, SAKARYA, TURKEY.

OBJECTIVES: Accurate initial assessment for the stage of disease is important for treatment selection and prognosis in gastric cancer. 18F-FDG PET/CT has been shown to be an important tool in the evaluation of gastric cancer. **AIM:** The aim of this study was to evaluate the role of 18F-FDG PET/CT in the staging of gastric cancer in comparison to histopathological results. **MATERIALS AND METHOD:** One hundred forty three patients (mean age:60.7 ±10.9 y) who underwent 18F-FDG PET/CT for primary staging of gastric cancer between May 2010 and December 2015 were included the study. Seventy one patients have been diagnosed by endoscopic and remaining 72 patients with surgical histopatological results. 18F-FDG PET/CT findings of primary lesions, lymph nodes and metastatic organs were compared with pathological results and/or follow-up imaging methods. **RESULTS:** In TNM staging of the patients 8 (11%), 7 (10%), 19(26%) and 38 (53%) were staged as T1, T2, T3 and T4, and 14 (20%), 9 (13%), 17(24%), 30(42%) and 2 (1%) were N0, N1, N2, N3a and N3b respectively. Distant metastasis was found in 57 (40%) patients (37 liver, 8lung, 7bone-bone marrow and 5multi-organ). Distant metastatic patients' primary tumor SUV max was calculated as 13.0±9.1. There was no statistically significant difference between distant metastatic and non-metastatic groups ($p>0.05$). According to analysis of histopathological types of primary tumors, SUV max of adenocarcinoma was calculated as 12.9±9.0, invasive adenocarcinoma as 13.1±9.1, signet ring cells carcinomaas 12.8±8.4 and mucinous adenocarcinoma as 12.2±8.6. There were no statistically significant differences between these groups ($p>0.05$). Fifty-five of 72 patients diagnosed lymph node metastasis with histopathological examination. In comparison with histopathological results 18F-FDG PET/CT was true positive (TP), false positive (FP), false negative (FN), true negative (TN) in 43, 6, 12 and 11patients respectively. Sensitivity, specificity, accuracy, positive predictive value (PPV) and negative predictive value (NPV) of 18F-FDG PET/CT were calculated as 78%, 65%, 75%, 88% and 48% respectively. **CONCLUSION:** Despite the low NPV of 18F-FDG PET/CT in detecting nodal metastasis of gastric carcinoma, relatively high sensitivity and PPV might contribute to accurate initial staging. Also our results suggested that 18F-FDG PET/CT has demonstrated a prominent role in detection of distant metastasis in initial staging of gastric cancer.

EPW29

The diagnostic usefulness of 18F-FDG PET/CT in radiological suspected cases of cholangiocarcinoma

B. R. Mittal, R. Kumar, A. Jois, A. Sood, A. Bhattacharya; Postgraduate Institute of Medical Education & Research, PGIMER, CHANDIGARH, INDIA.

Objective: This retrospective study was performed to evaluate the diagnostic yield of ¹⁸F-fluorodeoxyglucose positron emission tomography-computed tomography (¹⁸F-FDG PET/CT) in radiological suspected cases of cholangiocarcinoma **Material and Methods:** In this retrospective study, we evaluated data of patients with radiological suspicion of cholangiocarcinoma and who were referred for whole body ¹⁸F-FDG PET/CT from January 2011 to December 2015 to assess the disease status. The PET/CT images were evaluated by two experienced nuclear medicine physicians. Abnormal FDG uptake on PET images were correlated with the morphological abnormalities on corresponding contrast enhanced CT images and considered positive. The imaging results were compared with histopathological examination, clinical or imaging follow up. **Results:** A

total of 63 patients (32 males, 31 females) aged 29–78 years (median age of 56.7) data was analysed retrospectively. PET/CT results revealed positive findings in 47/63 patients (74.6%) while 16/63 patients (25.4%) were PET negative. Out of 47 PET positive patients, the intrahepatic lesions were localized in 29 patients while extra-hepatic lesions in 18 patients. On comparing with histopathological examination, FDG PET/CT was true positive (TP) in 43 patients, false positive (FP) in 4 patients, true negative (TN) in 15 patients and false negative (FN) in one patient. The overall sensitivity, specificity, positive predictive value (PPV), negative predictive value (NPV) and accuracy of FDG PET/CT for detection of malignant bile duct diseases was 97.7% (95% CI-87.9% -99.9%), 78.9% (95% CI-54.4% - 93.9%), 91.5% (95% CI-79.6% - 97.6%), 93.7% (95%CI- 69.7% - 99.8%) and 92.1% respectively. The sensitivity and PPV of FDG PET/CT for detection of intrahepatic disease was 100%, 93.10% respectively (TP-27, FP-2, FN-0 and TN-0) while for extra-hepatic disease 94.1% and 88.8% respectively (TP -16, FP-2, FN-1 and TN -0). By ROC curve analysis we found that SUV_{max} >3.6 had a sensitivity 100% and specificity 74.1% (AUC 0.843) for detection of intrahepatic lesions but for detection of extra-hepatic lesion SUV_{max} >7.1 had a sensitivity 75% and specificity 100% (AUC 0.781) respectively. FDG-PET detected distant metastatic lesions in 13 patients not found by other imaging studies and regional lymph nodes were noticed in 41 patients. **Conclusion:** FDG PET/CT had shown a high diagnostic performance in radiological suspected cholangiocarcinoma and promising tool in differentiating intra hepatic and extra-hepatic cholangiocarcinoma. FDG PET/CT also helps in detection of hidden distant metastases and can help in treatment planning.

E-PW4 – Monday, October 17, 2016, 08:30 - 09:30, e-Poster Area
e-Poster Walk 4 – M2M: Innovation in Imaging

EPW31

A New Method for Submillimeter Desktop Small-Animal SPECT Imaging using Tilted Detector

N. Zeraatkr¹, A. Rahmim^{2,3}, S. Sarkar^{4,5}, **M. Ay^{1,4}**; ¹Research Center for Molecular and Cellular Imaging, Tehran University of Medical Sciences, Tehran, IRAN, ISLAMIC REPUBLIC OF, ²Department of Radiology, Johns Hopkins University, Baltimore, MD, UNITED STATES, ³Department of Electrical and Computer Engineering, Johns Hopkins University, Baltimore, MD, UNITED STATES, ⁴Department of Medical Physics and Biomedical Engineering, Tehran University of Medical Sciences, Tehran, IRAN, ISLAMIC REPUBLIC OF, ⁵Research Center for Science and Technology in Medicine, Tehran University of Medical Sciences, Tehran, IRAN, ISLAMIC REPUBLIC OF.

Aim: During last decade, the role of molecular imaging in small-animal models has been highlighted in a variety of applications including pharmaceutical studies, radiopharmaceutical research, and exploring new approaches in cancer therapy. SPECT systems based on pinhole/multi-pin-hole collimators with a rotating gantry (or static gantry with a closed-structure multi-pin-hole collimator) are the most common design used. In this work, we introduce a new system for desktop small-animal SPECT imaging considering the primary goal of Submillimeter spatial resolution. **Materials and Methods:** The system consists of a detector equipped with a pinhole collimator. The detector-collimator set can rotate underneath a desk (imaging desk) with a tilt angle. The imaging desk has a determined region for placing the object to be scanned. The head acquires data in a step-and-shoot manner by rotating around the object underneath the desk maintaining its tilted angle. To evaluate the performance evaluation of the system, it was modeled using GATE Monte Carlo simulation. Also, some complicated phantoms including MOBY phantom were simulated, analytically. The acquired data were then reconstructed using an MLEM-based developed algorithm: Finite-Aperture-Based Circular Projection. For all GATE simulations in the

current work, pinhole diameter of 1 mm, pinhole-to-object distance of 18.5 mm, pinhole-to-detector distance of 300 mm, and tilt angle of 30° were applied. The data were reconstructed using 3 iterations. **Results:** The sensitivity was calculated as ~200 cps/MBq. Also, submillimeter tomographic spatial resolution with appropriate variation throughout the field-of-view (CV% of 9%) was obtained. The noise was quantified as 5.6% in terms of STD%. Non-uniformity was computed as about 25%. Moreover, using submillimeter pinhole diameter, images of the MOBY phantom were reconstructed with acceptable quality. **Conclusion:** The introduced system can provide images with comparable quality to the conventional small-animal SPECT systems while proposing a desktop method for tomographic scan. The system can be manufactured as a low-cost one regarding the application of simple design of the detection and mechanics. The dedicated image reconstruction algorithm developed for the system showed appropriate performance despite of complex geometry of the system.

EPW32

Feasibility of Ultra-low Dose Canine Imaging Using a Next Generation Digital PET System

M. I. Menendez, J. Zhang, K. Binzel, A. Siva, M. I. Knopp, M. Tweedle, T. Rosol, C. L. Wright, M. V. Knopp; The Ohio State University, Columbus, OH, UNITED STATES.

Aim: Molecular imaging using ¹⁸F-FDG positron emission tomography (PET) in veterinary subjects and patients is an important clinical and translational research tool. While imaging at as low as reasonable achievable doses (ALARA) is current practice in human patients, imaging at the lowest possible dose is even more critical to reduce staff exposure and to avoid the need for longer isolation housing. Veterinary subjects are imaged under anesthesia and therefore only physiologic motion needs to be considered. Associated with a project to develop and validate ultra-low human PET imaging, we initiated this pre-clinical project to demonstrate and validate the ability to perform ultra-low dose FDG using a next generation solid state, digital PET detector human PET/CT system. **Materials and Methods:** PET/CT imaging of anesthetized, healthy, skeletally mature beagles was performed using a next generation digital photon counting PET/CT system (Vereos, Philips) (dPET) that has excellent sensitivity and time of flight timing resolution (325ps). Combined dynamic and whole-body imaging over 110 min with a 120s per bed position acquisition time was acquired starting with injection and event data were recorded in listmode. A specialized reconstruction and *in silico* simulation computational environment was previously developed and utilized. Our current human standard of care dose is 3.5 - 7 MBq/kg. Canine dosing was performed and simulated in the range from 1 to 10 MBq/kg. Images were qualitatively analyzed by experienced blinded reader review and quantitatively by 3D ROI placement on reference tissues and SNR assessments. **Results:** Imaging was performed using 6 canine subjects with an average weight of 15 kg, evaluating total dose ranges from 15 to 111 MBq. In parallel, simulated lower dose whole-body scans were reconstructed in 10% dose reduction increments down to the 15 MBq. The quantitative analysis found consistent (less than 10% variability) SUV_{max} values when using the previously developed adaptive reconstruction approach over the assessed dosing range down to 1.0 MBq/kg. Visual quality was rated assessable for all dose ranges of 1.5 MBq/kg or above. **Conclusion:** Ultra-low dose canine FDG PET imaging can be accomplished at 1.5 MBq/kg using a digital PET/CT system and optimized reconstructions approaches. The considerable dose reduction supports increased opportunities of FDG PET for veterinary applications as the post procedure radiation dose has been a limiting factor necessitating subsequent isolation housing or undue exposures to support staff. Furthermore it creates new *in vivo* benchmark data for human patient dose reduction efforts.

EPW33**A Study on the Effect of Attenuation Correction in image Quantity in Small-Animal SPECT System**

S. Khorasani Gerdekoohi^{1,2}, N. Vosoughi¹, K. Tanha³, M. Assadi³, M. Ay^{2,4}; ¹Department of Energy Engineering, Sharif University of Technology, Tehran, IRAN, ISLAMIC REPUBLIC OF, ²Research Center for Molecular and Cellular Imaging, Tehran University of Medical Sciences, Tehran, IRAN, ISLAMIC REPUBLIC OF, ³Persian Gulf Nuclear Medicine Research Center, Bushehr University of Medical Sciences, Bushehr, IRAN, ISLAMIC REPUBLIC OF, ⁴Department of Medical Physics and Biomedical Engineering, Tehran University of Medical Sciences, Tehran, IRAN, ISLAMIC REPUBLIC OF.

Aim: Photon attenuation as an inevitable degradation factor affect the accuracy of quantitative measurements in single photon emission computed tomography (SPECT) images. Various attenuation correction methods have been evolved to compensate this degradation. We proposed a Chang based attenuation correction algorithm and then evaluated its effect on SPECT images of HiReSPECT scanner which developed in our department. Phantom and animal studies were performed to validate our method. **Materials and methods:** A post-processing Chang attenuation correction algorithm developed using extracting object contour from emission data. In our study due to small size of objects a uniform attenuation map with attenuation coefficient of water in 140 keV was used. Then a matrix calculated slice-by-slice and multiplied by reconstructed image to compensate the attenuation. Uniform cylindrical phantoms with various volumes from 1ml to 30ml and known activities were scanned to evaluate the influence of attenuation correction on different volumes of objects. Additionally, we scanned the NEMA NU-2008 image quality phantom and analyzed its uniform region and hot rods activity concentration before and after applying attenuation correction. At the end we performed rat renal scans (n=8 kidneys) to examine the validity of our correction method in non-uniform distribution of attenuating tissues in animal body. After each scan rat's kidneys were removed and counted with a dose calibrator to attain absorbed activity. Afterwards comparison of corrected and non-corrected images confirmed. Data analysis was done by drawing region of interests (ROI) in two ways: (a) manual ROIs for phantom images because of their simple shape and absence of background activity and (b) an iso-contour based ROI drawing for animal images. **Results:** In cylindrical phantoms, applying attenuation correction caused a reduction of 2.2% in relative error for phantom with 7mm diameter; whereas, it reduced the relative error 15.9% for 30mm phantom. So attenuation correction becomes more important when the size of the object and its self attenuation rises. In image quality phantom, applying attenuation correction improved the recovery coefficient (RC) 8% for hot rod with diameter of 2mm (smallest detected hot rod) and 19% for 5mm diameter hot rod (biggest one). Furthermore, relative error of activity concentration in uniform region reduced from -15% to 5% after correction. In animal studies, the quantitative error improved from -22.8% to +3.5% on average by applying attenuation correction. **Conclusion:** These results show that in small animals, a uniform attenuation map using only emission data can promise an acceptable image quantitative accuracy.

EPW34**A high-resolution hybrid gamma-optical camera for intraoperative imaging**

J. E. Lees¹, S. L. Bugby¹, M. S. Alqahtani¹, L. K. Jambi¹, N. S. Dawood¹, A. H. Ng², A. C. Perkins²; ¹University of Leicester, Leicester, UNITED KINGDOM, ²University of Nottingham, Nottingham, UNITED KINGDOM.

Introduction The development of compact low profile gamma-ray detectors has allowed the production of a small field of view, handheld

imaging device which could be used at the patient bedside and in operating theatres. The combination of an optical and a gamma camera, in a co-aligned configuration, provides an optical image overlaid with a scintigraphic image. This innovative introduction of hybrid imaging offers assistance in localising the site of uptake in procedures such as sentinel node detection. The hybrid camera concept can be extended to a multi-detector design which provides depth estimation of the gamma-emitting source. **Materials and Methods** The hybrid camera consists of a 1500 µm thick CsI(Tl) columnar scintillator coupled to an electron multiplying CCD with a tungsten pinhole collimator which gives a 40mm x 40mm nominal field of view for the 8mm x 8mm CCD detection area. An optical camera is aligned so as to provide the same field of view as the gamma camera. Optical and gamma images are taken simultaneously and fused to produce dual-modality images providing information from the gamma camera within an optical context. Images were obtained in laboratory simulations using a range of bespoke phantoms. Clinical images from patients attending the nuclear medicine clinic were also taken. **Results** The characteristics of the hybrid camera compared favourably with other portable SFOV cameras currently in use. High quality images from phantoms show that the hybrid system is particularly suited for sentinel lymph node detection. Experimental simulations demonstrated the ability to differentiate between adjacent hot sources (1:100 activity ratio) in close proximity, as would be required for differentiation of sentinel nodes from the injection site. Estimation of depths of radioisotope sources in a simple phantom were also achieved. We report on clinical results from lymphoscintigraphy, thyroid imaging and lacrimal drainage studies that show that the site of uptake could be visualised in the patient. **Conclusion** The hybrid camera has been used to produce dual-modality images in both laboratory simulations and in the clinic. In addition we have shown that the hybrid camera concept can be extended to estimate the position and depth of radionuclide distribution within an object.

EPW35**Portable hybrid gamma-near-infrared fluorescence imaging**

S. L. Bugby¹, J. E. Lees¹, A. H. Ng², M. S. Alqahtani^{1,3}, L. K. Jambi^{1,4}, M. A. Stammers^{5,6}, H. J. M. Handgraaf⁵, A. C. Perkins²; ¹University of Leicester, Leicester, UNITED KINGDOM, ²University of Nottingham, Nottingham, UNITED KINGDOM, ³King Khalid University, Abha, SAUDI ARABIA, ⁴King Saud University, Riyadh, SAUDI ARABIA, ⁵LUMC, Leiden, NETHERLANDS, ⁶Percurios, Leiden, NETHERLANDS.

Introduction: The first clinical study of targeted hybrid near-infrared (NIR) fluorescent-radioactive tracers was recently published. In addition, ICG-^{99m}Tc-nanocolloid is already being used by some centres for sentinel lymph node biopsy. Once exposed, the NIR fluorescence reporter can be imaged at very high resolutions while the radioactive component allows imaging at depths which would not be possible in NIR. Visualisation of NIR fluorescence during surgery requires a dedicated NIR camera, several of which are available commercially. Gamma detection may be carried out with a separate portable gamma camera or with a non-imaging probe. We describe a portable hybrid NIR-gamma small field of view camera, capable of displaying co-aligned images from both modalities which can be fused into one image or viewed separately. This study is a preliminary investigation of the performance of the fluorescence component of this camera, including phantom studies and first images from a preclinical pilot study. **Materials and Methods:** The hybrid camera consists of a 1.5mm thick CsI:Tl columnar scintillator coupled to an electron multiplying CCD. A 1.0mm diameter pinhole collimator gives a 40mm x 40mm nominal field of view for an 8mm x 8mm detector area. A fluorescence camera was aligned to provide the same field of view as the gamma camera with an LED ring as the excitation source. The performance of the fluorescence imaging was quantified in this study for the fluorophores ICG and IRDye800CW (CW800) using a number of phantom experiments.

Images are also presented for a preclinical study of a targeted hybrid tracer (cRGD-CW800-TCO + TCO-DOTA-¹¹¹In) in mice with HT29 colorectal cancer xenografts. These images have been used for a qualitative comparison between the hybrid camera and commercially available fluorescence imaging systems (Artemis, Quest; Pearl Impulse, LICOR). **Results and conclusions:** The hybrid camera prototype has been shown to successfully image the dual NIR-gamma tracers tested. With further development, this camera could be used intraoperatively, offering the benefits of high resolution surface NIR fluorescence imaging and the depth penetration of gamma imaging in a single imaging system.

EPW36

From compound library to lead compound selection via established ^{99m}Tc radiochemistry, high-throughput preclinical SPECT/CT imaging and automated analysis

S. Macholl¹, C. Finucane¹, S. Mather¹, J. Hesterman², D. Scully², E. Jouannot³; ¹inviCRO Ltd., London, UNITED KINGDOM, ²inviCRO LLC, Boston, MA, UNITED STATES, ³Sanofi-Aventis R&D, Chilly-Mazarin, FRANCE.

Feasibility and application of preclinical high-volume, high-throughput SPECT/CT imaging including automated analysis is presented, by example of a study comprising 25 tumor-targeting proteins. **Radiochemistry:** Each study day, 2 proteins were radiolabeled by ^{99m}Tc tricarbonyl technology followed by iTLC+HPLC for QC. **Imaging:** Tumor tissue was inoculated into mice in staggered batches. For each radiotracer, 3 mice were injected iv (20 nmol/kg; 100 MBq) and imaged simultaneously (Bioscan NanoSPECT/CT): whole-body SPECT scans at 1h, 4h, 24h (and 48h in pre-selected compounds) post-injection. For 10 preselected compounds, dynamic SPECT was done at 0-2 h p.i. Whole-body CT scans accompanied SPECT scans giving 291 scans in total. Reconstructed SPECT and CT images were split into single animals and analysed in VivoQuant (inviCRO). All data were stored on an iPACS study management system. Absolute radiotracer uptake in Bq was measured in tumor, skeletal muscle, heart, blood (left ventricle), liver and kidneys by manual and semi-automated segmentation. %ID, %ID/mL, SUV and %ID/mL ratio data were automatically generated and plots of all study data created by a Matlab script. QC images were generated automatically and inspected to verify injection quality, ROI placements and intersubject reproducibility. **Ex vivo:** Animals were dissected after imaging, tissue weights automatically stored into a spreadsheet, and this imported automatically into Matlab together with gamma counts (LKB-Wallac) to calculate and plot absolute radiotracer uptake in Bq, %ID, %ID/g, SUV and %ID/g ratios via Matlab script. QC included outlier detection. **Results:** A total of 507 single animal SPECT images were acquired for the 25 proteins in 5 weeks. Labeling quality was excellent and consistent for all compounds (radiochemical purity=(98.0±1.6)%). The analysis workflow was applied within hours to every incoming dataset and an updated set of plots generated comprising finally >3500 ROI and >1000 tissue data. SPECT/CT images clearly visualized uptake in tissues such as tumor (except controls), kidneys and liver, even at 48 h p.i. Tumor uptake was 0.5 to 13 %ID/mL. Intersubject variability for any compound was typically 10% COV. **Conclusion:** The large data set of tumor, blood, background and systemic uptake/clearance data from 75 mice and for 25 compounds allowed identification and ranking of lead compounds, with all experiments and analysis taking 3 months. QC results and a high level of automation throughout provide confidence in the data set. For even larger compound libraries, radiolabeling could be expedited and the number of imaging time points reduced to increase weekly throughput.

EPW37

Relationship Between 18F-FDG PET/CT Diagnostic Accuracy And Stimulated Thyroglobulin Levels In High/Intermediate Risk Differentiated Thyroid Carcinoma

E. TRIVIÑO-IBÁÑEZ^{1,2}, M. MUROS¹, E. TORRES-VELA¹, N. TESTART¹, A. GONZÁLEZ-JIMÉNEZ¹, R. SÁNCHEZ-SÁNCHEZ¹, M. BERMÚDEZ-MORALES¹, J. LLAMAS-ELVIRA¹; ¹Complejo Hospitalario Universitario de Granada, Granada, SPAIN, ²IBS, Granada, SPAIN.

INTRODUCTION: Multiple studies in the literature have analyzed the relationship between thyroglobulin (Tg) plasma levels and diagnostic accuracy of 18F-FDG PET/CT in the context of patients with TENIS Syndrome (elevated thyroglobulin and negative 131I-whole body scan). However, there is very little data available on the influence of Tg levels in the early evaluation with 18F-FDG PET/CT of patients with intermediate-high risk differentiated thyroid carcinoma (DTC) recurrence. **PATIENTS and METHODS:** A prospective study was carried out (June 2007 to December 2013) on 81 patients with high/intermediate risk of recurrence DTC, treated with surgery and radioiodine ablation (RIA). Our patient selection was not based exclusively on TNM classification and included broad risk criteria (ATA guidelines 2015, etc.), such as locoregional invasion, inadequate high Tg value and aggressive histological subtypes. We performed 18F-FDG-PET/CT just before or immediately after radioiodine ablation. We confirmed 18F-FDG-PET/CT results with other imaging techniques, pathology reports, first year whole body scans, neck ultrasounds or follow-up. **RESULTS:** 81 patients with high/intermediate-risk of recurrent DTC. Forty-one (50.6%) had positive uptake in 18F-FDG PET/CT, with negative 131I WBS. Sensitivity, specificity and diagnostic accuracy of PET/CT were 92.5%, 90.2% and 91.4% respectively. Considering Tg stimulated levels at the time of the ablative therapy with 131I, we observed a progressive increase in sensitivity and positive predictive value (PPV) of 18F-FDG PET/CT study. So with levels of Tg≤10 ng/mL the sensitivity was 92.8% and PPV 80%, with Tg>10 and ≤100 ng/mL sensitivity was 100% and PPV 80%, whereas above 100ng/mL both parameters values reach 100%. For ROC curves analysis, false positive and false negative cases of 18F-FDG PET/CT were excluded. The cutoff value of stimulated thyroglobulin at the time of ablation that showed a better relationship sensitivity/specificity was 9.3ng/ml, discriminated correctly to 83 % of patients with a sensitivity of 70.3% and a specificity of 86.1%. **CONCLUSIONS:** The diagnostic accuracy of 18F-FDG PET/CT in high/intermediate-risk of recurrent DTC is positively related with stimulated thyroglobulin levels. The cutoff value of stimulated thyroglobulin with best sensitivity/specificity relationship is 9.3ng/ml.

EPW38

Could Disappearance of Anti-thyroglobulin Antibody Predict Disease Persistence in Differentiated Thyroid Carcinoma Patients With Positive Anti-thyroglobulin Level After Total Thyroidectomy And Radioiodine Ablation

P. Lee¹, Y. Huang¹, S. Lee², L. Juan², Y. Hsu²; ¹Department of Nuclear Medicine, Koo Foundation Sun-Yat Sen Cancer Center, Taipei, TAIWAN, ²Department of Internal Medicine, Koo Foundation Sun-Yat Sen Cancer Center, Taipei, TAIWAN.

Background: Serum thyroglobulin (Tg) serves as an important marker in monitoring patients with differentiated thyroid cancer treatment. However, serum Tg measurement may be interfered by the presence of anti-Tg antibodies (TgAb), thus limiting the usefulness of Tg in surveillance of patients with positive TgAb. Recent articles demonstrated that TgAb may be used as a surrogate marker of disease persistence or response to treatment. The aim of this study was to evaluate if the disappearance of serum TgAb after ablation could predict disease persistence

in patients with differentiated thyroid carcinoma after thyroidectomy and radioiodine ablation. **Materials and Methods:** A retrospective review was performed on differentiated thyroid carcinoma patients who underwent total thyroidectomy and radioiodine ablation from 2006 till 2013, and were positive for TgAb before ablation. The change of serum TgAb before ablation (TgAb1) and after ablation (TgAb2), tumor pathologic status, patients' sex and age were all recorded. TgAb was considered positive or negative on the basis of specific assay cutoff values at our hospital. All of these parameters were correlated with disease persistence at 10-20 months after ablation. Disease persistence was defined as appearance of disease by diagnostic radioiodine scan, neck sonogram or stimulated Tg level of >1ng/ml. **Results:** A total of 53 patients with positive TgAb1 were included in this study. At 10-20 months after radioiodine ablation, 36 patients (67.9%) had persistent disease. TgAb2 was positive in 34 patients (64.2%) while TgAb2 declined to negative in 19 patients (35.8%). Of these 19 patients with negative TgAb2, disease persistence was still noted in 11 patients (57.9%). In the positive TgAb2 group, disease persistence was noted in 25 of 34 patients (73.5%). There was no statistical difference between TgAb2 negative and TgAb2 positive group ($p=0.242$). However, younger patients had a higher risk of persistent disease as compared to elder patients (mean age 40.3y/o vs 49.1y/o, $p=0.014$). Other parameters, such as sex, tumor number, extra-thyroidal extension, lymphovascular invasion, margin involvement, and lymph node involvement were non-predictive of persistent disease. **Conclusion:** Our results indicated that disappearance of serum TgAb2 at 10-20 months after ablation could not predict disease persistence in differentiated thyroid carcinoma patients after total thyroidectomy and radioiodine ablation. However, younger patients were more likely to have a higher rate of persistent disease.

EPW39

Investigation of the effect of BRAF^{V600E} mutation on the clinical outcome in the group of patients with papillary thyroid carcinoma

M. Hartmanova¹, K. Taborska, P. Sykora, T. Kracmerova, P. Vlcek, S. Dvorakova², V. Sykora²; ¹University Motol Hospital, Prague, CZECH REPUBLIC, ²Department of Molecular Endocrinology, Institute of Endocrinology, Prague, CZECH REPUBLIC.

This pilot study included 50 patients with papillary thyroid carcinoma (PTC) after total thyroidectomy or operation for relapse of the disease between 11/2006-1/2011. Parts of the frozen thyroid tissue were examined for the presence of BRAF^{V600E} mutation. All patients have been followed-up annually. In 2016, after receiving the results of the genetic screening, we were able to assess the clinical outcome both in patients with positive and with negative BRAF^{V600E} mutation findings. **Aim and methods:** The research was focused on the evaluation of the amount of remission or relapse of the PTC in both groups on the basis of: clinical examination, cervical ultrasonography, suppressed and stimulated level of thyroglobulin, presence of Tg antibodies and diagnostic or post-therapeutic whole-body ¹³¹I scintigraphy. Patients were considered to have complete remission if the clinical examination and ultrasonography were negative and suppressed level of hs (high sensitive) Tg was <0,2ug/l or the level of stimulated hsTg <2ug/l. **Methods:** We divided the patients into two groups according to the presence or absence of BRAF^{V600E} mutation and into groups considering their age (<45 years and older) and clinical stage. Then in each group of patients we assessed the number of iodine ¹³¹I administration and number of patients in remission or with persistent disease. **Results:** In the BRAF positive group (together 18 patients), there were one patient in the stage I and 2 patients in higher clinical stages, who have persistent disease inspite of repetitive radioiodine treatment. In the BRAF negative group (together 32 patients) all patients who were in stage I, even if they were treated repetitively, all reached complete remission. Only one out of 6 patients of higher clinical stage did not reach remission. Although there were more patients of higher

clinical stage in the BRAF negative group, the number of recidives was lower than in the BRAF positive group, where the majority of patients in higher clinical stage did not reach remission. Together, there were 33% BRAF^{V600E} positive and 77% BRAF^{V600E} negative patients in the group younger than 45 years. In the patients of the age 45 and older there were 41% BRAF^{V600E} positive and 59% BRAF negative. **Conclusion:** In conformity with previous published studies we demonstrated that the presence of BRAF^{V600E} somatic mutation is more common in elderly patients and is connected with more significant radioiodine resistance and higher risk of relapse of the PTC.

EPW40

Second Primary Cancer Risk Estimates in Differentiated Thyroid Carcinoma Patients Treated with Radioiodine

N. L. Correa¹, L. V. de Sá²; ¹Instituto Estadual de Diabetes e Endocrinologia, Rio de Janeiro, BRAZIL, ²Instituto de Radioproteção e Dosimetria - CNEN, Rio de Janeiro, BRAZIL.

Introduction: An increase in the incidence of second primary cancers (SPC) is the most feared late effect that can occur in differentiated thyroid carcinoma (DTC) patients treated with radioactive iodine (RAI). The decision to treat a patient with RAI should therefore incorporate a careful risk-benefit analysis. The objective of this work is to adapt the risk estimation models developed by the Biological Effects of Ionizing Radiation Committee (BEIR VII) to local epidemiological characteristics to assess the carcinogenesis risk from radiation in a population of Brazilian DTC patients treated with RAI. Absorbed radiation doses in critical organs were also estimated to determine whether they exceeded the respective thresholds for deterministic effects. **Material and Methods:** 416 DTC patients treated with RAI were retrospectively studied. Four organs were selected for absorbed dose estimation and subsequent calculation of carcinogenic risk: kidney, stomach, salivary glands and bone marrow. Absorbed doses were calculated by dose factors (absorbed dose per unit activity administered) previously established based on standard human models. The lifetime attributable risk (LAR) of incidence of cancer as a function of age, gender, and organ specific dose was estimated according to BEIR VII mathematical models, relating it to the activity of RAI administered in the initial treatment. **Results:** The salivary glands received the greatest absorbed doses of radiation ($1,567 \pm 0,431$ Gy), followed by the stomach ($1,022 \pm 0,738$ Gy), kidney ($0,315 \pm 0,089$ Gy) and bone marrow ($0,184 \pm 0,050$ Gy). None of these, however, surpassed the threshold for significant deterministic effects for a single administration of RAI. The LAR for stomach cancer incidence was by far the highest, followed in descending order by the salivary glands, leukemia and kidney cancer. The LAR for stomach cancer and leukemia incidence after RAI demonstrates a substantial reduction of risk for lower activities administered, especially in younger patients. **Conclusion:** RAI in single administration is extremely safe in terms of deterministic effects, because even high administered activities do not result in absorbed doses that exceed the thresholds for significant tissue reactions. The BEIR VII mathematical models allow a feasible quantification of SPC risk, demonstrating a marked decrease in risk for younger patients with the administration of lower RAI activities and suggest that only the smallest effective activities should be administered in low-risk DTC patients.

EPW41

Association Between 18F-FDG PET/CT and Thyroglobulin Doubling-Time in Differentiated Thyroid Carcinoma

G. Costa¹, P. Lapa¹, H. Martins¹, A. Albuquerque¹, J. Pedrosa de Lima^{1,2}; ¹Centro Hospitalar e Universitário de Coimbra, Coimbra, PORTUGAL, ²Instituto de Ciências Nucleares Aplicadas à Saúde, Coimbra, PORTUGAL.

Aim: Serum thyroglobulin doubling-time (Tg-Dt) and 18F-2-fluoro-2-deoxy-D-glucose (18F-FDG) PET/CT were recently proposed as important additional prognostic tools in differentiated thyroid carcinoma (DTC). Faster Tg-Dt and higher 18F-FDG uptake are associated with shorter survivor rates. We aimed to evaluate the relationship between Tg-Dt and the 18F-FDG PET/CT results. **Material and methods:** We review 64 PET/CT scans with 18F-FDG, performed in DTC patients (55 female, 9 male; 57.1±12.7 years). All patients were previously submitted to surgery and, at least, one course of radioiodine therapy. Indications for 18F-FDG PET/CT were elevated thyroglobulin (Tg) level in combination with negative 131I whole-body scintigraphy (WBS), unfavourable tumour histology or known distant metastases by any imaging modality. For Tg-Dt calculation, we collected 2 or 3 consecutive Tg measurements (always under suppressed TSH), taken before 18F-FDG PET/CT. Excluding the administration of levothyroxine, no thyroid carcinoma specific therapeutic procedure was done during that time. Tg-Dt was calculated by exponential curve fitting to the available data using nonlinear regression and the results were categorized in 3 groups: fast (Tg-Dt<1 year); slow (1<Tg-Dt<3 years); very-slow (Tg-Dt>3 years or negative value). 18F-FDG PET/CT were classified as true-positive (TP), true-negative (TN), false-positive (FP) and false-negative (FN) according to the histologic or clinical follow-up. PET/CT results were also analysed, based on the Tg-Dt. **Results:** Thirty two 18F-FDG-PET scans were classified as positive and 32 as negative. Of these, 31 were TP and 18 TN (sensitivity=69%; specificity=95%; accuracy=76%). Regarding Tg-Dt, we found 26 patients (40.6%) with a fast, 7 (10.9%) with slow and 31 (48.4%) with very-slow Tg-Dt. Most of the TP cases had a fast Tg-Dt (n=21; 67.7%) and most of the TN scan had a very-slow Tg-Dt (n=15; 83.3%). **Conclusion:** Our study shows a clear association between 18F-FDG results and Tg-Dt, suggesting that glycolytic metabolism is also linked to the Tg production rate.

EPW42

68Ga-DOTA-TATE PET-CT in differentiated thyroid cancer patients: comparison with 18F-FDG PET-CT

B. Vatankulu, B. Akovalı, S. Sağer, M. Halaç, L. Kabasakal, K. Sönmezoglu; İstanbul University Cerrahpaşa Medical Faculty, İstanbul, TURKEY.

Aim: We aimed to investigate the role of Ga-68 PET/CT in the patients with differentiated thyroid cancers (DTC) who had negative iodine- 131 (I-131) scan and elevated thyroglobulin (Tg) level and also to compare with FDG PET/CT. **Materials and method:** A total of 32 patients with DTC diagnosis who had negative I-131 scan and increased Tg level during follow-up were included in this study. All patients underwent both Ga-68 and FDG PET/CT imaging. The mean interval between the two scans was 14±3 days. PET/CT images were analyzed on a lesion-by-lesion, location-by-location and on a patient-by-patient basis. All lesions detected by PET/CT were divided into 4 groups as local, nodal, pulmonary or skeletal lesion. Final diagnosis was made by histopathological results, serial Tg measurement and clinical/radiological follow-up (at least 6 months). **Results:** While Ga-68 DOTA-TATE PET/CT detected recurrent/metastatic lesion in the 67% (21/32) of the patients, FDG PET/CT demonstrated in the 74% (23/32) of the patients. There was no statistically significant difference in the diagnostic ability between the two methods (p= 0,248). According to patient based analysis, the sensitivity and specificity was found to be 72,4% and 100% for Ga-68 PET/CT and 89% and 91% for FDG PET/CT. A total of 92 lesions were found by both imaging methods. Sixty-four of these were shown by Ga-68 PET/CT and 79 of the 92 lesions were detected by FDG PET/CT. Both methods were concordant in 60/92 lesions. There was high consistency in the detection of nodal metastasis between the 2 test ($\kappa=0.89$). On the other hand, it's lower for the pulmonary and skeletal lesions ($\kappa=0.65$). Ga-68 PET/CT changed therapy management in 21/32 patients while FDG PET/CT changed management in 18/32 patients.

Conclusion: We found that Ga-68 and FDG PET/CT had similar accuracy in the detection of DTC recurrence/metastasis according to patient based analysis. However, lesion based analysis showed that FDG PET/CT detected more lesion than Ga-68 study. Ga-68 PET/CT is a proper imaging technique for selecting DTC patients who are candidates for peptide receptor radionuclide therapy.

EPW43

Peptide receptor radionuclide therapy in non-neuroendocrine tumours - a field report

B. Nilica; Universitätsklinik für Nuklearmedizin Innsbruck, Innsbruck, AUSTRIA.

Purpose: To present observed impact of Peptide receptor radionuclide therapy (PRRT) in non-neuroendocrine tumours (non-NET) showing overexpression of somatostatin receptors (SSTR). **Methods:** On database research we found 50 patients who underwent PRRT with a progressive, histologically proven tumour other than NET but still SSTR-positive in 68Ga-DOTA-TOC PET which had no other convincing conservative option for treatment left. **Results:** All 50 patients showed tumour-progression and after evaluation with 68Ga-DOTA-TOC PET for SSTR-positive lesions were treated with PRRT. The main proportion were thyroid cancer (total 29, initially differentiated 17, medullary thyroid cancer 7, poorly differentiated / anaplastic 5) followed by paraganglioma (7), neuroblastoma (3), medulloblastoma (2), phaeochromocytoma, breast cancer, meningioma, merkel-cell carcinoma, mesothelioma, prostate cancer of possible neuroendocrine origin, sarcoma, thymoma, urothelial cell carcinoma (each 1). 43 Patients received one substance (e.g. 177Lu-DOTA-TATE) only, 7 patients two different treatment substances (e.g. 177Lu-DOTA-TATE or 90Y-DOTA-TOC). Of those 7, 5 patients were switched to another substance after fulfilling one full course of treatment (4 applications). Two patients switched due to problems of availability. The number of single applications ranged from 1 up to 16 treatments (median 3.5, mean 3.9), cumulative doses ranged inpatient from 759 MBq to 63190 MBq (median 14.6 GBq, mean 17.0 GBq), the age at first application from 3 to 87 years. The time between first and last application (40 patients more than one treatment) was up to 107 months in one case, median 6.5, mean 13.1, standard deviation 20.0. Taken together 31 patients were on treatment for 0.5 years (60%), 8 for one year, 5 for 2, 4 for 3.5 years and one for 5.4 and another one for 9 years. **Conclusion:** Patients with SSTR-positive progressive non-NETs with no or little conservative therapeutic options (side effects, contraindications) may benefit from PRRT. 40% of the patients treated by PRRT with SSTR-positive non-NETs were on treatment-course for more than 6 months with little side effects and remarking good quality of life in a palliative setting, suggesting that PRRT may offer a possible therapeutic option for these patients.

EPW44

¹⁷⁷Lu-DOTA-TATE therapy in patients with NETs: Response to treatment and long-term survival update

E. Demirci¹, O. Erdem Şahin², M. Ocak³, A. Aygün², I. Uslu², L. Kabasakal²; ¹Department of Nuclear Medicine, Sisli Etfal Training and Research Hospital, İstanbul, TURKEY, ²Department of Nuclear Medicine, Cerrahpaşa Medical Faculty, İstanbul University, İstanbul, TURKEY, ³Department of Pharmaceutical Technology, Pharmacy Faculty, İstanbul University, İstanbul, TURKEY.

Aim: We report the long-term survival results of patients with metastatic neuroendocrine tumors who were treated with ¹⁷⁷Lu-DOTA-TATE. Additionally, our secondary aim was to evaluate prognostic indicators. **Materials and Methods:** 234 patients with metastatic or inoperable well differentiated NETs who underwent ¹⁷⁷Lu-DOTA-TATE treatment during period of 2010-2015 included in this retrospective study. Response to

treatment evaluated according to RECIST criteria. Progression-free survival (PFS) and overall survival (OS) rates were calculated. **Result:** Patients were treated with an average 5.04 administrations and 4.45 ± 0.9 GBq of ^{177}Lu -DOTA-TATE. All patients had diagnosis of NET with primary localization of pancreas (n=90), non-pancreatic GEP-NET (n=45), lung (n=34), paraganglioma-pheochromocytoma (n=18) and other sites (n=12). In 34 patients primary tumor could not be identified. In 135 (57.9%) patients Grade 1 or 2 hematologic toxicity occurred after 36.5% and 52.9% of first cycle and second cycle (salvage) of treatment, respectively. Grade 3 hematologic toxicity occurred 0.6% and 1.2% after first and second cycles, respectively. Among 183 patients who had completed first cycle of treatment, 63 (27%) patients had progression, 37 (15.9%) patients had stable disease, 77 (33%) patients had partial response and 6 patients (2.6%) had complete response. Median overall survival rate was calculated 35 months (95% CI: 28.4–41.5) and 54.7 months (95% CI: 51.7–58.1) for all patients and for patients who had treated with at least 3 administration of ^{177}Lu -DOTA-TATE, respectively. Grade I NETs had a median survival of 51.3 months (95% CI: 44.9–57.7), grade II NETs had a median survival of 34.4 months (95% CI: 28.3–40.5) and grade III NETs had a median survival of 16.6 months (95% CI: 4.2–29). Overall survival rates according to primary site was 48.5 months for pancreas, 56.1 months for non-pancreatic GEP-NETs, 38.8 months for paraganglioma-pheochromocytoma, 43.5 months for lung and 38.4 months for unknown primary and 19.8 months for other sites. Patients who had bone metastasis had lower OS and PFS than those who did not (OS: 40.4 vs 54; $p < 0.005$). Patients who had stable disease or partial response after first cycle of treatment had a comparable survival rates with no statistically significant difference (OS: 57.7 vs 55.6; $p > 0.05$). However, patients who had progressive disease had significantly lower OS rates of 24.6 months with 95% CI of 8.3–21.5 ($p < 0.001$). **Conclusion:** Treatment with multiple cycles of ^{177}Lu -DOTA-TATE PRRT is safe and effective for patients with metastatic NETs. Response to treatment, progression free and overall survival rates compare favorably to the limited number of alternative treatments.

EPW45

Measurement of kidney absorbed dose using ^{177}Lu -DOTATATE in paediatric neuroblastoma

M. Aldridge¹, J. Gains², A. Smith¹, J. Bomanji¹, M. Gaze²; ¹Institute of Nuclear Medicine, UCLH, London, UNITED KINGDOM, ²Radiotherapy, UCLH, London, UNITED KINGDOM.

Introduction Neuroblastoma has been shown to express somatostatin receptor subtype 2 (sstr-2) as demonstrated by ^{68}Ga -DOTATATE imaging. Peptide receptor radionuclide therapy (PRRT) with ^{177}Lu -DOTATATE is therefore an option for therapy. However, avoidance of renal toxicity is essential for safety and a dose constraint is set at 23Gy for the kidneys. **Aims** In this study we calculate kidney absorbed dose for each fraction of treatment and cumulative dose to ensure safe tolerability of treatment. **Methods** Children with relapsed or refractory high-risk neuroblastoma were assessed for suitability for in-patient PRRT with ^{177}Lu -DOTATATE as assessed by ^{68}Ga -DOTATATE PET/CT. The intention was to administer 4 fractions of treatment. The administered activity of the first fraction of ^{177}Lu DOTATATE is weight-based (75MBq/Kg). Activity for subsequent administrations at 8 to 12 week intervals depends on the whole-body radiation dose received and the haematological and renal toxicity from previous administrations. Administered activity was escalated to 100MBq/Kg if whole body dose was $< 0.5\text{Gy}$ with minimal haematological and renal toxicity. Whole-body dose was determined by ceiling-mounted scintillation probe monitoring, performed regularly by carers over 4 days; and planar imaging, performed using a GE D670 gamma-camera at 6 time points with whole body and SPECT/CT imaging for critical organ dosimetry. **Results** 15 patients have been treated, with 36 fractions administered. Mean age was 6.2 years (range 1–16 yrs). 7

patients received 4 fractions of treatment, 1 patient received 2 fractions of treatment and 7 patients received a single fraction. Patients who received a single fraction of treatment were contraindicated for additional fractions due to disease progression and not toxicity. All patients receiving more than one fraction were escalated to 100MBq/Kg. 14/15 patients had imaging data appropriate for accurate dosimetry calculations. Mean whole body absorbed dose was 0.28Gy/fraction (range 0.19–0.38). Mean kidney dose was 4.02Gy/fraction (range 1.5–6.7). For those seven patients completing 4 fractions of treatments, mean cumulative kidney dose was 16.7Gy (range 12.0–22.6). Monitoring of GFR during and after treatment demonstrated no renal toxicity, although long-term data is yet to be obtained. **Conclusions** Treatment was well tolerated. No children exhibited renal toxicity and therefore PRRT in children with neuroblastoma is a safe therapeutic technique. As the cumulative kidney dose ranged from $< 50\%$ to $< 100\%$ of the kidney dose constraint of 23Gy, it is possible that personalised dose escalation based on the actual renal dose received might lead to better oncological outcomes.

EPW46

Can PET/CT ^{68}Ga -DOTA-peptides uptake predict the absorbed dose in peptide receptor radionuclide therapy (PRRT)?

A. Filice¹, F. Fioroni², E. Grassi², A. Tartaglione¹, A. Fraternali¹, M. Asti¹, C. Carnaghi³, N. Fazio⁴, A. Frasoldati⁵, A. Versari¹; ¹Nuclear Medicine Unit IRCCS-Arcispedale Santa Maria Nuova, Reggio Emilia, ITALY, ²Medical Physics Unit, IRCCS-Arcispedale Santa Maria Nuova, Reggio Emilia, ITALY, ³Medical Oncology Unit Humanitas Cancer Center, Milano, ITALY, ⁴Unit of Gastrointestinal Medical Oncology and Neuroendocrine Tumors, European Institute of Oncology, Milano, ITALY, ⁵Endocrinology Unit IRCCS-Arcispedale Santa Maria Nuova, Reggio Emilia, ITALY.

Purpose: it is well known that dosimetry was until now focused to normal organs in order to limit side effects while the absorbed dose-tumor response relationship has not been settled. However, knowledge about this relationship it's becoming crucial for a better understanding of PRRT. The purpose of this work is to demonstrate whether it is possible to predict absorbed dose on the basis of PET/CT ^{68}Ga -DOTATOC uptake. **Methods:** in our center a prospective PRRT clinical trial is ongoing. The dosimetric evaluation is performed at the first cycle of treatment. From 03/2014 to 11/2014, the first 20 consecutive patients were enrolled. We evaluated 50 lesions in the first 20 patients: liver (38), lymph node (7), and bone (5) and assessed the relationship between the PET/CT ^{68}Ga -DOTATOC baseline uptake, in terms of SUV max, and the absorbed dose (Gy) at the end of the treatment. **Results:** in our experience highest SUV max doesn't match always with highest absorbed dose. In a high number of lesions in the liver the absorbed dose is greater than SUV max, while in the lymph node and bone lesions SUV max is often greater than absorbed dose, perhaps because the kinetics in this tissues is more rapid than in the hepatic lesions. The mean values for absorbed dose (Gy) and SUV max in all lesions were respectively 132 (range 1–522) and 36 (range 6–89). If we consider the lesions according to the different localization, the mean absorbed dose values (Gy) are: liver 179 (range 24–522), lymph node 54 (range 4–270) and bone 38 (range 1–116). Mean SUV max values are respectively: liver 36 (range 8–89), lymph node 34 (range 10–89) and bone 37 (range 6–47). The mean kidney biological effective dose value (BED) was 26 Gy (range 11–48) and the tumour-to-kidney dose ratio was 5 (range 1–15). **Conclusion:** there is little attention to the relationship between uptake at PET/CT ^{68}Ga -DOTATOC baseline and absorbed dose but this is a very important aspect in PRRT because probably a better understanding of this relationship could give us the elements to be able to predict the therapeutic response. In our experience in a high number of liver lesions the absorbed dose is greater than SUV max while in the other tissues the data are more inhomogeneous. The kinetics of the radiopharmaceutical is important because the behavior is different in various tissues depending on many factors. More studies are needed to confirm these data.

E-PW6 – Tuesday, October 18, 2016, 08:30 - 09:30, e-Poster Area
e-Poster Walk 6 – Do.MoRe: Dosimetry (Best of Do.MoRe)

EPW47

Effective radiation dose estimate in volunteers recruited for renal transplant

I. Maamoun¹, M. Khalil²; ¹Intensive Care Unit (ICU), Faculty of Medicine, Cairo University Hospitals, Cairo, EGYPT, ²Department of Physics (Medical Biophysics), Faculty of Science, Helwan University, Cairo, EGYPT.

Aim: One of the categories that receive little attention in estimating radiation doses are kidney donor volunteers. They need comprehensive diagnostic examinations before clinical decision is made. Among those diagnostic testing are renal scintigraphy, CT renal angiography, and x-ray imaging. The aim of this work was to elaborate on the average effective dose received by this particular subjects group. **Methods:** Twenty patients (12 M and 8 F) who were considered potential kidney donors were retrospectively analyzed. All patients had undergone renal scan using Tc-99m labelled DTPA, CT renal angiography and planar x-ray imaging. DTPA scintigraphy was performed using an average dose of 3.1 ± 0.7 mCi. Scan parameters were 180 frames, 10 sec/frame and Lasix was co-injected with the tracer. The CT renal angiography protocol consisted of five phases namely non contrast phase, arterial phase, cortico-medullary phase, nephrographic phase and excretory phase. CT dose index (CTDIvol) and dose length product (DLP) were obtained from the scanning protocol performed for each patient. The scan length was determined using a scout image covering $400\text{mm} \pm 10\text{mm}$ in the abdominal and pelvis regions. CT scan was performed using 16 CT scanner, helical pitch of 24, detector collimation of $1.0 \text{ mm} \times 16$, slice thickness of 1.0 mm and $0.75 \text{ sec/rotation}$. The average mAs was 16386.8 ± 3140.7 and the average total scan time was 83.8 ± 17.0 sec. Contrast agent was injected before the arterial phase within 15-20 sec using 100-120ml of 350 mg/ml iodine solution. Planar x-ray image was taken at the end of the CT scan using 100-160 mAs at 70-80 kV tube voltage. All data were tabulated, descriptively summarized in terms mean \pm SD and statistically analysed. **Results.** On average, the effective dose measured due to renal scintigraphy was $0.53 \pm 0.03 \text{ mSv}$. However, a significant increase in effective dose calculations was revealed from CT angiography. The average CTDIvol was $203.7 \pm 32.5 \text{ mGy}$ and DLP calculations were $3268.3 \pm 604.3 \text{ Gy.cm}$. These measures resulted in a significantly higher effective dose of $49.0 \pm 9.0 \text{ mSv}$. Effective dose due to x-ray planar imaging was on average $0.7 \pm 0.2 \text{ mSv}$. **Conclusion:** Volunteer subjects who are recruited for donating kidneys are receiving a considerably high radiation effective dose. CT angiography is the potential player in this scenario and substantial efforts should be made toward dose reduction in clinical routine. Follow up of this patient category using nuclear or radiological imaging modalities would cause an incremental radiation burden. This will be further investigated in future studies.

EPW48

Simulation of ⁹⁰Y microspheres in Selective Internal Radiation Therapy (SIRT) reveals different heterogeneity profiles for glass and resin microspheres

J. Hemmingsson¹, J. Högberg², J. Svensson¹, J. Mölne¹, M. Rizell¹, P. Bernhardt¹; ¹The Sahlgrenska Academy at The University of Gothenburg, Gothenburg, SWEDEN, ²Department of Medical Physics, Linköping University Hospital, Linköping, SWEDEN.

Aim: Selective internal radiation therapy (SIRT) can supply normal tissue in the liver with radiation doses exceeding tolerance without causing toxicity, an effect possibly explained by microsphere clustering causing heterogeneity in the distribution. Using a simulation of microspheres transported through a simplified arterial structure, the aim of this study has been to

evaluate how the number of injected microspheres affect the dose distribution. **Materials and methods:** The simulation was based on observations in biopsies and autoradiographies from resected liver tissue receiving ⁹⁰Y-SIRT. Individual microspheres, with diameter and density from literature, were followed through a simplistic bifurcations model in which three parameters were introduced and optimised to obtain results consistent with observations: an artery coefficient of variation, a reduction parameter for the arterial diameter and a distribution volume parameter for the arterial tree. In the model the arterial diameter decreases for higher artery generations and the probability of microsphere clustering increases successively in the artery tree. After simulation a ⁹⁰Y dose kernel was applied to the 940 cm^3 sized 3D-matrix of microspheres and the dose distribution throughout the matrix was evaluated using varying resolutions and computing the coefficient of variation (CV). A smaller number of simulated microspheres (10^5) corresponds to the higher activity/sphere found in glass spheres while a larger number (10^7) resembles resin spheres. **Results:** As the number of microspheres increase from thousands to 10^6 the CV of the absorbed dose decrease from over 80 % to 32 % in a volume corresponding to a lobuli (2 mm^3) and at 10^6 microspheres a plateau was reached. The simulation was consistent with biopsy and autoradiography observations regarding the formation of clusters. A large majority of the clusters contain few microspheres and a minority of the clusters are significantly more numerous in microspheres. **Conclusion:** For the high microsphere concentrations used with resin microspheres the CV of the absorbed doses was constant (32 %) while for the lower microsphere concentrations used for glass spheres the CV varied between 90 % and 40 %. These results implies that small scale dosimetry for ⁹⁰Y-SIRT differs between resin and glass spheres.

EPW49

Improved dose-volume histograms for Y90-PET based dosimetry with partial volume effect and noise compensations by means of region sub-segmentation

M. Sanchez-Garcia¹, J. Strydhorst², H. Levillain¹, I. Gardin³, P. Buysse³, T. Carlier⁴, R. Lebtahi¹, I. Buvat², A. Dieudonné¹; ¹Department of Nuclear Medicine, Beaujon University Hospital, HUPNVS, APHP, INSERM 1149, Clichy, FRANCE, ²Imagerie Moléculaire In Vivo, IMIV, CEA, Inserm, CNRS, Univ. Paris-Sud, Université Paris Saclay, CEA-SHFJ, Orsay, FRANCE, ³Department of Nuclear Medicine, Henri Becquerel Cancer Center and Rouen University Hospital, & QuantIF – LITIS [EA 4108], Rouen, FRANCE, ⁴Department of Nuclear Medicine, University Hospital of Nantes, CRCNA-UMR 892 INSERM 6299 CNRS, Nantes, FRANCE.

Partial volume effects (PVE) and noise in ⁹⁰Y-PET images propagate in the absorbed dose calculation, producing biased dose-volume histograms (DVH). We propose a method to compensate for these effects. **Materials and methods:** The method consists in segmenting the region of interest (ROI) into sub-regions using super-voxels (SVs) defined by an eikonal region growing (ERG) (Buysse P *et al.* Image Vision Comput 2014). The SVs are generated on an image filtered using a median filter and are assumed to contain a homogeneous activity distribution to remove the noise. The optimal number of SVs n_{opt} is defined by the user. Geometric transfer matrix (GTM) inversion is then applied for PVE compensation. The absorbed dose computation is done on the corrected image. A realistic voxelized phantom was built using patient data. Lung and normal liver had uniform activity distribution. The liver lesion was divided into 4 sub regions, each with uniform activity. A 30-minute acquisition (5.4×10^{12} decays) with a Biograph mCT (Siemens) scanner was simulated using GATE and reconstructed using Siemens software (VG50, 2 iterations, 21 subsets, PSF modelling, TOF). Two median filters were tested: $2 \times 2 \times 2$ (med2) and $3 \times 3 \times 3$ (med3). For each, the calculation was performed with n_{opt} , the optimal number of SVs, $n_{opt}-1$ and $n_{opt}+1$. The resolution used for PVE compensation was a 3 mm FWHM. Theoretical, uncorrected and corrected DVHs were compared in terms of doses covering 5%, 20%, 50%, 80% and 95% of the lesion volume (D5, D20, D50, D80 and D95

respectively). **Results and discussion:** The uncorrected DVH deviated from the theoretical for D5, D20, D50, D80 and D95 by 15.2%, -7.5%, 7.1%, -20.7% and -38.1% respectively. With med2, $n_{opt}=5$. Using 4 SVs did not improve DVH estimates. Using 5 or 6 SVs resulted in a similar improvement with 5.7%, 0.4%, -6.7%, 9.1% and -10.2% errors. With med3 filter, $n_{opt}=4$. Using 3 SVs did not improve DVH estimates. For 4 and 5 SVs the results were improved similarly with 5.8%, 2.1%, -8.3%, -9.2% and -10.5% errors. These results show that the pre-filtering did not matter much when using the optimal number of SVs. Yet, for a given filter, the accuracy of the dose estimates depended on the number of SVs. **Conclusion:** We propose an approach to improve the DVH estimates in ^{90}Y -PET dosimetry, based on ROI segmentation using super-voxels and region-based PVE compensation.

EPW50

DNA Damage in Blood Lymphocytes after Personalised Peptide Receptor Radionuclide Therapy with High Activities

U. Eberlein¹, R. A. Werner¹, C. Lapa¹, C. Bluemel¹, M. Peper², A. K. Buck¹, H. Scherthan², M. Lassmann¹; ¹University of Würzburg, Department of Nuclear Medicine, Würzburg, GERMANY, ²Bundeswehr Institute of Radiobiology, Munich, GERMANY.

Objectives: Radiation-induced DNA double strand breaks (DSBs) cause, in their vicinity, the phosphorylation of the histone H2AX (then called γ -H2AX) and the accumulation of the 53BP1 protein that binds to and signals damaged chromatin at a DSB site. This leads to the formation of microscopically visible nuclear foci containing both markers, which thus mark radiation-induced DSBs. The aim of the study is to analyse the dose- and time-dependency of the DNA damage in blood lymphocytes in patients after a personalised high-activity ^{177}Lu -DOTATATE treatment. **Methods:** We investigated multiple blood samples of three patients up to 96h after peptide receptor radionuclide therapy (activity range: 14.4GBq-19.3GBq). The average frequencies of radiation-induced foci (RIF) containing both γ -H2AX and 53BP1 fluorescence were determined in the nuclei of two-colour immunostained γ -H2AX/53BP1 lymphocytes isolated from peripheral blood samples of patients before and after therapy. The foci containing both DSB markers were scored manually in a fluorescence microscope equipped with a red/green double-band-pass filter by an experienced observer. The individual background focus rate was determined in a sample taken prior to therapy. The results were compared to a previous patient study (Eberlein et al, EJNMMI 2015) and an in-vitro calibration curve (Eberlein et al, PlosOne 2015). **Results:** Blood samples of 3 patients receiving a personalised high activity therapy were evaluated for γ -H2AX and 53BP1. Compared to the standard therapy (7.7GBq) the absorbed dose to the blood after 48 h is higher (mean: 186mGy vs. 78mGy). In the first four hours after administration of the radiopharmaceutical there is a strong increase of the number of RIF/cell; the RIF/cell values are in accordance to the in-vitro calibration. The maximum foci numbers range from 0.8 RIF/cell to 1.1 RIF/cell. At $t=4$ h the mean standard therapy RIF/cell values normalised to the blood dose (0.019 RIF/cell/mGy) are higher than those of the high-activity patients (0.012 RIF/cell/mGy). 72 hours after application the patient who received the highest activity and the highest absorbed dose to the blood still shows increased levels of RIF/cell. For the two other patients the foci levels decrease similarly compared to the patients receiving a standard therapy (7.7GBq). **Conclusions:** This study provides a first RIF/cell analysis of Lu-DOTATATE patients receiving higher activities compared to the standard Lu-DOTATATE therapy. With the exception of the data of one patient at a late time-point the results are in accordance with our previous results.

EPW51

Effect of activity heterogeneity on the absorbed doses from Y-90 therapies

A. Divoli, J. Gear, I. Murray, G. Flux; Royal Marsden Foundation Trust, Sutton, UNITED KINGDOM.

Aim: Heterogeneous uptake is often observed in tumours treated with Y-90 therapies. A common uptake pattern observed in both PRRT and SIRT administrations is a ring of uptake, surrounding an inner section without activity. Generally, absorbed doses are calculated based on S-factors provided by OLINDA for spheres of various sizes. The aim of this work was to use Monte Carlo simulations to calculate the S-factors and the corresponding absorbed doses of typical heterogeneous tumours and to compare the results with those calculated when heterogeneity is ignored. **Material and methods:** Spherical “shell” lesions were simulated using two concentric spheres. Input files for the MCNPX2.5.0 Monte Carlo code were created with spherical lesions 40 and 50 mm in diameter with inner spheres of 20, 25, 30 and 40mm and lesion densities of 1.05g/cm³. The spectrum of Y-90 with all emissions was incorporated into the code as given by MIRD. Lesion geometries were voxelised into 0.5 mm bins and energy depositions at each voxel were recorded enabling the production of dose maps, dose volume histograms and segment specific S-factors. Typical cumulated activity values from patient data were used to translate the results into absorbed doses. **Results:** S-factors were generated for active areas of the lesion, non-active and for the whole lesion. As the percentage of non-active to active tumour increased a decrease in segment S-factor was observed. This decrease resulted in an increasing difference (10 - 50%) from the uniform model S-factors given by Olinda for the equivalent volume. This difference can be attributed to the deviation of the shell segment from a spherical shape and more absorbed dose being deposited outside the active segment. The observed cross irradiation from the active outer shell to the cold inner was not insignificant (up to 85%) and varied according to the size of the inner region; the smaller the inner region the larger the cross dose. It is therefore important to determine if the dose to the lesion as a whole or just to the active part is to be reported. **Discussion:** The heterogeneity of lesion uptake can cause errors in absorbed dose of up to 50% if not correctly accounted for. Further work is planned to study segmental S values under a larger variety of geometries aiming to provide S-factor values for these structures.

EPW52

A successful Y-90-microspheres radioembolization of the spleen in a case of primary myelofibrosis splenomegaly

A. Fernandes¹, A. Oliveira¹, N. Silva², J. Pereira¹, P. Morgado³; ¹Nuclear Medicine Department - Hospital de São João, Porto, PORTUGAL, ²Radiology Department - Hospital de São João, Porto, PORTUGAL, ³Interventional Radiology Department - Hospital de São João, Porto, PORTUGAL.

Introduction: Primary myelofibrosis (PMF) is a rare clonal disorder originated from the neoplastic transformation of early hematopoietic stem cells (50 to 60% of the patients presenting the JAK2 V617F mutation). Common clinical manifestations include splenomegaly, severe anaemia and cytopenias. Radioembolization with Y-90-microspheres of liver tumours (primary or metastatic), via the hepatic arterial route, is a safe, effective, established treatment, based on the fact that hepatic tumours typically have arterial vascularization (whilst normal hepatic parenchyma depends on portal irrigation). Due to its good results and low toxicity, this approach is rapidly expanding throughout the Nuclear Medicine and the Interventional Radiology communities, with different applications being sought after - treatments directed at the spleen, lungs and kidneys have been published. There is no ideal option for treating severe, symptomatic splenomegaly. The decision to use Radioembolization in this case was to provide an option with less associated morbidity and mortality than the alternatives - splenectomy, JAK inhibitors and external radiation therapy. **Case report:** We report a successful case of radioembolization with Y-90-glass microspheres of the spleen, in a 63-year-old, Caucasian woman, with primary myelofibrosis (with the JAK2 V617F mutation). The patient was experiencing increasing abdominal discomfort and night sweats, associated with an enlarging splenomegaly (23 cm, cranio-caudal), as well as the need for repeated, but ineffective, platelet transfusions - at the time of

evaluation for radioembolization, her platelet counts were $<10 \times 10^9/L$. The treatment was well tolerated, with no adverse events reported from radiation exposure. Follow-up, 16 weeks after the treatment, revealed a significant reduction of the spleen volume (43%), and its clinical effectiveness, with increasing platelet counts, without the need for further transfusions. **Conclusion:** We propose that, in carefully selected patients with primary myelofibrosis, radioembolization may be a viable alternative for the treatment of splenomegaly. The successful clinical and radiological responses suggest that achieving the necessary absorbed dose in the spleen is technically feasible and safe.

EPW53

Effect of image noise, respiratory motion, and motion compensation on quantitative accuracy of 90Y PET/CT based 3D absorbed doses following 90Y-microsphere therapy

W. Siman¹, O. Mawlawi¹, J. Mikell¹, F. Mourtada², S. C. Kappadath¹; ¹UT MD Anderson Cancer Center, Houston, TX, UNITED STATES, ²Christiana Care Health System, Newark, DE, UNITED STATES.

Aim: The liver is subject to motion due to respiration. Typical 90Y PET acquisitions 10-30 min/bed following SIRT introduce respiratory motion blur of in vivo 90Y activity concentration (AC); AC is proportional to absorbed dose. Our aim is to quantify the effects of image noise and motion blur on 90Y PET/CT 3D absorbed-dose distributions using AC volume histogram (ACVH) metrics; ACxx is the minimum AC that covers xx% of the tumor volume. We also investigated the efficacy of motion compensation using quiescent-period gating (QPG) as a function of tumor size and motion amplitude. **Materials and Methods:** An IEC phantom with SBR of 9.6 was prepared using 18F (0.8 kBq/mL background) to simulate clinical 90Y PET/CT (600 kBq/mL background) such that 47 s/bed with 18F corresponded to 30 min/bed with 90Y. List-mode PET data (GE D690) was acquired for 300 s/bed (high-count dataset) when the phantom was static and subject to periodic 1D-motion that simulated respiration with amplitudes of 1cm, 2cm, 4cm. PET emissions were binned into 6 independent datasets of shorter durations 47s-to-8s (100%-to-17%) to assess the effect of image noise on ACVH. PET acquisitions during motion was gated in real-time (RPM, Varian Medical System) and sorted into multiple phases to assess the effect of motion and QPG on ACVH. Images were reconstructed using 3D-OSEM with TOF and PSF corrections. **Results:** Decreased scan times increased the apparent non-uniformity of tumor doses by increasing the dispersion of ACVH metrics; these effects were severe for tumors <17 mm. AC20-AC60 was less sensitive (errors $<10\%$) to decreased scan times compared to AC80-AC90. ACmean errors were $<10\%$ when scan time reduction was $>50\%$ (>15 min/bed) for tumors >17 mm. Respiratory motion decreased the observed AC and skewed ACVH distribution to lower values; with degree of severity that depended on motion amplitude and tumor diameter. AC20-AC80 for 37mm/17mm tumors decreased by -20%/-30% and -50%/-55% for motion amplitudes of 2cm and 4cm. QPG that used 40-50% of respiratory phase was effective for improving AC quantification; AC20-AC80 showed errors $<20\%$ for motion amplitudes <4 cm. **Conclusion:** Biases and non-uniformities in absorbed dose estimates were introduced by 90Y PET image noise and respiratory motion; mean dose errors $<10\%$ were possible only for >15 min/bed and tumors >17 mm; AC80-AC90 were more sensitive than AC30-AC70. QPG techniques using 40-50% of respiratory phase was successful at reducing errors. Research support: NIH/NCI R01 CA138986.

EPW54

Optimizing Re-188 SPECT/CT: quantitative imaging for image-based dosimetry

P. L. Esquinas Fernandez¹, C. F. Uribe², J. Tanguay¹, M. Gonzalez³, C. Rodríguez-Rodríguez¹, U. Häfeli¹, A. Celler¹; ¹University of British

Columbia, Vancouver, BC, CANADA, ²British Columbia Cancer Research Centre, Vancouver, BC, CANADA, ³Vancouver Coastal Health Authority, Vancouver, BC, CANADA.

AIM: ¹⁸⁸Re is a promising isotope for radionuclide therapies, including trans-arterial radioembolization (TARE). The accuracy of image-based dosimetry calculations for ¹⁸⁸Re therapies relies on the quantification of activity using SPECT/CT. Our aim was to 1) optimize collimator, energy-windows settings and quantitative ¹⁸⁸Re SPECT reconstruction, and 2) evaluate the accuracy of ¹⁸⁸Re image-based dosimetry estimates. The methodology developed in this study will be applied to dose calculations for 40 patients undergoing TARE with ¹⁸⁸Re. **MATERIALS AND METHODS:** Experiments were performed using SymbiaT (Siemens) SPECT/CT camera with Medium Energy (ME) and High Energy (HE) collimators. A thorax phantom (with lungs and spine) containing six spheres (2mL-20mL) and two bottles (34mL-196mL) filled with ¹⁸⁸Re (3.8 MBq/mL) was scanned with three configurations: (A) empty phantom, (B) filled with water and (C) filled with ¹⁸⁸Re solution with signal-to-background ratio ~ 7 . Images were reconstructed using OSEM with attenuation, triple-energy window (TEW) scatter, and resolution recovery corrections. TEW was investigated using two sets of scatter windows. The sources were segmented using 1% threshold (air and water) and 40% threshold (hot-water). Quantification accuracy was evaluated by the percent difference between the reconstructed and the true activities for each source. Using these activities and CT-based volumes, the average absorbed dose-rates (AADR) for the spheres and bottles were estimated using OLINDA. Additionally, the voxelized S-Value (VSV) dose-map was calculated and AADR was estimated using again CT-based volumes. These AADR were compared to the “truth” calculated using the digital version of our phantom. **RESULTS:** The mean accuracy of activity quantification in A and B configurations was 7% (range 0.7%-12.5%) for both collimators. Images obtained with the ME collimator, however, had to be corrected for high dead-time. The 40% threshold resulted in underestimation of the true activity by $>15\%$ for both collimators. The use of wide scatter windows resulted in decreased accuracy (12% on average). For hot-water-scans, OLINDA and VSV underestimated the true dose by 27% and 19%, respectively. The results were comparable for both collimators. **CONCLUSIONS:** Our study demonstrates that ¹⁸⁸Re images reconstructed with corrections are quantitatively accurate (5.4% accuracy in total phantom activity). However, organ/tumour segmentation remains a challenge. Both 40% threshold (widely used in clinical studies) and the CT-based segmentation result in large activity underestimations. For ¹⁸⁸Re, the problem is exacerbated by poor resolution of ME or HE collimators. Since these inaccuracies strongly affect dose estimations, more research effort should be directed to accurate segmentation of nuclear medicine images.

EPW55

Comparison of Y90 and Ho166 3D-dosimetry for SIRT with collapsed cone superposition

A. Dieudonné¹, M. Sanchez-Garcia¹, I. Gardin², A. Siebert³, V. Vilgrain³, R. Lebtahi¹; ¹Department of Nuclear Medicine, Beaujon Hospital, HUPNVS, APHP, INSERM 1149, Clichy, FRANCE, ²Department of Nuclear Medicine, Henri Becquerel Cancer Center and Rouen University, QuantIF – LITIS [EA 4108], Rouen, FRANCE, ³Department of Radiology, Beaujon Hospital, HUPNVS, APHP, Clichy, FRANCE.

¹⁶⁶Ho has been proposed as an alternative to ⁹⁰Y for selective internal radiation therapy (SIRT). Both radionuclides disintegrate through a beta decay: ⁹⁰Y ($E_{max}=2.28$ MeV, $\Delta=933$ keV/des, 64.1 h) and ¹⁶⁶Ho ($E=1.87$ MeV, $\Delta=665$ keV/des, 26.8h). Additionally, ¹⁶⁶Ho has a photon emission (80.5 keV, 6.7%) allowing for imaging. This paper aims at comparing both radionuclides in term of dosimetry using a collapsed cone

superposition (CCS) algorithm. **Methods:** CCS takes into account tissue density heterogeneities by scaling linearly the energy deposition according to the radiological distance (Sanchez-Garcia *et al.*, Phys Med Biol 2014, 2015). We compared ^{90}Y and ^{166}Ho dosimetry based on SPECT/CT data, acquired 30 min after injection of $^{99\text{m}}\text{Tc}$ -macroaggregated-albumin, of a patient eligible for a SIRT. The VOIs were the normal liver, the lesion and the lung. All the calculations were done through the software tool VoxelDose. The absorbed dose coefficient, d in $\text{Gy}\cdot\text{GBq}^{-1}$, was calculated at the voxel level. The comparison was done in terms of mean absorbed d_{mean} in each VOI, and dose-coefficient-volume histogram ($d\text{VH}$) indices d_{80} , d_{50} , and d_{20} , irradiating respectively 80, 50 and 20% of the VOI. Additionally, $d\text{VH}$ indices were normalised by d_{mean} . **Results:** d_{mean} [$\text{Gy}\cdot\text{GBq}^{-1}$] in the normal liver equals 5.1 for ^{90}Y and 1.6 for ^{166}Ho , while d_{80} and d_{50} [$\text{Gy}\cdot\text{GBq}^{-1}$] equal 0 for both radionuclides and d_{20} respectively 4.5 and 1.4. In the lesion, d_{mean} equals 62 for ^{90}Y and 20 for ^{166}Ho , while d_{20} , d_{50} and d_{80} -values are equal respectively to 85, 53, 30 and 27, 17, 9.4 for ^{90}Y and ^{166}Ho . In the lung, d_{mean} equals 15 for ^{90}Y and 5.0 for ^{166}Ho , while d_{20} , d_{50} and d_{80} -values are equal respectively to 23, 14, 5.6 and 7.9, 4.4, 1.6 for ^{90}Y and ^{166}Ho . For $d\text{VH}$ indices normalised to d_{mean} , results are in the same order of magnitude for both radionuclides, indeed for the lesion, d_{20}/d_{mean} , d_{50}/d_{mean} and d_{80}/d_{mean} -values equal respectively 1.4, 0.84, 0.49 for ^{90}Y and 1.4, 0.84 and 0.48 for ^{166}Ho . For the lung, the normalised indices equal 1.6, 0.92, 0.38 for ^{90}Y and 1.6, 0.90 and 0.32 for ^{166}Ho . **Conclusion:** This dosimetry comparison of ^{90}Y and ^{166}Ho using a collapsed cone superposition algorithm shows that the absorbed dose coefficient in $\text{Gy}\cdot\text{GBq}^{-1}$ is around 3 times greater for ^{90}Y than for ^{166}Ho , while normalised $d\text{VH}$ indices show similar dose coverage for a given mean absorbed dose of each radionuclide.

EPW56

Monte Carlo calculated single-cell S -values using a stochastic atomic relaxation model for accurate nuclear data of Auger electron-emitting radionuclides

N. Falzone¹, B. Q. Lee², J. M. Fernández-Varea³, A. E. Stuchbery², T. Kibedi², K. A. Vallis¹; ¹University of Oxford, Oxford, UNITED KINGDOM, ²Australian National University, Canberra, AUSTRALIA, ³Universitat de Barcelona, Barcelona, SPAIN.

AIM: Auger electron- (AE) emitting radionuclides could be exploited for therapeutic purposes due to the high local energy deposition by low-energy Auger (and Coster-Kronig) electrons or may deliver an unintentional mean absorbed dose burden when used as medical imaging agents. The emission spectra of AE emitting radionuclides are essential for dosimetric calculations to quantify the biological damage to the target. The aim of this study is to compare single-cell S -values derived from the BrIccEmis radiation spectra of 14 AE emitting radionuclides to the corresponding MIRD data. **MATERIALS AND METHODS:** The radiation spectra of ^{67}Ga , $^{80\text{m}}\text{Br}$, ^{89}Zr , ^{90}Nb , $^{99\text{m}}\text{Tc}$, ^{111}In , $^{117\text{m}}\text{Sn}$, ^{119}Sb , ^{123}I , ^{124}I , ^{125}I , ^{135}La , $^{195\text{m}}\text{Pt}$ and ^{201}Tl were taken from the unabridged nuclear decay data of the MIRD RADTABS program^[2] and also generated using the BrIccEmis code, which implements a stochastic model for the atomic relaxation assuming either an isolated atom or condensed-phase approach. Dose-point kernels (DPKs) were calculated using event-by-event simulations with the general-purpose Monte Carlo (MC) code PENELOPE^[3]. The simulated DPKs and appropriate geometric reduction factors were then employed to calculate cellular S -values. **RESULTS:** Auger yields from MIRD are consistently higher than those calculated with the BrIccEmis code. The methodology adopted by MIRD did not account for variations in orbital binding energies during atomic relaxation and thus overestimated the intensity of low-energy electrons. S -values from BrIccEmis relative to MIRD data are up to 18% and 10% smaller for isolated and condensed phase approximations, respectively. A decrease in S -values is prominent when the cell size is small and the source is assumed to be uniformly distributed in the cell nucleus, as the differences

between MIRD and BrIccEmis data are most noticeable for electrons with energies below 2 keV. **CONCLUSION:** Overestimation in the total AE energy output by MIRD leads to higher predicted energy deposition by AE emitting radionuclides, especially in the immediate vicinity of the decaying radionuclides. However, the impact of different AE spectra becomes less noticeable at larger volumes ($> 1 \mu\text{m}$), and does not translate into significant differences in S -values. ^[1] Lee B *et al.* Comp Math Meth Med 2012; 651475. ^[2] Eckerman KF and Endo A, MIRD Radionuclide Data and Decay Schemes 2008. ^[3] Salvat F, Fernández-Varea JM, Sempau J, eds. PENELOPE-2011 OECD Nuclear Energy Agency.

E-PW7 – Tuesday, October 18, 2016, 08:30 - 09:30, e-Poster Area

e-Poster Walk 7 – M2M: Preclinical Multimodality Imaging

EPW57

Brain serotonergic and dopaminergic changes in a hot flash model with & without risperidone treatment

W. S. Huang¹, H. M. Wu², K. W. Chang³, Y. Y. Kuo⁴, C. Y. Shiu^{5,6}; ¹Taipei Veterans General Hospital, Department of Nuclear Medicine, Taipei, TAIWAN, ²Changhua Christian Hospital, Department of Neurology, Changhua, TAIWAN, ³Institute of Nuclear Energy Research (INER), Taoyuan, TAIWAN, ⁴National Defense Medical Center, Graduate Institute of Medical Sciences, Taipei, TAIWAN, ⁵National Taiwan University Hospital, PET Center, Department of Nuclear Medicine, Taipei, TAIWAN, ⁶National Taiwan University, Molecular Imaging Center, Taipei, TAIWAN.

Introduction: Hot flash remains a major problem worldwide affecting menopausal women that is thought to be related to central neurotransmitter derangement. This study observed brain serotonergic and dopaminergic changes in a hot flash model and its effects on risperidone, an antipsychotic medication using nuclear neuroimaging modalities. **Methods:** Home-made ^{18}F -Alterserin and ^{123}I -Epididone were applied to evaluate functional changes of central 5-HT_{2A} (HT_{2A}) and dopamine receptor-2 (D2). A hot flash rat model was created by ovariectomy (n=5) [Khajuria, 2012]. Sham operation group served as the controls (n=5). Imaging was performed using NanoPET (^{18}F -Alterserin, 37 MBq; dynamic for 60 min) or NanoSPECT (^{123}I -Epididone, 185 MBq; 30-60 min post-injection) with or without risperidone pre-treatment (0.005mg/kg, 2 weeks prior to imaging). Rectal temperature (RT), uterine weight (UW), plasma estradiol (E2), and NO₂/3 (NOx) were also measured. **Results:** Significant changes of RT, UW, E2 and NOx were found in the OVX group compared to the controls. The changes can be restored, at least in part with risperidone pre-treatment. The brain HT_{2A} uptake was significantly decreased in OVX group compared to the controls and partially restored with risperidone treatment. No significant decrease of D2 uptake between OVX and control groups but significantly decreased D2 uptake was noted after risperidone treatment. **Conclusions:** The results provide insight into the interplay among menopausal hot flash, central neurotransmission and its therapeutic effect that could be reflected by nuclear receptor imaging modalities and served as a platform for drug screening. **Key Words:** Hot flush, ^{18}F -Alterserin, ^{123}I -Epididone, 5-HT_{2A} receptor, Dopamine-2 receptor.

EPW58

Evaluation of [^{18}F]BR420 and [^{18}F]BR351 as potential PET ligands for in vivo imaging of MMP-9 activity in an animal model of traumatic brain injury

S. Missault, M. Chomet, N. Vazquez, D. Thomae, S. Deleye, I. Blockx, P. Van Der Veken, A. Van Der Linden, L. wyffels, S. Staelens, S. Dedeurwaerdere; University of Antwerp, Wilrijk, BELGIUM.

Aim: Matrix metalloproteinase-9 (MMP-9), a zinc-dependent endopeptidase, is a modulator of the brain extracellular matrix. Increased expression and activity of MMP-9 has been reported after traumatic brain injury (TBI) and is associated with blood-brain barrier disruption and inflammation. Due to its involvement in synaptic plasticity, a role for MMP-9 in the development of posttraumatic epilepsy has been proposed. This study evaluated the potential of radiolabeled broad-spectrum MMP inhibitors [^{18}F]BR420 and [^{18}F]BR351 for *in vivo* visualisation of MMP-9 after TBI. **Methods:** Adolescent male Sprague-Dawley (SD) rats were subjected to either Controlled Cortical Impact (CCI) injury over the left parietal cortex (impact depth: 2.5mm, velocity: 4m/s, dwell time: 500ms; n=10) or sham injury (craniotomy only; n=10). Metabolite studies were performed for both [^{18}F]BR420 (IC_{50} = 7nM) and [^{18}F]BR351 (IC_{50} = 50nM) in healthy rats sacrificed at 5min and 1h post-intravenous (iv) tracer injection (35.2±0.3MBq; n=3/time point). Plasma and brain were analysed by reversed-phase HPLC and collected fractions were counted in an automated γ -counter. CCI and sham-operated rats were subjected to T_2 -weighted MR imaging, followed by 60min dynamic PET-CT imaging at 7d post-injury. Rats were injected iv with either [^{18}F]BR420 (24.9±3.7MBq; n=7/group) or [^{18}F]BR351 (37.1±0.7MBq; n=3/group). After scanning, brains were resected, counted and processed for *ex vivo* autoradiography. Tracer uptake in different brain regions was quantified by region of interest (ROI) analysis using PMOD software and expressed as Standardised Uptake Values (SUV). **Results:** In plasma, [^{18}F]BR420 proved to be more stable than [^{18}F]BR351 (50.3±15.7% and 3.5±3.7% of intact tracer remaining 1h post injection (pi), respectively). However, both compounds presented a relatively fast metabolism in the brain with a polar brain penetrating metabolite ($\geq 40\%$) already present for both tracers 5min pi. Furthermore, at 1h pi, only 11.4±0.3% and 6.1±4.1% of intact [^{18}F]BR420 and [^{18}F]BR351 were measured. However, due to low brain extraction yields (respectively 43% and 46%) those results might be misinterpreted. PET imaging revealed no difference in [^{18}F]BR420 or [^{18}F]BR351 uptake at the lesion site, in perilesional cortex, ipsilateral hippocampus, contralateral cortex and contralateral hippocampus between CCI- and sham-injured rats. Brain uptake was 0.069±0.012 %ID/g and 0.055±0.002 %ID/g for [^{18}F]BR420 and [^{18}F]BR351 respectively. *Ex vivo* autoradiography revealed a homogeneous tracer distribution throughout the brain. **Conclusion:** Studies are ongoing to confirm the increase of MMP-9 at this time point in our model. Due to the rather fast metabolism of these tracers, it seems unlikely that they will be suited for *in vivo* brain imaging of MMP-9.

EPW59

Preclinical validation of synthetic peptide p5 plus 14 as a multi-platform molecular imaging agent for systemic amyloidosis

S. J. Kennel¹, A. Williams¹, E. B. Martin¹, T. Richey¹, A. Stuckey¹, S. Macy¹, X. Cheng², J. S. Wall¹; ¹UT GSM, Knoxville, TN, UNITED STATES, ²Oak Ridge National Laboratory, Oak Ridge, TN, UNITED STATES.

Background: Amyloid is comprised principally of protein fibrils and hypersulfated heparan sulfate proteoglycans. The fibrils can be of about 30 different proteins, but the most common are immunoglobulin light chain, transthyretin or serum amyloid protein. Systemic amyloid diseases are rare (~4,000 new cases per year in the US); thus, routine diagnosis is challenging resulting in delayed treatment and in high morbidity and mortality rates. At present, there are no routine clinical methods for imaging amyloid in these patients in the US. The glycosaminoglycans ubiquitously present in amyloid have a high degree of heparin-like hypersulfation. We have identified the heparin-reactive synthetic peptide, p5+14, as a potential amyloid-specific amyloid imaging agent. We present *in vivo* and *in vitro* preclinical data demonstrating the efficacy of ^{125}I - and $^{99\text{m}}\text{Tc}$ -labeled peptide p5+14 as an amyloid targeting agent. **Methods:** Peptide p5+14 was labeled with iodine-125 or biotin using

standard procedures. Technetium-99m labeling was achieved by reduction with SnCl_2 . The reactivity of ^{125}I - and $^{99\text{m}}\text{Tc}$ -p5+14 with amyloid was demonstrated in a pull-down assay. Binding to amyloid in formalin-fixed tissue sections was evidenced using biotinylated p5+14 or by addition of ^{125}I -p5+14 followed by microautoradiography. Specific colocalization of ^{125}I - and $^{99\text{m}}\text{Tc}$ -labeled peptide with amyloid *in vivo* was demonstrated in a mouse model of systemic inflammation-associated amyloidosis by using SPECT imaging and tissue radioactivity biodistribution. **Results:** Peptide p5+14 was shown by histochemistry and autoradiographic staining of patient tissue samples to react specifically with human amyloid deposits. In the solution phase pull-down assay, ^{125}I - and $^{99\text{m}}\text{Tc}$ -p5+14 bound synthetic fibrils, composed of distinct precursor proteins, as well as human amyloid extracts with high efficiency. Using small animal SPECT imaging, biodistribution measurements and microautoradiography we showed specific retention of radiolabeled peptide in amyloid affected organs, *in vivo*, as early as 1 h and as late as 72 h post-injection. Biodistribution data documented accumulation of ~10% injected dose per gram in the liver, spleen, and pancreas, sites of major amyloid deposition. In healthy, wild type mice the peptide was rapidly cleared via renal excretion with a whole body half-life of 1.5 h. Colocalization of the ^{125}I -labeled peptide with amyloid was documented using microautoradiography and Congo red staining. **Conclusion:** These studies demonstrate the reactivity of peptide p5+14 with numerous forms of human and murine amyloid. Given the specific localization of this radiotracer with visceral amyloid we have applied for support through the NHLBI/NIH to perform a first in man Phase 1 PET/CT imaging trial.

EPW60

Does early distribution of ^{18}F -FMISO reflect tumoral blood flow? Comparison study with quantitative ^{15}O -CO₂ gas inhalation PET

T. Watabe, Y. Kanai, H. Ikeda, G. Horitsugi, K. Matsunaga, H. Kato, K. Isohashi, K. Abe, E. Shimosegawa, J. Hatazawa; Osaka University Graduate School Of Medicine, SUITA/OSAKA, JAPAN.

[Objectives] The relationship between perfusion and hypoxia in the tumor is controversial. Previous study reported flow limited delivery might affect the uptake of the hypoxic region. The purpose of this study was to evaluate the early distribution of ^{18}F -FMISO reflects the tumoral blood flow (TBF) and its relation to hypoxic region by comparing ^{18}F -FMISO and ^{15}O -gas PET. [Methods] Six male Fischer rats with subcutaneous xenograft of C6 glioma (body weight=220 ± 18 g) were investigated. Early distribution of ^{18}F -FMISO was evaluated by the 5min PET frame data after intravenous administration of ^{18}F -FMISO (67.5 ± 10.6 MBq) and hypoxic region was evaluated by late static images 3hrs post injection. The TBF was measured by quantitative steady state inhalation method of ^{15}O -CO₂ gas PET with arterial blood sampling. Multiple volumes of interest (2 mm diameter sphere) were placed on the co-registered ^{18}F -FMISO and TBF images. The correlation between early uptake of standardized uptake value of ^{18}F -FMISO (eFMISO-SUV) and TBF were compared by Spearman's test and cluster analysis, in which VOIs were classified by global or lesional threshold of each median value of eFMISO-SUV and TBF. In the group analysis, VOI values were divided into two subgroups of non-hypoxic region (less than 1.0 in late ^{18}F -FMISO SUV) and hypoxic region (more than 1.0), in which the threshold was defined based on the background muscle uptake. [Results] Total 12 tumor lesions were evaluated. Mean value of eFMISO-SUV and TBF were 1.22 ± 0.43 and 44.9 ± 27.5 (ml/100ml/min) in the non-hypoxic region, and 0.96 ± 0.27 and 31.5 ± 17.0 in the hypoxic region, respectively. There was a significant positive correlation between eFMISO-SUV and TBF ($r=0.552$, $p<0.01$) in the global analysis. In the lesional analysis, 9 of 12 lesions also showed a significant positive correlation ($r=0.50 \pm 0.12$, $p<0.01$). Cluster analysis revealed regions with high eFMISO-SUV and high TBF were dominant in the non-hypoxic region (53.4 ± 38.6% and 33.5 ± 12.2%) and regions with low eFMISO-SUV

and low TBF were dominant in the hypoxic region ($35.9 \pm 26.3\%$ and $39.2 \pm 8.4\%$) using global and lesional threshold, respectively. [Conclusions] This study demonstrated significant positive correlation between eFMISO-SUV and the TBF. Cluster analysis revealed regions with low TBF with low eFMISO-SUV were dominant in the hypoxic region, indicating negative correlation between hypoxia and perfusion. Early distribution of ^{18}F -FMISO reflects TBF in the C6 glioma, suggesting the feasibility of dynamic ^{18}F -FMISO PET for perfusion imaging.

EPW61

Evaluation of whole-body biodistribution of ^{89}Zr -labeled antibodies in cynomolgus macaque with PET

T. Sasaki¹, S. Kimura², A. Noda², Y. Murakami², F. Takenaka¹, S. Miyoshi², E. Matsuura¹; ¹Okayama university, Okayama, JAPAN, ²Astellas Pharma Inc, Tukuba, JAPAN.

OBJECTIVES: To develop therapeutic antibodies, a set of pre-clinical pharmacokinetic studies in non-human primates (NHPs) is required due to their difficulty for extrapolating ADME data with non-primates. In the present study, we aimed pharmacokinetic evaluations of ^{89}Zr -labeled human irrelevant IgG and its metabolites, as with prior confirmed their non-specific/physiological accumulation in healthy NHPs. **METHODS:** Human IgG was conjugated to deferoxamine (DFO) and labeled with ^{89}Zr . The radiochemical purity was determined by size exclusion high performance liquid chromatography and thin-layer chromatography. Healthy cynomolgus macaques were injected with 9-16 MBq of ^{89}Zr -IgG; PET/CT images were acquired at 0, 1, 3, 6, and 10 days after the IgG injection and plasma was timely collected. We also analyzed with shortened antibody valiant, ^{89}Zr -Fab, in addition to ^{89}Zr -DFO and ^{89}Zr -oxalate as metabolites from ^{89}Zr -IgG. Regions of interest were drawn on organs, i.e., the heart, liver, spleen, kidneys, vertebral body, and muscles. **RESULTS:** The SUV in heart, vertebral body and muscle was decreased, depending on ^{89}Zr concentration in the circulation. Whereas the accumulation of radioactivity increased over time in kidneys and liver. Autoradiograph of renal sections indicated that most of radioactivity accumulated in the renal cortex. In addition, relatively high accumulation in kidney was also observed in ^{89}Zr -Fab injected macaques, and its renal autoradiograph showed the similar tendency to that of ^{89}Zr -IgG. Meanwhile, ^{89}Zr -DFO was rapidly excreted into urine, and ^{89}Zr -oxalate highly accumulated in epiphysis of long bone and vertebral body. Taken together, these data demonstrated that IgG itself and/or its metabolites physiologically accumulated in kidney and liver, although ^{89}Zr -DFO or ^{89}Zr metal did not accumulate in these organs. **CONCLUSION:** We demonstrated that the distribution kinetics of human IgG and its metabolites in NHPs. This preclinical pharmacokinetic study is of great significance for determining the basic distribution of ^{89}Zr -IgG using PET technique.

EPW62

Imaging p53 in Pancreatic Ductal Adenocarcinoma (PDAC)

S. Koustoulidou, J. C. Knight, V. Kersemans, E. O'Neill, B. Cornelissen; Department of Oncology, University of Oxford, Oxford, UNITED KINGDOM.

Aim: Pancreatic ductal adenocarcinoma (PDAC) is one of the most lethal tumours in the UK with a five-year survival rate of merely 3%. PDAC is characterised by a complex mutational landscape with four genes being the most prevalent: KRAS, TP53, CDKN2A/p16, and SMAD4/DPC4. Mutations of the p53 tumour suppressor, described as the “guardian of the genome”, appear at approximately 60% in the later stage PDAC development, which showed strong correlation with progression to invasive carcinoma characterised by severe dysplasia. The main treatment for PDAC remains, to date, surgical resection of the primary tumour.

However, the outcomes remain poor, mainly due to the lack of diagnostic biomarkers for early detection, patient staging, prognosis, and therapy evaluation. Previously, we demonstrated non-invasive imaging of intranuclear targets [1], using radioimmunoconjugates coupled to cell penetrating peptides with nuclear localisation sequence. The aim of this study is to develop a p53 imaging biomarker suitable for diagnosis and patient stratification. **Materials and Methods:** Anti-p53 antibodies were evaluated *in vitro*, using a panel of cell lines derived from a genetically engineered mouse model of PDAC (KPC), with high levels of mutated p53, confirmed by western blot, flow cytometry and immunofluorescence assays. The mouse monoclonal p53 (IC12) antibody, which binds to all forms of p53, was chosen for further *in vivo* experiments. IC12 antibodies or non-specific mouse-IgG1 control antibodies were modified by the addition of pSCN-benzyl-DTPA to allow labelling with ^{111}In . The cell penetrating peptide TAT was then conjugated to the antibody to enable nuclear translocation. After *in vitro* testing, the compounds were intravenously administered to mice bearing subcutaneous allografts of the KPC-derived B8484 cell line. SPECT/CT imaging was performed 24, 48, and 72 h post injection. **Results:** *In vitro* assays confirmed the specificity of the selected antibodies. Radiolabelling yields of ^{111}In -DTPA-p53 (IC12)-TAT and the isotype control ^{111}In -DTPA-mIgG1-TAT were determined as >99% by iTLC. *Ex vivo* biodistribution analysis, performed after the last scan, revealed significantly higher radioactivity uptake in p53-expressing tumours of ^{111}In -DTPA-p53 (IC12)-TAT (7.1 ± 3.0 %ID/g) over ^{111}In -DTPA-mIgG1-TAT controls (4.9 ± 1.4 %ID/g; $p < 0.05$), confirming the ability to image p53 *in vivo*. **Conclusions:** Our findings establish the proof of principle for a non-invasive p53-expression imaging method for tumours. Even though further research is needed, this method could have major significance for cancer patient management. 1. Cornelissen, B. *et al* (2011) Imaging DNA damage in vivo using gammaH2AX-targeted immunoconjugates, *Cancer research*, Vol. 71: 4539-49.

EPW63

Imaging of pancreatic tumours in mice using radiolabelled anti-Claudin4 antibodies

M. Mosley, J. C. Knight, S. Koustoulidou, B. Cornelissen; Oxford University, Oxford, UNITED KINGDOM.

Aim: Survival rates for pancreatic cancer patients, especially pancreatic ductal adenocarcinoma (PDAC) are particularly low, in large part because of late diagnosis and consequently untreatable metastatic disease. Identification of specific pancreatic tumour markers and the development of appropriate imaging tools provide hope for ameliorating the survival of these patients via early diagnosis and treatment. Claudin4 is increasingly expressed during early during tumour formation in PDAC, the most common type of pancreatic cancer (1). The aim of this study was to use an ^{111}In -labelled anti-Claudin4 antibody for SPECT imaging of a mouse model of pancreatic cancer. **Materials and Methods:** Claudin4-expressing PANC-1 cells (human PDAC), and Claudin4-negative HT1080 cells (human fibrosarcoma) were grown as subcutaneous xenografts in Balb/c nu/nu mice. A mouse monoclonal antibody recognizing an external epitope of human Claudin-4 (clone MAB4219) was conjugated to p-SCN-Bn-DTPA prior to labelling with ^{111}In (In). An isotype-matched mouse IgG (mIgG) was treated similarly and used as a negative control. Imaging agents (5 μg , 5 MBq) were injected intravenously and mice were imaged using SPECT/CT at 24, 48 and 72 hours post injection. After imaging, mice were sacrificed and selected tissues were removed, and the amount of ^{111}In in each tissue was measured using an automated gamma counter. Uptake was expressed as the percentage injected dose per gram of tissue (%ID/g). The xenograft tissue was then cryo-sectioned and its radio-label count monitored by autoradiography. **Results:** SPECT imaging of mice bearing Claudin4-positive PANC-1 xenografts showed high uptake in the xenograft after administration of ^{111}In -anti-Claudin4 (14.3 ± 2.6 %ID/g at 72 h post injection), compared to ^{111}In -mIgG (6.3

± 0.8 %ID/g; $p < 0.01$) or Claudin4-negative HT1080 xenografts (4.3 ± 3.0 %ID/g; $p = 0.001$). The PANC-1 xenograft sections from mice injected with ^{111}In -anti-Claudin4 antibody showed strong signal using autoradiography, whereas xenografts removed from mice injected with control ^{111}In -mIgG did not. In a separate study, using a genetically engineered KPC mouse (a mouse model of KRAS- and p53-mutation induced PDAC), SPECT/CT imaging after administration of ^{111}In -anti-Claudin4 antibody also showed high uptake in the tumour, whose location was confirmed by FDG-PET/MRI. **Conclusions:** This study shows the potential use of ^{111}In -anti-Claudin4 antibodies as an imaging tool for the timely diagnosis of pancreatic cancer. **I.** Mosley M, Knight J, Neesse A, et al. Claudin-4 SPECT Imaging Allows Detection of Aplastic Lesions in a Mouse Model of Breast Cancer. *J Nucl Med.* 2015;56:745-751.

EPW64

PET/MRI imaging of Aminopeptidase N (APN/CD13) expression of experimental hepatocellular carcinoma using ^{68}Ga -NOTA-c(NGR)

A. Kis¹, K. N. Enyedi², A. Farkas³, G. Nagy⁴, I. Garai^{1,4}, P. Kertai⁵, G. Mezö², I. Kertész¹, **G. Trencsényi**^{1,4}; ¹University of Debrecen, Department of Nuclear Medicine, Debrecen, HUNGARY, ²MTA-ELTE, Research Group of Peptide Chemistry, Budapest, HUNGARY, ³University of Debrecen, Department of Urology, Debrecen, HUNGARY, ⁴Scanomed Ltd., Debrecen, HUNGARY, ⁵University of Debrecen, Department of Preventive Medicine, Debrecen, HUNGARY.

Purpose: Aminopeptidase N (APN/CD13) plays an important role in neoangiogenic process. Our previous studies have already shown that ^{68}Ga -labeled asparagine-glycine-arginine (NGR) peptides specifically bind to APN/CD13 expressing mesoblastic nephroma (Ne/De) tumors in rats. The aim of this study was to investigate the APN/CD13 specificity of ^{68}Ga -NOTA-c(NGR) in chemically induced hepatocellular carcinoma (He/De) tumor models. **Methods:** c[KNGRE]-NH₂ peptide analogue was labeled with Ga-68-NOTA. He/De hepatocellular carcinoma cells were used for the induction of heterotopic transplanted (subcutaneously and under the left kidney capsule) tumor models in Fischer-344 rats (n=10). Ex vivo biodistribution studies and whole body PET/MRI (nanoScan PET/MRI, Mediso Ltd, Hungary) scans were performed 90 min after intravenous injection of 6.9 ± 0.2 MBq ^{68}Ga -NOTA-c(NGR) and two weeks after tumor cell implantation. The imaging of neoangiogenic process with ^{68}Ga -NOTA-c(NGR) was compared with $\alpha_v\beta_3$ integrin selective ^{68}Ga -NODAGA-[c(RGD)]₂ tracer. Aminopeptidase N receptor expression of primary He/De tumors was verified by western blot analysis. **Results:** ^{68}Ga -NOTA-c(NGR) was produced with high specific activity (5.52 ± 0.55 GBq/ μmol) and radiochemical purity (95% \leq). Biodistribution studies with ^{68}Ga -NOTA-c(NGR) showed lower uptake in abdominal organs than using ^{68}Ga -NODAGA-[c(RGD)]₂. After the quantitative analysis of PET/MRI images we found that ^{68}Ga -NOTA-c(NGR) accumulation in He/De tumors (SUVmean: 1.8 ± 0.2 , Tumor/Muscle ratio: 13.43 ± 2.1) was significantly ($p \leq 0,05$) higher than the ^{68}Ga -NODAGA-[c(RGD)]₂ accumulation (SUVmean: 0.7 ± 0.2 , Tumor/Muscle ratio: 5.52 ± 0.47) in the same tumor. **Conclusions:** In our preclinical studies ^{68}Ga -NOTA-c(NGR) showed specific binding to the APN/CD13 positive He/De tumors. Therefore, ^{68}Ga -NOTA-c(NGR) is a suitable tracer for the detection of APN/CD13 positive hepatocellular carcinoma tumors in vivo. This project was supported by the János Bolyai Research Scholarship of the Hungarian Academy of Sciences.

EPW65

Imaging EGFR In Head and Neck Cancer: Useful Prognostic and Treatment Monitoring Tool?

T. A. Burley, C. D. Martins, C. Da Pieve, L. Allott, R. Smith, D. M. Ciobota, G. Smith, K. Harrington, G. Kramer-Marek; Institute of Cancer Research, London, UNITED KINGDOM.

Aims: The human epidermal growth factor receptor 1 (HER1/EGFR) is targeted by a growing number of inhibitors. However, these drugs have shown limited success in the clinic so far, most likely due to the lack of a reliable method for patient stratification. Information about the potential biomarker status is routinely obtained *ex vivo* from biopsy specimens. However, receptor expression may be heterogeneous within and between tumours in the same patient. Therefore, an EGFR-targeted imaging biomarker could become an important tool measuring the receptor expression *in vivo* across the entire disease burden and help monitor receptor changes in response to treatment intervention. **Materials and Methods:** The ^{89}Zr was conjugated to the Z_{EGFR:03115}Affibody using the chelator desferrioxamine (DFO). The specificity of the radiotracer *in vivo* was investigated in mice bearing subcutaneous HNSCC and breast cancer tumours with varying EGFR expression CAL27(+++), DT562(++) and MCF7(+). Mice were injected with 100 μl (1.3-3.6MBq, 1-2 μg) of ^{89}Zr -Z_{EGFR:03115}Affibody and spiked with unlabelled Affibody. Biodistribution was undertaken 3, 24 and 48hr post tracer administration, the radioactivity within the organs was measured using a γ -counter. The *in vivo* imaging profile of the optimum dose of ^{89}Zr -Z_{EGFR:03115}Affibody was evaluated by PET at 3, 24 and 48hr post tracer injection. The EGFR expression and distribution of the tracer was assessed *ex vivo* by immunohistochemistry (IHC), Western blot and autoradiography. The tumour heterogeneity was further explored using texture analysis. To downregulate the EGFR level, treatment with AU922 was performed on CAL27 and DT562 cells *in vitro* and changes in receptor expression were monitored by FACS analysis using an Affibody conjugate. **Results:** *In vivo* studies demonstrated that the radiotracer can distinguish between the xenograft models with varying EGFR expression (CAL27 3.88 ± 0.18 %ID/g, DT562 2.42 ± 0.13 %ID/g and MCF7 1.67 ± 0.15 %ID/g) already 3hr post injection. Tracer was eliminated quickly from the blood and normal tissues, allowing high contrast images to be acquired (24hr T:B=2.5; T:M=16.0, 48hr T:B=9.34; T:M=13.56). A strong correlation was observed between PET analysis, *ex vivo* estimates of tracer concentration and the receptor expression in the tumour tissues. Additionally, texture analysis, which consisted of extracting first, second and higher order statistics of segmented tumours, allowed differentiation of tumours with varying receptor expression. Receptor downregulation due to AU922 treatment was confirmed by lower Affibody conjugate binding. **Conclusion:** ^{89}Zr -Z_{EGFR03115}Affibody can assess different levels of EGFR expression *in vivo* and has the potential to be used to stratify patients for treatment.

EPW66

Cardiac metabolic changes during doxorubicin treatment in mice

B. F. Bulten^{1,2}, M. Sollini³, R. Boni⁴, K. Massri⁴, L. de Geus-Oei⁵, H. W. M. van Laarhoven⁶, R. H. J. A. Slart⁷, P. A. Erba⁸; ¹Queen Beatrix Hospital, Winterswijk, NETHERLANDS, ²Department of Biomedical and Photonic Imaging, University of Twente, Enschede, NETHERLANDS, ³Humanitas University, Milan, ITALY, ⁴Department of Translational Research and New Technology, University of Pisa, Pisa, ITALY, ⁵Department of Radiology, Leiden University Medical Centre, Leiden, NETHERLANDS, ⁶Department of Medical Oncology, Amsterdam Medical Centre, Amsterdam, NETHERLANDS, ⁷Department of Nuclear Medicine and Molecular Imaging, University Medical Centre Groningen, Groningen, NETHERLANDS, ⁸Department of Translational Research and New Technology, University of Pisa, Pisa, NETHERLANDS.

Background: Although doxorubicin is a potent antineoplastic agent, it possesses distinct cardiotoxic attributes, of which the underlying pathologic mechanisms are not fully unraveled. It is important to elucidate the complex pathophysiology on a molecular level to allow early detection of cardiotoxicity and selection of prophylactic treatment strategies. **Methods:** The cardiac distribution of $^{99\text{m}}\text{Tc}$ -sestamibi, $^{99\text{m}}\text{Tc}$ -Annexin V, $^{99\text{m}}\text{Tc}$ -glucaric acid and ^{18}F -FDG was evaluated using a gammacounter

at baseline and after one, two, three or four cycles of 15 mg/kg DOX in healthy male BALB/c mice and controls. In addition, cardiac expression of nonimaging markers (Bcl-2, Caspase-3 and -8, TUNEL, HIF-1 α , p53) was assessed by Western Blot or immunohistochemistry and mitochondrial membrane potential was measured. Results: A total of 200 mice (100 treated, 100 controls) was evaluated. All radiopharmaceuticals showed a significantly increased uptake compared to controls, with peak cardiac uptake after one (^{99m}Tc -Annexin V), two (^{99m}Tc -sestamibi), three (^{18}F -FDG) or four (^{99m}Tc -glucaric acid) cycles of DOX. Strong correlations ($p < 0.01$) were observed between ^{99m}Tc -Annexin V, Caspase 3 and 8 and TUNEL and between ^{18}F -FDG and p53 and HIF-1 α . Conclusions: A significantly increased uptake all radiopharmaceuticals compared to controls was observed, depicting the metabolic changes following DOX exposure. The peak of apoptosis, represented by ^{99m}Tc -Annexin V, Caspase 3, Caspase 8 and TUNEL occurred at low levels of anthracycline exposure, as well as ^{18}F -FDG uptake corresponding with HIF-1 α expression, suggesting an adaptive response after low levels anthracycline exposure. The upregulation of Bcl-2 is underlined as a potential target for prophylactic therapy in AIC.

E-PW8 – Tuesday, October 18, 2016, 08:30 - 09:30, e-Poster Area
e-Poster Walk 8 – Clinical Oncology: PET in Oncology

EPW67

Clinical significance of focal parotid lesions incidentally identified on FDG PET/CT studies- what should we do?

K. Nakatani¹, K. Kitaguchi², K. Yoshino¹, T. Koyama¹; ¹Kurashiki Central Hospital, Kurashiki, Okayama, JAPAN, ²Kobe City Medical Center General Hospital, Kobe, Hyogo, JAPAN.

AIM: Incidental parotid lesions with significant focal uptake are often experienced in patients undergoing whole-body FDG PET/CT studies. However, their appropriate clinical decisions remain unclear, as they usually do not undergo histological confirmation of these lesions. The aim of this retrospective study was to find out the role of FDG PET/CT in the management of such incidental parotid lesions by investigating the outcome. **PATIENTS AND METHODS:** Our daily clinical reports between May 2012 and April 2015 were retrospectively reviewed, and a total of 232 patients were identified who had incidental focal FDG uptake in the parotid glands on the PET/CT scans. Exclusion criteria were those who underwent the scans for the work-up examination of known head and neck tumors, lymphoma, hematological malignancies, and systemic diseases that affect the salivary glands (e.g. Sjögren syndrome, IgG4-related disease), since parotid lesions in those patients should not be considered as true ‘incidental’ finding, and those whose follow-up period was less than one year. The confirmed diagnosis was made by histopathology or by the results of follow-up examination after one year or more. **RESULTS:** 60 patients (average age: 71 \pm 9.6, male/female = 51/9) were enrolled as study population. Among 21 patients who underwent biopsy or surgical excision for the parotid lesions, 19 had benign results (14 with Warthin’s tumor, 3 with pleomorphic adenoma, one with schwannoma, and one with intraglandular lymphadenopathy) and 2 patients had malignant parotid tumors, both of which are parotid gland metastasis (one from male breast cancer and one from esophageal cancer) with concurrent extensive visceral involvement. The remaining 39 patients had the follow-up examination, and none of the scan showed enlargement of the lesions; three of the lesions showed spontaneous regression, and the remaining 36 showed no significant change. Tumor SUVmax was 6.6 and 3.4 for the malignant cases and 1.5-26.9 (average 6.8 \pm 4.5) for the benign cases. There was no case identified with primary parotid cancer in this study. **CONCLUSIONS:** Except for the cases with extensive visceral tumor involvement, it seems that the majority of parotid lesions incidentally identified on FDG PET/CT scans are benign, regardless of the intensity of uptake. Follow-up observations are usually considered to be sufficient in these cases as far as the patients do not have any specific symptoms.

EPW68

Lesion analysis in PERCIST: Are we doing it right?

A. BHOIL¹, B. Mittal², N. Singh²; ¹Regional Cancer Centre, Shimla, INDIA, ²Postgraduate Institute of Medical Education and Research, Chandigarh, INDIA.

Objective: The standardized uptake value (SUV) is the most frequently used semi quantitative PET imaging parameter for response evaluation but this approach predicts metabolic activity only of single lesion. Newer response evaluation parameters a) Tumor Lesion Glycolysis (TLG) incorporating metabolic aggression and lesion volume b) Whole Body Metabolic tumor burden (MTB_{WB}) have been recently explored for response in various tumors. An effort to evaluate and compare response with different semi quantitative parameters as SUV_{peak} and TLG in single lesion, multiple lesions and total metabolic tumor burden (MTB_{WB}) in advanced NSCLC patients was made and association with the OS and PFS was analysed **Method:** Prospective serial 18F-FDG-PET /CT imaging was performed in twenty three patients (M=14, F=9, mean age=57.6 year) with Stage IIIB-IV advanced NSCLC before start of therapy, at 21 days (early) and at 42 days (late) after oral EGFR TKI treatment for response evaluation. The quantitative PET parameters as standard uptake lean body mass SUL_{peak}, SUV_{peak}, and TLG were measured in the single hottest lesion, multiple lesion (max of five) lesion and metabolic tumor burden whole body (MTB_{WB}). The TLG was calculated by fixed automated threshold while metabolic tumor volume (MTV) was calculated by automated summing of the lesions glycolysis. The SUV_{peak}, TLG and metabolic tumor burden whole body MTB_{WB} for response was compared for early response (21 days) and for late response (42 days). The overall survival and progression free survival were analyzed with Kaplan Meier analysis and log rank test. **Result:** No change in patients’ response was seen when evaluated with single hottest lesion, multiple lesions and the whole body tumor load in form of summed tumor lesion glycolysis. Change in response between disease control and no disease control was seen between early imaging (21 days) (DC- 22, NDC-1) and late imaging (42 days) (DC-20, NDC-3) which remained unchanged when the lesion was measured in the terms of hottest lesion, five hottest lesion or the whole body tumor load. The overall survival (OS) in the early imaging was statistically significant (p= 0.049) compared to the late imaging (p=0.115). **Conclusion:** Single hottest lesion shows similar disease response classification and overall survival compared to the five hottest lesions and whole body tumor burden (WB_{MTB}). Late imaging offered no significant advantage compared to that of early imaging in disease response evaluation. Thus early response evaluation with single hottest lesion with SUV_{peak} should be considered in clinical work setting.

EPW69

Adrenal mass in cancer patients: Comparison of total lesion glycolysis and conventional PET/CT parameters in differentiating between benign and malignant lesions

S. GUNGOR¹, F. DEDE², O. KUPIK³, M. ARPA⁴, A. H. AKTAN⁵, S. ASA³, E. OZER⁶; ¹Istanbul Medeniyet University Faculty of Medicine, Department of Nuclear Medicine, ISTANBUL, TURKEY, ²Marmara University Faculty of Medicine, Department of Nuclear Medicine, ISTANBUL, TURKEY, ³Recep Tayyip Erdogan University Training and Research Hospital, Department of Nuclear Medicine, RIZE, TURKEY, ⁴Recep Tayyip Erdogan University Training and Research Hospital, Department of Biochemistry, RIZE, TURKEY, ⁵Recep Tayyip Erdogan University Training and Research Hospital, Department of Internal Medicine, RIZE, TURKEY, ⁶Recep Tayyip Erdogan University Training and Research Hospital, Department of General Surgery, RIZE, TURKEY.

Objective: Benign adrenal lesions frequently encountered in oncologic imaging make difficulties in the diagnosis of metastatic disease. F18 FDG PET/CT is becoming widely used for differentiating benign from malignant adrenal masses. The purpose of this study was to determine the diagnostic performance of total lesion glycolysis (TLG) measured by PET/CT for characterizing adrenal masses in patients with cancer compared with conventional PET/CT parameters. **Methods:** A total of 48 adrenal masses in 48 patients with cancer (35 men; mean [± SD] age, 64.94 ± 10.5 years, and 13 women; mean [± SD] age, 66.38 ± 16.5 years) were retrospectively evaluated with FDG PET/CT. Diagnosis of adrenal malignant lesions was based on interval growth or reduction after chemotherapy. An adrenal mass that remained unchanged for over 1 year was the standard used to diagnose adrenal benign lesions. Metabolic (SUVmax, SUVmean, and tumor/liver SUVmax ratio), morphologic (size, Hounsfield Units (HU), and CT volume), and metabolovolumetric (total lesion glycolysis (TLG): SUVmean x metabolic tumor volume) parameters were calculated for each adrenal lesion. PET/CT parameters were assessed by using *Student t-test* and receiving operating characteristic (ROC) analysis. **Results:** There was a statistically significant difference between benign and malignant lesions for PET/CT parameters. All malignant lesions demonstrated FDG activity higher than liver. Among the PET/CT parameters, SUVmax, SUVmean, and tumor/liver SUVmax ratio revealed the best result in distinguishing benign and malignant lesions. The cut-off score, sensitivity, and specificity for the PET/CT parameters were presented in Table 1. **Conclusion:** We found that metabolic parameters showed the best result in distinguishing in benign and malignant adrenal lesions. However, TLG proposed as a new parameter in the literature did not reach the expected performance due to the negative impact of malignant but small and benign but large lesions on metabolovolumetric index. **Table 1:** The cut-off score, sensitivity, and specificity for the PET/CT parameters

EPW70

DOTATOC uptake in typical vertebral hemangiomas

N. Testart^{1,2,3}, M. Gauthé¹, F. Montravers¹, V. Nataf¹, J. Talbot¹; ¹Hôpital Tenon AP-HP et Université P& Marie Curie, Paris, FRANCE, ²Complejo Hospitalario Universitario de Granada, Granada, SPAIN, ³IBS, Granada, SPAIN.

Bone hemangiomas are frequent benign vascular tumors, usually asymptomatic and most frequently localized in the spine. There are few documented case reports describing an increased uptake of ⁶⁸Ga labeled peptides (DOTA-TATE) PET/CT in bone hemangiomas. The aim of our study is to evaluate the DOTATOC uptake in typical vertebral bone hemangiomas, derived from a large series. **PATIENTS AND METHODS** We retrospectively reviewed all ⁶⁸Ga-DOTATOC PET/CTs of a prospective cohort of patients who were referred to our department because of a neuroendocrine tumor. A masked image analysis of all CT scans was firstly performed independently by 2 nuclear medicine physicians in order to select patients with typical vertebral hemangioma pattern on CT i.e. “Polka Dot” appearance. The PET studies of those selected patients were secondarily analyzed, to measure SUVmax of the lesions and compare them to a healthy vertebra. A 1 cm diameter region of interest (ROI) in the liver right lobe was manually drawn to calculate the SUVmax ratios lesion/liver and healthy vertebra /liver. Comparison of the SUVmax values and SUVmax ratios were performed by paired Student’s t-test. **RESULTS** From the 536 patients who benefited from a DOTATOC PET/CT in our centre between February 2010 and March 2016, 16 (9 males and 7 females; mean age: 57 years [range: 29–72]) had a typical hemangioma in the spine (3% prevalence in our series). Two patients had 2 lesions. In a per lesion analysis (18 lesions), all hemangiomas had an increased uptake (mean SUVmax: 2.7 [95%CI 2.0; 3.6]; ratio: 0.36 [95%CI 0.26–0.48]), significantly higher than that of healthy vertebrae (mean SUVmax: 1.0 [95%CI 0.92–1.2] (p=0.001); ratio: 0.15 [95%CI 0.11–0.20](p<0.001)). **CONCLUSION** Our study showed an increased DOTATOC uptake in all typical vertebral hemangiomas that was

statistically higher than healthy vertebral uptake. The importance of our findings lies on the fact that, in a DOTATOC PET/CT study for staging of a neuroendocrine tumour, a bone hemangioma could be a cause of false positive for bone metastases, which emphasizes the need of a thorough evaluation of CT images, looking for a “Polka Dot” appearance in any focal vertebral uptake.

EPW71

Prognostic Significance of Metabolic Parameters by 18F-FDG PET/CT in Non-Small Cell Lung Cancer

G. Eren¹, S. Asa¹, O. Kupik¹, S. Güngör², S. B. Asa³; ¹Oncology Hospital of RTE University, Rize, TURKEY, ²Nuclear Medicine Department of Medeniyet University, İstanbul, TURKEY, ³Physics Department of İstanbul University, İstanbul, TURKEY.

PURPOSE: We evaluated the prognostic impact of metabolic and volumetric information by 18F-FDG PET/CT in non-small cell lung cancer (NSCLC) patients. **METHODS:** In this retrospective study we evaluated 18F-FDG PET/CT parameters of 67 patients with newly diagnosed NSCLC who had pretreatment 18F-FDG PET/CT scans between January and December of 2014. The metabolic tumor volume (MTV) of whole-body tumor (MTV_{WB}), of primary tumor (MTV_T), of nodal metastases (MTV_N), and of distant metastases (MTV_M); the total lesion glycolysis (TLG) of whole-body tumor (TLG_{WB}), of primary tumor (TLG_T), of nodal metastases (TLG_N), and of distant metastases (TLG_M); the standardized uptake value (SUV_{max}) of primary tumor (SUV_{maxT}), of nodal metastases (SUV_{maxN}), and of distant metastases (SUV_{maxM}), SUV_{peakT}, (SUV_{meanT}) and CT volume (CT_v) of primary tumor were measured. The MTV and TLG were measured using adaptive (adp) method. Histologic subtype, sex, age, TNM stage, clinical stage were registered. Kaplan-Meier, receiver operating characteristic (ROC) curve analysis were used to detect parameters influencing survival. **RESULTS:** The median overall survival (OS) was 10.1 months (95% confidence interval (CI) 6.2–14.0 months). MTV_{WB} (p:0.000), TLG_{WB} (0.005), MTV_T (p:0.006), CT_v (p:0.007), SUV_{maxM} (p:0.008), TLG_M (p:0.01), MTV_M (p:0.01), SUV_{maxN} (p:0.028), TLG_T (p:0.031), MTV_N (p:0.033), TLG_N (p:0.038) had impact on survival statistically significantly. SUV_{maxT} (p:0.73), SUV_{peakT} (p:0.83), SUV_{meanT} (p:0.27) did not predict survival statistically significantly. Significant cut-off values (sensitivity, specificity) were 360 for TLG_{WB} (72%, 67%), 60.5 cm³ for MTV_{WB} (72%, 81%), 29.5 cm³ for CT_v (72%, 67%). The 1 year median overall survival was 58% for patients with TLG_{WB} (<360) and 37% for patients with TLG_{WB} (>360) p:0.009, 67% for patients with MTV_{WB} (<60.5 cm³) and 31% for patients with MTV_{WB} (>60.5cm³) p:0.000, 64% for patients with CT_v (<29.5cm³) and 35% for those with CT_v (>29.5cm³) p:0.004. The median survival was 7.3 months in patients with distant metastases and 16.2 months in patients without distant metastases p:0.002. **CONCLUSION:** The metabolic tumor parameters; MTV_{WB}, TLG_{WB}, MTV_T, SUV_{maxM}, TLG_M, MTV_M, SUV_{maxN}, TLG_T, MTV_N, TLG_N and CT_v are statistically significant prognostic factors for survival in patients with newly diagnosed NSCLC. SUV_{maxT}, SUV_{peakT} and SUV_{meanT} did not influence survival statistically significantly. Further studies with larger patient populations are needed to explore these findings.

EPW72

The Role Of 18F-Fluorothymidine (18F-FLT) In Patients With Suspected Lymphoma Relapse

L. Zanoni¹, A. Broccoli², A. Lambertini¹, C. Pellegrini², V. Stefoni², F. Lodi¹, C. Fonti¹, R. Bonfiglioli¹, P. Zinzani², S. Fanti¹; ¹Nuclear Medicine, Azienda ospedaliero-universitaria di Bologna, Policlinico S.Orsola-Malpighi, Bologna, ITALY, ²Hematology “L. e A. Seragnoli”, Azienda ospedaliero-universitaria di Bologna, Policlinico S.Orsola-Malpighi, Bologna, ITALY.

AIM: Monocentric prospective study to evaluate the role of 18F-Fuorothymidine (FLT) PET/CT in lymphoma patients (pts) following a positive or equivocal 18F-Fluorodeoxyglucose (FDG) PET/CT at end-treatment or follow-up. **MATERIALS AND METHODS:** From May 2010 to April 2016, 46 patients were enrolled, all undergoing FLT within approximately 3 weeks from a previous positive/equivocal FDG scan and, if available, biopsy confirmation to define PET results. SUVmax and Tumor-to-background-ratio (TBR, using liver SUVmean) were recorded for the most avid lesion and then compared between the recurrent/residual disease group and the group in remission, for both tracers. **RESULTS:** Pts characteristics (n=46). Age: mean 55; median 60; range 20–76 27 males and 19 females 36 non-Hodgkin (NHL) and 10 Hodgkin lymphoma (HL) stage at diagnosis: 11 II, 10 III, 25 IV 6 pts were evaluated at end-treatment and 40 during follow-up. Only in 19/46 pts (41%) histological evidence was available. Biopsy was not an option in the remaining 27 due to practical/ethical reasons; in these cases, clinical judgment and subsequent laboratory and imaging follow-up was considered as standard of reference. Relapse/residual disease was excluded in 9 pts (20%), who were diagnosed as: 1 reactive follicular hyperplasia, 2 reactive-inflammatory tissue, 4 reactive nodes, 1 nodal sarcoid-like, 1 unspecified peri-caecal finding. 39 pts (85%) were FDG-positive, of whom 35 were true positive (TP) (90%); 32 pts (70%) were FLT-positive showing 30 TP (94%). 7 FDG pts showed inconclusive results, of whom 2 TP (29%), while 14 FLT pts were inconclusive, later showing 7 TP (50%). The majority of pts (31 pts, 67%) showed both FDG- and FLT-positivity with 29 TP (93%). 8 pts (17%) were FDG-positive but FLT-inconclusive (6 TP, 75%). 6 pts (13%) resulted both FDG and FLT inconclusive (1 TP, 17%). 1 patient (2%) was FDG-inconclusive but FLT-positive (1TP, 100%). FDG and FLT-TBR and FLT-SUVmax were significantly higher in recurrent/residual lymphoma pts than in the disease-free group ($p=0,0342$; $0,0377$; $0,0267$, respectively). On the contrary no statistically significant difference was found with FDG-SUVmax ($p=0,0578$). Re-staging (Ann-Arbor) according to FDG and FLT-PET images resulted concordant in 31 cases. In 1 case FLT upstaged whereas in 14 downstaged the disease-extent compared to FDG. Analyses on potential change in pts management are ongoing. **CONCLUSION:** Our preliminary data suggest that FLT might be complementary although not alternative to FDG. The elimination of inconclusive PET findings is still challenging. Further lesion/semiquantitative/ Ki67 correlation analyses are ongoing.

EPW73

The preliminary study of 18F-FLT and 18F-FDG PET/CT in predicting response to chemoradiotherapy in nasopharyngeal carcinoma

Z. Yang, Q. Shi, Y. Zhang, C. Hu, Nasopharyngeal carcinoma multidisciplinary team, Shanghai Cancer Center, Fudan University, Shanghai; Fudan University Shanghai Cancer Center, Shanghai, CHINA.

Aim: The main objective of this study was to explore the feasibility of 18F-Fluorothymidine (18F-FLT) and 18F-Fluorodeoxyglucose (18F-FDG) positron emission tomography/computed tomography (PET/CT) in monitoring and predicting treatment response of nasopharyngeal carcinoma (NPC). **Materials and Methods:** Patients with NPC of Stage II-IVB were prospectively enrolled, receiving 2 cycles of neoadjuvant chemotherapy (NACT), followed by concurrent chemoradiotherapy. Each patient underwent pre-treatment and post-NACT FLT and FDG PET/CT. SUVmax (maximal standard uptake value), SUVmean, PTV (proliferative tumor volume) and MTV (metabolic tumor volume) of primary tumor and lymph nodes were measured. Several threshold were tried to define the contouring margin around the target. Tumor response to NACT was evaluated before commencement of radiotherapy by MRI, and tumor regression at the end of radiotherapy was evaluated at 55Gy, according to RECIST 1.1 Criteria. **Results:** 20 patients have been consecutively enrolled into this prospective study. At the end of radiotherapy, 7 patients reached complete response while others were partial response. So far, no loco-regional recurrence or

distant metastasis has occurred. After 2 cycles of NACT, both FLT and FDG parameters declined remarkably. Parameters of FDG PET were more strongly correlated to tumor regression than those of FLT PET. In both FLT and FDG PET, 70% SUVmax was the best threshold to define the contouring margin around the target. Some residual lesions after NACT showed by MRI were negative in PET/CT. **Conclusion:** Both FLT and FDG PET could reflect the metabolic changes of tumor and predict tumor regression more early than MRI. They may play an important role in radiotherapy target volume delineation.

EPW74

⁶⁸Ga-DOTATOC PET/MRI for characterization of undetermined upper abdominal tracer uptake in ⁶⁸Ga-DOTATOC PET/CT

A. Sabet¹, J. Cohnen¹, K. Beiderwellen¹, S. Ezziddin², L. Umutlu¹, H. V. Grafe¹, A. Bockisch¹, T. D. Poeppel¹; ¹Universität Duisburg-Essen, Essen, GERMANY, ²Universität Saarland, Homburg, GERMANY.

Purpose: High density of somatostatin receptors (sstr) in the uncinate process of pancreas along with suboptimal soft tissue contrast of CT may hinder accurate assessment of pancreatic head and the adjacent organs in PET/CT imaging with ⁶⁸Ga-labelled sstr analogs. The aim of this study was to investigate the performance of simultaneous ⁶⁸Ga-DOTATOC PET/MRI in patients with undetermined increased DOTATOC uptake in upper abdomen in ⁶⁸Ga-DOTATOC PET/CT. **Methods:** 88 patients with well-differentiated neuroendocrine tumors (NET) and visually detectable DOTATOC Uptake were analyzed. PET/CT was followed by PET/MRI in all patients. Histopathology and follow-up served as reference standard. Diagnostic performances of the two modalities were compared. Quantitative assessments were also performed measuring standardized uptake value (SUV) parameters. Paired Students t-test was performed with a significance level of $p < 0.05$ to examine the differences in SUV_{max} between physiological and pathological uptake in both modalities. **Results:** 54/88 patients had a faint or irregular uptake with no morphologic correlate in either PET/CT, PET/MRI or during the follow up. Of 34/88 patients with focally increased uptake, PET/CT detected pancreatic tumors in 2, adjacent lymph nodes in 3, and duodenal lesion in 1 patients. PET/MRI defined corresponding pathologies in 10 of 34 patients, consisting of pancreatic tumor (n=4), adjacent lymph nodes (n=4), and duodenal lesions (n=2). Suspected uptake with no morphologic correlate proved duodenal NET in 1 patient during the follow-up. PET/MRI was superior to PET/CT in terms of sensitivity (91% vs 55%), negative predictive value (96% vs 82%), and diagnostic accuracy (97% vs 85%). The mean SUV_{max} was significantly higher in tumor lesions of uncinate process as compared to patients with physiological uptake. **Conclusions:** In this study, ⁶⁸Ga-DOTATOC PET/MRI could determine the entity (physiological vs pathological) and origin (pancreatic vs extra-pancreatic) of increased DOTATOC uptake in upper abdomen in significantly more patients compared to ⁶⁸Ga-DOTATOC PET/CT resulting in considerable reduction in inconclusive PET images.

EPW75

18F FACBC PET/CT for nodal staging in high risk prostate cancer: preliminary accuracy data

L. Zanoni¹, I. Bossert¹, C. Nanni¹, C. Pultrone², R. Schiavina², F. Giunchi³, M. Fiorentino³, C. Fonti¹, A. Matti¹, S. Ricciolino⁴, F. Lodi¹, A. Porreca⁵, E. Brunocilla², A. D'Errico³, S. Fanti¹; ¹Nuclear Medicine, Azienda ospedaliero-universitaria di Bologna, Policlinico S.Orsola-Malpighi, Bologna, ITALY, ²Urology, Azienda ospedaliero-universitaria di Bologna, Policlinico S.Orsola-Malpighi, Bologna, ITALY, ³Pathology, Azienda ospedaliero-universitaria di Bologna, Policlinico S.Orsola-Malpighi, Bologna, ITALY, ⁴Nuclear Medicine, Azienda ospedaliero-universitaria Federico II, Napoli, ITALY, ⁵Urology, Policlinico Abano Terme, Abano (PD), ITALY.

AIM: To evaluate the diagnostic performance of 18F-FACBC-PET/CT in nodal staging prior to lymph-node-dissection (LND) in high-risk primary prostate cancer (PCa). **MATERIALS AND METHODS:** 65 patients (pts), consecutively and prospectively enrolled, underwent 18F-FACBC-PET/CT. Inclusion Criteria were: high-risk biopsy-proven PCa; standard staging workup (including Choline-PET/CT); out of hormonal-therapy; eligible for LND. Any LN uptake greater than surrounding background was interpreted with a 5-point-scale (confidence of disease): 1-2 probably negative; 4-5 probably positive; 3 equivocal. Lesions' number, site and dimension, SUVmax and target-to-background-ratio were registered. PET/CT results were compared, on a per-patient basis, with histopathology from LND (39 pts). 26/65 pts were excluded from diagnostic-performance-analysis: 5 minimal lymphadenectomy; 3 not operated; 18 waiting for surgery. **RESULTS:** Overall pts characteristics (65pts). Age: Mean 65; Median 66; Range 47-76. PSA: Mean 10,30; Median 7,90; Range 2,56-30; BiopsyGS: 3+3 1; 3+4 3; 4+3 5; 4+4 32; 4+5 19; 5+4 4; 5+3 1. cT: T1c 6; T2n.s. 25; T2a 1; T2b 8; T2c 18; T3 7. **Diagnostic performance (39pts).** Overall 913 LN were removed in 39/65 pts (60%); mean 23; median 19; range 6-49. Despite a considerable risk for LNMs predicted by Briganti-Nomogram (mean 26%; median 22%; range 3-70%), only 4 pts (10%) resulted N1. Overall 14 LNMs were counted (10 in 1 pt; 1 in 2 pts; 2 in 1 pt), all showing millimetric deposits (range 1-5 mm). *Pts characteristics:* Age: Mean 65; Median 66; Range 47-75. PSA: Mean 10,42; Median 8; Range 2,87-30. Biopsy-GS: 3+3 1; 3+4 2; 4+3 1; 4+4 22; 4+5 10; 5+4 3. cT: T1c 3; T2 n.s. 12; T2a 1; T2b 2; T2c 15; T3 6. pT: T2b 1; T2c 11; T3a 21; T3b 6. pGS: 3+4 1; 4+3 9; 4+4 8; 3+5 1; 4+5 14; 5+4 2; 4+3(+5) 1; 4+4(+5) 3. *PET results:* 24 pts resulted negative (21 TN, 3 FN) and 8 positive (1TP, 7 FP) with both tracers; 1 positive with FACBC (1 FP) but negative with Choline (1 TN); 6 positive with Choline (FP) but negative with FACBC (TN). Sensitivity resulted 25% with both tracers; specificity 77 vs 63%, accuracy 72 vs 59%, PPV 13 vs 7%, NPV 90 vs 88% in favor of FACBC. **CONCLUSION:** FACBC demonstrated low sensitivity, equal to Choline, but slightly better overall diagnostic performance in nodal staging. Due to small size of LNMs, PET remains not ideal. Enrolment and further analyses (region-based/semi-quantitative/uni-multivariate-logistic-regression to search for relevant predictive factors) are ongoing.

EPW76

Evaluation of Effect of Intravenous Iodinated Contrast Enhanced Computed Tomography on Diagnostic Yield of PET/CT Scan in Recurrent Head and Neck Malignancies

S. BARAI¹, A. Singh², S. Gambhir²; ¹Department of Nuclear Medicine, Sanjay Gandhi Postgraduate Institute of Medical Sciences, Lucknow, INDIA, ²Sanjay Gandhi Postgraduate Institute of Medical Sciences, Lucknow, INDIA.

Aim: Iodinated contrast agents are routinely used in computed tomography (CT) and are acknowledged to provide additional information over a noncontrast CT. Iodinated contrasts are also increasingly being used in the CT component of Positron emission tomography (PET) with the assumption that contrast enhance CT will provide better diagnostic yield though the utility of contrast study for PET imaging is still being debated. Aim of the study was to evaluate the effect of contrast CT on diagnostic yield of PET/CT scan done in patients with suspected recurrent head, neck malignancies. **Materials and Method:** A total of 139 patients of head, neck malignancies having suspected tumour recurrence, undergoing FDG-PET scan were included in this study. Two sets of CT images were obtained. One set used standard noncontrast CT (80-130 mA, 120 kVp) for coregistration, and the other set used intravenous contrast (Iopromide 370) enhanced diagnostic quality CT (160-300mA, 120kVp) for coregistration. Two nuclear medicine physicians blinded to clinical details interpreted the results. Any difference in observation was resolved by consensus. **Results:** Both contrast and noncontrast PET/CT detected

recurrence at the primary site in 127 patients. In 33 of 127 patients histopathology of the primary recurrent site was available for analysis. The calculated sensitivity, specificity, accuracy and positive and negative predictive values of the noncontrast PET/CT protocol for detection of recurrence at the primary site were 91.6%, 66.6%, 84.8%, 88%, and 75% respectively and that of contrast enhanced PET/CT were 91.6%, 88.8%, 90.9%, 95.6%, and 88.8%, respectively. There was no statistical difference between PET/CT and PET/CECT protocols. However when compared to noncontrast PET/CT the contrast PET/CT resulted in better tumour margin delineation, resulting in disease status upstaging in 25 patients (17.9%) and downgrading in 3 patients (2.1%). Lymph nodes were also better visualised in contrast PET/CT allowing more accurate evaluation of nodal characteristics like shape, size, and presence of hilum, enhancement and presence of necrosis resulting in upstaging in 45 patients (32.3%) and down staging in 10 (7.1%) cases. Both contrast and non contrast PET/CT performed identically while deciding the M stage (distant metastases) of the disease, however in 3(2.1%) patients additional location of distant metastases were detected by contrast PET/CT. **Conclusion:** The contrast enhanced PET/CT protocol demonstrated a significantly better diagnostic performance in evaluation of tumour infiltration, margin and lymph nodal involvement, resulting in change in T stage in 20% and N stage in 39.4% patients of suspected recurrent head, neck malignancies.

E-PW9 – Sunday, October 16, 2016, 08:30 - 09:30, e-Poster Area

e-Poster Walk 9 – Radiopharmaceuticals & Radiochemistry: Radiopharmaceuticals

EPW77

Effects of Carbidopa on Kinetics of 6-¹¹C-Methyl-*m*-tyrosine and 6-¹⁸F-Fluoro-*m*-tyrosine into the Living Brain: A PET Study in Monkey

M. Kanazawa, H. Ohba, T. Kakiuchi, H. Tsukada; Hamamatsu Photonics K.K., Hamamatsu City, JAPAN.

Aim: We have recently developed a novel PET probe, 6-¹¹C-methyl-*m*-tyrosine (¹¹C-6MemTyr), to qualify presynaptic dopamine (DA) synthesis in the living brain (Kanazawa M., et al., *Bioorg Med Chem.* 2015;23:729). We reported that ¹¹C-6MemTyr, which has non-catechol structure, were not affected by pre-administration of carbidopa, a specific inhibitor of peripheral aromatic L-amino acid decarboxylase (AADC), at the clinical dose (Kanazawa M., et al., *J Nucl Med.* 2016;57:303). In contrast, PET measurements using 6-¹⁸F-fluoro-*L*-*m*-tyrosine (¹⁸F-6FMT), another non-catechol probe, are routinely conducted with preadministration of carbidopa. In the present study, we comparatively evaluated the effects of carbidopa on plasma metabolism and brain uptake of ¹¹C-6MemTyr and ¹⁸F-6FMT in the living normal monkey (*Macaca fascicularis*). **Materials and Methods:** ¹¹C-6MemTyr was synthesized by using a rapid Pd(0)-mediated crosscoupling reaction of ¹¹C-methyl iodide and corresponding alkenyl boronate precursor (Kanazawa M., et al., *Bioorg Med Chem.* 2015;23:729). ¹⁸F-6FMT was labeled by a highly enantioselective synthesis method using chiral phase-transfer alkylation as previously used for the labeling of no-carrier-added ¹⁸F-FDOPA (Lemaire C., et al., *Eur J Org Chem.* 2004:2899) with minor modifications. PET scans using ¹¹C-6MemTyr and ¹⁸F-6FMT were conducted in monkeys under isoflurane anesthetic state. In order to evaluate the effects of carbidopa, vehicle or carbidopa was orally administered 1 hr before the injection of ¹¹C-6MemTyr or ¹⁸F-6FMT. DA synthesis rates (Ki) in the striatum were calculated by Patlak plot analysis applying the TAC in the cerebellum as an input function. In addition, the effects of carbidopa on metabolic profiles of ¹¹C-6MemTyr and ¹⁸F-6FMT in plasma were assessed using radio-TLC method. **Results and Conclusion:** As previously observed using ¹¹C-6MemTyr, the striatal Ki value measured using ¹⁸F-6FMT was also not affected by carbidopa at clinical dose even with the slight changes in their plasma metabolic profiles. The present study demonstrated that ¹¹C-

6MemTyr and ^{18}F -6FMT could be potential PET probes for quantitative imaging of the presynaptic DA activity without pre-administration of carbidopa in the living brain with PET.

EPW78

In Vivo and In Vitro Metabolism of the new Translocator Protein PET Ligand [^{11}C]PBR170

M. Peyronneau¹, T. Bourdier², S. Eberl^{2,3}, C. Loch², L. Wen^{2,3}, D. Henderson², P. Lam², A. Mohamed^{2,4}, I. Greguric⁵, F. Mattner², A. Katsifis^{2,6}, M. Fulham^{2,3,4}; ¹IMIV, CEA, Inserm, Univ.Paris-Sud, CNRS, Université Paris-Saclay, CEA-SHFJ, Orsay, FRANCE, ²Department of Molecular Imaging (PET and Nuclear Medicine), Royal Prince Alfred Hospital, Missenden Road, Camperdown, NSW 2050, AUSTRALIA, ³Faculty of Engineering and Information Technologies, University of Sydney, Sydney, NSW 2006, AUSTRALIA, ⁴Sydney Medical School, University of Sydney, Sydney, NSW 2006, AUSTRALIA, ⁵Life Sciences, ANSTO, New Illawarra Road, NSW 2234., Lucas Heights, AUSTRALIA, ⁶Faculty of Pharmacy, University of Sydney, Sydney NSW 2006, AUSTRALIA.

Aim: The 2-(6,8-dichloro-2-(4-ethoxyphenyl)imidazo[1,2-a]pyridin-3-yl)-N-(2-fluoropyridin-3-yl)-N-methylacetamide has been previously synthesized and labelled with [^{11}C] for imaging the translocator protein (TSPO) with PET [1]. During preclinical imaging evaluation of this ligand in rats and non-human primates, our aim was to investigate the in-vitro and in-vivo metabolism of PBR170 and [^{11}C]PBR170 to determine the contribution of radiometabolites to the brain uptake and to evaluate species differences. **Materials and Methods:** The *in-vitro* metabolic study was assessed by incubation with rat, baboon and human liver microsomes followed by LC/MS and MS-MS analyses. PBR170 was radiolabelled by *N*-methylation of the corresponding des-methyl precursor with [^{11}C]methyl iodide in 30-45% radiochemical yield with radiochemical purity > 98% and specific activity of 90-190 GBq/ μmol . In-vivo metabolism was measured in arterial plasma samples by a validated solid phase extraction (SPE) method during dynamic brain imaging of [^{11}C]PBR170 in baboons (*Papio Hamadryas*) using a Biograph PET-CT. **Results:** LC-MS analyses of rat, non-human primate and human liver incubations identified 6 main metabolites generated by cytochrome P450-dependant *N*-demethylation, *O*-deethylation and hydroxylation of PBR170, forming: *N*-demethyl (*m/z* 459), *O*-deethyl (*m/z* 445), hydroxyl (*m/z* 489), *N*-demethyl, *O*-deethyl (*m/z* 431), *N*-demethyl, hydroxyl (*m/z* 475), *O*-deethyl, hydroxyl (*m/z* 461) and *O*-deethyl, hydroxyl, *N*-demethyl (*m/z* 447) derivatives of PBR170. The *N*-demethylated compounds (*m/z* 459 and 431) were the major metabolites in baboon and human liver microsomes whereas the *O*-deethylated (*m/z* 445) and hydroxylated (*m/z* 475) derivatives were the major metabolites in rat microsomes. In-vivo, [^{11}C]PBR170 slowly decreased in baboon plasma and contributed for more than 50% of the radioactivity 60 min after injection. The [^{11}C]N-demethylation leads to the formation of a non-radioactive *N*-demethylated compound, with lower affinity for the TSPO and [^{11}C]CO₂, which is excluded by the blood-brain barrier and therefore has little interference with brain measurements. *O*-deethylation results in non-radioactive acetate and a phenol with poor affinity for the PBR and CBR receptors. Finally, whole body PET-CT imaging, performed after 60 minutes, showed liver uptake and predominantly hepatobiliary elimination with little excretion through the kidneys. **Conclusions:** Species differences were observed in the metabolism of PBR170 between rat, non-human primate and human. In-vivo [^{11}C]PBR170 radiometabolites resulting from *N*- and *O*-dealkylation should not confound brain PET measurements.[1] Bourdier et al., Appl Radiat Isot, 2014;90:46-52.

EPW79

PET Imaging of HER2 Expressing Tumors using a Novel ^{18}F labeled Affibody with a Hydrophilic Linker

M. Yang, Y. Xu, Z. Bai, D. Pan, L. Wang, J. Yan, R. Yang; Jiangsu Institute of Nuclear Medicine, Wuxi, CHINA.

Human epidermal growth factor receptor 2 (HER2) is a potential target for diagnosis and therapy of the tumor. ^{18}F labeled HER2 targeting affibody, ZHER_{2:342}, has been developed for the noninvasive assessment of HER2 status in vivo through PET imaging. However, unfavourable abdominal background and laborious multiple-step synthetic procedure may hinder the widespread use of these agents. A new hydrophilic linker, GGGRDN, is benefit to improve the pharmacokinetic quality of peptides. In the present study, modified ZHER_{2:342} with the linker, ZHER_{2:342}-NDRGGG-Cys (denoted as MZHER_{2:342}), was designed and labeled using ^{18}F -Al-NOTA strategies. The imaging properties of the novel tracer were investigated in tumor models and also compared to those of unmodified counterpart. **Methods:** MZHER_{2:342} and ZHER_{2:342} were conjugated with MAL-NOTA under standard reaction conditions. The affibody molecules were then radiolabeled with Al ^{18}F complex. MicroPET imaging and biodistribution studies were performed in nude mice bearing HER2-positive human breast cancer JIMT-1 after iv injection. **Results:** ^{18}F -Al-NOTA-MAL-MZHER_{2:342} and ^{18}F -Al-NOTA-MAL-ZHER_{2:342} can be efficiently produced within 30 min with non-decay corrected yields of about 10% and radiochemical purities of more than 95%. PET imaging revealed that the JIMT-1 xenografts were readily visualized with high target to background contrast after administration of ^{18}F -Al-NOTA-MAL-MZHER_{2:342}. ROI analysis showed that the tumor uptakes were 8.75±0.83, 8.42±1.20 and 8.31±0.96 %ID/g and 1.71±0.31, 1.59±0.29, 1.41±0.29 %ID/g at 30, 60 and 120 min after administration of ^{18}F -Al-NOTA-MAL-MZHER_{2:342} and ^{18}F -Al-NOTA-MAL-ZHER_{2:342} respectively. Excessive unlabeled ZHER_{2:342} significantly inhibited the tumor uptakes at 60 min postinjection. The liver uptake of ^{18}F -Al-NOTA-MAL-MZHER_{2:342} was about 2 %ID/g, but the corresponding values for ^{18}F -Al-NOTA-MAL-ZHER_{2:342} was nearly 10% ID/g at all time points. Prominent uptake of ^{18}F -Al labeled affibodys were also observed in kidneys at early time points, suggesting that these tracers are mainly excreted through the renal-urinary routes. **Conclusions:** ^{18}F -Al-NOTA-MAL-MZHER_{2:342} can be prepared simply and GGGRDN linker greatly improved the pharmacokinetic performances in vivo. ^{18}F -Al-NOTA-MAL-MZHER_{2:342} is promising for detecting HER2 expression of cancers. **Acknowledgements** This work was supported by National Natural Science Foundation (51473071,81472749,81401450,21401084,21504034), Jiangsu Province Foundation (BE2014609), Health Ministry of Jiangsu Province Fund (RC2011095,Q201406 and H201529), 333 Project of Jiangsu (BRA2015476).

EPW80

Evaluation of two approaches for the [^{18}F]AIF radiolabeling of affibody Z_{HER3:8698} for PET imaging of HER3 status

C. Da Pieve, L. Allott, C. D. Martins, A. Vardon, D. M. Ciobota, G. Kramer-Marek, G. Smith; Institute of Cancer Research, Sutton, UNITED KINGDOM.

Background: HER3 is a member of the human epidermal growth factor receptor (EGFR/HER) tyrosine kinase family. HER3 is involved in the establishment of malignancy and its signalling has recently been identified as a prominent mediator of resistance to HER1 and HER2-targeted therapies. Radionuclide-based molecular imaging of HER3 receptor expression could guide patient stratification for HER3 targeted therapy and more importantly could aid monitoring early tumour response to therapeutic intervention. This study aimed to develop an efficient and reproducible radiolabelling of an affibody molecule having high HER3 affinity via the rapid and effective aluminium- ^{18}F -fluoride (^{18}F]AIF) method for the imaging of HER3 expression *in vivo*. **Materials and Methods:** The HER3-targeting Z_{HER3:8698} affibody (AffibodyAB, Sweden) was radiolabelled following two different strategies: a one-step radiolabelling performed at 100°C

using 1,4,7-triazanonane-1,4,7-triacetate (NOTA) as chelator for the [^{18}F]AIF complex; and a two-step alternative approach performed at room temperature based on the inverse electron demand Diels-Alder (IEDDA) reaction between a novel tetrazine functionalised 1,4,7-triazacyclononane-1,4-diacetate chelator (NODA-Tz) and a *trans*-cyclooctene (TCO) functionalised affibody. Binding affinity and specificities of the products were evaluated *in vitro*. High HER3-expressing MCF-7 tumour-bearing mice were used to assess the HER3 targeting *in vivo*. Results: NOTA- $Z_{\text{HER3}:8698}$ was radiolabelled with [^{18}F]AIF in a one-step reaction (38.8 ± 5.8 % radiochemical conversion). However, the exposure of the radioconjugate to the high temperatures required for radiolabelling formed a by-product. A purification procedure comprising of RP-HPLC followed by HLB-SPE was therefore developed to produce [^{18}F]AIF-NOTA- $Z_{\text{HER3}:8698}$ with a RCP higher than 98% and high stability. The alternative IEDDA reaction was performed by initially radiolabelling NODA-Tz with [^{18}F]AIF which was subsequently ligated to TCO- $Z_{\text{HER3}:8698}$ at room temperature to produce the [^{18}F]AIF-NOTA- $Z_{\text{HER3}:8698}$ radioconjugate. The binding affinities of both radioconjugates to HER3, using the overexpressing MCF-7 cell line, were found to be specific and in the subnanomolar range (ca 0.4–1.0 nM). Both radioconjugates display similar *in vivo* pharmacokinetic profiles when injected in MCF-7 tumour bearing mice. Tumour uptake was found to be 4.36 ± 0.92 and 4.96 ± 0.92 %ID/g for [^{18}F]AIF-NOTA- $Z_{\text{HER3}:8698}$ and [^{18}F]AIF-NODA- $Z_{\text{HER3}:8698}$ respectively at 1 h p.i. when 1 μg of protein (ca 0.8 MBq) was injected. Conclusions: [^{18}F]AIF radiolabelled HER3-targeting affibody molecule $Z_{\text{HER3}:8698}$ was efficiently achieved using two distinct approaches. Both radiotracers can provide specific PET imaging of HER3 expression in tumours. However, the simplicity of the synthesis and the *in vivo* data indicated [^{18}F]AIF-NOTA- $Z_{\text{HER3}:8698}$ as the most promising candidate for further investigation.

EPW81

Comparative evaluation of ^{177}Lu -HP2 and ^{111}In -HP2, secondary agents for affibody-based PNA-mediated radionuclide pretargeting

M. Altai¹, K. Westerlund², J. Vellella¹, H. Honarvar¹, A. Orlova³, A. Eriksson-Karlström², V. Tolmachev¹; ¹Immunology, Genetics and Pathology, Uppsala University, Uppsala, SWEDEN, ²DIVISION OF PROTEIN TECHNOLOGY, KTH, Stockholm, SWEDEN, ³Department of Medicinal Chemistry, Division of Molecular Imaging, Uppsala, SWEDEN.

Aim. The use of radiometal-labelled affibody molecules in targeted radionuclide therapy is hindered by the high uptake and retention of radioactivity in the kidneys. Commonly used methods for reduction of renal radioactivity were inefficient in the case of affibody molecules. We have recently developed a peptide nucleic acid (PNA) hybridization-mediated pretargeting approach to improve tumor-to-kidney radioactivity uptake ratios. The primary targeting agent is $Z_{\text{HER2}:342}$ -SR-HP1 affibody-PNA chimera. An anti-HER2 $Z_{\text{HER2}:342}$ affibody molecule provides localization of PNA hybridization probe HP1 in HER2-expressing tumours. The complementary PNA HP2 probe contains DOTA and can be labelled with a variety of radiometals. *In vivo* proof-of-principle was demonstrated using ^{111}In -labeled HP2. The radioactivity uptake in kidneys was ca. 2-folds lower than that in the tumour. In the current study we continue the optimization of our pretargeting approach using the therapeutic low-energy beta emitter ^{177}Lu . **Methods.** DOTA-HP2 was labelled with lutetium-177 in 1M ascorbate, pH 5.5. *In vitro* pretargeting was studied in HER2-expressing SKOV-3 and BT474 cell lines. Biodistribution of ^{177}Lu -HP2 and ^{111}In -HP2 was compared in NMRI mice at 1, 4 and 24h p.i. To test the possibility of further reducing the kidney uptake of ^{177}Lu -HP2, two groups of mice were co-injected with kidney reabsorption blocking agents, Gelofusine and lysine. **Results.** HP2 was efficiently and stably labelled with ^{177}Lu with a yield of 99.5 ± 0.4 % (n=5) and a specific radioactivity of 24.7 GBq/ μmol . SDS-PAGE analysis demonstrated minimal radiolytic damage during labeling. *In vitro*, ^{177}Lu -labeled HP2 bound specifically to HER2-expressing cells pretreated with $Z_{\text{HER2}:342}$ -SR-

HP1 and showed high cellular retention up to 24h. *In vivo*, ^{177}Lu -HP2 demonstrated significantly reduced retention in the blood in comparison to ^{111}In -HP2 (0.22 ± 0.1 vs. 0.68 ± 0.07 %ID/g). The low blood-borne radioactivity of ^{177}Lu -HP2 resulted in lower uptake in the well-perfused liver in comparison to ^{111}In -HP2 (0.1 ± 0.04 vs. 0.9 ± 0.3 %ID/g). No significant difference in the kidney uptake was observed. When mice were co-injected with Gelofusine and lysine, the kidney uptake of ^{177}Lu -HP2 was reduced 3- and 2- fold, respectively. **Conclusion.** ^{177}Lu -HP2 showed both favourable *in vitro* pretargeting and *in vivo* biodistribution properties. This study demonstrates the feasibility of further development of the ^{177}Lu -labelled HP2 for affibody-based PNA-mediated radionuclide pretargeting. Studies to evaluate the feasibility of *in vivo* pretargeting of HER2-overexpressing SKOV-3 ovarian carcinoma xenografts using ^{177}Lu -HP2 are ongoing.

EPW82

In vivo evaluation of pharmacokinetics, tumors targeting and therapeutic efficacy of a novel format of HER3-targeting affibody molecule with prolonged blood circulation

A. Orlova¹, M. Rosestedt¹, B. Mitran¹, T. Bass², F. Y. Frejd¹, J. Löfblom², V. Tolmachev¹, S. Ståhl²; ¹Uppsala University, UPPSALA, SWEDEN, ²Royal Institute of Technology, Stockholm, SWEDEN.

Aim. Surface expression of human epidermal growth factor receptor type 3 (HER3) and its heterodimerisation with other receptors of HER family is a cause of resistance of malignant tumors to anti-HER targeting therapies. We have developed affibody molecule with low picomolar affinity to HER3 for molecular imaging of HER3 expression. The anti-HER3 affibody molecule blocks its binding to the natural ligand heregulin, suppresses heregulin-induced HER3 phosphorylation *in vitro*, blocks heregulin-induced downstream signaling through the Ras-MAPK and the PI3K-Akt pathways, and demonstrates complete inhibition of heregulin-induced cancer cell growth. To increase further the therapeutic effect and to extend residence time of affibody molecule in circulation, we have developed a bivalent HER3-targeting construct containing two HER3-specific affibody molecules flanking the ABD (albumin binding domain), $Z_{\text{HER3}}\text{-ABD-}Z_{\text{HER3}}$. The aims of this study were to evaluate biodistribution and *in vivo* targeting properties of the new construct; to determine protein dose, administration pathway and injection frequency for pilot anti-HER3 therapy in murine model. **Materials and methods.** $Z_{\text{HER3}}\text{-ABD-}Z_{\text{HER3}}$ was coupled to DOTA chelator and labelled with indium-111. Its targeting properties were evaluated *in vitro* in HER3-expressing cell lines and *in vivo*. An experimental therapy was performed in mice bearing HER3-expressing xenografts, BxPC-3. **Results.** Radiolabeled $Z_{\text{HER3}}\text{-ABD-}Z_{\text{HER3}}$ preserved high affinity to HER3 ($K_D = 1.0 \pm 0.4 \times 10^{-10}$ M) and demonstrated HER3 specific uptake both *in vitro* and *in vivo*. The biodistribution of $^{111}\text{In-}Z_{\text{HER3}}\text{-ABD-}Z_{\text{HER3}}$ was quite similar after intravenous, subcutaneous and intraperitoneal injections. Biodistribution of $^{111}\text{In-}Z_{\text{HER3}}\text{-ABD-}Z_{\text{HER3}}$ was studied up to 168 h after intraperitoneal injection. The compound was efficiently taken up into blood circulation (7.9 ± 0.7 %ID/g blood 6 h pi). Residence time of the new affibody construct was extended by fusion with ABD in comparison to naked anti-HER3 affibody molecule (distribution phase 440-fold and elimination phase 3.5-fold). However, clearance of $Z_{\text{HER3}}\text{-ABD-}Z_{\text{HER3}}$ was rapid than for other ABD-fused affibody molecules. Increasing of injected protein dose significantly decreased radioactivity concentrations in organs expressing mErbB3 (murine counterpart of HER3) but not concentration in blood. Based on pharmacokinetic data, the pilot anti-HER3 *in vivo* therapy experiment was planned and performed in mice bearing HER3-expressing BxPC-3 xenografts. The growth of xenografts in the treated group was significantly slower than in the control group and treatment was well tolerated. **Conclusion.** The novel high-affinity affibody-ABD fusion protein $Z_{\text{HER3}}\text{-ABD-}Z_{\text{HER3}}$ provides efficient growth inhibition of HER3-expressing cancer cells *in vitro* and *in vivo*. Pharmacokinetic studies using radiolabeled construct allowed planning efficient therapy experiment.

EPW83

Imaging of EGFR Expression Using ^{99m}Tc-Labelled ZEGFR:2377 Affibody Molecule

M. Oroujeni¹, K. Andersson², J. Garousi¹, B. Mitran¹, A. Orlova¹, J. Löfblom², V. Tolmachev¹; ¹Uppsala University, Uppsala, SWEDEN, ²KTH-Royal Institute of Technology, Stockholm, SWEDEN.

Aim. Overexpression of the epidermal growth factor receptor (EGFR) is a driving force in proliferation of several carcinomas. Imaging of EGFR expression enables patients' stratification for hyperfractionated radiation therapy of head and neck carcinoma or for gefitinib treatment of non-small-cell lung cancer. Earlier, we have demonstrated that ¹¹¹In-labeled affibody molecule DOTA-ZEGFR:2377 enables specific imaging of EGFR-expressing xenografts in vivo. The use of ^{99m}Tc instead of ¹¹¹In permits to increase the resolution, improve sensitivity, decrease dose burden to patients and reduce costs of diagnostics. The goal of this study was to evaluate feasibility of EGFR imaging by ZEGFR:2377 affibody molecules labelled with ^{99m}Tc using C-terminal amino acid KVDC sequence as a chelator. **Materials and methods.** ZEGFR:2377 was labelled with ^{99m}Tc using a gluconate-containing kit. The labelling stability was evaluated in vitro by challenge with 300-fold molar excess of cysteine. In vitro binding specificity was checked in A431 and MDA468 EGFR-expressing cell lines using pre-saturation with non-labelled affibody molecules and anti-EGFR antibody cetuximab. The cellular processing of ^{99m}Tc-ZEGFR:2377 bound to A431 and MDA468 cells was evaluated using a modified acid wash method. Affinity was measured using LigandTracer. Biodistribution was measured in BALB/C nu/nu mice bearing A431 xenografts at 3 and 24 h after injection. In vivo specificity was checked by pre-saturation of receptors by cetuximab. Experimental imaging was performed at 3 and 24 h using Triumph SPECT/CT scanner for small rodents. **Results.** The conjugate was stable under cysteine challenge. In vitro-binding of ^{99m}Tc-ZEGFR:2377 to EGFR-expressing cells was receptor-specific and strong (KD=280 pM). Internalization of ^{99m}Tc-ZEGFR:2377 was relatively slow, and less than 35% of cell-associated radioactivity was internalized after 24h incubation at 37°C. In vivo, accumulation of ^{99m}Tc-ZEGFR:2377 in A431 xenografts was EGFR-specific. The tumour uptake was 3.6±0.9 and 2.5±0.9 % ID/g at 3 and 24 h after injection, respectively. Clearance of radioactivity from normal tissues was rapid than clearance from tumours, which resulted in significant increase of tumour-to-organ ratios at later time point. The tumour-to-blood and tumour-to-muscle ratios at 24h after injection were 8±3 and 18±4, respectively. Tumours were clearly visualized at both time points. **Conclusion.** The use of C-terminal amino acid KVDC sequence as a chelator provides stable labelling of ZEGFR:2377 with ^{99m}Tc. ^{99m}Tc-ZEGFR:2377 has high affinity to EGFR-expressing cells. Imaging of EGFR-expressing tumours using ^{99m}Tc-ZEGFR:2377 is feasible.

EPW84

New ⁶⁸Ga-HBED-CC conjugated GRPr targeted ligands for cancer imaging: a comparative study

C. Liolios¹, B. Buchmuller¹, A. Wacker¹, M. Schäfer¹, U. Bauder-Wüst¹, U. Haberkorn^{2,3}, M. Eder³, K. Kopka¹; ¹Department of Radiopharmaceutical chemistry, German Cancer Research Center (DKFZ), Heidelberg, GERMANY, ²Department of Nuclear Medicine, University Hospital, Heidelberg, GERMANY, ³Clinical Cooperation Unit Nuclear Medicine, German Cancer Research Center (DKFZ), Heidelberg, GERMANY.

Aim: Overexpression of the gastrin-releasing peptide receptor (GRPr) in many types of cancer (i.e. pancreatic, prostate and breast) renders GRP and its analogues attractive for peptide-mediated radionuclide imaging and therapy¹. In this study, three bombesin (BN) analogues, two agonists: H₂N-BN(2-14) (1), H₂N-PEG₂-[(R)-Tyr⁶,β-Ala¹¹, Thi¹³, Nle¹⁴]BN(6-14) (2) and one antagonist, 4-amino-1-carboxymethyl piperidine-[(R)-Phe⁶,Sta¹³]BN(6-14) (3) were conjugated to the acyclic chelator N,N'-

bis[2-hydroxy-5-(carboxyethyl)benzyl]ethylenediamine-N,N'-diacetic acid (HBED-CC), which allows fast and stable chelation of the short-lived positron emitter ⁶⁸Ga. Compounds (1), (2), (3) were labeled with ⁶⁸Ga and evaluated in vitro on PC-3 cells (GRPr +) and in vivo in PC-3 tumor-bearing mice. Methods: Syntheses were according to published solid-phase peptide chemistry methods^{2,3}. Radiolabeling with [⁶⁸Ga]Ga³⁺ eluate was accomplished within 10 min³. ⁶⁸Ga-1-3 were then investigated in vitro for their lipophilicity, GRPr-affinity, specific binding on and internalization in PC-3 cells, according to known methods³. The biodistribution was evaluated in PC-3 xenografted mice along with μPET imaging. Results: All peptides were labeled with RCY > 98 %. ⁶⁸Ga-2 presented the highest lipophilicity followed by ⁶⁸Ga-3 and ⁶⁸Ga-1 (logD = -1.13 ± 0.04; -1.54 ± 0.07; -1.91 ± 0.06, pH 7.4, respectively). All tracers showed specific binding on GRPr with binding affinities in the nanomolar range (1) 4.09, (2) 3.65, (3) 3.51 nM. Maximal cell uptake was achieved after 40-50 min of incubation. ⁶⁸Ga-2 and ⁶⁸Ga-3 presented higher cell binding than ⁶⁸Ga-1. The majority of the cell-bound radioactivity was internalized for ⁶⁸Ga-1 and -2 (60-70 %), while for ⁶⁸Ga-3 the radioactivity mainly remained on the cell surface (~80 %). Biodistribution experiments at 30 min p.i. showed the lowest tumor uptake for ⁶⁸Ga-2, 3.06 ± 0.28 % injected dose (ID)/g, while ⁶⁸Ga-1 reached 4.36 ± 0.90 % ID/g and ⁶⁸Ga-3, 4.32 ± 0.25 % ID/g. The uptake of the agonists significantly decreased at 60 min p. i., while for ⁶⁸Ga-3 it remained higher (4.74 ± 1.43 % ID/g). Also, antagonist ⁶⁸Ga-3 showed lowest off-target accumulation in muscle, intestines, kidneys and the pancreas. The μPET image of ⁶⁸Ga-3 was in accordance with these results, so that the tumor clearly was visualized. Conclusion: Of the three new tracers that were synthesized and evaluated, the antagonist ⁶⁸Ga-3 presented optimal pharmacokinetic characteristics, i.e. the highest tumor uptake and the lowest non-target organ accumulation. References: ¹Sancho V, et al. Curr. Drug Deliv. 2011;8(1):79-134; ²Liolios CC, et al. Eur. J. Inorg. Chem. 2012(17):2877-2888; ³Eder M, et al. Eur. J. Nucl. Med. Mol. Imaging 2008;35(10):1878-86.

EPW85

Does the use of protease inhibitors outperform the chemical stabilization approach on targeting the cholecystokinin 2 receptor in vivo with radiolabelled gastrin analogues?

A. W. Sauter¹, R. Mansi¹, I. Valverde¹, L. Del Pozzo¹, M. Béhé², D. Wild¹, M. Fani¹; ¹University Hospital Basel, Basel, SWITZERLAND, ²Paul Scherrer Institute, Villigen, SWITZERLAND.

Purpose: Systemic treatment options are limited in patients with metastatic medullary thyroid cancer (MTC). The cholecystokinin 2 receptor (CCK2) is a favoured target for imaging and therapy of MTC using radiolabelled gastrin analogues. These analogues are cleaved rapidly by proteases in vivo and therefore their potential therapeutic efficacy decrease. We aimed to evaluate the effect of protease inhibitors on the biodistribution and tumour uptake of different minigastrin analogues with varying in vivo stability in 2 xenograft models, to conclude on the preferable stabilization approach. **Materials and Methods:** The effect of the two protease inhibitors phosphoramidon (PA) and thiorphan (TH) on the stability of the radiotracers ¹⁷⁷Lu-MG11 (¹⁷⁷Lu-DOTA-D-Glu-Ala-Tyr-Gly-Trp-Met-Asp-Phe-NH₂), ¹⁷⁷Lu-PP-F11 (¹⁷⁷Lu-DOTA-(D-Glu)₆-Ala-Tyr-Gly-Trp-Met-Asp-Phe-NH₂) and ¹⁷⁷Lu-PP-F11N (¹⁷⁷Lu-DOTA-(D-Glu)₆-Ala-Tyr-Gly-Trp-Nle-Asp-Phe-NH₂) was assessed in non-tumour-bearing mice. Biodistribution studies were performed for first time in human medullary thyroid cancer MZ-CRC-1 xenografts and in the A431-CCK2 xenografts. All three radiotracers were evaluated alone (w/o) or in combination with the Inhibitors 4h post injection (p.i.). The results were expressed as injected activity per gram (%IA/g). **Results:** ¹⁷⁷Lu-MG11 is highly unstable in vivo (<4% intact peptide, 5 min p.i.) and is tremendously stabilized when co-injected with PA or TH (>70% and >90%, respectively). Diminished stabilization was found for the highest stable analogue in the series ¹⁷⁷Lu-

PP-F11N (intact peptide 39%, 5 min p.i.) after co-injection of PA or TH (60% and 66%, respectively). Due to improved stability the tumour uptake (%IA/g) of ^{177}Lu -MG11 increased from 1.2 ± 0.5 to 7.8 ± 0.8 by co-injection of PA and to 5.4 ± 1.4 with TH in A431-CCK2R tumours, and in MZ-CRC-1 from 3.2 ± 1.5 to 17.2 ± 4.8 and to 12.4 ± 4.2 co-injecting PA and TH, respectively. Less profound effect was found in the tumour uptake of ^{177}Lu -PP-F11 that increased as follows: A431-CCK2R: 6.7 ± 0.6 (w/o), 9.3 ± 1.1 (PA), 8.7 ± 1.2 (TH); MZ-CRC-1: 11.2 ± 0.6 (w/o), 19.7 ± 4.7 (PA), 11.8 ± 8.6 (TH). For ^{177}Lu -PP-F11N the effect is also small in A431-CCK2R tumours: 6.9 ± 0.8 (w/o), 8.5 ± 2.2 (PA), 10.0 ± 2.8 (TH) while no increase was found in the MZ-CRC-1 tumours: 18.8 ± 4.8 (w/o), 15.6 ± 3.8 (PA), 19.3 ± 7.1 (TH). **Conclusion:** The use of protease inhibitors impacts significantly on the *in vivo* stability and tumour uptake of highly unstable gastrin-based radiotracers (i.e. ^{177}Lu -MG11). However, this effect cannot be documented for “stabilized” analogues, such as ^{177}Lu -PP-F11N. The performance of ^{177}Lu -PP-F11N w/o inhibitors is as good as the performance of ^{177}Lu -MG11 in the presence of inhibitors. The human application of single compounds without additives is preferable, as it will facilitate licensing. A clinical phase 0/I study with ^{177}Lu -PP-F11N is already planned.

EPW86

Novel SPECT hypoxia imaging probes with unique retention mechanism

I. O. Umeda, S. Kimura, H. Fujii; National Cancer Center, Kashiwa, JAPAN.

Aim: Hypoxia is a characteristic feature of most solid tumor and closely related to tumor malignancy and treatment-resistance; therefore, *in vivo* visualization of tumor hypoxia promises to greatly contribute for optimization of cancer therapy. However, there is no general clinical probe for hypoxia imaging at present. Most available probes are nitroimidazole derivatives that are labeled with positron-emitters and unsuitable for general use. We herein developed new SPECT probes with a unique retention mechanism, differing from conventional nitroimidazole derivatives. **Strategy and Methods:** We designed new probes as compact compounds that consisted of $^{99\text{m}}\text{Tc}$ -binding ligand components and 4-nitrobenzyl ester or 4-nitrobenzyl sulfide groups. We postulated that, under excessive reductive conditions after the uptake in hypoxic cells, 4-nitrobenzyl ester or sulfide groups would be reduced and released from the original structure, resulting in production of hydrophilic and negatively charged $^{99\text{m}}\text{Tc}$ -complexes. These $^{99\text{m}}\text{Tc}$ -complexes will not be able to penetrate the cell membrane, consequently remaining inside hypoxic cells. To test this hypothesis, we synthesized some candidate compounds and evaluated them by using FM3A and EMT-6 tumor cells and tumor-bearing mice. Their biodistribution patterns were confirmed by *in vivo* SPECT/CT imaging. **Results:** We successfully synthesized some candidate compounds that consisted of $^{99\text{m}}\text{Tc}$ -binding ligand components [triamide mercaptide (N3S) or diamide dithiolate (N2S2)] and 4-nitrobenzyl ester or 4-nitrobenzyl sulfide groups, and labeled them with $^{99\text{m}}\text{Tc}$. In cell-based assay, they demonstrated significantly higher uptake in hypoxic cells than in normoxic cells, indicating the validity of our strategy. Animal studies revealed that their tissue distribution pattern including tumor accumulation after intravenous injection were greatly different depending on the structure of ligand components. By modifying them, the tumor uptake was improved as high as 1–2 % administered dose/g at 1 h after injection, yielding good tumor-to-background ratios. *In vivo* SPECT/CT images clearly depicted their accumulation in tumors. Additionally, intratumoral localization of our probes shown by autoradiography correlated well with positive areas stained with pimonidazole, a marker of hypoxia. **Conclusion:** Newly developed $^{99\text{m}}\text{Tc}$ -labeled probes successfully accumulated in the hypoxic region in the tumor according to our unique retention mechanism. $^{99\text{m}}\text{Tc}$ is the most common nuclide for nuclear medicine probes, therefore they are quite promising as general clinical probes for hypoxia imaging.

E-PW10 – Sunday, October 16, 2016, 08:30 - 09:30, e-Poster Area
e-Poster Walk 10 – Radiopharmaceuticals & Radiochemistry: Radiopharmaceuticals & Instrumentation

EPW87

Automated copper-mediated synthesis of ^{18}F -Flumazenil using the Ora Neptis® and the GE TRACERlab® MX Synthesizers

A. Hiensch¹, R. Martin¹, A. Zerges¹, S. Preshlock², S. Verhoog², M. Tredwell², V. Gouverneur², R. Smits¹, A. Hoepping¹, M. Müller¹; ¹ABX advanced biochemical compounds GmbH, Radeberg, GERMANY, ²University of Oxford, Chemistry Research Laboratory, Oxford, UNITED KINGDOM.

Aim: ^{18}F -Flumazenil (^{18}F -FMZ) is a ligand for the benzodiazepine binding site of the central GABA-A receptor. As a marker for neuronal density [^{18}F -FMZ] is a promising PET radiotracer for the localisation of the epileptogenic zone in drug-resistant epilepsy^[1] and the detection of neuronal loss in the hippocampus of patients with temporal lobe epilepsy.^[2] Until now, main approach for the synthesis of [^{18}F -FMZ] is the nucleophilic introduction of ^{18}F -fluoride into a mazenil precursor bearing a nitro leaving group.^[3] However, the synthesis requires high temperatures, is giving numerous side products and low yields. This makes the synthesis and purification a challenge to any radio chemist. Recently, V. Gouverneur and her co-workers reported a method for the nucleophilic introduction of fluorine into electron rich, neutral and poor aromatic systems. They used boronic acid esters as precursors and replaced them via a copper-mediated coupling with ^{18}F -fluoride.^[4] Based on these findings we aimed to develop an automated, feasible and high-yielding synthesis of [^{18}F -FMZ] using a pinacol boronate precursor on the Ora Neptis® and GE TRACERlab® MX synthesizers. **Methods:** ^{18}F -Fluoride labelling of ^{18}F -Flumazenil has been fully automated on the Ora Neptis® and GE TRACERlab® MX synthesizers including the following steps: (a) ^{18}F -fluoride fixation on a Sep-Pak® QMA Light cartridge and elution with a mild cryptofix solution, (b) azeotropic drying, (c) copper-mediated introduction of ^{18}F -fluoride into the precursor, (d) isolation of the labelled product on a tC18 cartridge, and (e) for the Ora Neptis® synthesizer: HPLC purification and final formulation of the product. For the GE TRACERlab® MX synthesizer, the crude product is easily obtained in order to proceed with a custom-made HPLC purification. **Results:** We established an automated and remotely controlled synthesis of ^{18}F -Flumazenil on Ora Neptis® and GE TRACERlab® MX synthesizers using a disposable kit system. For the Ora Neptis® synthesizer ^{18}F -Flumazenil was typically obtained in 15–20% non-decay-corrected yield. The chemical and radiochemical purities were >95% and >99% respectively (evaluated by HPLC). For the GE TRACERlab® MX synthesizer ^{18}F -Flumazenil was obtained as a raw product in 25–30% non-decay-corrected yield. **References:** [1] A. Hammers *et al.*, *Neurology* **2001**, *56*, 897–906. [2] B. Szeliés *et al.*, *Eur. J. Neurol.* **2000**, *7*, 393–400. [3] R. Schirmacher *et al.*, *Radiochemical Syntheses, Vol. 1: Radiopharmaceuticals for Positron Emission Tomography*, **13**, **2012**, John Wiley & Sons. [4] M. Tredwell *et al.*, *Angew. Chem.* **2014**, *126*, 1–6.

EPW88

Bisultones as attractive tools for the radiolabeling with fluorine-18 of native biopolymers for PET imaging under biocompatible conditions

A. Lafargue, C. Perrio; UMR 6301 ISTCT, LDM-TEP, CNRS, CEA, Univeristy Caen Normandie, CAEN, FRANCE.

Aim: Biopolymer-based radiopharmaceuticals are very attractive for PET imaging due to high affinity and specificity toward their biological molecular targets. However, the incorporation of fluorine-18 into biopolymers remains problematic. Recent advances in direct radiofluorination by formation of ^{18}F -Si, ^{18}F -Al or ^{18}F -B bonds involve functionalization of the macromolecular

object which is not always straightforward.¹ Radiolabeling strategies encompassing ¹⁸F–C bond formation, require radiofluorination of prosthetic groups followed by multiple steps of functional group transformations and purifications before conjugation to the native or modified biopolymer. Previously, we developed a new radiofluorination reaction based on the sultone ring opening with [¹⁸F]fluoride to afford easily purified ¹⁸F-labelled hydrophilic sulfonated products in high yields.² We extended this methodology to a two-step radiofluorination / conjugation sequence from a bis-sultone precursor as an original “double click” strategy for the radiolabeling of lysine, glucose and glucosamine residues as model substrates under biocompatible conditions. Method: Fluorination and radiofluorination of bispropanesultone and bisbutanesultone were performed using [^{19/18}F]fluoride in acetonitrile at room temperature, 50 or 75°C, and followed up by ¹⁹F NMR and HPLC respectively. Conjugation reactions to lysine, glucose and glucosamine were studied in buffer at pH ranging from 8 to 13. Finally, the overall radiofluorination / conjugation sequence was carried out using microfluidics based on staggered herringbone technology. Results: Bispropanesultone was found to be highly reactive for fluorination (quantitative yield after 1h at room temperature) and radiofluorination (about 60% radiochemical yield after 15 min at 50°C) leading to the corresponding [^{19/18}F]fluorosulfonatesultone. Conversion of bisbutanesultone was much more slower (quantitative fluorination after 30h at room temperature, no radiofluorination at 75°C after 15 min). Under non-radioactive condition, conjugation of monofluorosulfonatesultone was quantitative for lysine after 24h for all pH conditions, and for glucosamine after 24h at only pH 13. No conjugation to glucose was observed whatever the conditions. Under radioactive conditions, conjugation was successful only for lysine with optimum radiochemical yields (60%) obtained at pH 8 after 30 min at 50°C. The overall radiofluorination / lysine conjugation process in micromixers led to lysine ¹⁸F-conjugate in around 50% radiochemical yield from [¹⁸F]fluoride in less than 1 min at room temperature. Conclusion: The bis-sultone double ring-opening approach has been validated for ¹⁸F-radiolabeling of lysine containing biopolymers under biocompatible conditions. (1) K. Chansaenpak, B. Vabre, F. P. Gabbai, Chem. Soc. Rev. 2016, 45, 954. (2) Schmitt S, Bouteiller C, Barré L, Perrio C. Chem Commun 2011, 47, 11465.

EPW89

Evaluation of high polar ¹⁸F-Alanine for the labeling of a folate derivative

K. Kettenbach¹, H. Schieferstein¹, S. Pektor², G. Otto², L. M. Reffert³, R. Eckert¹, M. Miederer², F. Rösch¹, T. L. Ross³; ¹Johannes Gutenberg University Mainz, Mainz, GERMANY, ²Universitätsmedizin Mainz, Mainz, GERMANY, ³Hannover Medical School, Hannover, GERMANY.

Objectives: Many relevant biomolecules are based on amino acids what encouraged us to develop a novel ¹⁸F-labeled prosthetic group based on Alanine [1]. This highly polar ¹⁸F-Alanine derivative was used for ¹⁸F-labeling of azide-functionalized molecules, in particularly an azido-folate to improve its pharmacokinetic profile. **Methods:** The labeling precursor was obtained by alkyne-functionalization of *L*-serine using 3-bromo-1-(trimethylsilyl)-1-propyne. This enables the Alanine derivative to participate in CuAAC (copper-catalyzed azide-alkyne cycloaddition). For the ¹⁸F-radiolabeling we used the kryptofix/carbonate system and a chloro-precursor. The ¹⁸F-prosthetic group was isolated via HPLC and subsequently used for the reaction with an azido-functionalized folate derivative. The coupling was performed in PBS at 40 °C using CuSO₄ as catalyst. The ¹⁸F-Ala-folate was isolated via semi preparative HPLC and further evaluated in terms of lipophilicity and human serum stability as well as its binding and pharmacokinetic behavior. For *in vitro* and *in vivo* evaluation KB cells and xenografts in mice will be used for dynamic μPET and biodistribution studies. **Results:** The prosthetic group precursor was synthesized in good overall yields of 17% over 5 steps. The ¹⁸F-labeling was optimized using different bases and reaction conditions, leading to very good conversion rates of 77±6% after 5 min using a microwave-supported synthesis route. Complete deprotection of the ¹⁸F-prosthetic group was performed using

3.3 M HCl at 100 °C for 15 min followed by a semi preparative HPLC giving the final ¹⁸F-prosthetic group. The lipophilicity of the radiolabeled ¹⁸F-prosthetic group was determined as octanol-water-partition by shake flask. A logD value of -1.18±0.03 was calculated. The azido-functionalized folate was labeled via this novel ¹⁸F-prosthetic group using CuSO₄ and sodium ascorbate at 40 °C for 15 min followed by HPLC and SPE purification. **Conclusions:** This novel ¹⁸F-Alanine derivative promises an improved pharmacokinetic profile when coupled to biomolecules because of its amino acid structure having a high polarity. Especially, for peptide structures or very polar biomolecules this new ¹⁸F-radiolabeling method implies a very low influence on the biochemical properties. In summary, this approach offers the introduction of a hydrophilic ¹⁸F-prosthetic group with a minor effect on the physiological behavior of the ¹⁸F-labeled molecule since alanine is a biogenic amine of the amino acid aspartic acid. **Acknowledgements:** The authors thank the Max Planck Graduate Centre Mainz and the C13 cluster of excellence for financial support. **References:** [1] H. Schieferstein *et al.*, Eur J Org Chem, 2014, 3546

EPW90

Integrated microfluidic lab-on-a-chip systems for synthesis and purification of fluorine-18 radiotracers

P. He, M. D. Tarn, M. M. N. Esfahani, N. J. Brown, N. Pamme, **S. J. Archibald**; University of Hull, Hull, UNITED KINGDOM.

Aims: Dose-on-demand production of radiopharmaceuticals has the potential to revolutionise positron emission tomography (PET) medical imaging. Producing a single dose of a desired radiotracer on-site will allow facile adoption of a stratified approach to patient treatment with rapid access to an increased range of radiotracers. We aim to produce modules for lab-on-a-chip device design that can be used for isotope processing, synthesis and quality control tests on a microfluidic scale. Materials and methods: Modules for electrode trapping and release of [¹⁸F]fluoride, synthesis of [¹⁸F]FDG and [¹⁸F]FLT and purification were produced as prototypes using bespoke manufactured microfluidic glass chips with etched channels. [¹⁸F]fluoride was separated from [¹⁸O]water by means of a microfluidic electrochemical cell into dry MeCN solution (0.3 mL) containing KHCO₃ and K222. [¹⁸F]FLT was synthesized from 3'-N-Boc-5'-dimethoxytrityl-3'-O-nosyl-thymidine (10–15 mg) in capillary at 100 °C for 5 min followed acidic hydrolysis at room temperature for 2 min. Monolithic separation columns were produced in-house using a sol-gel process and chemically modified. Results: A process for highly efficient trap and release of [¹⁸F]fluoride from a low volume (< 200 μl) of aqueous solution allows trap and release into acetonitrile with an efficiency of up to 95% in both steps. [¹⁸F]fluoride activity of 95–99% (initial activity 10 mCi) can be efficiently trapped and 75–78% of trapped [¹⁸F]fluoride can be released into 0.3 mL of dry MeCN solution within 5 min, which is subsequently used for fluorination of FLT precursors at 100°C for 5 min and hydrolysis for 2 min at room temperature. Over 75% labelling yield and 100% hydrolysis yield can be obtained. Conclusions: Modules have been designed and tested for the synthesis of [¹⁸F]FDG and [¹⁸F]FLT. An efficient process for transfer of the [¹⁸F]fluoride into acetonitrile via electrode trapping allows synthesis of fluorine-18 containing radiotracers with high efficiency at low volumes. Separation modules using short in-house produced silica monolith columns were effective in providing sufficiently pure tracer samples for *in vivo* studies. Research Support: The authors thank the Daisy Appeal (grant no. DAhul0211) and the University of Hull (HEIF) for financial support. We would like to thank Dr Assem Allam for his generous support of this project.

EPW91

Rapid and cost effective SPE purification screening utilising 96 well plate technology

A. K. Kirjavainen¹, I. Khan², G. McRobbie², R. Fortt¹, J. Grigg², W. Trigg², S. K. Luthra², A. Gee¹; ¹King's College London, London, UNITED KINGDOM, ²GE Healthcare, Amersham, UNITED KINGDOM.

Aim: The aim of the study was to develop a solid-phase extraction (SPE) purification method as an alternative to the time-consuming HPLC purification of [^{18}F]GE-179. Several stationary and mobile phases were screened using a 96-well plate manifold. This enabled a SPE method to be rapidly developed. **Materials & Methods:** Decayed crude reaction mixture was diluted and spiked with GE-179 reference standard. This sample solution was loaded onto the conditioned plates. The plate manifold was connected to a vacuum pump and eluted dropwise. 96-well plates loaded with either ion exchange or tC18 (Waters) stationary phases were used to determine if GE-179 could be separated from the crude reaction mixture. Ion exchange well plates containing mixed cation (MCX), weak cation (WCX), weak anion (WAX) and mixed anion (MAX) ion exchange resins (24 wells each) were loaded with the crude solution. The loading was performed under acidic (pH 1), neutral (pH 7) and alkaline (pH 10) conditions. The existing published Waters 2x4 Method was employed to screen the ion exchange resins. For the tC18 well plate, the following variables were screened: organic mobile phase (MeCN or EtOH); pH (adjusted with TEA/H₃PO₄ to pH 4, 7 or 10) and wash volume. All loading, wash and elution samples were collected and analysed by HPLC (ca. 300 samples analysed). **Results:** MCX and WCX matrices trapped crude GE-179 but could not selectively elute the desired product from other guanidine-containing species. However, using tC18 cartridges, the crude reaction mixture could be trapped and purified using 40% MeCN at pH 7, where MeCN was found to be more effective than EtOH in washing away the less lipophilic impurities. GE-179 was then eluted into the product vial with acidified EtOH. **Conclusion:** The 96-well plate manifold was successfully used for screening of SPE purification of GE-179 in a rapid and cost effective way. Up to 96 different SPE purification conditions were tested in a single experiment. In 2-3 weeks, up to 300 samples were analysed by HPLC in order to determine the initial purification procedure. This technology provides an efficient means of screening SPE purification conditions for radiopharmaceutical products as an alternative to HPLC purification. **Acknowledgements:** This work was supported by European Commission, Marie Curie Fellowship FP7-PEOPLE-2012-ITN (316882, RADIOMI) and the National Institute for Health Research (NIHR) Biomedical Research Centre based at Guy's and St Thomas' NHS Foundation Trust and King's College London.

EPW92

Development of a simple kit-based method for the preparation of pharmaceutical grade ^{68}Ga -labelled radiopharmaceuticals

M. Asti, M. Iori, P. C. Capponi, S. Rubagotti, A. Fraternali, A. Versari; Arcispedale Santa Maria Nuova-IRCCS, Reggio Emilia, ITALY.

Background: The use of the $^{68}\text{Ge}/^{68}\text{Ga}$ generators is still limited if compared to the $^{99}\text{Mo}/^{99\text{m}}\text{Tc}$ counterpart, mainly because of the absence of commercial kits and of a kit-based method for preparing ^{68}Ga -radiopharmaceuticals in a reliable way. The present study aim to develop and optimize a reliable direct preparation of gallium-68 labelled radiopharmaceuticals through a kit-based approach. **Methods:** A fraction of the eluate of two different 1110 MBq commercial $^{68}\text{Ge}/^{68}\text{Ga}$ generators (EZAG, ITG) or the whole eluate of a 370 MBq of a IRE-Elit generator, were directly directed into a vial pre-filled with precursors (DOTATOC, DOTATATE, PSMA-11, PSMA-617) buffer and scavenger (the prototype of a potential lyophilized kit). The vial was directly warmed at 100 °C, or simply shaken at RT for HBED-CC-PSMA precursors, and then buffered with a 1.5 sodium ascorbate solution. Parameters influencing the reactions (reaction time, heating source, reaction pH, state of the reagents) were studied and optimized. The efficacy of the method in terms of incorporation yield and quality of the final radiotracers was compared to preparations performed with two commercial automatic synthesizers. For ^{68}Ga -DOTATOC the comparison was performed in terms of compliance to the Ph. Eur. Monograph. **Results:** In the optimal conditions, the incorporation yields were close to 98 % giving an overall radiochemical

yield of the kit-based process between 75±4 % and 90±2 % not decay corrected (depending on the generator used). The radiochemical purities were all > 95 %. The ^{68}Ga -DOTATOC preparations were compliant with all specifications reported in the pharmacopoeia monograph. **Conclusions:** RCY and RCP of the proposed gallium-68 labelled radiopharmaceuticals performed by a kit-based approach are comparable to those obtained by automatic synthesizers. The feasibility of a kit-based approach for the preparation of ^{68}Ga -DOTATOC / DOTATATE / PSMA-11 / PSMA-617 was proved and a first home-made version of a putative lyophilized kit was proposed.

EPW93

Chemoselective ligation of 2-cyanobenzothiazole with 1,2-aminthiol: a novel approach to label biomolecules

C. Ieritano, Y. Seimbille; TRIUMF, Vancouver, BC, CANADA.

Aim: Development of molecular imaging probes has not kept pace with the discoveries in biology, and the labeling of biomolecules (peptides, antibodies, oligonucleotides, etc.) is one of the major limitations hampering further development and deployment of functional imaging as experimental and clinical tool. Novel bioorthogonal chemistry, including Huisgen's cycloaddition (CuAAC) or inverse electron-demand Diels-Alder cycloaddition (IEDDA), have been recently explored and demonstrated that they are promising avenues to label biomolecules. Considering the biocompatibility and the fast kinetics of the naturally occurring chemoselective ligation between 2-cyanobenzothiazole (CBT) and 1,2-aminthiol to produce firefly luciferin, we have investigated if this specific chemical reaction could be an attractive alternative. **Materials and methods:** CBT reacts rapidly and specifically with 1,2-aminthiol. This chemical reaction adheres perfectly to 'click' criteria. We have envisioned a series of CBT-based chelating agents and a fluorescein-CBT derivative, and subsequently labeled a peptide containing a N-terminal cysteine residue with various radioisotopes to demonstrate the efficiency and versatility of our ligation approach. **Results:** We have synthesized a fluorescein, DOTA, NOTA and deferoxamine (DFO) derivatives containing a 2-cyanobenzothiazole moiety. Synthesis of fluorescein-CBT was accomplished in three steps from 6-hydroxy-2-cyanobenzothiazole, while DFO-CBT and the two macrocyclic chelating agents - DOTA-CBT and NOTA-CBT - were obtained in four and five steps from the same starting material, respectively. To test our labeling strategy, a cyclic RGD peptide has been functionalized with a polyethylene glycol spacer bearing the 1,2-aminthiol bioorthogonal click handle. Chemoselective ligation of the RGD peptide with fluorescein-CBT, and subsequently with Al18F-NOTA-CBT, ^{68}Ga -DOTA-CBT and ^{89}Zr -DFO-CBT have been successfully achieved under mild aqueous conditions. **Conclusions:** Our work is demonstrating the potential of the condensation reaction between CBT and 1,2-aminthiol to label sensitive biomolecules. As a proof of concept, it has been illustrated with a RGD peptide containing a N-terminal cysteine residue, but we anticipate that it could be applied to a large spectrum of biomolecules with wide imaging applications in Life Sciences.

EPW94

Metal Ion Selectivity of Novel Chelates with Application to PSMA Targeted Theranostics

J. M. Kelly, A. Amor-Coarasa, A. Nikolopoulou, D. Kim, C. Williams, Jr., S. Vallabhajosula, J. W. Babich; Division of Radiopharmaceutical Sciences, Department of Radiology, Weill Cornell Medicine, New York, USA, New York, NY, UNITED STATES.

Aim: Theranostic probes for prostate cancer are of potential value due to their ability to detect and treat lesions using a single ligand. DOTA is commonly the chosen chelator for such use. Quantitative labeling with DOTA requires the use of high temperatures and/or long labeling times. We compared three cyclen-based chelators: the octadentate, DOTA, and the decadentate (107) and dodecadentate (106) macrocycles, originally

described by Chong, conjugated to the PSMA-targeting Glu-urea-Lys (EuK) moiety via a thiourea bond to the lysine ϵ -NH₂. **Methods:** Labeling kinetics were assessed for a series of M³⁺ radiometals, including ⁶⁸Ga, ¹¹¹In, ¹⁷⁷Lu and ²²⁵Ac. Labeling was performed at pH 4.5–5.5 in NaOAc or NH₄OAc buffer using 5, 12.5 or 25 μ g of ligand. Complex formation was studied at 25°C, 50°C and 95°C at 1, 5, 10, 15 and 30 min incubation using radioTLC. In addition, each ligand was labeled with ⁶⁸Ga for μ PET/CT imaging studies in nude mice bearing LNCaP xenografts at 1 hr p.i. **Results:** EuK-**107** chelated each of the four metals with >90% efficiency after 1 min at 95°C. Near-quantitative chelation was observed for ¹¹¹In at 25°C. EuK-DOTA performed similarly to **107**, although chelation of ¹¹¹In, ¹⁷⁷Lu and ²²⁵Ac was slower. EuK-**106** achieved >90% chelation of ¹¹¹In at both 25°C and 95°C. In contrast, the maximum chelation of ⁶⁸Ga was >93% (95°C), chelation of ¹⁷⁷Lu was <40% after 30 min at 95°C and chelation of ²²⁵Ac never exceeded 10%. Chelation at 50°C showed considerable variability for all of the complexes with each metal ion studied. The ⁶⁸Ga-labeled complexes accumulated in LNCaP tumors in the order EuK-**107** > **106** > DOTA (5, 4 and 3 %ID/g respectively) displaying good contrast to surrounding tissue. **Conclusions:** Decadentate **107** chelates a range of radiometals of diagnostic and therapeutic interest in near quantitative yields at 95°C. A PSMA-targeting ⁶⁸Ga-labeled construct incorporating **107** showed good tumor uptake (comparable to ⁶⁸Ga-HBED-CC). Some residual blood pool activity was observed, suggesting that tumor uptake may continue to increase over time, which is potentially valuable when therapeutic radionuclides such as ¹⁷⁷Lu or ²²⁵Ac are coordinated. This property was not as evident for EuK-DOTA. On this basis, **107** merits further investigation as a potential chelating moiety for theranostics.

EPW95

68Ga vacuum elution approach for direct labelling of DOTA and NODAGA-conjugated peptides

R. BEN AZZOUNA^{1,2,3}, S. Leygnac^{1,2,3}, F. Al-Shoukr¹, F. Rouzet^{1,2,3}, D. Guilloleau⁴, D. Le Guludec^{1,2,3}; ¹Nuclear Medicine Department and DHU FIRE, Bichat-Claude Bernard University Hospital, AP-HP, Paris, FRANCE, ²UMR 1148 Inserm, Paris, FRANCE, ³Federation de Recherche en Imagerie Multimodale, Paris 7 University, Paris, FRANCE, ⁴Inserm, U930, Université de Tours, CHRU, Tours, FRANCE.

Background and objective: In the last few years ⁶⁸Ga-labelling have gained increased interest for clinical PET. With chemical ⁶⁸Ge/⁶⁸Ga generators, a costly synthesizer was necessary to concentrate and pre-purify the eluate from its metallic impurities. A European pharmaceutical-grade generator has recently received marketing authorisation. The compliance of its eluate with the Eur. Pharmacopeia specifications makes possible the direct labelling of vectors. With the recent advent of single vial formulations, production of ⁶⁸Ga-radiopharmaceuticals becomes readily accessible to all PET centres. However, manual handling of ⁶⁸Ga results in a high radiation dose to the hand. Moreover, the elution of ⁶⁸Ga/⁶⁸Ge generator with the recommended HCl volume leads to a low ⁶⁸Ga concentration which can disturb the labelling. Our approach aimed to circumvent these disadvantages by the use of a concentrated vacuum elution which avoids the radiation exposure and allows the production of ⁶⁸Ga-labelled peptides with high radiochemical (RCP) and radionuclidic purities (RNP), ready for injection without further purifications. **Methods:** Labelling was performed using “vacuum elution and concentration approach”. A vial containing 2.5 mL of 0.1M HCl and filled under nitrogen was connected to the inlet line of generator. A mixture of sodium acetate solution and DOTA or NODAGA-conjugated peptide was first transferred to an evacuated collection vial. The elution was then performed by the action of vacuum. The labelling of NODAGA-c(RGDyK) occurred instantly at room temperature (RT). DOTATOC labelling solution was incubated 7 minutes at 95°C. An evaluation of the radiation exposure using the manual elution with syringe vs the vacuum approach was done. **Results:** The “vacuum elution and concentration approach” makes possible the elution

of 95% of the available generator activity with 2.5mL of eluent (vs. the 5 recommended mL). The radiochemical purities exceed 99% for ⁶⁸Ga-NODAGA-c(RGDyK) and 97% for ⁶⁸Ga-DOTATOC (n=3). ⁶⁸Ge breakthrough ranged from 1.62.E-06 to 2.19E-06 % (Eur. Pharmacopeia specification <1.E-03%). When elution was performed manually, the estimated dose to the hand Hp(0.07) at the calibration date of a 50mCi generator was 39 μ Sv for RT preparation when collection vial is placed into a shielding and >117 μ Sv when heating is required and therefore the collection vial is placed into a dry-heater without further shielding. Hp(0.07)=0 μ Sv with vacuum approach. **Conclusion:** The ⁶⁸Ga vacuum elution and concentration approach allows production of ⁶⁸Ga-radiopharmaceuticals with high RCP and RNP and marked reduction in radiation dose comparatively to the manual approach, making the ⁶⁸Ge/⁶⁸Ga generator the “PET equivalent” of the ⁹⁹Mo/^{99m}Tc generator.

EPW96

Copper-mediated nucleophilic [¹⁸F]fluorination for [¹⁸F]FMTEB and [¹⁸F]flumazenil

A. Krzyczmonik¹, K. Grafinger^{1,2}, T. Keller¹, L. Pfeifer³, S. Forsback¹, F. R. Lopez-Picon^{1,2}, M. Haaparanta-Solin^{1,2}, V. Gouverneur³, O. Solin^{1,4,5}; ¹Turku PET Centre, University of Turku, Turku, FINLAND, ²MediCity Research Laboratory, University of Turku, Turku, FINLAND, ³Chemistry Research Laboratory, University of Oxford, Oxford, UNITED KINGDOM, ⁴Accelerator Laboratory, Åbo Akademi University, Turku, FINLAND, ⁵Department of Chemistry, University of Turku, Turku, FINLAND.

Aim: Copper-mediated nucleophilic [¹⁸F]fluorination of boronic esters is a new method of preparation of PET tracers [1,2]. [¹⁸F]Flumazenil [3] and [¹⁸F]FMTEB [4] are examples of such tracers which can be synthesized by this method. The aim of this project was to test the quality of the final products and evaluate both tracers in rats. **Materials and methods:** [¹⁸F]FMTEB and [¹⁸F]flumazenil were synthesized from boronic ester precursors by nucleophilic fluorination using tetrakis(pyridine)copper(II) triflate as a catalyst. The products were purified by preparative HPLC methods and formulated in saline solution containing 10% ethanol. The quality control of the final products were done by analytical radioHPLC and radioTLC. Sprague Dawley rats were injected with [¹⁸F]flumazenil (n=2; 21.5 and 15.6 MBq; 11.3 and 11.9 ng/kg, respectively) and with [¹⁸F]FMTEB (n=3; 14.7 \pm 6.9 MBq, 0.9 \pm 0.5 ng/kg). The dynamic PET/CT scan was carried out for 60 min. The specific uptake of [¹⁸F]flumazenil and [¹⁸F]FMTEB in brain was demonstrated by pre-treatment studies. Midazolam, that acts at the GABA_A receptor benzodiazepine modulatory site, and ABP688, a high affinity mGlu5 receptor antagonist, were injected 30 min before [¹⁸F]flumazenil and [¹⁸F]FMTEB injection. **Results:** [¹⁸F]flumazenil and [¹⁸F]FMTEB were successfully synthesized using copper-mediated nucleophilic [¹⁸F]fluorination. [¹⁸F]Flumazenil syntheses (n=4; 498 \pm 84 MBq) resulted in a final product with radiochemical purity (RCP) of 98 \pm 2 % and specific activity (SA) of 15 \pm 4 GBq/ μ mol. [¹⁸F]FMTEB (n=4; 251 \pm 195 MBq) was produced with a RCP of 99 \pm 2 % and SA of 153 \pm 63 GBq/ μ mol. In both cases the SA was high enough to provide high quality PET images and the pre-treatment studies in rats confirmed specific uptake in brain. **Conclusion:** Copper-mediated nucleophilic fluorination provides high quality tracers suitable for in vivo PET imaging. **Acknowledgement:** Funding was received from the European Union's 7th Framework Programme for Research, grant number 316882 and from the Academy of Finland, grant number 266891. **References:** [1] Tredwell M et al. *Angew. Chem. Int. Ed.* **2014**, 53, 7751-7755 [2] Enhanced Copper-Mediated ¹⁸F-Fluorination of Aryl Boronic Esters provides Eight Radiotracers for PET Applications, submitted for publication, Gouverneur et al., personal communication [3] Ryzhikov N N. et al. *Nucl. Med. Biol.* **2005**, 32, 109-116 [4] Hamill T. G. et al. *Synapse*, **2005**, 56, 205-216

Poster Walks

PW-1 – Sunday, October 16, 2016, 08:30 - 09:30, Poster Exhibition Hall
Poster Walk 1 – Conventional & Specialised Nuclear Medicine

PW01

Lymphatic system involvement in Klippel-Trénaunay syndrome detected by lower limbs lymphoscintigraphy with ^{99m}Tc-albumin nanocolloid

S. Capitanio¹, R. Dentici², C. Popescu¹, C. Coppola³, R. Mattassi⁴, C. Rossetti¹; ¹Nuclear Medicine Department, ASST Niguarda Hospital, Milan, ITALY, ²Nuclear Medicine Department, ASST Rhodense, Bollate Hospital, Bollate, (MI), ITALY, ³Nuclear Medicine Department, University of Milano-Bicocca, Milan, ITALY, ⁴Vascular Surgery Department, Humanitas Mater Domini Hospital, Castellanza (VA), ITALY.

AIM: Klippel-Trénaunay syndrome (KTS) is a rare congenital disease classically defined as the triad of vascular stain, soft tissue and/or bony hypertrophy, and venous varicosities more commonly affecting the lower limbs and usually isolated to one extremity. Lymphatic malformations are often associated to KTS but surprisingly difficult to diagnose with conventional imaging. Lymphoscintigraphy with ^{99m}Tc-albumin nanocolloid (LS) could represent a valid tool to easily detect lymphatic abnormalities in these patients improving their clinical management. The aim of our study was to determine the role of LS in the identification of lymphatic involvement in KTS patients. **MATERIALS AND METHODS:** we retrospectively analyzed 28 KTS patients (16 males and 12 females, age 30±16) who underwent a lower extremities LS between 2011 and 2015 at Nuclear Medicine Department of ASST Rhodense Hospital (Bollate, Milan). We performed a two-compartment LS in order to evaluate both deep and superficial lymphatic drainages. Firstly, we studied deep lymphatic circulation injecting about 15 MBq in a 0.3 mL dose using a 26-gauge needle in aponeurotic site of the soles of both feet. Images were recorded with a dual-detector instrument, using high-resolution parallel-hole collimators, in the whole-body scanning mode from the feet to the abdomen, at 5 and 30 minutes after plantar injections. Then, for the evaluation of the superficial lymphatic drainage, we performed 4 subcutaneous injections (about 9 MBq each) in the web space between the first and second and the fourth and fifth digits of the feet and in the medial and lateral retromalleolar regions of both limbs. Other series of images were subsequently acquired at 5 and 30 minutes after injections. Criteria for lymphatic dysfunction included delay, asymmetric or absent visualization of regional lymph nodes and/or lymphatic channels, the presence of “dermal flow”, collateral lymphatic channels, hyperplastic or irregular lymphatic channels. **RESULTS:** 23 of 28 patients (82%) showed lymphatic system anomalies. In 11 patients (39%) lymphatic abnormalities were bilateral involving also the limb without edema or other pathological features. In 13 of 28 patients (46%) the two-compartment technique allowed the identification of an altered deep circulation despite a normal superficial flow. **CONCLUSION:** Two-compartment LS showed that lymphatic abnormalities of the lower limbs are a common finding in KTS patients contributing to the limb swelling. This imaging technique could offer a reliable approach to diagnose and characterize the severity of lymphatic disease in these patients, leading to a more appropriate and effective treatment and preventing secondary effects.

PW02

Imaging of chronic recurrent multifocal osteomyelitis using ¹⁸F-NaF PET/MRI

M. Ø. Fosbøl¹, H. H. Johannesen¹, C. Myrup¹, T. Bjarnsholt¹, V. A. Kristensen², L. Borgwardt¹; ¹Rigshospitalet, Copenhagen, DENMARK, ²Næstved Hospital, Næstved, DENMARK.

Introduction: Chronic recurrent multifocal osteomyelitis (CRMO) is a rare inflammatory disorder in children and adolescents. Reliable imaging modalities are important to support diagnosis of CRMO and detect sub-clinical lesions. Aim of this study was to investigate the value of ¹⁸F-NaF PET/MRI in detecting CRMO lesions compared to standard ^{99m}Tc-diphosphonate bone scintigraphy with supplemental SPECT/low dose CT. **Methods:** ¹⁸F-NaF PET/MRI was performed in four patients (all females, age range 9-12 years) with CRMO verified by histopathology. PET/MRI was performed using a Siemens Biograph mMR 3 Tesla scanner 45 minutes after administration of ¹⁸F-NaF (2.2 MBq/kg, max 100 MBq). MR imaging: DIXON sequences for attenuation correction, coronal STIR and coronal T1 weighted sequences from skull base to toes for diagnostic imaging. Images were interpreted by experienced pediatric nuclear medicine physician and -radiologist. Lesions with increased tracer uptake and/or pathology identified on MRI were classified as symptomatic CRMO foci, subclinical CRMO foci, equivocal foci or classified as pathology not related to CRMO. PET/MRI results were compared to planar whole-body bone scintigraphy with supplemental SPECT/IdCT. Study was approved by the local ethical committee. **Results:** 21 lesions were identified (9 symptomatic CRMO foci, 8 subclinical CRMO foci, 1 equivocal focus and 3 foci not related to CRMO). The CRMO lesions were localized in the long bones (n=11), pelvis (n=3), calcaneus (n=2) and talus (n=1). All CRMO lesions had increased uptake of ¹⁸F-NaF, although one histopathological verified lesion presented as lower uptake in an epiphyseal plate with adjacent diffuse increased uptake. One symptomatic CRMO focus had no corresponding pathology on MRI. Bone scintigraphy identified 8 (89%) of the symptomatic foci and two (25 %) subclinical foci. **Conclusion:** Preliminary results suggest that ¹⁸F-NaF PET/MRI can be valuable in CRMO patients by increasing detection rate of foci compared to MRI and bone scintigraphy with supplemental SPECT/IdCT.

PW03

Differential diagnostic value of bone SPECT/CT versus SPECT alone in patients presenting with newly diagnosed cervical neck pain

L. D'hulst¹, D. Nicolaij², L. Nouwync³, O. Gheysens^{1,4}, I. Malfait³, A. Maes^{2,4}, C. Van de Wiele²; ¹Nuclear Medicine, AZ Groeninge Kortrijk and Nuclear Medicine and Molecular Imaging, University Hospital Leuven, Kortrijk, BELGIUM, ²AZ Groeninge, Kortrijk, BELGIUM, ³Catholic University Leuven, Kortrijk, BELGIUM, ⁴Department of Imaging and Pathology, Catholic University Leuven, Leuven, BELGIUM.

Aim of the study: To assess differences in diagnostic value between bone single photon emission computed tomography (SPECT) / computed tomography and SPECT alone in patients referred for newly diagnosed cervical neck pain. **Patients and methods:** All consecutive patients that were referred to our department between 04-2014 and 02-2015 with new onset of cervical neck pain and without history of cervical interventions, were retrospectively included in the study. All patients underwent diagnostic bone SPECT/CT imaging of the cervical spine 4h after injection of a weight-adjusted activity of ^{99m}Tc-HDP according to the EANM recommendations. SPECT and SPECT/CT images were independently interpreted by two experienced nuclear medicine physicians blinded to the clinical findings and other imaging results. Differences in image interpretation were resolved by consensus. Images were analyzed for the presence of abnormal findings and in case of a positive scan, the exact location was determined on SPECT and SPECT/CT. SPECT/CT imaging was used as gold standard for identifying the exact location of abnormal uptake. **Results:** Fifty-eight patients (13 men and 45 women) with a mean age of 49 years (range: 19 - 79 yrs) were included. In 21 patients (36%), both SPECT and SPECT/CT proved negative. In 11 patients (19%) both SPECT and SPECT/CT imaging showed facet joint arthropathy and/or discarthrosis that were concordant in terms of their exact level localization. In an additional 23 patients (40%) SPECT and SPECT/CT showed concordant pathological uptake in either disc or

facet joint but were discordant with regards to their location. Finally, in the remaining 3 patients (5%), SPECT findings were judged negative whereas SPECT/CT findings were considered positive. **Conclusion:** SPECT/CT imaging improves the accuracy for detection and localization of pathological bone uptake in patients presenting with newly diagnosed cervical neck pain. In our study, the location of active disease was changed in 40% of the patients when using SPECT/CT. Additionally, in three patients, SPECT/CT demonstrated pathology which was not detected on SPECT alone.

PW04

Canine NaF-18 PET/CT: Knee Assessment Using an Old Skeletal Radiotracer

M. I. Menendez, B. Hettlich, L. Wei, M. V. Knopp; The Ohio State University, Columbus, OH, UNITED STATES.

Osteoarthritis (OA) is a complex degenerative disease affecting the entire joint including synovium, menisci, ligaments and subchondral bone. It has been suggested that these subchondral bone changes are related to the severity of the cartilage lesions. Surgically-induced animal models of OA, such as an anterior cruciate ligament transection (ACLT) mainly involve inducing a mechanical instability within the joint, leading to pathological changes analogous to those observed in post-traumatic human OA. Sodium 18F-fluoride (18F-NaF) as a radiotracer per se in noninvasive *in vivo* imaging has been used to investigate musculoskeletal diseases. In clinical oncology, primary bone tumors, skeletal metastasis, benign bone diseases, and patellofemoral pain can reliably be detected by 18F-NaF PET. The aim of this study was to examine the use of 18F-NaF PET for the qualitative serially *in vivo* assessment of pathophysiological bone metabolism of induced OA in a canine model. Five skeletally mature Beagles underwent ACLT in one knee via arthroscopy, the contralateral knee served as control. Prior, 3 and 12 weeks after ACLT, under general anesthesia, the dogs underwent Na-F-18 PET-CT. Na-F-18 was injected (111 MBq) and PET/CT was performed using a Philips Gemini TF 64 PET-CT system (Cleveland, Ohio). Combined dynamic and whole-body imaging over 50 min were acquired. PET/CT parameters included 120KVp, 163mAs and 4 mm slice thickness, 90 seconds per bed position. Images were qualitatively analyzed by experienced blinded reader review and quantitatively by 3D ROI placement on the knee. The qualitative assessment of the scans performed prior to ACLT and post-arthroscopy, demonstrated significant differences in imaging characteristics. The knees that underwent ACLT showed a significantly higher Na-F-18 uptake than the contralateral uninjured knees at 3, 6 and 12 weeks. The higher Na-F-18 uptake found sequentially in the canine knees after ACLT is indicative of active bone turnover and altered bone metabolism. Thus, Na-F-18 PET/CT demonstrated to be a capable and reliable bone imaging marker detecting bone remodeling changes in the knee after a post-traumatic ACL transection in an *in vivo* canine model of OA. Na-F-18 PET provides insight into OA pathophysiology and appears to enable early diagnostic OA surveillance and therapy monitoring *n* pre-clinical studies.

PW05

The role of the scintigraphy using ^{99m}Tc-HMPAO labelled leucocytes in the diagnosis of inflammatory bowel disease in children with abdominal pain

D. Chroustova¹, N. El-Lababidi², J. Tmka³, V. Ptacnik¹, J. Kubinyi¹; ¹Department of Nuclear Medicine General University Hospital and 1st Faculty of Medicine, Charles University, Prague, CZECH REPUBLIC, ²Clinic of Paediatrics and Adolescent Medicine, General University Hospital and 1st Faculty of Medicine, Charles University, Prague, CZECH REPUBLIC, ³Department of Radiation Protection General University Hospital and 1st Faculty of Medicine, Charles University, Prague, CZECH REPUBLIC.

Introduction: Abdominal pain is one of the leading complaints in childhood. Its differential diagnosis is very broad. The possibility of inflammatory bowel disease (IBD) should be taken in mind. The clinical and laboratory findings are often unspecific. Imaging techniques can be helpful in setting the diagnosis. The first imaging method of choice is abdominal ultrasound and scintigraphy, due to their availability and non-invasive nature. The aim of this study was comparison of the results of scintigraphy using ^{99m}Tc-HMPAO (HexaMethylPropylenAmine Oxime) labelled leucocytes (LLE) and the final diagnosis in 69 children with suspected IBD and the evaluation of this method in the diagnostic scheme. **Patients and methods:** 69 children (30 boys and 39 girls, aged 4 to 18 years, average age 13.4 years) complaining of abdominal pain, examined between years 2010 and 2015 were included. After a detailed clinical and laboratory examination (in the majority of cases ASCA and fecal calprotectin levels were evaluated), scintigraphy using INFINIA Hawkeye 4 camera was performed after the administration of LLE. Early abdominal scintigrams were taken 40 minutes, abdominal SPECT 90 minutes and WB scans 180 minutes post LLE injection. The results were compared with the children's final diagnosis, which was established using other paediatric investigations and follow-up. **Results:** Corresponding scintigraphic findings and the final cause of abdominal pain were found in 92%. Using scintigraphy, 15 children were identified with IBD (in 14 cases Crohn's disease and in 1 case ulcerative colitis). IBD was verified in these children using MR enterography and endoscopies including biopsies. 48 children had a negative scintigraphic result. Their final diagnoses were mostly a different chronic GIT illness or another systemic diseases. 6 children (8%) had a disagreement between the scintigraphy outcome and the MR enterography and/or biopsy findings. 4 children had a positive scintigraphy finding but IBD was not confirmed on a histological level. 2 children had a negative scintigraphy outcome but enterography and histological findings admitted the presence of IBD. **Conclusion:** The corresponding findings using scintigraphy using LLE and the final cause of the abdominal pain in children confirm the importance of this method as a non-invasive screening tool for verifying the presence and the degree of inflammation with a high sensitivity. In many cases, when this examination's result marks the probability of IBD as unlikely, it saves the child from undertaking more invasive procedures.

PW06

Diagnostic performance of (18F)-Fluorocholine PET/CT in comparison to conventional scintigraphic imaging in primary hyperparathyroidism

A. Cuderman¹, S. Rep¹, M. Hocevar², K. Zaletl¹, M. Jensterle Sever³, T. Kocjan³, L. Lezaic³; ¹Department for Nuclear Medicine, University Medical Centre Ljubljana, Ljubljana, SLOVENIA, ²Department for oncological surgery, Oncology Institute, Ljubljana, SLOVENIA, ³Endocrinology, Diabetes and Metabolic Diseases, University Medical Centre Ljubljana, Ljubljana, SLOVENIA.

Background: Primary hyperparathyroidism (PHPT) is a common endocrine disorder characterized by parathyroid PTH overproduction with surgical removal of overactive gland(s) being its definitive treatment. Conventional nuclear medicine imaging currently remains the method of choice in preoperative localization of the causative gland(s), however sensitivity in cases of multiple gland disease (multiple adenoma or hyperplasia) is suboptimal. In several pilot series, (18F)-Fluorocholine PET/CT was suggested as superior imaging modality in comparison to conventional scintigraphic imaging. **Objective:** evaluation of (18F)-Fluorocholine PET/CT as the possible superior modality in preoperative hyperfunctioning gland localization in a larger patient series. **Methods:** 88 patients with PHPT were imaged preoperatively with (18F)-Fluorocholine PET/CT and conventional parathyroid scintigraphic methods consisting of ^{99m}Tc-sestaMIBI SPECT/CT, ^{99m}Tc-sestaMIBI/pertechnetate subtraction imaging and ^{99m}Tc-sestaMIBI dual-phase imaging. Imaging results were compared against histology as the

gold standard and postoperative Ca²⁺ and iPTH to calculate sensitivity and specificity; McNemar's test was used for comparison of imaging methods. **Results:** The sensitivity of (18F)-Fluorocholine PET/CT was significantly higher at 95% than conventional scintigraphic methods combined at 65% (53%, 43% and 37% for 99mTc-sestaMIBI SPECT/CT, 99mTc-sestaMIBI/pertechnetate subtraction imaging and 99mTc-sestaMIBI dual-phase imaging, respectively; McNemar < 0,05 for all comparisons). The diagnostic superiority of (18F)-Fluorocholine PET/CT was particularly evident in patients with multiple gland disease. Specificity was 100% in all modalities. **Conclusion:** (18F)-Fluorocholine PET/CT is a significantly superior imaging modality than currently widely used conventional scintigraphic imaging.

PW07

The value of FDG-PET/CT in diagnosis and during follow-up of 273 patients with chronic Q fever

I. Kouijzer¹, E.Aarntzen¹, L. Kampschreur², P. Wever³, C. Hoekstra³, M. van Kasteren⁴, M. de Jager-Leclercq⁵, M. Nabuurs-Franssen⁶, M. Wegdam-Blans⁷, L. de Geus-Oei⁸, W. Oyen¹, C. Bleeker-Rovers¹; ¹Radboudumc, Nijmegen, NETHERLANDS, ²University Medical Center Utrecht, Utrecht, NETHERLANDS, ³Jeroen Bosch Hospital, Den Bosch, NETHERLANDS, ⁴Elisabeth Hospital, Tilburg, NETHERLANDS, ⁵Bernhoven Hospital, Uden, NETHERLANDS, ⁶Canisius Wilhelmina Hospital, Nijmegen, NETHERLANDS, ⁷Laboratory for Pathology and Medical Microbiology (PAMM), Veldhoven, NETHERLANDS, ⁸Leiden University Medical Center, Leiden, NETHERLANDS.

Aim: Between 2007 and 2010, a large Q fever outbreak was observed in the Netherlands with over 4000 notified cases. In one to five percent of all acute Q fever infections, chronic Q fever develops, mostly manifesting as endocarditis, infected aneurysms, or infected vascular prostheses. Diagnosis is often difficult, because symptoms may be aspecific and infectious foci are often not visible with conventional imaging techniques. In this study, we investigated the diagnostic value of 18F-fluorodeoxyglucose positron emission tomography with combined computed tomography (FDG-PET/CT) in chronic Q fever at the time of diagnosis and during follow-up. **Materials and methods:** All Dutch adult patients suspected of chronic Q fever who were detected since the start of the Dutch Q fever epidemic in 2007 were retrospectively included until March 2015 when at least one FDG-PET/CT was performed. Clinical data and results from FDG-PET/CT scans at diagnosis and during follow-up were collected. **Results:** 273 patients suspected of chronic Q fever were included. Eventually, of 147 patients with proven chronic Q fever, 63 patients were diagnosed with infected vascular prostheses, 34 patients had an infected aneurysm, and 9 patients had definite endocarditis according to the revised Duke criteria. Of all 273 FDG-PET/CT scans performed at diagnosis, 31 scans (11.4%) led to a change in diagnosis (switch from probable to proven chronic Q fever). At diagnosis, 42 scans (15.4%), performed after blood and sometimes tissue PCR, led to treatment adjustment (start of antibiotic treatment in 37 patients, stop of antibiotic treatment in 2 patients, change of antibiotic treatment in 3 patients). Of all 175 scans performed during follow-up in 100 patients (median 2 scans per patient), 2 scans (1.4%) led to a change in diagnosis (switch from probable to proven chronic Q fever). Of 144 follow-up scans in patients with proven chronic Q fever, FDG-PET/CT led to a stop of antibiotic treatment in 12 (8.3%) of cases and 78 (54.2%) of FDG-PET/CT scans led to the decision of continuing antibiotic treatment. When adding FDG-PET/CT to the Duke criteria as major criterion, 15 more definite endocarditis were diagnosed. **Conclusions:** FDG-PET/CT is a valuable diagnostic technique in localizing chronic Q fever and during follow-up often leading to a change in diagnosis and/or adjustment of treatment.

PW08

Diabetic Patients With Suspected Foot Osteomyelitis: SPECT-WBC/MRI Versus SPECT-WBC/CT

M. Zorkaltsev, A. Kurazhov, V. Zavadovskaia, M. Zamyshevkaia, V. Udodov, E. Grigoriev; Siberian State Medical University, TOMSK, RUSSIAN FEDERATION.

Aim. To evaluate the diagnostic value of SPECT-WBC/MRI and SPECT-WBC/CT in detection of osteomyelitis in patients with various forms of diabetic foot (including Charcot foot). **Material and methods.** 80 patients (38 males and 42 females, aged 57.4 ± 12.1 years) with suspected diabetic foot bone infections were studied. Patients underwent 99mTc-HMPAO-labeled leukocytes scintigraphy (n=80, 370 MBq, SPECT Philips BrightView), MRI (n=54, Siemens Magnetom Essenza 1.5T), CT (n=26, GE Optima CT660 M40). Fusions of SPECT and MRI or CT were performed in program RView 9.06 (Colin Studholme). Diagnosis of osteomyelitis was established by pathologic specimen (n=31) and successful response to medical management (n=14). **Results.** When using SPECT-WBC/MRI (diagnostic criterion was a maximum accumulation of radiopharmaceutical in bone determined by MRI) were obtained 28 TP, 24 TN, 1 FP, and 1 FN results. SPECT-WBC/CT was demonstrated 15 TP, 9 TN, 1 FP, and 1 FN results. FP results in both methods were acquired in the case of neuroarthropathy (Charcot foot). Identified both FN results were due to the complexities of toes fusion. Summary, for SPECT-WBC/MRI in detections of osteomyelitis sensitivity, specificity, positive, negative predictive value and accuracy were 96.6%, 96.0%, 96.3%, 96.6%, and 96.0%, respectively, and for SPECT-WBC/CT 93.8%, 90.0%, 92.3%, 93.8%, and 90.0%, respectively. **Conclusion.** SPECT-WBC/MRI and SPECT-WBC/CT both demonstrated high sensitivity and specificity, and were comparable in detection of osteomyelitis in diabetic foot patients. FN results of SPECT-WBC/CT should be avoided if hybrid technic were used directly. But SPECT-WBC/MRI has potentially advantage in the indication of soft tissue infections.

PW09

Can we avoid early image at 30min on labelled leukocytes scintigraphy in the diagnosis of osteoarticular infection?

E. Noriega Álvarez¹, J. Rodríguez-Rubio Corona¹, I. Romero Zayas², M. T. Bajén Lázaro¹, A. M. Benítez Segura¹, M. P. Boya Román¹, A. Rodríguez-Gasén¹, G. A. Martínez-Pimienta¹, R. Jaller Vanegas¹, J. Suils Ramón¹, J. Mora Salvadó¹; ¹Nuclear Medicine Department, Hospital Universitari de Bellvitge-IDIBELL., Barcelona, SPAIN, ²Radiopharmacy and PET Units, Nuclear Medicine, IDI. Hospital U. de Bellvitge-IDIBELL, Barcelona, SPAIN.

Introduction and aim: Except for spine, white blood cell scintigraphy images (WBCS) is consider the first choice in Nuclear Medicine for bone infection diagnosis and the recommended protocol in literature includes images acquisition at 30min, 4h and 24h. The objective of this study is to demonstrate that it is possible to avoid early image at 30min in osteoarticular infection diagnosis in order to substantially shorten and simplify the exploratory protocol. **Material and methods:** 100 patients were studied (61 women, age 22-83 years) with suspected osteoarticular infection (e.g. axial osteomyelitis, peripheral osteomyelitis, joint prostheses, diabetic foot, etc.). Autologous leukocytes were radiolabelled with 740MBq of 99mTc-HMPAO following the EANM "Guidelines for the labelling of leucocytes with 99mTc-HMPAO." Acquisition of spot images at 30min, 4 and 24h p.i. with acquisition times of 5, 8 and 20 minutes respectively (based on the time correction acquisition decay). Two set of images were used: a) Group1: at 30 min, 4 and 24h b) Group2: only at 4 and 24h. The images were interpreted visually without any manipulations by two experienced nuclear medicine physicians. They classified WBCS

as: *Positive*: when there was an increase in intensity or extension of activity at 24h in comparison with earlier images. *Negative*: when there was no activity or there was a decrease in activity at 24h in comparison with earlier images. The clinical diagnosis was established by culture and/or biopsy in 52 cases and 6 months of clinical follow-up in the 48 remaining cases. Sensitivity, specificity, positive predictive value, negative predictive value and accuracy were analyzed in the two set of images. **Results:** Infection was confirmed by cultures/biopsy in 23 cases and infection was discarded in 77 cases (48 through follow-up and 29 by cultures). In Group1 WBCs were positive in 19 cases and negative for infection in 75 cases. In Group2 comparing with the Group1 there was not changes in visual analysis and the statistical data results are the same than Group1. **Conclusion:** Despite the small sample size in this preliminary study, the results both groups are the same, so it is possible to avoid 30min WBCs image without any changes in the scintigraphic diagnosis, in order to obtain a shorter acquisition protocol.

PW10

Usefulness of SPECT/CT in the diagnosis of posttraumatic and post-surgical peripheral bone osteomyelitis by Tc-99m-HMPAO-labeled leucocyte scan

S. Georga¹, V. Athanasiou¹, V. Vraggalas², G. Gkouvas³, D. Karapiperis⁴, D. Katsaboukas¹, I. Iakovou¹, V. Mpalaris¹, D. Lo-Presti¹; ¹3rd Dept of Nuclear Medicine, Aristotle University Medical School, Papageorgiou Hospital, THESSALONIKI, GREECE, ²2nd Orthopedic Dept of 424 General Military Hospital, THESSALONIKI, GREECE, ³1st Orthopedic Dept of 424 General Military Hospital, THESSALONIKI, GREECE, ⁴Infectious Diseases Dept of 424 General Military Hospital, THESSALONIKI, GREECE.

Introduction-Aim: Scintigraphy with in vitro labeled leucocytes has proven useful method for diagnosing complicated peripheral bone osteomyelitis. The aim of the study was to evaluate the contribution of SPECT/CT as an adjunct to planar images of ^{99m}Tc-HMPAO-labeled leucocyte scan (LS) for diagnosing posttraumatic and postsurgical peripheral bone osteomyelitis (OM). **Patients and methods:** Thirty two adult patients with clinical suspicion of peripheral bone OM in 36 sites, after trauma or fracture with or without metallic implants (n=24 sites), or after surgery (n=12) were enrolled in the study. Sites of suspected infection included: tibia (n=14), fibula (n=5), femur (n=4), calcaneus (n=5), other tarsal bones (n=3), metatarsus (n=3) and humerus (n=2). All patients underwent LS. Planar images were acquired 1 and 4 hours p.i. followed by a SPECT/CT scan. Bone marrow scan with ^{99m}Tc-tin-colloid (BMS) was additionally performed in 23 pts (26 sites). LS planar images were interpreted alone, in conjunction with SPECT/CT scans, and with BMS images. Persistent increased leucocyte bone uptake was compatible with OM. Incongruent LS/BMS images indicated OM. Final diagnosis was based on clinical follow-up or surgical results. **Results:** Final diagnosis was OM in 13/36 sites, soft tissue infection (STI) in 10/36 sites and no evidence of active infection in 13/36 sites. LS planar imaging results were: TP 11, TN 16, FP 7 and FN 2. The addition of SPECT/CT correctly localized infection to bone in 13/13 sites with OM and to soft tissues in 10/10 sites with STI, changing the interpretation of planar images in 6/36 sites (16.7%) and allowed better definition of the extent of infection in 17 more sites. SPECT/CT results were: TP 13, TN 19, FP 4 and FN 0. Sensitivity, specificity and accuracy of LS planar images for diagnosing posttraumatic and postsurgical OM were 84.6%, 69.6% and 75%, respectively, improved to 100%, 82.6% and 88.9%, respectively with the addition of SPECT/CT. The addition of BMS further improved specificity and accuracy of LS from 82.6% to 100% and from 88.9% to 96.1%, respectively, by reducing false positive results due to active bone marrow. **Conclusion:** SPECT/CT increases the diagnostic accuracy of LS for diagnosing posttraumatic and postsurgical peripheral bone OM, allowing accurate discrimination of bone from soft tissue infection and better definition of the

extent of infection. Combination with bone marrow scan, in cases of equivocal LS results, further improves accuracy of LS by enabling differentiation of active bone marrow due to healing processes from infection.

PW-3 – Sunday, October 16, 2016, 08:30 - 09:30, Poster Exhibition Hall
Poster Walk 3 – Cardiovascular System: Cardiovascular Imaging

PW21

PET Imaging In The Diagnosis Of Prosthetic Valve Endocarditis: Contribution Of The Standardized Uptake Value

A. Jiménez-Ballvé, C. Sánchez-Enrique, M. J. Pérez-Castejón, A. Ortega-Candil, M. Pedrera-Canal, I. Vilacosta, C. Olmos, I. Serrano García, J. L. Carreras-Delgado; Hospital Clínico San Carlos, Madrid, SPAIN.

Aim: The aim of this study was to assess the usefulness of the maximum Standardized Uptake Value (SUVmax) in ¹⁸F-FDG PET/CT scans for the diagnosis of prosthetic valve endocarditis (PVE). **Materials and methods:** We performed a prospective study including 45 patients (30 male and 15 female), with suspicion of PVE according to the Duke criteria from February 2013 to August 2015. SUVmax was measured in the suspicious foci (prosthetic material) and in two regions with physiological FDG uptake (mediastinal blood pool in ascending aorta and liver parenchyma in right hepatic lobe). We calculated two SUV ratios by dividing SUVmax prosthesis/SUVmax aorta and SUVmax prosthesis/SUVmax liver. The gold standard was the Duke pathological criteria (when tissue available) and in cases without surgery the final diagnosis was established by the endocarditis team decision after ≥ 4 month follow-up. **Results:** In the 45 PET/CT scans, we analyzed 62 prosthesis (35 mechanical and 27 biological); 64% localized in aortic valve, 31% in mitral valve and 5% in tricuspid valve. The abnormal uptake distribution on the prosthesis was 58% diffuse, 29% focal and in 13% non increased uptake was detected. The mean of SUVmax in the prosthesis, aorta and liver were 5.0, 2.0 and 3.5, respectively. Final diagnosis was PVE in 31 foci (50%). Mean values of SUVmax showed significant differences (p<0.001) between the group with final diagnosis of definitive and rejected infective endocarditis (6.7 vs 3.4 for SUVmax prosthesis; 3.6 vs 1.6 for SUV ratio aorta and 2.1 vs 0.64 for SUV ratio liver). The ROC curves showed an area under the curve of 0.85 for SUVmax prosthesis, 0.89 for SUV ratio aorta and 0.91 for SUV ratio liver. Semiquantitative parameters identified positives cases of infective endocarditis with a SUVmax prosthesis cutoff value of ≥4.5 (81% sensitivity and 65% specificity), SUV ratio aorta cutoff value of ≥2.3 (84% sensitivity and 74% specificity) and SUV ratio liver cutoff value of ≥1.3 (87% sensitivity and 74% specificity). Cutoff value ≥6.3 SUVmax prosthesis, ≥3.0 SUV ratio aorta and ≥1.8 SUV ratio liver, achieved a specificity of 97% to confirm infection. We did not found differences in the mean of SUVmax between mechanical and biological prosthesis (4.7 vs 5.5; p=0.273). **Conclusion:** Semiquantitative analysis of FDG uptake seems to be useful in distinguish presence from absence of infection in patients with suspicion of prosthetic valve endocarditis, not finding differences in the prosthetic material.

PW22

Doxorubicin Effect on Myocardial Metabolism: a ¹⁸F-FDG PET/CT and Echocardiographic Approach

M. Bauckneht¹, F. Fiz^{1,2}, G. Ferrarazzo¹, A. Ghidella³, P. Ameri³, P. Spallarossa³, S. Fiordoro¹, A. Bellodi⁴, L. Picori¹, G. Siclari¹, M. Miglino⁵, S. Morbelli¹, C. Marini⁶, G. Sambuceti¹; ¹Nuclear Medicine Unit, IRCCS AUO San Martino IST, Genova, ITALY, ²Nuclear Medicine Unit, Department of Radiology, Uni-Klinikum, Tübingen, GERMANY, ³Cardiology Unit, IRCCS AUO San Martino

IST and Department of Internal Medicine, University of Genova, Genova, ITALY, ⁴Department of Hematology and Oncology, IRCCS AOU San Martino – IST, Genova, ITALY, ⁵Haematology Clinic, Department of Internal Medicine (DiMI), University of Genoa, IRCCS AOU S, Martino-IST, Genova, ITALY, ⁶Institute of Bioimaging and Molecular Physiology, CNR, Milan, Genoa Section, Genova, ITALY.

Aim. Doxorubicin (DXR) induced cardiotoxicity is related to several mechanisms, including interference of mitochondrial respiratory chain and acceleration of glycolysis. We previously reported that this treatment may enhance myocardial FDG uptake. The present study aimed to verify whether this metabolic response on serial PET/CT imaging can predict myocardial function, non-invasively evaluated by follow-up echocardiography (ECHO). **Materials and Methods.** ¹⁸F-FDG PET/CT of 25 patients affected by Hodgkin Disease (HD), treated following ABVD scheme were analyzed. Inclusion criteria were: 1) availability of 4 consecutive PET/CT scan for staging (PET1), interim (PET2), post-therapy (PET3) and six months follow-up evaluation (PET4); 2) full remission after two ABVD cycles; 3) normal baseline EKG and ECHO findings and 4) no concurrent treatment with external thoracic radiotherapy. A volume of interest was manually drawn on the left ventricular myocardium. Average standardized uptake value within this region was normalized for the corresponding blood pool index measured in the inferior vena cava to obtain LV-SUV. All patients underwent a 12 months cardiological follow-up assessment encompassing clinical evaluation, EKG and ECHO. A cardiologist unaware of PET findings performed this procedure. **Results.** LV-SUV progressively increased from PET1 to PET4 in 6 patients (24%, 2 females, mean age 39±17, termed “increasers”) being 1.34±0.9, 3.34±2.6, 4.32±2.8 and 4.43±1.5 respectively. In the remaining 19 patients (76%, 7 females, 36±14), FDG uptake showed a largely variable response without any progressive increase. Accordingly, the ratio between PET4 and PET1 LV-SUV in the two subgroups was 3.85±0.8 and 1.06±0.4, respectively (p<0.001). Up to six months after therapy discontinuation, none of the 25 patients showed signs or symptoms potentially related to DXR cardiotoxicity. However, late follow-up ECHO detected the appearance of first-degree diastolic impairment with respect to baseline in 9 of the 25 examined patients (36%, 4 females, mean age 36±18). This finding occurred in 5/6 “increasers” (83%) and in only 4/19 non-increasers (21%) (p<0.001). **Conclusions.** The present data indicate that DXR related myocardial damage can be preceded by an enhanced glucose uptake. ¹⁸F-FDG PET/CT imaging might represent a useful tool to identify high-risk patients and to implement personalized program to monitor and prevent DXR-induced cardiotoxicity.

PW23

Quantitative and qualitative analysis to decide if perform only stress MPI protocol

A. Di Palo, A. Niccoli Asabella, C. Altini, F. Iuele, A. Cimino, G. Rubini; Nuclear Medicine Unit, D.I.M., University of Bari “Aldo Moro”, Bari, Italy, Bari, ITALY.

Aim: Myocardial perfusion imaging (MPI) is often employed to diagnose coronary artery disease (CAD) in patient with suspected angina. It is possible perform only stress MPI protocol (S-MPI) to saving time, costs and radiation exposure of patients and staff. We performed this study to establish a line of behavior to reduce significantly the radiation exposure but able to perform a reliable diagnosis of CAD. The aim of this study is evaluate if the choice to performing also the R-MPI is influenced by the qualitative or the quantitative analysis results in patients with the S-MPI. **Material and Methods:** We retrospectively analyzed S-MPI in 152 patients (57 female, 95 male), mean age 62,4 (range 12-84 years) who performed MPI according the standard protocol. We select patients with cardiac symptoms and without myocardial scar; among these 48/152 (31.5%) had a history for cardiovascular events, 31/152 (20%) had a

doubt echocardiography, 42/152 (48%) had a pre-test doubt (ECG-stress or coronarography), 27/152 (17%) both the events and 4/152 (2.6%) none. 82/152 (53%) had a maximal stress test during the S-MPI. Images were analyzed with qualitative perfusion and quantitative gated single-photon emission computed tomography (SPECT) (QPS/QGS) software. We performed a qualitative analysis of stress imaging (QA-SI) and considered the Summed Stress Score (SSS) for the quantitative assessment. The agreement between the QA-SI and the SSS analysis was calculated with Cohen’s Kappa. **Results:** Considering the qualitative analysis, the exam resulted positive in 81/152 (53%) and negative in 71/152 (47%); considering the SSS analysis 39/152 (26%) patients were positive while 113/152 (74%) were negative. Both the QA-SI and SSS analysis was positive in 28/152 (18%) patients; in 11/152 (7%) SSS analysis was positive and QA-SI was negative. SSS analysis was negative and the QA-SI was positive in 53/152 (35%) while SSS analysis and QA-SI were both negative in 60/152 (39%). The agreement between the qualitative analysis and the SSS analysis was considered to be poor (K=0.184;95%IC: from 0.054 to 0.314). **Conclusion:** The SSS analysis could be influenced by the presence of myocardial hypertrophy or dilatation or by no maximal ECG-stress-test; this explained the poor concordance. To avoid R-MPI is necessary know patients clinical history, pre-MPI test results but SSS analysis and especially QA-SI and a negative concordance of both evaluation permit to save about 50% of radiation exposure.

PW24

Implications of Residual Regional Myocardial Blood Flow and Perfusion/Metabolism Mismatch in Patients with Myocardial Infarction (MI)

E. Milan¹, L. Gallo¹, A. Pacchioni², L. Camoni³, R. Giubbini³; ¹S. Giacomo Hospital, Castelfranco Veneto - Treviso, ITALY, ²ULSS 13, Mirano - VE, ITALY, ³University of Brescia, Brescia, ITALY.

Perfusion and glucose metabolism mismatch as detected by PET is an accurate parameter for assessment of myocardial viability and it is used to evaluate the amount of viable recoverable myocardium. Absolute myocardial blood flow (MBF) provide additional diagnostic and prognostic information for coronary disease. Aim of our study was to investigate the role of residual MBF as compared to extension of mismatch in patients with previous MI. **METHODS** 16 pts (63±9 y; 14M) with previous MI (3 anterior, 12 inferior, 1 lateral) and multivessels coronary artery disease were evaluate. All Pts underwent rest dynamic ¹³N-NH₃ gated-PET and ¹⁸F-FDG gated-PET. Quantitative MBF evaluation was performed by using PMOD software, using 1-compartment model developed by DeGrado. Extension of perfusion/metabolism mismatch was quantify by using 4D-M PET software: both ¹³N-NH₃ summed rest score (SRS) and ¹⁸F-FDG SRS were calculated. **RESULTS** : 12/16 (75%) Pts received coronary revascularization (10 underwent PCI and 2 CABG). 14 vessel were revascularized by PCI and 5 by CABG. The median time from PET to revascularization was 10 (1, 28) days. ¹³N-NH₃ SRS was 13.42 ± 10.3 and ¹⁸F-FDG SRS was 9.58 ± 9.28 (p<0.05). In territories referred to vessel which were or were not revascularized ¹³N-NH₃ SRS was 5.06 ± 6.53 and 4.05 ± 7.09, respectively (p= N.S.). ¹⁸F-FDG SRS was 3.65 ± 5.98 and 2.61 ± 5.27 (p=N.S) in territories referred to vessel which were or were not revascularized. Rest MBF was reduced in 152/272 (56%) analyzed segments. Rest MBF was reduced in 11/14 (78%) vessels revascularized by PCI and in 4/5(80%) vessels revascularized by CABG. Rest MBF in segments attributed to LAD was 0.65 ± 0.17 in vessel revascularized vs 0.82 ± 0.23 in non revascularized (p<0.05). Rest MBF was 0.68 ± 0.14 vs 0.79 ± 0.18 (P= NS) in revascularized LCX and in non revascularized LCX, respectively. Rest MBF was 0.65 ± 0.12 vs 0.62 ± 0.23 (P= NS) in revascularized RCA and in non revascularized RCA, respectively. Analyzing the 4 pts whom didn’t received revascularization a reduced rest MBF was found in only one coronary territory. **CONCLUSION:** neither FDG nor NH₃ PET seem to influence the intention to treat in this group of pts. However the results of

PET scan can help Cardiologist in deciding which vessel need to be revascularized in multivessel diseased patients when partial revascularization is the therapy option

PW25

Rubidium-82 tracer activity optimisation for PET myocardial perfusion imaging

E. D. Huizing^{1,2}, J. D. van Dijk¹, J. A. van Dalen³, J. R. Timmer⁴, H. Arkies¹, C. H. Slump², P. L. Jager¹; ¹Isala Hospital, Department of Nuclear Medicine, Zwolle, NETHERLANDS, ²University of Twente, Enschede, NETHERLANDS, ³Isala Hospital, Department of Medical Physics, Zwolle, NETHERLANDS, ⁴Isala Hospital, Department of Cardiology, Zwolle, NETHERLANDS.

Introduction: Rubidium-82 PET/CT is increasingly being used for relative and quantitative myocardial perfusion imaging (MPI). However, recommended administered activities may be unnecessarily high for the present generation PET scanners. These high activities expose patients to higher doses and may interfere with blood flow quantification because of dead time effects. Our aim was to derive the minimum administered activity that allows reliable relative MPI assessment, using a present generation PET/CT scanner. **Method:** We included twenty-eight consecutive patients who underwent clinically indicated rest-stress MPI PET (Ingenuity TF, Philips) using an activity of 1110MBq Rb-82 per scan. List-mode data was reconstructed to create a reference scan, and was used to simulate scans with administered activities of 925, 740, 555 and 370MBq. The reference rest scan was compared to each simulated rest scan and differences in summed rest score (SRS) and total perfusion deficit (TPD) were derived. Differences in SRS \geq 3 or TPD $>$ 7% were considered to potentially influence diagnostic outcome. Experts scored the image quality of all simulation and reference scans as sufficient or insufficient for diagnostic interpretation. Next, the two simulated activities which showed the most potential for clinical adoption were selected. Stress-rest PET scans of these two simulations were interpreted by experts as being normal, containing reversible and/or irreversible defects, and were compared to the interpretation of the reference scan using 1110MBq Rb-82. **Results:** Differences in SRS \geq 3 between simulations of 925, 740, 555 and 370MBq and the reference scan occurred in zero (0%), two (7%), four (14%) and five (18%) patients, respectively. TPD changes $>$ 7% were found only in the 370MBq simulation in one patient. Image quality was the same between the reference scan and the 925MBq and 740MBq simulations but differed between the reference and 555MBq (p=0.046) or 370MBq (p<0.001) simulations. The two simulated activities with the most potential for clinical adoption were 740MBq and 555MBq. Interpreted diagnostic outcome only changed in one patient at 740MBq as well as at 555MBq. However, for this patient SRS and TPD did not change. **Conclusion:** For PET MPI an administered activity of 740MBq Rubidium-82 can safely be adopted in clinical practice without affecting image quality. Lowering the activity to 555MBq could be considered, as this does not affect diagnostic outcome, although image quality decreases.

PW26

Single Stress Dual-Isotope Myocardial Perfusion Imaging using ^{99m}Tc SPECT and ⁸²Rb PET: A Phantom Study

N. L. Christensen, L. C. Gormsen, L. P. Tolbod; Dept. of Nuclear Medicine and PET-Centre, Aarhus University Hospital, Aarhus N, DENMARK.

Aim: Technetium-99m SPECT and rubidium-82 PET are two well established MPI modalities that have been used for decades in the diagnosis of cardiovascular diseases. In previous comparison studies, the patients underwent pharmacological stress imaging in different days, thereby complicating the evaluation of the methods. A way to directly compare

the two modalities could be to use the same infusion of pharmacological stress agent for both exams, injecting ^{99m}Tc-sestamibi during the ⁸²Rb PET scan immediately after injection of ⁸²Rb. Our aim was to evaluate the technical aspect of having same-day PET and SPECT with a single episode of pharmacological stress. With this approach, we will be able to directly compare the diagnostic power of ⁸²Rb PET and ^{99m}Tc-sestamibi SPECT in patients with varying degrees of coronary artery disease.

Methods: A thorax-cardiac phantom underwent five 10 minute dynamic PET scans in the following setups; 1) injection of 1110 MBq ⁸²Rb in the left ventricle, 2) injection of 50 MBq ^{99m}Tc-sestamibi in the phantom background and injection of 1110 MBq ⁸²Rb in the left ventricle, 3) 50 MBq ^{99m}Tc-sestamibi in the phantom background and injection of 1110 MBq ⁸²Rb in the left ventricle, followed by a bolus injection of 500 MBq ^{99m}Tc-sestamibi in a tube across the phantom, 4) 50 MBq ^{99m}Tc-sestamibi in the phantom background, followed by an injection of 40 MBq ^{99m}Tc-sestamibi in the left ventricle and 5) 50 MBq ^{99m}Tc-sestamibi in the phantom background and 40 MBq ^{99m}Tc-sestamibi in the left ventricle followed by an injection of 1110 MBq ⁸²Rb in the left ventricle. CT scans were made for attenuation correction. Furthermore, a 15 minute SPECT scan was made to ensure, that the ^{99m}Tc-sestamibi was correctly injected into the left ventricle. PET scans were analyzed by evaluating true coincidences, scatter fraction factor and deadtime factor. Furthermore, visual inspection of the images was made. **Results:** The injection and presence of ^{99m}Tc-sestamibi in the phantom does not influence the image quality of ⁸²Rb PET, as no significant changes was seen in either deadtime or scatter fraction corrections. Furthermore, visual inspection of the images showed no influence from the ^{99m}Tc-sestamibi tracer in the PET images either. **Conclusion:** The ⁸²Rb PET images are not affected by the presence of ^{99m}Tc-sestamibi, allowing for single stress same-day protocols of dual-isotope/dual-modality MPI studies in both patients with coronary artery disease as well as in healthy volunteers.

PW27

New analysis tool for automatic and unsupervised analysis of dynamic cardiac PET studies

C. Velasco Jimeno, J. Mateo, J. Ruiz-Cabello, S. España; Centro Nacional de Investigaciones Cardiovasculares (CNIC), Madrid, SPAIN.

Introduction: Dynamic cardiac PET imaging provides valuable information of myocardium physiological state. Analysis of dynamic cardiac PET scans requires volumetric delineation (left ventricle, right ventricle, and myocardium), determination of the left ventricular long- and short-axis, kinetic modeling analysis, and generation of polar plots. This process is very time consuming and the results are user-dependent leading to an intra- and inter-observer variability, which prevent its implementation in the clinical routine¹. Thus, a tool for fully automatic analysis of dynamic cardiac PET studies has been developed in order to provide fast, robust and reproducible results. **Methods:** The analysis tool has been implemented in Python language using open source libraries for numerical and image processing. A series of dynamic PET images and a low-dose CT are loaded in order to perform the analysis. Left and right ventricles are automatically delineated applying k-means clustering to the early dynamic PET frames after tracer injection. Arterial input function is derived within the left ventricle. Myocardium is later segmented combining full dynamic PET and CT information including some anatomical constrains. According to the employed tracer a particular pharmacokinetic model is applied to derive the kinetic constants and to obtain parametric images. Short- and long-axis of the left ventricle are also obtained and images are resampled. In addition, myocardium delineation is used to generate polar plots of the results. The tool was tested on ⁶⁸Ga-DOTA PET/CT studies performed on a pig model of myocardial infarction. **Results:** Automatic delineation of left ventricle, right ventricle and myocardium as well as determination of short- and long-axis of left ventricle were validated against manually segmented and oriented contrast-CT images. Figure 1 shows the short- and long-axis views of perfusion of extracellular

volume fraction images obtained from the kinetic model as well as their polar plot representation. **Conclusions:** We have developed and validated a fully automatic tool for analysis of dynamic cardiac PET studies. Obtained results show the ability of this tool to obtain parametric images of myocardium without user intervention.

PW28

Response to Hemorheological Parameters and Relative to Oxidative Stress in Patients with Cardiac Syndrome X diagnosed by Myocardial Perfusion Scintigraphy

O. Yaylali, E. K. Toprak, T. Sengoz, Y. T. Yaylali, Y. Özdemir, Y. Ekbiç, D. Yuksel, H. Senol, M. B. Kucukatay, V. Kucukatay; Pamukkale University Medical Faculty, DENIZLI, TURKEY.

Introduction: Cardiac syndrome X (CSX) is a clinical interest, yet the underlying pathophysiological mechanisms have not been fully elucidated. The most current pathomechanisms suggested for CSX tend to emphasize endothelial dysfunction and chronic, low grade inflammation. Although abnormal hemorheologic parameters and increased oxidative stress play a pivotal role in different cardiovascular pathologies have been well-defined, no clear information is available about the effects of CSX. The aim of the current study was to determine alterations in blood rheology (erythrocyte aggregation and deformability) and relative to oxidative stress parameters [total oxidant/antioxidant status and oxidative stress index (OSI)] in CSX patients with abnormal myocardial perfusion scintigraphy (MPS) and normal coronary angiography. **Materials and methods:** The study comprised 26 CSX patients (55.77±12.33 years) with angina pectoris, positive exercise test, abnormal MPS (Philips Brightview XCT; Ohio, Cleveland, USA), normal coronary angiography and 37 age and sex matched (56.32±11.98 years) healthy controls. Elongation index (EI) which is the indicator of erythrocyte deformability and erythrocyte aggregation were measured by an ektacytometer. Total oxidant/antioxidant status (TOS, TAS) were measured using a commercial kit and oxidative stress index (OSI) was calculated. **Results:** Erythrocyte deformability measured at 1.69, 3.00 and 30.00 Pa were lower in CSX patients compared to control (p=0.001, 0.017 and 0.006 respectively). On the other hand, erythrocyte aggregation index (AI) (72.75±7.65 vs. 66.48±6.63, p=0.002); TOS (24.058±7.833 vs. 16.398±7.963, p=0.001); TAS (1.998±0.327 vs. 1.595±0.549, p=0.0001) were significantly higher in the CSX group compared to control group. **Conclusion:** In CSX, higher oxidative stress values appear to be related with lower erythrocyte deformability and higher erythrocyte aggregation. Abnormal hemorheological parameters and increased oxidative stress might be involved in the pathophysiology of CSX. Treatment modalities that decrease oxidative stress and modify rheological parameters might be beneficial for the management of CSX.

PW29

Real-World Evidence of the Safety of Pharmacologic Stress in Myocardial Perfusion Imaging

A. Sabra^{1,2}, M. Heatley¹, M. Martins³, R. Bidder³; ¹Cardiology Department, Singleton Hospital, Swansea, UNITED KINGDOM, ²Swansea University School of Medicine, Swansea, UNITED KINGDOM, ³Nuclear Medicine Department, Singleton Hospital, Swansea, UNITED KINGDOM.

Background: Myocardial perfusion imaging (MPI) is increasingly used as recommended by the National Institute for Health and Care Excellence (NICE) for patients with a 30-60% estimated likelihood of coronary artery disease. We aimed to investigate the safety of drugs used in patients undergoing pharmacologic stress MPI in our nuclear cardiology department. **Methods:** An 18-month (July 2014 - Feb 2016) retrospective study to investigate the incidence

of adverse effects (AE) in patients undergoing pharmacologic stress MPI. We employ standardized protocols (Tc-99m) using 4 agents: dipyridamole, regadenoson, adenosine and dobutamine. Clinical data including AEs were collected from cardiobase. Descriptive analysis and frequencies were calculated. AE in MPI were compared to those occurring in 165 patients who underwent conventional exercise tolerance testing (ETT) using chi-squared test. **Results:** Seven hundred fifty-one patients were included in this analysis. Of the 586 patients (mean age 67 years [SD 11]; 310 men, 276 women), who had pharmacologic stress agent administered, 268 (45.7%) became symptomatic: dyspnoea (21.8%), flushing (15.4%), chest discomfort (11.4%), cough (3.2%), chest pain (2.6%), headache (2.6%), pain elsewhere (2.6%), nausea (2.4%), wheeze (2.2%), dizziness (2%), vasovagal reaction (1.9%), vomiting (1%), abdominal discomfort (0.5%). The commonest symptoms were chest discomfort and dyspnoea for dobutamine, flushing and dyspnoea for adenosine and regadenoson, and mainly dyspnoea for dipyridamole. Adenosine had the highest incidence of AE (69%). No significant complications were recorded that required hospital admission. Interestingly, patients who underwent ETT were reported to have a significantly higher incidence of AE than MPI patients did (MPI 268/586 [45.7%], ETT 104/164 [63.4%]; p<.0001). **Conclusions:** This real-world data show that pharmacologic stress MPI is safe when performed within agreed clinical protocols. Given that technicians routinely perform ETT, well trained physicians who are confident in managing the side effects and reassuring patients can lead the MPI testing particularly in busy cardiac units as long as support is available from medical staff.

PW30

F-18-FDG-PET/CT does not detect atrial inflammatory activity in patients with atrial fibrillation under routine conditions

N. Avramovic¹, P. Lange², M. Schäfers¹, G. Frommeyer², K. Wasmer², C. Pott², L. Eckardt², C. Wenning¹; ¹Clinic for Nuclear Medicine, University Hospital Münster, Münster, GERMANY, ²Section Rhythmology, Department of Cardiology and Angiology, University Hospital Münster, Münster, GERMANY.

INTRODUCTION: Atrial fibrillation (AF) is the most common cardiac arrhythmia in developed countries. Increasing evidence both from preclinical and clinical studies support a role for inflammation in the development, maintenance and progression of AF. However, direct evidence of persistent inflammatory activity in the atria of AF patients is scarce. On the basis on previous case reports, F-18-FDG-PET/CT was assumed to detect inflammatory activity in the atrial walls. In this study we wanted to test this hypothesis in a larger cohort. **METHODS:** Routine 18-FDG-PET/CT scans of patients referred for various clinical indications were retrospectively analyzed. Patients with a history of AF (n=37, 25 men; mean age 70±7 years) were compared to a control group without AF (n=37, 24 men; mean age 71±7 years). Standardized uptake values (SUV) were obtained in the left and right atrial wall, as well as in the lateral wall of the left ventricular myocardium, by placing 5 regions of interest (ROI) of equal size. Background activity was measured by one ROI in the right ventricular blood pool. Target to background ratios (TBR) were determined by calculating the ratio of SUVmax in the atrial wall and the SUVmean in the right ventricular blood pool. **RESULTS:** TBR of the left atrial wall did not display significant differences between patients with and without AF (1,14±0,29 vs. 1,21±0,27; p=0,338). A weak, albeit significant difference was observed in signal intensities in the right atrial wall compared to control (0,96±0,20 vs. 1,14±0,45; p=0,028). However, the absolute SUV of the right atrial wall did not differ markedly. In addition, this difference could not be recapitulated visually. Moreover, SUVmax of the atrial myocardium correlated with SUVmax of the left ventricular myocardium (r=0,35; p<0,01) thereby pointing towards a metabolic correlation. **CONCLUSION:** PET/CT imaging did not detect a difference in inflammatory atrial activity in patients with AF. Contrary to previous reports, these results do not support a role for FDG-PET/CT imaging of inflammatory activity in the atrial wall under routine imaging conditions. Prospective clinical studies would be helpful to clarify if metabolic myocardial suppression techniques may unmask inflammation.

PW-4 – Tuesday, October 18, 2016, 08:30 - 09:30, Poster Exhibition Hall
Poster Walk 4 – Neurosciences: Basic & Clinical Neuroimaging

PW31

PET imaging with [¹¹C]ITDM, a selective radioligand for metabotropic glutamate receptor subtype 1 (mGluR1), in pilocarpine-induced epileptic rat brain

T. Yamasaki, III¹, J. Yui¹, M. Fujinaga¹, Y. Shimoda¹, W. Mori¹, Y. Kurihara^{1,2}, H. Wakizaka¹, M. Zhang¹; ¹National Institutes for Quantum and Radiological Science and Technology, Chiba, JAPAN, ²SHI Accelerator Service Co. Ltd., Tokyo, JAPAN.

Aim: Epilepsy is known as one of neurological diseases characterized by epileptic seizures induced via overstimulation of glutamatergic neurons. The metabotropic glutamate receptors (mGluRs) moderate in excitatory neurotransmission upon the central nervous system (CNS). Among mGluRs, mGluR1 is known as a trigger of neurotoxic cascades. In this study, we aimed to in vivo monitor regional changes of mGluR1 in pilocarpine-induced status epilepticus (PISE) model rat brains via longitude PET assessments. **Methods:** PISE model rats were induced by repeated pilocarpine hydrochloride treatments (10 mg/kg) after administration with lithium chloride (127 mg/kg). PET assessments with *N*-[4-[6-(isopropylamino)-pyrimidin-4-yl]-1,3-thiazol-2-yl]-*N*-methyl-4-[¹¹C]-methylbenzamide ([¹¹C]ITDM), a selective radioligand for mGluR1, were scheduled in acute (1 day), subacute (1 week), and chronic (3 weeks) periods after status epilepticus (SE). Acquired PET data were analysed with reference tissue models by PMOD software. To validate results of PET assessments, in vitro autoradiography with [¹¹C]ITDM was performed using PISE rat brain sections prepared in same experimental period used in PET experiments. **Results:** In PET assessments with [¹¹C]ITDM, binding potential (BP_{ND}) in the 1-3 cerebellar lobes significantly decreased ($P < 0.001$) in acute period (BP_{ND} = 3.2), subsequently recovering to normal level over subacute period (BP_{ND} = 4.6). Additionally, thalamic and hippocampal BP_{ND}s showed gradual declines with time after SE over chronic period. However, in vitro autoradiography showed no change of specifically bindings of [¹¹C]ITDM in the cerebellum in acute period, whereas bindings of [¹¹C]ITDM in the thalamus and hippocampus indicated a tendency of decrease with time after SE. **Conclusion:** Our study indicates that gradual declines of mGluR1 expressions in the thalamus and hippocampus of PISE model rat brain via longitude PET imaging. In vivo monitoring of mGluR1 using PET with [¹¹C]ITDM may enable to further understand mechanism involved in dysfunction of CNS.

PW32

Combined [¹⁸F]DPA-714 and [¹⁸F]FDG PET and autoradiography imaging of microglia activation in traumatic brain injury in mice

I. Israel¹, A. Ohsiek², E. Al-Momani¹, C. Stetter², C. Albert-Weissenberger², A. Buck¹, A. Sirén², S. Samnick¹; ¹University of Wuerzburg, Wuerzburg, GERMANY, ²Department of Neurosurgery, University of Wuerzburg, Wuerzburg, GERMANY.

Background: Traumatic brain injury (TBI) is a major cause of death and disability. Activated microglia contribute to acute damage after TBI and modulate long-term evolution of degenerative and regenerative responses to injury. In the present study, we correlated microglia activation to lesion severity and cellular identity of inflammatory cells in a murine closed head injury model using a combined approach of intra-individual *in vivo* μ PET imaging and *ex vivo* autoradiography with the specific 18-kDa translocator protein (TSPO) radioligand [¹⁸F]DPA-714. In parallel, [¹⁸F]FDG-PET was also performed in the same animals to evaluate the cerebral glucose metabolism. Imaging data with [¹⁸F]DPA-714 were correlated with immunohistochemical analysis. **Methods:** A closed head

TBI on C57BL/6N mice was induced by a falling weight onto the skull of mice. According to the height of the weight a diffuse or focal TBI was induced. The functional outcome was evaluated 1 h, 3 and 7 days after injury induction using a standardized neuroscore (NSS). [¹⁸F]DPA-714- μ PET imaging was performed on day 1, 7 and 16 and [¹⁸F]FDG- μ PET on days 2-5 after trauma using freshly synthesized radiotracers. On days 7 and 16, [¹⁸F]DPA-714-autoradiography was performed on brain cryosections prepared immediately after μ PET imaging. The sections used for autoradiography were subsequently exposed to antibodies against the activated microglia marker IBA-1. **Results:** Functional outcome in mice with a focal TBI was significantly worse than in sham operated mice or mice with diffuse TBI. [¹⁸F]FDG uptake was acutely reduced in the brains with focal lesions. Mice with diffuse TBI and less severe neurological deficits showed no significant reduction in [¹⁸F]FDG accumulation. Repeated μ PET imaging with [¹⁸F]DPA-714 showed increased radiotracer uptake in focal brain lesions on days 7 and 16 after TBI. In autoradiography [¹⁸F]DPA-714 uptake in focal trauma lesions correlated strongly with both NSS and the number of IBA1-positive microglia. After diffuse TBI microglia activation was detected in both hemispheres by immunohistochemical staining; however, it was not clearly observable by autoradiography or in μ PET imaging. **Conclusion:** [¹⁸F]DPA-714 uptake correlates with functional outcome and number of activated microglia after closed head TBI and can be used for repeated monitoring of neuroinflammation after TBI.

PW33

Biodistribution and metabolism of [¹⁸F]FMTEB in rats

F. R. Lopez-Picon^{1,2}, A. Krzyczmonik¹, K. Grafinger^{1,2}, T. Keller¹, L. Pfeifer³, S. Forsback¹, O. Solin^{1,4,5}, V. Gouverneur³, M. Haaparanta-Solin^{1,2}; ¹Turku PET Centre, University of Turku, Turku, FINLAND, ²Medicity Research Laboratory, University of Turku, Turku, FINLAND, ³Chemistry Research Laboratory, University of Oxford, Oxford, UNITED KINGDOM, ⁴Accelerator Laboratory, Åbo Akademi University, Turku, FINLAND, ⁵Department of Chemistry, University of Turku, Turku, FINLAND.

Aim In this study we aimed to study in rats the biodistribution and metabolism of [¹⁸F]FMTEB, a tracer for metabotropic glutamate subtype-5 receptors (mGluR5s), prepared via copper-mediated nucleophilic [¹⁸F]fluorination of boronic ester [1,2]. **Materials and methods** To study pharmacokinetics *ex vivo*, we injected 18 healthy adult Sprague Dawley rats (289±17 g) with [¹⁸F]FMTEB (injected dose, 15.9±5.1 MBq; injected mass, 0.7±0.3 ng/kg; SA, 153±64 GBq/ μ mol at the time of injection). The rats were sacrificed 5, 15, 30, 60 or 90 min post injection. Organs of interest were dissected, weighted, and measured for radioactivity. Retention and distribution of [¹⁸F]FMTEB in the rat brain was evaluated with *ex vivo* autoradiography. For three animals dynamic PET/CT scan was carried out for 60 min. The amount of intact tracer and its radioactive metabolites were analysed from blood and brain homogenates. The specificity of the synthesized [¹⁸F]FMTEB for mGluR5s, was tested blocking with ABP688, a high affinity mGluR5s antagonist. **Results** [¹⁸F]FMTEB was cleared rapidly from the blood, and in most tissues and organs the radioactivity uptake peaked at 5 min. The highest radioactivity was detected in the liver at 5 min, and later in the small intestine and urinary bladder. High levels of radioactivity were also recorded in the Harderian glands, brown adipose tissue and adrenals. Plasma metabolite analyses demonstrated that [¹⁸F]FMTEB was metabolized rapidly into three polar metabolites. One polar radioactive metabolite was found in brain, however its concentration at all analysed time points did not exceeded 10%. Both PET/CT scans and *ex vivo* brain autoradiography showed high uptake in the striatum, hippocampus and cortex. Using the cerebellum as a reference region, the uptake ratios of 22.6±3.2 and 16.5±2.4 (n=3) were obtained at 60 min for the striatum and hippocampus, respectively. Pre-treatment with ABP688 reduced the radioactivity uptake in striatum and hippocampus up to 85%. **Conclusion** PET/CT and *ex vivo* brain autoradiography studies demonstrated that [¹⁸F]FMTEB rapidly entered the rat brain, and specifically bound

to mGluR5s rich regions such as striatum, hippocampus and cortex. **Acknowledgement** Funding was received from the European Union's 7th Framework Programme for Research, grant number 316882 and from the Academy of Finland, grant number 266891. [1] Tredwell M et al. *Angew. Chem. Int. Ed.* **2014**, 53, 7751-7755 [2] Enhanced Copper-Mediated ^{18}F -Fluorination of Aryl Boronic Esters provides Eight Radiotracers for PET Applications, submitted for publication, Gouverneur et al., personal communication

PW34

Investigating the co-grafted effects of rat Sertoli cells and porcine VM tissue in a rat model of Parkinson's disease using [^{18}F]-DOPA/PET

K. Ma¹, **Y. Jhao**¹, **T. Liu**¹, **S. Weng**¹, **R. Yen**², **K. Tzen**³;
¹Department of Biology and Anatomy, National Defense Medical Center, Taipei, TAIWAN, ²Department of Nuclear Medicine, National Taiwan University Hospital, Taipei, Taiwan., TAIPEI, TAIWAN, ³Department of Nuclear Medicine, National Taiwan University Hospital, Taipei, Taiwan, TAIPEI, TAIWAN.

Aim: Parkinson's disease (PD) is a neurodegenerative disease characterized by a loss of dopaminergic neurons in the nigrostriatal pathway, leading to the progressive movement disorder. The cell therapy has been demonstrated a viable treatment in the late stages of PD. However, the usage of human fetal ventral mesencephalic (hfVM) tissue raises ethnic issues that remain unresolved. The xenograft strategy using porcine VM (pVM) tissue may be an alternative source for cell replacement, but the transplant rejection induced by pVM needs to be resolved. The Sertoli cells (SCs), also called nurse cells, may provide immunomodulatory effects for both allografts and xenografts and increase the survival rate of the grafted neurons. In this study, the rat SCs and pVM were co-grafted in the striatum of the PD rat, and the beneficial effects contributed by the SCs for xenograft were evaluated using apomorphine-induced behavioral test, immunohistochemistry, and [^{18}F]-DOPA/animal-PET. **Materials and methods:** The PD rat model were created by injecting 6-hydroxydopamine (6-OHDA) into right median forebrain bundle of the rats. The SCs were isolated from SD rats at postnatal 21 days and the pVM tissues were dissected from swine at 27 embryonic days. The rat SCs and pVM tissues were co-grafted into the striatum of the PD rat and the Apomorphine-induced rotational behavior was tested at 1 and 2 months after the transplantation. The [^{18}F]-DOPA/animal-PET was employed to evaluate the survival status of the dopaminergic neurons. Two months after transplantation, immunohistochemistry studies were performed to investigate the immunomodulatory effects of SCs in the grafted striatum. **Results:** In the test of drug-induced rotational behavior, the numbers of rotation were significantly reduced at 2 months after the co-grafted surgery. The images of PET showed that [^{18}F]-DOPA uptakes in the co-grafted area were increased at 2 months after the surgery of the PD rats. The immunohistochemistry data demonstrated that microglia (OX42 positive cells) in the striatum of co-grafted group were obviously less than that of pVM-grafted group. **Conclusion:** Our results suggested that the SCs may provide immunomodulatory effects on the grafted porcine dopaminergic neurons in the striatum of the rat brain.

PW35

Influence of reference regions in the performance to quantify 18F-Florbetapir studies

A. Fernandez-Leon^{1,2}, **F. Sampedro**³, **E. Vilapalana**^{4,5}, **J. Fortea**^{5,4}, **M. Carmona**^{4,5}, **D. Lopez Mora**¹, **D. Alcolea**^{4,5}, **A. Lleó**^{4,5}, **R. Blesa**^{4,5}, **I. Carrio**¹, **V. Camacho**¹; ¹Nuclear Medicine Department. Hospital de la Santa Creu i Sant Pau, Barcelona, SPAIN, ²Departament de Ciències Morfològiques. Universitat Autònoma de Barcelona, Barcelona, SPAIN, ³Faculty of Medicine. Universitat Autònoma de Barcelona, Barcelona, SPAIN, ⁴Memory Unit, Neurology Department. Hospital de

la Santa Creu i Sant Pau, Barcelona, SPAIN, ⁵Centre of Biomedical Investigation Network for neurodegenerative Diseases (CIBERNED), Barcelona, SPAIN.

The objective of this study was to evaluate different reference regions to quantify amyloid PET studies and correlate them with cerebrospinal fluid (CSF) measurements in 18F-Florbetapir studies. **Material and methods:** we included 50 consecutive patients (27 health control (HC), 12 with mild cognitively impairment and 10 with Alzheimer's disease AD) who underwent 18F-Florbetapir PET-CT. Studies were performed 50 minutes after injection of 370mBq of tracer. After transmission data was obtained, brain PET dynamic acquisition was performed (2x5min frames). The reconstruction method was iterative (LOR RAMBLA, 3 iterations and 33 subsets) with a 128x128 image size, 2mm pixel size and 2mm pixel slice thickness. Florbetapir PET images were visually assessed as positive and negative. For the quantitative analysis, Freesurfer segmented T1 MRI were coregistered to PET studies, which were subsequently used to extract weighted cortical retention means (SUVRs) using five different reference regions (whole cerebellum (WhCer), cerebellar gray matter (CGM), brainstem (B), eroded subcortical white matter (ESWM) and composite reference region (C). Also we determined the CSF measurements: A β 42, Tau, pTau and A β 42/Tau ratio. **Results:** To differentiate between HC and AD patients, the best SUVR cut-off points for each reference region: 1.102 using WhCer (AUC 0.95; S:90%, E:89%), 1.216 CGM (AUC 0.937; S:90%; E:89%), 0.947 B (AUC 0.948; S: 90%, E:96%), 0.74 ESWM (AUC 0.885; S:90%, E:96%) and 0.931 C (AUC 0.930; S:90, E:96%). No significant performance differences were obtained between the reference regions. Significant correlation between CSF measurements and SUVR values using different reference regions were observed. The A β /Tau ratio presented the highest correlation with the SUVR values in all reference regions (WhCer: -0.785;CGM:-0.776,B: -0.787; ESWM:-0.745; C: -0.789; p<0.01). **Conclusion:** Several reference regions may be used to quantify Florbetapir studies. Significant correlation between SUVR values using different reference regions and CSF measurements were observed; the highest correlation was observed between the A β /tau ratio and SUVR values obtained from all reference regions studied.

PW36

Optimal reference region to measure longitudinal amyloid-beta change with 18F-florbetaben PET

S. Bullich¹, **A. M. Catafau**¹, **V. L. Villemagne**², **C. C. Rowe**², **S. De Santi**³; ¹Piramal Imaging GmbH, Berlin, GERMANY, ²Department of Nuclear Medicine and Centre for PET, Austin Hospital, Melbourne, AUSTRALIA, ³Piramal Pharma Inc, Boston, MA, UNITED STATES.

Background: Accurate measurement of longitudinal changes of amyloid-beta (A β) deposition in the brain is important in anti-A β therapeutic trials. Optimal reference region (RR) selection is essential to reduce the variance of PET measurements, allowing early detection of treatment efficacy. The aim of this study was to determine the RR that allows earlier detection of subtle A β changes using 18F-florbetaben (FBB) PET. **Methods:** 18F-FBB PET scans from 45 mild cognitively impaired (MCI) patients (72.69 \pm 6.54 yrs., 29 male/16 female) who underwent three FBB scans were included (baseline (n=45), one-year (n=41) and two-years (n=36)). FBB scans were visually assessed as positive and negative. Cortical regions (frontal, lateral temporal, occipital, parietal, anterior cingulate and posterior cingulate) were quantified using the standardized AAL region-of-interest (ROI) atlas applied to the spatially normalized gray matter PET image obtained from the segmentation of the participant's baseline T1-weighted volumetric MRI. Four regions of reference (gray matter cerebellum (CGM), whole cerebellum (WCER), pons (PONS) and subcortical white matter (WM)) were studied. Cortical standardized uptake value ratio (SUVR) for each RR was calculated dividing cortex activity by the RR activity. A composite SUVR was calculated by averaging SUVRs from all cortical regions. SUVR at baseline to the SUVR from one- and two-years follow-up scans were compared using a T-test grouped

according to the anticipated pattern of change for the MCI patients. **Results:** Both CGM and WCER RRs enabled early detection of cortical SUVR changes in those scans that were positive at baseline. Average percent of A β accumulation per year (mean \pm SD) derived from composite SUVR in negative (-) and positive (+) scans was 0.13 \pm 1.68(-)/1.39 \pm 2.02(+) for CGM, 0.16 \pm 1.43(-)/1.36 \pm 1.79(+) for the WCER. Composite SUVR increase in positive scans was significantly larger than those in negative scans between baseline and 1-year follow-up (p(CGM)=0.04, p(WCER)=0.02) and between baseline and 2-years follow-up scans (p(CGM)=0.04, p(WCER)=0.02). PONS detected significant changes only at 2-years follow-up (p(1-yr)=0.71, p(2-yrs)=0.001) while SWM did not show significant difference either follow-up (p(1-yr)=0.50, p(2-yrs)=0.04). **Conclusions:** Reference region selection is essential to obtain reliable and early measurement of amyloid-beta changes. Cerebellar reference regions (CGM and WCER) are recommended as RR for 18F-FBB PET since they allow earlier detection of amyloid-beta change.

PW37

Brodmann 's areas agreement between the early acquisition of FLORBETABEN-PET and FDG-PET. Multicenter study

P. SOPENA-NOVALES; HOSPITAL 9 DE OCTUBRE, valencia, SPAIN.

Aim: The aim of this work, is to compare the uptake brain pattern between the early vascular phase of florbetapen-PET (eFBB) and FDG-PET based on the hypothesis that the eFBB represents regional brain perfusion and could be a surrogate of glucose brain metabolism measured by FDG-PET. **Materials and Methods:** Thirty-two patients with early and/or atypical onset of cognitive impairment from two different PET-CT centers were enrolled, 20 men; mean age 66.5 \pm 7.2 years. All patients were explored by FDG-PET (acquisition according to EANM procedure guidelines) and two acquisitions of FBB-PET: the early FBB-PET scan (eFBB), 0-10' p.i 3D, and a standard FBB-PET scan (sFBB), 90' p.i 3D. Performed by specific protocol and the following Manufacturer recommendations Data from FDG and eFBB were processed using an extraction algorithm that computes the mean intensity of 116 Brodmann 's areas (BAs). Afterwards data were analyzed for independent BAs, based on correlation analysis and two-sample t-test ($\alpha=0.05$) between both modalities. **Results:** Correlation analysis in 14 regions (including Rectus, Cingulum, Parietal, Angular, Precuneus, Caudate, Heschl, Temporal and Vermis regions) were found to be significant (p<0.05) between both uptakes. The p-value was computed by transforming the correlation to create a "t" statistic having N-2 degrees of freedom, where N is the number of samples. The complementary analysis based on two sample t-test for $\alpha=0.05$ (the type II error may be negligible due to the sample size), enabled to discard the BAs that are not statistically similar in both modalities. A total of 68 out of 116 regions couldn't be rejected under the test including Frontal, Insula, Cingulum, Hippocampus, Temporal, Cerebellum, etc. subregions. Moreover, when the image patterns were considered as inputs into a supervised learning system (i.e. PCA-based PETRA method), the classification accuracy, sensitivity and specificity were extremely low (<5%) and the system failed to predict the underlying classes (i.e. modalities). **Conclusion:** The eFBB uptake showed a significant correlation in the most of BAs and only different in a small fraction of BAs to FDG acquisition which prompted to supervised learning computed system to not tell if the study corresponded to eFBB or FDG.

PW38

FDG-PET and MRI study of default-mode network integrity in disorders of consciousness

G. Marotta¹, **C. Rosazza**², **A. Andronache**², **D. Sattin**², **M. Bruzzone**², **A. Nigri**², **S. Ferraro**², **R. Benti**¹, **M. Leonardi**², **L. D'Incerti**², **L. Minati**²; ¹Department of Nuclear Medicine, Fondazione IRCCS Ca' Granda Ospedale Maggiore Policlinico, Milano, ITALY, ²Neuroradiology Dept, Istituto Neurologico Besta, Milano, ITALY.

Introduction. Disorders of consciousness (DOC) encompass a spectrum of conditions ranging from coma, vegetative state/unresponsive wakefulness state (VS/UWS), minimally conscious state (MCS) to severe disability (SD). The default-mode network (DMN) is known to be dysfunctional, although correlation with level of consciousness remains controversial. We investigated DMN activity with resting-state functional MRI (rs-fMRI) and conducted separate analyses for independent component analysis (ICA), seed-based analysis (SBA), and FDG-PET. **Methods.** We enrolled 119 consecutive patients: 72 in VS/UWS, 36 in MCS, and 11 with SD. All underwent structural MRI and rs-fMRI, and a subset of 85 patients also underwent FDG-PET. Data were analyzed with manual and automatic approaches. DMN integrity was assessed multimodally: (1) functionally, based on ICA and SBA of rs-fMRI; (2) anatomically, based on visual ratings of anatomical damage in the DMN regions, as visualized by conventional MRI scans; and (3) metabolically, based on average SUV values in the DMN regions by FDG-PET scans. FDG-PET images were coregistered using SPM12 to individual volumetric T1-MRI series, which were segmented to generate the normalization deformation field to be applied to coregistered FDG-PET scan. Using the DMN mask, the average SUV values for PCC, LPC and MFC were computed. **Results.** DMN activity was decreased in VS/UWS compared to MCS (p<0.001), and correlated with clinical score. Independent-component and seed-based analyses provided similar results, although the latter and their combination were most informative. Structural MRI and FDG-PET were less sensitive to head movement and had better diagnostic accuracy than rs-fMRI when all cases were included. Excluding the quartile with largest head movement and considering only the subsample of patients who underwent FDG-PET, sMRI (AUC 0.72) and rs-fMRI (AUC 0.65) provided similar performance, and FDG-PET was slightly superior to both (AUC 0.75). Voxelwise analyses of SUV maps delineated a broader set of regions, which encompass the posterior DMN nodes; whereas correlation with the CRS-R yielded a clear and broader effect, comparison of MCS versus VS/UWS led to a more constrained difference than rs-fMRI. **Conclusion.** We investigated the integrity of DMN in relation to consciousness with rs-fMRI in the largest group of DOC patients, directly comparing rs-fMRI with sMRI and FDG-PET. We confirm a significant relationship between functional, anatomical, and metabolic integrity of the DMN and clinical status, and provide additional insight on the potential clinical contribution of each technique. Structural integrity across DMN regions also correlates with consciousness level, and FDG-PET yields the highest accuracy scores.

PW39

Evaluation of Parkinson's disease by neuromelanin-sensitive MR imaging and ¹²³I-FP-CIT SPECT

T. Ogawa, K. Kuya, Y. Shinohara, F. Miyoshi, S. Fujii, Y. Tanabe; Tottori University, Yonago, JAPAN.

Introduction: Neuromelanin-sensitive MRI can visualize the neuromelanin-containing neurons in the substantia nigra pars compacta (SNc), and its utility has been reported in the evaluation of parkinsonism. On the other hand, dopamine transporter imaging by ¹²³I-FP-CIT SPECT (DaTSCAN) is now an established method for evaluating parkinsonism, detecting presynaptic dopamine neuronal dysfunction. Both methods can assist the differentiation between the neurodegenerative parkinsonism and the other parkinsonisms. However, to our knowledge, there have been a few studies concerning a correlation between two methods. The aim of this study is to correlate the utility of neuromelanin-sensitive MRI and DaTSCAN for the diagnosis and management of Parkinson's disease. **MATERIALS AND METHODS:** Seventeen patients with Parkinson's disease who underwent both neuromelanin-sensitive MRI and DaTSCAN were included. We measured the volume of the neuromelanin-positive SNc region by manually contouring the high signal intensity region of the SNc on neuromelanin-sensitive MRI, and measured the specific binding ratio (SBR) on DaTSCAN. The asymmetry index of neuromelanin-positive SNc volume

(AI_{vol}) and the asymmetry index of the SBR (AI_{SBR}) were also calculated. We also evaluated the relationship between the Unified Parkinson's disease rating scale part III (UPDRSIII) score widely used for the clinical evaluation of Parkinson's disease and each of the volume of the neuromelanin-positive SNc region and SBR. **RESULTS:** The volume of the neuromelanin-positive SNc region showed significant correlation with the SBR (right: $p < 0.001$, $\rho = 0.77$, left: $p < 0.001$, $\rho = 0.86$). The AI_{vol} and the AI_{SBR} also showed a significant correlation ($p < 0.001$, $\rho = 0.64$). A significant negative correlation was found between the UPDRSIII score and mean of bilateral SBR ($p < 0.01$, $\rho = -0.56$), but there was no significant correlation between the UPDRSIII score and mean of bilateral volume of the neuromelanin-positive SNc region ($p = 0.27$, $\rho = -0.28$). **CONCLUSION:** Decrease of the high signal intensity region of the SNc on neuromelanin-sensitive MRI would indicate the damage of the nigrostriatal dopaminergic system as well as loss of the dopaminergic neurons itself. However, we conclude that DaTSCAN is more suitable for the evaluation of clinical severity of Parkinson's disease than neuromelanin-sensitive MRI.

PW40

^{18}F -FDG Uptake in the Healthy Brain as a Function of Age and Start of Acquisition

E. Pauwels¹, S. Bonte^{1,2}, A. Dobbela¹, S. Verleden³, K. Audenaert³, R. Van Hoen², I. Goethals¹; ¹Department of Radiology and Nuclear Medicine, Ghent University Hospital, Ghent, BELGIUM, ²Medical Imaging and Signal Processing (MEDISIP) - IBItech - Department of Electronics and Information Systems (ELIS), Ghent University, Ghent, BELGIUM, ³Department of Psychiatry, Ghent University Hospital, Ghent, BELGIUM.

Aim: ^{18}F -FDG positron emission tomography (PET) is a well-established tool in clinical practice for the diagnosis and evaluation of neuropsychiatric disorders. A thorough understanding of the healthy brain glucose metabolism - and thus ^{18}F -FDG uptake - including changes due to physiological processes and individual variations is essential for a correct interpretation of PET images. Healthy ageing for instance not only results in a global decrease of the cerebral glucose metabolism but also in significant regional brain metabolism decrease. Furthermore, time after injection will exert a probable influence on the distribution pattern of ^{18}F -FDG uptake. The aim of this study was to present regional normal values for ^{18}F -FDG uptake as a function of age and time after injection which can be used in clinical practice to detect abnormal brain metabolism. *Materials and methods:* 82 healthy subjects were carefully selected according to strict inclusion criteria. Each subject underwent an MRI and a dynamic brain FDG PET scan for a total acquisition time of 75 minutes. PET images were normalised to minimise inter-individual variation using three different reference regions: global mean, central white matter (WM) and cerebellum. Fifteen brain regions were defined using the Hammers Adult Brain Atlas 30 (30 subjects, 83 regions; <http://brain-development.org>). First, sex-related differences were studied. Subsequently, for each time frame a linear regression analysis of the uptake for each brain region as a function of age was performed. These data can be used to calculate the normal values for ^{18}F -FDG uptake. *Results:* In females, a significantly higher ^{18}F -FDG uptake is observed in the thalamus and striatum in a limited number of time frames. Since relative differences are small, the application of a mixed age-matched normative database is valid. The most prominent age-related decrease in ^{18}F -FDG uptake is observed in the frontal brain regions and the anterior cingulate. Global mean normalisation shows an increased uptake with age in the cerebellum, brainstem and thalamus. However, this is probably an artefact due to the use of the global mean as reference region. Indeed, using central WM and cerebellum as the reference region for normalisation no significant age-related differences are found in these regions. *Conclusion:* A mixed age-matched normative database of 82 carefully selected subjects is presented from which normal values of ^{18}F -FDG uptake as a function of age and time after injection (up to 75 minutes post injection) can be calculated and readily applied in clinical practice to detect abnormal uptake.

e-Posters

EP-01 – Sunday, October 16, 2016, during Exhibition hours, e-Poster Area
Clinical Oncology: Bone, Soft Tissues & Sarcoma

EP001

Frequency of skeletal metastasis in patients with germ cell tumors on bone scintigraphy as part of staging work up

M. Siddique, A. Hassan, H. Bashir, M. Nawaz; Shaukat Khanum Memorial Cancer Hospital and Research Centre, Lahore, Pakistan., Lahore, PAKISTAN.

Background: Germ cell tumors (GCT) are the most common malignant solid tumors in young male adults. Osseous metastases are rare at initial diagnosis and usually presents as a late event combined with synchronous nodal, pulmonary or hepatic metastases. Our aim is to determine the frequency of skeletal metastasis in patients with newly diagnosed germ cell tumors (GCT) on bone scintigraphy done as part of baseline staging work up. **Method:** Electronic medical records of 126 patients treated for histologically proven GCT of gonadal or extragonadal origin between October 2010 and September 2015 were retrospectively analyzed. Data was collected for histopathology, presence of bone metastasis on ^{99m}Tc-MDP bone scintigraphy at diagnosis, frequent sites of metastasis, association of osseous metastases with histologic subtypes and concurrent nodal/systemic metastasis. Bone metastases were further confirmed on the basis of clinical symptoms and correlative radiological imaging or histologic confirmation where available. **Results:** A total of 126 patients, 59(47%) females and 67(53%) males, who underwent bone scans were reviewed. Age range: 1 month-72 years (mean age=18 years). 105(83%) cases were of pediatric age group (<18 years) at the time of initial diagnosis. Of the total; 41(32.5%) had yolk sac tumor (27 of gonadal origin, 13 abdomino-pelvic masses and 1 mediastinal mass), 34(27%) had mixed germ cell tumors (24 of gonadal origin, 9 sacrococcygeal and 1 on femur biopsy), 16(13%) mature cystic teratoma, 14(11%) dysgerminoma of ovaries, 9(7%) seminoma of testis, 7(5.5%) immature teratoma of abdominopelvic masses, 3(2.4%) non seminomatous GCT of mediastinum and 2(1.6%) embryonal carcinoma. Osseous metastasis was detected in 12(9.5%) cases. 2 (17%) had solitary, and 10 (83%) multifocal skeletal metastases. Most frequent site of bone metastases was thoracolumbar spine (7,58%) with cord compression in 4 patients. Other sites included pelvis (6,50%), ribs (5,42%) and long bones (5,42%). Clinically, all patients had localized bone pain. Histologically bone metastases were more frequently associated with yolk sac tumor and primary mediastinal GCT. In patients with osseous metastases; additional sites of metastases included; lymph nodes (5,42%), lung (4,33%) and 42% had no other site of metastasis. None had concomitant hepatic metastases. 5/12, 42% died over a period range of 4-18 months. **Conclusion:** Distant osseous involvement was found in 9.5% of the GCT patients undergoing diagnostic skeletal scintigraphy. Based on our findings, baseline skeletal evaluation for metastases; especially in cases with bone pains or known systemic metastases should be done.

EP002

Assertiveness in Bone Scintigraphy: Is It a Matter of Faith?

A. S. Pinto, A. R. Fernandes, V. Alves, T. Vieira, T. Faria, A. Oliveira, M. Pérez, J. Pereira; Centro Hospitalar de São João, Porto, PORTUGAL.

Introduction: Bone Scintigraphy is a frequently performed Nuclear Medicine (NM) exam to evaluate bone metastasis (BM). Its specificity is relatively low, which leads to less assertive diagnostic answers by the NM doctors. **Aim:** To evaluate the diagnostic assertiveness of BM in

Bone Scintigraphy, to study the correlation between assertiveness and specificity and to compare the assertiveness between specialists and interns of specialization at our NM Department. **Materials and Methods:** Bone Scintigraphies of 50 consecutive patients with oncological pathology, performed in January 2014, were included. Besides the whole body images, SPECT of regions of interest were also performed in 24 patients. Five NM specialists and three interns (1st, 2nd and 4th years), without knowledge of the patients' clinical information, classified each bone scintigraphy as "positive - P", "probably positive - PP", "probably negative - PN" and "negative - N" for BM. To ascertain the existence of BM, the patients' clinical processes were later consulted. Two were excluded due to the impossibility of confirming BM. To calculate the sensitivity and specificity, the exams were considered "positive" when the bone scintigraphy was classified as "P" or "PP" and "negative" when the bone scintigraphy was "N" or "PN". The global assertiveness (GA) was studied calculating the proportion of "P" and "N" answers [GA=(P+N)/(P+PP+N+PN)*100]. The positive assertiveness (PA) [PA=P/(P+PP)] and negative assertiveness (NA) [NA=N/(N+PN)] were also calculated. The statistical analysis was performed with IBM-SPSS 22 [comparative test of Mann-Whitney U (p<0.05) and Spearman's correlation coefficient - r]. **Results:** The mean specificity was 78.96±11.94%. The sensitivity was 100%. The mean GA was 64.85±9.78%. Specialists and interns did not had values of GA significantly different (p=0.250) [specialists: mean=67.9±10.89%; interns: mean=59.77±6.00%]. The mean PA was 55.83±21.07% and the mean NA was 62.25±10.76%. There was no statistically significant differences between PA and NA, neither between specialists and interns. The correlation between GA and specificity was not statistically significant in the entire group (r=0.554;p=0.154), neither in the subgroups of specialists (r=0.100; p=0.873) or interns (r=0.866;p=0.333). There was a significant difference (p=0.036) between specialists and interns at the probability of hitting the diagnosis when the answer was globally non-assertive (specialists: mean=80.54±8.92%; interns: mean=59.43±10.64%). **Conclusion:** Non-assertiveness, even being associated with a high specificity, may imply a treatment delay, a greater anxiety in the patient and an increase in diagnosis costs, whereby it is crucial and potentially feasible to give a confident result.

EP003

Prospective study regarding the reliability of the detection of bone metastases using planar scintigraphy, whole-body SPECT, and a computer-assisted analysis software

M. Schubring, M. Zuhayra, M. Marx, Y. Zhao, M. Jüptner, U. Lützen; Universitätsklinikum Schleswig-Holstein, KIEL, GERMANY.

Aim Bone scintigraphy is a well-known method for detection of bone metastases. This study evaluates the sensitivity and specificity of planar whole-body scintigraphy (WBS), whole-body SPECT (WB SPECT) and a computer assisted evaluation program for detection of bone metastases. **Methods** In 64 patients (58 women and 6 men, mean age 61.7 (34 - 86) years) with malignant tumor disease (breast cancer n=46, malignant melanoma n=11, breast cancer and malignant melanoma n=3, prostate cancer n=2, malignant melanoma and lung cancer n=1, breast cancer and renal cancer n=1) prospectively a bone scintigraphy was performed, consisting of a planar whole-body scintigraphy (WBS) and a 5-position whole-body SPECT (WB SPECT) of each patient. The images were randomized and anonymized. Both the planar and SPECT data were analyzed by two nuclear medicine specialists (A and B) concerning the existence of bone metastases (classification 1 - 4, 1 = certainly yes, 2 = rather yes, 3 = rather no, 4 = certainly no). The WBS were additionally analyzed by the EXINI bone program. The evidence of bone metastases was verified by all available clinical information including diagnostic tools such as MRI, PET/CT and CT and was used as reference for each patient. **Results** Regarding the references 23 of the 64 patients (35.9 %) suffered from bone metastases. The evaluation showed a sensitivity of 78.3 % (A 82.6 %, B 73.9%) for

WBS, 84.8 % (A 82.6 %, B 87.0 %) for WB SPECT, and 78.3 % for EXINI bone software. The specificity of WBS was 87.8 % (A 90.2 %, B 85.4 %), of WB SPECT 73.2 % (A 75.6 %, B 70.7 %), and of EXINI-bone 90.2 %. Moreover the interobserver variability of the detection of bone metastases was significantly lower in the analysis of planar WBS compared to WB SPECT ($p=0.02$). **Conclusions** This study shows a higher sensitivity and a lower specificity for WB SPECT in comparison to planar WBS. Consequently it is not meaningful to perform only a WB SPECT without a planar WBS. The computer assisted evaluation offers a comparable sensitivity and specificity. The solely use of the program cannot be recommended but it is very helpful especially in training of students and young physicians.

EP004

Fluorocholine PET/CT Predicts Skeletal Progression, Skeletal Event and Cancer Specific Survival in Patients with Biochemical Relapse for Prostate Cancer

L. Evangelista¹, M. Hodolic², F. Zattoni³, A. Guttilla⁴, E. Pizzirani⁵, F. Zattoni³, G. Saladini¹; ¹Nuclear Medicine and Molecular Imaging Unit, Veneto Institute of Oncology IOV - IRCCS, Padua, ITALY, ²Nuclear Medicine Research Department, IASON, Graz, AUSTRIA, ³Department of Oncological and Surgical Sciences, Urology Clinic, University of Padua, Padua, ITALY, ⁴Urology Unit, Hospital of Camposampiero, Padua, ITALY, ⁵Radiology Oncology Unit, Veneto Institute of Oncology IOV - IRCCS, Padua, ITALY.

Objectives: the aim of our study is to evaluate the prognostic impact of 18F-Choline (FCH) positron emission tomography (PET)/computed tomography (CT), CT alone and bone scan (BS) in PCa patients with skeletal recurrences. **Methods:** we retrospectively selected 62 patients who underwent, between June 2010 and February 2013, both FCH PET/CT and BS within a span of six months. All patients had a biochemical PCa recurrence after radical prostatectomy and/or radiation therapy. Two independent observers reviewed PET/CT and BS images. The bone window of CT portion from PET/CT was separately assessed. Time to progression (TTP), skeletal event free survival (SES) and OS were defined as the length of time between imaging and progression of disease, skeletal related events and all-cause mortality, respectively. A patient based and a K agreement analysis were used to compare the findings of all three imaging modalities. Kaplan-Meier and log-rank analysis were computed for survival assessment. A multivariate Cox regression analysis was used to identify the independent predictors for OS and TTP. **Results:** bone metastases were detected in 25 (40%) patients at FCH PET/CT, in 30 (48%) at BS and in 27 (44%) at CT. The agreement between PET/CT and BS, CT and BS, and PET/CT and CT were fair/moderate (respectively, k : 0.513, 0.32 and 0.47; all $p<0.05$). After 36 months (IQR: 26-52 months) of follow-up, 36 (61%) patients had a new recurrence of disease, 13 (21%) had skeletal related events and 22 (35.5%) died. Three subjects (5%) were lost during the observational period. At survival analyses, a worse TTP, SES and OS were found in patients with a positive PET/CT at bone level than those with a negative scan (all $p= <0.05$). Conversely, any significant difference in TTP, SES and OS was found for patients with both a positive BS and CT scan. At univariate analysis, a positive PET/CT at skeletal level was associated with all events (all $p<0.05$). However, only a negative PET/CT at any site was an independent prognostic variable of TTP (HR: 0.29; CI 95%: 0.10-0.82; $p=0.02$). **Conclusions:** PET/CT should be preferred to CT and BS in the evaluation of bone metastatic PCa because it allows a better stratification of TTP, SES and OS compared to CT and BS. Additional studies are needed to compare the prognostic impact of FCH PET/CT with either magnetic resonance imaging or new radioactive tracers, such as radiolabeled prostate specific antigen membrane.

EP005

Multicenter prognostic registry for prostate cancer using bone scintigraphy and bone scan index: PROSTAT-BSI study design

K. Nakajima¹, A. Mizokami¹, M. Ueno², H. Horikoshi³, T. Ichikawa⁴, S. Takahashi⁵, H. Matsuyama⁶, H. Shiina⁷; ¹Kanazawa University Hospital, Kanazawa, JAPAN, ²Saitama Uro-Dermatol Clinic, Saitama, JAPAN, ³Gunma Prefectural Cancer Center, Ohta, JAPAN, ⁴Chiba University Hospital, Chiba, JAPAN, ⁵Nihon University Itabashi Hospital, Tokyo, JAPAN, ⁶Yamaguchi University Hospital, Ube, JAPAN, ⁷Shimane University Hospital, Izumo, JAPAN.

Purpose: In patients with prostate cancer, amount of bone metastasis has been considered to be an important prognostic factor to evaluate therapeutic effect, skeletal-related events, and mortality. While bone scan index (BSI) has been proposed as a quantitative measure of bone metastasis, few studies have validated the role of BSI in a prospective manner during standard hormonal therapy and chemotherapy. The objective of this study was to create a multicenter cohort registry and to evaluate the utility of BSI in the management of prostate cancer. **Methods:** The patient inclusion criteria included newly diagnosed prostate cancer with definite bone metastasis as evidenced by imaging modalities, such as bone scan, X-ray computed tomography and/or magnetic resonance imaging. Patients were classified into groups of hormonal therapy (Group H) and chemotherapy with Docetaxel due to resistance to hormonal therapy (Group C). Bone scintigraphy was performed using whole-body anterior and posterior imaging in each hospital before and after treatment every 3 months. The software BONENAVI (FUJIFILM RI Pharma/EXINI bone, EIXINI Diagnostics) used artificial neural network to determine locations and extent of bone metastasis. Using a Japanese multicenter database ($n=1,532$), the software was upgraded to provide the diagnostic sensitivity and specificity of 90% as validated previously. BSI was calculated to express percentage of bone metastasis divided by whole bone mass. The primary target of this study was to investigate the relationship between BSI and relapse-free survival and prostate specific antigen (PSA)-progression-free survival, as well as overall survival. Changes in BSI from the baseline condition to after treatment will be compared to those in PSA and other bone metabolic markers. **Results:** A total of 237 patients were registered from 30 hospitals in Japan, including 157 patients with hormonal therapy and 80 with chemotherapy. Based on the clinical data as of March 2016 ($n=174$), mean BSI calculated on-site was 3.1 ± 3.0 ranged from 0.02 to 13, and number of hot spots 29 ± 31 , ranged from 1 to 119. Lymph node metastasis was observed in approximately 70% at the time of entry. Median PSA was 285 and 30 ng/ml for Groups H and C, respectively. While incidence of lung metastasis did not differ between groups (12%), that of liver metastasis was higher in Group C (7%) than Group H (1%). **Conclusion:** Multicenter registry involving patients with prostate cancer with bone metastasis was designed, and the role of BSI in prostate cancer treatment would be clarified in this cohort study.

EP006

Whole body (WB) vs. Limited Field of View (LFOV) Sodium Fluoride (NaF) Positron Emission Tomography/Computed Tomography (PET/CT) Imaging; comparison of both techniques

S. Alratroot¹, A. Al-Dhafiri², A. Al-Tuwaijri², R. Al-Muslem³, A. Moin²; ¹King Fahad University Hospital, Dammam, SAUDI ARABIA, ²King Fahad Specialist Hospital Dammam, Dammam, SAUDI ARABIA, ³University of Dammam, Dammam, SAUDI ARABIA.

Purpose: NaF PET CT imaging is commonly used for osseous evaluation. Routinely the FOV for NaF follows the same technique as planar bone scintigraphy (BS) i.e. whole body imaging from vertex to toes with arms down. Here we evaluate the comparison of WB vs. LFOV from base of skull till proximal thighs with arms down. **Methods:** The study was approved by

institutional review board. We did retrospective review of NaF PET CT scans that were performed during three weeks. **Results:** 47 scans were performed. There were 41 females and 6 males, aged 26–84 years. Most of the scans were performed for breast cancer staging followed by prostate and thyroid cancers workup. 15 scans were positive for metastatic lesions. 4/15 patients had super scans. Remaining 11 scans showed lesions in the ribs, spine, base of skull, proximal humeri, scapulae, sternum and proximal femurs. Only one patient showed additional lesion in left distal femur (along with multiple others in axial and proximal appendicular skeleton) that was suspicious for metastatic disease. Out of 32 negative scans, 1 scan had CT lytic changes but did not show any NaF uptake and it was considered false negative. Remaining 31 scans showed mostly degenerative changes and traumatic lesions which could have been mostly visualized in LFOV imaging. **Conclusion:** We conclude that NaF PET CT can be used with limited FOV instead of WB imaging for tumor staging work up. This can avoid unnecessary radiation exposure to the patient, especially to the extremities and brain.

EP007

The Screening Potential of Bone Scintigraphy and Serum Bone Metabolic Markers for Early-stage Medication-related Osteonecrosis of the Jaw

S. Watanabe, K. Nakajima, A. Mizokami, N. Noguchi, S. Kawashiri, M. Inokuchi, S. Kinuya; Kanazawa University, Kanazawa, JAPAN.

Aim: Medication-related osteonecrosis of the jaw (MRONJ) is an important side effect of antiresorptive and antiangiogenic drugs. Early detection of MRONJ has been attempted by various methods. The aim of this study was to quantitatively evaluate the screening potential of bone scintigraphy and serum bone metabolic markers for early-stage MRONJ. **Methods:** A total of 68 cancer patients treated with antiresorptive drugs were evaluated retrospectively. All patients underwent bone scintigraphy, and tracer uptakes in the jaw were analyzed semiquantitatively by bone scan index (BSI) of the jaw related to MRONJ (BSI_{MRONJ}). The software BONENAVI (FUJIFILM RI Pharma, Japan; EXINIbone, EXINI Diagnostics, Sweden) could detect abnormal intensities and calculate each regional BSI (rBSI), which was defined by the fraction of abnormality to the entire skeleton (%). Using the regions detected by the software, we selected MRONJ-related regions manually. The largest rBSI in the jaw (BSI_{max}) and the BSI of the whole body were also calculated. The serum levels of bone alkaline phosphatase (BAP) and pyridinoline cross-linked carboxy-terminal telopeptide of type I collagen (1-CTP) were examined. **Results:** In 22 patients who developed stage 2 MRONJ, BSI_{MRONJ} and BSI_{max} showed significant correlation ($p < 0.05$). The BSI_{max} was significantly higher in patients who developed MRONJ than in those who did not, even 6 months before the diagnosis of stage 2 MRONJ ($p < 0.002$). The BSI_{max} was significantly higher in the maxilla than in the mandible in patients who did not develop MRONJ ($p = 0.02$) and in those who developed stage 2 MRONJ at 6 months before the diagnosis ($p = 0.03$). Using the cutoff value of 0.06%/0.10% in the mandible/maxilla, BSI_{max} for predicting stage 2 MRONJ showed sensitivity and specificity of 57%/71% and 80%/93%, respectively, at 6 months before the diagnosis. The BSI_{max} $\geq 0.06\%/0.10\%$ in the mandible/maxilla was much more frequently observed in patients who subsequently developed stage 2 MRONJ 6 months after bone scintigraphy than in those who did not ($p = 0.003/0.0004$, odds ratio = 7.6/35.8). In contrast, the serum bone metabolic markers (BAP and 1-CTP) did not correlate significantly with the incidence of MRONJ. The serum bone metabolic markers and the BSI of the whole body showed significant correlation ($p < 0.005$). **Conclusion:** The BSI provided a new index for evaluating MRONJ. For predicting occurrence of MRONJ, the threshold of BSI_{max} = 0.06%/0.10% in the mandible/maxilla may be used in patients treated with antiresorptive drugs, and a differential diagnosis of MRONJ is recommended. In contrast, serum bone metabolic markers reflect systemic bone metastasis rather than MRONJ.

EP008

Performance of SPECT/low dose CT imaging in the diagnosis of metastatic bone disease

T. Pipikos¹, F. Vlachou¹, A. Nikaki¹, K. Dalianis², D. Papoutsani¹, S. Merisoglou¹, V. Papoutsis¹; ¹Nuclear Medicine & PET/CT Department, Hygeia SA, Athens, Marousi, GREECE, ²Medical Physics Department, Hygeia SA, Athens, Marousi, GREECE.

AIM: Bone scintigraphy is a very sensitive imaging modality for whole body bone staging of cancer patients. Although the sensitivity of the method is high, specificity is rather low. Modern hybrid SPECT/low dose CT devices, give anatomic localization and further characterization of abnormal tracer uptake foci. In this study we evaluated the performance of SPECT/low dose CT in the diagnosis of metastatic bone disease.

MATERIAL AND METHODS: We reviewed the SPECT/low dose CT images of 43 patients, that underwent a bone scan for malignancy staging and had limited findings (solitary lesions) suggestive or highly suspicious of metastatic bone disease. We evaluated the findings of low dose CT in the site of abnormal tracer uptake. All patients were followed up with diagnostic CT/MRI, were re-evaluated in a period of 1 year and in some cases a bone biopsy was performed. **RESULTS:** From the total of 48 patients, 19 had a lytic corresponding lesion in low dose CT images, 15 of them had a sclerotic or mainly sclerotic lesion, 5 patients had lesions with mixed lytic-sclerotic characteristics, while 9 patients showed no corresponding abnormality. In the group of patients with lytic findings, one patient was proven to show uptake in an aneurysmal bone cyst. One sclerotic lesion was proven to be fibrous dysplasia and one patient had an osteoma. One lesion with mixed sclerotic-lytic appearance was finally attributed to an enchondroma. Two patients with no findings in low dose CT were proven to have benign lesions, a bone infarct and a femoral shaft stress fracture. Overall SPECT/CT correctly identified 42/48 (88%) patients with metastatic bone disease. **CONCLUSION:** SPECT/low dose CT imaging increases the specificity of bone scan, but abnormal uptake does not always correspond to a metastatic deposit. In our small group of patients, lytic appearance is the most specific pattern of a metastatic lesion. SPECT/CT imaging systems with a diagnostic CT component, are expected to further improve diagnostic performance.

EP009

Value of the EXINI Bone Scan Index as a Biomarker During Xofigo Therapy in Patients with high Tumor Load

M. Miederer¹, C. Thomas¹, V. Weyer¹, H. Buchholz¹, F. Luttrupp², M. Schreckenberger¹; ¹University Medical Centre Mainz, Mainz, GERMANY, ²EXINI Diagnostics, Lund, SWEDEN.

Objectives: Several promising drugs have been approved for treatment of mCRPC within the last years. One of them is Radium-223, an osteotropic radiopharmaceutical. Due to heterogeneity of disease, limited validity of blood based biomarkers and difficulties in quantification of tumour load on imaging, monitoring the therapeutic effect of Radium-223 remains challenging. Imaging with osteotropic tracers might be a viable option to visualize treatment induced reduction of osteoblastic activity. In the current study, we investigated the prognostic role of a new quantification technique for tumour load on bone scans in mCRPC patients undergoing Radium-223 treatment. **Methods:** In 15 consecutive mCRPC patients with multifocal/disseminated bone metastases baseline and interim bone scans were obtained and analyzed for tumor load using the commercial software EXINI bone scan. Changes in bone scan quantification were compared to Serum-PSA response and overall survival. The EXINI software was recently updated to ensure validity in particular in patients with high tumor burden up to a value of 13 (BSI 2.1). Based on the

validation of the software, statistical analysis as a biomarker for outcome was restricted to 12 patients displaying initial BSI between 3 and 13. Three additional patients with higher tumor loads were analyzed separately. Results: Manual corrections were necessary in one patient due to obstruction induced urine uptake in the upper urinary tract and in two patients due to incontinence induced urine contamination (3/30 scans). In one patient pelvic metastasis could not be discriminated from bladder activity. Comparison of BSI Version 1.8 and 2.1 for 15 patients revealed higher values in particular at higher tumor burden both for baseline (mean 6.3 vs 8.7) and for follow up (mean 7.1 vs 9.4). However, difference between baseline and interim-staging was not significant between both versions ($p=0.83$). 5/15 patients showed a decrease of bone scan index after the first two cycles of radium-223. In contrast, only two patients with initial low levels of serum PSA (<100 ng/ml) presented a PSA decline at this time point. Cox regression analysis showed a trend towards validity for bone scan index to serve a predictive marker similar to serum PSA ($p=0.035$ and $p=0.18$ for BSI version 1.8 and 2.1; $p=0.034$ for PSA) Conclusion: The bone scan index is a valuable and easily applicable tool to quantify tumor load and treatment response on bone scans in mCRPC patients undergoing Radium-223 treatment.

EP010

Multiple Non Ossifying Fibromas in 20 year old patient with Speckled Lentiginous Nevus syndrome; Jaffe-Campanacci syndrome?

I. Sisko Markos, M. Romić, P. Petranovic Ovcaricek, V. Gladic Nenadic, M. Franceschi, Z. Kusic; UHT Sestre Milosrdnice, Zagreb, CROATIA.

INTRODUCTION: Speckled lentiginous nevus syndrome is a recently described syndrome with male to female ratio of 4:3; usually present at birth but may appear during first years of life. Cafe au lait macules can be topped by either browns or black macules or papules. Patients usually present with musculoskeletal and neurological anomaly at ipsilateral site. Nonossifying fibromas (NOFs) are the most common benign bone tumor in children. The tumors affected long bones as the humerus, the tibia, the femur, the fibula. Approximately 8 % of people with NOF will have more than one tumor. It is uncommon to have more than two or three tumors except in certain very rare conditions like Jaffe - Campanacci 's syndrome. This syndrome can present only with skin patches and NOFs, but also as a part of more severe systemic presentation like cardiovascular, renal, ocular abnormalities and mental retardation. **CASE PRESENTATION:** a 20 year old female with a known diagnosis of Speckled lentiginous nevus Syndrome presented to our Department in 2012 for evaluation of prolonged discomfort in the right leg. Performed MRI showed atrophy in right leg and hyperintensive ovale zone (24x10 mm) in distal part of left femur. Three phase bone scan revealed decreased uptake in all 3 phases in right lower extremity, without focal lesions in the left and increased uptake in right humerus (initially evaluated as a bone infarct or eosinophilic granuloma). Bone scan performed in 2013 showed increased left - right asymmetry uptake between lower extremities. Since then she developed paresthesia in right arm. X-ray showed a 41x10 mm zone in proximal diaphysis of right humerus suspected for NOF. Bone scan performed in 2016 showed same changes in right humerus as 2012, but with new focal increased uptake in distal part of diaphysis of left femur with same scintigraphy pattern as in the right arm. Diagnosis of multiple non-ossifying fibromas was presumed. **CONCLUSION:** Regarding the clinical presentation and bone scan, diagnosis of Jaffe-Campanacci syndrome was presumed.

EP011

Volumetric FDG-PET indices for the assessment of histological response to neoadjuvant chemotherapy and outcome in paediatric patients with Ewing sarcoma and osteosarcoma

C. Bailly¹, L. Campion², E. Thebaud¹, N. Corradini¹, A. Moreau¹, D. Dansette¹, F. Kraeber Bodere¹, T. Carlier¹, C. Bodet Milin¹; ¹University Hospital, Nantes, FRANCE, ²Cancer Center ICO René Gauducheau, Nantes, FRANCE.

Aim: Response to chemotherapy is a prognostic factor in patients with Ewing sarcoma (EWS) and Osteosarcoma (OST). Several studies showed high diagnostic accuracy of positron emission tomography using 18F-fluoro-2-deoxy-glucose (FDG-PET) for response to initial chemotherapy (CHT) in these patients and a correlation with outcome. Despite a potential impact of age on the prognosis of bone sarcoma patients, most of these studies mixed adult and paediatric populations. The objective of this retrospective work was to evaluate the prognostic value of quantitative indices derived from FDG-PET in an homogeneous paediatric bone sarcoma population including EWS and OST. **Methods:** 31 paediatric patients with EWS (median age 14.7 years) and 31 with OST (median age 12.8 years) were included. All patients were treated with CHT, and underwent surgery for local control. All patients had FDG PET at diagnosis and after induction CHT, prior to surgery. Several parameters for assessment of response of the primary tumour to therapy by FDG PET were evaluated: SUV_{max} , SUV_{peak} , SUV_{mean} , metabolic tumor volume (MTV), total lesion glycolysis (TLG), Tumor to contralateral Background Ratio (TBR), 7 textural features (TF) and 3 shape features (SF). For each metric requiring a segmentation step, 3 delineation methods were compared including an adaptive approach, 40% of SUV_{max} and $SUV > 2.5$. Each pair of FDG-PET scan were also classified as responding (R) and non-responding (NR) according to PERCIST criteria. Results were then compared to histopathological regression of the resected tumour as defined by Salzer-Kuntschik and to the clinical follow-up for survival evaluation (median of follow-up: 5 years). **Results:** After CHT, the absolute SUVs, MTV, TLG, TF, SF or TBR, the reductions of SUVs, TF or SF, TBR and PERCIST criteria were neither significantly associated with histologic response nor overall survival or progression free survival for either EWS or OST. The MTV and TLG reduction (segmentation $SUV > 2.5$) were the only quantitative indices that significantly discriminated histopathological responders from non-responders using the entire patient population ($\Delta MTV_{2.5}$, $p=0.0109$; $\Delta TLG_{2.5}$, $p=0.0076$) as well as in the subgroup of OST patients ($\Delta MTV_{2.5}$, $p=0.0032$; $\Delta TLG_{2.5}$, $p=0.0040$), but not in the EWS subgroup. **Conclusion:** Only MTV and TLG reduction seem to enable accurate non-invasive assessment of histopathological reduction after CHT in the OST paediatric population but reveal limited additional prognostic value in paediatric patients with EWS.

EP012

Prognosis value of SUV-based metrics, textural and shape features derived from initial FDG-PET in paediatric patients with Ewing sarcoma and osteosarcoma

C. Bailly¹, L. Campion², E. Thebaud¹, N. Corradini¹, A. Moreau¹, D. Dansette¹, F. Kraeber Bodere¹, C. Bodet Milin¹, T. Carlier¹; ¹University Hospital, Nantes, FRANCE, ²Cancer Center ICO René Gauducheau, Nantes, FRANCE.

Purpose: Histologic response, measured by the percentage of tumor cells remaining after neoadjuvant chemotherapy (CHT) is the main prognostic factor in Osteosarcoma (OST) and Ewing sarcoma (EWS). Previous positron emission tomography using 18F-fluoro-2-deoxy-glucose (FDG-PET) studies tried to determine the value of FDG uptake as an accurate and non-invasive preoperative marker of response. Yet most of them explored heterogeneous populations mixing different histological

subtypes, CHT regimens or age groups. Our objective was to evaluate, retrospectively, the accuracy of FDG-PET for OST and EWS staging and to determine the prognosis values of quantitative parameters in a homogeneous paediatric bone sarcoma population. **Methods:** 31 patients with EWS (median age 14.7 years) and 31 with OST (median age 12.8 years) were included. All patients were treated with neoadjuvant CHT, and underwent surgery for local control. All patients were examined with conventional imaging (CI) modalities (CT, MRI, bone scintigraphy) and with FDG-PET at diagnosis. Several parameters were extracted from the main lesion: SUVmax, SUVpeak, metabolic tumor volume (MTV), total lesion glycolysis (TLG), 7 textural features (TF) using two different normalization and 3 shape features (SF). The segmentation was performed using an adaptive approach. Results were compared to histopathological regression of the resected tumour as defined by Salzer-Kuntschik using Spearman analysis and to the clinical follow-up and CI for survival evaluation (median of follow-up: 5 years) using univariate and multivariate Cox analysis. **Results:** FDG-PET and CI were equally effective in the detection of primary tumors (accuracy, 100%). FDG-PET was superior to CI for detection of bone metastases in both EWS (sensitivity, 80% vs. 60%) and OST (sensitivity, 100 vs. 20%), whereas CI was more reliable than FDG-PET in depicting lung metastases (sensitivity, 100% v 50%, respectively). For EWS, univariate analysis did not highlight any prognostic value on histological response, PFS and OS regardless of all the considered metrics and known prognostic factors such as anatomic primary site or presence of metastatic disease. For OST univariate analysis showed that presence of metastatic disease and one of the SF, namely elongation, were significantly associated with PFS and OS. Multivariate analysis confirmed that the presence of metastatic disease was an independent factor for OS whereas elongation was the only significant factor for PFS. **Conclusion:** Only a SF called elongation determined on initial FDG-PET has a potential interest as a prognostic factor of PFS in paediatric OST patients. All the metrics reveal limited additional prognostic value in paediatric EWS patients.

EP013

The physiological accumulation of FDG in the muscles in relation to the side of intravenous administration

Y. Otomi¹, T. Shinya¹, Y. Arai¹, K. Miyamoto¹, K. Takechi², N. Uyama¹, M. Harada¹; ¹Tokushima University Hospital, Tokushima, JAPAN, ²Tokushima Red Cross Hospital, Tokushima, JAPAN.

Purpose: The purpose of the present study was to evaluate the physiological accumulation of FDG in the muscles in relation to the side of intravenous administration. **Methods:** We retrospectively reviewed 1,423 FDG-PET/CT exams that were performed in our institution in 2015. Cases that involved hyperglycemia (over 140mg/dl), metastases to the muscles or subcutaneous tissues in the shoulder and arm, diffuse FDG accumulation in the arm muscles, cases of neurofibromatosis, cases in which the patients had arteriovenous fistulas for hemodialysis, the intravenous administration of FDG to the lower limbs, subcutaneous extravascular leakage of FDG, and cases in which the patients were not imaged in the supine position were excluded from the analysis. Thus, a total of 1,310 exams were included in the present study. We evaluated the physiological accumulation of FDG in the muscles of the shoulder and arm related to the side of intravenous administration. We investigated the association of the accumulation in the teres minor muscles and the side of administration. We also investigated the association of the accumulation in the muscles between the radioulna near the elbow and the side of administration. **Results:** Two hundred eighty-four of the 1310 (21.7%) exams showed the physiological accumulation of FDG in the teres minor muscle. Accumulation was seen on the side of administration in 223/284 (78.5%) exams. Accumulation was observed contralateral to the side of administration in 26/284 (9.2%) exams. Accumulation in the bilateral teres minor muscles was seen in 35/284 (12.3%) exams. Accumulation in the muscles between the radioulna near

the elbow was observed on the side of administration in 161/194 (83.0%) exams and contralateral to the side of the administration in 16/194 (8.2%) exams. Accumulation in the muscles between the radioulna near the elbow was observed bilaterally in 17/194 (8.8%) exams. The Cohen k coefficient was 0.791 when confined to cases with unilateral accumulation in the teres minor muscles. The Cohen k coefficient was 0.896 when confined to cases with unilateral accumulation in the muscles between the radioulna near the elbow. **Conclusion:** The present study reported that accumulation in the teres minor muscles and accumulation in the muscles between the radioulna near the elbow on the side of intravenous administration occurred significantly more frequent than accumulation on the contralateral side. Our results indicate that the accumulation in both the teres minor muscle and the muscles between the radioulna near the elbow was associated with the side of intravenous administration.

EP014

Role of ¹⁸F-FDG PET/CT for initial staging and restaging of sarcomas

C. Bentancourt, A. Banchemo, S. Rossi, O. Alonso, J. Gaudio, H. Engler; Uruguayan Centre of Molecular Imaging, Montevideo, URUGUAY.

Introduction: Sarcomas are a heterogeneous group of malignancies that can arise either from soft tissue or bone. They represent 1% of all cancers. Soft tissue sarcomas have an incidence 3-4 times higher than osseous. The role of MRI in local characterization and thorax CT in the diagnosis of distant metastasis (mainly pulmonary) is well known. However, the utility ¹⁸F-FDG PET/CT for both initial staging and restaging remains uncertain. **Objective:** The aim of our study was to investigate the clinical value of ¹⁸F-FDG PET/CT for staging and restaging in patients with sarcomas. **Material and method:** We retrospectively analyzed 164 patients who underwent PET/CT scans in the Uruguayan Centre of Molecular Imaging from January 2011 to March 2016. Fifty-six % of patients were women (mean age 46 ± 19 yr). Mean age for men was 45 ± 22 yr. Fourteen patients were under 14 yr. Scans were performed 60 minutes after the injection of 4.07 MBq/Kg ¹⁸F-FDG. Children were injected according the EANM pediatric dose chart. The study was performed for initial staging (n=17) or restaging (n=147) of a confirmed sarcoma. Forty-one patients (25%) were diagnosed with osteosarcoma and 123 (75%) with soft tissue sarcoma (11% initial staging in each group). **Results:** Overall, PET/CT shows a detection rate of 53% in patients for initial staging and 51% in patients for restaging. When performed as initial staging in osteosarcomas, PET/CT detected local lesions in 50% of patients, with no distant metastases. For initial staging of soft tissue sarcoma, PET/CT detected local lesions in 46% of patients, distant in 15% and both in 15%. The most important feature in defining local disease is surgical planning, allowing a better characterization of bone marrow involvement to define the surgical strategy. This is important due the existence of new conservative techniques such as hemicortical allograft reconstruction. In restaging of osteosarcomas, PET/CT was able to diagnose local recurrence in 11%, distant metastases in 24% and both in 13%, with 48% detection rate. In the case of soft tissue sarcomas PET/CT detected local recurrence in 7% of patients, distant in 30% and both in 9%, with a detection rate of 46%. **Conclusion:** Despite controversy, ¹⁸F-FDG PET/CT is useful in initial staging and restaging of sarcomas. We could characterize bone marrow involvement allowing surgical planning with a lesion detection rate of 53%. The diagnosis of local and distant metastases led to a more accurate treatment in 51% of patients.

EP015

FDG PET-CT Findings In Different Locations Synovial Sarcomas

J. BENOHOUD, S. CHOUKRY, S. TOUIL, A. GUENSI; CHU Ibn Rochd, Casablanca, MOROCCO.

INTRODUCTION: Synovial sarcomas are rare malignant tumors that encompass from 5 to 10% of soft tissue sarcomas. They affect mainly young adults and present as a painful slow growth mass located in deep soft tissues of extremities, near joints, even though their onset can be in any part of the body. We report FDG PET/CT findings in 5 patients with 5 different synovial sarcoma locations. **MATERIALS AND METHODS:** We collected all PET-CT examinations performed in the staging of a synovial sarcoma between September 2014 and March 2016 at the nuclear medicine department of the Ibn Rochd University Hospital, Casablanca, Morocco. We conducted our tests using a SIEMENS BIOGRAPH 6 engine starting in 2011. We achieved All body PET/CT scan examination 60 minutes after injection of 5 MBq / kg of 18-FDG. **RESULTS:** All patients were male, mean age was 30.4 years. Synovial sarcomas locations were: the forearm, elbow, thigh, popliteal and pleura. The mean SUVmax lesions were 4.8 with extremes of 2.5 and 6.4. A lymph node was found in 3 patients, she was axillary in 2 patients and in the other mediastinal. All patients had metastatic lung lesions, and 3 patients had secondary bone lesions. Pneumothorax was fortuitously discovered in one of the patients. Only two patients underwent resection surgery. **CONCLUSION:** In synovial sarcomas, a complete resection of the tumor is the best treatment. Tumors response to chemotherapy and radiation therapy is poor. The contribution of PET/CT to diagnosis and treatment sarcomas has not been identified properly yet. It seems show the involvement areas in whole body images. PET/CT may have a significant role managing synovial sarcoma. In fact, precociously diagnosis of lesion and metastasis may improve treatment strategy. Also, PET/CT scan may be an important tool in follow-up strategies in patient with synovial sarcomas by detecting the early metastatic disease.

EP016

Differential diagnose between hibernoma and liposarcoma, a case report

U. Jon, A. Perissinotti, A. Allende-Riera, C. Cardenas-Negro, E. Martinez-Gimeno, D. Cabello, O. Vilahomat, M. De Sequera-Rahola; Hospital Universitario Nuestra señora de la Candelaria, Santa Cruz de Tenerife, SPAIN.

Aim: Hibernomas are infrequent benign tumours that usually manifest in adults as a low growing painless mass located in the thigh, shoulder, back, neck, chest, arm or abdominal cavity/retroperitoneum. Hibernomas arise from fetal brown adipose tissue remnants and are highly 18F-FDG avid because of the elevated metabolic rate due to their high number of mitochondria for thermogenic purposes. Core needle biopsy is not recommended in cases of suspected hibernoma due to the tumor's hypervascularity and, in opposition to liposarcomas, hibernoma treatment consists of complete surgical resection and postoperative prognosis is excellent. The aim of this report is to present a case of patient with an unknown hibernoma which was mistaken for malignant lesions at initial diagnosis. **Materials, methods and results:** A 23 year old female was admitted to our centre with a right thigh mass. She referred tightness in right groin and anterior thigh with presence of a rapidly increasing size tumour. She denied history of prior trauma. TC and MRI scans performed at our centre revealed a fat-density bilobulated 8.7 cm mass located in the right thigh in close contact with tensor fascia lata, sartorius, minor and medius gluteus and vastus lateral and anterior muscles. Presumptive diagnose was reported as liposarcoma. 18F-FDG PET/CT scan was performed using a PET/CT camera (Gemini TF-16, Philips) with an injected activity of 2.6 MBq/Kg. PET/CT showed a high focal uptake in the right thigh mass with an homogeneous 14.2 SUVmax uptake value and no amebolic necrotic areas. No other abnormal foci or FDG uptake was present on the rest of the study and PET/CT results put forward the differential diagnose of hibernoma. Surgical resection of the mass was performed and histopathological study revealed a well delineated adipose tumour with presence of mature adipocytes with no atipia or mitosis

confirming the hibernoma diagnose. **Conclusion:** In the assessment of fatty tumours, usually low to intermediate glucose metabolism is associated to benign lipoma and low grade liposarcoma, while elevated 18F-FDG uptake suggest high grade liposarcoma. However, hibernoma should be considered in the differential diagnosis as PET/CT scan appearance can be worrying due to its high hypermetabolic rate and should not be confused with liposarcoma. Also, fluctuation in the SUVmax between PET/CT examinations has been described in hibernomas and is thought to be consequence of the influence of the external temperature.

EP017

Pathophysiology of Bone-Seeking Tracers in Patients with Disseminated Prostate Cancer: a SPECT/CT Study, Based on Computational Analysis

F. Fiz¹, S. Sahbai¹, C. Campi², M. Piana², G. Sambuceti³, C. la Fougère¹; ¹Nuclear Medicine Unit, Department of Radiology, University of Tübingen, Tübingen, GERMANY, ²Department of Mathematics, University of Genoa, Genoa, ITALY, ³Nuclear Medicine Unit, Department of Health Sciences, University of Genoa, Genoa, ITALY.

Rationale: Whole body ^{99m}Tc-DPD SPECT/CT is used for staging as well as response evaluation in patients with disseminated metastases from castration-resistant prostate cancer (CRPC) in which radionuclide therapy has become clinical standard recently. Understanding the interaction between bone density and tracer distribution might enable a personalized radionuclide therapy planning. In this study a computational approach was used, in order to analyze the relationship between bone density and tracer uptake. **Material and Methods:** Seventy-six ^{99m}Tc-DPD SPECT/CT scans, from CRPC patients suffering from bone metastases, were analyzed with a dedicated software application. The output included the volumes of total (TBV), compact (CBV) and trabecular (IBV). Average Hounsfield density was computed for IBV and CBV (iHU and cHU, respectively). Also blood-pool normalized counts were computed separately: this value was labeled target-to-background ratio (iTBR and cTBR for trabecular and compact bone, respectively). In the analysis, whole-body, axial and appendicular skeleton were considered separately. Presence and extent of intraosseous metastases was quantified as the percentage of CBV on total skeleton (CBV%). **Results:** iTBR directly correlated with iHU in the whole-body, axial as well as appendicular skeleton IBV (R=0,62, 0,59, 0,65, respectively, p<0,001). In the axial skeleton, iTBR also correlated with cHU, albeit with a parabolic pattern, peaking at about 600 Hounsfield units and dwindling thereafter (R=0,59, p<0,01). Furthermore, a direct correlation between axial cHU and cTBR was found (R=0,64, p<0,001). Moreover, cTBR directly correlated with CBV% in the whole-body and in the axial bones (R=0,53 and 0,58, p<0,01). When stratifying the population according to CBV% quartiles, cTBR was higher than iTBR (p<0,05) in all groups; the difference was most notable in the highest CBV% quartile (45±12 vs. 28±10, p<0,01). **Conclusion:** Our data highlight a direct correlation between bone density and tracer uptake in both trabecular and compact bone, as well as a cross-correlation between compact bone density and activity in the trabecular bone. Moreover, a higher percentage of compact bone was linked with higher uptake values, particularly in the compact bone. These data could be of use in clarifying the mechanisms of bone marrow toxicity and therapy effectiveness in patients who might be candidate for radionuclide treatments. In particular, should these distribution patterns be mirrored by bone-seeking alpha- or beta-emitting radiopharmaceuticals, it would follow that a higher bone density could entail a higher dose to both the skeletal lesions as well as to hematopoietic bone marrow.

EP-02 – Sunday, October 16, 2016, during Exhibition hours, e-Poster Area
Clinical Oncology: Brain

EP018**Diagnostic Accuracy for F18-FDG-PET/CT and C11-METHIONINE-PET/CT Co-registered with MRI For Differentiation of Recurrent Brain Tumor From Radiation Injury**

L. RODRIGUEZ-BEL¹, **C. GÁMEZ-CENZANO**¹, **J. GARCÍA-GARZÓN**², **A. SABATÉ-LLOBERA**¹, **J. VERCHER-CONEJERO**¹, **L. GRÀCIA-SÀNCHEZ**¹, **E. LLINARES-TELLO**¹, **C. MAJÓS-TORRO**³, **A. LUCAS-CALDUCH**⁴, **M. MACIÀ-GARAU**⁴, **J. BRUNA-ESCUER**⁵; ¹PET Unit. Department of Nuclear Medicine. IDI. Hospital U. de Bellvitge-IDIBELL, L'Hospitalet de Llobregat (Barcelona), SPAIN, ²PET ESPLUGUES Unit. CETIR-ERESA., Esplugues de Llobregat (Barcelona), SPAIN, ³RM Unit. Department of Radiology. IDI. Hospital U. de Bellvitge-IDIBELL, L'Hospitalet de Llobregat (Barcelona), SPAIN, ⁴Department of Radiation Oncology. ICO. Hospital Duran i Reynals-IDIBELL, L'Hospitalet de Llobregat (Barcelona), SPAIN, ⁵Department of Neurology. Hospital U. de Bellvitge-IDIBELL, L'Hospitalet de Llobregat (Barcelona), SPAIN.

Aim: Our purpose was to evaluate the ability of FDG-PET co-registered with MRI to differentiate recurrent tumor from radiation necrosis, in patients with inconclusive clinical and MRI findings. We also evaluated the additional role of ¹¹C-Methionine-PET (MET-PET) in the negative/equivocal FDG-PET scans. **Materials and Methods:** Retrospective study of 28 patients previously treated with radiotherapy after primary treatment for metastatic brain tumor (23) or glioma (5). A total of 33 FDG-PET scans were obtained (5 during follow-up). The mean interval between radiotherapy and FDG-PET was 15 months (range: 3-36). FDG-PET were co-registered with MRI and visually classified as: 1) negative when hypo or isoactivity was seen in the lesion, 2) positive when focal accumulation of FDG exceed any level of activity in the adjacent grey/white matter and 3) equivocal if an slightly increase homogeneous activity was seen at the margin around the irradiated lesion. FDG-PET images were also quantitatively assessed using T/N ratios (SUVmax tumor/SUVmax contralateral normal region). MET-PET was performed in 12 patients where FDG-PET was negative in 7, equivocal in 3 and positive in 2. MET-PET scans were visually assessed (evaluation of the grade of intensity and tracer uptake morphology) in PET/MRI co-registered images (Software-AGFA/SPM8) and quantitatively assessed using T/N ratios (SUVmax tumor/SUVmean contralateral region). The definitive diagnosis was based on clinical and radiological follow-up (median 17 months, range 4-51). Additional pathological confirmation was obtained in 6 patients. **Results:** FDG-PET sensitivity, specificity, positive predictive value and negative predictive value were 94%, 87%, 89% and 93% respectively. The results of MET-PET of the 12 patients were: true positive in 3 patients (with also FDG-positive scans), true negative in 9 patients (with also FDG-negative scans in 7 but 2 equivocal FDG-PET results). The interobserver agreement between FDG-PET and MET-PET was excellent (Kappa Coefficient: 1). The mean T/N ratios of positive FDG-PET scans was 1,28 (range, 0,86-2,06) and for the negative and equivocal ones was 0,91 (range, 0,71-1,2), and we found statistical differences in these two groups (t-Student test with a p less than 0,05). **Conclusions:** According to our results, MRI co-registration makes FDG-PET a more sensitive and useful test in differentiating brain tumor recurrence from radiation necrosis. The probability for disease detection is higher in patients with higher T/N ratios. In this scenario we considered MET-PET especially useful in equivocal and negative FDG-PET scans. These results must be confirmed by larger number of patients and biopsy-proven lesions.

EP019**Diagnostic Value of PET Using [¹¹C]Methionine in Suspected Glioma Recurrence**

T. Skvortsova, **Z. Savintseva**, **D. Zakhs**, **S. Medvedev**; **N. P. Bechtereva** Institute of the Human Brain of Russian Academy of Sciences, Saint-Petersburg, RUSSIAN FEDERATION.

The purpose of the study was to assess the diagnostic accuracy of positron emission tomography with [¹¹C]methionine (PET-Met) in distinguishing brain tumor recurrence from posttreatment radiation effect (PTRE) and to analyze prognostic value of PET imaging. **Material and method.** PET-Met was performed in 308 patients (median age 35 years) with glioma (n=304) or other tumors (n=4) previously treated with multimodal therapy. Entry criteria included new or progressive enhancing lesions on MRI after treatment and final diagnosis on the basis of pathological examinations (n=84) or MRI and PET follow-up on an average 18 months (range 1-108). PET examinations were assessed by visual inspection and calculating [¹¹C]methionine uptake index (UI) as the ratio of the mean lesion uptake (ROI 10 mm in diameter) to normal cortex. Imaging results were also related to progressive free survival (PFS) in 262 patients. **Results.** 313 PET detected abnormalities in 308 patients were classified into three groups: pure PTRE (102 lesions), recurrent tumors (n=115) and mixture of radionecrosis with recurrent/residual tumor (n=96). Analysis of Met uptake showed that 96% of lesions with negative tracer uptake (UI<1,2) represented PTRE or complete metabolic response of glioma. But 4% of negative cases were recurrence with small size of glioma or large cyst component. Lesions with UI range from 1,2 to 1,6 represented residual irradiated tumor or radiation necrosis (85% of lesions). However low UI could be detected in initial recurrence (16%). UI between 1,6 and 2,0 was most typical for mixed pathology (55%) but one was observed in 12% of PTRE and 33% of progressive tumor. 89% of lesions with UI>2,0 were recurrence. Additional use of MR-perfusion allowed differentiating lesions with equivocal uptake. Using cutoff value of UI >1,87 ROC analysis showed a sensitivity of 74% and a specificity of 96% for differentiating recurrence from non-progressive disease (including PTRE and residual irradiated glioma). UI of the lesion had also significant independent influence on PFS (cut-off >1,9, PFS 12,5 vs 44 months, p<0,0001) **Conclusion.** PET-Met seems to be a method of choice in the evaluation recurrent brain tumor but sometimes diagnostic conclusion can be made with complimentary MR-perfusion or by comparing the serial studies.

EP020**Imaging of tumor-associated system xc⁻ activity with 18F-fluoropropylglutamate (FSPG) PET/CT for intracranial malignancies**

I. Sonni¹, **R. Minamimoto**¹, **M. Jamali**¹, **N. Hatami**¹, **N. Koglin**², **M. Berndt**², **A. Stephens**², **F. Chin**¹, **N. Fischbein**¹, **G. Zaharchuk**¹, **S. S. Gambhir**¹, **E. Mittra**¹; ¹Stanford University, Stanford, CA, UNITED STATES, ²Piramal, Berlin, GERMANY.

Introduction: The glutamate-cystine exchanger system xc⁻ is an emerging target in oncology, balancing oxidative stress, providing a possible growth advantage for a variety of tumors, including those in the brain, and has been associated with higher-grade tumors. System xc⁻ activity can be non-invasively visualized by means of the investigational PET radiopharmaceutical ¹⁸F-FSPG. The aim of this study was to investigate the utility of ¹⁸F-FSPG PET/CT in the evaluation of intracranial malignancies. **Methods:** Patients with primary brain tumors or brain metastases were recruited for this study. A single dose of ¹⁸F-FSPG was injected intravenously (8.28 mCi ± 0.58). A dynamic PET/CT brain scan (0-30 min post-injection) was acquired, followed by a whole-body scan 60 min post-injection. Standard-of-care brain MRIs and, in some cases, ¹⁸F-FDG PET/CT scans, were also acquired. The PET images were visually and quantitatively assessed, compared with MRI and, when available, standard-of-truth histopathology. The MRI scans were also independently read and lesions assessed for malignancy and growth (malignancy and growth score) by two neuroradiologists. **Results:** Twenty-six patients with primary brain tumors (17) or brain metastases (9) have been enrolled in the study (average age 54 ± 12 yrs). The dynamic images show increasing concentration of FSPG over the first 30 minutes in the brain lesions, and decreasing uptake in background tissues. At 60 minutes post-injection, FSPG uptake in

suspected lesions had an SUVmax of 7.47 ± 7.15 in primary brain tumors, and 6.53 ± 5.07 in brain metastases. FSPG uptake was nearly absent in healthy brain parenchyma (SUVmax 0.27 ± 0.1 in patients with primary brain tumors, and 0.27 ± 0.9 in patients with brain metastases). For primary brain tumors, SUVmax on FSPG scans correlated usually well to the independent MRI scores, whereas for brain metastases, the FSPG results were more equivocal. However, there were also some instances where non-specific MRI signals were not seen with FSPG, or suspected malignancy is seen with FSPG but not MRI. Clinical follow-up, pathology evaluation and kinetic analysis are still ongoing. Conclusions: ^{18}F -FSPG is a potentially useful PET imaging agent for the detection of residual/recurrent disease in the brain in settings where MRI alone is not definitive or discriminant, and can inform about system x_{C} activity.

EP021

Contribution of 11C-Methionine PET/CT in the management of patients with brain tumors

J. L. López-Defilló, I. Martínez-Rodríguez, M. De Arcocha-Torres, J. Jiménez-Bonilla, R. Quirce, M. Jiménez-Alonso, F. Gómez-De La Fuente, C. Lavado-Pérez, N. Martínez-Amador, I. Banzo; Nuclear Medicine. Marqués de Valdecilla University Hospital. University of Cantabria, Santander, SPAIN.

Aim: Magnetic resonance imaging (MRI) is the current gold standard method for evaluation of brain tumors. However, MRI has known limitations in the differential diagnosis between brain tumor tissue and local post-therapy changes. The aim of this study was to evaluate the contribution of 11C-Methionine PET/CT (MET-PET) in the management of patients with suspected or known brain tumor in comparison with MRI findings. **Materials and methods:** This retrospective study included 47 MET-PET examinations (41 patients: 22 women, mean age: 46.3 ± 17.5 y.). Eight examinations were requested for suspicion of brain tumor, 6 for evaluation of brain tumor extent and 33 for suspicion of persistent or recurrent disease on MRI. MET-PET scan was obtained 20' after intravenous injection of 740 MBq of 11C-Methionine. MET-PET images were assessed by visual analysis and the results were compared with MRI and Ki67 index at diagnosis (available in 25 examinations). Final diagnosis was established by histopathological sampling in 12 examinations and by clinical and radiological follow-up in 35. **Results:** MET-PET was positive in 29 examinations (61.7%) and negative in 18 (38.3%). Twenty-eight out of the 29 positive MET-PET scans were true positive and only 1 was a false positive result. Thirteen out of the 18 negative MET-PET scans were true negative and 6 were false negative results (sensitivity 82.4%, specificity 92.3%, positive predictive value 96.5%, negative predictive value 66.6% and accuracy 87.2%). Previous MRI was positive for malignancy in 33 examinations, negative in 7 and non-conclusive in 7. MET-PET was positive in 22 out of the 33 positive MRI (all MET-PET were true positive) and negative in 11 (5 true negative and 6 false negative). MET-PET was true positive in 3 out of the 7 negative MRI and true negative in 4. Finally, MET-PET was positive in 4 out of the 7 non-conclusive MRI (3 true positive and 1 false positive) and negative in 3 (all true negative). Mean Ki67 index was higher in true positive MET-PET scans (26 ± 21.1) compared to false negative scans (13.7 ± 7.5), although the difference was not statistically significant ($p = 0.4959$). All MET-PET scans with Ki-67 index $>30\%$ were true positives. **Conclusion:** MET-PET provided useful information in brain tumor patients with high specificity and positive predictive value. In a high percentage of non-conclusive MRI scans, MET-PET established a definitive diagnosis. Our results suggest a correlation between MET-PET scan and Ki-67 proliferation index although further investigation applying a semiquantitative analysis would be desirable.

EP022

Comparison of 11C-methionine PET and perfusion-weighted MRI in malignant gliomas

A. Mestre Fusco¹, L. Del Carpio², S. Gonzalez Ortiz², S. Medrano², J. Capellades², S. Mojal³, G. Conesa⁴, M. Suárez Piñera¹, Neuro-oncology PSMar Group; ¹Nuclear Medicine. Hospital del Mar., Barcelona, SPAIN, ²Neuroradiology. Hospital del Mar., Barcelona, SPAIN, ³Statistics department. IMIM., Barcelona, SPAIN, ⁴Neurosurgery. Hospital del Mar., Barcelona, SPAIN.

Background: 11C-methionine PET (MET-PET) may help improve diagnostic procedures in malignance characterization of gliomas. In addition, perfusion-weighted MRI was used in gliomas to evaluate their vascularity. Recent studies suggest that perfusion-weighted MRI using regional cerebral blood volume (rCBV) may provide similar information to PET with amino-acid tracers. **Aim:** Compare methionine uptake ratio on MET-PET and rCBV perfusion on MRI in gliomas and evaluate their correlation. **Methods:** PET and MRI were performed in 22 patients diagnosed of glioma, who were consecutively included (12 male, mean:50.2, range:29-78). PET images were analyzed visually and quantitatively (ROI) and Ratio T/N was calculated of each lesion (SUVmax hot-spot-of-lesion/mean-cortical-uptake-in-healthy-brain). Gliomas were classified as low or high PET grade using a cut-off point of Ratio T/N=2.1. In case of Ratio T/N>2.1, glioma was classified as high PET grade. In addition rCBV perfusion score was calculated in the highest metabolic area on PET using MRWorkspace of Philips Healthcare software. In case of rCBV>2, glioma was classified as high rCBV grade. Gliomas were classified as low (II) or high (III-IV) grade depending on pathological criteria WHO classification. Association between PET grade and rCBV grade was analyzed (Chi-Square, Fisher test, $p < 0.05$). Moreover correlation between Ratio T/N and rCBV scores was assessed (Pearson correlation coefficient, $p < 0.05$). **Results:** Fifteen out of 22 gliomas were histopathologically classified as high grade: twelve glioblastomas, four anaplastic astrocytomas, and six grade II astrocytomas. Two grade II gliomas with negative perfusion showed Ratio T/N less than 1.4. Three astrocytomas were correctly classified as low grade according to Ratio T/N and rCBV. Thirteen glioblastomas were correctly classified as high grade according to Ratio T/N and rCBV. Nevertheless discordant grade classification between the two tests were found in 4 low grade gliomas: two of them were classified as high grade by PET and two of them were classified as high grade by perfusion. The rCBV value was higher in case of perfusion was evaluated on the point that PET has the highest uptake but rCBV was clearly lower in case of perfusion was measured on the borders of metabolic activity. An association between the two variables was found (Fisher test 2x2 table $p = 0.02$). Moreover, a significant correlation between Ratio T/N and rCBV of gliomas was observed ($r = 0.63$, $p = 0.02$). **Conclusion:** 11C-methionine PET may provide grading information in gliomas, with a correlation between metabolic activity and perfusion on MRI. Our data suggests an association between Ratio T/N and rCBV in gliomas.

EP023

Diagnostic utility of $^{99\text{m}}\text{Tc}$ labelled Methionine Brain SPECT/CT in differentiating residual / progressive disease and radiation necrosis in patients with primary brain tumors: A comparison with contrast enhanced MRI

H. Singh, B. Singh, B. R. Mittal, R. K. Basher; Postgraduate Institute of Medical Education and Research, Chandigarh, INDIA.

Aim: The aim of the present study was to assess the diagnostic utility of $^{99\text{m}}\text{Tc}$ labelled Methionine Brain SPECT/CT in differentiating residual / progressive disease from radiation necrosis in patients with primary brain tumors and to compare its efficacy with that of ceMRI (contrast enhanced

MRI). **Materials and methods:** In this prospective study, seventeen patients with previously treated primary brain tumors (surgical excision, ± chemotherapy / radiotherapy) referred for evaluation of residual / recurrent disease were enrolled. ^{99m}Tc -methionine brain SPECT and ceMRI were performed at the time of presentation and at 6 months follow up. The time interval between the two scans was less than 2 weeks in all the patients. Brain SPECT and ceMRI findings were validated by reference standard (clinical course and imaging follow-up). **Results:** A total of 26 studies of 17 patients were evaluated (13 males & 4 females; age range 19-65 years; mean age 45.05 years). All the cases were of high grade gliomas (WHO grade III and IV) and most common histological subtype (according to WHO classification) was Glioblastoma Multiforme (GBM) 76.4% (13/17). Of the 17 baseline studies, 9 had SPECT e/o residual / recurrent disease, while 8 scans showed no e/o disease. Based on the reference standard used for evaluation of this study, 10/17 patients showed disease recurrence while 7 were deemed disease free. In the present study, sensitivity, specificity, positive and negative predictive value were 94%, 100%, 100% and 90% for Methionine Brain SPECT and 100%, 88.8%, 94.7% and 100% for ceMRI respectively when compared to the reference standard. Excellent agreement (κ value = 0.83) was also found between Brain SPECT and ceMRI findings. **Conclusion:** ^{99m}Tc -methionine brain SPECT supplements ceMRI in diagnosis of recurrent disease due to its very high specificity and positive predictive value. Thus it has potential role in equivocal cases to confirm the presence of disease. Additional advantages of low cost, easy availability, imaging with a SPECT gamma camera and lower radiation burden encourage its promising utility.

EP024

Accurate Differentiation of Radiation Injury from recurrent Glioma by ^{99m}Tc -Tetrofosmin SPECT

G. ALEXIOU¹, S. Tsiouris¹, A. Papadopoulos¹, E. Levi², A. Fotopoulos¹; ¹UNIVERSITY HOSPITAL OF IOANNINA, IOANNINA, GREECE, ²proACTINA S.A., 20 Delfon St., 15125 Athens, Greece, Athens, GREECE.

Purpose: Treatment of high-grade gliomas involves surgery, radiotherapy and chemotherapy. After treatment, gliomas near always recur. Differentiation of recurrent glioma from treatment induced necrosis (TIN) is not always straightforward. Both entities have the same appearance on MRI. SPECT has the advantage of lower cost and wider availability compared to PET. We set out to investigate the ability of ^{99m}Tc -Tetrofosmin (TF) SPECT to detect recurrent glioma. **Material and Methods:** Thirty studies (21 men, 9 women, mean age 61.5 ± 11.1 years) were eligible for the study. All patients had high-grade gliomas, received previous surgery and chemoradiation and during the follow-up period presented with a suspicion of recurrent tumor. On TF SPECT, the portion of the tumor with the highest accumulation was selected as the region of interest (ROI), lesion-versus-normal ratio (LN) was defined as the ratio of average TF counts in the lesion divided by average counts per pixel in normal white matter. **Results:** Twenty-seven patients suffered from glioblastoma, 1 from anaplastic astrocytoma and 2 from anaplastic oligodendroglioma. Histological examinations in 2 cases showed recurrent glioma. Twenty-two cases were considered to have recurrence, whereas 6 were considered to have TIN based on stable neurological symptoms with no sign of massive enlargement of the lesion on follow-up MR after at least 6 months. There was a statistical significant difference in TF uptake between patients with recurrent glioma and TIN (12.29 ± 6.61 vs. 2.37 ± 1.27 respectively; $P = 0.002$). The L/N cut-off threshold value representatively discriminating the two clinical entities was 4 as indicated by the ROC analysis. **Conclusion:** Brain imaging by TF could offer useful information in the workup of treated gliomas. To validate the technical and diagnostic performance of TF/SPECT, a phase II multicentre clinical trial (EurtraCT No: 2015-005573-21) is ongoing,

as part of the clinical development of TF/SPECT for glioma diagnostic imaging. *This project has received funding from EU's Horizon 2020 research and innovation programme, grant agreement No673737. The above reflects only the authors' view; the Agency is not responsible for any use that may be made of the information it contains.*

EP025

Common malignant tumors of the brain: Can FDG PET/CT aid in differentiation ?

N. C. Purandare, S. Shah, A. Agrawal, C. Bongulwar, T. Gupta, V. Rangarajan; Tata Memorial Centre, Mumbai, INDIA.

Objectives: 1) To study the metabolic characteristics of common malignant space occupying lesions (SOL's) of the brain. 2) To determine the utility of FDG PET/CT in differentiating between the common types of malignant brain SOL's. **Materials and methods:** All patients with brain SOL's who were referred for a FDG PET/CT scan by a multidisciplinary team were included in this retrospective study. The metabolic characteristics of the brain lesions in the form of SUVmax was obtained and compared with the final diagnosis. Ratios of SUVmax of the primary tumor to that of the contralateral cortex as well as white matter were also calculated. All primary brain lesions underwent a surgical biopsy for histopathological confirmation whereas the diagnosis of metastasis was confirmed by performing biopsy from the primary or other metastatic sites demonstrated on PET/CT. The difference in SUVmax values and tumor to background activity ratios between the various pathologies were compared using non-parametric statistical tests. ROC curve analysis was used to evaluate the optimal SUVmax cut off for Lymphomas. **Results:** The study included 106 patients (M/F -70/36), median age 55.5 yrs (range 15-78). Glioblastoma multiforme (n=30), lymphoma (n=25) and metastases (n=46) accounted for most of the malignant tumors (95.2%). Majority of patients (66%) had a solitary brain lesion whereas 34% had multifocal disease. Amongst the patients with brain metastases, lung was the commonest site of primary malignancy (n=40). Four patients with brain lymphoma had extracranial disease on FDG PET. Lymphomas showed a significantly high metabolic uptake (median SUVmax-20.3, range 8.1-46.3) as compared to GBM's (median SUVmax-10.3, range 0-21.7) and metastases (median SUVmax-11.5, range 0-19.6) ($p=0.00$). Tumor to background activity ratios for lymphomas were also significantly higher. There was an overlap in the metabolic uptake of GBM's and metastases with no significant difference between their SUVmax values ($p=0.245$). A SUVmax ≥ 15.5 shows a 84% sensitivity and 80% specificity to diagnose lymphomas (AUC=0.876, $p=0.00$). **Conclusion:** 1)PET/CT can be useful in differentiating between the common malignant brain SOL's by virtue of their variable FDG uptake. 2)The high avidity of lymphomas on FDG PET/CT can help differentiate them from GBM's and metastases in majority of cases. 3)The ability of FDG PET/CT to detect primary malignancy in patients with metastatic brain SOL's and extracranial disease sites in patients with brain lymphoma provides additional benefit in their staging work up.

EP026

4'-[methyl- ^{11}C]thiothymidine positron emission tomography in patients with newly diagnosed glioma: Comparison with Gd-DTPA enhanced magnetic resonance imaging

Y. Fukuda¹, K. Tanaka¹, Y. Yamamoto¹, T. Hatakeyama², N. Kudomi³, J. Toyohara⁴, Y. Nishiyama¹; ¹Kagawa University Department of Radiology, Kita-gun, JAPAN, ²Kagawa University Department of Neurological Surgery, Kita-gun, JAPAN, ³Kagawa University Department of Medical Physics, Kita-gun, JAPAN, ⁴Research Team for Neuroimaging, Tokyo Metropolitan Institute of Gerontology, Tokyo, JAPAN.

Introduction: A novel radiopharmaceutical, 4'-[methyl- ^{11}C]thiothymidine (4DST), has been developed as an in vivo cell proliferation marker based on the DNA incorporation method. The purpose of this study was to evaluate 4DST uptake in patients with newly diagnosed glioma and correlate with gadopentetate dimeglumine (Gd-DTPA) enhancement in magnetic resonance imaging (MRI). **Methods:** 4DST studies in 23 patients with newly diagnosed glioma were retrospectively investigated. In the 4DST PET, metabolic tumor volume as defined as the volume with a threshold of 40 % of the maximum standardized uptake value for tumor (V_{PET}). In the MRI, regions of interest were manually placed over the Gd-DTPA enhancing part of the tumor, avoiding necrotic-appearing areas. The volume of the Gd-DTPA enhancing part of the tumor (V_{MR}) was calculated. **Results:** 4DST PET detected 20 of 23 gliomas. Three gliomas that were not visualized with 4DST had no Gd-DTPA enhancement. The mean (\pm SD) of the V_{PET} and V_{MR} was 25.03 ± 31.49 and 14.93 ± 21.24 , respectively. A significant correlation between V_{PET} and V_{MR} was found ($r=0.738$, $p<0.0001$). **Conclusion:** These preliminary results indicate that 4DST PET may be useful for the detection of glioma and the volume of 4DST uptake correlates to that of Gd-DTPA enhancement.

EP027

Correlation of F-18 FDG uptake with Histopathological grading in Meningioma

N. Shuke, C. Miyazaki, T. Kamibayashi, T. Aburano, A. Ando, T. Onishi, O. Saito, T. Inagaki, S. Irie, K. Saito; Kushiro Kojinkai Memorial Hospital, KUSIRO, JAPAN.

Objective: The objective of this study was to investigate the correlation of F-18 FDG uptake with histopathological grading in meningioma. **Methods:** Eleven patients (pts) with surgically proven meningioma (age 63 ± 6 , M/F= 5/6), who underwent FDG PET/CT before surgery, were retrospectively studied. As an index of tumor FDG uptake, SUV max was adopted. As histopathological parameters, WHO grade, Ki67/MIB-1 labeling index (MIB1LI), and peripheral tissue invasion (brain or bone) were adopted. Bivariate correlations of SUV max of the tumor with WHO grade and MIB1LI were evaluated by rank correlation. Also analyzed was multivariate correlation of SUV max of the tumor with WHO grade (MIB1LI was omitted because of its collinearity with WHO grade) and peripheral tissue invasion (brain or bone) by Hayashi's quantification theory class 1, which is a statistical method to investigate relationship between parametric objective variable and nonparametric explanatory variables. **Results:** Pathological examination revealed 8 pts had WHO grade 1 meningioma, 2 pts had grade 2, and 1 pt had grade 3. Brain and bone invasion were found in one pt each. Although bivariate rank correlations of SUV max of the tumor with WHO grade or MIB1LI were not statistically significant ($P > 0.05$), multivariate analysis showed significant correlations of SUV max with WHO grade and peripheral tissue invasion ($R^2=0.890$). Partial correlation coefficients of SUV max with WHO grade, bone invasion, and brain invasion were 0.819, 0.910, and 0.318, respectively, indicating significant correlation of SUV max with WHO grade and bone invasion. **Conclusion:** WHO grade and bone invasion were significantly correlated with degree of FDG uptake by meningioma. Bone invasion might be an independent factor of FDG uptake by meningioma.

EP028

Role of 18F-Fluorocholine PET-CT to improve radiotherapy planning in resected glioblastoma patients

N. Testart Dardel^{1,2}, M. Zurita Herrera¹, A. Jorques Infante¹, E. Triviño Ibáñez¹, R. Luque Caro¹, M. Pérez Rosillo¹, C. Santos Chamorro¹, M. Gómez-Río^{1,2}, J. Llamas-Elvira^{1,2}; ¹Complejo Hospitalario Universitario de Granada, Granada, SPAIN, ²IBS, Granada, SPAIN.

OBJECTIVES: Even though major improvements in the treatment of the glioblastoma have occurred in the past few years, the prognosis remains poor. The **aim** of our study is to evaluate the potential role of 18F-Fluorocholine PET/CT to define therapeutic targets prior to radiotherapy and its added value in the delimitation of treatment volumes. **PATIENTS AND METHODS:** Prospective study of adult patients with resected glioblastoma prior to radiotherapy. The standard protocol for determination of radiation therapy volumes is based on MRI: pre-surgical, early post-surgical (<72h) and delayed post-surgical (4 weeks). The proposed protocol includes the additional information provided by 18F-Fluorocholine PET/CT performed during the week before radiotherapy (integrated PET/CT system following the standard protocol including 6 h fasting, intravenously injection of 185 MBq of 18F-fluorocholine, 15 m resting and acquisition during 30 min; 168 matrix, zoom 2, FWHM 2 mm; reconstruction by iterative algorithm [OSEM, 14 subsets, 4 iterations]). The Nuclear Medicine specialist is asked to estimate the probability of tumour presence to determine treatment targets according to fluorocholine uptake and its relation with Gd-enhanced and/or oedema regions. The definitive radiotherapy target volumes are determined after the analysis of both imaging procedures (MRI and 18F-Fluorocholine PET/CT) separated and fused. A final consensual report is provided to the radiotherapist. **RESULTS:** Seven patients were included (4 males and 3 females; mean age: 58.7 years [range: 47-71]). In the analysis of fused images in all patients, no significant uptake was appreciated outside the margin of enhanced area in MRI-T1-Gd, neither in the surrounding oedema evaluated by T2F-MRI. In three patients there was total concordance between both image modalities. In 4 patients there were discrepancies between the intensity of the T1-MR-Gd-enhancement and the intensity of fluorocholine uptake: one patient showed a highly intense heterogeneous uptake and in the remaining three the area of fluorocholine uptake was smaller and comprised into the T1-MR-Gd-enhancement area. The planned volumes of treatment were not changed in any patient. **COMMENTS:** Our preliminary results showed discrepancies in the intensity of MR-T1-Gd-enhanced areas and the intensity of choline uptake. The addition of 18F-Fluorocholine PET/CT in the pre-RT evaluation of these patients has no impact in the expected treatment approach and does not modify the planned volumes for treatment.

EP029

Inter-observer variability of total hemispheric glycolysis ratio obtained at 1-hour and 3-hour FDG-PET/CT imaging in glioma patients

E. A. Segtnan^{1,2}, C. Constantinescu¹, J. Holm¹, P. Grupe¹, O. Gerke^{1,3}, P. F. Høiland-Carlson^{1,4}; ¹Odense University Hospital, Odense, DENMARK, ²University of Southern Denmark, Odense, DENMARK, ³Centre of Health Economics Research, University of Southern Denmark, Odense, DENMARK, ⁴Department of Clinical Research, Faculty of Health Sciences, University of Southern Denmark, Odense, DENMARK.

Aim: Total hemispheric glycolysis ratio (THGr) obtained by FDG-PET/CT may provide predictive value in glioma patients. We performed 1-hour (1h) and 3-hour (3h) time point FDG-PET/CT imaging in glioma patients to examine whether THGr had the same inter-observer variability at late (3h) compared to early (1h) imaging. **Material and methods:** Forty-eight FDG-PET/CT studies were prospectively collected at 1h and 3h after FDG-injection in 5 male and 9 female glioma patients, aged 35-77 (mean 63) years. The PET studies were performed before treatment, after resection/biopsy, after radio-chemotherapy, during and after chemotherapy. Two independent observers applied dedicated software (ROVER; ABX, Radeberg, Germany) for segmentation and calculation of the patients' cerebral (Ce) and cerebellar (Cb) total hemispheric glycolysis ratio (THGr). The two observers obtained IRV results by applying "top-down" procedures, *i.e.* a threshold of either 2 SUVs (T2) or 3 SUVs (T3) below the maximum SUV of Ce or Cb, respectively. The results, therefore represented the brain parenchyma and neurons with the highest level of glucose metabolism, *i.e.* the index of functionality. We also tested

IRV with the “top-down” thresholds 50% below SUVmax (T50), 4 SUVs (T4) and 3 SUVs (T3) below SUVmax, for Ce and Cb, Ce, and Cb, respectively. IRV was calculated with the coefficient of variation and compared to the IRV from 1h scan. **Results:** Cerebrum: IRV for T3-THGr(Ce) was in median 9.5%; Inter Quartile Range (IQR) 4.1–22.3, whereas 1h was 3.3%; IQR 1.9–4.2. IRV for T4-THGr(Ce) was in median 6.0%; IQR 2.3–14.5, whereas 1h was 2.7%; IQR 1.0–5.0. IRV for T50-THGr(Ce) was in median 3.2%; IQR 0.6–5.0, whereas 1h was 2.3%; IQR 1.0–4.2. Cerebellum: IRV for T2-THGr(Cb) was in median 16.9%; IQR 6–43, whereas for 1h it was 5.9%; IQR 3.0–14.3. IRV for T3-THGr(Cb) was in median 13.7%; IQR 6.8–28.8, whereas for 1h it was 4.5%, IQR 1.8–7.5. IRV for T50-THGr(Cb) was in median 7.3%; IQR 3.4–10.1, whereas for 1h it was 3.5%, IQR 1.7–5.4. **Conclusion:** Only two thresholds had median IRV above 10%. Inter-rater variability when using 3h THGr was lowest with the threshold T50. THGr at 3h had higher IRV than IRV at 1h. The reason for this might be the higher washout of FDG uptake at the 3h time point and, hence, a decrease in metabolic segmented volume and an increased sensitivity of mask delineations. Thus, it appears that high SUV cut-offs should be used with care at 3h time point imaging with FDG.

EP030

Prognostic value of 4'-[methyl-¹¹C]-thiothymidine PET in patients with newly diagnosed glioma

Y. Yamamoto¹, K. Tanaka¹, K. Mitamura¹, T. Norikane¹, Y. Fukuda¹, T. Hatakeyama¹, H. Yamamoto¹, J. Toyohara², Y. Nishiyama¹; ¹Kagawa University, Kagawa, JAPAN, ²Tokyo Metropolitan Institute of Gerontology, Tokyo, JAPAN.

A novel radiopharmaceutical, 4'-[methyl-¹¹C]thiothymidine (¹¹C-4DST), has been developed as an in vivo cell proliferation marker based on the DNA incorporation method. The purpose of this study was to evaluate ¹¹C-4DST uptake in patients with newly diagnosed glioma and to correlate the results with proliferative activity and patient prognosis. **Methods:** ¹¹C-4DST PET/CT was investigated in 20 patients with newly diagnosed gliomas. The maximum standardized uptake value (SUVmax), tumor-to-contralateral normal brain tissue (T/N) ratio, and metabolic tumor volume (MTV) were derived from ¹¹C-4DST PET images. Linear regression analysis was used to assess the proliferative activity as indicated by the Ki-67 index in tissue specimens. Kaplan-Meier curves and univariate and multivariate Cox regression were used to analysis of overall survival (OS). **Results:** Median OS was 21.5 months, with 15 survivors at the time of analysis. Linear regression analysis indicated a significant correlation between SUVmax ($r=0.52$, $p<0.03$) and MTV ($r=0.71$, $p<0.001$) using ¹¹C-4DST and the Ki-67 index. In univariable analysis, SUVmax (cutoff 3.0) and T/N ratio (cutoff 5.0) were significant prognostic factors for OS ($p<0.01$ and $p<0.03$, respectively), but these correlations did not hold in multivariate analysis. MTV (cutoff 15) was not predictive for OS ($p=0.58$). **Conclusion:** These preliminary results suggest that ¹¹C-4DST PET/CT may be useful in the noninvasive assessment of proliferation and survival in newly diagnosed gliomas.

EP031

¹⁸F-DOPA PET/CT imaging in brain tumors

D. Grigolato, L. Locantore, M. Cucca, M. Zuffante, M. Ferdeghini; Azienda Ospedaliera di Verona, VERONA, ITALY.

AIM: Amino acid transport imaging is a noninvasive imaging technique able to assess metabolic features of brain tumors. We wanted to analyze the added value of ¹⁸F-FDOPA PET when MRI gives uncertain diagnostic results. This study compares visual and semiquantitative analysis parameters for detection of lesions. **METHODS:** Twenty-one patients, 12

female, 9 male, age range 32–82 years, underwent ¹⁸F-FDOPA PET/CT imaging for suspected tumor recurrences (n.9), for differentiating dysplasia from low grade lesions (n. 8), low grade lesions from ischemic lesions (n. 3), low grade lesions from high grade ones (n. 1). All PET/CT of the brain were acquired at 5 and 60 minutes after radiotracer injection. PET studies were fused with contrast enhanced MR sequences. PET scans were analyzed visually and semiquantitatively: lesion-to-striatum (L/S) and lesion-to-normal brain tissue (L/N) ratios using SUV_{max} in early and delayed images. Uptake parameters were compared and correlated with histology, WHO tumor grade and patient follow-up with conventional imaging. **RESULTS:** Thirteen PET/CT were positive at DOPA imaging (SUV max range 2.2–8.8), the accuracies for detection of pathological lesions for visual and semiquantitative analysis were similar. Eight of them had higher value of L/S and L/N ratios (range 0.8–2.8 and 1.4–4.6 respectively): five patients were submitted to surgery with evidence of recurrences; one patient, suspected for ischemic lesion, had high grade astrocytoma; two patients demonstrated progression at MRI and CT. The remaining 5 positive patients had lower values of max L/S and L/N ratios and they were judged having low grade lesions. These patients were stable at a minimum follow up of six months. Eight patients with no or faint DOPA uptake in the suspected regions, even after image fusion with MR, were considered negative. None of them was submitted to surgery and at follow-up they did not evolve. **CONCLUSIONS:** When MRI is inconclusive DOPA PET/CT imaging can give functional relevant information to clinicians in the complex decision making. It seemed particularly useful in the discrimination between recurrences and radionecrosis/fibrosis. Visual and semiquantitative indices detected brain recurrences and high grade brain lesions with high accuracy. Lesion-to-normal-tissue ratios were the best discriminators.

EP032

Pooled Diagnostic Performance of Static ¹⁸F-FET PET Parameters in Differentiating Recurrent Brain Tumours from Nonneoplastic Treatment-related Changes

G. Treglia¹, B. Muoio², M. Reinert³, A. Richetti², G. A. Pesce², L. Giovannella¹; ¹Oncology Institute of Southern Switzerland, Nuclear Medicine and PET/CT Center, Bellinzona and Lugano, SWITZERLAND, ²Oncology Institute of Southern Switzerland, Radiation Oncology, Bellinzona and Lugano, SWITZERLAND, ³Neurocenter of Southern Switzerland, Neurosurgery, Lugano, SWITZERLAND.

Aim: to assess the pooled diagnostic accuracy of static ¹⁸F-fluoroethyl-L-tyrosine positron emission tomography (¹⁸F-FET-PET) parameters [maximal and mean lesion-to-background ratios (LBRmax and LBRmean)] in discriminating recurrent brain tumours (BTs) from nonneoplastic treatment-related changes. **Methods:** A comprehensive literature search of published studies on the role of ¹⁸F-FET-PET in this setting was performed (from inception up to February 2016) using Pubmed, Scopus and Google Scholar databases. Pooled sensitivity, specificity and diagnostic odd ratio (DOR) of static ¹⁸F-FET-PET parameters on a per lesion-based analysis were assessed. The area under the summary receiver-operating-characteristic curve (AUC) was calculated. Sub-analyses were performed whether significant heterogeneity was found ($I^2>50\%$). Pooled weighted mean difference (WMD) of ¹⁸F-FET-PET parameters among malignant and benign lesions was calculated. Pooled ROC analysis to assess the best LBRmax and LBRmean cut-off values to discriminate malignant from benign lesions was performed. **Results:** Ten articles including 422 patients with BTs were selected. Pooled sensitivity, specificity, DOR and AUC of static ¹⁸F-FET-PET parameters in discriminating recurrent BTs from nonneoplastic treatment-related changes were 84% (95%CI:80–88%), 80% (95%CI:71–88%), 34 (95%CI:15–77) and 0.92, respectively, for LBRmax, and 81% (95%CI:76–86%), 86% (95%CI:76–93%), 30 (95%CI:13–73) and 0.92, respectively, for LBRmean. As significant heterogeneity between the selected studies was found ($I^2>50\%$), a sub-

analysis including only patients with high-grade gliomas (HGG) was performed (for LBRmax only). This sub-analysis showed that pooled sensitivity, specificity, DOR and AUC of static ^{18}F -FET-PET in discriminating recurrent HGG from nonneoplastic treatment-related changes were 95% (95%CI:90-98%), 83% (95%CI:68-93%), 44 (95%CI:13-148) and 0.95, respectively, without significant heterogeneity ($I^2 < 50\%$). Pooled WMD among recurrent BTs and treatment-related changes were 0.93 (95%CI:0.6-1.3; $p < 0.0001$) for LBRmax and 0.59 (95%CI:0.3-0.8; $p < 0.0001$) for LBRmean. LBRmax and LBRmean values of 2.2 and 2, respectively, were the best cut-off values to discriminate recurrent BTs from nonneoplastic treatment-related changes at pooled ROC analysis. **Conclusions:** Evidence-based data show that static ^{18}F -FET-PET parameters are accurate in differentiating recurrent BTs from nonneoplastic treatment-related changes, in particular in patients with HGG. Large prospective multicenter trials and cost-effectiveness analyses are needed to substantiate the role of ^{18}F -FET-PET in this setting.

EP033

The Diagnostic Role of FDG PET/CT in Cancer of Unknown Primary Presented with Brain Metastasis

Z. P. Koç, P. Ozcan Kara; Mersin University, Mersin, TURKEY.

Aim: F-18 Florodeoxyglucose Positron Emission Tomography/Computed Tomography (FDG PET/CT) has an important role in determination of the primary of the patients with cancer of unknown primary (CUP). We investigated the role of this method in a special group of CUP patients presented with brain metastasis. **Materials and Method:** Thirteen patients (5M, 8F; mean: 57.7 \pm 12.9 years old) with diagnosis of brain metastasis according to histopathology and/or MRI were included into this retrospective study. **Results:** The patients presented with hypermetabolic (mean SUVmax: 8.6 \pm 1.14) or hypometabolic brain lesions with additional metastatic sites in 7 patients (mean SUVmax: 5.91 \pm 3.5). Two of these patients were documented to have benign brain disease. The primary tumor was determined by FDG PET/CT in 9/11 patients (69%) (lung (n=5), primary brain (n=3), renal cell carcinoma (n=1)) and two patients with suspicious primary site (colon (n=1), nasopharynx (n=1)) were determined. Seven of thirteen patients were out of follow up. Four patients had documented primary site which we pointed out in FDG PET/CT. **Conclusion:** Previous studies report 20-50% detection rate for identification of primary tumor in patients with CUP. However new generation multislice scanners may provide higher detection ratios. The detection rate of FDG PET/CT might be higher than previously reported according to this study however prospective studies in large series are warranted. **Key Words:** Unknown primary, brain, metastasis, FDG.

EP034

Hypoxic volume of malignant glioma by ^{18}F -fluoromisonidazole PET: a comparison with ^{11}C -methionine PET and Gd enhanced MRI-based tumor volume

K. KIRII, M. Kanoto, Y. Sugai, T. Hosoya; Yamagata university faculty of medicine, Yamagata city, JAPAN.

OBJECTIVE: In malignant glioma, few reports have examined a correlation between PET-based metabolic volume and hypoxic volume. The objective of this study was to assess hypoxic volume of malignant glioma by comparing between hypoxic tissue assessed by ^{18}F -fluoromisonidazole (FMISO), metabolic tumor volume by ^{11}C -methionine (MET) PET and morphological tumor volume by Gd enhanced MRI. **MATERIALS AND METHODS:** Eighteen patients with newly diagnosed glioblastoma multiforme (GBM) who had a pretreatment MET-PET, FMISO-PET and Gd-enhanced MRI were retrospectively reviewed. Metabolic tumor volume and hypoxic volume was estimated using an adaptive threshold-

based automatic method on MET (MET-volume) and FMISO (FMISO-volume) PET. Morphological tumor volume was delineated on the gadolinium (Gd) enhanced T1 weighted MRI (Gd-volume). **RESULT:** Mean MET-volume (42.6 cm³) was not significantly different from mean Gd-volume (35.3 cm³), mean FMISO-volume was (23.4 cm³) was significantly smaller than MET-volume and Gd-volume. Each MET-volume and FMISO-volume showed a strong correlation with Gd-volume ($r = 0.81$ and $r = 0.78$, respectively). FMISO-volume also showed a strong correlation with MET-volume ($r = 0.78$, $p < 0.01$). The percentage of FMISO-volume in Gd-volume was large at 63.4%. **CONCLUSION:** Hypoxic volume by FMISO-PET was different from metabolic volume and MRI-based tumor volume in GBM. However hypoxic volume was large depending on the metabolic volume.

EP035

Evaluation of recurrent primary brain tumors by ^{11}C Methionine PET/CT and $^{99\text{m}}\text{Tc}$ Methionine SPECT/CT A comparative analysis

N. Seniaryar, Sr.¹, A. Jaimini¹, M. D'Souza¹, D. Kumar¹, P. Panwar², A. Mishra², R. Sharma¹; ¹Department of PET Imaging, Institute of Nuclear Medicine and Allied Sciences (INMAS), New Delhi, INDIA, ²DCRS, Institute of Nuclear Medicine and Allied Sciences (INMAS), New Delhi, INDIA.

Introduction: ^{11}C Methionine is an amino acid tracer which has been widely used for evaluation of recurrent primary brain tumors. However, ^{11}C Methionine is a cyclotron produced radiopharmaceutical with a short half-life of 20 min, which increases the cost and limits its availability. $^{99\text{m}}\text{Tc}$ Methionine can overcome these limitations and can be used as an alternative tracer to ^{11}C Methionine in the evaluation of brain tumors suspected of residual or recurrence. We review our experience of ^{11}C Methionine and $^{99\text{m}}\text{Tc}$ Methionine in detection of recurrent primary brain tumor. **Materials and Methods:** 20 patients (12 males, 8 females) age 35-55 years' post therapy were sent for recurrence evaluation. All patients underwent ^{11}C Methionine PET/CT and $^{99\text{m}}\text{Tc}$ Methionine SPECT/CT scans on two different days. **Results:** ^{11}C Methionine images were assessed visually and by SUV calculation. $^{99\text{m}}\text{Tc}$ Methionine images were visually assessed and tumor to background ratio calculated. Both were found to show tracer accumulation at sites of residual/recurrent tumor in all cases. **Conclusion:** Our study reveals that $^{99\text{m}}\text{Tc}$ Methionine can be used as an alternative tracer to ^{11}C Methionine in the evaluation of brain tumors suspected of residual or recurrence.

EP036

Influence of different attenuation correction approaches on dynamic ^{18}F FET PET/MRI of recurrent glioma

I. Rausch¹, A. Haug¹, R. Aghamohammadi-Sareshgi², M. Fenchel³, M. E. Mayerhoefer¹, T. Beyer¹, T. Traub-Weidinger¹; ¹Medical University of Vienna, Vienna, AUSTRIA, ²General Hospital of Vienna, Vienna, AUSTRIA, ³Siemens Healthcare GmbH, Magnetic Resonance, Erlangen, GERMANY.

Aim: To evaluate the influence of different attenuation correction approaches in positron emission tomography (PET)/magnetic resonance imaging (MR) on clinical evaluation of dynamic ^{18}F FET imaging. **Methods:** Up to date, 12 patients who underwent a 40 min (0-40 min post injection) dynamic PET/MR (Siemens Biograph mMR) examination following the injection of 250 MBq ^{18}F FET were included in this ongoing study. Dynamic PET data was reconstructed using an OP-OSEM algorithm (3 iterations, 21 subsets, 3mm FWHM Gaussian post filtering) into 8 frames of 2x2 min, 4x4 min and 2x10 min using four different attenuation correction methods: (A) Standard implemented Dixon-based AC, (B) Standard implemented UTE-based AC, (C) a

model-based post-processing approach incorporating spatially variant bone attenuation values into the attenuation map from (A) (non-commercial prototype software by Siemens Healthcare) and (D) CT-based AC. For each reconstruction, a threshold-based volume of interest (VOI) was segmented using a threshold of 90% of the maximum pixel in the respective lesion on summed images (20–40 min). An additional spherical background VOI was placed on the contralateral side to calculate a lesion-to-background ratio (LBR). The VOIs were copied to the different timeframes to calculate the time activity curves (TAC). From the last time frame, volumes of the VOIs and LBR were extracted. An experienced reader with 5 y of experience in dynamic [18F]FET imaging assigned each TAC to two curve patterns: 1) constantly ascending or peaking followed by a plateau and 2) peaking followed by a descent. The volumes and LBRs were compared, and differences to (D) were calculated. For the TAC patterns, changes in assignments relative to the pattern found in (D) were investigated. **Results:** Extracted VOI volumes changed on average by (A): $-14\pm 29\%$, (B) $-7\pm 38\%$ and (C) $0\pm 23\%$ relative to (D). LBR were in general similar for all AC methods with an average difference to (D) of (A): $-2\pm 2\%$, (B) $-2\pm 5\%$, and (C) $0\pm 3\%$. The assignment of the TACs to the different uptake patterns changed for 2/12 cases for (A) and for (B). For (C), no change in uptake pattern assignment could be observed. **Conclusion:** The use of different AC methods in PET/MR can influence the clinical diagnosis in dynamic [18F]-FET glioma imaging. This is mainly attributed to changes in the segmentation of VOIs when using threshold-based segmentation approaches. Nevertheless, LBR seems to be comparable for all evaluated AC approaches.

EP037

Total hemispheric glycolysis ratio by FDG-PET/CT in gliomas; Evaluating diaschisis and potential prognostic information

E. A. Segtnan^{1,2}, P. Grupe³, O. Gerke^{3,4}, J. O. Jarden⁵, S. B. Christlieb³, C. Constantinescu³, J. E. Pedersen³, S. Houshmand⁶, S. Hess^{3,7,8}, M. Zarei⁹, A. Gjedde¹⁰, A. Alavi⁶, P. F. Højlund-Carlson^{3,8}; ¹Department of Nuclear Medicine, Odense University Hospital, Odense, DENMARK, ²University of Southern Denmark, Odense, DENMARK, ³Department of Nuclear Medicine, Odense University Hospital, Odense, DENMARK, ⁴Centre of Health Economics Research, Odense, DENMARK, ⁵Department of Neurology, Herlev University Hospital, Copenhagen, DENMARK, ⁶Division of Nuclear Medicine, Department of Radiology, Perelman School of Medicine, Hospital of the University of Pennsylvania, Philadelphia, PA, UNITED STATES, ⁷Department of Radiology and Nuclear Medicine, Hospital of Southwest Jutland, Esbjerg, DENMARK, ⁸Department of Clinical Research, Faculty of Health Sciences, University of Southern Denmark, Odense, DENMARK, ⁹National Brain Mapping Centre, Shahid Beheshti University (Medical and General Campus), Tehran, IRAN, ISLAMIC REPUBLIC OF, ¹⁰Department of Neuroscience and Pharmacology, Panum Institute, University of Copenhagen, Copenhagen, DENMARK.

Aim: Diaschisis denotes brain dysfunction remote from a focal brain lesion. We quantified diaschisis using cerebral and cerebellar hemispheric glycolysis ratios and tested the claim that these ratios have prognostic value in glioma patients. **Material and methods:** Fifty FDG-PET/CT studies collected prospectively in 5 male and 9 female glioma patients, aged 35–77 years, were compared to scans from 10 healthy controls, aged 43–75 years. Dedicated 3D-segmentation software (ROVER, ABX, Germany) provided “total hemispheric glycolysis” (THG), i.e., the product of segmented metabolic volume and SUVmean in each hemisphere. The hemisphere of likely diaschisis (i.e., the ipsilateral cerebral and the contralateral cerebellar hemisphere) was normalized to the opposite hemisphere to provide the “total hemispheric glycolysis ratio” of cerebrum and cerebellum, i.e., THGr(Ce) and THGr(Cb), respectively. Receiver operating characteristics (ROC) provided optimal cut-offs for these variables.

Two independent observers obtained data for reproducibility analysis, and quantitative scores were compared with visual interpretation done by a PET neuroimaging specialist. **Results:** The coefficient of variation for the two independent observers’ calculation of THGr(Ce) had a median of 3.3% (interquartile range (IQR) 1.9–4.2) and one of median 5.9%, (IQR 3.0–14.3) for THGr(Cb). Visual analysis confirmed cerebro-cerebellar diaschisis in 100% of glioblastoma PET studies performed within one year until death. Diaschisis was not observed in healthy controls, who had mean values of THGr(Ce) and THGr(Cb) that significantly exceeded those of patients, i.e., $p=0.0007$ and $p=0.02$, respectively. Median THGr(Ce) averaged 0.62, 0.71, 0.88 in patients surviving less than one year, one to three years, and more than three years, respectively, versus 0.98 in healthy controls. Median THGr(Cb) averaged 0.74, 0.88, 1.01, and 0.96, respectively. The finding of a low THGr (Ce < 0.62 or Cb < 0.84) agreed almost completely with the presence of diaschisis by visual assessment of cerebrum or cerebellum, i.e., in 16/17 (94%) and 25/26 (96%) of PET scans, respectively. The combination of THGr(Ce) < 0.62 and THGr(Cb) < 0.84 had a 100% sensitivity and a 78.6% specificity with regard to survival of less than one year for the glioblastoma patients. **Conclusion:** We present a novel and feasible quantitative approach for detection of diaschisis in glioma patients. THGr could demonstrate diaschisis in both cerebrum and cerebellum, and optimized cut-off values for THGr(Ce) and THGr(Cb) had a high sensitivity and fair specificity for prediction of survival of less than one year for these glioma patients. The presented semi-automated quantitative approach may allow comparison of similar data obtained at different institutions.

EP038

Towards early detection and personalized treatment monitoring of glioma: [68Ga]-DOTA-A2B1, a promising prognostic surveillance agent

H. Chiu, 333¹, W. Chang¹, S. Hsu¹, Y. Chung¹, Y. Lin¹, F. Huang², T. Yen^{1,3}, C. Huang¹; ¹Center for Advanced Molecular Imaging and Translation, Chang Gung Memorial Hospital, Taoyuan, TAIWAN, ²Department of Biochemical Science and Technology, National Taiwan University, Taipei, TAIWAN, ³Department of Nuclear Medicine, Chang Gung Memorial Hospital, Taoyuan, TAIWAN.

Purpose: Despite recent advances in diagnostic tools and aggressive surgery followed by adjuvant chemotherapy, the clinical outcome of patients with glioblastoma multiforme (GBM) remains dismal. The overexpression of integrin $\alpha 2\beta 1$ has been associated with increased radio-resistance and chemodrug-resistance in glioblastoma, making it a promising surveillance biomarker for not only early malignant glioma detection but also subsequent treatment effect monitoring. **Methods:** To prospectively verify the prognostic value of integrin $\alpha 2\beta 1$, the *in vitro* western blot was performed to validate the integrin $\alpha 2\beta 1$ expression level of human glioblastoma (U87MG) cells and its dose-dependent escalation after adding doxorubicin. The PET/MR hybrid brain tumor imaging were performed with novel integrin $\alpha 2\beta 1$ targeting PET tracer ([68Ga]-DOTA-A2B1) in orthotopic U87MG glioma xenograft mice (n=5) and the tumor regions of interest (ROIs) was determined by manually 50% of maximum minus minimum tumor activity. The follow-up PET/CT scans were performed just after 6 hours of the administration of effect dose of doxorubicin (5mg/Kg) in U87MG tumor-bearing animal to validate the treatment response capability of [68Ga]-DOTA-A2B1 PET tracer. The average radioactivity accumulation within a tumor or an organ was further analyzed in accordance with the pathologic data. **Results:** Extremely high expression level of integrin $\alpha 2\beta 1$ of glioblastoma U87MG cell correlated with its high tumorigenic potential in western blot results justifies its role as a potential prognostic marker. The [68Ga]-DOTA-A2B1 PET tracer longitudinally demonstrated prominent tumor uptake in orthotopic U87MG xenografts along with the steady growth of tumor size monitoring with MR imaging. The tracer uptake in malignancies

were 0.30±/0.05, 0.34±/0.05 and 0.58±/0.11 (%ID/g) at day 7, day 14 and day 21, respectively. Furthermore, due to the low normal brain uptake background, the tumor contrast ratio of tumor/contralateral region increased significantly from 2.22 (day 7) to 2.80 (day 14) and 3.11 (day 21), which can achieve precise whole brain tumor localization for preoperative planning and delineate the tumor margins with high sensitive and high spatial resolution from con-registered PET/MR imaging data. After administration of effect doxorubicin dose (5mg/Kg) in tumor bearing animals, the two-fold increase of [68Ga]-DOTA-A2B1 tracer uptake was observed in the tumor lesions, making treatment respond monitoring is possible. **Conclusion:** These results suggest that there is significant uptake in [68Ga]-DOTA-A2B1 accumulation along with the tumor growth monitoring by MR imaging. The specific uptake might offer a critical diagnostic imaging criterion in the identification of aggress phenotype of gliomas.

EP-03 – Sunday, October 16, 2016, during Exhibition hours, e-Poster Area
Clinical Oncology: Breast

EP039

Added value of SPECT/CT in patients with equivocal bony metastasis from breast cancer

D. BEN SELLEM, L. ZAABAR, B. DHAOUADI, B. LETAIEF, M. F. BEN SLIMENE; University of Tunis El Manar, Faculty of Medicine of Tunis, Salah Azaiez Institute, Department of Nuclear Medicine, Tunis, TUNISIA.

Aim: Planar bone scintigraphy lacks specificity. But single photon emission computed tomography/computed tomography (SPECT/CT), by clarifying anatomic localization of lesions in 3D and correlating to CT aspects, allows accurate diagnosis. The purpose of our study was to investigate the value of SPECT-CT in the assessment of solitary foci of increased bone metabolism classified as indeterminate on whole-body planar scintigraphy in patients with breast cancer. **Material and Methods:** Our prospective study included 100 patients aged 28 to 83 years (mean ± SD = 53.4±10) followed for breast cancer. All these patients underwent planar whole-body scintigraphy 2-3 h after intravenous injection of a mean activity of 740 MBq (20 mCi) 99m technetium- methylene diphosphonate (^{99m}Tc-MDP). Immediately after acquisition, these images were analyzed by a board-certified nuclear medicine physician. All of them had at most two indeterminate increased uptake on planar scintigraphy and therefore they underwent SPECT/CT scan and among them 80 (80 %) had solitary focus. We performed our studies on the same hybrid camera combining a dual-head γ-camera with a dual-slice spiral CT scanner installed within the same gantry (Symbia T2; Siemens Medical Solutions). Afterwards, the corresponding SPECT/CT images were analyzed and the findings previously considered as indeterminate were classified either as definitely benign, indeterminate, or definitely malignant. **Results:** SPECT-CT allowed us to classify these indeterminate lesions as malignant in 40 % of cases (48 foci) and benign in 51.7 % of cases (62 foci). However, 10 (8.3 %) remained indeterminate. This technique detected over them, 12 additional metastatic bone foci included in the field of SPECT exploration that were invisible on planar scan. In two other patients, spine lytic metastases were multiple. SPECT-CT was able so to clarify 91.7 % of planar findings classified as indeterminate, modifying the final report in 90 % of our patients. **Conclusion:** Our study highlighted the higher diagnostic value of SPECT-CT over planar skeletal scintigraphy in clarifying more than 91 % of solitary indeterminate lesions in oncologic patients. Thus, this technique modified the final report for almost 90 % of our patients, allowing early adequate therapeutic management.

EP040

Variations of FDG PET/CT SUV and textural indices in breast cancer according to lymph node status

S. Boughdad¹, C. Nioche², F. Orhac³, L. Champion¹, J. Alberini¹, I. Buvat²; ¹Institut Curie-Hôpital René Huguenin, Saint-Cloud, FRANCE, ²IMIV CEA, Inserm, CNRS, UnNiv Paris Sud, CEA-SHFJ, Orsay, FRANCE, ³IMIV CEA, Inserm, CNRS, UnNiv Paris Sud, CEA-SHFJ, IGR, Orsay, FRANCE.

Introduction: Breast cancer (BC) is a very common cancer and lymph node (LN) involvement is an important prognostic factor. The aim of our study is to identify variations of SUV and textural indices (TI) in BC according to the LN involvement status and also as a function of the grade and the Ki 67 expression. **Method:** We studied a population of 76 women who underwent a F18-FDG-PET/CT in our institution for initial staging of biopsy proven BC. Two groups of patients were defined: N+ (LN involvement) and N- (no LN involvement), according to the current guidelines: either cytology proven or on approved imaging techniques (MRI or F18-FDG-PET/CT). Volume (mL), SUV (max, mean and peak), TLG (total lesion glycolysis, mL) and TI (homogeneity, entropy, LRE, SRE, LGZE and HGZE) were measured in each VOI obtained using a threshold method (40% of SUVmax) and exceeding 1.5 mL in volume. We used a Mann-Whitney test to determine whether Volume, TLG, SUV and TI were significantly different in the VOI between the N+ and N- groups. We also compared the groups according to Ki 67 expression using a cut-off of 20% and the grade (grade I-II vs III). **Results:** Eighty VOI were drawn in our BC population: 43 VOI in 40 patients in the N- group and 37 VOI in 36 patients in the N+ group. Three N+ pts and one N- pt had a multifocal BC. There was no significant difference in SUV and TI between N+ and N- patients (p > 0.05) but there were significant differences in the volume between N+ and N- pts (p=0.003). When we compared N+ and N- pts in subgroups created from the Ki 67 expression and the grade, there were still significant differences in the volume (cf table) but no significant difference was found for SUV or TI. Besides, according to the metastatic status when comparing N+ patients according to the metastatic spread (M+ or M-), the only significant difference found was once again the volume (p 0.04). **Conclusion:** Our study did not show any significant difference in SUV or TI between N+ and N- patients in our BC population. The only significant difference was the tumor volume. This difference remained when we analyzed subgroups according to the grade and Ki 67 expression. Tumor volume appeared to be a strong prognostic factor at initial staging.

EP041

Is F-18-FDG-PET/CT useful to stage or predict progression-free survival in breast cancer patients?

M. Sollini¹, B. Zangheri², L. Calabrese², M. L. Di Paolo³, A. Versari³, M. Gasparini⁴; ¹Humanitas University, Rozzano, ITALY, ²IRCCS MultiMedica, Sesto San Giovanni (MILAN), ITALY, ³IRCCS Ospedale Santa Maria Nuova Reggio Emilia, Reggio Emilia, ITALY, ⁴IRCCS Multimedica Sesto S. Giovanni, Sesto San Giovanni, ITALY.

Aim: Breast cancer (BC) is the most commonly diagnosed cancer among women. The role of F-18-FDG-PET/CT in the management of BC is increasing. We aimed to evaluate the role of PET/CT to stage and to predict outcome in BC. **Methods:** 62 female (one bilateral) with histology proven BC who performed FDG-PET/CT during the staging were retrospectively analysed. FDG uptake in primary tumor (T), lymph node(s) (N) or distant (M) metastases was considered. According to PET/CT results patients were divided in group 1 (uptake in N and/or M, any T) and group 2 (negative N and M, any T). According to immunoistochemical characteristics, patients were grouped as A (any ER/PgR, Her2 - and Ki67<14%), B (any ER/PgR, Her2+ and

Ki67>14%), C (ER/PgR/Her2 all negative) D (ER/PgR - with Her2+), E (any ER/PgR, Her2 - and Ki67>14%). Histology was used as reference standard for FDG-PET/CT in all pre-operative cases for T/N parameters, in the post-surgical setting imaging and clinical follow-up (FU) were used. Progression-free survival (PFS) was calculated. Differences for variables were assessed by Chi-square test (or Fisher test); differences for survival were studied by Kaplan-Meier curves with log rank test. P-value <0.05 was considered significant. Results: patient were followed for 745 ±854 days. PFS was 635±440 days. Forty-four patients had no evidence of disease, 16 patients had progressive disease (group 1=13, group 2=3), while in 2 cases bone metastases (detected by PET/CT at diagnosis) were stable according to the RECIST criteria. FDG-PET/CT resulted positive and negative in 57/62 and 15/62 patients, respectively. FDG uptake was seen only in T and in N in 18 and 3 patients, respectively; in T + N in 14 cases, in T + M in 2 cases, in T + N + M in 8 patients, and in N + M in 2 cases. According to final diagnosis PET/CT resulted TP=41/63, TN=12/63, FN=10/63 and TP=26/63, TN=25/63, FN=11/63, FP= 1/63 for the T and the N status, respectively. PET/CT resulted positive for M in 12 cases (10 TP and 2 FP). PET/CT results did not differ significantly among categories A-E (p=0,263). Groups 1 and 2 significantly differed in terms of outcome (p = 0,005). Survival significantly differed in group 1 and group 2 (p=0.002). Conclusion: PET/CT resulted useful to stage and predict outcome in BC, supporting its clinical use. Staging PET/CT allows, in addition to having a more accurate and early diagnosis, an ever greater customization of therapy.

EP042

FDG PET parameters on primary tumor are prognostic factors of progression free survival for patients with initial metastatic breast cancer

L. Delcroix, A. Maillez, A. Olivier, E. Tresch, A. Oudoux, H. Kolesnikov-Gauthier; Oscar Lambret Center, Lille, FRANCE.

Aim: This study was performed in order to evaluate the prognostic relevance of ¹⁸F-DG PET/CT in patients with breast cancer who had distant metastasis at the diagnosis. **Materials and methods:** Between September 2011 and December 2015, 66 metastatic breast cancer patients underwent ¹⁸F-DG PET/CT at the time of initial diagnosis and before any treatment. Histological and clinical prognostic factors were reviewed. Different PET parameters such as maximum standardized uptake value (SUVmax), metabolic tumor volume (MTV) and total lesion glycolysis (TLG) were retrospectively measured on primary tumor (t). A 3D isocontour at 41% of the maximum pixel value was used to determine a volume of interest (VOI) for each lesion. We analyzed the relationship between these PET parameters and the progression-free survival (PFS). Univariate and multivariate analyses were performed with Cox and Kaplan-Meier hazards models. Optimal cutoff values (maximizing the log-rank test) were determined for variables which were significantly correlated with PFS. Results: Median age was 60 years (range: 33-88). According to clinical examination and mammography results, tumours were T1 (n=3), T2 (n=30), T3 (n=14), T4 non-d (n=8), T4d (n=11). Among the 66 patients, 12 had triple negative breast cancer, 9 a lobular invasive carcinoma and 26 visceral metastasis. Forty-nine patients (74%) progressed or died during the follow-up, (mean follow-up: 31 months; range: 2.8-50 months). Mean PFS was 10 months (range: 6.8-12.4 months). tSUVmax, tMTV and tTLG, were identified by univariate analysis as prognostic factors for PFS (p<0.01). We determined optimal cutoff values of tSUVmax (≤9.7 vs >9.7), tMTV (≤42.8 vs >42.8), tTLG (≤380 vs >380) for predicting PFS. Multivariate analysis revealed that tSUVmax [HR=2.9; IC95%: 1.5-5.6], tMTV [HR=5.0; IC95%: 2.2-11.2] and tTLG [HR=6.3; IC95%: 2.8-13.8] independently predicted PFS. Conclusion: tSUVmax, tMTV and tTLG values determined on initial ¹⁸F-DG PET/CT are independent prognostic factors for PFS in patients with metastatic breast cancer.

EP043

Role of prone high resolution PET CT in breast cancer

A. Baassiri, G. Berjawi, M. Abusamra, K. Gharzeddine, L. Nassar, M. Hourani, M. Haidar; American University of Beirut Medical Center, Hamra - BEIRUT, LEBANON.

Objective: The goal of this study is to determine if patient staging for breast cancer patients differs between prone position and supine position.

Methods: Thirty three patients had undergone a supine position PET/CT at standard resolution that was followed by a prone position PET/CT at high resolution acquisition. Images acquired in both positions of the same patient were compared. **Results:** We had a total number of 33 patients; 29 of them presented for staging and 4 for restaging. One patient had presented for restaging where both PET/CT positions had detected one axillary lymph node lesion with no primary breast lesion. The average value of SUVmax of the primary breast lesions detected on prone position PET/CT was 7.63 and in Supine position PET/CT the average value of SUVmax was 5.95. One case of classical invasive lobular carcinoma had been missed in the supine position but detected in the prone position. Axillary lymph nodes were detected in 20 out of 33 cases by prone position PET/CT while the supine position PET/CT detected them in 18 cases. The minimum number of lesions detected per case was 1 and the maximum was multiple (more than 10) for both PET/CT positions. The average value of SUVmax of the axillary lymph nodes detected on prone position PET/CT was 7.00, and for supine position the average value of SUVmax was 5.74. As for comparison between both PET/CT positions, in one case the prone position image detected multiple axillary lymph nodes while none of them were detected in the supine position. Internal mammary lymph nodes were detected in 3 cases in total. The prone position detected them all while the supine position missed one case. In this case, one lymph node had been detected in the prone position but missed in the supine position. Supra clavicular lymph nodes were detected in 3 cases in the prone position while they were detected in a single case in the supine position. No mediastinal lymph nodes were detected in either PET/CT positions in any of our patients. Bone lesions were detected in 3 cases out of 33 by both PET/CT positions. All three were osteolytic lesions. **Conclusion:** Our preliminary results showed that the high resolution prone position is a promising technique to detect primary breast lesions and metastatic lymph nodes which may be missed by traditional acquisition (supine position) which can lead to change in patient staging and management.

EP044

FDG PET-CT evaluation of the contralateral breast in patients with recently diagnosed breast cancer

R. Kumar, A. Mukherjee, M. Nadig, C. Bal; All India Institute of Medical Sciences, New Delhi, INDIA.

Objectives: Although breast cancer is one of the most common cancers in women, bilateral breast cancer is uncommon. Contralateral breast cancer can be synchronous and/or metachronous in patients with cancer of one breast. The present study evaluated the role of PET-CT in detecting contralateral breast cancer in patients with known breast cancer undergoing PET/CT scan for restaging. **Methods:** Data of 2197 breast cancer patients referred for PET-CT at our department were analysed over a period of eight year. **Results:** Incidence of bilateral breast cancers was 10.6% (233 of 2197 patients). Mean age of these patients was 46.1 ± 11.4 yrs (range 25-72 yrs). Out of 233 patients Synchronous tumors were found in 109 (47%) patients of which 66 (61%) were known to have bilateral tumors before being referred for PET and in rest 43 (39%) patient contralateral breast tumor was confirmed after noting abnormal FDG uptake in the other breast. Metachronous tumors were found in 124 patients (53%). Average time period between detection of 2nd lesion in this group was

18 months (range 8 months– 72 months). In this group 72 patients (58%) had been treated for cancer in one breast and presented with clinically or mammographically suspicious lump in the contralateral side and referred for further evaluation by PET/CT. Increased FDG uptake was seen in all of these lesions which were confirmed by histopathology later on. The remaining 52 (42%) patients suspicion of tumor was raised after noting abnormal intense 18F-FDG uptake in the other breast during follow-up study and confirmed by further evaluation. Thus 18F-FDG PET/CT detected unsuspected contralateral breast tumour in 4.3 % (95/2197) of patients and accounted for 40.7 % (95/233) of the bilateral breast tumors in this series. **Conclusions:** FDG PET-CT play important role in detection of cancer in contralateral breast in patients of known breast cancer.

EP045

Can PET/CT Volumetric Data Be Useful As Biomarkers Predictive Of Pathological Response To Neoadjuvant Treatment In Patients With Locally Advanced Breast Cancer?

M. Martínez de Bourio, A. Jiménez-Ballvé, O. Salsidua Arroyo, A. Serrano-Palacio, M. García García-Esquinas, C. Rodríguez-Rey, A. Ortega-Candil, J. A. García-Saénz, M. E. Fuentes Ferrer, J. L. Carreras-Delgado; HOSPITAL CLINICO SAN CARLOS, MADRID, SPAIN.

Objective: To investigate whether the different PET indexes, measured in the initial staging PET/CT scan, can be able to predict the pathological response to neoadjuvant treatment in patients with locally advanced breast cancer (LABC). **Materials and methods:** A retrospective study from January/2010 till March/2016 was performed. One hundred women (mean age 49 years old, range 25-75 years) with LABC treated with neoadjuvant chemotherapy (NAC), were included. 18F-FDG PET/CT scan for initial staging was performed prior undertaking neoadjuvant treatment, analysing different metabolic parameters: SUV_{max}, SUV_{mean}, metabolic tumour volume (MTV) and total lesion glycolysis (TLG) in the primary tumour (T), in local metastatic nodes (N) and all lesions. The histological response was analysed in the surgical specimen, and it was classified as pathological complete response when there was no evidence of tumour and non pathological complete response in the opposite case. **Results:** From all of the patients included in this study, twenty-nine per cent (29/100) showed pathological complete response whereas seventy-one per cent (71/100) showed non pathological complete response. From the different metabolic parameters measured in the initial staging PET/CT scan, only MTV in the primary tumour was related to pathological response, being higher in patients who did not show a pathological complete response compared to those who showed a pathological complete response (7.8 cm³ vs. 4.9 cm³; p=0.046). Differences observed in SUV_{max}, SUV_{mean} and TLG values (in the primary tumour, local metastatic disease and all lesions), as well as in MTV value (in local metastatic disease and all lesions), were not significantly correlated with response to NAC. In the ROC curve analysis, the best cut-off point of MTV in the primary tumour to predict a pathological complete response was ≥ 6.8 cm³ (sensitivity 61% and specificity 59%). **Conclusions:** In our study, the only PET parameter able to predict the pathological response in patients with locally advanced breast cancer who undergo neoadjuvant treatment, is metabolic tumour volume measured in the primary tumour. These results suggest that the inclusion of this parameter to clinical data could identify those patients who will have a better response to neoadjuvant treatment.

EP046

Prognostic value of primary tumor SUV_{max} on F-18 FDG PET/CT compared with semi-quantitative tumor uptake on Tc-99m sestamibi breast-specific gamma imaging in invasive ductal breast cancer

J. Yoo, H. Yoon, B. Kim; Ewha Womans University School of Medicine, Seoul, South Korea, Seoul, KOREA, REPUBLIC OF.

Objectives: This study aimed to evaluate the prognostic value of F-18 FDG PET/CT in comparison with Tc-99m breast-specific gamma imaging (BSGI) and previously established clinical prognostic parameters of invasive ductal breast carcinoma (IDC). **Methods:** We retrospectively included 149 female IDC patients (mean age: 49.1 years, range: 29-78) who underwent PET/CT and BSGI. Maximum standardized uptake value (SUV_{max}) and tumor-to-normal ratios (TNR) of primary tumor was measured on PET/CT and BSGI, respectively. Univariate and multivariate survival analysis was performed to evaluate the prognostic value of measured parameters and other clinical prognostic factors: pathologic tumor size (pTS), axillary nodal status (ANS), nuclear grade, histologic grade, hormonal receptor status of estrogen (ER) and progesterone receptor (PR) and C-erb-B2 expression. **Results:** Among 149 patients, recurrence occurred in 15 patients (10.1%). In univariate analysis, pTS (p < 0.001), ANS (p < 0.01), nuclear grade (p < 0.05), histologic grade (p < 0.01), ER status (p < 0.01), C-erb-B2 status (p < 0.01), primary tumor SUV_{max} (p < 0.001), and TNR (p < 0.001) were significant predictors of recurrence. Among them, pTS (p < 0.05) and primary tumor SUV_{max} (p < 0.01) were independent prognostic factors in multivariate regression analysis. **Conclusions:** In IDC patients, high primary tumor SUV_{max} of PET/CT and high TNR of BSGI were poor prognostic factors and especially primary tumor SUV_{max} was an independent prognostic factor along with pTS. (This research was supported by grants from the National Research Foundation (2015R1C1A1A02037051, 2012M3A9B6055379) of South Korea.)

EP047

Dual-time-point FDG-PET/CT: prognostic value of total metabolic tumour volume in patients with recurrent breast cancer

C. B. Petersen¹, M. G. Hildebrandt¹, O. Gerke¹, C. Baun¹, K. B. Falch¹, A. Alavi², P. Høilund-Carlsen¹; ¹Odense University Hospital, Odense C, DENMARK, ²Perelman School of Medicine, University of Pennsylvania, Philadelphia, PA, UNITED STATES.

Aim: The purpose was to examine the prognostic value of total lesion glycolysis (TLG) and metabolic tumour volume (MTV) measured by 18F-FDG-PET/CT in women with recurrent breast cancer. **Material and methods:** Twenty-two women (aged 37-76 years) diagnosed with disseminated recurrent breast cancer underwent dual-time-point (1h and 3h) FDG-PET/CT. The scans were evaluated using dedicated quantification software (ROVER®, ABX, Radeberg, Germany), with an iterative algorithm and threshold of 40% of maximum. Whole body MTV, TLG and TLG corrected for partial volume effect (cTLG) were calculated. Differences in mean values of measured variables between survivors and non-survivors were recorded. ROC analyses of these variables were made to find cut-off points for high and low risk of death and to serve as basis for Kaplan-Meier curves. Multiple COX-regression analyses were made to test for correlation between PET variables and baseline characteristics and survival during a follow-up period of 17-43 months, (mean 20 months). **Results:** Eleven of the 22 patients died during the follow-up period. Median MTVs for survivors and non-survivors at 1 h imaging were 26.7 cm³ (range: 8.1-372.3) and 83.0 cm³ (4.4-744.7), respectively; at 3 h 18.9 cm³ (6.4-393.6) and 58.3 cm³ (4.8-747.7), respectively, (all p-values < 0.05). No statistically significant difference was found for any of the other PET measures. ROC analyses showed that values below cut-off points of 44.1 and 34.7 for MTV at 1 h and 3 h imaging, respectively, were associated with longer survival. Multiple COX-regression analyses showed modest, but statistically significant, hazard ratios of 1.00346, 1.000708, and 1.000409, respectively, for MTV, TLG, cTLG at 1 h imaging and of 1.000506 for TLG at 3 h imaging. **Conclusion:** Significantly higher metabolic active tumour burden was found in non-surviving compared to surviving women with systemic recurrent breast cancer. Thus, semi-quantitative PET measures might be independent prognostic factors. Due to the limited number of patients, our results should only be seen as hypothesis generating. The potential clinical value of these measures needs to be documented in larger samples of patients.

EP048**Clinical significance of FDG uptake in invasive duct carcinoma of the breast - correlation with histopathological prognostic markers**

L. PUSHPALATHA SUDHAKAR, S. Praveen, P. Amber, M. Sailaja reddy, P. Raghuram; KRISHNA INSTITUTE OF MEDICAL SCIENCES, SECUNDERABAD, INDIA.

Aim: To evaluate the prognostic value of FDG uptake in Invasive Duct Carcinoma (IDC) of the breast in correlation with histopathological factors such as tumor grade, nodal involvement, immune histochemical (IHC) markers including estrogen receptor (ER), progesterone receptor (PR), and HER2/neu status. **Materials & Methods:** Study included 40 patients with surgically proven IDC. Maximum standardized uptake values (SUV max) for the primary lesions were evaluated retrospectively on preoperative F18 FDG PET-CT scans. Histopathology factors including tumor grade, lymph nodal involvement, ER, PR & HER2/neu receptor status were analyzed. SUV max was correlated with these factors. p values of less than 0.05 were considered statistically significant. **Results:** The average SUV max of forty lesions was 12.75 (SD±8.30). Grade 2 tumor was seen in 18 and grade 3 in 22. Lymph nodal involvement was seen in eighteen patients (45%). The mean SUV max value of ER+ and ER- lesions were 12.45 ± 8.24 and 13.70 ± 8.88 respectively. Mean SUV max of PR+ was 13.32 ± 8.85 and PR- was 10.00 ± 4.20. HER2/neu+ had mean SUV max of 12.23 ± 7.10 and HER2/neu- had 13.00 ± 8.91. The mean SUV max of grade 2 was 9.83 ± 7.74 and grade 3 was 15.04 ± 8.16. The lymph nodal involvement showed mean SUV max of 15.61 ± 7.29. Statistically significant correlation was noted between SUV max and the lymph nodal involvement as well as the tumor grade (p value less than 0.046). However there was no correlation between SUV max and ER, PR & HER2/neu status. **Conclusion:** Our study highlights the statistically significant correlation between FDG uptake and nodal involvement & tumor grade. SUV max can be used as one of the prognostic factors in nodal involvement and high tumor grade. However no correlation between the uptake and ER, PR, HER2/neu receptor status was found in our study.

EP049**New era of PET/CT in breast cancer: High resolution acquisition**

A. BASSIRI, G. Berjawi, M. Abusamra, K. Gharzeddine, L. Nassar, M. Hourani, **M. Haidar**; American University of Beirut Medical Center, HAMRA- BEIRUT, LEBANON.

Objective: The aim of this study is to determine the role of high resolution PET/CT in staging and management of breast cancer patients. **Methods:** 25 patients with breast cancer had undergone a supine position PET/CT at standard resolution that was reconstructed to high resolution acquisition. **Results:** According to the pathology results, we had 20 lesions of invasive ductal carcinoma, one lesion of granulation tissue, two cases of invasive mammary carcinoma, and a case of invasive mucinous carcinoma. The 25 breast lesions detected on PET/CT had an average size of 1.96 cm. The average value of SUVmax of the primary breast lesions detected on high resolution PET/CT was 5.83 versus 4.57 in standard acquisition. All these lesions were better characterized and visualized in high resolution acquisition. Axillary lymph nodes were detected in 13 out of 25 cases by both PET/CT resolutions. The intensity of uptake was higher with high resolution acquisition lead to better visualization of lymph node and decrease the grey zone. No internal mammary, supraclavicular, or mediastinal lymph nodes were detected by either PET/CT resolutions. Bone lesions were detected in 2 cases out of 25 by both PET/CT positions. All lesions were osteolytic lesions. No osteoblastic lesions were detected by either PET/CT positions. **Conclusion:** Our preliminary results showed no change in patient staging in any of the patients between both PET/CT resolutions but high resolution Images lead to be more comfortable for localization and decrease the number of grey zone lesion especially for the axillary lymph node.

EP050**Variations of FDG PET/CT SUV and textural indices in breast cancer according to metastatic status**

S. Boughdad¹, C. Nioche², F. Orhac³, L. Champion¹, J. Alberini¹, I. Buvat²; ¹Institut Curie-Hôpital René Huguenin, Saint-Cloud, FRANCE, ²IMIV CEA, Inserm, CNRS, UnNiv Paris Sud, CEA-SHFJ, Orsay, FRANCE, ³IMIV CEA, Inserm, CNRS, UnNiv Paris Sud, CEA-SHFJ, IGR, Orsay, FRANCE.

Introduction: Breast cancer (BC) is a very heterogeneous disease and the metastasis stage is of poor prognosis. We investigated whether SUV and textural indices (TI) in BC differed as a function of the metastatic status and also of the Ki 67 expression, grade and molecular subtype. **Method:** We studied a population of 122 women who underwent a F18-FDG-PET/CT in our institution for initial staging of biopsy proven BC. Two groups of patients were defined: M+ (metastatic spread) and M- (no metastatic spread), according to the current guidelines (biopsy proved or on approved imaging technique: MRI or F18-FDG-PET/CT). Volume (mL), SUV (max, mean and peak), TLG (total lesion glycolysis, mL) and TI (homogeneity, entropy, LRE, SRE, LGZE and HGZE) were measured in each VOI obtained using a threshold method (40% of SUVmax) and exceeding 1.5mL in volume. We used a Mann-Whitney test to determine whether Volume, TLG SUV and TI were significantly different in the VOI between the M+ and M- groups. We also compared the groups according to Ki 67 expression using a cut-off of 20%, grade (SBR II vs III) and the breast molecular subtype (classification of 2010). **Results:** We drew 132 VOI in our BC population: 84 VOI in 76 patients in the M- group and 48 VOI in 46 patients in the M+ group. There was no significant difference in SUV and TI between M+ and M- patients (p > 0.05). When limiting the analyses to patient subgroups based on a 20% cut-off for Ki 67 expression, or based on the grade or according to the luminal B subtype, SUV and TI were still not significantly different for M+ and M- patients. However, there were significant differences in TLG between M+ and M- patients: 101.8 ± 181.3 mL in M+ vs 53.3 ± 97.9 mL in M- (p=0.028), and the volume (mL) was also different (p < 0.05). We also found significant differences in volume in the 2 subgroups based on the Ki 67 expression: p=0.016 between M+ and M- in the Ki 67 >20% subgroup including 33 M+ and 53 M- pts. Similarly, volumes and TLG were significantly different between the 30 M+ and 50 M- pts with Luminal B tumors: 30 M+ vs 50 M- pts (p=0.00: volume and p=0.048: TLG). **Conclusion:** The only significant differences found between M+ and M- patients in our BC population were in the TLG and the tumor volume which remains a strong prognostic factor in BC.

EP051**The role of (18)F-Fluorodeoxyglucose Positron Emission Tomography/Computed Tomography (PET/CT) in patients with breast cancer recurrence: a comparison to conventional imaging (CI) techniques and clinical impact on patient management**

S. Panareo¹, I. Santi¹, I. Rambaldi¹, S. Taralli¹, A. Frassoldati², C. Cittanti¹; ¹University Hospital - Nuclear Medicine Unit, FERRARA, ITALY, ²University Hospital - Oncology Unit, FERRARA, ITALY.

AIM: The aim of this study was to evaluate the impact of PET/CT on clinical management in patients with breast cancer recurrence and compare PET/CT data with CI data (US, ceCT, MR). **METHODS:** we observed 70 consecutive patients (age 60.25 ± 6.2 yo) addressed to PET/CT scan from January 2015 to April 2016 for suspected recurrence of previously staged and treated breast cancer. All patients were studied with the same high performing PET/CT scanner with innovative image reconstruction algorithm (integrating parameters derived from "Point Spread Function" and "Time Of Flight" calculations). PET/CT findings were compared with CI data on a patient

basis. **RESULTS:** in 21 patients (30.0%) PET/CT revealed recurrence of breast cancer in the region of the primary tumor; CI detected local recurrence in 16 patients (22.9%) [p=ns]. In 2 cases (2.8%) PET/CT showed a focal radiotracer uptake in the contralateral mammary gland (final histology showed malignant tumor involvement). In 21 patients (30.0%) PET/CT showed lymph node metastases in the primary breast tumor ipsilateral axilla, while CI managed to do so in 15 (21.4%) [p<0.35]. Furthermore PET/CT showed lymph node disease relapse in other basins in 39 patients (55.7%) while CI in 23 (32.8%) [p<0.1]. Bone metastases were detected by PET/CT in 28 patients (40%) while by ceCT in 12 (17.4%) [p<0.01]. Lung involvement was detected by PET/CT in 17 cases (24.2%) while by ceCT in 15 (21.4%) [p=ns]. PET/CT showed liver metastases in 9 cases (12.8%) while CI in 8 (11.4%) [p=ns]. Adrenal metastases were seen on PET/CT in 6 cases (8.5%) while on CI in 3 (4.2%) [p<0.106]. In 22 patients (31.4%), PET/CT detected additional lesions not visible on CI. PET/CT had an impact on clinical management in 37 patients (52.8%) by detecting more extensive loco-regional disease or distant metastases. In 21 patients (30.0%) extensive surgery was not undertaken and treatment was changed (CHT and/or RT). The sensitivity, specificity, accuracy, positive and negative predictive values of PET/CT were respectively 97%, 92%, 95%, 94% and 96%. **CONCLUSIONS:** PET/CT proved to play an important role in restaging patients with breast cancer recurrence since its results changed the clinical management in a large percentage of patients. PET/CT showed better performance than CI in all evaluated recurrence sites -although the difference was mainly not statistically significant- therefore it could potentially replace conventional imaging in restaging patients with breast cancer recurrence -especially concerning bone involvement- to optimize diagnostic timing and even costs.

EP052

Correlation of hypoxia inducible transcription factor in breast cancer and SUVmax of F-18 FDG PET/CT

Y. Jeong, J. Jung, Y. Cho, S. Park, H. Oh, S. Kang; Catholic University of Daegu School of Medicine, Daegu, KOREA, REPUBLIC OF.

Background Tumor hypoxia induces the expression of several genes via the hypoxia-inducible transcription factors alpha (HIF-1 α), which is associated with the prognosis of several cancers. We studied the immunohistochemical expression of HIF-1 α in patients with invasive ductal breast cancer (IDC) and the possible correlation with SUVmax of the primary tumor (pSUVmax) as well as other biological parameters. Prognostic significance of pSUVmax for the prediction of progression-free survival (PFS) was also assessed. **Materials and Methods** Two-hundred seven female patients with IDC who underwent pretreatment F-18 FDG PET/CT were enrolled. The pSUVmax was compared with clinicopathological parameters including ER, PR, HER2, axillary lymph node (LN) metastasis, stage and HIF-1 α . The prognostic value of pSUVmax for PFS was assessed using the Kaplan-Meier method. **Results** pSUVmax was significantly higher in patients with HIF-1 α ≥ 2 compared to patients with HIF-1 α < 2 (5.2 \pm 4.5 vs. 3.7 \pm 3.1, P=0.008). pSUVmax was also significantly higher in higher stage (P<0.000001), ER-negative tumors (P<0.0001), PR-negative tumors (P=0.0011) and positive LN metastasis (P=0.0013). pSUVmax was significantly higher in patients with progression compared to patients who were disease-free (6.8 \pm 4.4 vs. 4.1 \pm 3.7, P=0.0005). A receiver-operating characteristic curve demonstrated a pSUVmax of 6.51 to be the optimal cutoff for predicting PFS (sensitivity; 53.6%, specificity; 86.0%, P<0.0001). **Conclusions** pSUVmax on pretreatment F-18 FDG PET/CT reflects expression of HIF-1 α and can be used as a good surrogate marker for the prediction of progression in patients with IDC. The amount of FDG uptake is determined by the presence of glucose metabolism and hypoxia in breast cancer cell.

EP053

Dual-time-point FDG Uptake Correlates with Prognostic Factors of Invasive Breast Cancer: Clinical Usefulness of Early Delayed Scanning

H. Song; Jeju National University School of Medicine, Jeju-si, KOREA, REPUBLIC OF.

Purpose This retrospective study investigated the correlation between FDG uptake on tumours assessed by modified dual-time-point FDG PET/CT and clinical, histopathologic, and immunohistochemical prognostic parameters of invasive breast cancer. **Subjects & Methods** Thirty-two women were enrolled. All the patients underwent mastectomies and pre-operative FDG PET/CT by modified dual-time-point scanning for invasive breast cancer. They underwent standard FDG PET/CT (PET1) followed by the early delayed acquisition (PET2) without repositioning and additional CT scanning. Maximal standardized uptake values on PET1 (SUV1) and PET2 (SUV2) were evaluated, and the percentage changes between SUV1 and SUV2 (retention index) calculated. Clinical factors (age, body mass index, and blood glucose level at the time of FDG injection) and pathologic features (tumour size, number of metastatic lymph nodes, and TNM stage) were assessed. Biologic prognostic parameters (histologic grade; tubular differentiation; nuclear pleomorphism; mitotic count; and expression of estrogen receptor (ER), progesterone (PR), HER-2, p53, epidermal growth factor receptor (EGFR), CK56, Ki-67, and E cadherin) were evaluated from primary tumours after mastectomy. Statistical analysis was performed to find the correlation of clinical features, pathologic factors, and biologic prognostic parameters with retention index. **Results** PET2 scans were conducted 17.7 \pm 1.5 min after PET1 without repositioning and additional CT scanning. Retention index showed a moderately positive relationship with the degree of Ki-67 expression (p < 0.001, rho = 0.629). Significant statistical differences between histologic grade (1 to 3, P = 0.016), nuclear pleomorphism (1 to 3, P = 0.002), mitotic count (1 to 3, P = 0.01) and ER (positive and negative, P= 0.023) were observed around the mean retention index. **Discussion & Conclusion** This modified dual-time-point FDG PET/CT has advantages including a low radiation exposure to patients and a shortened scanning time compared to a conventional dual-time-point FDG PET/CT (delayed acquisition on 120-180 min after FDG injection). This study demonstrated that retention index correlated with well-known biologic prognostic factors of invasive breast cancer and that early delayed scanning could possibly substitute for a conventional dual-time-point FDG PET/CT.

EP054

Dynamic uPAR-PET/CT imaging of breast cancer patients for establishing optimal scan time following injection of ⁶⁸Ga-NOTA-AE105

D. Skovgaard¹, M. Persson², N. Kroman¹, T. Tvedskov¹, A. Loft¹, A. K. Berthelsen¹, M. Brandt-Larsen¹, J. Madsen¹, L. Hojgaard¹, A. Kjaer¹; ¹Rigshospitalet, Copenhagen, DENMARK, ²Curasight ApS, Copenhagen, DENMARK.

Introduction Overexpression of urokinase-type plasminogen activator receptors (uPAR) represents an established biomarker for poor prognosis in many common malignant diseases including breast cancer. Accordingly, uPAR is an important target both for new therapeutic and diagnostic strategies. In a recent *first-in-human* uPAR PET study using the tracer ⁶⁸Ga-NOTA-AE105, which is based on the high affinity uPAR peptide antagonist AE105, we found high uptake in both primary breast cancer and lymph node metastases. However, no dynamic scans were performed in that study and accordingly, the best image contrast, i.e. tumor-to-background ratio, following injection of ⁶⁸Ga-NOTA-AE105 remains to be established. The aim of the present study was therefore to determine the optimal time to perform PET/CT following injection of ⁶⁸Ga-NOTA-

AE105 in breast cancer patients. **Materials and methods** Five patients with histologically confirmed breast cancer scheduled for lumpectomy/mastectomy underwent 60 minutes of dynamic PET and low dose-CT of the breast region starting at the time of injection of ^{68}Ga -NOTA-AE105 (≈ 200 MBq). PET data was reconstructed into 5-minutes time frames, resulting in 12 consecutive frames in total. Time activity curves were created for tumor lesions, background organs (muscle and normal breast tissue) and blood pool. Tumor-to-background ratios were calculated for all time frames. In addition, experienced readers evaluated the images for best visual tumor-to-background contrast. **Results** The primary tumors of all 5 patients and several bone metastases in one patient were clearly visualized on the ^{68}Ga -NOTA-AE105 PET/CT at all time frames (average SUV_{max} 3.7; range 1.9-5.1). Tumor-to-background ratio were higher than 2 across all time points (average $\text{SUV}_{\text{max}}(\text{tumor})/\text{SUV}_{\text{mean}}(\text{background})$: muscle 6.8; range 3.8-10.3 and normal breast 5.4; range 2.1-18.5). Due to an initial high blood pool activity, the tumor-to-blood pool ratio reached a level >1 at the time frames between 15-25 minutes. By visual judgment, tumor-to-background contrast was found to be best between 15-25 min. **Conclusion** Based on tumor-to-background ratios as well as visual judgment, the optimal time for conducting uPAR PET/CT imaging following injection of ^{68}Ga -NOTA-AE105 is suggested to be approximately 20 minutes.

EP055

Hybrid PET-MR imaging for accurate nodal staging prior to neoadjuvant chemotherapy in breast cancer patients - preliminary results

S. Vöö, B. Goorts, M. L. Smidt, T. J. van Nijnatten, J. Wildberger, M. B. Lobbes, F. Mottaghy; Maastricht University Medical Center, Maastricht, NETHERLANDS.

Purpose: To assess the clinical value of hybrid FDG PET-MR imaging for nodal staging prior to neoadjuvant chemotherapy (NAC) in breast cancer patients. **Methods and Materials:** In this prospective study, patients with primary invasive breast cancer with at least cT2 and/or a histopathologically confirmed lymph node metastasis undergoing NAC were included. A hybrid PET-MR breast protocol was performed before NAC. MR images were evaluated independently by one dedicated breast radiologist, PET images independently by one dedicated nuclear physician. Afterwards a combined PET-MR report was made. The number and localization of lymph nodes suspicious for metastases on PET-MR was compared to conventional nodal staging methods, i.e. ultrasound with core needle biopsy and MRI-only. The percentage of patients with a modified treatment plan based on PET-MR was studied. **Results:** In this ongoing study, 25 patients were included so far. In 16% (4/25) of the included cases, treatment plan altered based on PET-MR findings. In two patients, PET-MR showed an enlarged internal mammary lymph node with high FDG-uptake. One patient had five axillary lymph nodes suspicious for metastases on PET-MR, whereas initially only two were seen on ultrasound and none on MRI-only. For these three patients radiotherapy plan was extended. One patient had three axillary lymph nodes suspicious for metastases on PET-MR compared to more than three on ultrasound and MRI-only, resulting in a reduced radiotherapy plan. **Conclusion:** Pre-NAC hybrid PET-MR changed treatment plan in 16% of patients. Consequently, PET-MR might be more accurate for nodal staging, compared to conventional imaging.

EP056

The Prognostic role of Skeletal Tumor Burden on ^{18}F -Fluoride PET/CT in Metastatic Breast Cancer

A. E. Brito, C. Mosci, A. Santos, S. Q. Brunetto, C. D. Ramos, E. Etchebehere; University of Campinas, Campinas, BRAZIL.

Introduction Skeletal tumor burden determined by ^{18}F -Fluoride PET/CT has been shown to have a prognostic role in prostate cancer patients treated with Ra-223. **Objectives** This study aimed to correlate skeletal tumor burden determined by ^{18}F -Fluoride PET/CT with clinical outcomes in patients with breast cancer. **Methodology** Patients with breast cancer that underwent a ^{18}F -Fluoride PET/CT whole-body image for investigation of bone metastases were retrospectively analyzed. ^{18}F -Fluoride PET/CT PET images were quantified using METAVOL® software. Skeletal tumor burden was calculated using the threshold $\text{SUV}_{\text{max}} \geq 10$, to exclude normal bone. Abnormal sites not related to metastases (ex. urinary bladder, degenerative processes, etc) were manually excluded. The parameters total volume of fluoride avid bone metastasis (FTV_{10}), the total uptake of fluoride-avid bone metastasis (TLF_{10}), the highest SUV_{max} among all the metastases, and the mean SUV_{max} were calculated. The primary endpoint was overall survival (OS), established from the date of ^{18}F -Fluoride PET/CT until death or last follow-up. Secondary aims were time to progression (TTP), time-to-bone event (TTBE) and progression free survival (PFS). The tumor characteristics Ki-67, HER-2, Histology and nuclear grades were correlated with skeletal tumor burden. **Results** Twenty-eight female patients with breast cancer (25 invasive ductal carcinomas), ages 60.6 ± 11 years were studied. Median follow-up was 13.9 months (2 -31 months). At the end of follow-up, the mean TLF_{10} and FTV_{10} of patients that were alive was three times lower than of patients that were dead. Furthermore, the mean TLF_{10} and FTV_{10} was five times greater for patients that progressed when compared to those who did not progress. TLF_{10} and FTV_{10} values were shown to be highly correlated ($p < 0.05$; $P < 0.0001$). FTV_{10} was significantly associated with OS and TTP on univariable ($P < 0.0001$) and multivariable analyses ($p < 0.05$). There was no significant association between TLF_{10} , FTV_{10} , mean SUV_{max} or SUV_{max} with TTBE and PFS. The tumor characteristics (Ki-67, HER-2, histology and nuclear grades) were not independent predictors of survival. **Conclusion** These preliminary results show that TLF_{10} seems to be an independent prognostic imaging biomarker of OS and TTP in breast cancer patients. The analysis of a larger population can confirm these results.

EP057

Utility of Single-Photon Emission Computed Tomography (SPECT/CT) in selective Sentinel Lymph Node Biopsy (SLNB) in patients with melanoma

M. Pedrera-Canal, A. Ortega-Candil, M. J. Pérez-Castejón, C. Riola-Parada, A. Serrano-Palacio, O. Salsidua Arroyo, A. Jiménez-Ballvé, L. Lapeña-Gutierrez, J. L. Carreras-Delgado; HOSPITAL CLINICO SAN CARLOS, MADRID, SPAIN.

Objective: The aim of the study was to investigate the role of Single-Photon Emission Computed Tomography (SPECT/CT) in selective Sentinel Lymph Node Biopsy (SLNB) in patients with melanoma. **Material and Methods:** This is a retrospective study between April/2011 and November/2015. We consecutively included 44 patients affected of cutaneous melanoma (23 female and 21 male) with a mean age of 61,5 years old. Location of primary lesion was: head and neck (13.6%), trunk (43.2%), upper extremities (20.5%) and lower extremities (22.7%). All patients had indication for SLNB procedure. Initially all patients underwent primary excisional biopsy. Both SLNB and margins enlargement surgery were performed the same day. Dynamic images were acquired immediately after ^{99}Tc -nanocolloidal albumin peri-scar injection, secondly planar images of the injection-site 30 and 60 minutes post-injection were performed and finally SPECT/CT scanning was acquired (Low dose CT, 140 Kv, 2,5 mAs). SLNs excision was undertaken 3-6 hours after injection with a gamma probe and a portable gammacamera. **Results:** SLNs detection rate reached 95.4% (42/44 patients) using planar images and SPECT/CT. The mean number of radiotracer deposits visualized in the planar images and SPECT/CT was the same (2.51 deposits, range 0-6). We did not find significant differences between both images

($p=0.136$), with a good Kappa Index (0.767). The radiotracer did not migrate in 4.5% (2/44) patients, whereas, in 65.9%, lymphatic drainage was only in one nodal station and in 22.7% patients drainage reached two or more nodal stations. Migration distribution was ipsilateral to the primary lesion in 85.7% (36/42) patients and bilateral in 14.3% (6/42). A mean of 2.81 sentinel nodes were removed (range 0–10). In 71.4% (30/42) patients, SLNs were negative for malignancy and their Breslow Thickness (BT) mean value was 1.99 mm. However, in 28.6% (12/42) patients, SLNs were positive for malignancy, obtaining a BT mean value of 3.58mm. Surgeons considered SPECT-CT images very useful for a better anatomical localization. Conclusion: In our sample, planar lymphoscintigraphic and hybrid SPECT/CT imaging presented the same ability to detect SLNs. However SPECT/CT was very useful for surgeons to improve the correct anatomical localization, especially in those cases with more than one lymphatic drainage station and bilateral distribution.

EP058

SPECT-CT with 99m-Tc-MIBI in diagnosis of non-sentinel lymph node invasion by breast cancer

P. Krzhivitskiy, S. Novikov, S. Kanaev, P. Krivorotko, O. Ponomareva, L. Jukova, A. Chernaya, E. Turkevich; N.N. Petrov Institute Oncology, St Petersburg, RUSSIAN FEDERATION.

Purpose: to evaluate accuracy of SPECT-CT with 99m-Tc-MIBI in diagnosis of non-sentinel lymph node (LN) involvement in patients with early breast cancer (BC). **Material and methods:** 184 patients with clinically early (T1-3 N0 M0) BC were included in this study. All of them underwent SPECT-CT examination on Symbia-T16 scanner which consists of dual head gamma-camera combined with 16 slices diagnostic CT. SPECT-CT was performed 15 min after i/v injection of 740–860 MBq of 99mTc-MIBI. Experienced radiologist and specialist in nuclear medicine separately reported on CT and SPECT-CT data. The signs of metastatic lymph node involvement were: short axis more than 10mm, cortical thickness more than 4mm, solid structure (absent hilum), intensive tracer uptake (70% above background and more), more than 2 abnormally LN. All LN with tracer uptake on the level of background or less than 70% above background uptake were considered as normal or nonspecific LN. The size of primary tumor also was taken into consideration - more than 20mm. Final interpretation of the data was done according to histological verification of removed sentinel and non-sentinel LN. **Results:** In total 62 (34%) of 184 evaluated patients had axillary LN metastases on final histology: in 37 cases we revealed involvement of only sentinel LN and in remaining 25 patients (14%) - sentinel and non-sentinel LN. We determined high accuracy (88%) and sensitivity (96%) and moderate specificity (55%) of SPECT-CT in diagnosis of non-sentinel LN invasion. **Conclusion:** Our data demonstrated high sensitivity (96%) of SPECT-CT with 99mTc-MIBI in diagnosis of non-sentinel LN involvement by BC. At the same time we must also take into consideration high false positive rate (38%) of this test.

EP059

The preliminary study of 18F-FES PET/CT in predicting postmenopausal patients with ER/PR+, metastatic breast cancer receiving combination treatment of fulvestrant and docetaxel

Z. Yang, Y. Sun, J. Zhang, B. Wang, S. He, Y. Zhang, X. Xu, H. Yuan, Y. Zhang; Fudan University Shanghai Cancer Center, Shanghai, CHINA.

Aim: To investigate the clinical value of 18F-FES PET/CT in predicting postmenopausal patients with ER/PR+, metastatic breast cancer receiving combination treatment of fulvestrant and docetaxel. **Methods:** Postmenopausal patients with pathology confirmed ER/PR+, metastatic breast cancer were prospectively enrolled and randomly divided into two groups (D: docetaxel and D+F: docetaxel + fulvestrant). Each patient

underwent FES and FDG PET/CT before and after two cycles of treatment. SUVmax of all the metastatic lesions were measured. Patients were followed every 2 cycles for at least 1 year. Tumor response was evaluated according to RECIST 1.1 Criteria. The ER changes in different groups were performed by χ^2 test. The difference of SUVmax in two groups of various PFS (>1 year and <1 year) was validated by two-tailed t test. Results: Thirteen patients in group D and 9 patients in group D+F have been consecutively enrolled. However, 4 patients in group D were lost during follow up due to various reasons and they were not further analyzed for PFS; additionally, 2 patients in group D+F suffered from adverse effect in cycle 1 and quitted from our study, and another patient failed to undergo FES PET/CT. The ratio of PFS>1 year in group D and D+F were 4/9 and 4/6, respectively. FES PET/CT detected 7 patients with ER upgraded and 6 patients with ER downgraded in group D; nevertheless, all 6 patients were confirmed to be ER downgraded in group D+F. There was statistical difference between these two groups ($p=0.044$). In group D+F, SUVmax of FES in patients with PFS>1 year decreased significantly than those with PFS<1 year (>1 year: $79.5\pm 26.3\%$, <1 year: $8.5\pm 2.1\%$, $p=0.023$) after 2 cycles. However, there was no obvious change by FDG results (>1 year: $57.0\pm 55.0\%$, <1 year: $15.0\pm 87.7\%$, $p=0.495$). Besides, no statistical difference of both FES and FDG were detected in group D+F. Conclusion: Several preclinical studies demonstrated that fulvestrant could significantly reverse the ER mediated chemoresistance in vivo. Our preliminary study showed ER downgrade in all patients receiving combination treatment of fulvestrant and docetaxel by FES PET/CT. We might use the changes of SUVmax in predicting patients' outcome; therefore, individualized treatment strategy could be referred.

EP060

^{18}F -FDG PET/CT versus ^{18}F -Fluoride PET/CT for Detecting Bone Metastases in Patients With Breast Cancer and Equivocal Bone Scan

A. E. Brito, R. G. Almeida, C. Mosci, M. C. L. Lima, B. J. Amorim, A. O. Santos, T. F. Souza, S. Q. Brunetto, E. C. Etchebehere, C. D. Ramos; UNICAMP, Campinas, BRAZIL.

Introduction Whole-body bone scintigraphy (BS) is a sensitive procedure for diagnosis of bone metastasis (BM) in patients with breast cancer; however, it presents low specificity and significant rate of equivocal results. **Objectives** This study aimed to compare ^{18}F -FDG-PET/CT and ^{18}F -fluoride-PET/CT for detection of BM in patients with inconclusive BS. **Methods** We prospectively studied 18 female patients with breast cancer and no BM previously diagnosed (33–78 years of age, mean: 57 ± 12 years). All patients had BS performed for staging or restaging purposes with inconclusive findings and were submitted to true whole-body ^{18}F -FDG-PET/CT (4.5MBq/kg) and ^{18}F -fluoride-PET/CT (3.7MBq/kg) acquisitions, with a time interval of 20 ± 17 days between the procedures, without treatment. All abnormalities identified on BSs were compared with their appearance on both ^{18}F -FDG and ^{18}F -fluoride images. Inconclusive lesions on BSs and additional lesions on PET/CT images were classified as BM or not. The lesions defined as BMs were also classified as lytic, blastic, mixed or without any anatomical changes, according to their appearance on CT images. The final diagnosis of BM was defined by follow-up (clinical and imaging procedures) and established at least 1 year after the PET/CT studies. **Results** The final diagnosis after follow-up defined that 12/18 patients had BMs and 6/18 patients had only benign lesions. ^{18}F -fluoride-PET/CT identified all 12 metastatic patients, whereas ^{18}F -FDG-PET/CT identified only 9 (sensitivity 100% and 75%, respectively, for patient analysis). Thirty-three of the 50 inconclusive lesions on BSs were defined as BM. ^{18}F -fluoride-PET/CT identified 30/33 and ^{18}F -FDG-PET/CT 19/33 of these BMs (sensitivity of 91% and 58%, respectively, for lesion analysis). ^{18}F -fluoride-PET/CT detected 26 additional lesions in 5/12 metastatic patients and ^{18}F -FDG-PET/CT 48 additional BM in only 2 patients; therefore, the methods detected a total of 101 BMs. On CT images, 26/101 BMs were classified as blastic, 19/101 lytic, 4/101 mixed and 52/101 without anatomical changes (most of these in only one patient) and the sensitivity for these types of BMs were respectively 85%, 68%, 75% and 55% for ^{18}F -fluoride-PET/CT

and 42%, 68%, 50% and 88% for ^{18}F -FDG-PET/CT. **Conclusion** ^{18}F -fluoride-PET/CT is more sensitive than ^{18}F -FDG-PET/CT to detect BM in patients with breast cancer and inconclusive BS. ^{18}F -fluoride PET/CT is more sensitive than ^{18}F -FDG-PET/CT to identify blastic and mixed blastic/lytic lesions. The sensitivities of both procedures for pure lytic lesions were similar in the present study. Interestingly, ^{18}F -FDG-PET/CT was more sensitive than ^{18}F -fluoride PET/CT to detect lesions without anatomical changes found in one patient.

EP061

Locally Advanced Breast Cancer: Utility Of Volumetric Parameters In ^{18}F -FDG PET/CT Scans To Predict Recurrence And Overall Survival

M. Martinez de Bourio, A. Jimenez-Ballvé, O. Salsidua Arroyo, A. Serrano-Palacio, A. Ortega-Candil, C. Rodriguez-Rey, M. García García-Esquinas, J. A. García-Saénz, M. E. Fuentes Ferrer, J. L. Carreras-Delgado; HOSPITAL CLINICO SAN CARLOS, MADRID, SPAIN.

Objective: To evaluate the ability of PET volumetric parameters, such as metabolic tumour volume (MTV) and total lesion glycolysis (TLG) compared to Standardized Uptake Value (SUVmax and SUVmean) in the initial staging ^{18}F -FDG PET/CT performed in patients with locally advanced breast cancer (LABC), to predict the recurrence risk and overall survival. **Materials and methods:** This is a retrospective study of 100 LABC women who were treated with neoadjuvant chemotherapy from January/2010 till March/2016. We measured SUVmax, SUVmean, MTV and TLG in the primary tumour and MTV and TLG in all lesions (the sum of the primary tumour and lymph node metastases). **Results:** The median follow up was 52.5 months, 13% (13/100) presented recurrence, local disease (n=2), distant metastasis (n=10) and both (n=1), and 5% (5/100) died, all of them with recurrence. The only parameter related to recurrence was MTV in the primary tumour, which was higher in those patients with recurrence compared to those without it (20.5 cm³ vs 6.8 cm³; p=0.048). TLG in the primary tumour was also higher in the group with recurrence, almost reaching statistical significance (91.1 g vs. 24.5 g; p=0.079). We found statistical association between MTV, measured in the primary tumour and all lesions, and overall survival (31.3 cm³ vs. 7.1 cm³; p=0.003; and 36.2 cm³ vs. 8.7 cm³; p=0.006, respectively). Likewise, TLG in the primary tumour and all lesions was higher in those patients who died (126.9 g vs. 25.5 g; p=0.007 and 164.6 g vs. 33.8 g; p=0.009). However, neither SUVmax nor SUVmean in the tumour and all lesions were able to predict recurrence and overall survival significantly (p>0.05). In the ROC curve analysis, the best cut-off points of MTV in the primary tumour to predict recurrence and overall survival were: ≥ 9.35 cm³ (sensitivity 62 % and specificity 61%), and ≥ 27 cm³ (sensitivity 80 % and specificity 88%) respectively. **Conclusions:** Metabolic tumour volume in the primary tumour could be useful to predict both recurrence risk and overall survival in patients with locally advanced breast cancer. Other parameters associated with overall survival are metabolic tumour volume in all lesions, as well as total lesion glycolysis in the primary tumour and all lesions.

EP062

Fludeoxyglucose (^{18}F) PET/CT in breast cancer patients: evaluation of patient based diagnostic performance and of impact on patient management

L. Kaliska¹, M. Zacharovska¹, M. Vereb², S. Balogova³; ¹Institute of Nuclear and Molecular Medicine, Agel Diagnostic, Banska Bystrica, SLOVAKIA, ²Praxis für Radiologie, Nuklearmedizin und Strahlentherapie, Kassel, GERMANY, ³Nuclear Medicine Clinic, St. Elisabeth Cancer Institute Hospital, Bratislava, SLOVAKIA.

Aim: Breast cancer (BC) has a high prevalence among malignancies in woman. Prognosis and management of BC patients depends on both, histopathologic characteristics and spread of the tumour. Early diagnosis of recurrence is also important to allow appropriate treatment. The aim of this study was to prospectively assess the value of FDG PET/CT in terms of diagnostic performance and impact on patient management in various clinical situations of BC. **Material and Methods:** 434 patients were referred for a FDG PET/CT in following clinical situations: Initial staging: 1. Initial staging (n=8), 2. Staging after resection of primary tumour (n=6); Evaluation of primary curative treatment and systematic follow-up: 3. Evaluation at the end of treatment (n=12), 4. Systematic follow-up in asymptomatic patients (n=62); Localisation of recurrent BC: 5. Clinical suspicion from recurrence (n=21), 6. Suspicion of recurrence on conventional imaging (n=72), 7. Raise in serum tumour markers levels (n=98), 8. Restaging of BC (n=14); and Evaluation of palliative treatment: 9. Evaluation of effect of palliative treatment (n=141). The standard of truth for evaluation of diagnostic performance was either histology (45/434=10%) or follow-up more than 6 months (398/434=90%). The impact of FDG PET/CT on patient management was considered as major (change between main clinical modalities) or minor (within intended modality). **Results:** The patient based sensitivity, specificity and diagnostic accuracy of FDG PET/CT were 196/209=94%, 199/229=88% and 395/434=91% respectively. Overall the impact on patient management was observed in 194/434=45% of cases. The major impact was observed in 98/194=51%, minor impact in 95/194=49% patients. The most frequent impact on management was observed in group 9, 6 and 7. In a group of patients referred for systematic follow-up FDG PET/CT (group 4), the impact of FDG PET/CT on patient management was observed in 8/62=13% cases (Table 1). **Conclusion:** Our results show that FDG PET/CT plays a substantial role in the management of breast cancer patients, having considerable impact rate on the clinical management particularly in patients referred for localisation of recurrent disease in case of clinical, biochemical or imaging suspicion if recurrent disease.

EP063

PET/MRI in Staging of Breast Cancer: Correlation with Histological Findings

D. Franceschi, K. Airola, R. Matthews, R. Chimpiri, K. Yaddanapudi, N. Relan; Stony Brook University Hospital, Health Sciences Center, STONY BROOK, NY, UNITED STATES.

INTRODUCTION: F-18 FDG positron emission tomography (PET) combined with magnetic resonance imaging (MRI) is a new hybrid technology used in cancer imaging. We retrospectively evaluated its utility in the initial staging of patients with breast cancer and correlated with histological findings. **MATERIAL AND METHODS:** We identified 64 FDG PET/MRI studies performed in patients with breast cancer in period from January, 2014 to May, 2016. In 12 patients imaging was done for staging purposes, due to locally advanced cancer or postoperatively due to positive sentinel node surgery. Studies were reviewed by radiologist and nuclear medicine physician. **RESULTS:** In 10 patients histology was invasive ductal carcinoma and 2 patients had invasive lobular carcinoma. All 12 patients had hypermetabolic lymph nodes reflecting metastatic adenopathy. In 6 patients additional satellite hypermetabolic breast lesions and in 4 patients distant hypermetabolic lesions representing metastases are identified. Average SUV was 11.4 in ductal carcinoma ranging up to 31.8, and low SUV of 1.4 and 3.0 was found in patients with lobular carcinoma. One patient with lobular carcinoma had metastasis in the uterus without evidence of hypermetabolic activity. **CONCLUSIONS:** PET-MRI proved to be a feasible and effective modality in staging of patients with breast cancer capable of accurate primary lesion, metastatic adenopathy and distant metastasis identification.

EP064**Clinical efficacy of extensive and dual-time-point ¹⁸F-FDG PET/CT for breast cancer**

t. hamada¹, t. komori¹, y. tanaka¹, n. sato², y. narumi¹; ¹osaka medical hospital, takatsukishi, JAPAN, ²hokusetu general hospital, takatsukishi, JAPAN.

Purpose: Since there are significant false positives and false negatives in metabolic imaging with FDG, it has been attempted to improve diagnostic accuracy devising imaging acquisition. In case of breast cancer, although there are several reports on clinical efficacy of dual-time-point ¹⁸F-FDG PET/CT, only few extensive and dual-time-point are included in the studies. Our study is to verify the additional information acquired by delayed images (2 hour after) comparing with the early images (1 hour after FDG injection) in 77 case with 96 examinations. **Subjects & Methods:** 77 cases of breast cancer patient (age;36-84 years old) have undergone ¹⁸F-FDG PET/CT scan (GE Discovery-ST and 710Q.Suite Vision) with dual-time-point scan (early PET/CT (1 hour after FDG injection) [E] and delayed thoracoabdominal area (2 hour) [D]). The injection dose was 185-250Mq. The total number of examination was 96. This study performed from May 2007 through December 2015. We compared the diagnostic accuracy between early and delayed images. **Results:** Both E and D were positive in 36 cases, but one case of those was benign pulmonary granuloma. Diagnosis was changed in 13 cases at D. These were; three cases of increase in number of lymph node metastasis, three cases of increase in number of liver metastasis, two cases of increase in number of bone metastasis, and five cases of localized intestinal tract accumulation to physiological accumulation. This study showed that the sensitivity, specificity, and accuracy of E were 0.855(47/55), 0.854(35/41), and 0.854(82/96) respectively, whereas those of D were 1(55/55), 0.976(40/41), 0.99(95/96) respectively. D had better sensitivity, specificity, and accuracy than E (p=0.0047, p=0.0253, and p=0.0008 respectively). **Conclusion:** In breast cancer patient, dual-time-point ¹⁸F-FDG PET/CT improves diagnosis precision.

EP065**Accuracy of imprint cytology for intraoperative diagnosis of axillary sentinel node in Breast Cancer**

M. Luna, M. Solà, M. Fraile, J. Julian, E. Castellà, A. Mariscal, I. Pascual, J. Navines, A. Fernández, M. Framis; Hospital Germans Trias, Badalona, SPAIN.

Objective: The study aim was to establish Sensitivity, Specificity, Positive Predictive, Negative Predictive, and Accuracy Values of both imprint cytology (IC) and the OSNA assay for intraoperative assessment of axillary sentinel node (SN) involvement in breast cancer patients and if there were potential differences related to specific clinicopathological variables. We wished to find out if true positive and false negative results of imprint cytology in axillary lymphadenectomy (ALND) were associated to CK19 copy numbers. Also, we addressed a comparative cost analysis between techniques. **Methods:** 244 patients treated for breast cancer in the Breast Unit of Hospital Germans Trias i Pujol from March 2011 to May 2015 were prospectively included. A transversal, consecutive design was applied to assess the diagnostic test (IC) compared to the reference test (OSNA). Inclusion criteria were: T1 and T2 tumors with negative nodes, both clinical and on axillary US/FNA. Excluded were patients on neoadjuvant chemotherapy. **Results:** sensitivity of imprint cytology for macrometastases was 70% with an AUC 0,84. Considering all patients in whom ALND is not to be performed as true negative cases (negatives plus isolated tumour cells or micrometastases), the negative predictive value of IC was 95,75%. Accuracy of IC reached 96,12%. No significant differences in clinicopathological variables were detected between true positives and false negatives of IC. The false negative rate was acceptably

low (3.87%). The release time of results for OSNA doubled that of IC. In the comparative cost analysis, it was observed that OSNA was associated with an increased cost of € 370, which added to the extra surgical time required. **Conclusions:** IC makes a good technique for intraoperative sentinel node diagnostic as it has high sensitivity, high negative predictive value, and low false negative rate compared to the OSNA assay. It allows keeping the whole node tissue and thus the possibility of improved histopathological evaluation, which can be useful for adjuvant. Furthermore, IC offers the advantage of being less time consuming. Cost analysis shows a higher cost for OSNA, which may exceed the potential benefit of sorting out false negatives from IC.

EP066**The additional prognostic information of FDG PET/CT when added in pre-operative and post-operative setting of patients with high risk breast cancer**

L. Evangelista¹, V. Guarneri², T. Saibene³, S. Michieletto⁴, P. Conte²; ¹Nuclear Medicine and Molecular Imaging Unit, Veneto Institute of Oncology IOV - IRCCS, PADOVA, ITALY, ²Oncology Unit 2, Veneto Institute of Oncology IOV - IRCCS, PADOVA, ITALY, ³Brast Surgery Unit, Veneto Institute of Oncology IOV - IRCCS, PADOVA, ITALY, ⁴Breast Surgery Unit, Veneto Institute of Oncology IOV - IRCCS, PADOVA, ITALY.

Introduction. The aim of this study was to assess the prognostic information providing by ¹⁸F-FDG PET/CT in patients with high risk breast cancer, either before and after surgical approach. **Materials and methods.** Between 2011 and 2013, we prospectively enrolled 275 patients (age: mean±standard deviation=53±12 years) with a high risk breast cancer (stage I-III; triple negative and HER2 positive cancer). One-hundred forty-nine (54.2%) patients underwent ¹⁸F-FDG PET/CT before neoadjuvant therapy and 126 (45.8%) after surgery and before any additional adjuvant therapy. The patients were followed for a median period of 79 (2-157) months. The effects of PET/CT findings and prognosis was assessed by using Kaplan-Meier analysis, separately for each group of patients (pre-operative and post-operative setting, respectively) and by Cox-regression analysis for the identification of the predictors of poor prognosis. A statistical significance was set for a $p < 0.05$. **Results.** During the follow-up period, 4 patients were lost at follow-up. Forty patients had a recurrence of disease and 28 died (14.5% and 10.2%, respectively). A total of 46 events occurred. In pre-operative setting, the rates of recurrence and death were higher in patients with a positive PET/CT finding other than the site of primary cancer, although only the rate of recurrences were significantly different between patients with a positive than negative scan (27.4% vs. 0%; $p < 0.05$). Conversely, in the post-operative setting, any significant difference was found between positive and negative PET/CT results, neither for recurrence and death, (11.4% vs. 5.6% and 11.4% vs. 8.9%, respectively). After 120 months, in the pre-operative setting, at Kaplan-Meier analysis 95% of patients with a negative PET/CT other than the site of primary cancer were still alive, as compared to only 75% with a positive scan. Interestingly in the same length of time, 100% of patients with a negative scan were free of disease-recurrence. Unfortunately, any significant difference, in terms of survival curve was found in the post-operative setting. Similarly, at multivariate Cox-regression analysis, a positive PET/CT resulted a significant predictive factor of a poor prognosis (all events; HR: 0.117; $p = 0.036$), in patients in pre-operative setting. The significance was lost in the post-operative setting. **Conclusions.** In the pre-operative setting, PET/CT is able to provide additional prognostic information, being able to better stratify those patients who will develop a recurrence or die for breast cancer, from those who will be a long survivor. Conversely, PET/CT in post-operative setting did not add any prognostic value.

EP067**The new perspective of PET/CT for axillary node staging in breast cancer patients according to ACOSOG Z0011 trial**

E. Kong, K. Chun, I. Cho, S. Lee, S. Kang, J. Choi; Yeungnam University Hospital, Daegu, KOREA, REPUBLIC OF.

Purpose: According to the results of the ACOSOG Z0011 trial, the use of sentinel lymph node (SLN) dissection alone did not result in inferior survival compared with axillary lymph node dissection (ALND) in patients with limited SLN disease treated with breast-conserving surgery (BCS). We investigated the diagnostic performance of FDG PET/CT with respect to one or two ALN metastasis from three or more. **Methods:** We retrospectively analyzed preoperative contrast enhanced PET/CT images taken from Jan 2010 to June 2012. The patients had clinical T1-2 primary invasive ductal cancer without palpable adenopathy and was underwent BCS with ALND within 2 weeks from scan. We excluded the patients with neoadjuvant chemotherapy or distant metastasis at initial work up. We counted the number of suspicious LN, considering FDG avidity with morphologic change; Image analysis was as follows: FDG PET evaluation for any focally increased PET signal, then a morphologic evaluation was done. Images were considered positive if areas in the axillary basin took up more FDG than the surrounding tissues. The criteria for abnormal lymph nodes on CT included a round/ovoid, or cortical thickening with contrast enhancement. The sizes of the lymph nodes did not directly enter the final PET/CT finding criteria. **Results:** Fifty-three women (27-72 y-o) were enrolled and their mean tumor size was 2.09 (1.2-4.2 cm). All the patients had axillary metastasis: 1 or 2 (n=42; limited group), 3 or more (n=11; extended group). Four women had recurrence during follow up period. The mean tumor size was 2.19 in limited group and 2.07 in extended group. The mean SUVmax for tumor was 7.16 in limited group and 7.20 in extended group. PET/CT correctly predicted 41/42 in limited group and 7/11 in extended group. The diagnosis for extended group was 63.6% in sensitivity, 97.6 in specificity, 87.5 in PPV and 91 in NPV. Regarding 4 false negative patients, 5.89 in tumor SUVmax and 2.33 in tumor size. Regarding 4 recurred patients, 10.16 in tumor SUVmax and 2.1 in tumor size, the tumor SUVmax showed an evident trend (p=0.158) **Conclusion:** Preoperative PET/CT scan predict 3 or more positive ALN metastasis with high specificity and have evolving role to treat plan in patients with clinical T1-2 IDC and no palpable adenopathy.

EP068**Meta-analysis of 99mTc-Sestamibi Imaging for Neoadjuvant Chemotherapy Response in Locally Advanced Breast Cancer: More Consistent Results by Incorporating Standardized Quantification, SPECT/CT and Tumour Subtypes?**

A. Collarino¹, E. J. de Koster², R. A. Valdés Olmos^{1,3,4}, L. M. Pereira Arias-Bouda^{1,5}; ¹Nuclear Medicine Section, Department of Radiology, Leiden University Medical Center, Leiden, NETHERLANDS, ²Department of Radiology and Nuclear Medicine, Radboud University Medical Center, Nijmegen, NETHERLANDS, ³Interventional Molecular Imaging Laboratory, Department of Radiology, Leiden University Medical Center, Leiden, NETHERLANDS, ⁴Department of Nuclear Medicine, The Netherlands Cancer Institute –Antoni van Leeuwenhoek Hospital, Amsterdam, NETHERLANDS, ⁵Department of Nuclear Medicine, Alrijne Ziekenhuis, Leiderdorp, NETHERLANDS.

Aim: In recent years ¹⁸F-FDG has displaced ^{99m}Tc-Sestamibi as radio-tracer for breast cancer functional assessment. However, results of ¹⁸F-FDG PET/CT in early prediction of neoadjuvant chemotherapy (NAC) response in locally advanced breast cancer (LABC) remain contradictory and appear to be strongly influenced by breast tumour subtypes. The purpose of this meta-analysis was to determine whether and how ^{99m}Tc-

Sestamibi has been evaluated to predict NAC response in LABC. **Materials and Methods:** The literature search was updated up to February 15th, 2016. Studies with at least 10 women with LABC evaluating ^{99m}Tc-Sestamibi for NAC response with planar imaging, SPECT, and/or SPECT/CT taking histopathology and/or radiological imaging as reference standard were included. Meta-analysis was performed using Meta-DiSc, statistical software version 1.4. **Results:** Out of 162 references 17 studies concerning 588 women, were selected; 14 studies evaluated ^{99m}Tc-Sestamibi with conventional planar scintimammography and 3 with dedicated gamma cameras for breast imaging. No articles evaluating SPECT or SPECT/CT and tumour subtypes were found. Pooling of all studies was inappropriate because of heterogeneity in methodology and patient selection. Therefore, only the 14 studies with planar ^{99m}Tc-Sestamibi were analysed. Overall pooled sensitivity for correct prediction of tumour presence was 70% (95% CI 64-76%) and specificity for correct prediction of tumour absence was 77% (95% CI 70-83%). In relation to the timing of ^{99m}Tc-Sestamibi only two articles were found concerning in total 88 patients with sensitivities of 94-95% and specificities of 85-90% when assessment was effectuated early during NAC. **Conclusion:** Only conventional planar ^{99m}Tc-Sestamibi scintimammography has been used to predict tumour response in LABC with relatively low sensitivity and specificity. Preliminary results using ^{99m}Tc-Sestamibi early during NAC appear to be more sensitive but experience is limited. Other important factors, not or insufficiently evaluated, like SPECT/CT imaging, tumour subtypes and standardized ^{99m}Tc-Sestamibi quantification and timing need to be further investigated.

EP069**Cardiotoxicity Related To Trastuzumab In Breast Cancer: Influence Of Cardiovascular Risk Factors And Basal Cardiac Study With Multiple Gated Acquisition Ventriculography**

M. Garrido Pumar, Sr., M. Pombo Pasin, V. Pubul Núñez, S. Nieves Maldonado, B. Aradas Cabado, S. Argibay Vázquez, M. Fierro Alanis, A. Ruibal Morell; Clinic University Hospital of Santiago de Compostela, Santiago de Compostela, SPAIN.

OBJECTIVE: Cardiotoxicity is an important adverse effect in the treatment of breast cancer. Cardiotoxicity from the monoclonal antibody Trastuzumab, used in HER2-positive breast cancer differs from the cardiotoxicity caused by anthacyclines because the myocardial damage caused by trastuzumab is no dosage-dependent and it is reversible if detected in an early stage. Monitoring the cardiac function, usually by measuring the ejection fraction of the left-ventricle (LVEF) is extremely important to prevent the cardiotoxicity caused by trastuzumab. In this study we intend to analyze the influence of cardiovascular risk factors and the hemodynamic factors measured by a basal study with multiple gated acquisition ventriculography (MUGA), in patients that begins to receive trastuzumab for treatment of early breast cancer. **METHODS:** We studied 258 women with HER2-positive breast cancer that performed a basal MUGA and consecutive controls of LVEF during the therapy with trastuzumab. Cardiovascular risk factors included age, obesity, hypertension, diabetes, dyslipidemia, anemia and previous cardiopathy. Basal MUGA parameters include systolic data: LVEF, telesystolic and telediastolic volumes (TSV and TDV) and diastolic data: Peak filling rate (PFR) and time to peak filling rate (TPFR). We consider positive a study with a decline of LVEF <50% during the treatment with trastuzumab. **RESULTS:** 43 women had a <50% decline of LVEF during the trastuzumab administration. There were no significant relation with the presence of any cardiovascular risk factors and the decline of LVEF. The basal MUGA study however showed relation with lower values of basal LVEF (58 [55-62] vs 66 [62-71] p<0.001), VTS (45 [42-52] vs 34 [29-40] p<0.001), VTD (112 [97-139] vs 104 [91-118] p 0.019) and PFR (139 [112-168] vs 124 [111-152] p 0.31). In the group of 43 women with a significant decline of LVEF, 32 showed a recovery of LVEF after the modificatio/suspension of the therapy, and 4 developed clinical cardiac

insufficiency. **CONCLUSION:** Potential trastuzumab cardiotoxicity is a frequently observed during treatment and reversible in most cases if we made a good control of patients. The cardiovascular profile does not allow a stratification of the patients at risk. The basal study of cardiac function however showed that patients with lower basal systolic and diastolic function are more related to develop a significant decline of ejection fraction. The perform of a basal cardiac study if highly recommended in the treatment of breast cancer with trastuzumab.

EP070

Clinical-diagnostic implication of incidental mammary 18F-FDG uptake during PET/CT performed for other pathology

S. Panareo¹, I. Santi¹, I. Rambaldi¹, S. Taralli¹, P. Carcoforo², M. Rollo³, P. Querzoli⁴, C. Cittanti¹; ¹University Hospital - Nuclear Medicine Unit, FERRARA, ITALY, ²University Hospital - Radioguided Surgery Unit, University of FERRARA, ITALY, ³University Hospital - Senology Section, FERRARA, ITALY, ⁴University Hospital - Pathology Section, University of FERRARA, ITALY.

AIM: to investigate the clinical-diagnostic meaning of accidental breast uptake of 18F-FDG during PET/CT performed for other pathology, mainly cancer, correlating with radiological imaging and histopathology. **METHODS AND MATERIALS:** we retrospectively selected 43 patients (7 male, 36 female, mean age 66.28±14.7y/o) investigated for breast uptake of 18F-FDG, successively examined with mammography (MMX), UltraSound (US) and, if necessary, Magnetic Resonance (MR). Cases suspected for breast malignancy were studied with US-guided macro-biopsy (USMB). Patients were primitively affected by lung cancer (15), NHD (8), melanoma (4), head-neck cancer (2), other diseases (13) as well as ampullary cancer, Burkitt's lymphoma, CUP Syndrome, esophageal cancer, GIST, T lymphoma, occult tumour, sarcoma, thyroid cancer, tonsil cancer, rectal cancer, vasculitis. A correlation between PET/CT (SUV), radiology (imaging and BI-RADS classification), age, histopathology was done. PET/CT images were interpreted by one radiologist and one nuclear physician together. **RESULTS:** Of 43 patients analyzed, 19 performed US and MMX, 11 performed only US, 13 did not perform nothing because they did not carry on the follow-up. Of 11 patients who performed US, 6 did not perform USMB because unnecessary. Eight patients of 30 who carried out the study of the radiological findings on mammary gland did not show morphological abnormalities. Histopathology of 22 eligible patients showed: 9 infiltrating ductal carcinomas, 4 lymphomas (including 1 skin), 1 adenoidcystic cancer, 1 carcinomatous mastitis, 6 fibroadenomas and 1 phyllodes tumour. About 22 patients studied, we found 7 with SUVmax >2.5 and 15 with SUVmax <2.5 (average SUV=2.0233±2:38SD). There was not statistically significance (p=0.361) between SUVmax and histology. The incidence of malignancy was 68.2%. The incidence of benignity was 31.8%. We did not found a significant correlation (p< 0.106) between SUVmax and radiological imaging. We did not see a significant correlation (p<0.356) between patient age and tumour characterization. BI-RADS classification did not correlate with final histology. In 8 cases PET finding was not confirmed radiologically for the occurrence of artifacts from breast movement during PET or physiological distribution of 18F-FDG in the mammary gland related to menstrual cycle. **CONCLUSIONS:** The identification of an accidental mammary uptake during PET may represent an "alarm bell" inducing to deepen PET findings. It seems to have a clinical implication because the change of patient treatment. The diagnostic anticipation would have a favorable prognostic value and lead to a significant reduction in costs. Data must be confirmed in a more large casuistic.

EP071

Usefulness assessment of single photon emission tomography/computed tomography for localisation sentinel lymph node in breast cancer patients

A. Giżewska^{1,2}, A. Mazurek¹, Z. Stembrowicz-Nowakowska¹, M. Koza², M. Dziuk^{1,2}; ¹Military Institute of Medicine in Warsaw, Warsaw, POLAND, ²Affidea, Warsaw, POLAND.

Introduction Planar SLN scintigraphy yields functional data while hybrid SPECT/CT imaging provides information on both function and anatomy of the lymph node. **Aims** The aim of the study was to verify whether the routine performing of SPECT/CT in addition to planar imaging increases the SLN detection rate and yields more accurate SLN localization details in patients with early-stage breast cancer. The primary aim of the study was to compare diagnostic accuracy in SLN detection of SPECT/CT and planar imaging. **Materials and methods** There were 153 early-stage breast cancer patients referred to the Department of Nuclear Medicine of the Military Institute of Medicine in Warsaw for sentinel lymph node scintigraphy in years 2007-2013. Patients with T1-2N0M0 breast cancer were included - the primary tumor was ≤5 cm in diameter, the axillary lymph nodes were non-palpable and invisible in conventional imaging studies. Planar and SPECT/CT lymphoscintigraphy were performed on the day prior to the operation, 1.5-2 hours after periaxillary injection of 74-111 MBq (2-3 mCi) of 99mTc-Nanocol or 99mTc-Nano-albumin. Both planar and SPECT/CT examinations were performed using hybrid gammaceras. **Results** SPECT/CT identified SLN in 119/153 patients and planar scintigraphy in 114/153 patients which yielded an identification rate of 77,7% and 74,5% respectively. Lymph node assessment performed intraoperatively identified SLN in 76/126 patients with an identification rate of 60,3%. SPECT/CT identified SLN in more than one region in 17 patients. All the SLN with metastases were identified in SPECT/CT (n=22). They were localized in the axilla (95,5%) and by the sternum (4,5%). Metastatic SLN were also found in planar imaging (n=19) and during intraoperative lymph node detection procedure (n=18). Planar imaging yielded 170 uptake foci which were interpreted as SLN. Most of the foci were located in the axillary region (90%, n=153). Sensitivity and specificity of each assessed method was calculated basing on the results of histopathological examination. Sensitivity and specificity of SPECT/CT, planar imaging and intraoperative SLN detection were as follows: 91% and 93%, 62% and 55% and 46% and 61%. SPECT/CT sentinel lymph node detection yielded the highest positive and negative predictive values - they were 78% and 97% respectively. **Conclusions** 1. Hybrid SPECT/CT lymphatic mapping yields high SLN detection rate in patients with early-stage breast cancer and provides precise lymph node localization details. 2. SPECT/CT identifies more SLNs compared to planar imaging and intraoperative SLN detection. 3. SPECT/CT imaging is particularly recommended when the planar imaging is difficult to interpret or inconclusive.

EP072

Brown Fat In Breast Cancer Patients: Analysis Of Serial ¹⁸F-PET/CT Scans

A. GONZALEZ JIMENEZ, R. SANCHEZ SANCHEZ, A. C. REBOLLO AGUIRRE, N. TESTART DARDEL, E. M. TRIVIÑO IBAÑEZ, J. M. LLAMAS ELVIRA; Hospital Virgen de las Nieves, GRANADA, SPAIN.

AIM Brown adipose tissue (BAT) is present in at least a significant fraction of human adults; however its physiological importance requires further investigation. Recent studies suggest that BAT may play a key role in breast cancer progression. ¹⁸F-FDG Positron emission tomography/computed tomography (PET/CT) enables the study of metabolic active tissues on glucose substrates. The aim of this study is determine the prevalence of BAT in breast cancer

patients and to analyze whether a correlation exists between presence of BAT in ^{18}F -PET/CT and the different characteristics of this patient population. **MATERIAL AND METHODS** We retrospectively analyzed data from breast cancer patients who had ^{18}F -PET/CT scan between January-June of 2015. Data on distribution (bilateral upper neck, supraclavicular and paraspinal regions) of active BAT were evaluated by two nuclear physicians, blinded to the clinical history. ^{18}F -PET/CT scan were considered positive when diffuse, symmetrical, abnormal BAT uptake was detected. No SUVmax threshold value was set to define a positive BAT. Statistical analysis to determine whether correlation exists between ^{18}F -PET/CT results and the different characteristics of this population was done. **RESULTS** A total of 180 patients were included. The patient characteristic were: mean age (years)-56.95, Invasive ductal carcinoma-76.1%, Invasive lobular carcinoma-13.3% and other histology-10.5%, Grade of differentiation (G): GI-19.4%, GII-50.4%, GIII-30.2%, Molecular type: Luminal A-27.3%, Luminal B-54%, HER2-8.1% and Basal like-10.6%, Initial malignant tumor size (cm): <2 cm-35.7%, 2-5 cm-46.4%, >5 cm- 17.9%, 74.4% of patients had initial nodes metastases and 55.3% distant metastases. A total 180 of PET/CT images were analyzed. Nine scans (5%) showed abnormal BAT uptake. Abnormal BAT uptake was present on uncorrected and attenuation-corrected images. Statistical analysis showed that correlation exist between positive BAT in PET/CT and younger age (<40 years) ($p=0.002$) and the absence of initial distant metastases ($p=0.042$). **CONCLUSION** Our retrospective clinical data provide support to pursue prospective clinical and translational studies to further define the role of BAT in breast cancer development and progression.

EP073

Comparison of subareolar Injection lymphoscintigraphy with the 1 day and the 2 day protocol for the detection of sentinel lymph nodes in patients with breast cancer

J. Seok, E. Lee; Chung-Ang University Hospital, Seoul, KOREA, REPUBLIC OF.

Objectives: Lymphoscintigraphy and sentinel node biopsy were used for the detection of axillary lymph node metastasis in breast cancer patients. We compared the results of subareolar injections on the day of surgery (1 day protocol) with injections the day before surgery (2 day protocol). **Methods:** This study included 880 breast cancer patients who underwent surgery between 2001 and 2016. For the 1 day protocol 0.8 ml of Tc-99m Tin-Colloid (37MBq) was injected in 549 patients in the subareolar region on the morning of the surgery. For the 2 day protocol 0.8 ml of Tc-99m Tin-Colloid (185MBq) was injected in 331 patients on the afternoon before surgery. Lymphoscintigraphy was performed in the supine position and sentinel node identification was performed by hand-held gamma probe during surgery. **Results:** Among 549 patients with the 1 day protocol, 519 cases (94.5%) were identified by sentinel node lymphoscintigraphy, and 522 cases (95.1%) were identified by gamma probe. Among the 331 patients, in the 2 day protocol, 308 cases (93.1%) had the sentinel node identified by lymphoscintigraphy, and 298 cases (90.0 %) had the sentinel node identified by the gamma probe. There was no significant difference in the identification rate of the sentinel node between the 1 day and 2 day protocol by lymphoscintigraphy and the gamma probe. **Conclusions:** The results of the identification of the sentinel node according to 1 day or 2 day protocols showed no significant differences. Because the 2 day protocol allows for an adequate amount of time to perform the lymphoscintigraphy, it is a more useful protocol for the identification of sentinel nodes in patients with breast cancer

EP074

Value of FDG PET/CT in stage IV breast cancer

J. Duch, L. Del Carpio, T. Ramón y Cajal, A. Flotats, M. Estorch, D. López, A. Moral, I. Carrió; Hospital de la Santa Creu i Sant Pau, Barcelona, Barcelona, SPAIN.

Aim: The prognosis in patients with stage IV breast cancer is heterogeneous, including patients with only distant node metastasis diagnosed by FDG PET/CT. We aimed to compare the prognosis of these patients compared to the rest of stage IV breast cancer patients. **Methods:** Between January 2012 and June 2015 we retrospectively studied patients with locally advanced breast cancer (LABC) with FDG PET/CT. For prognosis stratification, in stage IV breast cancer we differentiated patients with only bone metastasis, with visceral metastasis and with only distant node metastasis. We compared progression free survival (PFS) and overall survival (OS) in these groups of patients. **Results:** We recruited 188 patients with LABC being 43 of these in stage IV (mean age 68). Baseline performance status (PS) was 0-1 in 81% and presurgical PS was 0-1 in 93%. 16 patients were T1, T2 or T3. In 9 patients (21%) FDG PET/CT only found distant node metastasis, in 16 patients (37%) only bone metastasis and in 18 patients (42%) visceral metastasis. No significant differences were found in progression free survival (PFS) and overall survival (OS) between group of only distant node metastasis (PFS 18 months; OS 35 months), only bone metastasis (PFS 28 months; OS 32 months) and visceral metastasis (PFS 24 months; OS 35 months). **Conclusions:** FDG PET/CT is useful in staging locally advanced breast cancer. If stage IV is found, the presence of only distant node metastasis (hardly diagnosed with procedures other than PET/CT) has the same prognostic value as the rest of stage IV.

EP075

$^{99\text{m}}\text{Tc}$ MIBI SPECT as a Tool for Effectiveness of Neoadjuvant Chemotherapy Evaluation

A. Medvedeva^{1,2}, V. Chernov^{1,2}, I. Sinilkin^{1,2}, R. Zelchan^{1,2}, Y. Belevich¹, S. Chizhevskaya¹, E. Slonimskaya¹, O. Bragina^{1,2}, E. Choyznov^{1,2}; ¹Tomsk Cancer Research Institute, Tomsk, RUSSIAN FEDERATION, ²Tomsk Polytechnic University, Tomsk, RUSSIAN FEDERATION.

Purpose: assessment of the role of SPECT with $^{99\text{m}}\text{Tc}$ -MIBI of neoadjuvant chemotherapy response prediction in patients with cancer. **Materials and methods:** The study included 27 breast cancer patients and 20 patients with cancer of the larynx and laryngopharynx. SPECT studies were carried out 20 minutes after the injection of 740 MBq of $^{99\text{m}}\text{Tc}$ -MIBI using ECAM-180 gamma-camera (Siemens), studies was conducted before treatment and after two courses of neoadjuvant chemotherapy. The images were quantitatively assessed using the tumor/background index (T/B index) for patients with breast cancer and indices tumor / submandibular salivary gland (T/SSG index) and tumor / parotid gland (T/PG index) for patients with cancer of the larynx and laryngopharynx. Indices were compared with clinical effect which was assessed by RECIST scale. **Results:** Partial response was registered in 20 (74%) patients with breast cancer and stable disease was observed in 7 (26%) patients by RECIST scale. After neoadjuvant chemotherapy T/B index decreased from 3.5 ± 1.7 to 1.6 ± 0.7 . Decreasing of T/B index more than 30% was observed in 24 (89%) breast cancer patients and no considerable change in 3 patients (11%). Partial response was registered in 12 (60%) patients with cancer of the larynx and laryngopharynx and stable disease was observed in 8 (40%) patients by RECIST scale. After neoadjuvant chemotherapy T/SSG index decreased from 0.49 ± 0.15 to 0.34 ± 0.12 and T/PG index from 0.51 ± 0.12 to 0.39 ± 0.1 . Decreasing of indexes more than 30% was observed in 15 (75%) patients with cancer of the larynx and laryngopharynx and no considerable change in 5 patients (25%). **Conclusion:** Thus, the present study demonstrated that SPECT with $^{99\text{m}}\text{Tc}$ -MIBI may be regarded as a method of assessing the state of malignant neoplasm of breast cancer, larynx and laryngopharynx during neoadjuvant chemotherapy. The T/B index is the most beneficial in response of breast cancer neoadjuvant chemotherapy evaluation and T/SSG and T/PG indices are useful in response of larynx and laryngopharynx cancer neoadjuvant chemotherapy estimation.

EP076**Comparison of the efficiency for Tc-99m Tin-colloid and Tc-99m Phytate in sentinel node detection in breast cancer patients**

J. Seok, E. Lee; Chung-Ang University Hospital, Seoul, KOREA, REPUBLIC OF.

Objectives: Lymphoscintigraphy and sentinel node biopsy has become a standard method for detection of axillary lymph node metastasis in breast cancer patients, but the standard radiopharmaceutical was not prepared. About detection of axillary lymph node metastasis by lymphoscintigraphy and sentinel node biopsy in breast cancer patient, we compared the results of Tc-99m Tin-colloid and Tc-99m Phytate by subareolar injection. **Methods:** This study included 880 breast cancer patients who were performed operation during 2001-2016. Four hundred twelve patients were injected 0.8 ml of Tc-99m Tin-colloid (37-185 MBq) by subareolar injection. Four hundred sixty eight patients were injected 0.8 ml of Tc-99m Phytate (37-185 MBq). Lymphoscintigraphy was performed in supine position and sentinel node localization was performed by hand-held gamma probe in operation. **Results:** Among 412 patients by Tc-99m Tin-colloid, 374 cases (90.8%) were localized the sentinel node by lymphoscintigraphy and 367 cases (89.1%) were localized by gamma probe. Among 468 patients by Tc-99m Phytate, 453 cases (96.8%) were localized by lymphoscintigraphy and 453 cases (96.8%) were localized by gamma probe. The detection rate by lymphoscintigraphy and gamma probe was superior for Tc-99m Phytate compared to that for Tc-99m Tin-colloid, with a statistically significant difference. ($p < 0.05$, $p < 0.05$) **Conclusions:** Tc-99m Phytate is a better choice for localization of sentinel node than Tc-99m Tin-colloid in breast cancer patients

EP-04 – Sunday, October 16, 2016, during Exhibition hours, e-Poster Area
Clinical Oncology: Colorectal Cancer

EP077**The value of ^{18}F -FDG PET/CT and CEA among patients with colorectal carcinoma in detecting disease recurrence**

A. Barrenechea, I. Bandong, F. Estrada; St. Luke's Medical Center-Quezon City, Quezon City, PHILIPPINES.

Surveillance for colorectal carcinoma recurrence in patients who have undergone surgery and adjuvant treatment with chemotherapy or radiotherapy is usually initiated with elevated serum carcinoembryonic antigen (CEA) levels. Previous studies have shown, however, that elevated CEA is less sensitive in detecting recurrence as recurrence is also seen in patients with normal CEA levels. We evaluated the utility of FDG-PET/CT in patients with suspected recurrence of CRC by comparing PET/CT performance to CEA levels. **METHODS:** An ambispective cross-sectional design was done on 183 adult patients diagnosed with colorectal adenocarcinoma and who had previous surgical resection, with or without chemotherapy or radiotherapy, and who underwent PET/CT using ^{18}F -FDG from July 2013 to September 2015 at a PET center of a local tertiary hospital. Eighteen patients (10 males, 8 females, with ages ranging from from 28 to 87 years and a mean age of 63.72 years) were included as these patients were the only ones who had histopathologic confirmation or clinical follow-up proving disease recurrence. **RESULTS:** The FDG-PET/CT study yielded a true positive in detecting recurrence in 11 (61%) out of the 18 patients, a true negative in 5(28%) patients, a false negative in 0 (0%) patients and a false positive in 2(11%) patients. The sensitivity, specificity, and positive predictive value (PPV) of the FDG-PET/CT study for establishing recurrence were 100, 71 and 85%, respectively. In contrast, these parameters were 82, 29 and 64%, respectively, for CEA levels. No significant association was noted between CEA levels and PET/CT scan as well as SUV_{max} . **CONCLUSIONS:** FDG PET/CT is a highly sensitive and specific tool for detecting recurrence in patients with colorectal carcinoma when compared to CEA and is able to provide a more accurate diagnosis even in patients that show a negative CEA on surveillance.

EP078**Prognostic value of initial and post-chemoradiotherapy FDG-PET in patients with anal carcinoma**

A. TESTARD¹, C. Guillerminet¹, L. Campion², M. Lacombe¹, S. Girault¹, O. Morel¹; ¹ICO Paul Papin, Angers, FRANCE, ²ICO Gauducheau, Nantes, FRANCE.

AIM : The objective of this study was to evaluate the prognostic value of FDG-PET-CT before and after definitive chemo-radiotherapy in patients with anal canal cancer. **MATERIALS AND METHODS :** This retrospective study included 31 patients treated for anal canal cancer with curative radiotherapy (+/- chemotherapy). Constitutive parameters (sex, age), T and N stage (TNM stage) evaluated on staging conventional imaging (CT, echography, +/-MRI) and N evaluated on initial PET-CT were recorded. Primary tumor SUV max, MTV (metabolic tumor glycolysis), TLG (total lesion glycolysis) were measured on the 31 pre-treatment PET and on the 25 post-treatment PET, and their percentage change were calculated. A visual metabolic response assessment was also performed. We correlated these different parameters (clinical and quantitative) with the event free survival (EFS). An event was a residual disease, a local recurrence or distant metastasis. **RESULTS :** Pre-treatment PET : univariate analysis showed that the male sex ($p=0.011$), lymph node involvement on PET ($p=0.006$) and TLG (using a 41% and a 35% SUV max threshold) had a worse impact on EFS. On multivariate analysis, only nodal status on PET was statistically significant, the 2-year EFS was 100% for patients without lymph node involvement and 56% for patients with lymph node involvement ($p=0.0147$). Post-treatment PET : univariate analysis showed that male sex ($p=0.011$), SUV max ≥ 5 ($p=0.04$), response index $\leq 67\%$ ($p=0.04$), MTV $\geq 3,5\text{cc}$ ($p=0.016$), TLG ≥ 10 ($p=0.037$) and δTLG (difference between pre-treatment TLG and post-treatment TLG) had worse impact on EFS. On multivariate analysis, only SUVmax was significantly correlated with EFS, the 2 year EFS was 89% for patients with SUV max < 5 on post-treatment PET and 22% for patients with SUV max ≥ 5 ($p=0.0006$). **CONCLUSION :** At initial staging, the nodal status evaluated by PET was the only independent predictor factor of EFS. After treatment, only SUV max (with cutoff at 5) calculated on PET was correlated with EFS on multivariate analysis. At our knowledge, it's the first study which presented that metabolic parameters calculated on post radiotherapy PET, were predictive of patient outcome.

EP079**The role of FDG PET-CT in the detection of local recurrence of rectal cancers**

Z. Kandemir, 06608, E. Özdemir, S. Yılmaz Aksoy, M. Keskin, N. Yıldırım, & Kılıncı Vicdan, S. Türkölmöz; Ankara Atatürk Training and Research Hospital, Ankara, TURKEY.

Aim: Fluorine-18 fluorodeoxyglucose positron emission tomography /computed tomography (^{18}F FDG PET/CT) is an important and useful imaging method in the evaluation of colorectal cancers (CRC). It can be used for detecting recurrence during follow-up after primary treatment and restaging. In this study, we aimed to evaluate the role of PET/CT in patients with presacral soft tissue density to detect local recurrence. **Materials and methods:** A total of 80 patients with diagnosis of rectum tm (52 male, 28 female, mean age: 59,1 [28-95]) who had soft tissue density during follow-up and referred for PET/CT between July 2010 and September 2015 were included in this study. PET/CT examinations were retrospectively analyzed. Final diagnosis was made by histopathologic analysis, serial CEA measurement or clinical-radiological work-up. **Results:** PET/CT detected recurrence in 49 of 80 (61,25%) patients. CEA levels were available in all patients. Sixty-seven patients also underwent CT imaging and 13 patients underwent MR imaging. PET/CT was performed 2 times in 6 patients and 3 times in the other 6 patients. Seven patients had histopathological

correlation. The sensitivity, specificity, negative predictive value (NPV) and positive predictive value of FDG PET/CT in differentiating a *fibrotic presacral* mass from *recurrent* disease were 92.8%, 71%, 64.2%, 78% and 82.5%, respectively. **Conclusion:** FDG PET/CT which give both metabolic and anatomic information, can effectively differentiate between fibrotic masses and soft tissue recurrences in patients with rectum tm. Hence, it helps early diagnosis of the disease allowing proper management.

EP080

Evaluation of FDG PET/MR in the restaging of colorectal cancer

S. Djelbani¹, C. Comtat¹, T. Aparicio², P. Wind³, B. Helal¹, I. Buvat¹, M. Soussan¹; ¹IMIV, CEA-Inserm, Univ Paris Sud, CNRS, Université Paris Saclay, Orsay, France, Orsay, FRANCE, ²APHP, Avicenne Hospital, department of gastroenterology, Bobigny, FRANCE, ³APHP, Avicenne Hospital, department of digestive surgery, Bobigny, FRANCE.

Objectives: FDG-PET/MR might be a powerful tool for restaging colorectal cancer (CRC), because it combines the excellent accuracy of liver MR for liver metastasis and the sensitivity of PET for extra-hepatic lesions. The aim of this study was to compare the detection rate and diagnostic confidence of PET/MR imaging with PET and liver MR alone for the restaging of CRC. **METHODS:** Eighteen patients with CRC underwent FDG-PET/MR (Signa, GE Healthcare) for restaging. FDG-PET/MR parameters were: head to mid-tight scan, 4MBq/kg, 3-6 min/bed position, time-of-flight OSEM reconstruction with 2 iterations/28 subsets, 5 mm post-reconstruction filter. MR sequences consisted in a Dixon sequence for attenuation correction, a thin section axial T2-weighted sequence from head to mid-tight, and diffusion-weighted (DWI) and post-contrast multiphase T1W sequences for liver imaging. Three image sets were analyzed: PET (read with only low resolution Dixon sequence for anatomical localization purpose), liver MR and PET/MR. A radiologist and a nuclear medicine physician independently assessed liver MR and PET, respectively. Double reading was performed for PET/MR. Metastatic lesion was defined on PET as a pathological increase of FDG uptake. On liver MR, lesions were rated as metastases when at least two of the three sequences (T2W, DWI, post-contrast T1W) were compatible with the diagnosis. Detection rate, lesion conspicuity (0=not visible, 1=barely visible, 2=clearly visible) and diagnostic confidence (1=uncertain, 2=rather certain, 3=very certain) were compared between the three sets of images. **RESULTS:** Detection rate of liver metastasis was the highest with PET/MR (n=34) compared to PET (n=28) and MR (n=32). For liver metastasis, lesion conspicuity increased in PET/MR (rate of grade 2: 97%, 33/34) and MR (88%, 30/34), compared to PET (74%, 25/34); diagnostic confidence increased in PET/MR (rate of grade 3: 94%, 32/34) and MR (97%, 31/32) compared to PET (82%, 23/28). PET detected 39 extra hepatic lesions: 20 lung nodules, 16 lymph nodes, 2 carcinomatosis nodules and 1 bone metastasis. Enhanced FDG uptake was present in measurable targets seen in T2W in 85% of extra hepatic lesions (33/39). In particular, T2W imaging identified 90% (18/20) of hypermetabolic lung nodules. **CONCLUSIONS:** PET/MR with full liver imaging is feasible in CRC restaging in less than 45 minutes. Although its precise role in the patient management still needs to be established, our preliminary results suggest that it might be a valuable option for a one-stop comprehensive patient assessment.

EP081

Association between FDG-PET/CT Findings and Tumor Markers in Patients with Colorectal Carcinoma

A. Hassanzadeh-Rad, M. Eftekhari, A. Kafshgar, A. Fard-Esfahani, B. Fallahi, A. Emami-Ardekani, D. Beiki, M. Saghari; Research Center for Nuclear Medicine, Tehran University of Medical Sciences, Tehran, IRAN, ISLAMIC REPUBLIC OF.

Aim: Patients with Colorectal Carcinoma (CRC) are followed up by serum tumor markers (i.e Carcinoembryonic Antigen (CEA) and CA19-9). FDG-PET/CT scans are often asked by the referring physician for staging, restaging or evaluation of response to treatment. We aim to correlate serum tumor markers levels with FDG-PET/CT findings to better delineate pathophysiology of CRC and relationship between tumor markers and metabolic activities of tumoral lesions. **Patients and Methods:** Patients with pathologically documented CRC who are referred to our center for FDG-PET/CT study and have results of recent CEA and CA19-9 tests (performed within 3 months of scan), are enrolled in the study. After injection of 6-12 mCi of FDG, fasting patients are asked to wait for 1 hour till PET/CT acquisition. PET/CT is performed using Siemens Biograph T6 @ device. CT electrical current and voltage are set for 30 mA and 120 kV respectively. Processing of tomographic data are done by iterative reconstruction method. Manufacturer's software is used for visualization of PET-CT images. Quantification part of the software is applied for drawing Regions Of Interest (ROIs) and calculating maximum Standardized Uptake Values (SUVmax) of lesions. All patients have been followed up for at least 6 months after the study. **Results:** Preliminary data consist of 40 patients with CRC (25 male and 15 female, Age= 58.32± 12.27 years). PET/CT results were negative in 6 (15 %) and positive in 34 (85 %) of the patients. Follow ups reveal True Positive and True Negative results to be 97.1 % and 83.3 % respectively. In patients with true positive results, there was a statistically significant positive correlation between CEA serum levels and maximum SUVmax of all tumoral lesions (r= 0.52, p-value=0.003). No significant correlation was found between CA19-9 levels and SUVmax of the lesions. There were no significant correlations between tumor markers and number or anatomical locations of metabolically active lesions either. **Conclusion:** Statistically significant positive correlation between CEA and maximum SUVmax of tumoral lesions in patients with CRC can better delineate association between tumor markers and metabolic activity of tumoral cells. By increasing number of patients in this study, a linear or non-linear relationship between SUVmax of tumoral lesions and CEA levels maybe proposed which can be used as an aid to visual interpretation of FDG-PET/CT scans in patients with CRC.

EP082

Demonstration of the effectiveness of neoadjuvant chemotherapy and radiotherapy by ¹⁸F-FDG PET-CT and MRI in patients with colorectal cancer

S. S. Gül¹, S. Rahatlı², G. Güler³, F. Sönmezgöz⁴, Z. Hasbek⁵; ¹Gaziosman Pasa University School of Medicine, Department of Nuclear Medicine, TOKAT, TURKEY, ²Gaziosman Pasa University School of Medicine, Department of Internal Medicine, TOKAT, TURKEY, ³Gaziosman Pasa University School of Medicine, Department of Radiation Oncology, TOKAT, TURKEY, ⁴Gaziosman Pasa University School of Medicine, Department of Radiology, TOKAT, TURKEY, ⁵Cumhuriyet University School of Medicine, Department of Nuclear Medicine, Sivas, TURKEY.

AIM: Colorectal cancer is one of the most common tumors of the gastrointestinal tract. It is more common in males with a peak age at the 5th decade. The primary treatment for colorectal cancer is surgery. The adjuvant therapy selected according to the stage and location of the disease affects the prognosis. Postoperatively administered radiotherapy and chemotherapy is effective on local and systemic recurrences, respectively. In our study, the effectiveness of preoperative chemotherapy and radiotherapy in patients with colorectal cancer was evaluated by using ¹⁸F-FDG PET-CT and MRI. **METHODS:** Twelve patients with a diagnosis of colorectal adenocarcinoma were included in the study (5females/7males; mean-age:68.1±11.8years). Patients were treated with concomitant chemotherapy and radiotherapy before the surgery. Preoperative and postoperative ¹⁸F-FDG PET-CT and MRI images were obtained. PET-CT

images were used to determine the tumor size, area and volume with the SUVmax and were compared to the tumor size, area and volume on MRI. **RESULTS:** All patients had the diagnosis of adenocarcinoma. Chemotherapy regimen of capecitabine 825 mg/m² two times daily for 5 days/week was given to 8 patients and 5-Fluorouracil 225 mg/m² with an infusion pump for 7 days was given to the remaining 4 patients. Simultaneous radiotherapy included a total of 45 Gy with a fractionated dose of 1.8 Gy/day to the areas with standard risk and a total of 50 Gy with a fractionated dose of 2 Gy/day to the high-risk areas. Preoperative and postoperative ¹⁸F-FDG PET-CT and MRI images were obtained (Figure1). Both imaging methods revealed a significant decrease in the tumor size, volume and area after the treatment (Table1). In addition, PET-CT images showed a significant decrease in SUVmax. **CONCLUSION:** Effect of perioperative chemotherapy and radiotherapy on survival rate is an important research area in terms of adjuvant therapy with no available clear conclusions. Results of the present study suggest that chemotherapy and radiotherapy given before the surgery is an effective treatment method resulting in a significant decrease in tumor size which was shown in both PET-CT and MR images. In conclusion, ¹⁸F-FDG PET-CT is considered to be a good alternative for conventional MRI. **Table 1.** Comparison of the decrease in tumor size after the neoadjuvant chemotherapy and radiotherapy by using MRI and PET-CT in patients with colorectal cancer. **Figure 1.** The decrease in tumor size (white arrow) on transaxial and sagittal ¹⁸F-FDG -PET-CT images obtained before and after the surgery in patients with colorectal cancer.

EP083

Features of 18 FDG PET application for recurrence detection and staging during radiation therapy planning and its effectiveness monitoring in patients with tumors of the anorectal localisation

O. Solodyannikova¹, A. Ashumkhin², Y. Kmetiuk²; ¹Institute of Oncology AMS of Ukraine, KIEV, UKRAINE, ²Ukrainian Radiosurgery Center of Clinical Hospital “Feofanyia”, KIEV, UKRAINE.

Background. Experience of 18f-FDG PET/CT clinical application confirms the usefulness of this imaging in oncology, namely: for the differential diagnosis, staging before surgery or radiation therapy, restaging after treatment. Also 18-FDG PET/CT showed high sensitivity for the efficacy monitoring of chemotherapy and radiotherapy. The numerous studies on the use of 18-of FDG PET/CT images for further dynamic control and radiotherapy planning proved higher results' accuracy of systemic and loco-regional staging compared with conventional CT and MRI techniques. It was found that the macroscopic tumor volume determined by PET/CT is statistically significantly larger in the CT MPO with mean difference of 25%. **Materials and methods.** Between 11/2011 and 01/2016 the 18 FDG PET/CT was performed in 277 patients with colorectal cancer. Of them men were 154, women - 123; patients age was from 24 to 82 years. In overall 388 examinations were performed in 277 patients, including 94 without contrast and 294 with contrast. Average activity per injection was 373.98 MBq; in men - 402.75 MBq, in women - 332.62 MBq. We used Cyclotron Siemens Eclipse RDS for obtaining radiopharmaceuticals 18-FDG; and PET/CT Scanner Siemens Biograph 64. **Results.** Functional 18-FDG PET/CT images were used during planning of radiotherapy for rectum and anal canal carcinomas. It is found that the PET/CT by sensitivity and specificity is more informative compared with conventional structural imaging techniques. Mean sensitivity and specificity of 18-FDG PET/CT for the main focus were 83% and 91%, respectively, while the corresponding indices for the basic CT method were respectively 64% and 74%. The sensitivity of lymph node involvement evaluation using CT method was 65% and PET/CT - 53%. It should also be taken into account the risks of false-negative results of PET/CT for lesions in the lungs less than 1.0 cm, small lesions in the upper sections of

liver, located predominantly subcapsularly, and in histological tumor type - mucinous adenocarcinoma. It was found that applying PET/CT for staging caused changes of the treatment tactics in 55.4% of patients, of them in 15 - due to higher disease stage, and in 5 - scheduled surgery was not performed. **Conclusions.** The 18 FDG PET/CT possesses significant advantages concerning the disease recurrence detection and restaging in the cases when CT and MRI data are inconclusive. It was proved that by sensitivity and specificity the PET/CT method is more informative for planning radiotherapy compared with conventional structural imaging techniques.

EP084

Prevalence of malignant and premalignant lesions on incidental focal colorectal uptake with dual time point (18)F-FDG-PET/CT images

A. G. GÓMEZ-GRANDE, P. Pilkington Woll, A. Hernandez Martinez, P. Sarandeses Fernandez, S. Ruiz Solis, J. Marroquin, M. Tabuena, A. Saviatto, J. Estenez Alfaro; HOSPITAL UNIVERSITARIO 12 DE OCTUBRE, MADRID, SPAIN, MADRID, SPAIN.

Aim: Analyze the prevalence of malignancy or pre-malignancy of incidental colorectal focal uptakes detected by 18F-FDG-PET/CT, using additional delayed images. **Materials and methods:** Retrospective analysis of 3264 PET/CT studies carried out consecutively in the Nuclear Medicine Department of our hospital from January 2015 to March 2016. The inclusion criteria were patients with incidental focal colorectal uptake. Patients suspected of colorectal carcinoma were excluded. Finally, a total of 61 patients were included in the analysis. Colonoscopy was recommended based on the persistence of the focal colorectal uptake in the delayed images, which were acquired approximately two hours post-injection. Colonoscopy with biopsy was established as a gold standard. The SUVmax value and histopathological results in these patients were evaluated. **Results:** In 44 of the 61 patients colonoscopy and biopsy was performed, confirming malignant or non-malignant pathology in 42 of these (95%). Eleven of these 42 patients (26%) were diagnosed of a primary unsuspected colorectal carcinoma (10 adenocarcinomas y 1 GIST), while 25 patients (60%) had premalignant lesions with different degree of dysplasia (11 tubular Adenoma, 12 tubulovillous adenoma, 1 serrated adenoma, 1 adenomatous polyp and 1 juvenile (retention) polyps). The remaining 6 patients (14%) had inflammatory findings (2 diverticulitis, 1 cytomegalovirus (CMV)-associated colitis, 1 lymphoid hyperplasia, 1 ulcerative colitis and 1 hemorrhoid). In all these cases focal uptake persisted on delayed images and SUVmax increased in most of them. Nevertheless, the SUVmax increase was not statistically different between malignant, pre-malignant and inflammatory/infectious lesions (p<0.05). The remaining 2 cases had a negative colonoscopy. SUVmax was ≤ 5 and decreased in the delayed images. The SUVmax average value was 17,10 for malignant lesion (carcinomas and high-grade dysplasia), 11,78 for premalignant lesion and 7,53 for inflammatory and infectious lesions. During the time of this analysis, the prevalence in the FDG-PET/TC image of malignant lesion, including adenoma with high grade dysplasia, was 36%. **Conclusion:** Presence of incidental focal colorectal uptake on a PET/CT justifies a colonoscopy to detect malignant and premalignant lesions. The dual time point images could help to confirm and better characterize these incidental findings. This protocol let early detection and treatment of malignant and premalignant lesions.

EP-05 – Sunday, October 16, 2016, during Exhibition hours, e-Poster Area
Clinical Oncology: External Beam Radiation Therapy Planning

EP085**Fluorodeoxyglucose-PET/CT in locally advanced head and neck cancer can influence the stage migration and nodal radiation treatment volumes**

R. Mazzola¹, P. Alongi², F. Richetti¹, A. Fiorentino¹, S. Fersino¹, N. Gaj-Levra¹, U. Tebano³, M. Salgarello⁴; ¹Division of Radiation Oncology, Sacro Cuore Don Calabria Cancer Care Center, Negrar (Verona), ITALY, ²Unit of Nuclear Medicine, San Raffaele G.Giglio Institute, Cefalù, ITALY, ³School of Radiation Oncology, University of Padova, Padova, ITALY, ⁴Division of Nuclear Medicine, Sacro Cuore Don Calabria Cancer Care Center, Negrar (Verona), ITALY.

Aim: Although [18F] fluorodeoxyglucose (FDG) positron emission tomography (PET/CT) is effective for the staging of locally advanced head and neck cancer (HNC), its role on patient management remains controversial. Present study analyzed the impact of PET/CT in the radiotherapy (RT) planning-strategy in HNC, focusing on neck-nodes treatment planning and correlating CT-scan and PET/CT performances. **Materials and Methods:** Inclusion criteria of this retrospective analysis were: age > 18 years old, histologically proven squamocellular HNC, patients candidate to curative RT ± chemotherapy, evaluation of stage of disease by means of PET/TC and CT-scan performed at our Institution. PET/CT scans were visually reviewed by experienced readers blinded to clinical data. Visual assessment was used to define the presence of primary lesion, local lymph node and distant recurrences. All cases in which a stage migration was recorded, in terms of differences in nodal involvement between CT and PET/CT, were discussed with the Nuclear Medicine Physician and Radiologist. Only in case of discrepancies of imaging interpretation between them it was discussed with the patient the utility of a fine needle aspiration cytology (FNAC). **Results:** sixty patients treated between October 2011 and February 2016 were included in the analysis. Primary tumor site was represented as follows: Nasopharynx in 8 patients (13%), Oropharynx in 25 (42%), Oral Cavity in 19 (32%) and Larynx non-glottic in 8 (13%). Oral cavity tumors revealed to be at particular risk of nodal stage migration, occurring in 21% of cases (5/19). PET/CT findings caused changes in the management of RT volumes in 10% of patients. In one case of nasopharynx cancer, it was detected the primary tumor previously unknown at CT-scan, in 5 cases of oral cavity tumors neck-nodes PET/CT positive from one side and/or the other (not detected at CT-scan) were included in the high-risk volumes and in 2 cases of oropharyngeal cancer RT was avoided because of distant metastases detection. **Conclusion:** Present findings showed that PET/CT images could be a guide in HNC in order to individualize the RT-curative strategy. Further investigations are advocated to evaluate if this strategy could impact on long-term outcomes in HNC.

EP086**Application of an Adaptive Thresholding Algorithm for ¹⁸F-FDG PET Head and Neck Lesion Segmentation**

L. L. Vigna, M. Paolini, E. Puta, L. Deantonio, R. Matheoud, G. Loi, M. Krengli, M. Brambilla, G. Sacchetti; A.O.U. Maggiore della Carità, Novara, ITALY.

AIM: ¹⁸F-FDG PET is used in radiation oncology for the delineation of gross target volumes (GTV) in the treatment planning. The aim of this work was to implement on the treatment planning system and to use in a clinical context an adaptive thresholding algorithm (ATA), previously derived and validated on a phantom. **MATERIAL AND METHODS:** forty-one patients (12F,29M) that underwent radical intensity modulated radiation therapy with simultaneous integrated boost (IMRT-SIB) for head-and-neck squamous cell carcinoma (3 oral cavity, 11 nasopharynx, 20 oropharynx, 6 hypopharynx and 1 larynx lesions), were included in the present analysis. 33/41 pts received concurrent radio-chemotherapy and 37/41 were in a locally advanced stage. Median age was 64 years (range 38-76 yrs). For all the patients FDG-PET/CT was performed in RT

treatment position with patients immobilized with a customized thermo-plastic mask. The lesions were outlined by means of ATA implemented on the iTaRT workstation (Tecnologie Avanzate, Italy). This algorithm uses calibration curves specific for each PET/CT scanner that depend on lesion-to-background ratio (LB) and amplitude of reconstruction smoothing filter (FWHM). The biological target volume segmented by means of ATA (BTV_{ATA}) was compared with the mean value of the gross tumour volume manually drawn by 2 expert radiation oncologists (GTV_{RO}) on the basis of the anatomical information provided by the simulation CT or pre-treatment MRI. The reproducibility of ATA in volume estimation was determined evaluating the volume overlap of multiple segmentation of the same lesions by different operators. **RESULTS:** lesion LB was in the range (4-30) and SUV mean (sd) was 14.8(9.5), respectively. Mean (sd) BTV_{ATA} and GTV_{RO} were 13(6) cm³ and 18(4) cm³, respectively. ATA thresholding values were in the range (39-51)%. Results showed high reproducibility (98%) of the algorithm implemented on workstation, with some limitations in the estimation of small volumes. **CONCLUSIONS:** the proposed adaptive threshold algorithm resulted robust and reproducible. The ATA used in the present study allows routine GTVs delineation on PET images clinically feasible. At present [¹⁸F]FDG-PET is routinely available and of interest also for focused dose escalation. A IMRT-SIB with dose painting by contours with a boost on BTV_{ATA} drawn by our algorithm can be feasible.

EP087**Variations in target volume definition and dose to normal tissue using anatomic biological imaging in the treatment of bone metastases**

D. Berwouts¹, K. De Wolf¹, W. De Neve¹, L. Olteanu¹, B. Lambert¹, I. Goethals¹, I. Madani², P. Ost¹; ¹Ghent University Hospital, Ghent, BELGIUM, ²University Hospital Zurich, Zurich, SWITZERLAND.

Purpose: To report the impact on target volume delineation and dose to normal tissue using anatomic versus biological imaging (¹⁸F-FDG-PET) for bone metastases. **Material and methods:** Patients with uncomplicated painful bone metastases were randomized (1:1:1) and blinded to receive either 8 Gy in a single fraction with conventionally planned radiotherapy (arm A) or 8 Gy in a single fraction with DPBN (dose range between 6 and 10 Gy) (arm B) or 16 Gy in a single fraction with DPBN (dose range between 14 and 18 Gy) (arm C). The primary endpoint was overall pain response at 1 month. Volumes of the gross tumor volume (GTV) - both biological (GTV_{PET}) and anatomical (GTV_{CT}), planning target volume (PTV), dose to the normal tissue and maximum standardized-uptake values (SUV_{MAX}) were analyzed (secondary endpoint). **Results:** Sixty-three percent of the GTV_{CT} volume did not show ¹⁸F-FDG-uptake. On average, 20% of the GTV_{PET} volume was outside GTV_{CT}. The volume of normal tissue receiving 4 Gy, 6 Gy and 8 Gy was at least 3x, 6x and 13x smaller in arm B compared to arm A and Arm C (p<0.05). **Conclusions:** PET-information potentially changes the target volume for bone metastases. DPBN between 6 and 10 Gy significantly decreases dose to the normal tissue compared to conventional radiotherapy.

EP088**Usefulness of 18F-choline PET/CT in treatment of oligometastatic prostate cancer recurrence using Stereotactic Body Radiation Therapy (SBRT)**

A. Franceschetto¹, A. Bruni², L. Massi¹, B. Lanfranchi², V. Rossetti¹, F. Lohr², N. Prandini¹; ¹Azienda Ospedaliero-Universitaria di Modena – Policlinico, Dipartimento ad Attività Integrata di Oncologia ed Ematologia, Struttura Complessa Medicina Nucleare, Modena, ITALY, ²Azienda Ospedaliero-Universitaria di Modena – Policlinico, Dipartimento ad Attività Integrata di Oncologia ed Ematologia, Struttura Complessa Radioterapia Oncologica, Modena, ITALY.

Aims: Currently the detection of oligometastatic prostate cancer (OI-PCa) recurrence is common in clinical routine due to imaging innovations, such as the 18F-/11C-choline PET. In these patients (pts) the use of aggressive local treatment, as radiotherapy, may be potentially justified rather than a systemic approach. We report clinical experience of a small group of pts with OI-PCa recurrence and treated with SBRT on positive lesions at 18F-choline PET/CT (18F-CH). **Materials and Methods:** From 2011 to September 2015, 18 pts with OI-PCa recurrence at 18F-CH, were treated with SBRT on PET-positive lesions (mean age: 69 years; range: 56-81). All pts underwent radical prostatectomy at time of first diagnosis and 11 of them also received adjuvant/salvage radiotherapy (RT). At staging, we found 3 high-risk PCa, 9 very high-risk PCa, and 1 intermediate-risk PCa; Gleason Score (GS) was less than 7 in 1 pts, equal to 7 in 8 pts, and exceeding 7 in 9 pts. Median time to clinical relapse after primary treatment (surgery +/- RT) was 26.2 months (range: 3-141). Nine pts received one or more lines of androgen deprivation therapy (ADT) before RT. Mean and median PSA before SBRT was 3.01 ng/ml and 1.9 ng/mL (range: 0.69-14.9), respectively. SBRT was delivered on 18F-CH positive nodal recurrence (N-MTS) in 16 pts, and in 2 pts with positive bone metastases (B-MTS); it was delivered in association with ADT in 6 pts, while the treatment was exclusive in the other 13 pts. We analyzed outcomes in terms of local control (LC), progression free survival (PFS) and overall survival (OS). **Results:** All pts were alive at a mean and median follow-up (15.5 and 18.3 months, respectively) (range: 2.5-58). Fourteen pts were treated with SBRT to 1 site (abdominal node: 12 pts; bone lesion: 2 pts), while 4 pts were treated to 2 different sites (all nodal). One-Year OS was 100% while mean and median PFS were respectively 19.7 and 13.1 (CI95% 5.3-21) months. One-year PFS were 52.7%, while LC was 100%. In terms of PFS, we have not found significant statistical prognostic factors: only adjuvant ADT and no concomitant treatments (SBRT exclusive) seemed to have a positive impact on PFS with a 1-year PFS of 60.0% for hormone-naive pts. **Conclusions:** In pts with OI-PCa recurrence, 18F-CH has proved to be useful in planning SBRT, a non invasive loco-regional approach, with the aim of reducing side effects of more invasive treatments.

EP089

18F-FDG PET/CT-guided SBRT planning in stage I-II unresectable NSCLC: a clinical experience

A. Franceschetto¹, A. Bruni², L. Massi¹, B. Lanfranchi², V. Rossetti¹, F. Lohr², N. Prandini¹; ¹Azienda Ospedaliero-Universitaria di Modena – Policlinico, Dipartimento ad Attività Integrata di Oncologia ed Ematologia, Struttura Complessa Medicina Nucleare, Modena, ITALY, ²Azienda Ospedaliero-Universitaria di Modena – Policlinico, Dipartimento ad Attività Integrata di Oncologia ed Ematologia, Struttura Complessa Radioterapia Oncologica, Modena, ITALY.

Aims: Positron emission tomography computed tomography with 18F-FDG (FDG-PET/CT) has proven to be a valuable diagnostic and staging tool for non-small-cell lung cancer (NSCLC). FDG-PET/CT has also been shown to have a significant impact on the treatment of these patients (pts), and, particularly, on radiation therapy target volume definition. We report our experience in a small group of pts with early-stage NSCLC treated with Stereotactic Body Radiation Therapy (SBRT) for coexisting diseases instead of standard surgery. **Materials and Methods:** From 2008 to 2014, 15 pts with stage I-II NSCLC were treated with SBRT exclusively on lung lesions on the basis of FDG-PET/CT and CT simulation using same immobilization devices for both studies. At staging, mean age was 73 years (range: 52-83); the histology was adenocarcinoma (ADK; 11 pts), squamous cell carcinoma (SCC; 3 pts), and large cell carcinoma (LCC; 1 pt). The pts follow-up was carried out by FDG-PET/CT and by chest and abdominal CT scans. We analyzed outcomes in clinical terms, and of progression free survival (PFS) and overall survival (OS). **Results:** At basal FDG-PET/CT, we found a mean SUVmax of 5.71 (median: 4;

range: 1.8-17) in ADK, of 4.1 (median: 2.8; range: 2-7.5) in SCC, and a SUVmax of 10.9 in the LCC. A lung toxicity due to SBRT was reported in 5 pts, one of whom required hospitalization. All but 8 patients were alive at mean and median follow-up, respectively of 22.3 and 23.8 months (range: 3.7-48.4). Mean time to TC and/or FDG-PET/CT relapse after SBRT was 19.5 months (median: 20.4; range: 3.6-45.5), while metastases appeared at a mean time of 20.8 months (median: 18.6; range: 1.4-45.5) only in 4 pts with ADK (lung: 3 cases; bone with liver: 1 case). One year after treatment, OS and PFS were respectively 67% and 60%, while overall mean and median PFS were both 18.4 months. Analyzing our population in statistical terms, no prognostic factors were found as statistical significant. **Conclusions:** In patients with early-stage unresectable NSCLC, FDG-PET/CT plays a important role in defining the radiotherapy planning and giving them a valid alternative to surgery.

EP-06 – Sunday, October 16, 2016, during Exhibition hours, e-Poster Area
Clinical Oncology: Gynaecological

EP090

Uterine cervical cancer: Diagnostic performance of F-18 FDG PET/CT for preoperative examination of regional lymph-node metastasis based on MR diagnosis of local staging

M. Nakabayashi¹, M. Nogami¹, T. Hashimoto¹, A. Kogiku¹, S. Hirabayashi², D. Takenaka¹, S. Adachi¹; ¹Hyogo Cancer Center, Akashi, JAPAN, ²Institute of Biomedical Research and Innovation, Kobe, JAPAN.

PURPOSE: The purpose was to evaluate the diagnostic performance of F-18 FDG PET/CT for preoperative examination of regional lymph-node metastasis in patients with uterine cervical cancer based on the interpretation of local extent on MRI. **MATERIALS AND METHODS:** Fifty-four consecutive patients with pathologically confirmed as squamous cell carcinoma of the uterine cervix and clinically diagnosed as T1b-2b N0 underwent PET/CT and pelvic MRI before operation. The SUVmax and size in short-axis of detected regional lymph nodes on PET/CT were separately measured on the workstation in 8 lymph-node regions in the pelvis. The primary lesion was also evaluated by SUVmax, SUVpeak, metabolic tumor volume (MTV), total lesion glycolysis (TLG) on PET/CT and by tumor size and extent on MRI. The reference standard of the regional lymph nodes was acquired histopathologically from lymph node dissections in the operation. To evaluate the relationship between PET/CT and/or MR findings and histopathological results, the logistic regression test was performed. The ROC analysis was performed to determine the diagnostic performance of PET/CT for regional lymph node metastasis. **RESULTS:** Eight (30 lymph-node lesions) in 54 patients were confirmed to be positive for regional lymph node metastasis histopathologically. The logistic regression test showed the SUVmax of the regional lymph node significantly correlated with pathological results (odds ratio 6.12, p=0.0023), whereas no correlation was found with the other parameters regarding primary lesion and lymph nodes. The diagnostic performance by SUVmax of the lymph node (Area under the curve (AUC) 0.81, sensitivity 66.7, specificity 90.0, cut-off SUVmax 1.8) was significantly higher than that by size (AUC = 0.54) in patients with T2 on MRI, however, there was no significant difference between SUVmax and size in patients with T1 on MRI and in overall subjects. **CONCLUSIONS:** In patients with T2a-b cervical cancer on MRI, diagnostic performance of SUVmax for the regional lymph-node metastasis is significantly higher as compared with T1b on MRI, suggesting diagnostic ability of PET/CT for regional lymph node metastasis is variable depending on the local extent evaluated by MRI.

EP091**Detection of pelvic lesions in patients with endometrial cancer with fused PET/MRI. Compared to PET/CT or MRI**

H. Juri, T. Komori, T. Hamada, Y. Tanaka, A. Higashiyama, G. Nakai, Y. Narumi; Osaka Medical College, Takatsuki, JAPAN.

Purpose: To evaluate the fusion image from pelvic magnetic resonance imaging (MRI) and ^{18}F -fluorodeoxyglucose positron emission tomography (FDG-PET) for detecting lesions in patients with endometrial cancer. **Materials and Methods:** Forty-eight patients with endometrial cancer underwent PET/computed tomography (CT) and pelvic MRI for staging. Two readers evaluated lymph node metastases, peritoneal disseminations, and other malignant lesions in the pelvis with PET/CT, MRI, and fusion images from PET and MRI (fused PET/MRI). The area of lymph nodes was divided into eight areas, consisting of common iliac, external iliac, internal iliac, and obturator area on the right or left sides. The final diagnosis were obtained by histopathological examinations or radiological imaging follow-up. Sensitivity, specificity and accuracy for detecting lesions were determined by comparing the results of consensus readings with the final diagnosis as per lesion analysis, and differences between each group were evaluated using McNemar test. **Results:** Sensitivity, specificity and accuracy for detecting lymph node metastases were 45.5% (5/11), 99.7% (372/373) and 98.4% (378/384) on PET/CT, 36.4% (4/11), 99.7% (372/373) and 98.2% (377/384) on MRI, and 36.4% (4/11), 99.7% (372/373) and 98.2% (377/384) on fused PET/MRI, respectively, and there was no significant difference between each group. Sensitivity, specificity and accuracy for detecting peritoneal disseminations were 42.9% (3/7), 100% (42/42) and 91.8% (45/49) on PET/CT, 28.6% (2/7), 100% (42/42) and 89.8% (44/49) on MRI, and 42.9% (3/7), 100% (42/42) and 91.8% (45/49) on fused PET/MRI, respectively, and there was no significant difference between each group. Sensitivity, specificity and accuracy for detecting other malignant lesions in the pelvis were 87.5% (7/8), 97.6% (40/41) and 95.9% (47/49) on PET/CT, 87.5% (7/8), 100% (41/41) and 98.0% (48/49) on MRI, and 87.5% (7/8), 97.6% (40/41) and 95.9% (47/49) on fused PET/MRI, respectively, and there was no significant difference between each group. Fused PET/MRI does not improve detection of all lesions in the pelvis in patients with endometrial cancer compared to PET/CT. Although fused PET/MRI improve detection of two lymph node metastases compared to MRI, it is not significantly different. **Conclusion:** Fused PET/MRI does not improve detection of lesions in the pelvis in patients with endometrial cancer compared to PET/CT or MRI.

EP092**FDG-PET/CT in early stage uterine cervical cancer: can SUVmax discriminate between malignant and benign lymph nodes?**

J. Holm, M. G. Hildebrandt, A. Thomassen, O. Gerke, P. F. Høilund-Carlsen; Odense University Hospital, Odense C, DENMARK.

Aim: The frequency of lymph node metastasis in early stage uterine cervical cancer is low. If positive pelvic lymph nodes are detected by the diagnostic FDG-PET/CT-scan, further staging by laparoscopic lymph node dissection is performed before radical hysterectomy or other treatment is initiated. Unfortunately, this set-up often drags out the staging process. PET specialists are urged to improve the segregation between lymph nodes suspected of true malignancy and those regarded as merely reactive to recent cervical conization, portio biopsy, or other benign causes. We retrospectively examined whether the distinction between true positive, false positive, and true negative lymph nodes could be assessed by SUVmax alone. **Materials and methods:** A total of 134 patients aged 25-81 years (median 42) with early stage cervical uterine cancer, FIGO stage 1A or 1B, who had undergone preoperative FDG-PET/CT during

the period 2009-2015 were retrospectively included. The scan result was compared to histopathology obtained by lymph node dissection. SUVmax was measured in PET-avid pelvic lymph nodes in the right side, left side or at the midline, and each assigned a separate SUVmax-value. The differences between the true positive, false positive and the true negative reactive lymph nodes were assessed by one-way analysis of variance, using Bonferroni's adjustment for multiple testing. **Results:** Thirty women had 44 lymph nodes with increased PET activity. Eight (18%) lymph nodes were true positive, twenty-five (57%) false positive, and eleven (25%) true negative, reactive nodes. The corresponding mean SUVmax values \pm SD were 3.1 ± 0.89 , 3.4 ± 0.78 and 2.1 ± 0.84 , respectively. We found a statistically insignificant difference of 0.3 ($p=0.96$) in SUVmax between the true positive and false positive group, but significant differences of 1 ($p=0.034$) between true positive and true negative nodes and of 1.3 ($p<0.0001$) between true negative and false positive nodes. **Conclusion:** SUVmax values obtained by preoperative FDG-PET/CT imaging in early stage uterine cervical cancers cannot discriminate PET-positive metastatic from non-metastatic lymph nodes. Diagnostic laparoscopic lymph node dissection should be performed in all lymph node PET-positive patients. The SUVmax of reactive lymph nodes was significantly lower than that of both true and false PET-positive lymph nodes. Nevertheless, correct PET/CT lymph node diagnostics in early stage cervical cancer remains a complex combination of several parameters, and the SUVmax value cannot stand alone.

EP093**Can preoperative PET/CT be used as an efficient tool in planning extent of surgical lymph node dissection in endometrial cancer patients?**

B. E. AKKAS¹, H. EFETURK¹, B. B. DEMIREL¹, G. UCMAK^{2,3},
¹ANKARA ONCOLOGY RESEARCH AND TRAINING HOSPITAL, DEPARTMENT OF NUCLEAR MEDICINE, ANKARA, TURKEY,
²HITIT UNIVERSITY ÇORUM RESEARCH AND TRAINING HOSPITAL, DEPARTMENT OF NUCLEAR MEDICINE, ÇORUM, TURKEY,
³ANKARA ONCOLOGY RESEARCH AND TRAINING HOSPITAL, DEPARTMENT OF NUCLEAR MEDICINE, Ankara, TURKEY.

Aim: The most important prognostic factor in endometrial cancer (EC) patients is lymph node metastasis. The primary therapeutic approach to EC is surgery. To avoid intraoperative complications and morbidity, lymphadenectomy (PPLND) is performed in selected patients. The aim of this study was to assess the role of preoperative PET/CT in detecting lymph node metastasis in EC patients and to assess its contribution to tailoring surgical therapy of patients. **Materials and methods:** Preoperative PET/CT was performed in 72 EC patients. Presence of lymph node (LN) positivity on PET/CT was compared to postoperative histopathology results. The FDG uptake in LN was evaluated according to visual uptake compared to background and was marked as present or absent. A true positive (TP) lesion was a LN detected on PET/CT and also found to be positive on histopathology; a false positive (FP) lesion was a LN detected on PET/CT but not positive on histopathology; a true negative (TN) lesion was a LN not detected on both PET/CT and histopathology and a false negative (FN) lesion was a LN not detected on PET/CT but positive on histopathology. Sensitivity, specificity, positive predictive value, negative predictive value and accuracy of PET/CT was calculated on a patient based criteria. **Results:** Of 72 patients 9 (12%) had histopathologically confirmed LN metastasis. PET/CT detected pelvic/para-aortic LN in 14 patients with positive FDG uptake. Of these, PET/CT was TP in 8, FP in 6 patients, PET/CT did not reveal any hypermetabolic LN in 58 patients. Of these 57 were TN, whereas 1 patient has a metastatic pelvic LN. The sensitivity, specificity, positive predictive value (PPV), negative predictive value (NPV) and accuracy was calculated as 88%, 90%, 57%, 98% and 90% respectively. The low PPV was attributed to inflammatory LN. The average size of TP LN's

was 0.7 cm (0.5–1 cm) and the average size of FP LN's was 0.7 cm (0.6–1 cm). There was no significant difference between SUVmax of TP and FP LNs. Conclusion: Our study showed high sensitivity, specificity, NPV and accuracy. These values show that PET/CT can successfully detect patients without LN metastasis. We considered that although PET/CT has a significant limitation in distinguishing metastatic LN from inflammatory processes in patients with EC, PET/CT is a valuable method to successfully select patients in whom extended surgery with lymphadenectomy, which may increase surgery based morbidity, can be avoided.

EP094

Predicting response for locally advanced cervical cancer

b. vendel; umcg, groningen, NETHERLANDS.

Purpose. Being able to identify noninvasively, prior to therapy, those patients with cervical cancer at highest risk of recurrence or compromised survival, allows for targeting this high risk population with more aggressive therapy, such as adjuvant chemotherapy or participation in a clinical trial. Additionally, the prognostic information offered by the PET-based prognostic nomograms could be used for risk stratification in clinical trials. The problem is that most nomograms are developed in a single institution following different local protocols. For this feasibility study, we evaluate the use of a previously developed FDG-PET-based prognostic nomograms for locally advanced cervical cancer assessed on pretreatment FDG-PET for predicting recurrence-free survival (RFS), disease-specific survival (DSS), and overall survival (OS) in the Netherlands. Patients and methods. The preliminary study included 20 cervical cancer patients, FIGO stage Ib1-IVa, treated with definitive radiation or chemoradiation therapy in the period 2010–2016. All patients underwent FDG-PET/CT at diagnosis, from which cervical tumor volume, SUVmax, SUV peak, SUV Mean, SUV min, tumor volume and LN status were recorded. Using the prognostic nomogram developed by Kidd et al 2012 RFS, DSS, and OS, were calculated. Results. 65 percent of patients had FDG-avid LN on PET; the highest level of nodal involvement was pelvic in 11, para-aortic in 2, The average cervix tumor SUVmax was 14.05 (range, 5.15–21.97) SUVpeak 12.43, SUV mean 8.48, SUV min 5.62 and PET tumor volume average was 52.89 cm³ (range, 6.38–253.6 cm³). PET LN status had the greatest influence on outcome. The average calculations were: RFS 1 year 0.78, RFS 3 year 0.62, DFS1 year 0.89, DFS 3 year 0.72 OS 1 year 0.87 OS 3 year 0.68. The patients who developed a recurrence in the first 2 years had an average RFS3 year of 0.58. Conclusions. Pretreatment FDG-PET LN status, cervical tumor SUVmax, and tumor volume combined in a nomogram create good models for predicting cervical cancer RFS, DSS, and OS. In the final study a larger cohort of 300 patients will be analyzed to establish the prognostic value of new SUV measurement and develop a new predicting model.

EP095

Assessment of nodal status by 18F-FDG PET/CT in early stage vulvar cancer

P. Guglielmo¹, C. Crivellaro², C. Dolci³, L. Baratto¹, F. Elisei⁴, L. Guerra⁴, A. Buda⁵, L. Montanelli¹, E. De Ponti⁶, C. Landoni²; ¹University of Milan Bicocca, Milan, ITALY, ²Nuclear Medicine Department, ASST - San Gerardo, Monza; Nuclear Medicine, University of Milan Bicocca, Milan, ITALY, ³Tecnomed Foundation, University of Milan Bicocca, Milan, ITALY, ⁴Nuclear Medicine Department, ASST - San Gerardo, Monza, Monza, ITALY, ⁵Gynecology Department, ASST - San Gerardo, Monza; Gynecology, University of Milan Bicocca, Milan, ITALY, ⁶Medical Physics Department, ASST Monza, Monza, ITALY.

Objectives In early stage vulvar cancer (clinical stage I-II) the involvement of regional lymph nodes (LN) is one of the most important prognostic

factor. A non-invasive imaging modality that allows an accurate LN staging could improve preoperative assessment and consequently therapeutic approach. Aim of this study was to evaluate the performance of 18F-FDG PET/CT in nodal staging of patients (pts) affected by early stage vulvar cancer. Methods 25 pts (mean age 68 years; range 51–83) with an apparent clinical early stage vulvar cancer underwent preoperative 18F-FDG-PET/CT scan followed by radical vulvectomy and bilateral (or monolateral in case of tumour > 2 cm from midline) inguinal lymphadenectomy. PET/CT images were analyzed by three examiners in consensus and correlated to histopathological findings according to a pt-based and a lesion-based analysis. Furthermore the highest SUVmax of the nodal uptake of each inguinal area (if present) has been calculated. Results PET/CT scan resulted negative at inguinal LN level in 15 pts (7 true negative -TN-, 8 false negative -FN-) and positive in 10 pts (5 true positive -TP-, 5 false positive -FP-). Mean number of dissected LNs was 12 per pt. Incidence of LN metastases resulted 52% (13/25), in particular with low-volume metastases in 23% of cases. On pt-based analysis, sensitivity, specificity, accuracy, negative and positive predictive value of PET/CT in detecting LN metastases were 38%, 58%, 48%, 47%, 50% respectively. On a lesion-based analysis, considering 46 LN-sites overall, these values were 42%, 80%, 67%, 73%, 53% respectively. The average value of SUVmax was 4.1 (range 0.7–9.3) for sites of metastatic LNs, whereas 1.6 (range 0.7 - 5.4) for site with negative LN at histology (p=0.007); however in 47% of nodal metastatic sites, a low FDG uptake (SUVmax less than 2.5) was observed. Conclusions In clinical early stage vulvar cancer patients, 18F-FDG PET/CT was not an accurate tool for the nodal status assessment. Although the average value of SUVmax in metastatic sites resulted higher, nodal metastases could occur also in sites with absent or low uptake. Sensitivity of PET/CT resulted low (38%) probably related both to the presence of low-volume or low glycolytic activity/necrotic lesions. In addition, FP findings may occur because inguinal LNs frequently undergo reactive changes.

EP096

Risk Stratification of Endometrial Cancer Patients into clinical Low-Risk or High-Risk Groups Based on Preoperative FDG PET/CT Parameters

H. EFETURK¹, B. E. AKKAS¹, B. B. DEMIREL¹, S. DEMIRTAS², G. UCMAC^{2,3}; ¹ANKARA ONCOLOGY RESEARCH AND TRAINING HOSPITAL DEPARTMENT OF NUCLEAR MEDICINE, ANKARA, TURKEY, ²HITIT UNIVERSITY ÇORUM RESEARCH AND TRAINING HOSPITAL DEPARTMENT OF NUCLEAR MEDICINE, ÇORUM, TURKEY, ³ANKARA ONCOLOGY RESEARCH AND TRAINING HOSPITAL DEPARTMENT OF NUCLEAR MEDICINE, Ankara, TURKEY.

Aim: Endometrial cancer is the most common gynecologic malignancy and the eighth leading cause of death from malignancy in women. Postoperative risk assessment for recurrence is generally based on prognostic factors determined by surgical and pathological staging which forms the basis of postoperative adjuvant therapy planning and follow-up. Functional imaging and quantification of 18-fluorodeoxyglucose positron emission tomography-computerized tomography (PET/CT) parameters of the primary tumor may have prognostic implications. The aim of this study was to determine whether metabolic PET/CT parameters can be used as a potential preoperative imaging modality to improve risk classification and guide a tailored surgical approach and therapeutic strategy. **Materials and methods:** Preoperative FDG PET/CT was performed in 72 women with endometrial cancer. 52 patients had stage I, 5 patients had stage II, 10 patients had stage III and 5 patients had FIGO stage IV disease. Tumors were classified as high or low-risk carcinomas postoperatively. Patients with FIGO stage I, endometrioid histology, histological grade 1 or 2 and invasion of less than half of the myometrium were included in low-risk group. The remaining patients were included in the

high-risk group. Maximum standardized uptake values (SUVmax), metabolic tumor volume (MTV) and total lesion glycolysis (TLG) of the primary tumor were compared to postoperative histopathology in order to evaluate whether these metabolic parameters can predict high-risk patients preoperatively. Receiver operating characteristics (ROC) curve analysis was performed to examine which metabolic parameters were able to differentiate high-risk from low-risk endometrial cancer. **Results:** SUVmax (15 ± 6.6 vs. 18.8 ± 7 , $p:0.02$), MTV (7.8 ± 5.7 vs. 28.4 ± 37.6 , $p:0.006$) and TLG (80.7 ± 85.6 vs. 355.5 ± 453.4 , $p:0.001$) were significantly higher in high-risk patients compared to low-risk group. The areas under ROC curves (AUCs) for distinguishing low-risk patients from high-risk groups were 65% for SUVmax, 75% for MTV and 73% for TLG. When metabolic indices were compared to FIGO clinical stages, both MTV and TLG were significantly correlated with higher FIGO stage ($p:0.02$). We did not observe correlation between SUVmax and FIGO stage in our patient group. **Conclusion:** Our study showed that a prognostic estimate can be obtained prior to surgery with metabolic parameters obtained by preoperative PET/CT. All SUVmax, MTV and TLG were found successful to predict high-risk patients. However, we found that TLG, which considers both the metabolic activity and tumor burden, was a stronger parameter that can be used to distinguish high-risk patients and may guide the surgeon deciding the extent of the surgical procedure preoperatively.

EP097

The Experience of $^{99m}\text{Tc-Al}_2\text{O}_3$ Using for the Detection of Sentinel Lymph Nodes in Cervical Cancer Patients

V. Chernov^{1,2}, I. Sinilkin^{1,2}, A. Medvedeva^{1,2}, R. Zelchan^{1,2}, A. Lyapunov¹, O. Bragina², A. Chernyshova¹, L. Kolomiets¹, V. Skuridin²; ¹Tomsk Cancer Research Institute, Tomsk, RUSSIAN FEDERATION, ²Tomsk Polytechnic University, Tomsk, RUSSIAN FEDERATION.

The purpose of the study was to evaluate the feasibility of using the new radiopharmaceutical, based on technetium-99m-labeled gamma-alumina ($^{99m}\text{Tc-Al}_2\text{O}_3$), for the detection of sentinel lymph nodes in cervical cancer patients. Materials and methods. Nanocolloid $^{99m}\text{Tc-Al}_2\text{O}_3$ with size of nanoparticles 80-100nm coated with organic covering was studied. During passage through the lymphatic way nanoparticles lose organic coating and strongly accumulate in the sentinel lymph nodes without redistribution. The study included 23 patients with cervical cancer $T_{1a}N_xM_x - T_{2b}N_xM_x$ stage. The day before surgery, four subcutaneous injections of $^{99m}\text{Tc-Al}_2\text{O}_3$ at a dose of 20 MBq per quadrant were made in each quadrant around the cervical tumor. SPECT study was performed at 18 hours after injection, intraoperative detection was executed by gamma probe at 20 hours after injection. Patients were then underwent iliac-pelvic lymph node dissection. After lymphodissection, the removed lymph nodes were re-examined with gamma probe to detect SLNs missed during intraoperative examination. Results. In all patients 27 SLN were identified by SPECT and 34 SLN by gamma probe. Accumulation of $^{99m}\text{Tc-Al}_2\text{O}_3$ in SLN was 3%-12% (average - 7%) by SPECT and 17%-29% (average - 24%) by gamma probe (in compare to spot of injection). The most common site for SLN detection was the external iliac region (57%), followed by the internal iliac, obturator, presacral and retrosacral regions (they amounted to 14%, respectively), and the parametrial region (1%). The excised SLNs were evaluated by imprint cytology with subsequent routine histological examination. All lymph nodes including SLNs and non-SLNs were metastasis-negative, there by indicating that there was no phenomenon of "jumping" nodal metastases. Conclusions. The clinical study of $^{99m}\text{Tc-Al}_2\text{O}_3$, a new radiopharmaceutical agent, have shown that the studied nanocolloid has high uptake level in SLN and can be successfully used for visualization of SLN in patients with cervical cancer. SPECT and intraoperative gamma probe-guided identification performed after paratumoral injection of $^{99m}\text{Tc-Al}_2\text{O}_3$ enable the detection of SLNs with 79 and 100% sensitivity, correspondently.

EP098

Sentinel lymph node biopsy in endometrial cancer in early stages: evaluation of results

J. Cordero Garcia, C. López de la Manzanara Cano, A. Palomar Muñoz, M. Talavera Rubio, M. Tello Galán, V. Poblete García, F. Pena Pardo, A. García Vicente, Á. Soriano Castrejón; Hospital General de Ciudad Real, CIUDAD REAL, SPAIN.

Objective: To evaluate the results of the application of the technique of sentinel lymph node (SLN) in endometrial cancer in early stages. **Material and methods:** Prospective study (research project with public funding PI-2009/31) which included 66 patients with endometrial adenocarcinoma, at presurgical clinical stage I, excluding the upper clinical stages and those patients diagnosed with endometrial sarcoma. To identify the SLN, 2 mCi of $^{99m}\text{Tc-Nanocolloid}$ were injected in two opposite points of the uterine cervix (total: 4 mCi), obtaining planar images and SPECT-CT of the pelvis at 30 min, and delayed planar images at 16 h when necessary. The SLN was identified intraoperatively using a conventional gamma-probe. All patients were treated with pelvic lymphadenectomy, hysterectomy and oophorectomy. The SLN were studied by conventional histology (H & E), as well as those lymph nodes obtained from the lymphadenectomy. **Results:** In 58 patients at least one SLN was identified both in the scintigraphic and in the intraoperative study (detection rate 88%). In 8 patients was not possible to find a SLN neither scintigraphically nor surgically. One SLN was found in 25 patients, 2 SLN in another 17, and 3 or more in the remaining 16. During the operation a total of 104 SLN were identified (median 1, mean 2). Histological study showed that only 2 of the patients had lymph node involvement, both by micrometastases (3.1%), and in both of them the SLN was the only affected node (100% true positives, 100% sensitivity). **Conclusions:** SLN identification in endometrial cancer in early stages is a simple and reliable technique with a good detection rate and histological correlation. Therefore, it may be considered as an alternative to systematic pelvic lymphadenectomy in these patients.

EP099

Lymphatic metastasis correlates with metabolic tumor burden detected by PET/CT in patients with endometrial carcinoma

B. E. AKKAS¹, H. EFETURK², B. B. DEMİREL², G. UCMAK^{3,4}; ¹ANKARA ONCOLOGY RESEARCH AND TRAINING HOSPITAL, ANKARA, TURKEY, ²ANKARA ONCOLOGY RESEARCH AND TRAINING HOSPITAL, DEPARTMENT OF NUCLEAR MEDICINE, ANKARA, TURKEY, ³HITIT UNIVERSITY ÇORUM RESEARCH AND TRAINING HOSPITAL DEPARTMENT OF NUCLEAR MEDICINE, ÇORUM, TURKEY, ⁴ANKARA ONCOLOGY RESEARCH AND TRAINING HOSPITAL, DEPARTMENT OF NUCLEAR MEDICINE, Ankara, TURKEY.

The presence of lymph node (LN) metastasis in endometrial cancer is well accepted to have a negative effect on prognosis. In this study, we investigated the association of clinical parameters and metabolic indices such as metabolic tumor volume (MTV), standardized uptake value (SUVmax) and total lesion glycolysis (TLG) with the presence of surgically proven LN metastasis in patients with primary endometrial carcinoma. A total of 72 patients with endometrial carcinoma, who were referred to our clinic for 18F-FDG PET/CT imaging for initial staging and pre-treatment evaluation were enrolled in this retrospective study. 59 patients had endometrioid type tumor, whereas 13 patients had non-endometrioid subtypes. All patients underwent surgical staging including hysterectomy, bilateral salphingo-oophorectomy, abdominal exploration and selective lymphadenectomy. 52 patients had FIGO stage I, 5 patients had stage II, 10 patients had stage III and 5 patients had stage IV disease. The

presence of LN metastasis was correlated with metabolic parameters such as SUVmax, MTV and TLG. Results: Nine patients had surgically proven LN metastasis. Six of 10 (60%) patients amongst stage III patients, and 3 of 5 (60%) patients amongst FIGO stage IV patients had LN metastasis. Apart from clinical stage, 6 of 13 patients (46%) with non-endometrioid type tumor had LN metastasis. Patients with LN metastasis had significantly higher MTV ($68.4 \pm 56.3 \text{ cm}^3$ vs. $14.2 \pm 17 \text{ cm}^3$, $p:0.0001$) and TLG (810 ± 651 vs. 160 ± 228.4 grams, $p:0.001$) compared to non-metastatic patients. On univariate analysis, the presence of LN metastasis was significantly correlated with non-endometrioid histology, advanced FIGO stage, high MTV and high TLG of the primary tumor. Conclusion: Non-endometrioid tumor type and advanced FIGO stages are known poor prognostic factors which are clinically associated with lymphatic involvement in patients with endometrial cancer. In addition to these well known clinical parameters, we observed that metabolic indices that considers metabolic tumor burden also correlate with LN metastasis in endometrial cancer. These findings support the use of PET/CT as a complementary approach to FIGO staging in the pre-treatment work-up of patients with endometrial cancer.

EP100

Comparison of integrated ^{18}F -FDG PET/contrast-enhanced CT and contrast-enhanced CT for pretreatment staging of epithelial ovarian cancer

M. Mayoral, P. Paredes, A. Saco, L. Buñesch, M. C. Sebastià, S. Martínez-Roman, A. Fernandez-Martinez, J. Ordi, J. Pavia, J. Pahisa, F. Lomeña; Hospital Clinic Barcelona, Barcelona, SPAIN.

AIM: Contrast-enhanced CT (ceCT) is the procedure of choice for preoperative staging of epithelial ovarian cancer (EOC). This study aimed to evaluate the diagnostic performance of integrated ^{18}F -FDG PET with ceCT (PET/ceCT) in comparison with conventional ceCT. **MATERIALS AND METHODS:** Thirty-two patients with suspected or newly diagnosed EOC underwent pretreatment PET/ceCT. An experienced nuclear medicine physician evaluated PET/ceCT and the ceCT component was interpreted by a radiologist separately. For each study, findings other than the primary tumour were categorized into four groups: peritoneum, abdominopelvic lymph nodes, supradiaphragmatic disease and metastasis in other organs. Histopathological findings, whenever possible, were the reference standard to determine the final diagnosis of disease status. The diagnostic performance of PET/ceCT and ceCT was calculated on a site-based analysis. For extra-abdominal areas not resectable during surgery, the agreement of the two imaging modalities was compared with the kappa coefficient. McNemar test was used to determine the significance of differences between both techniques. **RESULTS:** The median age was 62 years old (range 19-83 years). Papillary serous adenocarcinoma was the most common histological subtype, being present in 24/32 (75.0%) cases. The mean value of CA-125 serum levels was 1057.1 U/mL (standard deviation 1162.4 U/mL). Peritoneal biopsies were obtained from 21 patients and histopathology showed tumoral involvement in 19 (90.5%) patients. The two imaging modalities detected peritoneal implants in all these cases. Abdominopelvic lymph nodes status could be histologically evaluated in 15 patients, 6 (40.0%) of which had metastasis. The sensitivity, specificity, positive predictive value, negative predictive value and accuracy of PET/ceCT to detect abdominopelvic adenopathies was 83.3%, 77.8%, 71.4%, 87.5% and 80.0%. For ceCT, these values were 66.7%, 66.7%, 57.1%, 75.0% and 66.7%, respectively. PET/ceCT detected supradiaphragmatic disease in 13/32 (40.6%) patients and ceCT in 5/32 (15.6%) patients, all of them also detected by PET/ceCT. These differences between both techniques were statistically significant ($p=0.008$). The agreement between both techniques to detect supradiaphragmatic disease was fair ($\kappa=0.271$). PET/ceCT detected metastasis in other organs in 6/32 (18.8%) patients and ceCT in 4/32 (12.5%) patients. These

differences were not statistically significant ($p=0.5$). The agreement between both techniques to detect metastasis in other organs was substantial ($\kappa=0.684$). **CONCLUSION:** PET/ceCT was superior to conventional ceCT for the detection of supradiaphragmatic disease and abdominopelvic lymph nodes. Thus, integrated PET/ceCT is a more accurate imaging modality for staging EOC than ceCT.

EP101

Prognostic role of ^{18}F -FDG PET parameters in preoperative phase of endometrial carcinoma

E. Incerti¹, P. Mapelli¹, A. Bergamini², P. Rancoita³, A. Bonazzi⁴, F. Fallanca¹, E. Rossi², M. Petrone², E. Rabaiotti², A. Dell'Acqua², G. Mangili², L. Gianolli¹, M. Picchio¹; ¹IRCCS San Raffaele Scientific Institute, Nuclear Medicine, Milan, ITALY, ²IRCCS San Raffaele Scientific Institute, Obstetrics and Gynecology, Milan, ITALY, ³University Centre of Statistics in the Biomedical Sciences, Vita-Salute San Raffaele University, Milan, ITALY, ⁴University Of Milano-Bicocca, Milan, ITALY.

Aim: To explore the prognostic value of preoperative ^{18}F -FDG PET/CT in endometrial cancer by using ^{18}F -FDG PET-specific semi-quantitative tumour parameters. **Methods:** Preoperative ^{18}F -FDG PET/CT was performed from August 2009 to March 2015 in 32 women (mean age: 63 years, range: 49-81 years) with endometrial cancer. Mean and maximum standardized uptake values (SUVmean - max), metabolic tumour volume (MTV) and total lesion glycolysis (TLG) of primary tumours, at different thresholds of 40%, 50%, 60% (40-50-60), were retrospectively evaluated and compared with anatomical and pathological features. All ^{18}F -FDG PET-specific semi quantitative tumour parameters measured have been evaluated to assess their diagnostic performance in terms of differentiation of low-risk disease (pT1 or International Federation of Gynecology and Obstetrics - FIGO Stage I) from high-risk disease (pT2-pT3 or FIGO Stage II-III-IV). The Receiver Operating Characteristics (ROC) curve analysis was used to investigate the performance of PET parameters in predicting the tumour status. For each PET parameters, the optimal cut-off was derived using a standard method, consisting in choosing that value corresponding to the point on the ROC curve nearest to the upper left corner of the ROC graph. Logistic regression analysis was used to assess whether the PET parameters categorized with the optimal cut-off were able to predict the tumour status and only those which reached a statistical significance were reported (P -value <0.05). **Results:** MTV40 and TLG40-50-60 were significantly related to FIGO Stage I versus FIGO Stage II-III-IV ($P=0.0157$, $P=0.0246$, $P=0.0474$, $P=0.0474$, respectively). The optimal MTV40 cut-off value of 8.9, determined by ROC analysis, was found to have 70% sensitivity and 77% specificity for risk stratification. The optimal cut-off values of 85.6, 58.0, 40.0, for TLG40-50-60, determined by ROC analysis, respectively, were found to have 60%, 60%, 60% sensitivity, respectively, and 82%, 77%, 77% specificity for risk stratification, respectively. **Conclusions:** MTV40 and TLG40-50-60 of primary endometrial cancer show correlations with anatomical and pathological features, being more useful for differentiating low-risk from high-risk disease than SUVmean-max parameters that could not reach a statistical significance in our series. ^{18}F -FDG PET-specific semi-quantitative tumour parameters may represent a clinically valuable tool for preoperatively predict endometrial carcinoma.

EP102

Preoperative metabolic indices of FDG PET/CT correlate with deep myometrial invasion in clinical FIGO Stage I endometrial carcinoma

B. E. AKKAS¹, H. EFETURK¹, B. B. DEMIREL¹, G. UCMAR^{2,3}; ¹ANKARA ONCOLOGY RESEARCH AND TRAINING HOSPITAL DEPARTMENT OF NUCLEAR MEDICINE, ANKARA, TURKEY, ²HITIT UNIVERSITY ÇORUM RESEARCH AND TRAINING

HOSPITAL DEPARTMENT OF NUCLEAR MEDICINE, ÇORUM, TURKEY, ³ANKARA ONCOLOGY RESEARCH AND TRAINING HOSPITAL DEPARTMENT OF NUCLEAR MEDICINE, Ankara, TURKEY.

The prognosis of patients with FIGO Stage I endometrial cancer is favorable after radical surgery. Depth of myometrial invasion (MI) is one of the clinically significant prognostic factors in patients with endometrial cancer. In addition, prior knowledge of MI depth is important for surgical planning. Curative tumor resection is possible in superficial MI (<50% of myometrium), while patients with deep MI (> 50% of myometrium) may benefit from extended surgery with pelvic and/or paraaortic lymphadenectomy. The aim of this study was to evaluate the value of FDG PET/CT for estimating MI in endometrial cancer. Method: 52 patients with FIGO stage I endometrial cancer were included in this study. All patients underwent FDG PET/CT imaging prior to surgery. Standardized uptake values (SUV), metabolic tumor volume (MTV) and total lesion glycolysis (TLG) were calculated on the PET image. All patients underwent total hysterectomy and bilateral salpingo-oophorectomy (THBSO). Extended surgery was considered based on intra-operative findings and frozen section results. Metabolic data was compared to post-operative histopathology obtained from the surgical specimen. Results: The surgical stage was IA in 32 and IB in 20 patients. Nineteen patients (63.5%) had deep MI, 33 had superficial MI. SUVs in patients with deep MI were significantly higher than those with superficial MI (20.2±6.8 vs. 14±6.4, respectively, p:0.001). The area under ROC curves (AUCs) for distinguishing patients with deep MI from those with superficial MI was 77% for SUVmax. The best compromise between sensitivity (84%) and specificity (73 %) was reached at a cut off value of SUVmax:15.6. MTV in patients with deep MI was significantly higher than those with superficial MI (15.4±9.2 vs. 9.4±9.7, respectively, p:0.01). AUC for predicting patients with deep MI for MTV was 75% and a cut off value was calculated as 9.9 cm³ with a sensitivity of 72% and specificity of 73%. AUC for TLG was calculated as 77% which was higher than both SUVmax and MTV. The cut off for TLG was found as 108 grams with a sensitivity of 72% and specificity of 76%. Conclusion: Our study showed that all metabolic parameters obtained from preoperative PET/CT are successful to predict deep MI in patients with clinical stage I endometrial cancer. We considered that, after confirmed by larger prospective studies, SUVmax greater than 15.6, MTV greater than 9.9 cm³ and TLG greater than 108 grams can be applied preoperatively for risk stratification and deciding upon the optimal surgical therapeutic strategy.

EP103

The role of maximum standardized uptake value and minimum apparent diffusion coefficient of the primary tumor for predicting clinicopathological characteristics in endometrial cancer

F. AYDIN¹, E. SURER BUDAK¹, T. TOPTAŞ¹, A. ONER², C. CEVİKOL¹, T. ŞİMŞEK¹; ¹AKDENİZ UNIVERSITY, ANTALYA, TURKEY, ²KOCATEPE UNIVERSITY, AFYON, TURKEY.

Abstract Objective: To investigate relationships of maximum standardized uptake value (SUV_{max}) and minimum apparent diffusion coefficient (ADC_{min}) of the primary tumor to clinicopathological features, and to compare their predictive ability in patients with endometrial cancer (EC). **Methods:** A prospective case-series with planned data collection was conducted in a total of 45 patients who underwent staging surgery following a preoperative evaluation with ¹⁸F-fluorodeoxyglucose positron emission tomography combined with computed tomography (¹⁸F-FDG PET/CT) and diffusion-weighted magnetic resonance imaging (DW-MRI). Relationships between variables were analyzed using the multiple linear regression analysis. **Results:** The mean ADC_{min} and SUV_{max} were 0.72±0.22 and 16.54±8.73, respectively. In univariate analysis, while the potential factors associated with ADC_{min} were age, myometrial invasion (MI), and lymphovascular space involvement

(LVSI); the potential factors associated with SUV_{max} were age, stage, tumor size, MI, LVSI and number of metastatic lymph nodes. However, only MI remained to be an independent variable associated with ADC_{min} (P=0.007) as well as SUV_{max} (P=0.024) after adjustment for other confounders in multivariate analysis. Optimal cutoff values of ADC_{min} and SUV_{max} for predicting deep MI were found to be ≤0.77 [93.7% sensitivity, 48.2% specificity, and 93.0% negative predictive value (NPV)] and >20.5 (62.5% sensitivity, 86.2% specificity, and 81.0% NPV), respectively; although the comparison of two diagnostic tests revealed no significance (P=0.266). **Conclusions:** MI is the sole clinicopathological feature independently associated with SUV_{max} as well as ADC_{min}. However, predictive performances of both parameters are not high enough to support the routine use of ¹⁸F-FDG PET/CT or DW-MRI.

EP104

Value of (18)F-fluorodeoxyglucose PET/CT in the diagnosis of local recurrence uterine cancer: comparison with CT and MRI

S. Panareo¹, I. Santi¹, I. Rambaldi¹, S. Taralli¹, A. Stefanelli², C. Cittanti¹; ¹University Hospital - Nuclear Medicine Unit, FERRARA, ITALY, ²University Hospital - Radiotherapy Unit, FERRARA, ITALY.

AIM: To evaluate the accuracy of (18)F-fluorodeoxyglucose (FDG) PET/CT (PET/CT) in the diagnosis of suspected uterine cancer local recurrence after treatment (surgery, chemotherapy and/or radiotherapy) and to assess the impact of PET/CT findings on clinical management, compared with contrast enhanced CT alone and MRI. **METHODS:** we retrospectively studied 64 women (mean age 72±5.2 yo) who underwent treatment for histopathologically proven uterine cancer. For the clinical-diagnostic suspect of local cancer recurrence, all patients underwent PET/CT examination at least 3 months from the end of treatment. PET/CT results were correlated to contrast enhanced CT alone and MRI. Lesion status was determined on the basis of histopathology, radiological imaging and clinical follow-up for longer than 6 months. Differences among the three imaging modalities were tested using the Cochran Q test, followed by multiple comparisons using the McNemar test with Bonferroni adjustment. **RESULTS:** Patient-based analysis showed that PET/CT confirmed a local disease relapse in 35 patients (54.6%) out of 64. PET/CT data were confirmed by clinical-diagnostic and surgical follow-up. On the other hand CT alone showed a local recurrence of disease in 22 patients (34.3%). On the other hand MRI showed a relapse disease in 25 patients (39%). The sensitivity, specificity, and accuracy of PET/CT were, respectively, 91%, 93%, and 92%; whereas those of contrast enhanced CT alone were, respectively, 68%, 87%, and 78%. Finally, sensitivity, specificity and accuracy of MRI were, respectively, 82%, 91% and 90%. PET/CT findings resulted in a change of management in 21 of 64 patients studied (32%). **CONCLUSION:** PET/CT is a more accurate modality for assessing recurrence of uterine cancer and more appropriate than contrast enhanced CT alone in the restaging of patient with suspected uterine cancer recurrence. MRI seems to be better than contrast enhanced CT for the restaging of local recurrence of uterine cancer but not performing like PET/CT. PET/CT done at least 3 months from the end of treatment allows to differentiate between after treatment local inflammation and tumour recovery. The change of treatment management gives a better prognostic stratification and restraint of costs. Data must be confirmed in a more large casuistic.

EP105

The effect of dual phase PET/CT imaging on Standardized Uptake Value, Metabolic Tumor Volume and Total Lesion Glycolysis of the primary tumor in endometrial cancer patients

B. E. AKKAS¹, G. UCMAK^{2,3}, H. EFETURK¹, I. KERIMEL¹, B. B. DEMIREL¹; ¹ANKARA ONCOLOGY RESEARCH AND

TRAINING HOSPITAL, DEPARTMENT OF NUCLEAR MEDICINE, ANKARA, TURKEY, ²HITIT UNIVERSITY ÇORUM RESEARCH AND TRAINING HOSPITAL DEPARTMENT OF NUCLEAR MEDICINE, ÇORUM, TURKEY, ³ANKARA ONCOLOGY RESEARCH AND TRAINING HOSPITAL DEPARTMENT OF NUCLEAR MEDICINE, Ankara, TURKEY.

Aim: It is known that fluorodeoxyglucose (FDG) uptake continues to rise for several hours after the injection of radiotracer in various malignancies. Dual phase positron emission tomography/computed tomography (PET/CT) imaging has been shown to have impact on the differentiation of malignant lesions from benign inflammatory processes. Our aim was to evaluate the effect of dual phase PET/CT imaging of the primary tumor on the functional metabolic parameters that reflect metabolic tumor burden such as maximum standardized uptake value (SUVmax), metabolic tumor volume (MTV) and total lesion glycolysis (TLG) in patients with endometrial cancer and to investigate their role in risk stratification. **Methods:** Preoperative PET/CT results and postoperative histopathology results were retrospectively analyzed in 72 patients with endometrial cancer. Dual-phase pelvic imaging was performed on 16 of these patients. Clinical FIGO stages were as follows; stage I (n:5), stage II (n:5), stage III (n:4) and stage IV (n:2). Early imaging was done 1 hour after and delayed imaging was done approximately 2 hours after FDG injection. The SUVmax, MTV and TLG values were obtained from the primary lesion in the uterus in both early and delayed images. MTV was measured inside the tumor with margin thresholds set as 40% of SUVmax. **Results:** We observed a significant increase in tumor SUVmax on delayed image. The average of SUVs of the primary tumor were 17.2 ± 6.8 on the initial image whereas 20.8 ± 7.6 on delayed image ($p:0.002$). MTV ranged between 3.5–130 cm³ and TLG ranged between 25–1800 g in the patient group. We found no significant difference in MTV and TLG of the primary tumors with dual phase imaging. **Conclusion:** Dual-phase FDG PET offers information about the dynamics of glucose metabolism. We observed that, although malignant tumors continue to accumulate FDG over time, indices reflecting metabolic tumor burden are not affected by dual-phase PET imaging in this study of limited number of patients. We considered that both MTV and TLG are stable metabolic parameters that are not affected by timing of acquisition in patients with endometrial cancer.

EP106

Incidence and clinical Significance of bone metastasis detected using F-18 FDG PET/CT in Patients With Gynecologic Malignancy

S. Yoon; Dankook University College of Medicine, Seoul, KOREA, REPUBLIC OF.

Objective: Usually bone metastasis is rare in the gynecologic malignancy, therefore bone scan is not indicated. The prognosis of gynecological cancer patients with bone metastasis is poor. We performed F-18 FDG PET/CT for staging and evaluation of metastasis in 4242 patients with gynecologic malignancy. Therefore we evaluated the incidence of bone metastasis using F-18 fluorodeoxyglucose positron emission tomography (FDG-PET) in the patients with the gynecologic cancer patients. **Material and method:** Between 2009 and 2015, we retrospectively analyzed PET/CT scans with pathological-proven gynecologic malignancies including cervix cancer(3040 patients), endometrial cancer(805 patients) and ovarian cancer(397 patients). Bone metastases were proved by MRI following FDG PET-CT or clinical follow up. **Results:** Incidence of metastatic bone metastasis in all 4242 patients with gynecologic malignancy was 18 patients(0.4%). Eight patients (33%) among 24 patients with bone metastasis were pathologically diagnosed cervical carcinoma. Three endometrial and seven ovarian carcinoma showed bone metastases. Five patents (28%) among 18 patients showed only single bone metastasis on the PET CT. The most common type of gynecologic malignancy with bone metastasis by incidence was ovarian carcinoma ($1.8\% = 7/397$ patients) compared with

cervical carcinoma ($0.3\% = 8/3040$ patients) and endometrial carcinoma ($0.4\% = 3/805$ patients). **Conclusions:** We found that the incidence of bone metastases in the gynecologic malignancy were very low (0.4%). The most common type of gynecologic malignancy with bone metastasis by incidence was ovarian carcinoma more than four to six times compared with cervical carcinoma and endometrial carcinoma. Although some article reported the incidence of bone metastasis secondary to endometrial cancer was 6 to 15% through very long follow up including autopsy, usually bone metastasis is rare in the gynecologic malignancies.

EP107

Correlation of ¹⁸F-FDG uptake on PET/CT with Ki67 immunohistochemistry in pretreatment epithelial ovarian cancer

M. Mayoral, P. Paredes, A. Saco, A. Fernandez-Martinez, P. Perlaiza, A. Tapias, P. Fusté, M. C. Sebastià, J. Ordi, J. Pavia, J. Pahisa, F. Lomeña; Hospital Clinic Barcelona, Barcelona, SPAIN.

AIM: Metabolic tumor volume (MTV) and total lesion glycolysis (TLG) from ¹⁸F-FDG PET/CT are emerging prognostic biomarkers in various solid neoplasms. These volumetric parameters and the maximum standardized uptake value (SUVmax) have shown to be useful criteria for disease prognostication in preoperative and post-treatment epithelial ovarian cancer (EOC) patients. On the other hand, Ki67 is another known prognostic biomarker in EOC associated with tumour aggressiveness. The aim of this study was to evaluate the association between ¹⁸F-FDG PET/CT measurements (SUVmax, MTV and TLG) and Ki67 in pretreatment EOC to determine whether PET/CT parameters could non-invasively predict tumour aggressiveness. **MATERIALS AND METHODS:** Fifteen patients with suspected or newly diagnosed EOC underwent pretreatment PET/CT. Two nuclear medicine physicians assessed the images. The highest SUVmax among all the malignant lesions and volumetric parameters MTV and TLG with a threshold of 30% and 40% of the SUVmax were obtained. The sum of the MTV of every lesion was the whole-body MTV (wbMTV) and whole-body TLG (wbTLG) was the summation of the MTV of each lesion multiplied by its SUVmean. On the other hand, proliferative activity as indicated by the Ki67 index was estimated in tumoral tissue specimens. Mean and hotspot Ki67 were obtained. Immunohistochemical findings were correlated with PET parameters using linear regression analysis. Previously, Shapiro-Wilk test was used to determine if the variables under study followed a Normal distribution. **RESULTS:** In this group of 15 patients with pretreatment EOC, the median age was 60 years old (range 19-74 years). Serous cancer was the most common histological subtype, being present in 11/15 (73.3%) patients. The median values of SUVmax, wbMTV 30%, wbMTV 40%, wbTLG 30% and wbTLG 40% were 14.79 (range 4.33-24.42), 572.22 mL (range 171.14-1548.59 mL), 406.42 mL (range 130.28-1176.26 mL), 2468.29 g (range 389.96-7418.11 g) and 2027.61 g (range 326.61-6013.27 g), respectively. The median values of mean and hotspot Ki67 were 33.60% (range 5.60-79.00%) and 54.41% (range 22.5-95.9%), respectively. All variables under study followed a Normal distribution. A weak correlation was observed between PET parameters and Ki67. The highest correlation was obtained between mean Ki67 and SUVmax ($r^2=0.198$). **CONCLUSION:** SUVmax, wbMTV and wbTLG measured by ¹⁸F-FDG PET/CT were weakly correlated with Ki67. Thus, PET parameters do not seem to be predictors of tumour aggressiveness in patients with pretreatment EOC.

EP108

Comparison of ¹⁸F-FDG PET/CT or PET and CT in the diagnosis of metastatic lymph nodes in cervical cancer patients: a meta-analysis

H. Zhou; West China Hospital, Chengdu, CHINA.

Purpose: The study aims to perform a meta-analysis to compare the diagnostic performance of 18F-FDG PET/CT or PET and CT for detection of metastatic lymph nodes in cervical cancer patients. **Methods:** Articles of 18F-FDG PET/CT and CT on PC published in English from January 1990 to September 2016 was searched in the PubMed, EMBASE, Cochrane Library, Web of Science, and EBSCO databases to identify eligible studies on PET/CT or PET or CT of metastatic lymph nodes in cervical cancer patients. QUADAS was used to evaluate the methodological quality of the included studies. Pooled sensitivity, specificity, and diagnostic odds ratios (DOR) were calculated both on a per-patient basis. Summary receiver operating characteristic (SROC) curves were also drawn to obtain the area under curve (AUC) and Q* value. **Results:** 33 articles were included in the analysis. On a per-patient basis, the pooled sensitivity of PET/CT or PET (88%) was significantly higher than that of CT (62%), and the pooled specificity of PET/CT (92%) was higher than that for CT (89%). **Conclusions:** This meta-analysis indicated that FDG PET/CT or PET was better than CT on a per-patient basis for diagnosis of metastatic lymph nodes in cervical cancer patients.

EP109

FDG-PET/CT in the primary assessment of operability of women with ovarian cancer - experiences with incidental findings

S. E. Sponholtz¹, M. G. Hildebrandt¹, P. F. Høiland-Carlsen¹, O. Mogensen², P. T. Jensen¹; ¹Odense University Hospital, Odense, DENMARK, ²Karolinska University Hospital, Stockholm, SWEDEN.

Aim: The aim was to assess the clinical impact of pre-operative FDG-PET/CT in women with ovarian, fallopian tube, and peritoneal cancer (abbreviated to: OC) with special focus on consequences of identifying incidental findings (IFs). **Material and methods:** Pre-operative FDG-PET/CT scans in women with OC performed from January 2011 - December 2012 at our hospital were reviewed. All IFs were registered, and at the first succeeding multidisciplinary team conference it was decided whether an IF needed further examination or not. Subsequent procedures were tracked via medical records. The result of additional examination and the consequent delay in planned treatment was registered. **Results:** Of 209 included women, aged 16-95 years, 46 (22%) presented with one or several IFs. Further examination was recommended in all 46 and was actually performed in 35 (76%). Malignancy was identified in 12 (34%) of the 35 women, revealing metastases from OC (9 women) or a synchronous primary cancer (3 women). The identified metastases from OC were localized in lungs, uterus, colon, vagina, and breasts. Further investigation in the remaining 23 women with IFs, who underwent further examination, revealed two benign lesions and one pre-malignant lesion; no abnormality was found in 16 women, and findings were considered inconclusive in four. A significant delay in time until treatment of median four days (range 1-83) was found when an IF led to further examination ($p < 0.004$). **Conclusion:** About 1/5 to 1/4 of FDG-PET/CT scans detected IFs. Further examination led to a malignant diagnosis in about 1/3 of these cases, most often as metastases from OC, indicating that FDG-PET/CT may be considered a valuable tool in assessing metastases with rare locations in women with OC. Further examinations as a consequence of IFs delayed the time to treatment by median four days; the clinical implications of this must be balanced against the gain by detecting unrecognized malignancy in 12 of 209 patients (6%).

EP110

Incidence and clinical Significance of Neck Node metastasis in Patients With Gynecologic Malignancy : Tumor Marker vs PET/CT Correlation in 4242 patients with gynecologic malignancy

S. Yoon; Dankook University College of Medicine, Seoul, KOREA, REPUBLIC OF.

Objective: Usually node metastasis in the neck region is rare in the gynecologic malignancy. We performed F-18 FDG PET/CT for staging and evaluation of metastasis in 4242 patients with gynecologic malignancy. Therefore we evaluated the incidence of neck node metastasis using PET/CT in the patients with the gynecologic cancer patients. PET/CT finding correlated with tumor marker. **Material and method:** Between 2009 and 2015, we retrospectively analyzed F-18 FDG PET/CT scans with pathological-proven gynecologic malignancies including cervix cancer(3040 patients), endometrial cancer(805 patients) and ovarian cancer(397 patients). Neck node metastases were proved by sono guided biopsy of the neck nodes or clinical follow up. We compared the tumor marker according to the multiplicity of FDG uptakes outside of the neck and only single uptake in the neck. **Results.:** Incidence of metastatic neck node in all 4242 patients with gynecologic malignancy was 24 patients(0.6%). Fifteen patients (75%) among 24 patients with pathological proven neck node metastasis were cervical carcinoma. Three endometrial and six ovarian carcinoma were diagnosed as neck node metastases. Six patents (25%) among 24 patients showed only single uptake in the neck on the PET CT. Four patients among six single node metastasis was cervix carcinoma. Tumor marker of 5 patients (83%) among 6 patients with only single uptake and metastasis in the neck were within normal range. While, only 2 patients (11%) among other multiple focal FDG uptakes including neck node uptake showed the normal tumor marker. The most common type of gynecologic malignancy with neck node metastasis by incidence was ovarian carcinoma (1.5%= 6/397patients) compared with cervical carcinoma (0.5%=15/3040patients) and endometrial carcinoma(0.4%= 3/805patient). **Conclusions:** We found that the incidence of neck node metastases in the gynecologic malignancy were very low (0.6%). Sensitivity of tumor marker in patient with single neck node metastasis was very low (17%). The most common type of gynecologic malignancy with neck node metastasis by incidence was ovarian carcinoma more than three times compared with cervical carcinoma and endometrial carcinoma. We should rule out the neck node metastasis in case of neck node uptake on the PET/CT even though very lower incidence of neck node metastasis and normal tumor marker in gynecologic malignancy.

EP111

The Role of F-18 FDG PET/CT Scan in Evaluation of the Patients with Vulvar and Vaginal Cancers

I. AK SIVRIKOZ¹, E. VARDARELI², H. ONNER¹, S. OZALP³; ¹ESOGU SCHOOL OF MEDICINE DEPARTMENT OF NUCLEAR MEDICINE, ESKISEHIR, TURKEY, ²ACIBADEM UNIVERSITY SCHOOL OF MEDICINE DEPARTMENT OF NUCLEAR MEDICINE, ISTANBUL, TURKEY, ³ESOGU SCHOOL OF MEDICINE DEPARTMENT OF GYNECOLOGIC ONCOLOGY, ESKISEHIR, TURKEY.

Aim: The use of FDG-PET/CT in patients with vulvar cancer is unclear. There are a few reports suggesting that these tumors are FDG avid, however there is very little published data addressing the diagnostic impact of PET/CT in vulvar and vaginal cancers. The aim of this study was to assess the diagnostic yield of F-18 FDG PET/CT in the management of patients with vulvar and vaginal cancers. **Material and methods:** We retrospectively analyzed the data of 34 consecutive patients underwent F-18 FDG-PET/CT study for a known primary or suspected/recurrent vulvar/vaginal cancer from our institution and another centre had same PET/CT scanner. All patients underwent a staging evaluation with history and physical examination, routine laboratory studies, vulvar/vaginal biopsy, CT of the thorax, abdomen and pelvis, and whole-body F-18 FDG PET/CT scan (Siemens Medical Solutions, Biograph 6, Chicago, IL, USA). **Results:** A total of 34 patients with vulvar carcinoma (n= 28 patients) and vaginal carcinoma (n=6 patients) enrolled to the study. The mean age of the patients was 68.2 ± 2.18 years (range 45-91 years). Twenty four FDG PET/CT studies were from patients with a new diagnosis (70%) and 10 from patients with suspicion of recurrence due to previous vulvar/vaginal cancer (30%). The histological types of

the tumours were the Squamous cell ca in 29 patients, Malign Melanoma in 4 patients and Adenocarcinoma in one patient. F-18 FDG PET/CT scan was performed on pre-operative period in 18 of 24 patients. All of them showed increased FDG uptake at primary tumour localization (18/18). There were no sign of pelvic nodal involvement or distant metastatic disease in 7 of these 18 patients. However, inguinal/iliac lymph node involvements and distant metastasis (lung, liver and bone) were seen in 9 of 18 patients and in 2 of 18 patients, respectively. The PET/CT scan was performed in 6 patients after the excision of vulvar lesion for staging of diseases. There was no pathologic FDG uptake for suggesting nodal/distant metastatic involvement on whole body study. There were positive FDG results for only local recurrence and/or iliac/inguinal lymphatic involvements in 2 of 10 patients (10/34) with suspicion of recurrence due to previous vulvar/vaginal cancers. In remaining 8 patients, there were positive FDG results for distant metastasis (lung, bone, liver and adrenal gland). **Conclusion:** F-18 FDG PET/CT is postulated as a useful imaging modality for the management of vulvar/vaginal cancers, mainly in the identification of nodal metastases.

EP112

Standardizing SUV Measurements and Comparing With Other Parameters to Predict Treatment Failure of Cervix Carcinoma

L. A. Güner, E. Ozyar, B. Sahin, B. Atalar, T. Aksoy, E. Vardareli; Acibadem University Maslak Hospital, Istanbul, TURKEY.

There are reports of different SUV based measures estimating prognosis of cervix carcinoma. Since body weight normalization is only one of the approaches with its own shortcomings, we proposed further normalizations that may provide additional or more robust information for tumor characteristics that may be related to disease prognosis. **Methods:** We prospectively evaluated 41 patients referred to our department for chemoradiotherapy. 23 of 41 (56%) patients had pelvic and/or FDG avid abdominal lymph nodes before treatment. During follow up (median 21 months), 14/41 had recurrence (34%) of which 11/41 had distant recurrence (27%), 5/41 (12%) had local/regional recurrence, 2/41 had both. Using the pretreatment staging FDGPET scans, we calculated SUVmax of primary lesion, SUVmean, SUVmax normalized to cerebellum mean (SUVnormcerebellum), SUVmax normalized to liver mean (SUVnormliver), metabolic tumor volume of 40% of maximum FDG uptake, metabolic tumor volume of >2.5SUV, total lesion glycolysis (tlg), tlg normalized to cerebellum, tlg normalized to liver, standard deviation of primary lesion as a surrogate for heterogeneity and visual evaluation of heterogeneity (Hvisu). **Results:** Of all the parameters calculated, versus recurrence (local/distant) only SUVnormliver was significantly correlated ($p=0.047$). Versus only distant-recurrence, again only SUVnormliver was significant ($p=0.05$). When we analyzed the subgroup of patients with FDG-avid abdominal lymph nodes before treatment, none of the variables held significance. When patients without FDG-avid abdominal lymph nodes were selected, again none of the variables were significantly correlated, although p-value for SUVnormliver was 0.08. When plotted in a ROC curve, SUVnormliver of 7.2 was the optimal cutoff point for predicting recurrence (with 71% sensitivity and 50% specificity). For this threshold, odds ratio of having a recurrence was 2.1. On the other side, with a pretreatment FDG-avid abdominal lymph node, the odds ratio of having recurrence was 1.9. These two parameters; pelvic lymph node positivity and SUVnormliver were correlated ($p=0.027$) and ROC analysis showed SUVnormliver of 7.6 was optimum cutoff value (65% sensitivity, 79% specificity for pelvic lymph node). **Conclusion** Among the mentioned parameters of tumor burden, heterogeneity or metabolic activity, only SUVmax normalized to liver was predictive of treatment failure. When subgroup analysis was performed for node-negative disease, this parameter was weakly correlated, though still better than others. Node positivity is already established for predicting recurrence. Other SUV based parameters should be avoided, as our results show no correlation to recurrence. SUV normalized to liver may still have value in node negative subgroup. Larger sample sizes are required to establish its value.

EP113

Sentinel node biopsy in early endometrial cancer: preliminary results

A. Caresia Aróztegui, L. Ribot Luna, J. Martin Marimon, Q. Sun Lin, A. Rodríguez Revuelto, I. Costa Trachsel, B. Morillas Oliveras, Y. García García, J. Antoni Vives, L. Bernà Roqueta; Hospital Parc Tauli, Sabadell, SPAIN.

AIM: This study aims to evaluate our experience implementing sentinel lymph node (SLN) mapping in early stage endometrial cancer. **MATERIALS AND METHODS:** We included 22 patients with early stage endometrial cancer (preoperative FIGO stage Ia (n=7), Ib (n=14), and II (n=1)) on laparoscopic staging between 2010 and 2016. The SLN mapping technique included cervical injection of 99mTc-nanocolloid, preoperative lymphoscintigraphy (24 h before intervention), and intraoperative laparoscopic gamma probe SLN detection. After surgical removal of the SLN, all patients underwent systematic laparoscopic pelvic lymph node dissection. Ultrastaging of SLN was performed with haematoxylin and eosin stain (H&E) and immunohistochemistry (CAM 5.2). Lymphadenectomy samples were studied by conventional histopathological analysis with H&E. We calculated the detection rate and descriptive statistics for node- and patient-based analyses. **RESULTS:** The SLN mapping technique failed in two patients (1 without SLN drainage and 1 with intraperitoneal nanocolloid uptake); the SLN detection rate was 90% (20/22). A total of 29 SLNs were detected (mean, 1.45 per patient); 69% in the interiliac region (20/29) and 31% in the internal iliac region (9/29). One SLN had macrometastases, four had micrometastases, and two had isolated tumour cells. At lymphadenectomy, a mean of 14.8 nodes were dissected; all non-SLNs dissected were negative (0% false-negative rate). Of the 20 patients, 4 had positive SLN (1 macrometastases and 3 micrometastases). Ultrastaging of SLNs revealed lymph node metastases in 2 patients undetected by conventional histopathological analysis. In the patient-based analysis, the sensitivity was 100% and the negative predictive value was 100%. **CONCLUSIONS :** SLN surgical biopsy in early endometrial cancer is a feasible and useful technique for detecting metastatic node involvement. The high negative predictive value in our preliminary results suggests that it could be incorporated into routine clinical practice.

EP-07 – Sunday, October 16, 2016, during Exhibition hours, e-Poster Area
Clinical Oncology: Head & Neck

EP114

The role of oropharyngealoesophageal scintigraphy in the evaluation of swallowing function in nasopharyngeal and oropharyngeal cancer treated by radiotherapy: short-term results of a prospective study

E. Fiasconaro¹, M. Grosso¹, E. Tardelli¹, G. Aghakhanyan¹, B. Fattori², G. Puccini¹, M. Gennaro¹, R. Boni¹, F. Guidoccio¹, R. Raschilla¹, S. Ursino³, I. Paglianiti¹, D. Volterrani¹; ¹Department of Nuclear Medicine, University Hospital S. Chiara, Pisa, PISA, ITALY, ²Otorhinolaryngology-Audiology-Phoniatic Unit, University Hospital Cisanello, Pisa, PISA, ITALY, ³Department of Radiation Oncology, University Hospital S. Chiara, Pisa, PISA, ITALY.

Aim To report the initial results of a prospective trial aimed to assess instrumental deglutition function (Videofluoroscopy, OroPharyngealEsophageal and Fiberoptic Endoscopic Evaluation) for sparing the swallowing organ at risk in nasopharyngeal and oropharyngeal cancers after radio or chemoradiotherapy using intensitymodulated radiotherapy (IMRT). **Patients and Methods** Since 2012 to 2014, we enrolled 23 patients affected by Nasopharynx (7) or Oropharynx (16) cancer (Stage II-IVA), ECOG 0-2. Instrumental assessment of swallowing function included VFS, FEES and OPES at baseline, 1, 6 and 12 months after radiotherapy. The scores of dysphagia parameters, such as pre-deglutition penetration, aspiration, pharyngeal transit time (PTT) and hypopharyngeal retention index (HPRi), were

calculated after each assessment both with liquid (L) and semiliquid (SL) bolus intake. **Results** The examination of the relationships between the pre and post-treatment changes in HPRI score was found to be statistically significant both at FEES-L ($p=0,021$) and SL ($p=0,02$) and at VFS-L ($p=0,008$) and SL ($p=0,005$) and OPES-SL ($p=0,028$). In particular we found a SLHPRI worsening scores from the baseline to 1 month after treatment. Besides, a total of 12 (55%), 21 (95%) and 14 (62%) patients experienced poorer scores at FEES-L, VFS-L and OPES-L. All patients showed a poorer HPRI score at VFS-SL and OPES-SL, as well as 14 (70%) at FEES-SL. PTT resulted not significantly affected by RT at the three different exams both after L and SL bolus intake. Furthermore, the pre-deglutition penetration at 1 month was detected in only 1 patient at FEES-L and SL while aspiration at 1 month was detected in 1 only patient by OPES-L and FEES-SL. Finally, aspiration was observed in only 2 patients (10%) at OPES-L. **Conclusions** Our preliminary data seem to confirm a low percentage of major instrumental dysfunction (pre-deglutition penetration or aspiration) after IMRT and lack of severe side effects (PEG positioning or clinical aspiration). IMRT significantly limits acute severe deglutition sequelae in HN cancer treated patients compared to literature reports. Thus, the dysphagia assessment using solid bolus might show a higher percentage of HPRI worsening due to the requirement of a stronger muscular propulsion in this cohort. Indeed, longer follow-up and greater sample size are needed to further evaluate whether increase of HPRI by instrumental methods such as OPES, would be related to a high risk of developing late aspiration (6 and 12 months).

EP115

Sentinel lymph node procedure in squamous cell carcinoma of the oral cavity, comparison with subsequently performed elective neck dissection

D. Lobeek¹, W. L. J. Weijts¹, C. Coppen¹, A. I. J. Arens¹, M. C. van Rijk¹, M. Rijpkema¹, E. P. Mijnheere¹, J. Honings¹, M. A. W. Merks¹, H. Ghaemina¹, S. C. van den Bosch¹, O. C. Boerman¹, W. J. G. Oyen^{1,2}, R. P. Takes¹; ¹Radboud University Medical Center Nijmegen, Nijmegen, NETHERLANDS, ²Institute of Cancer Research, Royal Marsden NHS Trust, London, UNITED KINGDOM.

AIM: Several studies have been performed to study the feasibility and clinical applicability of the sentinel lymph node (SN) procedure in oral cavity squamous cell carcinoma (OCSCC). The SN-procedure is gaining more acceptance as a viable alternative to the conventional elective neck dissection (END) in T1-2N0 OCSCC. To introduce this SN-procedure in our institution, we performed a SN-procedure prior to the END to evaluate the feasibility of this procedure. **MATERIAL AND METHODS:** The day before surgery, 80 MBq ^{99m}Tc-nanocolloid was administered as four peritumoral injections in patients clinically classified as T1-2N0 OCSCC. The injection was followed by dynamic lymphoscintigraphy. Additional planar and SPECT/CT images were obtained 2-4 hours after injection. Pre-operatively, all images were used to identify the tumor draining lymph nodes and to discriminate them from second echelon nodes. These SNs were marked on the skin. During surgery the marked SNs were identified using a handheld gamma probe and excised. The SN-procedure was immediately followed by END and tumor resection. **RESULTS:** Sixteen patients with a cT1-2N0 OSCC (buccal mucosa (n=2), tongue (n=10), floor of the mouth (n=4)) were recruited from August 2015 till April 2016. In each patient, one to five SNs were identified pre-operatively. 82% (37/45) of all SN foci could be localized and resected, of which 22% (8/37) revealed metastasis. With the END a total of 374 nodes were excised. 1.9% (7/374) of the nodes in the END specimen, not identified and removed as SN, showed accumulation of ^{99m}Tc-nanocolloid, but did not contain metastasis. 0.53% (2/374) nodes of the END in two patients revealed metastasis at histology. One patient showed metastases in an ipsilateral node level III of a lateral tongue tumor and the other showed metastases in a level II node of a floor of the mouth tumor in

the midline. Both patients were within the first six of the performed procedures and in which not all SNs were harvested during the SN biopsy. The SNs found in these two patients did not contain metastasis. **CONCLUSION:** One to five nodes per patient were identified as SNs, but not all were identified and excised during the SN-procedure. For adequate SN-procedures, a close cooperation of all involved disciplines is essential. Also, a learning curve should be taken into account to identify, mark, and find SNs adequately. To intercept possible mishaps of the SN-procedure, the SN-procedure should be introduced while continuing the END in the first couple of patients.

EP116

Diagnostic accuracy of F18-FDG-PET/CT in patients with biochemical evidence of recurrent, residual or metastatic medullary thyroid cancer

L. RODRIGUEZ-BEL¹, A. SABATÉ-LLOBERA¹, J. VERCHER-CONEJERO¹, L. GRÀCIA-SÁNCHEZ¹, E. LLINARES-TELLO¹, M. COS-DOMINGO², P. MORENO-LLORENTE³, M. PÉREZ-MARAVÉ⁴, A. TEULÉ-VEGA⁵, I. GIL-VICIANO⁶, J. ROBLES-BARBA¹, M. CORTÉS-ROMERA⁶, C. GÁMEZ-CENZANO¹; ¹PET Unit. Department of Nuclear Medicine. IDI. Hospital U. de Bellvitge-IDIBELL, L'Hospitalet de Llobregat (Barcelona), SPAIN, ²Department of Radiology. IDI. Hospital U. de Bellvitge-IDIBELL, L'Hospitalet de Llobregat (Barcelona), SPAIN, ³Department of Surgery. Hospital U. de Bellvitge-IDIBELL, L'Hospitalet de Llobregat (Barcelona), SPAIN, ⁴Department of Endocrinology. Hospital U. de Bellvitge-IDIBELL, L'Hospitalet de Llobregat (Barcelona), SPAIN, ⁵Department of Medical Oncology. ICO. Hospital Duran i Reynals-IDIBELL, L'Hospitalet de Llobregat (Barcelona), SPAIN, ⁶PET Unit. Department of Nuclear Medicine. IDI. Hospital U. de Bellvitge-IDIBELL, L'Hospitalet de Llobregat (Barcelona), SPAIN.

AIM Medullary thyroid carcinoma (MTC) is a rare calcitonin and carcinoembryonic antigen (CEA)-secreting tumor of the parafollicular C cells of the thyroid. Calcitonin is the principal serum tumor marker. The aim of this study was to investigate the potential use of FDG-PET/CT in localizing MTC residual, recurrent or metastatic disease in patients with elevated calcitonin +/- CEA levels. **MATERIAL AND METHODS** From our database between 2003 to 2015 we retrospectively included 59 FDG-PET/CT studies in 44 patients with MTC. Final selection criteria with total thyroidectomy and elevated calcitonin levels resulted in 51 FDG-PET/CT scans in 44 patients. Serial follow-up scans (7) were included when there was an increase in calcitonin level by at least 20% and the prior study was negative or when positive after surgical resection of FDG-avid lesions in the interim and the calcitonin level did not normalize. PET/CT findings were classified as positive or negative on the basis of visual interpretation of the scan. Maximum Standardized uptake values (SUVs) were also calculated. FDG-PET/CT findings were confirmed by histopathological results, when available, or other imaging studies and clinical follow-up (mean 4 years, range 1-12). **RESULTS** The 51 FDG-PET/CT scans were classified as: 23 true-positive, 3 false-positive, 14 true-negative and 11 false-negative. The overall sensitivity specificity, positive predictive value and negative predictive value were 68%, 82%, 88% and 56% respectively, with a diagnostic accuracy of 72%. Calcitonin levels ranged from 49 to 28.000 pg/ml (mean in positive FDG-PET/CT scans of 3521 and in negative ones of 521). We found statistical differences on calcitonin levels between positive and negative FDG-PET/CT scans ($p<0,05$). The mean SUVmax of all lesions with FDG uptake was 4,7 g/ml (range 3-11; mean in metastatic disease: 5,6 and in locoregional disease: 3,5). There were statistical differences on SUVmax values between patients with locoregional and metastatic disease ($p<0,05$). **CONCLUSIONS** FDG-PET/CT can detect residual, recurrent or metastatic MTC with a reasonable sensitivity of

68% and diagnostic accuracy of 72% in patients with elevated calcitonin levels. The probability for disease detection is higher in patients with higher calcitonin levels. FDG-PET/CT has a therapeutic impact because of its high positive predictive value (88%). However, in negative FDG-PET/CT scans a strict clinical, serological, and radiological follow-up is mandatory because of the negative predictive value of the technique (56%).

EP117

Usefulness of ¹⁸F-FDG-PET-CT in Searching for the Primary in Cancer of Unknown Primary (CUP) of Head and Neck

C. Sampol¹, S. Rubi¹, A. Moll², M. Villar³, M. Toscano³, M. Oporto¹, C. Peña¹; ¹Hospital Universitario Son Espases. Nuclear Medicine Department., Palma de Mallorca, SPAIN, ²Hospital Universitario Son Espases. Radiology Department., Palma de Mallorca, SPAIN, ³Hospital Universitario Son Espases. Radiopharmacy Department, Palma de Mallorca, SPAIN.

AIM To analyze the usefulness of the ¹⁸F-FDG-PET/CT in detecting CUP of the head and neck after a malignant anathomopathologic result in a biopsy of a cervical lymph adenopathy as the only finding. **METHOD** Included 49p, all of them diagnosed with malignancy of head and neck lymphadenopathy. A CT with intravenous contrast and an endoscopic examination were done, without detecting any lesion suspicious of primary tumor. A ¹⁸F-FDG-PET/CT was performed on patients. Afterwards we proceed to confirm the results of the images by biopsy or by clinical follow-up. **RESULTS** Out of 49p included, median age 60yo, 42 were Squamous cell carcinoma, 4 Undifferentiated, 2 adenocarcinomas and 1 lymphoepitelioma. The PET-CT showed primary tumor in 24p, 22 located in head and neck (8 in base of tongue, 7 in amygdala, 2 in nasopharynx, 2 in piriform sinus and 3 in hypopharynx), and 2 located outside of head and neck (metastatic prostate cancer and lung). 3/24p were false positive: 2 amygdala and 1 hypopharynx, with negative biopsy result. The detection rate of primary tumor with PET-CT was 42.8%(21/49). In 25p PET-CT was negative of any focus suspicious of primary tumor, being negative the biopsy in 23(1p was diagnosed with metastatic parotid node of a cutaneous malignancy and 3p showed distant metastasis); 2/25p were false negative result of the image finding positive biopsy in left nasopharynx and lateral wall of hypopharynx. Out of 19p without primary tumor diagnosis, no tumor was detected or distant metastasis by any other technique during follow-up (average 24m). The PET/CT detected distant metastasis in 5p (bone, lung, brain and adrenal gland), as well as extracervical lymph nodes in 14p (12 of the supraclavicular). A second primary tumor was detected by PET in 2p, both in the colon (1p died the following month because of a perforation). One of the patients with Undifferentiated tumor result an anaplastic lymphoma on the finally anathomopathologic result after functional lymphadenectomy. The PET/CT in the detection of the primary tumor in CUP of head and neck showed a S, E, PPV, NPV of 91%, 88%, 87.5% and 92%, respectively. In 35% of cases thanks of PET/CT, the treatment strategy was modified. **CONCLUSION** The ¹⁸F-FDG PET/CT demonstrates a very strong capability in detecting primary tumor of head and neck CUP in patients with cervical lymph adenopathies that induces an important change in the therapeutic approach of this patients. It should be used as a guide of biopsy in the clinical handling of these patients.

EP118

Similar image of FDG PET-CT in lesion of palatine tonsils: in primary tonsillar cancer, Non Hodgkin Lymphoma and Chronic tonsillitis three cases

T. Y. P. Yordanova, Anelia Klisarova, Pavel Bochev, Borislav Chaushev, Zhivka Dancheva; MBAL St Marina, Varna, BULGARIA.

Aim: The aim of this study is to assess the usefulness of ¹⁸F-FDG PET/CT in lesion of palatine tonsils and cervical lymphadenopathy. F-FDG PET/CT has been used for the evaluation of various tumors. PET/CT is used to identify primary or synchronous secondary primary tumor of the Head and neck through changes in F-FDG uptake. However, both physiologic and abnormal lesions increase F-FDG uptake. **Methods:** We presented three cases of patients with biopsy confirmed various primary malignancies (Non-Hodgkin's Lymphoma, Oropharyngeal carcinoma and Lung carcinoma). The whole body T/CT scan presented similar image in head and neck in all of them- high FDG in palatine tonsil and increase glucose metabolic activity in regional lymph node. **Methods:** Before whole-body PET/CT two of patients had histological confirmation of primary malignancy of palatine tonsils (Non-Hodgkin's Lymphoma, Oropharyngeal carcinoma). The third patient has histological conformation of primary lung carcinoma and PET/CT detected high metabolic activity in palatine tonsil (SUVmax 7.9) and high FDG uptake in regional lymph node (SUVmax 3.5), which was suspicious for synchronous secondary primary tumor of Head and neck. In the patient with Non-Hodgkin's Lymphoma, PET/CT showed high ¹⁸F-FDG uptake in tonsil (SUVmax 3.8) and in regional lymph node (SUVmax 2.5). In patient with Oropharyngeal carcinoma PET/CT demonstrated very high FDG uptake in palatine tonsil (SUVmax 10.7) similar like those with primary lung carcinoma and incidental finding of high FDG accumulation in tonsil SUVmax 7.9 (which was suspected for synchronous secondary primary tumor of Head and Neck). Both patients presented with remarkable FDG uptake in palatine tonsil (SUVmax 10.7/ 7.9) and high glucose metabolism in regional lymph node (SUVmax 2.5/ 3.5). In third patient after tonsillectomy of the suspected malignant lesion the histology report revealed inflammation (chronic tonsillitis). The PET/CT result was false positive. **Conclusion:** ¹⁸F-FDG is not tumor specific marker. We presented three cases with various tumors: primary tonsillar lymphoma, primary oropharyngeal carcinoma (involved tonsil) and Lung carcinoma with chronic inflammation in palatine tonsil. The whole body T/CT scan presented similar image in head and neck in all of them- high FDG in palatine tonsil and increase glucose metabolic activity in regional lymph node. Our three cases illustrated that PET-positive lesions not always present malignancy (regardless of the degree of glucose metabolism SUVmax), and a tissue biopsy is mandatory to confirm the diagnosis.

EP119

Laryngeal tuberculosis mimicking laryngeal carcinoma on F-18 FDG PET/CT imaging

A. Cengiz¹, S. Göksel¹, Y. Başal², S. Taş Gülen³, Y. Yürekli¹; ¹Adnan Menderes University, Medical School, Department of Nuclear Medicine, Aydın, TURKEY, ²Adnan Menderes University, Medical School, Department of Otorhinolaryngology, Aydın, TURKEY, ³Adnan Menderes University, Medical School, Department of Chest Disease, Aydın, TURKEY.

Aim: Laryngeal tuberculosis is an infrequent manifestation of extrapulmonary tuberculosis but it is the most common granulomatous disease of the larynx. Usually, it is seen as a complication of pulmonary tuberculosis but sometimes only laryngeal involvement is possible. Clinical, laryngoscopic and radiological findings of laryngeal tuberculosis have a tendency to mimic laryngeal cancer. F-18 FDG PET/CT findings of extrapulmonary tuberculosis are not specific and also mimic malignancy. We present a case of laryngeal tuberculosis who had underwent F-18 FDG PET/CT imaging with prediagnosis of laryngeal carcinoma. **Case report:** A 51 year old woman was referred to our otolaryngology clinic with history of cough, hoarseness and sore throat. Laryngoscopy revealed diffuse swelling and a lesion involving both arytenoids and the marginal portion of the epiglottis suggesting carcinoma of the larynx. Her prior medical history was unremarkable. Histopathological examination of lesion demonstrated necrosis and suspicious for malignancy and a second biopsy was recommended. Contrast-enhanced computed tomography (CT) scan of the neck

demonstrated an edema and asymmetry of **epiglottic vallecula**. **Thorax CT showed multiple nodules which resembling pulmonary metastasis on both lungs. Patient underwent F-18 FDG PET/CT imaging for diagnosis and staging.** PET/CT imaging showed hypermetabolic focus on left aryepiglottic fold and interarytenoid area (SUVmax:8.9) which was not accompanied by anatomical finding. In addition, there were multiple hypometabolic nodules and hypermetabolic infiltrations (SUVmax:6) on both lungs and mildly hypermetabolic millimetric cervical lymph nodes. Second laryngeal biopsy revealed a necrotising granulomatous inflammation suggesting tuberculosis. Mycobacterium tuberculosis PCR assay was also positive. Patient diagnosed lung and laryngeal tuberculosis and antituberculosis medication was started. **Conclusion:** As a whole body scanning method, 18F-FDG PET/CT facilitates the detection of extrapulmonary tuberculosis. Although it is a rare condition, extrapulmonary tuberculosis in head and neck should be kept in mind in differential diagnosis.

EP120

Role of 18F FDG PET-CT in restaging of patients with malignant salivary gland tumors: - experience at a tertiary care hospital

D. Malik, T. K. Jain, R. Kumar, A. Bhattacharya, A. Sood, B. R. Mittal; Post graduate institute of medical education & research, Chandigarh, INDIA.

Objective: Salivary gland tumors are rare neoplasms comprising about 0.5% of all malignancies and about 5% of head and neck cancers that have not been studied extensively with FDG PET/CT. The aim of present study was to assess the clinical utility of 18F-Fluorodeoxyglucose (¹⁸F-FDG) positron emission tomography-computed tomography (PET-CT) for restaging patients with malignant salivary gland tumors. **Methods:** In this retrospective study we evaluated the data of 25 patients (Age: 44.9±23.2 years; male/female: 17/8) with histopathological proven malignant salivary gland tumor, who underwent ¹⁸F-FDG PET-CT for restaging between August 2008 and September 2015. After restaging ¹⁸F-FDG PET-CT majority of patients received chemotherapy (85%), followed by radiotherapy and surgery. ¹⁸F-FDG PET-CT images were reviewed by two nuclear medicine physicians in consensus who were blinded to all details except for primary diagnosis. Clinical/imaging follow up (minimum-12 months) with histopathology were taken as reference standard. **Results:** Of the 25 patients, 18 patients were presented with primary parotid tumors while 7 with submandibular gland tumors. All 25 patients underwent FDG PET/CT for restaging and found 19 (76%) were positive and 6 (24%) were negative for disease. FDG PET/CT detected loco-regional disease in 18 (72%) patients and distant metastasis in four (16%) patients. In all four patients with distant metastasis, the lesions distribution was lung in 2/4 (50%) patients and brain and skeleton in one patient each. Seventeen FDG PET/CT were true positive, 5 were true negative, two were false positive and one was false negative. The overall sensitivity of ¹⁸F-FDG PET-CT was 94.7% [95% CI: 73.9-99.8], specificity was 71.4% [95% CI: 29.0-96.3], positive predictive value 90.0% [95% CI: 68.3- 98.7] negative predictive value 83.3% [95% CI: 35.8- 99.6] and accuracy was 94%. Additionally FDG PET/CT detected 2nd primary malignancy in two patients (lung and larynx in one each). **Conclusions:** We concluded that 18F-FDG PET/CT had high diagnostic accuracy for residual/recurrent disease in malignant salivary gland tumor patients and also useful in detection of additional metachronous second primary.

EP121

Efficacy of 11C-MET-PET/CT in the restaging of adenoid cystic carcinoma of head and neck

F. SCALORBI¹, A. Matti¹, G. Lima¹, S. Diodato¹, A. Iannalfi², M. Bonora², B. Vischioni², P. Castellucci¹, S. Fanti¹; ¹S. Orsola-Malpighi Hospital-University of Bologna, Bologna, ITALY, ²Centro Nazionale Adroterapia Oncologica, Pavia, ITALY.

Aim: The aim of this retrospective study was to evaluate the role of 11C-MET-PET/CT (MET-PET) in the restaging of adenoid cystic carcinoma (ACC) of head and neck, after primary treatments (surgery, radiotherapy or both). **Materials and Methods:** Eleven patients (6 female, 5 male, mean age 60.5 years, range 23-79 years) underwent MET-PET, between May 2013 to November 2015, within 3.3 months from the last treatment (range 1-4; only one patient performed MET-PET after 14 months). Four of eleven (36%) were treated with Hadron Therapy, two (18%) with surgery and five (46%) with both therapies (surgery + Hadron Therapy). All the findings were validated by means of imaging and/or clinical follow up (FU) (mean value 9.8 months, range 3-20 months). MET-PET were evaluated visually by two experienced nuclear medicine physicians. MET-PET results were classified as positive, negative or doubt. SUV max was calculated but not used to achieve the final diagnosis. **Results:** MET-PET was positive in six (55%) of eleven patients, negative in four (36%) and doubt only in one case (9%). All the six positive cases were confirmed to be true positives (TP) by clinical and/or radiological FU. MET-PET Positive Predictive Value (PPV) was 100% for the localization of local relapse and for the detection of lateral-cervical lymph-nodes metastasis. In one of these cases MET-PET showed an increased uptake in temporal lobe, that was confirmed to be positive during FU. Four cases were negative on MET-PET, two of these were True Negative and two were False Negative (FN). The first FN case had local progression of disease after one year of FU. We consider this as typical long-term evolution that characterized this disease. The second FN patient showed faint uptake misinterpreted as post-actinic reaction but consistent with progression of disease, as confirmed three months later by FU. MET-PET was doubt in one patient, were it was not possible to distinguish between post surgical changes and persistence of disease. Finally we would like to underline that, in our small population, we didn't note any correlation between time elapsed from the end of primary treatment and the accuracy of MET-PET. **Conclusions:** MET-PET showed an excellent PPV (100%) and a low NPV (50%) to restage ACC. This is partially in contrast with what is generally observed in other head and neck tumors. Further studies are needed in order to assess the potential clinical impact of MET-PET to restage ACC.

EP122

A novel, objective interpretation method for dual-phase Technetium 99m-sestamibi parathyroid scan, measuring the degree of asymmetric parathyroid activity on bilateral thyroid beds, aids preoperative localization of single parathyroid adenoma for minimally invasive parathyroidectomy

D. Kim, J. Rhodes, J. Hashim, L. Rickabaugh, D. Brams, E. Pinkus, Y. Dou; Lahey Hospital and Medical Center, Burlington, MA, UNITED STATES.

Aim: Primary hyperparathyroidism affects approximately 1 in 1,000 people in the general population. Approximately 80% of these cases can be attributed to solitary parathyroid adenoma. Given this high incidence of solitary adenoma, surgical and imaging communities have searched for an accurate preoperative localizing test to select patients for minimally invasive parathyroidectomy (MIP) in lieu of traditional four-gland exploration. We hypothesized that Tc99m sestamibi scan interpretation incorporating numerical measurements on the degree of asymmetrical activity on bilateral thyroid beds can be useful in localizing single adenoma for MIP. **Materials and Methods:** We devised a novel two-step interpretation method for dual-phase Tc99m sestamibi scan, based on the degree of asymmetrical activity on early phase images and dichotomized interpretation of washout on delayed images. To measure asymmetrical activity on early phase images, the numerical ratio value of each scan was obtained by dividing the number of counts from symmetrically drawn regions of interest (ROI) over bilateral thyroid beds. To validate our new method, 109 sestamibi scans—previously performed for primary hyperparathyroidism—were reinterpreted and correlated with their final

pathology. **Results:** Among the 109 cases, there were 85 instances of non-ectopic single adenoma (78.0%), 2 ectopic adenoma (1.8%), 11 hyperplasia (10.1%), 2 multiple adenoma (1.8%), 2 parathyroid carcinoma (1.8%), and 3 normal parathyroid glands (2.8%). Using the ratio values obtained for each scan as above, an empirical Receiver Operating Characteristic curve was obtained and the area under the curve (AUC) was calculated to be 0.71 ($p=0.0032$), validating this method as a diagnostic tool. Using Youden indices, the optimal cut-off point with maximal combined sensitivity and specificity was found with a corresponding sensitivity of 67.45% (56.48% to 77.16%, 95% CI) and a specificity of 76.2% (52.83% to 91.78%, 95% CI). An additional higher cut-off with higher specificity and minimum possible sacrifice on sensitivity was also selected, yielding a sensitivity of 27.91% (18.77% to 38.62%, 95% CI) and a specificity of 90.48% (69.62% to 98.83%, 95% CI). The addition of delayed phase information also improved the specificity for localization, but to a lesser degree than the degree of asymmetrical activity on the initial phase. **Conclusion:** Our results demonstrated that more asymmetrical activity on the initial phase corresponded with greater success in the localization of single parathyroid adenoma on sestamibi scans. Using high cut-off ratio value obtained from initial phase sestamibi scan images, we were able to select patients for minimally invasive parathyroidectomy with 90% specificity.

EP123

Increased Tc99m-labelled Somatostatin Analogue Uptake in a Lymph Node Metastasis of Squamous Cell Carcinoma in the Head and Neck Region. Presentation of an Unusual Case

Z. Varga¹, L. Jorgov¹, É. Remenár², M. Gödény², E. Takács¹, I. Szilvási¹, G. Dabasi¹; ¹Semmelweis University, Budapest, HUNGARY, ²National Institute of Oncology, Budapest, HUNGARY.

In our case report we present intensive uptake of Tc99m-EDDA/HYNIC-TOC in a histologically verified lymph node metastasis of squamous cell cancer in the neck region. This is a very rare finding. To our best knowledge only one similar case report has been published up to now. Case report: A 70 year old male patient was admitted because of recent enlarged lymph node without any inflammatory changes on the right side of the neck. MRI revealed abnormal soft-tissue mass on the neck close to the right submandibular gland. US guided FNA was inconclusive. Based on MRI examination diagnosis of a glomus tumor was suspected. We performed Tc-99m-HYNIC-EDDA-TOC scintigraphy using SPECT/CT. Increased uptake of radiopharmaceutical was seen in the soft tissue mass with a diameter of 30x27x25 mm without any other abnormal uptake on the whole body scan. After a repeated MRI examination surgical excision biopsy was performed in July 2013. Histological finding was lymph node metastasis of grade III basaloid type of planocellular cancer. By immunohistochemistry chromogranin, synaptophysin, S100 were negative. Looking for the primary tumor MRI and contrast-enhanced CT of the head and neck, thorax, contrast-enhanced CT of the abdomen, pelvic region and FDG PET/CT examinations, biopsy from the tongue root and from the right tonsil were performed. No primary tumor was found. Based on the decision of the onco-team, regional radiotherapy was applied to the right neck region. In the follow up of the patient until February 2015 no recurrence or any sign of progression were observed by repeated imaging methods. The primary tumor remained unknown. Discussion: To our best knowledge there are just a few report on abnormally increased uptake by somatostatin receptor scintigraphy in squamous cell carcinoma and only one report has been published in a patient with squamous cell cancer of the head and neck region. Up to present, basaloid cancer has not been on the indication list of somatostatin receptor scintigraphy. We plan to start a prospective study to evaluate the possible clinical usefulness of Tc99m-EDDA/HYNIC-TOC scintigraphy in patients with squamous cell tumors of the head and neck region.

EP124

Diagnostic and prognostic values of 18F-FDG PET-CT in the management of adenoid cystic carcinoma of salivary glands

G. Bera, R. De Laroche, G. Hervé, C. Bertoia, M. Bandini, M. Habert, A. Giron, C. Bertolus, A. Kas; Groupe Hospitalier Pitié-Salpêtrière, PARIS, FRANCE.

Aim Adenoid cystic carcinoma of salivary gland is the most commonly reported malignant tumor of the minor salivary glands and one of the most common cancers of the major salivary glands. The difficulty in its management lies on its unusual relentlessly growing characterized by perineural invasion and multiple local recurrences. Moreover, in contrast to regional node metastases, hematogenous spread is common especially to lung, bone and liver. Solid or high-grade histological type is considered to be more aggressive with relatively poor survival. Only one publication has reported the prediction of distant metastasis based on pretreatment SUV_{max} of the primary tumor. The purpose of this study is to demonstrate the diagnostic and prognostic values of PET-CT in the management of this tumor. **Methods** 14 patients (5 parotides, 2 sub-mandibulars, 7 minor salivary glands) including 5 high-grades had initial pretreatment PET-CT. SUV_{max} , MTV and TLG were measured on the primary tumor by 2 reviewers. Patients were classified into 2 groups reflecting their status, *better prognosis* (without any recurrence, $n=6$) or *lower prognosis* (at least one recurrence to related death, $n=8$). Histological grading, status at last follow-up and follow-up duration were taken as gold-standard. **Results** Median follow-up period was 25 months (3-258). All PET-CT detected primary tumor and distant metastasis ($n=6$). Median time to first recurrence was 20 months (range 18-156) for 4 patients. Only 4 patients had nodal metastasis, 2 of them were not identified by PET-CT nor MRI and concerned a lymph-node fused to the tumor. SUV_{max} (median 5, range 2.8-14) was positively correlated with grading (high vs low cut-off 6.4, $p<0.001$) and the presence of a solid pattern tumors $>30\%$ (cut-off 5.4, $p<0.0002$). MTV (median 6.6, range 1.7-89) and TLG (median 31.5, range 3.6-206) separated correctly the 2 groups, cut-off 6.1 ($p<0.01$) and 19.6 ($p<0.05$) respectively and showed a non significant trend to negative correlation with follow-up duration ($p=0.07$). The distinction between *better prognosis* group and patients dead of disease ($n=3$) was in particular well defined with MTV and TLG, cut-off 16.8 ($p<0.0007$) and 45.4 ($p<0.003$) respectively. **Conclusion** This study supports the high diagnosis value of 18F-FDG PET-CT for adenoid cystic carcinoma of the salivary glands by detecting primary tumors and metastasis in all cases, with only 2 false negative findings for lymph-nodes fused to the primary tumor. In addition PET parameters of primary tumors such as SUV_{max} , MTV and TLG could be used as prognostic factors.

EP125

Functional vs morphological imaging in nasopharyngeal carcinoma : What agreement ?

S. Touil, H. Bendaoud, Y. Shimi, J. Benouhoud, H. Aschawa, A. Guensi; CHU IBNOU ROCHD OF CASABLANCA, Casablanca, MOROCCO.

Morocco is a country with intermediate risk of nasopharyngeal cancer with an incidence of 5 cases per 100,000 inhabitants per year. The diagnosis is often delayed in our context. Indeed locally advanced and metastatic forms represent 66.5% of cases according to the register of the cancers of Casablanca of 2007. The positron emission tomography (PET-CT) is now the investigation of choice for their staging. We conducted a prospective study spread from January 2013 to December 2015 for 19 patients followed for nasopharyngeal cancer T3 T4 N +, who having benefited PET-CT: 10 in the initial balance sheet and 9 at the time of local

recurrence. The aim of our study was to evaluate the correlation between PET-CT and morphological imaging (MRI and / or nasopharyngeal CT; Assessment of extension including thoraco-abdominal CT and bone scan) in the determination of the lymph node and metastatic status and its impact on the therapeutic strategy. 70% of patients who underwent PET during the initial assessment had nodal involvement (10% N1, 50% N2 and N3 10%) against 60% in morphological imaging (20% N1, N2 30% and 10% of N3). For the evaluation of distant metastasis, 10% of patients were metastatic at PET (lung metastases) versus 0% on morphological imaging. Among the nine patients who underwent a PET with local recurrence, 55.6% had cervical lymph node recurrence associated (against 22.2% for MRI nasopharyngeal) and 22.2% distant metastasis. No patient received thoraco-abdominal CT at the recurrence. PET-CT allowed the change of the therapeutic strategy concerning the lymph node status in 37% (14% in the initial assessment and 59.5% in local recurrence). It must be applied routinely before each recurrence of nasopharyngeal carcinoma and before all locally advanced tumors at the initial evaluation time

EP126

FDG PET/CT in staging of head and neck carcinoma and for detecting synchronous tumors and distant metastases

T. Yordanova, Anelia Klisarova, Pavel Bochev, Borislav Chaushev, Zhivka Dancheva; MBAL St Marina, varna, BULGARIA.

im: The role of PET-CT imaging in head and neck squamous cell carcinoma during pre-treatment staging, radiotherapy planning, treatment response assessment and post-therapy follow-up is reviewed with focus on current evidence, controversial issues and future clinical applications. Second primary tumors are notably the first cause of death with a decisive impact on overall survival rates of early stage HNSCC patients. In staging, the role of ^{18}F -FDG PET-CT is well recognized for detecting cervical nodal involvement as well as for exclusion of distant metastases and synchronous primary tumors. Accurate diagnosis of tumor extent is important. It is real advantage of early detection of distant metastases in asymptomatic patients. Materials: We describe a case of 54 years old man with pain in his throat from several months. After clinical examination, endoscopy and biopsy in the left region of oropharynx, the histopathology report revealed squamous cell carcinoma. The patient came in our department for pre-treatment staging before radiotherapy. Methods: ^{18}F -FDG PET-CT performed at pre-treatment staging a patient with carcinoma of left tonsil and root of the tongue. Whole body PET-CT shows intense ^{18}F -FDG uptake of the primary tumour as well as lot of lateral cervical lymph nodes. PET/CT demonstrated a tumor mass in the left kidney with high uptake and osteolytic lesion with soft tissue component in proximal femur with high glucose metabolism in the surrounded muscles. The conventional contrast CT of abdomen founded a tumor on the left kidney. After one week the patient underwent orthopedic surgery of right femur- hip replacement. Histopathological report establish metastasis in bone and femoral muscles from renal cell carcinoma. Then the patient was scheduled for surgery on the kidney and followed radiotherapy of the primary tumor in head and neck. Conclusion: Second primary tumours (SPTs) can occur in 5-10% of HNSCC patients and are more frequent in the head and neck region, oesophagus and lungs. We presented an interesting clinical case in patient with HNSCC and second primary tumor of the renal. In this context, a high accuracy of ^{18}F -FDG PET-CT for detection of distant metastasis and synchronous tumors, has been clearly demonstrated. Moreover, in approximately 13% of cases the improvement in detection of distant lesions leads to a change of management with important consequences for patient survival.

EP127

Diagnostic Value of 18F-FDG PET/CT in Patients with Cervical Lymph Nodes Metastases of Unknown Primary

J. A. Marroquín Gálvez, A. Saviatto, E. Martínez Albero, A. C. Hernandez Martinez, J. P. Pilkington Woll, S. Ruiz Solis, P. Sarandeses Fernandez, A. Gomez Grande, J. M. Estenoz Alfaro; 12 de Octubre University Hospital, Madrid, SPAIN.

OBJECTIVE 18F-FDG PET/CT is an essential tool in the initial and post-treatment evaluation of head and neck tumors, with an important role in the detection of occult primary tumors. The aim of this study was to determine the diagnostic value of 18F-FDG PET/CT in patients with cervical lymph node metastases of unknown primary. **METHODS** Retrospective study of patients with cervical lymph node metastases of unknown primary after endoscopic/physical examination and/or CT (contrast-enhanced CT of neck, thorax and abdominal was performed in 14/20 patients), in which 18F-FDG PET/CT was performed, between October 2009 and March 2015. A total of 20 patients were included, 18 men and 2 women, with age ranging from 45-80 years (mean 63.35 ± 9.77), history of smoking (18/20) and alcoholism (11/20). Pathological study of cervical lymph nodes were consistent with squamous cell carcinomas (17) and undifferentiated carcinomas (3). **RESULTS** The primary tumor detection rate of 18F-FDG PET/CT was 40%, finding the primary tumor in 8/20 patients: hypopharynx 4, nasopharynx 2, supraglottis 1 and oropharynx 1. In one patient PET/CT was false positive in the nasopharynx, without evidence of malignancy on the biopsy. PET/CT was negative in 11/20 patients, in 2 of these the primary tumor was detected during follow-up (cutaneous squamous cell carcinoma in pinna and bladder urothelial carcinoma). Finally 10 patients remained with diagnosis of unknown primary tumor. 18F-FDG PET/CT change the N staging in 6/14 patients with contrast-enhanced CT of neck: N1 to N2b (2), N2b to N2c (1), N2b to N3 (2) and N2c to N3 (1). PET/CT did not detect distant metastases in any patient, but found two synchronous tumors (colonic adenocarcinoma and carcinoma of the gastroesophageal junction). The obtained sensitivity, specificity, positive predictive value, negative predictive value and accuracy rates for the detection of the primary tumor were: 80%, 90%, 88.89%, 81.82% and 85%, respectively. **CONCLUSIONS** 18F-FDG PET/CT is a valuable tool in the detection of primary tumors in patients with cervical lymph node metastases of unknown origin. Its ability to improve node staging and detect distant metastasis or synchronous tumors can influence treatment management.

EP128

Hypertrophic osteoarthropathy linked to pulmonary metastasis secondary to undifferentiated nasopharyngeal carcinoma, an insight from bone scintigraphy and 18F-FDG PET/CT imaging

E. Fiasconaro¹, G. Aghakhanyan¹, E. Biasco², E. Papucci¹, C. Malvezzi¹, I. Paglianiti¹, M. Grosso¹, L. Galli², D. Volterrani¹; ¹Regional Center Nuclear Medicine, PISA, ITALY, ²Oncology Unit 2, University Hospital of Pisa, PISA, ITALY.

AIM Secondary hypertrophic osteoarthropathy (HO), also known as Pierre Marie-Bamberger syndrome, is a rare condition commonly associated with broncogenic malignancies. Extrathoracic causes are less frequent. Periostitis is the hallmark of HO and is accompanied with burning pain, swelling of limbs and clubbing of distal phalanges. The bone scan and clinical manifestations usually unveil the HO, nevertheless, atypical presentations may occur. Herein, we presented a rare case of HO due to progression of pulmonary metastatic disease secondary to nasopharyngeal carcinoma that underwent into comprehensive diagnostic work-up with bone scintigraphy and whole-body ^{18}F -FDG PET/CT imaging. **MATERIALS AND METHODS** A 69-years old woman referred to our center for bone scintigraphy due to diffuse pain in her upper and lower extremities last 8 weeks. Patient had a history of undifferentiated

nasopharyngeal carcinoma (cT3N1M1), treated 3 years ago with radiotherapy. Despite initial good response and post-treatment remission, two years follow-up revealed radiological and histopathological evidence of the disease dissemination with pulmonary and mediastinal lymph-nodes metastases. A chemotherapy has been initiated. The response evaluation one month post-treatment revealed metastatic disease progression. The patient developed overt pain involving the extremities and light clubbing. A bone scan using technetium hydroxymethane diphosphonate (99mTc-HDP) was performed. To restage the disease and corroborate the scintigraphic finding a whole-body 18F-FDG PET/CT was obtained. **RESULTS** The 99mTc-HDP bone scan showed bilateral patchy linear uptake along cortical margins of diaphysis of tubular bones both upper and lower extremities (“tramline” sign) with increased periarticular uptake on both sides. Whole-body 18F-FDG PET/CT, in comparison to previous PET study, revealed multiple new pulmonary mass lesions and widespread mediastinal lymphadenopathy with no recurrence of primary disease. Moderately increased periosteal FDG uptake was observed in the long bones of the upper and lower extremities. In line with mild soft tissue swelling in distal portion of the fingers (clubbing), the patient was diagnosed with secondary HO. **CONCLUSION** The intrinsic features of HO, such as clubbing, pain and periostitis of the long bones are well known, nonetheless, the pathogenesis of HO is still unclear. We reported a case of secondary HO in a patient with history of undifferentiated nasopharyngeal carcinoma, which draws a causal link between development of secondary HO and progression of pulmonary metastatic disease, but not with primary tumor. Occasionally, the bone scan might be misleading in atypical presentations or advance stages of underlying disease, thus 18F-FDG PET, elucidating the inflammatory nature of HO, may assist in diagnostic controversies.

EP129

Parathyroid Carcinoma: Clinical Cases with a favourable Outcome

S. Kusacic Kuna, H. Tomic Brzac, G. Horvatic Herceg, D. Huic; Clinical Department of Nuclear Medicine, Zagreb, CROATIA.

OBJECTIVES: Parathyroid carcinoma is a rare endocrine malignancy which usually secrete parathyroid hormone (PTH), thereby producing hyperparathyroidism. The majority of carcinomas are sporadic, but rare forms of genetic hyperparathyroidism-jaw tumor syndrome with mutations in the *HRPT2* gene are also reported. The etiology of cancer remains unknown, it could be associated with a history of neck irradiation, but some authors suggest long-standing secondary hyperparathyroidism as a provoking factor of disease. **PATIENTS AND METHODS:** The aim of report is to present a cases of a patients with favourable outcome of parathyroid cancer, with comparing the clinical and pathohistologic findings of each patient. The study included three female patients (mean age 51 years) with primary hyperparathyroidism due to parathyroid carcinoma managed at the Clinical Department of Nuclear Medicine during 5 years. All of them exhibit symptomatology of hypercalcemia at presentation with high levels of PTH, and two of them have previous anamnesis of multinodular goiter. All of them had renal impairment with significantly reduced bone density, and one of them has typical „brown“ tumours involving the long bones of the extremities. Patients underwent to surgery after improving of calcium laboratory results with adequate hydration, diuretics and bisphosphonates administration and after the amelioration of the general state. Preoperative imaging techniques such as neck ultrasound and 99mTc sestamibi scan help to localize disease, ultrasound-guided fine needle-aspiration biopsy (US-FNAB) revealed suspected cells in two of patients, but the definitive diagnosis was established only on the basis of pathohistological preparations. The imaging material with a demographic data and histopathological features of the tumor are presented. **RESULTS:** All of patients experienced long-term remission after the surgery with normalization of laboratory parameters as serum PTH and calcium levels. The brown tumors in one patient required no additional

surgical treatment. **CONCLUSION:** A parathyroid carcinoma is a rare form of endocrine cancer that sometimes could be difficult to diagnose preoperatively due to clinical features shared with benign causes of hyperparathyroidism. Complete surgical resection is the recommended treatment and offers the best chance of cure, although persistent or recurrent disease occurs in more than 50% of patients.

EP-08 – Sunday, October 16, 2016, during Exhibition hours, e-Poster Area
Clinical Oncology: Liver, Upper GI & Pancreatic Cancer

EP130

Ultra-High Definition Digital PET for Hepatic Malignancies and Metastases

J. Zhang¹, C. L. Wright¹, A. Siva¹, P. Bhatia¹, K. Binzel¹, C. Tung², M. V. Knopp¹; ¹The Ohio State University, Columbus, OH, UNITED STATES, ²Philips Healthcare, Cleveland, OH, UNITED STATES.

Purpose: To evaluate if FDG PET imaging of the liver can be qualitatively improved within whole-body acquisitions by using an ultra-high definition (UHD) reconstruction approach with 1mm³ voxel volume enabled by digital PET technology and compare the findings to current clinical reconstruction, standard definition (SD) of 64 mm³ voxel volume PET. **Materials and Methods:** Imaging was performed on a pre-commercial release, digital photon counting PET/CT system (Vereos, Philips) (dPET). 12 clinical patients receiving ¹⁸F-FDG whole-body dPET with a target dose of 480 MBq that had demonstrated hepatic lesions were included in this evaluation. A total of 79 hepatic lesions were identified and included in this assessment. dPET imaging was reconstructed in both traditional SD 4mm voxel length and investigational UHD 1mm voxel length using the 3D OSEM TOF algorithm. While the system default OSEM number of subsets was 29, we performed reconstructions with a range of subsets (S=1, 5, 9, 13, 17 and 25) leaving the number of iterations fixed at 3. ROIs were placed on normal liver background and the hepatic lesions. SUV, SNR and normal liver parenchyma uniformity were quantitatively measured with penalty scores from 1-10 being assigned based on noise levels. Blinded image reviews were performed by experienced readers. **Results:** Refining the reconstruction from the traditional SD 4mm to the investigational UHD 1mm led initially to increased noise in normal liver parenchyma with visible blobby liver texture when the default number of subsets was used. Subsequently, the assessment found that the optimal number of subsets was 17 for 4mm SD reconstruction and 9 for 1mm UHD. With the reduced number of subsets the overall image quality improved and led to an increased confidence level for lesion detection. The quantitative assessment showed that liver background noise was reduced by 56±8% for the UHD recon when changing from S=29 to S=9. Correspondingly, normal liver parenchyma uniformity was improved by 60±8%, while lesion SUV_{max} remained equivalent (p<0.01) and a significantly improved SNR by about 2x. We found a variability that led to the concept of a BMI adaptive # of subset approach where (BMI>28) benefited from even lower # of subsets (S=7). **Conclusion:** Ultra-high definition reconstruction was demonstrated to be feasible for FDG dPET after optimization and appears capable of considerably improving the detectability and characterization of hepatic lesions as well as the diagnostic confidence.

EP131

Role of FDG-PET/CT in Suspected Gallbladder Cancer: Preliminary Results

A. Sabaté-Llobera¹, L. Gràcia-Sánchez¹, J. Mestres-Martí¹, G. Reynés-Llompart¹, J. L. Vercher-Conejero¹, E. Llinares-Tello¹, L. Lladó-Garriga², T. Serrano-Piñol³, E. Ramos-Rubio², C. Gámez-Cenzano¹; ¹PET Unit, Department of Nuclear Medicine - IDI. Hospital U. de Bellvitge-IDIBELL, L'Hospitalet de Llobregat (Barcelona),

SPAIN, ²Department of Surgery, Hospital U. de Bellvitge-IDIBELL, L'Hospitalet de Llobregat (Barcelona), SPAIN, ³Department of Pathology, Hospital U. de Bellvitge-IDIBELL, L'Hospitalet de Llobregat (Barcelona), SPAIN.

AIM: Gallbladder cancer is an uncommon, fatal malignancy, sometimes found incidentally in image examinations. Our objective was to evaluate the additional information from FDG-PET/CT in patients with suspected gallbladder cancer based on clinical presentation, tumor markers (CA19-9) or conventional imaging (CT and MRI). **MATERIAL AND METHODS:** Whole-body FDG-PET/CT was performed in 22 patients (12 men, median age 68.5 years) with clinical/radiological suspicion of gallbladder cancer. FDG uptake in the gallbladder was assessed both visually (positive when higher than liver activity) and semiquantitatively (SUVmax and lesion-to-normal-hepatic-activity ratio (L/NHA)). We analysed the correlation between semiquantitative parameters and CA19-9 with definitive diagnosis (benign/malignant) based on histopathological findings or follow-up (9-40 months). **RESULTS:** Histopathology and CA19-9 levels were available in 15/22 and 20/22 patients respectively. Globally, median SUVmax and L/NHA in the suspected lesion were, respectively, 3.7 (1.1-15.3) and 1.14 (0.34-6.12). Visually 10/22 patients (45%) were PET-negative, with median SUVmax 1.8 and median ratio L/NHA 0.53, and were interpreted as benign findings. In the 12/22 PET-positive patients (55%), median SUVmax and L/NHA ratio were 8.5 and 2.66, respectively; all except one were interpreted as malignant. Surgery was performed in 15/22 patients (68%); 7 patients were not operated and follow-up confirmed benign lesions (adenomyomatosis). Of the 11 patients interpreted as benign, four were operated: 3 showed chronic cholecystitis and one an adenocarcinoma; the remaining 7 patients had adenomyomatosis. The 11 patients interpreted as malignant in the PET/CT were all operated: 10 had neoplastic lesions, while one had chronic inflammation. Sensitivity, specificity, positive and negative predictive values, and accuracy of FDG-PET/CT are 91%. In 5/20 patients (25%) CA19-9 levels were increased (72.3-3060 U/ml), all with histologically proven malignant lesions. However, 6/11 (54%) patients with gallbladder cancer had normal CA19-9 (<37 U/ml). Malignant lesions had significantly higher SUVmax and L/NHA ratio than benign disease ($p < 0.05$). When correlating the ratio L/NHA with histological results, logistic regression showed a perfect segregation (100% specificity) between benign and malignant pathology at a cut-off of 1.2. When analysing the correlation SUVmax-histopathology we found a cut-off of 5.4 to distinguish between benign and malignant lesions (probability of 90%). Moderate-low correlation was observed between CA19-9 levels and histopathology ($\phi = 0.53$). **CONCLUSIONS:** Despite the small number of patients, FDG-PET/CT seems to be a good technique to differentiate between benign and malignant lesions of the gallbladder. The ratio L/NHA shows better results than SUVmax, and both metabolic parameters have a better correlation with histology than CA19-9.

EP132

Clinical Impact of PET/MRI Dosimetry after Radioembolization

P. J. Parikh, N. Maughan, A. Weiner, K. Fowler, R. LaForest, N. Saad; Washington University School of Medicine, Saint Louis, MO, UNITED STATES.

Aim: To measure clinical changes in management after the implementation of Y-90-PET dosimetry **Methods:** Patients were scanned on the Biograph mMR (Siemens, Erlangen, Germany) within 36 hours of Y-90 radioembolization based on patient and scanner convenience. 20-40 min of PET data were acquired in a single station to cover the liver. Key MR sequences used were a 2-point DIXON for attenuation correction, dynamic arterial post-gadolinium contrast VIBE for hypervascular lesions, and

delayed post-gadoxetate contrast VIBE for hypovascular lesions. PET images were reconstructed with 3 iterations, 21 subsets, 172 x 172 matrix, post-processing Gaussian filter of 5 mm in full width at half maximum, and with resolution recovery, resulting in a voxel size of 4.17 x 4.17 x 2.02 mm. Individual lesions were segmented on the appropriate MR image, and then lesion specific dosimetry was calculated on a commercial software package with the dose-point kernel method (SurePlan, MIM Software, Cleveland, Ohio). Dosimetry was calculated on a per-voxel basis, and the Davg (average dose to the tumor) and the D70 (dose to 70% of tumor) were calculated off the dose-volume histogram for each segmented lesion. Results: 12 reports have been generated for 11 patients with primary or metastatic liver cancer since January 2016. Seven patients received resin microspheres (8-1.5 GBq, body surface area calculation) and 4 patients received glass microspheres (107-309 Gy, infused volume calculation). Two patients, with greater than 20 metastatic lesions from neuroendocrine or colorectal cancer, did not have the dosimetry completed due to the workload required. 29/42 lesions in the remaining patients showed adequate D70 or Davg based on recent publications in Y-90 PET dosimetry. Dosimetric results prompted changes in therapeutic management in 4 patients. Three patients (2 colorectal cancer, 1 hepatocellular carcinoma) received immediate salvage radiation therapy to 1-3 unexpected under-dosed lesions in the area of the radioembolization. The 4th patient received radioembolization by an experienced interventional radiologist (> 100 cases) to the left lobe for biphenotypic liver cancer. The catheter tip was in the left hepatic artery on radiograph prior to administration. However, post-treatment PET/MRI noted most of the dose going to the right lobe. This patient is being observed for liver toxicity and further liver directed therapy is postponed. **Conclusion:** Post-treatment radioembolization dosimetry resulted in changes to patient management in a third of patients, both in detecting lesions that are under-dosed and with a significant administration change as compared with intended treatment.

EP133

Quantitative FDG-PET parameters for the assessment of patients with oesophageal and gastrooesophageal carcinoma

E. Cong¹, M. Lee^{1,2,3}, A. Chicco⁴, M. Lin^{1,4,2}, J. Yap⁵, P. Lin^{1,5,2}, T. Tran³, I. Ho-Shon^{1,5,2}; ¹University of New South Wales, Sydney, AUSTRALIA, ²Western Sydney University, Sydney, AUSTRALIA, ³Cancer Therapy centre, Liverpool Hospital, Sydney, AUSTRALIA, ⁴Department of Nuclear Medicine and PET, Liverpool Hospital, Sydney, AUSTRALIA, ⁵Department of Nuclear Medicine and PET, Sydney, AUSTRALIA.

Aim: To assess the prognostic value of quantitative FDG-PET parameters collected before and after definitive or neoadjuvant radiotherapy and/or chemotherapy in patients with newly diagnosed oesophageal or gastro-oesophageal junction carcinoma. **Methods:** Ninety seven patients with endoscopically confirmed oesophageal or gastro-oesophageal junction carcinoma treated with definitive or neoadjuvant therapy received pre-treatment FDG-PET/CT scans, and of these, sixty seven received post-treatment FDG-PET/CT scans. Quantitative parameters (maximum standardized uptake value: SUVmax, mean standardized uptake values: SUVmean, metabolic tumour volume: MTV, and tumour lesion glycolysis: TLG) were obtained for both pre and post-treatment scans which were then used to derive absolute and percentage changes in these parameters. Cox regression was used to analyse the relationship between parameters and survival. ROC curves and log-rank analysis were used to identify optimal thresholds. **Results:** On multivariate analysis all post-treatment and percentage changes in quantitative FDG-PET/CT parameters were significant prognostic factors for overall survival (OS) and progression free survival (PFS) (e.g. post-treatment SUVmean, HR = 2.231, $p < 0.001$ for OS; percentage change in MTV, HR = 1.003, $p = 0.013$ for OS) whilst no pre-treatment parameters were significant prognostic factors. Patients with post-treatment SUVmean < 3 had median OS of 53.3 months

compared to 15.2 months for $SUV_{mean} \geq 3$ and patients with a reduction in MTV of 96% or more had median OS of 56 months compared to 15.1 months for patients with a reduction in MTV of less than 96%. **Conclusion:** Post-treatment quantitative parameters can be used to assess prognosis in patients with oesophageal or GOJ cancer undergoing curative therapy. Percentage change in parameters can be used to potentially assess for treatment response to guide subsequent management.

EP134

Potential prognostic value of ^{18}F -FDG-PET/CT imaging in patients with esophageal cancer using metabolic and anatomical parameters—exploratory analysis of retrospective data from 40 patients

T. S. Nakuz¹, B. Wallner¹, W. Wadsak¹, P. Anner¹, B. Fueger², A. Haug¹, M. Hacker¹, G. Karanikas¹; ¹Medical University of Vienna, Department of Biomedical Imaging and Image-guided Therapy, Division of Nuclear Medicine, Vienna, AUSTRIA, ²Medical University of Vienna, Department of Biomedical Imaging and Image-guided Therapy, Division of Radiology, Vienna, AUSTRIA.

Aim of the study: The objective of this study was to determine the prognostic value of relative changes in SUV_{max} , HU, size of the primary lesion by tumor length, and wall thickness obtained by ^{18}F -FDG-PET/CT to predict overall survival in patients with esophageal cancer. **Materials and Methods:** In this retrospective study, 40 patients (33 males and 7 females) 30 to 80 years of age (mean age, 61 years) were included. All patients underwent a pre-treatment ^{18}F -FDG-PET/CT-scan and a second scan before esophagectomy. For statistical evaluation, the median decrease in SUV_{max} , HU, length, and wall thickness of the primary lesion in patients was dichotomized using the median observed value. Overall survivals were computed by Kaplan-Meier method and then compared between the two groups. The significance of prognostic variables for outcome was calculated by the log-rank test. **Results:** The average timespan between the two scans was 89 days (42 to 286 days). Twenty-nine patients received chemotherapy, nine received radio-chemotherapy, and two received radiotherapy. The median decrease of SUV_{max} was 37% (range, an increase of 94% to a decrease of 89%). The two-year overall survival showed a significant difference for patients with a less than 37% decrease in SUV_{max} , at 55%, than for patients with a greater than 37% decrease, at 80% ($p=0.005$). For HU, the median decrease was 4%; thus, the two-year overall survival for patients with a decrease under 4% was 60%, and for patients with a HU decrease higher than the median, 73.7% ($p=0.340$). The median decrease in the length of the primary tumor was 8%. The two-year survival of patients with a lower than median decrease was 47.4% and 83.3% with a higher than median decrease ($p=0.014$). The median decrease in the thickness of the primary tumor was 30%. The two-year overall survival for patients was 55% with a less than 30% decrease in the thickness, and 80% for patients with a greater than 30% decrease ($P=0.084$). **Conclusion:** Based on our results, a combination of a functional variable, represented by SUV_{max} , and an anatomical variable, such as the length of the primary tumor, could provide an even more precise prognostic appraisal of outcome for patients with esophageal carcinoma.

EP135

Whole body ^{18}F -FDG PET/TC in comparison with CECT in the TNM evaluation in patients with suspected esophageal carcinoma recurrences

C. Altini, A. Niccoli Asabella, A. Di Palo, V. Lavelli, V. Loseto, C. Ferrari, G. Rubini; Nuclear Medicine Unit, D.I.M. – University of Bari “Aldo Moro”, Bari, ITALY.

Aim: To evaluate the role of whole body ^{18}F -FDG PET/CT and CT with contrast enhancement (CECT) in the TNM evaluation of patients (pts) with suspected recurrent esophageal cancer. **Materials and Methods:** 33 ^{18}F -FDG PET/CT were performed in 33 pts (27 males and 6 females; median age 58 years old, range 45-80 years). 22/33 pts previously underwent surgery and chemotherapy, 6/33 pts underwent only surgery and 5/33 pts underwent chemotherapy and radiotherapy. Both the techniques were performed at least 6 months after the end of therapy. All CECT were performed within 30 days from the ^{18}F -FDG PET/CT. The results of ^{18}F -FDG PET/CT and CECT were compared with clinical and instrumental follow-up of at least six months and with histology in pts who underwent subsequent surgery. Sensitivity (Se), specificity (Sp), diagnostic accuracy (DA), Positive Predictive Value (PPV) and Negative Predictive Value (NPV) of the two methods were calculated. The two techniques were compared with the McNemar test. **Results:** Concerning the T parameter, ^{18}F -FDG PET/CT and CECT resulted positive both in 10/33 (30.3%) pts. Se, Sp, DA, PPV and NPV of ^{18}F -FDG PET/CT and CECT were respectively 82%, 95%, 91%, 90%, 91% and 73%, 91%, 85%, 80%, 87%; no statistical difference between the two techniques was observed ($p=0.723$). Concerning the N parameter, ^{18}F -FDG PET/CT resulted positive in 9/33 (27.3%) pts and CECT resulted positive in 6/33 (18.2%) pts. Se, Sp, DA, PPV and NPV of ^{18}F -FDG PET/CT and CECT were, respectively, 100%, 89%, 91%, 67%, 100% and 50%, 89%, 82%, 50%, 89%; no statistical difference between the two techniques was observed ($p=0.505$). Concerning the M parameter, ^{18}F -FDG PET/CT resulted positive in 8/33 (24.2%) pts and CECT resulted positive in 9/33 (27.3%) pts. Se, Sp, DA, PPV and NPV of ^{18}F -FDG PET/CT and CECT were respectively, 75%, 92%, 88%, 75%, 92% and 75%, 88%, 85%, 67%, 92%; no statistical difference between the two techniques was observed ($p=1.000$). **Conclusions:** The two techniques demonstrated an optimal performance in whole body staging of patients with suspected esophageal cancer recurrence. Even if there is not differences statistically significant between them, ^{18}F -FDG PET/CT resulted better than CECT especially in the T parameter evaluation. Analysis of more numerous samples is necessary to refine these results.

EP136

Recommendations for radioembolization after liver surgery using yttrium-90 resin microspheres: an international consensus panel report

M. Samim¹, L. M. van Veenendaal¹, M. N. G. J. Braat¹, R. van Hillegersberg¹, S. Gómez-acebo², Y. Kao³, D. Liu⁴, J. D. Louie⁵, D. Y. Sze⁵, S. C. Rose⁶, D. B. Brown⁷, H. Ahmadzadehfard⁸, E. Kim⁹, M. A. A. J. van den Bosch¹, M. G. E. H. Lam¹; ¹University Medical Center Utrecht, Utrecht, NETHERLANDS, ²Clinica Universidad de Navarra, Pampola, SPAIN, ³Cabrini Hospital, Melbourne., AUSTRALIA, ⁴Vancouver General Hospital, Vancouver, BC, CANADA, ⁵Stanford University Medical Center, Stanford, CA, UNITED STATES, ⁶University of California, San Diego, San Diego, CA, UNITED STATES, ⁷Vanderbilt Cancer Center, Nashville, TN, UNITED STATES, ⁸University Hospital Bonn, Bonn, GERMANY, ⁹Icahn School of Medicine at Mount Sinai, New York, NY, UNITED STATES.

Introduction: For radioembolization (RE) using yttrium-90 (^{90}Y) resin microspheres (SIR-Spheres®, Sirtex, Sydney, Australia), the Body Surface Area (BSA) method is commonly used for calculation of the prescribed activity. Guidelines on how to adjust activity in patients with a history of liver resection are lacking. The primary aim of this study was to draw recommendations on activity planning for resin microsphere RE in patients with a previous history of liver surgery, based on clinical data and expert consensus. **Material and Methods:** Patients with a history of liver surgery undergoing ^{90}Y RE with resin microspheres between February 2009 and July 2015 were selected. Data on patient, disease and procedure characteristics were collected from the electronic medical records. The

mean absorbed dose across the target arterial territory (D_{Target}) was retrospectively calculated for each patient. In case of an available post-treatment ^{90}Y -PET/CT scan, the absorbed dose in the healthy liver tissue (D_{HL}) was also calculated. The dose-toxicity correlations were investigated for D_{Target} and D_{HL} . For evaluation of current expert opinion in activity reduction in the context of prior liver surgery, six representative post-surgical patients were selected and presented to ten international experts in the field of ^{90}Y RE. Results: A total of 43 patients were included. Activity reduction (range 20–50% decrease or target dose of 50 Gy) occurred in seven patients (16%), with surgery reported as a reason for dose reduction in five out of seven. There was a significant correlation between D_{Target} and D_{HL} ($R^2=0.293$; $P=0.004$), but a dose-toxicity correlation was only found for D_{HL} ($R^2=0.408$; $P=0.001$). Recommendations on activity reduction for the six presented patients were highly variable between the members of the expert panel. Across all presented cases, the desired D_{Target} advised by the expert panel members varied between 18–55 Gy. Activity reductions were recommended by the expert panel 40 times (67%); small liver remnant volume was the most common reason for recommending activity reduction (24 times, 37%). Conclusion: Although resin microsphere ^{90}Y RE could be safe in the majority of post-surgical patients, caution should be taken when using the BSA method for activity prescription because it does not account for the decreased remnant liver volume. Alternatively, a possible approach might be to use $D_{\text{Target}} \leq 50$ Gy as an interim guide, until dose-toxicity relationships using D_{HL} have been explored in further radiobiological detail.

EP137

Restaging of pancreatic cancer: clinical and prognostic value of FDG PET/CT

P. Alongi¹, **D. Familiari**², **V. Trono**³, **S. Pulizzi**¹, **R. Gentile**⁴, **S. Russo**², **A. Ruggeri**², **M. Fomito**², **M. Midiri**⁵; ¹San Raffaele G.Giglio Institute, Cefalù, ITALY, ²A.R.N.A.S GARIBALDI - Nesima, Catania, ITALY, ³University of Milano-Bicocca, Milano, ITALY, ⁴University of Messina, Messina, ITALY, ⁵University of Palermo, Palermo, ITALY.

Aim:The aim of this retrospective study, through a collaboration between San Raffaele G.Giglio Institute (Cefalù,Italy) and ARNAS Garibaldi (Catania,Italy), was to evaluate the clinical and prognostic impact of FDG-PET/CT in the restaging process of pancreatic cancer. **Materials and Methods:** data from 52 patients (pts) treated for primary pancreatic cancer, who underwent FDG-PET/CT for suspicious of recurrent disease were collected. Accuracy was assessed employing conventional diagnostic procedures, multidisciplinary team case notes, further PET/CT scans and/or follow-up. ROC curve and likelihood ratio (LH+/-) analysis were used for completion of accuracy definition. Progression-free survival (PFS) and overall survival (OS) were assessed by using Kaplan-Meier method. The Cox proportional hazards model was used to identify predictors of outcome. **Results:** sensitivity, specificity, positive predictive value, negative predictive value and accuracy of FDG-PET were 85%, 84%, 90%, 76%, 84%. AUC was 0.84 (95%IC 0.72-0.96; $p<0.05$). LH+ and LH- were 5.3 and 0.17 respectively. FDG-PET/CT findings influenced significantly the therapeutic management in 30% of pts revealing new metastatic foci in 5 pts and excluding suspicious lesions in 11 pts. Analysis of PFS revealed FDG-PET/CT positivity to be associated with a worse cumulative survival rate over a six months (6m) and 12 months (12m) period in comparison to FDG-PET/CT negativity (6m-PFS 63% vs 95%, $p<0.05$; 12m-PFS 43% vs 85%). Moreover, a negative study was associated with a significantly longer OS than a positive one (73% vs 14% after 2 years, $p<0.05$). In addition, a positive PET scan was associated with an increased risk of disease progression ($\text{HR}=3.4$; $p<0.05$) and an increased risk of death ($\text{HR}:2.5$ ($p<0.05$)). **Conclusion:**FDG-PET/CT showed high diagnostic accuracy for restaging process of pancreatic cancer, proving also its potential value in predicting clinical outcome after primary treatment.

EP138

Added diagnostic and prognostic value of FDG PET/CT in assessment of nodal metastasis in high risk patients with GIST

E. El-kholy¹, **G. El-Hennawy**¹, **H. Fathy**¹, **H. Moustafa**², **M. Maher**³; ¹Nuclear medicine unit, National cancer Institute (NCI) Egypt, Cairo, EGYPT, ²NEMROCK center, Cairo University, Egypt, Cairo, EGYPT, ³Medical oncology departement, National cancer Institute (NCI) Egypt, Cairo, EGYPT.

Aim: to evaluate the role of FDG PET/CT in detection of nodal metastases in GIST and to assess its response pattern to imatinib therapy and prognosis. **Materials and methods:** 47 patients (23 female, 24 male, mean age: 49.2 ± 12.7) with pathologically proven GIST in whom FDG PET/CT scan were retrospectively assessed. Nodal lesions analysis in total 66 PET/CT studies (18 pre-therapy and 48 follow up) scans during imatinib therapy were conducted in comparison to diagnostic CT. Pathological and clinical/radiological follow-up for 3–15 months duration served as standards of reference. **Results:** Lymph node (LN) metastasis is reported in 9 patients (19%), their mean age was 53.6 ± 13.8 . Stomach was the site of primary in 66.7% and spindle cell pathology was found in 7 among 9 patients (77.7%). The mean SUVmax value and size was 6.7 ± 4.5 and 2.7 cm (range, 1–9 cm), respectively. All 9 patients had double and triple site of metastases (liver and/or peritoneal deposits). A total of 40 lymph nodes (29 abdominal and 11 mediastinal), (19 ones at pre-therapy staging) were detected. FDG PET/CT had higher sensitivity, specificity, and accuracy of 97%, 71%, and 93% versus 82%, 57% & 78%; for diagnostic CT, with P-values of 0.35, 0.03 and 0.03; respectively. FDG PET/CT was true positive in 32 lesions (80%), compared to 27 lesions (67.5%) in diagnostic CT. FDG PET/CT showed false positive results in 2 nodal lesions (5%) that proved inflammatory in follow up. Finally 7 out of 9 patients with nodal metastases (77.7%) showed disease progression (1 patient died), compared to 3/13 patients (23%) with liver and/or peritoneal deposits without nodal metastases. **Conclusion:** In an incidence of 19%, lymph nodes metastasis is believed to be an adverse prognostic factor in patients with GIST. FDG PET/CT seems to be superior to diagnostic CT in nodal detection and assessment response to Imatinib therapy. **Key words:** FDG PET/CT, GIST, nodal metastases, Imatinib therapy, prognosis.

EP139

Differentiation of physiologic and pathologic uptake in histological proven pancreatic neuroendocrine tumours using ^{68}Ga -DOTA-TOC PET/CT

A. Kroiss, **C. Uprimny**, **L. Scarpa**, **L. Geraldo**, **L. Gruber**, **B. Neururer**, **I. Virgolini**; Nuclear Medicine, INNSBRUCK, AUSTRIA.

Purpose We wanted to establish the range of ^{68}Ga -DOTATOC uptake in pancreatic neuroendocrine tumours (NET). This would allow differentiation between physiological uptake and tumour-related somatostatin receptor (SST) expression in the pancreas (including the uncinate process). **Methods** 115 ^{68}Ga -DOTATOC PET/CT studies were performed in order to detect or exclude SST-expressing malignancy. Histopathology confirmed NET of the pancreas in 15 patients who underwent surgery after positive ^{68}Ga -DOTATOC PET/CT scan. Results: SUV_{max} (mean \pm standard deviation) values of ^{68}Ga -DOTA-TOC were 33.2 ± 15.1 in three NET of the uncinate process, 57.9 ± 67.6 in three NET of pancreas body and 47.2 ± 39.7 in nine NET of the pancreas cauda. Significant differences in SUV_{max} between nonmalignant and malignant tissue was found for the pancreas cauda ($p<0.03$). At a cutoff value of 17.1 the specificity and sensitivity for differentiating tumors in the uncinate process were 92.0% and 100% ($p<0.0001$) and 92.5% and 88.9% ($p<0.0001$) for the cauda at a cutoff value of 12.0, respectively. A cutoff value of 14.4 was evaluated for the pancreas body, resulting in a specificity and sensitivity of 100%

($p < 0.0001$), respectively. **Conclusion** ^{68}Ga DOTATOC is an excellent tracer for the imaging of pancreatic NET expressing SST on the tumour cell surface. The noninvasive PET/CT approach by measurement of regional SUV_{max} offers important clinical information to distinguish between physiological and pathological somatostatin receptor expression, especially in the case of unclear anatomical correlation of the pancreas.

EP140

Evaluation of diagnostic value of TOF- ^{18}F -FDG PET/CT in patients with suspected pancreatic cancer

S. Stanzel¹, F. Quehenberger², R. M. Aigner¹; ¹Medical University of Graz, Department of Radiology, Division of Nuclear Medicine, Graz, AUSTRIA, ²Medical University of Graz, Institute for Medical Informatics, Statistics and Documentation, Graz, AUSTRIA.

Aim: Evaluation of the advantages of time-of-flight (TOF) in ^{18}F -FDG-PET/CT in the detection and characterization of pancreatic lesions in patients with suspected pancreatic cancer. Furthermore, the maximum standard uptake value (SUV_{max}) was assessed. TOF should improve image noise, local resolution and thus the demarcation of small lesions. **Materials and methods:** TOF- ^{18}F -FDG PET/CT was prospectively performed in 30 patients with suspected pancreatic cancer. In all patients, a histopathologic confirmation was made. PET/CT images were performed 30 and 90 min. p.i. including a diagnostic CT of the upper abdomen with contrast medium and pancreas protocol. SUV_{max} of the lesions was measured and compared with and without TOF in the 30 and 90 min. p.i. images. Lesions with an increase of SUV_{max} on the delayed images were assessed as malignant, whereas lesions with a decrease of SUV_{max} were assessed as benign. The comparison of TOF-PET/CT with standard PET/CT images and the determination of cut-off values for malignant lesions were made using ROC-analysis. **Results:** Of 30 patients 17 patients had malignant and 13 patients a benign pancreatic lesion. In two patient IPMN was diagnosed correctly only with TOF. Based on the histopathologic findings sensitivity, specificity and diagnostic accuracy for TOF were 94% and 62% versus 82% and 92% without TOF. ROC analysis of SUV_{max} with TOF 30 and 90 min p.i. yielded a cut-off value of 4.3 and 4.4, respectively with a sensitivity and specificity of 67% and 82% and 82% and 92%, respectively. The area under the curve (AUC_{PET}) and AUC_{TOF} -values showed no significant difference neither in the early nor the delayed images. **Conclusion:** Among patients with suspected pancreatic cancer, the use of TOF-PET/CT correlated due to a better anatomical localization and identification of pancreatic lesions with higher sensitivity. However, TOF-PET/CT is of no additional use in differentiating malignant and benign pancreatic lesions. To what extent patients can benefit from the higher statistical weighting of the sensitivity should be examined in a greater patient population.

EP141

^{18}F -FDG PET Findings of Lymphoepithelioma like Gastric Carcinoma

J. Yoon, S. Lee, Y. An, D. Lee, Y. Kim, H. Hur, S. Han, S. Lim, K. Lee; Ajou University School of Medicine, Suwon, KOREA, REPUBLIC OF.

Lymphoepithelioma-like carcinoma (LEGC) is a rare type of gastric cancer that constitutes about 4% of all gastric cancers. In this study, the diagnostic performance and the findings of ^{18}F -fluorodeoxyglucose (FDG) PET/CT in LEGC were evaluated. **Methods:** A total of 26 patients (20 men, 6 women, age = 54 years) who underwent preoperative ^{18}F -FDG PET/CT were enrolled retrospectively. Seven patients underwent follow-up ^{18}F -FDG PET/CT. Pathologic information was obtained

through gastrectomy and the association with Epstein-Barr virus (EBV) was investigated in 24 patients. Maximum standardized uptake value (SUV_{max}) was measured from primary tumors. **Results:** Eighteen patients had advanced gastric cancers (AGC), while 8 patients had early gastric cancers (EGC). Tumors were located at upper in 11, mid in 13 and lower 3rd in 2 patients. Most of tumors (20/24, 83.3%) were EBV-associated. ^{18}F -FDG PET/CT detected 83.3% (15/18) of AGC and 12.5% (1/8) of EGC. The mean SUV_{max} of 16 primary tumors was 7.7 ± 3.0 (5.1–16.8). Lymph node metastasis was detected by histology in 50.0% (13/26) of all patients. The sensitivity and specificity of ^{18}F -FDG PET/CT for lymph node metastasis is 30.7% (4/13) and 100.0% (13/13), respectively. ^{18}F -FDG PET/CT also detected sarcomatoid carcinoma of liver in one patient with EGC. ^{18}F -FDG PET/CT falsely diagnosed as metastasis for eosinophilic infiltration of liver in one case. Of 7 patients, follow-up ^{18}F -FDG PET/CT revealed a multiple liver metastasis in one patient, which was missed by conventional CT, and metachronous cholangiocarcinoma in one patient. In addition, ^{18}F -FDG PET/CT correctly excluded a recurrent disease in the rest of the patients. **Conclusion:** ^{18}F -FDG PET/CT has a high sensitivity for AGC and high specificity for lymph node metastasis in patients with LEGC. Moreover, ^{18}F -FDG PET/CT diagnosed a recurrent disease correctly. ^{18}F -FDG PET/CT might be a useful tool in evaluating patients with LEGC.

EP142

Whole body ^{18}F -FDG PET/CT and CECT in comparison for the evaluation of patients with esophageal carcinoma

C. Altini, A. Niccoli Asabella, A. Di Palo, M. Fanelli, C. Ferrari, N. Merenda, G. Rubini; Nuclear Medicine Unit, D.I.M. – University of Bari “Aldo Moro”, Bari, ITALY.

Aim: To evaluate the role of ^{18}F -FDG PET/CT and CT with contrast enhancement (CECT) in the management of patients (pts) with suspected primary or recurrent esophageal cancer. Furthermore to evaluate the role of the semiquantitative parameters such as SUV_{max} , SUV_{mean} , Total Lesion Glycolysis (TLG) and Metabolic Tumor Volume (MTV) in relation to the tumor site (upper esophagus, middle esophagus, lower esophagus and surgical anastomosis) and histotypes. **Materials and Methods:** 55 ^{18}F -FDG PET/CT were performed in 55 pts (42 males and 13 females; median age 61 years old, range 36–83 years) for suspected esophageal carcinoma: 22/55 (40%) primitive, 33/55 (60%) recurrences. All total body CECT were performed within 30 days from the ^{18}F -FDG PET/CT. The results of ^{18}F -FDG PET/CT and CECT were compared with histology in 22 pts who underwent subsequent surgery, and clinical and instrumental follow-up of at least six months in the remaining 33 pts. Sensitivity (Se), specificity (Sp), Positive Predictive Value (PPV), Negative Predictive Value (NPV), and diagnostic accuracy (DA) of the two methods were calculated. The two techniques were compared with the McNemar test. The role of PET semi-quantitative parameters was evaluated by ANOVA and post-hoc. **Results:** The values of Se, Sp, PPV, NPV and DA of ^{18}F -FDG PET/CT and CECT were, respectively, 79%, 92%, 85%, 92%, 80% and 72%, 84.6%, 78%, 84%, 73%; no statistical difference emerged between the two techniques ($p > 0.005$). Only SUV_{max} (mean value 7.76; range 1.9–19.5) and SUV_{mean} (mean value 4.55; range 1.1–11.7) have an additional role in the identification of relapses in relation to the tumor site ($F=8.43$, $p=0.02$ and $F=7.35$, $p=0.03$). No differences between PET/CT semiquantitative parameters and histotype were observed. **Conclusions:** The lack of statistically significant difference between the two techniques suggests their combined use in the evaluation of suspected esophageal cancer. Furthermore PET semiquantitative parameters should be ever collected especially in case of suspected recurrences. It would be desirable to perform ^{18}F -FDG PET/CT with contrast enhancement, assessed jointly by a nuclear physician and a radiologist.

EP143**Prognostic Value of Psoas Muscle Area on Preoperative ¹⁸F-FDG PET/CT in Patients with Surgically Treated Esophageal Cancer**

S. Park, J. Yoon, S. Lee, Y. An, S. Haam, J. Jung; Ajou University School of Medicine, Suwon, KOREA, REPUBLIC OF.

Sarcopenia is a syndrome characterized by progressive and generalized loss of skeletal muscle mass and strength, which has been known as a poor prognostic factor in various cancers. ¹⁸F-fluorodeoxyglucose (FDG) PET/CT has been widely used in the evaluation of esophageal cancer. In this study, the prognostic significance of psoas muscle area (PMA) and the mean standard uptake value (SUV_{mean}) of psoas muscles measured on preoperative ¹⁸F-fluorodeoxyglucose (FDG) PET/CT were evaluated. **Methods:** A total of 131 patients (125 men, 6 women, age = 63.4 years) who underwent preoperative ¹⁸F-FDG PET/CT and esophagectomy with extensive lymphadenectomy were enrolled retrospectively. PMA was measured at third lumbar vertebra level on an axial section of a non-contrast CT part of PET/CT. SUV_{mean} was calculated on a transaxial plane of FDG PET. Locoregional and distant recurrences were determined based on the results of follow-up PET/CT, chest CT or tissue biopsy. **Results:** Pathological stages were I for 38 (29.0%), II for 41 (31.3%) and III for 52 (39.7%) of patients. The median follow-up period was 32.5 months. The mean body mass index (BMI), the mean PMA and SUV_{mean} of the psoas muscles were 59.5±10.1 kg/m², 14.4±4.3 cm² and 1.5±0.3 g/mL, respectively. Operative mortality developed in 7 (5.3%) patients. The BMI and the PMA were significantly lower in patients with operative mortality (19.2±1.8 kg/m² and 11.3±1.5 cm²) than those without operative mortality (21.7±3.0 kg/m² and 14.6±4.4 cm²). However, there's no significant difference in SUV_{mean} between 2 groups. The 3-yr overall survival (OS) and disease free survival were 14.4% and 42.0%, respectively. A multivariate analysis revealed that PMA was a risk factor for OS (hazard ratio=0.930, p=0.004); 37.1% in low-PMA patients (<15.8) and 64.9% in high-PMA patients. Akaike's information criterion decreased in the multivariate model including PMA versus the model without PMA. **Conclusion:** PMA measured on the preoperative ¹⁸F-FDG PET/CT was a significant prognostic factor for OS in patients with surgically treated esophageal cancer, however, SUV_{mean} of psoas muscles was not.

EP144**Efficacy of Ga-68 DOTATE PET/CT for detecting suspected or unknown primary neuroendocrine tumors**

U. Elboga, A. Sevinc, M. Ozkaya, Y. Celen; Gaziantep University, GAZIANTEP, TURKEY.

Objective: It has been reported that Ga-68 somatostatin analogue DOTATE PET/CT has higher diagnostic performance with higher affinity of somatostatin receptor 2 for detecting neuroendocrine tumors (NETs). The purpose of this study was to investigate the usefulness of Ga-68 somatostatin analogue DOTATE PET/CT in detecting clinically-suspected NET lesions. **Material and Methods:** A total of 36 patients were retrospectively analyzed. Fifteen patients underwent a Ga-68 somatostatin analogue DOTATE PET/CT scan for detecting unknown primary tumors after histopathological confirmation of NET (group 1), 7 patients for detecting suspected recurrence by a rising hormone level after surgery for NET (group 2), and the remaining 14 patients for detecting unknown primary tumors due to high chromogranin A levels (group 3). The detection rate was evaluated according to their situation. **Results:** In group 1, primary tumors were suspected by Ga-68 somatostatin analogue DOTATE PET/CT in 9 of 15 patients (gastrointestinal NET in 9 patients), all gastrointestinal NET were confirmed by histopathology. In group 2, Ga-68 somatostatin analogue DOTATE PET/CT described suspected lesions in all 7 patients (liver metastasis in 3 patients and nodal metastasis in

4 patient). In group 3, Ga-68 somatostatin analogue DOTATE PET/CT did not show any abnormal uptake in this all patients with high chromogranin A levels. **Conclusion:** Ga-68 somatostatin analogue DOTATE PET/CT was useful for detecting NETs, especially when recurrence was suspected due to high hormone levels after surgery for NET or primary tumors were suspected after histopathological confirmation of NET. However, no relevant information was achieved in patients who had no history of NET clearly when chromogranin A levels were high.

EP145**Early phase of 18F-FDG dynamic image to detect liver tumour**

L. Cai¹, C. Han², Y. Chen¹; ¹Department of Nuclear Medicine of West-South University Hospital, Luzhou, CHINA, ²Turku PET Centre and Turku University Hospital, Turku, FINLAND.

Introduction: Only parts (50-70%) of liver tumours exhibit glucose metabolism higher than that the liver parenchyma as uptake of 18F-FDG in clinical PET imaging. Early dynamic 18F-FDG has been shown to be useful for detecting different tumour, such as liver and prostate cancers. However, quantitative methods applied to early dynamic of FDG PET imaging data are confused. In the current study, we employed two simple quantitative methods, maximal upstroke and half time to peak, measured based on tissue-activity curves from tumour, normal liver tissue and abdominal aorta to investigate liver tumours. **Materials and Methods:** Five patients (four: hepatocellular carcinoma and one: hemangioma) were enrolled in this study. All patients were involved surgical operation and pathological examination confirmed the diagnosis. Before surgical operation, all patients underwent liver early 18F-FDG PET imaging (250 MBq bolus injection). Four frames at 15 seconds intervals, followed by 3 frame at 60 seconds. Regions of interest (ROI) on liver lesions (tumour and hemangioma), normal liver tissue and abdominal aorta were drawn. Tissue-activity curves (TAC) were extracted for each ROI. Two parameters were used: half time to peak (T1/2) and maximal upstroke normalized by abdominal aorta ROI (MU). Furthermore, a global index (EDindex), combining T1/2 and MU, was defined as EDindex=(normal T1/2 / tumour tissue T1/2)*(tumour MU / normal MU). All analysis were performed using Carimas2 (developed in Turku PET Centre, Turku, Finland. <http://www.turkupetcentre.fi/carimas>). **Results:** In liver cancer patients, T1/2: 26.8s(+/-5.40) and 40.25s(+/-4.52), MU: 11.60(+/-4.52) and 6.59(+/-1.50), in tumour and normal tissue, respectively, with statistical significant (p<0.01). Meanwhile, in hemangioma patient, T1/2: 61.2s and 60.0s, MU: 2.74 and 4.09 in lesion and normal tissue, respectively, with statistical significant (p<0.01). In four tumour patients, EDindex is 3.57, 2.74, 2.97 and 1.21, respectively, meanwhile, in hemangioma patient, EDindex is 0.66. **Conclusions:** Early dynamic 18F-FDG PET imaging provides useful information for identifying liver lesion. Based on simple quantitative analysis methods, it seems that parameters of T1/2 and MU, especially global parameter, EDindex, could be used to detect tumour lesion from liver parenchyma.

EP146**FDG PET/CT versus multidetector computed tomography in the initial staging of pancreatic carcinoma**

S. Sampath¹, B. Mittal², D. Bhasin², S. Rana², R. Gupta², A. Das², R. Nada²; ¹TamilNadu Government Multi Super Specialty Hospital, Chennai, INDIA, ²Post Graduate Institute of Medical Education and Research, Chandigarh, INDIA.

Aim: To compare MDCT and FDG-PET/CT in the initial staging of pancreatic carcinoma. **Materials and methods:** Staging MDCT and PET/CT records of 54 patients diagnosed with pathologically proven pancreatic malignancy were reviewed. The sensitivity, specificity,

PPV, NPV and accuracy of MDCT and PET/CT for nodal and metastatic staging were calculated. The statistical difference was calculated by McNemar's test. Results: Of 54 patients, 29 had nodal metastasis and 14 had distal metastasis. The sensitivity, specificity, PPV, NPV and accuracy of MDCT vs PET/CT for nodal staging were 52% vs 93%, 84% vs 100%, 79% vs 92%, 60% vs 92%, and 67% vs 96% respectively, $p < 0.001$. The sensitivity, specificity, PPV, NPV and accuracy of MDCT for metastatic staging were 77%, 90%, 67%, 60%, 85% whereas the accuracy of PET/CT was 100%, $p = 0.01$. By correctly identifying distant metastases, PET/CT can change management in 15% of patients. Conclusion: PET/CT achieves excellent accuracy in the staging of pancreatic carcinoma and may be considered in the initial staging evaluation.

EP147

Incidental findings on low dose CTs performed as part of SPECT-CT following Yttrium-90 resin microsphere treatment for liver cancer and metastases

D. Ersahin¹, **M. Chen**²; ¹Yale New Haven Hospital, New Haven, CT, UNITED STATES, ²Yale School of Medicine, New Haven, CT, UNITED STATES.

Introduction: Yttrium-90 (90-Y) resin microsphere treatment is often followed by a single-photon-emission computed tomography (SPECT) combined with low dose computed tomography (CT) to evaluate the distribution of the microspheres and potential immediate complications of the treatment. Despite low dose technique, unexpected or incidental CT findings are frequently encountered. The purpose of this study was to investigate the prevalence and significance of these unexpected findings. **Methods:** Reports from total 75 patients with post-treatment SPECT-CT scans performed between 1/1/2012 and 12/31/2015 at Yale New Haven Hospital were reviewed retrospectively. Abnormal CT findings other than known liver lesion(s) were recorded. For patients who had short interval repeat treatments, only one scan per patient was included in the study. Results: Forty-four scans of 75 patients (58.7%) demonstrated at least one incidental CT finding. The common encountered findings were lung atelectasis (28%), lung nodules (20%), splenomegaly (10.7%), pleural effusion (9.3%), and ascites (9.3%). Patients also had other findings such as lymphadenopathy, skeletal metastases, renal cysts, gallstones, etc. Two patients (2.7%) had soft tissue hematomas related to the procedure and they were managed conservatively. Thirty one scans (41.3%) did not reveal any incidental CT findings per reports. **Conclusion:** Low dose CT scans performed as part of post-treatment SPECT-CTs frequently reveal unexpected findings. Therefore, nuclear medicine physicians and radiologists should be aware of these potential findings which can be critical requiring immediate attention from the referring physicians. Patient management can also be potentially impacted when previously unknown metastatic lesions are detected during post-treatment SPECT-CTs.

EP148

Use of 18F-FDG uptake (SUVmax) and CT attenuation (HUmean) for detection of hepatocellular carcinomas (HCCs) : preliminary study

H. Lee, **S. Byun**, **S. Kim**, **K. Hwang**; Gachon University Gill Hospital, Incheon, KOREA, REPUBLIC OF.

Purpose: Hepatocellular carcinomas (HCCs) have been known to have variable 18F-FDG uptake and this was suggested due to the degree of differentiation of HCC. The detection of HCC is sometimes difficult because of this variety of 18F-FDG uptake. Both SUVmax and

Hounsfield Unit (HU) can be measured on PET-CT. We studied the detectability of HCCs when HU was considered as well as SUVmax. **Methods:** We retrospectively reviewed 18 patients who were newly diagnosed HCCs from January 2014 to December 2015. There were a total of 24 biopsy-proven HCCs. All PET, CT (no contrast), and fusion PET-CT images were analysed visually and both SUVmax and HUmean were measured for the areas of suspected abnormality on either PET-CT or CT. Locations of HCCs were confirmed by MRI or enhanced CT. **Results:** Average SUVmax of 14 HCCs were similar to those of normal liver (3.1 vs. 3.0, $P > 0.05$). Other 10 lesions were definitely distinguished from normal liver (SUVmax 9.2 vs. 2.8, $P < 0.05$). However, average HUmean was 42 for those 14 HCCs and was 41 for the rest 10 lesions, which showed no statistical difference ($P > 0.05$). Total HCCs showed average HUmean of 42 regardless of 18F-FDG uptake. Normal liver showed average HUmean of 58 on the other hand ($P < 0.05$). The ratio of HUmean to SUVmax were 13.7, 4.5, and 19.8 for non-FDG-avid, FDG-avid, and normal liver, respectively. Overall, the HUmean/SUVmax was 7.3 for all HCCs. **Conclusions:** In this preliminary study, HUmean of HCCs showed lower values compared with that of normal liver. As a result, the ratio of HUmean to SUVmax tended to be smaller for HCCs and this might have an influence on the detectability of lesions. Further study with greater number of samples is warranted for more such as cut-off. In addition, it is better to have a careful look of CT in PET-CT to detect abnormality especially when PET shows homogeneous 18F-FDG uptake in HCCs.

EP-09 – Sunday, October 16, 2016, during Exhibition hours, e-Poster Area
Clinical Oncology: Lung

EP149

Routinely including brain and use of contrast in whole body FDG PET-CT for staging NSCLC — its incremental value and comparison with MRI of brain for detection of asymptomatic brain metastases

S. RAY, **J. DAS**; TATA MEDICAL CENTER, KOLKATA, INDIA.

Aim: Brain MRI is the standard imaging to detect asymptomatic brain metastases (ABM) in non small cell lung cancers (NSCLC). In most centres, staging Fluorodeoxyglucose (FDG) PET-CT protocol for NSCLC doesn't include the brain. We investigated the incremental value of routinely including brain CT with contrast as a part of the PET-CT staging protocol in NSCLC and compared their asymptomatic brain metastases detection rates to MRI. **Materials and methods:**Data of the first 200 consecutive patients was retrospectively analysed. TNM staging information was tabulated. Comparison of brain image of the whole body PET-CT, non contrast plain CT and contrast enhanced CT images of the brain not fused with PET and dedicated brain PET images was performed in correlation with brain MRI as the standard. **Results:**T3/T4 primary lesions were found in 52% patients with 89.2% having N2/N3 nodal disease on PET-CT scan. 18% had ABM on MRI, 61.1% of whom had adenocarcinoma. Amongst adenocarcinoma 72.2% and 88.9% had T3, T4 lesions or N2, N3 disease respectively in the ABM group, compared to 45.1% and 64.6% in those without ABM. Similarly, in squamous cell carcinoma 100% versus 32.3% had either T3/T4 and/or N2/N3 disease respectively in the ABM versus non-ABM groups. Brain MRI detected ABM in 18% cases out of which 77.77% were also detected in both PET-CT and CECT, 50% were detected in non contrast CT and 83.33% ABM noticed in MRI were detected in dedicated brain PET-CT. 28.5% of brain metastases detected in PET-CT had FDG avidity and in other 71.5% cases it was photopenic. Out of all ABM patients in 16.6% metastases were detected in MRI alone and in no other imaging modality. **Conclusion:**Routine inclusion of brain CECT as a part of FDG-PET-CT protocol could detect asymptomatic brain metastases in approximately 78% cases therefore negating the requirement of an additional staging brain MRI in NSCLC. This could enable resource optimised use

of MRI staging in more advanced T/N stages. There is no significant difference in sensitivity between CECT brain and fused PET-CT image of the brain. Non contrast plain CT has very poor sensitivity (50% only) for detection of brain metastasis. Addition of dedicated brain PET to contrast enhanced CT enhances the sensitivity for identification of brain metastasis to 83%. We recommend routine inclusion of brain in the whole body protocol for staging PET-CT in NSCLC along with use of iodinated contrast and preferably an additional dedicated brain PET acquisition.

EP150

Evaluation of 18F-FDG PET/CT and non-imaging factors in predicting patient survival in small cell lung cancer: A single tertiary centre experience

A. Agahi, C. Leung, E. Nowosinska, H. Jan; Barts Healthcare Trust, London, UNITED KINGDOM.

Aim Small-cell lung cancer (SCLC) is an aggressive malignancy that accounts for 15-25% of lung cancers. SCLC is classified as limited disease (LD), confined to hemithorax, mediastinum or ipsilateral supraclavicular lymph nodes, or extensive disease (ED) spreading beyond the hemithorax and supraclavicular nodes. There is mixed evidence in the literature regarding metabolic activity of primary tumour on Fluorine-18-Fluorodeoxyglucose Positive Emission Tomography/ Computer Tomography (18F-FDG PET/CT) and patient survival. We aim to determine whether staging 18F-FDG PET/CT in patients would be predictive of patient survival in LD and ED SCLC. **Materials and Methods** We retrospectively collected data of all patients with histologically proven SCLC who underwent 18F-FDG PET/CT staging over the period of 2010 to 2013 at our tertiary referral centre. These patients were followed up until the end of 2014. Data was collected using Electronic Patient Record (EPR) system and Patient Archiving and Communication System (PACS). Statistical analyses were performed to identify correlation between prognostic factors (primary tumour size, primary tumour SUV max, number of metastases and the age at diagnosis) and patient survival in both LD and ED categories. **Results** A total of 31 patients were identified. Four patients who remained alive at the end of the follow-up period were excluded. A total of 27 patients were included. There were 13 male and 14 female patients with a mean age of 68 years (ranges from 48 to 84 years). In patients with LD, there was statistically significant correlation between primary tumour size, primary tumour SUVmax, number of nodal metastases and patients' age, and patient survival ($p < 0.0001$). Similarly in patients with ED, there was statistically significant correlation between primary tumour size ($p = 0.0225$), primary tumour SUVmax ($p = 0.0097$), number of nodal and distal metastases ($p = 0.0097$) and patients' age ($p = 0.0252$), and patient survival. **Conclusion** SCLC is predominantly diagnosed in the elderly population. 18F-FDG PET semi-quantitative analysis, size of the primary tumour, number of metastasis at staging and patient's age all carry important prognostic value in both LD and ED patients. Further analysis of the above prognostic factors is currently being evaluated in a larger patient cohort.

EP151

Evaluation of anterior mediastinal tumors using a standard deviation as a heterogeneity index on FDG-PET/CT

K. TAMURA¹, I. Sakata¹, K. Yoshikawa², Y. Tajima³, N. Shigematsu⁴, M. Jinzaki⁴, K. Murakami⁴, H. Usui⁵, K. Hayashi⁶, Y. Ozeki⁶, J. Ishida¹; ¹Tokorozawa PET Diagnostic Imaging Clinic, Tokorozawa, JAPAN, ²Tokyo Bay Advanced Medical Clinic, Chiba, JAPAN, ³Tokyo Medical University Hospital, Tokyo, JAPAN, ⁴Keio University Hospital, Tokyo, JAPAN, ⁵Saiseikai Utsunomiya Hospital, Utsunomiya, JAPAN, ⁶National Defense Medical College, Tokorozawa, JAPAN.

OBJECTIVE: Heterogeneity is one of the features in malignant tumors. The objective of this study is to investigate the intratumoral heterogeneity of 2-deoxy-2-[(18)F] fluoro-D: -glucose (18F-FDG) accumulation in patients with anterior mediastinal tumor. **METHODS:** Forty-six patients (18 females and 28 males, mean age 56.7±15.2) with anterior mediastinal tumor who had been referred to our clinic for PET/CT in Jul. 2006-Dec.2015, and besides had surgical removal or biopsy after PET/CT scan were evaluated. All PET/CT scans were performed both 60min and 120 min (delayed scan) after FDG injection. Standard Uptake Value (SUVmax) was calculated in all patients. Also, we placed circle ROIs (both 1cm and 2cm in diameter) in the tumor lesions, including the highest uptake area. We calculated standard deviations within the ROIs of 1cm (SD1) and 2cm (SD2) in diameter based on cumulative SUV-volume histograms as a heterogeneity index. **RESULTS:** Mean tumor size was 66.1±22.6mm (22 to 120 mm). Pathological findings (18 malignant and 28 benign) were thymoma in 25 patients, thymic carcinoma in 9, malignant lymphoma in 4, seminoma in 2, and the others in 6 (adenocarcinoma, germ cell tumor, malignant neuroendocrine tumor, mature teratoma, hyperplasia, and schwannoma). The mean SUVmax, d-SUVmax, SD1, and SD2 in the benign tumor group were 3.85±1.60, 4.44±2.19, 0.27±0.21, 0.39±0.18, while those in the malignant tumor group were 11.1±4.36, 13.9±6.30, 0.99±0.81, and 1.55±0.90. All parameters in malignant tumors were significantly higher than those in benign tumors ($p < 0.0001$). In a diagnosis of malignant tumor, sensitivity, specificity, and accuracy were 88.9% (94.4%), 89.7% (82.8%), and 89.4% (87.2%) respectively using an SUVmax (d-SUVmax) cutoff of 6. Also, by using cut-off SD1 of 0.4 and SD2 of 0.6, sensitivity were 88.9 and 94.4%, specificity were 79.0 and 93.1%, and accuracy were 80.9 and 93.6% respectively. **CONCLUSIONS:** The standard deviation of SUV within 20mm ROI that is calculated easily is considered to be a valuable tool for a differential diagnosis between malignant and benign tumors in anterior mediastinal tumors.

EP152

Nodal Staging in Patients with Pulmonary Malignancies using 18FDG-PET and EBUS

S. Angelides, A. Markewycz; Westmead Hospital, Earlwood, AUSTRALIA.

Up to 40% of 18FDG-positive mediastinal nodes are not due to metastatic disease. EBUS is increasingly employed to evaluate mediastinal nodal status prior to definitive therapy. **Aim:** To retrospectively compare 18FDG-PET scans and EBUS findings in patients with documented pulmonary malignancies. **Methods:** 65 patients with documented pulmonary malignancies underwent 18FDG-PET scintigraphy followed by EBUS within the ensuing 3 weeks. One-two nodes were assessed in each patient, determined by 18FDG-PET findings and accessibility of the FDG-positive nodes. The mediastinal nodal status from each procedure was compared. **Results:** 53 of 110 18FDG-positive mediastinal nodes did not demonstrate any malignancy upon fine needle biopsy performed during EBUS. Mediastinal nodal status downgrading occurred in 28 (43%) patients. No upgrading was noted. Downgrading most likely occurred when there several non-enlarged lymph nodes of similar 18FDG-avidity distributed randomly and bilaterally in the mediastinum, often with bilateral hilar uptake (20 of 28 patients). Further, only 2 of 19 patients exhibiting such a pattern of mediastinal tracer distribution were found to have lymph node metastases (10%), and both had metastatic disease elsewhere on the PET scan. 23 of 25 patients with positive EBUS findings demonstrated discrete 18FDG-avid lymph nodes ipsilaterally, with minimal-to-no 18FDG-avid nodes contralaterally. EBUS findings in 14 (22%) patients were inconclusive, despite multiple sampling. Enlarged, rounded lymph nodes with avid FDG uptake ($SUV > 4$) were also more likely to harbour metastatic disease. Conversely, a Hounsfield unit of > 55 was associated with benign disease. **Conclusion:** The pattern of

mediastinal 18FDG uptake was highly predictive of metastatic disease, and may circumvent the need for EBUS evaluation. Prospective analysis of these parameters will be undertaken.

EP153

18F-FLT PET/CT in patients with advanced Non-Small Lung Cancer (NSCLC) treated with Nivolumab: preliminary results

G. Polverari¹, V. Ambrosini¹, F. Gelsomino², S. Diodato¹, F. Ceci¹, F. Sperandi², A. Ardizzoni², S. Fanti¹; ¹Service of Nuclear Medicine, S.Orsola-Malpighi University Hospital, University of Bologna, Bologna, ITALY, ²Division of Medical Oncology, S.Orsola-Malpighi University Hospital, University of Bologna, Bologna, ITALY.

Aim: to evaluate the role of 18F-FLT-PET/CT in Non-Small Lung Cancer (NSCLC) patients candidated to Nivolumab therapy. **Materials and Methods:** we prospectively enrolled patients with advanced NSCLC progressed after at least one prior platinum-based chemotherapy and candidated to Nivolumab within a compassionate use program (EAP). 9/11 patients did not perform surgery as primary treatment while 2/11 underwent lung surgery. 18F-FLT-PET/CT and contrast enhanced computed tomography (ce-CT) scan were performed before Nivolumab as baseline imaging procedures in all patients. To date only 6/11 patients have completed 4 cycles of treatment. In these six patients, 18F-FLT-PET/CT and ce-CT were performed 2 months after the fourth cycle of Nivolumab. Response to Nivolumab was assessed according to RECIST criteria v1.1. **Results:** Overall 11 patients were included. 18F-FLT-PET/CT was positive in all cases detecting the primary lung lesion in 9/11 with a mean SUVmax=7.2 (range 3.1-14.2). 9/11 patients showed lymph nodes metastases with a mean SUVmax=6.1 (range 3.3-13.3), 7/11 extranodal metastases with a mean SUVmax=6.9 (range 1.9-13.3). Sites of extranodal metastases included bone (1/11), spleen (1/11), adrenal gland (1/11), contralateral lung (4/11) and pleura (2/11). In the 6/11 patients who completed 4 cycles of therapy, response assessment showed progressive disease (PD) in 2/6, partial response (PR) in 2/6 and stable disease (SD) in 2/6 patients. 18F-FLT-PET/CT pre-therapy SUVmax was higher than reference background uptake (mean SUVmean liver= 6.5; range= 4.8-9.6 and mean SUVmean L3= 7.6; range= 4.6-9.5) in patients who showed a partial response (mean SUVmax of lung primary=11.5; range= 8.8-14.2) while was lower in patients with SD/PD (mean SUVmax of lung primary=5.0; range 3.5-6.5). **Conclusions:** Nivolumab has become a standard of care in advanced pretreated NSCLC. To date, no predictive factors of clinical benefit have been identified. In our study, high 18F-FLT-PET/CT SUVmax value was associated with PR at 2 months, suggesting an attractive role as predictor of response. Further studies are needed to better assess the role of 18F-FLT-PET/CT imaging.

EP154

Can SUVmax or HU differentiated benign from malignant pleural effusion in FDG PET-CT scans?

H. Farghaly^{1,2}, S. Al Shaikh², A. Alqarni², H. Nasr^{3,2}; ¹Assiut University, Assiut, EGYPT, ²Radiology department, Prince Sultan Military Medical City, Riyadh, SAUDI ARABIA, ³Nuclear Medicine Unit, Cairo University, Cairo, EGYPT.

Aim: To evaluate the ability of SUVmax or/and HU to differentiate benign from malignant pleural effusions. **Material and Methods:** Total of 4111 FDG PET/CT scans were reviewed for presence of pleural effusions. Any FDG PET/CT scan with pleural effusions and tapping with cytology of the effusions were included in this study. A region of interest was drawn on the dependent region of pleural effusions in the trans axial plan without including the pleural edges and SUVmax and mean HU were recorded. The pleural effusion SUVmax to liver SUVmax ratio (P/L SUVmax) were calculated and recorded. The results of the pleural

effusion cytology were recorded and compared with the SUVmax and HU values. The pleural effusions were divided based on cytology into two groups, one positive and the other negative for malignancy. Comparison made between mean SUVmax, mean P/L SUVmax ratio and mean HU for each group by T-test for independent samples. The amount of pleural effusion divided into two groups, group one with mild effusion and group two with moderate to large effusion based on visual assessment and comparison made between mean SUVmax in each group. Results: Twenty two patients had pleural effusion tapping and cytology results revealed malignancy in 6 and no evidence of malignancy in the remaining 16 patients. The mean HU was significantly higher in patients with proved malignant effusion -2.17±6.52 vs. -16.13±12.64 in non-malignant effusion (p=0.02). Using ROC analysis there a cutoff point for mean HU value of >12 was able to differentiate malignant from benign effusion with a 100% sensitivity and a 73.3% specificity (AUC 0.878; p=0.0001). There was no significant difference in the mean SUVmax, mean P/L SUVmax ratio between patients with malignant effusion and those with no evidence of malignancy. The mean SUVmax was 2.03±1.28 in malignant pleural effusion vs. 2.03±1.06 (p=0.99) while mean P/L SUVmax ratio was 0.59±0.19 vs. 0.61±0.17 (p=0.90). The mean SUVmax was significantly lower in patients with moderate to large effusion compared to those with mild effusion (0.96 ±0.33 vs. 1.68±0.60; p=0.009), suggesting a possible dilution effect. **Conclusion:** The mean HU value could be helpful to differentiation between malignant and benign pleural effusions. On the other hand no significant statistical relation was found between effusion SUVmax and pleural effusion cytology with tendency of lower SUVmax values in patients with large to moderate effusions.

EP155

Metabolic parameters in [18F] FDG PET/CT as an early predictor of Stereotactic Body Radiation Therapy response in primary lung tumor

D. Lopez^{1,2}, A. Domenech¹, V. Camacho¹, A. Fernandez¹, N. Farre³, A. Flotats¹, J. Duch¹, M. Estorch¹, I. Carrió¹; ¹Hospital de la Santa Creu i Sant Pau. Nuclear Medicine Department, Barcelona, SPAIN, ²Universitat Autònoma de Barcelona, Barcelona, SPAIN, ³Hospital de la Santa Creu i Sant Pau. Oncology Radiotherapy Department., Barcelona, SPAIN.

PURPOSE: Distinguishing morphological changes from recurrence after Stereotactic Body Radiation Therapy (SBRT) in primary lung tumor remains challenging. To compare metabolic tumor parameters (Maximum Standard Uptake Value[SUVmax], Metabolic Tumor Volume[MTV] and Total Lesion Glycolysis[TLG]) derived from [¹⁸F]FDG PET/CT as predictors of clinical status at 1 year after SBRT in patients (p) with primary lung tumor. **MATERIALS AND METHODS:** Fifteen patients [14 male; mean age=82 y/o, range 67-86] with primary lung tumor (adenocarcinomas [7], squamous cell carcinoma [4], non-histology [3], non-small cell lung cancer [1]), who underwent baseline (before SBRT), early follow-up (1-3 months after SBRT) and late follow-up (6 months after SBRT)[¹⁸F]FDG PET/CT were retrospectively reviewed. Images were visually assessed by 2 nuclear medicine physicians identifying morphometabolic response to SBRT (local recurrence [LR], disease progression [DP], stable disease [SD] and complete response [CR]). Morphological changes post-SBRT (mc-pSBRT) were also considered in CR. Quantitative measurements to track changes in tumor volume and metabolic activity between baseline and follow-up scans were performed using Philips Tumor Tracking Application. SUVmax, MTV and TLG were determined to compare their value in predicting response to SBRT. Clinical assessments at 1 year after baseline PET/CT were reviewed to evaluate patients evolution. **RESULTS:** In visual analysis of follow-up scans, 12 of the 15p were considered in CR, 2 in SD and 1 in DP. Ten of the 12p considered in CR presented mc-pSBRT in the follow-up scans while the remaining 2p did not present mc-pSBRT. In

quantitative analysis of the follow-up scans, all the patients visually considered in CR presented a decrease in SUV_{max}. Patients in CR with mc-pSBRT showed an increase in MTV and TLG values. Patients in CR without mc-pSBRT demonstrated a decrease of all metabolic parameters. The 2p visually considered in SD did not present significant changes in the metabolic parameters. The patient in DP showed local CR with distant metastases. Clinical evolution assessed one year after the last PET/CT demonstrated that 13p were in CR, 1p in SD and 1p exitus. Overall, SUV_{max} helped to predict clinical status at 1 year after the baseline PET/CT in 87% (13/15) of the patients with primary lung tumor treated with SBRT. **CONCLUSION:** SUV_{max} is the only PET/CT metabolic parameter at 3 and 6 months that may be useful to predict clinical status in patients with primary lung tumor treated with SBRT. Patients in CR with mc-pSBRT show increase of MTV and TLG values probably related with morphological changes.

EP156

Mediastinal staging in non-small-cell lung carcinoma: 18F-FDG PET/CT compared to postoperative pathological findings: our experience

S. Casagrande¹, I. Schiorlin¹, F. Tanzi², N. Rotolo³, F. Berizzi³, A. Imperatori³; ¹Nuclear Medicine, Circolo Hospital, VARESE, ITALY, ²Health physics dept., Circolo Hospital, VARESE, ITALY, ³Dept. of Surgical and morphological sciences center for thoracic surgery, Insubria University, VARESE, ITALY.

AIM: 18F-F PET/CT plays an important role in hilar and mediastinal lymph node staging of patients with non-small cell lung cancer (NSCLC), because it is more accurate than contrast-enhanced computed tomography (ceCT). According to the literature, PET/CT for lymph node staging has 80-90% sensitivity, 85-95% specificity, and in patients with peripheral NSCLC has greater NPV than ceCT. The purpose of this study was to assess the accuracy of PET/CT for hilar and mediastinal lymph node staging of NSCLC patient eligible for potentially radical surgery according to the T stage, and to identify risk factors correlated to lymph node involvement. **MATERIAL S AND METHODS:** We reviewed 67 patients (73% male) with NSCLC [adenocarcinoma (ADK), n=44; squamous cell carcinoma (SCC), n=16; miscellaneous, n=7] and node status assessed by surgical pathological findings. From September 2014 to January 2016 all patients underwent preoperative ceCT and PET/CT. The maximum standardized uptake value (SUV_{max}) and metabolic tumor volume (MTV) of the primary lung cancer were measured. Mediastinal lymph node positivity on PET/CT was defined as focally increased FDG uptake higher than mediastinal blood pool. Multivariate analysis was performed separately in patients with ADK and SCC, for the following factors associated with lymph node metastasis: age, gender, tumor location, grading, SUV_{max}, MTV. **RESULTS:** The primary tumor SUV_{max} was significantly higher in SCC patients (range : 2.7-51) compared with ADK (range:1.5-31). The sensitivity, specificity, accuracy, NPV, PPV of regional lymph node metastasis were respectively 47%, 82%, 74%, 82%, 47% , with PET/CT and 41%, 63%, 58%, 75%, 29%, with ceCT. Multivariate analysis showed that SUV_{max} (p= 0.0028) and MTV (p=0.0097) were significant predictors of lymph node metastasis only in ADK group. Moreover, in ADK the ROC curve showed an area under curve better for SUV_{max}, 0.859 (95%CI: 0.717-0.947) than for MTV. No significant differences were found in the SCC group, possibly because of small sample size. For PET/CT, the false-negative incidence (N1 or N2) was 13.4% (14.9% for ceCT). Interestingly, occult N2 metastases were found in 3 of 44 ADK patients (7%) and all these occurred in peripheral ADK. CeCT showed a trend to overstaging (false-positive rate was twice that of PET/CT). **CONCLUSION:** In patients with lung ADK the SUV_{max} and MTV predicts mediastinal nodal involvement. In patients with peripheral ADK with high SUV_{max} and MTV, and PET-negative mediastinal lymph nodes, our results suggest the need of pre-surgical mediastinal lymph node biopsy to rule out false-negative N2 status.

EP157

Texture analysis of FDG-PET/CT images to characterize lung cancer lesions and to predict outcome in patients undergoing primary surgery: preliminary results

M. Kirienko^{1,2}, F. Gallivanone³, M. Sollini⁴, G. Veronesi², E. Voulaz², L. Antunovic², G. Testanera², I. Castiglioni³, A. Chiti⁴; ¹Università Milano-Bicocca, Milan, ITALY, ²Humanitas Research Hospital, Milan, ITALY, ³Laboratory of Innovation and Integration in Molecular Medicine of the Institute of Molecular Bioimaging and Physiology of the National Research Council, Milan, ITALY, ⁴Humanitas University, Milan, ITALY.

Purpose: to assess the correlations between FDG-PET/CT image features, histological data and outcome in patients affected by non-small cell lung cancer (NSCLC) undergoing surgery. **Methods:** we retrospectively analyzed 31 stage I-III NSCLC patients (19 adenocarcinoma, 9 squamocell carcinoma, 3 other; differentiation grade was: G1=1/31, G2=13/31, G3=16/31, not available = 1/31) submitted to FDG-PET/CT for staging purpose and underwent surgery within 1 month. Mean follow-up was 28 ±9 months. At 2-years follow-up, 18 patients had no evidence of disease, 9 patients experienced relapse, 2 patients were dead and 2 lost at follow-up. Statistical analysis was used to correlate PET features (primary tumour Metabolic Tumor Volume (MTV), SUV_{max}, SUV_{mean} corrected for partial volume effect (PVC-SUV), Total Lesion Glycolysis (TLG), 14 textural features and 4 shape-and-size features extracted within the MTV), with histological data and with outcome (local relapse free survival (LRFS), distant metastasis free survival (DMFS) and disease free survival (DFS)). **Results:** We found significant correlations between PET features (Mean Absolute Deviation, PVC-SUV, Spherical disproportion, Sphericity, MTV, Surface, Surface-to-Volume ratio, SUV_{max}, TLG, Maximum, Mean, Minimum, Kurtosis, Standard Deviation, Variance, and Energy) and grading, T parameter, N status and pathological stage. Both features Energy and Kurtosis resulted predictive for DFS and DMFS. The features PVC-SUV and SUV_{max} were predictive for DMFS. These four features were able to separate the whole population into two groups with different outcome. **Conclusions:** Texture analysis of FDG-PET images is able to characterize lung cancer lesions, suggesting the possibility of an *in vivo* "imaging biopsy" by routine baseline FDG-PET/CT. Moreover, texture analysis parameters were predictive of DMFS and DFS in treatment naïve NSCLC patients undergoing primary surgical resection.

EP158

No significant association between EGFR gene mutation and FDG-PET maximum standardized uptake value in early-stage lung adenocarcinoma

N. Chiu, B. Lee; Cheng Kung University Hospital, Tainan, TAIWAN.

Purpose Correlation between EGFR gene mutation and 18F-FDG uptake in advanced lung adenocarcinoma has been reported. To investigate the association between EGFR gene mutation and FDG-PET maximum standardized uptake value (SUV_{max}) in early-stage lung adenocarcinoma we underwent this study. **Subjects and methods** We retrospectively collected all patients with early-stage lung adenocarcinoma who had EGFR mutation analysis and underwent FDG PET/CT before any therapy between December 2014 and October 2015. We analyzed the association between EGFR mutation status and SUV_{max} of the primary lung tumor. **Results** Forty patients with early-stage lung adenocarcinoma (12 men, 28 women; age, 61.6 ± 13.4 y) were included. Thirty (75%, 7 men, 23 women) had EGFR mutation. The mean SUV_{max} of EGFR-mutant adenocarcinoma was (4.14 ± 3.36) and that of the wild-type adenocarcinoma was (5.83 ± 2.77). The differences in SUV_{max}, age, disease stage between the two groups of patients were not statistically significant. **Discussion** There is no significant association between EGFR gene

mutation and SUVmax of the primary lung tumor in early-stage lung adenocarcinoma. FDG PET seems not suitable to predict EGFR mutation in early-stage lung adenocarcinoma.

EP159

A possible role of F-18 FDG PET/CT scan in differentiation of malignant and benign pulmonary lesions that tend to show lower FDG affinities

E. Tatici¹, F. Demirag², I. Uslu Biner¹, Y. Erdogan³, U. Yılmaz³, G. Findik⁴, O. Ozmen¹, A. Ozturk³, A. Gokcek⁵; ¹Ataturk Chest Diseases and Thoracic Surgery Training and Research Hospital, dept. of Nuclear Medicine, Ankara, TURKEY, ²Ataturk Chest Diseases and Thoracic Surgery Training and Research Hospital, dept. of Pathology, Ankara, TURKEY, ³Ataturk Chest Diseases and Thoracic Surgery Training and Research Hospital, dept. of Chest Diseases, Ankara, TURKEY, ⁴Ataturk Chest Diseases and Thoracic Surgery Training and Research Hospital, dept. of Thoracic Surgery, Ankara, TURKEY, ⁵Ataturk Chest Diseases and Thoracic Surgery Training and Research Hospital, dept. of Radiology, Ankara, TURKEY.

Purpose/Introduction: International Association for the Study of Lung Cancer/American Thoracic Society/European Respiratory Society (IASLC/ATS/ERS) has recently proposed a new lung adenocarcinoma classification. New terms as lepidic predominant adenocarcinoma and invasive mucinous adenocarcinoma were defined for the carcinomas of the lung formerly known as non-mucinous bronchioloalveolar carcinoma (BAC) pattern and mucinous BAC pattern respectively. The purpose of the present study was to assess the ability of 18F-fluorodeoxyglucose (FDG) Positron Emission Tomography (PET)/Computed Tomography (CT) to discriminate hamartomas from lung tumors which tend to show low FDG uptakes such as pulmonary carcinoids, lepidic predominant adenocarcinoma and invasive mucinous adenocarcinoma. **Subject and Methods:** We retrospectively reviewed medical records of 79 patients with pathologically confirmed lepidic predominant adenocarcinoma, invasive mucinous adenocarcinoma, pulmonary carcinoid tumors and hamartomas between 2009 and 2015. All patients underwent preoperative 18F-FDG PET/CT. The maximum standardized uptake values (SUVmax) of the lesions were calculated for semiquantitative analyses. Kruskal-Wallis tests were used to compare differences in SUVmax values and the tumour size between lesions. This retrospective study was approved by Institutional Review Board Committee. **Results:** Of the 79 patients, 15 patients had low grade adenocarcinoma; 6 had lepidic predominant adenocarcinoma and 9 had invasive mucinous adenocarcinoma. Thirty-seven patients had pulmonary carcinoid tumors (12 atypical, 25 typical) and 27 patients had hamartomas. Tumor sizes were in a range from 0.7 to 13.5 (mean \pm SD, 2.7 \pm 1.9). Adenocarcinomas were greater in dimension than typical carcinoids and hamartomas ($P=0.007$). There was no significant difference in the lesion size between adenocarcinomas and atypical carcinoids. SUVmax of all lesions ranged from 0.86 to 11.2 (mean \pm SD, 3.6 \pm 2.48). The mean SUVmax values of the hamartomas were significantly lower than typical carcinoids, atypical carcinoids and adenocarcinomas ($p=0.0001$). There were no statistically significant differences in SUVmax between adenocarcinomas and carcinoids. **Discussion/Conclusion:** 18F-FDG PET/CT has an important role in distinguishing between benign and malignant lung lesions. However, 18F-FDG uptake depends on the histologic type of the tumor. It has been reported that FDG uptake may be low in BAC and pulmonary carcinoids. Differentiation of these tumors from benign nodules may be difficult. Pulmonary hamartomas are one of the most common benign tumours of the lung. We found that 18F-FDG uptake of hamartomas was significantly lower than typical carcinoids, atypical carcinoids and adenocarcinomas. 18F-FDG PET/CT findings may be helpful in the differential diagnosis of hamartomas from pulmonary carcinoid tumors, lepidic predominant adenocarcinomas and invasive mucinous adenocarcinomas.

EP160

Usefulness of 18FDG-PET/CT in the evaluation of lung tumors treated with stereotactic body radiotherapy: preliminary results

J. L. Vercher-Conejero¹, C. Gámez-Cenzano¹, A. Navarro-Martin², M. Cortés-Romera¹, J. Mestres-Martí¹, J. Robles-Barba¹, A. Sabaté-Llobera¹, E. Llinares-Tello¹, L. Rodríguez-Bel¹, L. Gràcia-Sánchez¹, E. Andia-Navarro², M. Arnaiz-Fernandez², F. Guedea-Edo²; ¹Hospital U. de Bellvitge-IDIBELL, L'Hospitalet de Llobregat, SPAIN, ²Hospital Duran i Reynals - ICO, L'Hospitalet de Llobregat, SPAIN.

Aim: Stereotactic body radiation therapy (SBRT) is a relatively new treatment modality whose main indications are inoperable non-small-cell lung cancer and oligometastases to liver and lung. The aim of our study was to evaluate the usefulness of FDG-PET/CT in monitoring treatment response and in the follow-up of patients with lung lesions treated with SBRT. **Materials and Methods:** We retrospectively reviewed 71 patients that received SBRT for stage I lung cancer or isolated pulmonary metastases of other tumors. Final analysis excluded 45/71 patients because of no baseline or follow-up PET was available or additional therapies were administered. We included 26 patients (76% male), mean age 73.3 y.o. (range 53-86) with lung lesions: 22/26 primary lung cancer and 4/26 colorectal metastases. SBRT dose ranged 34-60 Gy. FDG-PET/CT was performed at baseline (<1 month prior to SBRT) and post-SBRT to correlate metabolic to morphological response and clinical follow-up. The follow-up was performed in 3 timepoints after SBRT: early (<6 months), intermediate (6-18) and late (>18). SUVmax was recorded in every lesion. Clinical evaluation of response was classified as stable disease (SD) (including metabolic partial or complete response, independently of the lesion size) or progression disease (PD). **Results:** 92% had ≥ 1 FDG-PET/CT within first year and 32% had at least one FDG-PET/CT after 18 months post-SBRT. Primary lung tumors were adenocarcinomas (15) and squamous cell carcinoma (7), and adenocarcinomas (4) for colorectal cancer, presenting a baseline-SUVmax average of 6.9, 10.8 and 6.5 g/ml, respectively. At diagnosis, size of lesions ranged 7-42 mm with global SUVmax average of 7.9. 75% patients with SD already had a decrease of metabolic activity within early evaluation with no significant reduction of size. Diffuse low metabolic uptake was seen in most patients up to 18 months due to inflammatory changes. 25% had PD, both on PET and CT: 2 in early, 2 in intermediate and 1 in late evaluation. **Conclusion:** Although larger number of patients is required, these preliminary results show that metabolic response with FDG-PET/CT is more reliable than CT in monitoring lung tumoral lesions treated with SBRT, probably because SBRT-induced CT changes may have a consolidation/mass-like appearance and therefore, differentiation from tumor recurrence can be challenging. However, it's important to notice that moderate post-SBRT hypermetabolic activity may persist up to 18 months without definite evidence of recurrence. PET response correlated well with clinical response and appears to be a good early surrogate of outcomes following SBRT.

EP161

Role of late response evaluation in Non Small Cell Lung Cancer (NSCLC) treated with EGFR Tyrosine Kinase Inhibitor with PET quantitative parameters

A. BHOIL¹, B. Mittal², N. Singh², B. Singh²; ¹Regional Cancer Centre, Shimla, INDIA, ²Postgraduate Institute of Medical Education and Research, Chandigarh, INDIA.

Objective: To evaluate significance of late imaging for response evaluation of 18F-FDG PET/CT compared to early response imaging following treatment by EGFR TKI in non-small cell lung cancer (NSCLC). **Method:** Prospective serial imaging with 18F-FDG-PET/CT for response evaluation in 23 patients (14M, 9F; mean age 57.6) with Stage IIIB-IV advanced NSCLC was done before start of EGFR-TKI therapy, at 3week(early) & at 6week(late). The metabolic response was assessed

using modified PERCIST criteria for changes of SUV_{peak} , SUL_{peak} and TLG in hottest lesion. The statistical analysis using Kaplan-Meier analysis and the log-rank test were performed to analyze the association with the median overall survival (OS) and the progression free survival (PFS). **Results:** Disease was classified in patients at 6 weeks as disease control (DC=20) and no disease control (NDC=3) compared to that at 3 weeks (DC=22, NDC=1). The change in metabolic disease response in form of disease progression was seen in 2 patients at 6 weeks. The response evaluation with SUV_{peak} showed statistically significantly ($p=0.049$) median OS among DC-258 d was more compared to NDC-129d at 3 weeks and at 6 weeks (DC 271d vs NDC 172d; $p=0.115$). No statistically significant PFS was seen between the DC (172 vs 128 d; $p: 0.183$) and NDC at 3 weeks or at 6 weeks. (169 vs 172; $p: 0.461$) The response evaluation with TLG showed no change in disease classification in terms of DC=19 and NDC=4 in patients at 6 weeks compared to 3 weeks. The median OS time was similar at 3 weeks ($p=0.496$) and at 6 weeks with between DC-227d but was less compared to NDC-353d. No change in survival was seen at 6 weeks. No statistically significant PFS was seen between the DC (172 vs 165 d; $p: 0.172$) and NDC at 3 weeks or at 6 weeks (172 vs 165; $p: 0.172$) when evaluated with TLG. TLG analysis in progressive disease patients showed non-significant shorter time to progression (165 vs 172; $p: 0.172$) at 3 weeks and at 6 weeks **Conclusion:** Although the early imaging for response evaluation is highly recommended considering the cost effective results provided by early imaging. Our results suggest that late imaging may be of value in progressive prediction of treatment response especially in patients presenting with stable metabolic disease in early imaging. The semi-quantitative PET measures as TLG in early response assessment of NSCLC patients do not perform significantly better than the previously proposed SUV_{peak} .

EP162

Is there diagnostic and prognostic importance of serum anti-p53 antibody level in lung cancer?

Z. Hasbek¹, B. Turgut¹, O. T. Dogan², B. Yücel³, S. Berk², I. Sarı⁴, Y. Silig⁴, M. M. Seker⁵, S. A. Ertürk¹; ¹Cumhuriyet University School of Medicine, Department of Nuclear Medicine, SIVAS, TURKEY, ²Cumhuriyet University School of Medicine, Department of Chest Diseases, SIVAS, TURKEY, ³Cumhuriyet University School of Medicine, Department of Radiation Oncology, SIVAS, TURKEY, ⁴Cumhuriyet University School of Medicine, Department of Biochemistry, SIVAS, TURKEY, ⁵Cumhuriyet University School of Medicine, Department of Medical Oncology, SIVAS, TURKEY.

Aim: Lung cancer is the leading cause of cancer-related deaths worldwide. Survival rate in lung cancer is low especially in advanced diseased inoperable patients in spite of new treatment options like immunotherapy. So there are studies which aimed at new treatment options and early diagnostic options. p53 is one of the most studied tumor suppressor gene for this reason. Because p53 is mutated in 60-70% of cancer patients. Recent researches suggest that serum anti-p53 Ab level can be considered as biomarkers to detect many types of cancer, as ovarian cancer, esophageal cancer, breast cancer and lung cancer. In this study we aimed that are there any diagnostic and prognostic importance of serum anti-p53 Ab level in lung cancer patients. **Materials- Methods:** Patients were included who were referred to our department with the purpose of ^{18}F -FDG-PET/CT imaging for staging due to lung cancer diagnosis (LC) and patients who were performed ^{18}F -FDG-PET/CT for diagnosis in the cause of the suspected pulmonary nodule in thorax CT but not detected pathologic FDG accumulation (NAPN=pulmonary nodule with non-avid-FDG) and healthy volunteers. Serum anti-p53 Ab levels were measured with ELISA method in the all patients. **Results:** A total of 65 LC patients (age:37-80years;median age:63 years;58male/

7female), 47 patients with NAPN (age:22-80years;median age:57years;20male/27female), and a total of 34 healthy volunteers (age:44-89years; median age:63years;26male/8female) were included in this study. Median serum anti-p53 Ab levels are 3.4 ng/mL in LC patients, 3.77 ng/mL in NAPN patients, 3.07 ng/mL in healthy volunteers. There is no statistically significant difference for serum anti-p53 Ab level in LC and NAPN patients ($p=0.678$). Moreover there is no statistically significant difference for serum anti-p53 Ab level in patients and healthy volunteers ($p=0.377$). Two-year median survival of patients was 14 month. It has been found that there is no effect of serum anti-p53 Ab level whether >3.4 or <3.4 on the patient survival rate ($p=0.652$). **Conclusion:** Even though serum anti-p53 Ab is very important in carcinogenesis, we think that serum anti-p53 Ab level by itself is not important in lung cancer diagnosis and survival rate. There are multiple factors in carcinogenesis and this may be the reason of this situation. But we think that this study must be done with further patient number.

EP163

Potential prognostic value of ^{18}F -FDG-PET/CT imaging in patients with non-small cell lung cancer using metabolic and anatomical parameters—exploratory analysis of retrospective data from 25 patients

T. S. Nakuz¹, F. Gröller¹, W. Wadsak¹, P. Anner¹, B. Fueger², A. Haug¹, M. Hacker¹, G. Karanikas¹; ¹Medical University of Vienna, Department of Biomedical Imaging and Image-guided Therapy, Division of Nuclear Medicine, Vienna, AUSTRIA, ²Medical University of Vienna, Department of Biomedical Imaging and Image-guided Therapy, Division of Radiology, Vienna, AUSTRIA.

Aim of the study: The objective of this study was to determine the prognostic value of relative changes in SUV_{max} , HU, and size of the primary lesion obtained by ^{18}F -FDG-PET/CT to predict overall survival in patients with non-small cell lung cancer (NSCLC). **Materials and Methods:** In this retrospective study, 25 patients (18 males and 7 females) 43 to 87 years of age (mean age, 64.2 years) were included. All patients underwent a pre-treatment ^{18}F -FDG-PET/CT-scan and a post-therapy scan. For statistical evaluation, the median decrease in SUV_{max} , HU, and size of the primary lesion in patients was dichotomized using the median observed value. Overall survivals were computed by the Kaplan-Meier method and then compared between the two groups. The significance of prognostic variables for outcome was calculated by the log-rank test. **Results:** The average timespan between the two scans was 225 days (66 to 485 days). Twelve patients received chemotherapy, nine received radiotherapy, and four received radio-chemotherapy. Eleven patients had an adenocarcinoma, ten had a squamous cell carcinoma, and results for the remaining four patients were not available. The median decrease of SUV_{max} was 36% (range, an increase of 58% to a decrease of 80%). The two-year overall survival was not significantly different for patients with a less than 36% decrease in SUV_{max} , at 61.5%, than for patients with a greater than 36% decrease, at 66.7% ($p=.816$). For HU, the median decrease was 7.8%; therefore, the two-year overall survival for patients under 7.8% decrease was 66.7% and for patients with a HU decrease higher than the median 58.3% ($p=.215$). The median decrease in the length of the primary tumor was 3%. The two-year survival of patients with a lower than median decrease was 66.7% and 58.3% with a higher than median decrease ($p=.822$). **Conclusion:** Based on the results in our patient cohort, the functional and anatomical parameters (SUV_{max} , HU, and size of tumor) using ^{18}F -FDG-PET/CT imaging do not appear to provide prognostic value. Further prospective studies should elucidate the usefulness of these parameters in the early/late stages of NSCLC.

EP164**Delayed 18F-FDG PET imaging can improve detection of lesions in patients with advanced non-small cell lung cancer**

S. Krebs¹, M. Dunphy¹, J. Humm¹, J. Chaff¹, J. Fredrickson², W. A. Weber¹; ¹Memorial Sloan Kettering Cancer Center, New York, NY, UNITED STATES, ²Genentech, Inc., San Francisco, CA, UNITED STATES.

Objectives: For historic reasons, PET/CT imaging is usually started approximately 60 min after injection of 18F-FDG. However, there are only few data that have investigated if and to which extent lesion detection changes at later time points. The aim of this study was to investigate, whether delayed 18F-FDG-PET/CT improves image contrast and lesion detectability in patients with NSCLC based on changes in FDG uptake, tumor-to-normal tissue ratios, and signal-to-noise ratio (SNR). **Methods:** Retrospective review of 16 patients with advanced NSCLC who underwent FDG-PET/CT with a GE DSTE PET/CT. Each patient was scanned at 60 min and 180 min after injection of 12 mCi FDG (6–7 bed positions, 3 min each). Volumes of interest were placed over up to 5 FDG avid lesions (with typical CT features of metastases) on the 60 min images. The same lesions were identified on the 180 min images and maximum SUVs normalized to body weight (SUVmax) were determined. Image contrast was evaluated by dividing SUVmax of the lesions by the mean SUV of the liver. As a measure of the signal-to-noise ratio (SNR) we subtracted the average uptake in normal liver from the SUVmax of the lesion and divided by the standard deviation of FDG uptake in the liver. SUVmax, contrast and SNR were determined at early (E-SUVmax; E-C, E-SNR) and delayed (D-SUVmax, D-C, D-SNR) imaging and compared by a Wilcoxon signed-rank test. **Results:** A total of 71 lesions with an average E-SUVmax of 7.1 (1.1–18.2) were analyzed. At 180 min, SUVmax increased for 69 of the 71 lesions resulting in an average D-SUVmax of 9.3 (1.8–25.4, $p < 0.0001$). Contrast and SNR improved for 71/71 and 56/71 lesions, respectively: E-C 4.4 (0.6–11.2) and D-C 7.1 (1.5–19.8); E-SNR 62.7 (–4.2–240, $p < 0.0001$) and L-SNR 73.2 (3.8–221, $p < 0.0001$). An additional 32 lesions were identified in 11 patients on the 180 min images with an average D-SUVmax of 3.5 (2.6–4.7). **Conclusions:** Imaging at 180 min increases image contrast and SNR of FDG PET/CT scans and identifies more lesions than standard imaging at 60 min. Modification of current PET imaging protocols may be justified.

EP165**Identification of factors contributing to misdiagnosis in assessment of lymph node metastases among patients with NSCLC imaged by 18F-FDG PET/CT**

J. Teodorczyk¹, B. Brockhuis¹, G. Romanowicz¹, W. Cytawa¹, I. Wenzel-Duszynska¹, J. Kozłowska-Gładki¹, P. Lass^{1,2}; ¹Department of Nuclear Medicine, Medical University of Gdansk, Gdansk, POLAND, ²Division of Molecular Spectroscopy, Institute of Experimental Physics, University of Gdansk, Gdansk, POLAND.

Objective: Study aims to identify sources of errors in evaluation of lymphonodal metastases using 18F-FDG-PET/CT in NSCLC patients. **Material and methods:** Study included 89 patients and 436 nodal stations. Imaging results were compared to pathological status of operative material which served as the “gold standard”. **Results:** The most relevant source of erroneous false negative assessment seems to be associated with limited spatial resolution and partial volume effect of PET - in most false negative interpretations lymph nodes were relatively small (subcentimeter). Another important factor increasing the probability of false negative result was location - the hilar nodes were most frequently omitted due to pulsation and breathing blurring, which were most pronounced in the hilum. Another factor complicating hilar nodes evaluation

was relatively high vascular background activity reducing target-to-background ratio and chance for detection. Central, hilar location of the primary tumor increased the risk of false assessment of hilar nodes - both negative and positive. It seems to be due to Compton scattering of the primary tumor activity resulting in masking the nodal activity or misinterpretation of primary tumor broadly scattered activity as the nodal one. Frequent encasement of hilar nodes by the primary lesion makes imaging diagnosis of nodal involvement impossible, but can be reported by the pathologist being a source of false negative PET-CT result. Small group of false results seems to be related to inaccuracies in assignment to a particular nodal group by surgeon and nuclear medicine specialist. It especially affects nodes localized on the border of lymphonodal subgroups or in case of block resection (in one piece) of many lymphatic stations without detailed markings. Localization inaccuracies are aggravated by motion artifacts - both in low-dose-CT and PET. Interestingly some false positives with high uptake of radiotracer in lymph nodes were in cases with severe necrosis of the primary lesion probably due to intense inflammation reactive to tumor necrosis. **Conclusions:** Accuracy of 18F-FDG-PET/CT in nodal staging of NSCLC is negatively affected by many factors both technical and biological. Biological factors disturbing accurate nodal staging are better recognized. Numerous technical conditions can additionally impair accuracy of the nodal staging by PET-CT in NSCLC cases. Identification and constant awareness of all these factors can help reduce the risk of misdiagnosis.

EP166**Diffuse Increased Splenic FDG Uptake in Lung Cancer Patients: Accompanying Infection or Systemic Inflammation?**

L. Ege Aktas, A. Sarikaya, S. Soyloğlu Demir; Trakya University Medical Faculty Department of Nuclear Medicine, Edirne, TURKEY.

Objective: Chronic disease- inflammatory anemia is one of the common complications during cancer surveillance and it is multifactorial. Recently, a few studies suggested anemia, inflammations and infections were associated with increased splenic uptake on F-18 fluorodeoxyglucose positron emission tomography/computed tomography (FDG PET/CT) during cancer surveillance. The purpose of this study was to investigate the association of diffuse splenic FDG uptake on PET/CT with tumor maximal standardized uptake values (SUVmax), presence of distant metastases, hematological and inflammatory parameters to clarify the clinical significance of this event in lung cancer patients. **Material and Methods:** We retrospectively analyzed the reports of FDG PET/CT scans and selected 15 lung cancer patients, with diffuse splenic FDG uptake on their initial scan, as the patient group (Group1). Also a total of 12 patients who underwent FDG PET/CT scans for histopathologically proven lung cancer recently were enrolled as a control group (Group2). All the 27 patients had hematological data including CRP within 5 days before or after PET/CT survey. ROIs were placed on the tumor, liver, spleen and iliac crest, to determine the SUVmax's. The possible associations between the spleen/liver (S/L) and bone marrow/liver ratios (BM/L) and tumor SUVmax, presence of metastasis, various hematological parameters were evaluated. **Results:** S/L ratio and hemoglobin (Hg) values were different between the two groups ($p = 0,000$ and $0,05$ respectively). The number of patients with anemia were significantly higher in Group1 ($P = 0,02$). Although the mean Hg values were different between two groups, there was no correlation between Hg values and S/L ratios. There was not any significant difference between the numbers of patients which had an accompanying infection site in both groups. Twelve patients had not got any evidence of infection at the time of PET/CT survey. Eleven patients had accompanying pneumonia, 1 patient had meningitis, 1 patient had mastoiditis, 1 had lymphadenitis and another had osteomyelitis. Only CRP values were correlated with S/L ratios in Group1 among

various parameters ($r=0,559$, $p=0,05$). BM/L ratios were positively correlated with white blood cell (Wbc), neutrophil count (Neu) in all of the patients ($r=0,421$, $p=0,02$, $r=0,426$, $p=0,02$, respectively).

Conclusion: Our results suggest that, increased splenic FDG uptake in lung cancer patients is related with the spleen's function in humoral immunity and hematopoiesis, during cancer surveillance. It is correlated with the inflammation degree and enhanced by anemia rather than an accompanying infection site.

EP-10 – Sunday, October 16, 2016, during Exhibition hours, e-Poster Area
Clinical Oncology: Lymphoma, Leukaemia & Myeloma

EP167

Bone Marrow Involvement In Follicular Lymphoma; Correlation Between FDG-PET/CT And Bone Marrow Biopsy

M. CORTES-ROMERA¹, **S. MERCADAL-VILCHEZ**², **E. LLINARES-TELLO**¹, **I. CARRO**², **A. SABATÉ-LLOBERA**¹, **J. VERCHER-CONEJERO**¹, **L. GRÀCIA-SÁNCHEZ**¹, **F. CLIMENT-ESTELLER**³, **I. ROMERO-ZAYAS**¹, **E. GONZÁLEZ-BARCA**², **J. MESTRES-MARTIN**¹, **C. GÁMEZ-CENZANO**¹; ¹PET UNIT NUCLEAR MEDICINE. IDI. HOSPITAL U BELLVITGE-IDIBELL, L-HOSPITALET DE LLOBREGAT (BARCELONA), SPAIN, ²DEPARTMENT OF HEMATOLOGY. ICO. HOSPITAL DURAN I REYNALS-IDIBELL, L-HOSPITALET DE LLOBREGAT (BARCELONA), SPAIN, ³DEPARTMENT OF PATHOLOGY. HOSPITAL U BELLVITGE-IDIBELL, L-HOSPITALET DE LLOBREGAT (BARCELONA), SPAIN.

Aim: Bone or bone marrow focal FDG uptake in PET/CT in Hodgkin lymphoma (HL) and diffuse large B-cell lymphoma (DLBCL) is highly sensitive for bone marrow involvement (BMI) and may obviate need for bone marrow biopsy (BMB). By contrast, BMB is required in staging and re-staging follicular lymphoma (FL) patients due to limited FDG-PET sensitivity. The aim of this study was to assess the utility of FDG-PET/CT for BMI detection in patients with FL compared to BMB. **Material and Methods:** Sixty-six patients with FL were studied with FDG-PET/CT for staging or re-staging. As the reference standard was BMB (in the left iliac crest), 14 patients were finally excluded due to absent or unsuccessful BMB (insufficient material). Regarding BMI, a positive PET scan was considered as diffuse bone marrow uptake (BMU) higher than liver uptake or focal/multifocal/heterogeneous BMU pattern. Negative PET scan was considered as diffuse BMU lower than liver uptake or normal distribution. Kappa agreement index was performed between both techniques. Sensitivity, specificity, negative and positive predictive values were calculated. **Results:** Fifty-two patients (30/22; F/M), with a mean age of 59 years (range 30-80) were analyzed. FL histological types were: grade 1-2 (58.5%), grade 3A (19.5%), grade 3B (9.7%) and composite FL/DLBCL (12.2%). The stages were I (4%), II (17%), III (27%) and IV (52%). BMI was detected in 23 patients (44%) by FDG-PET/CT and in 17 patients (33%) by BMB. Concordant results were obtained in 38 (73%); 13 with positive PET scans (5 uni-/multifocal, 6 heterogeneous and 2 diffuse patterns) and BMB and 25 with negative PET/CT and BMB. Discordant results were obtained in 14 (27%), 10 of them with positive PET scans (4 diffuse and 6 multifocal patterns) and negative BMB (not performed in active sites). The remaining 4 discordant cases had negative PET scans and positive BMB. Diffuse BMU higher than liver uptake had positive BMB in 2/6 patients (33%). Kappa index was 0.54. Sensitivity, specificity, negative and positive predictive values were 76%, 71%, 56% and 86%, respectively. **Conclusion:** FDG-PET/CT detects more BMI in follicular lymphoma compared with BMB. Concordant results between FDG-PET/CT and BMB were found in 73% of patients. Kappa index was moderate. Positive PET scan with a diffuse pattern was found in 6 patients; 2 of them with a positive BMB.

EP168

Diffusely increased bone marrow uptake of 18F-FDG is significantly correlated with total metabolic tumour volume in patients with newly diagnosed Hodgkin Lymphoma

M. A. Pedersen¹, **L. C. Gormsen**¹, **P. H. Kamper**², **F. D'Amore**²; ¹Department of Nuclear Medicine and PET-center, Aarhus University Hospital, Aarhus, DENMARK, ²Department of Haematology, Aarhus University Hospital, Aarhus, DENMARK.

Background 18F-FDG PET/CT has become an established part of the initial staging process in patients with newly diagnosed Hodgkin Lymphoma (HL) and is recommended in international guidelines as the preferred imaging option. In a significant proportion of patients undergoing pre-therapeutic 18F-FDG PET/CT, diffusely increased 18F-FDG uptake is observed in the bone marrow (BMU). This is generally considered to be of benign aetiology but may also indicate para-neoplastic bone marrow activation. Recent studies have shown that pre-therapeutic metabolic tumour volume is a prognostic parameter in patients with newly diagnosed HL. However, evaluation of tumour burden is not done routinely since it is laborious and requires specialized tools for accurate quantification. Since BMU is easily evaluated on 18F-FDG PET/CT using widely available viewing tools, it was our aim to examine if there is a correlation between BMU and total tumour burden. **Material and methods** A total of 115 patients (median age 44, range 8-83) with newly diagnosed HL referred to 18F-FDG PET/CT for initial staging between 2008 and 2014 were retrospectively reviewed. 18F-FDG uptake was measured in the vertebral bone marrow (L3/L4) (SUVvertebra) and in the liver (SUVliver). BMU was calculated as SUVvertebra/SUVliver. In addition, the total metabolic tumour volume (TMTV) was measured using semiautomatic methods (Hermes Tumourfinder). A standardised uptake value (SUV) ≥ 2.5 in pathological lymph nodes and extranodal lesions were considered to represent lymphoma (TMTV2.5). For each lesion with SUV ≥ 2.5 , a new tumour volume was calculated using a recommended 41% SUVmax threshold (TMTV41%). First, the correlation between BMU and TMTV2.5 as well as TMTV41% was analysed and second, a multivariate regression analysis was performed to identify independent predictors of BMU. **Results** Mean BMU was 0.98 (SD 0.26, range 0.56-2.13). Mean TMTV2.5 was 401 ml (SD 469, range 0-2510) and 102 ml (SD 169, range 0-1121) when 41% SUVmax was used. Both TMTV2.5 and TMTV41% were significantly and positively correlated with BMU, however, the correlation was better for TMTV2.5 (Pearson $r=0.34$, $p<0.0001$). In a multivariate regression model with BMU as dependent variable and age, lymphocytes, haemoglobin and TMTV2.5 as independent variables, TMTV2.5 and age were independent predictors of BMU (combined model $r^2 = 0.36$, $p<0.0001$). **Conclusion** Diffusely increased 18F-FDG uptake in the bone marrow is significantly correlated with total tumour volume using both a SUV >2.5 and 41% of SUVmax threshold. Since BMU is easily measured, it could be a potential candidate parameter for evaluating prognosis at initial staging.

EP169

Bone Marrow FDG Uptake Predicts In Vitro CLL Cells Activation Through RANKL/RANK Loop

R. Piva¹, **S. Bruno**², **F. Fiz**^{1,3}, **M. Sicignano**¹, **M. Pennone**¹, **S. Matis**⁴, **G. Cutrona**⁵, **A. Ibatci**⁶, **A. Massone**⁷, **C. Campi**⁸, **M. Piana**⁸, **E. Gugliatti**², **F. Fais**², **G. Sambucetti**¹, **C. Marini**⁹; ¹Chair of Nuclear Medicine, Genoa University, IRCCS San Martino-IST, Genoa, ITALY, ²Department Experimental Medicine, University of Genoa, Genoa, ITALY, ³Nuclear Medicine Unit, Department of Radiology, Uni-Klinikum, Tübingen, GERMANY, ⁴Molecular Pathology Unit, Genoa University, IRCCS San Martino-IST, Genoa, ITALY, ⁵Molecular Pathology Unit, Genoa University, IRCCS San Martino-IST, Genoa, ITALY, ⁶Department of Haematology and Bone Marrow Transplants, IRCCS Martino-IST, Genoa, ITALY, ⁷CNR SPIN (Superconductors, oxides and other innovative materials and devices), Genoa,

ITALY, ⁸Department of Mathematics, University of Genoa, Genoa, ITALY, ⁹CNR Institute of Molecular Bioimaging and Physiology, Milan, Section of Genoa, Genoa, ITALY.

Aim. B-cell Chronic Lymphocytic Leukemia (CLL) combines progressive insensitivity to apoptotic stimuli with an accelerated proliferation of neoplastic lymphocytes. There is accumulating evidence that both features could be sustained by nuclear-factor κ B and its ligand (RANK/RANKL) overexpression whose interaction can generate an autocrine loop, increasing interleukin secretion and providing a shield against apoptotic signals and cytotoxic treatments. In the present study we tested the correlation between RANK/RANKL activation, response to RANKL-specific antibody (Denosumab, DNS) and bone marrow metabolism, using a computational analysis application on FDG-PET/CT images. **Materials and Methods.** FDG-PET/CT images of 22 consecutive CLL patients (6 Binet A, 11 Binet B and 5 Binet C, mean age 69 ± 13 years) were analyzed. The algorithm extracted the intraosseous volume (IBV) from whole-body PET/CT images. Mean IBV SUV, normalized by blood-pool (target-to-background ratio, TBR) was assessed from the co-registered PET images. CLL cells from each patient were cultured; vitality was defined as vital cells percentage after 96 hours of unstimulated culture. Proliferation (HDF) was defined by % of hyper diploid cells, i.e. cells in S+G2M cell cycle phases after five-days activation. Response to DNS was defined as % HDF reduction after DNS. Relative fluorescence intensity (RFI) was measured for both RANKL and RANK surface expression. **Results.** Viability of neoplastic clone did not correlate with bone marrow TBR ($R=0,18$, $p=ns$). By contrast, HDF directly correlated with TBR of the whole bone marrow ($R=0,55$, $p<0,01$) as well as TBR in axial ($R=0,57$, $p<0,01$) or appendicular segments ($R=0,59$, $p<0,01$). Patients with bone marrow TBR lower than the median value (1,21) showed a significantly lower neoplastic clone proliferating activity with respect to the remaining ones ($11 \pm 6\%$ vs. $18 \pm 7\%$, respectively, $p<0,05$). Moreover, HDF directly correlated with response to DNS ($r=0,71$, $p<0,01$). Finally, response to DNS correlated with RANK, but not with RANKL, expression ($R=0,52$, $p<0,01$). **Conclusions.** In CLL patients, analysis of FDG uptake in the bone marrow provides an index of leukemic clone proliferation. The relevance of this finding at least partially relies on the correlation between clone aggressiveness and RANK/RANKL loop activation, which might represent a potential therapeutic target.

EP170

Prognostic value of 18F-FDG PET-CT in patients with Lymphoma who underwent Allogeneic or Autologous Bone Marrow Transplantation. Preliminary results

L. G. Diaz¹, L. Lopez², B. Perez¹, C. Montes³, R. Ruano¹, D. Caballero², P. Tamayo¹; ¹Nuclear Medicine Department. Hospital Universitario de Salamanca, Salamanca, SPAIN, ²Hematology Department. Hospital Universitario de Salamanca, Salamanca, SPAIN, ³Radiological Protection Department. Hospital Universitario de Salamanca, Salamanca, SPAIN.

AIM: To study the role of 18F-FDG PET-CT in the evaluation of treatment response in those patients with Hodgkin and aggressive Non Hodgkin Lymphoma (HL and NHL, respectively) who underwent Bone Marrow Transplantation (BMT), making a difference between Allogeneic (AlloBMT) and Autologous (AutoBMT) transplantation. **METHOD** Prospective study of 22 patients (12 HL with 7 AutoBMT and 5 AlloBMT; 10 NHL, with 8 AutoBMT and 2 AlloBMT). In each patient, three 18F-FDG PET-CT were performed: immediately before BMT (PET0), to determinate patient status; and 100 days (PET1) and 1 year (PET2) after BMT, to evaluate early and late response to treatment, respectively. We considered as positive PET those ones with at least one hypermetabolic lesion with SUVmax bigger than Liver uptake. We evaluated HL from NHL patients separately.

RESULTS - 15 AutoBMT patients (7 HL; 8 NHL). 5 of them were positive PET0 and remained so in PET1 and PET2 (Predictive Value for no metabolic response: 100%). The other 10 patients who were negative PET0 remained negative in PET1 and 50% of them showed positive PET2 (50% of HL and 50% of NHL). - 7 AlloBMT patients (5 HL, 2 NHL), all of them negative PET0 and PET1. 80% of HL and 100% of NHL remained negative in PET2. **CONCLUSION** According to our preliminary results, 18F-FDG PET-CT has an excellent positive predictive value in those HL and NHL patients with positive PET0 and AutoBMT, and it is also a good predictor of complete metabolic response in those HL and NHL AlloBMT patients with negative PET0.

EP171

The importance of uptake time in FDG imaging of patients with lymphoma

J. T. Dunn¹, N. G. Mikhaeel², T. Puri^{1,3}, P. K. Marsden¹, M. J. O'Doherty¹, S. F. Barrington¹; ¹PET Imaging Centre, King's College London, London, UNITED KINGDOM, ²Department of Clinical Oncology, Guy's & St Thomas' Hospital, London, UNITED KINGDOM, ³Department of Oncology, University of Oxford, Oxford, UNITED KINGDOM.

Aim: EANM guidance recommends 60 minute uptake for FDG oncology scans, however uptake increases in several tumours beyond 60 minutes. The aim of this study was to determine the time course of FDG uptake in common lymphoma types after injection and how this might affect imaging assessment. **Methods:** Patients attending for routine staging FDG PET-CT scans with classical Hodgkin's lymphoma (cHL), diffuse large B cell lymphoma (DLBCL) or follicular lymphoma (FL) were recruited. The protocol involved dynamic imaging for 90 minutes after injection and subsequent 10 minute static scans at 120 and 180 minutes. Dynamic images were summed to create two static images representing uptake from 55-65 and 80-90 minutes. Four static images (55, 80, 120, 180 min) for each patient were visually assessed by an experienced nuclear medicine physician blinded to scan time. Images were viewed with Hermes Medical Hybrid Viewer and scored as good (4), satisfactory (3), suboptimal (2) or poor (1) and ranked in order of preference considering the number, uptake, extent and contrast of lymphomatous lesions. Tumours were segmented using in-house software using the standardised uptake value (SUV) = 2.5. SUVmax and SUVmean were calculated for each scan. Visual scores and ranks were analysed using the Skillings-Mack test. Quantitative parameters were analysed using a mixed model to assess effects of time and group. **Results:** Results are available for 36 patients with cHL (16), DLBCL(10) and FL (10). Means and ranges for SUVmax were 13.7, 4.4-27.5 (cHL), 35.6, 6.6-97.9 (DLBCL), 8.7, 1.4-24.0 (FL). Visual scores showed no difference between time points ($p=0.25$) with an overall mean score of 3.6 (s.d. 0.6). Ranks showed a highly significant effect of time ($p<0.0001$) with the later time points ranking highest (mean ranks: 3.3, 2.7, 1.6 and 1.4 for 55, 80, 120 and 180 minute images respectively) and was present across lymphoma subtypes ($p<0.002$). SUVmean time activity curves were observed to increase during dynamic imaging for most patients and quantitative analysis revealed significant effects of time and group for SUVmean ($p<0.0001$), SUVmax ($p<0.007$). The average increases in SUVmean between 55-180 minutes were 22% for the cHL group, 41% for the DLBCL group and 58% for the FL group. **Conclusion:** Imaging was satisfactory or good at all time points but optimal at 120-180mins post injection. Imaging later than EANM guidance suggests may be beneficial in some lymphoma subtypes.

EP172**Splenic involvement in diffuse large B-cell lymphoma: Diagnostic criteria for FDG PET/CT determined by reproducibility of volumetric analysis in the normal spleen**

M. Nogami¹, M. Nakabayashi¹, S. Hirabayashi², T. Hashimoto¹, D. Takenaka¹, S. Adachi¹; ¹Hyogo Cancer Center, Akashi, Hyogo, JAPAN, ²Institute of Biomedical Research and Innovation, Kobe, Hyogo, JAPAN.

PURPOSE: The purpose was to assess the reproducibility of FDG uptake and volume of the spleen in normal subjects and to determine the diagnostic criteria for splenic involvement in patients with diffuse large B-cell lymphoma (DLBCL). **MATERIALS AND METHODS:** Twenty normal subjects without hematological disorders and splenic impairments and 63 patients with DLBCL were retrospectively analyzed. For normal subjects FDG PET/CT was performed twice within 6 months, and the patients underwent PET/CT at initial staging and end of the therapy. SUV_{peak}, volume of the spleen on CT (CT volume) and spleen to liver- SUV_{peak} ratio (S/L ratio) were measured for both normal subjects and patients. To evaluate the reproducibility within same scan and limits of agreements between different scans, SUV_{peak}, CT volume and S/L ratio in normal subjects were statistically assessed by the Bland-Altman analysis in each normal subject. To determine the diagnostic criteria for splenic involvement, cut-off values for SUV_{peak}, CT volume and S/L ratio were defined from reproducibility coefficient for the normal spleen. The sensitivity and specificity by using each cut-off value and visual analysis according to the Lugano classification were then compared by the McNemar's test. The reference standard for splenic involvement was determined as the decrease in S/L ratio larger than reproducibility coefficient after therapy in each patient. **RESULTS:** The reproducibility of measurement of SUV_{peak}, CT volume and S/L ratio within same scan for normal subject was mean difference of 0.000, 0.38 [cm³] and 0.00, respectively, and reproducibility coefficient of 0.000, 9.228 [cm³] and 0.000, respectively. The limits of agreements of those values between different scans for normal subject was mean difference of 0.028, 10.96 [cm³] and 0.024, respectively, and reproducibility coefficient of 0.506, 43.53 [cm³] and 0.146, respectively. The sensitivity of S/L ratio (76.9%) was significantly higher than that of visual analysis (61.5%), CT volume (46.2%) and SUV_{peak} (53.8) ($p=0.0313$). **CONCLUSIONS:** The difference in CT volume between different scans for the same normal subject is relatively larger than that of SUV_{peak} and S/L ratio. Based on the cut-off values determined by reproducibility assessment of normal subjects, diagnostic performance of S/L ratio is significantly superior to the visual analysis, evaluation of CT volume and SUV_{peak} in patients with DLBCL.

EP173**Prognostic value of interim ¹⁸F-FDG PET/CT in DLBCL according to molecular profiles**

J. Kim, Y. Song, S. Kim; Seoul National University Bundang Hospital, Gyeonggi-Do, KOREA, REPUBLIC OF.

Purpose: Diffuse large B cell lymphoma is a pathologically heterogeneous disease with different prognosis according to its molecular profiles. Previous studies that have investigated the value of interim ¹⁸F-fluoro-2-deoxy-D-glucose (FDG) positron emission tomography/computed tomography (PET/CT) in DLBCL have reported conflicting results. The purpose of this study was to evaluate the prognostic value of interim PET/CT in DLBCL according to germinal center B-cell-like (GCB) and non-GCB molecular profiling. **Methods:** We enrolled 118 newly diagnosed DLBCL patients treated with rituximab, cyclophosphamide, doxorubicin, vincristine, and prednisolone (R-CHOP) retrospectively. Interim FDG-PET/CT scans performed after 2 or 3 cycles of R-CHOP treatment were evaluated based on the International Harmonization Project (IHP) criteria.

Patients were grouped as GCB or non-GCB molecular subtypes according to immunohistochemistry (IHC) results of CD10, BCL6 and MUM1, based on Han's algorithm. Results are as follows: 35% GCB, 65% non-GCB; interim PET/CT, 55% negative, 45% positive. Ann Arbor stage III or IV (HR = 5.12, 95% CI = 1.26 - 20.82, $p=0.02$) and positive interim PET/CT (HR = 2.20, 95% CI = 1.06 - 4.54, $p=0.03$) were significant prognostic factors for progression free survival (PFS) in multivariate analysis. During the median follow-up period of 23 months, the positive interim PET/CT group showed significantly inferior PFS compared to the negative interim PET/CT group ($p=0.03$) in entire patients. A subgroup analysis according to molecular profiling demonstrated similar significant difference in PFS between the positive and negative interim PET groups in GCB subtype of DLBCL ($p=0.02$). However there was no significant difference of PFS between the positive and negative interim PET groups in non-GCB subtype of DLBCL. **Conclusions:** Interim PET/CT scanning had a significant predictive value for disease progression in the GCB subtype of DLBCL, but not in the non-GCB subtype. Therefore, molecular profiles of DLBCL should be considered for interim PET/CT utilization.

EP174**Semi-quantitative parameters could improve positive predictive value of interim FDG-PET/CT in Hodgkin Lymphoma**

S. ANNUNZIATA¹, A. Cuccaro², S. Hohaus², A. Giordano¹, V. Rufini¹; ¹Institute of Nuclear Medicine, Università Cattolica del Sacro Cuore, Rome, ITALY, ²Institute of Hematology, Università Cattolica del Sacro Cuore, Rome, ITALY.

Aim. Interim FDG-PET/CT after first cycles of chemotherapy (iPET) has recognized to be the best prognostic factor in patients with Hodgkin Lymphoma (HL). Nevertheless, recent studies indicated that iPET has still some limitations to optimally identify patients with different prognosis. In particular, positive predictive value in terms of relapse and progression (PPV) of visual analysis with five-point Deauville Score (DS) is still suboptimal. Semi-quantitative parameters could improve PPV of iPET and help clinicians to early identify patients with worse prognosis. **Aim** of this study is to compare PPV of visual and semi-quantitative analysis of iPET in patients with HL. **Methods.** Sixty-seven patients with HL who underwent iPET after two cycles of ABVD were retrospectively evaluated. For visual analysis, DS was used, considering DS>3 or DS>4 as positive findings. Semi-quantitative parameters considered were: ratio between target lesion and liver SUV_{max} (rPET); ratio between target lesion and mediastinal blood pool SUV_{max} (mPET); ratio between target lesion SUV_{peak} and liver SUV_{mean} (qPET); target lesion metabolic tumour volume (MTV) and total lesion glycolysis (TLG). Two-years progression-free survival (PFS) and PPV were estimated, with relapse or progression recorded as adverse events. The receiver operating characteristic approach was applied to identify the optimal cut-point of semi-quantitative parameters with respect to events. Survival curves were estimated using the Kaplan-Meier product limit method. Log-rank tests were used to analyse for differences in PFS. A value of $p<0.05$ was considered statistically significant. **Results.** About visual analysis, DS was >3 in 25/67 patients, DS>4 in 14/67. PFS in patients with DS>3 and DS>4 was 53% and 27%, respectively. Nevertheless, patients with DS>3 and DS>4 had a low PPV (40% and 57%, respectively). About semi-quantitative parameters, SUV_{max}, rPET, mPET and qPET were prognostic factors in our population ($p<0.01$). Conversely, MTV and TLG were not prognostic factors ($p>0.05$). The most accurate cut-point in predicting adverse events for rPET, mPET and qPET were 1.14, 2 and 1.46, respectively. For values higher than the cut-point, PFS were 15%, 25% and 20%, respectively; PPV were 70%, 63% and 80%, respectively. **Conclusion.** iPET semi-quantitative parameters seem to have an incremental prognostic value over visual analysis in patients with HL. In particular, ratios between target lesion and background SUV (liver or mediastinal blood pool) could improve the predictive value in terms of relapse or progression. Further larger prospective studies are needed to evaluate the prognostic value of MTV and TLG.

EP175**Role of FDG-PET/CT in primary gastric diffuse large B-cell Lymphoma: a bicentric evaluation at staging and at the end of treatment**

P. Ferro¹, M. Bertoli², D. Albano², M. Spallino¹, G. Bosio², F. Bertagna², F. Fallanca³, R. T. Giubbini², L. Gianolli³, M. Picchio³; ¹Università Milano Bicocca, Milano, ITALY, ²Medicina Nucleare Spedali Civili di Brescia, Brescia, ITALY, ³Ospedale San Raffaele, Milano, ITALY.

AIM: Primary gastrointestinal lymphoma represents the most common type of extranodal lymphomas. One of the more frequent subtypes is diffuse large B-cell lymphoma (DLBCL). The aim of this double institution study is to evaluate the role of fluorine-18-fluorodeoxy glucose PET/CT (FDG-PET/CT) in staging DLBCL and its predictive value in the end of treatment (EOT) results. As far as we know this is the first study which deals with gastric DLBCL separately, and not as part of a heterogeneous group of gastric lymphomas or heterogeneous localizations of DLBCL. **MATERIALS AND METHODS:** We retrospectively analyzed 60 patients (35 men and 25 women, mean age 60 years, age range 23-83) who underwent from 2006 to 2016 at San Raffaele Hospital in Milan and at Spedali Civili in Brescia both staging and EOT (chemotherapy) FDG-PET/CT scans for the evaluation of histologically confirmed DLBCL. A qualitative (FDG avidity) and semi-quantitative (maximum standardized uptake value body weighted (SUV_{max}), lesion-to-liver SUV_{max} ratio and lesion-to-mediastinum SUV_{max} ratio) analysis was performed on both PET/CT studies, considering gastric, nodal and extra-nodal localization of disease. Deauville score (DS) was calculated and compared to the qualitative evaluation of the scans. Treatment failure was defined by a DS >3. Statistical analysis was carried out with chi-squared test. P-Value of ≤0.01 was considered as statistically significant. **RESULTS:** Staging PET resulted positive in 95% of the patients, 35% with gastric involvement, 43% with gastric and nodal involvement and 22% with gastric, nodal and extranodal involvement (average SUV_{max} was 25,58; lesion-to-liver SUV_{max} ratio 10,51; lesion-to-mediastinum SUV_{max} ratio 12,59). EOT scans were positive in 33% patients, 47% with only gastric involvement and 53% with gastric and lymphnodal involvement (average SUV_{max} was 4,55; lesion-to-liver SUV_{max} ratio 1,61; lesion-to-mediastinum SUV_{max} ratio 1,91). DS indicated in 58% of the patients treatment failure and no statistically significant difference was found with the qualitative analysis of the scans. Neither SUV_{max} of the lesion nor extragastric involvement in the staging scan showed statistically significant correlation to results of EOT scan considering both qualitative analysis and DS. **CONCLUSION:** FDG-PET is a useful tool in staging gastric DLBCL lymphoma, detecting successfully either gastric, nodal and extranodal localizations of disease. In our experience SUV_{max}, lesion-to-liver/blood pool SUV_{max} ratio, extranodal involvement in the staging scan are not capable of predicting EOT results. No statistically significant difference was found in the interpretation of EOT FDG-PET/CT between a qualitative analysis of the scans and the DS.

EP176**Utility of FDG-PET in initial assessment of primary central nervous system lymphoma**

M. Bertaux¹, A. Kas¹, C. Soussain², E. Veronique³; ¹Hospital Pitié-Salpêtrière, Paris, FRANCE, ²Hospital René-Huguenin, Curie, Saint-Cloud, FRANCE, ³Hôpital René-Huguenin, Saint-Cloud, FRANCE.

Introduction: Primary central nervous system lymphoma (PCNSL) is a rare form of non-Hodgkin lymphoma (diffuse large B-cell lymphoma (DLBCL) in more than 90% of cases) limited to the brain, eye and spinal chord. Initial systemic work-up is needed to exclude systemic localisations of DLBCL and is usually done with computed tomography (CT) and bone marrow biopsy (BMB). **Aim:** The aim of this study was to evaluate the utility of 18-fluoro-deoxy-glucose positron emission tomography (FDG-PET) in the initial assessment of PCNSL. **Materials and**

methods: In this bi-centric study, 70 patients who had an FDG-PET before chemotherapy for a PCNSL were included and had their imaging, pathological, clinical and biological data reviewed. **Results:** For 6 patients (8,5 %), the eyes were the only CNS structures involved and vitreous analysis showed large B-cells in all cases. In total, pathological analysis showed DLBCL in 64 patients/69 (92,7 %), immunoblastic B-lymphoma in 2 patients (2,8%), Lymphomatosis cerebri in two patients (2,8%) and T lymphoma none otherwise specified in one patient. In FDG-PET, systemic significant uptakes were seen in 12 patients and were considered as malignant lymphoma systemic involvement in 6 patients (8,5%): two patients with bone marrow involvement for which BMB were negative, one patient with bowel involvement, one with hepatic involvement, one patient with adrenal involvement and one patient with nodal, adrenal and splenic involvement. In initial brain MRIs there was enhancing lesions in 56 of the 64 patients with cerebral involvement (87,5%) and only FLAIR hypersignals in 8 patients (12,5%). Mean size of greatest enhanced lesion was 32 mm. There was one lesion in 29 patients (45%) and multiple lesions in 35 patients (55%). For patient with brain involvement, FDG-PET showed at least one abnormal uptake in 53 patients (83%) and none in 11 patients (17%). Visibility of lesions in FDG-PET was strongly correlated with their size in MRI (p < 0,001). Visibility of at least one cerebral pathological uptake was correlated with event-free-survival (p < 0,05) but intensity of tumoral hypermetabolism of visible lesions expressed as SUV_{max} or its ratio to contralateral, cerebellar or hepatic uptake was not. Corticosteroids therapy before FDG-PET was associated with the absence of visible uptake of brain lesions and lower tumoral SUV_{max}. **Conclusion:** FDG-PET is a useful imaging modality for initial staging of suspected PCNSL, especially in bone marrow. High initial tumoral hypermetabolism is not an independent pejorative prognosis factor in treated patients.

EP177**Can SUV_{max}-based Criteria accurately interpreting interim and end-of-treatment 18F-FDG PET/CT for the prognosis of patients with diffuse large B cell lymphoma?**

Y. Zhang¹, Y. Fan², Z. Yang², X. Wang²; ¹Peking university cancer hospital & Institute, Beijing, CHINA, ²Peking university cancer hospital, Beijing, CHINA.

Objective Our aim was to further investigate whether SUV_{max}-based criteria could be superior to the other two methods in analyzing interim and end-of-treatment PET. **Method** One hundred twenty six patients with DLBCL were recruited in the research and underwent baseline PET/CT scans. Eight-eight patients carried out PET/CT after 4 cycles of chemotherapy (PET-4), 91 ones performed end-of-treatment PET/CT (PET-end), and 53 ones were with both interim and posttherapy PET/CT scan. SUV_{max}-based criteria were adopted to analyze the interim and end-of-treatment PET/CT scans, comparing to five-point criteria and %ΔSUV_{max} criteria. The optimal threshold of SUV_{max}-based criteria was decided via interobserver agreements and prognostic accuracies. Residue SUV_{max} higher than the optimal threshold or new ¹⁸F-FDG avid lesions indicated the positive lesion in interim and end-of-treatment PET. Prognostic values of PET/CT interpreting with three criteria were compared via accuracy of survival analysis. Survival curves were obtained using Kaplan-Meier estimates compared using the log-rank test. Uni- and multivariate analysis of outcomes were performed using clinical variables and PET-4 and PET-end. **Results** The median follow-up was 19 months for 88 patients with PET-4 and 24 months for 91 patients with PET-end. Interobserver agreements were almost perfect (kvalue: from 0.824 to 1) when the threshold was set above 1.4 times of SUV_{max-liver}. In both PET-4 and PET-end, the better specificity, positive predictive value (PPV) and good negative predictive value (NPV) were achieved for progress free survival (PFS) and overall survival (OS)

using SUV_{max}-based criteria, comparing to 5-PS or % Δ SUV_{max} interpretation. The 3-year PFS and OS were 6.7% and 28.6% for PET-4 with positive lesion and 77.1% and 78.1% for negative PET-4, respectively. Also, all of patients with positive lesion in PET-end suffered the progression of disease, while 3-year PFS of negative PET-end was 79.3%. Three-year OS was 44.4% for positive PET-end while 90.6% for the negative. Univariate analysis suggested stage, level of LDH, IPI, and performance status were adverse factors for PFS and OS. Cox regression multivariate analysis showed positive residue interpreting with SUV_{max}-based criteria in PET-4 and PET-end was an independent prognostic factor for PFS and OS. **Conclusion** This retrospective research demonstrated SUV_{max}-based criteria were better than five-point criteria and % Δ SUV_{max} criteria in analyzing the interim and end-of-treatment PET imaging for the prognosis of DLBCL patients. Further test of SUV_{max}-based criteria will be investigated in HL and other NHL.

EP178

Utility Of Initial Staging ¹⁸F-FDG PET-CT Scan To Detect Bone Marrow Infiltration In Patients Diagnosed Of Lymphoma: Can We Avoid Bone Marrow Biopsy?

M. Pedrera-Canal, M. Martínez de Bourio, R. M. Couto Caro, L. F. León-Ramírez, C. Riola-Parada, A. Serrano-Palacio, O. Salsidua-Arroyo, E. Cala-Zuluaga, J. L. Carreras-Delgado; HOSPITAL CLINICO SAN CARLOS, MADRID, SPAIN.

Objective: To evaluate the ability of 2-fluorine-18-luoro-2-deoxy-D-Glucose (¹⁸F-FDG) positron emission tomography/computed tomography (PET/CT) performed for initial staging in patients with newly diagnosed lymphoma compared to bone marrow biopsy (BMB), to detect bone marrow infiltration. **Material and methods:** Retrospective study from December/2014 until February/2016 including 40 patients (21 male and 19 female), with a mean age of 57.2 years old. They all had been recently diagnosed of lymphoma, classifying them as Hodgkin's Lymphoma (HL) 22.5%, diffuse large B-cell lymphoma (DLBCL) 30%, mantle cell lymphoma 5%, follicular lymphoma 30%, T-cell lymphoma 7.5% and others 5%. ¹⁸F-FDG PET-CT scan for initial staging was performed in all of them, as well as a BMB, with a mean of 20 days between both. We compared right iliac crest Standardized Uptake Value (SUV_{max}) measured in PET/CT scan and the histology of the sample obtained from the BMB. PET/CT was considered positive in those cases with a right iliac crest SUV_{max} \geq 2.3. **Results:** PET/CT was negative for bone marrow infiltration in 72.5 % (29/40) and positive for it in 27.5% (11/40). However, BMB was negative for malignancy in 80% (32/40), positive in 17.5% (7/40), and doubtful in one case. In 85.7% (6/7) of the patients with a positive BMB, PET/CT scans as well as BMB were positive for bone marrow infiltration. In just 2.6% (1/29) of the patients with a negative PET/CT scan, BMB was positive and PET-CT was negative for malignancy, obtaining a good Kappa Index (0.685) between both techniques. Furthermore, we made the comparison between the different histological subtypes, dividing them into HL, aggressive B-NHL (DLBCL and mantle cell lymphoma), indolent B-NHL and T-cell NHL. In HL, both BMB and PET/CT were negative for malignancy in 75%, whereas in 25%, PET/CT was positive with a negative BMB. In aggressive B-NHL, PET/CT results corresponded to BMB results in 85.8%, whereas in 14.2 % did not. In indolent B-NHL and T-cell NHL, we obtained the same results in both techniques in 100% cases. **Conclusion:** In our study, PET/CT performed for initial staging in patients with lymphoma, was well correlated to BMB to detect bone marrow infiltration. From all the subtypes, indolent B-NHL and T-cell NHL had the best correlation between both tests. These results suggest that in those subtypes, we could avoid BMB using initial PET/CT scan as reference. However, we should make more studies with more patients.

EP179

PET/CT And Beta-2-Microglobulin In Lymphoma Patients After Standard Chemotherapy

D. Vassileva¹, B. Spassov¹, K. Mladenov², V. Hadzhiyska², M. Guenova¹, G. Mihaylov¹; ¹Specialized Hospital for Active Treatment of Hematological Diseases, Sofia, BULGARIA, ²Clinic of Nuclear Medicine, University Hospital "Alexandrovska", Sofia, BULGARIA.

Background: The detection of residual disease after standard chemotherapy using imaging methods and tumor markers in lymphoma patients (pts) is essential to determine which pts would benefit from additional treatment. Positron emission tomography/computed tomography (PET/CT) imaging has become a very sensitive technique for monitoring therapy response in lymphoma pts. Beta-2-microglobulin (β_2 M) is low molecular protein used as a major tumor marker in lymphoproliferative diseases. However the data regarding the detection of residual disease by PET/CT and serum β_2 M levels after standard chemotherapy in lymphoma pts are limited. **Aim:** The aim of the study was to assess the role of PET/CT and β_2 M in lymphoma pts after standard chemotherapy for determination of the further management. **Materials and methods:** A total 128 pts, aged 19-71 years, were analyzed - 45 and 83 pts with Hodgkin's disease (HD) and non-Hodgkin's lymphoma (NHL), respectively. These pts were examined 4-6 weeks after the end of the standard chemotherapy by ¹⁸F FDG PET/CT according to the accepted protocol. Serum β_2 M levels were also measured radioimmunologically for disease activity assessment. **Results:** By applying PET/CT results two pts' groups were formed: [1] pts with complete metabolic response (PET/CT negative results) and [2] pts with partial metabolic response or progressive disease (PET/CT positive results). Using Deauville criteria complete response was observed in 26 (58 %) HD and 39 (46%) NHL pts (Deauville score 1-3). Sixty three pts (49%) had partial response, stable or progressive disease (Deauville score 4-5); 16 of them had one hypermetabolic lesions and 47 - disseminated nodal or extranodal involvement located in the lungs, thyroid gland or bones. PET/CT revealed 3 previously unknown additional lesions in two pts undetected by conventional visualization methods. The pts with one hypermetabolic lesions were considered for radiotherapy, while pts with more than one nodal and extranodal lesions after completion of standard chemotherapy were considered for high dose chemotherapy \pm autologous stem cell transplantation (ASCT). The median serum β_2 M levels were significantly higher in HD and NHL pts with PET/CT positive results compared to those pts with PET/CT negative results (HD pts - 3.3 vs 1.6 mg/L and NHL pts 4.4 vs 1.8 mg/L) respectively. **Conclusion:** The combination of PET/CT and serum β_2 M levels was useful in lymphoma pts after standard chemotherapy for determination of those who need additional therapy: radiotherapy, chemotherapy or ASCT. These results should be confirmed in prospective clinical trials.

EP180

The role of 18 F-FDG PET/CT in identifying bone marrow infiltration in patients with non-Hodgkin's Lymphoma

T. Mannarino, C. Mainolfi, N. Frega, G. Rossi, S. Pellegrino, L. Marano, F. Trastulli, L. Simeone, O. Vitagliano, V. Russo, S. Del Vecchio, A. De Renzo, M. Petretta, A. Cuocolo; Federico II University, Naples, ITALY.

Aim: Bone marrow infiltration (BMI) evaluation plays a key role in lymphoma staging, treatment and prognosis. The role of PET/CT in the assessment of BMI is still controversial, especially in non-Hodgkin's lymphoma (NHL). We compared ¹⁸F-FDG PET/CT visual and

quantitative analyses with bone marrow biopsy in NHL patients. **Material and Methods:** Fifty patients with newly diagnosed NHL from February 2011 to February 2016 were retrospectively analyzed. Of these, 26 (group A) patients had aggressive NHL and 24 (group B) indolent NHL. To detect BMI on the posterior iliac crest 3 different PET/CT evaluation methods were used: 1) visual analysis, 2) maximal standardized uptake values (SUVmax, cut-off >2.5), and 3) Deauville score (categorical). Each method was applied in the whole patients cohort, in group A and in group B. Images were blindly reviewed separately by 3 nuclear medicine physicians. PET/CT results were compared with the bone marrow biopsy performed after imaging in all patients. Decision-curve analysis was used to evaluate the increment in net benefit (NB) obtained considering the Deauville score over a biopsy-all strategy. **Results:** The prevalence of a positive biopsy was 38% in whole cohort, 19% in group A and 58% in group B. In the whole cohort, sensitivity, specificity and accuracy were 21%, 84% and 60% for visual analysis; 58%, 55% and 50% for SUVmax; and 47%, 81% and 68% for Deauville score. In group A, sensitivity, specificity and accuracy were 0%, 76% and 62%, for visual analysis; 40%, 52% and 50% for SUVmax; and 20%, 71% and 62% for Deauville score. In group B, sensitivity, specificity and accuracy were 29%, 100% and 58% for visual analysis; 64%, 60% and 62% for SUVmax; and 57%, 100% and 75% for Deauville score. At probability threshold equal to the prevalence of a positive biopsy, the increase in NB by Deauville score was 0.11 in the whole cohort, 0.02 in group A and 0.33 in group B. In this latter group, biopsying patients on the basis of the Deauville score is a strategy that reduced the biopsy rate by 24%, without missing any BMI. **Conclusions:** FDG-PET/TC visual analysis has a limited value for detecting BMI in patients with NHL, while quantitative analysis by Deauville score provides a higher diagnostic performance. Noteworthy, the high positive predictive value in patients with indolent NHL suggests a potential role of FDG-PET/TC in avoiding bone marrow biopsy in this subtype of lymphoma.

EP181

Analysis of early interim PET/CT results for treatment individualization in patients with lymphoma: comparison between Deauville criteria and $\Delta\text{SUV}_{\text{max}}$

M. Khodjibekova, L. Tyutin, N. Kostenikov, N. Il'in; Russian research center of radiology and surgical technologies, Saint-Petersburg, RUSSIAN FEDERATION.

Aim: Treatment of lymphoma requires an early and accurate assessment of prognosis. This study aimed to assess the value and reproducibility of early PET/CT with ^{18}F -FDG after two-four cycles of chemotherapy using Deauville five-point scale and $\Delta\text{SUV}_{\text{max}}$. **Methods:** Sixty four patients with newly diagnosed Hodgkin and non-Hodgkin lymphoma were evaluated. All patients underwent PET/CT scan at baseline, after two-four cycles of chemotherapy and after completion of chemotherapy. Scans were interpreted using Deauville five-point scale, between baseline and interim PET/CT scans $\Delta\text{SUV}_{\text{max}}$ was calculated. **Results:** According to Deauville five-point scale 27 (42.2%) patients were scored as negative and 37 (57.8%) patients as positive. In all patients with interim PET-negative scan $\Delta\text{SUV}_{\text{max}}$ between baseline and interim examination was more than 71%. SUV_{max} in all patients with score 5 of PET-positive group was stable or didn't decrease significantly between studies. However the $\Delta\text{SUV}_{\text{max}}$ in most of the patients (58.8%) with score 4 of PET-positive group was more than 71% indicating a favorable prognosis of the disease. The prognostic value of PET/CT using Deauville score ≥ 4 was moderately inferior ($p=0,004$) than cut-off of $\Delta\text{SUV}_{\text{max}} \geq 71\%$ ($p=0,0002$). **Conclusion:** Combined application of visual and quantitative analysis in the evaluation of the early PET/CT results increases the accuracy of the method. Calculation of $\Delta\text{SUV}_{\text{max}}$ in patients with Deauville high score (≥ 4) leads to better outcome prediction.

EP182

18F-FDG PET/CT In The Initial Evaluation And Response Assessment In Primary Central Nervous System Lymphoma

R. FERNÁNDEZ LÓPEZ¹, Á. De Bonilla Damiá¹, J. Lojo Ramírez¹, I. Acevedo Bañez¹, L. Caballero Gullón¹, V. Pachón Garrudo¹, F. Capote Huelva², I. Borrego Dorado¹; ¹H.U. VIRGEN DEL ROCÍO, SEVILLE, SPAIN, ²H.U. PUERTA DEL MAR, CÁDIZ, SPAIN.

Objective: To evaluate the role of positron emission tomography combined with computed tomography with 18F-FDG (18F-FDG PET/CT) in the initial evaluation and response assessment in primary central nervous system lymphoma (PCNSL). **Material and methods:** A total of 16 patients (7 males and 9 females) with a median age of 56 years diagnosed of PCNSL between October 2011 and January 2015 were retrospectively analyzed from our institution. All patients presented a histological subtype of diffuse large B-cell lymphoma. A brain and whole body 18F-FDG PET/CT were performed in the initial evaluation. In 7 patients a PET/CT after treatment was performed in order to evaluate response and follow-up after treatment. Images data were collected, analyzed and correlated with outcome with an average of follow-up of 10,59 months. **Results:** 18F-FDG PET/CT showed at diagnosis a hypermetabolic focal lesion in 9 patients, multiple lesions in 6 patients and one patient did not evidence significant uptake. No patient showed hypermetabolic lesions outside central nervous system. The mean of maximum SUV (SUVmax) of the primary tumours was 17.86 (range: 9.2 - 29.5). The average follow-up was 10.59 months (0.5-43) with an overall mortality of 62.5% (10/16 patients). From the seven patients with PET/CT scan images after treatment: 3 developed complete metabolic response (CMR), 1 reached nearly complete metabolic response (NCMR) and 3 had progressive metabolic disease (PMD). The overall mortality in this subset of patients was of 57.1% (4/7 patients). Two out of the three patients with CMR died because of disease relapse with an overall survival (OS) of 25 and 22 months, respectively. Two out of the three patients with PMD died with an OS of 7 and 8 months, respectively. The remaining 3 patients (1 NCMR, 1 CMR and 1 PMD) are alive without evidence of disease with an OS of 19, 26 and 43 months, respectively. It seems to be unrelated between the type of metabolic response and survival although the data are limited. **Conclusions:** 18F-FDG PET/CT can be useful in the initial evaluation and may contribute as valuable information for the management of PCNSL, particularly in the assessment of the treatment response. Prospective studies are needed to confirm their possible prognostic value.

EP183

The clinical value of ^{18}F FDG Positron Emission Tomography in high risk Mycosis Fungoides

S. Usmani, F. Marafi, A. Esmail, F. al Kandari; Kuwait Cancer Control Center, Kuwait, KUWAIT.

The aim of the present study is to evaluate the possible role of 18F-FDG PET-CT in the management of high risk mycosis fungoides. **Materials and Method:** Twenty three patients (mean age, 41.5yrs; median age 42yrs; 18 males and 5 females) with risk of secondary lymph node involvement (those with large cell transformation, tumors, erythroderma, or enlarged LNs on physical examination) were included in the study. FDG PET-CT was performed at the time of initial diagnosis or suspected relapse. We excluded patients who had done scans at mid-treatment. All patients underwent PET-CT scan by injecting 0.06mCi/kg of F18 FDG. The maximum standard uptake value (SUV max) was recorded for each patient. **Results:** The 18F-FDG PET-CT was positive in 19 patients. PET-CT detected local cutaneous disease in 17 cases. The range of SUV max is 2.8-14.1. Out of 23 patients hypermetabolic adenopathy are in found in 12 patients and visceral involvement in one. **Conclusions:** Although the study population is small our findings suggests that 18F-FDG PET-CT

can detect cutaneous and extra-cutaneous lesions in mycosis fungoides and may guide biopsies especially in patients with risk of secondary lymph node involvement.

EP184

Clinical significance of FDG-PET negative residual masses in DLBCL patients treated with R-CHOP

Y. Ramirez Escalante¹, M. Coronado Poggio¹, P. Gómez², S. Rizkallah Monzón¹, S. Rodado Marina¹, C. Escabias del Pozo¹, G. Villoria Almeida¹, I. Santos Gómez¹, J. Guzmán Cruz¹, M. Orduña Diez¹, L. Dominguez Gadea¹; ¹Medicina Nuclear, Hospital Universitario La Paz, Madrid, SPAIN, ²Hematología, Hospital Universitario La Paz, Madrid, SPAIN.

INTRODUCTION FDG-PET/CT is the standard method for assessment of response at the completion of treatment in Diffuse Large B Cell Lymphoma (DLBCL) patients. Recent data suggest that patients with a complete metabolic response but a residual mass on CT (CMRr) may have different outcome to patients with CMR and no radiological residual lesions (CMR). **OBJETIVE** The aim of this study was to investigate the significance of PET negative residual masses in DLBCL patients treated with standard regimen. **MATERIAL AND METHODS** Fifty-two patients diagnosed of DLBCL between 2010 and 2014 who underwent PET before treatment (PET0) and final PET after 6 cycles of R-CHOP (PET6) were retrospectively reviewed. Age at diagnosis: 20-86 years old. Ann Arbor stage and IPI at diagnosis were recorded. PET6 result was defined as positive or negative, and negative PET patients were classified as CMR or CMRr following Lugano recommendations (*J Clin Oncol* 32:3048-3058). Follow up was made for 6 to 101 months (median: 41 months). Survival of CMR and CMRr groups was calculated. **RESULTS** From the total population, 39/52 patients (75%) were PET6 negative and 13/52(25%) patients were PET6 positive. 26 out of 39 negative PET6 patients were classified as CMR and 13/39 negative PET6 patients were classified as CMRr. Two patients relapsed from the CMRr group versus one patient from the CMR group. Mean free time survival was higher in the CMR group than in the CMRr one (p=0.064). One patient from CMRr died and no patients from CMR group were dead in the follow up time. Overall survival of CMR and CMRr groups could not be calculated due to the small number of patients. **CONCLUSIONS** DLBCL patients with negative PET after 6 cycles of R-CHOP seem to have a higher risk of relapse when there is residual lesion in CT. Larger series are needed to establish the prognostic value of PET negative residual masses in this population.

EP185

FDG-PET/TC in mantle cell non Hodgkin lymphoma: experience in our institution.

A. Perissinotti¹, A. Allende-Riera¹, J. Uña-Gorospe¹, M. J. Rodriguez-Salazar², J. M. Raya-Sanchez², D. Cabello¹, M. De Sequera-Rahola¹, E. Martínez-Gimeno¹, C. Cardenas-Negro¹, O. Vilahomat¹; ¹Hospital Nuestra Señora de la Candelaria, Santa Cruz de Tenerife, SPAIN, ²Hospital Universitario de Canarias, Santa Cruz de Tenerife, SPAIN.

Aim: Our aim is to report our experience in the assessment of patients with mantle cell non Hodgkin lymphoma (MCL) with ¹⁸F-Fluorodeoxyglucose positron emission tomography/computed tomography (FDG-PET/TC). **Materials and methods:** We retrospectively reviewed 27 patients (mean age 63, range 38-82. 19 male/9 female) with histologically proven MCL disease studied with 138 FDG-PET/TC scans (mean dose 2.76 MBq/Kg) during their initial staging, interim, end-of-therapy, surveillance or relapse phase of the disease. All patients were classified as WHO grade III or IV. A mean number of 5 (ranging from 1 to

13) FDG-PET/TC studies per patient were performed. **Results:** 70% (19/27) of patients showed at least one pathological FDG-PET/TC study showing hypermetabolic lesions during the course of the disease: FDG uptake in the most active lesion of all FDG-PET/TC studies had a mean SUVmax of 10.4 (ranging from 2.8 to 27). 8 out of 27 patients were studied with FDG-PET/TC as part of their initial staging and also were subsequently studied with FDG-PET/TC: all of them showed positive pathological scans with a mean SUVmax of 8.5 (ranging from 17.64 to 3.35) in the most active lesion. One of them showed unsuspected splenic involvement and two of them splenic and bone marrow compromise. Four out of this eight patients reached complete metabolic response after chemotherapy treatment. **Conclusion:** Despite the fact that FDG-PET/TC is not currently included in all mantle cell non Hodgkin lymphoma assessment guidelines, our experience suggests that FDG-PET/TC can be a valuable diagnostic tool because of its ability to detect hypermetabolic lesions at all stages of the disease and treatment monitoring evaluation; specially for the initial staging as all of our FDG-PET/TC staging studies showed positive pathological scans.

EP186

18F-FDG-PET/CT in the Staging and Prognostic Evaluation of Patients with Indolent Lymphoma

R. Fonti¹, S. Pellegrino², B. Salvatore¹, O. Vitagliano³, L. Simeone³, F. Cacace³, M. Memoli³, S. Leone³, A. De Renzo³, S. Del Vecchio²; ¹IBB-CNR, NAPLES, ITALY, ²Department of Advanced Biomedical Sciences, University "Federico II", NAPLES, ITALY, ³Haematology Division, University "Federico II", NAPLES, ITALY.

Indolent lymphomas are a group of low-grade non-Hodgkin lymphomas characterized by slow growth and chronic clinical course. Recent studies have reported that indolent lymphomas almost always show variable FDG avidity regardless of tumor grade thus providing a rationale for using 18F-FDG-PET/CT in the management of these patients. **Aim.** The aim of our study was to evaluate lymph node involvement in patients with indolent lymphomas by 18F-FDG-PET/CT and to correlate the derived imaging parameters with clinical, biochemical and haematological variables routinely used in the staging and prognosis of low-grade lymphomas. **Methods.** We evaluated retrospectively 43 patients (16 males, 27 females; mean age±SD, 60±10.2 years) with indolent lymphoma (27 with follicular lymphoma, 11 with marginal zone lymphoma and 5 with small lymphocytic lymphoma) who had undergone whole-body 18F-FDG-PET/CT and contrast-enhanced CT alone or as part of 18F-FDG-PET/CT examination at the time of diagnosis. All patients were staged according to standard criteria and were stratified in risk groups based on Follicular Lymphoma International Prognostic Index (FLIPI) 1 that include parameters such as age, stage, lactate dehydrogenase levels, haemoglobin levels and number of pathological nodal sites. **Results.** In the 43 patients studied, the number of positive lymph node basins at 18F-FDG-PET/CT ranged between 1 and 33 and the SUVmax of the lymph node with the highest tracer uptake varied from 2 to 19.9. While the number of positive lymph node basins at contrast-enhanced CT ranged between 1 and 28 and the maximum diameter of the largest lymph node varied from 11 to 80 mm. The number of pathological lymph nodes at both 18F-FDG-PET/CT and contrast-enhanced CT were significantly correlated with stage (Spearman rank correlation coefficient $r=0.42$, $P=0.0065$ and $r=0.37$, $P=0.0149$, respectively). In addition, also the size of the largest lymph node showed a significant correlation with stage (Spearman rank correlation coefficient $r=0.40$, $P=0.0153$). Moreover, the number of pathological lymph nodes at both 18F-FDG-PET/CT and contrast-enhanced CT was significantly correlated with FLIPI 1 score (Spearman rank correlation coefficient $r=0.48$, $P=0.0009$ and $r=0.54$, $P=0.0002$, respectively). **Conclusion.** 18F-FDG-PET/CT may contribute to the evaluation of lymph node involvement and thus may help in the staging and prognostic assessment of patients with indolent lymphoma.

EP187**Clinical importance of bone marrow 18F - FDG uptake after treatment in lymphoma patients**

V. Hadzhiyska¹, M. Garcheva², P. Nikolova¹; ¹University Hospital Alexandrovska, Sofia, BULGARIA, ²City Clinic, Sofia, BULGARIA.

A lot of examinations confirm the importance of 18F-FDG PET/CT for initial evaluation of bone marrow involvement in lymphoma. **The aim** of this study was to evaluate the clinical significance of the patterns of bone marrow uptake in different periods after the end of the chemotherapy. **Material and methods.** Sixty six patients, examined by the standard protocol of -FDG PET/CT were retrospectively evaluated: 36 with Hodgkin disease (HD), 17 with diffuse large B-cell lymphoma (DLBCL), 7 - with follicular lymphoma (FL) and 6 - with other lymphoma types. The exclusion criteria were patients with initially proved bone marrow involvement. Twenty patients (gr.1) were examined in one month, 26 (gr.2) - in the period between the 2nd and the 6th month and 20 pts (gr.3) - in one year period after chemotherapy. **Results.** In gr. 1 diffuse uptake was detected in 7 pts (35%), and in the rest 13 pts (65%) - negative bone marrow uptake. In gr. 2 diffuse uptake was found in 2 pts, (8%) and focal uptake abnormalities was detected in 1 pt (4%), twenty three, 88% of patients were with negative bone marrow uptake. In gr. 3 four of the pts (20%) were with diffuse uptake and other three (15%) with focal uptake abnormalities, 65% remained with negative bone marrow. The consequent biopsy proved in 2 out of 4 patients with diffuse uptake bone marrow involvement. **Conclusion.** While the diffuse bone marrow uptake early after the end of the chemotherapy can be attributed to post therapeutic activation, its presence in one year period after the end of the therapy parallels the increase of the rate of the focal uptake abnormalities and is highly suspicious for bone marrow involvement. We consider that these patients should be reevaluated by magnetic resonance imaging, or bone marrow biopsy.

EP188**Role of 18F FDG PETCT in Marginal Zone Lymphomas**

E. ABAMOR¹, A. Kucukoz Uzun², T. Cakir¹, A. Cakir³, A. N. Karadayi⁴, T. Atasever¹; ¹Medipol University, Faculty of Medicine, Department of Nuclear Medicine, ISTANBUL, TURKEY, ²Dr.Lutfi Kirdar Kartal Education ve Research Hospital, Department of Nuclear Medicine, ISTANBUL, TURKEY, ³Medipol University, Faculty of Medicine, Department of Pathology, ISTANBUL, TURKEY, ⁴Dr. Lutfi Kirdar Kartal Education and Research Hospital, Department of Pathology, ISTANBUL, TURKEY.

Aim: Role of FDG PETCT remains controversial in marginal zone lymphomas (MZL), due to variable F18-FDG avidity. We evaluated the value of FDG PETCT in a limited group of patients with diagnosis of marginal zone lymphoma (MALT, splenic and nodal subtypes). **Material and methods:** We reevaluated FDG PETCT findings in 15 patients with MZL. All patients were histopathologically diagnosed by biopsy of bone marrow or lymph node or primary solid lesion. Six women and 9 men, aged between 61 - 77 (mean age: 62,53) were reviewed. Six patients (% 40) had MALT, 6 patients had splenic involvement (% 33) and 11 patients had nodal involvement (% 73). All patients had FDG PETCT at baseline staging. **Results:** Six MALT lymphoma patients had primary lesions in orbita, eyelid, parapyranging region, larynx, colon and cervix with significant FDG uptake, SUV between 5,1 - 15,3 (mean: 10,25). One MALT patient had also spleen involvement by diffuse increased FDG uptake (SUV 4,5). Another MALT patient had hepatomegaly with diffuse increased FDG uptake (SUV 4,4). One patient with MALT had brain metastasis (SUV: 13,6) and 2 other MALT patients had lung metastasis (SUV: 4,2 - 6,2). Eleven patients had lymph nodes involvement, with SUV between 2,6 - 10 (mean: 6,51). Spleen involvement was observed

in 6 patients with SUV between 3,3 - 10,2 (mean: 5,96). Only 5 patients represented increased FDG uptake in bone marrow and at metastatic bone, SUV between 2,8 - 8,2 (mean: 5,26). Six patients had metastatic FDG uptake at liver, brain, lung or muscle tissue, in which SUV was between 3,1 - 13,6 (mean: 6,28). The overall mean SUV was 6,80 for all lesions. Primary and metastatic sites of MALT lymphoma had highest metabolic activity rates (the overall mean SUV: 8,89). FDG nonavidity was not detected in patients. Weak FDG affinity (SUV: 2,6 - 3,3) was observed in only 1 patient. The stage of disease was increased with splenic involvement, organ and bone metastasis by PET/CT. **Conclusion:** Although in limited number of patients, our data shows significant metabolic activity in marginal zone lymphoma lesions. MALT lymphoma lesions of primary and metastatic sites show higher FDG uptake than splenic and nodal MZL. But splenic and nodal MZL also tend to have significant FDG uptake. Though it needs a larger population with followup study, our data suggests a valuable role for PET/CT in all subtypes of MZL at baseline diagnostic and staging study.

EP189**18F-FDG PET-CT imaging in patients with cutaneous lymphoma: single institutional experience**

K. K. AGARWAL, A. MUKHERJEE, P. SHARMA, H. SINGH, R. KUMAR, C. BAL; ALL INDIA INSTITUTE OF MEDICAL SCIENCES, NEW DELHI, INDIA.

Purpose: To evaluate the role of 18F-FDG PET/CT in patients with cutaneous lymphoma. **Methods:** The data of 40 patients (Age: 52 ± 20.5 years; Male: 22) with cutaneous lymphoma who underwent total 60 18F-FDG PET/CT studies for staging (n=17) or restaging (n=43) were retrospectively evaluated. The primary histopathology was T cell lymphoma in 19, mycosis fungoides in 13, DLBCL in 3, ALCL in 2 and marginal zone B cell lymphoma in 3 patients. PET/CT studies were evaluated qualitatively and semiquantitatively (SUVmax) and interpreted as positive or negative for disease. The site of the lesions was also noted. Histopathology/cytology (when available) and clinical/imaging follow up of minimum 6 months was taken as reference standard. **Results:** 37 PET/CT studies were positive for active disease. Per study wise sensitivity, specificity, PPV, NPV and accuracy of PET/CT were 93.5%, 89%, 93.5%, 89% and 92%, respectively. The accuracy of PET/CT in staging group and restaging group was same, 92% (p=0.541). 32 Cutaneous lesions (unifocal-14, multifocal-18), 22 nodal lesions (single group-8, multiple groups-14), 5 splenic lesions and 2 liver lesions were noted. The sensitivity, specificity and accuracy of PET/CT for cutaneous lesions was 90%, 100% and 94%, and for nodal lesions was 100%, 94%, and 96%, respectively (p=1.00). The mean SUVmax of cutaneous lesions was 5.1±2.8, nodal lesions was 4.4±2.7 and splenic lesion was 5.4±2.8. **Conclusions:** 18F-FDG PET/CT has high diagnostic accuracy for staging and restaging patients with cutaneous lymphomas. It can detect both cutaneous and non cutaneous lesions with high sensitivity and specificity.

EP190**Prognostic Importance of Bone Marrow Uptake on Baseline 18F-FDG Positron Emission Tomography/Computed Tomography in Diffuse Large B-Cell Lymphoma**

C. Soydal¹, E. Koksoy², A. Yasar², E. Turgal³, B. Doganay Erdogan⁴, H. Akbulut², N. O. Kucuk¹; ¹Ankara University Medical Faculty Nuclear Medicine Department, Ankara, TURKEY, ²Ankara University Medical Faculty Medical Oncology Department, Ankara, TURKEY, ³Hittit University Medical Faculty Biostatistics Department, Corum, TURKEY, ⁴Ankara University Medical Faculty Biostatistics Department, Ankara, TURKEY.

Aim: To define prognostic importance of bone marrow uptake on pretreatment ^{18}F -Fluorodeoxyglucose (FDG) Positron Emission Tomography (PET)/Computed Tomography (CT) in Diffuse Large B-Cell Lymphoma (DLBCL) Patients. **Material and Methods:** Fifty-four (mean age: 55.5 ± 18.3 , 20F and 34M) DLBCL patients who underwent pretreatment ^{18}F -FDG PET/CT were included to the study. Prognostic effect of age, gender and serum LDH levels of patients, disease stage, presence of extranodal and bone marrow involvement, Deauville Score, SUVs to progression free survival (PFS) were analyzed by using Cox-Regression Analysis. **Results:** Mean PFS was calculated as 19.5 (min-max: 1-64) months. While extranodal FDG uptake was seen 36 (67%) (stomach in 6, lung in 6, spleen in 6, skin-soft tissue in 6, liver in 4, bowel in 4, tonsil in 4, nasopharyngeal region in 3, pancreas in 3, thyroid in 2, peritoneum in 1 patients), bone marrow uptake was observed in 8 (15%) patients. Female gender ($p=0.025$), presence of bone marrow uptake ($p=0.013$) and serum LDH levels ($p=0.001$) were found as significant factors to predict PFS. Additionally Negative Predictive Value (NPV) for bone marrow uptake was calculated as 100%. **Conclusion:** Bone marrow uptake in pretreatment ^{18}F -FDG PET/CT is an important prognostic factor in DLBCL patients. Moreover in consideration of high NPV, ^{18}F -FDG PET/CT could eliminate unnecessary bone marrow biopsy in FDG negative patients. Although pretreatment PET/CT could give useful information in staging of disease, in this analysis other parameters in PET/CT did not reach to prognostic significant level.

EP191

Optimization criteria for metabolic prognostic assessment in patients with lymphoma

M. Cozar Santiago¹, J. Garcia Garzon², M. Soler Peter², R. Sanchez Jurado¹, J. Aguilar Barrios¹, R. Sanz Llorens¹, R. Brisa Vazquez¹, J. Ferrer Rebolleda¹; ¹ERESA-GENERAL UNIVERSITY HOSPITAL, VALENCIA, SPAIN, ²CETIR-ESPLUGUES PET UNIT, BARCELONA, SPAIN.

AIM: to identify metabolic response evaluation criteria that optimizes a prognostic assessment of disease **MATERIALS AND METHODS:** there were included 138 patients affected by lymphoma (43 Follicular Lymphoma, 43 Hodgkin Lymphoma, 43 Diffuse large B-Cell Lymphoma) on whom three 18F-FDG PET/CT studies were performed: the first one for staging the disease or "basal PET" (bPET), the second one after three/four cycles of treatment or "interim PET" (ipet), and the last one at the end of the chemotherapy and/or radiotherapy, or "end PET" (ePET). Images were analyzed using 2 interpretation criteria: visual method using the Deauville scale and semiquantitative method or "percentage reduction SUVmax" (ΔSUVmax). Chi square (χ^2) was calculated to determine whether there were significant differences between DS and $\% \Delta\text{SUVmax}$ and the Kappa (K) concordance degree. iPET prognostic utility with both methods was assessed depending on the clinical status after at least 13 months of follow-up and if they are able to identify treatment failure patients who would be able to benefit from a second-line treatment. Survival curves (Kaplan Meier product test and long Rank test) were calculated. **RESULTS:** we saw a good correlation between the two methods of evaluation, for the three types of lymphomas; for ePET as well as for the iPET with a significant χ^2 (χ^2 : 52.12 $p < 0.05$) and good agreement between them (K : 0.60). Both methods proved to be useful for the prognostic assessment of iPET. Regarding to survival, both methods were useful for identifying potential relapse after the proposed PFS (long Rank test 23, 15, $p = 0.00$). **CONCLUSION:** metabolic criteria allow a correct assessment of patients with lymphoma obtaining similar values of agreement. Taking into account the potential utility of them in iPET, both methods have a similar reliability.

EP192

Variability in 18F-FDG avidity in extranodal marginal zone B-cell lymphomas

A. Sadija, N. Beslic, R. Milardovic, S. Ceric; University Clinical Center, Sarajevo, BOSNIA AND HERZEGOVINA.

Introduction: Most lymphomas are proven to be highly avid to 18F-FDG, but there are some lymphoma subtypes with lower avidity such as small lymphocytic lymphoma, peripheral T-cell lymphoma and extranodal marginal zone B-cell lymphoma. Current guidelines advise the use of 18F-FDG imaging for staging of lymphomas with already known high 18F-FDG avidity, but there are small amount of information on rare lymphomas. It is also advised that for other lymphoma subtypes considered as variably tracer-avid, 18F-FDG imaging is recommended only if patients are included in clinical trials with endpoint which mainly considers response rate. The aim of this pilot study is to investigate 18F-FDG avidity in different extranodal sites of marginal zone lymphomas by reviewing the reports of all 18F-FDG PET-CT studies. **Patients and methods:** PET-CT studies were performed in all 12 extranodal marginal zone lymphoma patients referred to University Clinical Center Sarajevo for initial staging. All information were analyzed retrospectively reviewing medical records and PET-CT scans performed in period from 8/2014 to 3/2016. All PET-CT scans were analyzed for the presence of 18F-FDG avidity measuring SUVmax values in all extranodal sites of lymphoma involvement, and all data recorded. 18F-FDG avidity was defined as the presence of at least 1 focus of 18F-FDG uptake in involved site. Non-18F-FDG-avidity was defined as disease proven by clinical examination and histopathology but with no 18F-FDG uptake in any of the involved sites. **Results:** There were 11 patients with extranodal marginal MALT lymphoma and one patient with splenic marginal zone lymphoma. Sites of MALT lymphoma involvement were stomach, lung, parotid gland, epipharynx, submandibular gland, maxilla, orbit and thyroid gland. Only two patients with biopsy proven MALT lymphoma were non-avid to 18F-FDG in initial staging, with stomach and lung as lymphoma involved sites. SUVmax values were in the range of 2.6 - 12.2 with lowest SUVmax values measured in lung and stomach MALT lymphoma and highest in submandibular gland, maxilla, orbit and epipharynx. **Conclusion:** This study suggests that imaging with 18F-FDG PET-CT is useful for both initial staging and also follow-up of patients with extranodal marginal zone B-cell lymphoma. We found out that certain sites of lymphoma involvement as lungs and stomach have lower FDG avidity comparing to sites of involvement localized in head region, and we are suggesting larger studies to investigate the heterogeneity of 18F-FDG avidity in different sites of involvement. **Key word:** extranodal, lymphoma, avidity, 18F-FDG PET-CT

EP193

Role of 18F-FDG PET-CT and MRI in diagnosis of smoldering multiple myeloma and plasmocytoma

A. Mestre Fusco¹, A. Senín², E. Abella², F. García-Pallarols², J. Ares³, A. Solano³, M. Suárez-Piñera¹; ¹Nuclear Medicine. Hospital del Mar., Barcelona, SPAIN, ²Hematology. Hospital del Mar., Barcelona, SPAIN, ³Radiology. Hospital del Mar., Barcelona, SPAIN.

Background: Smoldering Multiple Myeloma (SMM) is defined by more than 10% of clonal bone marrow plasma cells and serum monoclonal protein without end-organ damage (CRAB criteria). Solitary Plasmocytoma (SP) is characterized by presence of clonal plasma cells outside the bone marrow. The Revised International Staging System (RISS) stratifies patients in three prognostic groups. Magnetic Resonance Imaging (MRI) is used in SMM and SP as gold standard imaging modality in order to guide decision making. In addition, 18F-FDG PET-CT (FDG-PET) may upgrade SMM and SP to Multiple Myeloma (MM). **Aim:** 1.-To compare FDG-PET and MRI in SMM and SP and evaluate the

concordance between both imaging modalities. 2.-To study the sensitivity of FDG-PET compared to MRI. 3.-To evaluate an association between metabolic activity on FDG-PET (SUVmax) and R-ISS score. Methods: FDG-PET and MRI were performed in 27 patients diagnosed of SMM or SP who were prospectively included (11 males, mean:61.5 years, range:38-85). FDG-PET whole body studies were performed in a PET-CT (Siemens Biograph6). A positive PET-CT was defined of abnormal increased uptake of FDG and/or evidence of lytic bone destruction on CT. SUVmax was calculated of each lesion. MRI whole body studies were acquired in a 1.5 Tesla (Signa GE Healthcare) with T1-weighted and STIR-weighted sequences. In all patients MRI was performed within 45 days of PET-CT. Concordance kappa was calculated. FDG-PET sensitivity was estimated. Correlation between R-ISS and SUVmax was estimated (ANOVA). Results: Of the 16 patients who were diagnosed initially as SMM, eight of them (50%) were upstaged to MM based on FDG-PET and MRI. Of the 7 diagnosed initially as SP, three of them (43%) were upstaged to Multiple Plasmocytoma or MM. FDG-PET and MRI were both negative in seven patients. Three patients showed extra-osseous involvement only detected by FDG-PET. However, FDG-PET fails to detect bone disease in three patients with blastic pattern on MRI. Estimated FDG-PET sensitivity was 88%. A correlation between FDG-PET and MRI was found ($k=0.667$, $p<0.05$). In 12 out of 16 (75%) there was a discrepancy in the number of lesions detected by both techniques. No correlation between SUVmax and R-ISS was found. Conclusion: FDG-PET and MRI offer complementary information in diagnostic evaluation on SMM and SP. In addition, FDG-PET provides additional information of disease in areas not covered by MRI. On the other hand, MRI seems to be more sensitive than PET in case of focal or smaller osteoblastic lesions.

EP194

The Comparison Of F-18 FDG PET/BT VE Tc-99m MIBI SPECT/ BT In Multiple Myeloma

S. Razavi Khosroshahi¹, H. Sayman¹, S. Berk², O. Balkanay³, J. Nematyazar¹, B. Vatankulu¹, S. Sager¹, M. Halac¹, M. Demir¹, L. Kabasakal¹, I. Uslu¹, K. Sonmezoglu¹; ¹istanbul university, cerrahpaşa medical faculty, nuclear medicine department, istanbul, TURKEY, ²istanbul university, cerrahpaşa medical faculty, hematology department, istanbul, TURKEY, ³istanbul university, cerrahpaşa medical faculty, cardiovascular surgery department, istanbul, TURKEY.

Multiple myeloma (MM) is a malignant disease of plasma cells derived from B cells in the bone marrow. Different imaging methods for staging, evaluation of relapse, response to therapy and prognosis are used. Despite the role of Tc-99m MIBI planar whole body scintigraphy is demonstrated, it is replaced by F-18 FDG PET/CT. Considering that the sensitivity and specificity will increase after the introduction of the newly developed SPECT/CT technology and its cost-effectiveness let us to compare these two methods prospectively. With this purpose, in 40 patients diagnosed as MM and referred for F-18 FDG PET/CT for further examination, additional Tc-99m MIBI planar and SPECT/CT imagings were performed. The obtained data were statistically evaluated by using Chi-square test. When the lesions were evaluated on regional basis SPECT/CT had a dual positive rate of 80.6% and a dual negative rate of 90.5%. On the other hand, when the evaluation was done on patient base, these ratios were calculated as 93.1% and 72.7%, respectively. Similar results were obtained when both methods were evaluated in subgroups. When bone marrow biopsy was accepted as a gold standard method, PET/CT sensitivity, specificity, PPV and NPV were calculated as 86.7%, 87.5%, 92.9% and 77.8% respectively, whereas for SPECT/CT were 93.3%, 87.5%, 93.3 and 87.5% respectively. When Tc-99m MIBI scintigraphy planar whole body and SPECT/CT images were compared, of 18 patients without any lesion on whole body imaging, 8 had lesions on SPECT/CT. According to the study results, in all clinical evaluation steps of patients with MM, having less cost as well as same diagnostic value, Tc-99m MIBI SPECT/CT can be a replacement for F-18 FDG PET/CT.

EP195

Could 18F-Choline PET/CT scan be a new diagnostic tool in assessing bone involvement in patients with multiple myeloma?

Z. Meckova¹, L. Lambert², J. Kubinyi¹, I. Spicka³; ¹Institute of Nuclear Medicine, GUH Prague, Prague, CZECH REPUBLIC, ²Clinic of Radiodiagnostic, GUH Prague, Prague, CZECH REPUBLIC, ³First Internal Clinic, GUH Prague, Prague, CZECH REPUBLIC.

Background: Multiple myeloma is a clonal plasma cell disorder resulting in infiltration of bone marrow and osteolytic lesions of the skeleton. The diagnosis and staging of multiple myeloma are based on blood and urine tests, bone marrow biopsy and imaging (radiography, CT, MRI and 18 F-FDG PET-CT). The presence and extent of bone marrow involvement is an important factor influencing prognosis and clinical management. Therefore, the imaging is vital for making the decision on the treatment initiation. **Aim:** Due to the fact that bone and bone marrow infiltration is difficult to detect by standard imaging methods, the aim of this study was to find out whether imaging by ¹⁸F-Choline could be of any additional value to that of 18F-FDG PET/CT in a patient affected with multiple myeloma. **Methods:** Series of ten patients untreated with extra medullary extensive disease will undergo a standard ¹⁸F-Choline PET/CT and ¹⁸F-FDG PET/CT within ten days. The results of the two scans will be compared in terms of number, sites and SUV_{max} of lesions. **Results:** At this stage two patients had a positive ¹⁸F-Choline and ¹⁸F-FDG PET/CT scans and the scans identified different number of lesions. Choline showed a mean SUV_{max} of 13.94 while FDG showed a mean SUV_{max} of 9.9 ($p = 0.0004$). Overall, ¹⁸F-Choline PET/CT scans detected eight more bone lesions than ¹⁸F-FDG PET/CT scans but the difference was not statistically significant ($P = 0.29$). **Conclusion:** The preliminary data show that ¹⁸F-Choline PET/CT could be more sensitive than ¹⁸F-FDG PET/CT for the detection of bone myelomatous lesions. It is necessary to extend our study and if the data are confirmed then ¹⁸F-Choline PET/CT can be considered as more appropriate functional imaging method in association with MRI for MM bone staging.

EP196

Diagnostic accuracy of 18F-FDG PET/CT in detection of bone lesions in patients with Multiple Myeloma

B. Chaushev, I. Micheva, P. Bochev, J. Dancheva, C. Yordanova, A. Klisarova, I. Krasnaliev; MBAL`ST.MARINA`, VARNA, BULGARIA.

Multiple myeloma (MM) is the most common cause of primary malignancy in bones. Diagnostic imaging plays a pivotal role in staging and prognostic assessment as well as in planning and monitoring treatment. The aim of our study was to estimate the diagnostic accuracy of 18F-FDG PET/CT in 18 patients with MM in the evaluation of the extent of bone disease at the time of initial diagnosis. Materials and methods: 18 patients (9 males and 9 females; age range 42- 68 years) with newly diagnosed IgG MM were included in the study. PET/CT was used as staging procedure for the detection of the bone lesions and the stage was determined according Durie - Salmon PLUS Staging Systems. Correlative imaging data was available in most of the cases and included skeletal radiographic survey in 11, CT in 7 and MRI in 2. Results: In 13 patients 18F-FDG PET/CT detected higher number of bone lesions in comparison to the other imaging methods. In 5 patients there was no difference in the number of bone lesions, including the two cases where MRI was performed. According to Durie - Salmon PLUS Staging Systems 18F-FDG PET/CT detected 13 patients in stage I, 4 in stage II and 1 patient in stage III. Conclusion: 18F-FDG PET/CT has shown to have high sensitivity specificity and key prognostic value in patients with MM. It is a superior imaging modality for diagnosis of bone lesions in myeloma compared to conventional radiography.

EP-11 – Sunday, October 16, 2016, during Exhibition hours, e-Poster Area
Clinical Oncology: Melanoma

EP197

Cutaneous Melanoma: clinical and prognostic value of FDG PET/CT after surgery

D. Familiari¹, M. C. Fornito¹, R. Gentile², S. Russo¹, A. Ruggeri¹, M. Midiri³, P. Alongi²; ¹Nuclear Medicine Department - A.R.N.A.S. Garibaldi, Catania, ITALY, ²Nuclear Medicine Unit - San Raffaele G. Giglio Institute, Cefalù (Pa), ITALY, ³University of Palermo, Palermo, ITALY.

Aim: The aim of this retrospective study, through a collaboration between San Raffaele G. Giglio Institute (Cefalù, Italy) and ARNAS Garibaldi (Catania, Italy), was to evaluate the clinical and prognostic impact of FDG PET in the restaging process of melanoma after surgery. **Materials and Methods:** data from 74 pts surgically treated for cutaneous melanoma, who underwent FDG-PET for suspicious of recurrent disease were collected. The diagnostic accuracy of visually interpreted FDG-PET was obtained by considering histology (n=21pts), other diagnostic imaging modalities (ceCT in 52/74 pts and MRI in 18/74 pts) and clinical follow-up (n=74pts). Progression-free survival (PFS) and overall survival (OS) were assessed by using Kaplan-Meier method. The risk of progression (Hazard Ratio-HR) was computed by Cox regression analysis. **Results:** suspicious of recurrent melanoma was confirmed in 24/27 pts with a positive FDG-PET scan. Overall, the sensitivity, specificity, positive predictive value, negative predictive value and accuracy of FDG-PET were 82%, 93%, 88%, 89%, 89%. AUC was 0.87 (95%IC 0.78-0.97; p<0.05). FDG-PET findings influenced significantly the therapeutic management in 18 patients (modifying therapy in 10 pts; guiding surgery in 8 pts). After 2 years of follow-up, PFS was significantly longer in pts with a negative vs. a positive FDG-PET scan (90% vs 46%, p<0.05). Moreover, a negative study was associated with a significantly longer OS than a positive one (76% vs 39% after 2 years, p<0.05). In addition, a positive PET scan was associated with an increased risk of disease progression (HR=8.2; p<0.05). **Conclusion:** FDG-PET/CT showed a valuable diagnostic performance in pts with suspicious of recurrent melanoma. This method has an important prognostic value in predicting the survival outcomes and assessing the risk of disease progression.

EP198

Leakage monitoring method in Isolated Limb Perfusion. Our experience

C. Calvo Morón, A. Agudo Martínez, F. García Gómez, P. De la Riva Pérez, T. Cambil Molina, J. Castro Montaña; Hospital Virgen Macarena, Sevilla, SPAIN.

Aim: *Isolated limb perfusion* (ILP) by the use of extracorporeal circulation allows the infusion of high-doses of chemotherapeutic agents to avoid amputation of irresectable tumors of the extremities. Regional-to-systemic leakage is continuously monitored during the infusion procedure (60-minutes) since flow of the cytotoxic drug to the systemic circulation could result in a life-threatening situation. ILP have to be discontinued if leakage rates of 10-12% are detected. We report our experience in the leakage monitoring method through the continuous measuring of systemic ^{99m}Tc-human serum albumin (^{99m}Tc-HSA) with a portable gamma-camera. **Methods:** 15 patients underwent ILP: 14 patients were diagnosed of locally advanced malignant melanoma being treated with melphalan while 1 patient was diagnosed of undifferentiated pleomorphic sarcoma grade 3 being treated with melphalan and TNF-alpha. Two doses of ^{99m}Tc-HSA (20μCi for systemic and 200μCi for limb circulation measurements, respectively) are used. Systemic dose is injected once the limb is isolated. When basal plateau of precordial counts is reached, limb dose can be injected. Gamma-camera

detector is placed on the precordial for leakage monitoring during procedure. Counts measures are performed throughout the drug infusion, determining the percentage of leakage by calculating the increase of precordial activity from the basal plateau and adjusted to decay of the radiotracer. Local toxicity of ILP is classified by Wieberdink scale while systemic toxicity is directly related to percent of leakage. **Results:** Procedure was suspended in 1 patient because a significant leakage (25%) was detected before starting the infusion of chemotherapy agent. Subsequently, procedure was repeated with undetectable leak (0%). Leakage >15% was observed in 1 patient, 15-minutes after starting melphalan infusion, with no postoperative complications. Leakage >10% was detected in 2 patients, with no systemic or local complications after completing the procedure. Leakage <10% was demonstrated in the remaining patients. 1 patient suffered systemic complications -nausea, vomiting and sepsis- and local complications (Wieberdink IV), as well as only local complications was related in 4 patient (2 patients Wieberdink II-II, 1 patient Wieberdink IV). In the patient treated with TNF-alpha, 2% leakage was detected and evolving favorably with only local complications (Wieberdink I-II). **Conclusions:** ILP is an alternative procedure that can effectively be used as a palliative treatment which requires strict leakage monitoring to reduce systemic complications, possible thanks to advances in technology and the development of appropriate software. In our experience, control method allowed the treatment even in the leakage limits with satisfactory results.

EP199

Staging 18F-FDG PET/CT as a further determinant of prognosis in patients with cutaneous melanoma associated to Breslow thickness

S. Diodato¹, E. Dika², M. A. Chessa², G. Veronesi², S. De Vivo³, G. Polverari¹, S. Sanfilippo¹, I. Sandler¹, C. Nanni¹, P. A. Fanti², S. Vaccari², A. Patrizi², S. Fanti¹; ¹Service of Nuclear Medicine, S.Orsola-Malpighi Hospital, University of Bologna, Bologna, ITALY, ²Unit of Dermatology, S.Orsola-Malpighi Hospital, University of Bologna, Bologna, ITALY, ³Service of Nuclear Medicine, Bufalini Hospital, Cesena, Cesena, ITALY.

Aim: Breslow thickness (BT) is an important determinant of prognosis in cutaneous malignant melanoma (CMM). The aim of our study was to determine whether staging 18F-FDG PET/CT associated to BT could further stratify patients with CMM. **Materials and methods:** we retrospectively included 54 patients (mean age 62.8 years, range 28-88) with histologically proven CMM and BT available, who underwent staging FDG-PET/CT between November 2004 and November 2011 and had at least 6 months of clinical/imaging follow-up. We divided PET/CT results in positive and negative. Furthermore, two patient groups were defined according to BT: low-BT group (thickness < or = 2.0 mm, 22 patients) and high-BT group (thickness > or = 2.01 mm, 32 patients). A Kaplan-Meier survival analysis of melanoma-specific-survival (MSS) and disease-free-survival (DFS) with positive/negative PET/CT result and BT was performed. **Results:** the mean follow-up was 51 months (range 6-122 months). 46/54 PET/CT were negative and 8/54 were positive. A significant correlation between positive/negative PET/CT results and MSS was found (p=0.0007). On the contrary, no significant correlation between PET/CT results and DFS was reported (p=0.1520). An analysis per BT-group associated to PET/CT positive/negative was performed and a significant correlation was found for MSS and DFS (p=0.0001 and p=0.0129, respectively). Median SUVmax of true-positive lesions was 12.1 (range 6.4-19.6). No statistical analysis was performed for SUVmax due to the small number of positive findings. However, patient with the highest SUVmax had the shortest survival (2 months) and patient with the lowest had late recurrence (87 months). **Conclusions:** staging 18F-FDG PET/CT is significantly related to MSS. PET/CT positive/negative result can be used to further stratify patients risk within the standard BT groups. SUVmax could be associated with increased recurrence and death but further studies are needed to better assess its prognostic role in CMM and its correlation with BT.

EP200**Effectiveness of 18F-FDG-PET/CT in the staging and follow-up of patients with high-risk cutaneous melanoma**

J. Lojo Ramírez¹, R. Fernández-López¹, I. Acevedo-Báñez¹, V. Pachón-Garrudo¹, L. Caballero-Gullón¹, B. Russo^{1,2}, M. Sancho-Márquez¹, J. Domínguez-Cruz¹, T. Zulueta-Dorado¹, I. Borrego-Dorado¹; ¹Hospital Universitario Virgen del Rocío, Sevilla, SPAIN, ²Università Federico II di Napoli, Napoli, ITALY.

Objective: The aim of this study was to evaluate the effectiveness of fluorine-18 fluorodeoxyglucose (¹⁸F-FDG) positron emission tomography combined with computed tomography (PET/CT) in the staging and follow-up of the high-risk malignant cutaneous melanoma. **Material and methods:** A prospective cross-sectional cohort study was performed including 26 consecutive patients (17 males and 8 females with a median age of 59 years-old at the moment of the initial scan), with the inclusion criteria of being diagnosed with high-risk cutaneous malignant melanoma (stage IIB, IIC or III) and have underwent at least one FDG-PET/CT study between October 2012 and October 2015 (performing a total of 63 FDG-PET/CT). This criteria was established by the Melanoma Board at our hospital. **FDG-PET/CT results** (positive/negative) and location of disease (lymphatic-regional, local or distant metastasis) after qualitative and semiquantitative evaluation were correlated with histopathological confirmation or confirmation by clinical-radiological follow-up of at least 6 months. **Results:** Initial staging: In 23% patients (6/26) was demonstrated the existence of tumor disease at the time of initial staging. Regarding to the initial FDG-PET/CT, it was achieved 6/26 TP, 1/26 FP and 19/26 TN, with a sensitivity, specificity, PPV, NPV and accuracy of 100% (95%IC: 61-100%), 95% (95%IC: 76.4-99.1%), 85.7% (95%IC: 48.7-97.4%), 100% (95%IC: 83.2-100%) and 96.2% (95%IC: 81-99%), respectively. Follow-up: During follow-up it was demonstrated recurrence of tumor disease in 15% (3/20) patients in whom it had not been demonstrated its existence in the initial staging. It was achieved 3/20 TP, 1/20 FN and 16/20 TN, with a sensitivity, specificity, PPV, NPV and accuracy of 75% (95%IC: 30-95.4%), 100% (95%IC: 80.6-100%), 100% (95%IC: 43.8-100%), 94.1% (95%IC: 73-99%) and 95.0% (95%IC: 76.4-99%), respectively. Overall, it was obtained a global detection rate of disease of 34.6% (9/26), with a sensitivity, specificity, PPV, NPV and accuracy of 90% (95%IC: 59.6-98.2%), 93.8% (95%IC: 71.7-98.9%), 90% (95%IC: 59.6-98.2%), 93.8% (95%IC: 71.7-98.9%) and 92.3% (95%IC: 75.9-97.9%), respectively. **Conclusions:** 18F-FDG PET/CT in the initial staging and follow-up every six months is an effective and useful tool in the control and management of patients with high risk cutaneous melanoma.

EP201**FDG-PET/CT in Preoperative Staging of Sentinel Node Biopsy Positive Melanoma Patients: A One-Year Evaluation of a Novel Diagnostic Strategy**

E. Frary, D. Gad, L. Bastholt, P. Høilund-Carlsen, S. Hess; Odense University Hospital, Odense, DENMARK.

Aim: On April 1st 2015 the Region of Southern Denmark began a new diagnostic strategy wherein all malignant melanoma (MM) patients with positive sentinel lymph node biopsies (SLNB) undergo FDG-PET/CT prior to lymph node dissection treatment to reveal and localize remote metastases preoperatively. The aim of this study was to evaluate this new strategy by analyzing preoperative FDG-PET/CT findings and examine to what degree they altered treatment or triggered additional diagnostic tests. **Methods:** The patient population included an unselected retrospective cohort of all MM patients from the Region of Southern Denmark with positive SLNB, who from April 1st 2015 to March 31st 2016 underwent routine FDG-PET/CT, i.e., with scans from vertex of the skull to the proximal femurs or the entire body if the primary lesion was in the lower extremities. CT was low-dose and

non-contrast-enhanced. Clinical data were collected from the Danish Melanoma Database and cross-referenced with patient reports for basic information (e.g. about age and sex), primary tumor characteristics, and SLNB findings. FDG-PET/CT results were obtained as routine scan interpretations made by a nuclear medicine specialist. **Results:** A total of 47 patients, 27 male and 20 female with a median age of 61 years [range 26-82], were included. Median follow-up was five months [range 1-11]. Increased FDG-uptake suggestive of remote metastases was found in 7/47 patients (15%). One case was determined to be progression of preexisting concomitant carcinoma of the lungs and not a MM metastasis. In the remaining six patients, focal FDG-uptake was localized in the colon (n=3), thyroid gland (n=1), lungs (n=1), and hilar lymph nodes (n=1). These findings led to additional testing in the form of colonoscopy (n=3), ultrasound-guided biopsy (n=1), pulmonologist referral (n=1), and endobronchial ultrasound biopsy (n=1). Ultimately, no remote MM metastasis or anything else of relevance was found. **Conclusion:** Surprisingly and contrary to findings in the literature, this new diagnostic strategy revealed no remote MM metastases during its first year. FDG-PET/CT triggered a number of additional diagnostic procedures, none of which did lead to a change in treatment. Although results are preliminary and our population is limited, these findings seem to indicate a need for re-evaluation of the strategy including considerations about optimal scan protocol, i.e., scanning of the entire body in all patients, and CT procedure, i.e., low-dose versus diagnostic CT with contrast enhancement.

EP202**Diagnostic yield of selective sentinel lymph node dissection in melanoma, our experience between 2013-2015 La Paz Hospital, Madrid, Spain**

G. VILLORIA, C. Escabias del Pozo, I. Santos Gomez, Y. Ramirez Escalante, S. Rizkallal, Y. Guzman Cruz, M. Orduña Diez, L. Dominguez Gadea; LA PAZ UNIVERSITY HOSPITAL, MADRID, SPAIN.

OBJECTIVE: Assess the diagnostic performance of selective sentinel lymph node dissection to reduce the number of unnecessary lymphadenectomy in patients with malignant melanoma without clinical evidence of regional lymph nodes or distant metastases. Assess the value of monitoring and characterizing the tumors in our environment. **MATERIALS AND METHODS:** A retrospective, analytical study of 43 patients from September 2013 to July 2015 diagnosed with melanoma referred to our service for selective sentinel node biopsy (SLNB), with an average age of 57 years (14-92), 22 were men. Breslow index was 2.03 +/- 2.2 studied (0-9) and the Clark level was III (I-V), 14 (32.6%) had ulceration. The location of melanomas was: 6 (14%) head and neck, 22 (51.2%) trunk, 3 (7%) upper limbs, 9 (20.9%) lower limbs, and 3 (7%) in other locations. The time from diagnosis to performing SLNB time was 0.9 +/- 0.7 months. All patients underwent lymphoscintigraphy prior to surgery day, resulting in dynamic and static images according to location of drainage and SPECT-CT in all cases. The average follow-up time was 11.6 months (4-24). **RESULTS:** Most melanoma were histological type of Superficial spreading melanoma, in 76.7%. 1.6 +/- 0.7 GC were detected in lymphoscintigraphy, surgically analyzed GC 3.09 +/- 4, 8 (18.3%) were positive and 7 underwent lymphadenectomy. During lymphadenectomy 7 positive nodes extracted of a total of 156 nodes (4%) were obtained. The locations with the highest number of GC were Axillary 48% and inguinal in 32% of cases. 3 (7%) patients had locoregional and/or distant recurrence. **CONCLUSION:** Undoubtedly selective sentinel node biopsy in melanoma decreases the number of lymphadenectomy in our patients. Recurrence is low and monitoring is appropriate in our environment. It is confirmed that the sentinel node is a simple technique, low morbidity, with an important role in staging for the treatment of malignant melanoma.

EP203**The value of a non-dedicated brain PET/CT whole body protocol for evaluation of brain metastases of metastasized malignant melanoma under immune therapy**

H. Einhellig¹, A. Krackhardt², J. Kohlmeyer³, R. Hein³, M. Schwaiger¹, **M. Mustafa¹**; ¹Klinikum rechts der Isar, Dept. of Nuclear Medicine, Munich, GERMANY, ²Klinikum rechts der Isar, Dept. of Hematooncology, Munich, GERMANY, ³Klinikum rechts der Isar, Dept. of Dermatology, Munich, GERMANY.

Aim: FDG PET proves to be a growingly important tool in staging and restaging patients with metastasized melanoma - even more so in the age of immune therapy with novel checkpoint inhibitors. The ideal PET/CT protocol is including brain and lower extremities, although the usefulness of this total body approach has been questioned lately. The aim of this retrospective study is to investigate specificity and sensitivity of FDG-PET in diagnosing brain metastasis in comparison to serial ceMRI as a gold standard. **Methods:** We retrospectively evaluated 124 patients (pts) with metastasized malignant melanoma under immune therapy who were treated at the interdisciplinary melanoma group of our institution 05/2011 - 01/2016. They received contrast enhanced brain MRI within 8 weeks after every routine total body FDG- PET/CT-scan. Brain glucose metabolism of this non-dedicated FDG-PET was evaluated blinded to the outcome of consecutive MRI with regards to focal FDG-uptake or reduced regional FDG-metabolism. **Results:** Of 122 pts 20 pts developed cerebral metastases during follow-up (11%). FDG PET was able to identify 8 patients with suspicious glucose metabolism, of which 6 pts showed increased and 2 pts showed decreased FDG-uptake. Two pts who showed a regional decrease of FDG-uptake proved to have regional ischemic lesions in the consecutive cMRI without underlying metastatic disease. This results in a low sensitivity of 40% but an exceptionally high specificity of 98% for FDG-PET in detecting undiagnosed brain metastases (PPV 80%, NPV 89,5%). **Conclusion:** FDG-PET even in non-dedicated brain protocols is in spite of the physiological cortical brain metabolism a highly specific tool diagnosing cerebral metastases in a metastasized melanoma cohort. In conclusion, standard FDG-PET/ CT protocols should always include the brain, although the low sensitivity does not render it suitable for stand-alone restaging of high-risk melanoma patients. In this context FEG-PET/MR might prove more suitable for restaging and therapy monitoring.

EP-12 – Sunday, October 16, 2016, during Exhibition hours, e-Poster Area
Clinical Oncology: Neuroendocrine Tumours

EP204**Matched Pair Validation of Ultra-low-dose CT Compared to Low-dose CT for Oncologic ¹⁸F-FDG PET/CT**

N. C. Hall¹, C. L. Wright², N. Gortanla², V. Nagar², J. Zhang², M. V. Knopp²; ¹Philadelphia VA Medical Center, Philadelphia, PA, UNITED STATES, ²The Ohio State University, Columbus, OH, UNITED STATES.

Aim: To validate by matched pair assessment the equivalency of ultra-low-dose adaptive-current iterative reconstructed CT compared to low-dose CT in clinical oncologic ¹⁸F-FDG PET/CT. **Materials and Methods:** 65 consecutive patients receiving follow-up PET/CTs were retrospectively evaluated after a system upgrade (VA40A) enabling modulated ultra-low dose CT on a Siemens mCT 64 PET/CT. Three experienced reviewers evaluated the de-identified and blinded paired CT data sets (standard low-dose CT without VA40A [150 mAs] versus ultra-low-dose CT with VA40A [adaptive mAs with 100mAs as reference]) using a 4-point scoring system for clinical image quality. Assessment scores and CT radiation doses for each data set were independently recorded.

CTDIvol, DLP as well as EDE were calculated and analyzed for each data set. **Results:** 65 matched pair data sets were evaluable and were independently reviewed by the 3 readers. Equivalent diagnostic CT image quality was determined by every reader individually and collectively with no case identified in which the ultra-low-dose CT did not render diagnostic quality images. The CT radiation dose reduction was found to be: CTDIvol (mGy) from 13 ± 3 to 5 ± 2 ; DLP (mGy*cm) from 1367 ± 382 to 515 ± 231 ; EDE (mSv) from 21 ± 6 to 8 ± 4 (all $P < 0.01$). Minor notable observable differences included a more pixelated skin-subcutaneous fat interface. No significant differences ($P < 0.01$) in Hounsfield Units for tissues relevant for attenuation correction were noted. **Conclusion:** Significant radiation dose reduction ($P < 0.01$) was achieved with ultra-low-dose iterative reconstructive CT without compromising image quality in patients undergoing routine oncologic PET/CT. Given the increasing clinical need for repeated PET/CT imaging assessment in such oncologic patients, the findings support the implementation of ultra-low-dose CT for routine oncologic ¹⁸F-FDG PET/CT in order to promote and achieve ALARA.

EP205**PET/CT for primary staging of rectal cancer patients with and without extramural vascular invasion detected by MR (EMVI-MR)**

M. Queiroz, C. Ortega, T. Morita, P. Viana, M. Zagatti, R. Blasbalg, M. Menezes, C. Buchpiguel; Unviersity of Sao Paulo, Sao Paulo, BRAZIL.

PURPOSE To evaluate the use of PET/CT for primary staging of rectal cancer according to EMVI-MR status. **METHOD AND MATERIALS** Twenty-two patients with rectal cancer before neoadjuvant radio and chemotherapy were enrolled in this prospective study. All patients underwent contrast-enhanced CT of thorax and abdomen, pelvic MR, whole-body PET/CT and liver MR with DWI and Primovist®. Imaging analysis consisted on evaluation of the primary tumor on MR concerning T- and N-staging, mesorectal involvement and EMVI status. PET/CT, ceCT and liver MR were analyzed for the presence of distant metastases. Biopsy of rectal tumor was obtained in all patients before treatment. The patients were divided based on the presence of EMVI-MR and the detection rate of metastatic disease was compared between ceCT, PET/CT and liver MR. Additionally, quantitative analysis of the primary tumor was done using DWI (ADC) and PET parameters (SUV, TLG, MTV) and compared to histology. **RESULTS** Metastatic disease was found in 4/22 patients (18%) accounting for 28 lesions. There were 13/22 (59%) patients without EMVI-RM and 9/22 (41%) patients with EMVI-RM, which 4/9 (44%) presented distant metastases. PET/CT detected two more lesions than ceCT, which had high clinical impact, changing the patient management from curative to palliative intention. Liver MR did not identify any additional lesion to PET/CT or ceCT. Quantitative analysis showed an inverse correlation of TLG and grade of histological differentiation of the primary rectal tumor. **CONCLUSION** Positive EMVI-MR can be used to select patients that would benefit from whole-body staging with PET/CT. Quantitative data of PET/CT aid on the characterization of tumor aggressiveness. **CLINICAL RELEVANCE/APPLICATION** PET/CT might be preferred to stage rectal cancer with EMVI-MR due to higher detection rate of distant metastases and potential clinical impact on patient management.

EP206**Bone metastasis in neuroendocrine tumors. ⁶⁸Ga DOTA-TOC PET-CT vs CT alone: retrospective analysis**

A. Sartorello¹, R. Butini², E. Milan¹, S. Bissoli¹, V. Fiore¹, S. Medea¹, M. Gregianin¹; ¹UOC Medicina Nucleare Osp. S. Giacomo, Castelfranco Veneto TV, ITALY, ²UOC Radiologia Osp. S. Giacomo, Castelfranco Veneto TV, ITALY.

AIM: aim of the study was to evaluate retrospectively the role of 68Ga-DOTA-TOC PET-CT vs CT alone in the detection of bone metastasis in patients with neuroendocrine tumors. Materials and Methods: from January 2013 to July 2015 792 PET-CT with 68Ga-DOTA-TOC were performed. 51 Pts (24 M, mean age 63.92 y) showed bone lesions at first PET/CT evaluation. The primary site of the tumor was gastrointestinal (20), pancreas (11), lung (11), unknown (5), thyroid (3) and ovary (1). PET/CT scan was performed for evaluation after surgery or chemotherapy (12), during therapy (12), staging (7), marker increase (6), suspect of recurrence (12), detection of primary unknown tumor (2). PET/CT scan were performed 60 minutes after the i.v. injection of 3MBq/bw of radiopharmaceutical acquiring images from the base of the skull to the upper third of the thighs. PET/CT and CT alone images were independently evaluated by a Nuclear Physician and a Radiologist unaware of the results of the other modality and of patient history. Bone lesions were calculated in each patient for both PET-CT and CT alone and assigned to 8 regions: base of the skull, column, ribs, scapula, clavicle, sternum, pelvis, long bones. Moreover, Radiologist described the bone lesions as lytic, sclerotic or mixed. Results: PET-CT showed 610 bone lesions whereas CT only 147 (PET-CT vs CT): base of the skull 6 vs 2, column 168 vs 76, ribs 98 vs 24, scapula 24 vs 1, sternum 33 vs 6, clavicle 16 vs 1, pelvis 211 vs 34, long bones 54 vs 3. At CT 31 lesions were lytic, 115 sclerotic and 1 mixed; this technique showed 27 lesions PET-CT negative: 20 sclerotic and 7 lytic. Interestingly two positive PET-CT lesions were vertebral haemangioma at CT. Twenty-five patients were PET-CT positive and CT negative. Conclusions: In our retrospective study 68Ga-DOTA-TOC PET-CT enabled early evaluation of suspected metastatic site in the cortical bone, but also in bone marrow before cortical destruction has occurred. 68Ga-DOTATOC PET-CT results to be a reliable technique for early detection of bone metastasis regardless the characteristics of the lesions. PET scan confirmed its crucial role in the evaluation of NET patients and can lead to a change in their management and prognosis.

EP207

Esthesioneuroblastoma- evaluation of ⁶⁸Ga-DOTATATE PET/CT imaging efficacy in diagnosing and treatment monitoring-initial experience

G. Lapinska, A. Jarzabski, M. Dedecjus; Maria Sklodowska-Curie Memorial Cancer Centre and Institute of Oncology, WARSAW, POLAND.

Introduction: Esthesioneuroblastoma (olfactory neuroblastoma) is a rare primary sinonasal tumour with neuroendocrine differentiation originating from olfactory epithelium. It is often highly aggressive and leads to local recurrence and distant metastases. The aim of the study was to present our experience concerning the efficacy of 68Ga-DOTATATE in staging, restaging, treatment monitoring as well as its usefulness in radiotherapy planning. Materials and methods: From 2011 to 2016, PET/CT examination was performed on nine patients diagnosed with histological esthesioneuroblastoma (3 women, 6 men, aged 26-66, median 36 years). All of the patients underwent their first PET/CT after surgical resection of primary tumour. 2 patients were after, 1 during and 1 before chemotherapy (chth). 4 out of 9 were before radiotherapy (rth). So far, 3 of the patients had only one PET/CT scan, 5 underwent the examination 3 to 4 times in order to monitor the efficacy of the treatment or as a follow-up. The remaining one patient was examined 8 times with PET/CT. PET/CT was performed on Phillips Gemini 16TF PET/CT scanner. Images were obtained 60 minutes (+10 min) after i.v. administration of 111-185 MBq 68Ga-DOTATATE (depending on patient's weight). Results: First PET/CT scans were negative in 2 patients, in 4 patients before, during or after chth the primary tumour resection scans revealed metastases. In the remaining 3 patients moderate uptake of tracer was present in the postoperative localization. 2 patients (26 and 30 years old) that

underwent rth and chth died within a year of diagnosis due to the progression of disease visible on PET/CT scans (bone and liver metastases). The remaining patients are still undergoing treatment monitoring or follow-up using gallium PET/CT. PET/CT scan was used for radiotherapy planning for 3 patient. For the first time it was used for a patient with primary lesion located in nasal cavity, close to the optic nerve. The scan proved to be helpful in determining target volumes for radiotherapy which prevented the patient from losing his sight after therapy. Additionally, in 1 patient PET/CT scan revealed in the right breast small lesion with moderate increased uptake of the tracer, which was identified as a breast cancer. The patient is after tumorectomy and rth. Conclusion: 68Ga-DOTATATE PET/CT scan seems to be an effective tool in staging, restaging and therapy monitoring in esthesioneuroblastoma, however this it still requires further investigation.

EP208

Neurocrine Tumour Evaluation: ¹⁸F-FDG-PET/CT Versus Somatostatin Receptor Scintigraphy (SRS)

I. Cillero¹, A. Mendiola¹, A. Gomez¹, A. Lacasta², P. Santesteban¹, G. Rios¹, F. Rodriguez¹; ¹Fundación Onkologikoa, San sebastian, SPAIN, ²Hospital Universitario Donostia, San sebastian, SPAIN.

OBJECTIVE The aim of this study is to identify which imaging modality is the most appropriate in the evaluation of neuroendocrine tumours (NET) based on clinic, histologic and analytic parameters **MATERIAL AND METHODS** Between June 2013 and April 2016, 72 consecutive patients with neuroendocrine tumours were enrolled in the study. These patients had a somatostatin receptor scintigraphy (SRS) and ¹⁸F-FDG PET/CT. The scan result (positive or negative) was correlated with different variables: localization, tumour grade, Ki67, chromogranin A (Cg A) and serotonin. **RESULTS** All of 72 patients had a SRS and out of them 44, have performed both scans (¹⁸F-FDG PET/CT and SRS). The overall sensitivities (S) of SRS and ¹⁸F-FDG PET for detection of either primary tumour or metastases were 55,5% and 84,1%, respectively. Based on tumour grade (no available in 52%), the sensitivity for ¹⁸F-FDG PET/CT and SRS, was for grade 1, 63,6% vs 75%; for grade 2, 100%(n=2) vs 60%(n=5) and for grade 3, 100%(n=5) vs 55,67%(n=9) ($p=0,19$ and $p=0,5$ for PET/CT and SRS respectively). Taking into account the proliferation index, S of PET/CT and SRS respectively was: Ki67 $\leq 2\%$: 42,9% vs 57,1%; Ki67 2-20%: 90% vs 71,4% and Ki67 >math>20\%</math>: 100% vs 46,7% ($p=0,006$ and $p=0,31$). Cg A and serotonin values do not seem to influence in PET/CT sensitivity. For SRS, the sensitive is 76,9% when Cg A >math>109\text{ng/ml}</math> and 46,7% if Cg A $\leq 108\text{ng/ml}$ ($p=0,029$). When serotonin >math>401\text{ng/ml}</math> sensitivity is 90,9% and if serotonin ≤ 400 is 59,4% ($p=0,071$). The sensitivity for localization is the same for both SRS and PET/CT scans. **CONCLUSION** For choosing the best the imaging modality to assess TNE, the sensitivity of PET/CT is higher in grade 3/poorly differentiated and Ki67 values >math>20\%</math>. SRS has greater sensitivity in grade 1/well differentiated and Ki67 values $\leq 20\%$. Cg A and serotonin do not seem to influence the sensitivity of PET/CT. The sensitivity of SRS increases at higher values of serotonin and Cg A. The location of TNE does not influence the sensitivity in both tests.

EP209

Comparison of sensitivity and specificity of Tc-99m octreotide and I-131 MIBG scintigraphies in diagnosis and localization of pheochromocytoma and neuroblastoma

A. Fard-Esfahani, A. Emami-Ardekani, A. Mirzabeigi, B. Fallahi, A. Hassanzadeh-Rad, D. Beiki, P. Geramifar, M. Eftekhari; Research Center for Nuclear Medicine, Shariati Hospital, Tehran University of Medical Sciences, Tehran, IRAN, ISLAMIC REPUBLIC OF.

Introduction: Tc-99m octreotide scan and I-131 metaiodobenzylguanidine (MIBG), are both valuable agents in diagnosis and localization of neuroendocrine tumors. This study was performed to compare the sensitivity and specificity of these agents in detection of pheochromocytoma and neuroblastoma. **Materials and methods:** 40 patients with pathologically proven pheochromocytoma/neuroblastoma were enrolled and octreotide and MIBG scans were performed for every patient. A composite reference standard consisting of cytopathology, biomarkers, anatomical imaging and six-month follow-up data was used as a reference for final diagnosis to evaluate the scintigraphic imaging results. Lesion-based and patient-based analysis were performed. **Findings:** On the basis of lesion-based analysis, overall sensitivity of MIBG was better than octreotide study (94.44% vs 80.56%). Considering each disease separately, sensitivity of both scans for pheochromocytoma was 100%, but MIBG study showed a higher specificity (100%) than octreotide (87.5%). In neuroblastoma, MIBG sensitivity (100%) was better than octreotide (81.25%); however specificity was higher with octreotide study (100% for octreotide versus 92.85% for MIBG). On the basis of patient-based analysis, MIBG had equal sensitivity and specificity of 100% for both diseases. Although octreotide also had 100% sensitivity for pheochromocytoma, its specificity was 87.50%. For neuroblastoma, octreotide study had 81.25% sensitivity and 100% specificity. **Conclusion:** Both MIBG and octreotide scans show high sensitivity and specificity in detection of neuroendocrine tumors of pheochromocytoma and neuroblastoma. However, MIBG scan with its better sensitivity may be considered the first line functional imaging modality; octreotide can be used to provide complementary information. It is advisable that if any of these two scans becomes negative in a patient with high clinical suspicion, the other one is performed, so that no useful data is missed in patient's management.

EP210

Clinical Value of Serum Chromogranin A, Neuron Specific Enolase, CEA, and Calcitonin in Neuroendocrine tumors : Comparison by The 68Ga-DOTA-PEPTIDE PET-CT imaging SUVmax value

F. AYDIN¹, E. SURER BUDAK¹, S. BOZKURT¹, A. ONER², A. BOZ¹; ¹AKDENIZ UNIVERSITY, Antalya, TURKEY, ²AFYON KOCATEPE UNIVERSITY, AFYON, TURKEY.

Aim: Neuroendocrine tumors (NET) are malignant solid tumors originating from neuroendocrine cells dispersed throughout the body. Differentiated NET overexpress somatostatin receptors (SSTRs), which enable the diagnosis using radiolabeled somatostatin analogues. Most NET produce and secrete a multitude of peptide hormones and amines. In this study, our aim was to determine if there was a relationship between the SSTRs activity obtained from 68Ga PET imaging (SUVmax) and serum tumor markers (chromogranin A, neuron specific enolase: NSE, CEA, and calcitonin). **Materials and Methods:** Sixtyseven patients with histologically confirmed NET who had undergone 68Ga-DOTA-PEPTIDE PET/CT images were included in the study. Serum chromogranin A levels (n:36), NSE (n:17), CEA (n:15), and calcitonin (n:9) were measured. 68Ga-DOTA-PEPTIDE PET/CT images SUVmax values were compared with serum tumor markers, retrospectively. **Results:** The values of lesions SUVmax of the cases were seen that ranged between 4.3 to 181 (median: 24). Serum chromogranin A, NSE, CEA, and calcitonin levels were in the range of 7-817 (median:82), 5.3-278.3 (median:21.2), 0.9-2190 (median:4.5), and 4-13010 (median:800), respectively. There were statistically significant correlation between the SUVmax and serum chromogranin A level. The correlation coefficient value was calculated as $r=0.34$, ($p<0.046$). Any statistically significant correlation between SUVmax value and other serum tumor markers ($p>0.05$) could not be found. **Conclusion:** 68Ga-DOTA PEPTIDE is suited equally well for staging and patient selection for PRRT with 177Lu-DOTA PEPTIDE. Chromogranin A is considered the best general neuroendocrine serum marker available both for diagnosis and therapeutic evaluation and is increased in 50-100% of patients with various NET.

In literature is not found clinical value of serum tumor marker and 68Ga DOTA PEPTIDE. Our study is the first. Serum chromogranin A level together with 68Ga DOTA PEPTIDE PET/CT could be important in diagnosis, and management in NET. They may be an independent markers of prognosis in patients with NET.

EP211

Comparison of lesions detected on F-18 FDG PET-CT and Ga-68 DOTANOC PET-CT and their correlation with Ki-67 index in neuroendocrine tumour patients

A. Passah, M. P. Yadav, G. Kumar, R. Kumar; All India Institute Of Medical Sciences, New Delhi, INDIA.

Aim: To study the correlation between F-18 FDG PET-CT and Ga-68 DOTANOC PET-CT with Ki-67 index in patients with neuroendocrine tumours (NET). **Materials and Methods:** This is a retrospective study in which records of 21 patients diagnosed with NET were analysed. The study included patients sent for staging and response assessment after therapy. All patients had both F-18 FDG PET-CT and Ga-68 DOTANOC PET-CT done in any order. The scans were analysed qualitatively based on the sites of lesions detected or maximum standardised uptake value (SUVmax) of primary lesion or metastatic site, if primary has been resected, detected on one or both scans and correlated with Ki-67 index of each patient. The nuclear medicine physician was blinded to the results of either scan and Ki-67 index and each scan was assessed independently. **Results:** There were 4 patients in which both F-18 FDG PET-CT and Ga-68 DOTANOC PET-CT detected same sites of lesions. These patients had a median Ki-67 index of 7.5 (range 1.9 to 15). In 8 patients, more lesions were detected on F-18 FDG PET-CT compared to Ga-68 DOTANOC PET-CT. These patients had a median Ki-67 index of 21.5 (range 4.5 to 81). In 9 patients, more lesions were detected on Ga-68 DOTANOC PET-CT as compared to F-18 FDG PET-CT. These patients had a median Ki-67 index of 2 (range 0.9 to 35). However one patient had an unusually high Ki-67 index in this group. If this patient is excluded, then 8 patients in this group had a median Ki-67 index of 1.95 (range 0.9 to 7). **Conclusion:** This study shows a good correlation between molecular imaging using dual isotopes and a marker of cellular proliferation. Poorly differentiated cells with high index of proliferation show high uptake of F-18 FDG whereas well differentiated cells show high uptake of Ga-68 DOTANOC. This behaviour of cells can guide us in patient directed selection of isotopes and also plan for therapy.

EP212

Semiquantitative Analysis Of Physiological Biodistribution of ⁶⁸GA-DOTATATE and ⁶⁸GA-DOTANOC

E. S. Budak¹, A. Oner², S. Demirelli³, M. Erkişç⁴, A. Boz⁴, B. Karayalçın⁴; ¹Antalya Training and Research Hospital, Department of Nuclear Medicine, Antalya, TURKEY, ²Afyon Kocatepe University Faculty of Medicine, Department of Nuclear Medicine, Afyon, TURKEY, ³Denizli State Hospital, Department of Nuclear Medicine, Denizli, TURKEY, ⁴Akdeniz University Faculty of Medicine, Department of Nuclear Medicine, Antalya, TURKEY.

Objectives: In this study, in patients who underwent 68Ga-DOTATATE and 68Ga-DOTANOC PET/CT imaging modalities with the diagnosis of NET, it was aimed 1) to determine the areas of physiologic uptake and means (\pm SD) and value ranges (min. and max.) of these areas, using semiquantitative parameters as SUVmax and SUVmean(\pm SD) 2) to compare the data obtained with those of the literature so as to define helpful reference ranges for intermediate cases with the intention to discriminate between physiologic and pathologic uptakes. **Materials and methods:** Radiological images of 40 patients (female, n=23 and male, n=17; mean age, 52.50 \pm 15.82 years) who had undergone ⁶⁸Ga-DOTA labeled (TATE

and NOC) PET/CT imaging modalities with the diagnosis of GEP-NET, non-GEP-NET and thyroid cancer were retrospectively evaluated. Measurements were performed from areas of physiologic uptake including pituitary gland, parotid gland and submandibular gland, palatine tonsils, thyroid, lungs, blood pool (left ventricular cavity), thymus, lymph nodes, liver, pancreas (from head, body and tail parts), spleen, stomach (fundus and other parts), both adrenal gland, kidney (from cortex), small bowel and colon, bone marrow, prostate, glandular breast tissue and muscle tissue. **Results:** In spleen, adrenal glands, head of the pancreas, palatine tonsils and breast, a statistically significant intergroup difference was not detected as for SUVmax and SUV mean values. As for the lymph node measurements, SUVmax values were statistically significantly higher in the TATE group, while SUVmean value did not differ between groups. Due to scarce number of cases, statistical analysis between both groups could not be performed for prostate and thymus. In the TATE group, significantly higher uptake in the body and tail of the pancreas compared to the head, and significantly higher uptake in the gastric fundus was observed. For both TATE and NOC, a statistically significant difference was not found between SUVmax and SUVmean values of the right and left adrenal glands, and of small bowel and colon. A statistically significantly higher SUVmax and SUV mean values were detected in the TATE group relative to the NOC group in all other organs in the study. **Conclusion:** This study used SUVmax and SUVmean values to demonstrate semiquantitatively distribution pattern of ^{68}Ga -DOTATATE and ^{68}Ga -DOTANOC in normal organs. We think that determination of uptake patterns and related range of values we defined for both agents in many organs will aid in discrimination between physiologic and pathologic uptake during interpretation of images.

EP213

Comparison Of 18F-FDG PET/CT With 111In Penteotide Scan For Detection Metastatic Neuroendocrine Tumors

F. Iuele, A. Niccoli Asabella, C. Altini, C. Ferrari, A. Di Palo, F. Duni, G. Rubini; Nuclear Medicine Unit, D.I.M. – University of Bari “Aldo Moro”, Bari, ITALY.

AIM. To compare the 18F-FDG PET/CT and 111In pentetotide imaging (OCT) to characterize the metastatic neuroendocrine tumors (NETs) MATERIALS AND METHODS: we retrospectively analyzed 27 patients (pts) (13 female, 14 male, mean age: 65, range 39 - 81 years) with previously diagnosed NETs who underwent between January 2014 and March 2016 both 18F-FDG PET/CT and OCT imaging within 3 month interval. 7/27 pts had SCLC, 12/27 GEP, 4/27 NETs of unknown origin, one Merkel cell carcinoma, one NETs of adenohypophysis, one of thyroid, one of bladder. PET/CT and OCT abnormal uptake was evaluated, according the following anatomic district: lung, liver, bone, thoracic or abdominal lymph nodes and other sites. The comparison between the PET/CT and OCT results and abnormal uptake was performed by K of Cohen. RESULTS: The comparison between OCT and 18F-FDG PET/CT, regarding the overall district, showed that the two methods were concordant in 23/27 pts. The correlation was good (K: 0.684, 95% C.I.: 0.403-0.965). The comparison of lung lesions showed that the two methods were concordant in 26/27 pts and the correlation was very good (K: 0.899, 95% C.I.: 0.705-1). The comparison of hepatic lesions showed that the two methods were concordant in 23/27 pts and the correlation was good (K: 0.617, 95% C.I.: 0.289-0.952). The comparison of bone metastatic lesions showed that the two methods were concordant in 25/27 pts and the correlation was good (K: 0.710, 95% C.I.: 0.339-1). The comparison of mediastinal lymph node involvement showed that the two methods were concordant in 22/27 pts and the correlation was fair (K: 0.348, 95% C.I.: -0.085-0.780). The comparison of abdominal lymph node metastasis, showed that the two methods were concordant in 23/27 pts and the correlation was good (K: 0.614, 95% C.I.: 0.273-0.956). As regard the other sites of metastasis, the comparison showed that the two

methods were concordant in 21/27 pts and the correlation was moderate (K: 0.540, 95% C.I.: 0.217-0.863). PET/CT overall evaluation detected a greater number of lesions than OCT (44 versus 37) especially in bone and mediastinal lymph nodes. CONCLUSIONS: 18F-FDG PET/CT reflects the grade of malignancy and recognizes rapidly progressive tumors, while OCT reflects the grade of differentiation and somatostatin receptor. Although PET/CT detected a greater number of lesions, the concordance between the two methods was good, so we advice a combined use to improve the diagnostic accuracy.

EP214

SPECT-CT Somatostatin-Receptor Scintigraphy with ^{99m}Tc -Tektrotyd in Pulmonary and Thymic Neuroendocrine Tumors (NETs)

S. Sergieva¹, M. Dimcheva¹, A. Jovanovska¹, A. Fakirova², B. Robev¹; ¹Sofia Cancer Center, Sofia, BULGARIA, ²Military Medical Academy, Sofia, BULGARIA.

Pulmonary NETs and mediastinal NETs, developing from the thymus are unusual tumors that account for less than 5-6% of all lung/thymic neoplasms. Neuroendocrine tumors are classified according to the grade of biological aggressiveness (G1-G3) and the extent of differentiation (well-differentiated, poorly-differentiated). The well-differentiated neoplasms comprise typical (G1) and atypical (G2) carcinoids. Large cell neuroendocrine carcinomas as well as small cell carcinomas (G3) are poorly differentiated. The purpose of this study was to determine clinical role of SPECT-CT studies with ^{99m}Tc -Tektrotyd in patients with pulmonary and mediastinal NETs. Patients & Methods: 35 pts (31 with pulmonary/4 with mediastinal tumors) with neuroendocrine differentiation: 50%-100% positive-staining tumor cells, were studied: 8 were with Large cell NE carcinomas 7 were with SCLC 8 were with lung carcinoids (typical and atypical) 4 were with thymic NETs 4 were with metastatic lesions from tumor with unknown primary origin (UPO), expressed NE markers, suggestive for lung NE origin. • SPECT-CT gamma camera Symbia T2, Siemens with Low Dose CT was used. 58 examinations including SPECT-CT studies of the chest and/or abdomen were performed 2-6 hrs post i.v.inj. of 740 MBq ^{99m}Tc -HYNIC-TOC (Tektrotyd, Polatom). • Results: Primary lung NE tumors were visualised in 4 pts with UPO, proven histologically. Locoregional mediastinal and hilar lymphadenopathy were imaged in 17 pts. Distant liver, pulmonary, bone and/or suprarenal positive metastatic lesions were visualized in 15 pts, correlated with increased level of secret serum marker - CgA. There was not a tracer uptake in 3 pts with liver multiple secondary lesions due to metastatic dedifferentiation. Some of these patients were followed-up after the complex treatment. It can be summarized that main indications for SPECT-CT studies are as follows: • For diagnosis these studies have limited role only to depict the most appropriate tumor lesion for correct biopsy and to image primary tumor in cases with UPO. • To assess SSTR expression and thus could effectively influence the management of individuals with NETs. • For correct pre-treatment N-/M-staging of pulmonary and thymic NETs and to determinate treatment response. • To differentiate pathological lesions from benign and physiological uptake. • For early determination of recurrence in cases with negative anatomical imaging (CT,MRT) but with clinical and biochemical indices for NET. In conclusion SPECT-CT somatostatin - receptor scintigraphy imaging is a potential new technique for staging and follow-up of patients with pulmonary and thymic NETs in coming years.

EP215

Predictive value of Chromogranin A in the assessment of neuroendocrine tumors uptaking octreotide- ^{99m}Tc

S. E. Bouyoucef, M. Habbeche, C. Mahmoudi, s. Rahabi, A. Talbi, M. Tiar; CHU Bab El Oued, Algiers, ALGERIA.

Introduction : Chromogranin A (CGA) is an hydrophyle and acid protein of 439 amino acids (49KD) which is present in chromaffine cells of neuroendocrine tumors (NETS). High blood levels of CGA may reflect the well differentiation and the aggressiveness of NETS. However, the value of normal CGA blood level is still not well established and controversial. **Objective:** To compare and study the sensitivity of serum CGA in patients with positive octreotide-^{99m}Tc Patients and **method:** 58 patients have had a simultaneously an octreotide-^{99m}Tc scan and test of serum CGA. The serum of CGA was determined by radioimmunoassay techniques using sandwich method (Cis Bio, normal range: 20 to 115ng/ml). Whole body octreotide-^{99m}Tc followed by two tomographic acquisition in mode SPECT/CT were performed 4hours after injection of 560MBq of octreotide-^{99m}Tc with a SPECT/CT gamma camera Symbia T6 (Siemens). For the comparison, all selected patients have had a positive octreotide-^{99m}Tc scan. **Results** Among the 58 patients with positive octreotide scan, 19 patients have had a normal CGA level. Among those 19 patients, 10 which represents more than 52%, have had a unique lesion seen in octreotide scan and the other 7 patients have had a multiple lesions uptaking octreotide-^{99m}Tc (47%). The level of serum CGA was elevated in 39 patients. This level was ten times the normal values elevated in 17 patients and 15 of them presented metastatic disease of NETS meanwhile the two others presented an unique uptake on the primary tumor. The serum level of CGA raised to three time the normal level in 13 patients from whom 9 have had a metastatic disease of NETS and 4 only a primary. It was to note that when the level of CGA was higher than three times but less than ten times the normal value in 9 patients who presented all a metastatic disease of NETS. **Conclusion** Serum level of CGA has a good predictive value of NETS when the level is significantly high above three times the normal values and in those cases CGA level is well correlated with metastatic diseases of NETS. Unique uptake by the primary tumor of NET may also express high level of CGA. However, when the CGA level is normal it could not exclude a metastatic or a primary NET.

EP216

Role of somatostatin receptor scintigraphy in neuroendocrine G3 tumor imaging

M. Catalano, G. Annunziata, D. Scala, V. Ippolito, I. valenti, I. Sepe; AORN, Naples, ITALY.

Aim : Neuroendocrine tumors (NET) present pathological characteristics that can be investigated by different functional imaging modalities as somatostatin receptor scintigraphy (SRS) and PET-CT. Imaging technique choice depends on pathological tumor characteristics: well differentiated tumors can be investigated by SRS or ⁶⁸GaPET-CT, poorly differentiated tumors by ^{18F}-FDG-PET-CT and mildly differentiated tumor by both techniques. **Aim of the study** is to evaluate SRS **diagnostic role** in patients (pts) with histologically verified poorly differentiated NET and targeted specific treatment derived from SRS data. **Materials and Methods:** Between October 2013 and March 2016, 160 pts affected with NET underwent to SRS. Mean age was 59.6 ± 17. 16/160 pts (10%) were G3 NET, with Ki67 > 25% (ranging from 25% to 90%). Pathological diagnosis identified 6 NET of lung, 3 pancreas, 2 bladder, 2 stomach, 1 colon, 1 rectum, 1 Merkel. 166-269 MBq of ¹¹¹In pentetreotide (OctreoScan; Mallinckrodt) was intravenously injected. Whole-body scans at a speed of 5 cm/min and a matrix size of 256 × 1,024 using a dual-head γ-camera equipped with a medium-energy general-purpose parallel-hole collimator and static images over 15 min, with a matrix size of 256 × 256 were acquired after 4 h and 24 h from injection. SPECT was performed using 3° steps, 40 s/step, a 180° orbit, and a matrix size of 128 × 128 after 4h e 24h too. **Results:** 5/16 pts (68%) were SRS negative, 11/16 pts had SRS positive lesions, with low uptake score in all lung NET and in one pt with stomach tumor; score 3 in 3 pts with liver metastasis from pancreas and colon; score 4 in one pt with rectum tumor with diffuse metastatic involvement of liver, bone,

lymphonodes and rectum. **Conclusion** Although SRS has never been used on a routine basis for imaging of G3 NET and its diagnostic performance in these tumors is unsettled, it could be added in diagnostic protocol of this group of NET. Its complementary diagnostic information could influence therapy and follow-up of these tumors characterized by overexpression of somatostatin receptors and high proliferation index. We noted low uptake score in lung NET but higher indium pentetreotide uptake in metastatic more aggressive disease. The meaning of this data is still uncertain and the small sample size of the study requires further investigation about the real contribute of SRS in G3 NET diagnosis and therapy.

EP217

Intraindividual comparison of SUVmax, SUVmean and tumor volume results with ¹⁷⁷Lu-DOTA-TATE SPECT/CT and ⁶⁸Ga-DOTA-TOC PET/CT in neuroendocrine tumor patients

M. Rodrigues, E. Thorstensen, C. Uprimny, D. Kendler, I. Virgolini, B. Warwitz; Department of Nuclear Medicine, Innsbruck Medical University, Innsbruck, AUSTRIA.

Aim: to evaluate whether results obtained with ⁶⁸Ga-DOTA-TOC PET/CT - the current procedure for diagnostic, staging and restaging of neuroendocrine tumors (NET) - correlate with those gained with post therapeutic ¹⁷⁷Lu-DOTA-TATE SPECT/CT. **Patients and Methods:** 18 patients (9 males, 9 females; age: 42-85, mean 61.6 years) with histologically proven NET grade 1 (n=1), grade 2 (n=11) and grade 3 (n=6) were investigated with ⁶⁸Ga-DOTA-TOC PET/CT (79.5-154 MBq, mean 103 MBq ⁶⁸Ga; GE Discovery 690 time of flight PET/CT) and thereafter with ¹⁷⁷Lu-DOTA-TATE SPECT/CT (3.49-7.85 GBq, mean 5.67 GBq ¹⁷⁷Lu; Philips Brightview XCT). Both imaging modalities were performed within 21-33 (mean 29.1) days apart from each other. The SUVmax, SUVmean and tumor volumes obtained with these imaging modalities were compared in a total of 45 tumor lesions (3 primaries, 42 metastases). Furthermore, SUVmax and SUVmean in a liver region without metastases were calculated and used as reference in each patient. **Results:** SUVmax ranged 4.63-78.08 (mean 31.01) and 1.62-61.00 (mean 23.98), and SUVmean ranged 3.08-45.81 (mean 20.12) and 0.95-38.14 (mean 15.11) with ⁶⁸Ga-DOTA-TOC PET and ¹⁷⁷Lu-DOTA-TATE SPECT, respectively. Using tumor/liver ratio, SUVmax and SUVmean were significantly higher with ¹⁷⁷Lu-DOTA-TATE SPECT (1.22-44.2, mean 10.21, and 1.08-40.36, mean 11.25, respectively) than with ⁶⁸Ga-DOTA-TOC PET (0.52-7.88, mean 3.43, and 0.52-9.01, mean 4.68, respectively). Tumor volumes measured with ⁶⁸Ga-DOTA-TOC PET and ¹⁷⁷Lu-DOTA-TATE SPECT ranged 0.39-256.68 (mean 18.3) ml and 1.12-172.33 (mean 6.5) ml, respectively. No correlation was found between the SUV-values obtained with ⁶⁸Ga-DOTA-TOC PET and ¹⁷⁷Lu-DOTA-TATE SPECT while the measured tumor volumes correlated strongly. **Conclusions:** The SUV-values in tumor lesions are significantly higher and in tumor/liver lower with ⁶⁸Ga-DOTA-TOC PET than with ¹⁷⁷Lu-DOTA-TATE SPECT while tumor volumes correlate strongly between the two imaging modalities. Therefore SUV-results obtained with ⁶⁸Ga-DOTA-TOC PET should be used with precaution when planning further therapy with ¹⁷⁷Lu-DOTA-TATE.

EP218

The usefulness of ¹¹¹In-pentetreotide SPECT/CT in the diagnosis of non-functioning neuroendocrine gastroenteropancreatic (GEP) tumors and their metastases: a comparison with conventional imaging procedures (CIP)

A. Spanu¹, O. Schillaci², B. Piras¹, A. Falchi¹, R. Danieli², P. Ferro³, S. Nuvoli¹, F. Dore³, G. Madeddu¹; ¹University of Sassari, SASSARI, ITALY, ²University of Rome Tor Vergata, Rome, ITALY, ³Hospital of Trieste, Trieste, ITALY.

Introduction: Some GEP tumors can be non-functioning with absence of clinical symptoms due to polypeptide hormone or other substance over-production in respect of functioning tumors, also occurring later, with more elevated size and, in some cases, with exocrine carcinoma similar characteristics. We evaluated ^{111}In -Pentetreotide SPECT/CT usefulness in diagnosing non-functioning primary GEP tumors and their metastases compared with CIP, such as US, CT, MRI. **Methods:** We studied retrospectively 104 non-functioning GEP tumor patients, 30 in initial diagnosis phase and staging (DS), 74 in follow up (F) with previous ascertained primary tumors; 35 patients (18 DS, 17 F) were classified as inoperable for disseminated metastases and treated with octreotide or chemotherapy. Definitive diagnosis was performed by histology and, when not possible in recurrences and metastases, by CIP or radioisotopic procedures with follow up period of 6–36 months. According WHO 2010 digestive system tumor classification, the patients were classified as neuroendocrine tumor grade 1 (G1; 65 cases) and 2 (G2; 22 cases), neuroendocrine carcinomas (NEC; 12 cases) and mixed-ado-neuroendocrine carcinomas (MANEC; 5 cases). In all cases, SPECT/CT images were obtained using a hybrid variable-angle dual-head gamma camera, including low dose x-ray tube, 4th, 24th, 48th hours following i.v. injection of 148–222 MBq of ^{111}In -pentetreotide. SPECT was first acquired followed by CT and the images, reconstructed by iterative method, were fused with those of CT using a dedicated software package. **Results:** Both sensitivity and accuracy of SPECT/CT were higher than CIP in G1 patients (92.3 vs 74.4% and 95.4 vs 85.6%, respectively), G2 (88.2 vs 70.6 % and 90.9 vs 77.3%, respectively), NEC (88.9 vs 60% and 83.4 vs 66.7%, respectively) and MANEC (100 vs 75% and 100 vs 80%, respectively), but significantly ($p=0.0009$) only for G1. In all single patient groups SPECT/CT evidenced more lesions, primary and metastatic, than CIP, but significantly ($p=0.00006$) only for G1 group. Globally, SPECT/CT incremental value was 35.6%, correctly changing CIP classification and patient management in 27.9% of cases, while it down-staged the disease in 9.6% of cases than CIP. **Conclusion:** Our data show that ^{111}In -Pentetreotide SPECT/CT is useful in detecting non-functioning GEP tumors and revealing their neuroendocrine origin in patients without either clinical signs of hormone over-expression or characteristic secretion pattern in blood. In particular, SPECT/CT was significantly more sensitive and accurate than CIP, but their combined use achieved the highest accuracy values and gave the most accurate staging, thus suggesting their use together.

EP219

Impact of ^{68}Ga -DOTATOC PET Imaging to Assess SSTRs Expressing Lesions in a Tertiary Care Center

M. Scarlattei¹, G. Baldari¹, C. Cidda¹, M. Silvia¹, A. Sammartano¹, R. Dalla Valle², G. Missale³, L. Ruffini¹; ¹Nuclear Medicine Dept, University Hospital of Parma, Parma, ITALY, ²Surgery and Transplant Unit, University Hospital of Parma, Parma, ITALY, ³Haepatology Unit, University Hospital of Parma, Parma, ITALY.

Functional imaging with PET tracers is an evolving field for neuroendocrine tumors (NETs). Recently, somatostatin receptor (SSTR)-based imaging with gallium-68-based radiopharmaceuticals showed promising results in looking for primaries and determining the extent of metastatic disease. Aim of this work was to assess clinical impact of PET imaging with ^{68}Ga -DOTA-TOC in the decision making process of patients with known or suspected NETs. **METHODS** We prospectively enrolled all the PET studies performed with ^{68}Ga -DOTATOC since Dec 2014. PET studies were acquired using an integrated system (GE IQ) 60 min after i.v. tracer injection. ^{68}Ga -DOTATOC is produced on-site and on demand

by an automated module (Scintomics GRP®). All reagents used in the preparation of ^{68}Ga -DOTATOC are of pharmaceutical quality. Before administration, the quality of the final solution was analysed according to the European Pharmacopoeia. Patients receiving therapy with somatostatin analogues (SSAs), interrupted their analogues 24 h before PET/CT for short-acting SSAs, or 4–6 weeks before PET/CT for long-acting SSAs. Whole-body (WB) ^{68}Ga -DOTATOC PET/CT images from the head to mid-femur were acquired. All the PET studies were evaluated independently by two expert Nuclear physicians. **RESULTS** PET imaging with ^{68}Ga -DOTATOC was performed in 81 patients. Mean administered activity was 143 ± 29 MBq. Mean yield of labelling reaction was 63.78%, mean RCP 98.54% and the minimum specific activity 15.93 GBq/ μmol . PET issue was characterization of lesions detected by CT or MRI in 31 pts (of them, 7 were studied for pancreatic NETs and 4 for suspected insulinoma), staging in 22, restaging in 17, detection of primary tumor in 11 pts (of them, 2 for suspected insulinoma). PET showed SSTRs expressing lesions in 49/81 pts. Characterization PET detected SSTRs expressing tissue in 14/31 pts. Insulinoma was confirmed in 4/6 pts by imaging and surgery. All PET scans performed to identify hormone producing tumour resulted as negative ($n=6$). In 1 patient with SDHB mutation PET identified malignant metastatic paraganglioma. PET informations have driven patient management in 86% pts and changed treatment options or sequence in 30% of the cases (10% from surgery to medical drug, chemo-radiotherapy before surgery in 5%, debulking before radionuclide therapy in 15%). **CONCLUSIONS** Results demonstrate that a reliable and well suited ^{68}Ga -agents output for use in a hospital-based radiopharmacy allows high accuracy in NET's imaging and diagnosis with correct allocation and appropriateness use of resources in patient management changing or well driving treatment option in most of them.

EP220

Physiological uptake in the pancreatic head on SRS using ^{111}In -DTPA-octreotide; Incidence and Mechanism

T. Brabander, J. J. M. Teunissen, D. J. Kwekkeboom; Erasmus MC, Rotterdam, NETHERLANDS.

Purpose Physiological uptake in the uncinate process or pancreatic head has been described with Gallium-68 labelled PET tracers for somatostatin receptor imaging. ^{111}In -DTPA-octreotide is the only registered radiopharmaceutical for the imaging of neuroendocrine tumours. We studied the uptake in this region of the pancreatic head on somatostatin receptor scintigraphy (SRS) using ^{111}In -DTPA-octreotide in a large group of patients. **Methods** 407 patients underwent SRS using ^{111}In -DTPA-octreotide in our department in 2014. After excluding patients with a known malignancy in or close to the pancreas, as well as all scans without SPECT/CT of the upper abdomen, we reviewed 178 scans in total. The uptake was graded on a 4-point scale that correlates the uptake in the pancreatic head to physiological uptake in the liver. **Results** Uptake in the region of the pancreatic head, including the uncinate process, was seen in 46/178 patients (26%) on SPECT-CT and in 12 patients (7%) on planar imaging. On SPECT/CT uptake was lower than the liver in 26 patients (15%), equal to the liver in 17 patients (10%) and higher than the liver in three patients (2%). In patients with diabetes mellitus the incidence of uptake in the pancreatic head was 50% on SPECT/CT. **Conclusion** Physiological uptake in the pancreatic head is seen on SPECT/CT with ^{111}In -DTPA-octreotide in 26% of patients and the incidence is doubled in patients with diabetes mellitus. Previous case reports showed uptake in the pancreatic head due to histologically proven pancreatic polypeptide cell hyperplasia. Also, patients with DM have elevated serum PP concentrations, which is likely due to PP-cell hyperplasia. Since 90% of PP-cells are present in the pancreatic head, PP-cell hyperplasia is the most likely explanation for visualization of the pancreatic head on SRS in a substantial number of patients.

EP-13 – Sunday, October 16, 2016, during Exhibition hours, e-Poster Area
Clinical Oncology: Prostate 1

EP221

¹⁸F-FCH PET/CT disease detection rate in recurrent prostate cancer in relation to PSA level and PSA kinetic indexes

C. Ferrari, A. Niccoli Asabella, V. Lavelli, A. Di Palo, M. Fanelli, N. Merenda, G. Rubini; Nuclear Medicine Unit, D.I.M. – University of Bari “Aldo Moro”, Bari, ITALY.

Aim: To investigate the ¹⁸F-fluorocholine (¹⁸F-FCH) PET/CT reliability for the detection of recurrent prostate cancer in relation to the prostate-specific antigen (PSA) level and to evaluate if PSA doubling time (PSAdt) and PSA velocity (PSAvel) can improve the patient selection and the ¹⁸F-FCH-PET/CT performance. **Methods:** ¹⁸F-FCH-PET/CT was performed in 159 prostate cancer patients (mean age 75±7 years, range 49-88 years), who underwent to radical treatment and with rising PSA level at time of imaging. The last PSA dosage (PSAlast) was available in all patients while PSAdt and PSAvel were available in 103/159. ROC analysis was used to assess diagnostic capability and optimal cutoff points for PSAlast, PSAdt and PSAvel to predict ¹⁸F-FCH-PET/CT positive findings. Non-parametric Mann-Whitney-Wilcoxon test was used to assess differences between the median values of each PSA index. Spearman's coefficient correlation was then used to evaluate the relation among PSA indexes. Contingency tables were performed to test the association between ¹⁸F-FCH-PET/CT results and classes of age (≤50, 51-60, 61-70, >70), Gleason score (≤6, 7, ≥8) and PSAlast (<1, 1-2, >2), by using Chi-square test. *p*-value <0.05 was considered statistically significant. **Results:** In 159 patients, PSAlast median level was 3,49 ng/ml (range 0,20-1129,93); ¹⁸F-FCH-PET/CT was positive in 82/159 (51,6%) patients. In 103/159 patients PSAdt median level was 5,13 months (range 0,70-89,95) and PSAvel median level was 0,29 ng/ml/months (range 0,01-848,9); ¹⁸F-FCH-PET/CT was positive in 58/103 (56,3%) patients. Among PSA indexes, PSAlast (0.826; cut-off>4, sensitivity 68,3%, specificity 84,4%) and PSAvel (0.810; cut-off>0,4, sensitivity 67,2%, specificity 82,2%) demonstrated the best diagnostic capability with no statistically significant difference (*p*=0,557). For PSAlast >4 ng/ml the ¹⁸F-FCH-PET/CT detection rate was 65,8% and for PSAvel >0,4 ng/ml/months was 67,2%. Differences between the median values of each PSA index in ¹⁸F-FCH-PET/CT-positive and ¹⁸F-FCH-PET/CT-negative patients were statistically significant (PSAlast *p*=0; PSAdt *p*=0,008; PSAvel *p*=0). A statistically significant correlation was found between PSAdt and PSAvel (*r*s=-0,63; *p*=0), PSAdt and PSAlast (*r*s=-0,29; *p*=0,003), PSAvel and PSAlast (*r*s=0,89; *p*=0). A positive association was observed between ¹⁸F-FCH-PET/CT results and classes of age ($\chi^2=17,061$, *p*=0,001), Gleason score ($\chi^2=7,256$, *p*=0,027) and PSAlast ($\chi^2=29,616$, *p*=0). **Conclusion:** Our results suggest that ¹⁸F-FCH PET/CT is a reliable method for the evaluation of patients with biochemical recurrence of prostate cancer. The employment of PSAlast and PSAvel in clinical practice could improve patients' selection and correlate with ¹⁸F-FCH-PET/CT results. Moreover, higher age and Gleason score also represent positive predictive factors for recurrent disease.

EP222

Role of 18F Choline PET/CT in guiding biopsy in patients with risen PSA levels and previous negative biopsy for prostate cancer

G. A. Jimenez Londoño, Sr.¹, A. M. García Vicente¹, M. Amo Salas², M. A. Lopez Guerrero³, V. M. Poblete García¹, F. Funes Mayorga⁴, P. Gutierrez Martín⁵, M. J. Tello Galán¹, A. M. Soriano Castrejon¹; ¹Hospital General Universitario de Ciudad Real, Ciudad Real, SPAIN, ²Castilla La Mancha University, Ciudad Real, SPAIN, ³Hospital Virgen de la Salud, Toledo, SPAIN, ⁴Hospital Virgen de Altagracia, Manzanares, SPAIN, ⁵Hospital General Nuestra señora de la Reina, Talavera de la Reina, SPAIN.

Objective: To study 18F-Choline PET/CT in the diagnosis and biopsy guide of prostate cancer (pCa) in patients with persistent high prostate-specific antigen(PSA) level and previous negative prostate biopsy. To compare the clinical risk factors and metabolic variables as predictors of malignancy. **Methods:** Patients with persistently elevated level of PSA in serum (total PSA >4 ng/mL) and at least a previous negative or inconclusive biopsy were consecutively referred for a whole body 18F-choline PET/CT. Patient age, PSA level, PSA doubling time (PSAdt) and PSA velocity (PSAvel) were obtained. PET images were visually (positive or negative) and semiquantitatively (SUVmax) reviewed. 18F-choline uptake prostate patterns were defined as focal, multifocal, homogeneous or heterogeneous. Histology on biopsy using TRUS-guided approach was the gold standard and additional intraprostatic tissue samples were obtained by using PET findings as guidance. Sensitivity (Se), specificity (Sp) and accuracy (Ac) of PET/CT for diagnosis of pCa were evaluated using per-patient and per-prostate lobe analysis. Receiver-operating-characteristic (ROC) curve analysis was used to assess the value of SUVmax to diagnose pCa. Correlation between PET/CT and biopsy results per-prostate lobe was assessed using the Cohen's kappa statistic. Univariate and multivariate logistic regression analysis was applied to compare clinical risk factors and metabolic variables as predictors of malignancy. **Results:** Thirty six out of 43 patients with histologic confirmation were included. In 11 (30.5%) patients, pCa was diagnosed (Gleason score from 4 to 9). The mean values of patient age, PSA level, PSAdt and PSAvel were: 65.5 years, 15.6 ng/ml, 28.1 months and 8.5 ng/mL per year, respectively. Thirty three patients had a positive PET/CT; 18 had a focal pattern, 7 multifocal, 4 homogeneous and 4 heterogeneous. The Se, Sp and Ac of PET/CT were of 100%, 12% and 38% in the patient analysis, and 87%, 29% and 14% in the prostate lobe analysis, respectively. The ROC curve analysis of SUVmax showed an AUC of 0.568 (*p*=0.52). On a lobe analysis, poor agreement was observed between PET/CT findings and biopsy results (*k*=0.097). In the univariate/multivariate analysis, none of clinical and metabolic variables was statistically significant as predictor of pCa. **Conclusion:** 18-F Choline PET/CT could be offered as a screening option in the selection of patients in which the repetition of prostate biopsy should be considered. However, a high rate of false positive results should be expected.

EP223

¹¹C-choline PET/CT for restaging prostate cancer. Results in 4426 scans of a single-centre patient series

T. Graziani¹, F. Ceci¹, P. Castellucci¹, G. Polverari¹, G. M. Lima¹, J. J. Morigi¹, P. Ghedini¹, A. G. Morganti², R. Schiavina³, S. Fanti¹; ¹Service of Nuclear Medicine, S.Orsola-Malpighi Hospital, University of Bologna, Bologna, ITALY, ²Department of Radiotherapy, S.Orsola-Malpighi Hospital, University of Bologna, Bologna, ITALY, ³Department of Urology, S.Orsola-Malpighi Hospital, University of Bologna, Bologna, ITALY.

Aim: to evaluate the importance of ¹¹C-choline-PET/CT as a diagnostic tool for restaging prostate cancer (PCa), in a large, homogenous and clinically relevant population of recurrent PCa patients with biochemical relapse (BCR), after primary therapies. Secondary aim was to assess the best timing for performing ¹¹C-choline-PET/CT during BCR. **Material & methods:** we retrospectively analysed 9632 ¹¹C-choline-PET/CT performed in our institution for restaging PCa from January 2007 to June 2015. Inclusion criteria were: 1) proven PCa radically treated with RP or with primary EBRT; 2) PSA serum values available; 3) proven BCR: PSA>0.2 ng/mL after radical prostatectomy (RP) or PSA>2 ng/mL above the nadir after primary radiotherapy (EBRT), with rising PSA levels. 3203 recurrent PCa (rPCa) patients matching all the inclusion criteria were retrospectively enrolled and 4426 scans were analysed. **Results:** Overall, 52.8% of ¹¹C-choline-PET/CT scans (2337/4426) and 54.8% of patients (1755/3203) resulted positive. In 29.4 % of scans, at least one distant finding was observed. The mean and median PSA values were respectively 4.9 and 2.1 ng/mL at the moment of the scan (range 0.2-50 ng/mL). In our

series, 995 scans were performed with PSA levels between 1–2 ng/mL: in this subpopulation the positivity rate was 44.7%, with an incidence of distant findings of 19.2% and an incidence of oligometastatic disease (1–3 lesions) of 37.7%. PSA absolute value at the time of the scan and ongoing ADT were associated with an increased probability of a positive ^{11}C -choline-PET/CT ($p < 0.0001$). At ROC analysis, PSA=1.16 ng/mL resulted the optimal cut-off value. In patients with PSA < 1.16 ng/mL (1426 scans), ^{11}C -choline-PET/CT was positive in 26.8% of cases, with an incidence of oligometastatic disease in 84.7% of positive scans. **Conclusion:** ^{11}C -choline-PET/CT confirmed, in a large cohort of patients, its feasibility to detect the sites of metastatic disease in PCa patients with BCR. PSA resulted the main predictor of a positive scan with an optimal cut-off value of 1.16 ng/mL. In the majority of positive scans an oligometastatic disease, potentially treatable with salvage therapies, was observed.

EP224

11C-Choline uptake at initial diagnosis predicts patient outcome

M. Rodríguez-Fraile, L. Sancho, F. Guillén, B. García-García, G. Quincoces, M. Collantes, J. Richter; Clínica Universidad de Navarra, PAMPLONA, SPAIN.

Objective To investigate the potential utility of ^{11}C -Choline PET/CT semiquantitative parameters in the prediction of recurrence in patients with prostate carcinoma (PC) at initial diagnosis. **Materials and Methods:** 45 patients with biopsy-confirmed PC were prospectively followed after being studied by ^{11}C -Choline PET/CT before radical prostatectomy (RP). Choline uptake in the whole gland were measured by SUVmax, SUVmin and SUVmean. Two indexes were calculated: SUVmax-SUVmin and SUVmax/SUVmin. All this parameters were correlated with the biochemical relapse (BR) (PSA > 0.2 ng/ml after RP). Patients with less than 4 years of follow-up were excluded from the analysis. **Results:** 31 patients were finally included in the analysis. The mean follow-up time were 8 years (98.6 months \pm 39). During this period, 8 patients suffered BR. Only SUVmax, SUVmax/SUVmin and SUVmax-SUVmin at diagnosis showed correlation with BR ($p=0.003$, $p=0.005$ and $p=0.002$, respectively). SUVmax (AUC-ROC: 0.85) and SUVmax-SUVmin (AUC-ROC: 0.88) discriminated better those patients who suffered BR. A value of 4.76 for SUVmax and of 4 for SUVmax-SUVmin resulted in both cases in a sensitivity of 87.5% and a specificity of 83%. **Conclusion:** ^{11}C -Choline SUVmax and SUVmax-SUVmin at diagnosis, predicts the recurrence of prostate carcinoma with good diagnostic accuracy.

EP225

The value of ^{18}F -FDG PET-CT as a prognostic factor in penile cancer patients

A. L. Salazar¹, S. Lage², L. Salomão², M. Drummond², M. F. Cunha², E. P. Junior², P. G. Salles¹, E. A. Reis², M. Mamede²; ¹Mário Penna Hospital, BELO HORIZONTE - MG, BRAZIL, ²Federal University of Minas Gerais, BELO HORIZONTE - MG, BRAZIL.

Introduction: The penile cancer (PC) is a rare neoplasm in the world. This rarity is most evident in more developed countries, however, in developing regions, its incidence can be high. In Brazil, according to the Brazilian National Cancer Institute (INCA), PC represents up to 2% of cancers in men, reaching 17% in the North and Northeast regions. The dilemma in the treatment of penile cancer is the correct assessment and approach to regional inguinal nodes. This assessment is of utmost importance as directly impacts the prognosis. Clinical staging of the inguinal region is flawed mainly due to enlarged lymph nodes secondary to inflammatory reaction. Morphological imaging techniques have also conflicting results, while the use of ^{18}F -FDG PET/CT has shown promising results. **Objective:** The objective of this study was to investigate the role of ^{18}F -FDG PET/CT as a

prognostic factor in PC patients. **Methods:** Fifty-five patients with histological diagnosis of PC underwent ^{18}F -FDG PET/CT scans before surgery. SUVmax of PC (SUVmax-P) and of inguinal lymph node (SUVmax-L) were correlated with pathologic findings and clinical outcome for prognostic evaluation. **Results:** Two patients were excluded due to high blood glucose level. Thirty patients (60.0%) underwent inguinal lymphadenectomy and 13 (24.5%) died due to primary lesion. ROC analyses showed SUVmax-P higher than 11.5, 14.0, 14.0, 14.9 and 16.5 as significant cut-off values to differentiate patients pT1b ($p < 0.005$), cN ($p < 0.01$), perineural invasion ($p < 0.05$), death ($p < 0.0001$), and pN ($p < 0.05$), respectively. SUVmax-L higher than 5.1, 5.5, 6.2 and 6.5 as significant cut-off values to differentiate patients pT1b ($p < 0.05$), death ($p < 0.05$), pN ($p < 0.01$) and cN ($p < 0.05$), respectively. The best significant survival predictor value for SUVmax-P and SUVmax-L were 14.9 and 6.2, respectively ($p < 0.05$ for all). Multivariate logistic regression analyzes showed pathologic lymph node positive and SUVmax-P as significant variables to predict death with OR (95%CI) of 16.5 (2.4 to 114.1) ($p < 0.001$) and 1.2 (1.0 to 1.4) ($p < 0.05$), respectively. **Conclusions:** This study demonstrated that PET/CT with ^{18}F -FDG can be used as predictor value in PC patients. **Financial Support:** Fapemig, CNPq

EP226

Fluorescence camera navigation during sentinel node biopsy for penile cancer: A clinical pilot study

G. H. KleinJan¹, N. S. van den Berg¹, M. N. van Oosterom¹, T. Wendler², M. Miwa³, K. Hendricksen⁴, A. Bex⁴, S. Horenblas⁴, F. W. B. van Leeuwen¹; ¹LUMC, Leiden, NETHERLANDS, ²TUM, Munich, GERMANY, ³Hamamatsu Photonics, Hamamatsu, JAPAN, ⁴NKI-AVL, Amsterdam, NETHERLANDS.

Introduction The clinical introduction of indocyanine green (ICG)- $^{99\text{m}}\text{Tc}$ -nanocolloid, a hybrid tracer for sentinel node biopsy has resulted in the ability to directly translate preoperative imaging findings into the operation room. Here, the addition of the fluorescence signature allows the surgeon to perform fluorescence image-guided resection of the lesions of interest as seen on preoperative imaging. Lacking herein is the physical link between the fluorescence camera and the preoperative imaging. In the current pilot study we evaluated a SPECT/CT-based navigation concept that allows navigation of a fluorescence camera in preoperative SPECT/CT images to ICG- $^{99\text{m}}\text{Tc}$ -nanocolloid containing sentinel nodes in patients with penile cancer. **Methods** Five penile cancer patients scheduled for SN biopsy were injected with ICG- $^{99\text{m}}\text{Tc}$ -nanocolloid on the morning of surgery followed by lymphoscintigraphy (15 min and 2 h post-injection). SPECT/CT imaging was performed with a reference tracker fixed on the patient (2.5 h post-injection). In the operation room a sterile reference tracker was placed on the patient, and a second tracker on the fluorescence camera. Subsequently SPECT/CT images were uploaded into the navigation device. The fluorescence camera video feed was also uploaded into the navigation device which resulted in a real-time overlay of the preoperative SPECT/CT findings and the video output of the fluorescence camera on the patient. The error between SPECT/CT-based SN localization and the location of the SN as determined via fluorescence imaging was determined on a per SN base. **Results** Preoperatively 13 SNs were identified in 9 groins. Intraoperatively, fluorescence camera navigation in preoperative SPECT/CT images was successful for the identification of 12 SNs with a median error of 7.5 mm (range: 0–20 mm). Reference tracker placement, and the interference of the optical signal from the tracking-device of the navigation system with that of ICG- $^{99\text{m}}\text{Tc}$ -nanocolloid were of influence on the navigation accuracy. **Conclusion** Fluorescence camera navigation in preoperative SPECT/CT images is feasible with reasonable accuracy. Upon accuracy improvements the combined technique has the potential to further refine fluorescence image-guided surgery.

EP227**Automatic 3D-segmentation of the prostate gland**

E. Polymeri¹, M. Sadik¹, N. Hasani¹, F. Fejne², F. Kahl², C. Geronymakis³, L. Edenbrandt⁴; ¹Department of Clinical Physiology, Göteborg, SWEDEN, ²Dept of Signals and Systems Chalmers University of Technology, Göteborg, SWEDEN, ³Department of Radiology, Göteborg, SWEDEN, ⁴Department of Clinical Physiology, Göteborg and Malmö, SWEDEN.

Aim: PET/CT have been proposed as an imaging modality to increase accuracy in the management of prostate cancer patients. Uptake of different PET tracers can be used to assess the underlying altered biology in cancer in the prostate gland and for the detection of metastases. Our long-term aim is to develop imaging biomarkers for the analysis of PET/CT as indicators of prognosis. The aim of the present study is to develop an algorithm for automated segmentation of the prostate gland in CT images. **Materials and Methods:** CT images from 20 patients who had undergone FDG-PET/CT scans were selected as training group. Manual prostate gland segmentations performed separately by two physicians were used as training data. CT images from additional 50 consecutive patients who had undergone FDG-PET/CT scans were included as test group. All PET-CT images were obtained with a biograph 64 True V PET/CT scanner (Siemens 2008) using a low dose radiation CT (Helical scan, pitch 0.8, 120 kV, tube load 30 mAs). A multi-atlas registration based method was applied for automated segmentation of the prostate gland. A test image was registered separately to all the images in the training set and the result was used on the manual delineations to obtain 20 rough segmentations of the image. These segmentations were fused together using a random forest classifier and the final segmentation was obtained with graph cuts. The Dice index was used to quantitatively evaluate the similarity between the automated and the manual prostate segmentations. The automated segmentations in the training and test groups were also evaluated independently by two experienced radiologists who categorized each prostate segmentation as “optimal”, “acceptable” or “inadequate”. **Results:** In the training group the mean Dice index comparing the automated to manual segmentations was 0.73 (SD 0.09). The automated segmentations for the training and test groups were considered as optimal or acceptable by at least one of the two radiologists, (20/20) and (35/50) respectively. The two radiologists presented substantial visual agreement, percentage agreement (PA) 83% and Kappa (*K*) 0.72 for the whole group (70 patients). **Conclusion:** A completely automatic algorithm for 3D-segmentation of the prostate gland in CT images is proposed. This is the first step in the development of an objectively measured PET/CT imaging biomarker. The CT segmentations will for example be used for automated quantification of choline uptake in the prostate gland.

EP228**Contribution of Ga-68 PSMA PET/CT in primary staging of prostate cancer**

N. Ergül¹, T. F. Çermik²; ¹Istanbul Training and Research Hospital, Istanbul, TURKEY, ²Sakarya University Medical Faculty, Department of Nuclear Medicine, Sakarya, TURKEY.

Introduction: PSMA (prostate specific membrane antigen) is a surface antigen located on the prostate cell membranes. It is highly expressed on the prostatic adenocarcinoma cells and can be used to image the primary tumor, metastasis and the recurrence as well. We evaluated the role of Ga-68 PSMA-HBED-CC (Ga-68 PSMA) positron emission tomography/computed tomography (PET/CT) for primary staging in patients with prostate cancer (PCa). **Materials and Methods:** Thirty-one patients with histologically proven PCa were enrolled. Two patients were at low risk (Gleason score 6 and PSA<10), 15 patients were at intermediate risk (Gleason score 7 or PSA between 10-20 ng/mL) and 14 patients were at high risk (Gleason

score ≥ 8 or PSA ≥ 20). All patients underwent Ga-68 PSMA PET/CT imaging before operation and treatment. PET/CT findings were compared with other imaging and clinical findings. **Results:** In the intermediate risk group, pelvic lymph node metastases were detected in 5 patients, distant lymph node metastases in 2 patients, bone metastases in 6 patients and liver metastase in 1 patient. In the high risk group, in 7 patients pelvic lymph node metastases, in 3 patients distant lymph node metastases and in 6 patients bone metastases were detected. In 2 patients with low risk no metastases were detected. In 18 of 31 patients (58%) Ga-68 PSMA PET/CT detected M1 disease and changed the therapy management. In 27 patients the Ga-68 PSMA PET/CT findings were compared with bone scintigraphy findings. In 17 patients the findings of both imagings were congruent. However in 10 patients (37%), findings were discordant. In 6 patients the metastatic foci in bones detected by PET/CT were not detected by bone scan, and in 4 patients the suspected metastases in bone scan were not seen in Ga-68 PSMA PET/CT. **Conclusion:** 68Ga-PSMA PET/CT has a big potential to change the therapy management in patients with prostate cancer, especially with intermediate or high risk disease showing the distant metastatic foci. For detection of bone metastases it is more accurate than bone scintigraphy demonstrating both lytic and sclerotic metastases specifically.

EP229**Clinical application of ¹⁸F FDG PET/CT in evaluation of radiological suspected cases of renal cell carcinoma and comparison with conventional imaging: experience at a tertiary care center**

A. Sood, A. Jois, R. Kumar, T. K. Jain, B. R. Mittal, A. Bhattacharya; PGIMER, Chandigarh, INDIA.

Objective: The aim of this retrospective study was to analyze the diagnostic performance of ¹⁸F-FDG PET/CT for evaluation of renal masses with radiological suspicion of renal cell carcinoma and its comparison with conventional imaging. **Material and methods:** In this retrospective study, we evaluated 68 patients (median age = 53.9 years; range = 14-74 years; male = 44, female = 24) with radiological imaging (USG/ CT/MR) suspicion of renal cell carcinoma. All the patients underwent whole-body ¹⁸F-FDG PET/CT for characterization of the lesions. ¹⁸F FDG PET/CT findings was evaluated by two experienced nuclear medicine physicians and any abnormal FDG uptake on PET images was correlated with lesion on CECT and taken as positive. SUVmax values of the primary renal lesion and existing metastatic foci were also evaluated. For the validation of PET/CT results, histopathological examinations, clinical or imaging follow up were taken as reference standard. Conventional anatomical images (USG / CT or MR scans) were also evaluated for comparison with FDG PET/CT. **RESULTS:** Out of total 68 patients with suspicion of renal cell carcinoma on conventional imaging (CI), the final diagnosis of renal cell carcinoma was established in 50 patients. The CI had revealed a sensitivity, PPV of 100% and 73.5% respectively but non specific in establishing the final diagnosis. ¹⁸F-FDG PET/CT revealed positive findings in 58 patients and negative in 10 patients. Regional lymph nodal disease was noticed in 19 patients, regional and distant metastases in 22 patients and only distant metastases in 11 patients. Adrenal lesions were noted in 12 patients. Fifty patients were true positive, eight false positive, nine true negative, and one false negative. ¹⁸F-FDG PET/CT had shown sensitivity, specificity, positive predictive value, negative predictive values and accuracy of 98.0%, 52.9%, 86.2%, 90.0% and 86.7% respectively. On ROC analysis of uptake (SUVmax) in the primary lesion with respect to the results, a cutoff value of SUVmax > 3.2 (sensitivity 92.3%, specificity 76.5% and area under ROC curve 0.89) was obtained to establish the diagnosis. There was a weak correlation between the SUV max values in the primary lesion and distant metastatic disease (Spearman's coefficient rank correlation ρ 0.0180). **CONCLUSIONS:** ¹⁸F-FDG PET/CT had shown an

excellent diagnostic performance with high sensitivity, PPV and NPV for establishing the diagnosis of renal cell carcinoma as compared to CI which has no specificity. Additionally ^{18}F -FDG PET/CT also helped in the detection of regional as well as distant metastases.

EP230

Utility of ^{18}F -Choline PET-CT for detection of disease and outcome prediction in castration resistant prostate cancer, compared with PET-CT in patients with biochemical relapse

J. J. Robles-Barba¹, A. Sabaté-Llobera¹, J. Mestres-Martí¹, L. Gràcia-Sánchez¹, E. Llinares-Tello¹, J. L. Vercher-Conejero¹, E. M. Merino-Serra², A. M. Ferrer-Artola³, A. M. Boladeras-Inglada⁴, A. Arellano-Tolivar⁴, J. F. Suárez-Novos⁵, C. Gámez-Cenzano¹; ¹PET Unit. Department of Nuclear Medicine. IDI. Hospital U. de Bellvitge-IDIBELL, L'Hospitalet de Llobregat, (Barcelona), SPAIN, ²CT Unit. Department of Radiology. IDI. Hospital U. de Bellvitge-IDIBELL, L'Hospitalet de Llobregat, (Barcelona), SPAIN, ³Department of Pharmacy. Hospital U. de Bellvitge-IDIBELL, L'Hospitalet de Llobregat, (Barcelona), SPAIN, ⁴Department of Radiation Oncology. ICO, L'Hospitalet de Llobregat & Badalona, (Barcelona), SPAIN, ⁵Department of Urology. Hospital U. de Bellvitge-IDIBELL, L'Hospitalet de Llobregat, (Barcelona), SPAIN.

AIM: To assess the detection rate and recurrence location of ^{18}F -Choline PET-CT (FCH-PET) in castration resistant prostate cancer (CRPC) patients, compared to those with biochemical relapse (BR), as well as evaluate its possible role in outcome prediction. **MATERIAL AND METHODS:** This prospective study included 220 patients classified in 2 groups: 1) CRPC patients (n=30), 58-83 y.o., median PSA 10.4 ng/mL and the following D'Amico classification: 26 high risk (86%), 2 medium risk (7%), 2 low risk (7%). 2) BR patients (n=190), 50-83 y.o., median PSA 3.7 ng/mL and the following D'Amico Classification: 114 high risk (60%), 50 medium risk (26%) and 26 low risk (14%). All patients underwent FCH-PET scans. Results were categorized as negative or positive, indicating location of the recurrence (exclusively prostatic, pelvic nodes or distant metastasis) and SUVmax of the most FCH-avid lesion. A follow-up of CRPC patients (7-38 months) was performed including PSA levels and imaging studies, with diagnosis of improved/stable disease (SD) or progressive disease/exitus (PD). Outcome was correlated with recurrence location and SUVmax in PET-CT. **RESULTS:** Detection rate was 100% (30/30) in patients with CRPC and 81% (154/190) in patients with BR. CRPC patients showed also a significant higher percentage of distant metastatic recurrence (73% vs. 16% in BR). Those distant metastasis were more frequently bone/visceral in CRPC group (n=17/22) and nodal in BR group (n=17/31). Regarding BR patients, 36/190 (19%) showed negative FCH-PET studies, 66/190 (35%) presented exclusively prostatic recurrence and 57/190 (30%) pelvic node recurrence. In CRPC patients, 5/30 (17%) showed exclusively prostatic recurrence and 3/30 (10%) pelvic node recurrence. After PET-CT, most CRPC patients underwent treatment with abiraterone acetate +/- enzalutamide, or radiotherapy/surgery if localized disease. During the follow-up, SD was seen in 24/30 patients and PD in 6/30 (1 exitus). Patients with PD presented different FCH-PET patterns compared to patients with SD: percentage of distant metastatic recurrence (83% (n=5/6) vs. 71% (n=17/24) respectively), bone/visceral metastasis (66% (n=4/6) vs. 42% (n=10/24)) and a higher SUVmax (6.5 vs. 4.2). **CONCLUSIONS:** FCH-PET is a very useful technique for detection of disease in CRPC patients, with a higher detection rate than in BR patients, probably due to the more advanced stage of the disease. The pattern of recurrence in FCH-PET in CRPC patients was very often metastatic. Location of recurrence and a higher SUVmax could predict a worse outcome. Further studies with a larger number of CRPC patients and a longer follow-up are required.

EP231

Value of 18F-choline-PET/CT for re-staging prostate cancer patients with biochemical persistence / relapse: correlation with PSA, PSA doubling time, and Gleason

A. G. GÓMEZ-GRANDE, H. Perez-Montero, A. Campos Bonel, M. Cabeza Rodriguez, A. Rodriguez Antolin, S. Ruiz Solis, P. Sarandeses Fernandez, A. Hernandez Martinez, P. Pilkington Woll, J. Estenez Alfaro; HOSPITAL UNIVERSITARIO 12 DE OCTUBRE, MADRID, SPAIN, MADRID, SPAIN.

Aims and Purpose: Current NCCN guidelines suggest 18F-choline-PET/CT imaging (18F-Ch-PET) as a diagnostic study for the evaluation of patients with recurrent prostate cancer (PCa). The objective of this study was to evaluate the use of 18F-Ch-PET to restage patients with biochemical relapse (BR) and correlation with PSA, PSA doubling time and Gleason. **Material and Methods:** This is a prospective study (data collected between February/2014 and April /2016) in a cohort of 54 high-risk PCa patients (based on NCCN criteria) with BR (PSA doubling time (DTPSA) <8 months) after treatment with radiotherapy and/or prostatectomy. Pearson χ^2 test was performed. **Results:** The mean age of the cohort was of 67 years (range from 46 - 80). Mean PSA was of 3.11 +/-4.2 (0.15 - 21.39). Mean DTPSA of 7.19 +/- 9.1 (0.7 - 61.52). In most cases (57.5%) the Gleason score was ≥ 7 (4+3). Positive 18F-Ch-PET results were obtained in 63% of the scans performed, 62% showed local and/or regional disease and 38% had distant metastases. Scans were positive in 33% of patients with PSA<1 ng/mL and in 87% of patients with PSA ≥ 1 ng/mL (p<0.001). We found a statistically significant correlation between positive 18-F-Ch-PET studies and Gleason score ≥ 7 (4+3) (p=0.031). A positive scan and a DTPSA<3 months had a tendency to correlate. All patients with a positive 18F-Ch-PET had a negative TC and bone scan. **Conclusions:** 18F-Ch-PET seems to be a very useful diagnostic test for restaging recurrent PCa in selected group of patients. It can also modify treatment management in an important percentage, identifying which ones can be offered a potential curative treatment. In our series, like in the literature, PSA level is a strong predictive factor for positive 18F-Ch-PET.

EP232

Diagnostic performance of contrast enhanced PET/CT scan for restaging and recurrence in renal cell carcinoma

A. K. Singh, S. Gambhir, P. K. Pradhan, G. Shankar AP, A. Prashanth, M. Ravina, N. Kumar; SGPPI, LUCKNOW, INDIA.

Aim: The role of PET/CT is limited in the evaluation of renal cell carcinoma because of the urinary excretion of ^{18}F 2-fluoro-2 deoxyglucose (FDG). While demonstrating similar accuracy to CT in diagnosing primary renal cell carcinoma (RCC), PET/CT appears to be even more reliable in identifying local recurrence and distant metastasis as well as monitoring progression of disease and response to immunotherapy. The present study was undertaken to emphasize on evaluating the diagnostic performance of contrast PET/CT scan for restaging and recurrence in RCC. **Materials and Methods:** A total of 33 cases of histopathologically proven renal cell carcinoma for restaging and suspected recurrence were included in this study on the basis of clinical and pathological data. The IV contrast agent applied was Ultravist 370 (Bayer, Iopromide 370 mg I/ml, osmolality 607mOsm/kg, density 1.322 g/cm³ at 37°C). Infusion was given by using Medrad Intego PET/CT Infusion System. For whole body 3.0 ml/sec for 100-125 ml with 50 ml saline, 30 second delay was used. CT images were taken in cranial-caudal over roughly 8-30 seconds. Additional diagnostic contrast CT (CECT) images were obtained with 100 sec and 130 sec delay (Nephrogenic phase and delayed phase)

in region of interest (Top of liver to bottom of kidneys) using CT with 120 mA 120 kVp with 0.5 sec rotation, 4 detector rows, 5.0 mm thickness Pitch 0.8: 1 at a speed 8mm/rotation if required. Immediately after the CECT images were acquired, a PET emission scan was obtained from the vertex to mid-thigh. Two experienced nuclear medicine physicians interpreted the results. **Results:** Out of 33 patients with standard of reference as histopathology, true positive (TP), false positive (FP), false negative (TN) and true negative (TN) results were seen in 22, 1, 2, and 8 cases respectively. The sensitivity, specificity, accuracy, and positive and negative predictive values of the contrast PET/CT for identifying the primary recurrent tumour were 92%, 89%, 90%, 95%, and 80% respectively. **Conclusion:** The contrast PET/CT scan demonstrated a significantly good performance in detecting recurrence and restaging in renal cell carcinoma post-surgery. Based on the above findings combining contrast enhanced CT (CECT) and PET can be considered as a one-stop-shop imaging approach which can detect local and distant metastases with high accuracy in the recurrence of Renal cell carcinoma.

EP233

Evaluation of dualtracer multiparametric PET/MRI parameters in primary prostate cancer

M. Hartenbach¹, P. Baltzer¹, S. Hartenbach², M. Susani³, C. Seitz⁴, L. Kenner³, L. Papp¹, A. Haug¹, W. Wadsak¹, M. Mitterhauser¹, I. Rausch⁵, A. Pohnholzer⁵, M. Lamche⁶, S. Shariat⁴, M. Hacker¹; ¹Medical University of Vienna, Dep. of biomed. imaging and image guided therapy, Vienna, AUSTRIA, ²German Armed Forces Hospital, Institute of Pathology, Ulm, GERMANY, ³Medical University of Vienna, Institute of Pathology, Vienna, AUSTRIA, ⁴Medical University of Vienna, Dep. of Urology, Vienna, AUSTRIA, ⁵Medical University of Vienna, Dep. of Medical Physics and biomedical engineering, Vienna, AUSTRIA, ⁶Hospital St. John of God, Urology, Vienna, AUSTRIA.

Aim Retrospective analysis of multiparametric ⁶⁸Ga-PSMA^{HBED-CC} / [¹⁸F] Fluorocholine-PET / MRI (mp PSMA/FC-PET/MRI) in terms of detection, characterization and prognosis in primary prostate cancer. Method 43 lesions in 38 prostatectomy patients with preoperative PET/MRI were color-coded in histological whole-mount sections with respect to their Gleason patterns. In so far 18 patients, p14/STAT3-tissue microarrays for risk assessment of early biochemical relapse were performed. SUV, tumor-to-muscle ratios (TBR) and heterogeneity (COV, SUVmax / mean) were determined and percentiles for ADC and DCE (Ktrans, Ve, IAUC and kep). PSMA immunohistochemistry was used to verify PET-PSMA-negative lesions. ROC analyzes discriminated Gleason 3 vs. Gleason >3 pattern and STAT3/p14-loss. FC-SUVmax >3.0, deltaTBR after PSMA application >1.0 and 25th percentile ADC <1.0 * 10⁻³mm² / s served as cut-off for positive tumor detection. Results All lesions were FC-positive. 9 lesions each (21%) were PSMA and ADC negative. The AUC for Gleason 3 vs. Gleason >3 pattern for FC-COV, ADC and dualtracerSUVmax / mean was 0.86, 0.87 and 0.89 (P <0.001). At a cut-off of 1.54, dualtracerSUVmax/mean showed a sens/spec/acc/PPV/NPV of: 84%/75%/81%/88%/69% (P=0.001). A STAT3 and/or p14-loss of the tumor lesion was detected with an AUC of 0.8 by this parameter (p <0.05). iAUCmax demonstrated the largest AUC among DCE parameters: 0.70 (p = 0.06). Conclusions All lesions analyzed showed a significant choline metabolism. Significant PSMA-expression and water diffusion restriction was found in 79% of the lesions, however, contributed to a higher accuracy in the assessment of tumor aggressiveness and correlated with prognostic markers for an early biochemical recurrence (STAT3/p14). MRI DCE parameters should be considered critically in the protocol.

EP234

Value and efficacy of sentinel lymph node diagnostics in patients with penile carcinoma with palpable inguinal lymph nodes as a new multimodal, minimally invasive approach

U. Lützen, M. Marx, M. Zuhayra, Y. Zhao, K. Jünemann, M. Naumann; Universitätsklinikum Schleswig-Holstein, KIEL, GERMANY.

Introduction: The international guidelines recommend sentinel lymph node biopsy (SLNB) for lymph node staging in penile cancer with non-palpable inguinal lymph nodes (LN) but it is not recommended with palpable inguinal LN. As a new approach the aim of this study was to evaluate the reliability and morbidity of SLNB with radioactive labelling in combination with an ultrasound-guided resection of suspect inguinal LN as a multimodal, minimally invasive staging-technique in these patients. **Material and Methods:** We performed SLNB in 26 penile cancer patients with 42 palpable inguinal LN after using Tc 99m-nanocolloids. Prior to the combined staging procedures the patients underwent a ultrasound examination of the groins as well as planar lymphatic drainage scintigraphy and SPECT/CT-scans. During the surgical procedure, the radioactive-labelled sentinel lymph nodes (SLN), and in addition, sonographically suspect LN, were resected under ultrasound-guidance. Follow-up screening was done by ultrasound examination of the groins according to the guidelines of the European Association of Urology (EAU). **Results:** Staging of the primary tumor resulted T1: 14, T2: 9 and T3: 3 cases. Tissue differentiation was G1: 2, G2: 19 and G3: 4. For one patient, who had undergone primary surgery ex domo, the degree of tissue differentiation was unknown. 19 groins of 42 preoperatively palpable inguinal findings were histologically tumor-positive. SLNB alone showed lymphogenic metastases in 14 groins. Sonography revealed 5 further metastatic groins, which would not have been detected during SLNB due to a tumor-related blockage of lymphatic drainage or a so-called re-routing of the radioactive tracer. During follow-up, none of the 28 groins with tumor-negative LN status showed any LN recurrence in this combined investigation technique. The median follow-up period was 46 (24 to 92) months. Morbidity of this combined procedure was low at 4.76% in relation to the number of groins (2 out of 42) resp. 7.69% in relation to the number of patients (2 out of 26). **Conclusions:** Results from this study show that the combined procedure of SLNB after radioactive LN labelling and ultrasound-guided resection of suspect inguinal LN is a reliable multimodal diagnostic approach for treatment of penile cancer patients with palpable inguinal LN. This combined approach is associated with low morbidity rates. SLNB alone would lead to a significantly higher false-negative rate in these patients.

EP235

To evaluate the role of F 18 FDG PET CT in the metastatic work up in operated cases of penile squamous cell carcinoma

A. K. Jhajharia, A. Bhattacharya, U. K. Mette, N. Kakkar, B. Singh, B. R. Mittal; Post Graduate Institute of Medical Education & Research, Chandigarh, INDIA.

Background: Squamous cell carcinoma is the most common variant of penile cancer and post-surgical recurrence and metastatic disease progression is very frequent. Therefore, a close follow up using clinical examination, biochemical markers and molecular imaging for accurate disease diagnosis for improved prognosis and survival benefits is warranted. **Methods:** We retrospectively reviewed clinical and 18 F-FDG PET/CT data of thirty one patients of SCC penis after partial / total penectomy / circumcision. The reference standard was based on histopathology findings of biopsy/surgery, clinical and/or imaging follow up. **Results:** Thirty-one (mean age 57.6 years; range 35-75 years) operated patients of SCC of penis who were referred between 2010-2015 for PET/CT staging were included in the present study. Twenty-one patients had undergone partial penectomy, 7 complete penectomy and 3 patients underwent circumcision respectively.

Additionally, one patient received chemotherapy, 3 patients received radiotherapy and 9 patients received both chemo-radio treatment. The reconstructed 18 F FDG PET/CT imaging data demonstrated normal scan findings in 6/31 patients and these patients were found to be disease free on clinical follow-up during the follow-up period of 6-months. On the other hand, 13/31 patients were found to have penile residual/recurrent and ilioinguinal lymph nodal metastatic disease. The remaining 12/31 patients were observed to have multiple and distant lymph nodal metastatic disease. Seven (7/12) patients wide spread lymph nodal metastases died during follow-up. PET CT scan findings were false positive in 2 patients as they remained disease free without any intervention during the subsequent follow up. The sensitivity, specificity, PPV, NPV and accuracy of FDG PET/CT in detecting residual / recurrent / metastatic disease in SCC penis in the present were found to be 100%, 75%, 92%, 100% and 82.5% respectively. **Conclusion:** Our result suggest that ¹⁸F-FDG PET/CT is a very useful modality in detecting local recurrence, regional and distant lymph nodal metastases in operated cases of SCC of penis. These findings thus may guide the treating urologists in the further management of these patients by using appropriate therapeutic options.

EP236

¹⁸F-Fluoromethylcholine (¹⁸FCH) PET/CT compared with standard imaging in patients with recurrent prostate cancer

C. Ferrari, A. Niccoli Asabella, V. Lavelli, C. Altini, G. Bianco, N. Merenda, G. Rubini; Nuclear Medicine Unit, D.I.M. – University of Bari “Aldo Moro”, Bari, ITALY.

Aim: To assess the utility of 18F-Fluoromethylcholine (¹⁸FCH) PET/CT in recurrent prostate cancer compared to guidelines standard imaging (SI): bone scan (BS) and/or morphologic imaging (MI). **Methods:** 105 patients previously treated for prostate cancer, performed ¹⁸FCH-PET/CT and SI (81/105 BS, 57/105 MI and 38/105 both) within a 1-month for suspected recurrence. ¹⁸FCH-positive bone lesions were compared to BS while soft tissue lesions, both loco-regional recurrence (LRR) and distant lesions (DL) were compared to MI, by Cohen's K. **Results:** ¹⁸FCH-PET/CT resulted positive in 55/105 (52.4%) patients, SI in 65/105 (61.9%). In 81/105 patients who performed BS, ¹⁸FCH-positive bone lesions resulted in 25/81 (30.8%) patients while BS was positive in 34/81 (41.9%). The two methods resulted concordant in 56/81 (69.1%) patients -positive concordant (PC) in 17/81 (21%), negative concordant (NC) in 39/81 (48.1%) and discordant in 25/81 (30.8%). The strength of agreement was 'fair' (K=0.342). ¹⁸FCH-PET/CT showed additional soft tissue lesions in 33/81 (40.7%) patients (LRR in 21/81, DL in 6/81 and both in 6/81). In 57/105 patients who performed MI, ¹⁸FCH-positive lesions for LRR were found in 22/57 (38.6%) patients while MI-positive lesions in 20/57 (35.1%). The two methods were concordant in 37/57 (64.9%) patients -PC in 11/57 (19.3%), NC in 26/57 (45.6%) and discordant in 20/57 (35.1%). The strength of agreement was 'fair' (K=0.247). Considering DL, ¹⁸FCH-PET/CT resulted positive in 11/57 (19.3%) patients while MI was positive in 21/57 (36.8%). The two methods were concordant in 41/57 (71.9%) patients -PC in 8/57 (14%), NC in 33/57 (57.9%) and discordant in 16/57 (28%). The strength of agreement was 'fair' (K=0.330). ¹⁸FCH-PET/CT showed additional soft tissue lesions in 13/57 (22.8%) patients (LRR in 8/13, distant lesions in 3/13 and both in 2/13). In 38/105 patients who performed both BS and MI, ¹⁸FCH-PET/CT resulted positive in 22/38 (57.9%) patients while SI resulted positive in 32/38 (84.2%). The two methods resulted concordant in 26/38 (68.4%) patients -PC in 21/38 (55.3%), NC in 5/38 (13.1%) and discordant in 12/38 (31.6%). The strength of agreement was 'fair' (K=0.292). ¹⁸FCH-PET/CT showed additional lesions in 11/38 (28.9%) patients (LRR in 8/11, DL in 1/11, and LRR, bone and DL in 2/11 patients). **Conclusion:** ¹⁸FCH-PET/CT showed fair concordance with BS and MI, although it detected additional soft tissue and bone lesions in a significant percentage of patients, respect to SI. Thus, ¹⁸FCH-PET/CT could be a more complete whole-body diagnostic tool to evaluate patients with recurrent prostate cancer.

EP237

Should the head be included in 18F- Choline PET/CT scans of patients with prostate cancer ?

A. Nocuń, B. Chrapko; Chair and Department of Nuclear Medicine, Medical University of Lublin, Poland, LUBLIN, POLAND.

Introduction: There are no definitive procedure guidelines for 18F-Choline (FCH) positron emission tomography/computed tomography (PET/CT) imaging. The acquisition protocols vary between centers. The head is included or not included in the field of view (FOV) on the delayed scans. Inclusion increases the time of imaging and radiation exposure to the patient, however it may be speculated, that it improves the staging accuracy. The aim of the present study was to determine the incidence and clinical significance of abnormalities within the head on FCH PET/CT scans in patients with prostate cancer. **Materials and methods:** Retrospective analysis included 170 consecutive FCH PET/CT examinations in 150 patients with pathologically proven prostate cancer who underwent FCH PET/CT imaging in our institution between January 2014 and March 2016. Data acquisition was performed using a dedicated PET/CT system Biograph mCT S(64)-4R (Siemens, Germany). The delayed scans were acquired from the top of the skull to the mid-thigh level. Image evaluation was performed visually and by means of maximum standardized uptake values (SUVs). **Results:** Lesions in the head with increased radiotracer accumulation were seen in 5 patients (2.9% examinations): metastases in the skull (3 cases) and brain tumors (2 cases). In 2 patients with metastases in the skull, multiple lesions in other bones and various organs were observed. In one case, the lesion in the skull was solitary osteolytic metastasis (SUVmax 3.2). The diagnosis of brain tumors was meningioma in one case (SUVmax 3) and metastases from prostate cancer in the second case (four lesions, size from 10mm to 27mm, SUVmax from 5 to 16.1). Brain tumors in both patient were asymptomatic. The staging based on FCH PET/CT with the head in the FOV, was altered in two patients (1.2% examinations) when compared to the FOV from the base of the skull. **Conclusions:** In patients with prostate cancer examined by means of FCH PET/CT, the abnormalities within the head are very rare, however in some cases detection of such lesions may alter the staging of the disease (1.2% of scans in the present study).

EP238

Detection of local recurrence of prostate cancer after radical prostatectomy in patients with PSA ≤ 2ng/ml: Is there a role for early ¹⁸F-FCH PET/CT?

A. Chiaravallotti^{1,2}, F. Calabria³, A. Fiorentini¹, D. Di Biagio¹, P. Sannino², E. Di Giorgio⁴, M. Zinzi², M. Tavolozza¹, O. Schillaci^{1,2}; ¹Department of Biomedicine and Prevention, University Tor Vergata, Rome, ITALY, ²IRCCS Neuromed, Pozzilli, ITALY, ³Neuromimaging Research Unit, IBFM, National Research Council, Catanzaro, ITALY, ⁴IRCCS Neuromed, Rome, ITALY.

Aim: To investigate the diagnostic performance of early acquisition compared to late imaging for the detection of local recurrence of prostate cancer (PC) in a selected population with PSA ≤ 2ng/ml after radical prostatectomy by means of ¹⁸F-FCH PET/CT. **Materials and methods:** Forty-five patients (age 68 ± 11 years) with biochemical recurrence of PC following a previous radical prostatectomy were included in this retrospective study. The biochemical relapse was determined as a PSA level of 0.2 ng/mL or greater followed by another increased value during the time. None of the patients was subjected to radiotherapy for local or distant recurrence nor to hormonal therapy prior to PET/CT examination. The PSA level was determined from blood samples obtained during the fasting period 2 weeks (±2 days) prior to PET/CT scan. Early acquisition (8 minutes in dynamic modality, every frame lasting 30s in a 128 x 128 matrix) started after the in bolus injection of ¹⁸F-choline intravenously (4

MBq/kg). All patients were asked to empty their bladder before image acquisition. Late acquisition started 40 minutes after the injection of the tracer. First, a low-amperage CT scan for attenuation correction of PET images was taken. Immediately after the low-dose CT scan, whole body PET images were acquired in a 256 x 256 matrix (five to seven bed positions, 3 min/bed position, from the upper thighs to the vertex). **Results:** PSA resulted equal to 1.42±0.40 in the whole population examined. Twenty subjects (PSA=1.31±0.53) out of the 45 examined patients showed positive PET/CT findings for local recurrence. Among them, 4 patients were positive in both modalities (PSA=1.65±0.27), 5 shown a positive early and a negative late acquisition (PSA=1.33±0.86), while 8 shown a negative early and a positive late acquisition (PSA=1.50±0.44). We did not find significant differences in PSA values in subject with a positive PET/CT scan to subjects with a negative PET/CT scan (P=0.8). The analysis of sensitivity, specificity, diagnostic accuracy, positive predictive value and negative predictive value resulted equal to: 53.3%; 96.7%; 82.2%, 88.9 and 80.6% for early acquisition and 66.7%; 93.3%; 84.4%; 83.3% and 84.8% for late acquisition, respectively. Conversely, considering together the results of both scans, results were 93.3%, 90.0%, 91.1%; 82.4% and 96.4% respectively. **Conclusion:** The combination of early acquisition with late acquisition lead to an increase of the diagnostic accuracy of ¹⁸F-FCH PET/CT for the diagnosis of local recurrence in PC after RP with PSA ≤ 2ng/ml.

EP239

Radiation dosimetry of ⁶⁸Ga-PSMA-11 (HBED-CC) and preliminary evaluation of optimal imaging timing

A. Afshar-Oromieh¹, H. Hetzheim², W. Kuebler³, T. Hope⁴, C. Kratochwil¹, F. Giesel¹, M. Eder⁵, M. Eisenhut⁵, K. Kopka⁵, U. Haberkorn¹; ¹University Hospital of Heidelberg, German Cancer Research Center (DKFZ) Heidelberg, Heidelberg, GERMANY, ²Div. of Medical Physics in Radiology, German Cancer Research Center, Heidelberg, Germany, Heidelberg, GERMANY, ³Div. of Radiation Protection and Dosimetry, German Cancer Research Center, Heidelberg, Germany, Heidelberg, GERMANY, ⁴Dept. of Radiology and Biomedical Imaging, University of California, San Francisco, CA, UNITED STATES, ⁵Div. of Radiopharmaceutical Chemistry, German Cancer Research Center, Heidelberg, Germany, Heidelberg, GERMANY.

Aim: The clinical introduction of ⁶⁸Ga-PSMA-11 (“HBED-CC”) ligand targeting the prostate-specific membrane antigen (PSMA) has been regarded as a significant step forward in the diagnosis of prostate cancer (PCa). In this study we provide human dosimetry and data on optimal timing of PET imaging after injection. **Methods:** Four patients with recurrent PCa were referred for ⁶⁸Ga-PSMA-11 PET/CT. Whole-body PET/CT_{low-dose} scans were conducted at 5min, 1h, 2h, 3h, 4h and 5h after injection of 152-198 MBq ⁶⁸Ga-PSMA-11. Organs of moderate to high uptake were used as source organs; their total activity was determined at all measured time points. Time-activity curves were created for each source organ as well as for the remainder. The radiation exposure of a ⁶⁸Ga-PSMA-11 PET was identified using the OLINDA-EXM software. In addition, tracer uptake was measured in 16 sites of metastases. **Results:** The highest tracer uptake was observed in the kidneys, liver, upper large intestine and the urinary bladder. Mean organ doses were: kidneys 0.262 ± 0.098 mGy/MBq, liver 0.031 ± 0.004 mGy/MBq, upper large intestine 0.054 ± 0.041 mGy/MBq, urinary bladder 0.13 ± 0.059 mGy/MBq. The calculated mean effective dose was 0.023 ± 0.004 mSv/MBq (= 0.085 ± 0.015 rem/mCi). Most tumor lesions (n=16) were visible at 3h p.i., while at all other time points many were not qualitatively present (10/16 visible at 1hr p.i.). **Conclusion:** The mean effective dose of a ⁶⁸Ga-PSMA-11 PET is 0.023 mSv/MBq. A 3 hour delay after injection was optimal timing for ⁶⁸Ga-PSMA-11 PET/CT in this patient cohort.

EP240

Diagnostic value of F-18 FDG PET/CT compared to CE-CT for local and distant relapse surveillance in surgically treated RCC patients.

M. A. Abdelwahab, W. Omar, H. Elsayd; National Cancer Institute, Cairo, EGYPT.

Objective: to evaluate the diagnostic performance of combined fluorine-18 fluoro-deoxyglucose (18F-FDG) PET/ computed tomography compared to Ce-CT for the detection of local and distant disease relapse in surgically treated patients with renal cell carcinoma (RCC). **Patients and methods:** This retrospective study includes 94 patients with a clinical suspicion of renal cell carcinoma tumor recurrence referred to nuclear medicine department, Children's Cancer Hospital, Egypt (CCHE) to perform PET/CT study. Each patient underwent 18F-FDG PET/ computed tomography (CT) with low-dose CT, followed immediately by Ce-CT. Study-based analyses for a total of 94 scans were carried out. For each study, site based analysis was performed. Sites of relapse were categorized into 7 groups: local tumor site, lymph nodes, lung, brain, liver, bone and other soft tissue sites (e.g. adrenal, subcutaneous, intramuscular & pancreas). The final diagnosis of disease status was made on subsequent follow-up by conventional imaging (CT/MRI), 18F-FDG PET/CT, or histopathology whenever possible. **Results:** Out of the 94 evaluated patients, 69 (73.4 %) studies had local &/or distant recurrent disease and 25 (26.6 %) studies were disease free on the basis of the final diagnosis. 18F-FDG PET/CT and Ce-CT had a sensitivity, specificity, negative predictive value, and positive predictive value of 95.8 versus 100%, 100 % versus 98.5 %, 98.5% versus 100 %, and 100% versus 96 %, respectively for the detection of local recurrence and 92.4 % versus 94 %, 97.4 % versus 62.5 %, 80.9 % versus 78.1 %, and 99.1 % versus 88.1 %, respectively for the detection of distant metastases. 18F-FDG PET/CT was significantly more specific with significantly higher PPV for the detection of distant recurrence (specially in soft tissue sites as intramuscular, subcutaneous, adrenal, & pancreatic lesions) compared to Ce-CT, with P-values of <0.05. **Conclusion:** 18F-FDG PET/CT seems to have added value compared to Ce-CT alone in detection of distant metastatic lesions in the re-staging of surgically treated RCC patients.

EP241

Scintigraphic assessment of pelvic sentinel lymph nodes metastatic spread in oncurologic patients

V. Sukhov¹, K. Zaplatnikov², A. Marin¹; ¹Military Medical Academy, ST. PETERSBURG, RUSSIAN FEDERATION, ²maz, Nuremberg, GERMANY.

Purpose of the study was to evaluate ^{99m}Tc-colloid scintigraphy used as method of clarifying the routs of lymphatic cancer spread for lymph dissection and optimization of radiation therapy. **Materials and methods:** SLN scintigraphy was performed in 51 patients 17 - 47 y.o. with tumors of the testis (n=17) by administration of 37-74 MBq of ^{99m}Tc-colloid beneath tunica albuginea of the tumor-affected testis prior to its surgical resection or in the stump of spermatic cord, if the patient had earlier undergone orchiectomy and prostate cancer (n=34) - by administration of 37-74 MBq of ^{99m}Tc-colloid beneath capsule. Examinations were performed 45-60 minutes p.i. on gamma-camera "E.cam Var" (Siemens) in Anterior, Posterior, Left, Right and perineal projections. Sentinel lymph nodes were seen on scintigrams as foci of intensive accumulation of the radiopharmaceutical most closely to the site of tumor. **Results:** Pelvic SLN scintigraphy data were helpful for determining of the direction of lymph outflow from tumor-affected testis or the stump of spermatic cord and prostate to sentinel lymph nodes by normal or changed lymph collectors. Thus, SLN scintigraphy led to exact determination of local lymph node dissection or delineation of fields' size and configuration for local

radiation therapy. Conclusions: Clarifying of the lymph outflow routs with 99 mTc-colloid increases the validity of early lymphatic cancer spread detection, including or excluding cases of lymph nodes enlargement. This gives an opportunity to determine precise configuration of radiation fields within sites of 99 mTc-colloid accumulation.

EP242

Introduction of a molecular PI-RADS classification system for ^{68}Ga -PSMA-PET/MR imaging of primary prostate cancer

S. Lütje¹, A. Wetter², J. Cohnen¹, L. M. Sawicki³, A. Bockisch¹, T. D. Poeppel¹, B. Gomez¹; ¹Clinic for Nuclear Medicine, University Hospital Essen, Essen, GERMANY, ²Department of Diagnostic and Interventional Radiology and Neuroradiology, University Hospital Essen, Essen, GERMANY, ³Medical Faculty, Department of Diagnostic and Interventional Radiology, University Dusseldorf, Düsseldorf, GERMANY.

Aim: Multi-parametric magnetic resonance imaging (MRI) is the standard technique for non-invasive tumor staging of primary prostate cancer (PCa). First clinical studies indicate that positron emission tomography (PET)/MRI targeting the prostate-specific membrane antigen (PSMA) is a highly promising new technique for staging of patients with primary PCa. Here, the addition of a molecular component to the standard reporting system PI-RADS was introduced to allow metabolic classification of suspect prostate lesions and their differentiation from benign/inflammatory processes with ^{68}Ga -PSMA-PET/MRI. **Materials and methods:** In a retrospective study, six patients with primary PCa underwent ^{68}Ga -PSMA-PET/MRI for initial staging. Patients received intravenous injections of 113 ± 21 MBq of the ^{68}Ga -labeled PSMA ligand HBED-CC-PSMA at 121 ± 25 min p.i.. All tumor lesions were histologically proven by biopsy. Images were analyzed quantitatively (SUV_{max} and SUV_{mean}) and qualitatively using a three point scale from A (normal tracer accumulation) and B (moderate focal tracer accumulation) to C (suspect focal tracer accumulation) in addition to the original PI-RADS system. **Results:** Seven PET-positive lesions (mean SUV_{max} 6.5, range 3.6-10.5, mean SUV_{mean} 2.9, range 1.8-4.9) were identified with the PET component of ^{68}Ga -PSMA-PET/MRI. All seven lesions were visually concordant to suspect lesions in the MRI component (T2w and DWI) of the PET/MRI system. All visualized suspect lesions were histologically confirmed to be tumor lesions. Six tumor lesions were classified PI-RADS 4 (PCa likely to be present), while one lesion was PI-RADS 3 (presence of PCa is equivocal). All lesions were accompanied by the (m)PI-RADS classification score C as all lesions showed suspect focal tracer accumulation. In the patient with equivocal presence of PCa according to the original PI-RADS classification, ^{68}Ga -PSMA-PET/MRI showed a highly suspect focal tracer accumulation (score C), indicating malignant involvement, which was confirmed by histology. Therefore, the use of the new (m)PI-RADS classification system could clarify unclear findings, by adding a metabolic value to the original score. **Conclusion:** Here, a new (m)PI-RADS system was introduced, which adds a metabolic aspect to the original PI-RADS system, which could facilitate the differentiation between benign and malignant lesions within the prostate.

EP243

Diagnostic impact of 18F-Fluoromethylcholine PET/CT in biochemical relapse of the prostate cancer

A. Alvarez Alonso, C. Vigil Díaz, B. Fernández Llana, A. Álvarez Blanco, N. Martín Fernández, L. Díaz Platas, N. Pérez Castro, O. Rodríguez Fonseca, F. González García; Hospital Universitario Central de Asturias, Oviedo, SPAIN.

Objective: Evaluate the potential diagnostic of the 18F-Fluoromethylcholine (FCH) PET/CT in the diagnosis of the prostate adenocarcinoma recurrence. **Material and methods:** 87 patients with prostate adenocarcinoma treated with curative intent were retrospectively included from October 2014 to January 2016, with a median age of 68 years (range 52-86). Initial treatment was radical prostatectomy in 29 patients (33%), salvage radiotherapy in 51 (59%) and other treatments in 7 (8%). At the time of the study 22 patients were receiving hormonal treatment. The patients were referred for a 18F-FCH PET/CT study due to biochemical relapse (mean PSA: 14,1 ng/ml, 95% CI 9,3-18,9. Final diagnosis of recurrence was confirmed by clinical follow-up (median 188 days). Sensitivity (Se), specificity (Sp), positive (PPV), and negative predictive values were measured for 18F-FCH PET/CT, CT and bone scintigraphy. A T-Student test was performed to compare the value of PSA in patients with or without recurrence in the 18F-FCH PET/CT. **Results:** The 18F-FCH study was positive in 63 patients (72%). 18F-FCH findings showed local recurrence in 19 patients (22%), metastatic lymph nodes in 29 (32%), metastatic bone disease in 17 (22%) and negative in the remaining 20 patients (24%). The Se, Sp, PPV and NPV values for 18F-FCH PET/CT study were 95%, 74%, 94% and 46%, respectively. For CT study 30%, 80%, 87% and 20%, respectively. When the detection of bone metastasis was isolated analyzed, the values obtained were 31%, 99%, 99% and 84%, respectively. Statistically significant differences ($p < 0.002$) between the value of PSA in the negative and positive 18F-FCH studies were observed (4,5; 95% CI: 2-7,1 vs. 17,8; 95% CI: 11,3-24,2). Recurrence was detected more frequently in the group of patients initially treated with radiotherapy (40/51, 78%) than in the group initially treated with radical prostatectomy (15/29, 52%). Recurrence was detected in 20/22 (91%) of patients with hormone treatment and confirmed during the follow-up. **Conclusion:** The findings remarked the accuracy of 18F-Fluoromethylcholine PET/CT in the diagnosis of local and distant relapse of prostate adenocarcinoma, defining the location of the recurrence and surpassing conventional imaging techniques. The study showed a significant association between high levels of PSA and positive 18F-FCH and suggests that the presence of hormonal therapy is not a decisive factor in the outcome of this exploration.

EP244

Effects of Lutetium-177 PSMA-i and Radioiodine Therapy on Salivary and Lacrimal Glands

O. E. Sahin¹, B. Vatankulu¹, R. Akyel¹, J. Nematyazar¹, E. Demirci², H. Pehlivan¹, E. Karayel¹, A. Aygun¹, M. Ocak³, L. Kabasakal¹; ¹Department of Nuclear Medicine, Cerrahpasa Medical Faculty, Istanbul University, Istanbul, TURKEY, ²Sisli Etfal Training and Research Hospital Department of Nuclear Medicine, Istanbul, TURKEY, ³Department of Pharmaceutical Technology, Pharmacy Faculty, Istanbul University, Istanbul, TURKEY.

Aim: Lutetium177-PSMA-i is a new radiopharmaceutical for the treatment of castration-resistant prostate cancer (CRPC). Normal tissue dose rates and absorbed doses are very important to follow-up of the side effects in radionuclide therapy. Lu-177 PSMA-i dosimetry studies showed that absorbed doses of salivary glands and lacrimal glands are higher than kidneys. It is also known that radioiodine has higher uptake in salivary glands. Therefore we aimed to evaluate the effects of radioiodine and Lu-177 PSMA-i therapies on salivary and lacrimal glands. **Material-method:** Nineteen prostate cancer patients (mean age: 64 ± 8 years) who had PSMA-11 PET/CT imaging before and after Lu177 PSMA-i therapies (average of Lu177-PSMA dose: $25,4 \pm 6,14$ GBq) were included into the study. Additionally we included 7 differentiated thyroid cancer patients (mean age: 61 ± 7 years) who underwent RAI therapy (average of RAI dose: $26,04 \pm 12,8$ GBq) and who had PSMA PET for staging. Background corrected SUV_{max} values of parotid glands, submandibular glands, lacrimal glands, kidneys, liver and spleen

were obtained from initial and posttherapy PSMA PET/CT images of prostate cancer patients and average ratios of tissue/liver SUVmax were calculated and compared with each other by using wilcoxon matched pair test. Additionally, background corrected SUVmax values of aforementioned tissues were obtained from PSMA PET/CT images of thyroid cancer patients and calculated ratios of tissue SUVmax/liver SUVmax . **Results:** The most difference in ratio was seen in lacrimal glands [(Right(R)gland=Before Therapy(BT): 1.02± 0.56-After Therapy(AT): 0.68±0.27,p: 0,01);(Left(L)gland :BT: 0,93±0,41-AT:0,66 ±0,33,p:0.004)] and followed by parotid [(R= BT:1.53±0.62- AF:1.17 ± 0.46,p:0.02);(L= BT: 1.36±0.52 - AT: 1.05±0.37, p: 0.014)] and submandibular glands [(R= BT: 1.69±0.8- AT: 1.38±0.57,p: 0,048);(L=BT: 1.59 ±0.7-AT: 1.29±0.47,p:0.022)].No significant difference was shown in spleen [BT: 1.03±0.31 - AT: 0.94±0.32,p: 0.248] and kidneys [(R= BT: 5.6±3.74 - AT : 5.94±3.05, p: 0.810);(L=BT: 4.97±2.1,AT: 5.48 ±2.35,p:0.248)]. Significant reduction of PSMA uptake were demonstrated in salivary and lacrimal glands of 7 thyroid cancer patients with the ratios of tissue/liver SUVmax [parotis glands (R:0.53;L:0.48),lacrimal glands (R : 0 , 6 7 ; L : 0 , 6 6) , s u b m a n d i b u l a r g l a n d s (R:0.87;L:0.89),spleen(0.71),kidneys (R:5.81;L:5.73)] **Conclusion:** Lu-177 PSMA and radioiodine show higher uptake in salivary glands and lacrimal glands . It seems that the most effected tissues are salivary glands and lacrimal glands after Lu177-PSMAi therapy. No significant differences were shown in spleen-kidneys . Moreover radioiodine therapy have serious effect on salivary and lacrimal glands.These results show that both therapies can cause lacrimal and salivary gland dysfunctions as xerostomia.

EP245

Biodistribution patterns of Lu177-DKFZ-PSMA617 and Ga68-DKFZ-PSMA11 in the same patient group

N. Yeyin¹, O. E. Sahin¹, B. Vatankulu¹, T. Toklu², E. Demirci³, A. Aygun¹, E. Karayel¹, H. Pehlivan¹, N. A. Selcuk², M. Ocak⁴, L. Kabasakal¹; ¹Department of Nuclear Medicine, Cerrahpasa Medical Faculty, Istanbul University, İstanbul, TURKEY, ²Department of Nuclear Medicine, Yeditepe University Medical School, İstanbul, TURKEY, ³Department of Nuclear Medicine, Sisli Etfal Training and Research Hospital, İstanbul, TURKEY, ⁴Department of Pharmaceutical Technology,Pharmacy Faculty,Istanbul University, İstanbul, TURKEY.

Aim: Prostate-specific membrane antigen (PSMA) is increasingly recognized as a novel target and 68-Ga-DKFZ-11 (68-Ga-PSMA) has been suggested as a novel tracer for detection of PCa relapses and metastasis. As a theranostic approach its counterpart Lu-177 labelled ligand Ga-68-DKFZ-617 have a potential role for the treatment of castration resistant prostate cancer. However, both agents have different biochemical structures and may have different biochemical distribution. The aim of the study was to compare the biodistribution of Ga-68-DKFZ-11 and Lu-177-DKFZ-617 in patients who underwent Lu-177-PSMA therapy and Ga-68-PSMA imaging. **Material and Method:** For this purpose 10 patients were included to the study. Organ and tissue uptakes of Lu-177-DKFZ-617 were calculated from whole body images obtained at 4, 24, 48 and 120 hour after administration. In order to calculate the activity taken up in the kidneys, liver, parotid glands and left parotid, ROIS were drawn. The geometric mean of anterior and posterior counts were determined through ROI analysis, after that background subtraction and attenuation correction were applied using patients Ga-68-PSMA PET/CT images taking into account. Organ thickness, body thickness and Hounsfield unites from Computed Tomography scan. Average uptake values of organs and lesions at mentioned times were calculated by using activity values per unit. Also average of background corrected SUVmax values of kidneys, liver, parotid glands, lacrimal glands,

metastatic lymph nodes (n=5) and bone metastases (n=9) were obtained from PET images. **Results:** Analysing the uptake rates, the highest values were observed in metastatic lymph nodes, followed by bone metastasis, lacrimal glands while low activity were observed in kidneys and liver. When it comes to SUVmax values, highest rates were obtained in kidneys (SUVmax:44.4), in lymph nodes (SUVmax:19.9), bone metastasis (SUVmax:15.9), parotid glands (SUVmax:11.6), liver (SUVmax:8.0) and lacrimal glands (SUVmax:6.2). **Conclusion:** Ga-68 PSMA-11 and Lu-177-PSMA-617 have substantial different bio-distribution patterns., In order to make a therapy plan as a theranostic approach and predicting the therapy response Ga-68-PSMA-11 PET/CT imaging should be interpreted cautiously.

EP246

68Ga-PSMA PET/CT in Biochemical Relapsed Prostate Cancer - Initial Experience

R. Silva^{1,2}, A. Abrunhosa², A. Figueiredo¹, Â. Cruz², A. Xavier², D. Barroca², M. Castelo Branco², J. Pedroso de Lima^{1,2}; ¹Centro Hospitalar e Universitário de Coimbra, Coimbra, PORTUGAL, ²Instituto de Ciências Nucleares Aplicadas à Saúde, Coimbra, PORTUGAL.

AIM: The role of positron emission tomography/computed tomography (PET/CT) in prostate cancer imaging, either with F18-Fluorocholine (F18-FCH) or 68Ga-prostate specific membrane antigen (Ga68-PSMA), is gaining prominence. Current imaging strategies, despite having progressed significantly, have limitations. In particular, they lack sensitivity in the detection of metastatic lymph nodes. 68Ga-PSMA PET/CT has shown encouraging results, particularly in biochemical recurrent disease. In this study we meant to evaluate 68Ga-PSMA PET/CT detection rate in biochemical relapsed prostate cancer. The influence of PSA values was also analysed. **MATERIAL AND METHODS:** The clinical charts of the 19 patients submitted to 68Ga-PSMA PET/CT scans performed until March 2016 were retrospectively reviewed. Four patients were excluded (3 were scanned for initial staging, and 1 initiated hormonal therapy before scanning). Fifteen prostate cancer patients in biochemical relapse were included (65.2±6.9, 55-74 years). According to the European Association of Urology guidelines, 12 patients were classified as high risk and 2 as low risk for biochemical recurrence (1 patient was not classified due to insufficient information). Seven patients were previously submitted to radical prostatectomy (RP), 2 to radiotherapy (RT) and 6 to both RP and RT. At the time of scanning the average PSA value was of 4.6 (±7.5, 0.1-25) ng/ml. Statistical analysis was performed using IBM[®] SPSS[®] Statistics, version 22. **RESULTS:** Globally, Ga68-PSMA PET/CT detected lesions in 11/15 (73.3%) patients. Not excluding other disease sites, local recurrence was detected in 1/15 (6.7%) patients, pelvic lymph node metastasis in 6/15 (40.0%), distant lymph node metastasis in 5/15 (33.3%) and bone lesions in 5/15 (33.3%). The average PSA values for 68Ga-PSMA PET/CT positive and negative patients was 5.8 (±8.5, 0.1-25) and 1.5 (±1.5, 0.19-2.87) ng/ml, respectively (p>0.05, Mann-Whitney U test). In total, distant disease (lymph node metastasis or bone lesions) was detected in 8/15 (53.3%) patients. The average PSA values for patients with local and distant disease was 2.0 (±1.8, 0.2-5.1) and 7 (±9.8, 01-25) ng/ml, respectively (p>0.05, Mann-Whitney U test). **CONCLUSION:** In our sample, Ga68-PSMA PET/CT detection rate in biochemical relapsed prostate cancer was 73.3%. Distant disease, either extra pelvic lymph node metastasis or bone lesions, was detected in 53.3% of cases, with profound implications in treatment strategy. PSA values did not allow the distinction between 68Ga-PSMA PET/CT positive and negative patients or between local and distant disease.

EP247**Early and Late Imaging of Choline PET/CT for the Detection of Prostatic Fossae Recurrences in Prostate Cancer with a Biochemical Failure (PSA < 2 ng/mL)**

L. Evangelista¹, M. Hodolic², M. Burei¹, E. Pizzirani³, G. Ramondo³, G. Saladini¹; ¹Nuclear Medicine and Molecular Imaging Unit, Veneto Institute of Oncology IOV - IRCCS, Padua, ITALY, ²Nuclear Medicine Research Department, IASON, Graz, AUSTRIA, ³Radiology Unit, Veneto Institute of Oncology IOV - IRCCS, Padua, ITALY.

Introduction: biochemical recurrence of disease represents a failure of treatment in patients with prostate cancer treated with radical prostatectomy. 18F-Choline (FCH) PET/CT is often used to detect the presence of recurrence, although its detection rate is poor in case of prostatic fossae relapse, particularly in those patients with a PSA < 2 ng/mL. The aim of the present study was to assess the improvement in the detection rate of FCH PET/CT in the prostatic fossae in patients with low PSA values. **Materials and methods:** from an Institutional database of 100 patients undergoing FCH PET/CT from 1st January to 31st March 2016, we selected those who performed an early scan for the detection of prostate fossae recurrences and had a PSA levels < 2 ng/mL at PET time. Thirteen patients met the inclusion criteria (median age: 74 years; range: 45-86 years). All patients underwent an early static (after 2 minutes from the FCH injection; 1 bed; 5 minutes/bed) and late whole-body (after 60 min from FCH injection; 7 beds; 3 minutes/bed) PET/CT acquisition. A correlation among PSA levels, PSA doubling time (PSAdt), PSA velocity (PSAvel) and early/late PET/CT findings were assessed by using non parametric test. A $p < 0,05$ was considered statistically significant. **Results:** the median PSA level, PSAdt and PSAvel at the time of FCH PET/CT were 0.53 ng/mL (0.12-1.9 ng/mL), 8.1 months (2-12.5 months) and 0.5 ng/mL/year (0-1.9 ng/mL/year), respectively. A significant uptake of FCH at the early images was reported and interpreted as a local recurrence of prostate cancer, in 3 patients. However, in these latter subjects, late images were hardly interpreted due to the presence of bladder and therefore considered as negative. Conversely, 10 patients had a negative FCH PET/CT scan, either in the early and late images. The median levels of PSA and PSAvel were significantly higher in patients with a positive early PET/CT scan as compared those with a negative scan (0.88 vs. 0.52 ng/mL and 1.1 vs. 0.45 ng/mL/year, respectively; both $p < 0.05$). On the contrary, the median value of PSAdt was similar between positive and negative early scan (7.9 vs. 8.6 months; $p = \text{not significant}$). **Conclusions:** from this preliminary analysis emerges that an early FCH PET/CT acquisition should be considered in patients with very low PSA levels (< 2 ng/mL), low PSAdt (< 8 months) and high PSAvel (> 1 ng/mL/year), particularly in case of suspicious for prostatic fossae recurrence. However, a prospective, large observational study is warranted for providing final considerations.

EP248**18FDG-PET/CT hypermetabolic renal bed granuloma post-nephrectomy mimicking local recurrence in renal cancer**

G. L. BRUNO, G. L. BRUNO; FCDN, Buenos Aires, ARGENTINA.

AIM: To raise awareness about the existence of renal bed inflammatory granulomas frequently found in studies of 18FDG-PET/CT after post-surgical nephrectomy for kidney cancer, and try to avoid misinterpretation as local recurrence. **MATERIALS AND METHODS:** Retrospective study, were it was included and analyzed 20 patients between January 2009 and March 2016 with ages ranging between 36 and 78 years, who underwent radical nephrectomy for renal cancer and 18FDG-PET/CT post-surgically study, either as part of monitoring the disease or for other reasons. The patients presented as the only positive finding related to the disease, the presence of a hypermetabolic pseudonodular solid image in

the renal bed. Then the patients underwent biopsy/surgery or clinical follow-up and or conventional diagnostic methods or reexamination with 18FDG-PET/CT. All 18FDG-PET/CT studies were performed on a GE Discovery STE 16, between 4-151 months after surgery. The findings are described and correlated chronologically. **RESULTS:** The 20 patients selected, presented hypermetabolic pseudonodular solid images in the renal bed, 9 (45%) right-sided and 11 (55%) left-sided, respectively. Of these, 4 patients (20%) underwent confirmatory surgery for local recurrences, showing SUVmax values greater than 5, with an average size of 41.2 mm in diameter. The remaining 80 % (n= 16) patients presented SUVmax values between 1.2 and 6.7 and average size of 15.8 mm in diameter which was statistically significant ($p = 0.0004$). These patients were followed by clinical and/or conventional diagnostic method; and also some of them underwent 2 or more 18FDG-PET/CT studies showing decreased metabolic activity among subsequence studies, which were interpreted as granulomas. **CONCLUSION:** Post-nefrectomia inflammatory granuloma is a frequently false positive finding in 18FDG-PET/CT studies during restaging of renal cancer. They are usually difficult to characterized, whether morphologic or metabolically, being often misinterpreted as local recurrence. In our experience it is important to emphasize that lesions less or equal than 15mm in diameter were statistically significant and could guide the diagnosis of inflammatory granulomas, whereas the SUVmax values were not relevant. It may be important to keep in mind these results to avoid misdiagnosis and even sometimes, biopsies and/or unnecessary surgery.

EP249**Value of 18F-FDG PET/CT in patients with castration resistant prostate cancer**

M. Grmek, S. Hawlina, L. Lezaic; University Medical Centre Ljubljana, LJUBLJANA, SLOVENIA.

Different nuclear medicine investigations are used in patients with prostate cancer. The primary diagnostic investigations to evaluate disease progression in patients with castration resistant prostate cancer (CRPC) are bone scan, CT of thorax and abdomen. **The aim** of the study is to find out the value of 18F-FDG PET/CT in patients diagnosed with castration resistant prostate cancer. **Patients and methods:** 16 men having CRPC were included in the study. 14 men had Gleason score 9, one Gleason score 8 and one 7. Patients were on average 75 ± 5 years old. In all patients we performed initial 18F-choline PET/CT study followed by 18F-FDG PET/CT study within one week. After 108 ± 12 days we performed control 18F-choline PET/CT study followed by 18F-FDG PET/CT study. Injected activity per study was 2,5 MBq/kg of body weight for 18F-choline and 4 MBq/kg of body weight for 18F-FDG. Acquisition on PET/CT (Siemens, Biograph mCT) started 45 minutes after 18F-choline administration and 1 hour after 18F-FDG administration. A low dose CT scan followed by PET acquisition (two minutes per bed position with 45% overlap) was used. The results of the initial 18F-choline and 18F-FDG study were compared with the follow-up studies and classified in 3 groups - stable, slowly progressive and rapidly progressive disease. Each patient was classified as; Stable, if no new lesions suspected for prostatic cancer metastases were detected or if SUV max wasn't increased more than 25% in any of already known metastases; Slow progress, if combined number of new lesions suspected for metastases and already known metastases with SUV max increase of more than 25% was between one and three; Rapid progress, if combined number of new lesions suspected for metastases and already known metastases with SUV max increase of more than 25% was four or more. **Results:** Initial 18F-choline PET/CT study showed metastases in 12 of 16 patients and initial 18F-FDG PET/CT study in 6 of 16 patients. Results of disease progression are presented in the table. **Conclusion:** 18F-choline PET/CT study is more sensitive than 18F-FDG PET/CT study for metastasis detection in patients having CRPC. However, accuracy to detect patients in whom disease will progress was higher for 18F-FDG PET/CT study. Therefore we suggest that 18F-FDG PET/CT study should be used in therapy planning and follow up of patients with CRPC in addition to 18F-choline PET/CT.

EP250**18F-Choline PET-CT findings in prostate cancer recurrence and treatment modality**

L. Mohamed Salem, Sr., A. Abella Tarazona, M. Ibañez Ibañez, V. Godoy Bravo, R. Reyes Marles1, I. Sime Loayza, J. Navarro Fernandez, L. Frutos Esteban, M. Castellón Sanchez, F. Nicolas Ruiz, P. López Cubillana, F. López Soler, P. López González, M. Porras martinez, M. Claver Valderas; Hospital Clínico Universitario Virgen de la Arrixaca, Murcia, SPAIN.

AIM: To evaluate the relationship between the 18F-Choline PET-CT findings and treatment method in patients with prostate cancer recurrence after treatment with curative intent and the association between the PSA level and the detection rate. **MATERIALS AND METHODS:** Together with Urology and Oncological Radiotherapy departments of our Hospital, we study retrospectively 100 patients with prostate cancer (PCa) with biochemical relapse after treatment with curative intent, radical prostatectomy or external radiotherapy and negative conventional imaging techniques, all patients underwent a bone scan and a new determination of PSA level, if they had not one during the last month, PET-CT scan was carried out after I.V. injection of 4 MBq/Kg of 18F-Choline with acquisition of a pelvic bed one minute and a whole body PET-CT 60 minutes after injection. We analyze the association between the treatment method, radical prostatectomy or external radiation therapy (we excluded patients who had both modalities or brachytherapy) and 18F-Choline PET-CT findings in terms of the type of recurrence, whether it is only local or distant with or without local recurrence, as well as the PSA level and the detection rate. **RESULTS:** Mean PSA is 12,9213 ng/ml, median is 5,5100 ng/ml. 73 patients had a positive scan and 27 patients had a negative scan. Median PSA value was 3 in patients with negative scan and 7.83 in patients with positive one, comparing positive and negative scans according to PSA value, we find strong relationship between PSA value and positive 18F-Choline PET-CT scan, the association is statistically significant $P = 0.001$, the higher the PSA level is, the higher is the probability to have a positive scan. 32 of 38 (84,21%) patients who was treated by only external radiotherapy, had positive scan. 12 of 24 (50%) patients who was treated by only surgery (radical prostatectomy), had positive scan. 45 patients of 73 had local recurrence, which is 61,64% of patients with positive scan. **CONCLUSION:** There is a strong correlation between PSA level and the probability to have a positive 18F-Choline PET-CT scan. There is more recurrence among patients treated with external radiotherapy, than radical prostatectomy. The most frequent recurrence type is local recurrence.

EP251**Dual-Time Point Evaluation of Prostate Cancer Lesions detected by ⁶⁸Ga-PSMA PET/CT**

L. Sobral Violante, I. Sampaio, J. Teixeira, G. Ferreira, H. Duarte; Instituto Português de Oncologia, Porto, PORTUGAL.

Aim: The importance of dual-time point imaging has been described in several studies using ¹⁸F-FDG PET/CT. The aim of this study was to evaluate maximum standardized uptake value variation (Δ SUVmax) percentage in malignant lesions detected by ⁶⁸Ga-PSMA PET/CT in initial and late images and also to evaluate the clinical significance of this parameter. **Methods:** We performed a retrospective analysis on 44 consecutive patients (median age 70±6.7 years) who underwent ⁶⁸Ga-PSMA PET/CT between October 2015 and April 2016. Clinical indication was biochemical recurrence in the majority of cases (42 patients) and staging (2 patients). Mean prostate-specific antigen (PSA) level was 18.7±32.2 ng/ml ranging from 0.4 to 144.6 ng/ml. Gleason score (GSC) range was 6-9. Inclusion criteria: patients with pelvic recurrence/metastasis detected on ⁶⁸Ga-PSMA PET/CT and confirmed by histology or clinical follow-up. Pelvic region lesions were evaluated in two time points for

Δ SUVmax calculation: in the initial imaging (5 minutes bed immediately after radiotracer injection) and in whole-body imaging (acquired approximately 60 minutes post injection). **Results:** In 26 patients (59.1%) at least one lesion indicative of prostate cancer recurrence or pelvic metastasis was detected in ⁶⁸Ga-PSMA PET/CT scan. From those, 2 patients were excluded due to bladder interference in quantification and lack of histological/clinical confirmation, respectively. In the remaining 24 patients, a total of 27 focal lesions were detected in ⁶⁸Ga-PSMA PET/CT (16 prostatic bed/region; 8 lymph node; 2 bone; 1 seminal vesicle lesion) with an average SUVmax value of 6.6 (2.9-16.7) in the initial images and 13.5 (4.0-45.9) in the late images. Δ SUVmax Percentage Mean: prostate= 98.4% (22.1%-320.0%); lymph node=81.1% (9.1%-175.8%); bone= 108.8% (71.3%-146.4%). The seminal vesicle lesion SUVmax did not vary with acquisition time. **Conclusion:** The majority of lesions (96.3%) increased their uptake between initial and late acquisitions. These preliminary data suggests that ⁶⁸Ga-PSMA dual-time point imaging improves identification of local recurrent disease/ metastasis in prostate cancer disease. Further research is necessary to confirm these results.

EP252**Detection of primary and metastatic lesions of urinary tract tumors by ¹⁸F-FLT PET/CT**

K. Kato¹, Y. Koshiba¹, K. Kunimoto¹, M. Honda¹, A. Murai¹, S. Abe², T. Odagawa¹, S. Naganawa¹; ¹Nagoya University Graduate School of Medicine, Nagoya, JAPAN, ²Nagoya University Hospital, Nagoya, JAPAN.

Purpose: The aim of this study is to investigate the efficacy of ¹⁸F-FLT PET/CT for detection of primary and metastatic lesions of urinary tract tumors. **Methods:** Twenty-two (16 men, 6 women) patients were examined by ¹⁸F-FLT PET/CT (Siemens Biograph 16). All the patients received surgical operation or biopsy and the tumor was diagnosed histopathologically. **Results:** In 22 patients examined by ¹⁸F-FLT PET/CT, 13 were confirmed histopathologically to be urothelial cell carcinoma, 6 renal cell carcinoma, 2 retroperitoneal liposarcoma, and 1 bladder carcinoma. Five patients had lung metastases, 2 had lymph node metastases, and 1 had gallbladder cancer synchronously. In 7 of the 13 patients with urothelial carcinoma and 1 with bladder carcinoma, the primary tumor could not be detected due to retention of urine in the ureter and urinary excretion of ¹⁸F-FLT. In the other 6 patient with urothelial cell carcinoma, 2 with retroperitoneal liposarcoma, and 1 with renal cell carcinoma, the primary tumor could be detected due to lack of urinary excretion of ¹⁸F-FLT by renal insufficiency. ¹⁸F-FLT uptake in the tumor site expressed as SUVmax in ¹⁸F-FLT PET was 2.17-28.99 (mean±S.D. 8.51±11.50) in urothelial cancer, 1.65 in renal cell carcinoma, and 9.35 and 4.24 (6.8±3.61) in retroperitoneal liposarcoma. Lung metastases after nephrectomy for renal cell carcinoma in 5 patients could be detected (SUVmax: 3.24-6.44 (4.45±1.13)). Lymph node metastases in 5 patients also could be detected (SUVmax:2.16-6.35 (4.45±1.73)). **Conclusion:** Usually, ¹⁸F-FLT PET/CT is not suitable for detection of the primary lesions of urinary tract tumors because of its urinary excretion, whereas their metastatic lesions can be detected by ¹⁸F-FLT PET/CT. Nevertheless, in patients whose urinary excretion of ¹⁸F-FLT is disturbed by renal failures, ¹⁸F-FLT PET/CT is useful for detection of the primary lesions of urinary tract tumors.

EP253**C11-choline PET/CT is an effective tool in prostate cancer diagnosis**

I. Garai¹, A. Káplár¹, B. Farkas¹, C. Bercez²; ¹ScanoMed Ltd, University of Debrecen, Debrecen, HUNGARY, ²Department of Urology, University of Debrecen, Debrecen, HUNGARY.

C11 choline PET/CT is a sensitive method to reveal the early recurrence or metastatic spreading of prostatic cancer. C11 choline PET/CT has been introduced in human care since 2014 in Hungary. The aim of this study was to evaluate our experience with C11 choline. **Patients and Method:** We performed C11 choline PET/CT examinations on 97 patients and analysed the results retrospectively. We grouped the patients based on the primary indications. The groups were as follows: 1. screening (15 patients), 2. primary staging (16 patients) and 3. restaging (66 patients). 700-850 MBq C11 Choline was injected iv. and acquisition was started 5 minutes later with 120 sec./frame using Philips Gemini 64/Tof PET/CT camera from the mid thigh to the base of the skull. Low dose CT was also done (120 keV, 150mAs) for attenuation correction and anatomical localisation. We evaluated our results based on clinical data collected from the patients' medical history. **Results:** In the screening group, we found focal intense choline uptake in the prostate only in 3 cases and the biopsy proved malignancy in those cases. However in some cases, diffused uptake in the prostate caused uncertainty in the diagnosis. Metastasis was absent in this group. In the primary staging group the primary tumor was revealed in all cases on choline PET/CT in the same sites as MRI. Mean SUVmax was 7.4 in the primary lesion. However, the disease was upstaged in 7 cases due to lymphatic and bone metastasis. In the restaging group we classified patients based on sePSA level into three subgroups. Subgroup 1 had 16 patients with PSA <1 ng/ml and there was no pathological uptake. Subgroup 2 had 12 patients with PSA 1-2 ng/ml and in 4 cases showed disease recurrence. Subgroup 3 had 38 patients with PSA > 2 ng/ml and 27 cases showed choline positivity. We found a significant correlation between the choline positivity and PSA level. C11 choline PET/CT is an effective diagnostic method especially in restaging of prostatic cancer in cases of biochemical failure. Furthermore, it can provide additional information in primary staging too.

EP254

The Burden of Castrate-Resistant Prostate Cancer: Making a Case for PSMA Targeted Therapy in Southwest Nigeria

Y. A. Onimode^{1,2}, A. T. Orunmuyi^{1,2}, B. O. A. OSIFO²; ¹University of Ibadan, Ibadan, NIGERIA, ²Nuclear Medicine Centre, University College Hospital, Ibadan, NIGERIA.

Introduction: Prostate cancer (PC) is the leading male cancer in Nigeria, with an age-specific incidence rate of 62.35 per 100 000 men. The mean age of diagnosis of cancer in Nigerian men is 50.5 years. Globally, PC is said to be the fifth most common cancer, with a prevalence of 3.2 million. Lu-177-PSMA targeted therapy has recently become available for the treatment of CP. Prostate-specific membrane antigen (PSMA) is an ideal target in management of prostate cancer, which is overexpressed in metastatic PC and (castrate-resistant prostate cancer) CRP. However, Lu-177 PSMA is presently unavailable in Nigeria. **Aim:** To determine the prevalence of castrate-resistant prostate cancer (CRP) patients presenting for bone scintigraphy, to assess bone scan (BS) findings, and make a case for government and private sector provision of PSMA-therapy facilities. **Materials and Methods:** A retrospective review of Tc-99m hydroxymethylene diphosphonate (HMDP) bone scans for PC from 2013-2015 at a tertiary NM facility in South-West Nigeria. **Results:** Of 372 BS, 199 (53.4%) were for patients on anti-androgen therapy (AAT), aged 45 - 87 years. 121 BS showed metastases (60.8%), 30 had suspicious lesions (15.1%), three had metastatic and suspicious lesions (1.5%), while 45 (22.6%) had normal scans. Metastases were most common in the axial skeleton (50.4%), then the lower limbs (23.5%) and upper limbs (16.6%). A significant association was found between type of AAT (medical, surgical or combined) and BS outcome ($p=0.003$). No significant association was found between BS findings and type of treatment 1 (AAT/prostatectomy/adjunct or combination), between PSA level and duration of AAT, nor between age and bone scan findings. **Conclusion:** Of 199 BS for CRP patients, 61% had metastases despite AAT, of which 63.6% were extensive in nature, mainly involving the axial skeleton. Findings thus suggest that CRP is common among PC patients, and that a potential population exists for Lu-177 PSMA therapy in these patients. 2

EP255

Impact of 18F-Choline PET-CT on the selection of patients with oligometastatic prostate cancer recurrence candidates for local salvage treatments

I. L. Fernandez-Tercero, A. Gomez-Iturriaga, A. Sanchez-Salmon, F. Casquero, A. Urresola, A. I. Ezquerro, R. Llaraena, E. Rodeño; Cruces University Hospital, Baracaldo(Bizkaia), SPAIN.

Purpose: Patients with oligometastatic prostate cancer detected by (18F)-Choline PET-CT (Ch-PET) may benefit from targeted high-dose irradiation of the pathologic choline uptake sites associated with a short course of Androgen Deprivation Therapy (ADT). The objective of this study was to select candidates for salvage treatment of oligometastatic prostate cancer recurrence by Ch-PET. **Methods:** From 2013 to 2015, 30 consecutive prostate cancer patients diagnosed with oligometastatic-recurrence on Ch-PET have been prospectively treated. The recurrence occurred after radical prostatectomy in 22 (74%) patients, after radiotherapy(+/-ADT) in 7 (13%), and after cryotherapy in 1(3%) patient. All patients underwent pelvic multiparametric Magnetic Resonance Imaging to assess local failure. All Ch-PET-CT (contrast enhanced) were reviewed by two independent physicians. There was not biopsy confirmation of the pathologic choline uptakes. All patients with biochemical failure after salvage treatment were re-staged by Ch-PET scan. **Results:** Median follow-up was 12 months (range 8-26). The median prePET PSA was 3.96 ng/ml (1.51-36.4) and median prePET PSA-doubling-time was 4.5 months (1-47.4). Ch-PET showed pathologic uptake consistent with recurrence in lymph-nodes in 24 (80%) patients, bone in 4 (14%) patients, bone and nodes in 1 (3%) patient, and bone and prostate in 1 (3%) patient. A total of 64 lesions have been treated. The treatments administered to the initial oligo-recurrence uptakes were Intensity-Modulated-Therapy (IMRT) +/- ADT (23 patients; 77%) and Stereotactic- Body-Radiation (SABR) +/- ADT (7 patients; 23%). ADT was administered for no longer than 6 months in 18 patients. At last follow-up, 18 patients are free from biochemical failure and 12 patients showed biochemical failure. Median time to biochemical failure from first salvage treatment was 8 months (2-14). Four (30%) (3 nodal, 1 bone) out of the 12 patients with biochemical failure presented on a repeated Ch-PET oligometastatic disease, and were treated with a second salvage treatment (1 IMRT, 3 SABR). Two of them, are free from biochemical failure at last follow-up. Seven (58%) out of the 12 patients with biochemical failure developed progression on a repeated Ch-PET scan, and in one of them, macroscopic recurrence was not found. **Conclusion:** Early detection of oligometastatic prostate cancer recurrences with Ch-PET allows guiding local salvage radiation treatments. Follow up with Ch-PET in patients with biochemical failure detects subsequent oligometastatic recurrences suitable for further salvage treatment

EP256

qPET Distribution in Prostate, Lymphonodular and Skeletal FCH-PET Positivities in Biological Relapse of Prostate Carcinoma

c. Olianti¹, M. Di Russo¹, I. Laghai¹, M. R. Raspolini², F. Sessa³, A. Minervini³; ¹Nuclear Medicine Unit, FLORENCE, ITALY, ²Pathologic Histology Unit, FLORENCE, ITALY, ³Clinic Urology Unit, FLORENCE, ITALY.

We retrospectively evaluated 100 male asymptomatic patients [median age : 75 y - range : 54-91 y; PSA (ng/ml) median : 2,3 ; range: 0,13 - 203] with biological relapse of prostate carcinoma undergone to FluoroCholine-Positron Emission Tomography (FCH-PET). Of them 43 pts. (43%) had negative FCH-PET and 57 pts. (57%) had positive FCH-PET , on prostate 28% (P), lymph nodes 43% (LN) and bone 29% (SK). For each FCH-positivities we extracted qPet 3D value by an automatic selection of Voxel with highest SUV and subsequent extraction of mean SUV in a 4 voxel VOI around the highest SUV. Analysis of variance found significant differences

in qPet SUV mean VOI values (qPet) among P (mean +/- SD: 7.4 +/- 3.4), LN (mean +/- SD: 5.4 +/- 2.4) and SK (mean +/- SD: 4.2 +/- 2.5) positivities, $p < 0.001$ among all groups; Post Hoc test HSD di Tukey found significant differences between SK and Ln qPet with $p < 0.05$, between SK and P qPet with $p < 0.001$, between Ln and P qPet with $p < 0.02$. We also found on the basis of FCH-PET results a significative difference in mean PSA of patients with FCH-Pet positive and patients with FCH-Pet negative) non parametric test of Kolmogorov - Smirnov $Z = 2,8$; $p < 0.001$. RocAnalysis found a PSA cutoff-value between positive and negative FCH-Pet results corresponding to 2.845 ng/ml with a sensibility of 67 %, specificity of 80% and accuracy of 73%; VPP = 80 %; VPN = 67 %. We conclude that a qPet value seems correlated to a more FCH-expression in local relapse, than in LN and SK metastasis. Also PSA, as note in literature, is and useful index of presence of disease relapse or metastatic illness.

EP257

Computer-assisted analysis of skeletal lesions in the staging of prostate cancer: Prospective multicenter study

L. J. Petersen¹, J. C. Mortensen², H. Bertelsen¹, H. D. Zacho¹; ¹Aalborg University Hospital, Aalborg, DENMARK, ²Regional Hospital West Jutland, Herning, DENMARK.

Aim The purpose of this study was to compare the diagnostic properties of EXINI Bone^{BSI} versus expert reading in the initial bone metastasis staging in prostate cancer. **Materials and Methods** Bone scintigraphy was performed in 342 consecutive patients referred for the staging of newly diagnosed prostate cancer in a multi-center trial. The bone scan index (BSI) and the number of malignant lesions (hot spots) was calculated by EXINI Bone^{BSI}. Three imaging experts independently classified bone status by a dichotomous outcome (M1 for bone metastasis, M0 for no bone metastasis). **Results** The diagnostic characteristics of BSI>0/BSI=0 versus expert M1/M0 classification showed excellent sensitivity and negative predictive value (NPV) (96 - 98 %) but low to modest specificity (38 %) and low positive predictive value (PPV) (21 %). A BSI value of 0.3 was identified as the optimal diagnostic cut off by which sensitivity was 88 %, specificity 86 %, PPV 51 %, and NPV 98 %. Stratification based on individual risk classification did not improve the diagnostic performance of the software. A subgroup of patients were classified as true M0 (n=130) or M1 (n=12) based on supplementary imaging and/or clinical follow up. The software incorrectly showed malignant lesions in 64 % of the M0 patients but correctly identified malignant skeletal lesions in all M1 patients. **Conclusion** EXINI Bone^{BSI} presented excellent sensitivity and NPV, but specificity was modest, and PPV was low to modest. The diagnostic value of EXINI Bone^{BSI} in staging of newly diagnosed prostate cancer is limited.

EP258

The importance of whole body PET/CT with 18F-Choline in detecting unsuspected brain lesions in patients with prostatic cancer

L. Massi¹, A. Franceschetto¹, V. Rossetti¹, A. Bruni², F. Lohr², N. Prandini¹; ¹Nuclear Medicine, Modena, ITALY, ²Radiation Oncology, Modena, ITALY.

Aims: 18F-Choline (FCH) PET/CT is routinely performed in patients with biochemical relapse of prostate cancer. The PET/CT scan is usually performed from base of the skull to mid thigh. In this study we report our experience of PET/CT whole body scan, including the skull vertex, looking for brain metastases from prostate cancer. **Materials and Methods:** A total of 485 whole body 18F-CH PET/CT in patients with prostatic cancer and biochemical recurrence were performed from January 2013 to December 2015. All the patients were i.v. injected with 3.7 MBq/Kg of 18F-CH and immediately underwent to a PET/CT scan of the pelvis: 50 minutes later a PET/CT whole body scan including the head vertex was obtained. In five patients a focal brain uptake of 18F-CH was found. In 2 patients the FCH uptake was in sella turcica, in 1 patient was

in left corpus callosum region, in 1 patient in the left frontal region and in 1 patient in fronto-parietal bilateral regions. Results: All 5 patients were studied by brain MRI: in two of them an histological examination of the lesions was obtained whereas the remaining 3 patients underwent to a clinical and instrumental management. The final diagnosis was of two meningiomas and two pituitary adenomas (one resulted a prolactinoma at biopsy). The patient with prolactinoma was treated with medical therapy with subsequent reduction of the lesion at MRI imaging. The fifth patient had an uptake of 18F-CH in the left side of corpus callosum without other pathological uptake in the body; the MRI showed a cystic-necrotic parasagittal lesion (diameter of about 3 cm) with a compression in the frontal horn of the lateral ventricle with deviation of septum pellucidum suspected for an high grade glioma. The subsequent brain stereotactic biopsy has demonstrated a metastasis of prostatic adenocarcinoma. The lesion was then treated with stereotactic ablative radiotherapy. Conclusions: In the normal brain parenchyma FCH uptake is low. The inclusion of the brain study in 18F-CH PET/CT can detect unknown brain lesions, which sometimes are the only secondary localization of prostatic cancer.

EP259

Detection of bone metastases in patients with PSA progression: comparison [18F]Choline PET/CT with bone scintigraphy; our experience

M. Grivet Fojaja¹, B. Carabellese¹, M. Lago¹, F. Scarabeo², G. Giglio³; ¹Nuclear Medicine department "A.Cardarelli" Hospital, Campobasso, ITALY, ²Diagnostic Imaging department "A.Cardarelli" Hospital, Campobasso, ITALY, ³Oncology department "A.Cardarelli" Hospital, Campobasso, ITALY.

AIM: The purpose of this study was to evaluate the clinical usefulness of [18F]choline positron emission tomography PET/CT in comparison with bone scintigraphy (BS) in detecting bone metastases (BM) of patients with biochemical progression after radical treatment for prostate cancer. **MATERIALS AND METHODS:** 27 consecutive patients (mean age 74 years; range 56-84) with a biochemical relapse after radical prostatectomy were included in our retrospective study. These patients underwent a both [18F]Choline PET/CT and bone scintigraphy (BS) for restaging (range: 1 week to 8 months; mean: 3 months). The imaging were retrospectively analyzed using morphological and/or follow-up imaging as standards of reference. Validation of positive results for bone metastasis was established by a positive subsequent BS and/or 18F-choline PET/CT, and a normalization of 18F-choline bone uptake after systemic therapy. **RESULTS:** in 19/27 patients positive bone disease were found, both on [18F]Choline PET/CT and on BS; equivocal findings occurred in 2/27 patients on 18F-choline PET/CT, no equivocal finding occurred on BS; 6/27 negative patients for bone metastasis were findings on [18F]Choline PET/CT; in 8/27 patients negative bone disease on BS were findings. [18F]Choline PET/CT findings 164 bone metastatic localization vs 123 bone metastatic localization findings with BS. Concordant findings between [18F]Choline PET/CT and BS occurred in 20 of 27 (74%). Concordance rate for negative metastatic bone disease was 75%; concordance rate for positive metastatic bone disease was 84%. Sensitivity and specificity for [18F]Choline PET/CT and BS were 86%, 83% and 95%, 77%, respectively. For 3/27 patients (11%), with biochemical progression, BS and [18F]Choline PET/CT were negative ([18F]Choline PET/CT for no bone lesions too). For 2/27 patients (7%), with biochemical progression, BS and [18F]Choline PET/CT were negative for bone lesions but positive on [18F]Choline PET/CT for no bone lesions (lymphnodes and local recurrence) **CONCLUSION:** In clinical practice, [18F]Choline PET/CT may not replace BS because of its lower sensitivity. However, for its high specificity, [18F]Choline PET/CT, positive findings may accurately predict presence of bone metastasis. Also, there where the negativity for bone metastases does not explain the increased laboratory data, [18F]Choline PET/CT allows simultaneously the parenchyma and lymphnodes evaluation.

EP260**Is there a Role for 68-GaDOTATOC PET/CT in renal cell carcinoma? Our preliminary experience**

L. Locantore, D. Grigolato, M. Zuffante, M. Cucca, F. Sciumè, M. Ferdeghini; Nuclear Medicine Unit, University Hospital of Verona, Verona, ITALY.

Background/Aim: Renal cell carcinoma (RCC) may be a target for somatostatin receptor (SSTR) imaging, due to the reported SSTRs expression. Moreover, most of RCC are not 18F-FDG avid. PET/CT using 68Ga-labelled DOTA0-Tyr3 octreotide (DOTATOC) is one of the diagnostic imaging tools in SSTR imaging. We assessed if DOTATOC PET/CT could be helpful in patients with recurrent or metastatic RCC. **Patients/Methods:** Five consecutive patients (mean age 61.5 years, range 52-71) who had surgery for RCC, underwent 68Ga-DOTATOC PET/CT due to suspicion of recurrent/ metastatic lesions. Suspected relapse occurred at a median of 10 years after surgery. 68Ga-DOTATOC PET/CT was performed after contrast-enhanced CT (ceCT) scan; four patients also underwent 18F-FDG PET/CT (FDG) prior to 68Ga-DOTATOC PET/CT scan. Images were acquired 1 hour after 68Ga-DOTATOC intravenous administration with a PET/CT Philips Gemini TF Big Bore scanner (3 minutes/bed position, from skull-vertex to mid-thigh level). Images were analyzed both qualitatively and semiquantitatively (SUVmax). Results were compared both to ceCT and FDG PET/CT findings. Clinical and radiological follow-up data were also assessed. **Results:** 68Ga-DOTATOC PET/CT was positive in 3 patients, confirming disease in pancreas (=2) and lung (=1). Two patients had 68Ga-DOTATOC PET/CT scan negative (lung was the site of CT suspected recurrence). No uncertain results were found. SUV max of the lesions ranged from 4.3 to 19 (mean 9). In one patient an additional site of possible recurrent disease (parotid gland) was found. Compared to 18F-FDG PET/CT results, 2/4 patients were positive at 68Ga-DOTATOC PET/CT but negative at FDG scan (1 lung and 1 pancreas); 1 patient was classified as positive at DOTATOC but indeterminate at FDG (lung). One patient had both FDG and DOTATOC PET/CT scan negative (lung). Totally, 3/4 patients had FDG negative scan; in one case FDG results were rated as doubtful. 68Ga-DOTATOC PET/CT findings changed patients management in 4/5 cases. In patients candidate to surgery, histologic evaluation confirmed RCC origin in 100% of the lesions. One patient with negative DOTATOC underwent cytologic examination (lung), with negative results (1 year radiologic follow-up showed lesion stability, referable to non-neoplastic aetiology). **Conclusions:** At this time, experience with DOTATOC PET/CT in RCC is limited. When inconclusive findings are obtained by conventional imaging, 68Ga-DOTATOC PET/CT could be useful for confirming or excluding renal origin of the lesions. Thus, in our patient population the use of DOTATOC PET/CT led to a more accurate staging, impacting patients treatment-decision making.

EP-14 – Sunday, October 16, 2016, during Exhibition hours, e-Poster Area
Clinical Oncology: Prostate 2

EP261**Automated Bone Scan Index as an imaging biomarker to predict outcome in the Zeus/SPCG11 study**

M. Reza¹, M. Wirth², T. Tammela³, V. Cicaese⁴, F. Gomez Veiga⁵, P. Mulders⁶, K. Miller⁷, A. Tubaro⁸, F. Debryne⁹, A. Patel¹⁰, C. Caris¹¹, W. Witjes¹¹, O. Thorsson¹, P. Wollmer¹, L. Edenbrandt¹; ¹Department of Clinical physiology and nuclear medicine, Skåne university hospital, Malmö, Malmö, SWEDEN, ²University Clinic Carl Gustav Carus, Urology, Dresden, GERMANY, ³Tampere University Hospital and University of Tampere, Urology, Tampere, FINLAND, ⁴Azienda Ospedaliera "S. Giuseppe

Moscato", Urology, Avellino, ITALY, ⁵A Coruña University Hospital, Urology, A Coruña, SPAIN, ⁶Department of Urology, Radboud University, Nijmegen Medical Centre, Nijmegen, NETHERLANDS, ⁷Charité, Universitätsmedizin, Urology, Berlin, GERMANY, ⁸Sant'Andrea Hospital", Urology, Rome, ITALY, ⁹Andros Clinic, Urology, Arnhem, NETHERLANDS, ¹⁰Royal London Hospital At Bartshealth Nhs Trust, Urology, London, UNITED KINGDOM, ¹¹European Association of Urology, Research Foundation (EAU RF), Arnhem, NETHERLANDS.

Background: The Zeus/SPCG11 study is a randomized controlled clinical trial with the aim to assess the efficacy of zoledronic acid (ZA) in preventing bone metastases in high-risk prostate cancer (PCa) patients. Automated Bone Scan Index (aBSI) reflects the tumour burden in bone calculated from bone scintigraphy, and has recently been validated as an imaging biomarker in metastatic PCa patients. The purpose of this study was to investigate if change in aBSI during treatment may serve as a useful imaging biomarker to predict clinical outcome in the Zeus/SPCG11 study population. **Methods:** We retrospectively selected as our aBSI-study group all patients with bone scan image data of sufficient quality to allow for both baseline and 48-months follow-up aBSI-assessments. aBSI data from the resulting cohort was later obtained by using the automated quantification software EXINI bone^{BSI}, in a blind fashion, without knowledge of any clinical data or treatment randomization. Clinical data on age, overall survival (OS) and prostate-specific antigen (PSA) concentration in blood at baseline and upon follow-up was collected separately. Association between clinical data and aBSI-change during treatment was evaluated using Cox proportional-hazards regression models, Kaplan-Meier estimates of the survival function and Log rank test. Discrimination between prognostic variables was assessed using the concordance index (C-index). **Results:** From a total of 1,433 high-risk PCa patients who participated in the Zeus/SPCG11 study, 176 fulfilled the inclusion criteria. The patient-characteristics of the aBSI-study group (n=176) showed baseline characteristics similar to those of the final total Zeus study population ($p=0.83$). In our aBSI-study cohort (N=176), patients with a aBSI-change ≤ 0.3 had a significantly longer median survival time compared to patients with aBSI-change of > 0.3 (32.3 months and 18.2 months respectively) ($p < 0.001$). In the Cox analysis aBSI-change from baseline to follow-up was significantly associated with OS ($p < 0.01$ and C-index=0.6) while age and PSA change were not significantly associated with OS. **Conclusions:** aBSI-change during treatment was associated with OS in high-risk PCa patients from the Zeus/SPCG11 study. aBSI may be a useful imaging biomarker in future clinical trials involving PCa patients with bone metastases.

EP262**18F-choline PET/CT physiological distribution and pitfalls: a multicenter Southern Italian experience on 1000 patients examined for Prostate Cancer**

F. CALABRIA¹, A. Chiaravallotti², C. Ciccio³, V. Gangemi⁴, G. L. Cascini⁴, O. Schillaci^{2,5}; ¹IBFM Italian National Research Council - PET/MRI Unit., Catanzaro, ITALY, ²Department of Biomedicine and Prevention, University "Tor Vergata", Rome, ITALY, ³Department of Diagnostic Imaging, Sacro Cuore Hospital "Don Calabria", Verona, ITALY, ⁴Department of Diagnostic Imaging, Nuclear Medicine Unit, Magna Graecia University., Catanzaro, ITALY, ⁵IRCCS INM Neuromed, Molise, ITALY.

Introduction. The (¹¹C or ¹⁸F) labeled choline has become one of the mostly useful PET/CT radiopharmaceuticals, due to its capability to be enhanced in neoplastic lesions with low rate of glucose metabolism, as for prostate cancer (PC) cells. Similarly to the ¹⁸F-FDG, choline uptake can be observed in several physiological conditions, inflammatory processes and tumors other than PC. A satisfactory knowledge on the "in vivo" bio-distribution of the radiolabeled choline is essential for nuclear physicians, in order to recognize possible physiologic variants or pathologic false

positive findings. Moreover, being the experience with radiolabeled choline PET/CT largely linked to studies on PC patients, few information are available on the “*in vivo*” bio-distribution of this tracer in female patients. The aim of our study was to show and discuss false positive findings and diagnostic pitfalls documented in a multicenter experience in Southern Italy with ^{18}F -choline PET/CT in PC patients. Our secondary aim was to describe the “*in vivo*” ^{18}F -choline physiological bio-distribution in the female body. **Materials and Methods.** We collected a large series of false positive cases and diagnostic pitfalls in three PET centers performing PET/CT with ^{18}F -choline on an overall population of 1000 PC patients. Moreover, we performed a whole body PET/CT in 5 female patients undergoing brain PET/CT for suspicion of brain tumor relapse. Diagnostic pitfalls was ensured by follow-up, correlative imaging and/or histological sample. SUVmax analysis of the ^{18}F -choline uptake in the female body was done. **Results.** 169/1000 (16.9%) PC patients showed abnormal and unexpected PET/CT findings not owing to PC localizations. The majority of these findings were owing to inflammation. Few benign tumors were also observed. In a minority PC patients (1%) a concomitant malignant tumor was found (lymphoma, primitive bladder cancer, colon cancer, multiple myeloma, low-grade brain tumor, mesothelioma). SUVmax was significantly higher in malignant tumors than in inflammation and benign lesions. In the female body, the breast showed mild/low physiological uptake. **Conclusion.** A more confident diagnosis of PC secondary localizations can be achieved by nuclear physicians by the accurate knowledge of the bio-distribution, physiological variants and potential diagnostic pitfalls of ^{18}F -choline PET/CT. Semi-quantitative measurement of SUVmax can help to reach the final diagnosis but, especially when observing ^{18}F -choline uptake in lymphadenopathies and colon, correlative imaging and histological exam are of the utmost importance. In women, the uptake in the breast is physiologically due to the high gradient of ^{18}F -choline uptake in the exocrine glands.

EP263

Full-bladder with “cold” urine whole-body protocol for ^{18}F -fluorocholine PET/CT in patient with prostatic cancer

M. Gauthé, V. Huchet, J. Ohnona, O. Belissant, J. Zhang Yin, K. Kerrou, S. Balogova, F. Montravers, J. Talbot; Hôpital Tenon, Paris, FRANCE.

Purpose: to assess the feasibility and efficacy of a ^{18}F -fluorocholine (FCH) PET/CT whole-body acquisition without previous voiding of the bladder, in order to optimize image analysis of the pelvis, in patients with prostate cancer (PC). **Methods:** Patients with PC referred for FCH-PET/CT were prospectively evaluated. Two acquisition protocols were considered. The proposed “full bladder” protocol consisted in a starting PET acquisition immediately after FCH administration without previous voiding of the bladder, patient being positioned supine with arms crossed above head, speed 2 minutes per bed position, the upper limit of the first step being centered on the ischial tuberosity. The standard protocol consisted in a starting acquisition 10 minutes after FCH administration, patient having voided, positioned supine with arms crossed above head, from mid thighs to vertex, same speed. The interference of radioactive urine on visualization and quantification of uptake by foci was classified by two masked readers according to a 4-points scale, from no to major interference. This quotation was applied on 3 pelvic areas: prostatic bed, right and left ilio-obturator lymph nodes. The presence of radioactive urine and the radioactive urine interference on quantification between the acquisition protocols were compared using the non-parametric Kuskal-Wallis test, and the reproducibility of the reading between readers using non non parametric Wilcoxon matched pairs test. **Results:** 147 patients with PC were included. Thirty-seven (25.2%) underwent FCH-PET/CT for initial workup, 49 (33.3%) for biochemical recurrence, 32 (21.8%) for evaluation of therapeutic efficacy and 29 (19.7%) for another indication. Forty-one (27.9%) patients had history of prostatectomy. Fifty-one PET/CTs (34.7%) were performed according to the “full

bladder” protocol. “Full bladder” protocol resulted in a significant reduction in radioactive urine interferences compared to standard protocols, in all pelvic areas for both readers ($p < 0.001$). “Full bladder” protocol resulted in fewer urinary artifacts in the prostatic bed and fewer urinary artifacts in all pelvic areas when considering the whole group of patients and the biochemical recurrence subgroup respectively. In the subgroup of patients who underwent prostatectomy, “full bladder” protocol demonstrated less radioactive urine interferences than standard protocol, in all pelvic area for both readers ($p = 0.03$). **Conclusion:** the “full bladder” protocol allowed a better certainty in reading image of the pelvis by suppressing physiologic urinary accumulation in the bladder that can compromise the evaluation. It seems to be particularly interesting in patients presenting for biochemical recurrence and/or patients with history of prostatectomy.

EP264

Detection of liver lesions during ^{11}C -Choline PET/CT in relapsing prostate cancer patients

P. Ghedini¹, I. Bossert¹, T. Graziani¹, F. Ceci¹, F. Massari², E. Nobili², B. Melotti², P. Castellucci¹, S. Fanti¹, C. Nanni¹; ¹Nuclear Medicine Department, University Hospital S.Orsola-Malpighi, Bologna, ITALY, ²Medical Oncology Unit, University Hospital S.Orsola-Malpighi, Bologna, ITALY.

Aim: During our daily clinical practice using ^{11}C -Choline PET/CT for restaging patients affected by relapsing prostate cancer (rPCa) we noticed an unusual but significant occurrence of hypodense hepatic lesions with a different tracer uptake. Thus we decided to evaluate the possible correlation between rPCa and these lesions as possible hepatic metastasis. **Materials and Methods:** We retrospectively enrolled 528 patients (mean age 71yr) diagnosed with rPCa in biochemical relapse after a radical treatment (surgery and/or radiotherapy). Among these, 47 patients were excluded due to the occurrence of a second tumour or other benign hepatic diseases. All patients underwent ^{11}C -Choline PET/CT during the standard restaging workup of their disease. We analyzed CT images to evaluate the presence of hypodense lesions, and PET images to identify the relative tracer uptake. Patients were divided into 5 groups: 1-absence of lesions; 2-only one exam available, showing suspected lesions; 3-stable lesions in more than one PET/CT; 4-lesions showing modified dimensions/morphology on subsequent scans; 5-lesions confirmed as prostate liver metastasis by histopathology, triphasic CT, CEUS and clinical or biochemical evaluation. Furthermore we evaluated the relationship between these groups and PSA level at time of scan, SUVmax of lesions, presence of local relapse or non hepatic metastasis (lymphnodes, bone, other parenchyma), and presence of renal cysts. We also analyzed the ratio between SUVmax of the main lesion and SUVmean of the liver (SUVmax/SUVliv). **Results:** 396 (82,3%) patients were included in group 1, while 85 (17,7%) presented hepatic findings. Among these patients 19/481 (3,95%) were included in group 2, 12/481 (2,49%) in group 3, 37/481 (7,69%) in group 4, and 17/481 (3,5) in group 5. The mean SUVmax/SUVliv and PSA level were respectively: 4.5/8.4 and 7.9 for group 2; 4.2/7.3 and 10.4 for group 3; 4.8/7.4 and 14.4 for group 4; 5.9/8.8 and 14.7 for group 5; mean PSA of group 1 was 6.9 and mean SUVliv was 7.5. Though the majority of lesion was colder than SUVliv, in 3 patients lesions showed a higher SUVmax value. Presence of liver metastasis did not correlate with PSA levels, local relapse or other distant metastasis. **Conclusions:** Our results state that liver metastasis in relapsing prostate cancer occur, during restaging, with a significant incidence up to 17,6% (3,5% was confirmed by other techniques, and 14,1% was strongly suspected). On this basis we suggest to always investigate hepatic hypodense areas at ^{11}C -Choline PET/CT, given that a similar finding can radically change patient management.

EP265**The role of 18F-FACBC PET/CT in localizing aggressive intra-prostatic lesions in high-risk primary prostate cancer: comparison with MRI and 11C-Choline PET/CT**

L. Zanoni¹, I. Bossert¹, C. Nanni¹, C. Pultrone², R. Schiavina², F. Giunchi³, M. Fiorentino³, C. Fonti¹, C. Gaudiano⁴, R. Golfieri⁴, L. Bianchi², A. Porreca⁵, E. Brunocilla², A. D'Errico³, S. Fanti¹; ¹Nuclear Medicine, Azienda ospedaliero-universitaria di Bologna, Policlinico S.Orsola-Malpighi, Bologna, ITALY, ²Urology, Azienda ospedaliero-universitaria di Bologna, Policlinico S.Orsola-Malpighi, Bologna, ITALY, ³Pathology, Azienda ospedaliero-universitaria di Bologna, Policlinico S.Orsola-Malpighi, Bologna, ITALY, ⁴Radiology, Azienda ospedaliero-universitaria di Bologna, Policlinico S.Orsola-Malpighi, Bologna, ITALY, ⁵Urology, Policlinico Abano Terme, Abano (PD), ITALY.

AIM: To assess whether 18F-FACBC PET/CT could identify the most aggressive intra-prostatic malignant lesion in high risk prostate cancer (PCa) scheduled for radical surgery, compared to endorectal-MRI and 11C-Choline PET/CT. **MATERIALS AND METHODS:** 65 patients (pts) with biopsy-proven high risk primary PCa prospectively underwent 18F-FACBC-PET/CT prior to radical surgery. All pts received standard staging workup, including 11C-Choline-PET/CT in all cases and MRI in 36. Lesion location was assessed in PET by prostate-uptake-pattern (diffuse/focal; inhomogeneous/homogeneous) and SUVmax laterality, whereas in MRI by site of suspected predominant nodule, and finally confirmed by available prostatectomy pathology specimens. Readers were aware of full clinical history but blinded to histopathology. Overall, 20 pts were evaluable for analysis. **RESULTS: Pts characteristics (20pts):** Age: mean 65; median 66; range 47-75. PSA: mean 9,1; median 7,3; range 3,7-27,4. cT: cT2 n.s 6; cT2c 8; cT3 6. **Biopsy:** %positive-cores: mean 43; median 43; range 8-83. GS: 3+4 1; 4+3 1; 4+4 12; 4+5 6. **MRI:** Size predominant nodule (14pts): mean 17mm; median 16; range 5-30. PIRADS (13pts): mean 4; median 4; range 3-5. ECE (18pts): 11 neg; 7 pos. SVI (18pts): 17 neg; 1 pos. Perfusion-curves (6 pts): type2. **Histopathology:** Acinar (1 acinar+neuroendocrine) PCa. pT: pT2b 1; pT2c 7; pT3a 10; pT3b 2. Tumor (%): mean 24; median 20; range 6-60. Size predominant nodule (10pts): mean 25mm; median: 22,5; range 13-40. EPE (18pts): 9 neg; 5 focal; 4 extensive. Perineural invasion: 3 neg; 17 pos. 11 R0 and 9 R1. GSmax: 3+4 1; 4+3 4; 4+4 2; 4+5 8; 3+5 1; 4+3 (tertiary 5) 2; 4+4 (tertiary 5) 2. FACBC prostate pattern was very comparable to Choline (except for 1 case), differed in SUVmax and estimated disease extent (focal vs multifocal) in 16/20 pts. FACBC revealed the most aggressive malignant lesion in 14 pts (70%), Choline in 15 (75%) and MRI in 16 (80%), respectively. The 3 imaging modalities were all in agreement with pathological findings in 13 pts (65%). Among the 7 pts with discrepancies, all methods failed in 3, whereas MRI performed better than PET in 2, both Choline and MRI better than FACBC in 1 and PET better than MRI in 1. **CONCLUSION:** 18F-FACBC PET/CT may support intra-prostatic localization of the most aggressive PCa lesion. However combined clinical, morphological and functional modalities are warranted for better localization and risk stratification at initial staging. Enrolment and further semi-quantitative and predictive analyses are ongoing.

EP266**PSMA PET Index - Introduction of a new imaging quantitative biomarker for assessment of osseous tumor burden in patients with metastatic castration-resistant prostate cancer**

M. Krönke¹, M. Bieth^{1,2}, R. Tauber³, M. Retz³, B. Menze², J. Gschwend³, T. Maurer³, M. Schwaiger¹, M. Eiber¹; ¹Department of Nuclear Medicine, Technical University of Munich, Munich, GERMANY, ²Department of Computer Science, Technical University of Munich, Munich, GERMANY, ³Department of Urology, Technical University of Munich, Munich, GERMANY.

Introduction & Objectives Bone scintigraphy (BS) is performed in prostate cancer (PC) patients to evaluate osseous lesions and has been recommended for therapy response evaluation in patients treated with radium223. 68Ga-PSMA-PET/CT is an emerging technique for re-staging of PC offering a higher spatial resolution as well a superb specificity. Aim of this project was to create a semi-automatic and quantitative tool for assessment of patients' osseous tumor burden and compare it to the current standard of the bone scan using the bone scan index (BSI). **Material & Methods** 45 patients with castration resistant prostate cancer (mCRPC) underwent 68Ga-PSMA-PET/CT before initiation and after 3 or 6 cycles of Radium223-dichloride. 35 patients underwent additional BS. BSI was computed using the commercially available EXINI Bone BSI. An in-house developed software first segmenting the skeleton and secondly extracting the osseous tumor load was used for determining a PSMA-PET- Index (PPI). PPI(VOL) is defined as the percental bone volume affected by bone metastases. PPI(SUV) considers additionally the PSMA-expression measured by SUV in every voxel. The threshold for automatically identifying bone metastasis was determined by analysis of 15 patients without bone metastasis with the assumption that less than 0.1% false positive voxels would be accepted. Correlation between different thresholds, PPI(VOL) and PPI(SUV), PPI and BSI were performed. **Results** Semiautomatic identification of total bone volume as well as metastatic affected bone was feasible. A small amount of manual correction was necessary especially due to misalignment, calcification and endoprosthesis. There was a very high correlation between the PPIs(VOL) for different SUV-cutoffs ($r=0.95$, $p<0.0001$), PPIs(SUV) for different SUV-cutoffs ($r=0.99$, $p<0.0001$). PPI(SUV) and PPI(VOL) showed a high correlation ($r=0.89$, $p<0.0001$). The new volumetric parameter for 68Ga-PSMA-PET PPI(VOL) showed a highly statistical moderate correlation to the established BSI ($r=0.77$, $p<0.0001$). A weak to moderate correlation was found between the change in BSI and PPI(VOL) during Radium223-dichlorid treatment ($r=0.52$, $p<0.001$). **Conclusion** The assessment of bone metastases in PC using a novel semi-automatic tool for evaluation of PSMA PET as a new imaging biomarker is feasible. Preliminary analysis shows a good correlation between a newly introduced PSMA PET Index and the traditional Bone Scan Index regarding osseous bone involvement. Changes of both parameters during therapy seem to be less correlated. Further study evaluating the value of this new quantitative biomarker for 68Ga-PSMA-PET with clinical outcome in mCRPC are mandatory and ongoing.

EP267**Clinical impact of PSMA PET/CT for evaluation of patients with biochemical recurrence of prostate cancer**

A. Santos, **M. Queiroz**, P. Viana, F. Barbosa, A. Vicente, G. Cerri, E. Etchebehere; Hospital Sirio-Libanés, Sao Paulo, BRAZIL.

Purpose Analyze the clinical impact of PSMA PET/CT in patients with biochemical recurrence prostate cancer. **Materials and Methods** Twenty-four patients were included in the retrospective analysis approved by the local ethic committee. The inclusion criteria were biochemical recurrence of prostate cancer (defined as PSA > 0.2 ng/dL; three consecutive rises of serum PSA; PSA doubling time less than 6 months) and negative findings on conventional imaging diagnostic work-up (Bone scintigraphy, US, CT, MR and/or FDG PET/CT). All patients underwent a whole-body PET/CT 30 minutes after the injection of 185 MBq of PSMA-⁶⁸Ga. Positive lesions detected by PSMA PET/CT were confirmed by histopathology. Clinical impact was measured through a structured form applied to the referring physician and it was categorized as high, medium, low or nule, according to the therapeutic change determined by PSMA PET/CT. **Results** Twenty-four patients (mean age of 68 ± 10.8 years) were included. Mean PSA serum level was 3.98 (± 4,42). In 18 out of 24 patients (75%), PET/CT was detected lesions with abnormal PSMA uptake. Histopathology was available in 22/24 patients. The

detection rate for local recurrence was 14%, for regional lymph node metastasis 41% and for distant metastasis 36%. PSMA PET/CT determined change in therapeutic management in 82% of patients, all of them with high impact. Any adverse event was evinced. **Conclusion** PSMA PET/CT is capable to determine local, regional and distant recurrence in patients with biochemical recurrence of prostate cancer and equivocal findings in conventional diagnostic work-up. PSMA PET/CT has a high clinical impact in the therapeutic management.

EP268

F-18 PSMA-1007 - histopathological verification of a novel fluorinated low-molecular weight PSMA targeting PET tracer

F. Giesel¹, J. Cardinale², C. Kratochwil¹, J. Radtke³, B. Hadaschik³, K. Kopka², U. Haberkorn¹; ¹Department of Nuclear Medicine, University Hospital Heidelberg, Heidelberg, GERMANY, ²Division for Radiopharmaceutical Chemistry, German Cancer Research Center (dkfz), Heidelberg, GERMANY, ³Clinic of Urology, University Hospital Heidelberg, Heidelberg, GERMANY.

Introduction: The new PET tracer F-18 PSMA-1007 was chosen from a series of pre-clinically evaluated radiofluorinated PSMA ligands to demonstrate favorable characteristics in regard to tumor uptake and physiological biodistribution in comparison to Ga-68 PSMA-11. **Methods:** In this investigation about men (n=5) with prostate cancer at high risk F-18 PSMA-1007 PET/CT 1h and 3h p.i. were performed prior to surgery, which included pelvic lymphadenectomy. The diagnostic findings regarding localization of the dominant intra-prostatic lesion as well as lymphnode metastases were correlated with histopathology. **Results:** Already 1h p.i. F-18 PSMA-1007 presented with sufficient tumor-to-background ratios. In comparison to Ga-68 PSMA-11 the here presented new radiofluorinated PSMA ligand presented a significant portion of hepatobiliary excretion and in exchange a lower clearance in the urinary bladder. This presents preferable for diagnostics of primary tumors in the central or transitional zone of the prostate and pelvic lymph node metastases. **Conclusion:** F-18 PSMA-1007 seems a feasible alternative to Ga-68 PSMA-11 and could be produced in larger amounts if an on-site cyclotron is available to reduce the demand for multiple tracer synthesis per week.

EP269

Preliminary experience with Cu64PSMA PETCT in patients with intermediate and high risk prostate cancer (PC) before prostatectomy

V. Gangemi¹, R. Damiano², F. Calabria³, F. Barbato⁴, G. L. Cascini¹; ¹Nuclear Medicine- Università Magna Graecia, Catanzaro, ITALY, ²Urology- Università Magna Graecia, Catanzaro, ITALY, ³Institute of Molecular Bioimaging and Physiology, National Research Council, Catanzaro, Catanzaro, ITALY, ⁴Nuclear Medicine, Napoli, ITALY.

Aim To analyze the diagnostic performances of PET with PSMA labeled with Copper 64 (Cu64PSMA/PET) during the staging of patients with PC scheduled for radical prostatectomy (RP). **Materials and methods** From November 2015, 13 patients (age range, 67-81; median 71) with biopsy proven PC were enrolled into the study. Sums of Gleason Score (GS) were 9 in 2/13, 8 in 2/13, 7 in 4/13, and 6 in the other 5 pts. All patients were drug-naïve. PSA values were ranged between 2.9-65.0 median 7.1. Six pts were classified as High Risk (HR) whereas 7 as intermediate or Low Risk group (LR). Hybrid Cu64PSMA-PET/CT acquisition included static scan of the pelvis at the time of the injection (early images), and whole body scan after 1 and 4 hours by using a 5 min/bed duration. The administered dose was ranged between 259-370 MBq. SUVmax on early and delayed images was measured for any focal area of pathological uptake and into the liver as reference with a regular 1.5 cm ROI.

Changes SUVmax were analyzed. **Results** All pts underwent RP within 21 days from PET scan. In 6 pts according to the risk stratification extended pelvic lymph node (LN) dissection were performed. In all pts Cu64PSMA-PET detected an intense, focal hot spot into the prostate with an SUVmax ranged between 4-14, median 6.6. All focal areas were considered pathologic because of low physiological prostate uptake and low urinary excretion, particularly on 4h images. The SUVmax of primary prostatic lesions progressively increased from early to delayed images (30%) with an optimal tumor-background ratio at 4h. Median SUVmax of liver was 27.1 (range 19.5-40.5). PET findings well correlated to the site of primary tumor as well as to the lesion dimensions, GS and PSA values. In 3 out of 6 HR pts were also detected a focal PSMA uptake corresponding to 6 regional LNs on 1h and 4h images both. The average SUVmax was 5.2 (range 4.1-6.2). The LNs involvement detected by PET were confirmed by histology after the surgical removal in all patients and for all lesions. The average of LN dimensions were 1.0 mm (range 0.6-1.5). A false negative micrometastatic LN was reported. None of 13 pts showed distant pathological uptake. **Conclusion** Cu64PSMA-PET may represent an alternative to Ga68-PSMA in patients with PC because high quality delayed images due to low urinary excretion and the good physical properties.

EP270

F-18 PSMA-1007 - a novel fluorinated PET tracer structural similar to PSMA-617 as a theragnostic tandem

F. Giesel¹, J. Cardinale², O. Neels², C. Kratochwil¹, U. Haberkorn¹, K. Kopka²; ¹Department of Nuclear Medicine, University Hospital Heidelberg, Heidelberg, GERMANY, ²Division for Radiopharmaceutical Chemistry, German Cancer Research Center (dkfz), Heidelberg, GERMANY.

Introduction: Lu-177 PSMA-617 was recently clinically introduced as promising option for the treatment of mCRPC. The currently most used fluorinated PSMA ligand F-18-DCFpYl differs significantly in chemical structure. In contrast, PSMA-1007 shares structural similarity with PSMA-617 and, thus, we suggest PSMA-1007 to be a closer analogue to form a theragnostic tandem with PSMA-617. **Methods:** In this ongoing investigation, patients scheduled to PSMA targeted radioligand therapy with Lu-177-PSMA-617 received PSMA-PET/CT 1h and 3h p.i. after i.v. injection of 300-350 MBq F-18 PSMA-1007. The PET-scans were compared to the post therapeutic emission scans of the succeeding Lu-177 PSMA-617 therapy and the last PSMA targeted previous imaging (Ga-68 PSMA-11 PET or Tc-99m MIP-1427 SPECT). **Results:** The fluorinated PSMA ligand F-18 PSMA-1007 demonstrated a good agreement with the biodistribution of Lu-177 PSMA-617 in both tumor targeting and normal organs. In contrast, the other diagnostic compounds differed significantly regarding liver and kidney uptake. In regard to tumor delineation, the additive value of F-18 PSMA-1007 should be based on the physical advantages of F-18-PET (lower positron energy than Ga-68) rather than differences in targeting. **Conclusion:** A related chemical structure and similar biodistribution in men suggest F-18 PSMA-1007 as suitable theragnostic analogue to tailor patients for or against Lu-177 PSMA-617 therapy. Its diagnostic potential in comparison to other PCa PET-diagnostics has still to be evaluated.

EP271

Diagnostic efficacy of Ga-68 labelled PSMA ligand PET/CT in clinically and/or radiologically suspected cases of prostate cancer - A prospective study

B. R. Mittal, R. Kumar, S. K. Singh, J. Shukla, A. Bhattacharya, A. K. Mandal; Postgraduate Institute of Medical Education & Research, CHANDIGARH, INDIA.

Objective: To evaluate the diagnostic performance of Ga-68 labelled PSMA ligand PET/CT in patients with clinical and/or radiological suspicion of prostate cancer and a possible association between different clinical variables and the imaging results. **Material and Methods:** In this prospective study we evaluated 38 patients aged 45-80 years (median 66.4) with the clinical and/or radiological suspicion of prostate cancer and with raised PSA levels. All the patients underwent Ga-68 labelled PSMA ligand PET/CT imaging and the data was evaluated by two expert nuclear medicine physicians. Any abnormal tracer uptake on PET images was correlated with the corresponding CT images. SUVmax was measured in prostate region, pelvic and abdominal lymph nodes, bone and other lesions. The target to background ratio for all lesions was also evaluated. Histopathological examination was taken as gold standard to compare the results. PSA levels were also correlated with the PET results. **Results:** Histopathological examination showed prostatic carcinoma in 20 patients and no evidence of malignancy in 18 patients. PET/CT revealed positive findings in 26/38 patients (68.4%) while 12/38 patients (31.6%) were negative. Apart from primary lesion in the prostate, locoregional disease was noticed in 12 patients and distant metastases in 13 patients. On comparing the PSMA ligand PET/CT findings with HPE, 19 patients were true-positive, 7 false-positive, 11 true-negative and one false-negative. PET had shown a sensitivity, specificity, positive predictive value (PPV), negative predictive value (NPV) and accuracy of 95.00%, 61.1%, 73.08%, 91.67% and 78.9% respectively. We noticed a good correlation between PET findings and final diagnosis ($P=0.001$). The mean SUVmax value in the prostate in the prostate cancer group was 15.4 (3.3-61.3) while it was 4.4 (2.1-8.1) in benign group and there was strong correlation between SUVmax and final diagnosis ($P=0.003$). By ROC curve analysis we found that SUVmax >5.2 had a sensitivity and specificity of 85.0% and 88.2% respectively (AUC 0.90). Similarly lesion to background ratio >5.9 had a sensitivity and specificity of 100.0% and 88.2% respectively (AUC 0.92). The mean PSA value in the prostate cancer group was 92.8ng/ml (4.7-863.0 ng/ml) while 11.3ng/ml (0.3-36.3 ng/ml) in benign group. **Conclusion:** 68Ga-PSMA PET/CT has a high sensitivity in detecting prostate cancer in clinically or radiological suspected cases. It also localizes distant metastases helping in management strategy. More studies with larger patient population are required for further evaluating the diagnostic accuracy of 68Ga-PSMA ligand PET/CT imaging clinically suspected cases of prostate cancer.

EP272

Ga-68 PSMA PET/CT in metastatic or locally recurrent prostate cancer: Comparison to bone scan, CT or MRI

E. Acar, R. Bekiş, Ö. Özdoğan, B. Polack; Dokuz Eylül University, School of Medicine, Department of Nuclear Medicine, İzmir, TURKEY.

Aim: The purpose of this study was to evaluate the diagnostic role of Ga-68 PSMA PET/CT and to investigate its complementary role to the other imaging modalities such as bone scan, CT and MRI in local recurrence/metastatic prostate cancer patients. **Material and Method:** We retrospectively analyzed a total of 57 patients (the mean age 68.8 (range: 48-89), Gleason score 7.86 (range: 6-10), PSA level 214 ± 455 (0.01-1740) ng/ml who were referred to our department to investigate metastatic foci or recurrent disease. Patient based analyses were performed and compared to other images such as bone scan, CT and/or MRI. All scans of the each patient were performed within one month period. Bone scans, CT and MRI were available for comparison, in 31/57, 45/57 and 10/57 patients, respectively. **Results:** There was no abnormal Ga-68 PSMA uptake in 11 patients (19%). The mean PSA level of these patients was 2.6 (0-15.9) ng/mL. Ga-68 PSMA PET/CT showed increased uptake which was considered as metastatic or recurrent foci in 46 out of 57 (81%) patients. Lymph node, bone, liver, lung and adrenal gland metastases were detected in 24 (42%), 17 (30%), 6 (10%), 4 (7%), 3 (5%) patients, respectively. Local recurrence

was found in 8 patients. Peritoneal, penile and scrotal metastases were found in one of each patient. Ga-68 PSMA showed increased uptake in primary lesion in 3 patients who did not have a prostatectomy. All the lesions were detected by Ga-68 PSMA PET/CT were either suspicious for metastatic foci in the other imaging modalities or unknown for the clinicians. In one patient, a liver lesion evaluated as metastases by MRI did not show Ga-68 PSMA uptake. **Conclusion:** Ga-68 PSMA PET/CT seems to be a valuable imaging modality to evaluate local recurrence and/or metastatic disease in patients with prostate cancer patients who has a high PSA level and radiologically suspicious or negative for metastases.

EP273

Diagnostic Accuracy Of ⁶⁸Ga PSMA In High Risk Prostate Cancer & Its Comparison With CECT

V. Rangarajan, A. Agrawal, A. N, N. Purandare, S. Shah, G. Bakshi, G. Prakash, U. Mahantshetty, V. Murthy, S. Menon, A. Joshi; Tata Memorial centre, Mumbai, INDIA.

Aim - In the past few years ⁶⁸Ga PSMA has emerged as a useful investigational tool in evaluation of disease recurrence post biochemical relapse. Its usefulness lies in detection of small nodal disease which remains undetected by morphologic imaging like CT or MRI. The aim of this study was to evaluate the diagnostic efficiency of ⁶⁸Ga PSMA and compare its efficiency with CECT (contrast enhanced CT) in high risk prostate cancer. **Materials and Methods-** 75 consecutive patients with carcinoma prostate who underwent ⁶⁸Ga-PSMA PET/CECT at initial staging were retrospectively analyzed. All were high risk prostate cancer with PSA level >20 ng/ml. The age range was between 47-83 years. 68Ga PSMA scans were analyzed to look for lymph nodal and visceral metastases. Increased uptake more than the background which did not correlate with physiological uptake was taken as a positive finding on PSMA scan. On CECT - the following criteria were taken for node positivity - >1 cm size in short axis and/or, rounded shape and/or, enhancement and/or, presence of necrosis. **Results -** PSMA was positive for locoregional nodes in 11 patients and CECT in 5. PSMA was positive for metastatic disease in 51 patients - by virtue of retroperitoneal nodes in 33 and by CECT in 28. The remaining 18 patients had only skeletal metastases. None of the patients had visceral metastases. The detection rates (DR) of PSMA were 100% for the primary (75/75). CT was not assessed for this as MRI is the imaging modality of choice. DR of PSMA was 15% (11/75) for locoregional nodes and 6% for CECT (5/75). DR rate of PSMA was 44% (33/75) for metastatic retroperitoneal nodes and 37% (28/75) for CECT. PSMA PET/CT had incremental value over CT in 14 % (11/75) of patients. It upstaged the disease from organ confined to Loco-regional in 8% (6/75) patients and locoregional to metastatic in 6% (5/75) patients. **Conclusion -** ⁶⁸Ga PSMA proved to have better diagnostic accuracy in detection of locoregional and metastatic adenopathy over CECT in high risk prostate cancer.

EP274

Detection efficacy of hybrid ⁶⁸Ga-PSMA ligand PET/CT in 129 prostate cancer patients with suspected recurrence after primary radiation therapy

I. Einspieler, C. Hacker, I. Rauscher, M. Krönke, C. Rischpler, T. Maurer, M. Schwaiger, M. Eiber; TU München, München, GERMANY.

Purpose: The aim of this study was to investigate the detection rate of ⁶⁸Ga-PSMA PET/CT in a population of patients with suspected recurrence of prostate cancer, exclusively treated with external (photon or proton therapy) or internal beam therapy (brachytherapy) as primary treatment. **Methods:** We enrolled 129 patients for a retrospective analysis with proven biochemical recurrence using the ASTRO criteria. Median prostate-specific antigen (PSA) level was 6.1 ng/mL (range, 0-158 ng/mL). 87 and 42 patients had been treated by external (73 by photon and

14 by proton therapy) or internal radiation therapy, respectively. Of the 129 patients, 62 were receiving antihormonal treatment within at least 6 months prior to the PET/CT scan. The detection rates were correlated with different PSA levels. The contribution of primary Gleason score and antihormonal treatment to the final diagnosis was assessed. Results: 114 (88.4%) patients showed pathologic findings in ^{68}Ga -PSMA ligand PET/CT. The detection rates were 93.9% (31/33), 93.0% (40/43), 78.6% (33/42) and 90.9% (10/11) for PSA levels of ≥ 10 , 5 to <10 , 2 to <5 and 0 to <2 ng/mL, respectively. Remarkably, with regard to the ASTRO criteria, all patients with a PSA-value <2 ng/mL received antiandrogen therapy. ^{68}Ga -PSMA ligand PET/CT indicated local recurrence in 48 cases (42.1%), local and distant relapse in 28 cases (24.6%), only distant relapse in 38 cases (33.3%) and distant relapse with/without local recurrence in overall 66 cases (57.9%). No significant difference in detection efficacy was present regarding Gleason score ($p=0.4421$) and antiandrogen therapy ($p=0.2245$). Conclusion: Hybrid ^{68}Ga -PSMA ligand PET/CT demonstrates substantially high detection rates in patients with suspected recurrence of prostate cancer after primary radiation therapy. It was able to detect extraprostatic disease in 57.9% of patients, potentially having substantial impact on further clinical management.

EP275

The PSMA-Agent Tc-99m-MIP-1404 in the Primary Staging of Biopsy Proven Prostate Cancer - Preliminary Results

M. Beck¹, J. Reinfelder¹, P. Ritt¹, J. Sanders¹, T. Bartschat², P. Goebell¹, T. Kuwert¹; ¹University Erlangen-Nuremberg, Erlangen, GERMANY, ²Hospital Martha-Maria Nuremberg, Nuremberg, GERMANY.

Purpose: The prostate specific membrane antigen (PSMA) is a relatively new target for molecular imaging. The purpose of our study was to investigate the potential of the PSMA-ligand Tc-99m-MIP-1404 in biopsy proven prostate cancer (PC) prior to therapy. **Methods:** Thirty patients with biopsy-proven medium- and high-risk PC (median PSA 8.8 ;Range 4.5 - 59) were referred for PSMA whole-body scintigraphy and SPECT/CT of the abdomen prior to planned surgery. Scans were performed 3 to 4 hours after injection of 740 ± 19 MBq Tc-99m-MIP-1404. Two observers read the images for pathological uptake in the prostate, as well as for visceral and osseous metastases. Furthermore, standardized uptake values (SUV) were calculated based on quantitative SPECT/CT images. **Results:** The measured background activity in bone ($\text{SUV}_{\text{mean}} 1.1 \pm 0.1$) and soft tissue ($\text{SUV}_{\text{mean}} 0.5 \pm 0.1$) was low. In 28 patients, an increased focal or diffuse tracer uptake in the prostate gland was identified, with an average SUV_{max} of 16.5 ± 18.9 (Range 4.4 - 107.3). Prostate SUV_{max} correlated significantly with the serum concentration of prostate specific antigen (PSA; $r = 0.76$, $p < 0.01$). Lymph node filiae ($\text{SUV}_{\text{max}} 12.7 \pm 8.7$) were suspected in three patients and confirmed by histology or CT in two. One patient had PSMA-positive bone metastases in a thoracic vertebral body ($\text{SUV}_{\text{max}} 49.5$) and the pelvic region; another patient had diffusely increased skeletal uptake caused by polycythemia vera (left femoral head $\text{SUV}_{\text{mean}} 5.9$). An additional seventeen patients in whom pelvic lymph node dissection was performed had no evidence of lymph node metastasis in imaging, which was confirmed by histology. **Conclusion:** Tc-99m-MIP-1404 is a promising PSMA agent with high tracer uptake in prostate cancer and the potential to inform preoperative staging of PC.

EP276

Is the ^{68}Ga -PSMA PET-CT the new benchmark for lymphnode staging in high risk prostate cancer patients: A comparative study with MRI?

M. Gupta, P. S. Choudhury, D. Hazarika, S. Rawal; Rajiv Gandhi Cancer Institute and Research Centre, Delhi, INDIA.

Abstract: Introduction: Lymphnode staging is an important step in high risk prostate cancer patients before a potentially curative treatment. Using size criteria Computed Tomography (CT) and Magnetic Resonance Imaging (MRI) perform similarly with a poor sensitivity for metastatic pelvic lymphnode. We compared lymphnode detectability of ^{68}Ga -PSMA PET-CT to MRI in high risk prostate cancer patients taking histopathology as standard. Method: 39 high risk prostate cancer patients underwent staging ^{68}Ga -PSMA PET-CT in-between Dec-2014 to Dec-2015. 5 received radiotherapy & 2 high intensity focused ultrasound (HIFU) as primary treatments and 20 patients with distant metastasis on PSMA PET were excluded. 12 patients with radical prostatectomy (RP) with extended pelvic lymphnode dissection were analysed. Sensitivity, specificity, positive predictive value (PPV), negative predictive value (NPV) and accuracy of ^{68}Ga -PSMA PET-CT and MRI were calculated for numbers of patients and lymphnode metastasis. Chi Square test, McNemar's test and ROC analysis were also done. Results: ^{68}Ga -PSMA PET-CT and MRI diagnostic sensitivity, specificity, PPV, NPV and accuracy for number of patients detection were 100%, 80%, 87.5%, 100%, 91.67% and 57.14% 80%, 80%, 57.4%, 66.67% respectively. For metastatic lymphnode detection findings were 66.67%, 98.61%, 85.71%, 95.95%, 95.06% and 25.93%, 98.61%, 70%, 91.42%, 90.53% respectively. Lymphnode detectability was better and statistically significant on Chi square test for ^{68}Ga -PSMA PET-CT. On McNemar's test, P value was insignificant for number of patient detection (P value 0.250) but significant for lymphnode detection (P value 0.001) for ^{68}Ga -PET-CT. In ROC analysis, AUC was also significantly high for lymphnode detectability by ^{68}Ga -PSMA PET-CT. Conclusion: We conclude, ^{68}Ga -PSMA PET-CT is a promising imaging modality for lymphnode staging in high risk prostate cancer with overall sensitivity (66.67%). It has the potential to impact patient's initial management and can upstage and down stage the disease. Therefore, it's worthwhile to use it before RP to assess disease volume and distribution in high risk patients. Key Words: ^{68}Ga -PSMA PET-CT, MRI, High risk prostate cancer, pelvic lymphnode comparison

EP277

Utility of ^{68}Ga -PSMA-PET/CT in Prostate Cancer with Biochemical Recurrence with PSA ≤ 1

L. Geraldo¹, C. Uprimny¹, D. Kandler¹, A. Kroiss¹, B. Nilica¹, L. Scarpa¹, C. Decristoforo², A. Griesmacher³, P. Lukas⁴, W. Horninger⁵, I. Virgolini¹; ¹Nuklearmedizin Universitätsklinik Innsbruck, Innsbruck, AUSTRIA, ²Radiopharmazie Universitätsklinik Innsbruck, Innsbruck, AUSTRIA, ³Labordiagnostik Universitätsklinik Innsbruck, Innsbruck, AUSTRIA, ⁴Strahlentherapie Universitätsklinik Innsbruck, Innsbruck, AUSTRIA, ⁵Urologie Universitätsklinik Innsbruck, Innsbruck, AUSTRIA.

Aim ^{68}Ga -Prostate Specific Membrane Antigen (PSMA)-ligand-PET/CT is a new imaging method that allows the exploration of patients with biochemical recurrence (BR) of PC after curative primary treatment (mainly radical prostatectomy (RP) and radiation therapy (RT)). Up to 40% of PC patients will develop BR, evidenced by a rise in serum prostate-specific antigen (PSA) levels within 10 years after primary treatment. Hence, the importance of early detection and localization of recurrent disease. In this study we evaluated the utility of ^{68}Ga -PSMA-HPED-CC-ligand PET-CT in the detection of lesions in patients with PC and BCR with a PSA ≤ 1 . **Methods** 32 consecutive patients with recurrent PC after curative primary treatment and PSA ≤ 1 were included (mean age: 67, range: 40-81 years); mean time from initial diagnosis: 6 years). All patients underwent a ^{68}Ga -PSMA-HPED-CC-ligand-PET/CT whole-body acquisition at 60 min after intravenous injection of ^{68}Ga -PSMA-HPED-CC-ligand-PET/CT (mean dose 140, range: 103-159 MBq). 19/32 patients (26%) had PSA ≤ 0.5 . 31 patients had RP and 11 local RT as curative treatment after initial diagnosis. **Results** 14/32 patients (44%) demonstrated pathologic lesions in ^{68}Ga -PSMA-HPED-CC-ligand-PET/CT,

1/32 (3%) local relapse, 9/32 (28%) showed lymph node relapse and 4/32 (13%) patients had distant metastases. In 8 patients a doubtful uptake in the prostatic PET was observed, not considered as clear local relapse. 5/19 patients (26%) with PSA \leq 0.5 were pathological in ^{68}Ga -PSMA-HPED-CC-ligand-PET/CT imaging, 4/5 showed positive lymph nodes, and only one had a distant metastasis. **Conclusion** ^{68}Ga -PSMA-HPED-CC-ligand-PET/CT imaging can help to identify BR in PC patients, even with PSA \leq 1, and therefore has a significant implication for treatment strategy, also in this subgroup of patients.

EP278

Impact of ^{68}Ga -PSMA PET/CT in the Assessment of Prostate Cancer Patients with Biochemical Recurrence

M. Beheshti¹, C. Schiller¹, B. Aschacher², H. Geinitz², L. Imamovic¹, J. Kaufmann¹, C. Pirich³, W. Loidl⁴, W. Langsteger¹; ¹PET-CT Center Linz, St. Vincent's Hospital, Linz, AUSTRIA, ²Department of Radiation Oncology, St. Vincent's Hospital, Linz, AUSTRIA, ³Department of Nuclear Medicine, Paracelsus Medical University, Salzburg, AUSTRIA, ⁴Prostate Cancer Center Linz, Department of Urology, St. Vincent's Hospital, Linz, AUSTRIA.

Aim ^{68}Ga -PSMA (PSMA) PET/CT is introduced as promising imaging in assessment of prostate cancer (PCa). This study is planned to evaluate the value of ^{68}Ga -PSMA PET/CT in prostate cancer (PCa) patients with evidence of biochemical recurrence (BCR). **Material & Methods** In this prospective study 100 consecutive PCa patients (mean age 68 \pm 8) with evidence of BCR underwent ^{68}Ga -PSMA PET/CT. Radiotherapy and/or hormone therapy was performed in 36 patients while 54 patients had no treatment after radical prostatectomy (RPE). PET/CT imaging was performed 60 min. after intravenous injection of 140 MBq Glu-NH-CO-NH-Lys-(Ahx)-[^{68}Ga (HBED-CC)] (^{68}Ga -PSMA) with 3min./bed position acquisition time. Pathologic findings in each imaging modalities have to be clarified histopathologically or by conventional imaging modalities and/or clinical follow-up. **Results** ^{68}Ga -PSMA PET/CT was able to localize recurrent disease in 83% (83/100; 47 pts without previous treatment & 36 pts with previous and/or ongoing therapy; PSA range: 0.01 - 56.6 ng/ml) of the patients. PSA value was \leq 0.5, 0.6 - 1.0, 1.0 - 2.0 and $>$ 2.0 ng/ml in 24 %, 7 %, 11 % and 40 %, respectively, in ^{68}Ga -PSMA PET-positive patients. ^{68}Ga -PSMA PET/CT was negative in 17 % of the patients with a PSA range of 0.01 - 3.7 (10 pts under hormone therapy and 7 patients without any ongoing treatment). It was able to detect local recurrence (LR) in 33 %, lymph node metastases (LNM) in 35 % and bone metastases (BM) in 11 % of the patients. In 4 % of the cases all LR, LNM and BM were detected. **Conclusion** ^{68}Ga -PSMA PET/CT showed a sensitivity of 83 % in the detection of recurrent disease in prostate cancer. It seems to be a very promising diagnostic procedure even in low PSA level \leq 0.5.

EP-15 – Sunday, October 16, 2016, during Exhibition hours, e-Poster Area
Clinical Oncology: Sentinel Node

EP279

The Value of SPECT Lymphoscintigraphy for Sentinel Lymph Node (SLN) mapping in melanoma

A. Velidaki, A. Kolindou, M. Karkani, N. Prosotsianiotis, E. Dagrakis, E. Kitsou; Nuclear Medicine Dept., Laiko General Hospital of Athens, ATHENS, GREECE.

Introduction: Lymphoscintigraphy is a sensitive, inexpensive, non-invasive imaging modality that allows SLN identification in patients with malignant melanoma. Several techniques have been described: planar imaging (PL), tomographic imaging (SPECT) and more recently (where

available) SPECT/CT imaging. The aim of our study was to assess the benefit of SPECT to PL lymphoscintigraphy in presurgical SLN mapping. **Materials and method:** We studied 73 patients with melanoma (24women, 49 men, age 30 to 80 y.o.). The technique involved the peritumoral injection of 1-2 mCi Tc-99m-nanocolloid. Planar images according to the expected sites of SLN were obtained 5 minutes p.i. The first hot spot in the lymphatic drainage represents the SLN and it was marked to the skin as a guide to the surgeon. The same was performed if more than one SLN were detected. Sequentially, SPECT imaging was performed and the number of the SLNs detected from the reconstructed images was evaluated. PL and SPECT results were compared to the findings of the surgery. **Results:** A total of 196 SLNs were surgically resected in all 73 pts (1 SLN in 22 pts, 2 in 19 pts, 3 in 17 pts and $>$ 3 in 17 pts). The total number of SLNs identified by PL was 138 and by SPECT imaging was 189; 13/189 detected SLNs were near the injection site and they were not detected by PL. SPECT accurately identified at least 1 SLN in all 73 patients (identification rate of 100%). In a single case PL failed to image any SLN. Agreement between surgery and PL regarding the number of SLNs was in 32/73 pts, while SPECT accurately predicted the number of surgically identified SLNs in 64/73 pts. **Conclusion:** SPECT imaging detects more sentinel nodes than conventional planar imaging. Nodes near the injection site are more clearly identified with SPECT.

EP280

Selective lymph node biopsy in patients with adenocarcinoma of the prostate with intermediate and high-risk our experience

V. Vera Pinto; Hospital Universitario y Politécnico La Fe, Valencia, SPAIN.

OBJECTIVE To determine the effectiveness of Selective Lymph Node Biopsy (SLNB) in patients with adenocarcinoma of the prostate with intermediate and high risk. **MATERIAL AND METHODS** Descriptive study of 55 patients with mean age of 64,8 (50-75 years old) in which SLNB was performed between August 2012 to January 2016 after ruling out distant metastases with bone scintigraphy. All patients were diagnosed with prostate adenocarcinoma in intermediate or high risk stages with a mean serum PSA of 9.65ng/ml (range 4 - 46,39 ng/ml). The day before surgery, 10 mCi (370 MBq) of nanocolloids labelled with ^{99m}Tc were injected within the prostate guided by transrectal ultrasound while simultaneously abdominopelvic acquisitions were made with portable gamma camera (Sentinella®) to ensure intraprostatic deposit of the tracer. 2 hours later planar abdominopelvic acquisitions and SPECT / CT (Phillips BrightView XCT®) were performed to obtain definitive lymph node mapping. In all cases, standard pelvic lymphadenectomy was performed by Laparoscopic technique, however, it will become extended in cases where migration of the tracer reaches unusual lymphatic territories. Abdominopelvic acquisitions with Sentinella®, pre and post lymphadenectomy were also done in the operation room. All sentinel lymph nodes (SLNs) were removed and examined with haematoxylin and eosin staining and immunohistochemical techniques. **RESULTS** In 100% of cases there was migration of the radiotracer with positive scintigraphy. 25.4 % (14/55) of patients presented metastatic SLN infiltration. 74.5 % of patients (41/55) were true negatives, obtaining negative predictive value of 100%. 41 patients (74,5%) present unusual lymphatic drainage to paraaortic chains 41,8 %, , presacral chains 36,3 % and 43.8% common iliac chain. In this group of patients, 7.3% (3/41) presented metastatic infiltration of atypical SLN. **CONCLUSION** SLNB in prostate cancer is a reliable and useful tool, capable to identify first landing lymphatic chains of the prostate, allowing properly assessment of lymph node involvement in prostate cancer. It is also a useful technique to detect patients with atypical prostate lymphatic drainage. If SLNB wasn't performed a potential metastatic node would be involved but not resected, and that allows the surgeon to recognize when to perform an extended lymphadenectomy.

EP281**Radioguided Occult Lesion Localization in Reoperative Procedures of Patients with Locoregional Metastases of Papillary Thyroid Cancer**

I. SAHINER¹, G. U. VURAL¹, M. A. GULCELİK¹, I. KERIMEL¹, T. SENGEZER², S. ILGAN²; ¹Ankara Oncology Research And Training Hospital, ANKARA, TURKEY, ²Ankara Güven Hospital, ANKARA, TURKEY.

Purpose/Introduction : Surgery is the preferred modality of treatment in locoregional recurrences of papillary thyroid cancer (PTC) providing improved disease control. However, reoperative surgery in patients with previous neck exploration in either central and/or lateral compartments carries increased risks associated with surgery in addition to diminished operative success. The aim of our study was to determine if radioguided occult lesion localization (ROLL) technique was feasible in terms of surgical success and reduction in complication rates in reoperations of PTC recurrences. **Subjects and methods:** Sixteen consecutive patients (12 female, 4 male) who were previously operated for PTC with cytological proof of locoregional recurrences in the previously operated neck compartments were included in the study. Preoperative mapping and injection of Tc-99m labeled macroaggregated albumin into selected lesions were performed under guidance of ultrasonography (US). Surgical exploration was carried out according to the US map and labeled lesions were localized with a handheld gamma probe intraoperatively. After the excision of lesions; counts from the background, lesion and postexcisional site were compared to confirm the success of the procedure. All excised specimens were evaluated histopathologically and serum levels of thyrotropin (TSH), thyroglobulin (Tg), anti-Tg antibodies and calcium were recorded for each patient before and (minimum 45 days) after the surgical procedure. **Results:** Mean patient age was 47 (range: 17-69). Thirteen of the patients had previous therapies with radioiodine (cumulative activity range: 100-1150 mCi, median: 250 mCi). The smallest lesion injected was 5x5 mm and the largest was 16x18 mm in two dimensions. An average of 2.13 injections were performed per patient (range: 1-5). A total of 79 suspicious lesions were detected preoperatively, 143 lesions were excised and 75 were histopathologically proven to be infiltrated by PTC. Serum Tg and/or anti-Tg levels of 14 patients displayed reductions on similar pre- and post-operative TSH levels, whereas serum Tg levels of one patient rose after the surgery and lung metastases were detected in follow up. In the remaining no rise in Tg and/or anti-Tg serum levels were present before and after the surgery. Ductus thoracicus injury occurred only in 2 patients, without any chyle leak in the follow up period. **Discussion/Conclusion:** ROLL technique and lesion mapping under preoperative US guidance is a safe and efficient method in terms of surgical success with reasonable complication rates in reoperations of locoregional PTC recurrences.

EP282**Preoperative sentinel node visualisation in breast cancer using portable gamma cameras**

D. M. V. Huizing^{1,2}, L. J. de Wit - van der Veen¹, B. Pouw¹, C. H. Slump², M. P. M. Stokkel¹; ¹Netherlands Cancer Institute - Antoni van Leeuwenhoek hospital, Amsterdam, NETHERLANDS, ²University of Twente, Enschede, NETHERLANDS.

Aim Portable gamma cameras (PGCs) are routinely used during surgical radio-guided sentinel node (SN) procedures in our hospital. The high spatial resolution and sensitivity of these real-time imaging systems ensure precise visualisation of SNs during resection. Up-to-now the role of PGCs in a preoperative setting has been limited. Accordingly the aim of this study was to assess if PGC imaging could substitute conventional gamma imaging in preoperative breast cancer SN detection. **Materials**

and methods Sixteen patients scheduled for breast conserving surgery (BCS) and SN procedure were prospectively included. Conventional lymphoscintigraphy was performed 15 minutes and 3 hours after intratumoural injection of ± 140 MBq Tc-99m albumin nanocolloid. PGC acquisition and image interpretation were performed 2.5 hours post-injection by an experienced user blinded for conventional gamma imaging results. Additional PGC imaging was performed 22 hours (shortly before surgery) post-injection to evaluate the visibility of the SNs. The breast, axillary and parasternal regions were imaged from 15 cm distance (field-of-view 20x20 cm) and close to the skin. **Results** SNs were visualised in 81% of the patients by PGC, where conventional imaging showed nodes in 69% of the patients, performed 2.5 and 3 hours post-injection respectively. PGC visualised 9/10 axillary nodes detected by the conventional gamma camera. In two patients, PGC imaging showed an axillary SN which was not visualised on the conventional gamma camera. Axillary nodes were most important, since parasternal and intramammary nodes generally are not surgically removed in this group of patients. Twenty-two hours post-injection, SNs were visible in 56% of the patients using PGC. The main advantage of using the PGC for preoperative imaging was to assess the number and location of SNs, however intraoperative benefit of the PGC was limited. Preoperative breast cancer SN imaging using a PGC reduces time and costs compared to conventional gamma imaging. Furthermore, extra acquisition time for more complex gamma imaging is created. For this reason, PGC imaging would be best performed at the Nuclear Medicine department, and in this way also the possibility for reinjections remains. **Conclusion** The sensitivity of PGC imaging for SN detection in breast cancer patients is comparable to conventional gamma imaging; both performed 2.5 to 3 hours post-injection after ± 140 MBq of radiotracer administration. Preoperative SN detection using the PGC at the department of Nuclear Medicine reduces time and costs compared to conventional gamma imaging, enabling more conventional gamma acquisitions for other indications.

EP283**Feasibility of ¹⁸F-FDG PET/CT-guided Cytoreductive Surgery (CRS) and Hyperthermic Intraperitoneal Chemotherapy (HIPEC) in patients with peritoneal carcinomatosis : a Preliminary Experience**

S. Lee^{1,2}, D. Lee³, K. Oh⁴, D. Jeong⁴, C. Lee⁵, E. Kim³, S. Oh⁶, J. Choe^{2,7}; ¹Department of Nuclear Medicine, G Sam Hospital, Hyosan Medical Foundation, Gyeonggi-do, KOREA, REPUBLIC OF, ²Department of Medicine, Graduate School, Korea University, Seoul, KOREA, REPUBLIC OF, ³Department of Medical Oncology, G Sam Hospital, Hyosan Medical Foundation, Gyeonggi-do, KOREA, REPUBLIC OF, ⁴Department of General Surgery, G Sam Hospital, Hyosan Medical Foundation, Gyeonggi-do, KOREA, REPUBLIC OF, ⁵Department of Oncologic Surgery, G Sam Hospital, Hyosan Medical Foundation, Gyeonggi-do, KOREA, REPUBLIC OF, ⁶Department of Nuclear Medicine, National Police Hospital, Seoul, KOREA, REPUBLIC OF, ⁷Department of Nuclear Medicine, Korea University Anam Hospital, Seoul, KOREA, REPUBLIC OF.

The prognosis of patients with secondary peritoneal carcinomatosis (PC) remains poor, despite of the variable best standard treatment options. Recently, cytoreductive surgery (CRS) and hyperthermic intraperitoneal chemotherapy (HIPEC) has been developed to treat PC. But there reported considerable complications, morbidity, and mortality owing to the aggressiveness of the surgery. Therefore, exact pre-surgical determination of localization and extent of PC is crucial for the clinical outcome. This study aims to review our preliminary experience with ¹⁸F-Fluorodeoxyglucose (¹⁸F-FDG) PET/CT-guided CRS and HIPEC in patients with PC, which could be expected as less invasive technical procedures in the way that pre-surgical mapping and planning surgical procedure are possible. Seven patients (3 men and 4 women; mean age 62.3 years; range 60-72) with secondary PC from April 2015 to March 2016 were enrolled in this study. Underlying primary malignancy sites were ovarian cancer (n=2), colorectal cancer

(n=2), malignant peritoneal mesothelioma (n=1), and pancreatic cancer (n=2). All patients had been examined on pre-operative staging ^{18}F -FDG PET/CT. PET/CT image were assessed and analysed as positive or negative, regarding presence and localization of PC manifestations based on the peritoneal cancer index (PCI) by Sugarbaker et al. Patients underwent CRS and HIPEC within 10 days afterward of pre-op PET/CT. PET/CT images were assessed and correlated with surgical reports and pathologic confirmation. Post-surgical PET/CT exams were performed on one-month later for assessment of the residual tumor burden in three patients. Total 79 peritoneal segments in 7 patients were surgically removed and sampled during CRS HIPEC (PET positive segment n=62, PET negative segment n=17). PET/CT provided a reliable detection of PC. In summary, 1 peritoneal segment was classified as a false positive and 5 segments were as false negative group. Diagnostic performance of ^{18}F -FDG PET/CT-guided CRS HIPEC in patients with PC was sensitivity 92%, specificity 94%, PPV 98%, NPV 77%, and diagnostic accuracy 92% with lesion-by lesion analysis. Moreover, we could be notified a dramatically decreased metabolic tumor burden of PC after CRS HIPEC with comparison of pre- and post-surgical ^{18}F -FDG PET/CT in three patients who underwent post-surgical PET/CT examination. ^{18}F -FDG PET/CT-guided CRS HIPEC appears to be technically feasible and effective in patients with excessive peritoneal metastases. This is a pilot study with limited number so further studies are needed to elucidate its precise role in the patient-tailored multimodality management.

EP284

A novel device for true PET guided biopsies: First accuracy tests

J. Cortes-Rodicio¹, G. Sanchez-Merino¹, I. Tobalina Larrea², M. Garcia-Fidalgo¹; ¹S^o Fisica Medica, OSI Araba, Hospital Txagorritxu, Vitoria-Gasteiz, SPAIN, ²S^o Medicina Nuclear, OSI Araba, Hospital Santiago, Vitoria-Gasteiz, SPAIN.

INTRODUCTION AND OBJETIVES: PET/CT guided biopsy is a relative new technique in which metabolic information from a previously acquired PET/CT scan is integrated into a CT guided biopsy procedure. Besides, there are examples of real PET guided biopsy procedures in which a radioactive source is coupled to the biopsy needle and is introduced into the patient. Many drawbacks arise from both procedures: incorrect positioning of the patient, sterilization of radioactive needles, expensive radioactive sources, radiation protection of patients and staff... In this work we present a novel device to perform true PET guided biopsies avoiding the problems of previous procedures and improving the biopsy process. **METHODS AND MATERIALS:** A first prototype of the stereotactic frame has been built with a 3D printer. It consists of four main components: A fixed circular base, an outer circular rotating crown with a U-shaped fixed piece, a header that moves along the U-shaped piece and a needle holder. The primary base constrains three holders where radioactive markers doped with ^{18}F -FDG are introduced. Another marker is attached to the outer end of the needle. These four markers will be the only visible points of the device in PET images. Once the device is mounted, a spherical coordinate system is built with the entrance needle point in the skin as the origin of coordinates. Two in-house software programs have been written in ImageJ macro language. The first one obtains the spherical coordinates (θ , φ and $depth$) of the tumour tissue that want to be punctured with respect the stereotactic frame. After the puncture, a biopsy verification is performed to assess that the needle is placed at the desired point. To this end, the second program draws the inner end of the needle in the PET image. **RESULTS:** For testing purposes of the prototype, a gel tumour phantom was built to test the PET guiding device. It consists on a dissolution of FDG (2.5kBq/ml) in which a sphere of 10mm of diameter and an activity concentration of 4:1 with respect the background is settled. After all biopsy procedures we found the needle tip inside the tumour, with an accuracy of less than 5mm with respect the center of the sphere. **CONCLUSIONS:** A first prototype has been built and tested successfully. Anyway some improvements have to be developed and more trials have to be done to further characterize the device

EP285

Lymphatic drainage patterns in breast cancer recurrence with previous surgical interventions - our experience

A. Fernandes, T. Faria, A. Oliveira, M. Perez, V. Alves, A. Pinto, J. Pereira; Hospital São João, Porto, PORTUGAL.

Aim: The aim of this study was to determine the drainage patterns in patients with breast cancer recurrence who had been submitted to previous surgical interventions, and underwent a sentinel node procedure at our department. **Introduction:** Lymphoscintigraphy determines lymphatic drainage of the breast and identifies the sentinel node(s) (SLN). Lymphatic drainage of the breasts occurs predominantly to the ipsilateral axilla, but it can occur to other locations, especially in patients with prior interventions, like chest and axillary surgery. **Materials and Methods:** We reviewed data from all patients who underwent lymphoscintigraphy at our department from November 2009 to March 2016 (n=560), and selected the patients with breast cancer recurrence that had been submitted to previous surgical intervention. A total of 33 patients were enrolled. **Results:** In 11 of the 33 patients reviewed, no drainage was observed. The other 22 (detection rate of 67%) showed multiple drainage patterns: 13 ipsilateral axillary nodes, 7 contralateral axillary nodes, 6 ipsilateral internal mammary nodes, 1 contralateral internal mammary node, 3 intramammary nodes, 1 supraclavicular node, 1 infraclavicular, 2 intercostal nodes and 1 pectoral node. **Conclusion:** Our results demonstrate a diversity of drainage patterns in the patients with breast cancer recurrence who had been submitted to previous surgical intervention. Routine lymphoscintigraphy should therefore be mandatory in this group, as it may significantly impact staging, therapy approach and prognosis.

EP286

Clinical outcomes of sentinel lymph node biopsy in breast cancer patients. Our follow up experience

S. M. Nieves Maldonado¹, S. Argibay Vázquez², M. Garrido Pumar¹, P. Fierro Alanis¹, L. Souto³, B. Vidal⁴, V. Pubul Nuñez², B. Fernández⁵, O. D. Rodríguez Fónseca⁶, Á. Ruibal Morell²; ¹Nuclear Medicine Department. Hospital Clínico Universitario de Santiago de Compostela, Santiago de Compostela, SPAIN, ²Nuclear Medicine Department. Hospital Clínico Universitario de Santiago de Compostela. Grupo de Imagen Molecular e Oncología, Instituto de Investigación Sanitarias (IDIS), Santiago de Compostela, SPAIN, ³Gynecology Department. Hospital Clínico Universitario de Santiago de Compostela, Santiago de Compostela, SPAIN, ⁴General Surgery Department. Hospital Clínico Universitario de Santiago de Compostela, Santiago de Compostela, SPAIN, ⁵Pathologic Anatomy Department. Hospital Clínico Universitario de Santiago de Compostela, Santiago de Compostela, SPAIN, ⁶Nuclear Medicine Department. Hospital Central de Asturias, Oviedo, SPAIN.

Purpose: Our aim is to evaluate the clinical outcomes after a sentinel node biopsy in patients with breast cancer followed up at our institution. **Methods:** Our study involved 828 consecutive breast cancer patients who underwent isotopic detection of SLN in our department. Lymphoscintigraphic images were acquired after injection of 111 MBq of Te^{99m} nanocolloid for SLN mapping. SLN localization at surgery was performed using a hand-held gamma probe. Sentinel nodes were studied intraoperatively and axillary lymphadenectomy was indicated in SLN positive cases. **Results:** The median follow-up time for the study was 4.5 years (range 1-9 years). The mean age of patients was 58 years (range 28- 88 years), most of them were staged as I (47%, n: 386) and IIa (29%, n 237) according to TNM 7th edition. The most prevalent tumor type was infiltrating ductal carcinoma (77%), and the most frequent molecular diagnosis was Luminal A (68 %). The pre-surgical lymphoscintigraphic images showed tracer migration to the SLN in 91% of patients included

(755), showing lymphatic drainage to axillary region (n: 751 - 99.5 %), as well as the internal mammary chain (10%), clavicular region (6 %) and intramammary region (5%). A mean of 2,6 sentinel lymph nodes were resected per patient (range 1-6 SLN). The pathology results were negative for malignancy in 63% of cases (478). From the 277 positive for malignancy SLN, 108 presented micrometastases. Lymphadenectomies were performed in 268 positive for malignancy patients. The 32% of these lymphadenectomies were positive for malignancy (86). The breast cancer committee decided that 9 patients with micrometastasis should not receive lymphadenectomy, 5 of them were SLNB prior to neoadjuvant chemotherapy cases and the remaining 4 were derived to radiotherapy. Almost every patient included in the study presented a favorable follow up 94 % (780), 6 developed local recurrence (0.7%). Only one patient presented axillary recurrence (0, 1%), it was a positive for malignancy SN due to micrometastasis which was not considered for lymphadenectomy, and was detected as a recurrence at the sixth year of follow-up. Metastases appeared over time in 16 patients (1.9%). The 3% of patients died (25) due to different reasons, and only 8 of the deaths were secondary to the breast cancer. Conclusion: Our results allow us to indicate that adequate local control is achieved with favorable outcomes after many years of follow up by application of the SLN techniques as lymphatic staging tools for breast cancer patients.

EP287

Sentinel node biopsy after neoadjuvant therapy in breast cancer patients

J. Duch, F. Ascencio, B. García Valdecasas, E. Capdevila, A. Moral, A. Domènech, D. López, I. Carrió; Hospital de la Santa Creu i Sant Pau, Barcelona, Barcelona, SPAIN.

Aim: We previously validated sentinel lymph node dissection (SLND) after neoadjuvant therapy (NT) in a group of 30 breast cancer patients. We have evaluated the results 6 years after validation. **Methods:** Between february 2010 - december 2015, 170 breast cancer patients (T2-3, N0-1, M0) were treated with NT. After then all patients were N0. After the SLND, complete axillary lymph node dissection (ALND) was only performed in those with sentinel node metastases or not located. **Results:** 81 patients (48%) were N1 before NT, but all were N0 when the treatment was finished. Whole SLND identification rate was 92% (85% in initial N1 patients and 98% in initial N0 patients). In 14 patients (2 N0 and 12 N1) SLND was not found. Only 7 of these ALND was positive. Among located SN, 36 of them were positive. Among the 170 patients we have been able to avoid 120 axillary dissections (70%) (37 of them were initially N1). With the follow-up, only 1 patient has developed local recurrence and 11 patients distant metastases, but none of them has developed axillary recurrence. **Conclusion:** SLND after NT is safe and feasible in breast cancer patients, not only in initially N0 but also in initially N1. It accurately predicts the status of the axilla and avoids unnecessary ALND.

EP288

¹⁸F-FDG PET/CT Real Time guided biopsy: our experience

V. Rossetti^{1,2}, A. Cappelli³, T. Balbi⁴, A. Gasbarrini⁵, F. Mangiacotti¹, S. Brocchi³, L. Zanoni³, R. Golfieri³, S. Fanti¹, C. Nanni¹; ¹Azienda Ospedaliero-Universitaria S.Orsola Malpighi, Dipartimento di Medicina Specialistica, Diagnostica e Sperimentale, U.O. Medicina Nucleare, Bologna, ITALY, ²Azienda Ospedaliero-Universitaria Policlinico di Modena, Dipartimento di Oncologia ed Ematologia, S.C. Medicina Nucleare, Modena, ITALY, ³Azienda Ospedaliero-Universitaria S.Orsola Malpighi, Dipartimento Malattie Apparato Digerente e Medicina Interna, U.O. Radiologia, Bologna, ITALY, ⁴Azienda Ospedaliero-Universitaria S.Orsola Malpighi, Dipartimento di

Ematologia-Oncologia e Medicina di Laboratorio, U.O. Anatomia e istologia patologica, Bologna, ITALY, ⁵Istituto Ortopedico Rizzoli, Dipartimento Patologie Ortopediche-Traumatologiche Specialistiche, S.C. Chirurgia Vertebrale a indirizzo Oncologico e Degenerativo, Bologna, ITALY.

The clinical management of a suspect lesion relies not only on diagnosis of benign vs malignant, but also on tumor grading, immunohistochemistry and genetic information. Biopsy of suspect tissues is required for diagnosis and planning an adequate treatment. Open incisional biopsy (OIB) is traditionally the method of choice, providing an accuracy of approximately 100%, nevertheless is associated with several drawbacks. The development of imaging-guided biopsies (CT,US) has almost overcome these disadvantages: safe, easy to perform, less invasive and with a good accuracy. However, in recent literature a variable amount of non-diagnostic imaging guided procedures is reported. FDG PET/CT is a functional imaging technique capable of interrogating the metabolic characteristics of masses, with a very high sensitivity. Inherent advantages include early detection of malignancy, (sometimes before changes are evident morphologically), and concerning inhomogeneous tumors, FDG uptake is higher in the most malignant part of the lesion, lower in the most differentiated components and absent in necrotic/fibrotic areas. In the period 11/2014-10/2015 were selected 11 patients with unclear hypermetabolic findings (more lesions with variable SUVmax, small lesions, large inhomogeneous masses; 7F,4M, mean age 56). 9/11 had a suspect malignancy relapse (4 anorectal, 2NHL, 2 gynecologic, 1 Langherans Histiocytosis), 2/11 was a first diagnosis. 5/11 had a previous non diagnostic CT-guided biopsy. FDG PET/CT guided biopsy was performed by trained doctors (interventional radiologist/orthopedic, nuclear medicine and pathologist): after a PET/CT target on the lesion were identified its skin projections and local anaesthesia was performed. The biopsy needle was tracked by driving its progression towards the highest SUVmax through serial PET/CT acquisition (1bed/position; acquisition time 1'). On average, the procedure lasted 1h/patient. The sample was laid down on adhesive glass slide for cytological extemporaneous exam, were tested its adequacy (if not, repeated) and, sometimes, for an immediate diagnosis. 9/11 pts had a definitive diagnosis after PET/CT biopsy (1TBC, 1 sacral chordoma, 2 rectal ca relapse, 2NHL, 2 gynecological ca, 1 Langherans Histiocytosis) while 2 pt with suspect rectal relapse had non pathological findings (1 post-RT scar tissue, 1 muscular tissue). These pt are currently negative after 18 months follow-up. No pts had complications. FDG PET/CT guided biopsy is feasible and safe in the clinical practice. It impacted positively on the time to treatment onset, especially in pt with a previous non diagnostic procedure. Further issues to be discussed are the dose (pt and operators), scanner occupancy, real time/non real time acquisition, non FDG tracers.

EP289

The diagnostic performance of sentinel lymph node biopsy after neoadjuvant chemotherapy in patients with node negative and node positive breast cancer: prospective single centre trial

S. N. Novikov, S. Kanaev, P. Krivorotko, E. Trufanova, P. Krzhivitskiy, L. Jukova; N.N. Petrov Institute Oncology, St Petersburg, RUSSIAN FEDERATION.

Purpose: to evaluate diagnostic accuracy of sentinel lymph node (LN) biopsy (SLNB) after neoadjuvant chemotherapy (NAC) in patients with breast cancer (BC). The secondary end point was to determine whether SPECT-CT with 99mTc-MIBI can guide patient selection for SLNB. **Material & Methods:** From May 2014 to March 2016, 62 women with BC were accrued to the study. Before the start of NAC all patients underwent routine clinical staging with obligatory addition of SPECT-CT scintimammography (SMG) with 99mTc-MIBI. In 44 women with suspiciously abnormal axillary LN ultrasound examination was supported by

aspiration biopsy. According to clinical examinations 40 women were node-positive and 22 - node-negative. After 2-3 cycles of NAC and before surgery efficacy of treatment was evaluated by ultrasound and SMG. In all cases accuracy of SNLB was verified by standard axillary LN dissection. **Results:** All 62 women included in analysis underwent successful SLNB: metastases in SLN were revealed in 26 cases, false negative results obtained in 4, true negative - in 31 patients. False negative rate (FNR) was 13%. Average number of positive LN in SLNB positive group was 3.92: on axillary dissection 16 of 26 (61.5%) patients had 3 or more metastatic LN. In 25 women with prominent and complete scintigraphic response to NAC sentinel LN were positive in 7 cases, SLNB was true negative in remained 18 women, FNR - 0%. In 31 patients with negative LN on pre-surgery SMG SLNB revealed metastases in 6 of 7 women with positive LN diagnosed on axillary dissection: FNR - 14%. **Conclusion:** 1) High FNR of SLNB after NAC dramatically reduced to zero in women with prominent-complete BC response detected by SMG at the end of NAC. 2) Axillary dissection should be recommended in all patients with positive SLNB after NAC.

EP290

Sentinel Lymph Node Biopsy in penile squamous cell carcinoma: review of our experience

J. Rodríguez-Rubio Corona, R. Jaller Vanegas, J. Suils Ramón, M. Boya-Román, G. Martínez-Pimienta, A. Benítez Segura, E. Noriega Álvarez, J. Suárez Novo, J. Mora Salvadó, M. Bajén Lázaro; Hospital Universitari de Bellvitge - IDIBELL, L'Hospitalet de Llobregat, SPAIN.

AIM: To analyse our experience in the applicability of sentinel lymph node biopsy (SNLB) in patients with squamous cell carcinoma **METHOD:** Retrospective review. 18 p with previous primary surgery for penile cancer (T₁₋₄, G₁₋₂) were included (June 2002-April 2016). Two groups were performed based on clinical groin lymph node status previous SLNB: group A (patients with clinically negative lymph node, cN0) and group B (patients with unilateral clinically groin nodes metastases (cN+)). All patients underwent preoperative lymphoscintigraphy with 99mTc-Nanocolloid and radioguided surgery to evaluate the nodal status in group A, and contralateral nodal status in group B. Ipsilateral lymphadenectomy was performed in patients who had positive sentinel lymph node (SLN). Parameters analyzed: scintigraphy and surgical sentinel node detection; SLN status and lymphadenectomy status when it was performed, and lymph node recurrence in both groups after a median follow-up of 84,5 months (1 month - 168 months). **RESULTS:** 10/18 patients (p) (55.6%) were cN0 and SLNB was requested to study bilateral groin (group A). 8/18 p (44.4%) had unilateral cN + and SLNB was requested to study contralateral groin (group B). Scintigraphic and surgical detection was 100% in both groups. SLN was negative in 8/10p (80%) in group A and in 7/8p (87.5%) in group B. SLN was positive in 3/18p (16.7%) (2p in group A and 1p in group B) and lymphadenectomy was performed in 2/3 (only 1p had positive nodes). 1p of group B developed lymph node recurrence 6 months after SLNB. The scintigraphy showed multiple hot spots, but only two SLN were biopsied at surgery, so residual activity remained (>10%). **CONCLUSION:** Despite the short series of patients studied, SLNB is applicable in cN0 patients to stage bilateral lymph node involvement, and in unilateral cN+ patients to stage contralateral lymph node involvement. Both groups benefit of less morbidity associated to SLNB technique.

EP291

Usefulness of Radioguided Occult Lesion Localization for small intraparenchymal or non palpable lung lesions. Preliminary results

s. fuertes, J. Sanchez, J. Moradiellos, A. Villalba, S. Amor, M. Velasco, A. Varela, A. Maldonado; Quiron Madrid University Hospital, Pozuelo de Alarcon (Madrid), SPAIN.

Objectives: Peripheral subpleural solitary pulmonary nodules can be visualized and resected easily at thoracoscopy, but it is very difficult to localize deep non-palpable pulmonary nodules that lie in lung parenchyma. The aim of this study is to evaluate usefulness of Radioguided Occult Lesion Localization (ROLL) for intraparenchymal or non-palpable lung lesions. **Methods:** This is a prospective study performed from August 2014 to February 2016. 11 patients with suspicious small intraparenchymal or non-palpable lung lesions were offered and consented to the procedure as part of a single diagnostic-therapeutic minimally-invasive surgical approach. The day before or the same day, underwent computed tomography (CT)-guided injection of a solution, composed of 0.2 ml 99mTc-labeled human serum albumin microspheres (1-5 mCi) and 0.1 ml nonionic contrast, into the nodule or into the area just in contact with it, using a 25 G needle. The site of injection were confirmed by CT scan and scintigraphy image. Intraoperative lesions were localized and excised during surgery using a laparoscopic gamma probe, followed by frozen-section analysis. **Results:** No complications were reported after the injection. The diameter of lung lesions ranged from 4-23 mm as measured by CT. In 10/11 cases the gamma-detection was successful and 1 case was considered unsuccessful because the most of the activity was detected in the chest wall but a puncture mark in the lung allowed for a successful localization of the lesion. 4 of 11 cases, who revealed primary lung cancer after frozen-section examination underwent video-assisted thoracoscopic lobectomy except one case lobectomy were performed with a full robotic technique. 4 cases showed metastasis and 3 cases revealed benign lesion. **Conclusions:** Our initial results demonstrate that ROLL guided by CT is useful and simple technique for complete excision undiagnosed lung lesions, particularly in small intraparenchymal or non-palpable ones. It avoids problems such as wire-guide dislodgment and dye diffusion and it may be particularly useful for fully-VATS or robotic approaches, without need for digital palpation.

EP292

ROLL and SNOLL in breast carcinoma patients after NeoAdjuvant Chemotherapy (NAC) treatment

S. Maccafeo¹, S. Chiusaroli¹, F. Fiore Melacrinis¹, S. Ghinassi¹, A. Massari¹, A. Piccinetti¹, A. Ricci², E. Ruggeri¹, E. Pofi¹, P. Frittelli¹, R. Schiavo¹; ¹Belcolle Hospital, Breast Unit, Viterbo, ITALY, ²Belcolle Hospital, Medical Physics Unit, Viterbo, ITALY.

Aim: Surgical planning after NAC in breast cancer patients may be difficult as the clinical impact of imaging techniques based on pre-treatment “marker” insertion after a complete treatment response may be cumbersome in helping the surgeon to clearly detect the tumoral bed and perform total excision. The feasibility of ROLL (Radioguided Occult Lesion Localization) and SNOLL (Sentinel Node biopsy and Occult Lesion Localization) techniques in these settings was evaluated. **Methods:** From 2009 to 2015 we studied 26 patients (pts) undergoing breast cancer surgery after NAC. ROLL (9 pts) and SNOLL (17 pts) surgery was performed, after radiopharmaceutical administration (99mTc-albumin macroaggregate for ROLL, 99mTc-albumin nanocolloid for SNOLL). A 1-2 mCi activity was directly injected as close as possible to the pre-treatment “marker” using an ultrasound guide (12 pts) or a stereotactic mammography (14 pts). Scintigraphic images were then acquired in all pts to verify the absence of anomalous activity diffusion and the correct lymph node detection: subdermal periareolar 99mTc-nanocolloids were administered in SNOLL pts with no lymph node activity (4 pts) after deep interstitial injection. **Results:** In all treated pts (26/26), intraoperative detection was successful and allowed a precise tumoral bed excision. Sentinel node biopsy was correctly performed in 15/17 SNOLL pts: no significant lymphatic drainage was observed in 2 pts even after subdermal periareolar administration. **Conclusions:** ROLL and SNOLL techniques are both feasible in pts undergoing breast cancer surgery after a complete response to the NAC treatment. NAC-induced drainage derangements or secondary lymphatic involvement should be taken in account for those pts with a negative sentinel node identification.

EP293**Starting a ¹²⁵I radioactive seed localization program in nonpalpable breast lesions**

R. SANCHEZ SANCHEZ, A. GONZALEZ JIMENEZ, A. C. REBOLLO AGUIRRE, E. M. TRIVIÑO IBAÑEZ, N. TESTART DARDEL, S. MENJON BELTRAN, J. M. LLAMAS ELVIRA; Hospital Virgen de las Nieves, GRANADA, SPAIN.

AIM: To show our preliminary result in using of ¹²⁵I radioactive seed (RSL) for guidance during surgical resection of nonpalpable breast lesions. **METHODS:** Patients undergoing breast procedures after radiologic localization were included. RSL was performed with a 4.5 mm by 0.8 mm titanium seed containing 3.7–11.1 MBq of iodine 125. The radioactive seed is loaded into and 18G spinal needle after occluding the tip with sterile bone wax. RSL were preferentially conducted under ultrasound guidance and were performed under mammographic guidance if the lesion was no sonographically visible. The day selected was determined by radiology and operative suite scheduling (up to five days). At the time of operation a gamma probe is set to detect 27 KeV (¹²⁵I) source. The incision was made at the point of greatest activity. Seed removal within the specimen is assured by detecting the ¹²⁵I source of radioactivity within the excised specimen and no ¹²⁵I source remaining within the wound. Sentinel lymph node were performed in patients with no contraindication. Margins of excision were assessed delayed. Margins were considered negative if all were ≥ 1 mm from invasive carcinoma and ductal carcinoma in situ on final histology. **RESULTS:** A total of 16 consecutive patients with nonpalpable breast lesions were included. Five of them received neoadjuvant therapy previously. The patient characteristics were: mean age (years)- 60.43, malignant tumor size (cm) mean-1.4, Invasive ductal carcinoma-81.3%, Invasive lobular carcinoma- 12.5% and other histology- 6.3%. Concomitant SLN mapping and biopsy was performed in 14/16. SLN metastases were identified in one patient. In one patient there was an erroneous placement of the seed, a wire was successfully placed to localize the lesion correctly. No major complications occurred during surgery. All seed were removed. Specimen size mean was 4.8 cm; malignant tumor size mean was 1.44 cm. Margins in first specimen were negative in 14/16 (87.5%). Two patients showed margins affected but only one required a reoperation. **CONCLUSION:** In our institution RSL is a feasible procedure that shows promising results. RSL seems to improve our rate of negative margins of excision and shows advantages in scheduling surgery. It is necessary increased the number of patient and good preliminary results encourage us to continue working on it.

EP294**Pulmonary nodules radioguided surgery with gammadetector probe**

J. Suils Ramon¹, R. Jaller¹, I. Romero², J. G. Rojas¹, A. Rodriguez-Gasen¹, E. Noriega¹, G. A. Martinez-Pimienta¹, P. Boya¹, J. Rodriguez-Rubio¹, E. Carreño³, F. Rivas⁴, A. M. Benitez¹, M. Bajen¹, J. Mora¹; ¹Nuclear Medicine Department. Hospital Universitari de Bellvitge-IDIBELL, L'Hospitalet de Llobregat, Barcelona, SPAIN, ²Radiopharmacy and PETs Units. Nuclear Medicine. IDI. Hospital Universitari de Bellvitge-IDIBELL, L'Hospitalet de Llobregat, Barcelona, SPAIN, ³Radiodiagnostic Department. Hospital Universitari de Bellvitge-IDIBELL, L'Hospitalet de Llobregat, Barcelona, SPAIN, ⁴Toracic Surgery Department. Hospital Universitari de Bellvitge-IDIBELL, L'Hospitalet de Llobregat, Barcelona, SPAIN.

AIM: Assessment of radioguided surgery (ROLL) utility in the resection of pulmonary nodules. **METHODS:** Retrospective review of 56 pulmonary ROLL in 47 patients, since 30/03/2012 until 05/11/2015, with a pulmonary lesion potentially resectable. 14 patients without oncologic antecedent. Middle age 60,12 years old (range 34 - 82 y). 2 patients were excluded by disease progression. All patients had a thoracic CT between 2 days and

3 months before the surgical procedure. Scintigraphy detection (planar projection +/- SPECT - CT) and radioguided surgery after intra or peritumoral administration of the radiotracer (1,5 - 3 mCi / 0.2 mL / 0.3 mL air ^{99m}Tc-MAA) guided by CT the same or previous day before the surgery. We analyzed the scintigraphy detection, surgery detection, histological results and the size of the pulmonary lesion. **RESULTS:** Radiotracer administration could not be performed in 2 patients due to retrocostal localization in one patient and moderate symptomatic pneumothorax caused by puncture in other patient. Presurgical scintigraphy showed intrapulmonary focal uptake in 50/54 ROLL (94%), absence of pulmonary uptake in one patient caused by radiotracer pass to systemic circulation, and other patient showed pleural diffusion. In first studies we performed SPECT - TC which did not provided additional information and did not help in the surgical detection respect to planar images, for that reason only it was used in the establishment of the technique and in doubtful cases. The nodal surgical detection was possible in the 49/54 ROLL (90, 70%). The pathology anatomy results showed benignity in 14 nodules. The extracted nodules presented sizes between 4 and 17 mm (medium: 8 mm). **CONCLUSIONS:** ROLL technique in pulmonary nodule is easy and allow the localization of small nodules with safety resection margins. Planar scintigraphy is enough for surgical planning. SPECT - CT is useful in doubtful cases.

EP295**Lymphoscintigraphy (LS) in Oral Cavity Cancer (OCC) as a tool for a tailored surgical approach through selective and modified lymphadenectomy: preliminary report**

S. Panareo¹, N. Malagutti², I. Santi¹, I. Rambaldi¹, S. Taralli¹, S. Pelucchi², A. Pastore², C. Cittanti¹; ¹University Hospital - Nuclear Medicine Unit, FERRARA, ITALY, ²University Hospital - Othorynolaringoiatry Section, FERRARA, ITALY.

Aim: The purpose of the study was to assess the role of LS as a simple and widely accessible method with a favorable cost/benefit ratio in improving OCC staging and surgical appropriateness and implementing a tailored surgical approach to cervical lymph node dissection. The aim was to assess the lymphatic drainage in OCC through LS, in order to identify the percentage of patients with a lymphatic drainage beyond the compartments classically included in tumor surgery, and extend lymphadenectomy to the side of abnormal lymphatic drainage evaluating the metastatic status of excised lymph nodes. **Method:** we enrolled 7 consecutive patients (4 female, 3 male, median age 74±4.2 yo) affected by OCC scheduled for surgery. The day before surgery all patients underwent LS with planar and SPECT/CT images acquisition comprising head and neck regions, after the administration of ^{99m}Tc-nanocoll (median 74±2.1 MBq) divided into injections (median 3±1) performed around the OCC, with lymph nodal drainage identification. Patients underwent tumor excision and lymphadenectomy of usual laterocervical compartment (depending on tumor localization) and radioguided surgery of additional sites of lymphatic drainage as shown by LS. Anatomic-pathological analysis of tumor and lymph nodes was performed. **Results:** in 4 cases the tumor was in the tongue; in 1 case in the upper right dental arch and in 2 cases in the palate. Out of 7 patients, 3 (42%) showed laterocervical lymphatic drainage both ipsilateral and contralateral (LII, LIV and LIII respectively) to tumor. In 1 of these 3 cases (33%), metastasis was identified in the contralateral cervical lymph nodes (LIII). In the remaining 4 cases the lymphatic drainage was only ipsilateral to tumor and lymph nodes metastases were observed in 2 cases (50%). **Conclusions:** Although the results of this study are limited and preliminary, it has been possible to observe that the lymphatic drainage from OCC can be abnormal, namely contralateral to tumor site in cervical region, in a non-negligible percentage of cases (42% overall), with possible cervical lymph nodes metastatic involvement (33% of cases and 14% overall). Therefore LS could be a useful tool to properly map the lymphatic drainage from OCC, in order to perform a selective and modified

lymphadenectomy (different from classical one) with potential benefits for patients in terms of more accurate cancer staging and better disease control, and for health service in terms of costs. Of course, our data should be increased in order to obtain more reliable and reproducible results.

EP296

Is reliable Sentinel lymph node biopsy in axillary node-positive breast cancer patients after neoadjuvant chemotherapy?. Preliminary results

S. Fuertes, G. Hernandez, M. Velasco, S. Linares, R. Sainz de la Cuesta, V. Martínez de Vega, L. Gonzalez, A. Maldonado; Quiron Madrid University Hospital, Pozuelo de Alarcon (Madrid), SPAIN.

Aim: Sentinel lymph node biopsy (SLNB) has replaced conventional axillary lymph node dissection (ALND) in axillary node-negative breast cancer patients, but the use of SLNB remains controversial in patients after neoadjuvant chemotherapy (NAC). The aim of this study is to evaluate if is reliable SLNB after NAC in axillary node-positive breast cancer patients. **Material and methods:** This is a prospective study performed from April 2012 to February 2016. 23 breast cancer patients (p.) diagnosed with metastasis of the axillary lymph node by fine needle aspiration were enrolled in this study. All patients scheduled to receive NAC and patients undergoing SLNB after NAC, followed by ALND. The day before surgery an intrasional (21 p.) dose of 99mTc-nanocolloid (activity of 4 mCi and 0.2 ml volume) was injected guided with MRI (18 p.) or ultrasonography (3 p.) or periareolar (2 p.). The site of injection and lymphatic drainage were confirmed by scintigraphy image. Intraoperative lesion and sentinel lymph node were localized and excised during surgery using a gamma probe. **Results:** Sentinel nodes were identified in 19 p. (identification rate, 82.6%). The number of resection SLN were 36 (1.9 per p.). In 7 p. the SLN was positive however ALND showed metastasis in 5/7p. In 12 p. the SLN was negative with post-chemotherapy changes. In these cases, the ALND was negative with post-chemotherapy changes. The false negative rate was 0%. 4 p. didn't show lymphatic drainage. In 3 p. the ALND was negative with post-chemotherapy changes and 1 p. the ALND showed metastasis. **Conclusions:** Our results demonstrate that SLNB is reliable after NAC for node-positive breast cancer, with an acceptable identification rate.

EP297

Promising Results of RSL Technique to localize non palpable breast lesions

O. Ajuria Ilarramendi, A. L. Santos Carreño, A. P. Ortega Manrique, M. E. Rioja Martin, P. Paredes Rodriguez, J. M. Castro Beiras; Hospital Ramon y Cajal, Madrid, SPAIN.

The increase of the screening mammography rates and the improvement in breast cancer imaging has led to localize non palpable breast lesions (under 1mm). Radioguided Seed Localization (RSL) is a new technique that has replaced WL to localize these lesions. AIM Review of the experience of our Breast Cancer Unit in localization of non palpable breast lesions using Radioguided Seed Localization (RSL). MATERIAL AND METHOD All the patients in our database that underwent RSL surgery between 2013-2015 were considered. Specifically, 275 cases of RSL were reviewed, from which 226 were breast non palpable lesions. Out of these 226 cases, in 192 (84, 96%) the seed was deployed intratumour helped by ultrasonography, while in 29 (12, 83%) cases, radiography (either mammography, CT or MRI) was the elected technique. Just in 3 cases was necessary the combination of both techniques and there were 2 cases where the technique was not reported. RESULTS It must be highlighted that out of the 226 cases, 87,17% were correctly deployed

in the middle of the lesion, 5,75% were left on the tumour margin and only at 8 cases the RSL technique failed. When comparing the rates of deployment obtained with respect to the radiological technique, we observed that 90,63% were correctly set by using ultrasound, 5,21% were marginally set and only in 2,08% cases failed. When the procedure was guided by radiography technique, 68,97% were correctly set, 10,34% marginally, and the rate of failure amounts to 13,79%. It stands out a low rate of affected margins, being necessary to amplify them in only 54 cases and what is more relevant, reintervention was only needed at 6,64% of the cases. When the reintervention rates are analyzed concerning the radiological techniques, it can be noticed, on one hand that when ultrasonography was the elected technique, only 6,25% cases needed another surgery, while on the other hand, when radiography imaging was the preferred technique the rate of reintervention was slightly higher been of 10,34%. CONCLUSION To sum up, RSL is a novel procedure that has become the preferred technique among the surgeons due to the good outcomes, low rate of reintervention, its accuracy and safety. Furthermore, when using RSL guided by ultrasound, results were outstanding.

EP298

Comparison of first day and second day imaging in evaluating sentinel lymph node with SPECT/CT in breast cancer

B. Vatankulu¹, E. Akgün¹, M. Velidedeolu², S. Sağer¹, M. Halaç¹, K. Sönmezoglu¹; ¹Istanbul University Cerrahpaşa Medical Faculty Department of Nuclear Medicine, İstanbul, TURKEY, ²Istanbul University Cerrahpaşa Medical Faculty Department of General surgery, İstanbul, TURKEY.

Aim: Although sentinel lymph node biopsy (SLNB) is a certain method, the protocol of sentinel lymph node scintigraphy (SLNS) is not clear. Studies against the late imaging emphasized that washout of the activity from the lymph node was the main problem. On the other hand, several studies supported the second day imaging after SLNS that make surgeons free to decide the timing of surgery. We compared first day early imaging and second day late imaging in breast cancer patients who had SLNS with SPECT/CT. **Materials and methods:** Thirty-eight patients who referred to our clinic for SLNS before SLNB were included into the study. For whole patients, after injection of 1mCi Tc-99m nanocolloid dynamic imaging followed by first day early SPECT/CT and second day late SPECT/CT imaging were performed. The presence, morphology and activity uptake intensity of SLN and nonSLN were recorded in all imaging. Patients were divided into the two groups as early imaging (group A) and late imaging (group B). Each group were compared by using McNemar test. **Results:** SLN was detected in 18% of patients with dynamic imaging after injection and SLN was detected with late SLNS in whole patients. The number of lymph node compatible with SLN was equal in both group A and B. Although no significant differences in visual analysis of activity uptake intensity were seen in both groups, activity uptake intensity of SLN and nonSLN were decreased in group B patients (p=0.08). Moreover despite the number of nonSLN were higher in group A, no significant difference was showed (p=0.09). There is no difference of the localizations of lymph nodes compatible with SLN between group A and B. The localizations for SLN were; intra+internalmammary in 1 patient, level II in 1 patient and level I in 94% of patients. **Conclusions:** In the present study, no significant differences were observed in the number of SLN and activity uptake intensity between first and second day imaging. It is suggested that imaging performed 1 day before the surgery may help the surgeon free to decide the timing of SLNB.

EP-16 – Sunday, October 16, 2016, during Exhibition hours, e-Poster Area
Clinical Oncology: Therapy Response Assessment

EP299**TRAP substudy: assessment of 18-FLT PET/CT to examine tumour proliferation in patients with ASS1-deficient thoracic cancers treated with arginine deiminase (ADI)-PEG20, pemetrexed and cisplatin**

T. A. Szyszko¹, J. S. Bomalaski², V. Goh³, S. F. Barrington³, G. J. R. Cook³, P. W. Szlosarek⁴; ¹KCL and Guys and St Thomas PET Centre, London, UNITED KINGDOM, ²Polaris Pharmaceuticals Inc, San Diego, CA, UNITED STATES, ³Division of Imaging Sciences and Biomedical Engineering, KCL, London, UNITED KINGDOM, ⁴St Bartholomew's Hospital, London, UNITED KINGDOM.

Aim: Loss of argininosuccinate synthetase 1 (ASS1) sensitises malignant pleural mesothelioma (MPM) and non small cell lung carcinoma (NSCLC) cells to apoptosis following arginine (L-Arg) deprivation. L-Arg depletor pegylated arginine deiminase (ADI-PEG20, ADI) enhances the cytotoxic effect of pemetrexed (PEM) and cisplatin (CIS) in ASS1-negative tumour cells involving suppression of pyrimidine synthesis and the salvage pathway. The aim of this study was to explore the role of 3'-Deoxy-3'-(18)F-fluorothymidine (18-FLT-PET) as a biomarker for assessing disease response to ADI, PEM and CIS (ADIPEMCIS) compared to CT response using RECIST 1.1 criteria in NSCLC and MPM. **Materials and Methods:** 18-FLT-PET was performed to assess tumour proliferation at baseline (scan 1), 24 hours post first dose of ADI and prior to PEMCIS on day 3 (scan 2), post first cycle ADIPEMCIS and before cycle 2 on day 15 (scan 3) and at end of ADIPEMCIS (@ day 120) (scan 4). Baseline imaging was performed in 10 patients with MPM and 4 patients with NSCLC. 3 patients did not complete the study, due to ill health. This was a substudy of a larger phase 1 clinical trial (TRAP). Treatment response was measured using EORTC based PET response criteria (partial response or PR, stable disease or SD, progressive disease or PD). This was compared with the response on diagnostic CT using RECIST 1.1 (NSCLC) and modified RECIST (MPM) criteria at day 15 and also at the end of treatment. **Results:** At the end of cycle one, PET response in 11 patients (8 MPM and 3 NSCLC) was PR in 4/11 (36%) SD in 6/11 (55%) and PD in 1/11 (9%) CT (RECIST 1.1) response in the same 11 patients was PR in 4/11(36%) and SD in 7/11(64%). At the end of treatment, a complete data was only available for both PET and CT in 7 patients and in these PET revealed a PR in 6/7 (86%) and SD in 1/7(14%) whereas CT revealed a PR in 4/7 (57%), SD in 2/7 (29%) and PD in 1/7 (14%). **Conclusion:** 18-FLT-PET may provide early evidence of response to ADI therapy in ASS1-deficient thoracic tumours, equivalent to RECIST 1.1 response rate. The rate of metabolic PRs is maintained at the end of treatment. Our study confirms that L-Arg depletion impacts on tumour proliferation and warrants further investigation as a novel antimetabolite strategy with antifolate drugs for cancer therapy.

EP300**Role of GLCM-based Texture Analysis using FDG PET/CT in Evaluation of Response to Neoadjuvant Therapy in Patients with Locally Advanced Breast Cancer**

G. Kumar, A. K. Pandey, R. Kumar; All India Institute of Medical Sciences, New Delhi, INDIA.

Introduction Tumor heterogeneity assessment using texture analysis in various imaging modalities including PET/CT is evolving as an attractive option in various aspects of Oncology practice. **Aim**Our study assesses the possible role of texture parameters obtained on from FDG PET/CT using Gray Level Co-occurrence Matrices (GLCM) in evaluation of response in patients undergoing neoadjuvant chemo/hormonal therapy for locally advanced breast cancer (LABC). **Material and Methodology** Thirty female patients with histopathologically confirmed breast cancer were enrolled in this prospective study. At baseline FDG PET/CT evaluation, 13 patients had TNM stage II disease while 17 had stage III disease.

Following completion of three cycles of neo-adjuvant therapy, each patient subsequently underwent a post-therapy PET/CT. From each PET/CT scan, the following GLCM-based texture parameters were obtained from gray-scale image of that section of primary tumor with longest diameter: Angular Second Moment (ASM), Inverse Differential Moment (IDM), Contrast, Entropy and Correlation. Each texture parameter was extracted twice for test-retest reliability analysis. For comparison, routinely used metabolic parameters viz. SUVmax, SUVmean, Primary lesion metabolic Tumor Volume (PTV) and whole-body Metabolic Tumor Volume (MTV) were obtained. Appropriate statistical methods were further applied and results were obtained; P value of less than 0.05 was considered statistically significant. **Results** On test-retest reliability analysis, there was excellent linear correlation (Spearman's rho) and ranked correlation (Pearson's r) for all texture parameters with values approaching Unity in all of them. Response to therapy was assessed based on RECIST 1.1 criteria. Accordingly there were 16 responders (Partial Response=15, Complete Remission=1) and 14 non-responders (Stable Disease=6, Progressive Disease=8). On applying Mann Whitney U test, Contrast and Entropy, were statistically significant (P < 0.0001) between the responders and non-responders compared to the other three texture parameters. 'Delta' value (percent change between post-therapy and pre-therapy value) of each texture parameter was calculated and employed for ROC curve analysis. On ROC analysis, texture Entropy (AUC=0.902) and Contrast (AUC=0.879) again outperformed the other three texture parameters. Among the metabolic parameters, SUVmean (AUC=0.888), SUVmax (AUC=0.857) and MTV (AUC=0.821) outperformed PTV. Contrast, Entropy, SUVmean and SUVmax were employed as covariates for binary logistic regression analysis for predicting non-responders. The resulting model correctly classified 86.67% of patients (P=0.0003). Only texture contrast was statistically significant (P=0.0407) in predicting the non-responders. **Conclusion** Our study shows that GLCM-based texture parameters extracted using FDG PET/CT are reproducible, accurate and are valuable in identifying the non-responders in patients with LABC undergoing neo-adjuvant therapy.

EP301**Evaluation of metabolic response with 18F-FDG PET-CT in patients with advanced or recurrent thymic epithelial tumors**

S. Segreto¹, R. Fonti², M. Ottaviano³, S. Pellegrino¹, G. Palmieri³, S. Del Vecchio¹; ¹University of Naples Federico II, Naples, ITALY, ²Institute of Biostructures and Bioimages, National Research Council, Naples, ITALY, ³Rare Tumors Excellence Center, University Hospital Federico II, Naples, ITALY.

Aim: Thymic epithelial tumors are rare malignancies arising in the anterior mediastinum. Although surgery is the mainstay treatment, most of these tumors are unresectable or in advanced stage at diagnosis and require chemotherapy. Furthermore, despite radical resection, recurrence is common in those patients and multicourse therapy is often necessary. The aim of this retrospective study is to evaluate the usefulness of 18F-FDG PET-CT to monitor chemotherapy efficacy in patients with advanced or recurrent thymic epithelial tumors and to compare metabolic response with morphovolumetric reduction of tumor burden as assessed by RECIST criteria. **Materials and Methods:** We evaluated 27 consecutive patients (18 male and 9 female; age 56±11 y) with advanced (16 patients, Masaoka stage III, IVa and IVb) or recurrent (11 patients) thymic epithelial tumors. All patients underwent 18F-FDG PET-CT before and after at least 3 cycles of chemotherapy. 18F-FDG PET-CT scans were acquired after fasting for 8 h and 60 min after i.v. injection of 370 MBq of 18F-FDG using an integrated PET-CT system. SUVmax of all detected lesions was recorded and the most 18F-FDG avid lesion in each patient was selected for determination of percentage change in 18F-FDG uptake using the following formula: $\Delta\text{SUVmax} = \text{SUVmax post} - \text{SUVmax pre}/\text{SUVmax pre}$. Contrast-enhanced CT was performed at baseline and

at the end of the planned regimen to assess tumor response. On the basis of RECIST criteria, patients were allocated in classes of complete response (CR), partial response (PR), stable disease (SD) or progressive disease (PD). ROC curve analysis was performed to define the optimal threshold of deltaSUVmax discriminating responders (CR+PR) from nonresponders (SD+PD). **Results:** Objective response was observed in 17 patients (2 CR and 15 PR) whereas in the remaining patients, 8 showed SD and 2 had PD. Metabolic response expressed as deltaSUVmax was significantly correlated to morphovolumetric response ($r=0.645$, $p=0.001$). ROC curve analysis showed that a deltaSUVmax value of -25% could discriminate responders from nonresponders with a sensitivity of 88% and a specificity of 80%. Conversely, basal SUVmax values, although significantly correlated with the stage of disease ($r=0.521$, $p=0.008$), were not predictive of morphovolumetric tumor response. **Conclusion:** Our findings indicate that metabolic response assessed by 18F-FDG PET-CT may allow early identification of responders and non-responders thus guiding adaptation of therapy in patients with advanced or recurrent thymic epithelial tumors.

EP302

Early evaluation with 18FCH-PET/CT for response assessment among patients with metastatic castration-resistant prostate cancer treated with abiraterone

L. Pailhas¹, L. Vercellino², D. Pouessel³, C. Balouzet¹, E. Barré¹, C. Hennequin⁴, S. Culine³, P. Merlet²; ¹Radiopharmacy Unit, APHP, Hôpital Saint Louis, Paris, FRANCE, ²Department of Nuclear Medicine, APHP, Hôpital Saint Louis, Paris, FRANCE, ³Department of Medical Oncology, APHP, Hôpital Saint Louis, Paris, FRANCE, ⁴Department of Radiotherapy, APHP, Hôpital Saint Louis, Paris, FRANCE.

Abiraterone is a selective inhibitor of androgen biosynthesis used in metastatic castration-resistant prostate cancer manifesting disease progression during and after docetaxel chemotherapy. 18F-Fluorocholine (18FCH) is a cell membrane biosynthesis marker. 18FCH-PET/CT shows better sensibility and specificity than 18FDG-PET/CT in prostate cancer. Metabolic imaging with 18FCH-PET/CT could be an early indicator of therapeutic evolution in comparison to anatomic imaging. The aim of our study is to evaluate the prognostic value of 18FCH-PET/CT in response to abiraterone and its correlation with therapeutic responses. A retrospective study was conducted from January 2011 to December 2014 on patients treated with abiraterone. Patients had two 18FCH-PET/CTs: just before abiraterone treatment instauration and six weeks later. The Standard Uptake Value (SUVmax) relative variation between the two exams (Δ SUVmax) enables the evaluation of tumor response using criteria from the European Organisation for Research and Treatment of Cancer (EORTC). The therapeutic evaluation was conducted following the Prostate Cancer Working Group 2 (PCWG2) recommendations using the following criteria: biologic (Prostate Specific Antigen (PSA) level variation), clinical (treatment tolerance, pain, performance status) and imaging (bone scintigraphy, CT) twelve weeks after abiraterone initiation. Eight patients were identified. 18FCH-PET/CT results are consistent with therapeutic response for 6/8 patients: progressive disease (EORTC criteria) and non-responding (PCWG2 criteria) for 2/6, or stable (EORTC criteria) and responsive (PCWG2 criteria) for 4/6. Two patients' results are inconsistent. In one case, PSA level variation presents a stability indication value (Δ PSA = -12 percent) whereas PET interpretation gives a partial response. In the other, Δ PSA = +90 percent shows a biologic progression whereas the PET indicates stable disease. Average survival without progression is 4.4 months. Average duration of abiraterone treatment is 6.2 months. Causes for interrupting abiraterone treatment are biologic and/or radiologic progression for seven patients. One died. After interruption, patients are treated with cabazitaxel (4/8), docetaxel (1/8) or hormone therapy (1/8). One patient was lost from sight after abiraterone interruption. Economically, although the 18FCH-PET/CT exam is

expensive (550-1000€) it is justified if its predictive value is confirmed, compared to the monthly cost of abiraterone treatment (3200€). 18FCH-PET/CT seems to correctly identify responsive and non-responsive patients at an early stage, but some results show inconsistency. 18FCH-PET/CT and the clinical evaluation will remain complementary. A prospective study and a higher number of patients could give more exhaustive data and statistically confirm this tendency as found in literature.

EP303

Usefulness of 18F FDG PET CT in the assessment of neoadjuvant chemotherapy in Esophageal Cancer

J. Navarro Fernandez¹, L. Frutos Esteban¹, L. Mohamed Salem¹, M. Porras Martinez¹, V. Munitis¹, G. Ruiz Merino¹, M. Marin Vera¹, M. Alcaraz Baños², M. Claver Valderas¹; ¹HCU VIRGEN DE LA ARRIXACA, 30120, SPAIN, ²Universidad de Murcia, 30120, SPAIN.

Although 18F-FDG PET CT has a well-established role in the diagnosis and staging of esophageal carcinoma, it should not yet be used in routine practice to guide neoadjuvant chemoradiotherapy (NACR) decision in patients with this disease. Predicting complete pathologic response (CPR) preoperatively can significantly affect surgical decision making. Aim: to determine if 18F-FDG PET CT characteristics are associated with CPR in patients undergoing trimodality treatment for esophageal cancer. Materials and methods This is a retrospective analysis of 20 patients with Locally advanced oesophageal or junctional cancer underwent 18F-FDG PET CT at baseline and after NACR prior to planned surgical resection. Quantitative measurements of tumor FDG uptake were correlated with histopathologic response. Results On surgical pathology, there was complete or near complete regression of tumor in 12 patients (60% responders) and lack regression or partial response in 8 patients (40% no responders) The median of SUV decrease after finished of therapy was 0.6 ± 0.9 for histopathologic responders and 0.42 ± 0.23 for nonresponders ($p < 0.077$). In receiver operating characteristic analysis, the area under the curve was 0.719 At a threshold of 43% decrease of FDG uptake compared with baseline, sensitivity to detect response was 83.3, with a corresponding specificity of 62.5. The positive and negative predictive values were 82% and 62% respectively. Conclusion FDG PET is a valuable tool for the noninvasive assessment of histopathologic tumor response after NACR.

EP304

Value of 18F-FDG PET/CT in the characterization of indeterminate adrenal lesions

L. Zanoni¹, C. Nanni¹, A. Farolfi¹, E. Casadio², V. Vicennati², G. Zavatta², R. Pasquali², S. Fanti¹; ¹Nuclear Medicine, Azienda ospedaliero-universitaria di Bologna, Policlinico S.Orsola-Malpighi, Bologna, ITALY, ²Endocrinology, Azienda ospedaliero-universitaria di Bologna, Policlinico S.Orsola-Malpighi, Bologna, ITALY.

AIM: To assess the value of 18F-FDG PET/CT for the characterization of indeterminate adrenal lesions. **MATERIALS AND METHODS:** Records of patients (pts) referred to the Endocrinology Unit, between 2006 and 2016, for indeterminate adrenal lesions were retrospectively collected (113 pts). Only pts with at least one 18F-FDG PET/CT performed before diagnosis, available dicom files, histological proofs (or clinical diagnosis) of adrenal findings as Standard of Reference, were included for the analysis (48/113 pts). PET were blindly revised for visual uptake (negative or positive for malignancy, lesion laterality, homogeneity and focality) and semi-quantitative parameters (adrenal SUVmax, SUVmean; adrenal-to-liver-ratio (AL) using liver SUVmean; adrenal-to-controlateral-adrenal-SUVmax-ratio (AA). Adrenal enlargement was considered only when significant on corresponding low-dose CT images. Diagnostic performance was evaluated, cut-off values for optimal separation of benign from malignant

glands were proposed (ROC). **RESULTS:** Using visual interpretation PET resulted negative in 30 pts (all true-negative) whereas positive in 18 (8 true-positive, 10 false-positive) out of 48: sensitivity was 100%, specificity 75%, PPV 44%; NPV 100%, accuracy 79%. The population comprised 40 benign (25 adenoma, 12 hyperplasia, 1 Schwannoma, 2 eumorphic adrenals) and 8 malignant lesions (5 carcinoma, 2 pheochromocytoma, 1 lymphoma). In particular the 10 FP cases (mean SUVmax 6,5) were 4 atypical adenoma, 2 nonfunctioning adenoma, 4 bilateral macro-nodular hyperplasia. Malignant adrenal glands were all significantly enlarged and presented with diffuse and inhomogeneous pattern (1 homogeneous). Mean SUVmax was 10, 5 (median 10,6; range 3,3–18,5); mean SUVmean was 5,9 (median 5,7; range 2–9,7); mean AL-ratio was 4,8 (median 5; range 1,3–7,5); mean AA-ratio was 5,8 (median 4; range 2,5–16,8). On the other side benign lesion showed: mean SUVmax 3,3 (median 2,4; range 0,8–8,5); mean SUVmean 2,1 (median 1,6; range 0,4–5,4); mean AL-ratio 1,5 (median 1,2; range 0,4–3,9); mean AA-ratio 1,7 (median 1,4; range 0,9–3,7). These PET indices were significantly higher in malignant than in benign lesions (Mann-Whitney-U-test: SUVmax $p=0,0006$; SUVmean $p=0,0007$; AL-ratio $p=0,0002$; AA-ratio $p<0,0001$). SUVmax cut-off of 3 resulted in 100% sensitivity but 65% specificity; AL-ratio cut-off of 2,5 in 87,5% for both sensitivity and specificity whereas AA-ratio of 2,3 in 87,5% and 82,5% respectively. Their performance was similar (AUC 0,886; 0,923; 0,848; $p>0,4$). **CONCLUSION:** Our preliminary results suggest that 18F-FDG PET/CT is helpful in assessing the malignant potential of indeterminate adrenal lesions. However a “grey-zone” of benign avid lesions exists. Further analyses (including contrast-enhanced-CT features and hormonal profile) for more accurate multidisciplinary characterization, are ongoing.

EP305

18F-FDG PET/CT versus contrast enhanced (ce) CT versus PET/ceCT in patients with peritoneal carcinomatosis candidates to Hyperthermic Intraperitoneal Chemotherapy (HIPEC)

L. Evangelista¹, A. Cervino¹, G. Pintacuda², G. Ramondo², A. Sommariva³; ¹Nuclear Medicine and Molecular Imaging Unit, Veneto Institute of Oncology IOV - IRCCS, Padua, ITALY, ²Radiology Oncology Unit, Veneto Institute of Oncology IOV - IRCCS, Padua, ITALY, ³Surgery Oncology Unit, Veneto Institute of Oncology IOV - IRCCS, Padua, ITALY.

Introduction: to investigate the relationships between 18F-FDG PET/CT, ceCT, PET/ceCT and surgical evaluation in patients with peritoneal carcinomatosis from mucinous/non mucinous malignancies who were candidates to HIPEC. **Materials and methods:** from 2012 to 2016 we prospectively collected data from 27 patients (median age: 52 years; male: 13) with a clinical suspicious of peritoneal carcinomatosis candidates to HIPEC for the resolution of the disease (18 patients with no-mucinous and 9 with mucinous cancer). All patients underwent FDG PET/ceCT in a single session. The acquisition was started after 60 minutes from the administration of FDG. Two nuclear medicine physicians and 2 radiologists independently evaluated PET/CT and ceCT imaging, respectively. In case of discordance, the consensus was reached by a discussion between the specialists. Moreover, the combined images were evaluated by all the specialists in consensus. The images were qualitatively and quantitative analyses, by using the peritoneal cancer index (PCI). A 39-score was used. The PCIs obtained from surgical look, PET/CT, ceCT and PET/ceCT were compared each other. The coefficients of correlation (r) were calculated. **Results:** PET/CT showed a significant uptake of FDG in 20/27 (74%) patients, being focal in 11 cases, diffuse in 5 and focal+diffuse in 4. The r coefficients were 0.641, 0.639 and 0.99 between PCI at PET/CT vs. ceCT, PCI PET/CT vs. PET/ceCT and PCI PET/ceCT vs ceCT, respectively. Surgical PCI was available in 21 patients, due to a progression of disease in 6 subjects. The r coefficients between surgical PCI, PET/CT, ceCT and PET/ceCT were respectively, 0.528, 0.876 and 0.878. Out of 21 patients who underwent surgical look, 12 had a non-

mucinous cancer and 9 a mucinous one. The r coefficient between surgical PCI and PET/CT was higher in patients with a non-mucinous cancer than the counterpart (0.601 vs. 0.303) and the addition of ceCT significantly increase the correlation ($r=0.953$) (see Table 1). Moreover, at FDG PET/CT, peritoneal carcinomatosis from mucinous cancer showed more often a focal pattern. Conversely, the peritoneal carcinomatosis of non-mucinous cancer had a both a focal and diffuse FDG uptake. **Conclusions:** PET/ceCT as single examination seems more accurate than PET/CT and ceCT alone for the definition of PCI in patients candidates to HIPEC. However, a careful selection of histological pattern should be warranted, although a negative PET/CT scan would provide important prognostic information.

EP306

Characterization of malignant pleural effusion (MPE) with 11C-Methionine PET/CT before and after talc pleurodesis: interim evaluation of a prospective clinical trial

E. Lopci¹, P. Zucali¹, G. Ceresoli², A. Testori¹, E. Voulaz¹, K. Marzo¹, L. Leonardi¹, L. Olivari³, G. Ferraroli¹, E. Bottoni¹, A. Galeassi⁴, G. Veronesi⁵, M. Alloisio¹, A. Santoro¹, A. Chiti¹; ¹Humanitas Clinical and Research Hospital, Milano, ITALY, ²Humanitas Gavazzeni, Bergamo, ITALY, ³Milano University, Milano, ITALY, ⁴Humanitas Castellanza, Castellanza, ITALY, ⁵Humanitas Research Hospital, Rozzano, ITALY.

Purpose: Malignant pleural effusion (MPE) is a pathological condition associated to cancer and one the most frequent signs of mesothelioma presentation. 18F-FDG PET/CT has proved to be useful in detecting malignant pleural lesions, although unreliable results have been reported in early epithelioid mesothelioma and in patients receiving talc pleurodesis. 11C-methionine is expected to be less influenced by inflammatory reaction to pleurodesis. In this study we aimed to define the role of 11C-Methionine PET/CT in the characterization of MPE before and after talc pleurodesis. **Materials and Methods:** From September 2014 to February 2016, 30 consecutive patients referred to our Institution for MPE were prospectively enrolled. Patients were evaluated at baseline and after talc pleurodesis with two consecutive PET/CT investigations: 11C-methionine (experimental) and 18F-FDG (standard in our Institution). Semi-quantitative PET parameters were defined for both examinations: i.e. SUVmax, SUVmean, metabolic tumor volume (MTV) and metabolic tumor burden (MTB=MTV x SUVmean). During video-thoracoscopy for pleurodesis, all patients underwent pleural biopsy and imaging parameters were compared to pathological findings. A statistical analysis was performed to compare the impact of talc pleurodesis on 11C-Methionine and 18F-FDG PET. **Results:** The interim analysis was completed in 15 out of 30 patients (M:F= 13:2; mean age 73 years), all affected by malignant mesothelioma (12 epithelioid, 3 non-epithelioid). All tumors showed increased uptake of 11C-methionine at baseline: median SUVmax, SUVmean, MTV and MTB were 4.7 (range 3–10.1), 2.8 (range 1.5–4.6), 19.5 (range 0.9–464.3) and 45.2 (range 2–2052.2), respectively. MTV and MTB were significantly higher in non-epithelioid tumors compared to epithelioid histotype ($p=0.022$ and 0.03, respectively). For 11C-methionine PET, the median percentage of variation before and after talc pleurodesis was 12.8 for SUVmax (% Δ SUV) and 29.9 for MTB (% Δ MTB). Compared to 18F-FDG PET, the percentage of variation for MTB resulted significantly lower for 11C-methionine ($p<0.001$), but not for SUVmax. Interestingly, there was an inverse linear correlation between MTV for 18F-FDG PET at baseline and % Δ SUV or % Δ MTB after pleurodesis ($p<0.01$), whereas for 11C-methionine only for % Δ SUV. **Conclusion:** 11C-methionine PET/CT appears to be able to characterize malignant pleural effusion. This preliminary analyses shows that it might be less influenced by inflammatory reaction related to talc pleurodesis compared to 18F-FDG PET/CT.

EP307**A Paradigm Shift in PET Imaging Reconstruction Inspired by Digital PET**

M. V. Knopp, K. Binzel, A. Siva, R. Moore, C. L. Wright, J. Zhang; The Ohio State University, Columbus, OH, UNITED STATES.

Aim: Despite many advances in PET technology and reconstruction, as we moved from filtered back projection to iterative with time of flight correction, the image voxel volume remained unchanged using a 3–4 mm voxel length. Prior attempts to increase the reconstruction matrix, thus reducing the voxel volume, were impeded by the rapid increase in noise. With the introduction of solid state detectors, we realized that iterative convergence is strongly dependent upon count densities and changes in voxel volume may thus require a re-optimization of reconstruction parameters. With this experience, we reassessed the possibility of substantially improving image quality, even on conventional time of flight PET systems through rigorous reconstruction optimization. **Materials and Methods:** 30 previously acquired FDG whole body oncologic PET scans performed within standard of care and archived with complete listmode data were included in an optimization / assessment study. 10 cases were used for rigorous analysis by reconstructing listmode data using a 2mm voxel / 288x288 reconstruction matrix, using a comprehensive set of iterative reconstruction parameters. These images were compared against each other as well as the default 4mm voxel / 144x144 matrix images using visual and quantitative assessments. The ROC methodology was used to define the optimized parameter set that was subsequently utilized in 20 cases for intra-individual comparisons. **Results:** Surprisingly, higher matrix reconstruction was readily accomplished with improved and preferable image quality from standard clinical acquisitions. High definition reconstruction simply requires a re-optimization of iterative reconstruction parameters, as the reconstruction dependent image noise level otherwise impedes the benefits of reduced partial volume effects. Without optimization, decreasing voxel size leads to spuriously poor image quality. We found that reducing the number of iterative subsets reliably produces excellent image quality while simultaneously maintaining quantitative accuracy. **Conclusion:** Image quality can be considerably refined, even on current generation conventional time of flight PET/CT systems, if smaller voxel volume reconstructions are being used based on utilizing re-optimized reconstruction parameters. While the future of PET is evolving into solid state digital detection, which has many benefits, existing technologies still hold great potential for improving image quality through optimization of reconstruction.

EP308**Are the Clinical Indications Easily Retrieved from ¹⁸F-FDG PET-CT Request-Forms? Analysis of 200 ¹⁸F-FDG PET-CT Request-Forms from a Single PET-CT Centre**

M. Mattoli¹, V. Scolozzi¹, D. Ripani¹, L. Indovina², V. Rufini¹, A. Giordano¹, M. Calcagni¹; ¹Institute of Nuclear Medicine, Università Cattolica del Sacro Cuore, Rome, ITALY, ²Institute of Physics, Università Cattolica del Sacro Cuore, Rome, ITALY.

Introduction: In oncologic patients, the identification of clinical indication is of paramount importance to evaluate whether PET-CT is appropriate or not according to the EANM guidelines. **Aims:** to assess the accuracy of ¹⁸F-FDG PET-CT request-forms; to analyse the practical-organizational aspects. **Materials and methods:** We retrospectively evaluated 200 consecutive oncological ¹⁸F-FDG PET-CT request-forms. We assessed the accuracy of the request-forms (consisting on the form and the clinical information attached) and the clarity of the clinical indication reported on it. The request-form was defined as “correct” when filled-out in all parts or at least in those essential to identify the clinical indication; the clinical indication was defined as “clear” when it was well identified. In addition, we assessed the following practical-organizational aspects: presence of information attached; amount of in-

patients/out-patients; PET-CT requests with CT contrast medium; urgency. **Results:** Patients characteristics: 90 males; mean age 64±13years. Anatomical districts involved: lung (n=53), breast (n=33), gastrointestinal (n=33), pelvic (n=29), haematological (n=25), head-neck (n=11), double district (n=6); excretory system (n=5), skin (n=3), unknown primary malignancy (n=2). Request-forms judged as correct: 115/200 (58%); clear clinical indications: 124/200 (62%); correct request-forms with clear clinical indications: 111/200 (56%); correct request-forms with unclear clinical indications: 4/200 (2%); non-correct request-forms with unclear clinical indications: 72/200 (36%); non-correct request-forms with clear clinical indications: 13/200 (6%). Information attached: 74/200 (37%); in-patients: 3/200 (1.5%); contrast medium: 10/200 (5%); urgency (to be performed within 15days): 51/200 (25%). **Conclusion:** In our clinical practice, the accuracy of the request-forms was low because only half of them was properly filled-in. This can be attributed to a poor compliance of the referring clinician who selected none or more than one clinical indication. Inaccuracy implies an overload work for nuclear physicians to retrieve necessary information. Finally, PET-CT is a second-line exam, as demonstrated by the low requests of PET-CT with contrast medium (diagnostic CT had already been performed), and by the small number of PET-CT performed for in-patients. The need to perform PET-CT within 15 days is low, suggesting that the clinical indications considered really urgent (<15days) are few, such as staging, guiding biopsy, and unknown primary tumor. On the contrary, treatment evaluation and characterization of pulmonary nodule can be considered “not urgent”, while restaging can be performed within 15days, as well as after. This analysis allows to improve the organization of the PET-CT departments, and to reduce the waiting-list.

EP309**Repeatability of Quantitative ¹⁸F-FLT Uptake Measurements in Solid Tumors: A multi-centre Meta-Analysis**

G. M. Kramer¹, Y. Liu², A. J. de Langen³, E. P. Jansma⁴, I. Trigonis⁵, M. Asselin⁵, A. Jackson⁵, L. Kenny⁶, E. Aboagye⁶, O. S. Hoekstra¹, R. Boellaard¹, QuIC-ConCePT consortium; ¹Department of Radiology and Nuclear Medicine, VU university medical center, Amsterdam, NETHERLANDS, ²European Organisation for Research and Treatment for Cancer (EORTC), Headquarters, Brussels, BELGIUM, ³Department of Pulmonology, VU university medical center, Amsterdam, NETHERLANDS, ⁴Medical Library, VU university medical center, Amsterdam, NETHERLANDS, ⁵Institute of Population Health, Wolfson Molecular Imaging Centre, Manchester Academic Health Sciences Centre, The University of Manchester, Manchester, UNITED KINGDOM, ⁶Department of Surgery and Cancer, Imperial College London, Hammersmith Hospital, London, UNITED KINGDOM.

Objectives. ¹⁸F-Fluorothymidine (¹⁸F-FLT) positron emission tomography (PET) has potential as imaging biomarker of response to antitumor therapy. Before quantitative ¹⁸F-FLT uptake metrics can be used for evaluation of proliferative response, repeatability of these metrics have to be established. The aim of this study was therefore to determine repeatability of several ¹⁸F-FLT uptake metrics by analyzing available patient data from previously published reports. **Materials and Methods:** A systemic search was performed in PubMed and EMBASE.com from inception-January 2015 and revealed five ¹⁸F-FLT repeatability cohorts in solid tumors. ¹⁸F-FLT avid lesions were delineated using a 50% isocontour adapted for local background on the test and retest scans (in-house developed software). SUVmax (maximum SUV), SUVpeak (1.2cm³ spherical region positioned to maximize its mean value), SUVmean (mean SUV), proliferative volume (50% threshold of SUVpeak corrected for local background) and total lesion proliferation (TLP) (product of SUVmean and proliferative volume) were calculated. Repeatability of quantitative uptake metrics was assessed using repeatability coefficients (RC) calculated as 1.96 * SD, linear regression analysis and intraclass correlation coefficients (ICC). Analyses were performed to investigate the impact of different lesion selection criteria.

Results: Images from four datasets containing 30 patients with 52 lesions were obtained and analyzed (10 in breast cancer, 9 in head and neck squamous cell carcinoma and 33 in non-small cell lung cancer patients). Repeatability of SUV (RCs of 29.4% - 33.5%) was better than of TLP (76.4%) and proliferative volume (79.2%). Patients did not receive any therapeutic treatment between the test and test scans (interval <8 days). No significant differences in RCs were found between the different SUV metrics. With exception of proliferative volume, a good correlation was found between test and retest data for all ^{18}F -FLT uptake metrics ($R^2 > 0.86$; $\text{ICC} > 0.91$). Lesion selection methods based on size (tumor >4.2mL), SUV (>4.0), hottest lesion or primary tumor did not influence repeatability of any of the ^{18}F -FLT uptake metrics. **Conclusion:** We show that ^{18}F -FLT SUV metrics are acceptably repeatable in the meta-analysis of a multi-centre dataset, with proliferative volume and TLP being less repeatable. A $\geq 30\%$ change in SUV metrics represents a true change in ^{18}F -FLT uptake independent of the lesion selection strategy.

EP310

Diagnostic Value Of 18F-FDG PET/CT In Fever Of Unknown Origin. Our Experience

M. Fernández Rodríguez, P. García Alonso, C. Sandoval Moreno, A. Herrero Muñoz, L. Castillejos Rodríguez, C. Paniagua Correa, M. Balsa Bretón, A. Ortega Valle, F. Penín González; Hospital Universitario de Getafe, Getafe, SPAIN.

AIM: To assess diagnostic contribution of 18F-FDG PET/CT for evaluation of fever of unknown origin (FUO). **MATERIALS AND METHODS:** We retrospectively evaluated (August 2013-March 2016) 54 cases of patients investigated for FUO. All fulfilled the Durack and Street modified criteria for FUO and underwent a 18F FDG PET/CT. 12 patients were excluded by lack of data under follow-up. 42 cases were included in the analysis: 22 women (52.38%) and 20 men (47.62%); aged 59 ± 27 . Final diagnoses were based on integration of clinical, microbiological, radiological and histological data at follow-up (mean follow-up time 6.54 months). Studies showing at least one area of pathological FDG uptake ($\text{SUV}_{\text{max}} > 2.5$) were defined as PET positive. Studies showing FDG activity only in areas of physiologic tracer biodistribution were considered as negative. A PET/CT study demonstrating a focal, localized disease process confirmed by additional conventional techniques as representing the cause of FUO was considered as contributory for diagnoses and defined as true-positive (TP). A PET/CT study showing normal findings, when no localized disease process was further diagnosed by additional techniques, and there was no evidence of disease following at least 6 months of clinical follow-up, was regarded as contributory in excluding focal disease and defined as true-negative (TN). **RESULTS:** 19 (45.24%) PET/CT studies demonstrated pathological FDG uptake and were considered abnormal. 17 studies were considered TP (40.48%) and final diagnoses were: 9 infectious diseases (1 osteomyelitis, 1 pancreatitis, 1 hepatic abscess, 1 spondylodiscitis, 1 prosthetic joint infection, 3 vascular graft infections and 1 tuberculosis), 9 inflammatory/autoimmune diseases (3 lymphadenopathy of uncertain clinical significance, 2 temporal arteritis, 2 sarcoidosis, 1 Wegener's granulomatosis, 1 Ig G4-related disease) and 1 neoplasm (thymic carcinoma). FP included 2 cases: 1 increased FDG uptake in anal region (ultrasound and MRI demonstrated no pathological process) and 1 uptake in left ventricular outflow tract (normal cardiac MRI). PET/CT showed no pathological FDG uptake in 23 cases (54.76%): 19 (45.24%) were considered TN (FUO resolved with no etiologic diagnoses and no evidence of disease during at least a 6-month follow-up) and 4 FN (9.52%): 2 endocarditis, 1 renal vasculitis, and 1 patient died with no diagnosis. PET/CT had: accuracy 85.71%, sensitivity 80.95%, specificity 90.48%, a positive predictive value 89.47% and negative predictive value 82.61%. In 85.71% cases PET/CT was considered clinically helpful and contributory to diagnosis. **CONCLUSION:** PET/CT is a noninvasive diagnostic tool useful for the diagnosis of patients with FUO.

EP311

Is The Amount of Doubtful Reports Dependent on the Appropriateness of Clinical Indication? Analysis of 200 ^{18}F -FDG PET-CT Reports from a Single PET-CT Centre

M. Mattoli¹, V. Scolozzi¹, D. Ripani¹, L. Indovina², V. Rufini¹, A. Giordano¹, M. Calcagni¹; ¹Institute of Nuclear Medicine, Università Cattolica del Sacro Cuore, Rome, ITALY, ²Institute of Physics, Università Cattolica del Sacro Cuore, Rome, ITALY.

Introduction: PET-CT report is the most important final step in the diagnostic work-up. It can be positive, negative, or doubtful for malignancy. Since PET-CT is a second-line exam, the rate of doubtful reports should be low. **Aims:** to evaluate the rate of doubtful ^{18}F -FDG PET-CT reports; to match the report with the appropriateness categories according to EANM guidelines 2010 (v.1.0) and 2015 (v.2.0). **Materials:** We retrospectively classified as positive, negative, and doubtful for malignancy 200 consecutive oncological ^{18}F -FDG PET-CT reports drafted by six nuclear physicians. We matched them with the appropriateness categories, and the doubtful reports with clinical indications. **Results:** Overall, 92/200 (46%) PET-CT reports were positive, 92/200 (46%) negative, 16/200 (8%) doubtful. According to EANM guidelines v.1.0: 61/200 (31%) PET-CT were appropriate, 124/200 (62%) inappropriate, 15/200 (7%) promising. The reports of appropriate PET-CT group were positive in 34/61 (56%), negative in 22/61 (36%), doubtful in 5/61 (8%: all restaging). The reports of inappropriate PET-CT group were positive in 47/124 (38%), negative in 67/124 (8%), doubtful in 10/124 (8%: 7 follow-up, 1 restaging, 1 treatment response, 1 staging). The reports of appropriate PET-CT group were positive in 11/15 (73%), negative in 3/15 (20%), doubtful in 1/15 (7%: response evaluation). According to EANM guidelines v.2.0: 127/200 (64%) PET-CT were appropriate, 73/200 inappropriate. The reports of appropriate PET-CT group were positive in 78/127 (61%), negative in 40/127 (32%), doubtful in 9/127 (7%: 6 restaging, 2 treatment response, 1 staging). The reports of inappropriate PET-CT group were positive in 14/73 (19%), negative in 52/73 (71%), doubtful in 7/73 (10%: follow-up). **Conclusions:** Overall, the rate of doubtful PET-CT reports is very low (overall 8%) despite the reports were drafted by several nuclear physicians. This finding confirms that when all previous exams are available (PET-CT is a second-line exam) and clinic-anamnestic information are known, the chance to draft a doubtful PET-CT report is very low. The doubtful reports rate in each appropriateness category is almost equal, either for guidelines v.1.0 or v.2.0. The major incidence of doubtful reports were in follow-up and restaging and not in other clinical indications. Two examples for explaining these findings: during follow-up, a ^{18}F -FDG uptake without a corresponding morphological alteration not supported by clinical/instrumental suspicion can be doubt; for restaging, a ^{18}F -FDG uptake in a morphological alteration around the prosthesis implanted for previous malignancy can be doubt. Finally, the nuclear physician experience and temperament play an important role in the reporting.

EP312

Clinical implication of F-18 FDG PET/CT with Philadelphia chromosome-negative myeloproliferative neoplasms

S. Kang¹, J. Kim², H. Bom¹, J. Min¹, H. Song²; ¹Department of Nuclear Medicine, Chonnam National University Hwasun Hospital, Hwasun-Gun, KOREA, REPUBLIC OF, ²Department of Nuclear Medicine, Chonnam National University Hospital, Gwangju, KOREA, REPUBLIC OF.

Background: The objective of this study was to investigate the clinical implication of ^{18}F -FDG PET/CT in patients with Philadelphia chromosome-negative myeloproliferative neoplasms (MPNs). **Materials and methods:** Twenty-eight patients diagnosed with Philadelphia chromosome-negative MPNs who underwent FDG PET/CT from 2007 to 2013 were enrolled; 6 polycythemia vera (PV), 16 essential

thrombocytopenia (ET), 6 primary myelofibrosis (PMF). All patients underwent FDG PET/CT, hematologic tests, and bone marrow biopsy. FDG uptake was semi-quantitatively assessed using mean standardized uptake values (SUVmean) in the lower thoracic and lumbar vertebrae and mediastinal blood pool. The correlation between PET and clinical parameters were determined. The prognostic significance of following parameters were evaluated: age, sex, laboratory parameters, JAK2V617F mutation, splenomegaly, and bone marrow FDG uptake. **Result:** Among parameters, only the presence of JAK2V617F mutation and WBC count ($\times 10^3/\text{mm}^3$) were correlated with bone marrow FDG uptake. Bone marrow SUVmean to mediastinal blood pool SUVmean ratio ($\text{SUV}_{\text{BM/M}}$) was significantly higher in patients with JAK2V617F mutation and in patients with higher WBC count; 1.73 ± 0.37 vs. 1.06 ± 0.23 in $\text{SUV}_{\text{BM/M}}$ ($p < 0.0001$), 1.72 ± 0.38 vs. 1.32 ± 0.40 in $\text{SUV}_{\text{BM/M}}$ ($p = 0.007$), respectively. Furthermore, $\text{SUV}_{\text{BM/M}}$ showed a strong positive correlation with the allele burden of JAK2V617F ($\rho = 0.702$, $p = 0.005$) and the WBC count ($\rho = 0.643$, $p < 0.0001$). However, the allele burden of JAK2V617F was not correlated with the WBC count ($\rho = 0.344$, $p = 0.250$). High $\text{SUV}_{\text{BM/M}}$ ($p = 0.021$, log-rank test) and presence of JAK2V617F mutation ($p = 0.023$) were statistically significant poor prognostic factors in overall survival analysis but not in event free survival analysis ($p = 0.275$, $p = 0.087$, respectively). **Conclusion:** In Philadelphia chromosome-negative MPNs, bone marrow FDG uptake might imply JAK2V617F mutation status and predict prognosis.

EP313

Solitary and multiple metastases in the skeletal muscles on 18F-FDG PET/CT imaging

A. Nocuń, B. Chrapko; Chair and Department of Nuclear Medicine, Medical University of Lublin, Poland, LUBLIN, POLAND.

Introduction: Skeletal muscle metastases (SMM) are suggested to occur more frequently than it is usually recognized, however, currently available publications on SMM imaging contain a large number of case reports and only few comprehensive studies. The aim of the present study was to retrospectively investigate the features of SMM detected by 18-fluorodeoxyglucose (FDG) positron emission tomography/computed tomography (PET/CT) with particular attention to patterns of solitary and multiple intramuscular lesions, their frequency and impact on cancer staging. **Materials and Methods:** Our database was analyzed for patients with pathologically proven malignancy, who underwent FDG PET/CT in our institution. The subjects with SMM were included into the study group based on the final diagnosis confirmed by follow-up or histopathology. Images were acquired using a PET/CT system Biograph mCT S(64)-4R (Siemens, Germany). CT was performed without contrast enhancement. Image evaluation was performed visually and by means of maximum standardized uptake values (SUVs). **Results:** The selected group with SMM consisted of 31 patients (1.7% of the database), 18 females and 13 males. A total of 233 lesions were found with SUVmax ranging from 3.2 to 26.8 (average 10.6 ± 6.3). The prevalence of SMM evaluated in specific primary malignancies was the highest in melanoma (6.9%). The most common site of muscle metastases was the torso. Three patterns of skeletal muscle metastatic involvement were observed: 1) multiple SMM associated with extramuscular metastases (20 patients, 64.5%), 2) solitary SMM with other metastatic sites (9 patients, 29%) and 3) isolated SMM without other abnormalities on FDG PET/CT scans (2 patients, 6.5%). In the first and second pattern (93.5% of cases) the presence of SMM did not alter the staging. **Conclusions:** Solitary SMM are less common than multiple. On FDG PET/CT imaging SMM are usually associated with other metastases and their presence does not affect tumor staging. The cases of isolated SMM, detected as the only abnormality on FDG PET/CT scan, are very rare. Nevertheless, in patients with diagnosis of malignant disease, a solitary, FDG avid intramuscular focus should be suspected to represent metastasis. Biopsy is mandatory in such cases.

EP314

Role of ^{18}F -FDG PET/CT in the Diagnosis and Staging of Rosai-Dorfman Disease

S. Karunanithi^{1,2}, A. Mukherjee², R. Kumar²; ¹Malabar Institute of Medical Sciences, Calicut, INDIA, ²All India Institute of Medical Sciences, New Delhi, INDIA.

Aim: To evaluate the role of ^{18}F -Fluorodeoxyglucose (^{18}F -FDG) positron emission tomography/computed tomography (PET/CT) in the diagnosis and staging of Rosai-Dorfman disease (RDD). **Materials and Methods:** Study was a retrospective data analysis of histopathologically proven RDD who underwent FDG PET/CT in the department of Nuclear Medicine, AIIMS, New Delhi between July 2005 to August 2014. Twenty six patients (mean age-31.5 years, median-33 years, range: 3-48) with clinically suspected and/or histopathologically proven RDD underwent ^{18}F -FDG PET/CT imaging for staging and/or localisation of the disease. The scans were done with a dedicated PET-CT scanner (Biograph 2, Siemens, Germany). All patients fasted for at least 4-hours. Blood glucose was less than 140mg/dl. FDG PET-CT study was evaluated by two experienced Nuclear Medicine physicians. The PET-CT findings were grouped as nodal, extranodal and both. SUVmax of nodal and extranodal lesions were measured. Results were verified with clinical follow up and histopathology. Histopathological confirmation of the suspected lesion was taken as reference standard. **Results:** Age of patients ranged from 3-48 years [mean of 31.5 (± 1.25) years]. M:F ratio was 1:1. Of the 26 patients with RDD, PET/CT demonstrated pure lymph nodes (LN) involvement in 15 (57.7%), extranodal in 3 (11.5%) and both nodal & extranodal lesions in 8 (30.8%) patients. Pure LN involvement patients presented with generalised LN in 12 and with bilateral cervical LN in 3 patients. Retro-orbital mass was the extranodal site who presented with pure extranodal involvement. In patients with both nodal and extranodal involvement, skeletal and soft tissue lesions were the extranodal sites. The mean SUVmax of nodal and extranodal lesions were 6.8 and 5.7 respectively. PET/CT emerged as excellent imaging modality for assessment the disease burden with 100% sensitivity and PPV for detecting nodal and extranodal lesions. In our study extranodal in total was found in 42.3% of patients. It correlates with the literature which quotes extranodal involvement is seen in 25%-43% cases. We had 12 patients with generalised lymph nodes involvement which mimics lymphoproliferative disorders. In this scenario, FDG PET/CT findings are nonspecific for RDD, and a biopsy is needed to establish the diagnosis. This study was the first to evaluate the role of FDG PET/CT in RDD in a larger population till date. **Conclusion:** ^{18}F -FDG PET/CT is a very useful imaging investigation for diagnosing and staging in RDD. PET/CT emerged as excellent imaging modality for assessment the disease burden for detecting nodal and extranodal lesions.

EP315

Alert Management In Oncologic Unenhanced 18F-FDG PET-CT Studies

J. Mucientes, B. Rodríguez, A. Prieto, J. Cardona, M. Mitjavila; Hospital Puerta de Hierro Majadahonda, Madrid, SPAIN.

AIM The aim of this poster is to describe the most common findings in oncologic unenhanced 18F-FDG PET-CT studies which must be immediately or as soon as possible communicated to the referring physician. **MATERIAL AND METHODS** We revised unenhanced 18F-FDG PET-CT and described the most common findings encountered in oncologic patients which can be life-threatening or require a priority or immediate evaluation. We described these findings with supporting images. **RESULTS** When a PET-CT study is finished is useful a fast evaluation to assess the image quality and the possible findings which need a immediate or priority clinical evaluation. We divided the findings depending on

the location. Head and Neck Unsuspected brain metastases is one of the most frequent findings which may require a priority evaluation by the referring physician. If there is brain herniation, evaluation should be immediate. Neck airway obstruction or stenosis due a tumour needs to be evaluated clinically. Chest Pneumothorax is other of the most frequent findings in patients referred to a FDG PET-CT scan. Recent pulmonary biopsy is one of its causes. Severe pleural or pericardial effusion needs clinical evaluation and may need thoracentesis or pericardiocentesis. Unsuspected great vessels tumour infiltration may require a priority evaluation. Focal cardiac uptake may require a priority echocardiography. Abdomen Some infrequent findings as pancreatitis, cholecystitis or appendicitis may require clinical evaluation or surgical treatment. Patients should be explored to assess their clinical status. Skeletal Fracture risk assessment and evaluation of soft tissue masses which can produce spinal cord compression should be done in patients with bone metastases. CONCLUSION There are many findings to assess at the end of oncologic PET-CT scans. Some of this findings may require immediate or priority clinical/complementary evaluation even in unenhanced PET-CT studies.

EP316

Can 18F-FAMT replace 18F-FDG for malignancy detection? A meta-analysis of diagnostic accuracy

A. Achmad¹, A. Bhattarai¹, R. Yudistiro^{1,2}, T. Higuchi¹, Y. Tsushima¹; ¹Gunma University, Maebashi, JAPAN, ²Mochtar Riady Comprehensive Cancer Center, Jakarta, INDONESIA.

Aim: This meta-analysis evaluates the diagnostic accuracy of ³-¹⁸F- α -methyl tyrosine (¹⁸F-FAMT) PET in malignancy detection in comparison with that of ¹⁸F-FDG PET. **Material and methods:** Electronic search was performed for diagnostic test accuracy studies directly comparing ¹⁸F-FAMT and ¹⁸F-FDG PET for detection of malignant tumors from the inception of ¹⁸F-FAMT to August 2015. Study quality, the risk of bias and sources of variation among studies were assessed using the QUADAS tool. A separate meta-analysis was performed for diagnostic performance based on visual assessment and based on diagnostic cut-off. The meta-analysis method was applied according to the study availability after systematic review. Whenever possible, a bivariate random-effect model was used for analysis and pooling of diagnostic measures across studies. **Results:** Forty-two peer-reviewed basic science investigations and clinical studies were reviewed, and six eligible studies (272 patients, all were prospective studies) of various type of cancer were meta-analyzed. The diagnostic accuracy of both radiotracers were consistent under either univariate or bivariate meta-analysis. The diagnostic accuracy of ¹⁸F-FAMT was higher than ¹⁸F-FDG for malignancy based on both visual assessment (diagnostic odd ratio (DOR): 8.90 (95% CI 2.4-32.5) vs 4.63 (95% CI 1.8-12.2, area under curve (AUC): 87.8% vs 86.1%) and diagnostic cut-off (DOR: 13.83 (95% CI 6.3-30.6) vs 7.85 (95% CI 3.7-16.8), AUC: 87.0% vs 87.1%), respectively. Resultant data of accuracy based on visual assessment were only slightly heterogeneous. **Conclusion:** ¹⁸F-FAMT PET has a better diagnostic performance for malignancy detection compared to ¹⁸F-FDG PET.

EP317

18F-FDG PET-CT Appropriateness According to EANM Guidelines: Analysis of 200 18F-FDG PET-CT Request-Forms from a Single PET-CT Centre

M. Mattoli¹, V. Scolozzi¹, D. Ripani¹, L. Indovina², V. Rufini¹, A. Giordano¹, M. Calcagni¹; ¹Institute of Nuclear Medicine, Università Cattolica del Sacro Cuore, Rome, ITALY, ²Institute of Physics, Università Cattolica del Sacro Cuore, Rome, ITALY.

Introduction: The appropriateness for oncological ¹⁸F-FDG PET-CT is established by EANM guidelines published in 2010 (v.1.0) and updated in 2015 (v.2.0). A pre-requisite for evaluating the appropriateness is to have an evaluable request-form: it should report a clear clinical indication with all information attached. **Aims:** to assess whether the request-forms for PET-CT were evaluable in order to establish the appropriateness according to EANM guidelines v.1.0 and v.2.0; to analyse the most common clinical indication. **Materials and methods:** We retrospectively evaluated 200 oncological ¹⁸F-FDG PET-CT request-forms. We defined “evaluable” the request-form in which the clinical information was sufficient to evaluate the appropriateness. Otherwise, the nuclear physician retrieved other additional clinical information in the medical record. **Results:** EANM guidelines v.1.0: 117/200 (58.5%) request-forms were non-evaluable: in 76/117 (65%) the clinical indication was unclear, and in 41/117 (35%) additional information was needed despite a clear clinical indication. EANM guidelines v.2.0: 76/200 (38%) request-forms were non-evaluable because of unclear clinical indication. After retrieving the missing data, all clinical indications were identified. Significant difference ($p=0.01$, χ^2 test) between non-evaluable request-forms according to EANM guidelines v.1.0 and EANM guidelines v.2.0 was found. The clinical indications were: follow-up ($n=65$), restaging ($n=40$), staging ($n=32$), response evaluation ($n=35$), pulmonary nodule characterization ($n=22$), guiding biopsy/radiotherapy planning ($n=4$); unknown primary malignancy ($n=1$), screening ($n=1$). **Conclusions:** Applying the EANM guidelines v.1.0, more than half of the request-forms were not evaluable, while applying the EANM guidelines v.2.0 the rate of non-evaluable request-forms was significantly lower. The main reasons making the request-form non-evaluable were: 1) clinical indication missing or unclear, regardless the guidelines used; 2) missing of specific information (histotype; whether locally advanced; whether the relapse is potentially curable) only required by EANM guidelines v.1.0, that can be considered more restrictive than those of 2015. Finally, the most common clinical indication was “follow-up”, the only indication not present in both guidelines. This finding can be attributed to the precautionary attitude of the referring physicians and/or to “defensive medicine” attitude while it is known that PET-CT cannot be used to monitor oncologic patients. The consequences of this “malpractice” are: unnecessary exposure to radiations; longer waiting-list for patients needing an appropriate PET-CT; high healthcare costs; increased number of exams and reduced time for tumour-board discussions and for educational sessions, especially in an Academic centre. On the contrary, a clear clinical indication is mandatory, regardless from the guidelines’ version, reflecting the professional competences of referring physicians.

EP318

Improving Patient Accesibility to Nuclear Medicine and Radiation Therapy Services in Argentina: Challenges and Pitfalls Encountered in the Implementation of an Ongoing Nationwide Initiative

D. J. Passadore^{1,2}, J. C. Furnari¹, V. E. Ugarte³, L. Rovere⁴, V. J. Ugarte⁵; ¹Comisión Nacional de Energía Atómica, Buenos Aires, ARGENTINA, ²Fundación Centro Diagnóstico Nuclear, Buenos Aires, ARGENTINA, ³Fundación Escuela Medicina Nuclear, Mendoza, ARGENTINA, ⁴Comisión Nacional de Energía Atómica, San Carlos de Bariloche, ARGENTINA, ⁵Centro de Medicina Nuclear y Molecular de Entre Ríos, Paraná, ARGENTINA.

Aim. A national strategic plan for improving the availability and utilization of nuclear medicine and radiation oncology in our country is being carried on under the coordination of the Comisión Nacional de Energía Atómica (CNEA, the local National Atomic Energy Commission), in order to mitigate the uneven deployment of these technologies, which affects patients’ accessibility and equality in healthcare. The present article describes the challenges and pitfalls faced in implementing the initiative, which is ongoing, named Plan Nacional de Medicina Nuclear

(PNMN, i.e. National Plan of Nuclear Medicine). Materials and Methods. Seven new facilities are being built in different regions all over the wide geography of the country that currently don't have or have limited access to hybrid imaging technologies and the most modern radiation therapy (RT) techniques. Most of the new centers comprise the installation of PET/CT and SPECT/CT cameras as well as Cyclotron and PET Radiopharmacy, together with the RT devices. All new centers are planned to be operational during the biennium 2016–2017, although the different services will be available on a gradual basis, depending mainly on the availability of specialized human resources. The total amount invested in equipment sums up to approximately 90 million USD and another 82 million USD in buildings and service areas. The new centers are receiving on-site as well as remote support for different purposes but basically for training; equipment set-up, acceptance testing and maintenance and advice for achieving compliance with regulatory requirements, from previously existing centers and facilities, in operation for several years. Results. The crucial pitfalls originate from the short period of time assigned to the construction process and the necessary coordination with the specification and installation of the equipment, all of which must comply with the nuclear and pharmaceutical regulatory requirements together with the significant number of new centers to be built. The major challenge is to identify, recruit and establish teams of physicians, technologists, pharmacists and other essential human resources, especially in remote and therefore less populated regions of the country. Conclusions. Being a country with a long history of development of the peaceful applications of nuclear energy, it is considered to be a pending issue the federalization of access to nuclear medicine and radiotherapy. Nevertheless, the scale of the initiative entails such a number of specialized human resources that imposes a major challenge to its success, moreover if a homogeneous level of quality must be provided.

EP319

Intracardiac tumor thromboembolism initially detected by ^{18}F -FDG PET/CT

S. Lee^{1,2,3}, D. Lee⁴, J. Kim^{3,2}, J. Choe^{2,5}; ¹Department of Nuclear Medicine, G Sam Hospital, Hyosan Medical Foundation, Gyeonggi-do, KOREA, REPUBLIC OF, ²Department of Medicine, Graduate School, Korea University, Seoul, KOREA, REPUBLIC OF, ³Multimodal Imaging and Theranostic Lab, Cardiovascular Center, Korea University Guro Hospital, Seoul, KOREA, REPUBLIC OF, ⁴Department of Medical Oncology, G Sam Hospital, Hyosan Medical Foundation, Gyeonggi-do, KOREA, REPUBLIC OF, ⁵Department of Nuclear Medicine, Korea University Anam Hospital, Seoul, KOREA, REPUBLIC OF.

Cardiac ^{18}F -fluorodeoxyglucose (^{18}F -FDG) uptake with oncologic purpose FDG positron emission tomography/computed tomography (PET/CT) has been widely reported and accepted as variable. Thus, cardiac FDG uptakes are often not well assessed and evaluated during malignancy work-up. We report two cases of intracardiac tumor thrombi initially detected by FDG PET/CT. Case 1: Initial staging FDG PET/CT scan of a 36-year-old female for pancreatic cancer revealed focal hypermetabolism on left atrium. On the background CT images, there was no definite abnormal finding but PET finding suggested intracardiac tumor thromboembolism. Patient underwent transthoracic echocardiography for clarification of the FDG-avid lesion. The echocardiographic examination revealed a mass lesion in LA around MV annulus. Case 2: Patient underwent FDG PET/CT for malignancy of unknown primary origin (MUO) work-up. This patient suffered recurrent multiple embolic brain infarction without underlying disease. PET scan suggested primary site as lung cancer, with multiple lymph node metastases in mediastinum, and there noted irregular hypermetabolic lesion in the left atrium. Patient had undergone echocardiography 2 month earlier without abnormal finding. According to the PET finding, follow up echocardiography was done and

newly developed LA mass lesion was detected. Emergency operation was conducted for resection of LA tumor thrombi and pathologic result was metastatic squamous cell cancer from lung origin. Conclusion: ^{18}F -FDG PET/CT findings led to the diagnosis of unexpected intracardiac tumor thromboembolism in these two cases.

EP320

How Can We Use Digital Programmable LED Lighting in a Nuclear Medicine Environment?

M. M. Knopp¹, J. Milacek², M. I. Knopp², K. Binzel², C. L. Wright², M. V. Knopp²; ¹Emory University, Atlanta, GA, UNITED STATES, ²The Ohio State University, Columbus, OH, UNITED STATES.

While dedicated commercial solutions for ambient LED lighting have been available for years and are increasingly used in healthcare environments, broader utilization has been limited due to high costs. Fully digital, IP addressable lights have entered broadly into the consumer market and thus are economical and available in a large variety of LED configurations. We explored, assessed and report on experience of deploying such systems in a nuclear medicine environment. While there are several standards evolving from home automatization to bus based technologies, we focused on the broadly adapted standard of the ZigBee. A major advantage of such a consortium approach is interoperability of LED lights and control. Manufacturers support software development tools and have smart device apps available for local and remote control. Most devices are uniquely IP addressable and enable variation in intensity and hue. We focused on the programmability in hue for creating specific ambience such as a calming setting either in the dose injection rooms, the imaging suites, or the reading rooms, we also looked at the feasibility system interfaces to enable visual feedback for timing or procedure feedback. We utilized replaceable bulbs in recessed housings, lightstrips and standalone fixtures. Patient, subject and staff experiences and visual perception of LED intensity and hue was recorded by interview and questionnaire. The implementation of consumer level, IP addressable LED lighting proved to be simpler than anticipated and economical. While manufacturer software applications are available, complex applications do require customization. This can be achieved by software coding utilizing a large portfolio of developer toolkits which also enable vast flexibility including complex applications to support visual feedback approaches. We implemented several use cases e.g. remaining length of examination feedback and hue guidance for breath holding. Especially for patient instructions / feedback, traditional use of verbal communication can now be supplemented or replaced with visual guidance. The overall perception and acceptance of ambient LED lighting concepts was even more positive than originally anticipated in all areas of patient, imaging, and reading rooms. The deployment of consumer level programmable LED components was found to be feasible, robust, and economical. The feedback and acceptance has been exceptional as the inherent flexibility and customization enables new concepts to improve room ambience, thus patient and staff experience and its IP based programmability facilitate light hue and intensity as a nonverbal guidance and feedback tool.

EP321

Diagnostic performance of PET/CT or PET and CT for detection of peritoneal carcinomatosis: a meta-analysis

H. Zhou; West China Hospital, Chengdu, CHINA.

Purpose: The study aims to perform a meta-analysis to compare the diagnostic performance of ^{18}F -FDG PET/CT and CT for detection of peritoneal carcinomatosis (PC). Methods: Articles of ^{18}F -FDG PET/CT and CT on PC published in English from January 1990 to September 2016 was searched in the PubMed, EMBASE, Cochrane Library, Web of

Science, and EBSCO databases to identify eligible studies on PET/CT or CT of peritoneal metastases. QUADAS was used to evaluate the methodological quality of the included studies. Pooled sensitivity, specificity, and diagnostic odds ratios (DOR) were calculated both on a per-patient basis. Summary receiver operating characteristic (SROC) curves were also drawn to obtain the area under curve (AUC) and Q* value. Results: 27 articles were included in the analysis. On a per-patient basis, the pooled sensitivity of PET/CT (68%) was significantly higher than that of CT (60%), and the pooled specificity of PET/CT (95%) was markedly higher than that for CT (88%). Conclusions: This meta-analysis indicated that FDG PET/CT was better than CT on a per-patient basis for diagnosis of peritoneal carcinomatosis (PC).

EP322

18F-FDG PET-CT Appropriateness: Comparison between EANM Guidelines 2010 (v.1.0) and EANM Guidelines 2015 (v.2.0) in 200 Oncological Patients

M. Mattoli¹, V. Scolozzi¹, D. Ripani¹, L. Indovina², V. Rufini¹, A. Giordano¹, M. Calcagni¹; ¹Institute of Nuclear Medicine, Università Cattolica del Sacro Cuore, Rome, ITALY, ²Institute of Physics, Università Cattolica del Sacro Cuore, Rome, ITALY.

Introduction: The EANM guidelines 2010 (v.1.0) define the clinical indications for oncological ¹⁸F-FDG PET-CT as “appropriate” or “promising”; the EANM guidelines 2015 (v.2.0) define them as “appropriate”. **Aims:** to compare the ¹⁸F-FDG PET-CT appropriateness between the two EANM guidelines versions; to match the appropriateness with clinical indications. **Materials and Methods:** We retrospectively compared the appropriateness of 200 consecutive oncological ¹⁸F-FDG PET-CT applying EANM guidelines v.1.0 and EANM guidelines v.2.0. **Results:** For EANM guidelines v.1.0: 61/200 (31%) appropriate PET-CT for restaging (n=37), pulmonary nodule characterization (n=9), staging (n=8), guiding biopsy (n=3), response evaluation (n=3), unknown primary tumor (n=1); 15/200 (7%) promising PET-CT all for treatment response; 124/200 (62%) inappropriate PET-CT for follow-up (n=65), staging (n=24), response evaluation (n=18), pulmonary nodule characterization (n=13), restaging (n=3), and screening (n=1). For EANM guidelines v.2.0: 127/200 (64%) appropriate PET-CT for restaging (n=40), staging (n=32), response evaluation (n=36), pulmonary nodule characterization (n=15), guiding biopsy (n=3), unknown primary tumor (n=1); 73/200 (36%) inappropriate PET-CT for follow-up (n=65), pulmonary nodule characterization (n=7), and screening (n=1). **Conclusions:** The amount of inappropriate and appropriate PET-CT was specular: higher inappropriate for EANM guidelines v.1.0, and higher appropriate for EANM guidelines v.2.0. The main causes were: 1) clinical indication not present in both EANM guidelines (follow-up); 2) indications of EANM guidelines v.1.0 rather restrictive (few types of primary tumors, locally advanced, ¹⁸F-FDG avid). Although the EANM guidelines v.2.0 are less restrictive, we believe that some clinical indications in these guidelines deserve further clarifications: 1) “*differentiation of benign from malignant lesions*”: which are the characteristics of the lesions and in which organ? PET-CT performance is different on the basis of these two aspects; 2) “*Staging patients with known malignancies*”: how the malignancy was proved? Is it ¹⁸F-FDG avid? Several malignancies are not ¹⁸F-FDG avid. 3) “*Monitoring the effect of therapy on known malignancies*”: which therapy? Which timing? How often the effects have to be monitored? The response evaluation is completely different on the basis of the type and duration of therapy. 4) “*Detecting tumour recurrence, especially in the presence of elevated tumour markers*”: which is the proper level of increased markers? At first measure even if the level is borderline high? There are false positive results for tumour markers, as well as false negative results for PET-CT. It is hopeful that the EANM committee provides further information for each of these critical points in order to reduce the number of not-useful PET-CT.

EP323

Extra-pelvic extension of recurrent intra-pelvic tumor in FDG PET/CT : anatomical consideration

H. Munechika, T. Saginoya, Y. Miura, S. Takekawa, Y. Takano, Y. Teranishi, S. Hashimoto, Y. Fukaya, K. Watanabe; Southern Tohoku General Hospital, KORIYAMA, JAPAN.

Purpose ; Intra-pelvic malignancy can be detected easily by FDG PET/CT but an intra-pelvic tumor extending toward extra-pelvic space is not assisted adequately by FDG PET/CT alone in the setting of tumor recurrence. This is an educational exhibit to show extra-pelvic extension of a recurrent intra-pelvic tumor with anatomical consideration. **Material and Method ;** FDG PET/CT findings are correlated with enhanced-CT and MRI findings in a recurrent tumor after various treatment in cases with a rectum, uterus or bladder carcinoma. Anatomical landmarks are created to see which of the anatomical structures in the pelvic wall and floor can be passed through by a tumor to extent from the intra-pelvic to extra-pelvic space. The anatomical landmarks of the pelvic wall and floor indicate the following structures ; ①paces of the pelvic floor (urogenital triangle and rectal triangle) ②bones (pubic ramus, ischiopubic ramus, ischial ramus, ischial tuberosity, sacrum) ③muscles and ligaments (burbospongiosus muscle, ischiocavernosus muscle, transverse perineal muscle, perineal membrane, perineal muscle, obturator internus muscle, levator ani, piriform muscle, sacrospinous ligament) ④foramina and fossa (sciatic foramen, ischiorectal fossa, sacral foramen, obturator foramen) **Discussion and Conclusion ;** The landmarks of the pelvic wall and floor facilitate to recognize anatomically extra-pelvic extension of a recurrent intra-pelvic tumor in FDG PET/CT and it is convinced by enhanced-CT and MRI because of better delineation of the landmarks.

EP324

Gastric Hernia Mimicking Lung Mass in PET-CT: Case Report

G. Mutevelizade, Y. Parlak, G. Gumuser, D. Goksoy, E. Sayit; Celal Bayar University, Manisa, TURKEY.

Gastric Hernia Mimicking Lung Mass in PET/CT: Case Report A 54 years old male patient was referred to our clinic for PET/CT scan with the indication of primary esophagus carcinoma pre-treatment staging in November 2013. In 2011, he was treated for lung cancer and had received chemotherapy and radiotherapy in a different clinic. In June 2013 thorax CT showed progression in the dimensions of the lung mass and F-18 FDG PET/CT was performed for restaging. PET/CT had been reported as progression of size and metabolic activity of the mass located in the paravertebral area at the left lower lobe (SUV max:6.4). Also, newly formed malignant thickening of the wall at distal esophagus was reported. Primary esophagus adenocarcinoma had come as a result of the endoscopic biopsy. We reported malignant thickening at the lower end of esophagus in PET/CT examination in our clinic (SUV max:19.3). Also, rolling hernia was determined at the paramediastinum localization of the neighborhood of esophagus which had moderately increased FDG uptake at the gastric wall (SUV max:6.4). Thorax and abdominal CT was performed and the same lesion was reported as rolling hernia due to its wall structure similar to the gastric fundus and liquid content inside. Gastric barium X-Ray was done and gastric hernia presence was confirmed. While the evaluation of F-18 FDG PET/CT scan for oncologic patients, some non-oncological conditions may lead to incorrect assessments. It should be considered that this can affect the stage of the disease and management of medication. That's why we have to be very careful while interpreting PET/CT scans and multidisciplinary approach can be useful in case of suspense.

EP325**Role of FDG PET-CT in predicting response to Selective Internal Radiation Therapy (SIRT) in Hepatocellular carcinoma (HCC)**

M. Jreige, P. Mitsakis, A. Van-Der-Gucht, M. Nicod Lalonde, M. Silva Monteiro, A. Denys, J. Prior, N. Schaefer; Centre Hospitalier Universitaire Vaudois (CHUV), LAUSANNE, SWITZERLAND.

Aim of the study: To determine different conventional and functional imaging staging variables affecting response to SIRT in HCC patients. **Materials and methods:** We reviewed retrospectively imaging studies of patients with HCC referred in our institution for SIRT. FDG PET-CT images in the pre-therapeutic setting were analyzed and SUVmax for lesions and SUVmax and SUVmean of normal liver parenchyma were reported. T stage was determined for each case based on initial liver MRI results by analyzing number and size of lesions and vascular invasion. Results of different variables were correlated to progression-free survival (PFS) based on a Kaplan-Meier survival analysis and Log-Rank Test. **Results:** Sixty patients undergoing SIRT were enrolled retrospectively. All patients received prior FDG - PET and liver MRI. A positive correlation with PFS was shown with SUVmax using a threshold of 8g/ml corresponding to the mean value of the population ($p=0.049$) using the Log Rank test. However, morphologic criteria measured in MRI as singularity of lesions versus multiple lesion ($p = 0.071$), lesion size less or more than 3 cm ($p=0.274$), lesion size less or more than 5cm ($p=0.629$) or vascular invasion ($p=0.541$) did not predict PFS in our patient population. SUVmean outside lesions using a threshold of 2.5 g/ml was not predictive for further PFS as well. **Conclusion:** In our population only SUVmax in HCC lesions with a threshold of 8g/ml in the FDG - PET prior to SIRT therapy was predictive for PFS. Morphologic parameters as single vs multiple lesions, lesion size or vascular invasion were not predicting median PFS. Further studies using bigger sample or prospective approach are needed.

EP-17 – Sunday, October 16, 2016, during Exhibition hours, e-Poster Area
Clinical Oncology: Thyroid & Parathyroid

EP326**Protein expression heterogeneity between primary tumor and distant metastasis in differentiated thyroid cancer**

I. LIM, J. Choi, J. Myung, M. Lee, B. Byun, B. Kim, C. Choi, S. Lim; Korea Cancer Center Hospital, Seoul, KOREA, REPUBLIC OF.

Purpose: The aim of this study was to investigate the protein expression heterogeneity between primary tumor and distant metastasis in differentiated thyroid cancer (DTC) patients in terms of glucose metabolism and somatostatin receptor (SSTR). **Method:** We retrospectively reviewed 18 DTC patients (M : F = 7 : 11, Age; 56 ± 10) with bone or soft tissue metastases. The protein expressions were assessed as negative, weak positive, strong positive by immunohistochemistry in terms of glucose transporter 1 (GLUT-1), hexokinase 2 (HK-2), and somatostatin receptor 2 (SSTR-2) from surgical specimens. The correlations between protein expression and iodine avidity and FDG avidity were evaluated using radioiodine scan and 18F-FDG PET scan. These parameters were analyzed using Chi-squared test, Mann-Whitney test and spearman correlation. **Results:** Metastatic lesions showed higher GLUT-1 expression (65%, 11/17) than primary lesions (50%, 9/18). HK-2 were expressed highly in both primary (17/18) and metastatic (16/17) sites. Primary lesions revealed similar SSTR-2 expression (9/18) to metastatic lesions (7/17). The GLUT-1 expression tended to show positive correlation between primary and bone metastasis ($r=0.46$, $P=0.06$), but the HK-2 and SSTR-2 did not show the correlation between them respectively (HK-2 $r=0.21$, $P=0.42$; SSTR-2 $r=0.056$, $P=0.83$). Of the 8 patients who underwent surgery and PET imaging within 1 year, GLUT-1 positive

group showed higher SUVmax than GLUT-1 negative group ($p=0.046$), while HK-2 ($P=0.74$) and SSTR-2 ($P=0.65$) did not show significant difference. Regarding iodine avidity and SSTR-2 expression, no significant difference was observed in terms of SSTR-2 expression between iodine avid and iodine non avid patients ($P=0.32$). 1 of 6 patients showed SSTR-2 expression in case of iodine non avid patients. **Conclusion:** GLUT-1 expressions showed positive correlation between primary tumors and bone metastatic lesions of DTC, which was not observed for HK-2 and SSTR-2. Particularly, SSTR-2 targeted therapy could be applied for some iodide non-avid patients.

EP327**Thyroglobulin Doubling Time as a prognostic indicator in management of differentiated Thyroid cancer**

S. Fatima, S. T. Butt, M. Faheem; Nuclear Medicine , Oncology & Radiotherapy Institute (NORI), Islamabad, PAKISTAN.

Serum thyroglobulin (Tg) is most important disease predictor in post thyroidectomy differentiated thyroid cancer(DTC) patients. Raised Thyroglobulin indicates unsuccessful surgery or disease recurrence in post treatment patients. Objective of this study was to evaluate the prognostic value of the serum Thyroglobulin doubling-time in differentiated thyroid cancer patients. **Methods:** We retrospectively analyzed total of 431 patients with DTC presenting to department of Nuclear Medicine between January 2009 to December 2013. Patient having raised anti-Tg antibody were excluded from the study. Total 328 patients' data with 3 or more serum Tg measurements was finally submitted for analysis. The Tg doubling-time was computed using Tg values measured during routine follow-up. Patients were followed for a mean of 26.9 months and a median of 27.2 months. **Results:** Of the 328 patients, 119 patients had 4 or more measurements that revealed detectable serum Tg. The Tg doubling-time (Tg-DT), calculated using all available data, varied widely, and were grouped into those that were less than 1 year (9 patients), those that were 1-3 years (15 patients), and those that were more than 3 years (22 patients), as well as those with a negative value due to decrease in serum Tg (63 patients). There were also 83 patients who had three or fewer serum Tg measurements that showed detectable but stable Tg levels, as well as 177 patients in whom serum Tg measurements were below the lower limit of detection. In the group of patients with a Tg-DT of less than year the cause specific survival at 5 years was 50%, and in the group with a Tg-DT of 1-3 years it was 95%. In all other groups it was 100%. Many classical prognostic factors (age, gender, tumor type, tumor size and stage) as well as the Tg-DT were significant indicators of survival by univariate analysis, but Tg-DT remained the only independent predictor by multivariate analysis. Tg-DT was also the only independent predictor of distant metastases and loco-regional recurrence on multivariate analysis. **Conclusions:** Tg-DT is a very strong prognostic predictor superior to the classical prognostic factors in patients with DTC.

EP328**Is Thyroglobulin at Ablation a Good Predictor for Thyroid Remnant Size in Differentiated Thyroid Cancer?**

H. C. Martins¹, G. Costa¹, R. Silva^{1,2}, P. Gil¹, J. Isidoro¹, J. Pedroso de Lima^{1,2}; ¹Centro Hospitalar e Universitário de Coimbra, Cabeceiras de Basto, PORTUGAL, ²Instituto de Ciências Nucleares Aplicadas à Saúde., Coimbra, PORTUGAL.

Aim: Stimulated thyroglobulin (sTg), measured at radioiodine remnant ablation (RRA) in patients with differentiated thyroid cancer (DTC), is an

important predictive factor of persistent disease. However, Tg produced by normal thyroid cells may contribute to the sTg value. We aimed to study the relationship between sTg level in RRA period and the thyroid remnant size (TRs), using post-therapy whole-body scan (131I-ptWBS).

Materials and methods: We review DTC cases referred to our department for RRA, prepared with recombinant human TSH (rhTSH) and with low-iodine diet in the week preceding the treatment. Anti-thyroglobulin antibodies (TgAb) and sTg were measured on the fifth day after the first rhTSH injection. Patients with positive TgAb, with evidence of 131I-uptake outside the thyroid bed on 131I-ptWBS and suspected to have persistent disease on the first 6-12 month follow-up period ($Tg \geq 1 \text{ ng/mL}$ and suspicious neck ultrasound) were excluded. A total of 274 patients (225 woman, 49 men; average age \pm sd:48.7 \pm 14.4 years-old) were selected. For each patient, TRs was assessed by 131I-ptWBS, using a fixed-circular region of interest (ROI) placed in thyroid bed. The geometric mean (GM) of the total counts (cts) in the ROI was calculated, corrected for the thigh background and normalized according to the treatment activity (nGM). Based on nGM, remnants were classified into small(S)-nGM \leq 10cts/MBq; medium(M)-10cts/MBq $<$ nGM \leq 50cts/MBq and large size (L)-nGM $>$ 50cts/MBq. Spearman's rank correlation coefficient was used to test the association between sTg and the TRs. Statistical analyses were carried out using SPSS version-23. **Results:** 151 patients (55.1%) were included in group-S (average sTg=11.9 \pm 41.3ng/mL, range:0-357ng/mL); 93 (33.9%) in group-M (average sTg=48.6 \pm 137.3ng/mL, range:0-1161ng/mL) and 30 (11%) in group-L (52.9 \pm 95.2ng/mL, range:0-406ng/mL). When all patients were taken into account, a moderate positive correlation between nGM and sTg was found ($r_s=0.55, P<0.001$). When divided according to remnant size, a moderate positive correlation was found in group-S ($r_s=0.57, P<0.001$), however, we did not find a significant correlation between nGM and sTg values in group M and L ($r_s=0.05, P=0.66$ and $r_s=0.24, P=0.20$ respectively). **Conclusion:** Radioiodine-scintigraphy and sTg are important tools to evaluate the functional status of both normal and neoplastic thyroid tissue. However, in DTC patients, our results suggest that in the absence of clinical/imaging disease, a moderate correlation between TRs and TG was only found in small remnant size patients. Therefore, we hypothesize that TRs is not a good predictor of sTg values in patients submitted to less extent thyroidectomies.

EP329

Serum thyroglobulin concentration after rhTSH stimulation as a prognostic factor during adjuvant radioiodine treatment of differentiated thyroid cancer

D. Handkiewicz-Junak, A. Ledwon, A. Kropinska, J. Roskosz, E. Paliczka-Cieslik, Z. Puch, T. Gawlik, T. Olczyk, B. Jarzab; Centre of Oncology - MSC Memorial Institute, GLIWICE, POLAND.

Measurement of serum thyroglobulin (Tg) levels is a well established marker for monitoring patients with differentiated thyroid cancer (DTC). Tg concentration during adjuvant radioiodine treatment after thyroid hormone withdrawal is prognostic factor. However, if the adjuvant radioiodine treatment is performed after rhTSH stimulation there are no data when is the most appropriate time to measure Tg concentration. The aim of the work was to compare Tg concentration measured on 3rd and 6th after rhTSH stimulation as a prognostic factor during adjuvant radioiodine treatment. **Patients and Methods.** 279 patients with DTC treated with total/near total thyroidectomy and adjuvant radioiodine treatment after rhTSH stimulation were included into the study. Most patients were diagnosed with papillary thyroid cancer (91%). 37% had T3/T4 disease and 23% had lymph node metastases. Only patients with negative Tg antibodies were evaluated. Median time of observation in the studied group was 5 years. **Results.** Median Tg concentration during 1st, 3rd and 6th day of rhTSH stimulation was 0,9 ng/ml, 8 ng/ml i 16 ng/ml respectively. During follow-up structural recurrence was diagnosed in 17

(6%) of patients. Tg concentration on 1st, 3rd and 6th day of rhTSH stimulation was higher in patients diagnosed with recurrence during follow-up however the difference was statistically significant only for measurements performed on day 3rd of stimulation (median 15 ng/ml vs 40 ng/ml respectively in patients without and with recurrence). In all measurements Tg concentration was highly related to diameter of thyroid remnants. **Conclusions.** Preliminary results suggests that although during adjuvant rhTSH aided radioiodine treatment the highest Tg concentration is on day 6, results from day 3 of stimulation are more sensitive to predict disease recurrence.

EP330

¹³¹I-SPECT/CT usefulness in the follow up of patients thyroidectomized for thyroid papillary microcarcinoma (PTMC)

A. Spanu, I. Gelo, L. Mele, B. Piras, S. Nuvoli, G. Madeddu; University of Sassari, SASSARI, ITALY.

Introduction: PTMC present excellent prognosis in most cases, but it can be multicentric/multifocal and present neck lymph node metastases, local recurrences and also distant metastases. Thus, PTMC lesion identification is mandatory for the most precocious and appropriate treatment. In this study, we evaluated 131-SPECT/CT usefulness, in PTMC patients in follow up post-thyroidectomy. **Methods:** Among 704 follow up patients with differentiated thyroid carcinoma, we retrospectively selected 321 PTMC patients. At surgery, 19 patients were at high risk (H), 76 at low risk (L) and 226 at very low risk (VL); 94 patients had multicentric disease (47 bilateral). In 294 cases, 48 h after diagnostic 185 MBq ¹³¹I dose, and in 27 cases, 5 days after radioiodine therapeutic dose, planar WBS (5 cm/min) followed by SPECT/CT over neck/chest and other suspected regions was performed using hybrid dual-head gamma camera with high energy, parallel hole collimators and with low dose x-ray tube, for total 557 exams. **Results:** Both planar and SPECT/CT were negative in 196/321 patients, while planar evidenced 277 iodine fixing foci in 113/321 patients and SPECT/CT 332 in 125 patients confirming all foci evidenced by planar, but correctly characterizing 79 foci in the neck and outside classified as benign or unclear at planar and identifying 55 further occult foci. Globally, SPECT/CT correctly classified 80 malignant lesions in 23 patients (4H, 5L, 14VL), while planar, although evidenced 48 metastases in 11 patients (4H, 4L, 3VL), only characterized 15 in 2 patients (1H, 1L). Seventeen/23 patients (1H, 3L, 13 VL) only had neck lymph node metastases, 9 VL being T1a N0M0 with undetermined Tg, while in the remaining 8/17 Tg was <2.5 to >10 ng/ml; 2/23 patients (1L, 1VL) only had metastases outside the neck (lung and mediastinum) both of them with Tg <2.5 ng/ml; 4/23 patients (3H, 1L) had metastases in both the neck and outside with Tg levels from <2.5 to >10 ng/ml. In 6/23 cases PTMC was multifocal. **Conclusion:** This study confirms that PTMC can be aggressive since our follow up patients developed metastases in 7.8% of cases. 131I-SPECT/CT proved higher performance than planar to evidence and characterize malignant lesions, in particular in patients VL, T1aN0M0 and very low Tg levels, obtaining a global incremental value in positive patients of 43.2% than planar and changing planar classification and patient management in 24.8% of cases. SPECT/CT wider use is suggested in PTMC patient follow up.

EP331

The incremental value of ¹³¹IODINE SPECT/CT in the management of DTC patients

A. Ezzine^{1,2}, M. Ben Fredj^{1,2}, H. Regaieg¹, R. Sfar¹, S. Melki^{1,2}, H. Boudriga¹, M. Nouira^{1,2}, K. Chatti¹, S. Ajmi¹, M. Guezguez¹; ¹Nuclear medicine department, Sousse, TUNISIA., Sousse, TUNISIA, ²LR 12Es02, Faculty of Medecine Sousse, University of Sousse, Sousse, Tunisia, TUNISIA.

Aim: The aim of this study is to evaluate the incremental value of single photon emission computed tomography/computed tomography (SPECT/CT) over planar radioiodine whole-body imaging and to assess its clinical impact on the management of patients. **Materials and methods:** We retrospectively reviewed planar ^{131}I whole-body and ^{131}I -SPECT/CT imaging findings in 27 of differentiated thyroid cancer (DTC) patients (23 women and 4 men) with an average age of 49 years-old, who underwent ^{131}I therapy for thyroid cancer (22 papillary and 5 follicular) approximately 5 days after the therapeutic administration of 3,7 GBq (100 mCi) of ^{131}I . The foci of increased tracer uptake were identified in the neck, thorax and elsewhere. Serum thyroglobulin level, histopathology and other imaging findings served as the reference standard. **Results:** Planar imaging showed 57 foci of uptake and SPECT/CT showed 67 foci, confirming all foci seen on planar imaging but identifying an additional 10 occult foci in 8 of 27 patients. SPECT/CT correctly characterized 63 uptake foci unclear on planar imaging. It was a determinant in classifying as neoplastic 49 foci of 67 (73, 13%) and identified 14 foci of 67 as false positive findings. Only in 4 cases, SPECT/CT was insufficient and a complementary exploration was needed. Globally, SPECT/CT modified therapeutic management in 43.33% and avoided unnecessary treatment in 20, 89% of patients with only single benign lesions or physiologic uptake. **Conclusion:** ^{131}I -SPECT/CT is a valuable addition to standard post-therapy planar imaging. It improved diagnostic confidence and provided crucial clinical information leading to change of management for a significant number of DTC patients.

EP332

131I-SPECT/CT predictive value to the occurrence of radioiodine-positive cervical lymph node metastatic disease a year after ablation in patients with thyroid cancer

I. Iakovou, E. Giannoula, V. Mpalaris, V. Athanasiou, D. Katsaboukas, S. Georga, D. Lo Presti, K. Badiavas, G. Arsos; Academic Nuclear Medicine Department, Aristotle University, Papageorgiou General Hospital, THESSALONIKI, GREECE.

PURPOSE: To investigate the value of 131I-SPECT/CT performed at the first radioablation to predict the occurrence and/or persistence of radioiodine-positive cervical lymph node metastatic disease (CND) after a year. **METHODS:** All 87 consecutive DTC patients (23/64 men/women, 47.9+16.9 yrs, 54/4/29 - papillary/follicular/follicular variant of papillary DTC, 47/20/17/3 - T1/T2/T3/T4, 23 N1, 2 M1 stage) referred to our department for ablation in 2014 enrolled in the study. 131I-WBS and SPECT/CT just after ablation and 7-12 months later at TSH stimulation was performed. The outcome variable of the study was the detection or exclusion of 131I-positive CND. **RESULTS:** Of 65 patients without a SPECT/CT diagnosis of 131I-positive CND at ablation, 63 had no 131I-positive CND at follow-up (49 no uptake, 14 thyroid remnant persisted). In the 2/65 patients a new radioiodine-positive CND lesion was detected. In 20 of 22 patients with a SPECT/CT 131I-positive CND diagnosis there was no evidence of 131I-positive CND (15 no uptake, 5 thyroid remnant persisted) at the time of follow up. In almost all cases (19/20) where CND was treated with radioiodine, lymph nodes were smaller than 1ml, while lymph node size was bigger than 1.2ml in the 2 cases of persistent CND. **CONCLUSION:** 131I-SPECT/CT at ablation has a high negative predictive value with regard to the occurrence of radioiodine-positive CND a year after initial treatment. Even if the diagnosis of CND at ablation scan may consequence to an early surgical re-intervention, the fact that small size CND responds well to radioiodine treatment motivates for new studies to elucidate the parameters predictive of response to treatment of CND by 131I.

EP333

Clinical Significance of Follow-up I-131 Diagnostic Scintigraphy after Radioactive Iodine Ablation Therapy on Well-differentiated Thyroid Cancer

H. Song; Jeju National University School of Medicine, Jeju-si, KOREA, REPUBLIC OF.

<META NAME="author" CONTENT="송희성">**Purpose** This retrospective study researched for clinical significance of routine follow-up (F/U) I-131 diagnostic scintigraphy (Dx-scan) after radioactive iodine therapy (RI-Tx) on well-differentiated thyroid cancer. **Subjects & Methods** Three hundreds eighteen patients were enrolled. All underwent total thyroidectomy due to well-differentiated thyroid cancer and high dose RI-Tx to ablate remnant thyroid tissue. The definition of complete ablation was below 2.0 of F/U stimulated thyroglobulin (sTg) plus negative finding of F/U Dx-scan after RI-Tx. The rest except complete ablation was regard as incomplete ablation. Re-treatment performed when pathologic results of recurrence or clinical findings of highly suspicious recurrence. **Results** Five of complete ablation patients (n=185) were taken the re-treatment (2.7%). Main diagnostic modalities affecting the re-treatment were Dx-scan (n=2), contrast CT (n=1), ultrasonography (n=1) and sTg (n=2). 29 of incomplete ablation patients (n=133) performed the re-treatment (21.8%). Chief diagnostic tests affecting the re-treatment were FDG PET/CT (n=14), contrast CT (n=5), ultrasonography (n=9), Dx-scan (n=2), and sTg (n=2). Dx-scan influenced in 1.1% of complete ablation patients and 1.5% of incomplete ablation patients for the re-treatment. **Conclusion** F/U Dx-scan after RI-Tx is not useful for detecting recurrence especially in incomplete ablation patients, considering difficulties of the preparation of I-131 diagnostic scan compared to FDG PET/CT, ultrasonography and contrast CT.

EP334

Are TSH serum levels greater than or equal to 30 mIU/L prior to RAI a predictor of successful treatment of patients with differentiated thyroid carcinoma?

E. Vasilenko¹, D. Fomin¹, I. Guryanov²; ¹Russian Scientific Center of Roentgenoradiology, Moscow, RUSSIAN FEDERATION, ²National Research University Higher School of Economics, Moscow, RUSSIAN FEDERATION.

Aim: Comparative evaluation of combined treatment results in patients with DTC at different levels of TSH-stimulated prior to RAI. **Materials and Methods:** The study included 197 patients (36 female, 161 male) of the age group 18-75 years with a mean age of 47 years. In all cases DTC was confirmed by histological tests (154 papillary carcinoma cases and 43 follicular thyroid cancer cases, stage T1-T3, N0-N1, M0). 4 weeks prior to RAI all patients were suggested to follow an iodine-free diet with the abolition of L-T4 supplementation. Although recent ETA (2010) and ATA (2015) guidelines recommend that serum TSH levels should be ≥ 30 mIU/L for successful treatment, in 50 patients this level has not been achieved due to their severe physical condition or individual characteristics. Nevertheless, radical radioiodine activities from 3.0 to 4.2 GBq and posterior scintigraphy were carried out for all patients. A year after RAI a stimulation test with the abolition of L-T4 supplementation was performed for all patients. Test results were regarded as negative if the Tg level was less than 2 ng/ml and scintigraphy showed no disease. The data was analyzed using several statistical methods: analysis of variance (ANOVA), linear and logistic regression models. Linear regression and ANOVA allowed us to compare serum TSH levels and find significant differences between the two groups of patients (remission/no remission). The dependent variable was serum TSH level and the independent variable was treatment success. Logistic regression allowed us to estimate the impact of serum TSH level change on the success of treatment. **Results:**

Linear regression and ANOVA showed that mean serum TSH level in the no-remission group was 58.709 mIU/L and in the remission group it was 62.903, but the difference of these means was not statistically significant (t -value = 0.77, p -value = 0.442 at $p < 0.05$). Analysis of variance also confirmed it. Logistic regression showed that there was no impact of serum TSH levels on the treatment success (t -value = 0.771 p -value = 0.44 at $p < 0.05$). Based on this logistic regression model, it has been unable to predict the failure of a single treatment according to serum TSH levels (R^2 (Nagelkerke)=0.005). Conclusion: The resulting data from the analysis showed that there was no statistically significant association between serum TSH levels prior to RAI and DTC remission. If the standardized protocol for patient preparation for RAI is observed, it is not required to reach any fixed TSH threshold.

EP335

Comparison of FLT-PET/CT and FDG-PET/CT in detection of metastases of differentiated thyroid cancer

A. Murai¹, K. Kato², S. Iwano¹, S. Ito¹, S. Naganawa¹; ¹Nagoya University Graduate School of Medicine, nagoya, JAPAN, ²Nagoya University School of Health Sciences, nagoya, JAPAN.

Purpose: 3'-deoxy-3'-18F-fluorothymidine (FLT) has been recently developed as a PET/CT proliferation tracer. Up to the present, there have been few studies investigating its role in differentiated thyroid carcinoma (DTC). The aim of this study was to assess the efficacy of FLT-PET/CT for the detection of metastases in DTC in comparison with 2-deoxy-2-18F-fluoro-D-glucose (FDG)-PET/CT. **Materials and Methods:** We examined 17 patients (9 women, 8 men; mean age, 59.6±5.2 years) with DTC who had undergone total thyroidectomy and were hospitalized to be given I-131 therapy. All patients were examined by FLT-PET/CT and FDG-PET/CT before the therapy, and they were examined by I-131 scintigraphy after the therapy. Metastases in lymph nodes, bones and lungs were assessed in the 7, 16 and 2 divided segments, respectively. The sites of metastases were identified by I-131 scintigraphy, CT, MRI and clinical information. The positive findings for metastases at FLT-PET/CT and FDG-PET/CT were defined as areas of focally increased uptake, exceeding that of surrounding normal tissue. The sensitivity and specificity were calculated on a segment basis. **Results:** Lymph node metastases of DTC were confirmed in 10 of a total of 119 segments in 6 patients, bone metastases in 28 of a total of 187 segments in 10 patients, and lung metastases in 26 of a total of 34 segments in 13 patients. The sensitivities of FDG-PET/CT and FLT-PET/CT in detecting lymph node metastases were 100% and 20%, respectively ($p=0.013$), and both their specificities were 98% ($p>0.05$). Their sensitivities in detecting bone metastases were 39 and 57%, respectively ($p>0.05$), and their specificities were 100 and 97%, respectively ($p>0.05$). Their sensitivities in detecting lung metastases were 51 and 8%, respectively ($p=0.003$), and both their specificities were 100% ($p>0.05$). **Conclusion:** The sensitivities of FLT-PET/CT in detecting metastases of DTC in lymph nodes and lungs on a segment basis were significantly lower than those of FDG-PET/CT. However, the sensitivity of FLT-PET/CT in detecting bone metastases was higher than that of FDG-PET/CT, although the difference was statistically not significant.

EP336

Prognostic impact of 18F-FDG PET/CT in detecting residual or recurrent medullary carcinoma of thyroid in relation to rising calcitonin marker velocity

M. Siddique, A. Hasaan, H. Bashir, M. Nawaz; Shaukat Khanum Memorial Cancer Hospital and Research Centre, Lahore.Pakistan., Lahore, PAKISTAN.

Objective:The aim of this study is to evaluate the efficacy and clinical impact of the ¹⁸F-FDG PET/CT in localizing site of recurrence of

medullary thyroid cancer(MTC) in patients with rising serum calcitonin level. **Material and Methods:**Retrospective analysis of 77 consecutive patients with histological diagnosis of MTC from 1995 to 2015, registered at a single center. The association of gender, age at diagnosis, pathologic findings, the TNM stage and rising tumor marker levels were correlated with ¹⁸F-FDG PET/CT findings and overall survival. Results were confirmed by histopathological analysis in patients who underwent repeat surgery and by clinical followup - mean of 4 years(range: 6 months-8 years). **Results:** Seventy-seven(8.1%) of the total thyroid cancer patients registered at our centre had MTC. Mean age 37 years[range: 17 to 67 years]. Twenty-five females, 52 males. 17(22%) underwent partial thyroidectomy due to irresectable disease, 60(78%) had total thyroidectomy. By TNM staging; 10(13%) had stage II, 8(10.4%) had stage III disease and 47(61%) had stage IV disease. In 12(15.6%) histology was missing. Distant metastasis were present in 27(35%) at baseline. 10 pulmonary, 12 bone, 6 liver and one brain metastases. 12 of 77had MTC associated with MEN syndromes; 10 MEN IIA and two MEN IIB. On multivariate analysis, extrathyroidal extension, age greater than 40 years at diagnosis and distant metastasis were poor prognostic factors for survival (p -value: <0.05). 19 underwent ¹⁸F-FDG PET/CT due to elevated post thyroidectomy calcitonin levels at baseline measured at 4 weeks - 6 months. 5, 1, 5 and 7 has post-op serum calcitonin level <50 , 50-100, 100-1000, >1000 respectively. Post op calcitonin was unavailable in 1 patient. Serum calcitonin levels doubled in 13(62%) over 4 months-5 years. 7(37%) had declining calcitonin levels. Nine of 12 with rising tumor markers, were upstaged by ¹⁸F-FDG PET/CT findings. Hypermetabolic lesions were detected in 9/19(47.7%), with confirmation in 5 true positives (TP), 4 false positive(TP). Negative PET with no evidence of disease on follow up in 10/19(52.6%), indicating 10 true negatives (TN). In our series the sensitivity, specificity, PPV and NPV and accuracy was 100%, 71.4%, 56%,100% and 80% respectively. In addition, rate of change of calcitonin level over time showed no correlation with PET positivity. **Conclusion:** ¹⁸F-FDG PET/CT scan is a sensitive imaging tool for detection of MTC recurrence. Additional information is gained in nearly 50% of patients with raised calcitonin levels by detecting occult disease or confirming findings of other imaging tools.

EP337

18f-fdg pet/ct accuracy diagnosis in thyroid incidentalomas

F. ZELAYA REINQUET, Jr., A. RENDA ALCALDE, Jr., D. Ruiz Hernandez, M. Castrillon, Jr., C. Castillo Berrio, F. Loira Bamio, J. Nogueiras Alonso, L. Campos Villarino, R. Guitian Iglesias, A. Lopez Lopez; EOXI Vigo Hospital Meioxeiro, Vigo, SPAIN.

Thyroid incidentaloma (TI) in FDG-PET studies, is defined as pathological uptake of 18F-FDG by the thyroid gland in patients without known thyroid disease. According to current literature reports the prevalence of these findings in FDG-PET studies around 1.2% and 4.3%, with a malignancy rate between 25% and 50%. The diffusely increased FDG uptake is attributed to benign autoimmune thyroid disease, while the focal uptake may be associated with primary malignancy and less frequently to metastasis. **PURPOSE:** 1) Know the percentage of patients who underwent histopathologic thyroid study (HTS) through FNA, by finding TI in FDG-PET study in our Center. 2) Determine the type of thyroid disease (benign vs malignant) study confirmed by HTS and establish relationship with the TI uptake pattern in FDG-PET. **MATERIALS AND METHODS:** We have performed a retrospective review of 567 reports of HTS of our center during 72 months (Dec/2009-Dec/2015); and cross database and select those patients in which indication of HTS study was based on the TI FDG-PET findings.From 567 HTS reports we selected those that within the following inclusion criteria (IC):1) Uptake pattern of TI describing in the FDG-PET report. 2) Evaluate the HTS findings regarding PET-FDG in a time not exceeding three months from the acquisition of tomography. **RESULTS:** From 567 HTS, 20 patients reports(PR) had inclusion criteria

(IC).Of the 20 reports:• 8 men and 12 women• Average age 64.65 years. 18F-FDG focal uptake 14 patients: 8 with DTC (differentiated thyroid carcinoma) definitive diagnosis.5 with benign pathology(2 follicular benign nodule and 3 nodular thyroid hyperplasia) .1 patient in study. Medium SUV: 8.4g/ml.(range1,2-3,4g /ml) 18F-FDG diffuse uptake 6 patients:• 6/6 (100%) benign pathology (5 multinodular goitre/1chronic thyroiditis).• Medium SUV : 2.18g/ml.(range 2,8-36,6g/ml). **CONCLUSION:** We determined that in our series, 18F-FDG PET had a high sensitivity to detect thyroid disease in correlation with HTS (100%). In the focal uptake group, the sensitivity for detecting thyroid cancer was 61,53%. We found no relationship between the absolute value of the SUV and the likelihood of malignancy of the lesion. Although the sample is small and there is a selection bias of patients, the results of our study confirm those reported in the literature. It is advisable to enlarge explorations by the discovery of incidental FDG uptake in PET-CT studies especially in cases with focal uptake pattern.

EP338

Evaluation of the Thyroid Incidentomas of the Patients Detected on F-18 FDG PET/CT

f. s. simsek¹, z. p. koc², t. a. balci³, d. kuslu¹, y. narin⁴, e. dönder³, i. h. ozercan³; ¹elazığ training and research hospital, elazığ, TURKEY, ²mersin university, mersin, TURKEY, ³firat university medicine faculty, elazığ, TURKEY, ⁴elazığ medical park hospital, elazığ, TURKEY.

Background and Aims: The prognosis, meaning and risks of the patients with incidental thyroid nodules with FDG uptake is a challenging subject. There is no consensus about how to manage these kinds of patients. Aim of this study is to compare the lesion size and standardized uptake value (SUV) of the thyroid lesions of the patients with and without lymph node uptake and evaluate the results of the patients in follow up. **Materials and Methods:** 33 patients (14 Male, 19 Female; mean: 56±14,5 years old) who has increased uptake on F-18 FDG PET/CT examination were subjects of this study. In retrospective evaluation: mean size of the thyroid nodules were 1,9±1,2 cm; mean SUVmax value of these lesions were 7 ±4,5 and 11 patients among these 33 had additional lymph node involvement with lesion size of 1,8±0,9 cm and SUVmax of 6,8±3,2. Independent samples T test was performed and p<0.05 considered as significant. **Results:** In comparative analysis the age, lesion size and SUVmax value of the lesions of patients with and without lymph node involvement were not significantly different (p<0,05). Fine needle aspiration biopsy was performed to 10/33 patients (7/10; negative, 1/10; insufficient, 1/10; suspicious, 1/10; atypical aspirates) and total thyroidectomy/tru cut biopsy was performed to 5 of 33 patients (2/4 papillary thyroid carcinoma; 1/4 multinodular guatr; 1/4 malign mesenchimal tumor; 1/4 follicular adenoma). **Conclusion:** Additional lymph node uptake is not an indicator of higher SUVmax values or increased tumor size according to the results of this investigation. **Key Words:** thyroid, insidenteloma, F-18, FDG, lymph node.

EP339

Pre-ablation rhTSH-stimulated F-18 FDG PET/CT changes patient management in increased-risk thyroid cancer

G. Rendl, L. Rettenbacher, G. Schweighofer-Zwink, K. Hofstetter-Hörl, C. Pirich; Paracelsus Private Medical University Salzburg, SALZBURG, AUSTRIA.

Aim To evaluate the added-value of pre-ablation rhTSH-stimulated F-18 FDG PET/CT in comparison to the posttherapeutic whole body radioiodine scan in patients with advanced thyroid carcinomas. **Material and Methods** 53 sequential patients with moderate-to-high-risk thyroid carcinoma (31 females and 22 males) with a mean age of 58.5 ± 15.8 years were included in this

study. 34, 14 (2 Hurthle cell variant) and 5 patients had papillary, follicular and poorly differentiated thyroid carcinoma, respectively. The majority of patients had a pT3 stage (n=40), pT3(m) (4 pts.), T2 (2 patients), pT4a (6 patients) and pTxN0M1 (1 patient), respectively. All patients underwent FDG PET/CT with low dose CT on the day of their first radioiodine ablation (after administration of recombinant human TSH two days before), and a posttherapeutic whole body radioiodine scan (RIS) in planar and SPECT/CT technique. **Results** 12 out of 53 patients had a positive FDG PET/CT but negative RIS, of whom 5 patients had histologically verified metastases in lymph nodes. The treatment plan was changed to surgery in 4 patients while one underwent palliative radiotherapy and tyrosinkinase-inhibitor therapy. One patient refused to undergo surgery and progressed clinically. Posttherapeutic RIS was equivocal to FDG PET/CT in 39 patients and just 2 patients presented with RIS positive but FDG PET negative metastasis of whom one each had cervical lymph node metastases and pulmonary metastases. **Conclusion** About 23 % of patients with advanced thyroid cancer had rhTSH-stimulated FDG PET positive but radioiodine-negative metastases, leading to changes in patient management.

EP340

Role of ¹⁸F-Choline PET/CT in high-risk DTC patients. Comparison with ¹⁸F-FDG PET/CT

B. Dib, G. Bottoni, L. Foppiani, V. Altrinetti, M. Massollo, M. Massollo, M. Cabria, A. PICCARDO; AZIENDA OSPEDALIERA GALLIERA, GENOVA, ITALY.

Aim: to evaluate the sensitivity and clinical impact of ¹⁸F-Choline-PET/CT in patients affected by high-risk differentiated thyroid cancer (DTC) with suspected disease relapse during follow-up. We also compared ¹⁸F-Choline-PET/CT findings with those of ¹⁸F-FDG-PET/CT. **Materials and methods:** we prospectively evaluated 15 high-risk DTC patients who underwent total thyroidectomy and radioactive iodine treatment, and showed high/increasing thyroglobulin levels (median 8.1 ng/ml, range 1.6-340.0) under TSH suppression with L-thyroxine. All patients underwent ¹⁸F-FDG-PET/CT and ¹⁸F-Choline-PET/CT within 40 days from each other. For both imaging modalities we performed a both patient-based and lesion-based-analysis, and calculated the sensitivity. The standard of reference was based on clinical, imaging and histological data. In particular, histopathological results were available for 9 out of 15 patients. **Results:** the standard of reference confirmed disease relapse in all patients. On patients-based analysis, both ¹⁸F-FDG-PET/CT and ¹⁸F-Choline-PET/CT were positive in 10 out of 15 patients (sensitivity 67%). ¹⁸F-FDG-PET/CT was negative in 5 patients of which 4 affected by a non-virulent DTC subtype. ¹⁸F-Choline-PET/CT was negative in 5 patients of which 3 affected by a virulent DTC subtype. Indeed, mismatching findings between the two imaging modalities were shown in 4 patients. The diagnostic association of the two modalities was positive in 12 out of the 15 patients (sensitivity 80%). On lesion-based-analysis, ¹⁸F-FDG-PET/CT detected 22 out of 36 metastases (sensitivity 61%), ¹⁸F-Choline-PET/CT 17 out of 36 (sensitivity 51%) and the association of the two modalities showed 25 out of 36 (sensitivity 69%). A lesion-based analysis to determine the sensitivity of each modality in detecting lesions according to anatomical locations was also performed; ¹⁸F-Choline-PET/CT was more sensitive in detecting lymph-node relapse (13/19, 68 %) than ¹⁸F-FDG-PET/CT (11/19, 58%). ¹⁸F-FDG-PET/CT was more sensitive in detecting lung metastases (8/14, 57%), than ¹⁸F-Choline-PET/CT (1/14, 7%). The 3 bone metastases were correctly identified by both modalities (sensitivity 100%). The association of the two modalities slightly the identification of lung metastases (9/14, sensitivity 64%). When we looked at the therapeutic implications, ¹⁸F-Choline-PET/CT influenced treatment management in 3 out of 15 patients (20%). **Conclusion:** ¹⁸F-Choline-PET/CT may add important diagnostic informations during the follow-up of high-risk DTC patients. Although its sensitivity does not seem to be higher than that of ¹⁸F-FDG-PET/CT, ¹⁸F-Choline-PET/CT may be considered a useful complementary tool especially in patients affected by non-virulent DTC subtypes and/or with suspected lymph-node relapse.

EP341**Role of 18F-FDG PET/CT in the therapeutic management of DTC with cervical lymph nodes metastasis**

M. Larg^{1,2}, M. Saftencu², C. Pestean^{1,2}, E. Barbus^{1,2}, D. Piciu^{1,2}; ¹The Oncology Institute "Prof. Dr. Ion Chiricuta", Cluj-Napoca, ROMANIA, ²"Iuliu Hatieganu" University of Medicine and Pharmacy, Cluj-Napoca, ROMANIA.

AIM Differentiated thyroid carcinoma (DTC) is the most frequent endocrine tumor, having a 10-year survival rate over 90%. In some forms of DTC, radioiodine therapy might lose its sensitivity. In these patients, 18-F FDG PET/CT scan might bring additional information about the aggressiveness of the neoplasm. Our aim was to analyze the influence of 18F-FDG PET/CT scans in changing therapeutic approach for DTC patients with clinically and ultrasonographically detected cervical lymphadenopathies. **MATERIALS & METHODS** Our group consisted of 94 patients (n=94) with DTC and cervical lymph nodes metastasis. All patients had positive serum thyroglobulin (TG) levels (>5 ng/mL in stimulated conditions), negative TG-antibodies and negative whole body scan. Clinical and ultrasonographic exams were performed, showing swollen cervical lymph nodes. Data regarding age, gender, stage, TSH, TG and TG antibodies, previous CT scans, surgical treatment, RIT and hormonal substitutive treatment was analyzed. Patients fasted for 6 hours before undergoing 18F-FDG PET/CT examination and blood glucose levels were measured. Whole body scans were acquired 60 minutes after i.v. injection of 10 mCi 18F-FDG. **RESULTS** Out of 94 patients, 31 (31.95%) presented pathological 18F-FDG uptakes on their PET/CT scan in laterocervical lymphnodes, having the SUV (standard uptake value) lbm Max between 3-11.4. A group of 5 patients presented secondary tumors with various localizations (neck, mediastinum, lungs). Follow-up was indicated for the group of patients with normal PET/CT scans, while the patients with laterocervical lymph nodes metastasis had their therapeutic strategy changed. **CONCLUSION** 18F-FDG PET/CT examinations have an important role in patients with DTC and lymphatic metastasis, changing the therapeutic approach in 1/3 of the patients.

EP342**Role of recombinant human TSH in the diagnostic accuracy of 18F-FDG/scan-PET/CT in patients with differentiated thyroid carcinoma suspected of tumor recurrence**

J. M. Nogueiras Alonso, F. Zelaya, C. Castillo Berrio, M. Castrillón, A. Renda Alcalde, R. Guitián Iglesias, F. Loira, L. Campos Villarino, D. Ruiz Hernández; Hospital Do Meixoneiro, VIGO, SPAIN.

Introduction: Whole body scan (¹³¹I Na-WBS) in follow-up and identification of recurrent differentiated thyroid carcinoma (DTC) allows to guide the treatment. But 15-20% of patients with recurrence despite elevated Tg thyroglobulin, do not concentrated ¹³¹I Na with WBS negative. FDG uptake is linked to neoplastic dedifferentiation, losing the ability to capture and organify iodine, TSH receptor expression, which stimulate cellular uptake and glycolysis persist. It's postulated that TSH or rhTSH (human recombinant), stimulate cell metabolism accumulating more FDG. For some researchers the FDG-PET-CT sensitivity increases with TSH stimulation compared with suppressed TSH, detecting bigger FDG avidity, for other researchers the clinical impact is poor. Our objective was the prospective evaluation of 18-FDG-PET-CT locating pathological foci in patients with CDT and progressive elevation of Tg, and negative WBS, comparing the diagnostic yield with and without rhTSH in the same patient. **Materials and methods:** Study of 74 patients with DTC treated with thyroidectomy and ¹³¹I Na radio-ablation, which showing progressive increase of Tg and negative ¹³¹I Na-WBS, 16 patients were examined with 18F-FDG-PET/CT (GE Discover ST), with and without rhTSH, separated in 3 to 14 days, 15 patients

with positive Tg-antibody only were explored with rhTSH. The standard reference was the histopathology, if it wasn't possible they were followed by Tg, and response to treatment. **Results:** 90 FDG-PET/CT in 74 patients (24-81 years), 26 men and 48 women. In 16 patients it was acquired with and without rhTSH. With the suppressed TSH we got 5 positive PET and 11 negative (mean Tg/PET negative: 7.6ng/ml), SUVav: 2.65g/ml, S:33.33%, Sp:100%, PPV:100% and NPV:9.09 %. With rhTSH was positive in 15 and negative in 1, SUVav: 9.25 g/ml, S: 100%, Sp:100%, PPV and NPV of 100%. In 10/16 (62.5%) detection was possible only with rhTSH. In 74 patients with rhTSH the cut-off of Tg was 15 ng/ml, S: 58%; Sp: 76%; PPV: 75%; NPV: 59%. Accuracy: 66%. significantly higher (p <0.05) than unstimulated Tg with negative PET. The location of foci showed no significant difference in the same patient with or without rhTSH. **Conclusion:** The use of rhTSH significantly changed the management for 10/16 patients (NF without rhTSH), increasing the sensitivity of 18F-FDG PET/CT, especially in patients with relatively low value of Tg (<10 ng / ml).

EP343**The utility of ¹⁸F-FDG-PET/CT in differentiated thyroid cancer patients and elevated thyroglobulin after total thyroidectomy and ¹³¹I ablation**

K. Mladenov¹, B. Spassov², D. Vassileva²; ¹Clinic of Nuclear Medicine, University Hospital "Alexandrovska", Sofia, BULGARIA, ²Specialized Hospital for Active Treatment of Hematological Diseases, Sofia, BULGARIA.

Background: Whole-body ¹³¹I scintigraphy (WBS) and serial thyroglobulin measurement (Tg) are standard methods for detecting thyroid cancer recurrence after total/near total thyroidectomy and ¹³¹I ablation. Some patients with thyroid cancer recurrence have negative WBS scans (WBS-negative) but elevated Tg (Tg-positive). Positron emission computer tomography with ¹⁸F-fluorodeoxyglucose (¹⁸F-FDG-PET/CT) had been introduced in the clinical practice as an effective modality for detecting various cancer types. However data regarding the utility of ¹⁸F-FDG-PET/CT for detecting recurrent thyroid cancer in Tg-positive WBS-neg patients are limited. **Aim:** This study aimed to evaluate the role of ¹⁸F-FDG-PET/CT in recurrent differentiated thyroid carcinoma WBS-negative patients that are Tg-positive. **Material and methods:** We retrospectively reviewed 32 patients (8 men and 24 women), aged 31-67 years with histologically demonstrated differentiated thyroid cancer that underwent total/near total thyroidectomy followed by ¹³¹I ablation. WBS and ¹⁸F-FDG-PET/CT were performed according to standard operative protocols. Patients were WBS-negative but were suspected to have recurrence based on Tg levels. **Results:** ¹⁸F-FDG-PET/CT identified negative scans and FDG accumulating lesions in 9 (28%) and 23 (72%) patients, respectively. Reasons for negative scans were insufficient thyroid-stimulating hormone stimulation applied to the low diagnostic dose of ¹³¹I, very small tumor deposits to be detected by a gamma camera, a loss of concentration of iodine in the tumor and iodine-resistant metastases. In the positive group, 47.8% (11/23) had loco-regional disease (thyroid and local lymph nodes) while the remaining 52.2% (12/23) had distant metastases in mediastinum and lung. **Conclusion:** ¹⁸F-FDG-PET/CT enables detection and precise localization of loco-regional recurrence and distant metastases of differentiated thyroid cancer in patients with elevated serum thyroglobulin but WBS-negative. Patients with positive ¹⁸F-FDG-PET/CT accumulating lesions will probably need a change in their clinical management.

EP344**18-FDG-PET-CT the best diagnosis method in TENIS patients with elevated Tg-antibody**

J. M. Nogueiras Alonso, M. Castrillón, A. Renda Alcalde, C. Castillo Berrio, L. Campos Villarino, F. Loira, D. Ruiz Hernández, R. Guitián Iglesias; Hospital Do Meixoneiro, VIGO, SPAIN.

The differentiated thyroid carcinoma DTC has a good prognosis and high cure rate with survival rate at 10-year of 80-90%, but with a recurrence of 20%, it can be ruled by: negative cervical US, negative I-131 whole body scan (I-WBS) and undetectable thyroglobulin (Tg). With a negative I-WBS, the positivity of antiTg-Ab interferes and invalidates the proper determination of Tg, knowing that if the tissue is dedifferentiated and decreased iodine uptake ability by contrast increases glucose metabolism of the tumor cell, in this sense F18-FDG/PET able to locate disease. We analyzed prospectively the use of 18F-FDG-PET/CT in follow up of patients with elevated antiTg-Ab and negative I-131 WBS. Material and methods From 77 patients with DTC, negative I-WBS and detectable Tg followed for 4 years, we found 15 patients with detectable antiTg-Ab. 18F-FDG-PET/CT was made at 3rd day of stimulation with Thyrogen®, analytical (TSH, Tg and antiTg-Ab) basal and stimulated (3rd day), reviewed by two nuclear physicians. Results Patients: 15, papillary (10), follicular (4), (9♀-5♂) mean age 56,85y (31-79y). Eleven patients had metastatic lymph node involvement at initial diagnosis. After Thyrogen® all patients showed elevated TSH (25.30 to 173.4 mIU/ml) and detectable antiTg-Ab (61-2530ul/ml), Tg(0.5-391.7ng/ml). 31 Pathological hypermetabolism foci were obtained in 15 patients located in cervical region(25), supraclavicular(3), mediastinal(4), bone(1) with SUVmax of 1.5g/ml to 23.3g/ml. In 9 patients were confirmed metastatic DTC with pathological study (TP), one patient died and the result is pending in 5 patients. Conclusions 18F-FDG-PET/CT shows high sensitivity (100%), detecting tumor foci susceptible to cleavage with a good diagnostic accuracy it could be considered as a suitable diagnostic method in patients with elevated antiTg-Ab and negative I-WBS. The sample is still very small, and is required a larger sample to correlate the values of antiTg-Ab with sensitivity and specificity PET/CT.

EP345

Cytological and Histopathological Correlation of Follicular Neoplasms of the Thyroid: Fine-Needle Aspiration Biopsy Results of 985 Patients and a Single Center Experience

S. INCE¹, E. ALAGOZ¹, O. EMER¹, H. SAN¹, A. AYAN¹, K. OKUYUCU¹, A. O. KARACALIOGLU¹, S. DEVECİ², B. GUNALP¹, N. ARSLAN¹; ¹GULHANE MILITARY MEDICAL ACADEMY, DEPARTMENT OF NUCLEAR MEDICINE, ANKARA, TURKEY, ²GULHANE MILITARY MEDICAL ACADEMY, DEPARTMENT OF PATHOLOGY, ANKARA, TURKEY.

OBJECTIVE: Fine-Needle Aspiration Biopsy (FNAB) is a useful method for evaluation of thyroid nodules. However, it's not sufficient for the diagnosis of malignancy when follicular neoplasm is reported. We aimed to analyze final histopathological results of our follicular neoplasms in order to determine the prognostic value of FNAB. **MATERIAL AND METHOD:** Data from FNAB results of 985 consecutive patients were retrospectively analyzed. Patients with cytological diagnoses of follicular neoplasm who underwent thyroidectomy were evaluated. **RESULTS:** From 985 cases, 125 (12.69%) aspirates were non-diagnostic. 665 (67.51%) were benign; 60 (6.09%) were atypia of undetermined significance (AUS), 28 (2.84%) were follicular neoplasms; 4 (0.4%) had suspicion of malignancy; 44 (4.46%) were malignant tumors; 4 (0.4%) were parathyroid neoplasms; and 5 (0.5%) were Hurthle cell neoplasm on FNAB. Besides, 50 (5.07%) patients were underwent lymph node biopsy. Of 28 follicular neoplasms 16 were surgically treated: 10 (62.5%) were benign; 6 (37.5%) were malign. Benign cases included 8 follicular adenomas and 2 goiters; malign cases included 5 papillary carcinomas and 1 follicular carcinoma. The calculated risk of malignancy and positive predictive value in follicular neoplasm group was 37.5%. Of 5 Hurthle cell neoplasms 4 were surgically treated and all of them were benign: 2 were goiters; 2 were Hurthle cell adenomas. **CONCLUSION:** FNAB is a primary method for preoperative evaluation of thyroid nodules. Although it prevents unnecessary thyroidectomies, false positive ratio is somewhat high in follicular neoplasms. Although our result is a little higher than the

malignancy risk in follicular neoplasms reported in the literature (15-30%), it is still close proximity to the upper range. We think this is because all follicular neoplasms were not surgically treated and clinical properties of the study group were not got into account.

EP346

Clinicopathologic features and prognostic factors of tall cell variant of papillary thyroid carcinoma: comparison with classic variant of papillary thyroid carcinoma

K. Okuyucu¹, E. Alagoz¹, N. Arslan¹, O. Emer¹, S. Ince¹, S. Devci², A. Ayan¹, A. Taslipinar³, B. Gunalp¹, O. Azal³; ¹Gulhane Military Medical Academy, Department of Nuclear Medicine, Ankara, TURKEY, ²Gulhane Military Medical Academy, Department of Pathology, Ankara, TURKEY, ³Gulhane Military Medical Academy, Department of Endocrinology, Ankara, TURKEY.

Objective: Tall cell variant (TCV), an aggressive form of papillary thyroid carcinoma (PTC), frequently presents with extrathyroidal disease and recurrence. The aim of this study was to evaluate the clinicopathologic features and outcomes of patients with TCV by comparing them with a larger group of patients with classic variant of papillary thyroid carcinoma (cPTC). **Patients and methods:** A total of 2500 patients with differentiated thyroid carcinoma were treated and monitored during a 23-year period (1992-2015). Of them, 2250 (90%) had PTC and 235 (9.5%) had follicular thyroid carcinoma. Of the 2250 patients, 862 (38.3%) and 70 (3.1%) had cPTC and TCV, respectively. Cases of TCV and cPTC of PTC were compared on the basis of risk factors. **Results:** Patients with TCV were significantly older compared with cPTC patients (P<0.001). Tumor size was significantly bigger (P=0.01) and preablation thyroglobulin level was significantly higher (P<0.001) in TCV patients than in cPTC patients. The incidence of capsule invasion, extrathyroidal extension, and vascular invasion was significantly higher in TCV (P=0.003, <0.001, and 0.011, respectively). The incidence of initial lymph node metastasis was significantly higher in TCV (P<0.001). Patients with TCV were mostly at an advanced stage compared with patients with cPTC (P<0.001). Development of local or distant metastasis during the follow-up was significantly higher in TCV than in cPTC. Sex and multifocality were not statistically significant. **Conclusion:** TCV has a higher incidence of local or distant metastasis and mortality rate. Thus, it must be treated with the highest possible I-131 ablation doses and followed up carefully.

EP347

Clinical Value of Radioactive Iodine 131 Ablation Therapy in Postoperative Patients with Papillary Thyroid Microcarcinoma

J. Wang, S. Li, L. Zhang, X. Yao, R. Liu, F. Wang, Z. Wang; Nanjing First Hospital, Nanjing, CHINA.

Objective: To explore the clinical application value and the prognostic evaluation of patients with papillary thyroid microcarcinoma (PTMC) who underwent radioactive iodine 131 (I-131) ablation therapy after thyroidectomy. **Material and methods:** we collected 71 cases of patients with PTMC who underwent thyroidectomy, pathological examination, and I-131 ablation therapy in 2015, and analyse their data retrospectively. Measurement data were described with mean±standard deviation ($\bar{x}±s$), and using logistic regression to describe relation between the risk of PTMC recurrence and age, gender, foci number>1, extrathyroidal invasion, cervical lymph node metastasis >3. **Results:** Mean age of cohort was 41.46 years ±11.47; male/female ratio was 1:3.56; foci number >1 were 35, and others were 36. The mean tumor size was 0.47 cm ±0.39. Extrathyroidal invasion was seen in 14.08% of cases. Cervical lymph node metastasis was seen in 35.07% of cases, among them the metastatic rate of lymph node in neck central area was 52.15%, and other areas was

47.85%. All patients performed I-131 ablation therapy with 100mCi. Cervical lymph node metastasis and pulmonary metastases recurred in 9.86% of cases after I-131 ablation therapy, among them the metastatic rate of cervical lymph node was 7.04%, lung metastases were 2.82%. Univariate analysis showed that PTMC recurrence was associated with extrathyroidal invasion and cervical lymph node metastasis number >3 ($P < 0.05$). Age, gender and foci number were unrelated to PTMC recurrence ($P > 0.05$). **Conclusions:** It was revealed that extrathyroidal invasion, cervical lymph node metastasis >3 contribute to PTMC recurrence after I-131 ablation therapy. I-131 ablation therapy, serving as one main tool for targeted therapy of remanent thyroid, can display metastases sites and reduce recurrence rate.

EP348

Management of bone metastasis of differentiated thyroid cancer: Critical role of Iodine 131

S. E. Bouyoucef, D. mouas, A. Amimour, M. Habbeche, A. Talbi, A. Khelifa, s. Rahabi, F. Brahmi; CHU Bab El Oued, Algiers, ALGERIA.

Objective: To determine the role of Iodine 131 in the management of bone metastasis of differentiated thyroid cancer Patients and methods This is a retrospective study including 78 patients with bone metastasis of differentiated thyroid cancer (DTC) with a regular follow up at the department of nuclear medicine of CHU Bab El Oued. Those 18 men and 60 women with an average age of 52 years (range from 20yrs to 70yrs) presented bone metastasis of DTC with the following pathological variants: 60 follicular (pure or variant forms), 11 papillary (9 pure and 2 variants) and 7 indeterminate. From the 78 patients, bone metastasis were the onset of DTC in 31 patients and discovered during the follow up in 47 patients. Bone mets were associated with mets in other parenchymal sites in 41 patients (including 30 in lungs). The most common site of bone mets were spine (56) followed by pelvis (54) then skull (42). All patients were treated with radio iodine, 33 alone and 45 in association with other therapeutic modalities (Surgery, external radiotherapy and targeted chemotherapy). Results 78 patients received at least 11GBq with a global average of 18GBq. For patients who were treated by radio iodine alone average of cumulative dose was inferior than those patients who received additional therapy (16GBq versus 20GBq). Any complication of radio iodine treatment was noted for the 78 patients. Intrinsic stimulation alone was used in 57 patients and associated with recombinant TSH in 21 patients. 53 patients of 78 are well stabilized during 3 years by radio iodine and 40 patients have a survival of more than 5 years among them 13 patients with more than 10 years survival. All 60 patients are still stable and well controlled by radio iodine alone or associated with surgery and external radiotherapy. 8 Refractory cases for radio iodine were noted and moved to oncology to receive targeted or general chemotherapy. However, we have had 17 patients died and for 12 patients the reasons of their death were not linked to direct complications of bone metastasis. Conclusion Radio iodine treatment of bone metastasis under intrinsic alone or associated with external stimulation is an appropriate and safe therapy for bone metastasis of differentiated thyroid cancer. However active surveillance for at least twice a year is recommended for assessing regularly the status of bone mets and decide whether another complementary therapy is needed or not.

EP349

Treatment of malignant struma ovarii: report of 3 cases

A. Oudoux, A. Olivier, E. Leblanc, M. Jafari, J. Beaujot, H. Kolesnikov-Gauthier; CENTRE OSCAR LAMBRET, LILLE Cedex, FRANCE.

Struma ovarii (SO) is a rare tumor, mostly benign, defined as a predominance of thyroid tissue within a mature ovarian teratoma (approximately

3% of all ovarian teratomas). Malignant transformation occurs in less than 5% of all cases. After a local resection of the ovarian tumor, no consensus exists between surveillance alone and adjuvant therapy. We report our institutional experience. **Case report:** 3 patients (49, 67 and 56 years old) presented left ovarian mass (8, 4 and 6 cm respectively). One patient was asymptomatic and 2 patients presented metrorrhagia. They all underwent surgery. Because ovarian malignancies were suspected on imaging, two patients had a total hysterectomy with bilateral salpingo-oophorectomy, omentectomy and pelvic-aortic lymphadenectomy. Unilateral salpingo-oophorectomy was performed in the patient with a localized cystic lesion. On pathological examination, the ovarian mass was a papillary thyroid carcinoma (lesion sizes: 7, 5 and 2.5 cm respectively). One patient had metastatic retrocave lymph node (5 cm) and omental nodules. For adjuvant therapy, they all underwent total thyroidectomy (2-3 months later), with the intention to treat with ¹³¹Iodine. The thyroid consisted of normal tissue (2/3 patients) and 0.8 mm papillary micro-carcinoma (1 patient). Radioactive ¹³¹I therapy (3.7 GBq) was administered 5 to 8 weeks later. The stimulated serum thyroglobulin level was increased to 3.4 and 19 ng/mL for 2 patients and inferior to 1 ng/mL for the last one. ¹³¹I post-therapeutic scintigraphy only showed thyroid remnant uptake, without abnormal uptake for all patients. They were maintained on thyroid hormone suppression with thyroxine. Six months later, stimulated serum thyroglobulin, diagnostic ¹³¹I scintigraphy (185 MBq) and neck ultrasonography were normal for all patients. The subsequent follow-up consisted of a clinical examination and thyroglobulin measurements performed every six months for two years and annually thereafter. They remained free of disease respectively 5, 4 and 1 year later. **Conclusion:** If surgery is the first phase treatment of malignant SO, adjuvant therapy is not always proposed. In our institution, complementary ¹³¹I ablation is administered in case of lesions over 2 cm, disease outside the ovary or aggressive histological features. Total thyroidectomy is necessary before radioiodine therapy. Post-therapeutic ¹³¹I whole-body scintigraphy specifies the extent of the disease. After thyroid remnant ablation, serum thyroglobulin level can be used as a tumor marker. The clinico-biological monitoring of SO must be extended for 20 years, cases of late recurrence having been described.

EP350

Effect of adjuvant Lithium on Thyroxine (T4) concentration after radioactive iodine therapy

E. N. B. Hammond, M. W. H. Vangu; Charlotte Maxeke Johannesburg Academic Hospital, University of Witwatersrand, Johannesburg, SOUTH AFRICA.

Purpose: To study the effect of adjuvant lithium on serum T4 concentration in patients treated with RAI therapy in our environment. **Methods:** This was a prospective simple randomized comparative, experimental cohort study of hyperthyroid patients referred for radioactive ablation therapy in the two main academic hospitals in Johannesburg between February 2014 and September 2015. **Results:** Amongst the 163 participants submitted for final analysis, 75 received RAI alone whilst 88 received RAI with Lithium. Difference in mean T4 concentration at 3 months between RAI only (17.67pmol/l) and RAI with Lithium (11.55pmol/l) was significant with a small size effect ($U = 2328.5$, $Z = -2.700$, $p = 0.007$, $r = 0.01$). In participants who received RAI with Lithium, significant decrease in T4 concentrations observed as early as 1 month post RAI ($p = 0.0001$) whilst for those receiving only RAI, significant drop in T4 concentrations were observed only at 3 months post RAI therapy (0.000). Females and participants with Graves' who received RAI with adjuvant lithium also demonstrated significant drop in T4 concentrations at 1 month follow-up ($p = 0.002$ and $p = 0.003$ respectively). Also, there was statistically significant difference in mean T4 concentration across the 3 visits ($p = 0.001$) for participants with nodular disease who received adjuvant Lithium with RAI therapy whilst

those treated with only RAI showed no significant difference in T4 concentration ($p=0.607$). Conclusion: Adjuvant lithium leads to a prompt and better response to RAI therapy with lower T4 concentration at end of study which also is achieved faster. Also prompt response and decrease T4 concentrations associated with Graves' disease, nodular goiter and females who received adjuvant lithium therapy.

EP351

Disease-Related Deaths and its Predicting Factors in Patients with Differentiated Thyroid Carcinoma

J. Mihailovic; Department of Nuclear Medicine, Oncology Institute of Vojvodina, Sremska Kamenica, SERBIA.

The aim of the study was to analyze the mortality rate and predicting factors which influenced the disease-related deaths (DRD) in patients with differentiated thyroid carcinoma (DTC) in a 45-year follow-up study. Patients: From 1968 to 2000 363 DTC patients underwent initial thyroid surgery in different hospitals throughout the country. All of them underwent therapy with I-131 in our institution and were monitored until the end of 2015. Among 363 patients, 52 were lost to follow-up. Predicting factors were calculated by the Kaplan-Meier method and Log-rank test. Results: Out of 311, 96 (31%) patients have died during the course of the disease: 36 (37.5%) man and 60 (62.5%) woman aged from 8 to 74 years (mean, 52.9 years). Out of 311 DTC, there were 63 (20.3%) DRD, while 33 patients died due to other causes of deaths. DRD was significantly influenced by patients' age ($p=0.001$) and nodal and/or distal metastases ($p=0.000$), while following factors had no influence to cause of death: type of the initial treatment, gender, histology of the tumor and recurrent disease ($p=0.863$, $p=0.956$, $p=0.870$, and $p=0.827$, respectively). Conclusions: Disease-related deaths occurred significantly more frequent in patients older than 45 years than in patients younger than 45 years. Presence of nodal and distal metastases has also significant influence on DRD. Patients with DTC should be adequately treated and life-long monitored.

EP352

Long-term Prognosis of Follicular Variant of Papillary Thyroid Carcinoma: An Asian Single-Centre Retrospective Analysis

H. C. Low¹, Y. H. Kao², K. S. H. Loke¹; ¹Singapore General Hospital, Singapore, SINGAPORE, ²The Royal Melbourne Hospital, Melbourne, AUSTRALIA.

Background: The follicular variant of papillary thyroid carcinoma (FVPTC) is the most common variant of papillary thyroid carcinoma (PTC). The incidence of FVPTC has been increasing in recent years possibly related to ultrasound screening and earlier diagnosis. Several large multicentre studies had shown that FVPTC has similar or better prognosis than classical PTC. Others had reported excellent prognosis of non-invasive encapsulated FVPTC (EFVPTC). This study sought to compare the recurrence rate and long-term prognosis of patients with FVPTC (overall and different subtypes) at our Asian centre with that published in the medical literature. Methods: A retrospective clinicopathologic study of 110 patients with FVPTC from a single centre was performed. Variables evaluated include age at diagnosis, tumour size, tumour encapsulation, capsular and/or lymphovascular invasion, extrathyroidal extension, nodal and distant metastasis, treatment, recurrent or persistent disease and disease-specific mortality. All patients except six underwent total thyroidectomy; the six patients had subtotal or hemithyroidectomy. All patients except one also received adjuvant radioiodine treatment. The median follow-up duration was 92 months. Results: Our cohort consisted of 17 (15.5%) patients with non-invasive EFVPTC, 35 (31.8%) with EFVPTC with capsular and/or

lymphovascular invasion, 52 (47.3%) with non-encapsulated FVPTC, and 6 (5.4%) with unknown capsule status. In the non-invasive EFVPTC group, one patient had nodal metastasis and another had distant metastasis at diagnosis. The latter had persistent metastatic disease. No recurrence or disease-specific mortality occurred in this subgroup. In the invasive EFVPTC group, 10 (28.6%) patients had nodal metastasis and 4 (11.4%) had distant metastasis. Four (11.4%) patients had persistent/recurrent disease and 2 (5.7%) died from disease. In the non-encapsulated FVPTC group, 14 (26.9%) patients had nodal metastasis and 8 (15.4%) had distant metastasis. Six (11.5%) patients had persistent/recurrent disease and 1 (1.9%) died from disease. In the last group, 2 patients had nodal metastasis and 3 had distant metastasis. Two patients had persistent/recurrent disease and 1 died from disease. Overall, 27 (24.5%) patients had nodal metastasis, 16 (14.5%) had distant metastasis, 13 (11.8%) had persistent/recurrent disease and 4 (3.6%) died from disease. Information on the cause of death for 6 patients was unavailable. Conclusions: In our cohort, FVPTC behaved more like follicular thyroid carcinoma with higher rate of distant metastasis than classical PTC. Recurrence and mortality rates are also not significantly lower than classical PTC. However, patients with non-invasive encapsulated FVPTC had no recurrence or mortality on follow-up, in keeping with current evidence in the literature.

EP353

Lymphovascular invasion with metastasis (locoregional lymph node or distant) among adult Filipino patients with papillary thyroid carcinoma: A Case Control Study

E. Linchangco, **I. Bandong**, G. Goco; St. Luke's Medical Center- Quezon City, Quezon City, PHILIPPINES.

Papillary thyroid carcinoma is the most common type of thyroid cancer. Treatment includes surgery and remnant ablation with radioactive iodine therapy while follow-up monitoring includes whole body Iodine-131 scans and thyroglobulin monitoring. Lymphovascular invasion has been used as a predictor of metastasis in different cancers. Lymphovascular invasion therefore, might be useful in predicting metastasis in patients with papillary thyroid carcinoma since metastasis in this type of carcinoma travels via the lymphatic route. **Objective:** The purpose of this study is to determine the association of lymphovascular invasion with metastasis among patients with papillary thyroid carcinoma. Records of patients with papillary thyroid carcinoma (histopathologic reports, thyroglobulin levels and whole body Iodine-131 scans) were reviewed retrospectively. **Results:** A total of 108 subjects were recruited for this study, 47 (43.5%) of which had lymphovascular invasion. There was no association found between lymphovascular invasion and metastasis on baseline (p -value = 0.72) and follow-up scans (p -value = 0.07). However, there is an association between metastasis resolution on follow-up scans and high dose radioactive treatment (p -value = 0.02) regardless of presence or absence of lymphovascular invasion. Even though no association was seen between lymphovascular invasion and metastasis, a robust percentage of patients with lymphovascular invasion were positive for metastasis on whole body scans. **Conclusion:** There is significant association between the presence of LVI with elevated thyroglobulin levels (p -value = <0.0001). A significant association is also seen with LVI and dose activity with resolution of thyroid remnant, locoregional lymph node and distant metastasis (p -value = 0.02).

EP354

To ablate or not to ablate? The Question in Patients with Papillary Thyroid Microcarcinoma

M. URHAN¹, S. A. AY², A. I. FILIZ³, F. DENIZ², A. YONEM², Y. KURT³; ¹GATA HAYDARPAŞA TRAINING HOSPITAL DIVISION

OF NUCLEAR MEDICINE, ISTANBUL, TURKEY, ²GATA HAYDARPASA TRAINING HOSPITAL DIVISION OF ENDOCRINOLOGY, ISTANBUL, TURKEY, ³GATA HAYDARPASA TRAINING HOSPITAL DIVISION OF SURGERY, ISTANBUL, TURKEY.

Objective: Some suggest completion thyroidectomy and radioablation for patients with -mostly incidentally detected- papillary thyroid microcarcinomas while some others favor just follow-up. We assessed the prognosis of the disease in a group of patients with hemi-thyroidectomy only and in another with thyroidectomized but not ablated. Findings were compared with those of both thyroidectomized and radioablated patients. **Methods:** Two-hundred fifty-four patients with a proven diagnosis of thyroid cancer <10 mm among 1720 were enrolled. Any patient with capsular invasion, intrathyroidal spread, lymph node invasion and multicentricity was excluded. In group A (22 patients; 15 female, 7 male; mean age 74), patients were hemi-thyroidectomized only while in group B (56 patients; 37 female, 19 male, mean age 62) all cases had a total or near-total thyroidectomy. The preoperative diagnosis was nodular/multinodular goiter. The remaining 176 patients (118 female, 58 male; mean age; 56) had total/near total thyroidectomy and radioablated. All patients were monitored with serum Tg levels measurements for every 6 months and with ultrasound evaluation of the neck. Any lesion seen on ultrasound and an increase in serum Tg/ATg were noted for a period of 2 to 15 years **Results:** In group A, no other tumor or lymph node invasion was detected in the surveillance period. In group B, in 32 of 56 patients serum Tg levels were less than 2 ng/dl (range; 0.2 to 3.9 ng/dl). In the remaining 24, initial serum Tg level ranged from 2.0 to 9.8 but decreased to <4.0 ng/dl after 6 months. In 9 patients, pathological lesions were detected with ultrasound and lymph node invasion was confirmed with fine needle aspiration cytology. In 2 of these 9 patients; serum Tg values were less than 2.0 ng/dl. In group C, initial serum Tg levels ranged from 10.1 to 19.8 (mean; 14.8), but after radioablation, mean Tg level decreased to <0.8 ng/dl. In 19 patients, (Tg levels; 0.2- 19.8 ng/dl), lymph node invasion was detected and 12 of them had neck dissection. **Conclusion:** Approximately 1/10 of patients (11.5 %) with papillary thyroid microcarcinoma treated with total or hemi-thyroidectomy only presented with recurrent disease whereas 10.8% of patients treated with both total thyroidectomy and radioablation presented with recurrent disease in the surveillance period. As the difference is not significant between radioablated and not ablated groups, we do not recommend radioablation for patients with thyroid microcarcinoma with no unfavorable characteristics and follow-up.

EP355

¹³¹I-iodine dose planning in well differentiated thyroid cancer treatment by K-Means Clustering

L. Mijatovic¹, M. Selmic², D. Teodorovic³; ¹University of Kragujevac, Faculty of Medical Sciences, KRAGUJEVAC, SERBIA, ²University of Belgrade, Faculty of Transport and Traffic Engineering, Belgrade, SERBIA, ³Serbian Academy of Sciences and Arts, Belgrade, SERBIA.

Background: Thyroid cancers are the most frequent endocrine carcinomas. A range of clinical parameters (the patient's diagnosis, the patient's age, the tumor size, the existence of metastases in the lymph nodes and the existence of distant metastases) affect a physician's decision-making in dose planning. The choice of dose recommended by a physician is based on physician's expertise and experience. The physician's decision cannot be, without difficulty, explained by exact rules and/or mathematical algorithms. **Aim:** We developed the model that recommends the dose of I-131 iodine that should be given to the individual patient. **Materials and Methods:** The proposed model is based on the K-Means Clustering procedure (learning algorithm that solve clustering problem). By using the K-Means Clustering procedure we classify observed group of patients into a certain number of clusters that

are fixed a priori. The number of clusters is equal to the number of possible I-131 iodine doses. Every cluster represents one specific I-131 iodine dose. The developed model was tested on a group of 183 patients after total/near total thyroidectomy. All patients had well differentiated thyroid carcinomas. A patient's histopathologic diagnosis was one of the following: 1. Microcarcinoma papillare glandulae thyroideae; 2. Ca-papillare glandulae thyroideae multifocale; 3. Ca papillare-glandulae thyroideae; 4. Hurtle cell carcinoma glandulae thyroideae; 5. Ca folliculare gl. thyroideae (multifocale); 6. Ca folliculare gl. thyroideae; 7. Microcarcinoma papillare multicentricum. The dose of I-131 iodine that was given to the patients had the following four possible values: 1.85 GBq, 3.7 GBq, 5.5 GBq and 7.4 GBq. **Results:** The proposed approach was tested on the real data from patients treated in the Department of Nuclear Medicine, Clinical Center Kragujevac, Serbia. By comparing the results achieved through the proposed model with those resulting from the physician's decision, it was found that the proposed model is highly compatible with reality. In other words, the I-131 iodine doses suggested by the developed system are similar to the dose values recommended by the experienced nuclear medicine specialist. **Conclusion:** The developed model could be utilized for educational purposes, and with additional developments, it could help and direct young physicians.

EP356

Ablation with 100 mCi radioiodine and thyrotropin alfa in locally advanced thyroid cancer disease

S. Jeong¹, J. Jeong¹, J. Ha², S. Lee¹, B. Ahn¹, J. Lee¹; ¹Kyungpook National University School of Medicine, Daegu, KOREA, REPUBLIC OF, ²Chosun University Hospital, Gwangju, KOREA, REPUBLIC OF.

Background: It is unclear whether 100 mCi radioiodine (RI) with recombinant human thyrotropin (thyrotropin alfa) is as effective as 150 mCi RI with thyroid hormone withdrawal (THW) for RI ablation in patients with locally advanced thyroid cancer (DTC) disease underwent total thyroidectomy. We evaluated success rates and clinical outcomes by delayed risk stratification (DRS) treated either using 100 mCi RI with rhTSH or 150 mCi RI with THW. **Methods:** A total of 116 DTC patients with T4 or N1b by the 7th edition of the AJCC/UICC staging system were included. Ninety-six patients were treated using 100 mCi RI with rhTSH (LO group) and 80 patients using 150 mCi RI with THW (HI group). Successful RAI therapy was defined as (i) negative stimulated thyroglobulin (Tg) in the absence of Tg antibodies, and (ii) absence of remnant thyroid tissue and of abnormal cervical LNs on ultrasonography. Response to initial therapy was classified as excellent, indeterminate, or incomplete (biochemical or structural) by DRS. **Results:** RI ablation was successful in 59.3% in the LO group and 55.6% in the HI group. There was no significant difference in the rate of successful RAI therapy between the LO and HI groups ($p=0.55$). DRS demonstrated that excellent, acceptable or incomplete response was 58.6%, 24.1% and 17.2% in the LO group and 44.4%, 22.2% and 33.3% in the HI group, respectively. There was no significant difference in the rate of response to initial therapy between the LO and HI groups ($p=0.49$). **Conclusion:** Ablation using 100 mCi with rhTSH was as effective as 150 mCi with THW to treat locally advanced DTC patients with T4 or N1b disease.

EP357

Comparable Ablation Efficiency of 30 and 100 mCi of I-131 in Low to Intermediate Risk Thyroid Cancers Using Triple Negative Criteria

M. u. Zaman¹, N. Fa², A. Zaman³, U. Zaman³, R. Tahseen³; ¹AKUH, Karachi, PAKISTAN, ²Dr Ziauddin Hospital, Karachi, PAKISTAN, ³Dow University of Health Sciences, Karachi, PAKISTAN.

Background: There is a controversy about ablation efficacy of low or high doses of radioiodine-131 (RAI) in patients with differentiated thyroid

cancers (DTC). Purpose of this prospective study was to find out efficacy of 30 mCi and 100 mCi of RAI to achieve successful ablation in patients with low to intermediate risk DTC. **Materials and Methods:** This was a prospective cross sectional study which was conducted from April 2013 till November 2015. Inclusion criteria were patients of either gender, 18 years or older, having low to intermediate risk papillary and follicular thyroid cancers with T1-3, N0/N1/Nx but no evidence of distant metastasis. Thirty-nine patients were administered 30 mCi of RAI while 61 patients were given 100 mCi of RAI. Informed consents were acquired from all patients and counseling was done by nuclear physicians regarding benefits and possible side effects of RAI. After 06 months (range 6-16 months; after 2-3 weeks thyroxin withdrawal), these patients were followed up with stimulated TSH, thyroglobulin (sTg) and thyroglobulin antibodies, ultrasound neck (U/S) and a diagnostic whole body iodine scan (WBIS) for ablation outcome. Successful ablation was considered if stimulated Tg < 2 ng/ml with negative antibodies, negative U/S and a negative diagnostic WBIS (triple negative criteria). ROC curve analysis was used to find diagnostic strength of baseline sTg to predict successful ablation. **Results:** Successful ablation based upon triple negative criteria was 56% in low dose and 57% in high dose groups (non-significant p value). Successful ablation based on single criterion (follow-up sTg < 2 ng/ml) was 82% in low dose group than 77% in high dose group (p - non-significant). The ROC curve revealed that baseline sTg level ≤ 7.4 ng/ml has the highest diagnostic strength to predict successful ablation in all patients. **Conclusion:** We conclude that 30 mCi of RAI has similar ablation success to 100 mCi dose in patients with low to intermediate risk DTC. Baseline sTg ≤ 7.4 ng/ml is a strong predictor of successful ablation in all patients. Low dose RAI is safer, more cost effective and more convenient for patients and healthcare providers. **Key words:** Radioiodine ablation; differentiated thyroid cancer; successful ablation; low dose; high dose; stimulated thyroglobulin

EP358

Effectiveness of low radioiodine administered activity in patients with low risk differentiated thyroid cancer

I. YEDDES, Jr.^{1,2}, T. BEN GHACHEM¹, I. MEDDEB¹, K. LIMAM¹, M. SOMAII¹, I. SLIM¹, M. BEN SLIMENE¹; ¹SALA AZAIEZ INSTITUTE, tunis, TUNISIA, ²FACULTY OF MEDECINE OF t; university tunis el manar UNIS, Tunis, TUNISIA.

Background: the differentiated thyroid cancer (DTC) is deemed good prognosis tumors with a low potential for development provided to adapt the specific treatment. The postsurgical therapeutic management is still a controversial subject, but the radioiodine treatment is recommended for most patients. Indeed, there is no consensus on the dose of ¹³¹I to be administered, although the current trend towards therapy easing through mini-cures for patients with good prognosis. **Aim:** to confirm the non-inferiority in terms of effectiveness of an ablative mini-cure from 1.11 to 1.85 GBq, over a cure of 3.7 GBq, in patients with DTC operated for low and very low risk. **Methods:** We retrospectively studied 157 patients with very low and low risk DTC, followed in the Nuclear Medicine Department of the Salah Azaiez Institute between 2002 and 2012. These patients had a complementary radioiodine therapy with either low dose (group A) or high dose (group B) with an evaluation at six months post treatment and in long-term. **Results:** The average age was 42.8 ± 13.7 years with a female predominance (86.7%). The DTC papillary represented the most common etiology (95%) with a predominance of pure papillary (68%) on the follicular variant (27%). The first cure evaluation did not show statistically significant difference between the two approaches in terms of therapeutic ablative efficiency (p=0.13). The overall success rate was 77% (121/157), with 83% (54/65) in group A and 72.8% (67/92) in group B. The likelihood of having a remission from the first cure was 1.83 times greater for patients treated with low doses (OR = 1.83, 95% CI: 0.23-1.29). At the end of follow, we have noted one case of refractory disease. The male gender (adjusted OR = 2.71, 95% CI 0.51-

4.23, p=0.03), and the baseline Tg ≥ 10 (ng/ml) (adjusted OR = 3.48, 95% CI 1.25-9.67, p=0.01) were significantly independent predictors of successful first cure ablation. **Conclusion:** The results provide that mini-dose protocol is not less effective for ablation of the thyroid remnant than 3.7GBq activity. These results are consistent with the current strategy in the low risk DTC.

EP359

The Predictive Value of Postoperative Serum Thyroglobulin in the Outcome of Radioactive Iodine-131 Thyroid Ablation in Differentiated Thyroid Carcinoma

S. A. A. Elrasad¹, Y. G. Abdelhafez², A. Tawakol¹, A. Nawwar¹, S. M. A. El-Refaei¹; ¹Cairo university, Cairo, EGYPT, ²South Egypt Cancer Institute, Assiut University, Assiut, EGYPT.

Background: Thyroglobulin is commonly used to monitor patients with differentiated cancer thyroid. It has also become an excellent biological marker for tumor persistence or recurrence. **Aim of study:** To study the relation between the level of baseline serum thyroglobulin (Tg) and thyroid remnant ablation outcome using radioactive iodine-131 (RAI-131) in patients with differentiated thyroid cancer after surgical treatment. **Methods:** A prospective study involved 98 patients (age 20-70 years) with differentiated thyroid cancer, referred for post-surgical ¹³¹I ablation. All patients performed baseline serum Tg, anti-Tg-Ab's under TSH stimulation as well as neck ultrasonography, before receiving RAI-131 ablation dose 1110 - 3700 MBq (30 -100 mCi). Follow-up was performed 6-8 months later. Successful ablation was determined by negative whole body ¹³¹I scan, negative neck ultrasonography and stimulated serum thyroglobulin level less than 2 ng/mL. **Results:** Successful ablation was reported in 64 out of 98 cases (65.3 %). Baseline serum thyroglobulin level was significantly predictive of ablation outcome. ROC analysis identified a cutoff value of 3.7 ng/ml in predicting ablation outcome. Patients were divided into high and low baseline Tg groups using this cut-off point. Successful ablation was significantly higher in low Tg group 34 out of 44 patients (77.2 %) versus 30 out of 54 (55.5 %) in the high Tg group; P = 0.025. There was no significant difference between the two groups regarding their clinical and pathological data or the given 131-RAI ablative doses. **Conclusion:** Baseline serum thyroglobulin level is associated with ablation outcome. Serum Tg > 3.7 is linked to significantly higher rates of unsuccessful ablation.

EP360

Role of fluorine-18 fluorodeoxyglucose positron emission tomography/computed tomography in primary thyroid lymphoma

Y. Fan¹, Y. Zhang², Y. Zhi¹, N. Lin¹, J. Zhu¹, X. Wang¹; ¹Peking university cancer hospital, Beijing, CHINA, ²Peking university cancer hospital & Institute, Beijing, CHINA.

Objective: Primary thyroid lymphoma (PTL) is a rare malignancy, and this study aimed to investigate the usefulness of fluorine-18 fluorodeoxyglucose (¹⁸F-FDG) positron emission tomography integrated with computed tomography (PET/CT) imaging in PTL. **Methods:** We retrospectively reviewed the data of 1141 patients with lymphoma who had undergone ¹⁸F-FDG PET/CT. Of these, 17 patients (1.49%) were diagnosed with PTL via histological examination and Ansell criteria. The clinicopathological data were collected. Characteristic imaging features and metabolic information in baseline and interim ¹⁸F-FDG PET/CT scans were assessed and summarized by three experienced nuclear medicine physicians. Metabolic tumor volume (MTV) and total lesion glycolysis (TLG) in the baseline PET/CT were adopted as metabolic parameters. Treatment response was evaluated at the end of the first round of treatment or, in patients with progressive disease, at the time of

progression. Prognosis was estimated via the Kaplan-Meier method using clinical and metabolic parameters. **Results:** The mean age of PTL patients was 56 years (range, 37–74 years), and the female-to-male ratio was 1.83. Based on ^{18}F -FDG PET/CT images, the tumor appearances could be categorized into two types: a diffuse enlarged hypermetabolic thyroid (10 cases) and a solitary hypermetabolic nodule (7 cases). No necrosis or calcifications were found in the lesions. Of the 17 patients, 13 were at a limited stage and four were at an advanced stage. Of the 11 patients who underwent interim PET, eight ones showed complete response, two showed partial response, and one had no response. High whole-body TLG on baseline PET and positive residue on interim PET/CT were related to adverse prognosis ($P < 0.05$). Clinical factors, thyroid TLG, and MTV on baseline PET had no correlation with outcomes ($P > 0.05$). **Conclusions:** Baseline ^{18}F -FDG PET/CT may be helpful for characterizing and accurately staging lesions, evaluating the treatment response, and predicting the outcomes of patients with PTL.

EP361

Survival analysis of patients with locally advanced iodine-131 refractory papillary thyroid carcinoma treated with peptide receptor radionuclide therapy

M. Vlajkovic¹, M. Matovic², V. Artiko³, E. Matovina⁴, M. Rajic¹, M. Stevic¹; ¹Clinical Center Nis, NIS, SERBIA, ²Clinical Center Kragujevac, Kragujevac, SERBIA, ³Clinical Center of Serbia, Belgrade, SERBIA, ⁴Institute of Oncology, Sremska Kamenica, SERBIA.

Aim of the study: Somatostatin receptors are found over-expressed and broadly distributed in human differentiated thyroid cancer (DTC) cells, which provides a basis for their molecular localization and the selection of patients for peptide receptor radionuclide therapy (PRRT) as a possible treatment for iodine-131 refractory, dedifferentiated DTC (DeDTC). The aim of this paper is to emphasize the importance of combined somatostatin receptor scintigraphy (SRS) imaging using Technetium-99m-HYNIC-[D-Phe1,Tyr3-Octreotide](Tc-99m Tektrotyd), and fluorine-18 fluoro-deoxyglucose positron emission and computerized tomography (F18-FDG-PET/CT) in the detection of recurrent diseases and the selection of patients with DeDTC for the PRRT. The secondary goal is the evaluation of PRRT effectiveness in radioiodine-therapy-refractory thyroid cancer patients by means of analyzing the progression free survival period and overall survival rate. **Material and Methods:** The study enrolled 7 patients with locally advanced radioiodine-negative papillary thyroid carcinoma (4 women and 3 men; mean age 59.1 ± 14.0 years, range: 33–77 years). The inclusion criteria for PRRT were the presence of matched focal accumulation on Tc-99m-Tektrotyd and F18-FDG-PET/CT scan. Two out of seven patients who did not meet the criteria for PRRT were treated using chemotherapy. One out of 5 patients treated with PRRT received a single dose of 3.7GBq Y90-DOTA-Tyr3-octreotide (Y90-DOTA-TOC), while the other four were treated using combined 3.7GBq Y90-DOTA-TOC and 3.7GBq Lu177-DOTA0,Tyr3-octreotate (Lu177-DOTA-TATE) radiopharmaceuticals. Only one of the patients received 2 combined PRRT doses during the 3-month interval. **Results:** Response assessment (using RECIST criteria) was performed in all the patients and showed disease stabilization in 3 (42.8%), and complete remission in one patient. The remaining 3 patients (42.8%) showed progressive disease. Kaplan-Meier analysis revealed a post-PRRT mean progression free survival of 20.7months (95% CI, range 9.1–32.3) and mean overall survival rate of 23.2 months (95% CI, range 11.7–34.7). Overall survival in DeDTC patients after the initial treatment was 8 years (95% CI, range 4.3–11.6). **Conclusions:** Our results have shown that the Tc-99m Tektrotyd scan is a reliable method for detecting recurrent disease in radioiodine-therapy-refractory thyroid cancer patients. Combined with the findings of F18-FDG PET/CT, it can be extremely helpful in selecting patients with DeDTC for PRRT. Our results demonstrated that PRRT is a

promising therapeutical option in non-radioiodine-avid dedifferentiated thyroid cancer patients, considering mean progression free survival of 20 months. However, the overall survival rate of 8 years for the patients with locally advanced iodine-refractory disease was lower in comparison to the literature data for DTC.

EP362

Role of 18F DOPA PET CT in recurrence Medullary Thyroid Cancer (MCT)

E. Ignacio Alvarez, Arguelles Pérez David Antonio; Instituto Nacional de Cancerología, Ciudad de México, MEXICO.

Introduction: Medullary thyroid carcinoma (MTC) is a slow-growing neuroendocrine tumor originating from parafollicular C cells. MCT accounts for approximately 5% of thyroid carcinomas, this tumor is associated with a higher incidence of metastasis and poorer prognosis compared with the more frequently encountered well-differentiated papillary and follicular thyroid carcinomas. Most frequent sites of metastatic disease are cervical and mediastinal lymph nodes, lungs, liver, and bone. Early detection of this tumor may significantly improve chances of survival. Imaging plays a critical role in both early detection and accurate staging of MTC, which dictates surgical management. Several studies have compared the sensitivity of FDG and DOTANOC, FDOPA versus FDG PET-CT, with sensitivities of 94 vs 62%, 75.61 vs 63.4, respectively. **Case presentation:** We present 5 patients with a history of medullary thyroid cancer, following surgical resection of the thyroid gland, of which 2 had elevated calcitonin < 5000 pg/ml, 1 in values of 590 pg/ml and 2 with values < 500 pg/ml. The first two patients underwent PET-CT with 18F-FDOPA and 68Ga-DOTATOC, finding concordant injury and not concordant, between the two studies. The patient ranges calcitonin 590 pg/ml study with 68Ga-DOTATOC was negative, while 18F-FDOPA presented with focal uptake at the cervical level. The last 2 whose values calcitonin patients were less than 100 pg/ml, one both studies were performed whose result was negative and the other one is only performed PET-CT 18F-FDOPA, whose result was negative and decided not to the study of 68Ga-DOTATOC by low levels of calcitonin. **Discussion:** Although the number of patients is minimal, the results were similar to those reported in the world literature. That is, the levels of calcitonin are correlated in the expected results in studies PET-CT, as the sensitivity may be as low as 20% and when calcitonin levels are > 1000 pg/ml with a sensitivity up 90%. **Conclusion:** The 18F-FDOPA and 68Ga-DOTATOC dual studies are being complementary studies in these patients in whom it was found that can identify lesions not concordant between the two, which have greater sensitivity than 18F-FDG (55%).

EP363

Side effects of calcium stimulation test in patients with thyroid nodules: experience with 530 patients

T. Gincu, P. Ubl, A. Gessl, M. Krebs, A. Haug, M. Hacker, S. Li; Medical University of Vienna, VIENNA, AUSTRIA.

The aim of this study was to investigate the side effects of the calcium stimulation test in patients with thyroid nodules and increased basal calcitonin concentration. **Patients and Methods:** A total of 530 patients (276 females and 254 males, mean age of 58 ± 31 years) had calcium stimulation tests. All patients filled in a questionnaire regarding the side effects within 30 min after completion of the stimulation tests. The differences of side effects between female and male patients were evaluated. **Results:** Warmth feeling was the most frequent occurring side effect in all patients during the calcium stimulation tests, followed by nausea, altered gustatory sensation, and dizziness. The incidences of urgency to

micturate, warmth feeling and dizziness were significantly higher in the female patients as compared to male patients by calcium stimulation test. **Conclusion:** There is a significant gender-specific difference in side effects induced by calcium stimulation test. Female patients have more side effects as compared with male patients by calcium stimulation test. Therefore, more attention should be paid to female patients during the calcium stimulation test.

EP364

Detection of Papillary Carcinoma in Patients with chronic autoimmune thyroiditis

K. Zaplatnikow¹, V. Y. Sukhov²; ¹MÄZ, Department for Nuclear Medicine, NÜRNBERG, GERMANY, ²ARCEM n/a A.M.Nikiforov of MES Russia, St. Petersburg, RUSSIAN FEDERATION.

OBJECTIVE: Autoimmune thyroiditis (AIT) often associated with thyroid nodules. Unfortunately it is not fully examined at a time and we have no even background understanding. Increased thyroid dysfunction in regions with low iodine supply and additional radiation exposure led to increased incidence of thyroid gland diseases: e.g. AIT, nodular goiter (NG) and carcinoma. This study exploited multimodal approach as combination of nuclear medicine data and laboratory tests of AIT and NG. **MATERIALS AND METHODS:** 411 patients that were relocated to Germany between 2005 and 2015 from previous USSR weapon nuclear test region in North Kazakhstan were examined. Based on US-diagnosed goiter and thyroid nodules and RIA-evidenced AIT all patients underwent full in-vitro thyroid examination and scintigraphy. AIT patients with coexisting suspicious hypofunctional nodes were histologically verified after FNAB (n=39 pts - Gr. A) and compared with pts without suspicious NG and AIT (Gr.B, n=23 pts) and pts with cold nodes without AIT (group C, n=112) and typical AIT only (Gr. D - n=237 pts). **RESULTS:** From the whole cohort of 411 patients (11/6 F:M ratio; age 43+/-15 yrs) 17 had one type of carcinoma: multifocal papillary carcinoma (MPC) and coexisting AIT, remaining in eu/hypothyreotic state with levels of TSH 1,0-12,00 mIU/l and TU 0,3-3,2%. There were only 6 MPC patients in Gr. B with suppressed TSH (<0.01 mIU/L) and typical scintigraphic signs of autonomous nodes. Hyperthyroidism/or subclinical hyperthyroidism signs that not considered as AIT evidence were noticed in 37 pts of Gr. C. There were no histological confirmation of carcinoma in any pts in Gr. C and D. In group A there was shift to subclinical hypothyroidism (76 vs. 24%), opposite to group B (56 vs. 44%) (P=0.005). Maximal nodes diameter was down to 8% smaller in group A as compared with group B. A positive correlation between nodule size and age was found only in group B (P=0.015). **RESUME:** MPC is often pathology in regions with registered radioactive contamination and iodine deficiency, with background of thyroiditis and the nodular goiter. Presence of AIT led to inaccurate MPC detection because of very low difference in size of nodules (non-statistic significance between groups A and B) due to chronic thyroid lymphocytic infiltration and may blur the growth tendency of thyroid nodes and their functional activity.

EP365

Role of radioguided occult lesion localization (ROLL) in the management of Differentiated Thyroid Cancer, a single center experience

M. Menga¹, B. Elia¹, A. Codegone¹, G. Mensa², R. Pellerito¹; ¹Nuclear Medicine AO Ordine Mauriziano, Turin, ITALY, ²General and Oncological Surgery, Thyroid Unit AO Ordine Mauriziano, Turin, ITALY.

Aim: ROLL (Radioguided Occult Lesion Localization) is an established procedure widely used in localizing non palpable breast cancer. It has also been successfully employed in localizing differentiated thyroid cancer

(DTC) cervical recurrences, since reoperations in the neck can be affected by many side effects and by low probability of complete disease excision. We analyzed data of patients surgically treated for DTC by means of ROLL in our Institution. **Materials:** Data from 14 (4 M 10 F) consecutive patients from December 2013 to March 2016 were analyzed. All the patients were affected by DTC (11 papillary, 1 follicular, 2 Hurthle cell carcinoma). They had received prior total thyroidectomy and at least one radioiodine treatment. Disease persistence was suspected on the basis of persistent Thyroglobulin or AbTG and the patients showed ultra sonographic (US) features of enlarged lymph node or local recurrence. All them underwent ultrasonographically-guided fine needle aspiration (FNA) and cytology was consistent with DTC. Prior to surgical intervention was performed 99mTc-labeled macroaggregated albumin (MAA) injection in to the lesions (45 MBq in 0,2 ml) under ultrasound guidance. Planar scintigraphic images were also obtained in order to help localization. During surgery an intraoperative gamma probe was used for anatomic localization and to confirm complete excision of the lesions within the surgery field. All patients underwent subsequent radioiodine treatment post-surgery. **Results:** No side effects were observed after 99mTc injection. All the radiolabeled lesions were surgically localized and excised. Post-excision count also confirmed no significant activity within the surgical field and count-ratio was positive in the excised lesions. Pathology confirmed neck lymph nodes DTC metastases in 9 patients, neck soft tissues metastases in 4, and recurrences in both neck lymph nodes and soft tissues in 1 patient. After a median follow-up of 15 months 4/14 patients proved to be disease-free, 3/14 have Thyroglobulin or AbTG persistence without imaging localization (biochemical incomplete response), 3/14 showed persistence of Thyroglobulin or AbTG and US positive imaging (structural incomplete response), finally 4/14 patients are still being evaluated since they had surgery less than 6 months ago. **Conclusions:** Despite the small population presented, we confirm that ROLL in DTC patients is a simple, reliable and safe procedure that helps radical metastatic lymph node excision and correct localization of recurrences in the neck, therefore allowing a better control of persistent DTC.

EP366

Risk of incidental thyroid cancer is not increased in overweight or obese patients

S. Kim¹, K. Pak², S. Shin²; ¹Pusan National University Yangsan Hospital, Yangsan, KOREA, REPUBLIC OF, ²Pusan National University Hospital, Busan, KOREA, REPUBLIC OF.

Objectives: The relationship between obesity and several cancers including esophagus, colon, kidney, breast and skin have been reported. However, the role of obesity in thyroid cancer is controversial. We aim to evaluate the relationship between overweight and risk of malignancy in patients with thyroid incidentaloma detected by F18-Fluorodeoxyglucose (FDG) positron emission tomography/computed tomography (PET/CT). **Methods:** From January 2010 to December 2013, a total of 332 thyroid incidentalomas were detected by F18-FDG PET/CT. Patients with fine needle aspiration within 1 year interval with PET/CT were included. After reviewing the medical records, 246 patients were eligible in this study. Body mass index (BMI) was calculated by dividing the weight (kg) by the square of height (m). BMI less than 23.0 was defined as a normal weight (NW) group and 23.0 and more was defined as an overweight or obese (OVOB) group. Using the Bethesda system for reporting thyroid cytopathology, categories I-III (nondiagnostic, benign, and atypia of undetermined significance) were defined as a non-malignancy and categories V-VI (suspicious for malignancy and malignancy) were defined as a malignancy. **Results:** Among 246 patients, 105 (42.7%) patients were in NW group and 141 (57.3%) patients were in the OVOB group. Rate of malignancy in NW and OVOB groups were 29.1% and 20.0%, respectively. However, the difference of malignancy rate was not statistically significant (p=0.1055). When patients were categorized according to primary

malignancy, the difference of malignancy rate between OVOB and NW group in each primary malignancy was not statistically significant. **Conclusions:** We demonstrated that overweight and obesity did not increase rate of malignancy in patients with thyroid incidentalomas. Due to limitation of retrospective study, further large prospective study should be performed to validate this result.

EP367

Possibilities of comparative ^{99m}Tc-pertechnetate and ^{99m}Tc-MIBI scintigraphy in management of thyroid nodule pathology

O. Bessolova, O. Perfilova, Y. Kizhaev, V. Vidioukov, K. Teterin, N. Vyrenkova, S. Kozeev, T. Khalatyan, I. Samarkin; Russian Medical Academy of Postgraduate Education, Moscow, RUSSIAN FEDERATION.

Aim: To evaluate clinical usefulness of comparative ^{99m}Tc-pertechnetate and ^{99m}Tc-MIBI scintigraphy in assessment of thyroid nodules for malignancy. **Materials and methods:** A total of 50 patients (37 women and 13 men) with mean age of 59±7,4 years with solitary or multiple thyroid nodules were included in our study. All the patients were selected for surgery on the basis of clinical, laboratory, ultrasound and fine-needle aspiration biopsy (FNB) data. The size of nodules ranged from 8 to 40mm. The Bethesda System (BS) for reporting thyroid cytopathology was used. The first anterior neck scintigraphy was performed 20-30 min after intravenous administration of 74 MBq ^{99m}Tc-pertechnetate. Uptake of ^{99m}Tc-pertechnetate in thyroid nodules was compared with uptake in the surrounding normal thyroid tissue. In cases of cold, decreased and equal uptake ^{99m}Tc-MIBI scintigraphy was performed the same day 20-30 min after 555 MBq intravenous (GE Infinia Hawkeye 4, Siemens Symbia E Dual). LEHR collimator was used, acquisition 500 000 counts. Images were graded as “match” in cold, decreased or isointense ^{99m}Tc-MIBI uptake corresponding to ^{99m}Tc-pertechnetate scans, and “mismatch” - in nodule uptake on ^{99m}Tc-MIBI higher than on ^{99m}Tc-pertechnetate scan. Histopathology served as a gold standard. **Results:** In 34 patients was found benign and in 16 - malignant histology. “Match” status was meant as benign and “mismatch” - as malignant characteristic. For all patients of our study calculated sensitivity, specificity, PPV, PNV were 68,7%, 56,8%, 44,0%, 80,0% respectively. Majority of false negatives (4 from 5) were BS6 patients with malignant focus less than 10mm in size. Suggesting that the scintigraphy does not change the treatment tactic in BS6 patients we applied statistic evaluation to BS1-5 group (38). Calculated sensitivity, specificity, PPV, PNV for BS1-5 group were 80,0%, 58,8%, 22,2%, 95,2%. It is obvious that sensitivity and PNV data increased in such approach. It is useful for differentiated diagnostics of benign thyroid pathology. But in case of BS3-5 group we didn't get significant data cause of statistically small amount of patients (9). Application of scintigraphy in these patients for further management and treatment tactics still stays open to question. **Conclusion:** Comparative ^{99m}Tc-pertechnetate and ^{99m}Tc-MIBI scintigraphy is an appropriate diagnostic tool if combined with FNB and is most effective in management of BS1-2 group patients. Excluding malignancy with scintigraphy helps in avoidance of unnecessary radical approach in thyroid pathology management.

EP368

Management of Radio-iodine Refractory Thyroid Cancer with 13-cis retinoic acid

P. K. Pradhan, M. Ravina, G. Sankar, N. K. Yadav, A. Prashanth, A. K. Singh, A. Arya; SGP GIMS, Lucknow, INDIA.

Introduction and Aim: Differentiated thyroid cancer accounts for 95% of all thyroid cancers worldwide. The general management is by surgery,

radioiodine and levothyroxine suppression therapy. About 7-23% of these patients manifest metastasis. And out of these 2/3rd become refractory to radioiodine. We have evaluated the role of 13 cis retinoic acid as a redifferentiation agent in thyroid cancer. **Methods:** We administered 13 cis retinoic acid (RA) in 24 patients which were having persistent disease and were radioiodine negative on follow up I131 scan. The dose prescribed was 1.5 mg/kg for 6-12 weeks. Then a low dose iodine scan was performed post 01 month of levothyroxine withdrawal or recombinant human TSH. The patients who showed good response to the therapy indicated by a positive iodine scan were further continued on the therapy for 03 months. **Results:** We evaluated total 24 patients (12 male and 12 female). Out of these 20 were diagnosed papillary carcinoma thyroid (recurrence, pulmonary or cervical lymph nodal metastasis), 01 follicular carcinoma thyroid and 01 poorly differentiated carcinoma thyroid and 02 were hurthle cell variants. In an evaluation of 04 patients treated with RA showed increased tracer uptake, rest 20 patients were radioiodine negative. The patients which turned positive on iodine scan were treated with 100-150 mCi of radioiodine depending on the disease. Post radioiodine fall in serum thyroglobulin level was noted in addition to enhanced radioiodide transport and clinical improvement. **Conclusion:** These data suggest that RA redifferentiation therapy, considering especially its comparatively mild side effects (mucositis), may soon represent an alternative therapeutic approach to otherwise untreatable thyroid tumors. Our findings suggest that 13 cis retinoic acid therapy especially a 06 weeks protocol, may induce radioiodine uptake and reduce serum thyroglobulin levels in some patients with DTC, but whether this results in clinically significant response can only be ascertained on long-term follow-up.

EP369

Thyroid cancer in radiation exposed childhood cancer survivors: The influence of screening strategies on cancer-related morbidity

A. Heinzl¹, D. Müller², F. M. Mottaghy¹, F. A. Verburg¹; ¹UK Aachen, Aachen, GERMANY, ²UK Köln, Köln, GERMANY.

Aim: Childhood cancer survivors who received radiation therapy to the head or chest are at increased risk of developing thyroid cancer. Currently there is no agreement on which screening strategy is best in terms of reducing thyroid cancer related morbidity. The aim of the present study was to compare four strategies: No screening (NS), screening by ultrasound alone (SUS), screening by ultrasound followed by fine needle biopsy (SUSFNAB) and screening by palpation followed by ultrasound and fine needle biopsy (SPAUSFNAB). **Methods:** We built a decision-tree-model to compare the different strategies. The construction of the decision-tree-model and the sensitivity analyses were performed using TreeAge Pro 2009 software (TreeAge Software, Inc.). The input data for the model regarding diagnostic performance of the different strategies are derived from literature. Data on thyroid cancer related morbidity with regard to lymph node metastases, distant metastases, and local invasion (T4a/b) were extracted from the Würzburg Thyroid Cancer Database. We assumed annual screening until age of 45. Afterwards we would expect a risk comparable to the healthy population that would not require regular screening unless there were pathological findings. The 2.5-97.5% confidence interval surrounding the median morbidity was determined using Monte Carlo simulations. **Results:** Likelihood of lymph node metastases: NS 0.059 (0.13-0.014), SUS 0.01 (0.025-0.002), SUSFNAB 0.016 (0.037-0.003), and SPAUSFNAB 0.045 (0.043-0.016). Likelihood of local invasion (T4a/b): NS 0.055 (0.12-0.014), SUS 0.01 (0.025-0.002), SUSFNAB 0.015 (0.035-0.033), and SPAUSFNAB 0.044 (0.09-0.016). Likelihood of distant metastases NS 0.017 (0.038-0.004), SUS 0.001 (0.005-0.001), SUSFNAB 0.003 (0.008-0.001), and SPAUSFNAB 0.01 (0.02-0.004). **Conclusions:** Although cancer-related survival seems to be unaffected, different screening strategies have an impact on cancer-related morbidity in childhood cancer survivors. However, this has to be balanced against the morbidity induced by false positive results of the different screening strategies e.g. caused by unnecessary thyroidectomy.

EP370**Factors influencing the ablative activities of Iodine 131 in children and adolescents followed up for differentiated thyroid cancer. Experience of the Nuclear Medicine Department of Tunisian Center**

S. MELKI^{1,2}, M. NOUIRA^{1,2}, H. SAKRI², R. SFAR², A. EZZINE^{1,2}, H. BOUDRIGA², M. BEN FREDJ^{1,2}, K. CHATTI², S. AJMI², M. GUEZGUEZ²; ¹Lr12es02, Faculty of Medicine of Sousse, Sousse, TUNISIA, ²Department of Nuclear Medicine, University Hospital Sahloul, Sousse, TUNISIA.

Introduction: Radioactive iodine therapy has subvert the clinical and therapeutic history of differentiated thyroid cancer (DTC). The remission is indeed possible even at the stage of metastases. It is a cancer that can affect the child and the adolescent. The objective of this work is to determine the factors that influence the cumulative administered activities of Iodine 131 for thyroid remnant ablation in younger patients. **Materials and Methods:** We retrospectively studied 15 patients referred to the Nuclear Medicine Department of Tunisian Center, over a 19-year period from December 1991 until December 2010, presented with DTC. It was a papillary carcinoma in 14 cases and vesicular carcinoma in a one case. After surgery, the 15 patients in our series had received radioiodine therapy. The activity of Iodine 131 in each cure was 3700 MBq. An interval of 6 months has been maintained between the cures. The number of administered cures was conditioned by the results of the post therapeutic whole body scans and dosages of thyroglobulin. **Results:** The number of cure of radioactive iodine for thyroid remnant ablation was variable from one patient to another within our series. On average, the complete thyroid remnant ablation was obtained after 3.2 cures (with extremes from one to 7 cures). A single cure of iodine 131 was sufficient for the ablation of the thyroid remnant in 20 % of cases. In 26.6 % of cases two cures were necessary. In 53.4 % of cases three cures or more were needed. The ablative cumulative activity of the Thyroid remnant was superior to 7400 MBq in 55 % of patients presented with a tumor size equal to or exceeding 3 cm, in 75 % of patients presented with a locoregional invasion and in 60 % of patients having metastatic lymph nodes. **Conclusion:** The tumor size, the locoregional invasion and lymph node metastases seem to influence the cumulative administered activities of Iodine 131 for thyroid remnant ablation in children and adolescents followed up for DTC.

EP371**I-131 differentiated thyroid cancer therapy in pediatric patients based on I-123 pre-therapeutic red marrow dosimetry**

M. Pacilio^{1,2}, C. Orlandi¹, V. Cannata¹, S. Donatiello¹, M. C. Garganese³, E. Genovese¹, L. Lorenzon⁴, M. Pizzoferro³, M. F. Villani³, **M. Longo¹**; ¹Enterprise Risk Management/Medical Physics, Bambino Gesù Children's Hospital, IRCCS, Rome, ITALY, ²Department of Medical Physics, Azienda Ospedaliera San Camillo Forlanini, Rome, ITALY, ³Imaging Department, Nuclear Medicine Unit, Bambino Gesù Children's Hospital, IRCCS, Rome, ITALY, ⁴Post Graduate School of Medical Physics, Sapienza University of Rome, Rome, ITALY.

Aim: I-123-NaI radiopharmaceutical has several possible advantages for pre-therapeutic red marrow dosimetry in I-131 differentiated thyroid cancer (DTC) therapy: it reduces both radiation exposure and the possibility of stunning of remnant/metastatic tissue; it provides better image quality, localization and delineation of metastatic lesions for further dosimetric assessments. Unfortunately the brief physical half-time of I-123 (as compared to I-131) could be inadequate for dosimetric accuracy. We investigate the possibility of using I-123 for pre-therapy red marrow (RM) dosimetry of paediatric patients with metastatic or recurrent tumours, for the individual calculation of I-131 Maximum Tolerable Activity (MTA) associated with an absorbed dose to RM of 2 Gy. **Materials and methods:**

Five patients with recurrent or metastatic DTC were analysed. The biokinetics was studied with I-123 collecting blood samples and whole body (WB) images at 0.5-h (before micturition), 2-h, 4-h, 24-h, 30-h, 48-h and 54-h. The measurements were corrected for the difference between I-123 and I-131 physical half-time. Activities in blood and WB were determined with calibrated gamma counter and gamma camera, and absorbed dose (AD) to RM calculated according to the EANM guidelines. The individual time-activity curves in blood and WB were analytically fitted, calculating the cumulated activity either by integrating the fitting curve from zero to infinity (tau), or to the last experimental point and with physical decay from the last point to infinity (tau limit). The S factors of OLINDA/EXM were used, rescaling for the individual body mass. After I-131 therapeutic administration (performed with the standard administration regimen), RM dosimetry was achieved analogously, measuring at 2-h, 6-h, 24-h, 30-h, 48-h, 72-h and 144-h, and estimating WB activities using a probe at 2 m from the patient. **Results:** The results of I-123 pre-therapy dosimetry show that MTA calculated using tau limit is systematically less (from 2 to 47%) than that calculated using tau. These differences become negligible for I-131 post-therapy dosimetry because of the wider temporal observation window. With the tau limit method, the AD to RM calculated with I-123 pre-therapy dosimetry is systematically higher (from 16 to 57%) than that calculated with I-131 therapy; the differences obtained using the tau method do not always follow the same trend, but the mean AD was 35% higher. **Conclusion:** The I-123 may provide several advantages that are expected to impact I-131 therapy and, even if suboptimal, it may ensure cautionary quantitative evaluations of the I-131 MTA. Nevertheless, accurate dosimetric assessments require post-therapy evaluations.

EP372**Salivary scan can predict salivary dysfunction gland before high dose radioiodine therapy**

J. Park¹, J. Hwang¹, S. Park²; ¹Soonchunhyang Univ., Bucheon, KOREA, REPUBLIC OF, ²Soonchunhyang Univ., Seoul, KOREA, REPUBLIC OF.

Purpose : We investigated whether salivary scan (SS) before I-131 therapy in patients with differentiated thyroid cancer (DTC) could predict radioiodine retention in the salivary gland on post-therapeutic I-131 whole body scan. **Methods :** We evaluated 136 patients with DTC who underwent the SS before high dose I-131 therapy. Quantitative and visual assessments were used to analyze the SS including maximum salivary gland uptake ratio (SUMax) at 20 (SU20) and 40 (SU40) min, residual salivary uptake ratio on the washout image (RSw) in comparison with each golden standard (salivary uptake on the radioiodine therapeutic scan, 75 strong vs. 61 normal; 24 acute sialadenitis). **Results :** In SS, SUMax time showed at 20 min (mean 6.3±1.9, n=52), 40 min (mean 6.9±3.5, n=38) and similar SUMax between 20 and 40 min (mean 6.6±2.9, n=45), weak SUMax group (5.4±1.5) and strong SUMax group (10.7±2.1); complete RSw group (3.3±0.7) and incomplete RSw group (4.4±1.0). Strong SUMax group demonstrated stronger radioiodine retention in the salivary gland compared to that of weak SUMax group (87.1% vs. 45.7%, p<0.0001), incomplete RSw group showed stronger radioiodine retention compared to that of complete RSw group (66.3% vs. 36.0%, p=0.001). There was significantly different mean age between strong SUMax group and weak SUMax group (46.0±11.7 vs. 47.5±9.4, p=0.025). In applying acute sialadenitis for golden standard, strong SUMax group showed positive correlation (13.3% vs. 32.3%, p=0.03) and incomplete washout group showed negative correlation (8.0% vs. 23.3%, p=0.04). **Conclusion :** Radioiodine therapeutic scan is more sensitive than acute sialadenitis symptom for the evaluation of salivary dysfunction. Strong uptake of the salivary gland with incomplete washout on SS significantly is related to strong I-131 retention of salivary gland. The SS can predict salivary dysfunction before high dose radioiodine therapy.

EP373

Factors Predicting Early Release from Isolation Room of Thyroid Cancer Patients After Radioiodine-131 Treatment

M. u. Zaman¹, N. Fatima², A. Zaman³, U. Zaman³, R. Tahseen³, W. Shahid³; ¹AKUH, Karachi, PAKISTAN, ²Dr Ziauddin Hospital, Karachi, PAKISTAN, ³Dow University of Health Sciences, Karachi, PAKISTAN.

Background: Patients with differentiated thyroid cancers (DTC) who receive radioactive iodine-131 (RAI) are released from isolation when their dose rate is below the regulatory requirement. The purpose of this study was to find out predicting factors for early release from isolation facility after RAI administration in patients with DTC. **Material and Methods:** This was a prospective study which included 96 (58 females and 38 males) patients with DTC who had received RAI from April 2013 till August 2015. The study was duly approved by the ethical committee of the institute. Patients who had complete information of primary tumor size (PTS), serum TSH, stimulated thyroglobulin level [sTg] with antibodies (IU/ml) at the time of RAI treatment were included. All patients had normal serum creatinine level. To attain lower effective half-life good hydration and administration of soft laxative were ensured. Dose rate was measured (immediately, 24 h and 36 h) at 1 meter distance from anterior mid trunk and a dose rate <50 $\mu\text{Sv/h}$ at 1 meter was considered as releasing criterion. At 24 h 50 patients were released while remaining 46 patients were released at 36 h. A post-ablative whole body scan (PA-WBIS) was performed 5-8 days after RAI ablation in all patients. **Results:** Patients released after 24 h were significantly younger, had smaller lesions with higher proportion of papillary cancer, lower sTg, lower sTg/TSH ratio and had received a lower dose of RAI as compared to those who were discharged after 36 h. Serum TSH and gender were not found to have any significant correlation between two cohorts. ROC and multivariate analysis have shown age ≤ 37 years, PTS ≤ 3.8 cm, RAI ≤ 150 mCi, sTg ≤ 145 ng/ml and sTg/TSH ≤ 1.085 as strong independent predictors for early release. **Conclusion:** We conclude that younger age (≤ 37 years), smaller tumor size (≤ 3.8 cm), lower RAI dose (≤ 150 mCi), lower sTg (≤ 145 ng/ml) and a lower sTg/TSH ratio (≤ 1.085) are significant independent predictors for release at 24 h after RAI treatment in DTC patients. Effective utilization of these factors could help the treating physicians to use limited number of inpatient facilities with higher throughput, lower cost and lower psychological stress to patients. **Key words:** Radioactive iodine-131; differentiated thyroid cancer; isolation; early release; dose rate

EP374

Doses to members of the public from patients undergoing radioiodine ablation

F. H. Barrack, J. W. Scuffham, P. J. Hinton; Royal Surrey County Hospital, Guildford, UNITED KINGDOM.

Aim: To minimise doses to members of the public, radioiodine ablations are typically performed on an inpatient basis and discharged patients must avoid close contact with others. Many hospitals discharge patients when their estimated activity is less than 800MBq and give restrictions which last until this decreases to 150MBq and 30MBq for contact with people over and under 5 years old respectively. The aim of this work was to estimate doses if this activity based method was used and investigate the impact moving to a contact pattern based approach would have on inpatient stays. **Material and Methods:** Retrospective analysis was performed for 368 I-131 thyroid carcinoma treatments between 2009 and 2016 (81, 160 and 127 received 1.1GBq, 3.7GBq and 5.5GBq I-131 respectively). Count rate measurements were made using a Geiger

counter 2.5m above the bed immediately after administration, then twice daily until the patient was discharged. Exponential clearance was assumed and the time taken to reach 800MBq, 150MBq and 30MBq was calculated. Doses members of the public could receive was calculated from the estimated cumulated activity, dose rate of $1.2\mu\text{Sv}\cdot\text{d}^{-1}\cdot\text{MBq}^{-1}\cdot\text{m}^2$. and assumed contact patterns. The assumed contact patterns were: 15mins/day at 0.3m and 8hours/day at 1m during restrictions; 3h/day at 0.3m and 6h/day at 1m for over 5s afterwards; 8h/day at 0.3m and 8h/day at 1m for under 5s afterwards. Inpatient stays which would limit doses to under 5s to 0.3mSv and give patients restrictions that finished 14 days after administration were calculated using these contact patterns. The minimum inpatient stays required to discharge patients with no contact restrictions were also calculated. **Results:** Using the activity based method, 98% of over 5s and 97% of under 5s could receive >0.3mSv, with < 5% receiving >1mSv. The median inpatient stay using the activity method was 0.2d, 1.4d and 1.7d for 1.1GBq, 3.7GBq and 5.5GBq administrations respectively. For the contact pattern method the required inpatient stay was 0.3d, 1.6d and 1.9d for 1.1GBq, 3.7GBq and 5.5GBq administrations respectively with 14 day restrictions, increasing to 1.9d, 3.6d and 3.8d with 1.1GBq, 3.7GBq and 5.5GBq for no restrictions. **Conclusion:** When discharging based on activity, while only 5% could feasibly receive over 1mSv, 98% of over 5s and 97% of under 5s could receive over 0.3mSv. However, considering contact patterns could allow better tailoring of discharge date and restriction lengths so doses for members of the public could be reduced to less than 0.3mSv.

EP375

Therapeutic compliance improvement in patients who undergo ¹³¹I radioablation

M. Saftencu¹, C. Pesteau^{2,1}, M. Larg^{2,1}, E. Barbus^{2,1}, D. Piciu^{2,1}; ¹"Iuliu Hatieganu" University of Medicine and Pharmacy, Cluj-Napoca, ROMANIA, ²The Oncology Institute "Prof. Dr. Ion Chiricuta", Cluj-Napoca, ROMANIA.

AIM Therapeutic compliance is defined as the congruence between a patient's behavior and his personalized healthcare recommendations, as indicated by his physician. Radioiodine ablation (RIA) is a form of nuclear therapy for several thyroid conditions such as differentiated thyroid carcinoma or Graves' disease. It is safe and effective, but the patient has to follow strict rules in order to obtain the best therapeutic efficiency with a minimal risk. We wanted to evaluate and develop methods for increasing the therapeutic compliance in patients who undergo RIA. **MATERIALS & METHODS** We analyzed a prospective cohort of 40 patients (n=40) who were scheduled to undergo RIA therapy, out of which 20 patients received access to our website for thyroid-disease support, where they watched custom-made videos with instructions about patient preparation, radioiodine administration, radiation protection measures and also where they had the option to ask us further questions on-line. The access was provided a month before RIA. The other group of patients had access to the same kind of information, but only verbally or printed, in the morning prior to radioiodine administration. 7 days after RIA procedure, we analyzed the compliance and the anxiety levels for each patient through several questionnaires based on validated psychometric tools. Data regarding age, sex, primary diagnostic, surgical treatment, RIT and hormonal substitutive treatment were analyzed. **RESULTS** There was a significant increase of compliance levels in the group who had access to personalized information via internet (p=0.001), especially compliance related to radiation protection measures. Also, these patients had shown lower anxiety and hospital-related stress levels. **CONCLUSION** Well-instructed patients that undergo radioiodine ablation have a better therapeutic compliance, improving their quality of life. This can be achieved by using on-line interactive platforms, being a great step towards personalized medicine.

EP376**Evaluation of life quality in differentiated thyroid cancer patients from The Institute of Oncology, Cluj-Napoca, Romania**

E. Barbus^{1,2}, M. Saftencu², C. Pestean^{1,2}, M. Larg^{1,2}, C. Moisescu-Goia¹, D. Piciu^{1,2}; ¹The Oncology Institute "Prof. Dr. Ion Chiricuta", Cluj-Napoca, ROMANIA, ²"Iuliu Hatieganu" University of Medicine and Pharmacy, Cluj-Napoca, ROMANIA.

Aim: We wanted to identify if quality of life (QoL) is altered in patients with differentiated thyroid cancer (DTC) by using a dedicated thyroid cancer questionnaire that evaluates disease-specific and radiation protection data. **Materials & Methods:** We developed a specific questionnaire for DTC patients and we used it for QoL evaluation in several disease-related matters and radiation protection concerns about radioiodine ablation. 52 patients (n=52) with DTC took the questionnaire prior to radioiodine treatment administration. We evaluated the QoL in these patients based on their answers. The study was conducted in The Institute of Oncology "Prof. Dr. Ion Chiricuta" from Cluj-Napoca, Romania. The questionnaire consisted of two parts: the first part contained 30 questions about disease-specific issues (general aspects including surgery-related stress and classical hypothyroidism symptoms), while the second part had 20 questions regarding radioprotection measures for the patient and his family. The questionnaire was based on validated psychometric tools. **Results:** We identified the most important disease- and radioprotection-related factors among DTC patients: the most significant disease-related identified factors were fatigue, weight gain, anxiety, post-surgical voice alterations, edema/myxedema, lability of affect and post-surgical cosmetic appearance changes. Radioprotection-involved factors are mainly represented by anxiety triggered by taking the radioiodine pill and irradiation-linked stress. This can lead to worries related to birth carrying, hair loss and secondary tumors due to irradiation. **Conclusion:** Implementing a specific, thyroid-disease related questionnaire for DTC patients is a helpful tool for the physician, helping him in the improvement of disease management and patients' quality of life.

EP377**Impact of lymphocytic thyroiditis on the outcome of papillary thyroid carcinoma treated with radioactive iodine**

M. H. M. Sayed; Clinical Oncology and Nuclear Medicine Department, Faculty of Medicine, Assiut University, Assiut, EGYPT.

OBJECTIVES: A higher incidence of lymphocytic thyroiditis (LT) has been reported in patients with papillary thyroid carcinoma (PTC). However, the Impact of LT on the prognosis of PTC remains controversial. The aim of the current study was to assess the impact of LT on the outcome of radioactive iodine (I-131) treatment for patients with PTC. **METHODS:** 50 consecutive patients with PTC, underwent total or near-total thyroidectomy, followed by I-123 whole body scan (WBS), neck ultrasound (US), serum thyroglobulin (Tg) and serum Tg antibodies (TgAb) assay, and subsequent I-131 ablation after 40 days without thyroid hormone replacement (TSH > 30 µIU/ml) were retrospectively enrolled in current study. 6 months later follow up I-131 WBS, neck US, serum Tg and serum TgAb were performed following suspension of L-thyroxin for one month (TSH > 30 µIU/ml) in 39 patients and following rhTSH stimulation in 11 patients. Patients were classified into two groups according to the presence or absence of lymphocytic thyroiditis. **RESULTS:** Of the studied 50 PTC patients, 20/50 (40%) had LT. There was no significant difference regarding age, gender, histopathology, extent of surgery, and ablative dose of I-131 between both groups. 19/20, (95%) of patients with evidence of LT and 23/30 (76.7%) of patients without evidence of LT, had negative follow up I-131 WBS. However, one patient of those with evidence of LT, and 4 of those without evidence of LT who had a negative follow up I-131 WBS, had serum Tg > 5 ng/ml,

with US findings suggestive of residual disease in the neck. The overall successful ablation rate were 18/20, 90% in patients with evidence of LT compared to 19/30, 63.3% in patients without evidence of LT (P< 0.05). **CONCLUSION:** We found a significantly better outcome and higher successful I-131 ablation rate among PTC patients with histopathologic evidence of LT compared to those without evidence of LT.

EP378**Unusual False Positive Iodine Uptakes in Patients with Differentiated Thyroid Carcinoma**

A. Oral¹, B. Yazici¹, C. Eraslan², Z. Burak¹; ¹Ege University Medical Faculty, Department of Nuclear Medicine, Izmir, TURKEY, ²Ege University Medical Faculty, Department of Radiology, Izmir, TURKEY.

Aim: Radioiodine is the most specific radionuclide for differentiated thyroid carcinoma (DTC) imaging. Despite its high specificity and sensitivity false positive I-131 uptakes could be seen on whole body scintigraphy (WBS). Besides physiological sites unusual I-131 uptakes can be seen on I-131 WBS that may cause misdiagnosis and unnecessary radioiodine treatments. In this study, we aimed to present the I-131 WBS and concomitant SPECT/CT images of unusual false positive radioiodine uptakes and the patients' clinical outcomes. **Materials and Methods:** The I-131 WBS's of 1507 patients with DTC who were treated in our clinic between 2012 and 2015 were retrospectively reviewed. Expected false positive I-131 uptakes like in breasts or thymus were excluded from the study. Concomitant SPECT/CT imaging was performed to patients with unexpected I-131 uptakes on I-131 WBS. The unusual I-131 uptakes on WBS were accepted as false positive due to patients' concomitant SPECT/CT images, radiological findings, low serum thyroglobulin levels and negative follow-up scintigraphies. The unusual false positive I-131 uptakes were included in the study. **Results:** 21 patients (1.4%) had 23 unusual false positive I-131 uptakes on I-131 WBS and concomitant SPECT/CT imaging. The vast majority (87%) of the patients' unusual findings were seen on post-therapeutic I-131 WBS, the rest (13%) were seen on diagnostic WBS. The unusual findings were located in cranial, thoracic, abdominal and pelvic regions in 1, 15, 1 and 6 patients respectively. The I-131 uptakes were due to bronchiectasis in 2 patients, lung infection in 1 patient, subcutaneous injection into gluteal fatty tissue in 3 patients, aortic calcification in 2 patients, benign bone cyst in 1 patient, vertebral hemangioma in 1 patient, recent non-thyroidal surgical procedure site in 1 patient, rotator cuff injury in 1 patient, mature cystic teratoma in 1 patient and ovarian follicle cyst in 1 patient according to SPECT/CT, radiological and clinical findings. However the possible reasons of 9 false positive I-131 uptakes couldn't be explained by radiological findings. **Conclusion:** We suggest that the false positive I-131 uptakes and underlying mechanisms (inflammation, trapping, increased perfusion, etc.) must be kept in mind and unexpected findings must be considered together with serum thyroglobulin levels, SPECT/CT and radiological findings to avoid misdiagnosis and unnecessary radioiodine treatments.

EP379**Combination of radioiodine therapy and ultrasound-guided percutaneous radiofrequency ablation in benign thyroid disease**

A. Mader, C. Happel, H. Korkusuz, F. Grünwald, W. T. Kranert; University Medical Center, Frankfurt, GERMANY.

Aim: Radioiodine therapy (RIT) and thyroidectomy are standard treatment procedures for nodular goiters. Both are, however, associated with side effects. Especially goiters of large volume cannot be treated sufficiently by RIT in many cases due to increased required amounts of radioiodine-131 that may lead to radiation induced thyroiditis and tracheal

stenosis. Unfortunately, just in these cases also thyroidectomy involves high surgical risks especially in elder patients. Therefore a local ablation to reduce target volume prior to RIT may lead to a significantly reduced required therapy dose of radioiodine-131 and makes these patients treatable again. The aim of this study was to evaluate effectiveness of RIT in combination with radiofrequency ablation (RFA). Success criteria were volume reduction of the goiter and the resulting decrease in dose of radioiodine-131. **Material and Methods:** In ten patients (5 f. median age 53a) suffering from nodular goiters, a combined treatment of RFA and RIT was performed. RFA was performed directly prior to RIT under local anesthesia and sterile conditions with the CelonPower System® (Olympus Medical Systems Group) and cooled bipolar applicators. The system generates a variable output power of up to 250 W at a frequency of 470 kHz achieving a target temperature of 60–110°C. A trans-isthmus approach was chosen to position the probe. The patient was placed in a supine position with a hyperextended neck. The tissue destruction was imaged sonographically. The reduced vital volume was used to calculate the potential reduction of the necessary dose of radioiodine-131. **Results:** RFA led to a statistically significant median reduction of vital thyroid volume ($p < 0.01$) of 34% (median: 18 ml; range: 10–59 ml). Therefore the required dose of radioiodine-131 could potentially be reduced significantly ($p < 0.01$) by 438 MBq (range: 414–1,565 MBq). **Conclusion:** The bipolar radiofrequency system is safe to use without neutral electrodes. It provides a current flow and therefore a steady energy disposition between the tips of the applicator probe. Vital thyroid volume and therefore the necessary dose of radioiodine-131 can be significantly reduced by the performance of an RFA prior to RIT. Country-specific caps for discharge values can be met faster and the radiation exposure of healthy organs such as kidneys, bone marrow and bladder can be reduced significantly by the administration of reduced amounts of radioiodine-131. The combined treatment is a safe and effective alternative to surgical intervention in cases of large nodular goiters.

EP380

Radiation risk perception and quality of life in patients with thyroid cancer who receive radioactive iodine therapy

M. Robert¹, G. Fleury-Bahi¹, F. Kraeber-Bodéré¹, C. Rousseau², D. Rusu², A. Bonnaud-Antignac¹; ¹Université de Nantes, Nantes, FRANCE, ²ICO site René Gauducheau, Nantes, FRANCE.

Aim. Little is known about patient's nuclear risk perception during hospitalization, whereas emotional state can influence risk perception and that risk perception can also influence patient's emotional quality of life in return. This study investigates the evolution of patient's nuclear risk perception during the treatment and determine the influence of risk perception on the quality of life and coping with treatment and illness. **Materials.** The sample included 45 thyroid cancer patients who had total thyroidectomy interviewed before, during and after radioiodine therapy. Interviews were focused on nuclear risk perception, iodine 131 experience, anxiety, quality of life, coping with treatment and coping with illness. **Methods.** 135 interviews were audiotaped, transcribed and analyzed according to the categorical thematic analysis and a semiquantitative analysis. **Results.** The patients met had little knowledge about radioactivity, radiation protection measures and associated risks, consequently they developed anxious beliefs concerning the radioprotected environment before their hospitalization. Information about the treatment are fragmented between the different health care professionals and, for the patients, the search for a feeling of controllability before treatment is compromised. That is the reason why, during the hospitalization, patient's nuclear risk perception depends on caregiver's behavior toward radioactivity. Their perception of the seriousness of the risk and vulnerability evolve during the treatment. Foremost, seriousness of risk and vulnerability for those around them are discussed before the treatment and then, loneliness and radio-protection measures confront the patient to his

cancer and to nuclear risks. We can notice that, more than the radioactivity, the isolation affects the emotional quality of life of patients during their hospitalization. Results also demonstrate different factors of vulnerability such as the administered radioactivity (3,7 GBq or 1,1 GBq), the thyroid hormone withdrawal, the patients with toddlers, the number of treatments and experiences of previous treatments. **Conclusion.** The findings illustrate the importance of taking into account the development of beliefs and perception of nuclear risk throughout the support. A group information session should be proposed to educate the patient about radiation exposure and health risks, and nuclear medicine department should make caregivers aware of watchfulness toward treated patients.

EP381

Occurrence of papillary thyroid micro-carcinoma in an adolescent with congenital dysmaturational hypothyroidism

W. Amouri, D. Ghorbel, F. Hamza, I. Jardak, F. Kallel, S. Charfeddine, F. Guermazi; Habib Bourguiba hospital, sfax, TUNISIA.

AIM: to describe an unusual case of papillary thyroid micro-carcinoma in a boy with dysmaturational congenital hypothyroidism **MATERIALS AND METHODS:** the patient record was reviewed retrospectively. We analysed clinical outcomes and thyroglobulin rate as well as imaging findings after radio-iodine therapy. **RESULTS:** we report the case of 17-year-old adolescent diagnosed with congenital goitrous hypothyroidism at neonatal age. A familial history of dysmaturational goitre was found. The boy was treated by adequate thyroxine replacement until 17 years of age, when he presented with a large multi-nodular goitre. The patient underwent total thyroidectomy. Pathological examination revealed multifocal papillary thyroid micro-carcinoma. Serum thyroglobulin level after thyroidectomy was 5ng/ml. So, the patient was referred for radio-iodine ablation. The whole body scan post 100 mCi Iodine-131 showed cervical and physiologic thymus uptake. The patient was then maintained under suppressive daily dose of 150 µg of l-thyroxine. **CONCLUSION:** Papillary thyroid carcinoma complicating dysmaturational goitre has been rarely reported in the literature. The management of these cases is based on total thyroidectomy because future development of a second malignancy in thyroid tissue remains possible. In our case, ablative radio-iodine therapy was indicated since serum thyroglobulin rate was abnormal.

EP382

Quantitative ¹³¹I planar imaging of patients undergoing thyroid cancer treatment

R. Barquero¹, H. Pérez-García¹, A. Cardenas²; ¹Hospital Clínico Universitario Valladolid, Valladolid, SPAIN, ²Hospital Nacional Edgardo Rebagliati Martins, Lima, PERU.

Aim: Patients undergoing differentiated thyroid cancer (DTC) are treated (after ablation) with ¹³¹I. A post-treatment control acquiring a planar Gammacamera image is done seven-ten days after administration. The present study focused on the quantification of the activity uptake in these images. **Methods:** Ten patients undergoing ¹³¹I DCT treatment have been studied with administered activities from 3.7 to 4.44 GBq after a low dose of rhTSH. A static planar local image of each patient is obtained with a Siemens e-cam Gammacamera with HEGP collimator at 15 cm skin-collimator distance and with energy window of 15% centered at 364 keV. Sensitivity (cps/MBq) in each acquisition is calculated as the product of geometric efficiency and intrinsic efficiency. Geometric efficiency is estimated by Monte Carlo simulation with MCNPX and an accurate simulation of the lesion, collimator and the Gammacamera crystal. Intrinsic efficiency of device is previously obtained from the quantification of an image of a

reference source of calibrated activity in air. All images are analyzed with the free software ImageJ. A specific low pass filter is applied to eliminate collimator artifacts in each image previously to the quantification. The total counts rate for each patient's lesion is obtained drawing a ROI encompassing the lesion. In order to retain only the geometric component of events in the photopeak, the ROI size is delimited with a diameter as the full width at ten maximum (FWTM) of the central profile defined of the lesion. The attenuation correction is estimated with a simple exponential approximation with 2.5 cm thickness of tissue between lesion and skin of each patient. The method to quantify the activity uptake has been validated with a set of independent measurements using different phantoms and calibrated sources. **Results:** ROI radius from all lesions goes from 12 to 28 mm. The sensitivity value has a mean value of 26.5 cps/MBq with a standard deviation of 6%. The value of the activity uptakes of the patients goes from 0.05 MBq (1.56 μ Ci) to 1.86 MBq (50.20 μ Ci). No correlation between administered activities and activity uptakes has been found. **Conclusions:** Activity uptake of each lesion of patients in ^{131}I DTC therapy can be estimated with accuracy by means of an absolute quantification of each lesion. The procedure relies on the Monte Carlo simulation and an independent measurement to determine the intrinsic efficiency of the Gammacamera device. The activity uptake in all analyzed cases is always less than 0.06% of the administered activity.

EP383

Does the time of whole body scan affect to physiological hepatic visualisation after radioiodine remnant ablation?

Z. Hasbek¹, S. S. Gül², E. Çiftçi¹, B. Turgut¹, S. A. Ertürk³, A. Cakmakçılar³; ¹Cumhuriyet University School of Medicine, Department of Nuclear Medicine, SIVAS, TURKEY, ²Gaziosman Paşa University School of Medicine, Department of Nuclear Medicine, TOKAT, TURKEY, ³Cumhuriyet University School of Medicine, Department of Nuclear Medicine, Sivas, TURKEY.

Aim: Postoperative radioiodine remnant ablation (RRA) is routinely used at most institutions to destroy residual thyroid tissue and occult foci of neoplastic cells in differentiated thyroid cancer (DTC). Diffuse homogenous hepatic uptake in whole body scan (WBS) after RRA suggests that there is occult or visible remnant thyroid tissue and/or tumor tissue in the body. It is thought that the reason of this situation is hepatic metabolism of radioiodine (^{131}I) marked thyroglobulin fragments which are secreted by tumor tissue. Diffuse homogenous hepatic uptake after the low dose diagnostic ^{131}I WBS performed 8-12 months after RRA is suspected that the presence of metastatic focus anywhere in the body. The purpose of this study was to investigate whether or not early or late WBS after RRA has an effect on the physiological hepatic uptake. **Materials-Methods:** In this study 58 DTC patients were evaluated (46 female, 12 male, mean age: 48.5 (19-75 years old)) who referred to nuclear medicine department for RRA. The therapeutic ^{131}I dose ranged from 100 mCi to 200 mCi. WBS after RRA was performed earlier (in 1-3th day after RRA) in 24 patients (group 1); and was performed later (in 8-9th day after RRA) in 34 patients (group 2). Diffuse hepatic uptake of radioiodine were evaluated visually by two experienced nuclear medicine physicians. **Results:** 3 of group 1 (8.1 %) have diffuse hepatic uptake whereas all patients of group 2 (100%) have diffuse hepatic radioiodine uptake ($p < 0.0001$). There is not a statistically significant relationship between the hepatic uptake and thyroglobulin and TSH level during the WBS ($p > 0.05$). Also there is not a statistically significant relationship between the hepatic uptake and given radioiodine dose ($p > 0.05$). **Conclusion:** Physiological diffuse hepatic uptake of radioiodine in WBS after RRA may not be seen during the early (1-3 day) WBS. But it does not mean that there is any residual thyroid tissue or metastatic tissue. It is thought that half life of serum thyroglobulin affects this situation.

EP384

Low-Risk Papillary Microcarcinoma (PMC) Post-surgical Thyroablative rhTSH 1.1 GBq Radioiodine Therapy - Fact or Fiction?

P. Solný^{1,2}, T. Kráčmerová^{1,2}, L. Jonášová¹, P. Vlček¹; ¹Department of Nuclear Medicine and Endocrinology, Charles University 2nd Faculty of Medicine, Prague, CZECH REPUBLIC, ²Department of Dosimetry and Application of Ionizing Radiation, FNSPE, Czech Technical University in Prague, Prague, CZECH REPUBLIC.

Aim: It is discussed whether Papillary microcarcinoma (PMC) patients classified as low-risk based on the presence of lesion that is less than 10 mm in diameter should be even treated by radioiodine after surgical thyroablation. Moreover, recombinant human TSH (rhTSH) introduction becomes another option to judge in radioiodine therapy (RAIT) conception world-wide. The question to treat or not to treat is set and, sadly, mostly retrospective studies are given as answer. In case of conservative approach to thyroid carcinoma treatment post-surgical radioiodine therapy is preferred for most of PMC patients. Aim of this study was to investigate whether PMC patients stimulated with rhTSH will obtain a thyroablative (300Gy) absorbed dose when 1.1 GBq of ^{131}I is administered. **Materials and methods:** PMC patients for this study means a) stimulated thyroglobulin (Tg) lower than 6.5 $\mu\text{g/l}$ in the absence of Tg antibodies, and b) absence of larger (more than 0.5 ccm) remnant thyroid tissue and of abnormal cervical lymph nodes on ultrasonography. 17 PMC patient volunteers (15 F, 2 M) assisted to undergo up to 5 post-therapeutic scintigraphy examinations (5, 24, 30, 48, and 72 h after administration) and SPECT; if necessary, using Symbia S gamma camera. Whole body (WB) radioiodine activity was monitored by radiometer SVLD probe (relative measurements referred to data 1.5 h after administration). Gammacamera system was calibrated and quantitative imaging was done. Measured data were fitted and cumulated activity was determined up to 400 h after administration. Mass of the treated tissue was measured by sonography or estimated from SPECT volumetric analysis. Absorbed dose was determined for 200 h cumulated activity extrapolation. **Results:** For 18% of patients no or background similar accumulation was observed. For 24% of volunteers dosimetric evaluation confirmed radioiodine thyroablation (300Gy exceeded within accumulating remnants). For 29% sufficient absorbed dose was not unequivocally proved regarding the measurement errors. For 29% of patients absorbed dose was classified as insufficient to be named as thyroablative. During ongoing follow up no recurrence was observed for 15 patients one year after therapy. 2 of the patients have not been checked yet. **Conclusions:** Based on the dosimetric measurement 1.1 GBq radioiodine therapy was cancelled as potentially insufficiently thyroablative. PMC patients are now treated using 1.85 GBq according EANM guidelines. Further dosimetry measurements are being done to make evidence-based patient treatment if treated.

EP385

Calculation of Therapeutic Activity of Radioiodine in Graves' Disease by Means of Marinelli's Formula, Using Technetium ($^{99\text{m}}\text{Tc}$) Scintigraphy

P. Szumowski, S. Abdelrazek, M. Mojsak, M. Sykala, D. Jurgilewicz, J. Mysliwiec; Medical University, Białystok, POLAND.

The therapeutic activity of ^{131}I administered to patients with Graves' disease (GD) can be calculated by means of Marinelli's formula. The thyroidal iodine uptake ($^{131}\text{I}U_{\text{max}}$) needed for the calculation is usually determined with the use of ^{131}I . The purpose of the paper was to estimate $^{131}\text{I}U_{\text{max}}$ on the basis of technetium uptake in the thyroid at 20 minutes ($^{99\text{m}}\text{Tc}U_{20\text{min}}$). **Methods:** Eighty patients suffering from Graves' disease were qualified for radioiodine therapy with measurement of fT_4 , fT_3 , TSH and TRAb. Prior to the treatment, all the patients were euthyroid.

^{131}I U_{max} for each patient was determined according to the levels of ^{131}I after 24h (^{131}I U_{24h}), while effective half-life (T_{eff}) according to the measurements of ^{131}I U_{24h} and ^{131}I uptake after 48h (^{131}I U_{48h}). Additionally, on the day before measuring ^{131}I U_{24h}, $^{99\text{m}}\text{Tc}$ U_{20min} was calculated for each patient. **Results:** It was demonstrated that there existed a correlation, with statistical significance at $p < 0.05$, between the following pairs of values: TRAb and ^{131}I U_{24h}, TRAb and $^{99\text{m}}\text{Tc}$ U_{20min}, and $^{99\text{m}}\text{Tc}$ U_{20min} and ^{131}I U_{24h}. The interdependence between ^{131}I U_{24h} and $^{99\text{m}}\text{Tc}$ U_{20min} at the level of significance $p < 0.05$ is described by the following algorithms: ^{131}I U_{24h} = 17.72 \times \ln(^{99\text{m}}\text{Tc}U_{20\text{min}}) + 30.485, if TRAb < 10 IU/ml, and ^{131}I U_{24h} = 18.03 \times \ln(^{99\text{m}}\text{Tc}U_{20\text{min}}) + 38.726, if TRAb > 10 IU/ml.}}

Conclusion: It is possible to predict thyroid iodine uptake ^{131}I U_{24h} in Graves' disease on the basis of measuring the uptake of $^{99\text{m}}\text{Tc}$ U_{20min}. This shortens the time necessary for diagnosis, reduces

EP386

Development Of Radiation Protection Recommendations According To The Dose Rate And Social-Family Characteristics, In Hyperthyroidism Patients Treated With Iodine 131

J. OROZCO-CORTÉS¹, R. DÍAZ-EXPÓSITO¹, I. CASÁNS-TORMO¹, V. LÓPEZ-PRIOR¹, A. AMR-REY¹, H. BOWLES-ANTELO¹, N. LUQUERO-LLOPIS², C. ALAMAN-SÁNCHEZ², S. DÍEZ-DOMINGO²; ¹NUCLEAR MEDICINE SERVICE. HOSPITAL CLÍNICO UNIVERSITARIO DE VALENCIA, VALENCIA, SPAIN, ²RADIOLOGIC PROTECTION SERVICE. HOSPITAL CLÍNICO UNIVERSITARIO DE VALENCIA, VALENCIA, SPAIN.

OBJECTIVE Our objective was to evaluate the usefulness of developing individualized radiation protection recommendations, in patients with hyperthyroidism, based on social and family characteristics of the patient and in the measurement of a dose rate in $\mu\text{Sv/h}$ at 3 hours after iodine 131 treatment (DR). **MATERIAL AND METHODS** 95 patients (66 women), mean age (58±16), 21-88 y/o, 47 with diffuse goiter (DG), 48 multinodular goiter (MG). The administered activity was established by type of goiter, qualitative estimation of glandular size and thyroid uptake with previous scintigraphy, age and weight of the patient. The radiation protection recommendations were developed according to the norms of Spanish Society of Radiologic Protection and International Commission on Radiological Protection (ICRP), establishing the total days of restriction of close contact with children-pregnant (ChP)-R1 and with adults-R2, according to DR and social-family characteristics of the patients (group 1 (45): without ChP, partner age > 60 or without partner; group 2 (13): without ChP, partner age < 60; group 3 (37): patients with ChP. **RESULTS** Mean administered activity was 11.6±1.6 (8-15 mCi) without significant differences (SD) between men (11.4±1.6)-women (11.7±1.6). Mean DR was 23.5±6 (11-39) $\mu\text{Sv/h}$, and it was higher in men (26.4±5.4) than women (22.3±5.9, $p = 0.002$), and also R2 was higher in men (8.6±1.7) than women (7.6±2.2, $p = 0.02$). Mean activity administered to patients with MG (12.1±1.6) was higher than DG (11.2±1.4, $p = 0.008$), but without SD in DR, R2. The DR was higher when the administered activity was > 10 mCi (N=64) vs ≤ 10 (N=31) (24.4±5.6 vs 21.7±6.5, $p = 0.042$). When DR ≥ 23 (N=51), both R1 and R2 were higher than if DR < 23 (N=44) ($p < 0.0001$). Both groups 1 and 2 showed higher R2 ($p < 0.0001$) if DR ≥ 23 than if DR < 23 (8.5±1.7 vs 6.5±1.2). In group 3, R1 was higher, when DR ≥ 23, than if DR < 23 (16.3±3.3 vs 13.2±2.5, $p = 0.003$). Group 1 showed lower R2 than group 2 (7.3±1.8 vs 8.6±1.6, $p < 0.023$), although there was not SD in the DR between both groups (23.7±6.5 vs 24.6±6). **CONCLUSIONS** We confirm the usefulness of developing recommendations on radiation protection, according to the DR and the social-family conditions of patients with hyperthyroidism treated with iodine 131. The established days of restriction of close contact are higher in all patients if DR ≥ 23 $\mu\text{Sv/h}$ (mean value in our patients). But these days are also higher in the patients with determined social conditions (group 2 vs 1) independently of DR obtained, thus reinforcing the importance of establishing individualized recommendations.

EP387

Cytotoksyczne supresorowe limfocyty T zaburzenia w chorobie Gravesa-Basedowa po radiojodem 131 I Leczenia

M. Plazinska¹, E. Rosiak¹, R. Matyskiel¹, A. Czarnywojtek^{2,3}, M. Kobylecka¹, L. Królicki¹; ¹Department of Nuclear Medicine, Medical University of Warsaw, Warsaw, POLAND, ²Department of Pharmacology, Poznan University of Medical Sciences, Poznan, POLAND, ³Department of Endocrinology, Poznan University of Medical Sciences, Poznan, POLAND.

AIM: Activation or failure of apoptotic pathways can contribute to various autoimmune diseases, including Graves' disease (GD) and thyroid-associated ophthalmopathy. Radioiodine (^{131}I) is widely used for the treatment of Graves' hyperthyroidism but can induce alterations in immune response, and the development or worsening of Graves' orbitopathy (GO). The aim was to assess the apoptosis in peripheral blood (PB) lymphocyte subpopulations after 131I treatment of patients with Graves' disease and to examine its association with GO activity. **MATERIALS:** We included prospectively 54 patients (42 females, 12 males; mean age 37.2±10.2 years) with Graves' hyperthyroidisms after 131I treatment (20 ± 5.0 mCi). Clinical assessment, determination of serum TSH, fT3, fT4, thyroid autoantibodies levels were carried out at the onset and after 1, 3, 6, 9 and 12 months of 131I treatment. According to the severity and activity of GO all patients before 131I had NOSPECS score < 3 and CAS score < 3. Up to 4.5 months after 131I therapy and within one year of post-treatment follow-up all patients were euthyroid. **METHODS:** PB lymphocyte subpopulation were analysed by flow cytometry and FITC, PE-conjugated antibodies have been used: CD3 FITC/Anti-HLA DR, CD4 FITC/CD8 PE for surface phenotyping. The Annexin V/Propidium iodide protocol is used to assess apoptotic cells. Linear regression models was used to assess the association of CAS score and degree of apoptosis in CD8+ suppressor/cytotoxic T cells. **RESULTS:** 6 months after 131I treatment in 34 patients we observed significant increase in CD8+ suppressor/cytotoxic T cells in comparison with the initial evaluation (48% ± 3.90%, 95%, $p = 0.01$), but most of CD8+ T cells have undergone apoptosis (67% ± 8.15% (95% PU $p < 0.05$). Decreased levels of functional CD8+ suppressor/cytotoxic T cells resulted in an elevated CD4/CD8 ratio. There was a positively correlation between the increase of the percentages of apoptotic lymphocytes and the exacerbation GO in CAS score ($p < 0.05$). **CONCLUSION:** Graves' orbitopathy exacerbation after radioactive iodine therapy with may be associated with increased apoptosis of CD8+ suppressor/cytotoxic T cells. This result need further evaluation in larger group of patients.

EP388

The dose to bone marrow in small pool PTS during ^{131}I therapy for Hyperthyroidism

V. Longari, C. Canzi, M. Castellani, F. Buffoni, I. Martina; Fondazione IRCCS Cà Granda Ospedale Maggiore Policlinico, Milano, ITALY.

AIM: A higher iodine (I) uptake at 4 than at 24 h is the hallmark of the so called "small pool" pts with immunogenic hyperthyroidism. The rapid release of I in the blood leads to a decrease of the administered dose to the gland and to an increase of the extrathyroidal tissues irradiation. Aim of this study was to calculate the dose released to the bone marrow of "small pool" pts treated with high activities of ^{131}I necessary to achieve hypothyroidism. **MATERIALS and METHODS:** 7 hyperthyroid females (mean age 59.5; range 38-77y TSH 0.005±0 uIU/ml; FT3 20.3±8.3 pg/ml; FT4 47.5 ± 27.6 pg/ml; TRAb 40.3± 35.8 UI/L) identified by a previous ^{123}I dosimetric study as "small pool" pts, underwent ^{131}I therapy and a second dosimetric study. All pts had multiple thyroid scans (range 2-671 hrs) and blood samples (range 0.13-670 hrs) at different times; whole body scans were also acquired at the same

times of the thyroid images in 6 pts. The delivered doses to thyroid (DT) and bone marrow (DBM) were derived from ^{131}I uptake calculated on thyroid and whole body images and from ^{131}I levels in blood samples. DMB was calculated by summing the dose derived from the activity in circulating blood (BD) and in the whole body (WBD). The ablative target dose to the thyroid was set to 300 Gy. A mean ^{131}I activity of 604 ± 55 MBq was administered in order to reach the target dose. **RESULTS:** The rapid release of I in all “small pool” pts detected at ^{123}I scintigraphy, was confirmed by the ^{131}I therapeutic study (^{131}I uptake mean values at 4 and 24 hrs respectively $74,2\% \pm 6,3$ and $63,5\% \pm 10,7$; $p=0,01$). The mean of DT(mDT), DBM(mDBM), BD(mBD), WBD(mWBD) along with minimum and maximum values are reported in the table. Hypothyroidism occurred in 5 pts within a mean time of 3.7 months, while persistent hyperthyroidism was observed in 1 pt after 1 year. The last patient treated has still an extremely short follow up. **CONCLUSIONS :** In our pts, the dose to the bone marrow is much lower than the limit of 2 Gy and the main contribution is due to the Beta particles in circulating blood. These results show that in “small pool” pts the use of high activity is safe to achieve the clinical endpoint.

EP389

18F-DOPA PET/CT in the diagnosis and localization of cervical lymph node extension of medullary thyroid carcinoma

L. M. VIJA^{1,2}, A. Hitzel^{1,2}, M. Bauriaud^{1,3}, A. Salabert², L. O. Dierickx³, E. Gabiache³, S. Grunenwald⁴, P. Payoux^{1,2}, P. Caron^{1,4}, F. Courbon^{1,3}, S. Zerloud³; ¹Paul Sabatier University, Toulouse, FRANCE, ²Nuclear Medicine Department, Pierre Paul Riquet Hospital, Toulouse, FRANCE, ³Nuclear Medicine Department, IUCT-Oncopole, Toulouse, FRANCE, ⁴Endocrinology Department, Larrey Hospital, Toulouse, FRANCE.

Background: Medullary thyroid carcinoma (MTC) is a thyroid neuroendocrine tumor with frequent lymph node extension and recurrence. Patients with high initial or persistent calcitonin levels necessitate preoperative lymph node extensive staging for adequate cervical surgical management which systematically comprises cervical ultrasound. Conventional neck imaging (ultrasound, CT) sometimes fails to localise all recurrent or metastatic disease, leading to further functional explorations. 18F-DOPA PET/CT seems to be the best functional imaging examination for detection of present, persistent or recurrent MTC. **Aim:** To assess the impact of 18F-DOPA PET/CT on lymph node MTC staging and surgery. **Material and methods:** Twenty-five MTC patients (15 men, 10 women, median age 53.5 years), with increased calcitonin levels (median 270ng/ml [8-4270]) were prospectively explored with 18F-DOPA PET/CT (n=27 exams), CT (n=15) and neck US (n=24) in University Hospital of Toulouse PET Center (14 patients) and IUCT-Oncopole (11 patients) at diagnosis (n = 2) and in the post-operative follow-up (n = 23). Pathologic neck lesions were surgically removed, when possible (n=62 lesions; 3 patients). 18F-DOPA PET/CT sensitivity for pathologic lymph node detection was assessed comparatively to histopathological findings. **Results:** 18F-DOPA PET/CT presented an excellent concordance with neck ultrasound (K=0.9) and cervical CT (K=1) and higher sensitivity than cervical ultrasound (54% vs 48%) for lymph node detection. 18F-DOPA PET/CT performance for the characterisation of suspect cervical lymph nodes compared to histological findings was superior to cervical ultrasound on lesion analysis (sensitivity: 50% vs 31%). 18F-DOPA PET/CT sensitivity was 55% (5/9 patients) in patients with serum calcitonin levels below 150 pg/mL, detecting lymph nodes with plasma calcitonin levels as low as 28 ng/mL, 90% (9/10 patients) for calcitonin levels between 150-500 pg/mL and 100% for calcitonin levels higher than 500pg/ml (6 patients). ROC curve analysis confirmed an 18F-DOPA PET/CT specificity of 100% for calcitonin values greater than 200 pg/mL. Early (10 minutes post injection) cervical centered acquisitions

exclusively detected cervical lymph node uptake in three patients. **Conclusions:** 18F-DOPA PET/CT imaging could represent a useful complementary exam for better detection of cervical lymph nodes and preoperative lymph node classification. Although recent international guidelines do not recommend PET/CT evaluation if calcitonin levels are under 150 pg/mL, it would be interesting to evaluate the role of 18F-DOPA PET/CT for preoperative cervical lymph node detailed staging for both primary or recurrent CMT even for calcitonin levels between 20-150 pg/mL

EP390

Dual phase ^{18}F -DOPA PET/CT in medullary thyroid carcinoma

D. Grigolato, M. Cucca, M. Zuffante, L. Locantore, P. Brazzarola, M. Ferdeghini; Azienda Ospedaliera di Verona, VERONA, ITALY.

Aim: To evaluate the performance of ^{18}F -L-dihydroxyphenylalanine ^{18}F -DOPA PET/CT at 20 and 60 minutes post administration in the detection of medullary thyroid carcinoma (MTC), locoregional and distant MTC metastases. **METHODS:** We retrospectively evaluated 24 MTC patients (9 male, 15 female, age range 25 -82 years) with persistently high serum calcitonin levels. They underwent ^{18}F -DOPA PET/CT between January 2013 and December 2015 and in all of them a dual acquisition PET/CT was performed: early images (at 20 minutes) centered over the neck to half thorax (2 to 3 beds) and late total body images (at 60 minutes). The activity administered was 2,5 Mbq/kg. All scans were carried out on a 16-slice Gemini Big Bore TOF (Philips) with 2 minutes for bed position. Seven patients were studied for staging purpose before initial surgery and 17 patients underwent PET/CT for restaging and therapy control. They were followed up for at least 6 months after the PET/CT assessment. The results were compared with histological data or with complementary imaging modalities during follow-up. **RESULTS:** Early images were positive in 21 of the 24 patients, corresponding to a patient-based sensitivity of 87%, while the late study was positive in 19 patients with a sensitivity of 79%. In the preoperative staging all patients demonstrated high uptake in the known primary tumors at early imaging with decreased uptake from 20 to 80 % in the late acquisition, one patient had cervical pathological nodes. Distant metastatic disease was seen in 12 patients, all showed lymphadenopathy (laterocervical/subclavicular nodes in 5 patients and mediastinal nodes in 11 cases), one liver localization, two patients with pulmonary involvement and three cases with bone metastases. Three patients did not show any increased of ^{18}F -DOPA despite the elevation of s-calcitonin and they were also negative at radiological imaging. Four patients received different surgical approaches after ^{18}F -DOPA imaging. In the early acquisition two patients had bone lesions in the sternum and they both showed rapid wash-out. During therapy a patient demonstrated progression disease with an increased number of bone and pulmonary lesions, while the other three patients had stable disease. **CONCLUSION:** Although the limited number of patients in our study the results were promising: ^{18}F -DOPA PET/CT allowed early diagnosis of a noteworthy number of patients with distant metastasis, guiding surgical compartment approach of the neck when judged possible and enabled therapy assessment. The best diagnostic results were obtained with early imaging.

EP391

Quantitative Approach In Dynamic Parathyroid Scintigraphy And FCH PET For Evaluation Of Parathyroid Vs. Thyroid Anomalies

A. Koljevic Markovic, 1964.¹, M. Jankovic², J. Talbot³, M. Gauthé⁴, W. Langsteiger⁵, L. Imamović⁶, V. Miler Jerković⁷, M. Paskas⁸, G. Pupić¹, D. Popović², R. Džodić⁹; ¹National Cancer Research Center Serbia, Belgrade, SERBIA, ²University of Belgrade- School of Electrical Engineering of Serbia, Belgrade, SERBIA, ³Hospital Tenon, University

P&M Curie, Paris, FRANCE, ⁴Hospital Tenon, Paris, FRANCE, ⁵St Vincent's Hospital, Universities of Innsbruck | Graz | Vienna, Linz, AUSTRIA, ⁶St Vincent's Hospital, Linz, AUSTRIA, ⁷University of Belgrade- School of Electrical Engineering, Belgrade, SERBIA, ⁸Innovation Center University of Belgrade- School of Electrical Engineering, Belgrade, SERBIA, ⁹National Cancer Research Center Serbia, University of Belgrade Medical Faculty, Belgrade, SERBIA.

PURPOSE: Scan data novel processing and statistic analysis of time/activity/curves (TAC) in parathyroid were applied to evaluate hyper-functional lesions (HL), for differential diagnosis vs thyroid anomalies (TA) by different radiopharmaceuticals: MIBI and FCH as well as modifying time acquisition protocols. **METHOD:** In patients suspected for primary (PHPT) hyperparathyroidism (median age 58) preoperative ^{99m}Tc-MIBI scintigraphy (EANM guidelines 2009) was applied in 53pts and in four patients FCH PET two phase (early dynamic 8 min plus static acquisition) protocol. New designed software deals with region of interest in matrix and automatic preprocessing (linear fitted TAC logarithm, ensemble coupling) plus segmentation (automatic TACs clustering), as well as fractal analysis for TACs in order to analyze lesions and noise artifacts. **RESULTS:** 1. Scintigraphy PHPT histopathology: solitary- 44pts, hyperplasia: 8pts and one carcinoma; median lesion volume up to 1cm³; concomitant HL and TA in 36/53pts; findings had PPV 81%. PL had typical uptake pattern with late phase peak, independent to PTA volume and/or PTH levels. Ratio of HL-to-normal thyroid uptake was 1.35(±0.21). Parameters of optimal HL curve (associated with correlation matrix) enabled clear visual interpretation in time interval 10.-25.min after i.v. MIBI application. Fractal theory was helpful in matrix 5x5 designing classifier dimension 1.1-1.3 for automatic procedure. A new method raised PPV (97%). 2. FCH PET: autonomy 2pts, hyperplasia 2pts (one patient with concomitant thyroid nodule) median volume 1,1cm³. FCH had true positive results; following parathyroid time/uptake showed that in dynamic early phase after 5 minutes was maximal PL uptake as well as in thyroid (and thyroid nodule). The acquisition protocol of FCH visualize HL in early static as well as late static acquisitions. For now SUV values determined in static scans showed lower values for TA compared to HL and the pitfalls stay in parathyroid hyperplasia concomitant to thyroid anomalies. **CONCLUSION:** Quantitative approach facilitated the recognition of hyperfunctional parathyroid in the presence of concomitant thyroid anomalies, in scintigraphy but that was not the added value in FCH PET early dynamic acquisition protocol. Still, the benefit of quantification can be applied in modifying acquisition protocols in more efficient way in conventional as well as hybrid molecular imaging.

EP392

18F-fluorocholine PET/CT imaging is useful in localization of hyper-functioning parathyroid tissue in primary hyperparathyroidism: a comparative study with ^{99m}Tc-MIBI SPECT/CT and neck ultrasonography

K. Sönmezoğlu¹, B. Vatankulu¹, M. Ocak², R. Özcan Tutar³, H. Pehlivanoglu¹, E. Karayel¹, A. Karataş⁴, S. Teksöz⁴, L. Kabasakal¹, Y. Bükey⁴; ¹Istanbul University Cerrahpaşa Medical Faculty Department of Nuclear Medicine, İstanbul, TURKEY, ²Istanbul University Pharmacy Faculty, İstanbul, TURKEY, ³Istanbul University Faculty of Sciences, İstanbul, TURKEY, ⁴Istanbul University Cerrahpaşa Medical Faculty Department of General Surgery, İstanbul, TURKEY.

Aim: In patients with primary hyperparathyroidism (pHPT), preoperative localization of hyper-functioning parathyroid gland(s) is a very important issue in order to enable less invasive parathyroidectomy as well as to minimize post-surgical morbidity and cost. Several recent studies reported that ¹⁸F-fluorocholine (FCH) PET/CT imaging is an effective method to determine hyper-functioning parathyroid tissue. The aim of this study was to evaluate the

assessment of the diagnostic value of FCH-PET/CT for preoperative localization of hyper-functioning parathyroid tissue by comparing with ultrasound (US) and Tc-^{99m}-MIBI SPECT/CT imaging. **Materials and methods:** A single-institution prospective study was carried out in series of 28 consecutive patients with a biochemical diagnosis of non-familial pHPT, who undergone a neck US, Tc-^{99m}-MIBI SPECT/CT, and FCH-PET/CT as well. The diagnostic performance of the imaging methods was compared against histology as the gold standard and postoperative serum Ca and PTH values. **Results:** There were 19 (67%) female and 9 (33%) male patients with a mean age of 49 years. Preoperative mean PTH and Ca levels level were 167 ± 28.0 pg/ml (reference 10-55 pg/ml) and 11.4 ± 1.1 mg/dl (reference 9-10.5), respectively. Totally 30 lesions removed at surgery and histopathological examination revealed 21 parathyroid adenomas and 9 hyperplastic parathyroid glands. The sensitivity, specificity and positive predictive value of FCH-PET/CT imaging was 92.0 %, 100 %, and 100 %, respectively and superior comparing to neck US (63.2%, 56.6%, 78.3%) and MIBI SPECT/CT (76.4%, 100%, 91%). FCH-PET/CT was able to localize hyper-functioning parathyroid gland in 7 out of 28 cases with negative results on both neck US and MIBI SPECT/CT imaging. **Conclusion:** We agree that ¹⁸F-fluorocholine PET/CT is a promising imaging modality for the detection of hyper-functioning parathyroid tissue, most probably due to its superior spatial resolution. It has also some other advantages including low radiation burden and short scanning time, despite to its high cost. Therefore, it should be considered in cases with negative or discordant results on conventional imaging.

EP393

PARATHYROID SCINTIGRAPHY combining dual-isotope AND dual-phases imaging

K. LIMAM, I. Meddeb, I. Yeddes, M. Somai, A. Mhiri, I. Slim, M. Ben Slimane; salah aziez Institut, tunis, TUNISIA.

Introduction: Parathyroid scintigraphy is a reliable imaging for the diagnosis of parathyroid adenoma causing hyperparathyroidism. This exam can be performed by different procedures depending on the team experience and the available materials. The most common are dual-isotopes subtraction parathyroid scintigraphy and dual-phase imaging. Our purpose is to evaluate the results of combining both techniques on accuracy of the diagnosis. **Materials and methods:** This is a retrospective study in which we studied the cases of 35 patients with retained parathyroid adenoma diagnosis. Surgery, histological confirmation, and postoperative normalization of PTH was the reference standard. A parathyroid scintigraphy including a dual-isotope and a dual-phase imaging was performed. The imaging exploration starts with a thyroid Tc-^{99m} pertechnetate scintigraphy followed by a parathyroid Tc-^{99m} sestamibi scintigraphy with static cervical acquisition at 15 and 150 minutes and a thoracic acquisition at 30 minutes. **Results:** Twenty-seven out of thirty-five explorations (77%) were positive in both procedures and showed no significant difference. In fact, we noticed an increased uptake at the early images of the parathyroid Tc-^{99m} sestamibi scintigraphy compared to the thyroid Tc-^{99m} pertechnetate scintigraphy. These additional foci were still visible on late acquisitions of the parathyroid scintigraphy (late wash out). Seven exams (20%) had positive subtraction scintigraphy with a negative dual-phase imaging (early wash out). Only one exam concluded to a positive dual-phase imaging with a negative dual-isotope imaging. **Conclusion:** With a dual-isotopes subtraction we have nearly ninety-seven percent of positive diagnosis, but when we combine it to a dual-phase imaging we increase the accuracy of our parathyroid scintigraphy to show the parathyroid adenoma. These two methods of exploring the hyperparathyroidism are in fact complementary.

EP394**Radioguided Surgery With ^{99m}Tc-Sestamibi Primary Hyperparathyroidism: Experience in our institution**

U. Jon, A. Perissinotti, C. Cardenas-Negro, A. Allende-Riera, M. De Sequera-Rahola, E. Martinez-Gimeno, D. Cabello, O. Vilahomat; Hospital Universitario Nuestra señora de la Candelaria, Santa Cruz de Tenerife, SPAIN.

Aim: To report our experience in the use of ^{99m}Tc-Sestamibi for radioguided surgery in primary hyperparathyroidism and compare results of planar, SPECT/TC images and ultrasound with surgery, histopathological findings and also pre and post-surgery parathormone (PTH) and calcium blood levels. **Methods:** Radioguided parathyroidectomy surgery was performed in 18 patients with primary hyperparathyroidism. All patients were studied with ultrasound and ^{99m}Tc-Sestamibi scintigraphy before surgery. Planar and SPECT/CT ^{99m}Tc-Sestamibi scintigraphy images were acquired 15 minutes after radiotracer injection and planar delayed images at 120 minutes. Also pre and post-surgery PTH and calcium blood levels were measured. 185 Mbq of ^{99m}Tc-Sestamibi was injected on the day of the surgery for hand-held gamma probe radioguided parathyroid identification. Ultrasound and scintigraphy results were compared with histopathological findings and PTH and calcium blood levels. **Results:** In 16/18 (89%) cases histopathological findings of the radioguided resected tissue was compatible with parathyroid adenoma and serum calcium levels normalized after surgery. 12 out of this 16 patients (75%) showed at least a 50% reduction of their serum PTH levels with (mean reduction 57%). In one case histopathological results showed salivary gland tissue in what was thought to be an ectopic parathyroid adenoma; the patient continued with high serum PTH and calcium levels. Successful hand-held gamma probe radioguided resection of parathyroid adenoma showed an intense ex-vivo count rate with a 29% mean decrease activity of surgical bed activity. Planar ^{99m}Tc-Sestamibi scintigraphy imaging correctly identified the parathyroid adenoma in 11/18 (61%) cases and 7/18 (39%) were considered as normal studies. SPECT/TC successfully identified the parathyroid adenoma in 15/18 (83%). In two patients all imaging studies showed no abnormal findings, but in one of them parathyroid adenoma was successfully identified by hand-held gamma probe during surgery. The remaining case was considered a false positive SPECT/TC result as what was depicted as a probable ectopic parathyroid adenoma was histopathological reported as salivary gland tissue. Ultrasound correctly identified the pathologic parathyroid gland in 7/18 (39%) patients and was normal in 10/18 (56%) cases. In one case ultrasound showed incorrect localization of the parathyroid adenoma. **Conclusions:** Our experience showed that SPECT/TC ^{99m}Tc-Sestamibi scintigraphy in patients with primary hyperparathyroidism supplies crucial information for the successful identification of the hyperfunctioning parathyroid gland and is also of great value for surgery planning purposes. Furthermore, the use of hand held gamma probe during surgery allows to differentiate between the pathologic parathyroid glands and normal tissue.

EP395**Radioiodine kinetic in small pool hyperthyroid patients**

C. Canzi, V. Longari, M. Castellani, F. Buffoni, I. Martina, R. Benti; Fondazione IRCCS Ca' Granda Ospedale Maggiore Policlinico Milano, milano, ITALY.

Small pool (SP) patients are characterized by a high intrathyroidal iodine turnover. This results in thyroid uptake higher at early times (4-6h) than at 24h and, as a consequence, in an increment of radioiodine bound to protein circulating in blood and accumulating in liver that could increase dose to extrathyroidal tissues during therapy for hyperthyroidism. **Aim:** to study radioiodine kinetic in thyroid, blood, whole body(WB) and liver

in SP patients in comparison to non small pool (NSP) patients and to evaluate the contributions of blood self-irradiation and penetrating radiation from WB to mean absorbed dose to blood (D_{blood}) per unit of administered activity (A_0). **M&M:** After a pre-therapy dosimetry 7 hyperthyroid patients were classified as SP. After therapeutic administration blood samples were taken since 0.1h to about 168h and thyroid and WB images were acquired with a gammacamera at 2,5,24,48,96 and 168h to study iodine kinetic in blood, thyroid, WB and liver. The same study was performed on 3 NSP patients. **RESULTS:** Thyroid: in SP patients mean uptake at 5h was higher than at 24h: $74\pm 6\%$ and $64\pm 11\%$ respectively; in NSP it was the contrary: $34\pm 12\%$ and $49\pm 11\%$ respectively. Blood: up to 5h, there was no difference in radioiodine clearance between SP and NSP patients. After 24h, while in NSP patients there was a continuous decrease of ¹³¹I concentration, in SP there was a high increase, in correspondence of thyroid dismission, with a slow clearance. The contribution of blood self-irradiation to D_{blood} per unit of A_0 was $0.39\pm 0.20\text{Gy/GBq}$ and $0.06\pm 0.02\text{Gy/GBq}$ for SP and NSP patients respectively ($p=0.02$). WB: there was no difference between SP and NSP patients in radioiodine clearance rate. The contribution of penetrating radiation from WB to D_{blood} per unit of A_0 was $0.19\pm 0.05\text{Gy/GBq}$ and $0.15\pm 0.03\text{Gy/GBq}$ for SP and NSP patients respectively ($p=0.31$). Liver: in NSP patients liver wasn't visible on WB images at any time. In SP patients liver was clearly visible since 24h. Mean dose to liver per unit of A_0 was $533\pm 298\text{mGy/GBq}$. **CONCLUSIONS:** Radioiodine kinetic in SP hyperthyroid patients is quite different from NSP ones: in thyroid, uptake is higher at 5h than at 24h; in blood, after an initial fast clearance, there is an increment of concentration at 24h; in WB scans liver is clearly visible since 24h. In these patients the contribution of blood self-irradiation to D_{blood} per unit of A_0 is more important than the contribution of penetrating radiation from WB.

EP396**The interrelation of the blood absorbed dose and ablation success in thyroid cancer patients after ¹³¹I radioiodine therapy based on bi-phasic retention model**

F. Tabei, M. Dayagi, B. Shafiei; Shahid Beheshti university of medical sciences, Tehran, IRAN, ISLAMIC REPUBLIC OF.

Purpose: Radioiodine therapy with ¹³¹I is still a standard treatment of differentiated thyroid carcinoma patients post surgery. The required amount of radioiodine to achieve complete ablation is still subject to debate. The administered activity must be chosen with maximum ablation to target organ as well as minimal red marrow toxicity. The aim of this paper is to investigate the interrelation of the blood absorbed dose and ablation success of thyroid carcinoma patients after ¹³¹I radioiodine therapy. **Materials & Methods:** Total of 93 patients were arranged into three administered activity groups; 3.7 GBq (37.3 %), 5.55 GBq (56.6 %) and 7.4 GBq (6.0 %). The blood doses were calculated by external dose rate measurements of patients with an ionization chamber 2, 6, 12, 24 and 48 hours post administration of ¹³¹I. Ablation success defined as the negative ¹³¹I whole body scan and low Tg level after 6 months follow up post therapy. The whole body retention and residence times were determined by integrating biphasic decay curves fitted to the whole-body retention times. **Results:** Total of 70 male and 23 female patients aged 45±16 years had 6% follicular and 94% papillary thyroid carcinoma. Six months of follow up showed 58.0%, 38.3% and 20.0% ablation success in 3.7 GBq, 5.55 GBq and 7.4 GBq administered activity groups respectively. Average of the blood dose in 3.7, 4.62, and 5.55 GBq administered activity groups were 483 ± 15 , 491 ± 24 and 502 ± 38 mGy, respectively. Clearly there was no significant correlation between administered activity and ablation success in all groups. The blood dose distribution in 3.7 and 5.55 GBq groups showed significant correlation with ablation rates ($r=0.84$, $p=0.01$), but did not confirmed in 7.4 GBq group. **Conclusion:** This study clearly showed two important results. Increasing the

administered activity will not necessarily increase the ablation success and in the same administered activity patients the ablation success depends on the blood absorbed dose.

EP-18 – Sunday, October 16, 2016, during Exhibition hours, e-Poster Area
Do.MoRe: Data Analysis & Quantification

EP397

Procedural Errors and Their Impact on PET Quantification

T. Nguyen, C. Baun, P. F. Højlund-Carlsen; Dept. of Nuclear Medicine, Odense University Hospital, Odense, DENMARK.

Aim: In PET quantification, procedural variations and human errors will affect standardised uptake values (SUVs). Scan parameters extracted from DICOM image file metadata or patient records for SUV computation can contain data entry error that often unnoticed would yield faulty results. Practical deviations from protocol prescriptions also add to variability. We systematically assessed such inconsistencies and the impact on SUVs. **Materials and Methods:** Five research projects performed at our department from Jan 2015 to Jan 2016, totalling 201 patients, were retrospectively analysed. This included both FDG-PET/CT studies of various protocols (60 min and dual-time scans) and sodium fluoride (NaF)-PET/CT scans. Typed DICOM file entries of relevant parameters (patient weight, tracer dose, injection and scan time) were compared to corresponding registrations in handwritten records. Variations from protocol prescriptions were also recorded when applicable. Any whole number deviations were listed, from which variance estimates in terms of SUV ratios were calculated. **Results:** About 39% of studies had registration inconsistencies between DICOM and patient record entries. Discordance in patient weight (-1–100 kg) in these entries was seen in ~4% of studies, which would amount to a 0.99–41 factor difference in SUVs. Also, dissimilarity in tracer dose of -12–19 MBq ($p = 0.05$) and uptake time of -59–10 min ($p = 0.3$) would yield -5%–7% and -31%–7% SUV de/increment, respectively. Deviations from protocol prescriptions occurred in ~90% of studies with discrepancies in dose of -106–208 MBq ($p < 0.01$) and uptake time of -54–41 min ($p < 0.01$). These would translate into SUV variations by corresponding factors of 0.4–1.1 and 0.7–1.3. Errors collectively in each study would with DICOM entries give a 0.02–1.3 factor SUV difference and with patient record entries a factor of 0.4–1.3 difference compared to intended protocol parameters. **Conclusion:** Inconsistencies in parameter registrations found in routine PET/CT imaging practices are somewhat frequent. Both mainly small and a few highly discrepant DICOM and patient record entries would result in variable SUVs. Registered practical variations in tracer dose and uptake time compared to protocol prescriptions were most significant. This caused in worst cases SUV changes by more than 50% and variability to only increase significantly further with cumulative deviations. While most are expected practical variations, human errors are, therefore, in some instances not a negligible source of quantification bias.

EP398

A Comparison between Standard and Angular-Response-Function-Modeled GATE Simulations in Molecular SPECT: Focus on Computational Efficiency and Accuracy

M. R. Ay¹, H. Mahani², G. Raisali², A. Kamali-Asl³; ¹Tehran University of Medical Sciences, Tehran, IRAN, ISLAMIC REPUBLIC OF, ²Radiation Application Research School, Nuclear Science and Technology Research Institute, Tehran, Iran, Tehran, IRAN, ISLAMIC REPUBLIC OF, ³Radiation Medicine Engineering Department, Shahid Beheshti University, Tehran, Iran, Tehran, IRAN, ISLAMIC REPUBLIC OF.

Aim: While Monte Carlo modeling plays a crucial role nuclear medicine imaging, its performance is always challenged by a high computational demand, especially in high-resolution molecular SPECT simulations. In the current work, we compared standard GATE simulation with angular-response-function (ARF) modeled one based upon computational efficiency as well as accuracy. **Materials and Methods:** For this purpose, we modeled a dedicated molecular SPECT camera developed in our department, HiReSPECT scanner, in GATE. MC simulations were performed for low- (technetium-99m) as well as high-energy (iodine-131) collimators. The collimators were both high-resolution. The ARF allows the GATE to get rid of cumbersome photon transportation in the collimator by pre-calculating collimator-detector response. The ARF tables were extracted by a built-in function using a set of MC simulations at different energy-windows, and then implemented for simulation of NEMA image quality (IQ) phantom. To assess the performance of the ARF modeling, two NEMA IQ phantom simulation datasets (with and without the ARF incorporation) were acquired. Subsequently, each was iteratively reconstructed using a dedicated OSEM algorithm. There were 4 subsets and 3 full-iterations. **Results:** The ARF modeling results in an energy-dependent acceleration factor. The speed-up factor was 7.26 for the low-energy collimator and 12.82 for the high-energy one, considering the same noise-level of 5% for uniform part of the NEMA IQ phantom. Normalized mean square error (NMSE), as an index reflecting accuracy of the ARF modeling, between OSEM reconstructed images of hot-rods part of the NEMA IQ phantom (with and without ARF modeling) was 0.07 and 0.09 for the low- and high-energy collimator, respectively. System sensitivity was 1.32 cps/μCi for the low-energy collimator without ARF modeling, and a sensitivity of 1.24 cps/μCi was obtained when the ARF was modeled. In addition, the simulated system sensitivity (without ARF modeling) is consistent with that of experimental measurement, a 7.5% difference. **Conclusion:** The ARF modeling offered by the GATE makes it possible to dramatically shorten MC simulations of SPECT camera (by a factor between 7 and 13) without compromising accuracy of the data. The acceleration is substantial, especially when a high-energy molecular SPECT simulation is desired.

EP399

Improvement of the distortion effect in dual head PET scanner for breast imaging using an add-on Compton camera

H. Lin^{1,2}, C. Chiang¹, K. Lue¹, Y. Ni³, K. Chuang¹; ¹Department of Biomedical Engineering and Environmental Sciences, National Tsing Hua University, Hsin Chu, TAIWAN, ²Medical Physics Research Center, Institute for Radiological Research, Chang Gung University/Chang Gung Memorial Hospital, Taoyuan, TAIWAN, ³Health Physics Division, Institute of Nuclear Energy Research, Atomic Energy Council, Taoyuan, TAIWAN.

Aim Development of dedicated breast PET scanners is an active research area. Due to the limited angular coverage, fully 3D tomographic images without generation of distortion and artifact is very difficult without rotation of the detectors. In this work, we proposed a novel approach to improve the distortion effect by combining the PET and Compton imaging to achieve the 3D tomographic images without detector rotation. **Materials and methods** Stochastic origin ensembles (SOE) approach based on Markov chains is a good candidate for hybrid PET and Compton imaging since it's universal with any camera geometry. For each measured events (PET events or Compton events), the origins are randomly assigned on a conical surface or a line depending on the event type. During the reconstruction course, origins of the events are randomly moved at a condition of acceptance probability and finally those origins converges to the quasi-stationary state which can be voxelized in a reconstructed image. Monte Carlo simulation for the breast scanner design with a ring diameter and axial length of 15 cm is performed. The scanner comprises a dual head LSO PET detector and a Compton camera in

orthogonal directions. The Compton camera is composed of two double-sided silicon strip detectors as scatterers and LaBr3 scintillation detector as an absorber. A breast phantom embedded with several lesions of different sizes was used to evaluate the proposed system and reconstruction method. **Results** Preliminary simulation results suggest that the distortion and artifact is improved with the incorporation of Compton imaging, especially at the direction orthogonal to the dual head PET. The value for contrast recovery coefficient for small hot lesions of breast phantom can achieve similar performance with rotating dual head PET (full angular coverage). Furthermore, the addition of Compton camera can provide a ~10% gain in sensitivity compared to the dual head breast PET-only. **Conclusion** We conclude that the proposed method can reduce the artifact from the missing projections and improve the image quality of breast PET imaging.

EP400

Comparison of GE® Discovery IQ 5 rings vs Discovery IQ 4 rings physical performance of according to NEMA NU 2-2012

A. Loi¹, C. Ghetti², D. De Vittor¹, G. Serrelli², M. Carta¹, O. Ortenzia², M. Sireus³, S. Massa⁴, S. Loi⁴, G. Baldari⁵, G. Melis⁶, L. Ruffini⁵, M. Scarlattei⁵, S. Zucca⁴; ¹Alliance Medical, Cagliari, ITALY, ²Fisica Sanitaria AUO Parma, Parma, ITALY, ³Scuola di Specializzazione in Fisica Sanitaria, Università degli Studi di Cagliari, Cagliari, ITALY, ⁴Fisica Sanitaria AOB Cagliari, Cagliari, ITALY, ⁵Medicina Nucleare AUO Parma, Parma, ITALY, ⁶Medicina Nucleare AOB Cagliari, Cagliari, ITALY.

Aim: The purpose of the study was to compare the physical performance of two configuration (4 rings-*IQ4R* - and 5 rings-*IQ5R*) of the new integrated PET/CT system Discovery IQ (*DIQ* -GE Medical Systems). Measurements has been performed following the NEMA NU 2-2012 (*NU12*). **Materials and methods:** The *DIQ* combines a sixteen multi-slice helical CT scanner with a scalable PET tomograph which is available in configuration from 2 to 5 rings. Each ring consist of 18 double block of 8x8 BGO crystals. The crystal dimensions are 6.3x6.3x30 mm³. The *IQ4R* consists of 32 (4x8) rings of crystals allowing the acquisition of 63 images with an axial field of view coverage of 208 mm (63x3.27 mm). The *IQ5R* consists of 40 (5x8) rings of crystals allowing the acquisition of 79 images with an axial field of view coverage of 260 mm (79x3.27 mm). The low- and high-energy thresholds are set to 425 keV and 650 keV, respectively for *IQ4R* and *IQ5R*. The coincidence time window is set to 9.5 ns. **Results:** Spatial resolution was measured at different radial position (@1, 10, 20 cm) and along three main directions (radial -*rpr*, tangential- *tsr*- and axial-*asr*). The *rsr*, were 4.73, 5.22 and 7.94 mm @1, 10, 20 cm respectively (*IQ4R*); 3.80, 4.70 and 8.23 mm @ 1,10,20 cm respectively (*IQ5R*).The *tsr* were 4.92, 4.89 and 4.91 mm @1, 10, 20 cm respectively (*IQ4R*); 4.70, 4.74 and 5.19 mm @1, 10, 20 cm respectively (*IQ5R*). The *asr* were 4.90, 6.07 and 5.19 mm @1, 10, 20 cm respectively (*IQ4R*); 4.81, 5.79 and 6.50 mm @ 1, 10, 20 cm respectively (*IQ5R*).The sensitivity increased from 14.5 cps/kBq (*IQ4R*) to 22.4 cps/kBq (*IQ5R*) at radial position *r*=0 cm and from 13.4 cps/kBq to 20.1 cps/kBq at radial position *r*=10 cm. The scatter fraction was 39.93% (*IQ4R*) and 37.48% (*IQ5R*). The NECR peak was 75.9 keps at 9.1 kBq/cc in *IQ4R* and increased to 128.4 keps at 9.3 kBq/cc for *IQ5R*. Losses and random counts accuracy corrections were 3.22% for *IQ4R* and 4.34% for *IQ5R*. Also image quality, accuracy of the attenuation and scatter correction were evaluated for both systems. **Conclusion:** The new integrated PET-CT system Discovery IQ has excellent performances in both 4 and 5 rings with high sensitivity and a very good NECR response. Which configuration is better for own PET center depends mainly on the numbers of patients/year and the availability of a cyclotron in site.

EP401

Development of 18F-FDG doped alginate phantoms for advanced applications in Nuclear Medicine

J. Cortes-Rodicio, M. Hernandez-Garcia, M. Garcia-Fidalgo; Osakidetza, Vitoria-Gasteiz, SPAIN.

INTRODUCTION AND OBJECTIVES: The purpose of this work is to develop PET phantoms that simulate realistic geometrically situations we found in our nuclear medicine department. In particular, we developed phantoms for applications of true PET guided biopsies, for PET contour delineation verification, and in-body resolution measurements. **METHODS AND MATERIALS:** For all situations, we used a fast drying alginate powder dissolved in 18F-FDG doped water, with the FDG activity concentration of the phantom bulk similar to the clinical practice (2.5MBq/kg). According with the final usage, three different inserts were introduced inside the phantoms before the alginate was settled: (1) First, for testing purposes of a novel device for true-PET guiding biopsies, several spheres with diameters between 5 and 10mm and an activity concentration of 4:1 with respect the background were introduced inside the volume. In this case, the accuracy of the position of the biopsy needle tip with respect to the centre of the spheres can be measured after a PET guided biopsy procedure.(2) Second, a tumour phantom was built to verify the tumour delineation based on metabolic PET imaging for radiotherapy planning. In this case, the size of the 4:1 inserts was at least 4ml, with different shapes according with realistic tumour plaster moulds. The manual drawing contours of the inserts based on PET imaging were then compared with the real shape obtained from a previous CT scan of the phantom.(3) In the third case, we introduced FDG doped zeolites (diameter<1mm) with different activity concentrations (range 2:1 - 12:1) inside the phantom body. By this way, we can measure the resolution of our equipment in real clinical situations. **RESULTS:** All the alginate phantoms built were successfully used. First, the improvement of the precision and accuracy of the PET guided biopsies using the novel guiding device could be measured. Second, we provide a reliable training phantom for manual tumour delineation based on metabolic PET imaging. Finally, the real clinical resolution of our PET/CT equipment was characterized. **CONCLUSIONS:** Emerging nuclear medicine necessities require precise assessment and characterization prior the clinical implementation. In this context, we have successfully built different PET phantoms to meet the new challenges of our department. Anyway, the process of phantom elaboration has to be improved and the fields of application broaden.

EP402

Gated reconstruction in 18F-FDG PET-CT quantitative imaging: impact on SUV estimation of tumor motion inside the lung with dynamic thorax phantom

M. Zuffante¹, E. Zivelonghi¹, F. Sciumè¹, F. Dusi², P. Polloniato¹, D. Grigolato¹, M. Cucca¹, L. Pavanello¹, C. Cavedon¹, M. Ferdeghini¹; ¹AOU Verona, Verona, ITALY, ²Scuola Specializzazione in Fisica Medica, Università degli Studi di Milano, Milano, ITALY.

Introduction and purpose The methods based on SUV maps suffer from poor SUV and volume quantification due to respiratory motion. The aim of this study was to assess the impact of respiratory-gated PET-CT (4D-PET-CT) on SUV and SUV-based volume quantification in lung tumors using the respiratory track of patient and a dynamic thorax phantom. **Materials and Methods** 4D-PET-CT was performed by means of a Philips Gemini BigBore TOF scanner, using the Varian RPM gating system and a Dynamic Thorax Phantom. Administration and acquisition parameters were 5000 Bq/ml 18F-FDG in a sphere of 8 ml and 2 ml, 2 min/bed, retrospective-mode for both PET and CT modalities. The phantom was scanned at different motion amplitude ranging between 1.0 and 2.5 cm using the respiratory track of patient and cos4. Data were reconstructed in 1 (no sorting), 4, 5, 6, 7, 8, 9 and 10 phases. SUVmax values

within the lesion in max expiration (ph0) were studied as a function of the number of phases into which the breathing cycle was split. Lesion volumes were also obtained by three different methods: a) fixed SUV=2.2 threshold, b) 40% of SUVmax isocontour and c) gradient-based method. The volumes were also studied as a function of the number of phases in ph0. **Results** Comparison between the gated and the non-gated PET images showed a maximum 25% reduction in the total lesion volume calculated as 40% of SUVmax isocontour. Measurements of the maximum standardized uptake values in the gated mode showed an increase of up to 22% compared with that of the nongated measurements. Furthermore SUVmax value increases with the number of phase bins. The smaller sphere showed a greater drop in SUVmax than the larger sphere for the same motion amplitude. For the same sphere volume, the greater drop in SUVmax was obtained for the larger motion amplitude. **Conclusion** 4D-PET-CT offers a clear advantage in 18F-FDG SUV estimation for tumors that move with respiration. The effect of gating should depend on the lesion's size and lesion motion amplitude. A balance between acquisition time, SNR and SUV estimation accuracy seems to be achievable by using 4-6 phases, depending on lesion size and location. 4D-PET-CT might improve volume quantification as well; however, further research is needed in order to find the optimum segmentation method independently from tumor motion, as residual inconsistencies are observed after motion correction.

EP403

AniMate - An open source software for absolute PET quantification

C. Malbert; INRA, Saint-Gilles, FRANCE.

Image derived insulin sensitivity and glucose metabolic rate (MRglu) are essential to investigate whole body insulin resistance in type II diabetes and in obese individuals. PET imaging coupled with arterial input function measurement once correctly analyzed with compartmental kinetic modeling has been used to evaluate MRglu for the heart, liver, skeletal muscle, brain and more recently duodenum (Iozzo, 2015). While the workflow has been simplified by dedicated software such as Pmod (Switzerland), the calculation of the input arterial function is difficult, time consuming and prone to errors. Furthermore, calibration procedure is complex and the actual experiment requires exact timing with intermingled sampling. The aim of this work is to present an integrated open source software solution to streamline the workflow from the cross calibration down to the delivery of an arterial input function correctly formatted for data modeling. AniMate is a set of software modules written in Labview 2015 (National instruments, USA) that interact between each other to minimize user interaction to create a flexible automated workflow. All software modules have a comprehensive english user interface and are multiplatform aware. AniMate comprises four modules. One module aims at getting in line arterial counts and is directly interfaced with a Canberra 2007 photomultiplier tube and a WPI peristaltic pump. Another module is dedicated to get blood sample volume using a precision connected scale and plasma activity using a desktop gamma counter (2470 Wizard, PerkinElmer). These two modules have provision for cross calibration using PET as source calibrator. A third module serves as master timer. It extracts time frames from the PET machine and convert them into sampling time to automatically create a logbook of the experiment. A fourth module is dedicated to data integration for creation of the composite arterial input curve from inline data together with plasma samples. This module was also capable to build complex arterial input curves required when several organs are scanned sequentially. Finally, it extracts the endogenous glucose production from FDG fate. An additional module is mastering the automatic euglycemic clamp using an algorithm derived from Furler et al (1986). AniMate has been used successfully in more than 30 preclinical studies with miniature pigs and has been proved to be effective in reducing the work burden required for MRglu calculation both during the actual experiment and in analyzing the numerous pieces of informations that eventually will be used in data modeling.

EP404

Evaluation of auto-segmentation methods for the determination of skeletal tumor burden on F18-NaF PET/CT bone scans

A. Swallen, S. Chung, A. Nelson; MIM Software, Inc, Cleveland, OH, UNITED STATES.

Purpose/Objectives: Interpretation of F18-NaF PET/CT bone scans can be challenging due to the large number of lesions that can be present. Our goal is to evaluate different methods to automatically segment areas of high fluoride uptake for the determination of skeletal tumor burden on NaF PET/CT. **Methods/Materials:** Nine NaF PET/CT scans were processed using two auto-segmentation methods to identify areas of abnormal NaF uptake defined as > 10 SUV. Method 1 used an automated body segmentation method to outline the whole body. Method 2 identified bones by first outlining the whole body like Method 1, then thresholded the body to CT bone HU range, and used contour post-processing to finalize the bone contours. Areas > 10 SUV were then identified within the final region generated by each method. Comparison was made to a region created by applying a cutoff of 10 SUV to the manually created bone VOIs for each subject. Total lesion fluoride uptake (TLF10) and fluoride tumor volume (FTV10) were compared for each method. **Results:** The average TLF10 from the manual contours was 4648 SUV*mL with a range of 370-16436 SUV*mL. The average FTV10 from the manual contours was 292.67 mL with a range of 28.48-1167.37 mL. The percent difference in TLF10 and FTV10 for each method compared to the manual method were: Method 1 (137.18%, 90.10%), Method 2 (2.94%, 3.40%). **Conclusions:** The second method of auto-segmentation was found to produce the most accurate measurements of skeletal tumor burden as defined by areas within manually defined bone VOIs with >10 SUV.

EP405

Evaluation of quantitative parameter of Q.Clear, a new image reconstruction algorithm for PET, compared with conventional iterative reconstruction

T. Ishimori, Y. Nakamoto, K. Togashi; Kyoto University, Kyoto, JAPAN.

(Objectives) Quantitative analysis using standardized uptake value (SUV) is commonly used in oncological FDG-PET imaging. Recently, a new Bayesian penalized-likelihood reconstruction algorithm Q.Clear has been developed to generate images with lower noise compared to conventional OSEM. However, it is not clear how Q.Clear reconstruction affects quantification of clinical FDG-PET. We evaluated quantitative characteristics of Q.Clear reconstruction in terms of comparison of SUV on clinical images between Q.Clear and conventional OSEM. **(Methods)** Images of 40 FDG-PET/CT whole body scans with known or suspected malignancies were reconstructed by Q.Clear ($\beta=300$) and conventional OSEM (iteration 4, subsets 12) methods. SUVmax by Q.Clear (QSUV) and that by conventional OSEM (CSUV) were measured on the same region of interest placed on the liver, heart, brain. In 29 PET/CT scans, QSUV and CSUV of 40 malignant tumors (lung, colon, liver, lymph nodes, bone and soft tissue, etc.) with a diameter of 38.0 \pm 36.6mm were measured and compared with each other. In 5 scans, QSUV using various reconstruction conditions ($\beta=300, 400, 500$ and 600) were compared with one another. **(Results)** QSUV of the tumor (8.9 ± 6.3) was significantly greater than CSUV (8.3 ± 6.4) ($p < 0.01$). As for the brain and the heart, QSUV was significantly greater than CSUV (brain: QSUV= 13.7 ± 3.3 , CSUV= 12.8 ± 2.9 ; $p < 0.01$, heart: QSUV= 5.9 ± 3.4 , CSUV= 5.8 ± 3.3 ; $p = 0.02$), while the difference of QSUV and CSUV of the liver (QSUV; 3.2 ± 0.2 , CSUV; 3.2 ± 0.3) was not significant. Increasing β values reduced QSUV in the liver, heart, brain and tumor significantly. **(Conclusions)** Significant differences between QSUV and CSUV of the tumor and the normal organs should be noted in quantitative evaluation of PET images, while SUVmax of the liver is relatively

consistent regardless of reconstruction algorithms. When using Q.Clear reconstruction, appropriate β value should be selected in terms of not only image noise reduction but also SUVmax.

EP406

Amyloid Burden Clusters: An Exploratory Study

J. S. Oh¹, H. Moon^{1,2}, M. Oh¹, S. Oh¹, J. Roh³, J. Lee³, J. Kim¹; ¹Department of Nuclear Medicine, Asan Medical Center, University of Ulsan College Medicine, Seoul, KOREA, REPUBLIC OF, ²Department of Medical Science, University of Ulsan College of Medicine, Seoul, KOREA, REPUBLIC OF, ³Department of Neurology, Asan Medical Center, University of Ulsan College Medicine, Seoul, KOREA, REPUBLIC OF.

Aim The brain amyloid PET became one of representative imaging biomarkers for the investigation of amyloid- β associated cognitive and movement disorders. To the best of our knowledge there have been less literature that addressed the amyloid burden as clusters or networks in brain as compared to other brain imaging modality (e.g. anatomical/functional or metabolic connectome) studies. Therefore, we performed an exploratory investigation of the amyloid burden clusters using 60 visually diagnosed amyloid-positive patients among patients with Alzheimer's disease or mild cognitive impairment patients in our Neurology Clinics. **Materials and methods** All patients underwent 20min PET-CT scan on GE Discovery 690(Elite)/710 PET cameras 60 min after 185MBq i.v. of F-18 Florbetaben (FBB). 3D volumetric MRIs were also acquired for each subject for the anatomical precision of volume of interest (VOI) definition. Freesurfer-based parcellation of brain was conducted using these 3D MRIs resulting in sulcal/gyral parcellation of brain. Reference region was defined by cerebellar cortex for the purpose of uptake count normalization forming uptake ratio (also equivalent to standard uptake value ratio; SUVR). Seed regions were picked from representative VOIs of amyloid burden - PC square (posterior cingulate cortex and precuneus), bilateral middle frontal cortices (MFC)/ lateral temporal cortices (LTC). For an exploratory purpose, bilateral VOIs were used as different seed regions. Since global (nonspecific) mean uptake cause seemingly global high correlation, we corrected for all regional amyloid uptake by subtracting global mean uptake. Interregional correlation analysis was conducted using aforementioned seed regions and sulcal/gyral level parcellation of brain. **Results** Each seed region correlated with different regions of brain, forming many different clusters. All seed regions exhibited correlation with contralateral (mirrored) regions with lower correlation than in the ipsilateral ones. All seed regions but PC square exhibited correlation with themselves and their mirrored contralateral regions. PC square exhibited high correlation with itself and partial correlation with superior frontal cortex. **Conclusion** All representative amyloid burden-susceptible regions formed different clusters in terms of inter-regional correlation. Therefore, we suggest whole brain amyloid burden may be better described by a global (composite) VOI or a well-designed weighted sum of these subregions.

EP407

Radiomics of 18F-choline fusion PET/MRI for prostate cancer detection prior to targeted prostate biopsy

M. R. Piert, M. S. Davenport, J. Montgomery, L. P. Kunju, J. Siddiqui, V. Rogers, X. Shao, I. El Naqa; University of Michigan, ANN ARBOR, MI, UNITED STATES.

Objectives: MRI-guided (targeted) prostate biopsies are rapidly adapted to improve the diagnostic performance of prostate biopsies. We tested the value of texture analysis on 18F-choline PET/CT in conjunction with apparent diffusion coefficient (ADC) maps from diffusion-weighted

MRI to improve the detection of significant prostate cancer (Gleason \geq 3+4) over that from multi-parameter (mp) MRI alone. **Methods:** 18F-choline PET/CT (Siemens mCT PET/CT, HiRez, time-of-flight) and 3 Tesla mpMRI (Philips Achieva) of the pelvis were performed in 23 subjects with rising prostate specific antigen levels (PSA mean 7.9 ± 3.5 ng/mL) for known (n=17) or suspected (n=20) prostate cancer prior to a scheduled prostate biopsy procedure. PET and T2-weighted (T2w) MR volumes of the prostate were spatially co-registered (MIM software). Biopsy targets were selected based on visual appearance on MRI and graded as low, intermediate or high risk. Volumes-of-interest were defined to obtain 18F-choline SUV and ADC values. For texture analysis, a regularization and variable selection method (called elastic net) with 80% Lasso (L1 norm) to 20% ridge (L2 norm) penalty (binomial logistic model). Regularization parameter selection was done with 10-fold cross-validation and classification assessment using AUC with performance generalization using 1000 bootstrap re-sampling. Sampled image texture features (including global, GLCM, NGTDM, GLRLM, GLSZM) from 18F-choline PET, ADC and fused PET/MRI (normalized by peak signal) were applied. ROC analysis was performed for individual parameters (18F-choline maximum SUV, minimum ADC), and texture analysis from 18F-choline, ADC, and fusion PET/MRI. The biopsy procedure was performed after registration of real-time transrectal ultrasound (TRUS) with a 3D T2w MR sequence with embedded target information. Histology (Gleason scores) from image-guided (targeted) plus standard (systematic 12-core) biopsy cores, as well as from prostatectomy specimen (n=6) was used as reference. **Results:** A total of 37 lesions were identified by mpMRI (19 low; 10 intermediate; 8 high risk), and mpMRI-assigned risk was a good predictor of final pathology. Twelve subjects were ultimately identified with Gleason \geq 3+4 prostate cancer. The 18F-choline maximum SUV (AUC=0.79) and minimum ADC (AUC=0.68) as sole measurements were inferior to their respective texture analysis (AUC=0.82 and 0.86). Texture analysis of the combined PET/MRI classifier performed slightly better at AUC=0.88. **Conclusions:** Texture analysis of PET/MRI classifiers warrants further investigation for the identification of significant primary prostate cancer. Support: United States Department of Defense (DOD) GRANT10953301

EP408

Beth Israel Plugin for FIJI: A free and open source software tool for PET/CT processing in research

S. Kanoun^{1,2,3}, I. Tal⁴, J. Vrigneaud², A. Cochet^{1,2,3}; ¹LE2I, UMR CNRS 6306, Dijon, FRANCE, ²Centre Georges Francois Leclerc, Dijon, FRANCE, ³CHU Dijon, Dijon, FRANCE, ⁴Beth Israel Deaconess Medical Center, Boston, MA, UNITED STATES.

Aim: To develop a new collaborative free and open source software tool, provide image processing capabilities and facilitate data collection on PET/CT. **Presentation:** The software is developed by Beth Israel Deaconess Medical Center (Boston) in collaboration with other institutions. Based on FIJI (ImageJ distribution) and distributed with the General Public License (GPL), the software can be used with any operating system (Windows, Mac OSX, GNU/Linux). The project is open for any collaboration to provide a free software support for processing and data collection on PET/CT images. Software quantifications has been validated using a PET/CT phantom and with a clinical dataset and has shown identical results than commercial workstations. Functionalities: - DICOM compatibility: parsing and reading. - PET/CT display: PET and CT display, image fusion, LUTs availability, MPR and MIP reconstruction, image annotation, secondary capture. - Quantification: SUV (max, mean, peak, SD), SUL, MTV (absolute or relative threshold), TLG. Regular or irregular ROI drawing. - Results export in CSV files (global results and for each ROI), ROI coordinate saving. - Possibility to develop dedicated tool for specific research topics: data organization in local or remote database, advanced image processing, multi reader collaborative studies.... - Other: MRI registration, additional image processing using ImageJ/Fiji functions, automatic updates... **Conclusion:** Beth Israel Plugin for FIJI provides

free image processing and data collection services with personalized features capabilities. This free software solves usual software cost and availability issues. Based on a collaborative project, each researcher is welcome to suggest new image processing topics and participate in building an open source multipurpose software tool for scientific applications.

EP409

Method for accurate registration of PET and MRI to histopathology of the prostate

M. R. Piert, J. Siddiqui, V. Rogers, J. Montgomery, M. S. Davenport, L. P. Kunju; University of Michigan, ANN ARBOR, MI, UNITED STATES.

An exact co-localization of image data with pathology is needed to establish the accuracy of imaging to distinguish low risk (indolent) from intermediate/high risk (significant) primary prostate cancer and to determine tumor boundaries to guide focal prostate cancer treatments. Due to poor correlation of slice thickness and orientation between imaging and histology, verification of medical imaging results of smaller prostate lesions by pathology is challenging. Here we demonstrate an objective methodology using *ex-vivo* prostate specimen MRI and patient-specific 3D printed molds to facilitate registration. **Methods and results:** The registration process involves multiple steps. First, *in-vivo* PET is registered to a high resolution (0.75 mm³) 3D T2-weighted (T2w) MR sequence at 3 Tesla using commercially available software. The most difficult, second registration step is the mapping of pathology onto MRI, aided by *ex-vivo* prostate specimen MRI. Following prostatectomy, an *ex-vivo* T2w 3D specimen MRI is performed with the prostate immersed in perfluorocarbon solution to reduce susceptibility artifacts. Segmentation of the prostate then serves as mold design template. The scan also facilitates image registration utilizing embedded intra-prostatic imaging features. Mold sleds spaced 3 mm apart simplify later accurate gross sectioning of the specimen within the mold. Following complete fixation of the prostate, a second specimen MRI is performed; then the prostate is gross sectioned without repositioning in the mold. Volumetric 3 mm stacks of histology sections are then registered onto *ex-vivo* high resolution specimen MRI, providing a consistent registration of the *ex-vivo* MRI to pathology. All prostate cancer foci are outlined by the pathologist on whole-mount HE slices and lesion boundaries are transferred into the *ex-vivo* MRI. **Results:** The methodology allows the retrospective verification whether *in-vivo* imaging correctly identified and classified all tumor lesions identified at final pathology. Also, it is possible to determine the true tumor extension on *in-vivo* PET and MRI, thereby determining boundary errors based on visual image inspection as well as mathematical thresholding techniques. Furthermore, this methodology permits retrospective genomic and immunohistochemical analyses of specific imaging features. **Conclusion:** Additional expenses related to advanced registration techniques as described here are small in comparison to the overall costs of clinical trials. Employing such techniques improves the impact of imaging research, which is particularly true for prostate cancer, which often presents with multi-focal disease of varying clinical significance. Support: United States Department of Defense (DOD) GRANT10953301

EP410

Optimization of Filter Thickness in Filtering Technique for DISA Crosstalk Compensation

K. S. Chuang¹, H. H. Lin^{1,2}, Z. J. Wei¹, C. C. Chiang¹, Y. H. Lee¹, Y. F. Wang¹, C. S. Lin¹; ¹National Tsing-Hua University, Hsin-Chu, TAIWAN, ²Medical Physics Research Center, Institute for Radiological Research, Chang Gung University/Chang Gung Memorial Hospital, Taoyuan, TAIWAN.

Aim: Dual isotopes simultaneous acquisition (DISA) permits the imaging of two radiotracers in the same physiological state with perfect registration. However, crosstalk exists when the photopeak of the two photons from the dual isotopes are close. Artificial neural network (ANN) is the most used technique to toggle the crosstalk. However, it requires up to 26 energy windows which are not available in most SPECT. Recently, we used a filter on the collimator to alter the energy spectrum of the detected photons. It is possible to separate the two isotopes based on the attenuation differences in data from the two scans with and without the filter. In this study, we explore the effect of filter thickness on the decontamination and determine the optimal thickness. **Materials and methods:** A large filter thickness generated a larger attenuation difference between two photopeak windows and enabled a better separation between isotopes. A thicker filter absorbed more photons and caused an increase in image noise. The determination of filter thickness is a tradeoff between the noise and degree of decontamination. A figure of merit (FOM) was defined as the ratio between the attenuation difference in photopeaks of the two isotopes caused by the filter and Poisson noise in the projection data. We plotted FOM as a function of filter thickness and the one with largest FOM was regarded as optimal. **Results:** A thickness of 0.2 mm gold was found to be optimal for ¹²³I/^{99m}Tc DISA. The gold was selected for its high Z and excellent ductile property. The gold film is attached to the one of the two collimators of an E.CAM (Siemens, German) for DISA simulation. Preliminary results demonstrate that the proposed method improves image contrast and removes the artifacts caused by the energy crosstalk. The results show that quantitative recovery from mixed ^{99m}Tc and ¹²³I sources is comparable to that from matched single-isotope sources. **Conclusion:** In this study, a DISA SPECT technique to tackle the crosstalk using filter is proposed and the optimized thickness of the filter is determined. Projection data with and without filter are used to separate the energy spectrum. This method is simple to perform and yet generates promising results.

EP411

Improved Quantification of Preclinical ⁶⁸Ga PET studies with a CT-based Positron Range Correction

J. Cal-Gonzalez; Medical University of Vienna, Vienna, AUSTRIA.

Aim. Image quality of PET tracers that emits high-energy positrons, such as ⁶⁸Ga, ⁸²Rb or ¹²⁴I, is significantly affected by the “positron range” (PR) effect. PR effects are especially important in small animal PET studies, as they limit the spatial resolution and quantitative accuracy of the images. The aim of this study is to show how the quantitative results of ⁶⁸Ga-DOTATOC PET/CT imaging of neuroendocrine tumors in mice can be improved using a novel tissue-dependent and spatially-variant positron range correction (TDSV-PRC). **Materials and methods.** Monte Carlo simulations of the positron propagation in biological tissues were used to obtain the PR distributions for the most common radionuclides used in PET. These results were used to define voxel-dependent kernels which take into account the different materials that a positron may travel through until it annihilates. These kernels are computed before the PET reconstruction based on the associated CT scan, and they are incorporated in the forward-projection step of the iterative reconstruction. The performance assessment of the method has been carried out using two acquisitions of mice with xenografted neuroendocrine tumors injected with ⁶⁸Ga-DOTATOC and scanned in the Argus PET/CT system. Scan time was 60 minutes after 30 minutes of uptake, using an energy window of 100-700 keV. Image reconstruction was done using a 3D-OSEM algorithm with and without the proposed correction. Quality of the mice images was based on signal-to-noise ratio, measured by mean activity within the tumors and the standard deviation in a uniform region located within the liver. Activity profiles through the tumor and residual activity in the lungs and air surrounding the mice bodies were also evaluated. **Results.** We observed an activity recovery within the tumor of 106% (mouse 1) and 150% (mouse 2), from images at the same

noise level (12% in a uniform region). This level of noise was achieved after 250 (without PRC) and 100 (with PRC) image updates. A significant reduction of apparent tumor size was observed when PRC is applied, giving similar tumor delineations than the ones obtained from the CT images. Significant reduction of activity in lungs (27% for mouse 1 and 40% for mouse 2) was observed in the PRC images. **Conclusions and future work.** The proposed TDSV-PRC produces artifact-free images for large PR radionuclides such as ^{68}Ga . Further evaluations in a larger cohort of mice with neuroendocrine tumors are being performed and will be presented at the conference.

EP412

Clinical Impact of Anti-Thyroglobulin Antibodies & Hashimoto's thyroiditis In The Follow-up Of Differentiated Thyroid Cancer Patients

A. Zakir Ali, R. P. P. B; Basavatarakam Indo-American Cancer Hospital & Research Institute, Hyderabad, INDIA.

AIM To predict the prognosis of DTC patients from their anti-thyroglobulin trend & the status of Hashimoto's thyroiditis. **MATERIAL & METHODS** We evaluated about 102 patients retrospectively having only locoregional disease. A first follow-up (FFU) WBI scan alongwith serum thyroglobulin (Tg1) and serum anti-thyroglobulin antibody (TgA1) was performed after 6 months of radioiodine therapy (RIT). A second follow-up (SFU) WBI scan or whole body tumor scintigraphy was performed after 1.5 years post RIT alongwith serum thyroglobulin (Tg2) & serum anti-thyroglobulin antibody (Tg A2). The status of Hashimoto's thyroiditis (HT) were also noted. The patients having high serum TgA1 levels (> 18 IU/ml) were divided into two groups: Group A having negative FFU WBI scan (ablated or TENIS). Group B having a positive FFU WBI scan (residual or recurrence). The Group A were further divided into 2 subgroups based on the presence or absence of elevated Thyroglobulin levels: [a] Non-TENIS (Tg1 < 10 ng/ml) and [b] TENIS patients (Tg1 > 10 ng/ml). The group B patients underwent RIT +/- surgery. The subsequent serum anti-thyroglobulin antibody levels after 6 months were taken as TgA2 levels. **RESULTS** 24 out of 102 patients are positive for Hashimoto's thyroiditis (HT). 16 out of 102 patients have elevated TgA1. Only 6/16 TgA1 positive patients have HT. Out of the 16 patients who had elevated serum TgA1, 12 patients belonged to Group A and 4 patients belonged to Group B. Out of the 12 patients belonging to Group A, 10 belonged to Non-TENIS category & 2 to TENIS category. Out of 10 pts belonging to Non-TENIS category, 9 had a decreasing trend and 1 had an increasing trend of TgA2 as compared to TgA1. Out of the 9 having a decreasing trend, 5 had > 50% decrease (4 positive for HT) and 4 had < 50% decrease (1 positive for HT). The single patient with increasing trend of TgA2 had negative HT (diagnosed to have liver metastasis). Out of the 2 TENIS category patients (both negative for HT), one had a decreasing trend (< 50%) of TgA2 and the other an increasing trend. Out of the 4 patients belonging to Group B, all had a decreasing trend of TgA2 with one having > 50% decrease (negative for HT) and 3 having < 50% decrease (one positive for HT). **CONCLUSION** The trend of the serum TgA levels (increasing and < 50% decrease) alongwith a negative HT status predicts a poorer prognosis whereas a decreasing trend of > 50% with HT positivity suggests a good prognosis. It is especially useful in identifying occult TENIS syndrome patients.

EP413

Synthetic PET Image Modeling

C. HUERGA¹, P. CASTRO², L. ALEJO¹, R. PLAZA¹, E. GUIBELALDE³; ¹Medical Physics Department, Hospital Universitario La Paz, MADRID, SPAIN, ²Medical Physics Department, Hospital Universitario La Princesa, MADRID, SPAIN, ³Department of Radiology, Faculty of Medicine, Complutense University, MADRID, SPAIN.

Aim: To evaluate techniques of image processing is quite common to use synthetic images for its validation. In this work we show a model to generate synthetic PET images. The proposed model includes fundamental aspects for description of PET image: effect partial volume (EPV), noise (covariance) texture, and dependence with noise magnitude (variance). To compare synthetic PET images with real FDG-images, we apply a non-linear filtering based on wavelets. **Material and methods:** Synthetic images were produced simulating NEMA IEC Body Phantom which includes "hot" spheres. A dataset of 128 x 128 images with voxel size 3,906mm x 3,906mm x 4.25mm was performed where an ellipsoid simulates phantom section and a set of six spheres are embedded with the same diameter as the real ones. Image resolutions characteristics are obtained experimentally from recovery coefficient (RC) following the method proposed by Prieto [Prieto,2010]. RC is defined as the ratio of the activity concentration presented in the image and the real (introduced) activity. The mathematically images generated were convoluted varying SD kernel value until coincidence RC with experimental values. The noise texture is performed by random phase shift of noise power spectrum (NPS) [Fredenberg, 2010]. The NPS is obtained via Fourier transform of uniform phantom acquisition. The model also introduces the correlation intensity. Then, the expression for noise's model we propose is: $I_{noise}(x,y) = I_0(x,y) + f(I_0(x,y) * noise(x,y))$. Where I_0 is the synthetic image without noise and convoluted with the PSF. Function f represents dependence of variance with magnitude, we used expression proposed by Geng [Geng, 2003], the symbol * indicates a pixel by pixel product, and $noise(x,y)$ is the noise texture image defined above. Real images were acquired using PET /CT Discovery LS (GE Healthcare), with CT based attenuation correction using OSEM reconstruction. Images dataset using 18FDG and NEMA phantom was acquired. To compare real 18FDG-images (A) with synthetic (B) SURE wavelet filter with appropriate performance for PET images [Turkheimer,1999] was used. **Results:** Both A and B exhibit the same behavior. Global gain in SNR is about 30% in both A and B. Signal decrease in smallest spheres. With different sphere-background ratio (SBR): SBR=5-1 (low-contrast) -9% in A and -6.5% in B, decreasing when SBR is larger: SBR=20-1 (high-contrast) -2.8% in A and -2.2% in B. We show noise texture, real and synthetic phantom in order to evaluation. **Conclusions:** We show a model to generate synthetic PET image. It's a valid alternative to MC models.

EP414

Validation of an Automatic Segmentation Algorithm for SPECT/CT Based Tumour Dosimetry

M. Gray, I. Murray, G. Flux; Joint Department of Physics, Royal Marsden NHS Foundation Trust, London, UNITED KINGDOM.

Aims: To assess the performance of a novel user-independent automatic segmentation algorithm for SPECT/CT applications. The algorithm had been previously developed for PET/CT applications in external beam radiotherapy. **Method:** The Fuzzy Logic Automatic Bayesian (FLAB) segmentation algorithm developed by Hatt et al was initially coded and tested using experimental 2D PET data. A NEMA image quality phantom with fillable inserts of varying diameter from 37 mm to 10 mm was filled with 350 MBq of Tc-99m giving a target:background ratio of approximately 10:1. SPECT/CT acquisitions with varying projection time per view from 240 to 30 seconds were performed on a Philips Brightview XCT gamma camera. 128 x 128 and 256 x 256 acquisitions were set up to assess the impact on FLAB accuracy as a function of noise. All data sets were reconstructed using OSEM and with the Philips resolution recovery algorithm. FLAB code was generated and incorporated into a workflow set up on the Siemens Symbia.net. All inserts were segmented using this workflow. Accuracy of FLAB using OSEM was compared against FLAB with resolution recovery. Assessment of using smaller voxels was assessed. The addition of a low pass filter on pre-segmented data was also tested to determine its impact on FLAB accuracy.

Results: Preliminary results indicate FLAB is strongly dependent on the reconstruction algorithm and voxel size. Segmentation errors $e(\text{OSEM})$, and $e(\text{AST})$ ranged from 13% (37 mm sphere) to 245% (10 mm sphere) and 25% to 300% respectively. In terms of voxel size; segmentation with OSEM ranged from an accuracy of between 2 to 3 voxels difference for the 10 mm sphere and from less than 1 to 2 voxels for the 17mm and 37 mm spheres. Low pass filtering showed small changes in performance for all spheres for cut off frequencies between 0.4 and 1 cycles/cm. **Conclusion:** A systematic difference in segmentation performance was apparent between OSEM and resolution recovery. Smaller volumes could be delineated with better precision using resolution recovery. There was no significant difference between the segmentation accuracy using a 128 or 256 matrix indicating FLAB is robust to increasing statistical noise with SPECT. A degree of filtering with a low pass filter may improve delineation accuracy.

EP415

Automated segmentation of the skeleton in PET/CT scans

M. Sadik¹, **R. Kaboteh**¹, **N. Hasani**¹, **M. Landgren**², **L. Svärm**², **O. Enqvist**³, **F. Kahl**³, **L. Edenbrandt**⁴; ¹Department of Clinical Physiology, Göteborg, SWEDEN, ²Centre for Mathematical Sciences, Lund, SWEDEN, ³Dept of Signals and Systems Chalmers University of Technology, Göteborg, SWEDEN, ⁴Department of Clinical Physiology, Göteborg and Malmö, SWEDEN.

Aim: Hitherto there is no imaging biomarker included in the risk-stratification of prostate cancer patients even though it is well known that for example the extent of bone metastases assessed with diagnostic imaging methods is closely associated with survival. An automated method to calculate Bone Scan Index has recently been established as a first imaging biomarker in this field. The aim of this work is to develop new imaging biomarkers for the assessment of tumour burden to the skeleton from PET/CT images. The first step is to segment the skeleton in the CT images. **Materials and Methods:** The automated method was designed to specifically detect and segment the different bones of the thoracic and lumbar spine, pelvis, ribs, sternum, clavicle and scapula. For the classification of uptake as metastasis or benign, for example in fluoride-PET images, the exact localisation will be important. The first step of the automated method aims at approximate bone localization. A convolutional neural network is used to detect a set of anatomical landmarks. These landmarks together with a shape model are used to align an atlas to the query image. The atlas together with the image is input to a second convolutional neural network that performs the actual segmentation. CT images from 50 patients who had undergone FDG-PET/CT scans were used to develop and evaluate the segmentation method. Experienced image readers performed manual segmentations of the skeleton in the CT images. The PET/CT images were obtained with a Biograph 64/True V PET/CT (Siemens) using a low dose radiation CT. The Sørensen-Dice index was used to quantitatively evaluate the similarity between the automated and the manual segmentations as well as the similarity between two separate manual segmentations. For the purpose to compare the performance of the automated segmentation method, intra and inter observer variability in manual segmentations of the L1 vertebrae was studied. **Results:** The mean Sørensen-Dice index for comparison automated-manual methods were in these selected bones: Vertebra Th11=0.86, L1=0.87, L4=0.89, Sacrum-coccyx=0.91 Pelvic bone=0.95. The corresponding index comparing two manual L1 segmentations were 0.87 (same observer) and 0.86 (different observers). **Conclusion:** A completely automated method for 3D segmentation of the skeleton in CT images is proposed. The performance of the automated segmentation method is similar to that of experienced image readers. In future work we will use this segmentation method for the analysis of PET images based on for example sodium fluoride or choline.

EP416

Q.Freeze for Respiratory Motion Correction in PET/CT: Assessment and Optimisation with a 4D PET/CT phantom and patient data

G. Havariyoun, **E. Kalogianni**, **D. Ruiz**, **B. Corcoran**, **N. Mulholland**, **G. Vivian**; King's College Hospital NHS Trust, London, UNITED KINGDOM.

Background: PET/CT imaging of the lung and abdominal region is often affected by patient respiratory motion. This can lead to an apparent increase in tumour volume, an underestimation of tracer concentration and mismatched PET-CT images. **Purpose:** This study aimed to assess the efficacy and any optimisation requirements of a commercially available respiratory motion correction system in a clinical setting. **Materials and Methods:** The data of n=17 patients who had undergone standard 3D-PET/CT and 4D-PET/CT (n=15) or 4D-PET/4D-CT (n=2) acquisitions was retrospectively analysed. Overall n=33 lesions were considered for analysis. Furthermore, gated and un-gated acquisitions were performed with a dynamic phantom, and an in-house designed PET/CT insert, driven by patient specific respiratory traces to simulate liver and lung lesions in motion (in homogenous and heterogeneous environments). Reconstruction and acquisition parameters were varied to assess impact on image quality. Signal to Noise Ratio (SNR), Noise Equivalent Counts (NEC), maximum and peak Standardised Uptake Values (SUV) and lesion volume were assessed for gated and un-gated acquisitions. For the phantom acquisitions, results were compared to ground truth values obtained with the phantom motionless. **Results: Patient Data:** There was a significant ($p<0.05$) decrease in SUV_{max} (0.35 ± 0.70) and SUV_{peak} (0.20 ± 0.50) of the n=33 patient lesions with 4D-PET/CT (58% phase). Rejection of counts, due to non-periodic respiration, led to a significant ($p=0.006$) decrease in NEC (0.49 ± 0.64 Mcounts/m). There was a significant ($p<0.05$) decrease in SNR (2.30 ± 1.28) with 4D-PET/CT. Use of 9 or 12 subsets in the reconstruction of patient gated acquisitions increased SNR by 40% and 25% respectively. **Phantom Data:** Lung lesion: SUV_{max} increase of $2.0\pm 6.5\%$ (4D-PET/CT) and $1.8\pm 6.3\%$ (4D-PET/4D-CT). Volume decrease of $2.2\pm 6.7\%$ (4D-PET/CT) and $3.1\pm 6.4\%$. No significant difference between the SUV_{max} ($p=0.9$) and lesion volume ($p=0.06$) results obtained with 4D-PET/CT and 4D-PET/4D-CT. Liver lesion (lung-liver boundary): A statistically significant ($p=0.008$) difference in SUV_{max} obtained with 4D-PET/CT and 4D-PET/4D-CT. Excessive number of subsets used for reconstruction led to overestimation of SUV_{max} when compared to ground truth. Use of 9 or 12 subsets led to improved SUV_{max} results and decrease in background variability. **Conclusions:** The impact of respiratory motion in PET/CT is highly dependent on motion amplitude and lesion location. Results do not justify the extra radiation exposure implicated with the use of 4D-PET/4D-CT. Q.Freeze has indicated the ability to correct for respiratory motion in PET/CT imaging. However, appropriate setup and reconstruction settings are required in order to achieve this.

EP417

Performance characterization of a preclinical SPECT/MR scanner

M. Segbers, **J. de Swart**, **M. Bernsen**, **J. Haeck**, **M. de Jong**; Erasmus MC, Rotterdam, NETHERLANDS.

Aim: The Mediso nanoScan (Mediso, Budapest Hungary) SPECT/MRI integrates both modalities for the first time in a single imaging platform. In this study the performance of the SPECT subsystem has been characterized and the accuracy of MRI based attenuation correction was investigated. **Material and Methods:** For all scans $^{99\text{m}}\text{Tc}$ -pertechnetate was used. Resolution was measured using a micro Jaszczak phantom (rod sizes 0.7 - 1.5mm) at 12 different concentration levels (0.05 - 75 MBq/ml) for two sets of apertures: Standard-Whole-Body (SWB) and High-Sensitivity-Whole-Body (HSWB) apertures. We assessed system

linearity by scanning a 50-mL syringe at 24 different levels of radioactivity (between 0.03 and 50 MBq/ml) with both apertures, and the activity concentration range for which the system was linear (5% error margin). In addition, Signal-to-Noise Ratio's (SNR) were obtained for all scans by Region Of Interest (ROI) analysis. Five different syringes with varying diameters (between 1-ml and 20-ml) were scanned with the HSWB aperture using similar amounts of radioactivity (2.2 ± 0.4 MBq/ml). The Monte Carlo based reconstruction used a 3D Gradient Echo (TE/TR = 2.33/20) MRI as an attenuation map by segmenting air and water. A cylindrical ROI measurement was performed in the center of the reconstructed images, with and without attenuation correction. The ROI results were compared to the true concentration determined by a dose calibrator. **Results:** For activity levels higher than 3.2 MBq/ml in the Jaszczak phantom both apertures resolved the 0.9 mm rods, between 1.6 and 3.2 MBq/ml the SWB apertures still resolved the 0.9mm rods. Below 1.6 MBq/ml both apertures resolved the 1.0mm rods, but at 0.2 MBq/ml both collimators did not resolve any rods. The system was linear in the range between 0.07 - 54 MBq/ml and 0.2 - 64 MBq/ml for the HSWB and SWB apertures, respectively. For the HSWB apertures SNR was twice as high over almost the entire activity range (0.03 - 50 MBq/ml). Without MR attenuation correction the activity in the syringes was underestimated by on average 5%; the highest underestimation was found to be 13% for the 20-ml syringe. With attenuation correction, an overestimation of the activity concentration of on average 7% was found. **Conclusion:** The HSWB aperture showed only a small trade-off in resolution, while SNR improved by a factor of 2. The HSWB was capable of quantitative imaging for activity concentrations as low as 0.2 MBq/ml. MR-based attenuation correction led to a 7% overestimation of the activity concentration.

EP418

Evaluation of the use of 40% threshold contours for texture features computation on PET image

M. CARLES^{1,2}, I. TORRES-ESPALLARDO¹, U. NESTLE², L. MARTÍ-BONMATÍ¹; ¹Hospital Universitario y Politécnico La Fe, Valencia, SPAIN, ²University Hospital Freiburg, Freiburg, GERMANY.

Lesion heterogeneity has an impact on threshold-based segmentation on PET images. Frequently, PET studies used texture features (TF) for lesion heterogeneity characterization derived from threshold contours of 40% of tumor maximum intensity. We evaluated the use of 40%-contours for TF computation as bias in quantification of lesion heterogeneity. TF derived from 40%-contours, $TF_{40\%}$ for twenty-eight heterogeneous experimental phantoms, were compared with respect to TF derived from the ideal contour of the whole lesion, TF_{Ideal} . Heterogeneous phantoms were developed by a mixture of alginate and ¹⁸F-FDG. Imaging was performed with a PET/CT system using acquisition times of 15 min (PET) and 3.7 s (CT). Direct correspondence between alginate and FDG distribution permitted approaching VOI_{Ideal} by applying the growing region algorithm on CT image with a threshold interval of 65-135 HU. The comparisons of 8 TF (4 first order and 4 second order) were performed in terms of linear correlation (LC) and standard deviation (SD) of the relative deviation ($\delta 40\% - Ideal = 100(TF_{40\%} - TF_{Ideal}) / (TF_{40\%} + TF_{Ideal}) / 2$). $SD(\delta 40\% - Ideal)$ for conventional indexes, mean activity concentration (C_{mean}) and volume (V), was considered the criteria for reasonable stability. Results from the comparison showed that $SD(\delta 40\% - Ideal)$ for 5/8 TF were lower than for C_{mean} and for 6/8 TF were lower than for V. In addition, significant LCs ($p < 0.001$) were obtained for all TF under study, V and C_{mean} . In summary, this work presented the first evaluation of $TF_{40\%}$ with heterogeneous experimental phantoms. From the low deviation and high linear correlation obtained with respect to TF_{Ideal} , the current use of 40%-contours for heterogeneity quantification by TF could be concluded as a reasonable approach.

EP419

Optimized PET-CT acquisition and reconstruction based on patient morphology

D. Vallot^{1,2}, F. Courbon¹, L. Dierickx^{1,2}, E. Gabiache¹, S. Zerdoud¹, S. Brillouet¹, M. Bauriaud¹, O. Caselles^{1,2}; ¹Institut Claudius Regaud - IUCT Oncopole, Toulouse, FRANCE, ²SIMAD, Toulouse, FRANCE.

Aim: The aim of this study was to optimize image quality based on patient morphology and position using the new penalized-likelihood image reconstruction algorithm (Q.Clear). **Materials and methods:** In order to improve image resolution, the reconstruction field of view (FOV) was adapted to patient morphology during acquisition, based on the CT scout views (50, 60 and 70 cm). The β noise reduction factor of the Q.Clear algorithm was thus adapted to maintain homogeneous image quality for each FOV (in the range 250 to 450). First analysis was based on images acquired on a Discovery IQ PET/CT using a NEMA PET image quality phantom filled with 18F-FDG. Recovery coefficient (RC) and background variability (BV) were measured for the different reconstructions. 30 18F-FDG oncological patients exams were then analyzed. Acquisition and reconstruction protocols were as described above. Average injected activity was 159 MBq. Overall image quality comparison between optimized versus non-optimized reconstruction was evaluated by 3 experienced physicians in a blind way. **Results: Phantom study** The ratio of RC (or BV) measured for two different β values is nearly the same whatever the FOV. This result is observed for each of the six spheres. Taking into account the smaller sphere (10 mm in diameter), the statistical analysis clearly showed that both RC and BV were better adapting the β value to the FOV, confirming that spatial resolution is improved by this optimization. When comparing the different reconstructions, the higher RC for each sphere were obtained with the smaller FOV and β values, with BV values remaining in the lower specifications limits. **Clinical study** 64 % of the patients were scanned with a FOV of 60 cm. During the blinded comparison between optimized and non-optimized reconstruction, the nuclear medicine physicians always preferred the optimized one. **Conclusion:** Global image quality and image resolution have been improved adapting acquisitions and reconstructions protocols to patient specificities. Optimized settings are now implemented in clinical routine in our facility. This optimization will be evaluated in the near future for head and neck exams.

EP420

Investigation of possibilities for gamma camera imaging of patients injected with Targeted Thorium Conjugate TTC (²²⁷Th-labelled mAb)

E. Larsson¹, O. Lindén², T. Ohlsson¹, A. Cleton³, C. Hindorf¹; ¹Department of Radiation Physics, Skåne university hospital, Lund, SWEDEN, ²Department of Oncology, Skåne university hospital, Lund, SWEDEN, ³Clinical Science, Bayer Pharma AG, Berlin, GERMANY

Introduction Imaging of ²²⁷Th ($T_{1/2} = 18.7$ d) is challenging as: 1) the injected activity will be low (from 1.4 MBq), 2) the emitted photons have a relatively low yield (80-94 keV, 7%), (236 keV, 12%), (256 keV, 7%) and 3) the daughter ²²³Ra is also radioactive ($T_{1/2} = 11.4$ d). The most predominant photon energies emitted from ²²³Ra and its short-lived daughters are: ²²³Ra: (81-98 keV, 52%), (154 keV, 5.6%), (269 keV, 13.7%) and ²¹⁹Rn: (271 keV, 10.8%). The aim of this study was to investigate the possibility to separate between ²²⁷Th and ²²³Ra, and to determine acquisition settings to allow imaging of patients injected with ²²⁷Th labelled antibody-chelator conjugate. **Materials & Methods:** All acquisitions were performed on a GE Discovery 670 NM/CT gamma camera equipped with MEGP and HEGP collimators. All images were acquired in list-mode, which allows for optimization of energy windows after acquisition. Due to the low count rate, only planar imaging was evaluated. Two spheres were filled with 250 kBq/

L ^{227}Th and ^{223}Ra , respectively. Imaging was performed with the spheres placed in a Jaszczak phantom filled with air, water and with ^{227}Th (50 kBq/L) added to the water. A background image with no radioactive sources present was also acquired. **Results&Discussion:** As the signal-to-natural background is low, background subtraction has to be performed. Analyses of line profiles indicate that the HEGP collimator reduces scattered photons in the images. Four separate energy windows are identified for quantitative imaging: 1) 75-100keV; 2) 135-165keV; 3) 215-260keV; 4) 260-285keV. However, a summation of window 1 - 4 is desirable for qualitative imaging in order to improve count statistics. The phantom experiments demonstrate that ^{227}Th and ^{223}Ra can be distinguished from each other in images acquired in energy windows 3) and 4) when the sources do not overlap. The separation will improve if scatter correction is performed. In the First-in-Man trial of BAY 1862864, planar static patient images were acquired for 40 minutes at different points in time after a single injection of the TTC (1.4MBq). An X-ray scout image was acquired for fusion with the NM-image to facilitate anatomic localization. **Conclusion:** It is possible to image ^{227}Th in patients and to distinguish ^{227}Th from ^{223}Ra . Acquisition settings recommended for planar images are: HEGP collimator, 40 min acquisition time, energy windows: 1) 75-100keV; 2) 135-165keV; 3) 215-260keV; 4) 260-285keV and 5) the sum of windows 1-4. Background subtraction and filtration of the image is needed to reduce noise.

EP421

Compensation of Missing Data in Sinograms of a PET Scanner with Partial Geometry for Robust Image Reconstruction

S. Shojaeilangari, M. Ay; Research Centre for Molecular and Cellular Imaging, Tehran, IRAN, ISLAMIC REPUBLIC OF.

Purpose: Positron emission tomography (PET) is a noninvasive functional imaging technique to observe metabolic processes in the body with various clinical and preclinical applications such as cancer diagnosis, disease staging, therapeutic evaluation, and drug discovery. The partial geometry of scanners (less number of detectors for developing low cost systems) results projection incompleteness of data which leads to degraded image reconstructions. To preserve the quality of the reconstructed images, we applied an inpainting technique to projection data as a pre-processing stage before reconstruction. **Method:** The applied inpainting method is based on a penalized least squares approach using the discrete cosine transform to fill the missing data appeared in sinograms and suppress the artifacts as well. Then, various reconstruction approaches including FBP, MLEM, RAMLA, and OSEM were used to compare the quality of reconstructed images. We evaluated the method using both synthetic phantom images with simulated gap mask and real phantoms scanned in two scenarios: once with all detectors operational (baseline), and once with some detector blocks. Quantitative evaluations were performed by computing the root mean squared error and difference between the reconstructed images of non gapped and gapped sinograms, as well as computation time. **Results:** The simulation results demonstrate that the applied gap compensation approach prior to reconstruction is able to effectively control gap artifacts, as well as Poisson random noise. In particular, OSEM reconstruction after gap filling preprocessing showed promising robust results to different noise levels and gap structures. For the simulation study, the root mean squared error of recovered images for FBP, MLEM, RAMLA, and OSEM were 26.24%, 25.74%, 25.85%, and 10.56% respectively, when compared to the baseline. After adding Poisson noise and synthetic gapped structure to data without inpainting stage, these results changed to 85.11%, 35.08%, 34.95%, and 69.60% respectively. After applying the preprocessing stage, the results improved considerably which were 27.65%, 25.61%, 26.69%, and 13.53% respectively for the mentioned reconstruction algorithms. **Conclusion:** Sinogram inpainting approach prior to commonly used PET reconstruction algorithms was effective to decrease the occurrence of artifacts due to gaps between detector modules in a partial geometry PET scanner.

EP422

Detectability of small objects using digital PET

D. Koopman¹, M. L. Groot Koerkamp², H. Arkies¹, P. L. Jager¹, S. Knollema¹, C. H. Slump², P. G. Sanchez³, J. A. van Dalen⁴; ¹Isala, Department of Nuclear Medicine, Zwolle, NETHERLANDS, ²MIRA Institute for Biomedical Technology and Technical Medicine, Enschede, NETHERLANDS, ³Philips Healthcare, Eindhoven, NETHERLANDS, ⁴Isala, Department of Medical Physics, Zwolle, NETHERLANDS.

Background: Small lesion detection with FDG-PET/CT imaging is limited by the low spatial resolution of PET and the use of relatively large voxels. Recently, a prototype digital PET system (Philips Healthcare) was installed with an improved spatial resolution and faster time-of-flight performance, compared with analog PET systems. Based on the system acceptance data, we evaluated the small-object detectability of this system and compared it with a state-of-the-art analog system. **Method:** We performed a phantom study using a NEMA Image Quality phantom and a micro phantom, with sphere diameters 4-37 mm. Phantoms were filled with FDG with sphere-to-background ratio 10:1. PET/CT scans with 20 minutes scan duration were acquired on both digital PET prototype and analog PET (Ingenuity TF, Philips Healthcare). We reconstructed PET data using default reconstruction settings, with multiple voxel sizes: 4x4x4 mm³ and 2x2x2 mm³ voxels for both systems and additionally 1x1x1 mm³ voxels for digital PET. Mean and maximum contrast recovery coefficients (CRC_{mean} and CRC_{max}) were measured for all phantom spheres and percentage changes between analog and digital PET CRCs were calculated. **Results:** With digital PET, we found higher CRC_{mean} and CRC_{max} values for all spheres and all voxel sizes, in comparison with analog PET. CRCs increased more in smaller spheres and with smaller voxels. With 4x4x4 mm³ voxels, CRC_{mean} and CRC_{max} values increased with 5% and 7% respectively for spheres ≥ 13 mm while for spheres < 13 mm, these values increased with 11% and 35%, respectively. Furthermore, using 2x2x2 mm³ voxels, CRC values additionally increased up to 32% for the smallest spheres. Comparing digital PET using 1x1x1 mm³ voxels with analog PET using 2x2x2 mm³ voxels, we found CRC_{mean} and CRC_{max} increases up to 56% and 74% respectively for the smallest spheres. **Conclusion:** Digital PET produces higher CRCs as compared to analog PET, especially for small phantom spheres and with small voxel reconstructions. This suggests that the detection of small lesions may improve with digital PET. Clinical studies are needed to see the actual impact of digital PET imaging on lesion detectability.

EP-19 – Sunday, October 16, 2016, during Exhibition hours, e-Poster Area
Do.MoRe: Dosimetry

EP423

Evaluation Of Surgically Excised Non-Functioning Pan-Creatic Endocrine Tumours Followed By Radiopeptide Treatment; To Optimise PRRT, Aiming To A Longer Term Survival

G. S. Limouris¹, G. P. Fragulidis¹, I. Karfis¹, M. Paphiti², D. Voros¹, L. E. Mouloupoulou¹, R. V. McCready²; ¹National and Kapodistrian University of Athens, Athens, GREECE, ²Royal Sussex County Hosp, Brighton, UNITED KINGDOM.

Aim: We first report on adjuvant peptide receptor radionuclide therapy (PRRT) in 18 non-functional pancreatic neuroendocrine tumours (NF-PNETs) followed surgical lesion excision as an adopted technique in our Institution, aiming to optimize PRRT for a longer term survival. **Materials and methods:** Eighteen NF-PNETs received adjuvant PRRT i.a., after transhepatic infusions; 6 of them received ¹¹¹In-Octreotide, in a dosage of 4.0 -7.0 GBq, (12 cycles with treatment intervals of 5-8 weeks) and 12

n.c.a. ^{177}Lu -DOTATATE in a dosage of 7.4 GBq (6 cycles with treatment intervals also of 5–8 weeks), following their surgical excision as first-line treatment. Twelve patients underwent pancreato-duodenectomy and 6 distal pancreatectomy and splenectomy. Intraoperative Liver Ultrasonography was performed to enhance missed lesion detection. Liver metastases were present in 7 patients [3 bilobar, 4 unilobar]. The latter underwent hemihepatectomy or segmentectomy; in bilobar patients, concomitant major hepatectomy was planned and were subjected to pre-operative evaluation of the future liver remnant by Indocyanine Green clearance test. Prophylactic cholecystectomy was planned to obviate adverse events due to the use of somatostatin analogues. Response assessment was classified according to the RECIST criteria. Absorbed doses delivered to metastases, kidneys and red marrow were calculated according to OLINDA 1.0 program. CT/MRI were performed before and after the end of treatment and monthly US images for follow up. **Results:** In all 18 cases immediately resulted in a significant down slowing of the tumour aggressiveness clinically and biochemically confirmed, accelerating the therapeutic efficacy, prolonging the survival rate assessed by Kaplan-Mayer curves. Follow-up for 34 months compared to an other 17 patients cohort without surgical exeresis, the disease stabilisation was significantly lower in a 13% ($p < 0.05$) in favour to the partial remission. **Conclusion:** In pts with metastatic liver-lesions, scheduled for surgical exeresis complementary, adjuvant radiopeptide therapy slows down the tumour aggressiveness, accelerates the therapeutic efficacy and improves the patients RECIST score assessment in favour to the partial remission scoring. The drawback of the concept is that surgical lesion debulking lurks the danger of tumour dissemination. The latter drives us to the skepsis that P R R T should precede the scheduled surgical excision by a therapeutic scheme of 2–3 cycles of n.c.a. ^{177}Lu -DOTATATE for tumour ablation.

EP424

^{117m}Sn colloid as a potential candidate to replace ^{169}Er colloids in radiosynovectomy of small joints

K. Liepe¹, J. Lattimer², K. Selting², A. Bendele³, J. Simon⁴; ¹Klinikum Frankfurt, Frankfurt (Oder), GERMANY, ²University of Missouri, Columbia, MO, UNITED STATES, ³Bolder BioPath Inc, Boulder, CO, UNITED STATES, ⁴IsoTherapeutics Group, LLC, Angleton, TX, UNITED STATES.

Abstract: Radiosynovectomy or radiosynoviorthesis (RSO) is a common therapeutic treatment of arthritis in Germany and in many other countries. In this regard, ^{169}Er is universally used for the therapy of small joints but its availability is limited particularly outside of Europe. The dosimetry characteristics of ^{117m}Sn and ^{169}Er are very similar therefore making ^{117m}Sn an ideal replacement for this application. **Methods:** In a safety trial 5 dogs were injected the left elbow using 93 ± 2 MBq of ^{117m}Sn colloid. The animals were sacrificed after 49 ± 1 day's ($> 3 * t_{1/2, \text{phys}}$) and the amount of activity in the dissected tissue was measured. **Results:** $99.19 \pm 0.36\%$ of administered activity (%ID) was determined to be in the synovia of the treated joints despite multiple prior synovial punctures. The majority of the radiocolloid that was found outside the treated joint was in the liver ($0.70 \pm 0.36\%$ ID), significant lower are the %ID in local lymph node at treated site ($0.07 \pm 0.03\%$ ID) and spleen ($0.01 \pm 0.07\%$ ID). Over the follow-up period $0.06 \pm 0.02\%$ ID was found in blood, faces and urine within the first 14 days; $0.75 \pm 0.38\%$ ID in organs outside the joint after 45 days. In postmortem autoradiographic studies most of activity was found in the macrophages of sub-synovial tissue and less commonly in a few other locations (synovial lining cells, macrophage-like cells and macrophages). **Summary:** ^{117m}Sn colloid is useful in RSO of small joints with a high target dose and very limited dose outside the joint. Autoradiographic studies documented a fixed uptake in macrophages by phagocytosis. These macrophages were found in all layers of the synovium, which showed transportation of ^{117m}Sn colloid from the surface to varying depths. This opens up the possibility of treating larger joints.

EP425

Effectiveness of radiosynovectomy with Re-186 and P-32 colloid in a single study for chronic hemophilic synovitis : A Preliminary result

M. Amoui¹, R. Naghshine¹, P. Eshghi², S. Akhlaghpour³, M. Hakiminezhad¹, M. Hakiminezhad¹; ¹Shohada-e Tajrish Hospital-Shahid Beheshti University of medical Sciences, Tehran, IRAN, ISLAMIC REPUBLIC OF, ²Pediatric congenital hematologic disorders Research Center - Mofid hospital- Shahid Beheshti University of Medical Sciences, Tehran, IRAN, ISLAMIC REPUBLIC OF, ³Pardis-e Noor Medical Imaging center, Tehran, IRAN, ISLAMIC REPUBLIC OF, ⁴Students' Scientific Research Center-Tehran University of Medical Sciences, Tehran, IRAN, ISLAMIC REPUBLIC OF.

Bleeding in joint is a common complication of hemophilia. Repeated bleeding could lead to chronic synovitis followed by irreversible damage and severe loss of joint function within first or 2nd decades of life. Radiosynovectomy (RSV) is a non-surgical procedure to deactivate synovium and preserve joint function by beta emitting radiopharmaceuticals. The common radiotracers are P-32 and Y-90 in United States and Canada and Re-186, Y-90 and Er-169 in Europe. These agents are selected by accessibility, physical properties of radiocolloids and joint size. This ongoing study evaluates the efficacy of locally produced P-32 and Re-186 radiocolloids in chronic hemophilic arthritis. In addition, this is the first experience of RSV with Re-186 colloids in Iran and to our knowledge, the first analysis of these two radiocolloids in a single study. **M & M-**Hemophilic patients were referred for RSV with poor response to clothing factor prophylaxis. It has been performed with 10–37 MBq P-32 or 37–74 MBq Re-186 radiocolloids. Episodes of joint bleeding was assessed after one year (mean : 22 months). Appropriate response was defined as non-target joint. Clotting factor consumption and physical activity were evaluated, as well. **Results-**Thirty-seven patients (mean age: 14. yrs. - Range: 2–36 yrs.) with 51 joints were enrolled. Sonography-guided RSV was carried out with P-32 in 28 cases (knee:14, ankle:4, elbow:9, Shoulder:1) and Re-186 in 23 cases (ankle:15, elbow:8). Six cases were excluded (2 cases due to patient's decease secondary to intracranial hemorrhage and 4 others due to patient's unavailability). Appropriate response was seen in 29 cases (65%) and target joint remained in 16 cases (35%). This response rate doesn't correlate with joint type (P value=0.155), grade of synovitis (P value=0.068) or serum anti-factor (P value=0.959). No statistically difference was noted between two radiocolloids (P value=0.669 for identical joints). Presence of DJD correlated with poor response to therapy (P value=0.02). RSV was repeated in 7 cases which showed appropriate response in 4 cases (57%). More than 50% of factor reduction was noted in 84% of cases with complete stop in 25% of all cases. Physical activity was improved in 73% of cases. **Conclusion:** RSV is an effective method to stop or reduce episodes of bleeding, achieved with a single injection of radiotracer in an out-patient setting. It could be performed with Re-186 or P-32 radiocolloids depending on availability with similar results. Keywords: joints, orthopedics, radiation, phosphorus, radioisotopes

EP426

The Evaluation of Patients with Diffuse Pigmented Villonodular Synovitis of Knee with Functional Scoring Systems After Surgery and Radiosynovectomy

H. I. ATILGAN¹, M. SADIC², M. H. OZSOY³, M. KORKMAZ², O. FAKIOGLU⁴, A. A. BASKIN², K. DEMIREL², R. ORAK⁵, G. KOCA²; ¹Kahramanmaraş Necip Fazıl City Hospital, Kahramanmaraş, TURKEY, ²Ministry of Health Ankara Training and Research Hospital, ANKARA, TURKEY, ³Memorial Ankara Hospital, ANKARA, TURKEY, ⁴Hatay Dörtöyl State Hospital, Hatay, TURKEY, ⁵Istanbul Haydarpaşa Numune Training and Research Hospital, Istanbul, TURKEY.

Aim: To evaluate the symptoms and functional status of patients with pigmented villonodular synovitis (PVNS) of the knee using the modified Marshall scoring system and musculoskeletal tumor society (MSTS) rating scale before therapy and six months after radiosynovectomy (RS).

Materials and methods: Evaluation was made of 29 knee joints of 29 patients with DPVNS. Arthroscopic synovectomy was applied to all patients and additional posterior open synovectomy to five. Yttrium-90 (Y-90) citrate colloid was used in the RS procedure. RS was performed 11.8±13.3 weeks after the operation. In the six months after RS, patients were evaluated with the modified Marshall scoring system and MSTS rating scale. **Results:** The patients were 17 females and 12 males with a mean age of 31.8±12.9 years (range: 13–54 years). The preoperative modified Marshall score was poor in 24 patients and fair in five patients. In the follow-up period, the scores were excellent in 17 patients, good in 10 patients and fair in two patients. The mean modified Marshall scores increased after the operation and RS from 12.93±2.93 to 25.52±2.90 ($p<0.001$). The mean MSTS scores increased from 17.52±4.82 to 26.86±2.46 ($p<0.001$). In one of four patients with a score of 22 and three patients with a score of 24, maximum scores were obtained in the follow-up period with the effect of surgery and RS. **Conclusion:** RS with Y-90 citrate colloid after surgical excision in the treatment of PVNS is a reliable and efficient treatment method for the increase of functional capacity and decrease of symptoms.

EP427

Biological Therapy and Radiosynoviorthesis in Patients with Rheumatoid Arthritis and Psoriatic Arthritis

M. Szentesi, III, P. Géher, III; Semmelweis Univ., Budapest, HUNGARY.

Objectives: During biological therapy sometimes 1 or 2 joints could be affected by inflammation. In this cases always the question is how to solve the problem. Change of the biological or basic therapy, use surgical synovectomy or radiosynovectomy (RSO).

Patients and Methods: In our reumatological department 2100 patients with RA and PA were treated with biological therapy between 2002 and 2015. In 100 patients we applied RSO because of the inflammation of the knee joint during biological therapy. We made a long term follow-up in 72 patient. All participants provided written informed consent. 62 participants inflammatory knee joint disease was diagnosed on the basis of the American College of Rheumatology. 55 of 62 patients with rheumatoid arthritis were seropositive, 7 seronegative. Steinbrocker functional stadium II was observed in 52, stadium III in 10. 10 patients were psoriatic arthritis. Mean age of 13 male and 61 female patients was 51.4 years (range 24–79) years. In 38 patients the right knee, in 34 the left knee was treated by radiosynovectomy. Mean duration of disease was 7.3 years (range 0.5–25), of synovitis (6.3month (range 3–8) Mean number of punctions of the treated joint prior to radiosynovectomy was 4,2 per patient and of steroid administrations prior to radiosynovectomy 3,0. In 12 patients a systemic steroid therapy has been performed. **Results:** During the study period, inflammation decreased. In the first two years excellent and good results were recorded in 82,2%. Two years after radiosynoviorthesis 83.3% of patients did not need another puncture. Before the knee inflammation patients were in complete remission which status has been achieved after RSO as well. DAS: 2,4+–0,4. **Conclusions:** 1. RSO is an effective method to treat the inflammation of the knees. 2. The RSO performed during biological therapy is as effective as in the case of patients without biological therapy. 3. In case of a successful RSO there is no need for biological or basic therapy neither for surgical synovectomy. 4. However an intraarticular injection has a low risk for infection it is recommended to avoid the biological therapy during the RSO.

EP428

²²³Ra-dichloride SPECT and planar quantitative images for targeted alpha-emitting therapy of bone metastases

N. Benabdallah¹, M. Bernardini², C. de Labriolle-Vaylet³, D. Franck¹, A. Desbrée¹; ¹Institut de Radioprotection et de Sûreté nucléaire, Fontenay-aux-Roses, FRANCE, ²Nuclear Medicine Department, Hôpital Européen Georges Pompidou, Paris, FRANCE, ³UPMC, Univ Paris 06 Biophysics - Nuclear Medicine Department, Hôpital Trousseau, Paris, FRANCE.

Purpose: ²²³Ra-dichloride (Xofigo®, Bayer HealthCare) is the first alpha-emitter radiopharmaceutical that has received approval for the treatment of patients with castration-resistant prostate cancer metastasized to bones. This radiopharmaceutical mimics calcium and forms complexes with the bone mineral hydroxyapatite at areas of increased bone turnover such as bone metastases. To better determine the dose-limiting toxicities to bone marrow due to this new therapy and correlate absorbed dose to therapeutic response, patient-specific dosimetric studies are required. To that aim, it is necessary to compare ²²³Ra-dichloride uptake to bone lesion locations and its quantitative biodistribution into the bone by ²²³Ra emission images. The purpose of this study was to investigate the possibility of quantitative SPECT imaging of ²²³Ra to enable accurate activity quantification. **Methods:** The gamma camera imaging parameters were determined by measuring sensitivity, spatial resolution and energy spectrum, with a syringe containing 240 kBq of ²²³Ra. SPECT/CT images of a NEMA Phantom (60 projections, 360° rotation and 30s per view) were realized to determine the best reconstruction parameters available on clinical software. Finally, the accuracy of quantitative SPECT imaging was investigated using an anthropomorphic TORSO phantom containing a cylindrical insert and 3 spherical spheres. **Results:** The results from the basic imaging parameters showed that the 85 keV ± 20%, 154 keV ± 20% and 270 keV ± 10% energy windows are the more suitable for ²²³Ra imaging. The sensitivity of the gamma camera in the 3 combined windows was 155.4 cps/MBq. The parameters giving the optimal volumetric and the optimal quantitative reconstructions were determined. The phantoms study showed that activity could be quantified to within 36 % for a 3.7 cm diameter sphere without background activity and the lowest ratio (ratio of 6 between spheres and background) could be quantified to within 39%. **Conclusion:** Absolute quantitative ²²³Ra SPECT imaging is achievable with careful attention to the scatter and attenuation correction and system calibration. With this study, a clinical protocol has been established. Further studies on patient images will now be performed to confirm these findings, which will open the door for patient-specific ²²³Ra treatment planning.

EP429

Baseline ^{99m}Tc-DPD Distribution Can Predict Bone Marrow Toxicity in Patients Undergoing ²²³Ra-Dichloride Therapy

F. Fiz¹, S. Sahbai¹, C. Campi², M. Piana², G. Sambuceti³, C. la Fougère¹; ¹Nuclear Medicine Unit, Department of Radiology, University of Tübingen, Tübingen, GERMANY, ²Department of Mathematics, University of Genoa, Genoa, ITALY, ³Nuclear Medicine Unit, Department of Health Sciences, University of Genoa, Genoa, ITALY.

Rationale: ²²³Ra-Dichloride, owing to its prevalent alpha-emission, allows treating skeletal localizations from castration-resistant prostate cancer (CRPC), with limited bone marrow radiation exposure. However, given the impaired bone marrow (BM) reserve in patients with multiple CRPC bone metastases, hematologic toxicity is possible and relatively frequent. Predicting the occurrence of BM dysfunction would allow a better tailoring of treatment protocols. In order to do so, we applied a computational analysis application to ^{99m}Tc-DPD SPECT/CT images, to compare tracer distribution to trabecular bone to subsequent hematological parameters variation. **Patients and Methods:** Images from forty-two ^{99m}Tc-DPD SPECT/CT scans of CRPC patients before ²²³Ra-Dichloride

therapy were analyzed with a dedicated software application, which automatically separated trabecular bone from the remaining osseous components (including the external cortical compact bone and osteoblastic areas). It then extracted the blood-pool corrected counts (target-to-background ratio, TBR) from trabecular bone in the co-registered SPECT images. Axial and appendicular bones were considered separately. Thereafter, percent decrease of leukocytes and platelets was assessed after three/six ^{223}Ra -Dichloride cycles (%WBC3 and %WBC6; %PLT3 and %PLT6, respectively). These indexes were related to TBR within trabecular volume and to presence of appendicular disseminated disease (>5 foci at visual analysis). **Results:** Axial TBR was positively correlated with both %WBC3 and %WBC6 ($R=0,54$ and $R=0,53$, respectively, $p<0,01$); the same behavior was observed for appendicular TBR ($R=0,46$ and $R=0,42$, $p<0,05$). Correlation between TBR and %PLT3 was looser ($R= 0,34$ and $0,37$, for axial/appendicular bones $p<0,05$); yet, it became more evident at the %PLT6 time-point ($R=0,4$ and $R=0,5$; $p<0,05$ and $p<0,01$). Presence disseminated appendicular metastases purported a greater leukocytes decrease ($p<0,001$ and $p<0,01$ for %WBC3 and %WBC6, respectively). Moreover, standard deviation of TBR values in appendicular bones correlated with %PLT6 ($R=0,57$, $p<0,01$) and with %PLT3-6 ($R=0,49$ and $0,46$, $p<0,05$). **Conclusions:** Radiotracer uptake detected in correspondence of axial trabecular skeleton, where active BM is normally housed, correlates with occurrence of hematopoietic toxicity, especially in the long term. Tracer distribution to the appendicular trabecular bone seems to play a somewhat less important role in hindering hematopoietic turnover. Conversely, presence of active disease in the appendicular skeleton strongly predicted a worsened BM function after therapy, emphasizing the role of appendicular BM reactivation in patients with massive axial skeleton osteoblastic reaction. These data support the use of computational techniques in predicting the possible occurrence of BM toxicity and in dose tailoring.

EP430

Dosimetric evaluation of ^{177}Lu -exendin: feasibility for therapy of insulinomas

I. van der Kroon¹, T. Jansen¹, W. Wietske¹, M. Brom¹, L. Joosten¹, C. Frielink¹, M. W. Konijnenberg², D. Wild³, M. Gotthardt¹, E. P. Visser¹; ¹Radboudumc, Nijmegen, NETHERLANDS, ²Erasmus Medical Centre, Rotterdam, NETHERLANDS, ³University Hospital Basel, Basel, SWITZERLAND.

Aim: Although diagnosis of insulinomas is relatively easy, surgical removal is more difficult and is associated with a morbidity of 35%. The glucagon-like peptide-1 receptor, which is highly expressed on most insulinomas, is a promising target for non-invasive treatment. In this study, the potential of ^{177}Lu -exendin as a therapeutic radionuclide to treat insulinomas was investigated. To calculate the absorbed dose to the organs and to the islets of Langerhans, a combined organ scale and small scale dosimetry model was used. **Materials and Methods:** Time-integrated activity coefficients for whole body and kidneys were determined from time series of planar ^{111}In -exendin scintigraphy images acquired in a previous study of 5 healthy subjects and 5 type 1 diabetes patients. Tumor time-integrated activity coefficients were obtained from serial ^{111}In exendin SPECT/CT images ($n=2$). Finally, pancreas and islet time-integrated activity coefficients were obtained from a preclinical study in rats. Organ and tumor absorbed doses were calculated using OLINDA/EXM, whereas for islet doses Monte Carlo (MC) simulations were performed. To predict the doses delivered by ^{177}Lu -labelled exendin from the ^{111}In -exendin data, the biological behavior (biodistribution, clearance) for both radiopharmaceuticals was assumed to be equal. The differences in half lives, particles emitted with corresponding energies and relative yields between ^{111}In and ^{177}Lu were accounted for by adaptation of the time-integrated activity coefficients, by changing the S-values, and by using the results of ^{177}Lu -based MC calculations for the

islets. **Results:** The insulinoma absorbed dose per unit administered activity of ^{177}Lu varied between 3.9 and 9.3 mGy/MBq. For the kidneys, this range was 12.9 - 20.5 mGy/MBq. The ranges for the pancreas and the islets were 0.09 - 0.22 mGy/MBq, and 0.62 - 2.27 mGy/MBq, respectively. In case the kidneys are considered as the dose limiting organ with a maximum absorbed dose of 27 Gy [1], the maximum dose that could be delivered to the insulinomas would be about 19 Gy, obtained by administering 2.1 GBq of ^{177}Lu -exendin. The maximum islet absorbed dose would then approximately be 4.6 Gy, which is below the value of 10 Gy, as reported in ref[2] as the threshold above which 16% of the patients developed diabetes after >20 years due to beta cell damage. **Conclusion:** A maximum insulinoma dose of about 19 Gy could be reached using ^{177}Lu -labelled exendin, which could be sufficient for a treatment effect. [1] Wessels et al. J Nucl Med 2008;49(11):1884-99. [2] de Vathaire et al. Lancet Oncol 2012;13(10):1002-10.

EP431

Patient-Specific Dose Estimation of $^{99\text{m}}\text{Tc}$ -Hynic-Tyr³-Octreotide in Children

X. Hou¹, B. Birkenfeld², H. Piwowska-Bilska², A. Celler¹; ¹Department of Radiology, University of British Columbia, Vancouver, BC, CANADA, ²Nuclear Medicine Department, Pomeranian Medical University, Szczecin, POLAND.

Aim: Technetium-99m-hydrazinonicotinamide-Tyr³-octreotide ($^{99\text{m}}\text{Tc}$ -Hynic-TOC) is recognized as a promising alternative to ^{111}In -diethylenetriaminepentaacetic acid (DTPA)-octreotide for diagnosing neuroendocrine tumors (NETs). However, its radiation dosimetry information is limited and only concerns adults. As importance of pediatric radionuclide diagnostic procedures and therapies increases, similar dosimetric studies for children need to be performed. Thus, in this study we report the patient-specific 3-dimensional biodistribution and radiation dosimetry for children using $^{99\text{m}}\text{Tc}$ -Hynic-TOC. **Materials and Methods:** Eight children/teenage patients (ages 3-17 years) with suspected or diagnosed NETs were enrolled in this study. Patients imaging included a series of 2-3 whole-body planar scans and SPECT/CT performed using GE Hawkeye camera over 2-24 hours after the injections of $^{99\text{m}}\text{Tc}$ -Hynic-TOC. Additionally, one patient had a 30min dynamic scan. Patient and organ-specific time-activity curves for kidneys, liver, spleen and tumors (4 patients, 5 lesions) were determined from the series of whole-body scans. Our iterative adaptive threshold method was used to determine organs' volumes and absolute activities from images reconstructed using SPECT/CT data with quantitative corrections. Subsequently, the time-integrated activity coefficients (TIACs) were obtained by rescaling the time-activity curves based on the absolute activity values. Individual organ doses were calculated based on the Voxel-S value approach. All image analysis and dose calculations were performed using our dosimetry software, JADA. A hybrid planar/SPECT option was used to estimate TIAC for organs/tumors and to perform dosimetry analysis. Estimated children doses were compared with adults' dosimetry (Grimes et al JNM2011). **Results:** The average values of children's TIAC were 0.18 ± 0.08 (0.08-0.35), 0.33 ± 0.12 (0.17-0.53), 0.78 ± 0.26 (0.42-1.19) Bq·h/Bq for the kidneys, spleen and liver, respectively. The uptake time-activity curves, as determined by a 30-min dynamic planar scan, showed maximum uptake at 1 min to 1.5 min for spleen and liver, respectively, and slower, about 7min, for kidneys. The average doses per injected activity were 0.033 ± 0.010 (0.020-0.050), 0.024 ± 0.012 (0.011-0.048) and 0.016 ± 0.008 (0.004-0.027) mGy/MBq for kidneys, spleen and liver, and 0.008 ± 0.003 (0.006-0.012) mGy/MBq for tumors. In general, no statistical differences were noted between children of different

ages; however, significant dose differences were found between different patients. The children doses were very similar to those for adults. **Conclusion:** In this study, we report biodistribution and dosimetry information for children injected with ^{99m}Tc -Hynic-TOC for diagnosis of neuroendocrine tumors. No significant differences were found between children doses and those previously reported for adults. However, substantial disparity between different patients emphasizes the importance and necessity for patient-specific dosimetry.

EP432

Comparative Investigation of Internal Dose Calculation Methodologies

W. Lehnert, K. Schmidt, S. Kimiaei, M. Bronzel, A. Kluge; ABX - CRO advanced pharmaceutical services GmbH, Dresden, GERMANY.

Objectives The need for individual patient dosimetry is increasingly perceived as relevant for patient care in radionuclide therapy (2013/59/EURATOM). Different methodologies for dose calculation exist and their accuracy is an important factor in dosimetry. In this work we aimed (1) to compare two phantom-based safety dosimetry dose calculation tools, the ICRP-endorsed IDAC 1.0 package, and OLINDA/EXM 1.1, and (2) to investigate Voxel S dose calculation. All evaluations were performed using QDOSE, a comprehensive software solution allowing for direct comparison of different methodologies. **Methods** For safety dosimetry, the software tools IDAC 1.0 and OLINDA/EXM 1.1, which are both based on the stylized Cristy-Eckerman phantom series, were compared for patient data acquired with ^{177}Lu -Dotatoc (mean of large patient collective) and ^{177}Lu -Dotatate (3 patients with 4 therapy cycles each). For ^{177}Lu -Dotatate the absorbed doses to kidneys were also compared to Voxel S. **Results** Comparing IDAC 1.0 to OLINDA/EXM 1.1, the differences in absorbed doses to all organs for ^{177}Lu -Dotatoc were within 2%, except for the remainder body (4.8%) and red marrow (31.6%) when kidneys, spleen and remainder body were included as source organs. If red marrow was included as a source organ, the dose to red marrow calculated with IDAC was lower than with OLINDA/EXM, with a maximum difference of -27.5%. Absorbed doses to the kidneys for ^{177}Lu -Dotatate varied from -0.83% to 1.35% between IDAC and OLINDA/EXM. Differences of -24.2% to 27.1% were observed between OLINDA/EXM without and with individual kidneys mass adaption. Voxel S doses were -8.17% to -13.7% lower than doses calculated with OLINDA/EXM using kidneys mass adaption. **Conclusions** In general, the differences between IDAC 1.0 and OLINDA/EXM 1.1 are small, but in either case using individual target organ masses for dose calculation is advisable. The observed larger differences are related to a red marrow correction implemented in OLINDA/EXM while IDAC follows MIRD and assumes only self-absorption for electrons. The successor IDAC 2.0 uses the ICRP reference phantom and will incorporate measured absorbed fractions for electrons and therefore surpass the previous limitations. The differences in absorbed dose for Voxel S compared to OLINDA/EXM and IDAC could be partly related to differences in geometry between individual patients and the stylized reference phantom. However, similar differences were previously seen for spherical objects between Voxel S and the spherical model (OLINDA/EXM) indicating Voxel S to be more accurate due to improvements in the Monte Carlo code EGSnrc (DOSXYZnrc) used for the Voxel S Generation.

EP433

Patient dose comparison between GATE Monte Carlo voxelized dosimetry and MIRD method

J. Kim¹, M. Lee², K. Kim², J. Lee², C. Yi¹; ¹Korea Research Institute of Standards and Science, Daejeon, KOREA, REPUBLIC OF, ²Seoul National University, Seoul, KOREA, REPUBLIC OF.

The aim of this study was estimation of radiation dose using GATE voxelized dosimetry and compare the simulated dose results with dose from the MIRD method estimated by Olinda software. Three patient data (60.7 ± 10.7 kg, 53.7 ± 13.5 years old, 1F:2M) were retrospectively analyzed in this study. For all patient, PET/CT scans were performed after IV injection of 166.5 ± 14.0 MBq of ^{68}Ga -RGD. Eight serial PET emission scans (30, 30, 30, 45, 60, 180, 180 and 300 sec/bed; 5 beds) were performed during 90 min. Gate Monte Carlo (MC)-based voxelized dosimetry simulations were performed using CT images (attenuation information) and PET images (radio-pharmaceuticals distribution). Eight serial PET scans yield eight serial radiation dose map. Finally, we obtained patient dose distribution using dose maps and time information. For comparison, radiation dose from MIRD method were also accessed. Regions of interest (ROIs) were drawn for 5~7 organs, i.e. gall bladder, kidney, liver, lungs, pancreas, spleen and stomach. Radiation dose for each organs were evaluated by injected dose normalized cumulated activity (residence time) and OLINDA software. For the patient who have heavier weight than standard MIRD phantom (63 vs. 57 kg, female), the estimated dose from MIRD method were over-estimated by 7.6% than MC simulation. For the other two patients who have righter weight than standard MIRD phantom (49 vs. 57 kg, female; 70 vs. 73 kg, male), the estimated dose from MIRD method were severely underestimated by 47.5% and 40.5% than MC simulation. Estimated radiation dose from MIRD method were significantly under-estimated for righter patient than MIRD model. Fixed weight of standard MIRD phantom causes large estimation error. For the patient specific dosimetry for each individual, MC-based estimation is strongly recommended.

EP434

Biokinetics and Dosimetry of ^{99m}Tc -MAG3 scans in infants

J. Soares Machado, J. Tran-Gia, S. Schlögl, M. Lassmann; University of Würzburg, Department of Nuclear Medicine, Würzburg, GERMANY.

AIM: Renal scans are among the most frequent exams performed on infants. This patient group is classified as “high risk group” with a high probability for developing stochastic radiation effects. As there are only limited data on the biokinetics and dosimetry in this patient group, the aim of this study was to reassess the dosimetry for infants undergoing ^{99m}Tc -MAG3 renal scans based on a retrospective analysis of existing patient data. **METHODS:** Two physical kidney phantoms based on the data of MIRD pamphlet 19 (Bouchet et al., JNM 2003) (newborn: 8.6ml, 1-year-old: 23.4ml) were designed and fabricated with a 3D printer (Renkforce RF1000) for retrospectively calibrating planar gamma camera images (Siemens E-Cam Signature). The kidney phantoms were filled with ^{99m}Tc (newborn: 9.5MBq, 1-year-old: 22.9MBq) and placed inside a water-filled torso phantom (IEC 61675-1). For each acquisition, bed and detector were set to the same position whereas the kidney-depth inside the torso was varied between 8.2cm, 11.7cm and 15.2cm for determining a depth- and size-dependent calibration function. Were retrospectively analyzed data of 10 patients (8 males and 2 females; age: 1.6 to 13.2 months) with normal kidney function who had undergone renal scans (mean activity: 17.4MBq ^{99m}Tc). All scans were planar, dynamic, centered at the patients’ kidneys and started at the bolus injection with durations of up to 35 minutes. The activity in the planar images was quantified by inserting the counts obtained in a ROI analysis of the kidneys, the bladder and the whole-body (including adequate background ROIs) in the calibration function. The patient-specific organ sizes and depths were obtained from ultrasound data. The organ-specific time-activity curves were integrated to obtain the time-integrated activity coefficients (TIACs). Based on these data, absorbed-dose and effective-dose coefficients were assessed with OLINDA/EXM for the newborn and the 1-year-old phantoms. **RESULTS:** The mean TIAC values for kidneys, bladder and WB were 0.11 ± 0.08h, 1.29 ± 1.07h, and 0.75 ± 0.48h. The mean absorbed-dose coefficients of kidney and bladder were 0.06mGy/MBq and 0.36mGy/

MBq (newborn), and 0.03mGy/MBq and 0.24mGy/MBq (1-year-old), respectively. Compared to ICRP publication 128 (Ann. ICRP 44, 2015), the kidney absorbed-dose coefficients for the 1-year-old were 43.3% higher whereas the bladder absorbed-dose coefficients were 35% lower (no data is available for newborns). Related to the effective-dose coefficients, the mean value was 14.5% lower. **CONCLUSION:** By introducing a novel approach of quantitative planar imaging, this retrospective analysis provides new data on biokinetics and dose assessments to infants after renal scans with ^{99m}Tc -MAG3.

EP435

Evaluation of response of ^{90}Y citrate radiation synovectomy in hemophilic joint arthropathy

A. KAMRA, S. PAWAR, J. KALE, C. S. M. DESAI, S. MOHANTY; SETH GS MEDICAL COLLEGE AND KEM HOSPITAL, MUMBAI, INDIA.

Aim- Arthropathy is a frequent complication of repeated intra-articular bleeding in patients with hemophilia; causing pain, deformity, and disability. The purpose of study was to assess the response of intra articular ^{90}Y citrate therapy in hemophilic joint arthropathy and evaluate the reduction in the reaction of proliferated synovium and subsequently repeated bleeding episodes. **Materials and Methods-** 20 joints (17 knees, 2 elbows and 1 ankle) were selected for radiation-synovectomy with repeated (>3) intra-articular bleeds over six months causing disability and restriction of movement. They were injected intra-articularly with ^{90}Y -citrate (185MBq in knee joint and 111MBq in elbow and ankle joints). The intra-articular localization of ^{90}Y -citrate was confirmed using Bremsstrahlung radiation; planar and SPECT-CT images. The joints were immobilised for 72 hours in static splints using adequate compression and regular ice packs application. The patients were given cover of relevant and proportionate factor before and after the intra-articular injection. All patients were followed up for period of 6 to 18 months for response evaluation in terms of number of bleeding episodes, pain and movement pre and post therapy. **Results-** Out of 17 knees, in 10 knees number of bleeding episodes reduced from an average of 21 times per six month to 2 times in 6 months and in 7 knees number of bleeding episodes reduced from an average of 18.84 times per 6 months to no bleeding till date. Out of 2 elbows, bleeding reduced from an average of 12 times in 6 months to 2 times per 6 months. The single ankle joint treated, showed reduction in bleeding episodes from 12 times in 6 months to no bleeding. All joints show reduction in pain from 4-10 to 0-8 on the Visual Analogue Scale. Out of 17 knees, 8 knees showed improvement in mobility due to reduced frequency of bleeds, 9 knees showed no improvement in movements due to development of advanced stage of arthritis. Out of 2 elbows, one showed improvement and other showed no improvement in movement. The single ankle joint treated showed significant reduction in bleeds, also had significant improvement in the joint range. The two tailed test showed statistically significant results ($P < 0.0001$) for reduction in number of bleeding episodes post radiation-synovectomy. **Conclusion-** ^{90}Y -citrate therapy is an efficient treatment in the hemophilic joints in reducing the number of bleeds, reduction in pain and improvement in the mobility of the joint treated.

EP436

Sn-117m colloid distribution and autoradiography in the normal canine elbow

G. R. Gonzales¹, J. Simon², S. Gonzales², A. Bendele³, C. Doerr¹, N. R. Stevenson¹; ¹R-NAV, LLC, The Woodlands, TX, UNITED STATES, ²IsoTherapeutics, LLC, Angleton, TX, UNITED STATES, ³Bolder BioPATH, Boulder, CO, UNITED STATES.

OBJECTIVES: To determine the physical distribution and autoradiographic cellular distribution of a homogeneous Sn-117m colloid (HTC) injected into normal canine elbow joints. **METHODS:** Sn-117m ($t_{1/2} = 14\text{d}$) is considered to be a small sized joint radiosynoviorthesis (RSO) therapeutic with a conversion electron energy of ~140 keV and a tissue range of 300 μm . A HTC was injected into the elbows of 5 normal dogs at the University of Missouri School of Veterinary Medicine. The joints were then collected after ~3 half-lives for sectioning and microscopic evaluation. Elbows from the 5 dogs were decalcified for 14 days and processed for paraffin embedding and sectioning. Half of the sections were stained with Toluidine Blue. The remaining paired sections were dipped into KODAK Autoradiography (AR) Emulsion, air dried and placed into a light-tight box. Slides were then sequentially prepared and submerged in KODAK Developer D-19, distilled water, KODAK fixer and again in distilled water. Toluidine Blue stained slides were then paired with their adjacent AR slides and examined. **RESULTS:** Two of 5 elbow sections had mild and one of 5 had minimal, focal synovial and/or subsynovial macrophage infiltration in the anterior surface of the distal humerus opposite to the olecranon. The remainder of the synovium and subsynovial tissues were generally unremarkable and without inflammation, although a few small foci of macrophage accumulations were observed. There were no microscopic changes in articular cartilage or bone associated with the treatment. Based on AR results, the Sn-117m was most intense in macrophages that had migrated beneath the synovial lining in the subsynovial tissues mainly adjacent to the humerus in 3 of 5 elbows. It was also present within the normal type A (macrophage like) synovial lining cells in normal synovium in all elbows and occasionally noted in single cells (presumably macrophages) that were in the deeper connective tissues under the synovial lining. A few blood vessels contained AR positive cells. Sn-117m containing cells were generally absent in the cartilage, bone, and connective tissue. **CONCLUSION:** After ~3 half-lives the Sn-117m colloid was localized in synoviocytes throughout the joint in all 5 elbows. Macrophages were distributed in variable density in all layers of the synovium, and macrophages and synoviocytes contained the Sn-117m colloid. Retention of the HTC for ~3 half-lives and throughout the synovial layers in the elbow of the hounds suggests that Sn-117m is an appropriate RSO therapeutic isotope for small joints and possibly for intermediate and large joints.

EP437

Post I131-therapy planar scintigraphy. Is it sufficient for neck lymph node staging? Comparison to SPECT/low dose CT imaging

T. Pipikos¹, J. Koutsikos², F. Vlachou¹, A. Nikaki¹, K. Dalianis³, V. Papoutsis¹, E. Tsiakas¹, V. Prassopoulos¹; ¹Nuclear Medicine & PET/CT Department, Hygeia SA, Athens, Marousi, GREECE, ²Nuclear Medicine Department, NIMITS Hospital, Athens, GREECE, ³Medical Physics Department, Hygeia SA, Athens, Marousi, GREECE.

Aim: Post radioiodine therapy scan is of great importance in the staging and therapy decision making of DTC patients. Image resolution though and anatomical information provided is poor, reducing sensitivity and specificity. We evaluated the performance of planar post therapy scan in neck lymph node staging in patients with DTC, compared to SPECT/low dose CT hybrid imaging. **METHODS:** Twenty-eight patients with DTC and total thyroidectomy were studied after administration of 2775-3700 MBq of ^{131}I for thyroid remnants radioablation. A week after radioiodine administration a planar ^{131}I whole-body scintigraphy (WBS) was performed, followed by a ^{131}I SPECT/ low dose CT imaging the day after. Planar and SPECT/CT data were compared and correlated with ultrasound imaging (U/S), which was considered as gold standard for evaluation of thyroid or thyroglossal cyst remnants, or for pathological lymph nodes. The patients were under clinical surveillance in the next 16 months. **RESULTS:** WBS was false positive in 8/28 (28.5%) patients regarding neck lymph node involvement and also false negative in one

patient. False positive neck lymph node represented either thyroglossal duct cyst(2/8) or residual thyroid gland (5/8) or normal bio distribution(esophagus) (1/8), as it was confirmed from the SPECT/CT and U/S. SPECT/CT imaging identified correctly all above cases and moreover revealed a small pathologic lymph node in the lower neck, missed in planar imaging. Over all ^{131}I SPECT/CT in our study altered nodal stage from N1 to N0 in 8 from 28 patients and ustaged one patient. **CONCLUSION:** ^{131}I Planar imaging does not seem sufficient for neck lymph node staging in patients with DTC. SPECT/CT should be performed, since it is clearly superior , based on our results.

EP438

Head and neck pahntom for targeted radionuclide therapy calibrations and verifications

T. Kráčmerová, L. Jonášová, Z. Wolf, P. Solný; Department of Nuclear Medicine and Endocrinology Charles University 2nd Faculty of Medicine, Prague, CZECH REPUBLIC.

Aim Commercially available phantoms for nuclear medicine are quite expensive and many of them are only bespoke ones. Moreover; these phantoms are not usually very variable, though they are well reproducible. Aim of this work was to propose, develop and test an anthropomorphic (head, neck and shoulders), variable, reproducible and clinically achievable phantom for thyroid remnants simulations and gamma camera calibrations. Basic requirements were: water or tissue equivalence, safety during handling (robust, waterless, easily filled and source position system). **Materials and methods** Several materials available for phantoms were tested, however these materials were considered as unsuitable. A phantom contenting water may be split, leak through caps and cause damage to gamma camera. Radionuclide sources have to be adapted to the phantom and fastened well. Solid phantoms (PMMA etc.) are not so variable (limited variable positions for sources). The material is not easily accessible and not cheap. Our phantom consists of silhouette made of thermoplastic mask used in external beam radiotherapy and sonography gel which is basically water with organic supplement. The mask is fully filled with the gel. Other phantom components simulate cervical spine bones (adapted wild boar bones), a pharynx, a larynx, an esophagus, and blood vessels in the neck region. **Results and discussion** The homemade phantom was prepared and is tissue equivalent (CT checked). It is safe for handling and enable inserting the sources easily. The position system is also available which allows gamma camera system calibration in required settings. The phantom also enables individual patient source positioning simulations what may make dosimetry measurements more precise.

EP439

Is the asymmetrical mix of yttrium lutetium treatment more efficient than single radionuclide treatment of neuroendocrine tumours? - preliminary study

A. Mazurek¹, S. Piszczek¹, S. Osiecki¹, A. Gizewska¹, E. Witkowska-Patena¹, G. Kaminski², M. Dziuk¹; ¹Military Institute of Medicine, Department of Nuclear Medicine, Warsaw, POLAND, ²Military Institute of Medicine, Department of Endocrinology and Radioisotope Therapy, Warsaw, POLAND.

Background: Radionuclide therapy using yttrium (^{90}Y) or lutetium (^{177}Lu) labeled somatostatin analogues is one of the option for treatment of neuroendocrine tumors. There are no strict recommendations regarding which of the isotopes should be used. Yttrium is usually used for greater neoplastic lesions than lutetium but most patients have tumors of mixed sizes. **Aim** The goal of the study was to compare the treatment efficiency in neuroendocrine tumours with radionuclide labeled somatostatin

analogues in different combinations of radioisotopes. **Methods** The 35 patients were subjected to radionuclide therapy (19 female pts, mean age 65.4 years, mean therapeutic doses 4.1). The tumours were well (G1) and moderately (G2) differentiated according to WHO histopathologic classification. The primary tumour locations were as follows: of unknown location - 11, large bowel - 7, small bowel - 6, pancreas - 5, lung - 4, ovary - 2. The patients were subjected to intravenous administration of somatostatin analogues labeled with β -emitters. The mix composed of 150 mCi (5.55 GBq) ^{177}Lu and 50 mCi (1.85 GBq) ^{90}Y was administered to 23 patients. ^{177}Lu only of activity 200 mCi (7.4 GBq) was given to 10 patients. The two patients treated with 100 mCi yttrium only (3.7 GBq) labeled somatostatin analogues were excluded from analysis. The response to treatment was evaluated 6 months post radionuclide therapy by means of PET/CT with ^{68}Ga Gallium-labeled somatostatin analogues, contrast-enhanced CT and clinical assessment. **Results** The results of treatment in group of patients with mixed radionuclide treatment were as follows: stable disease (N= 9), partial response (N=10), progression (N=4). In a group of patients treated with lutetium only the results were: stable disease (N= 6), partial response (N=2), progression (N=2). The mixed yttrium/lutetium treatment resulted in greater number of patients with partial response (43%) comparing to lutetium only treatment (20%). **Conclusion** This comparison may indicate that 150/50 mCi mix of lutetium/yttrium is likely to result in better response than 200 mCi lutetium alone.

EP440

Standardized biodistribution template for nuclear medicine dosimetry collection and reporting

A. Kesner¹, G. Poli², S. Beykan³, M. Lassmann³; ¹University of Colorado, Anschutz Medical Campus, Department of Radiology, Aurora, CO, UNITED STATES, ²International Atomic Energy Agency, Vienna, AUSTRIA, ³University of Würzburg, Department of Nuclear Medicine, Würzburg, GERMANY.

Purpose: As the field of Nuclear Medicine moves forward with efforts to integrate radiation dosimetry into clinical practice we can identify the challenge posed by the lack of standardized dose calculation methods and protocols. All personalized internal dosimetry is derived by projecting biodistribution measurements into dosimetry calculations. In an effort to standardize organization of data and its reporting, we have developed, as a sequel to the EANM Dosimetry Committee guidance document of “good practice of clinical dosimetry reporting” (Lassmann M et al., EJNMMI 2011), a freely available biodistribution template, which can be used to create a common point of reference for dosimetry data. It can be disseminated, interpreted, and used for method development widely across the field. **Methods:** A generalized biodistribution template was built in a comma delineated format (.csv) to be completed by users performing biodistribution measurements. The template will be available for free download at <http://bitly.com/IAEA-BDT>. The download site includes instructions and other usage details on the template. The .csv-format was chosen as it can be easily edited by commercial spreadsheet software, while it can also be parsed easily by researchers or other developers interested in creating software tools to handle data. Examples of completed spreadsheets (I-131 radioiodine therapy, Lu-177 DOTATATE) are also available on the download site. **Results:** This is a new resource developed for the community. It is our hope that users will consider integrating it into their dosimetry operations. Having biodistribution data available and easily accessible for all patients processed is a strategy for organizing large amounts of information. It may enable users to create their own databases that can be analyzed for multiple aspects of dosimetry operations. Furthermore it enables population data to easily be reprocessed using different dosimetry methodologies. With respect to dosimetry-related research and publications, the biodistribution template can be included as supplementary material, and will allow others in the community to better compare calculations and results achieved.

Conclusion: As dosimetry in nuclear medicine becomes more routinely applied in clinical applications, we need to develop the infrastructure for handling large amounts of these data. Our organ level biodistribution template can be used as a standard format for data collection, organization, as well as to support dosimetry research and software development.

EP441

Dosimetry Evaluation Of Direct Radionuclide Cystography In Pediatric Patients

I. SIME LOAYZA, R. Moreno Cano, R. Reyes Marles, R. Padilla Muelas, M. Ibáñez Ibáñez, M. Godoy Bravo, J. Buades Former, L. Mohamed Salem, L. Frutos Esteban, M. Castellón Sánchez, J. Navarro Fernández, F. Nicolás Ruiz, G. Martínez Gomez, M. Claver Valderas; HOSPITAL VIRGEN DE LA ARRIXACA, MURCIA, SPAIN.

Aim: To evaluate the dosimetry of direct radionuclide cystography in pediatric patients and compare with the results obtained with the established recommended ranges in the literature. **Material and methods** We analyzed 44 patients with ages between 1 and 15 years, divided in 4 groups of age, who underwent direct radionuclide cystography for evaluation and monitoring vesicoureteral reflux, the results were analyzed according to the protocol recommended by the EAMN guidelines. All patients were given a dose of 20 MBq Tc-99m pertechnetate by direct bladder catheterization. The effective dose was calculated by multiplying the equivalent dose (HT) by a tissue weighting factor) by the duration of the test. Anova test was used to analyse the dose difference between different ages. **Results:** We found statistically significant differences between age groups, for the same administered dose. The average dose of all the patients in our study was 0,062 mSv. **Conclusions:** According to effective dose levels recommended by European Guidelines in this technique, our results are in the superior limit, although these differences are very insignificant and similar to those reported in recent publications we intend to try to reduce our radiation levels decreasing the duration of the test without losing diagnostic accuracy.

EP442

Dismal Awareness About Radiation Hazards Among Healthcare Radiation Workers: Point to Ponder?

N. Fatima¹, M. u. Zaman²; ¹Department of Nuclear Medicine, Dr Ziauddin Medical University, Karachi, PAKISTAN, ²Department of Radiology, Aga Khan University Hospital, Karachi, PAKISTAN.

Objectives: To find out core knowledge of healthcare radiation workers including physicians and technical staff as technologists, physicists and nurses and to measure knowledge-gained after attending a one day targeted symposium **Material and Methods:** Fifty-five participants (21 physicians, 25 technologists, 5 physicists and 4 nurses) attended a one day symposium on ionizing radiation and its hazards for healthcare workers at a tertiary care hospital. The participants were registered from 18 different healthcare facilities having radiology, nuclear medicine and radiation oncology services. Participants were solicited to fill a questionnaire comprised of 15 questions focused upon basic of ionizing radiation, their interaction, biological effects and radiation protection methods before and after the completion of session. **Results:** Mean scores of all participants in pre-session assessment was 45.472% which improved to 60.472% after attending session with a mean difference of 14.527% ($p < 0.0001$). Physicians scored significantly better (pre: 54.238%, post: 67.333%) than technical staff (pre: 39.471%, post: 55.088%). Importantly the knowledge-gained after attending session was greater in staff (15.617%) than physicians (13.095%) but not statistically significant ($p = 0.1183$). **Conclusion:** The level of knowledge about ionizing radiation hazards and radiation protection was not satisfactory in healthcare radiation workers. Physicians had significantly better pre and post session

scores than technical staff but knowledge-gained after attending session was not significantly different. Lack of knowledge among radiation workers is a global issue and this is the time to revamp their training programs in a meaningful strategy and International Atomic Energy Agency (IAEA) must take the lead.

EP443

Realistic single-cell geometry model: Cellular S-value calculations with Geant4, Geant4-DNA and PENELOPE

N. Falzone¹, R. Freudenberg², J. M. Fernández-Varea³, J. Malcolm¹, S. Able¹, K. A. Vallis¹; ¹University of Oxford, Oxford, UNITED KINGDOM, ²Universitätsklinikum Carl Gustav Carus an der Technischen Universität Dresden, Dresden, GERMANY, ³Universitat de Barcelona, Barcelona, SPAIN.

AIM: The MIRD monograph^[1] provides *S*-values for a spherical concentric single-cell model, however cells in culture assume a different morphology when plated that cannot realistically be described by a sphere model. The aim of this study is to compare single-cell *S*-values derived from Monte Carlo (MC) simulations for a realistic cell-in-culture geometry to the MIRD data. **MATERIALS AND METHODS:** The MC codes PENELOPE^[2] and Geant4-DNA^[3] were used to transport the full electron spectra of ⁹⁰Y, ^{99m}Tc, ¹¹¹In, ¹²³I and ¹³¹I in liquid water (mass density $\rho = 1 \text{ gcm}^{-3}$), by means of event-by-event simulations. Cellular *S*-values were calculated for a cell model with cell and nucleus radii $R_C = 5 \mu\text{m}$ and $R_N = 4 \mu\text{m}$ assuming both spherical and cell-in-culture geometries. The effects of cell eccentricity on *S*-values were evaluated for eccentric cell/nucleus arrangements in both geometries. Additionally, we compared the results to the standard Geant4 code (Livermore physics list). **RESULTS:** PENELOPE determined *S*-values for the spherical cell were generally within 10% of MIRD values for all radionuclides considered, when the source and target regions strongly overlap i.e. *S*(N←N) configurations, but greater differences were noted for *S*(N←Cy) and *S*(N←CS) configurations. However, Geant4-DNA cellular *S*-values for the realistic cell-in-culture geometry differed significantly from MIRD and PENELOPE derived *S*-values for all cell-nucleus targeting configurations. Furthermore, cell eccentricity greatly affected *S*-values in both models when the radiation sources are located on the surface of the cell (i.e. N←CS configurations). The comparison of Geant4-DNA to Geant4 (Livermore physics list) revealed differences up to 80% depending on the radionuclide and the source and target regions. **CONCLUSION:** Cellular geometry greatly affected calculated *S*-values. When micro-dosimetry is required to evaluate the effect of targeted radionuclides on cancer cells in culture, realistic cellular geometry models are required as well as detailed MC simulations. ^[1] Goddu SM, Budinger TF. MIRD Cellular S Values. SNM Inc. 1997. ^[2] Salvat F, Fernández-Varea JM, Sempau J, eds. PENELOPE-2011 OECD Nuclear Energy Agency. ^[3] Incerti S et al. THE Geant4-DNA project. IJMSSC 1 (2): 157-178, 2010.

EP444

The radiobiological effect of fractionation on molecular radiotherapy for bone metastases

A. M. Denis-Bacelar¹, S. Court¹, S. J. Chittenden², G. D. Flux²; ¹The Institute of Cancer Research, London, UNITED KINGDOM, ²The Royal Marsden Hospital NHS Foundation Trust, London, UNITED KINGDOM.

Aim: Repeated treatments of bone metastases with radiopharmaceuticals have been shown to improve survival. The optimisation of number and time-interval between administrations could potentially lead to improved treatment outcomes. The aim of this study was to investigate the effect of the number and time-interval between administrations on molecular

radiotherapy with ^{223}Ra -dichloride, ^{188}Re -HEDP and ^{177}Lu -PSMA-HBED-CC for prostate cancer metastatic to bone. **Materials and methods:** The linear quadratic model and the biological effective dose (BED) with the Lea-Catcheside factor were used to compare treatment schemes accounting for the repair of sub-lethal damage between administrations. The maximum tolerated administered activity was determined for a 2 Gy absorbed dose limit to the bone marrow as a function of the time-interval for 1-6 administrations. The bone lesion $\text{BED}_{\text{lesion}}$ was subsequently calculated from the maximum tolerated activity for every scheme. Patient-specific clinical bone lesion and bone marrow absorbed doses from available literature in ^{223}Ra -dichloride (Pacilio *et al*, EJNMMI 2015), ^{188}Re -HEDP (Lieve *et al*, JNM 2003) and ^{177}Lu -PSMA-HBED-CC (Baum *et al* JNM 2016) treatments were used in the calculations. Typical radiobiological parameters for prostate cancer and bone marrow cells were used. Uniform uptake distribution of the radiopharmaceuticals and a relative biological effectiveness of 5 for ^{223}Ra were assumed. **Results:** For a given total absorbed dose, the BED for repeated administrations increases as the time between fraction decreases, approaching the single fraction situation, indicating the effect of the dose rate overlap between administrations. The maximum $\text{BED}_{\text{lesion}}$ for ^{188}Re -HEDP and ^{177}Lu -PSMA-HBED-CC was obtained for a single administration of 3.28 GBq (13 Gy) and 128.9 GBq (837 Gy) respectively. For ^{223}Ra -dichloride, a maximum $\text{BED}_{\text{lesion}}$ of 921 Gy was obtained for 6 fractions of 167 MBq each, administered at 13 hour intervals. The relative differences between the minimum and maximum $\text{BED}_{\text{lesion}}$ for all the different fractionation schemes were 1.1%, 4.7% and 57% for ^{223}Ra -dichloride, ^{188}Re -HEDP and ^{177}Lu -PSMA-HBED-CC respectively. The $\text{BED}_{\text{lesion}}$ for ^{177}Lu -PSMA-HBED-CC administered at 50 hour intervals was on average 17% higher than for well separated administrations. **Conclusion:** From the radiobiological perspective, optimisation of ^{223}Ra treatments according to an absorbed dose limit to the bone marrow showed that the number and time-interval between administrations have a limited effect on the bone lesion biological effective dose. This result would justify a large number of administrations over a long time period to prolong pain palliation. Future work will include the effect of repopulation, in particular for long-lived radiopharmaceuticals and low dose rates.

EP446

Radioprotective Effect of Zinc on Major Salivary Glands

H. I. Atilgan¹, N. Yumusak², M. Sadic³, M. Korkmaz³, G. Koca³; ¹Kahramanmaraş Necip Fazıl City Hospital, Department of Nuclear Medicine, Kahramanmaraş, TURKEY, ²Harran University, Faculty of Veterinary Medicine, Sanliurfa, TURKEY, ³Ankara Training and Research Hospital, Clinic of Nuclear Medicine, Ankara, TURKEY.

Aim: To evaluate the radioprotective effect of zinc on the major salivary glands with histopathological examination after high dose of radioiodine (^{131}I). **Methods:** Sixteen Wistar albino rats were divided into two groups consist of eight animals in each group. The first group was the control group that was administrated ^{131}I and the second group was the zinc group that was administrated ^{131}I and zinc by gastric gavage. Zinc was started two days before ^{131}I and continued for five days after ^{131}I therapy. Twenty four hours after the last dosage of zinc animals were sacrificed and parotid, submandibular, and sublingual glands were removed bilaterally for histopathological examination. The slices were evaluated for oedema, vacuolization, panacinar inflammation, necrosis and atrophy in acinar epithelial cells; periductal fibrosis, periductal infiltration and periductal leakage in interstitial space; duct ectasia and squamous metaplasia in ductal system; sclerosis and stenosis (fibrin thrombi) in vascular system. **Results:** Oedema, vacuolization, panacinar inflammation, necrosis, atrophy, periductal fibrosis, periductal inflammation, periductal leakage, ductal ectasy, squamous metaplasia, sclerosis and stenosis were seen less in zinc group in all glands, except periductal inflammation in submandibular gland. But these data was not statistically significance, except atrophy in sublingual gland. Atrophy is significantly less seen in zinc group when

compared with the control group in submandibular gland. **Conclusion:** All of the parameters were less seen in the zinc group in all of the glands except periductal inflammation in submandibular gland that may show the beneficial effect of zinc on early damage of ^{131}I .

EP447

Preclinical assessment by Single Photon Emission Computed Tomography of various combinations of preparative measures on radioiodide thyroid uptake

C. Zwarthod^{1,2}, K. Chatti², J. Guglielmi², M. Hichri², C. Compin², J. Darcourt^{2,1}, G. Vassaux², D. Benisvy¹, T. Pourcher², B. Cambien²; ¹Service de médecine nucléaire, Centre Antoine Lacassagne, Nice, FRANCE, ²Equipe TIRO – UMRE 4320, Université Nice-Sophia-Antipolis, Nice, FRANCE.

Aim: MicroSPECT/CT imaging was used to evaluate quantitatively the influence of the route of iodine administration, of the injection of recombinant human TSH (rhTSH), and of low iodide diet in euthyroid and T3-treated mice. **Materials and Methods:** $^{99m}\text{TcO}_4^-$ and ^{123}I thyroid uptake on euthyroid and T3-treated animals, fed either on a normal-iodine diet (NID) or on a low iodide diet (LID), treated or not with rhTSH and administered either intravenously, subcutaneously, intraperitoneally or by gavage with the radiotracer were assessed using microSPECT/CT imaging. Western blot was performed to measure Na/I symporter expression levels in the thyroid. **Results:** Systemic administration of radioiodide resulted in a higher accumulation in the thyroid than the oral route (x2.35 in NID mice). LID further increased thyroid activity by 2-fold, thus resulting in a 5-fold increase compared to the standard NID/oral route. rhTSH injections stimulated thyroid activity both in euthyroid and T3-treated mice on NID regime, but in this later group uptake levels remained dramatically low compared to those of euthyroid mice. However, combining LID and rhTSH in T3-treated mice resulted in a 2.8 higher uptake compared to NID/T3/rhTSH mice and helped restoring a thyroid activity equivalent to that of euthyroid animals. **Conclusions:** Our data demonstrate the potential of SPECT/CT imaging in the study of thyroid physiology as well as to answer clinically-relevant questions. We show that systemic administration of radioiodide favors its accumulation in the thyroid compared to the oral route. These data highlight the importance of LID either in euthyroid- or in T3-treated-, rhTSH-injected-mice. Extrapolated to the human situation and in the context of the clinical guidelines for preparation of patients with differentiated thyroid cancer, our data emphasize the importance of LID to potentiate the efficacy of rhTSH treatment in T3-treated patients.

EP448

^{68}Ga -OPS202 and ^{177}Lu -OPS201 Dosimetry Assessment

S. Beykan¹, U. Eberlein¹, S. B. Jensen², J. Kaufmann³, R. Bejot³, B. Hakim³, M. Lassmann¹; ¹University of Würzburg, Department of Nuclear Medicine, Würzburg, GERMANY, ²Aalborg University, Department of Chemistry and Biochemistry and Department of Chemistry and Biochemistry, Aalborg University, DK-9000 Aalborg, Denmark, Aalborg, DENMARK, ³OctreoPharm Sciences GmbH, Ipsen Group, Berlin, Germany, Berlin, GERMANY.

Aim: ^{68}Ga -OPS202 and ^{177}Lu -OPS201 are the newest somatostatin receptor antagonists for diagnostics and therapy in patients with neuroendocrine tumor with the highest affinity towards the somatostatin receptor subtype sst2. In this study we present the results of two dosimetry studies in a pig animal model with the purpose of comparing biodistribution data of ^{68}Ga -OPS202 with ^{177}Lu -OPS201. **Materials and Methods:** In vivo biodistribution and dosimetry studies with approximately 175 MBq of ^{68}Ga -OPS202 (peptide mass: 27 μg) and 105 MBq of ^{177}Lu -OPS201

(peptide mass: 8 µg) were performed in 5 pigs for both tracers (3 female and 2 male). A series of whole-body PET/CT and SPECT/CT scans were conducted up to 6 hours for ^{68}Ga pigs and 10–12 days for ^{177}Lu pigs, respectively, after the intravenous injection. Blood samples were taken to determine the time-activity curves (TACs) in blood. Organ-specific and blood-based time-integrated activity coefficients (TIACs) were calculated by using NUKFIT (1) for the selected organs and the bone marrow. The ratios of the organ/tissue TIACs between the two groups of pigs (^{68}Ga -OPS202/ ^{177}Lu -OPS201) were assessed to show differences in the pharmacokinetics. Based on a two-compartment model, the biological elimination rates of the activity from the blood pool by kidney uptake (k_t , unit: d^{-1}) and the biological excretion rate from the kidney (k_b , unit: d^{-1}) were calculated and compared for both groups to distinguish differences in the pharmacokinetics of ^{68}Ga -OPS202 and ^{177}Lu -OPS201. **Results:** TIAC ratios of ^{68}Ga -OPS202 and ^{177}Lu -OPS201 for the kidney and bone marrow were similar (0.015 and 0.016). The higher TIAC ratio for the liver (0.029) denotes a difference in the biological behavior compared to kidney and bone marrow. In all pigs with both tracers unlike humans no spleen uptake was observed. The k_t value of the ^{68}Ga -OPS202 pigs (0.22 d^{-1}) was significantly higher (t-test, $p < 0.05$) compared to the ^{177}Lu -OPS201 pigs (0.08 d^{-1}), this is most likely caused by the amino acid kidney protection given iv. to the ^{177}Lu -OPS201 pigs. Although, a higher excretion rate k_b was observed for ^{68}Ga -OPS202 (0.55 d^{-1} vs. 0.002 d^{-1}) no statistical significance was reached (t-test, $p > 0.05$). **Conclusion:** The retentions of ^{68}Ga -OPS202 compound were higher in liver compared to kidney and bone marrow. Related to kidney kinetics, the kidney uptake rate in pigs administered ^{68}Ga -OPS202 was much higher than ^{177}Lu -OPS201 pigs which may be associated with differences of in-vivo pharmacokinetics due to the effectiveness of the amino acid kidney protection agent.

EP449

Metrology for clinical implementation of dosimetry in molecular radiotherapy: a new EURAMET project

V. Smyth¹, C. Bobin², M. Lassmann³, L. Struelens⁴, J. Tipping⁵, S. Judge¹; ¹National Physical Laboratory, Teddington, Middlesex, UNITED KINGDOM, ²Commissariat à l'Énergie Atomique, Saclay, FRANCE, ³University of Würzburg, Würzburg, GERMANY, ⁴SCK·CEN, Mol, BELGIUM, ⁵The Christie NHS Foundation Trust, Manchester, UNITED KINGDOM.

It is now widely accepted that routine nuclear medicine therapy (molecular radiotherapy - MRT) would be more effective if treatments were planned on the basis of individual normal and target tissue dosimetry (Strigari et al, 2014). The EURAMET funded project MetroMRT (<http://projects.npl.co.uk/metromrt/>), which ran from June 2012 to May 2015, demonstrated that it is both possible and practicable to measure the absorbed dose delivered by therapeutic radiopharmaceuticals in individual patients with the same rigorous traceability to primary standards as is required by dosimetry protocols for all other modalities of radiotherapy (eg. IAEA TRS 398, 2000). MetroMRT was the first large-scale European collaboration between clinical medical physicists and radiation metrologists. In June 2016 a new project, MRTDosimetry, was started as follow-on to MetroMRT, to continue the development of practical procedures for implementation of routine patient dosimetry in MRT clinics. The new project consortium is made up of 6 metrology institutes and 13 leading clinical MRT research centres. The project will include the following tasks: Development of a transfer instrument for calibration of clinical activity meters to enable measurement of therapeutic agents with greater accuracy; Development of a protocol for calibration and quality assurance of SPECT-CT and PET-CT based quantitative imaging (QI) systems; Development of radioactive test sources and 3D-printed quasi-anthropomorphic phantoms for validation of QI systems and absorbed dose measurements; Production of an open-access database

of test images that can be used for commissioning dosimetry systems; the images will cover a range of cases, and the contained activity and dose distributions will be made available; Development of a method for determining the optimum timing to take a sequence of QI measurements in order to maximise the accuracy of the activity-time integral; Development of a protocol for commissioning an absorbed dose measurement system. Each of the methods and protocols will be trialled extensively by the clinical partners in the consortium, as well as any other centres wishing to collaborate with the project. Details will be presented of the planned outputs, as well as opportunities to join the project as a collaborator. Strigari, L., et al. The evidence base for the use of internal dosimetry in the clinical practice of molecular radiotherapy Eur J Nucl Med Mol Imaging DOI 10.1007/s00259-014-2824-5 (2014) IAEA TRS 398, Absorbed Dose Determination in External Beam Radiotherapy: An International Code of Practice for Dosimetry Based on Standards of Absorbed Dose to Water, Technical Reports Series No. 398, Vienna (2000).

EP450

Energy Spectrum of Electrons Released in the Interaction of ^{60}Co Photons in Water; Comparison with Selected Beta Emitting Radioisotopes

P. Taheri, H. Rajabi, A. Rajabi; Tarbiat Modares University, Tehran, IRAN, ISLAMIC REPUBLIC OF.

Introduction: Recent advances in radioimmunotherapy (RIT) have led to a significant increase in medical applications of radioisotopes. However, absence of standard treatment planning procedure hindered application of the technique to the desired level. One of the most important reasons, is the lack of radiobiological information to predict the response of a given cell population to radiation dose from internal source of radionuclides. The major part of radiobiological information were derived from external source of radiation forming the bases of external beam radiotherapy. In recent years, efforts have been made to extrapolate external beam radiobiological information to internal radiation. However, considerable differences have been reported in biological response of equal macroscopic dose of radiation from external and internal sources. In the present work, physical bases of the two types of radiation in terms of electron density, electron energy distribution at the microscopic level were investigated and the results were compared. **Materials and Methods:** Assuming uniform distribution of the radionuclide in water, microscopic dose distributions as well as the energy spectrum of emitted electrons of four radioisotopes (^{131}I , ^{177}Lu , ^{111}In , and ^{90}Y) were determined using Monte Carlo simulation. Similar quantities were calculated for external source of ^{60}Co photons in water. We determined the differences between the microscopic dose distributions of Cobalt-60 and each one of the four isotopes when their macroscopic doses in water were equal. GATE/GEANT4 dedicated nuclear medicine package was used for Monte Carlo simulation **Results:** The results showed that electron energy distributions of four aforementioned sources were significantly different ($P < 0.01$) even though they generated almost the same number of electrons per unit volume of medium. The average energy of Cobalt-60 electron electrons was close to the average energy of Yttrium-90 electron spectrum. Normalizing the average dose transferred by Cobalt-60 and radioisotopes, the microscopic dose absorbed at various layers of the target volume were significantly different ($P < 0.01$) except for Yttrium-90 that dose variation with depth was not significantly different from Cobalt-60 ($P > 0.05$). **Conclusion:** The total number of events (ionisation/excitation) needed to achieve 1 mGy absorbed dose into target volume is almost equal. However, the average electron energy produced on water depends weakly on the type and energy of radiation, energy distribution of electrons and dose distribution for various radiation (^{60}Co photons and four radio-isotopes) are significantly different. **Keywords:** Radionuclide therapy, external radiotherapy, dosimetry, Monte-Carlo simulation.

EP451**Radiopharmaceutical dosimetry based on serial SPECT or PET images: comparison between the commercial software STRATOS and the Monte-Carlo-based OEDIPE software**

N. Benabdallah¹, M. Bernardini², T. Guitton¹, K. Ea¹, C. de Labriolle-Vaylet³, D. Franck¹, A. Desbrée¹; ¹Institut de Radioprotection et de Sûreté nucléaire, Fontenay-aux-Roses, FRANCE, ²Nuclear Medicine Department, Hôpital Européen Georges Pompidou, Paris, FRANCE, ³UPMC, Univ Paris 06 Biophysics - Nuclear Medicine Department, Hôpital Trousseau, Paris, FRANCE.

To determine dose-response relationship, either for preclinical and clinical purposes, there is a need to calculate personalized absorbed doses. Even for diagnostic radiopharmaceuticals, performing accurate specific dosimetry is of interest to assess the differences with respect to a standard dosimetry. With the availability of SPECT and PET images also dedicated to small animals, it is now possible to directly estimate the biokinetic of a radiopharmaceutical. For instance, the only commercially available software allowing dosimetric calculations based on the analysis of serial SPECT and PET images is STRATOS by Philips. Although the dose voxel kernel approach allows fast calculations, a most accurate dosimetry can be performed using Monte Carlo codes. In this context, we developed a new biokinetic module to the OEDIPE software that allows the determination of the cumulated activity at the voxel level based on SPECT or PET images. Serial PET ¹⁸F-FDG images of mice and ¹⁸F-choline images of human patients were used for this study. Standard dosimetry was realized using the OLINDA/EXM software. Personalized absorbed doses and dose-volume histograms were determined with the kernel approach using the STRATOS software and using with the MCNPX Monte Carlo code using the OEDIPE software. The differences in absorbed doses for the preclinical and clinical dataset will be discussed in terms of (i) standard versus personalized dosimetry, (ii) kernel versus Monte Carlo calculations and (iii) organ versus voxel level dosimetry and according to the biokinetic models used.

EP452**Dosage optimization in cadmium-zinc-telluride SPECT gamma camera gated tomographic radionuclide angiography**

J. Rydberg, T. Nguyen, B. Zerahn; Herlev Hospital, Herlev, DENMARK.

Purpose: To determine the influence of age, height, and weight on count rate on cadmium-zinc-telluride (CZT) SPECT gamma camera gated tomographic radionuclide angiography. **Methods:** From August to December 2015 a total of 549 patients referred for routine assessment of left ventricular ejection fraction (LVEF) were registered regarding age, height, weight, and count rate in addition to the standard variables: Left ventricular end systolic and end diastolic volumes (LVESV and LVEDV respectively) and LVEF. All radionuclide angiographies were performed on a dedicated cardiac CZT SPECT gamma camera, GE Discovery 530c (GE Healthcare, Milwaukee, WI, USA). A dose of 550MBq ^{99m}Tc-labeled human serum albumin was administered intravenously to each patient. An acquisition protocol for multigated acquisition, using 16 frames per R-R interval and requesting 600 accepted beats, was adapted and a 20% energy window centered on 140 keV was performed in all cases. Xeleris 3 Imaging workstation software (version no. 3.0562) was used for reorientation of the heart after applying a generic reconstruction algorithm and filtering. Assessment of standard variables was performed with Cedars-Sinai QBS processing software (revision 2009.0). Each acquisition was analysed by two experienced technologists. Four patients (0.7%) were excluded from the study. Three patients because it was impossible to focus their heart within the field of view due to a high thoracic circumference and one patient because of paravenously administered

radionuclide. **Results:** Count rate varied from 1.25 to 8.39 kcounts per second. Registered test variables, except age, were significantly correlated with count rate: age (adjusted R²: 0.003, P = 0.282) height (adjusted R²: 0.046, P < 0.0001) weight (adjusted R²: 0.628, P < 0.0001). A log-transformation was performed on count rate and weight to increase the linear relation. The influence of age in a linear multivariable regression model was negligible and this variable was subsequently excluded from the final model: $\log(\text{CountRate}) = \beta_0 + \beta_1 \cdot \text{Height} + \beta_2 \cdot \log(\text{Weight})$ Thus our model explains just below 70% of the variance (adjusted R²: 0.69) in log(count rate) with coefficients $\beta_0 = 6.075$, $\beta_1 = 0.012$ and $\beta_2 = -1.558$. **Conclusion:** Patient height and weight can be used to predict count rate when performing CZT radionuclide angiography and subsequently used for planning of tracer dosage. This provides the possibility to give a more patient specific dosage in radionuclide angiography.

EP453**SPECT/CT Quantification of Lu-177 Activity Using Phantom Images to Develop a Quantitative 3D Dosimetry for Molecular Radionuclide Therapy**

S. Wiessalla, C. Schuchardt, R. P. Baum; Zentralklinik Bad Berka GmbH, Bad Berka, GERMANY.

Aim: Scientifically developed or commercially available 3D dosimetry approaches are based on quantitative SPECT/CT images. The aim of this study was to determine the possibilities and limitations of SPECT/CT quantification of Lu-177 to develop a quantitative 3D dosimetry for molecular radionuclide therapy. **Methods:** Various phantom studies were acquired, which mainly served to optimize the recording protocol and reconstruction parameters. Herewith the existing Siemens Symbia T2 SPECT/CT was calibrated and recovery of activity under different geometric conditions was analyzed. Possibilities and limitations of the current technology were identified and compared. **Results:** The Phantom studies showed, that under ideal conditions, the activities can be obtained from target regions. The result largely depends on the manner of determining the volume-of-interest. When defining the contours with "expert knowledge" and exclusion of overlapping targets, a deviation of the detected activity of +/- 10% compared to the real activity was achieved. Contours obtained by anatomical demarcation of targets defined by CT, and subsequent calibration, demonstrated a deviation of 80% from the actual target activity. The long-term stability of the SPECT/CT system could also be determined, which remained consistent. **Conclusion:** Under certain conditions and constraints a quantified Lu-177 SPECT / CT scan can be used to supplement the planar dosimetry. A statement on the activity per voxel - and thus a voxel-based dosimetry - is not yet possible at the moment due to the variations in the use of CT volume. However, further studies are being performed to improve this concept of hybrid-dosimetry using SPECT/CT to overcome the shortcomings of 2D dosimetry.

EP454**Evaluation of Triple Energy Window scatter correction method in ¹³¹I imaging with Monte Carlo**

R. Barquero¹, H. Pérez-García¹, A. Cardenas²; ¹Hospital Clínico Universitario Valladolid, Valladolid, SPAIN, ²Hospital Nacional EdgardoRebagliati Martins, Lima, PERU.

Aim: In ¹³¹I Imaging high fractions of collimator scatter (s) and penetration events (p) appear that have to be corrected to retain only the geometric component in the photopeak. The currently used correction method in the clinic is the Triple-Energy Window (TEW) based in spectral analysis technics. This study presents an evaluation of TEW method using Monte Carlo simulation (MC) with MCNPX code. **Methods:** The

Gammacamera simulated in this study is a Siemens e-cam with HEGP collimator. The two geometries analyzed are point source ^{131}I in air, and 14 cm diameter Petri dish in air filled with radioactive water of ^{131}I . In both cases, the sources are centered with respect the crystal and are at 10 cm from the collimator face. Both simulations with MCNPX carry on with an accurate description of the source, crystal and collimator. The three main energy emission of ^{131}I 634, 637 and 723 keV are included as source terms. The hexagonal net of the HEGP collimator is realistically simulated with the repeated structure capability of MCNP using the FILL, U and LAT cards. Different energy bins, 308, 327, 400, and 424 keV for each source are conducted in the simulation such as the three TEW windows were covered: MAIN) a 20% energy window centered at 364 keV, LOWER) 6% energy window centered at 318 keV and UPPER) 6% energy window centered in 413 keV. The mean photon fluence per source particle is determined using $F4$ tally (mean track length) in the entire field of View (FOV). Total component of the counts is estimated from the simulation results for MAIN window. Counts for (s+p) component are estimated with the trapezoidal approximation: $c(s+p) = (c(\text{lower})/w(\text{lower}) + c(\text{upper})/w(\text{upper})) * w(\text{main})/2$, where $c(\text{lower})$ and $c(\text{upper})$ are the counts in the LOWER and UPPER windows, respectively, and $w(\text{main})$, $w(\text{lower})$ and $w(\text{upper})$ are the widths of the MAIN, LOWER and UPPER windows, 73, 22 and 23 keV. **Results:** The component of (s+p) counts is 24% of the total events for both sources, punctual and 14 cm diameter Petri dish. 73% has been estimated by others authors as a true value in the punctual source case. **Conclusions:** The TEW method can underestimate the s+p components in ^{131}I imaging because the trapezoidal approach doesn't fit well the shape for the background in the energy spectra. Other (s+p) correction methods could be investigated.

EP455

A dose radiation reduction strategy to patients in a Nuclear Medicine Department

R. Jover-Diaz, D. Martin-Rios, A. Martinez-Lorca, G. Salazar-Andia, C. Gonzalez-Roiz, J. Jimenez; Hospital Universitario Rey Juan Carlos, Madrid, SPAIN.

Objective: To reduce radiation rate exposure received by patients in a Nuclear Medicine Department, ensuring performance of proper quality of diagnostic tests. **Method:** We have calculated estimated effective dose per patient on each activity and technique employed. These are included in the Quality Assurance Nuclear Medicine Department Program which are based on the following Nuclear Security publications: ORISE (Oak Ridge Institute for Science and Education) and ICRP (International Commission of Radiologic Protection). **Results:** - Cardiology Department joint action protocol of patients submitted to a cardiac SPECT. Cardiac SPECT at rest was only obtained for those patients with perfusion abnormalities in stress test, after joint assessment with Cardiologist. Thus, a second part of the test has been avoided in approximately 29 % of patients who have undergone stress cardiac SPECT. Taking this into account, effective dose for each patient undergoing cardiac SPECT at rest with an administered activity of 23 mCi (851 MBq) of $^{99\text{m}}\text{Tc-MIBI}$ has been reduced by Nuclear Medicine in ~ 7.66 mSv (effective dose). Effective dose for each patient undergoing cardiac CT-SPECT at rest with a dose of 130 kVp and intensity modulation (DLP average of 30 mGy.cm), has been reduced by ~ 0.44 mSv (effective dose). This is a dose reduction of 53% - Dose reduction in patients who have undergone body scintigraphy with $^{111}\text{In-Pentetreotide}$. Since June 2015 only 24-hour SPECT- CT acquisition is performed. This is a dose reduction of 24% - Dose calculation of ^{131}I metabolic therapy in patients with hyperthyroidism. Usually ^{131}I fixed dose are employed of these patients, but since our department activity began, we calculate doses based on the data obtained from thyroid scintigraphy (weight, volume and degree of uptake radiopharmaceutical) - Safer practices using radiopharmaceuticals in Nuclear Medicine department has been pursued, titration to lower possible exposure radiation. However, quality of images obtained should be ensure, according to

ALARA criteria. Dose adjustment for pediatric population is mandatory following scientific societies recommendations. - It has sought to reduce patient dosimetry levels attending to appropriate medical indications of diagnostic and therapeutic nuclear medicine tests when performed. Example, assessment of the clinical record for justification by the specialist in Nuclear Medicine and validation of acquisition protocols for each patient at least twenty-four hours before according to Quality Royal Decree. **Conclusions:** We have achieved a significant dose reduction using different strategies for reducing dose administration without affecting quality diagnostic tests.

EP456

Radiation self-monitoring at home of patients receiving $^{177}\text{Lu-DOTATATE}$ peptide receptor radio-therapy for dosimetry informed radiation protection

L. Livieratos, T. Brothwood, D. Aniceto, R. Fernandez, C. Sibley-Allen, K. Adamson, S. Allen, V. Lewington; Guy's and St Thomas Hospitals, LONDON, UNITED KINGDOM.

Background: Targeted radionuclide therapy with $^{177}\text{Lu-DOTATATE}$ is increasingly used to treat inoperable, metastatic neuroendocrine tumours. Written radiation protection advice is provided for patients post-treatment based on 24 hour whole-body retention measurements. Measurement of external dose rates from patients beyond 24 hours would provide the evidence to review current radiation safety practice and generate more accurate data about whole-body retention and absorbed dose on an individual patient basis. This study aims to assess feasibility of self-monitoring at home for a cohort of non-local patients treated in our hospital over a period of minimum two weeks post-therapy. **Methods:** After a short demonstration of the monitoring procedure during their treatment visit (administration of $7400 \pm 10\%$ MBq), patients were issued with a portable energy-compensated GM monitor, simple instructions and a form to record twice-daily external dose rates at arm's length as point of reference for fixed measurement geometry. Cross-calibration for each patient was performed against retention measurements acquired while in hospital at a distance of 2m. Data were analysed on the basis of retention curves and external dose rate in order to calculate personalised whole-body dosimetry and collect a body of data of external radiation exposure for appraisal of radiation safety advice to patients, family members and the public. **Results:** Data were collected for a pilot cohort of 6 patients living up to 517km from our treatment centre. Compliance was excellent with each patient acquiring at least two measurements per day for 14-28 days post-therapy. Effective half-life of the slow component varied from 56 to 103 hours (2.3-4.3 days) non-corrected for isotope decay. Radiation exposure at arm's length from patient 14 days post-administration varied from 0.9 - 11.0 $\mu\text{Sv/hr}$ while the maximum exposure recorded 20 days post-therapy was 3.1 $\mu\text{Sv/hr}$. Whole-body retention at 14 days varied from 2.3 to $<1\%$ of injected dose. MIRD-based calculation of whole-body absorbed dose was within range of values (0.2-0.4Gy) calculated by whole-body imaging in a similar cohort of patients. **Conclusion:** Self-performed dose rate measurement at home is a feasible and realistic approach for data collection across centres for radiation protection, personalised whole-body retention and dosimetry purposes. For the first time, this initiative allows dose rate monitoring with patient participation beyond current limitations of geography and availability of fixed-site equipment. We feel this could have a significant impact upon both patient care and the safety advice given to patients and their families after Lu-177 radiopeptide treatment.

EP457

PET Imaging for Y-90 SIRT: Effect of Liver Motion on Dosimetry

M. D. Walker¹, C. A. Porter¹, D. R. McGowan^{1,2}; ¹Oxford University Hospitals NHS Foundation Trust, Oxford, UNITED KINGDOM, ²University of Oxford, Oxford, UNITED KINGDOM.

Purpose: Selective internal radiation therapy (SIRT) using Y-90 microspheres is increasingly used in the treatment of metastatic liver disease. Accurate verification of the dose to tumour and healthy tissue is crucial to allow treatments to be appropriately evaluated on a per-patient basis, and to enable treatment optimisation. We have performed phantom studies to assess the extent to which respiratory motion correction improves PET-derived dosimetry. **Materials and Methods:** A NEMA IQ and The Abdo-Man™ phantom (a 3D-printed liver phantom with fillable inserts) were imaged on a GE Discovery 710 PET scanner using our clinical protocols. Separate tests were performed using F-18 and Y-90. The phantoms were placed on a respiratory motion platform (QUASAR™; Modus QA) using realistic motion waveform and amplitudes. Respiratory gating signals were acquired using an infrared system (RPM; Varian Medical Systems). PET data were reconstructed using the manufacturer's Bayesian penalized likelihood reconstruction algorithm. Various motion correction methods were explored (quiescent period gating, phase-matched gating, phase matched gating combined with deformable image registration, and data driven gating). The resulting images were converted to dose maps (HERMES Hybrid Internal Radionuclide Dosimetry, HIRD™; HERMES Medical Solutions AB). Volumes of interest were placed over the hot spheres and used to generate dose-volume histograms. These DVH's were compared against the reference DVH found without motion. Dosimetry data were scaled such that the maximum dose in the reference DVH corresponded to 107% of the prescribed dose. The volume of the sphere receiving >95% (V_{95}), >80% (V_{80}) and >67% (V_{67}) of this prescribed dose was then calculated and compared for different motion amplitudes and correction strategies. **Results:** Results from the torso phantom using F-18 demonstrate large differences in the volume of the spheres that received "treatment doses" for the different motion amplitudes. For motion amplitudes of 10mm and reconstruction using quiescent period gating for motion compensation, the volume ratio V_{67}/V_{67-ref} for a 30 mm diameter sphere was unity indicating motion compensation was acceptable; V_{67}/V_{67-ref} was 1.08 without the use of motion compensation. The calculated ratios V_{95}/V_{95-ref} and V_{80}/V_{80-ref} for 10 mm motion amplitudes were however reduced to 0.84 and 0.94 respectively for quiescent period gating. These ratios were further reduced for motion amplitudes of 15 mm, to less than 0.5 in the case of V_{95}/V_{95-ref} (irrespective of the application of motion correction by quiescent gating). **Conclusions:** In this phantom study designed to represent post-SIRT PET imaging, motion correction improved the accuracy of DVHs.

EP458

Discrepancy between ^{99m}Tc -MAA SPECT and ^{90}Y glass microspheres PET lung dosimetry in radioembolization of hepatocarcinoma

C. Chiesa¹, M. Mira², M. De Nile², M. Maccauro¹, C. Spreafico¹, C. Zanette¹, G. Aliberti¹, T. Cascella¹, R. Romito¹, C. Sposito¹, E. Seregni¹, A. Marchiano¹, F. Crippa¹, V. Mazzaferro¹; ¹Foundation IRCCS Istituto Nazionale Tumori, MILAN, ITALY, ²Medical Physics School - University of Milan, MILAN, ITALY.

Aim: we quantitatively compared ^{99m}Tc -MAA predicted and ^{90}Y -PET absorbed dose to liver lesions, parenchyma, and lung. **Methods:** Two sequential groups (1 and 2) of 35 and 39 hepatocarcinoma patients were treated with ^{90}Y glass microspheres after planning based on attenuation and scatter corrected ^{99m}Tc -MAA SPECT images. Group 1 (2) was treated on Thursday (Monday of the 2nd week), i.e. 3.75 (7.75) days after the reference date, with 1 (2.8) million of particles per GBq respectively. We repeated the identical dosimetric method on peri-therapy ^{90}Y -PET images acquired with a PHILIPS GEMINI 64 TOF scanner. We applied the patient relative calibration method in both analysis. PET images were automatically coregistered to SPECT in order to apply identical VOIs. 4 (10) patients showing lung shunt fraction (LSF)>5% were studied as a separate group. Predicted and ^{90}Y -PET absorbed doses to 31 (29)

parenchyma and 38 (46) lesions were compared. **Results:** A dual phantom ^{90}Y -PET test followed by direct gammacounter measurement verified that the relative liver to lung concentration ratio was preserved in PET images. In the group 1, the ratio between the ^{90}Y -PET and the predicted parenchyma absorbed dose was median=1.02, range (0.69, 2.04), while for lesions we had median=0.99, range (0.42, 1.91); paired t-test was non significant. In the group 2, ratio for parenchyma was median=1.07, range (0.18, 3.83), and for lesions median=0.81, range (0.29, 2.32); t-test was significant (parenchyma $p=0.015$, lesions $p=0.004$). Preliminary liver toxicity data did not show any incidence increase in group 2. In 7 angiogram comparisons, noticeable absorbed dose discrepancy could not be attributed to differences between the two angiographic procedures. About lung, no matter the number of spheres, ^{90}Y -PET LSF was absolutely zero in 9/14 cases, and strongly reduced in 4/14. LSF was confirmed by ^{90}Y -PET only in one patient, who had a thromb in a sovrahepatic vein. **Discussion:** MAA overestimation of LSF is due to 10 micron MAA fraction, more penetrating in capillaries than 25 micron ^{90}Y microspheres, as found by Elshot et al with 30 micron ^{166}Ho microspheres. For the same reason we found an ^{90}Y -PET lesion absorbed dose reduction in group 2 (larger number of ^{90}Y microspheres), with a consequent increased ^{90}Y -PET parenchyma absorbed dose. **Conclusion:** MAA treatment planning for glass microspheres is safe, despite the presence of simulation-therapy discrepancies. However, an improved simulator should be developed, especially, but not only, to avoid unjustified activity reduction in cases with substantial MAA lung shunt.

EP459

A voxel-based correction method to allow quantitative dosimetry comparisons of pre- and post-therapy imaging in ^{90}Y -microsphere treatments

A. J. Craig¹, I. Murray¹, A. Denis-Bacelar², N. Khan³, A. Maenhout³, B. Rojas-Fisher⁴, L. Hossen⁴, G. Flux¹; ¹Royal Marsden Hospital, London, UNITED KINGDOM, ²Institute of Cancer Research, London, UNITED KINGDOM, ³Chelsea & Westminster Hospital, London, UNITED KINGDOM, ⁴Royal Brompton Hospital, London, UNITED KINGDOM.

Introduction Pre-therapy ^{99m}Tc -MAA SPECT scans are used to plan ^{90}Y -microsphere treatment of liver tumours based on calculations of absorbed dose to normal liver and tumour. Comparison of dosimetric values is limited by the different scan resolutions. Segmentation of normal liver and tumour should not be performed using SPECT due to the non-physiological microsphere uptake. Application of a delineated diagnostic CT to SPECT images for absorbed dose calculation result in inaccuracies due to the partial volume effect (PVE). The aim of this work is to develop a methodology to overcome PVEs allowing calculation and quantitative comparison of absorbed dose to normal liver for pre- and post-therapy imaging. **Methods** Simulation of SPECT scans of known activities for tumour burdens of 3-27% were performed based on delineated patient CT scans. Point spread functions (PSF) of ^{99m}Tc and ^{90}Y were measured and used to simulate different SPECT resolutions. Poisson noise was applied to the SPECT simulated images. An adaption of the modified Müller-Gärtner method was used to resolve SPECT scans into separate maps for normal liver and tumour values. This method is based on an assumption of uniform tumour uptake for the derivation of the normal liver map, and vice-versa. Errors were assessed by comparing total activity in each region to the known ground truth for this method and standard CT delineation. Normal liver absorbed dose maps from simulated pre- and post-therapy SPECT scans were obtained and mean absorbed dose and biological effective dose (BED) were compared. **Results** Calculations of total activity using CT delineation gave errors of 22% and 5% assigned to tumour and normal liver respectively for the ^{99m}Tc SPECT, and 35% and 13% for the ^{90}Y SPECT. This is compared to < 0.2% based on the derived maps. Comparison of livers with different tumour burden led to errors in the mean absorbed dose to normal liver of

4.7–39.9% from CT delineation compared to 0.007–1.1% from the normal liver map. Comparisons of pre- and post-therapy absorbed dose maps resulted in differences of 1.5–4.3% and 0.007–0.004% for CT outlines and the normal liver map respectively. Similarly for mean BED differences were 0.8–7.0% compared to 1.3–1.6%. **Conclusions** The methodology allows an accurate mean absorbed dose to be calculated for a normal liver distribution. Given knowledge of the tumour/normal liver segmentation and the PSF of both ^{99m}Tc and ^{90}Y SPECT, quantitative comparison of pre- and post-therapy dosimetry can be achieved.

EP460

The impact of missing attenuation or scatter correction on ^{99m}Tc MAA SPECT based dosimetry for ^{90}Y microsphere liver radioembolization

F. Botta¹, M. De Nile², S. Vitali³, M. Mira³, L. Lorenzon⁴, M. Ferrari¹, M. Pacilio⁵, C. Chiesa⁶, M. Cremonesi¹; ¹European Institute of Oncology, Milan, ITALY, ²Postgraduate School of Medical Physics, University of Milan, Milan, ITALY, ³Postgraduate school of Medical Physics, University of Milan, Milan, ITALY, ⁴Postgraduate school of Medical Physics, Sapienza University, Rome, ITALY, ⁵San Camillo Forlanini Hospital, Rome, ITALY, ⁶Istituto Nazionale per lo Studio e la Cura dei Tumori, Milan, ITALY.

Aim This study investigates the impact of missing SPECT attenuation and scatter corrections on dosimetric estimates for radioembolization.

Materials and Methods ^{99m}Tc -MAA SPECT of 63 patients undergoing radioembolization in 2 institutions (IEO and INT) were reconstructed with different combinations of attenuation (AC) and scatter (SC, Double Energy window subtraction) corrections: AC_SC, AC_NoSC, NoAC_SC, NoAC_NoSC (IEO:25 patients, metastasis, selective/lobar treatments; INT:38 patients, hepatocarcinoma, lobar treatments). “Total liver” (TL) and “lesion” (L) were drawn on CT aligned with SPECT. “Healthy liver” (HL) was TL-L. “Irradiated liver” (IL) included voxels perfused by ^{99m}Tc -MAA. “Irradiated healthy liver” (IHL) was IL-L. Relative calibration was adopted. Absorbed dose was calculated at voxel level. Average absorbed dose (D_m) and Equivalent Uniform Dose (EUD) were calculated for L; D_m for HL and IHL. Datasets obtained with different reconstructions were compared with Wilcoxon paired test. The difference $D\%$ was calculated between each dataset from AC_NoSC, NoAC_SC, NoAC_NoSC and the reference AC_SC. At IEO, comparison with AC_SC was performed at voxel and differential Dose Volume Histogram level calculating the Normalized Mean Square Difference ($\text{NMSD}_{\text{voxel}}$, NMSD_{DVH}). **Results** For all parameters of L, HL, IHL, differences between AC_NoSC and AC_SC were statistically significant. Difference between NoAC_SC and AC_SC was not statistically significant for HL (IEO and INT patients), while it was significant for L only for INT patients. For L: smallest range of $D\%$ (D_m) with AC_NoSC: [-20%,0]. With NoAC_SC: [-40%,+30%]. For HL: smallest range with NoAC_SC: [-5%,+7%] at IEO, [-13%,+11%] at INT. With AC_NoSC: [0,+30%] at IEO, [-21%,+34%] at INT. For IHL: smallest range with NoAC_SC: [-9%,+6%] at IEO, [-30%,+10%] at INT. With AC_NoSC: [-40%,0] at IEO, [-24%,+29%] at INT. NoAC_NoSC always yielded worst results. For HL and IHL, $\text{NMSD}_{\text{voxel}}$ was systematically lower for AC_NoSC, NMSD_{DVH} for NoAC_SC instead. No trend was observed for L. **Conclusion** Scatter correction significantly affects macroscopic dosimetric estimates and DVH, especially for HL. L: despite AC_NoSC parameters significantly differ from AC_SC, difference range is smaller with AC_NoSC, (systematic underestimation within -20%). HL: despite AC_NoSC parameters significantly differ from AC_SC, at voxel level AC_NoSC map is closer to AC_SC, while with NoAC_SC differences can be higher than noise fluctuations. With patient relative calibration, centers without Attenuation Correction can plan a safe treatment with HL dose difference - compared to AC_SC - within [-13%,+11%].

EP461

Efficacy of Yttrium-90 Time-of-Flight PET/CT in Post Radioembolization Imaging of Microsphere Biodistribution in Radiosynovectomy

M. Masoomi¹, H. Aldousari², S. Alenezi², N. Alnafisi², Q. Siraj³, I. Alshammeri¹; ¹Department of Nuclear Medicine, Adan Hospital, MOH, Kuwait City, KUWAIT, ²I.Jaber Al Ahmed Nuclear Medicine and Molecular Imaging Center, Kuwait City, KUWAIT, ³Department of Nuclear Medicine, Farwaniya Hospital, MOH, Kuwait City, KUWAIT.

Introduction & Purpose: ^{90}Y bremsstrahlung scintigraphy suffers from a low spatial resolution, ranging between 11 to 15 mm depending on the choice of energy window, collimator, and image processing. ^{90}Y bremsstrahlung activity on SPECT/CT often appears smooth and diffuse, with ill-defined margins, which are difficult to distinguish from closely adjacent activity foci. As a result, assessment of activity within sub centimetre tumours or tumour vascular thrombosis are often suboptimal on ^{90}Y bremsstrahlung SPECT/CT. Quantitatively, ^{90}Y bremsstrahlung scintigraphy is largely inaccurate, despite compensation techniques for attenuation, scatter, and collimator- detector response, making it unsuitable for dose-response analysis. PET/CT represents a technological leap from ^{90}Y bremsstrahlung SPECT/CT, both qualitatively and quantitatively, allowing direct imaging of ^{90}Y microspheres. The study is aiming to investigate feasibility of ^{90}Y PET-CT imaging as a proposed technique to improve overall detection accuracy of ^{90}Y distribution and leakage post radiation synovectomy. **Methods:** The radionuclide ^{90}Y liquid microspheres are used to perform all the phantom tests. A single dose of 185 MBq of ^{90}Y is used in a discrete and expanded ROI within the Knee phantom to imitate the clinical situation as much as possible. ^{90}Y PET/CT phantom test was performed on a conventional time of flight lutetium yttrium oxyorthosilicate scanner and on a state of art SPECT/CT. Images of the knee phantom with the embedded ^{90}Y will be acquired based on predefined acquisition and reconstruction parameters that are specific to the imaging modalities. Specific findings on ^{90}Y PET/CT will be corroborated by ^{90}Y bremsstrahlung SPECT/CT. PET/CT scans will be performed at zero and 60 minutes and 24 hours post injection. The CT scan will be used to map and delineate the ROI. **Results:** It is expected that the outcome of the pilot study establishes further a scientific platform for embarking more specially on the application of ^{90}Y in synovectomy. Equally, the investigators expected the specific phantom study utilizing new technology, namely TOF PET/CT provides an accurate overall detection setup and approach towards radiation synovectomy in relation to leakage and treatment efficacy. **Conclusion:** The study is ongoing and expected to provide a conclusive information about quantitative and qualitative assessment of ^{90}Y radionuclide imaging and establishes a platform for the follow up patient imaging utilizing the state of art TOF PET/CT at the molecular level. The outcome can be used to provide patient specific treatment planning for successive therapies and potentially improving response and therefore the quality patient care.

EP462

Comparison of ^{99m}Tc -MAA Planar Scintigraphy and SPECT/CT for treatment planning with ^{90}Y -labeled Microspheres

I. Torres-Espallardo, B. Ibáñez, M. Carles, M. Falgás, P. Oliván, C. Olivas, D. Pérez-Enguix, P. Bello; Hospital Universitario y Politécnico La Fe, Valencia, SPAIN.

Radioembolization using glass microspheres labeled with yttrium-90 (Therasphere®, MDS Nordion, Canada) is a locoregional treatment established in our center on March 2009. The treatment planning has been performed based on ^{99m}Tc -MAA planar scintigraphy since no SPECT/CT was available at that time in our center. After the acquisition of a SPECT/CT (Bright View XCT) system and provided that the European guidelines

recommend the use of attenuation-corrected SPECT scan for tumor-to-liver ratio (TLR) assessment, we intend to perform the treatment planning using SPECT/CT images. The aim of this work is to present a comparison study between the TLR obtained with both type of images. 22 patients with HCC treated with ^{90}Y glass microspheres were considered. Planar and SPECT acquisitions were performed in all the patients included in this study. The SPECT images were reconstructed using OSEM with attenuation, scatter and decay corrections applied. The TLR for the planar was calculated using manually-drawn regions of interest (ROIs) in the target and tumor areas. For the SPECT images a ROI was generated using a 40%-isocontour of the maximum value observed within the liver. Tumor (TuV) and target (TaV) volumes from SPECT were also compared with the ones obtained from CT. In addition, phantom acquisitions were performed to evaluate the best method for TLR estimation. We have employed alginate in order to reproduce different shapes, sizes and TLRs. Spheres from 11 to 27 cm^3 and cylinders of 250 cm^3 were used to mimic lesions. The inserted activities and TLRs (from 2.5 to 7) were selected to simulate clinical situations. From the analysis of the patient data we have observed that $\text{TLR}^{\text{SPECT}}$ is higher than $\text{TLR}^{\text{Planar}}$ in 64% of the cases. In 82% of the cases the $\text{TaV}^{\text{SPECT}}$ was larger than the one obtained based on CT. On the contrary, $\text{TuV}^{\text{SPECT}}$ were smaller in 68% cases in comparison with CT. When evaluating the phantom data, as expected, $\text{TLR}^{\text{SPECT}}$ were always closer to the reference value than $\text{TLR}^{\text{Planar}}$. In all the cases the TLR was underestimated. For the cylinders, it was observed that the relative error of the discrepancy was only 2.5% in the case of SPECT-images, whereas it was 33% for the planar-images. As suggested from the European guidelines and according to these initial results, attenuation-corrected SPECT images must be employed in TLR estimation. But, in order to reproduce the reference TLR, a better method to determine the tumor and target volume should be defined.

EP463

Late liver toxicity: a bad known complication of radioembolization

M. Mitjavila Casanovas, L. Gutierrez, S. Mendez, R. González, A. Prieto, J. Cardona, R. de Teresa, A. Ruiz; Hospital Puerta de Hierro Majadahonda, MADRID, SPAIN.

Introduction: selective internal radiation therapy (SIRT) allows the local treatment of colorectal cancer liver metastases (CRCLM) with Yttrium-90 microspheres. Although its use as salvage therapy in chemo-refractory liver disease is established, the progressive use in earlier stages (1st and 2nd line), could lead to poorly identified late toxicities. Radiation-induced liver disease (RIELD) is a sinusoidal obstruction syndrome which typically manifests 4-8 weeks post SIRT. Portal hypertension (PHT) is not considered an expected adverse event with SIRT. **Patients and methods:** A retrospective review of 20 cases followed in our hospital after SIRT of CRCLM is performed. Clinical variables, previous and post-SIRT treatments received are collected. A radiological assessment of the cases expressly seeking signs of HTP is made. **Results:** four/ 20 otherwise healthy patients with synchronous liver only CRC metastasis treated with SIRT in first to fourth line, developed late PHT. Two cases were extensively studied with transjugular liver biopsy and hepatic venopressure gradient. Hepatic failure was the final cause of death in three patients, two of them with demonstrated high figures of bilirubin (more than 20 mg/dl) with no bile duct obstruction. This hepatic failure occurred in later stages of the disease with long-term survivals after SIRT. **Conclusions:** Late hepatotoxicity after SIRT could be more common than described up to now. The use of oxaliplatin and SIRT could have additive effects regarding liver toxicity. It is important that radiologists pay attention to the signs of PHT (varices, splenomegaly, decreased liver volume) monitoring images, as it can be key to identifying this adverse effect.

EP464

Comparison of dosimetric methods in ^{90}Y microspheres hepatic radioembolization related to dose-response evaluation

E. Richetta, M. Manfredi, M. Pasquino, C. Cutaia, S. Valzano, L. Radici, M. Tabone, P. Carbonatto, R. Pellerito, M. Stasi; AO Ordine Mauriziano, Turin, ITALY.

AIM ^{90}Y microspheres radioembolization is considered an effective treatment for hepatocellular carcinoma. Even if the importance of a personalized dosimetry is known, which is the most useful dose parameter is still under debate. The aim of this work is to compare doses to tumor calculated with different methods in order to find the dosimetric parameter that best correlates with the patient-response finalized to address patients to surgery. **MATERIALS AND METHODS** 15 intermediate to advanced HCC patients were treated with ^{90}Y resin-microspheres: no dosimetric approach was used to determine the activity to be administered (BSA method). Dosimetry was performed retrospectively on pre-treatment SPECT $^{99\text{m}}\text{Tc}$ -MAA images: mean dose to tumor was calculated using both MIRD (D_{mird}) and Voxel method (D_{voxel} and D_{90}). Following EASL criterion, the response to therapy was evaluated after 1 and 6 months to investigate if some patients could be staged down to surgery. The statistical difference between groups was investigated using Mann-Whitney test; ROC analysis was also performed and significance of difference between AUC was tested (Hanley and McNeil). The same analysis was performed for the administered activity and Tumor-Non Tumor ratio (TNT). **RESULTS** After one month, 10 patients (67%) showed a preliminary complete or partial response (median dose $D_{\text{mird}}=418$ Gy, $D_{\text{voxel}}=454$ Gy, $D_{90}=195$ Gy), while 5 patients were stable or in progression (median dose $D_{\text{mird}}=121$ Gy, $D_{\text{voxel}}=106$ Gy, $D_{90}=68$ Gy). No patient was staged down to surgery. After 6 months, 5 of the 10 responding patients staged down to surgery (median $D_{\text{mird}}=880$ Gy, $D_{\text{voxel}}=570$ Gy, $D_{90}=310$ Gy), while the others 10 patients ($D_{\text{mird}}=152$ Gy, $D_{\text{voxel}}=125$ Gy, $D_{90}=98$ Gy) remained inoperable. Mann-Whitney test showed a statistical difference between groups (p -value: D_{mird} 0.0127, D_{voxel} 0.028 and D_{90} 0.024). AUC calculated on D_{mird} , D_{voxel} and D_{90} were 0.900, 0.860 and 0.870 respectively and when compared no statistical difference were observed among dose calculation methods. The best dose values to separate groups were $D_{\text{mird}}=418$ Gy, $D_{\text{voxel}}=213$ Gy and $D_{90}=160$ Gy. AUC calculated with the administered activity showed a lower value (0.710) and the p -value (0.198) showed no correlation to response, as well as TNT analysis, confirming the need of a personalized dosimetry. **CONCLUSION** Dosimetry can be useful to identify patients eligible for surgery and can be predictive of patient response. The results show that the investigated dosimetric methods are equivalent in calculating the activity to be administered to the patient.

EP465

Quality assurance of activity administration in Selective Internal Radiation Therapy (SIRT)

H. Levillain, G. Marin, B. Vanderlinden, T. Guiot, M. Vouche, P. Flamen; Jules Bordet Institut, Brussels, BELGIUM.

Abstract: SIRT dosimetry needs accurate and precise determination of administered ^{90}Y microspheres activity. With the assessment of ^{90}Y PET/CT, it is possible to quantify the administered activity. Our aim was to evaluate the difference between the computed administered ^{90}Y microspheres activity and the activity measured on PET/CT images. **Methods:** The study was based on 54 patients treated by liver ^{90}Y radioembolisation. Predictive treatment dosimetry was performed on $^{99\text{m}}\text{Tc}$ -MAA SPECT/CT, including the definition of $^{99\text{m}}\text{Tc}$ -MAA distribution volume and ^{90}Y microspheres activity prescription. Selected patients had no quantifiable $^{99\text{m}}\text{Tc}$ -MAA shunt to non-target organs. The activity to be injected was prepared in accordance with the prescription and measured with the radionuclide

calibrator CRC-15R, Capintec. Pre- and post-injection dose rates of injection box were measured to evaluate the residual activity and compute administered activity. PET/CT images were acquired on a Discovery 690 PET/CT (GE-Healthcare) with two bed positions of 30 minutes and voxels size: 2.7×2.7×3.3mm. The images were reconstructed with 3D OSEM algorithm (18 iterations, 3 subsets, 13.7mm FWHM Gaussian post-filtering) with all available corrections according to the Quantitative Uptake Evaluation in SIR-Spheres Therapy (QUEST) study recommendations. Image processing was performed with Pmod software v3.6. PET/CT was anatomically registered to SPECT/CT and ^{99m}Tc-MAA distribution volume contours were projected on PET. Registration was corrected in case of matching errors assessed by visual inspection. ⁹⁰Y microspheres activity was then quantified. Student test was performed and relative difference between computed injected activity and activity quantified on PET/CT was calculated. Mean ± SD of errors were computed. Plots of the errors as a function of treated volume size and as a function of the amount of injected activity were performed in order to study their correlations. **Results:** The mean relative difference was 4.7±13.9%. The differences between measured and quantified activities were not statistically significant, p=0.51. No correlation could be demonstrated between relative difference and either the treated volume or the amount of activity. **Conclusion:** Our study has shown that, despite known errors in radionuclide calibrator measurement and PET/CT quantification, the relative difference between them is relatively low. It demonstrates the feasibility of a quality assurance process to improve precision and accuracy of dosimetry.

EP466

Safety And Efficacy Of Radiation Segmentectomy

A. Ozgen¹, N. Alan Selcuk², T. Toklu², H. O. Ozdemir¹, L. Kabasakal³, ¹Yeditepe University Hospital, Dept. of Radiology, Istanbul, TURKEY, ²Yeditepe University Hospital, Dept. of Nuclear Medicine, Istanbul, TURKEY, ³Istanbul University, Cerrahpasa Medical School, Dept. of Nuclear Medicine, Istanbul, TURKEY.

Aim; To determine safety and efficacy of high dose superselective radioembolization in patients with primary or secondary tumors who were not suitable for surgery or percutaneous ablation. **Materials-methods;** 10 patients underwent radioembolization with ⁹⁰Y loaded microspheres with superselective catheterization. Three patients had cholangiocarcinoma, 3 patients had metastasis of colorectal carcinoma and 4 patients had metastatic breast carcinoma. Mean tumor diameter was 59 mm (range 32-87 mm). Four of the patients had liver only disease while rest had liver dominant disease. Radioembolization was the first choice of treatment in patients with cholangiocarcinoma while rest of the patients had systemic chemotherapy also. ^{99m}Tc macroalbumine aggregate injections were made for dose calculation and to explore extrahepatic activity. Mean tumor dose was calculated as 267 Gy (range, 210-450 Gy) and mean tumor free liver parenchyma dose was calculated as 82 Gy (range, 43-110 Gy) using Medical Internal Radiation Dosimetry (MIRD) formulation. Eight patients had single injection of ⁹⁰Y loaded microspheres while 1 had double injections and 1 had triple injections in the same session. Mean time of follow-up was 10 months (range 5-14 months). **Results;** Complete response were noted in 8 of 10 patients while partial response were noted in 2 which took 210 Gy of calculated tumor dose. In the follow-up period no recurrence was noted in enpatients with complete response. Progression was noted in non-responding areas in patients with partial response. No major complication was noted during or after the procedures. Liver function tests remained within normal ranges. Leukopenia and thrombocytopenia noted in second week disappeared in forth week in 3 patients. **Conclusion;** Considering our small group of patients, high dose superselective radioembolization might be a safe and effective method in the treatment of primary and metastatic malignancies of the liver. We also concluded that area of injection might have not covered the whole tumor in patients with partial response.

EP468

Comparison of Standard and Superselective Transarterial Radioembolization

N. Alan Selcuk¹, A. Ozgen², I. Karaaslan³, T. Toklu¹, O. Sonmez⁴, O. Eren⁴; ¹Yeditepe University Hospital, Dept. of Nuclear Medicine, Istanbul, TURKEY, ²Yeditepe University Hospital, Dept. of Radiology, Istanbul, TURKEY, ³Yeditepe University, Dept. of Physics, Istanbul, TURKEY, ⁴Yeditepe University Hospital, Dept. of Oncology, Istanbul, TURKEY.

Aim: To compare standard and superselective transarterial radioembolization (TARE) using microspheres loaded with Yttrium-90 in the treatment of primary and metastatic tumors of the liver in terms of safety, efficacy and technique. **Methods:** A retrospective analysis were performed on 39 adult patients with primary (4 patients) and secondary (35 patients) tumors of the liver who underwent standard TARE (28 patients) and superselective TARE (11 patients). Mean treatment doses, application techniques, complications and response to treatment in the second and sixth months were compared. Treatment doses were calculated using medical internal radiation dosimetry. Treatment results were categorized as total response, partial response, and no response or progression of disease in the targeted area. Follow-up of the patients were made by using PET-CT with contrast enhanced magnetic resonance imaging and/or computed tomography. **Results:** Total or partial response to treatment were observed in all patients in superselective group and 22 (79%) patients in standard group in the first and second follow-up. Mean tumor dose and mean healthy irradiated liver dose were significantly higher in superselective group while whole liver dose was significantly lower. Mean time for each treatment session for superselective group were significantly longer than standard group. Multiple injections were needed in two patients in superselective group. Mild angiographic complications were seen in 5 (45%) patients in superselective group and 3 (11%) patients in standard group. Mild to moderate liver toxicity was not seen in superselective group. Post-radioembolization syndrome were observed in 4 (36%) patients in superselective group and in 10 (36%) patients in standard group. Hospitalization was not required in any patient. **Conclusion:** Superselective TARE seems superior in comparison to standard TARE in terms of efficacy and safety and therefore might be preferred in suitable patients in the treatment of primary and metastatic malign tumors of the liver.

EP469

Calculation And Measurement Of Absorbed Doses For Non Uniform Activity Distributions In Liver Radioembolization Using 90Y-PET Imaging

M. D'Arienzo¹, M. Pimpinella¹, M. Capogni¹, M. Tapner², E. Spezi³, N. Patterson⁴, P. Chiaramida⁵, L. Filippi⁶, A. Fischer⁷, T. Paulus⁷, F. Mariotti⁸, P. Ferrari⁸, O. Bagni⁶; ¹ENEA, National Institute of Ionizing Radiation Metrology, Via Anguillarese 301, 00123, Rome, ITALY, ²SIRTEX, North Sydney 2060, NSW, AUSTRALIA, ³Cardiff University, Cardiff, UNITED KINGDOM, ⁴Department of Medical Physics, Velindre Cancer Centre, Cardiff, UNITED KINGDOM, ⁵GE Healthcare Medical Systems, Milano, ITALY, ⁶Nuclear Medicine Department, Santa Maria Goretti Hospital, Latina, ITALY, ⁷Philips Technologie GmbH Innovative Technologies, Research Laboratories Pauwelsstr. 17, 52074, Aachen, GERMANY, ⁸ENEA, Institute of Radiation Protection, Bologna, ITALY.

Introduction. Since the introduction of liver radioembolization with ⁹⁰Y-microspheres there has been an increasing interest in the assessment of absorbed doses. The recent availability of high-resolution ⁹⁰Y-PET images further stimulated research on this topic. The aim of the present phantom study is to investigate the accuracy of absorbed dose

calculations comparing various dose algorithms with experimental measurements. First we calculated the absorbed dose to the hepatic lesion of an anthropomorphic phantom using a number of well-established dose algorithms using ^{90}Y -PET images. Then we measured the absorbed dose to the tumour using LiF:Mg,Cu,P TLDs inside a cylindrical phantom filled with a homogenous $^{90}\text{YCl}_3$ solution. A comparison between calculated and measured absorbed dose was finally carried out. **Materials and methods.** Acquisitions were performed with a GE Discovery ST PET/CT scanner using an anthropomorphic phantom provided with a lesion insert. The first scan was performed with an activity concentration of 5.5 MBq/mL for the lesion and 0.89 MBq/mL for the liver background. The phantom was then acquired at days 4, 5, 6 and 12. Absorbed doses were calculated using different algorithms: I) Direct Monte Carlo (MC) using Raydose II) Kernel convolution using Philips Stratos III) Local-deposition (LD) IV) MC technique considering a uniform activity distribution V) MIRDO approach. Measurements of absorbed dose to the tumour region were performed using six home-made liver lesions each filled with an activity concentration of about 6.7 MBq/mL $^{90}\text{YCl}_3$. Three TLDs encapsulated by a waterproof envelope were placed into each simulated liver tumour. **Results.** Investigated dose algorithms provided dose estimates with deviations below 9%, except for dose calculations performed on day 1, where the standard deviation over the average absorbed doses was 20%. LD, MIRDO approach and Kernel-convolution methods provided comparable absorbed doses with average deviations below 6%. The measurement of absorbed dose to water from ^{90}Y using TLDs turned out to be a viable technique, providing a relative combined standard uncertainty on each absorbed dose measurement below 4%. Measured doses were consistent with absorbed doses calculated using full MC techniques with an agreement within 3%, well within the stated uncertainty. **Conclusions.** All dose algorithms provided comparable dose estimates within standard deviations. Due to its immediate use and ease of implementation LD dose algorithm may result practical in a clinical environment where resource-intensive computational systems are not always available. For the first time dose calculations performed on ^{90}Y -PET images were successfully compared with dose measurements performed with TLDs.

EP470

Personalized Dosimetry planning in Radioembolization with ^{90}Y -microspheres: Methodological Considerations

V. Moran, E. Prieto, A. Zubiria, L. Sancho, M. Rodriguez-Fraile, B. Barbés, L. Ramos, J. M. Martí-Climent; clinica universidad de navarra, pamplona, SPAIN.

Aim: Treatment planning based on proper dosimetry plays an important role in radioembolization outcomes. The aim of this study was to compare different currently available dosimetry methods based on ^{99m}Tc -MAA SPECT/CT and to evaluate the impact of the calibration factor of the SPECT scanner. **Materials and methods:** Retrospective dose quantification was performed on 14 patients with liver malignancy that had undergone ^{99m}Tc -MAA scan for planning radioembolization with ^{90}Y resin microspheres. Different dosimetry approaches were investigated, applying different calibration factors (CF) and calculation methods. The patient specific CF was extracted from the total counts in the SPECT planes containing liver tissue. Those counts were supposed to be proportional to the administered activity corrected by the lung shunt fraction, previously determined by planar scintigraphy. The experimental CF for the SPECT tomograph was obtained from total counts measured in a series of 10 phantom SPECT studies filled with ^{99m}Tc ($183 \pm 29\text{MBq}$). Two voxel-based dosimetry approaches were considered: Dose Point-Kernel (DPK) convolution with the kernels of Lanconelli database and Local Deposition Method (LDM) with a self-radiation factor of 1.35 mGy/(GBq.s). Differences between LDM and DPK methods were assessed by voxel based subtraction. CT scan was used to contour the whole liver.

The mean absorbed doses in the liver were calculated for each method. Statistical analysis was performed. **Results:** Experimental CF was estimated to be 4.07 ± 0.13 Bq/counts. Patient specific calibration factor was 5.48 ± 1.85 Bq/counts (U-Mann-Whitney-test $p < 0.01$). The mean deviation in absorbed dose due to the SPECT calibration method was $34 \pm 44\%$. Due to the uncertainty in the determination of the actual activity in the liver, experimental calibration should be more suitable. For LDM and DPK methods, mean absorbed dose in liver tissue (based on experimental CF) was 16.1 ± 10.8 Gy and 15.2 ± 10.6 Gy, respectively (paired t-test $p < 0.01$). Although global differences in the whole liver are small, important voxel-by-voxel differences have been observed. In fact, differences greater than 10 Gy were found in a maximum of 3.6% (mean 1.1%) of the whole liver volume. DPK tends to provide higher absorbed doses than LDM in outer edge of the uptake region and lower doses in the central area. **Conclusion:** The use of a proper calibration factor is more critical than the use of different dose deposition methods. Different 3D-dosimetry approaches yield important differences in final absorbed doses that can have a substantial impact in treatment planning.

EP471

Yttrium90 synovectomy in the management of chronic knee arthritis: results after 6 months

J. Navarro Fernandez¹, R. Asensio Sanchez², L. Frutos Esteban¹, L. Mohamed Salem¹, M. Ibañez Ibañez¹, V. Godoy Bravo¹, R. Reyes Marles¹, I. Sime Loayza¹, M. Castellon Sanchez¹, F. Nicolas Ruiz¹, M. Alcaraz Baños², M. Claver Valderas¹; ¹HCU VIRGEN DE LA ARRIXACA, 30120, SPAIN, ²Universidad de Murcia, 30120, SPAIN.

AIM: Radiation synovectomy has been used to treat chronically inflamed joints refractory to treatment using conventional agents. Aim to evaluate the effectiveness of radiosynovectomy with yttrium⁹⁰ in patients with rheumatic diseases, villonodular synovitis and other arthropathies. **Materials and methods:** We performed a retrospective study in which we reviewed the medical records of 20 patients who have been subjected to one radiosynovectomy radioactive yttrium⁹⁰ for a period of three years. Doses of 185 MBq were used in the all patients. **Results:** Altogether, 50% of the treated patients showed response: 10% of treated patients were more than 6 months without recurrence of the disease; 15% of patients were without inflammation or pain for a period of 3-6 months; and, 25% of patients had a local recurrence of the disease within three months after the application of treatment with radioactive isotope. **Conclusion:** Radiosynovectomy is a safe treatment for the patient can decrease the inflammatory joint pain patient for extended periods.

EP472

Development of ^{188}Re -Functionalized Microspheres as a Second Generation Radioembolization Agent for Hepatocellular Carcinoma Treatment

J. C. De La Vega¹, K. Saatchi¹, C. Rodríguez-Rodríguez^{1,2}, P. L. Esquinas², M. Bokharai¹, I. Moskalev³, A. S. Thakor⁴, D. Liu⁴, A. Celler⁵, U. O. Häfeli¹; ¹Faculty of Pharmaceutical Sciences, University of British Columbia, Vancouver, BC, CANADA, ²Department of Physics and Astronomy, University of British Columbia, Vancouver, BC, CANADA, ³Vancouver Prostate Cancer Centre and Department of Urologic Sciences, University of British Columbia, Vancouver, BC, CANADA, ⁴Department of Interventional Radiology, Vancouver General Hospital, University of British Columbia, Vancouver, BC, CANADA, ⁵Department of Radiology, University of British Columbia, Vancouver, BC, CANADA.

AIM: This study aims to develop and evaluate the efficacy and safety of monosized, biodegradable microspheres (MS) with ^{188}Re for radioembolization of hepatocellular carcinoma (HCC).

Radioembolization is the administration of MS labeled with a β^- -emitting radionuclide into the hepatic artery, which provides 80–90% blood supply to liver tumors. First generation radioembolization agents, TheraSpheres® and SIR-Spheres®, consist of non-uniformly sized MS with ^{90}Y , which can only be produced in nuclear reactors. Additionally, biodistribution studies are challenging due to the difficulty of imaging ^{90}Y 's bremsstrahlung emissions. **MATERIALS AND METHODS:** A microfluidic technology was used to produce MS made of a PLA-PEG copolymer functionalized with a customized chelator ("chelomer") for ^{188}Re binding. The effect of the chelomer concentration, PEG content, and reaction conditions on the labeling efficiency was evaluated. An orthotopic HCC animal model was developed in male Sprague Dawley rats. N1-S1 cells (ATCC® CRL-1604), a Novikoff HCC cell line, were injected below the capsule of the left lobe of liver. All injections were performed under ultrasound guidance using an ultra-high frequency transducer (32–56 MHz). A customized catheter for ^{188}Re -MS administration via hepatic intra-arterial catheterization was fabricated. A two-compartment partition model was used to determine a clinically relevant absorbed dose to conduct the study. **RESULTS:** Scanning electron microscopy (SEM) showed that our MS have a narrow size distribution ($D = 40.9 \pm 1.4 \mu\text{m}$, $\text{CV} = 3.4\%$). Thin layer chromatography (TLC) indicated $>80\%$ $^{188}\text{Re}(\text{CO})_3^+$ binding specificity and good stability ($>95\%$ over 24 h). A minimally invasive technique to induce HCC was developed via ultrasound-guided injections. The location, depth, and angle of the injections can be controlled reproducibly. We are currently growing 0.5 cm^3 tumors for treatment with up to 1.7 mCi of ^{188}Re -MS. Biodistribution of the MS and changes in tumor size will be monitored with a pre-clinical SPECT/CT imager (VECTor/CT, MILabs). Levels of hepatic enzymes and proteins will be measured at two different points to evaluate the short- and intermediate-term toxicity. **CONCLUSION:** A second generation radioembolization agent was developed and it is currently being evaluated in an animal model. As ^{188}Re decays by emission of γ photons in addition to β^- particles, ^{188}Re -MS can also be imaged. Hence, it is also feasible to conduct biodistribution studies. Future work revolves around evaluating the theranostic potential of ^{188}Re -MS, conducting MS degradation studies, and evaluating the outcome of using MS with different sizes. For this, we have already produced 20, 30, and $50 \mu\text{m}$ MS.

EP473

Monte Carlo Comparison between four beta-emitting Radionuclides of Interest for Targeted Radionuclide Therapy of Small Tumors: ^{177}Lu , ^{67}Cu , ^{47}Sc and ^{161}Tb

C. Champion¹, C. Morgat², M. A. Quinto¹, P. Zanotti-Fregonara², E. Hindie²; ¹CENBG-CNRS-IN2P3, Gradignan, FRANCE, ²Hopital Haut-Lévêque, Pessac, FRANCE.

PURPOSE: Radionuclide therapy is increasingly seen as a promising option to target micrometastases or minimal residual disease. Copper-67, scandium-47 and terbium-161 have a medium-energy beta-emission which is similar to that of lutetium-177. They offer the advantage of having diagnostic partner isotopes suitable for pretreatment imaging. The aim of this study was to compare the effectiveness of these isotopes at irradiating small tumor volumes. **METHODS:** Electron dose from uniform isotope distributions was assessed with the Monte Carlo code CELLDOSE in spheres of various sizes (from 5 mm down to $10 \mu\text{m}$ diameter). All electron emissions, including beta spectra, Auger and conversion electrons were included. As ^{177}Lu , ^{67}Cu , ^{47}Sc and ^{161}Tb differ in electron energy per decay, doses were compared assuming 1 MeV released per μm^3 , which would result in 160 Gy if totally absorbed. **RESULTS:** In a 5 mm sphere, the four isotopes yielded similar dose deposits per $\text{MeV}/\mu\text{m}^3$ (145 - 149 Gy). The absorbed doses decreased with decreasing sphere size, thus underscoring the difficulty of irradiating micrometastases. ^{161}Tb , however, delivered a higher dose compared to the other isotopes. For instance, in a $100\text{-}\mu\text{m}$ metastasis, dose deposits

were 24.5 Gy with ^{177}Lu , 24.1 Gy with ^{67}Cu , 14.8 Gy with ^{47}Sc and 44.5 Gy with ^{161}Tb . Auger and conversion electrons accounted for 71% of ^{161}Tb dose in this $100\text{-}\mu\text{m}$ metastasis. The differences between radionuclides further increased in cell-sized spheres. In a $10\text{-}\mu\text{m}$ cell, the dose delivered by ^{161}Tb was 3.6 times higher than that from ^{177}Lu , 4.1 times that from ^{67}Cu and 8.1 times that from ^{47}Sc . **CONCLUSION:** Terbium-161 can effectively target micrometastases and single tumor cells thanks to its decay spectrum that combines medium-energy beta emission and low-energy conversion and Auger electrons. These results are in agreement with some recent studies on cell cultures and tumor xenografts.

EP474

The development of materials for a practical use in additive technologies with specified Hounsfield indexes for the creation of individual radiotherapy phantoms

S. Stuchebrov¹, I. Miloychikova¹, V. Kudrina², A. Melnikov¹, M. Pereverzeva¹; ¹Tomsk Polytechnic University, Tomsk, RUSSIAN FEDERATION, ²Siberian State Medical University, Tomsk, RUSSIAN FEDERATION.

Currently, the planning of radiotherapy procedures is mainly carried out by computational methods based on the use of the Monte Carlo method. Modern dosimetric planning systems allow to model the character of the interaction of radiation and tissue. However, these methods are limited in accuracy as long as they allow to estimate the distribution of isodose curves in human tissues only approximately. The experimental planning of radiotherapy procedures with the use of individual anatomically precise phantoms will eliminate the inaccuracies of calculation methods. The purpose of this work is to develop a method which allows to create materials with specified HU suitable for rapid prototyping devices by Fused deposition modeling. The ability to carry out a rapid prototyping of organs of particular patients including simulated pathologies will allow to conduct the most accurate planning of gamma-radiation therapy procedures, which will reduce their negative consequences. The use of additive technologies allows to decrease the period of manufacturing of individual phantoms. It is necessary to develop a method which allows to manufacture consumables with specified HU in order to apply this technology. This problem can be solved by manufacturing a mixture of base material founded on ABS plastic and metal additives with different concentrations. The value of HU ranges from -900 to +1000 in human body. However for soft tissues it ranges from -150 HU to +100 HU. Thus it is enough to create filaments with specified Hounsfield units within at least 10 HU in the range of not less than -150 to +150. The mathematical model was created. It allows to calculate the interaction of radiation in plastics which have different impurity concentrations. The experimental samples of materials with different density have been prepared. The filaments for rapid prototyping were produced from these materials. The test samples were printed from these filaments. The values of HU of manufactured materials and printed samples were determined. The developed method allows to obtain materials with specified HU. The obtained filaments are suitable for 3D-printers. Tomography studies have shown that the material filling density is not 100% during the printing of test samples. This problem can be solved by adjustment the printing process. The further work will be aimed for the creation of phantom by the use of the FDM. The phantom will simulate human tissue of a real patient based on his tomogram.

EP475

Virtual CT for Improved Targeted Radionuclide Therapy Dosimetry

G. S. Mok, T. Li; University of Macau, Macao, CHINA.

Aim: Previously we showed that non-rigid registration on sequential CT images is superior to sequential SPECT in 3D targeted radionuclide therapy (TRT) dosimetry. However, sequential CT is not a common clinical

protocol due to the radiation concern. This study proposed a virtual CT (vCT) method for potential improved dose estimation with minimal increase of radiation dose. **Materials and methods:** We modeled 3 anatomical variations each with 3 In-111 Zevalin activity distributions, i.e., a population of 9 phantoms, using the digital 4D XCAT phantom with models of random local organ deformation, whole-body movement, normal respiratory and cardiac motion. We simulated SPECT acquisitions of 128 projections over 360° at 1, 12, 24, 72 and 144 hrs post-injection using an analytical MEGP projector. Attenuation, scatter and collimator-detector response were modeled in the realistic noisy projections which were then reconstructed using OS-EM with 128 updates incorporating full compensations. The corresponding attenuation maps of the phantoms served as the “real” CT (rCT) images. We generated vCT images by registering the whole-body 24-hr CT with the SPECT reconstructed images at other time points using the affine+b-spline method. Organ-by-organ non-rigid registrations for sequential SPECT, rCT and vCT images were performed after segmenting the organs-of-interest on the respective images. For CT-based registration, the acquired motion vectors were later applied to register the SPECT images. Voxel-by-voxel integration was applied on registered images over 5 time points, followed by convolution with a Y-90 dose kernel to generate dose images. Organ dose, differential and cumulative dose volume histograms (DDVH & CDVH) were generated for liver, spleen, kidneys and lungs. **Results:** For the organ dose, the results of vCT were superior to SPECT and were similar to those of rCT registrations with slightly larger SD, i.e., $-5.08 \pm 2.63\%$ vs. $-8.66 \pm 2.83\%$ vs. $-6.4 \pm 2.26\%$ for liver and $-6.02 \pm 4.28\%$ vs. $-14.81 \pm 4.91\%$ vs. $-6.28 \pm 3.29\%$ for spleen respectively. For kidneys and lungs where SPECT registration was not feasible due to low organ uptake, vCT registration also approached to rCT, i.e., $1.90 \pm 2.98\%$ vs. $1.33 \pm 2.81\%$ and $-2.61 \pm 2.66\%$ vs. $-2.21 \pm 1.16\%$ respectively. Results of DDVH and CDVH were consistent with the organ dose. **Conclusion:** The vCT eased the organ definition problem on the SPECT images especially for low uptake organs and its results were comparable with the rCT registration. It can effectively improve the TRT dosimetric results if there is only 1 CT available in the sequential imaging protocol, reducing the substantial increase of radiation burden from repeated CT scans.

EP476

Image-based internal dosimetry of Cu-64 and Tc-99m labeled radiopharmaceuticals in mice using Monte Carlo method

S. Woo¹, Y. Park¹, K. Kim¹, Y. Lee¹, B. Moon², B. Lee², J. Kang¹, S. Lim¹; ¹Korea Institute of Radiological and Medical Sciences, Seoul, KOREA, REPUBLIC OF, ²Seoul National University Bundang Hospital, Seoul, KOREA, REPUBLIC OF.

The aim of this study was to evaluate the image-based internal dose of radiopharmaceuticals in mice. We performed characteristics of radiopharmaceuticals in the mice organs and tumors using Monte Carlo simulation. The images of Cu-64 and Tc-99m labeled radiopharmaceuticals were acquired using a dedicated small animal PET/CT/SPECT scanner (Inveon, Siemens Healthcare, Malvern, PA). The tumor bearing mouse was injected with 3.7 MBq of Cu-64 labeled radiopharmaceuticals and the other mouse was injected with 18.5 MBq of Tc-99m labeled radiopharmaceuticals. Mice images were acquired at 6 time points after the radiotracer administration (Cu-64: 1, 2, 6, 24, 48, and 70 h, Tc-99m: 0.5, 1, 2, 3, 6, and 24 h). The image of tumor and lung were segmented by mean-based region growing 3D segmentation method and manually. Residence times were computed via time activity curves of the acquired region segmented PET and SPECT series data. The absorbed fractions were calculated using segmented CT images density information. S-values were calculated using Geant4 Monte Carlo method. Internal doses were calculated by residence times of PET and SPECT images and Monte Carlo-calculated S-values. In the case of Cu-64 labeled radiopharmaceuticals, representative residence time of the lung was 1.51 MBq-h/MBq and tumor was 4.72 MBq-h/MBq. Monte Carlo simulated S-value of the lung and tumor

were $1.31E-01$ and $3.28E-01$ mGy/MBq, respectively. An Estimated absorbed dose of the lung was $2.03E-01$ and tumor was $1.56E-01$ mGy/MBq. In the case of Tc-99m labeled radiopharmaceuticals, representative residence time of the lung was $1.10E-04$ MBq-h/MBq and tumor was $4.72E-02$ MBq-h/MBq. Monte Carlo simulated S-value of the lung and tumor were $3.88E-01$ and $6.15E-02$ mGy/MBq, respectively. An Estimated absorbed dose of the lung was $1.56E-01$ and tumor was $9.10E-02$ mGy/MBq. We performed the internal dose calculation of Cu-64 and Tm-99m labeled radiopharmaceuticals. Image-based Monte Carlo method will become available to calculate the object specific dose of theragnostics radiopharmaceutical in the total body.

EP477

Simulation of radioactive sources in a bone cavity to evaluated the activity quantification in bone marrow dosimetry

M. Salas, S. Schlögl, J. Tran-Gia, C. Kesenheimer, H. Hänscheid, M. Lassmann; University Würzburg, Department of Nuclear Medicine, Würzburg, GERMANY.

AIM: In diagnostic and therapeutic nuclear medicine, the determination of absorbed doses in the bone marrow is of great importance. Due to the tissue composition, the activity distribution in bone marrow can be highly inhomogeneous. Therefore, the aim of this study was to examine the general feasibility of an activity quantification of radioactive sources in a bone cavity using SPECT/CT and PET/CT imaging. **MATERIALS AND METHODS:** An in vitro phantom was built from a small fillable vial (volume: 0.32 ml) surrounded by a bovine femur segment. This setup was mounted in a 3D-printed (Renkforce RF1000) attachment system for a body phantom (IEC 61675-1). Activity distributions inside a human vertebra were simulated by filling the vial with different isotopes (SPECT: Tc-99m, Lu-177, I-131. PET: F-18, I-124) and filling the rest of the bone cavity with different fat/water ratios (100/0, 50/50, 0/100). SPECT/CT (Siemens Symbia T2) and PET/CT (Siemens Biograph mCT) imaging was performed with each of these combinations and the source activity for different VOIs (centered in the maximum of the activity distribution) was quantified. In addition, deviations between the image quantified activities and the activities measured in a dose calibrator (Venstra instruments VIK-202) or in a high purity Germanium Detector (Canberra, Germany) was performed. **RESULTS AND DISCUSSION:** A strong dependence of the quantification on the size and position of the VOIs was observed, which can be explained by partial volume effects caused by the small source volume. For 100% water inside the bone cavity, the Tc-99m quantification showed a deviation of -3.1% in a VOI of 3 ml, Lu-177 a deviation of -2.4% in a VOI of 15.9 ml, and I-131 a deviation of -4.2% for a VOI of 24.8 ml (the minus sign represents an underestimation of the activity). The increase in VOI is related with the sources size and the image resolution for each collimator. For the PET isotopes, fixed VOIs of 16.4 ml including the whole source and centered in the bone cavity were used. Deviations of 8.9% and 8.6% were registered for F-18 and I-124, respectively. No dependency of the activity quantification with respect to the fat/water concentration inside of the bone was found ($p=0.972$). **CONCLUSION:** This phantom study demonstrates the general feasibility of a quantification of radioactive sources in bone marrow dosimetry using SPECT/CT and PET/CT imaging. Furthermore, no dependency of the quantification on the fat/water ratio in the bone marrow was observed.

EP-20 – Sunday, October 16, 2016, during Exhibition hours, e-Poster Area
Do.MoRe: PSMA

EP478

Normal distribution of salivary gland tissue on ⁶⁸Ga-PSMA PET-CT

T. Klein Nulent¹, M. Valstar², B. de Keizer¹, A. Al-Mamgani², L. Smeets², R. van Es¹, W. Vogel²; ¹University Medical Center Utrecht,

Utrecht, NETHERLANDS, ²The Netherlands Cancer Institute, Amsterdam, NETHERLANDS.

Background: Functional imaging of prostate-specific membrane antigen (PSMA) with radiolabeled PSMA ligands with PET-CT is increasingly used for detection and (re)staging of prostate cancer. Remarkably, the PSMA epitope is also highly expressed in normal lacrimal and major salivary gland tissue. This results clearly in high tracer uptake in the major salivary glands (parotid, submandibular and sublingual glands) and lacrimal glands on PSMA-PET. In addition, the presence of minor mucosal salivary glands may be visualised, for example in the palate, the nasal cavity and the mucous glands of the supraglottic larynx. This study aimed to describe the distribution and characteristics of normal salivary gland tissue on PSMA-PET in order to facilitate interpretation of the head and neck area. **Methods:** The normal distribution of salivary gland tissue was analysed in 30 consecutive patients who underwent total body PSMA-PET for evaluation of disseminated prostate cancer. These patients did not have any known disorder of the salivary glands or history of irradiation in the head and neck area. Tracer uptake in the major and minor salivary glands and lacrimal glands was recorded by calculating the maximum standardized uptake value (SUV_{max}) on PET images reconstructed according to research guidelines of the European Association of Nuclear Medicine using the Lean Body Mass formula. **Results:** The PSMA-PET scan clearly depicts anatomical areas of salivary gland cell concentration by visualising high tracer uptake. The mean SUV_{max} for the major salivary gland locations were as follows: parotid gland 12.2 g/ml (range 5.2–22.9); submandibular gland 11.6 g/ml (6.0–19.3); sublingual gland 4.4 g/ml (1.4–9.6). PSMA uptake was also seen in the lacrimal glands: SUV_{max} 6.1 g/ml (range 2.5–13.6) and in oropharyngeal mucosal gland locations: Waldeyer's ring 4.3 g/ml (2.2–7.7); nasal cavity 3.4 g/ml (2.2–5.5); palate 2.3 g/ml (1.4–3.6) and the mucous glands of the supraglottic larynx 2.6 g/ml (1.7–3.8). The mean distribution in liver and kidneys were 3.7 g/ml (2.4–5.0) and 29.2 g/ml (16.9–44.5) respectively. **Conclusion:** PSMA-PET provides a very sensitive detection of salivary gland tissue including mucosal localisations. Familiarity with the normal distribution pattern outlined in this study can contribute to adequate interpretation of PSMA-PET imaging. Potential applications may also include: better analysis of salivary gland-sparing techniques in radiotherapy of the head and neck; quantification of salivary gland function; targeted therapy in salivary gland neoplasms; the visualisation of presumed ectopic or heterotopic salivary gland tissue and the detection of residual salivary gland tissue in recurrent plunging ranulas.

EP479

The ⁶⁸Ga/¹⁷⁷Lu-Theragnostic Concept in PSMA-Targeting of Prostate Cancer: A Long(er) Way to Go?

L. Scarpa, S. Buxbaum, D. Kendler, J. Bektic, C. Decristoforo, L. Gruber, L. Geraldo-Roig, B. Nilica, C. Uprimny, K. Fink, P. Lukas, W. Hominger, I. Virgolini; Department of Nuclear Medicine, Innsbruck, AUSTRIA.

Aim Progression to androgen independence is the first cause of mortality in castration resistant (cr) prostate cancer (PC) patients. For this reason a targeted theragnostic approach based on increased expression of prostate-specific membrane antigen (PSMA) on PC cells is an attractive treatment option. **Methods** Ten consecutive patients with progressive crPC were selected for ¹⁷⁷Lu-PSMA617-ligand therapy on the basis of PSMA-targeted ⁶⁸Ga-PSMA-HBED-CC-ligand PET/CT diagnosis showing extensive and progressive tumour load. Following dosimetry along with the 1st therapy cycle restaging (⁶⁸Ga-PSMA-HBED-CC ligand, ¹⁸F-NaF-PET) was performed after 2 cycles (each 6 GBq given via an intravenous infusion pump, 8 to 10 weeks apart). Further re-stagings were performed

at 8 to 10 weeks after 3 to 4 additional cycles (each 6 GBq, 8 to 10 weeks apart). PET/CT scans were compared to ¹⁷⁷Lu-PSMA617-ligand 24-hour whole body scans and contrast-enhanced dual phase CT. **Results** Dosimetry indicated high tumour accumulation of ¹⁷⁷Lu-PSMA617 (4.8±3.5 Gy/GBq; range 1.2–11.5 Gy/GBq) whereas the dose to all organs was acceptable in all patients for a calculated accumulated activity of 24 GBq. In 3/10 patients who had a partial remission ¹⁷⁷Lu-PSMA617-ligand therapy led to a significant decrease of PSA values (up to <50% of baseline) combined with decreased SUV_{max}-values obtained by ⁶⁸Ga-PSMA-HBED-CC-ligand PET/CT after 3 to 4 therapy cycles. Three other patients showed a mixed response and in 2 patients therapy was terminated after 2 cycles due to progression. ⁶⁸Ga-PSMA-HPED-CC-PET/CT-Response was well correlating to decline of ¹⁷⁷Lu-PSMA617-ligand uptake but not to follow-up with ¹⁸F-NaF PET/CT which in all patients suggested a flair phenomenon and had no relevance in clinical follow-up. The cumulated activity caused in 4/10 patients only a transient haematotoxicity (Grade less than or equal 2) but led to a 25% volume reduction of salivary glands. **Conclusion** Our data suggest that the ⁶⁸Ga / ¹⁷⁷Lu-PSMA-targeted theragnostic concept could evolve into an importance treatment option of metastasised crPC. We conclude that ¹⁷⁷Lu-PSMA617-ligand therapy in patients with crPC is clinically safe and can be effective in patients with progressive crPC. A prospective study is needed to better address the multitude of questions arising with this new treatment modality, especially to timing, dosing and response Evaluation.

EP480

Is Lu-177 PSMA radioligand therapy of prostate cancer safe for patients with single functioning kidney?

A. SINGH, C. Schuchardt, H. Kulkarni, R. P. Baum; ZENTRAKLINIK BAD BERKA GMBH, BAD BERKA, GERMANY.

Aim: Lu-177 PSMA radioligand therapy (PRLT) is a promising therapy option for the management of patients with metastatic castration-resistant prostate cancer (mCRPC). High post-therapy uptake in kidneys has been reported as a concern for nephrotoxicity, and a recent study has reported cases of grade 1–2 deterioration of renal function following Lu-177 PRLT. Hence, we aim to assess the safety of Lu-177 PRLT in patients with mCRPC possessing a single functioning kidney. **Methods:** Since April 2013, 119 patients with mCRPC have undergone 300 cycles of Lu-177 PRLT at our center. Two of 119 (1.68%) patients (P1, P2) had a single functioning kidney. Pre-therapy renal function test (RFT): urea, creatinine, eGFR, and MAG3-scintigraphy based tubular-extraction rate (TER) were performed within 1–2 days prior to PRLT, and follow-up RFT performed 2 weeks later. Dosimetry (MIRD scheme, OLINDA/EXM) was performed in 30 patients to assess renal kinetics of Lu-177 PSMA. **Results:** P1 received 3 cycles of Lu-177 PRLT with cumulative radioactivity of 20.1 GBq (mean 6.7 GBq) in 4 months. Baseline RFT: urea 7.3 mmol/L, creatinine 111.8 micromol/L; post-PRLT: urea 6.3 mmol/L; creatinine 102.7 micromol/L. TER reduced from baseline 140 to 129 ml/min (5%), and was clinically insignificant. P2 received 4 cycles of Lu-177 PRLT with cumulative radioactivity of 22.8 GBq (mean 5.7 GBq) in 6 months. Baseline RFT: urea 11.9 mmol/L, creatinine 82.7 micromol/L; post-PRLT, urea 9.1 mmol/L and creatinine 94.1 micromol/L. TER reduced from baseline 199 to 132 ml/min (26%). eGFR remained >60 for both patients persistently. Renal dosimetry revealed an effective half-life of 39 hours, mean absorbed dose of 1 mGy/MBq (mean 0.4–2.0 mGy/MBq), and mean absorbed dose of 6 Gy/cycle. **Conclusion:** In this small number of patients with a single functioning kidney each, no clinically significant acute

nephrotoxicity was observed. Despite a reduction of TER in one patient assessed prior to the fourth treatment, the renal function tests remained within normal limits. The dosimetry performed revealed favourable tracer kinetics. Long term follow-up of these and other similar patients is warranted to validate these findings.

EP481

Dose absorption estimates of the lower gastrointestinal tract during Lu-177 DKFZ-PSMA-617 therapy in patients suffering from mCRPC

I. Schatka, C. Bartel, U. Heimann, F. Wedel, V. Prasad, C. Furth, H. Amthauer, W. Brenner; Charité, Berlin, GERMANY.

Aim - Internal radiation therapy with lutetium (Lu) -177 labeled prostate-specific membrane antigen (PSMA) is a new therapeutic option in patients with metastatic castration-resistant prostate cancer (mCRPC). Of the organs at risk with high tracer accumulation, reliable dose estimations for the lower gastrointestinal tract (LGT) have not been presented so far. The objective of this study was to perform absorbed dose calculations of the LGT and kidneys during Lu-177- DKFZ-PSMA-617 therapy. **Methods** - Nine patients with mCRPC were treated by at least two cycles of Lu-177 DKFZ-PSMA-617 therapy and underwent a thorough clinical follow-up. Out of this cohort, a whole body dosimetry via a stationary dose rate monitor (LB 112 Micro Gamma, Berthold, Germany) has been conducted in three patients (mean age 67 yrs [range 61 - 72]) so far. Additional SPECT/CT images from the skull base to the pelvis were acquired at approximately 1, 4, 24, 48 and 72 h after administration of 3.6 GBq [range 3.5 - 3.7] Lu-177 DKFZ-PSMA-617. Time-dependent activities for the small, upper large and lower large intestines as well as the kidneys were determined by drawing volumes of interest in SPECT/CT images. Curve fitting, residence time calculation and absorbed dose calculation per organ were conducted using OLINDA/EXM.

Results - The calculated mean absorbed dose for the kidneys was 0.5 Gy/GBq [range 0.4 - 0.6], 0.13 Gy/GBq [range 0.12 - 0.15] for the small intestine, 0.44 Gy/GBq [range 0.42 - 0.45] for the upper large and 0.04 Gy/GBq [range 0.02 - 0.06] for the lower large intestine, respectively. Accordingly, there was no severe bowel obstruction, diarrhea, ulceration or perforation during the cause of therapy or follow-up (6 ± 1 month) within the nine patients. Likewise, there was no evidence of nephrotoxicity, as determined by serum creatinine levels and dynamic renal scintigraphy. One patient complained about mild, self-limiting constipation within three days after therapy. **Conclusion** - Based on the biodistribution and dose calculations, this preliminary data can be used as a first approximation for gastrointestinal risk assessment. Absorbed organ doses of the lower gastrointestinal tract appeared to be uncritical in Lu-177- DKFZ-PSMA-617 therapy.

EP482

Assessment of response, clinical evaluation and toxicity of radioligand therapy (RLT) with 177-Lutetium-DKFZ-617-labelled Prostate specific membrane antigen (177-Lu-DKFZ-617-PSMA) for metastatic castrate resistant prostate cancer (mCRPC): An initial experience in Jaslok

H. RATHORE, H. SHAH, P. ALAND, P. CHAUDHURI, T. BHARADWAJ, C. KALE, C. SHEKAR, A. PARAB, S. PALTRO, P. KOREPU, V. M. JAMES, V. LELE; JASLOK HOSPITAL, MUMBAI, INDIA.

OBJECTIVE: RLT with 177-Lu-DKFZ-617-PSMA is a novel targeted therapy for mCRPC. To assess the efficacy of single infusion of 177-Lu-DKFZ-617-PSMA RLT by prostate specific antigen (PSA) decline, clinical improvement, and early side effects. We present the first clinical experience of treating mCRPC using 177-Lu-DKFZ-617-PSMA.

METHODS: RLT with 177-Lu-DKFZ-617-PSMA was performed in 8 mCRPC patients, refractory to conventional treatment including hormonal, chemo and radiotherapy. 68Ga-HBED-CC PET-CT was performed in all patients prior to one cycle 177-Lu-DKFZ-617-PSMA RLT (Mean administered activity 7.03 GBq and range 6.67 - 7.4 GBq). In addition, early response was evaluated by serum PSA levels, complete blood counts, liver and renal function tests (LFT and RFT), serum electrolytes, lactate dehydrogenase (LDH) and ionised calcium prior to therapy and followed by 2, 4, and 6 weeks post therapy. All patients were contacted by telephone every week regarding the side effects and any positive or negative change. Study was approved by institutional board and informed consent was taken prior to therapy. **RESULT:** All lesions detected by 68Ga-HBED-CC PET-CT exhibited high 177-Lu-DKFZ-617-PSMA uptake on post therapy planar and SPECT images. Six weeks after therapy 5 patients (62.5%) experienced PSA decline of whom 2 patients (25%) experienced more than 50% PSA decline, 1 patient (12.5%) more than 30% PSA decline, and 2 patients (25%) any PSA decline. Three patients experienced rise in PSA out of which 2 patients (25%) experienced more than 25% raise in PSA with progressive disease, 1 patient (12.5%) experienced clinical improvement. Relevant hematotoxicity (ECOG common toxicity criteria) i.e. grade II/III anaemia and thrombocytopenia is showed by 2 patients (25%) with progressive disease, and the same 1 patient (12.5%) has experienced leucopenia in addition. 1 patient (12.5%) with more than 25% raise in PSA and 5 patients with decline of PSA did not experience any hematotoxicity. 1 patient (12.5%) with progressive disease experienced deranged LFT, RFT and serum electrolytes. Xerostomia was experienced by 3 patients (37.5%), which started within a week and resolved in about 6 weeks post therapy. **CONCLUSION:** 177-Lu-DKFZ-617-PSMA is a novel and promising RLT for mCRPC. Our initial results indicate that radioligand therapy with 177-Lu-DKFZ-617-PSMA is safe, effective and have low early side effect profile. A relevant PSA decline was detected in 62.5% of patients.

EP483

Radiation dosimetry of organs and tissues at risk from ¹⁷⁷Lu-DKFZ-PSMA-617 for prostate cancer therapy

M. Hohberg, W. Eschner, M. Schmidt, M. Dietlein, C. Kobe, T. Fischer, A. Drzezga, M. Wild; University Hospital of Cologne, Cologne, GERMANY.

Purpose: The calculation of the absorbed dose is crucial for the evaluation of possible risks against the therapeutic benefits of a new targeted radionuclide therapy. The absorbed dose for possible critical organs was calculated during in the first cycle of a peptide radioligand therapy with ¹⁷⁷Lu-DKFZ-PSMA-617 for patients with metastatic prostate cancer. **Methods:** Nine patients with castration-resistant prostate cancer and advanced metastases underwent radioligand therapy with 5.5 ± 0.16 GBq of ¹⁷⁷Lu-DKFZ-PSMA-617 therapy. Serial whole body scintigraphies acquired at 0.5/24/48/72 and 168 hours after application were analyzed by regions of interest and time-activity curves were generated for various organs. The cumulative activities and residence times were calculated by integrating a bi-exponential fits over the time-activity curves. Mean absorbed doses were finally estimated using OLINDA/EXM1.1™. Additionally the mean absorbed doses for each organ were determined when omitting the last measurement (168 hours p.i.) and compared with the results based on data from all measurement points. In a sub-study, the whole body uptake was supplementary measured by a probe counter. These measurements were used as additional monitoring of the absorbed whole-body doses and were compared to the ones obtained by planar scintigraphy. **Results:** The following mean absorbed doses were calculated: 2.82 mGy/MBq (SD= 0.76 mGy/MBq) for the lacrimal glands, 0.72 mGy/MBq (SD= 0.14 mGy/

MBq) for the salivary glands, 0.53 mGy/MBq (SD= 0.17 mGy/MBq) for the kidneys, 0.42 mGy/MBq (SD= 0.12 mGy/MBq) for the nasal mucous membrane and 63.0 μ Gy/MBq (SD= 22.9 μ Gy/MBq) for the whole body. Non-specific intestinal retention of activity was lower in patients with extended bone metastases. Omitting the last measurement resulted in a mean deviation of 10% to 30% for absorbed doses as compared to the ones received by analyzing all measurements. The whole body doses by probe counter measurements were in accordance with the ones obtained by planar scintigraphy. The mean deviation between the two methods was 2.36 %. **Conclusions:** After three therapy cycles absorbed doses are not likely to be critical for the kidneys, salivary glands and the nasal mucous membrane except for the lacrimal glands. The lacrimal glands may represent the dose-limiting organs, because critical exposure may result. Whole body scintigraphy appears sufficient for dose estimation but late measurements (168 hours p.i.) are mandatory, if accurate dose calculation is required. Further clinical studies based on a larger number of patients are necessary to validate these results.

EP484

Investigation of a hybrid image approach and a reduction in the number of blood samples for a decreased clinical workload for patient-specific bone marrow dosimetry in Lu-177-DKFZ-PSMA-617 therapy

A. Gosewisch, A. Delker, S. Tattenberg, L. Vomacka, F. J. Gildehaus, A. Brunegraf, P. Bartenstein, G. Böning; University Hospital Munich, Munich, GERMANY.

AIM: Bone marrow (BM) is a critical organ in radionuclide therapy, particularly in Lu-177-PSMA therapy, in which patients typically exhibit high burdens of bone metastases. However, while reliable organ and tumour dosimetry ideally requires sequential SPECT-imaging, BM dosimetry adds a series of planar acquisitions to the imaging protocol for dose estimation of the remainder of the body (ROB). This work aims at investigating a BM dosimetry protocol using a hybrid image approach based on a combination of a single planar image with sequential SPECT images, which still offers acceptable BM dosimetry estimates. Additionally, a possible reduction in the number of blood samples was studied for further minimization of clinical workload. **METHODS:** BM dosimetry was performed on four patients (eight cycles of 3.7GBq Lu-177-PSMA-DKFZ-617), using a full (FP) and a reduced (RP) dosimetry protocol (p.i. each: FP: SPECT/planar whole-body: 24/48/72h, blood: 20/30/40/60/80min and at each acquisition time-point; RP: SPECT: 24/48/72h, whole-body: 24h, blood: 20/60min and at each acquisition time-point). Images were acquired on a SPECT/CT-System (Siemens-Symbia-T2). Quantification included voxel-wise scatter and attenuation correction in case of planar and SPECT images and distance-dependent detector blur for SPECT. Calibration of planar images was done via known net-activity for the FP and via the quantitative 24h-SPECT for the RP. A monoexponential kinetic was assumed for all organs, tumours and the ROB and a biexponential for blood. Subsequent dosimetry was performed according to EANM guidelines. Determination of the ROB-to-BM dose for the RP was done by combining the effective half-life of the sequential SPECT with the planar image 24h to obtain a description of the ROB-time-activity-curve. **RESULTS:** Calibration factors derived from 24h-SPECT and net-activity showed strong correlation and similar means (Pearson's $r=0.74$, 24h-SPECT: 174 kBq/cps, net-activity: 175 kBq/cps). Results of both protocols showed very strong correlation and similar means concerning the total BM dose and the individual contributions: total BM dose: $r=0.91$, FP: 39.3+/-15.5mGy, RP: 40.8+/-17.2mGy; ROB-to-BM: $r=0.94$, FP: 26.3+/-14.4mGy, RP: 29.8+/-16.3mGy; blood-to-BM: $r=0.92$, FP: 13.0+/-8.7mGy, RP: 11.0+/-8.9mGy. **CONCLUSIONS:** Exploiting the information from sequential SPECT for reduction of planar images and clinical workload seems to be a promising approach. Thereby SPECT calibration of planar images offers a practical alternative to net-activity counting. The number of blood samples could be reduced from eight to five without a drastic change in the derived dose estimates.

EP485

The First Experience on Lutetium (Lu)-177 Prostate Specific Antigen (PSMA) Treatment in Castration Resistant Prostate Cancer Patients

C. Soydal, E. Ozkan, D. Nak, O. N. Kucuk; Ankara University Medical Faculty Nuclear Medicine Department, Ankara, TURKEY.

Aim: To report our first safety and efficacy data on Lu-177 PSMA treatment in castration resistant metastatic prostate cancer patients. **Material and Methods:** Totally 14 (mean age: 66.35 \pm 3.1) patients received Lu-177 PSMA treatment for castration resistant prostate cancer between the dates April 2015 and April 2016 in our department. Performance status and life expectancy was considered during pretreatment evaluation. Blood count, renal function tests, serum PSA measurement and pretreatment Gallium (Ga)-68 PSMA Positron Emission Tomography (PET)/Computed Tomography (CT) imaging was performed all the patients. Renal function tests and blood counts were repeated after each cycle to follow-up possible hematological and renal toxicity. All the patients who completed all cycles underwent posttreatment Ga-68 PSMA PET/CT for evaluation of treatment response. A scoring system based on number (1=no lesion, 2= 1 to 3, 3=4 to 10, 4>10) and SUV was used to evaluate pre and posttreatment Ga-68 PSMA images. **Results:** Gleason Scores of patients ranged 7-9. All the patients were received taxan based chemotherapy regimens. In pretreatment Ga-68 PSMA PET/CT images while 13 patients had multiple bone metastases, 7 patients had lymph nodes, 3 patients had liver and 2 patients had lung metastases. Mean pretreatment serum PSA level was calculated as 460.97 (min-max: 2.83-2044) ng/mL. Six patients completed 4 cycles of treatment. Treatment of 2 patients was discontinued after 2 cycles due to thrombocytopenia and neurological symptoms, respectively. While grade 2 anemia and grade 1 thrombocytopenia was observed in 1 patient, grade 1 anemia and grade 2 thrombocytopenia was seen in 1 and 1 patient. Significant renal toxicity was not developed in any patient. Complete remission was seen in one patient after 3 cycles. Finally 1 patient died after 3th cycle. Rest of the patients is still under treatment. According to Ga-68 PSMA PET/CT imaging, 4 patients responded to treatment. Additionally, PSA response was seen in 8 patients. Figure 1: Change of serum PSA levels. Conclusion: Based on our first experience, Lu-177 PSMA treatment seems to be safe and efficient in castration resistant metastatic prostate cancer patients.

EP486

Radiation Dosimetry of ¹⁷⁷Lu-PSMA; Results from a prospective clinical trial utilising automated voxelized dosimetry and comparison with PSMA PET/CT

J. A. Violet, P. A. Jackson, M. Scalzo, S. Sandhu, P. Eu, R. J. Hicks, M. S. Hofman; Peter MacCallum Cancer Institute, Melbourne, AUSTRALIA

Introduction: Retrospective series administering radiolabelled small molecules binding to prostate specific membrane antigen (PSMA) demonstrate a favourable therapeutic ratio in men with metastatic castration resistant prostate cancer (mCRPC). Toxicity and efficacy in radionuclide therapy is determined by absorbed dose in normal tissues and tumour and is controlled by adjustment of administered activity. We present regional dosimetry for men with mCRPC treated with ¹⁷⁷Lu-PSMA-617 and correlate with pre-therapy PSMA PET/CT. **Materials and methods:** The first ten men recruited in a single-arm prospective study (ACTRN12615000912583) were analysed following the first cycle of ¹⁷⁷Lu-PSMA-617 therapy. Administered activities for each cycle were adjusted according to tumour burden, body weight and renal function using a pre-defined method, and administered following oral hydration alone. Following cycle one of four planned therapies, quantitative SPECT/CT imaging was performed at 4, 24 and 96 hours. Series were deformably registered and voxel-specific time activity curves used to

derive three-dimensional absorbed dose maps based on Monte Carlo-determined voxel S-values at a combination of long and short ranges. Parotid gland and tumour dosimetry were correlated to pre-therapy ^{68}Ga -PSMA PET/CT SUVmax. **Results:** Dosimetry estimates to normal tissues following cycle 1 (median administered activity 8000 MBq, range 7300–8500) expressed as mGy/MBq \pm SD were kidney 0.43 \pm 0.11, parotid 0.52 \pm 0.25, submandibular 0.41 \pm 0.25, liver 0.08 \pm 0.01, spleen 0.08 \pm 0.03, spinal marrow 0.2 \pm 0.19, left ventricle 0.09 \pm 0.01. Lacrimal gland doses were excluded from the analysis due to limitation by partial volume effects but are qualitatively higher than those observed in parotids. Assuming mean biodistribution the estimated renal and parotid doses following 4 cycles of 800MBq would be 13.76 Gy and 16.64 Gy respectively. The mean dose to tumours with the highest uptake per patient was 37 Gy. The mean tumour absorbed dose in two most intense sites in bone, node and visceral tissue were 28.1 Gy (range 9.6–71.1), 29.2 Gy (range 10.6–53.1) and 38.3 Gy (range 4.2–68.3) respectively. Correlating SUVmax on pre-therapy PET/CT with parotid and tumour absorbed dose yielded squared Pearson correlation of 0.29 and 0.09, respectively. **Conclusions:** Absorbed dose was highest in salivary glands and kidneys. Assuming average biodistribution in this cohort administration of 4 cycles of therapy would not exceed conventional external beam tolerance doses. Tumour absorbed doses in index lesions are high. Pre-therapy PSMA PET/CT demonstrates high variability in correlation with parotid and tumour dosimetry indicating limited potential of using short half-life ^{68}Ga PET for prospective dosimetry.

EP-21 – Sunday, October 16, 2016, during Exhibition hours, e-Poster Area
Do.MoRe: Radiation Exposure & Protection

EP487

Concrete walls activation and scrap material in the decommissioning of a PET Cyclotron: preliminary results of Monte Carlo study

S. Vichi¹, A. Infantino¹, G. Cicoria², F. Zagni², A. Corazza², D. Mostacci¹, M. Marengo¹; ¹Montecuccolino Nuclear Engineering Laboratory, Department of Industrial Engineering, University of Bologna, Bologna, ITALY, ²Medical Physics Department, “S. OrsolaMalpighi” Hospital, Bologna, ITALY.

Introduction: During the operational life of a PET Cyclotron, the concrete walls of the cyclotron vault are activated by the secondary neutron flux interacting with rare earths and metals present in the concrete or in the reinforcement bars. For this reason when considering dismantling of such accelerators, a considerable amount of low level solid radioactive waste has to be taken into account. The aim of this work is to define a Monte Carlo approach for the assessment of activation levels of a cyclotron bunker. **Material and methods:** In this work The MC code FLUKA was used to simulate a GE PETtrace cyclotron (16.5 MeV) routinely used in the production of positron emitting radionuclides. The model of the cyclotron includes the magnet and magnet poles, the vacuum chamber, the coils and the target filling station panel (LTF). The target system modeled is the standard GE assembly including a Niobium chamber filled with O-18-water to produce Fluorine-18 by a (p,n) reaction. A detailed MC model of the cyclotron vault was implemented on the basis of the bunker’s original construction drawings; the model includes the ducts through the vault walls and the reinforcement rods. Experimental measurements inside the bunker were performed using a compact, portable CZT detector. A Monte Carlo model of the detector and of measurement geometry was developed in order to calibrate the detector for field measurements. **Results and conclusions:** Activation of the cyclotron vault walls and reinforcement rods was scored at different positions, depth and for different workload and life expectancy of the cyclotron. The principal long-lived radionuclides found in concrete were ^{152}Eu , ^{54}Mn , ^{60}Co , ^{154}Eu , ^{134}Cs , ^3H while in reinforced rods ^{55}Fe , ^{54}Mn , ^{60}Co were found.

After twenty years of cyclotron operation the expected activity concentration of this radionuclides in the concrete ranges from 0.001 Bq/g to 4 Bq/g. For short-lived radionuclides, it was possible to perform experimental measurements and to compare them with simulations. The results obtained are in agreement within uncertainties (e.g. ^{56}Mn standard deviation in activity concentration $< 10\%$). In conclusion, provided a detailed model is developed, Monte Carlo approach to the study of bunker activation level allows to characterize with satisfactory accuracy the radioactive waste from the decommissioning of a cyclotron facility. A preliminary evaluation of radioactive waste allows to identify any critical issue and possible countermeasures to be taken in order to decrease future dismantling costs.

EP488

Calibration of radiation detectors for air exhaust systems: an approach with Monte Carlo simulations

F. Zagni¹, S. Vichi², L. Pompignoli³, G. Cicoria¹, A. Corazza¹, D. Pancaldi¹, M. Marengo¹; ¹Medical Physics Department, University Hospital “S.Orsola – Malpighi”, Bologna, ITALY, ²Department of Industrial Engineering, Montecuccolino Laboratory, University of Bologna, Bologna, ITALY, ³Research and Development Coordinator, Tema Sinergie S.p.A, Faenza, ITALY.

Introduction. Air exhaust systems in cyclotron and radiopharmacy facilities involve the use of radiation detectors in order to monitor air contamination and comply with the concentration limits set by the regulations. The calibration of these devices is not straightforward; in this work we used Monte Carlo (MC) simulations in order to evaluate calibration factors for different detectors, in particular for a single-channel NaI scintillator probe. **Materials and methods.** We compared MC results with experimental measurements performed using the probe and a known activity. To do this, a cylindrical tube (1-meter long), similar to a real ventilation duct, was filled with water with a known, uniform, activity concentration of ^{18}F (assessed with a calibrated activity meter) and count-rate was recorded with the probe supported to the external wall surface. The same geometrical setup was modeled using MC simulations. The ratio between simulated and experimental results was used as a scaling factor for the subsequent calibration factors evaluated through simulations, in order to take into account the different count-rate between real and modeled probe, due to the intrinsic efficiency of the scintillation material, light and charge collection by the PMT. Calibration factors for different radionuclides, in particular positron emitters, were evaluated by simulating real measurement conditions, i.e. a duct filled with a uniform activity concentration in air. The difference between results obtained in air and water was analyzed, in particular the positron annihilation distribution in space. Factors for non-PET radionuclides were also estimated. Simulations were performed with both Geant4 and FLUKA toolkits and for each run statistical uncertainty was about 1%. **Results.** For the modeled NaI probe, the ratio between calibration factors for activity distributions in air and water gave 1.25 \pm 0.02. Simulations show that the difference is not explained only by the different material density, but also by the distribution of annihilation events, which changes significantly when positron are emitted in air. Factor for F-18 was 231 \pm 9 cps/(Bq/cm³). Other PET isotopes gave compatible results (thus different positron range was irrelevant for our setup). Geant4 and FLUKA gave compatible results within statistical uncertainties. **Conclusion.** MC simulations provide a feasible and accurate approach to the assessment of correction factors for a variety of radiation detection systems and geometrical setups. This work shows that both the MC toolkits used are able to properly support the calibration procedure of detectors dedicated to the monitoring of air exhaust systems.

EP489**FANC-survey of Administered Activity and Determination of Belgian Diagnostic Reference Levels for Radiopharmaceuticals in Daily Practice**

T. Vanaudenhove¹, M. Vandecapelle¹, K. Muylle², F. Jamar³, G. Moulin-Romsee⁴, B. Dehaes⁵, K. Bacher⁶, A. Fremout¹; ¹Health and Environment, Federal Agency for Nuclear Control, Brussels, BELGIUM, ²Department of Nuclear Medicine, UZ Brussel, Brussels, BELGIUM, ³Division of Nuclear Medicine, Cliniques universitaires Saint Luc, Université catholique de Louvain, Brussels, BELGIUM, ⁴Department of Nuclear Medicine, Sint-Andries ziekenhuis, Tielt, BELGIUM, ⁵Department of Nuclear Medicine, Ziekenhuis Oost-Limburg, Genk, BELGIUM, ⁶Division of Medical Physics, Ghent University, Ghent, BELGIUM.

Aim: To analyze the distribution of activity administered to patients in Belgian nuclear medicine (NM) departments and deduce national diagnostic reference levels (DRLs) for several types of scintigraphy procedures. **Materials and methods:** Since the 1st of January 2015, all NM departments in Belgium have to register their values of administered activity for one specific diagnostic procedure either during 3 months or for 30 patients. These data are collected by the Federal Agency for Nuclear Control (FANC) and used to determine the national DRL for that specific diagnostic procedure. This value is then compared to values from national and international recommendations. If adequate, the DRL is also calculated in function of the patient weight. First and third quartiles (Q1 and Q3) are computed and used to determine the relative position of an individual department. Belgian DRLs are determined as mean activity for an adult of 70 kg. So far distributions of the administered activity and DRLs were determined for five diagnostic procedures concerning adult imaging: bone scintigraphy (^{99m}Tc-phosphates), myocardial perfusion scintigraphy (^{99m}Tc-radiopharmaceuticals - single injection, one-day and two-day protocols - and ²⁰¹Tl-chloride), thyroid scintigraphy (^{99m}Tc-pertechnetate and ¹²³I-NaI), pulmonary perfusion scintigraphy (^{99m}Tc-MAA) and PET-scan (¹⁸F-FDG, based on incomplete data). **Results:** The Belgian DRL for bone scintigraphy was determined to be 750 MBq. For myocardial perfusion scintigraphy it was determined to be 740 MBq for single injections or two-day protocols and 380/980 MBq for one-day protocols (first/second injection) with ^{99m}Tc-radiopharmaceuticals and 110 MBq for single injections with ²⁰¹Tl-chloride. For thyroid scintigraphy it was determined to be 165 MBq with ^{99m}Tc-pertechnetate and 12 MBq with ¹²³I-NaI. For pulmonary perfusion scintigraphy it was determined to be 200 MBq. For PET imaging it was determined to be 265 MBq (based on incomplete data, can be reviewed). Approximately linear increase of the statistical quantities (average and quartiles) was observed in function of the patient weight for the bone, myocardial and PET procedures with no weight dependency for the thyroid and pulmonary procedures. **Conclusion:** Due to the large participation (close to 100% for the first four procedures), the determined DRLs are representative for Belgian NM departments. In order to optimize the administered activities in daily practice, every single NM department in Belgium was informed on how their administered activities were situated compared to the national DRLs to enable them, where needed, to take corrective actions and adapt their administered activities conform to the national and international guidelines.

EP490**Survey and decontamination of radium-223 dichloride for alpha-particle radionuclide therapy in clinical facilities**

M. Hosono¹, S. Hohara², M. Inagaki², H. Yamaniishi², G. Wakabayashi², T. Matsuda², K. Sakaguchi¹, K. Hanaoka¹, T. Ito²; ¹Kindai University, Faculty of Medicine, Osaka-Sayama, JAPAN, ²Kindai University, Atomic Energy Research Institute, Higashi-Osaka, JAPAN.

Aim: Radium-223 dichloride (Ra-223), a bone-seeking α -emitting radiopharmaceutical for radionuclide therapy, was developed and already incorporated in the management of castration-resistant prostate cancer with multiple bone metastases (mCRPC). Considering the impact of Ra-223 for mCRPC and potentially other bone metastatic diseases, issues concerning radiation control for Ra-223 still require investigation including monitoring using conventional detectors and radioactive decontamination in nuclear medicine facilities. We therefore conducted experiments on monitoring and decontamination of Ra-223, and constructed procedures and standards for handling Ra-223 in clinical facilities. **Methods:** A property of Ra-223 and its daughters of Rn-219, Po-215, At-215, Pb-211, Bi-211, Po-211, Tl-207, and stable Pb-207 is that, in addition to emission of α and β particles, they emit photons of γ -rays and characteristic X-rays that are detected by conventional GM detectors and NaI(Tl) scintillator detectors. Our studies consisted of 2 parts, 1) Monitoring with survey meters for Ra-223, and 2) Swab decontamination. 1) We made a mock contamination source, and conducted spectrum analysis of Ra-223 emission using High Purity Germanium detectors (HP-Ge), and then clarified characteristics of conventional GM detectors and NaI(Tl) scintillator detectors as well as a dedicated α detector for measuring Ra-223 by considering parameters of time constant, distance, and speed. 2) Swab decontamination rates were measured by dropping Ra-223 on materials including linoleum and pig skin, and decontaminating by swab technique with parameters as follows; with or without drying of materials, swab paper soaked with cleaners such as EDTA and commercially available cleaners, and swabbing pressure. **Results:** Regarding monitoring of Ra-223, photon spectrum was analyzed with HP-Ge, and then conventional GM detectors and NaI(Tl) scintillator detectors were more efficient than a dedicated α detector which showed remarkably decreasing counting rates with increasing source to detector distance. In decontamination of materials, drying of materials diminished decontamination rates, which suggested necessity of rapid coping in case of contamination. Swab paper soaked with cleaners provided good decontamination rates of more than 90% for linoleum material. **Conclusions:** An α -emitter Ra-223 should be handled in nuclear medicine facilities according to standard procedures for radiation protection. Characterizing survey detectors for responses to α particles is critical for optimization of measurements. Rapid decontamination of materials before getting dried and use of appropriate cleaners were recommended in case of contamination.

EP491**Radiation safety of intraoperative ¹⁸F-FDG Cerenkov Luminescence Imaging in breast cancer surgery**

C. Sibley-Allen¹, M. Grootendorst², P. Croasdale¹, A. Jones¹, S. Gould¹, E. Lee¹, S. Allen¹, A. Purushotham^{1,2}; ¹Guy's and St Thomas' NHS Foundation Trust, London, UNITED KINGDOM, ²King's College London, London, UNITED KINGDOM.

Aim: Breast-conserving surgery (BCS) with or without sentinel lymph node biopsy (SLNB) is the primary treatment for early-stage breast cancer. A key problem in BCS is that in the UK up to 25% of patients require a repeat operation due to positive or close tumour margins on postoperative histopathological analysis. ¹⁸F-FDG Cerenkov luminescence imaging (CLI) has the potential to assess tumour margins intraoperatively, with a view to reducing the re-excision rate. Good control of radiation safety is required for the successful implementation of this technique in an intraoperative setting. This study provides occupational radiation safety data from a first-in-human clinical trial assessing feasibility of ¹⁸F-FDG CLI-guided surgery in BCS. **Materials and Methods:** Research ethics committee approval and written informed consent were obtained (REC 12-EE-0493). Detailed written procedures and staff training for control of radiation dose were implemented. 150MBq ^{99m}Tc nano-colloid was administered for SLNB. 5 MBq per kg up to a maximum activity of 300MBq ¹⁸F-FDG was administered for CLI between 1-3 hours prior

to surgery. Staff performing injections in nuclear medicine, support staff accompanying the patient to theatre, theatre staff and recovery nursing staff were monitored for radiation exposure and contamination. Personal dose equivalent was recorded using calibrated electronic personal dosimeters. Extremity doses were measured with thermo-luminescent finger dosimeters. **Results:** Data from 24 patients provided the following mean and standard deviation radiation doses per procedure: surgeon, 33(15) μSv ; anaesthetist 11(5) μSv ; nursing 6(3) μSv and support staff 9(4) μSv . The maximum dose to the surgeon from one procedure was 74 μSv . The maximum extremity doses per procedure were 250 μSv and 150 μSv for the left and right hands respectively. A conservative estimate based upon the maximum procedural dose suggests surgeons could perform 270 procedures before exceeding the 20mSv UK classified radiation worker annual dose limit. No personnel were found to be contaminated with radioactivity after the procedure. Two to three clinical waste bags were generated per procedure with detectable radioactivity levels. Surgical equipment was found to have low levels of radioactive contamination and was stored between 1-3 days until contamination was no longer detectable. **Conclusion:** Radiation safety data shows that ^{18}F -FDG CLI is a low-risk procedure but there is a need for careful control of radiation safety. Radiation expertise in planning, training and procedure supervision ensures safe execution of this novel intraoperative technique.

EP-22 – Sunday, October 16, 2016, during Exhibition hours, e-Poster Area
Do.MoRe: Radioimmunotherapy (RIT)

EP492

Pre-Dosing with Cold Antibody (HH1) Reduces Red Bone Marrow Absorbed Doses in Patients Treated with the Novel Antibody-Radionuclide-Conjugate ^{177}Lu -DOTA-HH1

J. Blakkisrud¹, A. Løndalen², J. Dahle³, H. Holte⁴, A. Kolstad⁴, C. Stokke^{1,5}; ¹The Intervention Centre, Oslo University Hospital, Oslo, NORWAY, ²Department of Radiology and Nuclear Medicine, Oslo University Hospital, Oslo, NORWAY, ³Nordic Nanovector ASA, Oslo, NORWAY, ⁴Department of Oncology, The Norwegian Radium Hospital, Oslo University Hospital, Oslo, NORWAY, ⁵Oslo and Akershus University College of Applied Sciences, Oslo, NORWAY.

Aim: Red bone marrow is an organ that is often at risk in radioimmunotherapy, possibly leading to undesired haematological effects. ^{177}Lu -DOTA-HH1 is a novel anti-CD37 antibody-radionuclide-conjugate currently in a phase 1/2 study. Two pre-dosing regimens have been investigated, one with 50 mg unlabelled HH1 (Arm 1) and one without (Arm 2). The aim of this work was to compare red marrow absorbed doses for the two arms and to correlate absorbed doses with haematological toxicity. **Materials and Methods:** 8 patients with relapsed CD37+ indolent B-cell non-Hodgkins lymphoma were included for red marrow dosimetry. Four patients received pre-dosing with naked HH1 (Arm 1) four hours before a single injection of ^{177}Lu -DOTA-HH1, and four did not (Arm 2). Two patients in each arm received 10 MBq/kg of ^{177}Lu -DOTA-HH1 and two 15 MBq/kg. Adverse events were graded according to CTCAE v4. Uptake of ^{177}Lu -DOTA-HH1 in the red marrow was visible on SPECT/CT for both arms. SPECT/CT images from multiple time points were used to estimate activity concentration in the red marrow of lumbar L2-L4. Patient specific total marrow mass and cumulative activity were found by assuming that 6.7 % of total marrow is located in L2-L4. The absorbed doses, including both marrow self-dose and cross dose from remainder body, were calculated with OLINDA/EXM. **Results:** The mean absorbed doses to red marrow were 0.95 mGy/MBq for Arm 1 (with HH1 pre-dosing) and 1.52 mGy/MBq for Arm 2 (without HH1 pre-dosing). There was a statistically significant

difference between Arm 1 and 2 (student t-test, $p = 0.02$). Total absorbed marrow doses ranged from 0.67 - 1.29 Gy in Arm 1 and from 1.55 - 2.06 Gy in Arm 2. Patients with Grade 3/4 thrombocytopenia received significantly higher radiation doses to bone marrow than patients with Grade 1/2 thrombocytopenia ($p = 0.02$). A weaker and non-significant difference between Grade 3/4 and Grade 1/2 neutropenia was found ($p = 0.27$). **Conclusion:** Pre-dosing with unlabelled HH1 reduces the absorbed red bone marrow dose for ^{177}Lu -DOTA-HH1 patients. Haematological toxicity was more severe for patients receiving higher absorbed radiation doses, indicating that adverse events possibly can be predicted by the calculation of absorbed dose to red marrow.

EP494

Therapeutic efficacy of brief intraperitoneal radioimmunotherapy of ovarian cancer using ^{213}Bi -anti MISRII antibodies

R. LADJOHOUNLOU, Jr.¹, A. PICHARD¹, E. DEHAYES¹, V. Boudousq¹, F. Bruchertseifer², A. Morgenstern³, I. Navarro-Teulon¹, J. POUGET¹; ¹Inserm U1194, MONTPELLIER, FRANCE, ²European Commission, Joint Research Centre, Institute for Transuranium Elements, Karlsruhe, GERMANY, ³European Commission, Joint Research Centre, Institute for Transuranium Elements, Karlsruhe, GERMANY.

Hypothesis: We assessed in *in vitro* and *in vivo* models of ovarian cancer the therapeutic efficacy of 16F12 mAbs directed against Mullerian Inhibiting Substance type II receptor (MISRII) radiolabeled with ^{213}Bi **Methods:** *In vitro*, both direct and bystander cytotoxic effects were measured using clonogenic assay and standard medium transfer protocol. Typically, Clonogenic survival was assessed in SK-OV-3 donor cells expressing MISRII and exposed for 90 min to 0.06-0.5MBq/mL of 16F12 ^{213}Bi -mAbs. Bystander cytotoxicity was measured in recipient cells grown in non-radioactive culture medium preconditioned for 2 hours in the presence of donor cells. DNA double strand breaks (DSBs) were measured in both donor and recipients cells using immunofluorescent detection of gamma-H2AX and of 53BP1. *In vivo* we explored in athymic nude mice bearing intraperitoneal (IP) MISRII-expressing AN3CA tumor the therapeutic efficacy of brief-intraperitoneal radioimmunotherapy (BIP-RIT, 12.95 - 37 MBq; 37MBq/mg) or of intraperitoneal RIT (IP-RIT; 2.96-12.95 MBq; 37MBq/mg) using ^{213}Bi -16F12. BIP-RIT mimics hyperthermic intraperitoneal chemotherapy as used in clinic. It consists of intraperitoneal injection of high activities of radiolabeled mAbs followed 30 min later by wash of the peritoneal cavity with saline solution to remove unbound radioactivity. The biodistribution of radiolabeled antibodies following IP-RIT (12.95 MBq; 37MBq/mg) or BIP-RIT (37 MBq; 37MBq/mg) was assessed. **Results:** *In vitro* we showed in donor cells a strong direct cytotoxicity of 16F12 ^{213}Bi -mAbs. A significant bystander cytotoxicity was also measured in recipient cells. Genotoxic effects were also demonstrated as measured by the formation of DNA DSBs in both donor and recipient cells. *In vivo*, results of biodistribution indicated that tumour uptake of ^{213}Bi -16F12 during BIP RIT was higher than after IP RIT. The tumour-to-blood uptake ratio was 9 versus 3, respectively, one hour post RIT while it decreased down to 3 and 1, respectively, three hours post-RIT. Finally, a similar delay in tumor growth was observed in mice treated with 12.95 MBq of ^{213}Bi -16F12 following IP-RIT or treated with 37MBq using BIP-RIT. **Conclusions:** We confirmed *in vitro* the therapeutic efficacy of newly developed 16F12 ^{213}Bi -mAbs. *In vivo* results indicate that similar therapeutic efficacy and lower toxicity could be obtained with BIP-RIT compared with IP-RIT. BIP-RIT could be a new tool in the therapy of peritoneal carcinomatosis.

EP495**US DOE Tri-Lab (ORNL, BNL, LANL) Research Effort to Provide Accelerator-Produced ^{225}Ac for Radiotherapy**

K. D. John; Los Alamos National Laboratory, Los Alamos, NM, UNITED STATES.

A general overview of the US Department of Energy Isotope Program's Tri-Lab (ORNL, BNL, LANL) Research Effort to Provide Accelerator-Produced ^{225}Ac for Radiotherapy will be presented with focus on accelerator-production and final product isolation methodologies. In addition, associated impacts on the quality of the accelerator-produced ^{225}Ac product quality as well as the quality of the associated ^{225}Ac / ^{213}Bi generator will be presented. Specifics regarding ongoing evaluations of the accelerator-produced ^{225}Ac by independent end-users related to pre-clinical dosimetry and toxicity studies and broad logistical challenges associated with the accelerator-based production approach will also be discussed.

EP-23 – Sunday, October 16, 2016, during Exhibition hours, e-Poster Area
Do.MoRe: Radiopeptides

EP496**131I-mIBG treatment dosimetry: dependence on the fitting expression and the role of biodosimetry**

I. Torres-Espallardo, J. Balaguer, A. Montoro, N. Sebastián, J. Loaiza, C. Olivas, J. Bautista, M. Adrià, B. Ibáñez, V. Pascual, J. Campayo, J. Villaescusa, A. Cañete, V. Castel, P. Bello; Hospital Universitario y Politécnico La Fe, Valencia, SPAIN.

^{131}I -metaiodobenzylguanidine (^{131}I -mIBG) is a targeted radiopharmaceutical mostly used for patients with refractory or relapsed neuroblastoma. Recent studies indicate a better response using multiple infusions of high dose ^{131}I -mIBG. Our treatment protocol consists of a two infusions separated within 3-4 weeks. The goal is to provide a whole-body (WB) dose of 4 Gy. WB-dosimetry was performed according to MIRD schema, where the time-activity curve follows a multi-exponential expression. The aim of this work is to study the variability of the total dose according to the fitting expression and the role of the biodosimetry in supporting the physical dosimetry. **METHODS:** Three patients undergoing 2 administrations each were considered. The WB absorbed doses were calculated for all the patients and administrations. WB-dosimetry was based on external measurements of dose rate. Several fitting expressions were used for each case: bi-, tri-, and penta-exponential curves. For one of the patients of this study cytogenetic procedures were performed to carry out the dicentric chromosome (DC) assay. Blood samples were obtained the day before ^{131}I -mIBG administration (d0) and 7 days after (d7). Also, in vitro irradiation of blood samples was conducted to set-up a dose-effect curve. The frequency of dicentrics was obtained from the analysis of 100 first-division metaphases. WB-dose estimation was carried out taking into account the frequency of dicentric and the Chromosomal Aberration Calculation Software (CABAS) using the dose-effect calibration curve from Montoro et al. (2005). **RESULTS AND DISCUSSION:** The variability of the estimated WB-dose ranges from 4% to 15% when comparing the different fitting curves and it is lower for the second administration for all the patients. The frequency of dicentrics for d0 and d7 were 0.03 ± 0.017 and 0.44 ± 0.066 , respectively. Giving WB-doses of 0.47 ± 0.44 Gy for d0 and 2.71 ± 0.46 Gy for d7. The absorbed dose after fitting the dose rate measurements to a 3-phases exponential was 1.44 ± 0.15 Gy for d7. We do not expect the same value

obtained from both methods, but there is a good agreement. **CONCLUSION:** The biodosimetry tool DC-assay could help in estimating the second dose in case of sequential treatment since it takes into account the interindividual variability to radiation exposure and thus individual susceptibility to this type of treatment. Further studies with larger populations should be performed to evaluate the correlation between both methods and to elucidate whether biological dosimetry can be considered a tool for WB-dose assessment and predicting individual response following therapy with ^{131}I -mIBG.

EP497**A shared experience in the treatment of neuroendocrine tumors (NET) with ^{177}Lu dotatate**

G. LOBO¹, **M. VERAS**², **G. GOMES**¹, **C. TINOCO MESQUITA**², **J. MAGALHÃES**¹, **P. HUNGRIA**¹, **R. RAMOS**¹, **A. BARLETE**², **T. SANTOS**², **G. SADECK**², **W. KER**², **N. LAVATORI**², **A. COTRADO**²; ¹NUCLEOS, BRASILIA, BRAZIL, ²PROCARDIACO, RIO DE JANEIRO, BRAZIL.

Therapy with ^{177}Lu -dotatate has shown improvement in the outcome of patients with neuroendocrine tumors, especially for toxicity and progression free survival. To report a casuistry of two different nuclear medicine services in Brazil regarding the treatment of patients with NET and to evaluate the safety and progression free survival. We included patients with NET treated with ^{177}Lu -dotatate in two distinct Brazilian services from January 2008 until December 2015. Both services used the same protocol and were studied clinical, epidemiological, scintigraphic and progression free survival variables. In 48 patients (174 cycles), the average age was 58 years, 27 (56%) were women. Thirty-five (72%) completed 4 cycles. There was clinical deterioration in 1 patient, 6 died or had progression of the disease, and 5 lost follow-up (12 discontinued the treatment). Deaths were seen in 21 (43%) patients and progression free survival ranged from 1 to 129 months (mean 32 months). Progressive disease occurred in 4 cases. There was no interruption of the treatment with side effects. The most common ones were: alopecia, mild abdominal pain, nausea and vomiting and mild thrombocytopenia and leucopenia. In this studied population we found that treatment with ^{177}Lu -dotatate was safe and showed important benefit on progression free survival.

EP498**Relapse therapy with ^{177}Lu -octreotate: safety assessment of multiple repeated cycles peptide receptor radionuclide therapy**

A. Yordanova¹, **K. Mayer**², **M. A. Gonzales-Caramona**², **M. Essler**¹, **H. Ahmadzadehfar**¹; ¹Nuclear Medical Department of the University Hospital of Bonn, Bonn, GERMANY, ²Center for Integrated Oncology (CIO), University Medical Center Bonn, Bonn, GERMANY.

Peptide receptor radionuclide therapy (PRRT) is proved to be an effective therapy in patients with somatostatin receptor positive neuroendocrine tumors. Unclear is yet how many cycles of ^{177}Lu -octreotate can be repeated achieving an acceptable toxicity profile. The purpose of this study was to assess the safety of multiple repeated cycles PRRT with ^{177}Lu -octreotate in patients with recurrent neuroendocrine tumors. **Methods:** We summarized retrospective data from 15 patients treated with multiple repeated cycles of ^{177}Lu -octreotate between 2004 and 2015. The median of administrated activity was 63.8 GBq (53.9 - 96.6 GBq) in a median of 9 cycles with a range of 8 to 13 cycles. Nonhaematological and haematological toxicities were assessed by clinical reports and laboratory data. The occurrence of adverse events was then compared in three therapy groups.

The first group included side effects registered from cycle 1 to 4, the second: from cycle 5 to 8, and the third: cycle 9 to 13. We also compared the baseline laboratory assessments with data at the end of treatment. **Results:** We observed no life threatening adverse events (grade 4) during the treatment with ^{177}Lu -octreotate. Reversible haematological toxicity grade 3 occurred in 2 patients (13 %). No severe nephrotoxicity (grade 3/4) was registered. Surprisingly more grade 3 adverse events were recorded in the first therapy group (cycle 1-4) as in the other two groups (cycle 5-8 and cycle 9-13). Furthermore there was no significant change in the mean value of thrombocytes, leucocytes and plasma creatinine before and after the therapy. However, the mean haemoglobin fell from 14 g/dl to 11 g/dl. **Conclusion:** Relapse therapies with more than 8 cycles of ^{177}Lu -octreotate are well tolerated in patients with recurrent neuroendocrine tumors. **Keywords:** PRRT · ^{177}Lu -octreotate · neuroendocrine tumors · relapse therapy.

EP499

The effect of wrong organ volumes on the calculation of TIACs using a PBPK model in PRRT

D. Hardiansyah^{1,2}, N. J. Begum^{1,3}, P. Kletting⁴, F. M. Mottaghy^{5,6}, G. Glating¹; ¹Medical Radiation Physics/Radiation Protection, Universitätsmedizin Mannheim, Medical Faculty Mannheim, Heidelberg University, Mannheim, GERMANY, ²Department of Radiation Oncology, Universitätsmedizin Mannheim, Medical Faculty Mannheim, Heidelberg University, Mannheim, GERMANY, ³Digitale Signalverarbeitung, Information Technology Faculty, Hochschule Mannheim, Mannheim, GERMANY, ⁴Department of Nuclear Medicine, University Hospital Ulm, Ulm, GERMANY, ⁵Klinik für Nuklearmedizin, University Hospital, RWTH Aachen University, Aachen, GERMANY, ⁶Department of Nuclear Medicine, Maastricht University Medical Center (MUMC+), Maastricht, NETHERLANDS.

Aim: The aim of this study was to investigate the effect of erroneously chosen wrong organ volumes as fixed parameters in the physiologically pharmacokinetic (PBPK) model for peptide-receptor radionuclide therapy (PRRT) on the accuracy of the predicted time-integrated activity coefficients (TIACs). **Material and Methods:** The reference (*R*) settings from the literature were used for the estimation of unknown parameters of a PBPK model from the biokinetic data of 15 patients (152±15 MBq of ^{111}In -DTPAOC). In this reference setting the organ volumes of liver and spleen were fixed individually to the calculated true volumes, while the kidneys volumes were set to the reference man values, i.e. male $V_{\text{kidneys}}=0.31$ l and female $V_{\text{kidneys}}=0.27$ l. The fittings were repeated with the following wrong organ volumes: mean values of the 15 patients (*W1*), twice of the mean values (*W2*) and half of mean values (*W3*). One organ volume was changed for each *W* case and other volumes were fixed to the true individual values. Predicted TIACs of the kidneys, tumor, liver, spleen, remainder, whole body and serum were calculated for both *R* and the 3 *W* cases. The relative differences *RD* between TIACs from *R* and *W* cases were analyzed. Relative differences *RD* values ≤ 10 % were considered as an accurate prediction of TIACs. **Results:** The maximum *RD*s were < 10% for most of the *W* cases except for wrong liver and kidneys volumes, i.e. twice of mean liver volumes: $RD_{\text{liver}}=(-10\pm 8)\%$ and $RD_{\text{serum}}=(6\pm 4)\%$; twice of mean kidneys volumes: $RD_{\text{serum}}=(-0.3\pm 8)\%$, and half of mean liver volumes: $RD_{\text{liver}}=(6\pm 5)\%$. **Conclusions:** Estimation of predicted TIAC is little affected when using wrong organ volumes in the

PBPK model. Thus, inaccurate determination of individual organ volumes to use in the PBPK model may still be sufficient for treatment planning in PRRT. However, the calculation of absorbed dose could be highly affected due to wrong volume estimation.

EP500

Comparison of carrier-added and non-carrier added Lu-177 DOTATATE in patients with Neuroendocrine Tumours

P. Roach, S. Hain, E. Hsiao, A. Aslani, **D. Bailey**; Royal North Shore Hospital, St Leonards, AUSTRALIA.

Background: In Australia, carrier-added (ca) LuTate ([Lu-177]-DOTA-Octreotate) has been used for over a decade for the treatment of patients with neuroendocrine tumours (NETs). In recent years, non-carrier added (nca) LuTate has become commercially available. nca Lutate has several advantages over the ca product, including a higher specific activity and less generation of waste products, particularly Lu-177m. A comparison of the two products in the same patients has not been previously reported. **Aim:** To compare ca vs nca LuTate in the same patients being treated for NETs. **Methods:** Four patients receiving therapy with ca Lutate who received the nca product in their previous (n=3) or subsequent (n=1) treatment cycle were included in this study. The average time difference between the ca and nca treatments was 10 weeks (range 9-11 weeks). Lutate was obtained from IDB Holland (ca) and ITG Germany (nca). Two experienced Nuclear Medicine specialists independently and blindly reviewed the whole body geometric mean LuTate images obtained at 2 time points (4hrs and 96hrs) post treatment for both the ca and nca products, noting all sites of disease. In the event of disagreement between the readers, a consensus read was subsequently performed. Retained activity (% of injected dose) was also calculated for each product at each of the 2 time points. **Results:** There were 28 sites of disease documented from all imaging available. Reader 1 reported 27 sites of disease (26 true positive, 1 false positive, 2 false negative) on both ca and nca Lutate images. Reader 2 reported 25 sites of disease on ca Lutate scans (24 true positive, 1 false positive, 4 false negative) and 20 sites of disease on nca Lutate scans (20 true positive, no false positive, 8 false negative). There was no statistical difference between nca and ca LuTate in detecting sites of disease by either reader at either time point in the 4 patients. On the consensus read, there was 100% concordance between ca and nca scans in the detection of disease sites. On quantitative analysis, there was no significant difference in calculations of retained activity between ca and nca LuTate (p=0.89). **Conclusions:** On both visual and quantitative analysis, there was no significant difference in the detection of disease sites and overall scan interpretation between ca and nca Lutate performed in consecutive treatment cycles in the same patients. These results suggest that the biodistribution of ca and nca LuTate appears to be equivalent.

EP501

Comparison and Evaluation of n.c.a. ^{177}Lu -[DOTA⁰, Tyr3] TATE vs n.c.a. ^{177}Lu -[DOTA⁰, Tyr3] TOC in (GEP-NENs) Treated Patients

G. S. Limouris¹, M. Paphiti², M. Souvatzoglou¹, L. E. Mouloupoulou¹, R. V. McCready²; ¹National and Kapodistrian University of Athens, Athens, GREECE, ²Royal Sussex County Hosp, Brighton, UNITED KINGDOM.

Aim: To evaluate and compare the dosimetry profile and efficacy of n.c.a. Lu-177 DOTA-TATE vs n.c.a. Lu-177 DOTA-TOC in GEP-NEN patients, initially i.a. treated with DOTA-TATE and after a median progression-free-survival (PFS) of more than 39 mo further i.v. retreated with DOTA-TOC, to confrontate the relapse observed. **Materials and Methods:** The average dose of n.c.a. Lu-177 DOTA-TATE, [Groupe A: 12 cases (63 catheterizations of the hepatic artery)], and n.c.a. Lu-177 DOTA-TOC [Group B: 4 cases (13 i.v. infusions, antecubitaly)] administered to each patient was the same, i.e. 7.3 ± 2.3 GBq. For both groups repetitions did not exceed 6-fold with treatment intervals of 5–8 weeks to avoid a possible stunning effect. Blood samples were collected 2, 4, 8, 24 hrs p.i. to calculate the residence time in blood and in consequence the red marrow residence time; furthermore 24 hrs urine samples were collected too, to calculate the kidney excretion capability and the biological excretion half time. The % max uptake in organs and tumours was estimated by creating ROIs. Tumour Dosimetric calculations were performed using the OLINDA 1.0 code. **Results:** Non-carrier-added ^{177}Lu -[DOTA⁰,Tyr³]TATE blood and urinary radioactivity, expressed as a percentage of the injected dose was significantly lower compared as to non-carrier-added ^{177}Lu -[DOTA⁰,Tyr³]TOC, clearly depicted from the created time/activity curves; the tumour uptake (Bkg-corrected) was significantly higher as compared to non-carrier-added ^{177}Lu -[DOTA⁰,Tyr³] TOC. Absorbed dose kidneys' difference has been measured to be almost the same. The organ average radiation dose (mGy / MBq) of n. c. a. ^{177}Lu -[DOTA⁰,Tyr³] TATE / TOC was found as follows: (a) Liver tumour of 10 gr spherical mass was estimated to be 33.0/13.0 mGy/MBq, (b) Liver 0.19 / 0.55 mGy/MBq, (c) Kidneys 0.46/ 0.66 mGy/MBq, (d) Spleen 1.4 / 1.3 mGy/MBq and (e) Bone marrow 0.030 / 0.036 mGy/MBq. **Conclusion:** Comparing the i.a. infused, n.c.a. ^{177}Lu -[DOTA⁰,Tyr³]TATE vs the i.v. applied -TOC (a) 2.53-fold higher dose in tumour was found, (b) 0.69-fold lower dose to kidneys was observed and (c) 0.83-fold in bone marrow, advocating the efficacy profile of i.v. infused-TOC following the -DOTA-TATE tumour relapse and to feasibly continuation of the re-treatment procedure.

EP502

Effect of time-varying radioactivity volume versus static volume in kidney absorbed dose estimates during ^{177}Lu -DOTATATE therapy

M. Sandstrom, U. Garske-Roman, D. Granberg, A. Sundin, M. Lubberink; Nuclear medicine and PET, Uppsala, SWEDEN.

Aim: As in all therapies using ionizing radiation, a patient-specific optimization of the delivered radiation should be performed in therapy with ^{177}Lu -DOTA-D-Phe¹-Tyr³-octreotate (^{177}Lu -DOTATATE). To determine absorbed dose to the kidneys, where the self-dose gives the main contribution, the activity concentration in an organ needs to be determined at several occasions. As has been published previously by Sandstrom et al in EJNMMI physics 2015, the functional volume of the kidney varies over time after therapy with ^{177}Lu -DOTATATE. The aim of the present work was to study the influence of the change of the kidney volume over time on absorbed dose estimates during ^{177}Lu -DOTATATE therapy. **Materials and Methods:** Thirty patients (17 female and 13 male) with neuroendocrine tumors with high somatostatin receptor expression were included. SPECT/CT over the

abdomen were acquired at 24, 96 and 168 h after infusion of 7.4 GBq of ^{177}Lu -DOTATATE. Absorbed doses to the kidneys were calculated from these data in two ways and then compared. Total amounts of radioactivity in the each kidney at each time point were calculated using 42% and 50% isocontour volumes of interest over the entire organ in the SPECT/CT images. In method A, the absorbed dose was calculated directly from the radioactivity concentrations in each measurement. In method B, the radioactivity concentrations were calculated by division of the total organ radioactivity at each time point with the volume from the 24 h measurement. Absorbed doses were then calculated by integration of the time-activity curve and assuming self-dose only. Correlation and agreement between absorbed dose estimates based on method A and B were assessed using regression and Bland-Altman analysis. **Results:** No significant differences between left and right kidneys were found, so the remaining results include both kidneys in each patient. The percentage difference between absorbed dose calculation for the right kidney using method A and using method B was 6.0 (-9.3 - 50.3) (Median (Min-Max)) when a threshold of 42 % was used and 7.8 (-3.4 - 46.4) for a 50 % threshold. The difference between method A and B was statistically significant ($P < 0.0001$). **Conclusions:** The use of a single organ volume in patients receiving therapy with ^{177}Lu -DOTATATE can result in significant difference in kidney absorbed dose estimates when compared to using a time-varying radioactivity volume. Use of a single volume leads to significant underestimation of absorbed dose to the major part of the kidney.

EP503

Comparison and Evaluation of ^{111}In -Octreotide Relapsed GEP-NENs Patients, Re-Treated With n.c.a. ^{177}Lu -[DOTA⁰, Tyr³]-TATE

G. S. Limouris¹, M. Paphiti², I. Karfis¹, R. V. McCready²; ¹National and Kapodistrian University of Athens, Athens, GREECE, ²Royal Sussex County Hosp, Brighton, UNITED KINGDOM.

Aim: To evaluate and compare the activity/dose uptake profile, efficacy and toxicity of n.c.a. Lu-177 DOTA-TATE in GEP-NETS, initially i.a. treated with high doses of In-111 Octreotide with a median progression-free-survival (PFS) of more than 32 mo, and i.a. retreated with n.c.a. Lu-177 DOTA-TATE, to confrontate the relapse observed. **Materials and Methods:** The average dose of In-111 Octreotide administered to each patient [17 cases (193 catheterizations of the hepatic artery)] ranged from 4.07 GBq to 5.92 GBq for each patient; of them 5 pts relapsed and were retreated by extra therapy sessions with n.c.a. Lu-177 DOTA-TATE, in a dosage of 7.3 ± 2.3 GBq. Repetitions of infusions for pts treated with In-111 Octreotide did not exceed 12-folds with treatment intervals of 5–8 weeks to avoid a possible stunning effect. Blood samples were collected 2, 4, 8, 24 hrs p.i. to calculate the residence time in blood and in consequence the red marrow absorbed dose; furthermore 24 hrs urine samples were collected too, to calculate the kidney excretion capability and the biological excretion half time. The % max uptake in organs and tumours was estimated by creating ROIs. Tumour Dosimetric calculations were performed using the OLINDA 1.0 code. **Results:** Retreated pts showed a median progression-free-survival (PFS) of more than 50 mo up to date. The organ average radiation dose (mGy / MBq) of In-111 Octreotide vs n. c. a. ^{177}Lu -[DOTA⁰,Tyr³] TATE estimations were found as follows: (a) Liver tumour of 10 gr spherical mass was estimated to be 10.8/ 33.0 mGy/MBq,

(b) Liver 0.14 / 0.19 mGy/MBq, (c) Kidneys 0.41/ 0.50 mGy/MBq, (d) Spleen 1.4 / 1.2 mGy/MBq and (e) Bone marrow 0.030 / 0.040 mGy/MBq. **Conclusion:** Intra-arterially retreating relapsed GEP-NETs with n. c. a. ^{177}Lu -[DOTA0,Tyr3] TATE, followed a complete scheme of 12 sessions with In-111 Octreotide it is well achieved to control the disease and give a further survival time of 50 mo at least.

EP504

Peptide receptor radionuclide therapy in malignant pheochromocytoma and paraganglioma treatment

J. Nematyazar¹, B. Vatankulu¹, E. Demirci², S. Asa³, M. Ocak⁴, & Uslu¹, L. Kabasakal¹; ¹Istanbul University, Cerrahpasa Faculty of Medicine, Department of Nuclear Medicine, Istanbul, TURKEY, ²Sisli Etfal Education and Research Hospital Department of Nuclear Medicine, Istanbul, TURKEY, ³Recep Tayyip Erdogan University, Department of Nuclear Medicine, Rize, TURKEY, ⁴Istanbul University Faculty of Pharmacy, Istanbul, TURKEY.

Aim: Many of Pheochromocytomas (PCC) and paragangliomas (PGL) are benign however 10% of PCC's and 25% of PGL's behave as malignant tumors. The current situation of PRRT in PCC and PGL treatment is limited to a few cases and scarce findings is available in the literature. In this study we aimed to demonstrate the efficacy of PRRT in treatment of malignant PCC and PGL.

Materials and Methods: Lu-177 DOTA-TATE (PRRT) therapy applied for 17 patients who had no response to conventional treatments with intense diffuse lesion in Ga-68 DOTA-TATE PET-CT(SRS). Response to treatment evaluated with clinically by ECOG-WHO performance score, and follow up imaging results. Also hematologic-renal function results were followed. **Results:** 3,6-7,4 Mq ^{177}Lu -DOTA-TATE per cures in 1 to 10 cycles was given for 7 (41%) patients with mPCC and 10 (59%) patients with mPGL diagnosis. No hematologic and renal toxicity was seen in both groups in 6-38 months follow-up. One of 7 patient with PCC didn't show uptake in PRRT despite high uptake in SRS, therefore did not continue to PRRT. In the follow up of remaining 6 patients according to PERCIST criteria in SRS, 2 patients show stable disease, 2 partial response and 2 progression. Also in 10 patients with PGL received PRRT regression seen in 3 patients, stability in 2 patients and progression in 1 patient and 4 patients did not evaluated with SRS because of not completing their treatment cycles up to study date. In PCC patients evaluation according to the clinical performance score improvement in performance score seen in 4 patients in 1 patient with progressive disease who later died deterioration in score was detected and 2 patients had no significant change in performance score. In PGL patients, 2 bedridden patients became active in their daily life, disappearance of the symptoms seen in 5 patients and 1 case with initially extensive disease showed worsening of score and died finally. **Results:** Although PCC/PGL are indolent disease they can be fatal in the presence of metastasis. PRRT application in this patient group showed an improvement in patients' performance score without side effects. In addition with promising results in partial response or stability of disease we predict with more number of patients and long-term follow-up studies in the near future this type of therapy will be a selection in PCC and PGLs' treatment algorithms.

EP-24 – Sunday, October 16, 2016, during Exhibition hours, e-Poster Area
Do.MoRe: Radium

EP505

Bone marrow dosimetry for the ^{223}Ra radiopharmaceutical based on skeletal absorbed fractions for alpha in the adult male

N. Benabdallah¹, M. Bernardini², C. de Labriolle-Vaylet³, D. Franck¹, W. E. Bolch⁴, A. Desbrée¹; ¹Institut de Radioprotection et de Sûreté nucléaire, Fontenay-aux-Roses, FRANCE, ²Nuclear Medicine Department, Hôpital Européen Georges Pompidou, Paris, FRANCE, ³UPMC, Univ Paris 06 Biophysics - Nuclear Medicine Department, Hôpital Trousseau, Paris, FRANCE, ⁴Advanced Laboratory for Radiation Dosimetry Studies (ALRADS), J. Crayton Pruitt Family Department of Biomedical Engineering, University of Florida, Gainesville, FL, UNITED STATES.

Purpose: ^{223}Ra -dichloride (Xofigo®, Bayer HealthCare) is the first alpha-emitter radiopharmaceutical that has received approval for the treatment of patients with castration-resistant prostate cancer metastasized to bones. In this treatment, bone marrow is the organ at risk. Therefore, the evaluation of the dose to this region should be performed. However, accurate dosimetry to the bone marrow is difficult because of its heterogeneous and complex structure and because of the short path of alpha particles. Moreover, current dose models do not account for energy or bone-site dependence as shown by alpha-particle absorbed fractions given in ICRP Publication 30. The purpose of this study was to calculate the values of alpha absorbed fraction (AFs) accounting for both their bone-site and particle-energy dependence and to determine the S-value of ^{223}Ra for the bone marrow and bone endosteum. **Methods:** A standard voxelized model of the skeleton for adult male, developed by the University of Florida and realized from microCT images of 40 year male was used to calculate AFs for alpha particle between 2 and 12 MeV. Alpha particles transportations in 32 bone sites were simulated with the MCNP6 Monte Carlo code combined with the internal dose assessment OEDIPE software. The source regions were the trabecular bone volume, active marrow, inactive marrow and trabecular bone surface. The radiosensitive target regions were the active marrow and the endosteum. Then, as the marrow cellularity is dependent of the age and the gender, the evolution of AFs with the marrow cellularity was investigated. **Results:** Values of alpha absorbed fraction were determined for the 32 bone sites and the series of source-target organ couples. Significant differences in AFs were seen between different skeletal sites and energies. The S-values for ^{223}Ra to bone marrow and endosteum obtained using this model were compared to the approximations given in ICRP Publication 30 and exhibits some discrepancies. Finally, a strong dependence on marrow cellularity was observed. **Conclusion:** These results will allow better determining the dose-limiting toxicities to bone marrow due to this new alphanuclide and correlating absorbed dose to therapeutic response.

EP506

Lymphocyte function following Radium-223 therapy in patients with metastasized, castration resistant prostate cancer

V. Barsegian¹, S. Müller², D. Möckel¹, P. Horn³, A. Bockisch², M. Lindemann³; ¹Institute of Nuclear Medicine, HELIOS-Kliniken Schwerin, Schwerin, GERMANY, ²Department of Nuclear Medicine, University Hospital Essen, Essen, GERMANY, ³Institute for Transfusion Medicine, University Hospital Essen, Essen, GERMANY.

Therapy with the alphaemitter Radium-223 chloride (^{223}Ra) is an innovative therapeutic option in patients with metastasized, castration resistant prostate cancer. However, it has been described that this radiotherapy can lead to leukopenia and thrombocytopenia. Recent studies indicated that radiotherapy with beta and gamma emitting isotopes can not only induce numerical but also functional changes of leukocytes. The aim of our current study was to gain insight into the modifications that take place following a therapy with ^{223}Ra , an alpha emitting isotope, at the level of the lymphocyte proliferation as well as to identify a possible anti-microbial immunological impairment. Thus, in 11 patients treated with ^{223}Ra lymphocyte proliferation and the production of pro- and anti-inflammatory cytokines (interferon- γ and interleukin-10) after stimulation with mitogens and recall antigens were tested immediately prior to therapy and at day 1, day 7 and day 28 after therapy using lymphocyte transformation test and ELISpot. Our data indicate that lymphocyte proliferation and the production of interferon- γ and interleukin-10 remained unchanged after therapy. But a moderate reduction in the number of mononuclear cells (lymphocytes, monocytes, natural killer cells) could be observed, reaching a minimum at day 7. In conclusion, the results argue against an impairment of leukocyte functions after ^{223}Ra therapy. In consequence, anti-microbial immune responses most likely remain intact and allow an adequate immune response against pathogens.

EP507

Radium-223 dichloride bone-targeted therapy for metastatic salivary duct carcinoma: a case report

M. Manfredi^{1,2}, T. Angusti¹, M. Tucci¹, F. Vignani¹, C. Buttigliero¹, M. Airoidi²; ¹Azienda Ospedaliero-Universitaria San Luigi Gonzaga, Orbassano (TO), ITALY, ²Azienda Ospedaliero-Universitaria Città della Salute e della Scienza di Torino, Torino, ITALY.

Salivary duct carcinoma (SDC) is a rare pathology, frequently showing Androgen Receptor (AR) overexpression. Patients with this histologic variant benefit from the same androgen deprivation therapy (ADT) used in prostate cancer treatment. Radium-223 dichloride is a new radiopharmaceutical therapy approved for the control of bone pain in patients with castration resistant prostate cancer. Basing on the histological similarity between AR-overexpressing salivary duct and prostate carcinomas, we used Radium-223 treatment on a patient with castration-resistant SDC and osteoblastic bone metastases, achieving beneficial effects. A 75 years old male with AR positive SDC diagnosed in 2006, without other known comorbidity, was referred to our center in January 2015 for the control of bone pain via bone-targeted therapy, because of his incomplete response to analgesic therapy. Previous treatments included loco-regional radiotherapy, chemotherapy and ADT. Due to painful bone lesions, in 2013 the patient underwent palliative vertebral radiotherapy and in 2014 pain control therapy was added (paracetamol 3000mg/day, codeine 90mg/day). Radium-223 therapy was considered as a potential off-label therapeutic approach. A bone scan was performed to evaluate the extent of the pathology and the avidity for diphosphonates, confirming the presence of multiple bone metastases. A total of 6 administrations of 50 kBq/kg every 28 days of Radium-223 were given without delay or suspensions while continuing the planned ADT. During the treatment the patient reported a significant reduction of the bone pain, a better mobility and self-sufficiency with important upgrade in the quality of life. This improvement allowed us to initially reduce and then completely suspend the pharmacological painkiller therapy, even before the

end of the Radium-223 treatments. A bone scan analysis was repeated preformed after the therapy showing a remarkable reduction in concentration of HDP in the vertebrae, pelvis, ribs and sternum. The clinical case reported here is, to our knowledge, the first study suggesting a potential beneficial effect of the use of Radium-223 in the treatment of SDC. Given the low frequency of SDC, it is nearly impossible to start a prospective study for the approval of Radium-223 treatment. However, in our opinion, the off-label use of Radium-223 in this rare pathology is well founded, for the good long-time control of the bone pain achievable with minor side effects. Additional studies aimed to the approval of the use of Radium-223 in other than prostate oncologic pathologies, are desirable to further prove the positive effects of this therapy.

EP508

The Features of ^{153}Sm -oxabiphore Kinetics in Bone Metastases at Radionuclide Therapy

D. A. Dzhuzha; National Cancer Institute, Kyiv, UKRAINE.

Aim of the study was to investigate the features of a early kinetics of therapeutic activities of ^{153}Sm -oxabiphore (^{153}Sm -EDTPA analogue) in bone metastases and the possibility of using its for the optimisation of treatment. **Materials and methods:** Results of complex scintigraphic investigations of 36 patients aged 38-78 years (13 males, 23 females) with breast, prostate, renal, and pulmonary cancer who were undergoing radionuclide therapy (RT) of bone metastases with ^{153}Sm -oxabiphore were analysed. The radionuclide studies included subsequent implementation of a radionuclide angioscintigraphy during 1 min after intravenous injection of 4130-4950 MBq of radiopharmaceutical (RP), dynamic scintigraphy during 90 min, and delayed whole body scanning in 2 h after beginning study. **Results:** The feature of angiograms with ^{153}Sm -oxabiphore is the shorting of descending segment and the rapid transform it in "plateau" (I type), which is determined of RP fixation in metastases at first passing of RP bolus through the vessels. At intensive RP fixation the descending segment was absent and the ascending segment transformed directly in "plateau" (II type) or slowly ascending curve (III type). The level of RP fixation at first bolus passing was determined with help of fixation coefficient calculated according the formula: $C_f = 100h/H$, where C_f - fixation coefficient, %; H - the height of the peak of angiogram; h - the height of the peak of angiogram till a low point of the descending segment. The angiograms of I type were registered in 57.9 % of bone metastases, in these cases C_f consisted 51.0-93.6 %, in means - 79.6 ± 1.8 %. The angiograms of II type were determined in 17.5 % of bone metastases, angiograms of III type - in 24.6 %. At whole body scanning a relative accumulation of ^{153}Sm -oxabiphore in bone metastases consisted 105.0-957.0 %, the mean value - 212.8 ± 20.1 %. The significant correlation between the relative accumulation of ^{153}Sm -oxabiphore and ranged C_f was determined ($r=0.57$, $p<0.01$). The control osteoscintigraphies after 4-6 months were made in 10 patients. The significant correlation between types of angiograms and results of RT (progression, stabilization, partial regression) was determined ($r=0.86$, $p<0.01$). **Conclusions:** Considerable variability of the early ^{153}Sm -oxabiphore kinetics in bone metastases was determined. The features of angiograms from bone metastases with intensive accumulation of the radiopharmaceutical are a transitions from the ascending segment to "plateau" or slowly ascending curve. This character of the radiopharmaceutical fixation at angioscintigraphy may be a prognostic factor of the RT efficacy.

EP509**Radiation Protection Issues of liquid based alpha emitters**

P. J. O'Sullivan; Maidstone and Tunbridge Wells NHS Trust, Maidstone, UNITED KINGDOM.

Purpose: Radium 223 is being seen as a significant step forward in the treatment of prostate cancer patients with bone metastases. Many nuclear medicine departments across the UK are beginning to roll out services to provide the radionuclide to their patients. For many of these departments, it is the first time they will be dealing with liquid-based alpha emitters and the substantial risks they bring. This work aims to investigate the potential doses from inhalation, ingestion and sharps injuries as well as the potential methods in detecting such contamination. Methods: Volatile spills, sharps injuries, patient body waste and the cremation and resulting ashes of a patient will be studied to find the possible staff dose from radium 223. Monte Carlo simulations will be applied in the study, particularly in the case of sharps injuries to find the absorbed dose in the surrounding tissue. Possible methods such as the use intrinsic gamma camera, whole body scans and faecal measurements will be tested to see if they are a practical reality in detecting the presence of contamination. Results: Preliminary calculations show that the annual worker constraint will be breached upon inhalation of 0.869kBq (~0.001ml) and ingestion of 60kBq (~0.05ml). In most situations, the inhalation of radium 223 looks unlikely due to the very high vapour but other situations are being studied. Conclusion: The low activities show the need for this work to be carried out so departments can make accurate risk assessments on the use of radium 223.

EP510**Role of psychological status related to pain outcome and bone lesion dosimetry in patients with bone metastatic Castration-Resistant Prostate Cancer (mCRPC) treated with 223Radium**

V. Frantellizzi¹, G. A. Follacchio¹, B. Cassano¹, M. Pacilio², F. Proietti¹, R. Pani¹, R. Pellegrini¹, G. De Vincentis¹; ¹Sapienza University of Rome, Rome, ITALY, ²S. Camillo Forlanini Hospital, Rome, ITALY.

It has been well observed that in men with CRPC and symptomatic bone metastases, 223Radium-Dichloride (223Ra) has shown to improve Overall Survival. Pain is the most common symptom developed by patients with bone metastases with psychological status implications. The purpose of our study was to evaluate the psychological distress, (such as social support, functional status, depression and anxiety), related to trend of pain response and bone lesion dosimetry during 223Ra treatment. 55 consecutive patients affected by bone mCRPC were examined. A total of 195 cycles were administered with 50 KBq/Kg IVq4w of 223Ra. ECOG Performance Status mean value was 1.48 and Gleason Score average value was 8. Mean age was 76.2±6.07. Patients were evaluated with Brief Pain Inventory(BPI) Scale. To examine quality of life (QoL) endpoints, patients were asked to complete the EORTC QLQ-C30 questionnaire and the bone metastasis module, QLQ-BM22. Both were submitted at baseline and after every cycle of therapy. Edmonton Symptom Assessment Scale (ESAS) was used with the same timing to evaluate response to treatment. Absorbed Dose to selected bone lesions in a group of patients during 223Ra treatment was assessed through an image-based dosimetric approach. 55 patients underwent 1 cycle of therapy with 223Ra. Of these 47% had psychological distress, with an average value of 7.8 in BPI Scale for pain outcome. Second cycle was administered to 51 patients. Pain mean value of these was 7.13 and psychological distress was present in 39%. The evaluation of functional scales after third cycle showed that of 38 patients, 32% had psychological distress with a pain average value of 6.4. Analyzing patients that underwent 6 cycles, they showed that 27% had psychological distress and the mean value of BPI had fallen to 5.6. Preliminary data analysis on bone lesion dosimetry suggested a positive correlation between pain, psychological distress

and adsorbed dose: first ones decreased with adsorbed dose growing up. 223Ra therapy has an impact on QoL in all its dimensions, in particular as regards psychosocial aspects. In patients with painful bone metastases from prostate cancer there is a strong relationship between pain reduction and improvement of the subjective psychological distress. Even though bone lesion dosimetry is suitable only for single skeletal segments while pain response is a global evaluation parameter, future study on a large cohort of patients will help to understand the real role of internal dosimetry.

EP511**²²³Ra standardized image. Utility of bone scintigraphy in the response evaluation to treatment with ²²³Ra**

D. Balaguer, P. Abreu, H. Rodríguez, I. Latorre, T. Mut, M. Plancha, M. Guasp, M. Riera, D. Reyes, E. Caballero; Dr. Peset Hospital, Valencia, SPAIN.

Aim: ²²³Ra is indicated for the treatment of adults with castration-resistant prostate cancer with symptomatic bone metastases and not known visceral metastases. Due to its predominantly α -decay, a standardized distribution image of ²²³Ra has not been established yet. Response to ²²³Ra treatment has not been assessed by bone scintigraphy with ^{99m}Tc-HDP (BS) either, as it was not contemplated in the Alsympca study. This study aims to: 1. Obtain a standardized distribution image of ²²³Ra. 2. Evaluate qualitatively the therapy response to 223-Ra by BS. Material and methods: 1. To obtain a distribution image of ²²³Ra we detected the gamma emission of its decay (less than 2%). We searched, according to previous studies, the photons' photopeaks with high probability of emission and the energy intervals that were suitable for the gamma camera Siemens E.CAM 2H. Tests were done with different photopeaks, combining different parameters of the gamma camera, different time intervals from injection to image acquisition, and different acquisition times. All this was done looking for an image that we could correlate to the baseline BS. 2. A total of 13 patients were enrolled from 14/07/2015 to 01/04/2016, with 43 cycles administered. We evaluated response qualitatively (number and activity of the lesions) with BS after 3 and 6 cycles of treatment, classifying the response in relation to baseline BS in 4 categories: Response (R), stable disease (SD), improvement in some lesions and worsening of other (Imp / Wrs) and Progression (PD). Results: 1. The most suitable image was obtained 4 hours after the injection of 223-Ra, with the detection of 4 photopeaks (82, 154, 269 and 351 Kevs), the use of a high-energy collimator and an acquisition time of 10 minutes for static images, or 4 cm / min for whole body image. 2. We obtained 6 response evaluations after 3 cycles, with 16.7% of R, 16.7% SD, 50% of Imp / Wrs and 16.7% of PD. We need a longer follow up in order to obtain results after 6 cycles. Since this was an exploratory assessment, as it was not contemplated in the Alsympca study, the evaluations had no clinical implications themselves, they did not result in treatment discontinuation. Conclusions: The standardized scintigraphic image of ²²³Ra can be useful to visualize where the radiopharmaceutical is deposited and thus to assess its influence on the effectiveness. A correlation of these images with the BS after 3 and 6 cycles is necessary.

EP512**Initial experience with ²²³Ra-dichloride treatment**

A. M. Yepes Agudelo, P. Bello Arques, P. Borrelli, P. Olivan Sasot, V. Vera Pinto; HUP La Fe, Valencia, SPAIN.

Objective To present our experience with ²²³Ra-dichloride treatment in patients with prostate cancer castration-resistant with bone metastases, without visceral metastases evidence. Material and methods Treatment was administered to 14 patients, ages ranging from 50 to 82 years, with

prostate cancer painful bone metastases. Gleason score ranged from 5 to 10. All of them had positive bone scintigraphy, and were divided into 4 categories: 4 Superscan 8 > 20 metastases 1 between 6 - 20 metastases 1 less than 6 lesions. ²²³Ra treatment administration protocol used was one dose of 55 KBq/kg/4 weeks intravenous until 6 cycles were completed. Treatment was administered under supervision of a nuclear medicine specialist; patients were discharged with alpha emission radiopharmaceuticals radiological protection recommendations. Results Among the 14 patients treated: Three had finished treatment and are radiologically stable, clinically better and with levels of PSA and alkaline phosphatase diminishing: Three are still in treatment: Eight have abandoned treatment due to disease progression that in most of the cases included the onset of visceral metastases and just in one case sustained thrombocytopenia. Adverse effects most frequently presented were mild and transient, consisting in hematological alterations (anemia and thrombocytopenia) in 5 patients. Just one patient presented diarrhea. In 57% of the patients the usage of painkillers was diminished due to the less pain presented. In 29% of them no improvements in pain were achieved, and in 14% the pain was worsened due to bone metastases progression. Conclusion ²²³Ra-dichloride treatment has being a well-tolerated therapy, with few and mild adverse effects. Achieving a satisfactory pain management in the majority of the patients, therefore achieving a better life quality in those patients. Further analysis with a bigger patients sample and the introduction of this treatment in earlier disease stages is required.

EP513

The Use of Radium-223 Chloride Therapy in Patients with Castration-Resistant Metastatic Prostate Cancer: A District Hospital Experience

N. C. Mcaddy, H. H. Lee, P. O'Sullivan, P. Crawley, S. Beesley, M. Najji; Maidstone Hospital, Kent, UNITED KINGDOM.

Background The ALSYMPCA trial showed that treatment with Radium-223 resulted in improved survival and quality of life in patients with castration-resistant metastatic prostate cancer (CRPC) and symptomatic bone metastases. We report our one-year experience with Radium-223 in a district general hospital, to add to the body of data. We reviewed the pain evolution, symptomatic outcome, haematological profile and side effects on our patients and evaluated the potential use of biochemical markers for follow up. **Methods** Data was collected prospectively on eligible patients with symptomatic bone metastases, who were referred for Radium-223 therapy. A Radium-223 administration regime of 6 cycles in accordance with predefined protocols was used. Blood tests were performed before each treatment cycle. The haematological and general side effects were documented. The PSA, Albumin and ALP were also recorded. Patients were asked to record their pain using a visual analogue scale (VAS) and their quality of life on a scale of 1 to 10 (pre-treatment, mid treatment and post-treatment). Patients were contacted on regular basis to identify any adverse side effects. **Results** Patients, who completed the 6 cycles of Ra-223, reported a measurable improvement in pain with an average fall in pain score of 4. However, treatment effect on the quality of life was rather variable. Improvement was observed in some patients, but remained stable or deteriorated in others. Albumin on average fell by 0.8 points. The ALP dropped in most patients by an average of 270 points (Range 8-816) but the PSA responded variably. In 8 patients, the treatment had to be abandoned, 3/8 unfortunately deceased, 1/8 patient with pre-existing inflammatory bowel disease developed worsening diarrhea and had to stop the treatment. Treatment in the remainder was abandoned due to clinical deterioration. 5/8

patients of the abandoned group had chemotherapy prior to the Radium treatment. **Conclusions** Results in our DGH are comparable to those described in the literature. We observed an overall improvement in the pain score. ALP is shown to be a reliable biomarker but the PSA responded variably. Our data support the safety profile of Radium and only few patients developing significant haematological or general side effects. Our study supports the current indications that when referred early, possibly prior to chemotherapy, patients are more likely to complete 6 cycles and therefore may have better overall outcomes.

EP514

Advanced Prostate Cancer Treatment with ²²³Ra-dihloride: experience from Drammen, Norway

K. Nikoletic, F. Laszlo; Vestre Viken HF, Nukleærmedisinsk seksjon, Drammen, NORWAY.

Aim: Overview of the history and data regarding patients with advanced prostate cancer treated with ²²³Ra-dichloride (Xofigo). ²²³Ra-dichloride is an alpha-particle emitting radiotherapeutic drug used for the treatment of patients with castration-resistant prostate cancer (CRPC), symptomatic bone metastases and no known visceral metastatic disease. **Method:** We investigated total number of 14 patients (60-88 years old) treated with ²²³Ra-dichloride in Nuclear medicine Department. Since the most common adverse reaction is hematologic laboratory abnormalities, all patients were investigated for hemoglobin, neutrophil granulocytes and thrombocytes 10 days before each injection. If the values were within recommended, patient was administered with 50 kBq/kg by slow intravenous injection over 1 minute every 4 weeks for 6 doses. **Results:** Until now 5 of 14 patients completed the treatment with 6 injections. Among 5 patients who completed therapy, 2 had an excellent therapy response with significant decrease in bone pain; 2 had a good response and 1 patient characterized his condition as 'unchanged'. All 5 patients who completed therapy had significant fall in ALP values (median decrease of 34.2%), but PSA values before and after the therapy were inconclusive. The ²²³Ra-dichloride was discontinued in 8 patients. Out of these 8 patients 4 received 3 injections before the therapy was disclosed and each of the remaining 4 patients received 5, 4, 2 and 1 injection before the discontinuation. Treatment was discontinued because of radiologic progression in 5 patients, diarrhea in 1, development of kidney insufficiency of unknown origin in 1 and bone pain progression in 1. One patient is currently undergoing therapy. This patient has received 2 injections and is without complications. **Conclusion:** ²²³Ra-dichloride is an additional therapeutic option for patients with CRPC. In our limited group of patients who completed therapy, ²²³Ra-dichloride was well tolerated with positive effect on bone pain in 4/5 patients and a median decrease of 34.2% in ALP levels. Additional therapeutic results are necessary to estimate future possibilities of the use of ²²³Ra in patients with symptomatic bone metastases.

EP515

Radium-223: kinetics and therapeutic response against metastatic prostate cancer

I. A. Marques^{1,2,3}, A. M. Abrantes^{1,3,4}, A. S. Pires^{1,3,5}, G. Costa⁶, F. Caramelo^{1,7}, E. Tavares-Silva^{1,8}, M. F. Botelho^{1,3,4}; ¹Biophysics Institute, IBILI-Faculty of Medicine, University of Coimbra, Coimbra, PORTUGAL, ²Faculty of Pharmacy, University of Coimbra, Coimbra, PORTUGAL, ³CIMAGO, Faculty of Medicine, University of Coimbra, Coimbra, PORTUGAL, ⁴CNC.IBILI, University of Coimbra, Coimbra, PORTUGAL, ⁵Faculty of Sciences and Technology, Coimbra, PORTUGAL, ⁶Department of Nuclear Medicine, CHUC, Coimbra, PORTUGAL, ⁷Laboratory of Biostatistics and Medical Informatics, IBILI-Faculty of Medicine, University of Coimbra, Coimbra, PORTUGAL, ⁸Department of Urology and Transplantation, CHUC, Coimbra, PORTUGAL.

Aim: Study the effects of ^{223}Ra in prostate cancer (PCa) cell lines differing on hormonal receptors. Besides this the kinetics of Ra-223 and $^{99\text{m}}\text{Tc-HMDP}$ was also studied. An osteosarcoma (OS) cell line was used as control cell line. **Materials and methods:** Three tumor cell lines PC3 (metastatic PCa), LNCaP (non-metastatic PCa) and MNNG-HOS (OS) were incubated with the ^{223}Ra (0.5 $\mu\text{Ci/mL}$) or $^{99\text{m}}\text{Tc-HMDP}$ (25 $\mu\text{Ci/mL}$), in the presence or absence of calcium channel inhibitors. Samples at 5, 30, 60, 90 and 120 min were taken for separating sediment from supernatant. Retention studies were performed after cells radiopharmaceutical uptake. Uptake and retention percentage of ^{223}Ra and $^{99\text{m}}\text{Tc-HMDP}$ was calculated after measuring the radioactivity of both fractions in a well counter, in CPM. Clonogenic assay was performed by irradiating cells with increasing doses (0.25 to 30 mGy), plating 1500 (for PC3) or 2000 (for LNCaP) cells in 6-well plates and waiting for 12 to 20 days (depending on the cell line). At the end, colony formation was evaluated using crystal violet staining and survival factor (SF) calculation. **Results and discussion:** Results show that, at 180 minutes, the percentage of ^{223}Ra uptake by PC3 is twice higher (1.8 \pm 0.1%) than by MNNG-HOS (0.97 \pm 0.06%). A similar uptake profile was obtained for LNCaP cells (1.59 \pm 0.13%). The uptake of ^{223}Ra by PC3 is higher (1.8 \pm 0.1%) than the uptake of $^{99\text{m}}\text{Tc-HMDP}$ (0.2 \pm 0.05%). In MNNG-HOS cell line the same is observed. On the other side, LNCaP cell line showed an uptake profile similar between two radiopharmaceuticals. Preliminary studies show that retention percentage of ^{223}Ra is higher for all cell lines, compared to $^{99\text{m}}\text{Tc-HMDP}$. Preliminary results also suggest that, in presence of the inhibitor, the decrease of uptake it is not the same for all cell lines. Preliminary clonogenic assay results show that survival factor (SF) decreases with increasing ^{223}Ra doses (e.g. for 4 mGy, SF was 32.7 \pm 5.8%). **Conclusion:** These results suggest that, although both radiopharmaceuticals are analogues of calcium, the uptake and retention mechanisms may be different. Irradiations of CaP cell lines with ^{223}Ra decrease cell survival in a dose dependent way, at low doses. Thus, this study also enhances the therapeutic potential of ^{223}Ra in the treatment of metastatic PCa. The authors would like to thank Foundation for Science and Technology (FCT) (Strategic Project CNC.IBILI: UID/NEU/04539/2013), COMPETE-FEDER for financial support.

EP516

Considerations Following the Death of Recently Treated Radium-223 Patients

A. Smout, M. Pryor, **P. J. Hinton**; Royal Surrey County Hospital, Guildford, UNITED KINGDOM.

Aim Radium dichloride (Xofigo[®]) has been licensed for use in the management of metastatic prostate cancer since November 2013. Regularly treating near end of life patients is a new experience in nuclear medicine departments and if a patient dies whilst still radioactive, careful thought is needed about advice given to various groups coming into contact with the body. These groups consist of funeral workers, embalmers and cremation workers. Published excretion data is used as the basis for current advice given, but following count-rate measurements from the cremated remains of three patients we now have some initial data to validate the accuracy of assumptions used. **Methods** As of April 2016, 76 patients have been treated at the Royal Surrey County Hospital with 336 doses of radium-223. Seven patients have died before completing all six cycles and of these, four patients have died whilst still being radioactive. Three were cremated and one was buried. Excretion assumptions are based on published data which states 99% clearance from the blood at 24 hours, 5% urinary excretion, 44–77% bone uptake at 4 hours and a median of 76% whole body excretion at 7 days. Advice to staff handling the corpse is based on this data and simple assumptions involving the time of death after treatment. A calibration factor has been derived for standard contamination monitors using known Ra-223 activity in geometry applicable to patient remains. Assuming that all Ra-223 activity remains in the bones

after cremation, a simple model can be derived to estimate the activity remaining in the corpse at death to determine suitable radiation protection advice. **Results** Measurements were made at 30cm from the remains of 3 cremated patients using a standard contamination monitor. These patients died at 17, 39 and 45 days following their last treatment and had an estimated retained 450, 60 and 130 kBq at time of death. **Conclusions** A simple assumption of 25% of the administered activity, decay corrected to the time of death can be used to give an estimate of the activity remaining in the patient at time of death providing death occurs at least one week after treatment. This value can be used to assist in the provision of radiation protection advice to funeral workers, embalmers and cremation workers coming into contact with the corpse.

EP517

Radium-223 in mCRPC: Looking at patients, changes in quality of life and imaging results

M. L. De Rimini¹, G. Mazzarella¹, G. Borrelli¹, M. Bifulco¹, P. Muto¹, V. Montesarchio², L. Leo², F. Uricchio³; ¹Nuclear Medicine AO Ospedali dei Colli - Monaldi, NAPLES, ITALY, ²Oncology Dept AO Ospedali dei Colli - Monaldi, NAPLES, ITALY, ³Urology Dept AO Ospedali dei Colli - Monaldi, NAPLES, ITALY.

Introduction: Radium 223 dichloride (^{223}Ra -Alpharadin) is the first alpha particle emitting bone targeting agent approved for use in mCRPC patient (pts) with bone metastases and no visceral metastases. **Aim:** -to confirm ^{223}Ra feasibility in mCRPC pts affected with severe pain and impaired ECOG Performance Status (PS: n.v. = 0), -to report our results in terms of changes of quality of life and -to monitor Bone Scan (BS) imaging changes. **Methods:** 10 mCRPC pts (65–84 yrs; ECOG PS: -8/10 pts = 1-2; -2/10 pts = 3) with multiple bone metastases at baseline BS, no visceral metastases, severe pain with functional limitations, were enrolled for ^{223}Ra therapy (50 kBq/kg, 6 administrations, 4 weeks intervals/each other). Pts underwent WB - SPECT/CT BS at Baseline and 40 days after the end of therapy cycle. At baseline: -ALP \geq 115 U/L; -Gleason Score at diagnosis: >8 in all pts. **Results:** Alpharadin was generally well tolerated in all pts but, at the 5th dose, 2/10 pts, with severe impairment of physical status from the beginning, showed worsening of PS and thrombocytopenia. They were forced to discontinue therapy, so our results regard the last 8/10 pts. All of them showed pain relief, with a peak at the 3rd-4th week of therapy, and discontinue any pharmacological treatment for pain. No correlations were observed between PS improvement and changes in PSA or ALP, that were no significant anyway. 3/8 pts showing severe movement limitations at baseline underwent full remission of metastases at BS control, with full pain relief and functional recovery. Nevertheless, pain relief occurred in the last 5/8 pts, with no metastases improvement at BS. ECOG results: -2/8 pts PS pre ^{223}Ra = 3; post ^{223}Ra = 1; -6/8 pts: pre ^{223}Ra = 1-2; post ^{223}Ra = 0-1. **Conclusion:** In our experience Alpharadin is generally well tolerate. Worsening in the clinical status can occur in pts severely compromised already at baseline, due to disease and other therapies. ^{223}Ra can help pts affected with severe pain by inducing effective pain relief and functional PS recovery, modifying pts quality of life. The persistence of metastases at post Alpharadin BS control does not rule out the success of the therapy in terms of pain relief and improvement of quality of life.

EP518

Investigation into the feasibility of using EPDs to perform simple dosimetry modelling on Radium-223-dichloride therapy patients

A. H. Shaylor; Maidstone Hospital, Maidstone, UNITED KINGDOM.

Aim: The ability to quantify the dynamic activity distribution and the resulting organ and whole body doses in patients undergoing nuclear

medicine therapies may allow clinicians to monitor the likely efficacy and potential side effects associated with therapeutic procedures. The aim of this investigation is to determine whether Electronic Personal Dosimeters (EPDs) worn by the patient can gather sufficient information to provide useful dosimetric information by modelling the signal mathematically. Ra223 dichloride therapy was assessed in this investigation. **Materials and Methods:** All Ra223 patients assessed for treatment at Maidstone Hospital undergo a nuclear medicine Tc99m HDP bone scan within six weeks. For the purposes of this investigation the activity distribution of the bone scan is assumed to be the same as that of the Ra223 therapy distribution. The signal can then be modelled via Monte Carlo or analytical techniques to various EPDs located at different sites on the body (e.g. ankle, neck). The signal can be simulated for up to one week after administration to assess the cumulated activity of the therapy, and via the assumed tumour distribution, inferred by the bone scan, the total cumulated activity within specific tumours. Different EPD sites and number of EPDs were assessed in this study. **Results:** The cumulated activity distribution was converted to a dose distribution, including a whole body dose. Using EPDs simultaneously at different sites on the body enables the uncertainties associated with individual tumour doses to be substantially lowered. The assessment of whole body dose was adequate using one EPD. **Conclusion:** This investigation assesses the limitations and potential benefits of using EPDs to estimate dose distributions of Ra223 therapies. This work shows that EPDs have the potential to be used to monitor whole body dose and if extended to patient studies would not require additional hospital visits for the patient. Further work could combine early Ra223 gamma camera images with the EPD data. This study concludes that a pilot study is performed with real patient data to see if the potential benefits of this approach can be realised.

EP519

Xofigo therapy needs interdisciplinary cooperation

R. P. Jóna, S. Czibor, I. Szilvási; Medical Center - Hungarian Defence Forces, Budapest, HUNGARY.

²²³Radium dichloride (Xofigo) is an effective therapeutic option for patients with symptomatic multiple bone metastasis of castration-resistant prostate cancer without soft-tissue metastasis (mCRPC). Several clinical trials are going on to define pretreatment clinical criteria for the most optimal use of Xofigo in the dynamically changing therapeutic stage. **Objectives:** The aim of our study was to evaluate clinical data before, during and after Xofigo treatment. In the last 21 months 21 patients with mCRPC were treated in our department. The median follow-up period was 4,54±3 months. 7 patients had previous chemotherapy (docetaxel). **Methods:** Bone scintigraphy was performed before and after the last injection of Xofigo. The serum level of prostate-specific antigen (PSA) and alkaline phosphatase (SAP) were measured before and every eight weeks; hemoglobin, the absolute number of granulocytes and thrombocytes were measured before and every second week during the Xofigo treatment. Bone pain was monitored by a subjective scoring system. **Results:** Xofigo treatment had to be finished after 1-3 injection in 4 patients because severe granulo- and/or thrombocytopenia. In 3 patients Xofigo therapy was temporarily suspended (but continued 6-8 weeks later) due to reversible cytopenia. Xofigo-induced critical cytopenia occurred more frequently in patients with previous chemotherapy. Xofigo was also terminated in two other patients (due to newly developed brain metastasis and relapsed peptic ulcer respectively). 10 patients had a full course of Xofigo treatment. The average number of injections was 4,53 per patient. No death occurred during the treatment. In 20 out of 21 patients, metastatic bone pain has significantly decreased. However 2 patients presented severe ischialgia with neurological symptoms. Both patients had the same symptoms in their history long years before. We indicated MRI examination, and in both cases radical nerve compression was found. Serum PSA was slightly increased with the exception of 2 patients. SAP tended to be

decreasing continuously, however, it started to rise later in the follow-up period. Bone scintigraphy demonstrated diminishing of abnormally increased focal osteoblastic activity. **Conclusions:** Our experience with a limited number of patients underlines the importance of detailed knowledge of the history of the patients before the planned Xofigo therapy. It needs close interdisciplinary collaboration with uro-oncologists. In patients with previous low back pain and neurological symptoms in the history, neurological examinations MRI included are advised. Previous chemotherapy seems to be increase the risk of interrupting Xofigo treatment.

EP520

²²³Ra treatment: potential efficacy parameters and safety

D. Balaguer, P. Abreu, H. Rodríguez, I. Latorre, T. Mut, M. Plancha, M. Guasp, M. Riera, D. Reyes, E. Caballero; Dr. Peset Hospital, Valencia, SPAIN.

Aim: ²²³Ra is indicated for the treatment of adults with castration-resistant prostate cancer with symptomatic bone metastases and not known visceral metastases. Its approval came after demonstrating particular advantage in survival and control of bone pain. This study aims to: 1. Assess efficacy parameters of ²²³Ra. 2. Evaluate the toxicity of ²²³Ra. **Material and methods:** 1. A total of 13 patients were enrolled in the study from 14/07/2015 to 01/04/2016, with 43 cycles administered. The parameters used to assess efficacy were: alkaline phosphatase (AP) reduction, AP response, PSA response and pain response after treatment. AP reduction was defined as a decrease in AP compared to a baseline elevated value; AP response was reached when the decrease was ≥ 30%, measured 12 weeks after treatment initiation. The same criteria applied to PSA response. Pain response was measured by a visual analogue scale (VAS) before the administration of each cycle. 2. The safety of the ²²³Ra was assessed after graduating toxicity of each cycle by Common Terminology Criteria for Adverse Events (CTCAE) version 4. **Results:** 1. AP reduction after treatment initiation occurred in 85% of patients. AP response occurred in 100 % of the 3 patients that reached 12 weeks of treatment. Only a 16.7% PSA response was observed. The most important fact was the reduction of pain (VAS score) in 73% of patients, with an average decrease of VAS after 3 cycles of 69%. 2. ²²³Ra is safe, the most frequent toxicities were: anaemia (50%), followed by diarrhea (25%), nausea (16.7%) and thrombocytopenia (16.7%). But most of toxicity had a low grade. In fact, the only toxicities ≥ grade 3 were anaemia (8.3%) and thrombocytopenia (8.3%). A G2 dysgeusia was also observed in one patient, this had not been described by the EMA but in our patient it was clearly related to the treatment. **Conclusions:** 1. The AP response in treated patients, as well as the improvement in pain control may be subrogated factors of efficacy. Prospective studies are needed to assess these factors. 2. ²²³Ra, unlike other chemotherapeutic agents, has a good safety profile with a low rate of high-grade toxicity. It is important to remark dysgeusia as a previously non described adverse event.

EP521

From the physical to biological dose in patients undergoing to ²²³RaCl₂ therapy

L. Strigari¹, M. Balduzzi², V. Dini³, R. Sciuto¹, A. Soriani¹, A. Tabocchini³, A. Testa²; ¹Regina Elena NCI IFO, Rome, ITALY, ²ENEA, Rome, ITALY, ³ISS, Rome, ITALY.

Introduction: The exact correlation between blood dose and the information provided by biological assays is usually difficult to be determined in nuclear medicine treatments, according to the need to select an appropriate calibration curves for biological dosimetry. This study aims at estimating the correlation between the delivered dose to the blood and

the biodosimetry, i.e. the increment in the number of dicentric and micronuclei in lymphocytes after radium-223 chloride ($^{223}\text{RaCl}_2$) therapy in prostate cancer patients with bone metastasis. **Materials and methods:** Patients undergoing $^{223}\text{RaCl}_2$ therapy for skeletal diseases have been enrolled in this prospective trial. Imaging and blood samples collected before and at different times after the first treatment cycle were used to evaluate blood and non-target tissues doses. Calculated dose have been corrected for patient weight and for the quality of radiation using and RBE of 5.4 for Ra^{223} . Blood samples were also used to assess the number of dicentric and micronuclei from lymphocytes. Haematological toxicity parameters (blood cell count) have been monitored during therapy and analysed along with doses to blood and non-target tissues and results of biological dosimetry. **Results and conclusion:** Based on the calibration curve based on photon doses taking into consideration the RBE of radiation, the estimated dose was 10% lower than the physical ones to non-target tissues based on the number of dicentric. Moreover, the increase of binucleated cells with micronuclei was in average about 70% per Gy to non-target tissues. Our early results suggest that the “cumulative dosimetric index” reflects the delivered dose to the circulating lymphocytes (non target organ) before and after repeated treatments. The degree of chromosome radiation damage increases with the dose estimated with both physical and radiobiological methods.

EP-25 – Sunday, October 16, 2016, during Exhibition hours, e-Poster Area

M2M: Antibodies & Peptides

EP522

Evaluation of Affibody Molecules for Radionuclide Imaging of Carbonic Anhydrase IX Expression In Vivo

J. Garousi¹, H. Honarvar¹, K. Andersson², B. Mitran¹, A. Orlova¹, J. Buijs¹, F. Y. Frejd¹, V. Tolmachev¹; ¹Uppsala University, Uppsala, SWEDEN, ²KTH-Royal Institute of Technology, Stockholm, SWEDEN.

Aim. Carbonic anhydrase IX (CAIX) is overexpressed in tumours under chronic hypoxia and in normoxic renal cell carcinomas. Radionuclide molecular imaging of CAIX expression might identify radioresistant tumours for adjustment of radiation therapy protocols. It could be also used for discrimination of malignant and benign renal tumours. Affibody molecules have demonstrated high potential as imaging probes in preclinical and clinical studies. The aim of this study was to evaluate Affibody molecules and select the best one for imaging of CAIX. **Materials and methods.** Four affibody molecules, ZCAIX:1, ZCAIX:2, ZCAIX:3, and ZCAIX:4 were selected to bind with CAIX with high affinity. The Affibody molecules were labelled with $^{99\text{m}}\text{Tc}$ using HEHEHE-tag and with ^{125}I by conjugation with ^{125}I -para-iodo-benzoate. In vitro binding and cellular processing of the traces was studied using CAIX-expressing SK-RC-52 renal carcinoma cells. In vivo biodistribution and imaging experiments were performed at 4 h after injection in BALB/C mice bearing SK-RC-52 xenografts. **Results.** In vitro experiments demonstrated high stability of both labels. All radiolabelled variants demonstrated specific in vitro binding with low nanomolar affinity. In vivo, the tumour uptake of all radiolabelled variants was significantly ($p < 0.05$) and appreciably higher than the uptake of control Affibody molecule labelled using the same methods, suggesting highly specific targeting. All variants cleared rapidly from blood, but there were significant differences in biodistribution profiles and appreciable variation of the tumour uptake of different tracers for both labels. There was no correlation between tumour uptake and affinity, but there was correlation between tumour and blood uptakes of $^{99\text{m}}\text{Tc}$ -labeled variants. There was remarkable difference in renal retention between radioiodinated variants. $^{99\text{m}}\text{Tc}$ -(HE)₃-ZCAIX:2 (the tumour uptake of 16 ± 1 %ID/g and tumour-to-blood ratio of 44 ± 7) was the best for imaging of CAIX in disseminated cancer. The

variant ^{125}I -ZCAIX:4 (tumour uptake 10.3 ± 0.6 %ID/g, tumour-to-blood ratio of 23 ± 3 and tumour-to-kidney ratio of 2.1 ± 0.5) had the best prospects for imaging of primary renal cell carcinoma. **Conclusion.** Affibody molecules provide specific imaging of CAIX in vivo. The composition of binding site of Affibody molecules influences the blood clearance rate, the uptake in normal tissues and cellular processing in kidneys. $^{99\text{m}}\text{Tc}$ -(HE)₃-ZCAIX:2 is a potential candidate for development of a tracer for imaging of hypoxia in disseminated cancer. ZCAIX:4 with a non-residualizing label might be used for detection of renal cell carcinoma.

EP523

Structure and receptor affinity of DOTA-Gastrin analogue (CP04) complexes with radiometals

M. Maurin¹, A. Wodynski², M. Orzelowska¹, U. Karczmarczyk¹, P. Garnuszek¹, R. Mikolajczak¹; ¹National Centre for Nuclear Research, Radioisotope Centre POLATOM, Otwock, POLAND, ²Swierk Computing Centre, National Centre for Nuclear Research, Otwock, POLAND.

Introduction: Affinity of the chelator-peptide conjugates to the cell membrane receptors may vary depending on the metal incorporated into the complex. This phenomenon has been observed for the radiocomplexes of DOTA conjugated somatostatin and bombesin analogues [1,2]. So far, there are no such studies for gastrin/cholecystokinin receptor CCK2R. The interactions between the CCK2 receptor and a series of gastrin and mini-gastrin analogues have been investigated experimentally and theoretically and there seems to be a consensus that the last four N-terminal (-Trp-Met-Asp-Phe-) amino acids participate in the receptor binding process. Much less is known about peptides containing radionuclide-chelate carriers. The aim of our project was to investigate the influence of selected metals on the biological activity of radiocomplexes. **Materials & Methods:** The geometry optimization was carried out using DFT/B3LYP/6-311G(d,p) and semi-empirical (PM6). Molecular docking algorithm based on the shape complementarity principles, implemented in the Patchdock webserver, was used in preliminary docking procedure. The ^{68}Ga , ^{90}Y and ^{177}Lu radiolabelling of CP04 was performed in previously optimized conditions [4]. Biological activity of radiocomplexes was compared *in vitro* on human epidermoid carcinoma A431 cell line transfected to express the human CCK2R receptor (A431-CCK2R(+)) and on cells transfected with an empty vector (A431-CCK2R(-) [4]). The *in vivo* comparison was performed in tumour-bearing mice. **Results & discussion:** The results of docking simulation showed that interaction energy between M-CP04 and CCK2R is less negative for Lu-CP04 than for Ga-CP04. Additionally, comparison of patchdock scoring results confirms better shape complementarity of Ga-CP04 (5482) in respect to Lu-CP04 (5004). The *in vitro* cell investigations revealed the internalization of ca 75% with no significant differences between the complexes. A very similar biodistribution pattern with fast clearance with urine (> 90%ID after 1.5h p.i.v.) was observed for both ^{68}Ga -CP04 and ^{177}Lu -CP04. The uptake ratio of both complexes in CCK2R positive tumour was 1.5-times higher than in the negative one at 0.5h p.i.v. and increased to ca. 4 after 1.5h p.i.v. Due to a lower concentration of ^{177}Lu -CP04 in muscular tissue its T/M ratio was twice higher than for ^{68}Ga -CP04. **References** Reubi J.C., et al., *Eur J Nucl Med* **2000**, *27*, 273-282. Koumariou E., et al. *Eur J Nucl Med Mol Imaging* **2009**, *36*, S309 Maurin M., et al.; *Nucl Med Rev Cent East Eur* **2015**; *18*(2):51-5. Aloj L, Caraco C, Panico M, Zannetti A, Del Vecchio S, et al. *J Nucl Med* **2004**; *45*:485-494.

EP524

Biological Evaluation of radiolabeled Cetuximab and fragment for the PET imaging tracer of EGFR expression

S. Lee¹, Y. Kim², E. Cho¹, J. Chung¹, S. Kim¹, S. Oh¹; ¹ASAN Medical Center, Seoul, KOREA, REPUBLIC OF, ²SINIL Pharmaceutical Co, Gyeonggi-Do, KOREA, REPUBLIC OF.

Objectives: Generally, [^{18}F]fluoride has short half-life (109 min) to evaluate the intact mAb. Therefore metal radioisotopes such as Cu-64 ($t_{1/2}$, 12 hr) or Zr-89 ($t_{1/2}$, 3.3 day) are widely used for Immuno-PET study. However these radioisotopes show higher radiation exposure in patient than [^{18}F]F-labeled radiotracer. Recently, small size of protein such as affibody, nanobody and Fab fragment have been developed and labeled with Ga-68 or F-18 for the PET imaging because they have short half-life than intact mAb. We developed new [^{18}F]F-labeled Cetuximab fragment ([^{18}F]Fm-329 expressed from E-coli) for tumor imaging and evaluated the in vitro/in vivo properties. **Methods:** N-Succinimidyl 4-[^{18}F]fluorobenzoate ([^{18}F]SFB) was automatically synthesized using AIO chemistry module(Trasis). Three step synthesis and SPE (Solid phase extraction) purification method were used for the synthesis of [^{18}F]SFB. The [^{18}F]SFB which was dissolved in MeCN was obtained from chemistry module and MeCN was completely evaporated. Dried [^{18}F]SFB was dissolved in PBS (pH=7.8) and used to conjugated with Fm-329 and Cetuximab at room temperature for 30 min, respectively. The crude mixture was purified using centrifugal filtration with Amicon®Ultra centrifugal Filter (30K). After washing with PBS buffer, concentrated [^{18}F]Fm-329 was recovered from the centrifugal filter. After formulation, the radiochemical purity and quantification of [^{18}F]Fm-329 and [^{18}F]Cetuximab were evaluated with SEC (size exclusion chromatography)-HPLC and nanodrop, respectively. The binding affinity of radiolabeled Fm-329 and Cetuximab was evaluated with in vitro cell-binding assays with A431 cell line. The biodistribution in the nude mice model bearing A431 tumor xenografts were evaluated using PET/MR. **Results:** [^{18}F]Fm-329 and [^{18}F]Cetuximab were prepared with high labeling yield as $14.8\pm 7.0\%$ and $14.6\pm 2.8\%$ respectively. The in vitro cell uptake of [^{18}F]Fm-329 showed 86.57% binding compare with [^{18}F]Cetuximab which were normalized by protein quantity of cells, independently. The result of blocking study showed that cold Cetuximab inhibited the uptake of [^{18}F]Fm-329 and [^{18}F]Cetuximab to 4.85% and 2.93%, respectively. From the PET imaging analysis, tumor to muscle ratio of [^{18}F]Fm-329 at 2 hr, 3 hr and 4 hr after injection were 4.86, 5.11 and 7.87, respectively. [^{18}F]Cetuximab showed lower tumor to muscle ratio than [^{18}F]Fm-329 as 2.53, 3.45 and 3.58, at the same time point. **Conclusion:** [^{18}F]Fm-329 shows high affinity and good targeting to EGFR over expressed A431 cell line. It is a promising PET radioligand for imaging of EGFR expression.

EP525

In vivo imaging with retargeting immunotherapy components in prostate stem cell antigen-expressing tumor model

R. Bergmann¹, A. Feldmann¹, C. Arndt¹, S. Koristka¹, M. Cartellieri², A. Ehninger², J. Pietzsch¹, J. Steinbach¹, D. Máthé³, M. Bachmann¹; ¹Institute of Radiopharmaceutical Cancer Research, Dresden, GERMANY, ²GEMoaB Monoclonals GmbH, Dresden, GERMANY, ³Semmelweis University, Budapest, HUNGARY.

Aim: Retargeted immunotherapy is now becoming a promising modality of cancer treatment. Particularly the prostate stem cell antigen (PSCA) is a target of advanced prostate, bladder and, pancreatic tumors, as well as subgroups of mamma carcinoma, and glioblastoma. The immunotherapy via retargeting strategies requires modified T-cells, conventional and bispecific antibodies, scFv and nanobody based target modules. All these components were optimized for tumor killing efficiency, GMP production, and safety in application. The potential of these components for in vivo imaging were evaluated in a PSCA expressing tumor model using the different radiolabeled anti-PSCA antibody (Ab) formats (conventional Ab 155 kDa, bsAb 55 kDa, scFv based target module 33 kDa, and nanobody based target module 19 kDa). **Material and methods:** A xenotransplanted s.c. PC3-PSCA-Luc+ tumor model was in NMRI nu/nu mice established. The Abs were conjugated with DOTA and

NODAGA, and the average number of chelators per Ab was quantified by MALDI-TOF. The immunoconjugates were radiolabeled with ^{64}Cu , ^{68}Ga , and ^{177}Lu . Radioligand assays were performed to compare cellular binding, internalization and binding parameters for the immunoconjugates using the PSCA expressing cells. In the mouse model were small animal PET/CT, SPECT and biodistribution studies performed to compare the tissue uptake, the pharmacokinetics and the target to background ratios of the different Ab constructs. For anatomical characterization of the lesions were MRI and OI methods applied. **Results:** Tumors were specifically detected with the radiolabeled Abs already at fore hours after injection. The full mAb showed the highest accumulation in the tumor with a maximal target to background ratio at 48 h p.i. The engineered recombinant bsAb, scFv and target modules showed faster blood clearance, however, with high liver and kidney uptake but with clear visualization of the tumor xenografts after 24 h. **Conclusion:** The combination of molecular imaging modalities allowed studying the distribution of the radiolabeled components of this anti-PSCA-immunotherapeutic set up together with anatomical characterization. The radiolabeled anti-PSCA antibody formats showed in vivo favorable performance as imaging agents with good contrast and sensitivity for the xenotransplanted subcutaneous PSCA expressing tumors. The molecular weight determined the blood clearance and renal elimination. The full antibody showed excellent performance in visualization of the tumor in the mouse model and after optimization for imaging it should also be useful for radioimmunomonitoring of retargeting strategies in PSCA-positive cancer diseases.

EP526

Radiolabeling of a Cyclic RGD (cyclo Arg-Gly-Asp-d-Tyr-Lys) Peptide Using Sodium Hypochlorite As An Oxidizing Agent

K. Kumar, S. Doll, K. Woolum; Laboratory for Translational Research in Imaging Pharmaceuticals, The Wright Center of Innovation in Biomedical Imaging, Department of Radiology, The Ohio State University, Columbus, OH 43212, Columbus, OH, UNITED STATES.

Aim: Radiolabeling of a tyrosine residue in peptides and proteins is routinely performed by using various oxidizing agents such as Chloramine T, Iodobeads, and Iodogen reagent and radioactive iodide (I). The objective of the present study was to develop and optimize a novel radiolabeling method for a cyclic RGD (cyclo Arg-Gly-Asp-d-Tyr-Lys) peptide using sodium hypochlorite as an oxidizing agent. **Materials and Method.** A known amount of carrier-free ^{125}I Na activity was added to a 100 μL of 0.1 M Sodium Phosphate (pH 7.4) buffer solution in a 1.5 mL Eppendorf centrifuge tube followed by sequential addition of cRGDyK peptide and sodium hypochlorite solutions in PBS. The reaction mixture was incubated at room temperature for five minutes and the unreacted sodium hypochlorite was reduced by the addition of sodium metabisulfite. The crude reaction mixture was purified by using a Sep-Pak C₁₈ Light cartridge followed by a reversed-phase HPLC method. Final product was analyzed by a reversed-phase analytical HPLC method. **Results and Conclusions.** A rapid radiolabeling method for molecules and biomolecules containing tyrosine residue has been developed. Various parameters including ratio of reagents, reaction time, and pH of the reaction were studied. The study demonstrated that the radiolabeling of the cyclic peptide is fast (i.e, less than five minutes are sufficient) and pH independent. Mono- and di-iodinated cRGDyK formed under all conditions and varied with the ratio of the reagents. Total percentage of the iodinated cRGDyK (mono- and di-iodinated cRGDyK) varied between 40 to 90% depending on the conditions. Excess cyclic peptide over equal molar ratio of sodium iodide and sodium hypochlorite yielded in predominant amounts of mono iodinated cRGDyK, i.e., >60% under 2:1:1 ratio of cRGDyK: sodium iodide: sodium hypochlorite and >88% under 5:1:1 ratio of cRGDyK: sodium iodide: sodium hypochlorite.

EP527**Synthesis and evaluation of a ⁶⁸Ga-labeled affibody molecule for imaging carbonic anhydrase IX expression with positron emission tomography**

J. Lau, J. Pan, H. Kuo, C. Zhang, F. Benard, K. Lin; BC Cancer Agency, Vancouver, BC, CANADA.

Objective: Affibody molecules are a class of small proteins (MW = ~7 k) that have been explored extensively for targeted therapy and imaging. Tolerant to high temperatures, extreme pH, and structural modifications, these scaffolds typically exhibit nano to picomolar affinities to their targets of interest. An oncogene that has garnered significant interest as both a therapeutic and diagnostic marker for cancer is carbonic anhydrase IX (CA-IX). CA-IX is a cell surface enzyme that promotes survival under low oxygen conditions and is overexpressed within the hypoxic milieu of solid tumours. Z09781, a potent CA-IX-targeting affibody molecule, was previously radiolabeled with ^{99m}Tc for SPECT imaging and showed excellent tumour-to-background contrast (Honarvar et al. Eur J Nucl Med Mol Imaging 2014; 41 (Suppl. 2): S176). To explore the use of Z09781 for imaging with PET, herein we present the synthesis and evaluation of a ⁶⁸Ga-labeled Z09781 derivative (Cys[⁶⁸Ga-NOTA]Z09781) for CA-IX targeted imaging. **Methods:** The affibody molecule Cys-Z09781 was obtained by standard Fmoc solid-phase peptide synthesis. A cysteine residue was introduced at the N-terminal domain of the affibody to facilitate site-specific conjugation of maleimido-mono-amide-NOTA. For radiolabeling, Cys[NOTA]Z09781 was labeled with ⁶⁸GaCl₃ in 2 M HEPES buffer (pH 5.0) and 5% glycerol by microwave heating for 1 min. The radiolabeled product was subsequently purified by PD10 column before being used for in vivo evaluations. PET/CT imaging and biodistribution studies were performed at 2 h post-injection using HT-29 tumour xenograft-bearing immunodeficient mice. **Results:** Cys[⁶⁸Ga-NOTA]Z09781 was obtained in 64–73% decay-corrected radiochemical yields with 16.7 MBq/μg specific activity and > 99% radiochemical purity. Imaging and biodistribution studies showed that Cys[⁶⁸Ga-NOTA]Z09781 was predominantly excreted through the renal pathway, with the kidneys retaining majority of the radioactivity (96.1 ± 10.4 %ID/g at 2 h p.i.). Cys[⁶⁸Ga-NOTA]Z09781 allowed for clear delineation of HT-29 tumour xenografts in PET/CT images. With the exception of the kidneys and bladder, the highest uptake of activity was observed in tumour (1.05 ± 0.15 %ID/g at 2 h p.i.). The corresponding tumour-to-muscle and tumour-to-blood ratios were 11.8 ± 3.35 and 9.78 ± 1.59 respectively. **Conclusion:** We successfully synthesized and radiolabeled an affibody molecule with ⁶⁸Ga for CA-IX targeted imaging. Tracer pharmacokinetics and tracer uptake was assessed in a human hypoxia cancer model. Cys[⁶⁸Ga-NOTA]Z09781 enabled good visualization of HT-29 tumour xenografts with good contrast, and is promising for imaging CA-IX expression with positron emission tomography.

EP528**Physicochemical and biological characterization of SubstanceP fragments labeled with ¹⁷⁷Lu**

A. Majkowska-Pilip¹, E. Gniazdowska¹, A. Rawicz-Galińska¹, M. Bednarczyk¹, P. Koźmiński¹, T. Budlewski², A. Bilewicz¹; ¹Institute of Nuclear Chemistry and Technology, Warsaw, POLAND, ²Central Clinical Hospital of the Ministry of Interior, Warsaw, POLAND.

Aim: Gliomas, particularly WHO grade IV glioblastoma multiforme (GBM), is one of the most common and aggressive primary type of the cancer of the central nervous system. Despite of all current forms of treatment such as advanced surgery techniques, radiation therapy and chemotherapy, the life expectancy of patients diagnosed with GBM is only 12 to 15 months. The neuropeptide SubstanceP (SP) is the physiological ligand of the neokinin1(NK1) receptor consistently

overexpressed by glioblastoma cells. The aim of the work was to study physicochemical (lipophilicity, stability) and biological (K_D, IC₅₀) properties of different SP fragments labeled with β⁻ emitter - Lu-177. **Methods:** The ¹⁷⁷Lu-DOTA-SP fragments conjugates consist of central metal ion ¹⁷⁷Lu coordinated by macrocyclic ligand DOTA previously coupled with different SubstanceP fragments such as SP(1-11), [Thi⁸,Met(O₂)¹¹]SP(1-11), SP(4-11), SP(5-11), [Thi⁸,Met(O₂)¹¹]SP(5-11). The synthesized conjugates were characterized *in vitro* by partition coefficients (log P), in the *n*-octanol/PBS (pH 7.40) system. Stability of the complexes were investigated in different physiological solutions, namely phosphate buffered saline (PBS), histidine, cysteine, human serum (HS) and cerebral spinal fluid (CSF) using HPLC and ITC methods. The biological properties (K_D, IC₅₀) were characterized using cell line T98G. **Results:** All studied conjugates are formed with good yield and high radiochemical purity. The obtained lipophilicity values of the ¹⁷⁷Lu-DOTA-SP fragments are in the range from -2.5 to -5.0. The shorter SP fragments are characterized by higher lipophilicity values, while the replacement of amino acids in positions 8 and 11, respectively Phe and Met by the Thi and Met(O₂) leads to lipophilicity decreasing. The studied conjugates are stable in PBS buffer, as well as in 10 mM histidine and/or cysteine solutions. Stability studies in HS showed in the case of shorter SP fragments quicker enzymatic biodegradation comparing to that of SP molecules containing all 11 amino acids. However, stability studies in CSF showed no enzymatic biodegradation of tested compounds. All studied conjugates bind specifically to NK1 receptors expressed on glioblastoma cells with affinity in the nanomolar range. **Conclusions:** To summarize, the conjugates containing shorter SP fragments are characterized with higher lipophilicity values what can allowed more effective migration into GBM tissue or into the walls of post-surgery cavity. The disadvantage of these conjugates is their poor stability in HS, however due to their total stability in CSF, they can be considered as potential radiopharmaceuticals for local administration directly to glioblastoma tumours. Support by Grant 011/01/M/ST406756 is acknowledged.

EP529**¹⁸F-FDG-Aoe-LIKKP-Pyr-A: A new peptide radiotracer for apoptosis imaging**

D. Beiki¹, S. Khoshbakht², S. Shahhosseini³, F. Kobarfard³, O. Sabzevari², M. Amini⁴; ¹Research Center for Nuclear Medicine, Shariati Hospital, Tehran University of Medical Sciences, TEHRAN, IRAN, ISLAMIC REPUBLIC OF, ²Department of Radiopharmacy, School of Pharmacy, Tehran University of Medical Sciences, TEHRAN, IRAN, ISLAMIC REPUBLIC OF, ³Department of Medicinal Chemistry, School of Pharmacy, Shahid Beheshti University of Medical Sciences, TEHRAN, IRAN, ISLAMIC REPUBLIC OF, ⁴Department of Medicinal Chemistry, School of Pharmacy, Tehran University of Medical Sciences, TEHRAN, IRAN, ISLAMIC REPUBLIC OF.

Aim: Specific biochemical changes occur in cells undergoing apoptosis that provide potential targets for molecular imaging agents and imaging of apoptosis can provide a good way to predict effectiveness of cancer chemotherapy. Clinical information obtained from targeting of phosphatidyl serine (PS) would help to diagnosis and therapy of apoptosis related pathologies. A few LIKKPF peptides with acceptable affinity for PS have been already introduced for apoptosis imaging. We herein report the synthesis of a new LIKKPF peptide radiotracer with more affinity for PS for detecting apoptosis. **Materials and Methods:** The peptides were synthesized on solid phase using standard Fmoc strategy, conjugated with aminoxy (Aoe), and then was considered for the radiolabeling procedure with ¹⁸F-FDG. Biological properties were determined in vitro using camptothecin treated Jurkat cells and in vivo using liver apoptosis mouse model induced via intraperitoneal (IP) injection of lipopolysaccharide (LPS). Also, Log P values determination, biodistribution studies and PET/CT imaging were performed. **Results:** The radiochemical purity

was >95% (100°C, 30 min, pH 5-5.5). Log P value for ^{18}F FDG-Aoe-LIKKP-Pyr-A prepared by Fmoc-(4-pyridyl)-D-Ala-OH was -0.92. K_d of peptide was determined with value 0.52 μM . Biodistribution results showed 3 times liver uptake for apoptotic mice compared to normal mice. PET/CT images were in a good agreement with biodistribution results. The activity ratio of liver to kidney was 0.17 and 0.61 in normal and apoptosis mouse model, respectively. Conclusion: ^{18}F FDG-Aoe-LIKKP-Pyr-A showed good affinity to PS and might be a potential radiotracer for the detection of apoptosis.

EP530

Preparation and biological evaluation of $^{99\text{m}}\text{Tc}$ -HYNIC-LIKKPF for the detection of apoptosis

D. Beiki¹, S. Khoshbakht², S. Shahhosseini³, F. Kobarfard³, O. Sabzevari², M. Amini⁴; ¹Research Center for Nuclear Medicine, Shariati Hospital, Tehran University of Medical Sciences, TEHRAN, IRAN, ISLAMIC REPUBLIC OF, ²Department of Radiopharmacy, School of Pharmacy, Tehran University of Medical Sciences, TEHRAN, IRAN, ISLAMIC REPUBLIC OF, ³Department of Medicinal Chemistry, School of Pharmacy, Shahid Beheshti University of Medical Sciences, TEHRAN, IRAN, ISLAMIC REPUBLIC OF, ⁴Department of Medicinal Chemistry, School of Pharmacy, Tehran University of Medical Sciences, TEHRAN, IRAN, ISLAMIC REPUBLIC OF.

Aim: Radioligands that have affinity and bind to phosphatidyl serine (PS) are good candidates for noninvasive imaging of apoptosis. Because of limitations of Annexin V (as a most studied imaging agent for apoptosis), there is a need to develop radioligands with better biodistribution profile for this purpose. **Materials and Methods:** HYNIC-LIKKPF was successfully synthesized via Fmoc strategy and the compound was considered for the radiolabeling procedure with Tc-99m. Then, stability and Log P values of radiopeptide were determined. Finally, binding studies, biodistribution studies and SPECT/CT imaging were performed. **Results:** The radiochemical purity and Log P value were >95% and -0.92, respectively. $^{99\text{m}}\text{Tc}$ -HYNIC-LIKKPF was stable in human serum for at least 2 hr at 37°C. Although the affinity of radiolabeled LIKKPF was less than original phage peptide, the level of binding to apoptotic cells was 2.5 times higher than control cells. Biodistribution studies showed higher liver uptake of radiopeptide in apoptotic non-treated mouse model compare to normal and pre-treated mouse. The in vivo imaging results were consistent with biodistribution studies. **Conclusion:** $^{99\text{m}}\text{Tc}$ -HYNIC-LIKKPF has less affinity to PS compare to original phage peptide, but high enough for specific binding to apoptotic cells in vitro and in vivo. Less affinity of radiolabeled LIKKPF might be attributed to hydrophobicity of peptide. The future peptides should be more hydrophobic compare to LIKKPF.

EP531

Anti-VEGFR2 monoclonal antibody ramucirumab: comparison of selected radiolabeling methods

J. Janousek, P. Barta, F. Trejtnar; Faculty of Pharmacy in Hradec Kralove, Hradec Kralove, CZECH REPUBLIC.

Aim: Vascular endothelial growth factor (VEGF) is one of the most important regulator of angiogenesis, including tumor neovascularization. VEGF binds to two types of receptors with tyrosine-kinase activity of which VEGF receptor 2 (VEGFR2) is a key receptor in tumor neoangiogenesis. Ramucirumab (RAM) is a novel therapeutic anti-VEGFR2 monoclonal antibody (Mab) directed against the extracellular domain of VEGFR2 that inhibits binding of its natural ligand VEGF. Several types of cancer (e.g. gastric, pancreatic, lung or breast cancer) are known for their overexpression of VEGFR2. The MAb RAM labeled

with appropriate radionuclides could be potentially used for scintigraphic imaging and targeted radiotherapy of oncological diseases. The aim of this work was to develop convenient radiolabeling method for selected radionuclides and to evaluate radiochemical purity and stability of radiolabeled products. **Materials and methods:** Two methods of RAM radiolabeling were evaluated in experiments. The first tested method was the optimization of the direct labeling with $^{99\text{m}}\text{Tc}$ based on the reduction of disulfide bridges in RAM molecule with 2-mercaptoethanol. The second method was radioiodination (^{131}I) according to chloramine-T protocol. The radiochemical purity of the prepared antibody was tested by instant thin layer chromatography on silica gel (ITLC) immediately after labeling. To evaluate the stability the samples were analyzed on various times by size-exclusion high-performance liquid chromatography (SE-HPLC) with radiometric detection. The preparations were incubated 8-24 h at 4°C. **Results:** The introduced methods enabled effective labeling of RAM with either $^{99\text{m}}\text{Tc}$ or ^{131}I . The obtained radiolabeled preparations exhibited sufficiently high stability. Radioiodination method provided slightly higher radiochemical purity after labeling. However, we observed higher stability provided by direct labeling method with $^{99\text{m}}\text{Tc}$ under the used conditions. **Conclusion:** The tested methods are convenient for radiolabeling of RAM. The developed radiolabeled preparations may be used in further preclinical studies to evaluate biological behavior of labeled RAM in vitro or in vivo. This project was supported by Charles University: GAUK(998216/C/2016), SVV(260293) and PRVOUK P40.

EP-26 – Sunday, October 16, 2016, during Exhibition hours, e-Poster Area

M2M: Miscellaneous

EP532

Development of a new multimodal diagnostic nanosystem based on inorganic nanoparticles as a potential radiopharmaceutical in SPECT-MRI or PET-MRI imaging

A. Delgado Garcia, Sr., M. Cano Luna, R. Nuñez Lozano, S. Sanz Viedma, T. Amrani, E. Ramos Moreno, M. Martínez del Valle Torres, G. De la Cueva Méndez, J. Jiménez-Hoyuela García; INSTITUTO INVESTIGACIÓN BIOMÉDICA DE MÁLAGA (IBIMA), MÁLAGA, SPAIN.

Aim: Nanotechnology offers interesting tools that could help to overcome the handicaps of traditional radiopharmaceuticals: greater specificity through selective tropism to targeted tissues, and higher capacity of loading isotopes, to improve sensitivity and decrease toxicity and dosimetry in patients. The aim of this work is to develop a multimodal imaging system (PET - MRI or SPECT - MRI) based on inorganic nanoparticles (NPs) and assess their potential application as radiopharmaceutical. **Material and Methods:** Monodisperse NPs were synthesized, with a superparamagnetic iron oxide core (SPION) and silica coating, with different particle sizes (10-100 nm) and specific surface functionalization. These NPs were PEGylated to increase its circulation time and to provide a platform for subsequent functionalization with additional ligands that may improve their PK-PD and biodistribution. Magnetic properties were determined by measurements of magnetization and transverse relaxivity (T2), and its loading capacity of atoms of gallium, indium and zirconium was determined by two different methods: (1) cold, using chlorinated salts, determined by mass spectrometry with Inductively Coupled Plasma (ICP) and (2) labeling with radioactive isotopes Ga-67, In-111 and Zr-89, quantifying radiochemical purity (RCP) by thin layer chromatography (TLC) using a gamma-radioactivity single trace scanner. Loading kinetics was monitored at room temperature by performing measurements at different times (1, 3, 6, 24 and 48 hours). Moreover, the stability of said labelling was analyzed under physiological conditions, in PBS and fetal bovine serum (FBS). **Results:** Characterized NPs have shown good properties as

MRI T2 contrast agent. In addition, they have good intrinsic capacity for strong adsorption of metals (Ga, In and Zr), without using chelating agents, which allows a considerable loading of these isotopes. The union of these metals to the surface of the NPs is stable over time (up to 48h) in the tested conditions (PBS and FBS), and presents no variations of RCP during that period. Discussion: We have developed a potential multimodal diagnostic nanosystem (PET - MRI or SPECT - MRI) based on NPs composed made of SPION - Silica with intrinsic capacity for the adsorption of different radioisotopes (Ga, In and Zr). This system allows us to generate different particle sizes (10-100 nm) and to modulate its colloidal stability (PEGylation) and other PK-PD parameters through further functionalization, all of them key aspects of controlled biodistribution.

EP533

Development of a new purification protocol for radiosynthesis of 2-deoxy-2-[¹⁸F]fluoroacetamido-D-glucopyranose

M. Martinez Pozo, A. Makino, T. Mori, H. Okazawa, Y. Kiyono; University Of Fukui, FUKUI, JAPAN.

Aims: The diagnosis of infection and the ability to distinguish infection from inflammation by nuclear medicine remain as a challenge. A wide variety of radiotracers are under pre-clinical development, however the clinical imaging agents most currently employed, 2-[¹⁸F]fluoro-2-deoxy-D-glucose ([¹⁸F]FDG) and radiolabelled leucocytes, are non-specific and may accumulate at sites of sterile inflammation or other lesions, resulting in high rate of false positive results. We had reported the radiosynthesis of 2-deoxy-2-[¹⁸F]fluoroacetamido-D-glucopyranose ([¹⁸F]FAG) [1], which was able to distinguish infection from inflammation in animal models despite the final radiochemical yield and specific activity were low. Furthermore, we developed new precursors with same efficiency of [¹⁸F]fluoride incorporation under similar radiosynthesis conditions. The aim of the current study was to increase the final specific activity through modifications introduced to the original purification protocol. **Methods:** Non-radioactive FAG, as well as bromo and tosylate precursors were synthesized in our laboratory. Radiosynthesis of [¹⁸F]FAG was performed using microwave heating followed by alkaline hydrolysis. Final [¹⁸F]FAG was purified by high-performance liquid chromatography using: 1) an amino-bonded silica phase column or 2) an amino-bonded silica phase column plus a C18 bonded silica phase column. **Results:** Radiosynthesis of [¹⁸F]FAG using bromo or tosylate as a precursors showed similar radiochemical yields, radiochemical purities and synthesis times. Purification using only amino-bonded silica phase column gave specific activity values of $1.4 \pm 0.3 \times 10^{-3}$ and $2.1 \pm 0.2 \times 10^{-3}$ GBq/ μ mol for bromo and tosylate precursors respectively. Whereas, when amino column was followed by a C18 column the specific activity values obtained were $7.8 \pm 4.4 \times 10^{-2}$ and $8.0 \pm 1.9 \times 10^{-2}$ GBq/ μ mol for bromo and tosylate precursors respectively. Further analysis by ESI-MS found that purification using amino column was affected by a common by-product, identified as the deprotected mono-acetylated precursor, which co-eluted with [¹⁸F]FAG. A second purification through a C18 bonded silica phase column help to separate this by-product and can explain the observed increment by ten-fold in the final specific activity. **Conclusion:** There were not significant differences regarding the use of bromo or tosylate precursor for radiosynthesis of [¹⁸F]FAG. The inclusion of a C18 bonded silica phase column after the amino-bonded silica phase column help to increase by 10-fold the specific activity of final [¹⁸F]FAG. **Reference:** [1] ME Martínez et al. (2011) Nucl Med Biol; 38:807-17.

EP534

In-use stability of ^{99m}Tc-tilmanocept (Lymphoseek®), a sentinel lymph node detection agent

R. L. Green; Cardinal Health Nuclear Pharmacy Services, Dublin, OH, UNITED STATES.

Aim: ^{99m}Tc-tilmanocept (Lymphoseek®) is an US FDA and EMA approved agent for guiding sentinel lymph node biopsy in clinically node negative breast cancer, melanoma, and oral cavity squamous cell carcinoma. During the radiolabeling of tilmanocept, ^{99m}Tc sodium pertechnetate is added to the product vial and the mixture is allowed to stand at room temperature. According to the product information, the radiolabeled tilmanocept is then to be diluted with sterile normal saline (in the EU) or a phenol-stabilized phosphate-buffered saline (in the US) to bring the vial to the appropriate volume for the desired injection(s). The currently approved expiry time for the radiolabeled solution is 6 hours after compounding. The aim of this study was to evaluate the in-use stability by instant thin layer chromatography (ITLC) radiochemical purity (RCP) testing of ^{99m}Tc-tilmanocept beyond 6 hours, which may allow additional flexibility in surgical scheduling. **Material and methods:** Two different lots of product were radiolabeled using ^{99m}Tc sodium pertechnetate, followed by dilution using normal saline as the diluent in the preparation of ^{99m}Tc-tilmanocept. Vials from each lot were radiolabeled then tested over the following time points: 1, 3, 6, 9, 12, 15, 18, 21, 24 hours. RCP was determined in duplicate measurements by ITLC. **RESULTS:** Lymphoseek was stable throughout the course of the study with RCP values in excess of 99%, independent lot number. **CONCLUSIONS:** Based upon RCP results, ^{99m}Tc-tilmanocept solution for injection is stable in sterile normal saline diluent for at least 12 hours.

EP535

Improving of volumetric activity of the standard generator of technetium-99m

A. S. Rogov, V. S. Skuridin, E. S. Stasyuk, E. A. Nesterov, V. L. Sadkin, N. E. Villa, E. A. Ilina; National Research Tomsk Polytechnic University, Tomsk, RUSSIAN FEDERATION.

Introduction: Short-lived radionuclide technetium-99m is a daughter product β -decay of ⁹⁹Mo isotope. For its rapid separation of ⁹⁹Mo in everyday medical practice is used mobile generators of technetium-99m. The basis of the generator column filled with a chromatographic alumina, which is applied to the source of molybdenum-99 isotope. From daily generator allocate technetium-99m getting the eluate followed by a gradual decrease in activity. Generators based on the activation of molybdenum-99 produced by (n, γ) nuclear reactor IRT-T have an increased mass of sorbent. This leads to the necessity of increasing volume of NaCl needed to obtain the drug with a given activity. **Aim:** Development of the generator of technetium-99m-based activation molybdenum-99, with a minimum amount of NaCl used for the production of the drug. **Methods:** We know many different methods of application of molybdenum-99 to the surface chromatographic sorbent. However, for the manufacture suitable generators of technetium-99m from a less active as raw material using the method of charging the generator flow method. To increase the sorption mass of molybdenum-99 on our generator column were tested methods of pre-processing of sorbent to increase the active of adsorption centers. The dependence of the mass sorbed from solution passing time through the generator column. The dependence of sorbed mass from the solution passing time through the generator column. **Result:** The results showed that pre-acid treatment of the sorbent allowed to increase its capacity for molybdenum-99 by 15%. Slow flow rate of the solution through sorbent increases sorption performance by 10%. Considering the data suggested that a charging generator column with combining techniques. As an additional condition prompted to change the direction of the charging generator column. **Conclusions:** The combination of these techniques increase sorbent charging capacitance with a change direction it possible to increase sorption capacity of chromatographic alumina used by more than 38%. Due to changes in the direction of the charging generator appeared significant time interval, and the interaction of the sorbent solution containing molybdenum-99. Subsequent analytical studies have shown that the

content of active and inactive impurities in the product is at the upper limits of normal. The indicator radiochemical purity meets the requirements of the pharmaceutical articles on receiving the drug. Managed to increase the volumetric activity of generators technetium-99m is produced on the basis of activation of molybdenum-98 without the use of sophisticated methods of isotope concentration. Acknowledgment: The work was supported by the state on behalf of the Ministry of Education of Russia (RFMEFI57514X0034).

EP-27 – Sunday, October 16, 2016, during Exhibition hours, e-Poster Area

M2M: New Targets

EP536

Radioiodinated compounds for Auger therapy

E. Lemos Pereira^{1,2}, A. Paulo¹, M. Oliveira¹, F. Mendes¹, P. Raposinho¹, A. Belchior¹, I. Correia³, J. Lavrado⁴; ¹C2TN, Lisbon, PORTUGAL, ²FCT-UNL, Caparica, PORTUGAL, ³IST-UL, Lisbon, PORTUGAL, ⁴iMed-Ulisboa, Lisbon, PORTUGAL.

Aim: The design of Auger-emitting radiopharmaceuticals for DNA-targeted therapy is an emerging field in contemporary Radiopharmaceutical Chemistry. Our research work aimed to contribute for the progress of this field by studying the potential of ¹²⁵I-labelled Acridine Orange (AO) derivatives for Auger therapy. **Methods:** For this purpose, and based on the DNA-intercalation properties of AO, we've synthesized three new alkyl-iodobenzamide AO derivatives. The ¹²⁵I-labeled congeners were synthesized via the corresponding tributylstannyl derivatives, and were obtained in high *in vitro* stability and radiochemical purity (> 95%) after HPLC purification. The interactions of the compounds with calf thymus DNA and with plasmid DNA were evaluated. Cellular uptake assays, as well as radiocytotoxicity analysis were also conducted. **Results:** All three compounds showed high affinity to DNA, acting mainly as intercalators. Evaluation of ϕ X174 plasmid DNA showed induced double-strand breaks (DSB) yields in the range 0,07-0,09 and 0,05-0,04. Cellular uptake assays revealed good uptake rates, at 4 hours incubation. Preliminary radiocytotoxicity and DNA damage in living cells results suggested more than 35% cell death, which is certainly a consequence of its ability to produce DSB in the cellular DNA, as shown by the γ -H2AX assay. **Conclusion:** These results led us to conclude that the produced DNA damage from two of the synthesized compounds was mainly due to direct effects of emitted Auger electrons.

EP537

In Vitro Mouse and Human Serum Stability of A Heterobivalent Dual-Target Probe Which Has Strong Affinity To GRP and NPY1 Receptors on Tumor Cells

K. Kumar, A. Ghosh, V. Gaja, N. Raju, M. Tweedle; Laboratory for Translational Research in Imaging Pharmaceuticals, The Wright Center of Innovation in Biomedical Imaging, Department of Radiology, The Ohio State University, Columbus, OH 43212, Columbus, OH, UNITED STATES.

Aim. The objective of the present study was to determine the *in vitro* stability of a hetero bivalent dual-target probe (t-BBN-BVD15-DO3A), which has shown strong affinity to GRP and NPY1 receptors, in mouse and human serum at 37°C. **Materials and Method.** A hetero bivalent dual-target probe, t-BBN-BVD15-DO3A (where a GRP targeting ligand J-G-Abz4-QWAVGHLM-NH2 and Y1 targeting ligand INP-K [ϵ -J-(α -DO3A- ϵ -DGa)-K] YRLRY-NH2 were coupled)

that recognizes both GRP and Y1 receptors was synthesized, purified, and characterized. Mouse serum collected from fresh blood, Human Serum (MP Biomedicals), PBS (Gibco), and ¹⁵³GdCl3 (Perkin Elmer) were used in these studies. A known amount of a ¹⁵³Gd labeled (t-BBN-BVD15-DO3A) sample was mixed with mouse or human serum and incubated at 37°C. The degradation of the ¹⁵³Gd(t-BBN-BVD15-DO3A) was monitored with time by a Reversed-Phase HPLC method. The method involves using an Agilent HPLC which is interfaced with a Radioisotope Detector (RID) and a Chem Station software. Results and Conclusions. A ¹⁵³Gd labeling method and an analytical method for monitoring degradation of the dual-target probe in mouse and human serum were developed. Stability of the dual-target probe in mouse or human serum with time was monitored by the reduction in the main peak area. For example, the percentages of the main peak areas of the dual-target probe in mouse serum with time in minutes (in parenthesis) were: 92.4 (23), 94.9 (67), 75.7 (127), 66.8 (200) and 0.27% (1140). An estimated half-life of the dual-target probe in mouse serum is 3.2 hrs. In comparison, the dual-target probe is found to be more stable in human serum with estimated half-life > 5 hrs. A probable mechanism of degradation of the dual-target probe in mouse serum is proposed.

EP538

A systematic study of ⁶⁴Cu production on Ni target with 11 MeV protons

L. Auditore¹, E. Amato², R. Gentile², P. Coppolino², S. Baldari²; ¹University Hospital G. Martino, MESSINA, ITALY, ²University of Messina, MESSINA, ITALY.

Aim: ⁶⁴Cu is a promising theranostic nuclide for PET and nuclear medicine treatments of cancer. Relevant ⁶⁴Cu activities can be obtained by the nuclear reaction ⁶⁴Ni(p,n)⁶⁴Cu on (95%-99%) ⁶⁴Ni enriched targets. After irradiation, the target contains ⁶⁴Cu mixed with other isotopes such as ^{60,61,62}Cu and ^{55,57,58,61}Co. A valuable reduction of contaminants can be achieved by properly choosing beam parameters, target composition, thickness and shape, irradiation and cooling times. This work aims to provide a systematic study of the ⁶⁴Cu production with Ni enriched targets, evaluating the contribution of all the competing channels when changing proton energy (through a degrader), target thickness and irradiation/cooling times. Materials and methods: ⁶⁴Cu production from a 95% ⁶⁴Ni enriched target irradiated by protons (E_{max} = 11 MeV) was considered. Yields at the End Of Bombardment (EOB) were estimated using both the TALYS code and an analytical approach based on the EXFOR experimental data libraries and on a Bragg curve in Ni estimated with MCNPX. Yields_{EOB} were provided as a function of target thickness, beam energy and irradiation/cooling times. A validation of our theoretical estimations was obtained through a comparison with experimental data available in literature. Results: a good agreement was found between our calculation results and the experimental data; the observed deviations are attributable to the existing differences between TENDL and EXFOR excitation functions. For a thick target irradiated at 11 MeV, ⁶⁴Cu yields_{EOB} of 10.11/7.73 mCi/μAh were evaluated using TALYS and the analytical approach, respectively. ^{60,61,62}Cu and ^{55,57,58,61}Co contaminants are also produced. Reducing proton energy to 5 MeV, ⁶⁴Cu yields_{EOB} lowers to 0.92 mCi/μAh, ⁶⁰Cu and ^{55,57,58}Co are not produced or detectable, ⁶¹Cu and ⁶¹Co lowers to less than 1E-03 mCi/μAh, ⁶²Cu (T_{1/2}=9.67 m) lowers to about 1E-02 mCi/μAh, and can be reduced choosing a proper cooling time. Conclusion: ⁶⁴Cu production by means of the ⁶⁴Ni(p,n) reaction allows to obtain a ⁶⁴Cu yield of clinical interest. A theoretical systematic study like ours provides a pathway to optimize production while reducing contaminants acting on proton beam energy, target thickness, irradiation and cooling times.

EP-28 – Sunday, October 16, 2016, during Exhibition hours, e-Poster Area

M2M: PET/CT & Miscellaneous

EP539

Factors Influencing the Pattern and Intensity of Myocardial FDG Uptake in Oncologic PET-CT Imaging

B. Fallahi, B. Moasses Ghaffari, D. Beiki, A. Fard-Esfahani, M. Eftekhari; Research Center for Nuclear Medicine, Tehran University of Medical Sciences, Tehran, IRAN, ISLAMIC REPUBLIC OF.

Introduction: Myocardial FDG uptake is highly variable, ranging from quite intense to minimal distribution, in oncologic whole body FDG PET-CT studies. Intense or heterogeneous myocardial FDG uptake is undesirable as it may interfere with the visual or quantitative evaluation of tumoral invasion and metastases in pericardium, myocardium or adjacent mediastinal structures. The diet, as well as many other factors, is assumed to influence the myocardial FDG uptake. Using a multivariate model, we tried to identify and predict the main factors influencing cardiac FDG uptake in patients referred for oncologic PET-CT evaluation. **Methods:** A total of 214 patients referred for oncologic FDG PET/CT scan were enrolled in our study. Patients were randomly allocated into two groups according to the diet they were instructed to follow during 24-hour period before imaging. One hundred and seven cases with a routine diet (RD) and the same number of patients with a low carbohydrate high fat (LCHF) diet were included. All patients in both groups were also instructed to fast 6 hours before imaging. Weight, height, blood glucose, heart rate, systolic and diastolic blood pressure were measured before radiotracer injection. Visual and quantitative analysis were done after imaging and the pattern of FDG uptake as well as standardized quantitative value of cardiac uptake was determined for each case. **Results:** The frequency of undesirable cardiac FDG uptake in the LCHF group was significantly less than RD group (17% vs. 72%, $p < 0.001$). The univariate analyses showed male gender, BMI ≥ 30 as well as consumption of cardiochemotoxic agents, benzodiazepines and beta blockers were significantly associated with higher intensity of myocardial FDG uptake, while this undesirable finding was less evident in cases with diabetes mellitus. A multivariate logistic regression model including all of the mentioned variables revealed the diet was the only significant independent factor that predicted undesirable myocardial FDG uptake ($p < 0.001$). **Conclusion:** LCHF diet 24 hours before PET-CT imaging is the only controllable independent factor influencing the intensity and pattern of myocardial FDG uptake and is recommended to achieve optimal suppression of cardiac FDG uptake.

EP540

Prognostic Value of Volumetric Parameters of PET-CT With Stage IIIB-IV Non-Small Cell Lung Cancer

B. YUSUFOGLU¹, C. Bilir²; ¹RECEP TAYYIP ERDOGAN UNIVERSITY Teaching and Education HOSPITAL, RIZE, TURKEY, ²Sakarya University School of Medicine, Department of Medical Oncology, Sakarya, TURKEY.

Abstract Objective: PET-CT has been used for staging of lung cancer, particularly in case of exclusion and operability of distant metastasis. Although PET-CT is often used for response to treatment; clinically, prognostic and predictive importance of basal PET-CT haven't exactly been known. As well as TLG value in PET-CT is parameter associated with SUVmean and MTV values of tumoral region, information about its clinical importance is not sufficient yet. We investigated the relation of this parameter, which hasn't been specified in routine PET-CT reporting, with oncological outcomes in advanced stage NSCLC.

Methods: All patients TLG values of primary tumor, lymph nodes and measurable lesions in metastatic regions were calculated by being measured in accordance with RECIST criteria, reviewing basal PET-CT results of 76 NSCLC patients who was diagnosed and treated in our hospital between the years 2013-2015. SUVmax, SUV mean, MTV and TLG values were calculated for primary tumor, lymph nodes and metastatic regions separately. **Results:** The average of age of 76 patients was 64 (34-84) years and they consisted of 68 males and 8 females patients. While 41 patients were diagnosed with adenocarcinoma, 35 patients were diagnosed with squamous cell carcinoma. While there wasn't a significant difference between two groups in respect to their biochemical and hemogram parameters, which are among general characteristics; just the patients diagnosed with adeno Ca were younger (62 vs 67,8; $p = 0.03$). Among PET-CT parameters, a statistical relation of only SUVmax and SUVmean values was identified with PFS. But, PET-CT parameters were not related to PFS in subgroup analyzes of SCC tumor type. In adenocancer subtype, mediastinal TLG and WB TLG values were significantly correlated with each other in addition to the SUVmax value. Similarly, a relation of PET-CT parameter with only adeno Ca subtype was found. **Conclusion:** Although PET/CT has often been used for staging of lung cancer, prognostic importance of many PET parameters in exclusion of metastasis hasn't been known exactly. The most important finding of our study are that there is not prognostic and predictive importance of PET-CT in SCC; whereas, especially TLG values of primary tumor, WB TLG and mediastinal metastatic lymph nodes are significant and important for both PFS and OS in lung adeno Ca. As well as the number of our cases is small, provided it is supported with large-scale studies that PET-CT is more beneficial to patients diagnosed with lung adenocarcinoma; calculation of value of PET-CT indication and TLG value in this subtype may take an important place in terms of clinical practice.

EP541

Detection of Primary Tumor by FDG PET/CT in Cancer of Unknown Primary

P. Ozcan Kara¹, Z. Koc¹, E. Yaman Sezer²; ¹Mersin University Faculty of Medicine Department of Nuclear Medicine, Mersin, TURKEY, ²Mersin University Faculty of Medicine Department of Oncology, Mersin, TURKEY.

Abstract Aim: Cancer of unknown primary tumors is a heterogeneous group of patients who presented with metastatic involvement of a distant organ without a documented primary site despite detailed investigation. Aim of this retrospective study is to estimate the detection ratio of FDG PET/CT in cancer of unknown primary patients. **Materials and Method:** Twenty five patients (13M, 12F; mean: 61,84 \pm 12,16 years old) with diagnosis of distant metastasis according to histopathology and/or MRI/ultrasonography were included into this retrospective study. **Results:** The patients presented brain (n=10), bone lesion (n=3), liver (n=6), lymph node (n=5) and pleural lesions (n=1) with additional metastatic sites in 19 patients (mean SUVmax: 5,91 \pm 3,5). The primary tumor was determined by FDG PET/CT in 21/25 patients (84%) (lung (n=6), primary brain (n=2), renal cell carcinoma (n=2), thyroid (n=2), rectum (n=3), pancreaticobiliar (n=2), subcutaneous tissue (n=1), base of tongue (n=1), sinus priformis (n=1) and lymphoma (n=1)) and two patients with suspicious primary site (colon (n=1), nasopharynx (n=1)) were present. Eight patients were out of follow up. Four patients had documented primary site which we pointed out in FDG PET/CT. **Conclusion:** Previous studies report 20-50% detection rate for identification of primary tumor in patients with CUP. However new generation multislice scanners may provide higher detection ratio's. The detection rate of FDG PET/CT might be higher than previously reported according to this study however prospective studies in large series are warranted. **Key Words:** Unknown primary, metastasis, FDG, PET/CT.

EP542**The Value of ¹⁸F-fdg Pet/Ct and Cea Among Patients With Colorectal Carcinoma in Detecting Disease Recurrence**

A. Barrenechea, I. S. Bandong, F. G. M. Estrada; St. Luke's Medical Center, Quezon City, PHILIPPINES.

Surveillance for colorectal carcinoma recurrence in patients who have undergone surgery and adjuvant treatment with chemotherapy or radiotherapy is usually initiated with elevated serum carcinoembryonic antigen (CEA) levels. Previous studies have shown, however, that elevated CEA is less sensitive in detecting recurrence as recurrence is also seen in patients with normal CEA levels. We evaluated the utility of FDG-PET/CT in patients with suspected recurrence of CRC by comparing PET/CT performance to CEA levels. **METHODS:** An ambispective cross-sectional design was done on 183 adult patients diagnosed with colorectal adenocarcinoma and who had previous surgical resection, with or without chemotherapy or radiotherapy, and who underwent PET/CT using ¹⁸F-FDG from July 2013 to September 2015 at a PET center of a local tertiary hospital. Eighteen patients (10 males, 8 females, with ages ranging from from 28 to 87 years and a mean age of 63.72 years) were included as these patients were the only ones who had histopathologic confirmation or clinical follow-up proving disease recurrence. **RESULTS:**The FDG-PET/CT study yielded a true positive in detecting recurrence in 11 (61%) out of the 18 patients, a true negative in 5(28%) patients, a false negative in 0 (0%) patients and a false positive in 2(11%) patients. The sensitivity, specificity, and positive predictive value (PPV) of the FDG-PET/CT study for establishing recurrence were 100, 71 and 85%, respectively. In contrast, these parameters were 82, 29 and 64%, respectively, for CEA levels. No significant association was noted between CEA levels and PET/CT scan as well as SUV_{max}. **CONCLUSIONS:** FDG PET/CT is a highly sensitive and specific tool for detecting recurrence in patients with colorectal carcinoma when compared to CEA and is able to provide a more accurate diagnosis even in patients that show a negative CEA on surveillance.

EP543**Outcome of PET/CT ¹⁸F-Choline in high risk prostate cancer patients**

H. Lavados, R. PRUZZO, H. AMARAL, E. HERNANDEZ, B. MORALES, A. HAEGER, R. FERNANDEZ, A. HURTADO, R. GALAZ; Nuclear Medicine and PET/CT Center, PositronMed and Arturo Lopez Perez Foundation, Santiago, CHILE.

Introduction: Prostate cancer in high-risk patients (PSA >20 ng/mL, Gleason score ≥ 8 and T≥2 cm represent 20-30% of the total of this neoplasm. The lymph nodal involvement in this group is about 15-40%. One of the limitations is of the limitations is that conventional diagnostic tools (CT, bone scan) is the accurate staging. Positron emission tomography with ¹⁸F-Choline (PET/CT ¹⁸F-Choline) seems to be a more precise tool to evaluate these patients. However, there are few studies evaluating the outcome of this technique in the context of management protocols and study. **Objective:** To assess the outcome of PET/CT ¹⁸F-Choline in staging high risk prostate cancer patients. **Patients and method:** A total of 39 high risk prostate cancer criteria patients. 64 years old (53-74). PSA 18.9 ng/ml. Patients with histological diagnosis of high-risk prostate cancer. Radical prostatectomy performed and bilateral extended lymphadenectomy with PET/CT ¹⁸F-Choline as a method of pre-staging. Pre surgical PET/CT ¹⁸F-Choline and histopathology information were compared, including the resected lymph nodes. Sensitivity, specificity, positive predictive value and negative predictive value were calculated. **Results:** In this series the following values were obtained: sensitivity: 64%, specificity: 92%, positive predictive value: 77% and negative predictive value: 85%. **Conclusions:** Although this series represents a small

number of patients, PET/CT with ¹⁸F-Choline is a noninvasive test that provides more information about the lymph nodes involvement and presence of distant metastases in high-risk prostate cancer, allows a better staging than conventional techniques. Although the sensitivity in our series is low, it is higher than reported values for other conventional imaging techniques. Moreover the high specificity and negative predictive value allow foreseeing high degree of confidence if an abnormal PET/CT ¹⁸F-Choline, effectively presents lymph nodal involvement or distant metastases, which determines a more accurate clinical management.

EP544**Usefulness of 68Ga-PSMA as agent theragnostic in metastatic breast cancer**

S. S. MEDINA ORNELAS, F. O. GARCIA PEREZ; INSTITUTO NACIONAL DE CANCEROLOGIA, MEXICO CITY, MEXICO.

BACKGROUND Selective inhibition of angiogenesis is a key strategy in breast cancer. This process requires early identification when first-line therapy fails. Current research indicates that PSMA is related to angiogenesis of many solid tumors. However studies are limited in the use of this agent in metastatic breast cancer **PURPOSE** Demonstrate PSMA expression in tumor neovasculature of primary and metastatic breast cancer sites, to assess the potential use as theragnostic agent, regardless of the hormonal status and histology. **PATIENTS AND METHODS** Six patients of our institution with breast with estrogen receptors and progesterone (+) cancer, 3 patients were Her-2neu (+), and 3 patients Her-2neu (-), metastatic to bone confirmed by bone scintigraphy were evaluated by PET / CT with 68Ga-PSMA one month prior to receiving QT cycle; the purpose of assess the degree of avidity of metastatic lesions, under the hypothesis of the neovasculature of the tumor microenvironment of metastasis in breast cancer **RESULTS** Of the six patients evaluated similar uptake patterns were obtained in 3 of them: 1. Infiltrating ductal carcinoma; ki-67 30%, Her-2 (-) multiple bone metastases were observed 2. Infiltrating ductal carcinoma; ki-67 70%, Her-2 (+); multiple bone metastases were observed and primary lesion 3. Infiltrating ductal carcinoma; ki-67 40%, Her-2 (+); multiple bone metastases were observed and primary lesion 4. invasive lobular carcinoma; ki-67 5% Her-2 (-); not greedy bone metastases were observed PSMA, but two liver metastases unsuspected 5. invasive lobular carcinoma; ki-67 5% Her-2 (-); not greedy bone metastases were observed by PSMA 6.- Infiltrating ductal carcinoma; ki-67 70%, Her-2 (+); multiple bone metastases were observed and primary lesion **CONCLUSION** Expression levels in tumor neovasculature PLASMA differ between the primary site and metastasis. Our study showed expression of PSMA in the primary site in 50% of patients; while metastatic sites were observed in 100%. A PET / CT with 68Ga-PSMA demonstrating metastatic disease can help in the selection of tumors with high expression of PSMA to provide targeted therapy with 177 Lu-PSMA, particularly in patients with invasive ductal carcinoma regardless of the status of the Her-2neu, with failure to second-line treatment

EP545**Prognostic value of staging ¹⁸F-FDG PET-CT in patients diagnosed with non-small cell lung cancer**

P. García-Talavera¹, C. Montes², F. Gómez-Camino¹, L. Díaz¹, R. Ruano¹, B. Pérez¹, E. Martín¹, M. Martín¹, P. Tamayo¹; ¹Nuclear Medicine Department. Hospital Clinico Universitario de Salamanca, Salamanca, SPAIN, ²Radiation Protection Department. Hospital Clinico Universitario de Salamanca, Salamanca, SPAIN.

AIM Assessing the prognostic value of staging ¹⁸F-FDG PET-CT in patients with non-small cell lung cancer by means of SUV_{max} (maximum

standardized uptake value), MTV (metabolic tumour volume) and TLG (total lesion glycolysis). In addition, studying differences in these parameters depending on cell histology. **MATERIAL AND METHODS** Twenty patients were included (18 men). Mean age: 67.4 ± 8.3 years old (50–86). All of them were diagnosed with histologically proved non-small cell lung cancer. Histopathology: Adenocarcinoma (8), squamous cell carcinoma (9), others (3). Initial staging (AJCC 7th edition): IA (3), IB (1), IIB (1), IIIA (5), IIIB (3), IV (7). A PET-CT (Biograph mCT Flow) was performed in all patients, one hour after intravenous administration of ^{18}F -FDG (5MBq/kg). The following parameters were determined: SUVmaxT (tumour), SUVmaxN (nodes) and SUVmaxM (metastases) of the highest metabolic lesion, as well as sum of all MTVs and all TLGs. SUVmax was obtained by means of “syngovia” software and TLG and MTV, with a homemade software. The Kaplan-Meier method was used to perform survival analysis (overall and free progression survival) and the log-rank test was applied to compare survival curves. **RESULTS** Overall survival (OS) was 9.9 ± 3.8 (2–16 months) and free progression survival (FPS), 8.1 ± 4.7 (1–16). Regarding OS, there were statistically significant differences depending on MTV ($\chi^2=6.046$; $p=0.014$), with a cut-off value of 75. Regarding FPS there were statistically significant differences depending on MTV ($\chi^2=5.825$; $p=0.016$) and TLG ($\chi^2=6.793$; $p=0.009$), with cut-off values of 75 and 650, respectively. Results (mean \pm s.d), depending on histology, are shown in the table. There were significant differences (Kuskall-Wallis) among different types of histology in TLG ($p=0.003$) and SUVmaxT ($p=0.080$). Squamous cell carcinoma shows higher values of TLG and SUVmaxT than adenocarcinoma (Mann Withney’s test: $U=12.0$; $p=0.021$ and $U=9.5$; $p=0.011$, respectively). **CONCLUSIONS** This study indicates that staging ^{18}F -FDG PET-CT could be a prognostic tool in non-small cell lung cancer patients. Specifically, MTV could detect those patients at a higher risk of death; furthermore, MTV and TLG could indicate a higher probability of disease progression. Lesion histology has a significant influence on TLG and SUVmaxT, showing higher values in squamous cell carcinoma.

EP546

18F FDG PET/CT accuracy in the evaluation of residual axillary disease after neoadjuvant therapy depends on breast cancer subtypes

L. Gilardi¹, S. Baio¹, M. Colandrea¹, S. Fracassi¹, P. Rocca¹, L. Travaini¹, V. Galimberti¹, M. Colleoni¹, G. Paganelli², C. Grana¹; ¹European Institute of Oncology, Milan, ITALY, ²Istituto Scientifico Romagnolo per lo Studio dei Tumori IRST-IRCCS, Meldola, ITALY.

Purpose: The aim of our study was to prospectively investigate the role of pre-operative ^{18}F FDG PET/CT in the prediction of axillary lymph node response to neoadjuvant therapy (NT) in patients with breast cancer. **Methods:** Seventy patients with primary breast cancer clinically classified as cT2-T4a-c cN0-N3 M0 and with a positive baseline PET/CT scan in the axillary lymph nodes received neoadjuvant therapy. A second PET/CT was performed before surgery, with sentinel node biopsy (SNB) in the case of pathological FDG uptake disappearance in axilla (with subsequent axillary lymph node dissection - ALND - if the sentinel node was positive) and with a direct ALND in the case of persistent FDG uptake. **Results:** FDG PET showed high specificity and positive predictive value for the detection of axillary disease persistence (94% and 86%, with 95% confidence interval of 79–99% and 57–98% respectively), while sensitivity, negative predictive value and overall accuracy were only 31%, 52% and 59%, respectively. Stratifying for subtypes, higher negative predictive value and overall accuracy were significantly associated with non-luminal breast cancer ($p < 0.001$ and 0.0013 , respectively). **Conclusions:** Overall, PET/CT turned out to be inadequate to preclude surgical axillary staging after neoadjuvant treatment. However, the high specificity suggests that the procedure does have a role in the selection of patients who can directly undergo ALND, avoiding SNB. The overall accuracy of PET/CT in this setting depends on breast cancer subtypes.

EP547

Normal Distribution Pattern and Physiological Variants of Ga-68-PSMA PET/CT

E. Demirci¹, O. Sahin², M. Ocak³, B. Akovali², J. Nematyazar², L. Kabasakal²; ¹Department of Nuclear Medicine, Sisli Etfal Training and Research Hospital, Istanbul, TURKEY, ²Department of Nuclear Medicine, Cerrahpaşa Medical Faculty, Istanbul University, Istanbul, TURKEY, ³Department of Pharmaceutical Technology, Pharmacy Faculty, Istanbul University, Istanbul, TURKEY.

OBJECTIVES: Glu-NH-CO-NH-Lys-(Ahx)-[^{68}Ga (HBED-CC)] (Ga-68-PSMA) is a novel PET tracer and binds to extracellular component of Glutamate carboxypeptidase II, which is also called prostate specific membran antigen (PSMA) due to high expression in prostate cancer. Initial experience with Ga-68-PSMA suggests that PSMA PET/CT can be used for imaging of advanced prostate cancer. In this study we aimed to present detailed biodistribution of Ga-68-PSMA, as well as physiological and benign variants of this novel tracer. **METHODS:** We performed retrospective analysis of 40 patients who underwent PSMA PET/CT between January and August 2015 at our department and who had no evidence of residual or metastatic disease on PSMA PET/CT and conventional imaging methods. Additionally 16 patients who underwent PSMA PET/CT for any indications other than prostate cancer included in the study to evaluate physiological uptake in the normal prostate gland. Median, minimum-maximum, mean, standard deviation of SUVmax and SUVmean values were calculated for visceral organs, bone marrow and lymph nodes and mucosal areas. Any physiological variants or benign lesions with Ga-68-PSMA were noted. **RESULTS:** Ga-68-PSMA uptake was noted in kidneys, parotid and submandibular glands, duodenum, small intestines, spleen, liver, lacrimal glands, mucosal uptake in nasopharynx, vocal cords, pancreas, stomach, mediastinal blood pool, thyroid gland, adrenal gland, rectum, vertebral bone marrow, testes and calculated meanSD of SUVmax were 55.623, 19.66.5, 19.595.3, 18.36.6, 17.77.4, 13.515.87, 12.94.9, 11.44.1, 5.562.63, 5.641.87, 5.52.5, 5.12.3, 4.31.67, 4.21.96, 3.61.6, 3.62.25, 3.61.58, 2.860.93 respectively. Celiac lymph nodes showed slightly Ga-68-PSMA uptake in 24 of 40 patients without presence of any other pathologic lymph nodes in abdominal and pelvic areas and calculated meanSD of SUVmax were 3.62.02. Kidneys demonstrated DMSA-like high cortical uptake in 39 patients and showed reduced uptake in atrophic kidney of one patient. High uptake was observed in the gallbladder wall of 4 patients (SUVmax ranged from 10.7 to 40.1). In 2 of 40 patients, calcified choroid plexus showed minimal but visible uptake. Slightly elevated uptake was noted in breast parenchyma in 3 of 8 patients who had gynecomastia. Osteophytes of 2 patients showed slight uptake. Analysis of normal-sized prostate glands, in patient group who had PSMA PET/CT for indications other than prostate cancer ($n=16$), demonstrated a slight physiological uptake in prostate glands (SUVmax: 5.51.6, range: 3.5–8.3) **CONCLUSION:** This study demonstrates normal distribution pattern, range of SUVs and physiological variants of Ga-68-PSMA. Additionally, several potential pitfalls were documented.

EP548

A potential pitfall in 68 Ga-PSMA PET/CT: Anthracosis

T. Elri, M. Aras, Y. S. Salihoglu, R. U. Erdemir, M. Cabuk; Bülent Ecevit University School of Medicine, Department of Nuclear Medicine, Zonguldak, TURKEY.

Case Presentation: A 72 year-old prostate cancer patient with known bone metastases was referred to ^{68}Ga -PSMA PET/CT due to increased serum tumor markers [PSA = 21.36 ng/ml (normal levels = 0.04–4 ng/ml)] and newly detected liver metastases on recent abdominal CT. In addition to intense PSMA avid bone and liver metastases, PET/CT also revealed hilar

mass in the left lung and accompanying mediastinal lymphadenopathies with intense radiopharmaceutical uptake. The hilar mass was bronchoscopically biopsied to exclude second primary lung malignancy. The histopathological analyses of this mass was reported as anthracosis. The follow up 68 Ga-PSMA PET/CT performed three months after the initial scan revealed progressed lesions in the bone and abdomen. However significant regression was observed in the aforementioned thoracic lesions. Discussion: 68 Ga-PSMA PET/CT is a relatively new imaging modality, and there is no enough information about the PSMA avidity of extraprostatic malignancies and benign conditions yet. It was reported that 68 Ga-PSMA PET/CT alone could not give us the opportunity to reliably discriminate primary lung cancer from lung metastases of prostate cancer. On the other hand, although chronic inflammatory processes of the lung are well known reasons for false positive FDG PET/CT reporting, to our knowledge, 68 Ga-PSMA uptake in the benign conditions of the lung has not been reported yet. Our case showed that inflammatory conditions of the lung such as anthracosis may cause false positive reporting in 68 Ga-PSMA PET/CT. Conclusion: It should be kept in mind that benign conditions of the lung such as anthracosis may cause intense radiopharmaceutical uptake on 68 Ga-PSMA PET/CT and may lead to misdiagnosis. Histopathological analysis should be performed in the suspicion of second primary lung malignancy as this was the case in our patient.

EP549

The Detection of Prostate Cancer Relapse in Patients after Radical Prostatectomy with PSA Level < 2,0 ng/ml According to ¹¹C-Choline PET/CT

D. M. Pursanova¹, I. P. Aslanidis², O. V. Mukhortova², T. A. Katunina², V. I. Shirokorad³, D. A. Roshchin⁴; ¹A.N.Bakoulev Scientific Center for Cardiovascular Surgery of the Ministry of Health of the Russian Federation, Moscow, RUSSIAN FEDERATION, ²Bakoulev Scientific Center for Cardiovascular Surgery, Moscow, RUSSIAN FEDERATION, ³Moscow City Oncology Hospital №62, Moscow, RUSSIAN FEDERATION, ⁴N.Lopatkin Scientific Research Institute of Urology and Interventional Radiology – Branch of the National Medical Research Radiological Centre of the Ministry of Health of the Russian Federation, Moscow, RUSSIAN FEDERATION.

The detection of extrapelvic metastases in prostate cancer (PCa) patients with early biochemical relapse (PSA <1,0-2,0 ng/ml) after radical prostatectomy is crucial for selecting patients for salvage radiotherapy. **Purpose:** To evaluate the usefulness of ¹¹C-Choline PET/CT in patients after radical prostatectomy with low PSA level for detection of PCa relapse. To identify predictive factors of a positive ¹¹C-Choline PET/CT. **Materials and methods:** PET/CT was performed in 61 patients on PET/CT scanner (Biograph-64, Siemens) 10 min after injection of ¹¹C-Choline (400-700 Mbq). The mean PSA value in the group was 0.93 ± 0.54 (0.21-1.98) ng/ml, median - 0.91 ng/ml. **Results:** Overall, ¹¹C-Choline PET/CT detected PCa relapse in 30% (18/61) of cases. There was no statistical difference between PET-positive (n=18) and PET-negative (n=43) patients according to age, time to biochemical relapse after surgery, Gleason score and ongoing hormone therapy. The detection rate of relapse according to ¹¹C-Choline PET/CT showed correlation (p=0,007) with serum PSA: positive PET/CT results were obtained in 30% (18/61) patients with PSA <2,0 ng/ml, in 23% (12/53) - with PSA <1,5 ng/ml, in 17% (6/36) - with PSA <1,0 ng/ml, and in 20% (3/15) - with PSA <0,5 ng/ml. PSA doubling time <6 months, stage ≥T3 and N1 were significantly associated with an increased probability of positive PET/CT findings (<0,05 for all). All these parameters were found to be independent predictive factors for PET-positive result at simple linear regression analysis. The combination of mentioned predictors, except N1, was statistically significant in the prediction of a positive PET/CT at multiple linear regression analysis. Local relapse was detected in 61%

(11/18) patients: prostate bed (2) and pelvic lymph nodes (9). Distant metastases were identified in 28% (5/18) cases: lymph nodes (3), bone (1) and lungs (1). In 11% (2/18) cases both local and distant metastases were diagnosed: regional and extrapelvic lymph nodes (1), regional lymph nodes and bone (1). **Conclusion:** ¹¹C-Choline PET/CT was able to detect and correctly identify the localization of PCa relapse (local and distant) in 30% of patients with PSA <2,0 ng/ml, and therefore was useful in choice of further therapeutic approach. Pathological stage (≥T3, N1), trigger PSA and short PSA doubling time were found to be significant predictors for PET-positive result and should be considered in patient selection for ¹¹C-Choline PET/CT.

EP550

⁶⁸Ga-PSMA PET imaging of adenoid cystic carcinoma

T. J. W. Klein Nulent¹, S. M. Willems², R. de Roos³, G. C. Krijger³, F. F. T. Ververs³, R. J. van Es¹, B. de Keizer³; ¹department of oral and maxillofacial surgery, UMC Utrecht, Utrecht, NETHERLANDS, ²department of pathology, UMC Utrecht, Utrecht, NETHERLANDS, ³department of nuclear medicine and radiology, UMC Utrecht, Utrecht, NETHERLANDS.

Introduction: ⁶⁸Ga-PSMA PET imaging has been shown to be positive in several types of malignancies. We present the first results of ⁶⁸Ga-PSMA PET imaging in patients with local recurrence or metastatic adenoid cystic carcinoma (ACC), a rare tumour originating from the salivary glands. **Methods:** 5 patients with known or suspected local recurrence or metastatic ACC were retrospectively analysed. Also primary tumours were immunohistochemically (IHC) stained for PSMA expression. **Results:** All patients showed pathological PSMA binding in known or new sites of metastatic ACC. Mean SUVmax value of ACC was 7,73 (range 2,42 - 12,97). Mean SUVmax of the normal parotid gland in these patients was 14,04 (range 6,88 - 31,37). IHC was strongly positive for PSMA in 3/5 patients. **Conclusion.** ⁶⁸Ga-PSMA PET imaging might be a useful and better imaging modality in staging and follow-up of ACC. Due to the high PSMA expression of these tumours ACC might also be candidate for treatment with ¹⁷⁷Lu-PSMA.

EP551

The Impact of Time-of-Flight Acquisition on Shortened Dynamic 18F-FLT PET Quantification

X. Liu, J. Zhang, P. Subramanian, B. Ramaswamy, M. V. Knopp; The Ohio State University, Columbus, OH, UNITED STATES.

Aim: To investigate the impact of Time-of-Flight (TOF) information on kinetic ¹⁸F-FLT PET quantification combined with shortened acquisition. To establish an optimized dynamic FLT PET imaging protocol for accurate FLT kinetics quantification for therapy response assessment. **Materials and Methods:** 30min-dynamic and whole-body FLT PET were acquired on a Gemini TF 64 system (Philips). Dynamic PET data were reconstructed twice following a 26-frame protocol (8x15s, 6x30s, 5x1min, 5x2min, 2x5min), with and without TOF information separately. Maximum activity concentrations (Bq/mL) from tumors and plasma (descending aorta) were obtained via 3D ROI. Ki values were calculated from both TOF (Ki_TOF) and non TOF (Ki_NTof) data sets using Patlak Analysis by in-house developed software based on different data acquisition durations (Td) (10, 12, 14, 16, 20, 25, 30min) and different linear regression onset time (T0) points (1, 2, 3, 4, 5min). SUV_{max} of the tumors were collected from WB images (SUV_{max_TOF}). Ki_{_TOF} of the shortened data series were compared with Ki_{_TOF} as well as Ki_{_NTof} of the 30min-data sets. Ki_{_TOF} of the 30min-data sets and Ki_{_NTof} of the 30min-data sets were compared to each other as well as SUV_{max_TOF} values. Pearson product-moment correlation coefficient (R) of 0.9 was

chosen as a limit for the correlation coefficient. A total of 26 data sets were evaluated. Results: Ki_TOF from image series with shortened Tds compared Ki_TOF of the 30min series showed that the correlation increased as Td increased from 10 to 25min. It revealed weak correlation for series with $Td \leq 14$ min ($R=0.70 \pm 0.07$, 0.75 ± 0.05 , 0.86 ± 0.03 at $Td=10, 12, 14$ min) and excellent correlations when $Td \geq 20$ min ($R=0.97 \pm 0.00$, 0.99 ± 0.00 at $Td=20, 25$ min) regardless of T_0 value. When $Td=16$ min, strong correlation of Ki was shown only when $T_0 \leq 3$ min ($R=0.92$, 0.90 , 0.90 , 0.88 , 0.86 , 0.89 at $T_0=1, 2, 3, 4, 5$ min). Comparisons between Ki_TOF of all tested Tds and Ki_NTof from the 30min series revealed poor correlations independent from the T_0 value ($R=0.39 \pm 0.10$, 0.41 ± 0.10 , 0.50 ± 0.06 , 0.55 ± 0.05 , 0.67 ± 0.03 , 0.75 ± 0.02 , 0.81 ± 0.01 at $Td=10, 12, 14, 16, 20, 25, 30$). When comparing Ki_TOF and Ki_NTof of 30min data to SUV_{max_TOF} , strong correlations were discovered with Ki_TOF ($R=0.92 \pm 0.01$) while weak correlations were indicated with Ki_NTof ($R=0.86 \pm 0.03$) no matter of T_0 value (Fig. 1B). Conclusion: A 16min-long dynamic ^{18}F -FLT PET acquisition with TOF is capable of accurately estimating Ki values, which highly correlate to WB SUV_{max} . The use of TOF in dynamic FLT PET acquisition may introduce variation in Ki values when compared to non TOF.

EP552

Density-threshold for FDG-PET/CT-based N-staging in lung cancer patients

P. Flechsig¹, P. Frank¹, C. Kratochwil¹, L. Schwartz², U. Haberkorn¹, F. Giesel¹; ¹University Hospital Heidelberg, Heidelberg, GERMANY, ²Columbia University, New York, NY, UNITED STATES.

Purpose: Mediastinal N staging done by integrated ^{18}F -FDG-PET/CT in lung cancer patients is not always accurate. In order to reduce the need for invasive staging procedures, additional surrogate parameters for the detection of malignant lymph node infiltration would be helpful. The purpose of this study was to evaluate if semi-automated density measurements in mediastinal lymph nodes can improve pre-clinical N-staging, irrespective of the specific lung cancer entity. **Methods:** This retrospective study was approved by the institutional review board. 248 histologically proven lymph nodes in 122 lung cancer patients were investigated. Non-contrast enhanced ^{18}F -FDG-PET/CT was performed before surgery/biopsy. Lymph nodes analyses were performed on the basis of FDG-uptake and volumetric CT histogram analysis for metric lymph node sampling. **Results:** Of the 248 lymph nodes, 118 were benign, 130 malignant. Malignant lymph nodes had a significantly higher median CT density (>30 HU) compared to benign lymph nodes (9.3 HU, $p < 0.05$), irrespective of the histological subtype. The discrimination between different malignant tumour subtypes by means of volumetric density analysis failed. Irrespective of the malignant subtype, a possible cut off value of 20HU may help differentiate between benign and malignant lymph nodes. **Conclusion:** Density measurements in unclear mediastinal and hilar lymph nodes with equivocal FDG uptake in PET might serve as a possible surrogate parameter for N-staging in lung cancer patients, irrespective of the specific lung cancer subtype. This could also help to find possible high yield targets in cases where invasive lymph node staging is necessary.

EP553

Evaluation of the disease state and effectiveness of radiotherapy with F-18 FDG PET/CT in locally advanced cervical cancer

E. Acar¹, H. Durak¹, Z. Arican², & Görken², G. Çapa Kaya¹; ¹Dokuz Eylül University, School of Medicine, Department of Nuclear Medicine, İzmir, TURKEY, ²Dokuz Eylül University, School of Medicine, Department of Radiation Oncology, İzmir, TURKEY.

PURPOSE: The purpose of this study was to compare F-18 FDG PET/CT findings in patients with locally advanced cervical cancer before-and-after radiotherapy (RT). **METHODS:** We retrospectively evaluated 41 patients (mean age: 57.3, range:29-81) with cervical cancer referred to the Department of Nuclear Medicine between January 2009 and December 2015. There were 39 patients with squamous cell carcinoma, 1 with adenocarcinoma, 1 with poorly differentiated invasive carcinoma. All patients were treated with radiotherapy. F-18 FDG PET/CT was performed at baseline and at 12 weeks after the completion of RT. We compared the primary tumor area, regional lymph nodes and distant metastases before-and-after RT. **RESULTS:** For all patients, the average pre-treatment SUV_{max} was 12.7 ± 5.3 in the primary lesion area. 24 patients (58%) had regional lymph node metastases, and SUV_{max} values were 4.1 ± 5.1 . Four patients with mild F-18 FDG uptake in mediastinal lymph nodes were considered suspicious for metastasis. After treatment; 15 patients (36.5%) had no pathological uptake in the whole body, 21 patients (51%) had no pathological uptake in the cervix. Primary lesion area SUV_{max} was 2.6 ± 3.4 ($p < 0.01$). In 11 patients (27%) regional lymph node metastasis was observed, 10 of these patients (24.6%) had lymph node metastases at baseline F-18 FDG PET/CT imaging. After RT, SUV_{max} values of the regional lymph nodes decreased to 1.6 ± 3.2 ($p:0.004$). After treatment 11 patients (27%) showed distant metastatic disease, 1 patient (2.4%) was suspicious for distant metastasis. The most frequent metastatic sites were; bone, lung, liver, abdominal/mediastinal/cervical lymph nodes and intraabdominal implants. 1 patient showed spleen metastasis. **CONCLUSION:** In 51% of patients with cervical cancer complete response was observed after RT in primary tumor area. 27% patients developed metastatic disease in the short term. After RT, SUV_{max} value of primary lesion area and regional lymph nodes showed statistically significant reduction. Suggesting that the treatment is successful.

EP554

Breast Incidentalomas detected by ^{18}F -FDG PET/CT

I. P. Carvalho, R. Sousa, S. C. Vaz, P. Ratão, F. N. Brandão, M. R. Carvalho, T. C. Ferreira, L. Salgado; Instituto Português de Oncologia de Lisboa Francisco Gentil, Lisbon, PORTUGAL.

Aim: To evaluate the frequency and clinical significance of focal and unilateral breast lesions incidentally found on ^{18}F -fluorodeoxyglucose positron emission tomography (^{18}F -FDG PET/CT). **Material and Methods:** We retrospectively reviewed 5149 ^{18}F -FDG PET/CT performed at our department from January 2014 to January 2016, of which 2174 studies were performed on female patients (pts). All pts in whom the report mentioned unilateral and focal ^{18}F -FDG increased uptake and presence of findings on the CT component were selected. The reports from pts with the following criteria were excluded: under 18 years old (11 pts), known history of breast cancer (427 pts), occult primary tumors (23 pts), known breast disease from other malignancies (13 pts) and bilateral low-grade breast FDG uptake. We included 1699 study reports from 1642 women. In order to assess the clinical significance of breast lesions we recorded follow-up data (mammography, ultrasound and biopsy results). The data was analyzed using descriptive statistics. **Results:** On 1699 ^{18}F -FDG PET/CT studies performed, we identified 13 focal and unilateral breast lesions in 12 pts (incidence of 0.71%). The median age of the 12 women was 66 (range: 33-79 y). All the pts were referred for staging of tumours: malignant cutaneous melanoma (3/12), lung cancer (2/12), ovarian cancer (2/12), scapular chondrosarcoma (1/12), endometrial cancer (1/12), thyroid cancer (1/12), non-Hodgkin lymphoma (1/12) and Hodgkin lymphoma (1/12). The average of maximum

standard uptake value (SUVmax) of breast lesions was 3.37 (range: 1.5–13.8; median 2.59). The follow-up data was available in 6 out of 12 pts. Breast lesion biopsy was performed in 4 pts: 3 lesions were malignant (one moderately differentiated invasive breast carcinoma (SUVmax 2.4 and BI-RADS 6), one breast carcinoma not otherwise specified (SUVmax 13.8 and BI-RADS 6) and one poorly differentiated invasive breast carcinoma (SUVmax 3.2 and BI-RADS 6); the benign lesion was a fibroadenoma (SUVmax 2.6 and BI-RADS 4A). One patient did not require further follow-up (BIRADS 1) and one patient refused to perform biopsy. In the other 6 pts, breast lesions were not considered for further study in 4 and in the other 2 follow-up data were not available. Conclusion: According to our study, breast incidentalomas with focal increased FDG uptake on PET/CT are uncommon (incidence of 0.71%). From the 6 lesions studied, breast malignancy was confirmed in 3. However, the small size of the sample does not allow a definitive assessment of clinical significance. Further studies are needed.

EP555

Role of FDG - PET/CT in the diagnostics of changes in the lung parenchyma, suspicious of radiation pneumonitis

A. K. D. Demirev, Sr.^{1,2}; ¹City Clinic Oncology Sofia, Sofia, BULGARIA, ²University Hospital Aleksandrovska Sofia, Sofia, BULGARIA.

Radiation Pneumonitis /RP/ is an adverse complication of radiotherapy /RT/ and can sometimes limit the application of the already planned radiation dose. It is often associated with radiotherapy of lung carcinoma and is occasionally caused by radiation therapy of breast carcinoma and lymphomas located in the mediastinum, respectively in about 5–50%, 5–10%, and 1–5% of all cases. PET-CT with 18F - FDG hybrid imaging emerges lately as a prospective modality for early diagnostics of RP. Aim of this study was to summarize the initial data from the diagnostic application of PET-CT in patients suspicious of RP and to derive criteria, which can help differentiate RP from early recurrence of the disease and/or residual tumor. The current study included 23 patients (out of 220 patients with RT in the thoracic region) examined between 2012 and 2015, who had metabolic (PET) and morphological (CT) changes consistent with RP. We additionally defined the metabolic activity or the maximum standardized uptake value (SUVmax) in the lung parenchyma of 20 patients without RT. In our patient group 13/23 of the patients had serial examinations - 9/13 before and after RT, 4/13 more than 6 months after RT. The rest of the patients 10/13 had a single examination up to 6 months / more than 6 months after RT. All patients had considerably increased metabolic activity or a tendency towards increased metabolic activity in the lung parenchyma involved in the irradiated area with a mean of SUVmax3,45 /ranging between 1 and 7,1/. The control group had a physiological background metabolic activity of respectively SUVmax0.61 +/- 0.11. The difference in the metabolic activity between the two groups was statistically significant ($p < 0,0001$). The particular metabolic changes in the patients suspicious of RP involved diffusely increased metabolic activity coinciding with the morphological changes in the irradiated area. 3/23 patients had a proven recurrence of the primary neoplastic process in the irradiated area. The metabolic changes in those patients involved - increase in the metabolic activity at follow up or lack of tendency towards normalization after chemotherapy, which implied the existence of still viable tumor cells. Our initial experience in the diagnostic application of 18F-FDG PET/CT in patients suspicious of RP, allows us to summarize the following - PET/CT is a reliable imaging modality in the diagnostics of RP. Through its sequential use, we can differentiate inflammatory changes related to RP from early recurrence of the primary neoplastic process

EP556

Implications of PET/CT in radiotherapy treatment planning of Head&Neck disease

O. Ferrando¹, E. Giovannini², R. Leoncini², T. Scolaro³, F. Foppiano¹, A. Ciarmiello²; ¹Department of Medical Physics - ASL5 Spezzino, La Spezia, ITALY, ²Department of Nuclear Medicine - ASL5 Spezzino, La Spezia, ITALY, ³Department of Radiotherapy - ASL5 Spezzino, La Spezia, ITALY.

Aim. To evaluate the role of PET/CT respect to conventional CT in radiotherapy treatment planning for head and neck disease. Methods and Materials. We have analysed a set of 31 patients with histological diagnosis of head and neck cancer who underwent conformal-3D Radiotherapy. The anatomical area of this disease was divided in: oropharyngeal, laryngeal and oral cavity cancer. Gross tumour volumes were delineated on CT images (CT_GTVs) by an expert radiation oncologist blinded to PET data. Successively another set of target volumes was defined taking into account the combined PET/CT information (PET_GTVs). 3D-Radiotherapy planning was performed on CT_GTVs and the dose-volume histograms also for PET_GTVs were analysed at the aim to evaluate any changes in the dosimetric parameters. The study also analysed the difference between CT_GTVs and PET_GTVs volumes. Results. In the cohort of the analysed patient 9 had the nodal stage changed by inclusion of PET data. 1 patient had negative PET/CT and for 1 patient PET reveals distant metastasis. For two patients lymphonodal gross tumour volumes should not being identified without PET information. 3D-Radiotherapy planning implemented on CT_GTVs showed that, in 37% of the irradiated patients, PET_GTVs and BTVs (Biological Target Volume) underdosages would be in the range -69%±38% and -81%±20% of the prescribed dose respectively. Mean values of PET_GTV volumes were smaller than CT volumes: 109 ±110 cm³ versus 130 ± 98 cm³ ($p < 0.03$). The mean mismatching fraction between CT volumes and PET volumes was 0.41. Conclusions. In radiotherapy treatment planning of head and neck disease PET/CT provide a more precise target definition and prevent exclusion of pathologic areas. In our population addition of PET information to CT avoids significant underdosages of gross tumour volumes and biological tumour volumes in 37% of the patients. The most serious underdosages are observed in oropharyngeal and oral cavity cancer groups. In the laryngeal cancer group CT_GTVs overlaps PET_GTVs therefore for these patients the PET involvement allows a target volume reduction with a consequent better critical organ preservation and lower toxicity.

EP557

Low risk and high risk recurrent prostate cancer in 3D Volumetric lymph node assessment based on CT and PSMA11-PET/CT

M. Vinsensia¹, C. Kratochwil¹, J. Moltz², M. Eiber³, A. Afshar-Oromieh¹, U. Haberkorn¹, F. Giesel¹; ¹Department of Nuclear Medicine, University Hospital Heidelberg, Heidelberg, GERMANY, ²MeVis Fraunhofer, Bremen, GERMANY, ³Department of Nuclear Medicine, Technical University Munich, Munich, GERMANY.

Introduction PSMA11-PET/CT is a powerful method of detecting early nodal metastases in patients with biochemical relapse. On this retrospective investigation the volume, dimensions and SUVmax of nodes identified by Glu-urea-Lys-(Ahx)-[⁶⁸Ga(HBED-CC)] (⁶⁸Ga-PSMA11) was evaluated and identified alongside their initial risk profile. Methods All PET/CT images were acquired 60±10 min after intravenous injection of ⁶⁸Ga-PSMA-11 (mean dose 176 MBq). In 44 patients with recurrent prostate cancer and PSA relapse, 96 PSMA-positive lymph nodes were identified. These patients were classified based on their risk profile by the initial diagnosis in either low risk (Gleason Score≤6) or high risk group (Gleason Score>6). Fifty one PSMA-positive lymph nodes from 20 high

risk patients and 45 PSMA-positive lymph nodes from 22 low risk prostate cancer patients were identified. Using semi-automated lymph node segmentation software (MeVis, Bremen, GER), the node volume, short and long axis dimensions were measured and compared to the maximum standardized uptake value (SUVmax). By morphologic criteria alone, round nodes greater than or equal to 10 mm would be considered positive, meanwhile lymph node with PSMA uptake (SUVmax) more than 2.0 would be considered PSMA-positive. Results The mean volume of ^{68}Ga -PSMA-positive nodes in high risk group was 0.8 ml (range 0.3–38.0 ml) and 0.6 ml (range 0.1–7.8 ml) in the low risk group. The mean short axis diameter in high risk group was 8.8 mm (range 4.1–36.0 ml) and 7.5 ml (range 2.1–22.0 ml) in the low risk group. High risk group presented mean SUVmax of 17.5 (range 3.1–102.4), meanwhile the low risk group's mean SUVmax was 12.9 (range 2.7–74.3). From 51 PSMA-positive lymph nodes from the high risk group, 21 lymph nodes (41%) were positive based on diameter >10mm on CT. Meanwhile on the low risk group, only 14 out of 45 PSMA-positive lymph nodes (31%) were positive based on the morphologic criteria. Based on PSMA11-PET/CT, 4 out of 20 patients (20%) from the high risk group and 10 out of 22 patients (45%) from the low risk group were upstaged from N0 to N1. These patients had PSMA-positive nodal metastases that are smaller than 10 mm and therefore missed by the conventional morphologic criteria. Conclusion ^{68}Ga -PSMA-11 PET provides a better assessment of the nodal metastases status in patients with recurrent prostate cancer, especially in the low risk group. Morphological imaging strongly underestimates lymph-node involvement compared to PSMA-molecular staging in both, low- and high-risk group.

EP558

Biokinetic study of ^{18}F -fluorocholine uptake to differentiate malignant and physiologic uptake of ^{18}F -fluorocholine in prostate cancer metastases

M. Wondergem^{1,2}, R. J. J. Knol¹, F. M. Van der Zant¹, T. Van der Ploeg¹, J. Pruijm^{2,3}, I. J. De Jong²; ¹Noordwest Ziekenhuisgroep, Alkmaar, NETHERLANDS, ²University Medical Center Groningen, Groningen, NETHERLANDS, ³Stellenbosch University, Tygerberg Hospital, Stellenbosch, SOUTH AFRICA.

Introduction ^{18}F -fluorocholine-PET/CT is widely used in patients with prostate cancer. Knowledge of the biokinetic behaviour of ^{18}F -fluorocholine in malignant lesions and physiologic tissue is helpful in distinguishing malignant from physiologic ^{18}F -fluorocholine uptake and, furthermore, may elucidate the best time point after ^{18}F -fluorocholine administration for acquisition of PET/CT images. We studied characteristics of ^{18}F -fluorocholine uptake in tissues of importance to detect lymph node and bone metastases. **Methods** One hundred subsequent patients with histopathologically proven prostate cancer were prospectively included in the study. Dynamic PET/CT images of the pelvic area were acquired in the first 10 minutes followed by total body images at 45–60 minutes post injection. SUV measurements on different time-points were performed on lymph node metastases, normal lymph nodes, bone metastases, normal bone marrow, blood pool, adipose tissue, intestine and muscle. **Results** The dynamic data show a nearly stable ^{18}F -fluorocholine activity in all tissues from 2 minutes post injection. However significant changes in ^{18}F -fluorocholine uptake between early and late time-points are observed. A decrease in tracer uptake in non-malignant lymph nodes and blood pool is detected together with an increase in muscle, bone metastases and non-malignant bone. A statistically significant decrease of the tumour-to-background ratio (TBR) between bone metastases and muscle and malignant lymph nodes and muscle is observed at the late time-point compared to the early time-point. Conversely, an increase of the TBR between malignant lymph nodes and the blood pool is demonstrated. ROC-

analysis showed that $\text{SUV}_{\text{max,early}}$ is the best predictor of malignancy in lymph nodes (cut-off 2.0) and $\text{SUV}_{\text{max,early}}$ and $\text{SUV}_{\text{max,late}}$ (cut-off 2.5 and 2.9 respectively) are the best predictors of malignancy for bone lesions. **Conclusion** According to our data, a dual time-point acquisition protocol would be best for detection of lymph nodes metastases. The $\text{SUV}_{\text{max,early}}$ is the best characteristic to discriminate malignant from non-malignant lymph nodes. For detection of bone metastases data acquisition at an early time-point is favourable over a later acquisition which is hampered by accumulation of activity in muscle. Both $\text{SUV}_{\text{max,early}}$ and $\text{SUV}_{\text{max,late}}$ can be used to discriminate malignant bone lesions from non-malignant bone.

EP559

FDG-PET/CT in Multiple Myeloma: Correlation Between SUV and Standard Prognostic Scoring System in Multiple Myeloma

B. Østergaard¹, A. L. Nielsen², O. Gerke², J. T. Asmussen³, T. Plesner⁴, P. Holdgaard⁵, T. E. J. Ormstrup⁶, A. Alavi⁷, N. Abildgaard¹, P. F. Høiland-Carlsen²; ¹Department of Hematology, Odense University Hospital, Odense, DENMARK, ²Department of Nuclear Medicine, Odense University Hospital, Odense, DENMARK, ³Department of Radiology, Odense University Hospital, Odense, DENMARK, ⁴Department of Hematology, Vejle Hospital, Vejle, DENMARK, ⁵Department of Nuclear Medicine, Vejle Hospital, Vejle, DENMARK, ⁶Department of Radiology, Vejle Hospital, Vejle, DENMARK, ⁷Department of Radiology, Perelman School of Medicine, University of Pennsylvania, Pennsylvania, PA, UNITED STATES.

Aim: FDG-PET/CT is a promising methodology for staging, prognostication and response evaluation in multiple myeloma (MM). High intensity of FDG uptake at diagnosis is associated with more aggressive disease and reduced overall survival. However, it is unknown to which degree this type of functional information correlates with established clinical prognostic biomarkers in MM, including the international scoring system (ISS) and the revised ISS (R-ISS). We aimed to elucidate this. **Material and method:** As a part of an ongoing prospective study evaluating new imaging technologies in MM we examined data from the first 35 included patients with treatment demanding MM. Patients were enrolled at diagnosis and studied at baseline with ^{18}F -FDG-PET/CT prior to any given anti-myeloma treatment. The lesion with the highest FDG uptake was analysed by a semi-quantitative dedicated software (ROVER, ABX, Radeberg, Germany) to yield the values of lesion volume, SUVmax, SUVpeak, SUVmean and cSUVmean (SUVmean corrected for partial volume effect). Finally, SUVmax was standardized to the liver uptake of FDG according to the Deauville criteria. **Results:** One patient had incomplete ISS data. Thus, 34 patients were included. Of these, 19, 11, and 4 patients were stratified to ISS groups I, II and III, respectively, while 9, 24, and 1 patients were stratified to the revised ISS groups R-ISS1, R-ISS2, and R-ISS3, respectively. SUVmax values ranged between 3.6 MBq/ml and 27.8 MBq/ml. Six patients had Deauville score 3, 12 had Deauville score 4, and 6 had Deauville score 5. SUVmax standardized to liver uptake was inversely correlated with ISS ($p=0.03$), but not with R-ISS ($p=0.85$). This observation we interpret as an incidental finding. Absolute values of SUVmax, SUVpeak, SUVmean, and cSUVmean were not correlated to either ISS or R-ISS ($p = 0.3-0.8$). **Conclusion:** There were no significant correlations between FDG uptake and ISS or R-ISS scores. This indicate that the potential prognostic value of high FDG uptake is independent of conventional prognostic markers in multiple myeloma and raises the question whether serum biomarkers or quantitative molecular imaging provide the best and most accurate expression of MM disease activity and extent. We will examine this in detail when all data from the ongoing investigation will soon become available.

EP560**Vesicular Monoamine Transporter Expression in Pheochromocytomas and Paragangliomas according to Scintigraphy and Positron Emission Tomography behavior**

S. CHIACCHIO¹, A. Bacca², A. Pucci³, D. Lorenzini⁴, G. Puccini⁵, M. Gennaro⁵, E. Tardelli⁵, F. Betti¹, G. Bemini², D. Volterrani¹; ¹Regional Center of Nuclear Medicine-OSPEDALE SANTA CHIARA, PISA, ITALY, ²Department of Clinical and Experimental Medicine-OSPEDALE SANTA CHIARA, PISA, ITALY, ³Department of Histopathology-OSPEDALE SANTA CHIARA, PISA, ITALY, ⁴Department of Diagnostic, Interventional and Vascular Radiology and of Nuclear Medicine-OSPEDALE SANTA CHIARA, PISA, ITALY, ⁵Regional Center of Nuclear Medicine-University of Pisa, PISA, ITALY.

Aim: The expression of vesicular catecholamine transporters (VMAT1, VMAT2) in pheochromocytomas (PHEOs) and paragangliomas (PGLs) and relationships with 18F-DOPA PET/TC and 123I-MIBG uptake are unknown. Therefore the objective of this study was to correlate VMAT1 and VMAT2 expression with the functional imaging in patients with PHEOs, extra-adrenal abdominal PGLs (APGLs) and head/neck PGLs (HNPGs). **Patients and Methods:** This observational study involved 31 consecutive patients with PHEO (n=17) and PGL (n= 14) (14 men and 17 women), aged 40.7 yrs (age range 14-67 yrs) who undergone surgery over a 3-year (2010-2013) time. They had been admitted in our Hypertension Unit for signs and/or symptoms of catecholamine excess (n=20), mass incidentally discovered (n=3) or for mass-related disturbances (n=11). All patients underwent the same diagnostic work-up, including 24-h urinary methanephrines measurement, magnetic resonance (MR) and/or computed tomography (CT) and 123I-MIBG scintigraphy (n=20). Starting from 2011, 14/31 patients performed 18F-DOPA PET/TC. Three patients underwent both procedures. Histopathology and immunohistochemistry of the excised tumor was performed in all patients. The number of VMAT1 and VMAT2-immunoreactive cells in tumors was semi-quantitatively evaluated according to the immunoreactivity scoring system by Fottner et al. (2010). Human adrenal glands were used as positive controls. **Results:** VMAT1 immunostaining was found in all tumors, except two PHEOs. VMAT1 immunoreactivity was higher in PGLs than in PHEOs, though at not significant extent. VMAT2 was high in all but two negative tumors (PHEOs). Normal 123I-MIBG uptake was associated to either high, intermediate, low or absent VMAT1/2 immunoreactivity. Patients that underwent 18F-DOPA PET/CT had a high score level of both VMATs and were detected by the technique in all cases. **Conclusions:** VMAT receptors do not seem essential for 123I-MIBG uptake and other pathways for the vesicular storage of catecholamines might be hypothesized. Alternatively, an unknown interaction between VMAT and other transporters or surface receptors could be taken into account. Patients submitted to 18F-DOPA PET/CT (almost all with PGL) showed both VMAT highly expressed and the radiotracer uptake proved to be always present. Thus, we cannot know if this uptake would be observed also in presence of low or absent receptor immunoreactivity. In summary, VMAT1 and VMAT2 are highly expressed in most tumors, though VMAT1 immunoreactivity is predominant in PGLs rather than in PHEOs. VMAT1 and VMAT2 receptors play an important role but are not essential for radiotracer uptake, at least in 123I-MIBG scintigraphy.

EP561**Eomesodermin/Bcl6-expressing T-cells Play Essential Roles in Progressive State of Hashimoto's Thyroiditis**

M. Stefanic¹, S. Tokic², M. Suver Stevic², L. Glavas-Obrovac³; ¹Clinical Institute of Nuclear Medicine and Radiation Protection, Osijek University Hospital, Osijek, CROATIA, ²Dept. of Clinical Laboratory Diagnostics, Osijek University Hospital, Osijek, CROATIA, ³Dept. of Medicinal Chemistry and Biochemistry, School of Medicine Osijek, University J J Strossmayer, Osijek, CROATIA.

Introduction. There is an increasing appreciation for the role of cytotoxic CD8⁺ T-cells in Hashimoto's thyroiditis (HT), an autoimmune thyroid disorder manifesting in chronic thyroid inflammation, and subsequently, hypothyroidism. Recently, much has been learned on molecular mechanisms underlying cytotoxic T-cell development; however, the importance of several lineage master regulators that play a central role in the generation and preservation of terminally differentiated CD8⁺ T-cells has remained unknown in HT. **Subjects and Methods.** We assessed mRNA expression levels of several transcription factors, including eomesodermin (Eomes), Bach2, Bcl6 and Tcf7 in untouched T cells across three different outcomes of HT (hypothyroid, untreated HT-hypothyroid HT undergoing hormone replacement therapy-spontaneously euthyroid HT). Granzyme B (GZMB) mRNA expression was representative of cytolytic effector molecules. The study included 30 HT patients (56±13.8 yr) and 10 euthyroid, TPOAb-negative, age and body mass index-matched healthy controls (47±12.6 yr). T-lymphocytes were isolated from peripheral blood mononuclear cells, total mRNA was extracted from CD3⁺ T-cells and gene expression was studied in triplicate by TaqMan RT-qPCR relative to TBP products [2 (-delta delta Ct) method]. **Results.** Significantly higher expression levels of Eomes [P=0.044, Mann-Whitney test, median 2.15 fold, interquartile range 1.29-3.42], Bcl6 [P=0.001, 1.94 (1.37-2.49)] and GZMB mRNA [P=0.028, 3.12 (1.52-5.9)] were found in T-cells of the HT patients (n=30) when compared to the controls. For Bcl6, increased transcript abundance was observed in severely affected, hypothyroid patients, both L-thyroxine-treated [1.96 (1.37-2.61), n=10] and untreated [2.08 (1.67-2.46), n=9], but not in spontaneously euthyroid HT individuals [1.41 (1.13-1.99), n=11; Kruskal-Wallis P=0.0026, Bonferroni-Dunn's post-hoc test]. Both Eomes (Spearman's rho=0.34, P=0.034) and Bcl6 transcript levels (rho=0.35, P=0.026) increased with age. Increased T-cell Eomes mRNA expression was strongly associated with decreased residual thyroid volume (rho=-0.47, P=0.011) and high GZMB expression (rho=0.71, P=10⁻⁵) in the HT group. **Conclusions.** Our findings suggest potential novel functions for cytolytic/follicular helper T-cell transcription factors Eomes and Bcl6 in the context of HT, particularly in aged individuals and aggressive disease forms characterized by thyroid injury. Eomes⁺ T-cells may be associated with the development of thyroid atrophy. Integrating the role of CD8⁺ T cell subtypes will be an important new goal in understanding the pathogenesis of HT and in devising new therapeutic targets.

EP562**The Relationship Between Repeated Brown Adipose Tissue Evidence in Sequential PET/CT Examinations and Air Temperature Change**

S. Isgoren, T. hekimsoy, g. daglioz gorur, h. demir, Kocaeli University School of Medicine Department of Nuclear Medicine, KOCAELI, TURKEY.

AIM: The aim of our study was to investigate the rate of repeated brown adipose tissue (BAT) existence in sequential PET/CT scans and the affect of outdoor air temperature of the study date on BAT positiveness in this group. **METHODS:** PET/CT studies which are performed between 2012 and 2016 in our Nuclear Medicine unit were analyzed and 77 patients (29 male, 48 female) who underwent more than one PET/CT scans and had BAT existence in at least one of them were included in this study. A total of 219 PET/CT studies of these patients were investigated and 106 studies (48,4%) of them were BAT-positive while the remaining 113 studies (51,6%) were negative. Outdoor air temperature values on the days of PET/CT scans were evaluated for each group. **RESULTS:** In 10 patients (13%) BAT was detected in all their PET/CT scans (23 PET/CT studies) while the remaining 67 patients (87%) had both BAT-positive and negative PET/CT scans (196 PET/CT studies). When analyzing the effect of temperature on BAT-positive (106 studies) and negative (113 studies) studies, there was a significant temperature difference between these

two groups ($p < 0.01$). When PET/CT scan is repeated on patients with known BAT evidence, 48.4% of sequential studies were BAT-positive and outdoor air temperature was lower on the date of these studies (12.4 ± 5.6 °C) while it was higher (17.4 ± 6.8 °C) in BAT-negative study group. **CONCLUSION:** In summary, temperature is a highly affecting factor of persistence of BAT evidence on FDG-PET/CT in repeated studies. To prevent patients who are known to have a BAT in their previous PET/CT scans from being exposed to cold can be a solution to avoid existence of metabolically active BAT in sequential PET/CT studies.

EP563

A PRISMA based systematic literature review for revealing the impact of nuclear physicians' information behaviour on PET/CT oncological imaging

E. Persakis^{1,2}, P. Kostagiolas², I. Datsis¹, D. Niakas³; ¹Department of Nuclear Medicine - PET/CT, Evaggelismos General Hospital, Athens, GREECE, ²Department of Archives, Library Science and Museology, Faculty of Information Sciences and Informatics, Ionian University, Corfu, GREECE, ³School of Social Science, Hellenic Open University, Patras, GREECE.

Aim: Studying the information seeking behaviour and preferences of nuclear physicians is rather important for their everyday medical practices. This work aims to study the nuclear physicians' information seeking behavior and preferences to satisfy the information needs in order to explore the impact on PET/CT oncological imaging. Based on the above we discuss the essential role doctors' online literacy skills have in interpretation and documentation of the results of PET/CT. **Materials and Methods:** In terms of theoretically framing our research endeavor the macro model for information seeking behaviour by Wilson is employed. Through this methodology the three key information seeking layers of nuclear physicians are addressed and studied, i.e. medical practice information needs, utilization of information resources and presence of information seeking barriers. The analysis through the systematic literature review is based on PRISMA protocol. Therefore, a number of queries related to our research aims are formulated and addressed to Medline and other relevant databases in order to identify, select and critically appraise the relevant research studies for the impact of nuclear physicians' information preferences on PET/CT oncological imaging. **Results:** After the initial selection based on PRISMA method, a number of sixty eight papers have met the predefined inclusion criteria and included in the analysis. Overall, the most important information needs of nuclear physicians are related to differential diagnosis for a PET/CT finding, as well as the procedure of PET/CT oncological imaging. Nuclear physicians mostly utilize Internet and other online scholarly resources as well as electronic medical record (EMR). Barriers when seeking information mostly reported in the literature included information seeking skills, time constraints and cost. The literature emphasizes the need for an efficient utilization of healthcare information in PET/CT procedure. **Conclusion:** Medical schools and formal associations of Nuclear Medicine may develop educational programs for enhancing nuclear physicians' online information literacy skills. Internet and online scholarly resources are integrated into physicians' routines in PET/CT oncological imaging. Studying nuclear physicians' information preferences may contribute to the association between oncological imaging and other medical specialties, the communication between nuclear physician and referring physician, the relation of doctor - patient, prognosis and health related quality of life of oncological patients as well.

EP564

Consequences of 18F-FDG extravasation

C. Findlay¹, S. Allwood-Spires², C. McKeown¹, G. Gillen¹; ¹West of Scotland PET Centre, Glasgow, UNITED KINGDOM, ²Department of Clinical Physics, Glasgow, UNITED KINGDOM.

Aim Extravasation of 18F-FDG can cause image artefacts and localised tissue dose, potentially leading to tissue necrosis. A retrospective analysis of 25 patients who had tissue injections was made to quantify activity and localised tissue dose to the injection site. **Methods** Twenty-five patients with tissue injections were analysed. The radioactivity present at the extravasation site was quantified and tissue dose calculated using the specific dose factor for 18F. **Results** Radioactivity within the injection site ranged from 0.07MBq to 129MBq. Tissue doses ranged between 6mGy to 608mGy. Of the 25 cases, 8 had more than 10% of the injected activity at the extravasation site. In most cases where a high activity was tissue, the activity was spread over a large volume and so the localised tissue dose received was not high. The highest dose received from a tissue injection from this sample, estimated at 608mGy, is well below the level at which erythema is likely to occur. **Deterministic effects** of radiation on the skin are expected to occur from a dose of 2Gy upwards [1]. **Conclusions** Evidence from this patient sample has shown that despite what can sometimes be striking appearances on patient images, the dose from 18F-FDG tissue injections is unlikely to result in tissue necrosis. [1] Balter et al, "Fluoroscopically Guided Interventional Procedures: A Review of Radiation Effects on Patients' Skin and Hair." *Radiology* 2010 254:2, 326-341

EP565

Is Dual Time Point Imaging Necessary For Discrimination of adrenal benign lesions versus malignant masses: A Study Comparing Standart Methods with Dual Time Point FDG PET-CT Imaging

P. Ozcan Kara¹, Z. Koc¹, T. Kara², B. Kaya³; ¹Mersin University Faculty of Medicine Department of Nuclear Medicine, Mersin, TURKEY, ²Mersin University Faculty of Medicine Department of Radiology, Mersin, TURKEY, ³Necmettin Erbakan University Faculty of Medicine Department of Nuclear Medicine, Konya, TURKEY.

Objectives: Discrimination of adrenal benign lesions versus malignant masses is essential, especially in patients with cancer, for choosing the appropriate treatment approach and assessing prognosis. This prospective study was designed to investigate the clinical role of whole-body positron emission tomography/computed tomography (PET/CT) by using 2-[18F]fluoro-2-deoxy-D-glucose (FDG), for the evaluation of adrenal lesions and to compare the standart methods proposed in the literature such as SUVmax value, tumour/liver SUV (T/L SUV) ratio, visual analysis with dual time point imaging method to distinguish benign from malignant lesions in various cancer patients. **Materials and methods:** A total of 48 patients (26 male and 22 female) who had confirmed primary malignancies underwent PET/CT examinations for cancer screening, staging, restaging, and detection of suspected recurrence. A SUVmax cutoff value of 4.2 and T/L SUV ratio of 1.68 which have been identified in a recent study by our group were used. Of the 48 patients, 62 adrenal lesions (25 benign and 37 malignant adrenal lesions) were shown by CT. On visual analysis of PET/CT imaging, adrenal uptake was based on a three-scale grading system. For final assessment standards of references for adrenal malignant lesions was based on biopsy, interval growth, or reduction after chemotherapy. An adrenal lesion, which remained unchanged on clinical and imaging follow-up was decided as a benign lesion. **Results:** In adrenal malignant lesions maximum standardized uptake value (SUVmax: 7.89) was higher than that of adrenal benign lesions (SUVmax: 2.92, $P < 0.0001$). Dual time point imaging were performed in 19/48 patients. Of the 19 patients 14 had malignant and 5 had benign adrenal lesions. All 21 malignant adrenal lesions from 14 dual phase patients had higher SUVmax over time and all 6 benign lesions from 5 dual phase patients had lower SUVmax at the late image. **Conclusion** SUV or T/L SUV ratios per se are semiquantitative parameters that reflect metabolic activity, but are not specific markers of malignancies. As the uptake of 18F-FDG in malignancies is expected to increase over time, dual time point acquisition could be potentially useful in partially

overcoming the relatively low specificity of the SUVmax. Combined information obtained from PET/CT (SUVmax, T/L SUV ratio, visual analysis is recommended for better differentiation. Although, dual time point imaging of FDG PET/CT seems to be very effective especially in surreal lesions, addition of dual phase study is not necessary and recommended in only indetermined lesions.

EP566

Role of F-18 FDG PET-CT scan in evaluation of cases with unexplained weight loss

A. A. ZADE, S. RAI, V. A. R. B; NUCLEAR HEALTHCARE, NAVI MUMBAI, INDIA.

Aim: F-18 FDG PET-CT scan has an established role in staging, restaging and assessing treatment response of various malignancies. It also has a proven role in cases of metastases from unknown primary malignancy and Pyrexia of Unknown Origin. Unexplained weight loss (UEWL) is one of the presenting complains in cases suffering from granulomatous infection like tuberculosis and various malignancies. The present study was undertaken to evaluate the role of PET-CT scan as a one stop diagnostic imaging modality for identifying infective focus/malignancy in cases of UEWL **Materials & Methods:** This was a retrospective audit of 70 consecutive cases (43 males, 27 females) of UEWL. The mean age of the studied population was 59.4 ± 13.9 years. Each patient underwent a F-18 FDG whole body PET-CT scan using standard acquisition parameters. The scans were reviewed by two experienced nuclear medicine physicians and the findings were noted. Diagnosis was made by histopathological evaluation and/or other appropriate tests as deemed necessary on case to case basis. **Results:** During the study period, 70 patients were evaluated. One patient was lost to follow-up and hence not included in the final analysis. In 64 (44/69) patients, no focus of hypermetabolism was visualized on the scan. These patients were followed up for a mean period of 13 months during which no malignancy or infective focus was identified as a cause of weight loss. The PET-CT scan revealed hypermetabolic foci in 36 % (25/69) patients. They were further evaluated and were diagnosed with granulomatous infection (n=12), non-hematological malignancies (n=7) & lymphoma (n=4). In one case false positive FDG uptake was noted in base of tongue due to lymphoid hyperplasia and in another due to interstitial lung disease. The sensitivity, specificity, positive predictive value, negative predictive value & accuracy of F-18 FDG PET-CT scan was 100%, 96%, 92 %, 100% & 97 % respectively. **Conclusion:** F-18 FDG PET-CT scan has a promising role in evaluation of cases with unexplained weight loss.

EP567

18F-DOPA PET/CT physiological distribution and pitfalls: experience in 215 patients

F. F. CALABRIA¹, A. Chiaravalloti², M. Jaffrain-Rea³, M. Zinzi⁴, P. Sannino⁴, G. Minniti⁵, D. Rubello⁶, O. Schillaci^{7,4}; ¹IBFM Italian National Research Council - PET/MRI Unit., Catanzaro, ITALY, ²Department of Biomedicine and Prevention, University "Tor Vergata", Rome, Italy., Rome, ITALY, ³Department of Biotechnological and Applied Clinical Sciences, University of L'Aquila, Italy., L'Aquila, ITALY, ⁴IRCCS INM Neuromed, Molise, ITALY, ⁵Unit of Radiation Oncology, Sant'Andrea Hospital, University "La Sapienza", Rome, ITALY, ⁶Department of Nuclear Medicine, Santa Maria Della Misericordia Hospital, Rovigo, Italy., Catanzaro, ITALY, ⁷Department of Biomedicine and Prevention, University "Tor Vergata", Rome, ITALY.

Purpose of the report. F-18-DOPA Positron Emission Tomography/Computed Tomography (PET/CT) is an important diagnostic tool in the management of patients with low grade brain tumors, movement disorders or somatic neuroendocrine tumors. The purpose of our study

was to describe the physiological distribution of the tracer in the whole body to discuss the abnormal sites of F-18-DOPA uptake that we met in our clinical practice. **Materials and Methods.** We examined 215 patients with F-18-DOPA PET/CT. Among these, 161 were submitted to a brain scan and 54 undergone a whole body scan. **Results.** The physiological distribution was negligible in the brain, with the exception of basal ganglia, while greatest activity was noted in liver, pancreas, other exocrine glands and the urinary system. Several sites of tracer uptake (5.5%) were collected, not related to the diseases under study. Some of these findings were due to inflammation while in the majority of cases the uptake was linked to benign tumors of the brain or in the endocrine or exocrine glands. **Conclusion.** It is mandatory to consider the possibility of F-18-DOPA uptake in conditions such as inflammation or benign tumors. Correlation with history, physical exam, labs, CT, MRI and histology are necessary to obtain the correct diagnosis. **Keywords:** PET/CT; 18F-DOPA; brain tumor; pitfalls; tumor recurrence; molecular imaging.

EP568

Evaluation Of Factors Affecting On Development Of Brown Adipose Tissue Detected By F-18 FDG PET-CT

S. Isgoren, t. hekimsoy, g. daglioz gorur, h. demir; Kocaeli University School of Medicine, KOCAELI, TURKEY.

AIM: Brown adipose tissue (BAT) is a type of adipose tissue found in mammals and can be detected by PET/CT scan with high F-18 FDG uptake generally in cervical, supraclavicular, paraaortic, paravertebral and suprarenal area. The aim of our study was to investigate the factors affecting on development of BAT. **METHODS:** We retrospectively analyzed 3409 patients (mean age: 55 ± 18 ; 56,5% male, 43,5% female), who underwent PET/CT scan between the 1st January 2014 and 31st December 2015 in our clinic. Factors possibly affecting on development and metabolism of BAT including age, gender, body mass index (BMI), fasting blood glucose level, clinical indication for PET scanning, season, month and air temperature of the study date were evaluated. Additionally, maximum standardized FDG uptake values (SUVmax) of BAT and liver were determined in each BAT-positive study and SUVmax ratios of BAT to liver were calculated. **RESULTS:** Brown adipose tissue was detected 121 (3,5%) of all patients. When analyzing possible factors affecting on development of BAT, there was no significant difference with age, BMI, fasting blood glucose level and clinical indication for PET scanning between the BAT-positive and -negative patients ($p > 0,05$). When SUVmax ratios of BAT to liver and air temperatures of the study dates compared in BAT-positive patient group, no relationship was observed ($p > 0,05$). Nevertheless, incidence of BAT-positive patients was significantly correlated with gender, month, season and air temperature ($p < 0,01$). **CONCLUSION:** In this study, we found that BAT is more likely to develop in low temperatures especially in winter (46% of all BAT-positive patients) following autumn (35%) and spring (35%) while it is least seen in summer (4%). Also, BAT incidence is higher in women (66% of all BAT-positive patients) than men (34%) although the patient population is consisted of mostly men in our study.

EP-29 – Sunday, October 16, 2016, during Exhibition hours, e-Poster Area

M2M: PET/MR

EP569

Preoperative parallel PET/MR improves the prediction of the disease free survival in patients with breast cancer

I. LIM, J. Park, W. Noh, H. Kim, K. Park, S. Lee, I. Ko, K. Kim, B. Byun, B. Kim, C. Choi, S. Lim; Korea Cancer Center Hospital, Seoul, KOREA, REPUBLIC OF.

Aims: The aim of this study was to determine whether PET/MR could predict disease-free survival (DFS) in patients with operable breast cancer. **Methods:** Seventy-eight patients with breast cancer were enrolled. All patients underwent preoperative parallel PET/MR: whole body PET/CT at 1 h after 18F-FDG injection, breast dynamic contrast enhanced MR, and breast PET/CT at 2h after 18F-FDG injection sequentially in prone position. All patients were analyzed by diverse parameters (maximum SUV at 1 h [SUV1], maximum SUV at 2 h [SUV2], retention index of SUVmax [RI], metabolic tumor volume [MTV], total lesion glycolysis [TLG], initial slope of the enhancement curve [IS], transfer constant [K^{trans}], reflux constant [K_{ep}], extravascular extracellular space volume fraction [Ve], and initial area under the curve [iAUC]). A relationship between covariates and DFS after operation was analyzed using Kaplan-Meier method and multivariate Cox proportional-hazard regression method. **Results:** The median follow-up of 78 patients was 55 months (31-67 months), and 9 (11.5 %) patients developed recurrence or metastasis. Among parameters, higher RI ($p = 0.0010$), lower K^{trans} ($p = 0.0046$), and lower Ve ($p = 0.0035$) were significantly associated with poorer DFS. In contrast, SUV1, SUV2, MTV, TLG, IS, K_{ep} , and iAUC were not. On multivariate analysis, RI ($p = 0.016$; HR = 5.20; CI 1.4-19.7), and K^{trans} ($p = 0.035$; HR = 0.22; CI 0.054-0.89) were found as independent predictors of DFS. Patients with higher RI and lower K^{trans} revealed a significantly higher recurrence rate (66.7 %) than the rest of patients (6.9 %, $P < 0.0001$). **Conclusion:** RI and K^{trans} measured by preoperative parallel PET/MR can predict DFS in patients with operable breast cancer. The combination of these parameters could improve patients care because this application might specify the high risk group.

EP570

Reproducibility of MR-based Attenuation Maps in PET/MRI and the Impact on Response Evaluation in Lung Cancer

A. Olin¹, C. N. Ladefoged¹, N. H. Langer¹, S. H. Keller¹, J. Löfgren¹, A. E. Hansen¹, A. Kjer¹, S. W. Langer², B. M. Fischer¹, F. L. Andersen¹; ¹Dept. of Clinical Physiology, Nuclear Medicine & PET, Rigshospitalet, University of Copenhagen, Copenhagen, DENMARK, ²Dept. of Oncology, Rigshospitalet, University of Copenhagen, Copenhagen, DENMARK.

Aim: MR-based attenuation correction (MR-AC) in PET/MRI systems is a prerequisite in quantitative PET. Reliable PET images are strongly linked to the reproducibility of the attenuation maps (μ -maps). This study investigated the reproducibility of thoracic μ -maps by examining how potential inconsistencies and artifacts affected PET quantification in patients with non-small cell lung cancer (NSCLC). **MATERIAL AND METHODS:** Ten NSCLC patients underwent two to five chest PET-MRI examinations within ≤ 22 days using a Siemens Biograph mMR. Each examination consisted of two consecutive [¹⁸F]-FDG PET/MRI scans, where two vendor implemented Dixon-based μ -maps were acquired with fixed patient positioning. A total of 82 μ -maps were evaluated visually for quality and occurrence of categorized artifacts by two PET/MRI experienced physicians. Artifacts were rated on a scale from one to four, with three and four indicating artifacts with potentially severe impact on PET quantification. Only PET data from the first scan of each examination were used to analyze the quantitative effect of μ -map reproducibility. The μ -map acquired simultaneously with this PET data (μ -map_A) and the subsequently acquired μ -map (μ -map_B) were registered by rigid transformation, and two PET images (PET_A and PET_B) were reconstructed. Every tumor was outlined by a volume of interest (VOI) defined as a 40% isocontour of the maximum standardized uptake on PET_A. Minor manual VOI adjustments were done if considered appropriate, e.g. to exclude adjacent physiological uptake. The VOIs drawn on PET_A were transferred to the corresponding PET_B. The relative differences between mean (SUV_{mean}) and maximum

standardized uptake (SUV_{max}) in PET_A versus PET_B were calculated. **RESULTS:** All μ -maps included artifacts rated one or two. The frequency of μ -maps with artifacts rated three or four was 18/82 (22%) and involved six patients. Of these 18 μ -maps, eight were categorized with metal artifacts (one patient), two with body contour delineation and lung border artifacts (two patients), and eight with tissue misclassification artifacts (three patients). The average \pm SD relative difference between the SUV_{mean} in PET_A versus PET_B was 2.4 \pm 8.6% (min: -15.6%, max: 35.6%) across all patients. Similar results were found for SUV_{max} . **CONCLUSION:** Artifacts were frequently observed in the MR-based μ -maps causing potential impact on the PET-based tumor quantification. The quantitative evaluation showed a large variance and range in the relative difference between tumor uptakes (SUV_{mean} and SUV_{max}) in PET_A versus PET_B. Thus, inconsistencies of μ -maps may have an impact on the PET quantification and should be taken into consideration, especially in response evaluation.

EP571

18F-DOPA-PET/MRI image fusion for target volume definition in patients with recurrent glioblastoma treated with proton therapy

A. Palucci¹, D. Amelio², S. Agostini¹, A. Palermo¹, D. Donner¹, E. Bagatin¹, G. Carbone¹, M. Erini¹, M. Amichetti², F. Chierichetti¹; ¹Nuclear Medicine Dpt - S. Chiara Hospital APSS, Trento, ITALY, ²Proton Therapy Centre - Trento Hospital - APSS, Trento, ITALY.

Aim: Target volume definition for high grade gliomas is a crucial process when steep dose gradient techniques, such as proton therapy (PT), are employed. Aim of the study is to investigate the impact of 18F-DOPA on target volume definition in recurrent glioblastoma (rGBM) patients (pts) undergoing re-irradiation with PT, an advanced modality of external radiation therapy that allows to keep low the radiation burden on the healthy tissues. **Material and Methods:** We investigated the differences in volume and shape of MRI vs F18-DOPA-PET-CT-derived gross tumor volumes (GTVs) of 10 rGBM pts re-irradiated with PT between January and December 2015. All pts were previously treated with standard of care (surgery and adjuvant radio/chemotherapy). For target definition all pts received morphological MRI with contrast enhancement and 18F-DOPA PET-CT study. We used the pathological distribution of F-DOPA in brain tissue to identify the so-called Biological Tumor Volume (BTv). Such areas were assessed using a tumor to normal brain ratio > 2 . Moreover, any area of enhancing tumor on MRI was employed to identify the MRI-GTV. Definitive GTV included any area of contrast enhancement plus any pathological PET uptake regions. Clinical target volume (CTV) was generated by adding to GTV a 3-mm uniform margin. CTV was expanded by 4 mm to create Planning target volume (PTV). **Results:** Integrating 18F-DOPA-PET uptake into the delineation of GTVs allowed the detection of pathological uptake outside the enhancing tumor areas in all investigated pts yielding to larger treated volumes. Even though MRI- and DOPA-PET-derived GTVs show similar shape in most of the pts, the congruence of MRI and PET signals is mild. The PT irradiation of PET-integrated target volumes provided a median progression-free survival of 6.4 months, while the 3-, 6- and 9-month PFS rates were 80%, 67% and 22%, respectively. 6- and 12-month survival after PT rates were 100% and 60%, respectively. **Conclusions:** Target volume definition for rGBM undergoing PT re-irradiation may yield significantly differing results depending upon the imaging modality used for target contouring. The integration of both MRI and F-DOPA PET-CT may help to improve GTV coverage. Despite the small number of patients and the retrospective nature of the study clinical results seem promising suggesting that PT with multimodal imaging contouring process may be more effective for tumor control respect to the standard planning based to anatomical imaging only.

EP572**Evaluation of a fast MR-protocol for simultaneous ¹⁸F-FDG PET/MR imaging of patients with lymphoma**

J. Grueneisen¹, L. Sawicki², B. M. Schaarschmidt², A. Wetter¹, V. Ruhlmann¹, L. Umutlu¹; ¹University Hospital Essen, Essen, GERMANY, ²University Hospital Dusseldorf, Dusseldorf, GERMANY.

Aim: The aim of this study was to evaluate a diagnostic performance of a fast MR-protocol for integrated ¹⁸F-FDG PET/MR imaging, used for pretreatment staging, therapy monitoring and surveillance of patients with lymphoma in comparison to ¹⁸F-FDG PET/CT. **Material and Methods:** A total of 48 consecutive lymphoma patients underwent 52 clinically indicated PET/CT and subsequent PET/MR examinations. For PET/MRI readings, a whole-body fast MR-protocol was implemented, comprising (1) a transversal DWI (EPI) sequence, (2) a transversal T2w HASTE sequence and (3) a transversal post-contrast T1w VIBE sequence. Two readers separately evaluated both examinations and were instructed to identify the total number of tumor lesions. The standardized uptake value (SUV) for all ¹⁸F-FDG-avid lesions was determined in PET/CT and PET/MRI, using volume of interest (VOI) analysis. Agreement between PET/CT and PET/MRI regarding SUVmax and SUVmean was tested using Pearson's product-moment correlation. **Results:** Malignant lesions were present in 28 of the 52 examinations. Both, PET/CT and PET/MRI enabled correct identification of disease presence in all 28 cases. A total of 106 ¹⁸F-FDG-avid lymphoma lesions were analyzed for the comparison of the PET component in PET/CT and PET/MRI. Determined SUVs were significantly higher in PET/MRI than in PET/CT (SUVmax: 9.3 ± 6.1 vs 6.9 ± 4.3 ; $p < 0.05$; SUVmean: 5.1 ± 3.3 vs 4.1 ± 2.7 ; $p < 0.05$), however, there was a strong correlation between SUVmax and SUVmean of the two imaging modalities ($R = 0.87$, $p < 0.001$ and $R = 0.91$, $p < 0.001$). Estimated mean scan duration of whole-body PET/CT examinations as well as for the fast protocol for whole-body PET/MR imaging amounted to 17.3 ± 1.9 min and 27.8 ± 3.7 min, respectively. Furthermore, calculated mean effective-dose for a whole-body PET/CT scan was 64.4% higher than for a fast-PET/MRI examination. **Conclusion:** The FAST-protocol for PET/MR imaging offers an equivalently high diagnostic performance for staging lymphoma patients in comparison to PET/CT with only a slightly prolonged examination time. With regard to patient comfort related to scan duration and a markedly reduced radiation exposure, fast-PET/MRI may serve as a powerful alternative to PET/CT for a diagnostic work-up of patients with lymphomas.

EP573**The effect of discrete tissue classes and neglecting bone in soft tissue sarcoma PET/MRI patients: Evaluation with PET/CT data**

C. H. Holland¹, C. N. Ladefoged², A. Loft², K. F. Andersen², L. Højgaard², F. L. Andersen²; ¹King's College London, London, UNITED KINGDOM, ²Rigshospitalet, Copenhagen, DENMARK.

INTRODUCTION: A prominent difficulty with PET/MRI is inaccurate attenuation correction. Current standards discretise the tissue compartments into four tissue classes, disregarding variations within tissue types, and failing to segment both bone and tumour values. This study assesses the effect of this, using patients scanned on PET/CT by assessing each tissue class by itself, progressively bridging the gap between the gold-standard CT and the PET/MRI-simulated Dixon-sequence. **METHODS:** Four patients with FDG-avid histopathological verified high-grade soft tissue sarcoma scanned on a whole-body PET/CT system (Biograph TruePoint 64, Siemens Healthcare) were included in this study. The patients were injected with 300 MBq of [¹⁸F]-FDG. The PET/CT images were discretised into the classes: bone, lung, tumour, air, soft tissue and fat. These classes were combined to create four additional mu-maps: pseudoDixon (setting air, soft tissue, fat and lung to predetermined HU

values equivalent to Dixon, with bone to soft tissue value); Dixon+bone (as pseudoDixon with bone at original HU value); Dixon+tumour (as pseudoDixon with tumour at original value); CT-bone (original CT with bone at soft tissue value). Mean and variance %-deviation within the tumour relative to PET/CT were calculated for each of the four mu-maps, both globally as well as within ROIs extending consecutively away from bone. **RESULTS:** The average %-deviation in global mean PET signal was $-6.4 \pm 2.6\%$ (pseudoDixon), $-4.6 \pm 2.6\%$ (Dixon+bone), $-6.6 \pm 1.5\%$ (Dixon+tumour), and $-1.7 \pm 0.2\%$ (CT-bone) from PET/CT. ROI analysis in the tumours showed a clear gradient with the largest error close to the bone and smallest away from bone for pseudoDixon (-32.7% to -6.0%), Dixon+tumour (-24.2% to -6.3%) and CT-bone (-28.9% to -0.5%). The gradient was only significant within 2 cm of bone. No such marked gradient existed for Dixon+bone (-4.9% to -5.5%). **CONCLUSION:** The analyses of the global tumour signal showed a systematic underestimate of signal for all constructed mu-maps, greatest for those setting both bone and other tissues to Dixon values, though these errors were generally below 10%. Comparing results of different mu-maps also suggests the errors introduced by standardising different tissue classes is to first approximation summative, with standardising fat and soft tissue having a generally larger effect than setting bone to soft tissue value. However, ROI analysis demonstrated that setting bone to soft tissue value introduces overwhelmingly large errors in attenuation correction for signals in bone's immediate proximity indicating that in using Dixon maps, signals in and near bone should be interpreted with great caution.

EP574**Feasibility of using ZTE to generate an accurate MR-based attenuation map for head and neck PET/MR studies: Similarity analysis to CT-based attenuation map**

K. Lee, G. Zaharchuk, P. K. Gulaka, C. S. Levin; Stanford University, Stanford, CA, UNITED STATES.

Simultaneous PET/MR imaging systems have shown promise to provide simultaneous functional and morphological evaluation of a variety of pathophysiological conditions. However, challenges in MR-based attenuation correction (MRAC) methods still pose a problem for accurate quantification of PET images due to the difficulty of imaging and segmenting bone with MR sequences. To overcome this, the zero echo time (ZTE) MR sequence was introduced to acquire the fast-decaying MR signal from bone. Accurate attenuation coefficients for bone in the head and neck area are particularly important because a big portion of the head and neck area is bone, and lesions in the area are usually in or proximate to the bone. We investigate the feasibility of using MRAC incorporated with the ZTE sequence (ZTE-MRAC) by comparing the similarity of bone-added ZTE-MRAC to a CT-based attenuation map (CTAC), the gold standard for photon attenuation. This study is the first demonstration of similarity evaluation of a ZTE-MRAC μ -map to improve PET quantification accuracy in PET/MR for lesions in the head and neck area. Three patients with head and neck cancer underwent PET/CT scans (mCT PET/CT, Siemens Healthcare, TN), followed by PET/MR scans (SIGNA PET/MR, GE Healthcare, WI) that included ZTE- and Dixon-based MRAC sequences. Segmentation for bone was performed on the ZTE images and added on to Dixon-MRAC sequence to generate ZTE-MRAC. Multi-modality matching (MMM) registration between ZTE-MRAC and CTAC was performed before applying the similarity test. Using the segmented bone from the CT attenuation maps (μ -map), dice similarity coefficient (DSC) was calculated as the evaluation metric for the spatial overlap accuracy, being 1 for the perfect overlap and 0 for no overlap. We observed an average DSC of 0.65 (STD=0.18) when ZTE-based bone information was incorporated in the MRAC μ -map, compared to the CT-based μ -map. We found that PET quantification accuracy with ZTE-MRAC is superior to the Dixon-based bone-free MRAC. We also observed that it was difficult to distinguish air from bone

in certain regions leading to inaccurate ZTE-MRAC generation and lower DSC in those areas. Further improvements in quantification could be obtained by performing rigorous registration between ZTE-MRAC and CTAC. Future work will include the comparison of PET data quantification when Dixon-based bone-free MRAC, ZTE-MRAC, and CTAC are used for PET image reconstruction, respectively.

EP575

Strategies for acceleration of a new MLEM algorithm for emission-based photon attenuation correction in PET

A. Mihlin, C. S. Levin; Stanford University, Stanford, CA, UNITED STATES.

We have developed the first ever maximum likelihood expectation maximization method for joint estimation of emission activity distribution and photon attenuation map from PET emission data alone. We call this new method “EMAA” (expectation maximization estimation of activity and attenuation). The method is appealing since: (i) it guarantees monotonic likelihood increase to a local extremum, (ii) does not require arbitrary parameters, and (iii) guarantees the positivity of the estimated distributions. Such image estimation methods are typically very computationally intensive, due to the need to traverse all existing LORs. This is in contrast with estimation of just emission activity distribution, where only LORs with detected counts are traversed. Hence, acceleration is critical for clinically practical joint image estimation. We report on strategies for acceleration of EMMA, which include: graphics processing unit (GPU) based implementation, ordered subset expectation maximization (OSEM), use of time of flight (TOF) data, and “Adjusted OSEM” - an extension of OSEM for this joint image estimation problem. The methods are evaluated using a PET signal computationally generated via Monte-Carlo simulation of a three dimensional XCAT phantom, with no random- and scattered coincidences. For a Philips GEMINI LXL system geometry with 400 ps TOF resolution, these methods accelerate EMMA by 10^6 compared with a single CPU implementation. Thus, reducing joint estimation duration to just 7 minutes, for an estimated emission activity distribution root mean square error of 1%, compared with the true emission image.

EP576

A Radiofrequency-penetrable PET Insert for Simultaneous PET/MRI

C. Chang, B. J. Lee, R. D. Watkins, I. Kwon, C. S. Levin; Stanford University, Stanford, CA, UNITED STATES.

Objectives Simultaneous PET/MRI has shown great potential in disease characterization. However, the high cost of the commercial integrated PET+MR systems limits its dissemination, and hence its long-term impact. To address this challenge, we have developed a proof-of-concept radiofrequency (RF)-penetrable PET neural insert that may be inserted into (and removed from) any existing MR system. This work reports the performance characterization results of this insert system. **Methods** The PET insert consists of a ring of 16 detector modules, each shielded in a copper Faraday cage with 1 mm inter-module gaps for the RF field to leak through. PET detectors are powered by electrically-floating batteries. Inside each detector, the electrical signal of the photodetectors is converted into an optical signal and sent out through 20-meter length optical fibers to the data acquisition system in the next room. Eliminating long electrical cables and isolating the power line of the PET ring minimize the mutual interference between PET and MRI. Energy, timing resolution and phantom image quality were evaluated both outside and inside a 3T MRI bore with standard imaging pulse sequences [(spin-echo (SE), gradient-echo (GRE) and echo-planar

imaging (EPI)] running to study the impact of the operating MRI on PET performance. B_0 , B_1 maps, signal-to-noise ratio (SNR) and the uniformity of MRI phantom images were evaluated with and without the PET insert to study the impact of the operating PET on MRI. Simultaneous PET/MR phantom images were acquired with the built-in body coil serving as both RF transmitter and receiver. Results The energy resolution at 511 keV and the timing resolution of the PET insert are $15.6 \pm 0.2\%$ and 5.3 ± 0.2 ns FWHM, respectively, both outside and inside of MRI with insignificant differences for the spin-echo and gradient-echo pulse sequences. The B_0 field inhomogeneity is smaller than 0.02 ppm in 3T with or without the PET insert inside the MRI bore. Hot rods with 2.8 mm diameter can be resolved in the reconstructed images acquired with the insert outside or inside the MRI system. With the MRI auto-prescan procedure to calibrate the transmitter gain, simultaneous PET/MR images were successfully acquired using the built-in body coil with only -3.5 dB degradation of the MR image SNR. Further MR image SNR improvements are expected with a custom receiver coil located inside the PET insert rather than using the MR built-in body coil as receiver as well as transmitter.

EP577

Hybrid 18F-FDG PET/MR imaging usefulness in disease activity assessment in patients with sarcoidosis

D. Jurgilewicz¹, M. Mojsak¹, P. Szumowski¹, B. Kubas¹, B. Kuklinska², M. Hladunski¹, A. Amelian-Filonowicz¹, R. Mroz¹, J. Mysliwiec¹; ¹Medical University, Bialystok, POLAND, ²University Hospital, Bialystok, POLAND.

Background: Sarcoidosis is a multi-organ disease characterized by the appearance of inflammatory granulomas in various organs. Lungs and intrathoracic lymph nodes are the most common locations of the disease, but changes may be presented also in the eyes, skin, liver, spleen, muscles, bones and salivary glands. Hybrid imaging technic which enables simultaneous whole body molecular magnetic resonance and metabolic positron emission tomography (PET/MR) is a promising tool in evaluation of the stage of sarcoidosis. **Aim:** The purpose of the study is the evaluation the utility of 18F-fluorodeoxy-d-glucose (18F-FDG) PET/MRI in staging of sarcoidosis. **Materials and Methods:** 18F-FDG PET/MR study was performed in 31 patients (F/M: 12/19, mean age: 45 (25-69) treated in Department of Lung Diseases, with computed tomography (CT) diagnosed and histologically confirmed pulmonary sarcoidosis. PET scans were obtained 60 min after injection of 295 ± 45 MBq ¹⁸F-FDG). All patients underwent 18F-FDG PET/MR study with additional subsequent CE-MRI of the thorax at 3T in the prone position using Biograph mMR scanner (Siemens) with proper MR sequences: T1 VIBE, T2 HASTE, T2 BLADE. The obtained images were analyzed with visual and semi-quantitative methods. Disease staging based on presence and number of FDG-avid nodes was performed by two nuclear medicine and one radiology experienced specialists. Quantitative assessment was performed by calculation of SUV_{max} . **Results:** 18F-FDG PET/MR confirmed metabolically active disease in the lesions localized by CT in all patients. Eighteen (58%) patients were classified as phase I, thirteen (43%) as phase II pulmonary sarcoidosis. Increased 18F-FDG uptake in PET/MR study, with SUV_{max} : 2.43-9.00, as a new additional metabolically active foci were found in: abdominal lymph nodes in 10 patients (30%), cardiac left ventricle in 1 patient (3%), musculo-skeletal system in 1 patient (3%). Additionally, in nine patients with nonspecific neurological symptoms, mainly headache, changes in maxillary sinus were found on MR images. **Conclusion:** 18F-FDG PET/MR is useful method in the assessment of inflammatory activity of sarcoidosis and is promising diagnostic tool in clinical staging of the disease and patient selection for optimal treatment strategy.

EP578**Comparison of PET/CT and PET/MR-based ⁶⁸Ga-DOTATOC standardized uptake values**

E. Ilan^{1,2}, **A. Sundin**^{2,3}, **I. Velikyan**^{2,3}, **M. Sandström**^{1,2}, **H. Ahlström**^{2,3}, **M. Lubberink**^{1,2}; ¹Medical Physics, Uppsala University Hospital, SWEDEN, ²Department of Surgical Sciences, Uppsala University, SWEDEN, ³Medical Imaging Centre, Uppsala University Hospital, SWEDEN.

Objectives Quantitative imaging using PET/MR is challenged by the lack of bone visualisation in MR-based attenuation correction (MRAC). The geometry of integrated PET-MR scanners presents further challenges for quantification, especially for scatter correction for tracers with large uptake variations such as ⁶⁸Ga-DOTATOC. In most studies comparing PET/CT and PET/MR, both images were acquired after a single tracer injection, which compromises comparisons because of redistribution of the tracer between scans. The aim of this study was to compare standardized uptake values (SUV) in tumour and liver in patients with neuroendocrine tumors (NETs) imaged with ⁶⁸Ga-DOTATOC on PET/CT and PET/MR after separate injections on consecutive days. **Materials and methods** Four patients diagnosed with disseminated gastroenteropancreatic NETs underwent ⁶⁸Ga-DOTATOC whole-body PET/CT (Discovery ST) and PET/MR (Signa, both GE Healthcare) at 1 h post injection of circa 200 MBq ⁶⁸Ga-DOTATOC on consecutive days. Images were reconstructed using OSEM with settings optimized to provide similar image resolution across scanners. MRAC was based on a two-point Dixon gradient echo sequence. PET/MR images were reconstructed both with and without time-of-flight (ToF), whereas PET/CT was without ToF. Tumour volumes of interest (VOIs) were drawn using 50 % isocontours. A subsample of healthy liver was delineated using a spherical 20-ml VOL. Correlation and agreement between PET/CT and PET/MR SUV values was assessed using linear regression and Bland-Altman analysis. Results Mean time to imaging after ⁶⁸Ga-DOTATOC injection was 70 ± 2 min for PET/CT and 72 ± 5 min for PET/MR. Seven lesions could be delineated. Moderate correlation was found between PET/CT and PET/MR tumour SUV values, with Pearson correlation (R^2) 0.75 and 0.60 for non-ToF and ToF, respectively. On average, PET/MR SUV values were 1.2% (SD 22) lower and 23% (SD 14) higher than PET/CT values, without and with ToF, respectively. ToF consistently resulted in higher tumour SUVs. High correlation was found between PET/CT and PET/MR liver SUV values, with R^2 0.94 and 0.81 for non-ToF and ToF. On average, PET/MR liver SUV was 2.7% (SD 6.5) lower and 6.5% (SD 11) higher than PET/CT values, without and with ToF. **Conclusion** Our study showed moderate correlation between PET/CT and PET/MR ⁶⁸Ga-DOTATOC tumour SUV values based on a dual-injection protocol. Differences may be attributed partly to MRAC, but also to sub-optimal scatter correction for ⁶⁸Ga-DOTATOC. Along with the inclusion of more patients to allow for more robust conclusions, optimization of scatter correction will be part of further studies.

EP579**Evaluation of Psoriatic Arthritis of the Hands with Integrated ¹⁸F Fluoride PET/MRI**

T. D. Poeppe, **A. Koerber**, **M. Forsting**, **A. Bockisch**, **A. Sabet**, **N. Guberina**; Universitaetsklinikum Essen, Essen, GERMANY.

Aim: Psoriatic arthritis is a common comorbidity of psoriasis vulgaris and affects approximately 25% of all patients with psoriasis. Early and effective detection of psoriatic arthritis is essential to guide therapeutic management and to prohibit joint destruction. The purpose of our study was to evaluate the contribution of integrated ¹⁸F fluoride PET/MRI to the combined assessment of active inflammation and morphological features in psoriatic arthritis of the hands. **Methods:** 21 patients with a history of psoriasis vulgaris and active pain of joints of the hands were included. All patients underwent a dual time point protocol 5 and 90 min after

injection of 150 MBq of ¹⁸F fluoride in a Biograph mMR PET/MRI scanner (Siemens Healthcare, Germany). Estimation of inflammation was based 1) on a combined MRI score (0 = not present, 1 = moderate, 2 = extensive: synovitis, tendonitis, bone oedema, soft tissue oedema, bone erosions, joint space narrowing, joint subluxation, interphalangeal ankylosis, effusion), and 2) on ¹⁸F fluoride uptake in terms of maximal SUV (SUVmax). Results: 134/357 joints showed signs of inflammation in MRI. Joints most often affected were: distal interphalangeal joint (47%), carpometacarpal joint (28%), proximal interphalangeal joint (17%). Mean SUVmax was 4.9 ± 3.0. Pearson's correlation coefficient demonstrated significant correlation between MRI score and SUVmax ($p < 0.05$; $r = 0.525$). **Conclusions:** Integrated ¹⁸F PET/MRI provides information about inflammatory activity and morphological features in early as well as in advanced stages of psoriatic arthritis. Signs of inflammation in MRI and PET are closely related.

EP581**¹⁸F-FDG PET/MRI In Lymphoma: Discordance Between Standardised Uptake Value (SUV) and Apparent Diffusion Coefficient (ADC)**

A. Mallia¹, **U. Bashir**², **J. Stirling**¹, **S. Jeljeli**¹, **J. Joemon**¹, **V. Goh**³, **G. Cook**¹; ¹Cancer Imaging Department, King's College/St. Thomas' Hospital, London, UNITED KINGDOM, ²Cancer Imaging Department, King's College, London, UNITED KINGDOM, ³Cancer Imaging Department, King's College/Department of Radiology, Guy's & St Thomas' Hospitals NHS Foundation Trust, London, UNITED KINGDOM.

Introduction: PET/MRI systems have the potential to more accurately assess nodal and extra-nodal disease in patients with lymphoma. Evidence from other tumour types suggests there is a close relationship between diffusion weighted MRI derived apparent diffusion coefficient (ADC, reflecting cellular density) and PET derived standardised uptake value (SUV, measuring metabolic activity). Conflicting reports regarding the relationship of these two parameters remain in lymphoma. **Aim:** To explore the correlation between MRI ADC and PET SUV measurements in lymphoma patients at staging. **Methods:** Prospective patients with proven lymphoma were recruited and staged using ¹⁸F-FDG PET/MRI prior to commencement of therapy. Quantitative measurements were performed by drawing a region of interest (ROI) around lymph nodes ≥ 1 cm in short axis diameter within major nodal stations. A maximum of 2 nodes per involved nodal station were measured. A concordant node was defined as having an ADC minimum (ADCmin) measurement of ≤ 1 together with a SUVmax ≥ 2.5. Other combinations of measurements were considered as discordant and indeterminate. ADCmin, ADCmean, SUV maximum (SUVmax) and SUV mean (SUVmean) were recorded and correlation assessed using Spearman statistics. **Results:** 17 patients (mean age 56.4 years, 9 male, 8 female) were recruited of which 14 satisfied the inclusion criteria based on nodal size. 59 nodes were evaluated (12 Non-Hodgkin's Lymphoma (NHL), 32 Hodgkin's Lymphoma (HL), 1 Mantle, 2 MALT, 6 T-Cell Lymphoma (TL), 6 Follicular Lymphoma (FL). 52 nodes (88.1%) were concordant and 7 nodes (11.9%) were discordant (n=2, low ADC/low SUV all localised in the inguinal region, n=5, high ADC/high SUV all localised within the mediastinum). Overall, the SUVmax ranged from 0.8 to 40 mg/ml (median 8.95 mg/ml) and the ADCmin ranged from 215 to 2629 (median 662 × 10⁻⁶ mm²/s). No statistically significant correlation was found between pre-treatment SUVmax/ADCmin ($R = 0.004$) ($P = 0.9$), SUVmean/ADCmean ($R = -0.11$) ($P = 0.4$), and SUVmax/ADCmean ($R = -0.16$) ($P = 0.2$) with and without the discordant nodes ($R = -0.02$) ($P = 0.8$), ($R = -0.17$) ($P = 0.2$), ($R = -0.19$) ($P = 0.2$), respectively. A weak inverse correlation was found between the SUVmean and ADCmean when excluding the discordant nodes ($R = -0.39$) ($P = 0.03$) in patients with HL (29 nodes). **Conclusions:** No correlation was found between SUVmax and ADC in treatment naïve lymphoma patients even if discordant nodes were

excluded. Only a weak negative correlation between SUVmean and ADCmean in patients with HL was noted. Our results confirm that ADC and SUV represent different pathological processes.

EP582

Impact of overfeeding with saturated and polyunsaturated fat on hepatic [¹¹C]palmitate uptake and fat content using PET-MR

K. Heurling¹, A. Moreno¹, J. Kullberg¹, F. Rosqvist¹, G. Antoni^{1,2}, J. P. Eriksson², P. Nordeman², M. Sprycha², H. Wilking², A. Gronowski Edner², H. Ahlström¹, H. Ahlström^{1,2}, M. Lubberink^{1,2}, U. Risérus¹; ¹Uppsala University, Uppsala, SWEDEN, ²Uppsala University Hospital, Uppsala, SWEDEN.

Aim Obesity is characterized by an increase in the fatty acid oxidation pathway in the liver, which may be influenced by the type of fat in the diet. We have previously shown that overfeeding saturated fatty acids (SFA), promote liver fat accumulation in contrast to polyunsaturated fatty acids (PUFA). The present study aimed to investigate dietary effects of SFA vs PUFA on liver fatty acid uptake and liver fat content, using [¹¹C]palmitate PET-MR. **Materials and methods** Ten subjects underwent a baseline [¹¹C]palmitate PET-MR scan before randomization to one of two interventions: overfeeding with a diet high in either SFA or PUFA for 8 weeks. A single bed-position dynamic PET scan was performed during 60 min, covering the splanchnic bed, on a GE Healthcare Signa PET-MR. The protocol included collection of discrete arterial blood samples at 5, 10, 15, 20, 30 and 45 min post injection for measurement of whole-blood and plasma radioactivity concentrations and fraction of unmetabolized [¹¹C]palmitate. Quantification of [¹¹C]palmitate was performed using an image derived input function based on average radioactivity concentrations in ascending aorta and portal vein and corrected for metabolites and plasma-whole-blood ratio. The accumulation rate constant K_i was estimated using Patlak analysis using the 3-10 and 10-60 min post injection intervals. Liver fat content was determined using water-fat separated MRI and large region of interest analysis. After the intervention, the [¹¹C]palmitate PET-MR procedure was repeated. Changes in liver fat content, [¹¹C]palmitate K_i and standardized uptake values at 30 min were assessed, and differences between PUFA and SFA challenges were analyzed using the Mann-Whitney U test. **Results** There were no differences in [¹¹C]palmitate K_i change estimated using the 3-10 min ($p=0.548$) or 10-60 min intervals ($p=1.000$), or standardized uptake value change ($p=0.548$), between the two interventions. A tendency to larger increase in liver fat content was seen in the group receiving SFA compared to PUFA, though not statistically significant ($p=0.063$). **Conclusion** Despite the small sample size, a tendency of larger accumulation of liver fat was seen after SFA vs PUFA, in line with previously shown effects. However, neither SFA nor PUFA overfeeding affected [¹¹C]palmitate uptake, indicating that hepatic fatty acid uptake is not a main determining factor for palmitate-induced liver fat accumulation. Future studies are needed to address whether the proportion of [¹¹C]palmitate metabolism due to de novo fatty acid synthesis, oxidation or esterification were affected by the intervention, in spite of unaffected total uptake.

EP-30 – Sunday, October 16, 2016, during Exhibition hours, e-Poster Area

M2M: Preclinical Imaging

EP583

⁸⁹Zr-Trastuzumab-DM1: A Novel Probe for Positron-Emission Tomography (PET) Imaging of the Delivery of T-DM1 (Kadcyla) to HER2-Positive Breast Cancer

N. Al-saden, R. Reilly, C. Chan; University of Toronto, Toronto, ON, CANADA.

Background: Our aim was to construct a novel molecular imaging probe (⁸⁹Zr-labeled T-DM1) to visualize the delivery of trastuzumab-DM1 (T-DM1; Kadcyla, Roche) to HER2-positive breast cancer (BC) by positron-emission tomography (PET). T-DM1 is an antibody-drug immunoconjugate (ADC) approved for treatment of trastuzumab-resistant HER2-positive BC. **Methods:** T-DM1 was modified with desferrioxamine (DFO) for chelating ⁸⁹Zr by reaction with a 14-fold excess of p-NCS-Bz-DFO for 30 min at 37°C. The number of DFO per T-DM1 molecule was quantified spectrophotometrically at 430 nm following reaction with FeCl₃. Purity and homogeneity were assessed by SDS-PAGE and size-exclusion (SE)-HPLC. ⁸⁹Zr labeling was performed at a specific activity of 2μCi/μg in 2 M sodium carbonate/0.5 M HEPES buffer, pH 7.0 at RT for 60-90 mins. Radiochemical purity was determined by instant thin layer-silica gel chromatography (ITLC-SG) and SE-HPLC. HER2 immunoreactivity was measured in a saturation binding assay using SK-BR-3 human BC cells. **Results:** T-DM1 was modified with 3.0 ± 0.2 DFO chelators. SDS-PAGE and SE-HPLC revealed a pure and homogeneous immunoconjugate. The labeling efficiency with ⁸⁹Zr was >95%. ⁸⁹Zr-p-NCS-Bz-DFO-T-DM1 exhibited preserved HER2 immunoreactivity with high affinity binding ($K_d = 4.9 \pm 0.4$ nM). **Conclusions/implications:** A novel ⁸⁹Zr-labeled probe of T-DM1 was produced that exhibited high affinity binding to HER2 on human BC cells. This agent has application for PET imaging of the delivery of T-DM1 to tumours in patients with HER2-positive BC. Imaging may inform on those patients likely to benefit from T-DM1 treatment. Supported by the Ontario Institute for Cancer Research (OICR) Smarter Imaging Research Program.

EP584

Evaluation of radiolabeled NOTA-RGD-GE11 heterodimeric peptide as a probe for dual integrin and epidermal growth factor receptor-targeted tumor imaging in a lung tumor xenograft model

H. Yu, K. Lin, J. Chen, M. Wang, W. Lin; Institute of Nuclear Energy Research, Taoyuan, TAIWAN.

Objective: This study aims to evaluate ⁶⁸Ga-NOTA-RGD-GE11 heterodimeric peptide as a PET probe for dual integrin and epidermal growth factor receptor (EGFR)-targeted tumor imaging in lung carcinoma-bearing mouse model. **Methods:** ⁶⁸Ga-NOTA-RGD-GE11 was prepared by labeling the NOTA peptide conjugate with freshly eluted ⁶⁸Ga and purified using reversed-phase high-performance liquid chromatography. Subcutaneous tumor xenografts were produced by inoculation of NCI-H292 lung cancer cells in the left flank of 6-week-old nude male mice under anesthesia. Biological characterization studies of ⁶⁸Ga-NOTA-RGD-GE11 including in-vitro competitive binding assay, cellular uptake and dynamic nanoPET/CT imaging of NCI-H292 tumor-bearing mice were performed (0-2 h post-intravenous injection). **Results:** ⁶⁸Ga-NOTA-RGD-GE11 was prepared in high radiochemical yield (>85%, decay corrected) and radiochemical purity (>95%). The binding affinities of NOTA-RGD-GE11 to integrin and EGFR were confirmed by competitive binding assay. The accumulations of ⁶⁸Ga-NOTA-RGD-GE11 in NCI-H292 cells increased with time. Dynamic nanoPET/CT imaging studies in NCI-H292 lung carcinoma-bearing mice clearly delineated the tumor lesions. ROIs analysis showed that the accumulations of ⁶⁸Ga-NOTA-RGD-GE11 in NCI-H292 xenografts were increased with time. Tumor-to-muscle ratio was 3.23±0.98 at 2 h post-injection. **Conclusion:** In this study, the ⁶⁸Ga-NOTA-RGD-GE11 heterodimeric peptide was successfully prepared with high yield and radiochemical purity. Both results of cellular uptake and PET/CT imaging showed that ⁶⁸Ga-NOTA-RGD-GE11 was accumulated in tumor cells with desirable uptakes. ⁶⁸Ga-NOTA-RGD-GE11 is demonstrated as a potential radioprobes for dual integrin and EGFR-targeted tumor imaging. These results warrant further investigation of this heterodimeric peptide's biological characters.

EP585**18F-Fluorodeoxymannose (FDM) is a Potential New Tracer for Inflammatory Bowel Disease**

S. R. Christiansen^{1,2}, S. Hess^{1,2,3}, B. B. Olsen¹, C. Baun¹, N. Langkjær¹, P. Høilund-Carlsen^{1,2}; ¹Odense University Hospital, Odense, DENMARK, ²University of Southern Denmark, Odense, DENMARK, ³Hospital of Southern Jutland, Esbjerg, DENMARK.

AIM: Invasive endoscopies are the current gold standard in inflammatory bowel disease (IBD). PET/CT may be a viable alternative, but controversies remain regarding FDG for imaging bowel disease. Macrophages are predominant in chronic inflammation and 18F-Fluorodeoxymannose (FDM) has been suggested instead of FDG for macrophage imaging. We present preliminary results from a feasibility study comparing FDG and FDM uptake *in vitro* in macrophages and *in vivo* in an IBD-mouse model. **MATERIAL AND METHODS:** THP-1 monocytes were differentiated into naïve M0 macrophages with PMA (phorbol 12-myristate 13-acetate). The macrophages were then incubated with FDG and FDM (30 min, 45 min, 60 min, 75 min, 90 min, 120 min, 180 min) and the uptake quantified and compared. Male C57BL/6 mice were subjected to different concentrations (2% and 4%) of Dextran Sulphate Sodium (DSS) in a predetermined schedule over a period of 37 days, a well-established rodent model for IBD. Only the 2% mouse survived the entire study. On day 36, all mice underwent 15-minute static PET/CT scans with FDG (60–75 minutes after injection) and on day 37 all mice underwent a 90-minute dynamic PET/CT scan with FDM. Afterwards, the mice were sacrificed and used for biodistribution analysis. Tracer uptake in the bowel was assessed and quantified. **RESULTS:** *In vitro* there was no significant difference in macrophage uptake between FDM and FDG. The uptake for both tracers increased over time and after 180 minutes reached 0.52%±0.02% of added FDM vs 0.50%±0.03% of added FDG. Biodistribution in two normal control mice and one 2% IBD-mouse showed an increased uptake in the colon of the colitis mouse compared to the two controls (28.0% of IA/g (injected activity per gram) compared to 12.75%±2.95). Analysis of FDG and FDM scans at days 36 and 37 of a colitis mouse showed an increased uptake in absolute values of FDM compared to FDG. The ratios of organ specific values (intestine/liver, intestine/bladder) were similar in FDM compared to FDG, although the intestine/heart ratio was 61.8% larger in FDM compared to FDG. **CONCLUSION:** *In vitro*, macrophages showed similar uptake of FDM and FDG. *In vivo*, both FDM and FDG were able to visualize IBD. Preliminary biodistribution results showed higher overall FDM uptake including in the bowel of an IBD mouse compared to controls and, thus, potentially better target-to-background delineation for FDM. Overall, our results suggest FDM as a potential tracer for macrophage imaging in IBD, but further studies are needed.

EP586**RadTag a new biarsenical imaging probe for radiolabelling of biologicals**

M. Schou¹, J. Häggkvist¹, L. Tari¹, M. Tóth¹, A. Westermarck¹, H. Ingemyr¹, J. Malmquist¹, C. Halldin¹, P. Ström², A. Lundqvist³, V. Hruby⁴, M. Cai⁴, S. P. S. Svensson⁵; ¹Karolinska Institutet, Department of Clinical Neuroscience, Stockholm, SWEDEN, ²BioPercept AB, Lund, SWEDEN, ³Karolinska Institutet, Institute for Oncology, Stockholm, SWEDEN, ⁴Department of Chemistry, University of Arizona, Tucson, AZ, UNITED STATES, ⁵Department of Physics, Chemistry and Biology, Linköping, SWEDEN.

Aim The radiolabeling of biologicals for PET imaging has so far been hampered by a lack of generalised radiolabeling methodology. We have developed a novel approach for this purpose, RadTags, which enables rapid, specific, and simple radiolabeling of biologicals based on the

biarsenical-tetracystein system. One unique characteristic of the methodology is that RadTags may be labeled with any isotope of choice, using established radiolabeling technology, allowing imaging using the same constitutionally distinct molecular probe in a variety of settings, from the test tube to the clinic. The aim of the present study was to show proof-of-principle in a variety of studies, including *in vitro* radioligand binding studies and *in vivo* microPET nuclear imaging of melanoma tumors in xenograft mice. **Materials and methods** Melanin stimulating hormone (MSH) was modified to enable site-specific labeling using the biarsenical-tetracysteine methodology. Radiolabeled RadTag (³H or ¹¹C) was efficiently prepared by *O*-methylation of the desmethyl phenolic precursor using either or [³H]methyl nosylate or [¹¹C]methyl triflate under mild alkaline conditions. The modified MSH analog (NDP-MSH) was reacted with Radtag (³H or ¹¹C) in an aqueous buffer according to a published procedure. The radiochemical purity of [¹¹C]RadTag-NDP-MSH was >95%. *In vitro* radioligand binding characterization of [³H]-RadTag-NDP-MSH was performed using B16F10 melanoma cells or transfected cells. *In vivo* [¹¹C]RadTag-NDP-MSH microPET imaging of melanoma tumors was performed in B16F10 xenograft mice. **Results** The reaction of radiolabeled Radtag with NDP-MSH proceeded with near quantitative conversion after a ten minute incubation at room temperature. Both NDP-MSH and RadTag-NDP-MSH bind with low nM affinity to MC1 receptors, showing that modification of NDP-MSH does not influence the primary pharmacology of the peptide analogue. In the *in vivo* microPET experiment, [¹¹C]RadTag-NDP-MSH successfully visualized the melanoma tumor with a tumor/muscle ratio of about 1.5 at 60 minutes. **Conclusion** Our data shows that the new biarsenical RadTags may be successfully used for rapid multimodal radiolabeling of biologicals for *in vivo* molecular imaging.

EP587**Non-invasive determination of the beta cell mass with PET and SPECT with radiolabeled exendin in a spontaneous mouse model for type 1 diabetes**

L. Joosten, M. Brom, O. C. Boerman, M. Gotthardt; Radboud University Medical Center, Nijmegen, NETHERLANDS.

Aim The beta cell mass (BCM) plays a key role in the development and progression of diabetes, but the onset of beta cell loss and the relationship between loss of beta cell mass and beta cell function still needs to be unraveled. A non-invasive method to determine the BCM *in vivo* would allow measurement of the BCM during the development and progression of type 1 and 2 diabetes. Exendin-3 is a stable glucagon-like peptide-1 (GLP-1) analogue with high affinity for the GLP-1 receptor (GLP-1R). Recently, targeting of the GLP-1 receptor on beta cells was proven to be a successful method to determine the beta cell mass *in vivo* in rats with chemically induced beta cell loss. In a first clinical proof-of-principle study these preclinical data were confirmed. In this study we compared the *in vivo* BCM quantification of SPECT with PET in non-obese diabetic (NOD) mice and correlated this with exendin uptake determined *ex vivo* and with immunohistochemical determination of the BCM. **Materials and methods** NOD mice (n = 14) of 6, 12 and 18 weeks old were injected intravenously with 3–5 MBq ⁶⁸Ga-NODAGA-exendin-3 and 1 h p.i. PET/CT was acquired. Two days later mice received 15 MBq ¹¹¹In-exendin-3 and SPECT/CT images were acquired 1 h p.i.. Animals were euthanized after SPECT/CT and pancreas and relevant organs were dissected, weighed and the radioactivity in the organs was measured in a gamma counter. The pancreas was fixed in formalin, embedded in paraffin and sections were stained immunohistochemically to determine the BCM by morphometric analysis. **Results and conclusion** Both PET and SPECT visualized the pancreas. The correlation (Pearson) between the BC area (μm²) and pancreatic uptake of ¹¹¹In-exendin measured *ex vivo* (%ID/g) was 0.72 (p = 0.0036). Quantification of exendin uptake by SPECT resulted in a better correlation (Pearson r = 0.95, p < 0.0001)

with tracer uptake measured by ex vivo counting compared to quantification with PET (Pearson $r = 0.69$, $p = 0.0068$). Furthermore, a better correlation between BCM and image quantification was observed for SPECT than for PET (Pearson $r = 0.66$, $p = 0.0108$ and $r = 0.28$, $p = 0.32$, respectively). In conclusion, the BCM can be determined accurately with SPECT and PET. This study shows a preference for SPECT in preclinical imaging to achieve a more reliable measurement of the real BCM in this model for type 1 diabetes.

EP588

Radiolabeling and biodistribution study of engineered antibody-like protein with Tc-99m for tumor therapy

D. Lee, D. Choi; Korea Atomic Energy Research Institute, Jeongseup, KOREA, REPUBLIC OF.

Recently, antibody-like scaffold proteins have received a great deal of interest in diagnosis and therapy applications. Since antibody-like scaffold proteins possess intrinsic features that are often required for tumor imaging and therapy, they have potential to be used as platforms for integrating imaging and therapeutic functions. Intrinsic issues that are associated with therapeutic application of antibody-like scaffold proteins, particularly in cancer treatment, include an efficient and straightforward radiolabeling for understanding in vivo biodistribution and excretion route, and monitoring therapeutic responses. Herein, to investigate the biodistribution and blood clearance, antibody-like scaffold protein, rebody, was successfully radiolabeled with the $[^{99m}\text{Tc}(\text{OH}_2)_3(\text{CO})_3]^+$ (^{99m}Tc -tricarboxyl) by using a site-specific direct labeling method via hexahistidine-tag, which is a widely used for general purification of proteins with His-affinity chromatography. Rebody is antibody-like scaffold that consist of highly diverse leucine-rich repeat (LRR) modules, it has been constructed to bind to interleukin-6 for cancer therapy. For ^{99m}Tc labeling to rebody, we first prepared ^{99m}Tc -tricarboxyl. Synthesis of ^{99m}Tc -tricarboxyl precursor achieved yields more than 90%. The result of radio-TLC, the Rf value for ^{99m}Tc -tricarboxyl was 0.0 and 0.3–0.4 using a saline and solvent mixture (methanol 99%, HCl 1%) as the eluent, respectively. And then, the rebody was radiolabeled with ^{99m}Tc -tricarboxyl at 37°C for 1 h. After radiolabeling, for remove unconjugated ^{99m}Tc -tricarboxyl, simple purification step was performed using 10 kDa cut-off filter system. Radiochemical purity was determined by radio-TLC. The radiochemical purity of radiolabeled rebody with ^{99m}Tc (^{99m}Tc -rebody) was estimated to be greater than 99% and the specific activity was 925 MBq/mg. ^{99m}Tc -rebody was highly stable up to 24 h for both in vivo SPECT/CT and in vitro histidine challenge study. Biodistribution results showed that most of intraperitoneal doses of ^{99m}Tc -rebody were found in kidneys, and other organs were found with subsequent remaining. SPECT/CT images showed that most radioactivities were presented in the kidneys at early time point. These results were well matched with biodistribution data. These biodistribution studies of rebody will be useful for development of therapy strategy along with their systemic information.

EP589

A ^{99m}Tc radiolabeled tenascin-C binding aptamer for in vivo visualization of glioblastoma tumor

L. Kang¹, Y. Huo¹, R. Wang¹, X. Xu²; ¹Peking University First Hospital, Beijing, CHINA, ²Academy of Military Medical Sciences, Beijing, CHINA.

Objective: Aptamers are small molecule DNA or RNA fragments that fold into well defined 3D structures with high specificity and affinity towards target molecules. DNA aptamer, GBI-10 was found to bind with tenascin-C, an overexpressed extracellular protein in the tumor matrix. In this study, a new tumor-targeted agent of radiolabeled aptamer with technetium-99m

(^{99m}Tc) was developed, and its serum stability and in vivo imaging in glioblastoma tumor bearing mice was further evaluated. **Methods:** A six carbon amine group was linked at the 3' end of GBI-10 so that this aptamer could be radiolabeled with ^{99m}Tc via the conjugation to NHS-MAG3. Radiolabeled yield and purity were evaluated by HPLC. Agarose gel electrophoresis was performed to evaluate the stability of ^{99m}Tc -GBI-10 in human fresh serum. Cellular uptake assays were carried out in the U-251 cell line to evaluate tumor uptake in vitro. Further, in vivo imaging of ^{99m}Tc radiolabeled GBI-10 was performed in glioblastoma tumor models. **Results:** Aptamer GBI-10 was synthesized with CpG solid phase synthesis methodology. GBI-10 was modified with amine group and PS backbone. After conjugated with NHS-MAG3, GBI-10 was successfully labeled with ^{99m}Tc with high radiolabeling efficiency (95%) and radiochemical purities (>98%). Shown by gel electrophoresis, ^{99m}Tc -GBI-10 had high stability in fresh human serum. In cellular uptake assay, this radiolabeled aptamer showed significantly higher uptake in U-251 cells than ^{99m}Tc -pertechnetate. After system administration, ^{99m}Tc -GBI-10 showed high accumulation in tumor during 12 h. There was significant difference between radiolabeled GBI-10 and ^{99m}Tc -pertechnetate in U-251 tumor bearing mice, which suggested the specific binding ability of radiolabeled GBI-10 in glioblastoma tumor. **Conclusion:** ^{99m}Tc radiolabeled aptamer GBI-10 has good stability in serum and is considered a promising agent capable of detecting tenascin-C in tumors.

EP590

In vivo PET Imaging of the changes in a rat fluid-percussion-induced traumatic brain injury model with [^{11}C]PBR28 and [^{18}F]flumazenil: A preliminary study

Z. WANG¹, C. Yang¹, K. Ghosh¹, S. Kumar¹, P. Padmanabhan¹, C. Halldin^{2,1}, B. Gulyás^{1,2}; ¹Nanyang Technological University, Singapore, SINGAPORE, ²Karolinska Institutet, Stockholm, SWEDEN.

Background and Objectives: Lateral fluid-percussion-induced (LFPI) traumatic brain injury (TBI) model in rat is a commonly used experimental animal model to study the cellular and molecular changes of TBI observed in humans. It is capable of reproducing the physiological, pathological and behavioural aspects under different clinical conditions in rodents. It is also useful in tracking the longitudinal changes in the brain due to the primary and secondary injuries. Recent developments in Positron Emission Tomography (PET) imaging provide us with the possibility of qualitatively and quantitatively mapping of the cellular and molecular changes induced by TBI in both humans and animals in vivo. For instance, [^{11}C]PBR28, can monitor the neuroinflammatory response in a rat TBI model. Density changes of the γ -aminobutyric acid-type A (GABA_A) system can be detected with the [^{18}F]flumazenil radioligand. This study aimed to investigate (i) whether the combination of the two radiotracers ([^{11}C]PBR28 and [^{18}F]flumazenil) allows reliable quantification of the molecular changes *in vivo* in a rodent TBI model and (ii) whether there are any demonstrable changes related to the primary and secondary injuries which can be observed with the two radioligands. To our best knowledge, this could be the first rodent study that used two radioligands for the LFPI TBI rat model. **Materials and Methods:** Four Sprague-Dawley rats were used for this study. After the LFPI procedure, Day 3 post-op and Day 14 post-op 3D dynamic PET scans were performed using the nanoScan PET/MRI scanner (Mediso, Hungary) at SEMC Singapore. The animals were scanned first with [^{11}C]PBR28 for 60 minutes, followed 80 minutes later by a 90 minutes long PET scan with [^{18}F]flumazenil. The PET datasets were analyzed using the image fusion tool and Px Rat (W.Schiffner) template in PMOD (PMOD Technologies, Switzerland). **Results:** It is clear that there is an increased uptake of [^{11}C]PBR28 on Day 14 caused by the LFPI procedure in the right hemisphere, whereas the uptake of [^{18}F]flumazenil was decreased on Day 14. When comparing the left and right hemispheres using an area-under-the-curve measure, the differences between left and right hemispheres for [^{11}C]PBR28 were obvious. However, the differences

were not noticeable for [^{18}F]flumazenil. **Conclusions:** Although the PET datasets were limited in this study, our results demonstrate that it is possible to quantify the molecular changes with PET imaging with [^{11}C]PBR28 and [^{18}F]flumazenil in a TBI rodent model. Further studies are underway to explore the exact nature and timecourse of the changes.

EP591

xCT as Molecular Target for Oxidative Stress Imaging in PET

M. Colovic^{1,2}, H. Yang¹, H. Merckens², C. Zhang², K. Lin², F. Benard^{2,3}, P. Schaffer^{1,3}, ¹TRIUMF, Vancouver, BC, CANADA, ²British Columbia Cancer Research Centre, Vancouver, BC, CANADA, ³Department of Radiology, University of British Columbia, Vancouver, BC, CANADA.

Aim The system x_c^- , cystine/glutamate antiporter, has been shown to be upregulated under increased intracellular oxidative stress (OS), thus supplying the cell with cysteine, the rate-limiting substrate required for the synthesis of the antioxidant glutathione (GSH). We have developed a PET tracer targeting the transmembrane subunit of the system x_c^- , xCT. The goal of this study was to correlate 5-[^{18}F]fluoroaminosuberlic acid ($^{18}\text{FASu}$) uptake levels with xCT expression *in vitro* and *ex vivo*, as well as to understand xCT expression levels relative to other cellular markers of oxidative stress. **Materials and methods** xCT expression levels *in vitro* and in harvested tumour tissues and other organs, such as brain and pancreas, were determined using Western blot (WB) experiments. The protein expression levels were determined in untreated samples as well as under induced OS conditions. The $^{18}\text{FASu}$ uptake study was performed using an array of cancer cell lines, including 3 different types of breast cancers (MDA-MB-231, MCF7, ZR-75-1). Uptake was measured in the presence and absence of L-Asu and sulfasalazine (SSZ) as blocking agents. Thiols (GSH and cysteine) and reactive oxygen species (ROS) levels were determined in untreated cells lines as well as after treatment with diethylmaleate (DEM, an OS-inducing agent) and SSZ (system x_c^- inhibitor). Intracellular thiol levels were determined using commercially available fluorescence-based kit detecting free thiol groups on macromolecules. ROS levels were estimated using a 10-acetyl-3,7-dihydroxyphenoxazine-based assay. **Results** Our results to date indicate that xCT expression is positively correlated to ROS and thiol levels. Moreover, *in vitro* $^{18}\text{FASu}$ uptake seems to be following the same trend. In DEM-treated breast cancer cells, xCT protein expression increased, as did thiol content as well as $^{18}\text{FASu}$ uptake; while SSZ treated cells demonstrated reduced tracer uptake as well as a decline in cysteine and GSH content. Among the breast cancer cell lines studied, MDA-MB-231 had the highest xCT expression and also the highest $^{18}\text{FASu}$ uptake. More detailed ROS level measurements, *in vivo* tracer uptake, and its correlation to protein expression in tumour tissues are under investigation. **Conclusion** Our work suggests that xCT expression is positively correlated to increases in ROS and thiol levels. These increases are also correlated with increased $^{18}\text{FASu}$ uptake. Utilizing xCT as a molecular target, $^{18}\text{FASu}$ PET may provide functional information useful for clinical cancer care, including an ability to non-invasively establish cell and/or tissue OS responses for early detection, disease staging, and treatment monitoring for known and novel therapies.

EP592

In Vivo Biodistribution Of Labeled Adult Human Mesenchymal Cells ($^{99\text{m}}\text{Tc}$ - ahMSC_s) Administered Via Intra-Articular In Animal Model. Preliminary Results

A. Abella¹, E. Fernández¹, A. Montellano², T. Martínez¹, R. Rabadan³, P. Ros³, L. Meseguer-Olmo⁴, ¹Unidad de Radiofarmacia, Hospital Clínico Universitario Virgen de la Arrixaca., Murcia, SPAIN, ²Servicio de Medicina Nuclear. Clínica Belén, Murcia, SPAIN, ³Servicio de Traumatología. Hospital Clínico Universitario Virgen de la Arrixaca., Murcia, SPAIN, ⁴UCAM Universidad Católica San Antonio de Murcia., Murcia, SPAIN.

AIM Adult human mesenchymal stem cells from bone marrow (ahMSC_s) have an active role in cell therapy. Intravenous administration is currently in question due to drawbacks as the massive cell trapping in the pulmonary parenchyma and the lack of viability of these cells in the bloodstream. In previous study we compared the scintigraphic biodistribution of $^{99\text{m}}\text{Tc}$ -ahMSC_s after intravenously (IV) and intra-articular (IAR) administration in animal model. Surprisingly, pulmonary activity was not detected when the injection was performed by this second via. We intend to find out which route follows the extracavitary activity detected when using the IAR administration. **MATERIAL AND METHODS** Two New Zealand male rabbits (3.5-4k) were used. With an interval of two weeks, $2.9 \times 10^6 / 0.5 \text{ ml}$ of $^{99\text{m}}\text{Tc}$ -ahMSC_s (6.05 Bq / cell) and 74 MBq / 0.5ml of anhydrous sodium phytate (Phytacis®) were injected via intra-articular (knee joint) and $6 \times 9.2 \text{ MBq} / 0.1 \text{ ml}$ of $^{99\text{m}}\text{Tc}$ nanocolloidal human albumin (Nanocoll®) subcutaneously around the joint. After acquisition of dynamic images every 30 s for 25 min, whole body static images in previous projection at 1, 6 and 24 hours were acquired, previous sedation. Immunosuppressive agents were not administered. All animals survived the experiment. **RESULTS** Lymphatic drainage was observed with ipsilateral inguinal lymph visualisation without pulmonary or hepatic uptake in dynamic images obtained after subcutaneous administration of $^{99\text{m}}\text{Tc}$ - nanocolloidal human albumin around the joint. On the other hand, liver activity was observed after IAR injection of $^{99\text{m}}\text{Tc}$ -phytate as following administration of $^{99\text{m}}\text{Tc}$ -ahMSC_s. **CONCLUSION** Results seem to confirm that the activity detected in different organs after IAR administration migrates from the cavity through the circulatory system. However, the absence of pulmonary activity after IAR administration of $^{99\text{m}}\text{Tc}$ -ahMSC_s do not allow to establish a correspondence of this activity with the extracavitary cell migration.

EP593

Origin Of The Activity Detected By Scintigraphy After Intra-Articular Administration Of Labeled Adult Human Mesenchymal Stem Cells ($^{99\text{m}}\text{Tc}$ - ahMSC_s) In An Animal Model

A. Abella¹, E. Fernández¹, T. Martínez¹, C. Martínez², B. Revilla-Nuin³, R. Rabadan⁴, L. Meseguer-Olmo⁵, ¹Unidad de Radiofarmacia, Hospital Clínico Universitario Virgen de la Arrixaca., Murcia, SPAIN, ²Experimental Pathology Laboratory (LAPE). IMIB-Arrixaca and CIBERehd., Murcia, SPAIN, ³Unidad de genómica. IMIB-Arrixaca and CIBERehd, Murcia, SPAIN, ⁴Servicio de Traumatología. Hospital Clínico Universitario Virgen de la Arrixaca., Murcia, SPAIN, ⁵UCAM Universidad Católica San Antonio de Murcia., Murcia, SPAIN.

AIM Nuclear medicine imaging is an attractive technique in terms of non-invasive *in vivo* human mesenchymal stem cells (ahMSC_s) tracking after labeling with a radiopharmaceutical. Our previous work on intra-articular (IAR) administration of $^{99\text{m}}\text{Tc}$ ahMSC_s in an animal model pointed out that the extra-articular activity migrates from the cavity through the bloodstream; our purpose is to check the origin of such extracavitary activity by histological detection of ahMSC_s after IAR administration of ahMSC_s labeled with $^{99\text{m}}\text{Tc}$ -HMPAO in an animal model. **MATERIAL AND METHODS** Samples from synovial membrane and several organs (lung, heart, spleen, liver, stomach, intestine, colon, kidney, urinary bladder, gall-bladder and bone marrow) were analyzed by immunohistopathology and molecular biology in search of the presence of ahMSC_s. Paraffin embedded (for H&E and anti-CD90 examinations) and fixed RNA-later (for study the molecular expression of human GAPDH) samples were employed. **RESULTS** The presence of ahMSC_s was confirmed only in the synovial membrane. No signs of ahMSC_s, either by immunohistopathology or molecular biology, were observed in stated organs. **CONCLUSION** Histological analysis pointed out the absence of human ahMSC_s in extracavitary area, confirming the trapping of ahMSC_s in the cavity and the lack of migration to other organs. Scintigraphic activity detected outside the joint could be due to the efflux of $^{99\text{m}}\text{Tc}$ -HMPAO from the cells after administration.

EP594**Effects of intratumoral versus intravenous injection on the breast tumor targeting and tissue uptake distribution of ¹⁷⁷Lu-labeled bombesin peptide analog**

S. Okarvi, I. Jammaz; King Faisal Specialist Hospital & Research Centre, Riyadh, SAUDI ARABIA.

Aim: It is important to explore new and effective targeted routes of administration to enhance tumor targeting efficacy and reduce systemic toxicity. One main drawback of traditional intravenous (i.v) administration of radiopeptide is the high accumulation in nontarget tissues leading to low concentration in target tissue (tumor). Direct intratumoral (i.t) administration of radiopeptide is a new treatment exemplar which may be particularly beneficial for treating accessible solid tumors especially in early stages. The obvious rationale behind this approach is that the topical administration of radiopeptides improve the concentrations of agents in the target site while lowering their localization in healthy tissues. The purpose of the current study was to evaluate breast tumor targeting potential of ¹⁷⁷Lu-labeled bombesin (BN) analog in xenografted nude mice after i.t and i.v injection. **Materials and Methods:** In the present study a novel BN analog was synthesized by solid-phase synthesis following Fmoc/HBTU chemistry and manually coupled to DOTA ligand to facilitate labeling with ⁶⁸Ga/¹⁷⁷Lu. After labeling DOTA-GGC-BN(7-14) with ¹⁷⁷Lu in the presence of 0.1M NH₄OAc buffer (pH 4-5) in vitro cell binding was performed on various breast cancer cell lines including MCF7, T47D and MDA-MB-231. For in vivo tumor targeting the radiopeptide was administered by i.t and i.v injections in two groups of nude mice with subcutaneously grown MCF7 breast tumors. **Results:** ¹⁷⁷Lu-DOTA-GGC-BN exhibited a high and specific binding towards various human breast cancer cell lines with binding affinities below 20nM. Also a significant internalization (~20%) into cancer cell lines was observed. Following i.t injection into nude mice 36%ID/g of the radioactivity was localized in the breast tumor over 2 h whereas uptake in other major organs including kidneys was quite low (<1%ID/g). Tumor to blood, muscle and kidney ratios were found to be 252, 360 and 36. When i.v mode of administration was utilized a totally different and variable tissue uptake behavior was observed in terms of accumulation in nontarget tissues (up to 7%ID/g). The uptake in the tumor was below 2%ID/g. **Conclusion:** i.t administration of ¹⁷⁷Lu-DOTA-GGC-BN makes high amount of radioactivity retained in tumor with significantly lower radioactivity retained in normal tissues and provides a more effective targeting of BN receptor-expressing breast tumors. It is expected that direct i.t injection may offer less systemic exposure than i.v delivery and serve as an effective procedure to deliver high radiation dose specifically to tumors. Future studies should discover more usefulness of this inventive mode of administration.

EP595**Design and construction of a hybrid HER2/neu peptide for targeting human breast carcinoma**

S. Okarvi, I. Jammaz; King Faisal Specialist Hospital & Research Centre, Riyadh, SAUDI ARABIA.

Objectives: HER2/neu is a member of the epidermal growth factor receptor family of transmembrane tyrosine kinases. The HER2/neu gene is amplified and overexpressed in a variety of malignancies, including breast and ovarian cancers. This overexpression can result in ~200-fold increase concentration of the HER2/neu in tumor versus normal tissue. The E75 epitope (HER2/neu 369-377) is immunogenic peptide derived from HER2/neu protein, which is overexpressed in many breast cancer patients. Another peptide that has shown potential for targeting HER2/neu expressing tumors is based on KCCYSL sequence. In the current study, we have combined the sequences of these two important

peptides and formulate a hybrid HER2/neu peptide in an attempt to target breast tumors. **Methods:** The HER2/neu hybrid peptide (Ac-GGC-ALA-E75+KCCYSL) was synthesized by Fmoc/HBTU based peptide synthesis chemistry. The HER2/neu peptide was radiolabeled with ^{99m}Tc via GGC- chelating sequence by ligand exchange method. In vitro tumor cell binding was performed on HER2/neu expressing SKBR3 and MCF7 human breast cancer cell lines and in vivo tumor targeting was conducted on nude mice carrying MCF7 breast tumor xenografts. **Results:** The structure and purity of HER2/neu peptide was confirmed by mass spectrometry and HPLC analysis. The hybrid HER2/neu peptide radiolabeled efficiently with ^{99m}Tc (90%) and exhibited a high binding affinity to HER2/neu expressing SKBR3 and MCF7 cell lines (kd=<50 nM). In nude mice with MCF7 xenografts, the radiopeptide displayed efficient clearance from the blood and uptake in most of the major organs was low to moderate range (below 4%ID/g), with the exception of the kidneys, which retained the highest radioactivity (up to 14%ID/g). The accumulation in the tumor was found to be 2.10±0.67, with good tumor to blood and tumor to muscle ratios of 1.1 and 5.3. The excretion of radiopeptide was observed through the renal and hepatobiliary pathways. **Conclusions:** Our initial findings suggest that the hybrid HER2/neu peptide hold certain favorable in vitro and in vivo characteristics that may makes it useful for the diagnosis of HER2/neu positive tumors. Nonetheless further studies are required to assess the full diagnostic potential of this new emerging class of peptides for tumor targeting.

EP596**Investigation of experimental melanoma tumors using the novel melanin specific radiotracer ⁶⁸Ga-NODAGA-Procaïnamide (PCA)**

G. Trencsényi^{1,2}, G. Nagy², A. Vida^{3,4,5}, J. Angyal⁶, N. Dénes¹, J. P. Szabó¹, T. Kovács^{3,4,5}, I. Garai^{1,2}, P. Bai^{3,4,5}, I. Kertész¹; ¹University of Debrecen, Department of Nuclear Medicine, Debrecen, HUNGARY, ²Scanomed Ltd., Debrecen, HUNGARY, ³University of Debrecen, Department of Medical Chemistry, Debrecen, HUNGARY, ⁴MTA-DE Lendület Laboratory of Cellular Metabolism, Debrecen, HUNGARY, ⁵Research Center for Molecular Medicine, Debrecen, HUNGARY, ⁶University of Debrecen, Department of Periodontology, Debrecen, HUNGARY.

Aim: Malignant melanoma is the most aggressive form of skin cancer. The early detection of primary melanoma tumors and metastases using non-invasive PET imaging determines the outcome of this disease. Previous studies have shown that benzamide derivatives specifically bind to melanin pigment. The aim of this study was to synthesize and investigate the melanin specificity of the novel ⁶⁸Ga-labeled NODAGA-Procaïnamide (PCA) *in vitro* and *in vivo* using PET techniques. **Methods:** Benzamide derivative procaïnamide (PCA) was conjugated with NODAGA chelator and was labeled with Ga-68 (⁶⁸Ga-NODAGA-PCA). The melanin specificity of ⁶⁸Ga-NODAGA-PCA was investigated under *in vitro*, *ex vivo* and *in vivo* conditions using amelanotic Melur and melanotic B16-F10 melanoma cell lines. By subcutaneous and intravenous injection of melanoma cells tumor-bearing mice were prepared (n=20), on which 20 days after tumor cell inoculations (3x10⁶) biodistribution studies and small animal PET/CT scans were performed after intravenous injection of ⁶⁸Ga-NODAGA-PCA (11.3±0.2 MBq) and ¹⁸F-DG radiotracers (10.1±0.3 MBq). **Results:** ⁶⁸Ga-NODAGA-PCA was produced with excellent radiochemical purity (98%<) and with high specific activity (14.9±3.9GBq/μmol), at all cases. *In vitro* experiments showed that ⁶⁸Ga-NODAGA-PCA uptake of B16-F10 cells was significantly (p<0.01) higher than Melur cells. *Ex vivo* organ distribution and *in vivo* PET/CT studies using subcutaneous and metastatic tumor models showed significantly (p<0.01) higher ⁶⁸Ga-NODAGA-PCA uptake in B16-F10 primary tumors and lung metastases in comparison with amelanotic Melur tumors. In B16-F10 melanoma models more than 10-fold higher tumor-to-background ratios were found by using ⁶⁸Ga-

NODAGA-PCA when it was compared to the ^{18}F FDG accumulation. Conclusion: ^{68}Ga -NODAGA-PCA showed specific binding to the melanin producing experimental primary and metastatic B16-F10 melanoma tumors. Therefore, ^{68}Ga -NODAGA-PCA is a suitable diagnostic radiotracer for the detection of melanoma tumors and metastases *in vivo*.

EP597

Comparative *in vitro* and *in vivo* studies of Ga-68-labeled melanin-specific Procainamide (PCA) using different chelators

G. Trencsényi^{1,2}, G. Nagy², A. Vida^{3,4}, N. Dénes¹, J. P. Szabó¹, T. Kovács^{3,4}, I. Garai^{1,2}, P. Bai^{3,4,5}, J. Varga¹, I. Kertész¹; ¹University of Debrecen, Faculty of Medicine, Department of Nuclear Medicine, Debrecen, HUNGARY, ²Scanomed Ltd., Debrecen, HUNGARY, ³University of Debrecen, Department of Medical Chemistry, Debrecen, HUNGARY, ⁴MTA-DE Lendület Laboratory of Cellular Metabolism, Debrecen, HUNGARY, ⁵Research Center for Molecular Medicine, Debrecen, HUNGARY.

Purpose: Previous studies have shown that benzamide derivatives conjugated with different positron emitting radionuclides (Ga-68, F-18) specifically bind to melanin pigment of melanoma tumors. Ga-68 chelating agents have high influence on the radiochemical and physiological properties of Ga-68 labeled melanin-specific procainamide (PCA). The aim of this study was to compare the melanin specificity of ^{68}Ga -labeled PCA using HBED-CC and NODAGA chelators under *in vitro* and *in vivo* conditions. Methods: Benzamide derivative procainamide (PCA) was conjugated with HBED-CC and NODAGA chelators and was labeled with Ga-68. The melanin specificity of ^{68}Ga -NODAGA-PCA and ^{68}Ga -HBED-CC-PCA was investigated *in vitro* and *in vivo* using amelanotic (Melur) and melanotic (B16-F10) melanoma cell lines. Tumor-bearing mice (n=10) were prepared by subcutaneous injection of B16-F10 melanoma cells. 20 days after tumor cell inoculation and 90 min after intravenous injection of the radiotracers small animal whole body PET/MRI (Mediso nanoScan PET/MRI) scans were performed. Results: *In vitro* experiments showed that ^{68}Ga -NODAGA-PCA uptake of B16-F10 cells was significantly ($p < 0.001$) higher than the ^{68}Ga -HBED-CC-PCA accumulation after 30 and 90 min incubation time. *In vivo* PET/MRI studies using subcutaneous tumor models showed significantly ($p < 0.001$) higher ^{68}Ga -NODAGA-PCA uptake (SUVmean: 0.46 ± 0.05 , SUVmax: 1.96 ± 0.25 , T/M ratio: 40.69 ± 5.87) in B16-F10 primary tumors in comparison with ^{68}Ga -HBED-CC-PCA where the SUVmean, SUVmax and T/M ratios were 0.13 ± 0.02 , 0.56 ± 0.11 and 11.43 ± 0.45 , respectively. Conclusion: ^{68}Ga -labeled-PCA using NODAGA chelator showed specific binding to the melanin-producing experimental B16-F10 melanoma tumors. Because of its high specificity and sensitivity ^{68}Ga -NODAGA-PCA is a promising radiotracer for clinical and preclinical melanoma research.

EP598

Imaging response to therapy using PET imaging with the novel PSMA PET tracer, ^{68}Ga -THP-PSMA, in Du145-PSMA prostate cancer xenografts

A. Weeks, J. Young, N. K. Ramakrishnan, K. Sunassee, G. Mullen, V. Goh, P. Blower, G. Cook; King's College London, London, UNITED KINGDOM.

There are now several effective treatments for metastatic prostate cancer that prolong survival but response rates remain less than 50%. There is frequently a delay in changing therapy as current imaging methods are poor at differentiating responders from non-responders at an early enough time point to effectively guide therapeutic transition and limit toxicity in non-responders. Imaging of prostate specific membrane antigen (PSMA)

in prostate cancer is emerging as a specific and sensitive technique for the staging of prostate cancer but to date no data exists for therapy monitoring. Aim: The purpose of this pre-clinical study was to evaluate response to Docetaxel, a first line chemotherapeutic agent used in men with metastatic prostate cancer, using the novel PET tracer ^{68}Ga -THP-PSMA and our hypothesis was that measuring changes in PSMA expression can monitor therapeutic effect. Method: Expression of PSMA was confirmed in DU145-PSMA cells by flow cytometry. SCID-beige mice were injected subcutaneously in the right flank with DU145-PSMA cells. Tumours were measured 2-3 times per week until the mean diameter was 0.5-1cm. Mice then underwent a pre-treatment microPET/CT scan with ^{68}Ga -THP-PSMA 15 min after IV tail vein injection of 5-10 MBq. Mice were then treated on day 1 and day 5 with 3mg/kg clinical grade Docetaxel administered intravenously. Sham treated animals were administered sterile saline under the same regimen. PET/CT scans were repeated at 14 days after which mice were sacrificed and tumour and muscle samples were weighed and gamma counted to provide tumour to muscle ratios (TMR). Regions of interest were drawn manually on the whole tumour using PET and CT images and refined using global thresholding. ^{68}Ga -THP-PSMA uptake per unit volume was calculated from percentage of injected dose (%ID/mm³). Uptake in pre-treatment images were compared to 14 day images for change in uptake after therapy. Results: Ex-vivo gamma counting demonstrated reduced TMRs in Docetaxel treated mice (n=5) compared to sham-treated (n=3) (7.7:1 and 15.3:1, respectively, $p=0.048$). PET images of Docetaxel treated animals (n=5) showed a trend of a greater mean decrease in uptake compared to sham treated animals (n=3) (-4.7×10^{-4} %ID/mm³ and -1.0×10^{-5} %ID/mm³, respectively). Conclusions: These preliminary data demonstrate that ^{68}Ga -THP-PSMA uptake is reduced in prostate tumour xenografts treated with Docetaxel and may be suitable as an agent for PET imaging of therapy response.

EP599

Diagnosis with resource to image of bladder cancer: an *in vivo* evaluation of $^{99\text{m}}\text{Tc}$ -PEI-MP

S. M. Ferreira¹, A. M. Abrantes², M. Laranjo², J. Casalta-Lopes³, A. C. Goncalves⁴, A. B. Sarmiento-Ribeiro⁴, J. Zeevaert⁵, W. Louw⁵, C. Pais⁶, I. Dormehl⁷, M. F. Botelho²; ¹Biophysics Unit, Faculty of Medicine, University of Coimbra; Centre of Molecular and Environmental Biology, School of Sciences, University of Minho; Nuclear Medicine Course, School of Allied Health Technologies of Porto's Polytechnic Institute, Coimbra, Braga, Porto, PORTUGAL, ²Biophysics Unit, Centre of Investigation on Environment, Genetics and Oncobiology; Institute for Biomedical Research on Light and Image; Faculty of Medicine, University of Coimbra, Coimbra, PORTUGAL, ³Biophysics Unit, Faculty of Medicine, University of Coimbra, Coimbra, PORTUGAL, ⁴Centre of Investigation on Environment, Genetics and Oncobiology; Applied Molecular Biology and Hematology Group; Faculty of Medicine, University of Coimbra, Coimbra, PORTUGAL, ⁵Radiochemistry Department, NECSA, Pretoria, SOUTH AFRICA, ⁶Centre of Molecular and Environmental Biology, School of Sciences, University of Minho, Braga, PORTUGAL, ⁷Department of Internal Medicine, University of Pretoria, Pretoria, SOUTH AFRICA.

Introduction and Aim: Previous *in vitro* studies with $^{99\text{m}}\text{Tc}$ -PEI-MP (polyethyleneiminomethyl phosphonic acid) using a human cell line of transitional cell carcinoma of the bladder, demonstrated the affinity of PEI-MP to bladder cancer cells, revealing that $^{99\text{m}}\text{Tc}$ -PEI-MP could be an excellent agent for imaging *in vivo*. The aim of this work was to explore *in vivo* the potential of $^{99\text{m}}\text{Tc}$ -PEI-MP for diagnosis of bladder cancer. Material and Methods: The radiochemical purity of $^{99\text{m}}\text{Tc}$ -PEI-MP was evaluated hourly until 5 hours after the radiolabelling, using ascendant thin-layer chromatography (ITLC-SG/acetone and Whatman 3MM/citrate buffer). The *in vivo* studies were performed using 2 groups

of balb/c nu/nu mice without tumour and other 2 with xenografts of bladder carcinoma, injected with ^{99m}Tc -PEI-MP or ^{99m}Tc -Perthchnetate. After injection, were acquired dynamic (60 images/10 seconds each) and static images (10 minutes each, every 30 minutes until 120 or 240 minutes). For biodistribution proposes, mice were euthanized 120 and 240 minutes after injection and organ samples were weighted and counted in a well-counter to obtain percentage injected activity per gram of organ. The ratios tumour/muscle, tumour/bladder, tumour/liver, tumour/lung and tumour/bone were determined considering the origin of the bladder cancer and the target organs of distant metastasis. Results: The images and biodistribution studies demonstrated the uptake of ^{99m}Tc -PEI-MP by the kidneys and bladder. Also it was verified the uptake by the lungs. The biodistribution studies demonstrated the uptake by the liver, gallbladder and bilis indicating other route of excretion. It was verified the uptake by the xenograft of bladder carcinoma in the images and biodistribution studies. Tumour/muscle ratio was >1 for ^{99m}Tc -PEI-MP, but tumour/bladder, tumour/liver, tumour/lung and tumour/bone ratios were significantly <1 . Conclusions: ^{99m}Tc -PEI-MP is mainly excreted through the renal system, and a small part through the hepatobiliary system. The retention in the lung may be related with the large size of the complexes, being trapped in the blood capillaries. The uptake by the xenograft of bladder carcinoma demonstrated the affinity of PEI-MP by bladder cancer cells, and may be also related with the enhanced permeability and retention effect. The tumour/muscle ratio >1 may be an advantage for imaging with ^{99m}Tc -PEI-MP to determine the muscle invasiveness of the bladder cancer. The tumour/bladder, tumour/liver, tumour/lung and tumour/bone ratios <1 , theoretically would indicate that the tumour and metastases would appear as could lesions and possible to identify in the images with ^{99m}Tc -PEI-MP.

EP-31 – Sunday, October 16, 2016, during Exhibition hours, e-Poster Area

M2M: Radiometals

EP600

Performance evaluation for stable adsorbent in acidic eluent as a $^{68}\text{Ge}/^{68}\text{Ga}$ generator column material

J. Lee^{1,2}, J. Park¹, M. Hur¹, S. Yang¹, K. Yu³, S. Kim²; ¹korea atomic energy research institute, Jeollabuk-do Jeongeup-si, KOREA, REPUBLIC OF, ²Dongguk University-Gyeongju, Gyeongju, KOREA, REPUBLIC OF, ³Dongguk University-seoul, Seoul, KOREA, REPUBLIC OF.

Aim The adsorbent is the key component for radioisotope generator column system. Especially inorganic ion-exchangers such as amorphous zirconium phosphate (am-ZrP) were studied extensively for the application to the adsorption and desorption of $^{68}\text{Ge}/^{68}\text{Ga}$, due to their selectivity for the specific ions, acid resistant and radiation stabilities. In this study, various zirconium phosphates (ZrP) were synthesized to select acid resistant column material. **Materials and methods** Various ZrP derivatives were prepared using a common sol-gel and hydrothermal method. ZrP-1 was synthesized with 50 mL of 3 M zirconium (IV) propoxide solution and 100 mL of 5 wt% phosphoric acid then stirred for 20 h at room temperature. ZrP-2 was obtained in addition with sodium hydroxide based on solution of ZrP-1 as the following procedure. 5 mL of a 0.1 M NaOH solution was added to the ZrP-1 suspension. Crystalline ZrP-3 and ZrP-4 were prepared from ZrP-1 by refluxing and calcination at 450 °C for 24 h. The SEM-EDX was used in order to observe the morphology of ZrPs at the submicroscale. The crystal structure was measured with X-ray diffraction. N_2 gas adsorption and desorption were obtained using the BET. Finally, hydrodynamic size and zeta-potential of ZrPs were measured in 0.1N-HCl aqueous solution by Zeta-sizer. The stability of the ZrPs was evaluated in 0.1N-HCl aqueous solution as the acidic eluent.

The adsorption and desorption of ^{68}Ge & ^{68}Ga measured using the acid resistant am-ZrP by chromatography method. **Results and Conclusion** Am-ZrP and crystalline-ZrP were prepared as column materials with either sol-gel method or hydrothermal process to evaluate as $^{68}\text{Ge}/^{68}\text{Ga}$ generator column material. Am-ZrP showed good performances in stability, surface area as well as weight loss test. Am-ZrP also had the acceptable features in adsorption and desorption ability of Ga-68 $>70\%$ elution yield and Ge-68 $<10^{-3}\%$ breakthrough. This am-ZrP column material has a high potential as a $^{68}\text{Ge}/^{68}\text{Ga}$ generator adsorbent.

EP601

Preparation and preliminary evaluation of ^{90}Y -tropolonate-Lipiodol as a potential radiopharmaceutical for hepatocellular carcinoma therapy

N. Lepareur^{1,2}, J. Edeline^{1,2}, N. Noiret^{3,4}, V. Ardisson^{1,2}, E. Garin^{1,2}; ¹CLCC Eugene Marquis, Rennes, FRANCE, ²INSERM U991, Rennes, FRANCE, ³ENSCR, Rennes, FRANCE, ⁴ISCR UMR CNRS 6226, Rennes, FRANCE.

Aim Hepatocellular carcinoma (HCC) ranks third in terms of cancer mortality worldwide, with an increasing incidence in western countries. Due to often late detection and underlying hepatopathy, it is a pathology for which curative treatment is only accessible to a minority of patients. Radiolabelled Lipiodol has shown promising results for selective internal radiotherapy of inoperable hepatocellular carcinomas. Literature has shown that yttrium-90 is a radionuclide of choice for HCC treatment. We thus propose a new labelling of Lipiodol with yttrium-90 as a potential treatment modality for HCC. **Materials and Methods** Two tropolonate ligands have been investigated, tropolone and 4-isopropyltropolone (β -thujaplicine). Various conditions have been investigated (pH, temperature, reaction time...) to prepare yttrium-90 radiocomplexes based on these tropolonate ligands. Lipiodol labelling yield and *in vitro* stability have been determined by counting of organic and aqueous phases, over a period of 15 days. MTT assay has been done to assess efficacy of the yttrium-90 labelled compound. *In vivo* biodistribution in hepatoma bearing rats has also been investigated. **Results** Two lipid-soluble tropolonate radiocomplexes were successfully prepared and used to label Lipiodol. Preparation is quick and efficient, at room temperature, in just five minutes. These complexes were successfully extracted into Lipiodol. At 72h, 30 to 50% of the activity is released into the aqueous phase, indicating a lack of stability or a lack of lipophilicity of the complexes. *In vivo*, at 72h, the ID/g in the tumour is still $7.54 \pm 4.31\%$ with a 3.3 tumour/healthy liver ratio, indicating a preferential and sustained uptake in the tumour. **Conclusion** A new simple and reliable method for the ^{90}Y -labelling of Lipiodol has been demonstrated. Ligand optimisation is however still necessary to obtain a more stable complex.

EP602

Influence of ethanol on automated radiolabelling using NaCl post-processing

M. Meisenheimer, E. Eppard, S. Kürpig, M. Essler; University Hospital Bonn, Bonn, GERMANY.

Objectiv: Recent studies showed that addin ethanol to the reaction mixture improves radiolabelling with trivalent radiometals in terms of amount of precursor, reaction time, reaction temperature, specific activity and radiolysis. With regard to clinical application this effect is of practical interest in radiopharmacy. The aim of this study was to evaluate if it is possible to combine the positive effect of ethanol especially in terms of radiolysis and amount of precursor to automated systems with NaCl-post processing. **Methods:** ^{68}Ga was obtained from a 1 year old 1.85 GBq

$^{68}\text{Ge}/^{68}\text{Ga}$ -generator (iThemba South Africa). Radiolabelling was performed on an automated Ga-labelling cassette module (Gaia, Elysia-Raytest, Germany). PSMA-11 from ABX (Radeberg, Germany) and DOTATOC from ANASPECT (USA). The standard labelling protocol was used without modifications. Quality control was performed using radioHPLC and radioTLC. Results: Utilization of additional ethanol on an automated cassette module can be achieved by adding ethanol directly to the buffer solution without further modifications of the standard procedure. It was found that the amount of radiolysis side products was already decreased by adding 5 % ethanol to the reaction mixture. Further increase of the ethanol amount also effects the amount of precursor needed. Conclusion: The utilization of the effect of ethanol decreased radiolysis to a minimum. It was possible to combine the positive effects of ethanol on radiolabelling with the standard labelling procedure of an automated cassette module system. The whole process guarantees safe preparation of highly pure ^{68}Ga -Peptide for clinical application.

EP603

Development of a loop reactor system for the optimization of radiolabeling conditions

D. Szikra^{1,2}, G. Nagy², G. Trencsényi^{1,2}, J. Varga¹, I. Garai^{1,2}; ¹University of Debrecen, Debrecen, HUNGARY, ²Scanomed Ltd., Debrecen, HUNGARY.

Aim: The determination of optimal labeling conditions is important for efficient routine radiopharmaceutical production and for the comparison of newly developed chelators. Manual labeling is time consuming and the reproducibility of the results are often low. A capillary system was built to enable the fast optimization of labeling conditions of various chelators with ^{68}Ga and ^{44}Sc . It was designed to handle small (10 μl) reagent volumes for scouting experiments and to be able to scale up to several hundred microliters for production. **Materials and methods:** The system consists of three electronically actuated HPLC valves interconnected with teflon capillaries and controlled by an Arduino Mega card. The liquid is moved by the aid of a double syringe pump. The reagents are coinjected into a heated PEEK loop and - after the predetermined reaction time - injected onto a HPLC column for analysis or purification. **Results:** The dependence of RCY on pH and chelator concentration was determined for various chelators (DOTA, NOTA, NOPO) labeled with ^{68}Ga and ^{44}Sc . The effects of temperature and reaction time was also studied. $^{44}\text{Sc}^{3+}$ and $^{44}\text{ScDOTA}$ was separated on a reversed phase column, using 0.01 M oxalic acid eluent. DOTA could be labelled with ^{44}Sc in ammonium acetate buffer at pH 3 - 4 down to 3 micromolar chelator concentration.

EP604

Separation study of scandium radionuclides from excess of calcium

D. Pawlak, L. J. Parus, T. Dziel, P. Gamuszek, R. Mikołajczak; National Centre for Nuclear Research Radioisotope Centre POLATOM, Otwock, POLAND.

Introduction. Scandium is a chemical element with only one naturally occurring isotope of atomic mass 45, one +3 oxidation state and chemistry similar to lanthanides. ^{47}Sc could be used for therapy while ^{43}Sc and ^{44}Sc with the half-lives of 3.89h and 3.93h, respectively, longer than that of ^{18}F and ^{68}Ga , might be advantageous in diagnostic imaging. They can be produced in a cyclotron by reactions: $^{44}\text{Ca}(p,n)^{44}\text{Sc}$, $^{40}\text{Ca}(\alpha,n)^{43}\text{Sc}$, $^{43}\text{Ca}(p,n)^{43}\text{Sc}$ and $^{42}\text{Ca}(d,n)^{43}\text{Sc}$. Herein we present separation of the microgram quantities of Sc from milligrams of Ca using the commercially available resin DGA (Triskem International) which we proved earlier to separate Sc/Ti [1] pair and was used for separation of Ca/Sc [2]. **Methods**The studies were carried out using the 10 mL solutions containing 20 mg of Ca and 0.3, 2.3 or 10 μg of Sc and tracer amounts of ^{45}Ca

(600kBq) and ^{46}Sc (50kBq). Each solution was introduced on a column containing 100 mg of DGA resin with flow rate from 0.4 to 1.0 mL/min. The column was washed with 5 ml of 5 M HNO_3 to remove calcium and finally scandium was eluted with 10 mL of 0.1 M HCl or 0.15 M NaCl or 1:1 (v:v) mixture of 0.15 M NaCl and 0.3 M ascorbic acid. The contents of ^{46}Sc and ^{45}Ca were measured in each collected fraction. Results For all eluents used the recovery of scandium was high and amounted to $92.95 \pm 3.52\%$ for 0.1 M HCl, $81.15 \pm 4.65\%$ for 0.15 M NaCl and $85.59 \pm 4.02\%$ for a NaCl/ascorbic acid mixture. There was no significant effect of flow rate on the recovery of scandium or elution profile. However, for higher amount of scandium the elution volume was smaller. The content of ^{45}Ca in all scandium fractions was below detection limit (approx. 100 Bq) corresponding to the calcium content of less than 3 ppm. **Conclusion**The DGA resin seems to be promising for separation of Sc from Ca. The preliminary results obtained using mixture $\text{Ca}^{45}\text{Ca}^{46}\text{Sc}$ need to be verified on cyclotron irradiated targets. This work was supported by National Centre for Research and Development from public funds, realized within the Applied Science Program NCBiR No. PBS3/A9/28/2015 Reference 1. Pawlak D. et al. 2010 in ISBN 978-88-89884-14-0 2. Muller C. et al. J Nucl Med 2013, 54:2168-2174

EP-32 – Sunday, October 16, 2016, during Exhibition hours, e-Poster Area

M2M: Radiopharmaceuticals - PET

EP605

Accelerating PET tracer development: Establishment of a combinatorial-like, high-throughput development approach using condensation reactions and high-throughput screening

E. Nyberg L'Estrade^{1,2,3}, M. Palner², I. Nyman Petersen¹, S. H. Keller⁴, S. Lehel⁴, B. Dall⁴, J. Langgaard Kristensen¹, M. Erlandsson³, T. Olsson³, G. M. Knudsen², M. M. Herth^{1,2,4}; ¹Department of Drug Design and Pharmacology, Faculty of Health and Medicine, University of Copenhagen, Copenhagen, DENMARK, ²Neurobiology Research Unit, Copenhagen University Hospital, Rigshospitalet, Copenhagen, DENMARK, ³Strålningsfysik, Nuklearmedicinsk Fysik, Skånes Universitetssjukhus, Lund, SWEDEN, ⁴Department of Clinical Physiology, Nuclear Medicine & PET, Copenhagen University Hospital, Copenhagen, DENMARK.

The aim The development of new PET-tracers is still largely a “trial-and-error game”. Usually, it takes several years until the ideal tracer candidate is identified. In this work, we aim to accelerate this process combining more combinatorial-like labeling approaches with high-throughput *in vivo* screening. The feasibility of such a combinatorial-like approach was described within our group in 2014¹. In this work, we aim to expand the combinatorial-like labeling approach from reductive aminations to condensation reactions. Furthermore, we aim to establish a high-throughput screening methodology at our high-resolution tomograph (HRRT) and prove its feasibility to perform quantitative PET scans with 4 research animals simultaneously. **Materials and methods** Precursor building blocks and references compounds have already been published. ¹¹C-Labeling was performed at a phenylpiperazine building block and subsequently condensed with a set of halide-oxindole derivatives^{2,3,4,5}. High-throughput *in vivo* screening is conducted in a multi-rodent rack, making it possible to scan four rodents simultaneously. To evaluate the feasibility in respect to quantitative PET measurements of this approach, PET images reconstructed and evaluated towards their accuracy. **Results** The combinatorial-like approach could successfully be applied to condensation reactions. Compared with our previously published labeling strategy, the new strategy showed clear advantages in a preclinical set-up (faster and more efficient). High-throughput *in vivo* scanning using the newly developed multi-rodent rack resulted in satisfactorily PET data

even though a global underestimation of PET activity of $\pm 5\%$ was observed. This set-up allowed us to label and evaluate 4 compounds within one week. Each tracer was evaluated in 2 baseline and 2 blocking experiments. This set-up resulted in an extensive time reduction. **Conclusion** We believe that the proposed development set-up accelerates PET tracer development, at least in this specific synthesis and screening set-up. **References** 1) Herth *et al.*, *RSC Adv.*, 2014, 4: 21347–21350 2) Herth *et al.*, *ACS Chem. Neurosci.* 2012, 3: 1002–1007 3) Herth *et al.*, *J. Med. Chem.* 2015, 58: 3631–3636 4) Volk *et al.*, *J. Med. Chem.* 2008, 51, 2522–2532 5) Volk *et al.*, *J. Med. Chem.*, 2011, 54 (19): 6657–6669

EP606

Comparative studies on ^{64}Cu -complexing modern bifunctional chelator for $\alpha_v\beta_3$ integrin targeting and in vivo cancer imaging

P. T. Huynh¹, S. Sarkar¹, N. Soni¹, Y. S. Ha¹, W. Lee¹, H. Ahn¹, G. I. An², J. Yoo¹; ¹Kyungpook National University, Daegu, KOREA, REPUBLIC OF, ²Korea Institute of Radiological and Medical Sciences, Seoul, KOREA, REPUBLIC OF.

Abstract: Aim: Successful applications of copper radioisotopes towards metal based imaging or therapy have brought copper-based radiopharmaceuticals in focus of various researchers creating a need for the perfect bifunctional chelators (BFCs). An ideal BFC is capable of forming strong conjugation with disease-specific peptides or antibodies, and simultaneously have the ability to form stable complex with the central metal ion. The study presented here measured how the nature of BFCs affects various properties of ^{64}Cu -bioconjugates, ^{64}Cu -BFC-c(RGDyK), starting from its synthesis to biophysical nature, in vivo integrity, biodistribution pattern, or tumor targeting attitude which thereafter revealed the most appropriate chelator for radio-copper based medical applications. **Materials and methods:** ‘Available the best BFCs’, NOTA-Bn-NCS, TE2A-Bn-NCS, CB-TE2A, PCB-TE2A and PCB-TE2A-Bn-NCS was first conjugated with c(RGDyK) and consecutively radiolabeled with ^{64}Cu . All biophysical properties like specific activity, partition coefficient, integrin receptor binding affinity were measured under identical experimental condition for preliminary examination. In vivo stability studies were conducted subsequently in SD rat to evaluate the most robust ^{64}Cu -complex. Finally biodistribution and microPET imaging studies of ^{64}Cu -bioconjugates were accrued in U87MG xenograft tumor model to evaluate the most potent chelator. **Results:** Non cross-bridged chelators were radiolabeled at 50 °C whereas cross-bridged macrocycles required approximately 80 °C for quantitative radiolabeling. Various biophysical properties can provide insights towards the vivo biodistribution pattern and afford good preliminary indications in most of the cases. Current study highlighted that in vivo pharmacokinetics especially tumor targeting efficacy depends on the structural features of the bioconjugates specially the linker, aqueous solubility and in vivo stability of the bioconjugates. High in vivo stability of cross bridged compounds, ^{64}Cu -PCB-TE2A-Bn-NCS-c(RGDyK), ^{64}Cu -CB-TE2A-c(RGDyK) and ^{64}Cu -PCB-TE2A-c(RGDyK) leads to higher tumor uptake of these macrocycles in compare to non-cross bridged compounds. Clearance rate is highly depended on the water solubility of the compounds. The presence of extra NCS functionality in ^{64}Cu -PCB-TE2A-Bn-NCS-c(RGDyK) may provide additional stability, but simultaneously decreases clearance rate and hence not recommended for in vivo applications. For ^{64}Cu -CB-TE2A-c(RGDyK), although at initial time points tumor uptake was noticed to be higher but activity cleared out fast from tumor decreasing tumor to organ ratio. We found cross-bridged bioconjugates with excellent in vivo stability with no linker arm is more potent in designing ideal BFCs. **Conclusion:** In terms of higher tumor uptake and faster clearance from non-targeted organs, ^{64}Cu -PCB-TE2A-c(RGDyK) evolved to be absolutely potent for future peptide based clinical studies.

EP607

Automation of [^{18}F]AIF radiolabeling using a commercially available platform

L. Allott, C. Da Pieve, D. R. Turton, G. Smith; Institute of Cancer Research, Sutton, UNITED KINGDOM.

Background: The aluminium- ^{18}F -fluoride (^{18}F]AIF) method for radiolabelling biologically relevant molecules has generated significant interest owing to the capacity to combine metal-based radiochemistry with the excellent decay characteristics of fluorine-18. Many examples of peptides, proteins and biorthogonal reporters radiolabelled with [^{18}F]AIF methodology can be found in the literature. With translation to clinical application, our study aimed to devise a general method for the automated [^{18}F]AIF radiolabelling of azamacrocyclic-containing molecules (e.g. tetrazines, peptides and small proteins). **Materials and Methods:** The GE Tracerlab FX FN (GE Healthcare platform) was chosen for the study of automated radiochemistry development. The optimisation of the methodology was performed using a NODA containing tetrazine and then applied to a focused group of biomolecules. In a typical production: non-purified ^{18}F [F⁻] target water was diluted in sodium acetate (50 mM, pH 4); reservoir 3 was loaded with a solution containing the precursor (30 nmol), AlCl_3 (26 nmol in 0.5 M sodium acetate, pH 4) and sodium acetate (25 mM, pH 4); reservoir 4 was loaded with an organic co-solvent (1 mL); reservoirs 6 and 9 were loaded with water (5 mL). The buffered ^{18}F [F⁻] solution was transferred into the reactor followed by the addition of reservoir 3 and 4 contents. The reactor was heated to 105°C for 15 min followed by cooling with compressed air to 50°C (ca 3 min). Water was added to the reactor from reservoir 6 to dilute the reaction mixture which was transferred into a holding vessel attached at V12. The system was pressurised to allow slow loading of the reaction mixture (ca 8 mL) onto a pre-equilibrated HLB cartridge (1 mL, 30 mg). The HLB was subsequently washed with water from reservoir 9 and dried under a flow of nitrogen. The cartridge was removed and the pure product eluted by hand in a minimal volume of ethanol (ca 60 μL). **Results:** [^{18}F]AIF radiolabelling was performed using a commercial automated platform with a RCY of 25–46% (decay corrected at end of reaction). Total synthesis time was ca 30 min yielding products with radiochemical purities higher than 98%. **Conclusions:** The automated [^{18}F]AIF radiolabelling of various azamacrocyclic-conjugates was efficiently achieved and can be used to facilitate routine back-to-back production for clinical applications.

EP608

Preparation of ^{68}Ga labelled HBEDCCPSMA in a fully automated system using a cassette based module: our initial experience

C. Capelo, Sr.; IPO Porto, Porto, PORTUGAL.

Aim: During the past few years, the application of ^{68}Ga -labeled peptides has attracted considerable interest for cancer imaging due to the physical characteristics of ^{68}Ga ($t_{1/2}=68$ min, $\beta^+ = 1899$ keV) and the availability of reliable GMP-compliant $^{68}\text{Ge}/^{68}\text{Ga}$ generators. Moreover, the half-life of ^{68}Ga matches the pharmacokinetics of the small PSMA inhibiting peptides. PET imaging of the prostate-specific membrane antigen (PSMA) using [^{68}Ga]Ga-PSMA-HBED-CC has gained highest clinical impact. The aim of this work is to describe the preparation of ^{68}Ga labelled PSMA-HBED-CC using a fully automated cassette based system and report on our initial experience. All patients had an histopathological confirmation of prostate cancer **Material and Methods:** In [^{68}Ga]PSMA-HBED-CC we used a cassette based automated synthesis module (PharmTracer, Eckert&Ziegler); the $^{68}\text{Ge}/^{68}\text{Ga}$ generator (ITG) with nominal activity

of 1.11–1.85 GBq and elution solvent HCl 0.05M. Preconcentration: SCX cartridge, elution with NaCl/HCl mixture (3 ml) Labelling buffer: sodium acetate/hydrochloric acid buffer pH 4.5+/-0.1 (400 µl) Precursor amount: 10–20 µg Reaction time/Incubation: 5 min at 95°C at pH ~4 Purification by SepPak C-18 light, product elution from C18 cartridge with ethanol/water solution (50%) into product vial and dilution with saline PET/CT imaging: PSMA PET/CT images were obtained immediately after injection during 10 min (3 min/bed/1 bed) and 60 min after injection 3 min/bed/7beds with a dose of 120–185 MBq. The images were acquired with a *Siemens Biograph 6 PET/CT*. **Results:** Between October 2015 and April of 2016, we performed 16 synthesis of [⁶⁸Ga]Ga-PSMA-HBED-CC. We had better results achieving higher specific activity using precursor amount > 10 µg, the synthesis time was 14+/-3min. The success rate of the synthesis was very high (two of them failed). We performed PET/CT imaging in 44 patients and we could detect PSMA-positive lesions suspicious of recurrence in 26 of 44 patients with biochemical relapse after radical prostatectomy. **Conclusions:** Early detection of metastases or recurrent prostate cancer is very relevant in terms of clinical staging, prognosis and therapy management and the use of [⁶⁸Ga]Ga-PSMA-HBED-CC seems to be very promissory in this setting. The radiosynthesis of this radiopharmaceutical as described it prove to be a fast, reliable and robust method, with high reproducibility, which make it suitable for clinical use in Nuclear Medicine.

EP609

Development and Optimization of A Novel Automated Loop Method for Production of ¹¹C-Nicotine for Pharmacokinetics and PET Imaging Studies

K. Kumar, V. Gaja; Laboratory for Translational Research in Imaging Pharmaceuticals, The Wright Center of Innovation in Biomedical Imaging, Department of Radiology, The Ohio State University, Columbus, OH, UNITED STATES.

Aim: The objective of the present study was to develop and optimize a novel automated loop method for production of ¹¹C-Nicotine for Pharmacokinetics (PK) and Positron Emission Tomography (PET) imaging studies for uptake of nicotine in the human brain. **Materials and Method.** The ¹¹C-Carbon Dioxide, ¹¹CO₂, was produced by the ¹⁴N (p,α)¹¹C reaction using a GE PETtrace 880 cyclotron, 16.5 MeV, 25 uA beam for 30 minutes. In the automated synthesis process, the ¹¹CO₂ was trapped in a stainless steel coil at -180°C, converted into ¹¹C-methane by using H₂/Ni catalyst at 400°C, and finally ¹¹CH₄ was passed through an I₂ oven at 750°C to produce ¹¹CH₃I. The Porapak column adsorbed ¹¹C-methyl iodide was transferred into a stainless steel loop loaded with 2 mg (+) normnicotine dissolved in 1:1 DMF:DMSO (100 µL) mixture. The loop was heated at 100°C for 5 min, reaction mixture was cooled to room temperature, and injected into a semi-preparative reversed-phase (RP) HPLC system to remove unreacted ¹¹CH₃I and (+) normnicotine. The final product was analyzed by a RP-HPLC method. **Results and Conclusions.** In the present work, gas-phase produced ¹¹CH₃I precursor was used instead of ¹¹C-Formaldehyde or ¹¹CH₃I produced by the lithium aluminum/HI method. This method did not require using a base which resulted a clean reaction. The reaction conditions were optimized by varying purity and flow of the gases, reaction times and temperature. An efficient reversed-phase semi preparative HPLC method was developed for selectively removing ¹¹CH₃I and the starting material, (+) normnicotine. Additionally, a reversed-phase HPLC method with a shorter run time (<10 minutes) was developed and validated for the analysis of the final product, ¹¹C-Nicotine. Overall radiochemical yield of the reaction (from EOB and decay corrected) was 40% with a radiochemical purity (RCP) >99.9%.

EP610

Engineering and Evaluation of A Novel Antibody Fragment As A Potential PET Imaging Agent in Mice

K. Kumar¹, S. Doll¹, K. Woolum¹, S. Kothandaraman¹, H. Ding¹, M. Tweedle¹, M. Williams¹, N. Long², B. Sullivan², T. Magliery², E. Martin, Jr.³; ¹The Wright Center of Innovation in Biomedical Imaging, Department of Radiology, The Ohio State University, Columbus, OH, UNITED STATES, ²Department of Chemistry and Biochemistry, The Ohio State University, Columbus, OH, UNITED STATES, ³Department of Surgery, The Ohio State University, Columbus, OH, UNITED STATES.

Aim. The full size humanized antibody 3E8 binds tightly to the adenocarcinoma marker TAG-72, a mucinous glycoprotein, but is not suitable for PET and SPECT imaging due to slow blood clearance. The objective of the present study was to engineer, radiolabel with ¹²⁵I and ¹²⁴I, and evaluate a novel antibody fragment (3E8.G₄S) with a weighted average M.W. of 68 kD as a potential PET imaging agent. Evaluation parameters involved in this study were: pharmacokinetics, bio distribution, and PET imaging in mice. **Materials and Method.** The novel antibody fragment, 3E8.G₄S, was prepared by shortening the linker between the 3E8 variable domains from a previously constructed scFv. The engineered antibody fragment was characterized by gel permeation and the size-exclusion chromatography. Radiolabeling with ¹²⁵I (for pharmacokinetics studies) and ¹²⁴I (for bioD and PET/CT studies) was accomplished using the Iodogen method, the radiolabeled materials were purified by a PD-10 column, and analyzed for radiochemical purity and for stability using paper and size-exclusion chromatographic methods. All pharmacokinetics studies were conducted on normal balbC mice and bio distribution and micro PET/CT imaging studies were conducted on balbC nude mice bearing TAG-72 expressing LS174T human colon carcinoma xenograft tumors. **Results and Conclusions.** Gel Permeation and Size-Exclusion chromatography data showed that the fragment exists as a mixture of diabody and higher oligomers (i.e., mixture of tri- and tetra-body). Enriched diabody and oligomeric fractions were isolated. The fragment mixture, the enriched diabody, and the oligomer were radiolabeled. Stability of the radiolabeled fragment was assessed from 2–8°C storage for 50 days, and the fragment was found to be remarkably stable. Blood clearance kinetics of the ¹²⁵I labeled the fragment, the enriched diabody, and the oligomer showed fast clearance, almost complete within 24 h. The order of clearance rates of the three molecules was: enriched diabody > fragment mixture > oligomer. Bio distribution studies using ¹²⁵I labeled enriched diabody and fragment showed significant uptake in the tumor, (2.10±0.66%, at 44 h, n=3, for the enriched diabody) and (6.61±0.89%, at 48 h, n=5 for the fragment). PET imaging studies of the tumor bearing mice (n=3) using ¹²⁴I labeled fragment were conducted at 22 and 46 h.

EP611

Biodistributions of Copper-61 labelled Silica Nanospheres using NOTA, DOTA & SAR Bifunctional Chelators

A. H. Asad^{1,2}, L. Morandau¹, S. V. Smith¹, N. Zia³, P. S. Donnelly³, R. I. Price^{1,4}; ¹Sir Charles Gairdner Hospital, Perth, AUSTRALIA, ²Physics & Astronomy, Curtin University, Perth, AUSTRALIA, ³School of Chemistry and Bio21 Molecular Science and Biotechnology Institute, The University of Melbourne, Melbourne, AUSTRALIA, ⁴School of Physics, University of Western Australia, Perth, AUSTRALIA.

Aim: To evaluate the biological pathway of Cu-61 labelled silica nanospheres (Si NS) in healthy nude mice via µPET imaging and biodistribution. The new sarcophagine MeSar-Ph-NCS, NOTA-NCS and DOTA-NCS were conjugated the nanospheres and then radiolabelled with ⁶¹Cu. Methods: Cu-61 was produced from the ⁶⁴Zn(p,α)⁶¹Cu reaction and converted into ⁶¹Cu(OAc)₂, pH 6.5, followed by radiolabelling

of the conjugated MeSar-Ph-NCS-Si NS for 2 h at 37 °C. The same conditions were used for the other BFCs. The radiolabelled Si NS were then washed repeatedly with 0.1 NaOAc (pH 6.5) to remove any free ^{61}Cu and resuspended in the same buffer for injection in animals. Results: Radio-TLC and gamma counting confirmed the successful radiolabelling of BFC-NCS-Si NS with ^{61}Cu after washing step. *In vitro*; ^{61}Cu -radiolabelled BFC-NCS-Si NS were all found to be stable in saline (> 93% ; 4 h). However, incubation of the ^{61}Cu labelled BFC-NCS-Si NS in FBS at 37°C all showed a significant decrease of radiochemical purity to 84% at 4 h. Then mice were injected with Cu-61 labelled Si NS via retro-orbital and $^{61}\text{CuCl}_2$ was used the control. Animals were imaged at 1 and 4 then dissected and the organs counted in a gamma counter. The majority of the radioactivity was found in the liver and spleen; values of $(26.6 \pm 0.6[\text{SD}] \% \text{ID/g})$ $(12.3 \pm 3.1 \% \text{ID/g})$ respectively via μPET ROI analysis. When dissected organs were analysed the activities present were considerably higher. The liver was measured at 38.5 ± 8.1 , 48.1 ± 4.5 and $44.5 \pm 6.0 \% \text{ID/g}$ for ^{61}Cu -MeSar-Ph-NCS-Si NS, ^{61}Cu -NOTA-NCS-Si NS and ^{61}Cu -DOTA-NCS-Si NS, respectively. While the spleen was measured at 43.3 ± 9.3 , 63.6 ± 4.1 and $70.2 \pm 8.8 \% \text{ID/g}$ for ^{61}Cu -MeSar-Ph-NCS-Si NS, ^{61}Cu -NOTA-NCS-Si NS and ^{61}Cu -DOTA-NCS-Si NS, respectively. Each group of ^{61}Cu -radiolabelled BFC-NCS-Si NS plus controls ($^{61}\text{CuCl}_2$) were also evaluated by quantitative μPET imaging at 1h and 4h post-injection. The results were broadly similar between 1h and 4h time-points, particularly in liver and spleen. Conclusion: The novel sarcophagine MeSar-Ph-NCS conjugated to Si NS and labelled with Cu-61 for the first time. The behaviour of this radiotracer was compared with Si NS labelled using NOTA and DOTA. Overall biological profiles were similar. However, the spleen showed substantially higher accumulation of Cu-61 when radiolabelling with NOTA and DOTA compared to the new cage compound suggest the new compound is better suited for nanospheres labelling.

EP612

A Novel Cancer Imaging Tracer for Fumarate Respiration

Y. Nakagami^{1,2}, D. Kano¹, M. Kusumoto¹, Y. Kojima¹; ¹National Cancer Center, Chiba, JAPAN, ²Yokohama City University, Yokohama, JAPAN.

Aim: In recent years, cancer cells have been making the fumarate respiration does not in the normal cells of the mammalian cells are reported. Visualization of the fumarate respiration should be promising a new PET probe based on unique accumulation mechanism. In this study, we aimed to develop new imaging tracer for the fumarate respiration, ^{11}C -labeled fumaric acid was synthesized. **Materials and Methods:** Riss et al. elaborated novel carboxylation methods for the synthesis of ^{11}C -labeled carboxylic acids using boronic acid esters. In this approach, boronic acid esters are quite stable to air and moisture and therefore are easily handled and stored. Consequently, it is relevant to full automated PET tracer synthesis. The synthesis of ^{11}C -labeled fumaric acid was performed as follows. The precursor compound was prepared by copper-catalyzed mono-boration of ethyl propiolate. Radiosynthesis was achieved by copper-catalyzed ^{11}C carboxylation of boronic acid ester. No-carrier-added $^{11}\text{CO}_2$ was produced on a cyclotron. Production of ^{11}C -fumaric acid was performed at the automated multipurpose synthesizer. Cyclotron-produced $^{11}\text{CO}_2$, trapped on a column cooled with liquid N_2 , was released by purging the column with N_2 gas at room temperature and directed into a reaction vessel containing (*E*)-ethyl 3-(4,4,5,5, -tetramethyl-1,3,2-dioxabolan-2-yl) acrylate, CuI, Kryptofix-2.2.2, KF and TMEDA in DMF. The reaction mixture was, heated at 100 degrees centigrade for 5 minutes, and then rapidly cooled to room temperature, and then quenched with formic acid. The crude product was directed with water. Then the diluted solution was loaded onto two Sep-Pak Plus PS-2 cartridges connected in series. The cartridges were washed with water and the yielded ester was eluted with MeCN to second reaction

vessel. To the reaction vessel was added aqueous NaOH and heated at 80 degrees centigrade for 2 minutes. After cooled to room temperature, the reaction mixture was neutralized with KH_2PO_4 buffer. The crude ^{11}C -Fumaric acid was then loaded onto a semi-preparative HPLC column. The HPLC fraction containing ^{11}C -Fumaric acid was collected into product vial. The product obtained as an aqueous solution which can be administered directly. **Results and Conclusions:** The overall reaction takes about 25 minutes from the end of bombardment. The optimization of the reaction conditions resulted in radiochemical yield (4.2–8.6 percents). No radiochemical impurities were detected by HPLC. Biodistribution in tumor-bearing mice were examined. Furthermore, *in vivo* images were obtained using a small animal PET scanner. ^{11}C -Fumaric acid showed high uptake in the tumor tissue.

EP613

Evaluating A Thin Layer Chromatography Method To Separate ^{18}F -choline Of Its Main Metabolite ^{18}F -betaine

M. VILLAR¹, M. TOSCANO¹, M. GALMÉS², G. BARCELÓ³, F. VEGA¹, C. PEÑA^{1,4}, S. RUBÍ^{1,4}; ¹HOSPITAL SON ESPASES, PALMA DE MALLORCA, SPAIN, ²HOSPITAL QUIRONSALUD PALMAPLANAS, PALMA DE MALLORCA, SPAIN, ³INSTITUTO DE INVESTIGACIÓN SANITARIA DE PALMA (IDISPA), PALMA DE MALLORCA, SPAIN, ⁴INSTITUTO DE INVESTIGACIÓN SANITARIA DE PALMA (IDISPA), Palma de mallorca, SPAIN.

^{18}F -choline is a PET radiotracer used in diagnosis of prostate and brain neoplasms. After its intravenous injection, radiolabelled choline is oxidized by choline oxidase into its main plasma metabolite, ^{18}F -betaine. If PET quantification through kinetic modelling of ^{18}F -choline uptake is intended, the plasma input time-activity-curve of the parent tracer must be obtained, i.e., the fraction of the total plasma radioactivity corresponding to the nonmetabolized ^{18}F -choline at each time point has to be known. Hence our aim was to develop an easy-routine Thin Layer Chromatography (TLC) method to separate and quantify the relative fractions of ^{18}F -choline and ^{18}F -betaine. **MATERIALS AND METHODS** As a first step, we optimized a TLC-system to separate a cold standard solution of choline and betaine, using iodine vapor staining as visualization method. Based on previous knowledge about separation of these quaternary ammonium compounds, we tested Silica-Gel-60(SG60) and Aluminum-oxide as layers, and four eluents: (1)MeOH/0.5%NaCl/NH₃, (2)MeOH/Acetone/HCl, (3)MeOH/NH₃ and (4)MeOH/H₂O. We determined the R_f (retention factor) values for choline and betaine, after which SG60-MeOH/NH₃ was selected as the most suitable system because of its resolution. Thereafter, we proceeded to apply this TLC-system to radioactive ^{18}F -choline/ ^{18}F -betaine samples. We obtained ^{18}F -betaine through the chemical oxidation of an ^{18}F -choline sample with potassium permanganate and, at different incubation time points, aliquots were spotted on TLC plates for its analysis on a radio-TLC-scanner. The same were repeated diluting the oxidized samples in an acetonitrile-deproteinized plasma matrix before their TLC-analysis, in an attempt to simulate the *in-vivo* blood sampling conditions. **RESULTS** The R_f-values for choline and betaine cold standards on the selected TLC-system were R_f=0 and R_f=0.77 respectively. Radiochromatograms of ^{18}F -choline/ ^{18}F -betaine oxidation solution showed two separated and well-defined peaks, one at the origin (R_f=0) and the other one at R_f=0.82-0.89, both of them fairly in agreement with which had been previously observed in the TLC-analysis of cold standards. Radioactivity proportion of the first peak (^{18}F -choline) on radiochromatograms at 5, 20, 40 and 60 minutes oxidation times was 57%, 46%, 32% and 25% respectively, while the second peak (^{18}F -betaine) increased accordingly throughout the incubation period. Comparable results were obtained when the method was applied to ^{18}F -choline/ ^{18}F -betaine samples previously diluted in plasma matrix. **CONCLUSION** An easy-routine TLC method to separate ^{18}F -choline from ^{18}F -betaine and to measure their relative fractions is developed. The presented method is

suitable for being implemented in a conventional Radiopharmacy Unit and it may be a useful tool for metabolite correction in ^{18}F -choline-PET quantification.

EP614

Preparation of 18F-Fluoromethylcholine in a fully automated radiochemical synthesizer: a tertiary university hospital experience

E. KARAYEL¹, H. Pehlivanoglu¹, A. Aygün¹, R. Tutar², A. Kurt¹, M. Ocak³, L. Kabasakal¹, K. Sönmezoglu¹; ¹Department of Nuclear Medicine, Cerrahpasa Medical Faculty, İstanbul University, ISTANBUL, TURKEY, ²Department of Physicochemistry, Engineering Faculty, İstanbul University, ISTANBUL, TURKEY, ³Department of Pharmaceutical Technology, Pharmacy Faculty, İstanbul University, ISTANBUL, TURKEY.

Purpose: Choline is a quaternary precursor for the biosynthesis of phospholipids, which are essential components for all membranes. Within the cell, choline can be phosphorylated, acetylated or oxidized. The phosphorylation of choline is catalyzed by the enzyme choline kinase. Phosphorylcholine is an intracellular storage pool of choline and is further incorporated into phosphatidylcholine (Lecithin) a major phospholipid of all membranes. Tumor cells with high proliferation rate will have high uptake of choline to keep up with increased demands for the synthesis of phospholipids. Therefore, 18F Fluoromethylcholine was introduced as a potential PET tracer to image various cancers. We present our preliminary results of synthesizing and quality control by using a fully automated radiopharmaceutical synthesis device at Cerrahpasa Medical Faculty, Department of Nuclear Medicine, İstanbul since May 2015. **Materials and Methods:** The radiosynthesis was performed by using a fully automated synthesizer (Trasis, all-in-one, Belgium). Automated synthesis of fluorocholeline includes two synthetic steps: fluorination and purification. Radiochemical purity is determined by ITLC using Acetonitrile/NaCl (1:1) and RP-HPLC (Shimadzu) using 9mM H₂SO₄. The residual solution impurities are determined by Gas Chromatography (GC-Shimadzu). **Results:** The radiochemical impurity was higher than 95% by ITLC and RP-HPLC. The residual solution impurities were as follows: N,N-Dimethylformamide (DMF) <880ppm, Acetonitrile (ACN) <410 ppm, Dimethylaminoethanol (DMAE) <300 ppm, Ethanol <5000 ppm. Non-decay corrected yield was higher than 22%. **Conclusion:** The synthesiser and described methods allow us a satisfactory automated preparation of 18F Fluoromethylcholine with desired QC parameters that is a suitable radiopharmaceutical for human use.

EP615

Microwave-assisted ^{68}Ga -labeling of PSMA^{HBED-CC}

S. Pfaff^{1,2}, E. Schaier^{1,2}, M. Hartenbach¹, M. Mitterhauser^{1,3}, M. Hacker¹, W. Wadsak^{1,2}; ¹Department of Nuclear Medicine, Medical University of Vienna, Vienna, AUSTRIA, ²Department of Inorganic Chemistry, University of Vienna, Vienna, AUSTRIA, ³LBI for Applied Diagnostics, Vienna, AUSTRIA.

Aim: ^{68}Ga labeled radiotracers have gained remarkable interest during the last decade due to the good availability of this PET nuclide. As a result of the development of various new ^{68}Ga labeled radiotracers, several devices for their production have emerged as well. The motivation behind developing new synthesizers is increasing the efficiency in terms of radiochemical yield and reaction time. One technique for enhancing the conversion is microwave irradiation which enables faster and more efficient heating compared to the conventional heaters and moreover, impedes a temperature gradient from the surface of the vessel to the internal reaction mixture. Accordingly, microwave supported ^{68}Ga incorporation into DOTATOC was successfully accomplished by Veliky et al. (1). Hence, this study deals with microwave

assisted complexation of $^{68}\text{Ga}^{3+}$ to PSMA^{HBED-CC} and evaluation of the impact on conversion and reaction time. **Materials and methods:** The syntheses of ^{68}Ga -PSMA^{HBED-CC} (precursor PSMA-11 in GMP grade, ABX, Germany) were performed using a microwave synthesizer (petwave, CEM, USA). For pH adjustment a 1.5 M HEPES buffer solution (Sigma-Aldrich, Missouri) was used. $^{68}\text{Ga}^{3+}$ was obtained from a $^{68}\text{Ge}/^{68}\text{Ga}$ -generator (100 mCi, Obninsk, Russia; 50 mCi, GalliPharm, EZAG, Germany) using a fractionated protocol. $^{68}\text{Ga}^{3+}$ complexation was accomplished evaluating different parameters as power (25 W, 50 W, 75 W, 100 W) and precursor concentration in the reaction mixture (0.84 μM and 1.68 μM). The solution was exposed to microwave irradiation until a pre-selected temperature of 95°C was reached. **Results:** Preliminary experiments for a precursor concentration of 0.84 μM and power settings of 25 W, 50 W, 75 W and 100 W showed conversions of 68% (n=3), 59% (n=3), 61% (n=2) and 63% (n=2) could be obtained, respectively, within less than one minute. Likewise, the same conditions were tested for a concentration of 1.68 μM , with respective conversions of 86% (n=2), 95% (n=3), 96% (n=3) and 97% (n=3). **Conclusion:** Microwave heating is feasible for ^{68}Ga -labeling of PSMA^{HBED-CC} and achieves a striking conversion within a few seconds, which could make it an attractive tool for PET Tracer production. Especially the dramatically shortened reaction time gives reason to evaluate this approach further for clinical applications. (1) Veliky, I. *et al. Bioconjugate Chem.* 15, 554–560 (2004)

EP616

Evaluation of a novel radiolabeled anti-fibroblast activation protein (FAP) antibody fragment as a PET imaging agent

M. Martic¹, D. T. Ho², A. Lipman², A. M. Wu³, S. Chandra⁴; ¹Novartis AG, Basel, SWITZERLAND, ²ImaginAb Inc., Inglewood, CA, UNITED STATES, ³David Geffen School of Medicine at UCLA, Los Angeles, CA, UNITED STATES, ⁴Novartis Institute for Biomedical Research, Cambridge, MA, UNITED STATES.

Objectives: The objective of this work was to evaluate a novel fibroblast activation protein (FAP)-specific antibody fragment as a potential FAP imaging agent in a tumor xenograft-bearing mouse model. **Methods:** A panel of anti-FAP antibody fragments was isolated using phage display technology and screened by ELISA for positive FAP binding and lack of binding to dipeptidyl-peptidase 4 (DPP4). Selected clones were further engineered to support site specific radiolabeling. A single fragment with the most favorable properties was selected for subsequent *in vitro* and *in vivo* work. *In vitro* binding assessment was performed by ELISA on both FAP positive (LOX-IMVI) and non-expressing (Daudi) cell lines. FAP on- and off-rates were determined by Surface Plasmon Resonance (SPR). The antibody fragment was radiolabeled with Zr-89 via a site specifically conjugated bi-functional chelate, or I-124 (non-site specific labeling). PET imaging of isoflurane anesthetized mice carrying a single subcutaneous tumor xenograft (shoulder region) was performed at 0-2 hrs (dynamic scan), 4 (6), 8 and 20 hrs p.i. Following each PET scan, a 10 min CT scan was performed for anatomical reference. Biodistribution was performed at 8 hrs p.i. (Zr-89) and at 20 hrs p.i. (I-124). **Results:** 99% pure engineered antibody fragment was murine/human cross reactive with the binding affinity $K_D = 0.8\text{nM}$. The data show only a minor impact on FAP binding, depending whether site specific (Zr-89) or non-site specific radiolabeling (I-124) was performed. Radiolabeling efficiency with Zr-89 was 98-99% and radiochemical purity of the injected compound was 99.9%. For I-124, radiolabeling efficiency was 83% and radiochemical purity was 97%. The tumor-to-blood ratio at 8 hrs p.i. was approx. 4:1 for Zr-89 and approx. 1:1 for I-124 labeled variants. FAP+:FAP- tumor ratio at 8 hrs p.i. was approx. 2.5:1 for Zr-89 and approx. 5:1 for I-124 labeled variants. Results show predominantly renal excretion and rapid blood clearance with $t_{1/2} = 0.2$ hrs. Prior to translating this novel imaging tracer to humans, studies in additional FAP-relevant animal models will be conducted.

EP617**Sterility test of [18F]-Fluodeoxyglucose automatic infusion systems: Intego® (Medrad) and Posijet® (Lemer Pax)**

M. Lefebvre¹, C. Bianchi¹, C. Louet¹, C. Lemarie², O. Morel³, O. Couturier⁴, A. Vanniet-Cahouet¹, F. Lacoueille⁴; ¹CHU Angers Department of pharmacy, Angers, FRANCE, ²CHU Angers Department of bacteriology, Angers, FRANCE, ³ICO Paul Papin Angers Department of nuclear medicine, Angers, FRANCE, ⁴CHU Angers Department of nuclear medicine, Angers, FRANCE.

Intego and Posijet are PET (positron emission tomography) automated systems used for the fractionation and injection of [18F]-Fluodeoxyglucose (FDG). Fractionations are realized from a multidose vial, in a shielded compartment within the automated system and stored until the end of its use. Two sterile kits are needed for the fractionation and injection of FDG to the patient: A mother solution kit (one kit per vial) allowing to get the correct FDG activity and a single patient kit (one kit per patient) with or without 0,22 µm filter, linking the mother solution kit to the patient catheter. The aim of this work was to validate the aseptic conditions during the fractionation and the injection process for both automated systems. The microbiological controls of the samples were performed at two levels. Each day, FDG residual solution was withdrawn (1–4mL) under a laminar flow hood (n=25 samples). Others samples were realized by purging mother solution kits' catheter (n=20). All samples were inoculated into paediatric haemoculture vials. After the radioactive decay, all haemoculture vials were transmitted to bacteriology laboratory, for a ten days incubation. In parallel, the FDG vials utilization datas were collected in order to identify potential causes of contamination (time of utilization, quantity of injected patients, manual dilution of the vial, incident). During the study, an average of 6 patients (minimum 3, maximum 9) were injected per multidose vial. In order to decrease volumic activity (MBq/mL) for the first injected patients a manual dilution of FDG vials prior fractionation and injection by the posijet system was needed in 78% of the case. This dilution step can be a potential contamination source. The average time of utilization of a FDG vial were 214 min (± 60 min) and 198 minutes (± 44 min) for the Posijet and Intego systems respectively. No contamination due to aerobic germ was found on FDG vials originating from Posijet (n=12) or Intego (n=13), neither on mother solution kits used for Posijet (n=10) and Intego (n=10) systems. Our results show the maintaining of sterility of FDG solution in automatic injector environment and in medical devices needed for FDG administration.

EP618**Production of ⁶⁸Ga-DOTATOC, ⁶⁸Ga-DOTANOC and ⁶⁸Ga-PSMA-HBED-CC with an automated multi-purpose synthesis module**

S. Migliari¹, A. Sammartano¹, M. Scarlattei¹, G. Baldari¹, C. Cidda¹, G. Serreli², O. Ortenzia², C. Ghetti², L. Ruffini¹; ¹Nuclear Medicine and Molecular Imaging Department, University Hospital, Parma, ITALY, ²Medical Physics Unit, University Hospital, Parma, ITALY.

Development of new ⁶⁸Ga-based agents for in vivo visualization of specific molecular targets, along with important technical advances in isotope production and their labeling method is one of the driving forces of the expansion of clinical PET. Ga-68 has gained attention as one of the ideal research based PET radioisotopes because of on-site production from the ⁶⁸Ge/⁶⁸Ga generator and the automated synthesis systems of Ga-68 conjugated probes. These automated systems have advantages over the manual methods which have resulted in their increasing installation in radiopharmacies, but researchers are difficult to adapt them to synthesize their own radiopharmaceuticals. The aim was to investigate the flexibility and efficiency in synthesizing three different ⁶⁸Ga-radio-pharmaceuticals (⁶⁸Ga-DOTATOC, ⁶⁸Ga-DOTANOC and ⁶⁸Ga-PSMA-HBED-CC) using a unique multi-purpose automated synthesis module.

We validated the process of synthesis for ⁶⁸Ga-DOTATOC, ⁶⁸Ga-DOTANOC and ⁶⁸Ga-PSMA-HBED-CC, performing it with the automated synthesis module Scintomics GRP® (Good Radiopharmaceutical Practice). Reaction yield was calculated and the quality of the final product was assessed after each synthesis by ITLC-SG and HPLC methods to monitor the performance and efficiency of the synthesis. A TiO₂-based generator was eluted with 0.1M HCl and the ⁶⁸GaCl₃ purified using a cationic-exchange cartridge. Peptides were labeled at 95°C for 10min in HEPES buffer solution and the final product was purified with reversed-phase cartridge. RCP and CP were measured by instant thin-layer chromatography, high-performance liquid chromatography (Ultimate 3000 Thermofisher) and gas-chromatography (TRACE 1300 Thermofisher) according to Ph. Eur. We also evaluated pH, sterility/endotoxins and the radionuclidic purity using the HPGe detector (Ortec GEM30P4-76). The mean yield of labelling reaction was 63.78%, 60.43%, 65.53% and RCP was 98.54%, 100%, 99.90% for ⁶⁸Ga-DOTATOC, ⁶⁸Ga-DOTANOC and ⁶⁸Ga-PSMA-HBED-CC respectively. The Ge-68 breakthrough was 7.15*10⁻⁶%, 6.66*10⁻⁵%, 4.8*10⁻⁵%, and the specific activity was 15.93 GBq/µmol, 15.94 GBq/µmol, 15.46 GBq/µmol for ⁶⁸Ga-DOTATOC, ⁶⁸Ga-DOTANOC and ⁶⁸Ga-PSMA respectively. The pH was 7, the ethanol in the final product was less than 10%V/V as the spot of HEPES less intense than the corresponding reference solution (200µg/V) for all the batches. Bacterial endotoxin testing was accordant for the three radiopharmaceuticals as the LAL-test <0.25 EU/ml. The results showed a reliable ⁶⁸Ga-agents output with high labelling purity. Our system provides flexibility and efficiency of the same synthesis method using a unique automated synthesis module for ⁶⁸Ga-DOTATOC, ⁶⁸Ga-DOTANOC and ⁶⁸Ga-PSMA, through the same synthesis process, reagents and solvents, except peptides to label. The system is GMP compliant and well suited for use in a hospital based radiopharmacy.

EP-33 – Sunday, October 16, 2016, during Exhibition hours, e-Poster Area

M2M: Radiopharmaceuticals - SPECT

EP619**Preparation and preclinical evaluation of ¹¹¹In-tiuxetan-Anti MUC1 as a radioimmunoconjugate for diagnosis of breast cancer by SPECT**

B. Alirezapour¹, L. Mansoori², J. Solati², E. Maadi¹, N. Soltani¹, S. Abbas Abadi³, F. Bolorinovin¹, S. Moradkhan¹, A. Satari¹, G. Aslani¹, M. Pouladi¹; ¹Nuclear Science and Technology Institute, Tehran, IRAN, ISLAMIC REPUBLIC OF, ²Department of Biology, Karaj branch, Islamic Azad University, Karaj, Iran, Karaj, IRAN, ISLAMIC REPUBLIC OF, ³Faculty of pharmacy, University of Debrecen, Debrecen, HUNGARY.

Aim: Radioimmunoscinigraphy (RIS) has attracted considerable clinical application in tumor detection. Underglycosylated MUC1 antigen is one of the early hallmarks of tumor genesis and is overexpressed in more than 80% of breast cancers. PR81 is a new murine anti-MUC1 monoclonal antibody (mAb). In this study, as the first step, we have developed an efficient indirect labeling method of PR81 with ¹¹¹In ($T_{1/2} = 67$ h, gamma emitting major photo peak at 171 keV) through using tiuxetan (MX-DTPA) bi-functional chelator and performed preliminary biodistribution studies in mouse bearing breast adenocarcinoma. **Methods:** Anti-MUC1 (PR81) was conjugated with tiuxetan (MX-DTPA) (Macrocyclics), the average number of the chelator conjugated per mAb was calculated and total concentration was determined by spectrophotometrically. Tiuxetan-Anti-MUC1 was labeled with ¹¹¹In then Radiochemical purity and immunoreactivity, internalization study by MCF7 cell line and serum stability of ¹¹¹In-tiuxetan-Anti-MUC1 were determined. The biodistribution studies and radioimmunoscinigraphy were performed in female

BALB/c mouse bearing breast carcinoma tumor (^{111}In -tiuxetan-Anti-MUC1 i.v., 100 μl , 25 \pm 5 μg mAb, 12, 24, 48 and 72h). **Results:** ^{111}In -tiuxetan-Anti MUC1 was prepared (RCP >97% \pm 0.7, Specific activity 4.8 \pm 2.1 $\mu\text{Ci}/\mu\text{g}$). Conjugation reaction of chelator (50 molar excess ratio) to antibody resulted in a product with the average number of chelators attached to a mAb (c/a) of 3.7 \pm 0.9. Labeling yield with ^{111}In in 400 μg concentration of bioconjugate was 96.2% \pm 3.2. Immunoreaction of ^{111}In -tiuxetan-Anti MUC1 complex towards MUC1 antigen was determined by RIA and the complex showed high immunoreactivity towards MUC1. *In vitro* and *in vivo* stability of radioimmunoconjugate was investigated respectively in PBS and blood serum by RTLC method. *In vitro* stability was more than 92% \pm 1.43 in PBS and 83% \pm 2.82 in serum over 24 h. The Immunoreactivity of the radiolabeled Anti-MUC1 towards MCF7 cell line was done by using Lindmo assay protocol. Under these conditions, the immunoreactivity of the radioimmunoconjugate was found to be 0.79. The biodistribution of ^{111}In -tiuxetan- Anti-MUC1 complex in the mice with normal and breast tumor at 12, 24, 48 and 72 h after intravenous administration, expressed as percentage of injected dose per gram of tissue (%ID/g). Biodistribution and imaging studies at 12, 24, 48 and 72 h post-injection revealed the specific localization of complex at the site of tumors. **Conclusion:** ^{111}In -tiuxetan-Anti-MUC1 is a potential compound for molecular imaging of SPECT for diagnosis and follow up of MUC1 expression in oncology.

EP620

Formulation of a GMP Quality Kit for the Preparation of ^{111}In -DTPA-NLS-Trastuzumab Injection

V. A. Prozzo, C. Chan, R. M. Reilly; University of Toronto, Toronto, ON, CANADA.

BACKGROUND: ^{111}In -DTPA-NLS-trastuzumab is routed to the nucleus of HER2-positive breast cancer cells where Auger electrons emitted by ^{111}In are damaging to DNA. The gamma emissions of ^{111}In permit SPECT imaging to assess delivery of ^{111}In -DTPA-NLS-trastuzumab to tumours for radioimmunotherapy. Thus, ^{111}In -DTPA-NLS-trastuzumab is a potential theranostic agent for HER2-positive breast cancer. To advance ^{111}In -NLS-trastuzumab to a Phase I/II clinical trial, studies were conducted to develop a kit under GMP conditions to prepare clinical quality ^{111}In -DTPA-NLS-trastuzumab injection. The solubility and tendency of these immunoconjugates (ICs) to aggregate are major challenges in designing these kits. **METHODS:** Trastuzumab (Herceptin) was buffer-exchanged into 0.1 M NaHCO_3 , then reacted with a 10-fold molar excess of benzylisothiocyanate DTPA (bzDTPA). The ICs were then buffer-exchanged by ultrafiltration into 0.1 M NaPO_4 buffer with or without 0.01% polysorbate-20 (PS-20). Purified DTPA-trastuzumab was modified with maleimide groups for conjugation to nuclear localization sequence (NLS) peptides by reaction with a 5- or 10-fold molar excess of sulfo-SMCC in 0.1 M NaPO_4 buffer with or without 0.01% PS-20. Following re-purification, the ICs were reacted with a 50-, 60- or 75-fold molar excess of NLS peptides with a terminal thiol group. The DTPA-NLS-trastuzumab ICs were purified and buffer-exchanged into 0.1 M or 0.05 M NH_4OAc buffer with or without 0.01% PS-20. Final protein concentration was determined by measuring UV absorbance at 280nm, adjusted to 5.0 mg/mL and 1 mL aliquoted into single vials (kits). The kits were labeled with 111-137 MBq of ^{111}In . Desired specifications are 2-7 DTPA and 5-11 NLS per trastuzumab, >90% labeling efficiency, <5% aggregation assessed by SDS-PAGE and K_a and B_{max} values within 0.1-3.6 \times 10⁷ L/mol and 0.3-5 \times 10⁶ HER2/cell respectively. **RESULTS:** Eight kits (RG001-8) were manufactured. Production revealed addition of PS-20 to buffers reduced aggregate formation in the kits. Final reaction conditions of 10-fold molar excess of bzDTPA, 5-fold SMCC and 60-fold NLS peptides were finalized. DTPA substitution level ranged from 2-4 bzDTPA/trastuzumab, labeling efficiency was 75 \pm 16%, 0-11 NLS per trastuzumab, <5% aggregation, and the K_a and B_{max} were within 0.1-

3.6 \times 10⁷ L/mol and 0.3-5 \times 10⁶ receptors/cell respectively. **CONCLUSION:** Careful selection of reaction conditions was required to obtain a kit for preparation of ^{111}In -DTPA-NLS-trastuzumab injection exhibiting low (<5%) IC aggregation. Kits met specifications for DTPA and NLS substitution and exhibited preserved HER2 binding, but further optimization is required to increase the labeling efficiency to >90% for clinical use. This research was supported by the Canadian Breast Cancer Foundation

EP621

Radiolabeling and quality control of ^{111}In -CHX-A-DTPA-trastuzumab for Radioimmunoscinigraphy

B. Alirezapour¹, H. Hadad Dabaghi², H. Ansari Ramandi², A. Ghamoushi Ramandi², M. Hashemizadeh¹, E. Maadi¹, A. Jalilian¹, S. Rajabifar¹, S. Moradkhani¹, H. Masoumi¹, A. Rahiminejad¹; ¹Radiation Application Research School, Nuclear Science and Technology Institute, Tehran, IRAN, ISLAMIC REPUBLIC OF, ²Department of Science, Karaj Branch, Islamic Azad University, P.O. Box 31485-313, Karaj, IRAN, ISLAMIC REPUBLIC OF.

Radiolabeled monoclonal antibodies have shown great promise for cancer diagnosis and therapy. Trastuzumab (trade name; Herceptin) is a humanized IgG1 monoclonal antibody directed against the extracellular domain of the Human Epidermal Growth Factor Receptor2 (HER2). HER 2 receptor is overexpressed in 20-30% of the early-stage breast cancers and these patients may be candidates for Herceptin treatment. we attempted to label trastuzumab with ^{111}In ($T_{1/2}$ = 67 h, gamma emitting major photo peak at 171 keV) through using (CHX-A-DTPA) bi-functional chelator (CHX-A-DTPA) and performed preliminary biodistribution studies in normal mice. **Methods:** Trastuzumab was conjugated with CHX-A-DTPA (Macrocyclics), the average number of the chelator conjugated per mAb was calculated and total concentration was determined by spectrophotometrically. CHX-A-DTPA-trastuzumab was labeled with ^{111}In then Radiochemical purity and immunoreactivity, internalization study by SkBr3 cell line and serum stability of ^{111}In -CHX-A-DTPA-trastuzumab were determined. The biodistribution studies and radioimmunoscinigraphy were performed in normal mice (^{111}In -CHX-A-DTPA-trastuzumab i.v., 100 μl , 25 \pm 5 μg mAb, 12, 24, 48 and 72h). **Results:** ^{111}In -CHX-A-DTPA-trastuzumab was prepared (RCP >98% \pm 0.6, Specific activity 4.2 \pm 1.1 $\mu\text{Ci}/\mu\text{g}$). Conjugation reaction of chelator (50 molar excess ratio) to antibody resulted in a product with the average number of chelators attached to a mAb (c/a) of 4.1 \pm 0.8. Labeling yield with ^{111}In in 400 μg concentration of bioconjugate was 95.2% \pm 2.2. Immunoreaction of ^{111}In -CHX-A-DTPA-trastuzumab complex towards HER2 antigen was determined by RIA and the complex showed high immunoreactivity towards HER2. *In vitro* and *in vivo* stability of radioimmunoconjugate was investigated respectively in PBS and blood serum by RTLC method. *In vitro* stability was more than 91% \pm 1.3 in PBS and 81% \pm 2.5 in serum over 24 h. The Immunoreactivity of the radiolabeled trastuzumab towards SkBr3 cell line was done by using Lindmo assay protocol. Under these conditions, the immunoreactivity of the radioimmunoconjugate was found to be 0.75. The biodistribution of ^{111}In -CHX-A-DTPA-trastuzumab complex in the normal mice at 12, 24, 48 and 72 h after intravenous administration, expressed as percentage of injected dose per gram of tissue (%ID/g). The accumulation of the radiolabeled antibody in lungs, liver, spleen and other tissues demonstrates a similar pattern to the other radiolabeled anti-HER2 immunoconjugates. **Conclusion:** ^{111}In -CHX-A-DTPA-trastuzumab is a potential compound for molecular imaging of SPECT for diagnosis and follow up of HER2 expression in oncology. **Keywords:** Trastuzumab, Indium-111, Monoclonal Antibody, Bio-distribution, Breast Cancer cancer.

EP622

Comparison Between ^{99m}Tc Radiolabeled siRNA Singlet and Duplex in Serum Stability and Cellular Uptake by HepG2 Cells

L. Kang¹, Y. Huo¹, R. Wang¹, X. Xu²; ¹Peking University First Hospital, Beijing, CHINA, ²Academy of Military Medical Sciences, Beijing, CHINA.

Objective: The antisense single strand and small interference double strands RNA have been applied in some gene therapy studies. However the *in vivo* stability of these probes is important to their effect. This study was to compare the stability and activity between ^{99m}Tc labeled siRNA singlet and duplex *in vitro*. **Methods:** Both of sense and antisense RNA of siRNA were synthesized with 2'-OMethyl modification. The 21mer antisense RNAs were conjugated with bifunctional chelator S-Acetyl NHS-MAG3. Some antisense MAG3-RNAs were annealed with sense RNAs and then radiolabeled with ^{99m}Tc, while some antisense MAG3-RNAs were radiolabeled without annealing. The labeling efficiencies under different reaction conditions including reaction time and input of SnCl₂·2H₂O were evaluated. The serum stability and HepG2 cellular uptake was investigated at different time points. **Results** The labeling efficiency reached 73.4%±3% (n=5) at room temperature, and the RNA recovery rate was always higher than 98%. Longer reaction time than 1h seemed not improving the efficiency significantly, and much dose of SnCl₂·2H₂O could produce too much technetium collides to lead to decrease of labeling efficiency. In the incubation in fresh serum for 6h, the radiochemical purity of labeled duplex was no less than 90%, while that of singlet decreased to 76.4% in room temperature. The gel electrophoresis result showed more degradation of singlet probes than the duplex probes, especially at 6h. The uptake of ^{99m}Tc-duplex by HepG2 cells with and without liposome transfection increased quickly within 6 hours, and reached maximum separately 50.22±2.6% and 32.86±3.1% (n=4). However the uptake of ^{99m}Tc-singlet attained similar ratios compared to the duplex. There existed no significant difference in the cellular uptake between them (P>0.05). **Conclusions:** ^{99m}Tc-siRNA duplex showed higher serum stability than the ^{99m}Tc-singlet RNA, suggesting more suitable for the *in vivo* usage, while they have a similar cellular affinity.

EP623

Autoradiographic and Kinetic Evaluation of ^{99m}Tc-DTPA-can225IgG, a Tracer for the Canine EGFR-Receptor

N. Berroterán-Infante^{1,2}, J. Fazekas^{3,4}, C. Rami-Mark¹, J. Singer⁴, F. Andrae⁵, W. Wadsak^{1,2}, E. Jansen-Jarolim^{3,4}, M. Mitterhauser^{1,6}; ¹Division of Nuclear Medicine, Department of Biomedical Imaging and Image-guided Therapy, Medical University of Vienna, Vienna, AUSTRIA, ²Department of Inorganic Chemistry, University of Vienna, Vienna, AUSTRIA, ³Department of Comparative Medicine, Messerli Research Institute, University of Veterinary Medicine Vienna, Medical University of Vienna and University of Vienna, Vienna, AUSTRIA, ⁴Comparative Immunology and Oncology, Institute of Pathophysiology and Allergy Research, Center for Pathophysiology, Infectiology and Immunology, Medical University of Vienna, Vienna, AUSTRIA, ⁵piChem R&D, Graz, AUSTRIA, ⁶LBI for Applied Diagnostics, Vienna, AUSTRIA.

Background & Aim: The Epidermal Growth Factor Receptor (EGFR) has become an interesting target for cancer therapeutics and diagnostics, since its overexpression is associated in the formation and progression of several tumors. Therefore, identification of the expression status of EGFR in a tumor, is critical for patient selection for antibody-targeted therapy. In collaboration with the University of Veterinary Medicine, recently a caninized cetuximab-derived antibody for the EGFR (can225IgG) was synthesized and labeled with ^{99m}Tc [1,2]. In consequence, aim of this work was to evaluate the uptake of the newly developed tracer in canine

mammary carcinoma tissue as well the binding kinetics in cell lines expressing the EGFR. **Materials and Methods:** ^{99m}Tc-DTPA-can225IgG was prepared as previously reported [2]. For autoradiography experiments, canine mammary carcinoma frozen sections were incubated with the freshly prepared radiotracer and subsequently exposed to phosphor imaging. The same sections were stained with cresyl violet after 24 hours and two vicinal sections were stained with hematoxylin/eosin and for EGFR expression, respectively. Binding kinetics of the radiotracer were also evaluated in real-time using Ligand Tracer® (Ridgeview Instruments) with two cell lines expressing the EGFR (HT29: human colorectal carcinoma and SH1b: canine mammary carcinoma). Briefly, cells were cultivated on the oblique plane of a petri dish and an aliquot of the tracer was added; association of the tracer was evaluated over the time with addition of “cold” antibody at different concentrations. **Results:** Autoradiography experiments showed uptake of the labeled antibody to EGFR+ tumor sections and the radioactivity uptake was correlated immunohistochemically with the expression of the EGFR. Kinetic binding data showed a high dependency of the observed association rate constant and the radioligand concentration. Nevertheless, addition of “cold” antibody did not show any significant blocking, probably due to the typical low off-rate constant of antibodies. **Conclusions:** The presented results, together with previous *in vitro* evaluations [2], point towards a suitability of the new tracer, ^{99m}Tc-DTPA-can225IgG, for future *in vivo* evaluations. **References:** [1] Singer J, Fazekas J et al., *Mol Cancer Ther* 2014 7:1777-90. [2] Rami-Mark C et al., *EJNMMI* 2014 41(Suppl 2):S446.

EP624

Alternate radiolabelled meal formulations for assessing gastric emptying by scintigraphy for patients suffering from gastroparesis

A. Bodin-Hullin, P. Garrigue, Q. Sala, S. Gonzalez, A. Gouillet-Patiri, S. Gabriel, O. Mundler, V. Vitton, B. Guillet; APHM, Marseille, FRANCE.

Gastric emptying scintigraphy is the gold standard for the diagnosis of gastroparesis¹. [^{99m}Tc]technetium radiolabelled scrambled eggs (SE) are most often used as the ingested solid phase. Consequently, patients allergic or reluctant to eggs are not eligible to gastric emptying scintigraphy using this formulation. According to the absence of recommendation and poor literature for this purpose, we aimed at formulating two egg-free and soy-lecithin-based alternate meals: a microwave-baked chocolate mug-cake (MC) and a scrambled tofu (ST). Six healthy volunteers underwent gastric emptying scintigraphy after ingesting MC, ST or SE (control) radiolabelled with 37MBq [^{99m}Tc]technetium sulphur colloids on three consecutive days, and they were asked for their favourite meal formulation. The protocol was approved by our Institutional Review Board and we obtained informed consent from the subjects. Radiochemical purity of [^{99m}Tc]technetium sulphur colloids was ≥90%. Meals were prepared by the same person during the study period. Images were acquired 10min, 30min, 1h, 2h, 3h and 4h after ingestion. All SPECT images (Siemens Signature) were interpreted independently by two experienced, blinded nuclear medicine physicians. The interpretation resulted in the calculation of a gastric retention index for each time point, of emptying half-times and lag phase times for each scintigraphy using the Elashoff curve fit method. A two-way ANOVA test was used to compare gastric retention indexes obtained with the three formulations. Emptying half-times and lag phase times were finally compared between the test and control meals (MC vs SE and ST vs SE) by Kruskal-Wallis test followed by a Dunn's multiple post-hoc test. The alternate meals were well tolerated by all volunteers, although the MC was largely preferred. Scintigraphic images obtained with both tested formulations were overall similar to the control meal and gastric retention indexes did not change significantly between formulations (% of overtime variation to SE: MC 7.75±7.1%; ST 7.17±5.8%; P=0.6618, ns). Emptying half-times (SE: 79.0±20min; MC: 81.0±29min; ST: 70.5±24min) and lag phase times (SE: 23.5±6.1min; MC:

24.5±8.5min; ST: 16.5±5.3min) were not significantly different between formulations (respectively $P=0.6964$ and $P=0.1564$). As a conclusion, these formulations are interesting as solid phases, compared to liquid test formulations that have been recently experimented². In the absence of any commercialized and standardized formulation, we can consider both MC and ST as serious alternatives to classic SE for patients allergic or reluctant to eggs when gastric emptying scintigraphy is indicated. ¹Camilleri et al., Am J Gastroenterol 2013 ²Sachdeva et al., Dig Dis Sci 2013

EP625

In vivo tracking of ¹¹¹In-oxine labeled mesenchymal stem cells following infusion in rats with radiation skin lesions

O. E. Klementyeva, O. E. Klementyeva, T. A. Astrelina, A. O. Malysheva, K. A. Petrosova, K. E. Ternovskaya; Federal Medical Biological Agency Federal State Budget Institution State Research Center “Burnasyan Federal Medical Biophysical Center”, Moscow, RUSSIAN FEDERATION.

Studies on the biology of stem cells and regenerative medicine quickly displaced in the direction of their clinical application. Mesenchymal stem cells (MSCs) provide an opportunity to recovery the functions of organs by replacing damaged cells and tissues and can be a good alternative to other methods of treatment. However, many aspects of the biology of stem cells and their behavior in the body after administration is still beyond our understanding. Scintigraphy using cells labeled with a radionuclide is the most appropriate method for studying of cell tracking and whole-body biodistribution studies. Indium-111 oxine internalizes non-specifically into cells. Thanks to the long half life of Indium-111, SPECT tracking cell for 10 days after a single administration is possible. Given that Indium-111 oxine was approved for clinical application for labeling white blood cells to track sites of inflammation since more than 20 years ago, it was an acceptable extension to label stem cells for noninvasive tracking. **Aim.** Preparation of MSC's labeled by complex of ¹¹¹In-oxine and investigation of biodistribution in experimental animals. **Materials and methods.** 3.75 MBq of ¹¹¹In-oxine were added in MSC suspension (10⁶ cells). Resulting mixture was incubated for 30 min. During incubation, gently swirl the cell suspension periodically to prevent sedimentation of the cells. After the incubation, the cells were centrifuged. After centrifugation, remove the supernatant containing unbound ¹¹¹In-oxine and measure the amount of radioactivity in the pellet and in the supernatant to calculate the labeling efficiency. For biodistribution *in vivo* studying ¹¹¹In-oxine MSC were injected to the tail vein of rats with radiation skin lesions (110 Gy irradiation of skin surface for 380 s). The radiometry of dissected organs was made in 3 and 24 h post injection. **Results.** Labeled efficiency was 82.8±1.2%. After 3 h p.i the accumulation of ¹¹¹In-oxine labeled MSCs in liver, kidney and lungs was 4.4 ± 0.8%, 1.6% ± 0.1, 6.2 ± 1.4%, respectively. After 24 hours, the accumulation of these organs decreased by half. It should be noted that over time, the accumulation of ¹¹¹In-oxine MSC in foci of radiation injury increases. The ratio of pathology area/ normal skin was 1.2 - 1.4 after 24 hours p.i. **Conclusions.** From the preliminary results we can conclude that the ¹¹¹In-oxine can be used as promising agent for MSC tracing *in vivo*.

EP626

Radiolabeling and quality control of ⁶⁷Ga-DTPA-Cetuximab for Radioimmunosciintigraphy

B. Alirezapour¹, H. Hadad Dabaghi², A. Ghamoushi Ramandi², H. Ansari Ramandi², N. Soltani¹, M. Hashemizadeh¹, F. Bolorinovin¹, G. Aslani¹, P. Ashtari¹; ¹Radiation Application Research School, Nuclear Science and Technology Institute, Tehran, IRAN, ISLAMIC REPUBLIC OF, ²Department of Science, Karaj Branch, Islamic Azad University, P.O. Box 31485-313, Karaj, IRAN, ISLAMIC REPUBLIC OF.

Radiolabeled monoclonal antibodies have shown great promise for cancer diagnosis and therapy. Cetuximab monoclonal antibody is an epidermal growth factor receptor (EGFR) inhibitor used for the treatment of metastatic colorectal cancer, metastatic non-small cell lung cancer and head and neck cancer. we attempted to label cetuximab with radioactive gallium-67 (⁶⁷Ga) is cyclotron produced, decays by electron capture (EC) with $t_{1/2} = 77.9$ h accompanied with γ -rays, mainly 93, 184 and 296 keV, and is suitable for SPECT imaging. In the present study, ⁶⁷Ga labeled cetuximab through using bi-functional chelator (p-SCN-Bn-DTPA) was prepared followed by the cellular and biodistribution studies. **Methods:** Cetuximab was conjugated with p-SCN-Bn-DTPA (Macrocyclics), the average number of the chelator conjugated per mAb was calculated and total concentration was determined by spectrophotometrically. DTPA-Cetuximab was labeled with ⁶⁷Ga then Radiochemical purity and immunoreactivity by SW480 cell line and serum stability of ⁶⁷Ga-DTPA-Cetuximab were determined. The biodistribution studies and radioimmunosciintigraphy were performed in normal mice (⁶⁷Ga-DTPA-Cetuximab i.v., 100 μ l, 25±5 μ g mAb, 12, 24, 48 and 72h). **Results:** ⁶⁷Ga-DTPA-Cetuximab was prepared (RCP >98% ± 0.8, Specific activity 3.9 ± 1.1 μ Ci/ μ g). Conjugation reaction of chelator (50 molar excess ratio) to antibody resulted in a product with the average number of chelators attached to a mAb (c/a) of 3.8 ± 1.2. Labeling yield with ⁶⁷Ga in 400 μ g concentration of bioconjugate was 96.2% ± 2.7. Immunoreaction of ⁶⁷Ga-DTPA-Cetuximab complex towards EGFR antigen was determined by RIA and the complex showed high immunoreactivity towards EGFR. *In vitro* and *in vivo* stability of radioimmunoconjugate was investigated respectively in PBS and blood serum by RTLC method. *In vitro* stability was more than 90% ± 1.9 in PBS and 80% ± 1.5 in serum over 24 h. The Immunoreactivity of the radiolabeled cetuximab towards SW480 cell line was done by using Lindmo assay protocol. Under these conditions, the immunoreactivity of the radioimmunoconjugate was found to be 0.79. The biodistribution of ⁶⁷Ga-DTPA-Cetuximab complex in the normal mice at 12, 24, 48 and 72 h after intravenous administration, expressed as percentage of injected dose per gram of tissue (%ID/g). The accumulation of the radiolabeled antibody in lungs, liver, spleen and other tissues demonstrates a similar pattern to the other radiolabeled anti-EGFR immunoconjugates. **Conclusion:** ⁶⁷Ga-DTPA-Cetuximab is a potential compound for molecular imaging of SPECT for diagnosis and follow up of EGFR expression in oncology. **Keywords:** Cetuximab, ⁶⁷Ga, Monoclonal Antibody, Bio-distribution, Colon cancer.

EP627

The standard method for testing Radiochemical Purity of ^{99m}Tc-HMPAO is not compatible with its shelf life: validation of a quicker quality control method

T. Scotognella, V. Lanni, V. Nicoloso, D. Fortini, D. Di Giuda, A. Giordano; Institute of Nuclear Medicine, Università Cattolica del S. Cuore and Policlinico A.Gemelli, Rome, ITALY.

Technetium-99m exametazime (^{99m}Tc-HMPAO), prepared with the reconstitution of a cold kit, is widely used in the evaluation of regional cerebral blood flow with SPECT as well as in the investigation of inflammatory diseases by *in-vitro* leukocyte labelling. The Radiochemical Purity (%RP) assessment of ^{99m}Tc-HMPAO performed with the standard method, as specified in the product characteristics (SPC), is time consuming, exceeding the useful radiopharmaceutical shelf-life (30 minutes). Our aim is to propose an alternative quality control method of ^{99m}Tc-HMPAO in order to reduce the time required to test the radiochemical purity. **Materials and methods:** Our tests required the reconstitution of the kit with 5 ml (1,11 GBq) of fresh ^{99m}TcO₄⁻ freshly eluted from a ⁹⁹Mo/^{99m}Tc generator already used in the previous 24 hours. When necessary, preparations were diluted with sodium chloride solution 0.9% to obtain a 5 ml solution. According to the manufacturer instructions, the standard quality control technique consisted of two chromatographic systems: a TLC-SA

(Agilent) strip 2x20cm developed with methyl-ethyl-ketone (MEK) and a second strip (2x20cm) developed with an 0,9% sodium chloride solution. We compared the standard protocol, requiring approximately 30 minutes, with a quality control method employing the same TLC-SA and mobile phases, but with smaller strips, measuring 0,7x7cm (micro TLC-SA), requiring approximately 10 minutes. Three tests for each method were performed. For both procedures, the strips were analysed by autoradiography (Cyclone Plus®, Perkin Elmer); %RP and stability of ^{99m}Tc -HMPAO were calculated for each preparation immediately after the labelling and after 15, 30 and 45 minutes. The Wilcoxon test was employed to compare quality control results of the proposed method with the standard one. **Results** Similar mean values of % RP were obtained using the micro TLC-SA and the standard TLC-SA: $t_0=92,2\% \pm 2,6$, and $93,7\% \pm 3,4$, respectively, $p=0,75$; $t_{15}=93,4\% \pm 1,8$ and $90,3\% \pm 1,9$, respectively, $p=0,25$; $t_{30}=91,3 \pm 0,7$ and $88,7\% \pm 1,3$, respectively, $p=0,25$; $t_{45}=86,6\% \pm 5,7$ and $87,2\% \pm 4,2$, respectively, $p=0,75$. No significant differences were found between these two acquisition methods in the measurements performed at t_0 , t_{15} , t_{30} and t_{45} . **Conclusions:** We introduced a new method for the assessment of ^{99m}Tc -HMPAO radiochemical purity: a rapid, and accurate analysis technique, yielding optimal RP results before the administration of the radiopharmaceutical. If tested on a larger sample size and once demonstrated its reliability, the micro TLC-SA test could become a reasonable alternative to the registered SPC method.

EP628

Complete validation of the granulocytes radiolabeling method using Leukokit with introduction of a density gradient medium

C. MAUREL, R. de LEMPS, J. MARTI, M. RAZZOUK - CADET, C. GRANGEON; CHUN - Hopital de l'Archet, NICE, FRANCE.

Introduction: Scintigraphy with radiolabeled autologous White Blood Cells (WBCs) is a widely used method to detect infection sites. WBCs can be radiolabeled using a disposable medical device, Leukokit®, under Good Manufacturing Practices conditions. This kit contains all the material to realize the separation of leucocytes from the patient's blood and their labelling before re-injection. In order to increase scintigraphy specificity, we decided to introduce a GMP grade ready-to-use density gradient medium, Ficoll-Paque Premium®, to isolate granulocytes only. The aim of this study was to validate our Leukokit® process completed with Ficoll Plaque Premium® by carrying out routine quality controls, cell viability, cell subset recovery test and aseptic filling tests (sterility). **Material & Method:** Over a period of 3 months, 20 samples of blood intended for radiolabeled autologous WBCs scintigraphy were collected and treated with Leukokit®. Leucocyte-rich plasma was added to Ficoll Plaque Premium® after blood sedimentation. The cell pellet was labelled by ^{99m}Tc -HMPAO (950 MBq) obtained from a fresh eluate of ^{99m}Tc -pertechnetate. The labelling efficiency (LE) was determined by measuring the amount of radioactivity in the supernatant and the pellet of the labelling suspension after centrifugation. A LE between 40% and 80% was expected. Cell viability was performed using Trypan blue exclusion test. The number of granulocytes injected was quantified with a haemocytometer slide. Stained smears (May Grünwald Giemsa) were observed with a microscope under oil immersion at 100-fold magnification. Three consecutive sterility tests were performed according to the method described in the most recent European Pharmacopeia using media fills. **Results:** The mean of labelling efficiency was 70% and the cell viability was 97.7%. An average of 5.4×10^7 granulocytes was injected. Erythrocyte/WBC ratio was 1.8 and granulocytes/WBC ratio was 0.94. All media fill tests were sterile. **Conclusion:** These results confirm that we can validate the process of Leukokit® completed with Ficoll Plaque Premium®. According to the *Guidelines*

for the labelling of leucocytes with ^{99m}Tc -HMPAO of de Vries and al (2010), our quality controls were satisfactory: LE > 50%, sterility test (negative), cell viability (>96%) and cell subset recovery test (in final cell suspension erythrocyte/WBC ratio <3). Measurement of in vitro ^{99m}Tc cell efflux within the first hour after labelling (<10%) and in vivo lung uptake will be tested in a further study to complete our results.

EP629

Modification of radioactive labelling leukocytes from small volume of blood

M. Matějů; Charle University, Prague, CZECH REPUBLIC.

Introduction: Scintigraphy with labelled autologous white blood cells is used to detect suspected sites of acute inflammation or infection including also inflammatory bowel disease and fever of unknown origin- the most frequent indications to leukocyte scintigraphy in paediatric age. In adults leukocytes are obtained from 40-60 ml of venous blood. In children, the amount of blood depends on the patient weight. Aim: Description of radioactive labelling leukocytes with ^{99m}Tc -HMPAO from small volume of blood in childhood. Materials and methods: Procedure of radioactive labelling leukocytes includes some phases: collection of blood, isolation of mixed leukocytes, isolation of cell free plasma, labelling of leukocytes with ^{99m}Tc -HMPAO, quality control and reinjection. We used the auxiliary material supplied with the kits for labelling. Our modification of labelling white blood cells takes smaller amounts of blood for paediatric patients and adolescents. We usually took only twice 15 ml of blood (i.e. total of 30 ml) in adolescent patients. We took 16 ml of blood mostly for paediatric patients. We also added a smaller volume of auxiliary solutions for sedimentation of blood: ACD solution and 6 % hydroxyethyl starch solution. We identified the indication, the sedimentation time, sedimentation volume, radiochemical purity, activity of ^{99m}Tc -HMPAO used for the radiolabelling, the final activity injected and the labelling yield for each patient. Results: These results are based on our study group of 33 children weighing up to 35 kg and the group of 21 adolescents (with indications e.g. Crohn's disease, ulcerative colitis, fever, inflammation of unknown origin, etc.), who were administered autologous leukocytes labelled with ^{99m}Tc -HMPAO. The labelling efficiency of the radiopharmaceutical was $94.10\% \pm 3.38\%$, the yields of radiolabelled leukocytes were $71.90\% \pm 5.68\%$ and the average sedimentation's volume is $7.38\text{ ml} \pm 2.27\text{ ml}$ for children. The administered dose ranged between 150 - 350 MBq. The labelling efficiency of the radiopharmaceutical was $94.55\% \pm 3.82\%$, the yields of radiolabelled leukocytes were $69.91\% \pm 5.66\%$ and the average sedimentation's volume is $9.6\text{ ml} \pm 3.45$ for adolescents. The administered dose ranged between 350 - 500 MBq. **Conclusion:** Modification of labelling white blood cells means smaller amounts of blood. Our long experience has shown that this modification provides leukocyte labelling efficiency high above the limit values. The results of our method proved that our modification is functional. Our method is mainly used in paediatric patients and adolescents.

EP630

An Ornithine based Peptide motif: DO3A-Asp-Arg-Asp-Orn for SPECT imaging of $\alpha_v\beta_3$ integrin

S. Rangaswamy^{1,2}, R. Varshney¹, A. Kaul¹, S. K. Ghumman², A. K. Mishra¹; ¹Institute of nuclear medicine and allied sciences, Delhi, INDIA, ²Department of Chemistry University of Delhi, Delhi, INDIA.

Aim: The integrin are extracellular matrix (ECM) ligands and cell-surface ligands, constitute superfamily of cell adhesion receptors. They mainly constitute laminin basement formed from fibrillar networks of collagens are associated with active processes such as

wound healing and angiogenesis. Several *in vivo* and *in vitro* studies demonstrates the relationship between regulation of integrin expression and cancer. Integrins have been widely studied and formulated, integrin $\alpha_v\beta_3$ as a tumor progression marker. RGD a well-known marker for these integrin has been modified by replacing glycine *via* aspartic acid group and introduction of unnatural amino acid ornithine at C-terminal of the peptide chain, which will aid in better accumulation at tumor site and less susceptible to peptidic cleavage at the physiological conditions. **Methods:** The peptide sequence was synthesized manually using solid phase peptide synthesis (SSPS) with the help of Fmoc-chemistry on rink amide resin to yield Asp-Arg-Asp-Orn-sequence. The N-terminal of aspartic acid was alkylated with the help of chloroacetylchloride in the presence of DIPEA in solid phase. The chloro- derivative was conjugated to DO3A in presence of K_2CO_3 . After the completion of the synthesis, the peptide conjugate was cleaved from resin using TFA cocktail to give the desired ligand. The peptide conjugate (DO3A- Asp-Arg-Asp-Orn) was purified by HPLC to give the pure product at $R_t = 7.9$ min. DO3A- Asp-Arg-Asp-Orn was prepared with more than 75% yield by SSPS and was characterized using mass spectrometry giving $[M]^+$ peak at 904.4. **Results:** The synthesized ligand has been characterized by mass spectroscopic technique and purified by HPLC. Radiolabelling efficiency with ^{99m}Tc was achieved more than 98% and the radio conjugate did not exhibit any dissociation under physiological condition. The molecular modelling studies shows G-Score of -9.8 which is better in comparison with RGD (known for selectivity towards $\alpha_v\beta_3$ integrins). Cell uptake studies on U-87MG cell line suggests high specificity of the ligand towards $\alpha_v\beta_3$ integrins. The *in vivo* biodistribution and blood kinetics studies exhibited rapid clearance of the radiolabelled complex and follows hepatobiliary and renal route of clearance. The substantial accumulation at tumor site with tumor to muscle ratio being 1.92 ± 0.16 in 1 h which increases to 4.01 ± 0.21 in 4 h. **Conclusion:** We have successfully synthesized and characterized the ligand DO3A- Asp-Arg-Asp-Orn, which displays better binding with respect to cRGD a known $\alpha_v\beta_3$ integrin receptor imaging as displayed in molecular docking studies. The ^{99m}Tc - DO3A- Asp-Arg-Asp-Orn holds a promising future mammalian carcinomas expressed by $\alpha_v\beta_3$ integrin.

EP631

Particle size measurement by Dynamic Light Scattering of ^{99m}Tc -radiolabelled rhenium sulphide nanocolloids

R. Ramos-Membrive¹, N. Viedma², G. Quincoces¹, I. Peñuelas¹; ¹Clínica Universidad de Navarra, Pamplona, SPAIN, ²Universidad de Navarra, Pamplona, SPAIN.

Introduction & Aims ^{99m}Tc -nanocolloids are routinely used in nuclear medicine for Sentinel Lymph Node (SLN) localization and as detection tool in staging of breast cancer. SLN is influenced by several factors; being the particle size the most important. The aim is to evaluate particle size (PS) and the polydispersity (PdI) of ^{99m}Tc -labelled rhenium sulfide nanocolloids during the maximum time stated in the summary of product characteristics (SPC) and the possible effect of changing reconstitution physicals and chemical parameters. **Materials & Methods** Five rhenium sulfide nanocolloids kits (Nanocis®) were used. Two were prepared according to the manufacturers' instructions, incubated in a boiling water bath during 30' and cold up 5' in current water. We added to one of them 5 ml of 0.9% NaCl (NC) and to the other 1100 MBq of freshly eluted ^{99m}Tc sodium pertechnetate in 5 ml (^{99m}Tc -NC). Two kits were prepared as described but incubated for 30 min at 100°C using a dry heating system, or at RT respectively. A kit was prepared adding 5ml of NaCl 0.9% and incubated at RT. Radiochemical purity (% RCP) of all three ^{99m}Tc - NC was analysed by radio-TLC. PS and PdI were evaluated for all

kits by Dynamic Light Scattering (DLS) using a Zetasizer S90 system immediately after incubation and 30, 60, 90, 120 and 240 min later. Each measurement was performed in triplicate. **Results:** Radiochemical purity was >95% for all ^{99m}Tc - NC kits. The PS mean percentage distribution, throughout the period of validity, following manufacturers' instructions was 53.33 ± 0.91 nm for ^{99m}Tc - NC and 57.23 ± 1.85 nm for NC. ^{99m}Tc - NC showed 55.58 ± 0.68 nm using the dry heating system. ^{99m}Tc - NC incubated at RT showed higher mean percentage distribution (72.79 ± 0.71 nm) than the other two ^{99m}Tc -NC. NC incubated at RT presented the largest PS (86.81 ± 2.85 nm). The kits incubated 100°C presented similar PdI s 0.209 ± 0.003 . ^{99m}Tc - NC and NC reconstituted at RT showed PdI 0.180 ± 0.009 and s 0.211 ± 0.017 respectively. **Conclusions:** Particle size of all samples were similar throughout the period of validity and showed homogenous polydispersity in all cases. The summary of product characteristics of rhenium sulfide nanocolloid establishes the mean percentage of particle size distribution as 100nm. The results showed smaller particle size than 100 nm, significant differences between ^{99m}Tc - radiolabelled and unlabelled kits and a clear relationship of the particle size and the incubation temperature.

EP632

Development of radiopharmaceutical based on mini-antibody for early cancer detection

V. Skuridin¹, E. Stasyuk¹, O. Bragina¹, M. Usubov^{2,1}, V. Chernov^{3,1}, M. Larkina², R. Zelchan^{3,1}, A. Rogov¹, I. Similkin^{1,3}, L. Larionova¹; ¹Tomsk Polytechnic University, Tomsk, RUSSIAN FEDERATION, ²Siberian State Medical University, Tomsk, RUSSIAN FEDERATION, ³Tomsk Cancer Research Institute, Tomsk, RUSSIAN FEDERATION.

At present early detection and targeted intervention on cancer is the most important problem in modern functional medicine. The usage of specific antibody, beyond question, is one of the most perspective methods to achieve these purposes. The recombinant antibodies to HER2-neu-antigen, which belong to one of the most specific cancer marker, are regarded as the most perspective object for application in medical diagnostics. Aim: Technetium-99m labelling in the structure of the antibody, which is fixed with chelator, and obtaining on its basis new radiopharmaceutical is the most significant aim for cancer diagnostics. Methods: The bifunctional chelator was formed on the basis of 2,5-dioxypyrrolidin-1-yl-6-(di(pyridin-2-ylmethyl)amino)hexanoate to label mini-antibodies. On the one hand, the chelator containing nitrogen atoms, after its reduction up to IV/V valent state, is able to form stable coordinate link with technetium-99m. On the other hand, bifunctional chelator is able to form stable peptide link with antibody. The stannous chloride produced by Sigma-Aldrich (USA) was used as ^{99m}Tc reducing agent eluated from the technetium generator « ^{99m}Tc -GT-TOM». The 1% ascorbic acid solution produced by Merck (Germany) was introduced in the reaction feed as stabilizer. The radiochemical impurity determination was carried out by the thin-layer chromatography procedure on the silica gel plates of "Sorbfil" type. The distribution of ^{99m}Tc activity along the length in chromatograms was determined by the radiometer "GammaScan-01A". Result: The novel procedure of bifunctional chelator synthesis and the reaction of synthesized chelator addition to a mini-antibody were developed as the result of the conducted studies. Necessary and sufficient quantity of reducing agent and auxiliary components were determined for the effective ^{99m}Tc labelling into the structure of the obtained compound. The preliminary tests of the functional usefulness of the mini-antibody labelled with ^{99m}Tc were carried out using the positive and the negative Her-2/neo of breast adenocarcinoma cell lines. Conclusion: The conducted *in vitro* studies showed significant differences in the intensity of drug inclusion in benign and malignant cells, that indicates the functional usefulness of the obtained drug.

EP633**Synthesis and evaluation of [¹²³I]iodoanthraquinones for breast tumor**

J. Park¹, **B. Kim**¹, **J. Lee**¹, **M. Hur**¹, **K. Yu**², **S. Yang**¹; ¹Korea Atomic Energy Research Institute, Jeongeup, KOREA, REPUBLIC OF, ²Dongguk University-seoul, Seoul, KOREA, REPUBLIC OF.

Aim : As a specific inhibition of tyrosine inhibitor, anthraquinones are a natural chemotherapeutic compound and have a lot of the various biological activities such as anticancer, antiviral, anti-inflammatory, antiproliferative effect. In addition, recent studies showed that anthraquinones have been proven to inhibit estrogen receptor α expressing breast cancer cells as an anticancer agent. In this study, [¹²³I]anthraquinones (emodin and aloe emodin) have been synthesized and evaluated for cell uptake using an overexpressing estrogen receptor MCF-7. **Material and Method :** The labeling of [¹²³I]anthraquinones was carried out the each of emodin and aloe emodin (2 mmol) in 200 μ L of DMF was mixed with [¹²³I]NaI solution (37 MBq) at pH 12 and Chloramin T of 10 mg. And then mixture was stirring for 10 minutes at room temperature (27°C). [¹²³I]anthraquinones were purified by a RP-HPLC using ammonium acetate. In order to compare the biological evaluation of target agents (emodin and aloe emodin) and reference agents (iodoemodin, iodoaloe emodin), we were determined by morphological change and MTT assay using MCF-7. The growth of breast cancer MCF-7 cells were checked in the presence of various concentrations of target agents and reference agents ranging from 12.5 μ M -200 μ M for 24 hr. The cellular uptake of [¹²³I]anthraquinones were evaluated using tumor cell lines such as MCF-7, HepG2, CT26 cells. SPECT image was obtained with MCF-7 bearing balb/c mice **Results and Conclusion :** The radiochemical yield of product was approximately >85% and radiochemical purity was >98% by the analytical HPLC system. The results showed significant inhibition of MCF-7 proliferation in a dose and time dependent manner following treatment concentrations of target agents (emodin, aloe emodin) and reference agents (iodoemodin, iodoaloe emodin). While cell death of iodoemodin was smaller than emodin, cell death of iodoaloe emodin was larger than aloe emodin (emodin IC₅₀: 79.92 μ M, iodoemodin IC₅₀: 119.33 μ M, aloe emodin IC₅₀: 107.46 μ M, iodoaloe emodin IC₅₀: 82.86 μ M). In addition, the results of [¹²³I]anthraquinones were showed that [¹²³I]iodoaloeemodin (ID%: 4.63% at 15 min) was more significant uptake than [¹²³I]iodoemodin (ID%: 1.16% at 30 min) in MCF-7. Finally, the activity of [¹²³I]anthraquinones was concentrated on MCF-7 bearing left leg of balb/c mice. In this study, we successfully synthesized and evaluated [¹²³I]anthraquinones as inhibitors of estrogen receptor. This results suggests [¹²³I]anthraquinones is expected potent breast cancer imaging reagent.

EP634**Study of a Gglucose Derivative Labeled with Technetium-99m as Potential Radiopharmaceutical for Cancer Diagnosis**

R. Zelchan^{1,2}, **V. Chernov**^{1,2}, **A. Medvedeva**^{1,2}, **I. Sinilkina**^{1,2}, **E. Stasyuk**², **A. Rogov**², **E. Il'ina**², **V. Skuridin**², **O. Bragina**²; ¹Tomsk Cancer Research Institute, Tomsk, RUSSIAN FEDERATION, ²Tomsk Polytechnic University, Tomsk, RUSSIAN FEDERATION.

Purpose: to study possibility of using 1-thio-D-glucose labeled with 99mTc for cancer imaging in the experiment. **Materials and method:** study was performed in cell culture of normal CHO (Chinese hamster ovary cells CHO) and malignant tissues MCF-7 (human breast adenocarcinoma MCF-7). In the tubes with the cells in an amount of 3 million was added 25MBq 1-thio-D-glucose labeled with 99mTc and incubated for 30 minutes at room temperature. Thereafter, a centrifugation of the tube with the cells the supernatant was removed. Then radioactivity in tubes with normal and tumor cells was measured. In addition, the study included 10 mice of C57B1/6j lines with tumor lesion of the right femur. For neoplastic lesions model in mice was used carcinoma Lewis. Following anesthesia, mice

were injected intravenously with the 25MBq 1-thio-D-glucose labeled with 99mTc. After 15 minutes planar scintigraphy was performed in a matrix of 512x512 pixels for 5 minutes. **Results:** in measuring the radioactivity of normal and malignant cells after incubation with the 1-thio-D-glucose labeled with 99mTc it was found that the radioactivity of malignant cells is higher. The mean values of radioactivity levels in normal cells were 0.3 \pm 0.15MBq. The mean values of the level of radioactivity in the malignant cells were 1.07 \pm 0.6MBq. All examined animals were revealed increased accumulation of the 1-thio-D-glucose labeled with 99mTc at the tumor site. The accumulation of the 1-thio-D-glucose labeled with 99mTc in the tumor was on average twice as high as compared to the symmetric region. **Conclusion:** The present study demonstrated that 1-thio-D-glucose labeled with 99mTc is a prospective radiopharmaceutical for the cancer visualization. In addition, high accumulation of the 1-thio-D-glucose labeled with 99mTc in the culture of cancer cells and in animals tumor tissue demonstrates malignant tumor tropism of the radiopharmaceutical.

EP635**Experimental Studies of the ^{99m}Tc-PDA-DTPA Complex for Myocardium Imaging**

S. Sazonova¹, **E. Nesterov**², **V. Skuridin**², **S. Minin**³, **E. Stasyuk**², **E. Ilina**², **Y. Lishmanov**¹, **J. Ilushenkova**¹, **S. Tsibulnikov**¹; ¹Research Institute for Cardiology, Tomsk, RUSSIAN FEDERATION, ²Tomsk Polytechnic University, Tomsk, RUSSIAN FEDERATION, ³State Research Institute of Circulation Pathology, Novosibirsk, RUSSIAN FEDERATION.

Diagnosis of viable myocardium is an important task of cardiology influencing the treatment strategy of coronary artery disease. The ¹²³I-labeled fatty acids are the agents used clinically for myocardial metabolism imaging. High cost and limited availability of cyclotron-produced ¹²³I, makes ^{99m}Tc-labeled fatty acids more desirable for the purpose. **Purpose:** To perform experimental studies of new ^{99m}Tc-fatty chemical systems based on modified diethylene triamine pentaacetic acid (DTPA). **Methods.** We used DTPA as a chelate agent for radioactive technetium-99m labeling of pentadecanoic acid by previously described method (E.A.Nesterov et al // Eur J Nucl Med Mol Imaging 2015. V. 42 (Suppl 1) S1-924). The model for the assessment of functional suitability of the radiopharmaceutical included 5 rats with 45 minutes acute coronary occlusion, followed by 120 minutes of myocardium reperfusion. At 60 minute before the end of the reperfusion 70MBq of ^{99m}Tc-PDK-DTPA was injected to each rat into femoral vein. Zones of myocardial necrosis and hibernation were assessed by morphological staining techniques, following by radiometry of myocardial samples with varying degrees of damage. The radiometry of spleen, lung, liver and kidney was also performed. **Results.** The radiochemical purity of synthesized ^{99m}Tc-PDK-DTPA was 97 \pm 0.5%. The radiometry of internal organs showed maximum uptake in kidneys (16.8 \pm 0.2 %/g of injected dose). The uptake of ^{99m}Tc-PDK-DTPA in spleen, lung and liver was low (0.2 \pm 0.03%/g, 1.2 \pm 0.05%/g, 1.6 \pm 0.05%/g of injected dose respectively), in heart (healthy myocardium) - 2.1 \pm 0.07%/g. Heart/lung = 1.77; heart/liver = 0.52; heart/kidney = 0.12. The uptake of ^{99m}Tc-PDK-DTPA in necrotizing (0.2 \pm 0.02%/g) and hibernating (0.22 \pm 0.03%/g) myocardium did not differ significantly. The ratio hibernation/necrosis was 1.15. **Conclusion.** Eventually one can say that modified DTPA-molecules are functionally suitable for myocardial imaging, but it does not allow to differentiate necrotizing and hibernating myocardium. This work was supported by the Russian Federation represented by the Ministry of Education and Science of Russia (project № RFMEFI60414X0071).

EP-34 – Sunday, October 16, 2016, during Exhibition hours, e-Poster Area **M2M: Radiopharmacokinetics & Drug Development**

EP636**Targeting the human A3R in a mouse xenograft model using [¹⁸F]FE@SUPPY**

T. Balber^{1,2}, J. Singer^{1,3,4}, M. Dumanic¹, J. Fazekas^{3,4}, N. Berroterán-Infante^{1,5}, C. Vranka¹, E. Jensen-Jarolim^{3,4}, W. Wadsak¹, M. Hacker⁶, H. Viernstein², M. Mitterhauser^{1,7}; ¹Biomedical Imaging and Image-Guided Therapy, Division of Nuclear Medicine, Medical University of Vienna, Vienna, AUSTRIA, ²Department of Pharmaceutical Technology and Biopharmaceutics, Faculty of Life Sciences, University of Vienna, Vienna, AUSTRIA, ³Department of Immunology and Oncology, Institute of Pathophysiology and Allergy Research, Center of Pathophysiology, Infectiology and Immunology, Medical University of Vienna, Vienna, AUSTRIA, ⁴Department of Comparative Medicine, Messerli Research Institute of the University of Veterinary Medicine Vienna, Medical University Vienna and University Vienna, Vienna, AUSTRIA, ⁵Institute of Inorganic Chemistry, University of Vienna, Vienna, AUSTRIA, ⁶Division of Nuclear Medicine, Medical University of Vienna, Vienna, AUSTRIA, ⁷Ludwig Boltzmann Institute for Applied Diagnostics, Vienna, AUSTRIA.

Aim: The human adenosine-3-receptor (hA3R) is highly expressed in human colon cancer tissue as well as in colon cancer cell lines, suggesting this receptor as a tumor marker. The aim of the present study is the investigation of pharmacokinetics of [¹⁸F]FE@SUPPY, a hA3R antagonist, in mice and the design of a xenograft model to investigate the potential of [¹⁸F]FE@SUPPY to serve as a PET-tracer for oncology. **Methods:** *In vivo* blood stability was analyzed using radioHPLC. Therefore, 18MBq±2 [¹⁸F]FE@SUPPY were injected r.o. into healthy Balb-c mice and animals were sacrificed at different time points (10, 20, 40, 70 min). *Ex vivo* biodistribution was assessed after 70 minutes. To select appropriate human tumor cell lines, we analyzed their hA3R expression with Western Blot and flow cytometry. For the xenograft model, 2x10⁶ cells were injected s.c. into immunocompromised mice (SCID/beige). After 12 days, a tumor was formed and animals were injected with 13.8MBq±4 of [¹⁸F]FE@SUPPY r.o. *Ex vivo* autoradiography was performed with removed tumor tissue after 70 minutes. **Results:** Analysis of blood stability revealed 32.3% intact tracer after 5min and 11.4%, 5.6%, 2.4%, 2.3% after 10, 20, 40 and 70min, respectively (n=2). Highest %ID/g was found in organs of metabolism (2.7%ID/g ± 0.2 in kidney, 14.6%ID/g ± 0.2 in liver and 162.8%ID/g ± 37.5 in gall bladder, each n=3). The HT29 cell line (human colorectal adenocarcinoma) was identified to express high amounts of the hA3R protein (ΔMFI 53.6±22) and was therefore used for the xenograft model. *Ex vivo* autoradiography showed 1.96 fold higher uptake in tumor mass derived from HT29 cells compared to a hA3R-negative tumor (CHO-K1) (n=2). **Conclusion:** *In vivo* stability data in blood indicates metabolism in mice. The assessment of metabolism in organs of interest is in progress. Previous *in vitro* stability tests using human plasma and human liver microsomes suggested sufficient stability of [¹⁸F]FE@SUPPY for the time interval of a PET scan in humans. Uptake of [¹⁸F]FE@SUPPY in hA3R positive tumor, derived from HT29 cells, was not as prominent as expected. PET imaging and blocking experiments are in progress. Recently performed *in vitro* autoradiography revealed a 2.6 fold increased uptake of [¹⁸F]FE@SUPPY in human colorectal carcinoma tissue slices compared to healthy mucosa derived from the same patient, encouraging the potential of [¹⁸F]FE@SUPPY to serve as a PET-tracer for oncology.

EP637**Radiolabelling, SPECT/CT imaging and ex vivo studies of a nasal nano-vaccine for shigellosis based on S. flexneri Outer Membrane Vesicles**

R. Ramos Membrive¹, A. Camacho², G. Quinoces¹, Y. Pastor², J. Irache², C. Gamazo², I. Peñuelas¹; ¹Clínica Universidad de Navarra, Pamplona, SPAIN, ²Universidad de Navarra, Pamplona, SPAIN.

Introduction & Aims Shigellosis is one of the leading causes of diarrhea worldwide. The use of an acellular vaccine against shigellosis based on outer membrane vesicles (OMVs) obtained from supernatants of BEI-inactivated *Shigella flexneri* cultures showed full protection of mice against an experimental SF infection. OMVs can reach and activate lymph nodes in gastrointestinal tract by nasal administration. The aim is optimization of ¹²⁵I and ^{99m}Tc radiolabelling of OMVs and biodistribution studies by molecular imaging and *ex vivo* counting in BALB/c after nasal administration. **Materials & Methods** Two mg of OMVs were incubated with [¹²⁵I]NaI and iodo beads™. ¹²⁵I-OMV were purified using tangential filtration concentration unit (TFCU), tangential centrifugation or dialysis. Radiochemical purity (%RCP) was analyzed by radio-TLC. For biodistribution studies, 0.0074MBq of ¹²⁵I-OMV (n=6) and 0.16MBq of ¹²⁵I (controls,n=2) were used per animal by nasal administration. For *ex vivo* counting, 4mice (3¹²⁵I-OMV+1¹²⁵I) were perfused at 24h and 4 (3¹²⁵I-OMV+ 1¹²⁵I) at 48h, organs were extracted and activity was measured in a gamma counter. For ^{99m}Tc-radiolabelling, 10mg of OMVs were pre-tinned with SnCl₂·2H₂O and labeled for 30 minutes with freshly eluted ^{99m}TcO₄⁻. Different SnCl₂·2H₂O concentrations ranging from 0.005 to 1.0 mg/mL were used for radiolabelling optimization. %RCP was analyzed by radio-TLC. For biodistribution studies, 1.4MBq of ^{99m}Tc-OMVs (n=6) and 1.26MBq ^{99m}TcO₄⁻(controls,n=2) were used per animal. SPECT/CT studies were performed 1h and 24h post-administration. For *ex-vivo* counting, mice were sacrificed, perfused, organs excised and gamma-counted at 24h. **Results:** Tangential centrifugation and dialysis %RCP were not enough to be administered (<50%). Using TFCU purification %RCP was > 80% but most of ¹²⁵I-OMVs got blocked at the TFCU's membrane and low activity of ¹²⁵I-OMVs purified could be administered. After dissection+ counting nasal uptake was 0.2 and 0.05 % of injected dose (%ID) at 24h and 48h, while thyroid uptake was 0.70 and 1.30 of %ID respectively. RCP was >95% for ^{99m}Tc-OMVs using [SnCl₂]=0.5 mg/mL. SPECT/CT images showed nasal focal uptake and incorporation to intestine 1h post-administration; ^{99m}TcO₄⁻ presented abdominal focal activity. At 24h ^{99m}TcO₄⁻ had no biodistribution changes and ^{99m}Tc-OMVs nasal focal uptake remained, confirmed by dissection/counting ratios (0.45 %ID). **Conclusions:** The antigen complex could be hardly radiolabelled with ¹²⁵I with low radiochemical yield, while ^{99m}Tc-OMVs presented RCP >95% with no need of purification. The increase of thyroid uptake indicate ¹²⁵I-OMVs radiolabelling is not stable *in vivo*. Activity found in nose and intestine suggested OMVs were able to reach gastrointestinal lymph nodes.

EP638**Radiolabeling and Biodistribution study of GLP-1 with I-125**

M. Hernandez Fructuoso¹, C. Beltrán Gracia², B. Santos Montero¹, C. Hernández Pascual³, R. Simó Canonge³, S. Aguadé Bruix⁴, J. Castell Conesa⁴, J. Herance Camacho⁵; ¹Radiopharmacy Unit, Hospital Universitari Vall d'Hebron - Institut de Diagnòstic per la Imatge, Barcelona, SPAIN, ²Radiopharmacy Unit, Hospital Universitari Vall d'Hebron, Barcelona, SPAIN, ³Endocrinology Department, Hospital Universitari Vall d'Hebron, Barcelona, SPAIN, ⁴Nuclear Medicine Department, Hospital Universitari Vall d'Hebron, Barcelona, SPAIN, ⁵Hospital Universitari Vall d'Hebron, Institut de Recerca, ISCIII, Barcelona, SPAIN.

Aim: Retinal neurodegeneration is an early event in the pathogenesis of diabetic retinopathy (DR). Glucagon-like peptide-1 (GLP-1) receptor agonists have been proposed for the treatment of DR. The aim of this study is to label GLP-1 with I-125 and to determinate its biodistribution (BD) upon topical administration to the New Zealand white rabbits eyes. **Materials and Methods:** Standard chloramine T method was used to iodinate GLP-1. We checked different amounts of GLP-1 (100,200,300 and 400µg) at different times of reaction (1,2,5 and 7 minutes) at room temperature. Purification method was performed using size exclusion column (PD-10) and the elution profile was validated using GLP-1, ¹²⁵I-GLP-1 and ¹²⁵INa.

All the eluates were counted in a gamma-counter. (Cobra II, Packard). SA and RCP were determined using a HPLC (Agilent 1100 series). In vitro stability of GLP-1 radiolabelled in eye drop formulation was evaluated using PD-10 and HPLC. One 40- μ L drop of 125 I-GLP-1 was administered to 24 rabbits at right eye. BD studies were made using the cut&count technique by collecting tissues for ex vivo analysis and measured them in a gamma-counter during 5 minutes. Blood, right kidney, liver, stomach, urine, thyroid gland, testicles, crystalline lens right and left, retina right and left, sclera right and left, vitreous right and left, cornea right and left, iris right and left and Conjunctivae right and left were analysed. **Results:** 125 I-GLP-1 was proper labelled at 5 minutes using 300 μ g with 95% chemical yield. Isolation of 125 I-GLP-1 by PD-10 was efficient and RCP was > 95%. The SA was around 15Bq/ μ mol. BD studies demonstrated that 125 I-GLP-1 was distributed in different organs and tissues but principally in intraocular compartments (retina and crystalline lens). The BD results have been corrected by blank value, gamma radiation counter efficacy and normalized with non-treated group. **Conclusion:** The labelling of GLP-1 has been achieved with 125 I using a chloramine T method with high chemical yield and radiochemical purity. On topical administration, 125 I-GLP-1 is absorbed and distributed to all eye compartments, principally in retina. Based on this biodistribution, topical drops administration GLP-1 appears to be highly attractive for treatment of diabetic retinopathy.

EP639

68 Ga-labeled, zirconia-based nanocarrier systems for PET-nanomedicine and theranostic purposes

A. Polyak¹, L. Naszalyi Nagy^{2,3}, J. Mihaly³, S. Görres¹, I. Leiter^{1,4}, A. Wittneben¹, J. P. Bankstahl¹, M. Zrinyi², T. L. Ross¹; ¹Hannover Medical School, Hannover, GERMANY, ²Semmelweis University, Budapest, HUNGARY, ³Hungarian Academy of Sciences, Budapest, HUNGARY, ⁴University of Veterinary Medicine, Hannover, GERMANY.

Introduction. Biocompatible ceramic material zirconia is used for several biomedical applications, such as dental and surgical implants, but under certain circumstances this inorganic material can be formed to biodegradable pharmaceutical constituents, as well. Our research teams have developed a zirconia based drug delivery nanoparticle system which has been successfully tested as a SPECT-tracer base and beta-emitter radionuclide colloidal carrier candidate. In our latest studies we successfully developed a DOTA bifunctional chelator conjugated nanoparticle (NP) variant which proved to be suitable for further PET imaging and PET image guided therapeutic investigations. **Methods.** Solid zirconia nano-sized particles of 95 nm (\pm 19 nm; solid content = 2.45 mg/ml) have been synthesized in ethanol. Synthesis was based on a method previously described by Widoniak et al. (*Eur.J.Inorg.Chem.* 2005. 3149-55). DOTA bifunctional chelator was adsorbed on the surface of zirconia NPs in ethanol and the product was dialyzed into 1M ammonium acetate buffer pH4.1. For particle characterization, TEM and SEM (transmission and scanning electron microscope) and DLS (dynamic light scattering) methods were used. For 68 Ga-radiolabeling, DOTA-conjugated NPs were incubated for 20 mins at 95 °C in HEPES buffer (pH:4). Radiolabeling efficiency was checked by thin layer chromatography (TLC). For biodistribution studies, *Mus Musculus* C57BL/6N mice were injected with 18 MBq activity of the 68 Ga-labeled nanosystem. Animals were scanned Siemens Inveon μ PET/CT. **Results.** The 68 Ga-labeled NPs showed proper radiolabeling stability in their original suspension and in blood serum. Imaging studies of the new 68 Ga-nanosystem confirmed a RES-biodistribution profile characterized by nano-sized colloids. Most of the activity has been accumulated in the liver, while activities of kidneys and bladder have been increased slowly postinjection (p.i.). Low lung uptake could be observed during the tracing period, indicating the lack of *in vivo* aggregated colloid fraction. **Conclusions.** After a successful DOTA-chelated 68 Ga-labeling procedure of zirconia NPs, our first *in vivo* experiments with μ PET/CT confirmed that the new 68 Ga-DOTA-NP complex had durable radiochemical and colloidal stability p.i., therefore our new method offers the opportunity to

examine further specifically targeted and drug payload carrier variants of these zirconia NP systems using PET/CT imaging.

EP640

Targeted liposomal drug delivery system for radionucleosides - a theranostic approach

A. T. J. Vogt¹, R. Dóczy², K. Szigeti³, I. Horváth³, D. Máthé⁴, M. Roller¹, A. Morgenroth¹, N. Bornwasser¹, U. Königs⁵, F. M. Mottaghy¹, Z. Varga⁶; ¹University Hospital of the RWTH Aachen, Clinic for Nuclear Medicine, Aachen, GERMANY, ²Institute of Nuclear Techniques, Budapest University of Technology and Economics, Budapest, HUNGARY, ³Department of Biophysics and Radiation Biology, Semmelweis University, Budapest, HUNGARY, ⁴CROmed Translational Research Centers, Budapest, HUNGARY, ⁵FH Aachen, University of Applied Sciences, Campus Jülich, Jülich, GERMANY, ⁶Biological Nanochemistry Research Group, Institute of Materials and Environmental Chemistry, Research Centre for Natural Sciences, Budapest, HUNGARY.

Derivatized nucleosides have been used in basic cancer treatment since many years. This approach has highest therapeutical outcome if tumor cells exhibit a high proliferation associated with enhanced DNA related turnover. These therapies make higher serum levels mandatory which are paired with side effects especially in tissues with naturally elevated proliferation. In contrast, Auger electron emitter bearing nucleosides promise to reduce side effects since significantly lower concentrations of these radionucleosides already lead to an efficient therapeutic effect. The radionucleoside and thymidine analog [I-125]5-iodo-2'-deoxyuridine (IdUrd) has been reported already decades ago to efficiently drive proliferative cells into apoptosis. However, only a small fraction of that intravenously administered radionucleoside reaches the target cells due to both its extended metabolism and its rapid renal excretion. In order to reduce these two disadvantages, a targeted multimodal liposomal drug delivery platform has been developed for a theranostic approach. Self-assembled supramolecular structures like liposomes are suitable carriers for radionucleosides. They can be loaded with lipid-conjugated nucleosides simply by incorporation into the lipid bilayer. By this conjugation especially fast renal excretion is expected to be significantly reduced. In the present work we have used the lipid conjugate of [I-125]5-iodo-2'-deoxyuridine (IdUrd). Esterification was performed with both, hexanoic and oleic anhydride, and the conjugate was purified by reverse phase HPLC. Incorporation extent of the lipid-conjugated [I-125]IdUrd into the liposomes was monitored by size exclusion chromatography. Labeling of the liposomes with Ga-68/-67 for PET imaging was enabled by using a DTPA-conjugated phospholipid, while fluorescent labeling was achieved with a nitrobenzoxadiazole (NBD) fluorophore conjugated phospholipid with both building blocks being part of the liposomal construct. A specific targeting of the liposomal nanocarrier to cancer cells was enabled by covalent attachment of a prostate-specific membrane antigen (PSMA) ligand, basically comprising the peptide sequence Glu-urea-Lys. PSMA is highly overexpressed in prostate cancer, and therefore represents an excellent target for both, diagnostic and therapeutic treatments. The PSMA-ligand containing a primary amine-group was attached to the liposomes after having incorporated a N-hydroxy-succinimide activated polyethylene glycol - lipid conjugate (DSPE-PEG2000-NHS). In vitro binding with PSMA-targeted and fluorescently labelled liposomes in MDA-MB231 (PSMA positive) and PC-3 (PSMA negative) cell lines was evaluated by flow cytometric analysis, which verified a specific binding of the PSMA-targeted liposomes to the PSMA positive cells. This work was jointly supported by BMBF (Germany, grant 01DS14024) and NKFI (Hungary, grant TET_12_DE-I-2013-0013).

EP641

Labelling preparation of Rare-Sugar D-allose with 18 F for assessment of behavior in vivo

H. Yamamoto¹, N. Kudomi¹, K. Wada², Y. Yamamoto³, Y. Nishiyama³;

¹Department of Medical Physics, Faculty of Medicine, Kagawa University, Kagawa, JAPAN, ²Department of Chemistry for Medicine, Faculty of Medicine, Kagawa University, Kagawa, JAPAN, ³Department of Radiology, Faculty of Medicine, Kagawa University, Kagawa, JAPAN.

Aim: Applicability of rare sugars, such as D-allose, for diagnostic and therapy purpose is focused on recently. It would be important to make reveal their behaviors *in vivo*. Fluorinated D-allose derivatives, namely [¹⁸F]3-deoxy-3-fluoro-D-allose ([¹⁸F]3FDAllo) and [¹⁸F]6-deoxy-6-fluoro-D-allose ([¹⁸F]6FDAllo), are epimers of corresponding D-glucose derivatives with respect to carbon atom 3, [¹⁸F]3-deoxy-3-fluoro-D-glucose ([¹⁸F]3FDG) and [¹⁸F]6-deoxy-6-fluoro-D-glucose ([¹⁸F]6FDG), respectively. Preparation of [¹⁸F]3FDAllo and [¹⁸F]6FDAllo is of great significance because of their potential utility as probe molecules to investigate metabolic dispositions of a rare sugar, D-allose. **Materials and Methods:** A precursor of [¹⁸F]3FDAllo, 1,2,4,6-tetra-*O*-benzoyl-3-*O*-triflyl-β-D-glucopyranose, was prepared by 5-step reactions from 1,2,5,6-di-*O*-isopropylidene-α-D-glucofuranose, for the first time. On the other hand, a precursor of [¹⁸F]6FDAllo, 1,2,3,4-tetra-*O*-benzoyl-6-*O*-triflyl-β-D-allopyranose, was prepared via a new route consisting of 4-step reactions from D-allose. Preparation procedure of [¹⁸F]3FDAllo and [¹⁸F]6FDAllo are as follows: 50–60 MBq of [¹⁸F]fluoride was adsorbed on QMA and then extracted by K₂CO₃ (17 μmol)/K₂2.2 (53 μmol)/H₂O (0.2 mL)/CH₃CN (0.7 mL) mixture. After evaporation, another 1 mL of CH₃CN was added, and then it was evaporated again. 3 mL CH₃CN solution of a precursor (42 μmol) was added to it. The mixture was heated at 85 °C for 5 min, and concentrated. Deprotection reaction was carried in 0.3 M aq. NaOH/THF=1:1 at rt for 30 min. Then the reaction mixture was neutralized by 1 M aq. HCl and concentrated. [¹⁸F]3FDAllo and [¹⁸F]6FDAllo were purified by semi-preparative HPLC (column: Nakarai Sugar-D: ID10 x 20+250 mm, eluent: CH₃CN/H₂O=75:25, flow rate: 2 mL/min). The products were confirmed by HPLC and TLC. **Results:** [¹⁸F]1,2,4,6-tetra-*O*-benzoyl-3-deoxy-3-fluoro-β-D-allopyranose and [¹⁸F]1,2,3,4-tetra-*O*-benzoyl-6-deoxy-6-fluoro-β-D-allopyranose were obtained 85% and 70% radiochemical conversions (RCCs), respectively. [¹⁸F]3FDAllo and [¹⁸F]6FDAllo were obtained by 33% and 13% RCCs, respectively. RCCs were determined by radio-TLC. **Conclusion:** Basic synthetic procedures for [¹⁸F]3FDAllo and [¹⁸F]6FDAllo have been established and those would be applied to make reveal their behavior *in vivo*, though still some improvements of deprotection reaction process might be required.

EP642

Concentration of rhenium-188 for radiopharmaceutical synthesis

N. A. Konstantinov, A. Chagovets, A. Malysheva, G. Kodina; Burnasyan Federal Medical Biophysical Center FMBA Russia, Moscow, RUSSIAN FEDERATION.

In recent years more attention is attracted to rhenium-188 which can be obtained from generator directly in radiological departments. ¹⁸⁸Re is β-emitter, E_{βmax} = 2,1 MeV, E_γ = 155 keV, T_{1/2} = 17 h, maximum run of β-particles in tissues - 11 mm. Such properties allow using it in the development of new radiopharmaceuticals for radionuclide therapy. Currently, the following commercial generators are available in the world: “GREN-1” (Russia), 3,7 - 37,0 GBq, eluate volume 5 ml; generator IDB Radiopharmacy (Netherlands), 3,7 - 18,5 GBq, eluate volume 8 ml; generator from Oak Ridge National Laboratory (USA), 9,25 - 111 GBq, eluate volume 10-20 ml; POLATOM (Poland), 3,7 - 18,5 GBq, eluate volume 8 ml. Synthesis of radiopharmaceuticals used for radiotherapy, requires high activity in a small eluate volume (1 - 3 ml). In connection with these requirements the application of different methods of eluate concentration before it use for radiopharmaceutical preparation is important. **Aim:** Investigation of concentration systems after generator elution. **Materials and methods:** Na¹⁸⁸ReO₄ was obtained from domestic generator “GREN-1” (Institute of Physics and Power Engineering, Obninsk) and ¹⁸⁸W/¹⁸⁸Re generator with concentration module NEPTIS-TH (IRE

ELiT, Belgium). Radiochemical purity (RCP) of concentrated eluate was determined by TLC and ITLC in saline. **Results:** The concentration system, which consists of two columns with sorbents, was used for the concentration of perrhenate solutions, obtained from generator “GREN-1”. The cation-exchange resin DOWEX 50WX8 (100-200 mesh) in the Ag⁺-form was used for the selective deposition of trace amounts of chloride-ions. Further recovery of perrhenate-ions was performed on a column with weak acidic alumina oxide (pH 4). ReO₄⁻ can be easily desorbed by 1 ml of 0,9 % NaCl. The yield of rhenium-188 was 70 - 85 %. The losses of rhenium-188 were calculated at each stage of concentration and were about 10 - 18 % on the cation-exchange column and about 5 - 6 % on the anion-exchange column. RCP of the concentrated perrhenate solution was more than 99 %. Elution volume from Belgium generator was 100 ml. Concentration module allows to obtain perrhenate solutions with high volume activity in 2 - 5 ml with ¹⁸⁸Re-yield 73.4 - 85.8 %. We observed relatively low RCP at concentration in volumes less than 2 ml. **Conclusion:** The application of concentration system allows obtaining Na¹⁸⁸ReO₄ solutions with high volume activity and radiochemical purity, which can be successfully used in the synthesis of radiopharmaceuticals for radiotherapy.

EP-35 – Sunday, October 16, 2016, during Exhibition hours, e-Poster Area

M2M: Radiopharmacy

EP643

Tumor accumulation of ⁶⁸Ga-DOTA-NAPamid is increased by HPLC purification of the tracer after labeling

J. L. Körner, S. Erdmann, L. Niederstadt, A. Wagener, S. Prasad, S. Exner, N. Beindorff, E. J. Koziolok, W. Brenner, C. Grötzinger; Charité - Universitätsmedizin Berlin, Berlin, GERMANY.

Aim Cutaneous malignant melanoma is one of the most lethal forms of cancer. Its incidence is increasing rapidly, making it a significant public health threat. Melanocortin receptor 1 (MC1R) is overexpressed in most melanomas making it a promising molecular target for diagnosis and peptide radioreceptor therapy. Because of their low molecular weight, low immunogenicity and excellent tumor penetration, radiopeptides have attracted steadily increasing interest in receptor-mediated tumor targeting. ⁶⁸Gallium labeling of DOTA-conjugated peptides is an established procedure in the clinic for use in PET imaging. In the radiochemical process, a large molar excess of peptide over radiometal is usually used to reach high ⁶⁸Ga complexation yields. Aim of this study was to compare a standard labeling protocol against the ⁶⁸Ga-DOTA-peptide purified from the excess of unlabeled peptide. **Materials and Methods** The well-known MC1R-binding DOTA-peptide NAPamide was labeled with ⁶⁸Gallium using a standard clinical protocol. Radioactive peptide was then separated from the excess cold NAPamide by HPLC: immediately after the incubation of peptide and ⁶⁸Gallium (95 °C, 15 min), the reaction was loaded on a C18 column and separated by a water / acetonitrile gradient, allowing fractionation in less than 20 minutes. The radiolabeled products from the standard protocol and HPLC-purified peptide were compared in biodistribution studies and PET/MRI imaging using immunodeficient nu/nu mice, bearing MC1R-expressing B16-F1 xenograft tumors. **Results** In biodistribution studies, the unpurified ⁶⁸Ga-NAPamide was not found to accumulate in the tumor at 1 h post injection (around 1 %ID/g). With the additional HPLC step, the specific activity was raised around 10,000-fold by completely removing cold peptide. By using this rapid purification strategy, we were able to increase tumor uptake more than 8-fold without significant changes in the accumulation in any other tissue. The addition of unlabeled NAPamide to the purified product in various amounts led to a blocking effect and a decrease in specific tumor uptake, similar to the result seen with unpurified radiopeptide. In parallel, PET/MRI imaging was performed using the same tracers as in the biodistribution experiments. It was observed that purified ⁶⁸Ga-DOTA NAPamide shows superior tumor-to-background ratios.

Conclusion We showed that separation of radiolabeled and cold peptide via HPLC is technically feasible and beneficial, even for short-lived isotopes such as ^{68}Ga . Unlabeled peptide molecules can strongly compete with receptor binding sites in the target tissue. Purification of the radiopeptide improved tumor uptake as well as signal-to-background ratios in PET/MRI scans.

EP644

Resolving false-positive bacterial endotoxin test results obtained with some radiopharmaceuticals and cold kits due to the presence of cations, colloidal particles or fatty acids

A. Mitra, S. Lad, S. Kulkarni, **M. G. R. Rajan**; Medical Cyclotron Facility, Radiation Medicine Centre, BARC and BRIT, TMH Annexe, Parel, Mumbai, INDIA.

AIM: We have reported that certain ^{99m}Tc -radiopharmaceuticals (Tc-RPs) can give a false-negative BET due to the Ca^{++} in the lysate of the LAL reagent being trapped by the Tc-RPs (*JNMT,2014,42,278-282*). We now report instances where certain radiopharmaceuticals can give false-positive results due to the presence of cations, colloidal particles or fatty acids and how this effect can be overcome. **MATERIALS:** (a) Reagents: 9.6mM Ca^{++} and Mg^{++} free pH 7.1 PBS, LAL reagents (Sensitivity: 0.03EU/ml) used for BET including LAL-reagent water (LRW), Control Standard Endotoxin, Portable BET Test System (PTS) cartridges (Sensitivity:5-0.05EU/ml).(b) Radiopharmaceuticals studied: ^{99m}Tc -TRODAT, ^{99m}Tc -GHA, ^{99m}Tc -HSA-nanocolloid, ^{99m}Tc -Sulfur-colloid and their cold kits. ^{99m}Tc -carbonyl-DTPA-Rituximab, ^{99m}Tc -carbonyl-DTPA-Bevacizumab, ^{177}Lu -DTPA-Nimotuzumab, ^{177}Lu -DOTA-Nimotuzumab and their bi-functional chelated monoclonal antibody (BFCA-MoAb) cold kits, and ^{131}I -Lipiodol. **METHODS:** BET assays were performed for the RPs and cold kits using LRW or PBS as dilution agent by both gel-clot method (GCM) and kinetic chromogenic method (KCM) at various Maximum Valid Dilution (MVD) (400, 200, 100 and 50) taking care of maximum injection volume and endotoxin limits (EL: 6 EU/ml- RPs, 1 EU/mg - BFCA-MoAb). **RESULTS:** ^{99m}Tc -TRODAT, ^{99m}Tc -GHA and their cold kits, ^{177}Lu -BFCA-MoAb and its cold kit exhibited false-positive result (elevated-BET) by GCM when using LRW as diluting agent, but this was resolved using PBS instead. Elevated-BET in ^{99m}Tc -HSA-nanocolloid, ^{99m}Tc -Sulfur-colloid and their cold kits were resolved by filtering with 0.22 μm PES membrane filter before testing. Elevated-BET in ^{131}I -Lipiodol, by GCM, was avoided by vigorous vortexing at 1:400 MVD in LRW. KCM did not exhibit any difference in BET values (Recovery Positive Product Control < 200%) on using either LRW or PBS. KCM could not be performed on colloid-RPs or their cold kits. **CONCLUSIONS:** Radiolabeled compounds and cold kits with high cation concentration can cause unusual aggregation resulting in a pseudo-coagulation reaction due to disruption of ionic bonds between divalent cations and PO_4^- moiety of lipo-polysaccharide (LPS). Hence, PBS prevents this in GCM assay. We were successful in overcoming the elevated-BET seen in GCM-BET assays for the above mentioned radiopharmaceuticals and cold kits having interfering cationic salt concentrations, using PBS for dilution. Elevated-BET observed with RPs having fatty acids and colloids was successfully taken care of after increasing the dilution and filtering the product respectively before the assay. Elevated-BET was not observed with KCM as the assay is based on absorbance of released chromophore. However, KCM is not recommended to replace GCM for pharmaceuticals (including RPs) where interference in the latter method is observed.

EP645

Simplified Automation of the GMP production for Ga-68 and Lu-177-labelled PSMA

S. Maus; University Medical Center of the Johannes Gutenberg University, Mainz, GERMANY.

Objectives Imaging of the prostate-specific membrane antigen (PSMA)

for the detection of prostate cancer lesions and the therapy are more and more subject of intense research. With a view for the production of radiopharmaceuticals under GMP requirements the simplified automated processes for the GMP production of Ga-68-PSMA-11 and Lu-177-PSMA-617 using a cassette-based ModularLabPharmTracer® synthesizer (Eckert and Ziegler, Germany) in combination with the only recently pharmaceutically approved $^{68}\text{Ge}/^{68}\text{Ga}$ generator (GalliaPharm, Eckert & Ziegler Radiopharma GmbH, Germany) has been reported. **Methods** Ga-11-PSMA-11 labeling is conducted as follows: a Ge-68/Ga-68 generator (GalliaPharm, 50 mCi, Eckert & Ziegler Radiopharma GmbH, Germany) and cassettes (C4-Ga-68-PP) for [Ga-68]Ga-DOTA-peptides were used. 10 μg PSMA-11 precursor dissolved in 30 μl 0.25 M sodium acetate at pH of 4.5 was propounded in the reaction vessel and 2.2 ml generator eluat was transferred directly to the reaction vessel. After 5 minutes at 95° C the reaction mixture was diluted in 5 ml water and let passed a C18 cartridge. The product was eluted with 2 ml Ethanol:NaCl (50:50) and 8 ml 0.9 M NaCl and transferred to product vial via a 0.22 μm sterile filter. Lu-177-PSMA-617 labeling usually starts with of 9.0 GBq Lu-177-Cl₃ (Lumark, IDB-Holland, Baarle Nassau, Netherlands) using a C4-Y90-00-standard synthesis cassette (Eckert & Ziegler Eurotope, Berlin, Germany). 100 μg PSMA-617 precursor dissolved in 500 μl 0.5 M sodium-acetate at pH of 4,85 were propounded in the buffer vial. The activity was transferred directly into the reaction vessel. After 20 minutes at 95° C the reaction mixture was diluted in 5 ml water and let passed a C18 cartridge. The product was eluted with 4 ml Ethanol:NaCl (50:50) and 16 ml 0.9 M NaCl and transferred into product vial via a 0.22 μm sterile filter. **Results** Automated synthesis of ^{68}Ga -PSMA-11 resulted in radiochemical yields of $75 \pm 10\%$, purities of $> 98\%$ and stabilities of ≥ 4 h. For Lu-177-PSMA-617 we obtained yields of ($95 \pm 2\%$), purities ($>99\%$) and stabilities up to 72 hours at room temperature without adding any additionally quencher like ascorbic or gentisic acid. **Conclusion** In this work we could show the simplified automated processes for the GMP production of Ga-68-PSMA-11 and Lu-177-PSMA-617 using the cassette-based ModularLabPharmTracer synthesizer with standard cassettes, which reduces the costs and makes the introduction of new cassette types or the acquisition of new software unnecessary.

EP646

Liposome carried radioiodine probes for the detection of orthotopic pancreatic tumor

J. Jung¹, W. Lee¹, R. Pal¹, G. I. An², J. Yoo¹; ¹Kyungpook National University, Daegu, KOREA, REPUBLIC OF, ²Korea Institute of Radiological & Medical Sciences, Seoul, KOREA, REPUBLIC OF.

Aim: Pancreatic tumor is one of the most dreaded types of tumor, mainly because most of the cases are detected at advanced stage. So, an early diagnostic tool is extremely vital in order to provide proper treatment to patients with pancreatic tumor. Liposomes have been evolved as ideal drug delivery agents, but are rarely used to carry radiotracers for tumor imaging. This study focusses on the development of a liposome based radiotracer targeting orthotopic pancreatic tumor. **Materials and methods:** Hexadecyl-4-iodo benzoate was radiolabeled with 124/131I and consecutively loaded on liposome bearing DSPE-mPEG-2000-folate for active targeting of pancreatic tumor. The size of the liposome was measured using dynamic light scattering (DLS). The morphology of the liposomes was confirmed by transmission electron microscopy (TEM). Two different orthotopic pancreatic tumor models were prepared in BALB/c nu/nu mice using PANC-1 cells (folate receptor over-expressed cells, FR+) and MIA paca-2 (folate receptor deficient cells, FR-). Biodistribution studies were carried out in the tumor models. **Results:** The radiotracer was quantitatively radiolabeled with both isotopes of iodine, 124/131I. The TEM images clearly showed that the formed liposomes were of globular shape having a size of ~100 nm. The DLS measurements also showed good agreement with the TEM result having liposomes size distribution of mean diameter of 105 nm. Orthotopic pancreatic tumors

were well prepared by direct injection of the cells into the pancreas. In the biodistribution studies, at 24 h post injection, the pancreas uptake in the mice bearing PANC-1 cells (FR+) was about 2.7 times higher than that of the mice bearing MIA paca-2 cells (FR-). All other organs showed very similar uptake patterns between the two models. PET imaging study is going on. Conclusion: In this study, we developed a new radiotracer mediated active targeting of orthotopic pancreatic tumor in mice models.

EP647

Comparison of two radiopharmaceutical methods with $^{51}\text{CrEDTA}$ to calculate carboplatin dose

F. Alonso Zazo¹, C. Fernández García¹, B. Martínez de Miguel¹, D. Pérez Rodríguez¹, S. Rizkallal Monzón¹, A. Calviño Martínez²; ¹Hospital Universitario La Paz, Madrid, SPAIN, ²Dpto Estadística e investigación operativa III. Facultad Estadística. Universidad Complutense de Madrid, Madrid, SPAIN.

PURPOSE Determine the best radiopharmaceutical technique to estimate the renal function using $^{51}\text{CrEDTA}$ and decide the appropriate dose of drugs in paediatric oncology. **PATIENTS AND METHODS:** Retrospective study of 24 patients with neuroblastoma aged between 8 months, 16 years, and that will undergo treatment with Carboplatin. Carboplatin's pharmacokinetic depends on renal function, therefore it must be determined. To calculate the required dose of this drug we applied Newell's formula that requires renal function and body weight and, achieving an ideal AUC (6,6mg/mL.min). To measure renal function we used two methods of $^{51}\text{chromethylenediaminetetraacetate}$ ($^{51}\text{CrEDTA}$) clearance: Method 1: Glomerular Filtration Rate (GFR). One blood sample 120 minutes post-injection (Ham and Piepsz's method) Method 2: half life ($t_{1/2}$). Three blood samples 120, 180, 240 minutes post-injection (Brochner Mortensen method) The results were compared using the Statistical test of Pearson's correlation. **RESULTS** Dose interval of Carboplatin obtained by the Ham and Piepsz's method (GFR measurement) was [327,89 mg;1841,73 mg]. Dose interval of Carboplatin obtained by the Brochner-Mortensen's method (Half time measurement) was [102,45 mg;791,27 mg]. The average of the absolute difference of dose between both methods was 640,24 mg. The average of the relative difference was 3.4217 (342,17 %) with a confidence interval of 95% (2.3531; 4.4903). **CONCLUSIONS:** The calculation of Carboplatin dose by the GFR Method measurement would imply a dose between 235,31% and 449,03% higher in comparison to the $t_{1/2}$ measurement method, with a probability of 95 %, to obtain an AUC of 6,6 mg/ml.min. Therefore, in spite of the disadvantage of doing 3 extractions to the patient, it is preferable to use the half time measurement Method, since the ideal AUC will be achieved through the administration of less Carboplatin doses and, consequently, potential toxicity will be reduced.

EP648

A New And Facility Method To Preparation $^{188/186}\text{Re-EC}$ (Ethylene Cysteine Dimer) As Radiopharmaceutical To Prevention Of Restenosis Vascular After Endovascular Brachytherapy

H. Kamali, M. Karamivand, A. Gravand, F. Farajbakhsh, M. Davarpanah, H. Abbasi; Pars Isotope company, Tehran, IRAN, ISLAMIC REPUBLIC OF.

After surgery angiography, it is possible rapidly re-clogging blood vessels. To avoid this complication, use of therapeutic radioisotopes, is one of the effective methods. The radioactive rhenium isotopes, ^{188}Re (half-life: 90.64h) and ^{186}Re (16.98h), have been suggested as radiopharmaceuticals for cancer therapy because of their energetic beta(β). Regarding the lack of hydrolysis of active ingredients radiopharmaceutical, EC(Ethylene cysteine dimer), within the liver and the possibility of survival within the vascular system and rapidly excretion of renal so for this purpose, $^{188/186}\text{Re-EC}$ radiopharmaceutical was formulated with new and facility method. In this research, the preparation of [$^{188/186}\text{Re}$] Re complex of EC with a new method was presented. 1 ml of an

aqueous solution of EC, and 20 μl of $\text{SnCl}_2 \cdot \text{H}_2\text{O}$ in concentrated HCl were mixed together and $\text{ReO}_4^-/\text{saline}$ (3700-7000MBq) was added and adjusted pH. In this method, the complex of $^{188/186}\text{Re-EC}$ was formed at room temperature and the time of the labeling process was 15 minutes. Influencing various parameters for the preparation of radiopharmaceutical was investigated that include an amount of ligand and tin chloride, pH and the time of the labeling process. The best amount of parameters for this formulation method were 0.02 mmol of EC, $20\mu\text{l}(1 \times 10^{-3} \text{ mmol.ml}^{-1})$ of $\text{SnCl}_2 \cdot \text{H}_2\text{O}$ were used for these research. The best radiochemical purity yield of $^{188/186}\text{Re-EC}$ on optimum condition was achieved at 98%. The rate of clearance of $^{188/186}\text{Re-EC}$ from blood was very adequate (1.5%), low persistence in vital organs. The advantage of this new method formulation is that no heating at 100 °C for 30 minutes and reaches the maximum efficiency of complex formation only at room temperature for 15 minutes.

EP649

Validation of Quality Control Method for 6- ^{18}F fluoro-L-DOPA

J. G. Chan, K. Young, R. Mulligan, A. M. Scott, C. C. Rowe; Austin Health, HEIDELBERG VIC, AUSTRALIA.

Background: 6- ^{18}F Fluoro-L-DOPA (FDOPA) has found increasing clinical demand for imaging CNS disorders and other malignant diseases such as neuroendocrine tumours and pancreatic adenocarcinoma. More recently development of improved nucleophilic syntheses methods giving higher specific activities, yields and purity are replacing more complex electrophilic fluorination with its inherent problems. Our department decided to utilise the nucleophilic method released on the NEPTIS® synthesizer from ORA™ providing a reliable one-pot nucleophilic production with high SA for routine production. **Aims:** To develop a suitable quality control method for the testing of FDOPA and to validate the automated synthesizer installation and production method. **Methods:** The quality control method was based on pharmacopoeial monographs and also a method provided by ABX. Radiochemical / chemical purity was determined by HPLC (Shimadzu Prominence) using the following conditions: Phenomenex Kinetex EVO, 5 μm , 250 x 4.6 mm, 100A, eluent: 0.08% TFA/ACN gradient, flow: 1 mL/min, UV: 283 nm, radio-HPLC detector (Flow-Ram, LabLogic). Analytical standards tested: 6-fluoro-L-DOPA, 6-hydroxy-D,L-DOPA and 6-nitro-formyl-DOPA. Free [^{18}F]fluoride content was tested via radio-TLC (Raytest Rita-Star). Enantiomeric purity was tested with Chirale HPLC (Shimadzu) using the following conditions: Diacel Crownpak CR(+) chiral column, 5 μm , 150 x 4.0 mm, 100A, eluent: 20 mM perchloric acid pH 2, flow: 1 mL/min, UV: 283 nm, radio-HPLC detector. Residual solvents were tested with gas chromatography (Shimadzu GC-2010 Plus) using a Restek Rtx-624 column, 30 m, 0.32 mm ID, FID. **Results:** The production validation runs (x3) successfully passed tests for sterility and endotoxins. Radiochemical purity was > 95% and impurities were well below set limits. Problems arose when developing a suitable TLC method for free [^{18}F]fluoride content and various methods are compared to determine the most suitable. A method utilising ITLC-SG glass microfiber strips (Varian) and acetonitrile:normal saline 50:50 was finally chosen. **Conclusion:** Routine production of FDOPA was successfully introduced. A quality control method was validated and final analysis demonstrated compliance with set specifications.

EP650

Transfer of a radiolabelling process with gallium-68 from a manual method to a remote controlled method for clinical applications: the example of NODAGA-RGDfK

M. Chomet¹, C. Provost², V. Vega¹, A. Prignon², J. Talbot¹, V. Nataf¹; ¹APHP - Tenon Hospital, Paris, FRANCE, ²UPMC - Tenon Hospital - LIMP, Paris, FRANCE.

Aim: Various peptides have been ^{68}Ga -radiolabelled in research laboratories and clinical units. However, each team uses different conditions and equipment which raises the issue of transferring production processes from one team to another. We adapted the method of Knetsch et al. (2011) for ^{68}Ga -radiolabelling of NODAGA-RGDfK, a ligand of integrins, to our module used for clinical routine, i.e. following GMP conditions. **Materials and methods:** Radiolabellings were performed using an Elusynth module (Iason). Knetsch et al. starting conditions were first tested. Adapted to our 50 μg GMP vial of RGDfK (PiChem), 180 μL of 0.8 M sodium acetate solution were added to the reaction vial. The $^{68}\text{Ge}/^{68}\text{Ga}$ generator (Obninsk) was eluted using the fractionated elution approach, 1.2 mL were collected and the reaction mixture at $\text{pH}=3.5\text{--}4$ was heated 300s at 40°C . The reaction mixture was transferred on a tC18 light Sep-Pack (Waters) for final purification. All parameters involved were checked, to improve either the radiolabelling yield or the solid phase extraction (SPE) efficiency. **Results:** Following published conditions, radiochemical yield (RCY) mean values were $60.1 \pm 31.5\%$ ($n=7$). This method was not reproducible on our module. To improve the RCY we tested: • a higher temperature (95°C): the RCY increased to $98.5 \pm 0.5\%$ ($n=3$) but the SPE efficiency was $19.5 \pm 11.7\%$ ($n=2$). • an inversion in the order of introduction of reagents: the RCY increased to $98.9 \pm 0.4\%$ ($n=2$) with a 100% SPE efficiency. However this method was not applicable in an automatic mode with our module as it requires an intervention of the user during radiolabelling. • a higher pH (4.5–5): the RCY was 98.41% ($n=1$) with a SPE efficiency of $96.4 \pm 4.4\%$ ($n=4$). To improve the SPE efficiency at 95°C : • the reaction mixture temperature was lowered with an extra vial containing water before transferring on the SPE: the efficiency was above 95% **Conclusion:** A transfer of process from a manual to a remote controlled method as well as between two modules for the same radiolabelling is achievable if all parameters, especially those influencing the kinetics of the reaction, are described. Furthermore, depending on the module, user interventions might be limited. We decided to increase the pH of the reaction as it proved to be a robust and easily applicable method. By determining thoroughly all parameters involved, we guaranteed a successful transfer of process for daily clinical use of [^{68}Ga]NODAGA-RGDfK which could be extended to ^{68}Ga -radiolabellings of other tracers.

EP651

Comparison of two alternative methods for RCP determination of ($^{99\text{m}}\text{Tc}$ -EDDA-HYNIC-D-Phe(1), Tyr(3))-Octeotride

C. Beltrán Gracia¹, M. Hernández Fructuoso², B. Santos Montero², E. Miñana Olmo², J. Castell Conesa³; ¹Hospital Universitari Vall d'Hebron. Radiopharmacy Unit, Barcelona, SPAIN, ²Hospital Universitari Vall d'Hebron - Institut de Diagnòstic per la Imatge. Radiopharmacy Unit, Barcelona, SPAIN, ³Hospital Universitari Vall d'Hebron. Nuclear Medicine Department, Barcelona, SPAIN.

Aim: ($^{99\text{m}}\text{Tc}$ -EDDA-HYNIC-D-Phe(1),Tyr(3))-Octeotride ($^{99\text{m}}\text{Tc}$ -Tecktrotyd®) is a radioligand for somatostatin receptor used for neuroendocrine tumors diagnostic. During its preparation there are several potential impurities: $^{99\text{m}}\text{Tc}$ -pertechnetate, $^{99\text{m}}\text{Tc}$ -colloid and $^{99\text{m}}\text{Tc}$ -coligand. RCP (Radiochemical Purity) must be at least 90%, determined according to the Summary of product characteristics (SPC) through Instant Thin Layer Chromatography (ITLC); but it only separates $^{99\text{m}}\text{Tc}$ -pertechnetate and $^{99\text{m}}\text{Tc}$ -colloidal impurities. The aim of this study was to compare two methods to determine $^{99\text{m}}\text{Tc}$ -coligand impurity, and to obtain a faster and more accurate method of RCP testing compared with SPC procedure. **Materials and methods:** RCP was tested at different times: $t=0$ ($n=10$) and $t>6$ h (expiration time)($n=7$). ITLC silica gel was performed using a two strip and solvent system: Methyl ethyl ketone was used to determine the amount of $^{99\text{m}}\text{Tc}$ -pertechnetate ($\text{Rf}=1$) and Acetonitrile/

Water 1/1 for $^{99\text{m}}\text{Tc}$ -colloid ($\text{Rf}=0$). A third ITLC-SG strip with 0.1M sodium citrate $\text{pH}5$ as solvent was used to determine $^{99\text{m}}\text{Tc}$ -pertechnetate and $^{99\text{m}}\text{Tc}$ -coligand ($\text{Rf}=1$). The ITLC strips were measured in a dose calibrator and in a TLC Scanner (Mini Gita). Alternative method with Solid Phase Extraction (SPE) was evaluated: Sep-Pak C-18 was conditioned with 5ml 95% ethanol and 5ml saline. After the sample was loaded onto the cartridge, it was washed with 5ml saline to remove hydrophilic impurities ($^{99\text{m}}\text{Tc}$ -pertechnetate and $^{99\text{m}}\text{Tc}$ -coligand). $^{99\text{m}}\text{Tc}$ -Tecktrotyd® was eluted with 5ml 95% ethanol followed by 5ml saline. The radioactivity of the eluates and the column were measured in a dose calibrator. **Results:** The RCP was calculated expressing the activity of $^{99\text{m}}\text{Tc}$ -Tecktrotyd® as percentage of the total activity measured. The results from SPC procedure were higher ($t=0$ h; $97.9 \pm 1.6/t>6$ h; 91.5 ± 4.2) than the other two methods. The results with citrate method ($t=0$ h; $92.6 \pm 3.4/t>6$ h; 85.9 ± 5.1) showed higher RCP compared to SPE, that showed the lowest values ($t=0$ h; $89.3 \pm 5.3/t>6$ h; 84.9 ± 4.7). The paired t -test showed statistical significant RCP differences between the three methods: SPC vs Citrate $t=0$ h($p=0.00005$), $t>6$ h($p=0.00004$); SPC vs SPE $t=0$ h($p=0.00003$), $t>6$ h($p=0.00018$) and Citrate vs SPE $t=0$ h($p=0.00518$), $t>6$ h($p=0.04127$). **Conclusion:** Using the method recommended by the manufacturer, we overestimate the RCP value, as it do not detect the amount of $^{99\text{m}}\text{Tc}$ -coligand. Using the alternative methods, we detect RCP values under specifications even in the shelf life of the labeled product. We recommend the use of SPE method in the clinical routine as it seems to determine all the impurities and it is faster and simpler than three strips TLC method.

EP652

Radiolabelling of DOTA^{MZOL} on an automated module System using NaCl post-processing

M. Meisenheimer, E. Eppard, S. Kürpig, M. Essler; University Hospital Bonn, Bonn, GERMANY.

Objectives: DOTA^{MZOL} is a bisphosphonate which can be used for diagnostic or therapeutic applications by radiolabelling it with ^{68}Ga or ^{177}Lu . It shows promising results in patients suffering from bone metastases. The aim of this study was to evaluate if it is possible to adapt the radiolabelling on an automated module utilizing NaCl-post processing, with regard to clinical application under additional radiation protection point of view. **Methodic:** ^{68}Ga was obtained from a 1 year old 1.85 GBq $^{68}\text{Ge}/^{68}\text{Ga}$ -generator (iThemba South Africa). Radiolabelling was performed on an automated cassette module (Gaia, Elysia-Raytest GmbH, Germany). DOTA^{MZOL} was obtained from (ITG, Garching, Germany). Modifications were made in comparison to standard labelling procedures in terms of cassette setup and eluents. Quality control was performed using radioTLC. Reactor screening was necessary with different surfaces and coatings of glass and plastic vials. **Results:** The reactor screening showed DOTA^{MZOL} is sensitive to reaction vials and therefore in need of a specific preconditioned vial otherwise unplanned side products are obtained. Furthermore an automated method was obtained and tested. Radiochemical impurities could be separated by adding an anion exchanger before the sterile filtration of the final formulated radiopharmaceutical. **Conclusion:** A new syntheses route for DOTA^{MZOL} was developed with reduced handling of radioactive materials which reduces the radiation exposure of the operator. It was possible to reduce the effect of the used reactor to a minimum and to develop a purification method suitable for routine production. Also it was possible to adapt the synthesis on an automated module system. The whole process guarantees safe preparation of highly pure ^{68}Ga -DOTA^{MZOL} for clinical application. **Acknowledgement:** The bisphosphonate was made available from ITG, Garching, Germany.

EP653**Arteriovenous Fistula Influence on Glomerular Filtration Rate Results in Hemodialyzed Patients**

J. GARCIA-REDONDO¹, E. MORILLO-MARTINEZ¹, L. SANZ-CEBALLOS¹, A. RAMIREZ-NAVARRO¹, J. LLAMAS-ELVIRA²; ¹Radiopharmacy Unit. Nuclear Medicine Department. COMPLEJO HOSPITALARIO UNIVERSITARIO DE GRANADA, GRANADA, SPAIN, ²Nuclear Medicine Department. COMPLEJO HOSPITALARIO UNIVERSITARIO DE GRANADA, GRANADA, SPAIN.

Introduction: In our Department, glomerular filtration rate (GFR) with 51-Cr-EDTA by means of serial blood extractions is used to determine renal function in kidney transplant patients or potential donors, however, sometimes certain patients have higher plasma activity values in later times than in previous, contrary to expectations. **Aim:** Evaluate the possible relationship between patients presenting this device and the presence of arteriovenous fistula for having been subjected to hemodialysis. **Patients and methods:** Retrospective observational study of patients undergoing GFR test in our Nuclear Medicine Department from January 2012 until March 2016. Data if came from dialysis and what type of dialysis were collected. The procedure was to inject a dose of 51-Cr-EDTA along a via in one arm and the opposite arm drawing blood in time 0', 5', 10', 20', 120', 180' and 240' from the injection of the radiopharmaceutical dose. In case of arteriovenous fistula by the hemodialysis, the injection of the radiopharmaceutical was in this same arm. For the bivariate analysis of qualitative variables Chi-square or Pearson test was used, considering statistical significance when $p < 0.05$. **Results:** 231 patients were studied, 174 came from hemodialysis and the remaining 57 came from a reference group consisting of patients undergoing peritoneal dialysis and patients not on dialysis. No cases with this device were observed in the control group, however, in the group of 174 from hemodialysis patients were observed 18 cases with this device. These results indicate that 10.3% of patients undergoing hemodialysis have this disorder, which represents a significant correlation ($p = 0.012$). **Discussion:** These results confirm the relationship between this disorder in plasma activity in the early stages of extraction and the presence of arteriovenous fistula because of having undergone hemodialysis, which makes suppose that in those cases in which vein injection fall into the fistula, this would act as a reservoir of the radiopharmaceutical, thus increasing the time of distribution of the same and causing this change.

EP654**Pharmaceutical development of albuminum microspheres labeled by rhenium-188 for hepatocellular carcinoma**

A. Zverev¹, V. Petriev², V. Skvortsov²; ¹Federal center of nuclear medicine projects design and development, Moscow, RUSSIAN FEDERATION, ²A. Tsyb Medical Radiological Research Centre, Obninsk, RUSSIAN FEDERATION.

Purpose. Pharmaceutical drug development based on radionuclide rhenium-188 and microspheres of human albumin (radiopharmaceutical) is for liver cancer therapy. The mechanism of action is as follows - after intra-arterial introduction of albumin microspheres 20-40 micrometers in diameter, rhenium-188 labeled particles deposit in the tumor and remain in the tumor area for a long time (up to a complete disintegration of the radionuclide rhenium-188); in addition to that tumor tissue receives a therapeutic dose of radiation due to internal beta-rhenium-188 with minimal damage to healthy liver tissue, which leads to growth inhibition and tumor regression. **Materials and methods.** A method for obtaining human blood albumin microspheres is based on the principle of an aqueous albumin solution emulsification in olive oil. During vigorous stirring, albumin solution droplets are formed in the oil with dimensions depending on the

stirring rate. When heated, heat denaturation of albumin occurs with the formation of spherical particles, and the water evaporates. The formed microspheres are filtered, washed with acetone and dried. The microspheres are suspended in ethyl alcohol and fractionated using microsieve. Fraction is extracted in the range of 20 - 40 microns. It is dried out to constant weight. Rhenium-188 is obtained from the stationary centrifugal extractor. The extraction technique includes uploading irradiated tungsten oxide (¹⁸⁸WO₃) into the extractor dissolved in a mixture of hydroxide and alkali metal carbonate. Then, it is passed through an extractant (MEK). The received extract containing ¹⁸⁸Re, is evaporated to dryness and then it is dissolved by isotonic solution (0,9% NaCl solution), thereby obtaining a sodium perrhenate, ¹⁸⁸Re, required for the preparation of radiopharmaceuticals. **Results.** - microspheres size (20-40 microns); - the radiochemical purity of radiopharmaceutical - not less than 95%; - radiochemical impurities are not more than 5%; - stability of the labeled drug is not less than 5 hours from the time of production; - volume activity of radiopharmaceutical - 30-50 mCi /mL (1,11-1,85 GBq/ml); - safety - the forecast ratio of efficacy and toxicity will be positive. **Conclusion.** The composition and the form of the radiopharmaceutical preparation kit for the treatment of hepatocellular carcinoma and liver metastases is designed. Its main indicators of quality are offered. Theoretically and experimentally drug dosage form is developed. The prospects of development of the drug set conditions for the possibility of obtaining rhenium-188 from the sorption generator (¹⁸⁸W / ¹⁸⁸Re), allowing to apply the drug just before introducing it to the patient.

EP655**Evaluation of the accuracy and precision of a combine automatic system of FDG dose-dispensation and injection and its impact in operator radiation exposure.**

I. Romero-Zayas¹, P. Saldaña-Gutierrez², C. Gámez-Cenzano¹, G. Reynés-Llompart¹, S. Rustarazo-Losada¹, D. Mateo-Navarro¹, I. Ferrero-Febrer¹, I. Liarte-Trías¹, M. Albadalejo-Castaño¹, A. Cebrián-Leiva¹, D. Coca-Castro¹, C. Picón-Olmos², M. Roca-Engronyat¹; ¹Radiopharmacy and PET Units. Nuclear Medicine. IDI. Hospital U.de Bellvitge-IDIBELL, L'Hospitalet de Llobregat, Barcelona, SPAIN, ²Medical Physics.ICO.Hospital U.De Bellvitge-IDIBELL, L'Hospitalet de Llobregat, Barcelona, SPAIN.

AIM: The aim of this study was to evaluate the accuracy and precision of the dispensed FDG doses and the impact in operator radiation exposure using an automatic dose-dispensing and injector system. **MATERIAL AND METHODS:** KAR1100 (Temasinerjie) is an automatic motile dose-dispensing unit of FDG, which is used with a portable automatic injection pump, RAD-INJECT. The accuracy and precision was evaluated in 6561 dispensed doses (since September 2014 to December 2015), by using the difference between the requested activity dose and the dose dispensed automatically. The effective use of FDG supply was analysed measuring the residual dose in a sample of 150 after the loading procedure to the automatic system. The residual doses were also measured in a sample of 50 disposable syringes after patient infusion. The radiation exposure using a combined dose-dispensing and injection system was evaluated in 5 operators with the data from wrist, ring and badge dosimeters and it was compared with the manual dispensing and administration procedure. **RESULTS:** The mean accuracy (in absolute value) and precision of the dispensed doses was 0,15% (SD=3,59). The mean residual radioactivity in the manufacturer vial of FDG after the loading procedure was 174,6 MBq (SD= 191,5). It corresponds to the mean percentage of 3,10% (SD= 2,87). There was an inversely linear correlation with the amount of activity received ($r=-0,13$; $p<0,001$). The mean residual radioactivity in a sample of 50 syringes patient infusion was 0,67MBq (SD= 0,87). The mean effective dose received by the operators in 1 year using this system was: 1.63 mSv in ring dosimeter, 0.73 mSv in wrist dosimeter and 0.37 mSv in badge dosimeter. This corresponds to a decrease in 93.6%, 75.7%, 21.7% respectively when it is compared with a similar

period of time and clinical activity using a manual dispensing and injection technique. **CONCLUSION:** The combined automatic dose-dispensing and injection system has satisfactory accuracy and precision. An adequate effective use of the received FDG and dispensed/administrated FDG has been found (loss of FDG in the procedure loading and residual activity in the syringes are negligible). The radiation exposure of the operators is significantly reduced compared to manual protocol, especially in the extremities.

EP656

^{99m}Tc-Technetium radionuclide radiation measurements using a miniaturized gamma dosimeter

L. SANZ-CEBALLOS¹, J. CESARI², A. BARBANCHO², A. PINEDA², A. RAMIREZ-NAVARRO³, J. LLAMAS-ELVIRA⁴; ¹Radiopharmacy Unit Nuclear Medicine Department. Complejo Hospitalario Universitario de Granada, Granada, SPAIN, ²Integrated Circuits Malaga SL, Alaro, SPAIN, ³Radiopharmacy Unit Nuclear Medicine Department. Complejo Hospitalario Universitario de Granada, Granada, Spain, Granada, SPAIN, ⁴Nuclear Medicine Department Complejo Hospitalario Universitario de Granada, Granada, SPAIN.

Aim The aim of this work is to analyze the response of the miniaturized gamma dosimeter to see the sensitivity, linearity and other effects on the dosimeter to the ^{99m}Tc radionuclide. **Materials and methods** The materials used were two Floating gate (FG) gamma dosimeters integrated in one QFN32 package of 5x5 mm and mounted in a PCB and connected via USB to the computer. The computer was in charge via software to collect the data from both dosimeters with the rate of one sample every two seconds more or less. Samples of 5, 10 and 20 mCi of ^{99m}Tc were prepared in a five milliliter vial and measured with the reference activimeter (Atom Lab 400, Biodex). The measures were done during one, two or three hours depending on the dose. One run for each dose. This long time exposure was needed to see the Total Ionizing Dose (TID) accumulated by the dosimeter and also to have more relevant data as a first data measured from this kind of radionuclide with the dosimeter. The measures were carried out with the sensor attached to the external part of the vial. The measures from both dosimeters are compared and scaled versus the expected decay during the time from the ^{99m}Tc. All dosimeters were pre-characterized in temperature to remove the temperature effect from the measurements. The data collected from the dosimeters include the temperature for each sample and it permitted from the characterization curve in temperature to remove the temperature effect on the measures. **Results** The correlation with the data from the dosimeters and the expected decay curve from the radionuclide fits very well. The factor equivalency from mCi to TID is about 56,5 for the run one, 30.38 for the run two and 15 for the run three and the same equivalence factor for both dosimeters. From that values can be seen how the dosimeter has a lineal response for the different activities studied. **Conclusions** The dosimeters can measure linearly and with enough time the ^{99m}Tc radiation for activities ranges commonly used in a Radiopharmacy Unit. A coupling effect when the dosimeters are attached and unattached from the vial was observed and must be investigated. More investigation must be carried out to fix the sensitivity and limitations of the dosimeter for this radionuclide. Moreover other radionuclides should be studied.

EP657

On-chip gamma dosimeter measures comparison between ^{99m}Tc-Technetium and ⁶⁰Co radionuclides

L. SANZ-CEBALLOS¹, J. CESARI², A. BARBANCHO², A. PINEDA², A. RAMIREZ-NAVARRO¹, J. LLAMAS-ELVIRA³; ¹Radiopharmacy Unit Nuclear Medicine Department. Complejo Hospitalario Universitario de Granada, Granada, SPAIN, ²Integrated Circuits Malaga SL, Alaro, SPAIN, ³Nuclear Medicine Department. Complejo Hospitalario Universitario de Granada, Granada, SPAIN.

Aim To compare radiation measures on two different radionuclides (⁶⁰Co and ^{99m}Tc) using the same on-chip gamma dosimeter to the aim of finding future applications and upgrades on the dosimeter. **Materials and methods** The materials used were two Floating gate (FG) gamma dosimeters integrated in one QFN32 package of 5x5 mm and mounted in a PCB and connected via USB to the computer. The computer was in charge via software to collect the data from both dosimeters with the rate of one sample every two seconds more or less. Samples of 5, 10 and 20 mCi of ^{99m}Tc were prepared in a five milliliter vial and measured with the reference activimeter (Atom Lab 400, Biodex). The measures were done during one, two or three hours depending on the dose. One run for each dose. This long time exposure was needed to see the Total Ionizing Dose (TID) accumulated by the dosimeter and also to have more relevant data as a first data measured from this kind of radionuclide with the dosimeter. The measures were carried out with the sensor attached to the external part of the vial. The ⁶⁰Co radionuclide measures were done at different dose rates and time exposures using the same dosimeter. The dosimeter was at different distances from the gamma source depending on the dose rate desired. Three different dose rates were measured (20, 200 and 2000 rad/h). All dosimeters were pre-characterized in temperature to remove the temperature effect from the measurements. **Results** The measures from both radionuclides using the same dosimeter are discussed. The dosimeter shows a difference in terms of sensitivity response depending of the radionuclide. The output sensitivity for the ⁶⁰Co is around 300 Hz/rad and for the ^{99m}Tc 100 Hz/rad. The accuracy on the measure in terms of noise measured in the output is the same for both radionuclides. In addition when dosimeters are attached and unattached to the vial for the ^{99m}Tc measures an output coupling is observed. **Conclusions** The dosimeter behavior and performance measuring both radionuclides are the expected. The difference in terms of sensitivity between radionuclides measures must be because of the different energy emission for the gamma at each radionuclide (for ⁶⁰Co is about 1.1 MeV for the ^{99m}Tc is about 140 keV). More measures with similar dose rates and activities shall be performed. The coupling effect due to the measure attached to the ^{99m}Tc radionuclide must be investigated.

EP-36 – Sunday, October 16, 2016, during Exhibition hours, e-Poster Area

M2M: Technologies & Models

EP658

Image quality assessment of ALBIRA II PET system based on a range of positron-emitters

A. Attarwala¹, Y. Karanja¹, D. Hardiansyah¹, C. Romanó¹, M. Roscher², B. Wängler², G. Glattig¹; ¹Medical Radiation Physics/Radiation Protection, Universitätsmedizin Mannheim, Medical Faculty Mannheim, Heidelberg University, Mannheim, GERMANY, ²Molecular Imaging and Radiochemistry, Institute for Clinical Radiology and Nuclear Medicine, Medical Faculty Mannheim, Heidelberg University, Mannheim, GERMANY.

Aim: This study analyzes the performance characteristics of the Albira PET sub-system based on measuring the response of the system for the following positron-emitters: ¹⁸F, ⁶⁸Ga, ⁶⁴Cu and ⁸⁹Zr in small animal imaging. **Materials and Methods:** The Albira tri-modal system (Bruker BioSpin MRI GmbH, Ettlingen, Germany) is a pre-clinical device with a PET, SPECT and CT. The PET sub-system is made up of single continuous crystal detectors of lutetium yttrium orthosilicate (LYSO) coupled to position-sensitive photomultipliers (PSPMTs). The detector assembly consists of three rings and eight detector modules. The trans-axial field of view (FOV) is 80 mm and the axial FOV is 148 mm. NEMA NU-4 image quality phantom (Data Spectrum Corporation, USA) having five rods (Ø 1-5 mm) and uniform central region was used

to analyse the system sensitivity and recovery coefficients. Measurements with ^{18}F , ^{68}Ga , ^{64}Cu and ^{89}Zr were performed with a starting activity concentration of 700 kBq/ml. Spatial resolution (NEMA NU-4 2008 method) was calculated based on an in-house phantom developed of polymethylmethacrylate (PMMA) with dimensions of (60x60x10) mm³ containing cylindrical capillaries with a diameter of 1.2 mm, filled with a 1 μl point source solution of the respective radionuclide positioned at the geometric centre of the FOV. An energy window of 358–664 keV and a coincidence time window of 5 ns were selected. The data were reconstructed with a maximum likelihood expectation maximization (MLEM) algorithm; voxel size of 0.5 mm and iterations from 5 to 50 (step-size 5). All analyses were performed with PMOD software (PMOD Technologies Ltd., Switzerland) and MATLAB (R2015a, MathWorks, Natick, Massachusetts, USA). **Results:** The overall sensitivities for the entire FOV corrected for branching ratios were (3.78 \pm 0.05) %, (3.97 \pm 0.18) % and (3.79 \pm 0.37) % and (3.24 \pm 0.19) % for ^{18}F , ^{68}Ga , ^{64}Cu and ^{89}Zr , respectively. The spatial resolution in the x, y and z orientation was calculated and the median FWHM were 1.77 mm (^{18}F), 2.29 mm (^{68}Ga), 1.76 mm (^{64}Cu) and 1.74 mm (^{89}Zr). The image reconstruction algorithm converged after 25–30 iterations for all four radionuclides. The recovery coefficients for the 5 mm rod with an activity concentration of 400 kBq/ml were (0.77 \pm 0.13) ^{18}F , (0.51 \pm 0.08) ^{68}Ga , (0.89 \pm 0.20) ^{64}Cu and (0.58 \pm 0.11) ^{89}Zr , respectively. **Conclusion:** The Albira PET system has a comparable sensitivity range for the activity used for pre-clinical imaging for all the investigated radionuclides and the results indicate the system is a valuable tool for quantitative non-invasive small animal imaging studies.

EP659

Establishment of Hybrid Baculovirus-Sleeping Beauty 100 \times Vector-mediated Reporter Gene Imaging System

Y. Pan, J. Lv, Y. Zhang; Rui Jin Hospital, Shanghai Jiao Tong University School of Medicine, Shanghai, CHINA.

Reporter gene imaging can be used to non-invasively and repetitively monitor various cellular and intercellular events *in vivo*, like gene delivery, endogenous gene expression and cell trafficking, most of them required stable or long-term monitoring. The commonly used stable transgenic viral vector in reporter gene imaging system is retrovirus or lentivirus, which have their own instinct limitations. Recent years, baculovirus as a novel attractive viral vector with many distinctive superiorities has been developed and broadly accepted, however the short-term transgene expression was its shortcoming. In this study, we introduced a *Sleeping Beauty* 100 \times transposon gene and neomycin resistance gene into baculoviral vector to achieve a hybrid vector (BV-SB100 \times). A high titer BV-SB100 \times vector (higher than 10⁹ pfu/mL) was prepared according Bac-to-Bac system. The U87 cells and FTC-133 cells were infected by various types of BV-SB100 \times vector containing different reporter genes and selected by G418 for obtaining reporter gene stable-expressing cell lines. The results showed that these stable cell lines both maintained a long-term enhanced green fluorescent protein (eGFP) reporter gene expression for at least 180 days by the end of this study, with a stable expression level of more than 95% eGFP positive cells, compared with other constructed baculoviral vectors-mediated eGFP positive cells dropped to 10% in less than only 18 days. Reverse transcription PCR of different viral vector-infected cells in day1 or day 35 after infection also confirmed this result. CCK-8 cytotoxicity and proliferation assay indicated the biosafety of all different baculoviral vectors on two cell lines. BV-SB100 \times vector-mediated stable-expressed herpes simplex virus-1 thymine kinase could catalyze the ganciclovir, while the stable-expressed glucagon-like peptide-1 receptor (GLP-1R) could bind to its labelled ligand fluorescein-Trp²⁵-exendin-4. The eGFP fluorescent imaging showed a 35 days stable eGFP imaging *in vivo* after U87 cells transplantation, the further tumor frozen section analysis showed the high overlapping ratio of eGFP expression and DAPI nuclear staining in formed U87

tumors. At the end, GLP-1R radionuclide reporter gene imaging also confirmed the BV-SB100 \times vector-mediated long-term imaging *in vivo* for more than 50 days by nuclear medicine modality. In summary, the hybrid BV-SB100 \times vector could prolong the reporter gene expression as well as the reporter gene imaging, which would offset the drawback of transient transgene expression of baculovirus and broad the application of baculoviral vector.

EP660

Evaluation of Quantitative Accuracy of Tc-99m Small-Animal SPECT Imaging in Phantom Studies

S. Khorasani Gerdekoohi^{1,2}, N. Vosoughi¹, K. Tanha³, M. Assadi³, M. Ay^{2,4}; ¹Department of Energy Engineering, Sharif University of Technology, Tehran, IRAN, ISLAMIC REPUBLIC OF, ²Research Center for Molecular and Cellular Imaging, Tehran University of Medical Sciences, Tehran, IRAN, ISLAMIC REPUBLIC OF, ³Persian Gulf Nuclear Medicine Research Center, Bushehr University of Medical Sciences, Bushehr, IRAN, ISLAMIC REPUBLIC OF, ⁴Department of Medical Physics and Biomedical Engineering, Tehran University of Medical Sciences, Tehran, IRAN, ISLAMIC REPUBLIC OF.

Aim: The purpose of single photon emission computed tomography (SPECT) imaging is to determine absolute amount of activity in body. The goal of this study is to investigate the feasibility of absolute quantification of a small-animal SPECT images in HiReSPECT scanner, the developed scanner in our department. **Materials and methods:** Image reconstruction code of system is based on maximum likelihood expectation maximization (MLEM) method including a resolution recovery algorithm during the iterative reconstruction. Decay compensation is done during data acquisition too. We also applied a post-processing uniform attenuation correction to compensate degradation of photon attenuation. To convert image matrix values to activity concentration (MBq/ml) we achieved a calibration factor (CF) by scanning a point source. Distance dependence of CF calculated to obtain it in all needed radius of rotations (ROR). For evaluating quantitative accuracy thirteen point sources which were almost attenuation free with known activities were scanned. Six cylindrical tubes with different volumes were scanned in same acquisition parameters too. Furthermore, we performed an experiment on the NEMA NU4-2008 image quality phantom to examine the relative error in estimation of activity concentration of its uniform region and hot rods. **Results:** In point sources, correlation between activities those were achieved by the dose calibrator and those estimated values using image matrix showed that difference between these two methods is not significant ($p=0.98$). Images of cylindrical phantoms results in RCs from 0.60 for 1ml tube to 1.02 for 30ml tube which means that by increasing the size of scanned object and decreasing the influence of partial volume effect, the quantitative accuracy has improved. In image quality phantom, RCs of hot rods in attenuation corrected images obtained 0.38, 0.65, 0.80, and 0.88 for hot rods with diameters of 2, 3, 4, and 5mm, respectively and it was improved 19% by applying correction for rod with diameter of 5mm. Finally, the relative error in estimation of activity concentration reduced from -15.5% to +5.1% in the uniform region of the phantom after applying attenuation correction. **Conclusion:** Our results show that reliable quantitative analysis in HiReSPECT scanner is feasible and also attenuation correction has a crucial role in improvement of quantitative accuracy.

EP661

γ -eye: Forward to small animal in-vivo imaging

M. Georgiou¹, P. Papadimitriou¹, E. Fysikopoulos¹, K. Mikropoulos¹, G. Loudos²; ¹BioEmissionTechnology Solutions, ATHENS, GREECE, ²Technological Educational Institute of Athens, ATHENS, GREECE.

Introduction-Purpose Small animal imaging has been well proven as a robust tool to non-invasively study the biodistribution of various biomolecules. A number of imaging systems are commercially available but with high purchase and maintenance costs. For this reason, we present the “ γ -eye”, a dedicated γ -camera suitable for in-vivo scintigraphic molecular imaging. The “ γ -eye” is a unique benchtop system with $5 \times 10 \text{ cm}^2$ field-of-view for whole-body dynamic and static mouse imaging. **Materials & Methods** The “ γ -eye” is based on two Position Sensitive Photomultiplier Tubes H8500 coupled to a CsI_{Na} pixelated scintillator and a general purpose parallel hexagonal hole collimator. The external dimensions of the entire system, including all required electronics, are $45 \times 30 \times 30 \text{ cm}^3$. All studies can be stored as raw data and in DICOM format and are handled through a Database-Manager. The software supports a real-time viewer mode with selectable time frame and a post-processing mode, where various tools are adapted. **Results** The spatial resolution was measured $2 \text{ mm} @ 0 \text{ mm}$, the energy resolution for the 140 keV is 26% and the maximum sensitivity of the system is 200 cps/MBq . The quantification ability was assessed using a phantom of 4 tubes filled with $^{99\text{m}}\text{Tc}$ solution with different activities. Our results demonstrate accurate quantitative information even for 10sec scans. The system was tested using a mouse injected with $^{99\text{m}}\text{Tc}$ -MDP for bone imaging, a mouse injected with $^{99\text{m}}\text{Tc}$ -DMSA for kidneys imaging and finally a mouse injected with $^{99\text{m}}\text{Tc}$ -MIBI for heart imaging. **Conclusion** A new low-cost system, suitable for scintigraphic mouse imaging has been developed and evaluated using phantoms and small animals. Its dimensions and cost make it a unique solution for groups activated in the field of small animal nuclear imaging.

EP662

Abscisic acid improves glucose tolerance in rats. A FDG-microPET study

A. Nieri¹, A. Buschiazio¹, M. Magnone², F. Ticconi¹, L. Emionite³, A. Democrito¹, C. Ghersi¹, A. Bozzano¹, G. Bottoni¹, A. Oregno¹, L. Sturla², C. Marini⁴, E. Zocchi², G. Sambucetti¹; ¹Nuclear Medicine Unit, Department of Health Sciences, University of Genoa and IRCCS AOU San Martino-IST, Genoa, ITALY, ²Department of Experimental Medicine, University of Genoa, Genoa, ITALY, ³Animal facility, IRCCS AOU San Martino-IST, Genoa, ITALY, ⁴CNR Institute of Bioimages and Molecular Physiology, Milan, Section of Genoa, Genoa, ITALY.

Aims Abscisic acid (ABA) is a plant hormone, present also in mammals. In vitro, nanomolar ABA concentrations stimulate GLUT4-mediated glucose uptake in myoblasts and adipocytes. In vivo, oral glucose load increases serum ABA concentration in healthy human subjects, but not in diabetic patients. In the present study, we aimed to verify the effect of single oral ABA microdose (1 $\mu\text{g/Kg}$) on glycemic response to oral glucose load in rats and the mechanisms underlying this action by a dynamic microPET approach.

Materials and Methods All animal experiments were reviewed and approved by the Licensing and Ethical Committee of our Institute and by the Italian Ministry of Health. Eight male Wistar rats, fasted for 18 h, underwent glucose load without (control) or with ABA at 1 $\mu\text{g/Kg}$ of body weight in a random sequence. Immediately after gavage, rats were anesthetized with intra-peritoneal administration of diazepam (4 mg/kg) followed by intramuscular administration of ketamine (33 mg/kg)/xylazine (5 mg/kg). Serum glucose level was tested and animals were positioned on the bed of a dedicated micro-PET system (Albira, Bruker, US) centering the scanner field of view on the chest. A dose of 30–45 MBq of FDG was then injected through a tail vein, soon after start of a list mode acquisition lasting 50 minutes. A volume of interest (VOI) was manually drawn over the left ventricle to identify the arterial input function that was used to obtain parametric maps of glucose consumption (MRGlu) by Patlak analysis using the routine of a dedicated software (PMOD, Zurich, CH). **Results** At tracer injection, serum glucose level was significantly lower after ABA with respect to control conditions (211 ± 70 vs 263 ± 75 mg/dL, respectively, $p < 0.01$). In agreement with this observation, ABA administration markedly increased blood FDG clearance

(from 0.005 ± 0.002 to 0.011 ± 0.004 ml/min/g of body weight, respectively, $p < 0.01$) and thus overall whole-body glucose consumption (from 26.07 ± 8.5 to 46.31 ± 14.3 nMol/min/g of body weight, respectively, $p < 0.05$). This finding closely agreed with the metabolic response of skeletal muscles and brown adipose tissue whose MRGlu doubled after treatment with respect to control condition (from 32 ± 16 to 66 ± 20 nMol/min/g of body weight and from 100 ± 30 to 208 ± 100 nMol/min/g, respectively, $p < 0.01$). **Conclusion** Dynamic microPET studies indicate the capability of ABA in decreasing glycemia in response to an oral glucose load increasing the muscle and BAT glucose consumption.

EP663

Longitudinal SPECT studies on thyroid uptake in mice over a period of 24 months with respect to age, sex and circadian rhythm

N. Beindorff^{1,2}, A. Brönnner¹, E. L. Huang¹, K. P. Huang¹, M. Lukas¹, C. Lange¹, I. G. Steffen¹, W. Brenner^{1,2}; ¹Department of Nuclear Medicine, Charite - Universitaetsmedizin Berlin, Berlin, GERMANY, ²Berlin Experimental Radionuclide Imaging Center, Berlin, GERMANY.

Aim: The aim of this longitudinal exploratory study was to establish normal values for the thyroid uptake of Tc-99m-pertechnetate as a function of age, sex and circadian rhythm in healthy mice. **Materials and methods:** In isoflurane anesthetized 11 female and 11 male C57BL/6 mice 9 consecutive multi-pinhole SPECT images of 10 min duration each were acquired as quasi-dynamic acquisition (nanoSPECT/CTplus, Bioscan/Medisso) starting at 5 min after intravenous injection of approx. 80 MBq Tc-99m-pertechnetate. Each mouse was imaged in follow-up studies up to 24 months (A: 1 month, puberty; B: 3 months, sexual mature, but not fully grown; C: 6 months, fully grown; D: 12 months; E: 24 months). In order to monitor circadian rhythm, animals were imaged during light (sleeping phase (SP)) as well as during night conditions (awake phase (AP)). Image viewing and quantification were performed using PMOD 3.4. The percentage tracer uptake of the injected activity is expressed as median [interquartile range; IQR]. Differences between groups were analysed using Mann-Whitney-U test and paired Wilcoxon test. **Results:** Maximum thyroid uptake in mice occurred between 10 and 45 min after injection of Tc-99m-pertechnetate. Female mice showed a significantly higher uptake than males (female 1.7 [1.5-1.8], male 1.2 [1.1-1.2] $P < 0.001$). This effect could be observed up to an age of 12 months: A (female 1.6 [1.5-1.7], male 1.1 [1.1-1.3] $P < 0.001$), B (female 1.7 [1.5-1.9], male 1.2 [1.0-1.2] $P < 0.001$) C (female 1.8 [1.7-2.1], male 1.2 [1.1-1.3] $P < 0.001$), D (female 1.6 [1.5-1.7], male 1.2 [1.1-1.2] $P < 0.001$), E (female 1.1 [1.1-1.3], male 1.2 [1.1-1.2] $P = 0.79$). A sex-related impact of age on thyroid uptake cannot be excluded in females ($P = 0.059$) but in males ($P = 0.26$). No relevant effect of circadian rhythm could be observed both in females (SP 1.6 [1.5-1.8], AP 1.7 [1.5-1.9]) and males (SP 1.2 [1.1-1.3], AP 1.1 [1.0-1.2]). **Conclusion:** This study showed a significant influence of sex on thyroid uptake of Tc-99m-pertechnetate in mice. Sex seems also relevant for age-related effects, which could be observed in females but not in males. In contrast to sex and age, circadian rhythm had no relevant impact on thyroid uptake. Therefore, the design of thyroid studies in mice using Tc-99m-pertechnetate should consider sex, and age in females as relevant factors, while circadian rhythm seems to be negligible.

EP664

BODIPY: a highly versatile platform for the design of MonoMolecular Multimodal Imaging Probes

C. Goze¹, M. Ipy¹, N. Maindrion¹, D. Lhenry¹, C. Bernhard¹, M. Moreau¹, P. Provent², A. Oudot³, B. Collin³, J. Vrigneaud³, F. Brunotte³, F. Denat¹; ¹ICMUB-UMR CNRS 6302, Dijon, FRANCE, ²Oncodesign, Dijon, FRANCE, ³Centre G. F. Leclerc, Dijon, FRANCE.

Objectives. Due to their complementarity, combining fluorescence imaging with nuclear imaging techniques (PET or SPECT) can be advantageous both for preclinical and clinical use. The aim of our project is the elaboration of multimodal probes for optical/SPECT-PET imaging based on a BODIPY fluorophore. BODIPY derivatives appear as promising candidates for preclinical as well as clinical (surgery assistance) optical imaging applications owed to their excellent photochemical and photophysical properties, as well as a better stability when compared to the commonly used cyanines. **Methods.** Among the different approaches for the design of multimodal imaging agents, the MOMIP (Monomolecular Multimodal Imaging Probes) systems present numerous advantages compared to the conventional “dual labelling” approach. We synthesized two MOMIP based on a distyryl-BODIPY using two different amino acid platforms, which was coupled to three DOTA macrocycles (TBK-686 and TBY-684). The photophysical properties of the different compounds and their “cold metallated” complexes were investigated, as well as their stability in serum. The most promising MOMIP, TBK-686, was activated and bioconjugated to trastuzumab via the lysine residues of the antibody. ^{111}In radiometallation of the resulting imaging agent was investigated. Additionally, the ability of TBK-686 trastuzumab to target HER2+ expressing tumor was studied *in vivo* in a model of BT474 tumor bearing mice. Whole-body fluorescence images were recorded at 24h and 48h post injection. *Ex-vivo* imaging was performed to provide semi-quantitative information about the tracer biodistribution, when the tissue absorption and autofluorescence were reduced at minimum. **Results.** The BODIPY core did not affect the radiolabeling efficiency of the antibody conjugate (specific activity = 490 MBq/mg). The ^{111}In -conjugate remains fluorescent after radiolabeling, and is stable even in the presence of 2000-fold molar excess of DTPA. *In vivo* biodistribution studies revealed that the NIR fluorescence signal emitted by the BODIPY core can be easily detected at the tumor site. *Ex-vivo* imaging confirmed that a higher fluorescence intensity was observed in the tumor rather than in other organs, which demonstrates that the dual labeled trastuzumab is able to accumulate in the HER2-positive tumor. **Conclusion.** The BODIPY-based MOMIP TBK-686 reported herein is a valuable tool for bimodal imaging. A dual imaging study (SPECT-optical imaging) is currently investigated.

EP665

Pre-targeting of the chemokine receptor 4 via activatable and de-activatable fluorescent constructs

T. Buckle, S. van der Wal, D. M. van Willigen, C. M. de Korne, F. W. B. van Leeuwen; LUMC, Leiden, NETHERLANDS.

Background Internalization of receptor targeting imaging agents is a key aspect of their function, but can be hard to assess. “Traditional” activatable dyes can be used to provide enhanced fluorescence upon internalization and subsequent enzymatic cleavage. This concept is, however, complex to apply for targeting tracers. Using a pre-targeting concept we developed a de-activatable chemokine receptor 4 (CXCR4)-targeted tracer wherein the fluorescence of the extracellular portion of the tracer could be turned off via a secondary click chemistry. The efficacy of this approach was tested against an activatable tracer targeted against CXCR4. **Methods** Ac-TZ14011, a CXCR4 specific peptide, was coupled to 1) an activatable FRET dye construct wherein a Cy3 dye was linked to a Cy5 dye through a reduction-cleavable disulfide bond and 2) a Cy5 dye that contained a chemo-selective azide handle suitable for pre-targeting applications with a FRET and stacking inducing DBCO-containing Cy7 quencher dye. Besides tracer assessment in solution, receptor-specific binding of the tracers (1 μM) and subsequent visualization of cellular internalization was evaluated in CXCR4 over-expressing MDAMB231 X4 cells. **Results** The FRET efficiency of the disulfide-bridge containing activatable tracer ($K_d > 500 \text{ nM}$) was 55% and a limited 2.3-fold

increase in fluorescence was seen upon reduction in solution. Fluorescence imaging in viable cells revealed a similar effect; only a weak membranous staining and subsequent increase in the Cy3 signal in the cytoplasm of the cells was observed. In contrast, the de-activatable tracer set-up demonstrated that addition of the Cy7- quencher to the Cy5-azide labeled peptide ($K_d = 177 \pm 18.8 \text{ nM}$) resulted in a fast (2-5 minutes) and >90% reduction of the Cy5 signal in solution. Addition of the quencher resulted in an 80% decrease in the membranous staining within the first 10 minutes, while fluorescence of internalized tracer-component was preserved. **Conclusions** De-activatable fluorescence tracers were shown to provide a promising alternative for activatable tracers. Moreover, the click chemistry-based pre-targeting approach proved to be efficient and enabled clear assessment of the internalized fraction of the targeted tracer.

EP666

Pharmacokinetic of tumor FDG uptake in subcutaneous and orthotopic preclinical models of breast cancer - Influence of administration route

A. Oudot¹, J. M. Vrigneaud¹, O. Raguin², M. Guillemin¹, P. Provent², B. Collin^{1,3}, F. Brunotte^{1,4}; ¹CGFL Preclinical imaging platform, Dijon, FRANCE, ²OncoDesign, Dijon, FRANCE, ³ICMUB - CNRS 6302, UBFC, Dijon, FRANCE, ⁴Le2i - CNRS 6306, UBFC, Dijon, FRANCE.

Aim: Numerous studies evaluated FDG tumor uptake using microPET imaging in preclinical models. In parallel, many orthotopic tumors models were developed to better mimic human pathology. Our objective were i) to better characterize the kinetic of tumor uptake of FDG in subcutaneous and orthotopic models of breast cancer xenografts in mice, and ii) to evaluate alternative routes of administration of FDG injection that could be useful in preclinical studies involving repeated treatments with drugs via intravenous route. **Materials and methods:** NOD Scid mice were subcutaneously xenografted with BT-474 cells (HER2+ human breast cancer) and Balb/C mice were grafted in the mammary fat pad with 4T1 cells (triple negative mouse breast cancer). When tumors reached 200 mm³, mice were randomized in subcutaneous (sc), intraperitoneal (ip) or intravenous (iv) FDG injection groups. The pharmacokinetic of FDG tumor uptake was evaluated in fasted mice by a 90-min dynamic list mode PET imaging after a single injection of FDG (4-6 MBq). Analyses were performed in reconstructed PET-CT images after delineation of a region of interest corresponding to the entire tumor. **Results:** In mice bearing subcutaneous BT-474 tumors, FDG tumor uptake plateaued within 15-20 min after iv injection, 30-35 min after ip injection and 50-60 min after sc administration. Tumor FDG contents at 90 min were similar in iv- (0.68±0.09 SUV units) or sc- (0.69±0.09 SUV units) injected mice but lower in ip-injected mice (0.55±0.04 SUV units). In orthotopic 4T1 tumors, FDG uptake appeared to be slowed down for both iv and sc groups. In ip group, tumor delineation was delicate due the vicinity of ip cavity. As for subcutaneous tumors, orthotopic 4T1 tumor FDG content was similar in iv- (0.87±0.11 SUV units) or sc- (0.86±0.07 SUV units) injected mice at 90 min post-administration. In both tumor models, i) similar FDG uptakes (SUVmean and SUVmax) were measured in iv groups after 20, 30 or 45 min uptake period, ii) FDG tumor uptake measured 60 min post-sc injection was similar to that measured 30 min post-iv injection. **Conclusion:** The present work showed that the kinetic of FDG tumor uptake was different in subcutaneous and orthotopic mice models of breast cancer and that ip FDG administration may not be a relevant option to replace iv FDG injection. Subcutaneous administration of FDG can however be considered as an alternative route of administration, provided that the uptake period is extended to ensure that the uptake plateau is reached.

EP667**Feasibility of [¹⁸F]-FDG micro PET of resected, vital non-small cell lung cancer ex vivo**

J. de Swart, T. G. Meijer, N. S. Verkaik, G. N. Doeswijk, J. F. Veenland, D. C. van Gent, A. P. W. M. Maat, J. H. von der Thüsen, R. Kanaar, M. de Jong, S. F. Petit; Erasmus MC, Rotterdam, NETHERLANDS.

Aim: 2-deoxy-2-[¹⁸F]fluoro-D-glucose ([¹⁸F]FDG) is a well-known and often used radiopharmaceutical in PET imaging of, among others, tumour tissue *in vivo*. We investigated the feasibility of performing PET scans of small *ex vivo* non-small cell lung cancer (NSCLC) tissue slices as a prediction of tumour response to therapy. **Method:** After surgical resection, from three patients surplus material of the NSCLC tumour was cut in 300 µm thick slices. These slices were cultured using RPMI 1640 medium for 2–6 days at 37 degrees Celsius. Next, [¹⁸F]FDG 11.4 ± 5.2 MBq was added to the medium and incubated on an orbital shaker (60 rpm) for 30 minutes at room temperature, washed in PBS on the orbital shaker for 30 minutes, washed again with PBS and placed in a micro PET scanner (Siemens Inveon, Knoxville, USA). A 30 minutes emission scan of a single bed position was made, followed by a transmission scan using two ⁵⁷Co sources. To a number of the slices 1, 10 or 30 µg/mL cis-diamminedichloridoplatinum(II) (cisplatin) was added to the medium from the onset of the culturing period to eradicate tumour cells enabling discrimination between specific and non-specific uptake of [¹⁸F]FDG in the slices. The PET scans were reconstructed using the OSEM3D algorithm (2 iterations) and the Maximum A Posteriori (MAP) algorithm (18 iterations). The smoothing factor was set to 0.8 mm. **Results:** All slices showed a clearly heterogeneous [¹⁸F]FDG uptake pattern. The slices that had not been treated with cisplatin or with 1 µg/mL had uptakes of 6.4 ± 1.4% (mean ± SD) and 5.8 ± 2.1%, respectively, of the added [¹⁸F]FDG. In contrast, slices that had been treated with 10 or 30 µg/mL cisplatin showed a much lower uptake (0.68% and 0.44% respectively). **Conclusion:** It is feasible to image the specific uptake of [¹⁸F]FDG in small slices of NSCLC *ex vivo*. This model may serve as a tool to monitor the effect of (radio)therapy on human tumour tissue.

EP668**Texture analysis of tumour heterogeneity in response to anti-angiogenic therapy in a preclinical colorectal cancer model**

A. J. Weeks, J. Goda, M. Siddique, K. Shaw, S. Clarke, V. Goh, G. Cook; King's College London, London, UNITED KINGDOM.

Texture analysis refers to mathematical models that can be applied to an image to describe the relationship between voxel grey level intensities. Texture analysis may provide information about tumour heterogeneity that is not apparent from conventional image assessment. The purpose of this study was to assess multiparametric MR (mpMR) and ¹⁸F-FDG PET/CT changes in tumour heterogeneity after treatment of mice bearing human colorectal cancer xenografts with the anti-angiogenic agent Bevacizumab. We hypothesised that Bevacizumab treatment would lead to normalisation of tumour vasculature and changes in tumour heterogeneity. CD1 athymic mice were injected with 5 × 10⁶ LS174T cells (human colorectal carcinoma) and tumours were monitored until a mean diameter of 6–9 mm was reached. Tumour bearing mice were assigned to one of two groups; untreated control or Bevacizumab treated (5 mg/kg, IP, 3 times weekly, 2 weeks). Two days post treatment mice were subject to mpMR imaging (Bruker 9.4T, quantitative T1 +/- contrast 0.3 mMol/kg Magnevist, T2, T2* and apparent diffusion coefficient, ADC) and FDG-PET/CT (Bioscan nanoPET/CT, 5 MBq ¹⁸F-FDG) the next day. Texture features were analysed by Matlab-based in house software. Bevacizumab treated mice showed no significant differences in global first order texture features compared to control mice with the exception of T1 images which demonstrated higher mean and median values

($p=0.048$ and $p=0.027$). The treatment group demonstrated statistically significant differences in high order loco-regional texture features in T2, ADC, CT and ¹⁸F-FDG PET images compared to the control group. T2 images showed differences in grey-level co-occurrence matrix autocorrelation and grey-level zone matrix (GLZM) short zone emphasis ($p=0.021$ and $p=0.074$). ADC showed higher values in 4 GLZM parameters in the treatment group ($p=0.010$, 0.043, 0.015 and 0.015). In CT images the treated group showed lower values in 5 grey-level run length (GLRL) parameters ($p=0.026$, 0.026, 0.026, 0.026 and 0.018) and ¹⁸F-FDG PET showed lower values in 4 GLRL parameters in the treated group ($p=0.007$, 0.006, 0.015 and 0.006). The difference in tumour growth between control and treated mice during the treatment period was not statistically significant (351 and 312 mm³, respectively, $p=0.70$) indicating that standard size-related metrics of assessing treatment response are insensitive. Evaluation of image heterogeneity may provide additional novel parameters of response to anti vascular therapy with advantages over standard size-change.

EP669**High Throughput Rodent Imaging Using a Clinical Digital PET/CT System**

M. V. Knopp, K. Briley, M. I. Menendez, M. Williams, A. Siva, K. Binzel, J. Zhang; The Ohio State University, Columbus, OH, UNITED STATES.

Preclinical imaging, especially of rodents, has been a key element of molecular imaging. Compared to genome sequencing which exploded with the introduction of high throughput technology, molecular imaging has been limited to single subject per device imaging with relatively long acquisition times. As these limitations are increasing obstacles to efficient and fast pre-clinical cohort studies, we initiated this project to develop the capability of multi-subject, simultaneous whole-body PET/CT imaging using a next generation, digital PET detector based, clinical PET system. A pre-commercial release, next generation, solid state, digital photon counting clinical PET/CT system (Vereos, Philips) was used to perform simultaneous, multi-rodent PET and CT imaging. Previously, a system comparison was performed using micro phantoms with a dedicated small animal imaging PET/CT system (Inveon, Siemens). The clinical PET/CT allows z-axis coverage of 164 mm and has an effective trans-axial imaging width of up to 676 mm. Enabling the pre-clinical imaging was the prior development of ultra-high definition (UHD) reconstruction that facilitates a 1 mm³ voxel size leveraging the excellent time of flight timing resolution of 325 ps. CT imaging was also performed using a 1024 matrix size and reconstructed using 0.5 mm voxel length. In order to enable the simultaneous whole-body (WB) imaging of multiple mice, we developed a mouse hotel that can be variably configured to accommodate multiple animals. For the initial demonstration, we chose a 6 bed layout that was designed to consider also the TOF spatial resolution with only one bed within the resolution frame. Both CT and PET whole-body imaging was achievable within a single acquisition volume making even dynamic acquisitions readily feasible. The developed acquisition and reconstruction approaches led to surprisingly good image quality which was rated as fully acceptable for pre-clinical oncologic applications. No cross-interference from multiple beds was found. While the 6 bed layout appears practical, a higher number of beds is feasible without loss of spatial or quantitative quality. The multi to single bed comparison showed equivalent image and quantitative quality. Next generation digital detector, high performance time of flight clinical PET/CT systems can feasibly be used for high throughput, whole-body dynamic imaging of rodents in single bed to even more than 6 parallel bed configurations, with sufficient quality for oncologic molecular imaging. Special reconstruction and data handling approaches can be readily implemented making this a very effective approach for large rodent population imaging with effective radiotracer management especially for short half-life isotopes.

EP670**Genomic Profiling to Validate VPAC1 Expressing Liquid Biopsy Cells are Malignant**

M. L. Thakur; Thomas Jefferson University, Philadelphia, PA, UNITED STATES.

Objectives: Detecting cancer by liquid biopsy remains the most active translational cancer research. We have developed a technique in which we target VPAC1 receptors expressed on shed prostate cancer (PCa) cells in voided urine and detect PCa with >98% sensitivity (n=160). This investigation was to ascertain by genomic profiling that these VPAC1 receptors expressing cells shed in urine are malignant. **Method:** Non-DRE urine was collected from 4 PCa patients and 3 normal volunteers. Urine was centrifuged (10 min., 450xg), cells were washed, incubated with 1µg TP4303, washed, resuspended, and were subjected to fluorescence activated cell sorter (FACS). Cells with TP4303 fluorescence were collected, centrifuged, washed and lysed in cell lysis buffer (Norgen Biotek). RNA was then extracted from the cells (Norgen Biotek), quantified (nanodrop ND-100 spectrophotometer), and RNA quality was determined. (Agilent Technologies). Affymetrix gene chips, Human Transcriptome Array 2.0 (Affymetrix) were hybridized with 5 µg fragmented and biotin-labeled cDNA in 200 µl hybridization cocktail. Target denaturation was performed at 99°C for 5 min., at 45°C for 5 min, and followed by hybridization with rotation (60 rpm) for 16 hour at 45°C. Arrays were washed and stained (Gene Chip Fluidic Station 450). Chips were scanned (Affymetrix Gene Chip Scanner 3000) using Comman Console Software. Quality Control was performed by Expression Console Software. Experimental Group was compared with control group using Transcriptome array console software. Differentially expressed gene list was used for pathway analysis with IPA software. **Results:** Data showed that 5 coding PCa genes (AR, HSD17B, KLK3, KLK2 and ACTL6A) were upregulated and 19 coding PCa genes (PTEN, MR01, BACH1, etc.) were down regulated (>1.5 fold, P=<0.05). **Conclusion:** These genomic PCa fingerprint data confirmed that VPAC1 expressing cells shed in voided urine of PCa patients are malignant and validated our hypothesis that these malignant cells can be correctly detected by TP4303. Research Supported in part by, NIH CA 157372-02, (MLT).

EP671**Biological mechanisms of FDG uptake in non-small cell lung cancer**

S. B. Christlieb, B. B. Olsen, E. A. Segman, O. Gerke, K. E. Olsen, P. F. Høilund-Carlson; Odense University Hospital, Odense C, DENMARK.

Aim: 18-fluorodeoxyglucose (FDG) positron emission tomography (PET) visualizes the glycolytic activity in tissue, and increased glycolytic activity is known to be a hallmark of malignant cells. The aim of this study was to explore the underlying biological mechanisms of FDG uptake by assessing markers of proliferation, glucose metabolism, and hypoxia in non-small cell lung cancer (NSCLC). **Materials and Methods:** Thirty-six patients with NSCLC (13 with squamous cell carcinomas and 23 with adenocarcinomas) aged 41 to 83 years (median 68 years), who had undergone PET/CT prior to surgery and from whom fresh frozen tissue was available, were included in the study. Expression of Ki67, glucose transporter-1 (GLUT-1), hexokinase-II (HK-II), and hypoxia-inducible factor-1alpha (HIF-1alpha) was assessed with immunohistochemistry and categorized into three groups (<10%, 10% to <50% and ≥50%). Activity of HK and glucose-6-phosphatase (G6Pase) was determined by a colorimetric and spectrophotometric assay, respectively. The FDG-avid lesions were segmented to yield standardized uptake values (SUV), i.e., SUVmax, SUVmean, and total lesion glycolysis (TLG). **Results:** Ki67 correlated positively with GLUT-1 (Spearman's rho=0.41, p=0.01) and HIF-1alpha (rho=0.53, p<0.01), and GLUT-1 correlated positively with HIF-1alpha (rho=0.50, p<0.01). Furthermore, there

was a positive correlation between the enzymatic activity of HK and G6Pase (rho=0.48, p<0.01). The variation in measurements of FDG uptake was minimal with a median of 0% (range 0-10%) for SUVmean and of 1% (range 0-16%) for TLG for both intra- and interobserver variation. There was no variation in measurements of SUVmax between observers. SUVmax and SUVmean were moderately correlated with GLUT-1 (rho=0.53, p<0.01 and rho=0.39, p=0.02, respectively). TLG was moderately correlated with Ki67 and GLUT-1 (rho=0.44, p<0.01 and rho=0.50, p<0.01, respectively). There was no significant correlation between the expression of HK-II and HIF-1alpha or the activity of HK and G6Pase with the FDG uptake. In multivariable linear regression including all parameters, only GLUT-1 contributed statistically significantly to the SUVmax (R² adjusted: 0.22). **Conclusion:** There was but a moderate correlation of GLUT-1 and Ki67 with the FDG uptake, whereas there was no correlation between any of the other parameters and FDG uptake. These results suggest that the underlying biological mechanisms of FDG uptake in NSCLC are complex and warrant further investigations, i.e., in vitro studies of the interrelationship between the enzymatic pathways that governs the uptake of FDG in NSCLC.

EP672**Breast Cancer Immunophenotypic Heterogeneity. Evaluation By Molecular Imaging**

Q. G. Pitalúa Cortés, F. O. García Pérez; Instituto Nacional de Cancerología, Mexico City, MEXICO.

Background: Patients who develop distant metastases usually undergo systemic therapy with chemotherapy, hormonal therapy and/or human epidermal growth factor receptor 2 (HER2) targeted therapy. Choice of therapy is currently personalized on the basis of the immunophenotype of the primary tumor, since distant metastases are often not biopsied. However, previous studies have indicated that receptor status may differ from the primary tumor, generally denoted "receptor conversion". An alternative for taking biopsies could be molecular imaging methods that are currently being developed to functionally assess immunophenotype of breast cancer metastases. Published discordance rates between primary and recurrent disease are highly variable and range for example for the oestrogen receptors (ER) between 7.2 and 43.2% and for the HER2 between 0 and 64.3%. **Methods:** Ten patients with locally advanced or metastatic breast cancer were studied with ¹⁸F-FDG PET-CT, ¹⁸F-FES and ⁶⁷Ga-DTPA-Trastuzumab; tissue samples were collected post-imaging studies, and it was assessed ER and HER2 expression by IHC. We also correlated ¹⁸F-FES uptake (SUVmax) with ER expression measured by H-SCORE (0-210). ⁶⁷Ga-DTPA-Trastuzumab uptake was measured by a visual analysis based on the hepatic and blood pool uptake (-, +, ++, +++) and was compared with HER2 expression measured by IHC (positive or negative, ordering FISH only if the IHC results don't clearly show whether the cells are HER2-positive or negative. The percentage of receptor change status in the metastases immunophenotype was also evaluated in order to correlate with the primary lesion. **Results:** We included 28 lesions in 10 patients. Histology of primary lesion was 9 invasive ductal carcinomas and 1 invasive lobular carcinomas, ER positive=7, PR positive=8, Her2 positive=3; histology of metastatic disease was 7 ductal carcinoma, 1 lobular carcinoma, 1 neuroendocrine carcinoma, 1 without neoplasm evidence, ER positive=12 PR positive=10 Her2 positive=7; we found receptor discordances in 8 lesions; RE + to -: 1, RE - to +: 1, HER2 + to -: 1, HER2 - to +: 5. Final results were 8 receptor discordances in 18 studied metastatic lesions. ¹⁸F - FES SUVmax was correlated with ER H-Score (r: 0.7739, p: 0.0003); the uptake value of ⁶⁷Ga-DTPA-Trastuzumab was correlated with IHC (r: 0.8575, p: 0.0001). **Conclusion:** Molecular imaging in breast cancer is highly efficient to assess the receptor expression in metastatic lesions and any unsuspected change in these receptors, therefore leading change in the therapeutics.

EP673

Imaging neuroblastoma xenograft using [⁶⁴Cu]CuCl₂ for evaluation of novel treatment based on Dextran/Catechin conjugate

A. Parmar¹, O. Vittorio^{2,3}, A. Charil^{1,4}, M. Kavallaris^{2,3}, G. Pascali¹; ¹ANSTO, Camperdown, AUSTRALIA, ²Lowy Cancer Research Center, Randwick, AUSTRALIA, ³ARC Centre of Excellence for Nanomedicine, UNSW, Randwick, AUSTRALIA, ⁴Brain & Mind Center, University of Sydney, Sydney, AUSTRALIA.

Aim: Neuroblastoma is a very aggressive cancer with high mortality rate in children. Our group studies the effects of a novel treatment based on a Dextran-Catechin conjugate on animal models of neuroblastoma; survival and behavioural results have demonstrated the efficacy of this treatment. We have found evidence that the mechanism of action of this drug is linked to intracellular copper (Cu) trafficking and distribution. Our aim was therefore to employ [⁶⁴Cu]CuCl₂ to monitor Cu distribution *in-vivo* in neuroblastoma xenograft mouse models, both with and without treatment. **Materials and Methods:** A pilot study was carried out in normal healthy female BALB/c-Fox1nu/Ausb mice (n=4; 6-8 weeks of age) to understand the clearance of [⁶⁴Cu] over 2 days using 7-10MBq of [⁶⁴Cu]CuCl₂ in 100μL of PBS injected via the lateral tail vein. Scans were performed at the following time points: 0-2hrs, 5hrs, 24hrs and 48hrs, using a Siemens Inveon PET/CT scanner. We used the human neuroblastoma BE(2)-C xenograft mouse model in our study. On the day of imaging, 1hr prior to the PET scan, mice were intravenously treated either with saline (100μL) or Dextran-Catechin (300μg in 100μL of saline) and anaesthetised using 2% isoflurane. 7-10MBq of [⁶⁴Cu]CuCl₂ was injected via the lateral tail vein prior to PET/CT imaging at 0-2hrs and 5hrs post radiotracer injection. Following the imaging session, mice were sacrificed and tissues were collected for *in-vitro* analysis. Siemens Inveon IAW 2.0.0.1050 and IRW 4.2.0.8 software were used for image reconstruction and image analysis, as well as for obtaining kinetic curves for tumour and liver tissues. **Results:** The pilot study in normal mice demonstrated highest uptake of [⁶⁴Cu]CuCl₂ in the liver (20-30 %ID/g) followed by the kidneys and lungs. Interestingly there was high uptake in thyroid glands during the first 5hrs (4-7 %ID/g). The neuroblastoma tissues showed consistent uptake (2-4 %ID/g) in the saline group even after the 48hrs period, thus confirming high accumulation of Cu in the tumour mass. This [⁶⁴Cu] higher uptake was significantly reduced in Dextran-Catechin-treated animals. **Conclusion:** We have shown how Dextran-Catechin mediates its beneficial effects via copper metabolism, and this phenomenon could be highlighted by a relative lower uptake of [⁶⁴Cu]CuCl₂ in the tumour following the acute treatment of Dextran-Catechin in a neuroblastoma animal model. This opens the way to a deeper understanding of the molecular basis of Dextran-Catechin treatment and its potential applicability to other type of cancers.

EP674

Radiation-resistant cancer stem cells are sensitive to Auger-electron emission

B. B. Olsen, P. F. Højlund-Carlsen, H. Thisgaard; Odense University Hospital, Odense C, DENMARK.

Aim Cancer stem cells represent a clinical challenge, since they are involved in therapy resistance, recurrence and metastatic spread. Hence, successful treatment of cancer depends also on the elimination of cancer stem cells. The aim of this study was to investigate the radiation sensitivity of bulk cancer cells and cancer stem cells exposed to external ionizing radiation or Auger-electron emission. **Materials and Methods** Breast (MCF-7) and lung (NCI-H69) cancer cells were grown either as bulk cancer cells in 2D or as cancer stem cells in 3D. The cells were either irradiated with external irradiation (0, 2, 4, 6 and 8 Gy) or incubated with 0, 25, 100, 500, 1000, 2000 or 3000 Bq/ml of the Auger-electron emitting

thymidine analogue [125I]5-Iodo-2'-deoxyuridine (125I-UdR). In all experiments, the viability was determined after 7 days using the Cell-Titer Blue assay. **Results** Both cancer cell lines formed spheres when grown in the absence of serum. The lung and breast cancer stem cells were significantly more resistant to external irradiation (p<0.0001 for 4, 6 and 8 Gy) than the bulk cancer cells. For the lung cancer cell line, the difference was also significant at 2 Gy (p<0.005). Approximately 50% of the cancer stem cells survived the highest dose tested (8 Gy), while the bulk cancer cells were effectively killed. In contrast, when cells were incubated with (125I-UdR), there was no difference in cell survival between cancer stem cells and bulk cancer cells. IC50 values were 183 Bq/ml (145-231 Bq/ml) and 183 Bq/ml (146-229 Bq/ml) for lung and breast bulk cancer cells, respectively. For the cancer stem cells IC50 values were 172 Bq/ml (145-203 Bq/ml) and 247 Bq/ml (182-337 Bq/ml) for lung and breast cancer stem cells, respectively. **Conclusion** The external radiation-resistant cancer stem cells were sensitive to Auger-electron emission by 125I. These results show that Auger-electron emitters have the ability to kill both bulk cancer cells and otherwise therapy-resistant cancer stem cells in different cancer types and that Auger-electron therapy should be further explored for the development of successful cancer treatment.

EP675

Blood flow and glucose metabolism relationship between normal liver and tumor in patients with breast cancer

U. Abdulrezzak¹, H. Akgun², M. Kula¹, A. Tutus¹; ¹Erciyes University, School of Medicine, Department of Nuclear Medicine, Kayseri, TURKEY, ²Erciyes University, School of Medicine, Department of Pathology, Kayseri, TURKEY.

Aim: The purpose of the study was to determine whether an interrelationship between tumor and normal liver in terms of blood flow kinetics and glucose metabolism with dynamic and static 18F-fluorodeoxyglucose (FDG) positron emission tomography/computed tomography (PET/CT) in breast cancer patients. **Material and method:** Seventy six patients (75 female, 1 male; age: 50.89±12.89) with histologically confirmed breast carcinoma were analyzed immunohistochemically for estrogen receptor (ER), progesterone receptor (PR), human epidermal growth factor receptor 2 (cerb2), Ki67 index of proliferation. After the IV application of 296-444 MBq (8-12 mCi) of 18F-FDG, dynamic blood flow (*f*) study was performed over the breast region including the upper side of liver (L) for 10 minutes and a static acquisition 60-minute post injection were obtained for glucose metabolism imaging (*m*). The maximum standard uptake (SUV_{max}) values and mean activity concentration (AC) values (Bq/mL) of T (T-AC_f, T-AC_m) and L (L-AC_f, L-AC_m) were calculated on a spherical volume of interest (VOI) having a volume of ~1 cm³ in the hottest voxel from *f* and *m* images. The ratios of T to L (T/L-AC_f; T/L-AC_m) and the ratio of T-AC_m to T-AC_f (T-AC_m/*f*) were calculated. **Results:** L-AC_f was strongly negative correlated with the number of metastatic lymph nodes (r=-0.393, p=0.001). There were negative correlation between the L-AC_m and mitotic grade and between the L-AC_m and histologic grade (respectively r=-0.295, p=0.018 and r=-0.319, p=0.010). While T/L-AC_m values were positive correlated with tumor volume, mitotic grade and histological grade (respectively r=0.499, p<0.001; r=0.298, p=0.017 and r=0.302, p=0.015). In triple negative patients, T/L-AC_m and T-AC_m/*f* values were significantly higher than those of non-negative patients (p=0.003 and p=0.010). T/L-AC_f was positive correlated with cerb2 (r=0.246, p=0.036). ER positive patients showed significantly lower T/L-AC_f and T/L-AC_m values than those of negative patients (p=0.026 and p=0.007). In the PR positive patients, while L-AC_f was significantly higher than those of negative (p=0.050); T/L-AC_f, T/L-AC_m and T-SUV_{max} values were significantly lower (respectively p=0.018, p=0.005 and p=0.032). **Conclusion:** In patients with breast cancer, we claim that there is an interconnection between the blood flow-glucose metabolisms of normal liver and breast tumor. While the

blood flow and glucose metabolism of the tumor showed increasing, those of the liver showed decreasing. Further investigations may be helpful in determining which one is triggering factor.

EP676

Angiotensin AT₂ receptors promote differentiation and induce apoptosis in human uterine leiomyosarcoma cells by a peroxisome proliferator-activated receptor gamma - dependent mechanism

Y. Zhao¹, K. Lucht², M. Marx¹, M. Zuhayra¹, J. Culman², U. Lüthen¹; ¹Department of Nuclear Medicine, Molecular Imaging, Diagnostic and Therapy, UK-SH, Campus Kiel, Kiel, GERMANY, ²Institute of Experimental and Clinical Pharmacology, UK-SH, Campus Kiel, Kiel, GERMANY.

Angiotensin AT₂ receptors promote differentiation and induce apoptosis in human uterine leiomyosarcoma cells by a peroxisome proliferator-activated receptor γ - dependent mechanism. The biology of the uterine leiomyosarcoma, the most malignant tumour occurring in the uterus, is poorly understood. The present study clarifies the role of the AT₂ receptor and the peroxisome proliferator-activated receptor γ (PPAR γ) in proliferation, differentiation and apoptosis in the human leiomyosarcoma cell line, SK-UT-1 cells. Stimulation of AT₂ receptors was achieved by incubation of the cells with angiotensin II (Ang) II (10⁻⁷ M) in the presence of the selective AT₁ receptor antagonist, losartan. A 9 h stimulation of AT₂ receptors in SK-UT-1 cells increased the mRNA- and protein levels of smooth muscle differentiation markers, SM22 α and calponin. Blockade of the PPAR γ by the selective PPAR γ antagonist, GW 9662 completely prevented the AT₂ receptor-induced differentiation of SK-UT-1 cells. Activation of AT₂ receptors for 24 h did not alter the proliferation of leiomyosarcoma cells, assessed by ³H-thymidine incorporation and cell counting, but increased ^{99m}Tc-MIBI uptake. Stimulation of AT₂ receptors in SK-UT-1 cells for 48 h activated the intrinsic apoptotic pathway, as evidenced by increased levels of cleaved caspase-3 and Bax, down-regulation of the anti-apoptotic Bcl-2 protein and reduced ^{99m}Tc-MIBI uptake. Blockade of the PPAR γ by the GW 9662 prevented the AT₂ receptor-induced caspase-3 activation and the induction of Bax level indicating that activation of the PPAR γ is a prerequisite for the AT₂ receptor induced apoptosis in SK-UT-1 cells. These results demonstrate that Ang II acting at AT₂ receptors in leiomyosarcoma cells promotes differentiation at early stage of AT₂ receptor activation and apoptosis at later time points. Both processes are PPAR γ - dependent, i.e they require activation of the PPAR γ . Our findings provide the rationale for the use of AT₁ receptor antagonists and the PPAR γ agonist, pioglitazone, for the treatment of human leiomyosarcomas.

EP677

Effect of cholesterol rich diet on tumor growth in tumor-bearing rat models

E. Galgóczi¹, G. Trencsényi^{1,2}, A. Farkas³, G. Nagy², D. Szikra^{1,2}, M. Emri¹, I. Garai^{1,2}, P. Kertai⁴; ¹University of Debrecen, Department of Nuclear Medicine, Debrecen, HUNGARY, ²Scanomed Ltd., Debrecen, HUNGARY, ³University of Debrecen, Department of Urology, Debrecen, HUNGARY, ⁴University of Debrecen, Department of Preventive Medicine, Debrecen, HUNGARY.

Aim: Cardiovascular diseases and malignant tumors are the major causes of morbidity and mortality in developed countries. Several studies reported that high cholesterol level increases the risk of cancer. The aim of this study was to investigate the effect of cholesterol-rich diet on tumor growth in hypercholesterinaemia-dyslipidemia rat model using ¹⁸F-DG. Methods: Fischer-344 (n=12) and Long-Evans (n=12) rats were used in this experiments. For the induction of hypercholesterinaemia-dyslipidemia rat model animals were fed with cholesterol-rich diet for

two weeks. For the induction of syngenic tumor models My1/De (myelomonoblastic leukemia, 5x10⁶) or Ne/De (mesoblastic nephroma, 3x10⁶) cells were transplanted under the capsule of the left kidney using SRCA (subrenal capsule assay) technique. The tumor growth in control and dyslipidemic rats was followed with ¹⁸F-DG (11.2±0.2 MBq intravenously) imaging using the nanoScan PET/MRI (Mediso Ltd., Hungary). Two weeks after the tumor cell implantation animals were euthanized, the weights of the tumors were measured and blood samples were taken. Lipid profile (cholesterol, LDL, HDL, triglycerides) was determined from the blood. Results: By using cholesterol-rich diet the total cholesterol, LDL, HDL content of the serum significantly (p=0.001) increased in Ne/De and My1/De tumor-bearing animals. In tumor-bearing groups there were no significant differences in the weights and ¹⁸F-DG-SUV values of the tumors using different diets: standard diet-Ne/De tumor weight: 8.84±1.3g, SUVmean: 8.2±1.9; cholesterol-rich diet-Ne/De tumor: 9.21±1.4 g, SUVmean: 8.3±1.2). In case of My1/De leukemia animal model similar results were found. Conclusion: We have established a cancer-hypercholesterolemic animal model system in which large number of chemopreventive molecules can be tested quickly and relatively cheaply using small number of animals. In addition, cholesterol-rich diet had no effect on tumor growth in this model.

EP678

Up-regulation of key molecules for targeted imaging and therapy

P. Radojewski¹, V. Taelman¹, N. Marincek¹, A. Ben-Shlomo², A. Grotzky¹, C. I. Olariu¹, A. Perren³, C. Stettler¹, T. Krause¹, L. P. Meier¹, R. Cescato¹, M. A. Walter¹; ¹University Hospital Bern, Bern, SWITZERLAND, ²Cedars Sinai Medical Center, Los Angeles, CA, UNITED STATES, ³University Bern, Bern, SWITZERLAND.

Targeted diagnosis and therapy enable precise tumor detection and treatment. However, patients with tumors expressing low levels of the relevant molecular targets are deemed ineligible for targeted approaches. **Methods:** We performed a screen for drugs that up-regulate members of the somatostatin (sstr) and bombesin (bb) receptor families. Then, we characterized the effects of these drugs on transcriptional, translational and functional levels *in vitro* and *in vivo*. **Results:** We identified nine drugs that act as epigenetic modifiers, including the inhibitor of DNA methyltransferase (DNMT) decitabine as well as the inhibitors of histone deacetylase (HDAC) tacedinaline and romidepsin. *In vitro*, these drugs up-regulated sstr₂ and bb₂ on transcriptional, translational and functional level in a time- and dose-dependent manner. Thereby, their combinations revealed synergistic effects. *In vivo*, drug-based sstr₂ up-regulation improved the tumor-to-background and tumor-to-kidney ratios, which are the key determinants of successful sstr₂-targeted imaging and radiolabeled therapy. **Conclusion:** We present an approach that utilizes epigenetic modifiers to improve sstr₂-targeting *in vitro* and *in vivo*. Translation of this method into the clinic may potentially convert patients ineligible for targeted imaging and therapy to eligible candidates.

EP-37 – Sunday, October 16, 2016, during Exhibition hours, e-Poster Area
Molecular & Multimodality Imaging: PET/CT

EP679

¹⁸F-FDG PET and PET/CT findings in patients with polymyalgia rheumatica

Z. Rehak¹, P. Nemeč², Z. Fojtik³, J. Vasina¹, R. Koukalova¹, Z. Bortliceck⁴; ¹Masaryk Memorial Cancer Inst., Brno, CZECH REPUBLIC, ²St. Anne's University Hospital, Brno, CZECH REPUBLIC, ³University Hospital, Brno, CZECH REPUBLIC, ⁴Institute of Biostatistics and Analyses, Brno, CZECH REPUBLIC.

Aim: Polymyalgia rheumatica (PMR) is a disease presenting with pain and stiffness, mainly in shoulders, hip joints and neck. Laboratory markers of inflammation may bolster diagnosis. PMR afflicts patients over 50 years old, predominantly women, and may also accompany giant cell arteritis. **Patients and Methods:** 88 patients, who fulfilled Healey's criteria for PMR in the period between 2004 and 2015 and had positive FDG PET (PET/CT) findings were retrospectively evaluated. FDG uptake was assessed in large arteries, proximal joints (shoulders, hips and sternoclavicular joints), in extraarticular synovial structures (interspinous, ischiogluteal and praepubic area). **Results:** Articular/periarticular involvement (A) was detected in 80/88 (90.9%) patients and extraarticular synovial involvement (E) in 70/88 (79.5%) patients either individually or in combinations. Vascular involvement (V) was detected in 36/88 (40.9%) patients only in combination with articular (A) and/or extraarticular synovial (E) involvement. These combinations were: A+E involvement in 62/88 (70.4%) patients, A+V involvement in 8/88 (9.1%) patients, E+V involvement in 6/88 (6.8%) patients and A+E+V in 22/88 (25%) patients. **Conclusions:** PMR presents by articular/periarticular synovitis, extraarticular synovitis and can be accompanied by giant cell arteritis. All types of involvement have their distinct FDG PET (PET/CT) finding, which can be seen either individually or in any of their 4 combinations. FDG PET (PET/CT) examination seems to be an advantageous one-step examination for detecting different variants of PMR, for assessing extent and severity and also for excluding occult malignancy.

EP680

Usefulness of F-18 FDG PET/CT for Detecting the Extent of Disease in Patients with Sarcoidosis

A. Georgakopoulos¹, N. Pianou¹, E. D. Manali², S. Papiris², S. N. Chatziioannou^{1,3}; ¹Biomedical Research Foundation of the Academy of Athens, Clinical and Translational Research, Nuclear Medicine Division, PET/CT section, Athens, GREECE, ²2nd Pulmonary Department, "Attikon" University Hospital, Athens Medical School, National and Kapodistrian University of Athens, Athens, GREECE, ³2nd Radiology Department, "Attikon" University Hospital, Athens Medical School, National and Kapodistrian University of Athens, Athens, GREECE.

Aim: Sarcoidosis is a systematic granulomatous disease of unknown cause. Although lung is the most common site of disease, extrathoracic involvement occurs in 25%-50% of patients. Multi-organ involvement is often associated with a chronic and severe course, thus knowledge of the extent and severity of disease is crucial. The aim of this study is to determine the usefulness of F-18 FDG PET/CT for the detection of extrathoracic involvement in the sarcoidosis patients. **Material and Method:** Between 2013 and 2015, all biopsy proven sarcoidosis patients, from a tertiary referral center who then underwent F-18 FDG PET/CT were included in the study. 18F-FDG was injected intravenously (5.5 MBq/kg); and none of the patients had blood glucose levels >160 mg/dl. PET/CT images were obtained initially on the brain and then from the base of the skull to the feet. Positive findings were classified as thoracic and/or extrathoracic. Findings were described as positive-extrathoracic if there was increased 18F-FDG activity in one or more of the following: brain, peripheral lymph nodes, spleen, liver, bone/bone marrow, parotid glands, nasopharynx, skin, and muscle. **Results:** One hundred and ten patients, 66% female, mean age (\pm SD) of 52 \pm 12.08 years were included. Mean disease duration was 5.9 years and 36.3% of patients were under steroid treatment. Findings consistent with active extrathoracic disease were identified in 58 patients (52.7%). Almost all these patients (96%) also demonstrated active thoracic disease. In 26 patients (23.6%) PET/CT was negative for active disease, while another 26 patients (23.6%) demonstrated only active thoracic disease. A significant percentage (34 patients, 31%) revealed active disease in the musculoskeletal system (muscular 17%, bone 15% and skin 9%). Other very common extrathoracic disease sites there were in peripheral lymph node stations, mainly in

supraclavicular (25%), low cervical (17%), axillary (14.5%), retroperitoneal (17%), iliac (13%) and also in inguinal lymph nodes (32%). Active disease was also detected in organs such as the spleen (11%) and to a lesser percentage in the liver (5%) as well as in the parotid glands (3%). None of the patients revealed active brain disease. **Conclusion:** F-18 FDG PET/CT provides significant information in the assessment of extent and distribution of inflammatory activity in sarcoidosis, identifying in a large percentage of patients unsuspected and otherwise undetectable extrathoracic disease.

EP681

The Impact of 18F FDG PET/CT in Evaluating Thoracic Activity Disease in Patients with Sarcoidosis

N. Pianou¹, A. Georgakopoulos¹, E. Manali², S. Papiris², S. Chatziioannou^{1,3}; ¹Biomedical Research Foundation, Academy of Athens, Nuclear Medicine Division, Athens, GREECE, ²2nd Pulmonary Department, "Attikon" University Hospital, Athens Medical School, National and Kapodistrian University of Athens, Athens, GREECE, ³2nd Radiology Department, "Attikon" University Hospital, Athens Medical School, National and Kapodistrian University of Athens, Nuclear Medicine Division, Athens, GREECE.

Aim: Sarcoidosis is a systemic disease of unknown cause, characterized by the presence of granulomas in one or more organs, most commonly in the lungs. The ability to reveal unsuspected and persisting inflammatory activity may add in patient evaluation. The aim of the study is to investigate the role of 18F-Fluoro-deoxyglucose Positron Emission Tomography/Computerized Tomography (18F-FDG PET/CT) in the evaluation of disease activity in the thorax. **Material & Methods:** We evaluated patients with biopsy proven sarcoidosis with a whole body 18F-FDG PET/CT scan from the base of the skull to the feet, by intravenously injecting 18F-FDG (5.5 MBq/kg). In order to evaluate the myocardial involvement, we also performed a prolonged fasting and appropriate modification of low carbohydrate diet for 18 hours to suppress the 18F-FDG uptake from normal myocardial cells. **Results:** During 2014-2016 we studied 90 patients with known sarcoidosis, 53 women and 37 men (mean age 52y, range 31-81y). The average glucose values before the scan was 98 mg/dl (range 67-189 mg/dl). The thoracic involvement includes lung parenchyma, mediastinal and hilar lymph nodes, phrenic and axillary lymph nodes, as well as pleural, pericardial and left ventricle myocardial involvement. Findings consistent with active thoracic disease were identified in 27 patients (30%), in 20 patients (22.2%) PET/CT was negative for active disease, 23 patients (25.5%) demonstrated thoracic and also extrathoracic disease, while 3 patients (3.3%) had only extrathoracic disease. Based on 18F-FDG/PET/CT findings, 28 patients had lung active disease (31.1%). A significant percentage (49 patients, 54.4%) revealed bilateral lymphadenopathy consistent with active disease, while other very common sites of lymph node involvement included upper/anterior mediastinum (17 patients, 18.8%), upper and lower paratracheal area (73 patients, 81.1%), pretracheal area (19 patients, 21.1%), prevascular area (38 patients, 42.2%), subcarinal area (42 patients, 46.6%), aortopulmonary window (27 patients, 30%), paraoesophageal area (15 patients, 16.6%), phrenic area (9 patients, 10%), paracardial area (2 patients, 2.2%), internal mammary chain (7 patients, 7.7%) and axillae (18 patients, 20%). Other sites of involvement were pleura (3 patients, 3.3%), pericardium (2 patients, 2.2%) and left ventricle myocardium (6 patients, 6.6%). The SUVmax values of the hypermetabolic lesions of the lung parenchyma, the mediastinal and hilar lymph nodes showed a range of 1.4-10.0, 1.7-20.5 and 1.8-17.3 respectively. **Conclusion:** 18F-FDG PET/CT contributes significantly in the evaluation of thoracic disease activity in patients with sarcoidosis and could guide therapeutic decisions.

EP682**Assessment of the role of 18F-FDG PET/CT in the diagnosis of cardiac sarcoidosis**

M. GODOY BRAVO, L. FRUTOS ESTEBAN, J. GIMENO BLANES, M. IBAÑEZ IBAÑEZ, R. REYES MARLES, I. SIME LOAYZA, L. MOHAMED SALEM, J. NAVARRO FERNANDEZ, M. CASTELLON SANCHEZ, F. NICOLAS RUIZ, M. CLAVER VALDERAS; HOSPITAL CLINICO UNIVERSITARIO VIRGEN DE LA ARRIXACA, MURCIA, SPAIN.

AIM: Cardiac sarcoidosis (CS) is due to granulomatous infiltration of the myocardium, causing restrictive cardiomyopathy or heart failure, and it should be diagnosed by a combination of clinical, analytical, electrocardiographic, morphological, metabolic and histological findings. We evaluate the usefulness of the metabolic diagnosis of CS by 18F-FDG PET/CT (PET/CT). **MATERIALS AND METHODS:** We studied prospectively a number of 30 PET/CT carried out since January 2014 to March 2016, 27 of them at initial diagnosis and the other 3 for response assessment. All of them received a standard dose of 370 MBq 18F-FDG, in most of them preceded by heparin 50 UI/kg iv 15 minutes before. They followed the protocol of 12-18h of overnight fasting before study preceded by a low carbohydrate diet the day before. We performed acquisition of whole-body images at 60 minutes and delayed cardiac images 180 minutes respectively after 18F-FDG injection. **RESULTS:** 16 of the 30 PET/CT were negative, 10 were positive (classified according either patchy or focal pattern) and 4 could not be interpreted (deficient patient preparation or difficult assessment because of cardiac physiological uptake). 8 of the 10 positive PET/CT had patchy pattern (5 at initial diagnosis and 3 for response assessment) and 2 had focal pattern. All patients with patchy pattern PET/CT at initial diagnosis (5) were confirmed for CS: 4 were consistent with the endocardial biopsy and 1 with clinical evaluation. The 2 patients with focal pattern PET/CT were inconclusive for CS (1 patient with inespecific biopsy and 1 patient still under study). All patients with negative PET/CT (16) had favorable clinical course with no specific therapy for CS. In all patients with positive PET/CT that were confirmed for CS, delayed cardiac images showed a greater increase in FDG uptake than in early whole-body images. **CONCLUSION:** PET/CT is a powerful tool both for the diagnosis of CS and follow up in order to evaluate therapy response. PET/CT is useful for diagnosing CS with an adequate pre-treatment such as overnight fasting > 12h preceded by a low carbohydrate diet. According to our study: -A negative PET/CT allows excluding the diagnosis of CS and thus, it could avoid implementing an invasive procedure like endocardial biopsy. -A positive PET/CT strongly supports the diagnosis of CS.

EP683**Pulmonary mycobacterial solitary masses evaluated by FDG PET/CT**

K. Hayasaka, T. Saitoh, M. Fukasawa, H. Inoue, Y. Shiraishi, F. Kikuchi, T. Yoshiyama, A. Kurashima, H. Gotou; Fukujiji Hospital, Japan Anti-tuberculosis Association, Tokyo, JAPAN.

Purpose To define the features of pulmonary mycobacterial solitary masses on F-18 FDG PET/CT images. **Materials and Methods** This retrospective study reviewed the medical records, F-18 FDG PET findings and other data of 56 mycobacterial masses in 53 patients (male, n = 27; female, n = 26; age, 70.2 y; SD, 12.0 y) with pulmonary mycobacteriosis (*Mycobacterium tuberculosis* [TB], n = 16; *Mycobacterium avium-intracellulare* complex [MAC], n = 40). Mycobacteriosis was confirmed by biopsy (n = 27), surgery (n = 17) and bacterial culture (all) according to ATS/IDSA statement 2007. Maximum standardized uptake values (SUVmax) and ratios of changes in the SUVmax (%CR-SUVmax) were compared between F-18 FDG PET images of 56 and 39 lesions acquired at

one (E-SUVmax) and two (D-SUVmax) hours, respectively, after FDG injection. All data were statistically analyzed using SPSS Version 11.0 software (SPSS Inc., Chicago, IL, USA). Statistical significance was set at $p < 0.05$. **Results** The mean (SD) sizes of the TB and MAC masses were 24.7 (14.8) and 20.7 (8.0) mm, respectively. Differences in nodule size did not significantly differ ($p = 0.380$) between the two. The means (SD) of the E-SUVmax, D-SUVmax and the %CR-SUVmax in TB and MAC disease were 3.8 (2.2), 5.0 (2.8) and 28.4 (16.9), and 4.8 (3.1), 5.2 (3.8) and 17.5 (19.0), respectively. The E-SUVmax ($p = 0.721$), D-SUVmax ($p = 0.744$) and %CR-SUVmax ($p = 0.064$) did not significantly differ between TB and MAC disease. Pearson correlations between mass size and E-SUVmax, D-SUVmax and %CR-SUVmax were $r = 0.717$ ($p = 0.002$), $r = 0.576$ ($p = 0.010$) and $r = -0.268$ ($p = 0.377$) for TB, and $r = 0.478$ ($p = 0.002$), $r = 0.193$ ($p = 0.344$) and $r = -0.214$ ($p = 0.294$) for MAC disease, respectively. Differences were statistically significant between mass and E-SUVmax and D-SUVmax for TB, and between mass and E-SUVmax for MAC disease. **Conclusion** F-18 FDG PET/CT can help to evaluate the disease activity of TB and MAC disease, and might be useful for selecting appropriate anti-mycobacterial chemotherapy and assessing its effects on TB and MAC disease. However, this should be confirmed in further prospective studies.

EP684**Clinical Impact of 18F-FDG-PET/CT in Patients with Suspected Cardiac Device Infection**

B. Rodriguez-Alfonso, J. Mucientes-Rasilla, V. Castro, I. Zegri, A. Ramos-Martinez, A. Prieto Soriano, M. Mitjavila-Casanovas; Hospital Universitario Puerta de Hierro, Majadahonda (Madrid), SPAIN.

AIM: Infections related to cardiac implantable electronic devices (CIED) are increasing in incidence. CIEDs have intravascular and extravascular components. Infection can involve generator pocket, leads and/or native cardiac structures. It is mandatory to accurately diagnose the presence and extent of the infection as it affects the decision to completely or partially remove CIED or to manage it with antimicrobial therapy. The aim of this study was to analyse the diagnostic performance of ¹⁸F-FDG-PET/CT in suspected CIED infection and to assess its clinical impact on patient management. **MATERIALS AND METHODS:** All patients suspected of having CIED infection referred to our PET/CT department from 08/2011 to 02/2016 were retrospectively analysed. Patients were classified according to modified Duke criteria to determine the pre-PET probability of having CIED-related infective endocarditis (CIED-IE) and by clinical exam to determine superficial skin or pocket infection. ¹⁸F-FDG-PET/CT studies were visually analysed and interpreted as positive or negative for superficial infection, pocket infection or CIED-IE based upon the presence and location of ¹⁸F-FDG hotspots. Definite diagnosis was established by material cultures from the CIED in case of removal or by clinical follow-up and committee agreement in case of only antimicrobial treatment. Pre-test probability and PET/CT results were compared with final diagnosis to calculate sensitivity and specificity. Clinical impact of PET/CT on treatment decisions was also assessed. **RESULTS:** Twenty-nine patients were included (15 pacemakers and 14 cardioverter defibrillators). Definite diagnosis was obtained after CIED removal in 14 patients and by follow-up in 15. CIED-IE was established in 11 patients, pocket infection in 3 and infection was ruled-out or limited to the skin in 15. Sensitivity and specificity of PET/CT for the detection of CIED-IE were 81% and 94.7% respectively (pre-PET assessment according to modified Duke Criteria showed a sensitivity 63.6% and specificity 38.9%). Additionally PET/CT correctly detected an unsuspected aortic graft infection, a septic arthritis of hip and septic emboli to the lungs (2 patients). Also an unknown papillary thyroid carcinoma and low-grade colonic neoplasm were depicted. PET/CT information was essential to determine complete removal of 3 CIED. The overall impact on patient management was 17.2%. **CONCLUSION** ¹⁸F-FDG-PET/CT can accurately diagnose

IE and performs better than modified Duke criteria in patients suspected of having CIED infection. ^{18}F -FDG-PET/CT leads to changes on patient management, being sometimes the most robust evidence for the need of CIED removal. ^{18}F -FDG-PET/CT enables the detection of unsuspected secondary or concomitant relevant process, allowing early interventions.

EP685

Renal Kinetics of ^{11}C -Metformin

S. Jakobsen, O. L. Munk, A. K. O. Alstrup, J. Frøkiær; Aarhus University Hospital, Aarhus, DENMARK.

INTRODUCTION In the search for a PET tracer suitable for kidney studies, we recently synthesized ^{11}C -metformin and evaluated the tracer in healthy animals[1-2] and humans[3], as well as in a mouse model of chronic kidney disease[4]. Consistently, ^{11}C -metformin showed rapid renal kinetics, which could not be described by standard compartment models. Thus, our aim is to develop a physiologically based modeling of renal ^{11}C -metformin PET data, that gives information on renal plasma flow and mean parenchymal transit time. The ensuing model should also be able to handle the kinetics of other tracers, such as ^{15}O - H_2O and ^{15}O -CO. **METHODS** Anesthetized pigs with catheters placed in the femoral artery, left renal vein and both ureters allowed detailed analysis of renal tracer handling. A flow probe placed around the left renal artery allowed constant monitoring of renal blood flow. Dynamic PET scans with ^{15}O - H_2O , ^{15}O -CO and ^{11}C -metformin were performed with simultaneous blood and urine sampling. In parallel, constant infusion renal clearance of ^{131}I -hippurate was performed. Regions of interest (ROIs) of renal cortex and medulla were drawn on a contrast enhanced CT image which allowed us to generate time-activity curves (TACs) on the coregistered PET images. Furthermore, data from the initial human study with 5 volunteers consisted of plasma, whole blood and renal parenchymal TACs. **RESULTS** In its current form, our new model encompasses the renal cortex uptake processes (filtration plus secretion) and the urine flow which serve to remove activity from the ROI. In the single pig analyzed so far, cortical uptake of ^{11}C -metformin was fast ($K_1=2.2$ ml/ml/min), the renal extraction fraction of ^{11}C -metformin was 0.9-0.95 and that of ^{131}I -hippurate was 0.65-0.75. Blood flow from ^{15}O - H_2O PET scans (2.2 ml/ml/min) in agreement with flow probe measurements (220-245 ml/min/whole kidney) and the blood volume (^{15}O -CO PET) was determined to 16% (cortex) and 14% (medulla). Kinetic analysis also indicated that information on cortical urine outflow is necessary to model medulla ^{11}C -metformin TAC. **CONCLUSION** ^{11}C -metformin shows very attractive properties for renal PET application (no metabolism, < 0.5% plasma protein binding, very high extraction fraction) and with some adjustments we believe that the model can adequately describe the human kidney ^{11}C -metformin PET data. This will allow simultaneous determination of renal plasma flow and mean parenchymal transit time. [1] Jakobsen S *et al.* J Nucl Med 2016; 57:615-621 [2] Jensen JB *et al.* Diabetes 2016; doi:10.2337/db16-0032 [3] Gormsen L *et al.* J Nucl Med 2016; Submitted [4] Pedersen L *et al.* AJP/Renal Physiology 2016; Submitted

EP686

Effect of Reduced CT-Tube Current on Quantitative PET Values in Hybrid PET/CT

P. Ritt¹, T. Kuwert¹, M. Kramer²; ¹Clinic of Nuclear Medicine - University Hospital Erlangen, Erlangen, GERMANY, ²Institute of Radiology - University Hospital Erlangen, Erlangen, GERMANY.

Aim: It is known from phantom experiments, that the current of the CT's X-ray tube not only affects the CT image quality but also, to a small extent, the quantitative PET values of hybrid PET/CT. Unfortunately, studies using real patient data are still lacking. The aim of this work was to determine the influence of reduced CT tube currents onto attenuation correction and

quantitative PET values for patient acquisitions. **Methods:** 20 patients underwent a standard FDG-PET/CT examination. CTs were acquired at diagnostic quality with an average effective tube current time product of 168 mAs (100% = 7.3 mGy CTDIvol) at 100 kV tube voltage. Using a method which we validated on phantom scans, the patients' CT raw data were computationally modified in order to simulate scans with reduced tube current, without the actual need for additional scans. By this, CT images with 75% (126 mAs), 50% (84 mAs), 25% (42 mAs), and 5% (8.4 mAs) of the initial tube current were generated and applied for AC of the PET data. The differences between PET images based on attenuation correction with 100% tube current and the reduced currents were evaluated by determining liver SUVmean, SUVmax in FDG-positive lesions, and ratio SUVmean liver to SUVmax lesion. **Results:** Liver SUVmean, lesion SUVmax, and their ratio were marginally - but statistically significantly ($p<0.05$) - increased for reconstructions based on reduced CT currents. The average increase from 100% to 5% tube current was $1.3\pm 0.6\%$, $0.6\pm 0.4\%$, and $0.8\pm 0.7\%$ for SUVmean, SUVmax, and ratio, respectively. The maximal occurring changes for any patient were 2.2%, 1.4%, and 2.1% for SUVmean, SUVmax, and ratio, respectively. The deviations increased with decreasing tube current. **Conclusion:** We validated a method for computationally simulating datasets with reduced CT current. We applied that method on patient CTs and evaluated the influence on attenuation corrected PET images. We found that a reduced CT current and increase in image noise caused slight increase in PET SUVs. Although statistically significant, the effect is of such small extent that it'll most likely have no consequences for clinical routine.

EP687

Potential impact of different reconstruction algorithms on FDG PET-CT semiquantitative measurement: a correlation study between SUVmax and lesions volume

I. Rambaldi, I. Santi, S. Panareo, S. Taralli, V. Schincaglia, L. Lodi, L. Uccelli, C. Cittanti; Nuclear Medicine Unit, Ferrara, ITALY.

Aim: in oncological imaging the ^{18}F -FDG tissues accumulation evaluated with PET-CT is proportional to the amount of increased glucose metabolism. Its semi-quantitative measure (SUV) has quickly become the most common parameter used for detection, staging, restaging and therapy response evaluation in clinical oncology. The aim of this study was to compare PET-CT image reconstruction with standard iterative (IR) vs new True-X-TOF (Siemens Medical Solutions, Erlangen, Germany) method in order to assess their potential impact on quantification. **Methods:** we retrospectively analyzed 189 PET-CT lesions in lung cancer (92 pulmonary nodules, 67 metastatic lymph nodes) and lymphoma patients (30 Hodgkin or Non-Hodgkin pathologic lymph nodes). SUVmax and volume were calculated with IR and True-X-TOF. The distribution of SUVmax, in relation to the reconstruction method used, was statistically studied by linear regression (frequency distribution curves and scatter plots). The relationship between volume and ratio between SUVmax True-X-TOF and IR was evaluated and studied with box-plots. **Results:** True-X-TOF over iterative SUV ratios "x" were divided into three groups, I $1.0\leq x\leq 1.5$, II $1.5<x\leq 2.0$, III $x>2.0$, inside which regression correlation stays excellent ($R=0.996$, 0.996 and 0.993 respectively). Among the three groups a statistically significant stratification of ratios between lesion volumes and SUV ratio values was observed ($p<0.001$): smaller volumes are associated to greater SUV ratios while larger volumes ($>2\text{cm}^3$) are associated to SUV ratios closer to 1. Pulmonary lesions and lymph nodes represented 70% and 30% respectively of findings in group I, and 45% and 55% in group II and III combined. **Conclusions:** FDG PET-CT SUV is determined by a lot of parameters, among which acquisition and reconstruction techniques can play a pivotal role. Our preliminary data, obtained from a daily clinical setting, demonstrated that True-X+TOF shows greater SUV values in comparison to IR method. However, greater differential SUVmax values were identified in small lesions compared to larger ones, probably meaning that IR underestimates SUV in smaller

lesions. Therefore, True-X+TOF reconstruction algorithm seems to allow more sensitive metabolic characterization of small lesions in comparison to iterative methods making the impact of that feature more relevant in staging and prognostic stratification of lymph nodes than of generally larger pulmonary lesions. Moreover our study highlights the risk to compare PET-CT scans obtained with different reconstruction methods during clinical follow-up and so the importance of standardization in PET-CT imaging. Larger clinical prospective trials are mandatory to confirm these preliminary findings and to assess their potential impact in clinical practice.

EP688

Clinical Utility Of F-18 FDG PET/CT In Initial Evaluation And Response Assessment Of Langerhans Cell Histiocytosis

K. Shilpa, M. Indirani, S. Shelley, A. Jaykanth, J. Avani, K. Abhishek; Apollo hospital, Chennai, INDIA.

AIM/ OBJECTIVE: Langerhans cell histiocytosis (LCH) is a rare multi-system disorder caused by idiopathic proliferation of histiocytes. It represents a wide spectrum of disorders which varies from asymptomatic to severe, life-threatening complications. Frequently used indications for F-18 FDG PET/CT are in evaluation for malignancy and infection. Aim of this study is to evaluate the findings of F-18 FDG PET/CT and its utility role in this cancer like disease LCH. **METHODS:** Fourteen patients (9 children, 5 adults; 8 males, 6 females) who were diagnosed histopathologically as LCH were evaluated. After conventional imaging (MRI/CT/X-rays) all 14 patients had undergone F-18 FDG PET/CT scan before commencement of treatment with 3 patients also underwent post therapy follow-up F-18 FDG PET/CT scans. **RESULTS:** Out of the 14 patients in the study, 12 had skeletal lesions and 2 had extra-skeletal lesions- one each in choroid plexus and in parotid gland. All the lesions showed increased FDG uptake. In the 12 cases with skeletal involvement 5 were unifocal and 7 were multifocal. In the 5 unifocal cases, 3 showed additional metabolically active lesions on F-18 FDG PET/CT scan. In patients with multifocal skeletal involvement, F-18 FDG PET/CT scans showed numerous additional lesions compared to MRI/CT. In addition 4 out of these 12 patients had evidence of extra-skeletal involvement also, 2 in the lymph nodes and one each in liver and lung. In the patient with left parotid gland lesion, additional active lesions were noted in the thymus, submandibular glands whereas in the patient with choroid plexus involvement no other lesion was detected. In the 3 patients with post treatment follow-up F-18 FDG PET/CT scan, complete resolution was noted in 2 patients while 1 showed metabolically inactive residual lytic lesion. Overall F-18 FDG PET/CT was more sensitive and superior in lesion identification as compared to conventional imaging. **CONCLUSIONS:** F-18 FDG PET/CT is a sensitive tool for early identification of multiple skeletal as well as extra-skeletal active lesions helping in stratification and treatment of disease. F-18 FDG PET/CT acts as a single “one-stop” modality of imaging which demonstrates the dissemination of disease in the whole body and provides a clear picture of soft tissue involvement. It has an important role in monitoring response to treatment and detection of recurrence as well.

EP689

Do clinical and laboratory variables have any impact in the diagnostic performance of 18F-FDG PET/CT in patients with long-term fever?

M. TELLO GALÁN¹, A. GARCÍA VICENTE¹, J. ROS IZQUIERDO², M. AMO-SALAS³, B. LA ROSA SALAS², G. SERRANO PRADAS², G. JIMÉNEZ LONDOÑO¹, N. DISOTUAR RUIZ¹, J. CORDERO GARCÍA¹, A. PALOMAR MUÑOZ¹, Á. SORIANO CASTREJÓN¹; ¹NUCLEAR MEDICINE DEPARTMENT HGUCR, Ciudad Real, SPAIN, ²INTERNAL MEDICINE DEPARTMENT HGUCR, Ciudad Real, SPAIN, ³MATHEMATICS DEPARTMENT UCLM, Ciudad Real, SPAIN.

Objective: To assess the influence of clinical features and laboratory test results in the origin determination of the fever by means of 18F-FDG PET/CT. **Methods:** Retrospective and longitudinal analysis, including all the PET/CT studies requested for long term fever without a diagnosis performed in our department (2007-2015). Clinical pictures were classified as fever of unknown origin (FUO), inflammation of unknown origin or others. The existence of fever, 7 days before or after PET/CT, immunosuppressant risk factors, previous or active neoplasm and surgery or invasive procedures 3 months previous to PET/CT, among others, were extracted. Patients with a final diagnosis or a follow-up time greater than 12 months were included. Reference standard was established by serology, cultures or biopsy with other laboratory tests or clinical follow-up when necessary. Inflammation markers, protein analysis, serology and culture results, close to the PET scan were obtained. The final diagnosis was classified in 3 groups: group 1: focal aetiology (infection or neoplasm), group 2: diffuse aetiology (vasculitis, autoimmune disease or non infectious inflammatory disease) and group 3: others (auto-limited fever or fever persists without diagnosis). PET/CT scans were classified as positive (conclusive or unspecific findings) or negative and moreover in helpful or not in the diagnosis of the fever origin. The effect of clinical features and laboratory test variables in the PET/CT results was analysed. **Results** Sixty-seven patients met the inclusion criteria. The final diagnosis was: Group 1 (25), Group 2 (20) and Group 3 (22, 13 auto-limited). 64.2% of the patients was classified as FUO. 90.9% had positive inflammatory markers (79% of them ≥ 3), 31.7% protein alterations and 21.2% positive cultures. PET/CT was positive in 54/67 patients (44.8% conclusive and 35.8% unspecific findings). PET/CT helped in the establishment of the fever origin in 52.2% of the cases and was especially helpful in groups 1 and 2 ($p=0.035$). Sensitivity, specificity and accuracy of PET/CT were: 84%, 31% and 61%. PET results shown relations with the final diagnosis ($p=0.035$), cultures ($p=0.055$), inflammation markers ($p=0.029$) and protein analysis ($p=0.064$). No significant relations were observed with the rest of clinical or laboratory variables. **Conclusions:** 18F-FDG PET/CT had a high sensitivity although a low specificity in the diagnosis of the fever origin, probably due to the high rate of diffuse and auto-limited aetiologies. Patients most likely to benefit from the PET/CT study would be those with several positive inflammation markers reflecting a higher pre-test probability of active disease.

EP690

Inpatient Comparison of 18F-Fluodeoxyglucose Positron Emission Tomography/Computed Tomography (PET/CT) in Patients with a Driveline Infection after Left Ventricular Assist Device (LVAD) implantation

P. Kanapinn, R. Preuß, W. Burchert, J. Körfer; Heart and Diabetes Center North Rhine-Westphalia, Bad Oeynhausen, GERMANY.

Aim. Driveline infection (DI) after left ventricular assist device (LVAD) implantation is a challenging condition in longterm support of patients with chronic heart failure. While some studies evaluated the role of 18F-Fluodeoxyglucose (FDG) Positron Emission Tomography/Computed Tomography (PET/CT), little is known about the inpatient changes in PET/CT after DI. **Material and Methods.** Fourteen patients underwent a whole body FDG PET/CT at first in the context of a heart transplantation listing or because of fever of unknown origin - with no clinical signs of a DI. At a later date, these patients received a second PET/CT because of a clinically suspected DI. PET/CT findings were analysed qualitatively and quantitatively. The results of the two PET/CTs were compared. Clinical and microbiological data were obtained. **Results.** Qualitative comparison of the two PET/CTs revealed a superficial DI (above the transverse fascia) in five cases and a deep DI (below the transverse fascia, with additional signs of an infection of either the outflow cannula or the device) in nine cases. The mean time to infection was 521 days. Quantitative analysis of the SUV_{max} around the driveline showed an increase by the factor of 3.26

(mean SUV_{max} before infection 4.96; mean SUV_{max} after infection 16.18). However, the other sites of the LVAD showed no significant difference. **Conclusion.** FDG PET/CT is a frequently used diagnostic tool in the setting of a suspected DI. This study illustrates the inpatient changes in uptake pattern of a DI after LVAD implantation. It is implied that PET/CT can differentiate qualitatively between superficial and deep DI, but the quantitative analysis is only reliable for the area around the driveline.

EP691

Our experience of the clinical utility of F18-FDG PET/CT in the therapeutic response of cardiac sarcoidosis

K. L. Wallitt, S. R. Khan, S. Yusuf, N. Soneji, D. Gopalan, W. Svensson; Imperial NHS Trust, London, UNITED KINGDOM.

Aim: Review cases where F18-FDG PET/CT was utilized in the assessment of therapy for cardiac sarcoidosis (CS), and their outcomes. **Materials & Methods:** 57 cardiac F18-FDG PET/CTs (resting gated cardiac and whole body PET/CT following an 18 hour fast) have so far been performed at Imperial NHS Trust, UK in suspected/established CS. Of these, 4 patients with serial PET/CTs following a course of therapy for CS were selected. Individual cases were reviewed noting clinical manifestations of their cardiac disease, treatments received at baseline and follow-up imaging, and their PET/CT findings. The distribution of FDG uptake (focal, in-homogenous or diffuse, homogenous), maximum standardized uptake values (SUVs) and myocardial to blood pool ratios were recorded. **Results:** 4 patients had serial imaging to monitor disease response to therapy. All patients had active disease in a focal, in-homogenous distribution. One had concurrent pulmonary sarcoidosis. 2 patients had a permanent pacemaker (PPM), which precluded assessment with MRI. 2 patients had left ventricular dysfunction (LVD), of which one had severe heart failure; MRI could not be performed in this patient due to breathing difficulties. 1 patient had AV block, and 1 patient had both arrhythmogenic disease and LVD. All patients at baseline were receiving steroids, with or without immunotherapy. In 3 patients, there was a good response to therapy. In one of these patients, there was initially some disease response, but echocardiogram demonstrated worsening left ventricular function leading to a change in therapy. A subsequent PET/CT demonstrated complete metabolic response but the patient developed cryptococcal meningitis and reactive nodes from immunosuppression. Concurrent pulmonary disease responded in-line with cardiac disease in this patient. In the fourth patient there was disease progression, which led to a change in therapy. **Conclusion:** The role of F18-FDG PET/CT for disease response in CS has not yet been fully established, however we have found that in all 4 of our cases, F18-FDG PET/CT has had a positive role in optimizing therapy, with the aim of preventing end stage heart failure. Our experience also highlighted its use in patients with a PPM or breathing difficulties from severe LVD precluding assessment with MRI, and in assessing non-sarcoid

EP692

Usefulness of 18F-FDG-PET/CT in IgG4-Related Disease

B. Rodriguez-Alfonso, C. Field-Galan, J. Mucientes-Rasilla, J. Mulero Mendoza, R. Jimeno Pernet, J. Cardona-Arboniés, M. Mitjavila Casanovas; Hospital Universitario Puerta de Hierro, Majadahonda (Madrid), SPAIN.

AIM: To describe the most usual findings in IgG4-related disease in 18F-FDG-PET/CT and their correlation with the serum concentration levels of IgG4 as well as the use of PET/CT in monitoring treatment response. **MATERIAL AND METHODS:** We have retrospectively analysed all the PET/CT studies performed at baseline when IgG4-related disease

was suspected or performed as response to treatment. We included all patients with histological confirmation or high serum concentration levels of IgG4 and those with high suspicion although no histological or serum confirmation when no other entity could be assumed. Images were visually analysed. A positive PET/CT was considered when hot spots outside physiological uptake areas were detected. SUV_{max} of the most representative lesions were collected. The results were correlated with the clinical data and IgG4 levels. **RESULTS:** 13 patients have been referred for PET/CT since 2010 for IgG4-related disease suspicion. 4 have been excluded as the final diagnoses were others (sarcoidosis, lymphoma, amyloidosis and malignancy). The histological diagnosis was obtained in 6 patients, 2 of which had also high IgG4 serum concentration levels. One patient was exclusively diagnosed by elevated serum levels of IgG4 and 2 by high clinical suspicion. Nine patients underwent baseline PET/CT of which 5 had also PET/CT study for monitoring response. 6 PET/CT baseline studies showed positive findings. The most affected areas in accordance with the PET/CT images were retroperitoneum (4), lung (3), hilum/mediastinum (2), retro-orbital space (2) salivary glands (2). Higher levels of IgG4 were correlated with higher SUV_{max} at baseline. Negative PET/CT (3) were correlated with no increase in IgG4 levels. When monitoring response to treatment a negative PET/CT correlated with a normalization of the serum levels of IgG4 and in patients with no serum elevation of IgG4 at baseline, PET/CT was useful to assess disease progression (1 patient) and good treatment response (1 patient), determining in both cases further treatment (impact on patient management 22%). **CONCLUSION:** Our results suggest PET/CT is a useful tool in the diagnosis and extension assessment of IgG4-related disease and in monitoring treatment response, specially in patients with no elevated serum levels of IgG4.

EP693

Optimization and evaluation of low dose CT protocol for attenuation correction of PET data

Z. Mojabi^{1,2}, P. Ghafarian^{3,4}, H. Ghadiri^{1,2}, M. Bakhshayeshkaram^{3,4}, H. Jamaati³, M. Ay^{1,2}; ¹Department of Medical Physics & Biomedical Engineering, Tehran University of Medical Sciences, Tehran, IRAN, ISLAMIC REPUBLIC OF, ²Research Center for Molecular and Cellular Imaging, Tehran University of Medical Sciences, Tehran, IRAN, ISLAMIC REPUBLIC OF, ³Chronic Respiratory Diseases Research Centre, National Research Institute of Tuberculosis and Lung Diseases (NRITLD), Shahid Beheshti University of Medical Sciences, Tehran, IRAN, ISLAMIC REPUBLIC OF, ⁴PET/CT and Cyclotron Centre, Masih Daneshvari Hospital, Shahid Beheshti University of Medical Sciences, Tehran, IRAN, ISLAMIC REPUBLIC OF.

Purpose: It is obvious that among all imaging modalities, X-ray computed tomography (CT) has the highest patient adsorbed dose. The critical point of interest is the growth usage of CT lonely for diagnostic and also as attenuation correction (AC) for quantification and localization in PET/CT images. In this study, we aim to analyze and evaluate the possibility of using low dose CT for attenuation correction while keeping optimal image quality. **Materials and Methods:** Quality assurance (QA) and cylindrical phantom were scanned with Discovery 690 GE PET/CT scanner that equipped with 64-slice CT. Smart mA with various noise index (NI) and fixed mA method at various tube voltage (80, 100 and 120kVp), tube current (20-100mA), 1s rotation time and various pitch number was utilized. We also use the CT Dosimetry software which works based on Monte Carlo simulation to estimate organ absorbed dose. Optimization of low dose CT protocol was designed based on both quantitative factors such as modulation transfer function (MTF), contrast to noise ratio (CNR) and image noise and qualitative. **Results:** at 100kVp, 3.75 mm slice thickness and NI of 19 the CNR and image noise was 29.86 and 3.22HU when smart mA was applied, while fixed mA method (10mAs) can lead to 14.75 and 6.44 for CNR and noise respectively. With decreasing slice thickness from 3.75 to 2.5 mm and using smart mA method with

NI of 19 and 100 kVp tube voltage, CNR decline 53 %. MTF illustrated 97.6%, 93.06%, 72.96%, 49.86%, 34.19%, and 31.99%, when resolution were 1.6, 1.3, 1, 0.8, 0.6, 0.5mm respectively (100 kVp, smart mA, 3.75mm slice thickness). However when using 10 mAs, the value of 78.78%, 49.21%, 51.11%, 30.88% reported for MTF and the resolution bar of 0.6, 0.5mm disappeared. By decreasing tube voltage from 120 to 80, Dose length product (DLP) was declined 59%, meanwhile MTF, at 0.5 mm resolution increased 42%. **Conclusion:** This study demonstrates a possibility of reducing the dose of patients while maintaining image quality that meets diagnostic radiology goals. MTF increased by decreasing kVp from 120 to 80 when smart mA method was used while DLP was diminished. It should be noted that, utilizing low fixed mA in comparison with smart mA method can lead to miss smaller lesion. However combination of proper tube current and NI must apply when using smart mA method.

EP694

Role of FDG PET-CT in Distinction of benign thrombus and tumor thrombus in Oncologic Patients and Additional Contribution to Other Radiological Imaging Methods

P. Ozcan Kara¹, E. Yaman Sezer², Z. Koc¹, E. Yilmaz³; ¹Mersin University Faculty of Medicine Department of Nuclear Medicine, Mersin, TURKEY, ²Mersin University Faculty of Medicine Department of Oncology, Mersin, TURKEY, ³Mersin University Faculty of Medicine Department of Radiation Oncology, Mersin, TURKEY.

Aim: Accurate diagnosis of tumor thrombus and distinguishing benign thrombus from tumor thrombus avoid unnecessary anticoagulant treatment of oncological patients and it is important for the patient management. In this prospective study, we aimed to demonstrate the role of Fluorodeoxyglucose (FDG) PET-CT imaging for the distinction of benign thrombus from tumor thrombus and to compare it with other radiological methods. **Materials and Methods:** FDG-PET/CT imaging performed for staging, restaging and treatment response in oncological patients patients with thrombus were evaluated for accurate diagnosis of tumor thrombus and distinguishing benign thrombus from tumor thrombus by the examination of maximum standard uptake value (SUVmax). PET-CT imaging were evaluated both with visual assessment and increased metabolic activity. PET-CT findings were confirmed by clinical follow-up and biopsy in some cases. **Results:** PET-CT imaging findings of a total of 13 patients with suspected tumor thrombus (11 men, 2 women, mean age: 51-range: 22-82) were evaluated. Tumor thrombus in 5 segments in 5 patients (3 linear, 2 focal) and benign thrombus in 17 regions in the other 8 patients were reported in the evaluation of a total of 22 thrombi region in 13 patients on visual analysis and according to the increased metabolic activity. The most common region of thrombosis was defined as vena cava inferior. SUVmax values ranged from 9.27 to 19.45 in 5 tumor thrombus patients. Compared to mediastinal region increased metabolic activity was not detected in none of the 8 patients with benign thrombus and these patients were treated with anticoagulant agents. **Discussion:** In a similar study in the literature for distinguishing benign and malignant tumor thrombus reported 71.4% sensitivity and specificity values of % 90 with SUVmax cut-off value of 3.63, while in another study cut-off value has been reported as 2.25 (1-2). In this study, despite the limited number of patients, FDG PET-CT examinations were found useful in distinction of tumor thrombus & benign thrombus. As a conclusion, FDG PET-CT imaging may be useful in oncological patients when radiological imaging findings are suspicious for tumor thrombus. **Key Words:** FDG; PET-CT; Tumor thrombus **References** 1. Sharma P, Kumar R, Singh H, Jeph S, Patnecha M, Reddy RM, Naswa N, Bal C, Malhotra A. Imaging thrombus in cancer patients with FDG PET-CT. *Jpn J Radiol.* 2012 Feb;30(2):95-104. 2. Lee EY, Khong PL. The value of 18F-FDG PET/contrast-enhanced CT in detection of tumor thrombus. *Clin Nucl Med.* 2013 Feb;38(2):e60-5.

EP695

Detection of pleural and muscle involvement in Erdheim-Chester disease using FDG PET/CT

B. Seven¹, M. Turkeli², A. K. Ayan³, K. Cayir⁴, E. Orsal⁵; ¹Department of Nuclear Medicine, Amasya University Sabuncuoglu Serefeddin Training and Research Hospital, Amasya, TURKEY, ²Department of Internal Medicine, Division of Medical Oncology, Medical Faculty, Ataturk University, Erzurum, TURKEY, ³Department of Nuclear Medicine, Medical Faculty, Ataturk University, Erzurum, TURKEY, ⁴Department of Internal Medicine, Division of Medical Oncology, Numune State Hospital, Konya, TURKEY, ⁵Department of Nuclear Medicine, İstanbul Medeniyet University Göztepe Training and Research Hospital, İstanbul, TURKEY.

Erdheim-Chester disease, a rare form of non-Langerhan's cell histiocytosis with unknown specific etiology and pathogenesis, may present with focal or diffuse manifestation. While bone pain is the most common presenting symptom of the disease, extraskelatal manifestations are present in half of patients and are the main determinants of survival. The authors report the case of a 30-year-old man who was referred for evaluation of the extent of disease by F-18 fluorodeoxyglucose positron emission tomography/computed tomography (FDG PET/CT). The patient was received a treatment for diabetes insipidus for 8 years and was asymptomatic. Sagittal CT, FDG PET and fusion images from a PET/CT scanning demonstrate extensive pleural thickening and uptake in the pleura and muscles. Axial CT, FDG PET and fusion images also demonstrate skeletal involvement and uptake in the ribs, thoracic spine, and at muscles level. FDG PET/CT scan may be useful in assessing the extension of ECD and may detect extraskelatal involvement of ECD such as pleura and muscle.

EP-38 – Sunday, October 16, 2016, during Exhibition hours, e-Poster Area **Molecular & Multimodality Imaging: PET/MR & Biology (Benign Disease)**

EP696

Simultaneous Positron emission tomography (PET) with 18F-fluorodeoxyglucose (18F-FDG) with MRI enterography for monitoring activity of inflammation in patients with Crohns disease - a pilot study

B. Gomez¹, K. Beiderwellen², S. Lütje¹, A. Bockisch¹, T. Lauenstein², G. Gerken³, P. Heusch⁴, M. Ruenzi⁵, J. Langhorst⁶; ¹Clinic for Nuclear Medicine, University Duisburg-Essen, Essen, Germany, Essen, GERMANY, ²Department of Diagnostic and Interventional Radiology and Neuroradiology, University Hospital Essen, University Duisburg-Essen, Essen, Germany., Essen, GERMANY, ³Clinic of Gastroenterology and Hepatology, University Hospital Essen, University of Duisburg-Essen, Essen, Germany., Essen, GERMANY, ⁴Department of Diagnostic and Interventional Radiology, University of Duesseldorf, Duesseldorf, Germany., Duesseldorf, GERMANY, ⁵Department of Gastroenterology, Kliniken Essen-Sued, University Duisburg-Essen, Essen, Germany, Essen, GERMANY, ⁶Integrative Gastroenterology, Kliniken Essen-Mitte, University Duisburg-Essen, Essen, Germany, Essen, Germany, Essen, GERMANY.

Background: To assess the performance of combined PET/MR enterography in the non-invasive assessment of inflammatory bowel lesions in patients with Crohns disease (CD). **Materials and Methods:** The first 20 patients with confirmed CD (female: n=11; mean age: 46 ± 11 years; n=7 reported previous surgery; n=7 with current stenosis) underwent PET/MR enterography using an integrated PET/MR scanner

(Biograph mMR, Siemens Healthcare, Erlangen, Germany) with [18F]Fluorodeoxyglucose (FDG) in this ongoing study. For small bowel distension an oral contrast solution was ingested. The following sequences were acquired: a) TrueFISP coronar; b) T2w HASTE with fat saturation coronar; c) T1w VIBE coronar post gadolinium; d) T1w FLASH 2D coronar and axial post gadolinium. PET was acquired simultaneously in list mode with 8 min per bed. All datasets were reviewed by two readers in consensus with regard to the presence of active inflammation. For each segment SUVmax as well as SULmax (SUVmax/SUVmaxLiver) was determined. For a segment-based analysis the lower gastrointestinal tract was divided into 7 segments (rectum, sigmoid, descending, transverse and ascending colon, caecum, terminal ileum). A colonoscopy with a segment based analysis served as standard of reference. ROC analysis for diagnostic accuracy as area under the curve for SUVmax and SULmax was performed to determine an optimal cutoff value. Furthermore diagnostic accuracy, sensitivity and specificity for PET, MRI and PET/MRI were calculated. **Results:** A total of 122 ileocolonic segments were evaluated. According to the reference standard, active inflammation was present in 15 segments. A cutoff value for SULmax of > 1 was associated with the highest accuracy (SULmax > 1 : 0.77; SULmax >1.5 : 0.69; SULmax > 2 : 0.75; SULmax > 3 : 0.62) for the detection of inflammation. Using a cutoff value of SULmax < 1 sensitivity for PET was 87%, specificity 78%. MRI alone was associated with a higher specificity (sensitivity: 73%, specificity: 97%). Compared to MRI alone the combination of PET and MRI lead to an increase in sensitivity as well as decrease in specificity (sensitivity: 86%, specificity: 88%). **Conclusion:** 18F-FDG PET as well as MR enterography provide complementary approaches for the non-invasive assessment of inflammatory bowel lesions. The combination lead to an increase in sensitivity at a decrease of specificity in this ongoing study. Further studies investigating the integration of the different MR sequences as part of the PET/MR enterography protocol as well as the performance in the different segments should be performed.

EP697

Glucose uptake in visceral adipose tissue is decreased in obese type 2 diabetic subjects compared to healthy obese subjects, as measured by ^{18}F -FDG PET/CT

M. Boss, H. M. M. Rooijackers, M. Buitinga, M. Janssen, A. Arens, L. de Geus-Oei, L. Salm, B. E. de Galan, M. Gotthardt; Radboud University Medical Center, Nijmegen, NETHERLANDS.

Background and aims: The amount and distribution of adipose tissue are important risk factors for type 2 diabetes. Studies have shown decreased uptake of glucose in adipose tissue of non-diabetic obese-, compared to lean subjects, but no differences between healthy obese and type 2 diabetic obese subjects. This study was aimed to examine glucose uptake by ^{18}F -FDG PET/CT in adipose tissue of healthy obese and type 2 diabetic obese subjects under insulin-induced hypoglycemia. We hypothesize that hypoglycemic stress could elucidate differences not seen under physiological conditions. **Materials and methods:** 5 non-diabetic obese subjects and 5 BMI-matched ($\pm 2 \text{ kg.m}^{-2}$, mean BMI: $29.8 \pm 3.2 \text{ kg.m}^{-2}$) type 2 diabetic subjects underwent a hyperinsulinemic hypoglycemic clamp ($120 \text{ U.m}^{-2}.\text{min}^{-1}$). As a control, 5 BMI matched non-diabetic obese subjects underwent a hyperinsulinemic euglycemic clamp. When stable blood glucose levels were reached ($3.0 \pm 0.16 \text{ mmol/L}$ for hypoglycemia and $5.0 \pm 0.27 \text{ mmol/L}$ for euglycemia), $1.6 \text{ MBq/kg } ^{18}\text{F}$ -FDG was infused. After 60 minutes all subjects underwent a static whole body PET scan (4min/bp) (Siemens Healthcare). Uptake of ^{18}F -FDG in total adipose tissue, visceral-, subcutaneous- and gluteofemoral adipose tissue and skeletal muscle was quantified using Inveon Research Workplace software. **Results:** Uptake of glucose in all adipose tissue depots of healthy obese subjects was raised during hypoglycemia compared to euglycemia (visceral: 631.1 ± 51.5 versus $927.2 \pm 106.4 \text{ Bq/ml}$

resp. ($p=0.03$), subcutaneous: 284.6 ± 78.0 versus $513.0 \pm 114.1 \text{ Bq/ml}$ resp. ($p=0.007$), gluteofemoral: 415.0 ± 47.0 versus $634.0 \pm 71.4 \text{ Bq/ml}$ resp. ($p=0.04$). Under hypoglycemia, mean glucose uptake in visceral adipose tissue was lower in obese type 2 diabetic individuals than in healthy obese individuals (566.5 ± 36.4 versus $927.2 \pm 106.4 \text{ Bq/ml}$ resp., $p=0.011$). There was no difference in uptake in subcutaneous and gluteofemoral adipose tissue (subcutaneous: 324.1 ± 70.9 versus $513.0 \pm 114.1 \text{ Bq/ml}$ resp., gluteofemoral: 462.8 ± 116.3 versus $310.2 \pm 7.9 \text{ Bq/ml}$ resp., $p>0.05$ for all). Uptake in skeletal muscle was similar in all groups (euglycemia: 414.7 ± 47.0 , hypoglycemia: 634.3 ± 71.4 for healthy obese and 400.3 ± 33.1 for obese diabetic subjects, $p>0.05$ for all). **Conclusion:** Conditions of hypoglycemic stress, resulting in stimulated adipose tissue metabolism, elucidate a specific impairment of visceral adipose tissue glucose metabolism in type 2 diabetes. BMI matching ensures this impairment to be related to type 2 diabetes rather than obesity. This could indicate an important role of visceral adipose tissue in development of type 2 diabetes.

EP-39 – Sunday, October 16, 2016, during Exhibition hours, e-Poster Area

Molecular & Multimodality Imaging: SPECT & SPECT/CT

EP698

Quantification of Facet Joint Activity with Tc-99m MDP SPECT-CT

S. Razavi¹, R. Klein¹, D. Vu², L. Zuckier¹, W. Zeng¹; ¹The Ottawa Hospital, Ottawa, ON, CANADA, ²University of Sherbrooke, Sherbrooke, QC, CANADA.

Introduction Bone scintigraphy is commonly performed to identify active facet joint for cortisone injection in patients with back pain. SPECT-CT has the advantage of anatomical localization and soft tissue attenuation correction compared to planar images. The standard method of evaluating these patients has been visual inspection of the planar and SPECT-CT images. Recent availability of quantitative SUV SPECT enables absolute quantification of facet joint activity. The purpose of this study was to assess quantitative measurement of facet joint uptake and its correlation with visual subjective interpretations. **Methods** 48 consecutive patients who had undergone Tc-99m-MDP SPECT-CT for localization of facet arthropathy over 3 years were retrospectively reviewed. Patients were divided into having normal, mild, and moderate/severe facet uptake based on prior interpretation. Data were reconstructed using newly available quantitative SUV SPECT software (HERMES HybridRecon) including CT-based attenuation, scatter, and resolution recovery. For each facet joint with increased activity in the lumbar spine, a volume of interest (VOI) based on the measured maximum SUV was drawn and validated by a nuclear medicine physician. The VOI was then copied onto the contralateral or higher or lower ipsilateral level normal facet joint. Absolute mean SUV [g/mL] and VOI volumes [mL] were measured. Abnormal-to-normal facet ratios for each patient were also calculated. **Results** Of the 48 patients evaluated, 29 patients were visually diagnosed with facet arthropathy based on bone scan (19 female; mean age: 61 ± 11 years): 19 were interpreted as having mild disease (34 facets in total) and 10 (16 facets) as moderate/severe. Abnormal-to-normal facet uptake ratios were 2.43 ± 0.96 for the mild and significantly higher (4.75 ± 2.65 , $p=0.003$) for moderate/severe. Reference-normal facet mean SUV was 3.2 ± 1.2 , compared to mild abnormal (7.9 ± 3.6 , $p<0.001$) and to moderate/severe (11.6 ± 4.2 , $p<0.001$ vs. normal and $p=0.006$ vs. mild). Receiver-operating-characteristics (ROC) derived cutoff points (SUV=3.7 for mild and 9.2 for moderate) were used to classify facets into normal, mild and moderate/severe based on Mean SUV and had good concordance (Cohen's Kappa= 0.60) with visual classification. **Conclusion** Abnormal-to-normal facet uptake ratio can well differentiate abnormal

and normal facet as well as quantitatively characterize the severity of facet arthropathy. The value of the ratio may be useful to guide trainees in interpretation. Prior visual methods of facet assessment correlate well with new absolute measures of bone uptake. Furthermore, absolute mean SUV may be able to objectively classify severity of inflammatory arthropathy, but further validation would be required.

EP699

Quantitative assessment of femoral head ischemia using two-phase bone SPECT/CT in patients with proximal femoral fracture

K. Iwata¹, Y. Fukushima¹, S. Kumita¹, T. Hamana¹, H. Hashimoto², Y. Sugihara¹; ¹Nippon Medical School Hospital, Tokyo, JAPAN, ²Toho University Omori Medical Center, Tokyo, JAPAN.

Introduction: Proximal femoral fractures may cause femoral head ischemia associated with vascular injuries. Although femoral head necrosis caused by these fractures can be diagnosed using MRI, diagnostic procedures for the detection of femoral head ischemia remain unestablished. Furthermore, surgical indications are determined by the fracture site and the degree of fracture segment dislocation. Since the severity of femoral head ischemia is not allowed for the decision criteria, the criteria still remain some room to be improved. The aims of this study were to estimate the degree of femoral head ischemia and to assess the relationship between the proximal-femoral-fracture classifications and the degree of femoral-head ischemia in patients with proximal femoral fracture.

Materials and methods: A total of 20 consecutive patients (6 men and 14 women, 78 ± 6 years) between January 2013 and March 2016, who were diagnosed with proximal femoral fracture and underwent bone SPECT/CT before the treatment, were included in this study. In the procedure of bone SPECT/CT, perfusion and bone-metabolism images were acquired respectively 10 min and 2 hours after the administration of ^{99m}Tc-HMDP 740 MBq. The percentage of femoral-head perfusion-defect (%FHPD) was calculated by dividing femoral-head perfusion-defect volume derived from bone-perfusion SPECT images by femoral-head volume derived from CT images. All patients were divided into low- and high-classification groups based on surgical indications [Garden I-II or Evans Type 1 (group 1-2) and Garden III-IV or Evans Type 1 (group 3-4)-Type 2]. The relationship between the proximal-femoral-fracture classifications and %FHPD was analyzed. **Results:** Low and high proximal-femoral-fracture classification groups consisted of 14 and 6 patients, respectively. %FHPD was 67 (59-73) in the low group and 92 (84-99) in the high group (p = 0.009). The incidence of high %FHPD was higher in the high classification group than in the low group [odds ratio: 18.33 (1.51-222.89), p = 0.022]. **Conclusions:** The degree of femoral head ischemia was estimated by calculating %FHPD via two-phase bone SPECT/CT. In patients with proximal femoral fracture, the high classification can result in high %FHPD.

EP700

The Added Value of Hybrid SPECT/CT in Evaluation of Painful Orthopedic Implants and Fracture Healing Complications

B. Gunalp, S. Ince, A. Ayan, K. Okuyucu, N. Arslan; Gulhane Military Medical Academy and Medical Faculty, ANKARA, TURKEY.

PURPOSE: The aim of this study to investigate the added value of single photon emission computed tomography (SPECT)/computed tomography (CT) to three phase Tc-99m methylene diphosphonate (MDP) bone scan, Tc-99m hexamethylpropylene amine oxime (HMPAO) labeled leukocyte and Tc-99m nano-colloid (NC) bone marrow planar imaging in patients who complain pain after insertion of orthopedic implants (joint prostheses and internal fixation devices) and delayed fracture healing. **MATERIAL AND METHOD:** We retrospectively evaluated Tc-99m MDP bone and

Tc-99m HMPAO labeled leukocyte and in 7 cases Tc-99m NC bone marrow planar and SPECT/CT scans in 74 patients with orthopedic implants (24 knee, 16 hip and 34 internal fixation devices). The final diagnosis was made using bacteriologic data or clinical follow-up. Increased activity in all three phases of bone scan and increased activity bone-prosthesis interface and medulla in SPECT/CT, increased HMPAO leukocyte activity and decreased or absence of activity in NC bone marrow scan in similar areas defined as bone or orthopedic implant infection. **RESULTS:** Of the 74 patients, 14 patients (4 with knee prostheses, 2 with hip prostheses and 5 with fixation devices) had a diagnosis of prosthetic implant infections. In two suspicious cases Tc-99m NC SPECT/CT had an added value to bone and leukocyte SPECT/CT for identifying and excluding bone infection and further increased diagnostic accuracy. Diagnostic performances of planar, SPECT and combined tests (sensitivity, specificity and accuracy, respectively) have been found as follows: Three phase planar bone scan 81%, 37%, 44%; Bone SPECT/CT 90%, 45%, 52%; Leukocyte planar 72%, 35%, 41%; Leukocyte SPECT/CT 91%, 60%, 63%; Bone + Leukocyte + Bone Marrow SPECT/CT 100%, 100%, 100%. **CONCLUSION:** Correct diagnosis of orthopedic implant infections and other complications is very important in patient management. SPECT/CT offers additional information by providing not only precise localization of radiopharmaceutical accumulation but also anatomical information that can be critical for patient management. It is concluded that bone SPECT/CT should be the first line screening test for the investigation of causes of orthopedic implant failure and combine leukocyte and bone marrow SPECT/CT is the most accurate test for differential diagnosis of orthopedic implant infections.

EP701

The utility of ^{99m}Tc-Pyrophosphate SPECT in combination with left atrium 64-MDCT in diagnosis of latent myocarditis in patients with atrial fibrillation: a pilot study

Y. Ilyushenkova^{1,2}, S. Sazonova^{1,2}, R. Batalov¹, S. Popov¹; ¹Research institute of cardiology, Tomsk, RUSSIAN FEDERATION, ²National Research Tomsk Polytechnic University, Tomsk, RUSSIAN FEDERATION.

Aim: to compare results of ^{99m}Tc-Pyrophosphate myocardium SPECT in combination with left atrium 64-MDCT with histology data in patients with isolated persistent atrial fibrillation (AF). **Materials& methods:** We examined 15 patients (pts) (12 males and 3 females, mean age 44±7.5) with isolated persistent AF. After complete clinical and instrumental examination, all patients underwent SPECT with ^{99m}Tc-Pyrophosphate (^{99m}Tc-PYP) 18 hours post injection (delayed SPECT), following by left atrium 64-MDCT. Both images were then combined using 2 marks (radionuclide and radiopaque) to define more exactly the localization of ^{99m}Tc-PYP uptake in the heart and to exclude ventricles blood pool and bone elements. Endomyocardial biopsy (EMB) samples were taken during catheter ablation of AF. SPECT-CT results were compared with the EMB and immunohistochemical findings. **Results:** According to clinical and instrumental data only 11 pts repine of the arrhythmia, 7 pts- inspiratory dyspnea and in 6 pts was the relationship of AF and previously infectious disease. Any changes in the blood indicating inflammation have been identified in any pts. Moreover, in all patients LVEF was normal. According to histological data active lymphocytic myocarditis was verified in 13 pts (86%), in addition all pts had signs of cardiosclerosis different grading and staging. Immunohistochemical study detected the presence of viral antigens (herpes simplex of 1, 2 and 6 types, Epstein-Barr virus, enterovirus VP1) in myocardium samples of every patient with histologically confirmed myocarditis. The pathological uptake of ^{99m}Tc-PYP was found in 11 patients. The number of true-positive results was 11, true negative 2, false-positive - 0, false negative 2. The sensitivity was 84%, specificity 100%, accuracy 86%. **Conclusion:** The results of our study have shown that in 86% of patients with isolated

AF had latent myocarditis. Cardiac SPECT with ^{99m}Tc -PYP combined with left atrium 64-MDCT has a potential as an effective noninvasive tool of diagnoses of latent myocarditis in pts with isolated AF. Acknowledgment: This study was funded by Russian Science Foundation "The role of autonomic nervous system in pathogenesis and progression of ventricular and supraventricular arrhythmias" (grant number 15-15-10016)

EP702

A single region SPECT-CT along with a whole body bone scan provides a conclusive answer in solitary bone metastasis - an analysis of 140 bone scans with equivocal solitary bone lesions

J. DAS, Jr.; TATA MEDICAL CENTER, KOLKATA, INDIA.

Aim ^{99m}Tc -MDP whole body bone scan is the standard imaging method to detect bone metastases. Though radionuclide imaging is having an excellent sensitivity, the specificity is relatively low especially for solitary bone metastases. In this retrospective study we analyzed the incremental value of a single region SPECT-CT performed along with the whole body bone scan in 140 cases with equivocal solitary bone lesions. **Materials and methods** Data of the 140 patients was retrospectively analysed. The patients were administered 20 to 25 mCi of ^{99m}Tc -MDP approximately. In all of them a solitary lesion was identified which was indeterminate in nature. Immediately after the bone scan, a SPECT-CT of the same region was performed (360 degree, step and shoot, GE Infinia Hawkeye 4). In approximately 20% of the patients a single bed position diagnostic CT was obtained instead of SPECT-CT. Prior consent was obtained in all of them. **Results** In more than 90% cases SPECT-CT provided incremental additional information about the character of the solitary bone lesion which influenced the management. It helped to localize the lesion either in the bone or in the extraosseous soft tissue. The CT component could characterize the lesion by either identifying it as a physiological variant like bone island or by identifying structures and features like osteophytes, fractures, cortical destruction or associated soft tissue component which could classify the lesion as more likely to be benign or malignant. The study also informed whether image guided biopsy was possible or not. **Conclusion** Inclusion of SPECT-CT as a part of ^{99m}Tc -MDP whole body bone scan protocol could provide incremental information which had positive impact on the management and influenced decision making in approximately 90% cases with solitary bone lesions therefore negating the requirement of an additional imaging like ^{18}F -NaF bone PET, MRI or ^{18}F FDG PET-CT. This could enable resource optimised use of imaging equipment and minimize number of visits to the hospital. The cost of the investigation is also significantly less in comparison with other imaging modalities which could be utilized as a problem solving tool in solitary indeterminate bone lesions.

EP703

The effect of partial volume in quantitative pre-clinical imaging of ^{111}In -labelled antibodies

A. M. Denis-Bacelar¹, S. E. Cronin¹, C. Da Pieve¹, R. Paul¹, S. A. Eccles¹, T. Spinks¹, C. Box¹, A. Hall², J. K. Sosabowski³, G. Kramer-Marek¹, G. D. Flux²; ¹The Institute of Cancer Research, London, UNITED KINGDOM, ²The Royal Marsden Hospital NHS Foundation Trust, London, UNITED KINGDOM, ³Barts Cancer Institute, London, UNITED KINGDOM.

Aim: Standard pre-clinical imaging systems do not usually provide correction for partial volume effects. This can be of particular importance if results are compared with measurements from other methods, including *ex-vivo* gamma counting. The aim of this study was to explore the potential role of quantitative pre-clinical SPECT imaging as a substitute for

biodistribution studies. **Materials and Methods:** Six female CD-1 nude mice were injected with SK-OV-3 cells and 6-9.8 MBq of ^{111}In -labelled antibodies diluted in saline were administered via the tail vein. The mice were scanned using the Albira SPECT/PET/CT system (Bruker), with a 20% energy window width at 171 keV, default OSEM reconstruction and without attenuation, scatter or partial volume corrections. The mice were imaged at 4, 24, 48, 72 and 96 hours post-injection (pi) and two were additionally imaged at 168 and 197 hours pi. A CT and a 15 minute SPECT scan were performed at each time-point. Dead-time measurements were performed. Partial volume effects were investigated using four spherical phantoms with diameters of 3.8, 6, 13, and 20.2 mm, with a cold background and sphere to background ratios (SBR) of 3:1 and 4:1. The activity, mass and %IA/g of the tumour calculated from the last SPECT scan were compared with those obtained from the biodistribution study (gold standard). **Results:** A decrease in counts of 14% was observed for 13.5 MBq due to dead time. No differences in the calibration factors were observed between the different SBR when the data were corrected for dead time. A difference in calibration factors of 118% was obtained for the range of tumour masses measured (0.041-0.232 g). The measured SBR for the largest sphere was underestimated by 22-23%, highlighting that partial volume effects are still significant in large volumes. The median relative difference between the tumour mass determined from imaging and biodistribution was 17% (-31% - 52%). The tumour activity from the SPECT scan was underestimated in all mice, with a median relative difference of -16% (-27% - -6%). When the differences in activity and mass are compounded into the %IA/g calculation, no relationship between imaging and biodistribution uptake values was observed. **Conclusion:** Accurate tumour volumes are essential for image quantification and therefore dosimetry calculations. Partial volume effects were still significant for a sphere with radius of 10 mm and therefore should also be considered in studies with larger-size rodents.

EP704

Value of attenuation corrected SPECT in bone scanning of the spine - Comparison of SPECT vs SPECT/CT

L. Louw, M. H. W. Vangu; University of the Witwatersrand, SA, Johannesburg, SOUTH AFRICA.

Aim: A retrospective study undertaken to evaluate the additional diagnostic value of SPECT/CT imaging of the spine with ^{99m}Tc -MDP compared to CT attenuation corrected SPECT imaging, in patients with solid tumour malignancies. **Materials and methods:** A total of 192 adult patients (131 males, 61 females), aged 19-89 years, referred for bone scan from January 2013 - May 2015 were included. SPECT/CT reconstructed images of the spine were acquired for either better localization of abnormal foci on planar, or in the presence of back pain but unremarkable planar images. Attenuation correction for the SPECT images was done with the use of CT. CT attenuation corrected SPECT (M1) and fused SPECT/CT images (M2) were visually analyzed. Focal uptake in the posterior aspect of the vertebral body or pedicle, or diffuse uptake in the vertebral body was considered as likely malignant. **Results:** In the thoracic spine a total of 606 lesions were identified in M1 and 600 in M2. In M1, a total of 79 lesions were identified as potentially malignant in the thoracic spine and 68 in M2. Neither the difference in numbers ($p=0.223$) nor the increment ($p=1.0$) was significant from M1 to M2. Similar results were noted for the lesions that were seen in lumbar spine (580 lesions in M1 and 581 in M2). Furthermore, a total of 53 lesions were identified as potentially malignant in M1, and 46 in M2 in the lumbar spine. Once again neither the difference in these numbers between M1 and M2 ($p=0.414$), nor the increment of lesions from M1 to M2 ($p=1.0$) was significant. Using the CT component of the SPECT/CT images as reference, only 0.8% of affected vertebrae changed location from M1 to M2. The greatest impact in patients with probable metastatic disease (29 patients) was noted by down staging of 20 of them to "no metastatic

disease” from M1 to M2. **Conclusion:** Our study didn't find an overwhelming benefit of SPECT/CT as opposed to attenuation corrected SPECT imaging of the spine. However, the additional value of SPECT/CT was primarily found in down-staging a small number of patients. The use of this expensive modality in resource-limited settings has to be weighed carefully against added benefits, especially when diagnostic staging CT is often done as part of patients' investigations. A prospective study comparing SPECT/CT with non-CT based attenuation corrected SPECT is required.

EP705

Added value of ^{67}Ga SPECT-CT in the monitoring of antibiotic treatment in necrotizing external otitis

D. BEN SELLEM, L. ZAABAR, B. DHAOUADI, B. LETAIEF, M. F. BEN SLIMENE; University of Tunis El Manar, Faculty of Medicine of Tunis, Salah Azaiez Institute, Department of Nuclear Medicine, Tunis, TUNISIA.

Aim: Necrotizing external otitis (NEO) is an uncommon but severe and evolutive infection affecting mainly old diabetic. This osteitis spreads to the skull base at the temporal bone. Prognostic vital can be affected, treatment must be energetic, rapid and well adapted. Gallium 67 Citrate (Ga^{67}) scintigraphy is an early valuable tool to monitor the efficiency of antibiotic treatment. The aim of this study is to evaluate the additional diagnostic value of fused single photon emission computed tomographic (SPECT) and computed tomographic (CT) images (SPECT-CT), compared to planar ones. **Materials and Methods:** Forty diabetics with trailing otitis resistant to different treatments have benefited of 45 SPECT-CT, in order to monitor the efficiency of antibiotic treatment. These patients (22 men, 18 women) aged 66.2 ± 13.8 years (20 to 87 years, median 67 years) underwent, 72 h after intravenous injection of a mean activity of 185 MBq (5 mCi) Ga^{67} , static planar scintigraphy and SPECT/CT scan focused on skull, and whole body scan. Planar images and fused SPECT-CT ones were retrospectively and separately interpreted. **Results:** The qualitative analysis of the planar acquisition had shown an increased temporal uptake in 5 patients. The exam was negative in 40 cases. The qualitative analysis of the SPECT/CT has objectified a radiotracer uptake of the mastoid in 20 cases, indicating the continuation of antibiotic therapy. Also, the fused images allowed determining the extension of the osteitis: to the ipsilateral temporomandibular joint in 5 cases and to the deep spaces of the face, the skull base and the temporomandibular joint in another case. In 3 others cases, the temporal osteitis was inactive, but the SPECT/CT has diagnosed contra-lateral osteitis in one case and a persistent inflammation of the soft tissue in 2 cases. In the 22 last cases, the fused images were negative, showing a scintigraphic remission and allowing so stopping the antibiotic treatment. After analyzing the fused images, the final report was changed in 40 % of cases. **Conclusion:** The necrotizing otitis externa is a serious infection that can affect the vital prognostic. The monitoring of antibiotic treatment is crucial. Ga^{67} scintigraphy is an early valuable tool to monitor the efficiency of this treatment. The fused SPECT/CT images provided additional information in 40 % of cases, by detecting active infection imposing the prolongation of antibiotic therapy. It allowed also a better defining of the location and the extent of infection.

EP706

An Investigation into Metal Artefact Reduction Approaches in CT Attenuation Correction for SPECT/CT and PET/CT

J. A. Johnson; Cambridge University Hospitals NHS Foundation Trust, HERTFORDSHIRE, UNITED KINGDOM.

Background. Metal implants, and the artefacts which result from their CT imaging, pose an issue when acquiring attenuation correction data. The

high density and atomic number of the implant materials cause streaking, especially when FBP reconstruction is performed. This leads to erroneous attenuation correction and potentially mis-diagnosis. The aim was to quantitatively assess the severity of artefacts, assess existing MAR methods, and optimise the parameters used at acquisition to gain the most diagnostically useful CTAC images. **Methods.** A customised phantom was used to investigate the impact of different CT acquisition parameters and reconstruction techniques. The severity of the artefact was quantified both across the image FOV, and axially throughout the imaged volume for various acquisition parameters and CT reconstruction approaches. By positioning activity-filled syringes adjacent to the metal and at the phantom edge, the effect of the metal upon the visibility of a small feature was highlighted. **Results.** The data highlighted that no optimal technique exists for MAR. However, the artefact was shown to extend both across the field of view within a slice, and axially through the imaged volume. Iterative techniques appeared to marginally extend the artefact axially and decrease spatial resolution from the 1.4mm determined for FBP-reconstructed CT data. The visibility of lesions was affected by their proximity to the metal. The maximum counts/pixel was 18% lower adjacent to the hip in comparison to at the phantom edge. The use of a high kV CT scan for CTAC was shown to be beneficial for image quality. Therefore a new CT protocol was devised for imaging patients with metal hip implants, which is to be put into clinical practice for CTAC. **Discussion.** Evidently metal implants significantly affect image quality and the ability to make accurate diagnoses, with no existing CT reconstruction technique offered by GE providing an optimal solution. Acquisition parameters allow the artefact to be minimised, whilst quantifying the error provides awareness of the extent and impact of the artefact and highlights the shortcomings in the MAR techniques provided by manufacturers. **Conclusion.** It's clear that further work is needed to provide improved MAR approaches for CTAC. Further attempts to access CT reconstruction algorithm information from the scanners would allow novel approaches to be sought. Further investigation of the artefact's impact upon clinical images would also be valuable. It is clear, however, that regardless of the reconstruction technique used presently, the artefact has a noticeable impact upon the CTAC.

EP707

The Use of SPECT-CT with Besilesomab-99mTechnetium in Diagnosis of Actinic Enteritis: A Case Report

I. C. Palazzo, N. L. Correa, M. F. Veras, G. M. N. Sadeck, A. C. Y. Cotrado, w. K. d. Aguiar, M. M. M. Sabra, W. d. Ker, F. S. Costa, J. d. Azevedo, C. T. Mesquita; Hospital Pró-Cardíaco, rio de janeiro, BRAZIL.

A 67 years old male with hypertension, type 2 diabetes, diagnosed with rectal adenocarcinoma, which was surgically resected. The patient was receiving oral chemotherapy (Capecitabine associated with Docetaxel) and radiotherapy. After 20 sessions of external radiotherapy the patient developed fever, weight loss and diarrhea and was sent to the emergency room. The contrasted computed tomography (CT) demonstrated two thrombi in the infrarenal aorta, the largest measuring about 2 centimeters. In order to investigate a possible infection of the thrombi, scintigraphy with labeled leukocytes was requested. The scintigraphy was performed after the human anti-mouse antibody (HAMA) test to exclude the possibility of immune reaction to the radiotracer (besilesomab-99mTechnetium). The images were acquired in a hybrid gamma camera (Single-photon emission computed tomography), with low-dose computed tomography which allows attenuation correction and anatomic correlation. In addition to the low dose CT, the scintigraphic images were fused with the previous contrasted CT. The analysis of the images did not show radiotracer accumulation in the thrombi, however revealed reduced uptake in bone marrow lumbar vertebrae (post-radiotherapy effect) and high intensity uptake in the small intestine. A revision of the contrasted CT

demonstrated signs of distal small bowel inflammation. The radiotracer accumulation in the intestine was present in both early and late images, and confirmed the suggested clinical diagnosis of actinic enteritis. Inflammatory process of the bowel after radiation is not uncommon, up to 90% of patients undergoing radiotherapy for pelvic tumors develop altered bowel habits and 50% report reduction in quality of life. Despite being common, there are few publications that show this pathology through scintigraphy with labeled leukocytes. The scintigraphy with labeled leukocytes allowed the oncologists to rule out other causes of fever, directly impacting the care of the patient.

EP708

SPECT/CT Improves Inter-Observer Agreement of Equivocal Osseous Lesions Detected on Planar Bone Scan

Y. G. A. Abdelhafez¹, N. Bashank², L. Eloteify², M. Mekkawy²; ¹South Egypt Cancer Institute, Assiut University, Assiut, EGYPT, ²Faculty of Medicine, Assiut University, Assiut, EGYPT.

Aim To compare inter-reader agreement for planar and SPECT/CT interpretation of equivocal osseous lesions detected on bone scintigraphy in cancer patients. **Materials & Methods** This prospective study recruited patients known to have primary tumor referred for bone scintigraphy with their planar images showing solitary or few equivocal osseous lesions. Every patient underwent planar whole body scan followed by SPECT/CT for the concerned region(s). The gold standard was based on clinical/imaging follow-up for at least 6-12 months. Two experienced readers (reader 1 has 8-year experience & reader 2 has 12-year experience) scored each lesion on a subjective 5-point score for the possibility of being malignant (1=benign, 2= probably benign, 3 = equivocal, 4=probably malignant & 5 = malignant). True & false results were identified were identified in relation to the gold standard. Kappa measure of agreement was measured for both modalities. **Results** A total of 150 patients were included in this study (110 females ,40 males) with median age 54 years (range:7-84). On planar imaging, both readers successfully identified 48 true positive (TP) & 19 true negative (TN) patients. Both readers were false positive (FP) in 31 & false negative (FN) in 3 patients. They disagree in 2 patients. Moderate agreement was noted (kappa = 0.55). While on SPECT/CT imaging, both readers successfully identified 58 TP & 62 TN patients. Both readers reported FP results in 11 & FN in 2 patients. They disagree in a total of 9 patients. Perfect agreement was noted (kappa = 0.82). **Conclusion** SPECT/CT significantly improved inter-observer agreement among readers for equivocal osseous lesions detected on planar bone scintigraphy.

EP709

The role of gamma scintigraphy in the diagnosis of latent myocarditis in patients with atrial fibrillation

Y. Ilyushenkova^{1,2}, S. Sazonova^{1,2}; ¹Research institute of cardiology, Tomsk, RUSSIAN FEDERATION, ²National Research Tomsk Polytechnic University, Tomsk, RUSSIAN FEDERATION.

Aim: To evaluate the role of labeled ^{99m}Tc-HMPAO leucocytes (^{99m}Tc-HMPAO-L) myocardium SPECT in the diagnosis of latent myocarditis in patients with atrial fibrillation (AF). **Materials & methods:** We examined 70 patients (pts) (49 males and 21 females, mean age 48.72±6) with isolated persistent AF. After complete clinical and instrumental examination, all patients underwent SPECT with ^{99m}Tc-HMPAO-L 18 hours post injection (delayed SPECT), following by SPECT with ^{99m}Tc-MIBI at the rest condition. Both images were then combined to define more exactly the localization of ^{99m}Tc-HMPAO-L uptake in the heart and to exclude ventricles blood pool. In 50 pts Cardiac Magnetic Resonance (CMR) with gadolinium and immunobiochemical analysis of blood serum to

determine the concentration of proinflammatory cytokines were performed. Endomyocardial biopsy (EMB) samples were taken during catheter ablation of AF. All results were compared with the EMB findings. According to the results of statistical analysis of clinical and instrumental data, we have identified a number of clinical and radiological signs, with the highest informative value in the diagnosis of latent myocarditis in patients with AF. To determine the importance of gamma scintigraphy in the diagnosis of latent myocarditis have been developed 2 models of multinomial logistic regression, the diagnostic performance was calculated using ROC analysis. Model 1 included the diagnostic signs such as inspiratory dyspnea, low-grade fever, cardialgia, the link between the appearance of AF with infectious disease, late gadolinium enhancement at CMR and local contractility dysfunction of left ventricle. Model 2 included the full range of characteristics of model 1 and myocardial scintigraphy ^{99m}Tc-HMPAO-L. **Results:** According to the results of ROC analysis the sensitivity and specificity of model 1 in the diagnosis of latent myocarditis is 50% and 70% respectively, AUC= 0.662. The sensitivity and specificity of model 2 in the diagnosis of latent myocarditis was 70% and 96%, respectively, and the area under the ROC curve to 0.866. **Conclusion:** The results of our study have shown that adding to the diagnostic algorithm ^{99m}Tc-HMPAO-L myocardium SPECT increase the efficacy of diagnostics of latent myocarditis in patients with atrial fibrillation by 20%. **Acknowledgement:** This study was funded by Russian Science Foundation "The role of autonomic nervous system in pathogenesis and progression of ventricular and supraventricular arrhythmias" (grant number 15-15-10016).

EP710

Quantification of normal Sacroiliac joint to Sacrum Ratio with Tc-99m MDP SPECT/CT in Women

S. Bazarjani, S. Razavi, R. Klein, L. Zuckier, W. Zeng; The Ottawa Hospital, Ottawa, ON, CANADA.

Introduction Bone scintigraphy is commonly performed to identify sacroiliitis. Sacroiliac joint to sacrum (SIS) uptake ratio based on planar images has been used as a diagnostic aid. The SIS ratio quantification based on planar images may produce significantly variable values in even normal individuals due to body habitus such as the degree of soft tissue attenuation and variation of sacral curvature. SPECT/CT imaging may resolve these issues by providing soft tissue attenuation correction and precise anatomical delineation of sacral and SI joint components. The goal of this study was to quantify the SIS ratio with SPECT/CT in patients with normal sacroiliac joints and sacrum. **Methods** 18 patients referred to our department for ^{99m}Tc-MDP SPECT/CT bone scintigraphy were reviewed by 2 board certified nuclear medicine physicians. Patients with normal SI joint and sacrum on CT and no lumbar or hip symptoms to have significant effect on these joints were selected for the study. Male patients were excluded in this study due to limited numbers with normal SI joints. SPECT images were reconstructed using attenuation, scatter, and resolution recovery corrections with CT and quantified in SUV units using Hermes software. For each sacroiliac joint or sacrum, a volume of interest (VOI) based on the measured maximum SUV and the CT anatomy was drawn by experienced nuclear medicine physicians. Various parameters were evaluated including the mean SUV [g/mL], the integral SUV [g] within the VOI, and the SIS ratio. **Results** 18 female patients (mean age: 44.5 ± 12.3, range: 21-64) were evaluated in this study with the majority having breast cancer. Volumes (mL) of the right and the left SI joints and proximal sacrum were 67.8±18.4, 69.9±19.5, and 41.1 ±11.7, respectively. Mean SUVs were 4.44±0.88 for the right SI joints, 4.38±1.08 for the left SI joints and 3.49±0.82 for the sacra. Considerable size variation of the SI joint volumes was noted (SE=27%). However, SIS ratios remain relatively constant as expected, measuring 1.29 ± 0.16 (SE=13%) on the right and 1.26 ± 0.14 (SE=11%) on the left. There is no statistic difference between the right and the left SIS ratios (p=0.22) by paired t-test.

Conclusion The current study demonstrated the feasibility of quantifying the SI joints and sacral activity. The SIS ratios obtained in this study from subjects with normal SI joints and sacra are helpful as a reference in evaluating patients with suspected sacroiliitis.

EP711

SPECT/CT Characterization of Equivocal Osseous Lesions Detected on Tc-99m-MDP Planar Bone Scintigraphy

N. Bashank¹, Y. G. A. Abdelhafez², L. Eloteify¹, M. Mekawy¹;
¹Faculty of Medicine, Assiut University, Assiut, EGYPT, ²South Egypt Cancer Institute, Assiut University, Assiut, EGYPT.

Aim: To compare diagnostic performance of SPECT/CT versus planar imaging in characterization of equivocal osseous lesions in cancer patients detected on bone scintigraphy. **Materials & Methods:** This prospective study recruited patients known to have primary tumor referred for bone scintigraphy with their planar images showing solitary or few equivocal osseous lesions. Every patient underwent planar whole body scan followed by SPECT/CT for the concerned region(s). The gold standard was based on clinical/imaging follow-up for at least 6-12 months. The findings from both modalities were compared for diagnostic performance indices. **Results:** A total of 150 patients were included in this study (110 females, 40 males) with median age 54 years (range:7-84). The sensitivity, specificity and accuracy for planar scintigraphy versus SPECT/CT were (72% vs. 85%, 61% vs. 83% & 66% vs. 84%; respectively. The differences in sensitivity & specificity were statistically significant ($P = 0.04$ & 0.001); respectively. **Conclusion:** SPECT/CT significantly improved the diagnostic performance of planar bone scintigraphy in characterization of equivocal osseous lesions.

EP712

Validation of attenuation correction using SPECT/CT in MPI

L. Ali¹, S. Panchadar², Y. Al-Sayed², G. Biswas², M. Al-Garashi²;
¹Faculty of Allied Health, Kuwait University, KUWAIT, ²Chest Diseases Hospital, Ministry of Health, KUWAIT.

Gated SPECT (G-SPECT) myocardial perfusion imaging (MPI) using ^{99m}Tc-Tetrofosmin is used to evaluate coronary artery disease (CAD). Soft tissue attenuation in the anterior wall from breasts in female and inferior wall from diaphragm, leads to false positive studies. Computed tomography (CT) has recently been introduced for localization of lesions and correction for attenuation in hybrid SPECT/CT. The aim of this work was to use CT in a half dose-half acquisition protocol to correct for attenuation and investigate whether it imposes a great impact on the presence and severity of perfusion defects. **Methods:** Two hundred G-SPECT/CT MPI 2 days stress/rest studies were retrospectively selected. The acquisition was performed on hybrid (True Point Symbia SPECT/CT) equipped with SMATZOOM collimator. Uncorrected (NC) and attenuation corrected (AC) SPECT images were analyzed using 17 segments polar maps to obtain summed stress score (SSS), summed rest score (SRS) and summed difference score (SDS). Percentage perfusion defect and associated perfusion count was also evaluated. Two experienced NM physicians have assessed the abnormalities using visual scoring of 3-point scale (1 no difference in perfusion between AC and NC, 2 small difference in one or more segment, 3 marked difference in perfusion). **Results:** Out of 200 patients, 173 (86.6%), including 118 male (68.2%) and 55 female (31.7%) has shown significant improvement in perfusion by AC. 88 out of 131 male have defects in RCA territory in which 90.7 % have been modified whereas 57 out of 69 female have LAD defect in which 56.6 % have been modified after AC. The SDS for attenuation corrected stress and rest (3.12 ± 2.9) was significantly decreased compared to SDS for uncorrected data (6.72 ± 4.10), p

value=0.0003. The severity of lesions were shifted to normal from either mild, moderate, severe or absent in 44% (n=68), 16% (n=25), 5% (n=8) and 1% (n=2) respectively and were shifted from moderate to mild and severe to moderate in 22% (n=34) and 12% (n=18) respectively. McNemar test showed that visual improvement in perfusion with AC was seen in 122 out of 155 patients (79%) in which marked differences were seen in 45 patients (29%), p value=0.0001. Good agreement between observers with Kappa 0.73. **Conclusion:** Our results show that AC with CT is efficient in reducing the number of false-positive studies.

EP713

SPECT/CT lung perfusion study in Swyer-James-MacLeod syndrome: a case report

Z. Jurasinovic¹, A. Tabain², I. Bračić¹, G. Horvatic-Herceg¹;
¹University Hospital Centre Zagreb, ZAGREB, CROATIA, ²Outpatient Clinic Medikol, ZAGREB, CROATIA.

Swyer-James-MacLeod syndrome (SJMS), otherwise known as unilateral hyperlucent lung syndrome, is a rare disease occurring in childhood that is believed to be caused by bronchiolitis obliterans. Hypoplastic pulmonary arteries remain after such an event, leading to decreased vascularity and ultimately in reduced lung size. Nevertheless, this syndrome can remain unrecognized well beyond childhood due to an indolent course and than sometimes discovered in an adult. We scheduled a 42-year-old female patient for the lung perfusion study after she was treated for upper right lobe pneumonia, but the infiltrative lesion seen on her X-ray hasn't cleared after the treatment. Lung MSCT was performed before our study and showed localized emphysema in the upper and middle right lung, which raised the suspicion of SJMS. Six standard planar images were made after the administration of 148 MBq Tc-99m labelled macroaggregated albumin (MAA) and perfusion defects were noted in the right upper apical and anterior segments as well as a large defect in the middle lobe. SPECT study was additionally performed, combined with low-dose CT scan and hybrid images were generated so that it was possible to match perfusion defects with hyperlucent areas in the afore mentioned areas. We decided that lung ventilation study isn't warranted and concluded that MSCT angiography can also be omitted.

EP714

Abdominal SPECT/CT using Tc-99m-labelled autologous heath-denatured red blood cells after blunt abdominal trauma and splenectomy: a case report

Z. Jurasinovic; University Hospital Centre Zagreb, ZAGREB, CROATIA.

Twenty-nine years old female patient went to urgent splenectomy after blunt abdominal trauma and rupture of the spleen. On follow-up MSCT discovered a node measuring 0.8 cm in diameter located near the empty spleen bed, but also multiple nodes up to 4 cm in diameter throughout the left side of the abdomen, reaching front abdominal wall at the level of supravesical region. The patient was scheduled for abdominal scan with Tc-99m-labelled autologous heath-denatured red blood cells to confirm traumatic splenosis. We labelled red blood cells with Tc-99m and denatured the cells with heath using standard procedure and then performed SPECT/low-dose CT scanning of the abdominal and pelvic region. Hybrid images revealed multiple areas of splenosis not only in the upper left abdominal region and peritoneal surfaces of the entire left abdominal and pelvic region, but also one small focal lesion located in the upper right abdomen, between liver and diaphragm, not seen on CT slices.

EP715

Estimation of administered fluorodeoxyglucose activity in patients on the basis of dose equivalent rate on head by multiple regression analysis

M. Hosono, K. Sakaguchi, T. Imamura, N. Takahara, M. Hayashi, C. Hosokawa, M. Yamada, K. Ishii; Kindai University, Faculty of Medicine, Osaka-Sayama, JAPAN.

Aim: The aim of this study was to establish a method for estimation of administered dose of Fluorodeoxyglucose (FDG) of patients on the basis of variables including dose equivalent rate (DER) on the right temporal region of the head, sex, body weight (weight), blood sugar, elapsed time after administration, by using multiple regression analysis. Such estimation would be useful because intravenous injection is sometimes accidentally discontinued due to extravasation of FDG, complaint of pain, or trouble of injection devices during administration, and in such cases, estimation of already-injected FDG doses may help to know whether you should make another venipuncture and inject additional FDG or to estimate an eventual influence of underdose to standardized uptake values and image quality. **Methods:** Five hundred twenty patients (234 females, 286 males) undergoing PET examination with a single administration of FDG were prospectively enrolled in this study. FDG was prescribed as 3 MBq/kg, and administered into patients using an automated injector. The actual administered doses (ADs) were recorded as well as patients' characteristics. The correlation of AD with independent variables of DER on the right temporal region of the head, sex, weight, blood sugar, elapsed time after administration was analyzed using multiple regression analysis to obtain linear, quadratic, and cubic regression equations. In this process, DER was converted to corrected DER (CDER) by a plotting of DER/AD and weight, which was unaffected by the influence of weight. **Results:** Using CDER, regression equations were acquired as, Linear: $AD=L(1)\times CDER$, Quadratic: $AD=Q(1)\times CDER^2+Q(2)\times CDER$, Cubic: $C(1)\times CDER^3+C(2)\times CDER^2+C(3)\times CDER$, where $L(1)$, $Q(1)$, $Q(2)$, $C(1)$, $C(2)$, and $C(3)$ were regression coefficients. When these estimated ADs were compared with actual ADs, within an accuracy of $\pm 10\%$ using linear, quadratic, and cubic regression equations were included 60.77%, 61.92%, and 61.92% of all patients, and within an accuracy of $\pm 20\%$ were included 87.12%, 89.99%, and 90.20%, respectively. **Conclusions:** This method proved to be accurate for estimation of AD on the basis of DER and independent variables of sex, weight, blood sugar, and elapsed time after administration by adopting the cubic regression equation. We propose this method to know already-injected FDG dose in various clinical circumstances.

EP716

Does SUV normalization based on individual CT-based LBM calculation provide better SUVs?

J. Devriese¹, L. Beels², A. Maes², C. Van de Wiele², H. Pottel¹; ¹KU Leuven campus Kulak, Kortrijk, BELGIUM, ²AZ Groeninge, Kortrijk, BELGIUM.

Aim In positron emission tomography/computed tomography (PET/CT) semi-quantitative evaluation of tumour metabolic activity is possible through the standardized uptake value (SUV), which is usually normalized for body weight (BW). Other proposed normalizations include lean body mass (LBM) and body surface area (BSA). The purpose of this study was to determine patients' LBM and lean tissue (LT) mass using a CT-based method, and to compare SUV normalized by these

parameters to conventionally normalized SUVs. **Materials and methods** PET/CT examinations covering head to toe were retrospectively retrieved. LBM was determined using CT image segmentation (LBM_{CT}) based on tissue-specific Hounsfield unit (HU) thresholds, and again using the predictive formulas of James (LBM_{James}) and Janmahasatian (LBM_{Janma}). BSA was determined using the DuBois formula. LBM_{CT} was compared to formula-based estimates using the Bland-Altman method. SUVs in two healthy reference tissues, liver and mediastinum, were normalized for the aforementioned parameters and compared to each other in terms of variability and dependence on normalization factors and BW, and within-patient SUV variation was assessed in an independent dataset. **Results** LBM_{James} estimates are significantly higher than LBM_{Janma} with biases of 4.7kg (95%CI: 3.1 to 6.3) for females and 1.0kg (95%CI: 0.4 to 1.6) for male patients. Formula-based LBM estimates do not significantly differ from LBM_{CT} , neither for men nor for women. Variance of SUV normalized for LBM_{James} ($SUV_{LBM-James}$) was significantly reduced in liver compared to SUV_{BW} . All SUV variances in mediastinum were reduced, except SUV_{BSA} . Only SUV_{BW} and $SUV_{LBM-James}$ show independence from normalization factors. **Conclusion** No advantage of alternative SUV normalization over BW could be demonstrated.

EP717

Quantification of perfusion heterogeneity in patients with hypertrophic cardiomyopathy: evaluated by fractal analysis

K. Kiso¹, Y. Nishimura², Y. Takahasi³; ¹National Cerebral and Cardiovascular Center, Suita, JAPAN, ²Teikyo University, Ohmuta, JAPAN, ³FUJIFILM RI Pharma, Tokyo, JAPAN.

Backgrounds: Although patients with hypertrophic cardiomyopathy (HCM) showed heterogeneous perfusion distribution, there is no useful tool for quantitative assessment of such perfusion heterogeneity. "Fractal analysis" is known as one of the methods to evaluate the geometric self-similarity, which is applied for the assessment of heterogeneity of geometry or density. In this study, we investigated usefulness of "fractal analysis" for quantification of perfusion heterogeneity in HCM patients, and compared to that in normal subjects. Moreover, we also investigated the factors which influenced the perfusion heterogeneity in patient with HCM. **Methods:** Ten patients with HCM and 7 normal subjects (Normal) underwent ECG-gated myocardial perfusion SPECT at rest with ^{99m}Tc-MIBI. Polar map, which was generated from 3D-SPECT imaging, was analyzed with "box counting (BC)" and "pixel counting (PC)" methods, which were the procedures of fractal analysis to evaluate the degree of heterogeneity of geometry (BC) and density (PC). Then, we calculated and compared "fractal dimensions (FD)" of each method between HCM and Normal groups. Moreover, we investigated the relationship between FD and left ventricular (LV) functions (end diastolic volume: EDV, ejection fraction: EF), summed rest score (SRS), maximum wall thickness (MWT). **Results:** FD of both BC and PC methods, did not show significant differences between HCM and Normal groups. However, FD ratio of BC/PC was significantly higher in HCM than in Normal group ($P=0.01$). From further comparison of myocardial perfusion count profile between HCM and Normal, this significant difference of FD ratio between two groups might be derived from the difference of lower count distribution. In ROC analysis, AUC of detecting HCM by using this FD ratio was 0.9. In HCM patients, FD of BC and PC showed significant negative correlation with MWT ($r=-0.65$, $P<0.05$), and showed significant positive correlation with LVEDV ($r=0.78$, $P<0.01$). However, there were no significant correlation with LVEF and SRS. **Conclusions:** Fractal analysis might be useful for quantitative assessment of perfusion heterogeneity in HCM patients. Furthermore, this perfusion heterogeneity is influenced by MWT and LV volume.

EP718**Partial volume correction for improved PET quantification in 18F-NaF imaging of atherosclerotic plaques**

J. Cal-Gonzalez¹, X. Li¹, D. Heber¹, I. Rausch¹, S. C. Moore², K. Schäfers³, M. Hacker¹, T. Beyer¹; ¹Medical University of Vienna, Vienna, AUSTRIA, ²Harvard Medical School and Brigham and Women's Hospital, Boston, MA, UNITED STATES, ³University of Münster, Münster, GERMANY.

Aim. ¹⁸F-NaF PET uptake has been described as a marker of early calcium deposition in atherosclerotic plaques in the carotid arteries. However, due to the small size of these plaques, partial-volume effects (PVE) will compromise the quantification accuracy of the PET data. Therefore, our aim was to increase the accuracy of ¹⁸F-NaF PET uptake in carotid plaques following partial-volume correction (PVC). **Materials and methods.** The local projection (LP) method was implemented for PVC in clinical PET imaging. The performance and accuracy of the method was evaluated by using static acquisitions of a thorax phantom with three “plaque-type” lesions of 36mL, 31mL and 18 mL inserted, and lesion-to-background ratio (LBR) of 70:1. After the validation of the method with phantom data, LP-PVC was applied retrospectively to a cohort of 17 patients (12 m, 5 f. mean age: (64±9) y), each with at least one positive plaque in the carotid or ascending aortic arteries. In total, 51 calcified (HU>110 within the plaque) and 16 non-calcified plaque lesions (HU<110) were analyzed. For all calcified lesions, the tissue-segmentation required for the PVC was obtained from CT. In non-calcified plaque lesions and the thorax phantom data, a threshold-based segmentation of the PET image was performed by using the 3D isocontour halfway between the background and maximum lesion voxel values. The maximum HU value and the volume of the plaque were obtained from the CT images. The lesion-to-background ratio LBR (using the mean activity within the lesion) and the activity recovery within the lesions after PVC were measured on PET images. **Results.** For the phantom acquisitions we observed a significant increase in the LBR ratio when PVC was applied (42% to 109% for the three plaque lesions). In patient images, PVC led to a significant increase of the LBR in both calcified (mean = 38% [4%-116%]) and non-calcified plaques (mean = 43%, [9%-77%]). The inverse correlation of ¹⁸F-NaF uptake and HU values improved for the calcified plaques when PVC was applied. **Conclusions.** An LP-PVC method was evaluated in clinical NaF-PET/CT imaging of patients with carotid artery plaques. The PVC performance using the two proposed segmentation algorithms was evaluated in phantom experiments providing similar results in all cases. The PVC method performed well in phantom and patient data and led to improved quantification of atherosclerotic plaques in the carotids. Footnotes J. Cal-Gonzalez et al, Phys Med Biol. 2015; 60: 7127-49.

EP719**Comparison of an automatic method for the placement of a blood pool reference region compared to manual placement**

A. Nelson, S. Chung; MIM Software Inc., Cleveland, OH, UNITED STATES.

Purpose: To compare the mean SUV values of a manually placed blood pool reference region to a reference region placed using a completely automated method. **Methods:** 45 subjects with FDG-PET/CTs were chosen for this study. The upper portion of the descending aorta (DA) was manually segmented on the CT scan for each subject in the study. These subjects were combined into an atlas to automatically generate DA contours on each subject using a leave-one-out analysis. For the atlas-segmentation, the 5 most closely matched subjects are automatically found and then deformably

registered to the test subject. The 5 DA are then combined using STAPLE into a final atlas contour. An automatic method was used to search for the lowest coefficient of variation within a 1 cm sphere for the atlas-generated DA. The mean SUV value was then recorded and compared to PERCIST-based blood pool reference regions which had previously been manually placed in the DA. **Results:** The manually placed blood pool reference regions had an average mean SUV value of 1.91 with a standard deviation of 0.35, while the automatically generated blood pool reference regions had an average mean SUV value of 1.95 with a standard deviation of 0.38. The correlation between the two methods was 0.93, with an average difference of 0.11 (6.26%). The largest absolute deviation between automatic and manual was 0.40 SUV (20.62%). **Conclusions:** The automated method for blood pool reference region placement was found to agree well with manually placed reference regions and thus has the potential to save time when using criteria, such as PERCIST, that recommend reference to blood pool values.

EP720**Intra- and Interobserver Agreement with Quantitative PET Measures: Deriving Repeatability Coefficients from Variance Component Analysis**

O. Gerke¹, M. H. Vilstrup¹, E. A. Segtman¹, U. Halekoh², P. Høilund-Carlson¹; ¹Odense University Hospital, Odense C, DENMARK, ²University of Southern Denmark, Odense C, DENMARK.

Aim: Quantitative measurement procedures must be accurate and precise to be of clinical use. Accuracy refers to deviation of a measurement from the true value of the quantity being measured. Precision reflects deviation of groups of measurement from another. Closeness of comparable measurement sets is often expressed as proportions of agreement, standard errors of measurement, coefficients of variation, or the Bland-Altman (BA) plot. Applying the concept of variance component analysis (VCA), we estimated the variances due to errors caused by separate elements of a PET scan (scanner, time point, observer, etc.) to express the composite uncertainty of repeated measurements and obtain relevant repeatability coefficients (RC) for comparison with BA plots in a test-retest setting. The RC is the limit below which 95% of differences will lie. **Material and Methods:** For analysis we used data sets obtained in two different studies at our institution. In study 1, 30 patients with ovarian cancer were scanned pre-operatively, and SUVmax values were obtained twice by the same observer two months apart. In study 2, 14 patients with glioma were scanned up to 5 times before and during treatment, and resulting 49 images were assessed by three observers, who calculated total hemispheric glycolysis, i.e., the segmented metabolic volume times SUVmean. Thus, the two studies served as examples of intra- and interobserver variability assessment, respectively. In study 1, we treated ‘reading’ (1st vs 2nd) as fixed factor and ‘patient’ as random factor. In study 2, both ‘observer’ and ‘time point’ were considered fixed, whereas ‘patient’ and ‘scanner’ were treated as random effects. **Results:** In study 1, the within-subject standard deviation times 2.77 ($\sqrt{2} \times 1.96$) yielded a RC of 2.46 equaling half of the width of the BA band. In Study 2, the RC for identical conditions (same patient, same observer, same time point, same scanner) was 2392; allowing for different scanners resulted in a RC of 2543. The differences between observers were negligible compared to the other factors: estimated difference between observer 1 and 2: -10, 95% CI: -352 to 332; observer 1 vs 3: 28, 95% CI: -313 to 370. **Conclusion:** VCA appears to be a more informative and comprehensive approach to agreement studies that are conventionally tackled with simple measures only. VCA is built on various model assumptions; however, this has not been an obstacle to the extensive use of intraclass correlation coefficients in reliability analyses.

EP721**Evaluation of the clustering based image segmentation algorithms for nuclear medicine imaging**

D. Borys¹, M. Niezgodna¹, K. Szczucka-Borys², I. Gorczewska², M. Frackiewicz¹; ¹Silesian University of Technology, Gliwice, POLAND, ²Maria Skłodowska-Curie Memorial Cancer Center and Institute of Oncology, Gliwice Branch, Gliwice, POLAND.

Aim: A segmentation is a nontrivial and important step in an image analysis in every aspect of usage of imaging techniques. Especially in medical imaging, when tumour delineation is concerned, this task becomes a crucial challenge. In this work, with many segmentation algorithms, we used those, based on clustering. Standard k-means clustering technique was compared with neural gas clustering algorithm. The aim was to validate segmentation quality of those algorithms in PET segmentation imaging. **Materials and methods:** Data has been obtained with Philips Gemini hybrid PET/CT device at the Department of PET Diagnostics at Institute of Oncology in Gliwice. First phantom was a standard cylinder with five spheres of different radius and volume (diameter from 1.3 cm up to 4 cm). The second phantom was the Pro-NM SPECT performance phantom containing many internal structures for evaluating: pixel size, spatial resolution, etc. Spheres, in the first phantom, and the cylinder in the second one, have been filled with F-18 with constant concentration. For segmentation purpose, two clustering algorithms were tested. The first is a standard k-means clustering and the second is a neural gas algorithm. In both algorithms, the number of clusters was fixed to 2 as we are interested in discovering the borders between the lesion and the background. The Euclidean distance was used as a distance measure. For the neural gas algorithm, two parameters have to be set up: an adaptation step size A and neighbourhood size L. The number of iterations had to be determined as well and was set to 50. By maximising a Jaccard index values of parameters have been calculated and were A=0.3, L=0.96. We applied described methods to segment intensity images and to compare the results with other frequently used method based on the absolute SUV 2.5 level threshold. Results were compared to CT image based reference mask by using a Jaccard index ([0,1] where 1 corresponds to the full similarity of sets). Results: The mean values of the Jaccard index were: for the first phantom 0.65 (k-means), 0.7 (SUV 2.5) and 0.98 (neural gas), for the second phantom 0.79 (k-means), 0.22 (SUV 2.5) and 0.79 (neural gas). **Conclusion:** Neural gas method results with the highest Jaccard index in both phantoms. However, both methods obtained a reasonable result in the second case where standard SUV 2.5 threshold misclassified a lot of structures.

EP722**A Resolution and Noise Level Matching-Based Simulated SPECT Image Generation using PET**

H. Moon^{1,2}, J. S. Oh¹, J. Park¹, M. Oh¹, S. Oh¹, J. Kim¹; ¹Department of Nuclear Medicine, Asan Medical Center, University of Ulsan College of Medicine, Seoul, KOREA, REPUBLIC OF, ²Department of Medical Science, University of Ulsan College of Medicine, Seoul, KOREA, REPUBLIC OF.

Aim: Brain amyloid PET is a representative imaging biomarker in Alzheimer disease. We performed spatial resolution matching (SRM)- and noise level matching (NLM)-based generation of simulated SPECT images using phantom/clinical PET images, to explore the feasibility of Tc-99m-based amyloid SPECT. **Materials and methods:** To match PET resolution/noise onto those of SPECT, we acquired PET and SPECT images of Hoffman 3D Brain Phantom (HBP) using 18MBq fluorine-18 (F-18) and 185MBq Tc-99m, where both were reconstructed using iterative methods with clinically-used iteration/subset parameters for PET and SPECT in our institution. However, we did not apply post-smooth

filter to better explore the resolution/noise level differences. For the SRM of PET/SPECT, we used CT-based tissue label map (CTM), i.e., SPM8-based segmentation of a couple of best quality CT images of HBP. After morphologic image processing, we generated a label map valued four for Gray matter (GM) and one for White matter (WM) that correspond to the ideal uptake ratio in HBP PET. The CTMs were registered to individual PET and SPECT images of HBP using the transformations that project CTM onto CT images corresponding to PET and SPECT, respectively. After smoothing registered CTMs using Gaussian kernel with one-to-twenty mm FWHM (0.5mm interval), we found the resolution difference of PET and SPECT using best-fit kernels with the highest correlation coefficient for PET and SPECT. For the NLM of PET/SPECT, we added variable amplitudes (i.e., SD) of Gaussian noise before PET smoothing to find the additive noise level matching the coefficient of variation of smoothed PET in predefined GM VOI with that of SPECT. Using these matching parameters, we generated simulated patient brain SPECT using representative F-18 florbetaben (FBB) PET of patients with positive/negative/moderate amyloid deposition, followed by visual inspection of board-certified Nuclear Medicine Physicians (MO and JSK). **Results:** According to the estimated SRM/NLM factors (70% of mean PET GM count and 7.5mm FWHM), we could match resolution and noise level of PET onto those of SPECT by adding 70% noise and 7.5mm smoothing. Expert visual inspection-based diagnosis of positive/negative/moderate amyloid burden by F-18 FBB PET was not changed by SPECT-matched PET images. **Conclusion:** By conducting SRM and NLM, we could generate the simulated amyloid SPECT image on the basis of clinically-used amyloid PET image. The simulated SPECT images of patients using the clinical F-18 FBB PET images exhibited the feasibility of a new Tc-99m-based SPECT imaging in terms of consistent clinical diagnosis.

EP723**The Value of the 3hr SeHCAT Scan - Could we Estimate a Baseline Instead?**

A. Smout¹, A. Fullbrook², J. Ward², L. Wright², J. R. W. Hall², P. Hinton¹; ¹Royal Surrey County Hospital, Guildford, UNITED KINGDOM, ²Frimley Park Hospital, Frimley, UNITED KINGDOM.

The aim of this prospective audit was to see if an estimate of the 3 hour counts could be made instead of acquiring a baseline image. This would simplify the patient experience and avoids the use of an assumption that there is no clearance in the first 3 hours. A secondary aim of this audit was to investigate whether an episode of diarrhoea between administration and baseline imaging reduced the counts in the image. Patients are given a 0.37MBq Se-75 Tauroselcholic (SeHCAT) capsule and return 3 hours later for a 5 minute intrinsic acquisition using a gamma camera. The patients are asked if they have opened their bowels and if they are currently on anti-diarrhoeal medication - this information is noted in the clinical report. The decay and background corrected geometric mean counts from day 7 are compared to those of the baseline to calculate the percentage retained at 7 days and compared to published normal ranges. The counts in the baseline image are, in theory, a function of the activity in the patient, camera geometry and patient body habitus. For this audit of 67 patients the camera geometry was standardised, the capsule reference information was recorded to calculate the administered activity, and the patient height and weight were also recorded. A relationship between counts and the patient size was derived from the simple assumption that patients are homogenous cylinders of density 1 g/cm³. The effective radius was calculated and used within an exponential attenuation equation with attenuation coefficient for soft tissue of 0.1175 per cm. This simplistic approximation, which did not rely on any empirical factors, showed reasonable correlation (correlation coefficient 0.82) with the measured counts from imaging. A comparison between the measured counts and body mass index and again with body surface area gave correlation

coefficients of 0.78 and 0.60 respectively but gave increasing errors for more attenuating patients. The mean difference between the estimated and measured counts for patients that had opened their bowels (8 of 67) was -0.6% , suggesting that there had been no Se-75 excreted in the first 3 hours. The standard deviation of the difference between measured and estimated baseline counts was 8.0% , corresponding to a final standard deviation in the retained SeHCAT percentage of $\pm 0.8\%$ on a test result of 10% . This suggests that it may be viable to replace the 3 hour image with an estimate of the baseline counts.

EP724

Impact of the geometric mean calculation on the assessment of liver clearance with dynamic scintigraphy

Y. D'Asseler, R. Troisi, B. Lambert; Ghent University, Gent, BELGIUM.

Patients with liver tumors undergo a resection of the affected part of the liver as part of their treatment. In order to avoid complications, it is important to assess whether the liver function of the remaining part will be sufficient. This is done by dynamically scanning the patient with a gamma camera after injection of Tc-99m labeled Mebrofenin. Clearance from the blood by the liver is calculated according to the method proposed by Ekman et al. [Nuc Med Comm 1996, 17, 235-242]. In order to compensate for photon attenuation, the geometric mean of the anterior and posterior image was taken for construction of the time activity curves. In this paper, we investigate the sensitivity of the clearance calculation to the way this geometric mean is taken into account. 13 patients scheduled for liver surgery received a dose of approximately 180 MBq of Tc-99m-labeled Mebrofenin and were subsequently dynamically scanned for 10 min with 10 second time frames. For the first method, regions of interest (ROI's) of the liver and heart were drawn manually on the anterior image, and copied onto the posterior image. Time-activity curves (TACs) were constructed by taking the geometric mean of the anterior and posterior total counts in the ROI. These TAC's were then used as an input to calculate liver clearance using the method described in [1]. The second method consisted in calculating the geometric mean image pixel by pixel for each frame, and then drawing ROI's on these images to obtain the TAC's and calculate the liver clearance. For method 1, with geometric mean calculated on the total counts for each ROI, the average liver clearance was $(12.0 \pm 3) \%$ /min, for method 2, using a pixelwise geometric mean, liver clearance was $(14.5 \pm 4) \%$ /min. Calculating the relative difference in liver clearance for each patient, we obtained a mean difference between both methods of $(17.4 \pm 2.6) \%$, with a maximum observed difference of 22% . We observe a significant and large difference between calculated liver clearances if the pixel by pixel geometric mean calculation is performed instead of calculating the geometric mean on a ROI basis. Mathematically, a pixel by pixel calculation is the more correct method, however, not all clinical Nuclear Medicine processing packages allow this operation. Moreover, care should be taken in low count regions where pixels with zero counts in the posterior or anterior image may lead to a bias.

EP725

Quantitative Estimation of Activities in a Tc-99m/In-111 Small Animal SPECT Study

K. Ogawa¹, S. Endo¹, I. O. Umeda², H. Fujii²; ¹Hosei University, Tokyo, JAPAN, ²National Cancer Center, Kashiwa, JAPAN.

Aim: This study is aimed to develop a method to measure the distribution of two activities (^{99m}Tc and ¹¹¹In) simultaneously in a small animal SPECT study with multi-pinhole collimator. **Materials and Methods:** In the estimation of activities we applied an artificial neural network (ANN) with three layers: one input layer with three or four units, one

hidden layer with twice the number of units in the input layer, and one output layer with three units. For values input into the units in the input layer, we used a predefined number of ratios of counts calculated with several energy windows, which are the ratios of the count C_k acquired with the k -th window to the sum of the above counts C_s . That is, the value input into the k -th unit was the ratio R_k to C_s . The outputs were three count ratios defined as follows: R_{Tc} was the count ratio of primary photons for ^{99m}Tc (141keV), R_{In1} was that for ¹¹¹In (171keV), and R_{In2} was that for ¹¹¹In(245keV). With these ratios, each of the primary counts was estimated by multiplying R_{Tc} , R_{In1} , and R_{In2} with C_s . The ANN was trained with a back-propagation algorithm using the above data obtained with a Monte Carlo method. The data acquisition geometry was the same as that of the nano-SPECT/CT with four cameras each with a nine-pinhole collimator. To make training data, we used a cylinder (radius 20mm) filled with water, in which we located two small cylinders (radius 3mm) and emitted photons of ^{99m}Tc and ¹¹¹In. The number of emitted photons was 10Giga. The pixel size was $1.035 \times 1.035 \text{mm}^2$. The evaluated target was a cylinder (radius 15mm, length 10cm), inside which we located two small cylinders with a radius of 4mm. After separating the two radionuclides in the projection data, images were reconstructed with the ML-EM method. The accuracy of the estimation was evaluated by the root mean square error in the reconstructed images. **Results:** The results showed that the three-inputs ANN with three photopeak windows (^{99m}Tc: 1 and ¹¹¹In: 2) was suitable for the estimation of ¹¹¹In activities. And the four-inputs ANN including an extra energy window to measure scattered photons was suitable for the estimation of ^{99m}Tc activities. **Conclusions:** We applied the ANN method to quantitatively measure the distribution of activities with the ^{99m}Tc/¹¹¹In simultaneous data acquisition in a small animal SPECT study and determined the structure of the ANN.

EP726

Optimisation of time of flight FDG PET/CT for whole body imaging

E. Kalogianni, D. Ruiz, G. Havariyoun, C. Benjamin, G. Vivian; King's College Hospital, LONDON, UNITED KINGDOM.

Aim: The motivation of this project was to assess and optimise the relationship between FDG administered activity and accurate quantification as well as image quality in PET/CT whole-body (WB) imaging. **Method:** WB time-of-flight (TOF) PET/CT was performed in 32 patients, 64 ± 6 min after the injection of 336 ± 53 MBq (range 226-423 MBq) ¹⁸F-FDG, using a linear relationship between administered activity (A) and body mass (W) ($A(\text{MBq}) = 4.5 \times W(\text{kg})$). Median body mass was 73 ± 14 kg (47-105kg) and height was 1.7 ± 0.1 m (1.3 -1.8m). TOF reconstructions were created from simulated 1.5-min, 2-min and 2.5-min data taken from the 3-min per bed position (reference) acquired list mode data in order to create reduced count statistics. SUVmax from 93 FDG avid foci, from 24 patients was analysed using a 3-mm diameter VOI, autopositioned on all the reconstructed images. Bland-Altman plots were produced to assess the reproducibility of SUV measurements. Liver signal-to-noise-ratio ($\text{SNR}_{\text{liver}}$) that was determined from nine 3-mm diameter VOI placed in the uniform liver region and noise equivalent counts per axial length ($\text{NEC}_{\text{patient}}$) were used to assess the image quality. **Results:** SUV measurements showed high correlation between the reference acquisition and the 1.5-min, 2-min and 2.5-min acquisitions ($r > 0.99$). Reproducibility slightly worsened as acquisition time decreased; 95% confidence limits were $\pm 8\%$ (or ± 0.1 SUV) for the 1.5-min per bed position. $\text{SNR}_{\text{liver}}$ showed moderate correlation ($r > 0.5$) with body mass index (BMI) for all acquisitions. Median $\text{SNR}_{\text{liver}}$ was reduced by 27% for the 1.5-min per bed position from 11, as measured for the reference acquisition. 90% percentile of $\text{SNR}_{\text{liver}}$ of patients with $\text{BMI} < 25 \text{kg/m}^2$ scanned with at least 2.5-min acquisition was greater than 10, at 95% confidence. $\text{NEC}_{\text{patient}}$ was strongly correlated with body mass ($r > 0.7$). Median $\text{NEC}_{\text{patient}}$ decreased by 52% for the 1.5-min per bed position from 26 Mcounts/m, as measured for the reference acquisition. All median

NEC_{patient} values and median SNR_{liver} for the 3-min and 2.5-min acquisitions satisfied the Fukukita et al [1] image quality criteria. Conclusions: Reduced time acquisitions resulted in images with higher level of noise, but without significant bias in the SUV measurements. BMI was a better predictor of image noise. This study shows that time reduction up to 20% will not have significant impact to image quality, especially to patients with BMI < 25 kg/m². Visual assessment is needed to evaluate the findings. Reference: [1] Fukukita H, et al. *Ann Nucl Med* (2014) 28:693–705.

EP727

Quantification accuracy of PET images as a function of emission scan time in PET/CT and PET/MR

S. Wampl¹, I. Rausch¹, T. Traub-Weidinger¹, T. Beyer¹, M. Gröschl², J. Cal-González¹; ¹Medical University of Vienna, Vienna, AUSTRIA, ²Vienna University of Technology, Vienna, AUSTRIA.

Aim. To evaluate the effect of reduced emission times on the PET quantification accuracy in PET/CT and PET/MR. **Materials and methods.** Measurements were performed on a Biograph TruePoint-TrueView (TPTV) PET/CT and Biograph mMR PET/MR. Full acquisitions were split into time frames of (10, 5, 3, 2 and 1) min and reconstructed using iterative methods (OSEM, 4i21s, 5x5mm Gaussian post filtering) with and without resolution recovery (PSF, no post filtering). **Phantom evaluation:** A 20 min list mode acquisition of the NEMA NU-2 IQ phantom containing six spheres (10mm-37mm) was acquired. Quantification accuracy was evaluated by means of Signal-to-Noise-Ratios (SNR) and Recovery Coefficients (RC) for the maximum- (RC_{max}), and mean activity in a volume-of-interest defined by a background-corrected threshold at 50% of the maximum voxel (RC_{A50}). Time-dependent variations of segmented volumes were analyzed for the VOI used for RC_{A50} (V₅₀). **Patients:** 10-min dynamic data of ¹⁸F-FET brain scans (7 PET/CT, 4 PET/MR, 1 both) were processed similar to the phantom data. Quantification accuracy was evaluated using image noise, SNR and Standardized Uptake Values (SUV) for the maximum (SUV_{max}) and mean (SUV_{A50}) activity in V₅₀ VOI. **Results.** In phantom images, noise increases by up to 200% when reducing acquisition time (AcqT) from 20min to 1min, independent of the reconstruction method and PET system used. In PET/MR, reduction of AcqT introduced an increase of the RC_{max} in the biggest sphere for OSEM (+9%) and PSF (+60%). RC_{A50} demonstrated only half of these increases. The segmented volumes for the bigger spheres were reduced by up to 70% when shortening the AcqT. SNR decreased by 80% when reducing AcqT, independent of the sphere-size or reconstruction method. Reducing frame duration in patient studies (OSEM) using PET/CT and PET/MR increased image noise by 80% and 50%, thus, resulting in 15% and 9% higher SUV_{max}, respectively. PSF reconstructions revealed higher dependencies of SUV on the frame duration in PET/CT and PET/MR: 95% and 140% noise; 35% and 50% SUV_{max}, respectively. SUV_{A50} was less affected by reduction of AcqT. **Conclusions and outlook.** RC_{max} and SUV_{max} values are strongly affected by reduced emission scan times, thus, affecting quantification accuracy of PET images while RC₅₀ and SUV_{A50} show a more stable behavior.

EP728

Optimization of ²⁰¹Tl-SPECT Imaging in Brain Tumors Utilizing Simple Three 360° Rotational Acquisition and SPECT/MRI Hybrid Imaging

A. Abe¹, S. Abe², S. Oya¹, T. Matsui¹; ¹Saitama Medical University, Kawagoe, JAPAN, ²Shizuoka Medical Center, Shizuoka, JAPAN.

Background: ²⁰¹Tl-SPECT is useful in diagnosing brain tumors. The minimum radiopharmaceutical dosage of ²⁰¹Tl-chloride and the appropriate length of scan time for diagnosing brain tumors are, however, difficult

to determine and have not been precisely investigated. **Aim:** Validating the possibility of shortening the length of ²⁰¹Tl-SPECT scan time in patients with brain tumors is the primary purpose of this study. **Materials and Methods:** Ten cases of preoperative brain tumors: 5 intraaxial and 5 extraaxial, were included in this study. The early-phase imaging and delayed-phase imaging were started at 15 min and 3 hours 15 min after the injection of 111MBq of ²⁰¹Tl-chloride in a pre-filled syringe, respectively. One ²⁰¹Tl imaging took 27 min and consisted of three 360° rotational acquisition: one 360° rotation took 9min. The short length (9 min) scan data were acquired from the first 360° rotational scanning. The middle (18 min) and long (27 min) length scan data were acquired from the first and second and from the first to third 360° rotational scanning, respectively. The region of interest (ROI) was precisely placed on the uptake of the tumor (T) and its contralateral area as background uptake (N) on the ²⁰¹Tl-SPECT/MRI hybrid images obtained utilizing the NEUROSTAT-based multimodality fusion software. Thallium uptake indices of the early-phase imaging (ER) and delayed-phase imaging (DR) were defined as follows: thallium uptake index = mean counts per voxel in T / mean counts per voxel in N. The group of 9 min ERs, 18 min ERs and 27 min ERs were statistically compared with Friedman's χ^2 -test and the same comparison was also applied for 9 min DRs, 18 min DRs and 27 min DRs. **Results:** No statistically significant difference was observed among the groups of 9 min ERs, 18 min ERs and 27 min ERs (P = 1.34) and also among the groups of 9 min DRs, 18 min DRs and 27 min DRs (P = 1.48). **Conclusion:** ER and DR were invariable regardless of scan length: 9 min, 18 min and 27 min. The short length scan taking 9 min is, therefore, sufficient to calculate thallium uptake indices, i.e. ER and DR, which are essential to evaluate the degree of uptake of ²⁰¹Tl to brain tumors. These results also suggest the radiopharmaceutical dosage of ²⁰¹Tl-chloride can be reduced to a minimum of 37 MBq, one third of current 111 MBq, with the long length scan taking 27 min.

EP729

Fusion and Analysis of PET And CT Images of Patients with Non-Small Cell Lung Cancer

O. Ayyıldız¹, B. Yilmaz¹, S. Karacavus^{2,3}, O. Kayaaltı⁴, K. Eset³, C. Gazelolu¹, S. Icer³, E. Kaya⁵; ¹Abdullah Gul University, Department of Electrical and Electronics Engineering, Kayseri, TURKEY, ²Bozok University, Department of Nuclear Medicine, Yozgat, TURKEY, ³Erciyes University, Department of Biomedical Engineering, Kayseri, TURKEY, ⁴Erciyes University, Department of Computer Technologies, Kayseri, TURKEY, ⁵Acibadem University, Department of Nuclear Medicine, Kayseri, TURKEY.

Background: Non-small cell lung carcinoma (NSCLC) accounts for 85% of all cases of lung cancer. Use of positron emission tomography - computed tomography (PET-CT) imaging systems permits the acquisition of functional and morphological data within a single session. Recently, texture features obtained from PET/CT images that reflect the heterogeneity of the tumor are shown to be complementary to the quantitative assessment of the tumor. The texture analysis is mainly performed on only PET images. The number of studies that deal with fused images are very few. **Material and Methods:** In this work, we used PET/CT images of 67 NSCLC patients. We worked on PET slices with the maximum standard uptake value and the corresponding CT slices. The first step was to define the object boundaries and perform intensity based image registration to align the images. We applied principal component analysis (PCA) and discrete wavelet transform (DWT) to fuse registered PET and CT images. We compared fused images based on objective fusion metrics such as spatial frequency (SF), mutual information (MI), and fusion symmetry (FS). An experienced nuclear medicine expert also visually assessed the fusion performances. Then, we applied active contour segmentation method to segment the tumors in PET and CT images

separately and in images fused with PCA and DWT. Next, we extracted features using the gray level co-occurrence matrix (GLCM) and compared the texture features obtained from only PET images and images fused with DWT. **Results:** We found that the DWT was better than the PCA in terms of visual and objective metrics. We also found that there is no significant difference between textures features obtained from only PET and fused images ($p < 0.05$). **Conclusion:** Texture features determined from only 18F-FDG PET images can be used to evaluate the heterogeneity of the tumor in non-small cell lung cancer.

EP730

Assessment the Performance of Adding Risk Factors to Quantitative Analysis of Myocardial Perfusion Imaging

M. bordbar¹, S. Ghasemipoor²; ¹Department of Communication Engineering, Shiraz University of Technology, Shiraz, IRAN, ISLAMIC REPUBLIC OF, ²Alzahra Charity Hospital, Shiraz, IRAN, ISLAMIC REPUBLIC OF.

Although the regional and global quantitative analysis may improve the reproducibility and certainty of interpretation of SPECT myocardial perfusion imaging (MPI), but still there is not enough association between the quantitative values and physician's visual interpretations. In this study we assess if adding the risk factors as the complementary values to quantitative analysis, can improve the association to visual interpretations. In a retrospective study, all the patients (age: 51 ± 23 , 155 male, 306 female) with likelihood of coronary disease who underwent rest/stress 99mTc-sestamibi gated SPECT in our hospital during a month were selected. An expert interpreted the images visually while the quantitative data and risk factors were shown to him. The quantitative analysis results compared with the expert's decision about the patient's ischemia. According to our results, the sensitivity and specificity and area under curve of sum rest (SRS) and sum stress score (SSS) are 0.53 and 0.79, 0.74 and 0.63, 0.63 and 0.76 respectively. Adding the adequate risk factors to SRS and SSS analysis the total accuracy changes from 0.63 to 0.65 and from 0.71 to 0.63, and the precision grows dramatically from 0.67 to 0.87 and 0.68 to 0.78 for SRS and SSS respectively. The results of this study show that adding adequate risk factors as the complementary values to quantitative analysis can improve the diagnostic value of SRS and SSS. These findings suggest that computer aided diagnostic systems can effectively improve their performance by using quantitative parameters of MPI along with risk factors as the complementary values.

EP731

How much reduction in time can we go in myocardial perfusion SPCT Imaging? role of resolution recovery and correction of image degrading factors

M. M. Khalil¹, T. Ahmed^{2,3}, W. Elshemey⁴, A. ELfiky⁴; ¹Faculty of Science Helwan University, Physics Department, Cairo, EGYPT, ²Nuclear Medicine and Cyclotron department King Hamad University Hospital, Busaiteen, BAHRAIN, ³Faculty of science, Biophysics department, Cairo University, Cairo, EGYPT, ⁴Faculty of Science Cairo University, Biophysics Department, Cairo, EGYPT.

Objective:The aim of the present study was to evaluate the effect of reducing the acquisition time on the performance of Iterative Reconstruction (IR) algorithms accompanied with attenuation, scatter and resolution recovery corrections (IRACSCRR) on the quality of myocardial perfusion SPECT imaging. **Methods:**A standard cardiac phantom with solid inserts was used to simulate a routine myocardial perfusion SPECT/CT imaging. Two solid inserts were used; one placed in the mid anterior portion of the myocardium while the other was inserted in the basal inferior wall. The phantom was placed inside a uniform cylindrical

phantom. A clinically relevant count rate and acquisition time was used to avoid discordance with real data acquisition. Four SPECT scans were acquired using vendor standard cardiac protocol for resolution recovery applying different acquisition times (5, 10, 15 and 20 sec per frame). The CT attenuation map was acquired using 50 mA and 100 kV. Figures of merit used to evaluate the performance of the reconstruction algorithms were count uniformity, coefficient of variation (CoV) and Contrast to Noise ratio (CNR) calculated for normally perfused myocardium while percentage defect contrast was used to assess hypo-perfused segments represented by solid inserts. The slice uniformity and CoV were calculated using maximum count of 60 radial rays of circumferential profiles drawn over normal slices. Image reconstruction was carried out using FBP and IR (OSEM; IRACSCRR). **Results:** The image quality of (IRACSCRR) showed an improvement in terms of CNR and defect contrast resolution as we move towards longer acquisition time. CNR was improved in the direction of basal to apical slices while, there was significant improvement in defect contrast resolution for both defects at longer acquisition time. No large difference was found in the defect contrast of non-transmural relative to transmural defect for the same acquisition time. However, this was associated with slight increase in image noise as shown from image uniformity and CoV analysis. There was also improvement in CNR when using longer acquisition time but still not significant. **Conclusion:** The results showed that the image uniformity, CoV, defect contrast and CNR were improved by applying the higher acquisition time with slight differences appeared on apical versus basal slices and transmural versus non-transmural perfusion defects. In Comparison, the reduction in imaging time (down to one-third) was found non-significantly affecting the image quality. However, individualizing the acquisition parameters due to variable patient habitus could stabilize image quality among different subjects and/or scans. This is to be addressed in future studies.

EP732

Comparison of QGS, 4DM-SPECT, and MIMcardiac Left Ventricular Volumes for Tc99m SPECT to Cardiac Computed Tomography Angiography (CCTA) Volumes

A. Nelson, S. Pirozzi, A. Pilla, D. Nelson; MIM Software Inc., Cleveland, OH, UNITED STATES.

Purpose: To compare the left ventricular volumes generated by three commercially available software packages with reference to CCTA volumes for cardiac Tc99m sestamibi gated SPECT. **Methods:** CCTA images were collected for 15 patients with corresponding gated (8 frame) stress Tc99m sestamibi SPECT studies. The LV endocardial cavities were manually segmented on the CCTA's. The CCTA images were fused to the corresponding gated SPECT study and the most closely matched frame was identified prior to generating the SPECT contours. The gated SPECT scans were then processed using MIMcardiac, QGS, and 4DM to generate time volume curves. The volume from the frame that was previously determined to most closely match the CCTA was recorded. All processing was done completely automatically without any operator intervention. **Results:** MIMcardiac had correlation of 0.94 with an average volume difference of 31 mL (23% diff) compared to CCTA. 4DM had the next highest correlation of 0.90 and an average volume difference of 92 mL (63% diff). QGS had a correlation of 0.88 and an average volume difference of 64 mL (59% diff). Three of the fifteen QGS segmentations needed adjusted and after adjustment the results improved to a correlation of 0.93 and average volume difference of 48 mL (39%). All MIMcardiac and 4DM results were completely automatic. **Conclusions:** All three methods showed good correlation with CCTA volumes with MIMcardiac showing the highest correlation and least difference in volume. Additional studies are planned with comparison to gated cardiac MRI.

EP733**Usefulness of 18F-FDG PET/CT for the Diagnosis of Tuberculous Pericarditis**

T. Li, Z. Jiang; The First Affiliated Hospital of Nanjing Medical University, Nanjing, CHINA.

The diagnosis of tuberculosis as the aetiological cause is important. However, in a significant number of patients, a definite diagnosis cannot be established. Positron emission tomography (PET) can be a useful supplement to computed tomography (CT) because its depiction of metabolic activity in the pericardium or in pericardial fluid. When combined together, PET/CT may help with early diagnosis of tuberculous pericarditis. By far, only a few case reports have discussed the usefulness of ¹⁸F-FDG PET/CT for tuberculous pericarditis. Its value is not well determined. Therefore, we present the result with six cases of tuberculous pericarditis to analyze the clinical value of ¹⁸F-FDG PET/CT in diagnosis of tuberculous pericarditis and review the literature. **CONCLUSION:** 18F-FDG PET/CT features like pericardial thickening, pericardial enhancement of FDG uptake, mediastinal lymph nodes enlargement, mediastinal lymph nodes enhancement of FDG uptake may help to differentiate with idiopathic pericarditis. Mediastinal lymph nodes without hilar node involved may help to differentiate with malignant pericardial disease.

EP-41 – Sunday, October 16, 2016, during Exhibition hours, e-Poster Area
Physics & Instrumentation & Data Analysis: Image Reconstruction

EP734**Collimator-Detector Response Compensation in Preclinical SPECT using STIR Framework**

H. Mahani^{1,2}, G. Raisali², A. Kamali-Asl³, M. Ay^{4,1}; ¹Research Center for Molecular and Cellular Imaging (RCMCI), Tehran, IRAN, ISLAMIC REPUBLIC OF, ²Radiation Application Research School, Nuclear Science and Technology Research Institute (NSTRI), Tehran, IRAN, ISLAMIC REPUBLIC OF, ³Radiation Medicine Engineering Department, Shahid Beheshti University, Tehran, IRAN, ISLAMIC REPUBLIC OF, ⁴Department of Medical Physics and Biomedical Engineering, Tehran University of Medical Sciences, Tehran, IRAN, ISLAMIC REPUBLIC OF.

Aim: Ever growing need for high spatial resolution in quantitative molecular imaging of small-animals mandates to compensate the SPECT images for resolution degrading processes. The collimator-detector response (CDR) is well known as a primary function determining SPECT images resolution. Therefore, the principal objective of this study was to recover the lost resolution in molecular SPECT using STIR framework. **Materials and Methods:** To derive distance-dependent CDR functions, a set of point-source measurements at various distances from the collimator were conducted using HiReSPECT scanner, a dedicated small-animal SPECT camera developed in our department. Micro Derenzo as well as NEMA image quality (IQ) phantoms were analytically simulated (64 views over 360 degrees) with the STIR in order to acquire CDR-degraded projection data. The data were then corrupted by a Poisson noise to mimic a realistic data acquisition. Subsequently, the CDR-blurred sinograms were iteratively reconstructed with and without resolution modeling using an OSEM algorithm (4 subsets and 32 subiterations). Activity recovery coefficient for hot-rods part of the phantom, noise behaviors for its uniform part, and spill-over ratios for two cold cylinders inserted in the phantom were assessed in order to study how well the STIR compensates SPECT images for the CDR. The STIR study was validated by means of comparison with experimental measurements. **Results:** As a results of the CDR

compensation, a substantial gain in spatial resolution is yielded, and the rods with 1.6 mm diameter become resolvable in the micro Derenzo phantom reconstruction. The CDR compensation results in a significant increase in recovery coefficient up to a factor of 1.24 for the largest diameter rod. Spill-over ratio falls off from 0.24 to 0.16 (averaged for the two cold cylinders) as consequence of CDR modeling. A subtle reduction in coefficient of variation, as a metric indicating noise performance, from 8.4% to 6.7% was also observed. The CDR compensation mechanism outcomes a correlated blobby noise-texture compared with original Poisson one. In addition, a 15.5% overshoot at the edge of the uniform part, known as Gibbs ringing artifact, occurs as an unavoidable side-effect. The uncompensated recovery coefficients obtained using the STIR agree with those experimentally calculated, a maximum 11% difference for the 5-mm diameter cylinder. **Conclusion:** The STIR-provided results showed the importance of CDR modeling in preclinical SPECT. This modeling considerably corrects partial volume effect, but at the expense of Gibbs artifact as well as altering image noise-pattern.

EP735**The evaluation of the spatial dependence of noise correlation structure in SPECT images with and without resolution modelling**

I. S. Armstrong, M. J. Memmott; Central Manchester University Hospitals, Manchester, UNITED KINGDOM.

Aims. Lung SPECT has been shown to be superior to planar scintigraphy and a continued shift towards SPECT is anticipated. Resolution modelling (RM) has been shown to provide superior quality. Initial evaluations with Lung SPECT have shown promise but streak artefacts, primarily in sagittal and coronal planes, have prohibited its implementation. We believe these artefacts are due to spatial dependence of the noise correlation structure with RM. This work aims to quantify the degree of spatial dependence of noise structure in a uniform phantom. Methods. Gated SPECT data, generating 24 replicate images, of a 30cm diameter cylindrical phantom were acquired on a GE Optima with LEHR and ELEGP collimators. Attenuation-corrected images were reconstructed with and without RM; with 2, 5 and 10 iterations; 10 subsets and no post-filtering. Nine 17x17x17 voxel regions were extracted (8 radially offset and one central). For each region, Image Roughness (IR) was measured and a voxel correlation kernel was produced. A 2-dimensional Gaussian was fit to each kernel. The Coefficient of Kernel Elongation (CoKE) was expressed as the ratio of the FWHM of the Gaussian in orthogonal directions. A CoKE of 1 indicated a radially symmetric kernel and hence no directional noise structure. Results. With RM, average IR reduction relative to non-RM was 64%, 62% and 54% at 2i, 5i and 10i with LEHR collimators and 74%, 75% and 71% with ELEGP collimators. Correlation kernels from non-RM images showed very little elongation for all regions indicating no spatially dependent noise structure. Mean CoKE at 2i, 5i and 10i were: LEHR non-RM: 1.07, 1.04, 1.03; ELEGP non-RM: 1.08, 1.04, 1.03. Substantial radial kernel elongation was observed for both sets of RM data in the offset regions. This was less pronounced with LEHR collimators and was seen to decrease with increasing iteration for LEHR only. Mean CoKE at 2i, 5i and 10i were: LEHR RM: 1.49, 1.47, 1.45; ELEGP RM: 1.62, 1.63, 1.64. Conclusion. Voxel variance reduction due to RM is greater with ELEGP collimators than LEHR collimators. However, the broader point spread function of ELEGP collimators produces notably greater spatially dependent radial correlation structure when RM is used, compared with LEHR collimators. This study demonstrates RM, particularly with ELEGP collimators, is unlikely to be useful in lung SPECT and alternative methods of variance reduction such as isotropic post-filtering may be more appropriate than RM for either collimator.

EP736**Accuracy of Attenuation Correction in PET/MRI with Special Focus on Large Arteries**

A. Mota-Cobian¹, J. Alonso Farto^{1,2}, L. Fernández-Friera^{1,3}, J. Sánchez-González⁴, B. López Melgar^{1,3}, L. Jiménez-Borreguero^{1,5}, V. Fuster^{1,6}, J. Ruiz-Cabello^{1,7}, S. España^{1,7}; ¹CNIC (Spanish National Cardiovascular Research Centre), Madrid, SPAIN, ²Hospital General Universitario Gregorio Marañón, Madrid, SPAIN, ³Hospital Universitario Montepríncipe, Madrid, SPAIN, ⁴Philips Healthcare, Iberia, Madrid, SPAIN, ⁵Hospital Universitario La Princesa, Madrid, SPAIN, ⁶Mount Sinai School of Medicine, New York, NY, UNITED STATES, ⁷Ciber de Enfermedades Respiratorias (CIBERES), Madrid, SPAIN.

Introduction PET/MRI combines the capabilities of PET to provide functional information, with the anatomical information provided by MRI. Accuracy on quantitative PET image analysis, relies on the correct application of attenuation correction among others factors. In PET/CT scanners, reliable attenuation maps are obtained from CT images. However, obtaining an attenuation map from a MRI scan is one of the major challenges for PET/MRI that remains to be solved. The purpose of this study was to evaluate the effect of MRI-based attenuation maps and the use of flexible coils on the quantitative accuracy of PET images. We paid special attention to the use of FDG-PET for the assessment of vascular inflammation in atherosclerotic plaques. **Methods** PET/CT data from eight oncologic patients was used. PET data was reconstructed using attenuation maps with different level of detail emulating several approaches available on current PET/MRI scanners. PET images obtained with CT-based (CTAC) and MRI-based (MRAC) attenuation maps were compared to evaluate the quantitative accuracy obtained in different tissue types, and for the quantification on several arteries (carotid, iliac, femoral, aortic arch and abdominal aorta). In addition, the quantitative effect produced by the presence or absence of flexible MRI receiver coils in the attenuation maps was studied. **Results** Mean bias between CTAC and MRAC increased, as the attenuation map simplifies, in fat (-1.5 %, -1.2 %, 22.0 %), non-fat soft-tissues (-4.6 %, -5.2 %, 1.5 %) and bone (-5.5 %, -37.9 %, -36.5 %). Despite lung tissue is included in all MR-based attenuation maps, large deviations (18 % bias and 42 % RMSE) were obtained due to the high heterogeneity and inter-patient variability of the lung. The quantification of vascular inflammation using FDG-PET acquired with PET/MRI scanners had small deviations (*SUV* bias below 10%) except for the case when the flexible coil was added (up to 20%). On the other hand, *TBR* compensate quantitative errors produced by attenuation map simplification leading to lower biases than *SUV*. **Conclusions** In this study the effect of using simplified attenuation maps as provided by PET/MRI scanners on the quantitative accuracy of PET images has been studied. The quantitative accuracy of reconstructed PET images was gradually diminished as the attenuation map simplify. This degradation was especially significant for the quantification of lung and bones. However, the assessment of vascular inflammation using FDG-PET on PET/MRI scanners produce acceptable results, particularly when the *TBR* is considered.

EP737**Should the PET Reconstruction be Optimized in a Different Way for ¹⁸F-FLT?**

P. Subramanian, K. Binzel, P. Bhatia, B. Ramaswamy, J. Zhang, M. V. Knopp; The Ohio State University, Columbus, OH, UNITED STATES.

¹⁸F-fluorothymidine (FLT), is a promising marker to assess proliferation in tissue and the reticuloendothelial system, and is being explored as an alternative to FDG in PET imaging of advanced disease and response monitoring. In order to improve lesion characterization, we have previously validated and optimized the use of smaller voxel volume, high definition reconstruction for FDG acquisitions performed in parallel as

part of a dual tracer imaging trial. Our aim is to also advance the image quality of FLT acquisitions and the use of high definition reconstruction to further improve lesion conspicuity and quantitative accuracy. List mode raw data acquired previously for a FDG/FLT PET/CT breast cancer clinical trial for 10 patients were reconstructed using the default, standard definition (SD, 4 mm³ voxel volume, 3 iteration, 33 subset) protocol and an investigational high definition (HD, 2 mm³ voxel) protocol with varying numbers of subsets per iteration, 33, 29, 21, 15, 11, 9, and 7 subsets. The resulting images were visually assessed by 3 independent blinded reviewers and ranked in regard to clinical image quality. Quantitative assessment was performed by placing 3D ROI over lesions as well as liver and bone marrow, to compare default and HD quantification. ROC analysis was used to assess image quality performance in relationship to the modified reconstruction approaches. High definition FLT images revealed that using the standard 33 subsets improved visual detail, however increased image noise. Similar to the prior assessment of FDG parameters, we observed a substantial reduction in noise by lowering the number of subsets. The ROC analysis indicated that the optimization of the reconstruction parameters converged differently than seen in the same patient population for the FDG acquisitions. Images with higher subsets appear sharper, however are rated noisier. For FLT, the use of 9 subsets was rated most preferable with substantially more detail-containing images and markedly improved visualization of lesion heterogeneity. Quantification of the optimized images showed a significant increase in *SUV*_{max} while *SUV*_{mean} remained comparable in background. HD reconstruction greatly improves image quality, aiding in lesion detection and assessment of heterogeneity. Due to the different biodistribution of FLT, the optimization of image reconstruction revealed different characteristics, thus indicating that tracer specific reconstruction optimization is beneficial. It also appears to be preferential for quantitative robustness to assess clinical response.

EP738**A Software Motion-Correcting PET Reconstruction Reduces Nodule Size**

N. C. D. Morley¹, D. R. McGowan^{1,2}, K. M. Bradley¹, F. V. Gleeson^{1,2}; ¹Oxford University Hospitals NHS Foundation Trust, Oxford, UNITED KINGDOM, ²Oxford University, Oxford, UNITED KINGDOM.

BACKGROUND: Periodic respiratory motion can obscure focal activity in PET scans. Data Driven Gating (DDG) is used to detect this motion in the PET list data, without additional hardware. The technique has been further developed by gating the PET data into 5 respiratory phases. These phases can be individually corrected and then recombined, allowing data from all parts of the respiratory cycle to be used. Conventional DDG considers data only in the static part of the respiratory cycle. **AIM:** To compare a novel motion-correcting DDG reconstruction to our current clinical technique, using scans with FDG avid nodules affected by respiratory motion. **METHODS:** List mode data was retained for oncology FDG PET/CT scans (free-breathing studies, 90 mins after 4 MBq/kg FDG IV, with attenuation correction CT). After clinical reporting and identification of artefacts, the data was submitted to an additional retrospective DDG reconstruction using principal component analysis to detect motion. The data was divided into 5 respiratory phases which were then registered to a reference phase. The new reconstruction is compared to our current clinical standard using lesion measurements of the cranio-caudal diameter (manual, *SUV* window 0-6) and *SUV*_{max} (measured automatically within applied VOI). Both reconstructions use a Bayesian penalised likelihood algorithm with a beta of 400. Corrected data were normalised to the standard data to give relative values, and averaged to mean with 95% confidence interval (CI). 20 nodules have been assessed in 14 cases (max. 2 per case): 8 pulmonary, 11 hepatic, and 1 splenic. **RESULTS:** In most cases the nodules showed an increase in conspicuity, a decrease in lesion diameter and an increase in *SUV*_{max}. Mean lesion diameter decreased by

30% (CI 21 to 39%) and SUV_{max} increased by 7% (CI -4% to +17%).

CONCLUSION: Software detection of periodic respiratory motion in clinical PET data can be used to divide the data into phases, allowing subsequent motion correction with minimal data loss. This has improved conspicuity and quantitative assessment of nodules affected by respiratory motion. Improved lesion detection could increase the accuracy of staging and patient care. Better quantification could facilitate better assessment of therapeutic response.

EP739

Effect of Monte Carlo Collimator Modelling on ^{90}Y Bremsstrahlung SPECT Images

C. A. Porter¹, M. D. Walker¹, K. M. Bradley¹, D. R. McGowan^{1,2}; ¹Oxford University Hospitals NHS Foundation Trust, Oxford, UNITED KINGDOM, ²University of Oxford, Oxford, UNITED KINGDOM.

Aim: To investigate the effect of Monte Carlo collimator modelling (HybridRecon, Hermes Medical Solutions AB, Stockholm) on ^{90}Y Bremsstrahlung SPECT studies, with particular focus on the post-therapy imaging of ^{90}Y selective internal radiation therapy (SIRT) patients, and to compare the quality of such images with those acquired according to current local protocol. **Method:** A NEMA IQ phantom and the Abdo-Man™ phantom (a 3D-printed liver phantom with fillable inserts) [1] were imaged using a GE Discovery 670 SPECT/CT scanner with a number of different hot sphere to background ratios. Datasets were reconstructed twice using HybridRecon (Hermes Medical Solutions AB): using standard OSEM (5 iterations, 15 subsets) and using OSEM (5 iterations, 15 subsets) combined with Monte Carlo modelling of the GE MEGP collimators used in the acquisition. No filters were applied to any of the images. Regions were drawn in each of the hot spheres, with corresponding regions in the warm background. These were used to calculate contrast recovery (CR), background variability (BV) and contrast to noise ratio ($CNR = CR/BV$). Phantom images and ten patient images were also blind scored for image quality by a consultant radiologist. **Results:** With a sphere to background ratio of 4:1 in the Abdo-Man™ phantom, the CR for the 30mm diameter and 40mm diameter spheres was higher when Monte Carlo collimator modelling was used (by 14% and 11% respectively). No effect was observed on the CR for the 20mm diameter sphere. For the 20mm, 30mm and 40mm diameter spheres there was a decrease in BV of 2% when Monte Carlo collimator modelling was used. CNRs of the 20mm, 30mm and 40mm diameter spheres were increased when Monte Carlo collimator modelling was used (by 29%, 95% and 77%, respectively). **Conclusion:** In this study, it was shown that Monte Carlo collimator modelling improves CR, BV and CNR in ^{90}Y Bremsstrahlung SPECT images. **Reference:** [1] J.Gear et al EJNMMI,42(S1):Abs.P872

EP740

Computationally efficient method for fully 4-D voxel based direct estimation of time activity curve in dynamic myocardial SPECT

S. Entezarmahdi¹, A. Banani², A. Kamali-asl¹, R. Faghihi³, M. Haghghatafshar⁴; ¹Department of Medical Radiation, Shahid Beheshti University, GC, Tehran, IRAN, ISLAMIC REPUBLIC OF, ²Department of Nuclear Engineering, Isfahan University, Isfahan, IRAN, ISLAMIC REPUBLIC OF, ³Ray Medical Engineering Department, Shiraz University, Shiraz, IRAN, ISLAMIC REPUBLIC OF, ⁴Nuclear Medicine and Molecular Imaging Research Center, Shiraz University of Medical Sciences, Shiraz, IRAN, ISLAMIC REPUBLIC OF.

It has been shown that direct approach to estimating the dynamic parameters from inconsistent, as well as insufficient and truncated, image sequence of slow rotation SPECT projection data can reduce the bias and

variance. But the model assumption of blood pool and other segments should be appropriate to follow the dynamic behavior of different segments. On the other side, while the system matrix and dynamic model became more complicated the final dynamic parameters estimation may be impossible or at least the bias can rise up. In this study we suggest a computationally efficient model to represent the voxel-based dynamic behavior which is easy to be resolved by iterative optimization methods. We assumed that in a dynamic myocardial SPECT all the voxels can be modeled by a two terms exponential equation. Three different dynamic curves was extracted from published papers for each segment (blood pool, normal myocardium, and background) and tested to evaluate the suggested models. Five different generic optimization algorithms were used to solve the nonlinear equation and estimate the exponential equation coefficients. The proposed method was tested on a 32*32 matrix size image, simulated in MATLAB. Each voxel of simulated map belonged to known segment and had the dynamic behavior while projection data was acquired. The simulated dynamic SPECT acquisition consisted of just one rotation in 12 minutes with 90 views, each 6 seconds. Results show that the Levenberg-Marquardt algorithm was the superlative one to estimate each of the three input dynamic data for all of the segments (mean of three input data, blood pool: $R2=0.935 \pm 8\%$, $p<0.01$ - Myocardium: $R2=0.963 \pm 9\%$, $p<0.01$ - background: $R2=0.948 \pm 8\%$, $p<0.01$). We have implemented computationally efficient method for fully 4-D voxel based direct estimation of spatiotemporal distributions from dynamic myocardial SPECT projection data. Two terms exponential equation was used to model the time-activity curves for the blood pool and tissue volumes in a simulated cardiac data acquisition. Iterative Levenberg-Marquardt algorithm estimates of time-activity curves quickly and accurately. From these curves, kinetic parameters can be estimated accurately.

EP741

Data Driven Gating of Clinical List-Mode PET can Improve Lesion Detection and Quantification

N. C. D. Morley¹, D. R. McGowan^{1,2}, K. M. Bradley¹, F. V. Gleeson^{1,2}; ¹Oxford University Hospitals NHS Foundation Trust, Oxford, UNITED KINGDOM, ²Oxford University, Oxford, UNITED KINGDOM.

BACKGROUND: In oncology FDG PET/CT, respiratory motion can obscure focal uptake in the thorax and upper abdomen. This includes the liver and lung bases which are common sites of metastatic disease. Improved lesion detection could increase accuracy of staging and patient care. Better quantification could facilitate better therapeutic-response assessment. Data Driven Gating (DDG) is a deviceless technique to detect and gate respiratory motion from the list-mode data. **AIM:** Initial evaluation of a prototype DDG PET reconstruction, using FDG avid nodules affected by respiratory motion artefacts in clinical scans. **METHODS:** Standard oncology FDG PET/CT scans, 4 mins per bed-position, free-breathing, 90 mins after 4 MBq/kg FDG IV, with attenuation correction CT. After clinical reporting and identification of artefacts, the list-mode data was submitted to an additional retrospective DDG reconstruction, using principal component analysis (PCA). The new reconstruction is compared to our current clinical standard using lesion measurements of SUV_{max} (automatic within applied VOI) and craniocaudal diameter (manual, SUV window 0-6). Both reconstructions use a Bayesian penalised likelihood algorithm with a beta of 400. The gated data was normalised to the standard data for percentage and statistical analysis by mean with 95% Confidence Interval (CI). 18 nodules have been assessed in 12 cases (max 2 per case): 6 pulmonary, 11 hepatic, and 1 splenic. **RESULTS:** All 18 nodules examined showed a subjective increase in conspicuity, increase in SUV_{max} , and decrease in lesion diameter. In one case, a pulmonary nodule (6mm on CT) had identifiable uptake only after DDG. On average, SUV_{max} increased by 39% (CI 31-60%) of that in the standard reconstruction, and lesion diameter decreased by 34% (CI 25-42%). **CONCLUSION:** DDG using PCA can retrospectively identify and gate respiratory motion in clinical PET data without additional hardware or calibration. This can

improve image quality and quantitative assessment of lesions. We have observed an example of improved lesion detection.

EP742

Comparison of Quantitative Iodine-124 PET Imaging Accuracy between PET Systems

R. Gregory^{1,2}, I. Murray^{1,2}, M. Aldridge^{3,4}, S. Chua¹, G. Flux^{1,2}; ¹Royal Marsden NHS Foundation Trust, Sutton, UNITED KINGDOM, ²Institute of Cancer Research, Sutton, UNITED KINGDOM, ³UCL Institute of Nuclear Medicine, London, UNITED KINGDOM, ⁴UCL Hospitals NHS Foundation Trust, London, UNITED KINGDOM.

Aim: Several methods have been implemented to correct for PET noise introduced by 602 keV γ -photons emitted in cascade with over half the positrons of ¹²⁴I. These γ -photons can be detected in coincidence with one-another and/or annihilation photons. Prompt gamma compensation (PGC) on the Siemens Biograph systems corrects these events by fitting the estimated random and scatter distributions to the sinogram tails prior to subtraction. The other newer systems, for example GE Discovery 710, remove a uniform background fit to the sinogram tails. Older systems, such as the GE Discovery ST and VCT, can image in 2D mode with septa that discard γ -photons. The aim of this study was to compare the quantitative accuracy of ¹²⁴I imaging attained using each method. **Materials and Methods:** Measurements were made on 2 Siemens Biograph mCT systems and the GE Discovery ST, VCT and 710 PET/CT systems. A 20 cm long, 20 cm diameter cylindrical phantom was filled uniformly with 50 MBq ¹²⁴I. One 20 million true event PET scan was acquired to assess uniformity and the phantom was scanned repeatedly as its activity decayed. The NEMA image quality phantom was filled with ¹²⁴I to give a sphere-to-background ratio (SBR) of 21 and 6.5 MBq total activity. A 20-minute PET/CT scan was acquired at 1 bed position. The activity concentration accuracy was assessed along with recovery coefficients. **Results:** PGC consistently underestimated the activity concentrations in the uniform cylinder and background of the image quality phantom by 10%. The average recovery coefficient of the two largest spheres based on SUV peak was 0.90±0.04. Without γ -photon correction the cylinder and background of the image quality were non-uniform in 3D PET images giving an average 60% underestimation in activity concentration. These values were underestimated by 3% in the 2D images. However these images were noisier due to the low sensitivity of 2D PET. The SUV of the uniformly filled cylinder was within 1% with uniform background subtraction although the SUV in the background of the image quality phantom was overestimated by 17%. The largest sphere's SUV peak recovery coefficient was 0.97±0.05. **Conclusion:** The consistent 10% underestimation in ¹²⁴I activity concentration with PGC may be corrected by the same factor (1.11) for any activity distribution. Uniform background subtraction provides the correct SUV for the uniform SUV validation phantom and SUV peak of the larger spheres but under-corrects the counts in the background of the image quality phantom.

EP743

Performance evaluation of the step and shoot acquisition modality of the IRIS PET scanner

n. camarlinghi¹, C. Luongo¹, N. Belcar¹, D. Panetta², P. Iozzo², S. Burchielli³, P. Salvadori², G. Sportelli¹, A. Del Guerra¹; ¹Dipartimento di Fisica dell'universita' di Pisa & INFN sezione Pisa, 56127, ITALY, ²Institute of Clinical Physiology (IFC) CNR, Pisa, Italy, 56127, ITALY, ³CNR/Tuscany Foundation "G. Monasterio" (FTGM), 56127, ITALY.

AimThe IRIS PET/CT scanner (now distributed by Inviscan s.a.s., France) is a novel multimodal preclinical tomograph for high resolution PET/CT imaging of small animals. The PET component of the scanner features the

unique possibility of performing both static and "step and shoot" rotational acquisitions. This latter modality allows the user to obtain quantitative high quality images. However, in case of rotational scans, the image reconstruction becomes a very time-consuming task, thus hindering the use of this modality in clinical practice. To overcome this limit, we implemented a dedicated GPU CUDA-based 3D iterative reconstruction algorithm. In this work we present an assessment of the quantitative performance of both the static and rotational modalities obtained with the GPU algorithm. **Materials and methods** The PET component of the scanner consists of 16 modular detectors arranged in two octagonal rings. Each detector module comprises a matrix of 702 LYSO:Ce crystals of 1.6 mm×1.6 mm×12 mm with a pitch of about 1.7mm. The scanner features a total of 24 million of Lines Of Responses (LOR). The standard 3D quantitative image reconstruction of the IRIS/PET is implemented with a dedicated multi-core Maximum Likelihood Estimation Maximization (MLEM) iterative algorithm. The system response matrix is pre-calculated using a multi-ray "Siddon" algorithm and stored on file. The size of the system matrix is reduced using symmetries. As image reconstruction exhibits a high degree of parallelism, to improve the performance of the standard reconstruction software we ported it on a Graphics Processing Unit (GPU) using the NVIDIA CUDA programming model. The GPU reconstruction implements an "on-the-fly" calculation of the system model. In order to perform a quantitative evaluation of the different modalities, four NEMA quality phantoms were acquired: one was acquired with a stationary scan, while the others were acquired in "step and shoot" mode using 2,4,8 views spanning over 45 degrees. All the acquisitions lasted 20 minutes. The image quality of 18F-FDG imaging on mice and rats was also evaluated. **Results and Conclusions** We compared the results obtained with the GPU algorithm to those obtained with the reconstruction software included with the IRIS PET, obtaining no significant difference. Moreover, we achieved speedups in the reconstruction times up to 5x with respect to the original implementation.

EP744

Benefit of scatter limitation correction for cold artifacts caused by arm motion in whole-body PET/CT: physical phantom study

H. ONISHI¹, A. Furuta², Y. Kangai¹, N. Yada¹, T. Saho¹, H. Amijima³; ¹Program in Biological System Sciences, Graduate School of Comprehensive Scientific Research, Prefectural University of Hiroshima, MIHARA, HIROSHIMA, JAPAN, ²Program in Health and Welfare Sciences, Graduate School of Comprehensive Scientific Research, Prefectural University of Hiroshima, MIHARA, HIROSHIMA, JAPAN, ³Graduate school of nursing, Hyogo University of Health Sciences, Kobe, Hyogo, JAPAN.

Aims: Algorithms for scatter limitation correction in whole-body PET/CT systems have potential for mis-registration. The present study used physical phantoms to validate scatter limitation correction of mis-registered of CT and PET images caused by arm motion. **Methods:** We used a NEMA-IEC body phantom (simulated tumor targets comprised 10 and 37 mm spheres) and two peripheral bottles (7 cm ϕ) positioned laterally on either side of body phantom to represent arms. The ratios of the sphere to background and the two bottles containing 18-F solution were setting 4:1. We acquired PET/CT images in the 3D mode for 20 min with arms movement. To validate the performance of no-scatter (nonSC), scatter (SC), and scatter limitation correction (SLC) algorithms, the standardized uptake value (SUV) and scatter fraction factor (SFF) were measured in ROI on the 10 and 37 mm spheres in the PET images at the center and at 1 - 5 cm offset from the center with arm motion in 1 cm increments (inside, outside and topside). We compared SUV and SFF with nonSC, SC and SLC corrections for arms motion. **Results:** A cold artifact moved < 2 cm to inside, and < 5 cm to the topside of the arm in the PET images. Significant outside and topside (1 - 4 cm) cold artifacts did not occur. The cold artifact was improved by adapting itself in the SLC. The SUV of each target was increased by 5.13% (nonSC), 2.8% (SC), and 2.78% (SLC) by outside arm motion.

The SUV of nonSC was increased by 1.2%, whereas SC and SLC were decreased by 28.6% and 9.0% respectively by inside arm motion. The SUV of nonSC, SC, and SLC were increased with top-side arm motion. Outside SFF in SC and SLC was minimally affected by arm position. Inside SFF increased 2.5-fold (0.78) in SC and remained at 30% (0.45) of increment in SLC. The SFF of SLC did not exceed 0.45 under all conditions. **Conclusion:** The cold artifact caused by inside arm movement was improved in the SC algorithm using SLC. The finding results indicated that the optimal SFF setting in PET/CT systems should be 0.45.

EP745

Whole Body Dynamic FDG Acquisition : Validation of Static reconstruction Methods

P. M. Koulibaly; Centre Antoine Lacassagne, Nice, FRANCE.

Aim Whole Body Dynamic (WBD) acquisition has the promise of capturing variation of FDG uptake during conventional acquisition duration. This approach could replace dual point imaging in the future. This preliminary study investigates summation strategies of WBD reconstructions to show whether they can replace standard static reconstruction (STD) for conventional diagnosis and quantification. **Materials and methods** 20 oncology patients underwent WBD acquisition after (G1, 10 cases) or before (G2, 10 cases) conventional whole body static (WBS) FDG acquisition on a Siemens Biograph mCT camera. The WBD consisted in 3 1min/bed passes and WBS in one 2.5min/bed acquisition. Two static reconstructions were generated from each WBD acquisition: sum of 3 reconstructed dynamic frames (SRDF) and reconstruction from the summed sinograms (SSINO). The summed and STD images were assessed blindly and compared qualitatively and quantitatively. Two physicians rated image quality (equivalent or better) and assessed acceptance for clinical read and diagnostic interpretation. SUV max and peak of up to 3 lesions per case (51 in total) were compared, together with mean and standard deviation (SD) of ROIs in an area of uniform uptake in the liver. Correlation analyses were performed for quantitative parameters. **Results** The quality of all images was rated good for clinical read and diagnostic interpretation. Both SRDF and SSINO images had slightly better rating overall than WBS STD images, likely due to the 30s (20%) longer acquisition. The SSINO images had slightly better ratings than the SRDF, likely due to better noise modelling. The correlations of quantification parameters obtained from SRDF/SSINO vs static reconstruction were analyzed into two separated groups. SUVmax and SUVpeak were highly correlated in both groups. In G1, SUVs are higher due to increase of tracer uptake over time which would result in a slope >1 (G1_SUVmax (SRDF/SSINO): slope 1.23/1.19, R^2 0.99/1.00) (G1_SUVpeak: slope 1.19/1.14, R^2 1.00/1.00). In G2, the effect was reversed (G2_SUVmax: slope 0.75/0.76, R^2 0.99/0.94) (G2_SUVpeak: slope 0.77/0.75, R^2 0.96/0.95). Liver mean and SD values were also highly correlated except SD of G2 due to more counts in WBD (G1_SUVmean: slope 0.98/0.88, R^2 0.94/0.94) (G1_SUVstd_dev: slope 1.29/1.15, R^2 0.85/0.91) (G2_SUVmean: slope 1.06/0.99, R^2 0.99/0.94) (G2_SUVstd_dev: slope 0.92/0.46, R^2 0.29/0.60). Similar correlations were observed between SRDF and SSINO (results not shown). **Conclusion** WBD acquisition is feasible and the resulting summed images give identical image quality than conventional acquisition. This opens the way to collecting dynamic information during a single acquisition of standard duration.

EP746

Impact of non-specific normal databases on perfusion quantification of low-time myocardial SPECT studies in overweight or obese patients

C. Scabbio^{1,2}, M. Lecchi¹, A. Del Sole¹, G. Lucignani¹; ¹Department of Health Sciences, University of Milan and Nuclear Medicine Unit, ASST Santi Paolo e Carlo, Milan, ITALY, ²Medical Physics Postgraduate School, University of Milan, Milan, ITALY.

Aim. We have previously reported that stress myocardial perfusion quantification in overweight patients is negatively influenced when the acquisition time is reduced to a quarter of the reference while using standard-time databases of normality. This study was aimed at evaluating the impact of non-specific databases of normality on the estimates of the percent summed stress score (SS%) in overweight or obese patients. **Patients and Methods.** The study population comprehended 40 overweight/obese patients (mean BMI \pm standard error = 29.4 \pm 0.6 kg/m²) undergoing myocardial stress gated SPECT (BrightViewTM, general-purpose gamma-camera, standard acquisition time=16 min, 8 MBq/kg). Three simultaneous scans, started at the same time after tracer injection (^{99m}Tc]TetrofosminTM activity = 659 \pm 12 MBq), were acquired with three different acquisition-time/projections (30, 15 and 8 sec/step, i.e. full-time, half-time and quarter-time acquisitions, respectively). The three sets of projections were reconstructed using the AstonishTM iterative reconstruction algorithm with resolution recovery (default parameters: 4 iterations, 8 subsets and cut-off frequency = 1 cycles/pixel). Then, three different normality databases were used to estimate the SS% perfusion parameter: 1) full-time AstonishTM (full-time-A); 2) full-time iterative reconstruction algorithm provided by the manufacturer with 12 iterations and Butterworth filter (0.66 cycles/pixel and order=5) (full-time NOT-A) and, 3) half-time AstonishTM (half-time-A). The impact of database of normality on the SS% and acquisition-time/projections on the SS% was assessed by two-way ANOVA analysis and post-hoc test (Tukey pairwise for multiple contrasts). **Results.** Both the database of normality and the acquisition-time/projections influenced the SS% perfusion parameter in overweight or obese patients (F=42.3 and F=8.3, respectively). Whereas no significant differences were found between the SS% assessed with the two AstonishTM databases applied to the scans with different acquisition-time (SS%=3.88 \pm 0.98 for full-time-A and SS%=3.92 \pm 0.98 for half-time-A), significantly higher SS% values were observed with the full-time-NOT-A database (SS%=6.83 \pm 1.06). Significantly higher SS% values were also confirmed for quarter-time scans compared to half-time scans, even though a little reduction of the SS% overestimation was found by using half-time-A database compared to full-time-A database (mean SS% difference = +0.68% and +0.75%, respectively). **Conclusions.** Different reconstruction algorithms require the adoption of the specific database of normality developed for each reconstruction method. It is important to underline that a summed score for the stress exam higher than the real one could lead to wrong risk-stratification with regard to cardiac event-free survival.

EP747

Investigating the Operating Characteristics of Q.Clear Reconstruction

A. Hughes; Royal Preston Hospital, PRESTON, UNITED KINGDOM.

Aim To investigate the operating characteristics of Q.Clear (a fully convergent, noise constrained iterative reconstruction package) following the recent installation of a GE Discovery 710 PET/CT system. Reconstructed image quality was investigated as a function of the β value (a noise regularisation parameter) and bed overlap. **Method** Experiments were conducted using a NEMA PET (NU2) phantom filled with a uniform concentration of 5kBq/ml F18 and scanned over two bed positions using standard imaging parameters (192x192 matrix, ToF, scatter, randoms & attenuation corrections applied). The overlapping bed sections were positioned over the centre of the phantom. Reconstructed image noise was measured for a range of slice overlaps and different values of β . A NEMA Image Quality (IQ) phantom was filled with solutions of F18 at concentrations of 17.3kBq/ml and 4.8kBq/ml for the spheres and background respectively. This was scanned over two bed positions with the spheres (a) at the centre of the overlap and (b) at 3cm offset from the centre of the overlap. SUVmax and SUVmean were calculated for spheres ranging in diameter from 10 to 22mm at differing values of β . **Results**

Reconstructions of the NU2 phantom demonstrated a marked variation in image noise along the axis of the phantom in the vicinity of the overlapping sections. For an 11 slice overlap the noise increased from 6.9% on the central slice to 10.5% for slices at approximately 3cm either side of this position ($\beta=400$). The difference in noise values became more exaggerated at lower β values (8.8% on the central slice increasing to 12.8% 3cm to either side, $\beta=300$). Increasing the slice overlap reduced this axial variation in noise, with 15 slices being optimum. Q.Clear reconstructions of the IQ phantom demonstrated an increase in both the SUVmax & SUVmean at all sphere sizes over standard iterative techniques. However, SUVmax for the 10 and 17mm diameter spheres varied from 2.1 to 2.8 and 3.1 to 5.5 respectively ($\beta=300$, 11 slice overlap) depending on whether the spheres were positioned over the central slice of the bed overlap or offset from it axially by 3cm. Increasing the slice overlap to 15 slices reduced this variation in SUVmax with axial position. **Conclusion** Reconstructions using Q.Clear have the potential to improve image quality and increase the visibility of small lesions. However, slice overlap and β values must be carefully chosen to optimise its function. SUVmax should be used with caution, especially for small lesions.

EP748

Optimization of 90Y PET/CT imaging using an antropomorphic torso phantom with a gel suspension of glass microspheres in the liver

A. Zorz¹, A. Scaggion¹, L. Riccardi¹, A. R. Cervino², P. Reccia², G. Saladini², M. Paiusco¹; ¹Medical Physics Department, Veneto Institute of Oncology IOV-IRCCS, Padova, ITALY, ²Division of Nuclear Medicine, Veneto Institute of Oncology IOV-IRCCS, Padova, ITALY.

Because of its superior image resolution and quantitative capability, 90-yttrium PET/CT imaging is becoming part of the routine protocol to confirm the accurate delivery of radionuclide after radioembolization. The aim of this study was to optimize 90Y-PET/CT image quality in terms of absolute quantification and noise, comparing different reconstruction algorithms and parameters in images of an antropomorphic torso phantom. An antropomorphic torso phantom with lung, liver and spine inserts was filled with cold water. A plastic bottle with a mix of gel and 90Y glass microspheres was positioned inside the liver cavity in order to simulate a post-radioembolization small tumor activity concentration. The activity of the microsphere was measured with a dose calibrator before the phantom preparation. PET images were acquired with a Siemens Biograph mCT PET/CT scanner equipped with LSO crystals in 3D mode. Phantom scan was performed in two 40 minutes bed positions. All scan parameters were identical to a clinical scan protocol. Images were reconstructed with the standard 3D OSEM iterative algorithm with scatter, random, attenuation correction, resolution recovery (TrueX), 3 iterations, 21 subset, 168x168 matrix size and 4 mm gaussian filter. Different reconstructions were performed by varying the reconstruction algorithm (FBP) and OSEM parameters as the matrix size and the iteration number. For absolute quantification, a volume of interest (VOI) encompassing the entire microspheres sediment was generated by selecting a fixed volumetric isocontour threshold of 1%. All the data were corrected for the branching ratio of yttrium. The calculated activity in the VOI was compared to the actual value. To evaluate the background effects due to the random counts, a set of planar ROIs were positioned in different phantom areas outside the liver (3 in the lung, 6 in the body). Data were collected and compared for all the reconstructions. It was observed that the microspheres, even if mixed with gel, sedimented as an effect of their higher density. As a consequence, the microsphere sediment could be visible in the CT images with a mean HU number significantly higher than water (about 240 HU). Absolute quantification and background counts change according to different reconstructions. Minimal variations of the estimated activity were found with different matrix sizes, while the iteration numbers had a more appreciable effect. The study shows the feasibility of the 90Y-PET/CT absolute quantification provided that the optimal algorithm and reconstruction parameters are chosen.

EP749

Effect of kV changes in CT for Attenuation Correction on relative and absolute SPECT Quantification

N. A. Bebbington; Siemens Healthcare A/S, Aarhus, DENMARK.

AIMS: It is well known that lower kV reduces dose, but can alter CT HUs which could impact on attenuation maps for attenuation correction (AC). The aim was to assess how kV changes on AC CT affect relative and absolute quantification in SPECT. **MATERIALS AND METHODS:** Absolute quantification: Five spheres (13mm-37mm) in the NEMA-IEC image quality phantom were filled with Tc-99m, with water background. SPECT and 18 CT exposures with different kV (130, 110, 80) and mAs (100, 50, 30, 20, 12, 8) combinations were undertaken on a Siemens Symbia system. A second SPECT with 18 CTs was undertaken with greater attenuation (two sandbags (300-400 HU) under the phantom). Flash3D SPECT reconstructions were made with dual-energy-window scatter correction and AC with each CT. Total and maximum voxel counts for SPECT reconstructions made with 110kV and 80kV CTAC were compared with those using 130kV. Relative quantification: SPECT was undertaken with a Data Spectrum cardiac insert and phantom (inferolateral and septal defects) in two different attenuating conditions, each with 18 CT datasets as above, and reconstructed with Flash3D and CTAC. Scores used clinically in Cedars-Sinai QPS (SRS, extent (%) and TPD (%)) and defect contrast relative to the anterior wall were assessed. **RESULTS:** Absolute quantification: In the standard phantom, at 110kV CTAC sphere VOI and maximum voxel counts were underestimated by up to 0.17% and 0.12%, across the range of sphere sizes and mAs. At 80kV CTAC, sphere VOI and maximum voxel counts were overestimated by up to 0.64% and 0.59%. With additional attenuation, at 110kV sphere VOI and maximum voxel counts were overestimated by up to 0.60% and 0.43%. At 80kV, sphere VOI and maximum voxel counts were overestimated by up to 4.01% and 3.79%. Relative quantification: There were no differences in SRS (15), extent (26%), TPD (19%) or defect contrast (0.68) between 130kV, 110kV or 80kV CTAC reconstructions. **CONCLUSIONS:** Absolute quantification differences for SPECT reconstructed with 130kV and 110kV CTAC were minimal, but differences increased considerably for reconstructions using 80kV CTAC. Increasing differences were observed with increasing attenuation. kV reduction may therefore have significant implications for absolute SPECT quantification and further assessments should assess effects with materials of higher HU, and the advanced OSGC reconstruction which is recommended for absolute quantification. No differences in relative cardiac quantification measures were observed with reduced kV under the conditions in this study.

EP750

Stochastic origin ensemble image reconstruction algorithm for time-of-flight dual photons emission computed tomography system

C. C. Chiang¹, K. S. Chuang¹, H. H. Lin¹, Y. C. Ni²; ¹National Tsing Hua University, Hsin-Chu, TAIWAN, ²Health Physics Division, Institute of Nuclear Energy Research, Atomic Energy Council, Taoyuan, TAIWAN.

Aim: Stochastic origin ensemble (SOE) approach based on Markov chains theory is an iterative image reconstruction useful in photon-limited emission tomography. In this study, we apply SOE to a new time-of-flight dual photons emission computed tomography (TOF-DuPECT) system. Specifically, the main goal is to investigate its performance at different coincidence resolving time (CRT) of detectors by Monte Carlo simulation. **Method:** DuPECT is a system to image distribution of isotope that emits cascade photons simultaneously. In theory, the possible location of decay could be determined by TOF information and coordinates of detectors in spatial domain. When the coincidence

photons arriving detectors, the hyperbolic response curve can be directly described on the reconstructed space. During the process of proposed SOE reconstruction, the origins of each event are randomly assigned to locations on hyperbolic response curve. After a sufficient number of iterations, the possible origins can converge to actual position of emitters and then reaches a quasi-stationarity state. To validate and evaluate the proposed SOE algorithm, an in-house developed GATE/MPHG Monte Carlo software were used. The geometry of Siemens Biograph 6 PET scanner was considered and built in the simulation. The contrast phantom and the 19-rods phantom filled with selenium-75 were used to test the performance of proposed algorithm. **Results:** Results show that SOE method can be successfully employed for TOF-DuPECT system. The spatial resolution in the central field-of-view can achieve about 20 mm when CRT is under 100 ps. The results indicate that there is a strongly relationship between spatial resolution and CRT. Regarding to the reconstruction results of phantom studies, the SOE method seems practical for proposed system and can obtain well image quality. **Conclusion:** The conclusion is drawn that TOF-DuPECT system is feasible and potential technique and SOE method has been proved to be useful for the system. Furthermore, this technique would extend its usefulness to non-positron gamma-gamma coincidence imaging. Future works will include more phantom studies and correction techniques development for the TOF-DuPECT system (e.g., scatter correction and attenuation correction).

EP751

Improvement of PET/CT reconstructions by implementation of metal artifact reduction in CT

C. S. van der Vos^{1,2}, A. I. J. Arens¹, J. J. Hamill³, A. P. W. Meeuwis¹, L. de Geus - Oei^{1,2,4}, E. P. Visser¹; ¹Radboud university medical center, Nijmegen, NETHERLANDS, ²University of Twente, Enschede, NETHERLANDS, ³Siemens Healthcare, Knoxville, TN, UNITED STATES, ⁴Leiden University Medical Center, Leiden, NETHERLANDS.

In recent years different metal artifact reduction (MAR) methods have been developed for CT. MAR could be beneficial for interpretation and quantification of the PET/CT scan, however these methods have only very recently been implemented in PET/CT. In this study both phantom and patient data were used to analyze visually and quantitatively the effect of MAR CT data on PET scans. **Materials and Methods:** The phantom consisted of two types of hip prostheses in a solution of ¹⁸F-FDG and water, and was scanned in an mCT PET/CT scanner (Siemens). To analyze clinical relevance of MAR, ¹⁸F-FDG PET/CT scans of 14 patients with metal implants (either dental implants, hip or metal implants elsewhere) were scored by an experienced nuclear medicine physician. In all patients a lesion was located near the metal implant. For these scans the standard low-dose CTs were processed with the MAR algorithm. The PET data were reconstructed using the attenuation correction provided by both the standard CT and the MAR-processed CT. In addition to the 14 ¹⁸F-FDG PET scans a ⁶⁸Ga-PSMA scan was included to analyze the benefit of MAR for patients with metastasized prostate cancer (and who also have one or two hip prostheses). **Preliminary Results:** For the phantom scans, cold artifacts (where FDG concentrations are lower than expected, caused by metal) were visible in the FDG solution. There was a 30% deficit in FDG concentration which was restored by MAR processing, indicating that metal artifacts on the CT image influence the quantification of the PET data. So far, 10 (out of 15) patient scans were reviewed. In 9 out of 10 patients the MAR algorithm was helpful and increased the confidence. On average the confidence in interpretation improved by 29±30% (scored on a scale of 0 - 100% confidence) if MAR was used. The mean difference in SUVmean of the lesions was 9.0±8.2%. SUV increase or decrease was dependent on the type of metal artifact. **Conclusion:** So far, the metal artifact reduction algorithm increases the confidence of the interpretation of the PET/CT scan. The added value depends on the indication for the PET/CT scan, location of

the prosthesis and extent of the disease. For radiotherapy planning and therapy response monitoring, metal artifact reduction could be of relevance in specific cases where the implant has influence on tumor delineation and quantitative parameters.

EP752

MR-based attenuation correction in PET/MRI of the lungs: Clinical effect of truncation artifacts and ignoring bone

S. K. Øen¹, I. Rausch², M. L. Lassen², M. Fenchel³, T. Beyer², L. Eikenes¹; ¹Norwegian University of Science and Technology, Trondheim, NORWAY, ²Center for Medical Physics and Biomedical Engineering, Wien, AUSTRIA, ³Siemens Healthcare GmbH, Magnetic Resonance, Erlangen, GERMANY.

Aim: To evaluate the influence of different MR-based attenuation correction (MR-AC) methods used in PET/MRI and their effect on clinical lung cancer patient examinations. **Materials and methods:** 15 lung cancer patients were examined in a PET/MRI system (Siemens Biograph mMR) using two consecutive bed positions covering the thorax. PET emission data were reconstructed with four different AC maps: (A) Standard Dixon-based AC segmenting the body into four tissue classes; (B) Standard Dixon-based AC in combination with the implemented MLAA (maximum likelihood reconstruction of attenuation and activity) option to correct for truncation artifacts; (C) Prototype atlas based bone segmentation approach incorporating main cortical bone structures into the standard Dixon based AC and (D) CT based AC from a prior PET/CT scan from the same day. For the latter, the arms and shoulders from (A) were kept, as the arm position is different in PET/CT than in PET/MR. Reconstructions were performed in vendor-based non-product research software (e7tools, Siemens HC) with standard settings (ordered subsets expectation-maximization (OSEM), 21 subsets and 3 iterations). Mean standardized uptake values (SUV_{mean}) were derived from volumes-of-interest (VOIs) placed in a lung lesion (42% threshold) and two background regions (liver (14cm³) and mediastinum (3cm³)). Further, differences in the projected linear attenuation coefficients (pLACs) of the AC maps were calculated for (C) and (D) in the lung region. **Results:** Average differences in SUV_{mean} of lung lesions relative to (A) were 5.8±4.7% (p<0.01) (B), 0.2±0.2% (p<0.01) (C), and -1.5±6.2% (p=0.30) (D). Differences in background tissues were measured to be 11.2%±7.4 (p<0.01) (B), -0.1±0.2% (p=0.12) (C) and 2.9±5.3% (p=0.30) (D) for liver and 31.1±41.1% (p<0.01) (B), 0.4±1.5% (p=0.61) (C) and 3.6±8.5% (p=0.12) (D) for mediastinal VOIs. Average pLAC differences relative to (A) were 0.2±0.1% (p<0.01) and 1.2±0.8% (p=0.30) for (C) and (D), respectively, while the maximum relative difference was found to be 0.6% for (C) and 11.4% for (D). **Conclusion** Truncation cause a significant impact on SUV, which may have a clinical impact, while ignoring bone and segmentation of the AC maps in different tissue classes only cause minor changes in SUV for lung cancer patients.

EP753

Impact of PSF and Gaussian Filtering on SUV Assessment - A Clinical Study Using Digital PET

K. Binzel, A. Siva, T. Saif, C. Lehn, J. Zhang, M. V. Knopp; The Ohio State University, Columbus, OH, UNITED STATES.

Aim: Next generation digital PET/CT imaging systems provide a platform which allows for highly sensitive and precise molecular imaging. Advanced reconstruction options, such as point spread function (PSF) correction and Gaussian filtering, enable further improvements in the visual quality and quantitative accuracy of such imaging. We assessed the impact of these reconstruction options on images reconstructed using next generation digital PET. **Materials and Methods:** PET/CT images

for 35 patients were acquired on a pre-commercial release, next generation digital PET/CT system (Vereos, Philips). Patients were imaged for 90 seconds per bed position following a targeted 480 MBq dose of ^{18}F -FDG. Images were reconstructed with the default protocol, a 4 mm^3 voxel volume, using 3 iterations and 29 subsets. The images were further reconstructed using the same settings, with the addition of a system PSF correction, Gaussian filter, or both. The resulting image sets were quantitatively assessed, placing regions of interest over target lesions as well as in background areas. Taking the SUV_{max} and SUV_{mean} from the default reconstruction, the percent change in SUV was calculated for the three additional reconstructed image sets. Blinded image quality review was conducted as well. **Results:** The addition of the Gaussian filter decreased the SUV in all measured tissues, including target tumor lesions. The average change in SUV_{mean} of physiologic uptake in background areas was less than 10%. In target lesions, the SUV_{max} decreased between 6% and 22%, as compared to default readouts. The use of PSF correction had an opposite impact, leading to an increase measured SUVs in all tissues. For target lesions, the SUV_{max} increased between 12% and 33% with the use of the PSF correction. A combination of the PSF and Gaussian filter had a more balanced impact, in general leading to a minimal increase in SUVs. Image quality reviews revealed that PSF only images exhibited undesirable noise levels, while Gaussian only images appeared blurred, potentially impacting lesion detectability and characterization. In general, the combination PSF and Gaussian images were deemed most preferable. **Conclusion:** Phantom tests have shown that the use of PSF correction in image reconstruction leads to more accurate SUV measurements, however leads to noise. While the use of a Gaussian filter decreases quantitative values, it reduces visual noise. We conclude that a balanced optimization utilizing both methodologies appears to be the most robust and preferred approach for clinical FDG PET procedures.

EP754

Effect of TOF and PSF in detection of lymph node metastases in head and neck of PET/CT images

p. Ghafarian^{1,2}, **A. Ketabi**^{3,4}, **A. Doroudinia**^{1,2}, **M. Bakhshayesh Karam**^{5,2}, **M. R. Ay**^{3,4}; ¹Chronic Respiratory Diseases Research Center, National Research Institute of Tuberculosis and Lung Diseases (NRITLD), Shahid Beheshti University of Medical Sciences, Tehran, Iran., Tehran, IRAN, ISLAMIC REPUBLIC OF, ²PET/CT and Cyclotron Center, Masih Daneshvari Hospital, Shahid Beheshti University of Medical Sciences, Tehran, Iran, Tehran, IRAN, ISLAMIC REPUBLIC OF, ³Department of Medical Physics and Biomedical Engineering, Tehran University of Medical Sciences, Tehran, Iran., Tehran, IRAN, ISLAMIC REPUBLIC OF, ⁴Research Center for Molecular and Cellular Imaging, Tehran University of Medical Sciences, Tehran, Iran., Tehran, IRAN, ISLAMIC REPUBLIC OF, ⁵Pediatric Respiratory Diseases Research Centre, National Research Institute of Tuberculosis and Lung Diseases (NRITLD), Shahid Beheshti University of Medical Sciences, Tehran, Iran, Tehran, IRAN, ISLAMIC REPUBLIC OF.

Aim: Accurate staging in related to patients with head and neck cancer is essential for using proper therapy assessment. As reconstruction technique can affect contrast resolution, spatial resolution and noise level on the PET image, the aim of this work was to investigate the impact of time-of-flight (TOF) and point spread-function (PSF) along with various filter size and iteration number on lesion detectability and the standardized uptake value (SUV) of lymph node metastasis. **Materials and methods:** 20 patients with lymph node Metastases, uptake time 62 ± 3 min and injection of 310MBq (range 255-375MBq) ^{18}F -FDG were scanned with Discovery 690 GE PET/CT scanner, equipped with 64-slice CT. All PET images were retrospectively reconstructed with OSEM+PSF (3 iterations, 18 subsets) and OSEM+PSF+ TOF (2 iterations, 18 subsets) with various Gaussian filter size (1,3,4,5 and 6.4mm)

and 3min for each bed position. It should be emphasized that conventional method was OSEM+PSF (3 iterations, 18 subsets, 6.4 mm post filter). For comprehensive evaluation, we used NEMA image quality phantom with target to background ratio 4:1. A semi-quantitative analysis was performed with SUV_{max} and also coefficient of variance (COV), lesion to background ratio and signal-to-noise ratio (SNR) were considered for each lesion. The PET/CT images reviewed by two expert physicians blinded to the reconstructed methods. **Results:** In OSEM+PSF+TOF algorithm, with decreasing of Gaussian filter size, the relative difference of the SNR in lymph nodes were 11.57 ± 1.81 , 14.62 ± 8.60 , 15.77 ± 15.05 , 15.75 ± 20.11 and 15.83 ± 23.48 when compared with conventional reconstruction algorithm. In OSEM+PSF+TOF with 3 and 4mm post filter, the SUV_{max} were 31.73 ± 7.86 and 21.32 ± 5.65 in related to conventional reconstructed method respectively. The relative difference of lesion to background ratio increased with decreasing post filter from 6.4 to 3 mm in OSEM+PSF+TOF versus to conventional algorithms (2.63 ± 1.27 to 32.89 ± 6.25). According to balance among the lesion detectability, contrast, noise and visual assessment, the optimal images were observed with OSEM+PSF+TOF method along with post filter size between 3 to 5 mm. **Conclusion:** The presented results clarify that the conventional reconstruction method may not be convenient in the head and neck region. Major improvements can be achieved in lymph node metastases detectability and contrast to background ratio in OSEM+PSF+TOF in comparison with OSEM+PSF method with regard to decrease Gaussian filter size. It should be noted that this improvement can be achieved by increasing image noise and SUV values. **Key Words:** Time-of-Flight, Point-Spread Function, lymph node metastasis, Gaussian filter, Standardized Uptake Value, FDG-PET

EP755

Comparison of ten reconstruction algorithms in myocardial perfusion SPECT imaging: relative role of different degrading factors

T. Ahmed^{1,2}, **M. M. Khalil**³, **W. Elshemey**⁴, **A. ELfiky**⁴; ¹King Hamad University Hospital, Busaiteen, BAHRAIN, ²Faculty of Science, Biophysics department, Cairo University, Cairo, EGYPT, ³Faculty of Science Helwan University, Physics Department, Cairo, EGYPT, ⁴Faculty of Science Cairo University, Biophysics Department, Cairo, EGYPT.

Objective: The aim of the present study was to assess the relative performance of Iterative Reconstruction algorithms accompanied with different combinations of attenuation, scatter and resolution recovery corrections versus filtered back projection on the quality of myocardial perfusion SPECT imaging. **Methods:** The study was performed using standard cardiac phantom with two cold defects one anterior transmural and non-transmural positioned in the inferior wall. The phantom was placed inside the Jaczack cylindrical phantom. To simulate clinical count rate, an activity of 1.2 mCi was injected into myocardial walls whereas 11.8 mCi was used for background. SPECT/CT scan was acquired using vendor standard cardiac protocol for resolution recovery. The CT attenuation map was acquired using 50 mA and of 80 kV covering the whole length of the cylindrical phantom. Ten different algorithms were applied in image reconstruction namely FBP, FBPSC, IRNC, IRSC, IRAC, IRACSC, IRNCRR, IRSCR, IRACRR, IRACSCRR; where SC, AC, and RR refer to scatter, attenuation correction and resolution recovery respectively. NC denotes no correction was applied. Figures of merit used to evaluate the performance of the reconstruction algorithms were slice count uniformity, Coefficient of Variation (CoV) and CNR calculated for normally perfused myocardium while percentage defect contrast was used to assess hypo-perfused segments represented by cold inserts. **Results:** When compared to analytical techniques, IR showed better performance in terms of CNR and defect contrast resolution especially with gradual correction of SPECT degrading factors.

However, this was associated with slight increase in image noise as demonstrated by uniformity and CoV analysis. There was also a trend towards an improvement of defect contrast in transmural compared to non-transmural defect. On the other hand, CNR was not significantly different as applying different combinations of image degrading corrections (i.e. IRACSCRR, IRSCRR, and IRACRR) while there was noticeable improvement in defect contrast for both defects as we move towards the scheme (i.e. IRACSCRR) that considered all corrections in image reconstruction. Conclusion: The results showed more insights on how iterative (with different corrections) and analytical techniques handle image noise, defect contrast, CNR with remarkable differences appeared on apical versus basal slices and transmural versus non-transmural perfusion defects. This will have significant implications on quantitative perfusion parameters derived from the chosen reconstruction algorithm. Further investigations are underway to exploit the full potential of iterative based image correction techniques in myocardial perfusion imaging.

EP756

Validation of atlas-based head attenuation correction in the GE SIGNA PET/MR - initial results

G. Schramm^{1,2}, A. Rezaei^{1,2}, S. Willekens^{1,2}, R. Peeters^{1,3}, M. Koole^{1,2}, J. Nuyts^{1,2}, K. van Laere^{1,2}; ¹Department of Imaging and Pathology, KU Leuven, Leuven, BELGIUM, ²Division of Nuclear Medicine, University Hospitals Leuven, Leuven, BELGIUM, ³Division of Radiology, University Hospitals Leuven, Leuven, BELGIUM.

Aim Accurate attenuation correction (AC) of the head is crucial for absolute quantification of PET images. Due to the lack of signal from bone in MR images, AC is challenging in PET/MR brain examinations. In the GE SIGNA PET/MR, an atlas-based approach (GEAC) is used to generate attenuation images including a skull compartment with fixed bone attenuation values. In this study, we aimed to validate the accuracy of GEAC compared to CT-based attenuation correction (CTAC) in [¹⁸F]FDG brain examinations of healthy volunteers. **Methods** PET/MR raw data sets of 10 healthy subjects were reconstructed using GEAC (PET_{GEAC}) and CTAC (PET_{CTAC}) in the GE PET reconstruction toolbox v.1.22 (static TOF-OSEM reconstruction, 40 - 60 min p.i., 2 iterations, 28 subsets). The CTAC attenuation image including templates for the bed and MR-coils was derived from AC-CTs of PET/CT acquisitions performed immediately after the PET/MRI scan, using a Siemens HIREZ PET/CT. The AC-CT was rigidly co-registered and bilinearly scaled to PET attenuation coefficients. The alignment of the attenuation images was visually verified. Subsequently, relative differences in the mean [¹⁸F]FDG uptake of 86 anatomical regions of the Hammers atlas were calculated in PMOD v3.4 (PMOD, Zurich, Switzerland) and analyzed in R v.3.0.2 (R Foundation, Vienna, Austria). **Results** The bias (mean ± standard deviation) in the uptake of PET_{GEAC} compared to PET_{CTAC} was: 4.6 ± 2.6 % averaged over all regions, 4.6 ± 3.2% in grey matter, 5.5 ± 2.4% in white matter, 2.2 ± 1.6 % in the cerebellum, and 4.4 ± 1.3% in the striatum. In all regions the difference was significant (p < 0.05 using a Wilcoxon signed-rank test). The intra-regional variability was largest in the grey matter regions (-4.9% to 13.4%), and overestimation occurred especially in cranial regions (high frontal and parietal cortex). The highest intra-subject variability was found to be -1.2% to 13.3%. In 8 cases, the difference in the bias in the cerebellum compared to the bias in the superior gyri was larger than 5%. **Conclusion** GEAC leads to a small but significant region-dependent overestimation of the reconstructed [¹⁸F]FDG uptake in healthy volunteers, especially in cranial grey matter regions. Further patient studies are needed to verify if [¹⁸F]FDG uptake pattern interpretation is affected by the observed regional and intra-subject variability.

EP757

The impact of extending the acquisition time for quality of PET-CT examinations with 18F-FDG in obese patients on the LYSO TOF scanner

M. Koza¹, K. Buraczewska^{1,2}, A. Budzyńska^{1,2}, M. Dziuk^{1,2}; ¹Affidea, Warsaw, POLAND, ²Military Institute of Medicine, Warsaw, POLAND.

Background: The aim of the study was to quantitatively analyze the effect of extending the acquisition time by 25% in the PET-CT examinations in patients with the BMI above 30 (BMI_{mean} = 36.97, SD = 2.47). **Methods:** We evaluated 29 lesions in PET-CT exams with 18F-FDG in 15 patients. The average administered activity was 4MBq/kg, and the acquisition time was 2.5 min per bed position. The raw data were recorded in the List Mode, and then reconstructed retrospectively with the time of acquisition 2 min per bed position. In both cases the use of AC reconstruction with the Time of flight function and the PSF reconstruction (without TOF). The tumor to liver ratio (TLR) and tumor to background ratio (TBR) were calculated for SUV_{max}. The same measurements were performed for the SUV_{mean}. The statistics were made for the following pairs of dependent samples (SUV_{2.5min/bed} position and SUV_{2min/bed}) in a quantitative scale. None of the groups was characterized by a normal distribution, therefore Wilcoxon test as a test of significance was used in all cases. **Results:** There was significant improvement of TBR and TLR (p>0.05) in all cases for the PSF reconstruction for both SUVs. The value of TBR for AC reconstruction was statistically significant. The mean difference of TLR for AC and PSF reconstructions were -0.65 (SD=2,1) and 0,12 (SD=0,19) respectively. The TLR for SUV mean was 0,83 (SD=2,51) for AC reconstruction and -0.061 (DS=0,12) for PSF reconstruction. **Conclusions:** The prolonged acquisition time by 25 % is statistically significant in all cases TBR and TLR in TPR reconstruction. There is no statistical difference in TLR value in AC reconstruction.

EP758

Q.Clear - the new reconstruction algorithm of PET images in the analysis of lung tumours.

B. Grebieniow¹, S. Antczak¹, A. Wyszomirska², R. Giersz³, R. Czepczyński^{2,1}, W. Cholewiński^{2,4}, M. Ruchała²; ¹Affidea, Poznań, POLAND, ²Poznan University of Medical Sciences, Poznań, POLAND, ³Greater Poland Centre of Pulmonology and Thoracic Surgery, Poznań, POLAND, ⁴Greater Poland Centre of Oncology, Poznan, POLAND.

Q.Clear reconstruction algorithm based on the Bayesian penalized-likelihood and image noise control dependant on the activity level was introduced in order to improve quality of the images and parameters of the quantitative image analysis. The aim of this study was to evaluate the impact of this algorithm on the PET diagnosis of lung tumours. Material and methods. Patients with untreated lung tumours were qualified to the study. The patients were subjected to PET-CT 60 min after injection of 4 MBq/kg of 18F-FDG. The scans were registered by the Discovery IQ PET-CT scanner (GE Healthcare) using standard parameters. The images were analysed visually by two experienced observers. SUV_{max} values of the lung tumours were registered for both: Q.Clear reconstruction algorithm with the b parameter related to the noise level of the image equal to 350 and for the standard VPHD iterative 3D reconstruction algorithm. Patients with malignant tumours were operated. In case of negative PET scan, patients were followed-up with CT. **Results.** Sixty-seven patients aged 30-85 years (mean 64 yrs.), 52 men (60%) and 34 women were qualified to the study. In 37 patients with increased 18F-FDG uptake, the histopathology confirmed malignancy. Remaining 30 patients with slight or no 18F-FDG uptake were classified as benign and the follow-up did not show any progression. SUV_{max} measured using VPHD and Q.Clear was respectively: adenocarcinoma (n=19) 6.4±4.2 and 8.4±5.4,

squamous cell carcinoma (n=13) 8.8 ± 2.9 and 10.6 ± 3.7 , macrocellular carcinoma (n=5) 8.5 ± 1.5 and 10.7 ± 1.4 , benign lesions (n=30) 1.4 ± 0.7 and 1.7 ± 0.9 . In case of malignant tumours a positive correlation between tumour size and SUV_{max} was found in both reconstruction methods. The correlation was stronger for VPHD than for Q.Clear reconstruction algorithm ($r=0.5$ vs. 0.4). In case of benign disease this correlation was found only for Q.Clear algorithm. Conclusion. For both, benign and malignant tumours, Q.Clear shows higher SUV_{max} values than with VPHD method. The Q.Clear reconstruction algorithm improves the quality of the images and quantitative image analysis.

EP759

The influence of TOF and PSF techniques along with scan duration on respiratory artefact reduction in PET/CT images

p. Ghafarian^{1,2}, R. Sharif Pour^{3,4}, A. Doroudinia^{5,2}, M. Bakhshayesh Karam^{6,2}, M. R. Ay^{7,4}; ¹Chronic Respiratory Diseases Research Center, National Research Institute of Tuberculosis and Lung Diseases (NRITLD), Shahid Beheshti University of Medical Sciences, Tehran, Iran, Tehran, IRAN, ISLAMIC REPUBLIC OF, ²PET/CT and Cyclotron Center, Masih Daneshvari Hospital, Shahid Beheshti University of Medical Sciences, Tehran, Iran, Tehran, IRAN, ISLAMIC REPUBLIC OF, ³Department of Medical Physics and Biomedical Engineering, Tehran University of Medical Sciences, Tehran, Iran, Tehran, IRAN, ISLAMIC REPUBLIC OF, ⁴Research Center for Molecular and Cellular Imaging, Tehran University of Medical Sciences, Tehran, Iran, Tehran, IRAN, ISLAMIC REPUBLIC OF, ⁵Chronic Respiratory Diseases Research Center, National Research Institute of Tuberculosis and Lung Diseases (NRITLD), Shahid Beheshti University of Medical Sciences, Tehran, Iran., Tehran, IRAN, ISLAMIC REPUBLIC OF, ⁶Pediatric Respiratory Diseases Research Center, National Research Institute of Tuberculosis and Lung Diseases (NRITLD), Shahid Beheshti University of Medical Sciences, Tehran, Iran., Tehran, IRAN, ISLAMIC REPUBLIC OF, ⁷Department of Medical Physics and Biomedical Engineering, Tehran University of Medical Sciences, Tehran, Iran., Tehran, IRAN, ISLAMIC REPUBLIC OF.

Aim: The introduction of new techniques such as time of flight (TOF) and PSF modeling in reconstruction of PET images can alter respiratory artifact in diaphragmatic region. The aim of this study was to evaluate the influence of TOF+PSF reconstruction on decreasing of acquisition time per bed position while the white band respiratory artefact can be improved. **Materials and methods:** 29 patients with uptake time 61 ± 2 min and injection of 327.5MBq (range 261-350MBq) ¹⁸F-FDG were scanned with Discovery 690 GE PET/CT scanner, equipped with 64-slice CT. All of the lesions were in the diaphragmatic region and were in patients with extended white band artefact. For comprehensive evaluation we used NEMA image quality phantom with target to background 4:1. The PET images were retrospectively reconstructed using OSEM+PSF (3iterations, 18subsets) and OSEM+TOF+PSF (2iterations, 18subsets) with 4.4, 5.4 and 6.4 Gaussian filter size and 2.2:30 and 3min acquisition time per bed. A semi-quantitative analysis was utilized by SUV_{max} and SUV_{mean} with 45% threshold. For quantitative purpose, coefficient of variance, signal-to-noise ratio (SNR) and contrast to background evaluation were also considered. The PET/CT images reviewed by two expert physicians. **Results:** In the phantom study, the relative difference of FWHM in transverse view between OSEM+TOF+PSF (2iterations, 18 subsets, 6.4mm filter size, 3min) and conventional algorithm (OSEM+PSF with 3iterations, 18subsets, 6.4 mm post filter and 3min scan time) varied from -30.08% to -1.39% when the diameter sphere size increased from 13mm to 37mm, while the contrast ratio was still illustrated higher value in OSEM+TOF+PSF versus to OSEM+PSF in all sphere sizes. In clinical study, the combination of OSEM+TOF+PSF even in 2min acquisition time showed more SNR in related to OSEM+PSF with 3min scan time and 6.4mm post filter ($23.14\%\pm 14.62\%$) and the relative difference

of SUV_{max} and SUV_{45%} were 24.48 and 22.49 respectively. ICC correlation for SNR value in all OSEM+TOF+PSF algorithm with 6.4 and 5.4mm post filter and 2 to 2:30 min per bed position demonstrated excellent behavior with Cronbach's α values between 0.949 to 0.995. **Conclusions:** A significant lesion detectability and reduction of white band respiratory artifact was observed with combination of TOF and PSF versus to only PSF modeling. It is valuable that decreasing scan time from 3min to 2min still retained image quality and altered lesion size in PET images in the artifact region. It is suggested that decreasing of scan time is strongly depend on utilizing appropriate filter size along with convenient iteration number and subset in OSEM+TOF+PSF algorithm. **Key Words:** Time-of-Flight, Point-Spread Function, scan time, lesion detectability, respiratory artifact, Standardized Uptake Value, FDG-PET

EP760

Impact of advanced image reconstruction algorithm on qualitative and quantitative oncological 18F-FDG PET/CT

I. Shiri¹, P. Ghafarian^{2,3}, A. Bitarafan^{1,4}, M. Bakhshaesh Karam^{2,3}, M. AY^{5,6}; ¹Department of Medical Physics, School of Medicine, Iran University of Medical Sciences, Tehran, IRAN, ISLAMIC REPUBLIC OF, ²Chronic Respiratory Diseases Research Center, National Research Institute of Tuberculosis and Lung Diseases (NRITLD), Shahid Beheshti University of Medical Sciences, Tehran, IRAN, ISLAMIC REPUBLIC OF, ³PET/CT and Cyclotron Center, Masih Daneshvari Hospital, Shahid Beheshti University of Medical Sciences, Tehran, IRAN, ISLAMIC REPUBLIC OF, ⁴Cardiovascular Intervention Research Center, Rajaie Cardiovascular Medical and Research Center, Iran University of Medical Sciences, Tehran, IRAN, ISLAMIC REPUBLIC OF, ⁵Research Center for Molecular and Cellular Imaging, Tehran University of Medical Sciences, Tehran, IRAN, ISLAMIC REPUBLIC OF, ⁶Department of Medical Physics and Biomedical Engineering, Tehran University of Medical Sciences, Tehran, IRAN, ISLAMIC REPUBLIC OF.

Aim: New technology such as Time-of-Flight (TOF) and Point Spread Function (PSF) theoretically have led to higher signal to noise ratio (SNR) and improve spatial resolution. The aim of the current study was to investigate the effects of PSF and TOF reconstruction parameters on qualitative and quantitative oncological 18F-FDG PET/CT images. **Materials and Methods:** A complete set of measurements were performed with GE Discovery 690 PET/CT scanner using NEMA IEC body phantom containing 6 spheres (diameter 10 to 37mm) filled by F18-FDG with two sphere to background ratio (SBR) (2:1, 4:1). Phantom image were reconstructed into 3D-OSEM + PSF and 3D-OSEM+PSF + TOF and post-smoothing filters with FWHM 1 to 6.4 mm was applied to image. We evaluated lesion by qualitative parameters such as visual assessment, contrast and SNR. Each lesion, also was quantified with different parameters as follows: SUV_{max}, SUV_{mean}, SUV_{41%}, SUV_{50%} and SUV_{75%} (mean within a 41%, 50%, 75% isocontour). **Results:** For phantom spheres ≥ 13 mm, we found higher SNR (15-20%) using OSEM+PSF+TOF mode rather than OSEM+PSF. Also, in terms of post smoothing filter FWHM (1-6.4 mm), the highest value was obtained with increasing filter FWHM (increasing 26-40%) at all SBRs with the highest differences for SBR 4:1 decreasing to the lowest for SBR 2:1 (from 30% in difference to 10%). Both OSEM+PSF and OSEM+PSF+TOF reconstruction resulted in a substantial alteration ($\geq 35\%$) of SUV_{max} in phantom spheres ≥ 17 mm and SUV₅₀ was more accurate when activity measurements is performed. **Conclusion:** The implementation of PSF and TOF within the OSEM reconstruction algorithm clearly improves image quality. In quantitative analysis, advanced reconstruction techniques overestimate SUV_{max} while provide more accurate in quantification of SUV₅₀. SUV₅₀ has been shown as the best alternative in large lesion (≥ 13 mm) when using 3D-OSEM + PSF and 3D-OSEM+PSF + TOF reconstruction algorithm.

EP-42 – Sunday, October 16, 2016, during Exhibition hours, e-Poster Area
Physics & Instrumentation & Data Analysis: Instrumentation

EP761

Implementation of Correlated Signal Enhancement (CSE) Technique for Accurate Positioning in Gamma Camera

B. Teimourian Fard^{1,2}, M. Ay^{1,3}, S. Sajedi^{1,3}, A. Akbarzadeh¹, S. Kaviani¹, M. Farahani¹; ¹Research Center for Molecular and Cellular Imaging, Tehran University of Medical Sciences, Tehran, IRAN, ISLAMIC REPUBLIC OF, ²Department of Energy Engineering and Physics, Amir Kabir University of Technology (Tehran Polytechnic), Tehran, IRAN, ISLAMIC REPUBLIC OF, ³Department of Medical Physics and Biomedical Engineering, Tehran University of Medical Sciences, Tehran, IRAN, ISLAMIC REPUBLIC OF.

Aim: The most of modern gamma cameras are rectangular because of matching the FOV required for tomographic imaging. Despite the fact that square PMTs are completely compatible with the rectangular geometry and so they can minimize the dead zone in the camera, the use of them is limited due to the difficulty in implementation of conventional anger logic to estimate the position of interaction in the crystal. Because the main hypothesis in the anger logic is that the distances between the centers of neighboring PMTs is the same in all directions and this assumption is violated in square PMTs, therefore the uniformity of the images is destroyed. Different correction methods were applied to modify the uniformity of the distorted images. Since the correction methods in highly dependent to even small changes in PMT characteristics (such as gain), the correction methods are not useful enough. Therefore the need of existence of a positioning technique that can deliver an image with good uniformity characteristics is necessary. In this work, we applied the Correlated Signal Enhancement (CSE) to improve image quality in presence of square PMTs. **Materials and Methods:** CSE is a new positioning algorithm that could overcome the problem with the simple summation of signals of every row or column and the identical 1D center of mass (COM) calculation determines the position of photon in separate direction x or y. A gamma camera with the NaI(Tl) crystal, that has 40x25 mm² area and 9.5mm thickness, coupled with an array 24 square PMTs in 4x6 designed and developed to evaluate the performance of CSE algorithm. There are 6 values for rows and 4 values for columns that used to estimate the x and position of the interaction respectively. Results: The CSE method optimized for the proposed camera and intrinsic spatial resolution and the energy resolution were obtained 3.7mm and 8.5% respectively. The differential and absolute uniformity of the acquired flood field image (a point source of Tc-99 is located far from of camera face) were measured 0.99% and 1.56% in UFOV. Also a LEHR (Low Energy High Resolution) parallel-hole collimator was located over the camera face and the extrinsic spatial resolutions were calculated 7.6mm. **Conclusion:** The presented results that show the developed positioning method significantly improve the accuracy of photon detection in our developed detector.

EP762

A drop-in gamma probe for radioguided surgery in an -robot-assisted- laparoscopic setting

N. S. van den Berg¹, M. N. van Oosterom¹, H. Simon², L. Mengus², M. M. Welling¹, H. G. van der Poel³, F. W. B. van Leeuwen¹; ¹LUMC, Leiden, NETHERLANDS, ²EuroRad S.A., Strassbourg, FRANCE, ³NKI-AVL, Amsterdam, NETHERLANDS.

Introduction Other than in open surgery, during laparoscopic radioguided surgery procedures, the limited maneuverability of a

traditional laparoscopic gamma probe can hinder identification of (low-activity) lesions that are located near a high-activity background. To increase the maneuverability during laparoscopic procedures, a 'drop-in' gamma probe technology was developed. Such a drop-in gamma probe can be manipulated using the available and often flexible (robotic) laparoscopic surgical tools. **Methods** Taking general engineering restrictions such as detector surface, shielding, trocar-diameter, cable thickness, and patient safety into consideration, drop-in designs with 0°, 45°, 90°, and 135°-grip orientations were designed and 3D printed. Gripping was evaluated using both a laparoscopic and robotic forceps. In human-like phantoms, the maneuverability- and scanning direction of the different prototypes were evaluated and compared to a conventional laparoscopic gamma probe. Lastly the most potent grip designs were ex vivo evaluated in a clinical set-up. **Results** Phantom experiments showed that distinguishing a low objective from a high-activity background source (1:100 ratio) was only possible with the detector faced away >90° from the high background source. The best maneuverability- and resulting scanning range was obtained with the 90°-grip design (0-180° versus 0-111°, 0-140°, and 37-180° for 0°, 45° and 135°-grip designs, respectively). In the ex vivo clinical setup, during sentinel node biopsy for prostate cancer, the drop-in technology allowed accurate discrimination of the low-activity sentinel node from the nearby high-activity prostate. **Conclusion** The drop-in gamma probe technology provides and increases rotational freedom when using (robotic) laparoscopic surgical tools. This in turn improves probe-placement and increases the detectability of low-activity lesions.

EP763

Designing 14C-Urea Breath Test System for Detecting Helicobacter Pylori

A. Radnia¹, M. Farahani¹, M. Ay^{1,2}; ¹Research Center for Molecular and Cellular Imaging, Tehran University of Medical Sciences, Tehran, IRAN, ISLAMIC REPUBLIC OF, ²Department of Medical Physics and Biomedical Engineering, Tehran University of Medical Sciences, Tehran, IRAN, ISLAMIC REPUBLIC OF.

Aim: UBT is a painless, non-invasive and easy to use test method which detects the metabolically active bacteria, which makes the test suitable for pretreatment detection as well as for monitoring results after eradication treatment against Helicobacter pylorus (HP). In 14C-UBT method HP infection detection has 96.6% sensitivity and 100% specificity and has the best diagnostic performance compared with other methods like RUT, PCR, and HP-HE. In this work we designed, developed and evaluated a UBT system called HeliGuide based on 14C-UBT. **Materials and Methods:** In developed system the traditionally used liquid scintillator has been replaced with a detector containing two built-in Geiger-Muller counters operating in parallel mode. HeliGuide UBT consisting of two components, a breath-card and an analyzer. The patient exhales into the breath-card and the analyzer counts the activity of 14C in the breath-card. The absorbed 14C in the two pads mounted in Breath-Card emits low energy β-radiation. Two Geiger-Muller counters mounted in the Analyzer will detect and sum up all type of radioactive activity (α, β, and γ) reaching the sensors, so a shielding is designed to prevent penetration of background radiation. An optical sensor is designed in the shielding to detect insertion of breath-card. A DC high voltage is applied to detectors and the signals from them is amplified and then processed and counted. The microprocessor- controlled electronics in the analyzer steer the measurement cycle. Due to the short range of β-radiation, All activity registered by both sensors simultaneously, must originate from background activity, and thus all these activities are disregarded in the counting process in microprocessor. Finally the result is illustrated in LCD display. **Results:** The background error is omitted successfully; beta activity of breath-cards is measured properly and Maximum true count rate measuring of system is 20K count per second. 221 reference breath-cards have been analyzed with system and all results are matched with the reference.

Conclusion: The designed UBT system (HeliGuide) is a high accuracy UBT system which is adequate for detecting helicobacter pylori.

EP764

A Crosstalk Compensation for Simultaneous $^{99m}\text{Tc}/^{123}\text{I}$ Dual-isotope SPECT Imaging by Filtering Technique and Artificial Neural Network

K. S. Chuang¹, H. H. Lin¹, C. C. Chiang¹, Y. F. Wang¹, Z. J. Wei¹, Y. C. Ni², T. Y. Luo³; ¹National Tsing-Hua University, Hsin-Chu, TAIWAN, ²Health Physics Division, Institute of Nuclear Energy Research Atomic Energy Council, Long-Tan, TAIWAN, ³Isotope Division, Institute of Nuclear Energy Research Atomic Energy Council, Long-Tan, TAIWAN.

Aim Dual isotope simultaneous acquisition (DISA) can be used to visualize two radiotracer distributions at the same time to reduce scan time and avoid mis-registration artifact. However, DISA is marred by the crosstalk when the two photopeaks are close, e.g. ^{99m}Tc (140 keV) and ^{123}I (159 keV). Artificial neural network (ANN) is mostly employed to tackle the crosstalk. Conventional ANN techniques require more than 20 energy windows which are not supported by current SPECT. In this study, we incorporated ANN with attenuation information of a filter using only three energy windows to decontaminate the crosstalk. **Materials and methods** A metal filter is placed over the collimator to attenuate photons of different energy by various degrees. Based on the attenuation difference of the gamma from each isotope, we can separate the two isotopes. The constructed ANN consisted of three layers: input (6 nodes), hidden (9 nodes), and output (4 nodes). Photon counts in three energy windows from scans with and w/o filter are fed into ANN. The outputs are primary gamma of the two isotopes, w/ and w/o filter. The outputs of the ANN are then combined to form two primary data with crosstalk and scatter corrected each for the ^{99m}Tc and ^{123}I . A GATE Monte Carlo code is used for the DISA SPECT simulation. **Results** A gold filter with 0.2 mm thickness is attached to one of the collimator of a dual-heads E.CAM (Siemens, German) for the DISA simulation study. Preliminary results show that the crosstalk is successfully resolved by the proposed method. The results show that quantitative recovery from mixed ^{99m}Tc and ^{123}I sources is comparable to that from matched single-isotope sources. **Conclusion** In this study, a DISA SPECT technique to tackle the crosstalk using filter is proposed. Projection data with and without filter are inputted to an ANN to separate the energy spectrum of the two isotopes. Due to the extra information provided by the filtering, only 3 energy windows are needed. This method is simple to perform and yet generates promising results.

EP765

Channel Reduction in SiPM Array Using Fast Output for a PET Block Detector

S. Sajedi Toighoun¹, M. Taheri¹, N. Zeraatkar¹, S. Kaviani¹, M. Ay²; ¹Research Center for Molecular and Cellular Imaging, Tehran University of Medical Sciences, Tehran, IRAN, ISLAMIC REPUBLIC OF, ²Department of Medical Physics & Biomedical Engineering, Tehran University of Medical Sciences, Tehran, IRAN, ISLAMIC REPUBLIC OF.

Aims: By introducing PET/MR imaging in the early 2000s, Avalanche Photo-Diode (APD) and afterward SiPM based systems grew rapidly. By development and cost reduction in SiPM technology, more imaging detector configurations have been using this technology. In the imaging application, SiPM detectors are usually arranged in array form and because of high density of pixels in a detection area, the readout electronics is a challenging issue and efforts have been made to reduce number of readout channels with less performance degradation. The new developed SiPM series by SensL (Cork, Ireland) are equipped with ‘fast output’ as an extra output to improve timing resolution of detector. In this work, we

tried to reduce readout channels by implementing Scrambled Crosswire Readout (SCR) using ‘fast output’ signals. **Methods:** The utilized array is ArrayB-30035-144P-PCB having 12×12 pixels, each having 3×3 mm² active area with 4.2 mm pixel pitch. The SCR method, recommended by SensL, reduces 144 channels to 25 (9 tiles+16pixels) channels, where the array area is divided to 9 tiles each containing 16 pixels. This method multiplexes all anodes of similar pixels in different tiles, producing 16 Analog-to-Digital Converter (ADC) channels for positioning of the incident photon inside the tile. In addition, it multiplexes all cathodes of pixels in the same tile, producing 9 comparator circuits to allocate the fired tile. The fast output can be replaced for cathode in SCR method. In this arrangement, all fast outputs of the pixels inside a tile are multiplexed to one output which can be detected by the level threshold. Also, the fast output multiplexing is further required for time-pickoff discrimination. The arrangement was evaluated in a detector block using an array of LYSO crystal pixels with the size of $2 \times 2 \times 10$ mm³ and 2.1 mm pixel pitch. **Results:** The flood-field image has been taken to obtain enough counts per crystal pixel. The image showed admissible pixel resolution and the peak-to-valley ratio in different pixels varied between 10 to 17. The energy resolution of detector block was measured about 25% at 511 keV. **Conclusion:** The proposed readout method reduces 144 SiPM channels to 16 ADC channels, derived from ‘standard output’ signals, and 9 level threshold channels, derived from ‘fast output’ signals. Since in a PET detector block there is another effort to reduce 144 of ‘fast output’ channels to perform time-pickoff discrimination, we tried in this work to combine two channel reduction methods by one implementation.

EP766

Initial Evaluation of a New High Resolution Non-human Primate (NHP) PET System (LFER 150)

Z. Sarnyai¹, K. Nagy², G. Rosenqvist¹, A. Takano¹, R. Maior¹, M. Tóth¹, B. Gulyás¹, C. Halldin¹, A. Varrone¹; ¹Karolinska Institutet, Department of Clinical Neuroscience, Stockholm, SWEDEN, ²Mediso Ltd, Budapest, HUNGARY.

Aim The LFER 150 PET/CT by Mediso was developed for high-resolution imaging of the brain of non-human primates. The PET system uses LYSO crystals of $1.51 \times 1.51 \times 10$ mm, and has a field of view of 20 cm and 15 cm in the radial and axial direction, respectively. Gantry bore diameter is 26 cm. The objective of this study was initial performance evaluation of the system using the NEMA NU 4 standard protocol and *in-vivo* non-human primate (NHP) PET measurements. **Materials and Methods** Data were acquired and evaluated using the methodology of the NEMA NU4 standard for resolution, sensitivity, image quality and noise equivalent count rate (NEC). An additional Derenzo phantom scan was performed to test resolution using 3D OSEM reconstruction. Practical usability of the system was evaluated by NHP (cynomolgus monkey, weight: 4.5 kg) examination with a D2/D3 receptor radioligand, [¹¹C]raclopride (94 MBq). The NHP was anesthetized using I.V. administration of ketamine and Xylazine. List mode PET data were acquired for 65 min and reconstructed into 34 frames with the Tera-Tomo 3D engine using OSEM algorithm. **Results** Radial FWHM resolution was better than 2.2 mm and 3.2 mm in the central 60 mm and 160 mm diameter region, respectively. Maximum sensitivity in 400-600 keV and 250-750 keV energy window was 30.03 cps/kBq (absolute value 3.3 %) and 49.11 cps/kBq (5.4 %) respectively. Using the image quality phantom, the uniformity standard deviation was 6.2 % and the spill-over ratio for air and water was 0.06. Using the rat like phantom the NEC curve peaked at 399 kcps and 149 MBq. Using the Derenzo phantom, rods with 1.1 mm diameter could be visualised. In the NHP, the reconstructed 3D images of [¹¹C]raclopride were consistent with the known distribution of D2/D3 receptors and with the kinetic behavior of this radioligand. **Conclusion** The LFER 150 is a high-resolution PET-CT system suitable for molecular imaging studies of the brain in NHPs.

EP767**Optimal SPECT Detector Configuration for Myocardial Perfusion Scintigraphy in Patients with Small Body Habitus**

N. A. Bebbington: Siemens Healthcare A/S, Aarhus, DENMARK.

AIMS: In patients with very small body habitus, the standard 90° detector configuration used in Myocardial Perfusion Scintigraphy (MPS) can allow truncation of the heart, where part of the heart is outside of the field of view in some projections, creating artefactual perfusion defects. Siemens Symbia systems offer '90° NCO Prescan' and '76° NC' detector configuration/orbits to eliminate this effect. The aim was to assess which configuration is optimal for patients with small body habitus, considering truncation effects and image quality in a phantom. **MATERIALS AND METHODS:** The Data Spectrum cardiac insert was filled with Tc99m and underwent SPECT on a Symbia Intevo 6 with the standard 90°NC, 90°NCO Prescan, and 76°NC configurations, in two conditions: scan 1) unrealistic patient geometry with minimal adjacent tissue (with anteroseptal and inferolateral defects), to demonstrate worst case scenario truncation; scan 2) in cylindrical body phantom (with septal defect) to represent a patient with small body habitus. Number of projections with cardiac truncation and mean detector radius were recorded for each acquisition. SRS, Extent (%) and TPD (%) were measured in Cedars-Sinai QPS, and image quality determined by line profiles for septal and inferior walls. **RESULTS:** Scan 1 (unrealistic patient geometry): cardiac truncation was present in 28/64 projections for standard 90°, and was borderline in 10/64 for 90°NCO Prescan, but not present in 76°. True SRS in the truncated region was 4 (determined by 76° configuration without truncation), but increased to 10 for 90°NCO Prescan (possible truncation artefact), and to 31 for standard 90°. 76° gave smaller mean detector radius (225mm) than 90°Prescan (250mm). Minimum/maximum intensity on the line profiles demonstrated comparable defect contrast between 76° (0.58) and 90°Prescan (0.57). Scan 2 (realistic small body habitus geometry): cardiac truncation was present in 8/64 projections for standard 90° and was not present in 76° or 90° Prescan configurations. Defect scores were comparable between all configurations. 76° gave smaller mean detector radius (230mm) than Prescan 90° (259mm). Defect contrast was more favourable in the 76° configuration (0.60) compared with the Prescan 90° (0.67). **CONCLUSIONS:** 76°NC acquisitions guarantee no cardiac truncation in patients with small body habitus, and provided smaller rotation radii compared with 90° Prescan mode, which resulted in improved defect contrast in the phantom geometry representing a patient with small body habitus used in this study.

EP768**Monte Carlo Modeling of a Gamma Probe for Sentinel Lymph Node Biopsy**

A. Nikoogoftar^{1,2}, N. Zeraatkar², M. Shamsaie¹, **M. Ay^{2,3}**; ¹Faculty of Nuclear Engineering and Physics, Amirkabir University of Technology, Tehran, IRAN, ISLAMIC REPUBLIC OF, ²Research Centre for Molecular and Cellular Imaging, Tehran University of Medical Sciences, Tehran, IRAN, ISLAMIC REPUBLIC OF, ³Department of Medical Physics and Biomedical Engineering, Tehran University of Medical Sciences, Tehran, IRAN, ISLAMIC REPUBLIC OF.

Aim: Gamma probe is a small gamma detector with output of radiation count rate detected in addition to audio signal proportional to the count rate. The main application of gamma probe is in sentinel lymph node biopsy (SLNB). Radioactive colloid (mostly Tc-99m) is injected near the tumor. Then after a specific time passes, surgeon with the help of guidelines and protocols can find the location of Sentinel Lymph Node. Various gamma probe systems are available with different detector materials, detector sizes, and collimation for different type of application. The gamma probe performance is described by some quantitative parameters

e.g., sensitivity, spatial resolution, and shielding. The purpose of this study is to develop a Monte Carlo (MC) model for a gamma probe system (SUEGEOGUIDE II). Different quantitative parameters were measured using experimental and MC simulation according to NEMA NU3 protocol. **Materials and methods:** "The SUEGEOGUIDE II" is composed of two main parts: probe and control unit. The probe includes tungsten collimator, cesium iodide (thallium-activated) [Cs(Tl)] scintillator crystal, silicon photomultiplier (SiPM), and electronic boards. Sensitivity profiles were obtained using a point source placed on the long probe axis at distance of 10, 30, and 50 mm. The spatial resolution was determined by increasing lateral distance from a 30mm-far point source. Full-width at half-maximum (FWHM) was calculated after Gaussian fitting. For shielding calculation the source was moved all around the probe head in contact with, and the largest count rate was considered. We used Monte Carlo simulation MCNP4C code to model the system and then measurement of the abovementioned parameters with the same methods. **Result:** Sensitivity at distance of 10, 30, and 50 mm was calculated respectively as 7,120 cps/MBq, 1,830 cps/MBq, and 790 cps/MBq by practical measurements. The MC simulation result revealed sensitivity of 8540 cps/MBq, 2054 cps/MBq, and 890 cps/MBq for the same distances. Spatial resolution at distance of 30 mm with experimental and MC simulation was measured as 40 mm and 42 mm, respectively. Also, shielding was about 98% for both MC and practical methods. **Conclusion:** We developed an MC model for a gamma probe system. Then using practical experimental and the MC simulation, some performance parameters of the system such as sensitivity, spatial resolution, and shielding were measured. The result showed that the MC model is valid and can be used for other. We aim to optimize the crystal size and shielding thickness using the developed model.

EP769**Performance characteristics of NeuroPET system using GATE Monte Carlo simulation**

P. Sheikhzadeh^{1,2}, H. Sabet³, H. Ghadiri^{1,2}, P. Geramifar⁴, H. Mahani^{2,5}, P. Ghafarian^{6,7}, **M. Ay^{1,2}**; ¹Department of Medical Physics and Biomedical Engineering, Tehran university of medical science, Tehran, IRAN, ISLAMIC REPUBLIC OF, ²Research Center for Molecular and Cellular Imaging, Tehran University of Medical Sciences, Tehran, IRAN, ISLAMIC REPUBLIC OF, ³Massachusetts General Hospital, Harvard Medical School, Charlestown, MA, UNITED STATES, ⁴Research Center for Nuclear Medicine, Shariati Hospital, Tehran University of Medical Sciences, Tehran, IRAN, ISLAMIC REPUBLIC OF, ⁵Radiation Application Research School, Nuclear Science and Technology Research Institute, Tehran, IRAN, ISLAMIC REPUBLIC OF, ⁶Chronic Respiratory Diseases Research Center, National Research Institute of Tuberculosis and Lung Diseases (NRITLD), Shahid Beheshti University of Medical Sciences, Tehran, IRAN, ISLAMIC REPUBLIC OF, ⁷PET/CT and Cyclotron Center, Masih Daneshvari Hospital, Shahid Beheshti University of Medical Sciences, Tehran, IRAN, ISLAMIC REPUBLIC OF.

Aim: The aim of this study is to model the NeuroPET system using GATE simulation toolkit and compare the simulation result with reported data. **Materials and methods:** The NeuroPET scanner composed of 7 modules, 84 block detector and two LYSO scintillator detector layers in that the two layers are placed with half scintillator pixel offset with respect to each other. Crystal array including 2222 for outer and 21×21 for inner layer. Thickness of each layer is 10 mm and crystals dimension is 2.3 × 2.3 mm². We modeled NeuroPET geometry in GATE environment. An energy threshold of 400-650 keV and a 7 ns coincidence window was selected for the simulations to follow the published experimental results. The energy and timing resolution and dead time was set to real scanner electronic response to obtain accurate results. For absolute sensitivity assessment, a 700 mm line source uniformly Filled with 2.7 MBq 18F

and five concentric Aluminum sleeves around the line source was modeled according to the NEMA NU2-2012. The rate was normalized to the 70 cm line source. Final results were obtained by extrapolating the data to zero thickness using linear regression. To determine NECR, a 700 mm long, polyethylene scatter phantom was simulated. The phantom was centered in the FOV, and the 700 mm line source of F-18 being 45 mm below the transverse center was modeled. The NECR was calculated for different range of activities. In-house C++ code was developed to analyze the Root output from the simulated data. **Results:** Simulation results show that the sensitivity, 7.8 kcps/MBq (versus 7.5 kcps/MBq from experimental results) at center of FOV increases to 9.1 kcps/MBq (versus 8.8 kcps/MBq from experimental results) at a 10 cm center of FOV. The difference of the published experimental results and simulation sensitivities is reproduced to 3.8 and 3.2%, respectively. Also NECR curve was plotted against different activities and maximum NECR of 18.1 kcps was obtained for an activity of 3.1 kBq/ml (versus 19.5 kcps for an activity of 2.9 kBq/ml from experimental results). **Conclusion:** Our results show a good agreement between simulations and published experimental measurements with the NeuroPET scanner. The simulated system also provides insight for our ongoing research to develop brain-dedicated PET scanner with depth of interaction information using similar dual layer detector geometry.

EP770

Contrast Recovery Dependence on Activity Volume for a 1mm³ Resolution Clinical PET System

D. F. C. Hsu, D. L. Freese, D. R. Innes, C. S. Levin; Stanford University, Stanford, CA, UNITED STATES.

We are constructing the world's first 1 mm³ resolution clinical PET system dedicated to locoregional imaging (e.g. breast, head/neck, etc). The edge-on layout of densely-packed 8x8 arrays of 0.9x0.9x0.9 mm³ LYSO crystal elements provides high sensitivity and the capability to position the 3-D coordinates of one or more 511 keV photon interactions per event. In order to understand the ability of this system to visualize and quantify smaller lesions, contrast recovery (CR) performance, which provides a measure of how accurately regions of focal tracer accumulation in the field-of-view (FOV) are reconstructed, must be evaluated before quantitative clinical studies can be performed. Each panel of the built dual-panel system prototype has a sensitive area of 160mm by 33mm by 64mm. A micro-Derenzo phantom, having rods of 1.2/1.8/2.4/3.2/4.0/4.8 mm diameter, with 200 µCi of 18F-FDG, is placed inside an acrylic scattering medium covering the FOV and scanned for 30 minutes. A trimmed dataset of 5 minutes was derived from the original dataset, and 80 iterations of MLEM reconstruction was performed on both datasets with a reconstructed voxel size of 0.5mm. We define cylindrical regions-of-interests (ROIs) with a height of 33 mm and the same diameter as each of the rod sizes. The CR coefficient and normalized standard deviation are calculated as the mean and standard deviation of the voxel intensity in each ROI divided by the mean voxel intensity in the ROI of the 4.8 mm rod. Results show reconstructed CR of greater than 0.5 for 1 mm diameter rods, with the standard deviation in CR decreasing with increasing scan time.

EP771

Triple Head Multi Pinhole Brain SPECT System for striatal imaging

A. Forgács¹, A. Wirth², T. Bükki², J. Pechan³, S. Barna¹, L. Nagy², J. Hopin³, I. Garai¹, A. Verma⁴; ¹ScanoMed Ltd, Debrecen, HUNGARY, ²Mediso Ltd, Budapest, HUNGARY, ³InviCRO, Boston, MA, UNITED STATES, ⁴Biogen, Cambridge, MA, UNITED STATES.

OBJECTIVES: to present the optimization of the scan and reconstruction parameters based on phantom data, and to share the initial clinical experiences of a newly designed and developed triple head multi-pinhole

brain SPECT system optimized for striatal imaging. **METHODS:** helical brain SPECT and Low Dose CT scans were performed for both human and phantom studies. Quantitative image reconstruction was applied, including CT based attenuation correction and Monte-Carlo based scatter correction. Optimization was carried out using an anthropomorphic striatal head phantom filled with 123I solution. Patient preparation was performed following the procedure detailed in European DaTSCAN guideline. For comparison, each patient was also examined on a conventional SPECT system equipped with parallel hole collimators, using the routine clinical protocol. The reconstructed human brain images were registered with additional dedicated brain MR images for improved visual reporting and segmentation. The measurements were quantitatively evaluated using dedicated medical imaging software, with additional visual evaluation of the patient data performed by two experienced medical doctors. **RESULTS:** The acquisition and reconstruction parameters are optimized. The error of activity concentration in the reconstructed image is under 10% in the clinically relevant range of activity concentration of 123I. Qualitatively, the reconstructed human brain images measured by the multi-pinhole brain SPECT system show significant improvement in image quality compared to the images provided by a conventional SPECT system equipped with parallel hole collimators. **CONCLUSION:** The advanced multi-pinhole imaging technology may support higher accuracy for the clinician in the differential diagnosis of movement disorders related to parkinsonian syndromes and essential tremor. The improved image quality also lends itself to the development of a new normal database in the future.

EP772

Novel Cadmium Zinc Telluride (CZT) - based General Purpose Gamma Camera: Clinical Assessment and Comparison with a Standard Camera

Z. Keidar, R. Lugassi, I. Raysberg, A. Frenkel, O. Israel; Rambam Healthcare Campus, HAIFA, ISRAEL.

Objective: To prospectively compare the clinical performance of a newly designed Cadmium Zinc Telluride (CZT) based general purpose gamma camera (CZT-camera), with a standard Sodium Iodide (NaI) based device (NaI-camera). **Methods:** Fifty-five patients (25 men, age range 18 - 86y) referred for Nuclear Medicine procedures were prospectively recruited. The studies included Tc99m-MDP bone scintigraphy (23), one day, gated, rest-stress, single -(Tc99m-MIBI) or dual- (Tc99m-MIBI & Thallium 201) isotope myocardial perfusion imaging (10), Tc99m thyroid (5), Tc99m-MAA lung (4), Tc99m-DMSA renal (6), Tc99m-MIBI parathyroid (4) and Tc99m-HMPAO brain perfusion (3) scintigraphy. All patients underwent the standard scintigraphic procedure according to the specific routine protocol using both the dual head NaI-camera and the CZT-camera with the same acquisition protocols. The studies were performed sequentially at an average of 30 minutes time interval between the acquisitions on both devices. Forty-three patients were scanned on the NaI-camera first and rescanned with the CZT-camera while in 12 patients acquisition was completed first on the CZT-camera followed by imaging on the NaI-camera. Two readers scored all studies in consensus using a 5-point scale (1=non-diagnostic to 5=excellent) for perceived image quality and spatial resolution. The scores obtained for the two devices were compared using the Mann-Whitney test with p<0.05 considered as statistically significant difference. In addition a comparison of the above parameters was performed separately in the subgroup of patients in whom the acquisition was firstly performed on the NaI-camera and in those who were scanned initially on the CZT-camera. **Results:** Overall, 130 studies performed on each device in 55 patients were compared including 85 planar and 45 SPECT studies. The average image quality and spatial resolution scores in the CZT-camera studies were 4.63 and 4.74 respectively. These values were statistically significantly higher than the scores obtained with the NaI-camera (4.40 and 4.25 respectively, p<0.05). The

same statistically significant difference in image quality and spatial resolution scores was found when the CZT-camera images were obtained both after or before the scans on the NaI-camera. **Conclusions:** These initial results suggest that the CZT-based general purpose gamma camera has a higher diagnostic performance as compared to the standard NaI-based camera when using the same acquisition parameters. Future studies will assess whether time reduction and/or a decrease in the injected dose can be implemented for the CZT-camera acquisition protocols without any compromise in image quality and subsequent diagnostic accuracy.

EP773

Multimodal 4D cardiac imaging with the preclinical IRIS PET/CT scanner

N. Belcarì^{1,2}, N. Camarlinghi^{1,2}, D. Panetta³, P. Iozzo³, S. Burchielli⁴, P. A. Salvadori³, G. Sportelli^{1,2}, A. Del Guerra^{1,2}; ¹University of Pisa, Pisa, ITALY, ²INFN, Pisa, ITALY, ³Institute of Clinical Physiology (IFC) CNR, Pisa, ITALY, ⁴CNR/Tuscany Foundation “G. Monasterio” (FTGM), Pisa, ITALY.

Aim Cardiac phase-correlated (4D) imaging is employed in small animal models of cardiovascular diseases (CVD). When 4D-PET and 4D-CT are combined together, a comprehensive view of the cardiac function and morphology is obtained, allowing a motion artifact-free quantification of PET tracer regional distribution in the myocardium along with LV regional kinetics. This work presents the results of 4D-PET/CT imaging of small animals obtained with the IRIS PET/CT scanner (Inviscan, France). **Materials and methods** The PET component of the IRIS scanner consists of 16 modular detectors arranged in two octagonal rings. The PET field-of-view is 95mm axial × 80mm diameter. PET images are reconstructed with 3D-OSEM. The CT section is equipped with a X-ray source with tungsten anode (35-80kV, 80W) and a flat-panel CMOS-based detector. The FOV diameter of the CT is 90mm, and the maximum FOV length is 110mm. CT images are reconstructed using a Feldkamp algorithm. The PET ring and the CT components are placed on the same rotating gantry having a total rotation range of [+190°; -190°]. The offset between the centers of the PET and CT fields of view (FOV) is 120mm. For PET imaging ECG gating is used to extract the individual cardiac phases. The gating signal from the physiological monitoring system (SA instrument Inc. Model 1030) was fed into the PET acquisition system. For each cycle, 8 equally spaced frames are produced and then retrospectively rearranged to generate list-mode files corresponding to an equal number of phases. Respiratory gating is also applied, excluding from the list-mode file all events recorded in the end-inspiration phase. For CT, the gated scanning protocol consisted in a multi-arc rotating acquisition with 1000-20000 projections over the entire rotation (360°), with a total scan times from 2 to 6 minutes. The absorbed dose was 200-400 mGy. The physiological signals are derived analyzing the projection data, and the cardiac cycle was partitioned in 8-40 frames. Each projection was assigned to one or more cardiac phases with proper weights, excluding all projections in the end-inspiration respiratory phase. **Results and Conclusions** Phase-correlated cardiac images have been obtained on mice and rats with the IRIS scanner for both PET and CT modality. Multimodal 4D-PET/CT cardiac images are presented, along with example of quantification of cardiac morphofunctional parameters.

EP774

Clinical Results from a Novel CZT-based Digital SPECT System

E. Goshen¹, E. Stern², R. Goldkorn¹, S. Ben Haim¹; ¹Chaim Sheba Medical Center, Ramat Gan, ISRAEL, ²Molecular Dynamics, Caesarea, ISRAEL.

PURPOSE: Cadmium-Zinc-Telluride (CZT)-based digital gamma cameras can provide improved image resolution and greater sensitivity,

thereby allowing faster acquisitions and/or reduced administered dose compared to standard scintillator-based analog (Anger) systems. Evaluation of clinical feasibility, image quality, and diagnostic performance of a prototype of a novel CZT-based digital SPECT general purpose camera was performed. Results were compared to analog SPECT studies of the same patients. **MATERIALS AND METHODS:** The digital SPECT system (Valiance X12 prototype, Molecular Dynamics, Hamilton, Bermuda) is equipped with CZT detectors, fitted with a high-sensitivity collimator and mounted on a ring shaped gantry. The detectors are capable of independent motion to acquire data from multiple angular views. The flexible architecture also enables focusing the detection units on a specific region of interest to obtain enhanced images of a specific target. Data are reconstructed using an iterative reconstruction algorithm. Twenty-three digital SPECT scans were performed immediately following analog SPECT in 20 patients (14M, age 26-74yrs). The group consisted of 5 Tc-99m ECD brain scans, 2 Tc-99m MAA lung perfusion studies and 1 Tc-99m HMPAO labeled leukocyte study, while 12 patients underwent a total of 15 Tc-99m MDP bone studies (knees (n=7), lumbar spine/pelvis/hips (n=4) and ankles/feet (n=4)). Both sets of images were compared by experienced Nuclear Medicine physicians and were graded on a scale of 1 (poor) to 4 (very good) for sharpness, contrast, overall quality and diagnostic confidence. **RESULTS:** Digital SPECT studies were all diagnostic and were of good or very good quality. Mean grades for digital SPECT exceeded those of analog SPECT for sharpness (3.7 vs. 3.1), and contrast (3.9 vs. 3.3). Overall image quality and diagnostic confidence of digital and analog SPECT were comparable (3.7 vs. 3.6, and 3.8 vs. 3.9, respectively). **CONCLUSION:** The results indicate improved contrast and sharpness of digital SPECT compared to analog SPECT in several clinical settings. General purpose digital SPECT with high sensitivity collimators, together with improved sharpness and contrast as compared to analog SPECT technology are expected to have significant clinical impact. Further research will assess other general nuclear medicine applications, as well as the contribution of focused imaging, a unique capability of this CZT-based digital SPECT system.

EP775

Comparison of 3/8" and 5/8" NaI(Tl)-scintillation crystal (NaI) efficiency for different radioisotopes

C. Hoppel, M. Groothuis, A. Mader, B. Bockisch, F. Grünwald, W. T. Kranert; University Medical Center, Frankfurt, GERMANY.

Introduction: For scintillation cameras different NaI are available commercially. Common thickness of NaI for general purposes is 3/8". Thickness used to be attended by an improvement of efficiency, especially for high energy radionuclides due to the higher probability of interaction. Therefore, 5/8" NaI are available as well. Aim of this study was to evaluate the improvement in efficiency. **Material and Methods:** Measurements were performed on two identical uncollimated scintillation cameras (DST-XL/-XLi; GE) equipped with a 3/8" NaI and a 5/8" NaI respectively using ⁵⁷Co, ^{99m}Tc, ¹³¹I and ¹⁷⁷Lu due to their predominant use in nuclear medicine. Samples were placed centric on the lower detector with a distance of 68 cm to the upper detector. As ⁵⁷Co sample a calibration point source, for ¹³¹I sample a test capsule was used. ^{99m}Tc and ¹⁷⁷Lu were dissolved in liquid solution (50 µl). Doses ranged from 0.36 to 2.9 MBq. A 512x512 acquisition matrix and corresponding energy windows were used. Evaluation was performed by ROI analysis of the central field of view (56x56 pixel) due to the best comparability to the geometric conditions of a parallel hole collimator. **Results:** Efficiency was calculated decay and background corrected in [cps/kBq]. Efficiencies of the 3/8" NaI were 42 for ⁵⁷Co, 34 for ^{99m}Tc, 2.3 for ¹⁷⁷Lu (208 keV) and 7.9 for ¹³¹I respectively. In contrast, efficiencies of the 5/8" NaI were 47 for ⁵⁷Co (13% improvement), 40 for ^{99m}Tc (16%), 2.9 for ¹⁷⁷Lu (24%) and even 12 for ¹³¹I (49%). **Conclusion:** Due to different modes of decay, efficiencies are not directly comparable, but the percentage of

improvement is. For high energy isotopes, efficiency is significantly improved by the $5/8''$ NaI. Especially for ^{131}I -scans (370–1,100 MBq), an almost 50% improvement in efficiency leading to considerably improved count statistic and therefore image quality justifies the higher prizes of the $5/8''$ NaI. For diagnostic purposes with $^{99\text{m}}\text{Tc}$, a $3/8''$ NaI is adequate.

EP776

Detector performance evaluation for Cerenkov luminescence imaging

E. Ciarrocchi^{1,2}, N. Belcari^{1,2}, P. A. Erba³, A. Del Guerra^{1,2}; ¹Department of Physics, University of Pisa, Pisa, ITALY, ²INFN, Pisa, ITALY, ³Department of Translational Research and New Technologies in Medicine and Surgery, Azienda Ospedaliera Universitaria Pisana, Pisa, ITALY.

We are looking for a method for Cerenkov luminescence imaging to provide the absolute quantitative information on the source activity concentration. We believe that this goal can be obtained with the combination of a quantitative detection system and a Monte Carlo model to reconstruct the source activity from the measured signal. To this aim we are investigating the performances of two photodetectors, a conventional charge coupled-device (CCD) and an electron multiplying CCD (EMCCD) during Cerenkov luminescence measurements. Our final goal is to demonstrate that the number of photons impinging on the detector can be recovered from the measured quantity, and that the source activity can be reconstructed from this number with the Monte Carlo code. We are acquiring images with a lens in a light-tight box, with simple geometries that will be easily simulated to determine the quantitative capabilities. Two Na-22 point sources embedded in a 23.5 mm x 11 mm x 2 mm clear Plexiglass plate, with activity of 7 kBq and 15 kBq respectively, were imaged with both CCDs for exposure times between 1 and 5 minutes (reasonable for *in-vivo* applications). Preliminary results suggest that the EMCCD is more sensitive than the conventional CCD, since the EMCCD was able to detect the 7 kBq source by the Cerenkov radiation produced in its container, while the conventional CCD was able to detect only the 15 kBq source in the same experimental conditions. Lower and intermediate levels of Na-22 activities were not investigated. These two sources will be used also to study the spatial resolution of the two detectors. The measurements were repeated with F-18 diluted in 3 ml of water, and the minimum detectable activity with the EMCCD in this geometry was approximately 0.5 kBq, while lower activity levels produced a signal that depended on the acquisition settings (the differences between signals varied more than 20% with acquisition settings such as binning, exposure time and multiplication gain). To determine quantitatively the absolute number of photons impinging on the detection system, we will repeat the measurements with a set of filters and with a pure β^- emitter, to reduce uncertainties on experimental factors like the sensor efficiency and the focusing optics transmission and to remove noise due to high energy photons coming from the source. This experimental result for both CCDs will be compared with Monte Carlo predictions.

EP777

Image-based method for estimation of global calibration factor for SPECT images

A. Halty^{1,2}, J. N. Badel², D. Kryza³, A. L. Giraudet², D. Sarrut^{1,2}; ¹CREATIS, Villeurbanne, FRANCE, ²Centre Leon Berard, Lyon, FRANCE, ³LAGEP, Lyon, FRANCE.

Aims: Calibration is a key factor to perform quantification on SPECT images for dosimetry in Targeted Radionuclide Therapy (TRT). We investigated a new method to estimate a global calibration factor directly from image data, adapted to each patient and to the image acquisition

configuration, without requiring additional phantom acquisition. Materials and Method: We proposed to estimate the calibration factor (cps/MBq) by the total number of counts in the SPECT image divided by the patient total activity weighted by the Fraction of Activity in the FOV (FAF). The FAF corresponds to the percentage of the total activity inside the limited SPECT FOV. First, the dimensions and localisation of the SPECT FOV were projected onto the planar images, and the FAF was estimated by the number of counts in this FOV divided by the total number of counts. The total activity within the patient was estimated by the injected activity. This method was applied on 12 patients involved in a TRT clinical trial. The patients were intravenously injected with 187 ± 18 MBq of ^{111}In -OTSA101, a radiolabeled monoclonal antibody targeting a transmembrane receptor overexpressed in synovial sarcoma and developed by OncoTherapy Science. The SPECT/CT and whole-body planar scintigraphic (anterior and posterior) acquisitions were performed one hour post-injection. The SPECT FOV covers 92cm of the patient. The planar acquisitions were corrected for dead-time and scatter. The geometric mean was applied and the attenuation correction was performed by estimating the patients' thickness from the CT. Since the CT was not whole-body, the missing part, covering the inferior limbs, was estimated by extrapolation of the patient's legs thickness. SPECT images were reconstructed using attenuation corrected OSEM algorithm, and were also corrected from dead-time and scatter. Images were acquired before the urination of patients which limits strongly biological elimination. Patient-specific calibration coefficients were compared to those obtained by conventional source-based calibration. Results: The FAF varied from 76% to 92%. Among patients, the coefficient of variation of patient-specific calibration factor was reasonably low (4.32%). Source-based calibration estimated activities in the SPECT FOV 27% higher than our patient-specific calibration. It would mean that 105% of total injected activities is present in the SPECT FOV, which is unlikely. Conclusion: Image-based estimation of a global calibration factor may provide patient-specific calibration, adapted to the clinical configuration, without the need of an additional phantom acquisition. It only requires a whole-body planar scintigraphy and to prevent patient biological elimination.

EP-43 – Sunday, October 16, 2016, during Exhibition hours, e-Poster Area
Physics & Instrumentation & Data Analysis: Miscellaneous

EP778

Breast-Torso Phantom for Bimodal Nuclear-Optical Imaging Research

J. Peter; German Cancer Research Center, Heidelberg, GERMANY.

Objective: To propose an anthropomorphic breast-torso phantom for Monte Carlo simulation of radiolabeled (SPECT, PET, PEM) and/or near-infrared fluorescent tracer distributions for breast imaging research applications. **Methods:** The phantom consists of an upper torso including lungs (with optional respiratory motion dynamics affecting geometry of all organs), heart (with optional cardiac movement), liver, gallbladder, kidneys, rib cage, sternum, spine, and various breast attachments for prone as well as mammography specific geometries. There are various options for incorporating simple-geometry tumor lesions. To enable direct, un-discretized comparison of simulation results with experimentally acquired data of the same phantom geometry, planned at a later stage of this scientific project, phantom geometry is represented solely by superquadric shapes. Analytic shape representation has also been chosen because intersection calculations of photon trajectories with all involved surfaces can be performed in simulations at exceptional accuracy at comparatively low computational cost. All solids can be freely parameterized (e.g. radiotracer/energy distribution, fluorochrome/wavelength distribution, scatter and attenuation coefficients for light photon propagation). **Results:** Monte Carlo simulations have been performed for whole-body

(SPECT, PET) and dedicated breast imaging systems. For SPECT, cameras following arbitrary application-specific orbits were included for simulation. For PEM, simulation design was being tailored particularly towards the clearPEM system. Fluorescence optical imaging was simulated for conventional light cameras and, for the first time, for novel plenoptic detectors allowing for three-dimensional optical imaging. Photon trajectories were resolved with no discretization error involved which is particularly crucial for light photon propagation abandoning the breast and thorax shapes. **Discussion:** The proposed breast-torso phantom constitutes an intentional compromise between anthropomorphic realism on one hand and its intended use for prevailing imaging research such as the development and validation of bimodal image reconstruction algorithms or the optimization of data acquisition management involving either type of labelling component. Simulation setup, specifically phantom definition and modification, is straightforward as phantom shapes are being defined only by 5 or 7 geometric parameters, each, and is exact also with respect to predefined organ/tumor volumes because of the analytical phantom model. The anthropomorphic breast-torso phantom can be used directly within Monte Carlo simulation codes that accept super-quadric shape representation. The simulation code at hand is, in addition to tomographic and higher-order point mesh representation models, suitable for including super-quadric shapes. However, a discretization routine has been developed such that researchers can employ the breast-torso phantom in a voxelized form as well.

EP779

Semi-automated CT Image Segmentation Provides Accurate LBM Measurements

J. Devriese¹, L. Beels², A. Maes², C. Van de Wiele², H. Pottel¹; ¹KU Leuven campus Kulak, Kortrijk, BELGIUM, ²AZ Groeninge, Kortrijk, BELGIUM.

Aim Standardized uptake value (SUV), a semi-quantitative parameter used in positron emission tomography/computed tomography (PET/CT), is defined as the ratio of measured radioactivity concentration to the injected dose per distribution volume unit. It is usually normalized for body weight (BW) and other proposed normalizations include e.g. lean body mass (LBM) since ¹⁸F-FDG distribution in fatty tissues is limited. LBM can be estimated by predictive equations or measured by e.g. CT. Since cancer patients often experience weight loss during treatment or disease progression, their body composition may vary. LBM estimated by predictive, generalizing, equations may therefore introduce error at individual patient level. Accurate individual LBM measurements through CT might lead to more accurate and reproducible LBM, and consequently more accurate and reproducible LBM-normalized SUVs. The goal of this study was to segment human CT images into tissue types based on Hounsfield unit (HU) thresholds, and to test the validity of the LBM thus obtained. **Materials and methods** PET/CT examinations covering head to toe were retrospectively retrieved and semi-automatically segmented into tissue types based on thresholding of CT HU. The following HU ranges were used: 180 to 7 for adipose tissue (AT), 6 to 142 for LT, and 143 to 3010 for bone tissue (BT). Total body volumes (V) per tissue type were determined and tissue masses calculated, using tissue densities of 0.90, 1.05, 1.85 kg/L for AT, LT, and BT, respectively. Besides these literature tissue densities, other coefficient sets were determined through regression in order to compensate for e.g. partial volume effect (PVE) and uncertainty concerning bone tissue density. The segmentation method was validated in an independent dataset by comparing patient BW to total CT-estimated BW (BW_{CT}). **Results** Three regression equations were tested in an independent dataset, of which BW_{CT}(kg)=0.95*AT+0.99*LT+2.11*BT yielded the best results. Comparison of actual BW to BW_{CT}, shows a non-significant bias of 0.8 kg (95%CI: -1.3 to 4.1), with R² = 0.989, RMSE = 1.626 and Lin's concordance correlation coefficient (CCC) = 0.993. **Conclusion**

Although this is not a direct validation of our method, we are convinced that our segmentation method can reliably be used to accurately estimate AT, LT, and BT, and thus LBM, from CT images.

EP780

Tele Nuclear Medicine : Comparison of data transfer methods

W. PILLOY, V. Kritzinger, A. Van Niekerk, B. Ramjee; KVNR, Pretoria, SOUTH AFRICA.

Aim: To determine the advantages and disadvantages of three telemedicine methods, in terms of data transfer and compatibility. The issue of the transfer and storage of clinical data is not dealt with here. **Material and methods** Multi-sites private Nuclear Medicine (NM) firms collect NM data from various types of machines. Three telemedicine options are compared: P to P transfer; remote desktop; cloud computing. **P to P transfer of data:** Acquisition of data on a workstation and transfer to another workstation for processing and reporting. **Remote desktop:** One workstation accesses another workstation AND interacts with it. Two options: Remote desktop through direct (VNC) access to the framebuffer of the other station, and Remote desktop through Teamviewer™ (TV) proxy servers **Cloud computing:** Remote sites send their data to a central server; data can be accessed (thin client :VNC-like) by several users (floating licences). Servers can be local (Intranet) or remote (Internet). Experience based on Hermes. **Results: P to P: Disadvantages:** Requires some level of standardization between the sites- same dataset name & specifications; same software; standard identification of patient. **Advantages:** Speed, bandwidth, stability of the network is irrelevant (transfer is a background task). Screen size & resolution and processing power & speed of a workstation. Acquisition and interpretation on two distinct systems: no “cross-lines”. Duplication of archives **Remote desktop: Disadvantages:** Multiple interactions with the (acquisition) station: possibility of “cross-lines”, at the risk of confusing patients or data. VNC and TV image quality drops with low bandwidth: poor image resolution, refreshing rate, and control of commands. Cheap option: reporting often done on a monitor of small size with poor graphic card. Images spill over the edges and must be constantly shifted to see the whole picture. Archiving at the site of acquisition and no central archive **Advantages:** Reporting doctor can directly see the patient's images during the acquisition. No issue of compatibility of software **Cloud computing: Disadvantages:** Expensive system. Possible network problems (Internet) **Advantages:** Safety of the central storage of data on a secure server. All data processed by software stored on secure server. Always up to date software (Hermes: very flexible). Powerful database management system also checking patient ID. No cross-lines (floating licenses). **Conclusion:** Cloud computing is the better option, with the server close to the computer of the reviewing doctors. An add-on Remote Desktop option allows visualization of the acquisition.

EP-44 – Sunday, October 16, 2016, during Exhibition hours, e-Poster Area
Physics & Instrumentation & Data Analysis: Quality Control, Performance and Standardisation

EP781

Comparison of Ejection Fraction Values Measured by G-SPECT Studies with a use of Dynamic Heart Phantom Performed Both on Scintillation Gamma Camera and CZT Scanner

A. Budzynska¹, J. Gawel², I. Glowacka², M. Dziuk¹, D. Kluszczyński²; ¹Military Institute of Medicine, Warsaw, POLAND, ²National Centre for Radiation Protection in Health Care, Łódź, POLAND.

Aim: To optimize the procedure of evaluation of functional parameters of myocardial G-SPECT on the base of phantom studies and to test accuracy

of quantification algorithms available in different commercial applications for different types of cameras. **Material/Methods:** The dynamic heart phantom with automatic application assembly was used for 49 G-SPECT studies. Acquisitions were done on CZT solid-state scanner with ejection fraction (EF) settings from 45% to 70% (increment by 5%) and heart rate (HR) from 40 to 80 beats/min (increment by 10 beats/min). On standard SPECT-CT gamma camera one series of measurements programmed for 50 beats/min was acquired. All studies were performed with standard acquisition protocols. Data from SPECT-CT system were reconstructed with CT based attenuation correction. Two applications: Myometrix and Quantitative Gated SPECT (QGS) available on Xeleris workstation, were used for processing. **Results:** EF values [%] estimations were comparable with the phantom reference settings (mean absolute error was -0.54%; $p < 0.05$) for CZT scanner and QGS application. Estimations done with Myometrix were significantly underestimated (mean absolute error was -7.6%; $p < 0.05$) EF underestimation resulted from both lower end-diastolic volume (60.4 vs. 62.8; $p < 0.05$) and higher end-systolic volume (29.9 vs. 26.7; $p < 0.05$). Results of EF estimations for SPECT-CT gamma camera for QGS were significantly overestimated. For the same studies results from Myometrix, were comparable to the phantom settings (mean absolute errors were 6.5% and -0.3% respectively; $p < 0.05$). Overestimations were results of higher end-diastolic volume (47.2 vs. 43.7; $p < 0.05$), the differences in the end-systolic volume were not significant. Researches didn't observe relation between EF and heart rate ($p > 0.1$). **Conclusions:** Clinical interpretation of functional parameters of myocardial G-SPECT should be performed with awareness of correlation between acquisition system and processing software.

EP782

The influence of ^{18}F in ^{111}In images in dual isotope preclinical SPECT

J. de Swart, M. Segbers, M. W. Konijnenberg, M. de Jong, M. R. Bernsen; Erasmus MC, Rotterdam, NETHERLANDS.

Aim: Multi-pinhole preclinical scanners are capable of simultaneous imaging over a wide energy range. Imaging ^{18}F and ^{111}In simultaneously, inevitably creates down scatter from ^{18}F into the ^{111}In energy windows. We investigated the presence of ^{18}F on absolute quantification, resolution and contrast of the ^{111}In images in phantom studies. **Methods:** All experiments were performed with the VECTor (MILabs, Utrecht, the Netherlands). A 30mL plastic syringe was filled with 4.66mL water (solution) containing 17.0MBq [^{111}In]-diethylenetriaminepentaacetic acid ([^{111}In]-DTPA) and 73.2MBq 2-deoxy-2-[^{18}F]fluoro-D-glucose ([^{18}F]FDG) to determine camera sensitivity. The syringe was scanned in list mode for 16 frames of 45 minutes. A micro Jaszczak phantom with hollow rods (diameter range 0.7 - 1.5mm) was filled with 47.2MBq [^{111}In]-DTPA and 114.8MBq [^{18}F]FDG. It was scanned for 7 frames of 45 minutes to determine resolution by visual assessment. The ^{111}In energy window (171 and 245keV, width 20%, summed) and the ^{18}F energy window (511keV, width 16%) was reconstructed separately for all images. Scatter, including down scatter of ^{18}F , was corrected by using the triple-energy-method. 7keV, 10keV and 17keV scatter windows were placed adjacent to the 171keV, 245keV and 511keV energy window respectively. All images were iteratively reconstructed using the POSEM algorithm, 30 iterations, 4 subsets and 0.4mm voxel size. By drawing ROIs in ('hot') and between the rods ('cold') (1.0, 1.2 and 1.5mm) on the Jaszczak images contrast C was calculated using the formula $C = (\text{hot-cold}) / (\text{hot} + \text{cold})$. **Results:** From the syringe scans the measured ^{111}In activity in each frame was compared to the known activity (recovery coefficient (RC)), and was related to the $^{18}\text{F}/^{111}\text{In}$ ratio in radioactivity. The RC was within $\pm 10\%$ compared to the single ^{111}In RC for a $^{18}\text{F}/^{111}\text{In}$ activity-ratio ≤ 1 . A ratio > 1 showed a rise of the RC up to 1.66 at a ratio of 4.3. All rods were visible on the Jaszczak images using the ^{111}In window but with a noticeable higher background from a $^{18}\text{F}/^{111}\text{In}$ activity-ratio of 1.1 and higher. Contrast values were comparable for all measured rods and decreased from 0.87 at the lowest to 0.77 at the highest ratio.

Conclusion: The influence of ^{18}F in the ^{111}In images was limited when the activity of ^{18}F was lower or comparable to the activity of ^{111}In . Higher relative activity of ^{18}F lead to errors in absolute quantification of ^{111}In and decreased the image contrast. Triple energy window correction may be insufficient for (down) scatter correction for this activity ratio.

EP783

NEMA and Gaussian fit results for spatial resolution determination in PET

A. Attarwala¹, D. Hardiansyah¹, C. Romanó¹, M. Roscher², B. Wängler², G. Glatting¹; ¹Medical Radiation Physics/Radiation Protection, Universitätsmedizin Mannheim, Medical Faculty Mannheim, Heidelberg University, Mannheim, GERMANY, ²Molecular Imaging and Radiochemistry, Institute for Clinical Radiology and Nuclear Medicine, Medical Faculty Mannheim, Heidelberg University, Mannheim, GERMANY.

Aim: The National Electrical Manufacture Association (NEMA) based method to determine the spatial resolution of a system does not take into account the spatial distribution, quality check of the fitting and error of the estimated full width at half maximum (FWHM). A procedure based on three-dimensional Gaussian functions is investigated to develop a step-by-step approach to accurately determine the spatial resolution of a device. **Materials and Methods:** The spatial resolution of the ALBIRA II PET (Bruker BioSpin MRI GmbH, Ettlingen, Germany) sub-system was determined using a 370 kBq ^{22}Na point source. The measurement data were reconstructed with a maximum likelihood expectation maximization (MLEM) algorithm. Spatial resolution was calculated based on the NEMA NU-4 2008 protocol and the alternative method based on three 3-dimensional fitting functions: a 3-dimensional Gaussian function (3D Gauss) and convolutions of this function with pixel size (3D Gauss_p) of 0.5 mm and with the spherical source dimension of \varnothing 0.25 mm (3D Gauss_s). The Akaike information criterion (AIC) and Akaike weights were used for choosing the best-fit function. Simulation of convolutions between a mathematical source with Gaussian distributions using the FWHMs from all methods were performed to see the effect of calculated FWHMs on image quantification. **Results:** Based on the NEMA protocol, the FWHM in x, y and z directions were 1.68, 1.51 and 1.50 mm. The corresponding results using 3D Gauss and 3D Gauss_s functions were 1.87 ± 0.01 , 1.70 ± 0.01 and 1.50 ± 0.01 mm and for 3D Gauss_p were 1.84 ± 0.01 , 1.67 ± 0.01 and 1.47 ± 0.01 mm. All coefficients of variances of the fitted parameters were $\leq 0.50\%$ and the adjusted R² values were ≥ 0.98 . Based on Akaike weights, all 3D Gauss methods were similarly supported by the data. The simulation study showed relative error in quantification of spherical lesions up to 22 % with the FWHM calculated from the NEMA method. **Conclusion:** An alternative method to calculate the spatial resolution to overcome shortcomings of the NEMA methodology was demonstrated. The proposed methods include fitting of three dimensional functions, validation of fitting quality and choosing the best function based on the distribution of the data along with an estimation of the uncertainty. The corrections for pixel size and source dimensions would become more relevant for larger dimensions and should then be included in the calculation of the FWHM.

EP784

Method for spatial resolution description in preclinical PET using a sum of Gaussian functions

A. Attarwala¹, D. Hardiansyah¹, C. Romanó¹, M. Roscher², B. Wängler², G. Glatting¹; ¹Medical Radiation Physics/Radiation Protection, Universitätsmedizin Mannheim, Medical Faculty Mannheim, Heidelberg University, Mannheim, GERMANY, ²Molecular Imaging and Radiochemistry, Institute for Clinical Radiology and Nuclear Medicine, Medical Faculty Mannheim, Heidelberg University, Mannheim, GERMANY.

Aim: A method to determine the spatial resolution of a device based on multiple three-dimensional Gaussian functions, taking into account the complete data distribution, was investigated as an alternative to the currently used NEMA NU-4 protocol. **Materials and Methods:** A 370 kBq ^{22}Na spherical point source with a diameter of 0.25 mm was used to determine the spatial resolution of the ALBIRA II PET (Bruker BioSpin MRI GmbH, Ettlingen, Germany) sub-system. Image reconstruction was performed with a maximum likelihood expectation maximization (MLEM) algorithm. The full width at half maximum (FWHM) was calculated based on the NEMA NU-4 2008 protocol and the alternative method based on multiple three 3-dimensional fitting functions: a single 3-dimensional Gaussian function (3D Gauss₁), the sum of two 3-dimensional Gaussian functions (3D Gauss₂) and the sum of three 3-dimensional Gaussian functions (3D Gauss₃). The Akaike information criterion (AIC) and Akaike weights were used for choosing the best-fit function. A mathematical source simulation study was performed to see the effect of the spatial resolution model function calculated from the two methods on image quantification. **Results:** The FWHM based on the NEMA protocol in the x, y and z orientations were 1.68, 1.51 and 1.50 respectively. The corresponding values using the alternate method were 1.87±0.01, 1.70±0.01, 1.50±0.01 (3D Gauss₁), 1.78±0.01, 1.74±0.01, 1.83±0.01 (3D Gauss₂) and 1.76±0.03, 1.72±0.03, 1.78±0.03 (3D Gauss₃), respectively. Coefficients of variance of the fitted parameters were ≤ 29 % and the adjusted R² were ≥ 0.99. Based on Akaike weights, the 3D Gauss₃ function showed the highest probability to describe the data. The simulation study showed relative error in quantification of spherical lesions up to 46 % with the FWHM calculated from the NEMA method. However, no relevant difference in quantification was observed between the 3D Gauss₂ and 3D Gauss₃ functions. **Conclusion:** Different mathematical model functions for calculating the spatial resolution were investigated. The proposed methods include fitting sum of three dimensional functions to take into account the non-Gaussian tail, validation of fitting quality and choosing the best function based on the distribution of the data along with an estimation of the error. At least two Gaussian functions should be used to describe a point source when determining the spatial resolution of the system for quantification studies.

EP785

Multicentric ^{68}Ge phantom-based evaluation of quantification reproducibility with Block Sequential Regularized Expectation Maximization (BSREM) algorithm in PET

E. De Ponti¹, S. Morzenti¹, D. Vallot², C. Spadavecchia¹, O. CASELLES²; ¹Medical Physics Department - ASST, MONZA, ITALY, ²Institut Claudius REGAUD -IUCT Oncopole, TOULOUSE, FRANCE.

Aim: Accurate and reproducible SUV measurements in PET imaging are becoming mandatory for assessing therapy response and for reliable detection of lesion's uptake changes over time. The BSREM algorithm allows to reach full convergence without the detrimental effects of excessive noise found with OSEM and consequently with higher reproducibility in SUV quantification in small lesion. The performance of this regularized algorithm was evaluated in a phantom study in two European Centres. **Material and methods:** Acquisitions were performed with a ^{68}Ge -NEMA phantom based on standard NEMA-IQ phantom body, which adheres to the dimensions of NEMA-IQ phantom prescribed in the NEMA-NU2-2012 standard. Phantom filling was done by Eckert & Ziegler Isotope Products Inc. and fillable spheres were replaced with wall-less spheres of ^{68}Ge . The ratio of sphere to background activity was 4:1 and the lung insert was filled following the phantom manufacturer's procedure. Phantom was acquired 5 times in 5 different days with different repositioning and for each phantom positioning 5 iterations were acquired. Data from 25 different acquisitions for each Centre were averaged to evaluate statistical variability. NEMA-NU2-2012 contrast recovery (CR), background variability (BKG) and lung error from standard

OSEM and BSREM algorithm reconstructions were compared. **Results.** Results for all spheres are presented. 10mm sphere: CR was 39.0±4.6 and 29.1±3.8; BKG 9.3±0.9 and 8.5±0.9 (difference 9%) for BSREM and OSEM algorithms respectively. 13mm sphere: CR was 53.5±6.1 and 43.0±4.9; BKG 7.6±0.8 and 6.7±0.7 for BSREM and OSEM algorithms respectively. 17mm sphere: CR was 61.0±4.6 and 53.4±4.0; BKG 5.8±0.6 and 5.2±0.5 for BSREM and OSEM algorithms respectively. 22mm sphere: CR was 68.0±3.3 and 61.1±2.5; BKG 4.4±0.5 and 4.0±0.4 for BSREM and OSEM algorithms respectively. 28mm sphere: CR was 77.1±2.3 and 67.4±1.7; BKG 3.3±0.5 and 3.2±0.3 for BSREM and OSEM algorithms respectively. 37mm sphere: CR was 83.7±1.3 and 74.9±1.2; BKG 2.6±0.3 and 2.6±0.2 for BSREM and OSEM algorithms respectively. Lung error was 12.5±0.4 and 16.9±0.4 for BSREM and OSEM algorithms respectively. Anova test presented p<0.0001 for differences between BSREM and OSEM for all comparison. Coefficient of variability for CR was between 11% and 13% for 10mm and 13mm and less than 8% for bigger spheres. Coefficient of variability for BKG was between 9% and 15% for all spheres. **Conclusion:** CR were 11% to 38% higher with BSREM compared to OSEM algorithm while BKG remained statistically the same. Good reproducibility for both methods is probably associated to the high sensitivity scanners used for acquisitions.

EP786

Metrics for Assessing Quantitative Accuracy of PET/CT Systems

D. Byrd¹, S. Wollenweber², A. Alessio¹, C. Stearns², P. E. Kinahan¹; ¹University of Washington, Seattle, WA, UNITED STATES, ²GE Healthcare, Waukesha, WI, UNITED STATES.

The quantitative accuracy of PET/CT systems is typically not characterized or reported in a meaningful manner. We have developed quantitative performance measurements that relate to estimation of uptake of radiotracers by lesions for typical ^{18}F -FDG-PET/CT oncology scans. **METHODS:** We used the IEC 61675-1 / NEMA NU-2 body phantom, but activated with $^{68}\text{Ge}/^{68}\text{Ga}$ in epoxy, to enable estimation of ensemble variance across multiple scans. The activity level was 2.6 kBq/ml, roughly equivalent to a background SUV of 0.72 for a 370 MBq injection of ^{18}F -FDG followed by a 60 min uptake period. The sphere diameters were 10, 13, 17 and 22 mm, with an SUV of 2.75. Images were reconstructed using multiple reconstruction algorithms, including regular OSEM with eight iterations, OSEM with detector point-spread-function (PSF) modeling, and a convergent algorithm (BRSEM). We evaluated absolute and relative recovery coefficients (RCs), standard deviation (SDEV) using repeated scans and the IEC and NEMA protocols, the root-mean-square-error (RMSE), and total deviation index. The proposed measurements were evaluated using two time-of-flight PET scanners. The scanners used similar crystal sizes, but different timing resolutions (550 vs. 380ps) and axial length (15 vs. 25cm). The longer scanner utilized silicon photomultiplier technology. The 25cm system had a sensitivity that was approximately 3-fold higher than the reference system. Sets of 50 repeated scans of 2.5 min each were acquired on both systems. **RESULTS:** For mean regions of interest values, the least bias was with BRSEM, followed by OSEM+PSF, then OSEM. In all cases the bias was less for the 25cm+380ps system. The results for SDEV were consistent, although there were some variations. The summary RMSE values followed the same trends, ranging from 12% to 14.5% for the 10mm diameter sphere, down to 6% to 11% for the 23mm sphere. When image roughness noise was matched, the variability of the recovery coefficients for the spherical test objects was reduced by 33% for the 25cm+380ps system, averaged over a range of reconstruction parameters. **CONCLUSIONS:** These tests provide a clinically relevant methodology for comparing performance of current and next generation PET systems. As expected, the 25cm system with improved sensitivity and TOF timing resolution, but roughly equivalent crystal sizes, showed improved quantitative accuracy: 33% reduction in

estimation variability, and a 50% noise reduction for matched resolution. These tests and comparisons could be used to augment standards specifically for performance assessment of the quantitative accuracy of PET/CT scanners.

EP787

Optimization of acquisition and reconstruction parameters of combined CT angiography and 18F-NaF PET for preclinical assessment of vascular mineralisation in mice

G. Rucher¹, L. Camelière¹, A. Abbas², D. Nicolas³, A. Manrique¹; ¹EA4650, Université de Caen Normandie, Caen, FRANCE, ²Inserm UMR-S1077, Université de Caen Normandie, Caen, FRANCE, ³CNRS UMS 4308 - GIP Cycleron, Caen, FRANCE.

Introduction. Preclinical assessment of bone 18F-NaF uptake requires co-registration of high resolution anatomical and functional modalities. The aim of this study was to optimize acquisition and reconstruction parameters to favour the spatial resolution for both modalities. **Material and methods.** A custom-made resolution phantom consisting of 5 longitudinal line sources at 1-cm intervals filled with a 18F solution was imaged using a dedicated preclinical PET-CT (Inveon, Siemens). A 600 sec list mode acquisition was performed with low dose CT for attenuation correction, and reconstructed using filtered backprojection (FBP) and 3D-OSEM (4, 8 and 16 iterations), with and without scatter correction and with and without reconstruction zoom (factor 2). Using the FWHM of activity profiles across each line source, we determined the spatial resolution at the centre of rotation and the coefficient of variation of FWHM across the 5 line sources (COV). The CT resolution was calculated from the in-plane modulation transfer function curves measured as a function of detector binning (binning 1, 2 and 4) using a tungsten wire (18 microns diameter). All CT acquisitions were performed using a high acquisition magnification (FOV: 1.9x2.8 cm). Finally, a micro-CT resolution bar pattern phantom (QRM, GmbH, Möhrendorf, Germany) was used to qualitatively evaluate the cross-plane spatial resolution of the CT system. **Results.** Both central resolution and COV were improved by using 3D-OSEM vs. FBP (FWHM: 1.28±0.33 mm vs. 1.90±0.11, p<0.0001, and COV: 10.4%±1.42 vs. 7.57%±2.14, p=0.001 for 3D-OSEM and FBP respectively). A linear model analysis demonstrated that a zoom factor 2 but not scatter correction further improved the FWHM (p<0.0001) and COV (p<0.01) of 3D-OSEM reconstruction. Finally, using 3D-OSEM and zoom 2, FWHM was optimized using ≥8 iterations (FWHM = 0.9 mm). The CT in-plane spatial resolution was measured at 163 microns (binning 4), 87 microns (binning 2) and 62 microns (binning 1). The bar pattern phantom allowed the visualisation of bar pattern structures of 100 (binning 4) to 50 microns (binning 1 and 2). The acquisition time was reduced from 22 with binning 1 to 7 min with binning 4. **Conclusion.** Using 3D-OSEM with a reconstruction zoom (factor 2) without scatter correction optimized the spatial resolution of microPET. CT scan using a high acquisition magnification with binning 4 provided a good compromise between acquisition time and resolution. These parameters were confirmed on image quality in a mouse undergoing a combine assessment of 18F-NaF PET and bone CT scan.

EP788

Quantitative Imaging of Lu-177: Maximising counts from Lu-177 patients by using high count rate mode to reduce deadtime effects on a GE Optima 640 SPECT/CT gamma camera

J. Merrett^{1,2,3}, J. Scuffham^{3,1}, A. Fenwick², G. Schettino², A. Nisbet^{3,1}; ¹University of Surrey, Guildford, Surrey, UNITED KINGDOM, ²National Physical Laboratory, Teddington, London, UNITED KINGDOM, ³Royal Surrey County Hospital, Guildford, Surrey, UNITED KINGDOM.

Aim: GE SPECT/CT systems can be manually set-up in high count rate mode, which reduces deadtime losses when performing Nuclear Medicine imaging. The aim of this work was to assess the efficacy of using the high count rate mode for quantitative imaging of Lu-177 at the maximum likely administered activity (7.4GBq + 5% = 7.8GBq). **Materials and Methods:** The measurement procedure recommended by the National Electrical Manufacturers Association (NEMA) in report NU 1-2012 for measuring count rate performance in scatter was used. In this method a disc of liquid activity (170mm diameter, 20mm depth) is measured in the centre of an acrylic phantom (300mm diameter, 150mm depth) to provide scatter. The phantom is positioned such that it is in contact with the detector, and there is 50mm of acrylic between the disc of activity and the face of the detector. A further 80mm of acrylic is positioned behind the disc of activity. Locally, this test was also performed with the disc of activity measured in air at the same distance from the detector for comparison. The measurements were performed with the camera operating in both high and low count rate mode. The disc source was measured repeatedly over several weeks as it decayed, with an initial activity of 7.8GBq of radiochemically pure Lu-177. The observed count rate for each measurement was defined as the total counts acquired divided by the acquisition time. **Results:** Observed count rate was plotted against source activity. It was assumed that there were negligible deadtime losses at low count rates, and the linear relationship between observed count rate and source activity at these count rates were extrapolated back to the initial activity to allow quantification of deadtime losses. When imaging in low count rate mode, there were maximum deadtime losses of around 35%, whilst imaging in high count rate mode gave maximum losses of around 20%. Marginally reduced deadtime losses were observed for the scatter-free measurements, compared to the measurements made in the acrylic phantom. **Conclusion:** This work demonstrates a method by which deadtime losses can be reduced to around 20% at the maximum activity typically administered to a patient, resulting in higher count densities in the patient images. However, the remaining deadtime losses need to be compensated for in order to perform quantitative imaging. Further investigation into how to best perform deadtime corrections for both planar and SPECT/CT Lu-177 quantitative imaging is ongoing.

EP789

Image quality and acquisition time in integrated PET/MR scanner: a phantom study

A. Zorz¹, P. Turco², A. Scaggion¹, F. Roppo³, D. Cecchin², F. Bui², P. Zucchetta², M. Paiusco¹; ¹Medical Physics Department, Veneto Institute of Oncology IOV-IRCCS, Padova, ITALY, ²Division of Nuclear Medicine, University Hospital of Padua, Padova, ITALY, ³School for Radiology Technicians, University Hospital of Padua, Padova, ITALY.

Integrated PET/MR scanners reduce the overall patient dose if compared to PET/CT. Further potential for dose reduction resides in the possibility of decreasing the injected activity, taking advantage of the forced prolonged acquisition time of the MR acquisition. The aim of this study was to verify if an increased acquisition time could compensate for a reduced tracer activity. Tests were performed following the NU 2-2012 NEMA image quality protocol. The effect of different reconstruction parameters was also evaluated. The NEMA body phantom with different sphere to background ratio was acquired on Siemens Biograph mMR PET/MR integrated scanner, which uses lutetium oxy-orthosilicate scintillator crystals read out by avalanche photodiodes and a 3 T static magnetic field. A scatter line with 110 MBq was positioned contiguous to the IQ phantom. A 30 minutes list-mode PET image was acquired and reconstructed using 3D Poisson OSEM iterative algorithm with 3 iterations, 21 subset, 172x172 matrix size and 4 mm gaussian filter. A CT-based attenuation map was manually registered to the acquired data and used for the attenuation correction. A second acquisition was performed after a time

interval corresponding to the radioisotope half-life. Datasets with standard NEMA activity were retrospectively reconstructed at different times (12, 5, 2, 1 and 0.5 min); half activity images were reconstructed with double acquisition times (24, 10, 4, 2 and 1 min). On each image, the percentage of contrast and background variability were calculated according to NEMA protocol. In order to verify the effect of reconstruction parameters on the two datasets, 12 minutes images with standard and half radiotracer concentration were reconstructed with different iterations and matrix size. No significant differences were found comparing images with half radiotracer concentration and double acquisition time with the standard ones. Contrast of the standard activity images remained stable within the reconstructions of 12, 5, and 2 minutes datasets, with an acceptable noise level. All the spheres were almost visible also in the 30 seconds reconstruction. Contrast and background variability increased with the iteration number. Background variability increases from 128 to 256 matrix size, but no further variation is found when reconstructing with largest matrix size. The same trend was observed both in standard and half activity images. Increasing the acquisition time can compensate for reduced tracer activity injection. Image quality is acceptable until 2 minutes acquisition/bed. Changing the reconstruction parameters have the same effect on images with standard and half activity.

EP790

Development of a new phantom for spatial frequency response measurements of nuclear medicine imaging devices

A. Hoekstra, A. D. van het Schip, G. C. Krijger; Department of Radiology and Nuclear Medicine University Medical Center Utrecht, Utrecht, NETHERLANDS.

Objective. A key parameter of a nuclear imaging device is its spatial resolution response. This is usually measured with bar phantoms (planar gamma cameras) or with line sources (planar gamma cameras, SPECT or PET systems). For bar phantoms the spacing between lead bars (mm) is visually interpreted. For line sources results are expressed as FWHM (mm). As resolution depends on the spatial frequency response, a phantom was developed to measure the response at different frequencies to quantify the resolution. **Methods.** The new phantom is a box (220 x 125 x 17 mm) containing a 5 mm thick perspex plate with sinusoidal shaped free spaces each representing a geometrical frequency to simulate the modulation of a constant value. Modulation frequencies are: 0.25, 0.50, 0.75, 1.00, 1.25, 1.50, 1.75, 2.00 cycles/cm. The spaces were filled with a radionuclide to get a sinusoidal radionuclide-intensity distribution. Measurements were performed on a planar, SPECT and PET camera. The image data were analysed with the open source software ImageJ and a sinusoidal count distribution was created. The data were processed in Microsoft Excel to fit the frequency response. **Results.** A modulation index was calculated for each fitted image frequency result. This index was divided by the source modulation index resulting in a modulation factor. With these factors a modulation transfer function (MTF) was created and fitted as a polynomial curve. From this, a contrast function of the response data was calculated. The contrast is defined as the modulation depth of the response data to a square wave at different frequencies. A resolution criterion based on this contrast function is the frequency at a 20% contrast level, resulting in a resolution value and expressed in mm. The resolution value at 20% contrast for Tc-99m of the used gamma camera, with HR collimator, was 3.6 mm. For In-111 (ME) this value was 6.4 mm. A Tc-99m SPECT study with the same device resulted in 8.8 mm. An I-124 study with a PET/CT scanner resulted in a value of 5.6 mm. **Conclusion.** The inverse Fourier transform of our MTF data results in a Line Spread Function to determine the FWHM of the imaging devices. This value showed good agreement with specifications of the devices used, with the advantage of being the result of a more quantitative method. Therefore, this phantom has the potential to become a valuable tool for resolution specification determination of nuclear medicine imaging devices.

EP791

SUV Recovery on a Continuous Acquisition PET/CT: Influence of Table Speed, Noise Level and Reconstruction Settings

K. Jaspers^{1,2}, A. Talsma¹, R. Boellaard²; ¹Martini Hospital, Groningen, NETHERLANDS, ²University of Groningen, University Medical Center Groningen, Groningen, NETHERLANDS.

Aim: To investigate the impact of table speed settings, noise level and the use of point spread function (PSF) on SUV recovery on a continuous acquisition PET/CT using the EARL image quality protocol. **Materials and methods:** Measurements were performed according to EARL standard operating procedures on a Siemens Biograph mCT 20 Flow PET/CT (Siemens, Erlangen, Germany) using the NEMA NU-2 image quality phantom. The FDG-activity in the spheres equalled 20 MBq/L with a background activity of 2 MBq/L at time of first acquisition (T0). Datasets were acquired at T0, and after 1 and 2 half-lives (T1 and T2, respectively) with varying table speeds (0.5, 1, 2, 4 mm/s). The data were reconstructed with time-of-flight ordered subset expectation maximisation method using 2 iterations and 21 subsets, with and without the use of PSF (standard protocol and research protocol, respectively) and with a Gaussian filter of 5 mm. Reconstructed voxel size equalled 4x4x3 mm³. Analysis was performed using the EARL software tool providing maximum and mean SUV recovery coefficient (RC) curves (RC_{max} and RC_{mean}). To assess the influence of table speed, datasets with varying combinations of activity and table speeds were grouped based on noise level, determined by the coefficient of variation (COV) of voxel values in the background compartment of the phantom. **Results:** PSF reconstruction resulted in RC curves that exceeded the EARL criteria for both RC_{max} and RC_{mean}. The overshoot was most prominent for the smaller spheres. Without PSF, the EARL criteria were met for sufficiently low noise levels (COV < 15%). For sufficiently high statistics, recovery coefficients at a specific noise level were independent of the combination of activity and table speed. In the case of poorer statistics (COV > 15%), higher table speeds (≥ 2mm/s) resulted in higher RC that exceeded the EARL criteria. **Conclusions:** The mCT PET/CT can comply to EARL criteria regarding SUV recovery if no PSF is used. For sufficiently high statistics, table speed does not influence SUV recovery when scanning the phantom at matched noise levels. For poorer statistics, however, table speed appears to affect SUV recovery.

EP792

Validation and Optimization of Quantitative SPECT/CT

S. Razavi, R. Klein, P. Martineau, S. Dinning, M. Bryanton, W. Zeng, L. Zuckier; Dept of Nuclear Medicine The Ottawa Hospital, Ottawa, ON, CANADA.

Objective: To rigorously investigate factors influencing the accuracy and precision of quantitative ^{99m}Tc SPECT-CT under actual clinical conditions using known activity concentration phantoms. **Method:** Patients referred for ^{99m}Tc-MDP Bone or ^{99m}Tc- SestaMIBI parathyroid scans using SPECT-CT system were recruited for this REB approved study. After patient positioning on the scanner-bed and prior to image acquisition, 2-3 cylinders of varying sizes filled with a known concentration (MBq/cc) of ^{99m}Tc activity were placed under the armpits and/or between the legs. Patient image acquisition followed the clinical protocol. Quantitative (MBq/cc) tomographic images were reconstructed using Hermes HybridRecon and activity concentrations in the sources were measured using 10 mm diameter spherical volumes of interest (VOI) which were compared to known phantom concentrations and reported as percent-error. Accuracy and precision of measured activity was evaluated for intra-operator variability, acquisition types and reconstruction types. For operator-variability, VOIs were placed at the center of each of 38 phantoms (in 15 patients) on four different occasions. Acquisition

types (circular vs. contouring orbit and step-and-shoot vs. continuous) were evaluated in a physical phantom study with all sized phantoms in the field of view. To study the effect of OSEM reconstruction parameter the number of iterations was increased from 4 to 20 iterations, with and without collimator corrections. In a subset of 10 patients (27 phantoms) Maximum a-posteriori (MAP) reconstruction algorithms with smoothing, median root prior (MRP), anatomy-based (AMAP), and finite-impulse-response median hybrid (MRP-FMH) priors were compared along with our standard OSEM 4-iterations reconstruction. **Results:** Operator variability was excellent with 2.8% average standard-error. Based on a single phantom experiment with 4 cylinders of varying sizes, orbit type and camera-head motion did not significantly impact quantitative accuracy and no significant systematic quantification error was detected ($p>0.9$). Likewise, OSEM reconstruction parameters (4 iteration, 20 iteration, 20 iterations with collimator corrections) did not significantly change accuracy ($p>0.9$), but precision tended (6% vs. 9% for 4 vs. 20 iterations, $p=0.052$) to degrade with higher number of iterations. OSEM underestimated activity concentrations by 13% ($p<0.001$), whereas all MAP reconstruction methods improved on accuracy, with average MAP-MRP error at only 4% and not significantly greater than 0 ($p>0.1$). Precision was between 8% and 14% standard-error for OSEM 4-iterations and MAP-MRP respectively. **Conclusion:** Quantification of tracer concentrations in clinical applications is technically possible and robust to operator variability, acquisition types, and OSEM iterations. MAP reconstruction can achieve improved accuracy, but partial volume effects may persist.

EP793

Ge-68 based normalisation and SUV measurements on a Siemens PET-CT system: Implications of variations in Ge-68 cylinder source properties

S. J. McQuaid¹, J. W. Scuffham¹, J. R. W. Hall², V. Prakash³, P. J. Hinton¹; ¹Royal Surrey County Hospital NHS Trust, Guildford, UNITED KINGDOM, ²Frimley Park Hospital NHS Trust, Frimley, UNITED KINGDOM, ³Ashford and St. Peter's NHS Hospital Trust, Chertsey, UNITED KINGDOM.

Aim: Siemens mCT systems perform normalisation with a uniform Ge-68 cylinder. On one system, repeated low Ge-68-based SUV measurements (0.88 rather than the expected value of 1.00) were obtained, with potential implications for patient imaging quantification. The aim was to determine the cause of these anomalous measurements. **Materials and Methods:** The following were investigated as possible causes of the Ge-68 SUV error: 1) inaccurate reference activity 2) inaccurate stated cylinder volume 3) the presence of contaminants in the source (affecting the half-life) 4) non-uniformities in the cylinder construction and 5) differences in the source attenuation to that assumed by the PET-CT during normalisation. These were investigated by performing a normalisation followed by a 1-bed PET-CT acquisition for 8 Ge-68 cylinder sources: one manufactured by Eckhart & Ziegler (for which the error had been observed) and 7 manufactured by Siemens (for which SUV measurements were close to 1.00). The mean SUV and Hounsfield Units (HU) were measured from large regions-of-interest (ROIs) on 3 slices of the reconstructed PET and CT images respectively. Line profiles across the PET images of the cylinders were also compared. **Results:** Inaccuracies in source activity and volume may have been present in the E&Z source, but were ruled out as sources of Ge-68 SUV error, since the same values were used for the normalisation and SUV-check acquisition, cancelling out any errors present. Contaminants were also ruled out as the cause of the low SUV, since the E&Z source normalisation was repeated using the test-date activity (instead of the reference activity), which did not affect the result (0.88+/-0.07 using reference information, 0.87+/-0.08 using test-date information).

Variations in activity concentration were comparable between the sources (approximately 5%) and are largely mitigated in SUV measurements by averaging large ROI results over multiple slices. Mean HUs were 7.4 HU (E&Z source) and 64.7+/-1.6 HU (7 Siemens sources), which equates to attenuation differences of up to 12% over the gamma ray paths. This is comparable to the difference in SUV observed. **Conclusions:** Ge-68 SUV measurements are insensitive to errors in Ge-68 cylinder reference activity and source volume, but are affected by the attenuation of the Ge-68 cylinder. Ge-68 SUV errors due to attenuation effects could be indicative of F-18 SUV errors, due to inaccurate normalisation, which would affect image quantification. This should therefore be checked with a uniform F-18 cylinder and corrections applied to change the F-18 SUV to 1 where necessary.

EP794

How do French nuclear physicians deal with ethical aspects of communication results to patients after PET performed for oncological indications? A national french survey

S. Gonzalez, P. Le Coz, A. Loundou, A. Abdullah, C. Colavolpe, O. Mundler, D. Taieb; university-affiliated hospital Timone, Marseille, FRANCE.

Context: Delivery of information to patients in France is governed by regulated and non regulated obligations, the latter being very general. There exists no available guidelines or consensus regarding the content of information to be delivered, especially when taking into account the differences of each specialty. Current legislative texts require physicians to uphold the concepts of loyalty and transparency when dealing with patients. However, these texts do not well deep into the practical modalities of communicating information. The moment and method of breaking bad news varies according to the nature of the disease and the personal judgment of the physician. The patient-nuclear physician relationship is very unique. **Objective:** The goal of our study was to evaluate the practice of French nuclear physicians concerning the communication of results to patients undergoing PETs for oncological indications. **Methods:** An ad hoc questionnaire was developed in collaboration with the departments of public health and of medical ethics. All French nuclear physicians registered with the French Society of Nuclear Medicine, and all third and fourth year residents in nuclear medicine programs in France were contacted by email for completing an electronic questionnaire between the 25th of June 2015 and the 20th of July 2015. **Results:** 250 nuclear senior physicians and residents were included (31.3 % response rate). It was found that there was large heterogeneity among French nuclear physicians regarding their practice of information delivery post PET explorations for oncological indications. Concerning the consultations, 56 % see their patients systematically, while 35% adapt their practice on a case-to-case basis, and only 9 % state that they never see their patients. When it comes to orally communicating results to patients, 63 % adapt their approach on a case-to-case basis, 24 % never do, while 13% do so systematically. After multivariate analysis, the following factors were found to be associated with communicating results to patients; older age of physician ($p=0.0020$), more years of experience ($p=0.001$), private versus public practice ($p=0.033$), and the regular and systematic practice of consultations post PET ($p<0.001$). Finally, 80 % of physicians admit that current recommendations are not clear enough. **Conclusion:** This heterogeneity of practice methods among nuclear physicians concerning the communication of PET results to patients, stems from the lack of specific recommendations. An inter-collegial, ethical and multi-disciplinary reflection is needed in order to better guide nuclear physicians when it comes to communicating results to patients suffering from serious disease.

EP795**Administered dose optimization aiming for constant image quality in 3D 18F-FDG whole body PET/CT studies: Clinical implementation of the quadratic relation between dose and patient's body mass on two systems**

M. Kotzarslidou¹, M. Metaxas², A. Georgakopoulos², A. Pashali¹, N. Pianou², S. Hatzioannou², V. Hatzipavlidou¹; ¹Nuclear Medicine Dept., "THEAGENIO" Cancer Hospital, Thessaloniki, GREECE, ²PET-CT Department, Centre for Clinical, Experimental Surgery and Translational Research, Biomedical Research Foundation of the Academy of Athens, BRFAA, Athens, GREECE.

Quality of 18F-FDG PET/CT images, measured by the signal-to-noise ratio (SNR_L) in liver, depends on injected activity (A) and acquisition time, for certain scanning mode, percentage bed overlap and reconstruction parameters. According to EANM procedure guidelines, (version 2), quadratic scheme between prescribed FDG activity, patient's weight (w[kg]) and PET acquisition time per bed position (t[*min*]) results to constant image quality as patient weight increases. **Aim:** This study aims to determine the system specific quadratic relation between dose and patient's body mass for two PET/CT systems and evaluate its performance, when applied. **Method and materials:** Image quality was determined by SNR_L in 150 anonymized adult clinical data, (weight 45-125kg), who performed FDG-PET/CT scans, on two systems, GE Discovery PET/CT710 (ToF) and Siemens Biograph 6 (non ToF) applying a linear scheme between FDG dose (A) and patient's weight (w), $A=0.17*w$ using OSEM reconstruction and $A=0.07*w$, using 3-dimensional iterative reconstruction (3D-IR, 24subsets, 2iterations.) respectively. SNR_L was normalised for injected activity (A) and time per bed position (t), deriving $SNR_{norm} = SNR_L / (A*t)^{1/2}$. Data were fitted to a first order polynomial, $SNR_{norm} = a*w^d$. Parameters a, d were calculated. For constant image quality SNR_L should have an acceptable value, suggested equal to SNR_{mean}. Therefore optimized dose A [mCi], is given by the following equation: $A = (1/t) * (SNR_{mean}/a)^2 * w^{2/d}$. Optimized dose regimen was implemented for both PET/CT systems. 130 scans were analysed to investigate the effect on image quality, by comparing plots of SNR_L vs weight for linear and quadratic dose regimens. Statistical analysis for t-distribution was performed using SPSS Statistics 19. **Results:** For Discovery PET/CT 710, since $SNR_{mean} = 8.16 \pm 1.5$, parameters a, d were $a: 33.9 \pm 16.5$, $d: 0.655 \pm 0.11$ the derived formula was: $A [mCi] = 0.019 * w^{1.31}$. For Biograph 6, $SNR_{mean} = 6.79 \pm 1.5$, parameters a, d were $a: 78 \pm 35$, $d: 0.95 \pm 0.1$ the derived formula was: $A [mCi] = 0.0025 * w^{1.31}$. In both cases time per bed position, t, was set equal to 3min. Applying quadratic scheme to both systems SNR_L remained almost constant ($p < 0.05$). **Conclusions:** Application of the quadratic dose regimen is recommended in order to ensure constant image quality of 18F-FDG whole body PET/CT scans across a big range of patient weights. Comparing with linear model, it results to higher administered activities for patient weights less than 70kg but this fact can be compensated by increasing acquisition time per bed position (min-bed⁻¹).

EP796**Validation of an adaptive re-planning algorithm for delineation of an internal target volume**

C. GUILLERMINET, M. Lacombe, S. Girault, P. Gustin, A. Testard, O. Morel, D. Autret; ICO Paul Papin, Angers, FRANCE.

Aim: The delineation of internal target volumes (ITVs) in radiation therapy of esophageal tumors is commonly performed by the help of free-breathing positron emission tomography/computed tomography (FB-PET/CT) scan. Nevertheless, technologic advances in the field of radiation oncology have reinforced the importance of accurate target delineation. In this report we validate, in our routine tasks, the use of 4-dimensional (4D)-PET/CT for the delineation of target volumes in a

phantom using the new algorithm called «adaptive re-planning» of GE Medical System (GEMS). This algorithm permits to take in account the elastic deformation of the segmented lesion from a CT/scan to another. **Materials and methods:** A phantom with 3 hollow spheres was prepared surrounded by water. The spheres and the water were filled with 18F-FDG to obtain a background with an activity concentration of 5 kBq/mL and a contrast respectively of 2, 4 and 6. A 4D-PET/CT of the phantom scan was performed while moving in a cos4 breathing pattern. This scan was reconstructed under different phases (10, 6, 5 and 4). The spheres were contoured by 2 contouring method (41% of maximum and an objective segmentation based on a gradient algorithm) on the FB-PET/CT, the 4D PET/CT before and after the adaptive re-planning and the 4D/CT. The concordance between the different volumes was calculated using a DICE coefficient (DC). **Results:** The average DC in the phantom using the 2 contouring methods, respectively, was lowest for FB-PET/CT and highest for 4D-PET/CT. Non significant difference were noticed between the 2 contouring for 4D-PET/CT before and after the «adaptive re-planning». The number of phases has an impact on the contouring of the lesions. If consensus is a 6 phases 4D-PET/CT for the delineation with radiotherapy goal, 10 phases 4D-PET/CT has an interest in the case of small lesions. **Conclusion:** As expected, FB-PET/CT consistently underestimates the ITV when compared with 4D-PET/CT for a lesion affected by respiration. 4D-PET/CT replanned by the adaptive algorithm produces volumes with high concordance with 4D-CT across multiple contrast and lesion sizes. This work will continue with a focus on the use of different breathing patterns in order to take in account lung contrast and real patient breathing periods. Our 4D-PET/CT patient protocol will be modified according to the conclusions of this work and the impact of 4D-PET/CT will be investigated in delineation of patients lesions.

EP797**Noise characteristics of PET images reconstructed with OSEM algorithm**

P. Castro¹, C. Huerga², P. Chamorro¹, M. Roch¹, G. Pozo¹, L. Pérez¹; ¹La Princesa Hospital, Madrid, SPAIN, ²La Paz Hospital, Madrid, SPAIN.

Aim: The magnitude and structure of noise in PET can have various origins. The statistical nature of the emission process follows a Poisson model. Electronic noise, dead time and the loss of photons that do not reach the detector are other contributions associated with the detection system. Other important sources of noise in PET are the scattered counts generated in the patient and the random counts. The attenuation correction or the blank scan correction also assumes additional contributions to noise. Finally, the process of tomographic reconstruction determines the way in which the various sources of noise are presented in the image. The effect of adding all of these contributions of various statistical behaviors could result in the pixel values tend to have a Gaussian distribution (central limit theorem). The aim of the study is to characterize the noise present in PET images reconstructed with the Ordered-Subset Expectation Maximization (OSEM) algorithm through the standard deviation and the probability density distribution. **Materials and Methods:** The study is based on PET images acquired in 2D mode with a cylindrical phantom injected with 18FDG which provides a uniform activity distribution. Images are reconstructed with OSEM algorithm. Standard deviation provides information about the noise magnitude. Circular ROIs of 10 pixels diameter are used to analyse the spatial variation of noise magnitude. For axial dependence ROIs are centered on the phantom for each of the slices; for radial dependence the ROI position will vary from one end of the phantom to the opposite end through the centre, in different radial directions. Histograms of the experimental data are used to calculate the probability distribution. The obtained distribution is compared to different noise models (Poisson, Gaussian, Negative Binomial, Lognormal, and

Gamma). The Kolmogorov-Smirnov test is used to assess the goodness of fit. Results: There is an increase of noise at the edge slices consistent with the lower number of coincidence lines. The radial dependence shows a slight reduction in noise towards the edges of the phantom (<10%). The function that produces the best goodness of fit and lower differences with experimental statistical moments is the log-normal distribution. Results show the noise distribution is not well modeled by a Poisson model. Conclusion: The noise present in PET images, after all corrections and OSEM reconstruction algorithm have been applied, is non-Poisson. The OSEM reconstruction also tends to equalize noise over the entire phantom.

EP798

Alginate to simulate tumor lesions in phantoms for 3D SPECT and an alternative to Jaszak phantom in the quality assurance process

R. Ringler, M. Stich, K. Schuller, M. Lindner; Technische Hochschule Amberg-Weiden, Weiden, GERMANY.

MOTIVATION The quality assurance (QA) in nuclear medicine is defined by (inter-)national standards. During the ½ yearly QA to check the performance of the 3D resolution of SPECT system passive spheres in a phantom are used. The aim of our work was to develop a phantom with geometry similar to the patient and active alginate beads to simulate tumor structures. **MATERIALS & METHODS** Alginate beads with a six different diameters (31.8; 25.4; 19.1; 15.9; 12.7 and 9.5 mm) were placed in a cylindrical phantom. The physical properties of the spheres strongly dependent on the composition, structure and molecular size of the polymers of the alginate. With alginate spheres two different approaches can be chosen. One setup are alginate spheres with no activity in a water environment with Tc-99m (750, 600 and 50 MBq). The second approach are active alginate spheres with Tc-99m (35, 30 and 17 MBq). The data evaluation was done using MATLAB with various algorithms - Otsu, Fast Marching, Active Contour or edge enhancement - to segment the spheres and compare the calculated size to its original size. **RESULTS** In a watery environment the volume of the spheres increase in the first three hours for about 5% and continue to up to 9% of total volume increase in the next 2 days. The standard for QA demands that at least 4 of 6 cold spheres could be detected which was fulfilled. Active alginate showed a very good detectability (4 of 6 spheres) even with low activity (17 MBq). With increasing background activity, this number decreases. **CONCLUSION & DISCUSSION** The spheres made of alginate with Tc-99m could easily be used to simulate tumor structure in a phantom and perform the QA in terms of 3D resolution. With MATLAB and the Active-Contour or Otsu algorithm the spheres can easily segmented from the reconstructed SPECT image.

EP799

Performance Evaluation of the New Discovery IQ Five Rings PET/CT Scanner According to NEMA NU-2 Standard and the Image Quality Test with Low Activity Protocols

G. Reyes-Llompart¹, E. Montes², P. Saldaña², I. Romero-Zayas¹, S. Rustarazo-Losada¹, D. Mateo-Navarro¹, C. Picón², C. Gámez-Cenzano¹, J. Martí-Climent³; ¹PET Unit. Nuclear Medicine. IDI. Hospital U. de Bellvitge-IDIBELL, L'Hospitalet de Llobregat, Barcelona, SPAIN, ²Medical Physics Department. ICO. Hospital U. de Bellvitge-IDIBELL, L'Hospitalet de Llobregat, Barcelona, SPAIN, ³Nuclear Medicine. Clínica Universidad de Navarra, Pamplona, SPAIN.

Aim: The aim of this work was the assessment of the physical performance of the PET/CT Discovery IQ 5 rings of General Electric Healthcare (GE DIQ). **Material and Methods:** PET physical performance was measured following NEMA NU-2- 2012 procedures. For the image quality test

(IQ), initial radioactivity concentration was 5.5 kBq/cc. Data were acquired in list mode in order to study different time acquisitions and reconstructions, including NEMA specifications and clinical protocols; the latter were: VPHD, VPHD-S (12-subsets, 4-iterations, 8.8 mm FWHM) and Q.Clear with a beta value of 350. **Results:** Spatial resolutions on axial/tangential/radial planes were 4.8/4.7/4.2 mm at 1 cm, 4.8/5.1/5.6 mm at 10 cm and 4.8/5.5/8.5 mm at 20 cm. Sensitivity in the center and at 10 cm was 22.8 and 20.4c kps/kBq, respectively. The NECR peak was 124 kcps at 9.1 kBq/cc, with a 3D scatter fraction at NEACR peak of 36.2%. The accuracy of correction for the count losses and randoms was 3.9 % below the NECR peak. Average energy and timing resolution were 12.4% and 544 ps, respectively. The IQ test results for VPHD/VPHDS/Q.Clear, using 2 min acquisition were: Hot contrast for 10, 13, 17, and 22 mm spheres: 31/30/34, 40/44/47, 57/65/69, 63/67/75 for a contrast of 8:1, 35/31/25, 43/46/47, 54/59/61, 65/68/73, for a contrast of 4:1, and 16/17/13, 37/34/33, 68/68/67 and 70/73/76 for a contrast of 2:1. Cold contrasts for 28 and 37 mm spheres: 64/63/70 and 64/63/78 for a contrast of 8:1, 58/59/70 and 63/63/75 for a contrast of 4:1, and 60/60/71 and 65/64/77 for a contrast of 2:1. Lung residual: 25/26/12 for a contrast of 8:1; 24/25/11 for a contrast of 4:1, and 26/27/12 for a contrast of 2:1. Mean background variation: 7.0/6.2/4.7 for a contrast of 8:1, 5.6/5.0/4.0 for a contrast of 4:1 and 5.4/4.4/3.3 for a contrast of 2:1. For shorter acquisition times, simulating acquisitions with less activity concentration, Q.Clear has better performance than the other reconstruction methods, allowing to decrease the noise. A variation of the image quality parameters was found when changing the reconstructed field of view. **Conclusion:** Discovery IQ shows very good PET physical performance for all the standard NEMA NU-2-2012 measurements, especially for sensitivity an NECR. Furthermore, under simulated clinical conditions, the reconstruction algorithm Q.Clear available for PET data allows further improvement of the image quality performance that in further studies could be exploited in the clinical protocols.

EP800

Evaluation of the effects of different microCT parameters on microPET/CT imaging

W. McDougald, R. Collins, M. Green, A. Tavares; University of Edinburgh, Edinburgh, UNITED KINGDOM.

As the use of micro positron and computer tomography (microPET/CT) increases in preclinical small animal research so does the need for developing standardized acquisition and reconstruction protocols to ensure a reliable and consistent translation of preclinical findings to clinical use. Although there is a need for standardization of imaging protocols, in-depth analysis of the effects of different acquisition settings on image quality and biases is lacking. This study aims to investigate the effects of different microCT acquisition settings on image quality and data quantification. **Methods** All images were acquired using a Mediso nanoPET/CT scanner (Mediso, Hungary) and the following phantoms: air/water CT phantom and the CIRS model-91 water-filled tissue equivalent phantom (TEM). Collected imaging data was quantified and analyzed using PMOD image analysis software. **Results** Air/water CT phantom: Decreasing the microCT binning parameter resulted in an increase of the image noise (standard deviation (SD) of measured Hounsfield Units (HU) in water ranged from 33.15 to 215.27 for 1:16 to 1:1 binning). Increasing the exposure time resulted in higher bias compared with known HU for water (up to 27% for the highest exposure of 450 ms) and increased the noise (SD ranged from 33.15 to 46.89 for 170ms to 450ms). Tube voltage had minimal effect on the measured bias and image noise (SD of 77, 71 and 82 for 45, 55 and 75 kVp, respectively). TEM phantom: The greatest percent difference in measured HU for different tube voltage (ranging from 45 to 75 kVp) was determined in the adipose and muscle phantom rods and it was as great as ~60% in muscle and ~30% in adipose. Increasing the exposure time from 170ms to 300ms resulted in an increase of 230% of the measured HU values in the muscle,

while the HU difference in other TEM rods remained below 10%. Measured HU values in the TEM lung rod remained relatively consistent as the tube voltage or the exposure times increased (<5% difference). **Conclusion** The data has demonstrated the need to carefully evaluate the effects of different microCT settings on image quality and quantification. Increasing exposure time or tube voltage does not directly translate improvement of image results and, consequently, it will increase animal absorbed doses unnecessarily. Our data collected so far supports the need to assess the microCT parameters in a wider multi-center approach, while working towards standardization of scanning protocols for small animal imaging.

EP801

SPECT Characterisation and Quantification of Preclinical Scanners

T. J. Spinks¹, G. Flux¹, J. Sosabowski², C. Finucane², S. Macholl²; ¹Institute of Cancer Research and Royal Marsden NHS Trust Joint Department of Physics, Sutton, UNITED KINGDOM, ²Barts Cancer Institute, Queen Mary University of London, London, UNITED KINGDOM.

Introduction. Radionuclide imaging systems are routinely characterised using standard physical performance tests. Formalised (NEMA) tests have been published for preclinical PET but not for SPECT. Despite greatly improved spatial resolution, quantification for small structures remains a significant problem in preclinical imaging. In addition, spatial uniformity of response is a crucial parameter. The NEMA PET performance standards go some way to addressing these issues but it is pertinent to consider other approaches. The aim of this study was to carry out tests on two preclinical SPECT systems, based on NEMA PET and using alternative methods. **Methods.** Tests were performed on two preclinical systems: (i) an Albira Tri-Modal PET/SPECT/CT and (ii) a Mediso NanoSPECT/CT, using ^{99m}Tc and ¹¹¹In. Recovery Coefficients (RCs) were measured with (a) the NEMA Image Quality (NEMA IQ) phantom as defined for PET and (ii) a phantom consisting of multiple spheres of varying diameter (MS). Image uniformity was determined by defining a grid of spherical VOIs (diam 5 mm, spacing 5 mm) in the image of a uniform cylinder covering the FOV. **Results.** RCs were observed to reach a plateau, indicating full recovery, for a rod diam of 5 mm (NEMA IQ) and for a sphere diam of 8 mm (MS). The data were similar for ^{99m}Tc and ¹¹¹In. The coefficient of variation of the grid VOIs over the FOV was 4% (Albira) and 3% (NanoSPECT/CT). **Conclusion.** The NEMA preclinical standard tests for PET provide some basic parameters of a system but do have limitations, and suggestions for extending these are made in this study, specifically for SPECT. The NEMA RC values are determined from rod sources and so do not account for object size in the axial direction. Clearly significantly lower values are obtained in this study for the MS phantom, which is intended to represent spherical lesions. The pre-clinical NEMA PET prescription for image uniformity only encompasses a 10 mm axial range and it is proposed that a uniformity measurement using a grid of VOIS over the axial FOV occupied by an animal (e.g. about 50 mm for a mouse) is more realistic and interpretable, for example when tumours are located at different positions.

EP802

Survey on radionuclide therapy facilities in Japan with grants by Ministry of Health, Labour, and Welfare

M. Hosono¹, H. Ikebuchi², Y. Nakamura², N. Nakamura², S. Yanagida², A. Kitaoka²; ¹Kindai University, Faculty of Medicine, Osaka-Sayama, JAPAN, ²Japan Radioisotope Association, Tokyo, JAPAN.

Aim: The number of radionuclide therapy (RNT) has doubled from 2002 to 2012 in Japan. Yet the number per capita remains small (82.4 per

million inhabitants in 2012) as compared with 191 per million inhabitants (1993) in European Union. One of the reasons is attributable to shortage of RNT beds. **Methods:** To investigate the actual situations surrounding RNT in Japan, in the framework of a focused study granted by Ministry of Health, Labour, and Welfare (MHLW), we conducted a survey by sending questionnaire by mail during 3rd and 4th quarter in 2013. The subjects of the survey was 606 hospitals, consisting of 394 university hospitals or cancer base hospitals designated by MHLW, and other 212 hospitals providing radionuclide therapy, out of totally 1274 hospitals that carry out nuclear medicine practices across Japan. Among 14 survey items, main items included Q1) hospital bed capacity, Q5) monthly number of nuclear medicine examinations, Q6) number of RNT beds, Q7) number of RNT and breakdowns (thyroid cancer, hyperthyroidism, lymphoma, bone pain relief, etc.), Q9) what department leads RNT, Q11) licensed radionuclides and quantities for RNT, Q12) interest in new RNT procedures, Q13) exhaust ability of facility, Q14) drainage ability of facility, survey meters. **Results:** The recovery of the questionnaire was 72.6% (440 of 606). Q1) In the range of 300≤, <700 bed capacity were 303 hospitals (68.9%). Q2) Mean and median of monthly number were 165.1 and 150. Q6) Of 320 hospital providing RNT, 59 (18.4%) had RNT beds, and mean and median were 2.3 and 2.0 beds. Q7) Of 320 hospitals, 174 (54.4%) provided therapy with radioiodine, 273 (85.3%) with Sr-89, and 61 (19.1%) with Zevalin. Q11) Annual licensed radioactivity was 26,640 MBq (range:7,723 to 74,500) for I-131 in 235 hospitals, 8,460 MBq (5,460 to 15,600) for Sr-89 in 290, and 44,400 MBq (22,200 to 88,800) for Y-90 in 118. For 202 hospitals in which data were available, based on Q11, Q13 and Q14, capacity reserves of radioactivity were calculated by considering exhaust and drainage maximum capacity, and 152 showed a reserve of less than 20% of the actual capacity if without diluting drainage. **Conclusions:** Effective utilization of existing facility capacity through deregulation may contribute to increasing number of RNT, while further healthcare investments in RNT are eagerly anticipated by patients and healthcare professionals.

EP803

Using a 3D-printed anatomical pancreas-kidneys phantom in body casings of varying size to simulate beta cell imaging with ⁶⁸Ga-exendin PET/CT in obese patients

L. N. Deden¹, A. P. W. Meeuwis², F. J. Berends¹, M. Gotthardt², E. P. Visser²; ¹Rijnstate, Arnhem, NETHERLANDS, ²Radboud University Medical Center, Nijmegen, NETHERLANDS.

Aim To increase our knowledge of the role of beta cells in type 2 diabetes mellitus (T2DM), ⁶⁸Ga-exendin PET/CT can be used to quantify the pancreatic uptake of ⁶⁸Ga-exendin, which is considered as a measure for the beta cell mass. The occurrence of T2DM and body weight are correlated, therefore we examined the effect of increasing body weight on quantitative PET/CT with ⁶⁸Ga-exendin. In PET/CT imaging, several phenomena are body size dependent, among which are photon attenuation and scatter, and the ratio of random to true coincidences. In standard image quality (IQ) characterization of PET/CT scanners, normal sized phantoms, such as the NEMA NU2 IQ phantom are used. In our study, a 3D-printed pancreas-kidneys insert in the standard NEMA phantom casing and in two customized, larger casings were used. The sizes of the casings were chosen in correspondence with the subdivision into normal, obese and morbidly obese (MO) patients as derived from patient CT scans. **Materials and Methods** The standard, obese, and MO casings had circumferences of 86, 101, and 133 cm, respectively. The compartments were filled with a ⁶⁸Ga solution such that the activity concentration (AC) ratios of kidney-to-pancreas and pancreas-to-background were 16:1 and 540:1, respectively. Image reconstructions were performed using OSEM3D with TOF and PSF in 3 iterations and 21 subsets, using 10 and 20 min of list mode data. Volumes of interest (VOI) for the pancreas and both kidneys were delineated in the CT images. Recovery

coefficients (RC) for the pancreas and kidneys were calculated. Additionally, 10 cylindrical background VOIs were drawn to determine the background AC. **Results** For the 10 min reconstructions RC_{panc} were 0.68, 0.66 and 0.77, and RC_{kidn} were 0.80, 0.75 and 0.78 for the standard, obese, and MO casings, respectively. The background AC was comparable to the real AC for the standard and the obese phantom. In the MO phantom the background AC was 30 times higher than the real AC, with largest AC in the area around the kidneys. The 20 min reconstructions led to a small increase in RC_{panc} and to similar results in the kidneys and background. **Conclusion** RC_{kidn} was comparable for all phantoms. However, RC_{panc} was largest in the MO phantom. This may be the result of scattered photons originating from kidneys inaccurately attributed to the background and pancreas due to inadequate scatter correction. This effect will be further investigated.

EP804

The impact of using tube-current-modulation technique for attenuation correction of PET/CT images on image quality and patient dose

y. Salimi¹, P. Ghafarian^{2,3}, M. Deevband¹, M. Bakhshayesh Karam^{4,3}, H. Jamaati², M. Ay^{5,6}; ¹Department of Bioengineering and Medical Physics, Faculty of medicine, Shahid-Beheshti University of Medical Sciences, Tehran, IRAN, ISLAMIC REPUBLIC OF, ²Chronic Respiratory Diseases Research Center, National Research Institute of Tuberculosis and Lung Diseases (NRITLD), Shahid Beheshti University of Medical Sciences, Tehran, IRAN, ISLAMIC REPUBLIC OF, ³PET/CT and Cyclotron Center, Masih Daneshvari Hospital, Shahid Beheshti University of Medical Sciences, Tehran, IRAN, ISLAMIC REPUBLIC OF, ⁴Pediatric Respiratory Diseases Research Centre, National Research Institute of Tuberculosis and Lung Diseases (NRITLD), Shahid Beheshti University of Medical Sciences, Tehran, IRAN, ISLAMIC REPUBLIC OF, ⁵Department of Medical Physics and Biomedical Engineering, Tehran University of Medical Sciences, Tehran, IRAN, ISLAMIC REPUBLIC OF, ⁶Research Center for Molecular and Cellular Imaging, Tehran University of Medical Sciences, Tehran, IRAN, ISLAMIC REPUBLIC OF.

Aim: It is well known that the attenuation correction is vital in PET/CT imaging, however the radiation dose received during CT imaging is considerably high for patients in PET/CT examination. The aim of this study was to evaluate the impact of automatic tube current modulation technique for patient dose reduction with respect to optimal image quality for diagnostic purpose. **Materials and methods:** At the first, CTDI and DLP, were calibrated by head and body PMMA phantom. In the next step, QA and cylindrical Phantom with 20 cm and 30cm in diameter were scanned with Discovery 690 GE PET/CT scanner that equipped with 64-slice CT. CT images were reconstructed with slice thicknesses of 2.5 and 3.75mm. Smart mA technique with noise indexes of 18 and 19, tube voltage of 80, 100 and 120kVp, tube current between 50 and 120mA, pitch number 0.984:1 and 1s rotation time were utilized. Image quality was assessed both qualitative and quantitative. MTF, image noise, $CTDI_{\text{vol}}$ and DLP parameters were also considered. **Results:** With increasing of slice thickness from 2.5 to 3.75 mm, in noise index (NI) of 18 with regard to 80kVp and 100kVp, the image noise was decreased from 10.74 and 6.72 HU to 3.63 and 2.71 HU respectively, when tube current was 80mAs. With increasing of tube voltage from 100 to 120 kVp, at 70mAs, in NI of 19, the noise diminished 56.76% and 17.44% when slice thickness varied from 2.5 to 3.75mm respectively. It would be clarify that, the CTDI changed from 1.95 to 4.64 mGy when tube voltages varied from 80 to 120kVp. CT images with 2.5 mm slice thickness were considered for 1mm resolution in QA phantom. It was shown that, the MTF increased from 0.20 to 0.32, with decreasing of tube voltage from 120 to 100kVp. **Conclusion:** significant lower image noise was observed with increasing slice thickness, however with regard to clinical purpose, the image quality for diagnostic issue was also valuable. It should be clarified that, the noise

level was decreased with increasing of tube voltage and the intensity of this behavior is more prominent in the lower slice thickness. Our results illustrated that, 3.75 mm slice thickness with noise index 19 and tube voltage of 120 kVp could be one of the optimal images with consideration of image noise and diagnostic purpose. **Keywords:** Computed tomography, Tube current modulation, Dose, Image noise, MTF

EP805

National Survey of Radionuclide Dose Calibrators used in Nuclear Medicine Departments in Bulgaria

M. Dimcheva¹, P. Trindev²; ¹Sofia Cancer Center, Sofia, BULGARIA, ²QC in Nuclear Medicine Consultant, Sofia, BULGARIA.

The main objective of this national survey was to provide data on the accuracy of activity measurements of the radionuclide dose calibrators used in nuclear medicine departments. **Materials and Methods:** In 2015 over a period of two months, measurements were performed on 24 dose calibrators in all 18 nuclear medicine departments in Bulgaria. The dose calibrators included in the survey were delivered in the last 37 years by 7 manufacturers as follows: Picker - 2 pcs, Robotron - 1 pc, Isomed - 3 pcs, Atomlab - 1pc, Capintec CRC-15R - 1pc, Curiemontor - 12 pcs, Comcer - 4pcs). For the purpose of our survey, a certified source of Cs-137 with manufacturer serial number LB 165 was used. After correction the decay between the date of certificate and the time of measurement the difference between the expected activity and the measured activity was expressed as a percentage of expected activity. Twenty measurements were performed for each dose calibrators thus collecting data for precision estimation according to χ^2 criteria. **Results:** Bulgarian State Regulations require that deviation between measured and expected values must be within ± 5 percent of the average. Errors greater than ± 5 % in the interval from -20.5 % to +16 % were found in 18 of the 24 dose calibrators. It is interesting to note that the result which was close to the expected one (error of 0.3 %) was delivered by the oldest dose calibrator - Picker. The precision of measurement was estimated for each dose calibrator according to χ^2 criteria. An acceptable χ^2 for 20 measurements would be in the range $11.7 < \chi^2 < 27.2$ since this is the $0.9 > P > 0.10$ range. It is common convention that fixes the $P = 0.90 - 0.10$ range as acceptable. All results for χ^2 in our survey were less than 1 which means that too little variation is shown. **Conclusion:** According to the results of this survey, the accuracy of dose calibrators does not meet the requirements of National regulations and need special attention and immediate reaction.

EP806

Quantification of pancreatic uptake in beta cell imaging with ⁶⁸Ga-exendin PET/CT using a 3D-printed anatomical pancreas-kidneys phantom and the NEMA NU2 Image Quality phantom

L. N. Deden¹, M. Buitinga², A. P. W. Meeuwis², S. Ruiter³, D. Lobeek², M. Gotthardt², E. P. Visser²; ¹Rijnstate, Arnhem, NETHERLANDS, ²Radboud University Medical Center, Nijmegen, NETHERLANDS, ³University of Twente, Enschede, NETHERLANDS.

Aim Recently, ⁶⁸Ga-labeled exendin has become available for beta cell imaging using PET/CT. Quantification in PET/CT has extensively been described, mostly for FDG whole body scanning in oncology. Pancreatic beta cell imaging using ⁶⁸Ga-exendin differs in several aspects: (i) pancreatic uptake is much lower than the unspecific uptake in the nearby kidneys, which could lead to artifacts and quantification errors, (ii) uptake in the remainder of the body is extremely low, and (iii) the larger positron range of ⁶⁸Ga ($R_{\text{max}}=8.9$ mm) as compared to ¹⁸F ($R_{\text{max}}=2.4$ mm) may lead to decreased spatial resolution. To study image quality and to optimize quantification for ⁶⁸Ga-exendin PET/CT, experiments were performed using the NEMA NU2 phantom, and a 3D printed, realistic organ

phantom containing fillable pancreas and kidneys and a background compartment. **Materials and Methods** The NEMA-phantom was filled with ^{68}Ga solutions with 10:1 sphere-to-background ratio with activity concentrations as specified by the EARL criteria [1]. The pancreas, kidneys, and background in the pancreas-kidneys-phantom were filled with ^{68}Ga solutions of respectively 2.2, 35.5 and 4.1×10^{-3} kBq/ml (ratios 1:16:0.002), based on typical patient data. Both phantoms were scanned during 10 min in a Siemens mCT scanner. Image reconstruction was performed using OSEM3D with TOF and PSF using varying numbers of iterations and subsets. Recovery coefficients (RC) for the NEMA spheres were calculated using the EARL A50 VOI settings. The pancreas was delineated manually on CT. **Results** Using our standard settings (3 iterations, 21 subsets, TOF, PSF, Gaussian filter 3 mm FWHM, transaxial pixel size 2 mm), RC_{A50} were 0.48, 0.66, 0.69, 0.76, 0.77 and 0.81 for increasing sphere diameters. Recovery of the pancreatic activity was 0.69. However, when dilating the CT-based VOI by 6 mm, this increased to 0.89. Increasing the number of iterations resulted in an inhomogeneous distribution of pancreatic activity. **Conclusion** The RC_{A50} values are higher than the “maximum values” using the EARL settings, which can be attributed to our smaller Gaussian filter size, smaller pixels and the use of PSF, which is more in line with state-of-the-art PET/CT scanners. Accurate quantification for the pancreas ($\approx 10\%$ deviation from the real activity value), can be obtained for ^{68}Ga using our standard settings in the Siemens mCT scanner. However, to obtain the proper pancreatic activity, dilation of the VOI by 6 mm was necessary. This might partly be contributed to the larger positron range of ^{68}Ga as compared to ^{18}F . [1] <http://earl.eanm.org>

EP-45 – Sunday, October 16, 2016, during Exhibition hours, e-Poster Area
Physics & Instrumentation & Data Analysis: Radiation Exposure & Protection

EP807

Adaptative dosology: toward a new compromise between acquisition duration and administered activity with a new high sensitivity PET/CT

O. CASELLES¹, E. GABIACHE¹, B. Delpuech¹, D. VALLOT¹, S. BRILLOUET¹, V. ROBERT², S. ZERDOUD¹, L. DIERICKX¹, F. COURBON¹; ¹Institut Claudius REGAUD -IUCT Oncopole, TOULOUSE, FRANCE, ²CIMOF, TOULOUSE, FRANCE.

PURPOSE To take benefit of a new generation of high sensitivity BGO non-TOF PET/CT system, new prescription rules have been established for FDG exams mainly to reduce injected doses. A double benefit was expected: both reduction of patient exposure and staff safety. **METHOD AND MATERIALS** Dose prescriptions corresponding to 944 ^{18}F FDG PET scans were analyzed (480 men and 464 women). Dose calculation was based on average weight dosology of $1.9 \text{ MBq}\cdot\text{kg}^{-1}$, but adapted to patient's morphology. For this purpose, this dosology was multiplied by the ratio between patient's actual weight and an Ideal Body Weight (IBW) given by the Devine's formula. Thanks to a homemade online software linked to an SQL database, gender, weight, height and injected activity were recorded and further analyzed. Minimum and maximum doses were set respectively to 80 MBq and 400 MBq (due to French law restriction). Patient effective dose was estimated from ICRP 106 tables. Staff exposure was assessed using both electronic and passive whole body and extremities dosimeters during 1 month. **RESULTS** Patient's statistics are summarized in the following table: Average staff $\text{Hp}^*(10)$ were respectively 3 and $2 \mu\text{Sv}/\text{patient}$ using thermoluminescence and electronic personal dosimeters, leading to annual average individual exposures of 4.5 and 3 mSv. Extremity dose $\text{Hp}(0.07)$ was in average $40 \mu\text{Sv}/\text{patient}$ being 61.5 mSv per year and per technologist. **DISCUSSION** Devine's formula tends to give low ideal weights, in particular for short women.

For this reason, average weight doses are respectively 10% and 20 % higher than expected for men and women. This weight dosology remains significantly lower than recommended prescriptions from EANM guidelines: for our routine $2 \text{ min}\cdot\text{bed}^{-1}$, the injected dose should be $\text{FDG}(\text{MBq})=7\cdot\text{weight}(\text{kg})$ giving respectively 3.25 and 2.95 times our average dose for men and women. Staff exposure is well under applicable annual limits in France (respectively 20 mSv and 500 mSv for body and extremities), and were significantly lower than exposures recorded during previous studies performed in our facility. **CONCLUSION** New high sensitivity PET/CTs allow to dramatically reduce both patient and staff exposure, and it is now worth considering to increase patient per day workflow with no concern for staff radiation protection.

EP808

Evaluation of Radiation Exposure Dose Rates: A comparative study between the two commercially available Y-90 microsphere products TheraSphere and SIR-Spheres

H. Tanyildizi¹, M. Demir², M. Abuqebitah², I. Cavdar³, L. Kabasakal², K. Sonmezoglu²; ¹Istanbul Kemerburgaz University, Vocational School of Health Services, Istanbul, TURKEY, ²Istanbul University, Cerrahpasa Medical Faculty, Istanbul, TURKEY, ³Istanbul University, Science Faculty, Istanbul, TURKEY.

Aim: In this study, we aimed to measure Bremsstrahlung radiation dose rates which emitted into the environment in Y-90 radioembolisation and to evaluate the radiation safety precautions. **MATERIALS AND METHODS:** 19 patients were included in this study. The activity amounts to be applied for treatment was determined by making a specific radiation dosimetry. The results of the evaluation of physicians, 12 patients underwent with SIR-Sphere, 7 patients underwent with TheraSphere. The dose rate measurements were taken with Geiger Muller probe in activity preparation, in the course of injection to the patients, in occurring radioactive wastes and during the patients' being discharged. **RESULTS:** It was found that staff was exposed in Therasphere application per unit activity, $1,3 \cdot 10^{-4} \mu\text{Sv}/\text{MBq}\cdot\text{h}^{-1}$ in the stage of preparation, $2,4 \cdot 10^{-4} \mu\text{Sv}/\text{MBq}\cdot\text{h}^{-1}$ in the stage of injection, and SIR-Sphere application per unit activity $24,5 \cdot 10^{-4} \mu\text{Sv}/\text{MBq}\cdot\text{h}^{-1}$ in the stage of preparation, $10,1 \cdot 10^{-4} \mu\text{Sv}/\text{MBq}\cdot\text{h}^{-1}$ in the stage of injection. Mean effective dose per application of staff with considering the working time of them, $0,92 \pm 0,48 \mu\text{Sv}$ and $3,22 \pm 0,89 \mu\text{Sv}$ were calculated in TheraSphere and SIR-Sphere applications, respectively. The measurement of mean dose rate which was taken at 1 meter from patients to be discharged was found $4 \pm 0,28 \mu\text{Sv}/\text{h}$ in Therasphere, $3,2 \pm 0,15 \mu\text{Sv}/\text{h}$ in SIR-Spheres. The dose rate measured in the surface of plastic container in which the radioactive wastes were put was found $0,5 \pm 0,1 \mu\text{Sv}/\text{h}$ for Therasphere, $1,1 \pm 0,08 \mu\text{Sv}/\text{h}$ for SIR-Sphere. **CONCLUSIONS:** As a result, it was assigned that Y-90 Therasphere application provided the radiation safety, in Therasphere and SIR-Sphere applications dose rate measured around patient was low, and the short term storage of radioactive wastes was sufficient.

EP809

Occupational exposure incurring from PET/CT patients

P. Fragoso Costa, M. J. Reinhardt, B. Poppe; Pius Hospital Oldenburg, Oldenburg, GERMANY.

Introduction: In this paper we evaluate the whole body occupational exposure of Nuclear Medicine technologists to annihilation photon fields resulting from F-18-FDG administration in the context of PET/CT imaging. This study aims to assess the whole body exposure of a team of 6 nuclear medicine technologists, with no previous PET/CT work experience. Furthermore, it is intended to examine separately the exposure resulting from each procedural step of the PET/CT technique. **Methods:**

In our department personal dosimetry motorisation is performed using Electronic Personal Dosimeters (EPD - RADOS-60E, Hamburg, Germany) and film dosimeters (MPA - MPA NRW Gliding Shadow Dosimeter GD01, Dortmund, Germany). The assessed group consisted of 6 technologists involved in Nuclear Medicine conventional procedures (diagnostic and therapy) and PET/CT. To identify the PET/CT specific exposure, all 6 technologists were encouraged to register their whole body personal dose equivalent [Hp(10)] read on EPD referring to each PET/CT procedural step. The PET/CT examination was divided in its constituent steps, which included: F-18-FDG dispensing, F-18-FDG withdrawal F-18-FDG administration and patient positioning. Included in this study were all the monthly official dosimetry records in the period from 2009-2014 (both EPD and MPA) and the step-wise evaluation exposure resulting from 2142 PET/CT investigations in the same period. Radiation protection measures (i.e. syringe shielding, wall shielding and video surveillance) were applied constantly over the whole study. Results: The average yearly personal dose equivalent registered on MPA was $577 \pm 294 \mu\text{Sv}/\text{year}$ and EPD $840 \pm 346 \mu\text{Sv}/\text{year}$. The personal dose equivalent for the 6 technologists performing PET/CT ranged from 11.52 to 23.77 nSv/MBq, averaged over the 5-year period. Whole body radiation dose to health professionals originated mainly from radiopharmaceutical administration (41.5%) and patient positioning (51.1%). In the interval from 2009-2014 the yearly average PET/CT specific personal dose was, respectively 19.74, 19.66, 19.71, 17.65, 20.23 and 16.53 nSv per injected MBq. Conclusion: The final results showed that the existing radiation protection measures are sufficient to keep exposures below 1 mSv/year. The observed intra-technologist PET/CT exposure range is mostly related to personal experience and patient-care strategies. Results referring to the exposure evolution over time indicate that there is no increasing tendency with the passing of years. We suggest carrying out an internal quality assurance program for radiation protection in order to keep occupational exposures at a minimum.

EP810

Monte Carlo simulations of risky non-standard operations during handling radiopharmaceuticals

M. Fulop¹, J. Hudzietzova², J. Sabol³, P. Ragan⁴, P. Povinec⁵, D. Bacek⁵; ¹Slovak Medical University, Bratislava, SLOVAKIA, ²Faculty of Biomedical Engineering, CTU, Prague, CZECH REPUBLIC, ³Crisis Management Department, PACR, Prague, CZECH REPUBLIC, ⁴ABRS, Ltd., Bratislava, SLOVAKIA, ⁵Bratislava Ion Technologies, Bratislava, SLOVAKIA.

Aim: The aim of this work is to introduce an identifying the non-standard risky operations and determining the values of personal dose equivalent $H_p(0,07)$ at the point of maximum exposure on hands. **Materials and methods:** The non-standard risky operations have been identified by interviews with staff, by control of video records or by reading of personal ring dosimeter. The MCNPX code and three voxel phantoms simulating various hand operations were used for searching of locality on hand with point of maximum exposure. Validation of MCNPX simulations of the voxel phantoms were performed in comparison with experiments with the physical phantoms. The thermoluminescent dosimeters of type MCP-Ns for measurements of the dose equivalent $H_p(0,07)$ were used. **Results:** The proposed method for identification of the non-standard risky operations during the administration to patient the liquid ^{131}I in cup and ^{18}F -FDG in syringe has been used. The MC simulations of voxel phantom of hand holding unshielded syringe with ^{18}F -FDG have shown significant (more than 4-fold) increase of the dose $H_p(0,07)$ on the hands at the points of maximum exposure that were in different localities than these that were monitored by TLD. By simulations of the voxel phantom of the hand has been shown to penetrating of ^{18}F positrons through walls of unshielded syringe with ^{18}F -FDG and the contribution of positron dose to hand irradiation was determined. Similarly, the contribution to the local

electron irradiation of the skin in the palm handling unshielded cup with ^{131}I was calculated. **Conclusion:** A method of identifying and modelling of the non-standard risky operations by the Monte Carlo simulation of voxel hand phantoms and determining the values of the relevant personal dose equivalent at the point of maximum exposure was introduced. The method can introduce appropriate measures for improving radiation protection that lead to a significant reduction of radiation burden to workers handling radiopharmaceuticals. **Literature:** 1) P. Ferrari, M. Sans Merce, A. Carnicer, L. Donadille, M. Fülöp, M. Ginjaume, G. Gualdrini, M. Mariotti, N. Ruiz : Main results of Monte Carlo studies carried out for nuclear medicine practices within the ORAMED project, Radiation Measurement, ISSN 1350-4487, Vol. 46, Issue 11, Nov 2011. **Acknowledgements:** This work was partially supported by the project SGS15/114/OHK4/1T/17

EP811

Change of collective effective dose of patients examined for suspected pulmonary embolism after introduction of multislice CT (MDCT) into a diagnostic process - single center experience

O. Lang^{1,2}, I. Kunikova¹; ¹Charles Univ, 3rd Med Fac, Dept Nucl Med, Prague 10, CZECH REPUBLIC, ²District Hosp, Dept Nucl Med, Pribram, CZECH REPUBLIC.

Aim: To compare radiation burden of patients with suspected pulmonary embolism evaluated by lung perfusion scintigraphy and multislice CT pulmonary angiography (MDCTPA) and to evaluate change of number of negative scintigraphic results after introduction of MDCTPA in our teaching hospital. **Material and methods:** We recorded number of patients examined in our department per year from 1991 to 2015 before and after introduction of MDCTPA (2009 - this year was not included). Effective dose was determined according to National radiological standards and UNSCEAR report 2008. We consider dose equivalent to lung parenchyma and total body effective dose from scintigraphy using 150 MBq of $^{99\text{m}}\text{Tc}$ MAA per patient. Dose from MDCTPA was calculated from DLP and tables of UNSCEAR report, number of patients was hypothetical (difference between average number of scintigraphy patients before and after introduction of MDCT). Percentage of negative results of lung perfusion scintigraphy during 1 year before and after introduction of MDCT was also recorded. Values are expressed as a median (min-max). **Results:** Number of patients examined by scintigraphy per year was 1718 (1304-2411), collective dose equivalent was 17008 (12910-23869) mSv for lung parenchyma and collective effective dose was 2835 (2152-3978) mSv for total body from 1991 to 2008. Number of patients examined by scintigraphy per year was 369 (290-475), collective dose equivalent was 3648 (2871-4703) mSv for lung parenchyma and collective effective dose was 608 (479-784) mSv for total body from 2010 to 2015. Hypothetical number of patients examined by MDCT per year was then 1350 (1243-1428) with collective effective dose of 9447 (8701-9996) mSv from lung CT and 20243 (18645-21420) mSv from MDCTPA from 2010 to 2015. 77 % of all scintigraphic reports both 1 year before (1496 patients) and 1 year after (452 patients) introduction of MDCT were negative, excluded pulmonary embolism. **Conclusion:** Number of patients sent to our department for lung scintigraphy due to suspected pulmonary embolism was stable for many years, so we can assume it would be stable also after introduction of MDCTPA. This assumption was used to estimate collective effective dose from CT examination. It was more than 7 times higher per year comparing to scintigraphy and even more than 10 times higher if we assume performing lung CT together with CTPA. The percentage of negative scintigraphic results remained unchanged. We can, therefore, assumed that 77 % of all MDCTPA examinations was also negative and irradiation of these patients was unnecessarily high.

EP812**Radiation Risk Assessment In Preclinical Imaging: Protective Techniques And Handling Procedures Developed To Minimize Occupational Exposures**

S. PREVOT¹, A. OUDOT¹, M. GUILLEMIN¹, M. MOREAU², J. VRIGNEAUD¹, K. CHAPELIER³, O. RAGUIN³, L. HOUOT¹, A. COCHET¹, B. COLLIN^{1,2}, F. BRUNOTTE¹; ¹Centre Georges François Leclerc, Dijon, FRANCE, ²ICMUB - UMR CNRS 6302, Dijon, FRANCE, ³Oncodesign, Dijon, FRANCE.

Introduction: Introduction of PET in preclinical imaging gave rise to new radiation safety concerns. Specific protective techniques and handling procedures have been developed to optimize staff exposures. The aim of this study was to evaluate the protection benefit focusing on 2 steps: injections, gaining a good IV access before handling activity and dissections, using a preclinical custom-made lead bench screen. A series of measurements was performed when holding an antibody derivative labelled with ⁶⁴Cu. **Material & methods:** A prospective series of 20 mice was studied. A 27G catheter was placed in the lateral vein of the tail to minimize injection time. Activity was handled in a shielded syringe (W, 5 mm, Medisystem). Dissections were performed behind a bench screen (Pb, 30 mm, Orion) 24 hours post injection. Time was registered for all tasks. Individual Whole-body (WB) doses Hp(10) were monitored with electronic dosimeters (DMC2000 XB, Mirion). Screen attenuation was evaluated with 2 dosimeters: one in front of the lead glass, the other behind. TLD rings (Landauer) were used to investigate finger doses Hp(0.07). Exposure rates were measured with a dose ratemeter (fieldSPEC, Aries) during injections and dissections at distances of 1 & 30 cm. Mean activity of 5-dose syringes was 138.7 ± 6.4 MBq. Mean injected activity was 19.1 ± 4.3 MBq per animal. **Results:** Average time was 8 seconds per injection, 6 minutes per dissection performed by an experienced operator. Hp(10) without a shield was $11 \mu\text{Sv}$ for injections, $9 \mu\text{Sv}$ for dissections. WB dose was kept below $1 \mu\text{Sv}$ behind the bench screen. Mean exposure rates measured at short distances are high: $1500 \mu\text{Sv.h}^{-1}$ at 1 cm from the shielded syringe (5 doses), from 25 to $10 \mu\text{Sv.h}^{-1}$ at 30 cm during injections, $83 \mu\text{Sv.h}^{-1}$ at 1 cm from the animal during dissections. Finger dose Hp(0.07) at the left index was about $30 \mu\text{Sv}$ per injection, below $100 \mu\text{Sv}$ (minimum exposure range) for dissections. **Discussion:** Injection time was divided by a minimum factor of 8 since fine gauge catheters have replaced needles. This technique also contributes to minimize the number of sticks, the risk of needlestick injuries and the uncontrolled movements linked to the weight of the shield that can lead to extravasation. Despite activities injected to small animals are low compared to medical practice, appropriate shielded devices together with minimizing time spent at short distance from sources are key factors to maintain WB & finger doses ALARA.

EP813**Optimization of radiation shielding of ⁶⁸Ga sources for positron emission tomography**

L. Auditore¹, E. Amato², M. E. Stipo², E. Grassi³, F. Fioroni³; ¹University Hospital G. Martino, MESSINA, ITALY, ²University of Messina, MESSINA, ITALY, ³Arcispedale S. Maria Nuova - IRCCS, Reggio Emilia, ITALY.

Aim: The use of ⁶⁸Ga positron emitter is gaining diffusion due to the advantages of its compact generator source combined with the increasing variety of labeling kits. However, the high energy of positrons ($E_{\text{max}} = 1.898$ MeV) can request special precautions during handling. We studied the radiation shielding of that isotope by means of Monte Carlo simulations and experimental measurements. **Materials and Methods:** We set up two independent Monte Carlo simulations, in Geant4 and MCNPX, reproducing a glass vial containing 9 ml of ⁶⁸Ga solution enclosed in a

single lead shield or a double-layered shield made of PMMA plus lead; different thicknesses were tested. The dose was scored in 0.8-mm thick LiF detectors. We also set up a measurement to evaluate the contribution of different shielding materials on absorbed doses. We put a glass vial of ⁶⁸Ga solution in a double-layered shield and we measured the doses on the external shield surface with and without the inner layer. The doses measurements were performed by 0.8-mm thick LiF detectors (174 mg cm^{-2}) and thin active layer ultra-sensitive LiF dosimeters (8.5 mg cm^{-2}). **Results:** the dose rates estimated from simulations (Geant4/MCNPX) were: $12.0/12.8 \mu\text{Gy/GBq}$ s after 10 mm of lead, and $11.4/11.9 \mu\text{Gy/GBq}$ s after 6 mm of PMMA plus 10 mm of lead. The experimental measurements confirmed that the use of an adequate lead thickness is sufficient to stop the beta and any bremsstrahlung x-rays produced. **Conclusions:** Adding an inner layer of low-Z plastic material gives a negligible contribution in radiation protection, since the bremsstrahlung radiation originating from positron slowing down is effectively shielded by the high-Z layer devoted to the attenuation of annihilation radiation.

EP814**Dose optimization is feasible in PET-CT protocols**

E. Prieto, V. Morán, B. García-García, E. F. Guillén-Valderrama, L. Sancho, J. M. Madrid, M. Rodríguez-Fraile, M. J. García-Velloso, J. A. Richter, J. M. Martí-Climent; Clínica Universidad de Navarra, Pamplona, SPAIN.

The standard protocol for whole body FDG PET/CT examination in our center consisted of an administration of 5.18 MBq/Kg , a PET acquisition of 3 min/bed, and a CT acquisition with 120 kV and a reference current-time product of 120 mAs with automatic current modulation. **Objective:** To evaluate the impact in patient effective dose and image quality of the reduction of reference current-time-product for the CT scan and the PET tracer activity in PET/CT protocols. **Methods:** A Siemens Biograph mCT TrueV PET/CT tomograph is available in our center. In February 2016, PET/CT protocol was modified within recommendations of international guidelines. Particularly, FDG activity was reduced from 5.18 to 4.44 MBq/Kg and reference CT current-time-product was reduced from 120 to 100 mAs. A total of 197 consecutive patients referred for a clinical oncological FDG-PET/CT scan were evaluated in this retrospective study. For each patient, demographic data, clinical characteristics, CT parameters (kV, effective mAs, dose-length-product DLP) and actual FDG activity (MBq) were recorded. Effective dose associated to the CT examination was calculated from DLP using the AAPM conversion factors while the effective dose associated with the radiotracer was calculated based on the ICRP values. The overall image quality (IQ score) was subjectively rated by the referring physician on a 4-point scale: 1 meant excellent, 2 good, 3 poor but interpretable, 4 poor not interpretable. Analyses were performed with STATA/IC 12. **Results:** A comparison of patient characteristics revealed no differences in patient's age, weight and gender among groups. **CT Results:** Effective current-time-product was 84.85 ± 25.25 and 70.87 ± 20.18 mAs for the 120 ref.mAs group (N=99) and the 100 ref.mAs group (N=98) respectively, and the related effective dose was 8.12 ± 2.99 mSv and 6.69 ± 2.31 mSv (U-Mann-Whitney $p < 0.001$). However, there was a significant reduction in the IQ score (mean 1.55 vs 1.25, Chi-squared test $p < 0.001$). Specifically, the number of excellent images decreased (77% to 47%) while the number of good images increased (21% to 51%). The number of poor studies (IQ score >2) did not changed. **PET Results:** The final mean administered activity of FDG for each group was 4.83 MBq/Kg (N=102) and 4.21 MBq/Kg (N=99), leading to a mean effective dose of 6.61 ± 1.41 and 5.76 ± 1.38 mSv in each group (t-test $p < 0.001$). Both groups of images were graded of equal image quality (mean IQ score 1.22 vs 1.17, Chi-squared test $p = 0.189$). **Conclusions:** Dose reduction is feasible in PET/CT protocols without a substantial impact in clinical diagnosis.

EP815**18F-Fluorodeoxyglucose (18F-FDG) Dose in Paediatrics: Comparison between our Protocol and the EANM Recommendations**

P. C. Gil, J. Isidoro, P. Lapa, G. Costa, J. Pedroso de Lima; Centro Hospitalar Universitário de Coimbra, Coimbra, PORTUGAL.

Aim: Paediatric patient dose optimization is an important issue in nuclear medicine practice, because the risk to radiation exposure is much higher in children than in adults when the same effective dose is delivered. This is particularly relevant in PET/CT, where this technique combines two imaging modalities with potential high radiation dose to patients. With this work we aimed to compare the activities administered in our department, using our specific protocol, with the recommended values given by the EANM Paediatric Dosage Card (v 01.02.2014). **Material and methods:** By using our Protocol, FDG PET/CT procedures in adults are performed with 3minutes/bed acquisition time, 60 minutes after administration of 4-6MBq/kg. Paediatric protocols were designed in order to associate a risk equivalent to that for adults (not the effective dose). With this in mind (and ensuring good quality of the images), we reduced the administered activity in children and increased the acquisition time (using, if necessary, a vacuum bag to assure children immobilization). For the comparison, we used the data of 433 exams (patients <18 years-old) performed between 2012 and 2015 in a General Electric Discovery ST4 PET/CT scanner. Then, patients have been divided in 3 groups according to their weight: G1 (<14kg, 3MBq/kg and 4minutes/bed); G2 (14-40kg, 3.5MBq/kg and 3.5minutes/bed) and G3 (>40kg, 4MBq/kg and 3minutes/bed), the mean administered activities were calculated and compared with the mean theoretical activities given by the Paediatric Dosage Card (PDC). **Results:** The mean administered activity and the mean theoretical activity were, respectively, for each one of the 3 groups: G1 (15 cases) 3.5MBq/kg versus 7MBq/kg (50% reduction); G2 (224 cases) 3.6MBq/kg versus 6.1MBq/kg (41% reduction) and in G3 (194 cases) 3.7MBq/kg versus 5.5MBq/kg (32% reduction). **Conclusion:** Protocol optimization should take in consideration the PET scanner performance and acquisition settings. In our department, without any compromise of the image quality, the administered activities are significantly inferior to the EANM dosage card recommendations for all weight categories considered.

EP816**Dosimetry for ⁹⁰Y DOTATOC therapies, calculation of absorbed dose to kidney**

D. Krstic¹, M. Jeremic², D. Nikezic¹, M. Matovic², R. Krstic³; ¹University of Kragujevac, Faculty of Science, Kragujevac, SERBIA, ²Clinical Center Kragujevac, Kragujevac, SERBIA, ³KVARK Company, Kragujevac, Kragujevac, SERBIA.

Peptide receptor radionuclide therapy (PRRNT) is a molecular radiation therapy which is used for the treatment of neuroendocrine tumors (NET). Depending on the size of the tumor, ⁹⁰Y-DOTATOC ([⁹⁰Y-DOTA0,Tyr3]-octreotide), ¹⁷⁷Lu - DOTATATE ([¹⁷⁷Lu-DOTA0, Tyr3,Thr8] - octreotide, or their combination in the form of a cocktail is applied. The kidney is the organ which receive the large dose at the activities normally used for PRRNT. During the several successive applications of therapy the renal function of kidney are deteriorated with the time (Barone et al., 2005; Hindorf et al., 2007). Previously, human ORNL phantoms were developed and applied for dose calculation in various irradiation situations (Krstic and Nikezic 2007). In this work, absorbed dose in kidneys were calculated for ORNL human

phantom, by means of MCNP5/X software (Monte Carlo Neutron Particle transport code, version 5/X). One option is to calculate doses from left and right kidney separately, since any of them is a separate source of beta radiation. This could be overcome in MCNP by presenting the source as the union of two regions (left and right kidney). Absorbed dose per one emitted beta particle in kidney of $6 \cdot 10^{-14}$ Gy was obtained as result of calculation in this work. This result should be multiplied with the number of disintegration of beta emitter in kidney in order to estimate absorbed dose in this organ. To estimate the number of disintegration in organs, it is necessary to develop biokinetic model which describes behavior of radionuclide in human body. Parameters of such model should be determined based on activity of ⁹⁰Y measured in urine and blood of patients. **References** 1. Barone R, Borson-Chazot F, Valkema R, Walrand S, Chauvin F, Gogou L, Kvols LK, Krenning E P, Jamar F, Pauwels S. Patient-Specific Dosimetry in Predicting Renal Toxicity with ⁹⁰Y-DOTATOC: Relevance of Kidney Volume and Dose Rate in Finding a Dose-Effect Relationship. J Nucl Med 46:99S-106S; 2005. 2. Hindorf C, Chittenden S, Causer L, Lewington V J, Mäcke H R, Flux G D. Dosimetry For ⁹⁰Y-DOTATOC Therapies in Patients with Neuroendocrine Tumors. Cancer Biother Radio 22:130-135; 2007. 3. Krstic D, Nikezic D. Input files with ORNL-mathematical phantoms of the human body for MCNP-4B. Comp Phys Commun. 176:33-37; 2007. 4. X-5 Monte Carlo Team. MCNP-a General Monte Carlo N-Particle Transport Code, Version 5 Vol. I: Overview and Theory. Los Alamos, NM: Los Alamos National Laboratory; LA- UR- 03- 1987; 2003.

EP817**Estimation of radiation dose for Radiation worker staff in Nuclear Medicine department**

h. A. aldousari, m. Izzeldin.; jabeer alahmad for nuclear medicine and molecular imaging ministry of health, alsoblekat, KUWAIT.

Objective: The aim of this study was to estimate the radiation dose for the radiation workers staff in Nuclear medicine department (Jaber Al Ahmad center for Nuclear medicine & molecular imaging center) in order to determine whether rotation of the radiation workers staff, is necessary and if the staff need more training about the ALARA principle. **Materials and Methods:** The effective radiation dose was measured for Radiation workers staff (Physician -Medical Physicist -Technologist - Nurse) in Nuclear medicine department, using (Thermoluminescent dosimeter TLD) the data collected annually - month by month from (January to December 2015) .The total staff 24 , 3 Physician , 2 Medical Physicist , 8 Technologist and 11 Nurse) . **Results:** The results show that the values of annual reading radiation dose for 28 radiation workers in nuclear medicine department ,the result obtained between (2.624 msv to 0.979 msv) for the staff , to comparing this result with the annual dose recommended from the (IAEA) 20 msv per year. (13.12% - 4.895%) . Physician received the highest dose (2.624 msv - 2.401 msv - 2.310 msv) - (13.12% - 12.005% - 11.55 %) from the recommended dose from (IAEA) and 2 of the Technologist also received high dose (2.48 msv - 2.311 msv)- (12.4 % - 11.56 %) from the recommended dose from (IAEA). **Conclusion:** This study showed that effective radiation doses to the radiation workers staff were within the annual dose recommended from the (IAEA). The highest dose was received by the physician because they regularly performed radionuclide injection using the butterfly technique with a syringe without shielding. The technologist receive high dose from the patient during the scan acquisition and when handling the radionuclide dose from hot lab to the scan room. The two technologist work in both camera PET/CT and SPECT/CT. All the staff have high awareness of radiation safety

and ALARA Principle. **Key Words:** Radiation dose, Thermoluminescent dosimeter TLD, Nuclear medicine department, radiation safety, ALARA Principle.

EP818

Diagnostic nuclear medicine procedures and resulting radiation dose of Tehran population in 2011-2014

F. Tabeie¹, P. Honari¹, I. Neshandar Asli¹, B. Shafiei¹, M. Amoui¹, M. Ansari¹, M. Eftekhari², D. Beygi²; ¹Shahid Beheshti university of medical sciences, Tehran, IRAN, ISLAMIC REPUBLIC OF, ²Research center for nuclear medicine, Shariati hospital, Tehran university of medical sciences, Tehran, IRAN, ISLAMIC REPUBLIC OF.

Aim: Nuclear medicine diagnostic procedures has developed during the past four decades in Iran. This paper reports trends of diagnostic nuclear medicine procedures in Tehran and the resultant population effective dose during 2011-2014. **Materials and methods:** The data including type and number of procedures, type of radiopharmaceuticals used, range of administered activities for each examination were collected from 61 (out of 65) nuclear medicine centers in Tehran from 2011 to 2014. The gender and age distributions of the patients are also collected from 10 different centers. The effective dose for each examination was calculated based on the effective doses per unit administered activities given by ICRP publications 53, 80 and 106. **Results:** Total number of examinations increased from 155199 in 2011 to 264099 in 2014 with an increase of 70.16%. The annual number of examinations per 1000 population increased from 13.66 in 2011 to 22.59 in 2014 with an increase of 65.37% during four years. Most frequent were examinations of the cardiac (69.22%), the skeleton (9.54%) and the thyroid (7.06%) averaged over the five years. Also the contributions of these three procedures to the collective effective dose were 50.20%, 6.4%, and 2.22%, respectively. **Conclusion:** Compared to an earlier investigation in 2003 considerable changes were found in the trends of nuclear medicine in Tehran during a decade. The frequency of cardiac examinations increased from 43.2% in 2003 to 69.22% in 2014. Thyroid examinations with the relative frequency of 26.7% in 2003 decreased to 7.06% in 2014. The number of overall examinations per 1,000 population of Tehran increased from 8.8 in 2003 to 22.59 in this study. The decrease in relative frequency of thyroid examinations could be due to the decreased incidence of goiter and the introduction of new techniques for diagnosis of thyroid disease. The large increase in relative frequency of cardiac examinations could be due to two main reasons. Firstly the increased reliance of cardiologists on values of nuclear cardiology in diagnosis and follow up. Secondly the considerable decrease in frequency of several nuclear medicine examinations such as thyroid, liver/Spleen hepatobiliary and renal. The increase of collective effective dose from 529.76 person-Sv in 2003 to 1439.98 person-Sv and hence the effective dose per capita from 44.06 μ Sv in 2003 to 13.18 μ Sv in 2014, could be explained because of an about 70% increase of examinations but about 6.5% increase in Tehran population.

EP819

Remarks on using F18 automatic dispenser and injector system

F. Zenone¹, A. Bruno¹, G. Belli¹, A. Baldoncini²; ¹Medical Physics dep. USL SUDEST Toscana, Arezzo, ITALY, ²Nuclear Medicine dep. USL SUDEST Toscana, Arezzo, ITALY.

Aim: In Arezzo Nuclear Medicine Department, Karl-100 automatic dispenser, equipped with automatic injector, was used to prepare F-18 syringe. The aim of this work is to investigate the advantage on using automatic system, compared with traditional system, in terms of occupational exposure to radiation, injection time and patient comfort. **Materials and Methods:** For comparison of exposure levels, three personal

dosimeters Polimaster-PM1610 were assigned for a week to several people working with hot cells designed for manual preparation of doses of F-18. We sampled separately exposures in the phases of preparation (approximately 260MBq), administration and removal of needles, using three different dosimeters (43 measurements for each phase). Operators were asked to write down the duration of each exposure. Subsequently, during the training phase, the same measurements were repeated using the Karl system (34 measurements for each phase). To improve the protection of operators, we have monitored the dose rate with an ionization chamber around the dispenser and injector. After injection, the residual activity in syringe and in tube was measured with a dose calibrator. The duration of each phase was preset. A form was provided to operators for reporting any problems that could result in the lengthening of the exposure time. The interview was conducted with patients to register if they had experienced any discomfort during the automatic injection. **Results:** Based on the dose rate measurements, it was suggested operators: to place the bottom of the dispenser next to the wall, to stay near to the display only when necessary, far from the top and the sides especially when F-18 flows. Handling the injector is problematic for the bottom unshielded. No difference resulted between the manual and automatic methods for preparation, neither for exposure during needle extraction; while average dose rate measurements showed a decrease of about 83% during the preparation of syringes (21 μ Sv/h vs 122 μ Sv/h; [66 \div 10] μ Sv/h vs [256 \div 26] μ Sv/h) and about 79% during the injection stage (17 μ Sv/h vs 83 μ Sv/h; [66 \div 10] μ Sv/h vs [256 \div 26]). The residual activity contained in the waste was comparable with the background. Patients have felt comfortable and relaxed. Some problems related to automatic system occurred during the dispensing and the injection with a little increasing in working time, but still it showed an overall benefit. **Conclusions:** It was developed an appropriate protocol for exposure measurements relating to the dispensing system. The automatic system showed appreciable dosimetric advantages and comfortable for the patient.

EP820

The impact of selected factors on the exposure of hands of workers during handling radiopharmaceuticals in nuclear medicine in the Czech Republic

J. Hudzietzova¹, M. Fulop², J. Sabol³, J. Doležal⁴, J. Kubinyi⁵; ¹Faculty of Biomedical Engineering, CTU Prague, Kladno, CZECH REPUBLIC, ²Slovak Medical University, Bratislava, SLOVAKIA, ³Department of Crisis Management, PACR, Prague, CZECH REPUBLIC, ⁴Department of Nuclear Medicine, University Hospital, Hradec Králové, CZECH REPUBLIC, ⁵Institute of Nuclear Medicine, GUH, Prague, CZECH REPUBLIC.

Aim: The fingers of workers that prepare and apply radiopharmaceuticals at nuclear medicine departments are often the most exposed parts of their body. The paper analyses the effects of basic factors, such as the technological equipment, the maintaining of operating procedures and the duration of practice on the size of the local exposure of workers' hands. **Material and method:** In order to determine the maximum exposure to the skin in terms of the personal dose equivalent $H_p(0.07)$, thermoluminescent dosimeters (TLDs) were used in specific positions where higher exposure was normally expected and also in the position where finger dosimeters are usually worn. So far, some 176 measurements in 29 persons from PET centres in the Czech Republic have been carried out. All these centres were equipped with different technological equipment and different procedures for the administration of radiopharmaceuticals were also used. During the measurements video shots were taken; based on these shots risky operations were identified. **Results:** From the comparison and confrontation of the personal dose equivalent - $H_p(0,07)$ - received by individual workers, it appeared that to a large extent the exposure could be reduced by means of the automatic application of certain procedures (using a cannula), where the average exposure at the relevant workplaces monitored was lower by 3-7 times than in the case of manual

administration (when a cannula was not used). In the absence of the shielding on syringes when radiopharmaceuticals are applied manually, the exposure may be much higher, namely almost 10 times higher (this exposure was around 8 mSv/GBq) compared to average exposure with the shielding. As to the duration of practice, at the beginning of work the exposure is relatively higher than later, when the workers acquire some experience and the skill. However, after some years the exposure tends to go up, mainly due to declining caution after several years of repeated routine operations. Conclusion: Based on the results obtained, appropriate steps aimed at the optimization of radiation protection at the selected nuclear medicine departments have been recommended. In addition, the importance of using shielded syringes has been pointed out, the application of automated procedures (especially during the application) recommended, and the positive impact of the continuous training and education of workers emphasized. Acknowledgements: This work was partially supported by the project SGS15/114/OHK4/1T/17.

EP821

Equivalent dose to the extremities during ^{18}F -FDG dispensing - Influence of manual dose dispenser

J. Oliveira¹, J. Hunter², E. Carolino¹, F. Lucena¹; ¹Escola Superior de Tecnologia da Saúde de Lisboa, Lisboa, PORTUGAL, ²Clinical Imaging Sciences Centre, Brighton, UNITED KINGDOM.

The radiopharmaceuticals used in PET are beta plus-emitters (β^+) and radiate gamma photons (γ) with energy levels of 511 keV. This is considerably higher in comparison with conventional nuclear medicine (NM), implying that the conventional amounts of lead and tungsten in shields are not enough for an appropriate radiation protection of the NM practitioners (NMP). Therefore, the need arose to develop dose dispensers that enables withdraw the ^{18}F -FDG activity administering to the patient, reducing the occupational exposure to radiation. The main objective of this study is to compare two dispensers, in relation to the equivalent dose (ED) to the extremities, the time spent on each procedure and the precision and accuracy of the measured activities. Two different manual dose dispensers were compared (D_A and D_B). ED to the extremities was calculated from the measurements of an automatic electronic meter (data logger) and a calibration factor. Variables were analyzed with Statistical Package for the Social Sciences (SPSS) and non-parametric tests were applied: Wilcoxon test (ED-both hands; ED-left hand; ED-right hand; time of procedure), Kruskal-Wallis test (reproducibility) and Pearson Correlation (time/activity and ED). Differences were assumed statistically significant for p -values < 0.05. Accuracy and precision were evaluated through control chart. Although NMP received more ED with the D_B , there were no statistically significant differences ($p > 0.05$) between dispensers for both hands. Also, ED for right hand compared with left hand for D_A and D_B found $p > 0.05$. The dominant hand does not contribute to higher ED to the hands suggesting a bigger contribute to the ED from the practical procedure. There were statistically significant differences between the times of procedure with the two dispensers ($p = 0.007$), which is related with the lack of practice from NMP with D_B . It was found that both instruments are robust and accurate, although not precise.

EP822

Patient and staff radioprotection aspects in cardiologic nuclear medicine examinations

P. Saletti¹, M. Bartoli², L. Capaccioli¹, G. Belli¹; ¹Health Physics Unit - Azienda Ospedaliero-Universitaria Careggi, Florence, ITALY, ²University of Florence, Florence, ITALY.

Introduction: Cardiovascular diseases are nowadays spread pathologies and early diagnostic staging may support an adequate therapeutic

treatment. In nuclear medicine, both PET and SPET are currently used depending on clinical question with specific radiopharmaceuticals, activities and procedures resulting in significant absorbed doses by staff and patients. The aim of this work is an evaluation of dosimetric impact on patients and staff in nuclear medicine cardiologi by means respectively of ICRP 53 and 80 evaluations and measured dose rates from manipulated syringes and patients. **Materials and methods:** At our centre, cardiac scintigraphies are carried out with GE Venti gammacamera by means of 370MBq of ^{99m}Tc -MIBI administered for both rest and stress acquisition. PET cardiac examinations are instead performed at Philips Gemini TF PET/CT with 555-740 MBq of ^{13}N produced by a GE Minitrace cyclotron installed at radiopharmacy. For both procedures, a total amount of 10+10 patients were analysed, meaning that syringe and patient dose rate were measured at representative distances and normalised to 1GBq at measurement time. Moreover, permanence times in proximity to radioactive sources were recorded relating them to different actions (syringe manipulation, radiopharmaceutical administration, patient positioning...) in order to calculate absorbed dose by a simple multiplication. Patient dosimetry was assessed for ^{13}N and ^{99m}Tc -MIBI data from literature data. **Results:** Permanence times where measured for the whole process starting from syringe extraction from hot cell (10s), radiopharmaceutical administration (30s), patient preparation/assistance (300s) and positioning (70s) on scan bed for both PET and SPET procedures. Dose rate related to described operations was measured and equivalent doses was then calculated and normalized at 1GBq, ranging from 0.6 μSv to 12 μSv for total body exposure and from 25 μSv to 80 μSv for extremity exposure from ^{13}N , while, in case of ^{99m}Tc -MIBI, total body exposure and extremity were found to be respectively less than 1 μSv and 3 μSv . About patient internal dosimetry, effective dose from ^{99m}Tc -MIBI was found to be 4-9 mSv/GBq while, concerning ^{13}N , was less than 2mSv/GBq. **Conclusion:** A simple and practical method for staff exposure evaluation was assessed for cardiologic procedures in nuclear medicine, while literature data were used to account for patient internal dosimetry. Even if a small sample of patients was analyzed, it clearly appears that staff exposure is greater in PET cardiologic examinations with ^{13}N while, due to physical and pharmacological characteristics, is preferable in terms of patient radioprotection even if restricted to cyclotron-equipped centres.

EP823

First Impressions on a Commercial Patient Dose Management System in Nuclear Medicine

T. Tolvanen^{1,1}, A. Karlsson², C. Lafay³, F. Zanca³, M. Teräs^{1,4}; ¹Dep of Medical Physics, Turku University Hospital, Turku, FINLAND, ²Turku PET Centre, Turku University Hospital, Turku, FINLAND, ³GE Healthcare, Buc, FRANCE, ⁴Institute of Biomedicine, University of Turku, Turku, FINLAND.

Authorities require the use of ALARA principle and have developed Diagnostic Reference levels (DRL). EANM have launched guides like the paediatric dose chart and have efforts to standardise and harmonise protocols with the help of EARL (ResEARCh 4 Life). In Radiology several commercial or freeware dose management systems exist. The purpose of current study is to outline how the implementation of software for NM data management can help setting up best practices as it relates to injected activity and protocol standardisation, in order to achieve better patient outcomes. **Materials and Methods:** In November 2015 an existing dose monitoring system DoseWatch (GE Healthcare) was upgraded with a module for monitoring NM data and connected to two PET/CT scanners (GEDVCT, GED690). Between November 2015 and April 2016 data from more than 700 single-injection exams have been collected including radiopharmaceutical type, activity, effective dose, protocol and operator name associated with the exam. Protocol standardisation, protocol selection and administered activity for oncology follow up patients and impact of BMI on administered activity was assessed. **Results:** From present

reporting it is possible to compare protocol doses with DRLs. One difficulty is that although weight and height are present in database the reporting tool has BMI as preference. Data collection shows non-standardised protocol names across the scanners as well as some variability in administered activity for the same clinical indication for the two devices. For the D690 device, the most used Whole body protocol was analysed in more in details. The analysis of activity by BMI shows that the administered activity is not always tailored to the BMI: median activity is almost the same for [18,5 - 25] and [25 - 30] BMI categories (280 and 286 MBq respectively). Data from follow-up exams (oncology) have also been analysed. Although the same device is always used for the follow, the protocol changes in 50% of the case. Program development needs actions to handle dynamic studies where tracer information is normally set after the end of the study as well as IQ assessment. **Discussion:** The implementation of NM data management as complementary tool to dose management allows identifying variation within the same protocol, driving protocol optimization and standardization. The tool works best as the number of devices connected grows (hospitals or national database). The effort made so far is a good start as dose management will have a role in developing national and international standards.

EP-46 – Sunday, October 16, 2016, during Exhibition hours, e-Poster Area
Radiopharmaceuticals & Radiochemistry: Radiopharmaceuticals - PET

EP824

Abnormal PSMA Accumulation in Chronic Inflammation

K. Oksuzoglu, T. Ones, H. T. Turoglu, T. Y. Erdil; Marmara University School of Medicine, Nuclear Medicine Department, Istanbul, TURKEY.

Introduction: Prostate-specific membrane antigen (PSMA) is a specific type II membrane glycoprotein. 68Ga-PSMA PET/CT is a new modality for imaging prostate carcinoma. We present the case of a 72-year-old man with a history of prostatic adenocarcinoma who had a PSMA PET/CT scan for staging. 68Ga-PSMA PET images showed moderate uptake in the right hemithorax, corresponding to pleural thickening seen on the CT images. Histopathologic examination revealed the diagnosis of chronic inflammation. It is important to keep in mind other alternative diagnoses such as chronic inflammation when PSMA PET/CT identifies uptake at an atypical site. **Case Presentation:** A 72-Year-Old male patient with prostate cancer (PSA değeri:12.47ng/ml) underwent skeletal scintigraphy. Suspicious Tc-99m MDP uptake was seen on right hemithorax. 68Ga-PSMA PET revealed increased heterogeneous uptake in the right posterolateral segment of prostate gland compatible with prostate needle biopsy findings (adenocarcinoma). 68Ga-PSMA PET images showed non-expected moderate uptake in the right hemithorax too, corresponding to pleural thickening seen on the CT images (first intercostals space) and neighbourhood of the 4 and 6 rib. Thoracoscopic biopsy was performed to establish a definitive diagnosis. The results of histopathological examination indicated the features of chronic inflammation. **Conclusion:** Prostate-specific membrane antigen (PSMA) is a specific type II membrane glycoprotein and its expression is suppressed by androgen in prostate cancer. PSMA is a promising target for both therapy with monoclonal antibodies and imaging. PSMA is not specific to the epithelium of prostate gland and is expressed in normal other tissues too, for example urinary bladder, proximal tubules of kidney, liver, salivary glands, oesophagus, stomach, small intestine and neuroendocrine cells in the colon. Some malignant lesions such as transitional cell carcinoma, renal cell carcinoma, colon carcinoma, bronchial carcinoma, adrenocortical carcinoma, follicular and papillary thyroid carcinoma, glioblastoma, follicular lymphoma; and some benign lesions (schwannomas, thyroid and adrenal adenoma, desmoid tumour) can cause abnormal PSMA-ligand uptake that may be confused with metastases. Also, PSMA is expressed in non-neoplastic reparative and regenerative neovasculature tissues like

endothelial cells in keloids, granulation tissue from heart valves and pleura, and different phases of cycling endometrium. Chronic inflammation should be kept in mind when interpreting whole-body PSMA PET/CT images and PSMA-avid lesions should be confirmed with tissue biopsy before treatment. As far as we know, this is the first case report of a patient with PSMA accumulation associated with chronic inflammation.

EP825

Preclinical *In Vivo* and *In Vitro* Comparison of the Translocator Protein PET Ligands ¹⁸F-PBR102 and ¹⁸F-PBR111: Metabolism studies

M. Peyronneau¹, C. Loch², S. Eberl^{2,3}, L. Wen^{2,3}, D. Henderson², I. Greguric⁴, J. Verschuer², T. Pham⁴, P. Lam², F. Mattner², T. Bourdier², A. Mohamed^{2,5}, A. Katsifis^{2,6}, M. Fulham^{2,3,5}; ¹IMIV, CEA, Inserm, Univ.Paris-Sud, CNRS, Université Paris-Saclay, CEA-SHFJ, Orsay, FRANCE, ²Department of Molecular Imaging (PET and Nuclear Medicine), Royal Prince Alfred Hospital, Missenden Road, Camperdown, NSW 2050, AUSTRALIA, ³Faculty of Engineering and Information Technologies, University of Sydney, Sydney, NSW 2006, AUSTRALIA, ⁴Life Sciences, ANSTO, New Illawarra Road, Lucas Heights, NSW 2234, AUSTRALIA, ⁵Sydney Medical School, University of Sydney, Sydney, NSW 2006, AUSTRALIA, ⁶Faculty of Pharmacy, University of Sydney, Sydney, NSW 2006, AUSTRALIA.

Aim: [¹⁸F]PBR111 and [¹⁸F]PBR102 have been characterized as high affinity radioligands for imaging the translocator protein (TSPO) using PET in several animal models of neuroinflammation [1, 2]. Cerebral white matter inflammation has been recently assessed by PET with [¹⁸F]PBR111 in Multiple Sclerosis [3]. In this study, our aim was to evaluate and compare the *in-vitro* metabolic profile of PBR102 and PBR111 in rat and human microsomes to the *in-vivo* binding and metabolite uptake in the brain of non-human primates (Papio Hamadryas). **Materials and Methods:** The *in vitro* metabolism of PBR102 and PBR111 was carried out using rat and human liver microsomes followed by LC/MS and MS-MS analysis. [¹⁸F]PBR102 and [¹⁸F]PBR111 were prepared by nucleophilic substitution of their corresponding *p*-toluenesulfonyl precursors with ¹⁸F-fluoride. PET-CT brain imaging with arterial blood sampling and metabolite analysis [4] was performed in non-human primates, providing a metabolite-corrected input function for kinetic model fitting. Blocking and displacement PET-CT scans, using PK11195, were also performed. **Results:** Rat and human liver microsomal incubation-LC/MS analyses identified three main metabolites: O-dealkylated, hydroxylated and N-deethylated derivatives of PBR102 and PBR111. The O-dealkylated compounds were the major metabolites in both species; human liver microsomes were less active than those in rat. *In vivo*, the radiotracers decreased quickly in baboon plasma to 20% for [¹⁸F]PBR102 and 15% for [¹⁸F]PBR111 at 110 min post injection. The higher bone uptake for [¹⁸F]PBR111 observed during the displacement and blocking whole-body PET-CT studies (due to [¹⁸F]fluoride) may result from differences in the metabolism of [¹⁸F]fluoroacetate ([¹⁸F]PBR102) and [¹⁸F]fluoropropionate ([¹⁸F]PBR111), generated by O-dealkylation in the liver and further oxidation in plasma. Excretion of both tracers was through the urinary and biliary systems. Brain PET-CT studies showed similar kinetic parameters for baseline and blocking studies for tracer delivery to the brain (K₁) with low non-specific binding and lack of significant metabolite uptake in the brain. **Conclusions:** [¹⁸F]PBR102 and [¹⁸F]PBR111 display distinct metabolic profiles in rat and non-human primates, in agreement with *in-vitro* data. Whereas radiometabolites contributed to non-specific binding and confounded *in-vivo* brain analysis in rodents, their impact in primates was less pronounced and should be even less in humans. Hence, both [¹⁸F]PBR102 and [¹⁸F]PBR111 appear suitable for TSPO imaging with PET. *In-vitro* metabolite studies can be useful to predict *in vivo* radioligand metabolism and can assist in the improved design and development of radioligands for neuroreceptor imaging.[1]Fookes et al.,JMedChem,2008;51(13):3700-12. [2]Amhaoul et al.,NeurobiolDis,2015;85:526-539.

[3]Colasanti et al., JNuclMed, 2014;55(7):1112-8. [4]Katsifis et al., NuclMedBiol, 2011;38(1):137-48

EP826

Radiosynthesis of fluorinated quinuclidine 1,2,3-triazole derivatives to image $\alpha 7$ -nicotinic acetylcholine receptor by PET

J. Vercouillie¹, P. Tangpong¹, C. Mothes¹, A. Ouach², F. Suzenet², F. Buron², A. Domene¹, S. Routier², S. Chalou¹, D. Guilloteau¹; ¹INSERM 930, Tours, FRANCE, ²ICOA, Orléans, FRANCE.

Objective: Changes in brain alpha-7 nicotinic acetylcholine receptor ($\alpha 7$ nAChR) density has been associated with various disorders such as Alzheimer's disease, schizophrenia and depression. To understand pathophysiology of these disorders and to develop therapeutic approaches molecular imaging such as PET will be suitable. In this aim we developed fluorinated PET ligands of $\alpha 7$ nAChR based on a quinuclidine-1,2,3-triazole scaffolds^(1,2). The present study reports the radiosynthesis of six highly potent ligands (affinity for the target ranging from 0.18 to 16 nM) their radiochemical stability and their biological evaluation in rodents. **Method:** The ¹⁸F was prepared by nuclear reaction ¹⁸O(p,n)¹⁸F and then was transferred to a synthesizer module and was passed through a Sep-Pak® QMA cartridge. Reactivity of ¹⁸F was exalted by conventional procedure prior to the addition of the precursors diluted either in ACN or in DMSO. As two derivatives display an ortho fluoro pyridine moiety DMSO was used instead of ACN for the preparation of fluoroalkyls compounds. Reactions were conducted under conventional heating or under microwave when required. All tracers were purified, formulated and their radiochemical stability was checked up to 4h in the vehicle and in rat plasma solution. Radiotracers were evaluated by μ PET and/or biobistribution studies using sham and rats pretreated with methyllycaconitine (MLA), a selective alpha 7 receptor antagonist to determine their nonspecific binding. **Results:** Depending of the tracers, radioligands were obtained in low to moderate yields 7-30% (decay-corrected). Their radiochemical purity was >98% of all products and specific activity in the range of 10-86 GBq/ μ mol. All derivatives were radiochemically stable in the formulation media and in rat plasma up to 4h. Evaluation of the tracers demonstrated a moderate blood brain barrier uptake but a quite homogenous distribution in the CNS areas and a high nonspecific binding in comparison to the current ¹⁸F $\alpha 7$ reference ligand [¹⁸F]ASEM. **Conclusion:** We developed new high affinity $\alpha 7$ nAChR ligands that we radiolabeled with ¹⁸F. However, they showed a mainly nonspecific binding in vivo in rats in comparison to [¹⁸F]ASEM. This result will contribute to a better knowledge of the relationships between the chemical structure and in vivo brain binding of $\alpha 7$ nAChR tracers. **Research Support:** This research was supported by grants from the Région Centre (IMAD, BIALz), the ANR programs (ANR-10-MALZ-0004, ANR-11-LABX-0018-01) and France Alzheimer. References: 1-Routier S et al. 2012. WO2012143526. 2-Ouach A et al. Eur J Med Chem. 2016. 107:153-64.

EP827

Dosimetry and whole body distribution of [¹⁸F]PE2I in healthy volunteers

H. Lizana¹, L. Johansson¹, A. Larsson¹, J. Axelsson¹, J. Linder¹, M. Ögren¹, A. Varrone², C. Halldin², S. Jakobson Mo¹; ¹Umeå University, Umeå, SWEDEN, ²Karolinska Institutet, Stockholm, SWEDEN.

Aim: The recently developed radioligand [¹⁸F]FE-PE2I is a promising tracer for PET imaging of the dopamine transporter (DAT) in human brain. The higher DAT selectivity of the tracer compared to [¹²³I]FP-CIT and the higher temporal and spatial resolution in PET compared to SPECT offers detailed imaging of the DAT distribution in striatal and extrastriatal compartments. The aim of this study was to ensure that diagnostic imaging with

[¹⁸F]FE-PE2I is performed with acceptable radiation doses in patients. Effective dose estimation has previously been done in cynomolgus monkeys. This is the first whole body (WB) distribution and dosimetry study of [¹⁸F]FE-PE2I in humans, conducted within the clinical trial PEARL-PD (Eudra CT: 2015-003045-26). **Materials and methods:** Five healthy volunteers (>60 y), mean weight 69.5 kg, received a mean [¹⁸F]FE-PE2I activity of 2.40 MBq/kg. Three PET scans from head to thigh were performed within the first 30 minutes. PET/CT WB scans (head-feet) were performed at 30 minutes, 2 h, 4 h and 6 h post injection. The first PET/CT WB scan was done with low-dose CT (30mA) for attenuation correction and anatomical localisation, whereas ultra-low dose CT (10mA) were used for remaining scans. Blood radioactivity was sampled at each scan and total activity in voided urine was measured. VOIs were drawn around 17 organs and absorbed and effective doses were calculated using the IDAC software. **Results:** Preliminary analyses showed that immediately after injection the highest activity concentrations (10-20 kBq/ml) were seen in the stomach, liver and heart (4.5%, 14% and 1.8% of the injected activity, respectively). Thirty minutes post injection the activity concentration was highest in the gallbladder (15 kBq/ml, 0.2% of injected activity). The stomach and liver received the highest absorbed doses (0.03 mGy/MBq), followed by the kidneys (0.02 mGy/MBq). Within the first 7 hours about 9% of the injected activity was excreted with the urine. The effective dose was 0.017 mSv/MBq, resulting in an effective dose of 3.4 mSv for 200 MBq. **Conclusion:** The most frequently used ¹⁸F-labelled tracer [¹⁸F]FDG gives an effective dose of 0.019 mSv/MBq, similar to the 0.017 mSv/MBq calculated in this study. The effective dose mentioned above is in the same range as previously published data for [¹⁸F]FE-PE2I in non-human primates. The effective dose is somewhat lower than for 185MBq [¹²³I]FP-CIT (4.6 mSv). These preliminary human dosimetry data, together with the suitable imaging properties of [¹⁸F]FE-PE2I suggest its utility as a diagnostic agent for DAT imaging.

EP828

Demonstration of $\alpha_v\beta_6$ target engagement in healthy rat using [¹⁸F]IMAFIB

M. Onega, S. Tang, S. Ashworth, C. Plisson, C. Coello, L. Wells, J. Passchier; Imanova Limited, London, UNITED KINGDOM.

Background/ Aim: Expression of the epithelial-specific integrin receptor $\alpha_v\beta_6$ is up-regulated during the formation of scar tissue following injury as well as in certain carcinomas. Significant efforts are ongoing to develop new therapeutics for this target, particularly in the areas of lung, liver and kidney fibrosis. The fluorine-18 labelled peptide [¹⁸F]IMAFIB (aka [¹⁸F]A20FMDV2), was previously demonstrated to be a potent and selective ligand for delineation of $\alpha_v\beta_6$ receptors *in vivo* with PET^{1,2} and is currently under evaluation in patient populations in our institution to assess its clinical utility. Previous MicroPET studies with [¹⁸F]IMAFIB in healthy rat under baseline conditions and following administration of homologous block of IMAFIB (2 mg/kg; *i.v.*) demonstrated a reduction in V_T in the aforementioned tissues as assessed by quantitative kinetic analysis using the metabolite corrected plasma arterial input function.³ Evidence suggests $\alpha_v\beta_6$ receptors are expressed in healthy tissue such as liver, stomach and lung, albeit in low concentrations. The objective of the present work was to test if [¹⁸F]IMAFIB could be used in healthy animals using a simple and efficient tissue dissection protocol to demonstrate target engagement of novel therapeutics. **Materials and Methods:** [¹⁸F]IMAFIB was labelled using a GMP compliant and fully automated process as described previously.³ Anaesthetised Sprague-Dawley rats were injected with [¹⁸F]IMAFIB (*i.v.*) under baseline conditions (n=6) or following pre-dosing with 2 mg/kg unlabelled IMAFIB (n=6). Animals were sacrificed at 30 min post injection of [¹⁸F]IMAFIB and tissues and blood removed for measurement of radioactivity using an automated gamma counter. Subsequently, tissues were weighed and SUV values calculated. **Results and Conclusion:** Uptake of [¹⁸F]IMAFIB was significantly reduced in lung, liver, stomach wall and

kidney medulla following pre-treatment with unlabelled IMAFIB (SUV_R baseline vs post-dose ($mean \pm SD$): lung, 1.56 ± 0.76 vs 0.40 ± 0.06 ; liver, 4.08 ± 1.11 vs 2.45 ± 0.90 ; stomach wall 1.99 ± 1.05 vs 0.51 ± 0.17 and kidney medulla 115.1 ± 55.7 vs 41.6 ± 24.0 ; unpaired t-test $P < 0.05$). These results demonstrate a specific binding signal in healthy rats and support the data obtained from dynamic PET scans. In summary, this study shows that [^{18}F]IMAFIB may be used to demonstrate target engagement in healthy tissues such as lung, liver, stomach wall and kidney medulla without the need for an animal model of disease. **References:** [1] S. H. Hausner *et al.*, Cancer Research 2007, 67, 7833. [2] R. J. Slack *et al.*, Pharmacology, 2016, 97, 114–125. [3] M. Onega *et al.*, EANM 2015, P.279. *Manuscript for publication in preparation.*

EP829

High Affinity F-18 Labeled Prostate Specific Membrane Antigen (PSMA) Inhibitors: In Search of a Facile Approach to High Radiochemical Yield

A. Amor-Coarasa, J. M. Kelly, S. Ponnala, W. Qu, J. W. Babich; Division of Radiopharmaceutical Sciences, Department of Radiology, Weill Cornell Medicine, New York, USA, New York, NY, UNITED STATES.

Aim: Despite the value of an ^{18}F -labeled ligand targeting PSMA, few promising candidates have been reported to date. Furthermore, those currently in clinical use multiple step, prosthetic group labeling approach rather than direct fluorination. We sought to address these inconveniences by developing a high yield, high specific activity radiosynthesis of ^{18}F -labeled PSMA inhibitors while minimizing synthetic steps and time. **Methods:** Fluorination was carried out with no-carrier-added [^{18}F]fluoride on a range of substrates and prosthetic groups. Four strategies were employed to label a series of *EuK* containing PSMA inhibitors: direct [^{18}F]fluorination, [^{18}F]fluorination via isotopic exchange, [^{18}F]fluoroethylation using either 2-[^{18}F]fluoroethyltosylate ([^{18}F]FET) or 2-[^{18}F]fluoroethylbromide ([^{18}F]FEBr), and [^{18}F]fluorination via click chemistry with 2-[^{18}F]fluoroethylazide ([^{18}F]FEA). [^{18}F] incorporation was determined using radioHPLC. **Results:** Direct fluorination via nucleophilic aromatic or aliphatic substitution was unsuccessful, with decay corrected RCY (dcRCY) $< 1\%$. Isotopic exchange was attempted on an activated fluorophenylurea moiety and conversion was 2–5%. When a 4-nitrophenylurea was used as precursor, the labeling reaction underwent a series of color changes consistent with proton transfer from the urea to fluoride. [^{18}F]FET was prepared from ethylene ditosylate in 5 min at $100^\circ C$ in $> 70\%$ dcRCY. Reactivity towards primary and secondary amines was poor and evidence of base-catalyzed decomposition of [^{18}F]FET via elimination of TsOH. [^{18}F]FEBr was prepared from 2-bromoethyltriflate in 8 min and purified by distillation at $100^\circ C$ at approximately 30% dcRCY. Reactivity towards secondary amine groups remained low in both neutral and basic conditions. [^{18}F]FEA was prepared from 2-azidoethyltosylate ($> 90\%$ dcRCY) for later click reaction in 10 min at $80^\circ C$. [^{18}F]FEA was isolated by distillation at $130^\circ C$ in $> 60\%$ dcRCY and $> 97\%$ RCP. The subsequent reaction between [^{18}F]FEA and a PSMA-targeting alkyne precursor was achieved in 30–50% dcRCY at $100^\circ C/Cu^+$. A series of six PSMA inhibitors were [^{18}F]fluorinated by this approach and evaluated in preclinical mouse models. **Conclusions:** Direct [^{18}F]fluorination of urea-based PSMA inhibitors is highly disfavored due to the interaction between [^{18}F]fluoride and the urea protons. Therefore a prosthetic group approach to the [^{18}F]fluorination of PSMA inhibitors is preferred. Both the 2-[^{18}F]fluoroethyltosylate and [^{18}F]fluoroethylbromide synthons were prepared in reasonable dcRCY and high specific activity, but alkylation of precursors was unreliable and required extensive protection/deprotection chemistry. In contrast, the 2-[^{18}F]fluoroethylazide synthon was synthesized with high dcRCY and chemical purity and reacted rapidly with alkyne precursors without requiring protecting groups. This strategy was employed to synthesize six high affinity ($IC_{50} < 35$ nM) PSMA inhibitors for PET imaging of prostate cancer.

EP830

First-in-human studies of imidazopyridineacetamide, [^{11}C]CB184, as a novel 18 kDa translocator protein seeker

J. Toyohara¹, M. Sakata¹, K. Ishibashi¹, K. Wagatsuma¹, K. Hatano², K. Ishiwata^{1,3,4}, K. Ishii¹; ¹Tokyo Metropolitan Institute of Gerontology, Tokyo, JAPAN, ²University of Tsukuba, Tsukuba, JAPAN, ³Southern TOHOKU Research Institute for Neuroscience, Koriyama, JAPAN, ⁴Fukushima Medical University, Fukushima, JAPAN.

Aim: An imidazopyridineacetamide, *N,N*-di-*n*-propyl-2-[2-(4-[^{11}C]methoxyphenyl)-6,8-dichloroimidazol[1,2-*a*]pyridine-3-yl]acetamide ([^{11}C]CB184), is a potential radioligand for evaluation of 18 kD translocator protein (TSPO) overexpression in the brain by positron emission tomography (PET). In the present study, we performed safety evaluation and initial brain imaging of [^{11}C]CB184 in healthy human subjects. **Materials and methods:** Five healthy male subjects underwent 90-min dynamic [^{11}C]CB184 scans of brain regions with arterial blood sampling. For anatomic coregistration, T1-weighted magnetic resonance imaging was performed. Metabolites in plasma and urine were analysed by high performance liquid chromatography (HPLC). The total distribution volume (V_T) for [^{11}C]CB184 was evaluated by Logan graphical analysis ($t^* = 30$ min). **Results and conclusion:** The administered activity and mass of [^{11}C]CB184 were 571 ± 165 MBq and 4.1 ± 2.5 μg , respectively. There were no adverse or clinically detectable pharmacologic effects in any subjects throughout the study period. No clinically important trends indicative of a safety signal were noted for laboratory parameters, vital signs, or electrocardiogram parameters. A 90-min dynamic scan showed a rapid initial uptake of the radioactivity in the brain followed by prompt clearance. The [^{11}C]CB184 was homogeneously distributed in the grey matter. The V_T of [^{11}C]CB184 was highest in the thalamus (5.1 ± 0.4 ml/cm³) followed by cerebellar cortex (4.6 ± 0.3 ml/cm³) and others. The lowest V_T of [^{11}C]CB184 was observed in the head of caudate nucleus (3.2 ± 0.4 ml/cm³). Although regional differences were small, the observed [^{11}C]CB184 binding pattern was consistent with the TSPO distribution in the normal human brain. Furthermore, V_T values of [^{11}C]CB184 are 3 to 5 times higher than those of standard TSPO ligand (*R*)-[^{11}C]PK11195. Peripherally, [^{11}C]CB184 was metabolized in human: $34\% \pm 2\%$ of the radioactivity in plasma was detected as the unchanged form after 60 min. In urine obtained approximately 100 min post-injection, 0.3% of the total injected radioactivity was recovered. HPLC analysis of urine showed a major hydrophilic metabolite, and [^{11}C]CB184 itself was negligible. In this preliminary study, we could not observe low affinity binder of [^{11}C]CB184. These results demonstrate that [^{11}C]CB184 is a suitable radioligand to use in clinical trials for imaging TSPO in the human brain, providing acceptable pharmacological safety at the dose required for adequate PET imaging. Further clinical studies with [^{11}C]CB184 are needed to assess the added value of this new TSPO radioligand and to determine whether [^{11}C]CB184 could replace (*R*)-[^{11}C]PK11195.

EP831

Detection rate of PET/CT imaging in patients with biochemical relapse of prostate cancer using ^{68}Ga -PSMA I&T

C. Berliner¹, M. Tienken¹, T. Frenzel², Y. Kobayashi¹, A. Helberg¹, S. Klutmann¹, D. Beyersdorff¹, L. Budäus³, H. Wester⁴, J. Mester¹, P. Bannas¹; ¹Department of Interventional and Diagnostic Radiology and Nuclear Medicine, University Medical Centre Hamburg-Eppendorf, Hamburg, GERMANY, ²Department of Radiotherapy and Radiation Oncology, Hamburg, GERMANY, ³Martini Clinic, University Medical Centre Hamburg-Eppendorf, Hamburg, GERMANY, ⁴Pharmaceutical Radiochemistry, Technical University Munich, Garching, GERMANY.

Purpose: To evaluate 68Ga-PSMA I&T detection rates in biochemical relapse of prostate cancer. **Methods:** We performed a retrospective analysis in 76 consecutive men undergoing whole body 68Ga-PSMA PET/CT from July 2015 to April 2016. Only patients with documented biochemical relapse after definite treatment of prostate cancer were included. Median prostate specific antigen (PSA) was 1.1 (0.01 - 128) ng/ml. Median patient age was 68 (50-85) years. 68Ga-PSMA I&T was applied to patients via an intravenous bolus of 154±17 MBq (SD). PET scans with low dose and contrast enhanced CT scans were performed 60 minutes after injection. Subsequent CT image evaluation included multiplanar reconstruction in three standard planes. The detection rates were correlated with PSA levels. **Results:** PSMA positive lesions were detected in 64.5 % of all patients (49/76). Divided into subgroups no PSMA positive lesions was detected in patients with PSA below 0.2 ng/ml (0/6), in 39.1 % (9/23) of patients with PSA ≥0.2–<0.5 ng/ml, in 42.9 % with a PSA ≥0.5–<1.0 ng/ml (3/7), in 70 % (7/10) with a PSA of ≥1.0–<2.0 ng/ml, in 93.8 % (15/16) with a PSA of ≥2.0–<5.0 and in 100% in patients with a PSA ≥5.0–<10.0 (9/9) or ≥10 ng/ml (3/3). **Conclusions:** Our detection rates with PSMA I&T in patients with a PSA levels <1 ng/ml were below of those reported by Afshari et al. and Eiber et al using 68Ga-HBED-CC. Above PSA levels of 1 ng/ml the detection rates are comparable or even higher. Further improvement of detection rates is currently tested using forced diuresis one hour after tracer application and additional scanning after two hours. **References:** Eiber M et al. JNM 2015;56:668-74. Afshar-Oromieh A et al. Eur J Nucl Med Biol 2015;42:197-209.

EP832

Synthesis, radiochemistry and utilization of a novel 18F-synthron for indirect radiolabelling of biological vectors

B. Zhang^{1,2}, G. Pascali², L. Matesic², A. J. Robinson¹, B. H. Fraser²; ¹Monash University, Melbourne, AUSTRALIA, ²ANSTO, Sydney, AUSTRALIA.

AIM: Ethenesulfonyl fluoride (ESF) is one of the strongest Michael acceptor molecules reported in the chemical literature. ESF reacts with various nucleophiles including amines, thiols, enamines, dienes, phosphines and activated methylene groups under relatively mild conditions. Furthermore, the sulfonyl fluoride moiety is reported to be stable in biological conditions. Consequently, [18F]ESF has significant potential as a minimalistic prosthetic group for radiolabelling macromolecules that contain 'soft' nucleophilic groups such as lysine or free cysteine residues. In this work we aim to explore and optimise the synthesis of [18F]ESF and its utilisation in the radiofluorination of model amino acids and oligopeptides as one of the smallest 18F prosthetic groups available. **MATERIALS AND METHODS:** Radiolabelling of [18F]ESF was attempted using a microfluidic system (Advion NanoTek), either using a two-step route from 2-chloroethanesulfonyl chloride or by fluorine exchange on [19F]ESF. Exchange reactions were also performed under traditional vessel conditions and yields were compared with the microfluidic approach. These exchange reactions were performed in aqueous solvents (e.g. 0.9% saline) at 100°C. After cartridge purification of [18F]ESF, the coupling reaction was tested on several model amino acids (carboxy-protected) and oligopeptides in different solvent systems at room temperature. **RESULTS:** The 2-chloroethanesulfonyl chloride route was not successful in synthesizing [18F]ESF, while the exchange reactions in the microfluidic system provided high yields (>95%). The incorporation in vessel conditions was always lower yielding and required longer reaction times. All model amino acids and oligopeptides tested, with the notable exception of histidine, reacted with [18F]ESF in DMF/saline medium with incorporation yields over 40%. All the synthesized adducts were stable in their employed solvent over a period of 12 hours. **CONCLUSIONS:** We found a facile method to produce carrier added [18F]ESF via a 19F-18F fluoride exchange reaction in aqueous

solvents, using a microfluidic system. The cartridge purified prosthetic molecule was successfully used in coupling reactions with a set of model amino acids and oligopeptides at room temperature with good yields. Further studies are ongoing on the stability of the obtained radiofluorinated adducts in injectable formulations. In addition, novel routes leading to non-carrier-added [18F]ESF are being designed. These efforts would lead to a general, simple and minimalistic method for [18F]radiofluorinating biomolecules.

EP833

[11C]NS14444, a new radiotracer for alpha-7 nACh receptors. Synthesis and preclinical evaluation

K. Nägren¹, J. H. Dam¹, C. Baun¹, T. Andersen¹, A. Šačkus², O. Paliulis², D. Peters³; ¹Odense University Hospital, Odense C, DENMARK, ²Kaunas University of Technology, Kaunas, LITHUANIA, ³DanPET AB, Malmö, SWEDEN.

Introduction: The γ nAChRs are involved in neuropsychiatric diseases such as Alzheimer's disease, Parkinson's disease and schizophrenia. They are also located in the spleen, in various cancers and in vulnerable plaques in arteries. Although a number of γ PET tracers have been developed, none of them are in clinical routine use. NS14444, 2-(1,4-diazabicyclo[3.2.2]nonan-4-yl)-5-(1-methyl-indol-6-yl)-1,3,4-oxadiazole, developed by Dan Peters et al.,¹ is a high affinity (IC₅₀ 12 nM) ligand for the γ nACh receptor, and is selective over a wide range of receptors and transporters. **Methods:** Methylation of the indole nitrogen of NS14540 was attempted using [11C]methyl iodide or [11C]methyl triflate using a variety of bases. PET studies (a baseline and a blocking study) were performed in a Sprague-Dawley rat on a Siemens Inveon system after tail vein injection of 42 and 49 MBq (153 and 509 ng) of [11C]NS14444. For the blocking study, 10 mg/kg of SSR180711 was injected 16 min. before [11C]NS14444 administration. **Results:** The only successful methylation combination found was [11C]methyl iodide and NaH as a base in acetonitrile, with 3 min. heating at 90°C. The ¹¹C methylation yield was about 50%. Purification was performed on an Onyx HPLC column using ethanol in dilute phosphoric acid, giving 1.6-3.0 GBq of [11C]NS14444 with radiochemical purity higher than 99% and specific radioactivity of 60-180 MBq/nmol. A rather uniform and low uptake, max. 0.05% of injected dose, was obtained in the rat brain. Blocking with SSR180711 reduced the brain uptake at 45-60 min with 33%. In the baseline study, uptake in the spleen was relatively high, and this uptake was blocked almost completely by SSR180711 pre-administration. **Conclusion:** An effective method for the synthesis and purification of [11C]NS14444 was established. Although the low brain uptake in rat indicates that [11C]NS14444 might not be ideal for studies of neuropsychiatric diseases, it might be useful for studies of cancer, vulnerable plaques or diseases of the spleen. These topics will be addressed in future research. 1: Patent US 8,778,928, including NS14444, including isotopes.

EP834

Synthesis of N-[11C]methyl-rhodamine derivatives for Pgp-pump study

E. V. Németh¹, G. Horváth², T. Miklovicz¹, P. Mikecz¹, J. P. Szabó¹, A. Fekete¹, D. Szikra¹, G. Trencsényi¹, T. Márián¹, J. Varga¹; ¹Department of Nuclear Medicine, Faculty of Medicine, University of Debrecen, Debrecen, HUNGARY, ²Isotoptech Pty, Debrecen, HUNGARY.

Objective: Members of the rhodamine family are Pgp-pump substrates, which accumulate in the mitochondria; therefore the multidrug resistance can be tested using them. Earlier rhodamine was labeled by ¹⁸F and ¹¹C isotopes through the ester group. *In vivo* studies showed that the esterase

enzymes cut off the labeling part of the molecule. Our aim was to work out a synthesis for N-labeled derivatives, since they are expected to show higher stability *in vivo*. Direct methylation of amino group of rhodamine derivatives was unsuccessful, so we tested another way of labeling: the first step was N-acetylation followed by N-methylation, finally acid hydrolysis was performed to remove the acetyl groups. **Methods:** We produced our precursor N,N-diacetyl-R110 by the acetylation of R110 with acetic anhydride in pyridine. Its methylation with [^{11}C]CH₃OTf in DMF solution in the presence NaH as base gave N-[^{11}C]methyl-N,N-diacetyl-R110. After dilution with water, it was adsorbed on a C18 SepPak, purified by washing it with water, and eluted with ethanol. Following the addition of 3 M HCl, hydrolysis was carried out for 5 minutes at 120 °C, then the reaction mixture was neutralized with aqueous NaOH and Na-acetate. The resulting solution was injected onto a 250 mm long, 10 mm diameter Nucleodor C18 Pyramid 5µm semipreparative column, and eluted with ammonium formate (10 mM, pH=3): MeCN = 65:35; detection was performed at 254 nm. The fraction containing N-[^{11}C]methyl-rodamin110 was collected and identified by analytical HPLC, using a similar column (250 / 4.6 mm), and the purity was also determined. The solvent ratio was 70:30 in this case as well. For the *in vitro* tests KB-3-1 Pgp-negative and KB-V-1 Pgp-positive human epidermoid carcinoma cell lines were used. **Results:** The alkylation of the precursor with [^{11}C]MeTriflate to N-[^{11}C]methyl-N,N-diacetyl-R110 occurred with 60±5% yield. N-[^{11}C]methyl-rodamin110 was obtained with 94 ±3 % yield after acid hydrolysis. The radioactive end-product was isolated with semipreparative HPLC, the radiochemical purity was 97 ±2 %. Serum stability was studied by analytical HPLC for 55 min: no change was detected. The N-[^{11}C]methyl-rodamin110 accumulation in the Pgp-negative cells (KB-3-1) was approximately 2.5-fold higher than in the Pgp positive cells (KB-V-1), at all time points. Treatment with cyclosporin-A (CSA) - which is a Pgp-inhibitor - increased the N-[^{11}C]methyl-rodamin110 uptake of KB-V-1 cells close to the level of the KB-3-1 cells. **Conclusion:** We have successfully N methylation of rhodamine derivatives. This is a way useful to Pgp pump's functions test *in vitro* experiment.

EP835

Safety Analysis of a Novel Fatty Acid Analog 18-F FCPHA, Data from a Phase II Study

H. Strauss¹, O. Gheysens², R. Hustinx³, S. Goldman⁴, K. Eissler⁵, E. Lyons⁶, V. Roelants⁷; ¹Memorial Sloan Kettering, New York, NY, UNITED STATES, ²UZ Leuven, Leuven, BELGIUM, ³CHU Liege, Liege, BELGIUM, ⁴Hospital Erasme ULB, Brussels, BELGIUM, ⁵InsightRX Consulting LLC, Phoenixville, PA, UNITED STATES, ⁶FluoroPharma Medical, Inc., Montclair, NJ, UNITED STATES, ⁷Cliniques universitaires Saint-Luc, Brussels, BELGIUM.

Background: Myocardial perfusion imaging (MPI) is useful to detect myocardial ischemia and scar. Ischemia alters cardiac metabolism by converting from free fatty acid (FFA) to glucose. A Phase II study was conducted in Belgium to assess the safety and imaging characteristics of a novel FFA analog 18-F Fluoro-cyclopropylhexadecanoic acid (18-F FCPHA; CardioPET) in a population with known or suspected coronary artery disease (CAD), in comparison with Tc-99m SPECT and coronary angiography. Previous reports on safety and image quality did not reflect the full study cohort. **Methods:** Subjects referred for angiography after a positive SPECT MPI (sestamibi or tetrofosmin) or stress echocardiography underwent PET/CT imaging following 18-F FCPHA injection. Physical exam, vital signs, 12-lead ECG, hematology, chemistry and urinalysis were collected at baseline (day of study), at one hour after dosing with study drug and at 24-hours. Monitoring of vital signs via 3-lead ECG continued for 60-minutes during PET serial imaging. **Results:** Study cohort consisted of 31 subjects (mean age 67). CAD subjects presented with a variety of symptoms including dyspnea, angina and NYHA

II heart failure. 18-FCPHA was injected at either rest (n=14) or stress (exercise (n=14) and dipyridamole (n=3)); doses ranged from 136.9 to 358.9 MBq. Four adverse events (AE's) were reported (hyperventilation, anxiety, diarrhea, antiphospholipid antibodies positive); all were mild to moderate in severity; none were attributed to study drug. Three subjects with increased blood pressure deemed clinically significant (CS) at either 60 minutes or 24 hours were also CS at baseline. One subject had CS respiration at 60 minutes and was recorded as an AE. No other vital signs were considered to be CS by investigators. All ECG's flagged as potentially CS were medically monitored and considered to be within normal limits for the study population. Lab values out of range were examined by the medical monitor against the subjects' medical conditions and study drug, and determined to be unrelated to 18-F FCPHA. **Conclusions:** In this Phase II study, the FFA analog 18-F FCPHA could be safely administered in a high-prevalence CAD population. Four AE's were reported, but all of them were mild to moderate in severity. No other changes to vital signs or laboratory values were related to administration of the study drug.

EP836

Gold Nanoparticles with Stably Embedded Cu-64 and Their Use in Nanoparticle Research

A. I. Jensen¹, A. F. Frellsen¹, A. E. Hansen², R. I. Jølc³, G. W. Severin¹, S. Tietze¹, P. Kempen³, P. H. Rasmussen¹, A. Kjær², T. L. Andresen³; ¹Center for Nuclear Technologies (DTU Nutech), Technical University of Denmark, Roskilde, DENMARK, ²Nuclear Medicine & PET and Cluster for Molecular Imaging, University of Copenhagen, Copenhagen, DENMARK, ³DTU Nanotech, Center for Nanomedicine & Theranostics, Technical University of Denmark, Lyngby, DENMARK.

^{64}Cu is a popular radionuclide for PET imaging and when $^{64}\text{Cu}^{2+}$ is mixed with gold nanoparticles (AuNPs) it adheres to the gold surface. Taking advantage of this, we developed methods to trap the ^{64}Cu within the AuNPs by embedding under additional layers of gold. This resulted in radiolabeling efficiencies around 53 ± 6%. EDTA challenge for two days revealed the embedded ^{64}Cu to possess excellent stability with 94-98% of the radioactivity remaining associated with the AuNPs. Testing for two days against serum likewise showed no loss of ^{64}Cu from the ^{64}Cu -AuNPs. Accordingly, the technology was shown to yield a very stable radiolabel that can accurately trace AuNPs *in vivo*. Such chelator-free radiolabeling removes traditional concerns over the use of chelators for ^{64}Cu , notably instabilities of chelators, such as DOTA, and their ability to alter the surface and thus the biodistribution of the compounds onto which they are attached. Radiolabeled ^{64}Cu -AuNPs were prepared in biomedically relevant sizes of 20-30 nm and decorated with three different coatings, in order to investigate their *in vivo* performance by PET imaging in a murine xenograft model. We found the longest plasma half-life ($T_{1/2}$ about 9 hours) to result from a polyethylene glycol (PEG) coating, while faster elimination from the bloodstream was observed for both a Tween-20 stabilized coating and a zwitterionic coating based on sulfonic acids and quaternary amines. Accordingly, our data concluded the PEG coating to be most beneficial for long circulation *in vivo*. In the *in vivo* model, the ^{64}Cu was observed to closely follow the AuNPs for each coating, again attributing to the excellent stability of the radiolabel. Further, ^{64}Cu -AuNPs were prepared in three different sizes ranging from 30 to 70 nm and injected intravenously (I.V.) or intratumorally (I.T.) in murine xenograft models, either coated with PEG or stabilized by citrate (only 30 nm). In the I.T. experiments, citrate-stabilized ^{64}Cu -AuNPs were retained best in the tumors with about 100 %ID/g after 24 hours. For the PEG-coated ^{64}Cu -AuNPs, a tendency for increased retention as larger particles were injected was observed (30 nm: ~ 30 %ID/g, 70 nm: ~ 60%ID/g). In the I.V. experiments, the opposite tendency was observed, with smaller particles showing higher tumor accumulation and citrate-stabilized ^{64}Cu -AuNPs being rapidly taken up in liver and spleen. Our

group continues work with embedding of radionuclides in solid nanoparticles and further results will be presented as available.

EP837

Production of [^{18}F]F-Py-TFP as a secondary labelling precursor on a cassette based synthesis unit towards a GMP-compliant and convenient fluorosynthesis of [^{18}F]F-peptides and [^{18}F]F-peptidomimetics

O. C. Neels, Y. Remde, M. Schäfer, D. Burkert, K. Kopka, J. Cardinale; German Cancer Research Center, Heidelberg, GERMANY.

Aim: The synthesis and purification of prosthetic groups for the radiofluorination of peptides are sophisticated and therefore difficult to translate into routine production. The aim is to transfer the synthesis of [^{18}F]F-Py-TFP (6-[^{18}F]fluoronicotinic acid 2,3,5,6-tetrafluorophenyl ester) as reported by Olberg *et al.* onto a cassette-based radiosynthesis for large-scale GMP-compliant automated production ready for subsequent labelling of peptides. **Materials and Methods:** An aqueous solution containing [^{18}F]fluoride was obtained by nuclear reaction ($^{18}\text{O}(p,n)^{18}\text{F}$) from a Scanditronix MC32NI cyclotron, transferred to a Trasis All in One synthesis module, trapped on and eluted from a QMA cartridge using TBA-HCO₃ in water and acetonitrile as the eluent. After azeotropic drying, 10 mg of precursor *N,N,N*-trimethyl-5-((2,3,5,6-tetrafluorophenoxy)-carbonyl)pyridin-2-aminium trifluoromethanesulfonate in 1.2 mL tert-BuOH and 0.3 mL acetonitrile was added and heated. The reaction mixture was cooled down to room temperature and diluted with 5 mL of water. The crude mixture was trapped on a pre-conditioned Oasis MCX SPE cartridge and rinsed with 10 mL of water. Impurities were removed from the cartridge using the first fraction of acetonitrile. [^{18}F]F-Py-TFP was obtained by further elution with acetonitrile and dried using a Sep-Pak Dry Sodium Sulfate cartridge. [^{18}F]F-Py-TFP was then used to label the novel PSMA-ligand PSMA-1007 in a mixture of DMSO, acetonitrile and *N,N*-diisopropylethylamine at elevated temperature. The radiolabelled peptidomimetic was purified by HPLC and diluted with PBS buffer and sterile-filtered. **Results and Conclusion:** The secondary labelling precursor [^{18}F]F-Py-TFP was obtained within 30 minutes in dry acetonitrile and radiochemical yields higher than 25% (d.c.) on an automated cassette based synthesis module. The radiochemical purity of the product after simple cartridge extraction was sufficiently high and further investigations on the major impurity resulting from hydrolysis are in progress. Nevertheless, [^{18}F]F-Py-TFP was used on the same radiosynthesis for direct radiolabeling of a wide range of peptides including the novel small PSMA-ligand PSMA-1007 which was obtained in high radiochemical purity. Hence, this fully automated procedure represents a step forward towards the GMP-compliant production of promising F-18 labelled peptides and peptidomimetics.

EP838

In vitro and in vivo evaluation of ^{18}F -Labelled Chitosan-Based Nanoparticles to target folate receptor-positive tumor cells

A. LIMA OUBIÑA¹, J. SZABÓ¹, T. NAGY¹, G. TRENCSENYI¹, E. FAZEKAS², T. MIKLOVICZ¹, J. VARGA¹, J. BORBÉLY², P. MIKECZ¹; ¹Nuclear Medicine Institute, DEBRECEN, HUNGARY, ²BBS NanoTech, DEBRECEN, HUNGARY.

INTRODUCTION: Folate receptors (FR- α), are expressed on different epithelial malignant neoplasms, such as ovarian cancer, breast cancer, which represents a promising cell membrane-associated target for PET imaging of cancer. **AIM:** The purpose of this study was to label chitosan-based nanoparticles with F-18 via [^{18}F]F-4-fluorobenzaldehyde ([^{18}F]FBA) to target FR- α . These nanoparticles are composed of chitosan (polycation), and poly- γ -glutamic acid binding folic acid (polyanion, γ -PGA-FA) through 1-[3-(dimethylamino) propyl]-3-ethyl carbodiimide

methodide (EDC) technique. **METHODS:** Chitosan-Based Nanoparticles labelling was performed by direct reductive amination at 70°C during 30 minutes, reacting [^{18}F]FBA, synthesized from 3-4mg 4-Formyl-N,N,N-Trimethylanilinium triflate in DMSO, in a 5 minutes reaction at 80°C, with the free amine group of the polymer in a first step. After that [^{18}F]F-labelled chitosan 0.3mg/mL was self-assembled with the γ -PGA-FA 0.3mg/mL by gelation process through ion-ion interaction. Purification of labelled nanoparticles was achieved using PD10-column. Dynamic Light Scattering (DLS) measurements were done to study nanoparticles size. Radiochemical conversion (RCC) as well as radiochemical purity (RCP) were determined by radio-TLC. A parallel assay was performed between labelled chitosan and labelled nanoparticles to study the specific cellular accumulation in three different cell lines: KB(positive FR- α), MDA-MB-231(negative FR- α) and 4T-1(negative FR- α). The labelled nanoparticles was evaluated *in vivo* in normal mice BALB/C by PET-MRI, acquisition at 80 minutes post-injection. **RESULTS:** [^{18}F]F-labelled chitosan RCC via [^{18}F]FBA using direct reductive amination, was 79±9%. Nanoparticles labelling efficiency after purification no decay corrected was 16±8%. RCP 100% and nanoparticles size: 131±19nm. The *in vitro* studies showed non-specific binding, where [^{18}F]F-labelled chitosan as well as labelled nanoparticles presented similar profiles after 60 minutes of incubation: MDA-MB-231: 12±2% and 8±1%, and for 4T-1: 14±2% and 7±1% respectively. In regard to KB cells: [^{18}F]F-labelled chitosan 7±1% and 5±1% of injected dose for labelled nanoparticles. *In vivo* preliminary assay showed liver and spleen uptake with an unusual high renal cortical uptake after 80 minutes post-injection. **CONCLUSIONS:** [^{18}F]F-Labeling of Chitosan-Based Nanoparticles was performed successfully. Self-assembly between labelled chitosan and poly- γ -glutamic acid-Folic acid was confirmed by DLS, and nanoparticles were completely purified. Preliminary *in vitro* results showed unspecific binding to the FR- α . More biological studies are currently ongoing to achieve a clear conclusion about the behaviour [^{18}F]F-Chitosan-Based Nanoparticles to target folate receptor-positive tumor cells. **ACKNOWLEDGEMENTS:** This work was supported by FP7-PEOPLE-2012-ITN (316882 RADIOMI project).

EP839

Preliminary Biological Evaluation of ^{18}F -AIF-NOTA-MAL-Cys-Annexin V as a Apoptosis Imaging Agent

C. Lu, Q. Jiang; Jiangsu Institute of Nuclear Medicine, Wuxi, CHINA.

Objectives: One novel Annexin V derivative (Cys-Annexin V) with a single cysteine residue at its C-terminal and site-specific labeling of it with thiol-reactive prosthetic group such as [^{18}F]F-N-[2-(4-Fluorobenzamido)ethyl]maleimide (^{18}F -FBEM) have been developed. However, the synthesis of [^{18}F]F-FBEM-Cys-Annexin V was time consuming. To overcome this challenge, we developed a novel [^{18}F]F-AIF-NOTA-MAL-Cys-Annexin V as a apoptosis imaging agent, which has great potential for clinical translation. **Methods:** [^{18}F]F-AIF-NOTA-MAL was prepared as previously described using a semi-automatic method with some modification. [^{18}F]F-AIF-NOTA-MAL in 100 μL (185-370MBq) of 10% acetonitrile was added to a solution of Cys-Annexin V (50-100 μg in 100 μL) PBS, and the mixture was allowed to react at room temperature for 30 min and then was purified by using a PD-10 column. The radiolabeling yield (RLY) and radiochemical purity (RCP) of [^{18}F]F-AIF-NOTA-MAL-Cys-Annexin V were determined by high performance liquid chromatography (HPLC) with a TSK GEL column. In this study, eight male SD rats were divided into two groups, one group were treated with 10 mg/kg cycloheximide (CHX) to induce liver apoptosis and the other group were treated with saline as the control group. 3 h after the treatment, rats were injected via the tail vein with 0.2mL (7.4MBq) [^{18}F]F-AIF-NOTA-MAL-Cys-Annexin V. Ten-minute static scans were acquired at 1h after injection with a MicroPET, respectively. At the end of the scan the livers were harvested for terminal deoxynucleotide end-

labeling (TUNEL) staining. **Results:** The total synthesis time of ^{18}F -AIF-NOTA-MAL-Cys-Annexin V from [^{18}F]fluoride was about 60 min, however that of ^{18}F -FBEM-Cys-Annexin V was over 2h. RLY and RCP of ^{18}F -AIF-NOTA-MAL-Cys-Annexin V were over 78% and 95% (based on the starting ^{18}F -AIF-NOTA-MAL, non-decay corrected, $n=5$) respectively. HPLC retention time of ^{18}F -AIF-NOTA-MAL-Cys-Annexin V was about 10.7 min with the flow rate was 1.0mL/min. In rat models of hepatic apoptosis there were 6.23 ± 0.23 times ($n=4$) increase in hepatic uptake of ^{18}F -AIF-NOTA-MAL-Cys-Annexin V as compared to normal mice at 1h p.i. TUNEL staining showed good correlation of ^{18}F -AIF-NOTA-MAL-Cys-Annexin V uptake with TUNEL-positive cells. **Conclusions:** MicroPET studies combined with TUNEL staining showed that uptake of ^{18}F -AIF-NOTA-MAL-Cys-Annexin V correlates well with the level of apoptotic cells in this CHX induced liver apoptosis model. ^{18}F -AIF-NOTA-MAL-Cys-Annexin V is a potential apoptosis imaging agent and further study is needed. **Research Support:** Supported by Natural Science Foundation of Jiangsu Province (no.BK20151119) and Ministry of Health Foundation of China (W201207).

EP840

Fast Production of [^{11}C]Metomidate using Solid Phase Extraction Purification

E. Arponen, S. Helin, S. Forsback, P. Lehtikainen; Turku PET Centre, Turku, FINLAND.

Aim The objective of this work was to develop a rapid solid phase extraction (SPE) purification method for [^{11}C]metomidate and to validate the synthesis for clinical use according to GMP regulations at Turku PET Centre. Metomidate is an inhibitor of 11β -hydroxylase, a key enzyme in the biosynthesis of cortisol and aldosterone by the adrenal cortex. [^{11}C]Metomidate (O-[methyl- ^{11}C]-(*R*)-1-(1-phenylethyl)-1*H*-imidazole-5-carboxylic acid methyl ester) is used for PET imaging of the adrenal cortex and its tumours. **Materials and methods** [^{11}C]Metomidate production was done using a commercial GE Tracerlab FX_{C-pro} synthesizer placed in a validated clean room hot cell. [^{11}C]Metomidate was synthesized by ^{11}C -methylation of the desethyl-etomidate precursor with [^{11}C]methyl triflate prepared from cyclotron-produced [^{11}C]carbon dioxide. [^{11}C]Carbon dioxide was first converted to [^{11}C]methane. [^{11}C]Methyl iodide was synthesized from [^{11}C]methane and iodine in a gas phase reaction at 720 °C. [^{11}C]Methyl triflate was prepared online by passing [^{11}C]methyl iodide through a silver triflate/graphitized carbon column at 200 °C and bubbled into the reaction solution containing the precursor for metomidate. The reaction solution was diluted with 10% ethanol in sterile water and transferred through the SPE cartridge (Waters, Sep-pak C18 light), which retained the [^{11}C]metomidate fraction. The cartridge was then washed with 10% ethanol in sterile water. [^{11}C]Metomidate was eluted from the SPE cartridge with ethanol and formulated in ethanol/propylene glycol/0.1 M phosphate buffer (10/15/85). Finally, the product solution was filtered through a sterile non-pyrogenic single use syringe filter into a sterile vial. The filter integrity was assessed as a part of sterile filtration using a pressure hold test. **Results and Conclusion** An efficient and robust routine procedure for the production of [^{11}C]metomidate was developed using Tracerlab FX_{C-pro} module and SPE purification. The average synthesis time was 20 minutes including purification, formulation and online sterile filter integrity test. [^{11}C]Metomidate was purified by a SPE cartridge. The dilution of the reaction mixture and washing eluent for the cartridge were optimized to separate the precursor and other major chemical and radiochemical impurities from the end product. The SPE recovery yield for [^{11}C]metomidate was >95%. The identity, radiochemical purity and concentrations of the end product and desethyl-etomidate were determined using a validated analytical HPLC method. [^{11}C]Metomidate was obtained in high radiochemical yield, sufficiently for several clinical doses. The radiochemical purity exceeded 99% in all syntheses.

EP841

Automated synthesis of 4-[^{18}F]fluoroanisole, [^{18}F]DAA1106 and 4-[^{18}F]FpHe using Cu-mediated radiofluorination under “minimalist” conditions

J. Zischler^{1,2,3}, P. Krapf^{1,2,3}, R. Richarz^{1,2,3}, B. D. Zlatopolsky^{2,3}, B. Neumaier^{1,2,3}; ¹Forschungszentrum Jülich, Jülich, GERMANY, ²University Clinic Cologne, Cologne, GERMANY, ³Max Plack Institute for Metabolism Research, Cologne, GERMANY.

The growing clinical impact of PET imaging result in the increasing demand of large-scale cGMP-compliant syntheses of various PET-tracers in a safe and reproducible manner. Therefore, the novel preparation procedures have to be transferred to automated synthesis modules in order to be applied for the production of the clinically relevant probes. Recently, we showed that the Cu-mediated radiofluorination of (mesityl)aryl iodonium salts under “minimalist” conditions enables the operationally simple and rapid production of various radiofluorinated arenes. The aim of this work was to study amenability of this radiolabeling procedure to automation in commercially available synthesis modules and, consequently, its suitability for clinical PET applications. All radiosyntheses were carried out in a Scintomics hotbox^{three} module (Scintomics GmbH, Fürstfeldbruck, Germany). [^{18}F]Fluoride was trapped on a QMA cartridge and eluted with the corresponding iodonium salt precursor dissolved in MeOH. Afterwards MeOH was removed and (MeCN)₄CuOTf in DMF was added and the resulting mixture was heated at 85 °C for 20 min. The radiolabeled products were isolated by SPE or HPLC. In the case of 4-[^{18}F]Phe the *N,O*-protected intermediate, Boc-4-[^{18}F]FpHe-OMe was hydrolyzed with 12 M HCl at 140 °C for 10 min to give the desired PET-tracer. Under optimized reaction conditions 4-[^{18}F]fluoroanisole, 4-[^{18}F]FpHe and [^{18}F]DAA1106 were prepared in isolated radiochemical yields of 41–61% and radiochemical purities of > 95% within 30–60 min. 4-[^{18}F]FpHe and [^{18}F]DAA1106 could be purified by RP-SPE avoiding any HPLC purification steps. We have demonstrated that Cu-mediated nucleophilic aromatic radiofluorination under “minimalist” conditions can be easily transferred to a commercially available synthesis module. The utility of the developed procedure was confirmed by a successful preparation of [^{18}F]DAA1106 and 4-[^{18}F]FpHe in good RCYs and excellent RCPs. The evident simplicity as well as the high efficacy and versatility of the developed protocol enable a broad application of Cu-mediated radiofluorination in PET-chemistry in the very near future.

EP842

S-[^{18}F]THK-5117 production implementation at Turku PET Centre

J. Rokka, J. Uotinen, T. Saarinen, E. Kokkomäki, O. Solin; Turku PET Centre, University of Turku, Turku, FINLAND.

Aim The purpose of this work was to implement and validate the synthesis of S-[^{18}F]THK-5117 for clinical use according to GMP regulations at Turku PET Centre (TPC). S-[^{18}F]THK-5117 is an arylquinoline derivative developed for tau PET imaging of Alzheimer’s disease (AD). This tracer binds specifically to tau aggregates and has fast washout from the healthy brain, and longitudinal PET studies have shown that S-[^{18}F]THK-5117 binding is significantly higher in the AD patient brain compared to healthy controls [Okamura et al., 2013, Ishiki et al., 2015]. **Material and methods** S-[^{18}F]THK-5117 was synthesized using a two-step reaction. First, the precursor was ^{18}F -fluorinated using nucleophilic ^{18}F -fluorination, and then the protecting group was hydrolyzed. During the implementation, the amount of reagents, reaction temperature, and time for ^{18}F -fluorination and hydrolysis were optimized. The final product was separated from the reaction mixture by semi-preparative HPLC. The HPLC eluent containing the end-product fraction was removed by solid-phase extraction (SPE). HPLC and SPE eluents were adjusted to avoid

radiolysis and separate major chemical impurities. Finally, the end product was eluted from the SPE cartridge using ethanol and formulated in a 0.1 M phosphate-buffered solution (pH 7.4). The formulated product was sterile filtered using an in-house-built sterile filtration unit. S-[¹⁸F]THK-5117 synthesis was performed using a validated, in-house-built, remote-controlled device in a validated clean room hot cell. The device is fully automated and has a validated program to perform the synthesis from start to finish. The operator can intervene in the synthesis using the pause/continue and skip buttons. GM tubes are used to monitor the radioactivity during the synthesis steps. **Results and Conclusions** S-[¹⁸F]THK-5117 has been implemented and validated at TPC. By diminishing the amount of precursor, we can lower the chemical impurity of the final product without compromising the radiochemical yield of S-[¹⁸F]THK-5117. The radiochemical yield of S-[¹⁸F]THK-5117 is $19 \pm 8\%$, specific activity is >1 TBq/ μ mol, radiochemical purity is $>99\%$, and chemical purity is <0.3 μ g/ml. S-[¹⁸F]THK-5117 is currently in clinical use at TPC. This work received funding from the Academy of Finland (project 266891). We acknowledge Professor Okamura from Tohoku University for providing the precursor and reference compounds and for his knowledge and help in this implementation. Ishiki et al., PLOS ONE | DOI:10.1371/journal.pone.0140311; Okamura et al., *J Nucl Med.* 2013; 54:1-8

EP844

A fluorine-18 radiolabelled celecoxib-based PET probe for cyclooxygenase-2 monitoring - COX-2 affinity, radiosynthesis and in vitro studies

T. Knies, N. Bechmann, J. Steinbach, J. Pietzsch; Helmholtz-Zentrum Dresden-Rossendorf, Dresden, GERMANY.

Aim: Cyclooxygenase-2 is an inducible enzyme overexpressed in inflammatory conditions and is assumed to play a key role in carcinogenesis. Functional imaging of COX-2 with PET is a challenging approach e.g., for monitoring tumours with COX-2 expression and for characterization of inflammatory response in radiotherapy. Celecoxib is an established COX-2 inhibitor and a successful imaging of inflamed tissue was demonstrated using a celecoxib-based radiotracer [¹⁸F]1 (IC₅₀ COX-2 = 160 nM) having an aminosulfonyl group [1]. Since the aminosulfonyl functionality is known to cause slow blood clearance *in vivo* [2] we developed a [¹⁸F]fluoromethyl-substituted celecoxib analogue [¹⁸F]2, characterized by a methylsulfonyl moiety. **Materials and methods** Two fluoromethyl-substituted diaryl-1*H*-pyrazoles with an aminosulfonyl 1 and a methylsulfonyl moiety 2 were synthesized, and their COX-2 affinity was determined by a fluorescence-based assay. The appropriate tosylated precursor for fluorine-18 radiolabelling was received by a four-step synthesis sequence starting from 4-methyl-acetophenone. The radiotracer 3 - ([¹⁸F] fluoromethyl) - 5 - (4 - methyl phenyl) - 1 - [4 - (methylsulfonyl)phenyl] - 1*H*-pyrazole [¹⁸F]2 was obtained by nucleophilic [¹⁸F]fluoride substitution of the tosyl-precursor ([¹⁸F]Kf/K₂₂₂/MeCN, 10 min, 110°C) using an automated synthesiser module Tracerlab_{F_{XN}} (GE) and purified by semi-preparative HPLC. In preliminary *in vitro* studies [¹⁸F]2 was evaluated using pro-inflammatory stimulated human monocyte (THP-1) and COX expressing human melanoma cell lines (A2058, A375). **Results:** The *in vitro* COX assay of 1 and 2 revealed that submicromolar COX-2 inhibitory activity is preserved by replacing the aminosulfonyl function in 1 with a methylsulfonyl moiety in 2 (IC₅₀ = 100 nM / 170 nM). The COX-1/COX-2 selectivity ratio was found to be <1000 and <590 for 1 and 2, respectively. Automated radiosynthesis and purification yielded [¹⁸F]2 in 27-37% RCY (uncorrected, n=7) in $>95\%$ radiochemical and 88% chemical purity within 55 min overall synthesis time in a specific activity of 41-70 GBq/ μ mol at end of synthesis. The uptake of [¹⁸F]2 *in vitro* could be substantially blocked by both the reference 2 and by celecoxib, but was not shown to be correlated with varying cellular levels of COX-2 protein. **Conclusion:** A new [¹⁸F]fluoromethyl-substituted analogue of celecoxib [¹⁸F]2 with

submicromolar affinity to COX-2 was synthesized in good radiochemical yield and high purity. Cellular studies demonstrated an uptake and blocking of the radiotracer in COX expressing human melanoma cells. The pharmacological behaviour of [¹⁸F]2 *in vivo* regarding blood clearance and metabolic stability (¹⁸F-defluorination) have to be evaluated. [1] Uddin J., et al. *Cancer Prev. Res.* 4, (2011), 1536 [2] Kuge Y., et al. *Nucl. Med. Biol.* 33, (2006), 21

EP845

Synthesis and In Vitro Evaluation of ¹⁸F Radiolabeled AMO Targeting Tumor Overexpressed miRNA-155

L. Kang¹, Y. Huo¹, R. Wang¹, X. Xu²; ¹Peking University First Hospital, Beijing, CHINA, ²Academy of Military Medical Sciences, Beijing, CHINA.

Objective: MicroRNA-155 (miR-155) is first found frequently up-regulated in various malignant tumors and is reported as an oncogene biomarker. Antisense oligonucleotides have been used for effective target recognition and gene therapy studies. We previously labeled anti-miR-155 oligonucleotide (AMO-155) with ^{99m}Tc for *in vivo* visualization. PET imaging based on fluorine-18 gained high interest due to the favorable nuclear and physical characteristics of ¹⁸F. Therefore, we explored the optimized methods in the preparation of ¹⁸F radiolabeled AMO-155 with further *in vitro* evaluation. **Methods:** AMO-155 with chemical and structural modifications was designed and synthesized. This probe was radiolabelled with ¹⁸F using a direct Al¹⁸F labeling method. After conjugated with NOTA via an amine linker of NH₂ and six carbon, AMO-155 was successfully chelated with Al¹⁸F. Different reaction conditions were evaluated by HPLC for optimization. The product was identified by gel electrophoresis and gel imaging. Its serum stability and cellular uptake in MCF-7 cells were evaluated. **Results:** AMO-155 was synthesized with partial 2'-OMe and PS modification to improve its stability. Increasing the temperature in conjugation could improve the conjugated yield from 15% to 47%. After purification with HPLC, the conjugated product was labeled with ¹⁸F using Al¹⁸F method. The labeling is typically done at 100 °C for 15 min and the labeling efficiency reached to nearly 98%. Therefore, there is no need for further purification for labeled product. However, the labeling efficiency was only 35% when no purification was performed on NOTA conjugated AMO. The radiochemical purity of ¹⁸F-AMO in fresh human serum at 37 °C could maintain more than 95% during 6 h. The gel electrophoresis result showed that the location of radioactivity, which was imaged by micro-PET, coincided with the position of the AMO band and there was no degradation. The cellular uptake of ¹⁸F-AMO increased from 9% to 57% during the incubation of 6 h, whereas that of ¹⁸F did not increase significantly. **Conclusion:** The labeling efficiency can be improved greatly with optimized conjugation and reaction conditions. Moreover, this ¹⁸F labeled probe has a good serum stability and could be prepared easily and simply for *in vivo* imaging without further purification.

EP846

Simple and fully automatic production of [¹⁸F]THK-5351 using All-in-One chemistry module

S. LEE¹, S. OH¹, E. CHO¹, D. CHO¹, S. FURUMOTO², N. OKAMURA², J. KIM¹; ¹ASAN Medical Center, Seoul, KOREA, REPUBLIC OF, ²Tohoku University, Sendai, JAPAN.

Objectives: THK series radiotracers which have aryl quinolone chemical structure are promising radiopharmaceutical for imaging of tau protein in Alzheimer's Disease. [¹⁸F]THK-5351 is one of the THK series compounds with pure S-enantiomer. It has faster pharmacokinetics, higher contrast, and lower retention in subcortical white matter than previous

THK series compound such as [^{18}F]THK-5117. The purpose of our study was to develop the fully automatic preparation procedure with disposable cassette type chemistry module to have clinical feasibility. **Methods:** After trapping of 71.1 ± 11.1 GBq of [^{18}F]F $^-$ on QMA cartridge, we eluted it with KOMs (pH 7.8)/K $_{222}$ mixture as elution buffer and base. After completely drying, [^{18}F]fluorination was performed with 3 mg of precursor dissolved in 1000 μL of DMSO at 110°C for 10 min. After hydrolysis with 1 N HCl and neutralization with 0.8M AcOK, crude [^{18}F]THK-5351 was trapped on the C $_{18}$ cartridge and then the C $_{18}$ cartridge was washed using distilled water to remove reaction solvent. Trapped [^{18}F]THK-5351 was eluted from the C $_{18}$ cartridge with 60% ethanol and purified with HPLC. Isolated [^{18}F]THK-5351 was trapped in 2 $^{\text{nd}}$ C $_{18}$ cartridge to remove HPLC solvent and formulated with EtOH and ascorbic acid solution. Optimized reaction and purification condition were applied to All-in-One chemistry module (Trasis). **Results:** KOMs(pH 7.8)/K $_{222}$ and DMSO showed good [^{18}F] incorporation yield as $> 60\%$. $34.3 \pm 5.5\%$ (n=9) of non-decay corrected radiochemical yield was obtained with All-in-One chemistry module after complete synthesis. Total synthesis time including HPLC purification and formulation was 75 ± 5 min. Radiochemical purity and specific activity were $99.9 \pm 0.2\%$ and > 74 GBq/ μmol , respectively. **Conclusion:** We developed fully automatic synthesis method with disposable cassette for routine production of [^{18}F]THK-5351. Our method showed high radiochemical yield with high reproducibility and [^{18}F]THK-5351 could be used to clinical trial.

EP847

Fully automatic production of [^{18}F]FP-CIT with new chemistry including SPE purification

S. LEE 1 , E. CHO 1 , D. KIM 1 , H. LEE 2 , D. MOON 1 , J. KIM 1 , S. OH 1 ; 1 ASAN Medical Center, Seoul, KOREA, REPUBLIC OF, 2 Duchemio, Seoul, KOREA, REPUBLIC OF.

Objectives: [^{18}F]FP-CIT (fluoropropyl-carbomethoxyiodophenyl-nortropine) is a widely used radiopharmaceutical for dopamine transporter imaging in Korea. In our previous reports, we optimized production condition using protic solvent such as *t*-amyl alcohol and base for [^{18}F]fluorination step. The *t*-amyl alcohol is efficient reaction solvent for production of [^{18}F]FP-CIT but *t*-amyl alcohol does not mix with water and it is drawback for purification such as SPE purification. The purpose of our study was to develop the SPE purification method of [^{18}F]FP-CIT using All-in-One chemistry module from Trasis company. **Methods:** [^{18}F]Fluoride trapped on QMA was eluted with KOMs solution (pH=7.8) instead of inorganic base such as K $_2$ CO $_3$, KHCO $_3$. After evaporation of water, precursor (N-[3'-(mesyloxy)propyl]-2 β -carbomethoxy-3 β -(4'-iodophenyl)nortropine dissolved in 0.1 mL of CH $_3$ CN and 1-methoxy-2-methyl-2-propanol was added. [^{18}F]Fluorination was conducted at 100°C for 10 min. After fluorination, the crude mixture of [^{18}F]FP-CIT was diluted with 20 mL of water without reaction solvent drying and passed through the C18 cartridges for trapping of the [^{18}F]FP-CIT. After washing the C18 cartridge to remove the polar impurities, eluted it with EtOH solution passed through anion exchange cartridge (CM, WAX and MAX) to remove the organic impurities which have plus charge. Crude mixtures, waste solution, and final product were completely analyzed using HPLC to check the all amount of chemical impurities. Optimized reaction and purification condition were applied to All-in-One chemistry module from Trasis company. **Results:** After [^{18}F]fluorination, $28.7 \pm 2.9\%$ (n=7) of starting activity was trapped in the C18 cartridge and after SPE purification, non-decay corrected radiochemical yield was $16.3 \pm 4.9\%$ (n=3). Total synthesis time including SPE purification was 45 ± 5 min. In the crude mixture, main organic impurity was the precursor and 93.8% of precursor was remained after [^{18}F]fluorination. After purification with anion exchange cartridge (CM WAX and MAX), 2.7%, 7.6% and 0.92% of precursor was detected, respectively. Radiochemical purity was $> 98\%$ and the amount of residual precursor was 5.5–46.5 ppm.

Conclusion: We developed new automatic production method of [^{18}F]FP-CIT with new reaction solvent and SPE purification method. Our disposable cassette including SPE purification showed short preparation time and reasonable radiochemical yield without production failure.

EP848

Radiofluorination and characterization of a novel hybrid peptide analogs based on mucin and folic acid as potential breast/ovarian cancers PET imaging agent

I. Aljammaz, B. Al-Otaibi, S. Bin Amer, A. Abousekhrah, S. Okarvi; King Faisal Specialist Hospital and Research Centre, Riyadh, SAUDI ARABIA.

Epithelial mucin (MUC1) and folic acid (FA) are overexpressed by most epithelial cancers hence attracting increasing interest as potential targets for imaging and therapy. The high expression of MUC1 and FA on breast and ovarian cancers and low expression on normal tissues makes them potential targets for diagnosis and therapy of cancers. To develop an efficient ^{18}F -labeled radiopharmaceutical with enhanced breast/ovarian cancer targeting capacity we have designed and synthesized a novel MUC1-derived peptide and also conjugated MUC1 to FA in order to formulate MUC1-FA hybrid peptide conjugate for targeting MUC1/FA receptors. MUC1 and hybrid MUC1-FA were prepared by solid-phase synthesis following Fmoc/HBTU method. FA was attached to MUC1 via terminal Lys by manual conjugation. The synthetic approaches for radiofluorination of MUC1 and MUC1-FA entailed a one-step reaction through the primary amine of the Lys residues. The key precursors 4-N,N,N-trimethylammonium benzoate-MUC1 and MUC1-FA triflates were treated using catalyzed nucleophilic no-carrier-added ^{18}F in ACN at 80°C for 5 min. The radiofluorinated conjugates were purified by C18 Sep-Pak column. *In vitro* receptor binding was performed on T47D, MCF7 and KB cell lines and biological evaluation was done in normal and mice bearing MCF7 and KB cells xenografts. The structure and purity of conjugates were confirmed by mass spectrometry and HPLC. As determined by HPLC, the radiofluorination efficiency of these radioconjugates were $>70\%$ and radiochemical purities always $>95\%$ in less than 30 min. These synthetic approaches hold considerable promise as a rapid and efficient method amenable for automation for the radiofluorination of peptides with high radiochemical yield and short synthesis time. *In vitro* tests have shown that significant amount of the [^{18}F]MUC1 and [^{18}F]MUC1-FA associated with cancer cell fractions. *In vivo* characterization in normal mice revealed rapid blood clearance of hybrid [^{18}F]MUC1-FA with excretion by both urinary and hepatobiliary pathways. Biodistribution of [^{18}F]MUC1 and hybrid [^{18}F]MUC1-FA in mice bearing KB and MCF7 xenografts demonstrated significant tumor uptakes (6% and 11%, respectively). These uptakes were blocked by excess co-injection of FA and MUC1 suggesting receptor-mediated process. *In vivo* imaging using animal PET/CT is in progress and will be reported. These results demonstrate that [^{18}F]MUC1 and [^{18}F]MUC1-FA may be useful as molecular probes for detecting and staging of breast and ovarian cancers and their metastasis as well as monitoring tumor response to treatment and deserves further evaluation.

EP849

I-124 labeled diblock-co-polymeric micelles based on PLGA-PEG for drug delivery system

S. Lee 1,2 , J. Park 1 , J. Lee 1,2 , G. Kim 1,2 , M. Hur 1 , S. Yang 1 , S. Kim 2 ; 1 Korea Atomic Energy Research Institute, Jeongseup, KOREA, REPUBLIC OF, 2 Dongguk University, Gyeongju, KOREA, REPUBLIC OF.

Aim : We have developed folate conjugated biodegradable poly (lactide-co-glycolide)(PLGA) nanoparticles for targeted delivery by a modified solvent extraction/evaporation single emulsion method. The biodegradability and biocompatibility of PLGA have been approved by FDA. Polyethylene glycol(PEG) is used as the coupling agent in the composition of the systems, which bridges folate with PLGA to form a chain PLGA-PEG-Folate. Diblock-co-polymeric micells including I-124 labeled PLGA-PEG and folate conjugated PLGA-PEG was developed for the diagnosis of folate receptor overexpression in KB or CT-26 for drug delivery system. **Material and Methods :** Folate was conjugated with H₂N-PEG-NH₂ using a modified method described elsewhere. Folate was activated by EDC and NHS in the presence of pyridine. And final step was conjugated PEG-folate with activated PLGA in DMSO. Another step PEG conjugated PLGA and labeling of radioisotope at I-124 in DMF. PLGA-PEG-folate was characterized by spectroscopic analysis method and mass spectrometry(FT-IR, ¹H-NMR and ¹³C-NMR). Briefly, PLGA-PEG-¹²⁴I and PLGA-PEG-folate co-polymer were dissolved in ACN and vortexed as organic phase. And then, PLGA-PEG-¹²⁴I and PLGA-PEG-folate organic solution was slowly dropped into aqueous solution. To determine the lipophilicity test of PLGA-PEG-folate&¹²⁴I was dissolved in a mixture of saline and 1-octanol in the E.P tube. The in vitro stability test of PLGA-PEG-folate&¹²⁴I was measured by incubating a probe with human serum. The cellular uptake of PLGA-PEG-folate&¹²⁴I was evaluated using CT-26, KB and A549 cells. **Results and Conclusions :** The products were obtained in >65% radiochemical yields with a radiochemical purity of >91% as checked by radio-TLC. The partition coefficient (logP) was measured as -1.169, which is an indication of the hydrophilic nature of the agent. Cellular uptake values of PLGA-PEG-folate&¹²⁴I was KB, CT-26 and A549 cells over incubation periods of 15, 30, 60, 120 min and 12h(KB: 1.06 % at 15 min, 0.74 % at 30 min, 0.72 % at 60 min, 0.55 % at 120 min and 0.55 % at 12 h, CT-26 : 0.78 % at 15 min, 0.42 % at 30 min, 0.33 % at 60 min, 0.29 % at 120 min and 0.28 % at 12 h, A549 : 0.43 % at 15 min, 0.23 % at 30 min, 0.21 % at 60 min, 0.21 % at 120 min and 0.23 % at 12 h). The PLGA-PEG-Folate&¹²⁴I nanoparticles have greatly increased the folate receptor targeting efficiency and specificity. This study has reported their application in selective delivery of anticancer drug to the FR-overexpressed cancer cells.

EP850

Identification of the Precursor of [⁶⁸Ga]Ga PSMA-HBED-CC and Its Impurities by Mass Spectrometer

J. Laine¹, T. Lipponen¹, J. Parshintsev², G. Duporte², K. Bergström¹; ¹HUS Medical Imaging Center, Helsinki University Central Hospital, Helsinki, FINLAND, ²Laboratory of Analytical Chemistry, Department of Chemistry, University of Helsinki, Helsinki, FINLAND.

Aim Owing to its rapidly increasing clinical impact, we studied the stability of the precursor of [⁶⁸Ga]Ga-PSMA-HBED-CC (Ga-68 PSMA) and relevant aspects of its radiopharmaceutical production. During method development and validation, concern was raised since an impurity peak in a radio-HPLC chromatogram seemed to increase from synthesis to synthesis. The impurity was not detected when the precursor was diluted right before the synthesis, but it was more frequent and prominent the longer the precursor was diluted in water and stored in a freezer at -20°C before the synthesis. In this study, the precursor and the end product of Ga-68 PSMA were analyzed with radio-HPLC, and the precursor and its impurities were further identified with UHPLC-mass spectrometer. **Materials and methods** Ga-68 PSMA syntheses (n=20) were performed with a prepurification method using Eckert&Ziegler Pharmtracer and Ge-68/Ga-68 generator IGG100 or GalliaPharm. The PSMA-precursor was diluted in Trace select water (Fluka) 1 mg/ml and distributed to 20 µl quantities in Eppendorf tubes, after which it was stored in a freezer at -20°C. Chemical and radiochemical purity, including the ratio of the

stereoisomers of the Ga-68 PSMA-product, was analyzed with a Shimadzu Prominence LC-20A HPLC-UV instrument coupled with a Bioscan FC-3200 flow count detector. The Ga-68 colloids and hydroxides of the product were analyzed with a TLC method. The identification of the PSMA precursor and its impurities were further studied with a Thermo Ultimate 3000 UHPLC coupled with an Orbitrap Fusion Tribrid mass spectrometer (UHPLC-MS). **Results** The radiochemical purity (HPLC x TLC) of Ga-68 PSMA was decreased close to the acceptance criteria (90%) and the area of the impurity peak, following the Ga-68 PSMA in the radio-HPLC chromatogram, was increased from 0% to 7% when PSMA was diluted in water and stored in a freezer over one month. In the UHPLC-MS analysis, the main impurity peak of the PSMA precursor was separated, and the analysis of tandem mass spectra revealed a slow carboxylation of HBED-chelate, most probably in its phenol groups. **Conclusions** PSMA-HBED, a precursor of Ga-68 PSMA synthesis, is not stable when diluted in water and stored in a freezer. To improve the radiochemical purity of the Ga-68 PSMA product, PSMA-HBED should be freshly diluted to the buffer immediately before the synthesis.

EP851

HPLC and TLC methods for analysis of [¹⁸F]flumazenil and its metabolites from biological samples

K. Grafinger^{1,2}, T. Keller¹, A. Krzyczmonik¹, L. Pfeifer³, F. R. Lopez-Picon^{1,2}, S. Forsback¹, O. Solin^{1,4,5}, V. Gouverneur³, M. Haaparanta-Solin^{1,2}; ¹Turku PET Centre, University of Turku, Turku, FINLAND, ²MediCity Research Laboratory, University of Turku, Turku, FINLAND, ³Chemistry Research Laboratory, University of Oxford, Oxford, UNITED KINGDOM, ⁴Accelerator Laboratory, Åbo Akademi University, Turku, FINLAND, ⁵Department of Chemistry, University of Turku, Turku, FINLAND.

Aim: The radioligand [¹⁸F]flumazenil binds specifically to the central benzodiazepine receptor site of the GABA_A receptor. The aim of the study was to develop and compare radioHPLC and radioTLC methods for analysis of [¹⁸F]flumazenil and its radioactive metabolites in plasma and brain homogenate of rats. **Materials and methods:** [¹⁸F]Flumazenil was synthesized at the Turku PET Centre Radiopharmaceutical Chemistry Laboratory using copper-mediated nucleophilic [¹⁸F]fluorination of a boronic ester [1,2]. Sprague Dawley rats (n=15) were anaesthetized and 15 ± 3 MBq of [¹⁸F]flumazenil was injected into a tail vein. The rats were sacrificed at 5, 15, 30, 60, 90 min post injection. Cardiac blood samples were collected, centrifuged and plasma proteins were precipitated with acetonitrile. The brain samples were homogenized with the chromatographic mobile phase and centrifuged. The supernatants were analysed with both TLC combined with digital autoradiography (radioTLC), and HPLC combined with a radioactivity detector on the HPLC column outflow (radioHPLC). The amount of intact [¹⁸F]flumazenil and its radioactive metabolites was analysed as % of total ¹⁸F-radioactivity in the sample. **Results:** In plasma the amount of intact [¹⁸F]flumazenil rapidly decreased. At 15 min after tracer injection the amount of [¹⁸F]flumazenil in plasma was about 20%. Two major radioactive metabolites, one more polar and one less polar than [¹⁸F]flumazenil were found in plasma. The radioactive metabolites were not identified. In brain no radioactive metabolites were observed at any time point. RadioTLC and radioHPLC analysis results were comparable for all samples. **Conclusion:** RadioHPLC and radioTLC methods were developed for analysis of [¹⁸F]flumazenil and its radioactive metabolites in rat plasma and brain. Both methods are useful for the analysis of the [¹⁸F]flumazenil metabolic profile. With the radioHPLC method, [¹⁸F]flumazenil metabolites can be analysed with high resolution. RadioTLC enables analysis of multiple samples simultaneously and is preferred, when sample volumes are small and radioactivity concentrations are low. **Acknowledgements:** Funding was received from the European Union's 7th Framework Programme for Research, grant

number 316882 and from the Academy of Finland, grant number 266891. [1] Tredwell M et al. *Angew. Chem. Int. Ed.* 2014, 53, 7751-7755 [2] Enhanced Copper-Mediated 18F-Fluorination of Aryl Boronic Esters provides Eight Radiotracers for PET Applications, submitted for publication, Gouverneur et al., personal communication

EP852

[68Ga] peptide high-output production on commercially available MiniAIO® synthesizer

C. COLLET^{1,2}, S. Remy^{1,2}, R. Didier^{1,2}, N. Véran³, G. Karcher^{1,2,3}; ¹Nancyclotep, Vandoeuvre-les-Nancy, FRANCE, ²Université de Lorraine, Vandoeuvre-les-Nancy, FRANCE, ³CHRU Nancy-Brabois, Vandoeuvre-les-Nancy, FRANCE.

Introduction: Gallium-68 is a metallic positron emitter with a half-life of 68 min that is ideal for labelling small peptides as radiopharmaceuticals thanks to the use of a chelating agent with several clinical applications. Numerous gallium-68 labelled peptides (eg. [⁶⁸Ga]DOTA-TOC/-NOC, [⁶⁸Ga]HBED-PSMA-11, [⁶⁸Ga]NODAGA-RGD) have shown their interest [1,2]. Developing an easy, rapid and performant labelling method is important. Different methods for the pre-purification of the generator eluate have been explored in the literature, although recent improvement on some generator brands (i.e. low ⁶⁸Ge breakthrough and low metallic impurities content), makes this pre-purification unnecessary. Development of a labelling process, GMP-compatible and reproducible, using a commercial synthesis module for every peptide labelling is a real challenge for the nuclear medicine. The method presented herein uses a cassette-based approach and a MiniAIO (mAIO, Trasis®) module and has been tested with the IGG100 ⁶⁸Ge/⁶⁸Ga generators. **Materials & Methods:** Preclinical IGG100 was used as ⁶⁸Ge/⁶⁸Ga generator. Precursors of radiolabelling were bought from ABX. Automated ⁶⁸Ga-labelling was performed without pre-purification in mAIO module. Reaction parameters such as sodium acetate concentration, precursor quantity, temperature and time were optimized for each peptide. Labelling efficiency was determined on Waters HPLC system. **Results:** DOTANOC, DOTATOC, HBED-PSMA-11 and NODAGA-RGD were tested for ⁶⁸Ga-labelling without pre-purification. Optimal and reproducible conditions were determined for each peptide. ⁶⁸Ga-peptides were synthesised with excellent incorporation yields, (90-99%) and high synthesis yields > 60% in less than 15 min. **Discussion/Conclusion:** We developed an efficient automated strategy for peptide labelling with gallium-68. [⁶⁸Ga]DOTANOC, DOTATOC, [⁶⁸Ga]HBED-PSMA-11, [⁶⁸Ga]NODAGA-RGD were obtained in high radiochemical yield. Their preparation could be performed with this automation and their use in human could be done under clinical trial. **References:** [1] Breeman W, de Blois E, Chan HS, et al. [2011], *Semin Nucl Med*, 41: 314-321 [2] Velikyan [2014], *Theranostic*, 4(1): 47-80

EP853

The Use of [¹⁸F]Selectfluor bis(triflate) in Electrophilic Fluorination

S. Lahdenpohja¹, A. Kirjavainen¹, S. Forsback^{1,2}, O. Solin^{1,2}; ¹Turku PET Centre, University of Turku, Turku, FINLAND, ²Department of Chemistry, University of Turku, Turku, FINLAND.

Aim Various aryl molecules can be labelled with reasonable reaction times and conditions only by electrophilic ¹⁸F-fluorination. In electrophilic ¹⁸F-labelling with [¹⁸F]F₂-gas the major problems are low specific activity (SA) and possible formation of numerous by-products. Less reactive labelling reagents have been developed in order to better control the reactions. One novel “mild” ¹⁸F-labelling reagent is [¹⁸F]Selectfluor bis(triflate) ([¹⁸F]SF). It has been successfully used in the synthesis of several radiotracers. **Materials and Methods** [¹⁸F]SF was produced from

[¹⁸F]F⁻ produced [¹⁸F]F₂ [1,2]. 6-[¹⁸F]FDOPA, [¹⁸F]NS12137 and [¹⁸F]6-fluoro-marsanidine were produced by fluorodestannylation of suitable stannylated precursors [3-5]. ¹⁸F-labelled ketones and allylic fluorides were produced by fluorodesilylation [1] and ¹⁸F-labelled tri- and difluoromethylarenes by fluorodecarboxylation [6]. After ¹⁸F-labelling, protecting groups were removed if needed and the obtained radiotracers were purified by HPLC. Total synthesis times were ~60 minutes. [¹⁸F]NS12137 and [¹⁸F]6-fluoro-marsanidine were evaluated in animals (*in vivo* with PET and *ex vivo* by autoradiography) [4,5]. **Results** [¹⁸F]Aryl fluorides were obtained with >95 % radiochemical purity, radiochemical yields were 2 - 20 % and SAs were 1 - 6 GBq/μmol [1,3-5]. Additionally, the quality of 6-[¹⁸F]FDOPA produced from [¹⁸F]SF was comparable to the one produced for clinical use from [¹⁸F]F₂. ¹⁸F-labelled ketones and allylic fluorides were obtained with ~15 % radiochemical yields [1]. ¹⁸F-labelled tri- and difluoromethylarenes were obtained with radiochemical yields up to 18 % and SAs up to 2,5 GBq/μmol [6]. **Conclusions** [¹⁸F]SF is an excellent labelling reagent in electrophilic ¹⁸F-fluorination. With [¹⁸F]SF, it is possible to label tracers which could not be labelled selectively with [¹⁸F]F₂. Work is ongoing in our laboratory to explore further [¹⁸F]SF and its applicability in the preparation of clinically useful radiotracers. **Acknowledgments** This work was supported by the Academy of Finland (grant no. 266891). **References** [1] Teare H. et al. (2010) *Angew.Chem.Int.Ed.* 49:6821-6824 [2] Bergman J, Solin O. (1997) *Nucl.Med.Biol.* 24:677-833 [3] Stenhagen I. et al. (2013) *Chem.Commun.* 49:1386-1388 [4] Kirjavainen A. (2014) Thesis, University of Turku [5] Krzyczmonik A. et al. (2015) *J.Label.Compnd. Radiopharm.* 58:S208 [6] Mizuta et al. (2013) *Org.Lett.* 15:2648-2651.

EP854

The most stable and fully automatic production of [¹⁸F]FP-CIT using All-in-One chemistry module

S. LEE, E. CHO, D. KIM, J. KIM, S. OH; ASAN Medical Center, Seoul, KOREA, REPUBLIC OF.

Objectives: Radiolabeled FP-CIT (fluoropropyl-carbomethoxyiodophenyl-nor-tropane) is a widely used radiopharmaceutical for dopamine transporter imaging using SPECT or PET. The 1st full automatic production of [¹⁸F]FP-CIT was developed in our group with non disposable cassette type chemistry module and used for clinical diagnosis of Parkinson's disease in Korea since 2008. In our previous reports, we optimized production condition using protic solvent such as *t*-amyl alcohol and base for [¹⁸F]fluorination step. The purpose of our study was to develop the production method of [¹⁸F]FP-CIT using disposable cassette with new reactor design with All-in-One chemistry module from Trasis company for routine clinical application. **Methods:** Two kinds of reaction vessel were applied into the disposable cassette design. One is conventional type (long recovery tube which was reached to reactor bottom, generally, type A) and new type has short recovery tube (type B). The recovery tube in type B reactor does not reach to reactor bottom and it has 0.5mm gap from the end of tube to the bottom. After trapping of 70~150 GBq of [¹⁸F]F⁻ on QMA cartridge, we eluted it with KOMs (pH 7.8)/K₂₂₂ mixture as elution buffer and base. After completely drying, [¹⁸F]fluorination was performed with 4~8 mg of precursor dissolved in 100 μL of MeCN and 1000 μL of *t*-amyl alcohol at 100°C for 10 min. After fluorination, crude [¹⁸F]FP-CIT was purified using semi prep HPLC isolated [¹⁸F]FP-CIT was trapped in C₁₈ cartridge and formulated with EtOH and ascorbic acid solution. Optimized reaction with new type reaction vessel was applied to All-in-One chemistry module from Trasis company. **Results:** Type A reaction vessel with 4 and 8 mg precursor showed 4.6±3.3% (n=7) and 18.9±5.0% (n=7) of non-decay corrected radiochemical yield, respectively. Type B reaction vessel with 4 and 8 mg precursor showed 15.5±4.4% (n=7) and 28.9±4.0% (n=7) of non-decay corrected radiochemical yield, respectively. New synthesis method with disposable cassette and type B reactor showed never synthesis failure. Total synthesis time including HPLC purification and formulation was 65

± 5 min. Radiochemical purity and specific activity were $93.7 \pm 2.2\%$ and > 74 GBq/ μmol , respectively. **Conclusion:** We developed new type reaction vessel and fully automatic production method with disposable cassette and All-in-One chemistry module for [^{18}F]FP-CIT routine production. Our disposable cassette including new type reaction vessel showed high radiochemical yield as 28.9% without production failure.

EP855

Quality control procedure for [^{18}F]FECNT: A PET ligand for imaging of dopamine transporter (DAT)

J. Pijarowska-Kruszyna, A. Jaron, P. Garnuszek, R. Mikolajczak; National Center for Nuclear Research Radioisotope Center POLATOM, Otwock, POLAND.

Aim: Previously, we reported the rapid and efficient synthesis of 2 β -carbomethoxy-3 β -(4-chlorophenyl)-8-(2-[^{18}F]fluoroethyl)-nortropine ([^{18}F]FECNT), a dopamine transporter (DAT) ligand [1]. Prior to its administration to humans the appropriate quality testing needs to be performed. The aim of this work was to establish the quality specification and quality control methodology for the [^{18}F]FECNT final drug formulation, according to the Ph. Eur. and ICH requirements [2,3]. **Methods:** [^{18}F]FECNT was prepared by one-step automated synthesis from the chlorinated precursor as previously described [1]. The quality testing included: appearance (clarity, absence of color and particles; visually inspected), pH (4.5–8.5; indicator strip test), radionuclidic identity as an approximate half-life of ^{18}F (105–115 min; radioactivity measurement), radionuclidic purity ($>99.5\%$ of the observed γ -emission; gamma-ray spectrometry), radiochemical identity (comparison of [^{18}F]FECNT retention time with retention time of non-radioactive FECNT reference; HPLC), radiochemical purity (RCP $\geq 97\%$ of [^{18}F]FECNT, $\leq 2\%$ of [^{18}F]F and $\leq 1\%$ of α -isomer of [^{18}F]FECNT; HPLC), chemical purity as content of Kryptofix@2.2.2 (≤ 2.2 mg per maximum dose; spot test) and precursor (≤ 0.1 mg per maximum dose; HPLC), residual solvents ($\leq 10\%$ of ethanol, $\leq 0.04\%$ of acetonitrile; GC), specific activity (≥ 37 GBq/ μmol ; HPLC), sterility (sterile; membrane filtration) and bacterial endotoxins (≤ 175 IU/mL; Gel-Clot). Selection of analytical methods and acceptance criteria for each parameter was based on the official guidelines [2, 3]. Radiochemical and chemical purity, radiochemical identity and specific activity were determined using the same HPLC method (Luna C18(2) column and mobile phase consisted of ethanol:water (57:43) pH=8, flow rate 1.0 mL/min, detection at 220 nm). **Results and Discussion:** Three batches of [^{18}F]FECNT were examined. All tested parameters met the acceptance criteria for drug release. The final [^{18}F]FECNT products were clear and colorless with pH 5–7. The radiochemical and radionuclidic identity were confirmed. The HPLC analyses demonstrated RCP of more than 99%. The preparation was free from the starting precursor (<0.1 mg) and undesired [^{18}F]FECNT α -isomer. The amounts of Kryptofix@2.2.2 and residual solvents were below acceptance limits. The specific activity of [^{18}F]FECNT at the EOS was 55 GBq/ μmol . **Conclusions:** The quality specification for the radioactive preparation of [^{18}F]FECNT was established and testing performed according to it confirmed that product [^{18}F]FECNT was of proper quality and safe for application in human studies. **References:** [1] Pijarowska-Kruszyna J et al., [2016] J Label Comp. Radiopharm, 59:82–86; [2] European Pharmacopeia. General monograph 0125: Radiopharmaceuticals preparations; [3] ICH guideline Q3C (R5) on impurities: guideline for residual solvents;

EP856

^{68}Ga radiolabeling of minigastrin analogues and automation for possible clinical use

M. Kroselj, A. Socan, P. Kolenc Peitl; University Medical Centre Ljubljana, Ljubljana, SLOVENIA.

Aim Targeting of receptors, overexpressed in different cancers, has an important diagnostic and therapeutic potential in Nuclear medicine. Successful story of somatostatin analogues lead to a development of many different radiolabeled regulatory peptides, including gastrin analogues. For targeting cholecystokinin-2 receptors different minigastrin (MG) analogues have been developed, mostly ^{111}In radiolabeled. ^{111}In radiolabeled PP11 or CP04 is currently in Phase 1 clinical study. In pre-clinical studies in Balb/C animal model it was shown that ^{68}Ga -labeled PP11 has favorable characteristics over ^{111}In -labeled radiopeptide for imaging of CCK2R positive tumours (Roosenburg et al., 2014). Recently, we showed that norleucin congeners have similar in vivo characteristics to oxidation prone methionin analogues, so they could be potentially used in clinic. In this study we aimed to develop a robust automated method for ^{68}Ga labeling of different MG analogues. **Methodology** 20 μg of the MG analogues PP11 (CP04) and its Nle congener PP11B (DOTA-(D-Glu)₆-Ala-Tyr-Gly-Trp-Met/Nle-Asp-Phe-NH₂) and PP16B (DOTA-(D-Gln-D-Glu)₃-Ala-Tyr-Gly-Trp-Nle-Asp-Phe-NH₂) were used as a probes. $^{68}\text{Ge}/^{68}\text{Ga}$ generator (IGG100, EZAG) was eluted with 0.1M HCl. NaCl (Müller) method was used for prepurification and concentration of ^{68}Ga eluate. Reaction conditions such as buffers, pH range, radical scavenger, reaction temperature and time and volume of reaction solution were optimized for labelling MG analogues. Full automation of the processes was developed using self-shielded radiosynthesis box (MicroCell, EZAG). Quality testing of the final products was done. **Results** 500–650 μL of NaCl/HCl solution was needed to efficiently elute 300–400 MBq of ^{68}Ga from preloaded stron cation exchange column (Bond Elute SCX). Optimal pH of sodium acetate/HCl buffer for radiolabeling PP11 was 4.6 ± 0.1 and for PP11B and PP16B 4.3 ± 0.1 . Heating for 5 minutes at 95°C was sufficient to get radiochemical yields over 90%. A fully automated synthesis was developed for NaCl method using SepPak purification and final MB filtration. Total synthesis time was 18 minutes with radiosynthesis yields $>70\%$ and final radiochemical purities of $>95\%$ for all peptides. ^{68}Ge contamination in the final product was not detected and all other quality tests (pH, ethanol content, filter integrity, endotoxin testing, sterility) passed. **Conclusion** Due to well know advantages of ^{68}Ga and potentially better in vivo characteristics we successfully optimized ^{68}Ga radiolabeling conditions for 3 minigastrin analogues and developed a fully automated robust procedure for a possible clinical use. Clinical studies comparing ^{68}Ga vs. ^{111}In radiolabeled analogues ones are needed to explore possible advantages of ^{68}Ga MG analogues over ^{111}In ones.

EP857

GMP Compliant Automated ^{18}F -Flumazenil Production using Chemically Resistant Single-Use Disposable Cassettes

P. Lam, M. Aistleitner, R. Eichinger, C. Artner; IASON GmbH, Graz, AUSTRIA.

Introduction Production of ^{18}F -flumazenil from 2-nitroflumazenil under GMP conditions is primarily performed with manipulators or custom built radiosynthesis modules with fixed components, as the use of *N,N*-dimethylformamide (DMF) at 160 °C prohibits the use of commonly available disposable cassettes. Cassettes for the GE TRACERlab MX_{FDG} synthesis modules are commercially available in different materials, and it is known that most of the polymers used are not compatible with DMF. The aim of this work was to establish a robust automated radiosynthesis procedure for ^{18}F -flumazenil on the GE TRACERlab MX_{FDG} with the appropriate cassette material, where staff previously trained on the same equipment can easily perform the radiosynthesis. **Materials & Methods** Fragments of the ABX FDG cassette and chemically resistant manifolds were exposed for 1 or 24 h to various solvents including DMF at room temperature (RT) or 60 °C to assess its chemical resistance. A new synthesis sequence was written for the GE TRACERlab MX_{FDG}. A non-radioactive test run was performed with

the ABX FDG cassette, and radiosynthesis was carried out with the cassette components replaced by chemically resistance manifolds (ABX). **Results** Incubation of the ABX FDG cassette fragments in acetonitrile at RT showed no macroscopic influence on the polymer while the fragment became soft and mouldable at 60 °C. Visible changes occurred after 1 h incubation with DMF, with the polymer having completely dissolved after 24 h, regardless of temperature. To verify the implication of these results on a 1 h radiosynthesis, a test run was performed using the same cassette material and synthesis conditions without radioactivity. Parts of the manifold was found to have cracked, and a valve blockade was observed due to polymer melting. On the other hand, chemically resistant manifold showed no changes in DMF for up to 24 h at 60 °C. Radiosynthesis was carried out with the manifolds replaced by chemically resistant ones, and ^{18}F -flumazenil was successfully obtained in 4 % decay corrected yield. **Conclusions** Disposable cassettes assembled with chemically resistant manifolds is a requirement for the automated synthesis of ^{18}F -flumazenil from 2-nitroflumazenil using the GE TRACERlab MX_{FDG} synthesis module. Neither reagent kits nor program sequences are hitherto commercially available, but automated GMP grade production of ^{18}F -flumazenil with single-use cassettes can nonetheless be successfully carried out with minor modifications on existing equipment.

EP858

Preparation of (^{18}F)FDOPA in a fully automated radiochemical synthesizer: a tertiary university hospital experience

H. PEHLIVANOGLU¹, E. Karayel¹, A. Aygün¹, R. Tutar², A. Kurt¹, M. Ocak³, L. Kabasakal¹, K. Sönmezoğlu¹; ¹Department of Nuclear Medicine, Cerrahpaşa Medical Faculty, ISTANBUL UNIVERSITY, ISTANBUL, TURKEY, ²Department of Physicochemistry, Engineering Faculty, ISTANBUL UNIVERSITY, ISTANBUL, TURKEY, ³Department of Pharmaceutical Technology, Pharmacy Faculty, ISTANBUL UNIVERSITY, ISTANBUL, TURKEY.

Introduction: 3,4-dihydroxy-6- ^{18}F -fluoro-L-phenylalanine (FDOPA) has proven to be a useful radiopharmaceutical for the evaluation of presynaptic dopaminergic function in central nervous system. FDOPA is also taken up into cell by amino acid transporters (predominantly L-type), which are overexpressed in several types of cancer. Recently encouraging results with FDOPA PET imaging have been reported in neuroendocrine tumors particularly in medullary thyroid carcinomas and pheochromocytomas. FDOPA can be synthesized either via electrophilic or nucleophilic substitution reaction methods. In comparison to electrophilic synthesis, the nucleophilic method has several advantages. Here we present our preliminary results of synthesizing FDOPA with nucleophilic method using a fully automated radiopharmaceutical synthesis device at Cerrahpaşa Medical Faculty, Department of Nuclear Medicine, Istanbul **Material and methods:** The radiosynthesis was performed by using a fully automated synthesizer (Trasis, all-in-one, Belgium). Automated synthesis of FDOPA is consisted of five synthetic steps: fluorination, reductive iodination, alkylation, hydrolysis and purification. Purification was performed using a reversed phase semi-preparative HPLC. Radiochemical purity of FDOPA was determined by RP-HPLC using sodium dihydrogen phosphate adjusted to pH 2.4 with solution of phosphoric acid. Enantiomeric purity was determined by RP-HPLC using perchloric acid pH 2. Residual solvents purity determined by GC. **Results:** Both radiochemical purity and enantiomeric excess are higher than 95%. The non-decay corrected yield of the system is 30 ± 3 %. Residual solvents excess are follows: N,N-Dimethylformamide < 880 ppm, Dichloromethane < 600 ppm, Methanol < 3000 ppm, and Ethanol < 5000 ppm. **Conclusion:** The synthesizer and described methods allow us a satisfactory automated preparation of FDOPA with desired QC parameters that is a suitable radiopharmaceutical for human use.

Posters

P-02 – Sunday, October 16, 2016, 16:00 - 16:30, Poster Exhibition Hall
Cardiovascular System: Effect of (Cardiotoxic) Treatment

P011

Nuclear Medicine Assessment in management of Patients with Atrial Fibrillation Treated with PUFAs

V. Sukhov, K. Zaplatnikov, V. Nikiforov, P. Kirichenko, A. Ismailov, S. Grishaev; Military Medical Academy, ST. PETERSBURG, RUSSIAN FEDERATION.

Objective. This study examined the effects of polyunsaturated fatty acids (PUFAs) on myocardial perfusion and metabolism in patients with atrial fibrillation (AF) using well known in clinical practice myocardial gated single photon emission computerized tomography (G-SPECT) with ^{99m}Tc-tetrofosmine (TF) and ¹²³I-beta-methyl-iod-phenyl-pentadecanoic acid (BMIPP) as in vivo methods for diagnostics of different heart diseases. **Material and Methods.** 56 male patients 45-69 y.o. with persistent AF treated with standard anti-ischemic and anti-arrhythmic agents (control group) were compared with 51 male patients 44-66 y.o. with AF I-II FC NYHA treated with standard anti-arrhythmic + PUFAs. All of them underwent standard clinical investigation, Bruce protocol ETT, EchoCG and rest/stress G-SPECT with ^{99m}Tc-TF and ¹²³I-BMIPP. Both tracers SPECT data were analyzed with 17-segment model. **Results.** Definite regional abnormality of perfusion tracer uptake at rest/stress were concordant with metabolic defects at the same site. While comparing regions of repolarization disturbances, shifted metabolism and decreased perfusion tracer uptake in 95 patients, 93% of them were considered match (di=0,615-0,998), 7% - mismatch (di=0,002-0,385). Though sensitivity in detecting of impaired repolarization by ECG and decreased ^{99m}Tc-TF/¹²³I-BMIPP uptake regions by SPECT were 19.6% vs 87.1%./ 89.2%. Moreover, number of sectors with low ^{99m}Tc-tetrofosmine and/or ¹²³I-BMIPP uptake (<70%) and with EchoCG signs of cardiac insufficiency, ECG abnormalities and decrease of tracers uptake were equal. Repeated gated SPECT studies after treatment with PUFAs showed increase of perfusion tracer uptake in previously altered sectors compared to patients treated with only standard therapeutic scheme. **Conclusion.** Metabolic activity and myocardial perfusion as shown by ¹²³I-BMIPP and ^{99m}Tc-TF SPECT allow to perform adequate assessment of changing (decreasing) of myocardial metabolism (i.e. levels of beta-oxidation in cardiomyocytes) that together with perfusion data can fully represent the state of heart tissue impairments in AF patients. Therefore, this method is feasible and highly informative for assessment of PUFAs effects during metabolic treatment and follow-up.

P012

Early and late follow-up myocardial perfusion scan in patients with breast cancer after external radiotherapy

M. Eftekhari¹, A. Emami-Ardekani¹, F. Kalantari¹, M. Abbasi², S. Farzanefar², A. Fard-Esfahani¹, B. Fallahi¹, D. Beiki¹, A. Hassanzadeh-Rad¹; ¹Research Center for Nuclear Medicine, Shariati Hospital, Tehran University of Medical Sciences, TEHRAN, IRAN, ISLAMIC REPUBLIC OF, ²Research Center for Nuclear Medicine, Vali-Asr Hospital, Tehran University of Medical Sciences, TEHRAN, IRAN, ISLAMIC REPUBLIC OF.

Aim: Radiotherapy induced myocardial injury may increase cardiovascular morbidity and mortality especially in left sided breast cancer. To evaluate the prevalence of myocardial perfusion abnormalities following radiation therapy, in left and right-sided breast cancer patients, early and delay term myocardial perfusion imaging (MPI) findings were compared.

Materials and Methods: Patients with low 10-year Framingham risk scoring of coronary artery disease were included in the study. Modified radical mastectomy and postoperative 3D Conformal Radiation Therapy (CRT) were considered as the standard treatment for all patients. The surgical bed with an additional 1-cm margin was selected to deliver 46-50 Gy (in 2 Gy daily fractions) over a 5-week course and the same dose-adjusted chemotherapy regimen (including anthracyclines, cyclophosphamide and taxol) was administered. Three years after radiation therapy, all patients underwent MPI for the evaluation of myocardial perfusion. These patients also have been evaluated for possible early adverse effects 6 months after radiotherapy. General linear model for repeated measures was designed to assess the ischemic changes over time. **Results:** Forty patients with a mean age of 46±7.1 years [20 patients with left sided breast cancer (exposed) and 20 patients with right-sided cancer (controls)] were enrolled. Dose-volume histogram (DVH) [showing the percentage of the heart exposed to >50% of radiation] was significantly higher in patients with left-sided breast cancer. The prevalence of ischemia showed significant changes between groups in follow-up study (P value=0.001). The extent of ischemia decreased from the baseline to the second study in right sided mastectomy group. Apex and anterolateral walls were the most common segments demonstrating significant perfusion abnormality in the early study, while only apical abnormality was more prevalent at the delayed study (P value<0.05). **Conclusion:** Radiation induced myocardial perfusion injury is not uncommon in patients with left hemi thorax radiotherapy. It is recommended to apply precise radiation planning techniques to minimize the volume of the heart in the field of radiation therapy. MPI-SPECT is a sensitive and non-invasive technique for early detection and proper management of potential myocardial abnormality in these patients following radiotherapy.

P013

Prediction of symptomatic cardiac toxicity in the patients who underwent chemoradiotherapy for esophageal cancer by myocardial fatty acid metabolic imaging using I-123 BMIPP SPECT/CT

K. Takanami, A. Arai, R. Umezawa, K. Jingu, K. Takase; Tohoku University Hospital, Sendai, JAPAN.

Aim: The aim of this study was to determine the value of myocardial fatty acid metabolic imaging by using I-123-labeled long-chain fatty acid analogue, 15-(p-iodophenyl)-3-(R,S)-methyl-pentadecanoic acid (BMIPP), and SPECT/CT in the prediction of symptomatic cardiac toxicity in the patients who underwent chemoradiotherapy (CRT) for esophageal cancer. **Materials and methods:** We included 36 patients (29 men, 7 women; mean age, 64.3 years) with no history of heart disease who had undergone CRT for esophageal cancer. They underwent I-123 BMIPP SPECT/CT at a median of 463 days after the completion of CRT and have been followed up. Myocardial I-123 BMIPP summed defect scores were semi-quantified using a 17-segment 5-point system (normal, 0; absent, 4). The patients' data including the cardiac toxicity measured by RTOG and CTCAE v4.0 criteria were extracted from a prospectively collected database. Cox proportional hazards regression analysis was applied to determine the independent predictors of symptomatic cardiac toxicity as an endpoint. Statistical significance was defined as P < 0.05. **Results:** During a median follow-up period of 1048 days after SPECT/CT, 6 (16.7%) of 36 patients were identified with symptomatic cardiac toxicity, including myocardial infarction (n = 2), angina pectoris (n = 1), hypotension due to pericardial effusion (n = 1), and arrhythmia (n = 2). In the patients with symptomatic cardiac toxicity and the other patients, the median (interquartile range) of I-123 BMIPP summed defect score was 11 (6-14) and 6 (4-8), respectively, and that of the percentage volume of the left ventricle receiving 40 Gy or more was 16.6% (8.4% - 31.0%) and 20.5% (12.9% - 31.5%), respectively. Cox proportional hazards regression analysis showed that the most powerful predictor of symptomatic cardiac toxicity was I-123 BMIPP summed defect scores with hazard

ratio of 1.5 ($p < 0.05$). Conclusions: The results of this preliminary study indicate that myocardial fatty acid metabolic impairment found by I-123 BMIPP SPECT/CT may predict symptomatic cardiac toxicity in the patients who had undergone CRT for esophageal cancer.

P-03 – Sunday, October 16, 2016, 16:00 - 16:30, Poster Exhibition Hall
Cardiovascular System: Gated SPECT

P014

Introducing a pre-reconstruction cardiac motion compensation technique in gated myocardial perfusion SPECT

N. Salehi^{1,2}, M. Farahani², E. Fatemizadeh³, S. Farzanefer⁴, M. AY^{1,2};
¹Department of medical physics and biomedical engineering, Tehran university of medical sciences, Tehran, IRAN, ISLAMIC REPUBLIC OF,
²Research Center for Molecular and Cellular Imaging, Tehran University of Medical Sciences, Tehran, IRAN, ISLAMIC REPUBLIC OF,
³Electrical Engineering Department, Sharif University of Technology, Tehran, IRAN, ISLAMIC REPUBLIC OF, ⁴Department of Nuclear Medicine, Vali-Asr Hospital, School of Medicine, Tehran University of Medical Sciences, Tehran, IRAN, ISLAMIC REPUBLIC OF.

Introduction: Cardiac contraction and respiratory movement are two main factors which degrade gated myocardial perfusion SPECT images quality by inducing image blurring and quantification inaccuracies. As images are acquired in different time frames and gamma photons recorded in each time frame is limited the reconstructed “low-count” images, have poor statistical image quality. Therefore motion compensated temporal processing can have a major impact on gated images quality. **Material and Method:** In this study, mathematical four-dimensional NURBS-based Cardiac-Torso phantom of two heart sizes (124 ml and 100 ml left ventricular cavities) were constructed for male and female body, respectively. SIMIND Monte Carlo simulation package was used to simulate a clinical Tc-99m-mibi perfusion SPECT acquisition protocol on the dual headed Philips (ADAC-forte) gamma camera (Philips Medical Systems, Cleveland, Ohio), with Low Energy High Resolution (LEHR) collimators, 32 projection data of phantoms were obtained for each gate. We have warped each frame with respect to end diastolic frame, using a 3D dimensional non-parametric diffeomorphic algorithm based on Thirion demon registration technique in MATLAB 2015. 4D sequence of motion compensated projections and original projection data were reconstructed using OSEM algorithm. Myocardial thickness and myocardium versus ventricle contrast were measured in original different image phases and motion compensated image phases. Quantitative study of Image sequences were conducted after importing image sequences to cardiac SPECT system’s work station. Gated and summed image parameters were automatically derived and calculated on the basis of sex specific normal limits obtained from the same healthy population using standard Cedars-Sinai software. **Result:** The compensated images were less noisy. Compensated images has higher myocardium versus ventricle contrast than the corresponding summed images (18.63 vs. 14.89). Myocardial thickness between 8 phases were calculated, sum of squared difference between the wall thickness in end-systolic and end-diastolic phases were reduced from 0.44 to 0.16 after motion compensation. In QPS study original heart volume was 81 ml, 39 ml and the corresponding motion compensated volume was 92ml and 52 ml for male and female phantoms respectively. TPD (Total Perfusion Defect) was reported 11% and 31% for original male and female phantom images and the compensated data TPD was reported 9% and 28% respectively. **Conclusion:** Motion compensation increases image quality by increasing resolution and contrast and higher SNR is obtained due to summation of all morphed frames. It is highly recommended that with compensation we can improve defect detectability and diagnosis sensitivity.

P015

Comparison of phase dyssynchrony analysis among different software programs in patients with suspected or known coronary artery disease

S. Matsuo¹, K. Nakajima¹, K. Okuda², Y. Kunita¹, S. Kinuya¹;
¹Kanazawa University, Kanazawa, JAPAN, ²Kanazawa Medical University, Uchinada, JAPAN.

Cardiac dyssynchrony occurs during periods of post-stress myocardial ischemia. The feature of contractile discordance can be detected by phase analysis using gated myocardial perfusion SPECT (GMPS). Previous studies have shown that the histogram bandwidth (BW), phase standard deviation (SD) and phase entropy show good correlation with left ventricular (LV) dyssynchrony. In the evaluation of LV dyssynchrony, phase analysis of GMPS can be performed by commercially available different types of software. However, the comparison among programs has not been fully evaluated as yet. The aims of this study are to compare phase analysis parameters among software programs in patients with suspected or known coronary artery disease (CAD). Methods: Adenosine pharmacological stress myocardial perfusion imaging was performed in patients ($n=20$, aged 70.0 ± 10.1 , male 65%) with suspected or known CAD, using ^{99m}Tc-agents by a 1-day protocol. LV mechanical dyssynchrony was evaluated using the quantitative gated-SPECT (QGS) software of Cedars Sinai Medical Center, the Emory Cardiac Tool Box (ECTB) of Emory University, and cardioREPO (cREPO). The stress and rest defect scores were determined automatically. Ischemia was defined to exist when perfusion defects on post-stress images were completely or partially corrected on rest images, and summed difference score was more than one. The histogram BW, phase SD and phase entropy were calculated. Results: The fair correlation among software programs was observed. Mean values \pm SD of rest BW in QGS, cREPO and ECTB were 55.5 ± 47 , 54.2 ± 31.8 and 46.3 ± 17.5 , respectively. The values of phase SD in QGS, cREPO and ECTB were 11.0 ± 11.1 , 13.7 ± 7.9 , and 16.9 ± 7.8 , respectively. Delta BW (stress BW-rest BW) and delta phase SD (stress phase SD-rest phase SD) in QGS, cREPO, ECTB were 5.9 ± 38.4 , 13.6 ± 23.8 and 11.0 ± 41.3 , respectively. There was a difference between phase entropy of cREPO and that of QGS (48.4 ± 11.1 vs. 34 ± 15.9 , $p < 0.01$). Delta phase SDs of ECTB and cREPO were significantly higher than that of QGS ($p < 0.01$). The delta-SD of subjects with ischemia had higher than that without ischemia in cREPO ($p < 0.05$). There were no difference in delta-SD between subjects with ischemia and without on QGS and ECTB. In conclusion, phase analysis parameters derived from GMPS in CAD patients depend on software programs and ischemic phase expression may differ in each program. The results of phase analysis cannot be interchangeably used in the same CAD patients.

P016

Relationship between Tc-99m MIBI GATED SPECT myocardial perfusion, quantified functional analysis, and dyssynchrony assessment in patients with left bundle branch block (LBBB) and no evidence of Ischemic heart disease-An approach to the real facts

G. A. VILLORIA¹, S. Rodado Marina¹, P. catalan², J. Castro-Beiras², B. Lorente², Y. RAMIREZ¹, L. Dominguez Gadea¹, M. Gomez³;
¹LA PAZ UNIVERSITY HOSPITAL, MADRID, SPAIN, ²ramon y cajal UNIVERSITY HOSPITAL, MADRID, SPAIN, ³RAMON Y CAJAL UNIVERSITY HOSPITAL, MADRID, SPAIN.

objectives: The left bundle branch block (LBBB) is associated with increased overall mortality, and poses a challenge for the diagnosis of ischemic heart disease. It is often associated with a perfusion defect at the septal region during exercise. We evidenced this as an artifact due to conduction disorder but does not correspond to an actual or structural abnormality or perfusion. Our objective was to evaluate Tc-99mMIBI

GATED myocardial perfusion SPECT (GMPS) in patients with LBBB with normal coronary arteries, and thus determine the relationship between perfusion and functional quantification data in order to determine the possible value of the latter to rule out ischemic heart disease. We have also included analysis of dyssynchrony of the left ventricle in these patients to evaluate the possibility to be suitable candidates for resynchronization therapy. **Material and methods:** We studied 31 patients (mean age 70+/-9; males: 22+/-2). They underwent stress test followed by a myocardial perfusion and function quantified study with Tc-99mMIBI GATED myocardial perfusion SPECT (GMPS) in the territory of the left anterior descending artery (ADA). The absence of coronary disease was established by coronary angiography, echocardiography or angioCT. LV dyssynchrony assessment in 12 patients with LBBB compared with 18 patients without evidence of conduction anomaly with software corridor 4DM. **Results:** The perfusion defect in stress was 38%+/-21 and the rest of 33%+/-18 percent of total infarction (p = NS). The endocardial thickening defect was 12% +/- 14 in stress, 7% +/- 12 in rest (P = 0.033). Contractility defect 13% +/- 15, and 4% +/- 15 at rest. The perfusion defect was greater than abnormal thickening and contractility (p = 0.000). LV Dyssynchrony assessment was obtained for normal patients, EF: 72+/- 7, showing a mean peak of 45.3 +/- 5.6, mean SD = 4.7 +/- 2, Patients with LBBB had an EF: 46.3+/-9, mean peak = 48.7 +/- 6.2 NS between groups, and mean SD 10.15 +/- 3.2 with differences (P = 0.05). **Conclusions:** LBBB produces stress perfusion defects that may seem important in patients without evidence of heart disease. The perfusion defects also appear at rest. The size of the apparent defect is similar in stress and rest. Perfusion defects appeared in these patients were not related with thickening and contractility quantified values. LBBB patients have a degree of left ventricular dyssynchrony and dysfunction potentially significant for these patients.

P017

Assessment of Mechanical Dyssynchrony by Myocardial SPECT imaging is Predictor of Mortality in Congestive Heart Failure patients With Normal QRS Duration

S. T. BUTT; NORI, ISLAMABAD, PAKISTAN.

Researchers have assessed the prevalence of mechanical dyssynchrony in patients with CHF with normal QRS duration by echocardiography techniques such as tissue Doppler imaging. It is established now that mechanical dyssynchrony has some role in prognosis of congestive heart failure patients. In a developing country like Pakistan although echocardiography technique is widely available but lack of expertise in newer echocardiography techniques of dyssynchrony analysis such as TDI and Speckle tracking echo limits its use as predictor of future cardiac events. In comparison Myocardial SPECT imaging is not only widely available, its negligible interobserver variability can make it a valuable tool for assessment of myocardial dyssynchrony as a predictor of mortality and morbidity in CHF patients with normal QRS duration. Group A consisted of 50 patient with congestive heart failure with normal QRS complex who met the following criteria were retrospectively analyzed, Patients with NYHA function class II, III, IV for at least three months; bilateral pulmonary congestion on admission; and LV EF less than 35% and QRS duration more than or equal to 120 ms at the time of presentation. Patients having Atrial fibrillation, significant structural valvular disease, cardiac or cerebral ischemic event within the previous three months, coexisting malignant disease, coronary revascularization during the study period and with age above 80 years were excluded. Group B comprised control group. A total 50 age and sex matched normal patients were assessed as control for calculation of normal values of standard deviation (SD) and histogram bandwidth (HBW) in our population. Dyssynchrony analysis was performed in patients and control group. Patients record was analyzed at 6 months follow up for cardiac events and mortality and it was correlated with SD and HBW in CHF patients with normal QRS complex. Detection

of LV systolic dyssynchrony using Tc99m Myocardial SPECT was found an important independent predictor of clinical events and cause of mortality in CHF with normal QRS duration (significance value P less than 0.05) regardless of age, EF, QRS duration, etiology of CHF, and use of beta-blockers.

P018

Are echocardiography and radionuclide ventriculography reliable methods for left ventricle volume measurements? Significant underestimation of end-diastolic and end-systolic volumes of impaired left ventricle in 2D-echocardiography and tomographic SPECT radionuclide ventriculography in comparison with cardiac magnetic resonance as the golden standard

W. Cytawa¹, M. Gruchala¹, K. Dorniak¹, R. Galaska¹, P. Lass^{1,2}; ¹Medical University of Gdansk, Gdansk, POLAND, ²University of Gdansk, Gdansk, POLAND.

Aim: The aim of the study was to compare left ventricle volumes in patients with impaired contractile function measured by 2D-echocardiography, tomographic (SPECT) radionuclide ventriculography and cardiac magnetic resonance. **Materials and methods:** We examined 31 patients (20 males, 11 females, aged from 26 to 82, mean age 54, standard deviation (SD) 14,7), with various cardiac conditions leading to impaired systolic function (dilated cardiomyopathy, segmental contractile dysfunction or contractile dyssynchrony due to LBBB). Every patient had 2D-echocardiography (Echo), SPECT radionuclide ventriculography and cardiac magnetic resonance (CMR) with volume measurements, performed within one week. **Results:** The linear correlations between end-diastolic volumes in Echo (Echo EDV) and SPECT EDV comparing to CMR EDV were high and significant, with r=0,90-0,91. The mean values, however, were significantly different: mean Echo EDV was 189.4 ±91.2ml (range=74-410), mean SPECT EDV was 164.1±80.8ml (range=41-349) and mean CMR EDV was 283.8±127.9ml (range=112-603). The mean differences between CMR EDV and other modalities were considerable and significant: CMR EDV vs. SPECT EDV mean diff.=119,77 and CMR EDV vs. Echo EDV mean diff.=94.39. BA limits of agreement between CMR EDV and SPECT EDV were 12.48 252.02, and between CMR EDV and Echo EDV -22.9 211.67. Similar discrepancies were observed in case of end-systolic volumes. Linear correlations were high and significant: r=0.93-0.94. The mean values: mean Echo ESV 140.3±89.6ml (range=27-364), mean SPECT ESV 124.1±76.8ml (range=16-297), mean CMR ESV 214.4±129ml (range=55-534). Mean differences were again considerable and significant: CMR ESV vs. SPECT ESV mean diff.=90.29, BA limits: -37.83 218.41; CMR ESV vs. ECHO ESV mean diff.=74.06, BA limits: -32.36 180.49. r - linear correlation coefficient BA - Bland-Altman 95% limits of agreement **Conclusions:** In patients with cardiac conditions leading to impaired function of left ventricle precise volume measurement is necessary for ejection fraction calculation and hence proper clinical management. Our results revealed big discrepancies between 2D-echocardiographic and SPECT radionuclide ventriculography volume measurements comparing to cardiac magnetic resonance treated as the "golden standard". We reported systemic bias - both Echo and SPECT significantly and considerably underestimated EDV and ESV comparing to CMR.

P019

Evaluation of Diastolic Dysfunction in multivessel coronary artery disease using 16 Gated SPECT Myocardial Perfusion Imaging

M. Prabhu; Narayana Health City, Bangalore, INDIA.

INTRODUCTION: In the cascade of ischemia, after flow heterogeneity diastolic dysfunction precedes systolic dysfunction. We intended to

examine if this pathophysiological precedence can influence interpretation of myocardial perfusion imaging (MPI) in multivessel coronary artery disease (CAD). **AIMS AND OBJECTIVES OF THE STUDY:** 1. To detect the presence of Diastolic Dysfunction in multivessel coronary artery disease. 2. To evaluate the role of Diastolic Dysfunction in interpretation of MPI for detection of ischemia in multivessel CAD. **MATERIAL AND METHODS:** 100 coronary angiogram proven multivessel CAD patients were enrolled in this study. MPI was performed according to standard guidelines and images were acquired using dedicated CZT based cardiac gamma camera. Acquired data were processed on ECTool box and companion software on QGS. The cut off limits for PFR and TTPF for men were taken as 1.73 EDV/s and 211.4ms and for women, 1.87 EDV/s and 194.1ms. Two independent Nuclear Medicine physicians were made to interpret the perfusion images with and without diastolic parameters. Inter observer variability was assessed using kappa statistic. **RESULTS:** 24/100 patients developed stress induced diastolic dysfunction. 22 patients had diastolic dysfunction with preserved systolic function. Moderate agreement between observers was noted for interpretation of ischemia without diastolic parameters ($k = 0.49$) which improved to substantial agreement with the knowledge of diastolic parameters ($k = 0.66$). Also, 30% probable interpretation was changed to definite interpretation by observer 1 with the provision of diastolic parameters ($p < 0.001$). **CONCLUSIONS:** Diastolic dysfunction can occur at stress even in the absence of systolic dysfunction. Substantial agreement between the observers in interpretation of ischemia using diastolic parameters indicates its potential role in evaluation of multivessel CAD. Hence, identification of stress induced diastolic dysfunction in multivessel CAD adds value in identifying balance ischemia. **KEYWORDS:** CAD: Coronary artery disease, MPI: Myocardial Perfusion Imaging, PFR: peak filling rate, TTPF: Time to peak filling.

P020

Relationship between cardiac electrical and mechanical dyssynchrony

S. Sillanmäki^{1,2}, J. Lipponen³, T. Laitinen¹, M. Tarvainen³, T. Laitinen^{1,2}; ¹Department of Clinical Physiology and Nuclear Medicine, Kuopio University Hospital, Kuopio, FINLAND, ²Department of Clinical Physiology and Nuclear Medicine, University of Eastern Finland, Kuopio, FINLAND, ³Department of Applied Physics, University of Eastern Finland, Kuopio, FINLAND.

Aim: The aim of this study was to find vector electrocardiography parameters (VECG) which associate with mechanical dyssynchrony assessed by myocardial perfusion imaging (MPI) phase analysis. **Materials and Methods:** Study population consisted of 16 patients with left bundle branch block (LBBB) and 14 healthy controls. All subjects underwent a standard ECG-gated MPI. 12-lead resting ECG-data was collected using Mason-Likar leads and was analysed using custom made VECG analysis software. Gained VECG parameters were compared with MPI phase analysis parameters known to associate with left ventricular systolic dyssynchrony. VECG signals were analysed by estimating orientation, morphology and heterogeneity of depolarization wave front from the 5 minutes ECG-recording. X-, Y- and Z-leads were synthesized using Kors matrix and averaged beat segments (P-QRS-T) were produced for above-mentioned leads. Mean QRS vector loop angles were defined in frontal (α_{fro}), transverse (α_{tra}) and sagittal (α_{sag}) planes. Heterogeneity of the depolarization and repolarization sequences were parameterized using QRS-T angle. Also, QRS loop non-planarity measure (QRS_{σ3}) describing irregularity of the QRS complex were estimated. MPI studies were performed with Siemens Symbia SPECT-CT camera (^{99m}Tc-tetrofosmin, 64 angles, 25s/view, 128x128 matrix, 16 frame ECG). Reconstructions were done with HERMES HybridRecon Cardiology and data was analysed with Cedars-Sinai QGS2012 program. The bandwidth (BW), standard deviation (SD) and entropy% of the histogram were calculated as

mechanical dyssynchrony measures. **Results:** QRS vector loop of a typical LBBB subject is narrow and pointing towards the back of the subject. Healthy subject's QRS loop is on the other hand wider and pointing towards the left leg. Heterogeneity of the repolarization and depolarization sequences is also significantly increased in LBBB subjects. In both groups significant negative correlation was found between α_{sag} and SD ($r = -0.65$, $p < 0.05$) and positive between SD and QRS_{σ3} ($r = 0.53-0.69$, $p < 0.05$). In LBBB group, all mechanical dyssynchrony parameters showed strong negative association with mean QRS vector in sagittal plane ($r = -0.66 - -0.65$, $p < 0.01$) and positive in transversal plane ($r = 0.62 - 0.77$, $p < 0.01$). Also all mechanical dyssynchrony parameters in LBBB group correlated significantly with QRS_{σ3} ($r = 0.60 - 0.69$, $p < 0.05$) and α_{fro} ($r = -0.53 - -0.62$, $p < 0.05$). **Conclusion:** The form of QRS vector loop in LBBB group is different from control group's loop. Several VECG parameters correlate with MPI dyssynchrony parameters. This observation may help to understand electrical background of mechanical dyssynchrony in LBBB patients.

P021

Assessment of diastolic function in patients with type 2 diabetes mellitus with gated SPECT

A. Korkmaz¹, B. Caliskan¹, F. Erdem²; ¹Abant Izzet Baysal University Department of Nuclear Medicine, Bolu, TURKEY, ²Abant Izzet Baysal University Department of Cardiology, Bolu, TURKEY.

Aim Diabetes mellitus (DM) is one of the major risk factors for cardiovascular disease. In patients with DM, heart disease may remain silent until an advanced stage. Early identification of diastolic dysfunction of patients with diabetes is important in preventing cardiac events. In this study, we compared diastolic function parameters obtained with gated SPECT (G SPECT) in patients with DM without known coronary artery disease (CAD) and no ischaemia with those of individuals without DM. We assessed whether G SPECT can be used to evaluate both myocardial perfusion and systolic and diastolic functions in patients with DM with atypical cardiac symptoms. **Materials and methods** We examined 80 patients: 40 with and 40 without diabetes. The patients were compared in terms of systolic and diastolic parameters obtained using G SPECT. Tc-99m sestamibi was used to obtain 8-frame images in each cardiac cycle, with calculation of the left ventricular ejection fraction (LVEF), peak filling rate (PFR), mean filling rate during the first third of diastolic time (MFR3), and time to peak filling (TTPF) using the QGS software. **Results** G SPECT results were compared in 40 diabetic and 40 non-diabetic patients of similar age, sex and coronary artery disease risk factors. Of the diastolic function parameters, PFR was found to be lower in patients with than without diabetes (2.31 ± 0.68 vs. 2.76 ± 0.68 , respectively; $p = 0.004$). The TTPF and MFR3 in both groups were similar. PFR was negatively correlated with end-diastolic volume (EDV) and end-systolic volume (ESV) and positively correlated with LVEF. This correlation was stronger in patients with diabetes. **Conclusion** In conclusion, in the present study patients with DM with normal myocardial perfusion were shown to have disrupted cardiac relaxation and a low PFR compared with patients without DM using G SPECT. These results illustrate disruption in diastolic function in patients with DM in the early period and earlier occurring cardiac events. G SPECT is frequently used in daily practice at most nuclear medicine centres, and because it is a repeatable, highly accurate test independent of the operator, it can be used to evaluate diastolic function parameters in addition to myocardial perfusion with no time or financial loss. Thus, we believe that evaluation of diastolic function parameters with G SPECT may help to identify patients with DM requiring more aggressive treatment in the early period.

P022**Comparison between three different gated myocardial perfusion software programs in measuring left ventricular ejection fraction and volumes**

S. Alexiou^{1,2}, P. Georgoulis², V. Valotassiou², I. Tsougos³, D. Psimadas², A. Ziaka², E. Baniora², C. Ziogas², V. Lakiotis¹, D. Alexopoulos⁴, D. Apostolopoulos¹, P. Vassilakos¹; ¹Department of Nuclear Medicine, University Hospital of Patras, Patras, GREECE, ²Department of Nuclear Medicine, University Hospital of Larissa, Larissa, GREECE, ³Department of Medical Physics, Medical School, University of Thessaly, Larissa, GREECE, ⁴Cardiology Department, University Hospital of Patras, Patras, GREECE.

Purpose Left ventricular ejection fraction (LVEF), end diastolic volume (EDV) and end systolic volume (ESV) are functional parameters obtained using gated myocardial perfusion scintigraphy (G-SPECT). For the automatic calculation of the aforementioned variables, Emory Cardiac Toolbox (ECTb), Myovation and Quantitative gated single-photon emission tomography (QGS), are three of the most commonly used computer processing software packages. In the present study, we sought to evaluate and compare these three programs in measuring left ventricular quantitative parameters. **Materials and Methods** 634 consecutive patients (419 men and 215 women, mean age 64.0years \pm 10.6 years) comprised our study cohort. All patients were properly referred for myocardial perfusion imaging, for the evaluation of known or suspected coronary artery disease and patient risk stratification. Patients with valvular or congenital heart disease, cardiomyopathies, with low quality SPECT studies and those with inability to obtain gated SPECT data (atrial fibrillation or other severe arrhythmias) were excluded. Myocardial perfusion scintigrams were performed according to the one day stress/rest Tc99m Tetrofosmin protocol. The high-count rest scans were acquired as gated-SPECT studies (eight frames per cardiac cycle). Rest LVEF, EDV and ESV were calculated using ECTb, Myovation and QGS, on Xeleris 3 central workstation (GE Healthcare). The agreement between the three processing programs was assessed with the calculation of intraclass correlation coefficients (ICC) for random effects models. **Results** An excellent concordance was found between the three software algorithms according to ICCs values, ranging from 0.92 to 0.99. Nevertheless, pair comparisons among the software programs revealed some differences. Myovation software displayed lower values in all rest parameters compared to both ECTb and QGS algorithms. In addition, ECTb displayed higher values in all parameters except for LVEF as compared to QGS software. Rest LVEF were categorized as normal (>50%), mild-moderate (35-49%), and severe abnormal (<35%) and the agreement between the three software programs was examined. The overall concordance between the three software algorithms was 1.7% for severely abnormal rest LVEF, 5.9% for mild-moderately abnormal rest LVEF and 81.4% for normal rest LVEF, resulting in a 11.0% overall discordance. **Conclusion** ECTb, Myovation and QGS were highly correlated in evaluation of left ventricular functional parameters. Nevertheless, the differences in absolute values and categorization of LV systolic dysfunction, should be accounted for and the interchangeable use of software packages should be avoided in estimation of consecutive GSPECT studies.

P023**Assessment the impacts of the rejected heart beats on Left Ventricle Ejection Fraction and images quality in the gated SPECT cardiac perfusion imaging**

M. H. Khedr¹, M. A. Abd El Aziz², A. Soltan²; ¹Helwan University, Cairo, EGYPT, ²Cairo University, Cairo, EGYPT.

The impact of rejected heartbeats percentage on the evaluation of Left Ventricle Ejection Fraction(LVEF) from myocardial gated SPECT has

been assessed by comparing the gated SPECT by accepted beats dependent and time dependent acquisition with echocardiography data. Whether gating-related artifacts may have a clinically relevant on the evaluation of perfusion and Ejection Fraction in arrhythmic patients is still uncertain. **The aim** of this study was to examine the difference in Left Ventricle Ejection Fraction and images quality between simultaneously acquired gated SPECT dependent on time and gated SPECT dependent on accepted heartbeats data in arrhythmic and nonarrhythmic patients. **Methods:** In 51 consecutive patients classified into two group 40 nonarrhythmic patients (group 1) and 11 arrhythmic patients (Group 2) who underwent myocardial perfusion SPECT for standard clinical indications, both a gated SPECT dependent on time and gated SPECT dependent on accepted heartbeats study were simultaneously acquired and compared with Ejection Fraction from Echocardiogram. Perfusion was estimated in a masked manner on a 20-segment model using Total perfusion defect (TPD) and imaging quality was estimated by contrast. **Results** The mean LVEF was significantly different between gated SPECT dependent on time and Echocardiogram for arrhythmic patients $p < 0.005$ but not significantly different between gated SPECT dependent on accepted heartbeats and Echocardiogram $p = 0.62$ and not significantly different between both gated SPECT accepted heartbeats dependent and time dependent with Echocardiogram for nonarrhythmic patients. $p > 0.1$ Contrast and TPD significantly different between gated SPECT dependent on time and gated SPECT dependent on accepted heartbeats $p < 0.05$ **Conclusion:** time and accepted heartbeats parameter in gated SPECT acquisition have a clinically relevant impact on summed gated perfusion images and LVEF, in arrhythmic and nonarrhythmic patients Therefore, acquisition of a gated SPECT accepted heartbeats dependent study is imperative for accurate assessment of arrhythmic patients LVEF

P-04 – Sunday, October 16, 2016, 16:00 - 16:30, Poster Exhibition Hall
Cardiovascular System: Miscellaneous

P024**Feasibility of myocardial flow reserve prediction without using dynamic data of myocardial perfusion PET**

H. Hashimoto; Toho University Faculty of Medicine, Tokyo, Japan, Oomori-nishi/ootaku/tokyo, JAPAN.

Aim: The quantification of myocardial flow reserve (MFR) provides not only diagnostic value for detection of cardiovascular artery disease but also predictive value for major adverse cardiac events (MACE). ¹³N-ammonia myocardial perfusion positron emission tomography (MP-PET) can calculate MFR noninvasively. However, the common calculation method for MFR requires dynamic acquisition and specific software. The aim of this study was to estimate MFR using solely static images in ¹³N-ammonia MP-PET scans. **Materials and methods:** 34 consecutive patients suspected of ischemic heart disease and 6 healthy participants (28 men and 12 women, 70 \pm 11 years) were included in this study. All participants underwent adenosine stress and rest ¹³N-ammonia MP-PET. In the dynamic images, MFR in the entire-left-ventricular myocardium (ELV) and each of the 3 vessel-areas' MFR were calculated by dividing each stress myocardial blood flow (MBF) by rest MBF. In the static images, myocardium-to-background ratio (MBR) was calculated by dividing the entire-left-ventricular myocardial counts/voxel and each of the three vessel areas' counts/voxel by background upper thoracic aorta counts/voxel in both stress and rest images. Myocardium-to-background ratio increasing rate (MBR-IR) was calculated by dividing stress MBR by rest MBR. A relationship between MFR and MBR-IR in ELV and the three vessel areas was examined. Furthermore, the relationship between MFR and MBR-IR in ischemic myocardium and in non-ischemic myocardium was also examined. **Results:** Median MFR and MBR-IR in ELV were 1.84 (1.42-2.15) and 1.50 (1.16-1.83),

respectively. MBR-IR was correlated well with MFR in ELV ($r = 0.890$, $p < 0.001$). In the LAD territory, MBR-IR was the most correlated with MFR in 3-vessel area ($r = 0.900$, $p < 0.001$). MBR-IR was more correlated with MFR in non-ischemic coronary artery territory than in ischemic myocardium (0.930 , $p < 0.001$ vs. 0.862 , $p < 0.001$). Conclusions: This study demonstrated that MFR can be estimated using solely MP-PET static images.

P025

Rb-82 PET-CT Cold Pressor Test-CPT in the evaluation of the left ventricular flow reserve (VFR) in patients with metabolic syndrome(MS)

A. Fathinul Fikri, N. Abdul Jalil; University Putra Malaysia, Serdang, MALAYSIA.

Aims Rb-82 PET-CT image analysis is potentially valuable in evaluating risks of coronary artery disease (CAD) on the ventricular flow reserve(VFR; ml/g/m) of the left ventricle. We sought to determine the predictive markers for the VFR of the left ventricle in patient with MS. **Methods:** We considered 16 Rb-82 PET-CT CPT in (12 male, 4 female; $52.43 \pm 4.87y$) with mean BMI of $27.44 \pm 4.49kg/m^2$ in patients with MS (WHO 1999). The dual-phased CPT was performed during 5 minutes ice cube emersion (CPT) for the stress phase and at rest to underpin physiological changes of the left ventricular reserve flow being evaluated by the Rb-82 PET-CT. Utilising the acquisition of the list mode CT in static and dynamic phases to reconstruct CT images for attenuation correction and the dynamic data acquisition were processed to obtain quantification value of VFR of the left ventricle using FlowQuant software(Ottawa) on the PET polar map. Clinical risk factors (NIDDM, HPT, BMI) and doppler sonographic parameters [intima media thickness (IMT), peak systolic velocity(PSv)] of common carotid artery were analysed for potential predictors of the VFR. **Results:** There was a significant CPT-induced haemodynamic stress in all patients with (mean prestress BP: $126.25 \pm 16.37/77.75 \pm 6.06mm/Hg$ vs post stress BP: $163.00 \pm 20.53/91.50 \pm 10.43mm/Hg$, $p < 0.05$) respectively. There was a significant differences of the mean weight between group of VFR < 2.0 ml/g/m ($81.52 \pm 8.92kg$ vs $69.95 \pm 12.02kg$, $p < 0.05$). NIDDM was found as a sole predictor for VFR of the left ventricle($p = 0.039$; Mc Nemar Test)IMT $> 0.05mm$ is a good predictor in patient with low VFR($p < 0.05$). **Conclusion:** Rb-82 PET-CT CPT may be a useful tool as a surrogate marker for inotropic agents in evaluating risks of low left ventricular flow reserve in patient with metabolic syndromme.

P027

Clinical validation of the Shine 16 quantitative noise reduction in myocardial SPECT

P. Hannequin¹, P. BUFFAZ^{1,2}, C. GIULIANI¹, R. ZGIMOND¹; ¹Centre d'Imagerie Nucléaire d'Annecy, METZ-TESSY, FRANCE, ²Centre d'Imagerie Nucléaire d'Annecy, Metz-tessy, FRANCE.

Introduction: Statistical Poisson noise is one of the physical factors which degrades qualitative and quantitative properties of scintigraphic images. It implies that the higher the number of counts, the higher the signal to noise ratio. Administated activity and/or acquisition duration must be sufficient to produce scintigraphic images with an acceptable clinical quality. Shine 16, an original algorithm, enables to reduce statistical noise while preserving images properties (Phys Med Biol 60 (2015) 4581-4599). The first clinical myocardial SPECT results including 60 patients are presented. **Material and Methods:** Forty abnormal and 20 normal consecutive myocardial SPECT studies have been acquired with a one-day procedure: 220 MBq rest injection - 50 s/projection acquisition - 660 MBq stress injection - 30 s/projection acquisition. Number of counts in initial

reference data have been halved using a Poisson resampling method for simulating reduced counts (Phys. Med. Biol. 60 (2015) N167-N176). Halved data have been processed using Shine 16. Reference and Shine16-Halved slices have been reconstructed using the same parameters. They have been interpreted by two independent blind observers with a 17-segments display and quantitatively processed with QPS/QGS software. **Results:** Visual analysis: A difference superior to one ischemic segments between the Shine16-Halved and the reference visual scores occurs for two patients with observer n°1 and one patient with observer n°2. Quantitative analysis: The mean of the differences between Shine16-Halved and reference Sum Stress Scores and between Shine16-Halved and reference Reversibility Scores is 1.05 ($p = 0.03$) and 0.196 (NS) respectively. The correlation coefficient between Shine16-Halved and reference Stress Ejection fraction (EF), Rest EF and Stress Telediastolic Volume is 0.92, 0.88 and 0.94 respectively. **Conclusion:** Shine16 allows to decrease the number of counts in SPECT myocardial data while preserving their clinical value. Further studies are necessary to confirm these results and their practical interests : using lower dose to reduce patient irradiation or shortening acquisition duration to improve patient comfort, to minimize motion blur and to optimize camera throughout.

P028

^{99m}Tc-tetrofosmin myocardial perfusion imaging in patients with ischemic stroke

C. Sioka, K. Papadimitropoulos, M. Spiliotopoulou, S. Markoula, S. Zouroudi, K. Naka, L. Michalis, A. Behlioulis, A. Fotopoulos, A. Papadopoulos, A. Papadopoulos, A. Kyritsis, S. Giannopoulos; University Hospital of Ioannina, Ioannina, GREECE.

Aim: Single photon emission computer tomography (SPECT) with ^{99m}Tc-tetrofosmin (^{99m}Tc-TF) is an imaging technique for evaluation of myocardial perfusion (MPI). In our study, we evaluated myocardial status in patients with stroke. **Materials and methods:** We performed ^{99m}Tc-TF-SPECT MPI using polar map of 17 segments in 53 patients with ischemic stroke within 1 month after stroke. Myocardial ischemia (MIS) was defined as mild when the summed stress score SSS was 4-8, and moderate or severe when SSS was equal or more than 9. These MPIs were compared to patients with SSS less than 4, which was considered as nonsignificant MIS. Parameters such as age, BMI, abdominal perimeter, alcohol consumption, smoking habits and medical history (diabetes mellitus, dyslipidemia, etc) were evaluating according to MPI results. None of the patients had any history or symptoms of coronary artery (CAD) or other heart disease. **Results:** There was a significant number of stroke patients with abnormal MPI [32/52 (61.53%, p less than 0.05)] with the majority of patients exhibiting mild abnormalities (20/32, 62%) and 12/32 (38%) patients moderate or severe MPI abnormalities. Abdominal perimeter was found to be a risk factor in this group of patients independently of the severity of MIS (p less than 0.05). **Conclusion:** Most of the stroke patients (more than 50%) in our study had clinically silent MIS, with the majority of them mild, as depicted with ^{99m}Tc-TF-SPECT MPI. We recommend a thorough cardiological evaluation including MPI in stroke patients, in order to rule out MIS or diagnose it early for proper management and prevention of future symptomatic cardiac disease.

P029

Prospects Of Quantitative Scintigraphic Assessment Of Myocardial Blood Flow In Patients With Coronary Artery Disease

N. Krivonogov¹, A. Mochula¹, K. Zavadovsky^{1,2}, Y. Lishmanov^{1,2}; ¹«Research Institute for Cardiology», Tomsk, RUSSIAN FEDERATION, ²National Research Tomsk Polytechnic University, Tomsk, RUSSIAN FEDERATION.

Aim: The aim of the study was to evaluate capabilities of myocardial scintigraphy with Tc-99m-methoxyisobutylisonitrile (^{99m}Tc -MIBI) for assessment of myocardial perfusion in patients with coronary artery disease (CAD). **Materials and Methods:** The study comprised 12 patients diagnosed with CAD. Radionuclide angiopneumography (RNA) and myocardial perfusion scintigraphy with ^{99m}Tc -MIBI were performed. Cardiac output (CO) was calculated based on RNA data; myocardial perfusion was evaluated based on perfusion scintigraphy data; coronary fraction (CF) of radiopharmaceutical accumulation was determined by original method developed by authors. For verification of coronary ejection fraction (CEF) assessment with subsequent calculation of myocardial blood flow (MBF), the same patients received myocardial scintigraphy with macroaggregates of human serum albumin labelled with ^{99m}Tc (^{99m}Tc -MAA). ^{99m}Tc -MAA was introduced into the left ventricular cavity. Values of CEF and MBF were calculated using the following formulas: $\text{CEF} = \text{Cc}/\text{Ci} \times 100\%$, where Cc was scintigraphic count from the area of interest over the heart, Ci was scintigraphic count for the introduced dose of radiopharmaceutical; $\text{MBF} = \text{CO} \times \text{CEF}$ (mL/min). **Results:** For scintigraphic determination of myocardial blood flow, we proposed and evaluated the original method of RNA data processing consisting in summation of second-by-second frames corresponding to the first passing of the ^{99m}Tc -MIBI bolus and in determination of maximum amplitude of activity-time curve (counts/s) in the area of interest corresponding to the visual field of gamma-camera detector. According to data of scintigraphic studies, abnormalities of myocardial perfusion of various degrees were observed in all study patients. Coronary fraction of ^{99m}Tc -MIBI accumulation varied from 1.9% to 2.95% depended on myocardial perfusion. CEF obtained with ^{99m}Tc -MAA scintigraphy also directly depended on myocardial microcirculation. Minimum and maximum CEF values were 1.9% and 3.35%, respectively. Non-parametric Wilcoxon criterion did not detect significant differences ($p=0.866$) between ^{99m}Tc -MIBI-based CF accumulation and ^{99m}Tc -MAA-based CEF which allowed for considering ^{99m}Tc -MIBI-based CF accumulation a ^{99m}Tc -MIBI-based CEF. Values of CO calculated based on ^{99m}Tc -MAA-based CEF and ^{99m}Tc -MIBI CEF also did not significantly differ between each other ($p=0.886$) and ranged from 85 to 35 mL/min. **Conclusion:** Proposed method of quantitative ^{99m}Tc -MIBI-based scintigraphic evaluation of MBF in CAD patients is a non-invasive, affordable, and reproducible method for the detection of coronary insufficiency and may be used in diffuse atherosclerosis of coronary arteries as well as in non-coronary pathology of the cardiac muscle. The study was supported by a grant from the Russian Science Foundation (№14-15-00178).

P030

^{99m}Tc -Technetium tetrofosmin myocardial perfusion imaging in women with non specific cardiac complaints

C. Sioka, A. Papadopoulou, K. Papadimitropoulos, L. Lakkas, K. Pappas, E. Gkika, M. Spiliotopoulou, T. D. Kotrotsios, S. Tsiouris, X. Xourgia, J. al Boucharali, **A. Fotopoulos**; University Hospital of Ioannina, Ioannina, GREECE.

Purpose: To assess the myocardial status in female patients with non-specific cardiac complaints evaluated with ^{99m}Tc -Technetium-tetrofosmin (^{99m}Tc -TF) single photon emission computer tomography (SPECT) myocardial perfusion imaging (MPI). **Method-material:** Forty female were subjected to ^{99m}Tc -TF-SPECT MPI for evaluation of non-specific cardiac complaints. Various types of complaints were noted, such as chest wall pains, palpitations or shortness of breath. All patients had negative clinical cardiology examination and normal ECG. The patients' mean age was 58.4 years old (41 to 76 years). MPI was evaluated visually using polar map of 17 segments. Myocardial ischemia (MIS) was defined as mild when the summed stress score (SSS) was 4–8, and moderate or severe when SSS was equal or more than 9. According to MPI results, the role of factors such as obesity, diabetes mellitus, hypertension, dyslipidemia and cardiac heredity was assessed. **Results:** Abnormal MPI was found in 14/40 (35%) patients, all defined as

mild MIS. Hypertension was reported in the majority of them followed by obesity, dyslipidemia, medical history of cardiac heredity and diabetes mellitus [12/14 (86%), 8/14 (57%), 7/14 (50%), 7/14 (50%), and 4/14 (29%) patients respectively]. Furthermore, 11/14 (79%) patients had at least two and 7/14 (50%) at least three risk factors. None of the patients were smokers. **Conclusions:** The study suggested that adult females with non-specific cardiac complaints and a history of either hypertension or at least two cardiac risk factors are at risk for MIS and should have cardiological evaluation, including ^{99m}Tc -TF-SPECT MPI.

P031

SPECT imaging with 123I-BMIPP and ^{99m}Tc -MIBI in prediction of left ventricular remodeling after the surgical treatment of ischemic cardiomyopathy

M. Gulya^{1,2}, **K. Zavadovsky**^{1,2}, S. Andreev¹, Y. Lishmanov^{1,2}; ¹RI Cardiology, Tomsk, RUSSIAN FEDERATION, ²National Research Tomsk Polytechnic University, Tomsk, RUSSIAN FEDERATION.

Purpose of the study was to study perfusion and metabolism of the left ventricular (LV) myocardium in patients with ischemic cardiomyopathy (ICMP) and to identify the scintigraphic predictors of the efficacy of comprehensive surgical treatment of the left ventricular dysfunction. **Material and Methods.** The study comprised 32 patients with ICMP who underwent comprehensive surgical correction of the LV dysfunction (coronary artery bypass grafting + surgical ventricular reconstruction + mitral valve surgery if necessary). Inclusion criteria: >75% stenosis of coronary arteries; one and more myocardial infarctions in the medical history; heart failure (HF) III-IV NYHA functional class; LV ejection fraction (EF)60 mL/m²; and the presence of akinetic and dyskinetic areas of the LV according to data of echocardiography. Before surgical treatment, all patients received SPECT with ^{99m}Tc -MIBI and with 123I-BMIPP for evaluation of myocardial perfusion and metabolism, respectively. In early follow-up (four weeks) and 12 months after the surgery, all patients underwent echocardiography study to estimate intracardiac hemodynamics. **Results.** Twelve months after surgical treatment, patients were assigned to two groups: group 1 (n=18) patients with beneficial outcome of the operation that stopped the process of LV remodeling (increase LVESVI $\leq 15\%$ one year after surgery compared with the early postoperative period). Group 2 comprised patients (n=14) in whom LV remodeling was progressing despite successful performance of the surgery (increase LVESVI $> 15\%$ compared with the early postoperative period). Prior to surgery and in the early postoperative period LV contractile function (LVEF, LVESV, LVEDV) didn't significantly differ between groups. Also groups didn't significantly differ in the following scintigraphic parameters: myocardial perfusion defect size and metabolic defect size. Groups differed significantly in size of perfusion-metabolic mismatch ($13.23 \pm 11.7\%$ and $4.1 \pm 11.5\%$, $p < 0.01$). The best cut of value 12% for perfusion-metabolic mismatch size can predicted the efficacy of comprehensive surgical treatment for the left ventricular dysfunction with the sensitivity and specificity of 100% and 56%, respectively. **Conclusions.** The results of myocardial perfusion-metabolic scintigraphy can be used as a method for prediction of the progressing cardiac remodeling in the postoperative period of complex surgical correction of LV dysfunction in patients with ICMP. This work was financially supported by Federal Target Program №14.604.21.0071 (project unique identifier №RFMEFI60414X0071).

P032

The influence of hibernation volume according to PET/CT on the recovery of myocardial contractility, depending on the treatment type in patients with coronary artery disease

I. Shurupova, I. Aslanidis, L. Bockerija, E. Derevyanko, T. Katunina; Bakoulev Scientific Center for Cardiovascular Surgery, Moscow, RUSSIAN FEDERATION.

Purpose: to identify the dependence of the improvement of the left ventricle (LV) contractility from the original volume of hibernation myocardium (HM) and type of treatment - revascularization without plastics of the LV or common medical therapy (CMT).

Methods: we examined 63 patients with ejection fraction (EF) $\leq 55\%$ as a result of CAD and myocardial infarction (55,8±9.3 years), the functional class (FC) of heart failure (HF) by NYHA averaged 2.23±0.87. All patients underwent myocardial positron emission tomography with 18F-fluorodeoxyglucose (18FDG) and 13N-ammonium. HM was defined as the hypoperfusion area with the accumulation of 18FDG >math>\geq 50\%</math> and exceed the 13N-ammonium by more than 10%. In 26 patients with CMT 5 had HM >math>\geq 15\%</math> (1gr), 21 - HM $\leq 15\%$ (2gr), 38 patients with revascularization: 20 of them had HM >math>\geq 15\%</math> (3gr), 17 patients with HM $\leq 15\%$ (4gr). End diastolic and systolic volumes (EDV, ESV) and EF LV was calculated according to ECHO as the original and remote via 243.8±145.2 days after revascularization, and through 229.3±185.2 days of observation in CMT patients presented as median and percentiles. **Results:** significant increase in EF from 46%(40;50) to 50%(41;55) (p=0.03) was observed only in the 3 group of patients with revascularization and HM >math>\geq 15\%</math>. Non significant increase in EF from 40%(38;48) to 44%(42;50) (p=0,4) was observed in patients with revascularization and HM $\leq 15\%$. In CMT patients the increase of EF is not detected (40%(30;44) vs. 40%(29;47) in 1gr and 44%(35;46) vs. 44%(36;51) in 2gr). The most, but not significant reduction of EDV and ESV was also detected in 3 gr: with 165ml(142;192) to 147ml(126;192) and 90ml(76;113) to 72ml(60;112) (p=NA), respectively. In patients of 4thgr (HM $\leq 15\%$) EDV non-significant decreased after revascularization with 176ml(147;229) to 170ml(138;237), p=0,4, ESV has not changed (93ml(77;137) vs. 92ml(71;131), p=NA. Significant reduction of LV volumes in patients without revascularization (1 and 2gr) was not detected. When we have compared baseline severity of HF in patients group of with revascularization, the FCHF 3gr. was significantly less (1.6±1.0), than 4gr (2.41±0.8 p=0.015).

Conclusion: 1. Myocardial revascularization leads to a significant increase EF LV in the long-term observation only in patients with HM >math>\geq 15\%</math>. 2. Significant positive dynamics of LV volumes after revascularization were not observed in any of the groups with different amount of HM. 3. The weakest dynamics of LV contractility noted in the groups with CMT.

P033

The accumulation quantification of ^{99m}Tc-DPD in the myocardium of patients with transthyretin (TTR) cardiac amyloidosis

M. Buncová, J. Terš, A. Čepa, A. Krebsová, M. Kubánek; Institute for Clinical and Experimental Medicine, Prague, CZECH REPUBLIC.

Aim: comparison of 2 different ways of accumulation quantification of ^{99m}Tc-DPD ([^{99m}Tc] 3,3-diphosphono-1,2-propanedicarboxylic acid) in the myocardium in patients with TTR cardiac amyloidosis as instruments for diagnostics and evaluation of accumulation changes during the therapy. **Materials and Methods:** for the accumulation quantification of ^{99m}Tc-DPD (TECEOS®) a SPECT/CT scan of thorax 3-6 hours after the injection of 740 MBq was used. A quantitative index of local maximum accumulation of ^{99m}Tc-DPD in the myocardium (QMA) consisted of the determination of the ratio of the highest count/voxel in the area of the heart to the reference count density. The reference count density is the average value calculated from the highest count/voxel values estimated on the 2-8th ribs on the right side of the chest in the coronary plane identical to the localization of max. count/voxel value in the myocardium. QMA index reflects maximum accumulation of DPD in myocardium. The second way of quantification represents the ratio of accumulation

of ^{99m}Tc-DPD in the myocardium (RAM) and the total activity of the tracer in the part of thorax containing all transaxial myocardium slices. From the total 9 patients (78-90 years old) with TTR amyloidosis the scans were repeated in the distance of several months on 2 of those patients being treated with unspecified drug from drug study and on 1 man without any therapy treatment. The results of quantification using QMA and RAM were correlated and the indexes changes were observed in the course of repeated scans. **Results:** for the comparison of QMA and RAM a group of 13 patients positive on TTR amyloidosis was used. QMA index values in the range of 3.8-7.9 and RAM index values in the range of 16-36 % (13 pairs of index values) significantly correlated (correlation coefficient of R=0.81). Repeated examination of indexes of both patients undergoing unspecified treatment indicate decrease of accumulation in the myocardium. 1 man with TTR amyloidosis without any therapy treatment shows the growth of both indexes. **Conclusion:** the indexes of accumulation of ^{99m}Tc-DPD in myocardium correlate - QMA is better for the initial diagnosis of TTR, while RAM is more suitable for observation of long term therapy effects and the progressing disease. The advantage of both those quantification methods in contrast to the evaluation from whole body scans as presented in other articles is the limitation of subjective approach of the worker and more sensitive and wider numerical scale of the index values.

P034

Senile Transthyretin Amyloidosis And ^{99m}Tc-HDP Scintigraphy

A. HERRERO MUÑOZ, L. CASTILLEJOS RODRIGUEZ, P. GARCIA ALONSO, M. BALSAL BRETÓN, A. ORTEGA VALLE, C. PANIAGUA CORREA, C. SANDOVAL MORENO, M. FERNANDEZ RODRIGUEZ, F. PENIN GONZALEZ; HOSPITAL UNIVERSITARIO GETAFE, GETAFE, SPAIN.

Senile Transthyretin amyloidosis is an underdiagnosed cause of heart failure with preserved ejection fraction. Endomyocardial biopsy remains the gold standard for definitive diagnosis but, due to elderly patients, its not often possible. **AIMS** We try to determine utility of ^{99m}Tc-HDP scintigraphy in the diagnosis of senile transthyretin amyloidosis in elderly patients admitted due to heart failure with preserved ejection fraction, whom endomyocardial biopsy involves a high rate of adverse effects. **MATERIALS AND METHODS** We retrospectively screened 14 patients >65 years old admitted due to heart failure with preserved ejection fraction (left ventricular ejection fraction >50% with left ventricular hypertrophy). All eligible patients were offered a ^{99m}Tc-HDP scintigraphy. We administered 740 MBq intravenously and made planar images (antero-posterior, left lateral and left-oblique) and SPECT-CT 90 minutes later. Cardiac retention was assessed with a semi-quantitative visual score in relation to ribs uptake (0- no cardiac uptake; 1-less than ribs uptake, 2 similar uptake to ribs, 3- uptake greater than bone). We consider positive uptake equal to or greater than 2. **RESULTS** There were no differences in age, hypertension, diabetes and coronary artery disease between patients with senile transthyretin amyloidosis and patients with other causes of heart failure with preserved ejection fraction. A total of 3 patients showed severe uptake (3 scale) on the ^{99m}Tc- HDP scintigraphy and we considered them true positive cases. Endomyocardial biopsy was performed in one, confirming transthyretin amyloidosis. The other 11 patients didn't show pathological uptake on the ^{99m}Tc- HDP scintigraphy (0-1 scale). They were considered true negative cases and another causes of heart failure with preserved ejection fraction were finally diagnosed. Senile Transthyretin amyloidosis is an underdiagnosed disease that accounts for a significant number (21,4%) of heart failure with preserved ejection fraction **Conclusion** ^{99m}Tc- HDP scintigraphy is a good noninvasively method to diagnose senile transthyretin amyloidosis in elderly patients, whom endomyocardial biopsy involves a high rate of adverse effects.

P035**V/P SPECT perfusion gradients as a non-invasive method to follow-up patients with severe heart failure after heart transplantation. Validation with right-heart catheterization**

M. Al-Mashat¹, G. Rådegran², H. Arheden¹, J. Jögi¹; ¹Lund University, Department of Clinical Sciences Lund, Clinical Physiology, Skane University Hospital, Lund, Lund, SWEDEN, ²Lund University, Department of Clinical Sciences Lund, Cardiology, and The Section for Heart Failure and Valvular Disease, VO. Heart and Lung Medicine, Skane University Hospital, Lund, Lund, SWEDEN.

Background: Heart transplantation is the ultimate treatment alternative in patients with severe heart failure (HF). Right-heart catheterization (RHC), with the invasive measure of pulmonary artery wedge pressure (PAWP), is regarded as the reference method in diagnosing pulmonary congestion in HF. The non-invasive V/P SPECT method can be used in the assessment of pulmonary perfusion distribution in HF by quantitative perfusion gradients and qualitative visual assessment. It has not previously been investigated if V/P SPECT could be used to assess the treatment effect of heart transplantation. **Aim:** Therefore, the aim of the present study was to investigate if qualitative visual assessment of V/P SPECT and quantitative perfusion gradients can be used to follow-up effect on congestion in patients with severe HF who have undergone heart transplantation. **Method:** Nine patients with severe HF who were under consideration for heart transplantation were included. The patients underwent V/P SPECT and RHC before and 6 months after heart transplantation. The perfusion gradients were automatically derived from V/P SPECT images using a previously published algorithm. **Results:** Before treatment, seven out of 9 patients showed a redistribution of pulmonary perfusion to anterior parts of the lungs and/or positive dorso-ventral perfusion gradients. The perfusion gradients in seven patients were improved (normalized) after heart transplantation ($P=0.02$). After treatment, there was a significant decrease in mean PAWP ($P=0.01$) from 16.8 to 8.3 mmHg before vs. after heart transplantation, reflecting an improvement after transplantation. In three patients, the visual assessment of the images made by the clinical physicians was improved (normalized) after heart transplantation. For the rest of the patients, the visual assessment was unchanged. **Conclusion:** V/P SPECT perfusion gradients is a quantitative and non-invasive method that could have a role in the follow-up of patients who have undergone heart transplantation. Quantitative perfusion gradients seem to be more sensitive than qualitative visual assessment in the evaluation after heart transplantation.

P036**Usefulness of SPECT/CT fusion image of perfusion lung scan in patients with chronic thromboembolic pulmonary hypertension**

K. Hirose, T. Chikamori, S. Hida, Y. Igarashi, M. Watanabe, T. Saitoh, K. Suzuki, N. Koizumi, M. Yoshimura, H. Ogino, A. Yamashina; tokyo medical university hospital, tokyo, JAPAN.

Aim: We evaluated the effectiveness of fusion image of perfusion lung scan using ^{99m}Tc-MAA SPECT/CT for detecting lung perfusion abnormality and estimating the severity of chronic thromboembolic pulmonary hypertension (CTEPH). **Materials and methods:** Thirty-one patients with CTEPH underwent ^{99m}Tc-MAA SPECT/CT and right heart catheterization within 1 month intervals. Perfusion scores were assessed visually on a 4-point scale (0=normal perfusion, 1=mild hypoperfusion, 2=moderate-to-severe hypoperfusion and 3=absent perfusion) in 18 lung segments. Summed score was defined as total perfusion score adding each segmental perfusion score. Percentage of abnormal perfusion was calculated as summed score/36×100. Total lung volume and perfusion defect volume were calculated automatically with CT and SPECT using the threshold width from 25% to 100% of maximal counts of ^{99m}Tc-MAA on SPECT images. Percentage of defect volume

was calculated as (perfusion defect volume) / (total lung volume) ×100. Pulmonary vascular resistance (PVR), total pulmonary vascular resistance (TVR), mean pulmonary artery pressure (PAP) and mean pulmonary artery wedge pressure (PAWP) were measured by right heart catheterization. **Results:** The average age of patients was 60±14 years, and 8 patients were men and 23 women. Of these 31 patients, mean PAP was 37±11 mmHg, mean PAWP was 10±4 mmHg, mean PVR was 619±417 dyne/s/cm⁵, and mean TVR was 820±484 dyne/s/cm⁵. Average percentage of abnormal perfusion was 50±8.4%. Among 3 right and 2 left lung lobes, significant perfusion defects were visually observed in the right upper lobe in 29% of the patients, in the middle lobe in 58%, and in the lower lobe in 35%, whereas defects were observed in the left upper lung lobe in 6% of the patients and in the lower lobe in 13%. Total lung volume was 2578±468 ml. Although there were no significant correlations of percentage of abnormal perfusion with PVR, TVR and mean PAP (p for all=NS), there was significant correlation of percentage of perfusion defect volume with PVR ($r=0.41$, $P=0.02$). **Conclusion:** Fusion image of perfusion lung scan using SPECT/CT is useful not only to detect the distribution of perfusion abnormality, but also to estimate the severity of CTEPH.

P037**Quantitative perfusion gradients from V/P SPECT could be used to monitor treatment effect in patients with heart failure after receiving cardiac resynchronization therapy**

M. Al-Mashat¹, R. Borgqvist², H. Arheden¹, J. Jögi¹; ¹Lund University, Department of Clinical Sciences Lund, Clinical Physiology, Skane University Hospital, Lund, SWEDEN, ²Lund University, Institution for Clinical Sciences, Arrhythmia Dept, Skane University Hospital, Lund, SWEDEN.

Background: Currently, there is a lack of diagnostic methods to assess the effect of cardiac resynchronization therapy (CRT) in heart failure. Tomographic lung scintigraphy (V/P SPECT) can be used to quantify the redistribution of pulmonary blood flow in patients with heart failure using quantitative perfusion gradients and qualitative visual assessment of the images. The role of V/P SPECT in the assessment of CRT treatment effect is unknown. **Aim:** The aim of this study was therefore to investigate if V/P SPECT, with quantitative perfusion gradients and qualitative visual assessment of the images, could be used to monitor treatment effect in patients with heart failure before and after receiving CRT. **Material and methods:** Fourteen patients with heart failure who were candidates for receiving CRT were included. The patients were examined with V/P SPECT before and 6 months after the treatment. Of these, eleven patients have been followed up and 3 patients were lost to follow up. The perfusion gradients were automatically derived from V/P SPECT images using a 3D-regression algorithm that has previously been published. **Results:** Before treatment, a redistribution of pulmonary perfusion and/or positive dorso-ventral perfusion gradients were found in 7 of the CRT patients. After treatment, there was a significant decrease in perfusion gradients, reflecting an improvement in pulmonary perfusion distribution ($P=0.03$), although the visual assessment of the images made by the clinical physicians was unchanged. **Conclusion:** Quantitative perfusion gradients are more sensitive to the improvement in pulmonary perfusion pattern after CRT than the qualitative visual assessment of the V/P SPECT images, and could therefore have a role in monitoring treatment effect in patients receiving CRT.

P038**Isolated perfusion scan and SPECT/CT-angiography for pulmonary embolism diagnostic in chronic obstructive lung disease patients**

E. V. Migunova, N. E. Kudryashova, O. V. Nikitina, I. P. Mikhailov, G. A. Nefyodova; Sklifosovsky Inst.for Emerg. Medicine, Moscow, RUSSIAN FEDERATION.

Every year our hospital receives 450 patients with acute venous thrombosis and suspicion of PE. In most cases at clinical picture of PE it was enough to use the following diagnostic pattern: X-ray to exclude lung diseases and injuries → venous ultrasonography → pulmonary perfusion scan (PPS). However, in 10% cases there were doubts about PE diagnosis of the patients with COLD and fibrotic changes of lung tissue after perfusion scan, which required SPECT/CT lung angiography. **Purpose.** To define diagnostic significance rate of isolated PPS of the patients with massive PE on the background of COLD in comparison with lung SPECT/CT. **Materials and techniques.** Examined 44 patients, age 64,8 ±15,3 with venous thrombosis, clinical signs of PE, apparent respiratory distress on the background of COLD, perfusion edge defects and total perfusion deficiency of more than 45% according to isolated PPS. In all cases there remained doubts about the diagnosis and further examinations on hybrid system SPECT/CT «Discovery NM/CT 670» (GE, USA) with 120 MBq ^{99m}Tc-macroaggregated albumin and 70 ml of iso-osmolar nonionic contrast agent Iodixanol were performed. **Results and discussion.** SPECT/CT-angiography allowed to estimate kind and volume of lungs blood stream damage on subsegmental level. With diagnostic findings of SPECT/CT-angiography, which was performed for verification, PE diagnosis was confirmed in 30 cases of 44 total. In 14 cases after SPECT/CT-angiography conclusions were changed: 9 false positive results of isolated perfusion scan resulted from perfusion defect in COLD lung tissue fibrosis sites, 5 false negative resulted from presence of thromboembolism sites of segment level, which did not close the lumen. Diagnostic significance at PE after isolated PPS were: accuracy 68,2% (95% confidence interval 55,4%; 80,6%), sensitivity 83,3% (95% confidence interval 73,9%; 92,5%), specificity 35,7%. Besides refinement of PE diagnosis, results of SPECT/CT-angiography affected the treatment of the patients with contra-indications for system thrombolytic therapy. A number of patients with thromboembolia of major lung vessels got reological clot extraction. **Conclusions.** Isolated PPS in PE diagnostics of patients with COLD has low specificity and accuracy; it is advisable to perform lungs SPECT/CT-angiography for these patients, which helps to make accurate diagnosis, estimate total perfusion deficiency and exact localization of clots or rule out presence of clots on the lung artery system at lung perfusion defects of other origin. SPECT/CT method allows to choose the most suitable treatment at massive thromboembolia, i. e. to decide if system thrombolytic therapy or reological clot extraction is reasonable.

P039

Pulmonary perfusion in patients with hypoplastic left heart syndrome (HLHS) after surgical correction of the defect

K. Kovačević-Kušmirek¹, **A. Mazurek-Kula**², **T. Moszura**², **J. Moll**², **J. Moll**³, **A. Płachcińska**¹, **J. Kuśmirek**⁴; ¹Department of Quality Control and Radiological Protection Medical University of Lodz, Poland, Lodz, POLAND, ²Cardiology Department Polish Mother's Memorial Hospital, Research Institute Lodz, Poland, Lodz, POLAND, ³Cardiosurgery Department Polish Mother's Memorial Hospital, Research Institute, Lodz, Poland, Lodz, POLAND, ⁴Department of Nuclear Medicine, Medical University of Lodz, Poland, Lodz, POLAND.

HLHS can be treated with a multistage surgery including an anastomosis of superior vena cava and inferior vena cava with the right pulmonary artery. Aim: assessment of pulmonary perfusion in patients with HLHS after completion of a surgical treatment (Fontan operation). Material and methods: In 76 patients (52 boys and 24 girls) aged 3-20 (mean 9) years a planar lung perfusion study was performed twice (after administration of a radiopharmaceutical into upper and lower limb) in anterior and posterior projections after intravenous injection of activities of ^{99m}Tc-macroaggregates adjusted for body weight. Administration of a radiopharmaceutical into upper limb aimed at the assessment of blood distribution between both lungs through the anastomosis of superior vena cava with right pulmonary artery (SVC-RPA) and into lower limb - through

anastomosis of inferior vena cava with right pulmonary artery (IVC-RPA). Relative perfusion of both lungs was assessed with a software "Lung perfusion analysis" on Xeleris workstation as a geometric mean of percentages in anterior and posterior views. Distribution of perfusion not exceeding 50±10% was recognized as symmetrical. Results: Blood distribution between both lungs through SVC-RPA was diverse: in 27/76 (35%) patients it was symmetrical, in 28/76 (37%) hypoperfusion of the left and in 21/76 (28%) hypoperfusion of the right lung were observed. However, IVC-RPA provided lower relative perfusion of the left lung in 64/76 (84%) as compared with SVC-RPA (p<0,0001), symmetrical lung perfusion was observed in a lower percentage of patients - 12/76 (16%) as compared with SVC-RPA (p=0,015) and no cases of a relative hypoperfusion of the right lung were found. Moreover, in 9 (12%) patients an uptake of the radiopharmaceutical in kidneys was detected indicating right-to-left shunt, probably as a result of lung arteries malformations. Conclusions: Lung perfusion study revealed that in patients after surgical correction of HLHS blood distribution between both lungs is diverse, with predominance of a relatively lower perfusion of the left lung through the anastomosis of inferior vena cava with right pulmonary artery. Lung perfusion study additionally revealed right-to-left shunt in several patients.

P040

The role of serum 25 Hydroxy vitamin D levels, in patients with Coronary Artery Disease. Correlation with SPECT Myocardial scintigraphy

A. S. ZISSIMOPOULOS^{1,2}, **L. Baloka**³, **S. Floros**⁴, **P. Pavlidis**⁵, **A. Thomaidou-Ntanasel Antina**⁶, **O. Zissimopoulou**⁷, **A. Tsatsarakis**⁷, **R. Sotiropoulou**⁸, **A. Strataki**⁷, **E. Karathanos**⁷; ¹Democritus University of Thrace, Alexandroupolis, GREECE, ²Nuclear Medicine Dept., Alexandroupolis, GREECE, ³Molecular Biology and Genetics School Democritus University of Thrace, Alexandroupolis, GREECE, ⁴Cardiology Clinic 401 Army Hospital, Athens, GREECE, ⁵Laboratory of Forensic Sciences Democritus University of Thrace, Alexandroupolis, GREECE, ⁶Cardiology Clinic Democritus University of Thrace, Alexandroupolis, GREECE, ⁷Nuclear Medicine Dept Democritus University of Thrace, Alexandroupolis, GREECE, ⁸Medical School Democritus University of Thrace, Alexandroupolis, GREECE.

Introduction: Recent studies have reported that low serum vitamin D levels are associated with a variety of diseases, including cardiovascular disease and in particular ischemic heart disease (IHD). Possible mechanisms underlying this association include increased inflammation, renin-angiotensin system upregulation, insulin resistance, altered lipid metabolism, and altered vascular smooth muscle growth and function that lead to hypertension, diabetes, dyslipidemia and atherosclerosis. **Aim:** The aim of this study is to evaluate the serum levels of 25 hydroxy-vitamin D [25(OH) D] in patients with Coronary Artery Disease (CAD), as a prognostic factor of the severity of the disease, in correlation with SPECT myocardial scintigraphy. **Patients and method:** We study 78 patients (48 male and 30 female) aged between 37 and 73 years old (median age of 58 ±9 years) who suffer from CAD. 61 were patients of the University Cardiology Clinic of the University Hospital of Evros and the rest of other cardiologists. In all patient's blood samples were taken for (25-OH-D) determination and after this in everyone SPECT myocardial scintigraphy with ^{99m}Tc-MIBI and tomographic γ-camera was performed. The serum was collected and kept refrigerated at -70 °C. The vitamin D status was measured by radioimmunoassay (RIA) method with I¹²⁵[25(OH)D] kits Diasorin at in-vitro laboratory of Nuclear Medicine Dept. **Statistical analysis:** Was performed by the Pearson correlation test and statistical significance was considered to be p <0.005. **Results:** 37 patients with myocardial infarction had low values of vitamin D, 0-20 ng/mL, (p <0.005). In this group there is statistical significance in the relationship between very low values of

vitamin D and patients with extensive myocardial infarction. ($p < 0.005$). Therefore the very low prices associated with the severity of disease and the impending death of patients. These patients might need more intensive monitoring. 32 patients with reversible myocardial ischemia had low values of vitamin D 20–40 ng/mL. ($p < 0.005$). Therefore the very low levels associated with the progression of the disease. 9 patients who had normal myocardial scintigraphy had values of vitamin D to normal levels > 40 ng/mL ($p < 0.005$). **Conclusions:** In conclusion low vitamin (25-OH-D) levels may underlie established cardiovascular risk factors. The very low levels associated with the severity of (CAD) disease and the impending death of patients. The determination of vitamin D levels in patients with coronary artery disease is essential to monitor patients in the treatment and outcome of disease.

P041

99mTc-HMPAO SPECT For Evaluation Of The Renal Denervation Effects On Cerebral Perfusion: Correlation With Cognitive Function In Patients With Resistant Arterial Hypertension

N. Efimova^{1,2}, I. Efimova¹, V. Lichikaki¹, V. Mordovin¹, Y. Lishmanov^{1,2}; ¹«Research Institute for Cardiology», Tomsk, RUSSIAN FEDERATION, ²National Research Tomsk Polytechnic University, Tomsk, RUSSIAN FEDERATION.

Aim: The aim of the study was to elucidate the effects of radiofrequency ablation of renal arteries on regional cerebral blood flow (rCBF) and cognitive function in patients with resistant arterial hypertension (AH). **Materials and methods:** The study involved 21 patients (pts) with resistant AH examined by SPECT with 99mTc-HMPAO, 24-h blood pressure monitoring, and comprehensive neuropsychological testing before and after transcatheter renal denervation. Brain SPECT slices were divided into 14 symmetrical (right and left) regions of interest: inferior and superior frontal lobes, temporal, anterior and posterior parietal, occipital lobes, and cerebellar hemispheres. Regional cerebral blood flow (mL/100g/min) in these regions was calculated. Fifteen pts without angiographic signs of carotid atherosclerosis, coronary artery disease, AH, neurological and psychiatric disorders were investigated as control group. **Results:** Data showed decreases in rCBF in AH pts by 14.2% ($p=0.00003$) and by 16.0% ($p=0.0005$) in right and left inferior frontal lobes, respectively; by 12.1% ($p=0.006$) in right temporal brain region; and by 8.5% ($p=0.03$) in right and left occipital cortex in comparison with control group. The results of neuropsychological testing showed decreases by 13.1% in mentation ($p=0.0002$), by 42.4% in long-term verbal memory ($p=0.0003$), by 21.1% in long-term visual memory ($p=0.01$), by 21% in learning ($p=0.0005$), as well as decrease by 26.7% in attention ($p=0.001$) in pts with AH as compared with control group. Improvements of rCBF, 24-h blood pressure monitoring parameters, and cognitive functions were observed in patients with AH after 6 months of transcatheter renal denervation. Relationships between changes in rCBF, indices of 24-h blood pressure monitoring, and dynamics of cognitive function were found. Improvements of long-term verbal memory correlated well with increases in rCBF in left superior frontal region and right occipital region. Significant correlations between dynamics of mentation and attention and changes of rCBF in right posterior parietal region were demonstrated. **Conclusion:** Our results suggest that brain SPECT is a useful technique for the evaluation of cerebral perfusion and for understanding of cognitive disorder mechanisms in patients with resistant AH. Transcatheter renal denervation exerts beneficial effects on the levels of mean 24-h BP and load pressure and improves cerebral blood flow and cognitive function in patients with resistant hypertension. The study was supported by a grant from the Russian Science Foundation (№15-15-10016)

P042

Quantitative evaluation of bicompartimental lymphoscintigraphy in lower extremity lymphedema

G. Villa, G. Ferrarazzo, F. Ticconi, F. Boccardo, G. Sambuceti; IRCCS Osp Univ San Martino, Genova, ITALY.

Aim: Lymphoscintigraphy is a simple and noninvasive functional test for the evaluation of the lymphatic system. Quantitative approach offers an objective measure for lymphatic function and has been shown to have higher sensitivity and specificity. **Material and method:** Forty subjects suffering from monolateral or bilateral lymphedema of lower extremities underwent bicompartimental lymphoscintigraphy. It was performed in different days by injecting 30 MBq of technetium 99m-nanocolloid subcutaneously and 48 hours later subfascially, in order to explore respectively superficial and deep lymphatic circuits. Total body images were recorded after 1 hour. ROIs were drawn on injection sites, inguinal nodes and liver to quantify the tracer accumulation. Kleinhaus TI, percentual activity in the inguinal nodes and in the liver were calculated. Differences in continuous variables were evaluated using the Student's t-test and the Chi-squared test was used to evaluate categorical variables. **Results:** TI and inguinal nodes/sites of injection uptake ratio showed a very high statistical correlation ($r -0.79$ and -0.61). Average TI was respectively 22.3 ± 2.03 and 13.5 ± 3.1 , percentual nodal activity was 3.6 ± 0.84 and 13.5 ± 3.1 . Statistical correlation between hepatic uptake and TI was not demonstrated ($r -0.11$ and -0.12). On the other hand, sets of data from hepatic uptake after study of superficial (average 1.34 ± 0.35) and deep circuit (average 1.84 ± 0.26) are significantly different ($p < 0.01$). **Conclusion:** Inguinal nodes/injection site uptake ratio is significantly higher through the deep lymphatic circuit. This parameter demonstrate an high correlation with the TI in both circuits. The result is partially expected: TI calculation takes into account two objective parameters strictly related to the entity of nodal uptake. Hepatic uptake reflects the patency of the lymphatic ducts until the subclavian vein. This peculiarity allows to express different aspects than the lymphoscintigraphy of the lower limbs and may explain the lack of correlation with the studied parameters. Our study confirms TI as an objective scoring system and quantitative analysis, simply obtainable and well correlated with the inguinal lymph node uptake. Hepatic uptake probably provides different information, not necessarily related to the peripheral lymphatic pathways conditions.

P043

Impact of 18F-FDG PET/CT in patients with suspected infective endocarditis

A. Álvarez Alonso, C. Vigil Díaz, B. Fernández Llana, A. Álvarez Blanco, N. Martín Fernández, L. Díaz Platas, N. Pérez Castro, O. Rodríguez Fonseca, F. González García; Hospital Universitario Central de Asturias, Oviedo, SPAIN.

Objective: Evaluate the diagnostic impact of the high resolution 18F-Fluoro-2-deoxy-D-glucose (FDG) PET/CT in patients with clinical suspicion of infective endocarditis (IE) and negative results for echocardiogram (EC). **Material and Methods:** A retrospective study of 9 patients with clinical suspicion of IE was performed (range 79–92 years). Two patients were male and seven were female. Four of them had prosthetic valves (2 aortic, 1 double aortic and mitral) and the five remaining had native valves (three with implanted pacemaker and one with cardiac implantable electronic devices). All patients underwent a high resolution FDG PET/CT (GE Discovery 710) using specific cardiology protocol between October 2015 and February 2016 (average activity 5.4 mCi). Final diagnosis was established according to the modified Duke's criteria and clinical follow-up (median 4 months). **Results:** 6 of the 9 cases were classified as positive for EI according to the findings of the FDG PET/CT.

The global diagnostic concordance between final diagnosis and FDG PET/CT was 66% (6/9). Among the 6 cases with positive FDG PET/CT, the IE diagnosis was confirmed in 5 of them. Therefore, PET/CT diagnostic accuracy was superior to the EC and changed the clinical management in 55% of patients (5/9). Among the total patients, there were two false negatives and one false positive results of the FDG PET/CT study. **Conclusion:** In our pilot experience, the use of 18F-FDG PET/CT allowed to change the therapeutic strategy in 55% of patients with suspected infective endocarditis, due to the diagnostic information added to the conventional imaging techniques.

P-05 – Sunday, October 16, 2016, 16:00 - 16:30, Poster Exhibition Hall
Cardiovascular System: Myocardial Perfusion: CZT & IQ-SPECT

P044

Quantitative analysis of simultaneous dual-isotope SPECT imaging using a cardiac cadmium-zinc-telluride (CZT) camera: Comparison with conventional Anger camera

T. Niimi¹, M. Sugimoto¹, M. Nanasato¹, H. Maeda²; ¹Nagoya Daini Red Cross Hospital, NAGOYA, JAPAN, ²Nagoya University School of Health Sciences, NAGOYA, JAPAN.

Purpose: High-speed and high-energy resolution single-photon emission computerized tomography (SPECT), based on cadmium-zinc-telluride (CZT) detectors (D-SPECT; Spectrum Dynamics, Israel), enables high-sensitivity and high-energy resolution cardiac imaging. Moreover, high-energy resolution presents a new possibility for simultaneous dual-isotope (SDI) SPECT imaging (e.g., Tc-99m/I-123). However, SDI images can be misinterpreted owing to Compton scatter and radionuclide cross-talk artifacts. We performed image reconstructions with and without scatter correction in order to assess the influence of cross-talk when using Tc-99m/I-123 and Tl-201/I-123 SDI imaging and quantified the simulated transmural defect contrast. **Materials and Methods:** We evaluated the energy resolution for Tc-99m, I-123, and Tl-201 in phantom experiments using an SDI phantom (with a simulated transmural defect induced by a difference in energy). Data from Tc-99m/I-123 and Tl-201/I-123 imaging were simultaneously acquired in energy windows centered at 140 keV for Tc-99m, 159 keV for I-123, 167 keV for the upper Tl-201 line (10%), and 69–80 keV for the main Tl-201 emission. The data from these energy windows were concurrently obtained, using the CZT or Anger camera acquisition system. Image reconstructions were carried out with and without scatter correction, to assess the impact of cross-talk when performing use of Tc-99m/I-123 and Tl-201/I-123 SDI imaging. Differences in energy resolution were quantified by measuring the transmural defect contrast from the count value of the SDI images. **Results:** Upon calculation of CZT-SPECT data from the ratio of simulated transmural defect and myocardium images without scatter correction, the Tc-99m/I-123 SDI imaging improved 21.6%/56.6% and the Tl-201/I-123 improved 53.7%/19.3% compared to Anger-SPECT. In addition, visual inspection of the SDI phantom imaging failed to detect any cross talk on simultaneous dual Tc-99m/I-123 and Tl-201/I-123 CZT-SPECT SDI phantom imaging. Because the CZT detector was highly sensitive, the reduction in acquisition count had little effect, leading to an improvement of approximately 10% with both combination images after scatter correction was applied. **Conclusion:** The energy resolution of the CZT-SPECT system was largely superior to Anger-SPECT without scatter correction, and the Tc-99m/I-123 SDI SPECT imaging was also reliable. The CZT-SPECT system lowers the radiation dose by changing the nuclide from Tl-201 to Tc-99m, and could lead to greater patient throughput, providing further confirmation of the potential of the CZT camera for SDI acquisition.

P045

Assessment of Left ventricular Function in patients with Left Bundle Branch Block (LBBB) by means of Myocardial Perfusion Gated SPECT using CZT camera

C. Nganoa, D. Agostini, D. Legallois, A. Plane, B. Houdu, T. Salomon, A. Manrique; CHU Caen, Caen, FRANCE.

Background: The aim of our study was to assess the LV function of LBBB patients by means of CZT-gated myocardial SPECT compared to patients with low likelihood of CAD. **Methods:** 151 patients with LBBB undergoing a ^{99m}Tc sestamibi or tetrofosmin myocardial perfusion CZT SPECT from December 2011 to February 2014 were compared to 24 controls with low likelihood of CAD, normal perfusion SPECT and without LBBB. Stress (10 min post 2.4 MBq/kg IV) and rest (1h post 7 MBq/kg IV) acquisitions were underwent on CZT camera (D-Spectrum). LBBB patients were divided into 2 groups: “LBBB/MPI+”, 75 patients with myocardial perfusion imaging (MPI) showing ischemia, infarction or both and “LBBB/MPI”, 76 patients with normal MPI. LV function was assessed in post-stress and rest conditions using QGS software, including LV ejection fraction (LVEF), end-systolic and end-diastolic volumes (ESV and EDV). **Results:** Post-stress and rest LVEF were significantly decreased in LBBB patients compared to controls, with a mean difference of -14.4% in post-stress (IC95 [-17.9;-11] and -12.7% [IC95 [-16.3;-9.1] in rest conditions (p<0.0001). LV volumes from LBBB patients were significantly increased compared to controls. The mean difference was +35.5ml for post-stress EDV (IC95 [23.7;47.2]), +32.1ml for post-stress ESV (IC95 [23.9;40.3]), +34.1ml for rest EDV (IC95 [21.8;43.4]) and +31.1ml for rest ESV (IC95 [22.74;39.8]); (p<0.0001). LV function impairment was further exacerbated in patients with LBBB/MPI+ with a declined LVEF, increased EDV and ESV than in patients with LBBB/MPI-. LBBB/MPI- pts had significantly declined LVEF, increased EDV and ESV vs controls. **Conclusion:** LV function assessed by gated SPECT using CZT camera was significantly impaired in LBBB patients with or without myocardial ischemia.

P046

Dynamic single photon emission computer tomography with dedicated CZT camera in assessment of myocardial flow reserve in patients with three-vessel coronary artery disease

A. M. Mochula¹, K. Zavadovsky^{1,2}, S. Andreev¹, Y. Lishmanov^{1,2}; ¹RI Cardiology, Tomsk, RUSSIAN FEDERATION, ²National Research Tomsk Polytechnic University, Tomsk, RUSSIAN FEDERATION.

Purpose. The purpose of this study was to assess the myocardial flow reserve in patients with three-vessel coronary artery disease (MVCAD) by dynamic SPECT using semiconductor (cadmium-zinc-telluride)-based gamma camera. **Material and methods.** The study comprised fifteen patients (11 males and 4 females; mean age of 63.3±12.6 years) with MVCAD with the presence of coronary artery stenosis greater than 70% according to invasive coronary angiography. Control group consisted of 7 men and 2 women (25±4 years) without any cardiac diseases (healthy volunteers). All patients and volunteers underwent myocardial SPECT using (cadmium-zinc-telluride)-based gamma camera (GE Discovery NM/CT 570C). We used ^{99m}Tc-MIBI as a radiopharmaceutical. Acquisition protocol was as follows: (1) rest radiopharmaceutical injection (volume of 1 mL; dose of 185 MBq); 5-min list-mode acquisition; (2) stress radiopharmaceutical injection (volume of 1 mL; dose of 740 MBq) followed by two-minute adenosine infusion (160 mcg/kg/min); then additional two-minute adenosine infusion. List-mode (5-min duration) was started simultaneously with the injection of the radiopharmaceutical. Using dedicated software we received dynamic data on passage of the radiopharmaceutical in the walls and in the cavity of the left ventricle. To assess myocardial flow reserve, we calculated the ratio of

mean counts from the left ventricular myocardial region (apex, anterior, lateral, and septal walls) to the area under the curve from the left ventricular cavity. The index of myocardial flow reserve was calculated by dividing the ratio acquired in stress test by the ratio obtained at rest. Results. The average value of the global myocardial flow reserve (gMFR) index was lower in a MVCAD group. The gMFR indexes were 1.41 ± 0.48 versus 1.88 ± 0.43 in patients with three-vessel coronary artery disease and healthy volunteers, respectively ($p < 0.05$). Regional myocardial blood flow reserve (rMFR) indexes also significantly ($p < 0.05$) differed between patients with MVCAD and control group: 1.34 ± 0.43 versus 1.88 ± 0.38 for the apex; 1.44 ± 0.41 versus 1.95 ± 0.45 for the lateral wall; 1.32 ± 0.44 versus 1.63 ± 0.43 for the anterior wall; and 1.44 ± 0.77 versus 2.06 ± 0.38 for the septal wall, respectively. ROC analysis showed that the gMFR = 1.77 allowed for identifying MVCAD with the sensitivity and specificity rates of 81.8% and 66.7%, respectively. Conclusion. Dynamic myocardial rest-stress SPECT using semiconductor (cadmium-zinc-telluride)-based gamma camera allowed for identifying low myocardial flow reserve in patients with three-vessel coronary artery disease. This approach can be helpful in assessment of the severity of myocardial perfusion abnormalities in these patients. The study was supported by a grant from the Russian Science Foundation (№14-15-00178).

P047

Low dose thallium myocardial perfusion imaging using CZT camera

V. Kincl¹, M. Kamínek², J. Vašina³, M. Havel²; ¹St.Anne's University Hospital, ICRC, Brno, CZECH REPUBLIC, ²University Hospital Olomouc, Olomouc, CZECH REPUBLIC, ³Masaryk Memorial Cancer Institute, Brno, CZECH REPUBLIC.

Aim: To verify the feasibility of ultra low-dose thallium perfusion imaging using CZT SPECT camera. **Methods:** The study comprised 124 patients (86 men) referred for myocardial perfusion imaging. The one-day stress-redistribution protocol using 201-thallium chloride with administered activity 0.5 megabecquerel (MBq) per kilogram of body weight was performed. The quality of images was assessed by number of recorded counts and visually by 4-grade scale (1-poor quality, 4-excellent quality). The patients cohort was divided to obese ($n=43$) and non-obese patients ($n = 81$). **Results:** The average quality score was 3,97 for non-obese and 3,90 for obese patients. At stress both groups had similar number of counts (1100 for non-obese vs 1071 for obese patients, $p=NS$). At rest was recorded 1044 vs 1061 kilocounts respectively ($p=NS$). The mean administered activity was 39 MBq for non-obese and 49 for obese patients ($p < 0.0001$), that resulted in very low effective dose 4 and 5 millisievert respectively ($p < 0.0001$) for full stress- redistribution protocol. **Conclusion:** the ultra low-dose thallium myocardial perfusion protocol provides good quality of images with low radiation burden. The diagnostic accuracy will be in focus for further investigation.

P048

Influence of Different SPECT Systems And Radiotracers in Detecting the Presence and Extent of Myocardial Ischemia in the Left Anterior Descending Artery

T. Saitoh¹, T. Chikamori¹, K. Goto², S. Hida¹, M. Miyagawa³, T. Fukuyama⁴, T. Mochizuki³, Y. Igarashi¹, K. Hirose¹, A. Yamashina¹; ¹Tokyo medical university, Tokyo, JAPAN, ²Fukuyama cardiovascular hospital, Hiroshima, JAPAN, ³Ehime university graduate school of medicine department of radiology, Ehime, JAPAN, ⁴Shinkoga hospital, Fukuoka, JAPAN.

Background: In detecting the presence and extent of myocardial ischemia in the left anterior descending (LAD) arterial territory, few studies compared the cadmium-zinc-telluride (CZT) with the Anger cameras

using ²⁰¹Tl or ^{99m}Tc radiotracers. **Methods:** Pooled data of 95 patients having 1-vessel disease limited to LAD ($\geq 75\%$ diameter narrowing) who underwent stress myocardial SPECT using Discovery NM530c (D-camera), were extracted from the multicenter registry and were compared with the data of 63 patients using Anger camera (A-camera) from our own institution. Patients were divided into 4 groups; 62 patients studied by D-camera with ^{99m}Tc, 33 patients by D-camera with ²⁰¹Tl, 33 patients by A-camera with ^{99m}Tc and 30 patients by A-camera with ²⁰¹Tl. Patients with prior MI were excluded. SPECT image was analyzed using a 17-segment model; summed stress score (SSS) and summed difference score (SDS) were calculated, and a regional difference score (DS) limited to LAD territory were also calculated. Myocardial ischemia was defined if regional DS ≥ 1 was present. **Results:** Using ^{99m}Tc in 95 patients, SSS (6.7 ± 4.2 vs 9.9 ± 4.4 ; $P=0.001$), SDS (1.3 ± 5.1 vs 7.5 ± 3.0 ; $P < 0.0001$), and regional DS (0.6 ± 3.1 vs 5.7 ± 3.6 ; $P < 0.0001$) were less, and the detection of myocardial ischemia was infrequent (42 % vs 85 %; $P < 0.0001$) by the D-camera than by A-camera. Using ²⁰¹Tl in 63 patients, however, SSS (12.6 ± 7.1 vs 11.3 ± 4.0 ; $p=NS$), SDS (7.9 ± 6.6 vs 8.1 ± 3.2 ; $p=NS$), regional DS (5.5 ± 5.4 vs 5.4 ± 3.4 ; $p=NS$), and the detection of ischemia (88 % vs 83%; $p=NS$) were similar either by D-camera or A-camera. In addition, in 95 patients who underwent D-camera study, SSS (6.7 ± 4.2 vs 12.6 ± 7.1 $P < 0.0001$), SDS (1.3 ± 5.1 vs 8.0 ± 6.6 $P < 0.0001$), and regional DS (0.6 ± 3.1 vs 5.5 ± 5.4 $P < 0.0001$) were less, and the detection of myocardial ischemia was infrequent (42 % vs 88 % $P < 0.0001$) with ^{99m}Tc than with ²⁰¹Tl. **Conclusion:** These results based on the evaluation of single-vessel disease limited to LAD, suggested that the detection of the presence and extent of myocardial ischemia in the LAD territory may be underestimated with ^{99m}Tc-radiotracer using the CZT SPECT system.

P049

Impact of Cardiac Motion on Myocardial Blood Flow (MBF) using Dynamic SPECT-CZT Imaging in patients with Coronary Artery Disease

C. Nganoa¹, M. Maguet¹, A. Manrique¹, V. Roule¹, A. Plane¹, D. Peyronnet¹, R. Baavour², N. Roth², F. Beygui¹, D. Agostini¹; ¹CHU Caen, Caen, FRANCE, ²Spectrum Dynamics Medical, Caesara, ISRAEL.

Introduction. Quantification of myocardial blood flow is an emerging topic in nuclear cardiology with an expected diagnostic incremental value in patients with CAD. The advent of a novel CZT camera has introduced new perspectives for perfusion quantification using dynamic SPECT acquisitions. However, cardiac motion during acquisition can change estimations of MBF. Therefore, the aim of the study was to compare MBF with and without cardiac motion correction (MC) using a CZT camera in patients with stable angina. **Materials and methods.** 21 patients (17 M, 4 F; 64.5 ± 8 yo) with stable CAD (intermediate risk factors with angina and/or positive ischemia test) were prospectively included during the angiographic procedure. 6-min dynamic SPECT acquisitions using a contrast injector to deliver a bolus injection of ^{99m}Tc-sestamibi (3 MBq/kg at rest and 9 MBq/kg after regadenoson 400 μ g, IV) were performed using a CZT camera (D-SPECT, Spectrum Dynamics, Israel). Reconstructed frames were automatically segmented to extract the vascular input function and the myocardial uptake curve. One-compartment kinetic modeling was used to estimate global uptake values, and then MBF was derived using the Leppo correction. Global stress and rest MBF and MFR (as a ratio of stress MBF/rest MBF) were assessed using Corridor 4DM (INVIA-Ann Arbor, USA) with and without MC. **Results.** Rest vs stress injected activity was 310 ± 67 vs 817 ± 166 MBq, respectively; $P < 0.05$. The total injected dose was 1127 ± 228 MBq. Cardiac motion was identified in all patients on the sinogram and then corrected for left atrium ROIs positioning image-derived input function assessment. Global stress and rest MBF (with MC+ vs without MC-) by SPECT were not significantly different: stress (MC+) = 2.29 ± 0.76 vs (MC-) 2.73 ± 0.75 ml/min/g; rest

(MC+) = 0.89 ± 0.36 vs (MC-) 1.05 ± 0.35 ml/min/g; (P=NS, unpaired bilateral t-test). CFR was also not significantly different: (MC+) = 2.72 ± 0.81 vs (MC-) 2.77 ± 0.81 ; P=NS. **Conclusion.** Even with cardiac motion present during all dynamic SPECT acquisitions, the additional input of motion correction was not necessary to estimate global MBF and MFR in patients with CAD.

P050

Diagnostic impact of CT attenuation correction on CZT myocardial perfusion SPECT in patients with coronary artery disease compared to cardiac SPECT/CT hybrid imaging

Y. Fukushima, S. Kumita, H. Hashimoto, Y. Sugihara, K. Iwata, T. Hamana; Nippon Medical School Hospital, TOKYO, JAPAN.

Introduction: Cadmium-zinc-telluride (CZT) solid-state detectors have multiple advantages over conventional NaI cameras, such as higher spatial resolution, energy resolution, and sensitivity. However, CZT myocardial SPECT images show noticeable attenuation artifacts in the septal, inferoposterior, and posterolateral walls of the left ventricular myocardium. CT attenuation correction (CTAC) can improve the diagnostic accuracy of myocardial SPECT. Furthermore, myocardial SPECT/coronary CT angiography (CCTA) fused images provide true coronary artery distributions. The aim of this study was to determine the impact of CTAC on the diagnostic performance of CZT myocardial perfusion SPECT for patients with coronary artery disease (CAD) compared to cardiac SPECT/CCTA hybrid imaging. **Materials and methods:** The study between April 2015 and March 2016 included a total of 289 consecutive patients who were suspected of CAD and underwent a one-day rest-stress myocardial perfusion SPECT test using a CZT gamma camera: Discovery NM530c. The final study cohort was comprised of 46 patients (65 ± 15 years, 30 men and 16 women) who then underwent CCTA. Using a dedicated software for CTAC, SPECT images were coregistered with low-dose CT images acquired simultaneously with a separate device: Symbia T2. Using the 17-segment model, the summed rest scores (SRS), summed stress scores (SSS), and summed difference scores (SDS) were derived from both non-attenuation corrected (NAC) images and CTAC images. The presence or absence of myocardial ischemia in the left anterior descending artery (LAD), diagonal branch (Dx), left circumflex artery (LCX), or right coronary artery (RCA) territories was confirmed. The presence of CAD (> 50% coronary artery stenosis) was revealed using CCTA with SPECT/CCTA fused analysis, and the diagnostic accuracies of both NAC and CTAC images were compared. **Results:** There was a significant difference between NAC and CTAC images concerning both SRS and SDS (12 ± 6 vs. 9 ± 6 , $p = 0.0003$ and 2 ± 4 vs. 4 ± 4 , $p = 0.0009$, respectively) while SSS did not differ (14 ± 8 vs. 13 ± 8 , $p = 0.253$). CTAC improved accuracy globally and in the RCA territory (63% to 71% and 54% to 63%, respectively). Sensitivity was also improved in each individual territory (LAD: 50 to 63%, Dx: 44 to 58%, LCX: 25 to 50%, RCA: 36 to 58%). **Conclusions:** CTAC improves the diagnostic performance of CZT myocardial perfusion SPECT for patients with CAD. Furthermore, CTAC images can more accurately detect hemodynamically significant coronary lesions in cardiac SPECT/CCTA fused images.

P051

Myocardial Perfusion Imaging using IQ-SPECT, comparison with Coronary Angiography, Single Center Experience

M. Trogrlic, S. Tezak; University Hospital Centre Zagreb, Zagreb, CROATIA.

AIM: to evaluate the diagnostic performance of myocardial perfusion imaging (MPI) obtained with a multifocal collimator, IQ-SPECT, in the detection of coronary artery disease (CAD) by comparison with invasive

coronary angiography (CA). **MATERIALS AND METHODS:** 106 patients (60 males and 46 females; mean age 60 ± 9 years) with intermediate and high post stress coronary artery disease probability were included in this retrospective study. Patients showing only scar on MPI were excluded from study. All patients underwent two-day protocol perfusion scan (Gated IQ SPECT/CT) after stress test and at rest. Acquisition was performed on a Symbia T (Siemens) equipped with a dual-headed gamma camera system and with a multifocal smartzoom collimator. Acquisition was done in 128×128 matrix, 50 min after tracer injection (370 MBq Tc-99m sestamibi), 17 views per head, 20 sec/view. Flash 3D iterative reconstruction was done. Expert in nuclear cardiology assessed all myocardial perfusion images using 4D-MSPECT software. CAD was defined as $\geq 50\%$ stenosis of epicardial coronary arteries or their major branches detected on CA. **RESULTS:** On the basis of scintigraphic results, subjects were divided in two groups: Group A ($n=74$) with pathological findings on MPI, and group B ($n=32$) with normal MPI. 52 patients underwent CA within one year after MPI. In group A 64 patients (86.5%) had evidence of ischemia (showing at least one reversible defect - Summed Difference Score $SDS > 3$) while other 10 (13.5%) had evidence of scar with ischemia. The comparison between IQ SPECT and CA (available for 45 patients in group A) showed that in 24.4% (11/45) no evidence of stenosis $\geq 50\%$ in coronary arteries was found. 16 patients (35.5%) with multi-vessel CAD had more frequently severe ischemia on MPI. 18 patients (40%) had one-vessel disease. Despite no evidence of CAD on MPI in group B, 21.9% of patients (7/32) underwent CA showing no evidence of coronary artery stenosis in all cases. The comparison between MPI and CA showed that IQ-SPECT had sensitivity of 100% (89.72%-100%), specificity of 38.9% (17.30%-64.25%), accuracy of 78.8%, positive predictive value of 75.6% (60.46%-87.12%), and negative predictive value of 100% (59.04%-100%). **CONCLUSIONS:** IQ SPECT has excellent sensitivity, very good accuracy and high negative predictive value. Specificity is lower than expected probably due to changes in smaller coronary artery branches not detectable by CA, stenosis in coronary arteries less than 50%, or due to vasospasm. In our study we confirmed CAD in 34 out of 106 patients (32.1%).

P052

Tc99m Myocardial perfusion imaging using IQ SPECT: Prognostic comparison of stress only normal study and stress-rest normal study, one year follow up

F. ÇINARAL SAYIN, Ö. SAVAŞ DEN HARTIGH, M. ÖZHAN, H. MEMİŞ, Ö. MENĞİ; KARTAL KOŞUYOLU TRAINING AND RESEARCH HOSPITAL, İSTANBUL, TURKEY.

Aim: Guidelines for myocardial perfusion SPECT (MPS) recommend that if stress examination is performed first and reported as normal, the rest examination can be omitted. (MPS) Studies using IQ-SPECT Symbia S system (Siemens, USA) with SMARTZOOM™ collimators and with dedicated reconstruction software provides shorter scan time using lower levels of radioactivity compared to the conventional SPECT systems. We aimed to evaluate the prognostic value of stress only normal study compared to stress-rest normal study using IQ SPECT. **Methods:** Three hundred thirty nine patients underwent Tc99m myocardial perfusion scintigraphy with IQ SPECT on February 2013. Patients with abnormal studies were excluded. One hundred seventy four patients with normal MPS studies were enrolled in the study. Two days and stress first protocol was used. Patients with low likelihood of coronary artery disease that had normal stress study, did not have the rest study. Two days rest imaging was performed on patients with equivocal findings or with any abnormality on imaging after stress. The patients hospital data records were checked for follow up in one year. Myocardial perfusion GATED SPECT imaging results are compared with the clinical outcomes of the patients. **Results:** Stress

only protocole was used for 118 patients (85 Female, age 43-84, mean 63,4), (33 Male, age 42-81, mean 62,6) and two days stress-rest protocole was used for 55 patients (29 Female, age 45-77, mean 64), (26 Male, 38-80, mean 65,7). Among the stress only group 3 patients (2,5%) had cardiac events/ symptoms, one patient had LAD stenting, one patient had RCA stenting and one patient had coronary artery bypass surgery. One patient (1,8%) from the stres-rest study group had cardiac symptoms in one year of follow up and underwent coronary angiography revealing LAD lesion. Statistical analysis results revealed that there's no significant difference (p value < 0.01) between the two study groups prognosis for one year of follow up. Conclusion: Patients having normal stres imaging only have the same cardiac event rate with the patients having normal stres-rest imaging study. Stress only protocole can be used with the IQ SPECT gamma camera resulting in lower levels of radioactivity consumption and shorter scan time

P053

Keeping the reproducibility of functional parameters of the left ventricle between conventional system and IQ-SPECT

M. Havel, M. Kaminek, L. Henzlova, P. Koranda; Faculty of Medicine and Dentistry, Palacky University Olomouc and University Hospital Olomouc, Olomouc, CZECH REPUBLIC.

Introduction: Technological progress in myocardial perfusion imaging (MPI) brings to the market new dedicated tomographic devices but also additions to conventional Anger style cameras, such as "IQ-SPECT" system with multifocal "SMARTZOOM" collimators. The possibility to reduce the administered dose or acquisition time with this modern upgrade is progressive. However, in our daily practice we found there are significant differences when comparing results of the functional parameters of the left ventricle acquired with conventional camera equipped with Low Energy High Resolution collimators (LEHR) and "SMARTZOOM" collimators, as we referred previously. We tried to find easy way to keep the reproducibility of the results between the both systems by changing the filter parameters of the "IQ-SPECT" gated studies. **Materials and methods:** For this purpose we utilised random group of 31 patients, (19 males, 12 females, average age 62.4 +/- 8.4 years). All subjects were examined on both conventional (acquisition matrix 64x64, zoom 1.46) and "IQ-SPECT" (acquisition matrix 128x128, zoom 1.0) system. Acquisition was done on Symbia S dual head SPECT camera, data with LEHR collimators were processed and reconstructed with filtered back projection (applied Butterworth filter of order 5 with cut-off frequency 0.35). Data obtained with "SMARTZOOM" collimators were reconstructed with vendor's Flash3D iterative reconstruction (2 subsets, 15 iterations) and then filtered with the various settings of Butterworth (cut-off frequency range 0.2 - 0.4, order 1 - 8) and Gauss (FWHM 14 - 20 mm) filters - in total of 68 variations. The matrix of the "IQ-SPECT" study was changed to 64x64 prior filtering. The tomograms were processed in CORRIDOR4DM software. We compared ejection fraction values, end-diastolic and end-systolic volumes (EF, EDV, ESV) to find the best correlation between them. Results: Based on the Bland-Altman analysis we found the best agreement for the EF value from IQ-SPECT study processed with the Butterworth filter of order 2 and cut-off frequency 0.35 (mean difference -1.0%EF, the 95% limits of agreement were placed at -11.8%EF and +9.7%EF, Pearson correlation = 0.91). However, the width of the interval was still quite large. With this setting, the Pearson correlations for EDV was 0.96 and for ESV 0.97. Conclusion: The technological effort in MPI must keep the reproducibility of the results during the follow-up, with postprocessing there is possibility to adjust the the outcomes of "IQ-SPECT" to agree better with the conventional system.

P054

IQ-SPECT Positioning Uncertainty in Myocardial Perfusion Studies

T. Mäkelä^{1,2}, E. Hippeläinen^{1,2}; ¹HUS Medical Imaging Center, University of Helsinki and Helsinki University Hospital, Helsinki, FINLAND, ²Department of Physics, University of Helsinki, Helsinki, FINLAND.

Objective: Myocardial perfusion imaging is one of the most performed examinations in nuclear medicine. Pre-acquisition patient positioning can be challenging e.g. with large patients or if high liver or bowel uptake are present. The importance of correct centring is emphasized when using a cardio-centric orbit with multifocal collimators. Incorrect heart positioning can affect the image reconstruction and produce inaccurate semi-quantitative perfusion results. The aim of this study was to estimate the positioning accuracy in clinical practice. **Materials and methods:** Data from 379 clinical two-day stress-rest perfusion studies were retrospectively evaluated. Approximately 550 MBq of ^{99m}Tc labelled tetrofosmin (Myoview) was administered per day. If the scan was immediately repeated only the latest acquisition was included in the data set. The centring error was estimated as a distance from the SPECT centre-of-rotation (COR) to the middle point of the left ventricle. CORs were derived from the DICOM header values. The left ventricle middle points were determined from the perfusion images using MATLAB code particularly written for this project. The code was verified by comparing the output to ten manually determined ventricle centres. **Results:** The sample mean (\pm one standard deviation) distance between the program results and manual measurements was 6 \pm 3 mm. All automatically determined middle points were visually verified and one study (0.3 %) had to be manually corrected. The heart positions relative to the CORs had mean values of x=-9 \pm 12, y=5 \pm 9 and z=-1 \pm 9 mm for right-to-left, anterior-to-posterior and inferior-to-superior directions, respectively. The mean Euclidean distance was 17 \pm 10 mm for the stress and 18 \pm 9 mm for the rest images. In 9 % of the images the COR was positioned \geq 30 mm from the estimated ventricle centre. **Conclusion:** When considering typical heart sizes and the automated localization uncertainty only a minor directional bias was observed in the patient left-right direction. However, several individual outliers were present. It has been reported based on phantom studies that <2.5 cm offsets are unlikely to affect perfusion results (Caobelli et al. J Nucl Cardiol 2015;22:57-65). Further study is needed to assess at what distances mispositioning becomes clinically significant. Hopefully, a similar on-line verification will be implemented in the imaging systems giving the user instant feedback on positioning accuracy.

P055

A Comparative Study of Half Time Versus Full Time IQSPECT Acquisition in Patients Receiving Half the Standard Weight Based Dose

S. Panchadar, G. Biswas, Y. Al Sayed, M. HJ Garashi; Chest Disease Hospital, MOH, Kuwait, KUWAIT.

Aim: To evaluate IQSPECT semi-quantitative parameters and image quality at half time (HT-12Secs/frame) in comparison to full time (FT-20Secs/frame) in patients receiving standard weight based half dose.

Materials and Methods: Ninety eight (98) patients (62 males and 36 females; aged between 44-72 yrs) who had come for diagnosis of coronary artery disease (CAD), were randomly selected for myocardial perfusion studies with IQSPECT (SymbiaT16; Siemens) after being given standard weight based half dose (0.142mCi/Kg). Imaging was done 45mins after radiopharmaceutical administration initially with half time (HT) followed immediately by full time (FT) acquisition using single low dose CT for attenuation correction. Half of the Patients were imaged with initial HT acquisition followed immediately by FT acquisition and the other half were imaged with FT acquisition first followed immediately by HT acquisition. **Results:** Summed stress score (SSS), summed

difference score (SDS), summed rest score (SRS), total perfusion defect (TPD) and extent were significantly higher for IQSPECT-HT acquisition vis-à-vis FT acquisition ($p \leq 0.05$). Calculated left ventricular ejection fraction (LVEF) and left ventricular volumes (both end diastolic volume (EDV) and end systolic volume (ESV)) were similarly affected by HT acquisition ($p \leq 0.05$). Quality of images on HT acquisition were sub-optimal on visual analysis. **Conclusion:** Full time acquisition on IQSPECT is optimal for good quality images and reflects accurate semi-quantitative parameters in patients receiving half the standard weight based dose in comparison to half time (HT) acquisition in the same setting. Half time (HT) acquisition may be appropriate in patients receiving standard weight based full dose.

P056

Risk assessment using IQ SPECT myocardial perfusion scintigraphy in patients with coronary artery disease

G. Schweighofer Zwink¹, L. Hehenwarter¹, G. Rendl¹, M. Beheshti², C. Pirich¹; ¹Universitätsklinik für Nuklearmedizin und Endokrinologie, Salzburg, AUSTRIA, ²Abteilung für Nuklearmedizin, Krankenhaus der Barmherzigen Schwestern, Linz, AUSTRIA.

Aim: To assess the value of standard semiquantitative parameters for risk stratification in patients with manifested coronary artery disease undergoing accelerated myocardial perfusion imaging (MPI) using IQ SPECT. **Material and Methods:** Retrospective analysis of 204 patients with angiographically proven coronary artery disease (CAD) referred to our department for risk stratification with MPI performed using a two-day pharmacological stress protocol with adenosine or regadenoson and gated Tc-99m-Tetrofosmin SPECT (4 MBq per kg body weight). Data were acquired in 17 views (17 sec. each) using a Siemens Symbia T6 camera using IQ-SPECT collimators and the results were generated with Corridor 4DM software. The SSS, SRS, SDS, EF, TID, extent of ischemia and scar tissue in % of left ventricular area and time-to-peak values were analyzed statistically using SPSS software. **Results:** 204 patients (144 males, 60 females) with a mean age of 68±11 years were included into the study of whom 134 had multivessel disease. Comparing patients with single (SVD) versus multivessel disease (MVD) resting EF (46.4±11.3 % vs. 41.5±13.6 %, $p=0.01$) SSS (8.0±7.8 vs. 14.7±9.8, $p < 0.01$), and SRS (5.7±7.2 vs. 11.0±9.7, $p=0.01$) and the extent of ischemia (5.4±7.4 % vs. 8.6±8.2 %, $p < 0.01$) and scar tissue (5.8±10.4 % vs. 11.5±11.7 %, $p=0.02$) were significantly different in patients with SVD as compared to MVD. Neither TID nor SDS nor additional motion parameters showed a significant difference between those groups. **Conclusion:** The study employing accelerated MPS with IQ SPECT and a pharmacological stress protocol demonstrates that standard parameters i.e. EF, SSS, SRS and the extent of ischemia and scar tissue are significantly different in patients with SVD as compared to MVD and can be used for risk stratification while TID and time-to-peak analysis were not.

P-06 – Sunday, October 16, 2016, 16:00 - 16:30, Poster Exhibition Hall
Cardiovascular System: Myocardial Perfusion: SPECT

P057

General purpose collimators with resolution recovery enable significant dose reductions while maintaining image quality in myocardial perfusion SPECT

K. J. Saint, I. S. Armstrong, P. Chilra, S. Bartley, C. M. Tonge, P. Arumugam; Central Manchester University Hospitals, Manchester, UNITED KINGDOM.

Introduction. Increasing demand for myocardial perfusion SPECT (MPS) and continuing focus on dose reduction combined with forthcoming shortages of Tc-99m availability motivates a reduction in administered activity. Resolution Recovery (RR) enables reductions in either administered activity or imaging time. A recently published multi-vendor phantom study from our department demonstrates that more sensitive LEGP collimators with RR can provide comparable image quality to LEHR collimators with RR and allow for a reduction in administered activity. This work presents findings from a prospective follow-on patient study. **Methods.** 29 MPS scans were performed on a GE Infinia sequentially with LEHR collimators and then with LEGP collimators. Patients were administered tetrofosmin using a BMI-based protocol [280 MBq + 14 MBq × (BMI - 25)]. Based on the phantom work, pixel size was set at 6.8 mm for LEHR images and 4.4 mm for LEGP images. Counts in the myocardium were matched, being equivalent to a 40% reduction in administered activity in the LEGP images. Images were reconstructed with and without CT attenuation correction using GE Evolution for Cardiology with 6 iterations, 10 subsets and a Butterworth filter Fc 0.35 cycles/cm and power 10. Summed scores were extracted from a normal database comparison using Corridor 4DM. Functional data (EDV, ESV and LVEF) were analysed in Cedars Sinai QGS. **Results.** Image quality was comparable for images using each collimator. No significant differences were observed for the summed scores. On average, EDV and ESV were 16% ($P < 0.01$) and 26% ($P < 0.01$) greater in the LEGP images, respectively. On average, the LVEF was 3.1 percentage points lower ($P < 0.01$) in the LEGP images. The LVEF difference showed an inverse relation with the ESV. This is likely to be due to the smaller pixel size and reduced partial volume effects. **Conclusion.** MPS acquired using general purpose collimators with RR provides an excellent means of reducing administered activity and hence radiation dose, whilst maintaining image quality and quantitative perfusion results. The potential radiation dose for a two-day stress-rest protocol in our department would be between 3 to 4 mSv when using LEGP collimators. Furthermore the reduced Tc-99m usage will increase resilience against anticipated cost increases of radioisotope supply. As the majority of gamma cameras have LEGP collimators available, we believe that this is a highly accessible approach, which will facilitate a widespread reduction to population radiation dose from MPS.

P058

Role of Cardiac Hybrid Imaging (SPECT-CTCA) as a Prognostic Tool in Cardiomyopathy Patients

G. Sankar, S. Gambhir, P. K. Pradhan, N. K. Garg, A. Prashanth, A. K. Singh; SGPGIMS, Lucknow, INDIA.

Background and Aim of the study: Dilated cardiomyopathy (DCM) is a disorder characterised by enlargement of the left ventricular cavity along with systolic dysfunction. Idiopathic is the most common cause followed by myocarditis and ischemic heart disease. Single photon emission computed tomographic myocardial perfusion imaging (SPECT-MPI) shows high sensitivity in diagnosing ischemic component in DCM patients but it has moderate specificity. Similarly computed tomographic coronary angiography (CTCA) has high negative predictive value in ruling out ischemic disease. To incorporate the duality of morphology and function and to overcome individual limitations fusion imaging was done. The aim of this study was to know the value of fusion imaging as a prognostic tool in cardiomyopathy patients. **Materials and methods:** Thirty one patients clinically diagnosed by cardiologists to have DCM were included in this prospective study. They had no prior documented history of coronary artery disease (CAD). Initially they underwent stress-rest SPECT-MPI using Tc-99m labelled sestamibi. Of this only 28 patients underwent CTCA subsequently. Fusion imaging was successfully done using CardIQ software (GE Healthcare). Only those patients who had matched perfusion defects to stenotic segments in fusion imaging were labelled as having CAD. All the patients were followed up prospectively post fusion

imaging. Any cardiac events leading to hospital admission or cardiac death were considered as events. The effect of various parameters over event free survival was calculated using log rank test by Kaplan-Meier method. A p value of <0.05 was considered significant. **Results:** All the 31 patients who were initially included in the study were followed up for a median period of 6.5 months (range: 1 to 20 months; S.D: 6). Events occurred in five of the 31 patients (16%) the follow up period. Only three parameters, total calcium score (p=0.004), the nature of the perfusion defect (non viable, partially viable fixed defect, reversible ischemic and normal perfusion) noted in SPECT-MPI study (p=0.032) and the outcome of the fusion imaging (whether patient was labelled to have ischemic disease based on matched defects in fusion imaging or not) (p=0.038) were found to have a significant impact on event free survival in Kaplan-Meier survival analysis using log rank test. **Conclusion:** Fusion imaging may act as an independent prognostic marker in DCM patients, however longer median follow up period and larger multicentric prospective studies are required to validate these findings.

P059

SPECT MPI in the assessment of post infarct therapeutic attitude

S. E. Bouyoucef, A. Talbi, M. Habbeche, A. Khelifa, s. Rahabi, A. Amimour; CHU Bab El Oued, Algiers, ALGERIA.

Introduction: Prognosis following MI depends on a number of factors including geographic location, patient's health, extent of heart damage, and treatment given. However early risk stratification post-MI and therapeutic strategy is important to determine patients at increased risk for a recurrent ischemic event and those at increased risk for cardiac death (arrhythmic or non-arrhythmic). **Objective:** To assess the therapeutic approach by SPECT MPI Imaging and allows an accurate assessment of prognosis and guide patient post-MI management. **Patients and methods:** 430 patients in early phase of post myocardial infarct have been investigated in by SPECT/MPI. Patients have been classified in two groups: those who have received thrombolysis with or without revascularization and those who have not been thrombolysed. All patients recruited during two months underwent a two days protocols with physical/pharmacological stress/rest Gated SPECT MPI using tetrofosmine (Myoview) and a dual head gamma camera (Symbia T6) **Results:** Average age of patients was 60.6 years with a ratio Men/woman of 4 :1. Identified risk factors were : Hypertension (56%), Diabetes (43%) smoking (39%) and dyslipidemia (26%). 54% of patients did not received thrombolysis nor revascularization meanwhile 46% received thrombolysis treatment (14%) or revascularization by coronary artery bypass grafting (CABG, 12%) or percutaneous coronary intervention (PCI, 20%). Gated SPECT MPI showed in 357 patients (85%) fixed defects in 357 patients (85%) and reversible defects in 270 patients (63%). It was noted that more reversible defects were seen in patients who did not received thrombolysis (57%) than in those patients who did receive a thrombolysis or a revascularization. Patients who benefited from revascularization showed better summed stress score and less stress ischemia in other territories than patients who have not been thrombolysed (ratio of 0.7). Average post effort ejection fraction was better (59%) in patients who have been revascularized than in not thrombolysed patients. Average of transient index dilation (TID) was more elevated (>1.18) in non thrombolysed patients. **CONCLUSION:** SPECT/MPI is an important tool to assess post MI therapy and it is useful to stratify patients according the MPI findings in order to predict with better accuracy of the outcomes of post infarct therapy strategy.

P060

Gated myocardial perfusion SPECT-CT imaging with coronary calcium scoring in asymptomatic patients after percutaneous coronary intervention

A. Tzonevska¹, M. Garcheva¹, I. Kostadinova¹, L. Chavdarova², K. Tzvetkov²; ¹City Clinic, SOFIA, BULGARIA, ²HATO, SOFIA, BULGARIA.

Objective: Restenosis is the main problem in patients who have had percutaneous coronary intervention (PCI). Chest pain following PCI is a poor indicator of restenosis. The purpose of the present study was to assess the usefulness of gated single photon emission tomography/computed tomography ^{99m}Tc-tetrofosmin (gSPECT-CT) combined with coronary calcium scores (CAC) in asymptomatic patients after PCI. **Methods:** 57 asymptomatic patients (32 male and 25 female), mean age 49±16 years, 6 to 27 months after PCI with stent revascularization, were recruited. They were examined by technetium-99m-tetrofosmin gSPECT-CT and CAC scores and standard stress protocol. The quantitative analysis of the myocardial perfusion and function (QGS/QPS) and CAC score calculation with the Agatston method were used. **Results:** In 32 (56%) patients, normal myocardial perfusion and function was found. From twenty five patients with moderate to severe CAC, 9(16%) patients had mild to moderate hypoperfusion and were assessed as with low risk for coronary events and were referred to medical treatment and follow-up. In 16(28%) patients high risk for coronary events was diagnosed and they were referred to PCI. In 6(11%) patients in-stent restenosis was detected. In 8(14%) patients significant stenosis in unstented coronary vessel was assessed. In 2 patients no significant stenosis was found. Sensitivity and specificity were 93% and 84% respectively. **Conclusion:** ^{99m}Tc-tetrofosmin gSPECT-CT plus CAC scores provided combined cardiac assessment and can serve as a reliable screening method to assess asymptomatic patients, passed PCI and define risk stratification and management of these patients.

P061

The Association of Regadenoson and Isometric Exercise Significantly Improves Image Quality of Myocardial Perfusion Scintigraphy

j. Pinauy, Q. Ceyrat, H. Douard, L. Janvier, L. Bordenave; CHU BORDEAUX, BORDEAUX, FRANCE.

Background: Regadenoson is a selective A2a receptor agonist and it is widely used as vasodilator for the stress test of myocardial perfusion imaging (MPI). This study aimed at assessing whether adding an isometric exercise (i.e. handgrip) to Regadenoson injection would improve image quality and be well tolerated by patients. **Methods:** Patients referred for MPI were prospectively randomized in either the handgrip-Regadenoson group (HG-Reg, n= 50) or Regadenoson only (Reg, n = 50) group. A Nuclear Medicine physician, blinded to the stress test modalities and clinical characteristics of the patients, analyzed data. As a primary endpoint, the images were classified as good or bad. Secondary endpoints were: the hemodynamic changes, the recovery time and clinical side effects. **Results:** The images in the HG-Reg group were of significantly better quality than those in the Reg group (88% vs 52%, p<0.0001). Systolic blood pressure fell significantly less often in the HG-Reg group than the Reg group (p=0.0216). The other parameters (heart rate, maximum heart rate and percentage of age-predicted maximum heart rate, systolic blood pressure, recovery time) were not significantly different between the two groups. Fewer subjects in the HG-Reg reported at least one side effect in comparison to Reg subjects (70 vs. 92%, p=0.047). **Conclusions:** The association of handgrip exercise and Regadenoson administration is well tolerated and allows for a significant improvement in image quality of myocardial perfusion scans.

P062**Myocardial perfusion imaging for evaluation of the borderline coronary stenoses**

M. B. Garcheva-Tsacheva¹, V. Gelev²; ¹Cityclinic-Sofia, SOFIA, BULGARIA, ²Tokuda hospital-Sofia, SOFIA, BULGARIA.

Introduction. The stress myocardial perfusion imaging is important for visualization and quantification of the inducible hypoperfusion. The hemodynamic significance of borderline stenosis (BLS) is questionable, even in symptomatic patients. **Aim.** The aim of the study was to visualize and quantify the inducible ischemia by stress myocardial perfusion imaging (MPI) in patients with borderline stenoses, known from coronary angiography. **Material and methods.** Seventy six patients (49 men, 27 women aged from 45 to 87) with at least one borderline stenosis were examined by MPI after submaximal or symptoms limited stress. The examination was performed on Symbia 2T Siemens SPECT/CT with attenuation correction. Seven patients with previous myocardial infarction had also rest MPI. A quantitative evaluation was also done by QPS/QGS software with determination of the summed stress score (SSS), or summed differential score (SDS). The number of vessel territories with BLS was 126: 7 left main stenoses (LCA), 52 left anterior descendens (LAD), 29 right coronary arteries (RCA), 26 circumflex arteries (rCx) and 12 others. Thirteen vessels with in stent restenosis more than 40% were included. **Results.** Inducible hypoperfusion was visualized in 27.5% of patients and 18 % of lesions. Sixteen patients (from 21 with hypoperfusion) were with SDS between 4 and 8, the others had SDS 3. One patient received inducible left ventricular dysfunction. Two patients (from 13 with restenoses) had inducible ischemia. **Discussion.** The quantification by SSS, or SDS reflects the inducible hypoperfusion, while the total perfusion defect may include scar, or attenuation phenomenon. In our group of patients with BLS there were no patients with severe degree of hypoperfusion. **Conclusion.** MPI is important not only for visualization, but also for evaluation of the severity of the reversible perfusion changes, due to borderline coronary stenosis for determination of the further management of patients.

P063**The impact of attenuation correction in SPECT / CT on quantitative parameters of myocardial perfusion in patients with intact coronary arteries**

E. Khachirova¹, L. Samoylenko², O. Shevchenko¹; ¹Pirogov Russian National Research Medical University, Department of Cardiology FDPO, Moscow, RUSSIAN FEDERATION, ²Russian Medical Academy of Postgraduate Education Studies, Department of radiotherapy and radiology, Moscow, RUSSIAN FEDERATION.

The aim: to assess the impact of attenuation correction (AC) on quantitative parameters of myocardial perfusion and verification of myocardial ischemia in patients with chest pain and intact coronary arteries (CA). **Material and methods:** myocardial perfusion rest/stress SPECT/CT ^{99m}Tc-MIBI (SYMBIA T-16, SIEMENS) with and without AC was performed in 35 patients (male/female 15/20, mean age- 62.8 yrs) with a typical chest pain, a positive stress test, and intact CA. Patients with previous myocardial infarction, significant valvular disease, clinical heart failure or depressed systolic left ventricular function were not included. **Results:** In all patients stress-induced myocardial ischemia was detected both without and with AC images. However, quantitative parameters of myocardial perfusion were lower after the AC: SSS 6.9±1.2 vs. 7.7±1.1; SDS 4.0±0.8 vs. 4.9 ± 0.6; Stress ext. Total 11.2±1.8 vs. 13.0±1.9; Stress TPD total 9.3±1.2 vs.10.9±1.2; TPDi 4.1±1.0 vs.5.9±0.9 (for all p<0.05). For SRS, Rest ext. Total, and Rest TPD total difference was not significant. In women, significant difference was obtained for all parameters: SRS, SSS; SDS, Stress ext.Total, Stress TPD total, Rest ext.Total, Rest TPD total,

TPDi (2.8±0.8 vs. 3.7±0.9; 7.4±1.4 vs. 9.0±1.6 4;5±0.8 vs. 5.3±0.9; 12.3±1.4 vs. 14.7±2.1; 10.3±1.8 vs. 12.7±2.1; 4.5±1.1 vs. 5.6±1.4; 4.0±0.9 vs. 5.5±1.1; 6.4±1.2 vs. 7.1 ± 2.1, for all p<0.05), for men - only for the SSS, SDS, Stress ext. Total, Stress TPD total (6.4±1.3 vs. 7.9±1.1; 3.3±0.8 vs. 4.4±0.7; 12.2±1.6 vs. 14.1±1.8; 9.7±1.2 vs. 10.9±1.4; p<0.05). In patients with BMI ≥25 significant difference for all parameters was obtained: SRS 3±0.7 vs.4.5±0.8; SSS 7±1.8 vs. 9.9±2.2; SDS 4.0±0.9 vs.5.3±0.6; Stress ext.Total 13.5±1.8 vs.16.2±2.2; Stress TPD total 10.4±1.9 & 13.3±2.1; Rest ext.Total 5.5±1.6 vs. 7±1.7; Rest TPD total 4.8±1.1 & 6.5±0.8; TPDi 5.5±1.5 & 7±1.9 (for all p<0.05). However, patients with a normal BMI (18,5-24,9;WHO, 2004) significant difference was obtained only for Stress ext. Total, Stress TPD total (11.3±2.4 vs. 12.6±2.6; 9.6±1.6 vs. 10.7±1.8, p<0.05). **Conclusion:** Our results support better diagnostic ability with AC SPECT/CT for detection of the myocardial ischemia. Using AC one could decrease false-positive results and avoid overestimation of the extent and severity of perfusion defects, especially in women and obese patients.

P064**SPECT MPI finding in the prognosis of dilated cardiomyopathy**

S. E. Bouyoucef, s. Rahabi, A. Talbi, M. Habbeche, A. Khelifa, A. Amimour; CHU Bab El Oued, Algiers, ALGERIA.

Introduction: The prognosis for dilated cardiomyopathy (DCM) is very specific to an individual and their particular anatomy. Some people with the condition can lead a normal life and remain essentially asymptomatic. Others develop symptoms that can progress. MRI and SPECT/MPI are an important imaging modalities to assess and to establish a prognosis of the DC. **Objective:** To assess the role and the place of SPECT/MPI in the therapy management of DCM. **Patients and methods:** 84 patients have been referred to nuclear medicine department for DCM in 4 months. All patients recruited underwent a two days protocols with physical/pharmacological stress/rest Gated SPECT MPI using tetrofosmine (Myoview) and a dual head gamma camera (Symbia T6). A SPECT MPI analysis using the 4DM SPECT was done and comparison done between perfusion findings and clinical, risk factors and echocardiography results. **Results:** Average age of patients was 61 years with a ratio Men/woman almost equal to one (53% vs 47%). The risk factors were dominated by Hypertension (66%) than Diabetes (45%), dyslipidemia (26%), smoking (21%) and heredity (8%). 84% of patients were symptomatic and the dyspnea was the most frequent symptom (68%) followed by pectoris angina (42%). 26% of patients presented and LBBG and underwent a pharmacological stress SPECT MPI. Average ejection fraction obtained by echocardiography was 43%. SPECT MPI showed fixed defects in 66% of patients, reversible defect in 53% and normal patterns in 8% patients. Among patients with fixed defects, 60% have had more than 3 segments involved, 30% between 2 to 3 and 10% less than 2 segments. Regarding patients with reversible defects, 35% have had more than 3 segments involved, 40% between 2 to 3 and 25% less than 2 segments. Number of reversible defects as well as number of fixed defects were correlated to the clinical symptoms. SPECT MPI has helped in most cases to find out an appropriate therapeutic strategy. **Conclusion:** SPECT MPI in dilated cardiomyopathy is an important prognostic tool and has a major place in adjusting initial therapy in order to reduce cardiac events and improve quality of live.

P065**Assessment of myocardial perfusion in patients with chest pain and intact coronary arteries using ^{99m}Tc-MIBI SPECT/CT**

E. Khachirova¹, L. Samoylenko², O. Shevchenko¹; ¹Pirogov Russian National Research Medical University, Department of Cardiology FDPO, Moscow, RUSSIAN FEDERATION, ²Russian Medical Academy of Postgraduate Education Studies, Department of radiotherapy and radiology, Moscow, RUSSIAN FEDERATION.

The aim: assessment of myocardial perfusion and functional coronary flow reserve in patients with chest pain and unchanged coronary arteries (CA) using ^{99m}Tc -MIBI SPECT/CT. Material and methods: Myocardial perfusion rest/stress ^{99m}Tc -MIBI SPECT/CT (SYMBIA T-16, SIEMENS) was performed in 21 patients (male/female 8/13, mean age 61.6 yrs) with a typical chest pain and angiographically intact CA (the study group); in 14 patients (m/f - 8/6, mean age 57.4 yrs) with coronary atherosclerosis (the comparison group) in a two-day protocol. Results: All the patients from the study group showed transient ischemia during stress-test. 15 patients from the study group had arterial hypertension, of those 10 patients showed transient perfusion defects during positive stress-test, and 5 patients during negative stress-test. These findings in the latter patients were considered as secondary microvascular dysfunction associated with arterial hypertension. In 6 patients from the study group without arterial hypertension transient perfusion defects during positive stress-test were found. These findings were considered as primary microvascular dysfunction. Quantitative indicators of the extent and severity of perfusion defects showed moderate changes in the study group, however, they were significantly different vs. the comparison group: SRS 3.2 ± 2.25 vs. 4.7 ± 1.2 ; $p < 0.05$; SSS 7.3 ± 3.4 vs. 11.8 ± 2.3 , $p < 0.05$; SDS 4.3 ± 1.84 vs. 6.8 ± 1.8 , $p < 0.05$; Stress ext.Total 11.2 ± 7.2 vs. 21.5 ± 3.2 , $p < 0.05$; Stress TPD total 10.4 ± 4.2 vs. 17.8 ± 7.7 , $p < 0.05$; Rest ext.Total 4.2 ± 2.8 vs. 10.7 ± 2.0 , $p < 0.05$; Rest TPD total 4.8 ± 2.9 vs. 7.7 ± 2.8 , $p < 0.05$; TPDi 5.8 ± 1.6 vs. 10.3 ± 2.1 , $p < 0.05$. Conclusion: In patients with typical chest pain and intact coronary arteries transient ischemia due to primary or secondary microvascular dysfunction could occur. Myocardial perfusion SPECT/CT might be a useful tool for risk stratification and management decision in these patients.

P066

Relationship between MDCT coronary angiography and SPECT myocardial perfusion imaging in patients with intermediate and significant coronary artery stenosis

K. W. Zavadovsky^{1,2}, M. O. Gulya^{1,2}, E. V. Grakova¹, Y. B. Lishmanov^{1,2}; ¹Federal State Budgetary Institution «Research Institute for Cardiology» of Siberian Branch under the, Tomsk, RUSSIAN FEDERATION, ²National Research Tomsk Polytechnic University, Tomsk, RUSSIAN FEDERATION.

Aim. The aim of this study was to assess relationship between CT coronary angiography and SPECT myocardial perfusion imaging in patients with intermediate and significant coronary artery stenosis. Materials and Methods. We enrolled 70 consecutive patients (55 males and 15 females) aged 63.1 ± 7.1 years who were referred for hybrid cardiac SPECT/CT. All patients underwent MDCT coronary angiography and myocardial perfusion imaging at rest and in combination with pharmacological adenosine stress test. Based on MDCT data, we analysed the presence of coronary artery stenosis, its degree (by minimal diameter), and segment involvement score. Based on SPECT data, we analysed summed stress score (SSS), summed rest score (SRS), summed difference score (SDS), total stress (TSE%) and total rest extents (TRE%) of perfusion defects and their difference (TED%), extent of fixed perfusion defect (EFix%), and extent of reversible perfusion defect (ERev%). Based on MDCT data, all patients were divided in three groups with nonsignificant coronary artery stenosis $< 40\%$ (group I), intermediate coronary artery stenosis > 40 - $< 70\%$ (group II), and coronary artery stenosis $> 70\%$ (group III). Results. Except SRS and EFix%, SPECT indexes of myocardial perfusion statistically significantly differed between groups I, II and III. The incidence rates of reversible and mixed perfusion defects did not significantly differed between groups. Stable (fixed) perfusion defects were found significantly more often in patients of group III compared with group I. Normal myocardial perfusion was detected significantly more often in patients of groups I and II compared with patients who had stenosis $> 70\%$. Segment involvement score had weak and moderate correlation

relationships with SSS ($r=0.34$; $p=0.0015$), TSE% ($r=0.32$; $p=0.0026$), SRS ($r=0.30$; $p=0.009$); SDS ($r=0.42$; $p=0.0002$), and ERev% ($r=0.38$; $p=0.001$). Conclusions. Scintigraphic indexes (SSS; TED%, ERev%) had the maximum power for differentiating the perfusion abnormalities in the presence of intermediate and significant coronary lesions in stable coronary artery disease patients. The study was supported by a grant from the Russian Science Foundation (№14-15-00178).

P067

Long-term Follow-up of Patients after Coronary Stent Implantation by Gated Myocardial Perfusion SPECT

E. Takács¹, L. Jorgov¹, Z. Varga¹, M. Janecskó², I. Szilvási¹; ¹Semmelweis University, Dept. of Nuclear Medicine, Budapest, HUNGARY, ²Semmelweis University, Dept. of Anaesthesiology and Intensive Care Unit, Budapest, HUNGARY.

Aim: Coronary artery disease is a progressive disease even after percutaneous coronary intervention (PCI). Ischemia detected by myocardial perfusion SPECT has been shown to predict future cardiac events regardless of patient symptomatology. Aim of our study was to evaluate the clinical usefulness of ECG-gated myocardial perfusion SPECT (GSPECT) in long-term follow-up of patients after coronary stent implantation. Patient and methods: 27 patients (4 females, 23 males) were followed for 3 to 9 years (mean 5.9 ± 1.6 years) after coronary stent implantation. During this period all patients underwent at least two exercise/rest GSPECT using the one-day Tc^{99m}-tetrofosmin protocol. Summed stress score (SSS), summed difference score (SDS), total perfusion deficit (TPD) and left ventricular ejection fraction (LVEF) were measured by using a semi-quantitative software (QPS/QGS, 20 segments model, scoring system). The changes of these parameters of the GSPECT were correlated to clinical data of patients including late revascularization procedures as well. Results: 14 out of 27 patients showed worsening of detected ischemia. The mean SDS value increased significantly from 3.1 ± 1.3 to 7.5 ± 1.8 ($p < 0.05$). During the follow-up period no death or non-fatal myocardial infarction has occurred. Coronary angiography was recommended in 10 patients with severe ischemia or moderate ischemia and/or persistent angina (mean ΔTPD 7.1 ± 1.9). Percutaneous revascularization was performed in 5 patients: coronary angiography showed restenosis in 2 cases, new stenosis on previously untreated coronary vessel occurred in 3 cases. CABG procedure was necessary in one patient with severe restenosis. No significant stenosis was found on angiography in 4 cases. Significant decrease in LVEF was found only in patients with $\text{SDS} \geq 7$. Conclusion: Myocardial perfusion GSPECT is useful for long-term follow-up and risk-stratification of patients after PCI indicating repeated revascularization procedures.

P068

Normal Myocardial Perfusion In Left Ventricle Inferior Wall Identified By Supine-Prone Stress-Only Gated Spect Myocardial Perfusion And Low Risk Of Coronary Events

V. López-Prior, I. Casáns-Tormo, R. Díaz-Expósito, A. Amr-Rey, J. Orozco-Cortés, H. Bowles-Antelo; NUCLEAR MEDICINE, HOSPITAL CLINICO UNIVERSITARIO, VALENCIA, SPAIN.

OBJECTIVE Stress-only GATED SPECT myocardial perfusion is an efficient method to establish the existence of normal myocardial perfusion in some patients, with reduced radiation exposure, time and cost. Obtaining supine and prone acquisitions is a very simple method to improve accuracy of image interpretation, especially in obese patients with suspected diaphragmatic attenuation. Our objective was to investigate the prognostic value of combined supine-prone images in the identification of normal myocardial perfusion by isolated left ventricular

inferior wall defect that disappears from supine to prone. **MATERIALS AND METHODS** From a total of 65 consecutive patients with normal myocardial perfusion diagnosed by stress-only Gated SPECT, we retrospectively selected 18 of the 65 patients with normal myocardial perfusion in left ventricular inferior wall identified by reduction of hypoperfusion from supine to prone images, without other perfusion abnormalities. GSPECT was performed 1h after injection of a ^{99m}Tc -tracer (2 day-protocol, 20 mCi-70 kg), at the end of physical stress(S) in all cases. We have obtained visual and quantitative assessment (bull's eye) of myocardial segments perfusion, without attenuation correction, in supine and prone successive acquisitions. We obtained only in supine images left ventricular ejection fraction, end-diastolic and end-systolic volumes at post-S (SEF,SEDV,SESv) by QGS and wall thickening by visual assessment. All patients were followed for cardiac events (CE), considered as cardiac death, myocardial infarction and late (> 3 months after isotopic tests) myocardial revascularization. **RESULTS** The study group were 18 patients (17 m), mean age $64\pm 10(48-82)$ y/o, mean body mass index (BMI) 29.4 ± 4.5 , (72% with $\text{BMI}\geq 25$), submitted to investigate possible myocardial ischemia, all of them with GSPECT after treadmill exercise test with Bruce protocol, mean MPHR ($89.4\pm 17.3\%$), no angor-no ST depression (11) angor-no ST (1) ST-no angor (6). In all these cases we found inferior wall perfusion hypoperfusion in supine acquisition that showed complete recovery in prone images, so inferior defects were attributed to diaphragmatic attenuation and the patients were identified as normal. Global and regional functional parameters were normal. Mean SEF($60.4\pm 6.1\%$), SEDV(66.62 ± 1.9 ml) and SESV(27.4 ± 10.6 ml). After a mean follow-up of 31.6 ± 14.6 months (10–48) any patient showed CE. **CONCLUSION** Combined supine and prone myocardial perfusion images is a simple, accurate and inexpensive method to improve diagnostic certainty of normal myocardial perfusion in patients with left ventricular inferior wall hypoperfusion attributed to diaphragmatic attenuation with special benefit in obese men. This method can also identify patients with low risk of coronary events.

P069

Typical perfusion defects on myocardial perfusion SPECT in patients with left bundle branch block are related to myocardial wall motion but not to myocardial infarction or ECG characteristics

F. Hedeer, E. Ostfeld, B. Hedén, M. Carlsson, H. Arheden, H. Engblom; Lund University, Lund, SWEDEN.

Introduction: Patients with left bundle branch block (LBBB) can have fixed septal wall perfusion defects on myocardial perfusion single-photon emission computed tomography (MPS), resembling myocardial infarction. Late gadolinium enhancement (LGE) cardiac magnetic resonance (CMR) imaging is considered to be the reference standard for *in vivo* assessment of infarction and for evaluation of myocardial function. The aim of this study was to investigate if myocardial infarction, electrocardiogram (ECG) characteristics and myocardial wall motion in patients with LBBB are related to perfusion pattern on MPS. **Methods:** Patients with complete LBBB undergoing both MPS and CMR were retrospectively included. Using MPS images the patients were grouped depending on if typical LBBB septal perfusion pattern was present or not. The CMR images were evaluated for myocardial wall motion and presence and location of myocardial fibrosis. ECGs were analyzed using recently suggested strict criteria for complete LBBB. **Results:** Twenty-four patients (nine females) with complete LBBB were included in the study. Fourteen patients had a typical LBBB septal perfusion pattern on MPS of which three had signs of infarction by CMR. Only in one case the location of the infarction could be considered the cause of the septal perfusion defects. No differences in ECG variables were seen between the LBBB patient groups with and without typical LBBB perfusion pattern on MPS (QRS duration 153 ± 12 ms vs. 153 ± 16 ms, $p=1.0$). LBBB-patients with LBBB perfusion pattern on MPS showed significantly more dyskinesia in the

septal wall and significantly more hyperkinesia in the lateral wall compared to the LBBB-patients with normal septal perfusion pattern on MPS ($p=0.011$ and $p=0.007$, respectively). **Conclusion:** Differences in regional myocardial wall motion pattern can be a part of the explanation of why some patients with LBBB show perfusion defects in the septal wall on MPS without presence of underlying myocardial scar or fibrosis.

P070

The Logistics and Cost-Effectiveness of Performing Stress-Only Myocardial Perfusion Imaging (MPI) in a Busy Greek Nuclear Medicine Department

E. Kyrozi, A. Theodorakos, A. Iakovidou, A. Kalkinis, M. Koutelou; Onassis Cardiac Surgery Center, kallithea, GREECE.

Background: According to the European and American Guidelines for Myocardial Perfusion Imaging (MPI) rest SPECT images are not required when stress images are normal. The aim of this study is to evaluate the advantages of performing Stress-Only MPI protocol. **Method:** The study was carried out in the Nuclear Medicine Department of Onassis Cardiac Surgery Center. We analyzed data from a period of one calendar year (2015). With normal stress MPI, rest images provides no additional prognostic value and were therefore eliminated. The one-day protocol used a stress dose of 8-10 mCi Tc^{99m} Sestamibi and a rest dose of 18-20 mCi Tc^{99m} Sestamibi. **Results:** 3961 patients underwent MPI using Tc^{99m} Sestamibi, 887 of which (22.4%) performed a stress-only imaging protocol. The practice of omitting rest images has as a result the decrease of the test's duration (90 min compared to 2-3 hours) which is more convenient for the patient and staff and helps the logistics of the department. It also results in a lower radiation exposure to the patients 2.7mSv vs 9.3mSv (when both stress and rest imaging is performed). It is expected with the use of stress-only protocol a reduced occupational exposure to the staff of the nuclear medicine laboratory. In addition, this practice reduces the cost of the department as with the same number of vials we can examine more patients. **Conclusion:** Stress-only MPI provides only advantages. It helps the logistics of the department. Time saving, reduction of radiation exposure, and cost-effective examinations are the most significant benefits, without any compensation in the quality, the diagnostic accuracy and the prognostic value of the examination.

P071

Optimization physicals parameters for cardiac perfusion imaging

S. Alramlawy, M. Adel; Department of Critical Care medicine, Cairo University Hospitals, Faculty of Medicine, Cairo, EGYPT.

Objective myocardial perfusion imaging (MPI) has become an important tool and a substantial for diagnosis and management of heart disease. A new iterative reconstruction algorithm (flash 3D) has been recently proposed for (SPECT). The aim of work was to evaluate radiation exposure to practitioners and patients by reliance on reconstructions methods that aid in reducing the injected dose **Methods:** Forty-eight patients (30 M, 18F) who were referred to our department for MPI were randomly selected and divided into 3 groups: Group (1): contained two sub-groups, one scanned with full administrated dose (25 ± 3.2 mCi) and half dose (10 ± 2.5 mCi) Group (2): contained two sub-groups, one scanned with 32 projections per scan, the other with 16 projections per scan. Group (3): contained two sub-groups, one scanned at a time per projection of 20 s and the other scanned at 10 s per projection. The three groups were processed using 3D reconstruction algorithm (flash 3 D) (4 subsets, 13 iterations, FWHM=14 mm). Dose rate was recorded using a calibrated standard survey meter for all patients after dose administration. Besides, Dose calculations were also considered the time elapsed during staff exposure that included dose preparation, injection, patient imaging, and

release times.. Myocardial functional parameters such as Ejection Fraction (EF), End Diastole Volume (EDV), End Systole Volume (ESV) and Total Perfusion Defect (TPD) were compared for each group. **Results:** Qualitative assessments results from all groups showed which include (full dose (25±3.2mci) and half dose (10±2.5mci), one scanned with 32 projections per scan, the other with 16 projections per scan and a time per projection of 20 s and the other scanned at 10 s per projection Images were visually scored as very-good quality and sufficiently convergent and identical. Quantitative results using (3D) showed insignificant difference of the EF, EDV, ESV and TPD between the different groups. Dose rate reduced by 48%. when reducing to half dose (dose rate was 33±4.5 reduced to 14.8±3.6 along one meter from patient, also dose rate was reduced from 120±5.6 µSv/h to 67 ±3.9.6 µSv/h in patients' rest room) for that reason the effective dose 15.2 ± 2.4 was reduced to 7.1 ± 1.8 when using half protocols with 3D . **Conclusion:** New 3D enable reduction of dose administration or total acquisition time plays a significant role in staff exposure. Further investigations can be performed to assess these results on large patients cohort with further dose reduction.

P072

Cardiac Fusion Imaging (SPECT-CTCA) - better “Gate-Keeper” for Invasive Coronary Angiography

P. K. Pradhan, G. Sankar, S. Gambhir, N. K. Garg, A. Prashanth, A. K. Singh; SGPGIMS, Lucknow, INDIA.

Aim of the study: The aim of this study was to know whether fusion imaging (using both SPECT MPI and CTCA) is a better “gate-keeper” for segregating patients, with no prior history of coronary artery disease, who require further invasive evaluation than stand alone SPECT-MPI or CTCA. **Materials and methods:** Thirty one patients clinically diagnosed by cardiologists to have dilated cardiomyopathy (DCM) were included in this prospective study. They had no prior documented history of coronary artery disease (CAD). Initially they underwent pharmacological stress-rest SPECT-MPI using Tc-99m labelled sestamibi, using a dual head gamma camera (Infinia Hawkeye; GE healthcare). Low dose non contrast CT images were acquired after the SPECT images for the purpose of attenuation correction. Image analysis of SPECT images was done using commercially available software (EC toolbox; Xeleris workstation provided by G.E. Healthcare). Perfusion defects involving more than 20% of coronary artery territory were considered as significant. Of this only 28 patients underwent CTCA subsequently using 64-detector CT scanner (LightSpeed VCT; GE Healthcare). Coronary lesions were visually assessed for stenosis and those showing more than 50% stenosis were considered as significant. Fusion imaging was successfully done using CardIQ software (GE Healthcare). Only those patients who had matched perfusion defects to stenotic segments in fusion imaging were labelled as having CAD. **Results:** Significant perfusion defects (> 20%) were present in 22 of the 31 patients (71%). Mean total coronary artery calcium scoring was 291 Agatston score units (range: 0 - 2511; S.D: 641). Significant stenotic segments were seen in 51 segments (13% of all the segments analyzed). Significant stenosis (>50%) in one or more segments were present in 15 patients (54%). Only 10 patients showed significant perfusion defects which matched with the corresponding stenotic segments (36%) in the fusion imaging and only these patients were planned for invasive coronary angiography by the cardiologists. There was significant difference between the percentages of patients labelled to have CAD on the basis of SPECT-MPI, CTCA and that of fusion imaging (p value < 0.05). **Conclusion:** Fusion imaging may act as a better “gate-keeper”, especially in patients with dilated cardiomyopathy, in segregating the patients requiring further invasive evaluation than stand alone SPECT-MPI or CTCA. Larger multicentric prospective studies and different study populations are required to validate these findings.

P073

Diagnostic performance of regadenoson vs dipyridamole in patients undergoing myocardial perfusion scintigraphy

M. Catalano, G. Annunziata, D. Scala, A. Sasso, R. Gottilla, V. Ippolito, I. Valenti; AORN, Naples, ITALY.

Aim: Regadenoson is a vasodilator agent that binds more selectively to the coronary A2a adenosine receptors than dipyridamole or adenosine. At present, there are no reported studies investigating the clinical utility of regadenoson as a vasodilator stress agent for myocardial perfusion scintigraphy (MPS) . Aim of this study is to evaluate whether dipyridamole and regadenoson are comparable in detection coronary artery disease(CAD) in patients (pts) undergoing to MPS. **Materials and methods:** 55 pts, 33 male and 22 female (mean age 65.6±11.6) underwent pharmacological test because of left bundle block or limitation to exercise test; 27 pts were stressed with dipyridamole and 28 patients with regadenoson because of asthma and severe chronic obstructive pulmonary disease (COPD) . Baseline characteristics were similar in both groups. 8 pts were affected with myocardial necrosis, 14 pts had prior coronary revascularization, 9 pts had history of myocardial infarction treated with percutaneous transluminal coronary angioplasty and 24 pts with suspected CAD because of chest pain or multiple coronary risk factors. Images were interpreted semi-quantitatively using a standard 17-segment model and a 5-point (0-4) scoring system. Global summed stress score, summed rest score and summed difference score were computed (Quantitative perfusion SPECT software QPS, version 2008; Cedars-Sinai Medical Center, Los Angeles, CA) The extent and severity of ischemia was defined as the difference between summed stress score and summed rest score. A summed difference score <6 was considered mild, 7 - 12 moderate and >12 severe. **Results:** In the group of pts stressed with dipyridamole 13 scans were normal, a reversible or inducible myocardial perfusion abnormality was present in 11 pts , 2pts with severe ischemia, 6 pts with moderate ischemia and 3 pts with mild ischemia, 3 pts with fixed defects because of myocardial necrosis. In the group of pts stressed by regadenoson 13 pts had negative scans, 1 pt severe ischemia, 3 pts moderate ischemia, 7 pts mild ischemia and 5 pts were affected with myocardial infarction. We found omogeneous perfusion scores disease related in both group. No severe collateral effects and fatal or non-fatal cardiac events occurred in both groups too. Pts with scan positive for moderate or severe ischemia underwent coronary angiography that confirmed coronary vessels patency. **Conclusions:** Regadenoson and Dipyridamole are comparable as vasodilators for stress testing in pts with known or suspected CAD undergoing MPS, but Regadenoson is safe, well tolerated and accurate in pts affected with asthma and severe COPD.

P074

Quantitative Myocardial Perfusion Scintigraphy: a useful tool in the diagnosis, prognosis and risk stratification of patients undergoing investigation of chest pain

A. Oseni, L. Calovi Motschenbacher, E. Nowosinska, A. Haroon, K. Ranjan, H. Jan; Bart's Health NHS Trust, London, UNITED KINGDOM.

Objective: In England and Wales Coronary artery disease (CAD) is the most common cause of death. Despite advancements in modern medicine, CAD accounted for 15.4% of all male deaths in 2013. As a result, greater emphasis has been placed on accurate diagnosis, prognostication and risk stratification of patients who present with chest pain. Qualitative results from Myocardial Perfusion Scintigraphy (MPS) have been at the forefront of investigation of such patients, with CG95 NICE Guidelines recommending the use of functional imaging as first line. We evaluated whether semi-quantitative analysis of myocardial perfusion single computed tomography (SPECT) improves reliability of MPS results in the British population. **Method:** 200 patients underwent MPS with stress-rest protocol

between February and September 2014. Semi-quantitative data was extracted from these scans (ejection fraction and gated analysis) and correlated against patient symptoms, demographics, CAD risk factors and clinical pre-test probability scoring. Additionally, patients were followed up for one year and outcomes of further investigations and management recorded. **Results:** There was a positive correlation between low pre-test probability scores and normal MPS results both qualitative and quantitative. Patients with normal MPS results were more likely to have normal results from further investigation and no adverse outcome after 1 year ($p < 0.001$). Patients with a high pre-test probability had worse MPS results ($p < 0.05$). Poor MPS results were more commonly found in patients of Asian origin ($p < 0.05$). **Conclusion:** Semi-quantitative MPS analysis is a good negative predictor for the diagnosis of CAD. The use of semi-quantitative analysis improves the diagnostic and prognostic value of MPS in the investigation of patients with chest pain. Patients of Asian origin demonstrated abnormal MPS results more frequently when compare to other ethnic subgroups.

P075

Performance of stress-induced ST changes during exercise stress test in relation to stress-induced myocardial ischemia as determined by myocardial perfusion single photon emission tomography: aspects on gender differences

S. Akil, B. Heden, O. Pahlm, M. Carlsson, H. Arheden, H. Engblom; Clinical Science, malmo, SWEDEN.

Background: Exercise stress test (EST) is usually the first method of choice when diagnosing stable ischemic heart disease. Myocardial perfusion SPECT (MPS) has been used as the reference standard for evaluation of amount as well as the presence of stress-induced ischemia, due to its high diagnostic accuracy. Studies relating EST findings to MPS findings, in a patient population with a specific focus on gender differences, are to a large extent lacking. **Aim:** To determine the diagnostic accuracy of stress-induced ST segment changes as a biomarker for stress-induced myocardial ischemia as assessed by myocardial perfusion single photon emission tomography (MPS), with a special focus on gender differences, in patients with suspected or established stable ischemic heart disease. **Methods:** 941 patients (474 females) with bicycle EST, performed in conjunction with MPS, were retrospectively included. An EST interpretation of stress-induced ST segment response alone and ST response in addition to other EST variables (blood pressure- and pulse response as well as exercise capacity) was done by an experienced physician and the findings were related to MPS findings. A significant decrease in regional perfusion on MPS during stress not seen at rest was considered to indicate stress-induced ischemia. **Results:** The positive predictive value (PPV) was 28% in the total patient population (13% females/42% males), when stress-induced ST segment changes were used to diagnose presence of stress-induced ischemia. The negative predictive value of a normal ST response was 90% in the total population (92% in females/86% in males). PPV increased when blood pressure- and pulse response as well as exercise capacity were added to the EST interpretation (PPV= 40% in total population; 23% females/54% males). **Conclusions:** There is a significant difference between females and males with regard to accuracy of ST segment changes in diagnosing stress-induced ischemia as determined by MPS. The accuracy is improved in both genders by considering other variables in the EST interpretation in addition to the ST response.

P076

Is stress-only supine and prone myocardial perfusion SPECT evaluation feasible? One-year follow-up study in patients with CZT gamma camera perfusion imaging

S. Piszczek, S. Osiecki, E. Witkowska-Patena, A. Mazurek, M. Dziuk; Military Institute of Medicine, Warsaw, POLAND.

Aim The goal of the study was to evaluate the utility of stress-only myocardial perfusion SPECT (MPS) performed with a dedicated cardiac CZT (Cadmium Zinc Telluride) gamma camera in discriminating patients with low or increased risk of adverse cardiac events during a one year follow-up period. **Methods** Supine and prone stress MPS imaging using CZT gamma camera was performed in 203 consecutive patients. Both exercise and pharmacological stress tests were carried out with 8-16 mCi ^{99m}Tc -sestamibi. The images were evaluated independently by 3 physicians experienced nuclear cardiology using a three-point scale: 1 - rest study unnecessary, 2 - rest study can be useful, 3 - rest study necessary. Patients were assessed after 12 months, using a questionnaire regarding their medical history during the follow-up period. **Results** The one-year follow-up was completed by 151/203 (74%) patients. 31/151 (21%) patients had a history of myocardial infarction and 46/151 (30%) patients underwent invasive coronary interventions prior to the study. In 125/151 (83%) patients none or mild perfusion abnormalities were observed (the evaluation results were: 1 point - 92 patients, 2 points - 33 patients). Of these, 18 patients (14%) underwent coronary angiography after MPS and 9 of them were subsequently referred for invasive coronary intervention (6 for percutaneous coronary intervention [PCI] and 3 for coronary artery bypass graft [CABG]). The remaining 9 (7%) patients received 1 (n=1) or 2 (n=8) points in course of evaluation. Severe perfusion abnormalities (more than 10% of left ventricle myocardium) were observed in 26/151 (17%) patients. In all of them a necessity of rest study was emphasized (all patients were given 3 points). Significantly higher number of invasive procedures was observed in this group. Coronary angiography was performed in 20 patients (77%), 13 of them (50%) were referred for invasive coronary interventions (7 patients for PCI and 6 patients for CABG). Another 2 patients were scheduled for a CABG procedure. No cardiac deaths were observed in the study group during follow-up. Rest imaging was performed in 82/151 (54%) patients according to a two day protocol. **Conclusion** The study showed that stress-only supine and prone MPS evaluation is feasible and safe in patients with suspected and diagnosed coronary artery disease. However, the minority of patients will require rest myocardial perfusion imaging.

P077

Comparison of hemodynamic effects and negative predictive value of normal adenosine gated myocardial perfusion scan with and without caffeine abstinence

N. Fatima¹, M. u. Zaman², A. Zaman³, U. Zaman³, R. Tahseen³; ¹Department of Nuclear Medicine, Dr Ziauddin Medical University, Karachi, PAKISTAN, ²Dept. of Radiology, Aga Khan University Hospital, Karachi, PAKISTAN, ³Dow University of Health Sciences, Karachi, PAKISTAN.

Background: For vasodilator stress myocardial perfusion imaging (MPI) at least 12 hour caffeine is recommended as it attenuates cardiovascular hyperemic response of adenosine and dipyridamole. However, many published conflicting results have shown no significant effect upon perfusion abnormalities in MPI performed without caffeine abstinence. The aim of this study was to compare the hemodynamic changes and negative predictive value (NPV) of normal MPIs with adenosine stress performed with and without caffeine abstinence. **Material and Methods:** This was a prospective study which accrued 50 patients from May 2013 till September 2013 and followed till November 2014. These patients had a normal adenosine-gated-MPI with ^{99m}Tc -MIBI after 12 hour caffeine abstinence (No-caffeine). Next day, all patients had a repeat adenosine stress within 60 minutes after ingestion of a cup of coffee (about 80 mg of caffeine) followed by no MPI in 30 patients due to concern about radiation dose (Prior-caffeine adenosine No-MPI; Group A). Twenty patients opted for a repeat MPI (Prior-caffeine adenosine-MPI; Group B). Adenosine induced hemodynamic response and NPV of normal MPI with No-caffeine and Prior-caffeine protocols were compared. **Results:** The

mean age of the study cohort was 57 ± 09 years with a male to female ratio of 76:24% and mean body mass index (BMI) of 26.915 ± 4.121 Kg/m². Prevalence of hypertension, diabetes, dyslipidemia and positive family history was 76%, 20%, 22% and 17% respectively. Comparison of Group A with Group B revealed no significant difference in demographic parameters, hemodynamic or ECG parameters or left ventricular function parameters during adenosine intervention with Prior-caffeine and No-caffeine protocols. During follow no fatal MI was reported but 06 non-fatal MIs based upon history of short hospitalization for chest pain but without biochemical or ECG criteria for infarction (03/30 in Group A and 03/20 Group B). Event free survival (EFS) for fatal MI was 100% for both groups while EFS for non-fatal MI was 90% for Group A and 85% for Group B (non-significant p values). Kaplan Meier's survival plot also depicted non-significant EFS for non-fatal MI. **Conclusion:** This study did not find any significant attenuation effect upon adenosine induced hemodynamic response and similar negative predictive value of a normal GMPI in patients with and without caffeine abstinence. We assume that better designed prospective studies are required to validate findings of our study and provide justification for revision of guidelines about caffeine abstinence. **Key words:** Adenosine; Caffeine; Gated MPI; Negative predictive value; hyperemia

P078

Comparison of patient radiation doses in diagnostic and therapeutic cardiac imaging techniques

S. Alramlawy¹, M. Khalil², I. Maamoun¹, A. M. Hamed³; ¹Department of Critical Care medicine, Cairo University Hospitals, Faculty of Medicine, Cairo, EGYPT, ²Department of Physics (Medical Biophysics), Faculty of Science, Helwan University, Cairo, EGYPT, ³Department of Nuclear Medicine and Oncology, Ain Shams University Hospitals, Cairo, EGYPT.

Myocardial perfusion single photon emission computed tomography (SPECT), angiographic techniques based on x-ray computed tomographic (CT), and interventional cardiac procedures are different sources of radiation exposures to patients with coronary artery disease. It is always a good safety practice to avoid patient radiation dose if the diagnostic test wouldn't provide incremental diagnostic information. Therefore, it is critically important to understand the relative radiation risk of those diagnostic and/or therapeutic modalities. **Methods:** A retrospective analysis was performed on 165 patients with known or suspected coronary artery disease. They were consisted of 112 patients who underwent a two-day protocol Tc-99m sestamibi SPECT scans, 30 patients underwent CT angiography (12 using 64 slice CT and 18 subjects using 256 slice CT scanners), and 30 underwent interventional procedures. The later consisted of 12 patients who were referred to coronary angiography and occlusion assessment while 18 undergone percutaneous coronary intervention. Dose assessment of the myocardial perfusion SPECT was obtained using the ICRP dose coefficient. Dose estimate from CT were reported as CTDIvol using the conversion factor 0.016 mSv/mGy.cm. Dose estimates from Interventional procedures were obtained from protocol performed for each patient. Dose estimates for SPECT were derived using 0.01 mSv/MBq as combined (stress-rest) dose conversion factor. **Results.** Effective dose estimates (CTDI) revealed from CT was on average 32.0 ± 10.5 mSv provided that the DLP was 1974.5 ± 661.8 mGy.cm using mAs of 1467.1 ± 385.5 and 120 kV tube voltage. Dose estimates from SPECT data was on average 13.5 ± 1.7 mSv. Coronary catheterization showed effective dose levels of 4917 ± 255 μ Gy.m² and 16064 ± 6123 μ Gy.m² in diagnostic and therapeutic procedures respectively. These measures resulted in effective dose of 10.8 ± 3.79 mSv and 35.3 ± 13.4 mSv respectively. The average time of fluoroscopy and cine-mode in diagnostic sessions was 4.2 ± 1.8 min and 10.7 ± 2.9 min respectively whereas in therapeutic ones were 17.3 ± 7.1 min and 32.7 ± 9.8 min respectively. Dose from 256 multi-slice CT was significantly higher than

those produced from 64 slice CT (mean of 38.2 mSv vs. 21.4 mSv respectively, $p < 0.0001$) **Conclusion:** Patient dose levels in cardiac imaging using radiological as well as nuclear techniques vary considerably with special concerns placed on therapeutic and multislice CT scanning procedures. A risk estimate based on an experimental models designed specifically for cardiac procedures would be the best approach to address the radiobiological dose-effect relationship. This will be potentially considered in future studies.

P079

Optimal Stress-rest Tracer Activity Ratio in Single-day Myocardial SPECT. A Phantom Simulation Study

C. Marcassa¹, M. Lecchi^{2,3}, C. Rodella⁴, R. Mattheoud⁵, R. Campini⁶, O. Zoccarato⁶; ¹S. Maugeri Fnd, IRCCS, Veruno, ITALY, ²Department of Health Sciences, University of Milan, Milan, ITALY, ³Nuclear Medicine Unit, San Paolo Hospital, Milan, Milan, ITALY, ⁴Spedali Civili Hospital, Brescia, ITALY, ⁵Departments of Medical Physics and Nuclear Medicine, University Hospital, Novara, ITALY, ⁶Nuclear Medicine Dept. S. Maugeri Fnd, IRCCS, Veruno, ITALY.

Background. In single-day stress-rest, myocardial perfusion SPECT studies a 1:3 tracer activity ratio is currently recommended, although 1:2 to 1:4 ratios have been also proposed. **Aim.** To define the optimal tracer activities ratio for a single-day stress-rest SPECT protocol. **Methods.** An anthropomorphic phantom of the chest, with inserts simulating lungs, liver, LV wall and LV chamber was used. The following acquisitions were obtained: 1) **stress-equivalent**, with a tracer concentration equivalent to that obtained with an in-vivo stress study, using a low-dose approach. A solid insert filled with "cold" water was employed to simulate a transmural ischemia in septal location. 2) **rest-equivalent**, simulating a 3h stress-rest time delay. The phantom's chambers were filled with tracer activities simulating the stress residual concentration corrected for a 3h physical and biological half-life (different for normal, ischemic and liver tissues) plus a rest-equivalent solution with a ratio to stress equal to 1:1, 1:1.5, 1:2, 1:2.5 and 1:3. Wide Beam Reconstruction (UltraSpect, TM) was used to reconstruct SPECT images; attenuation and scatter correction were also applied. The defect contrast was calculated on the mid-ventricular short-axis slice best displaying the defect. Polar maps were scored by 3 independent observers using a 17-segments model; the septal-lateral ratio was also calculated. **Results.** From the stress-equivalent images to 1:1, 1:1.5, 1:2, 1:2.5 and 1:3 stress-rest activity ratio, respectively, the defect contrast reduced from 59.6% to 12.6%, 12.5%, 6.6%, 7.8%, and 8.7%; the summed score reduced from 8 to 5, 2, 1, 1, and 1, respectively, and the septal-lateral ratio increased from 47% on stress-equivalent images to 73%, 76%, 82%, 83%, and 85%, respectively on rest-equivalent images. **Conclusions.** According to our simulation study, no clinically meaningful differences were observed from 1:2 to 1:3 stress-rest activity ratios. A 1:2 ratio is lower than that currently suggested by EANM Guidelines; this would imply a more favorable patients' and staff radiation exposure. Clinical studies are required to confirm our experimental results

P081

Breast tissue attenuation in myocardial perfusion SPECT CT Imaging: Cardiac phantom study

F. BOGA¹, F. CANBAZ²; ¹Ondokuz Mayıs University Hospital, Faculty of Physics, KURUPELIT / SAMSUN, TURKEY, ²Ondokuz Mayıs University Hospital, Faculty of Medicine, KURUPELIT / SAMSUN, TURKEY.

Aim: The aim of our study is to investigate the effect of breast tissue in different size and density on myocardial perfusion imaging(MPI) and to

evaluate the changes after CT attenuation correction (CTAC) using a modeled breast cardiac phantom. **Material and Method:** The breast models in our study were designed using 400, 700, 1000 and 1300 milliliters of balloons filled with water, oil and liquid soap to simulate the breast tissues of different size and density. The cardiac part of the phantom was filled with diluted water of 37 MBq (1 mCi) Tc-99m pertechnetate activity. The breast models were attached to cardiac phantom respectively. Using a double detector hybrid SPECT/CT system, imaging was performed with the parameters used in routine clinical settings of MPI (64x64 matrix; 20 second/ projection, total of 32 projections). We used Cedars Sinai QPS perfusion quantitative software (V.2009) in processing and data collection. We analyzed the images, semi-quantitatively, using 17 segment model through polar maps. The analyzing of data belonging to standard and CT attenuation correction results were carried out via SPSS (V22.0) statistical program by using Wilcoxon, Mann-Whitney U, Kruskal-wallis tests on the base of myocardial segment, wall and level. **Results:** After CT attenuation correction, there were no significant differences (Δ) between the groups ($p > 0,05$) regarding the density and size but among the left ventricular walls, but the highest mean difference values between standard and CTAC images were detected on septum. The mean differences for myocardial septum wall were: $\Delta = 18,2 \pm 10,0$; $20,4 \pm 9,6$; $18,2 \pm 8,2$ for oil, water and liquid soap groups, respectively; and $\Delta = 19,1 \pm 10,8$, $19,0 \pm 9,5$, $19,6 \pm 9,0$ and $17,8 \pm 8$ were obtained for 400, 700, 1000 and 1300 volume groups, respectively. A heterogenic changing was seen on lateral wall $\{\Delta = [(-0,7 \pm 11,1) - (6,9 \pm 14,4)]\}$, after CTAC. **Conclusion:** The results in our study support that a considerable improvement was seen on left ventricle septum after CT attenuation correction without depending on the size and density of breasts; but the physicians should be aware that, although without SPECT/CT misregistration, new perfusion defects can occur after CTAC, especially on the lateral myocardial wall.

P082

Value of Tc-99m MIBI myocardial perfusion scintigraphy in predicting non-critical coronary stenosis

B. Dirlik Serim¹, M. Yilmaztepe², E. Yigit³, Z. Yigit⁴, G. Durmus Altun⁵; ¹Istanbul University, Cardiology Institute, Nuclear Medicine Department, Istanbul, TURKEY, ²Trakya University, Medical Faculty, Cardiology Department, Edirne, TURKEY, ³Umraniye Train and Research Hospital, Internal Medicine Department, Istanbul, TURKEY, ⁴Istanbul University, Cardiology Institute, Cardiology Department, Istanbul, TURKEY, ⁵Trakya University, Medical Faculty, Nuclear Medicine Department, Edirne, TURKEY.

Aim: Coronary angiography of most of patients with unstable angina pectoris showed that one or more critical stenosis are found in the coronary arteries. However, studies have revealed some non-critical stenosis on angiography in this patient group. Some evidences are available about the mechanisms that cause ischemia of the resting; these are temporary thrombosis settlement on unstable non-critical stenotic plaque or coronary vasoconstriction. The aim of this study is to show the value of Tc99m MIBI myocardial perfusion scintigraphy (MPS) in predicting non-critical coronary stenosis. **Material and method:** Data of the patients referred to our department in order to determine the presence and localization of ischemia were examined. The images and reports of patients were analyzed retrospectively. The reports of lesions that seemed as viable tissue or infarct region were excluded. Ischemia quantitation analysis was made by visually with Cedars-Sinai polar map. Angiography results of the patients who were reported only as ischemia, achieved from hospital automation system. One hundred sixty nine patients with non-critical stenotic lesions were included in this study. **Results:** The study included 64 women, 105 men a total of 169 patients; 50 of them have normal MPS. Age was 60.4 ± 10 years. The average number of 119 patients with defects in MPS was 5.03 ± 3.7 and MPS was performed 37 ± 44 days after

angiography. The number non-critical stenosis was 29 ± 18 as a result of angiography. The number of non-critical lesions according to vessels were; 45 of them was the only LAD stenosis, 8 of them was the only CX and 9 of them were the only RCA stenosis; 14 patients had on both LAD and Cx and 5 patients had on both RCA and Cx; 11 patients had on both LAD and RCA, 8 patients had on all LAD, Cx and RCA and in addition 3 patient had on LMCA. Stenosis was $43 \pm 14\%$ at LAD, $41 \pm 12\%$ at Cx and $44 \pm 15\%$ at RCA. The diagnostic value of MPS predicting non-critical coronary stenosis were calculated as 80.8%; sensitivity and specificity were calculated as 90.9% and 78.1%. According to the calculations positive predictive value was 87.7% and negative predictive value was 83.3%. **Conclusion:** Predicting non critical stenosis with MPS may provide a clearer way to put forward the risk group. Active and effective intervention can contribute to the damage-free nad disease-free survival. Studies of large series of patients will highlight the value of MPS predicting non-critical stenotic patient group.

P-07 – Sunday, October 16, 2016, 16:00 - 16:30, Poster Exhibition Hall
Cardiovascular System: Sympathetic Innervation

P083

Need for standardization of ROI definition in planar cardiac I-123-MIBG imaging

C. Schmitt^{1,2}, C. Jungen^{1,3}, K. Okuda^{4,5}, Y. Kobayashi^{1,2}, A. Helberg^{1,2}, J. Mester^{1,2}, C. Meyer^{1,3}, K. Nakajima^{4,6}; ¹UKE, Hamburg, GERMANY, ²Department for Interventional and Diagnostic Radiology and Nuclear Medicine, Hamburg, GERMANY, ³Department of Cardiology - Electrophysiology, University Heart Centre, University Medical Centre Hamburg-Eppendorf, Germany; DZHK (German Centre for Cardiovascular Research), partner site Hamburg/Kiel/Lübeck, Germany, Hamburg, GERMANY, ⁴Kanazawa University, Kanazawa, JAPAN, ⁵Department of Physics, Kanazawa Medical University, Kanazawa, JAPAN, ⁶Department of Nuclear Medicine, Kanazawa University Hospital, Kanazawa, GERMANY.

Background: Iodine-123-metaiodobenzylguanidine (MIBG) imaging has been established for risk assessment in patients with chronic heart failure or neurodegenerative diseases. Quantification of cardiac MIBG uptake using the heart-to-mediastinum ratio (HMR) is essential for the identification of pathologic loss of cardiac sympathetic nerve fibers. However, HMR is influenced by several technical factors, including the definition of region of interest (ROI). We aimed to investigate the comparability of different methods of ROI definition, to determine the inherent confidence interval of each method and to discuss the practical relevance of methodological uncertainties. **Methods and Results:** We retrospectively analyzed 32 planar images of 20 consecutive patients (63.5 years median; 2 females, 18 males) who were referred for MIBG imaging between January 2014 and October 2015 with cardiac arrhythmias (n=12) or with suspected neurodegenerative disease (n=8). Following intravenous application of 185 MBq (n=10) or 370 MBq (n=10) MIBG, patients underwent planar imaging at 15 minutes and 4 hours (n=12) or at 4 hours (n=8) only. The results of three different methods of ROI definition (manually during clinical routine (CLI), manually after simple standardization (STA) and semi-automated using a dedicated software (SAM)) were compared using Bland-Altman plots. Pairwise comparisons of HMR demonstrated significant mean differences (CLI vs STA 0.14, CLI vs SAM -0.22 and STA vs SAM -0.08, $p < 0.05$, two sided t-test). Inter-method standard deviations (SD) were 0.17, 0.19 and 0.08 respectively). SDs from the comparison of CLI with the other methods were significantly higher than the SD from STA vs. SAM (χ^2 test, $p < 0.05$). Intra-observer and inter-observer variabilities were

0.01 and -0.07 for STA and 0.01 and 0.01 for SAM, respectively. Considering a HMR of 1.60 as the lower limit of normal, and $\pm 1.96 \times \text{SD}$ as the width of the 95% confidence interval, 13 of 32 (41%) for method STA and 5 of 32 (16%) for method SAM of the measured HMR values in our study could not be classified to normal or pathologic cardiac sympathetic innervation. **Conclusion:** Different methods of ROI definition result in different widths of a zone around the normal limit, where definitive rendering of the results to normal or pathologic innervation is not possible (gray zone). As MIBG imaging analysis and the calculation of HMR is crucial for risk classification of patients with chronic heart failure or neurodegenerative diseases, internal validation of evaluation methods, e.g. by using standardized clinical data sets, is strongly recommended.

P084

SPECT myocardial perfusion and sympathetic innervation in patients with hypertrophic cardiomyopathy

A. Ansheles, V. Sergienko; Russian Cardiology Research and Production Complex, Moscow, RUSSIAN FEDERATION.

Objective: to determine the characteristics of myocardial perfusion and sympathetic activity (SA) assessed by single-photon emission computed tomography (SPECT) in patients with hypertrophic cardiomyopathy (HCM). **Material and Methods:** The study included 36 patients with a confirmed diagnosis of HCM. All patients underwent clinical status assessment, Holter ECG monitoring, rest echocardiography. All patients, as well as a group of healthy volunteers (n=20) underwent myocardial perfusion SPECT with ^{99m}Tc -MIBI at rest and after bicycle exercise test, and myocardial neurotropic SPECT with ^{123}I -MIBG, performed in 15 min (early phase) and 4 hours (delayed phase) after MIBG administration. Perfusion abnormalities were evaluated using standard quantitative parameters: Summed Stress Score (SSS) and Summed Difference Score (transient ischemia index, SDS). Global SA abnormalities were assessed with delayed heart/mediastinum ratio (H/M_d) and MIBG Washout Rate in 4 hours (WR). Regional SA abnormalities were assessed using early Summed MIBG Score (SMS_e). **Results:** All myocardial SPECT parameters, both perfusion and neurotropic, significantly differed in HCM patients compared to the control group (p<0.001). According to perfusion SPECT, reliable transient myocardial ischemia (SDS>4) in the main group was detected in 33% of cases, while it was diffuse and had no connection with certain regions of coronary arteries. The volume of regional innervation defects (SMS_e) in HCM patients was significantly higher than the total volume of perfusion defects (SSS), amounting to 15 (11-17) and 9 (8-11) points, respectively (p<0.001). SMS_e and SSS had a positive correlation (r=0.52, p=0.002), but perfusion and innervation defects did not match in localization clearly. The severity of LV hypertrophy was a factor of more severe perfusion and innervation defects: we detected direct correlation between posterior LV wall thickness and LV cavity pressure gradient, measured by echocardiography (r=0.31, p=0.07), between LV mass index and SSS (r=0.51, p<0.005), WR (r=0.51, p=0.002), SMS_e (r=0.34, p=0.03). No influence of LV outflow tract obstruction on parameters of Holter ECG, stress-test, perfusion and neurotropic myocardial SPECT was shown. SMS_e was higher in HCM patients with arrhythmias (p=0.046), and lower in HCM patients with angina and cardialgias (p=0.04). More severe perfusion and innervation abnormalities were detected in patients with nondiagnostic exercise test result (p<0.05). **Conclusion:** Combination of myocardial neurotropic and perfusion SPECT has a certain diagnostic value in patients with HCM, since sympathetic innervation abnormalities is one of the earliest marker of myocardial damage.

P085

Cardiac SPECT Imaging with Iodine-123 MIBG in Heart Failure Patients Qualified for an Implantable Cardioverter Defibrillator

A. Teresinska, O. Wozniak, A. Maciag, J. Wnuk, A. Czerwec, J. Jezierski, M. Madej, K. Biernacka; Institute of Cardiology, Warsaw, POLAND.

Introduction: The standard method of assessment of cardiac adrenergic nervous system with I-123 MIBG is semiquantification of MIBG uptake by calculating a heart-to-mediastinum ratio (H/R) in the planar anterior view. **Purpose:** The aim of this study was to determine the value of MIBG SPECT imaging in pts with post-infarction heart failure (IHf). **Methods:** We present a part of a single-center prospective study comprising consecutive patients with IHf qualified (on the basis of ESC Guidelines 2012) for undergoing implantation of ICD in the prevention of sudden cardiac death, i.e. pts with LVEF≤35%, NYHA class II-III, >40 d after infarction. Another inclusion criteria: age>50y, >3 mo from revascularization, signed informed consent. The 10-min-long planar studies were performed 15min and 3,5h after MIBG injection, and were followed by 30-min-long SPECT studies with dual-detector system and LEHR collimators. SPECT parameters: acquisition - 68 projections over 180°, 50 sec/projection, matrix 64x64; reconstruction - FBP with Butterworth filter, no scatter/attenuation correction. The image variables used in this analysis: late planar H/M and late SPECT summarized defect score (SDS; assessment in 17-segment model of the LV in a 5-step scale: 0-normal uptake, 4-lack of uptake). **Results:** Seventy-seven subjects were included (67 M): age 67±9y, weight 80±14kg, NYHA class 2.2±0.4, LVEF 26±9%, 17 (22%) of pts with diabetes mellitus; administered activity 9.3±1.1mCi. In 21/77 pts (27%, <18-38>) the assessment of SPECT studies was impossible because of very high lung uptake non-separating from LV walls. H/M values in this group were: 1.11-1.84 and the average (1.50±0.21) was lower than in the group of the others (p=0.035). In 56 pts submitted to planar and SPECT evaluation: H/M = 1.25-2.11 (av. 1.62±0.20), SDS = 8-52 (33±10), moderate correlation between H/M and SDS (-0,49). In 22 of those pts (22/77, i.e. 29% of all the pts), the assessment of SPECT studies was equivocal because of extracardiac uptake interfering with uptake in LV walls. Altogether, in 43/77 pts (56%, <45-67>), the SPECT quality was unacceptable or low. **Conclusions:** In pts with post-infarction HF qualified for implantation of ICD, with LVEF≤35%, NYHA class II-III and age>50y, the good-quality SPECT studies were achieved only in approximately half of cases. In relation to planar MIBG scintigraphy, SPECT can have additional prognostic value for improving selection of patients for ICD, but its usability is limited by frequent non-acceptable or borderline quality caused by high extracardiac MIBG uptake interfering with cardiac uptake.

P086

Cardiac MIBG scintigraphy in predicting the effectiveness of interventional treatment of atrial fibrillation

Y. Saushkina¹, V. Saushkin¹, K. Zavodovskiy^{1,2}, I. Kisteneva¹, R. Batalov¹, I. Kostina^{1,3}, G. Romanov^{1,3,4}, Y. Lishmanov^{1,2}, S. Popov¹, R. Karpov¹, D. Ryzhkova³, L. Maslov¹; ¹RI Cardiology, Tomsk, RUSSIAN FEDERATION, ²National Research Tomsk Polytechnic University, Tomsk, RUSSIAN FEDERATION, ³Federal Almazov North-West Medical Research Centre, St. Petersburg, RUSSIAN FEDERATION, ⁴S.M. Kirov Military Medical Academy, St. Petersburg, RUSSIAN FEDERATION.

Purpose. The aim of the study was to identify scintigraphic predictors of the effectiveness of interventional treatment of atrial fibrillation (AF). **Methods and Materials.** In this study were enrolled 35 patients with essential hypertension (EH) (the duration of EH 5-20 years): 17 patients with persistent AF and 18 patients with long-standing persistent AF. All

patients underwent single-photon emission computer tomography (SPECT) with 123I-metaiodobenzilguanidine (123I-MIBG) to evaluate cardiac sympathetic nervous system (SNS) activity before radiofrequency catheter ablation (RFCA). Evaluation of the effectiveness of RFCA was carried out after 12 months by means of twenty-four hour Holter monitoring. Results. Patients of both groups were divided into subgroups depending on the presence of recurrence of arrhythmia in a year after interventional treatment. In the group of patients with persistent AF, the arrhythmia recurrence 12 months after RFCA were detected in 7 people. In the group of patients with long-standing persistent AF, the arrhythmia recurrence 12 months after RFCA were detected in 8 people. By ROC analysis identified the main scintigraphic predictors of the effectiveness of interventional treatment of AF. Were investigated the preoperative scintigraphic characteristics of cardiac sympathetic activity for which subgroups with and without AF recurrence had significant differences. Optimal thresholds for predicting the effectiveness of RFCA in patients with persistent AF was $\geq 1,7$ for delayed heart-to-mediastinum ratios (HMR) (0,991 area under the ROC curve; sensitivity 100%, specificity 71%). Optimal thresholds for predicting the effectiveness of RFCA in patients with long-standing persistent AF were $\geq 1,69$ for early HMR (0,849 area under the ROC curve; sensitivity 100%, specificity 62%); $\geq 1,66$ for delayed HMR (0,938 area under the ROC curve; sensitivity 94%, specificity 23%). Conclusion. Thus, cardiac MIBG scintigraphy can be used to predict high risk of recurrence of atrial fibrillation after radiofrequency catheter ablation. The study was supported by a grant from the Russian Science Foundation No 15-15-10016.

P087

Cardiac MIBG scintigraphy in assessing the effectiveness of radiofrequency cardiac denervation

Y. Saushkina¹, V. Evtushenko¹, K. Smishlyaev¹, V. Saushkin¹, K. Zavadovskiy^{1,2}, I. Kostina^{1,3}, G. Romanov^{1,3,4}, Y. Lishmanov^{1,2}, A. Evtushenko¹, R. Karpov¹, L. Maslov¹, D. Ryzhkova³; ¹RI Cardiology, Tomsk, RUSSIAN FEDERATION, ²National Research Tomsk Polytechnic University, Tomsk, RUSSIAN FEDERATION, ³Federal Almazov North-West Medical Research Centre, St. Petersburg, RUSSIAN FEDERATION, ⁴S.M. Kirov Military Medical Academy, St. Petersburg, RUSSIAN FEDERATION.

Purpose. The aim of the study was to evaluate the role of radionuclide imaging with 123I-metaiodobenzilguanidine (123I-MIBG) in assessing of the cardiac radiofrequency denervation effectiveness. **Methods and Materials.** In this study were enrolled 32 patients with mitral valve (MV) disease: 21 patients with long-standing persistent atrial fibrillation (AF), who was undergone MV surgery and the «Maze» procedure (Maze+ group) and 11 patients with sinus rhythm (SR) and with MV surgery without the «Maze» procedure (Maze- group). All patients underwent cardiac 123I-MIBG imaging prior and 10 days after surgery. In addition, we determined the levels of norepinephrine, metanephrine, normetanephrine in plasma, obtained intraoperatively from the coronary sinus (CS) and the ascending aorta (Ao) before and after the main stage of the surgery. All patients were intraoperatively intake of histological material (atrial appendage) to determine the distribution density of nerve endings in the myocardium. **Results.** In patients with AF the early and delayed heart-to-mediastinum ratios (HMR) prior surgery were significantly lower compared to patients with SR ($p < 0.01$). The washout rate (WR) of 123I-MIBG prior surgery in patients with AF was greater compared to patients with SR ($p < 0.01$). The HMR after surgery was significantly lower vs baseline in both groups (early HMR: $1,78 \pm 0,17$ vs $1,56 \pm 0,19$; $p < 0,01$ and $2,12 \pm 0,25$ vs $1,79 \pm 0,18$; $p < 0,01$; delayed HMR: $1,69 \pm 0,21$ vs $1,47 \pm 0,19$; $p < 0,01$ and $2,0 \pm 0,22$ vs $1,74 \pm 0,19$; $p < 0,01$). The WR after surgery was significantly increased vs baseline in both groups ($27,3\% \pm 14,03\%$ vs $35,0\% \pm 14,18\%$; $p < 0,01$ and $17,1\% \pm 13,7\%$ vs $31\% \pm 16,15\%$; $p < 0,01$). After surgery sympathetic activity defect was increased only in the Maze+ group ($12,7\% \pm 7,3\%$ and $25,4\% \pm 8,5\%$; $p < 0,01$). The correlations between

the cardiac 123I-MIBG parameters and the levels of norepinephrine, metanephrine, normetanephrine in plasma were examined. Cardiac 123I-MIBG parameters had significant correlations with transcardiac gradients (CS-Ao) of the norepinephrine and normetanephrine. Cardiac 123I-MIBG parameters had significant correlations with the distribution density of nerve endings in the myocardium. **Conclusions.** Results of this study indicated that the more sympathetic innervation abnormality prior surgery was observed in patients with AF. In patients who had undergone MV surgery without the «Maze» procedure, there were no significant changes in sympathetic activity defect in the early stage. The MV surgery itself doesn't influence the regional cardiac sympathetic activity. The evaluation of the cardiac nervous activity using 123I-MIBG scintigraphy may be a promising tool to determine of effectiveness of the cardiac radiofrequency denervation. The study was supported by a grant from the Russian Science Foundation No 15-15-10016.

P088

Myocardial scintigraphy with 123I MIBG in a patient with Parkinson's

G. Sadeck¹, N. Lavatori¹, I. Palazzo¹, M. Veras¹, M. Sabra¹, F. Correa¹, A. Cotrado¹, W. K. Aguiar¹, W. Ker¹, C. Andre², C. Tinoco¹; ¹Hospital Pró-Cardíaco, Rio de Janeiro, BRAZIL, ²Sinapse Reabilitação, Rio de Janeiro, BRAZIL.

The meta-iodo-benzyl-guanidine (MIBG) is an analog of guanethidine, and a false neurotransmitter that is captured by adrenergic neurons and resembles norepinephrine. Myocardial perfusion imaging with iodine-MIBG is a scintigraphic examination able to evaluate the cardiac sympathetic nervous system in physiological and pathophysiological conditions. The indications for the exam range from ischemic heart disease to congestive heart failure (CHF), diabetes mellitus (DM) and any other medical condition that culminates with cardiac denervation, such as Parkinson's disease. **Case report:** MR, 78, male, caucasian. Patient with vertigo when diagnosed with Parkinson's in 2011. The Patient underwent clinical treatment without remission, and his clinical picture of atypical parkinsonism suggested alternative mechanisms to nigrostriatal degeneration. The past medical history includes arterial hypertension, previous smoking, COPD. Medications in use included L-DOPA and others. The patient had a previous brain scintigraphy demonstrating decreased presynaptic dopamine transport in the projection of the basal ganglia, more prominent in the right side. The scintigraphic images with I-123 MIBG showed functional impairment of the adrenergic nervous system of the heart with increased sympathetic tone. The patient presented a cardiac washout of 91.70% ($VN \leq 27\%$), and early heart / mediastinum ratio of 1.19 (normal value ≥ 1.80) and late heart / mediastinum ratio of 1.01 (normal value ≥ 1.80). **Conclusion:** Parkinson's disease can cause not only a motor disorder, but also cardiovascular dysautonomia. Thus, based on this case, we conclude that the worsening in the clinical condition and in the evolution of PD is directly related to the level of cardiac denervation. In this context, the heart scintigraphic study is of great value in monitoring these patients

P-08 – Sunday, October 16, 2016, 16:00 - 16:30, Poster Exhibition Hall
Cardiovascular System: Vascular Inflammation

P089

Comparison of FDG PET and aortic CT scan for the detection of aortitis in giant cell arteritis

M. Soussan¹, M. Hommada¹, S. Abad², R. Dhote², C. Larroche², O. Fain³, A. Mekinian³; ¹APHP, Avicenne Hospital, department of Nuclear Medicine, Bobigny, FRANCE, ²APHP, Avicenne Hospital, department of Internal Medicine, Bobigny, FRANCE, ³APHP, Saint-Antoine Hospital, department of Internal Medicine, Paris, FRANCE.

Objectives: Positron emission tomography (PET) scan is described as a very sensitive tool to detect aortitis in giant cell arteritis (GCA). Unfortunately, there is no consensus regarding the preferred scoring method and studies evaluating FDG-PET do not systematically compare the results with aortic CT scan, that is currently the reference for aortitis assessment. Visual vascular uptake higher than liver uptake might be a more reliable criterion than vascular wall SUV_{max}, and resulted in high specificity in recent studies. The objectives are to assess the detection rate of aortitis in GCA patients with visual criteria and to compare the findings with aortic CT scan. **Methods:** Forty-six GCA patients (ACR criteria > 3, positive temporal artery biopsy in 28/46) who underwent FDG PET were included (initial staging 32/46, relapse 9/46, remission 5/46). Aortic CT scan was performed in 27/46, in an interval < 1 month with PET and without interim start of therapy. Criteria for LV inflammation were vascular uptake > liver uptake for PET, and aortic thickening > 3 mm for CT. The agreement between PET and CT was evaluated by kappa coefficient. **Results:** Aortitis was detected in 17/46 (38%) with PET, and in 11/27 (42%) with CT. Agreement was very good between PET and CT for the diagnosis of aortitis (kappa = 0.85). Vascular segment-based analysis showed excellent agreement for thoracic aorta (k=0.90), and abdominal aorta (k=0.91), but agreement was poor for supra-aortic vessels (k=0.35). PET was positive in 6/8 patients with biological relapse, and negative in 5/5 patients in remission. **Conclusions:** Frequency of aortitis in GCA patients with PET is around 40%, a figure closed to those found in the literature with CT scan. Agreement between PET and CT is very good for aortic involvement, but not for supra-aortic vessels. PET imaging is suitable for assessing GCA relapse.

P090

Role of FDG PET/CT imaging in the measurements of inflammatory activity of atherosclerotic plaques in carotid artery

A. sinha, V. Sharma, S. kapur, S. Pillai; National University Hospital, singapore, SINGAPORE.

OBJECTIVE: Symptomatic carotid stenosis is associated with a 3-fold risk of early stroke recurrence compared to other stroke subtypes. FDG-PET/CT is exquisitely sensitive for detecting macrophage activity, an important source of cellular inflammation in vessel walls. More recently, we and others have shown that FDG-PET/CT enables highly precise, novel measurements of inflammatory activity of activity of atherosclerotic plaques in large and medium-sized arteries. Current carotid imaging techniques rely on estimating plaque-related lumen narrowing but do not evaluate intra-plaque inflammation, a key mediator of plaque rupture and thromboembolism. Using combined (18) F-fluorodeoxyglucose positron-emission tomography (FDG-PET)/computed tomography, we investigated the relation between inflammation-related FDG uptake and stroke recurrence in small group of the patients. **METHODS:** Consecutive patients with a recent stroke, symptomatic (since last one month) and ipsilateral carotid stenosis ($\geq 50\%$) were included in this study. FDG uptake was quantified as mean standardized uptake values (SUVs). Patients were followed prospectively for stroke recurrence. **RESULTS:** Forty one patients were included. Three patients had stroke recurrence within 90 days. FDG uptake in ipsilateral carotid plaque was greater in patients with early recurrent stroke (mean SUV, 2.5; standard deviation [SD], 0.44 vs 1.58; SD, 0.32, $p = 0.02$). On life-table analysis, 90-day recurrence rates with mean SUV greater than a 2.14 threshold were 80% (95% confidence interval [CI], 41.8-99.2) versus 22.9% (95% CI, 12.3-40.3) with SUV ≤ 2.14 (log-rank, $p < 0.0001$). In a Cox regression model including age and degree of stenosis (50-69% or $\geq 70\%$), mean plaque FDG uptake was the only independent predictor of stroke recurrence (adjusted hazard ratio, 6.1; 95% CI, 1.3-28.8; $p = 0.02$). **CONCLUSION:** Inflammation in a previously stable carotid plaque is an important event that leads to local

thrombosis and cerebral embolization. This phenomenon can be reliable imaged with F-18 FDG PET for better risk stratification and therapeutic strategizing in carotid stenosis.

P092

Comparison of tissue-to-background-ratio in major arterial vessels between 18F-fluorodeoxyglucose and 18F-fluoromethylcholine PET-CT - preliminary results of a pilot study

J. Jamsek, M. Grmek, S. Hawlina, L. Lezaic; Klinični center Ljubljana, LJUBLJANA, SLOVENIA.

AIM. During the last decade, numerous studies have evaluated ^{18}F -FDG as a potential molecular marker for vulnerable atherosclerotic plaque identification using PET-CT. However, little attention was directed to other molecular markers of atherosclerotic inflammation, such as ^{18}F -fluoromethylcholine (^{18}F -FCH), which was shown in preclinical studies to accurately depict inflammation of the arterial wall. The aim of our pilot study was to directly compare ^{18}F -FDG and ^{18}F -FCH mean maximum tissue-to-background ratio (mean TBR_{max}) in major arterial vessels to assess the suitability of ^{18}F -FCH as a molecular marker for vulnerable atherosclerotic plaque identification - preliminary results are presented. **MATERIALS AND METHODS.** We retrospectively evaluated ^{18}F -FDG and ^{18}F -FCH PET-CT examinations of 5 male patients (aged 76 years on average) who had had examinations with both PET tracers within one week, as part of a prostate cancer clinical trial. Imaging with both tracers was performed on a Siemens Biograph™ mCT PET-CT scanner: image acquisition started 60 min after administration of either ^{18}F -FDG (4 MBq/kg) or ^{18}F -FCH (2.5 MBq/kg). Following the EANM recommendations on PET imaging of atherosclerosis we measured mean TBR_{max} in the following great arterial vessels: ascending aorta (AscA), left and right common carotid arteries (LCC and RCC), thoracic aorta (TA), abdominal aorta (AA) and left and right common iliac arteries (LCI and RCI). We then compared the calculated mean TBR_{max} of the same anatomical segments using both tracers by performing a paired, two-tailed Student t -test ($\alpha = 0.05$). **RESULTS.** Arterial vessel mean TBR_{max} for ^{18}F -FDG and ^{18}F -FCH in the AscA was 1.50 and 1.88 respectively ($p = 0.013$), in the LCC 1.57 and 1.76 ($p = 0.173$), in the RCC 1.52 and 1.46 ($p = 0.849$), in the TA 1.50 and 2.13 ($p = 0.063$), in the AA 1.68 and 2.15 ($p = 0.234$), in the LCI 1.44 and 1.67 ($p = 0.226$) and in the RCI 1.64 and 1.51 ($p = 0.702$). **CONCLUSION.** ^{18}F -FCH appears to be a viable alternative to ^{18}F -FDG in molecular imaging of arterial vessels, yielding comparable information on metabolic activity of the arterial wall in most anatomical vascular segments. For a more comprehensive analysis additional data as well as prospective studies comparing ^{18}F -FCH and ^{18}F -FDG are needed.

P093

Contribution Of Cardiac Scintigraphy With $^{99\text{m}}\text{Tc}$ -DPD In The Differential Diagnostic Of Cardiac Amyloidosis Subtypes; Anatomical-Pathological Correlation

A. Cobo Rodríguez, J. Gomez Hidalgo, J. Villanueva Curto, A. Sainz Esteban, M. Gonzalez Selma, M. Ruiz Gomez, M. Alonso Rodriguez, C. Gamazo Laherran, R. Olmos Garcia; Hospital Clinico Universitario de Valladolid, Valladolid, SPAIN.

OBJECTIVE: To assess the contribution of cardiac scintigraphy with $^{99\text{m}}\text{Tc}$ -3, 3-diphosphono-1,2-propanodicarboxylic acid ($^{99\text{m}}\text{Tc}$ -DPD) in the diagnosis of different subtypes of cardiac amyloidosis (CA).

METHODS: We performed a prospective study in 11 patients (9 males and 2 females). The mean age was 73.6 (SD \pm 8.1). Patients were specifically referred to our department for the performing of cardiac scintigraphy with ^{99m}Tc -DPD, in order to differentiate between monoclonal immunoglobulin light chain amyloidosis (LC-CA) and transthyretin-related cardiac amyloidosis (ATTR-CA). Scintigraphy results were correlated with a biopsy (one of the patients refused the procedure). All patients underwent transesophageal echocardiography (TE) and 9 of them also cardiac MRI. Both TE and cardiac MRI were suggestive of infiltrative amyloid heart disease in all patients. We analysed each scan with a visual score from 0 to 3 to determine the existence and intensity of the radiotracer uptake in heart tissue. The lack of uptake was assessed as 0, less than the bone (adjacent rib) was assessed as 1, equal to bone as 2 and greater than the bone as 3. **RESULTS:** 5 out of 6 patients who showed a pattern 3 (myocardial uptake greater than bone) presented anti-transthyretin antibodies and / or positive immunohistochemistry for TTR-L. Patients with pattern 0-1 presented histological positivity for specific staining techniques (Congo Red and T-Thioflavine) but negative staining for anti-transthyretin antibodies and TTR immunohistochemistry. These findings corresponded to amyloid but not to the transthyretin-related one. **CONCLUSION:** Cardiac scintigraphy with ^{99m}Tc -DPD is a useful tool in the differential diagnosis between LC-CA and ATTR: scintigraphy with intense uptake of ^{99m}Tc -DPD would be indicative of ATTR, while a scan with no uptake rule it out.

P094

Application of the hybrid imaging methods in the diagnostics of patients suspicious for vascular graft infection

I. Kostadinova, A. Demirev; Medical University, Sofia, BULGARIA.

Although vascular graft infection is a rare complication, occurring in 2-6% of patients, it has a high rate of morbidity and mortality. The aim of the study was to evaluate the diagnostic value of “in vitro” labelled leucocytes, using SPECT-CT, in patients suspicious of vascular graft infection, determine the activity of the inflammatory process and compare obtained data with our first results from PET-CT application. We examined 25 patients (Pts), of whom 16 had aorto - bifemoral, 2-femoro - femoral, 2-axillo - femoral and 5-ileo - femoral bypass. Fourteen of the patients were still under the antibiotic therapy. We used labeled leucocytes with ^{99m}Tc -HMPAO and applied SPECT-CT. Results of all patients were verified microbiologically, surgically or by a follow-up. An index of accumulation (IA) was used for an evaluation of the activity of the infection process. IA was calculated as the activity of the suspected area divided by the activity of the contralateral area. Infection was ruled out when IA was below 1.1 (in 5 Pts), low grade activity was considered at IA of 1.1-1.3 (in 12 Pts) and active infection at IA above 1.3 (in 8 Pts). Use of CT, allowed for exact localization of the infectious process, differentiating infection along the vascular graft (in 13Pts) from infection in adjacent soft tissues (in 7 Pts). In 7/25 Pts, additional PET-CT with ^{18}F -FDG was performed. The sensitivity with labeled leucocytes was 84.2%, specificity of 83.3% and accuracy of 83.9%. According to results from PET-CT examinations, no difference in the final diagnosis was found, in comparison between the two imaging modalities, with the exception of 4 out of 7 patients, in whom a larger area of the grafts had FDG uptake. The infected segments had SUVmax 6,3 and in those without infection- 3.45. We consider that the higher FDG uptake in the last was a result of a chronic inflammation or reaction to the synthetic graft material, but more studies are needed to confirm these hypotheses. For 30% of the patients, both modalities have contributed important additional information, which changed the therapy. In summary, we suggest that “in vitro” labeled leucocytes, using SPECT-CT is a more specific, with a possibility for the measurement of the activity of infection, but time consuming modality. Therefore in heavily ill patients or in those without leukocytosis, PET-CT is preferable.

P-09 – Monday, October 17, 2016, 16:00 - 16:30, Poster Exhibition Hall
Conventional & Specialised Nuclear Medicine: Endocrinology

P095

Sensitivity and Specificity of Parathyroid SPECT/CT in Primary Hyperparathyroidism Detection in Relation to Parathormone and Calcium Levels

M. Trofimiuk-Müldner¹, A. Skalniak², L. Kluczyński³, A. Zapendowska⁴, A. Budek⁴, M. Buziak-Bereza¹, A. Sowa-Staszczak¹, A. Hubalewska-Dydejczyk²; ¹Chair and Department of Endocrinology, Nuclear Medicine Unit, Jagiellonian University Medical College, Krakow, POLAND, ²Chair and Department of Endocrinology, Jagiellonian University Medical College, Krakow, POLAND, ³Department of Endocrinology, University Hospital in Krakow, Krakow, POLAND, ⁴Department of Endocrinology, Nuclear Medicine Unit, University Hospital in Krakow, Krakow, POLAND.

Parathyroid scintigraphy and neck ultrasound are the main methods of primary hyperparathyroidism (PHP) imaging. The observed increasing frequencies of asymptomatic or oligosymptomatic PHP cases may increase the false negative imaging results rate. The aim of the study was to determine the level of PTH and calcium at which an enlarged parathyroid gland can be detected by parathyroid SPECT/CT. Material and methods. A retrospective analysis of 117 patients diagnosed with PHP (100 females and 17 males, aged 16-88 years, median age 62 years) was performed. In each patient parathyroid SPECT/CT after administration of 500 MBq of ^{99m}Tc -MIBI was conducted (Siemens Symbia T16). Serum calcium and parathormone (PTH) were measured in each patient, serum phosphate was estimated in 109 subjects. Statistical analysis was performed with Statistica 12 software. Results. Median serum calcium level was 2.77 mmol/L (LQ and UQ - 2.66 i 2.87 mmol/L respectively); median serum PTH level was 122.8 pg/mL (LQ and UQ - 97.2 i 191.9 pg/mL, respectively); median plasma phosphate was 0.84 pmol/L (LQ and UQ - 0.74 i 0.98 mmol/L, respectively). In 70 (59.8%) patients an enlarged parathyroid gland was detected with SPECT/CT, in the remaining 47 subjects results of radionuclide imaging were negative. There was a statistically significant difference in PTH levels (median 138.15 and 114.80 pg/mL, respectively, $p=0.02$) and serum calcium levels (median 2.74 and 2.67 mmol/L, $p=0.0003$) between patients with positive and negative parathyroid SPECT/CT. Serum phosphate levels did not differ significantly (median 0.83 and 0.85 mmol/L, respectively; $p=0.19$). Receiver-operator curves (ROCs) were drawn to establish PTH and serum calcium cut-off levels for positive parathyroid SPECT/CT imaging. Sensitivity and specificity of parathyroid scintigraphy are 38% and 89.6%, respectively, for PTH cut-off level of 191.9 pg/mL, and 52% and 79% respectively for serum calcium cut-off level of 2.74 mmol/L. Conclusions. Limiting parathyroid SPECT/CT to patients with significantly increased PTH and/or serum calcium levels, particularly if surgical treatment is not considered, may decrease false negative imaging rates and allows to avoid unnecessary radiation exposure. More precise determination of PTH and calcium cut-off levels requires analysis of larger patients group data.

P096

The Diagnostic Effectiveness of ^{18}F -FCH PET/CT in Detecting Hyperfunctioning Parathyroid Lesions for Primary Hyperparathyroidism with indeterminate ^{99m}Tc -sestamibi SPECT/CT and Thyroid Echography

R. Yen, W. CHiu, M. Wu, K. Chen, W. Yang; National Taiwan University Hospital, Taipei, TAIWAN.

Background: Hyperparathyroidism is a common endocrine disorder. Primary hyperparathyroidism is due to over-secretion of parathyroid hormone and subsequently hypercalcemia, hyperphosphatemia and osteoporosis with the prevalence of 1/500 in female and 1/2000 in male. Surgical approach is the major treatment modality for these. Pre-operative localization of hyperfunctioning glands may lead to minimally invasive surgery. The most commonly used imaging modality for this purpose is ^{99m}Tc -sestamibi (MIBI), and supplemented by ultrasonography (US) of the neck. However, the sensitivity and specificity is not satisfactory. Recently, some investigators reported cases of parathyroid adenoma discovered incidentally on choline PET images performed for prostate cancer. As a phospholipid analog, choline is integrated into newly synthesized membranes of proliferating cells by up-regulation of choline kinase. In addition, a previous study showed that the activity of phospholipid/Ca $^{2+}$ -dependent protein kinase was also higher in hyper-functioning parathyroid tissue than in atrophic parathyroid gland. Both mechanisms may be responsible for the uptake of choline tracers in hyper-functioning parathyroid tissue. The purpose of this prospective study was to evaluate the diagnostic effectiveness of ^{18}F -Fluorocholine (FCH) PET in detecting and localizing hyperfunctioning parathyroid lesions. **Materials and Methods:** ^{18}F -FCH PET/CT were performed for 9 patients with primary hyperparathyroidism and discordant/negative results on ^{99m}Tc -MIBI SPECT/CT and US. The diagnostic sensitivity of PET was evaluated according to pathological results and clinical outcome. **Results:** Table 1 lists the characteristics and serum parathyroid hormone levels of these patients (2 male and 7 female). Seven of them had parathyroid adenomas, 1 had adenomatous hyperplasia and 1 had hyperplasia for all 4 parathyroid glands. All patients showed normalization of serum PTH after operation. The diagnostic results of ^{18}F -FCH PET/CT, ^{99m}Tc -Sestamibi SPECT/CT and thyroid US are demonstrated in Table 2. PET only missed the case who had hyperplasia for all 4 parathyroid glands. The mean SUVmax of PET positive lesions was 4.6 ± 2.3 (range 2.8–9.9). The smallest PET positive lesion was less 100 mg (Fig. 1). Using clinical outcome as gold standard, ^{18}F -FCH PET/CT had 89% localization accuracy, while ^{99m}Tc -MIBI SPECT/CT showed 33.3% and thyroid echo showed 33.3% respectively. **Conclusion:** Our study demonstrates ^{18}F -FCH PET/CT is a sensitive and accurate diagnostic imaging tool in the localization of hyperfunctioning parathyroid lesions for patients with primary hyperparathyroidism and indeterminate ^{99m}Tc -MIBI SPECT/CT and thyroid US.

P097

Comparative efficacy of ^{18}F -Choline PET/CT, ^{99m}Tc Sestamibi imaging and neck ultrasonography for the preoperative localization of parathyroid adenoma in suspected cases of primary hyperparathyroidism

T. NTK, A. Sood, R. R. Kalathoorakath, R. Kumar, A. K. Reddy Gorla, B. R. Mittal, S. Bhadada, A. Behra; PGIMER, Chandigarh, INDIA.

Objective: To compare the diagnostic performance of ^{18}F -choline PET/CT (Choline PET), ^{99m}Tc sestamibi imaging (MIBI) and neck ultrasonography (USG) in the preoperative localization of parathyroid adenoma in patients with suspected primary hyperparathyroidism **Materials and methods:** A total of fifty-four patients with suspected primary hyperparathyroidism (PHPT) were included in this study. All the patients were evaluated using ^{18}F -Choline PET/CT, ^{99m}Tc -sestamibi (planar dual phase and SPECT/CT) and neck ultrasonography for the preoperative localization of parathyroid adenoma. Of the fifty-four patients, surgery was performed and final histology was available in twenty-four patients. Sensitivity, positive predictive value (PPV) and accuracy of these modalities were determined using histopathology as the reference standard. Also, correlation of histopathology with neck ultrasound, ^{99m}Tc -sestamibi imaging, ^{18}F -choline PET/CT and pre-operative serum iPTH was statistically analyzed. When statistically significant, cut off values were determined using ROC curves. **Results:** Mean age of the patient

population was 49.5 ± 15 years (Range: 27–72 years; 5 males, 19 females). All the patients showed uni-glandular involvement. Neck ultrasonography, ^{99m}Tc -sestamibi and ^{18}F -Choline PET/CT localized lesions in 16 (69.5%), 19 (79.1%) and 24 (100%) patients respectively. Choline PET was particularly useful in the accurate localization of ectopic lesions. Histopathology demonstrated adenoma in 23 out of 24 patients and remaining one detected by choline PET/CT had normal parathyroid tissue on histology, though patient had revealed clinical and biochemical improvement in postoperative follow up. Thus, sensitivity, PPV and accuracy were 71.4%, 93.7%, 69.6% for USG, 83.6%, 100%, 83.3% for MIBI imaging, and 100%, 95.8%, 95.8% for Choline PET respectively. Pre-operative serum iPTH (PRE-PTH) levels showed no statistically significant correlation (P= 0.180) with USG. However, significant correlation was noted between PRE-PTH and MIBI imaging (P=0.023; for a cutoff of 149 pg/ml with 84.2% sensitivity and 80% specificity on ROC analysis). Good correlation (Pearson correlation coefficient= 0.748) was noted between histology and normalization of iPTH status, thereby suggesting that there was no residual hyperfunctioning parathyroid tissue post-surgery. **Conclusion:** ^{18}F -choline PET/CT imaging is a promising imaging modality with higher sensitivity and accuracy as compared to conventional imaging (USG and MIBI imaging), especially in patients with ectopic lesions. Further validation of the results in larger cohorts is warranted to establish the utility of this technique.

P098

Factors affecting the sensitivity of Tc-99m MIBI Parathyroid SPECT

M. Araz, D. Cayir, M. Erdoğan, B. Ucan, E. Cakal; Ankara Diskapi Yildirim Beyazit Training and Research Hospital, Ankara, TURKEY.

AIM: The sensitivity of Tc-99m methoxyisobutylisonitrile (MIBI) SPECT is variable (43–96%). It has been reported that some medications, especially calcium channel blockers (CCB), have been reported to decrease the sensitivity of the study. However, literature is still lack of enough reliable data. In this study we aimed to investigate possible effect of coexisting thyroid diseases and regularly used medications on the sensitivity of Tc-99m MIBI parathyroid SPECT. **MATERIAL-METHOD:** 218 patients (190F,28M, mean age: 57 ± 14) with primary hyperparathyroidism who had undergone thyroid-parathyroid USG and Tc-99m MIBI SPECT were retrospectively investigated. Patients were divided into two groups: 119 patients (54.6%) who had a positive Tc-99m MIBI SPECT and 99 patients (45.4%) with a negative scan. The effect of sonographically detected thyroid diseases and use of CCB, beta blockers, Angiotensin converting Enzyme inhibitors (ACEI)/ angiotensin receptor blockers (ARB), oral antidiabetics, thyroid hormone preparates, non-steroid antiinflammatory drugs (NSAID) and proton pump inhibitors (PPI) on the sensitivity of Tc-99m MIBI SPECT studies were investigated in two groups. **RESULTS:** Overall sensitivity, specificity, positive predictive value (PPV) and negative predictive value (NPV) of Tc-99m MIBI SPECT were calculated 89.6%, 92.5%, 94.1% and 86.9%, respectively. The sensitivity was low in NSAID users (75.6%), compared to non-users (96.5%). No such difference was detected for the other drug groups (Table 1). The comparison results of the patients with positive and negative Tc-99m MIBI SPECT study showed that the frequency of NSAID usage was significantly higher in the negative scan group ($p < 0.001$). No significant difference was detected between two groups neither in terms of coexisting thyroid disease nor usage of other medications. In this context, the results of USG and Tc-99m MIBI SPECT were concordant (Table 2). First univariate and then multivariate logistic regression analysis were performed for possible variables indicative of the result of the scan. Only NSAID usage was in correlation with Tc-99m MIBI SPECT results (OR:0.262; CI: 0,128–0,538; $p < 0.001$). **CONCLUSION:** It has been reported that CCB usage decreased sensitivity of Tc-99m MIBI SPECT. In this study, among various drug groups, only NSAID were found to affect Tc-99m MIBI SPECT results. Because COX-2 expression has been

reported be increased in hyperplastic and adenomatous parathyroid glands, we state that NSAID may decrease the sensitivity of Tc-99m MIBI SPECT via this pathway.

P099

Pediatric Solitary Thyroid Nodules on Tc-99m Thyroid scan and their correlation with Histopathological Examination

M. Siddique, A. Hassan, H. Bashir, M. Nawaz; Shaukat Khanum Memorial Cancer Hospital and Research Centre, Lahore.Pakistan., Lahore, PAKISTAN.

Purpose: Although thyroid nodules are less frequent in paediatric population, but are more often malignant. Our aim was to evaluate the correlation between Tc-99m thyroid scan finding and histopathology of selected thyroid nodules in pediatric population. **Methods:** We retrospectively reviewed all pediatric patients who underwent thyroid scan for palpable thyroid swelling / deranged thyroid function tests at our center from 2007 to 2014. The scan findings were classified as diffuse goiter, Graves' disease and nodular goiter. Hot or cold nodules were assigned based on level of Tc-99m uptake. Cold nodules were further correlated with histopathological/ultrasound findings. **Results:** 227 cases with thyroid related signs and symptoms presented during the 8 years period. 177(78%) were females and 56(25%) were males. Mean age: 14.8 years (range= 1-18 years). 30 cases (13.2%) had nodular goitre on thyroid scan and the rest had diffuse goiter / hypothyroid / Graves' disease. Out of nodular glands, 23.3%(7/30) cases had toxic nodules. 76.7%(23/30) cases had cold nodules detected on thyroid scan; Out of 23 cases, 16 underwent ultrasound guided biopsy and seven were lost to follow up; Histopathological findings of fine needle aspiration cytology were categorized as Bethesda category I(n=0), 50% category II(n=8), category III(n=0), 18.75% category IV(n=3), 18.75% category V(n=3) and 12.50% category VI(n=2). Out of category II, three patients had thyroid cysts on further evaluation while five patients had follicular colloid nodule/hyperplasia. Among category IV and V, all six patients had papillary carcinoma (PTC) on subsequent total thyroidectomy. Of two cases with Bethesda category VI, there was one case each of PTC and medullary carcinoma of thyroid. Additionally, in two patients with unremarkable Tc-99m uptake pattern PTC was diagnosed on cervical nodal biopsy. **Conclusion:** According to our retrospective analysis, cold nodule on Tc-99m thyroid scan have a 50% chance of being malignant, therefore in the children with palpable thyroid nodules, an accurate multistep work-up is necessary.

P100

¹⁸F fluorocholin PET/CT as a complementary tool to MIBI SPECT/low dose CT for localisation of hyperproducing parathyroid tissue.

J. Kubinyi¹, M. Fialová², P. Libánský², S. Adámek², D. Chroustová¹, V. Ptáček¹, D. Zogala¹, P. Broulík¹; ¹General University Hospital, Prague, CZECH REPUBLIC, ²Motol Hospital, Prague, CZECH REPUBLIC.

AIM: Prove the utility of ¹⁸F-fluorocholine (FCH) PET/CT examination in the localization of hyper productive parathyroid tissue in cases of negative or equivocal finding with MIBI SPECT/low dose CT (MIBI) examination. Assess the accuracy of whole MIBI and FCH combining protocol when FCH is used only in negative and equivocal finding with MIBI. **METHODS:** During year 2014 and 2015 175 patients were examined in with MIBI (all) and 27 from them with FCH too because of localisation of hyperparathyroidism. Then the surgery was performed and scintigraphic localisation verified. All patients were with higher level of calcium and parathormone. Surgery, histology and normalisation of calcium and parathormone level were taken as confirmation of scintigraphic localisation of hyperproducing parathyroid tissue. MIBI - only

SPECT/low dose CT with scanner Infinia/Hawkeye GE after injection of 700 MBq (70kg) MIBI. Scans early 5-10 minutes and late 120 - 150 minutes post injection. Tc - only SPECT with the same scanner after injection of 200 MBq pertechnetate (70 kg). In all patient evaluation of wash out and then 3D subtraction MIBI minus Tc. FCH - neck and thorax 10 - 20 minutes after injection of 100 - 120 MBq fluorocholine with scanner Discovery 690 f. GE (bet time 7 minutes). CT was performed in standard conditions with Iomeron as contrast agent. 20 patients with negative or equivocal findings in 99mTc-MIBI scan and clear evidence of hyperparathyroidism (high level of calcium and parathyroid hormone - PTH) were examined with FCH PET/CT. PET scan was obtained 10 - 20 minutes after intravenous injection of 80 - 100 MBq FCH. Extent of scanning was from skull base to diaphragm. Time for bed was prolonged to 7 minutes for thyroid region and 5 minutes for the rest of chest. **RESULTS:** RESULTS: All surgery examined glands were 539 in 175 patients. 18 patients had hyperplasia and 157 patients had adenoma/s. Overall sensitivity was 85% and specificity 96%, for adenomas only the sensitivity was 97%. Sensitivity for hyperplasia is low, only about 45%. **SUMMARY:** Combined protocol used FCH only in negative or equivocal finding with MIBI examination seems to be very promising tool for localisation of hyper productive parathyroid tissue with very good accuracy. FCH can find small lesions bordered with thyroid and perhaps MIBI non avid lesions. On the other hand, for clear finding with MIBI is no need for FCH examination.

P101

Glucose Metabolism of hepatic, muscular, and adipose tissues in obesity Before and after bariatric surgery

W. Yao, C. Wu; College of Medicine, National Cheng Kung University, TAINAN, TAIWAN.

Introduction: Obesity has been linked to insulin resistance, hypertension, dyslipidemia, type 2 diabetes, and cardiovascular disease. Recently, bariatric surgery has been proposed to improve insulin resistance and glucose metabolism in obese patients, partially independent of weight loss. The aim of this study is to evaluate how bariatric surgery modifies the glucose metabolism of the whole body and different tissues in obese patients using F-18 FDG PET/CT. **Subjects and Methods:** We enrolled 14 obese subjects, aged between 22 and 61 years old, with Fat% 33.3 to 66.8. Both dynamic and whole body F-18 FDG PET/CT were done before and 6 months after bariatric surgery. Amount of abdominal visceral and subcutaneous fat was measured from CT at umbilical level. Semiquantitation of glucose metabolism (SUV-bw and SUV-lean) was measured by placing ROIs in each organ (liver, psoas muscle, quadriceps muscle, subcutaneous fat, and visceral fat). Body composition with DXA, serum glucose and insulin levels were also measured. **Results:** Bariatric surgery significantly lowered body weight, mostly adipose tissue, insulin and glucose levels. Using body weight for SUV calculation (SUV-bw), the glucose uptakes were decreased in the liver and muscles, while remained unchanged in adipose tissues after surgery. However, using SUV-lean, the glucose uptake remained unchanged in the liver (1.75±0.35 vs 1.81±0.34) and the psoas muscle (0.50±0.13 vs 0.49±0.07), while increased in fat tissues, both in visceral fat (0.22±0.11 vs 0.31±0.12) and subcutaneous fat (0.13±0.03 vs 0.21±0.07). **Conclusion:** Bariatric surgery increased glucose uptake in the visceral fat and subcutaneous fat in obese subjects. The underlying mechanism needs further investigation. SUV-lean may be more appropriate than SUV-bw for quantifying tissue glucose metabolism in obesity studies with F-18 FDG PET/CT.

P102

Minimally invasive radioguided surgery of primary hyperparathyroidism

V. Dedek, M. Havel, M. Kolacek, M. Formanek; Faculty hospital, Ostrava - Poruba, CZECH REPUBLIC.

Introduction: minimally invasive radio-guided surgery (MIRS) is accepted technique in patients (pts) with ^{99m}Tc -MIBI positive scintigraphy in primary hyperparathyroidism (PHPT). **Aim:** the gamma detecting intraoperative probe (C-Trak) and assessment of its contribution in the successful removal of PT adenoma. **Materials:** 87 pts underwent MIRS (75 women, 12 men). **Methods:** Dual-phase MIBI-scintigraphy to confirm PT adenoma was performed by the „separate-day protocol“. In the morning on the day of surgery we had administered i.v. 600 MBq ^{99m}Tc -MIBI and wrote in the report time interval to start operation (2,5 - 3 h). During MIRS surgeon was given auditory signals and digital counts (CPS-counts per second) to dissect the radioactive target tissue and placed upon record these facts: time of beginning and duration of MIRS, in vivo PT adenoma to thyroid ratio in CPS (A/T). We also estimated histological findings. **Results:** in 85/87 pts histological findings confirmed PT adenoma, once erroneously removed lymphatic node and in the second case papillary thyroid carcinoma. According to the surgeons the gamma probe detection was useful in 73/85 cases (86 %) and on the contrary the probe didn't help them in 12/85 cases (14 %), but in the end PT adenomas were successfully removed. Out of the gamma probe successful cases A/T ratio were in 8/73 1, 1-1,5, in 49/73 more than 1,5 and in the last 16/73 cases the ratios weren't specified by surgeon. We analyzed the possible reasons of gamma probe failure (12 cases). In 2 of them MIRS started too early (100, resp. 120 min. after MIBI administration), in 4 cases weren't MIBI uptake in scintigraphy significant, in the rest 6 cases we think about more factors: time to MIRS was too long (more than 240 min.), the sizes of PT adenomas were small (less than 1 cm), in two cases PT adenomas were ectopic (paraesophageal, resp. paravertebral). Duration of the operation in successful cases were 20–60 min in 72 pts and 70–160 min in 13 pts (included 7 cases of total thyroidectomy). **Conclusion:** In the PHPT pts MIRS is recommended technique in cases with high sestamibi uptake in dual-phase scintigraphy (included SPECT/CT). Our ORL surgeons were helped by gamma probe in 86 % out of the 85 PT adenoma dissections. In vivo A/T ratio was most often more than 1,5. We consider important to keep interval 2,5–3 h between sestamibi administration and MIRS. MIRS in the hands of experienced surgeon reduces time of surgery.

P103

Comparison of single-phase early SPECT/CT, dual-phase planar imaging with early SPECT and dual-phase planar imaging with early SPECT/CT Tc-99m Sestamibi Parathyroid Scintigraphy

JAVIER GÓMEZ HIDALGO, AMPARO COBO RODRÍGUEZ, A. SAINZ-ESTEBAN, CLAUDIA GAMAZO LAHERRÁN, JUAN GABRIEL VILLANUEVA CURTO, MARÍA ÁNGELES RUIZ GÓMEZ, MARÍA LUISA GONZÁLEZ SELMA, MERCEDES ALONSO RODRÍGUEZ, ROBERTO OLMOS GARCÍA; Nuclear Medicine Department. Hospital Clínico Universitario de Valladolid, VALLADOLID, SPAIN.

Aim: The purpose of our investigation was to directly compare diagnostic accuracies and confidences of various imaging protocols on same patients in the detection and localization of parathyroid adenomas. **Methods:** From January 2013 and December 2014 scintigraphy was performed on 337 patients with primary hyperparathyroidism. Of these, 45 had histologically proven single adenomas (40) or hyperplasias (5) and are the subject of this review. Planar imaging was performed at 15 min and 2 h after injection. Besides, SPECT/CT was performed after the early planar image. Three image sets (single-phase early SPECT/CT, dual-phase planar imaging with early SPECT and dual-phase planar imaging with early SPECT/CT) were reviewed for probability of adenoma on 5-point scale (1: definitely negative, 2: probably negative, 3: equivocal, 4: probably positive, and 5: definitely positive). Besides, the three image sets were also reviewed for adenoma localization at 7 possible sites. Each review was scored for location and certainty of focus by 2 reviewers. Surgical location served as the standard. **Results:** Dual-phase planar imaging with

early SPECT/CT detected 38 pathological parathyroids (84.4%) and correctly localized 28 (62.2%). False negative corresponded to two hyperplasia and five single adenomas. Single-phase early SPECT/CT detected 34 pathological parathyroids (75.5%) and correctly localized 27 (60%). Dual-phase planar imaging with early SPECT detected 34 pathological parathyroids (75.5%) and correctly localized 26 (57.7%). False negative corresponded to three hyperplasia and nine single adenomas. Regarding the equivocal cases, dual-phase planar imaging with early SPECT and single-phase early SPECT/CT presented 6 equivocal cases, while dual-phase planar imaging with early SPECT/CT only 4. **Conclusion:** Dual-phase planar imaging with early SPECT/CT allows more accurate detection and localization of parathyroid adenomas than single-phase early SPECT/CT and dual-phase planar imaging with early SPECT. However, the correct detection and localization of multiglandular hyperplasia remains difficult.

P104

Towards harmonization in parathyroid scintigraphy in Finland

V. Tunninen¹, P. Varjo¹, T. Kauppinen²; ¹Satakunta Central Hospital, PORI, FINLAND, ²Helsinki University Hospital, Helsinki, FINLAND.

AIM There is no consensus on how to perform parathyroid scintigraphy (PS), in terms of study method or acquisition techniques. This has led to a large variety of protocols worldwide, but also nationally. Finland has been working towards harmonization of PS since 2009, when a significant variability in PS protocols was revealed in our country. The aim of this follow-up study was to update the national status of in PS protocols. **MATERIALS AND METHODS** Our group published 2009 first results of national situation. All departments of nuclear medicine in Finland were now contacted in this study and the current status of PS methods and acquisition techniques were requested. **RESULTS** There are 25 departments of nuclear medicine in Finland. Current practices were received from all the departments which perform PS (n=19). There has been a significant change in the study methods used. Currently all hospitals use dual-isotope method using $^{123}\text{I}/^{99m}\text{Tc}$ -sestamibi as their primary method for PS (in comparison, 52,4% in 2009). ^{123}I activity ranged from 7,4 MBq to 30MBq (mean 18MBq), and iodine is given as an iv injection in all but one hospital (2009: 10–30MBq, 4 per os, 7 iv). ^{99m}Tc -sestamibi activity ranged from 400 MBq to 750MBq (mean 670MBq) (2009: 150–800MBq). The use of SPECT/CT acquisition technique has increased from 46% to 89,5% of hospitals using the dual-isotope method. At the same time, the use of planar imaging using the parallel-hole collimator has decreased from 100% to 47,4%, and with pinhole collimator from 46% to 36,8%. Additional acquisitions are performed in 16 of 19 hospitals (planar imaging with parallel-hole or with pinhole collimator). The late phase acquisition is still performed in 6 of 19 hospitals (all acquisition techniques are used). There still is variability in study protocols, but mainly in additional acquisitions and in the use of the late phase imaging. **CONCLUSION** Our follow-up study showed that the methods of PS have been harmonized significantly during the last seven years in Finland. We found two main reasons for this. First, 78,9% of hospitals have purchased new SPECT/CT equipment, so there is no instrumental limits for using modern acquisition techniques. Second, we have been working actively in this field (research, lectures in national meetings, active discussion between professionals). However, there still is need for studies to optimize the PS protocols, to minimize the time required for the study, the patient discomfort and the total cost of the study.

P105

Hyperfunctioning parathyroid lesions with rapid 99mTc-Sestamibi washout: more common than usually thought

J. G. Santos, M. R. Victor, A. I. Santos; Hospital Garcia de Orta, E.P.E., Almada, PORTUGAL.

Aim: Parathyroid scintigraphy with ^{99m}Tc -Sestamibi (PTS) is widely used to pre-operatively localize hyperfunctioning parathyroid lesions (HPTL). However, the biokinetic behaviour of this radiopharmaceutical is known to be variable, potentially causing false negative exams. The purpose of this work is to evaluate the frequency of rapid ^{99m}Tc -Sestamibi wash-out in parathyroid glands. **Materials and methods:** We retrospectively analysed a group of 40 PTS positive for HPTL followed by surgical confirmation, performed on 37 patients. Scintigraphy protocol included both early and late planar images and early SPECT imaging. Thyroid scintigraphy with ^{99m}Tc -Pertechnetate (TS) was performed if the reporting physician felt it was necessary to properly interpret PTS. HPTL with slow washout of ^{99m}Tc -Sestamibi (SW) were diagnosed by delayed imaging. HPTL with rapid washout of ^{99m}Tc -Sestamibi (RW) were identified by one or both of the following criteria: radiopharmaceutical uptake posterior to the thyroid in early SPECT images; ^{99m}Tc -Sestamibi uptake with no corresponding ^{99m}Tc -Pertechnetate uptake. Data was categorized according to type of hyperparathyroidism (primary - 1HPTL vs secondary/tertiary - 2/3HPTL), number of hyperfunctioning parathyroid lesions (single gland vs multiple gland) and radiopharmaceutical washout (SW vs RW). The chi-squared test of homogeneity was used. **Results:** Forty PTS cases were identified, performed on 16 males (mean age=56 years;SD=18,7;min=13,max=87) and 24 females (mean age=64 years;SD=12,7;min=27,max=80). 1HPTL accounted for 23 cases (57,5%) and 2/3HPTL for the remaining 17 (42,5%). There was a total of 26 SW cases (65,0%) and 14 RW cases (35,0%). Among 1HPTL, RW was present in almost half the cases (47,8%), but for 2/3HPTL only 17,7% of cases presented RW. This difference seems statistically significant (p -value=0.0479). Single lesions accounted for 75,0% of cases and multiple ones for 25,0%. There was only one multiple lesion case in the 1HPTL group (4,4%), while in the 2/3HPTL group these were a slight majority (52,9%). Among single lesions, there was a large minority of RW (43,3%), but for multiple lesions only one case of RW was identified (10,0%). This difference was not statistically significant (p -value=0.0556). Diagnosis of RW was achieved by SPECT in 6 cases, comparison with TS and a combination of both methods in 4 cases each. **Conclusion:** This series supports the idea that HPTL with RW are common, representing more than a third of our sample. This is most significant when considering patients presenting with 1HPTL. Still, one case of 2/3HPTL with RW was identified. Early SPECT is very useful in identifying these lesions.

P106

Impact of resolution recovery for improvement of image quality in $^{123}\text{I}/^{99m}\text{Tc}$ -MIBI parathyroid SPECT

M. VERSTRAETE, Y. R. PETEGNIEF, O. MOREL, C. UNGUREANU, G. LANDECY, L. COMAS, C. DROUET, H. Boulahdour; CHRU Jean Minjoz, BESANCON, FRANCE.

Introduction: The objectives of this study were to define a method for image reading of dual-isotope ^{99m}Tc -MIBI and ^{123}I -SPECT for the preoperative localization of parathyroid adenomas in the setting of primary hyperparathyroidism (PHPT) and to investigate the role of resolution recovery correction for iterative reconstruction. **Methods:** Twenty-eight consecutive patients who underwent imaging for PHPT over a 18-month period were retrospectively assessed. Visualisation of parathyroid adenomas in planar and SPECT dual-isotope studies was performed with subtraction of mean activity in thyroid gland on MIBI images to the mean thyroid activity on ^{123}I images. Thus, visual (K_1) and automatic (K_2) normalization coefficients were compared in planar and SPECT studies reconstructed with OSEM iterative reconstruction without (IR) and with collimator resolution correction (IRC). Neither scatter, nor attenuation correction were included in the reconstructions. Two readers rated planar and IR images and two readers rated IR and IRC images only. Images were graded on a 4-point scale : normal (0), probably normal (1),

probably abnormal (2) and definitely abnormal (3) with respect to intensity and location of the lesion. Contrast of lesions was compared between IR and IRC data. The preoperative results were compared to intraoperative findings obtained for 17 parathyroid lesions. **Results:** Visual and automatic normalization coefficients for SPECT correlated well ($K_2=0.99$ $K_1+0.05$, $R^2=0.78$) except for 3 patients with larger K due to the presence of thyroid pathology. For the two readers referred for planar and IR studies, sensitivity (S) was 0,94 and 1. For SPECT studies, S varied from 0,87 to 0,88 for all readers. Two false negative results with IR were not correctly rated with IRC. Contrast of inferior lesions was better with IRC than IR (2.0 vs 1.6) whereas in upper quadrants, contrast of adenomas was limited after IRC (1.6) due to the presence of higher background. **Conclusion:** The role of planar imaging in dual-isotope PHPT imaging is always important. Image quality of IRC globally improved readers' confidence in subtracted MIBI SPECT interpretation, but didn't change classification of SPECT results.

P107

Preoperative Parathyroid Lesion Detection: The Success of Ultrasonography, Technetium Tc-99m Methoxyisobutylisnitrile Parathyroid Planar Scintigraphy and SPECT-CT

Ö. Özdemir Başer, B. T. Okudan, D. Köseoğlu, P. Arıcan, D. Berker; Ankara Numune Hospital, Ankara, TURKEY.

Purpose: Autonomous over-production of parathormon with hyperfunctioning parathyroid glands is the most frequent cause of hypercalcemia in outpatient populations. Despite the various methods are available for preoperative localization of parathyroid lesions, there is still no certain preoperative imaging algorithm to guide a surgical approach. We aimed to find out and compare the efficacy of ultrasonography (USG), technetium methoxyisobutylisnitrile (Tc-99m MIBI) parathyroid planar scintigraphy and SPECT-CT in detecting the localization of parathyroid adenomas in patients with primary hyperparathyroidism (PH). **Methods:** In this study we retrospectively analyzed 700 patients with hyperparathyroidism which referred parathyroid scintigraphy and SPECT/BT to our department from 2013 to 2015. Two hundred forty of 700 patients had neck surgery with definitive histologic reports. The 211 patients were included which exact localization of parathyroid pathologies obtained at the operation. Of these patients USG, planar Tc-99m MIBI and SPECT-CT imaging performed before surgery was available in 205 patients. USG was not done in only 3 of these patients. For scintigraphy, after 20 minutes injection of 555 MBq Tc-99m MIBI early planar imaging, after 180 minute planar and SPECT-CT imaging were obtained. Preoperative parathyroid imaging with USG, planar Tc-99m MIBI and SPECT-CT were evaluated and compared with operative findings. **Results:** Between the time period this study was conducted, 254 patients underwent surgery for PH, and the pathological results were present in 240 patients. The pathological examination showed that 224 (88.2%) patients had parathyroid adenoma, 5 (2%) patients had carcinoma and 11 (4.3%) patients had parathyroid hyperplasia. The analysis of 14 patients (5.5%) showed no parathyroid tissue. USG detected the localization of the parathyroid pathology correctly in 174 patients (84.9%), whereas SPECT-CT and planar Tc-99m MIBI imaging were correct in 165 (79.3%) and 130 (62.5%) patients, respectively. The positive predictive value of USG, SPECT and MIBI were 92.1% (174/189), 85.5% (130/146), and 89% (165/193) respectively. **Conclusion:** Surgical treatment can be planned in patients with hyperparathyroidism, because of its complications due to high levels of parathyroid hormone. In particular, minimally invasive surgery is preferred for single adenomas. Therefore, preoperative localization of adenoma is important. Although, this study showed us USG is better than scintigraphic imaging techniques to correctly localize the parathyroid adenomas, it could be dependent to re-evaluation of USG following the SPECT/CT.

P108**Procalcitonin in the detection of medullary thyroid carcinoma**

J. Maffey-Steffan¹, R. Moncayo Nevada¹, A. Griesmacher², W. Prokop², I. Virgolini¹; ¹Department of Nuclear Medicine, Innsbruck, AUSTRIA, ²Department of Laboratory Medicine, Innsbruck, AUSTRIA.

Aim The aim of the present study was to investigate the usefulness of procalcitonin (PCT) as a diagnostic marker of medullary thyroid carcinoma (MTC). As the calcitonin (CT) radioimmunoassay (RIA) has relevant limits in the clinical praxis. **Methods** In 81 patients with multiple thyroid nodules CT and PCT were investigated in parallel. CT was measured by an Immuno Radiometric Test (Cisbio Assay) normal range: 0.1 ng/ml and PCT was measured by ECLIA (Electro Chemi Luminescence Immuno Assay, Elecsys BRAHMS PCT), normal range: 0.1 ng/ml before surgery. **Results** In 72/81 patients in whom no MTC was found the PCT was equal or less than 0.06 ng/ml and the CT was 13 pg/ml. In four patients with documented MTC the PCT and CT values were 0.4 ng/ml and 74.6 pg/ml, 3.36 ng/ml and 520 pg/ml (1:10), 4.72 ng/ml and 1160 (1:50) pg/ml, and 1.36 ng/ml and 370 (1:10) pg/ml, respectively. In one patient who was treated by chemotherapy PCT was 0.16 ng/ml and CT 11.3 pg/ml. In another patient treated by chemotherapy PCT was 3.44 ng/ml and CT was 400 pg/ml. In one patient with PCT of 0.07 ng/ml CT amounted to 16.6 pg/ml and in this patient a Ca²⁺-stimulation-test was positive. **Conclusion** Our data suggest that the determination of PCT is clinically useful as a quicker, cheaper and more practicable screening test than CT measurement in patients with nodular goiter to exclude MTC.

P109**Cost-effectiveness Analysis of Computed Tomography and Adrenal Scintigraphy in Primary Aldosteronism**

C. Lu¹, R. Chang², R. Yen¹; ¹National Taiwan University Hospital, Taipei, TAIWAN, ²Graduate Institute of Health Care Organization Administration, National Taiwan University, Taipei, TAIWAN.

Background Primary aldosteronism (PA) is the most common cause of secondary hypertension. The two main causes of PA are aldosterone-producing adenoma, which could be cured by surgical intervention, and bilateral adrenal hyperplasia, which should be medical-treated. Computed tomography (CT) is the initial imaging approach for lateralization with wide variation of sensitivity. Adrenal scintigraphy has limited role in lateralization during early days due to resolution. With the SPECT/CT fusion imaging technique, the accuracy of adrenal scintigraphy is significant improved. This study aimed on the comparison of the accuracy, average cost and cost-effectiveness analysis of four imaging modalities for differentiating the etiology of PA, including CT, NP-59 planar, NP-59 SPECT and NP-59 SPECT/CT. **Methods** We retrospectively included 27 clinical-confirmed PA patients from TAIPAI database. All of them had CT, NP-59 adrenal scintigraphy (planar, SPECT and SPECT/CT) studies and pathology reports of adrenal lesion. The accuracy and average cost of these four imaging modalities were analyzed. By decision tree and setting effectiveness as diagnostic accuracy and diagnostic utility, cost-effectiveness were also analyzed. Sensitivity analysis was performed to determine the impact on the average cost while the variables changed. **Results** NP-59 SPECT/CT is the most accurate study among four imaging modalities, with borderline significance as compared with NP-59 planar and CT. NP-59 SPECT/CT bares the lowest average cost, and NP-59 planar bares the highest average cost. By setting diagnostic accuracy as the effectiveness, NP-59 SPECT/CT has the lowest cost-effectiveness ratio. If setting diagnostic utility as the effectiveness, NP-59 planar is considered an ineffectiveness study.

In sensitivity analysis, if the sensitivity of NP-59 SPECT/CT decreases to 0%, the average cost of NP-59 SPECT/CT is still lower the average cost of CT. The average cost of NP-59 SPECT/CT is higher than the average cost of CT while the specificity of NP-59 SPECT/CT decreases to 59.5%. **Conclusion** Our study suggests that NP-59 SPECT/CT is the most accurate with the lowest average cost and the most cost-effective study among these four imaging modalities in differentiating the etiology of PA. It shows no significant impact on cost-effectiveness ratio as compared with CT while the sensitivity and specificity of NP-59 SPECT/CT changes. Aside from clinical concern, this result provides physicians consider the decision in another way to provide more effective management in PA.

P110**The role of preoperative imaging in localization of parathyroid adenoma - our experience**

V. Militano, N. Seshadri, S. Vinjamuri; Royal Liverpool and Broadgreen University Hospital NHS Trust, Liverpool, UNITED KINGDOM.

Introduction: Ultrasonography and 99mTc-MIBI scintigraphy are well recognized imaging techniques for preoperative parathyroid lesion localization. The aim was to determine the accuracy of planar and SPECT-CT MIBI scintigraphy in the preoperative localization in patients of suspected primary hyperparathyroidism in our center and its comparison with ultrasonography. **Materials and Methods:** We retrospectively reviewed 118 patients, who underwent Technetium-99m sestamibi scintigraphy with planar and SPECT/CT imaging at Royal Liverpool University Hospital, with diagnosis of suspected primary hyperparathyroidism between July 2014 and June 2015. 62 patients had parathyroid surgery and 46 patients of these, also, underwent high-resolution ultrasonography prior to parathyroid surgery. The diagnostic accuracies of both these techniques were evaluated using surgical and histological findings as the reference standard. **Results:** Following surgery the histology showed 77% [48/62] solitary parathyroid Adenoma(PA), 13%[8/62] parathyroid hyperplasia(PH), 5%[3/62] Dual parathyroid Adenoma(DPA) and 5%[3/62] normal parathyroid(NP). Of the 62 patients in whom histology was available planar imaging was true positive in 61%[38/62](33 PA, 1 DPA and 4 PH), true negative in 5%[3/62], false negative in 34%[21/62](16 PA, 4PH, 2DPA), false positive in 0% with a sensitivity of 64%, specificity of 100%, accuracy of 66%, PPV of 100% and NPV of 12.5%. Similarly SPECT/CT images was true positive in 74%[46/62](37 PA, 6 PH, 3 DPA), true negative in 5%[3/62], false negative in 21%[13/62](11 PA, 2 PH) and false positive in 0% corresponding to a sensitivity of 78%, specificity of 100%, accuracy of 79% with a PPV of 100% and NPV of 18.75%. Likewise Ultrasonography was true positive in 48%[22/46](21 PA and 1 DPA), true negative in 4%[2/45], false negative in 48%[22/46](15 PA, 5 PH, 2 DPA) and false positive in 0% corresponding to a sensitivity of 50%, specificity of 100% with accuracy of 52% PPV of 100% and NPV of 8.3%. There was significant difference in the weight of the glands on histopathology with a mean weight of 413 mg(970-80) for FN vs 1175 mg(3430-120) for TP studies on MIBI scintigraphy. However there was no correlation on MIBI scintigraphy study between Serum Ca FN 2.8(3.2/2.61) vs TP 2.8(3.2/2.5) and PTH levels FN 10.5(19.1/4.3) and TP 13.7(89/6). **Conclusion:** SPECT/CT was superior to planar imaging with an accuracy of 66%(planar) vs 79%(SPECT/CT). MIBI scintigraphy is more accurate than US in localizing parathyroid lesions with the latter adding little incremental benefit in localizing. The accuracy of MIBI scintigraphy is inversely related to the weight of the parathyroid lesion. However there is no correlation with Serum Ca and PTH levels.

P111**Utility of sestamibi ^{99m}Tc-SPECT/CT in the localization of the pathological parathyroid gland before surgery compared with other conventional imaging techniques**

M. OPORTO¹, C. SAMPOL¹, C. PEÑA¹, N. ORTA¹, M. TOSCANO², M. VILLAR², S. RUBI^{1,3}, J. MOLINA¹, F. CEPÁ¹; ¹HOSPITAL UNIVERSITARIO SON ESPASES. NUCLEAR MEDICINE DEPARTMENT, PALMA DE MALLORCA, SPAIN, ²HOSPITAL UNIVERSITARIO SON ESPASES. RADIOPHARMACY DEPARTMENT, PALMA DE MALLORCA, SPAIN, ³INSTITUTO DE INVESTIGACION SANITARIA DE PALMA (IdISPa), Palma de Mallorca, SPAIN.

Aim: To compare the capacity of Ecography, Planar scintigraphy dual-phase ^{99m}Tc-sestamibi and SPECT/CT ^{99m}Tc-sestamibi in the localization of parathyroid adenomas in patients diagnosed with hyperparathyroidism before surgery. **Material and methods:** We retrospectively evaluated the pre-operative studies of 46p with primary (n=44) and secondary (n=2) hyperparathyroidism. Ecography was performed in 44p before or after the planar scintigraphy. Dual-phase ^{99m}Tc-sestamibi planar scintigraphy was carried out in 46p, acquiring SPECT/CT in 41p (early phase n=30 and delayed phase n=11). The adenoma's localization for the 3 studies was compared with operative findings, histology and intraoperative PTH blood test (basal, 5' and 10'). **Results:** Out of 46p included, median age 58.5 years, 37 female and 9 male, all with high suspicion of hyperparathyroidism, with mean for PTH and calcium of 174 pg/ml and 10.9 mg/dl respectively. The Ecography detected image suspicious of adenoma in 26/44p and was negative in 18/46p (sensitivity 59%). Early phase planar scintigraphy with ^{99m}Tc-sestamibi was positive in 22/46p, negative in 15/46p and unclear in 9/46p (sensitivity 47.8%), delayed phase planar scintigraphy with ^{99m}Tc-sestamibi was positive in 32/46p, negative in 7/46p and unclear in 7/46p (sensitivity 69.5%) and SPECT/CT ^{99m}Tc-sestamibi was positive in 39/41p and negative in 2/41p. Sensitivity for SPECT/CT ^{99m}Tc-sestamibi was 95.1%. The accuracy for localizing pathologic parathyroid glands to the correct side of the neck was for ecography 25/44p (56.8%), Planar scintigraphy dual-phase ^{99m}Tc-sestamibi 32/46p (69.5%) and SPECT/CT ^{99m}Tc-sestamibi 41/41p (100%), 15 in the right and 26 in the left side, 4 superior and 37 inferior. Ecography detected 5/16p ectopic adenoma (sensitivity 31.2%), planar scintigraphy dual-phase ^{99m}Tc-sestamibi 9/16p (sensitivity 56.2%), and SPECT/CT 16/16p (sensitivity 100%): 9 in the anterior cervical region, 4 retrotracheal, 1 paraesophageal and 2 prevertebral. Out of 46p, 36p went to radioguided surgery and 10p to conventional surgery. The average intraoperative basal PTH was 202.3 pg/ml, 5' PTH 160.5 and 10' PTH 91.6. A total of 50 parathyroid glands were removed with a final diagnosis of parathyroid tissue and only 1p had unclear histology. A total of 41p (89.1%) were biochemically cured, 36/36p with radioguided surgery and 5/10p with conventional surgery. **Conclusion:** SPECT/CT ^{99m}Tc-sestamibi it is high recommended as a first-line imaging in patients diagnosed with hyperparathyroidism before surgery. It is superior to ecography and planar imaging for a more specific localization of the pathological gland and for the detection of ectopic adenoma, providing additional topographic information, which is crucial in order to achieve radioguided surgery success.

P112**The Relationship Between Disease Severity and Quantitative Parameters Derived From Tc-99m MIBI SPECT Images in Primary Hyperparathyroidism**

D. Cayir, M. Araz, A. Yalcindag, E. Cakal; Ankara Diskapi Yildirim Beyazit Training and Research Hospital, Ankara, TURKEY.

AIM: Tc-99m methoxyisobutylisonitrile (MIBI) parathyroid SPECT is the method of choice in detecting parathyroid pathology in primary

hyperparathyroidism. It has been previously reported that there was a relation between retention index (RI) and parathyroid washout parameters derived from parathyroid scintigraphy and serum intact parathormone (PTH) levels, size of the tumor and oxyphilic cell content. In this study, a possible correlation between multiple scintigraphic quantitative indices and clinical, laboratory and radiological data was investigated in a large population. **MATERIAL-METHOD:** 93 patients (14M, 79F, mean age: 59.61 ±13.55) were involved. They had been preoperatively investigated by Thyroid-parathyroid USG and Tc-99m MIBI SPECT and both imaging modalities revealed a single parathyroid adenoma. Histopathological confirmation of a parathyroid adenoma was made by single sided parathyroidectomy. Region of interests (ROI) of equal pixel numbers were drawn around the parathyroid adenoma (PT), neighbouring thyroid tissue (T) and background (BG) in early and late planar images and isocontour ROI were drawn around the adenoma in SPECT images (Figure 1 and 2). Following background activity correction, early and late PT, PT/T, PT-T, PT washout [(Early T-Late T)/Late T], RI [(Late PT/T - Early PT/T) X100 / Early PT/T] were calculated. The relationship between these parameters and serum PTH, Ca, P, urinary Ca levels, weight of the adenoma and urinary ultrasonography findings were investigated. **RESULTS:** Pearson correlation analysis revealed that there was a statistically significant relationship between the weight of the adenoma and serum PTH and Ca levels. Among the scintigraphic parameters, Early PT-T was correlated with serum CA levels and RI was correlated with serum PTH levels (p<0.05). When patients were divided into two groups, the patients who have findings of nephrolithiasis shown by Urinary USG and the patients who don't, the results of student's t test revealed that Early and Late PT values were significantly higher in the group with nephrolithiasis compared to the patients with no signs of nephrolithiasis. **CONCLUSION:** In this study, we state that some parameters derived from Tc-99m MIBI parathyroid SPECT study can be indicative of disease severity

P113**The Utility of Rapid Parathyroid Hormone Radioimmunoassay in the Surgical Management of Hyperparathyroidism**

J. Koutsikos¹, G. Angelidis¹, K. Kalogeropoulou¹, M. Vogiatzis¹, E. Iliá¹, A. Evagelatou², A. Velidaki², N. Dimakopoulos¹; ¹Nuclear Medicine Dept., Army Share Fund Hospital (417 NIMTS), ATHENS, GREECE, ²Nuclear Medicine Dept., Laiko General Hospital of Athens, ATHENS, GREECE.

INTRODUCTION: Primary hyperparathyroidism is a common disease caused by single or multiple parathyroid lesions. If treatment is necessary, surgery is the commonly used procedure. Before operation, hypercalcaemia and elevated PTH levels must be observed. Most failures in parathyroidectomies are associated with the inability to identify a multiglandular disease or an ectopic location. Intraoperative PTH measurement (i-PTH) aims to ensure parathyroidectomy success, as the half-life of PTH is approximately 5 min. In our institution, we use an immunoradiometric assay (ELSA-PTH, CISBIO, France) for PTH measurement. The standard PTH assay in the analyzer has an 18 hrs +/- 2 incubation time, not suitable for (rapid) i-PTH measurement. Furthermore, in the literature, the methodology of radioimmunoassays is seldom used today because of lengthy turnaround time and poor diagnostic utility. However, a rapid ELSA-PTH procedure characterized by 30 min incubation time is recommended by the manufacturers. The aim of our study was to define a possible diagnostic utility of rapid ELSA-PTH procedure, compared to standard method. **METHODS:** Twenty-eight plasma samples were collected from patients with suspected hyperparathyroidism in our hospital. The samples were analyzed according to both standard and rapid methodology. Findings were assessed by simple linear regression analysis. **RESULTS:** The mean PTH level using the rapid procedure was 170,3 nm/l (range 21.8 - 1153.4), while using the standard method was 125,2 (range 13.8 - 771.8). Higher PTH values were measured in 24/28 samples

with the rapid method. Significant coefficient correlation was found between the values measured with the two methods ($r=0.988$, $p<0.0005$). There was no normal measurement based on one of the two methodologies performed corresponding to an abnormal value, when the same sample was analyzed according to the other procedure. **CONCLUSION:** Our findings support the diagnostic value of rapid PTH radioimmunoassay methodology, suggesting a favourable clinical utility in the intraoperative setting given its short incubation time. Under a well-designed protocol, this procedure can lead to a close co-operation between the operating surgeon and the specialized laboratory staff, placing the nuclear medicine department at the immediate disposal of the surgical team.

P114

A Convenient Low Iodine Diet for Preparation of Radioiodine rhTSH Scanning in Korean Patients

M. Lee¹, Y. Ryu², I. Hyun¹; ¹Inha University Hospital, Incheon, KOREA, REPUBLIC OF, ²Gangnam Severance Hospital, Seoul, KOREA, REPUBLIC OF.

Introduction: A stringent LID for 2 weeks has been recommended in Korean patient with DTC prior to DxWBS. The reason is that the dietary iodine intake in Korea is higher than all other countries except for Japan and Canada. Seaweeds take up over 70% of the dietary iodine intake in Korea. Considering it, we make a hypothesis that the body iodine pool may be sufficiently depleted by seaweeds restriction. Based on this concept, we proposed a new protocol; a simplified LID protocol (seaweeds restriction only) for the patients with preparing DxWBS by using rhTSH. We want to evaluate the efficacy of this compromised plan and compare it with conventional protocol by using spot urine analysis. **Material & Methods:** Total 72 papillary thyroid cancer patients (53 females, 19 males) preparing for follow-up DxWBS with rhTSH were enrolled. In order to assess the impact of 2 weeks stringent LID (LID1) on urinary iodine excretion during the preparation of RAIT, morning spot urine specimen was obtained on the final day of LID1 from each patient and the urine iodine excretion (UIE1) was checked to evaluate the efficacy of LID1. For rhTSH DxWBS, they contributed morning spot urine 8 days (LID2) and 10 days (LID3) after a simplified LID prior to DxWBS; on the day of first and second rhTSH injections. The urine iodine excretion on LID2 (UIE2) and LID3 (UIE3) were also evaluated. **Results:** The median value of UIE after LID1 was 12.80 μ g/L. The median value of UIE after LID2 was 111.38 μ g/L. There was no significant difference in the median UIE values between gender. The median UIE value of LID3 and LID2 was not significantly different. The frequencies of excellent and good iodine deficiency did not differ between 8 and 10 days simplified LID. However, the median UIE value of LID1 was significantly lower than that of LID2 and LID3. **Conclusion:** A simplified LID protocol is acceptable to achieve an optimal level of body iodine depletion for rhTSH DxWBS.

P-10 – Monday, October 17, 2016, 16:00 - 16:30, Poster Exhibition Hall
Conventional & Specialised Nuclear Medicine: Gastroenterology

P115

Liver function assessed by 99mTc mebrofenin hepatobiliary scintigraphy to evaluate the gain of hepatic functional mass after portal vein stenosis preconditioning of living donor liver in swine

P. BRIGE¹, G. HERY², G. BAUDIN³, C. BUFFAT¹, A. ARCHIER⁴, A. MOYON⁵, A. COPPOLA¹, J. HARDWIGSEN⁶, Y. LE TREUT⁶, E. GUEDJ⁴, B. GUILLET⁵, V. VIDAL⁷, G. GORINCOUR⁸, P. ROLLAND¹, E. GREGOIRE⁹; ¹CERIMED_LIIE / Aix-Marseille university, Marseille, FRANCE, ²Department of general pediatric surgery and liver transplantation, Hôpital Timone, Marseille, FRANCE,

³Department of diagnostic and interventional medical imaging, Hôpital l'Archet 2, Nice, FRANCE, ⁴CERIMED_Nuclear medicine / Aix-Marseille university, Marseille, FRANCE, ⁵CERIMED / Aix-Marseille university, Marseille, FRANCE, ⁶Aix-Marseille University/ Department of General surgery and liver transplantation, Hôpital Timone, Marseille, FRANCE, ⁷CERIMED_LIIE / Aix-Marseille university/ Department of diagnostic and interventional imaging, Hôpital Timone, Marseille, FRANCE, ⁸CERIMED_LIIE / Aix-Marseille university/ Department of pediatric diagnostic and interventional imaging, Hôpital Timone, Marseille, FRANCE, ⁹CERIMED_LIIE / Aix-Marseille university/ Department of general surgery and liver transplantation, Hôpital Timone, Marseille, FRANCE.

In order to reduce the morbi-mortality risk for the donor in living donor liver transplantation (LDLT), we previously identified 20% left portal vein (LPV) stenosis as the effective preconditioning to induce cell proliferation in the contralateral lobe without the downstream ipsilateral atrophy. We report, here, the pathways involved in the first hours after the preconditioning and investigate the changes in liver volume and function. Fourteen pigs entered this study. Five of them were used to study the genetic, cellular and molecular mechanisms set up in the early hours after the establishment of our preconditioning. Nine pigs were equally divided into 3 groups: sham operated animals, 20% LPV stenosis and 100% LPV stenosis. Volumetric scanner and 99mTc-Mebrofenin hepatobiliary scintigraphy were performed before and 14 days after preconditioning in order to study morphological and functional changes in the liver. We demonstrated that liver regeneration triggered by 20% LPV stenosis in the contralateral lobe involves TNF-alpha, IL-6 and NOS2, by means of STAT3 and HGF. We confirmed that our preconditioning was responsible for an increase in the total liver volume. Finally, we demonstrated that this volumetric gain was associated with an increase in of hepatic functional capacity.

P116

Fatty meal substitute vs Intravenous CCK for hepatobiliary imaging, a large case volume retrospective analysis

C. Sinsabaugh, M. Tann; Indiana University School of Medicine, Indianapolis, IN, UNITED STATES.

Since the advent of functional hepatobiliary imaging, there has been continued debate over the appropriate assessment of gall bladder ejection fraction. The mainstay for induction of gall bladder contraction continues to be intravenous infusion of CCK analogue. Multiple studies have been conducted to assess oral alternatives to intravenous CCK analogues, although these studies are typically limited to relatively few imaging studies on relatively healthy individuals. Our institution made a concerted switch to performing functional hepatobiliary imaging with the use of a liquid, high fat content meal replacement supplement in February 2014. After 17 months of imaging was performed using this protocol, a retrospective analysis was performed of 463 examinations conducted with the use of a high fat content meal replacement supplement. Additional retrospective analysis was performed of 1384 biliary examinations conducted using our institutions' standard protocol with intravenous CCK. Comparison of the two agents' histogram data was performed, which yielded a right skewed, bell-shaped data set with a high fat content meal replacement including a mean ejection fraction of 73% with a standard deviation of 19%. The intravenous CCK data set revealed a non-normalized, random distribution of ejection fractions with a mean ejection fraction of 55% and a standard deviation of 30%. Using the widely agreed upon cut-off of 34% for an abnormal gall bladder ejection fraction, 28.6% of IV CCK examinations resulted in an abnormal gall bladder ejection fraction vs. 9.7% with the use of an oral, fatty meal supplement. This data set suggests that the use of a fatty meal supplement may generate a more normalized sample of ejection fractions that one might expect in a population and that the currently agreed upon 34% cut-off for abnormal gall bladder ejection fractions may be too

low. Continued analysis of this data set and further evaluation of the patients contained there-in, including final disposition of therapy (i.e. surgery vs. no surgery) and outcomes could help provide further elucidation of the most appropriate methods and use of functional hepatobiliary imaging.

P117

The utility of oro-pharyngeal-esophageal scintigraphy (OPES) to assess instrumental deglutition function in patients with idiopathic inflammatory myopathies (IIM): short-term results of an ongoing prospective study

G. Puccini¹, E. Tardelli¹, E. Fiasconaro¹, S. Barsotti², F. Guidoccio¹, M. Gennaro¹, S. Margotti¹, B. Dell'Anno¹, R. Neri³, M. Grosso¹, D. Volterrani¹; ¹Regional centre of nuclear medicine, PISA, ITALY, ²Rheumatology Unit, Department of Clinical and Experimental Medicine, University of Pisa, PISA, ITALY, ³Rheumatology Unit, Department of Clinical and Experimental Medicine, University of Pisa, PISA, ITALY.

Background Dysphagia represents a major burden in IIM patients. OPES is a safe, reliable and repeatable technique, which allow a semi-quantitative scoring of oropharyngeal (OP) and esophageal (E) involvement. **Aim:** To report the initial results of prevalence of upper gastrointestinal abnormalities in IIM patients using OPES and the correlation of abnormalities detected by OPES with disease activity and dysphagia. **Patients and Methods** Since 2014 to 2016, we enrolled 32 IIM patients (M:F=4:28; 12 dermatomyositis, 18 polymyositis, 2 inclusion body myositis; mean age: 61±12.6 years). Each patient underwent a disease activity evaluation: physician's and patients' visual analogue scale (phVAS and ptVAS), health quality assessment questionnaire, manual muscle test 8 (MMT8) and serum creatine kinase. Dysphagia was assessed by the "MD Anderson dysphagia inventory" (MDADI), which classifies dysphagia as not present, mild, moderate, severe and total disability. Dysphagia parameters, assessed by OPES after 10 ml liquid (L) and semi-solid (SS) bolus labelled with 99mTechnetium-nanocolloid, were: pre-deglutition penetration, aspiration, OP and E transit time (OPETT) and retention index (RI). OP-RI was classifiable by a 4 grade scale: no retention (<8% of the swallowed bolus), mild (9-20%), moderate (21-40%) and severe retention (>40%), while E-RI was classifiable by a 3 grade scale: no retention (<20%), mild (20-45%) and severe retention (>45%). **Results** According to MDADI score, 11 patients (35%) presented no dysphagia, 13 (41%) mild, 5 (15%) moderate and 3 (9%) severe disability. OPES showed a normal OPETT and absence of pre-deglutition penetration in all patients. RI were altered in almost all patients, and, both after L and SS bolus, RI was altered in 25 patients. In the 10 patients with no dysphagia symptoms, IR alterations for L and SS bolus were detected respectively in 9 and 7 patients. Correlations with statistical significance between disease activity parameters and MDADI index were found for phVAS and ptVAS ($p=0.032$ and $p=0.017$) and MMT8 ($p=0.014$), while E-RI correlated with MMT8 ($p=0.007$). Moreover, 14 patients presented uncoordinated movement at proximal and medium esophagus and 2 patients presented SL bolus inhalation. **Conclusions** Dysphagia represents a major disabling feature in 64% of IIM patients and is associated with disease activity. OPES could allow to identify subclinical involvement in almost all patients examined, even if no symptoms were reported. Greater sample size and, above all, prospective clinical follow-up will clarify the clinical meanings of the alterations detected by OPES and their prognostic value.

P118

Value of ⁷⁵SeHCAT in the diagnosis of bile acid malabsorption in Crohn's disease with chronic diarrhoea

L. Mena Bares, F. Maza Muret, E. Carmona Asenjo, E. Moreno Ortega, V. Guiote Moreno, E. Iglesias Flores, V. García Sánchez, J. Benítez Cantero, J. Vallejo Casas; Hospital Universitario Reina Sofia, Córdoba, SPAIN.

Aim: The objective of this study is to analyze the utility of ⁷⁵SeHCAT in patients with Crohn's disease and chronic diarrhoea with suspected bile acid malabsorption (BAM), and to assess whether there is a relationship between the malabsorption degree and the presence of ileal resection.

Material and Methods: We analyzed retrospectively 31 patients with Crohn's disease and chronic diarrhoea with and without ileal resection during the period between August 2015-April 2016. In all patients an inflammatory process was previously discarded. No patients had received treatment with bile acid sequestrants (Cholestyramine) before the study. We perform the test after the ingestion of a ⁷⁵SeHCAT capsule (0,37 MBq) prior fasting the night before. Three hours later an initial gamma measurement is taken from a large field of view gamma camera, equipped with high sensitivity and parallel-hole collimator. Abdominal retained activity was measured in anterior and posterior views for 5 minutes. Room background is also measured for 5 minutes before and after the patient has been scanned. Seven day measurements were compared with 3 hours activity to calculate the abdominal retention percentage. BAM was diagnosed when retention was <10% at seventh day. **Results:** We studied 16 women and 15 men with mean age of 43 years old. 24/31 patients had undergone ileal resection (ranged from 2 to 80 cm, average=27,87 cm). 96,8% of patients demonstrated abnormal values of ⁷⁵SeHCAT scan defined as < 10% abdominal retention of ⁷⁵SeHCAT after seven days. 24/24 patients with ileal resection and 6/7 patients without resection had BAM. 92% of patients with ileal resection had severe malabsorption and 8% moderate malabsorption. 72% of patients without resection had severe malabsorption, 14% moderate malabsorption and 14% had normal retention. We performed linear regression analysis and we found no significant association between ⁷⁵SeHCAT retention and performing surgery or not, type or length of resection. **Conclusions:** ⁷⁵SeHCAT is an useful procedure for diagnosing BAM in patients with Crohn's disease and chronic diarrhea, with and without ileal resection. There was no significant association between ⁷⁵SeHCAT retention and performing surgery or not, type or length of resection.

P119

Gastric Emptying at 2 Hours and 4 Hours: Sensitivity Depends on Severity of Delayed Gastric Emptying

P. Magnone, J. Fletcher, J. M. Wo, M. Tann; Indiana University, Indianapolis, IN, UNITED STATES.

Purpose. Gastric emptying (GE) scintigraphy has been recognized as the gold standard for the assessment of gastric motility. Imaging guidelines have been established concerning how to acquire images for evaluation of delayed gastric emptying (DGE) over a 4 hour period, and additional studies have suggested shortening this time period to 2 hours for many patients. However, the severity of DGE correctly or incorrectly identified at the 2 hour period has not been evaluated. We sought to determine how well the 2 hour criteria set by Bonta et al identified patients with different severities of DGE. Additionally, we sought to determine if the Bonta criteria were optimum for our patient population. **Methods.** We collected GE data on 900 patients over a 10 month period. After excluding patients aged 12 years or younger, patients with prior gastric surgery, and incomplete studies, 703 patients remained (ages 13-86, 185 males, 518 females). We calculated the sensitivity, specificity, accuracy, and percentage of exams that would be shortened with different cutoff values in addition to the Bonta criteria (35% and 55%). We then determined the severity of DGE in these patients by the amount of activity remaining at 4 hours (mild: >10% and <= 20%; moderate: >20% and <=35%; severe: >35%). **Results.** 166 patients (23.6%) demonstrated DGE at 4 hours (70 mild, 30 moderate, 66 severe). Using the Bonta criteria resulted in 86.8% sensitivity, 89.6% specificity, 89.0% accuracy, and 74.7% of exams that could be terminated after 2 hours. However, we found that using cutoffs of 30% and 60% resulted in 90.4% sensitivity, 91.4% specificity, 91.2% accuracy, and 61.5% of exams that could be terminated after 2 hours. Using either

criteria resulted in excellent sensitivity for moderate or severe DGE but relatively poor sensitivity for mild DGE. **Conclusion.** The 2 hour Bonta criteria performed fairly well, but not as well as reported elsewhere. However, this performance was primarily due to poor performance with mild DGE, while sensitivity with moderate or severe DGE was quite good. Given these results, we recommend close collaboration with referring gastroenterologists before instituting a change in the GE protocol, as treatment may vary depending on severity of DGE. While terminating some exams at 2 hours instead of 4 hours will result in some false positives and false negatives, the severity of DGE correctly or incorrectly identified at 2 hours may influence whether or not such a change in protocol is acceptable.

P120

Assessment of spleen size-function relationships by technetium-99m-heat altered red blood cells scintigraphy in cirrhotic patients

G. Arsos¹, S. Georga¹, L. Kirkiniska², D. Katsampoukas¹, E. Moravidis¹, A. Siozopoulos³, T. Vasiliadis²; ¹3rd Dept of Nuclear Medicine, Aristotle University of Thessaloniki School of Medicine, Papageorgiou Hospital, THESSALONIKI, GREECE, ²3rd Internal Medicine Clinic, Aristotle University of Thessaloniki Medical School, Papageorgiou Hospital, THESSALONIKI, GREECE, ³Department of Anatomy, Demokriton University of Thrace Medical School, ALEXANDROUPOLIS, GREECE.

Background and aim : Cirrhosis may be associated with splenic hypofunction (hyposplenism) despite the commonly seen splenomegaly in patients with portal hypertension. Radionuclide studies using image quantitation or kinetic, non-imaging, analysis, are best suited for splenic function assessment and with the recent advent of the hybrid imaging, for successful splenic size determination. In this frame, functional splenic volume (FSV) as the percentage of an amount of heat-altered red blood cells labelled with technetium-99m (Tc-99m-hRBC) trapped in the spleen (% uptake) divided by the spleen volume is considered a reliable index of splenic function. In order to explore the splenic size-function relationship across disease stages, we calculated FSV in a number of cirrhotic patients submitted to Tc-99m-hRBC scanning for splenic function assessment. **Patients and methods :** Thirty (33.3% F) adult cirrhotic patients (47% on stage A, 53% on stages B-C according to Child-Turcotte-Pugh), aged 61.4±10.7 years were evaluated. Autologous Tc-99m-hRBC were in vitro prepared and dynamic, static and combined tomographic single photon emission computed tomography and CT (SPECT/CT) scans were obtained for up to 2 hours post-injection. After splenic Tc-99m-hRBC uptake assessment from SPECT imaging and previous phantom-based calibration and splenic volume from CT slices using the interactive OSIRISX MD software, FSV was calculated. Between-variable differences and correlations were assessed by Mann-Whitney test and linear or non-linear regression analysis respectively. **Results :** Medians of splenic volume (ml), splenic uptake (%) and FSV (%/ml) for the stages A and B-C patients were 278 vs 686, p=0.07; 47 vs 55, p=0.07 and 0.16 vs 0.07, p=0.272 respectively. Splenic volume showed a moderate positive correlation with splenic uptake ($r = 0.640$, $p < 0.005$) but a strong inverse correlation with SFV ($r = 0.945$, $p < 0.0001$). **Conclusions :** In cirrhotic patients disease progression is accompanied by both splenic enlargement and Tc-99m-hRBC uptake increase. However, splenic function as expressed by the functional splenic volume is seriously suppressed.

P121

^{99m}Tc-Mebrofenin (HIDA) SPECT-CT: New Tricks for an Old Test? A Pictorial Review

S. Soares, N. Mulholland, N. Gulliver, B. Corcoran, A. Eccles, G. Vivian; King's College Hospital, London, UNITED KINGDOM.

Introduction: Advances in dynamic CT and MRCP liver imaging has resulted in dynamic ^{99m}Tc-trimethylbromo-iminodiacetic acid (TBIDA, mebrofenin) or HIDA cholescintigraphy being used less frequently in the investigation of hepato-biliary disorders. There have been anecdotal reports of the use of SPECT and SPECT-CT in the management of patients with trauma to the biliary tree. We aim to highlight the role of HIDA SPECT-CT in diagnosing hepatobiliary leak. **Methods:** We present the protocols and results of the dedicated HIDA SPECT-CT protocol in a single institution with a tertiary service liver transplant unit. **Results:** HIDA SPECT-CT is now considered a first line investigation. Between April 2015 and April 2016 we performed 27 examinations on patients suspected of having a biliary leak. Dynamic 60 minute supine examinations followed by SPECT-CT (low dose CT for AC and localization) were performed on a Siemens Symbia 16T or a Phillips Skylight followed by supine slide transfer to the Symbia for SPECT-CT. Tomography was performed before 60 min if a leak was seen on the dynamic images. Delayed static images were performed if no leak was seen. **Discussion:** The majority of patients were referred for iatrogenic leak but patients were also examined after liver sepsis and blunt trauma. 14 patients were shown to have a biliary leak. Two patients were found to have a very rare condition of broncho-biliary fistula. In one sequential studies were used to assess therapy, including microembolisation with glue particles. These are discussed in further detail as case studies. **Reference:** Hepatobiliary scintigraphy with SPET in the diagnosis of bronchobiliary fistula due to a hydatid cyst. *Hell J Nucl Med* 2015; 18(2): 160-162

P122

30 Minutes or 60 Minutes: Which is Optimal for the Assessment of Rapid Gastric Emptying

P. Magnone, J. Fletcher, J. M. Wo, M. Tann; Indiana University, Indianapolis, IN, UNITED STATES.

Purpose. Gastric emptying scintigraphy has been recognized as the gold standard for assessment of gastric motility. Imaging guidelines have been established concerning how best to acquire images for evaluation of delayed gastric emptying, however there is still some confusion concerning how best to detect rapid gastric emptying as both may show similar overlapping symptoms. We compared the sensitivity of measurement of gastric emptying at 30 minutes and 60 minutes post-prandial to determine which measurement time showed a higher detection rate. **Methods.** We collected gastric emptying data on 900 patients over a 10 month period. After excluding patients aged 12 year or younger, patients with prior gastric surgery, and studies with incomplete data, 622 patients remained (ages 13-86, 160 males, 462 females). The percentage of activity remaining in the stomach at 30 minutes and 60 minutes post-prandial was evaluated to determine how many patients met criteria for rapid gastric emptying (less than 70% remaining at 30 minutes or less than 30% remaining at 60 minutes). **Results.** A total of 152 patients (24.4%) demonstrated rapid gastric emptying, including 114 patients at 30 minutes only, 3 patients at 60 minutes only, and 35 patients at both 30 and 60 minutes. Thus, the 30 minute time point identified 149/152 (98%) patients with rapid gastric emptying, and the addition of the 60 minute time point resulted in the identification of an additional 3 patients with rapid gastric emptying. Comparatively, the 60 minute time point identified 38/152 (25%) patients with rapid gastric emptying. **Conclusion.** If the purpose of imaging at 30 minutes or 60 minutes post-prandial is to identify patients with rapid gastric emptying, then the 60 minute post-prandial time point is a less useful time point as it is significantly less sensitive and may be replaced by using the 30 minute time point alone.

P123**The Clinical Utility of ^{99m}Tc Technetium Red Blood Cell Scintigraphy in the Diagnosis of Gastrointestinal Haemorrhage: A Retrospective Study Between 2009 to 2016**

A. Saviatto, D. Marin Ferrer, J. Marroquin Galvez, E. Martinez Albero, M. Tabuenca Mateo, A. Gomez Grande, P. Pilkington Woll, A. Hernandez Martin, P. Sarandeses Fernandez, S. Ruiz Solis, J. Estenez Alfaro; University Hospital 12 de Octubre, Madrid, SPAIN.

OBJECTIVE: The aim of the present study was to evaluate the ^{99m}Tc-Technetium labelled red blood cell scintigraphy (RBCS) utility for detection and localization of gastrointestinal bleeding (GIB). **MATERIALS AND METHODS:** A retrospective review of 156 patients, mean age of 68.7 years (16-88), 65 females, who underwent a RBCS for the evaluation of GIB at our institution from 2009-2016. RBC were labelled with 740-925 MBq of ^{99m}Tc by the modified in vivo method. The patients were referred to the Nuclear Medicine Department for the following reasons: chronic anemia (63), rectorragia (27), melena (51), haematochezia (10), occult blood stool (3) and hematemesis (2). Additionally, 137 patients underwent colonoscopy, 126 gastroscopy, 42 capsule endoscopy and 3 arteriography. The findings of all these techniques were correlated, and treatments analyzed on those patients that tested positive for GIB. We have conducted a clinical follow up during a minimum three month period with all patients. **RESULTS:** We detected 40/156 (25.6%) patients with active GIB as follows: 13/40 (32.5%) tested positive with RBCS and also with some of the other techniques; 18/40 (45%) tested positive only for RBCS and the remaining 9/40 (22.5%) patients positive with the other techniques and negative for RBCS. The correct location of the bleeding site was identified in 11/40 (27.5%) patients: 6/11 (54.5%) were positive for RBCS and positive with some other technique; 3/11 (27.2%) positive with the other techniques and negative for RBCS, and the remaining 2/11 (18.1%) were positive only with the RBCS. On the 63 patients diagnosed of chronic anemia, haemorrhage was detected in only 9 (14.3%) of them. However, the other 93 patients which showed signs of haemorrhage, an active GIB was detected in 31 (33.3%). The bleeding sources were located in the colon (3), small intestine (14) and stomach (1). Out of 40 patients with evidence of GIB, 14 underwent conservative treatment, 5 surgical, 9 argon plasma coagulation, 2 octreotide, 2 embolization, 7 died and 1 patient requested voluntary discharge. In the 116 patients tested negative for GIB there were neither death nor signs of bleeding detected in the following 3 months. **CONCLUSION:** RBCS is an effective imaging modality for detecting and localizing active GIB, and it is complementary to other techniques. RBCS proved to be specially successful for detecting the bleeding location in the small intestine, on the other hand, it was less accurate when used on patients with chronic anemia.

P-11 – Monday, October 17, 2016, 16:00 - 16:30, Poster Exhibition Hall
Conventional & Specialised Nuclear Medicine: Imaging Guided Surgery (Benign)

P124**Is It Advisable To Perform A High Dose SPECT-CT For Minimally Invasive Radioguided Parathyroidectomy?**

M. Milá; Hospital Universitari Germans Trias i Pujol, Badalona, SPAIN.

AIM OF THE STUDY: SPECT-CT hybrid imaging has proved to offer advantages over planar acquisition in the diagnosis and anatomic location of hyperfunctioning parathyroid glands in patients with primary hyperparathyroidism (HPT). The aim of this study was to evaluate the feasibility of preoperative Sestamibi SPECT-CT before minimally invasive radioguided parathyroidectomy (MIRP). **MATERIALS AND**

METHODS: From 2013 to 2015, consecutive patients with primary HPT and positive Sestamibi SPECT/CT who underwent MIRP were included in this observational study. **Planar and SPECT/CT acquisition** were performed after ^{99m}Tc-Sestamibi injection (740 MBq). Diagnostic SPECT/CT (2-slice SPECT-CT, Siemens Symbia T2) was acquired 20 or 120 minutes after injection according to the findings on the planar scintigraphy. Acquisition parameters were: CT (70 mAs -care dose 4D-, 130 kV, 3 mm, 2x 2,5 mm), SPECT (128X128 matrix, 180° rotation, 32 frames, 15 s/frame). **Radioguided surgery** was planned according to SPECT/CT findings. MIRP consisted of a unilateral cervical exploration through minimal incision followed by radioguided and macroscopic identification of pathological parathyroid tissue. Surgical time and postsurgical morbidity were evaluated. **RESULTS:** Thirty four patients with primary HPT and positive Sestamibi SPECT/CT underwent surgery by MIRP (8 males; age mean 68 years, range 41-88): 31 glands were orthotopic and 3 ectopic. Pathology was consistent with parathyroid adenoma (n= 30) or hyperplastic gland (n=4). The average operating time was 42 min (range 20-80), the longest time for ectopic lesions. Surgery was successful in all patients with short-term income, less than 24 hours, without postoperative complications or remarkable late events. **CONCLUSION:** Preoperative diagnostic SPECT/CT is advisable for MIRP because it provides useful anatomic information which improves surgical outcome avoiding bilateral neck exploration and with a short surgical time.

P125**Intraoperative Radioguided Localization Of Non Palpable Lung Lesion Or Difficult Surgical Site**

M. D. Danús Laínez¹, J. Fuertes Manuel¹, M. Martin Domenech¹, M. Mendoza Pares¹, J. Garcia Bennett¹, D. Rodriguez Martinez², P. Rodriguez Taboada², G. Rosado², E. Baeta¹; ¹Hospital Universitario Sant Joan de Reus, Reus, SPAIN, ²Hospital Universitario Juan XXIII, Tarragona, SPAIN.

Objective Description of the technique used in the localization of nonpalpable lung lesion or difficult surgical site and our experience. **Material and methods** Radioguided technique intraoperative detection of nonpalpable lesions or difficult pulmonary localization was performed in 20 patients, removing a total amount of 22 lesions. The average age was 64.2 years (range 17-84 years), 13 men and 7 women. The technique was performed a few hours before surgery by injecting 0,5mCi Tc^{99m} macroaggregated albumin as a tracer, with posterior scintigraphic control, performing CT-guided (with or without fluoroscopy) marking, and gamma-detecting probe (thorascopic or not), during the surgical procedure. The types of lesions studied were 14 pulmonary nodules and 8 pulmonary lesions with ground-glass opacity. **Results** 21 of the 22 lesions studied (95.45%) were successfully located. The lesion not initially detected was localized by palpation. The types of excised lesions were 8 adenocarcinomas of colorectal origin (36.36%), 3 lung adenocarcinomas (13.6%), 3 atypical adenomatous hyperplasia (13.6%), 2 no mucinous bronchoalveolar adenocarcinomas (9.09%), 2 hamartomas (9.09%), 1 melanoma (4.5%), 1 necrotic nodule (4.5%), 1 lung squamous carcinoma (4.5%), and 1 emphysema (4.5%), the failure detection with subsequent detection of lung adenocarcinoma by palpation). Regarding the type of surgery, there have been 14 thoracotomies and 6 videothorascopies (after the acquisition of thorascopic probe). **Conclusions** The intraoperative radioguided localization of nonpalpable lung lesions or difficult surgical site is a reliable technique. It allows accurate and fast location of lesions, with minimization of aggression in surgical approaches in most cases (Performing videothorascopy instead of thoracotomy VATS). The learning curve of this technique is affordable after a few patients.

P126**Usefulness Of Radioguided Surgery By Intraoperative Scintigraphy In Patients With Primary Hyperparathyroidism And Not Conclusive Previous Scintigraphy**

J. OROZCO-CORTÉS¹, R. DÍAZ-EXPÓSITO, Sr.¹, I. CASÁNS-TORMO¹, H. BOWLES-ANTELO¹, V. LÓPEZ-PRIOR¹, A. AMRREY¹, A. ALMARCHA-GIMENO², R. JOVER-BARGUES³, N. CASSINELLO-FERNÁNDEZ³, J. ORTEGA-SERRANO³; ¹NUCLEAR MEDICINE SERVICE. HOSPITAL CLÍNICO UNIVERSITARIO DE VALENCIA, VALENCIA, SPAIN, ²RADIOPHARMACY UNIT. NUCLEAR MEDICINE SERVICE. HOSPITAL CLÍNICO UNIVERSITARIO DE VALENCIA, VALENCIA, SPAIN, ³SURGERY SERVICE. HOSPITAL CLÍNICO UNIVERSITARIO DE VALENCIA, VALENCIA, SPAIN.

INTRODUCTION We analyse the usefulness of the intraoperative scintigraphy (IS) in patients diagnosed with primary hyperparathyroidism, who were treated by minimally invasive parathyroidectomy (MIP), and presented a not conclusive previous parathyroid scintigraphy (PS). **MATERIAL AND METHODS** 30 patients (20 women), age 60+11 (29–79 y/o), with PS performed with 99mTc-MIBI (20 mCi–70 kg) and double phase protocol (Philips Brightview gammacamera). In 20 patients, the PS was considered unclear and in 10 negative for the presence of parathyroid adenoma (PA). In 18/30 (60%) cases, SPECT was performed. 19/30 patients presented morphological studies (sonography, CT and/or MR). 10 patients had thyroid disease. The value of pre and postoperative PTH was determined. MIP was performed using IS with a portable gammacamera Sentinella®, after administration of 99mTc-MIBI (5 mCi). We performed initial images 20 min after radiotracer administration, and after identification of the suspicious lesions, in vivo and ex vivo images of the removed piece as well as the surgical bed. Finally, it was performed later pathological confirmation. **RESULTS** After remove the lesion, in 25/30 (83.3%), the anatomopathological result was PA, in 3/30 (10%) parathyroid hyperplasia, 2 (thyroiditis, thyroid nodule). In the 16/20 cases with unclear PS, the IS was coincident with the previous PS, in the localization of the possible lesion. In 12 of these 16 cases (75%) the surgical localization was coincident, (finally PA in 10) and in 4/16 (25%) not (finally PA in 3). In the 10 patients with negative PS, 3 (30%) had a negative IS, although in those 3 cases, the removed piece was a PA (false negatives). The IS found a possible PA in 7 of these 10 (70%) patients. In 12/18 (66.6%) cases with suggestive PA in SPECT, in 9 (75%) the localization was coincident in relation with the IS. 12/19 patients with morphological study were suggestive of PA and the PS was coincident with a possible PA in 8/12 (66.6%). 7/8 (87.5%) cases were finally PA. Globally, when we analyzed the 25 patients who finally had a PA, the IS provided information for the localization and removal in 18 (72%). The mean value of preoperative PTH was 248.8 and the postoperative was 66.2. **CONCLUSIONS** When we perform MIP in patients with primary hyperparathyroidism and negative or unclear previous scintigraphy, the IS provided valuable information for the final localization of the PA in the majority of patients. There was a high probability to find a PA, when there was a coincident diagnostic between the morphological studies and PS. There was a high concordance between the PA localization with SPECT and IS.

P127**Use of SPECT/CT lymphoscintigraphy in the management of chylous ascites**

M. PRPIC, M. Franceschi, Z. Kusic; University Hospital Centre Sestre Milosrdnice, ZAGREB, CROATIA.

Introduction: Chylous ascites (CA) is characterized as accumulation of chyle containing lymphatic fluid within the peritoneal cavity. CA is usually secondary to disruption of the lymphatic duct derangement to cisterna

chyle. CA has various causes, as follows: trauma (including surgery), miscellaneous disorders and idiopathic. Lymphoscintigraphy is noninvasive method for evaluation of lymphatic drainage. The aim of our study is to elucidate the contribution of SPECT/CT in diagnosis and management of CA. **Case report.** A 34 years old lady, presents with one week history of distended abdomen, without upper or lower extremity swelling or dyspnea. She had mild abdominal pain with agitation and vertigo. She had cesarean section two months and laparoscopic extirpation of retroperitoneal right ovarian cyst 3 years before onset of symptoms. Lymphoscintigraphy was suggested after computed tomography (CT), ultrasound and abdominal paracentesis examinations. Whole body and additional static images were performed in differential time intervals (immediately, 20 min, 4h and 24h) after subcutaneous injections of 37 MBq 99mTc-nanocolloid between the 1th and 2nd dorsal interdigital spaces of both feet. Scintigraphic images showed accumulation of radiopharmaceutical in abdominal space and lymphatic leakage around right iliac lymphatic vessel, especially in SPECT/CT images after 24h. **Discussion.** CA is peritoneal lymphatic leakage. Determination of leakage localization is not always accurate and depends on functional status of lymphatic vessels and amount of lymphatic leak. The potential clinical problem could be a pain as a result of distension of the peritoneum, suggestive of an acute abdomen. **Conclusion.** The additional use of SPECT/CT can increase the sensitivity and specificity instead of planar lymphoscintigraphy. Thus, it can provide better anatomical localization of lymphatic leakage and direct surgical management. Hence, according to our presented case SPECT/CT improves the noninvasive assessment of determination of lymphatic leakage, especially in the case of damaged lymphatic vessels.

P128**Value of Radioguided Surgery in an Osteoid Osteoma case**

M. Solá¹, M. Minoves¹, P. Bassa¹, S. Mas², M. Fraile¹; ¹CETIR-ERESA, Barcelona, SPAIN, ²COT Clínica Sagrada Família, Barcelona, SPAIN.

Osteoma osteoid is the third most frequent benign tumor in bone, and accounts for the 10% of the cases. Osteoid osteoma shows a high prevalence in children and young adults, and is usually found in long bones. The most common localizations are the femur and the tibia which, when considered together, correspond to more than 50% of the cases. Bone scan is the most common procedure to confirm when osteoid osteoma is suspected, thus giving also a guide for the tomographic selective study, CT or MR, in order to exactly determine size of the nidus. Preferred definitive treatment of choice consists in percutaneous excision of the lesion by means of CT-guided radiofrequency. However, this procedure is not always available and percutaneous en-bloc resection is still a valid option for the orthopedic surgeon. We present the case of a 17-year-old female patient with symptoms and imaging procedures consistent with osteoid osteoma in her left tibia, which was excised by radioguided surgery after performing a bone scan. Intraoperative x-ray and subsequent pathological definitive exam both confirmed the final diagnosis. Implementation and advantages of radiosurgery location in this kind of benign lesions are discussed.

P-12 – Monday, October 17, 2016, 16:00 - 16:30, Poster Exhibition Hall
Conventional & Specialised Nuclear Medicine: Infection & Inflammation

P129**Emphasizing the pivotal role of F 18 FDG PET CT as an effective tool in evaluation of patients with pyrexia of unknown origin (PUO) in Indian population**

A. JAYKANTH, S. SHELLEY, E. INDIRANI, K. SHILPA, J. AVANI; APOLLO HOSPITALS, CHENNAI, INDIA.

Aim: In a densely populated country like India, in the background of ever increasing air and water pollution and lack of proper sanitation, people are more prone to recurrent microbial infections. Changing dietary habits, sedentary life style, use of tobacco, smoking, alcohol consumption and in era of foods with abundant preservatives and chemicals, the incidence of malignancy is becoming high. Patients presenting with PUO have become a challenging task for physicians to diagnose and treat. F18 FDG PET CT is being done as a last resort imaging in the workup of patients with PUO. F18 FDG PET CT has the advantage of being a one stop shop with high sensitivity and high negative predictive value to diagnose, exclude various causes of PUO and guides in further management by showing the appropriate metabolically active site to do biopsy. Objective of this study is to emphasize the pivotal role of F18 FDG PET CT as an effective tool in evaluation and management of patients with PUO. **Materials and Method:** A total of 42 patients (23 males, 19 females) with PUO who underwent F 18 FDG PET CT were studied prospectively during a period of 1 year. These patients were subsequently worked up and followed till final tissue diagnosis was confirmed. **Result:** Final diagnoses were categorised as infective and non-infective. 74% of patients had features of infective etiology and 26% had features of non-infective etiology. Tuberculosis was the predominant cause of infective etiology(90%) with various spectrum of presentation and rest were foci of microbial abscesses(10%). Non-infective causes include lymphomas/haematological malignancies(80%), vasculitis(10%), sarcoidosis(2%), carcinoma lung (3%), thyroiditis(2%), IgG4 related disease(2%) and cholecystitis(1%). **Conclusion:** In this study, we found more than 90% sensitivity and 60% specificity of PET CT findings in correlation with final tissue diagnosis. Almost 100% negative predictive value in excluding occult malignancy and infective foci. In an endemic country like India, various spectrum of presentation of tuberculosis was illustrated by F18 FDG PET CT which had significant impact on the further management. Hence F18 FDG PET CT can be an efficient, noninvasive technique for evaluation, management and follow up of patients with PUO with high sensitivity and high negative predictive value reducing the overall cost of hospitalization.

P130

FDG PET/CT in Tuberculosis: when and why?

D. Grigolato, M. Del Rizzo, M. Cucca, L. Locantore, M. Zuffante, E. Concia, M. Ferdeghini; Azienda Ospedaliera di Verona, VERONA, ITALY.

AIM: to assess the utility of functional imaging in the evaluation of patients with suspected tuberculosis (TB) and in monitoring therapy. **Method:** we retrospectively reviewed 88 patients (28 female, 60 male, age range 19 -78 years) who came in our department for diagnosing, staging and assessing therapy in TB between the beginning of 2014 to March 2016. Diagnosis of TB was based either on histology or microbiological assessment in 78 patients, on typical morphological features of TB in CT and improvement on antimycobacterial treatment in 10 patients. All scans were carried out on the 16-slice Gemini Big Bore TOF (Philips). **Results:** FDG PET/CT was performed in 42 patients for diagnostic purpose (48%), in 25 patients with previous history of TB (29%), in 10 patients during therapy (11%) and in 11 patients after treatment (12%). FDG PET/CT was positive in 74 patients and negative in 14 (all true negative). Among positive PET/CT, TB were found in 54 patients (73%): in 24 patients with suspicious TB (SUVmax range 1.7-26.2), in 15 patients with previous history of TB (SUVmax range 1.6-13.5), in 9 patients during therapy (SUVmax range 2.8-11.5) and in 6 patients after therapy (SUVmax range 1.5-5.7). FDG PET/CT identified 14 patients with exclusively lung involvement (SUV max range 1.5-10.9), 10 patients with extrapulmonary localizations and 30 patients with involvement of both sites. The most affected regions/organs were: lungs in 44 patients (bilateral in 35) and SUVmax range 1.5-19.9, lymph nodes in 36

patients with SUVmax range 2.7-20.4 (88% mediastinal nodes, 58% laterocervical nodes, 47% retroperitoneal nodes, 19% axillary nodes, 13% other basins), visceral organs in 11 patients, bone in three cases. In the remaining 20 patients with positive scans (23%), TB were ruled out after biopsy. There were four patients with tumors and 16 patients with infections (10 cases with pulmonary involvements and 5 patients with lymphadenopathy). **Conclusions:** metabolic imaging is valuable in the diagnostic work-up of patients with TB in patients with probable or confirmed TB to check disease activity, extension and monitoring response to therapy; it is appropriate in case of previous history of TB infection to distinguish latent from active TB. It can not differentiate tumors from TB but it guided biopsy and assisted to early diagnosis.

P131

Dual Time Point FDG PET/CT Imaging in Prosthetic Heart Valve Endocarditis

A. M. Scholtens¹, L. E. Swart², H. J. Verberne³, R. P. J. Budde², M. G. E. H. Lam⁴; ¹Meander Medical Center, Amersfoort, NETHERLANDS, ²Erasmus Medical Center, Rotterdam, NETHERLANDS, ³Amsterdam Medical Center, Amsterdam, NETHERLANDS, ⁴University Medical Center, Utrecht, NETHERLANDS.

Purpose: ¹⁸F-fluorodeoxyglucose positron emission tomography combined with computed tomography (FDG PET/CT) has been of increasing interest and clinical impact in the diagnostic workup of prosthetic heart valve endocarditis (PVE). Although some reports advocate later imaging times to improve the diagnostic accuracy for PVE, the optimal delay between FDG administration and image acquisition time has not been established yet. In this study, we compared standard and late FDG PET/CT images in patients under suspicion of PVE. **Materials and Methods:** Fourteen scans in 13 patients referred for FDG PET/CT for suspicion of PVE were performed at standard (60 min post injection) and late (150 min post injection) time points. Images were scored based on visual interpretation (PVE vs. no PVE) and semi-quantitatively with SUVmax and Target-to-Background Ratio (TBR, defined as [SUVmax valve/SUVmean blood pool]). Visual and semi-quantitative scores were compared for both time points. The imaging findings were related to the final diagnosis, based on surgical findings in all cases of infection (n=6) and unremarkable follow up after clinically rejected diagnosis of endocarditis in all others (n=8). **Results:** Compared to the standard time, TBR was higher in late images, mostly due to diminished activity in the blood pool (SUVmax standard 3.77 ± 1.06 vs. late 4.30 ± 1.64 , TBR standard 2.55 ± 0.93 vs. late 4.27 ± 1.89 , $P=0.0001$). Late images were more prone to false positive interpretation for both visual and semi-quantitative analyses. Visual analysis of the early images yielded 1 false negative and 1 false positive result. On the late images, no scans were false negative but 5 scans were false positive. ROC-analysis of the TBR showed a larger area under the curve for early measurements (0.87) compared to late measurements (0.79), though not significantly so ($P=0.22$). **Conclusion:** Late FDG PET/CT imaging for PVE seems to have a propensity for false positive results. Therefore late imaging should be interpreted with caution.

P132

Efficacy of 99mTc-UBI 29-41 scintigraphy in diagnosis of peri-prosthesis spinal infection

S. Fatima, S. T. Butt, N. Ahmed, M. Faheem; Nuclear Medicine , Oncology & Radiotherapy Institute (NOR), Islamabad, PAKISTAN.

Spinal surgery is associated with significant risks. Although several technical and operative improvements for surgical treatment of spinal problems especially the use of orthopaedic implants have recently been introduced. Infection rates after spinal surgery currently remain relatively high. In particular, postoperative spinal infection, is one of the most

serious complications after spinal surgery, is observed in up to 1% to 6% of all patients. The rate of implant associated infections is reported as high as 10% in various studies. Currently MRI is most reliable technique for diagnosing spinal infection however, prosthetic insertion may leads to false positive results. Objective: The purpose of the study was to evaluate the efficacy of Tc99-UBI for diagnosing vertebral prosthetic infection in comparison with MRI. Methods . All patients underwent UBI scans and contrast enhanced MRI. The scans were interpreted in a blind and independent fashion by 2 experienced observers. The final diagnosis was obtained with the histopathologic study or a microbiologic culture or with the clinical findings after a follow-up of at least 6 months. The sensitivity, specificity, positive and negative predictive values, and the positive and negative probability ratio were determined, always using a 95% confidence interval (CI). The concordance with the kappa index was determined. Results Fifteen patients with suspected post-prosthetic spinal infection were included; 9 males and 6 females, with a mean age of 50 years (SD = 16). Nine patients had a history if spinal infiltrations. The number of patients with a positive scan was 20. The sensitivity for detecting prosthetic infection was 100% (CI: 0.901-1) and the specificity was 86.5% (CI: 0.647-0.865). The positive predictive value was 0.95, and the negative predictive value was 1 (CI: 0.739-1). The intra- and interobserver kappa value was 1. Conclusion The UBI scan showed 100% sensitivity and 86% specificity for peri-prosthesis spinal infections. Although the role of this method in the diagnostic protocol of the patient with suspected post-implant spinal infection has not yet been defined We found a high diagnostic accuracy for ^{99m}Tc -UBI [29-41] scintigraphy in suspected orthopedic implants infections . Therefore, ^{99m}Tc -UBI [29-41] scintigraphy might be potentially recommended as a safe and promising imaging modality in these settings. However, further studies on larger number of patients and different pathologies are still needed.

P133

Qualitative and semiquantitative [^{18}F]FDG-PET/CT analysis in patients with IE: a strategy to enhance specificity?

r. boni¹, s. margotti¹, m. sollini², r. doria³, u. conti⁴, f. menichetti³, e. lazzeri¹, p. erba¹; ¹Centro Regionale di Medicina Nucleare, Pisa, ITALY, ²Umanitas University, Milano, ITALY, ³U.O. Malattie Infettive, Pisa, ITALY, ⁴U.O. Cardiologia 2, Pisa, ITALY.

AIM: The recent 2015 ESC Guideline for the diagnosis and management of infectious endocarditis (IE) included molecular imaging procedures such as radiolabeled leukocytes and [^{18}F]FDG-PET/CT as major criteria to establish the diagnosis of IE. Whereas in case of radiolabeled leukocytes the criteria for defining positive and negative scan are well established, in case of [^{18}F]FDG-PET/CT there is still unanimous consensus of the criteria that define a positive scan. MATERIALS AND METHODS: In this work prospectively evaluated a series of 76 patients (M:F=50:26, mean age 67±16 years, median age 72 years, range 18-88) that performed [^{18}F]FDG-PET/CT for suspected IE between January 2013 and January 2016 in our center to define which the pattern of uptake and the semiquantitative parameters (SUVmax, valve/liver, valve/lung and valve/mediastinum uptake ratio) with the highest diagnostic accuracy for diagnosis IE. Patients with permanent cardiac devices were excluded. PET/CT results were correlated with transthoracic (TTE) or transesophageal (TEE) echocardiography, blood culture, the Duke criteria. The new ESC criteria were also evaluated. RESULTS: globally PET/CT was true positive in 26/27 and false negative in 1/27 cases (96% sensitivity, 97% NPV, 75% specificity and 68% PPV). A focal pattern of uptake was found 15/26 patients with confirmed IE (mean SUVmax=5.29±1.8, median SUVmax=5.5) and only 2/49 patients without IE whereas a diffuse pattern of uptake was found in 11 patients with confirmed IE (mean SUVmax=8.1±3.5, median SUVmax=7.6) and in 10 negative scans (mean SUVmax=4.1±1.1, median SUVmax=3.3). No significant differences between the valve/liver ratio uptake and the valve/mediastinum uptake ratio were found between positive and negative

patients with either focal or diffuse pattern of uptake. Interesting, in presence of diffuse valve uptake both SUVmax and the valve/lung uptake ratio were significantly higher in patients with a final diagnosis of IE, including the group of patients under antimicrobial treatment (>90%). PET/CT confirmed its ability to identify extracardiac sites of [^{18}F]FDG uptake in presence of septic embolism (35%) and in patients with other diseases (vasculitis, vascular prosthesis infections, mediastinitis and cancer, particularly in patients with IE sustained by *Streptococcus Gallolyticus*). CONCLUSIONS: Our results confirmed the role of [^{18}F]FDG PET/CT in patients with IE to confirm or reject the diagnosis as well as in identifying septic embolic sites or alternative causes of infection/inflammation. The pattern of [^{18}F]FDG uptake more specific for valve infection in this series is a focal uptake or a diffuse uptake with a SUVmax>5 and a valve/lung ratio >8.

P134

The Value Of FDG PET/CT In The Diagnosis Of Aortic Stent Graft Infections

D. Zogala, V. Ptacnik, D. Rucka, V. Cerny, P. Varejka, J. Trnka, J. Kubinyi; General Teaching Hospital in Prague, Prague, CZECH REPUBLIC.

AIM: Endovascular aortic repair with stent graft (SG) insertion is a method of choice for the treatment of growing aortic aneurysm or dissection. FDG PET/CT is a recognized method for the diagnosis of infected surgical vascular grafts, but the literature evidence on its use in suspected stent graft infection (SGI) is scarce. Our aim was to analyse the value of FDG PET/CT in the diagnosis of SGI. MATERIALS AND METHODS: Two experienced nuclear medicine physicians have independently retrospectively analysed 11 FDG PET/CT examinations in 10 patients (8 males, 64 ± 10 years) referred with clinical suspicion of SGI between 2012-2016. The images were evaluated and scored visually (the pattern: diffuse, focal or inhomogeneous; the intensity of uptake: visual grading scale comparing the level of FDG uptake in the area of SG with accumulation in healthy liver parenchyma) and semiquantitatively (SUVmax in the area of SG, target-to-background ratio (TBR) comparing SUVmax in SG with average SUV of blood pool in the inferior vena cava). The SGI was defined as the presence of focal hyperactivity in the area of SG and eventually in adjacent tissues with the intensity exceeding the activity of the liver parenchyma. The CT images (mostly not dedicated vascular protocol) of PET/CT were independently assessed by one radiologist (blinded to PET). All images were evaluated in randomized and blinded manner. The clinical judgment of two angiologists based on thorough review of all available unblinded data in subsequent follow-up was used as a reference (the results of PET/CT were not taken in concern). The discrepancies between researchers were solved by confrontation and consent. RESULTS: 6/11 (55%) cases were interpreted as SGI by clinical review. FDG PET/CT correctly diagnosed SGI in 5/6 (83%) cases and yielded sensitivity of 83% and specificity of 80%. Mean SUVmax and TBR (average ± SD) were 8.4 ± 3.5 and 5.7 ± 1.6 resp. in the group of patients with true SGI and 4.6 ± 1.1 and 2.7 ± 0.5 resp. in true negative cases. Analysis of CT images resulted in sensitivity of 83% and specificity of 80% and was concordant with PET in 9/11 (82%) cases. CONCLUSION: In our limited patient group FDG PET/CT with visual assessment correctly identified 83% of cases of SGI and might be useful diagnostic tool in this clinical setting.

P135

The role of 18F-FDG PET/CT in patients with suspected infective endocarditis and echocardiographic inconclusive findings

C. E. Popescu¹, S. Capitanio¹, R. Sara¹, M. Milella¹, S. Fiorino¹, B. De Chiara², A. Moreo², C. Giannattasio², C. Rossetti¹; ¹Nuclear Medicine

Department, Niguarda Hospital, Milan, ITALY, ²“De Gasperis” Cardiovascular Department, Niguarda Hospital, Milan, ITALY.

AIM: The diagnosis of infective endocarditis (IE) can be difficult to make and in most institutions, the final diagnosis is established using the modified Duke criteria. The latest European Society of Cardiology guidelines have introduced nuclear imaging as a diagnostic test in patients with suspected IE. Compared to radiolabelled white blood cell imaging, the PET has the advantage of having a better spatial resolution and to have significantly lower acquisition times. The purpose of this preliminary study was to evaluate the role of 18F-FDG PET/CT in patients with suspected IE and echocardiography not conclusive. **MATERIALS AND METHODS:** Twenty-one patients (mean age 58 ± 16 years) hospitalized with suspected IE in our hospital from December 2013 to January 2016, underwent 18F-FDG PET/CT in the presence of echocardiographic findings doubts or inconclusive. PET/CT scan results were correlated with transthoracic or transesophageal echocardiography, blood cultures, and the Duke criteria. **RESULTS:** 10 (47, 6%) patients presented native valves, 8 (38%) had prosthetic valves after surgery (> 6 months) and 3 (14.4%) had cardiac implantable electronic device (CIED). Nine patients (43%) had positive blood cultures, 17 (81%) had hyperpyrexia and 18 (85.7%) performed the PET/CT scan during the antibiotic therapy. All patients with certain diagnosis had fever and 4 had positive blood cultures. The 18F-FDG PET/CT scan was positive in 5/21 (23.8%) patients. In 4 of these, PET/CT scan has allowed the diagnosis of definite endocarditis according to the modified Duke criteria. Among the 16 patients with negative results, the negativity of 18F-FDG PET/CT has ruled out the diagnosis of IE in 14 cases. None of the patients excluded from the diagnosis of endocarditis subsequently underwent surgery or died in follow-up (median 8 months, minimum one month, maximum 37 months). **CONCLUSIONS:** Our experience confirms the value of 18F-FDG PET/CT in the diagnosis of patients with suspected infectious endocarditis. Especially, for those cases where echocardiography is not conclusive, nuclear medicine proves a crucial role to conclude diagnostic procedure.

P136

PET/MR for evaluation of hepatic inflammation in patients with chronic hepatitis C virus infection

N. S. Nielsen, H. H. Johannesen, A. E. Hansen, E. Fallentin, J. Löfgren, M. S. Kjær, M. R. Clausen, A. Kjær, S. D. Nielsen, B. M. Fischer; University Hospital of Copenhagen/Rigshospitalet, Copenhagen, DENMARK.

AIM Chronic hepatitis C (CHC) infection is associated with systemic as well as hepatic inflammation, the latter contributing to the development of fibrosis, cirrhosis and hepatocellular carcinoma (HCC). Recently, direct-acting antiviral (DAA) agents have been introduced for treatment of CHC, resulting in sustained virological response (SVR) in the majority of patients. This pilot study examines the use of FDG PET/MR for evaluation of hepatic inflammation in patients with CHC, before and after treatment with DAA. **MATERIALS AND METHODS** The study is a substudy to a prospective study evaluating coagulation and inflammation in patients with CHC. FDG-PET/MR (Siemens Biograph mMR) was performed prior to and after DAA therapy. PET/MR included PET acquisition 60 and 90 min after FDG-injection, DIXON for AC, T2 and DWI (10 b-values between 0-700 s/mm^2). Three VOI of each 12-15 cm^3 were placed in the liver parenchyma, avoiding larger vessels. The following parameters were extracted: SUV_{mean60} , SUV_{mean90} , ADC_{total} , Perfusion Fraction (PF) and ADC_{slow} (perfusion free). Furthermore, HCV viral load, ALT and CRP was measured. Level of fibrosis was determined using transient elastography. **RESULTS** Ten patients completed PET/MR before and after DAA. Four patients had cirrhosis. Average HCV viral load prior to therapy was $1.7 \cdot 10^6$ IU/ml (SD $1.2 \cdot 10^6$). All patients obtained SVR. Average (SD) ALT decreased from 103(92) U/l to 22(12) U/l, $p=0.02$. CRP was within the normal range and did not change significantly

during therapy. Prior to therapy average SUV_{mean60} and SUV_{mean90} was 1.9(0.2) respectively 1.7(0.3). The ratio $SUV_{mean90}/SUV_{mean60}$ was 0.9 (0.1). Neither changed significantly during therapy, nor did ADC_{total} or ADC_{slow} (1017(55) and 1013(91) s/mm^2 respectively). PF increased from average 207(40) to 259(58) s/mm^2 , $p=0.001$. There was a trend towards higher SUV and lower PF in patients with cirrhosis. Plotting changes in the ratio $SUV_{mean90}/SUV_{mean60}$ against changes in PF suggests a correlation between the two parameters. **CONCLUSION** PET/MR in patients with CHC infection is feasible. In this study, all participants achieved SVR, and ALT decreased. Isolating PF on DWI-MR, an effect of therapy was found. However, all other PET/MR parameters including FDG-uptake were unchanged. A correlation between changes in FDG-uptake and PF is suggested, underlining that FDG-uptake is not only dependent on the presence of inflammatory cells, but also on perfusion. Whether or not PET/MR could be a useful tool to separate changes in FDG-uptake caused by changes in perfusion from changes in the number of inflammatory or malignant cells should be explored in future studies.

P137

The Role Of FDG-PET/CT In Infectious Processes

M. CORTES-ROMERA¹, E. LLINARES-TELLO¹, A. SABATE-LLOBERA¹, M. SANTIN-CEREZALES², L. RODRÍGUEZ-BEL¹, L. GRÀCIA-SÁNCHEZ¹, J. ROBLES-BARBA¹, F. MARTÍNEZ-TORRENTS³, J. VERCHER-CONEJERO¹, J. MESTRES-MARTÍ¹, C. GÁMEZ-CENZANO¹; ¹PET UNIT NUCLEAR MEDICINE. IDI. HOSPITAL U BELLVITGE-IDIBELL, L-HOSPITALET DE LLOBREGAT (BARCELONA), SPAIN, ²DEPARTMENT OF INFECTOLOGY/INTERNAL MEDICINE. HOSPITAL U BELLVITGE-IDIBELL, L-HOSPITALET DE LLOBREGAT (BARCELONA), SPAIN, ³DEPARTMENT OF RADIOLOGY. HOSPITAL U BELLVITGE-IDIBELL, L-HOSPITALET DE LLOBREGAT (BARCELONA), SPAIN.

AIM: To assess the utility of 18F-FDG-PET/CT in identifying the origin of infectious processes. **MATERIAL AND METHODS:** Fifty-one patients with suspected infectious processes were included in this study from 2011 to 2015. They were 18 women (36 %) and 33 men (64 %), with a mean age of 63 years (range 15-87). Patients were classified in 7 different groups according to the clinical suspicion: vascular graft infection (19), tuberculosis (9), renal or hepatic cyst infection in polycystic disease (7), abdominal or chest infection with lymph nodes (7), bacteraemia or sepsis of unknown origin (5), postoperative (3) and spinal infection (1). All patients underwent a whole body PET/CT at 60-120 minutes after intravenous administration of 3.7 MBq/Kg FDG. Nine patients were under antibiotics (including tuberculosis drugs). The results were compared with the final diagnosis based on the histopathology, microbiological assays, trans-thoracic echocardiography, morphological techniques, clinical and/or imaging follow-up after antibiotic treatment. Results were categorized as true-positive when abnormal 18F-FDG uptake was confirmed as infection. Normal test results were true-negative when no infectious process was confirmed or spontaneous remission. Accuracy, sensitivity, specificity, positive and negative predictive values were calculated. **RESULTS:** Forty-two out of 51 patients had a positive PET scan (82 %). In 38 of them (90%), PET/CT helped in identifying the cause of infectious processes (90 %) and these were classified in: abdominal infection (hepatic cyst in 4, hepatic and pelvic abscesses in 2), vascular or endovascular infection (endocarditis 3, mycotic aortic aneurysm 1, aortic prosthesis 4, catheter 1, pacemaker 1, femoro-popliteal bypass 1 and aorto-femoral bypass 2), spinal infection (2), postoperative infection (costochondritis 1, chronic osteomyelitis 1), mycobacterial (M) infection (tuberculosis 13, atypical M 1) and miscellanea (1). In the remaining 4 positive scans (9%), PET/CT helped to confirm the final diagnosis as an inflammatory process: sarcoidosis, choledocholithiasis, aortic aneurysm and postoperative changes. A negative PET scan was seen in 9/51 patients (18%), 2 of them during the course of antibiotic therapy due to

bacteraemia and were considered as false-negative. PET/CT contributed to the final diagnosis in 82% of the patients (42/51). Accuracy, sensitivity, specificity, positive and negative predictive values were 88%, 95%, 63%, 90% and 77%, respectively. **CONCLUSION:** FDG-PET/CT helped to identify the potential origin of the infection in 90% of patients with positive scans. Globally FDG-PET/CT contributed to the final diagnosis in 82% of the patients, but clinical scenario must be considered for a correct interpretation of the findings.

P138

Contribution of ¹⁸F-FDG PET-CT in diagnostic work-up of patients with fever of unknown origin.

M. Lavalle¹, P. Castaldi¹, M. Lorusso¹, R. Manna², A. Giordano¹;
¹Institute of Nuclear Medicine, Università Cattolica Sacro Cuore, Rome, ITALY, ²Institute of Internal Medicine, Università Cattolica Sacro Cuore, Rome, ITALY.

Aim. Fever of unknown origin (FUO) represents a challenge not only for the internists but also for other specialists due to time and resources consumed in its diagnosis and management. Despite recent advances in diagnostic techniques, an algorithm covering all possible causes of FUO does not exist and a final diagnosis can not be made in up to 50% of cases. Recently, the use of ¹⁸F-FDG PET/CT in the evaluation of patients with FUO is increasing. Aim of our study is to evaluate the diagnostic value of ¹⁸F-FDG-PET/CT in FUO and its place in the diagnostic algorithm of these patients. **Materials and methods.** All patients who underwent ¹⁸F-FDG-PET/CT because of FUO from 2008 to 2015 were enrolled in this retrospective observational study. PET/CT results were compared with the final diagnosis, which was established by additional procedures including histopathology, microbiological or serologic test, and clinical follow-up for more than 6 months. PET/CT results were definite “contributory to final diagnosis” when capable to correctly lead to further diagnostic investigations and the final cause of fever was identified or when a normal finding excluded other cause of FUO. **Results.** Seventy-six patients (54 ± 21 years, 34 women, 42 male) were retrospectively evaluated. Final diagnosis was made in 72/76 patients (95%), including non-infectious inflammatory disease (53%), malignant disease (17%), infectious disease (12%), and miscellaneous disease (13%). No diagnosis was reached in 4 patients. PET/CT was “contributory to the final diagnosis” in 60% patients (n=43), correctly leading to further diagnostic investigations and to the final diagnosis in 36 patients (large vessel vasculitis, neoplasms and infectious diseases) and excluding other cause in 7 patients. PET/CT was non “contributory to the final diagnosis” in 40% (n=29) of patients, resulting positive in 12 patients and negative in 7 patients. **Conclusion.** Our study supports the data that ¹⁸F-FDG PET/CT may be a useful diagnostic tool for the diagnosis of FUO guiding for further diagnostic investigations.

P139

Efficacy Of Radiological Methods In Diagnosing Diabetic Foot Infection

M. Zorkaltsev, V. Zavadovskaia, A. Kurazhov, V. Udodov, M. Zamyshevkaia, O. Kilina, E. Grigoriev; Siberian State Medical University, TOMSK, RUSSIAN FEDERATION.

Purpose: to compare the effectiveness of radiological methods for the establishment of osteomyelitis (OM) in the diabetic foot (DF). **Materials and methods:** In 211 patients (105 male (49.8%), 106 female (50.2%); mean age 56.8±14.2) with DF suspected OM were performed: X-ray (n=83), CT (n=83), ⁶⁷Ga-scintigraphy (n=47), ²⁰¹Tl-scintigraphy (n=40), WBC-scintigraphy (n=41), three-phase scintigraphy (n=83) and MRI (n=42). Study was performed by using Apollo Villa Sistemi Medicali (x-ray), Toshiba Xpress GX (CT), Philips BrightView (SPECT) and Siemens

MAGNETOM ESSENZA 1.5T (MRI). **Results:** Values of sensitivity, specificity and accuracy of X-ray and CT were 78.2%, 28.6%, 61.4% and 77.8%, 57.1%, 70.7% respectively. Low specificity of X-ray and CT was principally due to false positive results (FP) in Charcot foot. Also it should be noted poor visualization of soft tissues. Values of sensitivity, specificity and accuracy of ⁶⁷Ga-scintigraphy, ²⁰¹Tl-scintigraphy, WBC-scintigraphy, three-phase scintigraphy were 96.6%, 72.2%, 87.2%; 87.5%, 66.7%, 75.0%; 95.8%, 64.7%, 82.9% and 91.5%, 50.0%, 79.5% respectively. FP results of scintigraphy were caused by difficulty in determining the localization of the pathological accumulation of radiotracer due to the low resolution of the method. Values of sensitivity, specificity and accuracy of MRI were 90.9%, 80.0%, 85.7%. The specificity of MRI decreased due to the complexity of the differential diagnosis of bone marrow edema and inflammatory infiltration. **Conclusion:** Among the available methods of radiological diagnosis of osteomyelitis in the diabetic foot, priority is given MRI. However, we must remember the presence of FP results in neuropathic form of DF.

P140

Role of 18 F-FDG PET-CT in documenting the disease burden in Tubercular meningitis

S. GAMBHIR, M. RAVINA, N. KUMAR, M. DIXIT, S. C. KHERUKA, K. RANGAN, J. S. KALITA, U. K. MISHRA; S.G.P.G.I.M.S, Lucknow, INDIA.

AIM: The authors demonstrate the potential of F-18 Fluorodeoxyglucose Positron emission tomography (PET)/Computerized tomography (CT) and magnetic resonance imaging (MRI) at disease onset and its complementary role along with MRI in elucidating the brain involvement. This may have a possible role in planning duration of treatment in scenario of TB resurgence and reported increase in multi-drug resistance (MDR) and extensively drug resistant (XDR) tuberculosis (TB) in patients with past history of TB. **Materials and methods:** 10 patients with definite Tubercular Meningitis (TBM), based on clinical, CT/MRI scan and CSF criteria were prospectively studied and subjected to whole body 18F FDG PET CT imaging and MRI. ¹⁸F-FDGPET/CT results were independently reviewed and results were compared with MRI brain and other conventional imaging modalities (Ultrasound abdomen and Chest -X-Ray). The severity of TBM was graded into stage I to III meningitis. **Results:** There were 10 patients with TBM whose median age was 27 (range, 14-55) years and the median duration of illness was 4 (range, 0.5- 8.0) months. Two patients were in stage I; 6 in stage II; and two in stage III meningitis. ¹⁸F-FDG PET/CT confirmed the cranial MRI findings in 07 patients, revealed additional brain lesion in 01 and did not detect the existing MRI lesions in 02 patients. ¹⁸F-FDG PET/CT however detected additional lesions in vertebrae, spinal cord, lymph nodes in comparison to the conventional imaging. **Conclusion:** ¹⁸F-FDG PET/CT is complementary to conventional imaging modalities in documenting up-front disease burden in diagnosed cases of tuberculosis with further ramifications in long term management of these patients. **Keywords:** 18 F - FDGPET; Tubercular meningitis; stage; MRI; disease burden

P141

The Clinical Contributions of SPECT/CT in ^{99m}Tc-HMPAO-Labelled Leukocyte Scintigraphy For Bone Prosthesis Infections

T. Sengoz¹, O. Yaylali¹, D. Yuksel¹, F. Demirkan², O. Uluoyul¹;
¹pamukkale university, Faculty of Medicine, Department of Nuclear Medicine, denizli, TURKEY, ²pamukkale university, Faculty of Medicine, Department of Orthopedics, denizli, TURKEY.

Introduction: White blood cell scanning with ^{99m}Tc-hexamethylpropylene amine oxime (HMPAO) has proven a highly sensitive and specific imaging method in the diagnosis and follow-up of patients with suspected prosthesis infection. The aim of this retrospective study was to evaluate the usefulness

of SPECT-CT performed simultaneously using a hybrid imaging device of prosthesis infections. **Methods:** 99mTc-HMPAO scintigraphy was performed on 37 patients (11 men and 26 women; age range 38–84 years; mean age \pm SD, 65.7 \pm 5.6 years old). Planar scans were acquired 2, 4, and 24 h after injection. SPECT/CT was obtained 4 h after tracer injection, using a dual-head hybrid gamma camera coupled with a low-power x-ray tube (Philips Brightview XCT; Ohio, Cleveland, USA). In all patients, scintigraphic results were matched with the results of surgery or cultures and clinical follow-up. **Results:** Seventeen (45.9 %) out of 37 patients were prosthesis infection and 20 (54.1 %) out of 37 patients were non-infectious prosthesis pathologies (9 aseptic loosening (45 %), 11 prosthesis secondary degenerative changes (55 %)) with Tc 99m-HMPAO scintigraphy and SPECT/CT. The Tc 99m-HMPAO scintigraphy was true-positive for infection in 16 of 37 patients and true-negative in 20 of 37 patients. There was no infection in a patient considered as infectious disease by scintigraphic evaluation (false positive). SPECT/CT provided an accurate anatomic localization of all positive foci. With regard to the final diagnosis, SPECT/CT added a significant clinical contribution in 22 of 37 patients (59.4 %). There was no clinical contributions with SPECT/CT in 15 of 37 patients (40.6 %). SPECT/CT provided accurate anatomic localization and differentiated soft-tissue from bone involvement in 17 of 22 patients. Any pathological activity uptake was not detected on SPECT/CT images in 5 patients who were only mild activity uptake showed in static scintigraphic images. Thus, false positive results were prevented by addition of SPECT/CT. SPECT/CT was useful for differentiating soft tissue from bone tissue in patients with suspected prosthesis infection. SPECT/CT was contributed the localization of osteomyelitis in patients with structural alterations after traumatic process. **Conclusion:** Our results indicate that SPECT/CT performed using a hybrid device can improve imaging with 99mTc-HMPAO-labeled leukocyte scintigraphy in patients with suspected osteomyelitis by providing accurate anatomic localization and precise definition of the extent of infection. **Keywords:** 99mTc-HMPAO-labeled leukocyte scintigraphy; prosthesis infection; SPECT; SPECT/CT

P142

Role of ¹⁸F-FDG PET CT in detecting active disease and in management of patients with Takayasu arteritis

G. Sankar, S. Gambhir, A. K. Singh, A. Prashanth; SGPGIMS, Lucknow, INDIA.

Aim and objective: Takayasu arteritis (TA) is a systemic large vessel vasculitis involving aorta and its main branches. Serum inflammatory biochemical markers and angiography are the main investigations in diagnosis and follow up. ¹⁸F-fluorodeoxyglucose (FDG) is a glucose analogue and its uptake is noted in both malignancies as well as in inflammatory conditions. Aim of this study was to see if FDG can be used as a bio-marker in detecting active inflammatory lesions in TA patients and its role in management of these patients. **Material and Methods:** Whole body FDG PET-CT scan was done in 17 known or suspected case of TA over a period of two years (2013–2015) in this retrospective study. Serum inflammatory markers (ESR & CRP) work up was done prior to PET/CT. Semi-quantitative parameter, SUVmax, was calculated in all the active lesions. Correlation between inflammatory markers and SUVmax was also calculated and a p value <0.05 was considered significant. PET scan report leading to any change in the management was asked from the treating immunologists and was obtained only in 10 patients. Rest of the patients are yet to follow up. **Results:** A total of 17 including 15 females (88%) and 2 males (12%) were studied. The mean age of the patients was 29.9 years (range: 16–52). Twelve patients were already on steroid therapy prior to the PET-CT scan (71%). Four patients had prior angioplasty and stenting done at least in one major vessel (24%). Mean ESR value in patients having active lesions was 57.62 mm/hr (range: 25–100) and in others was 18 mm/hr (range: 8–26). CRP was done only in 14 patients. Mean CRP level was 2.46 mg/L (range: 0.26–16.6). A total of 28 active lesions were detected in

the FDG PET-CT scan. The mean SUVmax of these lesions was 3.03 (range: 1.4–5.9). There was significant correlation between SUVmax and ESR (p value: 0.01) as well as between SUVmax and CRP (p value: 0.01). FDG PET-CT scan lead to change in management in 7 out of the 10 patients who were followed up post PET-CT scan (70%). The most common change was addition of methotextrate or azathioprine in addition to steroids. **Conclusion:** SUVmax can be used as a bio-marker and shows significant co-relation with both ESR and CRP levels. FDG PET/CT scan can lead to change in management in TA patients. However larger prospective studies are required to validate these findings.

P143

Quantification of Ga67 in Necrotising Otitis Externa

D. O. Hall, L. Armstrong, A. Demmery, J. Kabala; UH Bristol NHS FT, Bristol, UNITED KINGDOM.

Aim: Necrotising Otitis Externa (NOE) is a rare but serious infection of the external ear and skull base. Clinical assessment is not always sufficient to diagnose the condition, or monitor the progress of disease and effect of treatment, so imaging is used, including MRI, CT and nuclear medicine bone and Gallium scans. Imaging however may remain abnormal even after the infection has subsided; for example nuclear medicine bone scans often show increased uptake in the healing phase of the disease. Gallium-67 citrate is a sensitive measure of the development and progress of the disease, and promises to be an early measure of disease response, as uptake should reduce as the infectious process resolves. This study was carried out to define a practical protocol for calculation of disease activity in NOE using Ga67 SPECT/CT, and to determine cut-offs to detect active disease and to decide whether disease has resolved. **Materials and Methods:** 22 patients had 33 SPECT/CT scans on a Symbia T16. 150 MBq Ga-67 Citrate was injected i.v., with imaging at 24 hours from injection. Studies were acquired on the Symbia T16 SPECT/CT scanner, Medium Energy Low Penetration (MELP) collimator, 128X128 matrix, no zoom, pixel size 4.8mm, 128 projections, 20s per projection. CT was acquired at 130kV, 120mAs with Automatic Exposure Control (Siemens Caredose). Ratios of abnormal to normal side and abnormal side to cervical spine were calculated using Siemens MI Apps Volumetric Analysis. 12 studies had active disease, 12 were normal, and 9 were equivocal. Cut-offs were determined using ROC analysis with the web-based utility Cutoff Finder [1]. **Results:** Results were calculated using both methods, i.e. ratios of abnormal to normal side and abnormal side to cervical spine. Inter-operator variability was significantly poorer for ratios of abnormal side to cervical spine than abnormal to normal side. Uptake in active disease was significantly higher than in equivocal or normal studies. For ratios of abnormal to normal sides, ratios of <1.215 were normal, 1.215–1.375 was equivocal, and >1.375 were abnormal, with sensitivity and specificity >95%. The use of these limits is demonstrated in patients who had repeated studies to monitor treatment. **Conclusion:** A practical method has been demonstrated for quantification of uptake of Ga67 SPECT/CT in NOE. **Reference:** 1. Budczies J, Klauschen F, Sinn BV, Gyorffy B, Schmitt WD, et al. (2012) Cutoff Finder: A Comprehensive and Straightforward Web Application Enabling Rapid Biomarker Cutoff Optimization. PLoS ONE 7(12): e51862. doi:10.1371/journal.pone.0051862. <http://molpath.charite.de/cutoff>

P144

Nuclear imaging and infective endocarditis: the diagnostic role of 99mTc-HMPAO-Labeled Leukocyte SPECT/CT in patients with inconclusive echocardiographic exam

C. E. Popescu¹, S. Capitanio¹, R. Sara¹, M. Milella¹, S. Fiorino¹, B. De Chiara², A. Moreo², C. Giannattasio², C. Rossetti¹; ¹Nuclear Medicine Department, Niguarda Hospital, Milan, ITALY, ²“De Gasperis” Cardiovascular Department, Niguarda Hospital, Milan, ITALY.

AIM: The diagnosis of infective endocarditis (IE) may be particularly challenging. The so-called modified Duke criteria, recommended for diagnostic classification, can be improved through functional imaging procedures. Compared to PET, scintigraphy with labeled leukocytes has the advantage of having a better specificity, especially in patients with chronic inflammatory states and previous cardiac surgery. The purpose of this preliminary study was to evaluate the role of ^{99m}Tc -HMPAO-Labeled Leukocyte SPECT/CT in patients with suspected IE and echocardiography not conclusive. **MATERIALS AND METHODS:** We assessed the value of ^{99m}Tc -HMPAO - Labeled Leukocyte scintigraphy including SPECT/CT acquisitions in 13 patients (mean age 50 ± 25 years) hospitalized in our hospital from March 2013 to November 2015, with suspected diagnosis of IE in the presence of echocardiographic findings doubts or inconclusive. ^{99m}Tc -HMPAO - Labeled Leukocyte scintigraphy results were correlated with transthoracic or transesophageal echocardiography, blood cultures, and the Duke criteria. **RESULTS:** 5 patients (38.5%) had native valves, 5 (38.5%) had prosthetic valves and 3 (23%) cardiac implantable electronic device (CIED). 8 (61.5%) patients presented positive blood cultures, 11 (84.6%) had hyperpyrexia, and 12 (92.3%) patients performed the exam during the antibiotic therapy. In 6 patients it was confirmed the diagnosis of definite endocarditis according to the modified Duke criteria. Scintigraphy was true-positive in 3 of 6 patients (23%) and had an important role to conclude the diagnosis, representing in 2 cases, the major criterion, along with positive blood culture results. In one case it was the minor criterion and was able to identify an extracardiac uptake indicating septic embolism. In 7 of the 10 patients with negative scintigraphy scan, was excluded the diagnosis of endocarditis. None of them had evidence of infected endocarditis in follow-up (mean duration 24 months, minimum 3 months, maximum 37 months). **CONCLUSION:** This study, even if having a limited number of cases, supports the use of ^{99m}Tc -HMPAO- Labeled Leukocyte scintigraphy in patients with high clinical suspicion of IE but inconclusive echocardiographic findings to confirm the diagnosis in unclear circumstances or to detect sites of septic embolism.

P145

Diagnostic Value of Fluorine-18 Fluorodeoxyglucose Positron Emission Tomography/computed Tomography In Fever of Unknown Origin

L. Kang, Y. Huo, R. Wang; Peking University First Hospital, Beijing, CHINA.

Objective: Fever of unknown origin (FUO) is a challenging problem in diagnosis in clinic. The diagnostic value of ^{18}F -FDG in malignant tumors has been well accepted. However, the differential diagnostic value of FDG PET/CT among tumors, infection and non-infectious inflammation still needs to be elucidated. This study is to evaluate the diagnostic value of ^{18}F -FDG PET/CT in FUO. **Methods:** We analyzed the records of 51 patients with FUO (32 men and 19 women; mean age of 54-year-old with a range between 3- and 81-year-old) retrospectively. All patients were examined by ^{18}F -FDG PET/CT and the results were compared to the final diagnosis established by additional procedures including pathology, laboratory examination and clinical follow-up for more than 3 months. The maximum of standard uptake value (SUVmax) in tumors and benign lesions was compared. T test was used for statistical analysis. **Results:** Final diagnosis were established for 48 patients, including 31 patients with infectious diseases, 9 with malignancies, and 8 with non-infectious inflammatory diseases. By FDG PET alone, the true positive (TP), false positive (FP), false negative (FN) and true negative (TN) rate was 52.9%, 27.5%, 17.6% and 2.0%, respectively. By FDG PET/CT, TP, FP, FN and TN rate was 70.6%, 27.5%, 2.0% and 0%, respectively. PET/CT had a sensitivity of 97.3% (36/37), a specificity of 0% (0/14) and an accuracy of 70.6% (36/51) in FUO, especially a high sensitivity and accuracy of 100% (9/9) in malignant tumor. Moreover, SUVmax in tumor was

significant higher than that in infection (3.7 ± 2.7 vs 7.7 ± 3.5 , $P=0.001$, $t=3.6$) and might be useful in differential diagnosis. **Conclusions:** ^{18}F -FDG PET/CT is a valuable imaging tool for the identification of the etiology in patients with FUO. It is helpful for locating the lesion, especially in the diagnosis of FUO cases with potential malignant lesions.

P146

Abdominal Tuberculosis in a low-incidence Country: a single-center experience on 13 patients investigated with ^{18}F -FDG PET/CT

L. Zanoni¹, V. Ambrosini¹, G. Vandi², G. Martelli², M. Tadolini², S. Brocchi³, J. Morigi¹, P. Viale², M. Zompatori³, S. Fanti¹; ¹Nuclear Medicine, Azienda ospedaliero-universitaria di Bologna, Policlinico S.Orsola-Malpighi, Bologna, ITALY, ²Infectious Diseases, Azienda ospedaliero-universitaria di Bologna, Policlinico S.Orsola-Malpighi, Bologna, ITALY, ³Radiology, Azienda ospedaliero-universitaria di Bologna, Policlinico S.Orsola-Malpighi, Bologna, ITALY.

AIM: To assess the role of ^{18}F -FDG PET/CT in the diagnosis of abdominal tuberculosis (ATB). **MATERIALS AND METHODS:** Clinical records, contrast-enhanced-CT and ^{18}F -FDG PET/CT findings of patients diagnosed with ATB between January 2013 and January 2016 at the Infectious-Diseases-Unit were retrospectively analyzed. Abnormal CT and PET/CT findings were independently documented, anatomically categorized and compared. **RESULTS:** A total of 289 pts were diagnosed with TB. 23/289 had ATB. 13/23 pts underwent ^{18}F -FDG PET/CT (12 before, 1 immediately after diagnosis) and were included in the analysis. **Clinical characteristics (13 pts):** 7 women, 6 men; median age 39 years (range 25-72). 12 foreigners, 1 Italian. All pts had no past history of TB. 2 HIV+; 11 seronegative. Common symptoms were: loss of body weight (12), abdominal pain (10), night sweats (7), fever (6); ascites (5), diarrhea (1). Clinical requests for imaging were: differential diagnosis between cancer and TB (4 pts); suspect of cancer (2), lymphoma (2) or TB (3) (n/a: 3). Abdominal nodes were identified in 12 pts (CT performed better in 1/12 and showed typical enlarged necrotic nodes with hypo-attenuating centers and hyper-attenuating enhancing rims in 7 cases; FDG uptake varied from faint/diffuse to intense/focal up to SUVmax 15.8). Peritoneal involvement (11 pts; 2 detected only by CT) markedly accumulated FDG (SUVmax: mean 9.6; median: 9.2; range 5.2-13.9) mimicking peritoneal carcinosis; in all cases, CT revealed smooth thickening and strong contrast-enhancement of the parietal peritoneum and ascites (UH: mean 21; median 21; range 10-253). Gastrointestinal-tract was affected in 3 pts (high PET metabolism and, in 1 case, typical ileocecal thickening on CT). Liver was involved in 1 pt (both PET and CT positive). Spleen involvement was detected in 1 case by CT but not clinically confirmed. Extra-abdominal localizations were depicted in lung in 5 pts (3/5 only CT positive), and other regions (i.e. intrathoracic nodes, pleural effusion/deposits, muscle) in 10 pts (2 only PET positive). Overall PET identified 44 affected regions whereas CT 46. Half of the population presented with disseminated disease (>10 lesions). PET report hypothesized malignancy rather than ATB in the majority of pts (6), correctly suspected infection in 3 cases, remained indeterminate in 4. Based on PET findings, focused biopsy led to bacteriological TB confirmation in 10/13 pts (77%) and histological confirmation in 3/13. **CONCLUSION:** PET seems to play an important role in ATB diagnosis, identifying the involved sites for focused biopsy. Larger studies are needed to confirm our observations.

P147

Brief experience of the clinical utility of three phase F-18 NaF bone PET for evaluation infected prosthesis

Y. Jeong, S. Choi, J. Jeong, H. Son, H. Yoon, D. Kang; Dong-A University Hospital, Busan, KOREA, REPUBLIC OF.

Purpose: Because F-18 NaF has a rapid kinetics than Tc-99m MDP, F-18 NaF bone PET has many advantages which are clear bone image, short imaging time and ability to quantify bone turn over. However, the usefulness of three phase NaF bone PET to diagnosis bone infection is not well known. In this study, we studied the clinical usefulness of three phase bone PET with F-18 NaF to identify the presence of prosthesis infection of joint. **Materials and Methods:** Five patients who presented symptoms suggesting infection of joint prosthesis after joint replacement surgery of knee (n=4) or hip (n=1) were enrolled. All patients performed three phase Tc-99m MDP bone scan and F-18 NaF bone PET on the same day. Three patients performed 3-time point PET acquisition (perfusion, blood pool and delayed images). Other two patients underwent F-18 NaF bone PET examinations as following protocol. First, list mode image was obtained for 20 min after injection of F-18 NaF. The list mode data was reconstructed into dynamic curve for 20 min, perfusion and blood pool images. Second, delayed static bone phase scanning was performed at around 60 min after injection of radiotracer. Ten normal controls who underwent joint replace surgery without symptom were also recruited for. Three volume of interest were drawn on artery, muscle, bone marrow and two different site of bone in patients and normal control. **Results:** Of five patients, infection of joint prosthesis was confirmed in 4 subjects. Non-infected joint prosthesis was revealed in another one patient and symptom of the patient gradually subsided with symptomatic treatment. As the patients with infected prosthesis, one patient without infection showed increased uptake in the peri-prosthesis area in delayed image. But pattern of tracer uptake was relatively even in patient with non-infected prosthesis. Time-activity curve for 20 min showed markedly different curve pattern between the patients with and without infected prosthesis. **Conclusion:** This preliminary data suggested that F-18 NaF bone PET showed clearer three phase images which helped to identify the site and extent of disease. Adding of dynamic curve could improve diagnostic accuracy.

P-13 – Monday, October 17, 2016, 16:00 - 16:30, Poster Exhibition Hall
Conventional & Specialised Nuclear Medicine: Miscellaneous

P148

Use of Ultra-Portable Ultrasound to Improve IV Access for Nuclear Medicine Dose Administration

M. I. Knopp, C. Odom, K. Binzel, C. L. Wright, M. V. Knopp; The Ohio State University, Columbus, OH, UNITED STATES.

Aim: IV access with no extravasation is essential for safe, precise and quantitative nuclear medicine imaging. As many procedures are performed on an outpatient basis for co-morbid patients with challenged venous access, optimal needle placement remains a top priority. Unfortunately, extravasations, though mostly minor, regularly occur. The miniaturization of ultrasound systems reached a new breakthrough with the clinical release of a smart device (tablet or phone) micro-USB attachable ultrasound transducer. We introduced and assessed the feasibility of such a device concept in nuclear medicine. **Materials and Methods:** An ultraportable, Android app-based FDA approved ultrasound system (Lumify, Philips) was purchased to explore innovative uses in nuclear medicine. The app runs on current generation tablets and smartphones. It installs like any app with a scan ready start up screen. For venous access imaging a linear array probe was used that also enables flow Doppler overlay on the morphologic image. Via settings, many characteristics can be customized including the setup of DICOM / network destinations that support direct upload to PACS via Wifi. Local storage of images and videos is supported as well as expected features for annotation or measurements. Overall operation is intuitive, fast and scaled to the size of display device. The app is fully integrated so that additional display casting options via Wifi are supported, enabling instantaneous sharing on a remote display. **Results:** Once the probe is attached

to the smart device, it is immediately usable making it extremely practical from fitting readily into a lab coat pocket to be ready for use. Most nuclear medicine technologists are not familiar with the use of ultrasound to find and place IV needles, but can be readily trained. The ability to cast images on PC/TV screens in the injection environment was found extremely helpful and convenient for training. While our prospective IV access performance collection is still ongoing, the clinical impact appears to evolve favorably and the operator, especially less IV experienced young professionals rate the availability of the system to be very helpful. One aspect that remains an inconvenience is that ultrasound gel remains necessary for coupling to the skin. Image quality consistently rated as excellent and operability as fully compatible within the nuclear medicine environment. **Conclusion:** Using ultrasound to improve IV access in nuclear medicine is considered inconvenient, inefficient, expensive and clunky. Ultra-portable, smart device-based probe technology overcomes these limitations. We observed very favorable acceptance and access quality improvements.

P149

Value 18F FDG PET CT in the assessment of Erdheim Chester disease

P. Gykiere¹, P. Ardies², G. Sery¹, H. Everaert², B. Van den Broeck¹; ¹University Hospital Ghent, Ghent, BELGIUM, ²University Hospital Brussels, Brussels, BELGIUM.

Objective: Erdheim-Chester disease (ECD) is a rare non-Langerhans form of histiocytosis of unknown etiology (1). ECD is a systemic disease and can present with a wide array of clinical manifestations involving many different organs, including the skeleton, central nervous system (CNS), cardiovascular system, kidneys, lungs and skin (1, 2). Because of this variable clinical presentation, diagnosis of ECD is often challenging. The aim of this study was to evaluate the use of FDG PET/CT in the assessment of the extent of the disease. **Methods:** We retrospectively reviewed PET/CT scans of 6 histological confirmed cases of ECD performed in two university hospitals between 2010 -2016. **Results:** After reassessment, the most common characteristic in our series (83%) is hypermetabolic skeletal involvement showing bilateral and symmetrical cortical FDG-avid osteosclerosis of the diaphyseal and metaphyseal regions in the long bones (typically sparing the epiphysis). Also, cardiovascular involvement with hypermetabolic sheathing of the aorta, retroperitoneal and perirenal involvement (“hairy kidney on CT”) was frequently observed (both 66%). In addition although less frequently, in some patients there was augmented activity in the lungs, adrenals, sinuses and CNS. These results correlate well with the known distribution of clinical manifestations of ECD (1, 3). **Conclusion:** Since ECD is a multisystemic disease, we found that whole-body FDG-PET scanning was able to depict the extent and activity of the ECD lesions. This is important because the clinical prognosis is dictated by the degree of organ involvement, especially the CNS (2). Secondly, PET/CT could help guide a safe and appropriate site of biopsy for definitive diagnosis. **References:** 1. Erdheim-Chester disease. Campochiaro C, Tomelleri A, Cavalli G, Berti A, et al. *European Journal of Internal Medicine* 2015; 26: 223-229. 2. Erdheim-Chester Disease: Characteristics and Management. Munoz J, Janku F, Cohen P, Kuzrock R. *Mayo Clin Proc.* 2014;89:985-996. 3. Erdheim-Chester disease. Haroche J, Arnaud L, Cohen-Aubart F, Hervier B, et al. *Rheum Dis Clin N Am* 2013; 13:299-311.

P150

Bone SPECT for the evaluation of condylar growth: comparison between different standardization methods

M. Silva¹, P. Gil¹, R. Silva^{1,2}, J. Isidoro¹, A. Albuquerque¹, F. Alban¹, P. Lapa¹, G. Costa¹, J. Pedrosa de Lima^{1,2}; ¹Centro Hospitalar da

Universidade de Coimbra, Coimbra, PORTUGAL, ²Instituto de Ciências Nucleares Aplicadas à Saude, Coimbra, PORTUGAL.

Aim: Hyperplasia of the mandibular condyle is a complex deformity of the mandible that may lead to important functional and aesthetic problems. Bone single photon emission computed tomography (SPECT) is an essential tool for assessing mandibular condylar uptake as a surrogate for mandibular growth. This study aimed to compare two different SPECT methods for the quantification of condylar uptake. **Material and Methods:** Eight patients (2 males and 6 females; 18–26 years of age, mean age:23.5±2.8 years) who performed ^{99m}Tc-MDP bone scans for indications not involving the skull, were asked to have an additional SPECT that included the mandibular condyles, with a source of known activity above the skull, included within the field of view (external standard). For each patient three dimensional (3D) regions of interest (ROIs) were drawn over both condyles, the clivus (internal standard) and the external standard. Maximum and total pixel values within the 3D ROIs were recorded and used to develop normal values for both quantification methods (average±2 standard deviations, 95% confidence interval). One hundred and thirty-eight bone SPECTs were performed for the assessment of mandibular condylar uptake (95 patients; 35 males and 60 females, 17–38 years of age, mean age:21.0±4.1 years). Condylar uptake was determined using both standards in all scans. Statistical analysis was performed using IBM[®] SPSS[®] Statistics, version 22. **Results:** Normal ranges were determined for the condylar uptake using both internal and external standards. All patients were classified as having normal or hyperplastic condyles, according to both internal and external standards and the normal values previously defined. A statistically significant correlation was found between the normal/hyperplastic classification using both methods (Pearson Chi-square < 0.05). Also, statistically significant correlations were found between internal and external condylar uptake in the right (p<0.01, r²: 0.459) and left clivus (p<0.01, r²: 0.255). **Discussion:** ^{99m}Tc-MDP bone SPECT provides a quantitative technique for assessing mandibular condylar uptake as a reflection of mandibular growth. However, several quantification methods can be used. In this study local normal ranges were determined for the condylar uptake using both internal and external standards and statistically significant correlations were found between them. We predict that the external standard may have significant advantages; however this thesis needs to be further evaluated.

P151

Is there anno 2016 still a role for quantitative salivary gland scintigraphy in suspected Sjögren Syndrome?

P. Kaldewey, E. ten Borg, E. M. W. van de Garde, J. B. A. Habraken, J. Lavalaye, M. M. C. van Buul; St. Antonius hospital, Nieuwegein, NETHERLANDS.

Purpose: Aim of this study is to evaluate the diagnostic value of semi quantitative parameters in salivary gland scintigraphy (SGS) in the diagnostic work-up in Sjögren's Syndrome (SS) using the AECC as gold standard. **Patients and methods:** Tc-99m pertechnetate-SGS was performed in 110 patients with suspected Sjögren's Syndrome. Uptake ratios (UR) and excretion fractions (EF) for all parotid and submandibular salivary glands were calculated. Patients were divided in SS-positive, SS-negative and SS-unequivocal groups based upon the AECC criteria, ocular and oral symptoms, Schirmer's test, labial biopsy and anti-SSA or anti-SSB antibodies. SGS semi quantitative parameters were compared per group and cut-off values were defined. **Results:** Ninety-six women (87%) and 14 men (13%) with a mean age of 51 years (range 18–77 years) were included. All patients underwent SGS, labial biopsy, Schirmer's test and antibody test (anti-SS-A and anti-SS-B). Twenty-four patients were SS-positive, 56 patients SS-negative and 30 SS-unequivocal. UR of the parotid glands did not differ between SS-positive and SS-negative groups (3.4 and 3.9, respectively), while UR of the submandibular glands were significantly lower in SS-positive patients (2.7 versus 3.5). EF in both

parotid and submandibular glands was significantly higher in SS-negative compared to SS-positive patients: parotid 44% and 56% respectively, submandibular 36% and 49%. Based upon a cut-off value of 2.0 for UR and 20% for EF, sensitivity, specificity, PPV and NPV were 0.67, 0.86, 86%, and 67%, respectively. Out of the 30 SS-unequivocal patients, 15 had a positive SGS and the other 15 were SGS negative. In both, there was no correlation with the results of AECC criteria IV (histopathology) and VI (antibodies). In these cases, the SGS result was decisive. **Conclusions:** Quantitative salivary gland scintigraphy is still a valuable tool in the diagnostic management of patients with suspected Sjögren's syndrome, especially in those in which the non-scintigraphic AECC criteria are not conclusive. The straightforward quantitative analysis of salivary gland scintigraphy used in this study can be implemented in any nuclear medicine department.

P152

Functional Recovery Of Patients With Secondary Lymphedema Treated With Lymphatic Venous Anastomoses And Lymph Node Transfer, Monitoring By Isotopic Lymphography. Value Of SPECT/CT

M. L. Lozano Murgas, L. Reguera Berenguer, J. Ardila Manjarres, A. Rotger Regí, J. Orcajo Rincon, C. Duran Barquero, R. Pascual Pérez, J. Lasso Vázquez, C. Pinilla Martínez, J. Alonso Farto; Hospital General Universitario Gregorio Marañón, Madrid, SPAIN.

AIM The aim of this cross-sectional descriptive study was to assess the functional recovery of lymphatic flow in patients with secondary lymphedema treated with microsurgical techniques (lymphatico-venous anastomosis and vascularized lymph node transfer) by isotopic lymphography. In addition, we wanted to evaluate the added value of single photon emission computed tomography/computed tomography (SPECT/CT) in medium term follow up of these patients treated with microsurgical techniques. **MATERIAL AND METHODS** A total of 16 consecutive patients (14 females; mean age 54 years, range 41–76) were studied. Eleven patients were operated with lymphatico-venous anastomosis (LVA) and 5 with vascularized lymph node transfer (VLNT). After injection of ^{99m}Tc-nanocolloid (about 96 MBq per limb) conventional lymphoscintigraphy was performed to obtain early (average 28 min) and late (2 h) images of both upper or lower limb according to the patient's condition (16 upper limbs and 16 lower limb). SPECT/CT delayed images were acquired in 8 inguinal and axillary regions respectively. **RESULTS** In 50% (8/16) of cases, lymphatic flow was restored, five of them had been treated with LVA and three with VLNT. Of these, 75% (6/8) showed lymph node appearance. In 2 of the remaining patients, additionally, radio-pharmaceutical dermal backflow was improved. From a total of 124 lymph nodes identified (upper limb, n=52; lower limb, n=72), 73,4% (91/124) were detected by conventional lymphoscintigraphy and 100% (124/124) by SPECT/CT. Therefore SPECT/CT provided 26,6% additional diagnostic information compared to planar lymphoscintigraphy, in the following anatomic sites: 8 axillary, 1 supraclavicular fossa, 4 infraclavicular fossa, 2 mid-arm, 1 right scapula, 1 elbow, 8 inguinal, 6 iliac and 2 para-aortic nodes. In cases undergoing LVA, 67,7% (84/124) of lymph nodes were detected while 32,3% were detected (40/124) after VLNT. **CONCLUSION** Our results, although preliminary, suggest an increase of lymph node recovery by ALV compared to VLNT microsurgical technique. SPECT/CT is complementary to conventional lymphoscintigraphy providing additional information regarding exact anatomic localization and improving the identification of lymph nodes.

P153

Evaluation of serum 25 Hydroxy vitamin D levels in patients with Diabetes Mellitus

A. S. ZISSIMOPOULOS¹, C. Tsigalou², D. Papazoglou³, N. Papanas⁴, O. Zissimopoulou¹, A. Pistola¹, M. Lambropoulou⁵; ¹Nuclear Medicine

Dept Democritus University of Thrace, Alexandroupolis, GREECE, ²Biopathology Lab Democritus University of Thrace, Alexandroupolis, GREECE, ³Diabetes Center- Second Department of Internal Medicine Dept Democritus University of Thrace, Alexandroupolis, GREECE, ⁴Diabetes Center- Second Department of Internal Medicine Democritus University of Thrace, Alexandroupolis, GREECE, ⁵Lab Histology-Embryology Democritus University of Thrace, Alexandroupolis, GREECE.

Introduction: Vitamin D deficiency is a condition of increasing prevalence worldwide. Diabetes mellitus (DM) is related to vitamin D levels. In recent studies there is association with vitamin D deficiency and the risk of developing diabetes and diabetes complications. **Aim:** The aim of this study is to evaluate the serum levels of 25 hydroxy- vitamin D [25(OH)D] in patients with type 2 diabetes mellitus. **Patients and method:** We study 108 patients (66 male and 42 female) aged between 43 and 70 years old (median age of 58±12 years) with type 2 diabetes mellitus with or without diabetes complications. All were in follow up at the University Hospital of Evros. In all patient's blood samples were taken for (25-OH-D) determination. After centrifugation the serum was collected and kept refrigerated at -70 ° C. The vitamin D status was measured by radioimmunoassay (RIA) method with I¹²⁵[25(OH)D] kits Diasorin at in- vitro laboratory of Nuclear Medicine Dept. University Hospital of Evros, Democritus University of Thrace. Also we studied 40 healthy individuals (blood donors) as control group. **Statistical analysis:** Statistical analysis was performed by the χ^2 - test (student test) and statistical significance was considered to be $p < 0.005$. **Results:** Diabetes mellitus patients had lower levels of 25(OH)D than controls ($p < 0.005$). In 62 patients with severe complications of the disease, the levels of [25(OH)D] were significantly low 0-20 ng/mL ($p < 0.005$), in 28 patients with mild complications of the disease the levels were 20-40 ng/mL (hypovitaminosis) and the rest 18 with no complications, had levels of [25(OH)D] > 40 ng/mL ($p < 0.005$). **Conclusions:** Diabetes mellitus patients had lower levels of 25(OH)-D than controls. Patients with severe complications of the disease had significantly low levels than the others. Vitamin D deficiency may be a risk factor for DM. Clinical trials with vitamin D supplementation are needed.

P154

^{99m}Tc-HDP Bone scintigraphy and ¹⁸F-sodiumfluoride PET/CT in primary staging of patients with prostate cancer

A. M. Burgers¹, M. Wondergem^{1,2}, R. J. J. Knol¹, I. J. de Jong², J. Pruijm^{2,3}, F. M. Van der Zant¹; ¹Noordwest Ziekenhuisgroep, Alkmaar, NETHERLANDS, ²University Medical Center Groningen, Groningen, NETHERLANDS, ³Stellenbosch University, Tygerberg Hospital, Stellenbosch, SOUTH AFRICA.

Introduction/Aim Correct staging of patients with prostate cancer is important for treatment planning and prognosis. In patients with high-risk primary prostate cancer bone scintigraphy with ^{99m}Tc-phosphonates (BS) is performed for detection of bone metastases. Due to the high rate of inconclusive BSs, new imaging techniques for bone metastases are being evaluated. Recent studies show better performance of ¹⁸F-sodiumfluoride PET/CT (NaF-PET/CT) compared to BS. The aim of this study is to evaluate the performance of both BS and NaF-PET/CT in primary staging of patients with prostate cancer. **Methods** Two cohorts were studied. The first, retrospective cohort consisted of patients who received a BS from January 2011 till December 2011 with a clinical follow-up of at least 18 months. The second, prospective cohort contained patients who received a NaF-PET/CT from January 2014 till October 2015 and had a follow-up of at least 6 months (6-28 months). The follow-up period was used as the reference standard and consisted of clinical, biochemical and radiological follow-up. **Results** Fifty-nine patients underwent NaF-PET/CT whereas 122 patients underwent BS. On a patient basis sensitivity of 97-100% and 88-96% and a specificity of 96-100% and 72-100% was found for

detection of bone metastases with NaF-PET/CT and BS respectively. The combination of NaF-PET with low-dose CT resulted in detection of extra-skeletal metastases in a large number of patients (lymphadenopathy in 47% and pulmonary metastases in 3%), even in 8 patients (14%) without bone metastases. In comparison to bone scintigraphy, NaF-PET/CT yielded less equivocal results requiring further evaluation (3% vs 22%). **Conclusion** NaF-PET/CT is an excellent tool for detection of bone metastases in patients with prostate cancer. Due to the combination of PET and low-dose CT the interpretation of foci with increased tracer-uptake is highly specific. Moreover, extra-skeletal metastases are found frequently on the low-dose CT.

P155

Simplifying the role of Lymphoscintigraphy for the assessment of lymphedema

D. Shivdasani; P D Hinduja Hospital, Mumbai, INDIA.

Introduction: Lymphedema is an under treated condition, causing swelling of the extremities. Misdiagnosis and/or delayed diagnosis are common. Lymphoscintigraphy is a specific radio-isotope technique to detect lymphatic causes of limb swelling from other causes like obesity, venous disease and hypoalbuminemia. **Materials and Methods:** Total of 113 patients (age 2-86y, mean 41.7y), 59 females, 54 males were referred to our Nuclear Medicine department for lymphoscintigraphy. One patient was excluded in view of intravascular tracer injection. 34 patients were referred to rule out chyle leak. 78 patients were referred for the evaluation of limb edema of which 75 patients had only lower limb edema, two children both 2 years of age were referred to rule out primary lymphedema and one patient suffered from upper limb edema following trauma. Lymphoscintigraphy was performed in all patients by intradermal injection of 0.1-0.2ml of 500microcuries of filtered Tc -99m sulphur colloid in the first web space. Whole body imaging was carried out 10-30 minutes post injection, followed by a second image at 1 hour and a delayed image (3-4 hours after injection) post- exercise of the injected limbs. Lymphatic obstruction was defined as absence of visualization of any tracer activity in regional (inguinal or axillary) nodes upto 4 hours post injection. Asymmetric delayed visualization of comparatively fewer nodes with either presence of dermal backflow or visualization of nodes of the deeper drainage system was defined as lymphatic dysfunction. **Results:** 32% patients referred to our center for evaluation of lymphedema had normal scans. 19% had lymphatic obstruction of which 11 scans were unilateral and 4 scans were bilateral. 36% patients with unilateral obstruction also demonstrated lymphatic dysfunction in the contra lateral asymptomatic limb. Lymphatic dysfunction was seen in 49% of which 30 patients had unilateral and 8 patients had bilateral dysfunction. Dysfunction in the form of dermal backflow was seen in 79% patients and 8 patients had visualization of deeper nodes either popliteal (n=6) or epitrochlear (n=2). 18% with dysfunction demonstrated both dermal backflow and abnormal nodes on their scans. **Conclusion:** The diagnostic utility of lymphoscintigraphy depends upon technical performance and accurate image interpretation. Our data reflects its simple, visual and qualitative interpretation using well defined criteria for classifying scans as normal, lymphatic obstruction or dysfunction. We suggest it can serve as a specific tool for differentiating lymphedema from other causes of limb swelling.

P156

¹¹¹Indium-DTPA-Scintigraphy Including SPECT-CT Can be Extreme Helpful in Solving Intrathecal Drug Delivery Failures. An Analysis of 15 Cases

A. Fröberg¹, E. Delhaas², F. Huygen², B. Harhangi³, A. van der Lugt¹, J. F. Verzijlbergen¹; ¹Erasmus MC, Department of Radiology & Nuclear

Medicine, ROTTERDAM, NETHERLANDS, ²Erasmus MC, Department of Pain Treatment, ROTTERDAM, NETHERLANDS, ³Erasmus MC, Department of Neurosurgery, ROTTERDAM, NETHERLANDS.

Aim: To assess the diagnostic potential of ¹¹¹Indium-DTPA-scintigraphy including SPECT-CT in patients suffering intrathecal baclofen (ITB) delivery failures. **Materials and Methods:** Our hospital is a referral center for ITB troubleshooting and for years ¹¹¹Indium-DTPA-scintigraphy has been one of the diagnostic tools in challenging cases. In the last two years we extended the standard planar investigations with Single Photon Emission Tomography in combination with computed tomography (SPECT/CT). The pumps are filled with a mixture of baclofen and ¹¹¹Indium-DTPA and both planar and SPECT/CT imaging of spine and head was performed at 24, 48, 72 and if warranted also at 96 hours and/or 8 days. Until now 15 consecutive patients referred for ¹¹¹Indium-DTPA-scintigraphy because of treatment failure had this extended procedure. Images were correlated with available radiographic examinations (like CT after intrathecal contrast administration and MRI) and clinical symptoms. **Results:** Though sometimes suffering from severe muscle spasms (because of delivery failure) all patients were able to complete the imaging procedure successfully. In 13 patients the cause of delivery failure could be demonstrated (hereby disapproving the assumption of tolerance for the intrathecal baclofen treatment). Discovered problems were (partial) catheter or spinal canal obstructions and CSF-leakage. Therapeutic interventions resulted in improvement of the symptoms in the majority of the patients. **Conclusion:** ¹¹¹Indium-DTPA-scintigraphy including SPECT-CT can be very helpful in the clarification of intrathecal baclofen delivery failures. This imaging technique can have a strong impact on the choice of treatment of these failures, thereby improving the quality of life of these patients enormously.

P157

The usefulness of salivary glands scintigraphy in the diagnostics of Sjögren's syndrome

D. BEN SELLEM, T. BEN GHACHEM, B. DHAOUADI, L. ZAABAR, B. LETAIEF, M. F. BEN SLIMENE; University of Tunis El Manar, Faculty of Medicine of Tunis, Salah Azaiez Institute, Department of Nuclear Medicine, Tunis, TUNISIA.

Aim: Sjogren's Syndrome (SS) is an autoimmune disease characterized by dryness of the mouth and eyes, defining the dry syndrome. SS can consequently be complicated by infections of the eyes, breathing passages, and mouth. The diagnostic confirmation is based on biopsy of the accessory salivary glands, and incidentally on the salivary glands scintigraphy that is not a routine test. The aim of this study was to demonstrate the contribution of salivary gland scintigraphy in SS suggested clinically without histological evidence. **Materials and methods:** This is a retrospective study of 167 patients (148 women, 19 men), collected over a period of 7 years. The average age was 47 ± 13.95 years (14 to 82). All these patients had a dry syndrome suggested clinically and were sent to our department for salivary glands scintigraphy. The protocol included dynamic acquisition contemporary to the injection of 74-111 MBq Technetium-99m Sodium Perchnetate and up to 40 minutes. Activity-time curves were plotted after making regions of interest on the parotid and submandibular glands. **Results:** Salivary glands scintigraphy was positive in 137 cases (82 %). Involvement was bilateral in 98 cases (58.7 %). The hypofunctioning interested both parotid and submandibular glands in 95 cases (56.9 %), only the parotid glands in 55 cases (32.9 %) and only the submandibular glands in 17 cases (10.2 %). **Conclusion:** Salivary glands scintigraphy is a simple, physiological and non-invasive test that evaluates salivary gland function. It plays an important role in the diagnosis of SS, 82 % of our cases, especially when salivary biopsy is unrealizable or remains equivocal.

P158

Use of workplace based assessment tools in nuclear medicine

K. Makhdomi; Aga Khan University Hospital, Nairobi, Kenya, Nairobi, KENYA.

OBJECTIVES: To document the introduction of two workplace based assessment tools in Nuclear Medicine for a Radiology residency program, and to assess its impact and resident feedback. **METHODS:** Two workplace based assessment tools, the direct observation of procedural skills (RAD-DOPS) and Mini Image Interpretation exercise (Mini-IPX) were modified from those used by RCR, and implemented in the Nuclear Medicine Section during the rotation of Radiology residents. Each resident underwent one assessment each with these two tools during their monthly rotations in Nuclear Medicine. The feedback provided was documented, including the opinions of the residents regarding the process. The subsequent assessments of the residents were compared with their previous ones and evidence of any change in performance noted based on comments from previous assessments. A total of twelve residents were involved over a one year period. **RESULTS:** The results revealed general acceptance of these tools by the residents as part of their workplace based assessment. Objective evidence of improvement in performance was noted in ten of the twelve residents, based on the feedback from the serial assessments. **CONCLUSION:** The study documents the utility of the workplace based assessment tools in the formative assessment of residents in Nuclear Medicine, and also their acceptance by the residents.

P159

Scintigraphic assessment of the Indium 111-DTPA transit in patients with an intrathecal baclofen delivery system

A. SHER¹, M. DINOMAIS², F. FREMONDIERE², I. RICHARD², P. MENEI³, O. COUTURIER¹, F. LACOEUILLE¹; ¹Department of Nuclear Medicine, University of Angers, Angers, FRANCE, ²Department of Physical Medicine and Rehabilitation, University of Angers, Angers, FRANCE, ³Department of Neurosurgery, University of Angers, France, Angers, FRANCE.

Introduction: In case of increased spasticity in patients with intrathecal baclofen infusion system, a resistance to treatment, an intercurrent disease and a mechanical or non-mechanical device malfunction should be considered. The aim of this work was to study the interest of Indium 111-DTPA scintigraphy combined with SPECT/CT in case of suspected malfunctioning of the intrathecal baclofen delivery system. **Patients and Methods:** Seven scintigraphic examinations were performed in 6 patients (4 men and 2 women, age min 27 years, max 73 years). A median dose of 30 MBq (min 18MBq, max 35MBq) of Indium 111-DTPA was injected into the pump reservoir without interrupting the delivery of baclofen. Static and SPECT/CT images were acquired at different times until 7 days after injection. **Results:** Three cases of catheter (n = 2) or pump (n = 1) malfunction, 2 cases of abnormal distribution in the cerebrospinal fluid and one normal appearance were observed in scintigraphy and confirmed by clinical follow-up and operating data. SPECT/CT helped localize and identify the cause of the dysfunction. The calculation of the theoretical arrival time of the radiotracer, which depends on the flow of baclofen, appeared necessary to adjust the acquisition times. **Conclusion:** Indium 111-DTPA scintigraphy combined with SPECT/CT could be usefull for the understanding and management of spasticity recurrences in patients with intrathecal baclofen pumps.

P160

Positioning for positron emission tomography/ computed tomography in public hospitals in Nigeria

A. T. Orunmuyi¹, Y. A. Onimode¹, K. S. Adedapo², I. A. Lawal³, J. E. Eje⁴, B. O. A. Osifo²; ¹Nuclear Medicine Centre and Radiation Oncology

Department, University College Hospital (UCH) and College of Medicine, Ibadan, Ibadan, NIGERIA, ²Nuclear Medicine Centre and Chemical Pathology Department, University College Hospital (UCH) and College of Medicine, Ibadan, Ibadan, NIGERIA, ³Radiopharmacy Unit, Nuclear Medicine Centre, University College Hospital (UCH) Ibadan, Ibadan, NIGERIA, ⁴Medical Physics Unit, Nuclear Medicine Centre, University College Hospital (UCH) Ibadan, Ibadan, NIGERIA, ⁵Nuclear Medicine Centre, University College Hospital (UCH) Ibadan, Ibadan, NIGERIA.

Background: The importance of positron emission tomography/computed tomography (PET/CT) in diagnosis and choice of cancer treatment strategy in Nigeria is unknown. Presently, medical tourism is the only source of PET/CT imaging in Nigeria. Since the establishment of Nigeria's first Nuclear Medicine centre in 2006, the centre has provided short-lived radionuclide scans and therapies daily to patients from all over the country. Developing a vision for PET/CT is critical to the introduction of a public PET/CT service in Nigeria. The aim is not to replace existing technical reports for developing countries. It is directed at establishing a formal reference for the Nuclear Medicine Institution in Nigeria with the objective to catalyse a framework for public PET/CT services in Nigeria. **Materials and Methods:** Primary data from Nigeria's first nuclear medicine centre was compared with country statistics from the International Agency for Research on Cancer (IARC). References were made to PET/CT experiences from South Africa and Egypt. The results are a descriptive epidemiology of cancers, nuclear medicine referrals, challenges and recommendations based on the experience of the authors towards a vision for PET/CT services in Nigeria. **Conclusion:** Gathering evidence for sustainable and cost-effective provision of public PET/CT services in Nigeria is a major contribution to the development of Nuclear Medicine in the country. Education and training of regulators, oncologists and other clinicians on new PET/CT tracers particularly more tumour specific and generator based Ga68-PSMA and Ga-68 DOTATATE/DOTATOC may be crucial to the initial realisation of the Nigeria PET/CT Vision. We welcome a private initiative to commission a cyclotron in Lagos, Nigeria as this will undoubtedly enhance the growth of Nuclear Medicine.

P161

Green way

I. Marikova, L. Cema, L. Baierova; Prague Medical Care Department s.r.o., Prague, CZECH REPUBLIC.

Structure: Presentation of common project of the Ministry of Defence of Czech Republic and Military University Hospital Prague. Nuclear medicine department is participating on this project. The project Green way is determined primarily for soldiers, military veterans, police officers, firemen or people from areas endangered by war. **Aim:** The aim is to show the usage of nuclear medicine in military health service in conditions of closely specialized Medical department of Military Hospital. **Material and methods:** Presentation is based on case interpretations of typical patients integrated in project of „Green way“. **Results and conclusion:** Relatively small and often discussed medical discipline as the nuclear medicine may be used in environment of military hospital. Multidisciplinary cooperation is possible in conditions of civil and military health service as well and everything is dependent of mutual cooperation of civil and military medical doctors.

P162

Assessment of thyroid uptake in dynamic salivary gland studies correlated with diagnostic ultrasound findings in patients with connective tissue diseases

A. Renda Alcalde, Jr., F. S. Zelaya Reinquet, Jr., D. M. Ruiz Hernández, M. A. Castrillón Sánchez, C. Castillo Berrio, F. J. Loira Bamio, L. M.

Campos Villarino, J. M. Nogueiras Alonso, A. M. Lopez Lopez, R. Guitián Iglesias; EOXI-VIGO-Hospital Meixoeiro, VIGO, SPAIN.

Salivary gland scintigraphy (SGS) is useful to assess the uptake and excretion of radiotracer in the major salivary glands (MSG). It is widely used in the diagnosis of xerostomia. In the standard technique, the thyroid gland (TG) is included in FOV. **AIM:** To determine the value of thyroid uptake pattern as an additional contribution to SGS tests at our department and correlating it with ultrasonographic (US) findings in patients with connective tissue diseases. **MATERIAL AND METHODS:** Retrospective review of 95 SGS performed at our centre among a period of 14 months (January/2015–February/2016), in patients with connective tissue diseases, mainly Sjögren's Syndrome. All the SGS were performed in fasting patient, after administering 5–10 mCi (185–370 MBq) of ^{99m}Tc-O₄. Dynamic scintigraphy was performed within the first 20 minutes post injection. Lemon juice stimulation was delivered at 10 minutes and the study ended with projections of the anterior and lateral views. In all test the thyroid gland was included in the FOV. To interpret the tests, we assessing the salivary incorporation and secretion in dynamic phase, as well as overall uptake, in the planar images. In addition, we classified thyroid uptake according to the following patterns: P1-high-uptake, P2-low-uptake, P3-normal uptake, and correlating them with US findings. **RESULTS:** We reviewed a total of 95 studies (95s), 89 woman–6 men; mean age 55, 78s (82%) with salivary gland malfunction. 52s (54.7%) revealed thyroid uptake alteration (TUA) and 43s (45.3%) normal uptake. Of the total, only 26s (27.4%) had additional cervical US. Subsequently, the studies were classified according to three thyroid uptake patterns: Pattern 1: 32s (33.7%), Pattern 2: 20s (45.3%) and Pattern 3: 43s (45.3%). P1-high uptake 32s, which 7 US: 4 nodules, 1 thyroiditis, 2 normal. P2-low uptake 20s, which 9 US: 4 nodules, 3 thyroiditis, 1 normal, 1 absence because of surgery. P3-normal uptake 43s, which 10 US: 3 nodules, 5 normal, 1 non assessable, 1 glandular atrophy. **CONCLUSION:** The assessment of thyroid gland visualized in SGS let us detecting unknown pathology. It is possible that we had over estimated the number of P1 in our sample which was of 32s (33.7%) mainly due to the significant amount of impair SGS 78s (82%). Although our review has a small sample size, we observed a good correlation between altered thyroid uptake and US findings (81.25%).

P-14 – Monday, October 17, 2016, 16:00 - 16:30, Poster Exhibition Hall
Conventional & Specialised Nuclear Medicine: Musculoskeletal (Benign)

P163

The role of the three phase bone scintigraphy in the evaluation of the patients with idiopathic carpal tunnel syndrome

M. Ceber¹, E. Sahin², B. Topcu³, R. Alp⁴; ¹Namik Kemal University Hospital, Department of Plastic, Reconstructive and Aesthetic Surgery, Tekirdağ, TURKEY, ²Namik Kemal University Hospital, Department of Nuclear Medicine, Tekirdağ, TURKEY, ³Namik Kemal University Hospital, Department of Biostatistics, Tekirdağ, TURKEY, ⁴Namik Kemal University Hospital, Department of Neurology, Tekirdağ, TURKEY.

Purpose/Introduction: Considering the anatomy of the carpal tunnel, the median nerve carries main sympathetic supply of the hand. Although sympathetic autonomic innervation of bones is an intriguing topic, its effects in the carpal bones in patients with carpal tunnel syndrome (CTS) is unknown. In this preliminary study, we aimed to investigate blood supply disorders and its effects in the wrist bones in patients with idiopathic CTS with the three-phase bone scintigraphy. **Subjects & methods:** A total of 90 hands (75 affected and 15 non-affected hands) in forty-five patients (age range: 29–65 years old, gender: 15 male, 30 female) with idiopathic CTS were analysed in the study. To analyse the changes in blood supply to the bones of the wrist, three-phase bone scintigraphy with ^{99m}Tc-MDP was applied to patients before surgical

treatment. Perfusion, blood-pool, delayed images were evaluated quantitatively-qualitatively in three-phase bone scintigraphy. Bone scintigraphy values for non-affected hands were used as controls for comparison with affected hands. **Results:** In patients with unilateral CTS, it was observed in all phases of increased radiopharmaceutical uptake in three-phase bone scintigraphy in affected carpal bones regions. There were a statistical significance for delayed phase related areas when compared to the non-affected hand and affected hand quantitatively in patients with unilateral CTS ($p=0,071$). However, it was observed no significant difference in radiopharmaceutical uptake in all phases and there were not statistical significance for delayed phase related areas when compared to the each of two affected hand quantitatively ($p=0,000$), in patients with bilateral CTS. **Discussion/Conclusion:** We believe that three-phase bone scintigraphy is a useful technique for the demonstration of the evolving circulatory disorders and its effects in the wrist bones in patients with unilateral CTS. **Key words:** Carpal Tunnel Syndrome; Radionuclide Imaging; Median Nerve; Wrist

P164

Radionuclide imaging in hemophilic arthropathy: Positive blood pool imaging on pretherapeutic bone scintigraphy is not a predictor of treatment success

A. Sabet¹, A. C. Strauss², J. Schmolders², R. Bornemann², A. Sabet³, J. Oldenburg², P. H. Pennekamp², H. J. Biersack², S. Ezziddin¹; ¹Saarland University, Homburg, GERMANY, ²University of Bonn, Bonn, GERMANY, ³University of California, Riverside, CA, UNITED STATES.

Purpose: Increased articular ^{99m}Tc-MDP uptake on blood pool imaging (BPI) of patients with rheumatologic conditions is indicative of active inflammatory changes and has been suggested as a strong predictor of response to radionuclide therapy (RTO). In this study we aimed to assess the value of pretreatment BPI positivity (i.e. scintigraphically apparent hyperaemia) for successful RTO in hemophilic arthropathy. **Methods:** 34 male patients with painful hemophilic arthropathy underwent RTO after failure of conservative treatment. Treated joints were comprised by the knee in 8, elbow in 5, and ankle in 21 patients. Pretreatment triple-phase bone scintigraphy showed hyperemic joints (positive BPI) in 17 patients, whereas 17 patients had no increased tracer uptake on BPI. Response to RTO was evaluated 6 months post-treatment measuring changes in intensity of arthralgia according to the visual analogue scale (VAS), bleeding frequency, and range of motion. The association of hyperemia (positive BPI) and treatment outcome was examined using nonparametric tests for independent samples. **Results:** Evident pain relief occurred in 26 patients (76.5 %) and the mean VAS decreased from 7.7 ± 0.1 to 4.6 ± 0.5 ($p<0.001$). The joint bleeding frequency (hemarthrosis) decreased from 4.5 ± 0.6 to 2.1 ± 0.4 during the first 6 months after RTO ($p<0.001$). According to both parameters (pain relief and bleeding frequency) patients benefited similarly from RTO regardless of pretreatment BPI: Arthralgia ($p=0.312$) and frequency of hemarthrosis ($p=0.396$). No significant improvement was observed for range of motion, but it was significantly more restrained in hyperemic joints both before ($p=0.036$) and after treatment ($p=0.022$). **Conclusions:** Hemophilic arthropathy can be effectively treated with RTO regardless of pretherapeutic BPI. Patients with no scintigraphically detectable articular hyperemia may have similar (outstanding) outcomes and should thus not be discarded from treatment.

P165

Hepatic HMDP tracer uptake on bone scintigraphy: report of two cases

A. Ezzine^{1,2}, R. Sfar¹, S. Melki^{1,2}, H. Boudriga¹, M. Nouria^{1,2}, M. Ben Fredj^{1,2}, K. Chatti¹, S. Ajmi¹, M. Guezguez¹; ¹Nuclear medicine department, Sousse, TUNISIA., Sousse, TUNISIA, ²LR 12Es02, Faculty of Medicine Sousse, University of Sousse, Sousse, TUNISIA.

Aim: Hepatic uptake of hydroxyl-methyl-diphosphonate labeled to ^{99m}Tc (^{99m}Tc-HMDP) is an accidental and unusual findings with multiple mechanisms. The purpose of this paper is to report two cases of abnormal hepatic accumulation and to discuss their pathophysiology. **Materials and methods:** We report the cases of two patients who were referred to our nuclear medicine department in order to search a bone infection site. The first patient was a newborn baby of 26 days old, who presented a limitation on the mobilization of the left hip evolving with fever. Laboratory tests showed elevated CRP and positive blood culture for Klebsiella. Ultrasound of the left hip was normal. The second case was a patient aged 16, suffering from a major beta thalassemia, hospitalized for red blood cell transfusion. Both patients underwent planar bone scan with acquisition of static tissue phase images followed by a whole body scan two hours after the injection of 10 MBq/kg of ^{99m}Tc-HMDP. **Results:** The initial bone scintigraphy did not find any suggestive sign of infectious bone location, but there was a diffuse hepatic uptake of ^{99m}Tc-HMDP despite a normal quality control of the preparation. Complementary exploration revealed a very high ferritin levels for both patients. For the first patient, a scintigraphic control after three months showed a normal bone scintigraphy with the normalization of the hepatic uptake correlated with a normal ferritin levels. For the second patient, a repeat bone scan performed three weeks later showed a better skeletal uptake with the persistence of an abnormal renal and hepatic radiotracer accumulation. It also showed the presence of bone uptake foci that can be related to infectious site. **Conclusion:** Knowledge of ^{99m}Tc-HMDP hepatic uptake mechanisms in bone scans, improves the interpretation of the examination. In this context, obtaining a relevant medical history can clarify incidental soft-tissue findings.

P166

Three phase bone scintigraphy in diagnosing stress fractures

M. Somai, I. Yeddes, I. Meddeb, K. Limam, A. Mhiri, I. Slim, M. F. Ben Slimene; institut Salah Azaiez, Tunis, TUNISIA.

Introduction : Stress fractures are an uncommon but important source of pain and disability in young. It is caused by sustained and submaximal physical activity. It is frequent among athlete. The diagnosis is suspected in case of a progressive onset of bone pain, that contrasts with the poverty of physical examination and radiographic signs. In such case, triple phase scintigraphy finds all its importance, it allows to detect metabolic changes few days after the beginning of this symptoms. **Methods** This was a retrospective study of 27 patients who were suspected to have a stress fracture. Standard radiography was noncontributory. These patients were referred to the department of nuclear medicine for a bone scintigraphy. This exam has included 3 phases: an angiographic phase, applied immediately after injection of 555 to 740mBq Hydroxy - Methylene Diphosphonates-Tc^{99m} (Tc^{99m} - HMDP), a tissue phase after 5 minutes of injection and a bone phase, on average 2 hours after. During these three phases, the acquisitions of images were focused on the painful area, taking both right and left sides. The late time also included a full-body scan in search of other bone alterations. **Results** Among these 27 patients, 52% were females. The average age was 31 years [13-67]. They had all initially been seen because of a progressive onset of a mechanical bone pain of the lower limb that is unresponsive to analgesics. 9 patients were athletes. All the patients had benefited standard radiographs of the painful area that has not objectified any abnormalities. Two patients underwent magnetic resonance imaging (MRI), that has showed signs for stress fracture. The triple phase Bone scintigraphy confirmed the diagnosis of stress fracture in 13 cases. It has objectified signs of periostitis in 5 cases. Scintigraphy was negative in 6 cases and it was inconclusive in three cases. In one case MRI has showed stress fracture signs that were not identified in bone scintigraphy. These fractures interested the lower limb especially the tibia followed by metatarsal bones. **Conclusion** Because it demonstrates subtle changes in bone uptake before changes are seen on conventional radiographs and high cost of MRI, the triple phase bone

scintigraphy is the choice procedure to diagnosis stress fracture. This exam is highly recommended in order to achieve early diagnosis, especially that the improvement of instrumentation has enhanced very significantly its diagnostic performance.

P167

Quantitative surgical criteria of bone scintigraphy in patients during hip arthroplasty

P. Korol^{1,2}, M. Tkachenko², V. Bondar¹; ¹Kiev's Clinical City Hospital #12, Kiev, UKRAINE, ²A.A. Bohomolets National Medical University, Kiev, UKRAINE.

Aim. Define the quantitative surgical criteria using bone scintigraphy in patient with deforming osteoarthritis during hip arthroplasty. **Material and methods.** Retrospective descriptive study (2005 - 2015): 468 patients with hip arthroplasty were imaged by a standard method of whole body bone scan. Intestinal uptake was observed visually 3 hours after the intravenous administration of 740 MBq ^{99m}Tc MDP. A whole body bone scan; anterior, posterior, oblique spot views of the hip joint region were obtained. **Results.** All patients were divided into three groups. The first group included 169 (36 %) patients who at bone scintigraphy the percentage accumulation of radiopharmaceuticals in the projection of the affected joint to 10% - 110%, and in the projection of the proximal femur 5% - 50%, relative to symmetric parts. The second group included 187 (40 %) patients whose accumulation rate indicator in the projection of the affected joint complex was 110% - 180%, and in the projection of the proximal femur 50% - 100%. The third group consisted of 112 (24 %) patients with accumulation indicator in the projection of the affected joint set of more than 180%, and in the projection of the proximal femur over 100%. In patients of first group on postoperative imaging in projection of the paraprosthesis area of joint percent accumulations of the indicator was equal 5% - 65%, in projections the proximal area of hip consisted 5% - 20%, to symmetrical area of the study. In patients second group - percent accumulations of the indicator in projections of the paraprosthesis area of joint was 160% - 250%, in projection the proximal area of hip consisted 55% - 120%. In patients third group in projection of the paraprosthesis area of joint was 215% - 380%, in projection the proximal area of hip consisted 90% - 200%. In 67 (22 %) patients two and three diagnostic groups were diagnosed with postoperative complications operated hip (inflammation, sprains). **Conclusion.** For avoiding the postoperative complications during hip arthroplasty, percent of the accumulation of the indicator on diagnostic imaging, in projections hip joint with osteoarthritis, must be within 10% - 110%. The percent of the accumulation of the indicator in projections of proximal area of hip must be consisting 5% - 50%, to symmetrical area of the study.

P168

Basal glucose metabolism in skeletal muscles measured by FDG-PET as a non-activated muscular activity: preliminary result

I. Chun¹, H. Park², S. Baik¹, K. Ahn², D. Lee², J. Park²; ¹Kangwon National University, School of Medicine, Chuncheon-Si, KOREA, REPUBLIC OF, ²Kangwon National University Hospital, Chuncheon-Si, KOREA, REPUBLIC OF.

Purpose/Introduction: ¹⁸F-fluorodeoxyglucose (FDG) is an analogue of glucose which is one of important energy substrates for most cells including cancerous, inflammatory, neuronal cells, and so it has been widely used in positron emission tomography (PET) imaging for evaluation of oncologic, neurologic, and sometimes inflammatory diseases. Recently, it was reported FDG-PET could detect activated muscles which might be related with musculoskeletal diseases.

However, it is not clear what degree of radioactivity within muscles on FDG-PET is closely related with activated muscles. Herein we tried to estimate glucose metabolism in the non-activated skeletal muscles by FDG-PET and to extract a threshold value of muscular glucose metabolism to distinguish activated muscles from non-activated ones. **Subjects & Methods:** Health screen-purpose FDG-PET images in seven healthy male subjects (age=37.42.3y, range=33-39y) were retrospectively reviewed. Each PET emission scan was obtained about 1 hour after intravenous injection of ¹⁸F-FDG (370.618.3MBq) and then non-contrast CT scan was obtained for attenuation correction. A muscular volume of interest (VOI) was obtained by manual delineation of paraspinal back muscles on the non-contrast CT image and it was copied on FDG-PET image to extract mean (SUV_{mean}) and standard deviation (SUV_{sd}) of standardized uptake value. Normal distribution was assumed in all SUV data and the normal distribution of non-activated muscular SUV was obtained by applying kernel density estimation (KDE). **Results:** Averaged SUV of seven subjects were 0.756, 0.186, 1.128, and 1.313 for SUV_{mean}, SUV_{sd}, SUV_{mean+2sd}, SUV_{mean+3sd}, respectively. On the other hand, predicted SUVs were 0.747, 0.165, 1.077, 1.242, respectively after kernel density estimation. **Discussion/Conclusion:** SUV_{mean} of 1.242 is the threshold value that can distinguish basal muscular glucose metabolism from activated one for 99.6% significance. This result can be a used as a reference for evaluation of muscular function by FDG-PET in various musculoskeletal diseases.

P169

Evaluation of of the results of PTH, Vitamin D and Calcium in Osteoporosis

R. Alimanovic-Alagic^{1,2}, **R. Alimanovic-Alagic**¹; ¹University Clinical Centre Sarajevo, sarajevo, BOSNIA AND HERZEGOVINA, ²Clinic for Nuclear Medicine, University Clinical Center of Sarajevo, Sarajevo, BOSNIA AND HERZEGOVINA.

Objective(s): Osteoporosis is a serious, life-threatening disease in both men and women. Vitamin D deficiency can contribute to bone loss from decreased vitamin D-mediated intestinal calcium absorption and resultant secondary hyperparathyroidism (HPTH). The parathyroid glands control of calcium and phosphorus in the blood and they do this by making a hormone called parathyroid hormone (PTH). **Material and Methods:** As a part of the investigational project 873 participants were examined of the University Clinical Center of Sarajevo and Public Medical Care Institution, Canton Sarajevo, age 20 to 80 during 6 months. For each patient we did personal history, age, medications, BMI, family history. We established presence of vitamin D deficiency, calcium levels, high level PTH, DXA higher than -2.5 SD. **Results:** In investigated group of 873 patients. The frequency of occurrence of osteoporosis is most common 44% between the ages of 40-59 years. Elevated levels of PTH at 64% patients, the patients have a vitamin D deficiency 77% and low-normal calcium levels 69%. Analysis of BMI obesity 52% as a potential factor for osteoporosis. **Conclusion(s):** Vitamin D deficiency is associated with increased parathyroid hormone (PTH) and also associated with low bone mineral density in patients who have diagnosed osteoporosis. Nutrition and BMI affect the metabolism and osteoporosis. Vitamin D and calcium supplementation reduces the risk of hip fractures and other peripheral fractures.

P170

Persistent muscular uptakes of rhabdomyolysis in ^{99m}Tc-HMDP scintigraphy after normalization of creatinine kinase levels

F. Hives, F. Demailly, F. Vandici, S. Hiroual, A. Besson, R. Hassad Ben Ticha, **G. Collet**; CH Valenciennes, Valenciennes, FRANCE.

AIM: Many causes can be suspected with a muscular uptake in bone scan. Rhabdomyolysis is a classic cause of muscular uptake in bone scan. Usually, creatinine kinase (CK) blood dosage and clinical examination are sufficient to confirm rhabdomyolysis. There is no evidence in literature of persistent muscular uptake in bone scan after normalization rate of CK. **MATERIALS AND METHODS:** A 85 year-old patient was admitted for rhabdomyolysis (CK: 25559 U/L, normal < 145 U/L) in a context of repeated falls. The rhabdomyolysis was complicated of acute kidney injury, hyponatremia and hypokalemia. Also, patient presented inflammatory syndrome, consequence of endocarditis and spondylodiscitis at staphylococcus aureus well treated by cefotaxime - ornidazole then clindamycin - levofloxacin. During hospitalization, CK level decreased, and was normal after nine days (CK: 70 U/L). We performed a ^{99m}Tc -HMDP scintigraphy to research signs of hip prosthesis infection, the same day as normalization of CK dosage. **RESULTS:** ^{99m}Tc -HMDP scintigraphy found muscles uptakes: right pectoralis major, gluteus maximus, sartorius, adductors, tibialis anterior, and bilateral sacral insertion of gluteus maximus. It found no pathologic uptake in contact with prosthesis. Laboratory tests days after bone scan showed no elevated CK levels. **CONCLUSION:** This case showed muscular uptake in bone scan and normal CK blood test level, because of a delay between normalize CK blood test level and disappearance of muscular uptake in bone scan. A negative CK blood test is not sufficient to eliminate a rhabdomyolysis as a cause of muscular uptake in bone scan. Clinical history is essential in the evaluation of muscular uptake.

P171

Value of ^{18}F -NaF PET/CT imaging in the assessment of Gorham-Stout disease activity

G. Z. Papadakis¹, C. Millo², U. Bagci³, N. J. Patronas¹, M. T. Collins⁴,
¹Department of Radiology & Imaging Sciences, Clinical Center (CC), National Institutes of Health (NIH), Bethesda, MD, UNITED STATES, ²Division of Nuclear Medicine, Clinical Center, National Institutes of Health (NIH), Bethesda, MD, UNITED STATES, ³Center for Research in Computer Vision (CRCV), Electrical and Computer Science Department, University of Central Florida (UCF), Orlando, FL, UNITED STATES, ⁴Craniofacial and Skeletal Diseases Branch, National Institutes of Dental and Craniofacial Research, Bethesda, MD, UNITED STATES.

AIM: To assess the application of ^{18}F -NaF PET/CT imaging in monitoring the activity of Gorham Stout disease (Vanishing Bone Disease). **PATIENT AND METHODS:** A 44 year-old male diagnosed with Gorham Stout disease underwent whole body PET/CT scan after intravenous administration of 3.29 mCi ^{18}F -NaF. PET acquisition commenced 65 minutes post injection, while a non-contrast low dose CT scan was performed for attenuation correction and co-registration. Maximum Standardized Uptake Values (SUVmax) were normalized to body weight and were obtained from Time-of-Flight (TOF) PET images. The patient had presented with worsening pain and movement limitation in the right shoulder joint, while CT and MRI scans of the chest revealed absence of the largest portion of the right scapular body with preservation only of the scapular spine. **RESULTS:** The remnant upper portion of the affected right scapula showed markedly increased ^{18}F -NaF uptake (SUVmax:27.3) compared to the corresponding portion of the unaffected left scapula. Furthermore, multiple foci of intensely increased ^{18}F -NaF activity were observed on the right posterior ribs, associated with areas of incipient bone resorption seen on CT scan. **CONCLUSION:** ^{18}F -NaF is a PET agent which is deposited on bone tissue via ^{18}F -ions exchange with hydroxyl (OH⁻)-ions on the surface of the hydroxyapatite matrix leading to formation of fluoroapatite. ^{18}F -NaF bone uptake and retention reflects osseous blood flow and bone remodeling. At the same time, Gorham-Stout disease is characterized by proliferation of endothelial-lined vessels in bone, and by progressive replacement of bone with fibrous tissue.

These underlying processes which are present in Gorham Stout disease result in increasing the bone surface exposed to blood flow providing high availability of binding sites for ^{18}F -NaF. This data suggests ^{18}F -NaF as the optimal bone-seeking PET-radiopharmaceutical to assess Gorham Stout Disease activity as well as monitor treatment response.

P-15 – Monday, October 17, 2016, 16:00 - 16:30, Poster Exhibition Hall
Conventional & Specialised Nuclear Medicine: Paediatrics

P172

Detecting More Reliable Time Period for the Calculation of Relative Renal Function in Assessing Response to Pyeloplasty in Children with Hydronephrosis

N. C. M. Gulaldi, N. Altun Yologlu, S. Ozyurt; Department of Nuclear Medicine, Dr. Sami Ulus Maternity and Children's Health and Diseases Training and Research Hospital, ANKARA, TURKEY.

Aim: The aim of the study is to evaluate 60-90 seconds period or 90-120 seconds period compared to 60-120 seconds period using ^{99m}Tc -MAG3 for the calculation of relative renal function for assessment of better prediction of surgery effect in hydronephrotic kidneys in pediatric patients. As a hypothesis, if one time period would better delineate relative kidney function correlated with other parameters such as residual activity and size of the pelvis, these could be used as to avoid any early collecting system activity within the ROIs. **Methods:** Twenty children (8 female, 12 male) (1 month-17 years of age mean=50±15,3 months) diagnosed as unilateral hydronephrosis because of narrowing in ureteropelvic junction level were included into the study. Dynamic renal scintigraphies using ^{99m}Tc -MAG3 were done before and after open pyeloplasty to all patients. Post-operative MAG3 scans were performed 292,7±39,7 days after pyeloplasty. Relative renal functions were calculated from the frames summed between 60-120 seconds, 60-90 seconds and 90-120 seconds images to evaluate any difference or comparative advantage between them. Background corrected ROIs drawn over kidneys were used and counts/pixel values within those ROIs were noted for each period. **Results:** Paired t-tests were used to compare results of counts/pixel values between the time periods. A p-value <0.05 was considered statistically significant for the difference. Relative kidney functions did not differ statistically (p>0,05) with regard to ROIs drawn for different time periods between 1-2 minutes. Pre-op and post-op relative kidney functions were in accordance with size of the kidneys and overall kidney functions in 17 patients. Three patients showed deteriorating relative function in spite of better diuretic response after pyeloplasty. However those patients also did not show statistically significant difference in correlation calculated for 3 time periods (p>0,05). **Conclusions:** Hydronephrosis in children requires ^{99m}Tc -MAG3 to be used for the scintigraphy in detecting kidney functions. However rapid excretion of the tracer may sometimes be cumbersome for the interpretation of the studies. In this study we showed that several time periods could be used before 2 minutes of the study to calculate relative renal function and this chosen period should be the same for the calculation in serial studies. We suggest using relative kidney function with the excretion parameters of the kidneys when deciding the operation or detecting the effect of surgical procedure.

P173

Interest of the renal dynamic scintigraphy with MAG3 in exploration of infant hydronephrosis About 70 cases

S. Touil, H. Aschawa, Y. Shimi, F. M'hamdi, H. Bendaoud, J. Benouhoud, A. Guensi; Faculty of Medicine and Pharmacy, Nuclear medicine service, Ibn Rochd University Hospital Center, Casablanca, MOROCCO.

Renal scintigraphy using ^{99m}Tc -MAG3 with diuresis has an important role in the exploration of hydronephrosis in infants. This non-invasive and low-radiating exploration allows both to specify the quality of drainage and the separate evaluating renal function. We report, through this work, a retrospective descriptive study including 70 patients referred for scintigraphic exploration of their hydronephrosis or uretero-hydronephrosis between January 2012 and March 2014. The renal dynamic scintigraphy using ^{99m}Tc -MAG3 (RDS) and diuresis test of furosemide F + 20 protocol was performed in all patients, supplemented by static acquisitions post-micturition and verticalisation. The interpretation takes into account the semi-quantitative and qualitative parameters of isotopic renogram obtained after treatment of dynamic sequential images. Of the 70 cases studied (11 F/59 M), the mean age was 5.44 months, with a range of 2-24 months. Data from the scintigraphic exploration with ^{99m}Tc -MAG3 allowed to classify our patients into three groups. Group I: absence of drainage alteration, with preserved function (group Ia) in (30%) and without preserved function (group Ib) in (4.3%) of patients. Group II: presence of altered drainage, with functional conservation (group IIa) in (38.6%) and without functional conservation (group IIb) in (11.4%) patients. Group III: represented by an equivocal response (comprising 15.7% of cases). Renal dynamic scintigraphy with MAG3 (radiotracer of choice, particularly in neonates and infants) and furosemide test F + 20 (protocol allowing sufficient diuresis) has, through this study, judged the quality of permeability ureteropelvic and specifying the relative contribution of each kidney in global function. Such information remains crucial to guide the surgeon to choose between a surgical or endoscopic therapy or no treatment and close monitoring well codified. Currently, it is recognized that any restriction on urinary excretion, which untreated, cause renal injury and that surgery should only be considered if the function is altered. So, this exploration occupies a specific place in the care decision in the hydronephrosis infant.

P174

Agreement Between Renal Length Measurements by Planar DMSA Scintigraphy and Ultrasonography

V. Marković, A. Barić, V. Čapkun, A. Punda, D. Eterović, A. Pranić-Kragić, A. Marović, A. Arapović; University Hospital Split, Split, CROATIA.

AIM: Renal length measurements (RLM) are considered as a surrogate measure for kidney function. Measurement by ultrasonography (US) is accepted as a standard procedure in nephrourological practice, while the role of planar ^{99m}Tc -DMSA scintigraphy is underestimated and neglected. The purpose of this study is to compare RLM by these two methods and to examine if there is agreement between them? MATERIAL AND METHODS: This was a retrospective study of 43 patients (83 kidneys), 25 females and 18 males with a median age of 3.67 years (range: 3 months to 51 years) with various nephrourological pathologies, and who had RLM by both methods. Agreement between RLM by US and posterior DMSA scintigraphy were evaluated by Pearson's correlation, Wilcoxon test and Bland-Altman Plot analysis. RESULTS: Median value of right kidney length measurements (KLM) by US was 75 mm (min-max:43-124 mm) and by DMSA scintigraphy 75 mm (43-128 mm) ($z=0.747$; $p=0.455$). Pearson correlation coefficient $r=0.922$ ($p<0.001$). Median value of left KLM by US was 84 mm (45-124 mm) and by DMSA scintigraphy 79 mm (47-142 mm) ($z=0.023$; $p=0.455$). Pearson correlation coefficient $r=0.907$ ($p<0.001$). Average value of differences between measurements by these two methods for right kidneys lengths was 0.983 ± 15 mm with 95% limit of agreement from -15 to 17 mm. Average value of differences between measurements by these two methods for left kidneys lengths was 1.41 ± 10.3 mm with 95% limit of agreement from -21.6 to 19 mm. Differences of measurements were tested by one sample t-test with test value zero for the average bias. We did not find average bias neither for right kidneys ($t=0.971$; $p=0.337$) nor for left kidneys ($t=0.689$; $p=0.945$). We also made linear

regression analysis where the independent variable was average and dependent variable was differences of measurements for each kidney separately by these two methods (proportional bias). We didn't find proportional bias neither for right kidneys ($p=0.966$) nor for left kidneys ($p=0.476$). After this results we put all measurements for right and left kidneys together and made same analysis. Average value of differences between measurements by these two methods for left and right kidney lengths together was 0.756 ± 9.26 mm with 95% limit of agreement from -18 to 18.2 mm. There was not average bias ($p=0.941$) and proportional bias ($p=0.573$). CONCLUSION: RLM on posterior planar scintigraphy with ^{99m}Tc -DMSA are in agreement with ultrasound measurements and we recommend it to be a routine procedure.

P175

^{99m}Tc -DMSA scan in assessing acute pyelonephritis

S. E. Bouyoucef, M. Habbeche, s. Rahabi, A. Khelifa, D. mouas, I. Kellou; CHU Bab El Oued, Algiers, ALGERIA.

Introduction Acute pyelonephritis (AP) is a potentially organ- and/or life-threatening infection that often leads to renal scarring. The diagnosis is based on clinical symptoms including fever and biological findings of bacteriuria ($>100\,000$ bacterias/ml). ^{99m}Tc -DMSA scan has a good negative predictive value in case of febrile urinary tract infection Objective Assessing the role of ^{99m}Tc -DMSA scan in acute pyelonephritis in children and defining the clinical, biological and morphological predictif factors for a positif ^{99m}Tc -DMSA Patients and methods : 192 children aged from 1 year to 16 years have been referred to the department for suspicion of AP after one or more episode of febrile urinary tract infection. All children presented fever above 38° and bacteriuria ($>100\,000$ bacterias/ml). Those children with obstructive uropathy were excluded. Each child underwent two ^{99m}Tc -DMSA scan, the first within the 10 days following the onset acute episode of urinary tract infection and the second 6 months later. Both ^{99m}Tc -DMSA scan were reported by two experienced nuclear physicians and compared to the findings of ultrasonography, urethrocytostcopy and complete biological inflammatory tests. Results: 110 girls and 82 boys have had urinary tract infection with a causal agent of E. Coli (94.79%). Abdominal US were normal. Initial ^{99m}Tc -DMSA scans were positive in 102 patients (53.13%). 6 months after, the second ^{99m}Tc -DMSA scans showed a persistence of cortical DMSA abnormalities in 45 children (45/102). Those cortical abnormalities were reported as kidney scar post pyelonephritis. Among those children with a scar, 21 have had VUR identified by urethrocytostcopy. 57 patients among the 102 with a positive first ^{99m}Tc -DMSA scan have had a negative second ^{99m}Tc -DMSA scan 6 months later with only 11 VUR seen on urethrocytostcopy. After statistical analysis, VUR was found as a strong predictive value for renal scar ($p=0.004$) meanwhile the female sex is at the limit value of predicting kidney scar ($P=0.06$). The age, the temperature, and inflammatory factors and even the grade of VUR were not predictive for kidney scars ($P=0.05$). Conclusion: The VUR was present in more than 25% patients with febrile urinary tract infection. The VUR has a good predictive value for kidney scars meanwhile age, temperature, and biological inflammatory parameters and even the grade of VUR were not predictive for kidney scars ($P=0.05$). ^{99m}Tc -DMSA scan was very useful for better management of the AP and permitted a targeting the populations of children who have highest risk of developing kidney post infection complications.

P176

Accuracy of 18F-FDG PET/CT versus bone marrow biopsy in assessing bone marrow involvement in paediatric Hodgkin's Lymphoma. Accuracy in a multicenter series of 156 patients

a. cistaro¹, l. cassalia², c. ferrara³, m. bianchi⁴, f. fagioli⁴, g. bisi⁴, m. pillon⁵, a. zanella⁶, p. zuchetta⁶, m. burei⁷, l. evangelista⁷, c. ferrari⁸, C. Altini⁹, T.

Perillo⁹, n. quartuccio¹⁰; ¹centro PET IRMET, torino, ITALY, ²università di messina, messina, ITALY, ³ospedale Umberto I, siracusa, ITALY, ⁴università di torino, torino, ITALY, ⁵coematologia pediatrica A.O.Padova, padova, ITALY, ⁶università di padova, padova, ITALY, ⁷IOV, padova, ITALY, ⁸università di bari, bari, ITALY, ⁹Università di Bari, Bari, ITALY, ¹⁰università di manchester, manchester, UNITED KINGDOM.

Objectives. To assess the utility of F-18-fluoro-2-deoxy-D-glucose (18F-FDG) positron emission tomography/computed tomography (PET/CT) in assessing bone marrow involvement (BMI) compared to bone marrow biopsy (BMB) in newly diagnosed pediatric Hodgkin's lymphoma (HL). **Materials and Methods.** 171 pediatric patients (range 5-18 years) with HL were retrieved from the hospital database of 6 different nuclear medicine departments. The patients were referred for completion of staging and evaluation of bone marrow involvement and underwent a baseline 18F-FDG PET/CT. The diagnostic distribution for stage disease at the time of the PET/CT exam was: stage I = 9 pts; stage II = 77 pts; stage III = 47 pts; stage IV = 38 pts. 18F-FDG PET/CT scans were performed in all the patients within 10 days from BMB, performed in the iliac crest. **Results.** Out of 171 cases, 8 patients had positive BMB. Among these 8 pts, 6 had evidence of lymphomatous involvement on PET/CT, one showed a pattern of diffuse and disomogeneous 18F-FDG distribution and the other one resulted PET/CT negative. In 131 of the remainder 163 patients presenting with negative BMB, PET/CT resulted negative (80.3%), positive in 19 patients (11.7%) (stage II=1, stage III= 2, stage IV= 16) and doubtful in 13 cases (8%) disomogeneous 18F-FDG distribution (stage II= 6, stage III= 6, stage IV=1). In 16/19 patients with positive PET/CT and negative BMB bone marrow involvement was confirmed by MRI, bone scan or CT images. The remaining 3 pts (stage III=1, stage IV=2) resulted to be false negative at BMB and true positive at PET/CT. The doubtful 18F-FDG PET/CT cases (uptake with diffuse and heterogeneous pattern of distribution) could be considered as functional bone marrow activation or as expression of bone marrow involvement. In our experience, if we had considered this FDG PET pattern as negative, the overall sensitivity, specificity, positive predictive value (PPV) and negative predictive value (NPV) of 18F-FDG PET/CT for BMI detection would have been, respectively, 91.6%, 98.6%, 76%, 98.6%. On the contrary, considering the imaging pattern as positive, the overall sensitivity, specificity, PPV and NPV would have changed in 95.8%, 89.1%, 58.9%, 99.2%, respectively. **Conclusions** 18F-FDG PET/CT shows a good agreement with BMB results in early and advanced stages disease. Further data are warranted to confirm whether BMB should be omitted in patients with negative or positive PET/CT scan and reserved exclusively for patients with doubtful 18F-FDG uptake in bone marrow.

P177

18FDG PET-CT in the diagnosis of GIT Graft versus Host Disease (GvHD) in Children

M. Seng, N. Kisiel, E. Turner, K. London, P. Shaw, T. O'Loughlan, R. Howman-Giles; The Childrens Hospital at Westmead, Sydney, AUSTRALIA.

Background: Gastrointestinal tract graft-versus-host disease (GIT-GvHD) is a common and potentially life threatening complication after allogeneic hematopoietic stem-cell transplantation. GIT-GvHD has been related to poor response to treatment and higher mortality. The diagnosis maybe difficult and may require endoscopy/biopsy. These procedures are invasive and morbid in patients who are already medically compromised. ¹⁸F-FDG PET/CT may be able to stratify patients who require endoscopy and biopsy. **Aims:** To evaluate the performance of ¹⁸F-FDG PET/CT in differentiating no or mild disease compared to moderate or severe disease in pediatric patients with suspected GIT-GvHD. **Methods:** Paediatric patients referred for ¹⁸F-FDG PET/CT with suspected GIT-GvHD were reviewed. Clinical follow-up, endoscopy and biopsy findings were

correlated with ¹⁸F-FDG PET/CT. Regional SUV parameters were extracted by placing ROIs around stomach, duodenum, distal ileum, caecum, ascending colon, transverse colon, descending colon, recto-sigmoid colon and rectum. Regional, and average large and small bowel SUV data were statistically compared between patients with no or mild GIT-GvHD versus moderate to severe disease. **Results:** 47 scans in 35 patients were analysed (age range 6months to 18years; 36 with no or mild GvHD and 11 with moderate to severe disease). Transverse colon SUVmax was significantly higher in the moderate to severe group compared to no or mild disease (Mann-Whitney-U p<0.05). There was a non-significant trend for average large bowel SUVmax to be higher in the moderate to severe group than the no or mild disease group (mean SUVmax 2.83 compared to 2.03, p=0.07). **Conclusion:** Large bowel ¹⁸F-FDG PET/CT may be higher in patients with moderate to severe GIT-GvHD, and transverse colon SUVmax could have the ability to differentiate children with no or mild GvHD from those with moderate to severe disease and allow triaging of patients who would be more likely to benefit from more proceeding to more invasive endoscopy and biopsy.

P178

¹⁸F FDG PET/CT Pitfalls and Artifacts in Paediatric Malignancies

A. A. Nawwar, M. Abu Gabal, A. Tawakol, H. Moustafa; Faculty of medicine, Cairo University, Cairo, EGYPT.

Paediatric malignancies have been on the rise over the last decade and early detection and accurate follow-up is key for better prognosis. F18-FDG PET/CT used requires consideration of particular challenges that are common to paediatrics but uncommon to adults, such as cooperation, fasting, intravenous access and sedation. Also, normal distribution of F18-FDG in "children" differs than adults'. **Aim:** Determine the prevalence, location and appearance of the non-tumoural F18-FDG focal uptakes (potential pitfalls) and various artifacts in pediatric malignancies. **Methods:** Over 2 years, 253 pediatric patients of both genders and various primary malignancies underwent F18-FDG PET/CT at CCHE using the standardized protocol for the hospital. Scans were prospectively reviewed by 2 nuclear medicine physicians. Detailed clinical history was obtained. Visual and quantitative image analyses were done. Pitfalls and artifacts were characterized into physiological uptakes, technical artifacts, benign lesions and therapy-related artifacts. **Results:** When the patients were examined on lesion-based analysis, 1098 pitfall and artifact sites were encountered. Physiological uptake was the highest (75.9%) followed by technical artifacts (15.8%), benign lesions (3.1%) and finally, therapy-related artifacts (5.3%). The commonest site of physiological uptake was the head and neck (279 sites); the nasopharynx (29%) with mean SUV max of 6.4 ± 1.1. It was noted in our study that uptake in brown adipose tissue was significantly higher in the >5 age group (P=0.01) which opposes to Park et al's results that state that BAT detection rate was higher with younger age (7.94% vs. 0.73%). Respiratory movement was the commonest technical artifact (24.2%). Bone marrow and splenic hyperplasia were the commonest therapy-related pitfall (61.2%), average SUV max of 1.4 ± 0.6. Benign lymph nodal uptake was found in 36.7% with mean SUV max 1.9 ± 0.5, representing the commonest benign lesion encountered. **Conclusion:** The prevalence of pitfalls and artifacts in pediatric PET/CT are high, mainly attributed to various physiological uptakes followed by misregistration, mainly due to failure of patients of such age group to hold their breath (respiratory motion). Many of the normal variants in children are similar to adults' but nevertheless unique, such as uptake in lymphatic tissue. It is vital to know the incidence of such pitfalls and artifacts, in order to avoid misinterpretation; for better prognosis. Therefore, correlation with clinical history is crucial alongside experienced nuclear medicine physicians. The CT component also provides vital information; localization and accuracy. Also, relaxed, child-oriented environment, and staff experienced in paediatric venipuncture and management are important.

P179**Correlation Between the Number of Acute Pyelonephritis Episodes and the Presence and Severity of Renal Scarring, Evaluated by ^{99m}Tc-DMSA Scintigraphy****J. RODRIGUEZ ALBAN;** CHUC, Coimbra, PORTUGAL.

Aim: To evaluate the correlation between the number of acute pyelonephritis (APN) episodes and the presence and severity of renal scarring, evaluated by renal scintigraphy with dimercapto-succinic acid labelled with ^{99m}Tc (^{99m}Tc-DMSA). **Material and Methods:** We reviewed the clinical charts of 950 children with history of APN, submitted to renal ^{99m}Tc-DMSA scintigraphy in our department, between September-1995 and July-2014. The minimum interval between the APN and the scintigraphy was, at least, 6 months. We selected only the cases with positive uroculture and with a recent ultrasound study. Then, we created 2 groups concerning the number of APN episodes (Group-1: 1; Group-2: >1). The renal scans were divided into 3 groups according to the number of scars (DMSA₀:0; DMSA₁:1; DMSA₂:2; DMSA₃: ≥3) and into 2 groups according to the absence/presence of functional impairment, considering an asymmetry of 20% or more in the differential renal function (DRF) (Group-A:<20% ; Group-B: ≥20%). Cases with doubtful results on the scintigraphy were excluded. **Results:** We selected 135 studies [59 boys (43.7%) and 76 girl (56.3%); age: 2.8±3.6], 99 from Group-1 (73.3%) and 36 from Group-2 (26.7%). Concerning the scintigraphy, 77 did not show any abnormality (DMSA₀) and 58 revealed scars (DMSA₁: 26; DMSA₂: 20; DMSA₃: 12). A hundred and sixteen cases (86%) had an asymmetry of DRF<20% (Group-A) and in 19 (14%) the asymmetry was ≥20% (Group B). We found a strong statistical correlation between the number of APN episodes and the number of scars (p=0.000) and functional impairment (p=0.000). In Group-1, 27 (27.3%) patients had at least 1 scar and 7 (7%) had already a significant function loss. Among the 58 children with renal scar, only 17 (23.9%) showed ultrasonographic changes consistent with scars. *Escherichia Coli* was the pathogenic agent isolated in the majority of the cases. **Conclusions:** Our results point towards a positive correlation between the number of APN episodes and the presence and severity of renal scarring. Children with one APN episode are less likely to develop renal scars than children with more episodes. Our study also confirms the low sensitivity of renal ultrasound in scar detection, with a sensitivity of only 29.3%.

P180**Congenital Ureteropelvic Junction Obstruction: which renographic parameter is used by the surgeon for deciding about surgery?**

A. I. Santos^{1,2}, M. Bernardo^{1,3}, P. Calhau^{1,3}, G. Costa⁴, G. Mimoso⁴, A. Vaz-Silva⁵, M. Knoblich⁵, I. Conde⁶, I. Vieira¹, M. T. Neto^{5,2}, A. Piepsz⁷; ¹Hospital Garcia de Orta, E.P.E., Almada, PORTUGAL, ²Nova Medical School - Faculdade de Ciências Médicas de Lisboa, Lisboa, PORTUGAL, ³Faculdade de Medicina de Lisboa, Lisboa, PORTUGAL, ⁴Centro Hospitalar e Universitário de Coimbra, E.P.E., Coimbra, PORTUGAL, ⁵Hospital Dona Estefânia - Centro Hospitalar Lisboa Central, E.P.E., Lisboa, PORTUGAL, ⁶Quadrantes - Grupo Joaquim Chaves, Miraflores, PORTUGAL, ⁷CHU St Pierre – Université Libre de Bruxelles, Bruxelles, BELGIUM.

Aim: In congenital hydronephrosis it is not consensual which renographic parameters influence more the clinicians for their surgical decision. The present study aims to evaluate the differences on renogram parameters between two groups of children, one operated immediately after a first renogram and another with two or more renograms performed before surgery. **Population and methods:** Retrospective analysis of a series of 38 children with unilateral congenital hydronephrosis submitted to pyeloplasty, 21 immediately after a first diuretic renogram (median age and interquartile range - 1.6[1.3;5.6]months) [Group 1] and 17 after a follow-up period in which 2 to 4 diuretic renograms were performed (median age and interquartile range - 2.6[1.9;5.6]months) [Group 2].

There was one horseshoe kidney on each group and there were no children with single kidneys. For the kidney with pyeloureteral obstruction, differential renal function (DRF) and normalized residual activity at post-micturition image (NORAPM) on the first performed renogram were compared between the two groups, using T-Student test for DRF and the Mann-Whitney Test for NORAPM. For the 17 children on Group 2, these same parameters were compared between the first and the last pre-operative renogram, using the Sign Test for DRF and the paired Samples t-Test for NORAPM. The presence of visually determined delayed cortical transit (CT) of the radiopharmaceutical was also analysed in the same groups. **Results:** No statistical significant difference was found for the initial DRF between the two groups (p= 0.16). There was a statistical significant difference for initial NORAPM between these same groups (p<0.001). For Group 2, considering the comparison between the first and the last pre-operative renogram, there were no statistical significant differences for none of these parameters (p=0.21 for DRF, and p=0.16 for NORAPM). The initial CT was delayed in the majority of children in both groups (17/21 operated after the first exam, and 11/17 scheduled for follow-up). Five of the children in Group 2, which had initial normal CT, presented delayed CT on the last pre-operative study. **Conclusion:** In this study, compromised kidney drainage seems to have been the most influential parameter for our clinicians to decide to perform the surgical procedure.

P181**Can the new renal imaging agent L -ethylenedicycysteine replace MAG 3 in children dynamic scintigraphy?****M. C. Fornito,** S. Russo, A. Ruggeri, D. Familiari, R. A. Balzano; Nuclear Medicine Department - ARNAS GARIBALDI, Catania, ITALY.

AIM: Search for the ideal radiopharmaceutical to measure ERPF is still underway. ^{99m}Tc-mercaptoacetyltriglycine (MAG3), the agent of choice, is not the perfect replacement for ^{131I}-Orthoiodohippurate (OIH). ^{99m}Tc-ethylene dicycysteine (EC), a metabolite of ethylene cysteine dimer (ECD), is a new technetium-labelled renal tubular function tracer alternative to OIH, with imaging qualities similar to ^{99m}Tc-MAG3. Preclinical and clinical studies in adult volunteers and patient showed that ^{99m}Tc-EC is a good tubular agent as well as ^{99m}Tc-MAG3. Only few studies with ^{99m}Tc-ED have been done in the paediatric population and all have used it as cortical agent for static scintigraphy. The aim of this study is to demonstrate the potential usefulness of ^{99m}Tc- EC in paediatric dynamic renal scintigraphy. **MATERIALS AND METHODS** 55 children (ranging 0.2-5 years) with various kidney disorders underwent conventional dynamic scintigraphy after intravenous injection of ^{99m}Tc-EC (EAMN paediatric guidelines). The most frequent disorders were ipo-dysplasia, pyelo-ureteral stenosis, megaureter, vesico-ureteral reflux, and obstructive nephropathy. Furosemide was administered in case of excretory disorders. No adverse effects were noted. Quality control (radiochemical purity and stability) was performed immediately at the preparation and after 2, 3, 4 and 5 hours. **RESULT** ^{99m}Tc-EC provided high-quality images similar to ^{99m}Tc-MAG3, even in newborns (2 or 3 months), with a low/negligible extra-renal clearance and high kidney-to-background ratio similar to DMSA. These properties allow good delineation of the kidneys and the detection of renal parenchymal lesions.. The lower liver and intestinal activity respect to ^{99m}Tc-MAG3, makes ^{99m}Tc-EC particularly attractive because the possibility of a clear delineation of right kidney from liver can affect the interpretation of the study, particularly in newborn babies. ^{99m}Tc-EC shows a good renal uptake in the smallest babies (8/12 weeks) comparable to that of the older children as well as the renogram shape and the diuretic time of response. These favorable characteristics depend on the significantly lower plasma protein-bound fraction (30%) and the lowest red blood cell binding (5.7%) The labelling procedure is easy, radiochemical purity is high (99.8%) and the complex is stable in the quality controls up to 5 hours or more. **CONCLUSION** Our experience showed that ^{99m}Tc-EC

has excellent imaging characteristics similar to ^{99m}Tc -MAG3 and excretion properties similar to OIH. Despite its use is not currently recommended in leaflet for children dynamic studies, our experience showed the radiopharmaceutical safety and that it can be used routinely to evaluate paediatric patients, particularly newborns, for the easier interpretation of the renogram.

P182

The levels of serum 25 Hydroxy vitamin D in pediatric patients with Bronchial Asthma

A. S. ZISSIMOPOULOS¹, A. Tsalkidis², E. Maziotis³, E. Parashakis², O. Zissimopoulou¹, D. Benti³, A. Pistola¹, C. Christofis⁴; ¹Nuclear Medicine Dept Democritus University of Thrace, Alexandroupolis, GREECE, ²Pediatrics Clinic Democritus University of Thrace, Alexandroupolis, GREECE, ³Molecular Biology and Genetics School Democritus University of Thrace, Alexandroupolis, GREECE, ⁴Department of Anaesthesiology Democritus University of Thrace, Alexandroupolis, GREECE.

Introduction: Bronchial asthma is a serious childhood disease which can cause discomfort in young patients and may have severe effects in their later life. The control of the aggravating factors of bronchial asthma may lead to the discovery of better treatments that will relief the young patients. **Aim:** The aim of this study is to evaluate the serum levels of 25 hydroxy- vitamin D [25(OH)D] of children patients and to correlate them with the severity of the disease's symptoms, in order to modify the pharmaceutical treatment which will improve the patient's condition. **Patients and method:** 85 pediatric patients (44 boys and 41 girls) was studied aged between 3 and 13 years old (median age of 8±3 years old). The most of them (62) were patients of the University Pediatrics Clinic of the University Hospital of Evros and the rest were patients of other pediatricians. All of the children had bronchial asthma because of different reasoning (mostly due to allergic reasoning and other lung diseases). In all children blood samples were taken and after centrifugation the serum was collected and kept refrigerated at -70 ° C. The vitamin D status was measured by radioimmunoassay (RIA) method with ^{125}I [25(OH)D] kits Diasorin at in- vitro laboratory of Nuclear Medicine Dept. University Hospital of Evros, Democritus University of Thrace. **Statistical analysis:** Statistical analysis was performed by the χ^2 - test (student test) and statistical significance was considered to be $p < 0.005$. **Results:** In 52 patients with severe symptoms of the disease, the levels of [25(OH)D] were significantly low 0-20 ng/mL (0-50 nmol/L), in 21 patients with mild symptoms of the disease the levels were 20-40 ng/mL (50-100 nmol/L) (hypovitaminosis) and the rest with no symptoms, had levels of [25(OH)D] > 40 ng/mL (>100 nmol/L). **Conclusions:** According to our results it is concluded that a statistically significant number of children who have vitamin D deficiency show severe symptoms of asthma ($p < 0.005$). Pediatric patients with mild asthma have hypovitaminosis ($p < 0.005$). While pediatric patients with adequate vitamin D levels had no symptoms. The levels of serum vitamin D is statistically significantly associated with the severity of the symptoms of asthma. It is possible to administer vitamin D supplements in pediatric patients with bronchial asthma in order to cause a reduction in the severity of disease symptoms. Clinical trials with vitamin D supplementation are needed.

P183

A Single Center's 5 Year Experience Regarding Relative Renal Function in Children, ^{99m}Tc DTPA versus ^{99m}Tc DMSA

I. C. Grierosu, Sr.^{1,2}, M. Starcea^{3,2}, M. Munteanu³, R. Russu³, I. Pasarica², A. Statescu¹, M. M. Gutu^{1,2}, C. Stefanescu^{1,2}; ¹Emergency Clinical Hospital Sf. Spiridon, Iasi, ROMANIA, ²Faculty of Medicine, UMF Gr. T. Popa, Iasi, ROMANIA, ³Emergency Children Clinical Hospital Sf. Maria, Iasi, ROMANIA.

Aim: The study was realized in the single Nuclear Medicine Department, who deserves the entire North-East region of Romania. **Materials and methods:** This is a retrospective study on five years period of time (2011-2015), with 69 cases of congenital hydronephrosis who undergoes both scintigraphic methods: ^{99m}Tc DTPA and ^{99m}Tc DMSA. We took into the consideration only 46 cases for which there was one day difference between the two methods. ^{99m}Tc DTPA dynamic scintigraphy with diuretic administration was performed to determine the type of obstruction and to calculate the relative renal function (RRF). ^{99m}Tc DMSA static scintigraphy was realized in cases with history of urinary infection to localize the scars and to measure the RRF. **Results:** Related to the age we classified them in: group A (under 3 years old) = 17 cases (36.96 %) and B (3-16 years) = 29 cases. The main diagnostics were: congenital ureteropelvic junction obstruction, vesicoureteral reflux, megaureter uni- or bilaterally and renoureteral duplication. In relation with the severity of the disease, meaning degree of hydronephrosis (HN) and degree of vesicoureteral reflux (VUR) we found: group 1 (HN and VUR < IV) = 26 cases (56.52 %) and group 2 (HN and VUR > IV) = 20 cases. The RRF for left kidney with ^{99m}Tc DTPA was compared with the same kidney with ^{99m}Tc DMSA using Pearson correlation factor (r). We found a strong positive correlation for both groups of age: $r_A = 0.947$ (with $p < 0.00001$) and $r_B = 0.9789$. High correlation with minimum differences were mentioned also in others two groups, classified after the disease severity: $r_1 = 0.9909$ and $r_2 = 0.9446$ ($p < 0.00001$). We notice a difference higher than 10 % for RRF between two kidneys: in 21 cases (45.66 %) with ^{99m}Tc DMSA and 18 cases (39.13 %) with ^{99m}Tc DTPA. **Conclusion:** The minor difference of RRF mentioned until 3 years old was, most probably, in relation with the maturation of kidneys. Also the minimum difference noticed in the cases of hydronephrosis and vesicoureteral reflux with degree higher than IV was related with urinary stasis in the pelocaliceal system. We conclude that when a scintigraphy with ^{99m}Tc DMSA is done for a patient in order to characterize renal parenchyma, the relative renal function can be taken into the consideration.

P184

Predictives factors of positive discharge perchlorate test in new born with congenital hypothyroidism

A. LEGENDRE, Jr., G. PETYT, G. COLLET, G. LION, B. Dimitri, F. SEMAH, H. LAHOUSSE; CHRU de Lille, LILLE, FRANCE.

AIM : Performing a perchlorate discharge test (PDT) in diagnostic of congenital hypothyroidism is not so easy between duration of the test and succeed to have perchlorate. **MATERIEL AND METHOD :** We evaluated retrospectively 48 new born under one month who had PDT after thyroid scintigraphy with 123 iodine in CHRU of Lille between 2004 and 2014. We analyzed four pre test variables: sex, TSH on Guthrie test, thyroid area and iodine fixation rate. Then we analyzed 3 of these variables in 3 under groups depending of percent of decreasing of iodine rate after PDT : negative inferior to 15%, positive shared itself in two groups 15-50% and superior to 50%. **RESULTS :** Thyroid area is the only pre variable test wich is statistically higher $p < 0,0001$ (Wilcoxon two-sample Test) when PDT is positive. Bigger is thyroid area more test has chance to be positive. Under 514 mm² all tests are negative and beyond 960 mm² all tests are positive. Thyroid area can help to well isolate 40% of patients. Sex, TSH on Guthrie test and 123 iodine fixation rate are not predictive on positive PDT. Furthermore, sex is not different between 3 under groups but different between negative and positive superior 50% PDT with more girls when test PDT is positive. TSH on Guthrie test is not statistically different between 3 under groups of PDT for $p = 0,0573$. Thyroid area is statistically higher in positive group than negative group $p = 0,02$, but not different between two positive group $p = 0,11$. **CONCLUSION :** Thyroid area is correlate with positive PDT but not enough to not perform PDT. We can't discriminate only with thyroid area PDT positive with 15-50 percent of decreasing than beyond 50 percent. We will continue to perform PDT.

P185**Lesion detectability in neuroblastoma children by mIBG planar images: could it be partially related to the display performances and the diagnostic expertise?**

M. Castellani, A. Lorenzoni, R. Luksch, C. Cavatorta, M. Lualdi, S. Meroni, F. Crippa; Fondazione IRCCS Istituto Nazionale Tumori, MILAN, ITALY.

Aim To test the diagnostic variability related respectively to display monitor performances and medical expertise in a Nuclear Medicine Unit. **Materials and Methods** Between mIBG scans performed in children (2m-8y old) with neuroblastoma, 78 planar mIBG images with different levels in difficulty of interpretation were selected by a senior Nuclear Medicine Physician (NMP). 26 images presented 3 uptake areas, 26 more than 3 and 26 no uptake areas, respectively. All images were blindly evaluated, during two different sessions, by the senior-NMP and a junior-NMP with a lower level of expertise using three models of color displays from NEC Company with different calibrated luminance values and display functions, DICOM or not. For each of the 234 evaluations, the observers were asked to complete a record form, stating the presence or the absence of uptake areas and their location and to grade the difficulty of interpretation of the images. The agreement coefficient Kc from Cohen Kappa statistic was computed in order to evaluate the reproducibility in identifying the presence of uptake areas between monitors and within/between observers; the correctness in the interpretation of the images was evaluated with respect to senior evaluation. **Results** Regarding the between-monitor agreement, a high reproducibility was found for the senior-NMP (Kc \geq 0.80), whereas lower values were found for the junior-NMP (range 0.60-0.78). Preliminary results for the DICOM display with the highest luminance show the lowest values of misclassified case for the junior-NMP with respect to the senior evaluation with 8% and 7% mistake rate in the two reading sessions. The number of misclassified cases increases when using the not-DICOM display with the lowest luminance, with a percentage of misclassified cases of 6% for senior-NMP, and of 24% and 21% for junior-NMP, in the two reading sessions, respectively. **Conclusion** A proper DICOM display function and a high contrast ratio seem to facilitate the detection of low uptake areas thus optimizing the diagnostic information that can be obtained from mIBG scintigraphic images. Our preliminary results confirm the importance of display settings in the medical decision process even when images with poor spatial resolution were considered as in nuclear medicine examinations.

P186**SPECT and SPECT-TC increase the sensitivity of 123I-mIBG for the evaluation of primitive tumour and soft tissue-lymph nodal lesions in patients on treatment for neuroblastoma.**

M. Castellani, R. Luksch, M. Testoni, G. Aliberti, M. Maccauro, C. Zanette, D. Mansi, A. Lorenzoni, F. Crippa; Fondazione IRCCS ISTITUTO NAZIONALE TUMORI, MILAN, ITALY.

Aims To investigate if I-123-MIBG SPECT/ SPECT/TC, prospectively performed at diagnosis and during therapy in neuroblastoma, has superior sensitivity than standard acquisition not only for the bone metastases, but also for assessing the primary tumour and for detecting the recurrences in the so-called soft tissue(ST) lesions : regional or distant lymph-nodes and viscera (liver, lung, skin, CNS) . **Method** From January 2011 to April 2016, 94 neuroblastoma patients consecutively underwent MIBG scan study. 33 pts were 2- 18 months old; 32pts were 19-59 months;18 pts 5-18 year old;11 pts>18 year old. 22/33 pts less than 18 months old were excluded from the present study due the lack of SPECT/SPECT-TC (SPECT) in adding to the standard MIBG (S-MIBG) acquisition (planar static or WB)). The remaining 72 evaluable patients were studied with a total of 247 scans (range 1-13, median 4) . The SPECT acquisition was in

most cases centred to the abdomen +/- thorax +/- skull. Co-registered SPECT/ CT consisted in CT low-dose acquisition (80 kVp, 33 mAs) with attenuation correction. SPECT was compared with S-MIBG results and confirmed by not co-registered TC or MR. **Results** At diagnosis SPECT recognized the Primitive Tumour in 67/69 (97%) vs S-MIBG in 63/69 pts (91%): The FN S-MIBG vs VP SPECT were 4 pts with respectively dominant photopaenia of T, the retro vesical or cervical site, the intense lumbar bone uptake. In the case of retrovesical tumor, SPECT confirmed the clinical suspect of neuroblastoma due to the opsomyoclonus ataxia syndrome . SPECT identified 26/28 (92%) of the regional loco-regional lymph-nodal lesions vs 11/28 (39%) of the S-MIBG ; 17/20 vs 8/20 of mediastinal lesions, 9/10 vs 6/10 of left supraclavicular lesions and 5/7 vs 3/7 of the cervical nodes. Liver lesions were identified in 4 babies <12 m old with lesions more than 1 cm . Skin lesions were seen in 3/3 cases. During the follow-up , SPECT showed in the cases S-MIBG negative the persistence of disease (or relapse) in soft tissue disease in 4 patients, in 2 patients in CNS and in 2 pts in spine (BM thin spots). **In conclusion:** In our experience SPECT/SPECT-TC significantly raised the MIBG sensitivity in the diagnosis of soft tissue lesions, so far considered as near silent in S-MIBG.

P187**Value of MIBG scan in the diagnosis & initial staging in patients with neuroblastoma**

A. SELLEM, W. ELAJMI, K. TRABELSI, H. HAMMAMI; MILITARY HOSPITAL, TUNIS, TUNISIA.

Introduction and purpose Neuroblastoma (NBL) is the commonest extra-cranial solid tumor in children. The purpose of this study was to evaluate the usefulness in a clinical setting of iodine-123-metiodobenzylguanidine (123I-MIBG) scintigraphy in patients with neuroblastoma as detected by a mass screening survey. **Methods** Fifty patients provisionally diagnosed by clinical and imaging criteria to have neuroblastoma were included. Each patient had imaging by ultrasound, CT and/or MRI. **Results** The age of patients ranged from 2 months to 11 years with a mean of 32.9 months. They were 33 boys and 17 girls. In all cases, 123I-MIBG whole body images was performed and revealed 14 (28%) patients had normal iodine-123 MIBG scans, and histology showed a malignancy other than a neural crest tumour. The remaining 36 patients (72%) showed abnormal iodine-123 MIBG scans. The location of the primary site was retro-peritoneal in 63.8 % of cases, thoracic in 16.6 %, pelvic in 11.1 % and 8.3 % in cervical. 16 of the 36 patients had metastasis : 9 (25%) with bone metastasis, 2 (5.5%) with liver metastasis, 2 (5.5%) with liver and bone metastasis, and 3 (8.3%) with both bone and lymph nodes metastasis. **Conclusion** 123I-MIBG scintigraphy has an excellent ability to discriminate between neuroblastoma and other small round cell paediatric tumours and it is a powerful tool for initial staging which is crucial for effective management.

P188**FDG PET/CT Versus I-131 MIBG in Neuroblastoma Osseous Infiltrates**

M. A. Abdelwahab¹, M. H. Kotb¹, H. Mostafa², W. M. Omar¹, H. Elsayd¹, M. Fawzy¹; ¹National Cancer Institute, Cairo, EGYPT, ²NEMROCK, Cairo University., Cairo, EGYPT.

Purpose: To compare diagnostic performance of 18F-FDG PET/CT & I-131 MIBG in neuroblastoma (NB) osseous lesions. **Patients and methods:** Comparative study with 63 pathologically proved NB patients who were referred to Nuclear Medicine department, Children's Cancer Hospital, Egypt (CCHE) from Oct., 2009 till Jan. 2014, their age ranged from 2 to 156 months, with male to female ratio 1.4:1 & dominating high risk category (~65.1 %). They underwent paired F-18 FDG PET/CT and

I-131 MIBG scans (with maximum 2 weeks interval) using standard techniques and results of all scans were correlated to bone marrow biopsy, and follow up clinico-radiological data. **Results:** On lesion based analysis of neuroblastoma bone metastases, statistically significant higher sensitivity was seen with 18F-FDG PET/CT (73.1%) compared to 55.2 % for I-131 MIBG (*p-Value=0.03*). Higher yet comparable specificity of 100% was seen with I-131 MIBG compared to 92.5% for 18F-FDG PET/CT (*p-value=0.95*). **CONCLUSION:** 18F-FDG PET/CT seems to have an added value in detection of NB osseous infiltrates with considerable specificity, compared to I-131 MIBG, yet further larger scale studies are needed.

P189

True Whole-Body versus Standard 18F-FDG PET/CT Acquisition for Staging Pediatric Lymphoma

E. Etchebehere¹, A. E. Brito², C. Mosci², A. Santos¹, S. Aguiar³, L. Cristofani¹, A. Vicente¹, V. Buccheri⁴, J. Soares Junior⁴, P. Lymphoma Group⁵, T. Pascual⁵; ¹Sirio Libanes Hospital, Sao Paulo, BRAZIL, ²University of Campinas, Campinas, BRAZIL, ³Centro Infantil Domingos A. Boldrini, Campinas, BRAZIL, ⁴University of Sao Paulo, Sao Paulo, BRAZIL, ⁵INTERNATIONAL ATOMIC ENERGY AGENCY, Vienna, AUSTRIA.

Introduction: The role of 18F-FDG PET/CT in lymphoma staging is well established mainly in the adult population. Standard (eyes to thighs) 18F-FDG PET/CT acquisition is performed when staging lymphomas in adults, but guidelines recommend true whole-body acquisition in children. However, this acquisition is time consuming, increases radiation exposure and is not cost-effective especially as it requires sedation. These disadvantages limit the use of 18F-FDG PET/CT in developing countries. **Objectives:** This study aimed to evaluate the clinical impact of performing true whole-body versus standard (eyes to thighs) 18F-FDG PET/CT for pediatric lymphoma staging in developing countries. **Methodology:** True whole-body 18F-FDG PET/CT acquisitions were performed for staging patients with histological diagnosis of Hodgkin's (HL) or Non-Hodgkin's lymphoma (NHL). Inclusion criteria consisted of patients between 0-18 (inclusive) years of age at the time of the baseline scan. Patients that were pregnant, lactating, had prior radiation therapy, prior chemotherapy and/or prior history of cancer were excluded. 18F-FDG PET/CT acquisition parameters and administered doses were performed according to SNM or EANM guidelines. True whole-body (vertex to feet) acquisitions were performed with a minimum of 2 min per-bed position for torso and 1 min per-bed position for extremities, in 3D MODE. CT parameters were: 80 - 120 kVp; dose modulation (mAs); iterative reconstruction; 2.5 - 4.0 mm slices. The true whole-body 18F-FDG PET/CT images for each patient were compared to a standard (eyes to thighs) acquisition. The clinical impact among the two were evaluated. **Results:** True whole-body 18F-FDG PET/CT acquisitions were performed in 19 patients (15 males), mean age=10±4 years-old, 12 HL. Four patients (21%) (1 HL and 3 NHL) had metastases outside the eyes-to thighs field-of-view, although none of them had disease only in the arms or legs. Since these patients also had multiple extranodal sites (bone, pleura, lung and peritoneum) within the eyes-to thighs field-of-view, management was not altered based on the lower limb results. **Conclusion:** Staging of pediatric lymphoma with a true whole-body 18F-FDG PET/CT acquisition protocol does not seem necessary as there is no clinical impact in patient management. A standard 18F-FDG PET/CT acquisition may be sufficient. Exceptions may be in bone lymphomas, although these cases correspond to a minority of patients and must be analyzed individually. Standard 18F-FDG PET/CT reduces examination time, the need for sedation, radiation exposure and is therefore more cost-effective in the pediatric population. These results will optimize the use of 18F-FDG PET/CT imaging in developing countries.

P190

The Role of ¹²³I-mIBG Scintigraphy in Kinsbourne Syndrome

D. BEN SELLEM, L. ZAABAR, B. DHAOUADI, B. LETAIEF, M. F. BEN SLIMENE; University of Tunis El Manar, Faculty of Medicine of Tunis, Salah Azaiez Institute, Department of Nuclear Medicine, Tunis, TUNISIA.

Aim: Kinsbourne syndrome or opsoclonus-myooclonus syndrome is very rare. It is characterized by opsoclonus (fast, multidirectional, conjugate eye movements), a jerky ataxia sometimes with a myoclonic component, marked irritability and/or sleep disturbance. It may be associated with occult neuroblastoma. MIBG scintigraphy is needed then. The aim of this study is to demonstrate the contribution of the ¹²³I-mIBG scintigraphy in the detection of neuroblastoma in the case of Kinsbourne syndrome. **Materials and methods:** Five girls and 2 boys aged from 10 months to 10 years (median 6 years) presenting Kinsbourne syndrome with increased serum neuron-specific enolase, were addressed to our department for ¹²³I-mIBG scintigraphy to search a neuroblastoma. Static acquisitions and fused images with SPECT/CT hybrid gamma-camera, equipped with low-energy collimators, were acquired 24 hours post injection of ¹²³I-mIBG. **Results:** In four cases, ¹²³I-mIBG scintigraphy not objectified abdominal or ectopic neuroblastoma. In the fifth case, the SPECT/CT demonstrated a left paravertebral focus of moderate uptake at D11 level, evoking a thoracic neuroblastoma. In the sixth case, the SPECT imaging showed a left posterior focal hot spot concluding to adrenal neuroblastoma. In the last case, the ¹²³I-mIBG scintigraphy has objectified asymmetric uptake depending on the right adrenal gland without anatomical correlation, compatible with poorly differentiated right adrenal neuroblastoma. **Conclusion:** Kinsbourne syndrome is exceptional. The mIBG scintigraphy allows the search for an underlying neuroblastoma, changing so prognosis and therapeutic management of this syndrome.

P-16 – Monday, October 17, 2016, 16:00 - 16:30, Poster Exhibition Hall
Conventional & Specialised Nuclear Medicine: Pulmonology

P191

Comparison of cigarette and ecigarette smoking to alveolocapillary membrane by dynamic ventilation scintigraphy

S. Barna¹, I. Garai¹, D. Rózsa², J. Varga³, A. Fodor⁴, M. Szilasi⁴, L. Galuska³; ¹ScanoMed Ltd, University of Debrecen, Debrecen, HUNGARY, ²BBS Nanotechnology Ltd, Debrecen, HUNGARY, ³Dept. of Nuclear Medicine, University of Debrecen, Debrecen, HUNGARY, ⁴Dept. of Pulmonology, University of Debrecen, Debrecen, HUNGARY.

Aims: Dynamic ventilation scintigraphy (DIT) has proved to be a suitable method for the staging and follow up of the damages of alveolo-capillary membrane (ACM) system of the lungs. The e-cigarette is a new smoking device producing vapor from nicotine solution. Here we present the first comparative DIT results of e-cigarette users, who returned for one week to the usual cigarette smoking. **Patients:** We included 13 healthy man volunteers (age 20-40) in the study, who regularly used e-cigarette, containing 10 or more mg nicotine/mL concentration fluid.. **Methods:** First we acquired a baseline DIT study, calculating the separate clearance half time (CT_{1/2}) values of the lungs, and performed respiration tests (FVC, FEV1, PEF, FEV1/FVC) as well as measured CO and COHg concentrations from exhaled air at e-cigarette use. Then we asked the volunteers to return to traditional cigarette smoking for a week's period. After that we repeated the above-mentioned tests, and statistically compared the results, using paired t-test for normally distributed variables, and Wilcoxon's test for the rest. **Results:** There was no significant change in the results of respiration tests, except for the exhaled CO and COHg levels, which were significantly higher at cigarette use (*p*<0.01), and increased in every case (CO: from a median value of 2 to 15 ppm;

COHg: from a median value of 1.0 to 3.0%). The DIT $CT_{1/2}$ times were lower at traditional cigarette smoking compared with e-cigarette use in every case ($p < 0.0001$): from 69.3 ± 13.8 min decreased by 31.1 ± 11.0 min), on average to 55.0% of the base value (95% confidence interval: 44.4 - 65.6 %). **Conclusion:** We first compared at the same persons the direct effect of traditional smoking vs. e-cigarette upon the lung ACM. Our results confirmed the known toxic (especially CO) effect of traditional cigarette smoking causing persistent alveolitis. The normal $CT_{1/2}$ values at e-cigarette use prove that it has no similar effect, there is no sign of alveolitis. So it could be recommended for heavy smokers who are unable to stop smoking, to switch to e-cigarette use, which is more tolerable for the lungs, for the ACM.

P192

Importance of V/P SPECT in Diagnosing COPD and Pulmonary Comorbidities

M. Bajc¹, Y. Chen², X. Li³, C. Wang⁴, H. Huang⁵, A. Lindqvist⁶, X. He⁷, X. He⁷; ¹University Hospital Lund, LUND, SWEDEN, ²Changzheng Hospital, Shanghai, CHINA, ³Hua Dong Hospital Shanghai, Shanghai, CHINA, ⁴Xin qiao Hospital Chongqing, Chongqing, CHINA, ⁵Changzheng Hospital Shanghai, Shanghai, CHINA, ⁶Helsinki University Hospital, Helsinki, FINLAND, ⁷Suzhou University Affiliated Tumor Hospital, Wuxi, Wuxi, CHINA.

Objective: To assess the degree of obstructivity in COPD patients and identify pulmonary comorbidities. **Methods:** 66 stable patients with a clinical diagnosis of COPD were included in this prospective, multi-centre study. They were classified according to GOLD criteria, spirometry, and symptom evaluation. Ventilation and perfusion tomography (V/P SPECT) was performed and interpreted according to European Nuclear Medicine guidelines. Obstructivity was evaluated blindly and semi-quantitatively using V/P SPECT¹. **Results:** Two patients showed no obstructivity with spirometry or V/P SPECT. However, V/P SPECT demonstrated pulmonary embolism (PE) in one and signs suggestive of tumour in the other. Mild obstructivity in V/P SPECT was found in 2 patients: both showed signs of suspected tumour and one chronic PE and emphysema. Among 23 patients with moderate obstructivity in V/P SPECT (post-bronchodilation FEV% $63 \pm 18\%$ and FEV1 $63 \pm 15\%$ of predicted), 17 patients had emphysema (74%), 14 PE (61%), 6 left heart failure (LHF) (26%), 5 of whom also had both LHF and PE, and finally 7 (31%) had parenchymal changes. Thirty-nine patients had severe obstructivity in V/P SPECT (post-bronchodilation FEV% $47 \pm 10\%$ and FEV1 $39 \pm 11\%$ of predicted) and emphysema was present in 38 (97%), 11 had LHF (28%), 2 had PE (5%) and 4 demonstrated other parenchymal changes (11%) in V/P SPECT. **Conclusions:** To our knowledge this is the first time that a prospective study has been conducted on COPD patients which focusses on pulmonary comorbidities using V/P SPECT. Most importantly V/P SPECT is not contraindicated in the diagnostic evaluation in COPD patients and can even grade its severity. Emphysema was a frequent finding and always present in patients with severe COPD. Regardless of the severity of COPD, V/P SPECT was able to demonstrate PE, LHF and other parenchymal changes difficult to see on planar images. These findings may explain the variety of complex patient symptoms and heterogeneity of the disease. V/P SPECT might play an important prognostic tool in COPD patients and have an impact on patient treatment. ¹Bajc et al, Ann. Nucl. Med. 2015; 29: 91.

P193

V/Q SPECT/CT findings of residual emboli and lung diffusion impairment after surgical embolectomy compared to thrombolysis in acute pulmonary embolism

J. Mortensen, P. Lehnert, J. Kjærgaard, P. S. Olsen, C. J. H. Møller, J. Carlsen; Rigshospitalet, COPENHAGEN, DENMARK.

Aim: To investigate the long-term amount of residual emboli and pulmonary diffusion impairment after acute high- and intermediate-risk pulmonary embolism (PE) treated with surgical embolectomy and thrombolysis. **Methods:** Prospective follow-up of a retrospective cohort treated between 1998 and 2014 at Rigshospitalet. Follow-up evaluation at least 3 months after the acute PE included ^{81m}Kr ventilation / ^{99m}Tc-MAA perfusion SPECT/CT and lung function tests of CO diffusion capacity. **Results:** A total of 136 patients (high-risk: 64; intermediate-risk pulmonary embolism: 72) were included, 80 were eligible for clinical follow-up, while 40 had deceased. Median clinical follow-up time was 31 months. For high risk PE patients, V/Q mismatch was found in 31% of cases treated with surgical embolectomy compared to 76% of cases treated with thrombolysis ($p=0.01$): The following no. of V/Q. mismatch defects was detected in the two patient groups: 1-3 segments in 3 and 12 patients, resp.; 4-6 segments in 0 and 3 patients, resp.; and 7-10 segments in 1 from each group. Pulmonary diffusion impairment was identified in 31% cases treated with surgical embolectomy and in 71% cases treated with thrombolysis ($p=0.02$). In the intermediate-risk PE patients, no difference in V/Q mismatch (5/11 vs. 18/35, $p=0.73$) or in diffusion capacity impairment (6/11 vs. 8/35, $p=0.07$) was found. **Conclusions:** Surgical embolectomy for acute high-risk PE seems to result in less residual PE and lung diffusion impairment when compared to treatment with thrombolysis. In intermediate-risk PE patients no difference was seen.

P194

Quantitative ventilation/perfusion SPECT - Initial experience

S. Carmona, J. G. Santos, A. Prata, J. A. Sequeira, M. R. Victor, A. I. Santos; Hospital Garcia de Orta, ALMADA, PORTUGAL.

Ventilation/perfusion SPECT scintigraphy (V/P SPECT) is presently the gold standard technique to perform ventilation/perfusion scintigraphy. Some authors defend that the determination of the perfusion percentage affected by pulmonary embolism (PE) can be an important adjuvant to decide pulmonary embolism treatment. But how easy is it to perform quantitative ventilation/perfusion SPECT? **Aim:** To analyse interobserver reproducibility in ventilation/perfusion SPECT, regarding the quantification of perfusion impairment, in pulmonary embolism. **Materials and methods:** We analysed 30 V/P SPECT performed in 30 patients (7 men and 23 women), median age and interquartile range $64[43;70]$ years. 28 patients were referred for PE diagnosis and 2 patients had already an angio CT confirming PE. Each study was analysed independently by 4 Nuclear Medicine specialists. PE quantification was made by counting segments or sub-segments of ventilation/perfusion mismatches compatible with PE, according to the method proposed on literature (Bajc M. et al). A sub-segmental defect was attributed 1 point, and a segmental defect 2 points (both lungs comprising 18 points). Mismatch defects were expressed as mismatch points, and after division by 36 gave the percentage of the lung that was embolized. Intraclass Correlation Coefficient was used for assessment of multiple raters agreement on the percentage of embolized lung. Non parametric tests for paired samples (Wilcoxon and sign tests), were used to evaluate the difference of embolized lung percentage for each observers pair. **Results:** For the 30 exams, the total mismatch points considered in both lungs and the number of exams with no mismatch defects were, for observer 1: 59 mismatch points and 5 (17%) exams with no defects; for observer 2: 86 mismatch points and 2 (7%) exams with no defects; for observer 3: 69 mismatch points and 7 (23%) exams with no defects; for observer 4: 62 mismatch points and 4 (13%) exams with no defects. The interobserver agreement, regarding the percentage of embolized lung was moderate (ICC = 0.43). For each pair of observers, regarding the percentage of embolized lung, there was only a statistically significant difference between observers 1 vs 2 ($p=0.033$) and 2 vs 4 ($p=0.024$). **Conclusion:** Although quantitative ventilation/perfusion scintigraphy is a powerful tool to evaluate the extent of perfusion affected by PE, care must be taken performing this technique. Our

initial experience revealed a moderate interobserver concordance quantifying perfusion mismatch defects in ventilation/perfusion scintigraphy, leading us to conclude that an initial learning process is needed to standardize the quantification results.

P195

Added value of low-dose CT coupled to Ventilation /Perfusion SPECT in acute pulmonary embolism

W. Amouri, F. Hamza, I. Jardak, F. Kallel, S. Charfeddine, F. Guermazi, Habib Bourguiba hospital, sfax, TUNISIA.

Introduction: There is increasing evidence of the improved accuracy of single photon emission CT (SPECT) and SPECT combined with low-dose CT (SPECT/CT) compared to planar Ventilation/Perfusion (V/Q) lung scintigraphy for the diagnosis of pulmonary embolism (PE). In this work, we aim to compare V/Q SPECT with perfusion SPECT/CT scan and to assess the additional information provided by this hybrid technique for accurate diagnosis of PE. **Materials and Methods:** In a retrospective study, 22 patients (13 men and 9 women with mean age of 54 years) were referred for suspicion of PE. 2 days protocol was conducted on Symbia T6 gamma camera. The first day, perfusion SPECT acquisition was performed after injection of 185 MBq 99mTc-labelled macro aggregated human albumin (99m Tc-MAA), followed by low dose CT acquisition without contrast iodine injection. The second day, ventilation SPECT was acquired after inhalation of 99mTc-labelled Technegas. The reconstructed images were interpreted according to the EANM criteria (2009). Correlations between V-SPECT and CT were studied. PE is diagnosed when there is more than one sub segment showing a V/Q mismatch representing an anatomic lung unit. **Results:** According to the criteria of the EANM, PE was excluded in 9 cases and confirmed in 12 patients. One case (4.5%) was classified no conclusive given the presence of one sub-segment mismatch on both V/Q and Perfusion SPECT/CT. The concordance rate between clinical probability and scintigraphic results was of 68%. The comparison of Perfusion SPECT/CT and V/Q SPECT showed a concordance in 100% of cases. CT allowed however a better anatomical localization of perfusion defects, as well as a best characterization of abnormalities related to non-embolic etiologies such as pneumonia lesion, pleural effusion and calcification, COPD and recognized pulmonary infarction. **Conclusion:** This study demonstrates that Perfusion SPECT/CT obtained with hybrid camera could be used for PE diagnosis with performances similar to V/Q SPECT. In addition, SPECT/CT improves test specificity by identifying non-embolic etiologies and allows accurate localization of perfusion defects.

P196

Continuous acquisition mode gives comparable images to step-and-shoot in lung perfusion SPECT

P. C. Holdgaard; Nuclear Medicine Dept., Vejle Sygehus, Vejle, DENMARK.

AIM: EANM guidelines recommend a 5 minute lung perfusion SPECT. Step-and-shoot mode (SS) acquisitions increase scan time by >3 minutes compared with continuous mode (CONT) where data is acquired during detector motion. If image quality is comparable it would give the possibility to reduce camera time or acquire longer and improve image quality with 60 %. We have previously made a thorough phantom study and found CONT equivalent to SS in cold lesions, but should be evaluated in the patient setting prior to clinical implementation. **MATERIALS AND METHODS:** Twenty two consecutive patients suspected for lung embolism were scanned first with SS and immediately after with CONT. Both SPECTs were acquired with 5 minutes sampling time (60 projections of 10 seconds), dual-head, LEAP collimator and 128 matrix, and OSEM

reconstructions (30 iterations and 2 subsets) made with resolution recovery and scatter correction. Prior to the perfusion study, all patients had a Technegas® ventilation study. The two SPECT modes were compared side by side for each patient by a nuclear medicine physician. Number of perfusion defects, localisation and difference between the two modes were recorded. **RESULTS:** There were 7 patients with lobar and/or several segmental perfusions defects, 7 with one sub-segmental or non-segmental defects and 8 with normal perfusion. All defects seen in SS were also seen in CONT and no new defects were introduced. It was visually observed that CONT acquisitions were slightly less homogenous, but had slightly greater contrast between defects and normal perfused areas compared with SS. The minor visual difference was considered negligible in a clinical setting, especially compared with the lower count ventilation studies. **CONCLUSION:** The distribution of defects is the same in CONT and SS acquisitions in lung perfusion SPECT. This gives the possibility to reduce scan time or improve image quality with CONT. If ventilation is also acquired with CONT, a total of 6-7 minutes can be saved. It is also possible to reduce doses if the perfusion/ventilation count ratio is still adequate.

P197

Comparison between V/Q Lung Scintigraphy and Computed Tomography Pulmonary Angiography in the Diagnosis of pulmonary embolism

D. A. M. Hassanin, Maryam Qaw, Sara Abdulwahab, Jenan Al-Awami; South Egypt Cancer Institute, Assiut, EGYPT.

Abstract : Pulmonary embolism is a disease characterized by a blockage of the pulmonary artery . It can be diagnosed using ventilation/perfusion scintigraphy (V/Q) or using CT pulmonary angiography (CTPA). The aim of our study was to compare between the properties of V/Q and CTPA and to propose when to perform each. **Method:** A questionnaire was published to a total of 150 radiologists, nuclear medicine technologists and physicians. And the results were compared with research papers comparing between V/Q and CTPA. **Results:** 74% of the sample said that V/Q is more effective in diagnosing PE and 53% said that CTPA is more. 63% said that CTPA is more available and widely used. 62% said that CTPA used more in emergency cases. 59% said that CTPA is more accurate with less mistake ratio and 41% said that V/Q is more. 77% said that in V/Q patients will have less radiation exposure than CTPA. 66% said that CTPA gives more quick results than V/Q. 64% that CTPA may cause allergic reaction, complications or side effects. 37% said that CTPA is sufficient alone to diagnose PE, 17% said that V/Q is sufficient alone and 45% said that both can be sufficient alone. **Conclusion:** V/Q will provide accepted diagnostic results for PE with low radiation dose and no side effects. CTPA with similar diagnostic results in a shorter procedure time but a higher radiation dose and a probability of some side effects. In general both CTPA and V/Q provide results with satisfactory sensitivity and accuracy, so exclusion or inclusion of PE will be better using the combination of these two tests. **Keywords :** Pulmonary embolism, ventilation/perfusion scintigraphy (V/Q), CT pulmonary angiography (CTPA).

P198

Diagnosing PE with V/P SPECT in the presence of COPD

A. Nasr, M. Bajc; Clinical Physiology and Nuclear Medicine, Lund, SWEDEN.

Background: The presence of Chronic Obstructive Lung Disease (COPD) is generally considered as a contraindication to perform lung scintigraphy in patients suspected for pulmonary embolism (PE). These facts were based on planar imaging technique and mainly Xenon gas was

used for the ventilation study. Tomographic technique (SPECT) for ventilation/perfusion scintigraphy, make detecting of PE possible even in the very obstructive patients. This is through use of the smallest aerosol-Technegas with very good periphery penetration. Aim: To determine the diagnostic value of VP SPECT in detecting PE in the presence of COPD. **Methods and materials:** We retrospectively analysed 1485 consecutive patients referred to V/P SPECT during a one year period. 1274 (86%) of those patients were referred for suspected pulmonary embolism (PE). The number of segments and sub-segments indicating PE typical mismatch were counted and expressed in percentage of the total lung parenchyma. Furthermore, areas with ventilation abnormalities were recognized which allowed the degree of total lung malfunction to be estimated. In the report to the clinicians the extent of PE was given as well as other sign of ventilation disturbances. These were described and interpreted in accordance with EANM Guidelines. **Results:** Among 1274 patients included in this study, 353 patients (28%) were detected with PE. More than a half of the patients (55%) showed signs of airway obstruction (from the sign of uneven ventilation to deposition of Technegas in small and large airways as well as areas of absent ventilation, mild-severe). Among the 353 patients with PE, 90 patients were also diagnosed as obstructive. In the group of obstructive patients, majority (87%) had small PE, <25%, of the total pulmonary perfusion, 10 patients (11%) had medium size PE (<50 %) and 2 (2%) had extensive PE (>50%). All examinations in patients with both PE and COPD were diagnostic even in the most severe grade of obstruction which was identified in 28% of these patients. **Conclusion:** COPD is not a contraindication to use pulmonary ventilation/perfusion tomography for PE diagnosis even in the most severe grade of COPD. All studies were diagnostic. The method is applicable to all patients and could explain patient symptoms.

P199

Inclusion of SPECT-CT in Assessment of Chronic Thromboembolic Pulmonary Hypertension

B. PEREZ LOPEZ, F. GOMEZ-CAMINERO LOPEZ, P. GARCIA-TALAVERA SAN MIGUEL, R. RUANO PEREZ, M. E. MARTIN GOMEZ, L. G. DIAZ GONZALEZ, E. MARTIN GOMEZ, M. P. TAMAYO ALONSO; HOSPITAL UNIVERSITARIO CLINICO DE SALAMANCA, SALAMANCA, SPAIN.

Objective: To establish the role of pulmonary perfusion SPECT-CT in patients with suspicion of chronic thromboembolic pulmonary hypertension as a complement to ventilation/perfusion scintigraphy. **Methods:** Chronic thromboembolic pulmonary hypertension has an incidence of 4% after suffering an acute pulmonary thromboembolism. It is caused by incomplete resolution of the thromboembolism that produces increased pulmonary vascular resistance. We reviewed all patients derived to our department with clinical suspicion of chronic thromboembolic pulmonary hypertension. Pulmonary perfusion SPECT-CT was performed depending on health status. Ventilation scintigraphy with Technetium-labeled (Tc-99m) - DTPA and perfusion scintigraphy and perfusion SPECT-CT with Technetium-labeled (Tc-99m) - MAA were performed to all patients. Acute pulmonary thromboembolism at the moment of the study was exclusion criteria. **Results:** 27 patients were analysed, 10 were men and 17 women, with average age of 71 years old. 67% of them were derived with known pulmonary hypertension and 33% without pulmonary hypertension diagnosis. Combining ventilation/perfusion scintigraphy and perfusion SPECT-CT, 18.52% of patients presented positive result for chronic thromboembolic pulmonary hypertension, 74% showed normal perfusion, and just 7.4% were not conclusive. Perfusion defects found in positive studies were mainly localized in left upper lobe. **Conclusion:** Pulmonary perfusion SPECT-CT is a very important tool that shows complementary information to ventilation/perfusion scintigraphy and allows to localize and define better perfusion defects. SPECT-CT is useful in diagnosis, follow-up and treatment response of chronic

thromboembolic pulmonary hypertension. SPECT-CT should be performed when chronic thromboembolic pulmonary hypertension is suspected.

P-17 – Monday, October 17, 2016, 16:00 - 16:30, Poster Exhibition Hall
Conventional & Specialised Nuclear Medicine: Thyroid (Benign)

P200

Serum Thyroglobulin Concentration as a Predictive Factor for Nodule Size and Malignancy in Patients with Thyroid Nodules

S. Gaberscek^{1,2}, S. Kukman³, A. Biček¹, A. Oblak¹, E. Pirnat¹, K. Zaletel¹; ¹Department of Nuclear Medicine, University Medical Centre Ljubljana, LJUBLJANA, SLOVENIA, ²Faculty of Medicine, University of Ljubljana, Ljubljana, SLOVENIA, ³Faculty of Medicine, University of Ljubljana, LJUBLJANA, SLOVENIA.

AIM. According to latest guidelines, measurement of serum thyroglobulin (Tg) concentration in the diagnostics of thyroid nodules is not recommended. In some studies, serum Tg concentration was associated with the nodule size. In papillary thyroid cancer, serum Tg concentration has no significant predictive value. In follicular and Hürthle-cell neoplasms, however, preoperative serum Tg concentration was reported either as a poor or as a useful predictor of thyroid malignancy. Therefore, our aim was to establish the value of Tg measurement in our patients with thyroid nodules. **MATERIALS AND METHODS.** In this retrospective study we reviewed medical records of all patients who were first diagnosed with thyroid nodules between May 2014 and December 2015 at our thyroid department. In all patients, a volume of thyroid nodules was measured by ultrasound (US), and a serum concentration of Tg was measured. In patients with thyroid nodules, which were larger than 1 cm and not active on thyroid scintigraphy, US-guided fine-needle aspiration biopsy (FNAB) was performed. The cytology report was categorized as suspicious or unsuspicious. Patients with cytology report suspicious for papillary thyroid cancer were not included in the study. **RESULTS.** Out of 801 consecutive patients with thyroid nodules (603 women and 198 men), 107 patients with the Tg concentration above 100 ng/mL had significantly higher volume of thyroid nodules than 694 patients with the Tg concentration below 100 ng/mL (median (range), 11.1 (0.02-95.5) and 1.1 (0.003-84.7) mL, respectively, p=0.006). We found a significantly positive correlation between the serum Tg concentration and the volume of thyroid nodules (R=0.469, p<0.001). Out of 413 patients with cytology reports, 41 patients with thyroid nodules suspicious for follicular and Hürthle cell neoplasm had significantly higher Tg concentration than 372 patients with unsuspicious thyroid nodules (median (range), 65.0 (7.0-34,650.0) and 23.5 (0.0-6,248) ng/mL, respectively, p=0.001). When applying a cut-off level of 200 ng/mL, the sensitivity and the specificity of the serum Tg concentration as a predictor for the suspicious or unsuspicious cytology report were 27% and 93%, respectively. Furthermore, the positive and the negative predictive values for the serum Tg concentration as a predictor were 32% and 91%, respectively. **CONCLUSIONS.** In our patients with thyroid nodules, serum concentration of Tg turned out to be a useful predictive factor of nodule size and malignancy. With more than 90% negative predictive value, a serum Tg concentration below 200 ng/mL was able to predict unsuspicious cytology report.

P201

Association of established hypothyroidism associated genetic variants with Hashimoto's thyroiditis

A. Baric¹, L. Brcic², S. Gracan¹, V. Torlak Lovric¹, I. Gunjaca², M. Simunac¹, M. Boban², T. Zemunik², O. Polasek³, M. Barbalic², A. Punda¹, V. Boraska Perica²; ¹Department of Nuclear Medicine, University Hospital Split, Split, CROATIA, ²Department of Medical Biology, University of Split, School of Medicine, Split, CROATIA,

³Department of Epidemiology, University of Split, School of Medicine, Split, CROATIA.

Aim: Hashimoto's thyroiditis (HT) is a chronic autoimmune disease of the thyroid gland, with 8 times higher incidence in women. It is the most common cause of hypothyroidism. Recently, two genome-wide association analyses showed association of several genetic variants with hypothyroidism. Since HT and hypothyroidism are closely related, the main aim of this study was to explore the association of established hypothyroidism single nucleotide polymorphisms (SNPs) with HT. **Materials and methods:** The case-control dataset included 200 HT cases and 304 controls. Diagnosis of HT cases was based on clinical examination, measurement of thyroid antibodies (TgAb, TPOAb), hormones (TSH and FT4) and ultrasound examination. We genotyped and analysed 11 known hypothyroidism associated genetic variants. Case-control association analysis was performed in order to test each SNP for the association with HT using logistic regression model. Additionally, each SNP was tested for the association with thyroid related quantitative traits (TPOAb levels, TgAb levels and thyroid gland volume) in HT cases only using linear regression. Power of the study was calculated using Quanto and all association analyses were performed using Plink and R statistical software. **Results:** We identified two genetic variants nominally associated with HT: rs3184504 in SH2B3 gene ($P=0.0135$, $OR=0.74$, $95\% CI=0.57-0.95$) and rs4704397 in PDE8B gene ($P=0.0383$, $OR=1.32$, $95\% CI=1.01-1.74$). The SH2B3 genetic variant also showed nominal association with TPOAb levels ($P=0.0163$, $\beta=-0.46$, $SE=0.19$) and rs4979402 inside DFNB31 gene was nominally associated with TgAb levels ($P=0.0443$, $\beta=0.41$, $SE=0.2$). There were no significant associations with thyroid gland volume. **Conclusion:** Our findings suggest that SH2B3 and PDE8B genetic variants are associated with HT. SH2B3 gene has previously been associated with susceptibility to several autoimmune diseases, whereas PDE8B has been associated with TSH levels and suggested to modulate thyroid physiology that may influence the manifestation of thyroid disease. Identified loci are novel and biologically plausible candidates for HT development and represent good basis for further exploration of HT susceptibility.

P202

Color Flow Doppler Sonography In Patients With Amiodarone-Induced Thyrotoxicosis

G. Horvatic Herceg, I. Bracic, S. Kusacic-Kuna; Clinical Department of Nuclear Medicine and Radiation Protection, University Hospital Center Zagreb, Zagreb, CROATIA.

It is well known that excess of iodine intake may alter thyroid function, presented as amiodarone-induced hypothyroidism (AIH) which is more frequent in iodine sufficient areas or amiodarone-induced thyrotoxicosis (AIT) which occurs more frequently in areas with low iodine intake. AIT may arise from iodine-induced excessive thyroid hormone synthesis in patients with underlying functional thyroid autonomy (type 1) or destructive thyroiditis in apparently normal thyroid glands with release of hormones (type 2). Also, mixed forms characterized by coexistence of these two phenomena exist. Distinguishing thyrotoxicosis types 1 and 2 is important to plan therapy. AIT type 1 usually responds to thionamides and potassium perchlorate, while type 2 responds to glucocorticoids. **Aim:** To evaluate the utility of color-flow Doppler sonography (CFDS) in the differential diagnosis of AIT. 94 patients (pts) on chronic amiodarone treatment (6 months-2 years) were included in this study. All patients (m: 60, f: 34, mean age 53 y) were on long-term therapy with amiodarone at maintenance doses ranging from 200 to 400 mg daily. The mean value of urinary iodine excretion was $423.5 \mu\text{g/l}$ (min. $256.9 \mu\text{g/l}$, max. $592.1 \mu\text{g/l}$). AIH was found in 28% and AIT in 31% of pts. In 29 hyperthyreotic pts with nodular or diffuse goiter, 21 (72%) had CFDS increased glandular vascularity diagnostic for type 1 AIT and in 8 pts (28%) glandular

vascularity was absent (type 2 AIT) ($p<0.0001$). 2-h I-131 uptake (RAIU) in 28 pts was low (range 2.09-5.6%) and in 1 pt was normal (11.4%). There were no patients with elevated RAIU. In the group of 21 pts with AIT type 1, nodular changes were found in 15 cases and diffuse changes in 6. In all pts with type 2 we have found diffuse changes of echostructure. Tc 99-m thyroid scans in all pts showed very low or absent uptake, consistent with either thyroiditis or blockade of uptake by iodine excess. **Conclusion:** CFDS can accurately distinguish between type 1 and type 2 AIT, but is not always concordant with the thyroid RAIU. Low uptake is of no differential value. Identification of the different subtypes of AIT helps to choose the appropriate therapy.

P203

Methimazole Treatment Influences Thyroid Vascularity in Patients with Graves' disease

K. Zaletel¹, P. Klavžar², A. Kisovar², S. Gaberšček^{1,2}; ¹University Medical Centre Ljubljana, Department of Nuclear Medicine, Ljubljana, SLOVENIA, ²University of Ljubljana, Faculty of Medicine, Ljubljana, SLOVENIA.

OBJECTIVES. In untreated Graves' disease (GD), significantly increased thyroid vascularity most likely reflects the action of thyroid stimulating autoantibodies (TSAb). Since less data is available on thyroid vascularity during the treatment of hyperthyroidism, our aim was to evaluate the effect of methimazole on thyroid blood flow in GD patients. **METHODS.** In our prospective clinical study, which was performed between November 2014 and November 2015, we enrolled 23 consecutive newly diagnosed hyperthyroid patients with GD (19 females and 4 males), aged between 26 and 78 years (mean, 50.7 ± 13.9 years). All patients were prescribed with initial dose of methimazole between 20-40 mg per day, which was reduced to 10 mg per day during the follow-up. Before as well as 7 weeks, 4 months and 7 months after initiation of treatment we determined thyroid function and TSAb. We measured thyroid volume and the peak systolic velocity (PSV) at the level of intrathyroid arteries. We compared the measurements during the treatment and determined correlations. **RESULTS.** Before treatment, patients had TSH 0.008 ± 0.0004 mU/L, fT_4 48.68 ± 18.73 pmol/L, fT_3 21.68 ± 8.08 pmol/L and TSAb 7.58 pmol/L (range, 2-60 pmol/L). Thyroid volume was 20.52 ± 9.43 mL and PSV was 18.77 ± 4.84 cm/s. During treatment with methimazole, initial PSV significantly decreased to 13.38 ± 2.01 cm/s at 7-week follow-up ($p<0.001$), to 12.00 ± 1.94 cm/s at 4-month follow-up ($p<0.001$), reaching 10.43 ± 0.77 cm/s by the 7-month follow-up ($p<0.001$). Before treatment, a significant correlation between PSV and TSAb was confirmed ($R=0.608$, $p=0.002$), whereas no correlation with thyroid hormones was found. During the follow-up, no correlation with TSH, thyroid hormones or TSAb was found until the final evaluation when the laboratory tests showed TSH 2.49 ± 3.30 mU/L, fT_4 14.36 ± 3.35 pmol/L, fT_3 5.56 ± 2.68 pmol/L and TSAb 2.50 pmol/L (range, 0.0-45.19 pmol/L). **CONCLUSIONS.** Our findings indicate that during treatment of GD patients with methimazole thyroid vascularity significantly decreases. Therefore, estimation of thyroid vascularity represents an additional useful tool to estimate the progress of treatment.

P-18 – Tuesday, October 18, 2016, 16:00 - 16:30, Poster Exhibition Hall
Conventional & Specialised Nuclear Medicine: Uro-nephrology

P204

Lycopene for Renal Ischemia Reperfusion Injury: Scintigraphic, Histopathologic and Biochemical Evaluation

M. SADIC¹, H. I. ATILGAN², A. AYDIN³, G. KOCA¹, M. KORKMAZ¹, T. KARAKAN¹, H. SURER¹, P. BORCEK⁴; ¹Ministry

of Health Ankara Training and Research Hospital, ANKARA, TURKEY, ²Kahramanmaraş Necip Fazıl City Hospital, Kahramanmaraş, TURKEY, ³Sanliurfa Mehmet Akif Inan Training and Research Hospital, Sanliurfa, TURKEY, ⁴Baskent University, Faculty of Medicine, ANKARA, TURKEY.

OBJECTIVE: Medical protection of kidney against ischemia reperfusion injury is very important. Many agents were used for the protection of ischemia reperfusion renal tissue injury. We aimed to evaluate the radioprotective effect of lycopene on the kidney in ischemia reperfusion injury with histopathological, biochemical and scintigraphic parameters. **METHODS:** Twenty one Wistar male albino rats were divided in three groups as lycopene, control and sham group. In lycopene group, lycopene was started 3 days before right renal ischemia reperfusion injury and continued for 15 days. In the control group, right renal ischemia reperfusion injury was applied with no medication. In the sham group, which neither right renal ischemia reperfusion injury nor medication were applied. On 15th day, all rats were sacrificed after DMSA scintigraphies were taken. Histopathological, biochemical and scintigraphic evaluations were made. **RESULTS:** The histopathological score was lower in the lycopene group. In biochemical analysis, MPO level was lower in the lycopene group than in the control group, but not statistically significant. The MDA and nitrite levels were lower in the lycopene group than in the control group. The postoperative mean Tc-99m DMSA uptake values were 44.82 ± 1.84 in the lycopene group, 38.92 ± 1.17 in the control group and 50.21 ± 1.35 in the sham group. DMSA uptake values were higher in lycopene group than in control group. **CONCLUSION:** Lycopene seems to be an effective agent for protection of the kidney in ischemia reperfusion injury as demonstrated by the histopathological, biochemical and scintigraphic parameters.

P205

Calculation of percent cardiac output to kidneys by implementation of Rutland-Patlak plot on initial part of renogram

S. BEATOVIĆ¹, M. Janković², D. Sobić Saranović¹, E. Jaksic¹, M. Blagić³, V. Antić³, V. Artiko¹; ¹University of Belgrade Faculty of Medicine, Center for Nuclear Medicine, Clinical Center of Serbia, BELGRADE, SERBIA, ²University of Belgrade Faculty of Electrical Engineering, BELGRADE, SERBIA, ³Center for Nuclear Medicine, Clinical Center of Serbia, BELGRADE, SERBIA.

The aims of this study were a) to evaluate whether renal blood flow (RBF) could be accurately estimated by the analysis of vascular transit of Tc-99m MAG3 by the use of the Rutland-Patlak (RP) analysis and b) to determine the sensitivity of this technique in assessing perfusion of native and transplanted kidney. **Subjects and Method:** Investigation was carried out in 54 subjects: 20 healthy potential kidney donors (Group A, control group), 20 patients with well-functioning kidney transplant (Group B) and 14 patients with transplanted kidney and suspicion on acute graft rejection (Group C). 74 kidneys were analyzed in total. Dynamic scintigraphy was done 22 minutes after injection of 370 MBq Tc-99m MAG3. For the first 40 seconds two frames per second were recorded. Regions of interest were outlined over left ventricle, right lung and kidneys. Lung region serves to eliminate lung activity in posterior view of left ventricle. For transplanted kidney, regions are outlined over kidney and abdominal aorta. RBF was estimated from a derived first pass activity plateau in renal region of interest as the difference between maximal slopes of renal and arterial TA curves. RBF was generated in units of percentage cardiac output (CO). **Results:** In group A, mean values of RBF were $18.28 \pm 3.65\%$ CO for both kidneys and $9.14 \pm 2.15\%$ CO for one kidney. Transplant blood flow (TBF) in group B was $13.99 \pm 2.29\%$ CO. This was 53% higher than one kidney RBF and 23% lower than global RBF in group A. TBF in group C was $6.11 \pm 2.27\%$ CO. It was 66% lower than in group A and 56% lower than in group B.

Statistical difference between A/C and B/C was significant ($p < 0.005$). There was no overlapping between groups C and B: the highest value in group C of 7.93% CO was lower than the lowest value in group B (9.62% CO). **Conclusion:** Fractional RBF, derived from the first-pass activity plateau as upslope ratio of kidney curve and arterial curve is sensitive method for quantifying renal perfusion. Method is independent of time interval between arterial and kidney time-activity curves. In healthy individuals physiological values of RBF were obtained. Well functioning transplants receive a fraction of CO similar to that delivered to two normal kidneys. Flow to rejecting allograft is significantly reduced.

P206

Predictive value of cortical transit time on MAG3 for the need of surgery in antenatally detected unilateral hydronephrosis due to ureteropelvic junction stenosis

J. Lee¹, S. Jeong¹, S. Lee¹, M. Cho¹, J. Jeong¹, J. Ha², S. Lee¹, S. Chung¹; ¹Kyungpook National University School of Medicine, Daegu, KOREA, REPUBLIC OF, ²Chosun University Hospital, Daegu, KOREA, REPUBLIC OF.

Background and purpose: Unilateral ureteropelvic junction (UPJ) stenosis is the most common prenatally detected disease leading to hydronephrosis. The aim of management is to preserve renal function by selecting the children who require early surgical intervention from those for whom watchful waiting may be appropriate because of spontaneous resolution without a significant loss of renal function. Some studies showed that cortical transit time (CTT) could successfully predict functional deterioration in children with UPJ stenosis. We assessed the impact of initial CTT on Technetium-99m mercaptoacetyl triglycerine (MAG3) diuretic renogram for the need for surgery in children with antenatally detected unilateral hydronephrosis due to UPJ stenosis. Materials and Methods: We retrospectively reviewed the medical records of 33 antenatally detected unilateral hydronephrosis (anteroposterior diameter (APD) > 10mm) due to UPJ stenosis patients who managed at our institution between 2006 and 2014. Delayed CTT was defined by absence of activity in the subcortical structures within 3 minutes of tracer injection on MAG3 diuretic renogram. This study analyzed and compared the initial level of society of fetal urology (SFU) grade, APD, split renal function (SRF), drainage pattern on diuretic renogram, and CTT with the need for surgery. Results: Of the 33 children, 16 were classified as the delayed CTT group and 17 were placed in the normal CTT group. During follow-up period (31.8 months), the surgery was performed in 75.0% (12/16) of delayed CTT group and in 5.9% (1/17) of normal CTT group ($p < 0.001$). Multivariate analysis showed that delayed CTT on initial MAG3 scan and APD on initial ultrasonography were independent predictive factors of the need for surgery. Conclusion: CTT on initial MAG3 scan was found to be a predictive factor of the need for surgery in children with antenatally detected unilateral hydronephrosis due to UPJ stenosis. Our findings indicate that CTT should be considered a priority in the management of congenital unilateral hydronephrosis due to UPJ stenosis.

P207

Correlation of quantitative indices of basal renal transplant scintigraphy with same day and 1-week graft function

B. Yazıcı, A. Oral, A. Akgün; Ege University Medical Faculty, Department of Nuclear Medicine, Izmir, TURKEY.

Aim: The aim of this study was to evaluate the correlation of quantitative indices of renal transplant scintigraphy (RTS) performed 2-days after transplantation with same day and 1-week post-operative serum creatinine (sCr) and estimated glomerular filtration rate (eGFR) levels.

Materials and Methods: A total of 221 patients (110 female, 111 male, mean-age 45.5) underwent kidney transplantation at Ege University Medical Faculty between October 2011 and January 2016 and to whom RTS with Tc-99m DTPA was performed within 2-days after transplantation were analyzed retrospectively. Hilson's perfusion index (HI), time between peak perfusion of graft and iliac artery (ΔP), peak-to-plateau ratio (P:Pl), ratio of peak graft perfusion to peak iliac artery (P:A), T $\frac{1}{2}$ of graft washout (GW $\frac{1}{2}$), peak perfusion to peak uptake ratio (P:U) and Graft Index (GI= $\Delta P \times A \times Pl / (P \times U \times \frac{1}{2})$) were obtained. A 1-week sCr of >2.5mg/dl and eGFR of <30ml/min and decreasing of sCr ratio <30% and increasing eGFR ratio <50% in one week were considered to be abnormal. Spearman's coefficient of correlation, Mann-Whitney U tests and receiver-operating characteristic (ROC) curve analysis were used for statistical analysis. $P < 0.01$ was accepted significant. **Results:** Graft index had the strongest correlation with same day and 1-week sCr and eGFR ($r = 0.54$ for same day sCr, $r = -0.58$ for same day eGFR, $r = 0.70$ for 1-week sCr and $r = -0.69$ for 1-week eGFR). Correlation coefficient of other indices with same day sCr/eGFR were <0.40 and 1-week sCr/eGFR were <0.50. In predicting 1-week graft function, all indices were significant ($P < 0.01$). Using the ROC curve analysis, the most accurate index was GI in predicting 1-week sCr of >2.5 mg/dl (AUC=0.88) and eGFR of <30 ml/min (AUC=0.87) and for prediction of decreasing sCr ratio of <30% (AUC=0.76) and increasing eGFR ratio of <50% (AUC=0.75) in one week. In predicting 1-week sCr of >2.5mg/dl and eGFR of <30ml/min, the AUC of other indices were <0.80. For prediction of decreasing sCr ratio of <30% and increasing eGFR ratio of <50% in one week, the AUC of other indices were <0.70. **Conclusion:** Assessing of the parameters of ΔP , A, Pl, P and 3rd minutes uptake (U_3) with the formula of GI increased the accuracy of RTS. Among the quantitative indices of basal RTS, GI had the best correlation with graft function. In addition, correlation of GI with 1-week graft function was better than its correlation with same day graft function. We considered that GI could be used as quantitative definition of graft function for RTS.

P208

Comprehensive Assessment Of Renal Function In Patients With Type 1 Diabetes Mellitus According To Dynamic Renal Scintigraphy And Doppler Ultrasound Of Renal Arteries

V. Zavadovskaia, A. Kurazhov, M. Zorkaltsev, A. Merinov, T. Saprina; Siberian State Medical University, Tomsk, RUSSIAN FEDERATION.

Aim. To study renal function in patients with type 1 diabetes mellitus used to dynamic renal scintigraphy and doppler ultrasound of renal arteries. **Material and methods.** The study based on 83 patients with type 1 diabetes mellitus (T1DM) (52 male, 31 female, aged from 18 to 56 years). According identified stage of diabetic nephropathy (DN) patients were assigned into 3 subgroups: subgroup 1 included DN patients with normoalbuminuria (NAU) (n=27, 32.5%); subgroup 2 consisted of patients with microalbuminuria (MAU) (n=35, 42.2%); and subgroup 3 included DN patients with proteinuria (PU) (n=21, 25.3%). Comparison group consisted of 15 patients with essential hypertension; control group consisted of 30 healthy volunteers. Cystatin C level was measured in all groups. **Results.** The analysis of clinical and laboratory data demonstrated that the values of cystatin C in control and comparison groups were significantly higher than the corresponding values in T1DM group ($p = 0.007$ and $p = 0.027$, respectively). The cystatin C level was significantly higher in MAU and PU subgroups compared NAU subgroup ($p = 0.02$ and $p = 0.003$, respectively). Analysis of duplex Doppler ultrasonography of renal arteries showed a statistically significant increase in the resistivity index (RI) at level of segmental renal arteries in both kidneys in T1DM group compared control group ($p = 0.001$ for right kidneys, and $p = 0.03$ for left kidneys). Intragroup analysis demonstrated a significant decrease in Vmin in PU subgroup compared NAU and MAU subgroups ($p = 0.006$ and

$p = 0.04$, respectively). Disease duration caused a statistically significant Vmin reduction and RI increase in T1DM patients ($p = 0.01$). Glomerular filtration rate (GFR) increasing on dynamic renal scintigraphy data were revealed in all groups. Intragroup comparison revealed a significant increase in T $\frac{1}{2}$ and T $\frac{1}{2}$ in PU subgroup compared with NAU subgroup ($p = 0.01$). An increase in the duration of T1DM was significantly associated with a decrease in GFR ($p = 0.03$). **Conclusion.** Leading radiological signs of renal dysfunction in patients with type 1 diabetes mellitus were resistivity index increase on duplex Doppler ultrasonography data and decreasing of glomerular filtration on dynamic renal scintigraphy data. Besides Cystatin C level duplex Doppler ultrasonography and renal scintigraphy data seems available tools for assessment of renal function in T1DM patients.

P209

The Protective Effect of Lycopene on Kidney against Experimentally Induced Unilateral Ureteral Obstruction

H. I. ATILGAN¹, A. AYDIN², M. SADIC³, M. KORKMAZ³, T. KARAKAN³, E. OGU³, P. BORCEK⁴, G. KOCA³; ¹Kahramanmaraş Necip Fazil City Hospital, Kahramanmaraş, TURKEY, ²Sanliurfa Mehmet Akif Inan Training and Research Hospital, Sanliurfa, TURKEY, ³Ministry of Health Ankara Training and Research Hospital, ANKARA, TURKEY, ⁴Baskent University, Faculty of Medicine, ANKARA, TURKEY.

Purpose: To investigate the possible protective effect of lycopene on kidney after unilateral ureteral obstruction. **Methods:** Twenty one Wistar albino rats were divided into 3 groups. In lycopene group, lycopene was administered 2 days before left ureteral ligation and was continued for 15 days. In control group, left ureteral ligation was applied with no medication. In sham group, a midline incision was made to abdomen and then closed. Histopathological, biochemical and scintigraphic evaluations were made. **Results:** Microscopic score was 50.56 ± 34.32 in lycopene, 97.22 ± 39.14 in control and 28.33 ± 12.58 in sham group. Microscopic score was lower in lycopene group than control group ($p = 0.033$). In biochemical analysis, mean value of MPO, MDA and nitrite levels were 0.05 ± 0.03 , 4.64 ± 1.49 and 0.06 ± 0.01 respectively in lycopene group, 0.10 ± 0.03 , 8.37 ± 3.31 and 0.14 ± 0.09 in control group and 0.04 ± 0.01 , 18.76 ± 9.30 and 0.05 ± 0.01 in sham group. MPO, MDA and nitrite levels were lower in lycopene group than in control group ($p = 0.033$, $p = 0.007$ and $p < 0.001$, respectively). Postoperative mean Tc-99m DMSA uptake values of left kidneys were 6.26 ± 5.17 in lycopene, 2.09 ± 1.03 in control and 49.17 ± 1.37 in sham group. There was no statistically significant difference between lycopene and control groups in respect of postoperative DMSA uptake values ($p = 0.063$). **Conclusion:** Lycopene is effective for the protection of kidney after ureteral obstruction as shown by microscopic parameters and decreased reactive oxygen species.

P210

Feasibility and advantages of ^{99m}Tc-DTPA dynamic SPECT renogram combined with a SPECT/CT session

M. Spiliotopoulou¹, E. Papachristou², P. Kalidonis³, A. Fotopoulos⁴, T. Spyridonidis¹, D. J. Apostolopoulos¹; ¹University of Patras, Medical School, Department of Nuclear Medicine, Patras, GREECE, ²University of Patras, Medical School, Department of Nephrology, Patras, GREECE, ³University of Patras, Medical School, Department of Urology, Patras, GREECE, ⁴University of Ioannina, Medical School, Department of Nuclear Medicine, Ioannina, GREECE.

Aim: This study addressed the feasibility and the advantages of ^{99m}Tc-DTPA SPECT renogram combined with SPECT/CT for attenuation correction and correlation of functional with anatomical data. **Method:** 20

patients aged 38–77 y.o. were examined. The imaging protocol included: Day 1: Conventional planar renogram with 74–111 MBq of ^{99m}Tc -DTPA for 30–40 min (lasix was given at 20 min) followed by 74–111 MBq of ^{99m}Tc -DMSA administration and SPECT/CT imaging (Infinia hawkkey-4, GE Healthcare) 3 hrs post-injection. Day 3: Dynamic SPECT (D-SPECT) renogram after injection of 222–370 MBq of ^{99m}Tc -DTPA (no lasix was given), immediately followed by a SPECT/CT session (VG hawkkey, GE Healthcare). GFR was calculated at the same day by the clearance method with blood samples taken at 2 and 4 hrs post-injection. D-SPECT was performed as follows: Consecutive SPECT sessions were acquired over 360° arc with continuous acquisition mode, $140\pm 30\%$ KeV energy window, on 64x64 matrix, 2 sec/frame (SPECT time=1 min) for the first 8 min and 4–8 sec/frame afterwards. A total of 14 SPECT groups was acquired for 26 min. CT-derived maps were used for attenuation compensation of D-SPECT data [D-SPECT(AC)], while CT slices were fused with SPECT images. Renal activity was measured in the whole kidney volume by ROIs manually drawn on consecutive transaxial CT slices which were then copied on each of the 14 SPECT series. The reference method for split renal function measurement was ^{99m}Tc -DMSA SPECT/CT. **Results:** a) D-SPECT(AC) images were of good quality. b) 26-min renographic curves obtained by planar renogram were quite similar in shape to those created by D-SPECT(AC). c) Split renal function calculation by D-SPECT(AC) correlated perfectly ($r=0.98$) with the reference method, whereas planar renogram was less accurate ($r=0.87$). Planar-SPECT inconsistencies were often in case of ectopic kidneys ($n=2$) and marked size differences between the two kidneys ($n=12$). d) Anatomic information provided by contrast-enhanced CT (calcium-containing calculi, parenchymal cysts, renal pelvis and ureter dilation, etc) offered an integrated structural-functional view valuable for the final diagnosis. e) D-SPECT(AC) kidney uptake at 2–3 min as a fraction of injected dose correlated better with reference GFR ($r=0.87$) than that estimated by the Gates method ($r=0.73$). **Conclusion:** 3-D ^{99m}Tc -DTPA renogram corrected for attenuation and fused with CT images is feasible with conventional gamma-cameras incorporated into hybrid SPECT/CT systems. It allows accurate split renal function measurement, is enriched by useful anatomical information and can be used for closer approximation of GFR compared with Gates method.

P211

Scintigraphic evaluation of renal protective effects of trimetazidine

Z. V. Vesnina^{1,2}, E. O. Vershinina¹, Y. B. Lishmanov^{1,2}; ¹Institute of Cardiology, Tomsk, RUSSIAN FEDERATION, ²National Research Tomsk Polytechnic University, Tomsk, RUSSIAN FEDERATION.

Introduction. One of the adverse effects of the x-ray angiography and endovascular procedures can be contrast-induced kidney dysfunction. In this connection, it requires the use of therapeutic approaches and pharmacological agents having high nephroprotective efficiency during radiocontrast procedures. **Aim.** Scintigraphic evaluation of the renoprotective efficacy of trimetazidine in patients undergone endovascular revascularization (ER) of the myocardium. **Material and methods.** The study included 48 patients with ischemic heart disease (42 men and 6 women, mean age 56.98 ± 1.40 years) who underwent ER (stenting of the coronary arteries). All patients were randomized into 2 groups: patients (20 men) who took trimetazidine before angiographic procedures (group I), and patients (28 men) who underwent ER without nephroprotection (group II). Dynamic radionuclide renoscintigraphy with ^{99m}Tc -DTPA were performed before and 2–3 days after the ER with the calculation of the parameters of filtration and excretory renal functions. **Results.** Patients of Group II after ER had the negative dynamics of renal filtration function parameters. Thus, there has been a significant decrease in the mean value of the total GFR, mainly by reducing the filtration activity of the left kidney. In patients of this group we observed a significant increase of radiopharmaceutical clearance half-time from the renal pelvis system (RPS), from the parenchyma of both kidneys and decrease

of cortical delay index of the left kidney. In the group of patients treated with trimetazidine (group I), mean values of parameters of filtration activity of the kidneys did not significantly change compared with the baseline (before ER) data. Compared to the filtration activity, in Group I adverse changes in the processes of renal excretion were observed frequently. However, in patients of Group I average changes of scintigraphic parameters that reflect the evacuation function of the kidney parenchyma and RPS were insignificant. **Conclusion.** It is shown that trimetazidine prevents contrast-induced renal dysfunction in patients undergone coronary procedures. **Key words:** contrast-induced renal dysfunction, trimetazidine, radionuclide renoscintigraphy. Funding This work was supported by a grant from the Russian Science Foundation (№ 14-15-00178).

P212

Glomerular Filtration Rate Measurement by Means of the Slope-Intercept Method - Do We Really Need the Standard Solution?

M. Silva¹, R. Silva^{1,2}, J. Isidoro¹, P. Gil¹, A. P. Moreira^{1,2}, P. Lapa¹, G. Costa¹, J. Pedroso de Lima^{1,2}; ¹Centro Hospitalar da Universidade de Coimbra, Coimbra, PORTUGAL, ²Instituto de Ciências Nucleares Aplicadas à Saude, Coimbra, PORTUGAL.

AIM: Glomerular filtration rate (GFR) is an accepted measure of renal function. It is routinely assessed using tracers that are cleared exclusively by glomerular filtration, the most common being ^{99m}Tc -diethylenetriaminepentaacetic acid (^{99m}Tc -DTPA). For all routine clinical purposes GFR can be satisfactorily estimated using 2 blood samples taken from the latter of the 2 exponential components of the plasma clearance curve (slope-intercept method). Although simpler than inulin infusion or the multiple blood samples technique, it is still labour intensive and involves the preparation of a standard solution (SS). The SS may, however, be discarded if the high accuracy and precision of the well counter guarantee a robust activity to counts ratio. In this study we mean to compare the classic slopeintercept method with a simplified version, that disregards the SS. **MATERIAL AND METHODS:** Twenty-eight consecutive patients (18 males and 15 females, 18–87 years of age, mean age: 57.0 ± 18.9 years), referred to our department between January and April 2016 for GFR measurement, were included. The GFR was estimated, after the injection of 114.3 ± 6.3 MBq, according to the British Nuclear Medicine Society guidelines. Additionally, the well counter's (CAPINTEC[®] CAPTUS3000[®]) activity to counts ratio was calculated and used to estimate the GFR without the SS for all patients. Statistical analysis was performed using IBM © SPSS © Statistics, version 22. **RESULTS:** On average, the GFR calculated without the SS was 1.04 ± 1.47 ml/min higher than the conventional method (65.32 ± 24.88 ml/min vs 64.28 ± 24.57 ml/min, respectively). A statistically significant correlation was found between both methods (Pearson $r:0.998$, $p<0.01$). **CONCLUSION:** In this study the GFR calculated with and without the SS solution were nearly identical and very strongly correlated, calling into question the need for a SS solution and opening the possibility of simplifying the technique.

P213

Comparison Of ^{99m}Tc Ethylene Dicysteine And ^{99m}Tc Dimercaptosuccinic Acid Scintigraphy For The Evaluation Of Renal Cortical Scarring And Differential Function In Patients With Urinary Tract Infections

A. Dharmalingam; Seth G.S Medical College and KEM Hospital, Mumbai-4000012, INDIA.

COMPARISON OF ^{99m}Tc ETHYLENE DICYSSTEINE AND ^{99m}Tc DIMERCAPTOSUCCINIC ACID SCINTIGRAPHY FOR THE EVALUATION OF RENAL CORTICAL SCARRING AND

DIFFERENTIAL FUNCTION IN PATIENTS WITH URINARY TRACT INFECTIONS Dr. D. Anitha, Dr. Shweta Ghule Pawar, Dr. G. H. Tilve Seth G. S. Medical College and K. E. M Hospital, Mumbai-400 012, India

AIM OF THE STUDY: The aim of this study was to assess the ability of Tc-99m Ethylene Dicycysteine (EC) scintigraphy to detect renal cortical scarring over Tc-99m Dimercaptosuccinic Acid (DMSA) and also to compare the difference between the renal split function obtained by both the radiopharmaceuticals in patients with urinary tract infections.

MATERIALS AND METHODS: 45 patients (age range of 15 days–12 years) presented with features of urinary tract infections with the kidneys located in the normal position were included in this study. The two studies, i.e. Tc-99m DMSA and Tc-99m EC scintigraphy as per the EANM guidelines, were performed on two separate days within an interval of 10 days of each other. Tc-99m EC images were acquired in 128×128 matrix after administering activity of 3.7 MBq/kg of body weight (minimum of 37 MBq) and Tc-99m DMSA study was acquired in both the 128×128 and 256×256 matrices after administering activity of 1.85 MBq/kg (15 MBq). The images of the 2–3 minutes of the dynamic study of the EC study were summed and compared with that of DMSA scan using same matrix size. The presence and the distribution of the scars in the upper, middle and lower poles were compared in 128×128 matrix of both the studies and was confirmed on 256×256 matrix images of DMSA study as gold standard. The split function values were calculated with Tc-99m EC were compared with Tc-99m DMSA. Both studies were performed on the same gamma camera, and reviewed by a single nuclear medicine physician to eliminate bias due to technical factors or inter-observer variability.

RESULTS: In the detection of cortical scars EC showed a positive predictive value was 100%, negative predictive value was 93.71%, sensitivity was 92.48% and specificity was 100% as compared with Tc-99m DMSA as the gold standard. Differential function of both the kidneys calculated by using Tc-99m EC was found concordant with that of Tc-99m DMSA which is the gold standard.

CONCLUSION: This study indicates that EC is comparable with DMSA in evaluating the cortical defects and differential function. By doing a single scan, there are added advantages of lower cost, convenience and low radiation exposure to the patient.

P214

^{99m}Tc-DMSA scan in child's uropathies

S. E. Bouyoucef, A. Khelifa, S. Rahabi, M. Habbeche, E. Atia, K. Chentli; CHU Bab El Oued, Algiers, ALGERIA.

Objective: To determine the role of ^{99m}Tc-DMSA scan when reporting the ^{99m}Tc-EC renogram in children with uropathy.

Material and methods: It is a retrospective study done between January and March 2016 with a total of 200 children with uropathy who underwent in a two days protocol a ^{99m}Tc-EC renogram and a ^{99m}Tc-DMSA scan. 131 boys and 69 girls aged from 20 days to 15 years (average age of 4.47 years) with uropathy were all referred in nuclear medicine for assessment of function and the drainage. Pyelo-ureteral junction (PUJ), mega ureter and vesico-ureteral reflux (VUR) were the most common indications. The injected activities for dynamic F0 ^{99m}Tc-EC scan were (20–90 MBq) and for static ^{99m}Tc-DMSA (20–74 MBq). For each kidney, the results of ^{99m}Tc-DMSA scan were compared to those of ^{99m}Tc-EC renogram before writing the final reporting. Both EC renogram and DMSA scan were reported separately by two experienced nuclear physicians.

Results: 253 kidneys have had normal renograms, 115 kidneys have had abnormal renograms and 32 kidneys were not functioning. 275 kidneys have had a normal DMSA scan and 125 kidneys and abnormal DMSA scan. Among the 125 abnormal DMSA scans, 49 were seen in kidneys with abnormal ^{99m}Tc-EC renogram including an impaired drainage (49/115). In other hand, the 253 kidneys with normal ^{99m}Tc-EC renogram presented 76 abnormal DMSA scans (76/253). Those abnormal DMSA scans with normal EC renograms, were seen essentially in VUR

followed by PUJ. DMSA scan confirmed the also the cases of non functioning kidneys and revealed additional morphological abnormalities such as horseshoe kidney.

Conclusion: The ^{99m}Tc-DMSA scan is essential when assessing an uropathy in children and allows better follow up and contribute for adapting a better management of the disease.

P215

Normalized residual activity: diagnosis of kidneys obstruction

D. BEN SELLEM, B. LETAIEF, B. DHAOUADI, L. ZAABAR, M. F. BEN SLIMENE; University of Tunis El Manar, Faculty of Medicine of Tunis, Salah Azaiez Institute, Department of Nuclear Medicine, Tunis, TUNISIA.

Aim: Normalized residual activity (NORA) is a parameter proposed for the estimation of renal emptying during renography with ^{99m}Tc-MercaptoAcetylTriGlycine (^{99m}Tc-MAG3) or ^{99m}Tc-Diethylene Triamine Pentaacetic Acid (^{99m}Tc-DTPA) on dilated kidneys. This parameter allows, in many cases, the differentiation between simple dilatation urinary tract requiring simple monitoring and obstruction whose treatment is surgical. The aim of this study was to evaluate the value of NORA in the diagnosis of obstructive dilated kidneys.

Materials and methods: This is a retrospective study of 300 patients referred to our department to evaluate kidney obstruction. Dynamic data acquisition was started at the moment of injection of a maximal activity of 100 MBq, adapted to body-surface. The patient was in the supine position and the collimator is posteriorly positioned. Furosemide was injected at 20 minutes (F+20). Data were processed in order to generate renogram curves. When the curves were suggestive of obstruction, delayed acquisition of dynamic images was performed to evaluate late emptying and to calculate the NORA. A total of 330 NORA was calculated. NORA is considered normal if its value is lower or equal to 1, abnormal if superior to 2 and equivocal if between 1 and 2.

Results: The NORA was normal in 63.94 % of cases (211/330), abnormal in 12.12 % of cases (40/330) and equivocal in 23.94 % of cases (79/330). The NORA has allowed a good classification of the obstruction in 76% of cases, thus guiding referring clinicians in their therapeutic decision.

Conclusion: Evaluation of renal emptying is crucial in the exploration of dilated kidneys. In fact, obstruction is managed surgically; while absence of obstruction needs a medical follow up. NORA is a simple parameter for the estimation of renal emptying during renography. In our study, it allowed the diagnosis of obstruction under the dilated renal tract in 12.12 % of cases and guided the therapeutic decision of clinicians in 76% of cases. Any suggestive signs of obstruction on renal curves must indicate delayed images in order to calculate the NORA.

P216

Comparison of Methods for Estimating Glomerular Filtration Rate in Head and Neck Cancer Patients Treated with Cisplatin

L. Lindberg, B. Kristensen, B. Zerahn; Department of Clinical Physiology and Nuclear Medicine, Copenhagen University Hospital, Herlev Hospital, Herlev, DENMARK.

Introduction: Cisplatin is a chemotherapeutic agent widely used in the treatment of various solid tumours. Cisplatin induces nephrotoxicity in a dose-dependent manner and may lead to long-term reduction of kidney function. Subsequently, determination of glomerular filtration rate (GFR) is used to monitor potential kidney damage during treatment. ⁵¹Cr-EDTA clearance (CrCl) is the clinical gold standard for determination of GFR. However, estimation of GFR from plasma creatinine applying different equations is widely used owing to the simplicity of the method. This study aimed to compare CrCl with two commonly used algorithms for estimating GFR (eGFR) from plasma creatinine.

Materials and Methods: Retrospective single center study of 94 head and neck cancer patients

treated with cisplatin at a maximum cumulated dose of 420 mg. CrCl was performed once before, during, and after treatment. CrCl was performed according to the principles of one sample clearance a.m. Broechner-Mortensen. Plasma creatinine was measured six times, concurrently. eGFR was assessed from plasma creatinine applying the Cockcroft-Gault (CG) equation that includes weight, and the Chronic Kidney Disease-Epidemiology Collaboration (CKD-EPI) equation. Agreement between the methods was assessed applying the statistical methods of Bland and Altman. A predefined limit of variation between CrCl and eGFR of 14% was applied in order to decide whether eGFR derived from the two equations would be useful in a clinical setting. **Results:** Comparison of CrCl and eGFR_{CKD} revealed a positive slope of the linear regression line, suggesting proportional bias ($p < 0.001$). No systematic bias was found between CrCl and eGFR_{CG}. Concerning the precision of each equation, 49 (54%) and 43 (47%) observations exceeded the clinically acceptable limit of variation for eGFR_{CKD} and eGFR_{CG}, respectively. Weight changes ranged from -17.0 kg to 4.7 kg. Median weight change was -0.6 kg/week, significantly different from zero ($p < 0.001$). **Conclusion:** Estimated GFR_{CKD} cannot sufficiently replace CrCl in the assessment of GFR in head and neck cancer patients during treatment with cisplatin. If CrCl is unavailable, then weight-corrected eGFR_{CG} is the better choice (probably due to its ability to compensate for changes in bodyweight during treatment) provided proper attention to the large variation between methods.

P217

Low level of GFR at baseline renal scan can predict postoperative 1 year function regardless of BMI

J. Ha¹, A. Chong¹, S. Jeong²; ¹Chosun University Hospital, Gwangju, KOREA, REPUBLIC OF, ²Kyungpook National University Hospital, Daegu, KOREA, REPUBLIC OF.

Introduction On previous research of our group, we found low level of GFR at baseline renal scan could predict abnormal Cr level at postoperative 1 years follow-up. In that study, patient's factor of body weight and height showed difference between normal and abnormal groups of serum Cr(reference 1). The aim of this study was to find out whether body weight, height, or BMI affect the relationship between baseline GFR and function of transplanted kidney. **Materials and Methods** Baseline Tc-99m DTPA scan (within 8 days after transplantation) of 86 patients were analyzed retrospectively. Serum creatinine (Cr) levels at the timing of postoperative 1 year, GFR of renal scan, height, weight, and BMI at the timing of renal scan were also analyzed. $P < 0.05$ was considered as significant. **Results** Baseline GFR correlates with serum Cr level at the timing of postoperative 1 year. Among clinical variables, height and weight showed difference between groups (serum Cr > 1.5 or not at the timing of postop 1 year). However, partial correlation analysis showed significant correlation between baseline GFR and serum Cr level of postop 1 year with covariates of BMI, height and weight. Cut-off value of baseline GFR to predict abnormal serum Cr level at postop 1 year were 65.6 ml/min (sen 90.5% and spe 52.4%). **Conclusion** Lower GFR of baseline renal scan could predict abnormal Cr of postoperative 1 year follow-up regardless of patients BMI, height and weight.

P218

Comparison of Single Sample and Two Sample Methods for Measuring Glomerular Filtration Rate (GFR) Using Tc99m DTPA Plasma Clearance Method

N. R. AKEPATI; JAWAHARLAL INSTITUTE OF POST GRADUATE MEDICAL EDUCATION AND RESEARCH, Pondicherry, INDIA.

AIM: The study aimed to assess the level of agreement between GFR values obtained with single plasma sample method (SPSM) and two

plasma sample method (TPSM) using plasma sampling technique. **MATERIALS AND METHODS:** Consecutive subjects referred to our department for GFR measurement between the period June 2014 to March 2016 were included in the study. 1 mCi of Tc-99m DTPA was injected intravenously to each subject and venous blood samples were withdrawn at approximately 60 and 180 minutes. Plasma was separated and counted after 24 hours. GFR was measured using Russel's two plasma sample technique formula (60 and 180 minutes samples) and single sample technique formula (180 minutes). GFR values obtained with SPSM and TPSM were normalised for body surface area and were expressed as median and interquartile range (IQ) Agreement between GFR values obtained with SPSM and TPSM was measured with Wilcoxon Signed Rank Test. Strength of agreement between SPSM and TPSM was carried out using Bland Altman analysis. P value less than 0.05 was considered significant. **Results:** 209 subjects (113 males, 96 females) with mean age of 41.28 years (SD 13.15 years, range 18-65 years) were included in the study. Out of 209 subjects, 70 were voluntary kidney donors, and 28 were transplant recipients. Chronic kidney disease patients with TPSM GFR values less than 30 ml/min were not included in the study. Mean GFR values for TPSM and SPSM were found to be 74.75 ml/min (IQ range-36.09) and 78.31 ml/min (IQ range-49.13) respectively. Wilcoxon Signed Rank Test showed no significant difference between median values of TPSM and SPSM values. On Bland-Altman analysis, GFR values calculated by SPSM were concordant with TPSM (Gold standard) in 95% confidence interval (average ± 1.96 SD). **Conclusion:** GFR values obtained with SPSM correlates well with TPSM in subjects with measured GFR values more than 30 ml/min. SPSM is a more convenient method since it involves a single blood sample and can be used in subjects who are expected to have GFR more than 30 ml/min.

P219

Diuretic Renography is a Gold Standard Method for Radiological Diagnosis of Urinary Obstruction: Optimal Timing of Diuresis Injection

H. M. Gad¹, A. Elgendy², S. Mansour¹, H. Abdelkader²; ¹Urology and nephrology center- Mansoura University, al mansura, EGYPT, ²Biophysics Department- Faculty of Science, al mansura, EGYPT.

Diuresis renography is widely accepted as a useful test for investigating the dilated urinary tract, evaluation of kidney function & urinary drainage and discriminating between obstructed and non-obstructed systems. The test achieve popularity because of its simplicity and noninvasiveness. **Purpose:** The aim of this study is to assess the optimum timing of furosemide injection in diuretic renography to gain the most accurate diagnosis. **Patients and Methods:** One hundred patients with suspected urinary obstruction due to presence of hydronephrosis underwent F+10 min diuretic renography. Forty patients gave no response to diuresis, diagnosed as obstructed kidneys however twenty patients showed delayed excretion but improved in response to diuresis and diagnosed as non obstructed kidneys. The remaining forty patients showed equivocal response to diuresis were enrolled in this study and underwent F-15 min .The results were classified into obstructed and non-obstructed according to images, T_{1/2} and curves of renogram after F-15 min diuretic renography. **Results:** The Results obtained for one hundred patients by F+10 min protocol showed that forty were obstructed and twenty were non-obstructed with sensitivity 60% , however the remaining forty patients with equivocal response to diuresis underwent F-15 min diuretic renography with thirty-one patients were proved to be obstructed and the other nine were non obstructed with sensitivity 100%. Obstruction was found in 71 out of 100 patients with mean \pm SD T_{1/2} values 31.39 min \pm 10.63. The mean kidney split function was 43.7% \pm 2.6. Twenty nine patients were non-obstructed with mean \pm SD T_{1/2} values 9.76 min \pm 3.31 min and there mean kidney split function was 45.59% \pm 3.34 %. As regard the forty patients with equivocal response to diuresis at F+10 min; thirty one patients were proved to be obstructed by F-15 min study with mean \pm SD T_{1/2} values 29.77 min \pm 8

which was $16.63 \text{ min} \pm 2.28$ by F+10 min ($p=.001$), however the other nine patients were proved to be non-obstructed with mean \pm SD $T_{1/2}$ values $12.89 \text{ min} \pm 3.22$ min in F-15 min study and it was 24.89 ± 10.8 min in F+10 min ($p=.01$). A p value less than .05 was considered significant. Conclusion: The optimum timing of diuretic injection is 15 min prior to renography study with the exact $T_{1/2}$ min and so F-15 min renal scintigraphy can be considered as the most sensitive method for diagnosing urinary obstruction and can be taken as a gold standard in this matter.

P220

Tc-99m DMSA Absolute renal uptake: Is it a reliable quantitative parameter to assess the degree of renal impairment in patients with chronic kidney disease

H. Nasr^{1,2}, H. Farghaly^{3,2}, A. Al Qarni², A. Kheder²; ¹Nuclear Medicine Department, Cairo University, Cairo, EGYPT, ²Radiology Department, Prince Sultan Military Medical City, Riyadh, SAUDI ARABIA, ³Nuclear Medicine Unit-Clinical Oncology Department, Assiut University, Assiut, EGYPT.

Objectives: To determine the accuracy of Tc-99m DMSA absolute renal uptake (ARU) in assessment of the severity of chronic kidney disease (CKD) in comparison to Cr-51 EDTA GFR. **Methods:** We retrospectively analyzed 66 patients with CKD (mean age 62.8 ± 15.07 , 35 males and 31 females). All patients had Tc-99m DMSA renal scans, Cr-51 EDTA GFR and serum creatinine, all three studies performed within less than 6 months period (mean 30.69 ± 63.06 days) and within less than 1 month in 86% of patients. Total (left + right) DMSA ARU was calculated using posterior view images performed after 3 hours of Tc-99m DMSA injection. For purpose of attenuation correction the depth of the kidneys was estimated using Tonnensen equation. Stages of CKD were based on GFR values according to KDOQI guidelines. Patients were classified into 3 groups; Group 1: GFR ≥ 60 (13 pt.), Group 2: GFR 30-59 (30 pt.) and group 3: GFR < 30 (23 pt.). The mean total ARU was compared between groups using ANOVA with post Hoc test. Pearson's correlation was performed between ARU, GFR and creatinine. Equation to estimate the GFR from the ARU was generated using regression analysis. **Results:** There was significant differences between the study subgroups as regards the mean ARU (group 1= 41.4 ± 10.8 , group 2= 19.7 ± 5.7 , group 3= 7.9 ± 4.2 ; $p < 0.001$) as well as for creatinine (group 1= 89.1 ± 25.9 , group 2= 132.1 ± 39.9 , group 3= 242.8 ± 109.3) with p values between all groups < 0.001 except for creatinine between group 1 and group 2 ($p=0.072$). The GFR for the entire study group was better correlated to the ARU than to creatinine ($r=0.914$ vs. $r=0.713$). The correlation of GFR with ARU in patients with GFR ≥ 40 ml/min was better than with creatinine ($r=0.827$ vs. $r=-0.423$), however in patients with GFR < 40 ml/min correlation of GFR was comparable for both ARU and creatinine ($r=0.716$ vs. $r=-0.708$). The equation for rough GFR estimation from ARU was: $\text{GFR} = 14.11 + 1.40 \text{ ARU}$. **Conclusions:** The ARU is well correlated to Cr-51 EDTA GFR and can be considered a reliable and more sensitive indicator than serum creatinine to detect renal impairment specially in early stages of CKD during which serum creatinine is relatively low and is not well correlated to GFR values.

P221

Evaluation of 99mTc DMSA's efficiency as a radiopharmaceutical in dynamic renal scans

i. M. A. abd-elfadil, Sr., Heba M Fahmy¹, Hossam M Yassin², Islam M Muhamed¹, Samar E Mohamed¹, Shima S Hassan¹ 1: Biophysics; science, cairo, EGYPT.

Background: Dynamic and static renal scanning are considered the routine techniques for the preoperative, postoperative and follow-up evaluation of renal functions. In dynamic renal Tc-99m diethylenetriamine

pentaacetic acid (DTPA) is much used and give information about the renal blood-flow and excretory function. Tc-99m dimercaptosuccinic acid (DMSA) is employed for static renal imaging and can show also the renal cortical structure. **Aim of work:** The purpose of this work was to evaluate whether DMSA can be utilized as a radiopharmaceutical in dynamic renal scans. The aim extends also to compare the results obtained from DMSA with those obtained with DTPA scans. **Materials and methods:** A total of 47 subjects (patients and normal kidney function cases) that had 99mTc-DMSA and 99mTc-DTPA dynamic scintigraphies using the same protocol. **Results:** Estimation of the total GFR from 99mTc-DTPA and 99mTc-DMSA renograms showed a strong positive correlation. Moreover, estimation of the time to the peak height from 99mTc-DTPA and 99mTc-DMSA renograms for right and left kidneys showed non-significant changes and strong positive correlation. **Conclusion:** In the light of the results obtained from the present study, it could be suggested that 99mTc-DMSA could be successfully replaced 99mTc-DTPA in dynamic renogram. This will be money and time consuming, and will lower the radiation dose. In addition, the same qualities of results are obtained with both radiopharmaceuticals.

P222

Testicular Scintigraphy as a Post-Surgical Evaluation Exam

A. S. Pinto, V. Alves, T. Vieira, A. R. Fernandes, T. Faria, A. Oliveira, M. Pérez, J. Pereira; Centro Hospitalar de São João, Porto, PORTUGAL.

Introduction: Testicular Scintigraphy (TestSci) is a Nuclear Medicine (NM) exam with proved utility in the setting of acute scrotal pain. It is used to distinguish between a variety of entities, namely testicular torsion, orchitis and epididymitis. In our NM Department, it is also requested as a follow-up exam after testicular surgical intervention, in order to evaluate testicular viability and atrophy. **Aim:** To evaluate the utility of TestSci as a post-surgical exam in our NM Department. **Materials and Methods:** We reviewed data from all patients who underwent TestSci at our Department from 2005 to 2015 ($n=44$) and selected the patients whose exam was requested for post-surgical evaluation. A total of 22 patients were included. **TestSci Protocol:** in adults, a dose of 185 MBq of ^{99m}Tc-pertechnetate is administered by intravenous injection; in children, there is an adjustment of the dose according to the "Administration of Radioactive Substances Advisory Committee" standards. Image acquisition begins immediately, with 1 minute dynamic phase followed by planar static images (anterior projection) of the pelvis and inferior abdomen during 15 minutes. When necessary, SPECT/CT is performed. **Results:** Our patients had a mean age of 7.7 ± 5.41 years old. Testicular torsion ($n=9$) and cryptorchidism ($n=9$) were the most frequent pre-surgical diagnosis, leading to orchiopexy as the most frequent surgery ($n=18$), followed by hemiorrhaphy to repair strangulated hernia ($n=3$) and a varicocele repair ($n=1$). TestSci was required to evaluate testicular viability in 5 patients, atrophy in 12 and both of these characteristics in 17 patients. In the majority of patients ($n=16$), the exam was requested 6 months after the surgical procedure. TestSci was considered "normal" in 9 cases, positive for atrophy in 9 cases and positive for non-viable testicle in 4 cases. In 15 patients it was also requested a Testicular Doppler Ultrasound, whose results matched with those of TestSci in 14 cases. There was a discordant result between TestSci and Doppler Ultrasound. Based on the results of both exams, 7 patients were submitted to a new surgery, which was an orchiectomy in all cases. **Conclusion:** TestSci allows the evaluation of blood perfusion and location of the testicles, which makes it useful in the post-surgical context at the evaluation of testicular atrophy and ischemia as possible sequelae, being a good option as a routine post-surgical exam.

P224**Using ^{99m}Tc -HMPAO SPECT as tool to compare two Transcranial Magnetic Stimulation protocols and their long-term effects in dogs**

R. Dockx¹, C. Baeken¹, L. Vlerick², R. Duprat¹, F. De Vos³, B. De Spiegeleer³, A. Dobbeleir², J. H. Saunders², I. Polis², E. Achten¹, K. Audenaert¹, K. Peremans²; ¹University of Ghent, Faculty of Medicine, Ghent, BELGIUM, ²University of Ghent, Faculty of Veterinary Medicine, Ghent, BELGIUM, ³University of Ghent, Faculty of Pharmaceutical Sciences, Ghent, BELGIUM, ⁴University of Ghent, Department of Radiology, Ghent University Hospital, Ghent, BELGIUM.

A single day protocol of repetitive Transcranial Magnetic Stimulation (rTMS) elevates the regional cerebral perfusion in dogs. Optimization of this rTMS protocol is necessary to use this technique as a treatment for anxiety in dogs. We hypothesize that a 4 day stimulation protocol will elicit a higher and longer response compared to a single day protocol. **Aim:** To assess the effects and their duration on the regional cerebral bloodflow between two High Frequency Accelerated Repetitive Transcranial Magnetic Stimulation (HF-rTMS) protocols on the normal canine left frontal cortex. **Material and Methods:** Eight dogs were included in a crossover study. They underwent a 3 Tesla MRI scan at the Ghent University Hospital. This scan was the basis for pointer-based neuronavigation (Brainsight 2, Rogue Resolutions, LTD) a technique used to externally locate the stimulation site. Each dog was subjected to two protocols. Protocol 1: a single stimulation day applying 5 consecutive aHF-rTMS (20 Hz) sessions and Protocol 2: the same stimulation protocol for 4 consecutive days. Stimulation was applied with a figure - of - eight coil (Magstim Company Limited, Wales, UK) over the left frontal cortex. The stimulation intensity was set at 110% of the motor threshold. One day prior to, one day after and 12 weeks after the last stimulation day, a ^{99m}Tc -HMPAO SPECT scan was acquired under general anesthesia. SPECT data were acquired with a triple head gamma camera (Trionix, Triad) 30 minutes after tracer injection (step and shoot, 120 steps of 3°, 10" per step). The data were reconstructed with OSEM reconstruction (Hermes, NUD, Sweden). A BW filter was applied (cut-off 1.6 cycles/cm, order 5). The perfusion indices (PI) in the frontal, parietal, temporal as well as subcortical regions (thalamus, striatum) were obtained by semi quantification (normalization to total brain counts). **Results:** Both protocols elicited a significant difference in perfusion at the stimulation site 24h post stimulation. The stimulation responses between both protocols did not differ in intensity. After stimulation the regional perfusion returned to baseline within three months. **Conclusions:** The performed aHF-rTMS protocols of the frontal cortex in dogs provoke an increase in rCBF at the stimulation site. Shorter ^{99m}Tc -SPECT scans acquisitions intervals could reveal differences in response duration. Determining the response duration may help refine an aHF-rTMS protocol to treat anxious dogs.

P225**PET for Neurology: Short Acquisition Neuro-PET Enabled by Digital Photon Counting**

K. Binzel, R. Revan, J. Zhang, D. Scharre, M. V. Knopp; The Ohio State University, Columbus, OH, UNITED STATES.

Aim: Positron emission tomography (PET) is increasingly being used as an imaging biomarker for neurologic applications, such as traumatic brain injury, dementia, and Alzheimer's disease. Standard acquisition times for PET neuro imaging can be quite long, typically greater than 10 minutes. For these specialized patient populations, motion during imaging can become a significant problem for such long imaging over a single anatomic area. We explored the feasibility of shortening neuro PET acquisitions, as enabled by the improved sensitivity of next-generation digital PET. **Materials and Methods:** 10 patients recruited for various neuro related trials with acquisition times ranging from 10-20 min over the brain, following injection of 185-555 MBq ^{18}F -imaging agents. Images were acquired on a pre-

commercial release next-generation digital photon counting system (Vereos Philips). Listmode data from the full acquisition were clipped into increments from 15 s to 5 min for re-reconstruction using the standard definition 4 mm voxel length methodology with point spread function correction. Images were then quantitatively evaluated using an atlas based z-score and SUV measurement. Visual quality was reviewed by 2 blinded reviewers, and the patient motion over the entire acquisition duration was tracked. **Results:** We found that excellent visual quality is maintained for time clipped reconstructions up to a[MVK1] 50% reduction in reconstructed acquisition time. Quantitative accuracy was robust as well, there were no significant differences in either z-score or SUV measures for 50% time clipped images as compared to full duration images (p>0.5). Motion tracking revealed that patients exhibited most motion beyond the 10 minute point of the acquisition despite using a firm head positioning device. Image sets of shorter than 10 minute duration markedly reduced the amount of motion within the images. After optimization of reconstruction that used a combined PSF, Gaussian filtering approach with a reduced number of subsets in the iterative recon, full visually and quantitatively equivalent brain images were obtained with even improved delineation of cortical area observed, likely due to less motion. **Conclusion:** PET for neurologic applications uses traditionally longer acquisition times. We are able to demonstrate, that using a next generation digital PET/CT system enables a substantial reduction of acquisition times with preserved visual quality and quantitative accuracy. Overall reduction by 50% can be readily achieved. Shorter acquisition enables noticeable reduction in patient motion. [MVK1]There could be more data here

P226**Changes of Some Resting State Networks in Patients with Dysexecutive Syndrome**

D. Susin, G. Kataeva, Y. Khomenko, I. Zavolokov, Y. Irishina; Institute of Human Brain of the Russian Academy of Sciences, Saint-Petersburg, RUSSIAN FEDERATION.

Introduction. The executive function (EF) is a set of abilities that allows us to control voluntary behavior responses. The dysexecutive syndrome (DES) is a disability of EF. One of the possible reason of DES is difficulties for some reason to switch attention between dorsal attention network (DAN) and ventral attention network (VAN), the first of these networks is responsible for voluntary (top-down) attention, the second responds to relevant external environmental stimuli. The goal of the study is to estimate the changes in attention networks in patients with DES and their interconnection with the default mode network (DMN) working. **Methods:** 31 patients (age 53-77) with DES (14 person with Parkinson's disease (PD) and 17 with chronic cerebral ischemia), 26 patients (age 41-77) without DES (17 person with PD and 9 with chronic cerebral ischemia) and 19 healthy controls with normal EF (age 20-29) were investigated with PET-FDG, performed on PC2048-15D Scanditronix scanner and standard protocol. Relative estimation of regional glucose cerebral metabolic rate (rCMRglu) in regions of interest (ROI), corresponding to Brodmann's areas (BA), were calculated by WFU PickAtlas after spatial normalization by SPM8. Psychological examination of EF was performed with frontal assessment battery (FAB). The functional connectivity of brain structures, resting state networks (RSN) were revealed by factor analysis of PET data. **Results.** In our research of PET data, we focus on four groups of ROIs, which belong to four networks, namely DMN, DAN, VAN and visual network. Healthy controls and patients without DES show similar structures of RSNs, consisting of the same four typical groups of ROIs. The patients with DES show the structural changes of the dorsal and ventral attention systems: the combination of the part of dorsal attention system and visual cortex with posterior cingulate cortex (PCC) (main element of DMN). We have also registered disintegration of ventral attention system. Our study gives the reason for the assumption that DES is based not only on the frontal cortex dysfunction, but also on some complicated reorganization of the attention networks.

P227**Astrocyte Involvement in TSPO Signal After Microglia Depletion in mice**

M. Tóth, L. Harald, J. Häggkvist, A. Forsberg, A. Varrone, C. Halldin, R. Harris, L. Farde; Karolinska Institutet, Stockholm, SWEDEN.

Aim In the newly developed CX3CR1Cre-ERxRosa26-DTA mice, we aimed to study the changes of [¹¹C]PBR28 signal after specific depletion of CX3CR1-expressing microglia. With the longitudinal follow up we have focused on the TSPO signal changes shortly after microglia depletion (7 days) and after re-population (30 days) in the brain. As TSPO signal might not only originate from microglia, but also from binding to other cell types such as astrocytes and from non-displaceable binding, we have investigated the astrocyte involvement in vitro as well as conducted pretreatment experiments with PK11195 in different cohorts of animals. **Materials and Methods** Seven CX3CR1-CreER(+/-) x Rosa26-DTA (+/-) and four control mice [CX3CR1-CreER(+/-) x Rosa26-DTA (-/-)] were imaged at baseline condition and 7 and 30 days after tamoxifen treatment. Additionally, we also performed pre-treatment experiments with PK11195 after baseline in three mice. All PET measurements were done using the NanoScan PET/MRI and PET/CT systems (Mediso Ltd, Budapest Hungary) after a tail vein bolus injection of [¹¹C]PBR28. PET scans were co-registered to an inbuilt MRI brain atlas in PMOD 3.7 (Zurich, Switzerland) and the corresponding template VOI set was used for time activity curve generation. As a primary outcome value the area under the curve (AUC) was used. **Results** In contrast to the expected outcome based on immunohistochemistry results, injection of tamoxifen did not result in the reduction of [¹¹C]PBR28 uptake at day 7, but resulted in a non-significant increase. At day 30 the striatum, thalamus, hippocampus, CAG and superior colliculi have shown a significant uptake increase of 32-37% compared to the baseline AUC in microglia depleted mice. Pretreatment with PK11195 resulted in a significant decrease of AUC values ranging from 27% in the striatum to 45% in the cerebellum compared to baseline. Preliminary immunohistochemistry results indicate an upregulation of astrocytes after microglia breakdown at day 7, but not at day 30. **Conclusion** The involvement of astrocytes in the general TSPO signal is often neglected or regarded as non-significant. The results presented here, show the possibility of a large enough increase in astrocyte related TSPO signal after total microglia depletion, that hides the depletion of brain microglia. Therefore care should be taken when interpreting the results of TSPO in vivo imaging in mice, regarding the contribution of microglia and astrocyte related signal changes.

P-20 – Tuesday, October 18, 2016, 16:00 - 16:30, Poster Exhibition Hall
Neurosciences: Data Analysis & Quantification

P228**Quantification of Brain Glucose Metabolism by ¹⁸F-FDG PET in Diabetic Mice**

P. Branger¹, M. Joubert¹, D. Bellevre², A. Manrique¹; ¹University Hospital of Caen, Caen, FRANCE, ²University Hospital of Lille, Lille, FRANCE.

Introduction. Brain glucose exposure has been implicated in cerebral dysfunction and cognitive impairment. We assessed brain glucose metabolism with dynamic and static ¹⁸F-FDG-PET in type 1, type 2 diabetic mice model and control. **Materials and Methods.** Nine male Swiss mice with streptozotocin induced diabetes (type 1 diabetes model) (D1), 5 control Swiss mice (C1), 6 male C57BL/6 seipin KO mice (type 2 diabetes model) (D2) and 6 control C57BL/6 mice (C2) were studied. A 60-min dynamic PET (Inveon micro-PET/CT scanner) was performed on isoflurane anesthetized mice after intravenous injection of ¹⁸F-FDG

(15-20 MBq in 50-100µL). Quantitative analysis was assessed by ¹⁸F-FDG uptake constant (K_i) using a vena cava image-derived input function and time-activity data from the 15- to 60-min. Cerebral metabolic rate of glucose (CMR_{Glu}) was then calculated using K_i and the lumped constant. Static analysis was performed estimating mean and maximum standardized uptake values (SUV) from the 45- to 60-min frame. **Results.** K_i and CMR_{Glu} were significantly lower in D1 (0.004 and 9.560 respectively) than in C1 (0.012 and 25.646, P<0.05) and higher in D2 (0.010 and 19.018) than in C2 (0.006 and 9.372, P<0.05). There was no difference on SUV_{mean} or SUV_{max} between D1 (1.078 and 2.171 respectively) and C1 (1.218 and 2.427), and between D2 (1.424 and 2.318) and C2 (1.406 and 2.087). K_i were negatively correlated to glucose level (R=-0.73, P<0.05) in D1 but not in D2. Animal weight, which is an indirect marker of insulin secretion (the more insulinopenic animals displaying the lower body weight), was positively correlated to K_i in D1 (R=0.74, P<0.05) but not in D2. **Conclusion.** Brain glucose metabolism differ between diabetic and non-diabetic mice, and between type 1 and type 2 diabetes. Our results suggest that insulin level might be a key determinant of brain glucose metabolism with a decreased CMR_{Glu} in insulinopenic type 1 animals whereas this parameter was increased in hyperinsulinemic insulin resistant type 2 animals. These different behaviour of brain glucose metabolism in response to blood glucose and insulin levels may lead to a potential neurotoxicity and cognitive impairment.

P229**Effects of Random, Scatter, Attenuation, and Partial Volume Corrections on the Quantification of Dopaminergic PET imaging**

K. H. Lue¹, H. H. Lin^{1,2}, C. S. Lin¹, C. C. Chiang¹, K. S. Chuang¹; ¹Department of Biomedical Engineering and Environmental Sciences, National Tsing Hua University, Hsinchu, TAIWAN, ²Medical Physics Research Center, Institute for Radiological Research, Chang Gung University/Chang Gung Memorial Hospital, Taoyuan, TAIWAN.

Aim Quantitative analysis of nigrostriatal dopamine function is important for the differential diagnosis of parkinsonian disorders in dopaminergic PET imaging. However, the accuracy of quantitative measurements is limited by a number of image degrading factors. This study investigated the effects of random events, scatter events, attenuation, and partial volume effect (PVE) on the quantification of striatal subregional uptake in dopaminergic PET images. **Materials and methods** Monte Carlo simulations were performed using an in-house integrated GATE and SimSET software. The Siemens BiographTM 6 PET scanner was built. A modified Zubal MRI head phantom was used to model realistic healthy and neurodegenerative radioactivity distributions. The simulated sinograms were sorted to mimic ideal random correction (RC) or scatter correction (SC). Attenuation correction (AC) was executed on the basis of the non-uniform attenuation maps. The random-, scatter-, and attenuation-corrected sinograms were reconstructed using an OSEM algorithm. The reconstructed images considered the PVE based on the recovery coefficients, which were derived from a combination of conventional image analysis and the technique of large regions of interest. The binding potential (BP) values for the entire striatum and its subdivisions were calculated for different correction schemes. **Results** Without any correction, the BPs were underestimated by 45.5% and 44.7% on average for healthy and neurodegenerative conditions, respectively. Given the low counting rates, the accuracy of BP estimates did not improve after only RC was carried out. The BPs remained the same as those observed without any correction. Adding SC to RC decreased the average bias in BP estimates. The bias values were 42.5% and 42.6% on average for healthy and neurodegeneration, respectively. The association of AC, RC, and SC was not adequate for the accurate quantification of BPs, which remained underestimated by more than 27.2% for each simulated conditions. The key correction for obtaining accurate BP estimates was partial volume correction (PVC). When PVC was combined with AC, RC, and SC, the

average bias values of BPs were 0.1% and 2.2% for healthy and neurodegeneration, respectively. **Conclusion** Our results indicate that the highest error in BP estimates was induced by PVE, the second largest source of error was attenuation, followed by scatter, and random coincidences. The correction of these image degradations can improve quantitative accuracy. PVC plays a major role in the quantification of dopaminergic PET imaging.

P230

There is more to “Lassen” plots than Lassen’s plot

M. S. Vafae¹, J. Araj Khodaei², M. Araj Khodaei³, A. Gjedde⁴; ¹University of Southern Denmark, Odense, DENMARK, ²Amirkabir University of Technology, Tehran, IRAN, ISLAMIC REPUBLIC OF, ³Shahed University, Tehran, IRAN, ISLAMIC REPUBLIC OF, ⁴University of Copenhagen, Copenhagen N, DENMARK.

Introduction: Neuroreceptor studies by PET often compare radioligand binding potentials in baseline and inhibition states in cases where an apparent reference region of no binding is unknown. The purpose is to obtain separate estimates of receptor saturation and non-displaceable radioligand volume of distribution, according to an equation linearized by Turton et al (1995), Gjedde & Wong 2000, and Cunningham et al (2010), as the Saturation, Inhibition, and Occupancy plots. The Saturation plot uses ΔVT as the X component, and VT(b) as the Y component, while the Occupancy plot uses ΔVT as the Y component, and VT(b) as the X component, yielding similar trend and regression accuracy parameter values. We determined the linearization with the best convergence to measured data of the fraction of receptors occupied (s) and the volume of distribution of non-displaceable radioligand (VND). **Methods:** We subjected 24 published reports of 98 sets of data to reanalysis. In six cases, the authors submitted data, and for the remaining 18 reports, we extracted the data from published graphs. We used two linear regressions, the Least Squares (LSM) and Deming methods to obtain parameter estimates by calculating s (fraction of receptors occupied) and VND. In LSM, the R2 value is the linearization accuracy. When the R2 value is closer to unity, the results are more accurate. In the Deming II method, Sigma X2 is the standard error. When the Sigma X2 value is closer to zero, the results are considered more accurate. As example, values of VT(b) and ΔVT were extracted from the report of Kågedal et al. 2013, and VT(i) values were calculated from the digitization. We obtained the parameter values from the Inhibition, Saturation, and Occupancy plot linearizations and the LSM and Deming method regressions. **Results:** The comparisons revealed that the mean value of R2 (for 86 samples) was closest to unity for the Inhibition plot, and the mean value of Sigma X2 in the Deming Method was closest to zero also for the Inhibition plot, as the most accurate of the three plots. **Conclusions:** Linearizations were derived from the equation of receptor availability. In comparison of 98 cases from the literature, the accuracy for each of the linear regressions was evaluated by Least Squares and Deming methods of regression. Due to the absent commingling of dependent and independent variable, the Inhibition plot emerged as the most accurate of the regressions.

P231

Delayed damage of cerebral tissue after hypoxic-ischemic encephalopathy in immature rats as observed in longitudinal hybrid MR/PET scanning with spontaneous ¹⁵O-oxygen inhalation

M. Oshima, M. Tsuji, J. Enmi, M. Yamazaki, H. Iida; National Cerebral & Cardiovascular Ctr - Res Inst, Suita City, Osaka, JAPAN.

Backgrounds: Hypoxic ischemic encephalopathy (HIE) is a common type of brain damage in infant, causing severe developmental and

cognitive delays, or motor impairments. The primary causes of HIE are hypoxemia and/or reduced oxygen supply, to which hypothermia is the only evidence-supported therapy for neonatals earlier than 6 hours of the birth. Other treatment techniques are currently under investigation, but variation of disease progression even in animal models makes systematic investigation difficult. This study was aimed at assessing sequential changes of disease status in an immature rat model of acute HIE. Particularly intention was to detect the longitudinal alterations using hybrid MR/PET system with spontaneous ¹⁵O₂/C¹⁵O₂/C¹⁵O inhalation procedures. **Methods:** Scans were carried out on 9 immature rats using PET (MicroPET Fucus120, Siemens) and MRI (Biospec 70/30, Bruker) at 0, 1, 2, 7 and 42 days after the ischemic hypoxic stress as presented previously (Oshima et al, Exp Neurol 2012). Series of PET scans were carried out during spontaneous inhalation of ¹⁵O-labeled gases, then followed by MRI scan for T2WI, FA, DTI images. Functional images of CBF, CMRO₂, OEF and CBV were calculated by the 3-step autoradiography using the left-ventricular input function. **Results:** At day 0 immediately after onset of HIE, CBF in the left hemisphere was reduced to 38.8 ± 22.2 % compared with the contralateral hemispheres, but CMRO₂ was normal, suggesting preserved cerebral tissue. CBF was restored on day 1. CMRO₂ became reduced to 29.9 ± 27.4 % at day 7, and the reduced area was further expanded after 2days. T2WI indicated high intensity at day 1 and turned to low density after day 2. FA showed no changes at the beginning, and then turned to low intensity after day 2. Defect volume in CBF, CMRO₂, T2WI and FA at day 42 agreed with the infarct volume estimated from histochemical analysis. **Conclusion:** Despite large variation of brain damage among animals, the present study demonstrated that the delayed damage of the cerebral tissue was present after acute HIE. Repeat MR/PET imaging for quantitatively assessing CBF, CMRO₂, OEF, and CBV, together with series of MR parametric images may be useful in evaluating/optimizing various new therapeutic approaches for HIE in immature rats.

P232

Transferring a brain imaging protocol from PET-only to PET/MR imaging: Implications for kinetic modeling

M. L. Lassen¹, J. Cal-Gonzalez¹, O. Langer¹, I. Rausch¹, O. Muzik², T. Beyer¹, M. Bauer¹; ¹Medical University of Vienna, Vienna, AUSTRIA, ²Wayne State University, Michigan, MI, UNITED STATES.

Objectives. In this study we investigate the feasibility of transferring a validated neuropharmacological imaging protocol from a PET-only to a fully-integrated PET/MR system. **Methods** Five subjects underwent dynamic PET-acquisitions using (R)-[¹¹C]verapamil to study P-glycoprotein transport activity at the blood-brain barrier. All subjects underwent a single-day, dual-injection dynamic imaging protocol in a (a) PET system (GE-Advance) and (b) a PET/MR system (Siemens Biograph mMR). All subjects had arterial blood-sampling for kinetic modelling in both imaging sequences. An additional low-dose CT was acquired on a PET/CT (Siemens Biograph TPTV) for all subjects for attenuation correction purposes. The PET-data was reconstructed in a dynamic set-up (1x15, 3x5, 3x10, 3x30, 2x150, 2x300 and 2x600 s) using the Transmission-based attenuation correction in (a) (aTX), and DIXON (bDi) and CT (bCT) in (b). All data were reconstructed using 2i28s followed by a subsequent post-filtering (6mm FWHM Gaussian). We report %-wise differences ((b-aTX)/aTX*100) for rate constants describing transport of (R)-[¹¹C]verapamil across the blood-brain barrier (K_1 and k_2) estimated with a 1-tissue-2-rate constant compartment model using PMOD for three regions of interest (whole-brain gray-matter (WBGm), insula and cerebellum). Average soft-tissue attenuation correction values were calculated for all attenuation correction maps in a 5cm³ VOL. **Results.** In WBGm, relative cross-subject differences in K_1 values were +15.0% (bDi:aTX) and +42.6% (bCT:aTX) and differences in k_2 values were +12.5% (bDi:aTX) and +19.1% (bCT:aTX). Relative differences for K_1 values

were +16.8% (bDi:aTX) and +42.3% (bCT:aTX) for cerebellum and +13.8% (bDi:aTX) and +34.9% (bCT:aTX) for the insula. Differences in k_2 values were -1.6%(bDi:aTX) and +9.5% (bCT:aTX) for cerebellum and -10.7% (bDi:aTX) and -3.3% (bCT:aTX) for insula. Average attenuation correction values were measured to be 0.087cm^{-1} (TX), 0.1cm^{-1} (DIXON) and 0.0983cm^{-1} (CT) **Conclusion.** Significant differences were observed between kinetic modelling outcome parameters obtained in a stand-alone PET and a PET/MRI system when using CT-based attenuation correction in the PET/MR. However, differences in outcome parameters between DIXON and transmission based reconstructions were acceptably small, thus, suggesting the possibility to transfer the scan-protocols.

P233

Individual Patient Contribution to Group-based Cerebral Blood Flow and Gray matter volume Co-variance Networks in Mild Cognitive Impairment

C. A. Sánchez-Catasús^{1,2}, A. Willemsen^{1,3}, R. Boellaard^{1,3}, L. Melie-García⁴, J. Samper-Noa⁵, A. Aguila-Ruiz⁶, P. De Deyn^{1,3}, R. Dierckx^{1,3}; ¹University Medical Center Groningen, Groningen, NETHERLANDS, ²University of Groningen, University of Groningen, NETHERLANDS, ³University of Groningen, Groningen, NETHERLANDS, ⁴Centre Hospitalier Universitaire Vaudois (CHUV), Lausanne, SWITZERLAND, ⁵Cuban Neuroscience Center, Havana, CUBA, ⁶Center for Neurological Restoration (CIREN), Havana, CUBA.

Graph theoretical analysis of co-variance networks derived from neuro-imaging data provides measurements of brain connectivity. However, due to the group-based nature of this methodology, it is not possible to assess the relationship between brain connectivity and patient characteristics and/or underlying pathophysiological conditions at the individual level. Although methods for extracting individual patient contribution have been recently reported, these have not yet been widely applied. **Aim:** We aimed to explore whether the individual contributions to cerebral blood flow (CBF) and gray matter volume (GMV) co-variance networks of patients with amnesic mild cognitive impairment (MCI) correlate to global cognitive function. **Materials and Method:** CBF SPECT, corrected for partial volume effect, and volumetric MRI (for GMV estimation) were obtained from 26 amnesic MCI patients (14 females; 64.7 ± 6.9 years; MMSE: 26.9 ± 1.24). Two group-based co-variance networks were constructed based on the AAL atlas (90 ROIs): one using CBF data and another one using GMV data. The individual contribution of each patient to each group-based network was operationalized as the change in the global correlation strength (CS) when the patient was excluded from the dataset (the “leave-one-out” approach). The global CS is the average of the regional CS (mean of Pearson’s correlation coefficients between a particular ROI and each ROI in the network). Global cognitive function was evaluated through to the Mini-Mental State Examination (MMSE) and the association between estimated individual contributions to each network and the MMSE score was calculated. The same analysis was performed for a subset of ROIs that correspond to the two subsystems (dorsal medial and medial temporal) of the default mode network (DMN) due to their relevance in MCI. **Results:** Individual contributions to the CBF co-variance network were the only ones that showed a significant and positive correlation with the MMSE score ($R=0.45$, $p=0.02$ for global CS; and $R=0.40$, $p=0.04$, for CS of the dorsal medial subsystem). The medial temporal subsystem showed no significant correlation in both co-variance networks. **Conclusions:** Our results suggest that MCI patients who have better cognitive performance contribute more to the global CS of the CBF co-variance network (i.e. more “connectivity” of the whole network). We have also documented this phenomenon for the dorsal medial subsystem of the DMN. Our results warrant further research into the potential utility of the individual patient contribution as a “network connectivity”-based biomarker in patients with MCI.

P234

Assessment of Training Efficacy in Scoring and Reporting 18F-Fluorbetaben PET Imaging

M. Scarlattei¹, G. Baldari¹, C. Cidda¹, S. Migliari¹, A. Sammartano¹, G. Serrelli², O. Ortenzia², C. Ghetti², L. Ruffini¹; ¹Nuclear Medicine Dept, University Hospital of Parma, Parma, ITALY, ²Medical Physics, University Hospital of Parma, Parma, ITALY.

Amyloid imaging by PET (Amy-PET) can assist in the early and accurate diagnosis of Alzheimer disease and other dementias. Training for accurate image interpretation is essential for clinical use. Current clinical method for interpretation of 18F-florbetaben (18F-FBB) beta-amyloid PET is visual assessment. Reader training is performed before starting clinical activity and required by Italian Medicines Agency (AIFA). Aim of this work was to test training efficacy, intra- and inter-readers’ agreement and compliance in assessing 18F-fluorbetaben PET. **METHODS** In-person reader training (n=2) and electronic training (n=1) were administered to the medical staff. Training modules were identical in approach and content focused on brain anatomy to identify normal white matter using MRI and coregistered PET images to detect white-gray matter boundaries. Positive scan demonstrates tracer uptake beyond cortical white matter to adjacent gray matter in reference regions. 18F-FBB PET scans were assessed visually by all readers, blinded each other, using a three-grade scoring system comparing regional cortical tracer uptake (RCTU) in gray matter (frontal, parietal and temporal cortex, posterior cingulate cortex/precuneus) with adjacent white matter. RCTU scores (1 no binding, 2 minor, 3 pronounced) are condensed into a single three-grade scoring system, BAPL score (1 no beta-amyloid load, 2 minor, 3 significant) and BAPLs condensed into a binary interpretation (score 1 negative; 2 or 3 positive). Intra- and inter-reader agreement were assessed by a re-evaluation session (30 random selected images) and Cohens’ kappa, compliance by a questionnaire. **RESULTS** 18F-FBB PET was performed in 83 patients, 82 classified equally by in-person trained readers: 47 B.P. 3, 9 B.P. 2 and 26 B.P. 1. The e-trained reader results were different: 44 B.P. 3, 11 B.P. 2, 28 B.P. 1. RCTUs were classified equally in frontal and parietal regions, different in the precuneus (8 pts) and in the temporal lobe (11 pts) in pts with severe atrophy. Different RCTUs did not change global assessment of amyloid plaque burden (BAPL). Reader’s compliance and confidence were evaluated optimal independently from training method. Inter- and intra-reader agreement were excellent ($k=0.98$) for in-person training group. **CONCLUSIONS** Results demonstrate good efficacy of the reader training; a supervision seems to be necessary for e-trained staff at starting. Inter- and intra-readers agreement was excellent for global scoring (BAPL) in the in-person trained group. More complex appears regional assessment suggesting the need of a quantitative method particularly necessary when it’s critical to establish relationship between anatomy, memory and extra-amnesic disorders and amyloid deposition.

P235

Computation strategy for CBV estimation from a single PET scan with sequential administration of ¹⁵O₂ and C¹⁵O₂

N. Kudomi¹, Y. Maeda², H. Yamamoto¹, Y. Yamamoto¹, T. Hatakeyama¹, Y. Nishiyama¹; ¹Faculty Of Medicine, Kagawa University, KAGAWA, JAPAN, ²Clinical Radiology, Kagawa University Hospital, KAGAWA, JAPAN.

Objectives: PET with ¹⁵O-labeled tracers is capable of providing unique and essential information in patients with cerebro-vascular disorders, and has been promoted as a clinical diagnostic tool. A novel DBFM method, allowing an extremely shortened examination period of <10 min, has been developed to assess parametric images of cerebral blood flow (CBF), oxygen extraction fraction (OEF) and metabolic rate of oxygen (CMRO₂), from a dynamic single PET scan in conjunction with

sequential administration of $^{15}\text{O}_2$ and H_2^{15}O [1]. The DBFM, however, misses information of cerebral blood volume (CBV) because of elimination of C^{15}O scan. This study was intended to develop a further improved computation strategy for estimating CBV image, from the single PET scan data. **Methods:** The computation formula applied involves differential term which allows for improving sensitivity to CBV estimation. The CBV image was computed with the developed formula after correction for blood appearance time [2]. Validity was tested on subjects with ($n=12$) and without ($n=12$) cerebro-vascular disorders. Regions of interest (ROIs) were placed on frontal, temporal, occipital cortical regions, white matter regions and sinus regions. Also, ROIs were placed on ischemic region for subjects with disorder. The CBV values were extracted from CBV image by the present method ($V_{B,\text{Dual}}$) and CO scan method ($V_{B,\text{CO}}$), and were compared between the methods. **Results:** The mean of CBV values in cortical region for subjects without disorder were 0.042 ± 0.030 and 0.039 ± 0.011 ml/g, for $V_{B,\text{Dual}}$ and $V_{B,\text{CO}}$, respectively. Those with disorder were 0.043 ± 0.027 and 0.039 ± 0.015 ml/g, respectively. Those for ischemic region were 0.035 ± 0.010 and 0.040 ± 0.025 ml/g, respectively. Differences between $V_{B,\text{Dual}}$ and $V_{B,\text{CO}}$ were not significant for all regions. Regression analysis showed tight correlations between $V_{B,\text{Dual}}$ and $V_{B,\text{CO}}$, namely, $r=0.92$ and $r=0.89$, for subjects with and without disorders, respectively. The obtained V_B images seemed to be similar between $V_{B,\text{Dual}}$ and $V_{B,\text{CO}}$, particularly CBV elevated regions due to ischemia were identical between the methods. **Conclusion:** The present method is of use for assessing CBV as well CBF, OEF and CMRO_2 rapidly in clinical settings. [1] Kudomi et al JCBFM (2013) 33; 440-448 [2] Kudomi et al EJNMMI Res (2013) 3; 41

P236

Comparison of delay of appearance time of blood in brain region with elevation of oxygen extraction fraction

N. Kudomi¹, Y. Maeda², H. Yamamoto¹, Y. Yamamoto¹, T. Hatakeyama¹, Y. Nishiyama¹; ¹Faculty Of Medicine, Kagawa University, KAGAWA, JAPAN, ²Clinical Radiology, Kagawa University Hospital, KAGAWA, JAPAN.

Objectives: PET with ^{15}O -labeled tracers is capable of providing unique and essential information in patients with cerebro-vascular disorders, and quantitative images of cerebral blood flow (CBF), oxygen extraction fraction (OEF), and metabolic rate of oxygen (CMRO_2) have been promoted as a clinical diagnostic tool. We have recently developed a novel DBFM method, allowing extremely short examination period <10 min for CBF and OEF [1], and also a computation method for appearance time of blood in arterial territories (ATB) [2]. SPECT, so far, can only provide CBF, but not OEF. This study was intended to compare elevation of OEF with delay of ATB from PET data and also that from SPECT CBF examination data. **Methods:** PET measurement was performed for patient subjects with suspected disorders, and the subjects were separated to two groups with OEF elevated (G1, $n=71$) and without that (G0, $n=221$). Two of subjects received SPECT $^{99\text{m}}\text{Tc}$ -ECD examination for each group. From the PET data, OEF and ATB images were obtained, and from the SPECT data, ATB images were obtained. Regions of interest (ROI) were placed on both hemispheres in temporal region in G0, and in G1, ROI was placed on OEF elevated region and its contralateral region. OEF values and ATBs were extracted from the placed ROIs. Differences of OEF (ΔOEF) and ATB (ΔATB) between hemispheres were calculated, and differences between ΔOEF and ΔATB were compared. **Results:** The obtained OEF values were 0.42 ± 0.04 and 0.42 ± 0.04 , and ATBs were 0.0 ± 1.9 s and 0.0 ± 2.0 s, for left and right hemispheres in G0, respectively. Differences were not significant between hemispheres. In G1, apparent delayed regions were seen in the ATB images similar to the OEF elevated regions, the OEF values were 0.43 ± 0.06 and 0.53 ± 0.08 , and ATBs were 0.1 ± 2.1 s and 2.2 ± 2.3 s, for contra- and ipsi-laterals, respectively. Differences were significant between hemispheres. Regression analysis

showed weak correlation: $r=0.16$, in G0 and moderate correlation: $r=0.39$, in G1 between ΔOEF and ΔATB . In ATB image from SPECT data, apparent delay was seen in the similar region of PET ATB image, and ATB was around 3 s in disease region. **Conclusion:** The present results suggest that ATB could provide similar information as OEF, and that the ATB can be also estimated from SPECT scan data. [1] Kudomi et al JCBFM (2013) 33; 440-448 [2] Kudomi et al EJNMMI Res (2013) 3; 41

P237

Semi-quantitative CBF parameters derived from ^{15}O]H₂O studies

T. Koopman¹, D. F. R. Heijtel², M. Yaqub¹, E. Bakker¹, A. J. Nederveen³, B. N. M. van Berckel¹, A. A. Lammertsma¹, R. Boellaard¹; ¹VU University Medical Center, Amsterdam, NETHERLANDS, ²Philips Healthcare, Best, NETHERLANDS, ³Academic Medical Center, Amsterdam, NETHERLANDS.

Aim: Quantification of cerebral blood flow (CBF) using ^{15}O]H₂O positron emission tomography (PET) requires the use of an arterial input function. Invasive arterial sampling, however, is not always possible, for example in ill-conditioned or paediatric patients. Therefore, it is of interest to explore the use of non-invasive (simplified) methods for the quantification of CBF. The purpose of this study was to investigate and compare the performance of several simplified quantification methods. **Methods:** Data from 16 healthy volunteers were included in this study. For each subject five dynamic ^{15}O]H₂O brain PET studies of 10 min duration and including arterial sampling were acquired. At baseline a test-retest study was performed followed by a study at hypercapnia (increased perfusion). After three to four weeks the same subject underwent two further studies, one at baseline and the other at hypercapnia. Hypercapnia was achieved by switching air delivery from normal medical air to a pre-mixed gas mixture of 5% CO₂ and 95% air. For each study absolute CBF within 67 cerebral volumes of interest were calculated using full kinetic analysis. In addition, various simplified methods, such as area under the curve (AUC) integrated over several time intervals, time-to-peak, peak height, wash-in and wash-out slopes, were used. Performance of these simplified methods was assessed using correlation and Bland-Altman analysis of simplified CBF parameters with fully quantitative CBF values. These analyses were repeated with normalization to cerebellar CBF, providing relative regional CBF (rCBF). **Results:** For relative rCBF, best overall (pooled over all scans and subjects) correlation between simplified and full quantitative CBF data was obtained for the 0-60 s AUC method ($R^2=0.89 \pm 0.01$). Corresponding correlations of time-to-peak, peak height, whole AUC, wash-in and wash-out slopes were $R^2=0.09 \pm 0.02$, $R^2=0.78 \pm 0.01$, $R^2=0.46 \pm 0.02$, $R^2=0.55 \pm 0.02$ and $R^2=0.09 \pm 0.02$, respectively. For absolute rCBF, the 0-60 s AUC method also showed good correlation per individual scan ($R^2=0.86 \pm 0.09$), but with variable regression slopes, i.e. with low reproducibility between scans and patients. **Conclusion:** Simplified quantification of relative rCBF is reasonable using the 0-60 s AUC method. Reliable absolute rCBF values could not be obtained with any of the simplified methods, due to the uncertainty and variability in the input functions. This variability was probably magnified by variance in the amount of injected activity.

P238

In vivo PET imaging of the cerebellar cholinergic innervation using ^{18}F -FEOBV: preliminary quantitative evaluation

J. Mazère^{1,2,3}, J. Debatisse^{2,3}, F. Lamare^{1,2,3}, D. Vimont^{2,3}, P. Fernandez^{1,2,3}, P. Burbaud^{4,5}, W. Mayo^{2,3}; ¹Service de médecine nucléaire, CHU de Bordeaux, F-33000, Bordeaux, FRANCE, ²Univ. Bordeaux, INCIA, UMR 5287, F-33000, Bordeaux, FRANCE, ³CNRS, INCIA, UMR 5287, F-33000, Bordeaux, FRANCE, ⁴Univ. Bordeaux,

Institute of Neurodegenerative Disorders, UMR 5293, F-33000, Bordeaux, FRANCE, ⁵CNRS, Institute of Neurodegenerative Disorders, UMR 5293, F-33000, Bordeaux, FRANCE.

INTRODUCTION The cerebellum plays a role in regulating the cognitive and emotional processes (1,2) and post-mortem, the cholinergic innervation of the human cerebellum was evidenced (3), highlighting the interest to explore *in vivo* cerebellar cholinergic innervation in various neurological disorders. ¹⁸F-fluoroethoxybenzovesamicol (¹⁸F-FEOBV) is a highly selective PET radioligand for a pre-synaptic cholinergic marker, the Vesicular Acetylcholine Transporter (VAcHT). However, quantification of ¹⁸F-FEOBV requires the use of the cerebellar hemispheres as a reference region (4), thus preventing any possible VAcHT quantification in this part of the cerebellum. We propose to validate a reference region based method allowing the quantification of ¹⁸F-FEOBV in the whole brain including several cerebellum sub-regions, by testing two reference regions: the visual cortex and the white matter of the posterior cingulate cortex (PCC-WM). **MATERIALS AND METHODS** Three healthy human volunteers underwent a dynamic brain PET imaging 0-80 and 130-150 min after injection of ¹⁸F-FEOBV and a magnetic resonance imaging (MRI) scan. Segmentation of MR images using Freesurfer® and SPM® softwares provided several extra-cerebellar and cerebellar regions of interest (ROI). PET data were partial-volume effect corrected and for each ROI, a complete pharmacokinetic analysis based on both Multilinear (MRTM2) and Simplified (SRTM2) Reference Tissue Models allowed to calculate the ¹⁸F-FEOBV nondisplaceable binding potential (BP_{ND}). **RESULTS** In the cerebellum sub-regions, only the PCC-WM provided standard error values of BP_{ND} (BP_{ND} % COV) lower than 10%, the highest BP_{ND} values being found in vermis and lobule X and the lowest in crus I-II. Goodness-of-fit R2 values greater than 0.90 were found in any sub-regions except the lobule X. In the rest of the brain, only the PCC-WM provided BP_{ND} % COV lower than 10 % in all ROIs and R2 values were greater than 0.90 in any ROIs except the amygdala for MRTM2. BP_{ND} values strongly correlated with those calculated using the cerebellar hemispheres as reference region. **DISCUSSION-CONCLUSION** The use of PCC-WM allows a reliable ¹⁸F-FEOBV quantification in the whole brain. The cerebellar distribution of ¹⁸F-FEOBV we find is consistent with previous histochemical results indicating the greatest cholinergic innervation in the vermis, lobule X, IX and VIII and the lowest in the remaining lobules (3). This ongoing study demonstrates that ¹⁸F-FEOBV is relevant for evaluating *in vivo* the involvement of cerebellar cholinergic deficit in cognition and emotion. **BIBLIOGRAPHY** 1. Habas et al., 2001 2. Schmahmann et al., 2010 3. De Lacalle et al., 1993 4. Petrou et al., 2014

P239

Can Spatially Inaccurate CT Based Attenuation Correction of EEG Electrodes Create Artificial Foci in Subtraction SPECT Images of Epilepsy Patients?

O. Sipilä, M. Pitkonen, A. Loimaala; HUS Medical Imaging Center, Clinical Physiology and Nuclear Medicine, University of Helsinki and Helsinki University Hospital, Helsinki, FINLAND.

Aim: Epilepsy patients may have EEG electrodes on the scalp during ictal and/or interictal SPECT/CT imaging. Impact of spatially mismatched attenuation correction (AC) CT data, with our currently used electrodes and their typical distribution, on the reconstructed SPECT image and thus on the subtraction analysis of the ictal and interictal images was studied. **Materials and Methods:** A Siemens Symbia T SPECT/CT-camera was utilized with the following parameters: LEHR collimators, imaging matrix 128x128, pixel size 3.3 mm, 60 frames over 180°, frame time 20 s, AC-CT with 35 mAs and 110 kV. In ictal imaging of three patients, 40-50

Ambu Neuroline 720 Ag/AgCl electrodes were present. Before interictal imaging, the electrodes were removed. In addition to the properly reconstructed ictal and interictal SPECT images, the following test images were reconstructed with Flash 3D, scatter correction, CT-AC, 4 iterations, 6 subsets, Gaussian filter 8.4 mm: 1) Interictal SPECT image, attenuation corrected with the coregistered ictal CT, simulating effects of adding attenuation correction in areas where no attenuation caused by the electrodes exists. 2) Ictal SPECT, attenuation corrected with the coregistered interictal CT, simulating the effects of missing attenuation correction in areas where the electrodes cause attenuation. 3) For one patient, the interictal SPECT was reconstructed with both the interictal and coregistered ictal AC-CT transferred 10 mm in x, y, or z direction or rotated 10 degrees to check the relative effects of wrong placement of the electrodes and head tissues. The SPECT images from these reconstructions were subtracted from the corresponding proper reconstructions for A) statistical analysis using the BioImage Suite Differential SPECT Tool (bioimagesuite.yale.edu) and B) detecting foci with SD of 1.0, 1.5 and 2.0 in the brain (in-house-developed module for Siemens SyngoMI). Results: Image reconstruction errors due to 1) falsely added electrode information in CT-AC and 2) to missing electrode attenuation information did not produce significant foci (p<0.05) in statistical analysis (A). Significant foci were detected in the brain with all SDs (B), but they usually had peculiar shapes and extended outside the brain, evident when reviewed with different SDs and slice directions. However, wrongly placed head tissues (3) caused significant foci (both A and B) totally inside the brain. Conclusion: Electrodes in spatially mismatched AC-CT data did not cause significant foci totally inside the brain in SPECT subtraction images. To recognize artificial foci, subtraction images should be carefully reviewed with different SDs and slice directions.

P240

Repeat assessment of total hemispheric glycolysis by FDG-PET/CT: Variability with reuse of baseline masks defined by dedicated software

E. A. Segtnan^{1,2}, S. B. Christlieb¹, P. Grupe¹, O. Gerke^{1,3}, P. F. Høiland-Carlsen^{1,4}; ¹Department of Nuclear Medicine, Odense University Hospital, Odense, DENMARK, ²University of Southern Denmark, Odense, DENMARK, ³Centre of Health Economics Research, University of Southern Denmark, Odense, DENMARK, ⁴Department of Clinical Research, Faculty of Health Sciences, University of Southern Denmark, Odense, DENMARK.

Aim: The dedicated PET processing software tool ROVER (ABX, Radeberg, Germany) targets problem of quantitative 3D ROI evaluation of PET scans including repeat studies. We wanted to investigate if automated reuse of baseline masks for processing of follow-up PET scans caused serious deviations in measured variables. **Material and methods:** Prospectively, cerebral FDG-PET/CT was performed in seven patients with glioblastoma, each of whom underwent two to five examinations during their treatment course resulting in a total of 21 FDG-PET/CT scans obtained before and after tumour resection, radio-chemotherapy, and chemotherapy alone. 3D-masks needed for measuring cerebral total hemispheric glycolysis (THG) and to circumscribe the entire cerebellum were defined at baseline, i.e., at the preoperative scan, and stored. These masks were automatically reused at all ensuing scans in the same patient to yield SUVmax, SUVmean, metabolic volume (ccm), THG, partial volume corrected SUVmean and THG, i.e., cSUVmean and cTHG, respectively. For validation of this automated procedure (A), each of the 21 PET studies was also segmented independently (I), meaning that the operator manually aligned the baseline mask to the follow-up PET scan, when this was processed. Mixed effects regression test was used to compare the two methods. Visual analysis was also performed for validation of the location of the interpolated masks. **Results:** The mean differences calculated from

all time points (with 95% CI) in absolute quantitative measures obtained by methods A and I were 0.01 (-0.10 to 0.13), 0.012 (-0.06 to 0.08), 0.03 (-0.12 to 0.2), 5.77 (-24.7 to 36.3), -0.19 (-4.2 to 3.8), and 12.25 (-30.2 to 54.7) for SUVmax, SUVmean, metabolic volume, THG, cSUVmean, and cTHG, respectively. No statistically significant differences between methods was observed ($p > 0.05$). We also compared reuse of baseline masks stratified to any specific treatment intervention, i.e., post-operation or post chemotherapy; no statistical significant difference was found either (p -value range 0.055–0.96). According to visual assessment, the automatically reused cerebral hemispheric and cerebellar 3D-masks delineated the respective target structures excellently on follow-up PET scans. **Conclusion:** The ROVER software furnishes reliable automated reuse of cerebral hemispheric and cerebellar baseline mask for processing of follow-up FDG-PET scans. The large size of the masks and the anatomically relatively fixed shape of the target structures could be an explanation of these good results, which indicate that the automated reuse of cerebral hemispheric and cerebellar masks provided the ROVER software is applicable for routine clinical use.

P241

Errors in data recording in cerebral FDG-PET/CT scans: Consequences for quantitative outcome when measuring whole brain glycolysis

E. A. Segtnan^{1,2}, S. B. Christlieb¹, O. Gerke^{1,3}, P. F. Høilund-Carlsen^{1,4},
¹Odense University Hospital, Odense, DENMARK, ²University of Southern Denmark, Odense, DENMARK, ³Centre of Health Economics Research, University of Southern Denmark, Odense, DENMARK, ⁴Department of Clinical Research, Faculty of Health Sciences, University of Southern Denmark, Odense, AUSTRIA.

Aim: We analysed data recordings used in PET/CT research protocols to examine consequences of errors for calculation of whole brain glycolysis (WBG) derived from FDG-PET/CT scans in glioma patients. **Material and methods:** Prospectively, 14 glioma patients, aged 35–77 years, were enrolled in a research protocol with FDG-PET/CT performed before any treatment intervention. Dedicated software (ROVER, ABX, Radeberg, Germany) was used for delineation of the whole brain, excluding the cerebellum. WBG was calculated as the product of the segmented volume (cm^3) of cerebral FDG uptake and the partial volume corrected SUVmean (cSUVmean). Firstly, segmentation was applied on PET scans in the DICOM format. Secondly, information stored in the DICOM format, i.e. tracer dose, injection time and time of scan, was compared with the hand written reports for each scan. If information deviated between the hand written report and the DICOM file, the hand written report was used as reference, and thus, information was corrected in the DICOM file. Values of quantitated WBG obtained before and after correction were compared. **Results:** Overall, the mean WBG was 5942 and 6208 before and after correction. By comparing each patient's values head to head, the two largest deviations were 2379 (30%) and 3604 (41%) in WBG due to injection time being typed 60 and 45 minutes incorrectly in the DICOM file, respectively. Two other patients had large deviations in WBG, i.e., -771 (-17%) and -667 (-18%), respectively, due to incorrectly typed injection dose, -19 and -6 Mbq, respectively. The other 10 patients, after correction of information from the handwritten reports, had deviations in WBG below 10% (-8% to -2%). This was either because the injection time had been incorrectly (maximum 11 minutes) entered, and/or because the injection dose had been incorrectly (-18 to -5 MBq) entered. **Conclusion:** This example, in a small sample, elucidates how typing errors may result in huge and minor deviations in calculated quantitative outcome, in this case WBG. Thus, the challenge of transferring information correctly from paper to digital format should not be neglected and should be taken into account for single and repeat studies and comparison of data obtained at different institutions.

P242

Impact of reconstruction algorithms and CT-based attenuation correction in I-123-Ioflupane SPECT

E. Richetta¹, M. Balma², A. Guida¹, A. Codegone¹, M. Manfredi², C. Cutaia¹, S. Valzano¹, L. Radici¹, R. Pellerito¹, M. Stasi¹,
¹AO Ordine Mauriziano, Turin, ITALY, ²Città della Salute e della Scienza, Turin, ITALY.

AIM Dopamine transporter scintigraphy with ¹²³I FP-CIT is an established part in the diagnosis of parkinsonism. The consistency between qualitative and semi-quantitative analysis are still under debate. In this study SPECT images were analyzed in order to evaluate the variability among different attenuation correction techniques and reconstruction algorithms, as well as intra-operator dependence. **MATERIALS AND METHODS** Integrated SPECT-TC acquisitions (Siemens SymbiaIntevo, 128x128, 120 views, 40s/view; 130 kV,3mm) were performed on 16 patients (8M,8F) with suspected Parkinson's disease after the administration of ¹²³I-iodoflupane. Images were reconstructed both with FBP algorithm without any attenuation correction (FBP_NOAC) and Iterative algorithm (Flash3D, #8iterations, #8subset) with CT low-dose attenuation correction map (IT_AC) or with uniform Chang's matrix (IT_Chang). Two experienced physicians, unaware of the reconstruction-attenuation correction methods, inspected qualitatively the images and assigned a negative, positive or doubtful score. Percentage differences between physicians as well as among methods were calculated. To investigate the possibility to distinguish positive to negative patients in a semi-quantitative way, specific-to-background ratios in caudate and putamen were calculated by drawing volume of interest in these areas. The diagnostic power was tested using ROC analysis. AUC results were compared (Hanley and McNeil z-values) in order to find statistical significant discrepancies and to individuate the best images processing method. **RESULTS** In the qualitative analysis the first physician gave an assessment other than the second one in 3/16 (19 %) images reconstructed with FBP_Chang ; these value increased to 4/ 16 (25%) for FBP_NOAC method and up to 6/16 (38%) for IT_AC method. Also comparing images within the same observer differences were found. For the first physician FBP_Chang and FBP_NOAC showed discrepancies in 1/16 (6,3%) patient and 3/16 (19%) for IT_AC; for the second assessor IT_Chang variability was the same (1/16) and becomes greater in patients comparisons with FBP_NOAC 3/16 (19%) and IT_AC 4/16 (25%) methods. Similar AUC values were found among the three methods both for caudate and putamen with a slightly higher value for IT_Chang method (caudate right 0.714 and left 0.746, putamen right 0.937 and left 0.999). When AUCs were compared z-values always lower than 1.96 confirmed that low-dose CT attenuation correction method hasn't significantly improved the diagnostic power. **CONCLUSION** The impact of CT-based attenuation correction compared to other methods (Chang or FBP_NOAC) on the interpretation of ¹²³I-iodoflupane SPECT images is negligible. Therefore CT-based AC cannot be recommended for routine use in clinical patient care, not least because of the additional radiation exposure.

P243

Unsupervised quantitative assessment of Beta amyloid images using Florbetaben(18F)

E. Giovannini¹, M. Riondato¹, R. Leoncini¹, C. Passera², E. Carabelli¹, O. Ferrando¹, A. Tartaglione², A. Mannironi¹, A. Ciarmiello¹,
¹S. Andrea Hospital, La Spezia, ITALY, ²Memory Laboratory CNS-ONLUS, La Spezia, ITALY.

Background Amyloid PET imaging is used to detect brain amyloid accumulation which is considered a key event in the onset of Alzheimer's disease. There are no standard methods for unsupervised assessment of tracer binding. Brain segmentation procedures are limited by poor signal differences between gray (GM) and white matter (WM). This work is

aimed to propose an automated method for brain tissues segmentation and unsupervised quantification of brain amyloid binding. **Methods** Subjects were recruited within a prospective study (EudraCT number: 2015-001184-39) at Neurology Unit of S.Andrea Hospital and Memory Laboratory CNS-ONLUS of La Spezia. Subjects underwent a neuropsychological battery for assessing different cognitive domains, executive functions and attentional systems. So far a population of 11 patients was enrolled in the study (Age 74±10; MMSE, 25±6). PET images were acquired in 3D mode 90 to 110 minutes after intravenous injection of 300 MBq of Florbetaben (¹⁸F) (NeuraceqTM) on a DISCOVERY TM 710 PET/CT scanner (GE Medical Systems, Milwaukee, WI). PET scans were converted to standardized uptake values (SUV) and normalized into MNI space using SPM8 T1 template (<http://www.fil.ion.ucl.ac.uk/spm/software/SPM8>). Image analysis procedure was implemented under Matlab 7.14 (MathWorks Inc., Sherborn, MA). PET images were evaluated by two trained independent readers who were blinded to the clinical results. Whole brain analysis resulted in a scores condensed into a binary interpretation of 0,1 for negative and positive scan respectively. Amyloid PET images were segmented by using hybrid segmentation technique incorporating apriori brain tissues probability distribution and gradient-based approach. GM and WM segmented tissues were used for extracting regional mean SUV values. Data extracted from each patient were grouped according to visual rating results. One-Way analysis was used to test group differences. The linear dependence of SUVs values on MMSE and age was determined by a simple regression. A significance level of $p < 0.05$ was chosen. Results Visual rating of PET images led to the diagnosis of 6 positive and 5 negative subjects. WM-to-GM ratio was 1.1 ± 0.09 and 1.3 ± 0.03 in positive and negative patients respectively (Anova, $F=7.1$, $P=0.025$). We found a significant correlation between GM-SUVs and MMSE ($R=0.52$; $P=0.01$) in contrast WM-SUVs did not show significant correlation on MMSE. We found positive correlation between WM-to-GM SUVs ratio with MMSE ($R=0.73$, $P=0.0008$), whereas no correlation of GM and WM-SUVs on age was found. Conclusion Our findings suggest that unsupervised quantitative assessment of PET amyloid binding may be useful to improve diagnosis and predict disease progression in Alzheimer's disease.

P244

Biodistribution Analysis of a Labeled Exogenous Protein Following Intranasal Delivery in Cynomolgus Macaques Using PET/CT Imaging and Autoradiography

C. M. Finucane¹, D. Kentala², A. W. Novicki¹, M. Qutaish¹, H. Dobson¹, H. Huttunen³; ¹inviCRO, Boston, MA, UNITED STATES, ²MPI Research, Mattawan, MI, UNITED STATES, ³Herantis Pharma PLC, Helsinki, FINLAND.

The aim of this study was to assess the kinetics and biodistribution of a ¹²⁴I-labeled exogenous protein in the brain of Cynomolgus monkeys after intranasal administration using a commercial nasal administration device. The success of intranasal administration into the brain is important due to the potential neuroprotective and neuroregenerative effects of this compound for use as a potential therapy administration procedure. Following radiochemistry development to radiolabel the protein at the required specific activity and mass dose, four female Cynomolgus monkeys received an intranasal administration of 0.5 mCi ¹²⁴I-protein (400 µg) in 2 actuations per nostril (200 µl total volume). Immediately after administration a focused brain scan was acquired for 3.75 hours, followed by a whole body PET scan and a whole body CT for anatomical registration. The focused PET scan was binned into 45 x 5 minute frames. Focused and whole body scans were also acquired at 24 hours post-administration. The administration technique was improved on advice from the commercial device manufacturer to improve the delivery of the dose to the upper nasal epithelium upon review of the initial results. Changes were made to the time between administration, the angle of administration and the position of the device in the nostril. In addition, autoradiography was performed

on the brain of one monkey following the 4 hour time point. A Cynomolgus brain atlas was registered to the data to quantify uptake brain regions and regions of interest (ROIs) were drawn in the upper nasal cavity, throat and thyroid. Quantitative ¹²⁴I autoradiography was performed on sagittal sections of the brain encompassing the area between both eyes. The qualitative analysis of the PET images revealed that any visible brain uptake was below the detectable range of the PET/CT system. A quantitative comparison showed signal in the brain (approximately 4% injected dose) of which over 90% was cleared by 24 hours. It is possible that high signal in the nasal cavity may also have affected the accuracy of PET quantitation. Autoradiography was performed to confirm the uptake in the brain and clearly showed signal in the lateral ventricles, indicating transport of the ¹²⁴I-protein across the cribriform plate into the CSF. *In vivo* imaging is a useful technique to evaluate the success of an intranasal administration and provides important information on tracer kinetics and biodistribution. Autoradiography is a valuable complementary assay to confirm that the brain signal detected by quantitative analysis is real.

P-21 – Tuesday, October 18, 2016, 16:00 - 16:30, Poster Exhibition Hall
Neurosciences: Dementia

P245

18F-Florbetaben SUVR cutoff quantification across reference regions and standards of truth and comparison to visual assessment

S. Bullich¹, A. M. Catafau¹, J. Seibyl², H. Barthel³, O. Sabri³, S. De Santi⁴; ¹Piramal Imaging GmbH, Berlin, GERMANY, ²Molecular Neuroimaging, New Haven, CT, UNITED STATES, ³Department of Nuclear Medicine, University of Leipzig, Leipzig, GERMANY, ⁴Piramal Pharma Inc, Boston, MA, UNITED STATES.

Background: Thresholds of 18F-florbetaben (FBB) standardized uptake value ratios (SUVRs) to categorize scans as positive or negative between 1.39 (Barthel et al., Lancet Neurol 2011;10:424-35) and 1.48 (Sabri et al., Alzheimers Dement. 2015;11(8):964-74) have been reported using cerebellar grey matter (GCER) as the reference region (RR). The aims of this study were 1) to generate 18F-Florbetaben (FBB) SUVR cutoff values for different reference regions (RRs) using blinded visual assessment (VA) as standard of truth (SoT); 2) to validate them in a different clinical population and SoTs and 3) to compare VA and SUVR cutoffs. **Methods:** For aim 1, SUVR cutoff was generated using FBB scans from 143 subjects (69.5 ± 7.5 yrs; $n=75$ Alzheimer's disease (AD), $n=68$ healthy volunteers (HVs)) who were visually assessed by 3 readers. SUVR was calculated using cerebellar gray matter (GCER), whole cerebellum (WCER), pons (PONS), and subcortical white matter (SWM) as RRs. A SUVR cutoff value for each RR was generated using Receiver Operating Characteristic analysis, VA as the SoT, and highest Youden's index as the selection criteria. For aim 2, SUVR cutoffs were validated in 78 end-of life subjects (80.1 ± 10.4 yrs) using VA from 8 readers and histopathological confirmation of the presence of neuritic beta-amyloid plaques as SoT. For aim 3, FBB scans from 78 subjects were visually assessed by 8 readers. The number of correctly or incorrectly classified scans according to pathology results using VA and SUVR cutoffs for each RR was compared. **Results:** Aim 1: Composite SUVR cutoffs were 1.43 (GCER); 0.96 (WCER); 0.78 (PONS); 0.71 (SWM). Aim2: Accuracy values were high and consistent across SUVR cutoffs and VA methods and SoTs (range 83-94% for histopathology, and 86-94% for VA). Aim 3: A range of 63-71 cases were correctly classified by both SUVR cutoff (across RRs) and VA, while 1-3 cases (across RRs) were incorrectly classified by both SUVR cutoff and VA. SUVR cutoff method misclassified more cases (range: 3-10 cases) than VA (range: 1-3 cases) for any RR. **Conclusion:** VA and SUVR cutoff quantification perform similarly in classifying FBB scans. These results indicate that VA is a robust method for the correct classification of FBB scans. However, the

use of SUVR cutoff did not improve VA classification of FBB scans independently of the RR used in this end-of-life population.

P246

Initial feedback on hybrid brain PET-FDG/MR imaging in the clinical evaluation of cognitive disorders

M. O. Habert¹, A. Bertrand², G. Bera¹, B. Law-Ye², N. Yeni¹, P. David¹, D. Dormont², A. De Villanueva², A. Kas¹; ¹Hopital Pitié Salpêtrière, Nuclear Medicine, PARIS, FRANCE, ²Hopital Pitié Salpêtrière, Neuroradiology, PARIS, FRANCE.

Introduction - Hybrid PET/MRI allows for accurately combining PET molecular information with a large variety of MRI sequences. The acquisition of both modalities in a single session minimizes the disagreements for the patient while maximizing collected information thanks to the spatial and temporal fusion of both modalities. Our objective was to evaluate the feasibility and, through pictorial examples, the potential interest of PET/MRI in the routine evaluation of patients with cognitive disorders. **Patients and methods**: - 274 patients underwent a PET-FDG/MRI for the evaluation of a cognitive impairment from October 2015 to March 2016. Patients were referred for suspicion of Alzheimer's disease (AD, n=107), fronto-temporal degeneration (FTD, n=38), primary progressive aphasia (n=34), Lewy body disease (n=27), mild cognitive impairment (n=48), posterior cortical atrophy (PCA, n=6), vascular dementia (n=4), or other rare diagnoses (n=10). Images were performed with the PET/MR SIGNA 3T (GE Healthcare). A dose of 2 MBq/kg was administered 30 minutes before the acquisition. The protocol included simultaneous PET list-mode acquisition and MRI sequences (3DFLAIR, 3DSWAN, 3DT1 and axial diffusion) for a 25 minutes duration. PET images were reconstructed with the Vue Point FX algorithm (8 iterations, 28 subsets) including spatial resolution and time of flight corrections. Attenuation correction was based on a MR Dixon-based sequence and a pseudo CT atlas-based method. Both a nuclear medicine physician and a neuroradiologist were present for interpretation, with a joint conclusion. **Results**: - PET and MR images were of good quality. Although not entirely accurate, attenuation correction did not yield artefacts hindering visual assessment. In early onset AD and its clinical variants such as logopenic aphasia or posterior cortical atrophy, PET usually showed a marked hypometabolism while MRI was normal or showed a moderate non specific atrophy. In more focal pathologies, such as FTD or semantic dementia, MRI and PET abnormalities were usually associated. Vascular lesions (leucopathy, microbleeds, ischemic lesions) were easily detected on 3D FLAIR and magnetic susceptibility sequences. In such cases, PET images often showed evidence of an associated neurodegenerative component, or even the remote impact of a subcortical lesion (deafferentation). **Conclusion**: - Our results highlight the clinical feasibility and the performance of hybrid PET/MRI in the clinical evaluation of dementia. The fusion of high-resolution PET images with morphological images improved the confidence in PET assessment. The simultaneous interpretation by two specialists provided to the clinicians an optimized diagnosis, particularly in complex cases.

P247

Dementia with Lewy body and Alzheimer's disease: a continuum? First results of a striatal [18F]Fluorodopa Positron Emission Tomography pilot study

A. Pallardy¹, P. Olivier¹, T. Carlier¹, T. Lebouvier², S. Le Dily¹, H. Courtemanche¹, F. Kraeber-Bodéré¹, C. Boutoleau-Brettonnière¹; ¹Nantes University Hospital, Nantes, FRANCE, ²Lille University Hospital, Lille, FRANCE.

Aim : Dementia with Lewy bodies (DLB) is the second neurodegenerative dementia in autopsy series. Concomitance of Lewy pathology with

AD pathology is the main cause of the poor sensitivity of DLB diagnosis. Current diagnostic criteria for MCL do not reflect the clinical and pathological overlap between MCL and Alzheimer disease (AD). DLB syndrome is indeed at the end of a pathological spectrum spanning from AD with occasional Lewy pathology to 'pure' DLB. The improvement of diagnostic tools is a challenge. We presented the initial results of a clinical study ongoing at Nantes (France), assessing the correlation between the amount and intensity of DLB features evaluated by a clinical score in validation in Nantes, and dopaminergic nigrostriatal function. **Materials and methods** : A clinical score (Lewy pathology Screening in COgnitive Disorders LESCOD) was constructed from a selection of 36 putative clinical features of Lewy pathology divided into 9 categories (genitourinary dysfunction, orthostatic hypotension, olfactory dysfunction, REM sleep behavior disorder, Parkinsonism, fluctuations, visiospatial/attention deficits and illusions/hallucinations). Patients with possible or probable AD, possible or probable DLB or considered as coexisting mixed AD - DLB pathology were included in the study and underwent (1) a LESCOD score assessment and (2) a [18F]fluorodopa Positron Emission Tomography (PET). Cerebral [18F]fluorodopa PET consisted of one single 'static' 20-min PET acquisition starting 70 to 90 min after injection. Patients received 2 MBq/Kg of body weight [18F]fluorodopa. Antiparkinsonian medication, haloperidol and reserpine were discontinued. PET data were assessed by volume-of-interest (VOI) analysis using the software PMOD - Dopasoft (IBA®). Caudate and putamen striatal to occipital ratio of [18F]fluorodopa were measured. **Results** : Of the first 10 patients included, one presented with probable AD, 5 with possible or probable DLB, and 4 were considered as mixed AD-DLB. There was a correlation between the number of pathological categories (LESCOD dissemination score) and [18F]fluorodopa uptake values in the putamen ($r=-0.88$, $p < 0.01$) and in the caudate ($r=-0.81$, $p < 0.05$). There was a correlation too between the sum of pathological clinical features (LESCOD severity score) and [18F]fluorodopa uptake values in the putamen ($r=-0.83$, $p < 0.01$) and in caudate ($r=-0.81$, $p < 0.01$). No significant correlation was observed between MMSE and dopaminergic binding. **Conclusion** : These initial results pave the way to new perspectives on the assessment of Lewy pathology burden in the AD - DLB spectrum through [18F]fluorodopa PET quantification of nigrostriatal dysfunction.

P248

Differentiation of dementia with Lewy bodies and Alzheimer disease using standardized I-123 metaiodobenzylguanidine heart-to-mediastinum ratio based on Japanese multicenter study

K. Nakajima¹, J. Komatsu¹, M. Yoshita², M. Samuraki³, K. Okuda⁴, S. Kinuya¹, M. Yamada¹; ¹Kanazawa University Hospital, Kanazawa, JAPAN, ²National Hospital Organization Hokuriku National Hospital, Nanto, JAPAN, ³Hirata Chuo Hospital, Hirata, JAPAN, ⁴Kanazawa Medical University, Uchinada, JAPAN.

Purpose: I-123 metaiodobenzylguanidine (MIBG) has been used for differentiating dementia with Lewy bodies (DLB). While heart-to-mediastinum ratio (HMR) has been used for quantification of myocardial MIBG uptake, camera-collimator difference has hampered creating common databases in multicenter study. The aim of this study was to investigate diagnostic ability of MIBG for differentiating DLB from Alzheimer disease (AD) using standardized HMRs. **Methods**: A total of 133 patients (male/female = 59/74, age 76 ± 6 years) were registered in Japanese multicenter study involving ten hospitals. The definitive diagnosis was made as probable DLB (n = 61), possible DLB (n = 26) and probable AD (n = 46) at the end of 1-year follow-up, and reevaluated in a subset of patients with complete 3-year follow-up (n = 65). After administration of I-123 MIBG (111 MBq), myocardial MIBG uptake was quantified using HMR in the core center. Four types of collimators were used in this study including low-energy (LE) high-resolution, LE general-purpose, extended-LE general purpose and low-medium-energy collimators. All

HMRs were calibrated using phantom experiments and converted to medium-energy (ME) collimator-comparable values (stdHMR) (conversion coefficient of 0.88). Probable DLB and probable AD patients were compared excluding patients with possible DLB. Results: Using the 3-year data, late HMRs for LE and ME collimator groups were 2.2 ± 0.2 and 3.1 ± 0.6, respectively ($p < 0.0001$) in AD patients. However, late stdHMR became 3.0 ± 0.4 and 3.2 ± 0.6 for LE and ME groups, respectively ($p = ns$), and the collimator difference disappeared. In DLB patients, no significant difference was observed before and after standardization (stdHMR = 1.8 ± 0.7 and 1.7 ± 0.7 for LE and ME groups). When stdHMR was compared in the 1-year data, late HMR was 2.9 ± 0.7 and 1.9 ± 0.8 ($p < 0.0001$, F ratio = 46) for AD and DLB patients, whereas it was 3.1 ± 0.6 and 1.7 ± 0.7 ($p < 0.0001$, F ratio = 75), respectively for the 3-year data. Diagnostic accuracy of late stdHMR using the 3-year data, demonstrated receiver operating characteristic curve-area under the curve of 0.92: sensitivity 77% and specificity 97% using a threshold of stdHMR = 2.2. Conclusion: DLB could be differentiated from AD using I-123 MIBG HMR. Standardization of HMR eliminates differences in camera-collimator systems and might be used effectively in multicenter comparison.

P249

Higher metabolism in the mesial temporal lobe is associated with poorer performance in verbal semantic fluency in patients with cognitive impairment

I. Apostolova¹, C. Lange², A. Maurer³, P. Suppa⁴, L. Spies⁴, E. Steinhagen-Thiessen², R. Buchert²; ¹University Hospital Magdeburg, Magdeburg, GERMANY, ²Charite - Universitatsmedizin Berlin, Berlin, GERMANY, ³Evangelisches Geriatriezentrum Berlin, Berlin, GERMANY, ⁴jung diagnostics GmbH, Hamburg, Hamburg, GERMANY.

Background: Alzheimer's disease (AD) is associated with disruption of functional connectivity between the mesial temporal lobe (MTL) and cortical brain regions which results in increased intra-MTL connectivity and increased MTL metabolism. The present study tested MTL metabolism as measured by FDG PET for correlation with neuropsychological performance scores in cognitively impaired geriatric inpatients and in ADNI MCI subjects. Methods: The sample of geriatric inpatients included 80 subjects (82.0 ± 5.4 y, 54 females) with mild cognitive impairment or mild dementia hospitalized in a geriatrics unit for an acute indication. FDG PET and MRI of the brain as well as detailed neuropsychological testing had been performed as part of a prospective study. The etiological diagnoses included non-neurodegenerative etiology ($n = 15$), AD ($n = 17$), cerebrovascular disease (CVD, $n = 23$) and mixed disease (MD, defined as concurrence of AD and CVD, $n = 25$). Unilateral FDG uptake ratios (SUVR) in the MTL were derived by region of interest (ROI) analysis using predefined standard ROIs for left and right MTL and with the pons as reference. Atrophy and partial volume effects were taken into account by correcting for hippocampus volume estimated from the individual MRI. The maximum of the corrected MTL-SUVR over both hemispheres was tested for associations with subscores of the CERADplus battery (z-scores corrected for age, gender and education). The Spearman test and multivariate linear regression were used for this purpose. The same analyses were performed in a sample of 634 ADNI MCI subjects. Results: There was a significant negative correlation between MTL-SUVR and several CERADplus subtests, most pronounced for the animals subtest ($\rho = -0.389$, $p < 0.0005$ uncorrected for multiple comparisons). Pons-scaled FDG uptake in an AD-signature meta-ROI (comprising posterior cingulate / precuneus and parietotemporal cortex; AD-SUVR) showed a positive correlation with the CERADplus animals z-score ($\rho = 0.341$, $p = 0.001$). Stepwise linear regression of the CERADplus animals score

with MMSE z-score, AD-SUVR and MTL-SUVR included all 3 parameters in the final model ($\beta = 0.346, 0.254, -0.336$; $p = 0.001, 0.013, 0.001$). This was confirmed in the ADNI cohort ($\beta = 0.181, 0.146, -0.135$; $p = 0.000, 0.001, 0.002$). Conclusion: In cognitively impaired patients, higher mesial temporal glucose metabolism is associated with poorer verbal semantic fluency performance, independent of overall cognitive performance and glucose metabolism in AD-characteristic brain regions.

P250

Automated FDG-PET data analysis for AD diagnosis in the prodromal phase: a comparison between statistical mapping software tools

S. TROMBELLA¹, L. ANTELMINI², H. LIM¹, P. BOSCO³, A. REDOLFI⁴, C. TABOURET-VIAUD⁵, O. RAGER⁶, G. GOLD⁷, P. GIANNAKOPOULOS⁷, EADC-PET Consortium, O. RATIB⁷, G. B. FRISONI⁷, V. GARIBOTTO⁷; ¹University of Geneva, Geneva, SWITZERLAND, ²IRCCS Istituto Neurologico C.Besta, Milano, ITALY, ³IRCCS Fatebenefratelli, BRESCIA, ITALY, ⁴IRCCS Fatebenefratelli, Brescia, ITALY, ⁵University Hospitals of Geneva, Geneva, SWITZERLAND, ⁶Institut IMGE (Imagerie Moleculaire de Geneve), Geneva, SWITZERLAND, ⁷University and University Hospitals of Geneva, Geneva, SWITZERLAND.

Aim: Aims of this study are to evaluate: 1) Extent and severity of the regional hypometabolism detected in single subjects by two software tools used in their standard settings: GridSPM and Hermes BRASS; 2) The diagnostic properties of metabolic deficit detection when software-assisted by the two programs. **Methods:** We included in the study 41 healthy controls and 101 MCI patients (followed-up until conversion to dementia or for at least 36 months) from the EADC PET Dataset. We investigated the accuracy of software-assisted diagnosis (by three independent expert readers) versus the clinical diagnosis at follow-up. 1) SPMgrid is the implementation of SPM8 into neuGRID. With SPMgrid, the FDG-PET scans are voxel-wise analyzed for hypometabolism, by testing the single scan versus a control group of 106 healthy subjects from the EADC PET Dataset (only subjects not belonging to the software control group were included). Results are provided by means of an unthresholded statistical 3D Students' T-map of the brain in the ICBM152 atlas space. 2) With BRASS, abnormalities are quantified voxel-wise against a database of 30 normal subjects on a voxel-by-voxel basis. Results are provided by means of an unthresholded statistical 3D Gaussian Z-map of the brain. 3) Mean z-values and t-values were computed for every anatomical VOI defined in the AAL Atlas. Each VOI mean value from BRASS was plotted against the corresponding value from SPMgrid, and a Pearson's R correlation coefficient computed as a measure of agreement. A histogram of frequencies for all R coefficients was produced. 4) Inter-reader agreement among readers was evaluated when supported by each of the two software tools using Fleiss' kappa test; 5) Statistical values of the two software tools were evaluated for the majority rating obtained across the three readers. **Results:** An excellent regional correlation between the two software tools was found when studying mean statistical map values over defined VOIs ($R = 0.73 \pm 0.16$). Higher inter-rater agreement was observed for GridSPM ($k = 0.48$) than for BRASS ($k = 0.36$). The two tools showed nearly equivalent AUC (GridSPM: 0.72, BRASS 0.67), however, BRASS revealed higher sensitivity (0.82 vs 0.58) and SPMGrid higher specificity (0.87 vs 0.52). **Conclusions:** The results of this study: (i) Confirm the validity of automated-assisted metabolic deficit detection in MCI, (ii) Show similar accuracy but differences in inter-rater agreement and diagnostic performance between tools, (iii) Represent the basis to develop guidelines on the use of these tools in the diagnostic workup of MCI patients.

P251**First Experience of 100 Clinical F-18 Florbetapir (Amyvid) PET/CT Scans in the Investigation of Cognitive Impairment: Imaging Characteristics, Inter-observer Agreement, Confidence of Read and Clinical Outcomes**

S. R. Khan, N. H. Patel, K. L. Wallitt, N. D. Soneji, D. Fakhry-Darian, C. J. Carswell, P. A. Malhotra, R. Perry, K. S. Nijran, S. Khan, W. Svensson, T. D. Barwick, Z. Win; Imperial College NHS Healthcare Trust, London, UNITED KINGDOM.

Aim: Amyvid brain PET/CT is a powerful new tool in the investigation of suspected Alzheimer's disease in vivo. As one of the 1st global institutions to perform in excess of 100 clinical Amyvid PET/CT examinations, we aim to assess the imaging characteristics of positive or negative scans, inter-observer agreement, reader confidence and clinical outcomes. **Materials and Methods:** 70 (100 examinations to be reviewed prior to presentation) F-18 florbetapir PET/CT examinations were subtyped into positive or negative type A (typical features) or non-type A (atypical features) scans. The examinations were anonymised, randomised and independently reviewed by 3 experienced PET radiologists, blinded to the subtype of scan. The radiologists were asked to perform a binary read, stating a confidence level of 1-5 (1- not confident, 3- moderate confidence, 5- very confident) and the results compared to the final report. Clinical follow-up at the Imperial Cognitive Clinic and subsequent management was documented. **Results:** 46% of scans were reported positive and 54% negative in the final consensus clinical report. Overall, there was good/excellent inter-reader concordance between the 3 readers [$k = 0.84$ (reader 1 & 2), $k = 0.77$ (reader 1 & 3), $k = 0.74$ (reader 2 & 3)], and to the final report [$k = 0.80$ (reader 1), $k = 0.71$ (reader 2), $k = 0.97$ (reader 3)]. Inter-observer agreement improved when analysing type A scans alone [$k = 0.91$ (reader 1 & 2), $k = 0.94$ (reader 1 & 3), $k = 0.92$ (reader 2 & 3)]. Overall, 87% of cases were interpreted with high confidence (4-5), of which 70% were type A and 17% non-type A scans. The percentage of cases interpreted with high confidence increased when reading type A scans (90%) compared to non-type A scans (75%). 25% non-type A scans were interpreted with low confidence (1-3), compared to 9% of type A scans. F-18 florbetapir PET/CT confirmed clinical suspicion in 68% of patients, caused a change in diagnosis in 32% and induced a change in management in 47%. **Conclusion:** The vast majority of type-A/typical scans can be read with excellent inter-observer concordance and with high confidence. Atypical/non-type A scans can be more difficult to interpret, with lower inter-observer agreement and confidence highlighting the importance of optimising image acquisition and having at least one 2nd reader. Amyvid imaging commonly confirms diagnostic suspicion when investigating dementia, and leads to change in diagnosis in 32% and management in 47%.

P252**Amyloid load and cognitive performances in non-demented elderly population: preliminary results of a ¹⁸F-Flutemetamol PET study**

M. MEYER¹, **P. ZANOTTI-FREGONARA**¹, **F. LAMARE**², **G. CATHELIN**², **C. HELMER**³, **K. PERES**³, **M. ALLARD**², **J. DARTIGUES**³, **P. FERNADEZ**¹; ¹Nuclear Medicine department CHU of Bordeaux, BORDEAUX, FRANCE, ²INCIA, University of Bordeaux, BORDEAUX, FRANCE, ³ISPED, University of Bordeaux, BORDEAUX, FRANCE.

Background: In the early stages of Alzheimer's disease, the impact of amyloid load on cognitive performance is variable, in particular in subject with high level of education due to the cognitive reserve. Previous studies have shown that between 20 and 50% of asymptomatic elderly subjects had high amyloid load. **Purpose:** To explore the relationship between amyloid load and cognitive performances, and its modulation by educational level in a non-demented elderly population. **Methods:** This is the preliminary

results of the EDUMA study, including 89 subjects. The amyloid load was assessed by ¹⁸F-flutemetamol PET-CT. We also collected for each subject: age, sex, ApoE status, educational level, the scores of MMSE test, Grober and Buschke test (episodic memory) and Isaacs set-test (semantic memory). We also performed a subgroup analysis on 36 subjects, for which we have evaluated the cognitive decline during the 10 years before the passage of PET examination. **Results:** 24% of the subjects had a positive ¹⁸F-Flutemetamol PET-CT. These were significantly older ($p=0.003$), had a mutation of the ApoE ($p=0.035$), and alterations of episodic and semantic memories ($p=0.028$ and $p=0.013$, respectively). Subjects with higher level of education had better cognitive performance, even though they were older ($p=0.003$) and they had a comparable amyloid load ($p=0.272$). Finally, in the subgroup analysis, high amyloid load is associated with cognitive decline ($p=0.018$). **Conclusion:** In non-demented elderly subjects, the impact of the amyloid load on cognitive performance is modulated by the level of education. These results confirm the interest of amyloid PET imaging in the early diagnosis of Alzheimer's disease.

P253**Metabolic differences in posterior cortical atrophy with and without amyloid pathology**

G. Marotta¹, **A. Arighi**², **P. Basilico**², **M. Longo**¹, **G. Fumagalli**², **D. Galimberti**², **E. Scarpini**², **R. Benti**¹; ¹Department of Nuclear Medicine, Fondazione IRCCS Ca' Granda Ospedale Maggiore Policlinico, Milano, ITALY, ²Department of Neurology, Fondazione IRCCS Ca' Granda Ospedale Maggiore Policlinico, Milano, ITALY.

Introduction. Posterior cortical atrophy (PCA) is a rare variant of Alzheimer's disease characterized by predominant complex visuo-spatial deficits and parieto-occipital or temporo-occipital cortical atrophy. As in typical Alzheimer's disease, amyloid cascade with deposition of plaques and tangles seems to play a key role in pathogenesis of PCA. However, a minority of cases without evidence of amyloid deposition may present with similar clinical manifestation. **Materials and methods.** We studied 16 patients with a clinical diagnosis of PCA, according to 2012 UCL criteria. All the patients underwent a neurological examination, neuropsychological evaluation, brain imaging with brain MRI or CT, lumbar puncture and brain FDG-PET. FDG-PET images were analyzed using statistical parametric mapping (SPM8, Wellcome Department of Imaging Neuroscience, London). **Results.** All patients had predominant visuo-spatial deficits on neuropsychological evaluation and posterior (parieto-occipital or temporo-occipital) atrophy on brain imaging (MRI or CT) or hypometabolism on FDG-PET in posterior cortical areas. CSF analysis showed a pattern of amyloid pathology in 10 cases, while 6 patients had normal A β 42 levels. The two groups were not significantly different from a clinical point of view. Using SPM8, the two groups showed a different pattern on FDG-PET ($p<0.001$): patients with normal A β 42 levels had a higher temporal and insular hypometabolism bilaterally, while patients with low A β 42 had a higher right posterior parietal and left mesial parietal hypometabolism. Moreover, considering all the patients together, occipito-parietal hypometabolism on FDG-PET correlates significantly ($p<0.001$) with low A β 42 CSF levels. **Conclusion.** There are cases of PCA without evidence of amyloid pathology and they have a different hypometabolism pattern on brain FDG-PET, involving insular and temporal region. Patients with amyloid pathology have a higher hypometabolism in parietal areas respect patients without amyloid pathology. The occipito-parietal hypometabolism is correlated with low A β 42 in CSF in all PCA.

P254**Brain perfusion pattern in semantic variant of primary progressive aphasia with Alzheimer's disease CSF profile**

G. Bera, **R. Migliaccio**, **T. Michelin**, **F. Lamari**, **M. Teichmann**, **A. Kas**; Groupe Hospitalier Pitié-Salpêtrière, PARIS, FRANCE.

Background and Objective Semantic variant of primary progressive aphasia (SvPPA) is nearly always associated with underlying non-Alzheimer pathology, such as TDP-43 (TAR DNA-binding protein 43) pathological aggregates (75%–100% in clinicopathological series). Very few anatomopathological studies have found the presence of other underlying pathologies, such as Alzheimer's disease (AD) in a very low percentage. Here, we aim at investigating *in vivo* cerebrospinal fluid (CSF) biomarkers profiles (AD vs. non-AD) and corresponding brain hypoperfusion patterns in SvPPA patients. **Methods** We included 21 SvPPA patients (mean age 64 ± 7.9 years, symptom duration 3.4 ± 2.5 years) who underwent lumbar puncture and brain perfusion SPECT (ECD-Tc99m). The PPA patients were classified into two subgroups according to the profile of CSF biomarkers, suggestive of AD (SvPPA-AD, $n=3$, age $79/63/60$ years, symptom duration $3/7/2$ years) or not (SvPPA-nonAD, $n=18$, mean age 63.5 ± 7.7 years, symptom duration 3.6 ± 2.5 years). We compared the brain perfusion profiles of the SvPPA subgroups with that of twenty-four healthy subjects (mean age 69 ± 7 years), and 24 amnesic, typical AD patients (mean age 65.1 ± 11 years, symptom duration 3.8 ± 2.1 years), on the voxel-basis using the Statistical Parametric Mapping software. **Results** All SvPPA patients had a severe left-side temporopolar hypoperfusion. In the SvPPA-AD, the hypoperfusion also extended to the left parietal associative cortex including the posterior cingulate ($p < 0.001$ uncorrected) while the SvPPA-nonAD patients had additional hypoperfusion in the anterior cingulate and orbitofrontal cortices ($p < 0.001$ uncorrected). **Conclusion** We observed a specific hypoperfusion pattern in SvPPA with AD pathology involving not only the temporal pole but also the left associative parietal lobe and the posterior cingulate cortices. These results highlight the critical role of the parietal cortex in the AD pathology irrespectively of the clinical presentation.

P255

Probability of conversion to Alzheimer's dementia (AD) in long-term non converters mild cognitive impairment (NC-MCI) patients: a volume of interest-based multivariate approach to 18F-FDG PET

M. Bauckneht¹, M. Pagani^{2,3}, A. Giuliani⁴, J. berg⁵, A. Chincari⁶, D. Arnaldi⁷, A. Picco⁷, F. Bongioanni¹, A. Nieri¹, E. Pomposelli¹, S. Maggio¹, F. Peschiera¹, G. Sambuceti¹, F. Nobili⁷, S. Morbelli¹; ¹Nuclear Medicine Unit, IRCCS AOU San Martino IST, Genova, ITALY, ²Institute of Cognitive Sciences and Technologies, CNR, Roma, ITALY, ³Department of Nuclear Medicine, Karolinska Hospital, Stockholm, SWEDEN, ⁴Environment and Health Department, Istituto Superiore di Sanità, Roma, ITALY, ⁵Department of Hospital Physics, Karolinska Hospital, Stockholm, SWEDEN, ⁶Istituto Nazionale di Fisica Nucleare, Sezione di Genova, Genova, ITALY, ⁷Clinical Neurology, Department of Neuroscience (DINOEMI), University of Genoa and IRCCS AOU San Martino-IST, Genova, ITALY.

AIMS: to identify those baseline variables influencing the probability of having an 18F-FDG-PET pattern classified as MCI due to AD, by means of a volume of interest-based multivariate approach, in a group of MCI patients still non-converted to AD after a minimum follow-up (FU) of 4 years. **METHODS:** 121 subjects were included: 44 normal aged subjects (CTR; mean age 69 ± 10), 28 NC-MCI at 4 years follow up after PET scan (mean age 72 ± 6), 36 MCI-AD converters more than 2 years later (earlyMCI, eMCI; mean age 75 ± 7), 58 MCI-AD converted within 2 years since PET scan (lateMCI, lMCI; mean age 76 ± 7) and 54 patients with mild-AD dementia (AD; mean age 73 ± 7). Mean 18F-FDG-PET uptake was computed on normalized images in 45 anatomical volumes of interest (VOIs) bilaterally as defined by the AAL Atlas. An in-house Matlab-based script automatically processed mean 18F-FDG uptake from each of the 90 VOIs normalizing them on cerebellar metabolism. Regions with similar anatomo-functional characteristics were merged into meta-VOIs and Area Under the Curve (AUC) differentiating NC-MCI from the other groups was computed through ROC analysis. Analysis of variance was

used to compute the influence of age, gender, years of formal education and baseline MMSE on the probability of each of the 121 subjects to be classified as normal aging (p(CTR)). Pearson Correlation Coefficients was used to assess the correlation between the tested variables and p(CTR). **RESULTS:** AUC differentiating NC-MCI from the other groups was 84% for eMCI, 98% for lMCI and 100% for AD. None among the tested variables demonstrated significant influence on p(CTR) in CTR, lMCI, eMCI as well as in mild-AD. By contrast, years of education, age and gender but not baseline MMSE significantly affected p(CTR) in NC-MCI ($p=0.006$, $p=0.02$ and $p=0.02$, respectively). In particular, education (the higher the educational level, the lower p(CTR)) showed the most significant effect and was able to influence p(CTR) even when included alone in the model ($p=0.0013$). **Conclusion:** this approach to 18F-FDG-PET was able to tell apart long-term NC-MCI from mild-AD patients and both eMCI and lMCI, all undergoing 18F-FDG-PET at first visit. In this framework only in NC-MCI, even after a long-term FU, higher education (reflecting higher cognitive reserve) may affect the residual risk of conversion to AD-dementia. Older age and female gender have a milder effect. These results reflect the role of cognitive reserve as one of the main determinants of long-term clinical stability in NC-MCI.

P256

Aging effect on F-18 florbetaben uptake in cognitive normal and visually PET negative older adults

K. Shin, J. Oh, M. Oh, H. Moon, J. Hwang, J. Roh, J. Lee, J. Kim; Asan Medical Center, Seoul, KOREA, REPUBLIC OF.

Objectives : Amyloid positive rate in cognitively normal adults is known to be depending on the age of the cohort and the threshold for defining positivity on amyloid PET. But, it is unknown there is an aging effect on tracer uptake in amyloid PET negative normal adults. We investigated the aging effect on F-18 florbetaben (FBB) uptake of cerebral cortex and deep white matter in cognitive normal and visually PET negative older adults. **Methods and materials:** F-18 FBB PET of 33 healthy subjects (54-79 yrs old, median 67, M:F = 6:27) with normal cognitive function, were analyzed visually by using the Brain Amyloid Plaque Load (BAPL) score and quantitatively using FreeSurfer software. We assessed the association of age and standardized uptake value ratios (SUVRs, reference: cerebellar cortex) of cerebral cortex and deep white matter. **Results:** Among 33 healthy subjects, 29 (88%) showed negative (BAPL score 1) and four (12%) showed positive (BAPL score 3) amyloid PET finding. In total 33 cases regardless of BAPL score, composite cortical SUVRs showed increasing tendency with age but not statistically significant ($r=0.239$, $p=0.09$). In 29 cases with visually negative PET finding, age were positively correlated with composite cortical SUVR ($r=0.559$, $p=0.001$) as an incline of 0.5% per yr. Regional cortical SUVRs (e.g. cingulate) also showed significant age-related increase ($p<0.05$). But, there was no correlation between age and deep white matter SUVRs ($r=-0.015$, $p=0.469$). **Conclusion:** FBB uptake of cerebral cortex increased with age in cognitively normal older adults with visually negative PET finding. This result may reflect preclinical amyloid deposition rather than hemodynamic effect.

P257

What ^{99m}Tc-HMPAO SPECT adds to memory function assessment in predicting conversion from amnesic Mild Cognitive Impairment (MCI) to Alzheimer's disease (AD)

D. Di Giuda¹, F. Coccilillo¹, D. Quaranta², D. Maccora¹, V. Rizzo¹, D. Fortini¹, C. Marra², G. Gainotti², A. Giordano¹; ¹Università Cattolica del Sacro Cuore - Nuclear Medicine Institute, Rome, ITALY, ²Università Cattolica del Sacro Cuore - Research Center for Neuropsychology - Neurology Institute, Rome, ITALY.

Aim: Identifying pre-clinical AD in MCI subjects is a major issue in clinical diagnosis. In this follow-up study we assessed if the ability to predict conversion from amnesic MCI (aMCI) to AD is improved by considering, at baseline, SPECT abnormalities in addition to delayed recall defects. **Materials and methods:** Forty-two aMCI patients (22 females, mean age: 69.6±7.2 years) underwent neuropsychological assessment. The Episodic Memory Score, EMS (Marra et al., J Alzheimers Dis. 2015), was obtained by integrating results from immediate and delayed recall as well as delayed recognition of the Rey Verbal Learning Test and delayed recall of the Rey-Osterrieth Complex Figure Test. ^{99m}Tc-HMPAO SPECT was performed within two weeks from the baseline evaluation. Every six months patients underwent neuropsychological assessment for a two-year follow-up. Baseline SPECT scans in patients converted to AD (aMCI-conv) and patients with stable aMCI (aMCI-stable) were compared using SPM8 and two-sample *t*-test. Region masks were extracted from significant clusters through the MarsBaR toolbox. Receiver Operating Characteristic (ROC) curves and areas under ROC curves (AROCs) were obtained for ROI and EMS results. Reliability indices of single and combined investigations were calculated. Analyses were performed using three EMS cut-off points (e.g., 7, 8, 9), whereas SPECT cut-off was set at ROI activity value displaying the highest sum of sensitivity and specificity. **Results:** During the two-year follow-up, 15 patients (36%) progressed to AD. SPM8 analysis showed hypoperfusion in the left posterior cingulate cortex (PCC) of aMCI-conv group, compared to aMCI-stable subjects (height threshold of $p < 0.005$). The mean activity extracted from the left PCC ROI differed between the two groups ($p = 0.002$). The AROC was 0.79 (95%CI=0.65-0.93); the best cut-off point corresponded to 91.5, showing the highest sum of sensitivity (0.87) and specificity (0.63). The EMS AROCs were: 0.77 (95%CI=0.64-0.91) for EMS<7 (sensitivity=0.73; specificity=0.81); 0.80 (95%CI=0.55-0.78) for EMS<8 (sensitivity=0.93; specificity=0.67); 0.67 (95%CI=0.68-0.91) for EMS<9 (sensitivity=0.93; specificity=0.41). The combination of EMS cut-off (<7, <8, <9, respectively) with SPECT data (left PCC perfusion<91.5) yielded fair results in sensitivity (range: 0.60-0.80) and good results in specificity (range: 0.74-1.00), with a high percentage of subjects properly classified (range: 76% to 90%). **Conclusion:** We showed that the combination of results from available and low-cost investigations, such as memory function assessment (EMS) and perfusion SPECT, allows to predict aMCI conversion with a high percentage of patients properly classified. If our results are replicated with different neuropsychological tests, significant advances could be achieved in this important area of public health.

P258

Influence of Education on Cognitive Performance and Dopamine Transporter Binding in Dementia with Lewy Bodies

G. Lamotte, C. Nganoa, P. Branger, R. Morello, G. Bouvard, V. De La Sayette, G. Defér, D. Agostini; CHU Caen, Caen, FRANCE.

Objectives. Dementia with Lewy bodies (DLB) and Alzheimer's disease (AD) are the two most common forms of dementia. These two diseases share some clinical and pathological similarities, yet the loss of dopaminergic neurons confirmed by 123-I-Ioflupane Single Photon Emission Computed Tomography (SPECT) is a suggestive feature of DLB. Current evidence suggests that higher education has a protective effect on the risk of developing clinical AD. However, how education influences cognitive performance and the presynaptic dopamine transporter marker in DLB is unknown. **Materials and Methods.** We reviewed 56 consecutive patients with DLB who underwent a 123-I-Ioflupane SPECT from January 2009 to August 2013 at the University Hospital of Caen. We collected clinical and neuropsychological data from medical files and 123-I-Ioflupane SPECT data for all patients. **Results.** There was no correlation between education and global cognitive performance in patients with DLB. However, there was a positive correlation between education and

tests exploring visuoconstructive functions (Rey complex figure copy and recall) and verbal retrieval strategies (Grober and Buschke free recall test). There was also a positive correlation between education and dopamine transporter binding. Higher educated patients had higher binding in the striatum, putamen and caudate nucleus ($p = 0.001$ for each regions of interest). Dopamine transporter binding in the striatum, putamen and caudate nucleus was lower in the subgroup of patients with REM sleep behavior disorder, but was not associated with other DLB symptoms. **Conclusion.** Higher education may have a protective effect on visuoconstructive performance and verbal retrieval strategies and may influence dopaminergic nigrostriatal neurodegeneration in patients with DLB.

P259

Florbetapir PET/CT in the evaluation of patients with Parkinson dementia: a preliminary study

D. Volterrani, G. Puccini, G. Tognoni, S. Mazzari, F. Guidoccio, M. Gennaro, G. Manca, R. Ceravolo; University of Pisa, Pisa, ITALY.

Cognitive impairment is a common non motor complication of Parkinson's disease (PD) which increases in severity and frequency over time leading most patients with PD to an overt clinical picture of dementia (PDD). Over the past 10 years, there was a growing evidence of a possible synergistic role of Alzheimer-type brain lesions containing β -amyloid (A β) and tau proteins in determining a PDD. Moreover, several clinical and pathological studies have stressed the co-existence of Lewy- and Alzheimer-type pathologies in PDD suggesting the correlation between greater cortical A β plaques and cortical α -syn load. Aim of this study was to find correlates between the pattern of deposition of A β and the variable expression of cognitive impairment in patients with PDD. of the cognitive deficits in PD. Ten patients (age 62.4±6.6) was enrolled at the Neurology Unit of the University of Pisa. The diagnosis of PD will be made according to UK Brain Bank criteria and PDD according to the Movement Disorder Society criteria. All patients performed neuropsychological tests exploring memory, executive, visuospatial, language and praxis and underwent a [¹⁸F]Florbetapir PET/CT. All PET/CT scans of (20 min acquisition) were acquired starting 40±5 min after intravenous injection of [¹⁸F]Florbetapir using a scanner GE Discovery 710. [¹⁸F]Florbetapir PET/CT images were visually and semiquantitatively analyzed. After spatially transformation of each scan into Montreal Neurological Institute (MNI) space, cortical-to-cerebellum mean standard uptake values (SUVr) were calculated for each subjects. Results: 3/10 patients resulted clearly positive on the visual analysis of [¹⁸F]Florbetapir PET/CT for the presence of cortical A β deposition. An inverse statistically significant correlation was found between global SUVr and the MMSE score, assessed at the time of PET/CT scan. A positive correlation was found between left and right putamen SUVr and the age of onset of PDD. Conclusions: few studies are available on the use of PET imaging in assessing cognitive deficits in PD. Although our data should be considered preliminary because of the limited number of studied patients in our series, the uptake of [¹⁸F]Florbetapir PET/CT seems to be related to the severity of cognitive impairment. More data are needed to understand the aetiology of cognitive deficits in PDD and the differing patterns and degrees of amyloid deposition.

P-22 – Tuesday, October 18, 2016, 16:00 - 16:30, Poster Exhibition Hall
Neurosciences: Miscellaneous

P260

Brain SPECT with ^{99m}Tc-HMPAO in assessing the effectiveness of surgical treatment of patients with occlusion of the carotid arteries

N. E. Kudryashova, V. A. Lukyanchikov, I. M. Godkov, O. G. Sinyakova, O. S. Kozmina; Sklifosovsky Inst.for Emerg. Medicine, Moscow, RUSSIAN FEDERATION.

AIM: Assessment of cerebral perfusion changes in the zone of occlusion of the carotid artery after surgery using brain SPECT with 99mTc-HMPAO. **MATERIAL AND METHOD.** The object of studying - 61 patients with occlusion of the internal carotid artery (ICA), preferably with one side (78.7%). 50 patients before surgery suffered stroke of various prescription and 11 had repeated transient ischemic attack (TIA). 13 patients (21.3%) had bilateral carotid atherosclerotic lesions. All patients before surgery performed SPECT with 99mTc-HMPAO (740 MBq) and vasodilatory breakdown (acetazolamide), based on the indications for surgical treatment: carotid endarterectomy (CEA) or extra-intracranial mikroanastomosis (EICMA) in terms of three days to one and a half years (from 45.9% - up to 1 month) after stroke or TIA. Again through 6-14 days after surgery of brain perfusion as assessed by SPECT. The regional CBF was determined by the formula $N \cdot Lassen$, where the reference area was cerebellum (CBF 55 ml/100g/min). **RESULTS.** Before the surgical intervention was found the place of hypo/aperfusion in the zone of occluded carotid artery with an average $CBF=27,54 \pm 6,75$ ml/100g/min. Test with acetazolamide was positive (increased perfusion to 12-33%) in 13 patients with critical stenosis of ICA - were performed CEA (group 1). The last 48 patients with negative vasodilatory breakdown ("steal syndrome" or increase less than 10%) imposed EICMA between the branches of the superficial temporal artery and a cortical branch of the middle cerebral artery (group 2). After surgical treatment the most of perfusion (from 20 to 90%) in the ischemic area was found in 68.8% of patients whom made EICMA (group 2, 33 of the 48 people.), and 15.4% after CEA (group 1, 2 of 13 people.). No effect or a slight increase perfusion (0 to 17%) was observed in 26 patients with bilateral carotid atherosclerosis, and prolonged ischemia: 84.6% in group 1 (11 of 13 patients) and 31.3% in group 2 (15 of 48 patients). Increase in perfusion after surgery in group 1 (CEA) on average amounted to 15.5% (Med = 11.0%; 95% CI, 8.1%, 22.9%) in group 2 (EICMA) - 31.4% (Med = 27.0%; 95% CI, 24.8%, 38.0%). Obtained a significant difference in the increase of perfusion as a result of two kinds of surgery ($p < 0,05$). **CONCLUSION.** The results of brain SPECT with 99mTc-HMPAO showed high efficiency EICMA with a significant strengthening of perfusion in the ischemic area in 68.8% of patients with occlusion of the ICA.

P261

Audit of DaTSCAN™ Referrals at East Kent University Hospitals, UK, According to the Current Guidelines and Financial Impact on Health System

R. Vickers, G. Shabo; East Kent University Hospitals Foundation Trust, Canterbury, UNITED KINGDOM.

To assess the appropriateness of DaTscan™ (^{123}I -Ioflupane) requests to our department in line with the current British NICE and the European Association of Nuclear Medicine (EANM) guidelines and the sufficiency of provided clinical information for accurate reporting. DaTscans come at significant financial cost, around £1000 per scan, and as such must be used appropriately, particularly in the current difficult economic climate. **METHODS** Retrospective review was carried out of 64 referrals between 1/10/14-31/12/14 and 85 referrals between 1/10/15-31/12/15, to look at any change in trend. They were assessed as regards the appropriateness of referrals and the content of clinical information using a combination of the electronic records and ordering system as well as electronic radiology and imaging systems (CRIS and PACS). The referrals were divided into three groups: 'Good' meeting guidelines with sufficient clinical information, 'Poor' lacking clinical details or 'Inappropriate' *i.e.* not in line with the guidelines. **RESULTS** 44/64 scans (68.75%) in the 2014 study group were deemed 'good' whereas 20/64 scans (31.25%) were 'poor' or 'inappropriate'. 11/20 scans (55%) were subsequently negative for evidence of Parkinson's disease or dementia. In the 2015 study group, there were 85 scans, an increase of 32.8% on the same period of the previous year. 54/85 scans (63.53%) were deemed 'good' whereas 31/

85 scans (36.47%) were deemed 'poor' or inappropriate. 21/31 (67%) scans were subsequently negative for evidence of Parkinson's disease or dementia. **CONCLUSION** There are a large number of inappropriate referrals resulting in negative scans. In these two small study groups; 32 scans were performed over a total of 6 month period that were poor/inappropriate referrals with negative results, at a cost of more than £30,000. At an approximate cost of £5000 per month, this equates to more than £60,000 per year to the Trust. It also appears that the number of inappropriate referrals is increasing, however this is a trend seen only in two sets of year on year results and therefore may be an anomaly. This does however present an opportunity for expansion of this audit to other years. In recommendation, it would be prudent to design a specific referral pro-forma that has mandatory clinical information section, requiring the referring clinician's signature before considering the request. This would provide an opportunity to cut down on unnecessary and expensive scans that are not clinically indicated.

P262

Role of 99mTc-HMPAO brain perfusion SPECT in the clinical management of autoimmune brain vasculitis (ABV)

V. Frantellizzi, M. Pontico, A. Farcomeni, A. Francia, M. Morreale, F. Monteleone, G. De Vincentis, M. Liberatore; Sapienza University of Rome, Rome, ITALY.

Vasculitis of the central nervous system (CNS) is a rare event and generally occurs as a manifestation of a systemic disease or as primary form of the CNS. Brain SPECT seems to be useful in the diagnosis and monitoring of the disease. The purpose of our study was to evaluate, with this investigation, the trend of brain perfusion in relation to the treatment duration. Fifty consecutive patients with ABV were enrolled in this study. 18 were affected by Systemic Lupus Erythematosus (LES), 22 by Undifferentiated Vasculitis (UV), 5 by Behcet's disease (BD) and 5 by Sjogren's syndrome (SS). All patients underwent a full neuropsychiatric investigation, objective examination and various serological tests. A brain SPECT was carried-out before the onset of appropriate treatment and was repeated during the follow-up at different time interval (12, 24 and 36 months). Brain SPECT with 99mTc-HMPAO, was performed by a dual-head gamma camera equipped with high-resolution low-energy collimators. Image analysis was performed using a specific software capable of providing for each cerebral area the mean and the SD of the counts recorded expressed as a percentage of the maximum count registered on the encephalon. Ten regions of interest were selected for each patient (entire right and left emicortex, parietal, temporal, frontal and occipital regions). Basal SPECT results were compared with those obtained during the treatment. In BD and SS results demonstrate an increase of the cerebral perfusion after treatment in agreement with clinical evaluation, even if no statistical analysis was performed due to the limited number of patients studied. The differences between the overall means and SDs calculated on the areas of interest before and after the treatment gave the following results. No significant differences resulted at 12, 24 and 36 months in the LES group. In the UV group no significant differences were found at 12 months, while such differences became significant at 24 ($p = 0.027$) and 36 months ($p = 0.001$). Similar results were obtained taking into account LES and UV together (p values: 12 months = 0.128, 24 months = 0.009, 36 months < 0.001). Even these results are consistent with the clinical course observed in patients. The results obtained with brain SPECT in this study suggest that a global improvement of brain perfusion can be achieved in UV only after a prolonged period of treatment.

P263

Brain FDG-PET quantification after chronic administration of benzodiazepines . An animal study

J. Silva-Rodríguez¹, L. García-Varela¹, E. López-Arias², I. Domínguez-Prado³, J. Cortés³, J. Pardo-Montero², A. Fernández-Ferreiro¹, A.

Ruibal³, T. Sobrino², P. Aguiar²; ¹Fundación Ramón Domínguez, Santiago de Compostela, SPAIN, ²Health Research Institute (IDIS), Santiago de Compostela, SPAIN, ³Nuclear Medicine Department, University Hospital, Santiago de Compostela, SPAIN.

Introduction: In order to minimize unspecific radiotracer uptake, patients undergoing brain FDG-PET are usually told to rest, lying down and with their eyes closed, for about 45 minutes before the examination. On this context, benzodiazepines might be useful when dealing with non-collaborative patients, which may be the case on several applications of brain PET such as dementia. Different authors have studied the effect of the acute administration of benzodiazepines on brain glucose uptake, reporting a decrease on global uptake around 20%. Due to this, current guidelines for brain PET imaging recommend to avoid the injection of diazepam prior to brain FDG-PET examination. Nevertheless, many patients undergoing PET studies are likely to be under chronic treatment with benzodiazepines due to the use of different medications such as sleeping pills. This chronic consumption of benzodiazepines has been related to cognition impairment even after stopping the treatment, and its impact on brain PET imaging remains to be studied. Animal studies may provide an extensive and accurate estimation in a well-defined and controlled framework. **Aim:** We are aimed at evaluating the impact of the chronic administration of benzodiazepines on brain FDG uptake and its evolution after the discontinuation of the treatment. **Methods:** Twelve healthy rats were randomly divided into two groups, one treated with diazepam and the other one used as control group. All the subjects underwent PET/CT examinations on basal state, after single-dose administration and chronic administration (during twenty-eight days) of diazepam (treated) or saline (controls), and one week after stopping the treatment. Different quantification methods were applied to evaluate the differences on total brain FDG uptake and uptake patterns of FDG between both groups. **Results:** Our analysis revealed a significant reduction of global FDG uptake after acute (-16.2%, $p < 0.02$) and chronic (-23.2%, $p < 0.03$) administration of diazepam. Moreover, a strong trend pointing to differences between acute and chronic administrations ($p < 0.08$) was also observed. Uptake levels returned to normal after interrupting the administration of diazepam. On the other hand, patterns of FDG uptake were not affected by the administration of diazepam. **Conclusions:** The administration of diazepam causes a progressive decrease of the FDG global uptake in the rat brain, but it does not change regional patterns within the brain.

P264

Is cerebral glucose metabolism related to blood brain barrier dysfunction and intrathecal IgG synthesis in Alzheimer Disease?

A. Chiaravalloti^{1,2}, A. Fiorentini¹, F. Ursini³, A. Martorana⁴, P. Sannino⁵, G. Koch⁴, M. Bozzali⁶, B. Di Pietro¹, E. Di Giorgio², O. Schillaci^{1,5}; ¹Department of Biomedicine and Prevention, University Tor Vergata, Rome, ITALY, ²IRCCS Neuromed, Rome, ITALY, ³Rheumatology Research Unit, University Magna Graecia, Rome, ITALY, ⁴Department of Neurosciences, University Tor Vergata, Rome, ITALY, ⁵IRCCS Neuromed, Pozzilli, ITALY, ⁶IRCCS Santa Lucia, Rome, ITALY.

Aim: To investigate the relationships between blood brain barrier (BBB) dysfunction, intrathecal IgG synthesis and brain glucose consumption as detectable by means of Serum/Cerebrospinal fluid (CSF) albumin index (Q_{alb}) and IgG index [(CSF IgG/serum IgG) x Serum albumin/CSF albumin] and 2-deoxy-2-(¹⁸F) fluoro-D-glucose (¹⁸F-FDG) Positron Emission Tomography/Computed Tomography (PET/CT) in a selected population affected by Alzheimer's Disease (AD). **Material and methods:** The study included 134 newly diagnosed AD patients according to the NINCDS-ADRDA criteria. The mean (\pm SD) age of the patients was 70 (\pm 6) years; 60 were male and 64 were female. Mini mental State Examination was equal to 18.9 (\pm 7.2). All patients underwent serum and

CSF assay for IgG index and Q_{alb} . Contextually we measured amyloid ($A\beta_{1-42}$) and tau [phosphorylated-tau (p-tau) and total-tau (t-tau)]. A Magnetic Resonance before ¹⁸F-FDG PET scanning was performed as well. The relationships were evaluated by means of statistical parametric mapping (SPM8) using sex, age, MMSE, scholasticity and CSF amyloid and tau values as covariates. **Results:** We found a significant negative correlation between the increase of Q_{alb} and ¹⁸F FDG uptake in the Brodmann Area 42 and 22 that correspond to the left superior temporal gyrus, with higher Q_{alb} values being related to a reduced glucose consumption in these areas (p FEW-corr=0.001; p FDR corr=0.000). Cerebellum-normalized ¹⁸F FDG PET values for BA 42 and 22 resulted equal to 1.05 \pm 0.12 (mean \pm standard deviation) and were not normally distributed ($K^2=32.2$ and $P < 0.001$). Spearman correlation analysis showed a good correlation between albumin ratio levels and normalized ¹⁸F FDG uptake further showing that low levels of albumin ratio were related to lower levels of ¹⁸F FDG uptake ($r=-0.22$ and $P=0.009$). No significant relationships were found between brain glucose consumption and IgG index. **Conclusions:** The results of our study suggest that BBB dysfunction is related to reduction of cortical activity in the left temporal cortex in AD subjects.

P265

Does F-18-choline PET/CT Have a Role in Primary Brain Tumor Characterization?

M. Nicod Lalonde, V. Dunet, G. Allenbach, P. Mitsakis, A. Van-der-Gucht, N. Schaefer, B. Lhermitte, P. Maeder, A. Hottinger, J. Bloch, J. O. Prior; Lausanne University Hospital, Lausanne, SWITZERLAND.

Study Aim: To determine whether F-18-choline (FCH) PET/CT can contribute to lesion characterization in patients with suspected primary brain tumors on MRI. **Materials and Methods:** We enrolled 42 consecutive patients from July 2009 to March 2016 presenting with a suspicion of primary brain lesion on MRI and with an intention to biopsy this lesion. FCH PET/CT was performed on all patients and lesion SUVmax were measured. The tumor-to-background ratio (TBR) was calculated by dividing lesion SUVmax by contralateral normal brain tissue SUVmean. The patients then underwent a biopsy or a resection of the tumor. Association between SUVmax (respectively TBR) and gadolinium (Gd) enhancement on MRI was examined by student t-test. One-way ANOVA was used to determine the relationship between MRI enhancement, SUVmax (respectively TBR) and tumor grade. **Results:** In total, 42 patients (30M, 12W) with a mean age of 47 y (range: 24-76) were enrolled. Histological findings showed WHO grade II brain tumor in 18 patients, grade III tumor in 16 patients and grade IV tumor in 8 patients. In 21 lesions, there was no Gd enhancement. SUVmax was significantly lower in patients with no Gd enhancement compared to patients with Gd enhancement on MRI: SUVmax 0.55 \pm 0.44 g/ml versus 1.47 \pm 1.11g/ml ($p=0.001$). Likewise TBR was significantly lower in patients with no Gd enhancement (3.29 \pm 2.17 vs. 7.59 \pm 5.74); $p=0.003$). SUVmax significantly increased with tumor grade (grade II: 0.72 \pm 0.52, grade III: 0.94 \pm 0.79, and grade IV: 1.8 \pm 1.55; $p=0.02$). The same was true for TBR (grade II: 4.18 \pm 2.53, grade III: 4.67 \pm 3.26, and grade IV: 9.81 \pm 8.34; $p=0.01$). When taking into account Gd enhancement on MRI, FCH uptake was also useful in characterizing brain lesions. In patients with Gd enhancement, TBR helped to predict brain tumor grade, as TBR increased with tumor grade (grade II: 6.46 \pm 1.93, grade III: 5.09 \pm 3.82, and grade IV: 12.25 \pm 8.3; $p=0.05$). Patients with no Gd enhancement had a similar TBR for all tumor grades (grade II: 2.73 \pm 1.66, grade III: 4.25 \pm 2.78, and grade IV: 2.5 \pm 0.71; $p=0.29$). **Conclusion:** As predicted, when using FCH PET/CT for characterization of primary brain tumors, our study shows a significant increase in SUVmax and TBR with tumor grade. Interestingly, when used in combination with MRI, FCH PET/CT helps in determining tumor grade only in patients with Gd enhanced lesions.

P267**Is cerebral glucose metabolism related to TSH, fT3 and fT4 in Alzheimer disease? A 18F FDG PET/CT study with cerebrospinal fluid amyloid and tau correlates**

A. Chiaravallotti^{1,2}, A. Fiorentini¹, F. Ursini³, A. Martorana⁴, P. Sannino², C. Di Russo¹, E. Palombo¹, O. Schillaci^{1,2}; ¹Department of Biomedicine and Prevention, University Tor Vergata, Rome, ITALY, ²IRCCS Neuromed, Pozzilli, ITALY, ³Rheumatology Research Unit, University Magna Graecia, Catanzaro, ITALY, ⁴Department of Neurosciences, University Tor Vergata, Rome, ITALY.

Aim: To investigate the relationships between thyroid stimulating hormone (TSH), freeT3(fT3) and freeT4 (fT4) and brain glucose consumption as detectable by means of 2-deoxy-2-(¹⁸F) fluoro-D-glucose (¹⁸F FDG) Positron Emission Tomography/Computed Tomography (PET/CT) in a selected population with Alzheimer disease (AD). **Materials and methods:** 87 subjects (47 males and 50 females, mean age 70 (±6) years old) with AD according to the NINCDS-ADRDA criteria were enrolled in this study. Mini mental state examination (MMSE) was 18.9 (±7.2). All of them were subjected to TSH, fT3 and fT4 assay and to cerebrospinal fluid amyloid (A β_{1-42}) and tau [phosphorylated-tau (p-tau) and total-tau (t-tau)] assay prior PET/CT examination. Mean values for TSH, fT3 and fT4 were 1.38 (±0.84), 3.34 (±0.33) and 1.16 (±0.17). Mean values for A β_{1-42} , p-tau and t-tau were 344.28 (± 134.31), 96.7 (± 76.9) and 679.15 (± 330.5). The relationships were evaluated by means of statistical parametric mapping (SPM8) using age, sex, MMSE, scholarship and CSF values of amyloid and tau as covariates. **Results:** We found a significant positive correlation between TSH values and cortical glucose consumption in a wide portion of the anterior cingulate cortex bilaterally (BA 32) and left frontal lobe (BA25) (p FEW-corr=0.001; p FDRcorr=0.000; cluster extent 66950). No significant relationships were found between cortical ¹⁸F FDG uptake and T3 and T4 serum levels. A significant relationship was found between t-tau levels and cortical glucose consumption in right BA32 (r=-0.25, P=0.019) and left BA32 (r²=0.054 and P=0.033) while no significant relationship was found in BA25 (r=-0.11;P=0.29). No significant relationships were found between cortical ¹⁸F FDG uptake and p-tau and A β_{1-42} in these sites. **Conclusions:** the results of our study suggest that a cortical dysfunction in anterior cingulate and frontal lobes affects serum values of TSH in AD patients. Pathological accumulation of tau protein could play a role in this phenomenon.

P268**Value of cerebral perfusion SPECT in HaNDL Syndrome**

L. Reguera Berenguer, J. Orcajo Rincón, A. Rotger Regí, C. Durán Barquero, R. Pascual Pérez, M. L. Lozano Murgas, J. Ardila Manjarrez, J. C. Alonso Farto; HGU Gregorio Marañón, Madrid, SPAIN.

HaNDL syndrome or pseudomigraine with pleocytosis is a benign and autolimited disease characterized by severe headache with at least one transient neurologic deficit and spontaneous resolution in less than 4 months. In addition, it is accompanied by cerebro spinal fluid (CSF) pleocytosis with lymphocytic predominance and negative etiological studies. In neuroimaging, cerebral perfusion SPECT with ^{99m}Tc-HMPAO has shown local blood flow alterations consistent with focal neurological deficits that tend to normalize in the period of clinical remission, although there is currently insufficient bibliographic support. **Aim:** To describe the perfusional pattern of this disease in the acute phase, assessing possible patterns relating symptomatology with perfusion SPECT findings and their normalization in the resolution phase. **Materials and methods:** Descriptive analysis of a series of 4 patients treated at HGU Gregorio Marañón from December 2009 to April 2016, in which HaNDL syndrome was suspected. All patients underwent EEG,

CSF puncture and conventional imaging tests (CT and MRI), in addition to brain perfusion SPECT with ^{99m}Tc-HMPAO in the symptomatic phase and at clinical remission. **Results:** All patients (2 males and 2 females) had lymphocytosis with protein concentration in CSF with no pathologic results in conventional imaging, whereas cerebral SPECT showed perfusional abnormalities consistent with the clinical manifestations, consisting of marked hemispheric hypoperfusion, contralateral to the neurological symptoms, showing reversibility in the control study. **Conclusions:** Cerebral perfusion SPECT appears to be an effective tool, not only in the early confirmation of the diagnosis of HaNDL syndrome, but also in monitoring its resolution.

P269**Assessment of collateral circulation in chronic cranial arterial occlusive disease using 123I-IMP CBF SPECT: delayed accumulation through collateral formation in dynamic phase**

K. Sohara¹, S. Mizumura², T. Kuwako¹, T. Kiriya¹, Y. Fukushima¹, N. Sugo³, S. Kumita¹; ¹Nippon Medical School, Tokyo, JAPAN, ²Dept of radiology, Omori Medical Center, Toho University, Tokyo, JAPAN, ³Dept of neurosurgery, Omori Medical Center, Toho University, Tokyo, JAPAN.

<The aim> The collateral circulation plays a pivotal role in the hemodynamics of cerebral ischemia in chronic cranial arterial occlusion disease. This study investigated the effects of collateral circulation using 123I-Iodoamphetamine (IMP) CBF SPECT. <Materials and methods> Twenty five patients with chronic cranial arterial obstruction, diagnosed by angiography, were performed with dynamic (0-8min) and static (15-40min) SPECT after the injection of 123I-IMP. Sixteen patients of them showed three types of the collateral circulation (positive case): the pathways of 1) arterial segments of the circle of Willis, 2) extracranial sources, 3) leptomeningeal anastomosis. The other 9 had no collateral circulation (negative cases). Stereotactic voxel-based VOIs were drawn on 7 vascular territories in a hemisphere: anterior cerebral artery (ACA), middle cerebral artery (MCA), internal carotid artery (ICA), and the central and peripheral zones of these vascular territories. To evaluate the VOI accumulation difference between affected and unaffected hemispheres in dynamic phase, “dynamic uptake ratio” was defined as the ratio of VOI values (count-standardized by VOI values on static image) in affected hemisphere to in unaffected hemisphere. We compared the dynamic uptake ratios of 7 sets of vascular territories in the positive and negative cases, and employed the receiver operating characteristic (ROC) curves when discriminating collateral formation positive and negative cases. <Results> The dynamic uptake ratios in all vascular territories of the positive cases tended to be lower than of the negative cases, but in all vascular territories, except for the central zone of MCA, there was no significant difference. The dynamic uptake ratios of the central zone of MCA in the positive cases were significantly lower than in the negative cases (p<0.05), while those of the peripheral zone of in the positive cases was not in the negative cases. In ROC curves, the dynamic uptake ratio in the central zone of MCA is exhibited the highest areas under the curves of 0.718, accuracies of 79%, sensitivity of 69% and specificity of 100% with cut off values of 0.99. <Conclusion>The patients with collateral formation would have a retrograde filling of patent but proximally obstructed branches. The delayed uptake in the central zone of MCA territory would reflect the existence of collateral circulation.

P271**Brain perfusion SPECT in Myalgic Encephalomyelitis: Normal database comparison for improved interpretation**

S. Neubauer¹, B. M. HYDE²; ¹Clinica Las Condes, Santiago, CHILE, ²Nightingale Research Foundation, Ottawa, ON, CANADA.

Myalgic encephalomyelitis (ME) and Chronic Fatigue Syndrome (CFS) are acquired complex syndromes including a variety of symptoms and physical findings affecting multiple systems of the body like severe, debilitating, unexplained fatigue for many months often a lifetime, frequent cognitive dysfunction and symptom flare-up in relation to physical or cognitive effort. ME may occur as an epidemic outbreak (e.g. 1905 Sweden, 1934 California) or may only affect individuals. Most investigators agree that the disorder can be related to an abnormal immune system and brain function in response to an infection or virus. There are no universally accepted diagnostic tests. Regional cerebral blood flow has consistently been abnormal on brain perfusion SPECT and different from depression. **Aim:** Based on previous experience of perfusion brain SPECT in ME/CFS patients with conventional 2D transaxial, coronal and sagittal projections, we evaluate the added value of a normal database comparison for analysis. **Material and Method:** We report on brain perfusion SPECT rCBF findings in 11 ME/CFS patients diagnosed according to the Canadian Consensus Criteria by one of the investigators (BH). They all were injected with Tc99m-HMPAO in resting condition, five of them also during exercise (Treadmill stress), one additionally during symptom triggering stimulus (inhaling certain perfume) and 4/5 also at 24 hours post-stress (recovery). All studies were compared against a normal age matched data base in Chile. Results are expressed in standard deviations of the normal mean in each of 14.000 voxels and are visually analyzed. **Results:** At rest all patients showed hypoperfusion in the lateral temporal lobes and multifocal hypoperfusion in the parietal lobes. There was also hypoperfusion in the posterior cingulate gyri in 9/11 patients, in the anterior cingulate gyri in 8/11 and in the occipital lobes in 8/11. During stress 5/5 patients had significant worsening of perfusion in the same areas and 3/5 had additionally hypoperfusion in the anterior frontal lobes. **Conclusions:** Brain perfusion SPECT comparison to a normal data base showed abnormal temporo-parietal perfusion in all ME/CFS patients by simple visual analysis of the images. Exercise caused worsening of brain perfusion abnormalities as expected from clinical data. Normal data base comparison is useful for intrasubject comparison of rest versus stimulated brain perfusion.

P272

Role of Ictal SPECT in medically refractory epilepsy: Post-surgical correlation

A. S. Manglunia¹, S. Pawar², S. Ravat², D. Mazumdar²; ¹Bombay Hospital & Medical Research Centre, Mumbai, INDIA, ²KEM hospital & Seth G. S. Medical College, Mumbai, INDIA.

Introduction: An epileptic seizure is a manifestation of abnormal and excessive paroxysms of involuntary activity of neurons in the brain. Seizures are controllable with medication in about 70% of cases. For the others, surgery remains an appealing treatment option. The common methods of seizure focus localization include electroencephalography (EEG), neuropsychological testing, and magnetic resonance imaging (MRI). As far as brain perfusion SPECT is concerned, there is large variation in the stated sensitivity of this technique. Also, the relationship between SPECT and surgical outcome has not been established. The purpose of this study was to evaluate the role of ictal brain SPECT in localization of the epileptogenic focus in patients with epilepsy. **Materials & Methods:** The study included patients referred to our department for ictal SPECT. The patients were subjected to a Brain MRI, inter-ictal EEG and video-EEG monitoring. Ictal and inter-ictal Brain Perfusion SPECTs were acquired. The patients then underwent surgery and were followed-up for 1 year, when their post-surgical outcome was classified according to Engel's system. **Results:** 30 patients, comprising of equal number of males and females were included. Mean age of the patients was 24.4 years (SD 9.8 years). MRI could localise the seizure focus in 15 patients, inter-ictal EEG in 12 patients, whereas ictal-EEG was localizing in 21 patients. SPECT could localize the seizure focus in 24 patients out of 30. Pre-

operative comparison of SPECT results with that of MRI, inter-EEG and ictal EEG showed concordance of 33.33%, 30.00% & 50.00% respectively. However, the differences were statistically insignificant. When using Engel's system as the standard of reference for post-operative state, SPECT showed maximum concordance rate of 80% (24/30). The difference in the concordance rate of SPECT when compared to both MRI and Inter-ictal EEG was statistically significant ($P < 0.01$). Of the patients with normal MRI (2/30), ictal EEG showed concordance with the resected site in 2/2 cases. MRI showed bilateral abnormal findings in 13 patients. SPECT in these patients correctly localized the lesion in 92.3% (12/13). **Conclusions:** In epilepsy cases with bilaterally abnormal MRI findings, brain SPECT is a useful modality for pre-surgical evaluation. Also, in cases with discordant results, SPECT can be employed as a supplementary tool for confirmation. SPECT also has a role in localizing the epileptogenic focus in patients with normal MRI finding.

P-23 – Tuesday, October 18, 2016, 16:00 - 16:30, Poster Exhibition Hall
Neurosciences: Movement Disorders

P273

Comparison of the diagnostic performance of two methods of semi-quantitative analysis of ¹²³I-FP-CIT brain SPECT images in mild Parkinson's disease

B. Palumbo¹, S. Nuvoli², S. Cascianelli³, A. Santonicola¹, M. L. Fravolini³, N. Tambasco⁴, M. Scialpi⁵, A. Spanu², G. Madeddu²; ¹Section of Nuclear Medicine and Health Physics, Dept of Surgical and Biomedical Sciences, University of Perugia, PERUGIA, ITALY, ²Unit of Nuclear Medicine, University of Sassari, SASSARI, ITALY, ³Dept of Engineering, University of Perugia, PERUGIA, ITALY, ⁴Unit of Neurology, Perugia University Hospital, PERUGIA, ITALY, ⁵Section of Diagnostic Imaging, Dept of Surgical and Biomedical Sciences, University of Perugia, PERUGIA, ITALY.

Aim: To investigate the differential diagnosis between Parkinson's disease (PD) and healthy subjects the diagnostic performance of two methods of semiquantitative analysis of ¹²³I-FP-CIT brain SPECT data, Basal Ganglia V2 software (BasGan) and Neurotrans3D (Segami Corp.), was compared by using a Support Vector Machine classifier (SVM), a powerful supervised classification algorithm based on ground-truth training data. **Materials and Methods:** ¹²³I-FP-CIT brain SPECT with semiquantitative analysis (according to EANM guidelines) with the two semiquantitative methods was performed in 91 patients with mild symptoms (bradykinesia-rigidity) to confirm or exclude PD, resulted 49 PD and 42 normal subjects. A clinical follow up of at least six months confirmed final diagnosis. Each patient was described by 4 descriptors (caudate-nucleus left/right - CL, CR- putamen left/right - PL, PR -) and a class label: 'PD' for PD and 'N' for normal subjects. For each semiquantitative method a nonlinear SVM with Radial Basis Function kernel was trained to predict the diagnostic categories. A 10-fold cross-validation was performed on the training set for SVM parameters tuning. The same protocol was used in further subsequent classification experiments, either on the entire feature set and on specific subsets of the initial features to assess their prediction capabilities: the first one using only caudate-nucleus left/right, the second one using only putamen left/right. **Results:** Both methods were able to correctly classify labels in the experiment using all the 4 descriptors; BasGan and Neurotrans3D showed respectively specificity of 96.16±7.98% and sensitivity of 86.43±13.38% and specificity of 98.49±5.26% and sensitivity of 87.79±12.43%. When using only putamen left/right as descriptors, both methods disclosed higher performances values, namely specificity of 96.37±7.63% and sensitivity of 90.48±11.96% for BasGan and specificity of 99.01±1.09% and sensitivity of 88.27±12.55% for Neurotrans3D. Conversely, using only caudate-

nucleus left/right as descriptors, performances decreased for both methods: BasGan achieves specificity of $80.79 \pm 14.62\%$ and sensitivity of $77.17 \pm 18.80\%$, while Neurotrans3D obtains specificity of $82.76 \pm 15.35\%$ and sensitivity of $74.98 \pm 18.01\%$. Therefore, putamen descriptors alone were able to correctly discriminate patients and controls. **Conclusion:** Both BasGan and Neurotrans3D were accurate in identifying PD in early phase, presenting a similar diagnostic performance. Furthermore, in our group of patients, among the different features used to classify subjects, putamen (either left or right) resulted as the most discriminative descriptor for mild disease using both semiquantitative methods.

P274

[¹⁸F]-FDG PET-CT identifies extraorbital muscle impairment in progressive supranuclear palsy

G. Petyt¹, A. Jaillard¹, G. Collet², D. Bellevre¹, H. Lahousse¹, F. Semah¹; ¹CHU Lille, Lille, FRANCE, ²CH Valenciennes, Valenciennes, FRANCE.

Vertical supranuclear gaze palsy is a key symptom for the diagnosis of progressive supranuclear palsy (PSP, Steele-Richardson-Olszewski syndrome). PSP neurofibrillary tangles affects the mesencephalic motor nucleus of the oculomotor nerves (N.III). N.III controls superior rectus muscle (>RM), inferior rectus muscle (<RM), medial rectus muscle (MRM) and inferior oblique muscle. Superior oblique muscle (>OM) and lateral rectus muscle (LRM) are respectively under control of trochlear nerve (N.IV) and Abducens nerve (N.VI), not involved in PSP. Ocular symptoms earlier affects down glaze by <RM involvement. **AIM:** Our work evaluate the ability of high definition FDG PET-CT to identify the ocular muscle hypometabolism in patient with possible or probable PSP on brain FDG scans. **Patients, Materials and Methods:** Five patients with PSP diagnosis were enrolled and compared to 33 successive FDG brain scans (10 epilepsy, 19 other neurodegenerative disorders (ND), 4 patients without evidence of ND). Images were acquired for 10 min, 30 min after injection of 185 MBq of [¹⁸F]-FDG, on mCT flow 20 (Siemens). UHD iterative algorithm (gaussian 2mm FWHM post filter) was applied. SUVbw max of extraocular muscles were measured (>RM, >OM, MRM, <RM, LRM). Relative uptake of each muscle were computed after normalization to the mean SUVmax for both eyes. Ratios between <RM uptake (earlier involved muscle) and LRM uptake (not involved in PSP) were computed for each eye. For each patient, lowest <RM/LRM ratio was recorded (Rmin). Relative uptake for each muscle, <RM/LRM ratio for each eye and Rmin for each patient were compared by unpaired t test with Welch's correction. **Results:** On patient based analysis, minimal ratio between <RM and LRM was lower in PSP patients than non PSP controls ($p=0.026$, respective mean 1.07 and 1.29). On eyes based analysis, <RM uptake was lower in PSP group (mean = 1.14 vs 1.42 in controls; $p=0.0001$). <RM/LRM ratio was lower in PSP patients (1.13 vs 1.39 in controls; $p=0.02$). Mean relative uptake of >RM, >OM, MRM and LRM were respectively 0.95 ($p=0.10$), 0.77 ($p=0.61$), 1.02 ($p=0.9$) and 1.05 ($p=0.19$) in PSP versus 0.82, 0.79, 1.01, 1.38 and 0.99 in controls. **Conclusion:** FDG scan identifies specific involvement of inferior rectus orbital muscle in PSP patients.

P275

¹²³I-FP-CIT brain SPECT: tracer uptake values of right putamen are the most discriminant to diagnose Parkinson's disease

B. Palumbo¹, S. Cascianelli², A. Santonicola¹, M. Ministrini¹, T. Buresta¹, M. L. Fravolini², N. Tambasco³, M. Scialpi⁴, S. Nuvoli⁵, A. Spanu⁵, G. Madeddu⁵; ¹Section of Nuclear Medicine and Health Physics, Dept of Surgical and Biomedical Sciences, University of Perugia, PERUGIA, ITALY, ²Dept of Engineering, University of Perugia,

PERUGIA, ITALY, ³Unit of Neurology, Perugia University Hospital, PERUGIA, ITALY, ⁴Section of Diagnostic Imaging, Dept of Surgical and Biomedical Sciences, University of Perugia, PERUGIA, ITALY, ⁵Unit of Nuclear Medicine, University of Sassari, SASSARI, ITALY.

Aim: Classification Tree algorithm (CIT) is an automatic classifier composed of a set of logical rules, organized as a decision tree to produce an optimised threshold based classification of data, thus providing discriminative cut-off values. We applied a CIT to 123I-FP-CIT brain SPECT semiquantitative data, to obtain cut-off values of radiopharmaceutical uptake ratios in basal ganglia able to identify PD and other conditions. **Materials and Methods:** 123I-FP-CIT brain SPECT (Millenium VG, G.E.M.S.) was performed using semiquantitative analysis with Basal Ganglia (BasGan) V2 software according to EANM guidelines in 141 patients with mild movement disorders. Among them 99 resulted as PD [51M and 48 F; range of age: 60-81 yrs, Hoehn and Yahr score (HY): 0.5-1.5; Unified Parkinson Disease Rating Scale (UPDRS) score: 6-38] and 42 resulted as non-PD (Essential Tremor and drug-induced PD, 20 M and 22 F; range of age 60-80 yrs). The final diagnosis was confirmed by a clinical follow-up of at least 6 months. A 10-fold cross validation was applied by repeating 1000 random experiments. This allowed the statistical evaluation the "average performance" of CIT. **Results:** According to CIT, the probability of correct classification in patients with PD was $85.38 \pm 13.17\%$ (mean \pm SD) and in non-PD patients $93.96 \pm 8.57\%$. For CIT, the first decision rule gave a value for the right putamen (RP) of 2.23 ± 0.14 , thus meaning that if RP values were lower patients were classified as PD, while if RP values were higher patients were classified as non-PD. More complex CIT structures, including caudate nuclei and left putamen values, were tested to refine the classification performance, but in our data these additional features appeared to be less significant. **Conclusion:** CIT accurately classified PD and non-PD patients by means of 123I-FP-CIT brain SPECT data, allowing to obtain cut-off values able to differentiate these groups of subjects. Furthermore RP uptake values in our patients resulted as the most discriminant to provide the diagnosis, probably due to a certain number of patients with initial prevalence of left clinical symptoms.:

P276

The utility of the combination of a SPECT study with I-123-ioflupane (DaTSCAN) and I-123 MIBG myocardial scintigraphy in differentiating Parkinson disease from other degenerative parkinsonian syndromes

N. Uyama¹, H. Otsuka², T. Shinya¹, Y. Otomi¹, M. Harada¹; ¹Tokushima University Hospital, Tokushima, JAPAN, ²Department of Medical Imaging/Nuclear Medicine, Institute of Biomedical Sciences, Tokushima University Graduate School, Tokushima, JAPAN.

Objectives: The molecular imaging of presynaptic nigrostriatal neuronal degeneration and sympathetic cardiac innervation with SPECT (DaTSCAN and MIBG scintigraphy) are useful tools for differentiating idiopathic Parkinson disease (PD) from other degenerative parkinsonian syndromes (non-PD) in the clinical setting. Nevertheless, these imaging modalities are often not sufficient to diagnose PD. The aims of this study were to semi-quantitatively evaluate the diagnostic capacities of DaTSCAN and MIBG scintigraphy and to explore the diagnostic accuracy of the combination of these modalities in degenerative parkinsonian syndromes. **Materials and Methods:** The SPECT radiotracers 123I-2 β -carbomethoxy-3 β -(4-iodophenyl)-N-(3-fluoropropyl) nortropane (FP-CIT) and meta-123I-iodobenzylguanidine (MIBG) were used to research presynaptic membranes of the terminals of dopaminergic projections (DaTSCAN) and myocardial adrenergic innervation (MIBG scintigraphy), respectively. Patients with PD (n=16; male 5, female 11; age 59.8 ± 13.1 years) and patients with non-PD (n=20; male 12, female 8; age 62.1 ± 14.8 years) who underwent both DaTSCAN and MIBG

scintigraphy were enrolled in this retrospective study. We used the ROC analyses in setting the cut-off values of specific binding ratio (SBR) in DaTSCAN and the heart to mediastinum ratio in delayed scan (delayed H/M ratio) in MIBG scintigraphy for differentiating PD from non-PD. The sensitivity, specificity, and test accuracy for the individual imaging methods were calculated. In addition, we compared these diagnostic accuracies with that of the combination of two modalities. Results: The sensitivity and specificity of SBR were 81.5% and 45.0%, respectively, with the cut-off value of 3.245. The sensitivity and specificity of delayed H/M ratio were 68.8% and 65.0%, respectively, with the cut-off value of 2.23 on MIBG scintigraphy. The analyses showed low accuracies for differentiation of PD and non-PD using each molecular approach, respectively (DaTSCAN, 61.1%; MIBG, 66.6%). In contrast, the accuracy was increased by the combined use of the two semi-quantitative analyses using a cut-off value of SBR of <3.245 and a cut-off value of delayed H/M ratio of <2.23. These indices distinguished PD from non-PD with a sensitivity of 68.7%, specificity of 85%, accuracy of 77.8%, predictive positive value of 77%, and predictive negative value of 78.5%. Conclusion: These results suggested that the combination of DaTSCAN and MIBG scintigraphy may improve the diagnostic accuracy in differentiating PD from non-PD.

P277

The Loss of Extrastriatal As Well As Striatal [¹²³I]FP-CIT Binding Is More Pronounced in MSA-P and PSP Than in Parkinson's Disease

M. Joling¹, C. Vriend¹, O. A. Van den Heuvel¹, P. G. H. M. Raijmakers¹, H. W. Berendse¹, J. Booij²; ¹VU University Medical Center, Amsterdam, NETHERLANDS, ²Academic Medical Center, Amsterdam, NETHERLANDS.

Purpose: [¹²³I]FP-CIT SPECT is a well-validated technique to assess dopamine transporter (DAT) binding in vivo, and it can be used to detect dopamine cell loss in parkinsonian syndromes like Parkinson's disease (PD), progressive supranuclear palsy (PSP) and multiple system atrophy (MSA). In addition to its affinity for DAT, [¹²³I]FP-CIT has modest affinity for the serotonin transporter (SERT). Extrastriatal [¹²³I]FP-CIT binding, for example in the diencephalon and the midbrain/pons, predominantly represents SERT binding. A growing body of evidence suggests that DAT and SERT binding in the midbrain of PSP and the parkinsonian variant of MSA (MSA-P) patients is lower than in patients with PD, indicating a possible use to improve differential diagnostics. In this light, we hypothesised that in addition to striatal DAT binding, extrastriatal [¹²³I]FP-CIT binding in SPECT scans may contribute to the differentiation between PSP, MSA-P and PD in clinical practice. **Methods:** We included 9 MSA-P, 7 cerebellar variant of MSA (MSA-C), 13 PSP and 30 PD age- and gender matched consecutive cases from the outpatient clinic for movement disorders at the VU University Medical Center in Amsterdam, The Netherlands. The [¹²³I]FP-CIT SPECT images were acquired 3 hours after bolus injection on a dual-headed system using a fanbeam collimator. [¹²³I]FP-CIT binding was analysed with region of interest (ROI) and voxel-based methods in the DAT-rich caudate nucleus and posterior putamen (striatum) and SERT-rich hypothalamus, thalamus and pons (extrastriatal). Non-specific binding was determined by assessing cerebellar binding. The specific to non-specific binding ratio was used as the outcome measure. **Results:** In ROI- or voxel-based analyses we observed lower striatal [¹²³I]FP-CIT binding in the caudate nucleus in PSP ($P=0.001$ left; $P=0.010$ right) than in PD patients, and a trend in MSA-P ($P=0.078$ left, $P=0.081$ right). PSP patients showed lower caudate binding than MSA-C patients ($P=0.004$ left; $P=0.005$ right). In the posterior putamen we observed lower binding in PSP ($P=0.001$ left; $P=0.003$ right), MSA-P ($P=0.001$ left; $P=0.002$ right) and PD (left: $P=0.020$) than in MSA-C. Furthermore, voxel based analysis of extrastriatal [¹²³I]FP-CIT binding showed lower binding in the hypothalamus of MSA-P and PSP patients than PD patients ($P=0.003$, $P<0.001$

respectively). **Conclusion:** In addition to striatal DAT, hypothalamic SERT binding in MSA-P and PSP patients was significantly lower than in PD and MSA-C patients. Consequently, combining information on striatal and extrastriatal [¹²³I]FP-CIT binding to DAT and SERT, respectively, may increase the role of SPECT imaging in the differential diagnosis of parkinsonian syndromes.

P278

Combined 123I Ioflupane SPECT and 123I MIBG cardiac scintigraphy use in Parkinson Disease (PD) and Vascular Parkinsonism (VP) differential diagnosis

S. Nuvoli¹, M. Piras², A. Mulas¹, S. Contu¹, B. L. J. Pung¹, B. Piras¹, B. Palumbo³, A. Spanu¹, G. Madeddu¹; ¹Unit of Nuclear Medicine, Clin. and Experimental Medicine DPT, University of Sassari, Sassari, ITALY, ²Unit of Neurology; Clin. and Experimental Medicine DPT, University of Sassari, Sassari, ITALY, ³Section of Nuclear Medicine, Surg. and Biomed. Sciences DPT, University of Perugia, Perugia, ITALY.

AIM: Despite 123I Ioflupane SPECT clinical relevance in PD and VP differential diagnosis, vascular damage (Vd) in basal ganglia or correlated cortical areas could reduce its specificity. In this study we evaluated 123I Ioflupane SPECT and 123I MIBG cardiac scintigraphy clinical usefulness in differentiating PD from VP, occurring Vd. **METHODS:** We studied 38 patients with Vd at MRI who underwent brain SPECT, 3-4 hrs after 148 MBq 123I Ioflupane i.v. injection, using dual head gammacamera. SPECT images were evaluated by qualitative and quantitative analyses, the latter by dedicated software which quantifies specific dopaminergic activity as Binding Potentials (BP) with cut-off value of 3.3. After 15-21 days, cardiac planar scintigraphy in anterior and left anterior oblique views in both early (15 min.) and delayed (240 min.) phases, was performed after 111 MBq 123I-MIBG i.v. injection. Qualitative and semi-quantitative analyses were evaluated, the latter calculating heart/mediastinum (H/M) ratio by mean count density measurement in manually drawn ROIs in anterior view (cut-off value: 1.56). **RESULTS:** 123I Ioflupane SPECT showed reduced tracer uptake in 33/38 patients (86.9%; Group A) and normal in 5/38 cases (13.1%; Group B). In Group A, 123I MIBG cardiac uptake, in early and delayed phases, was homogeneous in 18/33 cases (54.5%; Group A1) and reduced in 15/33 (45.5%; Group A2). H/M values were >1.56 in Group A1 and <1.56 in Group A2 cases, in both early and delayed phases. Group A1 early and delayed H/M mean values (1.71±0.10 and 1.74±0.08, respectively) were significantly ($p<0.001$) higher than Group A2 values (1.31±0.021 and 1.34±0.16, respectively). No statistical difference was found between early and delayed H/M mean values in the two groups. In Group B, 123I MIBG cardiac uptake was homogeneous in 5/5 cases, in both early and delayed phases, and H/M was >1.56 in all cases. No statistical difference was found when early (1.70±0.04) and delayed (1.82±0.09) H/M mean values were compared. Groups A1 and B cases (23/38; 60.5%) were clinically considered as VP, while Group A2 (15/38; 39.5%) as PD. **CONCLUSION:** 123I MIBG cardiac scintigraphy with H/M ratio calculation proved a useful tool in PD and VP differential diagnosis in our cases occurring basal ganglia Vd, while 123I Ioflupane SPECT alone showed lower performance. Cardiac scintigraphy with H/M ratio, also in early phase alone, combined with 123I Ioflupane SPECT can be considered a valid support to achieve correct diagnosis, to better define disease progression and prognosis and to perform appropriate treatments.

P279

Dopamine transporter imaging using ^{99m}Tc-TRODAT-1 SPECT in Parkinson's disease with and without levodopa-induced dyskinesias

F. A. Pitella, L. A. Santos, A. Trevisan, E. Itikawa, M. Kato, L. Wichert-Ana; HC-FMRP-USP, Ribeirão Preto, BRAZIL.

Levodopa is the most effective and common drug for treating Parkinson's Disease (PD). However, long-term use of levodopa is often complicated by significantly disabling fluctuations and dyskinesias. Younger age of Parkinson's disease onset, disease severity, and high levodopa dose increase the risk of development of levodopa-induced dyskinesias (LID). The underlying mechanisms for LID are unclear. Some authors have shown evidence that presynaptic dopaminergic denervation in PD plays a role in the development of LID. Objective: To evaluate the dopamine transporter (DAT) density in Parkinson's disease patients with ^{99m}Tc -TRODAT-1 and compare with other clinical data. Methods: This study included 60 volunteer patients, 20 healthy and 40 patients of the Clinical Hospital of Ribeirão Preto Medical School, University of São Paulo (HC-FMRP-USP), with confirmed PD by UK Parkinson's Disease Society Brain Bank Clinical Diagnostic Criteria. All patients were evaluated by an expert neurologist in extrapyramidal disease and underwent SPECT with ^{99m}Tc -TRODAT-1. The images analysis and DAT quantification were performed blindly and separately by two experienced nuclear physicians (examiner 1 and 2). RESULTS: The preliminary results shows: 34,4 % of patients with PD developed LID. LID group (group 1): mean age = 61,2 years (SD = 9,3), mean duration of the PD = 8,9 years (SD = 7,2), mean L-dopa dose = 1060 mg (SD = 340), mean number of daily doses of levodopa = 3,6 (SD = 1,6), UPDRS-3 = 20,75 (SD = 12,8), mean binding potential (BPI) of ipsilateral striatum: 0,41 (SD = 0,28), mean binding potential (BPI) of contralateral striatum: 0,42 (SD = 0,16). DP without dyskinesias (group 2): mean age = 56,9 years (SD = 8,4), mean duration of the PD = 8,3 years (SD = 5,9), mean L-dopa dose = 498 mg (SD = 340), mean number of daily doses of levodopa = 6,3 (SD = 1,8), mean UPDRS-3 = 23,9 (SD = 17), mean binding potential (BPI) of ipsilateral striatum: 0,56 (SD = 0,28), mean binding potential (BPI) of contralateral striatum: 0,52 (SD = 0,31). Healthy patients: mean binding potential (BPI) of ipsilateral striatum: 1,17 (SD = 0,22), mean binding potential (BPI) of contralateral striatum: 1,20 (SD = 0,23). Conclusion: Decrease of dopamine transporter density in Parkinson's disease patients seems to correlate with LID.

P280

Use of 123I-MIBG SPECT in association with 123I-FP-CIT in patients with Early Parkinson's Disease: a new point of view

V. Frantellizzi, M. Ullo, G. A. Follacchio, M. Pontico, M. Ricci, S. Sollaku, B. Berloco, M. Filauri, M. Liberatore, F. Monteleone, G. De Vincentis; Sapienza University of Rome, Rome, ITALY.

Early diagnosis of Parkinson's disease (PD) is often difficult. In the differential diagnosis of PD from parkinsonisms, Single Photon Emission Computed Tomography (SPECT) using 123I-FP-CIT (Ioflupane, DaTSCAN) is recommended. Myocardial innervation imaging using 123I-MIBG (Iobenguane, AdreView) has emerged as a useful method to support the clinical diagnosis of PD. However, recent studies have shown that Heart to Mediastinum (H/M) ratio, derived from 123I-MIBG scan, is not always helpful to identify Early PD while the role of Late Summed Scores (LSS) has never been assessed. Purpose of our study was to evaluate the role of LSS derived from 123I-MIBG SPECT, combined with 123I-FP-CIT in these patients. 15 consecutive patients affected by suspected PD were staged by using the Hoehn-Yahr classification. No patient had evidence of cardiac disease, diabetes mellitus, cerebrovascular diseases or other Central Nervous System disorders. Patients were given an intravenous injection of 185 MBq of 123I-FP-CIT and brain SPECT images were obtained 3 hours after injection. Semiquantitative analysis was performed by selecting three consecutive slices with the highest striatal uptake. Regions of interest of a fixed size were bilaterally drawn over the striatum (caudate nucleus and putamen); the occipital cortex was used as the reference region and Striatum/occipital lobe ratio (R/L) was calculated. Within 2 months from the previous study, patients underwent 123I-MIBG study. 20 and 240 minutes after i.v. administration of 123I-MIBG (185 MBq), planar and SPECT cardiac images were obtained. On planar images, Late H/M ratio was calculated. SPECT studies were

processed with Myovation software (GE Healthcare) and raw data for each one of the 17 segments of a standard polar map were obtained. Using a 5-point visual scoring model, data were semi-quantified and LSS was obtained. All patients presented a H-Y stage 1. 123I-FP-CIT images were normal in 3 out of 15 cases (R/L>3.5). Of them, 2 patients showed normal MIBG scan (H/M>1.43; LSS<26), whereas the last patient showed normal late H/M ratio, but pathological LSS value. Among the 12 patients with pathological 123I-FP-CIT, LSS resulted >26 in all cases, while only 8 patients showed a late H/M ratio<1.43. Early differentiation of PD and other neuro-degenerative parkinsonism is crucial, so there is an important need to improve the diagnostic accuracy. Our data shows how the extent of cardiac MIBG distribution, expressed in terms of LSS, appears as a sensitive marker for early detection of PD. Those preliminary data should be validated in a larger cohort of patients.

P281

Computed tomography guided anatomic standardization for quantitative assessment of dopamine transporter SPECT

K. Yokoyama¹, E. Imabayashi², T. Sako¹, D. Sone¹, Y. Kimura¹, N. Sato¹, H. Matsuda²; ¹National Center of Neurology and Psychiatry, Kodaira, JAPAN, ²Integrative Brain Imaging Center, National Center of Neurology and Psychiatry, Kodaira, JAPAN.

PURPOSE: For quantitative assessment of dopamine transporter (DAT) using 123I-FP-CIT SPECT (DaTscan), anatomic standardization is preferable for achievements of objective and user-independent quantification of striatal binding using a volume-of-interest (VOI) template. However, low accumulation of DAT prominently in posterior striatum in Parkinson's disease (PD) would lead to deformation error stretching anterior striatum posteriorly when using DaTscan-specific template without any structural information for anatomic standardization. To avoid this deformation error, we applied computed tomography (CT) data obtained from SPECT/CT equipment to anatomic standardization of DaTscan. METHODS: We retrospectively analyzed DaTscan images of 130 patients (67 women and 63 men, 66.5 ± 11.9 y.o.) with parkinsonian syndromes (PS): 80 PD (36 women and 44 men, 67.5 ± 10.4 y.o.) and 50 non-PD patients (31 female and 19 male, 64.9 ± 13.8 y.o.). First we segmented grey matter (GM) from CT images using statistical parametric mapping (SPM) 12. Then these GM images were anatomically standardized using the diffeomorphic anatomical registration using exponentiated Lie algebra (DARTEL) algorithm. Next, DaTscan images were warped with the same parameter as used in the CT anatomic standardization. The target striatal VOIs for decreased DAT in PD were generated from the SPM12 group comparison of 20 DaTscan images from each group. We applied these VOIs to DaTscan images of remaining patients of both groups and calculated the specific binding ratios (SBR) using nonspecific counts in a reference area. In terms of differential diagnosis of PD and non-PD groups using SBR, we compared the present method with other two methods, which have been already released as software programs for quantitative assessments of DaTscan images, DaTQUANT and Tossici-Bolt's methods. RESULT: SPM12 group comparison showed significant DAT decrease in PD patients at bilateral whole striatum. Of all three methods the present CT-guided method showed the greatest power for discriminating PD and non-PD groups, completely separating the two groups. CONCLUSION: CT-guided anatomic standardization using DARTEL algorithm was promising for quantitative assessment of DaTscan images.

P282

Different roles of dopamine transporter SPECT and I-123 MIBG myocardial scintigraphy to assess clinical severity in patients with Parkinson's disease

N. Okano¹, T. Sasaki², K. Takahashi², N. Araki², T. Yamamoto², M. Niitsu¹, S. Nishimura³, I. Matsunari⁴; ¹Department of Radiology,

Saitama Medical University Hospital, Saitama, JAPAN, ²Department of Neurology, Saitama Medical University Hospital, Saitama, JAPAN, ³Department of Cardiology, International Medical Center, Saitama Medical University, Saitama, JAPAN, ⁴Division of Nuclear Medicine, Saitama Medical University Hospital, Saitama, JAPAN.

Purpose: The aim of our study was to comparatively investigate the roles of dopamine transporter (DAT) single photon emission computed tomography (SPECT) and I-123 metaiodobenzylguanidine (MIBG) myocardial scintigraphy in the clinical severity of the Parkinson's disease (PD), especially focusing on impaired motor function affecting the activity of daily living (ADL). **Materials and Methods:** Data for 65 consecutive PD patients who underwent both DAT and MIBG SPECT imaging were reviewed. Associations between the imaging variables, and the Hoehn and Yahr (H&Y) and the self-supportive care (SSC) scale were investigated. Univariate and multivariate regression analyses were performed to determine the factors associated with dependent ADL. **Results:** After applying the exclusion criteria, 45 patients were analyzed (age, 73.1 ± 9.3 years; 23 male; H&Y stage 1: $n = 12$, stage 2: $n = 14$, stage 3: $n = 10$, stage 4: $n = 5$ and stage 5: $n = 4$; SSC scale dependent ADL: $n = 29$). DAT SPECT variables were significantly associated with the clinical severity of PD as assessed by H&Y staging, while MIBG variables were not. After dividing the H&Y stages into 2 groups, both DAT and MIBG uptakes in the severe stage group were lower than in the mild-to-moderate stage group; because DAT variables gradually changed throughout progressive stages, while the MIBG variables only changed in the advanced stage. In multivariate analysis that included clinical and imaging variables, a lower average specific binding ratio for DAT SPECT and early heart-to-mediastinum ratio for MIBG myocardial scintigraphy were significantly associated with dependent ADL. **Conclusions:** Both DAT and MIBG findings are associated with the clinical severity and dependent ADL. In the early and middle stages of PD, DAT SPECT is a stronger indicator of the severity than MIBG myocardial scintigraphy.

P283

Quantitative Structure-Activity Relationship Study to Elucidate the Structural Requirements for Positron Emission Tomography Tracers in Neuroimaging of Parkinson's Disease

M. salahinejad¹, Z. Tamiji², A. Niazi², M. Aboudzadeh¹; ¹Nuclear Science and Technology Research School, Tehran, IRAN, ISLAMIC REPUBLIC OF, ²Department of Chemistry, Arak Branch, Islamic Azad University, Arak, IRAN, ISLAMIC REPUBLIC OF.

Parkinson's disease (PD) as a serious neurological disorder has attracted great interest due to fail current manner of treatment to achieve long-term control. Since adenosine receptors antagonists have been shown to restore the deficits arise from decline of the striatonigral dopamine system, which is compromised by the loss of striatal neurons in this disease, A_{2A} antagonism provides a possible treatment for PD. Positron emission tomography (PET) is non-invasive medical imaging modality for in vivo imaging and eventual diagnostic central nervous system. Quantitative structure activity relationship (QSAR) technique is one of the significant research fields in drug design and medicinal chemistry. The QSAR approach assumes that differences in the structural or physical properties measured experimentally account for differences in the observed biological or chemical properties. In the present investigation, we perform quantitative structure activity relationships (QSAR) analysis for a series of 35 Xanthine ligands as PET tracers for mapping adenosine receptors as probes for diagnosis PD's disease. Several hundred numbers of molecular descriptors was used as independent variables and binding affinity of ligands to A_{2A} R receptors was considered as dependent variable. Several variable-selection techniques were applied to choose the best subset of molecular descriptors that would lead to good regression

equations. Multi linear regression (MLR) was applied to model construction. Among several models developed, the best model was a five-variable MLR model with a leave one out cross-validated correlation coefficient (Q^2) of 0.84 ± 0.02 and a correlation coefficient (R^2) of 0.90 ± 0.01 for prediction power of A_{2A} R binding. The QSAR model identified the molecular properties such as van der Waals surface area combination with the electrostatic property, the number of double bonds and rotatable bonds, partial charge, hydrophilic properties and molecular potential energy played important roles in the prediction models of A_{2A} R antagonist PET tracers. We expect the provided model to be a helpful tool in the prediction of the A_{2A} R Binding affinity and A_{2A} R-selectivity, in a fast and costless manner, for any future studies that may require an estimation of these important characteristics of A_{2A} R antagonist PET tracers.

P284

18F-DOPA for Multipurpose PET Imaging to Detect Amino Acid Metabolism and to Assess Brain Dopamine Function

M. Scarlattei¹, G. Baldari¹, C. Carla¹, S. Migliari¹, A. Sammartano¹, R. Dalla Valle², S. Calzetti³, L. Ruffini¹; ¹Nuclear Medicine Dept, University Hospital of Parma, Parma, ITALY, ²Surgery and Transplant Unit, University Hospital of Parma, Parma, ITALY, ³Neurology Unit, University Hospital of Parma, Parma, ITALY.

Functional PET imaging has been growing rapidly developing different radiopharmaceuticals (with different uptake mechanisms) to provide accurate staging of catecholamine-secreting tumours. In particular, 18F-DOPA has been proposed as a useful PET imaging tool to detect neuroendocrine cells able to take up, decarboxylate and store amino acids and their amines. Moreover, 18F-DOPA is a viable radiotracer for glioma imaging and treatment planning and to investigate presynaptic dopaminergic function. This study aimed to assess clinical settings for 18F-DOPA PET/CT utilization as highly sensitive non-invasive diagnostic tool for early detection of mass lesions in patients with catecholamine-secreting tumours and brain tumor. Moreover, we evaluate DOPA-PET imaging as simple method of image analysis in routine clinical studies, associated with more complex approaches revealing hidden aspects of brain dopamine in the pathophysiology of Parkinson's disease. **METHODS** We prospectively enrolled all the PET studies performed with 18F-DOPA since Dec 2014. The intravenously injected dose of 18F-DOPA (IasoDOPA®, Iason GmbH, Austria) was 260 MBq. The radiochemical purity exceeded 95% in every case. Whole body PET studies were acquired using an integrated system (GE Discovery ST and GE IQ) 60 min after i.v. tracer injection, from the skull basis to the middle thigh. A dynamic 90-min brain PET study was performed, in a 3D mode, for pts with Parkinson's disease. **RESULTS** PET imaging with 18F-DOPA was performed in 38 patients: 9 pts with brain tumor, 15 pts with suspicion of catecholamine-secreting tumours (pheochromocytoma, paraganglioma, insulinoma, medullary thyroid carcinoma) and 11 pts with rest-less leg syndrome and Parkinson disease to characterize dopaminergic transmission. PET showed residual neoplastic tissue in 4/9 brain tumors with doubtful MR. Pheochromocytoma and paraganglioma were confirmed by imaging and surgery in 8 cases. Insulinoma was detected in 3 cases. In Parkinson's disease DOPA-PET allowed characterization of basal ganglia function and subregional activity assessment (i.e. hypothalamus). PET informations have driven patient management in all pts with neoplastic lesions, and changed treatment options or sequence in 5 pts with brain tumor and 9/15 pts with catecholamine-secreting tumors. **CONCLUSIONS** Results demonstrate that 18F-DOPA is a flexible multipurpose tracer for clinical routine and pathophysiology investigation. In the oncologic setting DOPA-PET allows appropriate use of resources in patient management, changing or well driving treatment option in most of them. In the motor syndrome PET with 18F-DOPA PET is a particularly useful tool for the *in vivo* assessment of dopamine terminal density and dopamine neurotransmission.

P-24 – Tuesday, October 18, 2016, 16:00 - 16:30, Poster Exhibition Hall
Neurosciences: Neurodegeneration

P285

Quantification of time-related decline of dopamine transporter from consecutive DaTSCAN images

H. Fayolle¹, P. Gantet², A. Salabert³, J. Delrieu¹, C. Brefel-Courbon¹, T. Voisin¹, P. Payoux³; ¹CHU Toulouse, Toulouse, FRANCE, ²University Paul Sabatier, Toulouse, FRANCE, ³Toulouse neuro-imaging center ToNIC, Toulouse, FRANCE.

BACKGROUND: Dopamine neurodegeneration has been widely studied in population as for example in the international multicentric database of PPMI (*Parkinson's Progression Markers Initiative*). However, such studies has been realised on population mainly as transversal analysis. The aim of this longitudinal study is firstly to compare by innovative quantification tool the evolution of dopaminergic neurodegeneration between a normal (NG) and a pathological groups (PG), and secondly to test the impact of the antiparkinsonian treatment. **METHODS:** 60 patients who underwent two consecutive DaTSCAN were enrolled in this retrospective study in the Nuclear Medecine Department of Toulouse from 2002 to 2016. We have analysed the evolution of the striatum binding ratios (SBR: mean counts of Striatal ROI – mean counts of Background ROI) / (mean counts of Background ROI) with DaTsoft3D®, a software using an innovative self-calibrated based correction of partial volume effect. SBR were compared to PPMI database to be classify as NG or PG (SBR <1.7). We found 25 patients in NG, (age :63 ± 10.4 yo, sex ratio 11F/14M, delay between the 2 scans : mean 2,4 years, SD 2,2 years), and 35 patients in PG (age :68 ± 10.6 yo, sex ratio 11F/35M, delay : mean 3,3years, SD 2,6 years). In PG, we analyzed patients receiving treatment (PG1 group, 18 patients, treatment duration : 4 ± 3 yo) or not (PG0 group, 17 patients). **RESULTS:** The variation of SBR in NG did not significantly differ from 0 (1% per year, p=0.54), while it declined significantly in PG (-11% per year, p=0.0003). DaTsoft3D has shown significantly differences (-12%, p=0.0007 for Welch-test assuming unequal variances) between NG and PG, while PG0 (mean -11%) and PG1 (-9%) did not differ significantly (2,2%, p=0.74). **CONCLUSION:** DATSoft3D software was effective for the monitoring of dopaminergic presynaptic loss. The decrease of the SBR value observed in NG is closer that one observed in the literature (6.8% by decade p=0.34, Nicasastro et al. 2016) and PG differs from physiological value (p=0.0007). Unexpectedly in our study the dopamine loss rate was more important in the pathological group compared to the PPMI database which have not consider the loss for single patients (-11% vs -0,006% per year). Probably due to the low number of patients, we could not demonstrate a benefit from the antiparkinsonian treatment on the presynaptic neurodegeneration. DATSoft3D may be helpful for prospective studies comparing the impact of various treatments on dopamine loss slowdown.

P286

Evaluation of a novel extracellular matrix radiotracer: expression of proteases uPA and KLK8 is correlated with seizure outcome in an animal model of acquired epilepsy

S. Missault, H. Amhaoul, D. Thomae, A. Van Eetveldt, P. Van Der Veken, J. Joossens, S. Staelens, S. Dedeurwaerdere; University of Antwerp, Wilrijk, BELGIUM.

Aim: Serine proteases urokinase-type plasminogen activator (uPA) and kallikrein-8 (KLK8) are modulators of the extracellular matrix. They may play an important role in plasticity following an insult and hence the development of epilepsy. In order to assess uPA/KLK8 following brain insult, a new SPECT probe, [¹¹¹In]MICA-401 with high affinity for both proteases was recently developed. This study evaluated the radiotracer

post-mortem and *ex vivo* in animal models of acquired epilepsy. **Methods:** a) The tracer was implemented in an *in vitro* autoradiography (ARG) study in two rat models, the kainic acid-induced *status epilepticus* (KASE) and controlled cortical impact (CCI) models. KASE and control rats were sacrificed at 7d (n=11, n=6 respectively) and 12w post-SE (n=9, n=6 respectively); CCI and sham rats at 4d post-injury (n=5/group). Brain sections were incubated with 50nM [¹¹¹In]MICA-401 to assess total binding. 1mM of UAMC-01162, from which the cold standard is derived, was added to assess non-specific binding. b) Three CCI and sham rats were injected with radiotracer at 3d post-injury (39.1±2.2MBq). 7d post-injury, brains were resected for *ex vivo* ARG. **Results:** a) In the KASE model a significant decrease of [¹¹¹In]MICA-401 binding was observed in the latent phase of epileptogenesis in CA3 subregion of the hippocampus (p≤0.05) and extrahippocampal temporal lobe (p≤0.01) vs controls. Decrease in [¹¹¹In]MICA-401 binding further progressed in the chronic phase when spontaneous seizures were present in CA1/CA2, dentate gyrus, parietal cortex (p≤0.05), and temporal lobe (p≤0.001) vs controls. A correlation was observed between specific binding of [¹¹¹In]MICA-401 in hippocampus and i) the number of seizures and ii) the seizure severity in KASE rats at 12w post-SE (p≤0.05). In the CCI model a significant signal decrease was found in perilesional cortex and ipsilateral dentate gyrus (p≤0.01) vs shams. b) On the contrary, an increased tracer uptake was observed in the perilesional cortex and ipsilateral hippocampal formation of CCI rats vs shams at 4d post-injection (p≤0.1), confirmed by *ex vivo* ARG. This is due to an increase in blood-brain barrier (BBB) penetrability. **Conclusion:** KASE rats with a high number of seizures or proportion of generalised convulsive seizures showed a more pronounced decrease in uPA/KLK8 expression compared to rats with low number of seizures or less severe seizures. This decrease in uPA/KLK8 may be due to interictal hypometabolism, which has to be further investigated. While [¹¹¹In]MICA-401 is an interesting tracer for *post-mortem* assessment of uPA/KLK8, its *in vivo* implication is hindered by limited BBB penetrability.

P287

Changes in Cerebral Metabolism in Parkinson's Disease: Combined PET and MRS Study

I. G. Khomenko¹, G. V. Kataeva¹, E. A. Gromova¹, D. S. Susin¹, A. A. Bogdan¹, I. V. Milukhina², M. N. Karpenko²; ¹N.P.Bechtereva Institute of the Human Brain, RAS, St.Peterburg, RUSSIAN FEDERATION, ²Institute of Experimental Medicine, RAMS, St.Peterburg, RUSSIAN FEDERATION.

Introduction. Novel neuroimaging techniques allow getting valuable information about brain metabolism *in vivo*. A large amount of studies dedicated to the evaluation of the diagnostic role of proton magnetic resonance spectroscopy (H-MRS) and positron emission tomography (PET) data in neurodegenerative diseases, but there are only few studies matching these findings. We consider that such combined studies could contribute to the understanding of neurodegeneration pathogenesis. The aim of the current research was to investigate regional cerebral metabolism according to the FDG PET and H-MRS data in patients with Parkinson's disease (PD). **Methods.** 26 patients suffered from PD (age 62,8±9,6; 14 males; 1,0-3,0 stages by Hoehn and Yahr scale) were examined. Multivoxel H-MRS was performed on Achieva 3T scanner, Philips (2D PRESS, TE/TR=53/1500 ms) and included supraventricular white matter (WM) and medial cortex. Anatomical localization: the area of MRS study (8*9 voxels (10*10*15 mm), whole volume 80*90*15 mm) was divided into 9 ROIs: 6 in WM (3 ROIs: anterior, medium and posterior for each hemisphere) and 3 ROIs in medial cortex. NAA/Cr, NAA/Cho, Cho/Cr. Glx/Cr ratios (NAA - N-acetylaspartate, Cr -

creatine, Cho - choline, Glx - glutamin + glutamate) were analyzed. FDG PET study was performed with GE Discovery-710. PET images were normalized with SPM8, cerebral glucose metabolism rate (CMRglu) in Brodmann areas (BA) were calculated using WFU Pickatlas. Results. Correlations of H-MRS data and CMRglu in frontal and parietal cortex bilaterally were revealed: CMRglu in BA 8,9,10,47 and 39 correlated negatively with Cho/Cr in WM of semioval centers of the ipsilateral hemisphere ($r = -0.6 - 0.8$; $p < 0.01$). CMRglu in left and right cingulate cortex correlated positively with NAA/Cho ratio ($r = 0.6 - 0.7$; $p < 0.01$) in ipsilateral WM. Conclusions. NAA is commonly considered to be the neuronal integrity marker, so the obtained correlations of its concentration with glucose metabolism can be easily explained. However, the clinical significance of Cho/Cr ratio obtained in spectroscopy of visually intact neural tissue is not so clear: different studies found both its elevation and decrease in neurodegenerative diseases. Increase of Cho/Cr ratio coupled with the decreased CMRglu revealed in the present study can be related to the neurodegeneration process (neuron membranes degradation causes elevation of Cho in WM and decrease of cortex glucose metabolism). Further research should be performed to clarify the diagnostic role of the revealed metabolites interrelations.

P288

Effect of noradrenergic denervation on alpha2-adrenoceptor binding in rat brain in vivo

J. Phan¹, S. Jacobsen¹, A. Gjedde²; ¹Aarhus University, Aarhus, DENMARK, ²University of Copenhagen, Copenhagen N, DENMARK.

Introduction: Disrupted noradrenergic neurotransmission is implicated in Parkinson's and Alzheimer's diseases. However, the relative effects on noradrenaline levels and receptor density in vivo are uncertain. Tracer [11C]yohimbine is a radioligand of alpha2 adrenoceptors with sensitivity to noradrenaline release in pigs and rats. Here, we use measures of [11C]yohimbine binding to alpha2 adrenoceptor sites and noradrenaline release in rat brain in vivo to test the hypothesis that noradrenaline levels decline more than the available receptors in selected brain regions after noradrenergic denervation. Methods: Noradrenergic denervation was induced by IP treatment (50 mg/kg) of the selective neurotoxin (N-(2-chloroethyl)-N-ethyl-2-bromobenzylamine (DSP-4)) 7 days prior to positron emission tomography (PET). We determined [11C]yohimbine binding potentials at two levels of receptor occupancy, at baseline followed by amphetamine challenge (2 mg/kg) in DSP-4 pretreated and naïve animals. We calculated [11C]yohimbine binding potentials as bound vs. free ratios, using the yohimbine partition coefficient (VND), obtained from the Inhibition plot, a linearization of the Michaelis Menten equations applied to baseline and inhibition. Results: The binding potentials in naïve animals were greatest in striatum, followed in descending order by thalamus, frontal cortex, pons and cerebellum. Amphetamine challenge significantly reduced the binding potentials with a uniform magnitude of 38% in all regions of interest, indicating uniform noradrenaline increase. DSP-4 denervation exhibited significantly lower binding potentials than naïve animals, suggesting acute decline of alpha2 adrenoceptor density. The effect of amphetamine challenge after DSP-4 treatment was greater than in naïve animals but with regional heterogeneity. With amphetamine, the binding potentials declined 51-67%, indicating variable and regionally differential release from surviving projections. Conclusion: The greater decline of receptors than of noradrenaline levels is at variance with the original hypothesis stated above.

P289

FDG-PET pattern of C9orf72 positive and Amyotrophic Lateral Sclerosis

P. SOPENA-NOVALES; HOSPITAL UNIVERSITARIO Y POLITECNICO La FE, valencia, SPAIN.

Aim: Under the hypothesis that C9orf72 positive and amyotrophic lateral sclerosis (C9ORF72-ALS) patients could have a distinctive FDG-PET findings, the aim was to evaluate FDG-PET pattern of ALS-C9orf72 positive patients. **Materials and Methods:** ALS patients were screened for the C9ORF72 mutation in the ALS Unit of Hospital La Fe between January 2014 and June 2015. In those who tested positive for this mutation and accepted to participate, clinical data were collected, a brain MRI and a FDG-PET were performed. Healthy relatives of C9ORF72 mutation patients, carrying the same mutation were also offered to participate. The genetic analysis done by repeat primer PCR and confirmed by Southern blot. Neuroimaging FDG-PET acquisitions was made according the EANM procedure guidelines on PET-CT Philips Gemini TF. The data were processed using 3.5 software version of NeuroQTM which through the quantification of the average values of pixel of regions of interest identifies those with a standardized uptake below or upper 1.65 standard deviations of the mean regard to database normal subjects with pons as reference region. Also we used the OASISTM software for the 3D representation of the brain. **Results:** A total of eighty-one patients accepted to be subjected to screening the hexanucleotide repeat expansion in the C9orf72 gene, only 5 were carriers including one healthy carrier. Patients were two men and two women with a mean age at onset of symptoms 63 years old. Symptoms onset was bulbar in one patient and spinal in three (two in lower limbs and one in upper limbs). Two patients associated mild cognitive impairment. The asymptomatic case was a female 48 years old and had been previously diagnosed of schizophrenia and mild mental retardation. The analysis shows hypometabolism in bilateral inferior frontal cortex, left Brocca's area and left posterior cingulate cortex in all patients. Instead of patients, the healthy carrier not had alteration uptake in right inferior frontal cortex and left posterior cingulate cortex. The two patients with mild cognitive impairment were more deeply affected in bilateral frontal (inferior, medial y middle) cortex, right lateral temporal cortex, right parietal cortex and right anterior cingulate gyrus. The patient with bulbar onset was the only with hypometabolism in right superior frontal cortex, right parietotemporal cortex, left lentiform and left thalamic nucleus. Not hypermetabolism areas were found. **Conclusion:** The C9ORF72-ALS gene mutation carriers show a marked hypometabolism in bilateral inferior frontal cortex, left Brocca's area and left posterior cingulate cortex.

P290

Different pattern of brain glucose consumption in Alzheimer disease. Is cerebral glucose metabolism related to epsilon phenotype?

A. Chiaravalloti^{1,2}, A. Fiorentini¹, A. Martorana³, A. Cimini¹, R. Giacipoli¹, P. Sannino², M. Zinzi², E. Di Giorgio², R. Danieli¹, O. Schillaci^{1,2}; ¹Department of Biomedicine and Prevention, University Tor Vergata, Rome, ITALY, ²IRCCS Neuromed, Pozzilli, ITALY, ³Department of Neurosciences, University Tor Vergata, Rome, ITALY.

Aim: The aim of our study was to investigate the impact of epsilon phenotype in brain glucose consumption in a population with Alzheimer disease. **Materials and methods:** Statistical Parametric Mapping (SPM8) was used in order to investigate differences in brain glucose consumption (as detectable by means of 18F FDG PET/CT) in the population examined. A total of 140 patients (77 females and 63 males) with a diagnosis of probable AD according to the NINCDS-ADRDA criteria underwent the PET/CT examination. The mean (SD) age of the patients was 70 (± 7) years; mean mini mental state examination was 19(± 5.6). 59 expressed epsilon 4 phenotype (E4), 70 the epsilon 3 phenotype (E3) and 12 the epsilon 2 phenotype. Cerebro spinal fluid

amyloid, tau and t-tau have been measured resulting equal to 367.4 (± 149.1), 584.7 (± 312.1) and 79.2 (± 45.9) pg/ml respectively. Age, sex, MMSE, scholarship and CSF parameters were used as covariate in the SPM analyses. **Results:** We did not find significant differences in age, gender, MMSE and CSF values among groups. As compared to E3, E4 subjects show a significant reduction of brain glucose consumption in frontal lobe bilaterally and in the right insula (BA 47, 11, 13). As compared to E2, E4 showed a reduction of brain glucose consumption in the left frontal lobe (BA6). As compared to E4, E3 subjects showed a significant reduction of brain glucose consumption in right parietal lobe (BA7, 40). We did not find significant differences in brain glucose consumption when comparing E3 vs. E2 and when subtracting E2 to E4. **Conclusion:** epsilon phenotype is related to different metabolic patterns in Alzheimer Disease. In particular, E4 is related to a major involvement of frontal cortex while E3 is related to a major involvement of parietal cortex.

P291

Glucose metabolism in subcortical cerebral structures and its interrelation with cognitive state in patients with Parkinson's disease

E. Gromova, G. Kataeva, J. Khomenko, D. Susin, J. Irishina, I. Zavolokov; Institute of Human Brain RAS, Saint-Petersburg, RUSSIAN FEDERATION.

Introduction. Cognitive impairment is a frequent symptoms of Parkinson's disease (PD). Better understanding of brain mechanisms underlying cognitive impairment in PD is of great importance because of their negatively influence on the patients' life quality and social adaptation. The aim of this research was to investigate interrelations of cerebral glucose metabolism in subcortical structures and cognitive state and disability degree in PD. **Methods.** 27 patients with PD (11 male, 16 female, age 41-77) were examined. Positron emission tomography (PET) with ^{18}F -fluorodesoxyglucose (FDG) was performed in Scanditronix 2048 tomograph and standard protocol. All patients underwent clinical and neuropsychological examination including Unified Parkinson's Disease Rating Scale (UPDRS), Mini Mental State Examination (MMSE), clock drawing test and Frontal Assessment Battery (FAB). All patients received the antiparkinsonic medications. PET images were normalized with SPM8. Regional cerebral glucose metabolism rate (rCMRglu) were calculated using WFU Pickatlas. **Results.** UPDRSoff scores («off» - measured in the period of cessation of antiparkinsonic medication) correlated negatively with rCMRglu in dorsal nuclei ($r=-0.5$; $p=0.01$) and globus pallidus ($r=-0.5$; $p<0.01$) bilaterally; nucleus lenticularis ($r=-0.6$; $p<0.001$) and putamen ($r=-0.5$; $p<0.01$) in right hemisphere. Positive correlation of FAB scores and rCMRglu in nucleus caudatus were revealed in right hemisphere ($r=0.7$; $p<0.001$). No significant correlations were revealed with clock drawing test and MMSE scores. Also we found that rCMRglu in nucleus caudatus correlated positively with rCMRglu in a number of ipsilateral cortical areas: Brodmann areas (BA) 9,10, 23,24,31,32, 39, 45,46,47 ($r=0.6-0.7$; $p<0.001$) and BA 8,11,40,44 ($r=0.5$; $p<0.01$). In the previous study (Khomenko et al., 2015) correlations of the similar cortical areas and FAB scores in PD patients were revealed. **Conclusions.** Obtained correlations of UPDRSoff scores with rCMRglu in a number of subcortical structures could be easily explained because of wellknown role of subcortical nuclei in PD pathogenesis. However, the fact that only UPDRS «off» scores (measured during the antiparkinsonic medications cancellation) correlated with rCMRglu could indicate that antiparkinsonic medications did not influence on the glucose metabolism of subcortical structures, but to confirm this assumption further study is required. Significant positive correlation of FAB scores and rCMRglu in nucleus caudatus could indicate that the pathogenesis of

cognitive dysfunction was related with the degradation of the frontostriatal network. Revealed correlations between rCMRglu in nucleus caudatus and a number of cortical areas known to be associated with the cognitive functions in PD confirm this conclusion.

P292

$2\text{-}^{18}\text{F}$ -fluoroacetate as an imaging biomarker cerebral ischemia

H. Onoe¹, H. Mizuma¹, S. Kagawa², M. Ohno¹, K. Kakumoto^{1,3}, Y. Matsumoto¹, H. Yamauchi², T. Higashi², R. Nishii⁴, ¹RIKEN Center for Life Science Technologies, Kobe, JAPAN, ²Shiga Medical Center Research Institute, Moriyama, JAPAN, ³Foundation for Biomedical Research and Innovation, Kobe, JAPAN, ⁴Molecular Imaging Center, National Institute of Radiological Science, Chiba, JAPAN.

Aim: Fluoroacetate (FACE), a metabolic toxin that acts by blocking the tricarboxylic acid (TCA) cycle, is known to be preferentially incorporated into astrocytes mediated by monocarboxylic transporter (MCT). FACE was known to be accumulated in astrocyte by PET with ^{18}F -FACE using rat models of stroke and glioma (Marik et al., 2009). Recently, astrocyte has been reported to play an important role in neuronal cell death after ischemic injury in response to intracellular acidosis driven by its emergent lactate production (Beppu et al., 2014). To investigate changes in glial metabolism during ischemia, we performed PET imaging with ^{18}F -FACE in rat model of ischemic/reperfusion injury. **Materials and Methods:** ^{18}F -FACE-PET scan was conducted in the rats after ischemic /reperfusion injury by occluding in the right middle cerebral artery under isoflurane anesthesia. In comparison with ^{18}F -FACE, we measured ^{11}C -acetate uptake in the ischemic rats by PET. We also assessed neuronal cell death and astrocytic activation by immunohistochemical analysis. **Results:** ^{18}F -FACE was highly accumulated in the ischemic region during MCA occlusion with low cerebral flow, whereas ^{11}C -acetate was decreased as compared with that in the contralateral region. Immunohistological analyses revealed that ^{18}F -FACE accumulation was not associated with appearance of reactive astrocyte. **Conclusion:** These findings indicate that ischemia causes ^{18}F -FACE accumulation by changing in astrocyte energy metabolism and transportation, in other words ^{18}F -FACE can be a promising PET probe for the early detection of cerebral ischemia.

P293

Evaluation of Lewy bodies disease for the differential diagnosis of patients with parkinsonism using DAT SPECT, MIBG cardiac scintigraphy, and cerebral perfusion SPECT

T. Yoneyama, K. Yokoyama, S. Tuji, T. Michigishi; Department of Radiology, Public Central Hospital of Matto Ishikawa, Ishikawa, JAPAN.

Aim: We investigated the usefulness of dopamine transporter (DAT) SPECT and the relationship between DAT SPECT, ^{123}I -MIBG cardiac scintigraphy, and cerebral perfusion SPECT for the diagnosis of Lewy bodies disease (LBD). **Methods:** Of 112 cases who had undergone DAT SPECT, 79 cases who could be confirmed diagnosis were subjected. The diagnostic values (sensitivity, specificity, positive predictive value, negative predictive value, and accuracy) of DAT SPECT and ^{123}I -MIBG scintigraphy were calculated. Patients evaluated by DAT SPECT and ^{123}I -MIBG scintigraphy were divided into 4 groups based on the result of both studies for the diagnosis of LBD. A correlation between Specific Binding Ratio (SBR) calculated in DAT SPECT images and Heart/Mediastinum (H/M) ratio on early and delayed

^{123}I -MIBG planar images were determined in Parkinson's disease (PD) patients and PD patients considered as Yahr's stage 3 and above. Patients diagnosed as LBD were evaluated by DAT SPECT, ^{123}I -MIBG scintigraphy, and cerebral perfusion SPECT. Results: The diagnostic values of DAT SPECT in 79 cases were 98.3%, 72.7%, 91.9%, 94.1%, and 92.4%, respectively. In 39 out of 79 cases evaluated by both DAT SPECT and ^{123}I -MIBG scintigraphy, those of DAT SPECT were 96.8%, 87.5%, 96.8%, 87.5%, and 97.4%, and those of ^{123}I -MIBG scintigraphy were 80.6%, 87.5%, 96.2%, 53.8%, and 82.1%, respectively. In 39 cases divided into 4 groups, 7 cases were in a group of DAT normal/MIBG normal (Normal Pressure Hydrocephalus (NPH) 1, Amyotrophic lateral sclerosis 1, Alzheimer's disease 1, Mild Cognitive Impairment 1, psychiatric disorder 3), 1 in DAT normal/MIBG decrease (dementia with Lewy bodies (DLB) 1), 6 in DAT decrease/MIBG normal (PD 6), 25 in DAT decrease/MIBG decrease (PD 22, DLB 2, NPH 1). There was no significant correlation between SBR and H/M ratio in this study, however a moderate correlation was found between SBR and delayed H/M ratio in PD patients considered as Yahr's stage 3 and above. In 21 cases diagnosed as LBD (PD 18, DLB 3), hypoperfusion of occipital cortex on cerebral perfusion SPECT image was detected in 17 cases (PD 15, DLB 2: DAT decrease/MIBG decrease 14, DAT decrease/MIBG normal 2, DAT normal/MIBG decrease 1), and 4 cases with DAT decrease/MIBG decrease (PD 3, DLB 1) had no hypoperfusion of occipital cortex. Conclusions: DAT SPECT was superior to ^{123}I -MIBG cardiac scintigraphy for the diagnosis of LBD. Hypoperfusion of occipital cortex in cerebral perfusion SPECT was highly detected in patients with LBD who had decrease of DAT and/or MIBG uptake.

P-25 – Tuesday, October 18, 2016, 16:00 - 16:30, Poster Exhibition Hall
Neurosciences: Neurotransmission

P294

Dopamine transporter levels in mice with over expression of GDNF in striatum and midbrain studied using dynamic SPECT-imaging of ^{123}I - β -CIT

M. Pitkonen^{1,2}, E. Hippeläinen^{1,2}, J. Andressoo³, J. García-Horsman⁴, K. Bergström^{1,4}; ¹HUS Medical Imaging Center, Helsinki University Central Hospital, Helsinki, FINLAND, ²Department of Physics, University of Helsinki, Helsinki, FINLAND, ³Program of Molecular Neurobiology, Institute of Biotechnology, University of Helsinki, Helsinki, FINLAND, ⁴Real Time Imaging Unit, Faculty of Pharmacy, University of Helsinki, Helsinki, FINLAND.

Aim Glial cell line-derived neurotrophic factor (GDNF) promotes survival of dopamine neurons *in vitro* and *in vivo*. In previous studies using voltammetry measurements in acute striatal slices of GDNF hypermorphic mice it was found that enhanced GDNF levels up-regulated striatal dopamine transporter (DAT) activity. The aim of the current work is to compare DAT levels in striatum and midbrain, measured with ^{123}I - β -CIT SPECT between mice with over-expression of GDNF (hypermorphs) and littermate controls. The kinetics and binding of ^{123}I - β -CIT into striatum and midbrain regions was analyzed using Logan graphical analysis method. **Materials and methods** Five healthy wild type and five GDNF mice were scanned dynamically after intravenous tracer injection (39.7 ± 7.3 MBq, mean \pm SD) of ^{123}I - β -CIT (MAP Medical Technologies Oy, Finland). Dynamic SPECT acquisitions were performed with NanoSPECT/CT system (Mediso, Hungary). Dynamic imaging begins within 15 minutes post tracer injection.

Scanning time varied between 7.5 to 25 minute per scan, depending on the time point and protocol used. Latest imaging point was between 4-7.4 hours post tracer injection. Data was reconstructed, masked, and co-registered with the mice SPECT-brain atlas. Atlas defined four volumes of interest: both striata, cerebellum and midbrain regions. In those regions, time-activity curves were calculated and further analyzed using Logan Plot method, giving estimates of the distribution volume ratio (DVR). Cerebellum time activity curve was used to represent tracer in the non-specifically bound brain area. **Results and Conclusion** In the striatal areas, hypermorphs DVR values (10.0 ± 0.7) compared to controls (13.2 ± 2.7) was statistically different ($p = 0.032$, t-test). Also, in the midbrain, DVR values were significantly different between the groups (DVR = 3.3 ± 0.3 and = 3.8 ± 0.5 for hypermorphs and controls respectively; $p = 0.044$). Significantly different DVR value refers that there is less DAT binding in the striatum and midbrain of hypermorph mice. In conclusion, by using SPECT and ^{123}I - β -CIT, we are able to study central DAT density in genetically modified GDNF mice.

P295

Visual Cortex Reactions to Light in Humans: Functional Activity in Visual Cortex Stimulated at Different Light Complexities

A. Gjedde¹, S. Marrett²; ¹University of Copenhagen, Copenhagen N, DENMARK, ²McGill University, Montreal, QC, CANADA.

Objectives. Functional imaging of the visual cortex is based on the premise that changes of flow and energy metabolism are linked to the same incremental excitation of neurons. The baseline conjecture holds that a default mode of brain function is the baseline for added and coupled changes of blood flow and oxidative metabolism, both when activity falls and when activity rises. To locate the hypothetical baseline in visual cortex in relation to functional demands, we compared increments of (rCBF) and oxidative metabolism (rCMRO2) during visual stimulation of humans with light at three different levels of complexity. **Methods.** Healthy volunteers underwent positron emission tomography (PET) with [^{15}O] water and [^{15}O] oxygen while they viewed three stimuli in random order; a cross-hair fixation stimulus without color or spatial frequency (FX), an achromatic white disc stimulus with an 8 Hz on-off rate (WD), and a circular yellow-blue chromatic checkerboard with an 8 Hz color-reversing frequency (YB). For the baseline conjecture to hold, the sum of any pair of contrasts must equal the third at any site of significant change, such that the sum of the contrasts [YB-WD] and [WD-FX] must equal the contrast [YB-FX]. **Results.** The rCMRO2 and rCBF changes averaged 21% and 52% of the whole-brain average, implying excitation by increasing stimulus complexity. The color reversal contrast ([YB-WD]) revealed bilateral sites of significant change of rCMRO2 and a single left hemisphere site of significant rCBF change in the general region of Brodmann's areas (BA) 17 and 18 of the lingual gyrus. The spatial frequency contrasts ([YB-FX] and [WD-FX]) revealed single sites of significant change of rCMRO2 and rCBF also in the lingual gyrus but close to the midline. For the midline sites, the [YB-FX] and [WD-FX] contrasts were identical and revealed a baseline between the FX and WD/YB stimulus conditions. For the lateral sites, the [YB-WD] stimulus contrast revealed a baseline between the YB and WD stimulus conditions. **Conclusions.** The intermediate positions of the baselines indicated the existence in BA 17/18 of at least two populations of cells, a lateral group responding to the absence or presence of color reversal in the presence of a spatial frequency, and a midline group responding only to the absence or presence of spatial frequency.

P296**Hypoglycemia Reduces Cognitive Performance with Changes of Cerebral Blood Flow in Subjects with Type 1 Diabetes.**

A. Gjedde¹, M. Gejl², B. Brock², A. Møller², E. Van Duinkerken³, H. Haahr⁴, C. Hansen⁵, P. Chu⁶, K. Stender-Petersen⁴, J. Rungby¹; ¹University of Copenhagen, Copenhagen N, DENMARK, ²Aarhus University, Aarhus, DENMARK, ³VU University Medical Center, Amsterdam, NETHERLANDS, ⁴Novo Nordisk A/S, Søborg, DENMARK, ⁵Novo-Nordisk A/S, Søborg, DENMARK, ⁶Novo Nordisk, Inc, Princeton, NJ, UNITED STATES.

This randomized single-blinded, two-period cross-over trial investigated cognitive performance and associated regional cerebral blood flow (rCBF) during hypoglycemia. Subjects (n=26) with type 1 diabetes (T1D) underwent hypoglycemic and euglycemic clamps with target plasma glucose concentrations of 2.8±0.2 mM and 5.5±0.55 mM, respectively. Working memory was scored with a modified digit symbol substitution test (DSST), adjusted for sight and finger movements (control DSST [cDSST]) at both visits. During DSST and cDSST, rCBF was measured in 19 pre-specified brain regions with positron emission tomography of tracer water uptake. DSST scores and response times were analyzed using a linear mixed-effect model with glycemic condition and period as fixed factors and subject as random factor. All rCBF values were normalized to cerebral cortex and we compared these values by ANOVA with glycemic condition, period, and subject as fixed factors. DSST scores were significantly lower (estimated treatment difference [ETD]: -0.63, P=0.014) and the response times significantly longer (ETD: 2.86 s, P=0.0126) in hypoglycemia vs euglycemia. During DSST, rCBF was significantly lower (P<0.05) in medial temporal lobe and hippocampus, and significantly higher (P<0.05) in dorsolateral prefrontal cortex, middle and inferior frontal gyrus, superior parietal lobe and thalamus during hypoglycemia vs euglycemia. During cDSST, rCBF measures were significantly lower (P<0.05) in hippocampus, medial temporal lobe, parahippocampal gyrus and striatum, and significantly higher (P<0.05) in the regions of the frontal lobe, orbitofrontal cortex, superior frontal gyrus, ventromedial prefrontal cortex, superior parietal lobe and thalamus during hypoglycemia vs euglycemia. When the DSST was adjusted for control movement (DSST-cDSST), rCBF was elevated only in the striatum during hypoglycemia vs euglycemia. We conclude that even hypoglycemia at plasma glucose levels just below 3.1 mM reduced cognitive performance, accompanied by significant changes of rCBF, indicating raised activity in the attention network, at the expense of activity in the default mode network.

P-26 – Tuesday, October 18, 2016, 16:00 - 16:30, Poster Exhibition Hall
Neurosciences: Psychiatry

P297**Evaluating neuroprotective effects of Radix Scutellaria in depression-like rat model using 4-[¹⁸F]-ADAM/animal PET**

C. Cheng¹, K. Ma², S. Lu^{1,3}, C. Shiu¹; ¹Department of Nuclear Medicine, Tri-Service General Hospital, National Defense Medical Center, Taipei, TAIWAN, ²Department of Biology and Anatomy, National Defense Medical Center, Taipei, TAIWAN, ³Graduate Institute of Medical Sciences, National Defense Medical Center, Taipei, TAIWAN.

Aims: Depression may lead to an enormous loss to society and economy. Previous studies have reported that depression may cause a decrease in brain serotonin transporter (SERT)

density. Further understanding of the pathogenesis and finding of the treatment are imperatively needed. The aim of this study was to evaluate neuroprotective effects of *Radix Scutellaria* (a Chinese herbal medicine) in chronic mild stress (CMS)-induced depression-like rat model using the animal positron emission tomography (animal-PET) coupled with 4-[¹⁸F]-ADAM. **Materials and methods:** Eighteen male Sprague-Dawley rats (weighted in 350±10 g) were divided into the control, CMS, and CMS+RS (CMS with *Radix Scutellaria* treatment) groups. A thirty-five-day protocol of unpredictable CMS was applied to CMS and CMS+RS groups, respectively. The body weight measurement and force swimming test (FST) were carried out to evaluate the depression-like symptoms in groups of CMS and CMS+RS rats. The 4-[¹⁸F]-ADAM (a selective radioligand for SERT) coupled with animal positron emission topography (animal-PET) was used to examine the status of SERT in depression-like rat model and the images were calculated and expressed as specific uptake ratios (SURs). **Results:** Five weeks after the operation of CMS protocol, CMS+RS rats showed less body weight loss than that in CMS rat. The data of FST showed that CMS+RS rats had less depression-like behavior compared to that of CMS rats. We also found that the SURs of 4-[¹⁸F]-ADAM in various brain regions of CMS+RS rats were obviously higher than those of CMS rats. **Conclusion:** These results suggest that *Radix Scutellaria* may have neuroprotective effects against SERT loss in CMS rat brain. In addition, the CMS-induced depression-like rat model coupled with 4-[¹⁸F]-ADAM/animal-PET may be a feasible platform to evaluate the new neuroprotective drugs.

P298**Brain metabolic changes after psychodynamic psychotherapy**

G. Allenbach¹, N. Sierro¹, G. Ambresin², Y. de Roten², P. Marquet³, J. Prior¹, J. Despland²; ¹Nuclear medicine and molecular imaging department, Lausanne University Hospital, Lausanne, SWITZERLAND, ²University Institute of Psychotherapy, Lausanne University Hospital, Prilly, SWITZERLAND, ³Center for psychiatric neurosciences, Lausanne University Hospital, Prilly, SWITZERLAND.

Objective: To determine the effects of an intensive psychodynamic psychotherapy on brain metabolism in moderately to severely depressed patients. **Methods:** Patients belong to randomized controlled trial examining the efficacy of an intensive and brief psychodynamic psychotherapy (IBPP) in hospitalized depressed patients in adjunction to treatment as usual (TAU). Patients admitted to the psychiatric hospital for a moderate to severe episode were included and randomized in two groups (TAU and IBPP). Montgomery-Asberg Depression Rating Scale (MADRS) rating was obtained before inclusion. After informed consent, participants to this neuroimaging sub-study underwent 3 F-18-FDG PET scans before treatment (t=0), at the end of the treatment (t=1 month) and at distance to the treatment (t=3month). We presently analyzed the two first PET scans. Images were matched to a standardized atlas, normalized and a voxel analysis using SPM12 and regional uptake analysis using PMOD were performed. Changes between 1st and 2nd scans were computed for each patient separately and then analyzed as a group. Responders were defined as a decrease of ≥50% in MADRS. **Results:** Out of 42 patients included in the neuroimaging study, 40 completed the first two PET scans and MADRS assessments. At the baseline scan, a correlation between depression severity and metabolism was measured in the left parahippocampal gyrus (R=0.39, p=0.021), the left putamen (R=0.36, p=0.035) and pallidum on both sides (Left: R=0.47, p=0.005; Right: R=0.42, p=0.012). The comparison

between IBPP and TAU groups after treatment, (significance level $p < 0.001$, 10 voxels) showed significantly higher metabolism in the TAU group in the left frontal medial cortex ($z = 4.26$) and higher metabolism in the IBPP group in the left temporal anterior ($z = 3.77$) as well as in the posterior parietal area ($z = 3.50$). Responders were 5/21 (24%) in the TAU group and 6/19 (32%) in the IBPP group ($p = 0.6$). Comparisons of responders in both groups found significant differences in the precentral right area ($p = 0.024$) and in the left superior motor area ($p = 0.048$). Conclusions: In a group of moderately to severely depressed inpatients, depression severity at baseline was associated with an increased metabolism in different cortical and subcortical areas. Metabolic changes after adjunctive IBPP differed from those after TAU alone, suggesting different mechanisms of response.

P299

Regional cerebral blood flow, prolactin and cortisol levels changes in acute and transient psychotic disorders

R. Petrovic¹, A. Golubic¹, M. Rojnic², T. Samardzic¹; ¹Clinical Department of Nuclear Medicine and Radiation Protection, University Hospital Zagreb, ZAGREB, CROATIA, ²Psychiatry Clinic, University Hospital Zagreb, ZAGREB, CROATIA.

Aim: To assess and evaluate brain perfusion single-photon computerized tomography (SPECT), together with stress-related biomarkers prolactin and cortisol, as part of a continuing effort to understand the pathophysiology of the brain in acute and transient psychotic disorders (ATPD) and to correlate any found abnormalities with psychopathology of these disorders. They present as an acute psychosis associated with acute stress, with sudden onset and polymorphous symptomatology, including psychotic symptoms such as hallucinations and delusions. **Method:** 45 newly referred patients with an ATPD diagnosis underwent regional cerebral blood flow (rCBF) examination brain SPECT (25 female, mean age 30,8, range 18-63). Brain rCBF SPECT data from age- and sex-matched healthy volunteers were used as controls. Patients were diagnosed following ICD-10 criteria and were off psychoactive medication. SPECT scans were started 30 minutes after administration of 740 MBq of ^{99m}Tc-HMPAO in resting state, eyes closed and with low ambient noise. Tomograms were normalized to the mean brain activity and analyzed visually by two independent observers, unaware of clinical diagnosis. **Results:** Majority of scanned patients - 39 pt - 86,7% had brain perfusion changes, from small regions of decreased perfusion to widespread global cortical hypoperfusion and disseminated cerebral blood flow defects. Almost half (48,8%) had right/left asymmetries, and most (88,8%) had more than one region affected, predominantly prefrontal cortex and the temporal lobes. Half had frontal lobe hypoperfusion (53,3%). We had prolactin and cortisol measurements for 38 patients - 33 patients (86,84%) had elevated levels of prolactine, mean 64,5 ug/l, 12 patients (32,43%) had elevated cortisol levels, and 12 patients had both, cortisol and prolactin levels elevated. All 12 patients with elevated prolactin and cortisol levels had pathological rCBF. All but one patients with elevated prolactine levels had pathological rCBF. Additionally, detailed neurologic and laboratory examinations were within normal limits in all patients. **Conclusions:** Compared with the normals, majority of patients with ATPD were characterized by abnormal rCBF, predominantly affecting prefrontal cortex and the temporal lobes, and, in some cases, whole cerebral cortex. Different factors might explain pathological brain rCBF, partially as the consequence of neurophysiological changes which reflects dysfunction in neuronal activity responsible for psychotic symptoms - hallucinations and delusions, and/or the result of some associated symptoms such as acute stress. Our study also underscores the role of stress-related biomarkers in the pathogenesis of psychosis and their correlation with changes in rCBF.

Technologist Posters

TP-01 – Tuesday, October 18, 2016, 08:00 - 09:30, Poster Exhibition Hall
Technologist Poster Session 1

TP001

Upgrading Siemens software from Caredose mAs to both Caredose mAs and kV: Impact on patient radiation doses

B. Dall, C. Schulze, C. S. Knudsen, A. E. Ljunggren; Rigshospitalet, Copenhagen, DENMARK.

Background and Aim: Dose modulation based on the overview (Topogram) with respect to mAs and standard kV (120 kV) has been used in CT scans for many years by different companies. In Siemens terminology this function is called Caredose. In 2013 the software on Siemens Biograph mCT was upgraded, which made it possible also to adjust kV based on the Topogram. The standard 120 kV was adjusted to either 100 kV or 140 kV. We wanted to examine the impact from Care kV on radiation doses based on the calculated doses in Siemens software. **Materials and methods:** 102 consecutive patients were included in the study. The patients' height and weight were recorded in order to calculate Body Mass Index (BMI). The Topogram was conducted, and the desired scan area was adjusted. Dose in mGrey (mGy) with Care mAs and standard 120 kV was recorded. The Care kV function was then turned on, and the kV that the scan would be performed with, was recorded. The estimated dose in mGy was recorded as well. **Results:** For 67 patients the Voltage was downgraded from 120 kV to 100 kV, which led to a dose reduction (mGy) of 17 percent for this group. 19 patients were scanned with 120 kV, which was unchanged compared to the previous software, resulting in an unchanged dose (mGy). The Voltage was upgraded for 16 patients from 120 kV to 140 kV, resulting in an increased dose (mGy) of 17 percent for this group. The Voltage was correlated with BMI. The dose (mGy) for the total group was reduced by 5 percent. **Conclusion:** Upgrading Siemens software from Caredose mAs to both Caredose mAs and kV resulted in a dose reduction (mGy) of 5 percent for the total group. For patients with low or normal BMI, there was an average dose reduction of 17 percent. However, patients with high BMI had an average increase in dose of 17 percent.

TP002

Calculating the Effective Dose from the CT Component of a SPECT/CT Study

A. M. Cheetham, G. Havariyou, E. Kalogianni, D. Ruiz, L. Devlin, N. Gulliver, A. Eccles, N. Mulholland, G. Vivian; King's College Hospital NHS Foundation Trust, London, UNITED KINGDOM.

Introduction SPECT/CT is part of routine practice. The CT may be a low-dose localisation study or a relatively higher dose diagnostic acquisition. The effective dose (ED) from the radionuclide is well described, based on MIRD methodology. However, a CT will increase the total radiation dose. **Aim** To calculate the effective dose from the CT component of the SPECT/CT study, for a range of nuclear medicine procedures. **Method** 428 SPECT/CT studies from Dec-2014 to Dec-2015 were analysed. The patient's weight and Dose-Length Product (DLP) were recorded and studies categorised by examination procedure and CT scan anatomical location. Median DLP was calculated for patients weighing 50-90kg, and the ED calculated using conversion factors from Huda (2011). **Results** Parathyroid: Median DLP=196mGycm, ED=2.4mSv. Hepatobiliary: Median DLP=74mGycm, ED=1.2mSv. ¹³¹I Post-Therapy scans: Median DLP=95mGycm, ED=1.2mSv. Neuro-Endocrine Tumour imaging: DLP and ED is dependent upon the scan volume: Abdo Pelvis, median DLP=77mGycm, ED=1.3mSv. Chest Abdo Pelvis, median DLP=171mGycm, ED=3.2mSv. Head to Pelvis, median DLP=269mGycm, ED=4.1mSv. Bone scans: DLP and ED is dependent

upon the volume scanned and choice of CT (localisation versus diagnostic): Torso localisation CT, median DLP=84mGycm, ED=1.6mSv. Feet diagnostic CT, median DLP=462mGycm, ED=0.4mSv. Knees diagnostic CT, median DLP=395mGycm, ED=0.3mSv. Hips diagnostic CT, median DLP=388mGycm, ED=2.9mSv. Pelvis diagnostic CT, median DLP=276mGycm, ED=3.9mSv. Lumbar spine diagnostic CT, median DLP=446mGycm, ED=7.6mSv. Thorax diagnostic CT, median DLP=352mGycm, ED=7.2mSv. **Discussion** For comparison the ED due to the radionuclide (administered activities taken from UK guidelines): 8.1mSv from 900MBq ^{99m}Tc-MIBI. 2.4mSv from 150MBq ^{99m}Tc-T-BIDA. 11.9mSv from 220MBq ¹¹¹In-Octreotide. 2.6mSv from 200MBq ¹²³I-MIBG. 3.9mSv from 800MBq ^{99m}Tc-HDP. The percentage increase in ED due to the CT is: Parathyroid scans=30%. Hepatobiliary scans=50%. NET studies with ¹¹¹In-Octreotide=11-34%. NET studies with ¹²³I-MIBG=50-158%. Bone scans=8-195%. **Conclusion** The effective dose is dependent upon the choice of CT (localisation or diagnostic) and the anatomical volume scanned. The CT contributes a significant percentage to the total effective dose of SPECT/CT studies. **Reference** Huda W., Magill D., He W. (2011) CT effective dose per dose length product using ICRP 103 weighting factor Med. Phys. 38, 1261-1265

TP003

Dosimetry of absorbed doses of Radioiodine-131 in Therapy for Hyperthyroidism

Y. Koshiba¹, S. Abe², N. Fujita², T. Nishimoto², Y. Sakuragi², K. Kunimoto¹, M. Honda¹, T. Odagawa¹, K. Kato¹; ¹Nagoya University Graduate School of Medicine, Nagoya-shi, JAPAN, ²Nagoya University Hospital, Nagoya-shi, JAPAN.

Purpose: It is important to evaluate accurately absorbed doses of ¹³¹I in therapy for patients with Graves' disease. The purpose of this study was to evaluate the absorbed dose of ¹³¹I in therapy for patients with Graves' disease using the SPECT/CT images acquired after the therapy. **Patients and Methods:** 13 patients (11 females, 2 males; age range, 27 - 79 years; mean age ± SD, 48.9 ± 15.7 years) with hyperthyroidism who received ¹³¹I therapy between December 2014 and September 2015, were enrolled. SPECT/CT scans were taken 1 day after the therapy. The count density map from the SPECT/CT image was converted into an activity concentration map with a calibration phantom approach. Using this map and the effective half life, an accumulated activity map was obtained. This map was then convolved with ¹³¹I voxel S values which were given in MIRD pamphlet to yield three-dimensional distribution of absorbed dose. We compared the virtual absorbed dose obtained with the SPECT/CT images and the expected absorbed dose calculated according to the Quimby formula, and evaluated the effect of ¹³¹I therapy for the patients with hyperthyroidism. **Results:** The virtual absorbed dose was 55.4±4.4 Gy, and the expected absorbed dose was 194.4±47.7 Gy. The ratio of the volume which was irradiated over 50 % of the expected absorbed doses to the total volume of the thyroid gland was 21.7±8.7%. The therapeutic effect of ¹³¹I therapy was found in all the study patients. In 12 (92%) of the total 13 study patients, the thyroid function became euthyroid and the ¹³¹I therapy was finished. **Conclusion:** Although the virtual absorbed dose was lower than the expected absorbed dose, high therapeutic effect was observed. We will examine the absorbed dose of ¹³¹I obtained with SPECT/CT images by using more clinical data.

TP004

Radiation exposure of patients with primary hyperparathyroidism with SPECT/CT and subtraction scintigraphy

S. Rep¹, S. Sustar¹, B. Simonic¹, M. Hocevar², L. Lezaic¹; ¹Department for Nuclear Medicine, Ljubljana, SLOVENIA, ²Department for oncological surgery, Ljubljana, SLOVENIA.

Introduction: Parathyroid scintigraphy is based on the accumulation and distribution of radiopharmaceutical ^{99m}Tc -MIBI. Subtraction scintigraphy is performed using the combination of tracers ^{99m}Tc -MIBI and ^{99m}Tc -pertechnetate; SPECT/CT is performed using a single tracer, ^{99m}Tc -MIBI in combination with low-dose computerized tomography (SPECT/CT) for precise anatomical localization of parathyroid adenomas. **Objective:** The aim of the study was 1) to evaluate the performance of early and delayed (5 and 60 min after administration) SPECT/CT scintigraphy for localization of parathyroid adenomas in comparison to subtraction scintigraphy using histology as the gold standard; 2) to compare the radiation exposure to patients after administration 600MBq of ^{99m}Tc -MIBI, 150 MBq of $^{99m}\text{TcO}_4$ and after low-dose CT acquisition (25mAs and 130keV). **Materials and methods:** The study included 41 patients in whom we performed early and delayed SPECT/CT imaging and subtraction scintigraphy. Radiation exposure after administration of radiopharmaceuticals was calculated on the basis of dose coefficients obtained from the ICRP (International Commission on Radiological Protection) and the ImpACT CT dosimetry calculator. **Results:** The sensitivity and specificity of early SPECT/CT, delayed SPECT/CT and subtraction scintigraphy was 65.1% and 97.5%, 67.4% and 95.5% and 51.1% and 98.3%, respectively. Combined early and delayed SPECT/CT had sensitivity and specificity of 74.4% and 95.1%. The radiation exposure was significantly higher after subtraction scintigraphy (mean 7.37 ± 0.40 mSv) in comparison to early SPECT/CT (mean 6.13 ± 0.38 mSv), delayed SPECT/CT (mean 6.11 ± 0.36 mSv) and combined early and delayed SPECT/CT (mean 6.81 ± 0.44 mSv) ($p < 0.05$). **Conclusion:** The most sensitive method of preoperative localization of parathyroid adenomas is combined early and delayed SPECT/CT. The highest radiation exposure occurs with subtraction scintigraphy.

TP005

Radiation dose of nurses during the care of thyroid cancer patients treated with I-131 in isolation room

T. Lin, P. Lee, Y. Huang; Department of Nuclear Medicine, Koo Foundation Sun-Yat Sen Cancer Center, Taipei, TAIWAN.

Background: I-131 is widely used to treat patients with differentiated thyroid cancer. However, nurses may be subjected to radiation exposure during in-patient care of these patients due to emission of gamma ray by I-131. The objective of this study was to evaluate the radiation dose of nurses during the care of patients treated with I-131 in isolation room. **Materials and Methods:** A prospective study was conducted at our hospital from January 2014 to June 2015. Thermoluminescent detectors (TLD) were used to measure radiation-related whole body doses of nurses. One TLD was provided to all nurses every month. The nurses were required to wear the TLD upon entering isolation room, and placed the TLD in the background area after leaving the room. In addition, lead apron was worn by nurses on the first day of treatment upon entering the isolation room. Purpose of entering the room, duration of stay in the room and distance from patient were recorded. The TLD was sent to the Institute of Nuclear Energy Research every month for radiation dose measurement, and a new TLD was given to the nurses each month. **Results:** A total of 192 patients were admitted for I-131 treatment during this period. Seventy-four of 192 patients were treated with 100mCi, 113 patients with 150mCi, and 5 patients with 200mCi. The hospital stay ranged from 2–3 days. One-hundred and five patients (54.6%) were released on the second day after treatment, and 87 patients (45.4%) were released on the third day after treatment. During this period, 21 nurses were involved in the care of these patients. The purposes of entering the room were as follow: delivering discharge instruction (96%), administration of medication (1%), unknown (3%). The average frequency of entering isolation room was 7.3 times/month. The average duration of stay was less than 5 minutes in 1.0 times/month, between 5–10 minutes in 6.1 times/month and more than 10 minutes in 0.2 times/month. The average distance from the patient was approximately 30cm in 7.2 times/month and approximately 100cm in 0.1 times/month. A total of 18 TLDs were measured in our study. The radiation dose of nurses measured by all 18 TLDs were within background level. **Conclusion:** Based on our

study, radiation dose of nurses during the care of thyroid patients treated with I-131 in the isolation room is within background level, which is much lower than the annual dose limit for general public ($<1\text{mSv}$).

TP006

A comparison of the left- and right hand skin dose in nuclear medicine

R. Kraack; Department of Nuclear Medicine & PET Centre, Aarhus University Hospital, Aarhus, DENMARK.

Aim: There is an increasing focus on monitoring finger dose on staff who works in radiopharmacy. Radiation exposure of the hands of personnel in nuclear medicine is a real concern, and therefore it is important that the staff use ring dosimeters to monitor the radiation dose to fingers. The aim of this study is to demonstrate why ring dosimeters on both the dominant and the non-dominant hand seem to be preferable. **Materials and methods:** We have collected data using finger ring dosimeters from 2013 to 2016. At Aarhus University Hospital we use finger rings one month at a time. We use the rings on the palmar base of the left- and right forefinger under a pair of gloves. Each technologist use the same finger rings when working with radioactivity for diagnostics or radionuclide therapy. I have used my own fingerdosimeter data to the results, but I will also use my 2 colleagues' results to substantiate my results. **Results:** I have compared my own and my 2 pharmacy colleagues finger doses and found, that we all acquire more dose on our non-dominant hand, than on our dominant hand. In a period of 23 months with preparing and administering both ^{99m}Tc and ^{90}Y , I have received radioactivity on my non-dominant hand: 5,0 mSv/month and on my dominant hand: 2,3 mSv/month. In a period of 12 months without handling ^{90}Y , I received on my non-dominant hand: 4,5 mSv/month and on my dominant hand: 2,1 mSv/month. It is particularly important to use finger rings on the non-dominant hand when preparing and administering ^{90}Y , since we are receiving a higher dose per GBq activity handled, compared working with ^{99m}Tc . **Conclusion:** All of our data show, that we receive a higher dose on our non-dominant hand compared to the dominant hand. Therefore it seems important to use rings on both hands when handling radioactivity. While Laffont *et al.* [1] suggests using only a dosimeter on the forefinger of the dominant hand, this study indicates the relevance of using a finger ring dosimeter on both hands. Failing that, the forefinger of the non-dominant hand, rather than on the dominant hand is preferred. **References:** [1] Sophie Laffont *et al.* Eur J Nucl Med Mol Imaging (2016) 43:824–831

TP007

Worker dose evaluation result from cardiac scan

H. M. Yassin, I. Kamal, R. M. Abdel-Halim; Cairo Univeristy, cairo, EGYPT.

Introduction Reducing radiation exposure has become an important aim for nuclear cardiology in nuclear medicine departments the purpose of this study was to Measurement of effective dose to cardiology staffs who operate near the patient and are exposed to non-uniform radiation field due to patient scattered radiation. **Materials and Methods:** This study was performed in nuclear medicine department of Kasr EL- Eini Hospital for 6 months and 455 cardiac scan procedures studied. Doses were recorded with thermoluminescence dosimeter (TLD) for 5 cardiologists, 12 nurses and 4 physicists and the effective dose were estimated using the Niklason algorithm. **Results:** Mean annual effective dose (μSv) to cardiologist and nurses and physicists from scans procedures were 475.5 (53.9 - 1711.7) μSv and 138.1 (48.4 - 235.9) μSv respectively. Mean effective dose (μSv) per cardiology procedure for cardiologist and nurses and physicists were 1.98 and 0.299 μSv respectively. **Conclusion:** The results indicate large variation in radiation exposure between staffs. No correlation was found between the number of procedures and effective dose. None of the annual effective dose appear to exceed the annual effective dose limit of 20 mSv. **Keywords:** TLD, worker dose, Nuclear Medicine.

TP008**Radiation Exposure Analysis of Female Nuclear Medicine Radiation Workers**

J. Lee¹, **H. Park**²; ¹Chungbuk National University, Chungbuk, KOREA, REPUBLIC OF, ²Shingu College, Seongnam, KOREA, REPUBLIC OF.

In this study, radiation workers who work in nuclear medicine department were analyzed to find the cause of differences of radiation exposure from General Characteristic, Knowledge, Recognition and Conduct, especially females working on nuclear medicine radiation, in order to pave the way for positive defense against radiation exposure. The subjects were 106 radiation workers who were divided into two groups of sixty-four males and forty-two females answered questions about their General Characteristic, Knowledge, Recognition, Conduct, and radiation exposure dose which was measured by TLD (Thermo Luminescence Dosimeter). The results of the analysis revealed that as the higher score of knowledge and conduct was shown, the radiation exposure decreased in female groups, and as the higher score of conduct was shown, the radiation exposure decreased in male groups. In the correlation analysis of female groups, the non-experienced in pregnancy showed decreasing amount of radiation exposure as the score of knowledge and conduct was higher and the experienced in pregnancy showed decreasing amount of radiation exposure as the score of recognition and conduct was higher. In the regression analysis on related factors of radiation exposure dose of nuclear medicine radiation workers, the gender caused the meaningful result and the amount of radiation exposure of female groups compared to male groups. In the regression analysis on related factors of radiation exposure dose of female groups, the factor of conduct showed a meaningful result and the amount of radiation exposure of the experienced in pregnancy was lower compared to the non-experienced. The conclusion of this study revealed that radiation exposure of female groups was lower than that of male groups. Therefore, male groups need to more actively defend themselves against radiation exposure. Among the female groups, the experienced in pregnancy who have an active defense tendency showed a lower radiation exposure. Thus, those who have never been pregnant need to have a more active defensive conduct for the future possibility of pregnancy.

TP009**The impact of scatter subtraction coefficient on the image quality**

S. Rep., **S. Sustar**, **B. Simonic**, **L. Lezaic**; Department for Nuclear Medicine, Ljubljana, SLOVENIA.

Introduction: Detection of scattered radiation degrades image contrast of single-photon emission computed tomography (SPECT) imaging. Traditionally scatter correction methods were limited in accuracy, noise properties and were not very widely applied. This contrasts with phantom or patient imaging where better accuracy can lead to significant improvement of image quality. In concert with the increasing number of energy windows on modern SPECT systems and excellent attenuation maps provided in SPECT/CT, some of these methods give new opportunities to remove degrading effects of scatter with improved noise properties. **Aim:** The aim of our presentation is determine the impact of scatter subtraction coefficient on image quality **Method:** The phantom which was used for the determination the impact of scatter subtraction coefficient on image quality were filled with technetium. After acquisition, the reconstruction were performed with the different scattered subtraction coefficient (between 10% and 100%). We compared the average number of counts in the region of interest for the hot sphere and the background. OASIS SEGAMI® processing software was used for reconstruction and measurements analysis. **Results:** Our results showed that the average value of counts decies when the scatter subtraction coefficient increase. When the scattered subtraction coefficient increase more than 20% the results were statistically significant ($p < 0.05$). The scattered subtraction coefficient improve image contrast and were statistically significant ($p < 0.05$) when we use all coefficient. **Conclusion:** We concluded that the image quality is improved by using scattered subtraction.

TP010**Studies on the Effect of Scattered Radiation Out of Field of View on Tau Imaging**

M. Honda¹, **H. Yamaguchi**², **Y. Sakuragi**³, **S. Abe**³, **N. Fujita**³, **Y. Koshihira**¹, **K. Kato**¹; ¹Department of Radiological and Medical Laboratory Sciences, Nagoya University Graduate School of Medicine, Nagoya, JAPAN, ²Brain and Mind Research Center, Nagoya University, Nagoya, JAPAN, ³Department of Radiological Technology, Nagoya University Hospital, Nagoya, JAPAN.

Background and Purpose: Tau imaging is an important imaging method for accurate diagnosis and clinical evaluation of Alzheimer's disease. A degree of ¹⁸F-THK-5351 uptake into brain tau varies due to progress of the disease, and it is hardly accumulated in healthy brain. Thus, there is a possibility that scattered radiation out of field of view (FOV) affects the images and makes accurate detection of tau difficult. In this study, we determined the content of scattered radiation out of FOV at the detector which was located at various distances from the cylindrical phantom which mimiced the trunk (liver) by using PET system with 3D acquisition modes. In addition, we determined the influence of scattered radiation out of FOV when the radioactivity of the cylindrical phantom was increased and also examined whether the effect of scattered radiation from out of FOV was reduced by using a lead-made neck shield. **Materials and Methods:** A solution of ¹⁸F was enclosed into the brain phantom and the cylindrical phantom which mimiced the trunk (liver). The brain phantom was placed on the headrest, and the cylindrical phantom was placed on the bed. Distances between the brain phantom and the cylindrical phantom examined were 0, 10, 20, and 30 cm with or without a neck shield. PET data were acquired with 3D modes, and reconstructed under the same conditions as used in a clinical setting. Circular ROIs were drawn on the axial images and the total counts were measured. The content of scattered radiation out of FOV was estimated. **Results:** The maximum content of scattered radiation in the images obtained was 7.84%. As the distance between the cylindrical phantom and the detector increased, the content of scattered radiation in the images decreased. When the distance was longer than 25cm, the content of scattered radiation was close to about 1.0%. Scattered radiation from out of FOV was not reduced by using a lead-made neck shield in the images. **Conclusion:** When the distance between the cylindrical phantom and the detector was longer than 25 cm, there was no influence of scattered radiation out of FOV in 3D acquisition mode. The same results were obtained when the radioactivity of the cylindrical phantom was increased. Even when a lead-made neck shield was used, scattered radiation from out of FOV was not reduced.

TP011**A simulation study for estimating scatter fraction of human body in FDG-PET/CT**

S. Hosokawa; National Cancer Center East, Chiba, JAPAN.

In the FDG-PET/CT examination, the quality of an image depends on body size of the subject. Although It has been reported that constant image quality without depending on body type is obtained by adjusting the imaging time with Noise Equivalent Count density ($NEC_{density}$) Noise Equivalent Count Rate (NECR) divided by the imaging volume, to be constant, decrease of visual score is observed at a higher BMI subject. It is assumed that calculating the NECR using device-specific fixed Scatter Fraction(SF) is the cause. The purpose of this study is to clarify the difference between the estimated SF of various phantoms using Monte Carlo simulation and device-specific fixed SF. To simulate the 3D-PET device, code (*Geant4*) was used. A sinogram was drawn by identifying Line of Response (LOR) with coincidence counting. Scattered radiation was defined as those scattered within the subject and a source more than 20 mm in distance from LOR. Cylindrical phantoms (length:70 cm, a diameter: 10-50 cm), NEMA/IEC Body Phantom (Scatter phantom nonuse and use) and the human body phantom in which radiation sources were uniformly placed were used as scatterer. The imaging range of

the human body simulation phantom has a length for 5 beds and estimated each bed and average SF. The estimated SF of the cylindrical phantom (10–50 cm) which line source was inserted in was 32.1–74.1% of device-specific fixed SF. In accordance with the diameter increases, the rate of increase in SF became smaller. This is considered to be because the effect of absorption was increased. In the case of use of scatter phantom and nonuse, the SF of the body model was 34.3 % and 39.5 %, respectively. The average SF of each bed of the human body simulation phantom was 38.7 %. There was a difference between the maximum 13.3% in each bed. It can be said that device-specific fixed SF is assuming standard body types. The value of SF varies greatly depending on the size and shape of the scatterer, and impact on the visual score by SF was suggested

TP012

Evaluation of Quantitative Accuracy of Trans-PET® BioCalibur® System for *in Vitro* Study

J. Li, L. Wan, X. Liang, S. Han, Q. Xie; Huazhong University of Science and Technology, Wuhan, CHINA.

Aims: Recently, the small animal positron emission tomography (PET) has been employed for *in vitro* cell uptake studies. In cell uptake studies, the radioactivity of the tracers is usually below 1 μCi , which is two orders of magnitude lower than *in vivo* studies (50–200 μCi in mice, 500–2000 μCi in rats). Therefore, for *in vitro* experiments using small animal PET, the activity of the source which is enough for achieving data statistic and accurate quantitative results need to be measured. Hence, we aim to assess the measuring range of the activity when using the Trans-PET® BioCalibur® system for *in vitro* studies. **Materials and Methods:** The 96-well plate experiments and the Monte Carlo (MC) simulation studies were performed respectively to evaluate the quantitative accuracy of the Trans-PET. Eight wells of a 96-well plate was filled with ^{18}F -FDG (12.5 kBq, 5.43 kBq, 2.85 kBq, 1.47 kBq, 685 Bq, 361 Bq, 196 Bq, 102 Bq for 96-well plate tests and 2560, 1280, 640, 320, 160, 80, 40, 20 Bq for MC tests). The data acquisition time of MC simulations and 96-well plate experiments were both 20 min. And the ROI value of PET images were calculated for quantification. The results generated from 96-well plate experiment were compared with gamma counter. While the MC simulation results were compared with the known true values. **Results:** High degree of correlation was observed between the real activities and the ROI value of the PET image ($r^2 = 0.9998$ for the 96-well plate tests and $r^2 = 0.9998$ for the MC tests). Meanwhile, the Trans-PET system also demonstrated a wide available measuring range, from 12.5 KBq to 685 Bq (the fractional errors of these 5 wells are under 3%, while the fractional errors of the 3 wells under 314 Bq are over 10%) for the acquisition of 96-well plate test and from 2.56 Kq to 320 Bq (the fractional errors of these 4 wells are under 6%, while the fractional errors of the 4 wells under 160 Bq are over 10%) for the MC test. **Conclusions:** The available measuring range can reach ~ 700 Bq for the Trans-PET® BioCalibur® system detected in the *in vitro* experiment with data acquisition time of 20 min.

TP013

Simulation and theoretical calculation for production of ^{63}Zn by neutron induced reaction

M. Rostampour¹, S. Hamidi¹, M. Aboudzadeh Rovais², M. Sadeghi²; ¹Arak University, Arak, IRAN, ISLAMIC REPUBLIC OF, ²Nuclear Science and Technology Research Institute, Tehran, IRAN, ISLAMIC REPUBLIC OF.

Introduction The ^{63}Zn is a short lived beta emitter, which is very suitable for using in PET. It is proposed to produce ^{63}Zn via neutron induced reaction. The primary purpose of this investigation is to quantify the production yield of ^{63}Zn nuclei via $^{64}\text{Zn}(n,2n)^{63}\text{Zn}$ reaction by utilizing the Monte Carlo codes and theoretical method. **Method** In the present study, a cylindrical target having a

diameter of 1 cm has been implemented into the simulation code. The thickness of cylindrical ^{64}Zn target was calculated using SRIM-2013 code. The beam was designed to reach the target at 90° angle and impinge on the target in the z-direction. The residual nuclei were estimated using model option in “FT8 RES” card in MCNPX and G4HadronPhysics INC LXX, G4NeutronHP and G4Photo Nuclear Process have been used as physics list in the Geant4 code. Subsequently, estimated residual nuclei were used to calculate the simulated excitation function. Based on the available neutron induced reactions experimental data, a set of optical potential parameters and the level densities parameters has been obtained for evaluating reaction cross section for this reaction. Based on the available neutron induced reactions experimental data of ^{64}Zn , a set of neutron optical potential parameters at $E_n=12.5\rightarrow 14.5$ MeV has been obtained. With adjusting the level densities parameters, the reaction cross sections of $^{64}\text{Zn}(n,2n)^{63}\text{Zn}$ is calculated. The yields of $^{64}\text{Zn}(n,2n)^{63}\text{Zn}$ reaction were estimated by using the simulated and calculated excitation functions and stopping power calculations. **Results and discussion:** The theoretical method and the Monte Carlo codes, MCNPX and Geant4, reproduced experimental data and theoretical values from the TENDL-2015 library for the incident energies from 12.5 MeV to 14.5 MeV. The average of the production yields of ^{63}Zn via $^{64}\text{Zn}(n,2n)^{63}\text{Zn}$ reaction over the energy range $E_n=12.5\rightarrow 14.5$ MeV are 0.1675, 0.1665, 0.167, 0.167 MBq/ μAh for experimental, MCNPX, Geant4, theoretical based cross sections. **Conclusion** The theoretical method could be applied to provide a useful tool for calculating the $^{64}\text{Zn}(n,2n)^{63}\text{Zn}$ reaction cross section for the incident energies from $E_n=12.5\rightarrow 14.5$ with good accuracy. Also, MCNPX and Geant4 codes can be used for estimating the production yield of beta emitter nuclides. **Keywords:** ^{63}Zn , Cross-section, GEANT4, MCNPX, Optical potential, Level density

TP014

Characterisation & implementation of pinhole collimator for thyroid scintigraphy

N. Nielsen, K. Lajgaard, A. Arveshoug, P. Staantum; Dept. Nuclear Medicine & PET-Centre, Aarhus University Hospital, Aarhus C, DENMARK.

Aim The clinical value of thyroid and parathyroid scintigraphy can be improved by using a pinhole collimator rather than a high-resolution parallel hole collimator. The purpose of this study was, firstly, to characterise a newly installed gamma camera (Mediso Nucline TH45) equipped with pinhole collimator. Secondly, to implement a procedure for thyroid scintigraphy based on this characterisation. **Materials and Methods** Magnification and spatial resolution were determined by imaging of ^{99m}Tc in two parallel capillary tubes 3 cm apart and subsequent determination of their imaged distance and full-width-at-half-maximum (FWHM). Sensitivity was measured for ^{99m}Tc as a point-source and in a Petri dish. Pinhole-aperture diameters of 3, 4 and 6 mm and object-aperture distances between 5 and 13 cm were applied. All measured parameters were compared to theoretical models. For estimation of the most suitable object-aperture distance in thyroid scintigraphy, images of a thyroid phantom were recorded at various distances. For a direct comparison of pinhole collimator and parallel hole collimator, comparative images of a thyroid phantom and selected patients were recorded. **Results** For the employed range of distances the magnification was 1–3 and inversely proportional to object-aperture distance. For large magnifications, images of 3-dimensional objects like the thyroid phantom were heavily distorted due to the distance-dependent magnification. FWHM was reduced with about 1/3 from the largest to the smallest applied distance. FWHM was approximately proportional to the pinhole aperture diameter. The sensitivity was higher for the point source than the distributed source due to the reduced sensitivity for activity located off-centre. The point-source sensitivity dropped by a factor of about 8, when the distance increased from 5 cm to 13 cm, while the drop was less for the distributed source. A pinhole-aperture diameter of 4 mm yields a good compromise between spatial resolution and sensitivity, while an imaging distance of 7–10 cm is most appropriate with respect to magnification and spatial resolution. For the chosen

parameters the magnification was 1.4–1.9, the spatial resolution 5.3–4.6 mm and the point-source sensitivity 185–87 cps/MBq. **Conclusion** The gamma camera with pinhole collimator was characterized, and a suitable pinhole size and imaging distance was determined for thyroid scintigraphy. Judged from the determined parameters and visual evaluation of comparative images, the pinhole images represent an improvement compared to parallel hole collimator images in particular with respect to spatial resolution.

TP015

When is less more. Small but dedicated

B. Hoyer Mathiasen, D. L. Nielsen; Vejle Hospital, Vejle, DENMARK.

Aim: To explore the possibility of reducing costs, but increasing output, by (re)introducing simple planar imaging. **Background:** The European field of Nuclear Medicine has had a significant increase in the number of procedures performed over the last decade. This has resulted in an increase in the number of multi-purpose cameras. [1] These multi-purpose cameras, have special demands regarding shielding, cooling and ambient consistency. They have large footprint, and require a large amount of space. Space and money are two sparse resources in the current public healthcare service. This leads departments of Nuclear Medicine to seek new ways to meet the growing demand for nuclear imaging. In the Department of Nuclear Medicine, Vejle Hospital, Hospital Lillebaelt, this growing demand of imaging, and the fact that money within healthcare is sparse, has led to an increase in the number of dedicated and more simple gamma cameras for renal, heart and thyroid imaging. The current dedicated modalities include: NephroCam & SoloMobile (booth DDD-Diagnostic A/S) and CardioMD III (Philips Denmark A/S, Healthcare), primarily used for renal, thyroid and heart imaging respectively. **Results:** The price of the simple dedicated modalities, varies from 75.000€ to 130.000€ which is often up to 1/10 the price of a SPECT/CT. The price for a full service agreement, range from 1/10 to 1/20 of the price of a SPECT/CT. The more simple cameras reduce or eliminate the need for motions of the camera prior to the acquisition, and therefore give a better patient flow, with less idle time at the modality. A price comparison shows that if a single detector study (>41 minutes a day), is moved from a moved from a multipurpose camera. The purchase and service of a simple and dedicated camera is feasible. With the Danish reimbursement rates only 1 kidney scan a day can make the simple camera purchase feasible. Where a multimodality SPECT/CT needs to conduct >7 kidney scan a day to be economical feasible. **Conclusion:** The simple and less expensive gamma cameras, does have the ability to increase production at a lower cost, if production is moved from a multi-purpose camera. The less often demand for periodic maintenance gives more available camera time, also helping to boost production. Therefore the small simple gamma camera is, and should continue to be, the production workhorse for supplementing the more and more frequent multi-purpose gamma cameras. [1] http://www.fsnm.org/home/wp-content/uploads/2011/12/Results_EANM_Survey_20101.pdf (31.03.2015)

TP016

Comparison of calculated attenuation corrected FDG brain scans with CT

J. Wiegers, A. Willemsen, D. Vázquez García, R. Dierckx; UMCG, Groningen, NETHERLANDS.

Without attenuation correction (AC) PET images exhibit strong artifacts and do not allow quantitative imaging. Therefore, current PET-CT systems perform a low-dose CT-AC scan. Although of low dose, this still increases the total radiation dose to the patient which is a special concern when scanning children. In addition, patient motion between or during the CT-AC scan and the PET scan can introduce motion AC artifacts. For brain scans a calculated AC is possible which alleviates both problems. **Aim:** To compare the calculated AC corrected brain scans, using the Siemens Neuro-AC tool, with the

gold-standard i.e. CT-AC. **Methods:** For Alzheimer suspected patients, 10 FDG brain scans were included. (Age: 55–77, M: 6, F: 4) Subjects were positioned using a CT scout scan after which a CT-AC was performed (80 kV, 40 mAs). Scans of 5 min duration were made, 30 min after the injection of 200 MBq FDG. During the uptake period, patients remained in a darkened and quiet room. The scans were reconstructed using the CT-AC scan and the Neuro-AC tool. The reconstructions resulted in different dimensions of the data. Therefore, the scans were first co-registered and then both absolute and relative error images were calculated (Vinci). To prevent extra-cranial voxels to influence the analysis, the different images were masked using the CT-AC corrected FDG scan. The current analysis is based on a visual interpretation of the data, displayed in transaxial, coronal and sagittal sections. **Results:** Relative errors were largest in areas with low uptake which is a direct result of the division by low values. This is particularly evident for the skull. The smallest relative errors were observed for the cortical regions particularly the more cranial slices. More caudal structures, particularly at the level of the nasal cavities were more susceptible for errors. **Conclusion:** Calculated AC using the Neuro-AC tool may give large relative errors, although these are usually in low uptake areas. For a visual interpretation of FDG brain scans, particularly of cortical areas, its use seems appropriate. The same holds for the quantitative assessment (i.e. using SUV) of follow-up scans of patients. Generally, the use of SUV ratios is advised since this will reduce potential systematic errors. However, more research is required if this approach is to be used in a research setting.

TP017

Datscan® (123I-FP-CIT) brain SPECT: comparative analysis of different quantification methods

R. Correia¹, L. Roldão Pereira¹, D. Faria^{2,3}, L. Vieira^{4,5}, J. Vale^{2,3}, A. Martins², J. Patrino², J. Fernandes², J. Teixeira², D. Sousa², J. Oliveira²; ¹Licenciatura em Medicina Nuclear - Escola Superior de Tecnologia da Saúde de Lisboa, Lisbon, PORTUGAL, ²HPP-Medicina Molecular, SA; Lenitudes SGPS, SA, Lisbon, PORTUGAL, ³ESSUA - Escola Superior de Saúde de Aveiro, Lisbon, PORTUGAL, ⁴Área Científica de Medicina Nuclear, Escola Superior de Tecnologia da Saúde de Lisboa, Instituto Politécnico de Lisboa, Lisbon, PORTUGAL, ⁵Instituto de Biofísica e Engenharia Biomédica, Faculdade de Ciências, Universidade de Lisboa, Lisbon, PORTUGAL.

INTRODUCTION DaTSCAN® (¹²³I-FP-CIT) brain SPECT studies are of extreme importance on differential diagnosis of movement disorders in the assessment of dopaminergic degeneration in the nigrostriatal pathway. Quantitative algorithms have great impact on obtaining more objective data and to enable higher confidence in the diagnosis, inter-group analysis and longitudinal evaluation of patients. **PURPOSE** To investigate the impact of different types of quantitative algorithms in the quantification of specific uptake binding (SUB). **MATERIALS AND METHODS** Retrospective quantification of 37 DaTSCAN® (¹²³I-FP-CIT) brain SPECT individual studies (22 female, 15 male, mean age 61 years) was performed using the commercial software Quantispect®, a computational solution for automated quantification (CSAQ) and a manual method (Costa's Method - CM). **RESULTS** Our results show a positively strong Pearson correlation between all three methods, better for CM and CSAQ (0.90, P<0.0001) than for automatic method (0.80–0.88, P<0.0001). Friedman test showed statistically significant differences between all the methods (P<0,05). ROC curve with Youden maximization pointed out high sensitivity for all (mean of 88,4%, STD of 0,02%), with Quantispect® presenting the lowest specificity (83,33% vs 91.67% demonstrated by the others). **CONCLUSION** Preliminary results indicate that automatic quantification of the SUB in DaTSCAN® SPECT is more consistent and that quantification method choice is clinically relevant in the delivery of reliable patient care. The study is still ongoing and we hope to include more commercially available programs and a larger validated database of normal and abnormal individuals.

TP018**Discovery IQ - Acquisition and reconstruction optimization of ¹⁸F-FDG PET-CT Brain studies**

S. Ferreira¹, D. Faria², J. Fernandes³, A. Martins³, J. Teixeira³, D. Sousa³, J. Patrino³, J. Vale³, L. Vieira⁴, F. Silva³, J. Oliveira³; ¹ESTSL-IPL - Lisbon School of Health Technology, Lisbon, PORTUGAL, ²HPP-Medicina Molecular, SA; Lenitudes SGPS, SA; ESSUA- Aveiro University's Health School, Porto, PORTUGAL, ³HPP-Medicina Molecular, SA; Lenitudes SGPS, SA, Porto, PORTUGAL, ⁴Instituto de Biofísica e Engenharia Biomédica, Faculdade de Ciências, Universidade de Lisboa, Lisboa, Portugal, Lisbon, PORTUGAL.

Introduction PET-CT scanner Discovery IQ (GE D-IQ) represents the latest advance of GE in Molecular Imaging with 6.3mm x 6.3mm x 30mm BGO crystals and a dual energy acquisition channel that is able to reduce dead time and pileup at high-count rates providing the highest sensitivity among commercial scanners. Along with the improvement in hardware, GE introduced Q.Clear, a Bayesian penalized-likelihood reconstruction algorithm for PET, providing more accuracy in PET quantitation. **Aim** Acquisition and reconstruction optimization of ¹⁸F-FDG PET-CT brain studies in order to determine the optimum penalization factor β (beta) of Q.Clear, according to image acquisition parameters. **Methods** Images were obtained of a 3D-Hoffman phantom, filled with 35-90 MBq of F18, varying from 5 seconds to 30 minutes of duration, with a total number of 60 images reconstructed with Q.Clear algorithm with β values of 100-600. Maximum and mean SUV values were accessed for the left, right, anterior and posterior cortex, striatum and white matter. The right to left cortex (RL), anterior to posterior cortex (LP), caudate to white matter (CW), putamen to white matter (PW), putamen to caudate (PC) and grey to white matter (GW) ratios were obtained. Final images were visually evaluated by 2 scorers for overall image quality, contrast and noise level. **Results** Preliminary results showed a loss in contrast and overall image quality as β value is increased. β values above 400 have a significant impact in CW, PW and GW ratios affecting the overall image quality. Results also showed an inverse linear relation between image duration (number of prompts obtained) and β value used in the reconstruction algorithm, with higher β values for studies with poor statistics. **Conclusion** Study is still ongoing and preliminary results show a significant impact of β value on the overall image quality. Optimum penalization factor β of Q.Clear needs to be adjusted according to image statistic obtained.

TP019**A comparison study on acquisition counting with SPECT tomography**

Y. Wang; Huashan Hospital, Fudan University, Shanghai, CHINA.

Objective: To compare "Both, Either" different acquisition method parameter count in nuclear medicine SPECT tomography scan in clinic. **Methods:** 100ml water and 2ml radioactive nuclide ^{99m}Tc (2mCi) liquid were poured into three cylindrical sealed container respectively. The container was placed on headrest of Siemens Symbia T16 SPECT examination bed, bed height was adjusted and fixed, a circular and step-fault method was used to collect. Tomographic imaging were divided into A, B, C groups, the collection counts were "Both 50kcts", "Either 50kcts", "Either 52kcts" counts per frame respectively, and 64 frames were collected totally. Radionuclide was added before each imaging and ensure that the error between the three containers of less than 1%. Repeat and each sealed container was measured after adjusting the dose and repeated five times. **Results:** The acquisition time of three different modes was spent 2896.3 ± 3.4 seconds, and 2648 ± 2.3 seconds, and 2784.5 ± 2.8 seconds. Total acquisition counts of dual probe were 64075 ± 23counts, 62971 ± 43counts, 65796 ± 53counts. A pairwise comparison was carried on all these data. Acquisition duration was groups A > C > B, t = 59.497, P < 0.001, t = 46.694, P < 0.001, t = 62.071, P < 0.001. Acquisition count was groups B > A > C, t = 36.523, P < 0.001, t = 57.234, P < 0.001, t = 53.827, P < 0.001. The

counts of group C previous ten frames was low and count exceeds 50Kcts. **Conclusion:** If select "Both" to collect in the actual collection process, the probe A reaches the specified count and B has not reached the probe, the probe A will stop counting until the probe B reaches the count. When you select "either" acquisition, any probe reaches the specified count, the two probes will stop counting. Although there was "Both, Either" acquisition mode, the second half of the radioactive probe and can not reach the set count in 30 minutes collecting process, the acquisition program have logic design and assign acquisition time rules after acquisition starts, and the collecting results met the objectives not because of set "Both, Either". From the statistical results, Group C results were the highest efficiency and it can be recommended. In clinical practice, we can set the acquisition "Either" parameter, the count is slightly higher than the objectives and requirements, the amount of information will be enough reasonable acquisition time data.

TP020**Influence of CT attenuation correction on image quality of reconstructed SPECT image on stress Thallium-201 SPECT-MPI using CZT detector SPECT device**

K. Shogo¹, S. Tomiguchi², R. Matsuda¹, N. Katsuta³, S. Shiraishi⁴, Y. Yamashita⁴; ¹Graduate School of Health Sciences, Kumamoto University, Kumamoto-shi, JAPAN, ²Faculty of Life Sciences, Kumamoto University, Kumamoto-shi, JAPAN, ³Division of Medical Technology, Kumamoto University Hospital, Kumamoto-shi, JAPAN, ⁴Department of Diagnostic Imaging, Faculty of Life Sciences, Kumamoto University, Kumamoto-shi, JAPAN.

Object: In a single-photon emission-computed tomography myocardial perfusion imaging (SPECT-MPI) using CZT detector SPECT device (CZT camera), a decrease in radiation exposure to patient or shortening of data acquisition time is obtained by its high count sensitivity. However, attenuation is considered to be one of the factors deteriorating the image quality of reconstructed Thallium-201 SPECT-MPI image (SPECT image) obtained by CZT camera. The aim of this study was to evaluate the influence of CT attenuation correction (AC) on image quality of SPECT image in patients with visually normal myocardial perfusion. Optimal data acquisition time for SPECT-MPI was also assessed. **Methods:** Twenty-six consecutive patients without perfusion abnormality on visual assessment were enrolled in this study. They were 14 males and 12 females with their mean age of 73.1 years. Stress Thallium-201 SPECT-MPI and CT were performed in all patients. SPECT data were acquired for 7 minutes with list mode on CZT camera (NM530c: GE) and CT data on SPECT/CT device (NM/CT670: GE). Three SPECT images were reconstructed by iterative reconstruction algorithm. They were SPECT image without attenuation and scatter correction (NC), that with attenuation correction (AC) and that with attenuation and scatter correction (ACSC), respectively. Image quality of uniformity was evaluated by using a coefficient of variance (CV) of count distribution on polar map of each SPECT image. In addition, SPECT data acquired for 7 minutes were reconstructed every one minute to calculate normalized mean square errors (NMSE). Optimal data acquisition time was determined by NMSE of each acquisition time from 1 to 6 minutes SPECT image showing under 0.05 as compared with reference value (NMSE of 7 minutes SPECT image). **Results:** CV of SPECT images were 0.178±0.024 on NC, 0.135±0.022 on AC and 0.130±0.020 on ACSC, respectively. Significant statistical difference was observed between NC and AC image (p<0.01), but was not between AC and ACSC image. Artificial decrease in count of inferior wall was found on NC image. However, this was not observed on both AC and ACSC image. NMSE under 0.05 was obtained by 5 and 6 minutes data acquisition in three images. **Conclusion:** Uniformity of SPECT image on CZT camera is significantly increased by AC and ACSC. AC is necessary for improving a specificity of diagnostic performance in case of using CZT camera. In addition, optimal data acquisition time is considered to be 5 minutes.

TP021**Comparison of the dual-energy window method and the triple-energy window method for quantitative single photon emission computed tomography**

Y. ITO, M. KUNIYOSHI, M. SUETAKE, K. MOCHIZUKI, K. MATSUMOTO, K. ENDO; Kyoto College Of Medical Science, KYOTO, JAPAN.

Aim: Several factors adversely affect quantitative analysis in the single photon emission computed tomography (SPECT). Among these, the most significant are Compton-scattered photons mixing into the preset energy window. However, the energy resolution of the sodium iodide used gamma camera-based SPECT is relatively poor. Therefore, several techniques have been proposed for Compton scatter compensation. The dual-energy window (DEW) method is easy to implement in the clinical studies and has been shown to produce an improvement in image quality. On the other hand, the triple-energy window (TEW) method obtained the counts from three windows and estimates the amount of scattered photons mixing into the main window and this method is widely used in the cerebral blood flow SPECT. The purpose of this study was to compare the DEW method and the TEW method in the brain SPECT image. **Methods:** A gamma camera, GE Healthcare Millennium MG with a low-energy high resolution collimator, was used to scan images of a Hoffman 3-D brain phantom filled with Tc-99m. The main window of the DEW method was set at 130-151 keV (nominally 15%) and the scatter window was set at the same width (100-116 keV). The main window of the TEW method was 24% (set at 123-157 keV), the lower and upper scatter rejection window were 4% (set at 118-122 keV and 158-164 keV, respectively). A total of 128 projections were acquired at 40 sec per view, resulting in a total scan time of 45 min. The DEW method was changing the weight coefficient ("k"). Image reconstruction was done using filtered back projection and attenuation correction was not performed. Quality of the reconstructed images was evaluated in terms of a contrast and a two dimensional power spectrum analysis. The program was implemented using C (Cygwin: version 2.4.1) and a personal computer (Core i5 4300U, 1.9 GHz, 8 GB memory). **Results:** As for the DEW method, the contrast became high-valued in a bigger "k" setting, and the pixel counts decreased with increasing "k". In the TEW-corrected images, the contrast was approximately 16% higher than that the without correction images. The contrast of TEW method was comparable with the DEW method at k=0.8. **Conclusions:** The TEW method allows easily reliable scatter correction for SPECT system. Further work is necessary to validate the method for different phantom imaging and different radionuclide tracer.

TP022**Inpatient Variability in Blood-Pool and Liver SUV for 18F-FDG PET/CT**

Y. Parlak, D. Goksoy, G. Gumuser, E. Sayit; Celal Bayar University, Manisa, TURKEY.

The purpose of the study was to show variations in blood-pool and liver SUVmax between two 18F-FDG PET/CT scan of an individual patient to make true evaluation of therapy response. Two hundred fifty oncology patients had PET/CT scans using a Philips True Flight Select 16 PET/CT scanner. Patient preparation, acquisition parameters and reconstruction protocols for all patients were standardized. All patients were divided into ten cancer groups, including 25 patients (esophagus, stomach, colon, rectum, larynx, lung, breast, endometrial, ovarian and lymphoma cancer) in each group. SUVs were obtained from 2-dimensional regions of interest in the aortic arch blood pool and in the right lobe of the liver. The group's mean serum glucose level for first and second scan was 5.5, 5.7mmol/L, respectively. The group's mean blood-pool and liver SUVmax for firsts can were 2.55±0.2; 1.79±0.2, respectively. The group's mean blood-pool and liver SUVmax for second scan were 3.13±0.2; 2.03±0.2, respectively. The reference range, in all patient groups, for inpatient variation was 0 to 1.5 for blood pool SUV max and 0 to 1.8 for

liver SUVmax. These ranges are applicable in clinical practice as they indicate practical limitation on qualitative tumor response assessment or tumor to background ratios in comparison of 18F-FDG PET/CT images.

TP023**Correlating Time per Frame and Injected Activity in bone SPECT/CT scanning: the case for consistent practice**

A. C. A. Gomes Moura, D. G. Sharp, A. Nunes, F. Ul-Hassan, V. Lewington; Guy's and St Thomas NHS Foundation Trust, London, UNITED KINGDOM.

Aim: The recommended activities for ^{99m}Tc MDP bone scintigraphy in the UK are 600MBq (+/-10%) for planar and wholebody imaging and 750MBq(+/-10%) for SPECT/CT. Bone SPECT/CT scanning is a common procedure in our department accounting for 10% of all scans performed during 2015 but, as the decision to proceed with tomographic imaging is often taken following review of planar images, not all patients having SPECT/CT scans are injected with 750MBq. This study's objective is to establish whether SPECT/CT operators take the injected activity into consideration when choosing the time per frame used for scanning. **Method:** Injected activities and SPECT/CT acquisition parameters were retrieved from electronic records for all patients who underwent SPECT/CT scanning in 2015 and data analysis was done on Microsoft Excel. **Results:** Data from 532 consecutive patients was analysed of whom 162 (Group 1) were injected with 600 MBq (range : 546-659 MBq) and 370 patients (Group 2) were injected with 750MBq (range: 690-824 MBq). For group 1, the average time per frame was 12.61 sec/frame and the mode was 10 sec/frame. For group 2, the average time per frame was 12.95 seconds/frame with a mode of 15 seconds/frame. **Conclusion:** Although it was expected that operators would select longer acquisition times for patients undergoing ^{99m}Tc MDP SPECT CT following injected activities of 600 MBq (+/-10%) compared with those receiving 750 MBq (+/-10%), our study shows that this was not always the case. On the basis of this data, we have changed our bone scan acquisition protocols to improve consistency and ensure that injected activity is always considered when selecting the time per frame used for bone SPECT/CT scanning. Adherence to this protocol and impact upon workflow will be assessed prospectively.

TP024**Halo artefacts around kidneys and bladder in [⁶⁸Ga]PSMA PET/MRT scans: Influence of different scatter correction settings**

A. Kanzog, S. Milachowski, F. Büther, T. Krähling, L. Stegger; University Hospital Münster, Münster, GERMANY.

Introduction: [⁶⁸Ga]PSMA PET is becoming an established imaging technology to assess prostate cancer. However, scanning with this tracer on current PET/MRT systems often leads to apparent extinction zones ("halos") around highly-active structures, especially kidneys and bladder. This can be attributed to imperfections in the current scatter correction algorithm. To analyse these artefacts, we reconstructed affected datasets with different scatter correction algorithms. **Methods:** Data for this study was acquired on an mMR scanner (Siemens, Erlangen, Germany). 30 Patients were scanned one hour after injection of 2 MBq/kg [⁶⁸Ga]PSMA tracer. The PET scan comprised 5 - 7 bed positions that were scanned for 3 minutes each. Standard DIXON MR sequences with MLAA-based extension of the field-of-view were performed to calculate PET attenuation maps for air, lung, fat, and soft tissue attenuation. As a standard, scatter correction was performed using a relative scaling of the simulated scatter estimate to the scatter tails outside the patient. Additionally, both an absolute scaling of the scatter based solely on the scatter estimate and a non-scatter-corrected reconstruction were performed. Reconstruction was done using OSEM with 3 iterations and 21 subsets. The whole-body images were afterwards analysed for visual halo artefacts around kidneys and bladder. **Results:** Distinct halo artefacts were present in the relatively-scaled images in

13 out of 30 studies. Of these, 9 were around the kidneys and 10 around the bladder. Absolute scaling of the scatter estimate did not improve image quality; instead, the artefacts were often just relocated to slightly different positions. Images without scatter correction did not show halo artefacts, although the scatter background in the images makes quantitative PET values difficult to obtain. **Conclusion:** Halo artefacts around hot structures are a prominent problem in current state-of-the-art PET/MRT. This seems to be caused by imperfect scatter estimates, probably based in part on limited attenuation map quality and ^{68}Ga -specific prompt gamma emission that is not accounted for in the current software. Absolute scaling of the scatter estimate - although implemented by the vendor as a remedy for this kind of artefacts - does not lead to a substantial improvements. In cases where quantification is not important, images reconstructed without scatter correction might help to get image information from halo areas.

TP025

Sparkling water for better visualisation of the myocardium and reduction of extra cardiac activity in patients for PET-CT with rubidium-82

H. Slootweg, V. J. W. Slender, P. C. M. Pasker-de Jong, J. J. Boer, J. P. Esser; Meander Medical Centre, Amersfoort, NETHERLANDS.

Introduction During myocardial perfusion imaging with rubidium-82 (PET) extra cardiac activity often occurs in stomach, intestines and liver. This may lead to difficulties in visualization and interpretation of the inferior myocardium. The aim of this study is to assess whether ingestion of sparkling water prior to imaging would improve the image quality by reducing activity in the stomach. **Methods** The study group consists of 77 patients: 44 males (age range 50-83 mean 65) and 33 females (age range 32-89 mean 70) who were referred for myocardial perfusion imaging by PET. Caffeine (including derivatives) and dipyridamol is discontinued 12 hours and theophylline is discontinued 48 hours before acquisition. 27 patients had nothing to drink prior to the scan, 26 had sparkling water, and 24 had tap water. The examination protocol begins with a topogram and low dose CT. Then two acquisitions follow during rest and stress (the latter after intravenous administration of regadenoson 400 mcg) both after injection of 1110 MBq rubidium-82 followed by 7 minutes of acquisition in list mode. There is a break of several minutes between rest and stress acquisition to allow recovery of the strontium-82 generator. For both rest and stress images, physicians scored for stomach activity, scoring 'yes' when having trouble interpreting the image because of interfering stomach activity. **Results** During the rest phase interfering stomach activity was found in 28% of the cases after sparkling water, 38.1% after tap water and 46.2% after drinking nothing. During the stress phase interfering stomach activity was found in 20% of the cases after sparkling water, 18.2% after tap water and 23.1% after drinking nothing. There was a higher occurrence of stomach activity compared to females $\text{OR}=3.5$ [1,1 - 11,4] The size of the study group will be expanded to increase the statistical significance and power. **Conclusion** During rest phase image quality is improved by prior administration of sparkling water resulting in better interpretation when compared to drinking nothing. Prior administration of tap water yields worse results compared to sparkling water. Statistical significant differences could not be found for the stress phase. During stress there is more myocardial activity as compared to rest, while stomach activity remains the same in both situations, thus increasing discrimination during stress. Male patients had higher occurrences of extra cardiac activity than female patients.

TP026

Experience from the first two years of Radium-223 treatment in Denmark

M. M. Joergensen, S. Holm, J. Mortensen; Rigshospitalet, Copenhagen, DENMARK.

Ra-223 is an alpha-emitting radionuclide approved for treatment of patients with castration-resistant prostate cancer and symptomatic bone metastases based upon a phase 3 study showing prolonged survival, time to bone-related complications, and improved quality-of-life (QoL). As calcium mimic Ra-223 binds into newly formed bone tissue, and accumulates in bone metastases. 95% of the emitted Ra-223 energy is alpha-radiation with a high linear energy transfer, while 1.1% of the radiation energy is X-ray and gamma radiation that can be detected with gamma monitors, gamma cameras and whole body counters (WBC). Method: Since the dose coefficient for intake is high (1.0×10^{-7} Sv/Bq) it is essential during handling the Ra-223 to avoid internal contamination either from inhalation, ingestion or adsorption. Therefore, the staff needs to apply special safety precautions. If an accumulated activity of > 300 MBq is handled over a year by a staff member in Denmark, a potential exposure of 0.5 mSv or more on a monthly basis must be detectable. This can be achieved by measurement in our WBC immediately after handling the Ra-223 to the patients. Also to avoid internal contamination a protective dress is used and control measurement of gloves/hands are performed after each handling, both dispensing and injection, of the dose. Results: As yet, Rigshospitalet is the only centre in Denmark providing Ra-223 treatment. Through the first two years we have administered 430 Ra-223 doses to 120 patients on 48 treatment days (1-16 patients each day). At each treatment day two of the three Ra-223 dedicated technicians and one of the three physicists handle between 36 to 96 MBq Ra-223. The accumulated Ra-223 activity handled by each staff member was 300-1400 MBq over the last year. The level of handling 300 MBq is reached by handling 10-14 patients (~ max. 50 vials of 6 MBq each) per staff member yearly. Alternatively, our patient through-put could be served by at least 5 pairs of two technicians plus one physicist dedicated to Ra-223 treatment. At each treatment day minor spillage of Ra-223 (Bq-amounts) is usually detected and gloves need to be changed regularly (1-6 times per treatments day). However, the WBC measurements have demonstrated no internal contamination to any staff member. **Conclusion:** When special radiation safety precautions are used Ra-223 is a safe treatment for the dedicated staff and no internal contamination occurs.

TP027

Comparisons of quantitative data between anterior and posterior views in sialoscintigraphy

C. LIN; Taipei Veterans General Hospital, TAIPEI, TAIWAN.

Introduction: Sialoscintigraphy is an invasive and useful examination for evaluation of salivary gland function. Either anterior or posterior view is applied in clinical procedure. The purpose of the study was to compare the quantitative data of sialoscintigraphy acquired in anterior and posterior views. Materials and methods: Thirty-three patients (5 males, age 61 ± 14 y/o) underwent sialoscintigraphy. After $5\text{mCi } ^{99\text{m}}\text{Tc}$ pertechnetate intravenous injection, both anterior and posterior views of dynamic images (10 seconds/frame) were simultaneously acquired by Siemens E.Cam Gamma Camera for 30 minutes. At the 20th min, 10ml lemon juice was given as an oral salivary stimulant. Patients were instructed to keep it in mouth for 2 minutes before swallowing. Data were analyzed by Siemens E-soft software. Bilateral parotids, oral cavity and partial cerebrum were measured as the regions of interest (ROIs). Time-activity curves were then derived from these ROIs. During the time period from 18 to 24 min, the following functional parameters of bilateral parotids were calculated: Excretion fraction (EF), T_{max} (time of maximum count), T_{min} (time of minimum count), C_{max} (the maximum count rate), C_{min} (the minimum count rate). In ROI of oral cavity, T_{max} and C_{max} were recorded. Comparisons of those quantitative sialoscintigraphy data between anterior and posterior views were evaluated. Results: Of the right parotid, there were no differences between anterior and posterior views in T_{max} (19.03 ± 0.67 vs. 19.12 ± 0.54 min, p=ns) and T_{min} (22.19 ± 0.98 vs. 22.09 ± 0.99 min, p=ns), respectively. Of the left parotid, there were no differences between anterior and posterior views in T_{max} (19.36 ± 0.85 vs. 19.23 ± 0.53 min, p=ns) and T_{min} (22.17 ± 0.95 vs. 22.37 ± 0.94 min, p=ns), respectively. The calculated EF of anterior view was higher than that of posterior view in right (68.04

± 14.69 vs. $64.11 \pm 14.89\%$, $p=0.005$) and left (70.44 ± 13.93 vs. $65.45 \pm 12.41\%$, $p=0.004$) parotids, respectively. C_{max} and C_{min} of bilateral parotids were significantly higher in posterior than in anterior views ($p<0.05$). In oral cavity, there was a difference between anterior and posterior views in T_{max} (21.22 ± 1.23 vs. 21.56 ± 1.23 min, $p=0.033$). The C_{max} of anterior view was significantly higher than that of posterior view (178.45 ± 87.58 vs. 73.82 ± 23.68 counts/sec, $p<0.001$) Conclusion: The detector orientation does not affect the T_{max} and T_{min} in time-activity curve of bilateral parotids in sialoscintigraphy. Using anterior view leads to a higher excretion fraction of bilateral parotids and oral activity, whereas the posterior view causes a higher count rate of bilateral parotids.

TP-02 – Tuesday, October 18, 2016, 08:00 - 09:30, Poster Exhibition Hall
Technologist Poster Session 2

TP028

DOPA PET-CT In Medullary Thyroid Cancer: Early Vs Late Acquisition

F. Sciume, L. Pavanello, D. Grigolato, M. Zuffante, M. Cucca, M. Ferdeghini; AOUI VERONA, Verona, ITALY.

AIM: This study wants to show the importance of the early acquisition at 20 minutes in the restaging of patients with medullary thyroid cancer (MTC). **MATERIALS AND METHODS:** We have studied 51 patients with MTC from 2013 to 2016. PET-CT Philips Gemini TF Big Bore has been used for the acquisition scans with [^{18}F]fluorodopa (^{18}F DOPA). The protocol foresaw: an early acquisition of the neck and mediastinum (3–4 beds) and the standard total body acquisition at 60 minutes after administration of 2.5 MBq/kg of ^{18}F DOPA. The CT parameters used for the acquisition of the neck and mediastinum/total body were: 120 KV, 60–80 mAs pitch 0.813, 16×1.5 mm collimation, thickness 1.5, FOV 600. PET parameters: 2 min bed position, FOV 576 mm. We had to arrange our scheduled resources in MBq (range 590–740) towards three patients for each daily section, it inserted between them without delayed the each acquisition. While early scanning of a particular anatomical region (neck-mediastinum) lasts about 6–10 minutes and the 20 to 30 minutes for the total body scan, the better strategy in the overall timing organization was the following: Patient one was injected at time zero and acquired 20 min later; patient two injected immediately after 10 min and acquired at 30° min; the third patient was injected 30 min later and acquired at 50° min. Immediately after the completion of all the early scans we started the total body PET-CT acquisition at 1 hour. **RESULTS:** It was evident that images at 20 minutes showed better visual definition and higher SUVmax values compared to the ones obtained in the whole body at one hour. In fact, the uptake of 18F-FDOPA decreased by 40% between the two acquisitions in all the regions of interest (ROIs). **CONCLUSION:** In all the patients with MTC, the early acquisition with 18FDOPA PET-CT (20 minutes) seemed to be more appropriate in the detection of lesions with respect to the late scan, because these tumors usually show a rapid wash-out, so we suggest to usually perform an early study.

TP029

Sequential dual time point PET-CT scan in the evaluation of physiologic, benign and malignant 18F-FDG uptake in head and neck region

A. Pietrzak, M. Smolen, P. Cegla, W. Cholewinski; Greater Poland Cancer Centre, Poznań, POLAND.

INTRODUCTION: 18F-FDG has been widely used for cancer diagnosis, however 18F-FDG is not a tumor specific agent. It can accumulate in benign lesions as well as in various organs not affected by any disease, making a proper diagnosis more complicated and demanding. Several approaches were made for increase the specificity of FDG-PET scan, including a variety of dual time point scanning. The aim of this study was to assess whether

sequential dual-time-point (18F)-fluoro-2-deoxyglucose-PET/CT imaging may be helpful in differentiation of physiologic, benign and malignant structures. **METHODS:** Eighty nine patients with suspected malignancy were investigated by performing two sequential PET/CT static acquisitions started at 60min and 90min after intravenous injection of 18F-FDG (370MBq). In each patient nine normal structures were evaluated (cerebellum, parotid, neck muscle, tongue, thyroid, tonsils, larynx, vertebra and carotid arteries) as well as any benign and malignant foci of abnormal 18F-FDG uptake, visualized during scan evaluation. All lesions were verified by histology or 2 years of follow-up. Visual and semiquantitative analysis was performed on both sets of images based on VOI technique with metabolic activity of chosen structure/lesion assessed by SUVmax value. **RESULTS:** Normal structures of head and neck showed in majority similar 18F-FDG uptake at 60min and 90min post injection. There was marked but not significant decrease in SUV value at 90min in vessels and larynx (-4.5% and -4.5%, respectively) and pronounced increase in cerebellum and thyroid (+2.8% and +4.7%, respectively). Benign lesions showed at 60min significantly lower average SUVmax value than malignant (3.09 ± 2.29 vs. 5.88 ± 3.80 , 7.08 ± 3.00 $p<0.01$). Analysis of SUV change between 60min and 90min post injection showed decrease of average SUV value in benign foci (3.09 ± 2.29 vs 2.88 ± 1.78 , ns) while malignant lesions showed significant increase in SUV value (5.88 ± 3.80 vs 6.77 ± 4.04 , $p<0.05$). In benign lesions average relative change in SUV values ranged from -55.5% to +30.0% ($1.6 \pm 0.3\%$) but in malignant ranged from -5.0% to +132.0% ($17.0 \pm 0.2\%$), and the difference was statistically significant ($p<0.05$). **CONCLUSIONS:** Sequential, dual time point PET/CT scan may increase the specificity of 18F-FDG in management of benign and malignant lesions in head and neck cancer. Additionally, the sequential scanning allows to avoid time delays and repositioning of the patients for acquiring delayed set of images.

TP030

[^{18}F]Fluoride for clinical use

P. Saipa, N. Savisto, A. K. Kirjavainen, S. Forsback, O. Solin, R. Puranen, E. Kokkomäki, T. Saarinen, S. Vauhkala; Turku PET Centre, Turku, FINLAND.

Aim: [^{18}F]Fluoride (^{18}F]NaF) is a highly sensitive bone imaging PET tracer used for detection of skeletal abnormalities. The aim was to automate the production of [^{18}F]NaF for clinical use in Turku PET Centre (TPC). The new production method required a new synthesis device and analysis method for quality control. In a GMP environment all production processes and quality control procedures have to be validated. **Materials & Methods:** An automated synthesis device, enabling a synthesis in a closed system, was designed and built at TPC. The synthesis device was placed in a qualified hot cell located in cleanroom class C. An existing automated sterile filtration unit was connected to the device. The synthesis device was qualified according to the quality system at TPC. A new HPLC analysis method for [^{18}F]NaF was developed to ensure the quality of the end product. The method described in the European Pharmacopoeia was not applicable. Chemical and radiochemical purity of the end product were determined using a radioHPLC method. The same method was used to detect impurities as a limit test. The validation parameters for the method were specificity and detection limit with UV and radioactivity detectors. The manufacturing process was validated in compliance with our quality system. Three consecutive batches of [^{18}F]NaF were produced and all quality control tests were performed on the final product according to the method description. In addition to the parameters determined using the HPLC method, pH, shelf-life for six hours, residual solvents, sterility and bacterial endotoxins were analysed. One bioburden batch was produced to determine if the end product has a microbiological effect on sterilization. **Results:** All process validation batches complied with the product specifications and the process was confirmed to be appropriate for the production of [^{18}F]NaF. **Conclusion:** The new automated production method was taken into clinical use. The new production method is user-friendly, quick and safe from the viewpoint of radiation protection and sterility of the end product.

TP031**Could the image quality for 18F-Choline PET in obese patients be improved by prolonged acquisition time?**

B. Olsson¹, J. Hagerman¹, A. Stenval², F. Hedeer¹, H. Almquist¹, C. Hindorf², J. Oddstig²; ¹Clinical Physiology and Nuclear Medicine, LUND, SWEDEN, ²Radiation Physics, LUND, SWEDEN.

Aim Patients with prostate cancer are in clinical routine examined with ¹⁸F-Choline PET. The administered activity is 4 MBq/kg body weight, maximum 400 MBq, and images are acquired for 2 min/bed position. For patients with a body mass index (BMI) >30 a decreased image quality can be expected. The aim of this study was to investigate if the image quality could be improved with increased acquisition time for patients with BMI>30. **Material and Methods** 21 patients (11 patients with BMI>30) were included in the study. The patients received 4MBq/kg (maximum 400 MBq) of ¹⁸F-Choline and were imaged on a GE Discovery PET/CT690 60 minutes after administration. The acquisition time for patients <105kg was 2.0min/bed. For patients with a weight over 105kg the acquisition time per bed was prolonged: 105-125kg, 2.5min/bed; 126-150kg, 3.0min/bed. Acquisition in listmode allowed studies for patients with BMI>30 to be truncated to correspond to a study of 2.0min/bed. Three regions of interest were drawn in consecutive sections in the liver. The mean value of kBq/ml and the standard deviation of the kBq/ml were used as input to obtain the SNR (signal-to-noise ratio), calculated as the mean kBq/ml divided by the standard deviation of the kBq/ml. One expert reader scored the image quality. Scores were given by a five grade image quality scale (1=unacceptable image quality and 5=very high image quality). **Results** After increasing the acquisition time per bed for patients with BMI>30 the SNR increased from 11.1 to 12.0 (p<0.05) and the score of the image quality increased from 2.7 to 2.9 (p<0.05). For patients with BMI<30 the SNR was 14.0 and the score of the image quality was 3.5. **Conclusions** Increasing the acquisition time per bed for patients with BMI>30 will significantly increase the SNR and the scored image quality. However, both the SNR and the scored image quality will still be significantly lower than for a population with a BMI<30.

TP032**Comparison of metabolic activity of metastatic bone lesions assessed in vivo by 18F-FDG-PET/CT and 99mTc-phosphonates bone scan**

A. Pietrzak¹, M. Smoleń¹, E. Wierchoslawska¹, R. Czepczynski², W. Cholewinski¹; ¹Greater Poland Cancer Centre, Poznań, POLAND, ²Poznan University of Medical Sciences, Poznań, POLAND.

Background: The presence of bone metastases characterizes the advanced stage of cancer disease in over 70% of patients. There is a noticeable conviction that molecular imaging of metastases with 18F-FDG-PET/CT is an important tool in diagnosis and monitoring treatment response as more sensitive, accurate and specific than bone scintigraphy. However, 99mTc-phosphonates bone scintigraphy is still performed as a method of choice in detecting bone metastases. The aim of this study was to assess the difference between these two methods in detecting bone metastases with special focus on the comparative analysis of skeletal activity and glucose utilization in metastatic foci. **Material and methods:** 54 patients (26 male and 28 female), mean age of 62±12 (between 34-84 years) with confirmed neoplastic disease of prostate and breast and suspected bone metastases were included in this study. All patients underwent two studies on separate days - bone scan with 99mTc-phosphonates (activity of 740 MBq, WB scan 150 minutes post injection) and 18F-FDG-PET/CT (activity of 370MBq, WB scan 60 minutes post injection) within 4 weeks time. Number of metastatic foci was evaluated and the semiquantitative analysis based on the assessment on tracer uptake within abnormal foci was performed. Analysis was based on comparison of count rate in metastatic and physiologic area (R factor) on bone scan images. The metastatic glucose metabolism was evaluated based on SUVmax value on the corresponding 18F-FDG-PET scans. **Results:** The mean R value within bone

metastatic foci was 2.11±0.84 and it was higher but not significant in patients with prostate cancer than in breast cancer patients (3.37±3.66 vs 1.87±0.60; ns). The SUVmax average in whole group was 2.11±0.84 and it was significantly higher in breast patients than in prostate cancer patients (5.61±3.52 vs 4.74±1.76; p<0.05). Analysis of correlation showed no significant correlation between R and SUVmax values (correlation coefficient in whole group, prostatic and breast patients was 0.004, 0.11 and 0.16, respectively). 18F-FDG-PET/CT detected more bone lesions in 27 patients than scintigraphy, however the difference was statistically insignificant. **Conclusion:** No significant correlation was observed between osteoblastic activity and glucose utilization in metastatic foci and this observation validate the independent value of analyzed diagnostic methods and suggests negligible influence of glucose utilization in bone modeling cells.

TP033**The added value of ^{99m}Tc-Nanocolloid SPECT to ⁶⁸Ga-DOTApeptide PET/CT in pancreatic neuroendocrine tumors (NETs)**

L. Pavanello, F. Sciume', M. Zuffante, D. Grigolato, M. Cucca, M. Ferdeghini; AOUI, Verona, ITALY.

AIM: to clarify with ^{99m}Tc-nanocolloid SPECT doubtful lesions at ⁶⁸Ga-DOTApeptide imaging located in pancreatic tail or perisplenic. Pancreatic NETs, both primary or secondary lesions have usually high uptake of ⁶⁸Ga-DOTApeptide. There are some areas with elevated uptake of the somatostatin analog, perisplenic with or without splenectomy, or in the pancreatic tale, which are not NETs but only accessory or atypical spleens. In these cases it could be useful to demonstrate the presence of reticuloendothelial splenic tissue before surgery to exclude NET and to avoid massive surgery. **MATERIALS AND METHODS:** ⁶⁸Ga-DOTApeptidi PET/CT Philips Gemini TF Big Bore has been used for acquisition scans. We analyzed 11 patients that presenting suspicious lesions with elevated ⁶⁸Ga-DOTApeptidi in the pancreatic tail or in the splenic area (generally after splenectomy). All patients underwent PET/CT at one hour post injection in supine. The CT parameters used for the acquisition: 120 KV, 60-80 mAs pitch 0.813, 16x1.5mm collimation, FOV 600. The PET parameters were: 2 min bed position, FOV 576 mm, 1.5/2.5 MBq/kg of ⁶⁸Ga-DOTApeptidi. In another day we performed a ^{99m}Tc-Nanocolloid SPECT, dispensed activity of 740 MBq, patient in supine position, acquisition started 15min after injection, we acquired planar static images of the abdomen, followed by SPECT. We used a Gamma-camera Marconi Irix 3 heads with parallel holes LEHR collimator and a computer Odyssey Fx. The SPET parameters: orbit circular type, motion step and shoot, matrix 128 x 128 with zoom 1, angular step 3° at 25 secs/step, FOV includes the upper abdomen. In the image reconstruction we applied iterative algorithms (OSEM), in the image reading we gave importance to sagittal, coronal and axial sections, looking for sites of accumulation of the radiopharmaceutical. In addition we performed image fusion between PET/CT and SPET to reach the best clarifying results. **RESULTS:** In 3 of 11 patients studied with these methods we obtained important results which helped the surgeons to decide a personalized approach, sometimes avoiding unnecessary splenectomy because the areas in pancreatic tales or closed to the spleen with elevated ⁶⁸Ga-DOTApeptidi had also high ^{99m}Tc-Nanocolloid concentration, demonstrating atypical endothelial pattern, which stayed for accessory spleen. **CONCLUSION:** ^{99m}Tc-Nanocolloid SPECT correctly identifies the doubtful lesions located in pancreatic tale or perisplenic, positive with ⁶⁸Ga-DOTApeptide, which could be accessory spleen.

TP034**Quantification of myocardial glucose uptake for viability assessment in routine clinical setting**

M. Mortensen, N. L. Christensen, H. J. Harms, K. Bouchelouche, L. C. Gormsen, L. P. Tolbod; Dept. of Nuclear Medicine and PET-Centre, Aarhus University Hospital, Aarhus N, DENMARK.

Purpose: 18F-fluorodeoxyglucose (18F-FDG) PET has been used for decades to characterize the myocardial metabolism non-invasively. The identification of viable myocardium is important for the patients' further qualification for medical or surgical treatment. So far only static imaging has been used for this purpose clinically, thus only providing relative values for the myocardial glucose uptake (MGU). Our purpose was to implement a protocol to perform dynamic imaging clinically. This way, instead of measuring the relative myocardial glucose uptake, we are able to measure the absolute myocardial glucose uptake. **Method and results:** We have had 31 patients undergo a 60 minute 18F-FDG dynamic viability PET scan. One hour prior to the injection of 18F-FDG, a hyperinsulinemic-euglycemic clamp was performed. A low-dose CT scan was performed prior to the 18F-FDG injection for attenuation correction and anatomical localization. The total duration of the exam was two hours, during which blood glucose (BG) was measured every 10 minutes. Analysis of the scans was done using a Patlak-Gjedde model and an image derived input function in the Cardiac VUer software. MGU was determined as $BG \times lc \times Ki$, where a value of 1 was used for the lumped constant (lc) and Ki was the Patlak influx rate. Global MGU ranged from 0,09 $\mu\text{mol/g/min}$ to 0,41 $\mu\text{mol/g/min}$ with a mean of 0,24 $\mu\text{mol/g/min}$. **Conclusion:** We were able to perform dynamic viability exams with hyperinsulinemic-euglycemic clamp without prolonging the total examination time; actually the examination time was shortened by 15 min, compared to standard static viability exams. However, on-scanner time was increased from 15 min to 60 min. We did not experience any issues with patient compliance. This tool will be used to assess the added value of the hyperinsulinemic-euglycemic clamp over simple glucose loading.

TP035

The Comparison of the F18 FDG SUV Value of Lesion Depending on the Depth, Size and Time Using Pet Phantom

T. ERTAY¹, I. EVREN¹, M. ALSALEM², H. DURAK¹; ¹DOKUZ EYLUL UNIVERSITY, DEPARTMENT OF NUCLEAR MEDICINE, izmir, TURKEY, ²DOKUZ EYLUL UNIVERSITY, INSTITUTE OF HEALTH SCIENCES, DEPARTMENT OF MEDICAL PHYSICS, izmir, TURKEY.

PET imaging is unique technique that describes chemical and metabolic changes in the body. SUV (standard uptake value) is important for differentiating malignant and benign lesion. In this study PET/CT imaging studies were performed (Philips Medical Systems GEMINI TF 16) using PET phantom. Phantom as soft tissue, different size spheres (9.5, 12.7, 15.9, 19.1, 25.4, 31.8 mm) as lesion models were used. Imaging was performed at 1., 2. and 3. hours. Imaging times were during 30 s, 60 s, 120s. F-18 FDG activity concentration was adjusted as 30.4 MBq/mL in the spheres and of 3.8 kBq/ml in the phantom. Phantom was imaged by the same protocol with the patients. The rate of the total radioactivity of the phantom to total weight of phantom was calculated as SUV for each lesion at 1., 2. and 3. hours. Repeated Measure Anova (RMA) and Friedman Pearson Correlation analysis as statistical methods were applied to the data of the experimental study results. The values of the lesion location, size and concentrations were obtained. Display time did not create difference in assessments, lesion size and depth have created significant differences in SUV. In evaluation benign and malignant differentiation the size and depth of lesion localization should be considered.

TP036

The utility of PET-CT “breath-hold” protocol in the study of solitary pulmonary nodules. Preliminary results of a small case-series

J. Molina, J. Chinchilla, M. Oporto, S. Rubí, C. Peña, E. Perez, M. Gimenez; Hospital Universitario Son Espases. Departamento de Medicina Nuclear, Palma de Mallorca, SPAIN.

Aim: To evaluate the utility of a short PET acquisition “breath hold” protocol in a better definition of the pathologic FDG uptake in solitary pulmonary nodules

(SPN) suspicious of malignancy. **Methods:** 6 patients with a SPN detected on lung CT were studied: 1 suggestive of primary lung tumor, 1 indeterminate and 4 suspicious of lung metastasis (3 from rectal and thyroid malignancies and 1 from an osteosarcoma). After the standard whole-body (WB) PET-CT acquisition (GE Discovery PET-CT 600) at 50-80 min post-injection, a delayed (77-150 min) lung image centered on the PN was obtained with the “breath-hold” technique: the patients held their breath (apnea) at a medium expiration during the acquisition of a low-dose CT (10 sec) followed by a PET image of 1 bed of 20-30 sec of duration. In three out of 6 patients, an additional PET-CT lung image was acquired immediately after the “breath-hold protocol” with a conventional free respiration protocol (3min/bed). Then, PET images were evaluated on a visual and semiquantitative basis (SULmax). **Result:** Based on standard WB PET-CT images, 3 SPN in 3/6 patients were reported as visually positive (SULmax between 3-4.7), and all of them showed a marked increase of uptake in the “breath-hold protocol” images (SULmax between 7.9-8.3). In 2 out of these 3 SPN, a delayed respiration-free lung image also showed an increase FDG uptake, though it was less marked than in the “breath-hold protocol” (SULmax between 2.8-5.6). In 2/6 patients neither the standard WB PET-CT images nor the late “breath-hold protocol” images showed any significant uptake in the SPN. In 1 of these 2 patients a very mild positivity was reported on an additional respiration-free delayed PET image (SULmax=1.2). The remaining patient had a SPN suspicious of a thyroid cancer metastasis, and it showed no noticeable changes between the initial WB standard (SULmax=2) and the delayed “breath-hold” image (SULmax=2.2). **Conclusion:** A short PET-CT “breath-hold protocol” seems useful in the better evaluation of SPN, as significant increase in the uptake value was observed in some patients, without elevating the timing of image acquisition. Nevertheless, its clinical role compared to a delayed conventional respiration-free images remains uncertain so far in our small case-series, for which further research are needed.

TP037

Hanging Breast technique scan

D. M. J. Luikel-Hooghof; Spaame Gasthuis, Hoofddorp, NETHERLANDS.

Introduction: In the comparison of prone MR images with supine PET images the loss of normal landmarks is a limitation. It has been proved that a Hanging Breast technique scan (HB scan) followed by the routine (supine) 18F-FDG PET acquisition, can achieve a better visualization and localization of lesions for patients who have been diagnosed with breast cancer. These results support the inclusion of Hanging Breast scans in the acquisition guidelines of PET/CT imaging in breast cancer patients. **Aim:** This poster describes a simple method to make the PET Hanging Breast technique scan, in order to obtain better visualization and localization of the breast tissue for a side-by-side comparison with MRI. **Material&Methods:** Patients diagnosed with breast cancer, who have small or multiple lesions, are selected to make HB scans. A *Mamma Matrass* is used to position the patient for prone studies and can be placed on the scanner couch. The arms of the patient should be in an upward position, besides the patient head, resting on pillows. The HB study (surview(40 cm.)- lowdose CT- PET(1 bed position)), starts approximately 45 min. after FDG injection, so the FDG is distributed in the patients body. Followed by a routine PET whole body scan and if necessary a diagnostic CT with contrast agent. In this way, the patient is not repositioned between the WB PET and diagnostic CT. Side-by-side comparison with MR images are performed by a nuclear medicine physician. **Results:** Photos of few case examples that visualize the difference between a prone scan and supine in comparison to MRI. **Evaluation:** Using the HB method adds 5 minutes to the acquisition protocol, however it proves useful in lesion visualization and localization due to the corresponding position of the patient. **Footnotes:** Added value of prone position technique for PET-TAC in breast cancer patients. *Esp Med Nucl* 2010, 29(5):230-235. Improved breast cancer detection of prone breast FDG-PET in 118 patients. *NuclearMedicineCommunications*. October 2008- Volume 29-issue10-pp 885-893 VANDERWILT techniques by (886.019A)

TP038**The Importance on Lesion Detection of Arm Position for PET/CT Imaging**

Y. parlak, D. Goksoy, G. Mutevelizde, G. Gumuser, E. Sayit; Celal Bayar University, Manisa, TURKEY.

In many clinical PET/CT studies, PET/CT acquisition is commonly performed with the patient's arms raised above the head. For patients who can not raise arms, PET/CT scan is usually performed arms by the patient's side. For CT, this positioning increases the incidence of beam hardening artifacts and can give rise to striking artifacts on PET images. A 53-year-old male patient with lung cancer underwent PET/CT imaging for restaging in December 2014. The lumbar and thoracic spine metastasis were observed. Therefore, the patient received chemotherapy and PET / CT imaging as response to treatment was taken in December 2015. The PET/CT imaging was performed with the arms positioned patient's side because of his widespread body pain. Approximately 60 min later, a PET/CT examination was obtained from mid thigh to skull base with a Truflight Select PET/CT system (16 slices, 120 kV, 50mAs, Philips Medical Systems, USA). Striking artifacts, evident at the abdomen level, were detected on PET/CT images the arms down. A second image obtained as arms positioned above a rolled blanket. The second scan revealed increased F-18 FDG uptake at T12 (first scan SUV max; 3.7, second scan SUV max; 7.1) and L2 (first scan SUV max; 3.4, second scan SUV max; 4.9) regions. In the first scan, due to the artifact, SUV max were underestimated. When we compare the both PET/CT scan images, new multiple costal metastasis observed and metabolic progression of spine metastasis were detected. Arms down introduce CT artifacts depending on arm position. It is advisable to take notice of the positioning if there is a special region of interest. We suggest that the arm positioning above a rolled blanket is essential especially in the assessment of column vertebrae, in patients who can not raise arms.

TP039**Impact of Harderian Gland Uptake in the Quantification of ¹⁸F-FDG PET Studies in Rat Brain**

X. Liang, S. Han, J. Li, L. Wan, Q. Xie; Huazhong University of Science and Technology, Wuhan, CHINA.

Aims: The aim of the study was to evaluate the effect of the high accumulation of radioactivity in the Harderian glands on ¹⁸F-FDG-PET quantification of rat brain images. The evaluation was based on Monte Carlo simulation. **Materials and Methods:** Small animal PET was performed with the scanner Trans-PET BioCalibur LH (Raycan Technology Co., Ltd.). An adult male Sprague Dawley rat weighing 340 g was injected with ¹⁸F-FDG (14.8 MBq), and taken a 10 min static scan centered over the brain 70 min after ¹⁸F-FDG injection. After scanning, the PET image was reconstructed by using 3D ordered subsets expectation maximization (OSEM) method. Images were analyzed using AMIDE to quantify the tissue activity concentration (Bq/ml) and standardized uptake values (SUVs) over the following regions of interest (ROIs): olfactory bulb, cortex motor, cortex somatosensory, cortex visual, caudate putamen, thalamus, midbrain and Harderian glands. In the Monte Carlo simulation study, we used several phantoms modeling according to the rat imaging data to represent the ROIs calculated above. The data were acquired with and without the Harderian glands phantom using the same scanner and acquisition protocols as the animal imaging. The methods of reconstruction and quantitation were also the same as the animal study. We compared the ratio of the same ROI in two kinds of background to evaluate the effect. **Result:** The animal study showed that Harderian glands had high accumulation of ¹⁸F-FDG (ratio of ROI-gland/ ROI-other was 1.64–2.12). The simulation study revealed that ROIs in brain had different values with and without Harderian glands phantom and the ratio of each other also had changed. Among them, both the ratio of cortex somatosensory and caudate putamen to the whole brain are of

significant difference ($p < 0.05$). **Conclusions:** The high accumulation of radioactivity in the Harderian glands has an effect on the ¹⁸F-FDG-PET quantification of rat brain images. It should be considered in the quantification of brain, especially in the quantification of cortex somatosensory and caudate putamen.

TP040**Positron-Emission Tomography In The Diagnosis Of Solitary Pulmonary Nodules: Relation Of The SUV Measurement With The Histopathologic Types Of Lung Cancer And Clinical Outcome**

M. Pombo Pasín, Ms., M. Garrido Pumar, V. Pubul Núñez, A. Bejarano García, J. Cortés Hernández, I. Domínguez Prado, A. Golpe Gómez, Á. Ruibal Morell; Clinic University Hospital of Santiago de Compostela, Santiago de Compostela, SPAIN.

OBJECTIVE: The Positron Emission Tomography (PET) is a useful tool for the diagnosis of the nature of pulmonary nodules. The aim of this study is to establish the possible influence of the semiquantitative valuation in the PET of solitary pulmonary nodules (SPN) by measuring the Standard Uptake Value (SUV) with the different histopathological types of lung cancer, and with the posterior outcome of the patients. **METHODS:** From 334 patients that performed a PET for the characterization of a SPN, we selected 213 that had positive visual uptake in PET. We used the higher value of SUV in the nodule (SUVmax). The final diagnosis of the nodule came from histopathological analysis or radiological follow-up in cases with low risk of malignancy. The histopathological classification of the pulmonary nodules included benign nodules, squamous-cell carcinoma, adenocarcinoma, neuroendocrine carcinoma, small-cell carcinoma, metastasis from extra-pulmonary cancer, and other types/unclassified lung cancer. Patients were followed after the PET and clinical outcome data included cancer recurrence, metastatic disease and exitus. Statistical analyses included ANOVA and t-student tests. **RESULTS:** Median SUV was significantly higher in squamous cell carcinoma (Median SUV 13.6 [10–19]), followed by small cell cancer (Median SUV 12.8 [9.2–16.4]), the other type/unclassified lung cancer (Median SUV 10.2 [7.5–15.7]), neuroendocrine cancer (9.5 [6.7–13.4]), metastasis (8.3 [4.3–10.9]) and adenocarcinomas (7.4 [3.9–11.35]). Benign nodules had the lower SUV values (Median SUV 3.2 [2.2–4.6]) ANOVA/Kruskal-Wallis $p < 0.001$. In the posterior outcome, higher SUV values showed relation with recurrence (11.3 ± 5.8 vs 7.2 ± 6.4; $p < 0.003$), metastasis (10.5 ± 7.1 vs 7.2 ± 5.7; $p < 0.001$) and exitus (10.4 ± 6.5 vs 6.6 ± 5.3; $p < 0.001$). **CONCLUSION:** SUV values had significant relation with histopathological types, specially establishing differences between benign and malignant lesions. From malignant nodules, squamous-cell carcinomas showed the highest SUV values, and adenocarcinomas were the lesions with lower SUV values.

TP041**¹⁸F-Choline PET/CT vs Bone Scintigraphy for bone metastasis detection in patients underwent radical prostatectomy and radiotherapy.**

I. Baeta¹, H. Delgado¹, R. Oliveira¹, L. Vieira¹, E. Carolino¹, M. Vazquez², J. Alonso²; ¹Escola Superior de Tecnologias da Saúde de Lisboa, Lisboa, PORTUGAL, ²Departamento de Medicina Nuclear MD Anderson Cancer Center, Madrid, SPAIN.

AIM: Prostate Carcinoma (PC) is one of the most common malignancies pathologies in male, with high recurrence rates even after radical prostatectomy or radiotherapy. Positron Emission Tomography/Computed Tomography (PET/CT) with ¹⁸F-Choline and Bone Scintigraphy (BS) are currently used to detect PC recurrence in addition to the information provide by biochemical analysis, biopsy and other image modalities. The aim of the present study is to evaluate and compare both imaging techniques, PET/CT and BS, for the detection of bone metastasis. **MATERIAL AND METHODS:** It was performed a

retrospective analysis of 42 ^{18}F -CholinePET/CT studies and BS studies in 42 patients underwent radical prostatectomy and/or radiotherapy with evidence of biochemical recurrence. The conclusions of imaging and pathologic studies results were obtained through the patient history and medical reports of PET/CT and BS. A database was formulated with the collected data in SPSS (Statistical Package for the Social Sciences), version 22.0. Spearman statistical test was applied, as also many other correlations related with the number of lesions detected and PSA values. **RESULTS:** In 35.7% of the population bone metastatic lesions were detected by BS. Otherwise, only 30.9% of the population presents evidence of bone metastasis in PET/CT scan. After being applied Spearman statistical test, a percentage of 64.2% were obtained in terms of an equal number of detected lesions in both image techniques. Concordant findings between PET/CT and BS occurred in 64.2% of the population. In addition, a low-intensity positive correlation was found between the number of lesions detected by BS and PET/CT ($r_s=0.448$, $p=0.003$). In this study, BS detected more lesions than PET/TC in 19.04% of cases. **CONCLUSIONS:** Both image techniques are useful for the detection of bone metastasis caused by PC. In the present study, BS revealed more efficiency in the detection of bone metastasis than PET/CT. **Keywords:** Radical Prostatectomy, PSA, Biochemical recurrence, ^{18}F -Choline PET/CT, Bone Scintigraphy.

TP042

Salivary glands uptake from FDG PET/CT in the patients with IgG4-related disease

Y. Chen, Y. Wu, H. Wang, R. Yen, C. Ko, M. Cheng; National Taiwan University Hospital, Taipei City, TAIWAN.

Aim: The immunoglobulin G4-related disease (IgG4-RD) is associated with elevated serum IgG4 concentration and commonly involves the salivary glands. However, FDG activity from salivary glands in healthy subjects and patients diagnosed with IgG4-RD have not been compared. This study aims to establish clinical useful PET indices in identifying patients diagnosed with IgG4-RD affecting the salivary glands. **Materials and Methods:** From August 2008 to August 2014, 47 patients with IgG4-RD prior to steroid therapy and 134 health volunteers were enrolled. Images of the parotid and submandibular glands obtained using FDG PET/CT were analyzed. Parotid and submandibular glands were measured for standardized uptake values by placing volumes of interest (VOI) in the salivary glands seen in the coregistered CT images. All placed VOIs were corrected for blood pool activity. The results were also correlated with serum IgG4 level. **Results:** IgG4-RD group showed higher SUVmax in salivary glands compared with healthy group (parotid: 2.44 ± 1.12 vs 2.01 ± 0.43 ; submandibular: 3.19 ± 1.78 vs 2.63 ± 0.49 , both $P < 0.05$), regardless whether symptoms of sialadenitis were present. The serum IgG4 level showed better correlation with SUVmax of submandibular glands than with parotid glands ($r=0.52$ and 0.32 , respectively; $P < 0.05$) while there was no significant correlation with serum IgG. IgG4-RD group with submandibular SUVmax ≥ 2.63 (mean value from the healthy group) had higher serum IgG4 level than SUVmax < 2.63 (1590.72 mg/Dl vs. 592.43 mg/Dl, $P < 0.05$). **Conclusion:** Salivary glands uptake, especially submandibular glands, were significantly higher in patients with IgG4-RD than in healthy subjects, regardless whether symptoms or signs of IgG4-RD sialadenitis was present.

TP043

Influence of smoking on ^{18}F -Choline uptake in normal lungs

A. L. L. Canudo, B. Freitas, D. Dantas, V. Santos, S. Chaves, C. Oliveira, J. Castanheira, D. Costa; Champalimaud Foundation, Lisboa, PORTUGAL.

Introduction Choline is a phosphatidylcholine precursor, necessary for the cell membrane synthesis. Malignant tumors show increased synthesis of cell membranes, reflecting cellular proliferation. Malignant tissues show high uptake of ^{18}F -Choline compared to normal tissues. This enables the identification

and localization of malignant lesions. Unfortunately ^{18}F -Choline uptake is not specific to cancer cells and can occur in granulomatous tissue. It is possible that reduced ^{18}F -Choline uptake may be observed in other diseases with reduced viability and/or function of the phospholipid cell membranes. **Objective** To investigate the relationship between tobacco smoking and ^{18}F -Choline lung uptake in individuals with no known lung disease. **Material and methods** Retrospective analysis of 25 consecutive patients referred for staging and restaging of prostate cancer without known lung disease. According to the clinical history, patients were divided into 3 groups: smokers (S=8), never-smokers (nS=8) and former, but no more, smokers (fS=9). VOIs (28mm diameter) were drawn in the left (upper and lower lobes) and right lungs (upper, middle and lower lobes) in 3 consecutive axial, sagittal and coronal slices of the whole body images acquired 15minutes after injection. Measured maximum and average SUVs were compared between the three groups. **Results** There were no differences in the measured SUVs for the different lobes within each study group. However, it was interesting to note that SUVs in the lower lobes showed the highest uptake of ^{18}F -Choline in all 3 groups. Despite no statistically significant differences, we found the lowest SUVmax (1.36) in the group S (smokers). The fS group revealed SUVmax of 1.92 and the SUVmax (2.11) was recorded in the nS (never-smokers) group. **Discussion/ Conclusion** This quantitative mapping of pulmonary ^{18}F -Choline lung uptake in patients without a known pulmonary disease demonstrates greater uptake of ^{18}F -Choline in the lower lobes, most probably due to physiological pattern. The lower ^{18}F -Choline uptake in the lungs of smokers may be due to reduction of metabolic viability and/or function (phospholipid) of the alveolar-capillary membranes. Ongoing work is underway to better understand the relationship between tobacco smoking and lower ^{18}F -Choline lung uptake.

TP044

PET/MRI in clinical routine: initial experience in Brazil

S. A. Nogueira, T. Vitor, K. M. Martins, M. F. Barboza, A. F. Thom, J. Wagner; Hospital Israelita Albert Einstein, São Paulo, BRAZIL.

PET/CT is already an established imaging technique in various areas of oncology, as well as in neuroimaging. Recently, the integration of positron emission tomography (PET) and magnetic resonance imaging (MRI) has been ongoing research. Due to their ability to obtain anatomical, functional and metabolic information in a single examination, this combination provides significant advantages over PET/CT such as less ionizing radiation and better soft-tissue contrast that facilitate the differentiation between normal tissue and disease. In September 2015 we received the first full integrated PET/MRI scanner in Brazil. The aim of this study is describe the first clinical PET/MRI cases and discuss some of the areas of PET/ MRI imaging application and its relevance in the Albert Einstein Hospital clinical routine. The scans were performed in a Biograph mMR PET/MRI scanner (Siemens Medical Solutions, Erlangen, Germany). Cases described herewith include whole body, abdomen, pelvis, hip, prostate, chest, breast, brain and head and neck examination performed with ^{18}F -FDG, ^{18}F -FNa, ^{68}Ga -DOTATATE or ^{68}Ga -PSMA-11. In this study the protocols used the main MRI sequences for association with PET acquisition, looking for the shortest time and better resolution in both methods. The majority of our studies were indicated as a complement to PET/CT imaging. The scan time varied 30 - 90 minutes, resulting in high anatomical resolution and excellent soft tissue contrast. Despite the complexity of its operation, PET/MRI is proving to be a valuable tool in clinical practice.

TP045

Variations in the Indications of Myocardial Perfusion Gated-SPECT After the Inclusion of a Coronary-CT In Clinical Practice

B. PEREZ LOPEZ, R. RUANO PEREZ, M. DIEGO DOMINGUEZ, A. DIEGO NIETO, L. G. DIAZ GONZALEZ, F. GOMEZ-CAMINERO LOPEZ, P. L. SANCHEZ FERNANDEZ, M. P. TAMAYO ALONSO;

HOSPITAL UNIVERSITARIO CLINICO DE SALAMANCA, SALAMANCA, SPAIN.

Objective: To evaluate changes in number and indications of myocardial perfusion gated-SPECT after the inclusion of coronary CT in diary clinical practice in our hospital in April 2015. **Methods:** Patients from July-2014 to December-2015 were classified in two groups: A-group : pre CT-CR and B-group: post CT-CR. We considered as variables: amount of patients, gender, age, hospitalized status, indication (diagnosis, ischemia severity, ischemia follow-up, postinfarction, post- unstable angina pectoris, viability, incomplete PTCA) and gMPS result. Statistical analysis was made with SPSS, significance level considered was $p < 0.05$. **Results:** A-group: 572 patients (401 males, 171 females), average age 69.4 years old, 15.6% hospitalized. B-group: 581 patients (392 males, 189 females), average age 69.1 years old, 15.1% hospitalized. There were not statistically significant differences ($p > 0.05$) between amount of patients, proportion of patients hospitalized, age or gender. Regarding indication for gMPS in males, there was a reduction in ischemia follow-up studies (from 20.2% to 12.8%), viability studies (5.2% vs 2.6%) and postinfarction (4.4% vs 1.8%), differences statistically significant ($p = 0.000$). On the other hand, there was an increase in post-PTCA incomplete (1.2% vs 7.3%), diagnostics and evaluating ischemia severity (67.8% vs 75.2%). Furthermore, there were not statistically significant differences between the other indications. When evaluating gMPS result there was a significant rise in normal studies, in males from 36.1% to 50.1% ($p = 0.000$); and a non-significant rise in females: 47.3% vs 54.2% ($p = 0.192$). However when ischemia was detected the proportion of moderate to severe ischemia was similar ($p = 0.294$). **Conclusion:** Inclusion of coronary CT in clinical practice has not changed the amount of g-MPS studies, however there has been an increase in the number of normal gMPS. There were variation in indications of gMPS in males, mainly in myocardial viability studies and in those patients with recent heart attack.

TP046

The added value of SPECT/CT at Whole body bone scintigraphy performed for staging in detecting skeletal metastasis from prostate cancer

K. Schouten-Stadnik, A. van Dongen, M. Lakeman; Department of Nuclear Medicine, Westfriesgasthuis, Hoorn, NETHERLANDS.

Introduction: Prostate cancer is the most common cancer among men in The Netherlands. Prostate cancer often metastasizes to bone. The malignant cells from the prostate spread mainly to bones in the hips, pelvis and spine. Bone metastases lead frequently to bone pain and pathological fractures. Early detection of metastatic bone disease is critical for accurate staging and can help determine the most effective treatment strategy. Whole body bone scintigraphy is a standard technique used in many hospitals to detect bone metastases. Aim: The aim of this study was to investigate the additional value of Single Photon Emission Computed Tomography with CT (SPECT/CT) at each first Whole bone scintigraphy performed for staging, in detecting skeletal metastasis from prostate cancer. **Materials en methods:** This study is based on data from 40 patients with prostate cancer (mean age 74 years) who underwent ^{99m}Tc -hydroxymethane diphosphonate (HDP) Whole body bone scintigraphy and SPECT/CT of the lumbar spine and pelvis between march 2015 and march 2016. The images were evaluated by nuclear medicine physician. The reviewer used 4 - points diagnostic scale (1, malignant; 2, probably malignant; 3, benign; 4, probably benign) to score each lesion with abnormal tracer uptake. All lesions were double analyzed and scored. The first time using only the planar bone images and the second time the SPECT/CT images. **Results:** The analysis of the planar images showed that reviewer rated 10 % of lesions as malignant, 18% as probably malignant, 31% as benign and 41% as probably benign. The analysis of the SPECT/CT images showed that reviewer rated 18 % of lesions as malignant, 5% as probably malignant, 70% as benign and 7% as probably benign. **Conclusion:** The addition of SPECT/CT at first staging Whole bone scintigraphy improved higher accuracy in detecting skeletal metastasis from

prostate cancer. Furthermore, using of SPECT/CT resulted in a substantial reduction of equivocal bone lesions.

TP047

Characteristics of single- and dual-energy images with thallium-201 myocardial IQ-SPECT-CT system

T. Shibutani¹, M. Onoguchi¹, H. Yoneyama², T. Konishi², S. Matsuo³, K. Nakajima⁴, S. Kinuya⁴; ¹Department of Quantum Medical Technology, Graduate School of Medical Sciences, Kanazawa University, Kanazawa, JAPAN, ²Department of Radiological Technology, Kanazawa University Hospital, Kanazawa, JAPAN, ³Department of Nuclear Medicine, Kanazawa University Hospital, Kanazawa, JAPAN, ⁴Department of Biotracer Medicine, Graduate School of Medical Science, Kanazawa University, Kanazawa, JAPAN.

Objectives: Although dual-energy (DE) acquisition with conventional thallium (Tl)-201 myocardial perfusion SPECT has several advantages such as improved attenuation of the inferior wall and increased acquisition counts, characteristics of IQ-SPECT have not been fully evaluated. The aim of this study was to evaluate the difference of characteristics between single-energy (SE) and DE imaging using Tl-201 myocardial IQ-SPECT. **Methods:** Myocardial phantoms created in this study were normal and abnormal patterns simulating infraction of the inferior wall. SPECT scans were acquired with a Siemens dual-head SymbiaT6 SPECT-CT scanner equipped with multifocal SMARTZOOM collimators. Energy windows were set on 70 keV $\pm 10\%$ for SE, and additional 167 keV $\pm 15\%$ for DE. SPECT images were reconstructed using ordered subset conjugate gradient minimization method using order 3 and iteration 13, and a Gaussian filter (FWHM 9.6 mm) was used as a post filter. Three kinds of myocardial images were created; namely (1) without scatter and attenuation correction (NC), (2) with attenuation correction (AC), and (3) with both attenuation and scatter corrections (ACSC), while DE image with ACSC could not be created due to system limitation. The SE and DE images were assessed visually using a five-point (1 worst to 5 best) scale and quantitatively assessed with a 17-segment polar map. **Results:** The average scores of the SE and DE images for the normal myocardium were 3.9 and 4.4 for NC, and 4.5 and 4.7 for AC, respectively, and that of the SE image of ACSC was 3.4. Although the defect score was more than 4 for both of the SE and DE images with NC and the SE images with ACSC, the DE image with AC showed a significantly lower score than the SE image. Furthermore, the percentage uptake values of the SE and DE image in the inferior wall (segments 4 and 10) were 50% and 55% with NC, 69% and 77% with AC, respectively, and 65% for the SE image with ACSC. The SE image with ACSC showed high defect detectability; however, the visual score of normal myocardium was the lowest. **Conclusion:** The DE image with NC can improve attenuation of the inferior wall. DE image with AC, however, showed low defect detectability. Thus, myocardial image with AC should be SE rather than DE. Furthermore, while SE image with ACSC can detect the defect, it needs to be carefully interpreted, including the possibility of artificial inhomogeneity even in the normal myocardium.

TP048

Inter-Operator Variability in Assessing and Planning Bone SPECT/CT

A. C. A. Gomes Moura, D. G. Sharp, A. Nunes, F. Ul-Hassan, V. Lewington; Guy's and St Thomas NHS Foundation Trust, London, UNITED KINGDOM.

Background Published guidelines for ^{99m}Tc MDP bone SPECT/CT scanning lack specific information regarding the optimal length of time per frame, mainly due the variety of acquisition systems and reconstruction software available. Although our local protocol stipulates acquisition parameters according to the body area under investigation, there is scope for individual operators to tailor procedures to suit individual patients' circumstances. We studied

differences in inter-operator SPECT/CT practice by asking 5 experienced operators to define the acquisition parameters they would use when provided with detailed information regarding patients referred for SPECT/CT scan. **Method** 10 Whole body bone scans and accompanying static images were shown to 5 experienced SPECT/CT operators. Each data set included relevant clinical information such as patients' age, comorbidities, mobility, body mass index, analgesic requirements, urinary continence, and mental state. Operators were asked to state the time per frame that they would use for each SPECT/CT scan and how this varied from the department protocol. The scans chosen represented the 5 most commonly scanned anatomical areas. **Results** For head and neck scans, there were some inconsistencies between operators' responses with respect to patient specific factors such as claustrophobia. Lower variability was observed in adapting protocols for limb extremity and pelvic scans but higher inter-operator variability was recorded for spine SPECT/CT. Factors contributing to these decisions were analysed. **Conclusion** Inter-operator variability in acquiring bone SPECT/CT images reflects operator experience, interpretation of clinical information provided, and adaptation to patient's condition. While our study confirms the value of specific protocols to support decision making, it also demonstrates the importance of clinical judgement in optimising bone SPECT/CT scan acquisition.

TP049

The importance of SPECT/CT for abdominal blood pool scintigraphy: a case study

M. Koehner, C. Rischpler; Rechts der Isar, Munich, GERMANY.

Aim: The abdominal blood pool scintigraphy is a well-established method for localizing the source of blood loss in a patient. Although other methods like CT and Ultrasound have proved themselves as good and fast methods for finding severe bleedings the abdominal blood pool scintigraphy is the most sensitive method of finding small bleedings. The newer technology of SPECT/CT imaging has been able to further increase the sensitivity of the method as well as to provide better localization. **Method:** With a case study of a patient who was suffering of chronic blood loss, the importance of the abdominal blood pool scintigraphy for the clinic routine could be demonstrated. The patient had been undergoing several colonoscopies, angiograms as well as a camera colonoscopy with the aim of finding the source of his blood loss. All of those methods did not show the actual source of the bleeding. The patient underwent an abdominal blood pool scintigraphy in order to find the source of the bleeding problem. Dynamic images and planar images were acquired as well as SPECT/CT's. **Findings:** The planar images as well as the dynamic images themselves proved inefficient in finding the source of bleeding. SPECT images alone were able to show a bleeding in the upper intestines but only the utilization of SPECT/CT allowed the exact localization.

TP050

Multimodal Neurophysiology in presurgical evaluation of Epilepsy at the University Hospital in Lund, Sweden

A. Melin, I. L. Erlandsson; Neurofysiologiska kliniken, Lund, SWEDEN.

Purpose: Presenting neurophysiological tests used for epilepsy surgery evaluations preformed at the Department of Neurophysiology at the University Hospital in Lund, Sweden. **Methods:** • Electroencephalography (EEG) • Extra cranial video-EEG (EvEEG) • Single-photon emission computed tomography (SPECT) • Subtraction ictal SPECT co-registered to MRI (SISCOM) • Invasive intracranial video-EEG (IvEEG) • Co-registration: localization of intracranial electrodes using CT, co-registered to MRI • Electrical Brain Stimulation (EBS) **Results:** To illustrate the methods, we are using a case of a 16 year old female who has had seizures with feelings of discomfort and fear since age 12. For identifying the epileptogenic focus we preformed EEG, EvEEG, SPECT, SISCOM, IvEEG and EBS. Routine-EEG was normal, EvEEG showed in 50 % of the seizures low voltage rhythmic theta activity

over the right hemisphere, otherwise no typical epileptic activity. At SPECT examination Tc^{99m} -HMPAO was injected, 7 sec after clinical seizure onset. SISCOM showed a hotspot located in the right Cingulate gyrus. MRI was initially interpreted normal, after SISCOM, MRI was re-examined and a cortical lesion was found close to the SISCOM hotspot. Invasive electrodes were placed. Co-registration with MRI showed strip-electrodes over medial interhemispheric fissure and depth electrode in the right medial frontal hotspot. IvEEG revealed epileptic seizure activity in depth electrode 5 sec before clinical seizure onset, spreading after 10 sec to one of the strips. Interictal activity and high frequency discharges were seen in the depth electrode. EBS, stimulating depth electrodes induce the same aura as the patient experience at spontaneous seizures. Surgery was performed and a volume including the hotspot was removed. PAD showed focal cortical dysplasia type. The girl has been seizure free since 3 months. **Conclusion:** SISCOM and intracranial electrodes co-registered to MRI is an important tool in presurgical epilepsy evaluation.

TP051

Preoperative localisation of hyperfunctioning parathyroid glands; A preliminary comparison between ^{99m}Tc -sestaMIBI / ^{123}I scintigraphy and ^{18}F -fluorocholine PET/CT

E. Jansen, M. Wondergem, F. M. Van der Zant, R. J. J. Knol; Noordwest Ziekenhuisgroep, Alkmaar, NETHERLANDS.

Introduction/Aim Preoperative localisation of hyperfunctioning parathyroid glands is essential before minimally invasive surgical extirpation. Recent literature suggests improved sensitivity of ^{18}F -fluorocholine PET/CT over the conventional combined ^{99m}Tc -sestaMIBI / ^{123}I parathyroid scintigraphy. Other important advantages of ^{18}F -fluorocholine PET/CT include that it does not require withdrawal of certain medications, sometimes needed for up to 2 months prior to conventional scintigraphy, while the whole procedure can be completed in merely 2 hours instead of 2 days, which is typical for conventional parathyroid scintigraphy protocols. **Patients and Methods** Two cohorts were compared. Cohort A included 56 patients who underwent ^{99m}Tc -sestaMIBI / ^{123}I scintigraphy and cohort B included 50 patients who underwent ^{18}F -fluorocholine PET/CT for detection of hyperfunctioning parathyroid glands. Both cohorts were compared regarding to sensitivity of the scan procedure, number of patients that went for surgical intervention, pathological findings after surgery and effects of surgery on PTH and serum calcium levels. **Results** In cohort A and B respectively, 44.6% and 66.0% of the scans showed a parathyroid adenoma, 0.0% and 2.0% showed hyperplasia, 26.8% and 14.0% were negative and 28.6% and 18.0% were equivocal. For cohort A 15/56 patients underwent surgery, while preliminary analysis of cohort B revealed that 20/40 patients were found suitable for surgery. For 10/50 patients decisions on further treatment were not made at time of evaluation. In cohort A pathological findings showed a parathyroid adenoma in 10/15 (66.7%), in 3/15 (20.0%) hyperplasia and in 2/15 (13.3%) no parathyroid tissue was found. In cohort B 12 patients had been operated at the time of the preliminary evaluation. In 9/12 (75.0%) patients a parathyroid adenoma was found while in 3/12 (25.0%) patients a normal parathyroid was detected. In cohort A normalisation of serum PTH and calcium was found in 12/15 (80.0%) of the patients operated, in cohort B normalisation was found in 12/12 (100%) of the patients. **Conclusion** In the present data, ^{18}F -fluorocholine PET/CT localises more hyperfunctioning parathyroid glands than ^{99m}Tc -sestaMIBI / ^{123}I scintigraphy. The preliminary analysis of cohort B indicates that already more patients went for surgery after ^{18}F -fluorocholine PET/CT in whom normalisation of serum PTH and serum calcium was detected more frequently. These data will be updated upon completion of all surgical procedures.

TP052

Clinical Application Specialist

W. Lin¹, C. Lee², Y. Liang³, Y. Hsu¹; ¹Nuclear Medicine department of Jan-Ai Hospital DaLi Branch, Taichung, TAIWAN, ²Philips Health

Systems, Taipei, TAIWAN, ³PET Center of Jan-Ai Hospital DaLi Branch, Taichung, TAIWAN.

1. Introduction A pheochromocytoma is a rare, catecholamine-secreting tumor and paragangliomas arising from neural crest tissue is meant extra-adrenal tumor. Because of excessive catecholamine secretion, pheochromocytomas may precipitate life-threatening hypertension or cardiac arrhythmias. If the diagnosis of a pheochromocytoma is overlooked, the consequences can be disastrous, even fatal however, if a pheochromocytoma is found, it is potentially curable. Approximately 10% of pheochromocytomas and 35% of extra-adrenal paragangliomas are malignant. Only the presence of metastases defines malignancy. The clinical manifestations of a pheochromocytoma result from excessive catecholamine secretion by the tumor. Tumors in patients with gemline mutations of succinate dehydrogenase subunit genes (SDHB and SDHD), which cause familial paraganglioma, principally produce dopamine

2. Case Report A 39-year-old man without hypertension or heart disease complained with left flank pain for several months. He visited to ER and CT showed left huge tumor and several bony metastasis was noted, bone scan also showed radioactivity increased of upper and lower T-spine and left shoulder area. With surgery recession, radiotherapy and chemotherapy, the tumor was confirmed paraganglioma which invades to renal parachyma. Before surgery dissection, the imaging study was performed as description, CT study showed visualized 15x12x12cm hypodense mass in left upper kidney with central necrosis and multiple bony metastases at T-spine Bone scan showed high radioactivity in left humeral head, T4-T5, T10-T11, and right femoral neck. (In OP finding: Multiple, diffuse metastatic tumor almost over both the thoracic and lumbar spine and pathologic fracture and severe spinal cord compression at T4-5 and T9-11) In 2016 Feb, CT and Bone Scintigraphy were highly suggested a new bony metastasis in left femoral neck, the patient was arranged the F-18 FDG PET scan for further evaluation. The FDG PET showed multiple FDG-avid bony foci were noted, at right C2, right 10th rib, the coccyx and left proximal femur and an extra-ordinary brain focus at right hemisphere. **3. Discussion** I-131 MIBG is frequently used in cases of familial pheochromocytoma syndromes, recurrent pheochromocytoma, or malignant paragangliomas. But with shortage of I-131-MIBG in Taiwan, the diagnosis of pheochromocytomas and paraganglioma is still depended on CT and scintigraphy for evaluation. FDG PET wholebody scan with higher specificity and sensitivity will be the most valuable tool for diagnosis pheochromocytomas and paraganglioma with metastasis. With genetic study development in pathology, PET/CT will become approaching 100% sensitivity in SDHB-related metastatic paraganglioma and excellent in detecting primary, recurrent and metastases pheochromocytomas and paraganglioma.

TP053

Establishment of a simple simultaneous production of two different ¹¹C radiopharmaceuticals using two precursors in one reactor and HPLC

J. Lee, Y. Cho, Y. Lee, H. Park, C. Yoon, Y. Lee, H. Lee, J. Kim, K. Kang, J. Jeong; Seoul National University Hospital, Seoul, KOREA, REPUBLIC OF.

Aim: We have reported a method for producing two ¹¹C radiopharmaceuticals simultaneously using two HPLC loops and HPLC systems in 2012. In order to simplify this method further, we tried to label two different precursors by reacting with [¹¹C]CH₃I in a single HPLC loop and purify the resulting products using one HPLC system in the present study. **Materials and Methods:** [¹¹C]CO₂ was produced by a PETtrace cyclotron, converted to [¹¹C]CH₄ and [¹¹C]CH₃I in a TRACERlab FXC Pro successively. Precursors of flumazenil (0.3 mg) and PBR28 (1 mg) were dissolved in N,N-dimethylformamide (30 μL) and dimethyl sulfoxide (150 μL), respectively. And then 1 M potassium hydroxide solution (1.5 μL) and sodium hydride (7 mg) were added as bases. The mixture was vortexed and loaded into a HPLC loop (2 mL). Prepared [¹¹C]CH₃I as described above was delivered to the HPLC loop for 5 min and then the reaction mixtures was purified using one semi-preparative HPLC column (Waters, XTerra Prep RP18, 10 μm, 10 × 250 mm). Each

[¹¹C]flumazenil and [¹¹C]PBR28 peak was collected into a glass vial. **Results:** The syntheses were performed 5 times. The retention times of [¹¹C]flumazenil and [¹¹C]PBR28 were 11.1 ± 0.75 and 22.8 ± 0.78 min, respectively (Figure 1). The non-decay corrected yields of [¹¹C]flumazenil and [¹¹C]PBR28 were 25.2 ± 4.3% and 16.3 ± 3.3%, respectively. Radiochemical purities of both of the compounds were higher than 95%, and no cross-contamination by each compound was observed. The specific activities of [¹¹C]flumazenil and [¹¹C]PBR28 were 221 ± 102 and 509 ± 346 GBq/μmol, respectively. **Conclusion:** We established a straightforward preparation system of [¹¹C]flumazenil and [¹¹C]PBR28 simultaneously using one synthesis module and one HPLC system.

TP054

Preliminary evaluation of ⁸⁹Zr-labeled Affibody for PET imaging of Tumors Expressing HER2

Y. Xu¹, Z. Bai², D. Pan¹, L. Wang¹, J. Yan¹, R. Yang¹, M. Yang¹; ¹Jiangsu Institute of Nuclear medicine, Wuxi, CHINA, ²Nanjing Medical University, Nanjing, CHINA.

Aims: Human epidermal growth factor receptor 2 (HER2) is a biomarker in diagnosis, therapy and prognosis of cancers. PET imaging with HER2 specific agents could provide non-invasive assessment of target expression level with better sensitivity and accuracy. Affibody is a new type of imaging probes because of high affinity and rapid blood clearance. ⁸⁹Zr exhibits a long half-life, which allows for tracking and quantification biological processes for longer periods. Herein, the ⁸⁹Zr-labeled modified HER2 affibody, ⁸⁹Zr-DFO-MAL-CGGGRDN-ZHER_{2;342} (denoted as ⁸⁹Zr-DFO-MAL-MZHER), were prepared and its biological properties were preliminarily evaluated in tumor models using microPET imaging. **Materials and Methods:** MZHER was conjugated with MAL-DFO and then labeled with ⁸⁹Zr under mild reaction conditions. The stability of ⁸⁹Zr-DFO-MAL-MZHER was also determined in PBS and human serum. The HER2 targeting potential and pharmacokinetic profile of the ⁸⁹Zr labeled tracer were analyzed by in vivo studies in SKOV-3 human ovarian cancer models via small animal PET. **Results:** ⁸⁹Zr-DFO-MAL-MZHER can be efficiently produced within 20 min. The non-decay corrected yield was greater than 90% and the radiochemical purity was more than 95%. The tracer was stable in PBS and human serum after 120min in vitro incubation. Excellent tumor-to-background contrast were clearly observed at 30min p.i. and kept even at 48h after administration. The uptake values in SKOV-3 cancer xenografts ranged from 6.29 ± 1.20 %ID/g at 30min p.i. to 3.41 ± 1.31 %ID/g at 48h p.i. respectively. The tumor to muscle uptake ratios were 12.80 ± 3.23 and 30.91 ± 11.56 at the corresponding times. Co-injection of the excess non-labeled ZHER with the probe specifically reduced the SKOV-3 tumor uptake to 1.75 ± 0.53 %ID/g at 1h postinjection. Besides, the tracer showed low liver uptake (~1%ID/g) and high kidney accumulation at the early time points (125.47 ± 23.16 %ID/g at 30min p.i.) then dropped significantly afterward (72.56 ± 15.16 %ID/g at 48 h p.i.), indicating rapid renal clearance. **Conclusion:** ⁸⁹Zr-DFO-MAL-MZHER is a potential probe for monitoring HER2 receptor expression. Favorable preclinical data showing specific and effective tumor targeting suggest that the further trial should be undertaken to test its diagnostic utility in clinical imaging. **Research Support:** This work was supported by National Natural Science Foundation (51473071, 81472749, 81401450, 21401084, 21504034), Jiangsu Province Foundation (BE2014609), Health Ministry of Jiangsu Province Fund (RC2011095, Q201406 and H201529), 333 Project of Jiangsu (BRA2015476).

TP055

Excitation function evaluation of ⁶³Zn producing reactions by charged particles

M. Rostampour¹, S. Hamidi¹, M. Aboudzadeh Rovais², M. Sadeghi²; ¹Arak University, Arak, IRAN, ISLAMIC REPUBLIC OF, ²Nuclear

Science and Technology Research Institute, Tehran, IRAN, ISLAMIC REPUBLIC OF.

Introduction: The ^{63}Zn is a short lived beta emitter, which is very suitable for using in PET. Cyclotron based methods of ^{63}Zn production are investigated by many researchers. There are seven principal routes to produce ^{63}Zn at cyclotrons: $^{63}\text{Cu}(p,n)^{63}\text{Zn}$, $^{65}\text{Cu}(p,3n)^{63}\text{Zn}$, $^{nat}\text{Cu}(p,n)^{63}\text{Zn}$, $^{64}\text{Zn}(p,n+p)^{63}\text{Zn}$, $^{63}\text{Cu}(d,2n)^{63}\text{Zn}$, $^{62}\text{Ni}(\alpha,3n)^{63}\text{Zn}$, and $^{60}\text{Ni}(\alpha,n)^{63}\text{Zn}$. In the radioisotope production procedure, the nuclear reaction data are mainly needed for respective optimization of production rates. This process involves a selection of the projectile energy range that will maximize the yield of produced isotopes and minimize the radioactive impurities. This study was intended to give a suitable reaction to produce ^{63}Zn via cyclotron. **Method:** In the present study, excitation functions of ^{63}Zn for cyclotron based production methods were calculated by the nuclear model codes, TALYS-1.6 and EMPIRE-3.2.2. The results were compared with the reported experimental data and with the theoretical values obtained from the TENDL-2014 database. And the excitation functions for impurities in different proton induced reactions were calculated. Subsequently, for each reaction stopping power is calculated using SRIM 2013 code. The integral yields for the production of ^{63}Zn via seven reactions were obtained on the basis of cross section values obtained by nuclear model codes and stopping power values calculated by SRIM 2013. **Results and discussion:** Although the cross section for $^{65}\text{Cu}(p,3n)^{63}\text{Zn}$, $^{nat}\text{Cu}(p,n)^{63}\text{Zn}$, $^{64}\text{Zn}(p,n+p)^{63}\text{Zn}$, and $^{62}\text{Ni}(\alpha,3n)^{63}\text{Zn}$ reactions are considerable, the isotopic impurities are produced in these reactions. Thus these reactions are not desirable to produce carrier free ^{63}Zn . The energy and intensity of commonly available deuteron beams are low. Therefore, $^{63}\text{Cu}(d,2n)^{63}\text{Zn}$ reaction is not practical. There is no isotopic impurity in the $^{60}\text{Ni}(\alpha,n)^{63}\text{Zn}$ reaction. Nevertheless, the low natural abundance of ^{60}Ni hinders using this reaction for producing ^{63}Zn . In addition handling of an irradiated ^{60}Ni target has to be performed in highly radiation-shielded cells due to the neutron radiation produced from (α,n) reaction. **Conclusion:** By considering available cyclotrons, the isotopic impurities, and the production yields of seven Cyclotron based methods for producing ^{63}Zn , it has been verified that the $^{63}\text{Cu}(p,n)^{63}\text{Zn}$ is an optimal reaction for the cyclotron production of ^{63}Zn . **Keywords:** ^{63}Zn production • Excitation function • Production yield • EMPIRE-3.2.2 • TALYS-1.6

TP-03 – Tuesday, October 18, 2016, 08:00 - 09:30, Poster Exhibition Hall
Technologist Poster Session 3

TP056

Mycardial perfusion imaging using dedicated CZT-SPECT: acquisition time optimization

L. Camoni¹, G. Damini², A. Fierro³, G. Zobbio², R. Giubbini¹; ¹Univesity and Spedali Civili di Brescia, BRESCIA, ITALY, ²Univesity of Brescia, BRESCIA, ITALY, ³Spedali Civili di Brescia, BRESCIA, ITALY.

Aim: Aim of this study was to evaluate if time reduction of double dose rest acquisition during single day MPI by CZT SPECT can influence the Summed Rest Score (SRS) **Material and methods:** Single-day stress-rest Gated-SPECT with 185+370 Mbq of Tc-labeled compounds were performed using a CZT-based gammacamera (GE D530Alcyone) in 100 patients, randomly selected. The standard acquisition time was 9 minutes for both stress and rest acquisitions. The rest acquisition was retrospectively reconstructed by list-data as a 4 minutes and 30 seconds acquisition. The quantitative data obtained after SPECT reconstructions were evaluated by QPSv2009 using a 17 segment model. The SRS was obtained for the entire LV and from each coronary territory: LAD, LCX and RCA. *Statistical analysis was performed using SPSS v.21 (IBM Corp., Armonk, NY, USA) by Wilcoxon paired test.* **Results:** The data were expressed as means \pm standard deviation. The 9 minutes SRS was 2.65 \pm 4.4; LAD 1.58 \pm 2.9; LCX 0.57 \pm 1.6; RCA 0.5 \pm 1.3;

conversely the 4'30" minutes SRS was 2.81 \pm 4.57; LAD 1.67 \pm 2.9; LCX 0.58 \pm 1.7; RCA 0.6 \pm 1.4. p =ns. The SSS was 4.93 \pm 5.7 and the SDS for 9 minutes and half-time were respectively 2.59 \pm 2.77 and 2.49 \pm 2.76. p =ns.

Conclusion: after injection of 185+370 MBq of Tc-labelled compounds for stress/rest MPI, rest acquisition can be shortened as half time acquisition does not affect SRS and SDS results.

TP057

Comparisons of ejection fractions derived from different preset parameters of count and heartbeat in multiple gated acquisition scan

C. LIN; Taipei Veterans General Hospital, TAIPEI, TAIWAN.

Introduction: The acquisition parameters of presetting count and heartbeat are optional in multiple gated acquisition (MUGA) scan. The study aimed to investigate the ejection fractions (EFs) derived from different preset parameters of count and heartbeat. **Materials and methods:** Under the in-vivo labeling technique with 20 mCi ^{99m}Tc pertechnetate, 32 consecutive patients (3 males, age 57 \pm 12 y/o) received the MUGA scan. To obtain the optimal imaging angle of separating the right and left ventricles, the SPECT mode was applied first. Three groups of MUGA scan data were then serially collected from each patient by Siemens Symbia E Gamma Camera and defined as three groups: Group 1 (preset count:8000K), Group 2 (preset count:4000K), Group 3 (preset heartbeat: 500 beats). Images were processed to obtain the following data: EDC (End-diastolic count), EDA (End-diastolic area), ESC (End-systolic count), ESA (End-systolic area) and BGC (Background count/pixel). Left ventricular EFs were then calculated according to three formulas: (1) $EF = (EDC' - ESC') / EDC' * 100$ (2) $EDC' = EDC - BGC * EDA$ (3) $ESC' = ESC - BGC * ESA$. Comparisons among the EFs from the three groups were evaluated. Correlations between EFs and other variables were also checked, including age, accepted heartbeats, imaging angles, EDC, EDA, and BGC in each group. **Results:** There were no differences of EFs (Group 1 vs. 2 vs. 3: 67.91 \pm 6.34 vs. 67.46 \pm 7.44 vs. 67.93 \pm 6.01 %, p =ns) among three groups. In each group, there were no correlations between EFs and age, accepted heartbeats, imaging angles, EDC, and EDA. There were positive correlations between EFs and BGC in Group 1 ($p=0.001$), Group 2 ($p<0.001$) and Group 3 ($p=0.019$), respectively. After excluding the time of rejected heartbeats, the mean acquisition time were 14.26 \pm 3.7 min in Group 1, 7.36 \pm 2.03 min in Group 2 and 7.14 \pm 0.69 min in Group 3. **Conclusion:** The acquisition parameters of presetting count or heartbeat do not affect the left ventricular EFs in this study. The positive correlation between EFs and background counts indicates that poor efficiency of the in-vivo labeling technique causes higher left ventricular EFs in MUGA scan. Our finding is beneficial for unstable or arrhythmic patients by adjusting parameters to 4M counts or 500 heartbeats to save the acquisition time without changing the EFs in MUGA scan.

TP058

Effect of the Angle of Ventricular Septal Wall on Left Anterior Oblique View in Multi-Gated Cardiac Blood Pool Scan

Y. You, C. Lee, Y. Seo, H. Choi, Y. Kim, Y. Kim, W. Won, J. Bang, S. Lee, T. Kim; Nation Cancer Center, Goyang-si, KOREA, REPUBLIC OF.

Purpose : In order to calculate the left ventricular ejection fraction (LVEF) accurately, it is important to acquire the best septal view of left ventricle in the multi-gated cardiac blood pool scan (GBP). This study aims to acquire the best septal view by measuring angle of ventricular septal wall (θ) using enhanced CT scan and compare with conventional method using left anterior oblique (LAO) 45 view. **Subjects and Methods:** From March to July in 2015, we analyzed the 253 patients who underwent both enhanced chest CT and GBP scan in the department of nuclear medicine at National Cancer Center. Angle (θ) between ventricular septum and imaginary midline was measured in transverse image of enhanced chest CT scan, and the patients whose difference between the angle of θ and 45 degree was more than 10 degrees

were included. GBP scan was acquired using both LAO 45 and LAO θ views, and LVEFs measured by automated and manual region of interest (Auto-ROI and Manual-ROI) modes respectively were analyzed. Results : Mean \pm SD of θ on total 253 patients was $37.0 \pm 8.5^\circ$. Among them, the patients whose difference between 45 and θ degrees were more than ± 10 degrees were 88 patients ($29.3 \pm 6.1^\circ$). In Auto-ROI mode, there was statistically significant difference between LAO 45 and LAO θ (LVEF 45 = $62.0 \pm 6.6\%$ vs. LVEF θ = $64.0 \pm 5.6\%$; $P = 0.001$). In Manual-ROI mode, there was also statistically significant difference between LAO 45 and LAO θ (LVEF 45 = $66.7 \pm 7.2\%$ vs. LVEF θ = $69.0 \pm 6.4\%$; $P < 0.001$). Intraclass correlation coefficients of both methods were more than 95%. In case of comparison between Auto-ROI and Manual ROI of each LAO 45 and LAO θ , there was no significant difference statistically. Conclusion : We could measure the angle of ventricular septal wall accurately by using transverse image of enhanced chest CT and applied to LAO acquisition in the GBP scan. It might be the alternative method to acquire the best septal view of LAO effectively. We could notify significant difference between conventional LAO 45 and LAO θ view.

TP059

Studies on simultaneous myocardial imaging with dual radionuclides (^{123}I and ^{201}Tl) using cardiac focusing collimator

K. Kunimoto¹, S. Abe², N. Fujita², Y. Sakuragi², T. Odagawa¹, Y. Koshiba¹, M. Honda¹, K. Kato¹; ¹Nagoya University Graduate School of Medicine, Nagoya, JAPAN, ²Department of Radiological Technology, Nagoya University Hospital, Nagoya, JAPAN.

Purpose: Recently, a cardiac focusing-collimator (CF)(variable-focus collimator) designed for cardiac studies has been developed and enables to acquire the SPECT data faster than conventional SPECT studies. At present, in simultaneous myocardial imaging with ^{123}I and ^{201}Tl , the conventional parallel-hole collimator has been generally used instead of CF. If CF will be generally used for simultaneous myocardial imaging with ^{123}I and ^{201}Tl , the image acquisition time is shortened and patients' burden is reduced. In this study, we investigated the usefulness of CF in simultaneous myocardial imaging with ^{123}I and ^{201}Tl in the phantom experiment. **Materials and Methods:** ^{123}I and ^{201}Tl solutions were separately enclosed into the torso phantom, and the SPECT data were acquired using a low-medium energy general purpose collimator (LMEGP) and CF. Using the short-axis images, the crosstalk rate was examined. And both solutions were enclosed in together into the torso phantom and the SPECT data were acquired. The attenuation and scatter corrections were performed. On the short axis images, the accurate counts were determined using crosstalk rate. Using a profile curve obtained in the short-axis images, the full width half maximum (FWHM) was determined. This operation was conducted on the images acquired in each energy window. **Results:** In the SPECT images of ^{201}Tl , FWHM acquired with CF was better than that acquired with LMEGP. In the SPECT images of ^{123}I , FWHM acquired with CF was improved compared with that before scatter and attenuation corrections, but it did not surpass that acquired with LMEGP. This fact is considered due to the effect of 167 keV gamma rays from ^{201}Tl , and the septal thickness of CF was thin compared with LMEGP. **Conclusion:** In the SPECT images of ^{201}Tl after scatter and attenuation corrections, FWHM acquired with CF was better than that acquired with LMEGP. In the SPECT images of ^{123}I , however, FWHM acquired with CF did not surpass that acquired with LMEGP even after scatter and attenuation corrections. Further studies will be needed to search for more appropriate acquisition and reconstruction conditions when CF is used.

TP060

Study of Clinical Cases for the Standardization and Unification of the ^{123}I -metaiodobenzylguanidine Heart-to-Mediastinum Ratio

D. Ogura¹, H. Shimada², M. Kanou¹, M. Mochiki¹, T. Ino¹, T. Toyama³, K. Koyama¹; ¹Gunma Prefectural Cardiovascular Center, Maebashi,

JAPAN, ²Gunma University Hospital, Maebashi, JAPAN, ³Toyama Cardiovascular Clinic, Maebashi, JAPAN.

[Objectives] Using a simple phantom developed by Nakajima et al., Kanazawa University, the heart-to-mediastinum ratio (HMR) collected and processed differently can be corrected to a specific value so that ratios from different tests can be compared (Nakajima K, et al. J Nucl Cardiol. 2014;21:970-978). In our hospital there are two different devices for imaging. Therefore, correction was required for comparison. Only a few clinical studies have evaluated the use of this phantom, and none using a medium energy (ME) collimator, or where early and delayed values were reported individually. In this study, we used HMRs of the same patient taken with two different imaging devices to calculate the corrected values for standardization and unification. [Methods] PRISM-IRIX (LEHR/MEGP) (Shimadzu) and Infinia 8 Hawkeye 4 (ELEGP) (GE) were used. Early images were taken 15 minutes after ^{123}I -metaiodobenzylguanidine administration, and delayed images after 4 hours. A phantom experiment was conducted for each imaging condition to calculate a transformation coefficient. Imaging was performed using LEHR and ELEGP in 224 heart failure cases, and MEGP and ELEGP in 50 heart failure cases. Using the coefficient, correction values were calculated for the HMRs and compared each other. [Results] Bland-Altman analysis showed the following mean differences with LEHR and ELEGP, respectively: early: -0.60 ± 0.53 , delayed: -0.59 ± 0.67 (before correction); and early: -0.24 ± 0.47 , delayed: -0.24 ± 0.53 (after correction). The following mean differences were obtained with MEGP and ELEGP, respectively: early: 0.21 ± 0.24 , delayed: 0.34 ± 0.36 (before correction); and early: 0.04 ± 0.27 , delayed: 0.18 ± 0.34 (after correction). After correction, mean differences were reduced for both early and delayed values, showing a favorable correspondence. [Discussion] As reported previously, Sufficient correction was made for both early and delayed values in either collimator. However, scattered rays frequently penetrated the septum with LEHR; a higher HMR was associated with a greater correction deficiency. Therefore, the use of an iodine-specific or ME collimator seems desirable. HMR variation caused by differences between models by device updating or facility differences could have resulted; it might be improved by standardization. Furthermore, as cutoff values by disease are generated from the hospital's own data, standardization of evaluation criteria is expected to occur between facilities. [Conclusion] Corrected values calculated by a simple phantom experiment were designed to resolve differences between imaging models, collimators, and imaging conditions, and to be adaptable to early and delayed values, respectively. Phantom correction is expected to enable standardization of HMR between hospitals, with subsequent standardization to national and international levels.

TP061

Pharmacological Stress Agents in Myocardial Perfusion Scintigraphy - What to use in clinical practice

D. Teixeira¹, E. Sousa²; ¹NHS Greater Glasgow and Clyde, Glasgow Royal Infirmary and Stobhill Hospital, Glasgow, UNITED KINGDOM, ²Escola Superior de Tecnologia da Saúde de Lisboa, Lisboa, PORTUGAL.

Purpose/Introduction: Myocardial perfusion scintigraphy (MPS) with stress is an effective technique to detect disorders of left ventricle perfusion and function. However, development of new techniques and drugs to perform stress protocols are required to increase specificity, accuracy and sensibility of scans and still make the process simpler and more agreeable for the patients. This work aims to conduct a review about the use of different stress agents in clinical practice, respective advantages/disadvantages, comparison with physical stress and review of combined protocols of stress agents with low level of physical stress. **Subject/Methods:** Bibliographic research was made using "B-On", "PubMed" and "The knowledge network" platforms. The boolean connector "AND" was used combined with words such as "pharmacologic stress", "combined protocols", "myocardial perfusion stress", "adenosine", "dobutamine", "ATP", "dipyridamole" and "regadenoson". **Results/Discussion:** Adenosine, Adenosine Triphosphate (ATP) and dipyridamole are non-specific vasodilators given by infusion with several adverse effects identified in more than 50% of

the cases. Patients with restricted airways cannot be submitted to these agents since they may cause bronchoconstriction. However, regadenoson is a specific vasodilator and can be used safely in these cases, being administered in a standardized single dose. Dobutamine is an adrenergic agonist of the receptors β_1 and β_2 and is given as an infusion. This product can be used in patients with pulmonary diseases but because it promotes the contractility of the myocardium directly, it is a more dangerous drug and the stress test is a procedure which is harder to control. Secondary effects associated with dobutamine affect around 75% of the patients, however these can be controlled with drugs. Combined protocols work in similar ways for the several agents, combining the pharmacological agent with low level of physical stress. The combined protocols are safe, have reduced side effects and increased the image quality. **Conclusion:** In conclusion all the methods are safe although all have some side effects that can be controlled. Regadenoson should be the drug of choice since it is a vasodilator, used as a single standardized dose with no need for an infusion pump, can be used in the middle of a physical protocol, is safe for patients with pulmonary disease and it is associated with less side effects.

TP062

Reproducibility and reliability of two processing software for Cardiac Gated Scintigraphy

E. Lemos Pereira, M. Fernandes, G. Proença, L. Oliveira; NuclearMed - Hospital Particular Almada, ALMADA, PORTUGAL.

Aim: Several software packages for processing Cardiac Gated Scintigraphy provide more than one processing program. Usually, at the same department, only one is routinely adopted, but results tend to be more accepted if correlated to echocardiogram results. The aim of this study was to evaluate our departments two software for processing Cardiac Gated Scintigraphy. Moreover, we also compared both of our software's with echocardiogram results. **Methods:** A total of 100 consecutive patients (pt) that performed Myocardial Perfusion Scintigraphy between December 2015 and March 2016 were retrospectively analyzed. Pt characteristics like age, sex, body mass index, clinical indication and cardiovascular risk factors were analyzed. Myometrix™ and ECTollbox™, both Xeleris® software packages, were used to study ejection fraction (EF) and end diastolic and end systolic volumes (EDV and ESV), as well as wall motility. Results were also compared with previous echocardiogram parameters. Data was statistically analyzed with Microsoft Office Excel® and IBM SPSS®. **Results:** Although preliminary results indicated a good correlation between both gating processing software, as well as with echocardiogram results in the majority of cases, we found that for some pt, great discrepancy on the results was observed. **Conclusion:** Our results suggest that both cardiac gated processing packages are very reproducible and reliable when compared with echocardiogram. Nevertheless, cardiac gated analysis at Myocardial Scintigraphy must always take in consideration the pt clinical information.

TP063

Gated Myocardial Perfusion Single-Photon Emission Computed Tomography Imaging with Multifocal Collimator

K. Takahashi¹, T. Takeuchi², Y. Hosokai³, H. Odagiri², A. Usui¹, H. Saito¹; ¹Tohoku University, Sendai, JAPAN, ²Tohoku University Hospital, Sendai, JAPAN, ³International University of Health and Welfare, Ohtawara, JAPAN.

Introduction: Combining the functional information of myocardial perfusion single-photon emission computed tomography (SPECT) and the morphological information of computed tomography angiography (CTA) is an established technique for the non-invasive evaluation of coronary artery disease (CAD). Myocardial perfusion SPECT (MPS) using thallium-201 is a 3D-fused SPECT image that is currently combined using non-gated MPS including heart-motion and gated CTA. Gated MPS images are not used owing to insufficient counts available to diagnose CAD. However, a highly sensitive MPS with multifocal

collimator, the IQ•SPECT, is available. We aimed to evaluate the optimal reconstruction parameters in gated MPS images using the IQ•SPECT. **Methods and Materials:** We used a cardiac phantom with a lateral perfusion defect. The left ventricular myocardium, liver, and background were filled with 72, 14, and 7.0 kBq/ml of thallium-201, respectively. The heart rate was set to 60 beats per minute by the ECG checker. Gated SPECT was performed with a dual-head gamma camera equipped with a SMARTZOOM collimator, and the images were acquired with 17 views/detector, 56 beats/view in 8 frames per R-R interval. The gated MPS images were reconstructed by ordered subset conjugated gradient modified (OSCGM) with subset: 1-5, iteration: 1-60. We assessed the image quality using the coefficient of variation (%CV), contrast and the normalized mean squared error (NMSE) to determine the optimal reconstruction parameters. We evaluated %CV with the region of interest (ROI) setting on the anterior, septal, inferior, and lateral walls. Furthermore, we evaluated contrast with ROI setting on the septal and lateral walls. **Results:** The %CV in the anterior and septal walls converged in update (subset × iteration): 40, while the %CV in the anterior and septal walls in subset: 5 was slightly higher. There was no convergence in the %CV in the inferior and lateral walls. Contrast converged in update: 40 and was slightly lower than that in subset: 5. Iterations at which the NMSE demonstrated a minimum showed a low value with increasing subsets. The minimum NMSE values in subset: 1, 2, and 3 were similar, while subset: 5 was slightly higher. **Conclusion:** The results of the gated MPS images using IQ•SPECT suggest that the optimal OSCGM reconstruction parameters are subset: 3 and iteration: 14. Gated MPS images with IQ•SPECT may provide improved 3D-fused SPECT images, aiding in the non-invasive evaluation of coronary artery disease.

TP064

Myocardial Perfusion and Sympathetic Activity of the Heart in Professional Deep-water Divers

V. Sukhov, G. Kutelev, A. Chumakov, V. Nikiforov, P. Kirichenko, D. Cherkashin; Military Medical Academy, ST. PETERSBURG, RUSSIAN FEDERATION.

Background and purpose: Currently, state of cardiovascular system in professional deep-water divers is not clear enough. According to several authors, problems with cardiovascular system in divers remain at leading positions: arterial hypertension, neuro-circulatory asthenia, arrhythmias and conduction disturbances, ischemic heart disease, degenerative changes of the myocardium, etc. We need to clarify that. **Material and Methods:** We examined 20 men (26-42 y.o.) working under increased gas-mixture pressure in water environment. In all of them rest-stress myocardial perfusion and sympathetic activity were assessed using scintigraphy with 99mTc-tetrofosmin and 123I-MIBG. Such pathology as myocardial hypertrophy, dilatation of the heart chambers, reduced ejection fraction, myocardial ischemia in these persons were excluded. **Results:** We found diffusely heterogeneous perfusion at rest and widespread transient decreased of 99mTc-tetrofosmin uptake at stress, and also decline in the heart/mediastinum ratio and negative values of 123I-MIBG washout index. 123I-MIBG and 99mTc-tetrofosmin distribution data were largely concordant. Although all of them showed high tolerance to exercise and aerobic performance, even when compared with non-professional divers. **Resume:** We suggested retardation of myocardial metabolism, sympatholytic effect at the level of peripheral nerve endings, atherosclerosis of small coronary arteries branches. Coronarospastic effects, and degenerative changes in cardiomyocytes. Disturbances in cellular metabolism and sympatholytic effects may be a manifestation of sustainable adaptation of divers' organism to impact of hyperbaric environment factors.

TP065

Comparison between each institution using a 2-Layer Double-Pump Dynamic Cardiac Phantom

R. Hashimoto¹, M. Onoguchi¹, T. Shibutani¹, N. Hara²; ¹Department of

Quantum Medical Technology, Graduate School of Medical Sciences, Kanazawa University, Kanazawa, JAPAN, ²Department of Radiology, Sumitomo Hospital, Osaka, JAPAN.

Purpose: A conventional dynamic myocardial phantom fixed to the size of the outer membrane (epi-cardium) has reported. However, this phantom has the structure that only the inner membrane (end-cardium) can move in the antero-posterior directions. The volume of end-diastolic volume (EDV) and end-systolic volume (ESV) are fixed, and a real movement of the heart is not expressed. Recently, the new myocardial dynamic phantom which can change the myocardium and the left ventricle volume were developed. The aim of this study was to evaluate cardiac function analysis between different institutions whether this phantom can use as the standardization tools. **Methods:** Tc-99m was filled in the myocardial part of the phantom, and acquired two dual-detector SPECT-CT (Precedence 16; Philips, Symbia T6; Siemens) systems. Acquisition parameters were set on 16 frames per cardiac cycle, main window 140 keV±10%, 64×64 matrix, a rotation angle of 360, 64 projections. Acquisition time was different in each device, but the average count for myocardium was approximately 100 counts per pixel. The phantom fixed heart rates in 60 beats per minute and changed only the stroke width of the left ventricle. Reconstruction was performed with filtered back projection, and the attenuation, scatter and resolution corrections were not performed. The true volume calculated from enhanced CT Images. The ESV, EDV were analyzed using a quantitative gated SPECT (QGS), and the left ventricular ejection fraction (LVEF) were calculated from EDV and ESV. Then those values were compared between each institution. **Results:** The volume for EDV and ESV were different between each institution, however, the correlation between the true and measured values showed the same tendency to both EDV and ESV. The correlation coefficient for each institution were 0.98 and 0.95 for EDV, 0.87 and 0.95 for ESV, 0.98 and 0.95 for LVEF, respectively. The relative error was less than 30% both EDV and ESV. **Conclusion:** The calculation value was compared and examined between each institution by the myocardial dynamic phantom which can change the myocardium and the left ventricle volume. It was suggested that the novel myocardial dynamic phantom may be possible to the standardization.

TP066

Clinical usefulness of ²⁰¹Tl myocardial uptake at stress with ²⁰¹Tl SPECT-MPI on a Cadmium Zinc Telluride (CZT) camera

R. Matsuda¹, S. Tomiguchi², S. Kudo¹, N. Katsuta³, S. Shiraishi⁴, Y. Yamashita⁴; ¹Graduate School of Health Sciences, Kumamoto University, Kumamoto, JAPAN, ²Faculty of Life Sciences, Kumamoto University, Kumamoto, JAPAN, ³Division of Medical Technology, Kumamoto University Hospital, Kumamoto, JAPAN, ⁴Department of Diagnostic Imaging, Faculty of Life Sciences, Kumamoto University, Kumamoto, JAPAN.

Aim/Purpose Measurement of myocardial flow reserve (MFR) on single photon emission computed tomography myocardial perfusion imaging (SPECT-MPI) needs the dedicated SPECT camera. There is the problem in measurement of MBF that a patient's exposure increases with the twice dosage of the radiotracer in case of ²⁰¹Tl SPECT-MPI. ²⁰¹Tl myocardial uptake at adenosine stress (²⁰¹Tl myocardial uptake) is considered to reflect the MFR, because adenosine induces maximum dilatation of coronary arteries. The aim of this study was to evaluate a clinical usefulness of ²⁰¹Tl myocardial uptake in patients without visually myocardial perfusion abnormalities and to clarify the influence of an attenuation correction (AC) on ²⁰¹Tl myocardial uptake. **Material and Methods** Forty patients without visually myocardial perfusion abnormalities on stress ²⁰¹Tl SPECT-MPI were enrolled in this study. They were consisted of 8 without coronary arterial disease (CAD) and 32 with subclinical CAD. Adenosine stress ²⁰¹Tl SPECT-MPI was performed in all patients using a CZT camera (NM530c, GE). Outlines of the left ventricular myocardium were delineated by the count threshold determined visually. A total count of whole left ventricle (LVC) was then derived from summing

counts of all trans-axial myocardial images. Finally, ²⁰¹Tl myocardial uptake was calculated by dividing the myocardial radioactivity converted from LVC using cross-calibration factor by total injected dose. **Result** Mean value of ²⁰¹Tl myocardial uptake was 5.1% without AC and 9.2% with AC in 8 patients without CAD, while they were 3.1% without AC and 6.6% with AC in 32 patients with subclinical CAD. Mean value of ²⁰¹Tl myocardial uptake in patients without CAD is higher than that in patients with subclinical CAD and ²⁰¹Tl myocardial uptake with AC is higher than that without AC. **Conclusion** ²⁰¹Tl myocardial uptake is considered to be useful for the diagnosis of subclinical CAD. Further study is necessary for the evaluation of the prognosis to clarify a clinical significance.

TP067

Normal Myocardial Perfusion CZT-SPECT databases comparison

L. Camoni¹, G. Damini², A. Fierro³, G. Zobbio², I. Marchina², R. Giubbini¹; ¹Univesity and Spedali Civili of Brescia, BRESCIA, ITALY, ²Univesity of Brescia, BRESCIA, ITALY, ³Spedali Civili of Brescia, BRESCIA, ITALY.

Aim: Aim of this study was to evaluate any significant difference in quantitative MPI analysis, using two different commercially available software with different normal databases. **Material and methods:** Single-day stress-rest Gated-SPECT with 150+300 Mbq of Tc-labeled compounds were performed using a CZT-based gammacamera (GE D530Alcyone) in 100 patients, randomly selected. The standard acquisition time was 9 minutes for both stress and rest acquisitions. The quantitative data obtained after SPECT reconstructions were evaluated by QPS v.2009 and Corridor 4DM v.2012 using a 17 segment model. The SSS, SRS and SDS were obtained for the entire LV. Statistical analysis was performed using SPSS v.21 (IBM Corp., Armonk, NY, USA) by Wilcoxon paired test. **Results:** The data were expressed as means ± standard deviation. The QPS v.2009 results were: SSS:4.93±5.7; SRS:2.65±4.4; SDS:2.59±2.77; the Corridor 4DM v.2012 were SSS:6.95±8.5; SRS:5.59±7.5; SDS: 2.32±3.44; The statistical analysis was significant for all parameters (p<0.05) except for SDS (p=ns) **Conclusion:** Despite presence of significant differences in both SSS and SSR by QPS v.2009 and Corridor 4DM v.2012 there is a substantial overlap in quantification of myocardial ischemia by MPI using widely adopted commercial softwares.

TP068

Quantification of Heart-to-Mediastinum Ratio of I-123-MIBG Scintigraphy in a Cardiac Phantom: influence of collimator choice and of diverse energy window for scatter correction

S. Chaves, A. Faria, T. Vieira, J. Pereira; Centro Hospitalar S. João, Porto, Porto, PORTUGAL.

There is a good tendency of standardization of I-123-metaiodobenzylguanidine (MIBG) cardiac sympathetic imaging in order to become possible to compare different studies. The aim of this work is to compare the value of the Heart-to-Mediastinum ratio (H/M) acquired with different collimators and different energy windows for scatter correction (SC) by comparison with the true H/M in a cardiac phantom. We used a cardiac phantom filled with a I-123 solution. The absolute activity was 10.33 kBq/mL in the heart and 2.16 kBq/mL in the background. SPECT scans were consecutively acquired. For the SPECT/CT (Infinia-Hawkeve 4, GE®) were used LEHR and ME collimators, in L-configuration, rotation of 180°, 60 projections, 30 seconds/projection, 64x64 matrix; 20% energy window (143.1-174.9 KeV) centered on the isotope photopeak (159 KeV). In the acquisitions with LEHR collimators were used six different windows to apply SC by Dual-Energy window (DEW): DEW1=79.6-111.1 KeV; DEW2=111.3-143.1 KeV; DEW3=184-216 KeV; DEW4=174.9-207 KeV; DEW5=174.9-216 KeV; DEW6=DEW2+DEW3. From the first to the fifth, the energy windows were defined with the same width. For all, we used two different multiplication factor (k): 0.8 and 1. OSEM

reconstruction method was adopted and all images were submitted to CT-based attenuation correction. After image reconstruction, an elliptical VOI was drawn around the heart and a cuboid VOI in the background of the phantom (AMIDE®), in order to obtain the total counts (decay correction). We determined the system volume sensitivity using a Jaszczak phantom filled with a uniform concentration of I-123 activity. The H/M ratio was calculated for each SPECT acquired and compared with the true H/M calculated using the calibration factor. It was determined a relative error between true H/M and the calculated H/M. H/M is underestimated by 36% if no SC was applied. DWE1, DEW3, DWE4, DWE5, DWE6 presented high relative error independently of the k used in the SC. DWE2 showed a relative error of -1% and -8% for k equal a 1 and a 0.8, respectively. Concerning ME collimators the H/M is underestimated by 8%. This research confirm that collimator choice influences the calculation of H/M. When using LEHR collimators SC is needed for I-123-MIBG scintigraphy. The 111.3-143.1 KeV energy window shows better results and a k equals to 1 seems the best.

TP069

Simulation to solve the artifacts and pitfalls myocardial SPECT using data mining

K. Asakura, S. Kazuhiro, K. Miho, O. Akihito; Department of Radiology, Tottori Prefectural Central Hospital, ezu,tottori, JAPAN.

the aim SPECT myocardial perfusion imaging using ^{99m}Tc -sestamibi (MIBI) plays a central role in the diagnosis and prognosis of cardiovascular disease. However, there is a possibility that limits the clinical utility by a variety of artifacts and pitfalls. In particular, the filtered-backprojection (FBP) reconstruction method is known to produce streak artifacts from very intense area of activity (e.g., the gallbladder). The aim of this simulation is to examine the FBP method which is not affected by the streak artifacts using data mining. **Materials and Methods** MIBI was 7 MBq sealed in the heart part of the phantom (HL20 type). This normal myocardium was defined as the model A. We acquired SPECT images using a rotating digital gamma camera and a low energy high resolution collimator with an energy window of 141keV $\pm 10\%$ and 64×64 matrix. The images were collected over 360 deg (6 deg every 40 sec) and 60 frames of raw data were generated. Model B was designed on the FBP reconstructed short axis images containing from 1 to 10 times of cardiac radioactivity overlapping with other organs. Further, four types of occlusion model (front wall, bottom wall, side walls, septum) were defined as the model C. The combination of three types of models, we created 81 kind of sinogram as a teacher signal. The sinograms had 32 matrix on the horizontal axis in the channel direction. The vertical axis was arranged in a vertical projection data as the sampling angle. We applied back-propagation-method (BPM) of the artificial-neural-network (ANN) to data mining. As the input data of the ANN, seven directions were used from the sinogram signal which consisted of the samples of 32 directions. Then, short axis images of the myocardium were obtained by the optimal solution of the ANN. In this study, scatter and absorption were not corrected. **Results and Conclusion** Accuracy rate of this technique achieved almost 100%. We confirmed short axis images of the myocardium which is not affected by the streak artifacts in this phantom simulation. However, when this approach without attenuation correction is applied to clinical, some errors may occur. Furthermore, we have to make the ANN learn more teacher signals. If we solve these problem, this method will be useful for clinical.

TP070

The usefulness of Flash 3D Applications to shorten scan time for Gated Myocardial Perfusion SPECT

Y. parlak, D. Goksoy, G. Gumuser, E. Sayit; Celal Bayar University, Manisa, TURKEY.

Inaccurate image reconstruction impacts image quality and can result in both false positives and false negatives. Most reconstructed images are created using algorithms that do not account for the physical characteristics of the image acquisition system. Flash 3D Technology is a sophisticated new SPECT tomographic reconstruction algorithm. Flash 3D adds a post filter after reconstruction for noise reduction. The aim of this study is to compare rest and stress defects in gated MPS, functional parameters in half time flash 3D and full time Filtered Back Projection (FBP). Twenty patients (mean age: 60 ± 5 years; 11 female, 9 male) were imaged with Siemens Evo Excel gamma camera (Knoxville, USA). Patient preparation, acquisition parameters and reconstruction protocols for all patients were standardized. Half-time (32 projections) and full time (64 projections) SPECT data were acquired for both stress and rest imaging protocol. Full-time data were reconstructed using Standard filtered backprojection reconstruction, whereas half time data were reconstructed using Flash 3D software. The data were evaluated by two Nuclear Medicine specialist blinded to each other. The full-time and half-time data were evaluated and found differences (especially in rest images) in image quality assessed, LV function measured. Statistical analysis were performed between full time FBP and half time Flash 3D. The increased noise in the half-count projections increased the difficulty of assessing on images. We suggest that if we use half time flash 3D in MPS, increased activity should be administered to the patients especially in rest imaging.

TP071

Technical improvement of Continuous Dynamic SPECT in Epilepsy study

P. SUNMYUNG, P. JIN YUNG, Y. JOON HO; SAMSUNG MEDICAL CENTER, Seoul, KOREA, REPUBLIC OF.

Purpose : Epilepsy is a group of neurological diseases characterized by epileptic seizure. During Brain Epilepsy SPECT study, critical factor for proper study with ^{99m}Tc -ECD or ^{99m}Tc -HMPAO is one of the important causes to patient's movement caused by Inter-ictal or Ictal. It causes both improper diagnosis and examination failure. In this study, we evaluated the effect of Dynamic SPECT Acquisition compared to SPECT to raise efficacy and reject the data set with movement, as well as, be reconstructed in certain criteria. **Methods**: Deluxe Jaszczak phantom and Hoffman 3D Brain phantom were used to find proper standard data set and exact time. SPECT and Dynamic SPECT Acquisition were performed with SymbiaT16. Firstly, Deluxe Jaszczak phantom was filled with $\text{Na}^{99m}\text{TcO}_4$ 370MBq and obtained in 60 minutes to check spatial resolution compared with SPECT and Dynamic SPECT. The second, the Hoffman 3D Phantom filled with $\text{Na}^{99m}\text{TcO}_4$ 74 MBq was acquired for 15 Frame/minutes to evaluate visual assessment and quantification. Finally, in the Deluxe Jaszczak phantom, Spheres and Rods were measured by MI Apps program as well as, checking counts with the frontal lobe, temporal lobe, occipital lobe, cerebellum and hypothalamus parts was performed in the Hoffman 3D Brain Phantom. **Results**: In Jaszczak phantom, Sphere and Background Ratio was measured $0.41 \pm 0.0\%$ with SPECT and $0.36 \pm 0.0\%$ with Dynamic SPECT in 31.8, 25.4 19.1 15.9 mm except for unseen 12.7 mm and 9.5 mm Spheres in Jaszczak phantom which is acceptable differences to use Dynamic SPECT instead of SPECT. And visual evaluation for Rods was also performed and found no differences in 12.7, 11.1, 9.5, 7.9 mm except for 6.4, 4.8 mm in both. In Hoffman 3D Brain Phantom, Approximately the count value of frontal lobe 2660, 2816, temporal lobe 2336, 2720, occipital lobe 3240, 3418, cerebellum 3004, 3290, hypothalamus 1348, 1450 in SPECT and Dynamic SPECT respectively in full acquisition. Removing 8 frame/min in dynamic SPECT was acceptable. However, removing 9frame caused remarkable low image quality and differences. **Conclusion** : Dynamic SPECT in epileptic seizure condition enhances effects compared to SPECT image. And also is powerful method to reduce reacquisition rate caused by patient movement. The findings further indicate that it suggest rejection limit to maintain clinical value with certain reconstruction factors compared with Tomo data set. Further examination to improve spatial resolution, SPECT/CT should be the answer for that.

TP072**Dynamic supine renal imaging - the importance of standing**

M. G. G. Silva, S. Teixeira, A. Canudo, D. Dantas, D. Costa, C. Oliveira, A. Silva; Champalimaud Foundation, Lisboa, PORTUGAL.

Introduction Nephroptosis is a condition in which kidney descends more than 5cm (or two vertebral bodies) between supine and orthostatic (standing) positions. In 10 to 20% of cases it is clinically symptomatic, manifesting frequently with a renal colic. Sometimes, it can be accompanied by excessive rotation of the kidney. **Material and methods** A 78 year old female with a history of right breast carcinoma surgically removed three years before was referred due to pain in her right posterior ribcage. A bone scan was performed in July 2015 screening for secondary bone involvement. There were no osteoblastic bone metastases. However, marked retention of the tracer excretion in the pelvis of the right kidney was observed and prompted the performance of a renogram that was undertaken with MAG3. Previous renal ultrasound (October/2014) had shown both kidneys of normal size and good parenchymal differentiation and no nodular lesions. However, there was marked dilatation of the right pelvis with abrupt transition to the ureter but no definition of an obstructive cause. A pelvico-ureteric junction (PUJ) syndrome was suggested on the right. There were no signs of obstruction despite some retention on the left. Following intravenous administration of 269MBq of ^{99m}Tc-MAG³ a dynamic renal study was performed supine for 30 minutes. Furosemide was administered 15 minutes within the renal study acquisition. Subsequently, a standing pre-voiding image was obtained and additional standing and supine post-micturition images were acquired. **Results** The renal flow/perfusion was preserved bilaterally. Good concentration of the left kidney and delayed parenchymal transit on the right kidney was recorded. On the left there was pelvicaliceal retention responding promptly to furosemide. On the right there was continuous and progressive accumulation of the radiotracer in the pelvis, with poor and delayed response to diuretic overload, but no obstructive pattern. The left kidney contributed 55% and the right 45% to the total renal function. Pre and post-micturition standing images revealed marked ptosis with tilt of the right kidney (around 120° internal rotation of its upper pole). In the supine post-micturition image the right kidney returned to its initial non-ptotic anatomical position. **Discussion/ Conclusion** The herein reported right renal ptosis and internal rotation may explain the right posterior ribcage pain. Standing and not only supine pre and post-void renal images should always be acquired for completion of renogram studies.

TP073**Correlation between parathyroid scintigraphy, size of parathyroid adenomas and biomarkers**

S. Sustar¹, S. Rep¹, B. Trebec¹, I. Slodnjak¹, M. Hocevar², L. Lezaic¹; ¹Department for Nuclear Medicine, Ljubljana, SLOVENIA, ²Department for oncological surgery, Ljubljana, SLOVENIA.

Introduction: Primary hyperparathyroidism is an endocrine disorder that develops as a result of increased and uncontrolled formation of parathyroid hormone. Subtraction scintigraphy and SPECT/CT is the most established method for the preoperative localization of parathyroid adenomas. Most commonly used radiopharmaceutical for the purpose is ^{99m}Tc-MIBI. **Objective:** The aim of the study was 1) to assess diagnostic performance of preoperative localization of parathyroid adenomas in the early and delayed (5 min and 60 min after administration) SPECT/CT method with subtraction scintigraphy in patients with biochemically proven primary hyperparathyroidism using histology as the gold standard and 2) to determine whether size of parathyroid adenomas, serum PTH, Ca and P are correlated to successful localization. **Materials and methods:** The study included 41 patients in whom we performed early and delayed SPECT/CT imaging and subtraction scintigraphy (addition of ^{99m}Tc-pertechnetate). Correlation between size of the parathyroid adenomas, serum Ca, P and PTH levels was assessed using

Spearman correlation coefficient. The volume of surgically removed parathyroid adenomas was calculated as (length×width×height)×π/6. Receiver Operating Characteristic analysis (ROC analysis) were used to express relationship between scintigraphy results and size of the parathyroid adenomas, serum Ca, P and PTH levels. **Results:** The sensitivity and specificity of early SPECT/CT, delayed SPECT/CT and subtraction scintigraphy was 65.1% and 97.5%, 67.4% and 95.5% and 51.1% and 98.3%, respectively. Combined early and delayed SPECT/CT had the sensitivity and specificity of 74.4% in 95.1%. There was a good correlation (Spearman r=0.828, p<0.05) between iPTH and serum Ca²⁺ and a fair correlation between the gland volume and serum Ca²⁺ (Spearman r=0.641, p<0.05) and iPTH (Spearman r=0.606, p<0.05). **Conclusion:** The most sensitive method of preoperative localization of parathyroid adenomas was combined early and delayed SPECT/CT. There was a good correlation between iPTH and serum Ca²⁺ and a fair correlation between the gland volume, serum Ca and iPTH.

TP074**A new parameter for the calculation of Thyroid uptake by Thyroid area**

S. A. Abdulrasool; Fujairah hospital, MOH, UAE, Fujairah, UNITED ARAB EMIRATES.

Introduction: Thyroid scintigraphy using Tc-99m is an excellent method of evaluating the function of Thyroid gland and its uptake. A thyroid scan may be ordered by a physician when the gland becomes abnormally large. The scan can be helpful in determining whether the enlargement is caused by a diffuse increase in the total amount of thyroid tissue or by a nodule or nodules. When other laboratory studies show an overactive thyroid (Hyperthyroidism) or an under active thyroid (Hypothyroidism), a Thyroid scan uptake is often used to confirm the diagnosis. A normal scan will show a thyroid of normal size, shape, and position. The amount of radionuclide uptake by the thyroid will be normal according to established nuclear medicine figures. There will be no areas where radionuclide uptake is increased or decreased. **Objective & Aims:** The objective of this study is to measure the thyroid uptake by area. 1-To calculate the normal range of thyroid uptake by thyroid area (Counts/Pixel) 2-In patients with high Thyroid uptake this parameter will be useful to give an idea whether it is due to Hyperthyroidism or due to big-sized Thyroid gland. **Results:** Calculation of mean value was carried for all the 500 patients. Results show the following: 1-Normal Range between 6-34 counts/pixel 2-Hyperthyroid patients >35 counts/pixel 3-Hypothyroid patients 4 and counts/pixel was >40 4-Group (3) 100 patients with hypothyroidism, thyroid uptake measured was =<0.2 and counts/pixel was <5-Group (4) 30 patients with thyroid enlargement with thyroid uptake was =>4 high uptake and counts/pixel was between 6-30 which was normal. **Conclusion:** The thyroid uptake is performed to evaluate the function of the thyroid gland. In Fujairah hospital, we add new, simple and important parameter to thyroid scan by calculating uptake of thyroid. By area (counts per pixel) this useful parameter is applied in all thyroid scan studies. Some cases as a result of large thyroid gland size, the uptake give result higher than the real uptake to know to the real uptake using uptake by area (count per pixel) method.

TP075**Targeting VPAC1 Genomic Receptors for Optical Imaging of Lung Cancer**

M. L. Thakur; Thomas Jefferson University, Philadelphia, PA, UNITED STATES.

Objectives: Lung Cancer (LC) accounts for nearly 20% of all cancer deaths in the USA. Low dose CT scan of the chest as a screening strategy for high risk LC subjects has a very high false positive rate and a specific diagnosis of sub-cm lesions is challenging. In recent years, detecting circulating tumor cells (CTC) in liquid biopsy has drawn considerable attention to diagnose primary disease and even to determine effectiveness of therapy and to predict

disease recurrence. VPAC1 receptors are expressed in high density on LC cells at the onset of oncogenesis. The goal of this pilot study is to target VPAC1 using our receptor specific fluorophore TP4303 to optically image LC cells in lung lavage. **Methods:** Routine diagnostic bronchoscopy was performed in patients with suspected lung cancer and a 5-10 ml residual lung lavage sample was cytospun, cells were fixed, incubated with TP4303 (Ex=633nm, Em=754nm), washed and cell nuclei were stained with DAPI (Ex=350nm, Em=470nm). Slides were then read using confocal microscope. The protocol was IRB exempt as no health record was required to be collected. To validate the presence of VPAC1 on LC cells receptor blocking studies were performed, using human LC cell line A549. **Results:** As of this writing, seven lavage samples from seven subjects were analyzed. Histological examinations of lavage led to positive diagnosis for LC in all patients. Cells from 11 patients, under the microscope showed bright orange fluorescence around the cell nucleus, indicating the presence of malignant cells with dense expression of VPAC1 receptors on cell surface. All cells from one patient with Asthma but without LC, were normal without fluorescence. Receptor blocking studies validated the presence of VPAC1. **Conclusion:** The results (100%) of this small (n=11) feasibility study are highly encouraging and warrant studies of sputum obtained non-invasively from patients with known LC and those scheduled for bronchoscopy. Research Support: In part, by NIH CA 157372-02, (MLT)

TP076

Study of the lacrimal glands in Nuclear Medicine

D. Peña Torres, P. Villen Trinidad, Y. Said Criado, M. Torres Jimenez, D. Cid Jimenez; COMPLEJO HOSPITALARIO DE JAEN, JAEN, SPAIN.

INTRODUCTION The nasolacrimal duct carries tears from the lacrimal sac into the nasal cavity. The opening of the nasolacrimal duct leads into the inferior nasal meatus and is partially covered by a mucosal fold. Excess tears flow through the nasolacrimal duct, which drains into the inferior nasal meatus. 1. Dacryoscintigraphy is a grossly underutilized nuclear medicine procedure for assessing the patency of nasolacrimal ducts. 2. Nuclear Medicine scan is a means of demonstrating how well tears are cleared from the eyes and drain away **OBJECTIVES** The aim of the study is to gain and expand professional knowledge in the process of the preparation of radiopharmaceuticals and imaging. **MATERIAL AND METHOD** We carried out an observational descriptive study analyzing the process regarding the lacrimal glands scintigraphy **RESULTS:** Lacrimal duct scintigraphy: Preparation of the radiopharmaceutical: load 2 syringes of 1ml, with one drop (about 200µCi/10µl) of sodium pertechnetate Tc solution for injection Recommended for children and adults equally are 0.2 mCi activities in each eye. LEHR collimator Used (Low Energy High Resolution) First stage: dynamic acquisition followed by instillation, obtaining a phase of dynamic imaging with 20 shots to 15 seconds per image, creating five simultaneous static shots of 60 seconds per image, with a zoom 2,29 and 64x64 matrix in dynamic and 256 in static. A late phase at 2 hours radiopharmaceutical administration is performed with the same characteristics as the first phase. The gamma camera is placed in upright position to encourage the instillation of radiopharmaceutical. The patient is treated in sitting position, proceeding to the administration of the radiopharmaceutical, taking care to avoid possible contamination that may occur. Therefore a blotter is placed just below the lower eyelid. Then the patient is approximated with its face to the detector centering the field of vision in both eyes. Two factors play an important role for the examination: patient's age and its thus resulting cooperation (to avoid contamination of the work area and image artifacts caused by patient movement) For the examination of children the assistance of their parents might be necessary. **CONCLUSIONS** After all, top priority for all Specialist Technician in Nuclear Medicine entrusted with the preparation of radiopharmaceuticals is to ensure that their progress benefits the patients, so that the diagnosis of possible functional disorders of the lacrimal duct, which is indicated in suspected functional or partial blockages, can be performed correctly.

TP077

An Semi-liquid Imaging Analysis of Gastric Emptying in Adult Diabetics

Y. Wang; Huashan Hospital, Fudan University, Shanghai, CHINA.

Objective: Diabetes can cause autonomic disorders of the gastrointestinal tract and gastroparesis, so it is of great important to pay more attention to gastric emptying in diabetic patients. Gastric emptying scintigraphy is the gold standard for measuring gastric emptying. This research was to explore the relationship between food and half-time gastric emptying with the method of semi-liquid imaging study. **Methods:** A retrospective analysis was carried on four diabetic patients with delayed gastric emptying aged 20 to 40 years old and had a history of diabetes over five years. Three cases mixed ^{99m}Tc-DPTA (2mCi ~ 3mCi) with 500ml yogurt mix, one mixed in a mixture of protein flour (300g) and water (300ml). Patients kept a fast from last night, sat and perched on the probe at the time of acquisition. Dynamic acquisition continued 40 minutes including imaging from the mouth to the gastropyloric. Started the collection and oral administrated the semi-liquid food mixed with drugs, then drank water (about 500ml) immediately in order to fill the stomach to reach two-thirds. Use First Derivative to speculate gastric emptying time. **Results:** Patients taking yogurt mixed meal finished in 1 minute, and patient taking protein mixed meal finished in three minutes. Half-time of 3 patients taking stomach yogurt mixed meal were 35min, 37min, 48min respectively and that of patient with stomach taking protein mixed meal half time was 38min after calculated by built-in formula. **Conclusion:** gastric emptying imaging in patients with diabetic showed that the average half-time of semi-liquid meal was 39.5min. There was no significant difference between the half-time of these two semi-liquid gastric emptying. There were several advantages perched sitting imaging. First, the back can be supported by the probe to ensure long time examination. However, the spine will block part of the count theoretically. Second, it can avoid the risk of pollution probe when eating if faced the probe or partial scan missing. Third, sitting imaging is in line with the human physiological gastric emptying and it avoids the risk of shake and fall. The probe angle can be adjusted in order to obtain a good imaging position when necessary. Although protein mixed meal is more suitable for semi-liquid diet, yogurt mixed meal has a sample preparation and convenient eating and easier measuring of image gastric emptying peak on gastric emptying. It is recommended to use a yogurt mixture in nuclear medicine stomach empty semi-liquid measurement in clinic.

TP078

Radiochemical Purity and Stability control in Technescan MAG3

A. PALMIERI¹, C. DAOLIO¹, S. COLA¹, C. CATTINI²; ¹SANTA MARIA NUOVA HOSPITAL, REGGIO EMILIA, ITALY, ²UNIVERSITY OF MODENA AND REGGIO EMILIA, REGGIO EMILIA, ITALY.

Background: Technescan MAG3 Kit for the Preparation of Technetium Tc^{99m} Betiatide (Benzoilmercaptoacetiltriglicina) is a renal imaging agent for use in the diagnosis of congenital and acquired abnormalities, renal failure, urinary tract obstruction, and calculi in adults and pediatric patients. It is a diagnostic aid in providing renal function, split function, renal angiograms, and renogram curves for whole kidney and renal cortex. **Aim:** The aim is to verify the stability in vitro of Tc^{99m}-MAG3, analyzing the radiochemical purity. **Material and Method:** We verified stability for 8 sample of ^{99m}Tc-MAG3 instant kit formulation of Technescan MAG3. Tc^{99m} -MAG3 was prepared using 1 ml of fresh eluate; the activity should not exceed 1110 MBq (30 mCi). The calculated amount of Tc^{99m} was diluted to a volume of 10 ml with saline 0.9%. This volume was added to Technescan MAG3 vial using a G20 hypodermic needle. The kit was placed in upright position into boiling water bath for 10 minutes. After heating, we cooled the vial in cold water. Tc^{99m} -MAG3 should not be used more than four hours after preparation. We controlled radiochemical purity (RCP)

analysis 4 time: at preparation time and a 4, 5, 6 hours after kit reconstitution. RCP of Tc^{99m} -MAG3 was determined using Thin-Layer Chromatography (TLC) based on instant thin-layer silica gel strips as stationary phase for checking the main impurities, free pertechnetate and reduced hydrolysed $99mTc$. The radiochemical purity should not be less than 95% (Ph. Eur). **Results:** Mean of RCP calculated was: 97.95 (+/- 1.42) at preparation time; 96.85 (+/- 1.13) a 4 h; 95.72 (+/- 0.6) a 5 h; 92.07 (+/- 3.36) a 6 h after MAG3 Kit preparation.. **Conclusion:** TLC strip showed adequate RCP with acceptable free and hydrolysed Tc^{99m} percentages until 5 hours after kit reconstitution.

TP079

Comparative Study Of Two Chromatographic Methods For Radiochemical Purity Determination Of $99mTc$ -HMPAO

Y. Said Criado, D. Peña Torres, P. Villen Trinado, J. Diaz Alarcon, M. Torres Jimenez; COMPLEJO HOSPITALARIO DE JAEN, JAEN, SPAIN.

OBJECTIVE Compare the results of the PRQ (radiochemical purity) of $99mTc$ -HMPAO obtained by column chromatography versus those obtained by paper chromatography. **MATERIAL AND METHODS** 17 samples the radiopharmaceutical $99mTc$ -HMPAO for determination of radiochemical purity by two different chromatographic methods were used: Method 1: Column Chromatography; Stationary phase: Column Sep-Pak®, Mobile phase: Physiological saline Method 2: Paper chromatography; Stationary phase: Whatman™-17 Mobile phase: Ethyl acetate It was calculated mean value and standard deviation of the results of the radiochemical purity (%) of $99mTc$ -HMPAO by both chromatographic methods. **RESULTS** Method 1: Mean (average) = 91.50 and Standard Deviation = 2,857 Method 2: Mean (average) = 92.57 and Standard Deviation = 2,249 **CONCLUSIONS** Similar results are observed by both methods, although by paper chromatography a higher mean (average) and a lower standard deviation is obtained.

TP080

Radioiodinated L-Phenylalanine Conjugated Boron Nitride Nanotubes and In vitro Evaluation of Glioblastoma Cells

O. Kozgus Guldu, 35100, P. Unak, V. Tekin, G. Takan, E. Medine, S. Timur; Ege University, İzmir, TURKEY.

Introduction: Boron nitride nanotubes (BNNTs), isosteres of CNTs with unique physical properties, are inherently noncytotoxic. The ideal properties of Boron Neutron Capture Therapy (BNCT) agents are low toxicity, high brain tumor uptake, rapid clearance from blood and persistence in tumor during the therapy. Therefore, several BNCT agents has developed in 50 years. [(L)-4-dihydroxy-borylphenylalanine] (BPA), sodium mercaptoundecahydro-closododecarborate (BSH), sodium salt of closo- $B_{10}H_{10}^{2-}$ (GB-10), β -5-o-carboranyl-2'-deoxyuridine and 3-(dihydroxypropyl-carboranyl-pentyl) thymidine derivative N_5 -2OH etc, are most popular agents so far. **Methods:** In this study, we synthesized BNNts by using chemical vapor deposition (CVD) method. Synthesized BNNt/PAMAMs were conjugated with L-Phe compounds using *N*-(3-Dimethylaminopropyl)-*N'*-ethylcarbodiimide hydrochloride/*N*-Hydroxysuccinimide (EDC/NHS) conjugation method. BNNt/PAMAM/L-Phe nanobioconjugates were radioiodinated with $^{131}I/^{125}I$. *In vitro* biological affinities of characterized nanobioconjugates were investigated on mouse astrocyte brain cells (CRL2541) and human brain glioblastoma cells (U87-MG). 24, 48 and 72 hours toxicities of conjugates on CRL2541 and U87-MG were examined via WST-8 method. Samples at IC_{50} concentration were studied by TUNEL assay to reveal the apoptotic effect of the samples. Time and specific activity dependent cell uptake levels of ^{125}I labeled

compounds were determined. Cell binding and uptake affinities of FITC labeled samples were analyzed by fluorescence microscopy. **Results and Discussion:** BNNt's were synthesized via CVD method with a good yield. Radioiodination yields were over 97%. 8 hours was the optimum for time dependent U87-MG and CRL2541 cells uptake and 74 kBq/ μ g was an optimum radioactivity amount for the experiment. **Conclusion:** As a result, the synthesized BNNt/PAMAM/L-Phe compounds have the potential of being used as a BNCT agent like BPA. When the nanobioconjugate is compared with commercial BPA superior affinity to the glioblastoma cells are obtained. **Keywords:** L- Phenylalanine, Boron Nitride Nanotube, $^{125/131}I$, Radioiodination, Radiolabeling.

TP081

Correlation between two analyses programs for specific binding ratio in 123 I-FP-CIT SPECT in patients with Parkinsonism

T. KIMURA¹, M. Matsuura², T. Nakajima¹, I. Fujisawa¹; ¹Kishiwada City Hospital, Osaka, JAPAN, ²Saiseikai Noe Hospital, Osaka, JAPAN.

INTRODUCTION: It is known that Parkinson's disease cause reduction in the number of dopamine transporters in the nerve endings. Until recently, there was no practical way to visually assess reduction in intracranial dopamine. However, due to changes in the national healthcare insurance system in 2014 in Japan, 123I-Ioflupane was used. The dopamine transporter imaging by (123I)-*N*-*v*-fluoropropyl-2b-carbomethoxy-3b-(4-iodophenyl) nortropane (FP-CIT) SPECT (DaTSCAN) is now an established method for evaluating parkinsonism, detecting presynaptic dopamine neuronal dysfunction. The goal of our research is to consider how the differences in analytic methodology of two DaTSCAN image analysis programs affect the specific binding ratio (SBR). **METHODS:** 45 patients suspected of Parkinson's disease participated in this study from August 2014 to August 2015. We used two types of analysis programs, mask processing (mp) and non-mask processing (non-mp), angle correction (ap) and non- angle correction (non-ap) for non- attenuation processing (non- AC) and attenuation processing (AC). We compared both programs looking at correlation on each data. **RESULTS:** The correlation of mp and non- mp was good with SBR in non- AC ($r^2 < 0.939$). This was good correlation with SBR in AC ($r^2 < 0.914$). In non- AC, ap and non-ap showed very good correlation with SBR ($r^2 < 0.972$). The correlation of these was good with SBR in AC ($r^2 < 0.970$). **CONCLUSIONS:** The two DaTSCAN image analysis programs suggested good correlation with SBR on all condition.

TP082

1123 I FP-CIT Reconstruction Software Change in Clinical Practice

M. Hansen¹, C. Turner², N. Fullerton¹, R. Jampana¹, C. Santosh¹, A. Nicol²; ¹Institute of Neurological Sciences, Glasgow, UNITED KINGDOM, ²Queen Elizabeth University Hospital, Glasgow, UNITED KINGDOM.

1123 FP-CIT scans are performed at our centre for the evaluation of dopamine transporters in patients with movement disorders or Lewy body dementia. These are currently reconstructed using the Hermes HOSEM Iterative Reconstruction package. This is to change to the new Hermes Hybrid Recon package. Aim: To examine reconstructed images for visual differences between both reconstruction programmes, and to investigate which parameters to set using Hybrid Recon in order to optimise final displayed images available for reporting. Method: 15 patients (7 M, 8 F, mean age 73, age range 55-93) with scans ranging from normal through to grossly abnormal were reconstructed using both HOSEM and Hybrid Recon iterative reconstruction packages. Iteration / subsets numbers were the same for both packages and Chang attenuation correction was used for both. Hybrid Recon images were smoothed using two Butterworth post reconstruction filters (A, B). These reconstructed images were then reviewed

alongside the original HOSEM images by three experienced NeuroRadiologists in a random & blinded manner. The NeuroRadiologists were asked to choose which scans were, in their opinion, the preferred images. Results: All three Neuroradiologists agreed that both data sets A & B would result in the same clinical report as the original data. All three had an overall preference for images reconstructed using post reconstruction filter B. Conclusion: A method has been devised to facilitate the transfer of the reconstruction package for I123 FP-CIT procedures at our centre.

TP-04 – Tuesday, October 18, 2016, 08:00 - 09:30, Poster Exhibition Hall
Technologist Poster Session 4

TP083

Managing Radium-223 Therapy in patients with Metastatic Castration-Resistant Prostate Cancer - Developing a multiprofessional team

M. Botelho Cruz, D. Aniceto, A. Nunes, C. Mills, V. Lewington, H. Fahim, S. Allen; Guys and St. Thomas NHS Trust, London, UNITED KINGDOM.

Background: The alpha particle emitter Radium-223 dichloride ($^{223}\text{RaCl}_2$) prolongs survival in men with bone metastases arising from castration-resistant prostate cancer (CRPC). Unlike other bone targeting radiopharmaceuticals, $^{223}\text{RaCl}_2$ is prescribed as a course of 6 monthly injections. In order to manage predicted workload, we developed a new treatment protocol to meet individual patients' clinical needs within a busy nuclear medicine department. A multiprofessional radium team comprising nuclear medicine clinicians, nurse specialists, radiopharmacists, physicists and technologists was created to set up the service. The team discusses individual patients' management before each treatment cycle in a weekly multidisciplinary meeting. A review of the $^{223}\text{RaCl}_2$ therapy pathway at our hospital was conducted to assess service efficiency and identify opportunities to streamline workflow 2 years after the introduction of $^{223}\text{RaCl}_2$ at our centre. **Method:** Each step of the therapy pathway was analysed from initial referral, to pre-treatment assessment and follow up after each treatment cycle. Options to streamline processes and tailor care to an individual patient's requirements while running an efficient therapy service were reviewed. **Results:** 69 men with metastatic CRPC age range from 49 to 89, received $^{223}\text{RaCl}_2$ therapy in our centre. Having analysed each step in the treatment pathway, we developed a flowchart that incorporates all the points of contact with patients and subsequent procedures. This document clearly identifies the requirements of each team member at each contact and is accessible to all members of the therapy team. The weekly multiprofessional team meeting emerged as an important opportunity to pre-empt difficulties in a complex patient population, avoid $^{223}\text{RaCl}_2$ waste, ensure staff efficiency and strengthen team collaboration. **Conclusions:** 1. Multiprofessional teamwork is critical to support the development of a routine $^{223}\text{RaCl}_2$ service for CRPC patients. 2. A flowchart specifying every point of contact with patients undergoing $^{223}\text{RaCl}_2$ treatment improves service efficiency and has a positive impact upon demand management. 3. Weekly multiprofessional team meetings ensure that treatment can be adapted to an individual patient's circumstances, to ensure the best care and the optimal outcomes.

TP084

Utility of the SeHCAT Procedure: May Improve the Quality of Life of Patients Affected of Bile Acid Malabsorption?

M. Martínez Sánchez, A. Ruiz Rodríguez, M. Negre Busó, I. Trias Davesa, M. Sánchez García, N. Ferran Sureda, X. Aldeguer Mante, A. Rubió Rodríguez; Hospital Josep Trueta Girona, Girona, SPAIN.

AIM: Chronic diarrhea (CD) may have multiple etiologies, both benign and malignant diseases. Different physiopathological mechanisms could produce them, among those are bile acid malabsorption (BAM). In general,

patients with CD due to BAM respond well to treatment with bile acid sequestrants (such as cholestyramine) with significant reduction in bowel frequency and a better quality of life. The aim of the study was to verify that SeHCAT (radiolabelled bile acid analog) procedure is a simple test for the diagnosis of CD produced by BAM and helps to establish a treatment that improves the quality of life of patients affected. **MATERIAL AND METHODS:** A prospective study was performed from January 2013 to December 2015. In this period we studied 29 patients with suspicion of BAM. A SeHCAT procedure was done in all of them. The procedure consists in the oral ingestion of a capsule with 0.01 mCi of $^{75}\text{Selenium}$ Tauroselcholic acid, previous fasting of 7 hours. Anteroposterior images of the abdominal region were acquired (300 sec) at 3 hours, 4 days and 7 days, with acquisition of background activity before and after the study, in a dual head gammacamera Philips Forte. From these measurements, the percent abdominal retention (AR) of SeHCAT at 4 and 7 days were calculated. The test was considered positive if AR to 4 days was $<25\%$ and AR to 7 days $<10\%$. Clinical follow-up of patients with positive test was made (4 - 6 months), assessing if symptoms had improved. **RESULTS:** Of the 29 patients, 5 were men and 24 women (mean age 62 ± 13.6 years; range of 28 to 78 years). In 10 patients test were negative and in 19 positive (18 women and 1 man). Seventeen patients with positive test began treatment with cholestyramine. At follow-up, 6 manifested asymptomatic and 11 showed a decrease in the number of bowel movement and improved abdominal pain. **CONCLUSION:** SeHCAT is an easy technique that allows diagnosing BAM as a cause of DC and treat it easily. The treatment improves symptoms, leading to an increase in the quality of life of patients.

TP085

Management of Breast Cancer Patients after a Positive Sentinel Node. In the Road to Avoid Axilla Lymphadenectomy in Conservative and Non-Conservative Surgery

B. PEREZ LOPEZ, R. RUANO PEREZ, M. RAMOS BOYERO, T. RAMOS GRANDE, L. G. DIAZ GONZALEZ, M. P. TAMAYO ALONSO; HOSPITAL UNIVERSITARIO CLINICO DE SALAMANCA, SALAMANCA, SPAIN.

Aim: to evaluate the feasibility of avoiding the axilla clearance in patients with a positive sentinel node (SN) no matter if a conservative or non-conservative surgery of the breast is performed. **Method:** 641 patients with invasive breast cancer and indication of SN biopsy after a clinical and ultrasound axilla examination from 2010 to 2015 were included. The SN evaluation was done with CK19 expression by OSNA (macrometastasis >5.000 copies; micrometastasis 250-5.000 copies). T1 and T2 unifocal or multifocal tumors were analyzed separately. Conservative or non-conservative surgery was considered. Statistical analysis was done with SPSS program. **Results:** conservation of the breast was feasible in 100% T1a-T1b, 80.1% T1c, and 54.3 T2 tumors. In 409 T1 unifocal cancers, SN was positive for macrometastasis in 86 (21.0%), without statistical difference between tumorectomy or mastectomy ($p=0.299$). Also, axillary clearance was positive in 14/86 (16.3%) without statistical difference ($p=0.204$). 6/86 (6.9%) classified as pN2. In 54 T1 multifocal cancers, SN revealed macrometastasis in 21 (38.9%), being the axillary clearance positive in 4/21 (19.1%) without difference between tumorectomy or mastectomy ($p=0.305$). 2/21 (8.0%) classified as pN2. However in T2 tumors, mastectomy was significantly associated with a greater proportion of SN macrometastasis and positive axillary clearance than tumorectomy ($p=0.045$). In 118 T2 unifocal cancers, SN was positive for macrometastasis in 42 (35.6%), being the axillary clearance positive in 17/42 (40.5%). 7 of classified as pN2 (16.6%). In 17 T2 multifocal cancers, SN was positive in 8 (47.3%). The axillary clearance was positive in 4/8 (50.0%), 2 (25.0%) of them classified as pN2. **Conclusion:** after a positive sentinel node the remaining tumoral charge in the axilla is greater in T2 than T1 tumors. Up to now, to avoid axillary dissection when mastectomy is performed without planned adjuvant radiotherapy could be considered in invasive T1 tumors but should not be recommended in T2 tumors.

TP086**Patient experience of 18F-FDG-PET/CT in a mask fixation**

C. Andersson¹, B. Johansson²; ¹Nuclear Medicine & PET, Uppsala University, Uppsala, SWEDEN, ²Oncology, Uppsala University, Uppsala, SWEDEN.

Objective: The 18F-FDG-PET/CT examination is a valuable diagnostic tool for radiation treatment planning but the knowledge about patients experiences of the examination is scarce. The aim of this study was to explore how patients with known or suspected head- and neck cancer experienced undergoing an 18F-FDG-PET/CT examination in a mask fixation. **Methods:** A qualitative phenomenology methodology according to Max van Manen and the four existential; lived space, lived body, lived time and lived relation, a validated method for small sample sizes, was used. A convenience sample of nine patients, seven men and two women ranging in age from 48 to 75 years with known or suspected head- and neck cancer and who were scheduled for an 18F-FDG-PET/CT examination in a fixation mask for the first time was included February 2012 to August 2015. **Inclusion criteria** were that the participants could speak and understand Swedish, was 18 years or older and outpatients. The patients were asked to participate in the study after the examination was completed. If the patient agreed to participate a conversational interview was conducted either directly after the examination or within one week. The interviews started with the open-ended question “You have now gone through an 18F-FDG-PET/CT examination in a mask fixation. How did you experience the examination?” The interviews were tape-recorded and transcribed verbatim and read through thoroughly and analyzed separately. **Results:** Different themes regarding the patients’ experience of the 18F-FDG-PET/CT examination in a mask fixation and suggestions to improve patient satisfaction was identified. The period during the subsequent uptake phase, PET/CT camera and the time the patient spend in the mask fixation may all be experienced physical and emotional negative. Patients experienced that they were trapped in the mask which caused both physical and mental discomfort. The PET/CT camera was experienced as narrow and uncomfortable. Also feelings of being abandoned were experienced during the time in the camera. **Conclusion:** To undergo an 18F-FDG-PET/CT examination in a mask fixation may be a physical and emotional negative experience for the head- and neck cancer patient. Improved strategies to prepare the patients for the examination and possibilities to communicate if necessary and reassurance that they are not forgotten may be ways to improve patients’ experience of an 18F-FDG-PET/CT examination.

TP087**Briefing for implementation of patient safety in a nuclear medicine service**

M. Torres Jimenez, Y. Said Criado, P. Villen Trinado, D. Cid Jimenez, D. Peña Torres; COMPLEJO HOSPITALARIO DE JAEN, JAEN, SPAIN.

AIM: Ensure patient safety by conduction briefing to prevent adverse events. **MATERIAL AND METHODS:** The briefing is informative, short and multidisciplinary meetings where health service professionals, exchange information concerning patient safety. The patient safety is a fundamental principle of health care and a critical component of quality management. At these meetings possible risks to patients or incidents during attendance are discussed. Experiences on patient safety are openly shared, thence the importance of their implementation in any service. In the briefing we do in our service, the topics we discussed are the following, response to the main types of incidents that may occur: Identification of patients and alert to similarities in names., Communication with other services and other hospitals during the patient’s transference and derivation., Performance of correct procedure, at the correct organ and in the right patient. Improve communication among professionals responsible for the patient’s health., Reduce the risk of falls in

patients to position them in the gammacámara, taking special care to elderly and child., Reduce the risk of infection by washing hands., Safe handling and right administration of treatments., Responsibility of all professionals regarding patient., Provide a safety climate to the patients through clear communication., Resource management for grater effectiveness of radiation protection measures. **RESULTS:** The results of these meetings have been effective in relation to patient safety, reducing the incidence of adverse events. **CONCLUSION:** The briefings channel the efforts of professionals who care for the patients to ensure their safety.

TP088**A Novel Approach to Radiation Safety Advice for Hospital Staff**

L. A. Henderson¹, K. P. Eberhard¹, I. Badr²; ¹The London Clinic, LONDON, UNITED KINGDOM, ²The Radiological Protection Centre, St George’s University Hospitals NHS Foundation Trust, LONDON, UNITED KINGDOM.

Aim: Fears and misconceptions surrounding radiation exposure from Nuclear Medicine patients can present a challenge to non-nuclear medicine staff within a hospital setting. In our hospital, patients often attend more than one department during their hospital visit and many non-nuclear medicine staff did not have a good understanding of radiation safety. The objective was to alleviate fear and avoid unnecessary confusion by introducing a clear and effective method of communicating standardised radiation safety precautions to staff who may come into contact with nuclear medicine patients. **Materials and methods:** A traffic light colour coded system of cards was created in line with local legislation, guidelines and ‘as low as reasonably practicable’ (ALARP) principles. Nuclear medicine studies were categorised into three classifications (red, amber and green) based on the isotope properties and activity reference level of each study. For example; red cards for post Iodine131 therapies, amber cards for F18FDG studies and green cards for Tc04- thyroid studies. Information relating to pregnant staff members as well as recommended distance and time spent with a patient was outlined on the cards as well as a time limit for when the instructions cease to be relevant. The cards were designed for out-patients to take to any other appointments they had within the hospital. More detailed nurse oriented information for in-patients was updated to reflect similar guidance. A thorough roll out of the hospital wide policy was implemented which included training of nuclear medicine and radiology staff, awareness sessions for hospital staff and incorporation into the induction package for new starters. An audit by way of survey on staff understanding will be performed after the policy has been in place for 3 months. **Results:** Initial feedback from staff is very positive. Responses suggest staff feel more confident when dealing with nuclear medicine patients post radioactive administration. Full audit results will be discussed on completion. **Conclusion:** This is a new and simple approach to educating non-nuclear medicine staff in the hospital. Preliminary feedback suggests successful education of hospital staff.

TP089**Implementation of a software ASTRIM for quality assurance management in Nuclear Medicine Department (PET, SPECT and Therapeutic Radiopharmaceuticals) complying with the Italian Current Regulation**

C. MALIZIA, C. STEFANO, L. MORA, G. CICORIA, M. MARENGO, S. FANTI, F. LODI; Policlinico S.Orsola Malpighi Bologna, Bologna, ITALY.

Introduction And Purpose ASTRIM software is currently used in many Nucleare Medicine Centres to manage quality assurance of conventional SPECT radiopharmaceuticals. The current version is not able to manage the production of PET clinical trials and traditional PET radiopharmaceuticals like FDG. Up-date software ASTRIM was developed in our facility for

management the quality assurance of PET clinical trial and traditional PET radiopharmaceuticals production. Since the Nuclear Medicine Unit of the Bologna S.Orsola performance, about 12000 examinations/year and the new software was necessary to manage the amount of data and and to be compliant with Italian Current Regulation. **Materials And Methods** The change to a computerized management with Software ASTRIM it was possible thanks to the collaboration of all the professional role in Nucleare Medicine such as Nuclear Medicine Doctors, Radiopharmacist, Nuclear Medicine Technicians, Nurse, Physicist together with the Application Technologist of ASTRIM. The change come off for following steps involving every time different professional roles. - Analysis the specific procedures regarding the PET clinic trial and the PET radiopharmaceuticals splitted in several phases to be compliant with the software. - Training of the Nuclear Medicine Staff (50 people). - Routine use of the new developed software. The software implementation work for 10 PET radiopharmaceuticals lasted about six months covering all following phases: 1) storage and registration of devices, isotopes and any other reagent for radiolabelling; 2) preparations of devices for radiolabelling; 3) production of isotopes and preparation of reagents for radiolabelling; 4) radiolabelling; 5) dilution and sterilization of the final product; 6) quality control; 7) pre-release of radiopharmaceuticals; 8) fractionation into single dose for patients; 9) release of radiopharmaceuticals. The training of the staff (50 people) continued for about six months and during this time maintaining the management of quality assurance with both the old system and the new software. **Results and Conclusion** The developed ASTRIM Software for quality assurance management allowed to optimize the time especially in pre-release phases of radiopharmaceuticals, because of the complexity of the structure with about 80-90 patients daily divided into PET radiopharmaceuticals (3 preparations daily) and SPECT radiopharmaceuticals (5 preparations daily) as well as the radiopharmaceuticals for therapy (one preparation daily) all splitted into 4 PET/CT scanner and 3 Gamma Cameras. Moreover the up-date software allowed better management and monitoring reducing errors, of all the aspect of radiopharmaceuticals preparations, quality control and release.

TP090

4D-PET/CT Imaging Implementation at Oslo University Hospital, Ullevål

J. Ellingsen¹, R. DAGESTAD¹, J. HOLTEDAHL¹, H. L. STOKMO²;
¹OSLO UNIVERSITY HOSPITAL, ULLEVAAL, Oslo, NORWAY,
²OSLO UNIVERSITY HOSPITAL, Oslo, NORWAY.

Introduction Since January this year, we have had a test license for 4D-PET/CT (Siemens Phase-Match) at Oslo University Hospital, Ullevål. **Hardware:** Siemens Biograph mCT (40-slice) with Varian Real-time Position Management™ (RPM) Respiratory Gating. With 4D-PET/CT, the breathing cycle is divided into the desired number of phases from amplitude to amplitude. This is done *both* with CT and PET. Each phase of the PET uptake is attenuated with the corresponding phase of the CT. With our current CT-settings this 4D-protocol contributes an additional radiation dose of 2,3 mSv. **Purpose** 4D-PET/CT is a recently acquired technology in Nuclear Medicine. Previously, 3D-PET/CT and 4D-CT have been used in radiotherapy to observe tumour motion and to draw gross target volume (GTV). The former method tends to underestimate the FDG-uptake due to the localization and movement of the tumour. In addition, the FDG-uptake for small lesions are often underestimated and it becomes difficult to delineate the GTV. 4D-PET/CT provides a more accurate semi-quantitation of the FDG-uptake. This is due to a more accurate attenuation correction, as well as a sharper defined lesion. **Implementation / Protocol** A small block with reflectors is placed on the patient in a location suitable for detection and recording of breathing movements (e.g. upper abdomen). The movement of the block is registered and infrared light is reflected from the block, and detected and recorded by a camera that is located at the end of the patient table. When the breathing registration is completed, the breathing data is exported from Varian RPM to the modality computer for analysis. In our protocol, one static image is generated from the expiration phase. Furthermore, eight phases of attenuated PET uptake are generated. This is

played as a cine, so that all the phases of the lesions natural motion are shown on the fused images.

TP091

Operational Strategies and Policies of Nuclear Medicine Departments - Service Managers' view

S. Soares, C. Quintal; Faculty of Economics-University of Coimbra, Coimbra, PORTUGAL.

Introduction: The operational management of a Nuclear Medicine department (NMD) is dependent on factors such as: management style, knowledge and professional experience of the service manager; policies and features of the hospital in which the NMD belongs to. This study will explore the importance that the NMD service managers' give to their different tasks, and department policies regarding: workflow configuration; service improvement; incorrect preparation of inpatients and managing appointment DNAs. **Methods:** Semi-structured interviews were conducted with 10 NMD service managers of the NHS, based in the London area. Confidentiality and anonymity was guaranteed. A thematic analysis was chosen to analyse the results, and the dominant themes highlighted. **Results:** According to the interviewees, providing patient care and safety is their top priority. However, the management of the workload and workflow, staff, budget and resources is crucial for the proper functioning of the departments. Some of the most important and difficult tasks include compliance with the waiting targets and radiation regulations, and having sufficient staff with the necessary skills to perform the required job tasks. All interviewees agree on a semi structural workflow. Workflow configuration can be dependent on: radiopharmaceuticals supply and delivery prices; staff and facilities availability; scan duration; ARSAC restrictions and other procedures. This arrangement maximizes the use of the radiopharmaceutical vial, the equipment and all the human resources involved, achieving a smoother workflow (with the inconvenience of generating a disproportional waiting list). Although all interviewees undertook service improvement, only two of them consciously applied process mapping or a lean approach. Interviewees felt that the incorrect preparation of inpatients is mainly due to lack of communication, aggravated by turnover of ward staff. Therefore, assessing the patient beforehand, emphasizing costs involved, and cross charging the wards were methods suggested to minimize this problem. A department choose to outsource work, that requires complex patient preparation, to other Trusts. DNA policies were very similar across departments. Patients with a plausible excuse were re-booked, if not the referral was returned to the referrer. **Conclusion:** Greater knowledge about service improvement methods may help patient workflow and minimize existing barriers. Optimal strategies vary, and each NMD should adopt methods that best suit its needs. Whilst acknowledging this diversity, the sharing of these results may contribute to wider discussions on best practice.

TP092

Increasing the capacity of MPI IQ-SPECT. Changing the workflow?

M. Dini, N. Weel; Institute Verbeeten, Tilburg, NETHERLANDS.

Aim Over the past few years, the number of patients referred to our institution for myocardial perfusion imaging (MPI) has increased significantly. This year, compared to 2013, the number of studies has increased by more than 20% and further growth is expected. In order to cope with this growth, our department had to critically evaluate and optimize its current workflow process. Our goal was to increase our capacity by 20% in 2016 while maintaining the following conditions: All studies performed within working hours (8:00 - 17:30), With the same equipment, The technicians do not have to work faster. **Method** We have visualized the patient-routing throughout an exam. The duration of each step in this process was timed to evaluate where time losses occurred (at different points in the process). A distinction was made into 2 major components during the process: a stress test and the examination. We have a stress-test room, a gammacamera, 3 technicians and an additional technician at our disposal. At

each room there were 2 dressing rooms available. We use the IQ-SPECT acquisition method to exam patients. **Results** In the old situation, we could only perform a total of 71 exams (32 stress + 39 rest). In the new situation we are able to perform 92 exams (46 stress + 46 rest). To achieve this we use a rotation system between technicians. 2 technicians work at the camera and 1 is doing the stress test. After 3 patients the technicians rotate. The additional technician (technician 4) places the venflon needle before the stress test. Technician 4 places a venflon needle and puts the patient in a dressing room. Stresstest: Both the doctor and technician 1 stay in the room. This way there is no delay and there is a constant flow of patients. Technician 1 takes the first three charts with him to the scan room. Examination: Technician 2 operates the computer during an exam and technician 3 performs the exam. Technician 3 places the next patient in the dressing room during the CT scan. **Conclusion:** By using a rotation system between technicians the patient sees only 1 person at each step in the exam. In our experience this is very patient friendly. The acquisition time is reduced from 30 min per patient to 20 min per patient. By introducing the rotation system, we've accomplished a *rise* of 25 % of patients.

TP093

Data recording in PET/CT routine research protocols: Could we do better?

C. Baun, T. Nguyen, P. F. Høilund-Carlsen; Odense University Hospital, Odense, DENMARK.

Aim: To examine errors in data recording in a routine PET/CT workflow from which many patients enters into research studies. In our daily work we accept variations of +/- 10% in administered tracer dose and of +/- 5 min in acquisition time point. Such variations influence quantitative PET measurements. Therefore, we identified errors of this type to elucidate the extent of the problem. **Methods and materials:** A retrospective analysis of 201 patients included in five PET/CT research projects performed January 2015 - January 2016. These comprised 158 patients scanned with FDG in a 1h protocol and 24 scanned in a dual-time protocol, 10 patients scanned with sodium fluoride (NaF) in a 45 min and 9 scanned in a 60 min protocol. Recorded data were obtained from handwritten pre-scanning reports, the automatic tracer injection report (when used) and DICOM information from the PET/CT scanner and compared to research protocol requirements regarding tracer type, dose, injection time, and scan time. Basic data regarding patient weight, height, and blood sugar in handwritten reports were compared to registrations typed in by the technologist. **Results:** Among 1h FDG studies, errors were found in 143 cases (91%) and among dual-time FDG scans, in 22 cases (96%). With the two (45 and 60 min) NaF protocols, errors were found in all patient studies (100%). Errors mainly consisted in discrepancies between prescribed and injected tracer dose. This was found in 176 patients (88%). The error range for the FDG dose was -38 - 97 MBq and for the NaF dose -106 - 208 MBq. Errors in registered scan time were seen in 54 patient studies (27%) with a range of 1-59 min. Typing errors in patient height and weight registration were seen in 6 (3%) and 8 (4%) of studies, respectively. Only 4 patient studies had missing information regarding blood sugar. **Conclusion:** The overall absolute accuracy of data registration in routine research protocols appears rather low. Errors mainly concerned administration of correct tracer dose and scan time in accordance to prescribed time points. Although the number of errors is relatively large, it should be taken in consideration that any registration discrepancies regardless of size counted as an error in this study. In the daily routine, a small variation margin is allowed for practical purposes, which, however, reduces the accuracy and reproducibility of quantitative PET measurements. Attention should be taken to optimize reproducibility in routine workflows generating research data.

TP094

Patients not attending, how to reduce them

B. Hoyer Mathiasen, M. Adler, P. C. Holdgaard; Vejle Hospital, Vejle, DENMARK.

Aim: At the Department of Nuclear Medicine, Vejle Hospital, technologists experience a large proportion of outpatients not attending for their appointment. In 2014, 846 of 15471 patients (5,5%) did not attend their appointment. The hypothesis was is was patients in follow up that had received their written information a long time ago that did not attend. We wanted to investigate whether we could reduce the numbers of non-attending patients, who had received their written information more than 90 days by sending the patients a reminder letter. If more patients turn up, it would reduce the waste of resources, shorten waiting lists and improve overall economy. **Materials and methods:** To conduct this study, we registered all patients that had received their written information more than 90 days ago. These patients were sent a reminder letter 14 days prior to their time of examination. The patients not attending recorded. The letter consisted of a text, telling the patients to remember their examination, and referring to information in the original appointment letter, and contact information to our department, in case of any questions. The patients from the same months of 2015 were chosen as a control group. **Results:** 443 patients was included over a period of 3 months in 2016, 18 of these (4,1 %) did not attend and did not cancel their appointment. The control group for the same period in 2015, was 397 patients, 37 of these (9,3 %) did not attend. The results show a significant reduction ($p=0,002$) in the number of non-attending patients, in the group that received the reminder letter compared to the control group. **Conclusion:** We find that the patients attendance percentage can be strongly improved with a reminder letter prior to the time of the examination, in the patient group that have received their written information more than 90 days prior to the exam date. It has reduced the proportion of non-attending patients by more than 50 %. At the Department of Nuclear Medicine, we will therefore continue to send reminder letters to this patient group, and as of now (April 2016) it has been possible for the patients to subscribe to a reminder SMS.

TP095

Fast tracking of PET research studies that fits in your white coat pocket

E. S. Saxtoft; Copenhagen University Hospital, Rigshospitalet, Copenhagen, DENMARK.

Introduction The Department of Clinical Physiology, Nuclear Medicine & PET performs over 5000 PET/CT scans per year. About a fifth of these are part of highly specialized research projects. Each project has an associated protocol, which is created in collaboration with scientists, project leaders physicians and nuclear medicine technologists. The number of research projects have been increasing in recent years and the need for an electronic project catalog arose. The implementation of an online project catalog has facilitated the management of PET research studies and at the same time some other work processes as the fast track of tracers. The updated easy access to documents has ensured that the quality of research data has increased and we can save time and resources in every day work life. **Materials and Methods** We researched the market for tablets and found a solution that suited our needs. Using a NEXUS 7 Tablet, we have the perfect blend of both technology and mobility in the coat pocket. With a fast connection to the network, we have solved several challenges at once. Fast and useful access to important information and project data as: -Online project catalog -Tracershop overview and tracer release time -Patient transport service follow-up -Netradio for the patients -Mutual activity calendar -Document Management System **Results** We have covered the need to support our own knowledge on the various projects and their study criteria, which benefits the patients, the research studies and the staff on the ward. A clear and user-friendly overview of the various research studies has reduced the possibility of making errors among projects and we can thus feel more secure about the management of project data. The new tablet has contributed to a greater search-experience, as it turns out that the staff can save time and resources by taking the tablet around when the need for quick access to fully updated information is crucial. The tablets are a streamlined solution that is easy to synchronize and ensures that the staff is always working with information that is continuously updated. **Conclusion** The implementation

of the electronic tool benefits primarily the patient studies, quality assurance and the staff. The access to project data and other information on-the-go is probably the best argument for any further development and optimization of the mobile tool. A high specialized department with a large repertoire of project protocols requires an effective tool that can match the demand.

TP096

Do Fasting Hours, Blood Glucose Level and Diabetes Mellitus Influence Uptake of FDG in the Myocardium?

D. Mateo-Navarro¹, A. Sabaté-Llobera¹, M. Cortés-Romera¹, S. Rustarazo-Losada¹, I. Ferrero-Febrer¹, I. Liarte-Trias¹, M. Albadalejo-Castaño¹, A. Cebrián-Leyva¹, D. Coca-Castro¹, L. Gràcia-Sánchez¹, M. Ribas-Sitjas², G. Reynés-Llompant¹, C. Gámez-Cenzano¹; ¹PET Unit, Department of Nuclear Medicine - IDI. Hospital U. de Bellvitge-IDIBELL, L'Hospitalet de Llobregat (Barcelona), SPAIN, ²Department of Cardiology, Hospital U. de Bellvitge-IDIBELL, L'Hospitalet de Llobregat (Barcelona), SPAIN.

AIM: To correlate myocardial uptake of FDG with fasting hours (FH), blood glucose level (BGL) and diabetes mellitus (DM). **MATERIAL AND METHODS:** Retrospective evaluation of 208 patients (115 male, mean age 59 years) referred for whole-body FDG-PET/CT. Information about FH and BGL was collected. Forty-eight patients had DM (23%). One DM patient was excluded due to previous cardiac surgery. Myocardial FDG uptake was analysed semiquantitatively (SUVmax, SUVmean) placing a ROI on the left ventricle, and correlated to FH and BGL. Additionally, patients were divided in 2 subgroups according to FH (<12 and ≥12 hours), and differences between subgroups were tested. To rule out the potential influence of DM, other 2 subgroups were evaluated (DM and non-DM) and correlated to myocardial FDG uptake. **RESULTS:** Patients fasted for at least 6 hours (mean 10.3, range 6–20). Mean SUVmax and SUVmean was 5.4 and 3.1, respectively. No correlation was found between FH and myocardial FDG uptake, neither with SUVmax nor with SUVmean (Pearson's $r=-0.07$ for both parameters). However, higher SUV values were observed with less FH. Analysing the two subgroups (<12 and ≥12 hours) significant differences were obtained ($p=0.022$ for SUVmax; $p=0.015$ for SUVmean); yet, this results could be influenced by the number of outliers and a positively skewed distribution around low fasting times. To have more consistent data, values with $SUV \geq \text{mean} + 1.9 \times SD$ were eliminated. In this setting, we did not find neither correlation between FH and myocardial FDG uptake ($r=0.08$ for SUVmax and SUVmean), nor differences between subgroups ($p=0.962$ for SUVmax; $p=0.933$ for SUVmean). BGL was not available in 8 patients. Mean BGL was 5.6 mmol/L (3.8–12.9). No correlation between BGL and myocardial FDG uptake was observed, neither for SUVmax ($r=0.02$), nor for SUVmean ($r=0.03$), though most of the patients (88%) were normoglycemic. Of the hyperglycemic patients, 69.5% had DM. When comparing DM and non-DM patients, no differences regarding FDG uptake in the myocardium were observed ($p=0.399$ for SUVmax; $p=0.424$ for SUVmean). **CONCLUSION:** According to our study, FH and BGL do not seem to influence FDG uptake in the myocardium in standard conditions. However, significant differences appear between patients with <12 and ≥12 FH, even if they could be influenced by the number of outliers, as higher SUV values are observed in shorter fasting periods. No differences between DM and non-DM were observed, but additional variables may influence the results. Equalizing the number of patients in the subgroups could lead to different conclusions.

TP097

Does an automatic PET infusion system actually deliver the prescribed dose?

J. C. Gam-Hadberg, C. Baun, O. Gerke, P. F. Høilund-Carlson; Odense Universitetshospital, Odense, DENMARK.

Aim In an effort to reduce the radiation dose to the staff, many departments have implemented the use of automatic infusion systems for PET tracers. In our daily work we accept variations of $\pm 10\%$ in administered tracer dose; errors beyond this limit can have consequences for image quality and influence PET quantification measurements especially in research protocols. Therefore, we aimed to assess the accuracy of our PET infusion system and to elucidate any reduced performance during the years of use. **Materials and methods** Our retrospective analysis included 491 tracer doses delivered to patients by the Intego™ PET Infusion System (Medrad, Inc., Indianola, PA). Data were obtained from the printed label delivered by the Intego system post injection and comprised 341 delivered doses in 2011 and 150 in 2015. The differences regarding prescribed dose and delivered dose were calculated using Bland-Altman limits of agreement and paired t-tests, also stratified by year. Equivalence testing was performed by the 'two one-sided testing procedure' (TOST), using log-transformation. The equivalence limit was 10%, implicating critical boundaries of 0.9 and 1.11 of a respective 90% CI. **Results** The overall data showed a mean difference between prescribed and delivered dose of 0.22 MBq [95% CI: -0.70 to 1.15], with Bland-Altman limits -20.20 and 20.65 MBq. For the data obtained in 2011 the mean difference was -2.00 MBq [-2.39 to -1.62; $p<0.0001$], range -9.11 to 5.11 MBq; for data obtained in 2015: 5.27 MBq [2.53 to 8.02; $p=0.0002$], range -28.12 to 38.66 MBq. Prescribed and delivered doses were found equivalent at the 10% level in both 2011 and 2015. The ratio 'delivered/prescribed dose' was estimated to be 0.999 for both years [90% CI: 0.997 to 1.002]. The Intego performance changed statistically significantly ($p<0.0001$), but not clinically relevantly from 2011 to 2015. In 2011, 0.6% of doses were beyond the accepted 10% limit by a mean -2.39 MBq, range [-15.34 to 10.56]; for 2015, 4.6% of the doses exceeded the 10% limit by a mean of 23.6 MBq, range [10.84 to 32.01]. **Conclusion** The automatic Intego PET Infusion System delivered the prescribed dose within a 10% equivalence limit, actually within a 5% equivalence limit, although the results suggested that system performance decreased slightly over time. Attention should be paid to ensure accuracy of administered radioactive doses, and performance of automated system should be monitored over time from a quality control perspective.

TP098

Score cards for standardized comparison of myocardial perfusion imaging reports

J. D. Jensen, C. M. Hoff, K. Bouchelouche, N. L. Christensen, M. R. Jochumsen, M. A. Pedersen, L. P. Tolbod; Dept. of Nuclear Medicine and PET-Centre, Aarhus University Hospital, Aarhus N, DENMARK.

Background: When optimizing scan protocols or comparing modalities in myocardial perfusion imaging, it is necessary to compare the current method to the new method. This can be achieved by a comparison based on hard numbers such as MBF, summed rest and stress scores, total perfusion deficit etc. However, what is of importance to the patient is the total evaluation of these scores and the weight and confidence ascribed to each by the reporting physician. We suggest a standardized method summarizing the observations and the confidence of the physician in simple scores. We tested the developed score cards in a pilot project using a training scenario where 3 observers with varying experience (1 month, 5 months and 3 years, respectively) scored static rest/stress Rb-82 PET scans. **Method:** 10 patients with known ischemic heart disease were included. Using the 17-segment AHA cardiac model, each patient will get one or more of the five clinical scores (0) Insufficient pharmacological stress, (1) normal, (2) reversible ischemia, (3) irreversible ischemia and (4) 3-vessel and/or sub endothelial disease. The certainty of the clinical score will be marked as (0) equivocal, (1) probable or (2) certain. Furthermore, the degree of the defect will be defined (0) <10%, (1) 10–20%, (2) >20%. In addition, scan quality will be rated as (1) unacceptable, (2) poor or (3) good. In the test, the scoring process is performed by each observer. **Results:** Summed certainty score was similar for all three observers (15.3±1). A high summed scan quality score was given by the most and least experienced observers (18 and 19

respectively, 20 being the maximum summed score), but lower by the observer with medium experience (15). The average score deviation from the most experienced observer to the least and medium experienced observers was 0.7 and 0.4, respectively. Perfect agreements on extend of defect by medium and most experienced observers, whereas the least experienced observer tended to overestimate defect size. **Conclusion:** The test of the score card in a training situation was successful and results reflected the varying experience of the participating observers. However, deviations on quality score and defect size, illustrate the importance of supplying the observers with clear instructions and definitions. The score card will be used for optimizing cardiac PET protocols in the department.

TP099

First experiences of using segmentation and SPECT SUV tool

B. Mirocha, A. Sackiewicz; Maria Skłodowska-Curie Memorial Cancer Center and Institute of Oncology, Warsaw, POLAND.

Aim of this poster is to present our experiences of using software for SUV calculation for SPECT/CT studies. The use of new software solution for quantitative estimation of radiopharmaceuticals uptake and calculation of concentration in volume of interest (VOI) given in MBq/ml allow us to classify lesion characterization using SPECT SUV. The studies was made with use of GE Healthcare hybrid γ -camera Discovery NM/CT 670 equipped in special software called Q.Metrix. Use of that software for segmentation SPECT/CT studies needs some camera preparation with specific calibration. Studies acquisition data is iterative reconstructed with available corrections (AC, SC, RR) and presented in 3 standard planes (coronal, sagittal, axial). With this software it is possible to do three-dimensional segmentation and spatial localizations based as well on CT or SPECT and further mutual transformation from CT to SPECT and vice versa. At the end system calculate SUV in ROI/VOI and presents it with statistics. Given specification of The Maria Skłodowska-Curie Institute of Oncology and our experience it is possible to predict that Q.Metrix software will be helpful tool in high dose I-131 (3700 MBq) thyroid therapy studies and lesions assessment in follow up studies in bone tumor. Determine the value of SPECT SUV allows to compare statistics of studies in relation to follow up studies or after therapy.

TP100

3d-ssp implementation in nuclear medicine service as tool accessory for interpretation of brain spect 99mTc-hmpao

F. ZELAYA REINQUET, A. Renda Alcalde, J. Outomuro, D. Ruiz Hernandez, M. Castrillon, C. Castillo Berrio, F. Loira, L. Campos, R. Guitian, A. Lopez; Complejo hospitalario de vigo hospital meioxeiro, vigo, SPAIN.

Three-dimensional analysis of stereotactic surface projection(3D-SSP)has been widely used as imaging tool in dementias. It is an analysis method that evaluates cortical perfusion after anatomical standardization by calculating the maximum activity for the corresponding areas of cerebral cortex, assigning a value for each pixel of surface; the algorithm compensates individual differences in cortical thickness and depth of gyri using a standard stereotactic system. **OBJECTIVES:**1. Determine the degree of concordance of diagnostic interpretation between expert and novice observer with the help of the 3DSSP.2.Determine whether the use of 3DSSP adds value to diagnostic expert and novice observer. **MATERIALS AND METHODS:** We randomly selected 30 studies of brain perfusion SPECT with 99mTc-HMPAO, done between January and December 2015 at our hospital, with age between 50-79years (determined by the design of the program).Image processing was carried out according e-soft Siemens standardized reconstruction algorithms clinical applications package. Subsequently, the 3D-SSP processing was performed. The images were evaluated by two Nuclear Medicine experts, and nuclear medicine physician in training.The study was divided into two phases.1st phase:

Conventional processed image were evaluated, knowing only the reason for the request of the Brain SPECT.2nd Phase: 15 days later, images were reevaluated with help of processed images obtained with 3D-SSP. We delivery to the observer a template with the brain divided into anatomical sub-regions(prefrontal, orbitofrontal, parietal, frontotemporal, mesial and lateral temporal, and occipital), corresponding to both hemispheres, the observer assigned a value according to the semiquantitative perfusion grade: 0 normal; 1 minor involvement; 2 moderate involvement; 3: severe involvement.For interobserver statistical comparison we use the EPIDAT software, obtaining the Kappa Correlation index between the two interpretations. **RESULTS:**The kappa coefficient of correlation between the novice and expert observers was as follows:1st phase: 0.8159 with 95% CI (0.7645 to 0.8673).2nd Phase: 0.8860 with 95% (0,8440- 0,9280). **CONCLUSION:**Our series confirms what has been reported in the literature, 3D-SSP tool helps to improve visual assessment by physician in training. Instead of the 3DSSP contribution provided by the 3DSSP to senior observer is not statistically significant. We believe to train doctors in training is an interesting alternative to implement the training program MIR in the Services tool.

TP101

Standardizing image quality for ⁶⁸Ga-DOTA-TATE PET/CT

M. Cramer, S. Z. M. van Lierop, C. P. W. Cox, M. Segbers, R. Valkema; Erasmus MC, Rotterdam, NETHERLANDS.

Aim: The European Association of Nuclear Medicine procedure guidelines recommends a dose of at least 100 MBq for ⁶⁸Ga-DOTA-TATE PET/CT. This poorly defined dose regimen leads to differences in image quality between patients due to body composition and attenuation. Our aim is to propose a dose regimen that standardizes image quality for all patients. **Methods:** Retrospectively 20 ⁶⁸Ga-DOTA-TATE PET scans were analyzed. All scans were acquired 58 minutes (± 2.09) post injection (91 \pm 14 MBq) on a Siemens Biograph mCT. Time per bed position was dependent on the body mass and varied between 3 and 6 minutes. Iterative image reconstruction was performed using Time-Of-Flight and point spread function recovery (True-X). To assess image quality a volume of interest (VOI) with a diameter of 3 cm was drawn in a homogenous part of the liver. The mean pixel value and standard deviation were measured to calculate the signal-to-noise ratio (SNR). To investigate the relationship between SNR and patient dependent parameters (body mass, length, body mass index (BMI), body mass per body length and lean body mass), the SNR was normalized for variation in injected dose and time per bed position by assuming Poisson statistics for the VOI measurements. The SNR was normalized to 3 min/bed and a dose of 100 MBq which is currently recommended in the EANM guidelines. The relationship between the best correlating parameters and normalized SNR was used to propose an optimized dose regimen. **Results:** Three patient dependent parameters (Body mass, BMI and body mass per body length) show a significant ($p < 0.01$) decreasing linear correlation with the normalized SNR. Pearson r is respectively -0.766, -0.827, -0.823. The normalized SNR is proportional to the square root of the time per bed position and the amount of injected activity. This implies that injected dose or time per bed position should be varied quadratically with one of the patient dependent parameters to achieve standardized image quality. Or a combination of both can be used. **Conclusion:** Following the current EANM guidelines will result in decreasing image quality for patients with a higher body mass, BMI or body mass per body length. To achieve a standardized level of image quality a quadratic change of the [dose x time per bed position] product with one of these three parameters should be implemented.

TP102

Colonic transit scintigraphy using ⁶⁷Ga Citrate: establishing a department guideline

D. M. P. S. Neves, B. X. Lourenço, M. Faria Joao; Diaton S.A., Leiria, PORTUGAL.

Introduction: Colonic Transit is defined as the time required to excrete ingested substances that have reached the colon. Measuring colon transit time could be helpful in the evaluation of colonic motility disorders, namely in constipation cases. Radiopaque marker test (radiology), is the most widely used technique, although, colonic transit scintigraphy could represent an alternative. Scintigraphy is based on the oral administration of a non absorbable radiopharmaceutical in the bowel, such as liquid $^{111}\text{In-DTPA}$, ^{111}In - labeled activated charcoal capsules, or $^{67}\text{Ga-Citrate}$. To our knowledge, aqueous $^{111}\text{In-DTPA}$ or capsules, aren't commercially available in Portugal, therefore, $^{67}\text{Ga-Citrate}$ is the plausible option. SNMMI and EANM guideline for small-bowel and colon transit study mention this option, but it isn't addressed for $^{67}\text{Ga-Citrate}$ use. Additionally, there's a lack of standardization of this method within the literature. **Aim:** The aim of this work is to present a colon transit scintigraphy guideline using $^{67}\text{Ga-Citrate}$, established according to our department work. **Material and Methods:** Between 2009 and 2015, 16 patients (12 females and 4 males) were investigated. One patient (normal colon transit) was considered control. All patients were addressed by a surgery consult, with the clinical information of constipation. After preparation, 5.5 to 7.4MBq (150 to 200 mCi) were orally administered. Images were obtained at AP views, at 4-6 hours, 24 h, 48h, 72h, 96h, and in the 7th day if necessary. Images were all acquired in the same dual-head gamma camera. Processing activities included visual analysis, half-clearance time ($T_{1/2}$) calculation, and segmental analysis assessed by geometric center calculation. Results: The average half-clearance time for constipation patients occurred between 72 and 96 hours, and between 24 and 48 hours for the control. According with established interpretation criteria, several image patterns were observed, namely: normal colon transit, generalized slow colon transit, functional rectosigmoid obstruction, and segmental retention. **Conclusion:** The use of $^{67}\text{Ga-Citrate}$ revealed several advantages such as: non absorption in the bowel; price and availability; handling simplicity; good image quality; low administered activity; and suitable physic half-life ($T_{1/2}=3.3$ days), allowing for late imaging if necessary. No secondary effects were reported. The major limitations for its use is the absent standardization and the lack of dosimetry data comparing it with the $^{111}\text{In-DTPA}$. Data processing was also a challenge. Therefore, in our experience, when other validated radiopharmaceuticals aren't available, $^{67}\text{Ga-Citrate}$ could be a good option to perform colon transit scintigraphy. Nevertheless, more comparative studies (with $^{111}\text{In-DTPA}$ or/and radiology methods) are needed.

TP103

A Guide to Setting up a Ga68-PSMA PET/CT Service in the United Kingdom

L. A. Henderson¹, R. Pasternick¹, R. Maria¹, R. T. Meades², S. Khan¹, T. D. Barwick¹; ¹The London Clinic, LONDON, UNITED KINGDOM, ²Radiological Sciences Unit, Imperial College Healthcare NHS Trust, London, LONDON, UNITED KINGDOM.

Aim: Prostate specific membrane antigen (PSMA) labelled to Ga68 for PET/CT imaging of prostate cancer patients was unavailable in the United Kingdom prior to August 2015. However, due to the success of Ga68-PSMA in Europe demand from urologists was high. The service was setup, with our first patient scanned on the 28/09/2016 and in the following 6 months we successfully scanned 33 patients. Our objective is to summarise our experience of establishing and running this service in the UK to provide other centres with an insight into the challenges and considerations involved. **Method and materials:** Many challenges can arise when trying to implement a new service in a UK nuclear medicine department and for our non-NHS department these were compounded by the fact that the service was not yet offered anywhere else in the country. Availability of the short lived Ga68 isotope was limited and local legislation requires consultant reporting training prior to obtaining a license to use the product. A structured plan was established and executed over the months prior to radiopharmaceutical availability. The separate processes required to setup the Ga68-PSMA PET/CT service included appropriate equipment selection, understanding of regulations, radiopharmaceutical availability, staffing, refining imaging protocols, standard operating procedures, doctor and

staff training, referrer education, physics expertise, administration and finance support services. **Results:** Over a six month period 33 patients were scanned and during this time positive feedback was received from referrers. A reference level of 200MBq of Ga68-PSMA using the radiometal chelator HBED-CC was used. Patients were imaged on a Siemens Biograph mCT PET/CT scanner and imaging parameters included uptake period of 1hour. Imaging was performed over a scan range of skull vertex to knees using CT parameters dose reduction software set at a reference level of 70mAs, and a kV at reference level of 120. PET acquisition was performed for 3 minutes per bed, 3 PET reconstructions were created utilising CT for attenuation correction. A pelvis post micturation image was also performed on all patients. Studies were dual reported by Nuclear Medicine trained Radiologists. Challenges were faced to do with radiopharmaceutical availability and the department learned from this by introducing clear patient information to manage expectations. **Conclusion:** We successfully implemented this new service in our department by beginning with a structured and detailed plan. This work has provided a summary of the challenges and considerations experienced in setting up a Ga68-PSMA PET/CT service in the UK.

TP104

Importance of PET TAC Valuation in Oncology

M. Barrera Gonzalez, E. Ariza Cabrera, M. Valderas Montes, A. Benítez Morera, E. López Martínez; Servicio Andaluz de Salud, Cadiz, SPAIN.

Aim: - To implement a data collection system for assessing the patient at baseline. - To establish a protocol to the patient prior information as to the next steps for the diagnosis, evaluation and treatment. -To evaluate the quality of care, ensuring that patients are treated in nuclear medicine for PET procedure are properly prepared, informed, cared for and in a state of comfort. **Materials and Methods:** We have done an observational, descriptive cross-sectional study, all participating patients and their families. They served a total of 32 patients referred for PET -CT during the months of March and April 2016 in the Nuclear Medicine Hospital Puerta del Mar of Cadiz. To perform this test we used a radiopharmaceutical that it is a derivative of glucose (fluorodeoxyglucose) labeled with fluorine-18 (18F-FDG), which it will study the metabolic activity of the disease process. The gamma camera used is a Siemens PET CT, together with the availability of comfort rooms. We decided to make a collection of data using in an Excel spreadsheet and nursing assessment. **Results:** According to data obtained from patients seen in the sample, they indicate that 50% are men and the rest are women, the aged are approximately between 45 and 70 years. They have a majority of medical diagnosis of lung cancer, cervical cancer and melanoma. Glycemic indices indicate us that 90% are non-diabetic patients, since not altered capillary glycemia. **Conclusion:** The creation of this spreadsheet has served as an element of reflection and evaluation of quality in information handling. The deal is personal, one of the qualities that motivates the patient and decreases anxiety. Before the examination, patients have been cared for by nurses and performing a nursing assessment to them, much needed for data collection.

TP105

Local Recurrence in Breast Cancer, Which is the Role of Sentinel Lymph Node Biopsy?

B. PEREZ LOPEZ, R. RUANO PEREZ, T. RAMOS GRANDE, L. G. DIAZ GONZALEZ, F. GOMEZ-CAMINERO LOPEZ, M. RAMOS BOYERO, M. P. TAMAYO ALONSO; HOSPITAL UNIVERSITARIO CLINICO DE SALAMANCA, SALAMANCA, SPAIN.

Objective: To evaluate the utility of SNB in local recurrence of breast cancer in patients with previous surgery treatment. **Methods:** We reviewed all women with local recurrence from January-2002 until

December-2015. Indication for SNB was preoperative axilla node negative. The exclusion criteria were previous axillary lymph node dissection (ALND) or axillary radiotherapy. Lymphatic mapping was performed by a peri-tumoral intradermal injection of Technetium-labeled (Tc-99m) nanocolloid, considering where was the previous surgical scar. Surgical detection was done with a hand-held gamma probe. ALND was done when SN informed of macrometastasis or not located. **Results:** 59 women with local recurrence were analysed. 23 with previous ALND received no axilla examination. SLNB was not indicated in 4 cases with positive axilla. Also 9 patients directly went to ALND despite SLNB indication because of surgeon decision. Therefore the SLNB was done in 23 patients. Detection was feasible in 15 patients (65.2%), 13 of them had negative SN and 2 presented micrometastasis (13pN0, 2pN1mic) so no ALND was performed in any of them. In the 8 patients without detection of the SN, ALND was done resulting in 6pN0 and 2pN1a (one node). We found no relation between the previous surgical scar localization (external quadrants) and the absence of drainage. In the cases where ALND was directly performed, metastases were found just in the 4 patients with previous clinically suspicious of malignancy. **Conclusion:** SNB in women with local recurrence is technically feasible and permits to avoid axillary clearance. We believe that axillary lymph node dissection should not be performed if sentinel lymph node is not detected due to low probability of axillary lymphatic disease after a correct clinical and ultrasound examination of the axilla.

TP106

Is it possible to minimize time of uptake for SeHCAT patients without compromising the diagnosis?

A. Flensburg, G. Zulfovski, J. Nielsen; Bispebjerg Frederiksberg Hospital, Copenhagen, DENMARK.

Introduction: The SeHCAT test for bile acid malfunction is performed differently in different nuclear medicine departments according to time of counting, collimators, background measurement and distance between the patient and the detector(s). In our department we use 10 mins scans for background and measurement of patients using a camera with two uncollimated detectors placed as close as possible to the patient. We decided to find out if it is possible to minimize the measurement time without compromising diagnosis as well as count statistics. **Materials and methods:** Siemens Symbia Gamma Camera with two detectors. The lower detector is shielded with a thin plexiglass plate for protection. 75-SeeleniumHomoTauroCholicAcid capsules (GE HealthCare) 20 patients referred to the test. Detectors were placed far from the patient and as close as possible to the patient. Time of measurement was 1, 5 and 10 mins. In addition to the patient tests, background was measured another day while 99mTc and 81mKr was present in the vicinity of the room. **Results and discussion:** There is no significant difference in the retention % whether we use measuring time of 1, 5 or 10 minutes. However, the background counts are lower (approxim. 5, 30 or 60 kcts) when the detectors are placed in the position close to the imaginary patient, while the patient counts are higher when the detectors are close to the patient. This is not surprising, as the background radiation is minimized due to the closeness of the detectors. Background does not vary during the day, and more important: The diagnosis does not vary in any of the setups. This is probably because the only other isotopes used in the department, 99mTc and 81mKr have entirely different gamma energies (140 KeV and 190 KeV), whereas the window is set to 272 KeV, 20% during the SeHCAT-scans, according to one of the 75Se-energy peaks. **Conclusion:** We suggest that the counting time is reduced from 10 mins to 2 mins (The 2 mins count is in order to obtain acceptable background count statistics) and the detectors placed as close as possible to the patient. Background should be measured before the first and after the last patient. This will save time in our busy department and it will also not compromise the count statistics.

TP107

GC analysis of radiopharmaceuticals for residual solvents

E. Saksa, O. Solin, T. Viljanen; Turku PET Centre, Turku, FINLAND.

Aim Since there is no therapeutic benefit from residual solvents, all residual solvents should be removed to the extent possible to meet product specifications, good manufacturing practice, or other quality-based requirements. Drug products should contain no higher levels of residual solvents than can be supported by safety data. Testing should be performed for residual solvents when production or purification processes are known to result in the presence of such solvents. The aim of this study was to set up a method for residual solvent analysis of radiopharmaceutical patient injections. **Materials & Methods** The method is based on Agilent USP <467> application note.¹⁾ We use an Agilent 7820A gas chromatograph with a flame ionization detector (FID), automatic injector, liquid (split) injection and an Agilent DB-624 column. The method is validated for each radiopharmaceutical preparation as different solvents and formulation solutions are used. This is a limit test and therefore parameters to be validated are specificity and limit of detection (LOD). The validation sequence consists of blank, LOD-solution, water and standard solution runs. The concentrations of solvents in the standard solution are added in the concentration maximum limit values. The run time is 20 minutes. After the method validation, radiopharmaceutical sample runs are made. The run sequence consists of two replicate runs from the standard solution, one water run and two replicate runs from the sample. **Results** In validation the resolution factor for all used solvents in the chromatogram were > 1.5 and the LOD calculated from the signal to noise ratio was more than 3:1. Limit of detection is the lowest concentration which can be distinguished from the baseline noise. In radiopharmaceutical samples the concentrations of solvents were under the concentration limit values. **Conclusion** The method is accurate and fast enough to be used in quality control for determination of residual solvents in radiopharmaceuticals with half-lives longer than ~1h. The method is also useful for process validation. For quality control of carbon-11 radiopharmaceuticals faster run times are needed. ¹⁾ Agilent Technologies, Inc., 2012, 5990-7625EN

TP108

Quality, stability and robustness of ⁶⁸Ga-HBED-CC-PSMA and ⁶⁸Ga-HA-DOTATATE preparations for nuclear medicine applications using an automated system

R. de Roos, F. F. T. Ververs, B. de Keizer, G. C. Krijger; University Medical Center, Utrecht, NETHERLANDS.

Aim: ⁶⁸Ga-HBED-CC-PSMA and ⁶⁸Ga-HA-DOTATATE have been developed as PET tracers to detect (metastases of) prostate and neuroendocrine carcinoma, respectively. The quality, stability and preparation method robustness of these radiopharmaceuticals were studied. **Materials and methods:** Gallium-68 (⁶⁸Ga³⁺) was eluted from a registered 1110 MBq ⁶⁸Ge/⁶⁸Ga generator and ⁶⁸Ga-radiopharmaceuticals were prepared with the automated Modular-Lab easy system and accompanying buffers and cassettes (Eckert & Ziegler, Germany). Radiochemical purity, radionuclidic purity, pH, sterility, endotoxins and yield were determined according to European Pharmacopoeia procedures. The stability in time was analyzed using both ITLC and HPLC. **Results:** A total of 162 preparations were analyzed within expiration date of the ⁶⁸Ge/⁶⁸Ga-generator (1 year). 4 preparations were rejected (technical failure), 2 failed the radiochemical requirements. 156 preparations were released for administration. The mean radiochemical purity of ⁶⁸Ga-HBED-CC-PSMA was 98.1% ±0.8 and 97.2% ±1.9 using ITLC and HPLC, respectively. For and ⁶⁸Ga-HA-DOTATATE the mean radiochemical purity was 96.1% ±2.3 and 98.1% ±1.9. All preparations met the required specifications for radionuclidic purity, pH, sterility, endotoxins and radionuclidic purity. Both ⁶⁸Ga-HBED-CC-PSMA and ⁶⁸Ga-HA-DOTATATE were sufficiently stable after preparation for 3 hours. **Conclusions:** The Modular-lab easy is a stable system for ⁶⁸Ga-HBED-CC-PSMA and ⁶⁸Ga-HA-DOTATATE preparations to be used in routine health care and clinical trials.

TP109**Financial Management of Nuclear Medicine Departments from their Service Managers' Perspective**

S. Soares, C. Quintal; Faculty of Economics-University of Coimbra, Coimbra, PORTUGAL.

Introduction: Many financial and political changes have been affecting the efficiency and organizational structure of the National Health System (NHS) England. In addition, departments have to cope with new technological demands that require investment. The goal of this study is to determine those factors, which service managers feel have the greatest impact on the financial stability of their departments. **Methods:** 14 out of 21 Nuclear Medicine department service managers, London-based and belonging to the NHS, were invited to participate in this study. Individual in-depth interviews were performed with 10 participants. The intention was to evaluate the reality experienced and felt by the service leaders in their midst and according to their perception. The interviews were semi-structured, using the face-to-face model, and analysed by theme. Confidentiality and anonymity was guaranteed. **Results:** A number of service managers did not have access to departmental budgets or participate in financial meetings. According to the majority of interviewees, changes in the NHS financial model do not affect the quality of the service provided to patients, the way of working or the number of patients. To achieve the Trust Cost Improvement Plan target, service managers are trying to reduce costs and improve the department performance. Common strategies include optimization of appointments, radiopharmaceuticals and equipment usage, as well as extending the working day. Staff organizational structure is also being affected: no overtime payment is allowed and pay bands have been changed. More patients mean more income (especially higher profit examinations: therapies and PET/CT). Increasing the number of low cost examinations and repatriation of work back to the department are all factors that contribute to increased productivity. **Conclusion:** For some service managers, it is difficult to meet the financial demands. Constant actions to increase income and decrease expenditure need to be taken. However, these actions need to be monitored to not interfere with the service quality provided to the patient. The vast majority of the interviewees did not know which financial model was in operation previously or the characteristics of the current one. To fulfil their responsibilities, service managers should take a greater role in the financial aspects of the department, such as: attending financial meetings, acknowledge of the budget status and having the opportunity to take more financial decisions.

TP110**Advanced Practice in Nuclear Medicine: The Changing Role of the Clinical Technologist and Current Practical Problems**

M. Casanova Martins¹, R. Bidder¹, P. Davies², S. Stace², P. Ali¹; ¹ABMU HB, Swansea, UNITED KINGDOM, ²Hywel Dda NHS Trust, Swansea, UNITED KINGDOM.

The needs of a nuclear medicine department warrant continuous professional progression and innovation from the clinical technologist, driven by long waiting lists, financial restrictions and lack of staff availability or even deficiency of highly specialized trained people like consultant medical staff. Advanced practice such as cardiac stress testing as part of myocardial perfusion scintigraphy (MPS), or even issuing reports for imaging studies, is therefore beginning to constitute common practice amongst technologists. Working under DAGs (Delegated Authorization Guidelines) to authorise nuclear medicine procedures or to refer patients for additional radiology is also within the scope of advanced practice and is common practice in many departments since IR(ME)R 2000. However, there is a legal requirement for this to be undertaken by registered healthcare professionals. In the UK, there is no statutory register for clinical technologists, which may prevent the full development of their advanced practice responsibilities. Radiographers, on the other hand, are working under the professional guidelines laid down by the HCPC (Health and Care

Professions Council) and perform within their technical competencies. Current registration and the various ionising radiation regulations already permit radiographers to undertake these tasks after appropriate training. The aim of this paper is to outline training needs and legal requirements to the safe and high quality delivery of highly specific tasks designated as advanced practice for clinical technologists. The training needs for cardiac stress testing as part of MPS include a thorough training plan which has already been established in 2007 by the BNMS. This training plan comprises, for example, "in house" performance of at least 100 tests using the existing stressing agents (exercise, vasodilators and inotropic tests). Ideally, however, advanced practice training and practice should be certified and accredited. Though, there aren't mechanisms in place for the formal assessment of the advanced practitioner in this field by BNMS/BNCS and/or EANM/ESC. An active involvement of EANM and the ESC would be highly desirable in order to promote standardized training/requirements across Europe. The reporting training for nuclear medicine technologists relies, in the UK, on accredited courses provided by few universities. Involvement of EANM and the ESNM would promote standardization of reporting across Europe, as well as providing robust credibility in achieving a desired professional standard. The legal requirements for advanced practice from clinical technologists are not yet fulfilled or available. Adopting a similar framework to HCPC or the incorporation of clinical technologists within the HCPC could be the solution.

Authors Index

- Aalbersberg, E. A. **OP293**, OP483
- Aarntzen, E. **PW07**
- Aaron, V. OP012
- Aarts, E. O. OP365
- Aasheim, L. B. OP254
- Abad, S. P089
- Abamor, E. **EP188**
- Abbas, A. EP787
- Abbas Abadi, S. EP619
- Abbasi, H. EP648
- Abbasi, M. P012
- Abd El Aziz, M. A. P023
- Abd-Elfadil, I. M. A. **P221**
- Abdelhafez, Y. G. EP359, **EP708**, **EP711**
- Abdel-Halim, R. M. TP007
- Abdelkader, H. P219
- Abdelrazek, S. EP385, **OP540**
- Abdelwahab, M. A. **EP240**, **P188**
- Abdollahi, H. OP498
- Abdul Jalil, N. P025
- Abdullah, A. EP794
- Abdulrasool, S. A. **TP074**
- Abdulrezzak, U. **EP675**
- Abe, A. **EP728**
- Abe, K. EPW60
- Abe, S. EP252, EP728, TP003, TP010, TP059
- Abella, A. **EP592**, **EP593**
- Abella, E. EP193
- Abella Tarazona, A. EP250
- Abgral, R. OP181, **OP193**
- Abhishek, K. EP688
- Abildgaard, N. EP559
- Able, S. EP443
- Aboagye, E. EP309, OP341
- Aboudzadeh Rovais, M. P283, **TP013**, **TP055**
- Abousekhrah, A. EP848
- Abraham, M. R. OP611
- Abraham, T. OP611
- Abrantes, A. M. **EP515**, EP599, OP673
- Abreu, C. **OP215**
- Abreu, P. EP511, EP520
- Abrunhosa, A. EP246
- Abu Gabal, M. P178
- Abuqbeith, M. EP808, **OP679**
- Aburano, T. EP027
- Abusamra, M. EP043, EP049
- Acampa, W. OP460, OP461, OP467, OP604, OP607
- Acar, E. **EP272**, **EP553**
- Acevedo Bañez, I. EP182, EP200
- Achmad, A. **EP316**
- Achten, E. P224
- Adachi, S. EP090, EP172
- Adámek, S. P100
- Adamson, K. EP456
- Adamzek, K. OP587
- Adebahr, S. OP596
- Adedapo, K. S. P160
- Adel, M. P071
- Adens, A. **OP603**
- Adler, M. TP094
- Adrada, B. OP496
- Adrià, M. EP496
- Afshar-Oromieh, A. **EP239**, EP557, **OP552**, OP556
- Agahi, A. **EP150**
- Agarwal, K. K. **EP189**
- Agarwal, R. OP427
- Ager, A. OP227
- Aghakhanyan, G. EP114, EP128
- Aghamohammadi-Sareshgi, R. EP036
- Agostini, D. OP558, **OP559**, P045, **P049**, **P258**
- Agostini, S. EP571
- Agrawal, A. EP025, EP273, OP123, OP124
- Agrogiannis, G. OP417
- Aguadé Bruix, S. EP638
- Agudo Martinez, A. EP198
- Aguiar, P. OP070, P263
- Aguiar, S. P189
- Aguiar, W. K. EP707, P088
- Aguilar Barrios, J. EP191, OP278
- Aguila-Ruiz, A. P233
- Aguilera-Grijalvo, C. OP374
- Ahlström, H. EP578, EP582, EP582, OP252
- Ahmad, R. OP426
- Ahmadzadehfar, H. EP136, EP498, EPW12, EPW14, OP109
- Ahmed, I. OP060
- Ahmed, N. P132
- Ahmed, S. OP089
- Ahmed, T. EP731, **EP755**
- Ahn, B.-C. EP356, OP537
- Ahn, H. EP606
- Ahn, K. P168
- Ai, F. OP638
- Aid, R. OP423
- Aigbirhio, F. I. OP062
- Aigner, R. M. EP140, OP128
- Airaksinen, A. J. OP234
- Airola, K. EP063
- Airola, M. EP507
- Aistleitner, M. EP857
- Ajdinovic, B. OP368
- Ajmi, S. EP331, EP370, P165
- Ajuria Illarramendi, O. **EP297**, OP572
- Akbarzadeh, A. EP761, OP218
- Akbulut, H. EP190
- Akdemir, Ü. Ö. **OP261**
- Akepati, N. R. **P218**
- Akgün, A. P207
- Akgün, E. EP298, OP223
- Akgun, H. EP675
- Akhlaghpour, S. EP425
- Akihito, O. TP069
- Akil, S. OP477, **P075**
- Akkas, B. E. EP093, EP096, EP099, **EP102**, **EP105**
- Akkaya, T. S. OP668
- Akovali, B. EP547, EPW42

Ak Sivriköz, I.	EP111	Alongi, P.	EP085, EP137 , EP197, EPW22 , OP221
Aksoy, T.	EP112	Alonso, J.	TP041
Aktan, A. H.	EPW69	Alonso, M.	OP255
Akyel, R.	EP244	Alonso, O.	EP014, OP458
Akyüz, C.	OP684	Alonso Farto, J.	EP736, P152, P268
Alagoz, E.	EP345, EP346, OP141	Alonso Rodriguez, M.	P093
Alaman-Sánchez, C.	EP386	Alonso Zazo, F.	EP647
Aland, P.	EP482	Al-Otaibi, B.	EP843, EP848
Alanne, E.	OP688	Allothman, M.	OP462
Alan Selcuk, N.	EP466, EP468 , OP014	Alp, R.	P163
Alavi, A.	EP037, EP047, EP559, OP273	Alqahtani, M. S.	EPW34, EPW35
Albadalejo-Castaño, M.	EP655, TP096	Al Qami, A.	P220
Álban, F.	P150	Alqarni, A.	EP154
Albano, D.	EP175, OP539 , OP682	Alramlawy, S.	P071 , P078
Alberini, J.-L.	EP040, EP050, EPW01, OP516	Alratroot, S.	EP006
Albersen, M.	OP554	Al-saden, N.	EP583
Albert, N.	OP032, OP317, OP650	Alsalem, M.	TP035
Alberti, V.	OP693	Al Sayed, Y.	EP712, P055
Albertsen, S.	OP350	Al Shaikh, S.	EP154
Albert-Weißberger, C.	PW32	Alshammeri, I.	EP461, OP090
Al Boucharali, J.	P030	Al-Shoukr, F.	EPW95
Albuquerque, A.	EPW41, P150	Alstrup, A. K. O.	EP685
Alcaraz Baños, M.	EP303, EP471	Altai, M.	EPW81 , OP172, OP591
Alcolea, D.	PW35	Altini, C.	EP135, EP142, EP213, EP236, P176, PW23
Aldeguer Mante, X.	TP084		
Al-Dhafiri, A.	EP006	Altrinetti, V.	EP340
Aldousari, H.	EP461, EP817	Altun Yologlu, N.	P172
Aldridge, M.	EP742, EPW45	Al-Tuwaijri, A.	EP006
Alejo, L.	EP413	Álvarez Alonso, A.	EP243 , P043
Aleksyniene, R.	OP350, OP358	Álvarez Blanco, A.	EP243, P043
Alenezi, S.	EP461	Alves, F.	OP447
Alessio, A.	EP786	Alves, V.	EP002, EP285, OP044, P222
Alexanderson, E.	OP610	Al-Yanbawi, S.	EP843
Alexiou, G.	EP024	Amaddeo, G.	OP030
Alexiou, S.	P022	Amaral, H.	EP543
Alexopoulos, D.	P022	Amarencu, P.	OP418, OP419
Algarrarondo, V.	OP192	Amato, E.	EP538, EP813
Al-Garashi, M.	EP712	Amber, P.	EP048
Alhammad, M.	OP462	Ambresin, G.	P298
Ali, L.	EP712	Ambrosini, V.	EP153, OP035, P146
Ali, P.	TP110	Amelian-Filonowicz, A.	EP577
Aliberti, G.	EP458, OP011, P186	Amelio, D.	EP571
Alimanovic-Alagic, R.	P169, P169	Amer, H. A.	OP462
Alirezapour, B.	EP619 , EP621 , EP626	Ameri, P.	OP421, PW22
Aljammaz, I.	EP843 , EP848	Ametamey, S. M.	OP398
Al Kandari, F.	EP183	Amhaoul, H.	P286
Allard, M.	P252	Amichetti, M.	EP571
Allavena, P.	EPW25	Amijima, H.	EP744
Allen, S.	EP456, EP491, OP479, TP083	Amimour, A.	EP348, P059, P064
Allenbach, G.	P265, P298	Amini, M.	EP529, EP530
Allende-Riera, A.	EP016, EP185, EP394	Amini, N.	OP303, OP316
Alloisio, A.	OP127	Amiras, D.	OP569
Alloisio, M.	EP306, EPW25	Amit, M.	OP363
Allott, L.	EP607 , EPW65, EPW80	Amor, S.	EP291
Allwood-Spires, S.	EP564	Amor-Coarasa, A.	EP829 , EPW94, OP021, OP024, OP025, OP401
Almairac, F.	OP203	Amorim, B. J.	EP060
Al-Mamgani, A.	EP478	Amorim, I.	OP126
Almarcha-Gimeno, A.	P126	Amorin, I.	OP428
Al-Mashat, M.	P035 , P037	Amo Salas, M.	EP222, EP689
Almeida, A.	OP211	Amoui, M.	EP425 , EP818
Almeida, R. G.	EP060	Amouri, W.	EP381 , P195
Al-Momani, E.	PW32	Amparo Cobo Rodríguez,	P103
Almquist, H.	OP281, TP031	Amrani, T.	EP532
Al-Muslem, R.	EP006	Amr-Rey, A.	EP386, P068, P126
Alnafisi, N.	EP461	Amthauer, H.	EP481
Al-Nahhas, A.	OP341		

An, G. I.	EP606, EP646	Ardila Manjares, J.	P152, P268
An, Y.-S.	EP141, EP143	Ardisson, V.	EP601
Anagnostopoulos, C. D.	OP417 , OP420	Ardizzoni, A.	EP153
Andersen, F. L.	EP570, EP573, OP248	Arellano-Tolivar, A.	EP230
Andersen, J. B.	OP197	Arena, G.	OP604
Andersen, K. F.	EP573	Arens, A.	EP697
Andersen, T.	EP833	Arens, A. I. J.	EP115, EP751, OP683
Anderson, R. L.	OP521	Ares, J.	EP193
Andersson, C.	TP086	Argibay Vázquez, S.	EP069, EP286
Andersson, K.	EP522, EPW83, OP114	Arguelles Pérez David Antonio,	EP362
Andia-Navarro, E.	EP160	Arheden, H.	P035, P037, P069, P075
Ando, A.	EP027	Arias, T.	OP229
Andre, C.	P088	Arighi, A.	P253
Andre, M.	OP406	Ariza Cabrera, E.	TP104
Andreae, F.	EP623	Arkies, H.	EP422, OP493, OP534, PW25
Andreeff, M.	OP678	Arlandini, A.	OP535
Andreev, S.	P031, P046	Armstrong, I. S.	EP735, OP497 , P057
Andresen, T. L.	EP836	Armstrong, L.	P143
Andressoo, J.-O.	P294	Armaiz-Fernandez, M.	EP160
Andronache, A.	PW38	Arnaldi, D.	P255
Andrzejewski, P.	OP253	Arndt, C.	EP525
Angelides, S.	EP152	Aronen, H. J.	OP354
Angelidis, G.	P113	Arpa, M.	EPW69
Angusti, T.	EP507	Arponen, E.	EP840
Angyal, J.	EP596	Arslan, E.	EPW28
Aniceto, D.	EP456, OP479 , TP083	Arslan, N.	EP345, EP346, EP700,
Anizan, N.	OP170, OP423		OP141, OP573
Anner, P.	EP134, EP163	Arsoos, G.	EP332, P120
Annunziata, G.	EP216, P073	Artigas, C.	OP456
Annunziata, S.	EP174 , OP226, OP693	Artiko, V.	EP361, OP040, OP042, P205
Ansari, M.	EP818	Artner, C.	EP857
Ansari Ramandi, H.	EP621, EP626	Artom, N.	OP421
Ansheles, A.	P084	Arumugam, P.	OP497, P057
Ansquer, C.	OP407	Arun, B.	OP182
Antczak, S.	EP758	Arveshoug, A.	TP014
Antelmi, L.	P250	Arya, A.	EP368
Antic, V.	OP040, P205	Arzberger, T.	OP059
Antoni, G.	EP582, OP065, OP190, OP232, OP517	Asa, S.	EP504, EPW69, EPW71
Antoni Vives, J.	EP113	Asad, A. H.	EP611
Antunovic, L.	EP157, OP243	Asaka, T.	OP177
Antwi, K.	OP083	Asakura, K.	TP069
Aparicio, T.	EP080	Ascencio, F.	EP287
Apicella, F.	OP033	Aschacher, B.	EP278, OP555
Aplin, M.	OP333	Aschawa, H.	EP125, P173
Apostolidis, C.	OP148, OP454, OP520	Asensio Sanchez, R.	EP471
Apostolopoulos, D.	P022, P210	Ashtari, P.	EP626
Apostolova, I.	P249	Ashumkhin, A.	EP083
Appel, L.	OP252	Ashworth, S.	EP828
Arad, M.	OP191	Aslani, A.	EP500
Aradas Cabado, B.	EP069	Aslani, G.	EP619, EP626
Arai, A.	P013	Aslanidis, I.	EP549, P032
Arai, Y.	EP013	Asmussen, J. T.	EP559
Araj Khodaei, J.	P230	Assadi, M.	EP660, EPW33
Araj Khodaei, M.	P230	Assante, R.	OP460, OP467, OP604 , OP607
Arakawa, R.	OP303, OP316	Asselin, M.-C.	EP309
Araki, N.	P282	Asti, M.	EPW46, EPW92
Arapović, A.	P174	Astrelina, T. A.	EP625
Aras, M.	EP548	Atalar, B.	EP112
Araz, M.	P098, P112	Atasever, T.	EP188
Arbizu, J.	OP016, OP377	Atay Kapucu, L. Ö.	OP261
Arican, P.	P107	Athanasiadis, E.	OP417
Arican, Z.	EP553	Athanasious, V.	EP332, PW10
Archibald, S. J.	EPW90 , OP488	Atia, E.	P214
Archier, A.	P115	Atilgan, H. I.	EP426, EP446 , P204, P209
Ardenfors, O.	OP166	Attarwala, A.	EP658, EP783, EP784 , OP392
Ardies, P.	P149	Audenaert, K.	P224, PW40

Auditore, L.	EP538, EP813	Balaguer, D.	EP511, EP520
Autret, D.	EP796	Balaguer, J.	EP496
Auvity, S.	OP315, OP618	Balber, T.	EP636
Avani, J.	EP688, P129	Balbi, T.	EP288
Avramovic, N.	OP695, PW30	Balci, T. A.	EP338
Awais, R. O.	OP062	Baldari, G.	EP219, EP400, EP618, P234, P284
Axelsson, J.	EP827	Baldari, S.	EP538, EPW22, OP536
Ay, M.	EP398, EP421, EP660, EP693, EP734, EP769, EP754, EP759, EP760, EP761, EP763, EP765, EP768, EP804, EPW31, EPW33, OP218, OP301, OP302, OP359, OP498, P014	Baldoncini, A.	EP819
Ay, S. A.	EP354	Balduzzi, M.	EP521
Ayan, A. K.	EP695	Balkan, E.	OP573
Ayan, A.	EP345, EP346, EP700, OP573	Balkanay, O.	EP194
Aydin, A.	P204, P209	Ballardini, B.	EPW06
Aydin, F.	EP103, EP210	Balma, M.	P242
Aydin, B.	OP684	Balogova, S.	EP062, EP263
Aydos, U.	OP261	Baloka, L.	P040
Aygün, A.	EP244, EP245, EP614, EP858, EPW44	Balouzet, C.	EP302
Ayyildiz, O.	EP729	Balsa Bretón, M.	EP310
Azad, G.	OP602	Balsa Bretón, M.	P034
Azal, O.	EP346	Baltzer, P.	EP233, OP500, OP551
Azevedo, J. D.	EP707	Balzano, R. A.	P181
Azoulay, D.	OP030	Banani, A.	EP740
Baas, F.	OP283	Banchero, A.	EP014
Baassiri, A.	EP043	Bandholtz, S.	OP487
Baavour, R.	OP558, OP559, P049	Bandini, M.	EP124
Babich, J. W.	EP829, EPW94, OP021, OP024, OP025, OP401, OP424, OP556	Bandong, I.	EP077, EP353, EP542
Bacca, A.	EP560	Bang, J.-I.	TP058
Bacek, D.	EP810	Bangma, C. H.	OP107
Bachawal, S. V.	OP503	Baniora, E.	P022
Bache, S.	OP496	Bankstahl, J. P.	EP639, OP313, OP319
Bacher, K.	EP489	Bannas, P.	EP831
Bachmann, M.	EP525	Banzo, I.	EP021, OP195, OP431
Badel, J. N.	EP777	Barai, S.	EPW76, P223
Badel, J. N.	OP298	Baranski, A.-C.	OP022
Badiavas, K.	EP332	Baratto, L.	EP095, EPW09, OP082
Badr, I.	TP088	Barbalic, M.	P201
Badulescu, C.	OP220	Barbancho, A.	EP656, EP657
Baeken, C.	P224	Barbato, D.	OP340, OP547
Baeta, E.	P125	Barbato, F.	EP269
Baeta, I.	TP041	Barbés, B.	EP470
Baete, K.	OP677	Barbier, V.	OP353
Bagatin, E.	EP571	Barbos, O.	OP220
Bagci, U.	P171	Barbosa, F.	EP267
Bagni, O.	EP469	Barboza, M. F.	OP274, TP044
Baguña Torres, J.	OP400	Barbus, E.	EP341, EP375, EP376, OP220
Bai, P.	EP596, EP597	Barceló, G.	EP613
Bai, Z.	EPW79, TP054	Bardiès, M.	OP513
Baierova, L.	P161	Barelli, P.	OP024
Baik, S.-R.	P168	Bargalló, N.	OP200
Bailey, D.	EP500	Barić, A.	P174, P201
Bailly, C.	EP011, EP012, OP407, OP681	Barlete, A.	EP497
Baio, S.	EP546, EPW06, OP332, OP680	Barna, S.	EP771, P191
Bajc, M.	P192, P198	Barnardt, P.	OP037
Bajén, M.	EP290, EP294, PW09	Barnhart, T. E.	OP308, OP402, OP638
Bak, M.	OP395	Baroni, R. H.	OP274
Bakhshayeshkaram, M.	EP693, EP754, EP759, EP760, EP804, OP498	Barquero, R.	EP382, EP454
Bakker, E.	P237	Barrack, F.	EP374, OP138
Bakker, I. L.	OP107, OP351, OP547	Barré, E.	EP302
Bakrin, N.	OP601	Barrenechea, A.	EP077, EP542
Bakshi, G.	EP273	Barrera Gonzalez, M.	TP104
Bal, C.	EP044, EP189, OP597, OP651	Barret, O.	OP063
		Barrington, S. F.	EP171, EP299, OP686
		Barrios Treviño, B.	OP518
		Barroca, D.	EP246
		Barsegian, V.	EP506
		Bar-Shalev, A.	OP191
		Barsotti, S.	P117

Barta, P.		EP531	Beindorff, N.	EP643, EP663 , OP487
Bartel, C.		EP481	Bejarano García, A.	TP040
Bartenstein, P.	EP484, EPW15, OP088, OP032, OP111, OP314, OP317, OP378, OP425, OP650		Bejinariu, N.	OP220
Barthel, H.		OP378 , P245	Bejot, R.	EP448, OP289
Bartley, S.		P057	Bekiş, R.	EP272
Bartoli, M.		EP822	Bektic, J.	EP479
Bartolozzi, C.		OP167	Belcari, N.	EP743, EP773 , EP776
Bartschat, T.		EP275	Belchior, A.	EP536
Barwick, T.	OP260, OP341, OP652, P251, TP103		Belda-Sanchis, J.	OP600
Başal, Y.		EP119	Belevich, Y.	EP075
Baselli, G.		OP495	Belissant, O.	EP263
Bashank, N.		EP708, EP711	Bélissant Benesty, O.	OP292
Basher, R. K.		EP023	Bellafore, S.	OP598
Bashir, H.	EP001, EP336, OP086, P099		Bellevre, D.	OP091, OP603, P228, P274
Bashir, U.		EP581, OP602	Belli, G.	EP819, EP822
Basilico, P.		P253	Bello, I.	EPW07
Baskin, A. A.		EP426	Bello, L.	OP655
Bass, T.		EPW82	Bello, P.	EP462, EP496
Bassa, P.		P128	Bello Arques, P.	EP512
Bassi, F.		EPW06	Bellodi, A.	PW22
Bassiri, A.		EP049	Bellón Guardia, M.	OP369
Bastholt, L.		EP201	Beltrán Gracia, C.	EP638, EP651
Batalov, R.		EP701, P086	Benabdallah, N.	EP428, EP451, EP505
Báth, M.		OP132	Benali, K.	OP194, OP696
Bauckneht, M.	OP288, OP373, OP408, OP409, OP421, P255 , PW22		Benard, F.	EP527, EP591, OP020
Bauder-Wüst, U.		EPW84, OP022	Ben Azzouna, R.	EPW95 , OP192, OP560, OP605
Baudin, G.		P115	Ben Bouallégue, F.	OP507
Bauer, M.		P232	Bendaoud, H.	EP125, P173
Bauer, W. R.		OP189	Bendele, A.	EP424, EP436
Baum, E.		OP312	Benešová, M.	OP022, OP023
Baum, R. P.	EP453, EP480, EPW16, OP112, OP113, OP150, OP394, OP459		Benetos, A.	OP201
Bauman, A.		OP149	Benetos, G.	OP417, OP420
Baun, C.	EP047, EP397, EP585, EP833, OP273 , TP093 , TP097		Ben Fredj, M.	EP331, EP370, P165
Bauriaud, M.		EP389, EP419, OP494	Bengel, F.	OP202, OP313, OP319
Bautista, J.		EP496	Ben Ghachem, T.	EP358, P157
Bayarri-Lara, C.		EPW24	Ben-Haim, S.	EP774, OP191 , OP362
Bayrak, S.		EPW28	Benisvy, D.	EP447, OP203, OP429
Bazarjani, S.		EP710	Benitez, A. M.	EP294
Beatovic, S.		OP040 , OP042 , P205	Benítez Cantero, J.	P118
Beaujot, J.		EP349	Benítez Morera, A.	TP104
Beaumont, T.		OP165	Benítez Segura, A.	EP290, PW09
Beaurain, M.		OP255	Benjamin, C.	EP726
Bebbington, N. A.		EP749 , EP767 , OP361	Benoit, D.	OP197
Becher-Boveleth, N.		OP219	Benouhoud, J.	EP015 , EP125, P173
Bechmann, N.		EP844	Ben Sellem, D.	EP039 , EP705 , P157 , P190 , P215
Beck, E. M.		OP061, OP310	Ben-Shlomo, A.	EP678
Beck, M.		EP275 , OP018	Ben Slimene, M.	EP039, EP358, EP393, EP705, P157, P166, P190, P215
Beck, R.		OP314, OP317	Bentancourt, C.	EP014
Becker, G.-A.		OP617	Benti, D.	P182
Bedmutha, A. S.		OP245	Benti, R.	EP395, OP214, OP495, P253, PW38
Bednarczyk, M.		EP528	Bera, G.	EP124 , OP183, P246, P254
Beels, L.		EP716, EP779	Berzi, C.	EP253
Beer, A. J.		OP110	Berding, G.	OP202 , OP313, OP319
Beesley, S.		EP513, EPW18	Berends, F. J.	EP803, OP365
Begley, P.		OP333, OP480	Berendse, H. W.	P277
Begum, N. J.		EP499	Bergamini, A.	EP101
Behe, M.		EPW85, OP367	Bergmann, R.	EP525
Beheshti, M.	EP278 , OP348 , OP553, OP555 , P056		Bergström, K.	EP850, P294
Behlioulis, A.		P028	Beriollo Riedinger, A.	OP681
Behra, A.		P097	Berizzi, F.	EP156
Beiderwellen, K.		EP696, EPW74	Berjawi, G.	EP043, EP049
Beiki, D.	EP081, EP209, EP529 , EP530 , EP539, P012		Berk, S.	EP162, EP194
Beilin, L.		OP362	Berker, D.	P107
			Berkowitz, Y.	OP569
			Berliner, C.	EP831

Berlaco, B.	P280	Binzel, K.	EP130, EP307, EP320, EP669, EP737, EP753 , EPW32, OP017, OP184, OP295, OP521, OP567 , P148, P225
Bermúdez-Morales, M.	EPW37	Bird, N.	OP137
Bernal, M.	OP584	Birkenfeld, B.	EP431, OP225
Bernardini, M.	EP428, EP451, EP505	Bisi, G.	P176
Bernardo, M.	P180	Bissoli, S.	EP206
Bernà Roqueta, L.	EP113	Biswas, G.	EP712, P055
Berndt, M.	EP020, OP348	Bitarafan, A.	EP760, OP498
Bernhard, C.	EP664, OP588	Biurrun Manresa, J. A.	OP350
Bernhardt, P.	EPW48, OP132, OP391, OP522	Bizzi, A.	OP655
Bernini, G.	EP560	Bjarnsholt, T.	PW02
Bernsen, M.	EP417, EP782, OP671	Bjelic-Radisic, V.	OP128
Berriolo-Riedinger, A.	OP246, OP406	Blagic, M.	OP040, P205
Berroterán-Infante, N.	EP623 , EP636, OP286	Blakkisrud, J.	EP492
Bertagna, F.	EP175, OP535, OP539, OP682	Blanco-Cano, J.	EPW07
Bertaux, M.	EP176 , OP183	Blasbalg, R.	EP205
Bertelsen, H.	EP257, OP358	Bleeker-Rovers, C.	PW07
Berthelsen, A. K.	EP054	Blesa, R.	OP379, PW35
Berthold, F.	OP084	Bloch, J.	P265
Bertoia, C.	EP124	Blockx, I.	EPW58
Bertoli, M.	EP175, OP535, OP682	Blot-Chabaud, M.	OP344
Bertolus, C.	EP124, OP183	Blower, P.	EP598, OP163, OP400
Bertrand, A.	P246	Blüher, M.	OP617
Berwouts, D.	EP087	Blümel, C.	EPW50, OP290
Beslic, N.	EP192	Bluth, T.	OP694
Besombes, J.	OP255	Boban, M.	P201
Bessias, N.	OP417	Bobin, C.	EP449
Bessolova, O.	EP367	Boccardo, F.	P042
Besson, A.	P170	Bochev, P.	EP196
Besson, F. L.	OP144	Bockerija, L.	P032
Betti, F.	EP560	Bockisch, A.	EP242, EP506, EP579, EP696, EPW74, OP219, OP222, OP641
Betts, H. M.	OP062	Bockisch, B.	EP775
Bex, A.	EP226	Bode, A.	OP455
Beyer, T.	EP036, EP718, EP727, EP752, OP241, OP247, OP249, OP500, OP648, P232	Bodet Milin, C.	EP011, EP012, OP407, OP681
Beyersdorff, D.	EP831	Bodin-Hullin, A.	EP624
Beygi, D.	EP818	Boehm, A.	OP179
Beygui, F.	OP558, OP559, P049	Boellaard, R.	EP309, EP791, OP066, OP296, OP599, P233, P237
Beykan, S.	EP440, EP448 , OP289	Boer, J. J.	OP606 , TP025
Bhadada, S.	P097	Boerman, O. C.	EP115, EP587, OP119, OP173, OP175, OP306 , OP343, OP489, OP640, OP641
Bhalla, A. S.	OP597	Boersma, H. H.	OP610
Bharadwaj, T.	EP482	Boga, F.	P081
Bhasin, D.	EP146	Bogdan, A. A.	P287
Bhatia, P.	EP130, EP737 , OP184	Bögemann, M.	OP455
Bhatt, A. D.	OP184	Boisgard, R.	OP318
Bhattacharya, A.	EP120, EP229, EP235, EP271, EPW29, OP125	Bokharaci, M.	EP472
Bhattarai, A.	EP316	Boladeras-Inglada, A. M.	EP230
Bhoil, A.	EP161 , EPW68	Bolch, W. E.	EP505
Bhoori, S.	OP011	Bolorinovin, F.	EP619, EP626
Bianchi, C.	EP617, OP478	Bom, H.-S.	EP312
Bianchi, L.	EP265	Bomalaski, J. S.	EP299
Bianchi, M.	P176	Bomanji, J.	EPW45, OP191
Bianco, G.	EP236	Bonaffini, P. A.	EPW09
Biasco, E.	EP128	Bonazzi, A.	EP101
Bidder, R.	PW29, TP110	Bondar, V.	P167
Biček, A.	P200	Bondiau, P.-Y.	OP203
Biernacka, K.	P085	Bonfiglioli, R.	EPW72
Biersack, H. J.	P164	Bongarzone, S.	OP397, OP399
Bieth, M.	EP266	Bongioanni, F.	OP262, P255
Bifulco, M.	EP517	Bongulwar, C.	EP025
Bihin, B.	EPW08	Boni, G.	EPW20
Bilbao, J.	OP016	Boni, R.	EP114, EPW66, P133
Bilewicz, A.	EP528, OP445 , OP672 , OP675	Böning, G.	EP484, EPW15, OP111, OP650
Bilir, C.	EP540	Bonnaud-Antignac, A.	EP380
Billard, T.	OP058, OP063	Bonora, M.	EP121
Bin Amer, S.	EP848		

Bonte, S.	PW40	Brabander, T.	EP220
Booij, J.	OP427 , P277	Bracard, S.	OP201
Bora, A.	OP583	Bracic, I.	P202
Boraska Perica, V.	P201	Bradley, K. M.	EP738, EP739, EP741
Borbély, J.	EP838	Bragina, O.	EP075, EP097, EP632, EP634
Borcek, P.	P204, P209	Brahmi, F.	EP348
Bordbar, M.	EP730	Bračić, I.	EP713
Bordenave, L.	P061	Brambati, N.	OP478
Borg, M.	OP429	Brambilla, M.	EP086
Borges-Neto, S.	OP465	Brams, D.	EP122
Borgqvist, R.	P037	Branco, M. N.	OP676
Borgwardt, L.	PW02	Brandão, F. N.	EP554
Bormans, G.	OP426, OP615	Brandt-Larsen, M.	EP054
Bornemann, R.	P164	Branger, P.	P228, P258
Bornwasser, N.	EP640	Braune, A.	OP694
Borowiecki, A.	OP225	Brazzarola, P.	EP390
Borrego Dorado, I.	EP182, EP200	Brcic, L.	P201
Borrelli, G.	EP517	Breeuwsma, A. J.	OP349
Borrelli, P.	EP512	Brefel-Courbon, C.	P285
Borsatti, E.	EPW20	Bremmer, F.	OP492
Borsò, E.	OP145	Brendel, M.	OP317 , OP425
Bortliceck, Z.	EP679	Brenner, P.	OP550
Bortolus, R.	EPW20	Brenner, W.	EP481, EP643, EP663, OP487
Borys, D.	EP721	Brianzoni, E.	OP167
Bos, D.	OP364, OP640	Brice, P.	OP406
Boschetti, F.	OP588	Brige, P.	OP344, P115
Boschi, S.	OP077	Briley, K.	EP669
Bosco, P.	P250	Brillouet, S.	EP419, EP807, OP494
Bosio, G.	EP175, OP682	Brink, A.	OP041
Boss, M.	EP697 , OP365, OP367	Brinkert, M.	OP463
Bossert, I.	EP264, EP265, EPW75,	Brisa Vazquez, R.	EP191, OP278
	OP335, OP535	Brito, A. E.	EP056 , EP060 , P189
Botelho, M. F.	EP515, EP599, OP673	Brito, R.	OP126
Botelho Cruz, M.	OP479, TP083	Brocchi, S.	EP288, P146
Botta, F.	EP460	Broccoli, A.	EPW72
Böttcher, Y.	OP617	Brock, B.	OP372, P296
Bottoni, E.	EP306	Brockhuis, B.	EP165
Bottoni, G.	EP340, EP662, OP288, OP535	Brodney, M. A.	OP061, OP303, OP316
Bouabdallah, R.	OP406	Broggio, D.	OP165
Boubaker, A.	OP085	Broinger, G.	OP348, OP555
Bouchelouche, K.	TP034, TP098	Brom, M.	EP430, EP587, OP173, OP175, OP364, OP365, OP367
Boudousq, V.	EP494, OP545	Brönner, A.	EP663
Boudriga, H.	EP331, EP370, P165	Bronzel, M.	EP432
Boughdad, S.	EP040 , EP050 , EPW01 , OP516	Brothwood, T.	EP456
Boulleret, V.	OP318	Broulík, P.	P100
Boulahdour, H.	OP356, OP508, OP509, OP510, P106	Brown, D. B.	EP136
Bourdier, T.	EP825, EPW78	Brown, N. J.	EPW90
Bourg, V.	OP203	Bruchertseifer, F.	EP494, OP148, OP309, OP454, OP520, OP590
Bourgeois, S.	OP426	Brucker, S.	OP130
Bourhis, D.	OP181	Brulon, V.	OP081, OP251
Bouter, C.	OP492	Brumberg, J.	OP290
Bouterfa, H.	OP149, OP289	Bruna-Escuer, J.	EP018
Boutley, H.	OP563	Brunegraf, A.	EP484, OP111
Boutoleau-Bretonnière, C.	P247	Brunetto, S. Q.	EP056, EP060
Bouvard, G.	P258	Bruni, A.	EP088, EP089, EP258
Bouyoucef, S. E.	EP215 , EP348 , P059 , P064 , P175 , P214	Brunner, T.	OP596
Bowles-Antelo, H.	EP386, P068, P126	Bruno, A.	EP819, OP478
Box, C.	EP703	Bruno, G. L.	EP248 , EP248
Boya, P.	EP294	Bruno, S.	EP169, OP409
Boya-Román, M.	EP290, PW09	Brunocilla, E.	EP265, EPW75
Boz, A.	EP210, EP212	Brunotte, F.	EP664, EP666, EP812, OP246, OP250,
Bozkurt, S.	EP210		OP287, OP300, OP353, OP588
Bozzali, M.	P264	Bruzzozone, M.	PW38
Bozzano, A.	EP662, OP233, OP288	Bryanton, M.	EP792
Bozzao, A.	OP654	Bryanzeva, Z.	OP481
Braat, M. N. G. J.	EP136	Buades Former, J.	EP441

Buccheri, V.	P189	Caballero, D.	EP170
Bucerius, J.	OP422	Caballero, E.	EP511, EP520
Buchert, R.	P249	Caballero Gullón, L.	EP182, EP200
Buchholz, H.	EP009	Cabello, D.	EP016, EP185, EP394
Buchmuller, B.	EPW84	Cabeza Rodriguez, M.	EP231
Buchpiguel, C.	EP205	Cabrejo, L.	OP418, OP419
Buck, A. K.	EPW50, OP290, PW32	Cabria, M.	EP340, OP535
Buckle, T.	EP665, OP639	Cabuk, M.	EP548
Buckley, C. J.	OP376	Cacace, F.	EP186
Buda, A.	EP095, EPW09	Cai, H.	OP174
Budak, E. S.	EP212	Cai, L.	EP145, OP117
Budäus, L.	EP831	Cai, M.	EP586
Budde, R. P. J.	OP146, P131	Cai, W.	OP308, OP402, OP592, OP638
Budek, A.	P095	Caillé, F.	OP315, OP618
Budlewski, T.	EP528	Cakal, E.	P098, P112
Budzynska, A.	EP757, EP781	Cakmakçılar, A.	EP383
Buffat, C.	P115	Cakir, A.	EP188
Buffaz, P.-D.	P027	Cakir, T.	EP188
Buffoni, F.	EP388, EP395	Calabrese, L.	EP041
Bugby, S. L.	EPW34, EPW35	Calabria, F.	EP238, EP262 , EP269, EP567
Bui, F.	EP789	Calais, J.	OP181, OP696
Buijs, J.	EP522	Calamia, I.	OP233
Buitinga, M.	EP697, EP806, OP364 , OP365, OP367	Cala-Zuluaga, E.	EP178
Bükey, Y.	EP392	Calcagni, M.	EP308, EP311, EP317, EP322
Bükki, T.	EP771	Caldarella, C.	OP226
Bullich, S.	OP378, P245, PW36	Caldeira Ideias, P.	OP165
Bulten, B. F.	EPW66	Cal-Gonzalez, J.	EP411, EP718 , EP727, P232
Buncová, M.	P033	Calhau, P.	P180
Bundschuh, R.	OP109, OP189	Caligiuri, G.	OP170
Buñesch, L.	EP100	Caliskan, B.	OP043 , P021
Buongiorno, P.	OP467, OP607	Calovi Motschenbacher, L.	P074
Buraczewska, K.	EP757	Calviño Martínez, A.	EP647
Burak, Z.	EP378	Calvo Morón, C.	EP198
Burbaud, P.	P238	Calzetti, S.	P284
Burchert, W.	EP690	Camacho, A.	EP637, OP250, OP300
Burchielli, S.	EP743, EP773	Camacho, V.	EP155, OP379 , PW35
Burei, M.	EP247, P176	Camarda, M.	OP167
Buresta, T.	P275	Camarlinghi, N.	EP743 , EP773
Burger, J. W. A.	OP342	Cambien, B.	EP447
Burgers, A. M.	P154	Cambier, J.-P.	OP080
Burggraaff, C. N.	OP683	Cambil Molina, T.	EP198
Burke, B. P.	OP488	Camelière, L.	EP787
Burkert, D.	EP837	Camoni, L.	PW24, TP056, TP067
Burley, T. A.	EPW65	Camp, S.	OP652
Buron, F.	EP826	Campana, D.	OP035
Buschiazzo, A.	EP662, OP233 , OP262, OP288, OP373	Campayo, J.	EP496
Bushnell, D.	OP394	Campdelacreu-Fumado, J.	OP374
Bussink, J.	OP079	Campenni', A.	OP536
Busstra, M. B.	OP107, OP351	Campi, C.	EP017, EP169, EP429, OP135, OP262, OP421
Büther, F.	TP024	Campini, R.	P079
Butini, R.	EP206	Campion, L.	EP011, EP012, EP078
Butt, S. T.	EP327, P017 , P132	Campos, L.	TP100
Buttigliero, C.	EP507	Campos Bonel, A.	EP231
Buvat, I.	EP040, EP050, EP080, EPW01, EPW49, OP081, OP251, OP315, OP318, OP516, OP618	Campos Neto, G. C.	OP274
	EP479, OP294, OP457	Campos Villarino, L.	EP337, EP342, EP344, P162
Buxbaum, S.	EPW49	Canbaz, F.	P081
Buyssens, P.	P095	Canepa, M.	OP421
Buziak-Bereza, M.	OP428	Cañete, A.	EP496
Buzó, R.	OP061	Cannatà, V.	EP371
Buzon, L. M.	OP061	Cano Luna, M.	EP532
Byrd, D.	EP786	Cantoni, V.	OP460 , OP461
Byun, B.	EP326, EP569	Can Trábulus, F. D.	EPW28
Byun, S.	EP148	Canudo, A.	TP072, TP043
Caan, G.	OP211	Canzi, C.	EP388, EP395
		Caobelli, F.	OP221, OP463

Capaccioli, L.	EP822	Casasnovas, R.-O.	OP406
Çapa Kaya, G.	EP553	Casati, R.	OP495
Capdevila, E.	EP287	Cascella, T.	EP458
Capellades, J.	EP022	Cascianelli, S.	P273, P275
Capelo, C.	EP608	Cascini, G. L.	EP262, EP269
Capitanio, S.	P135, P144, PW01	Caselles, O.	EP419, EP785, EP807 , OP165, OP494
Çapkun, V.	P174	Casquero, F.	EP255
Caplin, M.	OP394	Cassalia, I.	P176
Capogni, M.	EP469	Cassano, B.	EP510, EPW19, OP336
Caponnetto, C.	OP262	Cassinello-Fernández, N.	P126
Capote Huelva, F.	EP182	Cassou-Mounat, T.	OP292
Cappelli, A.	EP288	Casta, N.	OP291
Capponi, P. C.	EPW92	Castaldi, P.	P138
Carabellese, B.	EP259	Castanheira, J.	TP043
Carabelli, E.	P243	Castel, V.	EP496
Caramelo, F.	EP515	Castellà, E.	EP065
Carapella, C.	OP653	Castellani, M.	EP388, EP395, OP085, P185, P186
Carbonatto, P.	EP464, OP013	Castell Conesa, J.	EP638, EP651, EPW07
Carbone, G.	EP571	Castellón Sanchez, M.	EP250, EP441, EP471, EP682
Carcoforo, P.	EP070	Castellucci, P.	EP121, EP223, EP264, OP035, OP077, OP335
Cardenas, A.	EP382, EP454	Castelo Branco, M.	EP246
Cardenas-Negro, C.	EP016, EP185, EP394	Castiglioni, I.	EP157, OP243
Cardinale, J.	EP268, EP270, EP837, OP022	Castillejos Rodríguez, L.	EP310, P034
Cardona, J.	EP315, EP463	Castillo Berrio, C.	EP337, EP342, EP344, P162, TP100
Cardona-Arboniés, J.	EP692	Castino, G.	EPW25
Caresia Aróztegui, A.	EP113	Castrillón, M.	EP337, EP342, EP344 , P162, TP100
Carideo, L.	OP654	Castro, P.	EP413, EP797
Caris, C.	EP261	Castro, R.	OP126
Carla, C.	P284	Castro, V.	EP684
Carles, M.	EP418 , EP462	Castro Beiras, J.	EP297, OP572, P016
Carlier, T.	EP011, EP012, EPW49, OP407, OP681, P247	Castro Montaño, J.	EP198
Carlsen, J.	P193	Catafau, A. M.	P245, PW36
Carlson, K.	OP190	Catalan, P.	P016
Carlsson, M.	P069, P075	Catalano, M.	EP216, P073
Carmo, S.	OP447	Catheline, G.	P252
Carmona, M.	PW35	Cathomas, R.	OP149
Carmona, S.	OP371, P194	Catrambone, U.	OP535
Carmona Asenjo, E.	P118	Cattini, C.	TP078
Carmona-Iragui, M.	OP379	Causser, L.	OP217, OP482
Carnaghi, C.	EPW46	Cavatorta, C.	P185
Carnero-Pardo, C.	OP375	Cavdar, I.	EP808
Caroli, A.	OP033	Cavedon, C.	EP402
Carolino, E.	EP821, TP041	Cawthorne, C.	OP488
Carollo, A.	OP332	Cayir, D.	P098, P112
Caron, P.	EP389	Cayir, K.	EP695
Carp, L.	OP080	Çędrowska, E.	OP590
Carreño, E.	EP294	Ceber, M.	P163
Carreras-Delgado, J. L.	EP045, EP057, EP061, EP178, OP698, PW21	Cebrián-Leiva, A.	EP655, TP096
Carril, J. M.	OP431	Ceccharini, J.	OP069, OP257, OP426, OP615
Carrió, I.	EP074, EP155, EP167, EP287, OP379, PW35	Cecchin, D.	EP789
Carroll, L.	OP341	Ceci, F.	EP153, EP223, EP264, OP035, OP077 , OP335
Carson, R. E.	OP312	Cegla, P.	OP280 , TP029
Carswell, C. J.	P251	Celen, Y.	EP144
Carta, M.	EP400	Celichowski, G.	OP672
Cartellieri, M.	EP525	Celik, F.	OP683
Cartron, G.	OP513	Celler, A.	EP431, EP472, EPW54
Carvalho, I. P.	EP554	Celoria, G.	OP145
Carvalho, M. R.	EP554	Cengiz, A.	EP119
Casadio, E.	EP304	Čępa, A.	P033
Casagrande, S.	EP156	Cępa, F.	P111
Casalta-Lopes, J.	EP599, OP673	Ceravolo, R.	P259
Casanova Martins, M.	TP110	Ceresoli, G.	EP306
Casáns-Tormo, I.	EP386, P068, P126	Ceriani, L.	OP337
		Ceriani, V.	OP421

Ceric, S.	EP192	Chereches, G.	OP220
Çermik, T. F.	EP228, EPW28	Cherkashin, D.	TP064
Cerna, L.	P161	Chernaya, A.	EP058
Cerny, V.	P134	Chernov, V.	EP075, EP097 , EP632, EP634
Cerovic, S.	OP368	Chernyshova, A.	EP097
Cerri, G.	EP267	Cherubini, A.	OP376
Cervino, A.	EP305, EP748	Chessa, M. A.	EP199
Cesari, J.	EP656, EP657	Chiacchio, S.	EP560
Cescato, R.	EP678	Chiang, C. C.	EP399, EP410, EP750 , EP764, P229
Cevikol, C.	EP103	Chiararamida, P.	EP469
Ceyrat, Q.	P061	Chiaravallotti, A.	EP238 , EP262, EP567, OP221, OP653, P264, P267, P290
Chaft, J.	EP164	Chicco, A.	EP133, OP036
Chagovets, A.	EP642	Chierichetti, F.	EP571
Chalaye, J.	OP030	Chiesa, C.	EP458 , EP460, OP011
Chalon, S.	EP826	Chikamori, T.	P036, P048
Chaltiel, L.	OP494	Chilra, P.	P057
Chamorro, P.	EP797	Chimpiri, R.	EP063
Champion, C.	EP473	Chin, F.	EP020
Champion, L.	EP040, EP050, EPW01	Chincarini, A.	P255
Chan, A. B.	OP642	Chinchilla, J.	TP036
Chan, C.	EP583, EP620	Chio', A.	OP262
Chan, J. G.	EP649	Chiotellis, A.	OP398
Chan, S.-C.	OP178	Chiotis, K.	OP065
Chandra, S.	EP616	Chiribiri, A.	OP514
Chang, C.	OP303, OP310, OP316	Chiti, A.	EP157, EP306, EPW25, OP145, OP243, OP355, OP655
Chang, C.-M.	EP576	Chittenden, S.	EP444, OP164, OP136
Chang, K.-. W.	EPW57	Chiu, H.	EP038
Chang, R.-E.	P109	Chiu, N.-T.	EP158
Chang, W.-C.	EP038, OP491	Chiu, W.-Y.	P096
Chapelier, K.	EP812	Chiusaroli, S.	EP292
Chappie, T.	OP310	Chizhevskaya, S.	EP075
Chaput, A.	OP181	Cho, D.	EP846
Chardès, T.	OP545	Cho, E.	EP524, EP846, EP847, EP854
Charfeddine, S.	EP381, P195	Cho, I.-H.	EP067
Charil, A.	EP673	Cho, M.	P206
Chasen, B.	OP394	Cho, S.-G.	EPW26
Chatti, K.	EP331, EP370, EP447, P165	Cho, Y.-H.	TP053
Chattopadhyay, A.	OP143	Cho, Y.-Y.	EP052
Chatzioannou, S.	EP680, EP681	Choe, J.	EP283, EP319
Chau, A.	OP352	Choi, C.	EP326, EP569
Chaudhuri, P.	EP482	Choi, D.	EP588
Chaumet-Riffaud, P.	OP144	Choi, H.	TP058
Chaushev, B.	EP196	Choi, J.	EP067, EP326
Chauveau, F.	OP058	Choi, S.	P147
Chavdarova, L.	P060	Choiński, J.	OP445, OP675
Chaves, S.	TP043, TP068	Cholewiński, W.	EP758, OP280, TP029, TP032
Cheetham, A. M.	TP002	Chomet, M.	EP650, EPW58
Chemin, A.	OP298	Chong, A.	P217
Chen, D.	OP304, OP669	Chosia, M.	OP225
Chen, F.	OP402, OP638	Choudhury, P. S.	EP276
Chen, J.-H.	EP584	Choukry, S.	EP015
Chen, K.-Y.	P096	Choynzonov, E.	EP075
Chen, L.	OP061, OP303, OP310 , OP316	Chrapko, B.	EP237, EP313
Chen, M.-K.	EP147, OP312	Chris, E.	OP083
Chen, X.	OP199, OP307	Christ, E.	OP149
Chen, Y.-C.	TP042	Christensen, M. H.	OP350
Chen, Y.	EP145, OP230, P192	Christensen, N. L.	PW26 , TP034, TP098
Cheng, C.-Y.	P297	Christiansen, S. R.	EP585
Cheng, J.	OP486	Christlieb, S. B.	EP037, EP671 , P240, P241
Cheng, M.-F.	TP042	Christofis, C.	P182
Cheng, X.	EPW59	Chronis, J.	OP463
Cheng, Z.	OP503	Chroustová, D.	P100, PW05
Chentli, K.	P214	Chu, P.-L.	P296
Cheon, G.	OP571	Chua, S.	EP742
Cheow, H.	OP137		
Chequer, R.	OP192 , OP560, OP605		

Chuamsaamarkkee, K.		OP163	Conesa, G.	EP022
Chuang, K. S.	EP399, EP410 , EP750, EP764 , P229		Cong, E.	EP133, OP036
Chumakov, A.		TP064	Constantinescu, C.	EP029, EP037
Chun, I.		P168	Conte, P.	EP066
Chun, K.		EP067, OP537	Conti, U.	P133
Chung, J.		EP524	Contreras, J.	OP193
Chung, J.-K.		OP571	Contu, S.	P278
Chung, S.	EP404, EP719, P206		Cook, G.	EP299 , EP581, EP598, EP668, OP602
Chung, Y.-H.	EP038, OP491		Coppen, C.	EP115
Cianci, C.	EPW20		Coppola, A.	P115
Ciarmiello, A.	EP556, OP145, P243		Coppola, C.	PW01
Ciarrocchi, E.		EP776	Coppolino, P.	EP538
Cicalese, V.		EP261	Corazza, A.	EP487, EP488
Ciccio, C.		EP262	Corcoran, B.	EP416, P121
Cicone, F.		OP654	Cordero García, J.	EP098 , EP689, OP369
Cicoria, G.	EP487, EP488, TP089		Cormier, L.	OP353
Cidda, C.	EP219, EP618, P234		Cornelisse, A. C.	OP683
Cid Jimenez, D.	TP076, TP087		Cornelissen, B.	EPW62, EPW63, OP490
Çiftci, E.		EP383	Coronado Poggio, M.	EP184, OP180
Cillero, I.		EP208	Corradini, N.	EP011, EP012
Cimini, A.	P290, PW23		Correa, F.	P088
Çinaral Sayin, F.		P052	Correa, N. L.	EP707, EPW40
Ciobota, D. M.	EPW65, EPW80		Correia, I.	EP536
Cistaro, A.	OP262, P176		Correia, R.	TP017
Cittanti, C.	EP051, EP070, EP104, EP295, EP687		Corroyer-Dulmont, A.	OP584
Civantos, F.	OP123, OP124		Corso, G.	EPW06
Claessens-Joosten, L.		OP364	Cortés, J.	OP070, P263
Clarke, A. R.		OP490	Cortese, N.	EPW25
Clarke, S.		EP668	Cortés Hernández, J.	TP040
Claudin, M.		OP563	Cortes-Rodicio, J.	EP284, EP401
Clausen, M. R.		P136	Cortés-Romera, M.	EP116, EP160, EP167 ,
Claver Valderas, M.	EP250, EP303, EP441, EP471, EP682			OP031, P137 , TP096
Clemente, G.		OP488	Cortot, A.	OP603
Cleton, A.		EP420	Corwin, C.	OP424
Climent-Esteller, F.		EP167	Cos-Domingo, M.	EP116
Clinch, P.		OP676	Cossu Rocca, M.	OP332
Coaguila, C.		OP509, OP510	Costa, D.	TP043, TP072
Cobo Rodríguez, A.		P093	Costa, F. S.	EP707
Coca-Castro, D.	EP655, TP096		Costa, G.	EP328, EP515, EP815, EPW41 ,
Cocciolillo, F.		P257		OP140, P150, P180, P212
Cochet, A.	EP408, EP812, OP246, OP287, OP353		Costa, P.	OP447
Codee-van der Schilden, K.		OP448	Costa Trachsel, I.	EP113
Codegone, A.	EP365, OP013, P242		Costentin, C.	OP030
Coelho, R. V.		OP310	Costes, N.	OP616
Coello, C.		EP828	Cotrado, A.	EP497, EP707, P088
Cohnen, J.	EP242, EPW74, OP222		Cottureau, A.-S.	OP406
Cohrs, S.		OP589	Courbon, F.	EP389, EP419, EP807
Cola, S.		TP078	Court, S.	EP444
Colandrea, M.	EP546, EPW06, OP332 , OP680		Courteau, A.	OP250, OP513
Colavolpe, C.		EP794	Courtemanche, H.	P247
Collantes, M.		EP224	Couto Caro, R. M.	EP178
Collarino, A.		EP068	Couturier, O.	EP617, P159
Colleoni, M.		EP546	Cox, C. P. W.	TP101
Collet, C.		EP852	Cozar Santiago, M.	EP191 , OP278
Collet, G.	OP091, OP603, P170 , P184, P274		Craig, A. J.	EP459
Collin, B.	EP664, EP666, EP812, OP287 , OP588		Cramer, M.	TP101
Collins, J.		OP064	Crawley, P.	EP513, EPW18
Collins, M. T.		P171	Créhange, G.	OP353
Collins, R.		EP800	Cremonesi, M.	EP460, OP680
Colloc'h, N.		OP612	Crippa, F.	EP458, OP011, P185, P186
Colovic, M.		EP591	Cristofani, L.	P189
Comas, L.		P106	Crivellaro, C.	EP095, EPW09
Compin, C.		EP447	Croasdale, P.	EP491
Comtat, C.	EP080, OP081, OP251		Cromphout, L.	OP554
Concia, E.		P130	Cronin, S. E.	EP703
Conde, I.		P180	Crunelle, C. L.	OP615

Cruz, Á.		EP246	Davarpanah, M.	EP648
Cucca, M.	EP031, EP260, EP390, EP402, P130, TP028, TP033	EP174	D'Avenia, P.	OP167
Cuccaro, A.		PW06	Davenport, M. S.	EP407, EP409
Cuderman, A.		OP600	Davey, N.	OP569
Cufi, M.		EP302	David, P.-M.	P246
Culine, S.		OP332	Davidsson, A.	OP562
Cullurà, D.		EP676	Davies, P.	TP110
Culman, J.		EP225	Dawood, N. S.	EPW34
Cunha, M. F.		OP274	Dayagi, M.	EP396
Cunha, M. L.		EP180, OP460, OP461, OP467, OP604, OP607	De Angelis, F.	OP167
Cuocolo, A.		OP600	Deantonio, L.	EP086, OP033
Curull, V.		EP464, OP538, P242	De Arcocha-Torres, M.	EP021, OP195, OP431
Cutaia, C.		EP169, OP408, OP409	Debatisse, J.	P238
Cutrona, G.		EPW09	De Bernardi, E.	OP495
Cuzzocrea, M.		EP165, P018	De Blois, E.	OP305, OP351, OP547
Cytawa, W.		EP387	De Boer, H.	OP365
Czarnywojtek, A.		EP758 , OP280, TP032	De Bonilla Damiá, Á.	EP182
Czepczyński, R.		P085	Debruyne, F.	EP261
Czerwiec, A.		EP519	Decarie, J.-C.	OP198
Czibor, S.		EP123	Decarolis, B.	OP084
Dabasi, G.		OP416	De Chiara, B.	P135, P144
Daemen, M. J.		OP139	Decristoforo, C.	EP277, EP479, OP343, OP345, OP457
Daeter, E.		TP090	Dede, F.	EPW69
Dagestad, R.		EP562, EP568	Dedecjus, M.	EP207
Daglio Gorur, G.		OP355	Dedek, V.	P102
D'Agostino, G.		EP279	Deden, L. N.	EP803, EP806, OP365
Dagrakis, E.		EP492, OP513, OP548	Dedeurwaerdere, S.	EPW58, P286
Dahle, J.		EPW08	De Deyn, P.	P233
Daisne, J.-F.		OP214	Deevband, M.	EP804
D'Alessio, A.		EP008, EP437	Defer, G.	P258
Dalianis, K.		OP569	De Galan, B. E.	EP697
Dalili, D.		EP605, TP001	De Geeter, F.	OP080
Dall, B.		EP219, P284	De Geus-Oei, L. F.	EP697, EP751, EPW66, OP079, OP297, OP642, PW07
Dalla Valle, R.		OP171, OP305 , OP340, OP547	De Groot, J. R.	OP282
Dalm, S. U.		EP833	Dehaes, B.	EP489
Dam, J. H.		OP428	Dehayes, E.	EP494
Damian, A.		EP269	Deheneffe, S.	EPW08
Damiano, R.		TP056, TP067	De Herder, W. W.	OP342
Damini, G.		EP168	De Jager-Leclerque, M.	PW07
D'Amore, F.		EP196	De Jong, I. J.	EP558, OP349, P154
Dancheva, J.		OP425	De Jong, M.	EP417, EP667, EP782, OP150, OP171, OP305, OP340, OP342, OP351, OP547, OP581, OP671
Danek, A.		OP252	De Jong, P. A.	P091
Danfors, T.		OP503	De Keizer, B.	EP478, EP550, OP683, TP108
Daniel, B.		OP461, OP467	De Klerk, J. M. H.	OP606
Daniele, S.		EP218, P290	De Korne, C. M.	EP665
Danieli, R.		OP377	De Koster, E. J.	EP068
Danilenko, A.		EP011, EP012	De Laat, B.	OP615
Dansette, D.		TP043, TP072	De Labriolle-Vaylet, C.	EP428, EP451, EP505
Dantas, D.		P125	De La Cueva Méndez, G.	EP532
Danús Láinez, M. D.		TP078	De La Fuente, A.	OP023
Daolio, C.		OP509, OP510	Delamare, J.	OP612
Daou, D.		EP607, EP703, EPW65, EPW80	De Langen, A. J.	EP309
Da Pieve, C.		EP447, OP203 , OP429	De La Riva Pérez, P.	EP198
Darcourt, J.		EP469	De Laroche, R.	EP124, OP183
D'Arienzo, M.		P252	De La Santa Belda, E.	OP369
Dartigues, J.-F.		EP146	De La Sayette, V.	P258
Das, A.		OP597	De La Vega, J. C.	EP472
Das, C.		EP149, EP702	Delbosc, S.	OP170
Das, J.		EP724	Del Carpio, L.	EP022, EP074
D'Asseler, Y.		EP563	Delcroix, L.	EP042, OP129
Datseris, I.		OP466	Delcroix, N.	OP507
Datta, D.		EPW17	Delemasure, S.	OP287
Daugaard, G.			De Lempers, R.	EP628

Deleye, S.	EPW58	Despland, J.-N.	P298
Delgado, H.	TP041	De Swart, J.	EP417, EP667 , EP782
Delgado Garcia, A.	EP532	De Teresa, R.	EP463
Del Guerra, A.	EP743, EP773, EP776	De Toterò, D.	OP409
Delhaas, E.	P156	Dettmann, K.	OP108
D'Elia, A.	OP653	Detyniecki, K.	OP312
Delker, A.	EP484, EPW15 , OP111	Deu, M.	EPW07
Dell'Acqua, A.	EP101	Deveci, S.	EP345, EP346
Dell'Anno, B.	P117	De Vet, H. C. W.	OP683
Dell'Aquila, A.	OP695	De Villanueva, A.	P246
Del Pozzo, L.	EPW85	Devillers, A.	OP681
Delpuech, B.	EP807	De Vincentis, G.	EP510, EPW19, OP334, OP336, P262, P280
Delrieu, J.	P285	De Vittor, D.	EP400
Del Rizzo, M.	P130	De Vivo, S.	EP199
Del Sette, M.	OP145	Devlin, L.	TP002
Delso, G.	OP252	De Vos, F.	P224
Del Sole, A.	EP746	De Vrey, E. A.	OP606
Del Vecchio, S.	EP180, EP186, EP301 , OP116, OP120	De Vries, E. F. J.	OP613
Demailly, F.	P170	Devriese, J.	EP716 , EP779
De Miguel-Pérez, D.	EPW24	De Vringer, T.	OP107
Demir, H.	EP562, EP568	Devrome, M.	OP069
Demir, M.	EP194, EP808, OP679	De Weerd, V.	OP171
Demirag, F.	EP159	DeWees, T.	OP015
Demirbas, S.	OP141	De Wit-van der Veen, B. J.	OP216, OP483, OP484, OP593
Demircan, K.	OP544	De Wit - van der Veen, L. J.	EP282
Demirci, E.	EP244, EP245, EP504, EP547 , EPW44 , OP223	De Wolf, K.	EP087
Demirel, B. B.	EP093, EP096, EP099, EP102, EP105	Dhafer, R.	OP312
Demirel, K.	EP426, OP544	Dhaouadi, B.	EP039, EP705, P157, P190, P215
Demirelli, S.	EP212	Dharmalingam, A.	P213
Demirev, A.	EP555 , P094	Dhillon, S.	OP602
Demirkan, F.	P141	Dhilly, M.	OP612
Demirtas, S.	EP096	Dhote, R.	P089
Demmery, A.	P143	Dhote, T. V.	OP411
Democrito, A.	EP662, OP233	D'hulst, L.	PW03
Denat, F.	EP664, OP588	D'huys, T.	OP488
Dénes, N.	EP596, EP597	D'Huyvetter, M.	OP590
De Neve, W.	EP087	Diallo, D.	OP170, OP423
Deng, B.	OP199	Diaz, L.	EP170 , EP545
De Nila, M.	OP011	Diaz Alarcon, J.	TP079
De Nile, M.	EP458, EP460	Díaz-Expósito, R.	EP386, P068, P126
Denis-Bacelar, A.	EP444 , EP459, EP703	Diaz Gonzalez, L. G.	P199, TP045, TP085, TP105
Deniz, F.	EP354	Diaz Platas, L.	EP243, P043
Denkova, A.	OP671	Dib, B.	EP340, OP535
Dente, A.	OP167	Di Biagio, D.	EP238
Dentici, R.	PW01	Di Castro, E.	OP336
Denys, A.	EP325	Didic, M.	OP373
De Paola Chequer, R.	OP565	Didier, R.	EP852
Depardon, E.	OP246 , OP353	Diederichsen, L. P.	OP568
De Ponti, E.	EP095, EP785 , EPW09	Diego Dominguez, M.	TP045
De Renzo, A.	EP180, EP186	Diego Nieto, A.	TP045
Derevyanko, E.	P032	Diehl-Schmid, J.	OP147
De Rimini, M. L.	EP517	Dierckx, R.	OP066, OP610, OP613, OP700, P233, TP016
De Roos, R.	EP550, TP108	Dierickx, L.	EP389, EP419, EP807, OP494
Deroose, C. M.	OP554	Dietlein, M.	EP483
De Rosa, V.	OP116, OP120	Dietz, A.	OP179
De Roten, Y.	P298	Dieudonné, A.	EPW49, EPW55 , OP631
D'Errico, A.	EP265, EPW75	Díez-Domingo, S.	EP386
De Sá, L. V.	EPW40	Di Giorgio, E.	EP238, P264, P290
Desai, M.	EP435	Di Giuda, D.	EP627, P257
De Santi, S.	OP378, P245, PW36	Dignat-George, F.	OP344
Desbrée, A.	EP428 , EP451 , EP505	Dika, E.	EP199
De Sequera-Rahola, M.	EP016, EP185, EP394	DiMugno, S.	OP024
Deshayes, E.	OP545	Dimakopoulos, N.	P113
De Smet, B. J. G. L.	OP606	Di Mauro, F.	OP536
De Spiegeleer, B.	P224		

Dimcheva, M.	EP214, EP805	Dreher, M. R.	OP012
Dimitri, B.	P184	Dresel, S.	OP378
Dimitriadi, E. Z.	OP636	Driscoll, B. D.	OP275
D'Incerti, L.	PW38	Drouet, C.	OP356, P106
Ding, H.	EP610	Drude, N.	OP546
Dini, M.	TP092	Drummond, M.	EP225
Dini, V.	EP521	Drzezga, A.	EP483, OP084, OP373
Di Nicola, E.	OP167	D'Souza, M.	EP035
Dinning, S.	EP792	Du, Y.	OP217, OP482
Dinomais, M.	P159	Duan, H.	EPW11
Diodato, S.	EP121, EP153, EP199	Duarte, H.	EP251, OP396
Di Palo, A.	EP135, EP142, EP213, EP221, PW23	Dubash, S. R.	OP341
Di Paolo, M. L.	EP041	Dubreuil, J.	EPW21 , OP601, OP699
Di Pietro, B.	P264	Dubroff, J.	OP427
Dirlík Serim, B.	P082	Duch, J.	EP074 , EP155, EP287
Di Russo, C.	P267	Ducrocq, G.	OP605
Di Russo, M.	EP256	Dufour, M.	OP203
Disotuar Ruíz, N.	EP689, OP369	Dugonjic, S.	OP368
Dittmann, H.	OP130	Duhovic, A.	OP500
Divoli, A.	EPW51 , OP163	Dumanic, M.	EP636, OP286
Divoux, J.-L.	OP366	Dumortier, O.	EPW21
Dixit, M.	P140	Dunet, V.	P265
Dizdarevic, S.	OP064, OP333 , OP480	Duni, F.	EP213
Djaballah, W.	OP563	Dunn, J. T.	EP171 , OP686
Djelbani, S.	EP080, OP081, OP251	Dunphy, M.	EP164
Dobbeleir, A.	P224, PW40	Dupont, P.	OP614
Dobson, H.	P244	Duporte, G.	EP850
Dockx, R.	P224	Duprat, R.	P224
Dóczy, R.	EP640	Dupuis, J.	OP406
Džodić, R.	EP391	Durak, H.	EP553, TP035
Doerr, C.	EP436	Durán Barquero, C.	P152, P268
Doeswijk, G. N.	EP667, OP305, OP547	Durand, E.	OP144
Dogan, O. T.	EP162	Durmus Altun, G.	P082
Doganay Erdogan, B.	EP190	DUR SUN, N.	EPW28
Doi, T.	OP284	Dusi, F.	EP402
Dolci, C.	EP095	Dutra, J.	OP061, OP303
Doležal, J.	EP820	Duval, X.	OP696
Doll, S.	EP526, EP610	Duvoux, C.	OP030
Domene, A.	EP826	Dvorakova, S.	EPW39
Domènech, A.	EP155, EP287	Dweck, M. R.	OP193
Domínguez-Ayala, M.	OP518	Dygai-Cochet, I.	OP246
Domínguez-Cruz, J.	EP200	Dzhuzha, D. A.	EP508
Domínguez Gadea, L.	EP184, EP202, OP180, P016	Dziawer, L.	OP672
Domínguez Prado, I.	P263, TP040	Dziel, T.	EP604
Donaire, A.	OP200	Dziuk, M.	EP071, EP439, EP757, EP781, P076
Donatiello, S.	EP371		
Dönder, E.	EP338	Ea, K.-M.	EP451
Dong, P.	OP174	Eade, T.	OP550
Donnarieix, D.	OP298	Eberhard, K. P.	TP088
Donnelly, P. S.	EP611	Eberl, S.	EP825, EPW78
Donner, D.	EP571, OP221	Eberlein, U.	EP448, EPW50
Doorduyn, J.	OP066, OP613	Eccles, A.	OP279, P121, TP002
Doran, S.	OP303, OP310, OP316	Eccles, S. A.	EP703
Dore, F.	EP218	Eckardt, L.	PW30
Doria, R.	P133	Eckert, R.	EPW89
Dormehl, I.	EP599, OP673	Edeline, J.	EP601
Dormont, D.	P246	Edeline, V.	OP406
Dorniak, K.	P018	Edenbrandt, L.	EP227, EP261, EP415
Doroudinia, A.	EP754, EP759	Eder, M.	EP239, EPW84, OP022
Doruyter, A.	OP614	Eder, V.	OP030
Dos Santos, G.	OP458	Eek, A.	OP343
Dottorini, M.	OP373	Efeturk, H.	EP093 , EP096 , EP099 ,
Dou, Y.	EP122		EP102, EP105
Douard, H.	P061	Efimova, I.	P041
Dougherty, C. A.	OP304	Efimova, N.	P041
Drabe, M.	OP617	Eftekhari, M.	EP081, EP209, EP539, EP818, P012

Ege Aktas, L.	EP166	Erdem, F.	P021
Eggert, A.	OP084	Erdem Şahin, O.	EPW44
Ehninger, A.	EP525	Erdemir, R. U.	EP548
Eiber, M.	EP266, EP274, EP557, OP074	Erdil, T. Y.	EP824
Eichinger, R.	EP857	Erdmann, S.	EP643, OP487 , OP585
Eid, T.	OP312	Erdoğan, M.	P098
Eidherr, H.	EPW11	Erdogan, Y.	EP159
Eikenes, L.	EP752, OP254	Eren, G.	EPW71
Eikens, L.	OP247	Eren, O.	EP468, OP014
Eilles, E.	OP314	Ergül, N.	EP228
Einhellig, H.	EP203	Eriksson, J. P.	EP582
Einspieler, I.	EP274	Eriksson, O.	OP232
Eiriksdottir, B.	OP548	Eriksson Karlström, A.	OP589
Eisenhut, M.	EP239	Eriksson-Karlström, A.	EPW81
Eissler, K.	EP835	Erini, M.	EP571
Ejeh, J. E.	P160	Erkiliç, M.	EP212
Ejlersen, J. A.	OP350, OP358	Erlandsson, I. L.	TP050
Ekbic, Y.	PW28	Erlandsson, M.	EP605
Ekim, S.	OP641	Ersahin, D.	EP147
Ekinci, O.	OP544	Ertay, T.	TP035
Elajmi, W.	P187	Ertürk, S. A.	EP162, EP383
El-Antabily, I.	OP089	Escabias del Pozo, C.	EP184, EP202, OP180
Elboga, U.	EP144	Escala-Ramirez, Y.	OP688
ELfiky, A.	EP731, EP755	Eschner, W.	EP483
El-Galaly, T. C.	OP686	Eset, K.	EP729
Elgendy, A.	P219	Esfahani, M. M. N.	EPW90
El-Hennawy, G.	EP138	Eshghi, P.	EP425
Elia, B.	EP365	Eskola, O.	OP354
Elisei, F.	EP095, EPW09	Esmail, A.	EP183
El-kholy, E.	EP138, OP089	España, S.	EP736, OP229 , PW27
El-Kilini, N.	OP089	Esquinas, P. L.	EP472, EPW54
El-Lababidi, N.	PW05	Esser, J. P.	TP025
Ellingsen, J.	TP090	Essler, M.	EP498, EP602, EP652, EPW12,
El-Nadi, E.	OP089		EPW14, OP023, OP109
El Naqa, I.	EP407	Estellat, C.	OP560
Eloteify, L.	EP708, EP711	Estenoz Alfaro, J.	EP084, EP127, EP231, P123
Elrasad, S. A. A.	EP359	Estorch, M.	EP074, EP155
El-Refaei, S. M. A.	EP359	Estrada, F.	EP077, EP542
Elri, T.	EP548	Etchebehere, E.	EP056, EP060, EP267, P189
Elsayd, H.	EP240, P188	Eter, W. A.	OP364
El-Sayed, M. A.	OP087	Eterović, D.	P174
Elshemey, W.	EP731, EP755	Eu, P.	EP486
Elsner, A.	OP686	Eugene, T.	OP407
Emami, A.	OP301	Evagelatou, A.	P113
Emami-Ardekani, A.	EP081, EP209, P012	Evangelista, E.	OP030
Emer, O.	EP345, EP346	Evangelista, L.	EP004, EP066, EP247,
Emionite, L.	EP662, OP288		EP305 , OP221, P176
Emmett, L.	OP550	Evens, A. M.	OP082
Emri, M.	EP677	Evens, J.	OP430
Emsen, B.	OP194	Everaert, H.	OP142, P149
Endepols, H.	OP422	Everaerts, W.	OP554
Endo, K.	TP021	Evers, S.	OP593
Endo, S.	EP725	Evren, I.	TP035
Engblom, H.	OP477, OP511, P069, P075	Evtushenko, A.	P087
Engelen, M.	OP134	Evtushenko, V.	P087
England, C. G.	OP308, OP592	Exner, S.	EP643, OP487, OP585
Engler, H.	EP014, OP458	Expósito Rodríguez, A.	OP518
Engvall, J.	OP562	Ezquerro, A. I.	EP255
Enmi, J.	P231	Ezziddin, S.	EPW74, P164
Enqvist, O.	EP415	Ezzine, A.	EP331 , EP370, P165
Entezarmahdi, S.	EP740		
Enyedi, K. N.	EPW64	Fa, N.	EP357
Eppard, E.	EP602, EP652 , EPW12, EPW14, OP023	Fabre, J.-E.	OP423
Eraslan, C.	EP378	Faccini, R.	OP680
Erba, P.	EP776, EPW66, P133	Faghihi, R.	EP740
Erbas, B.	OP684	Fagioli, F.	P176

Faheem, M.	EP327, P132	Ferdeghini, M.	EP031, EP260, EP390,
Fahim, H.	OP479, TP083		EP402, P130, TP028, TP033
Fain, O.	P089	Ferdinandus, J.	EPW12
Fais, F.	EP169, OP408, OP409	Ferme, C.	OP406
Fakhry-Darian, D.	OP260 , P251	Fernandez, P.	P252
Fakioglu, O.	EP426	Fernandes, A.	EP002, EP285 , EPW52 , OP044 , P222
Fakirova, A.	EP214	Fernandes, B.	OP655
Falch, K.	EP047, OP273	Fernandes, J.	TP017, TP018
Falchi, A.	EP218	Fernandes, M.	TP062
Falgás, M.	EP462	Fernandez, A.	EP065, EP155, OP494
Fallahi, B.	EP081, EP209, EP539 , P012	Fernández, B.	EP286
Fallanca, F.	EP101, EP175, OP682	Fernández, E.	EP592, EP593
Fallentin, E.	P136	Fernandez, P.	P238
Falls, T.	OP064	Fernandez, R.	EP456, EP543
Falzone, N.	EP443 , EPW56 , OP584	Fernandez, S.	OP344
Familiari, D.	EP137, EP197 , P181	Fernández-Alarza, F.	OP600
Fan, K.-H.	OP310	Fernández-Ferreiro, A.	P263
Fan, Y.	EP177, EP360, OP685	Fernández-Friera, L.	EP736
Fanelli, M.	EP142, EP221	Fernández García, C.	EP647
Fanggiday, J.	OP139	Fernandez-Leon, A.	OP379, PW35
Fani, M.	EPW85, OP083, OP149, OP289	Fernández Llana, B.	EP243, OP403
Fanti, P. A.	EP199	Fernández López, R.	EP182 , EP200
Fanti, S.	EP121, EP153, EP199, EP223,	Fernandez-Martinez, A.	EP100, EP107
	EP264, EP265, EP288, EP304,	Fernández Rodríguez, M.	EP310 , P034
	EPW20, EPW72, EPW75, OP035,	Fernandez-Tercero, I. L.	EP255
	OP077, OP335, P146, TP089	Fernández-Varea, J. M.	EP443, EPW56
Farahani, M.	EP761, EP763, OP218, P014	Fernando, A.	OP507
Farajbakhsh, F.	EP648	Ferrando, O.	EP556 , P243
Farcomeni, A.	P262	Ferrando, R.	OP428
Farde, L.	P227	Ferran Sureda, N.	TP084
Fard-Esfahani, A.	EP081, EP209 , EP539, P012	Ferrante, D.	OP033
Farghaly, H.	EP154 , P220	Ferrara, C.	P176
Faria, A.	TP068	Ferrazzo, G.	OP288 , OP409, OP421, P042, PW22
Faria, D.	TP017, TP018	Ferrari, C.	EP135, EP142, EP213,
Faria, T.	EP002, EP285, OP044, P222		EP221 , EP236 , P176
Faria Joao, M.	TP102	Ferrari, E.	OP127
Farkas, A.	EP677, EPW64	Ferrari, M.	EP460, OP680
Farkas, B.	EP253	Ferrari, P.	EP469
Farnesi, A.	EPW20	Ferraro, S.	PW38
Farolfi, A.	EP304	Ferraroli, G.	EP306
Farrar, G.	OP259	Ferreira, G.	EP251, OP396
Farre, N.	EP155	Ferreira, S.	TP018
Farzanefar, S.	OP218, P012, P014	Ferreira, S. M.	EP599 , OP673
Fatemizadeh, E.	P014	Ferreira, T. C.	EP554
Fathinul Fikri, A.	P025	Ferrer-Artola, A. M.	EP230
Fathy, H.	EP138	Ferrero-Febrer, I.	EP655, TP096
Fatima, N.	EP373, EP442 , P077	Ferrer Rebolleda, J.	EP191, OP278
Fatima, S.	EP327 , P132	Ferro, P.	EP175 , EP218, OP682
Fattori, B.	EP114	Ferrolí, P.	OP680
Fattori, S.	OP167	Fersino, S.	EP085
Fawzy, M.	P188	Fialová, M.	P100
Fay, R.	OP201	Fiasconaro, E.	EP114 , EP128 , P117
Fayad, Z. A.	OP193	Field-Galan, C.	EP692
Fayolle, H.	P285	Fierro, A.	TP056, TP067
Fazekas, E.	EP838	Fierro Alanis, M.	EP069
Fazekas, J.	EP623, EP636	Fierro Alanis, P.	EP286
Fazio, N.	EPW46	Fieux, S.	OP063, OP616
Fejne, F.	EP227	Figueiredo, A.	EP246
Fekete, A.	EP834	Figueiredo-Pereira, M. E.	OP424
Feldmann, A.	EP525	Figueroa, R.	OP410
Feldmann, G.	EPW12	Filauri, M.	P280
Felt, S. A.	OP503	Filice, A.	EPW46 , OP598
Fenichel, M.	EP036, EP752, OP249	Filippi, L.	EP469
Fendler, W.	EPW15, OP111	Filis, K.	OP417
Fenwick, A.	EP788, OP136	Filiz, A. I.	EP354
Fenwick, J. D.	OP068	Fillesoye, F.	OP612

Fimmers, R.	EPW12	Franceschi, D.	EP063
Findik, G.	EP159	Franceschi, M.	EP010, P127
Findlay, C.	EP564	Francia, A.	P262
Fink, K.	EP479	Francis, R.	OP550
Finnema, S. J.	OP312	Franck, D.	EP428, EP451, EP505, OP165
Finucane, C.	EP801, EPW36, P244	Frank, P.	EP552
Fiordoro, S.	PW22	Frank, S. J.	OP338
Fiore, V.	EP206	Franken, A.	OP534
Fiore Melacrinis, F.	EP292	Franssen, G.	OP343, OP345
Fiorentini, A.	EP238, OP653, P264, P267, P290	Frantellizzi, V.	EP510 , EPW19, OP334, OP336, P262 , P280
Fiorentino, A.	EP085	Franzese, C.	OP355
Fiorentino, M.	EP265, EPW75	Frary, E.	EP201
Fiorino, S.	P135, P144	Fraser, B. H.	EP832
Fioroni, F.	EP813, EPW46, OP598	Frasoldati, A.	EPW46
Fischbein, N.	EP020	Frassoldati, A.	EP051
Fischer, A.	EP469	Fraternali, A.	EPW46, EPW92
Fischer, B. M.	EP570, P136	Fratino, L.	EPW20
Fischer, M.	OP179	Fravolini, M. L.	P273, P275
Fischer, T.	EP483	Fraysse, M.	OP699
Fiz, F.	EP017 , EP169, EP429 , OP127 , OP130, OP135 , OP288, OP408, OP409 , OP421 , PW22	Frederic, C.	OP494
	EP465, OP393, OP456	Fredrickson, J.	EP164
Flamen, P.	OP567	Freese, D. L.	EP770
Flanigan, D.	EP552	Frega, N.	EP180
Flechsigg, P.	OP350, OP358	Freitas, B.	TP043
Fledelius, J.	OP311	Frejd, F. Y.	EP522, EPW82
Fleetwood, F.	OP039	Frellsen, A. F.	EP836
Fleming, J.	TP106	Fremont, A.	P159
Flensburg, A.	P119, P122	Frenkel, A.	EP489
Fletcher, J.	EP380	Frenzel, T.	EP772
Fleury-Bahi, G.	P040	Freundenberg, R.	EP831
Floros, S.	EP074, EP155	Frielink, C.	EP443, OP678
Flotats, A.	EP414, EP444, EP459, EP703, EP742, EP801, EPW51, OP131, OP136, OP164, OP217, OP360, OP482	Frilling, A.	EP430, OP364
Flux, G.	P191	Frings, V.	OP341
	EP679	Frisoni, G.	OP599
Fodor, A.	EP510, EPW19 , OP334 , OP336, P280	Frittelli, P.	OP373, P250
Fojtik, Z.	EP334	Fröberg, A.	EP292
Follacchio, G. A.	OP350	Frøkiær, J.	OP342 , OP351, P156
Fomin, D.	EP265, EPW72, EPW75, OP077	Frommeyer, G.	EP685
Fonager, R. F.	EP186 , EP301	Fröss-Baron, K.	PW30
Fonti, C.	EP340, OP535	Frutos Esteban, L.	OP291
Fonti, R.	EP556	Fudim, M.	EP303, EP250, EP441, EP471, EP682
Foppiani, L.	EP771 , OP212	Fueger, B.	OP465
Foppiano, F.	P102	Fuentes Ferrer, M. E.	EP134, EP163
Forgács, A.	OP598	Fuentes, S.	EP045, EP061, OP698
Formanek, M.	EP137, EP197, P181	Fuertes Manuel, J.	EP291 , EP296
Formisano, D.	EP840, EP851, EP853, EPW96, PW33, TP030	Fujii, H.	P125
Fornito, M. C.	P227	Fujii, S.	EP725, EPW86
Forsback, S.	EP579, OP501, OP502	Fujinaga, M.	PW39
	OP379, PW35	Fujisawa, I.	PW31
Forsberg, A.	EP627, P257	Fujita, N.	TP081
Forsting, M.	EPW91	Fukasawa, M.	TP003, TP010, TP059
Fortea, J.	EPW17 , PW02	Fukaya, Y.	EP683
Fortini, D.	EP024, P028, P030 , P210	Fukuda, Y.	EP323
Fortt, R.	EP132, OP015	Fukunaga, M.	EP026 , EP030
Fosbøl, M. Ø.	EP546, EPW06, OP332, OP680	Fukushima, Y.	OP213
Fotopoulos, A.	EP721	Fukuyama, T.	EP699, P050 , P269
Fowler, K.	EP809	Fulham, M.	P048
Fracassi, S.	EP423	Fullbrook, A.	EP825, EPW78
Frackiewicz, M.	EP065, P128	Fullerton, N.	EP723
Fragoso Costa, P.	EP065	Fulop, M.	TP082
Fragulidis, G. P.	EP088 , EP089 , EP258	Fumagalli, G.	EP810 , EP820
Fraille, M.		Fumoleau, P.	P253
Framis, M.		Funes Mayorga, F.	OP246
Franceschetto, A.		Furnari, J. C.	EP222
		Furth, C.	EP318
			EP481

Furtner, J.	OP649	García Sánchez, V.	P118
Furumoto, S.	EP846	García-Talavera, P.	EP545 , P199
Furuta, A.	EP744	García Valdecasas, B.	EP287
Fusté, P.	EP107	García-Varela, L.	P263
Fuster, V.	EP736, OP193	García-Vargas, J.	OP338
Fysikopoulos, E.	EP661, EPW05	García-Velloso, M. J.	EP814, OP410
Gabersček, S.	P200 , P203	García Vicente, A.	EP098, EP222, EP689, OP075 , OP240 , OP369
Gabiache, E.	EP389, EP419, EP807	Gardberg, M.	OP688
Gabriel, S.	EP624	Gardin, I.	EPW49, EPW55, OP631
Gad, D.	EP201	Garg, A.	OP651
Gad, H. M.	P219	Garg, N. K.	P058, P072
Gaetano, A.	OP332	Garganese, M. C.	EP371
Gainotti, G.	P257	Garibotto, V.	P250
Gains, J.	EPW45	Garin, E.	EP601
Gajja, V.	EP537, EP609	Garnuszek, P.	EP523, EP604, EP855
Galanakos, S.	OP420	Garousi, J.	EP522, EPW83, OP172
Galaska, R.	P018	Garrido Pumar, M.	EP069 , EP286, TP040
Galaz, R.	EP543	Garrigue, P.	EP624, OP344
Galeassi, A.	EP306	Garske-Roman, U.	EP502, OP291
Galetta, G.	OP214	Gärtner, F.	EPW12, OP109, OP189
Galgóczy, E.	EP677	Gasbarrini, A.	EP288
Galimberti, D.	P253	Gascón-Bayarri, J.	OP374
Galimberti, V.	EP546, EPW06	Gasparini, M.	EP041
Gallazzini Crepin, C.	OP681	Gasparini, N.	OP167
Galli, L.	EP128, EPW20	Gasser, G.	OP587
Gallivanone, F.	EP157, OP243	Gaudiano, C.	EP265
Gallo, L.	PW24	Gaudiano, J.	EP014
Galluzzi, S.	OP373	Gaudieri, V.	OP460, OP461, OP467 , OP604, OP607
Galmés, M.	EP613	Gauthé, M.	EP263 , EP391, EPW70, OP292
Galuska, L.	P191	Gawel, J.	EP781
Gama de Abreu, M.	OP694	Gawlik, T.	EP329
Gamazo, C.	EP637	Gaze, M.	EPW45
Gamazo Laherran, C.	P093, P103	Gazeloglu, C.	EP729
Gambhir, S.	EP020, EP232, EPW76, OP466, OP504, P058, P072, P140 , P142, P223	Ge, J.	OP199
Gámez-Cenzano, C.	EP018, EP116, EP131, EP160, EP167, EP230, EP655, EP799, OP031, OP374 , P137, TP096	Gear, J.	EPW51, OP136, OP164, OP217, OP360 , OP482
Gam-Hadberg, J. C.	TP097	Gee, A.	EPW91, OP397, OP399
Gancitano, P.	OP262	Geerlings, M.	OP022
Gangemi, V.	EP262, EP269	Géher, P.	EP427
Ganne-Carrie, N.	OP030	Geinitz, H.	EP278, OP553, OP555
Gantet, P.	P285	Geist, B. K.	OP038
Gao, S.	OP117	Gejl, M.	OP372, P296
Garaboldi, L.	OP233	Gelderblom, A. E.	OP541
Garai, I.	EP253 , EP596, EP597, EP603, EP677, EP771, EPW64, OP212, P191	Gelev, V.	P062
Garashi, M.	P055	Gelo, I.	EP330
Garcheva, M.	EP187, P060, P062	Gelsomino, F.	EP153
García, B.	OP410	Geluk-Jonker, M.	OP483
García, C.	OP456	Genissel, M.	OP366
García Alonso, P.	EP310, P034	Gennaro, M.	EP114, EP560, P117, P259
García Bennett, J.	P125	Genova, A.	OP467
García-Fidalgo, M.	EP284, EP401	Genovese, E.	EP371
García Fontes, M.	OP458	Gentile, R.	EP137, EP197, EP538, EPW22
García García, Y.	EP113	Georg, D.	OP253
García-García, B.	EP224, EP814, OP377	Georga, S.	EP332, P120, PW10
García García-Esquinas, M.	EP045, EP061	Georgakopoulos, A.	EP680 , EP681, EP795, OP417, OP420
García Garzon, J.	EP018, EP191	Georges, J.	OP366
García Gómez, F.	EP198	Georgi, T. W.	OP179
García-Horsman, J.	P294	Georgiou, M.	EP661 , EPW05
García-Pallarols, F.	EP193	Georgoulas, P.	EPW05, P022
García Pérez, F. O.	EP544, EP672	Geraldo, L.	EP139, EP277 , OP457
García-Redondo, J.	EP653	Geraldo-Roig, L.	EP479
García-Saénz, J. A.	EP045, EP061	Geramifar, P.	EP209, EP769, OP301
		Gerardo, L.	OP294
		Gereloni, C.	OP127
		Gerke, O.	EP029, EP037, EP047, EP092, EP559, EP671, EP720 , OP273, P240, P241, TP097

Gerken, G.	EP696	Gjertsson, P.	OP132, OP391
Geronymakis, C.	EP227	Gkika, E.	OP596, P030
Gessl, A.	EP363	Gkouvas, G.	PW10
Geworski, L.	OP202, OP313, OP319	Gladic Nenadic, V.	EP010
Ghadiri, H.	EP693, EP769, OP301, OP302	Glatting, G.	EP499, EP658, EP783, EP784, OP110, OP392, OP632, OP634
Ghaemini, H.	EP115	Glaudemans, A. W. J. M.	OP700
Ghafarian, P.	EP693, EP754 , EP759 , EP760, EP769, EP804, OP301, OP302, OP498	Glavas-Obrovac, L.	EP561
Ghamoushi Ramandi, A.	EP621, EP626	Gleeson, F. V.	EP738, EP741, OP068
Ghanem, G.	OP456	Glehen, O.	OP601
Gharzeddine, K.	EP043, EP049	Glick, D.	OP275
Ghasempoor, S.	EP730	Gloor, B.	OP083
Ghedini, P.	EP223, EP264 , OP335	Gniazdowska, E.	EP528
Gherzi, C.	EP662, OP233	Gobitti, C.	EPW20
Ghetti, C.	EP400, EP618, P234	Goco, G.	EP353
Gheysens, O.	EP835, OP282, OP554, PW03	Goda, J.	EP668
Ghidella, A.	PW22	Gödény, M.	EP123
Ghidini, P.	EPW20	Godkov, I. M.	P260
Ghilardi, A.	OP478	Godoy Bravo, M.	EP441, EP682
Ghinassi, S.	EP292	Godoy Bravo, V.	EP250, EP471
Ghorbel, D.	EP381	Goebell, P.	EP275
Ghosh, A.	EP537	Goel, S.	OP402
Ghosh, K.	EP590	Goethals, I.	EP087, PW40
Ghumman, S. K.	EP630	Goethals, L.	OP142
Giaj-Levra, N.	EP085	Goffin, K.	OP257, OP554
Giammarile, F.	EPW21, OP601	Goh, V.	EP299, EP581, EP598, EP668, OP602
Giancipoli, R.	P290	Gokcek, A.	EP159
Giannakopoulos, P.	P250	Göksel, S.	EP119
Giannattasio, C.	P135, P144	Goksoy, D.	EP324, TP022, TP038, TP070
Giannoni, P.	OP409	Gold, G.	P250
Giannopoulos, S.	P028	Goldenberg, D.	OP640
Giannoula, E.	EP332	Goldkorn, R.	EP774, OP362
Gianolli, L.	EP101, EP175, OP682	Goldman, S.	EP835
Giarika, A.	OP150, OP340	Golfieri, R.	EP265, EP288
Giersz, R.	EP758	Golino, P.	OP604
Giesel, F.	EP239, EP268 , EP270 , EP552, EP557, EPW13, OP022, OP148, OP454, OP552, OP556	Golpe Gómez, A.	TP040
Gizewska, A.	EP071	Golubic, A.	P299
Giglio, G.	EP259	Gomes, G.	EP497
Gil, P.	EP328, EP815 , P150, P212	Gomes Moura, A. C. A.	TP023 , TP048
Gil, T.	OP456	Gomez, A.	EP208
Gil, Z.	OP363	Gomez, B.	EP242, EP696 , OP222
Gilardi, L.	EP546 , EPW06, OP332, OP680	Gomez, J. D. C.	OP487
Gilardi, M.	EPW22	Gomez, L.	OP144
Gildehaus, F.	EP484, EPW15, OP111, OP317	Gomez, M.	P016
Gillen, G.	EP564	Gómez, P.	EP184
Gillett, D.	OP137	Gómez-Acebo, S.	EP136
Gil-Viciano, I.	EP116	Gómez-Caminero, F.	EP545, P199, TP045, TP105
Gimenez, M.	TP036	Gómez-De La Fuente, F.	EP021
Gimeno Blanes, J.	EP682	Gomez Grande, A.	EP084 , EP127, EP231 , P123
Gincu, T.	EP363	Gomez Hidalgo, J.	P093
Giordano, A.	EP174, EP308, EP311, EP317, EP322, EP627, OP226, OP693, P138, P257	Gomez-Iturriaga, A.	EP255
Giorli, E.	OP145	Gómez Palacios, A.	OP518
Giovanella, L.	EP032, OP337, OP535	Gómez-Río, M.	EP028, EPW24, OP375
Giovannini, E.	EP556, OP145, P243	Gomez Veiga, F.	EP261
Giraudet, A. L.	EP777	Gonçalves, A. C.	EP599, OP673
Girault, S.	EP078, EP796	Gonzales, G. R.	EP436
Giron, A.	EP124	Gonzales, S.	EP436
Giubbini, R.	EP175, OP539, OP682, PW24, TP056, TP067	Gonzales-Caramona, M. A.	EP498
Giuliani, A.	P255	Gonzalez, L.	EP296
Giuliani, C.	P027	Gonzalez, M.	EPW54
Giuliani, M.	OP275	González, R.	EP463
Giunchi, F.	EP265, EPW75	Gonzalez, S.	EP624, EP794
Gizewska, A.	EP439	González-Barca, E.	EP167
Gjedde, A.	EP037, OP372 , OP619 , P230 , P288 , P295 , P296	González García, F.	EP243, P043
		Gonzalez-Gay, M.	OP195
		González Jiménez, A.	EP072, EP293, EPW37, OP375

Gonzalez Ortiz, S.	EP022	Gröller, F.	EP163
Gonzalez-Roiz, C.	EP455	Gromova, E.	P287, P291
Gonzalez Selma, M.	P093	Gronowski Edner, A.	EP582
Goorts, B.	EP055	Grootendorst, M.	EP491
Gopalan, D.	EP691	Groothuis, M.	EP775
Gorczevska, I.	EP721	Grootjans, W.	OP297
Gorincour, G.	P115	Groot Koerkamp, M. L.	EP422, OP493
Görken,	EP553	Gröschl, M.	EP727
Gormsen, L. C.	EP168, OP686, PW26, TP034	Grosso, M.	EP114, EP128, P117
Görres, S.	EP639	Grosu, A.-L.	OP596
Gortanla, N.	EP204	Grötzinger, C.	EP643, OP487, OP585
Gosewisch, A.	EP484 , EPW15, OP111, OP650	Grotzky, A.	EP678
Goshen, E.	EP774 , OP191, OP362	Gruber, L.	EP139, EP479
Goto, K.	P048	Gruchala, M.	P018
Gotou, H.	EP683	Grueneisen, J.	EP572, OP501, OP502, OP505
Gotthardt, M.	EP430, EP587, EP697, EP803, EP806, OP173, OP175, OP222, OP364, OP365, OP367, OP641	Grunenwald, S.	EP389
Gottilla, R.	P073	Grünwald, F.	EP379, EP775
Gouillet-Patiri, A.	EP624	Grupe, P.	EP029, EP037, P240
Gould, S.-M.	EP491	Gschwend, J.	EP266, OP074
Goutal, S.	OP315	Guameri, V.	EP066
Gouveia, P. B.	OP126	Guasp, M.	EP511, EP520
Gouverneur, V.	EP851, EPW87, EPW96, PW33	Guberina, N.	EP579
Głowacka, I.	EP781	Guedea-Edo, F.	EP160
Goze, C.	EP664 , OP588	Guedj, E.	OP373, P115
Gracan, S.	P201	Guenova, M.	EP179
Gracia-Sánchez, L.	EP018, EP116, EP131, EP160, EP167, EP230, OP031, OP374, P137, TP096	Guensi, A.	EP015, EP125, P173
Grafe, H. V.	EPW74	Guermazi, F.	EP381, P195
Grafinger, K.	EP851, EPW96, PW33	Guerra, L.	EP095, EPW09
Grakova, E. V.	P066	Guezguez, M.	EP331, EP370, P165
Grall, N.	OP696	Gugiatti, E.	EP169
Grana, C.	EPW06, EP546, OP332, OP680	Guglielmi, J.	EP447
Granberg, D.	EP502	Guglielmo, P.	EP095 , EPW09
Grangeon, C.	EP628	Guibelalde, E.	EP413
Gräslund, T.	OP591	Guida, A.	P242
Grassi, E.	EP813, EPW46	Guidalotti, P.	OP035
Grasso, R.	OP033	Guidoccio, F.	EP114, P117, P259
Gravand, A.	EP648	Guidoux, C.	OP418, OP419
Graves, S. A.	OP592	Guillaud, O.	EPW21
Gray, M.	EP414 , OP131	Guillemetz, L.	OP366
Graziani, T.	EP223 , EP264, OP077, OP335	Guillemin, M.	EP666, EP812, OP250, OP287, OP588
Grebieniow, B.	EP758	Guillen, E. F.	OP377 , OP410
Grech-Sollars, M.	OP652	Guillén, F.	EP224
Green, M.	EP800	Guillén-Valderrama, E. F.	EP814
Green, R.	EP534 , OP460, OP461	Guillerminet, C.	EP078, EP796
Greenman, J.	OP488	Guillet, B.	EP624, OP344, P115
Gregianin, M.	EP206	Guilloteau, D.	EP826, EPW95
Gregoire, E.	P115	Guiot, T.	EP465, OP393
Gregory, R.	EP742 , OP136	Guiote Moreno, V.	P118
Greguric, I.	EP825, EPW78	Guitian, R.	TP100
Greisen, G.	OP197	Guitián Iglesias, R.	EP337, EP342, EP344, P162
Grierosu, I. C.	P183	Guittou, T.	EP451
Griesmacher, A.	EP277, P108	Gül, S. S.	EP082 , EP383
Grigg, J.	EPW91	Gulaka, P. K.	EP574, OP503
Grigolato, D.	EP031 , EP260, EP390 , EP402, P130 , TP028, TP033	Gulaldi, N. C. M.	P172
Grigoriev, E.	P139, PW08	Gulcelik, M. A.	EP281
Grillea, G.	OP653	Guldu, O. K.	OP668
Grimmer, T.	OP147	Güler, G.	EP082
Grimwood, A.	OP138	Güler, R.	OP311
Grishaev, S.	P011	Gulliver, N.	OP279 , P121, TP002
Grivet Fojaja, M.	EP259	Gulya, M.	P031, P066
Grizzi, F.	EPW25	Gulyás, B.	EP590, EP766
Gmnek, M.	EP249 , P092	Gumuser, G.	EP324, TP022, TP038, TP070
Grobelyny, J.	OP672	Gunalp, B.	EP345, EP346, EP700 , OP141, OP573
		Güner, L. A.	EP112
		Gungor, S.	EPW69 , EPW71
		Gunjaca, I.	P201

Günther, L.	OP314	Hallmann, S.	OP487
Gupta, M.	EP276	Halty, A.	EP777
Gupta, R.	EP146	Hamana, T.	EP064 , EP091, EP699, P050
Gupta, S.	OP651	Hamed, A. M.	P078
Gupta, T.	EP025	Hamidi, S.	TP013, TP055
Gupta, V.	OP444	Hamill, J. J.	EP751
Guryanov, I.	EP334	Hammami, H.	P187
Gustin, P.	EP796	Hammond, E. N. B.	EP350
Gutierrez, L.	EP463	Hamza, F.	EP381, P195
Gutiérrez Martin, P.	EP222	Han, C.	EP145, OP609
Gutiérrez Rodríguez, T.	OP518	Han, S.	TP012, TP039
Guttilla, A.	EP004	Han, S.-U.	EP141
Gutu, M. M.	P183	Hanaoka, K.	EP490
Guzmán Cruz, J.	EP184, OP180	Handgraaf, H. J. M.	EPW35, OP642
Guzman Cruz, Y.	EP202	Handkiewicz-Junak, D.	EP329
Gykiere, P.	OP142, P149	Hannequin, P.	P027
		Hannestad, J.	OP312
Ha, J.-M.	EP356, P206, P217	Hänscheid, H.	EP477
Ha, S.	OP571	Hansen, A. E.	EP570, EP836, P136
Ha, Y. S.	EP606	Hansen, C.	P296
Haahr, H.	P296	Hansen, J.	OP273
Haam, S.	EP143	Hansen, M.-T.	TP082
Haaparanta-Solin, M.	EP851, EPW96, PW33	Hansen, N. L.	OP506, OP512
Haas, H.	OP345	Happel, C.	EP379, EP775
Haass, C.	OP317	Hara, N.	TP065
Habbeche, M.	EP215, EP348, P059, P064, P175, P214	Harada, M.	EP013, P276
Haberkorn, U.	EP239, EP268, EP270, EP552, EP557, EPW13, EPW84, OP022, OP025, OP108, OP148, OP454, OP552, OP556, OP557	Harald, L.	P227
	EP124, OP183, P246	Hardiansyah, D.	EP499 , EP658, EP783, EP784, OP110, OP392 , OP634
Habert, M. O.	OP541, P151	Hardwigsen, J.	P115
Habraken, J. B. A.	EP274	Harhangi, B.	P156
Hacker, C.	EP134, EP163, EP233, EP363, EP615, EP636, EP718, EPW11, OP032, OP038, OP115, OP241, OP253, OP286, OP403, OP405, OP500, OP551, OP648, OP649	Harms, H. J.	TP034
Hacker, M.	OP068	Haroon, A.	P074
	EP621, EP626	Harrington, K.	EPW65
Hackett, S. L.	EP268	Harris, R.	P227
Hadad Dabaghi, H.	EP179, EP187	Hartenbach, M.	EP233 , EP615, EPW11, OP032 , OP405, OP500, OP551
Hadaschik, B.	EP417, OP305	Hartenbach, S.	EP233, OP032, OP500, OP551
Hadzhiyska, V.	EP543	Hartmanova, M.	EPW39
Haeck, J.	OP463	Hasaan, A.	EP336
Haeger, A.	EP472, EPW54	Hasani, N.	EP227, EP415
Haenny, G.	OP089	Hasbek, Z.	EP082, EP162 , EP383
Häfeli, U.	OP024	Hasenclever, D.	OP179
Haféz, H.	OP281 , TP031	Hashemizadeh, M.	EP621, EP626
Hage, D.	EP586, P227	Hashim, J.	EP122
Hagerman, J.	EP740	Hashimoto, H.	EP699, P024 , P050
Häggkvist, J.	OP391	Hashimoto, M.	OP285
Haghighatafshar, M.	OP249	Hashimoto, R.	TP065
Hagmarker, L.	EP043, EP049	Hashimoto, S.	EP323
Hahn, A.	EP500	Hashimoto, T.	EP090, EP172
Haidar, M.	OP399	Hassad Ben Ticha, R.	P170
Hain, S.	EP448	Hassan, A.	EP001, OP086, P099
Haji Dheere, A.	EP425	Hassanin, D. A. M.	P197
Hakim, B.	EP194, EP298, EPW42, OP223	Hassanzadeh-Rad, A.	EP081 , EP209, P012
Hakiminezhad, M.	OP544	Hassing, C.	OP248
Halaç, M.	EP720	Haste, P.	OP012
Halacli, S. O.	OP565	Hatakeyama, T.	EP026, EP030, OP256, P235, P236
Halekoh, U.	EP703	Hatami, N.	EP020
Halkovich, A.	P143	Hatano, K.	EP830
Hall, A.	EP723, EP793	Hatazawa, J.	EPW60
Hall, D. O.	EP204 , OP687	Hatzioannou, S.	EP795
Hall, J. R. W.	EP586, EP590, EP766, EP827, OP303, OP316, P227	Hatzipavlidou, V.	EP795
Hall, N. C.		Haufè, S.	OP556
Halldin, C.		Haug, A.	EP036, EP134, EP163, EP233, EP363, EPW11 , OP032, OP241, OP405, OP551, OP649

Hauser, S.		EPW12, EPW14	Hesse, S.	OP617
Havariyoun, G.	EP416 , EP726, OP279,	OP676 , TP002	Hesterman, J.	EPW36
Havel, M.		P047, P053 , P102	Hettlich, B.	PW04
Hawlina, S.		EP249, P092	Hetzheim, H.	EP239
Hay, T.		OP490	Heurling, K.	EP582 , OP065
Hayasaka, K.		EP683	Heusch, P.	EP696
Hayashi, K.		EP151	Heydorn Lagerlöf, J.	OP132
Hayashi, M.		EP715	Heye, T.	OP083
Hazarika, D.		EP276	Heyerdahl, H.	OP513, OP548
Hazenberg, B. P. C.		OP700	Hichri, M.	EP447
He, P.		EPW90	Hicks, R. J.	EP486
He, S.		EP059	Hida, S.	P036, P048
He, X.		P192, P192	Hienzsich, A.	EPW87
Heatley, M.		PW29	Higashi, T.	P292
Heber, D.		EP718	Higashiyama, A.	EP091
Hedeer, F.	OP281, OP477, OP511,	P069 , TP031	Higgie, J.	OP428
Hedén, B.		P069, P075	Higgins, G. S.	OP068
Hedenstierna, G.		OP517	Higuchi, T.	EP316, OP290
Heemskerck, J.		OP142	Hildebrandt, M.	EP047, EP092, EP109 ,
Hehenwarter, L.		OP485 , P056	Hill, P. J.	OP062
Heijtel, D. F. R.		P237	Himmelreich, U.	OP615
Heikkonen, J.	OP390, OP633		Hinderberger, P.	OP617
Heimann, U.		EP481	Hindié, E.	EP473
Hein, R.		EP203	Hindorf, C.	EP420, OP281, OP477, OP511,
Heinzel, A.		EP369	Hinton, P.	EP374, EP516 , EP723, EP793
Hekimsoy, T.		EP562, EP568	Hippeläinen, E.	P054, P294
Hekman, M.	OP119 , OP640 , OP641		Hirabayashi, S.	EP090, EP172
Helal, B.	EP080, OP081, OP251		Hirakawa, H.	EPW03
Helberg, A.		EP831, P083	Hirata, K.	OP029, OP177
Helbich, T. H.		OP241	Hirose, K.	P036 , P048
Helin, S.		EP840	Hiroual, S.	P170
Hellingman, D.		OP643	Hitzel, A.	EP389
Helmer, C.		P252	Hives, F.	P170
Helsen, M. M.		OP306	Hladunski, M.	EP577
Helsen, N.		OP080	Ho, D. T.	EP616
Hemmingsson, J.	EPW48 , OP132, OP391		Hobday, T.	OP394
Henderson, D.	EP825, EPW78		Hober, S.	OP172
Henderson, L. A.		TP088 , TP103	Hocevar, M.	PW06, TP004, TP073
Hendifar, A.		OP394	Hodolic, M.	EP004, EP247
Hendricksen, K.	EP226, OP643		Hoekstra, A.	EP790
Hennequin, C.		EP302	Hoekstra, C.	PW07
Henninger, B.		OP294	Hoekstra, O.	EP309, OP080, OP593, OP599,
Henry, C.		OP366	Hoeping, A.	EPW87
Hentic, O.		OP631	Hoff, C. M.	TP098
Henzlova, L.		P053	Hoffmann, F.	OP346
Herance Camacho, J.		EP638	Hofman, M. S.	EP486
Hermann, R.		OP522	Hofstetter-Hörl, K.	EP339
Herms, J.		OP317	Högberg, J.	EPW48
Hernandez, E.		EP543	Höglinger, G.	OP059, OP425
Hernandez, G.		EP296	Hohara, S.	EP490
Hernandez, R.		OP308	Hohaus, S.	EP174
Hernández Fructuoso, M.	EP638 , EP651		Hohberg, M.	EP483
Hernandez-Garcia, M.		EP401	Hohn, A.	OP118
Hernandez Martin, A.		P123	Høilund-Carlsen, P.	EP029, EP037, EP047, EP092,
Hernandez Martinez, A.	EP127, EP231, EP084			EP109, EP201, EP397, EP559, EP585,
Hernández Pascual, C.		EP638		EP671, EP674, EP720, OP242, OP273,
Hero, B.		OP084		OP568, P240, P241, TP093, TP097
Herranz, F.		OP229	Højgaard, L.	EP054, EP573, OP197, OP248
Herrero Muñoz, A.		EP310, P034	Holden, D.	OP312
Herrmann, K.		OP290	Holdgaard, P.	EP559, OP361, OP570 , P196 ,
Herth, M.		EP605	Holgersson, K.	TP094
Hervé, G.	EP124, OP183		Holland, C. H.	OP522
Hery, G.		P115	Holm, J.	EP573
Heskamp, S.	OP489 , OP641		Holm, S.	EP029, EP092
Hess, P.		OP465	Holmberg, B.	EPW17, TP026
Hess, S.	EP037, EP201, EP585, OP242		Holness, J.	OP562
				OP037 , OP039

Holte, H.	EP492	Hubber, J.	OP277, OP569
Holtedahl, J.	TP090	Huchet, V.	EP263
Homans, F.	OP080	Hudyana, H.	OP426
Hommada, M.	P089	Hudzietzova, J.	EP810, EP820
Honari, P.	EP818	Huegli, S.	OP587
Honarvar, H.	EP522, EPW81, OP172, OP589	Huerga, C.	EP413 , EP797
Honda, M.	EP252, TP003, TP010 , TP059	Hughes, A.	EP747
Honeyfield, L.	OP652	Huiban, M.	OP341
Hong, F.	OP082	Huic, D.	EP129
Hong, H.	OP304 , OP669	Huijbregts, J. E.	OP683
Hong, S.	OP571	Huisman, M.	OP593
Honings, J.	EP115	Huizing, D. M. V.	EP282
Hooshyar Yousefi, B.	OP059	Huizing, E. D.	PW25
Hope, T.	EP239	Humbert, O.	OP246, OP353
Hopin, J.	EP771	Humm, J.	EP164
Horenblas, S.	EP226, OP643	Hungria, P.	EP497
Hori, M.	OP285	Hunter, J.	EP821
Horikoshi, H.	EP005	Huo, Y.	EP589, EP622, EP845,
Horitsugi, G.	EPW60		OP121, P145
Horn, P.	EP506	Hur, H.	EP141
Horninger, W.	EP277, EP479	Hur, M.	EP600, EP633, EP849
Horváth, G.	EP834	Hurkmans, C. W.	OP296
Horváth, I.	EP640	Hurtado, A.	EP543
Horvatic Herceg, G.	EP129, EP713, P202	Hussein, A. E. M.	OP087
Ho-Shon, I.	EP133, OP036	Hustinx, R.	EP835
Hosokai, Y.	TP063	Huttunen, H.	P244
Hosokawa, C.	EP715	Huygen, F.	P156
Hosokawa, M.	OP029	Huylebrouck, M.	OP142
Hosokawa, S.	TP011	Huynh, P. T.	EP606
Hosono, M.	EP490 , EP715 , EP802	Hvidsten, S.	OP568
Hosoya, T.	EP034	Hwang, H.	EPW02
Hossein Foucher, C.	OP091, OP603	Hwang, J.	EP372, P256
Hossen, L.	EP459	Hwang, K.	EP148
Hossu, G.	OP201	Hyafil, F.	OP194, OP418, OP419, OP423, OP560 ,
Hosur, A.	OP333		OP565, OP605 , OP696
Hottinger, A.	P265	Hyde, B. M.	P271
Hou, X.	EP431	Hyun, I.	P114
Houdu, B.	P045		
Houot, L.	EP812	Iagaru, A.	OP076 , OP504
Hourani, M.	EP043, EP049	Iakovidou, A.	P070
Houseni, M.	OP034	Iakovou, I.	EP332 , PW10
Houshmand, S.	EP037	Ialongo, P.	OP336
Houzard, C.	EPW21, EPW21	Iampietro, E.	OP478
Hoving, B. G.	OP216 , OP484	Iannalfi, A.	EP121
Howman-Giles, R.	P177	Ibáñez, B.	EP462, EP496
Hoyer Mathiasen, B.	TP015 , TP094	Ibáñez Ibáñez, M.	EP250, EP441, EP471, EP682
Hruby, G.	OP550	Ibatici, A.	EP169, OP408
Hruby, V.	EP586	Icer, S.	EP729
Hsiao, E.	EP500, OP550	Ichikawa, T.	EP005
Hsu, C.-L.	OP178	Ieritano, C.	EPW93
Hsu, D. F. C.	EP770	Iftode, C.	OP355
Hsu, S.-T.	EP038, OP491	Igarasahi, Y.	P048
Hsu, Y.-J.	TP052	Igarashi, Y.	P036
Hsu, Y.-L.	EPW38	Iglesias Flores, E.	P118
Hu, B.	OP024	Ignacio Alvarez, E.	EP362
Hu, C.	EPW73	Iida, H.	P231
Hu, J.	OP586	Ikebuchi, H.	EP802
Huang, C.-W.	EP038, OP491	Ikeda, H.	EPW60
Huang, E. L.	EP663	Ilan, E.	EP578
Huang, F.-T.	EP038, OP491	Ilgan, S.	EP281
Huang, H.	P192	Ilhan, H.	EPW15
Huang, K. P.	EP663	Ilija, E.	P113
Huang, W.-S.	EPW57	Il'in, N.	EP181
Huang, Y.	OP312	Il'ina, E.	EP634
Huang, Y.-Y.	EPW38, TP005	Ilina, E.	EP535, EP635
Hubalewska-Dydejczyk, A.	P095	Ilushenkova, J.	EP635

Ilyas, H.	OP686	Jackson, A.	EP309
Ilyushenkova, Y.	EP701, EP709	Jackson, P. A.	EP486
Imabayashi, E.	P281	Jacobsen, S.	OP568, P288
Imamović, L.	EP278, EP391, OP553	Jacobson, A.	OP284
Imamura, T.	EP715	Jafari, M.	EP349
Imaz, L.	OP377	Jaffrain-Rea, M.-L.	EP567
Imbert, L.	OP508, OP560, OP563	Jaffray, D. A.	OP275
Imberti, C.	OP400	Jager, P. L.	EP422, OP493, OP534, PW25
Imbriaco, M.	OP461	Jaillard, A.	P274
Imperatori, A.	EP156	Jaimini, A.	EP035
Inagaki, M.	EP490	Jain, T. K.	EP120, EP229
Inagaki, T.	EP027	Jakobsen, S.	EP685
Iñárraeraegui, M.	OP016	Jakobson Mo, S.	EP827
Ince, I.	OP668	Jaksic, E.	OP040, OP042, P205
Ince, S.	EP345, EP346 , EP700, OP141 , OP573	Jakuciński, M.	OP520
Incerti, E.	EP101	Jalilian, A.	EP621
Indirani, E.	P129	Jalkanen, S.	OP517
Indirani, M.	EP688	Jaller, R.	EP290, EP294, PW09
Indovina, L.	EP308, EP311, EP317, EP322	Jamaati, H.	EP693, EP804
Infantino, A.	EP487	Jamali, M.	EP020
Ingemyr, H.	EP586	Jamar, F.	EP489
Innes, D. R.	EP770	Jambi, L. K.	EPW34, EPW35
Ino, T.	TP060	Jambor, I.	OP354, OP688
Inokuchi, M.	EP007	James, V. M.	EP482
Inoue, H.	EP683	Jamet, B.	OP407
Installé, J.	EPW08	Jammaz, I.	EP594, EP595
Iommelli, F.	OP116 , OP120	Jampana, R.	TP082
Ionescu, T. M.	OP274	Jamsek, J.	P092
Iori, M.	EPW92	Jan, H.	EP150, P074
Iozzo, P.	EP743, EP773	Janecskó, M.	P067
Ippolito, V.	EP216, P073	Janica, M.	OP540
Ipuy, M.	EP664	Jankovic, M.	EP391, OP040, OP042, P205
Iqbal, R.	OP599	Janousek, J.	EP531
Irache, J.	EP637	Jansen, E.	TP051
Irie, S.	EP027	Jansen, T.	EP430
Irishina, J.	P291	Jansen-Jarolim, E.	EP623
Irishina, Y.	P226	Jansma, E. P.	EP309
Isaac, S.	OP601	Janssen, I. M. C.	OP365
Isgoren, S.	EP562, EP568	Janssen, M.	EP697
Isgro', M.	OP226	Janvier, L.	P061
Ishibashi, K.	EP830	Jardak, I.	EP381, P195
Ishida, J.	EP151	Jarden, J. O.	EP037
Ishii, K.	EP715, EP830	Jarlier, M.	OP545
Ishimori, T.	EP405	Jaron, A.	EP855
Ishiwata, K.	EP830	Jarzab, B.	EP329
Isidoro, J.	EP328, EP815, P150, P212	Jarząbski, A.	EP207
Ismailov, A.	P011	Jasiakiewicz, K.	OP225
Isnardi, V.	OP298	Jaspers, K.	EP791
Isohashi, K.	EPW60	Jastrzębski, J.	OP445, OP672, OP675
Israel, I.	PW32	Javaid, A.	OP090
Israel, O.	EP772, OP697	Javier Gómez Hidalgo,	P103
Itikawa, E.	P279	Jaworska, A.	OP317
Ito, S.	EP335	Jaykanth, A.	EP688, P129
Ito, T.	EP490	Jeans, S.	OP136
Ito, Y.	TP021	Jedlicka, M.	OP521
Itoh, K.	OP029	Jegade, O.	OP082
Itoh, M.	EPW03	Jeljeli, S.	EP581
Itoh, S.	EPW03	Jensen, A. I.	EP836
Itti, E.	OP030	Jensen, J. B.	OP108
Iuele, F.	EP213, PW23	Jensen, J. D.	TP098
Iung, B.	OP696	Jensen, P. T.	EP109
Iwano, S.	EP335	Jensen, S. B.	EP448
Iwanowski, J.	OP225	Jensen-Jarolim, E.	EP636
Iwata, K.	EP699 , P050	Jensterle Sever, M.	PW06
Izzeldin., M.	EP817	Jeong, D.	EP283
		Jeong, J.	EP356, OP537 , P147, P206, TP053

Jeong, S.	EP356 , OP537, P206 , P217	Jünemann, K.-P.	EP234, EPW04
Jeong, Y.	P147	Jung, J.-W.	EP052
Jeong, Y.-J.	EP052	Jung, J.	EP143
Jeremic, M.	EP816	Jung, J.-M.	EP646
Jessop, A.	OP496	Jungen, C.	P083
Jessop, M.	OP333, OP480	Junior, E. P.	EP225
Jeziarski, J.	P085	Jüptner, M.	EP003, EPW04
Jhahharia, A. K.	EP235	Jurasinovic, Z.	EP713, EP714
Jhao, Y.-T.	PW34	Jurgilewicz, D.	EP385, EP577
Jiang, Q.	EP839	Juri, H.	EP091
Jiang, Z.	EP733, OP486	Jyrkkiö, S.	OP688
Jimenez, J.	EP455		
Jimenez, L. D.	OP392, OP634	Kabala, J.	P143
Jiménez-Alonso, M.	EP021, OP195 , OP431	Kabasakal, L.	EP194, EP244, EP245, EP392, EP466, EP504, EP547, EP614, EP808, EP858, EPW42, EPW44, OP014, OP223, OP679
Jiménez-Ballvé, A.	EP045, EP057, EP061, OP698 , PW21		
Jiménez-Bonilla, J.	EP021, OP195, OP431		
Jiménez-Borreguero, L.	EP736	Kaboteh, R.	EP415
Jiménez-Hoyuela García, J.	EP532	Kacperski, K.	OP357
Jiménez Londoño, G.	OP075, OP240, OP369, EP222 , EP689	Kadokami, T.	OP284
Jimeno Permett, R.	EP692	Kaeding, C.	OP567
Jingu, K.	P013	Kaehkoenen, E.	OP348
Jin Yung, P.	TP071	Kaekelae, M.	OP348
Jinzaki, M.	EP151	Kafouris, P.	OP420
Jiskrova, H.	OP041	Kafshgar, A.	EP081
Jóba, R. P.	EP519	Kagawa, S.	P292
Jochumsen, K.	OP242	Kagna, O.	OP697
Jochumsen, M. R.	TP098	Kähkönen, E.	OP354
Joemon, J.	EP581	Kahl, B.	OP082
Joergensen, H. B.	OP361	Kahl, F.	EP227, EP415
Joergensen, M. M.	TP026	Kakiuchi, T.	EPW77
Jögi, J.	P035, P037	Kakkar, N.	EP235
Johannesen, H. H.	P136, PW02	Kakumoto, K.	P292
Johansson, B.	TP086	Kalantari, F.	P012
Johansson, L.	EP827	Kalathoorakath, R. R.	P097
John, K. D.	EP495 , OP590	Kaldeway, P.	P151
Johnson, J. A.	EP706	Kale, C.	EP482
Johnson, M. S.	OP012	Kale, J.	EP435
Jois, A.	EP229, EPW29	Kalidonis, P.	P210
Jölck, R. I.	EP836	Kaliska, L.	EP062
Joling, M.	P277	Kalita, J. S.	P140
Joly, L.	OP201	Kalkinis, A.	P070
Jon, U.	EP016, EP394	Kalle, F.	EP381, P195
Jonášová, L.	EP384, EP438	Kalogeropoulou, K.	P113
Jonasson, M.	OP065	Kalogianni, E.	EP416, EP726 , OP676, TP002
Jones, A.	EP491	Kaloudi, A.	OP150, OP340
Joniau, S.	OP554	Kamal, I.	TP007
Joon Ho, Y.	TP071	Kamali, H.	EP648
Joossens, J.	P286	Kamali-Asl, A.	EP398, EP734, EP740, OP359
Joosten, L.	EP430, EP587 , OP173 , OP175	Kamibayashi, T.	EP027
Jorgov, L.	EP123, P067	Kamínek, M.	P047, P053
Jorques Infante, A.	EP028	Kaminska, A.	OP085
Joshi, A.	EP273	Kaminski, G.	EP439
Jouannot, E.	EPW36	Kamoun, T.	OP456
Joubert, M.	P228	Kamper, P. H.	EP168
Jovalekic, A.	OP378	Kampschreur, L.	PW07
Jovanovska, A.	EP214	Kamra, A.	EP435
Jover-Bargues, R.	P126	Kanaar, R.	EP667
Jover-Diaz, R.	EP455	Kanaev, S.	EP058, EP289, OP481
Jreige, M.	EP325	Kanai, Y.	EPW60
Juan, L.-Y.	EPW38	Kanapinn, P.	EP690
Juan Gabriel Villanueva Curto,	P103	Kanazawa, M.	EPW77
Juárez-Orozco, L.	OP610 , OP613	Kandee, A. A.	OP087
Judge, S.	EP449	Kandemir, Z.	EP079
Jukova, L.	EP058, EP289, OP481	Kanegae, K.	OP029
Julian, J.	EP065	Kang, D.-Y.	P147
Julka, P. K.	OP597		

Kang, J.	EP476	Kaya, B.	EP565
Kang, K.	OP571, TP053	Kaya, E.	EP729
Kang, L.	EP589, EP622, EP845, OP121, P145	Kayaalti, O.	EP729
Kang, S.-R.	EP312	Kaygisiz, O.	EPW23
Kang, S.-H.	EP067	Kazuhiro, S.	TP069
Kang, S.	EP052	Kearney-Schwartz, A.	OP201
Kang, Y.	OP424	Keat, N.	OP341
Kangai, Y.	EP744	Keidar, Z.	EP772 , OP697
Kannan, P.	OP064	Keijsers, R.	OP139
Kano, D.	EP612	Keinänen, O.	OP234
Kanoto, M.	EP034	Keizman, D.	OP338
Kanou, M.	TP060	Keller, H.	OP275
Kanoun, S.	EP408, OP246, OP353, OP406	Keller, S.	EP570, EP605
Kanzog, A.	TP024	Keller, T.	EP851 , EPW96, PW33
Kao, Y.	EP136, EP352	Kelloff, G.	OP687
Káplár, A.	EP253	Kellou, I.	P175
Kapp, T. G.	OP346	Kelly, J. M.	EP829, EPW94, OP021, OP024 , OP025, OP401
Kappadath, S. C.	EPW53, OP496	Kempen, P.	EP836
Kapur, S.	P090	Kemppainen, J.	OP348, OP354 , OP688
Kara, T.	EP565	Kendler, D.	EP217, EP277, EP479, OP294, OP457
Karaaslan, I.	EP468	Kennedy, J. A.	OP363
Karaaslan, S.	OP014	Kennel, S.	EPW59 , OP674
Karabacak, N.	OP261	Kenner, L.	EP233, OP500, OP551
Karacalioglu, A. O.	EP345, OP141	Kenny, L.	EP309
Karacavus, S.	EP729	Kentala, D.	P244
Karadayi, A. N.	EP188	Ker, W.	EP497, EP707, P088
Karagiannis, S.	OP400	Kerimel, I.	EP105, EP281
Karakan, T.	P204, P209	Kero, T.	OP190
Karakas, A.	OP141	Kerrou, K.	EP263
Karakatsanis, N.	OP193	Kerseman, V.	EPW62
Karakok, E.	OP544	Kertai, P.	EP677, EPW64
Karamivand, M.	EP648	Kertész, I.	EP596, EP597, EPW64
Karanikas, G.	EP134, EP163, OP241, OP649	Kesenheimer, C.	EP477
Karanja, Y.	EP658	Keskin, M.	EP079
Karapiperis, D.	PW10	Kesner, A.	EP440
Karataş, A.	EP392	Kessler, H.	OP346, OP566
Karathanos, E.	P040	Kessler, M.	OP202, OP313, OP319
Karayalçin, B.	EP212	Ketabi, A.	EP754
Karayel, E.	EP244, EP245, EP392, EP614 , EP858	Kettenbach, K.	EPW89
Karcher, G.	EP852, OP508, OP563	Khachirova, E.	P063, P065
Karczmarczyk, U.	EP523	Khalatyan, T.	EP367
Karfis, I.	EP423, EP503, OP393	Khalil, M.	EP731 , EP755, EPW47, P078
Karkani, M.	EP279	Khan, I.	EPW91
Karlberg, A. M.	OP254	Khan, M. U.	OP090
Karlsson, A.	EP823	Khan, N.	EP459
Karpenko, M. N.	P287	Khan, S. R.	EP691, OP260, P251
Karpov, R.	P086, P087	Khan, S.	OP260, OP277, OP569, OP652, P251, TP103
Karunanithi, S.	EP314	Kheder, A.	P220
Kas, A.	EP124, EP176, OP183, P246, P254	Khedr, M. H.	P023
Kataeva, G.	P226, P287, P291	Khelifa, A.	EP348, P059, P064, P175, P214
Kato, H.	EPW60	Kheruka, S. C.	P140
Kato, K.	EP252 , EP335, TP003, TP010, TP059	Khodjibekova, M.	EP181
Kato, M.	P279	Khomenko, I. G.	P287
Katsaboukas, D.	EP332, PW10	Khomenko, J.	P291
Katsampoukas, D.	P120	Khomenko, Y.	P226
Katsifis, A.	EP825, EPW78	Khorasani Gerdekoohi, S.	EP660, EPW33
Katsuta, N.	TP020, TP066	Khoshbakht, S.	EP529, EP530
Katunina, T.	P032, EP549	Khurshid, Z.	OP109
Kaufmann, J.	EP278, EP448, OP149, OP289	Kibedi, T.	EPW56
Kaul, A.	EP630	Kieboom, J.	OP352
Kaul, F.	OP149	Kiesewetter, D.	OP307
Kauling, R.	OP139	Kikuchi, F.	EP683
Kauppinen, T.	P104	Kilina, O.	P139
Kavallaris, M.	EP673	Kim, B.	EP633
Kaviani, S.	EP761, EP765, OP218	Kim, B.	EP046
Kawashiri, S.	EP007	Kim, B.	EP326, EP569

Kim, C.	OP196	Klaver, E. I.	OP534
Kim, D.	EP847, EP854	Klavžar, P.	P203
Kim, D.	EP122	Klebermass, E.-M.	OP403
Kim, D.	EPW94, OP021, OP024, OP025, OP401, OP424	Klein, C.	OP306
Kim, E.	EP136	Klein, I.	OP419
Kim, E.	EP283	Klein, R.	EP698, EP710, EP792, OP168
Kim, G.	EP849	Kleinberger, G.	OP317
Kim, H.	OP196	KleinJan, G. H.	EP226, OP134, OP643
Kim, H.-A.	EP569	Klein Nulent, T.	EP478, EP550
Kim, J.	EP406, EP722, EP846, EP847, EP854, P256	Klementyeva, O. E.	EP625 , EP625
Kim, J.	EP312	Klette, I.	OP150
Kim, J.	EP173	Kletting, P.	EP499, OP110 , OP392
Kim, J.	TP053	Klisarova, A.	EP196
Kim, J.	EP319	Kilinc Vicdan,	EP079
Kim, J.	EP433	Klonaris, C.	OP417
Kim, J.-W.	EPW26	Kluczyński, L.	P095
Kim, K.	EP476	Kluge, A.	EP432
Kim, K.	EP569	Kluge, R.	OP179
Kim, K.	EP433	Kluszczyński, D.	EP781
Kim, L.-S.	EPW02	Klutmann, S.	EP831
Kim, M.	OP354	Kmetiuk, Y.	EP083, EPW27
Kim, S.	EP173	Knäusl, B.	OP253
Kim, S.	EP600, EP849	Kneebone, A.	OP550
Kim, S.	EP148	Kniess, T.	EP844
Kim, S.	EP366	Knight, J.	EPW62, EPW63, OP490
Kim, S.	EPW26	Knoblich, M.	P180
Kim, S.-Y.	EP524	Knol, R. J. J.	EP558, P154, TP051
Kim, T.-H.	OP670	Knollema, S.	EP422, OP493
Kim, T.-S.	TP058	Knopp, M. M.	EP320
Kim, Y.	TP058	Knopp, M. U.	OP567
Kim, Y.	EP524	Knopp, M. V.	EP130, EP204, EP307 , EP320, EP551,
Kim, Y.-B.	EP141		EP669 , EP737, EP753, EPW32, OP017,
Kimiaei, S.	EP432		OP067, OP184, OP295, OP521, OP567,
Kimura, S.	EPW61, EPW86		OP687, P148, P225, PW04
Kimura, T.	TP081	Knopp, M. I.	EP320, EPW32, P148
Kimura, Y.	P281	Knudsen, C. S.	TP001
Kinahan, P. E.	EP786	Knudsen, G.	EP605
Kincl, V.	P047	Knuuti, J.	OP608, OP609
Kinuya, S.	EP007, OP285, P015, P248, TP047	Ko, C.-L.	TP042
Kirchner, J.	OP502	Ko, I.	EP569
Kirichenko, P.	P011, TP064	Kobarfard, F.	EP529, EP530
Kirienko, M.	EP157 , OP243	Kobayashi, K.	OP029
Kirihara, Y.	OP285	Kobayashi, Y.	EP831, P083
Kirii, K.	EP034	Kobe, C.	EP483
Kiriyama, T.	P269	Kobylecka, M.	EP387
Kirjavainen, A.	EP853, EPW91 , TP030	Koç, Z.	EP033 , EP338, EP541, EP565, EP694
Kirkineska, L.	P120	Koca, G.	EP426, EP446, OP544, P204, P209
Kis, A.	EPW64	Koch, G.	P264
Kisiel, N.	P177	Kocjan, T.	PW06
Kiso, K.	EP717	Kodina, G.	EP642
Kisovar, A.	P203	Koehner, M.	TP049
Kiss, A.	OP286	Koenders, M. I.	OP306
Kiss, T.	OP694	Koerber, A.	EP579
Kisteneva, I.	P086	Kogiku, A.	EP090
Kitagawa, Y.	OP177	Koglin, N.	EP020, OP378
Kitaguchi, K.	EPW67	Kohlmeyer, J.	EP203
Kitamura, C.	OP285	Koizumi, N.	P036
Kitaoka, A.	EP802	Kojima, Y.	EP612
Kitsou, E.-V.	EP279	Kokkomäki, E.	EP842, TP030
Kiviniemi, A.	OP688	Koksoy, E.	EP190
Kiyono, Y.	EP533	Kolacek, M.	P102
Kizhaev, Y.	EP367	Kolenc Peitl, P.	EP856
Kjær, A.	EP054 , EP570, EP836, P136	Kolesnikov-Gauthier, H.	EP042 , EP349, OP129
Kjær, M. S.	P136	Kolindou, A.	EP279
Kjærgaard, J.	P193	Koljevic Markovic, A.	EP391
Klaver, C.	OP587	Kolomiets, L.	EP097

Kolstad, A.	EP492	Kraeber-Bodéré, F.	EP011, EP012, EP380, OP407, OP681, P247
Komatsu, J.	P248	Krähling, T.	TP024
Koźminski, P.	EP528, OP672	Krainer, M.	EPW11
Komori, T.	EP064, EP091	Kramer, G.	EP309 , EPW11, OP551, OP599
Kong, E.	EP067 , OP537	Kramer, M.	EP686
Königs, U.	EP640	Kramer-Marek, G.	EP703, EPW65, EPW80
Konijnenberg, M. W.	EP430, EP782, OP547, OP581	Kráčmerová, T.	EP384, EP438
Konishi, T.	TP047	Kranenborg, E. J.	OP541
Konnert, J.	OP455	Kranenburg, G.	P091
Konno, T.	OP284	Kranert, W. T.	EP379, EP775
Konstantinou, M.	OP490	Krapf, P.	EP841, OP422
Konstantinov, N. A.	EP642	Krasnaliev, I.	EP196
Kooi, M. E.	OP416	Kiratli, P. Ö.	OP684
Koole, M.	EP756 , OP066, OP069, OP257, OP426	Kratochwil, C.	EP239, EP268, EP270, EP552, EP557, EPW13, OP148 , OP454 , OP552, OP556
Koopman, D.	EP422 , OP493	Krause, B. J.	OP118
Koopman, T.	P237	Krause, T.	EP678
Kopka, K.	EP239, EP268, EP270, EP837, EPW13, EPW84, OP022, OP023, OP444, OP552	Krebs, M.	EP363
Kopschina Feltes, P.	OP613	Krebs, S.	EP164
Koranda, P.	P053	Krebsová, A.	P033
Kordan, Y.	EPW23	Kreissman, S.	OP085
Korepu, P.	EP482	Krengli, M.	EP086, OP033
Körfer, J.	EP690	Krenning, E.	OP150, OP394
Koristka, S.	EP525	Krijger, G. C.	EP550, EP790, TP108
Korkmaz, A.	OP043, P021	Kristensen, B.	OP564, P216
Korkmaz, M.	EP426, EP446, P204, P209	Kristensen, V. A.	PW02
Korkusuz, H.	EP379	Kritzinger, V.	EP780
Körner, J. L.	EP643 , OP487	Krivonogov, N.	P029
Korol, P.	P167	Krivorotko, P.	EP058, EP289, OP481
Köseoğlu, D.	P107	Kroiss, A.	EP139 , EP277, OP457
Koshiba, Y.	EP252, TP003 , TP010, TP059	Królicki, B.	OP520, OP582
Kos-Kudla, B.	OP395	Królicki, L.	EP387, OP395, OP520 , OP582
Kostadinova, I.	P060, P094	Kroman, N.	EP054
Kostagiolas, P.	EP563	Krönke, M.	EP266 , EP274
Kostenikov, N.	EP181	Kropf, S.	OP405
Kostina, I.	P086, P087	Kropinska, A.	EP329
Kotb, M. H.	P188	Kroselj, M.	EP856
Kothandaraman, S.	EP610	Krstic, D.	EP816
Kothari, P.	OP401, OP424	Krstic, R.	EP816
Kotrotsios, T. D.	P030	Kryza, D.	EP777
Kotzasarlidou, M.	EP795	Krzhevitskiy, P.	EP058 , EP289, OP481
Kotzerke, J.	OP678, OP694	Krzyszmonik, A.	EP851, EPW96 , PW33
Kouijzer, I.	PW07	Kubánek, M.	P033
Koukalova, R.	EP679	Kubas, B.	EP577
Koulibaly, P. M.	EP745	Kubinyi, J.	EP195, EP820, OP041, P100 , P134, PW05
Koustoulidou, S.	EPW62 , EPW63	Kucuk, N. O.	EP190, EP485
Koutagiar, I.	OP417, OP420	Kucukatay, M. B.	PW28
Koutelou, M.	P070	Kucukatay, V.	PW28
Koutsikos, J.	EP437, P113	Kucukler, N.	OP611
Kovacic, J. C.	OP193	Kucukoz Uzun, A.	EP188
Kovács, T.	EP596, EP597	Kudo, S.	TP066
Kovačević-Kušmirek, K.	P039	Kudomi, N.	EP026, EP641, OP256 , P235 , P236
Koyama, K.	TP060	Kudrina, V.	EP474
Koyama, T.	EPW67	Kudryashova, N. E.	P038, P260
Koza, M.	EP071, EP757	Kuebler, W.	EP239
Kozeev, S.	EP367	Kuisma, A.	OP354
Kozgus Guldu, O.	TP080	Kuklinska, B.	EP577
Koziara, H.	OP520, OP582	Kukman, S.	P200
Koziolek, E. J.	EP643	Kula, M.	EP675
Koziolek, E. L.	OP487	Kulkarni, H.	EP480, EPW16, OP112, OP113 , OP150, OP459
Kozłowska-Gładki, J.	EP165	Kulkarni, S.	EP644
Kozłowski, K.	OP341	Kulke, M.	OP394
Kozmina, O. S.	P260	Kullberg, C.	OP477
Kp, H.	OP651	Kullberg, J.	EP582
Kraack, R.	TP006	Kumakura, Y.	OP619
Krackhardt, A.	EP203	Kumar, D.	EP035

Kumar, G.	EP211, EP300 , OP597	Lai, S. Y.	OP123 , OP124
Kumar, K.	EP526 , EP537 , EP609 , EP610	Laine, J.	EP850
Kumar, N.	EP232, P140	Laitinen, T.	P020
Kumar, R.	EP120, EP229, EP271, EPW29, OP125 , P097	Lajgaard, K.	TP014
Kumar, R.	EP044 , EP189, EP211, EP300, EP314, OP597	Lakeman, M.	TP046
Kumar, S.	EP590	Lakhani, P.	OP427
Kuśmieriek, J.	OP464, P039	Lakiotis, V.	P022
Kumita, S.	EP699, P050, P269	Lakkas, L.	P030
Kunikova, I.	EP811	Lalande, A.	OP287
Kunikowska, J.	OP395 , OP520	Laloux, M.	EPW08
Kunimoto, K.	EP252, TP003, TP059	Lam, M.	EP136, OP146, P091, P131
Kunita, Y.	P015	Lam, P.	EP825, EP857 , EPW78
Kuniyoshi, M.	TP021	Lamare, F.	P238, P252
Kunju, L. P.	EP407, EP409	Lamari, F.	P254
Kunz, P.	OP394	Lambert, B.	EP087, EP724, OP085
Kuo, H.-T.	EP527, OP020	Lambert, L.	EP195
Kuo, P.	OP427	Lambert, R.	OP198
Kuo, Y.-Y.	EPW57	Lambertini, A.	EPW72
Kupik, O.	EPW69, EPW71	Lambrecht, M. L.	OP296
Kurash, M.	OP697	Lambropoulou, M.	P153
Kurashima, A.	EP683	Lamche, M.	EP233, OP551
Kurazhiov, A.	P139, P208, PW08	Lammertsma, A. A.	P237
Kurch, L.	OP179	Lamotte, G.	P258
Kurihara, Y.	PW31	Lamprou, E.	EPW05
Kürpig, S.	EP602, EP652, EPW12, EPW14, OP023	Lancelot, S.	OP058
Kurt, A.	EP614, EP858	Landau, D.	OP602
Kurt, S.	OP313, OP319	Landecy, G.	P106
Kurt, Y.	EP354	Landgren, M.	EP415
Kurth, J.	OP118	Landkilde, N. C.	OP108
Kurzawski, M.	OP225	Landoni, C.	EP095, EPW09
Kusacic Kuna, S.	EP129 , P202	Lanfranchi, B.	EP088, EP089
Kusic, Z.	EP010, P127	Lang, O.	EP811
Kuslu, D.	EP338	Lange, C.	EP663, P249
Kusumoto, M.	EP612	Lange, P.	PW30
Kuszpit, K.	OP310	Langer, N. H.	EP570
Kutelev, G.	TP064	Langer, O.	OP315, P232
Kutluk, T. M.	OP684	Langer, S. W.	EP570
Kuwako, T.	P269	Langgaard Kristensen, J.	EP605
Kuwert, T.	EP275, EP686, OP018, OP515	Langhain, M.	OP428
Kuya, K.	PW39	Langhorst, J.	EP696
Kwee, R.	OP416	Langkjær, N.	EP585
Kwekkeboom, D.	EP220, OP394	Langsteger, W.	EP278, EP391, OP348, OP553 , OP555
Kwon, I.	EP576	Lanni, V.	EP627
Kyritsis, A.	P028	Langzenberger, R.	OP249
Kyrozi, E.	P070	Lapa, C.	EPW50, OP189, OP290
Laan, A.	OP671	Lapa, P.	EP815, EPW41, OP140, P150, P212
Lacasta, A.	EP208	Lapeña-Gutierrez, L.	EP057
Lacoeuille, F.	EP617, P159	Lapinska, G.	EP207
Lacombe, M.	EP078, EP796	Laranjo, M.	EP599, OP673
Lad, S.	EP644	Larg, M.	OP220, EP341, EP375, EP376
Ladefoged, C. N.	EP570, EP573, OP197, OP248 , OP249	Larionova, L.	EP632
Ladenstein, R.	OP085	Larivière, D.	OP194
Ladjohounlou, R.	EP494 , OP513, OP545	Larkina, M.	EP632
Ladno, W.	OP064	Laroche, T.	OP012
Lafargue, A.-E.	EPW88	La Rosa Salas, B.	EP689
Lafay, C.	EP823	Larroche, C.	P089
La Fontaine, M.	OP296	Larsen, H. C.	OP570
LaForest, R.	EP132, OP015	Larsson, A.	EP827, OP517
La Fougère, C.	EP017, EP429, OP130, OP135	Larsson, E.	EP420 , OP252
Lage, S.	EP225	Larsson, H. B. W.	OP197
Laghai, I.	EP256	Lass, P.	EP165, P018
Lago, M.	EP259	Lassen, M. L.	EP752, OP247, P232
Lahdenpohja, S.	EP853	Lasserre, M.	OP246
Lahousse, H.	OP091, OP603, P184, P274	Lassmann, M.	EP434, EP440 , EP448, EP449, EP477,
Lahoutte, T.	OP590, OP594		EPW50, OP289, OP290, OP635

Lasso Vázquez, J.	P152	Lee, S.	OP196
Laszczyńska, M.	OP225	Lee, S.	EP849
Laszlo, F.	EP514	Lee, S.	EP569
Latorre, I.	EP511, EP520	Lee, S.	EP283, EP319
Lattimer, J.	EP424	Lee, S.	EPW38
Lau, J.	EP527, OP020	Lee, S.	TP058
Lauenstein, T.	EP696	Lee, S.	EP141, EP143
Lavado-Pérez, C.	EP021, OP195	Lee, S.-J.	EP067
Lavados, H.	EP543	Lee, S.-M.	P206
Lavalaye, J.	P151	Lee, S.-W.	EP356, OP537, P206
Lavalle, M.	OP693, P138	Lee, W.	EP606, EP646
Lavatori, N.	EP497, P088	Lee, Y.	EP476
Lavelli, V.	EP135, EP221, EP236	Lee, Y. H.	EP410
Laverman, P.	OP306, OP345	Lee, Y.-S.	TP053
Lavrado, J.	EP536	Lees, J. E.	EPW34, EPW35
Law, I.	OP197, OP248	Lefebvre, M.	EP617
Lawal, I. A.	P160	Legallois, D.	P045
Lawson, G.	EPW08	Legendre, A.	OP091, P184
Law-Ye, B.	P246	Legouevéc, F.	OP366
Lazzeri, E.	P133	Le Gouill, S.	OP681
Lazzeri, P.	OP145	Le Guludec, D.	EPW95, OP170, OP192, OP418, OP419,
Le Bars, D.	OP616		OP423, OP560, OP565, OP605, OP696
Leblanc, E.	EP349, OP129	Lehel, S.	EP605
Lebouvier, T.	P247	Lehikoinen, P.	EP840
Lebron, L.	OP244	Lehn, C.	EP753
Lebtahi, R.	EPW49, EPW55, OP631	Lehnert, P.	P193
Lecchi, M.	EP746, P079	Lehnert, W.	EP432
Leccisotti, L.	OP693	Leisser, A.	OP405
Le Coz, P.	EP794	Leiter, I.	EP639
Le Dily, S.	P247	Lele, V.	EP482
Ledwon, A.	EP329	Lemarie, C.	EP617
Lee, B.	EP476	Lemos Pereira, E.	EP536, TP062
Lee, B.-F.	EP158	Leo, L.	EP517
Lee, B. J.	EP576	Leonardi, L.	EP306
Lee, B. Q.	EPW56	Leonardi, M.	PW38
Lee, C.	TP058	Leoncini, R.	EP556, P243
Lee, C.-N.	TP052	Leone, S.	EP186
Lee, C.-Y.	EP283	León-Ramírez, L. F.	EP178
Lee, D.	EP283, EP319	Leotta, K.	OP022
Lee, D.	EP141	Lepareur, N.	EP601
Lee, D.	P168	Leprince, C.	OP129
Lee, D.	OP571	Lescano, A.	OP428
Lee, D.-E.	EP588	Lesèche, G.	OP418
Lee, E.	EP073, EP076, EP491	Letaief, B.	EP039, EP705, P157, P190, P215
Lee, H.	EP148	Le Treut, Y.	P115
Lee, H.	EP847	Leung, C.	EP150
Lee, H.	OP196	Leurquin-Sterk, G.	OP615
Lee, H. H.	EP513, EPW18	Leva, L. M.	OP033
Lee, H.-J.	TP053	Levi, E.	EP024
Lee, J.	EP406, P256	Levigoureux, E.	OP058
Lee, J.	TP053	Levillain, H.	EP465, EPW49, OP393
Lee, J.	EP433	Levin, C. S.	EP574, EP575, EP576, EP770
Lee, J.	EP356, OP537	Levin, J.	OP425
Lee, J.	OP064	Lewington, V.	EP456, OP085, OP479, TP023, TP048, TP083
Lee, J.	P206	Lewis, J. S.	OP234
Lee, J.	EP600, EP633, EP849, OP670	Leygnac, S.	EPW95, OP560, OP605
Lee, J.	TP008	Lezaic, L.	EP249, P092, PW06,
Lee, K.	EP141		TP004, TP009, TP073
Lee, K.	EP574	Lhenry, D.	EP664
Lee, M.	EP133, OP036	Lhermitte, B.	P265
Lee, M.	EP433	Li, B.	OP586
Lee, M.	P114	Li, J.	TP012, TP039
Lee, M.	EP326	Li, J.	OP230
Lee, P.	EPW38, TP005	Li, L.	OP174
Lee, R. E.	OP488	Li, R.	OP338
Lee, S.	EP524, EP846, EP847, EP854	Li, S.	EP347

Li, S.	EP363	Liu, Y.	EP309
Li, T.	EP733	Liu, Z.	OP020, OP307
Li, T.	EP475	Livieratos, L.	EP456 , OP138, OP163
Li, X.	P192	Lizana, H.	EP827
Li, X.	EP718, OP286	Ljungberg, M.	OP299
Li, Y.	OP117	Ljunggren, A. E.	TP001
Li, Z.	OP486	Lladó-Garriga, L.	EP131, OP031
Liang, J.	OP638	Llamas-Elvira, J. M.	EP028, EP072, EP293, EP653, EP656, EP657, EPW24, EPW37, OP375
Liang, X.	TP012, TP039	Llarena, R.	EP255
Liang, Y.-T.	TP052	Lleó, A.	OP379, PW35
Liarte-Trías, I.	EP655, TP096	Llinares-Tello, E.	EP018, EP116, EP131, EP160, EP167, EP230, OP031, OP374, P137
Libánsky, P.	P100	Loaiza, J.	EP496
Liberatore, M.	OP334, P262, P280	Lobbes, M. B.	OP055
Lichikaki, V.	P041	Lobeek, D.	EP115 , EP806, OP343
Liepe, K.	EP424	Lobo, G.	EP497
Lim, H.	P250	Locantore, L.	EP031, EP260 , EP390, P130
Lim, I.	EP326 , EP569	Loch, C.	EP825, EPW78
Lim, S.	EP141, EP326, EP476, EP569	Lochner, C.	OP614
Lima, G.	EP121, EP223, OP035, OP335	Lococo, F.	OP598
Lima, J. P.	OP140	Lodi, F.	EPW72, EPW75, OP077, TP089
Lima, M. C. L.	EP060	Lodi, L.	EP687
Limam, K.	EP358, EP393 , P166	Lodi Rizzini, E.	OP335
Lima Oubiña, A.	EP838	Loening, A.	OP076, OP504
Limouris, G. S.	EP423 , EP501 , EP503 , OP636	Löfblom, J.	EPW82, EPW83, OP114, OP311
Lin, A.	OP275	Löffroy, R.	OP353
Lin, C.	TP027 , TP057	Löfgren, J.	EP570, P136
Lin, C. S.	EP410, P229	Loft, A.	EP054, EP573
Lin, H. H.	EP399 , EP410, EP750, EP764, P229	Lohr, F.	EP088, EP089, EP258
Lin, K.-L.	EP584	Loi, A.	EP400
Lin, K.-S.	EP527 , EP591, OP020	Loi, G.	EP086
Lin, M.	EP133, OP036	Loi, S.	EP400
Lin, N.	EP360	Loidl, W.	EP278, OP348, OP553, OP555
Lin, P.	EP133, OP036	Loimaala, A.	P239
Lin, S.-F.	OP312	Loira, F.	EP337, EP342, EP344, P162, TP100
Lin, T.	TP005	Lojo Ramírez, J.	EP182, EP200
Lin, W.-J.	EP584	Loke, K. S. H.	EP352
Lin, W.-Y.	TP052	Lomeña, F.	EP100, EP107, OP200
Lin, Y.-W.	EP038, OP491	Lo Moro, G.	OP538
Linares, S.	EP296	Lomperta, K.	OP540
Linchangco, E.	EP353	Løndalen, A.	EP492
Lindberg, L.	P216	London, K.	P177
Lindberg, U.	OP197	Long, N.	EP610, OP244
Lindbo, S.	OP172	Longari, V.	EP388 , EP395
Lindemann, M.	EP506	Longo, M.	EP371 , P253
Lindén, O.	EP420	Longton, E.	EPW08
Linder, J.	EP827	Looijen-Salamon, M. G.	OP079
Lindner, M.	EP798	Look, M. P.	OP171
Lindner, S.	OP317, OP425	Lopci, E.	EP306 , EPW25 , OP355 , OP655
Lindner, T.	OP118	Lopera Sierra, M.	OP394
Lindqvist, A.	P192	Lopes Alves, I.	OP066
Lindström, E.	OP311	Lopez, A.	TP100
Liolios, C.	EPW84	Lopez, B.	OP496
Lion, G.	P184	López, D.	EP074, EP155 , EP287, OP379
Lipman, A.	EP616	Lopez, L.	EP170
Lipponen, J.	P020	López-Arias, E.	P263
Lipponen, T.	EP850	López Cubillana, P.	EP250
Lishmanov, Y.	EP635, P029, P031, P041, P046, P066, P086, P087, P211	López-Defilló, J.	EP021 , OP195
List, A.	OP277	López de la Manzanara Cano, C.	EP098
Listewnik, M.	OP225	López González, P.	EP250
Liu, C.	OP503, OP685	Lopez Guerrero, M. A.	EP222
Liu, D.	EP136, EP472	Lopez Lopez, A.	EP337, P162
Liu, H.	OP591	López Martínez, E.	TP104
Liu, R.	EP347	López Melgar, B.	EP736
Liu, T.-T.	PW34	Lopez Mora, D.	PW35
Liu, X.	EP551 , OP567, OP584		

Lopez-Picon, F. R.	EP851, EPW96, PW33	Ma, M. T.	OP343, OP400
López-Prior, V.	EP386, P068 , P126	Maadi, E.	EP619, EP621
López Soler, F.	EP250	Maamoun, I.	EPW47, P078
Lo Presti, D.	EP332, PW10	Maaß, C.	OP632
Lorente, B.	P016	Maat, A. P. W. M.	EP667
Lorenz, R.	OP179	Maccafeio, S.	EP292
Lorenzini, D.	EP560	Maccauro, M.	EP458, OP011 , P186
Lorenzon, L.	EP371, EP460	Maccora, D.	P257
Lorenzoni, A.	P185, P186	Macholl, S.	EP801, EPW36
Loricera, J.	OP195	Maciag, A.	P085
Lorusso, M.	P138	Macià-Garau, M.	EP018
Loseto, V.	EP135	Mackie, S.	OP143
Loubinoux, I.	OP255	Macpherson, R. E.	OP068
Loudos, G.	EP661, EPW05	Macy, S.	EPW59
Louedec, L.	OP170	Madani, I.	EP087
Louet, C.	EP617	Madaschi, L.	OP478
Louie, J. D.	EP136	Madeddu, G.	EP218, EP330, P273, P275, P278
Loundou, A.	EP794	Madej, M.	P085
Lourenço, B. X.	TP102	Mader, A.	EP379 , EP775
Louw, L.	EP704	Madrid, J. M.	EP814
Louw, W.	EP599, OP673	Madsen, J.	EP054
Low, H. C.	EP352	Maecke, H.	OP149
Lozano Murgas, M. L.	P152 , P268	Maeda, H.	P044
Lozza, C.	OP545	Maeda, Y.	OP256, P235, P236
Lu, C.	EP839	Maeder, P.	P265
Lu, C.-C.	P109	Maenhout, A.	EP459
Lu, J.	OP486	Mäenpää, H.	OP390, OP633
Lu, S.-W.	P297	Maes, A.	EP716, EP779, OP080, PW03
Lu, W.	OP669	Maffey-Steffan, J.	P108
Lualdi, M.	P185	Magalhães, J.	EP497
Lubberink, M.	EP502, EP578, EP582, OP065, OP190, OP252, OP517	Maggio, S.	P255
Lucas-Calduch, A.	EP018	Magliery, T.	EP610
Lucena, F.	EP821	Magnander, T.	OP132 , OP391
Lucht, K.	EP676	Magnone, M.	EP662
Luciani, A.	OP030	Magnone, P.	P119 , P122
Lucignani, G.	EP746	Magnussen, R.	OP567
Lue, K. H.	EP399, P229	Magometschnigg, H. F.	OP241
Lugassi, R.	EP772, OP363	Magri, G.	OP539
Lugtenburg, P. J.	OP683	Maguet, M.	OP558, OP559, P049
Luikel-Hooghof, D. M. J.	TP037	Mahani, H.	EP398, EP734, EP769, OP359
Lukas, M.	EP663	Mahantshetty, U.	EP273
Lukas, P.	EP277, EP479	Maher, M.	EP138
Luksch, R.	P185, P186	Maheshwari, D.	OP064
Lukyanchikov, V. A.	P260	Mahida, B.	OP192, OP194, OP696
Luna, M.	EP065	Mahmoudi, C.	EP215
Lund, A. A.	OP242	Maier, A. K.	OP515
Lundqvist, A.	EP586	Maillez, A.	EP042
Luo, H.	OP592	Maina, T.	OP342, OP351, OP547
Luo, T. Y.	EP764	Maina-Nock, T.	OP150 , OP340
Luongo, C.	EP743	Maindron, N.	EP664
Luque Caro, R.	EP028	Mainolfi, C.	EP180
Luquero-Llopis, N.	EP386	Maior, R.	EP766
Luthardt, J.	OP617	Mairinger, S.	OP315
Lüthen, U.	EP676	Mairs, R.	OP545
Luthra, S. K.	EPW91	Maisonnette, P.	EPW06
Lütje, S.	EP242 , EP696, OP222 , OP641	Maite, F.	OP200
Luttrupp, F.	EP009	Majkowska, A.	OP445, OP675
Lützen, U.	EP003, EP234 , EPW04	Majkowska-Pilip, A.	EP528 , OP672
Luursema, G.	P091	Majós-Torro, C.	EP018, OP374
Lv, J.	EP659, OP228	Mäkelä, T.	P054
Lyapunov, A.	EP097	Makhdomi, K.	P158
Lymperis, E.	OP150, OP340	Makino, A.	EP533
Lyons, E.	EP835	Makis, W.	OP519
Ma, K.-H.	P297, PW34	Malagutti, N.	EP295
		Malbert, C.-H.	EP403 , OP366
		Malcolm, J.	EP443

Maldonado, A.	EP291, EP296	Marini, C.	EP169, EP662, OP127, OP233, OP262,
Malfait, I.	PW03		OP288, OP408, OP409, OP421, PW22
Malhotra, P. A.	P251	Marin Vera, M.	EP303
Mali, W. P. T. M.	P091	Mariotti, F.	EP469
Malik, D.	EP120	Mariscal, A.	EP065
Malizia, C.	TP089	Marjamäki, P.	OP688
Mallat, A.	OP030	Markewycz, A.	EP152
Mallia, A.	EP581	Markoula, S.	P028
Malmquist, J.	EP586	Marković, V.	P174
Maltsev, O. V.	OP346	Markovina, S.	OP015
Malvezzi, C.	EP128	Marotta, G.	P253, PW38
Malysheva, A.	EP625, EP642	Marović, A.	P174
Mamach, M.	OP202, OP313, OP319	Marques, I. A.	EP515
Mamede, M.	EP225	Marques da Silva, A.	OP066
Manabe, O.	OP029	Marquet, P.	P298
Manali, E.	EP680, EP681	Marra, C.	P257
Manca, G.	P259	Marrett, S.	P295
Mandal, A. K.	EP271	Marroquin, J.	EP084
Manfredi, M.	EP464, EP507, OP013 , P242	Marroquin Gálvez, J. A.	EP127 , P123
Manfrinato, G.	OP243	Marsden, P.	EP171, OP514
Manganelli, M.	OP460	Marshall, C.	OP227
Mangiacotti, F.	EP288	Martelli, G.	P146
Mangialardi, N.	OP693	Martens, J. W.	OP171
Mangili, G.	EP101	Marti, J.	EP628
Manglunia, A. S.	OP411, P272	Marti-Bonmatí, L.	EP418
Mango, L.	OP336	Martic, M.	EP616
Mani, V.	OP193	Martí-Climent, J.	EP470, EP799, EP814, OP016, OP377
Maniawski, P.	OP017, OP521	Martin, E.	EP545, EPW59
Manitto, M.	OP127	Martin, G.	OP300
Manna, R.	P138	Martin, Jr., E.	EP610
Mannarino, T.	EP180 , OP604, OP607	Martin, M.	EP545
Mannironi, A.	OP145, P243	Martin, R.	EPW87
Manresa, J. B.	OP358	Martina, I.	EP388, EP395
Manrique, A.	EP787, OP507, OP558 , OP559,	Martin Domenech, M.	P125
	P045 , P049, P228	Martineau, P.	EP792, OP198
	P186	Martinez, C.	EP593
Mansi, D.	EPW85	Martinez, T.	EP592, EP593
Mansi, R.	EP619	Martínez Albero, E.	EP127, P123
Mansoori, L.	P219	Martínez-Amador, N.	EP021
Mansour, S.	EP101, OP341	Martínez de Bourio, M.	EP045, EP061 , EP178, OP698
Mapelli, P.	OP200	Martínez del Valle Torres, M.	EP532
Mar, C.	EP183	Martínez de Miguel, B.	EP647
Marafí, F.	EP180	Martínez de Vega, V.	EP296
Marano, L.	P079	Martínez-Gimeno, E.	EP016, EP185, EP394
Marcassa, C.	OP513	Martínez Gomez, G.	EP441
Marcatili, S.	EPW25	Martínez-González, A.	OP075, OP240
Marchesi, F.	EPW25	Martínez-Lorca, A.	EP455
Marchetti, S.	EP458, OP011	Martínez-Lorca, A.	EP290, EP294, PW09
Marchianò, A.	TP067	Martínez-Pimienta, G.	EP533
Marchina, I.	OP410	Martínez Pozo, M.	EP021, OP195, OP431
Marcos, M.	EP487, EP488, TP089	Martínez-Rodríguez, I.	EP100
Marengo, M.	P117, P133	Martínez-Roman, S.	TP084
Margotti, S.	OP587	Martínez Sánchez, M.	P137
Mari, C.	TP103	Martínez-Torrents, F.	OP016, OP016
Maria, R.	P103	Martínez-Urbistondo, D.	EP243, P043
María Ángeles Ruiz Gómez,	OP338	Martín Fernández, N.	P199
Mariados, N.	EP834	Martin Gomez, E.	OP431
Márian, T.	OP507	Martín-Laez, R.	EP113
Mariano-Goulart, D.	OP201, OP508, OP560, OP563	Martin Marimon, J.	EP455
Marie, P.-Y.	P161	Martin-Rios, D.	TP017, TP018
Marikova, I.	P103	Martins, A.	EPW65, EPW80
María Luisa González Selma,	EP241	Martins, C. D.	EP328 , EPW41
Marin, A.	EP465, OP393	Martins, H.	OP274, TP044
Marin, G.	EP678	Martins, K. M.	PW29
Marincek, N.	P123	Martins, M.	OP511
Marin Ferrer, D.		Martinsson, E.	P264, P267, P290
		Martorana, A.	

Marx, M.	EP003, EP234, EP676, EPW04	Mazzaferro, V.	EP458, OP011
Marzo, K.	EP306	Mazzarella, G.	EP517
Mas, S.	P128	Mazzari, S.	EPW20 , P259
Maslov, L.	P086, P087	Mazzola, R.	EP085
Masoomi, M.	EP461	McAddy, N. C.	EP513 , EPW18
Masoumi, H.	EP621	McCarthy, M.	OP550
Massa, S.	EP400	McCarthy, T.	OP061, OP303, OP316
Massari, A.	EP292	McCready, R. V.	EP423, EP501, EP503, OP636
Massari, F.	EP264, EPW20	McDougald, D.	OP594
Massi, L.	EP088, EP089, EP258	McDougald, W.	EP800
Massollo, M.	EP340, EP340, OP535	McEwan, A. J. B.	OP519
Massone, A.	EP169, OP262	McGowan, D. R.	EP457, EP738, EP739, EP741, OP068
Massri, K.	EPW66	McGrath, J.	OP300
Matanza, D.	OP699	McKeown, C.	EP564
Mateo, J.	OP229, PW27	McLaughlin, M. F.	OP674
Mateo-Navarro, D.	EP655, EP799, TP096	McMullen, T.	OP519
Matesic, L.	EP832	McQuaid, S. J.	EP793
Máthé, D.	EP525, EP640	McRobbie, G.	EPW91
Matheoud, R.	EP086	Meades, R. T.	TP103
Mather, S.	EPW36	Meazza, R.	OP127
Mathieu, I.	EPW08	Meckova, Z.	EP195
Matis, S.	EP169, OP408, OP409	Mecocci, P.	OP373
Matějů, M.	EP629	Meddeb, I.	EP358, EP393, P166
Matovic, M.	EP361, EP816	Medea, S.	EP206
Matovina, E.	EP361	Medhus, J. B.	OP361
Matsuda, H.	P281	Medina Ornelas, S. S.	EP544
Matsuda, R.	TP020, TP066	Medine, E.	TP080
Matsuda, T.	EP490	Medini, I.	OP191
Matsui, T.	EP728	Medolago, G.	OP478
Matsumoto, K.	TP021	Medrano, S.	EP022
Matsumoto, Y.	P292	Medvedev, S.	EP019
Matsunaga, K.	EPW60	Medvedeva, A.	EP075 , EP097, EP634
Matsunari, I.	P282	Meeuwis, A. P. W.	EP751, EP803, EP806, OP297
Matsuo, S.	OP284, OP285, P015 , TP047	Mégarbane, B.	OP618
Matsutomo, N.	OP213	Meier, L. P.	EP678
Matsuura, E.	EPW61	Meier, R.	OP566
Matsuura, M.	TP081	Meignan, M.	OP406, OP681
Matsuyama, H.	EP005	Meijer, T. G.	EP667
Mattassi, R.	PW01	Meintjes, M.	OP217, OP482
Matthay, K.	OP085	Meisenheimer, M.	EP602, EP652
Mattheoud, R.	P079	Mekinian, A.	P089
Matthews, R.	EP063	Mekkawy, M.	EP708, EP711
Matti, A.	EP121, EPW75, OP035, OP335	Mele, L.	EP330
Mattner, F.	EP825, EPW78	Melhus, K. B.	OP548
Mattoli, M.	EP308 , EP311 , EP317 , EP322	Melie-Garcia, L.	P233
Matyskiel, R.	EP387, OP582	Melin, A.	TP050
Maughan, N.	EP132, OP015	Melis, G.	EP400
Maurel, C.	EP628	Melki, S.	EP331, EP370 , P165
Mäurer, A.	P249	Meller, B.	OP492
Maurer, T.	EP266, EP274, OP074	Meller, J.	OP492
Maurin, M.	EP523	Melnikov, A.	EP474
Maus, S.	EP645	Melo, I.	OP480
Mauxion, T.	OP012	Melotti, B.	EP264
Mawlawi, O.	EPW53	Memiş, H.	P052
Mayer, K.	EP498	Memmott, M. J.	EP735, OP497
Mayerhöfer, M.	EP036, OP405	Memoli, M.	EP186
Mayo, W.	P238	Mena, R.	OP149, OP289
Mayoral, M.	EP100 , EP107	Mena Bares, L.	P118
Maza Muret, F.	P118	Mendes, F.	EP536
Mazar, A. P.	OP304	Mendez, S.	EP463
Mazère, J.	P238	Mendiola, A.	EP208
Mazighi, M.	OP418, OP419	Mendler, C.	OP346
Maziotis, E.	P182	Mendoza Pares, M.	P125
Mazumdar, D.	P272	Menci, P.	P159
Mazurek, A.	EP071, EP439 , P076	Menendez, M. I.	EP669, EPW32 , PW04
Mazurek-Kula, A.	P039	Menezes, L.	OP191

Menezes, M.	EP205	Mikell, J.	EPW53
Mengi, Ö.	P052	Mikhaeel, N. G.	EP171, OP686
Menga, M.	EP365	Mikhailov, I. P.	P038
Mengus, L.	EP762	Miklovicz, T.	EP834
Menichetti, F.	P133	Miklovicz, T.	EP838
Menjon Beltran, S.	EP293	Mikołajczak, R.	EP523, EP604, EP855, OP395
Menon, S.	EP273	Mikropoulos, K.	EP661, EPW05
Mensa, G.	EP365	Milá, M.	P124
Menze, B.	EP266	Milacek, J.	EP320
Menke-van der Houven van Oordt, C. W.	OP593	Milachowski, S.	TP024
Mercadal-Vilchez, S.	EP167	Milan, E.	EP206, PW24
Mercier, J.	OP312	Milardovic, R.	EP192
Merenda, N.	EP142, EP221, EP236	Milella, M.	P135, P144
Merino-Serra, E. M.	EP230	Miler Jerković, V.	EP391
Mercedes Alonso Rodríguez,	P103	Milicevic Sephton, S.	OP062
Merinov, A.	P208	Militano, V.	P110
Merisoglou, S.	EP008	Mille, E.	OP650
Merkens, H.	EP591, OP020	Miller, K.	EP261
Merkle, E.	OP083	Miller, M.	OP295
Merkx, M. A. W.	EP115	Milliner, M.	OP560, OP605
Merlet, P.	EP302	Millo, C.	P171
Meroni, S.	P185	Mills, C.	OP479, TP083
Merrett, J.	EP788 , OP136	Miloychikova, I.	EP474
Meseguer, E.	OP418, OP419	Milukhina, I. V.	P287
Meseguer-Olmo, L.	EP592, EP593	Mimoso, G.	P180
Mesquita, C. T.	EP707	Min, J.-J.	EP312
Mester, J.	EP831, P083	Minamimoto, R.	EP020, OP076, OP504
Mestre Fusco, A.	EP022, EP193 , OP600	Miñana Olmo, E.	EP651
Mestres-Martí, J.	EP131, EP160, EP167, EP230, OP031, P137	Minati, L.	PW38
Metaxas, M.	EP795, OP420	Mindt, T. L.	OP398, OP587
Metello, L. F.	OP447	Minervini, A.	EP256
Metselaar, J. M.	OP306	Minestrini, M.	P275
Metsler, U.	EPW10	Mínguez-Gabiña, P.	OP518
Mette, U. K.	EP235	Minin, S.	EP635
Meyer, C.	P083	Minn, H.	OP348, OP354, OP688
Meyer, M.	P252	Minniti, G.	EP567, OP654
Mező, G.	EPW64	Minoves, M.	P128
Meza-Escobar, D.	OP195	Mira, M.	EP458, EP460, OP011
M'hamdi, F.	P173	Mirabile, A.	OP461
Mhiri, A.	EP393, P166	Miran, T.	OP546
Miao, Y.	OP586	Miranda, C. S.	OP488
Michalis, L.	P028	Mirocha, B.	TP099
Michaud, L.	OP292	Mirzabeigi, A.	EP209
Michelin, T.	P254	Mirzadeh, S.	OP674
Micheva, I.	EP196	Mirzaei, S.	OP282
Michieletto, S.	EP066	Mishra, A.	EP035, EP630
Michigishi, T.	P293	Mishra, U. K.	P140
Micholopoulou, S.	OP136	Misiak, R.	OP445
Michon, P.	OP699	Missale, G.	EP219
Midiri, M.	EP137, EP197, EPW22	Missault, S.	EPW58, P286
Miederer, M.	EP009 , EPW89	Mistry, A.	OP676
Mier, W.	EPW13, OP556	Mitamura, K.	EP030
Migliaccio, R.	P254	Mitjavila, M.	EP315
Migliari, S.	EP618 , P234, P284	Mitjavila Casanovas, M.	EP463 , EP684, EP692
Migliano, M.	OP408, PW22	Mitra, A.	EP644
Migunova, E. V.	P038	Mitran, B.	EP522, EPW82, EPW83, OP114, OP172, OP311
Mihailovic, J.	EP351	Mitsakis, P.	EP325, P265
Mihaly, J.	EP639	Mittal, B.	EP023, EP120, EP146, EP161, EP229, EP235,
Mihaylov, G.	EP179		EP271, EPW29 , EPW68, OP125, P097
Mihlin, A.	EP575	Mitterhauser, M.	EP233, EP615, EP623, EP636, EPW11, OP115,
Miho, K.	TP069		OP286, OP403, OP405, OP551, OP648, OP649
Mijatovic, L.	EP355	Mittra, E.	EP020
Mijnheere, E. P.	EP115	Miura, Y.	EP323
Mijnhout, S.	OP534	Miwa, M.	EP226
Mikail, N.	OP418, OP419 , OP565, OP605	Miyagawa, M.	P048
Mikecz, P.	EP834, EP838	Miyakoshi, M.	OP177

Miyamoto, K.	EP013	Moral, A.	EP074, EP287
Miyazaki, C.	EP027	Morales, B.	EP543
Miyoshi, F.	PW39	Morales, M.	OP410
Miyoshi, S.	EPW61	Moralidis, E.	P120
Mizokami, A.	EP005, EP007	Morán, V.	EP470 , EP814, OP016, OP410
Mizuma, H.	P292	Morandean, L.	EP611
Mizumura, S.	P269	Mora Salvadó, J.	EP290, PW09
Mladenov, K.	EP179, EP343	Morbelli, S.	OP127, OP233, OP288, OP373, OP408, OP409, OP421, P255, PW22
Moasses Ghaffari, B.	EP539	Mordovin, V.	P041
Mochiki, M.	TP060	Moreau, A.	EP011, EP012
Mochizuki, K.	TP021	Moreau, M.	EP664, EP812, OP588
Mochizuki, T.	P048	Moreau, P.	OP407
Mochula, A.	P029, P046	Moreira, A. P.	P212
Möckel, D.	EP506	Morel, O.	EP078, EP617, EP796, P106
Modzelewski, R.	OP181	Morelec, I.	OP699
Moens, M.	OP142	Morello, R.	P258
Mogensen, O.	EP109	Moreno, A.	EP582
Mognetti, T.	OP298	Moreno Cano, R.	EP441
Mohamed, A.	EP825, EPW78	Moreno-Llorente, P.	EP116
Mohamed Salem, L.	EP250 , EP303, EP441, EP471, EP682	Moreno Ortega, E.	P118
Mohan, A.	OP597	Moreo, A.	P135, P144
Mohanty, S.	EP435	Moret, M.	OP699
Mohring, M.	OP059, OP423	Morgado, P.	EPW52
Moin, A.	EP006	Morganti, A.	EP223, EPW20, OP335
Moinfar, F.	OP553, OP555	Morganti, S.	OP680
Moisescu-Goia, C.	EP376	Morgat, C.	EP473
Mojabi, Z.	EP693	Morgenroth, A.	EP640, OP422, OP546
Mojal, S.	EP022	Morgenstern, A.	EP494, OP148, OP309, OP454, OP520, OP590
Mojsak, M.	EP385, EP577, OP540	Mori, T.	EP533
Mok, G. S.	EP475 , OP133	Mori, W.	PW31
Molina, J.	P111, TP036	Morigi, J.	EP223, P146
Molina-Garcia, D.	OP075, OP240	Moriguchi-Jeckel, C. M.	OP613
Molkenboer-Kuenen, J. D. M.	OP343, OP489	Morillas Oliveras, B.	EP113
Moll, A.	EP117	Morillo-Martinez, E.	EP653
Moll, J.	P039	Morita, T.	EP205
Møller, A.	P296	Morley, N. C. D.	EP738 , EP741
Møller, C. J. H.	P193	Morosi, C.	OP011
Møller, H.	OP686	Morreale, M.	P262
Mölne, J.	EPW48	Morrish, D. W.	OP519
Moltz, J.	EP557	Mortensen, J.	EP257, EPW17, P193 , TP026
Monari, F.	EPW20, OP335	Mortensen, M.	TP034
Moncayo Nevada, R.	P108	Morzenti, S.	EP785
Mondot, L.	OP203	Mosci, C.	EP056, EP060, P189
Montanelli, L.	EP095	Moskalev, I.	EP472
Montani, L.	OP167	Mosley, M.	EPW63
Monteleone, F.	OP334, P262, P280	Mostacci, D.	EP487
Montellano, A.	EP592	Mostafa, H.	P188
Montes, C.	EP170, EP545	Moszura, T.	P039
Montes, E.	EP799	Mota-Cobian, A.	EP736
Montesarchio, V.	EP517	Mothes, C.	EP826
Monteverde, E.	OP262	Mottaghy, F.	EP055, EP369, EP499, EP640, OP276, OP392, OP416, OP422, OP546, OP632
Montgomery, J.	EP407, EP409	Mouas, D.	EP348, P175
Monti, M.	OP116, OP120	Moulin, M.	OP353
Montini, G. C.	OP335	Moulin-Romsee, G.	EP489
Montoro, A.	EP496	Moulopoulou, L. E.	EP423, EP501
Montravers, F.	EP263, EPW70, OP292	Mounier, N.	OP406
Moon, B.	EP476	Mourtada, F.	EPW53
Moon, D.	EP847	Moustafa, H.	EP138, P178
Moon, H.	EP406, EP722 , P256	Moyon, A.	OP344 , P115
Moore, R.	EP307, OP567	Mpalaris, V.	EP332, PW10
Moore, S. C.	EP718	Mroz, R.	EP577
Mora, J.	EP294	Mu, L.	OP398
Mora, L.	TP089	Mucientes, J.	EP315 , EP684, EP692
Moradiellos, J.	EP291		
Moradkhani, S.	EP619, EP621		

Mueller, A.	OP348	Nakagami, Y.	EP612
Mueller-Herde, A.	OP398	Nakai, G.	EP091
Mukherjee, A.	EP044, EP189, EP314	Nakajima, K.	EP005 , EP007, OP217, OP284 , OP285, P015, P083, P248 , TP047
Mukhortova, O. V.	EP549		
Mulas, A.	P278	Nakajima, T.	TP081
Mulder, E.	OP593	Nakamoto, Y.	EP405
Mulders, P.	EP261, OP119, OP640	Nakamura, N.	EP802
Mulero Mendoza, J.	EP692	Nakamura, Y.	EP802
Mulholland, N.	EP416, OP279, P121, TP002	Nakata, T.	OP284
Mullen, G.	EP598	Nakatani, K.	EPW67
Müller, C.	OP589	Nakuz, T. S.	EP134 , EP163 , OP241
Müller, D.	EP369	Nanasato, M.	P044
Müller, M.	EPW87	Nanni, C.	EP199, EP264, EP265, EP288, EP304, EPW75
Müller, S.	EP506	Nappi, C.	OP460, OP461 , OP467, OP604, OP607
Mulligan, R.	EP649	Naranjo, A.	OP085
Mundler, O.	EP624, EP794	Narducci, F.	OP129
Munechika, H.	EP323	Narin, Y.	EP338
Munitis, V.	EP303	Narula, J.	OP193
Munk, O. L.	EP685	Narumi, Y.	EP064, EP091
Muñoz, D.	OP428	Narvesh, K.	OP466
Munteanu, M.	P183	Nasr, A.	P198
Muoio, B.	EP032	Nasr, H.	EP154, P220
Murai, A.	EP252, EP335	Nassar, L.	EP043, EP049
Murakami, K.	EP151	Naszalyi Nagy, L.	EP639
Murakami, Y.	EPW61	Nataf, V.	EP650, EPW70, OP292
Murby, B.	OP136	Nault, J.-C.	OP030
Mure', M.	OP536	Naumann, M.	EP234, EPW04
Muros, M.	EPW37	Navab, N.	OP134
Murray, D.	OP519	Navales, I.	EPW07
Murray, I.	EP414, EP459, EP742, EPW51, OP131 , OP136, OP164, OP217, OP482	Navarra, P.	OP655
		Navarro Fernández, J.	EP250, EP303 , EP441, EP471 , EP682
Murthy, V.	EP273	Navarro-Martin, A.	EP160
Musaieva, K.	EPW27	Navarro-Teulon, I.	EP494, OP513, OP545
Mustafa, M.	EP203 , OP088	Navines, J.	EP065
Mut, T.	EP511, EP520	Nawaz, M.	EP001, EP336, OP086, P099
Mutevelizade, G.	EP324 , TP038	Nawaz, S.	OP400
Muto, P.	EP517	Nawwar, A.	EP359, P178
Muylle, K.	EP489	Nayak, T. K.	OP306, OP593
Muzik, O.	P232	Nederveen, A. J.	P237
Myoujin, M.	OP029	Neels, O.	EP270, EP837 , OP022
Myrthue, M. O.	OP247	Nefyodova, G. A.	P038
Myrup, C.	PW02	Negre Busó, M.	TP084
Mysliwiec, J.	EP385, EP577, OP540	Nekolla, S.	OP423
Myung, J.	EP326	Nelson, A.	EP404 , EP719 , EP732 , OP258
		Nelson, D.	EP732
Nabulsi, N. B.	OP312	Nematyazar, J.	EP194, EP244, EP504 , EP547
Nabuurs-Franssen, M.	PW07	Nemec, P.	EP679
Nada, R.	EP146	Németh, E.	EP834
Nadig, M.	EP044	Neri, R.	P117
Nag, S.	OP303, OP316	Neshandar Asli, I.	EP818
Naganawa, S.	EP252, EP335	Nesterov, E.	EP535, EP635
Nagar, V.	EP204	Nesterov, S. V.	OP608
Nagara, T.	OP177	Nestle, U.	EP418, OP596
Nagarajah, J.	OP219	Neto, M. T.	P180
Naghshine, R.	EP425	Neubauer, S.	P271
Någren, K.	EP833	Neumaier, B.	EP841, OP422
Nagy, G.	EP596, EP597, EP603, EP677, EPW64, OP212	Neumaier, C.	OP408
Nagy, K.	EP766	Neururer, B.	EP139
Nagy, L.	EP771	Neves, D. M. P. S.	TP102
Nagy, T.	EP838	Newman-Tancredi, A.	OP063, OP616
Naia, M. D.	OP447	Ng, A. H.	EPW34, EPW35
Nair, A.	OP245	Ng, S.	OP178
Naji, M.	EP513, EPW18	Nganoa, C.	OP558, OP559, P045, P049, P258
Nak, D.	EP485	Nguyen, D.	OP318
Naka, K.	P028	Nguyen, Q.	OP550
Nakabayashi, M.	EP090 , EP172	Nguyen, T.	EP397 , TP093

Nguyen, T. Q.	EP452, OP564	Nogueiras Alonso, J.	EP342 , EP337, EP344, P162
Ni, Y. C.	EP399, EP750, EP764	Noh, W.	EP569
Niakas, D.	EP563	Noiret, N.	EP601
Niaz, K.	OP462	Nolan, C.	OP061, OP303, OP316
Niazi, A.	P283	Nolè, F.	OP332
Niccoli Asabella, A.	EP135, EP142, EP213 , EP221, EP236, PW23	Nonnekens, J.	OP581
Nickles, R. J.	OP592	Noordman, B. J.	OP078
Nicod Lalonde, M.	EP325, P265	Noordzij, W.	OP700
Nicol, A.	TP082	Norberg, P.	OP562
Nicolaj, D.	PW03	Nordberg, A.	OP065
Nicolas, D.	EP787	Nordeman, P.	EP582
Nicolas, G.	OP083, OP149 , OP289	Noriega, E.	EP290, EP294, PW09
Nicolas, V.	OP563	Norikane, T.	EP030
Nicolás Ruiz, F.	EP250, EP441, EP471, EP682	Notni, J.	OP309, OP346, OP566
Nicoletti, A.	OP170	Nouira, M.	EP331, EP370, P165
Nicolosi, S.	OP145	Nouwynck, L.	PW03
Nicoloso, V.	EP627	Novicki, A. W.	P244
Nics, L.	OP403	Novikov, S.	EP058, EP289, OP481
Niederstadt, L.	EP643, OP487	Nowosinska, E.	EP150, P074
Nielsen, A. L.	EP559	Ntk, T.	P097
Nielsen, D. L.	TP015	Nunes, A.	OP479, TP023, TP048, TP083
Nielsen, J. B.	OP108, OP557	Núñez Lozano, R.	EP532
Nielsen, J.	TP106	Nunez-Santos, M.	OP424
Nielsen, N.	TP014	Nuvoli, S.	EP218, EP330, P273, P275, P278
Nielsen, N. S.	P136	Nuyts, J.	EP756
Nielsen, S. D.	P136	Nyberg L'Estrade, E.	EP605
Niemeyer, M.	OP239	Nyholm, D.	OP252
Niepsch, K.	OP459	Nyman Petersen, I.	EP605
Nieri, A.	EP662 , OP288, OP408, OP409, OP421, P255	Öberg, J.	P255
Nieuwenhuijzen, G. A. P.	OP078	Oberg, K.	OP394
Nieves Maldonado, S.	EP069, EP286	Oblak, A.	P200
Niezdoda, M.	EP721	Ocak, M.	EP244, EP245, EP392, EP504, EP547, EP614, EP858, EPW44, OP223
Nigam, S.	OP488	Ochoa-Figueroa, M.	OP562
Nigri, A.	PW38	Odagawa, T.	EP252, TP003, TP059
Niimi, T.	P044	Odagiri, H.	TP063
Niitsu, m.	P282	Odano, I.	EPW03
Nijran, K. S.	OP260, OP277, P251	Oddstig, J.	OP281, OP477, OP511 , TP031
Nikaki, A.	EP008, EP437	O Doherty, J.	OP514
Nikapota, A.	OP333	O'Doherty, M. J.	EP171
Nikezic, D.	EP816	Odom, C.	OP067 , P148
Nikiforov, V.	P011, TP064	Oehme, L.	OP694
Nikitina, O. V.	P038	Øen, S. K.	EP752, OP247
Nikoletic, K.	EP514	Ogawa, K.	EP725
Nikolopoulou, A.	EPW94, OP021, OP024, OP025, OP424	Ogawa, T.	PW39
Nikolova, P.	EP187	Ogino, H.	P036
Nikoogoftar, A.	EP768	Ögren, M.	EP827
Nilica, B.	EP277, EP479, EPW43 , OP294, OP457	Ogura, D.	TP060
Nilsson, J.	OP166	Ogus, E.	P209
Niñerola-Baizán, A.	OP200	Oh, H.-K.	EP052
Nioche, C.	EP040, EP050, EPW01, OP516	Oh, J.-M.	OP670
Nisbet, A.	EP788	Oh, J.	EP406 , EP722, P256
Nishii, R.	P292	Oh, K.	EP283
Nishimoto, T.	TP003	Oh, M.	EP406, EP722, P256
Nishimura, S.	P282	Oh, S.	EP283, EP406, EP524, EP722, EP846, EP847, EP854
Nishimura, Y.	EP717	Ohba, H.	EPW77
Nishiyama, Y.	EP026, EP030, EP641, OP256, P235, P236	Ohga, N.	OP177
Niu, G.	OP307	Ohlsson, T.	EP420
Nobili, E.	EP264	Ohme, J.	OP227
Nobili, F.	OP262, OP373, P255	Ohno, M.	P292
Nock, B. A.	OP150, OP340, OP342, OP351, OP547	Ohnona, J.	EP263, OP292
Nocuñ, A.	EP237, EP313	Ohsiek, A.	PW32
Noda, A.	EPW61	Okamoto, S.	OP177
Noël, N.	OP144	Okamura, N.	EP846, OP425
Nogami, M.	EP090, EP172		
Noguchi, N.	EP007		
Nogueira, S. A.	OP274, TP044		

Okano, N.	P282	Orlova, A.	EP522, EPW81, EPW82 , EPW83, OP114, OP172, OP311, OP591
Okarvi, S.	EP594, EP595 , EP843, EP848	Ormstrup, T. E. J.	EP559
Okazawa, H.	EP533	Oroujeni, M.	EPW83
Oksuzoglu, K.	EP824	Orozco-Cortés, J.	EP386 , P068, P126
Okuda, K.	OP217, OP285 , P083, P015, P248	Orrico, M.	OP693
Okudan, B. T.	P107	Orsal, E.	EP695
Okuyucu, K.	EP345, EP346, EP700, OP141, OP573	Orselik, A.	OP573
Olariu, C. I.	EP678	Orsini, F.	OP033
Olczyk, T.	EP329	Orta, N.	P111
Oldenburg, J.	P164	Ortega, C.	EP205
Olesen, O. V.	OP197	Ortega-Candil, A.	EP045, EP057, EP061, OP698, PW21
Olianti, c.	EP256	Ortega Manrique, A.	EP297, OP572
Olin, A.	EP570	Ortega-Serrano, J.	P126
Olivan, P.	EP462, EP512	Ortega Valle, A.	EP310, P034
Olivari, L.	EP306, EPW25, OP655	Ortenzia, O.	EP400, EP618, P234
Olivas, C.	EP462, EP496	Orunmuyi, A. T.	EP254, P160
Oliveira, A.	EP002, EP285, EPW52, OP044, P222	Orzelowska, M.	EP523
Oliveira, C.	TP043, TP072	Oseni, A.	P074
Oliveira, J.	EP821 , TP017, TP018	O'Shea, A.	OP548
Oliveira, L.	TP062	Oshima, M.	P231
Oliveira, M.	EP536	Osiecki, S.	EP439, OP76
Oliveira, R.	TP041	Osifo, B. O. A.	EP254, P160
Olivencia Palomar, P.	OP369	Ossenkoppele, R.	OP373
Olivier, A.	EP042, EP349, OP129	Ost, P.	EP087
Olivieri, P.	P247	Ostenfeld, E.	P069
Olmos, C.	PW21	Østergaard, B.	EP559
Olmos Garcia, R.	P093	Ostrowski, M.	OP225
O'Loughlan, T.	P177	O'Sullivan, P.	EP509 , EP513, EPW18
Olsen, B. B.	EP585, EP671, EP674	Otomi, Y.	EP013 , P276
Olsen, J.	OP015	Otsuka, H.	P276
Olsen, K. E.	EP671	Ottaviano, M.	EP301
Olsen, P. S.	P193	Otte, F.-X.	OP456
Olsson, B.	OP281, TP031	Otto, G.	EPW89
Olsson, E.	OP562	Otto, T.	OP118
Olsson, T.	EP605	Ouach, A.	EP826
Olteanu, L.	EP087	Oudot, A.	EP664, EP666 , EP812, OP250, OP287, OP588
Omar, W.	EP240	Oudoux, A.	EP042, EP349 , OP129
Omar, W. M.	P188	Outomuro, J.	TP100
Omar, W. S.	OP087	Ouvrier, M.	OP203
Onega, M.	EP828	Ovtchinnikova, V.	OP361
O'Neil, B.	OP303	Owsianski-Hille, N.	OP202
O'Neill, B. T.	OP061	Oya, S.	EP728
O'Neill, K. S.	OP652	Oyen, W.	EP115, OP079, OP119, OP343, PW07
O'Neill, E.	EPW62	Ozalp, S.	EP111
Oner, A.	EP103, EP210, EP212	Ozcan Kara, P.	EP033, EP541, EP565, EP694
Ones, T.	EP824	Özcan Tutar, R.	EP392
Onimode, Y. A.	EP254 , P160	Özçelik, M.	OP261
Onishi, H.	EP744 , OP213	Özdemir, E.	EP079
Onishi, T.	EP027	Ozdemir, H. O.	EP466
Onner, H.	EP111	Özdemir, Y.	PW28
Onodera, Y.	OP029	Özdemir Başer, Ö.	P107
Onoe, H.	P292	Özdoğan, Ö.	EP272
Onoguchi, M.	TP047, TP065	Ozeki, Y.	EP151
Oos, R.	OP314	Ozer, E.	EPW69
Oosterwijk, E.	OP119, OP640	Ozercan, I. H.	EP338
Oporto, M.	EP117, P111 , TP036	Ozgen, A.	EP466 , EP468, OP014
Orak, R.	EP426	Özhan, M.	P052
Oral, A.	EP378 , P207	Ozkan, E.	EP485
Orcajo Rincon, J.	P152, P268	Ozkaya, M.	EP144
Ordi, J.	EP100, EP107	Ozmen, O.	EP159
Ordidge, K. L.	OP652	Ozmerdiven, G.	EPW23
Orduña Diez, M.	EP184, EP202, OP180	Ozsoy, M. H.	EP426
Orengo, A.	EP662, OP233, OP408, OP409	Ozturk, A.	EP159
Orlandi, C.	EP371	Ozyar, E.	EP112
Orlandi, F.	OP340, OP547		
Orlhac, F.	EP040, EP050, EPW01, OP516		

Ozyurt, S.	P172	Papazoglou, D.	P153
Pacchioni, A.	PW24	Paphiti, M.	EP423, EP501, EP503, OP636
Plachcińska, A.	OP464, P039	Papi, S.	OP332, OP680
Pachón Garrudo, V.	EP182, EP200	Papiris, S.	EP680, EP681
Paci, M.	OP598	Papo, T.	OP194
Pacilio, M.	EP371, EP460, EP510, EPW19, OP336	Papoutsani, D.	EP008
Padilla, M.	OP193	Papoutsis, V.	EP008, EP437
Padilla Muelas, R.	EP441	Papp, L.	EP233, OP109, OP241, OP500, OP648
Padma, S.	OP182 , OP370	Pappas, K.	P030
Padmanabhan, P.	EP590	Paprottka, P. M.	OP032
Paeng, J.	OP571	Papucci, E.	EP128
Paepen, J.	OP677	Parab, A.	EP482
Paepke, S.	OP239	Parashakis, E.	P182
Paganelli, G.	EP546	Pardo-Montero, J.	P263
Pagani, M.	P255	Paredes, P.	EP100, EP107
Paglianiti, I.	EP114, EP128	Paredes Rodriguez, P.	EP297, OP572
Pahisa, J.	EP100, EP107	Parente, A.	OP066
Pahlm, O.	P075	Parikh, P. J.	EP132 , OP015
Pailhas, L.	EP302	Parisi, M.	OP085
Paillas, S.	OP545	Park, H.-H.	TP008
Pais, C.	EP599, OP673	Park, H.-W.	P168, TP053
Paisey, S. J.	OP227	Park, H.	EPW26
Paiusco, M.	EP748, EP789	Park, J.	OP196
Paja Fano, M.	OP518	Park, J.	OP503
Pak, K.	EP366	Park, J.	EP722
Pal, R.	EP646	Park, J.	EP600, EP633 , EP849, OP670
Palazzo, I.	EP707 , P088	Park, J.	EP569
Palazzo, M.	OP631	Park, J.	OP085
Palermo, A.	EP571	Park, J.	EP372
Paliczka-Cieslik, E.	EP329	Park, J.-H.	P168
Paliulis, O.	EP833	Park, K.	EP569
Pallardy, A.	P247	Park, S.	EP143
Pallissa, E.	EPW07	Park, S.	EP372
Pallwein-Prettner, L.	OP553, OP555	Park, S.-H.	EP052
Palmieri, A.	TP078	Park, Y.	EP476
Palmieri, G.	EP301	Parlak, Y.	EP324, TP022, TP038, TP070
Palner, M.	EP605	Parmar, A.	EP673
Palomar Muñoz, A.	EP689, EP098	Parshintsev, J.	EP850
Palombo, E.	OP653, P267	Parus, L. J.	EP604
Paltro, S.	EP482	Pasaoglu, H. E.	EPW28
Palucci, A.	EP571	Pasarica, I.	P183
Palumbo, B.	P273, P275 , P278	Pascali, G.	EP673, EP832
Pamme, N.	EPW90	Pascovich, C.	OP428
Pan, D.	EPW79, OP228, TP054	Pascual, I.	EP065
Pan, J.	EP527, OP020	Pascual, T.	P189
Pan, Y.	EP659 , OP228	Pascual, V.	EP496
Panareo, S.	EP051, EP070, EP104, EP295 , EP687	Pascual Pérez, R.	P152, P268
Panarotto, M.	OP539	Pashali, A.	EP795
Pancaldi, D.	EP488	Paskas, M.	EP391
Panchadar, S.	EP712, P055	Pasker-de Jong, P. C. M.	TP025
Pandey, A. K.	EP300, OP597	Pasquali, R.	EP304
Panetta, D.	EP743, EP773	Pasquino, M.	EP464, OP538
Pani, R.	EP510, EPW19, OP336	Passadore, D. J.	EP318
Paniagua Correa, C.	EP310, P034	Passah, A.	EP211
Panico, M.	OP116, OP607	Passchier, J.	EP828, OP060
Panwar, P.	EP035	Passera, C.	P243
Paolini, M.	EP086	Passot, G.	OP601
Paone, G.	OP337	Pasternicki, R.	TP103
Papachristou, E.	P210	Pastor, Y.	EP637
Papadakis, G. Z.	P171	Pastore, A.	EP295
Papadimitriou, S.	OP252	Pastorino, F.	OP288
Papadimitropoulos, K.	P028 , P030	Patel, A.	EP261
Papadimitroulas, P.	EP661	Patel, C.	OP597
Papadopoulos, A.	EP024, P028, P028, P030	Patel, N.	OP602
Papanas, N.	P153	Patel, N. H.	OP260, OP277, P251
		Patrina, J.	TP017, TP018

Patrizi, A.	EP199	Perkins, A. C.	EPW34, EPW35, OP062
Patronas, N. J.	P171	Perlaza, P.	EP107
Patt, M.	OP617	Perneczky, R.	OP373
Patterson, N.	EP469	Pernthaler, B.	OP128
Paul, F.	EPW13	Perren, A.	EP678
Paul, R.	EP703	Perrin, D. M.	OP020
Paulo, A.	EP536	Perrin, M.	OP563
Paulus, T.	EP469	Perrio, C.	EPW88, OP612
Pauwels, E.	PW40	Perry, R.	P251
Pavanello, L.	EP402, TP028, TP033	Persakis, E.	EP563
Pavia, J.	EP100, EP107, OP200	Persohn, S.	OP012
Pavlidis, P.	P040	Persson, M.	EP054
Pawar, S.	EP435, P272	Pesce, G. A.	EP032
Pawlak, D.	EP604 , OP395, OP520	Peschiera, F.	P255
Payoux, P.	EP389, OP255, P285	Pessina, F.	OP655
Plazinska, M.	EP387	Pestean, C.	EP341, EP375, EP376, OP220
Pechan, J.	EP771	Petegnief, Y.	OP356 , OP508, P106
Pedersen, J. E.	EP037	Peter, J.	EP778
Pedersen, M. A.	EP168 , TP098	Peters, A.	OP420
Pedraza-Canal, M.	EP057, EP178 , PW21	Peters, D.	EP833
Pedroso de Lima, J.	EP246, EP328, EP815, EPW41, P150, P212	Petersen, C. B.	EP047
Peer, A.	OP338	Petersen, L. J.	EP257 , OP108, OP350, OP358, OP557, OP686
Peeters, R.	EP756	Petersen, P. M.	EPW17
Pegg, R.	OP300	Peterson, D.	OP652
Pehlivan, H.	EP244, EP245	Peterson, M.	OP299
Pehlivanoglu, H.	EP392, EP614, EP858	Petit, S. F.	EP667
Pektor, S.	EPW89	Petranovic Ovcaricek, P.	EP010
Pellegrini, C.	EPW72	Petretta, M.	EP180, OP460, OP461, OP467, OP604, OP607
Pellegrini, R.	EP510, EPW19, OP336	Petriev, V.	EP654
Pellegrino, S.	EP180, EP186, EP301	Petrone, M.	EP101
Pellerito, R.	EP365, EP464, OP013, OP538, P242	Petrosova, K. A.	EP625
Pellico, J.	OP229	Petrovic, R.	P299
Pelucchi, S.	EP295	Petyt, G.	OP091, OP603, P184, P274
Peña, C.	EP117, EP613, P111, TP036	Peyronneau, M.-A.	EP825, EPW78
Pena Pardo, F.	EP098, OP075, OP240	Peyronnet, D.	OP558, P049
Peña Torres, D.	TP076 , TP079, TP087	Pfaff, S.	EP615 , OP405
Pende, D.	OP127	Pfeifer, L.	EP851, EPW96, PW33
Penín González, F.	EP310, P034	Pfisterer, M. E.	OP463
Pennekamp, P. H.	P164	Pham, T.	EP825
Pennone, M.	EP169, OP262, OP288	Phan, J.-A.	P288
Peñuelas, I.	EP631, EP637	Philippe, C.	OP115, OP286
Peper, M.	EPW50	Piana, M.	EP017, EP169, EP429, OP135, OP262, OP408, OP421
Pereira, J.	EP002, EP285, EPW52, OP044, P222, TP068	Pianou, N.	EP680, EP681 , EP795, OP417, OP420
Pereira, M.	OP245	Piccardo, A.	EP340 , OP535
Pereira Arias-Bouda, L. M.	EP068	Picchio, M.	EP101, EP175, OP682
Peremans, K.	P224	Piccinetti, A.	EP292
Peres, K.	P252	Picco, A.	P255
Pereverzeva, M.	EP474	Pichard, A.	EP494, OP513 , OP545
Pérez, B.	EP170, EP545	Piciu, A.	OP220
Perez, E.	TP036	Piciu, D.	EP341, EP375, EP376, OP220
Pérez, L.	EP797	Picker, W.	OP352
Perez, M.	EP002, EP285, OP044, P222	Picón, C.	EP655, EP799
Pérez-Beteta, J.	OP075, OP240	Picori, L.	PW22
Pérez-Castejón, M. J.	EP057, OP698, PW21	Picq, C.	OP366
Pérez Castro, N.	EP243, P043	Piekarski, E.	OP192
Pérez-Enguix, D.	EP462	Piepsz, A.	P180
Pérez-García, H.	EP382, EP454	Piert, M. R.	EP407, EP409
Pérez-García, V.	OP075, OP240	Pietrzak, A.	TP029, TP032
Perez Lopez, B.	P199, TP045, TP085, TP105	Pietzsch, J.	EP525, EP844
Pérez-Maraver, M.	EP116	Pignata, S.	OP536
Perez-Montero, H.	EP231	Pijarowska-Kruszyna, J.	EP855
Pérez Rodríguez, D.	EP647	Pijuan, L.	OP600
Pérez Rosillo, M.	EP028	Pike, L. C.	OP215
Perfileva, O.	EP367	Pilkington Woll, P.	EP084, EP127, EP231, P123
Perillo, T.	P176	Pilla, A.	EP732
Perissinotti, A.	EP016, EP185 , EP394, OP200		

Pillai, S.	P090	Popov, S.	EP701, P086
Pillon, M.	P176	Popović, D.	EP391
Pilloy, W.	EP780	Poppe, B.	EP809
Pimpinella, M.	EP469	Porras martinez, M.	EP250, EP303
Pinaquy, j.-B.	P061	Porreca, A.	EP265, EPW75
Pineda, A.	EP656, EP657	Porter, C. A.	EP457, EP739
Pinilla Martínez, C.	P152	Pötsch, N.	OP648, OP649
Pinker, K.	OP241	Pötschger, U.	OP085
Pinker-Domenig, K.	OP244	Pott, C.	PW30
Pinkus, E.	EP122	Pottel, H.	EP716, EP779
Pintacuda, G.	EP305	Pottier, G.	OP618
Pinto, A.	EP002 , EP285, OP044, P222	Poty, S.	OP588
Piper, J.	OP258	Pouessel, D.	EP302
Pipikos, T.	EP008 , EP437	Pouget, J.-P.	EP494, OP513, OP545
Piras, B.	EP218, EP330, P278	Pouladi, M.	EP619
Piras, M.	P278	Pourat, J.	OP234
Pires, A. S.	EP515	Pourcher, T.	EP447
Pires, L. M. P.	OP140	Poussier, S.	OP563
Pirich, C.	EP278, EP339, OP485, P056	Pouw, B.	EP282
Pirnat, E.	P200	Povinec, P.	EP810
Pirozzi, S.	EP732	Pozios, I.	OP611
Pistola, A.	P153, P182	Pozo, G.	EP797
Piszczek, S.	EP439, P076	Pozueta, A.	OP431
Pitalúa Cortés, Q. G.	EP672	Pozzi, L.	OP478
Pitella, F. A.	P279	Prabhu, M.	P019
Pitkonen, M.	P239, P294	Pradhan, P. K.	EP232, EP368 , P058, P072
Piva, R.	EP169 , OP408 , OP409, OP421	Prakash, G.	EP273
Piwowarska-Bilska, H.	EP431, OP225	Prakash, V.	EP793
Pizarro, C.	OP189	Prakken, N.	OP610
Pizzirani, E.	EP004, EP247	Prandini, N.	EP088, EP089, EP258
Pizzoferro, M.	EP371	Pranić-Kragić, A.	P174
Plancha, M.	EP511, EP520	Prasad, S.	EP643, OP487
Planche, L.	OP407	Prasad, V.	EP481, OP487, OP585
Plane, A.-F.	P045, P049	Prashanth, A.	EP232, EP368, P058, P072, P142
Plaza, R.	EP413	Prassopoulos, V.	EP437
Plesner, T.	EP559	Prata, A.	OP371, P194
Plisson, C.	EP828, OP060	Pratt, B. E.	OP164
Ploetz, T.	OP617	Praveen, S.	EP048
Poblete García, V.	EP098, EP222, OP369	Pregartner, G.	OP128
Podesser, B.	OP286	Preshlock, S.	EPW87
Poel, E.	OP217	Preuß, R.	EP690
Poepfel, T. D.	EP242, EP579 , EPW74, OP222	Prevot, S.	EP812
Pofi, E.	EP292	Price, R. I.	EP611
Polack, B.	EP272	Prieto, A.	EP315, EP463, EP684
Polak, A.	OP540	Prieto, E.	EP470, EP814 , OP016, OP377
Polasek, O.	P201	Prignon, A.	EP650
Polei, S.	OP118	Principi, E.	OP233
Poli, G.	EP440	Prior, J.	EP325, P265, P298
Polis, I.	P224	Procopio, G.	OP338
Polloniato, P.	EP402	Proença, G.	TP062
Polverari, G.	EP153 , EP199, EP223, OP035	Proietti, F.	EP510
Polyak, A.	EP639	Prokop, W.	P108
Polymeri, E.	EP227	Prosotsianiotis, N.	EP279
Pombo Pasin, M.	EP069, TP040	Provent, P.	EP664, EP666
Pommé, S.	OP677	Provost, C.	EP650
Pomper, M.	OP611	Prozzo, V. A.	EP620
Pompignoli, L.	EP488	Ptpic, M.	P127
Pomposelli, E.	OP127, OP262 , OP421, P255	Pruim, J.	EP558, OP349, P154
Ponholzer, A.	EP233, OP551	Pruszyński, M.	OP590 , OP672
Ponnala, S.	EP829, OP021	Pruzzo, R.	EP543
Ponomareva, O.	EP058	Pryma, D.	OP427
Pons-Escoda, A.	OP374	Pryor, M.	EP516
Pontico, M.	P262, P280	Psimadas, D.	P022
Ponzoni, M.	OP288	Ptáčník, V.	OP041, P100, P134, PW05
Poot, A. J.	OP587	Pubul Núñez, V.	EP069, EP286, TP040
Popescu, C. E.	P135 , P144 , PW01	Pucci, A.	EP560

Puccini, G.	EP114, EP560, P117 , P259	Ramadan, S.	OP354
Puch, Z.	EP329	Ramakrishnan, N. K.	EP598
Puig-Povedano, I.	OP031	Ramaswamy, B.	EP551, EP737
Pulizzi, S.	EP137	Rambaldi, I.	EP051, EP070, EP104, EP295, EP687
Pulkkanen, K.	OP338	Rami-Mark, C.	EP623, OP115
Pultrone, C.	EP265, EPW75	Ramirez, Y.	EP184 , EP202, OP180, P016
Punda, A.	P174, P201	Ramirez-Navarro, A.	EP653 , EP656, EP657
Pung, B. L. J.	P278	Ramjee, B.	EP780
Puntoni, M.	OP535	Ramondo, G.	EP247, EP305
Pupić, G.	EP391	Ramón y Cajal, T.	EP074
Purandare, N.	EP025 , EP273	Ramos, C. D.	EP056, EP060
Puranik, A. D.	OP411	Ramos, L.	EP470
Puri, T.	EP171	Ramos, R.	EP497, OP410
Pursanova, D. M.	EP549	Ramos Boyero, M.	TP085, TP105
Purtanen, R.	TP030	Ramos-Font, C.	EPW24
Purushotham, A.	EP491	Ramos Grande, T.	TP085, TP105
Pushpalatha Sudhakar, L.	EP048	Ramos-Martinez, A.	EP684
Putra, E.	EP086, OP033	Ramos Membrive, R.	EP631 , EP637
Pyatigorskaya, N.	OP183	Ramos Moreno, E.	EP532
		Ramos-Rubio, E.	EP131, OP031
Qu, Q.	OP586	Rana, S.	EP146
Qu, W.	EP829, OP401, OP424	Rancoita, P.	EP101
Quaranta, D.	P257	Raneri, F.	OP655
Quartuccio, N.	P176	Rangan, K.	P140
Quehenberger, F.	EP140	Rangarajan, V.	EP025, EP273
Queiroz, M.	EP205 , EP267	Rangaswamy, S.	EP630
Querzoli, P.	EP070	Ranjan, K.	P074
Quincoces, G.	EP224, EP631, EP637	Rapiceta, C.	OP598
Quintal, C.	TP091, TP109	Raposo, P.	EP536
Quinto, M. A.	EP473	Raschillà, R.	EP114
Quirce, R.	EP021, OP195, OP431	Rasmussen, P. H.	EP836
Quon, A.	OP082	Raspollini, M. R.	EP256
Qutaish, M.	P244	Rasul, S.	OP038
		Ratão, P.	EP554
Rabadan, R.	EP592, EP593	Rathke, H.	EPW13 , OP556
Rabaiotti, E.	EP101	Rathore, H.	EP482
Racz, T.	OP115	Ratib, O.	P250
Radchenko, V.	OP590	Ratto, G.	OP127
Rådegran, G.	P035	Rauch, G.	OP496
Raderer, M.	OP405	Rausch, I.	EP036 , EP233, EP718, EP727, EP752, OP247, OP249 , OP253, OP500, OP649, P232
Radhakrishnan, R. K.	OP125	Rauscher, I.	EP274, OP074
Radici, L.	EP464, OP538, P242	Ravat, S.	P272
Radnia, A.	EP763	Ravina, M.	EP232, EP368, P140
Radojewski, P.	EP678	Rawal, S.	EP276
Radtke, J.	EP268	Rawicz-Galińska, A.	EP528
Rafaat, T.	OP089	Ray, S.	EP149
Ragan, P.	EP810	Raya-Sanchez, J. M.	EP185
Rager, O.	P250	Raysberg, I.	EP772
Raghuram, P.	EP048	Razavi, S.	EP698, EP710, EP792 , OP168
Raguin, O.	EP666, EP812, OP588	Razavi Khosroshahi, S.	EP194
Rahabi, s.	EP215, EP348, P059, P064, P175, P214	Raziee, H.	OP275
Rahal, D.	EPW25	Razzouk - Cadet, M.	EP628
Rahatli, S.	EP082	Rebollo Aguirre, A. C.	EP072, EP293
Rahbar, K.	OP455	Reccia, P.	EP748
Rahiminejad, A.	EP621	Reddy, K.	OP339
Rahman, F.	OP686	Reddy Gorla, A. K.	P097
Rahmim, A.	EPW31, OP498	Redolfi, A.	P250
Rai, S.	EP566	Reffert, L. M.	EPW89
Raijmakers, P. G. H. M.	P277	Regaieg, H.	EP331, OP192, OP560, OP565, OP605
Raisali, G.	EP398, EP734, OP359	Regenthal, R.	OP617
Rajabi, A.	EP450	Reguera Berenguer, L.	P152, P268
Rajabi, H.	EP450	Rehak, Z.	EP679
Rajabifar, S.	EP621	Reich, D.	OP346
Rajan, M. G. R.	EP644	Reijonen, V.	OP390 , OP633
Rajic, M.	EP361	Reilly, R.	EP583, EP620
Raju, N.	EP537		

Reinert, M.	EP032	Rizkallal, S.	EP184, EP202, EP647, OP180
Reinfelder, J.	EP275	Rizzo, V.	P257
Reinhardt, M. J.	EP809	Roach, P.	EP500, OP550
Reis, E. A.	EP225	Robert, M.	EP380
Reiter, T.	OP189	Robert, V.	EP807
Relan, N.	EP063	Roberto Olmos García,	P103
Remde, Y.	EP837	Robertson, D.	OP674
Remenár, É.	EP123	Robev, B.	EP214
Remy, S.	EP852	Robin, P.	OP181
Renda Alcalde, A.	EP337, EP342, EP344, P162 , TP100	Robinson, A.	EP832, OP333
Rendl, G.	EP339 , P056	Robles-Barba, J. J.	EP116, EP160, EP230 , OP031, P137
Reñé-Ramírez, R.	OP374	Robson, P. M.	OP193
Rep, S.	PW06, TP004 , TP009 , TP073	Roca-Engronyat, M.	EP655
Repetto-Llamazares, A.	OP513, OP548	Rocca, P.	EP546, EPW06, OP332, OP680
Retamal, J.	OP517	Roch, M.	EP797
Rettenbacher, L.	EP339	Roch, V.	OP201, OP563
Retz, M.	EP266	Rockall, A.	OP341
Reubi, J.	OP083, OP149	Rodado Marina, S.	EP184, OP180, P016
Revan, R.	P225	Rodari, M.	OP355
Revilla-Nuin, B.	EP593	Rodella, C.	P079
Reyes, D.	EP511, EP520	Rodeño, E.	EP255, OP518
Reyes Marles, R.	EP250, EP441, EP471, EP682	Rodrigues, M.	EP217 , OP294
Reynés-Llompart, G.	EP131, EP655, EP799 , TP096	Rodríguez, B.	EP315
Reza, M.	EP261	Rodríguez, F.	EP208
Rezaee, A.	OP553	Rodríguez, H.	EP511, EP520
Rezaei, A.	EP756	Rodríguez Alban, J.	P179
Rhodes, J.	EP122	Rodríguez-Alfonso, B.	EP684 , EP692
Riaz, S.	OP086	Rodríguez Antolin, A.	EP231
Ribas-Sitjas, M.	TP096	Rodríguez-Bel, L.	EP018 , EP116 , EP160, OP031, OP374, P137
Ribeiro, A. S. F.	OP217 , OP482	Rodríguez de Dios, N.	OP600
Ribot Luna, L.	EP113	Rodríguez-Fernández, A.	EPW24, OP375
Riccardi, L.	EP748	Rodríguez Fónseca, O.	EP243, EP286, P043
Ricci, A.	EP292	Rodríguez-Fraile, M.	EP224 , EP470, EP814, OP016
Ricci, M.	P280	Rodríguez-Fuster, A.	OP600
Ricciolino, S.	EPW75	Rodríguez-Gasen, A.	EP294, PW09
Richard, I.	P159	Rodríguez-Martínez, D.	P125
Richarz, R.	EP841, OP422	Rodríguez-Osorio, X.	OP070
Richetta, E.	EP464 , OP013, OP538 , P242	Rodríguez Pérez, S.	OP677
Richetti, A.	EP032	Rodríguez Revuelto, A.	EP113
Richetti, F.	EP085	Rodríguez-Rey, C.	EP061
Richey, T.	EPW59	Rodríguez-Rodríguez, C.	EP472, EPW54
Richter, J.	EP224, EP814, OP410	Rodríguez-Rodríguez, E.	OP431
Rickabaugh, L.	EP122	Rodríguez-Rubio, J.	EP290 , EP294, PW09
Riedinger, J.-M.	OP246	Rodríguez-Salazar, M. J.	EP185
Riedl, C.	OP244	Rodríguez Taboada, P.	P125
Rieger, S.	EPW15	Rodríguez Taroco, M.	OP458
Riemann, B.	OP224	Rodríguez-Rey, C.	EP045
Riera, M.	EP511, EP520	Roelants, V.	EP835
Rigatou, A.	OP420	Roeleveld, D. M.	OP306
Rijpkema, M.	EP115, OP119, OP343, OP640	Rogers, V.	EP407, EP409
Ringler, R.	EP798	Rogov, A.	EP535 , EP632, EP634
Rioja Martin, M. E.	EP297, OP572	Roh, J.	EP406, P256
Riola-Parada, C.	EP057, EP178	Roivainen, A.	OP517
Riondato, M.	P243	Rojas, J. V.	OP674
Rios, G.	EP208	Rojas, J. G.	EP294
Ripani, D.	EP308, EP311, EP317, EP322	Rojas-Fisher, B.	EP459
Rischka, L.	OP249	Rojnic, M.	P299
Rischke, H.-C.	OP596	Rokka, J.	EP842
Rischpler, C.	EP274, TP049	Roldão Pereira, L.	TP017
Risérus, U.	EP582	Rolland, P.-H.	P115
Ritt, P.	EP275, EP686 , OP018 , OP515	Roller, M.	EP640
Riva, M.	OP655	Rollo, M.	EP070
Rivas, F.	EP294	Romano, A.	OP654
Riverol, M.	OP377	Romanó, C.	EP658, EP783, EP784
Rivier, J.	OP149	Romanov, G.	P086, P087
Rizell, M.	EPW48	Romanowicz, G.	EP165

Romero, I.	EP294	Rufini, V.	EP174, EP308, EP311, EP317, EP322
Romero Zayas, I.	EP167, EP655 , EP799, PW09	Ruggeri, A.	EP137, EP197, P181
Romić, M.	EP010	Ruggeri, E.	EP292
Rominger, A.	OP317, OP425	Ruggeri, R.	OP536
Romito, R.	EP458, OP011	Ruhlmann, V.	EP572, OP501, OP502, OP505
Roncali, M.	OP598	Ruibal, Á.	EP069, EP286, OP070, P263, TP040
Roncalli, M.	OP655	Ruiter, S.	EP806
Roncaroli, F.	OP652	Ruiz, A.	EP463
Ronchey, S.	OP693	Ruiz, D.	EP416, EP726, OP279, OP676, TP002
Rooijackers, H. M. M.	EP697	Ruiz-Cabello, J.	EP736, OP229, PW27
Roppo, F.	EP789	Ruiz Gomez, M.	P093
Ros, P.	EP592	Ruiz Hernández, D.	EP337, EP342, EP344, P162, TP100
Rosado, G.	P125	Ruiz Merino, G.	EP303
Rosazza, C.	PW38	Ruiz Rodríguez, A.	TP084
Rösch, F.	EPW89, OP023	Ruiz Solis, S.	EP084, EP127, EP231, P123
Roscher, M.	EP658, EP783, EP784	Rullmann, M.	OP617
Rose, S. C.	EP136	Rumià, J.	OP200
Rosenbaum-Krumme, S.	OP222	Rungby, J.	OP372, P296
Rosenqvist, G.	EP766	Runser, A.	OP399
Rosenström, U.	OP232	Runz, A.	OP444
Rosestedt, M.	EPW82, OP114	Rushforth, D. P.	OP164
Roshchin, D. A.	EP549	Russo, B.	EP200
Rosiak, E.	EP387, OP582	Russo, G.	EPW22
Ros Izquierdo, J.	EP689	Russo, S.	EP137, EP197, P181
Roskosz, J.	EP329	Russo, V.	EP180
Rosol, T.	EPW32	Russu, R.	P183
Rosqvist, F.	EP582	Rustarazo-Losada, S.	EP655, EP799, TP096
Ross, T. L.	EP639, EPW89, OP313, OP319	Rusu, D.	EP380
Rossetti, C.	P135, P144, PW01	Ruszniewski, P.	OP394, OP631
Rossetti, V.	EP088, EP089, EP258, EP288	Ruurda, J. P.	OP078
Rossi, E.	EP101	Ruuska, T.	OP688
Rossi, G.	EP180, OP167 , OP604	Rybalov, M.	OP349
Rossi, L.	OP214	Rydberg, J.	EP452 , OP564
Rossi, S.	EP014	Ryu, Y.	P114
Rossmann, A.	OP239	Ryzhkova, D.	P086, P087
Rostampour, M.	TP013, TP055		
Rota, R.	OP478	Saad, N.	EP132, OP015
Rotger Regí, A.	P152, P268	Saarinen, T.	EP842, TP030
Roth, N.	OP558, OP559, P049	Saatchi, K.	EP472
Rotmensz, N.	EPW06	Sabaté-Llobera, A.	EP018, EP116, EP131 , EP160, EP167, EP230, OP031 , P137, TP096
Rotolo, N.	EP156		OP356, OP508, OP509, OP510
Roule, V.	OP558, OP559, P049	Sabbah, R.	EP579, EPW74 , OP219, P164
Rousseau, C.	EP380	Sabet, A.	EP769, OP302
Roussel, P.	EPW21, OP601	Sabet, H.	EP810, EP820
Routier, S.	EP826	Sabol, J.	PW29
Rouzet, F.	EPW95, OP170, OP192, OP560, OP565, OP605, OP696	Sabra, A.	EP707, P088
	EP318	Sabra, M.	OP179, OP378, OP617, P245
Rovere, L.	EP649, PW36	Sabri, O.	EP529, EP530
Rowe, C. C.	P191	Sabzevari, O.	EP086, OP033
Rózsa, D.	EP170, EP545	Sacchetti, G. M.	OP632
Ruano, R.	P199, TP045, TP085, TP105	Sachs, J.	TP099
Ruano Perez, R.	EPW92	Sackiewicz, A.	EP833
Rubagotti, S.	EP567, OP601	Šačkus, A.	EP100, EP107
Rubello, D.	OP337	Saco, A.	OP194
Ruberto, T.	EP117, EP613, OP200, P111, TP036	Sacré, K.	EP707, EP497, P088
Rubí, S.	EP135, EP142, EP213, EP221, EP236, PW23	Sadeck, G.	TP013, TP055
Rubini, G.	TP084	Sadeghi, M.	OP446
Rubió Rodríguez, A.	EP758	Sader, J. A.	EP426 , EP446, OP544 , P204 , P209
Ruchala, M.	EP787	Sadic, M.	EP192
Rucher, G.	P134	Sadija, A.	EP227, EP415
Rucka, D.	OP290	Sadik, M.	EP535
Rudelius, M.	EP696	Sadkin, V. L.	OP503
Ruenzi, M.	OP488	Saenz, Y.	EP298, EPW42, OP223
Ruest, T.	OP596	Sađer, S.	OP225
Ruf, J.	EP219 , EP400, EP618, P234 , P284	Safranow, K.	OP225
Ruffini, L.		Saftencu, M.	EP341 , EP375 , EP376 , OP220

- Sager, S. EP194
Saghari, M. EP081
Saginoya, T. EP323
Sagona, A. OP243
Sahbai, S. EP017, EP429, **OP130**, OP135
Sahin, B. EP112
Sahin, E. **P163**
Sahin, O. E. **EP244, EP245**, EP547
Sahiner, I. **EP281**
Sahli-Amor, M. OP183
Sahlmann, C. O. OP492
Saho, T. EP744
Saibene, T. EP066
Said Criado, Y. TP076, **TP079**, TP087
Saif, T. EP753
Sailaja reddy, M. EP048
Saint, K. J. **P057**
Saint-Aubert, L. OP065
Sainz de la Cuesta, R. EP296
Sainz Esteban, A. P093, **P103**
Saipa, P. **TP030**
Saito, H. TP063
Saito, K. EP027
Saito, O. EP027
Saitoh, T. EP683, P036, **P048**
Sajedi, S. EP761, **EP765**, OP218
Sakaguchi, K. EP490, EP715
Sakata, I. EP151
Sakata, M. EP830
Sako, T. P281
Sakri, H. EP370
Saksa, E. **TP107**
Sakuragi, Y. TP003, TP010, TP059
Sala, Q. EP624
Salabert, A.-S. EP389, **OP255**, P285
Saladini, G. EP004, EP247, EP748
Salahinejad, M. **P283**
Salas, M. **EP477**
Salaün, P.-Y. OP181
Salazar, A. L. **EP225**
Salazar-Andia, G. EP455
Salcedo-Pujantell, M. **EPW07**
Saldaña, P. EP655, EP799
Saldarriaga Vargas, C. **OP677**
Saleem, A. OP341
Salehi, N. P014
Saletti, P. **EP822**
Salgado, L. EP554
Salgarello, M. EP085
Salihoglu, Y. S. EP548
Salimi, y. **EP804**
Salles, G. OP406
Salles, P. G. EP225
Salm, L. EP697
Salomão, L. EP225
Salomon, T. OP559, P045
Salsidua Arroyo, O. EP045, EP057, EP061, EP178
Salvadori, J. OP508
Salvadori, P. EP743, EP773
Salvatore, B. EP186
Samal, M. **OP041**
Samardzic, T. P299
Samarkin, I. EP367
- Sambuceti, G. EP017, EP169, EP429, EP662, OP127, OP135, OP233, OP262, OP288, OP373, OP408, OP409, OP421, P042, P255, PW22
Samim, M. **EP136**
Samiri, H. OP462
Sammartano, A. EP219, EP618, P234, P284
Sammur, E. OP514
Samnick, S. OP290, **PW32**
Samoylenko, L. P063, P065
Sampaio, I. EP251, OP396
Sampath, S. **EP146**
Sampedro, F. OP379, PW35
Samper-Noa, J. P233
Sampol, C. **EP117**, P111
Samuraki, M. P248
San, H. **EP345**
Sanches, P. G. OP493
Sanchez, J. EP291
Sanchez, P. G. EP422
Sánchez-Catasús, C. A. **P233**
Sánchez-Enrique, C. OP698, PW21
Sanchez Fernandez, P. L. TP405
Sánchez-Font, A. OP600
Sánchez García, M. **EPW49**, EPW55, OP631, TP084
Sánchez-González, J. EP736
Sanchez Jurado, R. EP191, **OP278**
Sanchez-Merino, G. EP284
Sanchez-Rodriguez, V. OP562
Sanchez-Salmon, A. EP255
Sánchez-Sánchez, R. **EP072, EP293**, EPW24, EPW37
Sánchez Vañó, R. OP375
Sancho, L. EP224, EP470, EP814, **OP016**
Sancho-Márquez, M. EP200
Sanders, J. EP275, OP018, **OP515**
Sandhu, S. EP486
Sandler, I. EP199
Sandoval Moreno, C. EP310, P034
Sandstrom, M. **EP502**, EP578
Sanfilippo, S. EP199
Sangro, B. OP016
Sankar, G. EP368, **P058**, P072, **P142**
San-Miguel, J. OP410
Sannino, P. EP238, EP567, OP653, P264, P267, P290
Santesteban, P. EP208
Santi, I. EP051, EP070, EP104, EP295, EP687
Santín-Cerezales, M. P137
Santini, C. **OP671**
Santonicola, A. P273, P275
Santoro, A. EP306, EPW25
Santos, A. EP056, EP060, EP267, P189
Santos, A. I. OP371, P105, **P180**, P194
Santos, J. G. OP371, P105, P194
Santos, L. A. P279
Santos, T. EP497
Santos, V. TP043
Santos Carreño, A. L. EP297, **OP572**
Santos Chamorro, C. EP028
Santos Gómez, I. EP184, EP202, OP180
Santosh, C. TP082
Santos Montero, B. EP638, EP651
Sanz, J. OP193
Sanz-Ceballos, L. EP653, EP656, EP657
Sanz L.Lorens, R. EP191
Sanz Viedma, S. EP532
Sapin, N. OP429
Saprina, T. P208

Sari, I.	EP162	Schiazza, A.	OP203, OP429
Sara, R.	P135, P144	Schibli, R.	OP398, OP589
Sarandeses Fernandez, P.	EP084, EP127, EP231, P123	Schick, U.	OP181
Sarikaya, A.	EP166	Schieferstein, H.	EPW89
Sarkar, S.	EP606, EPW31	Schillaci, O.	EP218, EP238, EP262, EP567, OP653, P264, P267, P290
Sarmiento-Ribeiro, A. B.	EP599, OP673	Schiller, C.	EP278, OP553, OP555
Sarmiento Soto, M.	OP584	Schincaglia, V.	EP687
Sarnyai, Z.	EP766	Schindler, T.	OP611
Saro, J.	OP593	Schiorlin, I.	EP156
Sarparanta, M.	OP234	Schlesinger-Irsch, U.	OP189
Sarrut, D.	EP777	Schleyer, P.	OP514
Sartor, O.	OP338	Schlögl, S.	EP434, EP477, OP635
Sartorello, A.	EP206	Schmidt, K.	EP432
Sasaki, T.	EPW61 , P282	Schmidt, M.	OP426
Sasso, A.	P073	Schmidt, M.	EP483, OP084
Satari, A.	EP619	Schmitt, C.	P083
Sato, H.	EPW03	Schmitt, S.	OP612
Sato, J.	OP177	Schmolders, J.	P164
Sato, N.	EP064, P281	Schoder, H.	OP687
Sattin, D.	PW38	Schols, D.	OP488
Sattler, L.	OP552	Scholtens, A. M.	OP146, P131
Saunders, J. H.	P224	Schonecker, S.	OP425
Saushkin, V.	P086, P087	Schoots, I.	OP351
Saushkina, Y.	P086, P087	Schottelius, M.	OP074
Sauter, A. W.	EPW85	Schou, M.	EP586
Savaş Den Hartigh, Ö.	P052	Schouten-Stadnik, K.	TP046
Saveur, L. J.	OP293	Schrader, L. D.	OP519
Saviatto, A.	EP084, EP127, P123	Schramm, G.	EP756
Savintseva, Z.	EP019	Schramm, N.	OP300
Savisto, N.	TP030	Schreckenberger, M.	EP009
Sawicki, L.	EP242, EP572, OP501, OP505	Schreiter, N.	OP149
Sawyer, M. B.	OP519	Schreuder, F.	OP416
Saxtoft, E. S.	TP095	Schrijver, W. A. M. E.	OP171
Sayed, M. H. M.	EP377	Schubring, M.	EP003
Sayit, E.	EP324, TP022, TP038, TP070	Schuchardt, C.	EP453, EP480, EPW16, OP112 , OP459
Sayman, H.	EP194	Schuller, K.	EP798
Sazonova, S.	EP635 , EP701, EP709	Schulze, C.	TP001
Scabbio, C.	EP746	Schwaiger, M.	EP203, EP266, EP274, OP059, OP074, OP088, OP239, OP346, OP423, OP566
Scaggion, A.	EP748, EP789	Schwartz, A.	OP338
Scala, D.	EP216, P073	Schwartz, L.	EP552, OP687
Scalorbi, F.	EP121 , OP221	Schwarz, T.	OP128
Scalzo, M.	EP486	Schwarzenböck, S. M.	OP118
Scarabeo, F.	EP259	Schweighofer Zwink, G.	EP339, OP485, P056
Scaringi, C.	OP654	Schweitzer, S.	OP444
Scarlattè, M.	EP219, EP400, EP618, P234, P284	Scialpi, M.	P273, P275
Scarpa, L.	EP139, EP277, EP479 , OP457	Sciumè, F.	EP260, EP402, TP028 , TP033
Scarpini, E.	P253	Sciuto, R.	EP521
Scarsbrook, A. F.	OP143	Scolaro, T.	EP556
Schaarschmidt, B. M.	EP572, OP501, OP505	Scolozzi, V.	EP308, EP311, EP317, EP322
Schaefer, N.	EP325, P265	Scopinaro, F.	OP654
Schäfer, M.	EP837, EPW84, OP022, OP444	Scorsetti, M.	OP355
Schäfers, K.	EP718	Scotognella, T.	EP627
Schäfers, M.	OP224, OP695, PW30	Scott, A.	EP649, OP550
Schaffer, P.	EP591	Scuffham, J.	EP374, EP788, EP793, OP136, OP138
Schaier, E.	EP615	Scully, D.	EPW36
Schaitel, B. A.	OP519	Sebastià, M. C.	EP100, EP107
Scharre, D.	P225	Sebastián, N.	EP496
Schatka, I.	EP481	Segars, P.	OP507
Scheidhauer, K.	OP088	Segbers, M.	EP417 , EP782, OP211, TP101
Schellens, J. H. M.	OP593	Segreto, S.	EP301, OP461
Scherthan, H.	EPW50	Segtnan, E. A.	EP029, EP037 , EP671, EP720, P240, P241
Schettino, G.	EP788	Seibyl, J.	OP378, P245
Scheurlen, M.	OP290	Seidl, C.	OP309
Schiariti, M.	OP680	Seimbille, Y.	EPW93
Schiavina, R.	EP223, EP265, EPW75		
Schiavo, R.	EP292		

Seitz, C.	EP233, OP500, OP551	Shegani, A.	EPW05
Seker, M. M.	EP162	Sheikh, M.	OP462
Selcuk, N. A.	EP245	Sheikhzadeh, P.	EP769, OP302
Selivanova, S. V.	OP446	Shekar, C.	EP482
Sellem, A.	P187	Shelley, S.	EP688, P129
Selmic, M.	EP355	Sheng, Y.	OP486
Selting, K.	EP424	Shepherd, T.	OP217, OP482
Semah, F.	P184, P274	Sher, A.	P159
Semiglazova, T.	OP481	Shevchenko, O.	P063, P065
Sen, F.	EPW23	Shi, Q.	EPW73
Senemaud, J.	OP170	Shi, S.	OP402, OP592
Seng, M.	P177	Shibutani, T.	TP047 , TP065
Sengezer, T.	EP281	Shiga, T.	OP177
Sengoz, T.	P141 , PW28	Shigematsu, N.	EP151
Seniaray, N.	EP035	Shiina, H.	EP005
Senin, A.	EP193	Shilpa, K.	EP688 , P129
Senol, H.	PW28	Shimada, H.	TP060
Seo, Y.	TP058	Shimi, Y.	EP125, P173
Seok, J.	EP073 , EP076	Shimoda, Y.	PW31
Sepe, I.	EP216	Shimosegawa, E.	EPW60
Sequeira, J. A.	OP371, P194	Shin, K.	P256
Seregni, E.	EP458, OP011	Shin, S.	EP366
Sergienko, V.	P084	Shindoh, M.	OP177
Sergieva, S.	EP214	Shinohara, Y.	PW39
Seror, O.	OP030	Shinya, T.	EP013, P276
Serrano, M. J.	EPW24	Shiraishi, S.	TP020, TP066
Serrano García, I.	PW21	Shiraishi, Y.	EP683
Serrano-Palacio, A.	EP045, EP057, EP061, EP178	Shiri, I.	EP760 , OP498
Serrano-Piñol, T.	EP131, OP031	Shirokorad, V. I.	EP549
Serrano Pradas, G.	EP689	Shiue, C.-Y.	EPW57, P297
Serrelí, G.	EP400, EP618, P234	Shivdasani, D.	P155
Serry, G.	P149	Shogo, K.	TP020
Serry, O.	OP087	Shojaeilangari, S.	EP421
Seshadri, N.	P110	Shuke, N.	EP027
Sessa, F.	EP256	Shukla, J.	EP271
Setoain, X.	OP200	Shulkin, B.	OP085
Seven, B.	EP695	Shurupova, I.	P032
Severi, S.	OP338	Sibley-Allen, C.	EP456, EP491
Severin, G. W.	EP836, OP304	Sibson, N. R.	OP584
Sevinc, A.	EP144	Sicignano, M.	EP169, OP127
Sewing, C.	OP587	Siclari, G.	PW22
Sfar, R.	EP331, EP370, P165	Siddique, M.	EP001 , EP336 , EP668, OP086 , OP602, P099
Shabo, G.	P261	Siddiqui, J.	EP407, EP409
Shafiei, B.	EP396, EP818	Siebert, A.	EPW55
Shah, H.	EP482	Sierro, N.	P298
Shah, S.	EP025, EP273	Sieuwert, A. M.	OP171
Shahhosseini, S.	EP529, EP530	Silig, Y.	EP162
Shahid, W.	EP373	Sillanmäki, S.	P020
Shahinfar, M.	EPW16, OP112	Silva, A.	TP072
Shamsaie, M.	EP768	Silva, F.	TP018
Shankar AP, G.	EP232	Silva, M.	P150 , P212
Shanmuga Sundaram, P.	OP182, OP370	Silva, M. G. G.	TP072
Shao, X.	EP407	Silva, N.	EPW52
Shapouri, Z.	OP218	Silva, R.	EP246 , EP328, OP140, P150, P212
Shariat, S.	EP233, EPW11, OP500, OP551	Silva Monteiro, M.	EP325
Sharif Pour, R.	EP759	Silva-Rodríguez, J.	OP070 , P263
Sharma, A.	OP015, OP597 , OP651	Silvia, M.	EP219
Sharma, M. C.	OP597	Siman, W.	EPW53
Sharma, P.	EP189	Sime Loayza, I.	EP250, EP441 , EP471, EP682
Sharma, R.	EP035, OP341	Simeone, L.	EP180, EP186
Sharma, V.	P090	Simó Canonge, R.	EP638
Sharp, D. G.	TP023, TP048	Simon, H.	EP762
Shaw, K.	EP668	Simon, J.	EP424, EP436
Shaw, P.	OP490, P177	Simon, T.	OP084
Shawky, O.	OP089	Simonds, H.	OP037
Shaylor, A. H.	EP518	Simoncic, B.	TP004, TP009

Simonsen, J. A.	OP568	Smith, D.	OP686
Simó-Perdigó, M.	EPW07	Smith, G.	EP607, EPW65, EPW80
Simsek, F. S.	EP338	Smith, R.	EPW65
Şimşek, T.	EP103	Smith, S. V.	EP611
Simsekyilmaz, S.	OP422	Smits, R.	EPW87
Simunac, M.	P201	Smoleń, M.	TP029, TP032
Sindermann, J.	OP695	Smout, A.	EP516, EP723
Singer, J.	EP623, EP636	Smyth, E. J.	OP060
Singh, A.	EP232 , EP368, EPW76, P058, P072, P142	Smyth, V.	EP449
Singh, A.	EP480 , EPW16, OP112, OP113, OP150, OP459	Soares, S.	P121, TP091, TP109
Singh, B.	EP023, EP161, EP235	Soares Junior, J.	P189
Singh, H.	EP189	Soares Machado, J.	EP434
Singh, H.	EP023	Sobic Saranovic, D.	OP040, OP042, P205
Singh, M.	OP651	Sobral Violante, L.	EP251 , OP396
Singh, N.	OP245	Sobrinho, T.	P263
Singh, N.	EP161, EPW68	Socan, A.	EP856
Singh, S. S.	OP561	Soffientini, C.	OP495
Singh, S. K.	EP271	Sohara, K.	P269
Sinha, A.	P090	Sola, M.	EP065, P128
Similkin, I.	EP075, EP097, EP632, EP634	Solano, A.	EP193
Sinsabaugh, C.	P116	Solati, J.	EP619
Sinyakova, O. G.	P260	Soler Peter, M.	EP191
Sioka, C.	P028, P030	Solfaroli Camillocci, E.	OP680
Siores, E.	OP417	Solin, O.	EP842, EP851, EP853, EPW96, PW33, TP030, TP107
Siozopoulos, A.	P120	Sollaku, S.	P280
Sipilä, O.	P239	Sollini, M.	EP041 , EP157, EPW66, OP243, P133
Siracusa, M.	OP536	Solný, P.	EP384, EP438
Siraj, Q.	EP461	Solodyannikova, O.	EP083 , EPW27
Sirén, A.-L.	PW32	Soltan, A.	P023
Sireus, M.	EP400	Soltani, N.	EP619, EP626
Sironi, S.	EPW09	Soma, M.	EPW03
Sisic, M.	OP368	Somai, M.	EP393, P166
Sisko Markos, I.	EP010	Somaii, M.	EP358
Sitarz, M.	OP445, OP675	Sommariva, A.	EP305
Siva, A.	EP130, EP307, EP669, EP753, EPW32	Sommer, P.	OP566
Siwowska, K.	OP543	Somsen, G. A.	OP217, OP282, OP283
Sjögreen Gleisner, K.	OP522	Son, H.	P147
Skaddan, M. B.	OP310	Sone, D.	P281
Skalniak, A.	P095	Soneji, N.	EP691, OP277, OP569 , P251
Skanjeti, A.	EPW21, OP601 , OP699	Song, B.-I.	OP196
Skibova, D.	OP041	Song, H.	EP053, EP333
Skoumas, J.	OP420	Song, H.-C.	EP312
Skovgaard, D.	EP054	Song, Y.	OP571
Skowasch, D.	OP189	Song, Y.	EP173
Skuridin, V.	EP097, EP632, EP634, EP635	Soni, N.	EP606
Skvortsov, V.	EP654	Sonke, J.	OP296
Skvortsova, T.	EP019	Sonmez, O.	EP468
Sladojevich, F.	OP398	Sönmezgöz, F.	EP082
Slama, M.	OP192	Sönmezoglu, K.	EP194, EP298, EP392, EP614, EP808, EP858, EPW42, OP223, OP679
Slart, R. H. J. A.	EPW66, OP610, OP700, P091	Sonni, I.	EP020 , OP076, OP504
Slender, V. J. W.	TP025	Sood, A.	EP120, EP229 , EPW29, OP125, P097
Slim, I.	EP358, EP393, P166	Sopena-Novales, P.	P289, PW37
Slodnjak, I.	TP073	Sorbets, E.	OP560, OP605
Slonimskaya, E.	EP075	Sörensen, J.	OP190, OP252, OP517
Slootweg, H.	TP025	Soret, M.	OP183
Sluimer, J.	OP416	Sorg, C.	OP147
Slump, C. H.	EP282, EP422, OP493, PW25	Soriani, A.	EP521
Smalley, M.	OP490	Soriano Castrejón, Á.	EP098, EP222, EP689, OP075, OP240, OP369
Smechov, M.	OP191	Soriano-Mas, C.	OP374
Smeele, L.	EP478	Sosabowski, J.	EP703, EP801, OP545
Smidt, M. L.	EP055	Sosef, M. N.	OP078
Smishlyaev, K.	P087	Sotiropoulou, R.	P040
Smit, E. F.	OP599	Sousa, D.	TP017, TP018
Smith, A.-L.	EPW45	Sousa, E.	OP480, TP061

Sousa, J. M.	OP252	Steinhagen-Thiessen, E.	P249
Sousa, R.	EP554	Stembrowicz-Nowakowska, Z.	EP071
Soussain, C.	EP176	Stender-Petersen, K.	P296
Soussan, M.	EP080, OP081, OP251 , OP315, OP516, P089	Stenvall, A.	OP281, TP031
Souto, L.	EP286	Stenzel, J.	OP118
Souvatzoglou, M.	EP501	Stephens, A.	EP020, OP348, OP378
Souza, E.	OP277	Stern, E.	EP774
Souza, T. F.	EP060	Stetter, C.	PW32
Sowa-Staszczak, A.	P095	Stettler, C.	EP678
Soydal, C.	EP190, EP485	Stevanovic, V.	OP294
Soyluoğlu Demir, S.	EP166	Stevenson, N. R.	EP436
Spa, S. J.	OP639	Stevic, M.	EP361
Spadavecchia, C.	EP785	Stich, M.	EP798
Spaepen, K.	OP080	Stipo, M.	EP813, OP536
Spallarossa, P.	PW22	Stirling, J.	EP581, OP514
Spallino, M.	EP175, OP682	Stokke, C.	EP492
Spanu, A.	EP218, EP330 , P273, P275, P278	Stokkel, M. P. M.	EP282, OP293, OP593
Spasic, E.	OP298	Stokmo, H.	TP090
Spassov, B.	EP179, EP343	Stolarz, A.	OP445, OP672, OP675
Speirs, C. K.	OP015	Strataki, A.	P040
Spencer, D. D.	OP312	Strauss, A. C.	P164
Sperandi, F.	EP153	Strauss, H.	EP835
Spezi, E.	EP469	Streefkerk, E. C.	OP484
Spicka, I.	EP195	Stricker, P.	OP550
Spielman, D. M.	OP503	Stricker, S.	OP444
Spiering, W.	P091	Strigari, L.	EP521
Spies, L.	P249	Ström, P.	EP586
Spiliotopoulou, M.	P028, P030, P210	Stroobants, S.	OP080
Spinks, T.	EP703, EP801	Strosberg, J.	OP394
Sponholtz, S. E.	EP109	Struelens, L.	EP449, OP677
Sportelli, G.	EP743, EP773	Strydhorst, J.	EPW49
Sposito, C.	EP458, OP011	Stuchbery, A. E.	EPW56
Spreafico, C.	EP458, OP011	Stuchebrov, S.	EP474
Sprycha, M.	EP582	Stuckey, A.	EPW59
Spyridonidis, T.	P210	Stuffins, M.	OP136
Spyrou, G.	OP417, OP420	Sturla, L.	EP662
Sreenivas, V.	OP597	Suárez Novo, J.	EP230, EP290
Staanum, P.	TP014	Suárez-Piñera, M.	EP022, EP193, OP600
Stace, S.	TP110	Suarez-Sipmann, F.	OP517
Stadhouders, T.	OP147	Subramanian, P.	EP551, EP737, OP067, OP184
Staelens, S.	EPW58, P286	Suchorska, B.	OP650
Ståhl, S.	EPW82, OP114, OP311	Suetake, M.	TP021
Stakhiv, O.	OP480	Sugai, R.	EPW03
Stalin, J.	OP344	Sugai, Y.	EP034
Stamatoullas, A.	OP406	Sugihara, Y.	EP699, P050
Stammes, M. A.	EPW35, OP642	Sugimoto, M.	P044
Stanzel, S.	EP140, OP128	Sugo, N.	P269
Starcea, M.	P183	Suils Ramón, J.	EP290, EP294 , PW09
Stasi, M.	EP464, OP538, P242	Sukhov, V.	EP241 , EP364, OP412, P011 , TP064
Stasyuk, E.	EP535, EP632 , EP634, EP635	Sulikowski, T.	OP225
Statescu, A.-M.	P183	Sullivan, B.	EP610
Staudenherz, A.	OP038	Summer, D.	OP345
Stearns, C.	EP786	Summers, S.	OP217, OP482
Stebner, V.	OP219	Sun, A.	OP275
Stefanelli, A.	EP104	Sun, H.	OP308
Stefanescu, C.	P183	Sun, Y.	EP059
Stefanic, M.	EP561	Sunaert, S.	OP257
Stefano, A.	EPW22	Sunassee, K.	EP598
Stefano, C.	TP089	Sundin, A.	EP502, EP578, OP291
Steffen, I. G.	EP663	Sundlöv, A.	OP522
Stefoni, V.	EPW72	Sun Lin, Q.	EP113
Stegger, L.	OP224, OP455, TP024	Sunmyung, P.	TP071
Steiger, K.	OP239, OP346, OP566	Suppa, P.	P249
Stein, D.	OP614	Surer, H.	P204
Steinbach, J.	EP525, EP844	Surer Budak, E.	EP103, EP210
Steiner, B.	OP403		

Skuridin, V. S.	EP535	Takenaka, F.	EPW61
Susani, M.	EP233, OP500, OP551	Takes, R. P.	EP115
Susin, D.	P226 , P287, P291	Takeuchi, T.	TP063
Sustar, S.	TP004, TP009, TP073	Taki, J.	OP285
Suver Stevic, M.	EP561	Tal, I.	EP408, OP246, OP406
Suzenet, F.	EP826	Talavera Rubio, M.	EP098
Suzuki, K.	P036	Talavera Rubio, P.	OP369
Svärm, L.	EP415	Talbi, A.	EP215, EP348, P059, P064
Svensson, J.	EPW48, OP132, OP391, OP522	Talbot, J.-N.	EP263, EP391, EP650, EPW70, OP292
Svensson, S. P. S.	EP586	Taljaard, L.	OP614
Svensson, W.	EP691, OP260, P251	Talsma, A.	EP791
Swallen, A.	EP404, OP258	Tam, H.	OP277, OP569
Swart, L. E.	OP146, P131	Tamagnan, G.	OP063
Švitlik, D.	OP357	Tamaki, N.	OP029
Sykala, M.	EP385	Tamayo, P.	EP170, EP545
Sykorova, V.	EPW39	Tamayo Alonso, M. P.	P199, TP045, TP085, TP105
Szabó, J.	EP596, EP597, EP834, EP838	Tambasco, N.	P273, P275
Szczucka-Borys, K.	EP721	Tamiji, Z.	P283
Sze, D. Y.	EP136	Tammela, T.	EP261
Szentesi, M.	EP427	Tamura, K.	EP151
Szigeti, K.	EP640	Tanabe, Y.	PW39
Szikra, D.	EP603 , EP677, EP834	Tanaka, K.	EP026, EP030
Szilasi, M.	P191	Tanaka, Y.	EP064, EP091
Szilvási, I.	EP123, EP519, P067	Tang, C.	OP550
Szkliniarz, K.	OP672, OP675	Tang, S.	OP060
Szlosarek, P. W.	EP299	Tang, S.-P.	EP828
Szoliková, M.	OP212	Tangpong, P.	EP826
Szumowski, P.	EP385 , EP577, OP540	Tanguay, J.	EPW54
Szysko, T. A.	EP299	Tanha, K.	EP660, EPW33
Tabain, A.	EP713	Tann, M.	OP012 , P116, P119, P122
Tabeie, F.	EP396 , EP818	Tanyildizi, H.	EP808
Tabocchini, A.	EP521	Tanzi, F.	EP156
Tabone, M.	EP464, OP013	Tapia, A.	OP200
Taborska, K.	OP085	Tapias, A.	EP107
Tabouret-Viaud, C.	P250	Tapner, M.	EP469
Tabuena, M.	EP084, P123	Taralli, S.	EP051, EP070, EP104, EP295, EP687
Taddei, C.	OP397 , OP399	Taran, F.-A.	OP130
Taddei, S.	OP598	Tardelli, E.	EP114, EP560, P117
Tadolini, M.	P146	Tari, L.	EP586
Taelman, V.	EP678	Tarn, M. D.	EPW90
Tafari, M.	OP255	Tartaglione, A.	EPW46, OP598, P243
Tagliabue, G.	OP011	Tarvainen, M.	P020
Taha, G.	OP089	Taş Gülen, S.	EP119
Tahari, A.	OP611	Tashiro, M.	EPW03
Taheri, M.	EP765	Taslipinar, A.	EP346
Taheri, P.	EP450	Tatci, E.	EP159
Tahseen, R.	EP357, EP373, P077	Tattenberg, S.	EP484
Taieb, D.	EP794	Tauber, R.	EP266
Taimen, P.	OP348, OP354	Taus, A.	OP600
Tajima, Y.	EP151	Tavares, A.	EP800
Takács, E.	EP123, P067	Tavares-Silva, E.	EP515
Takahara, N.	EP715	Tavella, S.	OP233
Takahashi, H.	OP029	Taviani, V.	OP503, OP504
Takahashi, K.	TP063	Tavolozza, M.	EP238
Takahashi, K.	P282	Tawakol, A.	EP359, P178
Takahashi, S.	EP005	Tebano, U.	EP085
Takahasi, Y.	EP717	Tedesco, M.	OP340, OP547
Takan, G.	TP080	Teichmann, M.	P254
Takanami, K.	P013	Teimourian, B.	EP761, OP218
Takano, A.	EP766, OP303 , OP316	Teixeira, D.	TP061
Takano, Y.	EP323	Teixeira, J.	TP017, TP018
Takase, K.	P013	Teixeira, J. P.	EP251, OP396
Takechi, K.	EP013	Teixeira, R.	OP126
Takekawa, S.	EP323	Teixeira, S.	TP072
Takenaka, D.	EP090, EP172	Tekin, V.	TP080
		Te Kolste, H. J.	OP146

Teksöz, S.		EP392	Tokic, S.	EP561
Tello Galán, M.	EP098, EP222, EP689 , OP075, OP240, OP369		Toklu, T.	EP245, EP466, EP468, OP014
Ten Borg, E.		P151	Tolbod, L. P.	PW26, TP034, TP098
Tennvall, J.		OP522	Tolmachev, V.	EP522 , EPW81, EPW82, EPW83, OP114, OP172, OP311, OP398, OP589, OP591
Teodorczyk, J.		EP165	Tolvanen, T.	EP823
Teodorovic, D.		EP355	Tomaszewska, E.	OP672
Terš, J.		P033	Tomic Brzac, H.	EP129
Teranishi, Y.		EP323	Tomiguchi, S.	TP020, TP066
Teräs, M.		EP823	Tong, C.	OP062
Teresinska, A.		P085	Tonge, C. M.	OP497, P057
Ternovskaya, K. E.		EP625	Topcu, B.	P163
Terry, S. Y. A.		OP343, OP400	Topping, G.	OP566
Tesselaar, M. E. T.		OP293	Toprak, E. K.	PW28
Testa, A.		EP521	Toptaş, T.	EP103
Testanera, G.		EP157	Torlak Lovric, V.	P201
Testard, A.		EP078 , EP796	Torrente, S.	OP033
Testart Dardel, N.	EP028 , EP072, EP293, EPW37, EPW70 , OP375		Torres-Espallardo, I.	EP418, EP462 , EP496
Testoni, M.		P186	Torres Jimenez, M.	TP076, TP079, TP087
Testori, A.		EP306	Torres-Vela, E.	EPW37
Teterin, K.		EP367	Toscano, M.	EP117, EP613, P111
Teulé-Vega, A.		EP116	Toschi, L.	EPW25
Teunissen, J. J. M.		EP220	Tosco, L.	OP554
Tezak, S.		P051	Tóth, M.	EP586, EP766, P227
Thaker, N. R.		OP411	Touati, A.	OP418, OP605, OP696
Thakor, A. S.		EP472	Toubeau, M.	OP246
Thakur, M. L.		EP670 , TP075	Touil, S.	EP015, EP125 , P173
Thebaud, E.		EP011, EP012	Tournier, N.	OP315 , OP618
Thelen, P.		OP492	Tousoulis, D.	OP417, OP420
Thellenberg Karlsson, C.		OP338	Toutouzas, K.	OP417, OP420
Theodorakos, A.		P070	Touzeau, C.	OP407
Thisgaard, H.		EP674	Towey, D.	OP652
Thivolet, C.		OP699	Toyama, T.	TP060
Thøgersen, K. F.		OP568	Toyohara, J.	EP026, EP030, EP830
Thom, A. F.		TP044	Trabelsi, K.	P187
Thoma, A.		OP088	Tran, T.	EP133, OP036
Thomae, D.		EPW58, P286	Tran-Gia, J.	EP434, EP477, OP635
Thomaidou-Ntanasel Antina A.		P040	Trastulli, F.	EP180
Thomas, C.		EP009	Traub-Weidinger, T.	EP036, EP727, OP249, OP648, OP649
Thomas, D.		OP189	Travaini, L.	EP546, EPW06, OP332, OP680
Thomassen, A.		EP092	Traxl, A.	OP315
Thompson, B.		OP550	Trebec, B.	TP073
Thompson, J. A.		OP488	Tredwell, M.	EPW87
Thorsson, O.		EP261	Treglia, G.	EP032 , OP337, OP535
Thorstensen, E.		EP217	Trejtmar, F.	EP531
Thulkar, S.		OP597	Trencsényi, G.	EP596 , EP597 , EP603, EP677 , EP834, EP838, EPW64
Thureau, S.		OP181	Tresch, E.	EP042, OP129
Thyroff, A.		OP018	Trevisan, A.	P279
Tian, J.		OP638	Trias Davesa, I.	TP084
Tiar, M.		EP215	Trigg, W.	EPW91
Ticconi, F.	EP662, OP233, OP288, P042		Trigonis, I.	EP309
Tienken, M.		EP831	Trigo Perez, J. M.	OP338
Tietze, S.		EP836	Trindev, P.	EP805
Tiling, R.		OP032	Tripathi, M.	OP651
Timmer, J. R.		PW25	Trivieri, M. G.	OP193
Timur, S.		TP080	Triviño Ibáñez, E.	EP028, EP072, EP293, EPW24, EPW37 , OP375
Ting, S.		OP219	Trnka, J.	P134, PW05
Tinoco, C.		EP497, P088	Trofimiuk-Müldner, M.	P095
Tio, R. A.		OP610	Trogrlic, M.	P051
Tipping, J.		EP449, OP136	Troisi, R.	EP724
Tirel, O.		OP612	Trojan, L.	OP492
Tkachenko, M.		P167	Trombella, S.	P250
Tobalina Larrea, I.		EP284	Trono, V.	EP137
Todica, A.		OP088	Trufanova, E.	EP289
Togashi, K.		EP405		
Tognoni, G.		P259		

Truffier, A.	OP170	Uricchio, F.	EP517
Trzcińska, A.	OP675	Urresola, A.	EP255
Tsalkidis, A.	P182	Ursini, F.	P264, P267
Tsartsarakis, A.	P040	Ursino, S.	EP114
Tsiakas, E.	EP437	Uslu, I.	EP194, EP504, EPW44
Tsiamis, E.	OP417	Uslu, L.	OP223, OP679
Tsibulnikov, S.	EP635	Uslu Biner, I.	EP159
Tsigalou, C.	P153	Usmani, S.	EP183 , OP090
Tsiouris, S.	EP024, P030	Usubov, M.	EP632
Tsougos, I.	P022	Usui, A.	TP063
Tsuji, M.	P231	Usui, H.	EP151
Tsukada, H.	EPW77	Uyama, N.	EP013, P276
Tsushima, Y.	EP316	Vaccari, S.	EP199
Tubaro, A.	EP261	Vach, W.	OP596
Tucci, M.	EP507	Vadrucci, M.	OP221
Tuji, S.	P293	Vafae, M. S.	P230
Tuncel, M.	OP684	Vag, T.	OP239
Tung, C.-H.	EP130	Vagne, B.	OP565
Tunninen, V.	P104	Vahrmeijer, A. L.	OP642
Turco, P.	EP789	Vaidyanathan, G. V.	OP594
Turgal, E.	EP190	Vaidyanathan, S.	OP143
Turgut, B.	EP162, EP383	Vašina, J.	P047
Turkeli, M.	EP695	Vaittinen, S.	OP688
Turkevich, E.	EP058, OP481	Valderas Montes, M.	TP104
Türkölmez, S.	EP079	Valdés Olmos, R. A.	EP068, OP643
Turner, C.	TP082	Valdovinos, H. F.	OP308, OP402
Turner, E.	P177	Vale, J.	TP017, TP018
Turoglu, H. T.	EP824	Valenta, I.	OP611
Turón-Sans, J.	OP374	Valenti, I.	EP216, P073
Turpin, S.	OP198	Valette, P.-J.	EPW21
Turri, L.	OP033	Valkema, M. J.	OP078
Turton, D. R.	EP607	Valkema, R.	OP078, OP107 , OP342, TP101
Tutar, R.	EP614, EP858	Vallabhajosula, S.	EPW94, OP424
Tutus, A.	EP675	Vallejo Casas, J.	OP338, P118
Tvedskov, T.	EP054	Vállez Garcia, D.	OP066, OP613, TP016
Tweedle, M.	EP537, EP610, EPW32	Vallinga, M. S.	OP349
Twyman, F.	OP341	Vallis, K. A.	EP443, EPW56, OP584
Tyczynska, K.	OP280	Vallot, D.	EP419 , EP785, EP807, OP494
Tyutin, L.	EP181	Valluru, K. S.	OP503
Tzen, K.-Y.	PW34	Valotassiou, V.	P022
Tzonevska, A.	P060	Valstar, M.	EP478
Tzvetkov, K.	P060	Valverde, I.	EPW85, OP398, OP587
Ubl, P.	EP363	Valzano, S.	EP464, OP538, P242
Ucan, B.	P098	Van Ammel, R.	EP677
Uccelli, L.	EP687	Vanaudenhove, T.	EP489
Ucmak, G.	EP093, EP096, EP099, EP102, EP105	Van Berckel, B.	OP373, P237
Udodov, V.	P139, PW08	Van Berge Henegouwen, M. I.	OP078
Ueno, M.	EP005	Van Brummelen, E.	OP593
Ugarte, V. E.	EP318	Van Buul, M.	OP139, P151
Ugarte, V. J.	EP318	Van Dalen, J. A.	EP422, OP493, PW25
Uiters, J.	OP149	Van Dam, M.	OP064
Ul-Hassan, F.	TP023, TP048	Van Damme, P.	OP069, OP430
Ullo, M.	P280	Vandecapelle, M.	EP489
Uhuyol, O.	P141	Van de Garde, E. M. W.	P151
Umeda, I. O.	EP725, EPW86	Van den Berg, N. S.	EP226, EP762, OP134 , OP639, OP643
Umezawa, R.	P013	Vandenbergh, S.	OP393
Umutlu, L.	EP572, EPW74, OP222, OP501, OP502, OP505	Vandenbergh, W.	OP426
Uña-Gorospe, J.	EP185	Vandenbos, F.	OP203
Unak, P.	OP668 , TP080	Van den Bosch, M. A. A. J.	EP136
Ungureanu, C.	P106	Van den Bosch, S. C.	EP115
Unterrainer, M.	OP650	Van den Broeck, B.	P149
Uotinen, J.	EP842	Van den Huel, O. A.	P277
Uprimny, C.	EP139, EP217, EP277, EP479, OP294, OP457	Van den Weyngaert, D.	OP080
Urbano, N.	OP653	Van den Wyngaert, T.	OP080
Urhan, M.	EP354	Van der Boor, R.	OP541
Uribe, C. F.	EPW54		

Vander Borgh, T.	EPW08	Varga, Z.	EP123 , EP640, P067
Van der Geest, T.	OP306	Varjo, P.	P104
Van der Gucht, A.	EP325, OP201, P265	Varona, D.	EPW07
Van der Kroon, I.	EP430	Varrone, A.	EP766, EP827, P227
Van Der Linden, A.	EPW58	Varshney, R.	EP630
Vanderlinden, B.	EP465, OP393	Vartzokas, M.	OP569
Van der Lugt, A.	P156	Vasanawala, S.	OP076, OP504
Van der Meulen, N.	OP589	Vasilenko, E.	EP334
Van der Ploeg, T.	EP558	Vasiliadis, T.	P120
Van der Poel, H. G.	EP762, OP134	Vasina, J.	EP679
Van Der Veken, P.	EPW58, P286	Vasquez, N.	OP611
Van der Vos, C. S.	EP751, OP297	Vassaux, G.	EP447
Van der Wal, S.	EP665, OP639	Vassilakos, P.	P022
Van der Zant, F. M.	EP558, P154, TP051	Vassileva, D.	EP179, EP343
Van Deurzen, C. H. M.	OP171, OP305	Vatankulu, B.	EP194, EP244, EP245, EP298 , EP392 , EP504,
Van de Velde, C. J.	OP134, OP642		EPW42 , OP223 , OP679
Van de Vondervoort, R. H. A. M.	OP489	Vauhkala, S.	TP030
Van de Wiele, C.	EP716, EP779, PW03	Vaysse, L.	OP255
Vandi, G.	P146	Vaz, S. C.	EP554
Vandici, F.	P170	Vazquez, M.	TP041
Van Diest, P. J.	OP171	Vazquez, N.	EPW58
Van Dijk, J. D.	PW25	Vaz-Silva, A.	P180
Van Dongen, A.	TP046	Vedin, O.	OP190
Van Dongen, G. A. M. S..	OP587, OP593	Veenland, J.	EP667, OP351
Van Duinkerken, E.	P296	Vega, F.	EP613
Van Eck-Smit, B. L. F.	OP217, OP282, OP283	Vega, V.	EP650
Van Eetveldt, A.	P286	Velasco, C.	OP229
Van Es, R.	EP478, EP550	Velasco, M.	EP291, EP296
Van Gent, D. C.	EP667, OP581	Velasco Jimeno, C.	PW27
Van Gils, K. A. J.	OP541	Velidaki, A.	EP279 , P113
Vangu, M.-D. H. W.	EP350, EP704	Velidedeoğlu, M.	EP298
Van het Schip, A. D.	EP790	Velikyan, I.	EP578, OP232 , OP517
Van Hillegersberg, R.	EP136	Velletta, J.	EPW81, OP172
Van Holen, R.	PW40	Vendel, B.	EP094
Van Kasteren, M.	PW07	Vendelbo, M. H.	OP686
Van Kronenburg -Rooze, L. A.	OP484	Ventroni, G.	OP336
Van Laarhoven, H. W. M.	EPW66	Vera, D.	OP423
Van Laere, K.	EP756, OP069, OP257, OP426,	Vera, P.	OP181
	OP430, OP554, OP615	Véran, N.	EP852
Van Lanschot, J. J. B.	OP078	Vera Pinto, V.	EP280 , EP512
Van Leenders, G. J. L. H.	OP351	Veras, M.	EP497, EP707, P088
Van Leeuwen, F. W. B.	EP226, EP665, EP762, OP134, OP639, OP643	Verberne, H. J.	OP146, OP217, OP282, OP283, P131
Van Lierop, S. Z. M.	TP101	Verburg, F. A.	EP369
Van Nederveen, F.	OP342	Vercellino, L.	EP302
Van Niekerk, A.	EP780	Vercher-Conejero, J. L.	EP018, EP116, EP131,
Vanniet-Cahouet, A.	EP617		EP160 , EP167, EP230,
Van Nijnatten, T. J.	EP055		OP031, OP374, P137
Van Oostenbrugge, R.	OP416	Vercouillie, J.	EP826
Van Oosterom, M. N.	EP226, EP762, OP134, OP643	Verdurand, M.	OP058
Van Rheenen, R. W. J.	OP700	Vereb, M.	EP062
Van Rijk, M. C.	EP115	Verger, A.	OP201 , OP563
Van Veenendaal, L. M.	EP136	Verhagen, A. F. T. M.	OP079
Van Velthoven, R.	OP456	Verheij, M.	OP296
Van Weehaeghe, D.	OP069, OP430	Verheul, H.	OP593
Van Weerden, W. M.	OP351	Verhoog, S.	EPW87
Van Willigen, D. M.	EP665, OP639	Verkaik, N. S.	EP667
Van Zon-Meijer, T. W. H.	OP079	Verleden, S.	PW40
Vaqas, B.	OP652	Verma, A.	EP771
Varasteh, Z.	OP423	Vermeulen, S.	OP142
Vardareli, E.	EP111, EP112	Vernooij, M. W.	OP342
Vardon, A.	EPW80	Veronesi, G.	EP157, EP199, EP306
Varejka, P.	P134	Veronesi, P.	EPW06
Varela, A.	EP291	Veronique, E.	EP176
Varelogianni, G.	OP562	Verri, E.	OP332
Varga, J.	EP597, EP603, EP834, EP838, P191	Versari, A.	EP041, EPW46, EPW92, OP598

Verschuer, J.	EP825	Vitalkar, S. D.	OP411
Verschure, D. O.	OP217, OP282 , OP283	Vitor, T.	OP274, TP044
Vershina, E. O.	P211	Vitton, V.	EP624
Verstraete, M.	OP356, P106	Vittorio, O.	EP673
Ververs, F. F. T.	EP550, TP108	Vivas, D.	OP698
Verzijlbergen, J. F.	OP107, OP351, P156	Vivian, G.	EP416, EP726, OP279, OP676, P121, TP002
Vesnina, Z. V.	P211	Vlachou, F.	EP008, EP437
Viale, P.	P146	Vlajkovic, M.	EP361
Viana, P.	EP205, EP267	Vlček, P.	EP384
Vicedo Gonzalez, A.	OP278	Vlemmings, W. E.	OP139
Vicennati, V.	EP304	Vlerick, L.	P224
Vicente, A.	EP267, P189	Vodovar, D.	OP618
Vichi, S.	EP487 , EP488	Voets, E.	OP276
Vickers, R.	P261	Vogel, M.	OP678
Victor, M. R.	OP371 , P105 , P194	Vogel, W.	EP478
Vida, A.	EP596, EP597	Vogg, A. T.	EP640 , OP546
Vidal, B.	EP286, OP063 , OP616	Vogiatzis, M.	P113
Vidal, V.	P115	Vogt, F.	OP422
Videla, S.	OP379	Voisin, T.	P285
Vidioukov, V.	EP367	Vollmar, B.	OP118
Viedma, N.	EP631	Volterrani, D.	EP114, EP128, EP560, EPW20, P117, P259
Vieira, I.	P180	Vomacka, L.	EP484, OP111 , OP650
Vieira, L.	TP017, TP018, TP041	Von der Thüsen, J. H.	EP667
Vieira, T.	EP002, P222, TP068	Von Guggenberg, E.	OP345, OP457
Viernstein, H.	EP636	Vöö, S.	EP055 , OP276, OP416
Vigil Díaz, C.	EP243, P043	Voros, D.	EP423
Vigna, L. L.	EP086	Vosoughi, N.	EP660, EPW33
Vignani, F.	EP507	Vouche, M.	EP465
Vigne, J.	OP170 , OP423, OP559	Vouillarmet, J.	OP699
Vija, A. H.	OP515	Voulaz, E.	EP157, EP306
Vija, L. M.	EP389	Vrachimis, A.	OP224
Vilacosta, I.	OP698, PW21	Vraggalas, V.	PW10
Vilahomat, O.	EP016, EP185, EP394	Vraka, C.	EP636, EPW11, OP115
Vilaplana, E.	OP379, PW35	Vriend, C.	P277
Vilches-Moure, J. G.	OP503	Vriens, D.	OP079
Vilgrain, V.	EPW55	Vrigneaud, J. M.	EP408, EP664, EP666, EP812, OP246, OP250 , OP287, OP298, OP300 ,
Viljanen, T.	TP107		OP353, OP588
Villa, E.	OP355	Vu, D.	EP698
Villa, G.	OP127, P042	Vugts, D. J.	OP587 , OP593
Villa, N. E.	EP535	Vultaggio, V.	OP607
Villaescusa, J.	EP496	Vural, G. U.	EP281
Villalba, A.	EP291	Vyrenkova, N.	EP367
Villalobos, A.	OP061, OP303, OP310		
Villani, M. F.	EP371	Wacker, A.	EPW84
Villani, V.	OP653	Wada, K.	EP641
Villanueva Curto, J.	P093	Wadsak, W.	EP134, EP163, EP233, EP615, EP623, EP636, EPW11, OP115, OP286, OP403, OP405, OP551, OP648, OP649
Villar, M.	EP117, EP613 , P111		
Villemagne, V. L.	PW36	Wagatsuma, K.	EP830
Villen Trinidad, P.	TP076, TP079, TP087	Wagener, A.	EP643, OP487
Villien, M.	OP616	Wagner, J.	OP274, TP044
Villoria, G.	EP184, EP202 , OP180, P016	Wagner, K.	OP596
Vilstrup, M. H.	EP720, OP242	Wagner, K.-H.	OP115
Vimont, D.	P238	Wain-Hobson, J.	OP558, OP559
Vines, D. C.	OP275	Waitz, D.	OP294
Vinjamuri, S.	P110	Wakabayashi, G.	EP490
Vinsensia, M.	EP557	Wakizaka, H.	PW31
Violet, J. A.	EP486	Walczak, R.	OP445, OP675
Virgolini, I.	EP139, EP217, EP277, EP479, OP294, OP457, P108	Waldman, A. D.	OP652
Vischioni, B.	EP121	Walgreen, B.	OP306
Visser, E. P.	EP430 , EP751 , EP803, EP806, OP079, OP297	Walker, M. D.	EP457 , EP739
Visser, M. G. W.	OP276	Walker, P.	OP250, OP287, OP353, OP588
Visvikis, D.	OP079	Wall, A.	OP065
Vitagliano, O.	EP180, EP186	Wall, J. S.	EPW59
Vitali, S.	EP460	Wallitt, K.	EP691 , OP260, OP569, P251

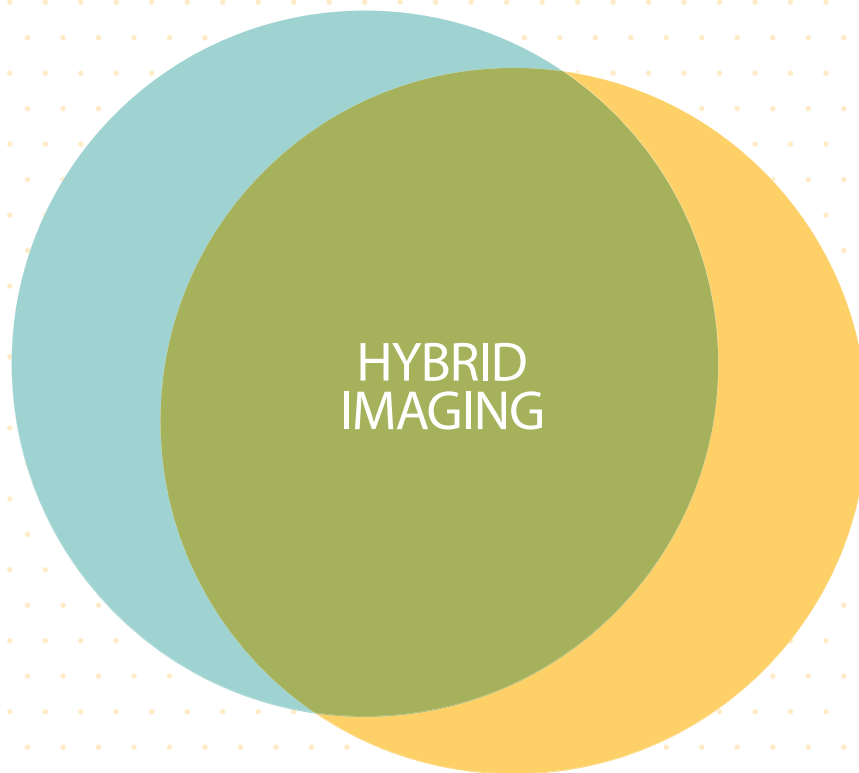
Wallner, B.	EP134	Weyer, V.	EP009
Wallwiener, D.	OP130	Wichert-Ana, L.	P279
Walter, M. A.	EP678	Wichmann, G.	OP179
Wampl, S.	EP727	Wieggers, J.	TP016
Wan, L.	TP012, TP039	Wieler, M.	OP519
Wanek, T.	OP315	Wierls, R.	OP416
Wang, B.	EP059	Wierzchoslawska, E.	TP032
Wang, C.	P192	Wiesinger, F.	OP252
Wang, F.	EP347	Wiessalla, S.	EP453 , EPW16, OP112
Wang, H.-P.	TP042	Wietske, W.	EP430
Wang, J.	EP347	Wijnhoven, B. P. L.	OP078
Wang, L.	EPW79, TP054	Wikström, G.	OP190
Wang, M.-H.	EP584	Wild, D.	EP430, EPW85, OP083, OP149, OP289
Wang, R.	EP589, EP622, EP845, OP121, P145	Wild, M.	EP483
Wang, X.	EP177, EP360, OP685	Wildberger, J.	EP055
Wang, Y.	OP117	Wilhelm, D.	OP649
Wang, Y.	TP019, TP077	Wilke, F.	OP202, OP319
Wang, Y. F.	EP410, EP764	Wilking, H.	EP582, OP190
Wang, Z.	EP590	Willekens, S. M. A.	EP756, OP175, OP257, OP430
Wang, Z.	EP347	Willems, S. M.	EP550
Wängberg, B.	OP522	Willemsen, A.	OP066, P233, TP016
Wängler, B.	EP658, EP783, EP784	Williams, A.	EPW59
Ward, J.	EP723	Williams, C.	EPW94, OP021, OP024, OP025
Ward, P.	OP352	Williams, M.	EP610, EP669
Warren, D.	OP024	Willmann, J. K.	OP503
Warwick, J.	OP037, OP039, OP614	Willoch, F.	OP352
Warwitz, B.	EP217, OP294	Wilson, W. H.	OP687
Wasmer, K.	PW30	Wimana, Z.	OP393, OP456
Watabe, T.	EPW60	Wimberley, C.	OP318
Watanabe, K.	EP323	Win, Z.	OP260, OP277, P251
Watanabe, M.	P036	Wind, P.	EP080
Watanabe, S.	EP007	Winz, O.	OP422
Watanabe, S.	OP029 , OP177	Wirth, A.	EP771
Watkins, R. D.	EP576	Wirth, M.	EP261, OP074
Weber, M.	OP649	Witjes, W.	EP261
Weber, S.	OP032	Witkowska-Patena, E.	EP439, P076
Weber, W. A.	EP164, OP244	Witoszynskij, S.	OP253
Weckesser, M.	OP224	Wittneben, A.	EP639
Wedel, F.	EP481	Wnuk, J.	P085
Weeks, A.	EP598, EP668	Wo, J. M.	P119, P122
Weel, N.	TP092	Włodarczyk, M. M.	OP464
Weerasekera, A.	OP615	Wodynski, A.	EP523
Wegdram-Blans, M.	PW07	Wöhler, A.	OP649
Wegen, S.	EPW14	Wolf, Z.	EP438
Wei, L.	PW04	Wolin, E.	OP394
Wei, Z. J.	EP410, EP764	Wollenweber, S.	EP786
Weich, A.	OP290	Wollmer, P.	EP261
Weichert, W.	OP346, OP566	Won, K.	OP196
Weijjs, W. L. J.	EP115	Won, W.	TP058
Weiler-Sagie, M.	OP363	Wondergem, M.	EP558 , P154, TP051
Weiner, A.	EP132	Woo, S.-K.	EP476
Weissinger, M.	OP135	Woodward, J. D.	OP674
Welling, M. M.	EP762, OP639	Woolum, K.	EP526, EP610
Wells, L.	EP828, OP060	Wozniak, O.	P085
Wen, L.	EP825, EPW78	Wright, C. L.	EP130, EP204, EP307, EP320,
Wendler, T.	EP226, OP134		EPW32, OP017 , OP067,
Weng, S.-J.	PW34		OP184, OP521 , P148
Wenning, C.	OP224, OP695, PW30	Wright, L.	EP723
Wenzel-Duszynska, I.	EP165	Wu, A. M.	EP616
Werner, R. A.	EPW50, OP290	Wu, C.-H.	P101
Wester, H.-J.	EP831, OP059, OP074, OP118, OP239,	Wu, H.	OP669
	OP290, OP309, OP343, OP346, OP566	Wu, H.-M.	EPW57
Westerlund, K.	EPW81, OP589	Wu, M.-H.	P096
Westermark, A.	EP586	Wu, Y.	OP586
Wetter, A.	EP242, EP572, OP502, OP505	Wu, Y.-W.	TP042
Wever, P.	PW07	Wurzer, A.	OP309

Wüstemann, T.	OP024, OP025	Yeyin, N.	EP245, OP679
Wuthrick, E.	OP017	Yi, C.-Y.	EP433
Wyffels, L.	EPW58	Yigit, E.	P082
Wyszomirska, A.	EP758	Yigit, Z.	P082
		Yilmaz, B.	EP729
Xavier, A.	EP246	Yilmaz, E.	EP694
Xia, Q.	OP231	Ying, Z.	OP685
Xie, Q.	TP012, TP039	Yildirim, N.	EP079
Xiong, G.	OP314	Yilmaz, U.	EP159
Xourgia, X.	P030	Yilmaz Aksoy, S.	EP079
Xu, X.	EP059, EP589, EP622, EP845, OP121	Yilmaztepe, M.	P082
Xu, Y.	EPW79, TP054	Yokoyama, K.	P281
		Yokoyama, T.	P293
Yada, N.	EP744	Yonem, A.	EP354
Yadav, M. P.	EP211	Yoneyama, H.	TP047
Yadav, N. K.	EP368	Yoneyama, T.	P293
Yaddanapudi, K.	EP063	Yoo, J.	EP046 , EP606, EP646
Yakushev, I.	OP147	Yoo, M.	OP571
Yalcin, H.	OP611	Yoon, C.	TP053
Yalçin, F.	OP611	Yoon, H.	P147
Yalcindag, A.	P112	Yoon, H.-J.	EP046
Yamada, M.	EP715, P248	Yoon, J.-K.	EP141 , EP143
Yamada, T.	OP284	Yoon, S.-N.	EP106 , EP110
Yamaguchi, H.	TP010	Yordanova, A.	EP498 , EPW12, EPW14
Yamaki, T.	P266	Yordanova, C.	EP196
Yamamoto, H.	EP030, EP641 , OP256, P235, P236	Yordanova, T.	EP118 , EP126
Yamamoto, S.	EPW03	Yoshikawa, A.	EPW03
Yamamoto, T.	OP213, P282	Yoshikawa, K.	EP151
Yamamoto, Y.	EP026, EP030 , EP641, OP256, P235, P236	Yoshimura, M.	P036
Yamanishi, H.	EP490	Yoshino, K.	EPW67
Yaman Sezer, E.	EP541, EP694	Yoshita, M.	P248
Yamasaki, T.	PW31	Yoshiyama, T.	EP683
Yamashina, A.	P036, P048	You, Q.	OP230
Yamashita, Y.	TP020, TP066	You, Y.	TP058
Yamauchi, H.	P292	Young, J.	EP598, OP400
Yamazaki, M.	P231	Young, J. M.	OP310
Yan, J.	EPW79, TP054	Young, K.	EP649
Yanagida, S.	EP802	Young-Mylvaganan, T.	OP483 , OP484
Yanai, A.	EPW03	Younis, A.	OP089
Yang, C.-T.	EP590	Yu, H.-W.	EP584
Yang, D.	OP304, OP669	Yu, J.	OP427
Yang, H.	EP591, OP117	Yu, K.-H.	EP600, EP633
Yang, M.	EPW79 , OP228, TP054	Yuan, H.	EP059
Yang, R.	EPW79, TP054	Yücel, B.	EP162
Yang, S.	EP600, EP633, EP849	Yudistiro, R.	EP316
Yang, S.-W.	EPW26	Yue, F.	OP230
Yang, W.-S.	P096	Yui, J.	PW31
Yang, Y.	OP308	Yuksel, D.	P141, PW28
Yang, Z.	EP059 , EP177, EPW73 , OP685	Yumusak, N.	EP446
Yanik, G.	OP085	Yürekli, Y.	EP119
Yano, F.	EPW03	Yusuf, S.	EP691, OP569
Yao, W.-J.	P101	Yusufoglu, B.	EP540
Yao, X.	EP347		
Yap, J.	EP133, OP036	Zaabar, L.	EP039, EP705, P157, P190, P215
Yaqub, M.	P237	Zacharovska, M.	EP062
Yasar, A.	EP190	Zacherl, M.	OP032
Yassin, H. M.	TP007	Zacho, H. D.	EP257, OP108, OP350, OP358 , OP557
Yavascaoglu, I.	EPW23	Zade, A. A.	EP566
Yaylali, O.	P141, PW28	Zagatti, M.	EP205
Yaylali, Y. T.	PW28	Zaghloul, M. S.	OP089
Yazici, B.	EP378, P207	Zagni, F.	EP487, EP488
Yeddes, I.	EP358 , EP393, P166	Zaharchuk, G.	EP020, EP574
Yen, R.-F.	P096 , P109, PW34, TP042	Zakhs, D.	EP019
Yen, T.-C.	EP038, OP491	Zakir Ali, A.	EP412
Yeni, N.	P246	Zaletel, K.	P200, P203 , PW06
Yepes Agudelo, A. M.	EP512	Zalutsky, M. R.	OP594

Zaman, A.	EP357, EP373, P077	Zhi, Y.	EP360
Zaman, M. U.	EP357, EP373 , EP442, P077	Zhou, H.	EP108, EP321
Zaman, U.	EP357, EP373, P077	Zhou, N.	OP685
Zampella, E.	OP460, OP467, OP604, OP607	Zhou, Y.	OP611
Zamyshevkaia, M.	P139, PW08	Zhou, Z.	OP594
Zanca, F.	EP823	Zhu, J.	EP360, OP685
Zanella, A.	P176	Zhuang, X.	OP230
Zanette, C.	EP458, P186	Zia, N.	EP611
Zanette, M.	OP259, OP376	Ziaka, A.	P022
Zangheri, B.	EP041	Ziangas, C.	P022
Zanoni, L.	EP265, EP288, EP304, EPW72, EPW75, P146	Zidan, L.	OP034
Zanotti-Fregonara, P.	EP473, P252	Ziebarth, B.	OP168
Zapendowska, A.	P095	Ziegler, S.	OP566
Zaplatnikov, K.	EP241, EP364, OP412 , P011	Ziel-van der Made, A. C. J.	OP171
Zarei, M.	EP037	Zijlstra, J. M.	OP683
Zasadny, K.	OP310	Zimmer, L.	OP058, OP063, OP616
Zattoni, F.	EP004	Zinzani, P.	EPW72
Zavadovskaia, V.	P139, P208 , PW08	Zinzi, M.	EP238, EP567, OP653, P290
Zavadovskiy, K.	P029, P031 , P046, P066 , P086, P087	Zipper, W.	OP675
Zavatta, G.	EP304	Zischler, J.	EP841
Zavolokov, I.	P226, P291	Zissimopoulos, A. S.	P040, P153, P182
Zeebregts, C. J.	OP610	Zissimopoulou, O.	P040, P153, P182
Zeevaart, J.	EP599, OP673	Zito, F.	OP214, OP495
Zegri, I.	EP684	Zivelonghi, E.	EP402
Zeinyeh, W.	OP058	Zlatopolskiy, B. D.	EP841, OP422
Zelaya Reinquet, F. S.	EP337 , EP342, P162, TP100	Zobbio, G.	TP056, TP067
Zelchan, R.	EP075, EP097, EP632, EP634	Zoccarato, O.	P079
Zellweger, M. J.	OP463	Zocchi, E.	EP662
Zemunik, T.	P201	Zogala, D.	P100, P134
Zeng, W.	EP698 , EP710, EP792, OP168	Zompatori, M.	P146
Zenone, F.	EP819	Zorkaltsev, M.	P139, P208, PW08
Zentai, M.	OP212	Zorz, A.	EP748, EP789
Zeraatkar, N.	EP765, EP768, EPW31	Zouroudi, S.	P028
Zerahn, B.	EP452, OP506, OP512, OP564, P216	Zrinyi, M.	EP639
Zerdoud, S.	EP389, EP419, EP807, OP494	Zsótér, N.	OP109
Zerges, A.-M.	EPW87	Zubiria, A.	EP470
Zgimond, R.	P027	Zucali, P.	EP306
Zhan, Y.	OP638	Zucca, S.	EP400
Zhang, B.	EP832	Zuccarino, F.	OP600
Zhang, C.	EP527, EP591, OP020	Zucchetta, P.	EP789, P176
Zhang, D.	OP133	Zuckier, L.	EP698, EP710, EP792, OP168
Zhang, J.	EP059, EP130 , EP204, EP307, EP551, EP669, EP737, EP753, EPW32, OP017, OP067, OP184, OP295 , OP521, OP687 , P225 OP061 , OP303, OP310, OP316	Zuffante, M.	EP031, EP260, EP390, EP402 , P130, TP028, TP033
Zhang, L.	EP347	Zuhayra, M.	EP003, EP234, EP676, EPW04
Zhang, I.	PW31	Zulfovski, G.	TP106
Zhang, M.-R.	EP659, OP228	Zulueta-Dorado, T.	EP200
Zhang, Y.	EP059, EPW73, OP486	Zuo, C.	OP199
Zhang, Y.	EP177, EP360, OP685	Zurita Herrera, M.	EP028
Zhang Yin, J.	EP263	Zverev, A.	EP654
Zhao, Y.	EP003, EP234, EP676 , EPW04	Zwaagstra, O.	OP448
Zheng, X.	OP024	Zwarthoed, C.	EP447 , OP203, OP429
		Zwergal, A.	OP314
		Zyuzin, A.	OP446

ESMIT

European School of Multimodality Imaging and Therapy



The ESMIT initiative represents ESNM's response to huge changes in the educational needs of the nuclear medicine community and the rising demand for greater multimodality content.

The EANM/ESNM decided to review and modernise its educational system, since the community needs not only to be educated on all modalities that are used in imaging, but also to be well prepared in the therapeutic applications of our discipline.

www.eanm.org



Each level will be led by the mentioned chairs and working groups consisting of specialists from different backgrounds, including radiologists, clinicians and scientists.

EANM'17

WORLD LEADING MEETING



Annual Congress of the European Association of Nuclear Medicine

October 21 – 25, 2017
Vienna, Austria

www.eanm.org

 Visit us on
[.com/officialEANM](https://www.facebook.com/officialEANM)